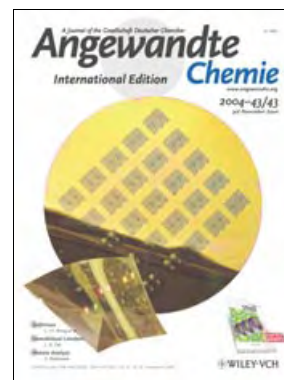


Cover Picture

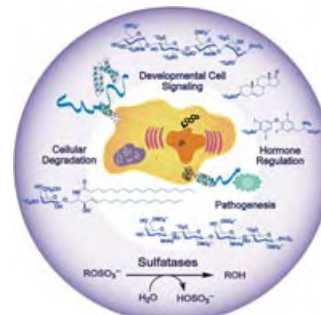
Jason P. Rolland, Erik C. Hagberg, Ginger M. Denison, Kenneth R. Carter,* and Joseph M. De Simone*

High-performance imprint lithographic applications are ideally suited for perfluoropolyether-based elastomers. The cover picture shows sub-100-nm sized features replicated by these materials whose successful application comes from their remarkably low surface energy and their high flexibility. The performance of the materials suggests that replication at even smaller sizes may be possible. For more information, see the Communication by J. M. De Simone, K. R. Carter, and co-workers on page 5796 ff.



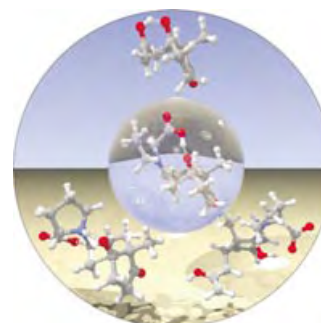
Enzyme Chemistry

The enzymatic cleavage of sulfate esters is the crucial process in the regulation of sulfation patterns. The current state of research is summarized by C.-H. Wong and co-workers in their Review on page 5736 ff.



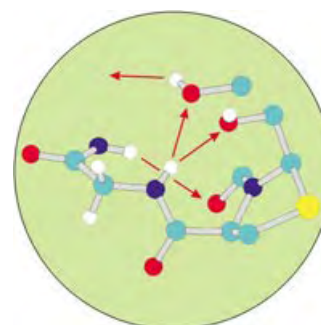
Reaction Mechanisms

The mechanism of the Hajos–Parrish–Eder–Sauer–Wiechert reaction, the prototype for asymmetric organocatalytic reactions, is discussed by K. N. Houk and F. R. Clemente in their Communication on page 5766 ff.



Peptide Mimetics

In their Communication on page 5789 ff., A. Geyer and P. Tremmel describe how highly functionalized bicyclic dipeptide analogues in oligopeptide mimetics form an ordered network of hydrogen bonds.



Angewandte EarlyView®

The following Communications are available online (in Wiley InterScience). You can find them, as well as forthcoming Reviews, Highlights, and Essays, at www.angewandte.org, under Early View.

T. J. Lowery, S. M. Rubin, E. J. Ruiz, A. Pines, D. E. Wemmer*:
Design of a Conformation-Sensitive Xenon-Binding Cavity in the Ribose-Binding Protein
 DOI: 10.1002/anie.200460629
 Published online: October 11, 2004

A. Tsuda,* E. Hirahara, Y.-S. Kim, H. Tanaka, T. Kawai,* T. Aida*:
A Molybdenum Crown Cluster Forms Discrete Inorganic–Organic Nanocomposites with Metalloporphyrins
 DOI: 10.1002/anie.200460990
 Published online: September 23, 2004

Articles judged by the referees or the editor as being either very important or very urgent are immediately edited, proof-read, and electronically published once the manuscript has arrived in the editorial office in its final form. As long as there is no page number available these articles should be cited in the following manner:

Author(s), *Angew. Chem. Int. Ed.*, online publication date, DOI.

News

Nobel Prizes 2004: Protein degradation, Olfactory system, Strong interaction _____ 5722

Books

The Chemistry of Nanomaterials	C. N. R. Rao, Achim Müller, Anthony K. Cheetham	<i>reviewed by U. Simon</i> _____	5723
Nanotechnology	Michael Köhler, Wolfgang Fritzsche	<i>reviewed by M. R. Bockstaller</i> _____	5723
Life, Death, and Nitric Oxide	Anthony Butler, Rosslyn Nicholson	<i>reviewed by B. Mayer</i> _____	5724

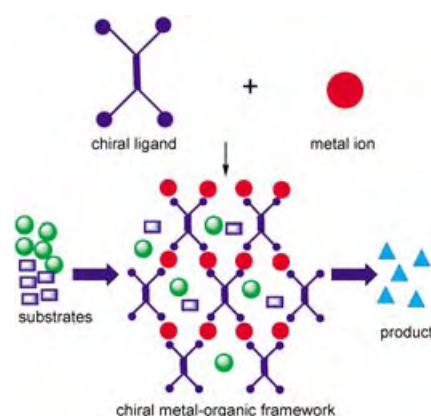
Highlights

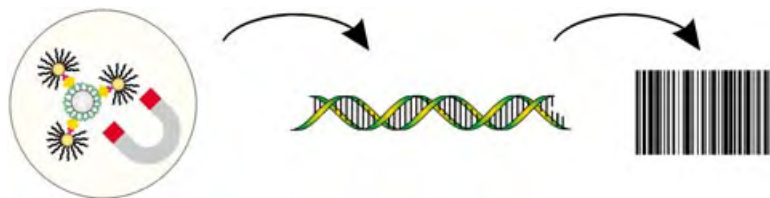
Immobilized Catalysts

L.-X. Dai* _____ 5726 – 5729

Chiral Metal–Organic Assemblies—A New Approach to Immobilizing Homogeneous Asymmetric Catalysts

Beyond classical immobilized catalysts, metal–ligand polymers self-assembled through coordination are easily prepared, have a robust chiral structure, and display a high density of catalytically active units. These heterogeneous catalysts give excellent results for enantioselective reactions and can be recovered and recycled without significant loss of selectivity.





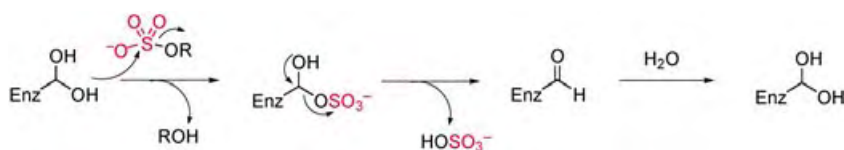
Beyond the shadow of a doubt: Detecting antigens, antibodies, pathogens, tumor markers, and potential therapeutics on the femto- to attomolar concentration level is still challenging. Nanostructured

materials and the innovative combination of immunoassays with (real-time) PCR and magnetic separation techniques hold promise for the field of ultrasensitive protein analytics.

Protein Analysis

S. Brakmann* _____ 5730–5734

DNA-Based Barcodes, Nanoparticles, and Nanostructures for the Ultrasensitive Detection and Quantification of Proteins



Through the cleavage of sulfate esters sulfatases modulate the activity of a broad range of small molecules and proteoglycans (see picture). These enzymes play critical roles in a number of biological events, including lysosomal degradation,

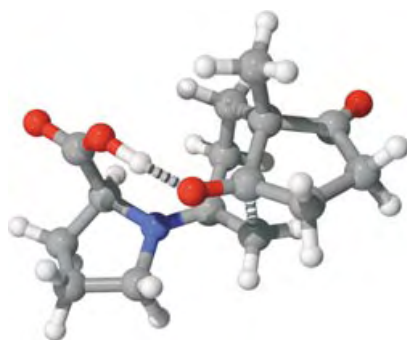
hormone regulation, and signaling processes. The structures of sulfatases, their mechanisms of action, their potential as targets for small-molecule intervention, and applications in synthesis are discussed.

Reviews

Enzyme Chemistry

S. R. Hanson, M. D. Best, C.-H. Wong* _____ 5736–5763

Sulfatases: Structure, Mechanism, Biological Activity, Inhibition, and Synthetic Utility



A comparison of previously proposed models of the C–C bond-forming step of the title reaction with density functional methods indicate that the most favored one involves an enamine intermediate undergoing a concerted aldol cyclization with proton transfer from the proline carboxylic acid group (see structure). This step is equal in energy to the intramolecular deprotonation leading to the enamine, and both are partially rate-determining steps.

Communications

Density Functional Calculations

F. R. Clemente, K. N. Houk* _____ 5766–5768

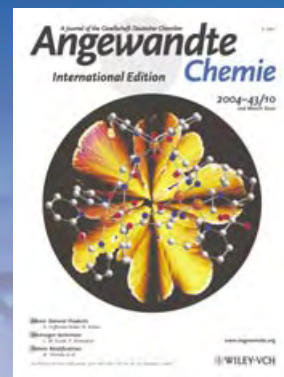
Computational Evidence for the Enamine Mechanism of Intramolecular Aldol Reactions Catalyzed by Proline

For the USA and Canada: ANGEWANDTE CHEMIE International Edition (ISSN 1433-7851) is published weekly by Wiley-VCH PO Box 191161, D 69451 Weinheim, Germany. Air freight and mailing in the USA by Publications Expediting Inc. 200 Meacham Ave., Elmont, NY 11003. Periodicals

postage paid at Jamaica NY 11431. US POSTMASTER: send address changes to *Angewandte Chemie*, Wiley-VCH, 111 River Street, Hoboken, NJ 07030. Annual subscription price for institutions: Europe € 3760.00/3418.00; outside Europe US\$ 4948.00/4498.00 (valid for print and electronic/print or electronic delivery); for

individuals who are personal members of a national chemical society, or whose institution already subscribes, or who are retired or self-employed consultants, print only: Europe € 258.00/outside Europe US\$ 394.00. Postage and handling charges included. All Wiley-VCH prices are exclusive VAT.

The best in chemistry – for more than a hundred years



A Journal of the Gesellschaft Deutscher Chemiker
**Angewandte
Chemie**
International Edition

www.angewandte.org

1888: The beginning
of a success story

Constant Innovations

- 1962:** First issue of the International Edition
- 1976:** Graphical abstracts
- 1979:** Cover pictures
- 1988:** Centenary of Angewandte
- 1989:** Routine use of color
- 1991:** New section: Highlights
- 1992:** Computerized editorial tracking system
- 1995:** Internet service for readers
- 1998:** Regular press service; full-text online
- 2000:** New section: Essays; EarlyView: Communications available online ahead of the printed version
- 2001:** New section: Minireviews
- 2002:** Online submission of manuscripts
- 2003:** Weekly publication; new section: News; new layout
- 2004:** Backfiles (1962-1997); ManuscriptXpress: Online system for authors and referees



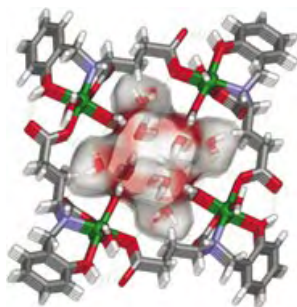
Angewandte's advisors...

Martin Quack
Physical Chemistry,
ETH Zürich

» **Angewandte Chemie** is my favourite journal covering all aspects of chemistry, from theoretical and physical chemistry to inorganic, organic, and biochemistry. It is by far the best journal worldwide for an overview of current research in chemistry as a whole. Beyond just publishing the best research in chemistry, it also helps us to fight the trend of too narrow specialization. «

Angewandte Chemie International Edition is
a journal of the German Chemical Society (GDCh)



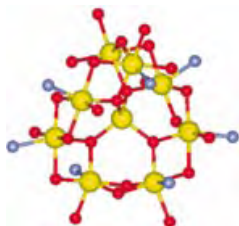


A stream of water molecules, held together by hydrogen bonding, forms a left-handed helix within the helical channels of a left-handed staircaselike metal coordination polymer. The result is a novel helix-in-a-helix structure. The water-filled channel can be seen on viewing the coordination polymer along the *b* axis (see picture; C gray, N blue, Ni green, O red).

Helical Water Chain

B. Sreenivasulu, J. J. Vittal* — **5769–5772**

Helix inside a Helix: Encapsulation of Hydrogen-Bonded Water Molecules in a Staircase Coordination Polymer



Mimicking magnetic minerals: Controlled hydrolysis of iron(III) salts leads to all-ferric molecular fragments with the iron and oxygen topology of magnetite and large spin ground states (see structure; yellow Fe, red O, blue N, gray C).

Magnetic Properties

G. W. Powell, H. N. Lancashire, E. K. Brechin,* D. Collison,* S. L. Heath,* T. Mallah, W. Wernsdorfer — **5772–5775**

Building Molecular Minerals: All Ferric Pieces of Molecular Magnetite

Tetrathiometalates [WS₄]^{2−} are the nodal building blocks in a new kind of heterometallic interpenetrating three-dimensional cluster coordination polymer (see picture) that has interesting nonlinear optical properties. The polymer exhibits optical self-focusing behavior and reverse saturable absorption effects.

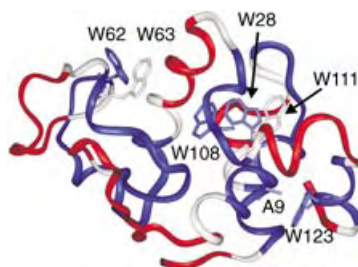


Coordination Polymers

K. Liang, H. Zheng,* Y. Song, M. F. Lappert, Y. Li, X. Xin, Z. Huang, J. Chen, S. Lu — **5776–5779**

Self-Assembly of Interpenetrating Coordination Nets Formed from Interpenetrating Cationic and Anionic Three-Dimensional Diamondoid Cluster Coordination Polymers

The non-native states of the model protein hen lysozyme (native state shown in picture) were investigated by using site-directed mutagenesis in combination with high-resolution NMR spectroscopy. The disruptions of the interactions between hydrophobic clusters by single point mutations dramatically alter the overall compactness of the unfolded state: single point mutations can turn a compact unfolded state into an extended state.



Protein Interactions

J. Wirmer, C. Schlörb, J. Klein-Seetharaman, R. Hirano, T. Ueda, T. Imoto, H. Schwalbe* — **5780–5785**

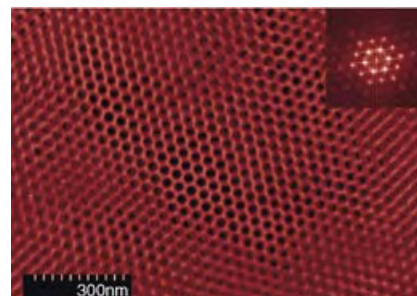
Modulation of Compactness and Long-Range Interactions of Unfolded Lysozyme by Single Point Mutations

Nanoporous Films

C. Liang, K. Hong, G. A. Guiochon,
J. W. Mays, S. Dai* — 5785 – 5789

Synthesis of a Large-Scale Highly Ordered
Porous Carbon Film by Self-Assembly of
Block Copolymers

Made to order: The synthesis of well-defined porous carbon films involves four steps: 1) monomer–block copolymer film casting, 2) structure refining through solvent annealing, 3) polymerization of the carbon precursor, and 4) carbonization. The resulting films, such as that depicted, have potential as separation membranes, chemical sensors, and catalysts.

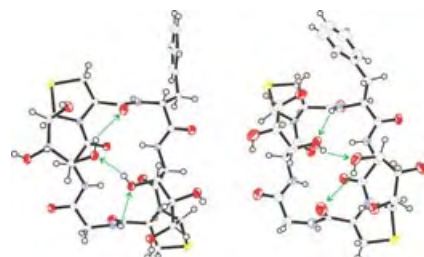


Peptidomimetics

P. Tremmel, A. Geyer* — 5789 – 5791

Coupled Hydrogen-Bonding Networks in
Polyhydroxylated Peptides

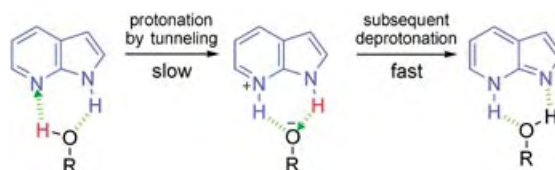
Information transfer: Crystal structures of bicyclic dipeptide analogues within oligopeptides are described for the first time. The bicyclic dipeptides occupy the i to $i + 1$ positions of either β I or β II turns. The rigidified dipeptides form hydrogen-bonding networks which transfer structural information along chains of ambident proton donors and acceptors over several Å (see structures; arrows: hydrogen bonds, red O, blue N, yellow S).



Proton Transfer

O.-H. Kwon, Y.-S. Lee, H. J. Park, Y. Kim,
D.-J. Jang* — 5792 – 5796

Asymmetric Double Proton Transfer of
Excited 1:1 7-Azaindole/Alcohol
Complexes with Anomalously Large and
Temperature-Independent Kinetic
Isotope Effects



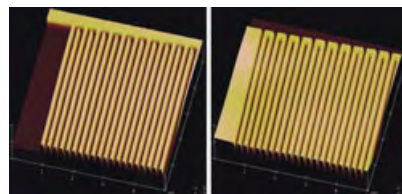
Bridging alcohols, tunneling protons: The intrinsic proton-transfer dynamics of cyclic H-bonded 1:1 7-azaindole/alcohol complexes in n -alkanes has been investigated at the lowest-lying excited singlet state with variation of alcohol, solvent,

isotope, and temperature by using static and time-resolved spectroscopy. The proton transfer occurs asymmetrically, and the rate is governed by tunneling although it is assisted by heavy-atom motions.

Lithography

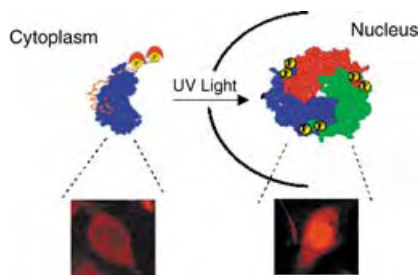
J. P. Rolland, E. C. Hagberg,
G. M. Denison, K. R. Carter,*
J. M. De Simone* — 5796 – 5799

High-Resolution Soft Lithography:
Enabling Materials for
Nanotechnologies



Making a good impression: Photocurable, liquid perfluoropolyethers (PFPEs) are ideal materials for high-resolution (< 100 nm) pattern transfer and imprint lithographic processes (see pictures). PFPEs possess attributes of both elastomers and rigid materials, exhibit a remarkably low surface energy, mold extremely small features with high fidelity, resist swelling by organic solvents, and endure repetitive molding procedures.

Expressed-protein ligation has been used for the semisynthetic preparation of a Smad2 protein with caged activating phosphoserine residues. Biochemical and cell biological experiments show that the caged protein is activated upon irradiation with UV light (see scheme). This sets the stage for the detailed kinetic analysis of Smad2 function in living cells.

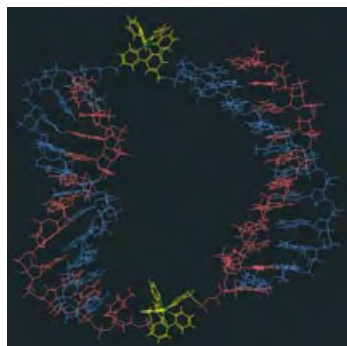


Bioorganic Chemistry

M. E. Hahn, T. W. Muir* — 5800–5803

Photocontrol of Smad2, a Multiphosphorylated Cell-Signaling Protein, through Caging of Activating Phosphoserines

A discrete cyclic nanostructure was obtained through the self-assembly of oligonucleotide-branched metal complexes. The picture shows the metal–DNA nanostructure, which contains two DNA double-helical arms and two relatively rigid redox- and photoactive $[\text{Ru}(\text{bpy})_3]^{2+}$ vertices.

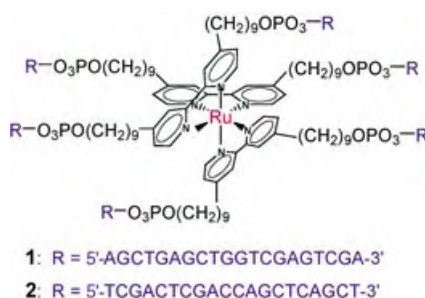


DNA Superstructures

D. Mitra, N. Di Cesare,
H. F. Sleiman* — 5804–5808

Self-Assembly of Cyclic Metal–DNA Nanostructures using Ruthenium Tris(bipyridine)-Branched Oligonucleotides

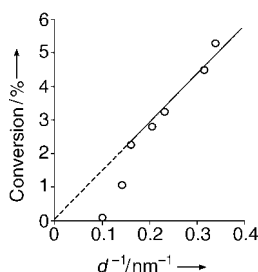
The 3D starshaped Ru–bpy–DNA complex pictured comprises a ruthenium(II) tris(bipyridyl) center with six DNA 20-mer sequences tethered through linkers at its 4- and 4'-positions. The complexes **1** and **2** hybridize with six complementary 20-mer strands to form duplex arms. Alternatively, the complementary DNA strands in **1** and **2** hybridize with each other to form larger nanoscale assemblies.



DNA Superstructures

K. M. Stewart, J. Rojo,
L. W. McLaughlin* — 5808–5811

Ru(II) Tris(bipyridyl) Complexes with Six Oligonucleotide Arms as Precursors for the Generation of Supramolecular Assemblies



Reducing size helps to oxidize: Unsupported gold particles behave as an efficient catalyst for the aerobic oxidation of glucose, showing a similar activity to enzymatic systems. The catalytic activity is inversely proportional to the particle diameter (d , see graph). With carbon-supported gold, no gold–support interaction is found; however, the use of a support avoids particle aggregation thus preserving the original activity for longer.

Heterogeneous Catalysis

M. Comotti, C. Della Pina, R. Matarrese,
M. Rossi* — 5812–5815

The Catalytic Activity of “Naked” Gold Particles

Host–Guest Systems

P. de Hoog, P. Gamez,* I. Mutikainen,
U. Turpeinen, J. Reedijk* — 5815–5817

An Aromatic Anion Receptor:
Anion– π Interactions do Exist

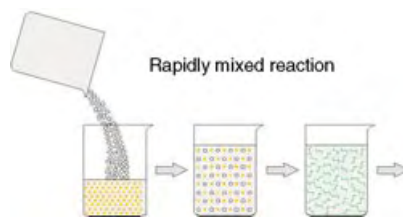


A particularly challenging task is the design of anion receptors, because anions are larger than cations and are pH- and solvent-sensitive. The first host for anionic guests is a dendritic octadentate N ligand, which upon reaction with CuCl_2 , encapsulates chloride ions (Cl_6 , see picture) as guests by means of anion– π interactions in an electron-deficient cavity formed by four pyridine rings.

Nanostructures

J. Huang, R. B. Kaner* — 5817–5821

Nanofiber Formation in the Chemical
Polymerization of Aniline: A Mechanistic
Study

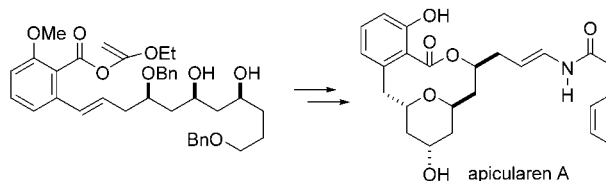


Stirring stuff: The morphological evolution of polyaniline from nanofibers to agglomerates during its chemical polymerization shows that the key to producing pure nanofibers is to suppress secondary growth after formation of the nanofibers. A simple and effective method for the synthesis of nanofibers was thus developed in which the polymerization is carried out in a rapidly mixed single-phase reaction (see scheme).

Natural Products Synthesis

A. F. Petri, A. Bayer,
M. E. Maier* — 5821–5823

Total Synthesis of Apicularen A through
Transannular Pyran Formation



A macrocyclization–transannulation strategy is the crux of an efficient total synthesis of the benzolactone enamide apicularen A (see scheme; Bn = benzyl). Key steps include a four-component coupling, a Stille cross-coupling to introduce

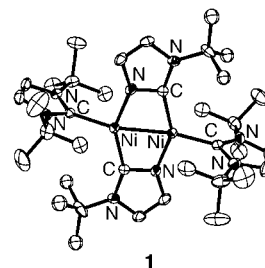
the aromatic moiety, and the formation of the enamide from a hemiaminal. The size-selective macrolactonization of the ethoxyvinyl ester shown was followed by transannular etherification in excellent yield.

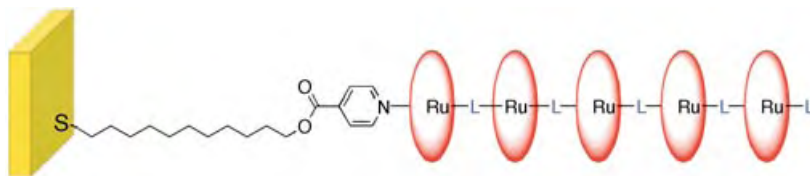
C–N Activation

S. Caddick,* F. G. N. Cloke,*
P. B. Hitchcock,
A. K. de K. Lewis — 5824–5827

Unusual Reactivity of a Nickel N-Heterocyclic
Carbene Complex: *tert*-Butyl Group
Cleavage and Silicone Grease Activation

Reaction lubrication? The reaction between $[\text{Ni}(1,5\text{-cod})_2]$ (cod = cyclooctadiene) and 1,3-bis-*tert*-butylimidazol-2-ylidene in the presence of silicone grease affords the siloxane bridged dimer $[\{\text{Ni}[\text{C}(\text{N}t\text{BuCH})_2][\text{O}(\text{Me}_2\text{SiOSiMe}_2)\text{-}\mu\text{-O}]\}_2]$. In a greaseless apparatus, the same reaction yields the dimer **1** (see structure), via two structurally characterized intermediates.





The modular assembly of metalloporphyrin oligomers through the stepwise addition of Ru–porphyrin units and a bidentate linking ligand (L, see graphic) onto a surface-confined isonicotinate

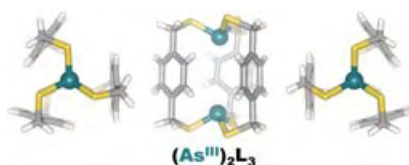
ligand is reported. Electrochemical measurements of the resulting oligomer show that electrons are transported along the length of its backbone.

Multilayer Assemblies

H. Van Ryswyk,* E. E. Moore, N. S. Joshi, R. J. Zeni, T. A. Eberspacher, J. P. Collman* — 5827 – 5830

Surface-Confined Metalloporphyrin Oligomers

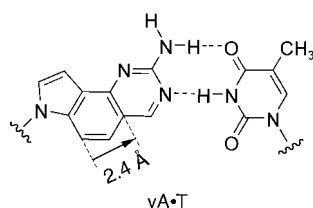
An As_2L_3 metallocryptand is the result of a new predictive design strategy for forming self-assembled supramolecular arsenic complexes. The assembly is remarkably stable to a variety of competing metal ions, harsh acid, and excess ligand. X-ray crystallographic studies and density functional calculations suggest that a strong arsenic– π interaction adds stability to the structure.



Metallocryptands

W. J. Vickaryous, R. Herges, D. W. Johnson* — 5831 – 5833

Arsenic– π Interactions Stabilize a Self-Assembled As_2L_3 Supramolecular Complex

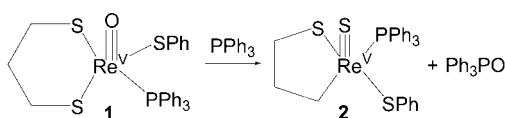


Room for expansion: Insertion of a benzene ring into the natural adenine heterocycle to generate the analogue yA results in the formation of base pairs that are 2.4 Å wider than natural ones (see structure). Melting temperature and free energy data show that yA•T and T•yA pairs can self-assemble into cooperative helices that are considerably more stable than natural DNA. Thus, yDNA may be a candidate for a new genetic system.

DNA Structures

H. Lu, K. He, E. T. Kool* — 5834 – 5836

yDNA: A New Geometry for Size-Expanded Base Pairs



Rhenium reactions: A reaction under mild conditions between oxo(dithiolato)rhenium(v) complex **1** and triphenylphosphine gives **2**. In the reaction a $\text{Re}\equiv\text{O}$ bond is cleaved, $\text{P}=\text{O}$ and $\text{Re}\equiv\text{S}$ bonds are

formed at the expense of a $\text{CH}_2\text{S}-\text{Re}$ bond, and a new $\text{Re}-\text{C}$ bond is formed converting a six-membered chelate ring into a five-membered one.

C–S Bond Cleavage

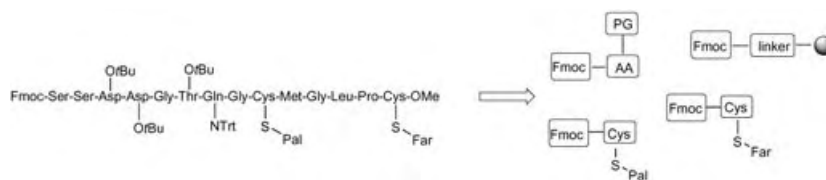
M. Li, A. Ellern, J. H. Espenson* — 5837 – 5839

Phosphine-Promoted Conversion of Oxo(dithiolato)rhenium(v) into Thio(thiolatoalkyl)rhenium(v) Compounds

Protein Synthesis

G. Kragol, M. Lumbierres, J. M. Palomo,
H. Waldmann* ————— 5839 – 5842

Solid-Phase Synthesis of
Lipidated Peptides



Blockers, anchors, and reporters: A solid-phase method for the synthesis of lipidated peptides (see scheme) relies on the base-labile Fmoc group to block the N-terminus, an oxidation-labile hydrazide

linker for anchoring to the solid support, and lipidated amino acid building blocks incorporating labels or photoactivatable groups.

Polymers

M. Ballauff,* L. Li, S. Rosenfeldt,
N. Dingenouts, J. Beck,*
P. Krieger-Beck ————— 5843 – 5846

Analysis of Poly(carbon suboxide) by
Small-Angle X-ray Scattering

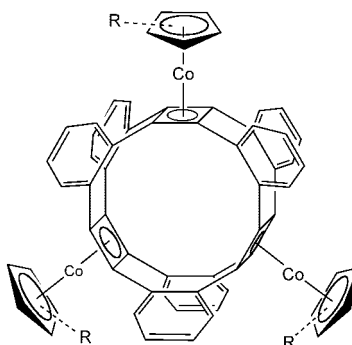
Band substances: The polymerization of C_3O_2 (see picture left, at $-10^\circ C$) into a red-brown, solid polymer (right) having identical composition has been known for almost 100 years. However, the constitution of the polymer remained unknown. Small-angle X-ray scattering studies of the dissolved polymer show that it forms a stiff bandlike molecule with approximately 40 monomeric units, thus confirming the predicted α -pyrone rings.



Cyclophanes

B. Hellbach, F. Rominger,
R. Gleiter* ————— 5846 – 5849

Synthesis of Beltenes by Reactions of
5,6,11,12-Tetrahydridibenzo[*a,e*]cyclooctene with $[CpCo(CO)_2]$ Derivatives

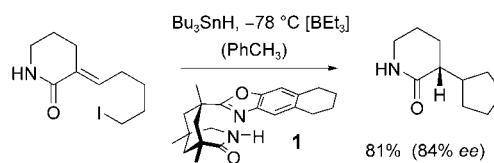


Cobalt studs the beltenes shown ($R = H, CO_2Me, SiMe_3, 5 Me$), which consist of annelated, conjugated four- and eight-membered rings. These strained molecules were synthesized in a one-pot reaction by a template supported trimerization of 5,6,11,12-tetrahydridibenzo[*a,e*]cyclooctene.

Asymmetric Synthesis

T. Aechtner, M. Dressel,
T. Bach* ————— 5849 – 5851

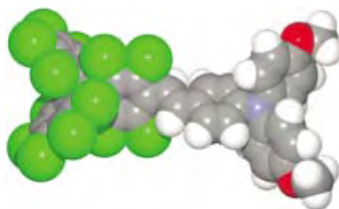
Hydrogen Bond Mediated Enantioselectivity of Radical Reactions



The chiral complexing reagent 1 used in the reductive cyclization of 3-(ω -iodoalkylidene)piperidin-2-ones in the presence of Bu_3SnH and with BEt_3 as the initiator (see scheme) leads to good enantioselectivities thanks to its hydrogen

bond mediated association with the radical intermediate. As this example shows, high stereoselectivities are possible for radical reactions proceeding through H-bonded intermediates.

Maintaining neutrality: A perchlorinated triarylmethyl radical and a triarylamine redox center were combined in the design of a neutral organic mixed-valence compound (see picture). The neutral character of this compound facilitated a detailed study of its solvatochromic behavior and the direct determination of the electronic coupling and the dipole moments in the ground and excited state by electroptical absorption measurements.



Electron Transfer

A. Heckmann, C. Lambert,* M. Goebel,
R. Wortmann _____ **5851–5856**

Synthesis and Photophysics of a Neutral
Organic Mixed-Valence Compound



Communications labeled with this symbol have been judged by two referees as being “very important papers”.

Looking for outstanding employees?

Do you need another expert for your excellent team?

...Chemists, PhD Students, Managers, Professors, Sales Representatives...

Place an advert in the printed version and have it made available online for 1 month, free of charge!

Angewandte Chemie International Edition

Advertising Sales Department: Marion Schulz

Phone: 0 62 01 - 60 65 65

Fax: 0 62 01 - 60 65 50

E-Mail: MSchulz@wiley-vch.de

Service

Keywords _____ **5858**

Authors _____ **5859**

Preview _____ **5861**

Apology

Nanofibers from Functionalized Dendritic
Molecules**

M. Ornatka, K. N. Bergman, B. Rybak,
S. Peleshanko, V. V. Tsukruk* **5246–5249**

Angew. Chem. Int. Ed. **2004**, 43

DOI 10.1002/anie.200460315

This Communication contains content that overlaps significantly with a Full Paper by the same group “Assembling of Amphiphilic Highly Branched Molecules in Supramolecular Nanofibers” *J. Am. Chem. Soc.* **2004**, 126, 9675–9684. Although submitted at the same time the authors did not provide the Editors of *Angewandte Chemie* with a copy of the Full Paper. This oversight resulted in the simultaneous appearance of the same information in two publications. The authors apologize for this mistake.



Nobel Prize in Chemistry 2004

The Nobel Prize in Chemistry is awarded to Aaron J. Ciechanover (Technion, Haifa, Israel), Avram Hershko (Technion, Haifa, Israel), and Irwin A. Rose (University of California, Irvine, USA) for the discovery of ubiquitin-mediated protein degradation. Ciechanover, Hershko, and Rose



A. Hershko and A. J. Ciechanover (right)

have demonstrated that the cell functions as a highly efficient checking station where proteins are built up and broken down at a very high rate. Far less research has been done on protein degradation than on protein synthesis. The degradation is not indiscriminate but takes place through a process that is controlled in detail so that the proteins to be broken down at any given moment are given a



I. A. Rose

molecular label: ubiquitin, a protein which consists of 76 amino acid residues. This unit fastens to the protein to be destroyed, accompanies it to the proteasome where it is recognized as the key in a lock, and signals that a protein is on the way for disassembly. Shortly before the protein enters the proteasome, its ubiquitin label is disconnected for re-use. Thanks to the work of the three laureates it is now possible to understand at the molecular level how the cell controls a number of central processes by breaking down certain proteins and not others. When the degradation does not work correctly, diseases result, such as certain forms of cancer.^[1]

Ciechanover (b. 1947) obtained an M.Sc. degree (1971) and a doctorate in medicine (M.D., 1974) from Hadassah Medical School in Jerusalem. He obtained a D.Sc. from Technion in

Haifa in 1982 and was appointed professor of biochemistry at its Rappaport Institute for Research in the Medical Sciences, as was Hershko (b. 1937). Hershko obtained M.D. (1965) and Ph.D. (1969) degrees from Hadassah Medical School. Rose (b. 1926) has been an emeritus professor at the Department of Physiology and Biophysics of the University of California in Irvine since 1997, and is a member of the US National Academy of Sciences. A major part of the research was done during a series of sabbatical leaves in the late 1970s and

early 1980s that Hershko and Ciechanover spent as visiting scientists in Rose's laboratory at Fox Chase Cancer Center in Philadelphia, where he was employed from 1963 to 1995. Rose earned a Ph.D. in biochemistry in 1949 from the University of Chicago. Subsequently, he worked as a Post-Doc at Case Western Reserve University in Cleveland and New York University and served on the faculty of the Department of Biochemistry of Yale Medical School from 1954 to 1963. This is the first time a Nobel Prize in science has been awarded to Israelis.

Physiology or Medicine

Richard Axel (Columbia University, New York, USA) and Linda B. Buck (Fred Hutchinson Cancer Research Center, Seattle, WA, USA) were awarded the Nobel Prize in Physiology or Medicine 2004 for their discoveries of odorant receptors and the organization of the olfactory system. They discovered a large gene family, which consists of some 1000 different genes (three per cent of our genes) that give rise to an equivalent number of olfactory receptor types. These receptors are located on the olfactory receptor cells, which occupy a small area in the upper part of the nasal epithelium and detect the inhaled odorant molecules.

Physics

Their research on the very fundamentals of physics has brought this year's Nobel Prize in Physics to David J. Gross (University of California, Santa Barbara, USA), H. David Politzer (California Institute of Technology, USA), and Frank Wilczek (Massachusetts Institute of Technology, USA): The particle physicists are recognized for the discovery of asymptotic freedom in the theory of the strong interaction, which keeps the quarks in neutrons and protons together. In a way that resembles releasing a rubber band, this force weakens when the particles move closer together. Eventually, they behave almost like free particles. This discovery was formulated in an elegant mathematical way in 1973 and led to a completely new theory: quantum chromodynamics.

This year, the Prizes are worth 1.1 million Euros each. They are given traditionally on December 10, the anniversary of Alfred Nobel's death.

Photos: Technion / P. R. Kennedy (UCI)

[1] a) A. Ciechanover, A. L. Schwartz, *Hepatology* **2004**, 35, 3, b) A. Ciechanover, A. Orian, A. L. Schwartz, *BioEssays* **2000**, 22, 442.

Chiral Metal–Organic Assemblies—A New Approach to Immobilizing Homogeneous Asymmetric Catalysts

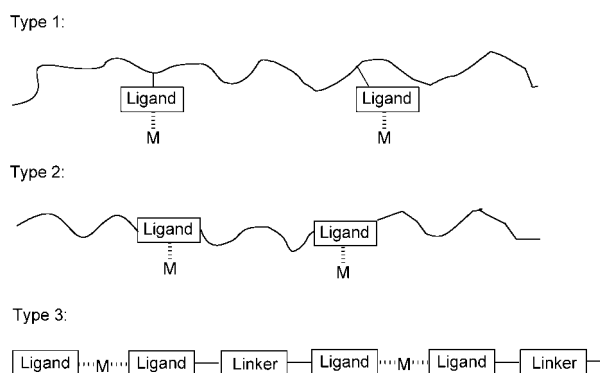
Li-Xin Dai*

Keywords:

asymmetric catalysis · bridging ligands · heterogeneous catalysis · immobilization · self-assembly

Homogeneous asymmetric catalysis has the advantages of high enantioselectivity and catalytic activity for a variety of asymmetric transformations conducted under relatively mild reaction conditions.^[1] However, since the catalyst loadings employed in most cases have ranged from 1 to 10 mol %, homogeneous methods remain impractical due to the high cost of the chiral noble metal catalysts and the difficulty of their recovery and reuse.^[2] The other problem with homogeneous catalysis stems from the trace contaminants leached from the catalysts in the products, which is particularly unacceptable for pharmaceutical production. The immobilization of homogeneous catalysts should resolve the problems of recovering and recycling.^[3,4] Many approaches have been employed with this aim, including using inorganic materials, organic polymers, dendrimers, and membranes as supports, as well as conducting the reactions in ionic liquid and biphasic systems.^[3,4]

In the classical immobilization with organic polymers,^[3,4] the chiral ligands or the catalytically active units are anchored randomly onto irregular polymers (Type 1, Scheme 1). The resulting immobilized catalysts often display reduced enantioselectivity and less efficiency than their homogeneous counterparts. The incorporation of chiral ligands on the main chain of the polymers



Scheme 1. Three types of polymer-immobilized chiral catalysts.

Type 1: Pendant ligands anchored on a polymer; prepared by polymer reaction. Type 2: Ligands on the backbone; prepared by copolymerization. Type 3: Ligand and metal on the backbone; prepared by coordination.

is another approach (Type 2, Scheme 1). Here, the chiral ligand unit is copolymerized with a specific linker.^[5] Although the use of chiral polymers for asymmetric catalysis has a long history,^[3] successful examples were realized at the end of last century by incorporating the rigid binaphthyl skeleton in the main chain. For example, Chan and Fan et al. incorporated the binap skeleton (binap = 2,2'-bis(diphenylphosphanyl)-1,1'-binaphthyl) into a polyester chain,^[6] and Lemaire et al. used a polyamide to copolymerize with the binap skeleton.^[7] On the other hand, the backbone of the catalyst developed by Pu and co-workers was a wholly rigid aromatic system, comprising a large portion of the binaphthyl skeleton.^[5] All of these catalysts showed excellent enantioselectivity. Moreover, Chan and Fan et al. also showed that the leaching of metal from the polymer-supported catalyst is almost negligible (< 16 ppb).^[6] This strategy is indeed successful,^[8] but it is necessary to

synthesize the polymeric ligands beforehand.

Very recently, the third type of polymer-immobilized chiral catalyst (Type 3, Scheme 1) was described.^[9] Several examples showed very high enantioselectivity and efficiency.^[10–12] This type of catalyst is called a metal–ligand polymer^[13] for the sake of simplicity and in the context of asymmetric catalysis.

The concept is to transform a ligand from a homogeneous catalysts which has one coordination site into a ligand with two or more coordination sites and then react it with metal species to ensure the self-assembly of the metal–ligand polymer (or oligomer).

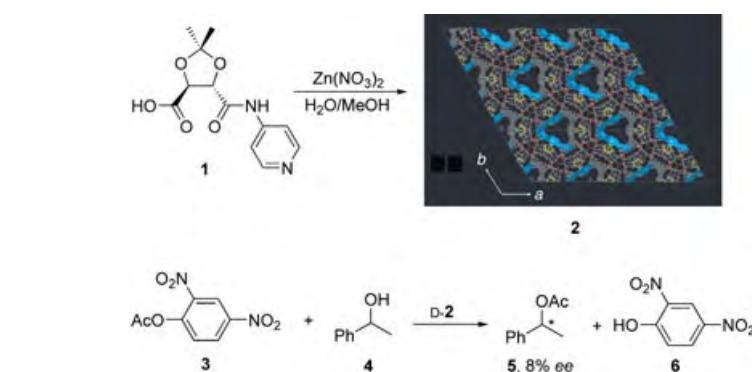
Recent extensive research on the design and synthesis of metal–organic frameworks has led to the increasing numbers of such metal–organic assemblies. Accordingly, many novel metal–organic assemblies with high stability, organic functionality, and porosity have been reported in the last decade. The research groups led by Lehn,^[14] Yaghi,^[15] Stang,^[16] and Fujita,^[17] among others^[18] have significantly forwarded the development of this challenging area and have demonstrated that these metal–organic assemblies based on discrete or infinite networks with well-defined coordination geometries and functions can be rationally designed and synthesized by the combination of organic bridging ligands and metal ions. Aoyama and co-

[*] Prof. L.-X. Dai
State Key Laboratory of Organometallic Chemistry
Shanghai Institute of Organic Chemistry
Chinese Academy of Sciences
354 Fenglin Road
Shanghai 200032 (China)
Fax: (+86) 21-6416-6128
E-mail: dailx@mail.sioc.ac.cn

workers have demonstrated the catalytic properties of nonchiral metal–organic materials for Diels–Alder reactions.^[19] With a few exceptions,^[20] homochiral metal–ligand polymers have not been tested for applications in asymmetric catalysis up to the beginning of this century. In any case, the design and synthesis of chiral metal–organic frameworks or polymers might provide a new strategy for asymmetric heterogeneous catalysis, because the chiral bridging ligand can spontaneously form a chiral environment inside the cavities of the materials or on the surface of the solids for enantioselective control of the reaction, and the metal ion acts as the catalytically active center. These solid-state metal–organic materials usually have extremely low solubility in the reaction medium even when other supports are not used and thus fulfill one of the basic prerequisites of heterogeneous catalysis. Accordingly, the use of chiral metal–ligand assemblies can be considered as a “self-supported” strategy^[21] for the heterogenization of homogeneous catalysts in enantioselective reactions. This type of chiral metal–organic assembly would not only have the advantages of heterogeneous catalysts, such as easy recovery and convenient recycling, but also of facile preparation and robust chiral frameworks, as well as high density of the catalytically active units.

Kim and co-workers first demonstrated the application of a homochiral metal–organic porous material to enantioselective separation and catalysis in 2000.^[9] The homochiral open-framework solid having the formula of $[\text{Zn}_3(\mu_3\text{-O})(\text{1-H})_6]\cdot 12\text{H}_2\text{O}$ (**2**) was prepared by the reaction of Zn^{2+} with the enantiopure chiral building block **1** derived from D-tartaric acid (Scheme 2). Although the enantiomeric excess in the product of transesterification was rather low ($\approx 8\%$ ee), the enantioselectivity was unprecedented because this asymmetric induction was observed for a reaction promoted by a modular porous material. This creative work triggered interest in using self-supported metal–organic systems to immobilize homogeneous catalysts.^[22]

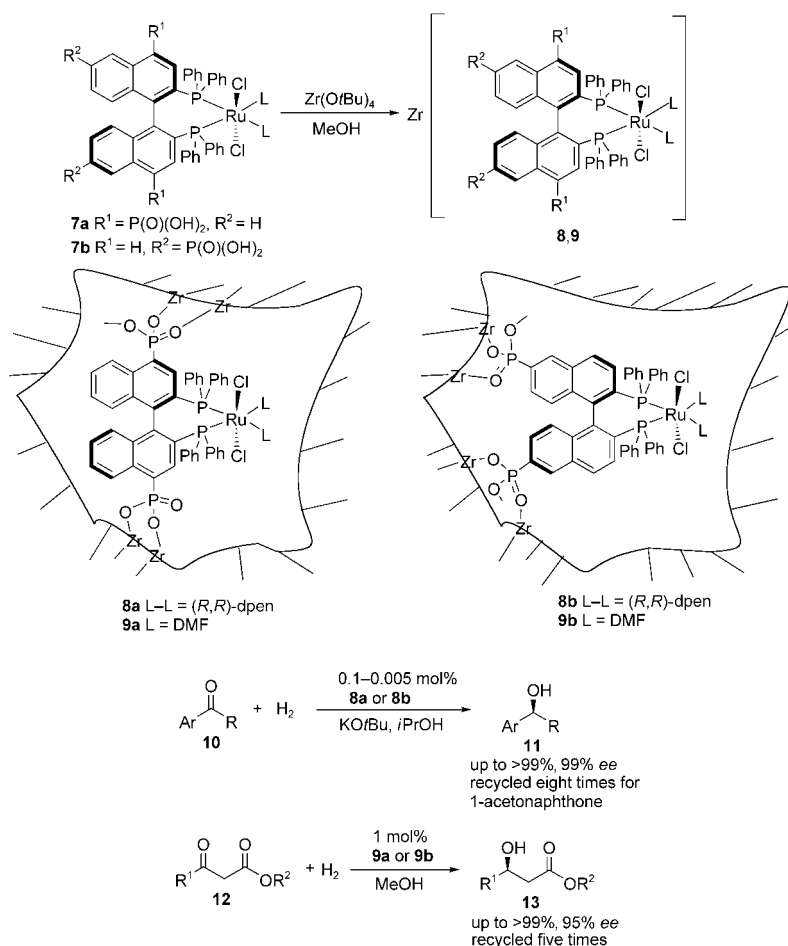
The success of asymmetric catalysis with this kind of metal–ligand polymer was realized only very recently. Lin and co-workers reported that the heteroge-



Scheme 2. Chiral metal–organic porous materials for the enantioselective transesterification of **3** with racemic **4**.

nization of Noyori’s catalysts could be achieved by in situ formation of chiral porous hybrid solids such as **8** and **9** through the reaction of zirconium *tert*-butoxide with chiral bisphosphine/Ru complexes functionalized with phosphonic acid groups (**7**) (Scheme 3).^[10a]

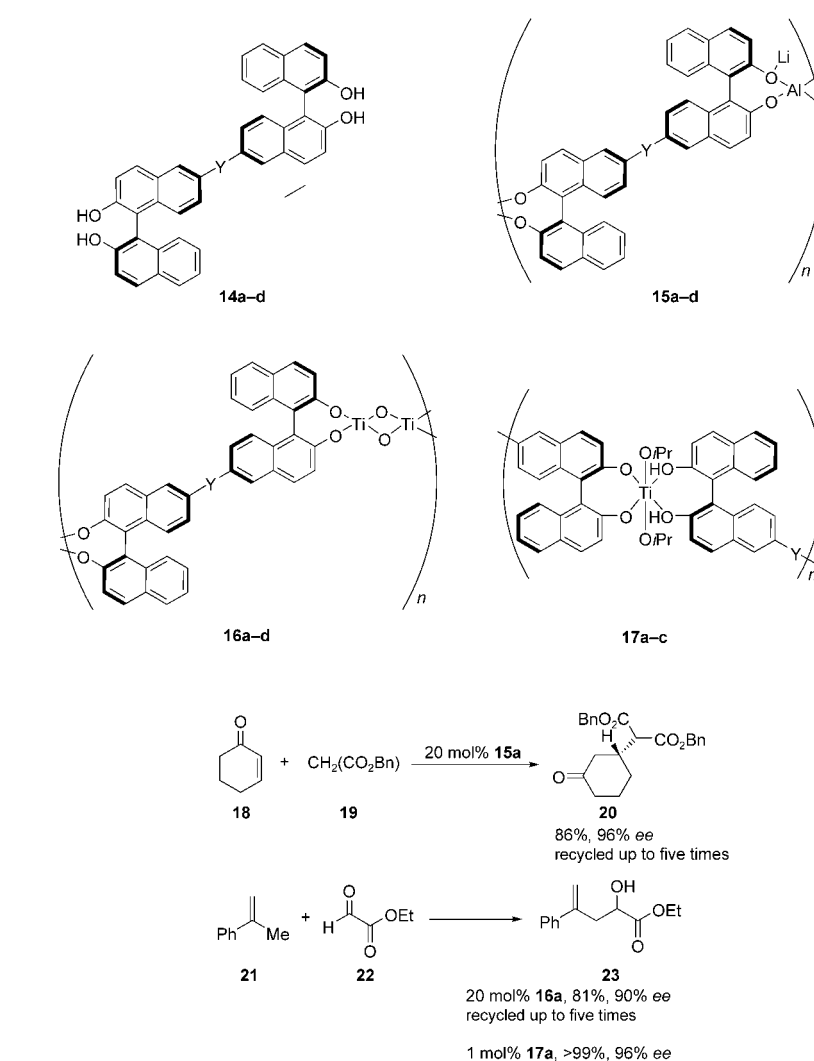
Nitrogen adsorption measurements demonstrated that these hybrid solids are highly porous with rather wide pore-size distributions. The total BET surface areas of the solids range from 328 to 475 m^2g^{-1} with microporous surface areas of 60–161 m^2g^{-1} and pore volumes



Scheme 3. Chiral metal–ligand polymer in the catalysis of enantioselective hydrogenation of ketones.

of $0.53\text{--}1.02\text{ cm}^3\text{ g}^{-1}$. The heterogenized catalysts **8a** and **8b** exhibited exceptionally high activity and enantioselectivity in the hydrogenation of aromatic ketones. With 0.1 mol % of catalyst **8a**, the conversion of the substrates was quantitative and the enantioselectivity approached 99% *ee*. Particularly, the catalyst loading can be reduced to 0.005 mol % without significant loss of the enantioselectivity. Remarkably, these binap-derived porous Zr phosphonates provide enantioselectivity superior to that of the parent homogeneous counterpart, the binap/RuCl₂/dppe system developed by Noyori et al.^[23] The other two catalyst systems, **9a** and **9b**, were also used for the asymmetric hydrogenation of a series of β -keto esters. Under optimized conditions, the hydrogenation with 1 mol % of **9b** afforded the corresponding β -hydroxy esters in quantitative yield and good to excellent enantioselectivities.^[10b] For the asymmetric hydrogenation of methyl acetoacetate the catalyst **9b** could be recycled five times without significant loss of enantioselectivity. Catalysts **8a** and **9b** showed better catalytic activity and enantioselectivity than catalysts **8b** and **9a**, respectively, which demonstrates the importance of the position of the linker on the backbone of binap in the formation of the microporous catalyst.

Almost at the same time, the research groups led by Sasai^[11] and Ding^[12] independently reported an alternative approach to generating chiral metal-organic coordination polymers for enantioselective catalysis. As shown in Scheme 4, the rigid chiral ligands having two 1,1'-2,2'-binaphthol (binol) units react with metal ions, resulting in the spontaneous formation of assembled metal-organic polymers in which the metal ions not only play the role of the bridging linker, but also act as the catalytically active sites. Moreover, the chirality of the binol units in the ligands can provide the asymmetric environment around the catalytically active centers in the polymers. These assembled metal-organic coordination polymers are insoluble in common organic solvents. This offers an excellent opportunity for running heterogeneous catalysis with these "self-supported" cata-



Scheme 4. Self-supported chiral metal-ligand polymer as catalyst in Michael addition and carbonyl-ene reactions. Bn = benzyl. Y = single bond (a); 1,4-phenylene (b); 1,3-phenylene (c); 1,2-phenylene (d).

lysts. The metal-ligand polymer of the Sasai and Ding groups is somewhat different from that of Lin et al. In the latter, the catalytic metal center, Ru, is situated as a pendant group on the Zr-linked backbone,^[10] while the catalytically active metal of Sasai, Ding, et al. is located on the backbone of the polymer.^[11,12]

The success of this strategy was demonstrated in asymmetric Michael additions^[11] and carbonyl-ene reactions.^[11,12] The heterogeneous Al-bridged polymers **15** prepared by the reaction of LiAlH₄ with bis(binol) ligands **14** was employed in the enantioselective Michael addition of dibenzyl malonate (**19**) to 2-cyclohexenone (**18**) in THF. Adduct **20** was obtained with results comparable to those obtained with a homogeneous

Al-Li-bis(binaphthoxide) (ALB) catalyst (100% yield, 97% *ee*). After the reaction was complete, catalyst **15a** could be recovered conveniently and reused at least three times with a slight decrease of enantioselectivity (from 96% *ee* for the first run to 85% *ee* for the third run). Similarly, the heterogeneous Ti-bridged catalysts (**16** and **17**) prepared by the reaction of ligands **14** with Ti(OiPr)₄ (**14**:Ti = 1:2 or 1:1) gave excellent enantioselectivity (up to 96.5% *ee*) in the carbonyl-ene reaction of **21** with **22**.^[11,12] The reusability of this type of catalyst (**16a**) in the carbonyl-ene reaction was also demonstrated by Sasai et al. After being reused five times the Ti-bridged polymer exhibited consistent catalytic selectivity, affording **23** with an *ee* value of 88% at a catalyst

loading of 20 mol%. It seems that catalyst **17a** prepared with **14**:Ti = 1:1 (1 mol%, up to 99% yield and 96% ee) possesses higher activity and enantioselectivity than **16a** prepared with **14**:Ti = 1:2 in the presence of 1 equiv of H₂O (20 mol%, up to 72% yield and 92% ee). This phenomenon probably arises from the activating effect of additional binol unit in **17a**.^[24] In both the Michael addition and carbonyl-ene reaction, the linkers between two binol units in the ligands have significant impact on the enantioselectivity of the assembled catalysts prepared from them. The heterogeneous catalysts derived from **15a,b** and **17a,b**, in the pairs of the phenolic hydroxy groups are situated at opposite sites in the symmetric, multidentate ligands, gave the Michael adduct or carbonyl-ene adduct with higher enantioselectivity than that attained with the catalysts from ligands **15c,d** and **17c**, respectively. The dramatic influence of the linking spacer on the enantioselectivities of the reactions reflects that the linkers between two binol units of the ligands probably significantly alter the supramolecular structure of the assemblies in the catalysts. Therefore, the frameworks of assembled catalysts can be optimized by the rational design of chiral ligands to improve the catalytic activity and enantioselectivity of the “self-supported” catalyst.

Obviously, the “metal–ligand polymer” strategy for the immobilization of homogeneous catalysts developed by the Lin,^[10] Sasai,^[11] and Ding groups^[12] represents a significant breakthrough in the heterogeneous asymmetric catalysis, since it satisfies many requirements for the immobilized catalysts. Their performance is comparable to or better than that of the parent catalysts, they are easy to separate and reuse, and there is minimum leaching of the catalyst. Furthermore, the metal–ligand polymer was prepared by an in situ self-assembling process, a really simple manipulation. This strategy might provide a new direction in asymmetric catalysis, particularly for the development of practical syntheses of optically active compounds. Meanwhile, the use of chiral “metal–ligand” assemblies for chiral recognition

and separation may be another exciting area in chiral chemistry.^[25]

- [1] a) *Chirality in Industry: The Commercial Manufacture and Applications of Optically Active Compounds* (Eds.: A. N. Collins, G. N. Sheldrake, J. Crosby), Wiley, Chichester, **1992**; b) *Chirality in Industry II: Developments in the Commercial Manufacture and Applications of Optically Active Compounds* (Eds.: A. N. Collins, G. N. Sheldrake, J. Crosby), Wiley, Chichester, **1997**; c) R. A. Sheldon, *Chirotechnology: Industrial Synthesis of Optically Active Compounds*, Dekker, New York, **1993**.
- [2] For comprehensive reviews on asymmetric catalysis, see for example: a) R. Noyori, *Asymmetric Catalysis in Organic Synthesis*, Wiley-Interscience, New York, **1994**; b) *Catalytic Asymmetric Synthesis*, 2nd ed. (Ed.: I. Ojima), Wiley-VCH, Weinheim, **2000**; c) *Comprehensive Asymmetric Catalysis, Vols. I–III* (Eds.: E. N. Jacobsen, A. Pfaltz, H. Yamamoto), Springer, Berlin, **1999**; d) G. Q. Lin, Y. M. Li, A. S. C. Chan, *Principles and Applications of Asymmetric Synthesis*, Wiley-VCH, Weinheim, **2002**.
- [3] *Chiral Catalyst Immobilization and Recycling* (Eds.: D. E. De Vos, I. F. J. Vankelecom, P. A. Jacobs), Wiley-VCH, Weinheim, **2000**.
- [4] For a special issue on recoverable catalysts and reagents, see: *Chem. Rev.* **2002**, *102*, 3215–3892.
- [5] L. Pu, *Chem. Eur. J.* **1999**, *5*, 2227.
- [6] Q. H. Fan, C. Y. Ren, C. H. Yeung, W. H. Hu, A. S. C. Chan, *J. Am. Chem. Soc.* **1999**, *121*, 7407.
- [7] R. ter Halle, B. Colasson, E. Schulz, M. Spagnol, M. Lemaire, *Tetrahedron Lett.* **2000**, *41*, 643.
- [8] T. Arai, T. Sekiguti, K. Otsuki, S. Takizawa, H. Sasai, *Angew. Chem.* **2003**, *115*, 2194; *Angew. Chem. Int. Ed.* **2003**, *42*, 2144.
- [9] J. S. Seo, D. Whang, H. Lee, S. I. Jun, J. Oh, Y. J. Jeon, K. Kim, *Nature* **2000**, *404*, 982.
- [10] a) A. Hu, H. L. Ngo, W. Lin, *J. Am. Chem. Soc.* **2003**, *125*, 11490; b) A. Hu, H. L. Ngo, W. Lin, *Angew. Chem.* **2003**, *115*, 6182; *Angew. Chem. Int. Ed.* **2003**, *42*, 6000.
- [11] S. Takizawa, H. Somei, D. Jayaprakash, H. Sasai, *Angew. Chem.* **2003**, *115*, 5889; *Angew. Chem. Int. Ed.* **2003**, *42*, 5711.
- [12] H. Guo, W. Wang, K. Ding, *Tetrahedron Lett.* **2004**, *45*, 2009.
- [13] It was designated in the literature as metal–organic framework, metal–organic coordinated network, metallosupramolecular assembly, metal-bridged polymer, or hybrid solid.
- [14] a) P. N. W. Baxter, J.-M. Lehn, G. Baum, D. Fenske, *Chem. Eur. J.* **1999**, *5*, 102; b) P. N. W. Baxter, J.-M. Lehn, B. O. Kneisel, G. Baum, D. Fenske, *Chem. Eur. J.* **1999**, *5*, 113.
- [15] O. M. Yaghi, M. O’Keeffe, N. W. Ockwig, H. K. Chae, M. Eddaoudi, J. Kim, *Nature* **2003**, *423*, 705.
- [16] a) S. R. Seidel, P. J. Stang, *Acc. Chem. Res.* **2002**, *35*, 972; b) S. Leininger, B. Olenyuk, P. J. Stang, *Chem. Rev.* **2000**, *100*, 853.
- [17] a) M. Fujita, *Acc. Chem. Res.* **1999**, *32*, 53. b) W.-Y. Sun, M. Yoshizawa, T. Kusukawa, M. Fujita, *Curr. Opin. Chem. Biol.* **2002**, *6*, 757.
- [18] a) *Molecular Self-Assembly—Organic versus Inorganic Approaches, Vol. 96* (Ed.: M. Fujita) Springer, Berlin, **2000**; b) O. R. Evans, W. Lin, *Acc. Chem. Res.* **2002**, *35*, 511; c) C. A. Schalley, A. Lützen, M. Albrecht, *Chem. Eur. J.* **2004**, *10*, 1072.
- [19] T. Sawaki, T. Dewa, Y. Aoyama, *J. Am. Chem. Soc.* **1998**, *120*, 8539; T. Sawaki, Y. Aoyama, *J. Am. Chem. Soc.* **1999**, *121*, 4793.
- [20] For an early example of using polymeric metal–ligand assembly for aldol reactions, attaining product enantioselectivities of up to 60% ee, see: X. T. Zhou, PhD Dissertation, Shanghai Institute of Organic Chemistry, **1999**.
- [21] For the concept of “self-supported” heterogeneous catalysts for the hydrogenation of ethylene, see: a) C. Bianchini, E. Farnetti, M. Graziani, J. Kaspar, F. Vizza, *J. Am. Chem. Soc.* **1993**, *115*, 1753; for self-supported achiral catalysts in chiral matrices, see: b) R. Dorta, L. Shimon, D. Milstein, *J. Organomet. Chem.* **2004**, *689*, 751.
- [22] O. R. Evans, H. L. Ngo, W. Lin, *J. Am. Chem. Soc.* **2001**, *123*, 10395.
- [23] T. Ohkuma, R. Noyori, *Angew. Chem.* **2001**, *113*, 41; *Angew. Chem. Int. Ed.* **2001**, *40*, 40, and references therein.
- [24] a) K. Mikami, M. Terada, T. Korenaga, Y. Matsumoto, M. Ueki, R. Angelaud, *Angew. Chem.* **2000**, *112*, 3676; *Angew. Chem. Int. Ed.* **2000**, *39*, 3532; b) K. Mikami, S. Matsukawa, *Nature* **1997**, *385*, 613.
- [25] Remarkable results were obtained for the enantioseparation of racemic organic compounds, see: a) C. J. Kepert, T. J. Prior, M. J. Rosseinsky, *J. Am. Chem. Soc.* **2000**, *122*, 5158; b) R.-G. Xiong, X.-Z. You, B. F. Abrahams, Z. Xue, C.-M. Che, *Angew. Chem.* **2001**, *113*, 4554; *Angew. Chem. Int. Ed.* **2001**, *40*, 4422.

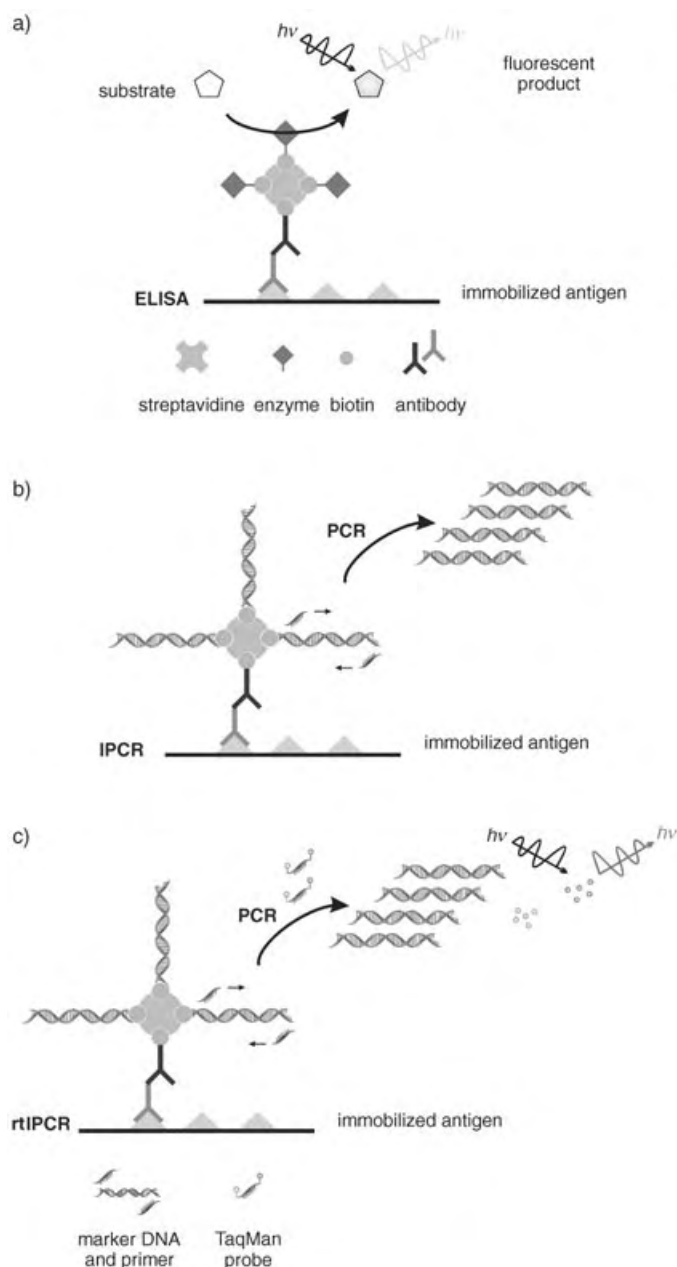
DNA-Based Barcodes, Nanoparticles, and Nanostructures for the Ultrasensitive Detection and Quantification of Proteins

Susanne Brakmann*

Keywords:

antibodies · antigens · immunoassays · proteins

Immunoassays are techniques that employ labeled or nonlabeled antibodies for the quantitative assessment of analytes. These techniques have become most popular in clinical and medical research laboratories because they are precise, sensitive, and relatively inexpensive. Increasingly important, however, is the detection of proteins at extremely low concentrations, especially in biofluids containing very low titers of disease markers and in food or environmental samples containing toxic or ineligible proteins. Although classical tests such as ELISA (enzyme-linked immunosorbent assay; Figure 1 a) and RIA (radioimmunoassay) are capable of providing relatively high sensitivity and very low limits of detection (1 fmol), they may not be applicable to all possible samples, for example, antigenic species present at very low concentrations. Currently, this is the problem with prion diseases. A major improvement in the sensitivity of immunoassays was achieved by Cantor and his colleagues about ten years ago: Rather than coupling the detection antibody to an enzyme, these researchers linked the antibody to one or more DNA fragments, which can then be amplified specifically by polymerase chain reaction (PCR) before detection, for example, by gel electrophoresis (Figure 1 b). Instead of the



[*] Priv.-Doz. Dr. S. Brakmann
Applied Molecular Evolution
Institute of Biology II
University of Leipzig
Liebigstrasse 18, 04103 Leipzig (Germany)
Fax: (+49) 341-97-37838
E-mail: sbrakma@rz.uni-leipzig.de

Figure 1. a) Principle of the ELISA assay. b,c) Principle of immuno-PCR with conventional detection of the PCR product (b) and with quantitative detection using a FRET probe (c, real-time IPCR).

linear signal amplification achieved by the ELISA test, the PCR process yields an exponential amplification, thus lowering the detection limit by three to four orders of magnitude.^[1]

Since then, this technique, called immuno-PCR (IPCR), has proved to be suitable for the highly sensitive detection of antigens, antibodies, pathogens, tumor markers, and potential therapeutics in the femto- to attomolar concentration range and therefore, is of interest predominantly for clinical diagnostics. A number of different IPCR protocols have been developed showing that this technique can be adapted for a broad range of analytes and immunoassay techniques (a recent review is found in ref. [2]). Due to the tremendous amplification power of PCR, IPCR is extremely sensitive not only in detecting specific proteins but also in detecting cross-contaminations of extrinsic nucleic acids or false-positive signals resulting from unspecific binding of the antibody. Application of IPCR as a routine method thus requires the elimination or inactivation of impurities to the greatest possible extent and the use of highly standardized protocols.

In combination with “real-time” PCR techniques^[3] that have become highly popular during the past years, IPCR has been extended to a robust technique for the quantitative detection of antigens and is suited for routine diagnostics as well as for the parallel analysis of large numbers of samples. For these applications PCR mixtures are supplied with DNA intercalators like SYBR-Green or FRET probes like Taqman that bind to the nascent DNA chain and consequently, fluoresce. Since machines exist that can monitor fluorescence directly during amplification and evaluate the data relative to a calibration curve, real-time IPCR (rtIPCR) can be used for the reproducible and quantitative detection of analytes in microplate formats (96 wells, or 384 wells) and also, for the recording of melting curves that support the characterization of amplicons.

An important example that illustrates the sensitivity and impact of the rtIPCR technique was recently presented with the detection of only 30 000 molecules of the potent cytostatic anticancer drug rViscumin (concentration

ca. 100 fg mL⁻¹) in standardized human serum samples.^[4] Supramolecular IPCR reagents—oligomeric conjugates made from streptavidine, bisbiotinylated dsDNA, and biotinylated antibodies that were recently developed by Niemeyer and colleagues^[5]—made the impressive sensitivity possible because they enabled the binding to multiple analytes, which resulted in an entropic advantage. Additionally, the authors improved their rtIPCR assay by adding a competitively replicating DNA fragment that serves as an internal standard and also, increases the signal-to-noise ratio (Figure 1 c).^[6]

Unfortunately, rtIPCR has not as yet found its way into routine diagnostics despite impressive sensitivity and successful demonstration of its efficiency in highly reproducible analyses. This could be due to the still-complex preparation of IPCR probes. These conjugates of DNA and antibodies are typically strongly bound either through covalent interactions or streptavidine–biotin binding. While DNA–antibody conjugates are synthesized by means of the sulfhydryl and amino functions of DNA or the antibody,^[7,8] streptavidine–biotin conjugates are usually made starting from biotinylated antibody and biotinylated DNA.^[5,9] Both approaches require complex modifications to link DNA and antibody proteins that are only occasionally commercialized.

Nanoparticle-Based Barcodes for the Identification of Proteins

Further improvements in IPCR sensitivity could be limited by the low ratio of detection antibody to DNA identification sequence (usually 1:1) as well as slow target-binding kinetics that are due to the heterogeneous nature of the target-capture procedure.^[10] For this reason many new concepts concerning amplified biosensing combine the immunoassay with techniques for the immobilization of biopolymers at the surfaces of micro- and nanoparticles. The combination is advantageous not only for the formation of recognition complexes in suspension; commercially available and meanwhile widespread magnetic microparticles can also be

used for the physical isolation of the immunocomplexes using an external magnet. Therefore these techniques are ideally suited for the separation and enrichment of antigen–antibody conjugates from complex mixtures (see ref. [11] and references therein).

In a recently published approach, Mirkin and colleagues demonstrated the detection of a tumor marker (PSA, prostate-specific antigen) with a system of antibody-linked microparticles and gold nanoparticles functionalized with anti-PSA antibodies and double-stranded DNA.^[14] In the presence of PSA a specific complex forms connecting the magnetic microparticles and gold nanoparticles (Figure 2). The functionalization of gold nanoparticles with a combination of both DNA and antibody had already been described.^[12] Mirkin et al. were able to show that 180 molecules (concentration 30 aM) of free PSA, usually present at (sub-)femtomolar concentration in the sera of breast cancer patients,^[13] can be detected without PCR amplification, while ten times less, that is, a minimum of 18 molecules (concentration 3 aM) were detectable with amplification.^[10]

Mirkin’s astonishingly sensitive approach is characterized not only by an enrichment of the immunocomplex by means of magnetic separation techniques but also by a high ratio of recognition antibody to marker DNA (approx. 1:100). The signaling immunocomplex is a “sandwich” of magnetic microparticles functionalized with PSA monoclonal antibodies (mABs), antigenic PSA, and gold nanoparticles functionalized with one or a few copies of a polyclonal antibody directed against PSA as well as multiple copies of double-stranded marker DNA. After formation of the sandwich complex, all magnetic particles or particle complexes are separated by application of an external magnet, leaving unreacted nanoparticles and antigens in solution. Marker DNA that is attached to the enriched complexes serves as a template in PCR amplifications and can be detected easily by standard techniques (such as gel electrophoresis and staining with ethidium bromide). However, Mirkin achieved greater sensitivity in detecting DNA by melting the double-stranded marker DNA, optional PCR

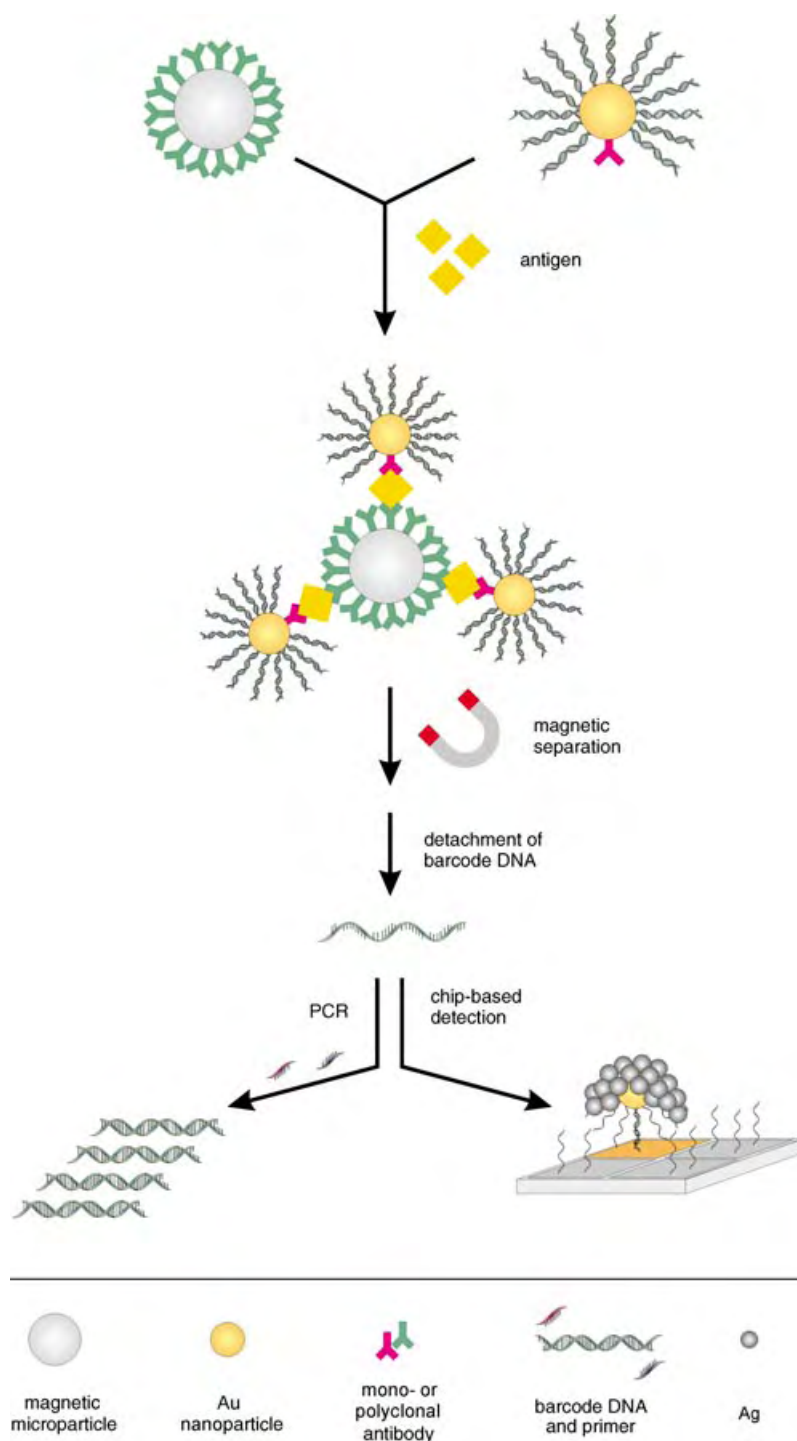


Figure 2. Essential steps in a bio-barcode immunoassay. The first (monoclonal) antibody is linked to the surface of magnetic microparticles, which are employed for separating and enriching the protein from the sample solution. The second (polyclonal) antibody is bound to gold nanoparticles, which also are functionalized with multiple double-stranded DNA fragments. Following formation and magnetic separation of the sandwich complex, these DNA strands are detached and can be detected either after PCR amplification or by using DNA chips.

amplification, and chip-based detection, which comprises the hybridization of marker DNA with immobilized complementary strands, silver staining of the

resulting double-stranded DNA, and scanometric detection. The assay is also suited for the parallel analysis of multiple analytes if every antigen is coded by

a distinct marker DNA sequence. Therefore, these DNA sequences were called “bio-barcodes” by Mirkin.^[14]

Similar to rtIPCR, the bio-barcode approach requires the synthesis of antibody conjugates such as the noncovalent, equimolar coupling of gold nanoparticles to polyclonal antibody prior to the covalent coupling with a 10- to 100-fold excess of barcode DNA. Both compliance with the desired stoichiometry as well as stabilization and handling of the resulting conjugates are exceedingly difficult. The immobilization of monoclonal antibody on the surface of magnetic microparticles can be achieved in a straightforward fashion using well-established glutaraldehyde–amine coupling chemistry (efficiency 90 %).

Another difficulty associated with Mirkin’s procedure may arise from the utilization of polyclonal antibodies for the recognition of the antigen. This type of antibody can also bind to other proteins. The resulting reduction in the signal-to-noise ratio would lead to a loss of sensitivity and, in particular, would compromise the parallel detection of analytes. However, it will be tantalizing to see whether the ultrasensitive bio-barcode technique will be suitable for “real life”.

Bioelectronic Coding and Detection of Proteins

Promising alternatives to optical detection techniques are possible with electronic approaches, which in addition can be triggered and controlled using magnetic microparticles.^[11] These techniques are based on the electroactivity of nucleic acids, which adsorb strongly to electrodes where they undergo charge-transfer reactions.^[15] Thereby, predominantly the nucleobases are reduced at mercury electrodes and oxidized at graphite electrodes. Because nucleobases that accumulate at the electrode surface come off during oxidation, they can be detected using potentiometric stripping analysis (PSA) at very low concentrations (nM).^[15]

Wang and colleagues utilized this DNA property for the development of a highly sensitive immunoassay-based method to detect proteins that is closely related to the technique presented by

Mirkin et al.^[16] The “bioelectronic” protocol also is based on the formation of a sandwich immunocomplex starting from antibody-linked magnetic microparticles and DNA-functionalized polystyrene particles which also are coupled to the detection antibody. Following magnetic separation and enrichment of particle-bound immunocomplexes, marker (barcode) DNA is detached by alkaline denaturation of the double-stranded DNA and subsequently submitted to acid-catalyzed depurination. Free purines (adenine, guanine) can then be detected quantitatively using chronopotentiometric stripping analysis at a pyrolytic graphite electrode (Figure 3).

The authors demonstrated that they were able to detect as few as 40 000 molecules of an analyte (concentration 13 fM) by their bioelectronic approach without amplification, for example, by PCR. By including an amplification step, the already high sensitivity could be increased additionally by two orders of magnitude. Due to high sensitivity, selectivity (that is, no background signal in the absence of analyte or in the presence of a 1000-fold excess of bovine serum albumine) as well as high reproducibility (standard deviation of ca. 5% in six analogous experiments), the electronic detection of barcode DNA appears promising. However, it remains to be seen whether the probes will become commercially available so that this approach could become a routine method for diagnostics or proteome analysis. Ultimately, the market for new technologies, which almost always responds slowly to innovations, will be decisive for the distribution of all three methods, rtIPCR, bio-barcode, and bioelectronic barcodes.

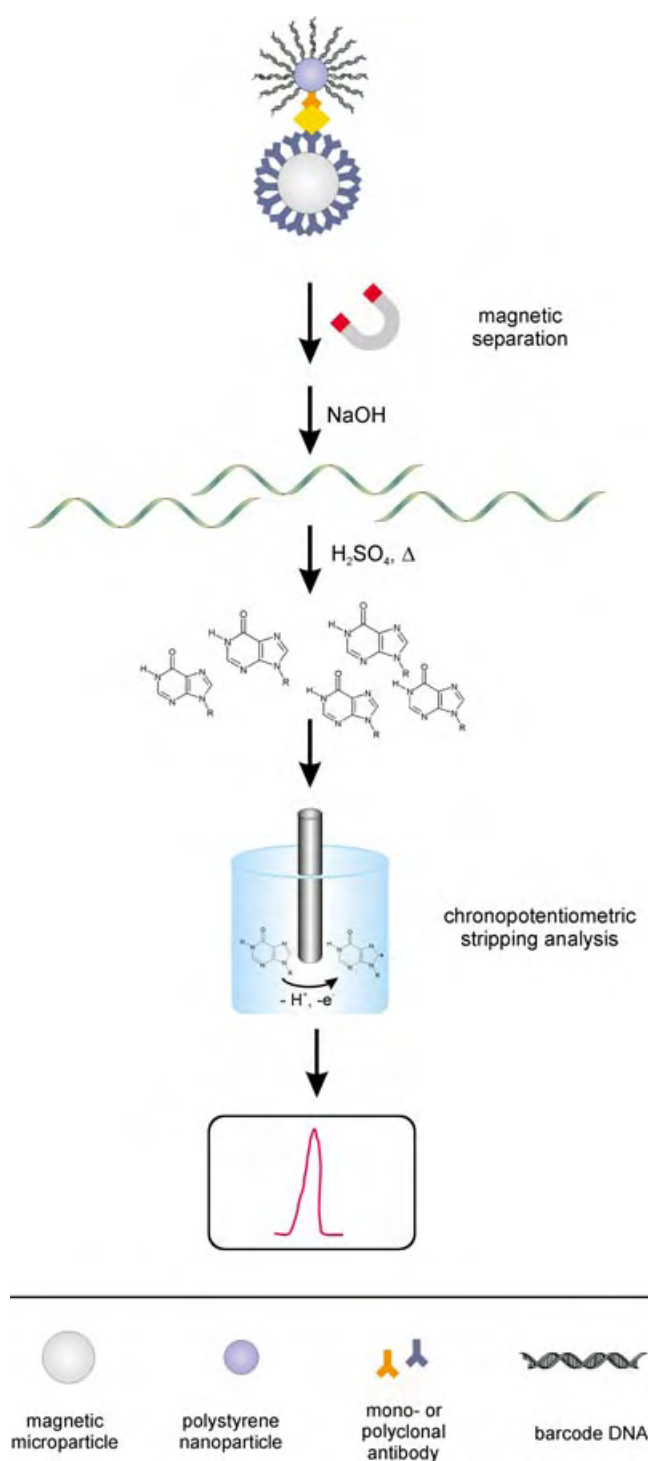


Figure 3. In the case of the bioelectronic barcode assay, the second antibody is coupled to plastic beads which, again, are functionalized with many short DNA fragments. After detachment of the DNA, the purines adenine and guanine are released and can be detected by electrochemical analysis, by which adenine is clearly distinguishable from guanine.

- [1] T. Sano, C. Smith, C. Cantor, *Science* **1992**, 258, 120–122.
- [2] S. Schiavo, A. El-Shafey, N. Jordan, C. Orazine, X. Zhou, N. H. L. Chiu, I. S. Krull, *PharmaGenomics* **2004**, 36–45.
- [3] A. Guilletti, L. Overbergh, D. Valckx, B. Decallonne, R. Bouillon, C. Mathieu, *Methods* **2001**, 25, 386–401.
- [4] M. Adler, M. Langer, K. Witthohn, J. Eck, D. Blohm, C. M. Niemeyer, *Biochem. Biophys. Res. Commun.* **2003**, 300, 757–763.
- [5] C. M. Niemeyer, M. Adler, B. Pignataro, S. Lenhert, S. Gao, L. Chi, H. Fuchs, D.

Blohm, *Nucleic Acids Res.* **1999**, 27, 4553–4561.

- [6] M. Adler, R. Wacker, C. M. Niemeyer, *Biochem. Biophys. Res. Commun.* **2003**, 308, 240–250.

[7] H. C. Wu, Y. L. Huang, S. C. Lai, Y. Y. Huang, M. F. Shaio, *Lett. Appl. Microbiol.* **2001**, 32, 321–325.

[8] R. D. Joerger, T. M. Truby, E. R. Hendrickson, R. M. Young, R. C. Ebersole, *Clin. Chem.* **1995**, 41, 1371–1377.

- [9] P. P. Sanna, F. Weiss, M. E. Samson, F. E. Bloom, E. M. Pich, *Proc. Natl. Acad. Sci. USA* **1995**, 92, 272–275.
- [10] J. M. Nam, C. S. Thaxton, C. A. Mirkin, *Science* **2003**, 301, 1884–1886.
- [11] I. Willner, E. Katz, *Angew. Chem.* **2003**, 115, 4724–4737; *Angew. Chem. Int. Ed.* **2003**, 42, 4576–4588.
- [12] C. M. Niemeyer, B. Ceyhan, *Angew. Chem.* **2001**, 113, 3798–3801; *Angew. Chem. Int. Ed.* **2001**, 40, 3685–3688.
- [13] M. H. Black, M. Gai, R. Ponzzone, P. Sismondi, H. Yu, E. P. Diamandis, *Clin. Cancer Res.* **2000**, 6, 467–473.
- [14] J. M. Nam, S. J. Park, C. A. Mirkin, *J. Am. Chem. Soc.* **2002**, 124, 3820–3821.
- [15] E. Palecek, M. Fojta, *Anal. Chem.* **2001**, 73, 75A–83A.
- [16] J. Wang, G. Liu, B. Munge, L. Lin, Q. Zhu, *Angew. Chem.* **2004**, 116, 2210–2213; *Angew. Chem. Int. Ed.* **2004**, 116, 2158–2161.

Why Wait to Make Great Discoveries

When you can make them in an instant with
Wiley InterScience® Pay-Per-View and ArticleSelect™

Now you can have instant, full-text access to an extensive collection of journal articles or book chapters available on Wiley InterScience. With Pay-Per-View and ArticleSelect™, there's no limit to what you can discover...

ArticleSelect™ is a token-based service, providing access to full-text content from non-subscribed journals to existing institutional customers (EAL and BAL)

Pay-Per-View is available to any user, regardless of whether they hold a subscription with Wiley InterScience.

Benefits:

- Access online full-text content from journals and books that are outside your current library holdings
- Use it at home, on the road, from anywhere at any time
- Build an archive of articles and chapters targeted for your unique research needs
- Take advantage of our free profiled alerting service, the perfect companion to help you find specific articles in your field as soon as they're published
- Get what you need instantly, no waiting for document delivery
- Fast, easy, and secure online credit-card processing for Pay-Per-View downloads
- Special, cost-savings for EAL customers: whenever a customer spends tokens on a title equaling 115% of its subscription price, the customer is auto-subscribed for the year
- Access is instant and available for 24 hours

www.interscience.wiley.com



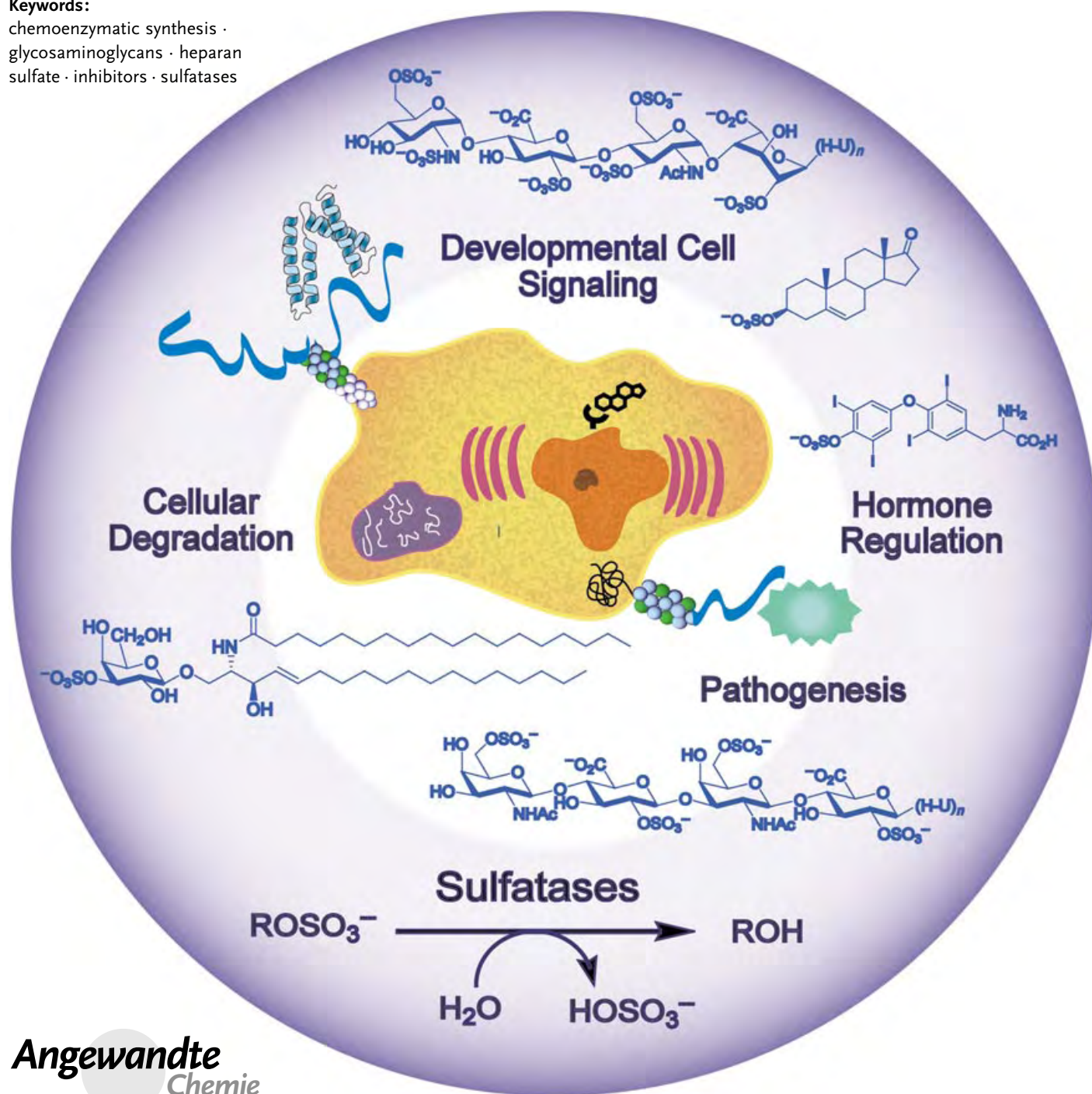
Enzyme Chemistry

Sulfatases: Structure, Mechanism, Biological Activity, Inhibition, and Synthetic Utility

Sarah R. Hanson, Michael D. Best, and Chi-Huey Wong*

Keywords:

chemoenzymatic synthesis ·
glycosaminoglycans · heparan
sulfate · inhibitors · sulfatases



Angewandte
Chemie

Sulfatases, which cleave sulfate esters in biological systems, play a key role in regulating the sulfation states that determine the function of many physiological molecules. Sulfatase substrates range from small cytosolic steroids, such as estrogen sulfate, to complex cell-surface carbohydrates, such as the glycosaminoglycans. The transformation of these molecules has been linked with important cellular functions, including hormone regulation, cellular degradation, and modulation of signaling pathways. Sulfatases have also been implicated in the onset of various pathophysiological conditions, including hormone-dependent cancers, lysosomal storage disorders, developmental abnormalities, and bacterial pathogenesis. These findings have increased interest in sulfatases and in targeting them for therapeutic endeavors. Although numerous sulfatases have been identified, the wide scope of their biological activity is only beginning to emerge. Herein, accounts of the diversity and growing biological relevance of sulfatases are provided along with an overview of the current understanding of sulfatase structure, mechanism, and inhibition.

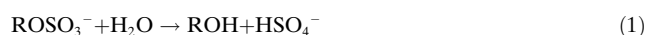
1. Introduction

Whereas sulfotransferases have been the subject of intense investigation for the past several years, sulfatases have received considerably less attention. Sulfatases were discovered sporadically in eukaryotes and prokaryotes throughout the 20th century, but for a long time this class of enzymes was undervalued, as their biological function was thought to be limited mainly to the degradation of organic sulfates in soil. An abundance of new information regarding human sulfatases became available in the 1960s after it was discovered that sulfatase deficiencies led to a number of inherited lysosomal disorders. Since then, sulfatases have emerged as important components in processes such as hormone regulation (and deregulation in hormone-responsive cancers), gamete interactions, and proper bone and cartilage development.

Most recently, sulfatases have been implicated in the modification of sulfate moieties on glycosaminoglycans (GAGs),^[*] which dictate developmental cell signaling and patterning phenomena in the extracellular matrix (ECM). Furthermore, new functions of invertebrate and prokaryotic sulfatases have been discovered, including potential roles in bacterial pathogenesis. This Review takes a comprehensive look at the sulfatase family, examining structure, mechanism, and inhibition. Information on the substrates and biological roles of sulfatases, focusing on emerging topics and potential therapeutic targets, is also provided. Finally, the synthetic utility of these enzymes for probing the biological interactions of sulfated carbohydrates and GAGs within the extracellular matrix is discussed.

2. The Sulfatase Family

Sulfatases (EC 3.1.5.6) catalyze the hydrolytic desulfonation of sulfate esters (CO–S) and sulfamates (CN–S) [Eq. (1)



and (2), respectively].



They comprise a class of enzymes that is highly conserved sequentially, structurally, and mechanistically across eukaryotic and prokaryotic species. The remarkable similarities shared by sulfatases include: 1) 20–60 % sequence homology over the entire protein length, 2) a highly conserved N-terminal region containing the consensus sulfatase motifs, and 3) a unique active-site aldehyde residue, α -formylglycine (FGly), which is installed post-translationally.

The high degree of sequence and structural likeness observed thus far amongst sulfatases has led to the proposal that they emerged long ago from a common ancestral gene.^[1,2] The human enzymes (15 are known, 13 genes have been cloned, Table 1) and the invertebrate, lower eukaryotic, and prokaryotic enzymes (many are known, 13 genes have been cloned, Table 2) are typically between 500 and 600 amino acids in length; the newly discovered human Sulf enzymes

From the Contents

1. Introduction	5737
2. The Sulfatase Family	5737
3. Structure	5740
4. Mechanism	5742
5. The Post-Translational FGly Modification	5744
6. Substrates and Biological Functions of Eukaryotic Sulfatases	5746
7. Substrates and Biological Functions of Prokaryotic Sulfatases	5750
8. Sulfatase Inhibition	5753
9. Synthetic Utility	5755
10. Conclusion and Outlook	5758

[*] S. R. Hanson, Dr. M. D. Best, Prof. C.-H. Wong
Department of Chemistry and
The Skaggs Institute for Chemical Biology
The Scripps Research Institute
10550 North Torrey Pines Road, BCC 357
La Jolla, California 92037 (USA)
Fax: (+1) 858-784-2409
E-mail: wong@scripps.edu

[†] Frequently used abbreviations are listed at the end of the Review.

Table 1: Substrates and subcellular location of human sulfatases.

Sulfatase ^[a]	Abbr.	Physiological substrate	Subcellular location ^[b]	Ref. ^[c]
aryl sulfatase A	ARSA	sulfatide	lysosome	[67]
aryl sulfatase B	ARSB	dermatan sulfate, chondroitin sulfate	lysosome	[2, 68]
aryl sulfatase C	ARSC	steroid sulfates	ER	[121]
aryl sulfatase D	ARSD	unknown	ER	[129]
aryl sulfatase E	ARSE	unknown	Golgi network	[129]
aryl sulfatase F	ARSF	unknown	ER	[130]
aryl sulfatase G	ARSG	unknown	ER	[133]
galactosamine-6-sulfatase	GalN6S	chondroitin sulfate, keratan sulfate	lysosome	[69]
glucosamine-3-sulfatase*	GlcN3S	heparan sulfate	lysosome	[92, 93]
glucosamine-6-sulfatase	GlcN6S	heparan sulfate, keratan sulfate	lysosome	[70]
glucouronate-2-sulfatase*	GlcA2S	heparan sulfate	lysosome	[91]
heparan-N-sulfatase	GlcNS	heparan sulfate	lysosome	[71]
iduronate-2-sulfatase	IdoA2S	heparan sulfate, dermatan sulfate	lysosome	[72]
endo sulfatase 1	Sulf1	heparan sulfate	ECM	[22]
endo sulfatase 2	Sulf2	heparan sulfate	ECM	[22]

[a] The genes for human sulfatases marked with asterisk have not yet been cloned. In addition to human genes, orthologues with equivalent roles have been cloned from many other vertebrates (mice, rats, cats, pigs, quails, and goats). [b] ER=endoplasmic reticulum, ECM=extra cellular matrix. [c] References for gene cloning or discovery (*).

have a slightly longer sequence of around 800 residues (Figure 1). In eukaryotes, sulfatases are targeted for the secretory pathway and are extensively glycosylated before being transported to the extracellular matrix (ECM) or to subcellular locations, such as the endoplasmic reticulum

(ER), Golgi complex, and lysosome (Table 1). The lysosomal and extracellular sulfatases are soluble, whereas the residents of the ER and Golgi network are membrane bound. All known invertebrate, lower eukaryotic, and bacterial sulfatases are soluble and have been found to reside in cytoplasmic, periplasmic, and extracellular regions (Table 2).^[3]

Sulfatases catalyze the hydrolysis of a diverse range of sulfate ester substrates, including hydrophobic glucosinolate, steroid, and thyronine sulfates; amphiphilic sulfated carbohydrates found in GAGs, proteoglycans, and glycolipids; and water-soluble mono- and disaccharide sulfates. The identification of physiological substrates of sulfatases has often trailed behind the initial discovery of these enzymes by using small aryl substrates; hence, many of them carry the generic name aryl sulfatase (ARS).^[3–5] Eight disorders

in humans are known that result from a deficiency in a single sulfatase (Table 3).^[1, 6, 7] Furthermore, a rare autosomal recessive disorder known as multiple sulfatase deficiency (MSD) results from severely decreased activity in all sulfatases.^[8]

Table 2: Sulfatases from genes cloned from invertebrates, lower eukaryotes, and prokaryotes.

Organism	Sulfatase	Substrate	Subcellular location	Physiological role	Ref.
Invertebrates and lower eukaryotes					
<i>Helicoverpa erythrogramma</i>	HeARS	unknown	extracellular	developmental	[115]
<i>Hemicentrotus pulcherrimus</i>	HpARS	unknown	extracellular	developmental	[116]
<i>Strongylocentrotus purpuratus</i>	SARS	unknown	extracellular	developmental	[118]
<i>Helix pomatia</i>	HeSulf1	unknown	unknown	unknown	[155]
<i>Plutella xylostella</i>	PGSS	unknown	gut lumen	detoxification	[152]
<i>Chlamydomonas reinhardtii</i>	CARS	glucosinolates	periplasm	sulfur scavenging	[160]
<i>Neurospora crassa</i>	NARS	tyrosine O-sulfate	extra-/intracellular	sulfur scavenging	[158]
<i>Volvox cateri</i>	VARS	unknown	periplasm	sulfur scavenging	[161]
Prokaryotes					
<i>Flavobacterium</i>	FHS2S	heparan sulfate	periplasm	HS degradation	[58]
<i>Klebsiella pneumoniae</i>	KARS	unknown	periplasm	sulfur scavenging	[63]
<i>Prevotella sp. RS2</i>	PMdS	unknown	periplasm	mucin degradation	[60]
<i>Pseudomonas aeruginosa</i>	PARS	unknown	cytoplasm	sulfur scavenging	[173]
<i>Sinorhizobium meliloti</i>	SChoS	Choline O-sulfate	cytoplasm	sulfur scavenging, osmoprotection	[181]



Chi-Huey Wong received his B.S. and M.S. degrees from the National Taiwan University and completed his PhD in chemistry at the Massachusetts Institute of Technology. After a postdoctoral year at Harvard University, he moved to Texas A&M University in 1983, and became Professor of Chemistry at The Scripps Research Institute in 1989 (Ernest W. Hahn Chair). His research interests include bioorganic and organic methods in synthesis, as well as biocatalysis with a particular focus on the study of carbohydrate-mediated biological recognition.



Sarah R. Hanson received her B.S. in chemistry in 1999 at the University of California, Berkeley, with research on antiproliferative purine derivatives with Prof. Peter G. Schultz. She also spent a summer as an NSF Undergraduate Fellow with Prof. Maria C. Linder. After graduating, she took an industrial position at Diversa, where she was involved in the development of novel enzyme catalysts. Since 2002, she has been enrolled in the Chemistry Graduate Program at The Scripps Research Institute under the guidance of Prof. Chi-Huey Wong.

	1*	2	3	4	5	6	7	8	9	10	11	12	Position of FGly (1*)	Length	Accession No. [a]
Human Sulfatases															
ARSA	C	T	P	S	R	A	A	L	L	T	G	R	69	507	P15289
ARSB	C	T	P	S	R	S	Q	L	L	T	G	R	75	533	NP_000037
ARSC	C	T	P	S	R	A	A	F	M	T	G	R	83	583	P08842
ARSD	C	T	P	S	R	A	A	F	L	T	G	R	89	593	CAA58555
ARSE	C	T	P	S	R	A	A	F	L	T	G	R	86	589	I37187
ARSF	C	S	P	S	R	S	A	F	L	T	G	R	79	591	X97868
ARSG	C	S	P	S	R	A	S	L	L	T	G	R	82	525	[130]
GalN6S	C	S	P	S	R	A	A	L	L	T	G	R	79	522	P54793
GlcN6S	C	C	P	S	R	A	S	I	L	T	G	K	91	552	CAA78164
GlcNS	C	S	P	S	R	A	S	L	L	T	G	L	70	502	P51688
IdoA2S	C	A	P	S	R	V	S	F	L	T	G	R	84	550	P22304
Sulf1	C	C	P	S	R	S	S	M	L	T	G	K	87	871	AAM76860
Sulf2	C	C	P	S	R	S	S	I	L	T	G	K	88	870	AAM76861
Invertebrate and Lower Eukaryotic Sulfatases															
HeARS	C	T	P	S	R	S	A	I	M	T	G	R	106	559	AAC27821
HpARS	C	T	P	S	R	S	A	I	M	T	G	R	100	551	P14000
SARS	C	T	P	S	R	S	A	I	V	T	G	R	115	567	P50473
HpSulf1	C	T	P	T	R	S	Q	L	M	S	G	R	80	508	AAF30402
PGSS	C	S	P	A	R	T	A	V	L	T	G	K	70	532	CAC86342
CARS	C	C	P	S	R	T	N	L	C	A	A	S	73	646	KJKM
NARS	C	C	P	A	R	V	S	L	W	T	G	K	89	639	AAC02716
VARS	C	C	P	S	R	T	N	L	W	R	G	Q	72	649	Q10723
Prokaryotic Sulfatases															
FHS2S	C	T	P	S	R	S	A	I	F	S	G	K	82	464	[58]
KARS	S	A	P	A	R	S	M	L	L	T	G	N	72	577	T45548
PARS	C	S	P	T	R	S	M	L	L	T	G	T	51	533	P51691
PMdS	S	T	P	A	R	A	C	L	L	T	G	L	79	517	AAF72520
SChoS	C	A	P	A	R	A	S	F	M	A	G	Q	54	512	AAC13371

Figure 1. Signature sequences of sulfatases. Partial alignment of sulfatases from all sulfatase genes cloned shows a homology of the sulfatase signature sequences (PS00523). This consensus sequence is important for directing the first amino acid residue to the catalytically active FGly for oxidation. Highly conserved residues are shown in white letters on a black background; other significantly conserved residues are shown in gray. The accession codes for ExPASy are given, or the reference to the literature for those proteins not deposited with ExPASy.

Two highly homologous amino acid motifs, recognized as the sulfatase signature sequences I and II, are found within the first third of the N-terminal sequence of all known hydrolytic sulfatases.^[9] The signature sequence I, comprising the 12 amino acids C/S-X-P-S/X-R-X-X-X-L/X-T/X-G/X-R/X, is critical for directing the post-translational modification of the initial cysteine or serine residue into the catalytically active residue FGly.^[10,11] The specialized role of these residues is underscored by their highly conserved nature from eukaryotic to prokaryotic organisms, as shown by the partial alignment of sequences Figure 1. The core motif C/S-X-P-X-R is conserved throughout the entire enzyme class. The arginine residue in this pentapeptide sequence has been shown to act as: 1) an important director in FGly modifica-

Table 3: Inherited disorders resulting from deficiency in a single sulfatase.^[a]

Subcellular location	Sulfatase	Genetic disorder ^[b]
lysosome	ARSA	metachromatic leukodystrophy (MLD)
	IdoAS	Hunter's disease (MPS II)
	GlcNS	Sanfilippo A (MPS IIIA)
	GlcN6S	Sanfilippo B (MPS IIIB)
	GalN6S	Morquio A (MPS IVA)
	ARSB	Maroteaux-Lamy (MPS VI)
ER, Golgi	ARSC	X-linked ichthyosis (XLI)
	ARSE	chondrodysplasia punctata (CDPX)

[a] In addition to the diseases resulting from a deficiency in a single sulfatase, a rare genetic disorder known as multiple sulfatase deficiency (MSD) shows markedly diminished activity in all sulfatases. [b] MPS = mucopolysaccharidoses.



Michael Best received his B.S. in chemistry in 1997 from Boston College, where he worked with Prof. Lawrence T. Scott on the synthesis of fullerene derivatives. He completed his PhD in 2002 at the University of Texas at Austin on the design and synthesis of fluorescent sensors for biomolecules in the research group of Prof. Eric V. Anslyn. He has since been carrying out postdoctoral research with Prof. Chi-Huey Wong at The Scripps Research Institute on the development of small organic molecules which perturb biological systems.

tion,^[10] 2) an integral member of the active site that stabilizes the FGly residue,^[12] and 3) a critical structural element.^[11] The conserved proline residue also plays a key role in directing FGly modification^[10] and is believed to be part of an α helix that precisely situates FGly within the active site.^[11] Interestingly, two enzymes that are not sulfatases, a phosphate monoester hydrolase (U44852) and an alkaline phosphatase (AF047381), have also been found to contain the core directing sequence C/S-X-P-X-R. Given the potential evolutionary link between sulfatases and the alkaline phosphatase,

tases,^[13] these enzymes could be the most likely candidates outside the sulfatase class to harbor an FGly residue. The second sulfatase signature sequence contains the 12-mer consensus sequence G-Y/V-X-S/T-X-X-X-G-K-X-X-H. The conserved lysine and histidine residues within this motif are active-site residues that are important for sulfate ester catalysis.^[14]

3. Structure

The structures of four sulfatases have been solved to date by X-ray crystal-structure analysis: HARSA (2.1 Å),^[15] HARSB (2.5 Å),^[16] and HARSC (2.6 Å)^[17] from humans, as well as PARS (1.3 Å) from the gram-negative bacterium *Pseudomonas aeruginosa*.^[12] The structures are strikingly similar, revealing a nearly spherical globular monomer with mixed α/β topology, which is divided into two domains (Figure 2). ARSC additionally contains a unique transmembrane domain from which the soluble domain “sprouts”, giving the enzyme a “mushroomlike” morphology. The larger, N-terminal domain consists of α helices surrounding a large mixed β sheet, which consists of 10 strands in the HARSA, HARSB, and PARS structures and 11 strands in HARSC. The smaller, C-terminal domain contains a four-stranded antiparallel β sheet tightly packed against a long, solvent-exposed C-terminal α helix. As is typical for the α/β family of enzymes,^[18] the active-site cavity is nestled at the C-terminal end of the large β sheet, with the FGly residue located at the bottom of a narrow cleft lined with charged amino acids. The catalytic N-terminal domain of sulfatases shows a high degree of structural similarity to that of the alkaline phosphatases (APs) but differs dramatically in sequence.^[19] When the structures of ARSA and AP are superimposed, 169 contiguous C $^{\alpha}$ atoms overlap, including the large β sheets and several key active-site residues, with a root-mean-squared deviation (rmsd) of 1.9 Å. Similar values are obtained when comparing HARSB and PARS.^[15]

Crystallographic and mutagenesis studies have provided valuable information about the active site of sulfatases (Figure 3). In each of the structures solved thus far the catalytic residues and geometry are conserved to a remarkable extent (rmsd < 0.45 Å), which supports the notion of a

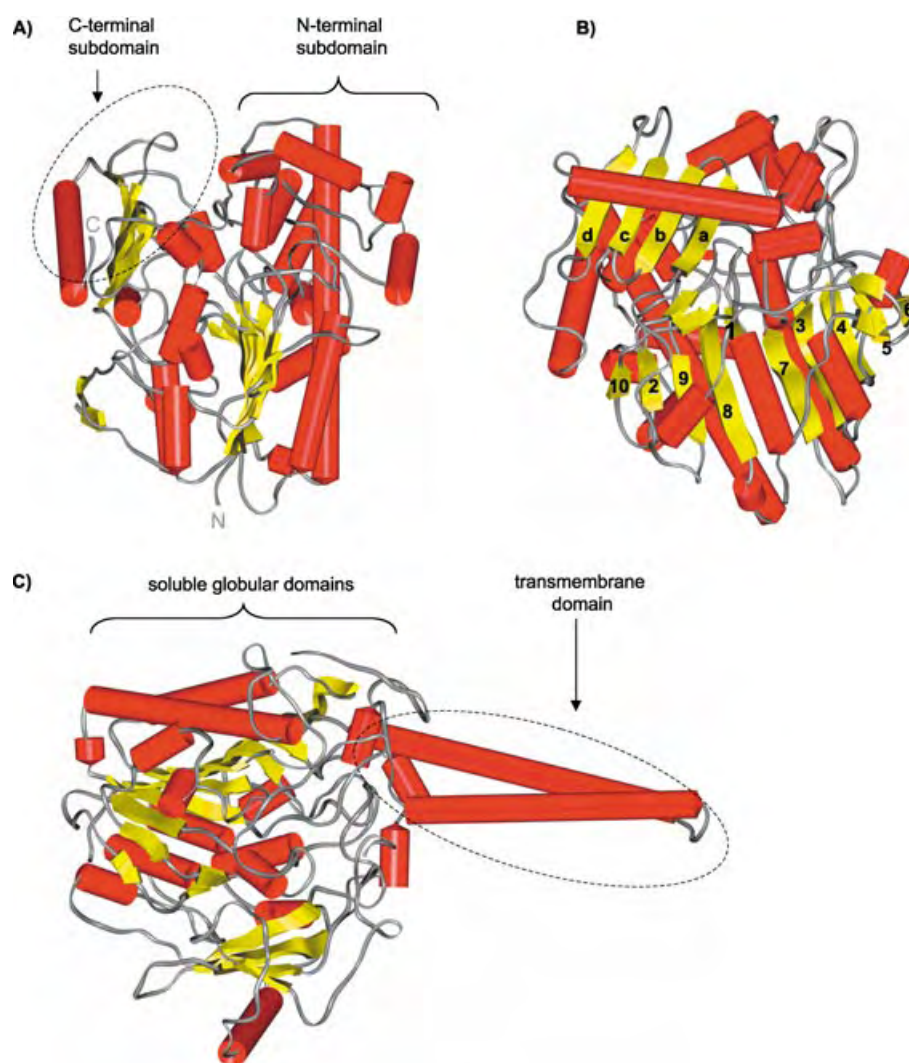


Figure 2. Crystal structures of sulfatases (red cylinders: α helices, yellow arrows: β sheets). A) Structure of PARS, characterized by two subdomains with mixed α/β topology. B) Same structure of PARS, rotated 90°; the strands of the large β sheet within the N-terminal domain (numbered 1–10) and the small β sheet in the C-terminal domain (labeled a–d) are visible. C) Structure of HARSC, which shares high structural homology with PARS within the globular domains. This ER-resident protein also contains a transmembrane domain comprising two highly hydrophobic helices of 40 Å in length.

conserved mechanism for sulfate ester hydrolysis. The active site is comprised of 10 highly interconnected polar residues and a divalent metal cation; the positions and proposed functions of these components are summarized in Table 4. In the case of HARSA, the importance of each of these residues was further established in a mutational scanning experiment.^[14] A metal-binding region is formed by the generic residues AspA, AspB, AspC, and AsnA, which is conservatively replaced by a glutamine residue in ARSC. In HARSB, HARSC, and PARS these metal-binding residues, along with FGly and an oxygen atom of the sulfate (or water in its absence), coordinate a Ca²⁺ cation heptavalently; in HARSA an Mg²⁺ ion is coordinated octahedrally. However, in the latter case it can not be excluded that the magnesium ions, which were present in high concentrations during the purification of the enzyme, replaced the native cation,^[15] as was observed in a more recent refinement of the ARSA

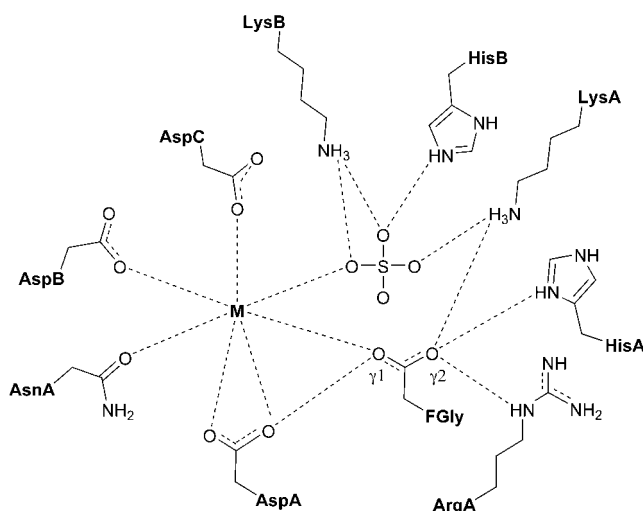


Figure 3. A generic rendition of the sulfatase active site depicting the highly conserved residues found in the crystal structures. Key hydrogen-bonding interactions are shown with dotted lines. For the sake of clarity some details are not shown in the diagram, including localized charges, some double bonds, and several interactions, such as a salt bridge between LysA and the noncoordinated oxygen atom of AspC, a hydrogen bond between sulfate and the nitrogen atom in the main chain of FGly, and several sulfate–FGly interactions. Table 4 lists the positions and proposed functions of the residues in each solved structure.

structure by another research group.^[20] Severe decreases in binding and catalytic activity were observed upon mutation of any of the metal-binding residues in HARSA, underscoring the central role the metal plays in cleaving sulfate esters, presumably by both binding the substrate and activating it for nucleophilic attack.^[14]

The catalytic pocket is lined with several positively charged residues, including LysA and LysB, which are involved in binding the anionic sulfate. Along with the divalent metal ion and HisB, these residues probably neutralize the sulfate anion and withdraw electron density to create an electrophilic sulfur center. They also position the tetrahedral sulfate for an in-line nucleophilic attack by FGly.^[21] Furthermore, HisB and LysB are implicated in the protonation of the exocyclic oxygen atom on the alcoholate leaving group released in the transesterification. The catalytic

FGly residue rests at the bottom of the pocket as an FGly hydrate (FGH). The geminal diol performs two distinctive functions: FGH-Oγ1, which interacts with the metal center and AspA, is orientated ideally for nucleophilic attack on the sulfur atom of the substrate; FGH-Oγ2, which is anchored by HisA, ArgA, and LysA, points toward the center of the pocket and is involved in the elimination of the enzyme–sulfate ester intermediate. The critical functions of the geminal hydroxy groups are thought to be mediated by protons, shuffling between AspA and FGly-Oγ1, in addition to HisA and FGly-Oγ2 (Section 4).

To date, no crystal structures of sulfatases bound to their natural substrates have been solved, leaving the residues that play a role in substrate specificity largely unknown. Presumably, the recognition of natural substrates must occur outside the narrow cleft containing the conserved active-site residues. The cocrystal structure of Cys69Ala-HARSA (a mutant with the catalytic FGly residue replaced by alanine) with *p*-nitrocatechol sulfate (pNCS, a general substrate for sulfatases) exhibited a tightly bound sulfate group (coordinated by the metal center, LysA, LysB, and HisA; Figure 3) and a highly disordered phenyl ring outside the sulfate-binding pocket.^[21] Indeed, the fact that many sulfatases accept small aryl substrates could mean that extensive binding sites on their surfaces discriminate between and properly align large substrates, but do not necessarily hinder access to the active site.

Typically, the C-terminal region of sulfatases bears the highest structural diversity and is a likely candidate for a substrate-discerning region. Interestingly, the HSulf sulfatases and HGlcN6S, which catalyze the hydrolysis of glucosamine-6S (GlcNAc_{6S}) residues, contain C-terminal stretches of amino acids that exhibit high homology with a region of the GlcNAc transferase from *Arabidopsis thaliana*, suggesting that this region may play a role in the recognition of the GlcNAc substrate.^[22] The C-terminal region of the membrane-bound sulfatases may also serve an additional purpose. According to the crystal structure of ARSC, the small subdomain is involved in several key interactions between hydrophobic loop structures and the lipid bilayer. These polypeptide segments could potentially act as “swinging doors” to recognize substrates and lead them to the active-site gorge, which is buried near the membrane surface. The active-site gorge of ARSC contains a host of nonpolar

Table 4: Positions and proposed functions of amino acids and metal cations in the active site.

Residue ^[a]	PARS	HARSA	HARSB	HARSC	Proposed function
FGly	51	69	91	75	catalytic nucleophile as FGH
M	Ca ²⁺	Mg ²⁺	Ca ²⁺	Ca ²⁺	substrate binding and activation, stabilization of FGH
AsnA	Asn318	Asn282	Asn301	Gln343	metal coordination, activation of FGH
AspA	Asp317	Asp281	Asp300	Asp342	metal coordination
AspB	Asp14	Asp30	Asp54	Asp36	metal coordination
AspC	Asp13	Asp29	Asp63	Asp35	metal coordination
ArgA	Arg55	Arg73	Arg95	Arg79	stabilization of FGH
HisA	His115	His125	His147	His136	stabilization of FGH, elimination of FGS
HisB	His211	His229	His242	His290	substrate binding and activation, alcohol protonation
LysA	Lys113	Lys123	Lys145	Lys134	substrate binding and activation, stabilization of FGH
LysB	Lys375	Lys302	Lys318	Lys368	substrate binding and activation, alcohol protonation

[a] Generic residues are depicted schematically in Figure 3.

residues that are capable of forming hydrophobic interactions with the steroid backbone when the sulfate is properly aligned in the sulfate-binding cleft.^[17]

4. Mechanism

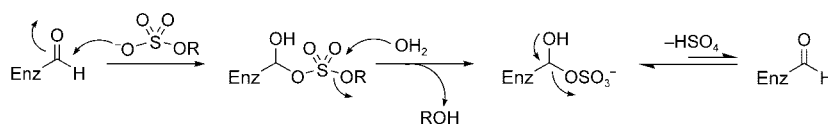
4.1. Sulfate Ester Hydrolysis

The most salient feature of the sulfatase family of enzymes is the presence of the FGly residue (2-amino-3-oxopropanic acid, α -formylglycine) in the active site. FGly is present in the active site of all prokaryotic and eukaryotic sulfatases characterized to date and is essential for catalytic activity.^[23] Its importance was initially identified by von Figura and co-workers during their extensive studies on multiple sulfatase deficiency (MSD).^[8] The researchers correctly speculated that a common structural feature in the sulfatase active site, generated by a post-translational modification, was deficient in MSD patients, thus resulting in the global inactivation of sulfatases.^[24] In a landmark study, the novel aldehyde modification was detected in the position in which a cysteine residue was encoded in the cDNA for HARSA and HARSB enzymes.^[25] Later, it was determined that the residue destined for modification can be either cysteine in eukaryotes^[25,26] and prokaryotes,^[27] or serine^[28] in prokaryotes. Prokaryotic sulfatases are therefore further categorized as Cys-type or Ser-type.^[29–32]

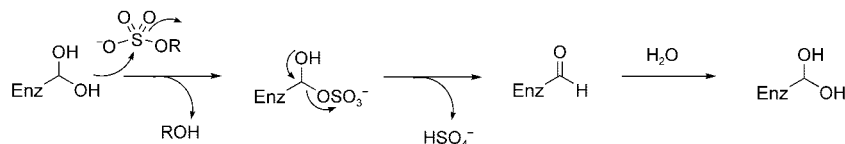
The mechanism of sulfate ester hydrolysis remained a mystery for years, as nothing was known about the underlying post-translational modification required to generate the key active-site aldehyde. The elucidation of the mechanism was greatly facilitated by the discovery of this modification and by the crystal structures of the sulfatases.^[12,15–17] Although it was immediately clear that the novel FGly residue was crucial for catalysis,^[25,33] its mode of action was the subject of debate for some time.^[23] Structural similarity with the alkaline phosphatases (APs) provided initial insight into the mechanism of the sulfatases, and after the first sulfatase structure was solved in 1995 (HARSB) an addition–hydrolysis (AH) mechanism was proposed.^[16] As depicted in Scheme 1a, the mechanism begins with a nucleophilic attack by a sulfate group oxygen atom at the electrophilic aldehyde group of FGly to form a sulfate diester. The alcohol conjugate is then released through the action of a nucleophile, such as an activated water molecule (akin to the AP mechanism). The FGly–sulfate adduct (FGS), which was observed in the HARSB crystal structure, was proposed to be the resting state of the catalytic cycle, although equilibrium with the aldehyde was assumed.

The HARSA resting-state structure was interpreted differently: Its structure showed a twofold-disordered electron-density pattern at the FGly residue, leading to the postulation that the FGly functions catalytically as an

a) Addition–Hydrolysis Mechanism



b) Transesterification–Elimination Mechanism



Scheme 1. Proposed mechanistic schemes for the hydrolysis of sulfate esters by the active-site aldehyde FGly. a) An addition–hydrolysis (AH) mechanism was proposed based on the interpretation of a sulfate hemiacetal (FGS) in the crystal structure of HARSB as the resting state of the catalytic cycle. b) A transesterification–elimination (TE) mechanism was presented for hydrated aldehyde group (FGH) present in the crystal structure of HARSA. See text and Scheme 2 for details.

aldehyde hydrate.^[15] Based on these data, a transesterification–elimination (TE) mechanism was presented, in the first step of which one of the geminal hydroxy groups of the FGly hydrate (FGH) acts as a nucleophile. As shown schematically in Scheme 1b, an S_N2 attack at the sulfur atom of the sulfate hydrolyzes the conjugate alcohol and creates a transient FGS. The second geminal hydroxy group then reacts to eliminate sulfate and re-form the aldehyde. Finally, the catalytic cycle is completed by hydration of the aldehyde to reform the FGH. Unfortunately, poor resolution within the vicinity of the crucial FGly residue in both structures left the general model for sulfate ester hydrolysis open for debate.

Support for the TE mechanism was provided by studies of HARSA and HARSB mutants containing a serine residue in place of FGly. When exposed to [³⁵S]-*p*-nitrocatechol sulfate, the serine mutants released *p*-nitrocatechol, but the labeled sulfur atom remained bound, whereas wild-type enzymes showed no residual radioactivity.^[34] These results suggested that the first step of the TE enzymatic process, namely transesterification of the substrate by serine to form a sulfoenzyme intermediate, was possible. However, the second step was not. Serine mutants were unable to eliminate sulfate, underscoring the importance of the second FGH hydroxy group for sulfate ester catalysis. The experiment also provided strong evidence against the AH mechanism, as nucleophilic attack at serine by an oxygen atom of the sulfate group is highly unlikely. Further evidence for the TE mechanism was provided when a cocrystal structure of an FGly-alanine HARSA mutant with pNCS was superimposed with wild-type HARSA: The comparison showed that the sulfate group was optimally orientated for an in-line nucleophilic attack by the O γ 1 hydroxy group, which was positioned 2.85 Å from the sulfur center.^[21]

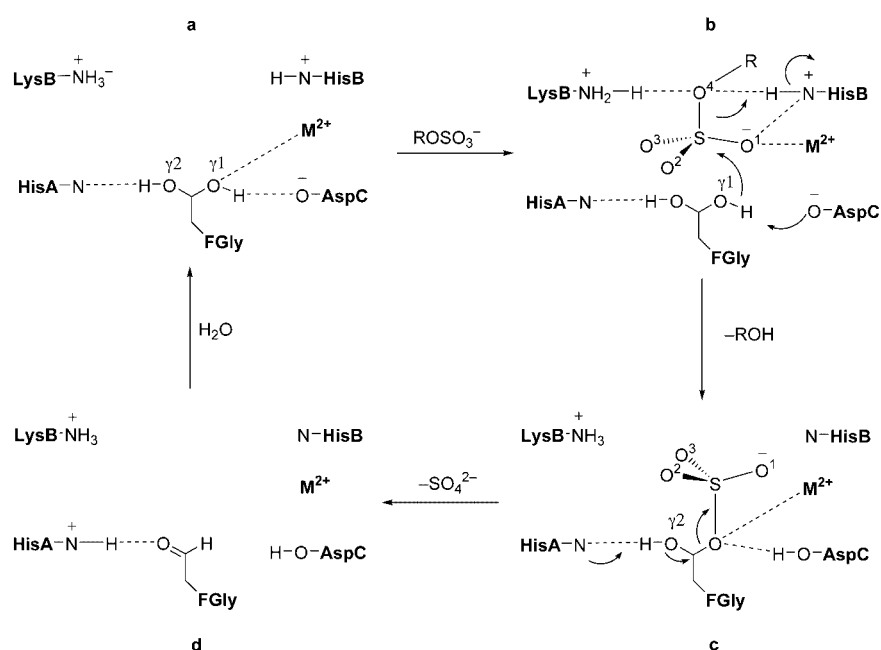
Another key discriminating feature between the two mechanisms is the configuration of the chiral sulfate released from the substrate after catalysis. The TE mechanism would

cause an inversion of configuration at the sulfur atom, as it proceeds through a pentagonal intermediate in the S_N2 transition state. In contrast, the AH mechanism, which proceeds without chemical modification at the sulfur center, would produce a sulfate group with retention of configuration. In a study of chiral sulfates as the substrates for an aryl sulfatase from *Aspergillus*, inversion of configuration was observed, thus providing further evidence for a TE mechanism.^[35] To date, the experiment has not been reproduced with other better characterized sulfatases.

Particularly strong support for the TE mechanism was derived from the elucidation of the X-ray crystallographic structure of PARS at atomic resolution (1.3 Å).^[12] The structure clearly showed that the FGly hydrate was near to, but independent of, a coordinated inorganic sulfate. The sulfate moiety is probably present as a result of the high concentrations of exogenous sulfate used to procure the PARS crystals. Not surprisingly, high sulfate concentrations are well known to inhibit hydrolytic sulfatases.^[3,5] Again, the orientation of the sulfate was found to be optimal for nucleophilic attack, with one face of the tetrahedron situated at a distance of 2.96 Å from FGH-Oγ1, similarly to the pNCS-Cys69Ala-HARSA cocrystal.^[21] Presently, it is believed that the sulfate hydrolysis proceeds by the TE mechanism depicted in Scheme 2.

The question of whether the transition state of sulfate ester hydrolysis is primarily associative (S_N2 -like) or dissociative (S_N1 -like) has not been addressed directly. However, several studies have shown that the nature of the alcohol leaving group is important. In studies with bacterial sulfatases, linear free-energy relationships were established that showed a strong correlation between substrates with better phenolic leaving groups and improved binding and catalysis (see the review by Dodgson et al.).^[3] These results were mirrored in more recent studies on the inhibition of ARSC with aryl and alkyl sulfamates.^[36] Irreversible inhibition by these compounds occurs after the rate-limiting hydrolytic step, although the exact course of events leading to the dead-end adduct is unknown. The results showed that the presence of electron-withdrawing groups (EWGs) at the α position of alkyl groups or on the phenolic chain resulted in much better inhibition, indicating that a better stabilized leaving group is important for the initial hydrolysis and subsequent inhibition. This behavior closely mirrors the trends observed for the dissociative mechanisms of APS, which have benefited from over 25 years of biochemical probing.^[37]

Recently, the uncatalyzed hydrolysis of sulfate esters has also been found to be more dissociative than associative in nature.^[38] In a dissociative transition state for sulfate ester hydrolysis, the bond forming between the incoming nucleophile and the sulfur atom would be expected to be weak,



Scheme 2. The TE mechanism involving FGly and key active-site residues based on the crystal structure of PARS and mutagenesis studies on HARSA. a) In its resting state the FGly residue forms an FGly hydrate (FGH) stabilized by hydrogen bonds. a→b: Positively charged residues and the metal center bind, orientate, and activate the substrate sulfate for in-line nucleophilic attack by one of the FGH geminal hydroxy groups, HOγ1, which is positioned 2.96 Å from the sulfur center. The transesterification is promoted by proton transfer between Oγ1 and AspC. b→c: An S_N2 substitution (shown by arrows in (b)) proceeds through a pentacoordinated intermediate with inversion of configuration at the sulfur center and release of the conjugate alcoholate, which accepts a proton from HisB and diffuses from the pocket (LysB, Oγ2, and H₂O could also serve as proton sources, depending on the pH). Elimination of the sulfate hemiacetal (FGS) is favored by the electron-withdrawing groups coordinated to the sulfate. c→d: Abstraction of the H-Oγ2 proton by HisA induces the elimination of sulfate and regeneration of the aldehyde, which is subsequently rehydrated to complete the catalytic cycle (d→a). See Table 4 for the numbering of the residues and Figure 2 for a schematic of the residues in the active site.

whereas a more pronounced bond dissociation between the sulfonyl group and the leaving group would result in the accumulation of negative charge on the phenolate oxygen atom. Electron-withdrawing groups would help delocalize this charge, thereby stabilizing the dissociative transition state. The results accumulated to date seem to support the model of a dissociative transition state for sulfate ester hydrolysis, implying that the mechanism proceeds with some S_N1 character, probably with the assistance of the nucleophilic FGly hydrate. However, this interpretation should be treated with caution, as only limited studies have been carried out.

4.2. Other Sulfatase Mechanisms

At least two other mechanisms for sulfate ester cleavage have been identified in prokaryotes. Several bacterial alkyl sulfatases have been found that cleave the C–OS bond of sulfate esters, as opposed to the CO–S bond cleaved by hydrolytic enzymes.^[39,40] Interestingly, some of these secondary alkyl sulfatases have been reported to produce an inversion of configuration at the stereogenic carbon center.

suggesting a nucleophilic attack takes place at this position (see the review by Dodgson et al.^[3]). Making use of this stereoinversion, one research group has recently developed a method for deracemizing secondary alkyl sulfates.^[41–43] The oxidative cleavage of alkyl sulfate groups to aldehydes and inorganic sulfate has also been reported.^[44–46]

Genes for C–O cleaving^[47,48] and oxidative sulfatases have been cloned.^[46] Not surprisingly, these enzymes do not share significant sequence homology with the hydrolytic S–O cleaving sulfatases and do not contain the characteristic consensus sequences for FGly modification. Several other S–O cleaving alkyl sulfatases are known,^[49,50] but information on their sequences is not yet available, and it is unclear if they operate by a FGly-mediated hydrolytic process or by other mechanisms of sulfate ester cleavage. Another potential mechanism for sulfate cleavage may be at work in the aryl sulfatases isolated from *A. Carrageenovora* and *Campylobacter jejuni*.^[51,52] These enzymes do not contain the sulfatase consensus sequence required for FGly generation and bear little overall sequence similarity to the hydrolytic aryl sulfatases. At this point, the mechanistic details pertaining to these enzymes have not been elucidated.

5. The Post-Translational FGly Modification

5.1. The Cys–FGly Modification in Human ARSA

The catalytic integrity of sulfatase enzymes rests in the FGly residue. Normally, this unique residue is generated through the oxidation of a cysteine precursor found in the encoded peptide sequence of all human sulfatases. However, in multiple sulfatase deficiency (MSD) this critical modification is absent, resulting in categorically inactive sulfatases and severe clinical manifestations.^[25] The MSD factor (MSDF) was postulated to be a defect in the post-translational modification machinery or in the FGly-generating enzyme (FGE).^[7] Recently, a major breakthrough occurred when the FGE gene was identified and characterized as the causative agent of MSD.^[31,32]

As components of the secretory pathway, sulfatases are directed to the ER during protein synthesis where the key catalytic residue, FGly, is generated from a cysteine residue.^[53,54] All the information necessary to initiate modification is contained in the autonomous linear sequence C-T-P-S-R-A-A-L-L-T-G-R, which begins with the cysteine residue destined for modification.^[10,53] Mutation and truncation of this targeting sequence revealed that a core motif, C(X/T)P(X/S)R, is the minimum sequence required to direct modest amounts of oxidation. Mutations of P and R within this motif greatly reduced efficiency, whereas mutations of T and S were tolerated individually, but not simultaneously. Of the seven auxiliary residues, the LTGR sequence was found to be the most important, and it is hypothesized that this sequence plays a role in molecular recognition. Apart from mutations of the cysteine residue, no single mutation was capable of abolishing modification activity altogether.^[10,11]

Several experiments have demonstrated that the oxidation event occurs during late co- or post-translation, after

translocation to the ER, and before protein folding.^[10,11,53–55] The modification of ribosome-bound nascent polypeptide chains (RNCs) in vitro occurred after translocation to microsomes or after they had been exposed to soluble extracts from the ER. These results show that translocation and exposure to the luminal components of the ER are required to initiate the transformation. In translocation-arrested RNCs containing engineered N-glycosylation sites, the FGly residue was created after glycosylation and chemical release from the ribosome, and even after the cleavage of the signal peptide. These observations indicate that the oxidation step takes place during a late cotranslational phase. Finally, the finding that FGly is also expressed in truncated and heterologous protein constructs implies that the conversion is not influenced greatly by other portions of the peptide or by protein folding. That modification occurs in a largely unfolded state was also supported by the fact that small exogenous peptides comprised of the targeting sequence effectively inhibit FGly expression in RNCs.^[55] In vitro oxidation of these small peptides (ARSA65–80) has even been observed recently as well, which provides further evidence for an autonomous interaction of the linear directing sequence with the FGE.^[31]

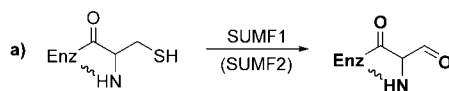
Recently, the long-sought-after FGE was discovered by two research groups independently.^[31,32] The FGE gene, *sumf1* (sulfatase-modifying factor 1), encodes for an ER-localized protein with 374 amino acids belonging to a class of proteins of previously unknown function. Preliminary biochemical characterization suggests that SUMF1 acts as a mixed-function oxygenase that is both essential and limiting for the expression of active sulfatases (Scheme 3a).^[31] Highly conserved SUMF1 homologues were found in many eukaryotic and prokaryotic species, which is not surprising given the importance of the FGly modification.^[31,32] Catalytic and functional conservation among FGE homologues was demonstrated by the production of active human sulfatases coexpressed with SUMF1 cDNAs from mice and *Drosophila*.^[32] Paralogues of SUMF1, known as SUMF2, were also identified by sequence homology. These proteins also showed FGE activity, albeit much less efficient than that of SUMF1, and it is postulated that they are responsible for the weak, residual sulfatase activity observed in MSD.^[32]

5.2. The FGly Modification in Prokaryotes

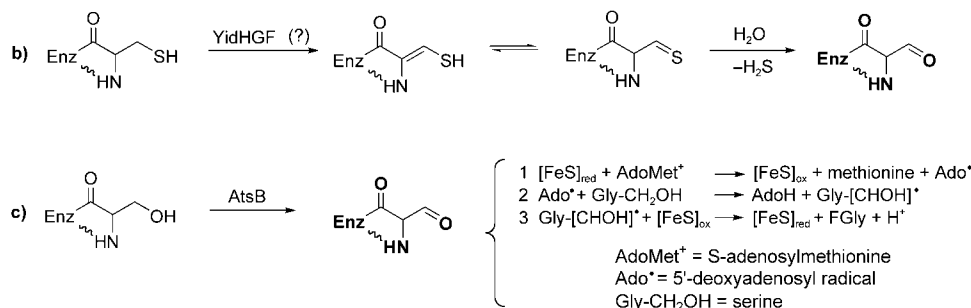
Several sulfatase genes from prokaryotes have been cloned and characterized (Table 2). The sequences show a high degree of similarity with those of eukaryotic sulfatases, especially within the FGly-targeting signature sequence. However, unlike in the case of eukaryotic enzymes, which exclusively encode cysteine as their FGly progenitor, prokaryotic sulfatases derive FGly residues from serine as well as cysteine precursors. The modification of the Ser-type and Cys-type enzymes occurs by different routes, and several studies have been designed to identify and characterize the underlying FGE.

The bacterial Cys-type FGE (C-FGE) is likely to be a homologue of the conserved family of SUMF1 proteins, which were recently discovered in eukaryotes (Scheme 3a).^[31,32]

Eukaryotes and Prokaryotes



Prokaryotes



Scheme 3. Mechanisms for FGly generation by eukaryotic and prokaryotic FGEs. The SUMF genes have been preliminarily characterized as mixed-function oxygenases that are essential for the generation of FGly residues from cysteine progenitors in eukaryotes (route A). FGly residues in prokaryotes can be generated from cysteine and serine precursors by C-FGE and S-FGE, respectively. The C-FGE might be of the same type as the eukaryotic FGE; however, other pathways have also been suggested (route b; see text for details). The S-FGE (route c) has been identified as the iron-sulfur protein AtsB, which catalyzes the transformation by the proposed redox process outlined in steps 1–3.

Putative SUMF1 genes were detected in some bacteria by sequence analysis; however, the cloning and characterization of a bacterial C-FGE has not yet been achieved. Most of the information available about the bacterial Cys-modification system has been garnered from the recombinant expression of sulfatases in *Escherichia coli*, which does not produce an endogenous aryl sulfatase.^[56] Although an active sulfatase has not been isolated from *E. coli*, both Cys- and Ser-type genes and putative activity have been described.^[29,57] It is clear that the bacteria have an active C-FGE, which installs FGly residues exclusively from cysteine precursors. The recombinant expression of Cys-type PARS and FHS2S (FHS2S = heparan-2-sulfatase from *Flavobacterium heparinum*) in *E. coli* results in active enzymes,^[27,58] whereas Ser-type sulfatases are inactive.^[59,60] Likewise, the mutation of PARS and FHS2S to Ser-type enzymes also renders inactive proteins.^[27,61]

The efficiency of the C-FGE in prokaryotes appears to differ dramatically from that in eukaryotes. The modification of PARS proceeds to completion in native and *E. coli* hosts.^[27] In contrast, the human FGE has been found to be a limiting factor^[62] where efficient modification requires the co-overexpression of SUMF1, and even then, oxidation is incomplete.^[31,32] Such a discrepancy indicates some fundamental differences in the C-FGEs of bacteria and eukaryotes.

It is even possible that another FGE, distinct from SUMF1, is harbored in some bacteria. One bioinformatics study located a gene cluster, *yidHGF*, in *E. coli* near a putative Cys-type sulfatase, *yidJ*. Based on the sequence homology and mechanistic similarity, the cluster has been proposed to catalyze the oxidative desulfurization of the sulfanyl group of cysteine to an aldehyde, in analogy with the

oxidative deamination of aspartate to oxaloacetate (Scheme 3b).^[29]

Relatively more is known about the Ser-type FGE (S-FGE) in bacteria. Early experiments on the expression of the aryl sulfatase from *Klebsiella pneumoniae* (KARS) showed that the production of an active enzyme in *E. coli* required the coexpression of an adjacent gene, *astB*, which forms a bicistronic operon with the KARS gene.^[63] Initially, AstB was speculated to be a positive regulator of KARS or a transcriptional factor.^[64] Later, it was recognized to have high homology with oxidoreductases and was found to be critical for the expression of FGly residues, indicating that it might be the S-FGE.^[27,59] The possible role of AstB homologues as S-FGEs was further substantiated by the fact that the Ser-type sulfatase PMdS (PMdS = mucin sulfatase from *Prevotella* sp. RS2) was inactive when expressed in *E. coli*, but active during heterologous production in *Bacterioides thetaiotaomicron*.^[60] *B. thetaiotaomicron* harbors the gene *chuR*, which encodes for a protein that is highly homologous with AstB. Indeed, endogenous sulfatase activity is inhibited when *chuR* is knocked out.^[65] Sequence analysis of the regions flanking the PMdS gene showed that it has an adjacent gene which encodes for an AstB homologue. It is tempting to speculate that the coexpression of this gene in *E. coli* might produce active PMdS. In fact, similar operons were identified when the sequences of several putative Ser-type sulfatases were analyzed, suggesting that the S-FGE is commonly bicistronic with the sulfatase that it modifies.^[29] In each case, the second gene encodes for an iron-sulfur protein that contains conserved cysteine clusters. These proteins have recently been linked with oxidoreductase activity and are capable of oxidizing a serine residue to an aldehyde (Scheme 3c).^[29,30]

The role of AstB in modulating the transformation of serine residues into FGly was firmly established when KARS was expressed independently and with AstB in *E. coli*.^[59] FGly was only formed in the presence of AstB. The observed modification efficiency of 60 % corresponds to the yield with natively expressed KARS.^[28] More recently, AstB was shown to be a cytoplasmic enzyme that directly interacts with the FGly-targeting sulfatase signature sequence in a serine-dependent manner, and was proposed to catalyze the transformation through oxidoreductase activity (Scheme 3c).^[30] The transformation process is facilitated by the presence of a signal peptide that targets protein translocation to the periplasm. Removal of this sequence dramatically decreased the efficiency of the FGly modification of the periplasmic KARS enzyme. Also the FGly transformation was introduced into a mutant Ser-PARS when the enzyme was also recombinantly adorned with the KARS signal sequence.^[28] All known and several putative Ser-type sulfatases contain N-terminal signal peptides which direct the enzyme to the periplasm; most Cys-type sulfatases, however, are localized in the cytoplasm.^[29]

The fact that bacteria are capable of the post-translational generation of FGly from both cysteine and serine residues by separate mechanisms is intriguing, as the sequences surrounding the FGly progenitors are essentially identical.^[29] According to an early theory the enzymes do not differentiate between the nearly identical targeting sequences on the basis of binding processes, but instead implement specific catalytic domains that oxidize the cysteine and serine residues to FGly.^[59] Indeed, in the purification of the mammalian (Cys-type) FGE a binding matrix containing the Ser-targeting sequence was exploited.^[51] It appears that subcellular distribution might also have an influence on which FGE is operative in bacteria. The periplasmic targeting sequence helps to facilitate a fruitful connection between Ser-type sulfatases and the S-FGE, and it is possible that other translocational components are also involved in this process.^[30]

6. Substrates and Biological Functions of Eukaryotic Sulfatases

Many eukaryotic sulfatases were initially identified based on their enzymatic activity with small aromatic sulfates, such as *p*-nitrophenol sulfate (pNPS), *p*-nitrocatechol sulfate (pNCS), and 4-methylumbelliferone sulfate (4MUS). This activity led to a long-running misunderstanding about the physiological roles of sulfatase enzymes, but is now used for the general classification of sulfatases into ARS and non-ARS types.^[4,5] Both classes of enzymes are active with aryl substrates, but the ARS type effect hydrolysis at much higher rates. Steroid sulfates and a variety of sulfonated carbohydrates, including monosaccharides, oligosaccharides, proteoglycans, and glycolipids, count among the natural substrates of the human sulfatases (Table 1). As shown in Table 5, the enzymes show a strong specificity for their biological substrates despite their promiscuity with aryl substrates.

Human sulfatases have been found in several subcellular locations, where they play key roles in important biological processes, including the synthesis of hormones in the ER, the degradation of glycosaminoglycans and glycolipids in the lysosome, and the modulation of developmental-cell signaling in the ECM. Several other human sulfatases have been identified, but their biological functions are unknown. Potentially these enzymes might be involved in the desulfonation of other important biomolecules, such as sialyl Lewis^x-6S (sLe^x-6S) and tyrosine *O*-sulfate. The sulfatases of invertebrates and lower eukaryotes are largely unexplored. Several genes have been cloned (Table 2), and in some cases exhibit activities, including a role in the development of sea-urchin embryos, the inactivation of endogenous plant toxins, and involvement in the sulfur metabolism in algae and fungi.

6.1. Lysosomal Sulfatases

The lysosomal sulfatases were the first to be associated with physiological functions and are by far the best characterized of human sulfatases. They are ubiquitous housekeeping enzymes that are synthesized in the secretory pathway and are targeted to the lysosome through the mannose 6-phosphate receptor pathway.^[66] Characteristic of their subcellular location, the enzymes exhibit pH optima in the acidic region (Table 5). They also demonstrate exquisite substrate specificity and little functional redundancy. Catalytic desulfonation is critical to the catabolism of several sulfate-bearing metabolites. Indeed, six physiological disorders in humans are known to arise from the accumulation of toxic levels of nondegradable sulfated compounds, owing to deficiencies in single lysosomal sulfatases (Table 3).^[24] Because of their role in certain diseases, a number of lysosomal genes from humans^[2,67–72] and other mammals have been cloned and characterized extensively.^[1,7,8]

As shown in Table 5, ARSA hydrolyzes a number of sulfated substrates.^[73,74] The major physiological substrates are sulfatides, specifically sphingolipids with galactose-3S (Gal-3S) head groups.^[75,76] It has been suggested that ascorbic acid 2S is another natural substrate.^[77] ARSA has been associated with the inherited genetic disorder metochromatic leukodystrophy (MLD), which is characterized by extensive demyelination in the nervous system.^[7] This disorder results from improper catabolism of the sulfatide cerebroside-3S (**1**, Figure 4), which is one of the major structural components of the myelin sheath. The cleavage of the cerebroside-3S ester in vivo requires the presence of the solubilizing agent, sphingolipid activator protein B (sapB), which forms a 1:1 complex with the substrate prior to hydrolysis.^[78] More recent studies indicate that ARSA may also play a role in non-lysosomal environments as well: It has been detected on sperm surfaces, where it is thought to adhere to sulfated egg glycoproteins and modulate steps in the fertilization process.^[79–82]

The human lysosomal sulfatases ARSB, GalN6S, GalN3S, GlcN6S, GlcA2S, GlcNS, and IdoA2S have been studied extensively. They play a role in mucopolysaccharidosis (MPS), a group of lysosomal storage disorders resulting from deficiencies in GAG catabolism (Table 3).^[1] GAGs are

Table 5: Catalytic properties of human sulfatases.

Enzyme	Substrate ^[a]	Rate ^[b]	K_m ^[c]	pH optimum	Ref.
ARSA	4MUS	40 000	12 500	5.7	[73, 74]
	pNCS	160 000	400	5.5	
	ascorbic acid 2S	85 000	2800	4.8	
	cerebroside-3S	6600	105	4.5	
	seminolipid-3S	5000	180	4.5	
	psychosine-3S	3000	200	4.5	
	tyrosine-S	6700	3500	5.5	
ARSB	4MUS	48 500	1180	5.6	[74, 89, 94]
	GalN_{4S}-(CS/DS)*	2000	60	5.6	
	tyrosine-S	871	< 300 000	5.5	
ARSC	4MUS	7000	800	7.0	[122]
	pNPS	4000	400	7.0	
	estrone-S	2900	0.8	7.0	
	pregnolone-S	1600	0.6	7.0	
	cholesterol-S	1400	2	7.0	
	DHEA-S	1000	1.7	7.0	
	testosterone-S	1	40	7.0	
	vitamin D3 S	< 1	N/A	7.0	
ARSD	4MUS	n.d.		7.0	[129]
ARSE	4MUS	663		7.0	[129, 130]
ARSF	4MUS	1356		7.0	[129]
ARSG	4MUS	n.d.		7.0	[133]
GalN6S	4MUS	120	4400	4.7	[88, 89]
	GalNAc_{6S}-(CS)*	1990	15	4.0	
	Gal_{6S}-(KS)*	100	50	4.0	
GlcNS	4MUS	114	4800	5.4	[95]
	GalN₅-(HS)*	930	10.3	5.6	
	GalN ₅ -IdoA _{2S}	60	4.1	3.8	
	GalN ₅	0.04	0.7	5.6	
GlcN6S	4MUS	10	5800	5.2	[70, 95]
	GlcNAc_{6S}-(HS)*	218	0.25	4.1	
	GlcNAc_{6S}-(KS)*	4.5	1	3.9	
	GlcNAc _{6S}	1.6	7.1	5.7	
IdoA2S	4MUS	300	12 400	5.6	[89, 96]
	IdoA_{2S}-(HS)*	3400	3	4.5	
Sulf-1	4MUS	1000–2000		7.5	[22]
	GlcN_{6S} (endo)	0.088		7.5	
Sulf-2	4MUS	1000–2000		7.5	[22]
	GlcN_{6S} (endo)	0.097		7.5	

[a] Physiological substrates are in bold face. Asterisks denote activity at the nonreducing end of the glycosaminoglycan in parenthesis. [b] Rate expressed as nmol substrate per min per mg enzyme. n.d. = no detectable activity. [c] Values reported in μM .

comprised of long chains of repeating disaccharide units consisting of uronic acid (U) and hexosamine (H) sugars. These chains are highly polydispersed owing to their varying length, glycosidic connections, epimerization, *N*-acetylation, and the degree of *O*- and *N*-sulfation (Figure 5).^[83, 84] Table 1 lists the substrates of the various lysosomal sulfatases, most of which are named based on their residue specificity within the GAG chain. The exceptions are ARSB, heparan *N*-sulfatase,

and galactosamine-6-sulfatase. ARSB, originally regarded as a generic aryl sulfatase,^[85] is now known to specifically cleave sulfate esters at the 4-position of *N*-acetyl galactosamine (GalNAc) residues found in dermatan sulfate (DS) and chondroitin sulfate (CS).^[86, 87] Heparan *N*-sulfatase (GlcNS) catalyzes the hydrolysis of *N*-linked sulfamates of glucosamine residues in heparin and heparan sulfate (HS).^[62] GalN6S, initially named for its ability to hydrolyze the GalNAc_{6S} residues of DS and CS, is also responsible for the hydrolysis of galactose-6S (Gal_{6S}) residues of keratan sulfate (KS).^[88, 89]

Within the lysosome, degradation pathways involve sulfatases and glycosidases that act sequentially to break down GAG structures from the nonreducing ends.^[90] Figure 6 depicts some generic GAGs; the sites of sulfate ester cleavage by lysosomal sulfatases are marked with arrows. Although several sites are indicated on the GAG structures for the sake of brevity, it must be emphasized that each lysosomal sulfatase acts on the GAG in an exoenzymatic fashion, only as specific residues are exposed at the nonreducing terminus by a glycosidase. The glycosidases, in turn, require desulfonation of the nonreducing residue before the next processing step can occur. Table 5 lists some kinetic parameters known for specific substrates of these sulfatases.^[91–96]

6.2. Extracellular Sulfatases and Developmental Signaling

Recently, a new class of ECM sulfatases, known as the Sulfs, have been attributed a pivotal role in signaling and embryonic development based on the modulation of interactions between GAGs and signaling molecules. Initially, QSulf1 was discovered in the search for sonic hedgehog (shh) responsive genes in quail embryos.^[97] Shh is an extracellular signaling molecule that influences the development of stem cells into specific tissues and organs.^[98] QSulf1 is induced by Shh, but does not participate directly in Hedgehog (Hh) signaling. However, it was shown to induce Wingless/Int (Wnt) signaling and is

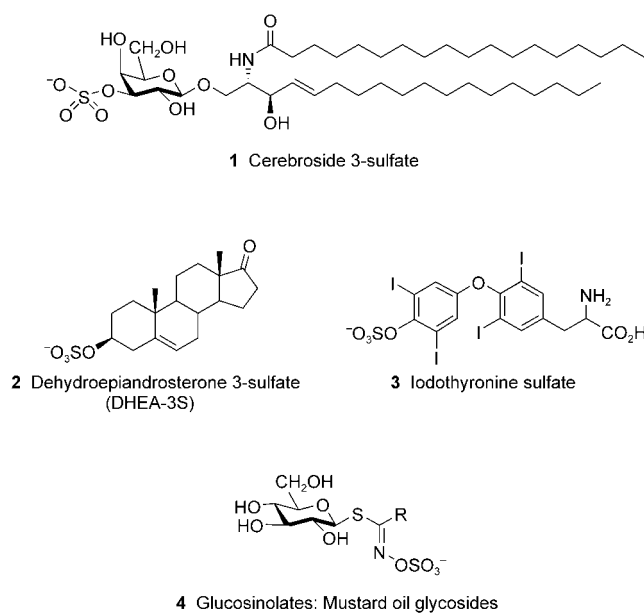


Figure 4. Representative sulfatase substrates. Cerebroside-3S (**1**) is a physiological substrate for ARSA; DHEA-3S (**2**) is one natural substrate for ARSC; iodothyronine sulfate (**3**) is a possible substrate for one of the ER sulfatases; glucosinolates (**4**) are substrates for PGSS.

GAG	Disaccharide unit	H	U	Modifications
Heparan and heparan sulfate	$H_{2N}Y_{5X,6X}-(\alpha1,4)-U_{2X}-(\alpha\beta1,4)$	GlcN	GlcA IdoA	N-sulfonation N-deacetylation O-sulfonation C5-epimerization
Chondroitin and dermatan sulfate	$H_{2N}AC_{4X,6X}-(\beta1,4)-U_{2X}-(\alpha\beta1,3)$	GalN	GlcA IdoA	O-sulfonation C5-epimerization
Keratan sulfate	$H_{2N}AC_{6X}-(\beta1,3)-Gal_{6X}-(\beta1,4)$	GlcN	Gal	O-sulfonation

Representative monosaccharide units			
D-Glucosamine (GlcN)	D-Galactosamine (GalN)	D-Glucuronic acid (GlcA)	L-Iduronic acid (IdoA)

Figure 5. GAG disaccharide units with modification sites indicated. The GAGs are sophisticated polydisperse macromolecules that consist of unbranched repeating disaccharide units of uronic acid (U) and hexosamine (H). The GAG sulfate esters are separated into three major classes distinguished primarily by the identity and linkage of the sugar residues; examples are heparan sulfate (HS) and heparin sulfate (HSGAG, which generally contains more sulfates on average than HS), keratan sulfate (KS), and chondroitin and dermatan sulfate (CS and DS). Several modifications can be introduced into the disaccharide units, including the C5 epimerization of GlcA residues to IdoA, N-acetylation, and O- and N- sulfonation. Subscripted symbols are used to denote positions that are sulfated or unsubstituted (X); or sulfated, acetylated, or unsubstituted (Y).

suspected to participate in the signaling of fibroblast growth factor (FGF) and epidermal growth factor (EGF).^[97,99,100]

The extracellular Wnt and FGF signaling molecules, which are intimately linked with proper cell differentiation and embryo patterning, are known to bind heparan sulfate

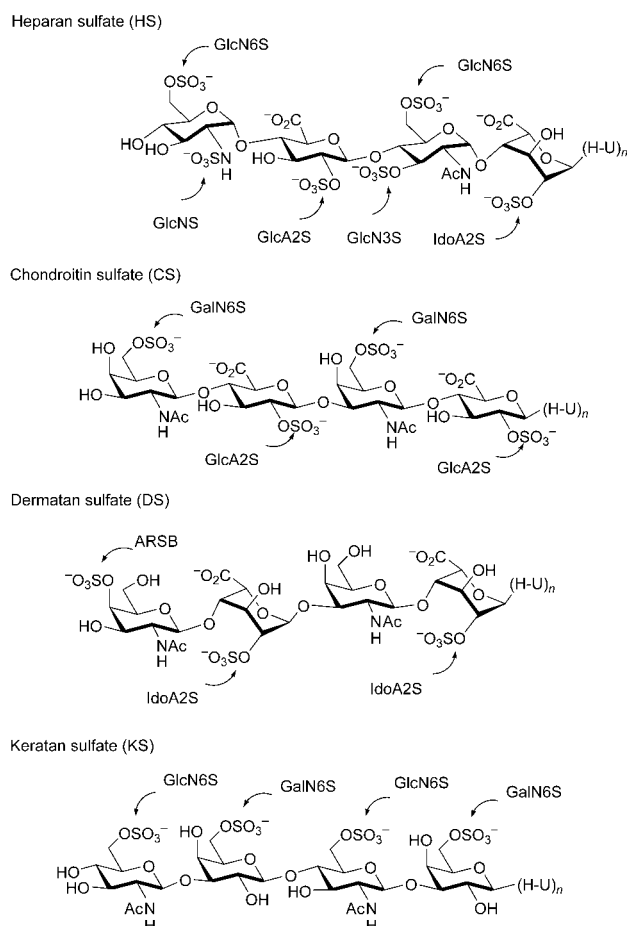


Figure 6. Generic glycosaminoglycans with sites for sulfate ester cleavage indicated by arrows. Note that in the lysosome cleavage only occurs exoenzymatically from the nonreducing end.

proteoglycans (HSPGs) in the ECM.^[101,102] Specifically, their interactions with HS have been associated in part with the 6-*O*-sulfate groups on GlcNAc residues.^[103–106] As enzymes targeted for the cell surface, Sulf1 is poised to play a role in remodeling these critical sulfates in the ECM.^[97,100] Indeed, overexpression of QSulf1 has been directly correlated with an increase in Wnt signaling, and this activity was shown to depend on catalytic sulfatase activity. Based on these results, Dhoot et al. speculated that HSPG-bound Wnt was released for signaling after 6-*O*-sulfate cleavage by QSulf1 (Figure 7).^[97] Recently, this hypothesis was substantiated and further characterized in biochemical and cell-expression studies wherein a two-state “catch and present” model was suggested for the regulation of Wnt signaling by QSulf1.^[99] In this model, desulfonation by QSulf1 is proposed to stimulate a shift from a high-affinity HS–Wnt complex (the catch phase) to a low-affinity HS–Wnt complex, which interacts with Frizzled receptors (the present phase) to initiate the Wnt signaling cascade. Desulfonation of HSPGs by HSulf1 also influences other signaling pathways, including EGF and FGF.^[100] In the past, HS-based signaling was thought to be primarily controlled by sulfonation of HS during biosynthesis in the Golgi.^[107] The Sulf1 represent a new pathway for dynamically regulating these sulfonated ligands.

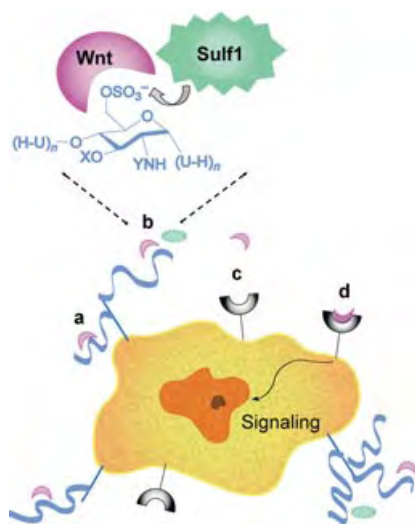


Figure 7. Proposed mechanism for the amplification of Wnt signaling by Sulf1. In the extracellular matrix (a), Wnt (purple) binds to HS proteoglycans (blue) at the glucosamine-6S residues. Sulf1 (green) cleaves the GlcN₆S sulfate (b), thereby releasing HS-bound Wnt (c) and allowing the interaction of Wnt with Frizzled receptors (shown generically in gray). Upon binding, important signaling cascades begin. Recent experiments suggest that HS may also interact with the receptor in the form of a low-affinity HS–Wnt complex.

Extracellular *Sulf1* orthologues from rats, mice, and humans have been identified and cloned.^[22,108] An analogous gene, *Sulf2*, was also isolated from mice and humans.^[22] Studies showed that HSulf1 and HSulf2 hydrolyze the substrate 4MUS more slowly than typical ARSs, but at least an order of magnitude faster than non-ARSs (Table 5). The high sequence similarity with lysosomal GlcN6S and the key signal modulation by GlcN₆S residues in HS strongly suggested that the Sulfs would be active with these substrates. Indeed, such activity was observed. The Sulfs display endo activity at neutral pH values (Table 5). Functional selectivity for a subset of 6-*O*-sulfates in HS, including the trisulfated motif IdoA_{2S}-GlcN_{6S} and the doubly sulfated GlcA-GlcN_{6S} disaccharide unit, was identified in biochemical studies of both human and quail enzymes.^[97,99] Interestingly, the IdoA_{2S}-GlcN_{6S} sequence is known to be important in both the binding of FGF and the dimerization of the FGF-dependent receptor.^[109,110] Thus, desulfonation by a Sulf enzyme would be expected to negatively regulate this process, although the exact nature of this relationship remains to be established.

In addition to their roles in proper growth and development, growth factors, such as FGF, and morphogens, such as Wnt, have been implicated in pathophysiological conditions including tumor onset and progression.^[111] The involvement of these molecules in both normal and disease processes is highly regulated by the HSPGs, which bind these agents and modulate their activity.^[112] As the Sulfs are key players in regulating these binding events, they might also be involved with deregulation during disease states, such as cancer. As such, they might serve as novel candidates for therapeutic intervention in the future.

Sulfatases have been implicated in the development of sea-urchin embryos, although their direct involvement in cell

signaling events has not yet been demonstrated. Three highly similar ARS genes cloned from the distinct sea-urchin species *Hemicentrotus pulcherrimus*, *Strongylocentrotus purpuratus*, and *Helicodaris erythrogramma* (Table 2), were shown to localize on cell surfaces in a cell-lineage-specific and cell-stage-specific manner during embryosis.^[113–115] Their expression was found to coincide with important cell-differentiation events.^[116,117] It has been suggested that sulfonated proteoglycans are the substrates of these extracellular ARSs, but this activity has not been verified.^[118] The sea urchin has long been a model system for the study of embryonic patterning,^[119] and it might prove useful to investigate a possible role of the sea-urchin aryl sulfatases in HS-related signaling pathways.

6.3. Steroid Sulfatase

The levels of steroid hormones are modulated in part by the microsomal sulfatase ARSC, also commonly known as steroid sulfatase (STS).^[120] ARSC is a ubiquitously expressed, membrane-bound, lumen-oriented protein, which is primarily localized in the rough ER.^[121] It has a neutral pH optimum and processes several aryl and steroidal substrates efficiently (Table 5).^[122] The broad range of substrates hydrolyzed by ARSC has raised the question of whether multiple ARSC isoforms, or even distinct enzymes, are involved in processing the different sulfate conjugates. However, convincing evidence from several studies points to a single housekeeping ARSC protein that is fully capable of hydrolyzing disparate steroid sulfates.^[6] ARSC releases systemic steroid precursors from inactive 3-*O*-sulfate conjugates, such as estrone and dehydroepiandrosterone sulfate (2, Figure 4), that feed into pathways for hormone-based signaling.^[123] Upregulation of ARSC activity has been implicated in hormone-dependent breast cancer,^[124–126] whereas a deficiency in the enzyme has been observed in the inherited disorder X-linked ichthiosis.^[6] The former has made ARSC an attractive target for small-molecule therapeutics (see Section 8).^[127,128]

6.4. Novel Sulfatases of the ER and Golgi Network

Several recent additions to the human sulfatase family have been reported. The ARSD, ARSE, and ARSF genes, for example, were isolated from a positional cloning experiment aimed at mapping the causative gene(s) for the congenital disorder chondrodysplasia punctata (CDPX).^[129,130] The genes are located together with the gene for ARSC in a cluster on the distal short arm of the X chromosome (Xp22.3) and have a similar genomic organization, suggesting an evolutionary duplication event.^[131,132] The gene for another sulfatase, ARSG, was also cloned recently after being identified in bioinformatics searches.^[133] All four of these newly discovered genes encode for membrane-bound sulfatases of the ER and Golgi network with a neutral pH optimum. Each of these sulfatases received the ARS designation because of structural similarities with known ARSs, even though only ARSE and ARSF have shown activity with

aromatic substrates.^[130,133–135] The natural substrates of these sulfatases are as yet unknown.

A deficiency in ARSE alone was found to be responsible for the disorder CDPX (Table 3).^[134,136] Interestingly, ARSE is inhibited by warfarin, the causative agent of warfarin embryopathy, which has clinical manifestations strikingly similar to CDPX.^[129,130] Both disorders are characterized by bone and cartilage dysplasia, suggesting that ARSE plays a critical role in the proper development of these tissues.^[6,137] Given the subcellular location of ARSE and the critical roles that GAGs play in bone and cartilage structure and development, it is tempting to speculate that ARSE might function along with other anabolic enzymes of the Golgi network in the construction of GAGs and cell-surface HSPGs.^[138–140]

Iodothyronine sulfate (**3**) is a potential substrate of ER sulfatases (Figure 4). Recent research has indicated that the biological activity of thyroid hormone might be modulated by sulfonation akin to steroid hormones.^[141] A reversible sulfonation pathway has been proposed in which the action of a sulfatase leads to the release of active thyroid from inactive sulfonated conjugates.^[142,143] The steroid-hormone regulator ARSC possesses some ability to hydrolyze iodothyronine sulfate; however, recent studies showed that the hydrolysis is primarily carried out by a sulfatase (or possibly several sulfatases) isolated from human liver microsomes that are biochemically distinct from ARSC.^[142,144] A likely candidate for iodothyronine sulfatase activity is ARSD, which shows a similar gene expression pattern to that of ARSC.

6.5. Sulfatases of Invertebrates and Lower Eukaryotes

Few sulfatases from invertebrates have been characterized. However, sulfatases have been identified in a number of gastropods and echinoderms (including the ARSs from sea urchins), and it is likely that many more exist and have analogous roles to those in vertebrates.^[3,145–151] Furthermore, some divergent roles for sulfatases in invertebrates have come to light. In recent studies on herbivore–plant interactions, a unique sulfatase was isolated from *Plutella xylostella*, an insect commonly known as the diamondback moth. Diamondback moths are able to feed on cruciferous plants by circumventing an inbuilt defense mechanism of the plant that releases toxic isothiocyanates, nitriles, and thiocyanates from a precursory glucosinolate sulfate (GS, **4**, Figure 4) upon insect feeding.^[152] Diamondback moth resistance results from the activity of a glucosinolate sulfatase (GSS), which efficiently desulfonates several GSs to innocuous by-products. The GSS gene has not been formally identified in other pests, but GSS and ARS activity in *Helix pomatia*, the common garden snail, is known.^[153,154] One gene and a partial gene (*HpSulf1* and *HpSulf2*, which have no established relation to the Sulf enzymes involved in signaling) were recently cloned from *Helix pomatia*, but neither appeared to encode for the GSS enzyme.^[155] As an enzyme common to pests, the novel GSS sulfatase might serve as a potential target for pesticides.

Sulfatase activity has been identified in several lower eukaryotic organisms,^[156,157] and three aryl sulfatase genes from fungi^[158] and algae^[159–161] have been cloned and partially

characterized (Table 2). These enzymes are upregulated during sulfur starvation and are believed to play a role in sulfur scavenging. For example, NARS and choline sulfatase (ChoS) isolated from the filamentous fungus *Neurospora crassa* are known to hydrolyze tyrosine-*O*-sulfate and choline-*O*-sulfate under sulfur-limited conditions.^[162,163] The NARS enzyme has also been shown to be 30 times more active during germination, regardless of sulfur availability, suggesting that it might play a developmental role.^[164]

7. Substrates and Biological Functions of Prokaryotic Sulfatases

High levels of ARS, alkyl sulfatase, and glycosulfatase activity have been identified in many different types of bacteria.^[3,50] However, only a handful of bacterial sulfatase genes have been cloned and characterized (Table 2). These enzymes typically function as scavengers, removing sulfate groups from exogenous substrates to provide sulfur and carbon sources for their hosts.^[3] Recent studies have demonstrated further functions of bacterial sulfatases in osmoprotection and pathogenic processes.

7.1. Sulfate Scavenging in Bacteria

ARS activity has been identified in several species of enterobacteria (*Klebsiella*,^[63,165] *Salmonella*,^[166,167] *Proteus*,^[146,168] *Pseudomonas*,^[169] and *Serratia*^[170]), aquatic bacteria (*Alteromonas*^[52]), pathogenic bacteria (*Mycobacteria*^[171,172] and *Pseudomonas*^[173,174]), extremophilic bacteria (*Plectonema*^[175]), and soil bacteria (*Comamonas*^[176] and *Pseudomonas*^[176]). Indicative of their role in scavenging, most of the bacterial ARS enzymes are upregulated during sulfur starvation.^[3,50] Although their preferred substrates are unknown, it is thought they may be sulfated carbohydrates. The most thoroughly characterized ARS enzymes are from *Pseudomonas aeruginosa*^[173] and *Klebsiella pneumoniae*^[63] (formerly classified as *Klebsiella aerogenes* and *Aerobacter aerogenes*). Early studies on these enzymes focused on genetic induction under sulfur-limited conditions, whereas recent studies have probed KARS involvement in sulfate transport.^[50,177] Studies of the PARS and KARS enzymes have provided invaluable mechanistic and structural information on the sulfatase enzyme class as a whole.^[12,27,59]

One bacterial alkyl sulfatase traditionally categorized as a sulfate scavenger has been shown to have an additional role. Choline-*O*-sulfatase (ChoS) is primarily involved in breaking down choline sulfate into carbon, nitrogen, and sulfur sources,^[178–180] but it also participates in the synthesis of an osmoprotectant.^[181] The *bet* operon in the rhizobium *Sinorhizobium meliloti* encodes for several enzymes that orchestrate the synthesis of glycine betaine, a common bacterial osmoprotectant derived from choline.^[182] In a cloning scheme for this operon, a ChoS homologue was isolated unexpectedly, thus indicating that the versatile ChoS enzyme can perform two functions: the assimilation of nutrients as needed and the synthesis of osmolytes to protect the organism.^[181]

7.2. Glycosaminoglycan-Degrading Sulfatases

The ability of bacteria to survive on glycosaminoglycans (GAGs) as a sole nutrient source has long been known.^[3] It was also recognized early on that bacterial degradation pathways might prove useful in deconvoluting the complex nature of GAGs, thus prompting the characterization of several enzymes from *Proteus Vulgaris*, *Bacteriosides theitomicron*, and *Flavobacterium heparinum* (Table 6). Much of the research on GAG-degrading enzymes has focused on bacterial lyases,^[183–185] but sulfatases have also been characterized.^[3,50] Generally, the degradation is initiated by several unique lyases that cleave GAG chains at the hexosamine–uronate (H-U) linkage by elimination to give $\Delta 4,5$ -U-H (dU-H) disaccharide units. (Note that the stereochemical information that distinguishes IdoA from GlcA is lost upon formation of the dU unit.)^[183] The sulfatases then desulfonate these units in an order that depends on the nature of the glycosaminoglycan (Figure 8).

In the processing of HS, the disaccharide units must be desulfonated at the dU2S position by the HS2S enzyme before it is cleaved by a hydrolase into monosaccharide units.^[186] Any sulfate groups remaining on GlcN units are then sequentially cleaved by the monosaccharide sulfatases HS3S, HS6S, and HSNS.^[187–189] In the degradation of CS, CS6S and CS4S act on the nonreducing end of GalNAc residues before it is cleaved into monosaccharide units.^[190,191] Additionally, it has been shown that CS6S is capable of endoenzymatic cleavage on larger CS chains.^[192] CS also contains uronic acid residues with 2-*O*-sulfate groups, although fewer than HS. The activity of a sulfatase specific for disaccharides, trisaccharides, and tetrasaccharides with dU2S residues, irrespective of the sulfation profile, has been reported.^[186,192–195] It is

believed that the dU2S residues of HS and CS substrates are processed by the same sulfatases; indeed, the FHS2S enzyme from *F. heparinum* recently showed activity for both substrates.^[58,61] FHS2S cleaves the 2-*O*-sulfate functionality of the HS disaccharide unit dU_{2S}(β -1,4)H_{NS,6S} preferentially, but is also active for substrates with a lesser degree of sulfation and different glycosidic connections, such as the α -1,3 linkage of CS. This behavior shows that the enzyme is primarily specific for dU_{2S} residues at nonreducing ends of GAG chains.

7.3. Mucin Sulfatases

Mucin sulfatases (MdSs, mucin-desulfating sulfatases) are bacterial enzymes that cleave the sulfate esters on the mucin proteoglycans in the gastrointestinal (GI) lining. Like glycosaminoglycans, mucin oligosaccharides contain numerous sulfate groups that collectively influence their physical properties.^[196] Sulfate esters have been identified on interior and exterior GlcNAc, Gal, and occasional GalNAc residues at the 3-, 4-, or 6-positions of mucins.^[197] Mucins contain blood-group antigens, including various sialyl and sulfosialyl groups that are known to be involved in bacterial recognition processes and leukocyte trafficking.^[198] One of the primary functions of mucins is to act as a protective barrier between endothelial cells and potentially harmful agents in the GI lumen, such as colonizing bacteria.^[199] Accumulating evidence suggests that sulfonation might preserve mucin structures against bacterial breakdown, as desulfonation by MdSs is the rate-limiting step in bacterial degradation.^[200] This might be the link between the increased levels of sulfate esters in mucins (known as sulfomucins) that are the most heavily inhabited by bacteria, such as the colon and mouth.^[201]

Table 6: Bacterial sulfatases involved in the degradation of glycosaminoglycans.

Organism	GAG	Sulfatase ^[a]	Residue specificity ^[b]	pH optimum	K_m [μ M]	Position, type of cleavage	Ref.
<i>Flavobacterium heparinum</i>	HS	HS2S	dU _{2S} -GlcNS	6.5	1060	nonreducing end, exo	[58, 186]
			dU _{2S} -GlcNS _{6S}		87		
			dU _{2S} -GlcNAc _{6S}		515		
		HS3S	GlcNAc _{3S}	8.0	42	monosaccharide	[186]
			GlcNS _{3S}		7.5		
		HS6S	GlcN _{6S}	7.5	1350	monosaccharide	[187]
			GlcN _{6S}		16		
<i>Flavobacterium heparinum</i>	CS	HSNS	GlcNAc _{6S}	7.0	54	monosaccharide	[189]
			GlcN ₅		8.3		
		CS2S	dU2S-GlcNAc _{6S}		> 10 000	nonreducing end, exo	[58, 192, 195]
			CS4S*				
			CS6S*				
<i>Bacteriosides theitomicron</i>	CS	CS4S	dU-GlcNAc _{4S}	7.0			[191]
		CS6S	dU-GlcNAc _{6S}				
<i>Proteus vulgaris</i>	CS	CS4S	dU-GlcNAc _{4S}			reducing end, endo, exo	[192]
		CS6S	dU-GlcNAc _{6S}			reducing end, exo	

[a] Enzymes marked with an asterisk have been detected, but not isolated. [b] Enzymes are specific for the sulfate residues shown in bold.

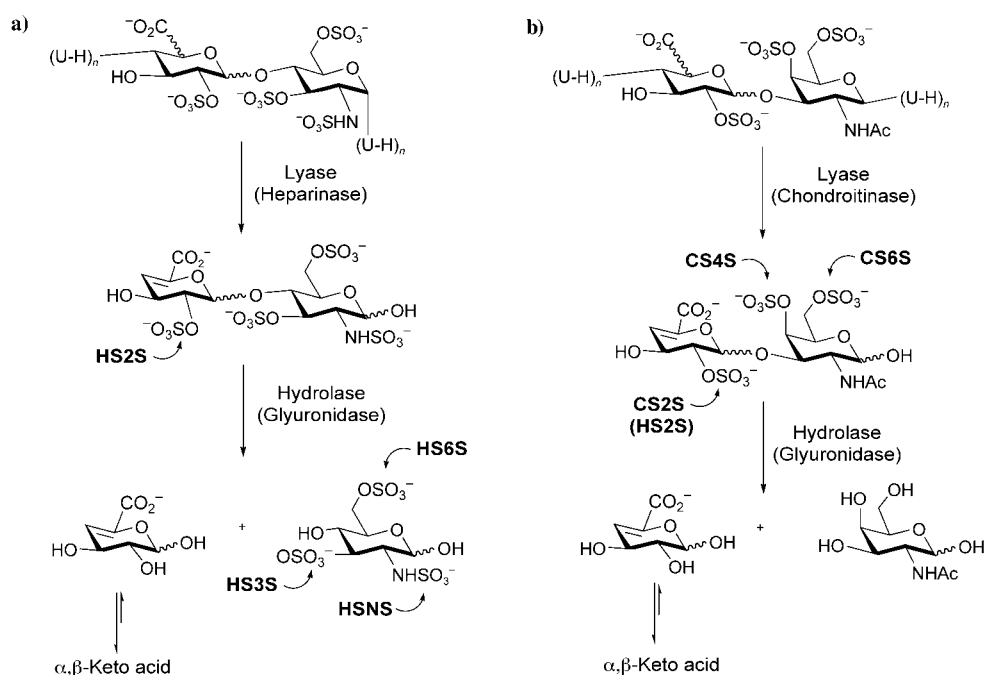


Figure 8. The role of bacterial sulfatases in the degradation of HS (a) and CS (b). The sites of sulfate ester hydrolysis are demarked by arrows.

MdS enzymes have been identified in strains of enterobacteria capable of growing on ^{35}S -labeled mucin as the sole carbon source (Table 7).^[202–204] Three enzymes with unique characteristics have been purified to date. The first, a 30-kDa protein isolated from the extracellular environment of a *Helicobacter pylori* culture, has a pH optimum of 5.7 and catalyzes the desulfonation of $\text{GlcNAc}_{6\text{S}}$ and $\text{Gal}_{6\text{S}}$ in mucins, as well as $\text{Glc}_{6\text{S}}$ in glyceroglucolipids.^[205] Another 15-kDa enzyme, purified from fecal extracts, has a pH optimum of 4.5

and cleaved approximately 25 % of the radiolabelled sulfate from a human colonic mucin.^[206] The third, isolated from *Prevotella* RS2, is a 58-kDa periplasmic enzyme with a pH optimum of 7.0 that removed 33 % of the radiolabelled sulfate from a human colonic mucin.^[207] This enzyme, whose gene was recently cloned, was shown to be an exoenzyme specific for $\text{GlcNAc}_{6\text{S}}$ residues.^[60,208]

With crude cell extracts from *Prevotella*, 79 % of the radiolabelled sulfate could be cleaved from mucin substrates,

Table 7: Bacterial mucin sulfatases.

Organism	Host, substrate ^[a]	Residue specificity	pH optimum	Subcellular location ^[b]	Infection	Ref.
<i>Prevotella</i> RS2	S*-rat, gastric mucin	$\text{Glc}_{6\text{S}}$, $\text{GlcNAc}_{6\text{S}}$	7.4	periplasm		[60,207–209]
<i>Bacteroides thetaiotamicron</i>	S*-human, colonic mucin	$\text{Gal}_{6\text{S}}$	7.0	cytoplasm		[202,206]
<i>Bacteroides fragilis</i>	human, colonic mucin	$\text{Glc}_{6\text{S}}$	5.0	extracellular		[208,209]
unknown (human feces)	S*-human, colonic mucin	$\text{Glc}_{6\text{S}}$	4.5	extracellular	ulcerative colitis	[206,210,211]
<i>Helicobacter pylori</i>	S*-human, gastric mucin	$\text{Glc}_{6\text{S}}$, $\text{GlcNAc}_{6\text{S}}$	5.7	extracellular	peptic ulcer, gastric cancer	[205,212]
<i>P. aeruginosa</i> , <i>Burkholderia cepacia</i>	S*-human, colonic mucin	$\text{Gal}_{6\text{S}}$	7.0		necrotizing pneumonia	[57]
<i>Streptococcus mitis</i> , <i>S. mutants</i> , <i>S. salivarius</i>	S*-human, colonic mucin			extracellular	dental plaque	[203]
<i>Ruminococcus torques</i> , <i>Bifidobacterium</i> VIII-210	$\text{Gal}_{6\text{S}}$ -(b1,4)-glucitol	$\text{Gal}_{6\text{S}}$	5.0	extracellular		[204]
<i>E. coli</i>	S*-human, colonic mucin					[57]

[a] S* = radioactive ^{35}S isotope used to label the mucin. [b] Extracellular location was assumed based on the presence of enzymatic activity in supernatants of the culture and/or of feces.

suggesting that more than one MdS enzyme may exist in this organism.^[207] *Prevotella RS2* possibly contains another MdS enzyme specific for Gal_{6S}, as lysates harvested from cells grown on colonic mucin showed increased activity for both Glc_{6S} and Gal_{6S} substrates.^[209] Two separate MdS enzymes that desulfonate Gal_{3S} and Gal_{6S} substrates were also found in partially purified extracts from *Bacteriodes fragilis*.^[208,209] Other sulfated carbohydrates within the GI tract (i.e. glycosaminoglycans and sialyl substrates) have certain sugar residues in common with mucins. The mechanisms by which mucin sulfatases differentiate between these substrates remains to be clarified.^[197,200]

7.4. Bacterial Sulfatases and Pathogenicity

Accumulating evidence suggests that MdS enzymes might be involved in numerous clinical manifestations. For example, they have been implicated in the phenomenon of bowel inflammation.^[200] Elevated MdS activity was observed in the fecal extracts of patients with ulcerative colitis (UC).^[210,211] This observation is consistent with the results of another study that correlated increased mucin degradation with increased MdS activity in UC patients.^[210] Additionally, decreased sulfomucin levels were observed in gastric samples of patients infected with *H. pylori*, a causative bacteria in gastric diseases.^[212] Although it is not known if mucin degradation by mucin sulfatases is the primary contribution to these conditions, it is thought to contribute to their severity.^[201] It has also been suggested that MdS enzymes may play a role in the invasion of opportunistic pathogens *P. aeruginosa* and *Burkholderia cepacia* in lung tissue, especially in patients with impaired mucosal clearance, which is common in cystic fibrosis (CF).^[57,213]

In addition to providing access to sources of sulfur and nutrients, it has been proposed that these sulfatases expose sites of adhesion. For example, *P. aeruginosa* may use MdSs to remove the sulfate groups shielding its requisite mucin-binding motifs, Gal(β-1,3)GlcNAc and Gal(β-1,4)GlcNAc.^[57,214,215] Sulfomucin inhibits the binding of *H. pylori* to its normal adhesion elements (galactosphingolipid-3S), suggesting that the desulfonation of mucins might be critical for initial pathogenic colonization.^[216] This assumption was substantiated by the finding that two common antiulcerative drugs, nitecapone and sulcrasulfate, which are efficacious against infection by *H. pylori*, significantly decrease desulfonation activity by MdSs.^[205,212]

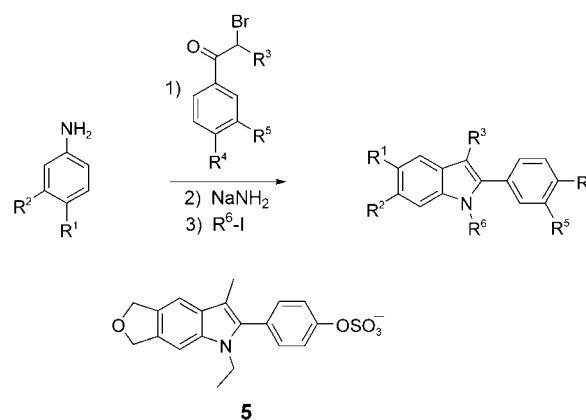
Remodeling of the sulfate structure has also been proposed as a mechanism for the pathogenicity of certain strains of *Mycobacterium*. A bioinformatics study suggested that the ubiquitous sulfatase sequences found in these organisms could potentially encode for enzymes that modify glycosaminoglycans to generate binding sites required for infection.^[217] Such an adaptation would give a competitive edge to especially pernicious bacteria. A quick search of the Entrez database^[310] reveals that putative sulfatase genes are harbored by many pathogens, including *Yersinia pestis* (bubonic and pneumonic plague),^[218] *Salmonella enterica* (typhoid fever),^[219] *Enterococcus faecalis* (vancomycin-resist-

ant pathogen),^[220] *Bacillus anthracis* (anthrax, potential biological weapon),^[221] and *Streptococcus agalactiae* (leading cause of sepsis, pneumonia, and meningitis in neonates), to name a few.^[222] Interestingly, a putative sulfatase gene identified in *E. coli* K1, one of the causative agents of meningitis, endows the bacteria with an increased ability to colonize cerebrospinal fluid.^[223] Although the exact role of the putative sulfatase is unknown, this work establishes another intriguing link between bacterial sulfatases and pathogenicity. As more connections between infections and bacterial sulfatases are established, it seems increasingly likely that these enzymes might serve as targets for therapeutic intervention.

8. Sulfatase Inhibition

Most studies on the inhibition of sulfatases have focused on blocking the activity of estrone sulfatase (ARSC), which releases active steroid hormones from inactive sulfate conjugates, such as estrone sulfate (E1S) and dehydroepiandrosterone (DHEAS). Increased release of E1 and DHEA has been connected with the development of mammary tumors, and upregulation of ARSC has been noted in several forms of cancer. As a result, steroidal sulfatase inhibitors show potential as therapeutics for these hormone-dependent cancers. The treatment of breast cancer, in particular, with small-molecule therapeutics aimed at ARSC inhibition has been under intense investigation over the past several years.^[36]

After 2-(hydroxyphenyl)indoles were recognized as inhibitors of mammary tumors,^[224,225] sulfate derivatives of 2-phenylindoles were evaluated as inhibitors of steroid sulfatases.^[226] Combinatorial synthesis (Scheme 4) yielded compound **5** as the most potent inhibitor with an IC₅₀ value of 120 μM. The inhibitors were assayed by detection of the amount of 6,7-[³H]estrone sulfate that was hydrolyzed by liquid scintillation counting. More recently, a sulfamoyloxy-substituted derivative was found to inhibit ARSC with an IC₅₀ value of 200 nM. The antiestrogen tamoxifen and related metabolites,^[227] as well as daidzein sulfoconjugates^[228] and danazol,^[229,230] have also been reported as ARSC inhibitors.



Scheme 4. Combinatorial synthesis of 2-(hydroxyphenyl)indole inhibitors.

Estrone 3-phosphonates and thiophosphonates were analyzed for their activity as inhibitors of steroid sulfatases.^[231,232] The best inhibitor was found to be the methylthiophosphonate (**6**, E1-3-MTP, Figure 9) with an IC_{50} value of less than

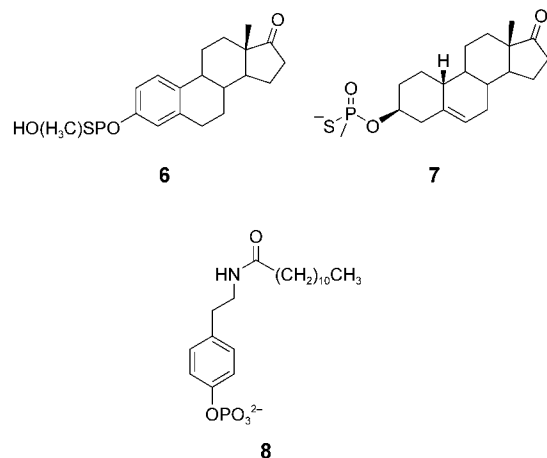


Figure 9. Steroidal and nonsteroidal phosphonate and thiophosphonate inhibitors.

100 nM. The pure R_p diastereomer was obtained through selective digestion of the S_p stereoisomer with snake-venom phosphodiesterase. The pure R_p inhibitor was less active than the original mixture, suggesting that the S_p isomer was more potent. In general, hydrophobicity, basicity, size, and charge were found to affect the potency of this class of inhibitors.^[233] Dehydroepiandrosterone phosphate (**7**) was reported to have an IC_{50} value of 140 nM at pH 6.0. It has a higher activity than the corresponding sulfate analogue, but is not susceptible to enzymatic hydrolysis.^[234] In a study of nonsteroidal phosphate esters, hydrophobicity was again found to be an important factor in the activity of the inhibitor. A K_i value of 520 nM was reported for *n*-lauroyltyramine phosphate (**8**) at pH 7.0.^[235]

Another series of compounds that were evaluated as ARSC inhibitors were 17 α - and 17 β -alkylated or benzylated estradiols.^[236] It was determined that the introduction of alkyl and substituted benzyl groups at these positions led to increased activity. The most potent inhibitor, **9**, had a 3'-bromobenzyl substituent and an IC_{50} value of 24 nM (Figure 10). Inhibitory activity increased when sulfamate groups were added to these compounds, as evidenced by the IC_{50} value for **10** against ARSC of 150 nM.^[237,238] The effect of long alkyl chains on the activity of estradiol was also determined. The potency increased with increasing chain length up to octyl substitution (IC_{50} = 440 nM).^[239] In later work, the 4'-benzyloxybenzene derivative **11** was found to have an IC_{50} value of 22 nM. Benzyl-substituted analogues of androstane and pregnane were also synthesized and analyzed.^[240] More recently, 17 α -substituted estradiol sulfamates were prepared by split-pool combinatorial synthesis on a solid phase.^[238] As illustrated in Scheme 5, a piperazine group was attached to the steroid to provide a core structure for the library. Sequential acylations were then performed by adding an amino acid followed by a carboxylic acid. The compound

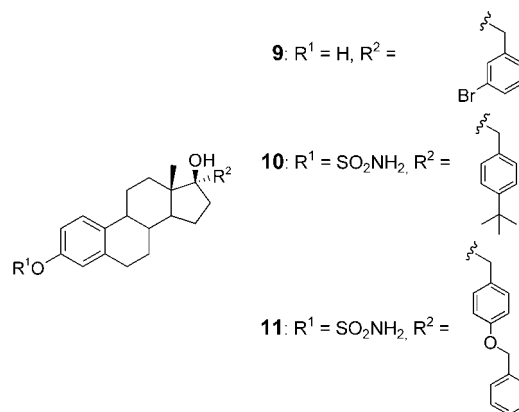
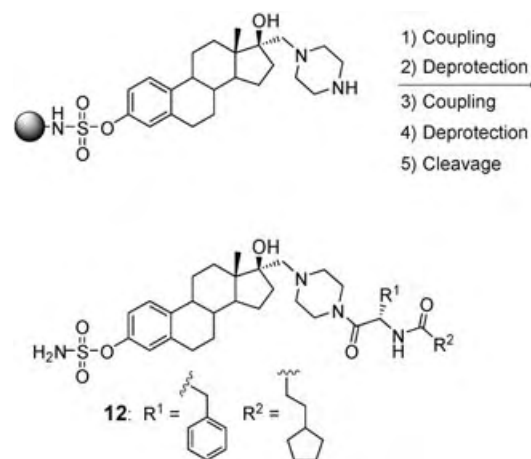


Figure 10. Benzylated estradiol inhibitors.



Scheme 5. 17 α -Substituted inhibitors of estradiol sulfamate.

containing the most hydrophobic groups, **12**, was once again the best inhibitor.

The substitution of estrone with a sulfamate group yielded the potent, irreversible inhibitor EMATE (**13**, Figure 11), which irreversibly inhibits ARSC with an IC_{50} value of 80 nM.^[241,242] The bridging oxygen atom of the sulfamate group was found to be important for the activity, as the corresponding thiophosphonate, *N*-sulfamate, and *S*-sulfamate analogues all exhibited decreased inhibition.^[243] *N*-Alkylation of the sulfonamide group also led to weaker, reversible inhibitors. A shift in research towards nonsteroidal inhibitors took place after EMATE was found to be an estrogen-receptor agonist.^[244] A study of coumarin sulfamate scaffolds uncovered the potent non-estrogenic, irreversible ARSC inhibitor COUMATE (**14**, IC_{50} = 380 nM).^[245] This motif was enhanced through the introduction of increased hydrophobic character: the tricyclic coumarin sulfamate **15** has an IC_{50} value of 8 nM.^[246] Other efforts towards nonsteroidal inhibitors have focused on sulfamate derivatives of tetrahydronaphthalene, indanones, and tetralones.^[247] Modifications to a known aromatase inhibitor, including the introduction of sulfamate groups, led to the development of dual estrogen sulfatase/estrogen aromatase inhibitors.^[248] The best inhibitors were **16** ($IC_{50}(STS)$ = 2.3 nM, $IC_{50}(aroma-$

tase) = 20 nM) and **17** ($IC_{50}(\text{STS}) = 0.82 \text{ nM}$, $IC_{50}(\text{aromatase}) = 39 \text{ nM}$, Figure 11).

Other nonsteroidal estrone sulfatase inhibitors are chromen-4-one sulfamates. The most potent compounds had highly branched aliphatic substituents diagonally opposite to the sulfamate moiety, as evidenced by the good inhibitory activity of 2-(1-adamantyl)-4*H*-thiochromen-4-one-6-*O*-sulfamate (**18**, $IC_{50} = 340 \text{ pM}$, Figure 11).^[249,250] Benzophenone sulfamates were also prepared, including 4,4'-benzophenone-

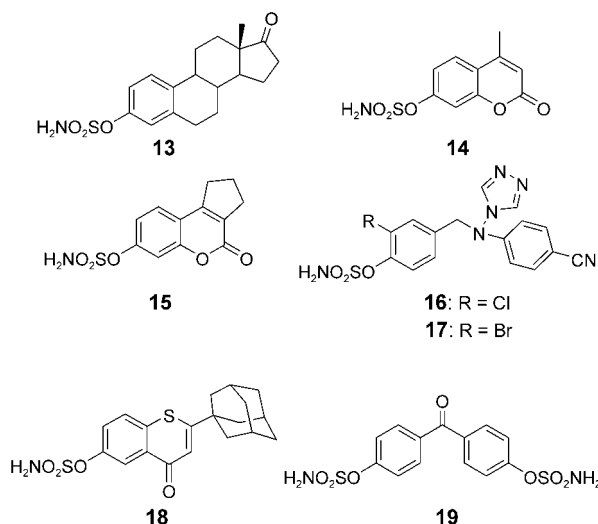
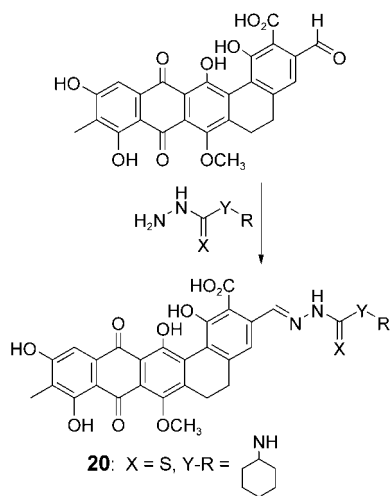


Figure 11. EMATE (**13**), COUMATE (**14**), and nonsteroidal sulfamate inhibitors.

O,O'-disulfamate (**19**, Figure 11) with an IC_{50} value of 190 nM.^[251] Finally, thiosemicarbazone derivatives of madurahydroxylacetone, a secondary metabolic product produced by the soil bacterium *Nonomuria rubra*, were studied.^[252] The most potent compound was the cyclohexylthiosemicarbazone **20** (Scheme 6) with a K_i value of 350 nM. This inhibitor was found to act in a noncompetitive fashion and showed low acute toxicity.



Scheme 6. Thiosemicarbazone inhibitors.

An alternative approach to the discovery of ARSC inhibitors has focused on developing a better understanding of the active site and transition state through modeling and structure–activity relationships.^[253] One study suggested that a sulfonate group at C3 was necessary for tight binding, whereas a polar group at C17 may not be required.^[254] Analysis of a series of phenol sulfamates with different substituents showed a correlation between the basicity of the phenoxide leaving group and inhibition.^[36,255,256] The most effective inhibition was observed for sulfamates with phenolic leaving groups with a pK_a value of 8. In a related study on a series of 4-sulfamated phenyl alkyl ketones, the best IC_{50} value found was 3.4 μM (octyl substituents).^[257] Structure–activity relationships for phenyl ketones^[258–260] and biphenyl sulfamates^[261,262] indicated the importance of hydrophobicity for activity.

Most work on sulfatase inhibition has focused on ARSC because of its involvement in hormone-dependent cancers. Several potent inhibitors with various hydrophobic scaffolds have been developed. Although permutations of the core structure have been shown to affect substrate binding, it is ultimately the presence of the sulfamate moiety that leads to irreversible inhibition of the enzyme. Several theories have been proposed for the mechanism of the affinity label; however, the precise dead-end product is unknown.^[36,246] It would be helpful to discern the location of the affinity label, as this position would certainly give telling information about the mechanism of sulfate ester hydrolysis.

The inhibition of sulfatases other than ARSC by sulfamate-based inhibitors has yet to be demonstrated. Because of the conserved mechanism and the general acceptance of small aryl substrates by sulfatases, it is tempting to speculate that a phenyl sulfamate pharmacophore would be a good general sulfatase inhibitor. The design of specific inhibitors might be a much more difficult task, but one of great importance, as therapeutic targets must be selectively disabled in the presence of critical sulfatase activity, such as lysosomal catabolism (see Table 5). The development of specific inhibitors is certainly not an unreasonable goal. Warfarin, for example, has been shown to inhibit ARSE selectively, without affecting other ARSs in the ER.^[129,130] Cocrystal structures of sulfatase–substrate or sulfatase–inhibitor complexes would supply critical information about substrate-binding regions within the sulfatase structure and would facilitate avenues for optimizing inhibitor specificity.

9. Synthetic Utility

9.1. Sulfatases in Glucosaminoglycan Sequencing

Sulfated oligosaccharides are receiving a great deal of attention as a result of their involvement in numerous biological processes.^[139,263,264] Heparan sulfate (HS) in particular serves as an important mediator in many biological processes, including embryogenesis and developmental signaling,^[140,265] inflammation,^[266,267] coagulation,^[268,269] angiogenesis,^[270] cancer metastasis,^[111] and microbial and viral adherence and invasion.^[271–273] With a growing list of interesting interactions to study, the development of analytical tools

for the structure determination of complex oligosaccharides has become a primary objective.^[274,275] The sequencing of complex oligosaccharides is by no means a trivial task. For example, HS contains 32 unique disaccharide units owing to variations in glycosidic connection, epimerization, and sulfonation (Figure 5). This structural diversity qualifies HS as one of the most information-dense biomolecules. By way of comparison, DNA is made up of just four and proteins of 20 different units. Furthermore, unlike these well-studied biomolecules, HS and GAG sequences are not templated and are non-amplifiable, necessitating the quantification of sub-milligram samples. Finally, the highly anionic character of these molecules has made them notoriously difficult to purify. It has become increasingly apparent that specific epitopes within the HS sequence are generated in a tissue-specific manner for selective interactions with certain important proteins, including growth factors, cytokines, receptor proteins, and enzymes.^[139,276] Many sequencing strategies have therefore targeted HS to enable the characterization of these interactions.^[274,277]

Several techniques in which sulfatase enzymes are invaluable tools have been developed to decode HS sequences. Two recent advances, integral glycan sequencing (IGS)^[278] and property-encoded nomenclature in conjunction with matrix-assisted laser desorption mass spectrometry (PEN-

MALDI),^[279] have proved very useful in the rapid determination of HS structures from small amounts of pure sample. The IGS sequencing format entails fluorescent labeling of the reducing end of the HS chain followed by iterative chemical and enzymatic degradation steps that are analyzed by gel electrophoresis (Figure 12). After labeling, the oligosaccharide is partially cleaved at GlcN-(α -1,4)-H residues by treatment with nitrous acid to generate several intermediate-sized fragments. These fragments are then subjected to stepwise degradation with a series of exoenzymes that cleave monosaccharide units (glycosidases) or sulfate groups (lysosomal sulfatases) from the nonreducing end. Characteristic electrophoretic shifts after each step can be used to decipher the original HS sequence. Similar methods utilize high-performance liquid chromatography (HPLC) and capillary electrophoresis (CE) for analysis of the fragments. Methods for the radiolabeling of HS from in vivo samples have also been reported.^[280–282]

PEN-MALDI uses a slightly different approach, incorporating mass spectrometry and bioinformatic techniques with chemical and enzymatic degradation.^[279] The enzymes used in this process include exoglycosidases and sulfatases from eukaryotic sources in addition to bacterial lyases, hydrolases, and sulfatases from *F. heparinum*. The process begins with an initial mass spectrometric reading from which

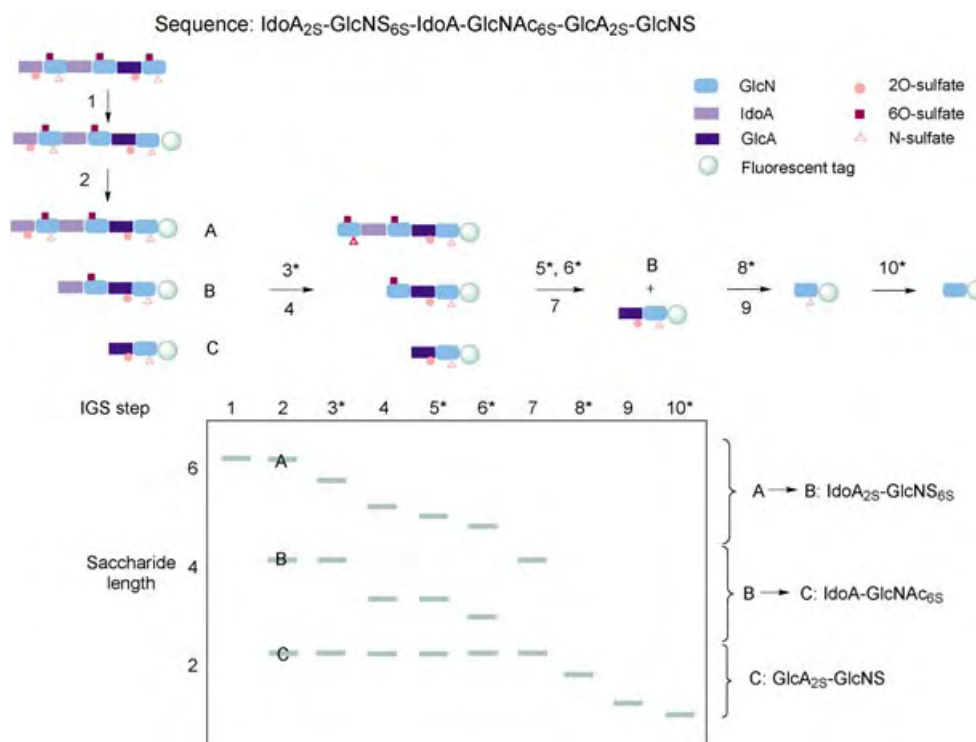
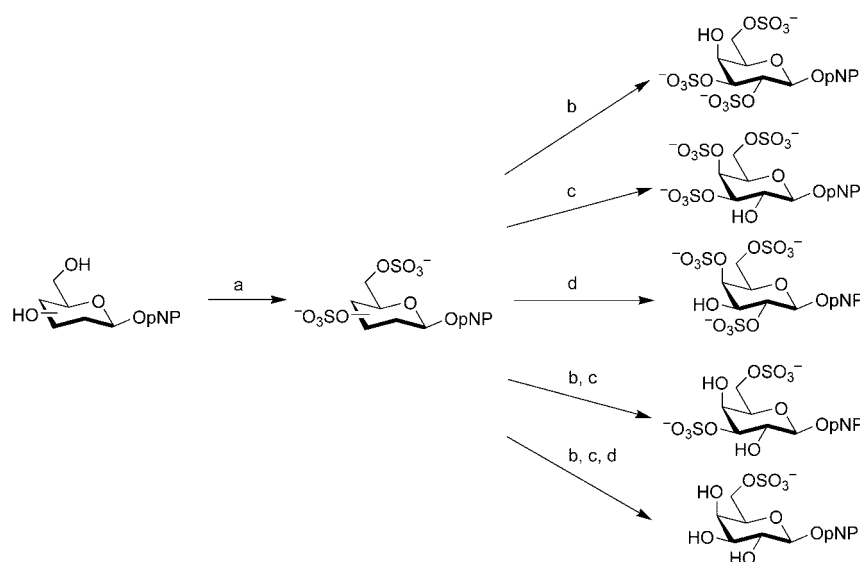


Figure 12. The integral glycan sequencing (IGS) strategy for decoding heparan sulfate (HS) sequences. Isolated HS saccharides can be sequenced rapidly through a combination of chemical and enzymatic steps followed by electrophoretic separation of the products. This schematic example shows the elucidation of a simple hexasaccharide sequence (top). The saccharide is labeled at its reducing end with a fluorescent tag (step 1). Partial chemical cleavage at GlcN residues with nitrous acid creates fragments A, B, and C, each differing in size by a disaccharide unit (step 2). In steps 3–10, specific sulfate groups or monosaccharide residues are removed from the nonreducing end of A, B, and C by specific exosulfatases (labeled with an asterisk) and exoglycosidases. The enzymes used are the lysosomal sulfatases IdoA2S (step 3), GlcN6S (step 6), GlcA2S (step 8), and GlcNS (steps 5 and 10) and the appropriate glycosidases. The separation of the enzymatic products on a high-density polyacrylamide gel produces fluorescent band patterns that are characteristic for the saccharide sequence.

a master list of all possible HS sequences is generated. The list is rapidly whittled down as the iterative actions of well-defined chemical and enzymatic agents provide new constraints for the sequence. The power and utility of these HS sequencing methods have been demonstrated in several important studies that have helped elucidate the interactions of HS with FGF^[278,283,284] antithrombin III (AT-III),^[285–287] and herpes simplex virus.^[288] These sequencing methods can also be adapted for the study of other glycosaminoglycans. Several similar techniques have been developed for the analysis of chondroitin sulfate and dermatan sulfate,^[289,290] and it is conceivable that the further characterization of mucin-degrading enzymes and mucin sulfatases could aid in the sequencing of biologically pertinent sulfomucin sequences.



Scheme 7. Use of sulfatases to generate different sulfation patterns on monosaccharide donors. Following global sulfonation by chemical and/or enzymatic synthesis (a), sulfatases can be used independently or in combination to generate the desired sulfation pattern. The sulfatases used are a 4-O-sulfatase from abalone (b), a 2-O-sulfatase from the limpet (c), and a 3-O-sulfatase from the snail (d).

9.2. Sulfatases in Synthesis

With the increased sophistication of the sequencing strategies, several key HS-binding motifs have emerged. There are also many well-described sulfonated carbohydrate structures, such as sLe^x-6S, that are of biological interest.^[291] Often, it is desirable to explore the biological activity of these molecules through the combinatorial synthesis of libraries that facilitate the establishment of structure–activity relationships. Another approach that is also frequently used is the targeted synthesis of analogous structures as potential therapeutic agents. The bottleneck in such endeavors consistently lies in the notoriously difficult synthesis of oligosaccharide libraries,^[292,293] and the use of enzymes is often sought.^[294,295] In this regard, there are a number of ways in which sulfatases might be exploited to facilitate the chemical synthesis of sulfate-bearing oligosaccharides.

As is the case for many processes in carbohydrate chemistry, the sulfonation of saccharides in a regioselective manner often requires arduous protecting-group manipulations. Although a few methods for regioselective sulfonation already exist,^[291,296–299] the use of sulfatases has recently been shown to be a viable alternative. Uzawa et al. synthesized *p*-nitrophenol galactose derivatives with multiple sulfate groups and subjected them to enzyme-catalyzed desulfonation with commercially available sulfatases from mollusks.^[300,301] By studying the activity of several enzymes, conditions were found under which various sulfation patterns could be generated selectively, thus providing facile access to a library of sulfated monosaccharides. These compounds could be subsequently converted into glycosyl donors for the construction of more complex sulfated oligosaccharides (Scheme 7).^[302]

The discovery of the Sulf enzymes provided further possibilities for the application of sulfatases in synthesis. Most GAG-specific sulfatases known prior to Sulf discovery demonstrate strict exo specificity, which has proven useful in sequencing schemes and in the synthesis of sulfated monosaccharide donors. The Sulfs, on the other hand, show unique endo activity.^[22] Their ability to cleave sulfate esters in a regioselective manner within GAG chains might be useful for the generation of diversity in libraries or in the custom synthesis of oligosaccharide epitopes of interest.^[275] For example, a sensitive gel shift assay was recently used to quantify the binding of proteins to HS targets by coupling sulfates enzymatically to an unadorned oligosaccharide backbone.^[303] A complementary sequence could potentially be generated with specific sulfatase enzymes by beginning with a known ligand and HS target and systematically cleaving the sulfate residues. In fact, the interaction between Wnt, HS, and Sulf1 is a prime candidate for investigation by using the gel shift assay. Such a study could provide solid evidence that Sulf1 directly modulates the binding affinity of HS for Wnt by cleaving a key sulfate ester (Figure 7).^[97] Clearly, the discovery and development of novel sulfatases with distinct specificities would greatly add to the potential of this method; one can envisage the use of an assortment of enzymes, including sulfatases and sulfotransferases, for the dynamic manipulation of sulfated oligosaccharide structures with the aim of elucidating HS activities at the cell surface.

Several other applications of sulfatases have been established. One chemoenzymatic approach took its cue from the functional role of sulfatases in the body. In a procedure patented by Bristol-Myers Squibb, a tumor-specific sulfatase-conjugated antibody and a sulfated prodrug were used for tissue-specific drug delivery.^[304] In this process the active therapeutic is released only in the vicinity of the tumor cell

requiring treatment, thus limiting nonspecific activity. The glucosinolate sulfatases from the diamondback moth and the snail *H. pomatia* have been used to help analyze and classify glucosinolates (**4**, Figure 4) from various plant sources.^[152] Extracts from *H. pomatia* have been used in many other analytical applications, from the examination of soil organic matter^[305] to the identification of steroids and psychotropic drugs from urine and hair samples.^[306,307] Other applications of prokaryotic sulfatases include the bioremediation of alkyl sulfate waste products^[48,308,309] and the deracemization of secondary alkyl sulfates.^[41–43]

10. Conclusion and Outlook

A primary aim of this Review was to provide a comprehensive overview of the various areas of sulfatase research. Sulfatases are intriguing in many respects, and their scope is rapidly expanding. Regarding their catalytic activity, a key active-site aldehyde group endows sulfatases with the unique ability to hydrolyze sulfate esters. The post-translational generation of this residue, which is lacking in multiple sulfatase deficiency, is of great clinical interest and requires further mechanistic investigation.

Regarding their structure, the sulfatases exhibit a highly similar three-dimensional fold and highly similar catalytic-cleft geometry, underscoring their functional conservation from prokaryotes to eukaryotes. Such mechanistic homogeneity is interesting given the wide range of substrates and pH optima over which sulfatases operate. Currently, little is known regarding the nature of the catalytic transition state or the basis for substrate specificity. Such information would undoubtedly provide valuable insight for the development of potent, specific inhibitors for sulfatases.

Sulfatases play important roles in a number of biological processes. However, it is becoming clear with the discovery of novel sulfatases and the elucidation of new biological roles that a great deal of research will be necessary to complete the functional picture of this enzyme class. One of the most exciting new areas in which sulfatases are emerging is in the remodeling of important sulfonation states on HS chains, which govern crucial signaling pathways and molecular-recognition events. The study of heparan sulfates is a challenging field in which sulfatases have already proven to be of great value in HS-sequencing strategies. Sulfatases also have the potential to serve as powerful tools in synthetic endeavors with biological and therapeutic objectives.

A diverse range of biological interactions are known to be dependent on sulfate groups, including 1) the participation of heparan sulfate and other sulfated glycosaminoglycans in developmental signaling, as well as bacterial and viral infections, 2) the role of protein tyrosine-*O*-sulfate in the activity of peptide hormones and the entry of HIV into cells, and 3) the role of sLe^x-6S in inflammation. The physiological synthesis of these sulfonated biomolecules by sulfotransferases has been under intense investigation in recent years. It will be very interesting to see if eukaryotic, prokaryotic, or viral sulfatases can also participate in the modulation of these processes.

Abbreviations

AP	alkaline phosphatase
ARS	aryl sulfatase
ECM	extracellular matrix
EGF	epidermal growth factor
ER	endoplasmatic reticulum
FGE	FGly-generating enzyme
FGF	fibroblast growth factor
FGH	α -formylglycine hydrate
FGly	α -formylglycine
FGS	FGly-sulfate adduct
GAG	glycosaminoglycan
HS	heparan sulfate
HSPG	heparan sulfate proteoglycan
MSD	multiple sulfatase deficiency
MSDF	MSD factor
pNCS	<i>p</i> -nitrocatechol sulfate
SUMF	sulfatase-modifying factor
Wnt	Wingless/Int

This work was supported by the NIH. SRH acknowledges a fellowship from the ARCS Foundation.

Received: September 1, 2003

Published Online: October 18, 2004

- [1] E. F. Neufeld, J. Muenzer in *The Metabolic & Molecular Bases of Inherited Disease*, Vol. III, 8th ed. (Ed.: C. R. Scriver), McGraw-Hill, New York, **1999**, p. 3421.
- [2] C. Peters, B. Schmidt, W. Rommerskirch, K. Rupp, M. Zuhlsdorf, M. Vingron, H. Meyer, R. Pohlmann, K. von Figura, *J. Biol. Chem.* **1990**, 265, 3374.
- [3] K. S. Dodgson, G. F. White, J. W. Fitzgerald, *Sulfatases of Microbial Origin*, CRC, Boca Raton **1982**.
- [4] A. B. Roy in *The Enzymes*, Vol. V (Ed.: P. D. Boyer), Academic Press, New York, **1971**, p. 1.
- [5] R. G. Nicholls, A. B. Roy in *The Enzymes*, Vol. V (Ed.: P. D. Boyer), Academic Press, New York, **1971**, p. 21.
- [6] A. Ballabio, L. J. Shapiro in *The Metabolic and Molecular Bases of Inherited Disease*, Vol. III, 8th ed. (Ed.: C. R. Scriver), McGraw-Hill, New York, **1999**, p. 4241.
- [7] K. von Figura, V. Gieselmann, J. Jaeken in *The Metabolic and Molecular Bases of Inherited Disease*, Vol. III, 8th ed. (Ed.: C. R. Scriver), McGraw-Hill, New York, **1999**, p. 3695.
- [8] J. J. Hopwood, A. Ballabio in *The Metabolic and Molecular Bases of Inherited Disease*, Vol. III, 8th ed. (Ed.: C. R. Scriver), McGraw-Hill, New York, **1999**, p. 3725.
- [9] See the website: <http://us.expasy.org/cgi-bin/prosite> (PDOC00117).
- [10] T. Dierks, M. R. Lecca, P. Schlotterhose, B. Schmidt, K. von Figura, *EMBO J.* **1999**, 18, 2084.
- [11] A. Knaust, B. Schmidt, T. Dierks, R. von Bülow, K. von Figura, *Biochemistry* **1998**, 37, 13941.
- [12] I. Boltes, H. Czapinska, A. Kahnert, R. von Bülow, T. Dierks, B. Schmidt, K. von Figura, M. A. Kertesz, I. Usón, *Structure* **2001**, 9, 483.
- [13] According to the Prosite website (<http://us.expasy.org/prosite>), there are two sulfatase signature sequences (PS00523, PS00149).
- [14] A. Waldow, B. Schmidt, T. Dierks, R. von Bülow, K. von Figura, *J. Biol. Chem.* **1999**, 274, 12284.

- [15] G. Lukatela, N. Krauss, K. Theis, T. Selmer, V. Gieselmann, K. von Figura, W. Saenger, *Biochemistry* **1998**, *37*, 3654.
- [16] C. S. Bond, P. R. Clements, S. J. Ashby, C. A. Collyer, S. J. Harrop, J. J. Hopwood, J. M. Guss, *Structure* **1997**, *5*, 277.
- [17] F. G. Hernandez-Guzman, T. Higashiyama, W. Pangborn, Y. Osawa, D. Ghosh, *J. Biol. Chem.* **2003**, *278*, 22989.
- [18] C. I. Branden, *Q. Rev. Biophys.* **1980**, *13*, 317.
- [19] J. M. Sowadski, M. D. Handschumacher, H. M. K. Murthy, B. A. Foster, H. W. Wyckoff, *J. Mol. Biol.* **1985**, *186*, 417.
- [20] M. Chruszcz, P. H. Laidler, M. Monkiewicz, E. Ortlund, L. Lebioda, K. Lewinski, *J. Inorg. Biochem.* **2003**, *96*, 386.
- [21] R. von Bülow, B. Schmidt, T. Dierks, K. von Figura, I. Uson, *J. Mol. Biol.* **2001**, *305*, 269.
- [22] M. Morimoto-Tomita, K. Uchimura, Z. Werb, S. Hemmerich, S. D. Rosen, *J. Biol. Chem.* **2002**, *277*, 49175.
- [23] G. Uhlhorn-Dierks, T. Kolter, K. Sandhoff, *Angew. Chem.* **1998**, *110*, 2591; *Angew. Chem. Int. Ed.* **1998**, *37*, 2453.
- [24] K. von Figura, B. Schmidt, T. Selmer, T. Dierks, *Bioessays* **1998**, *20*, 505.
- [25] B. Schmidt, T. Selmer, A. Ingendoh, K. von Figura, *Cell* **1995**, *82*, 271.
- [26] T. Selmer, A. Hallmann, B. Schmidt, M. Sumper, K. von Figura, *Eur. J. Biochem.* **1996**, *238*, 341.
- [27] T. Dierks, C. Miech, J. Hummerjohann, B. Schmidt, M. A. Kertesz, K. von Figura, *J. Biol. Chem.* **1998**, *273*, 25560.
- [28] C. Miech, T. Dierks, T. Selmer, K. von Figura, B. Schmidt, *J. Biol. Chem.* **1998**, *273*, 4835.
- [29] A. Schirmer, R. Kolter, *Chem. Biol.* **1998**, *5*, R181.
- [30] C. Marquardt, P. H. Fang, E. Will, J. H. Peng, K. von Figura, T. Dierks, *J. Biol. Chem.* **2003**, *278*, 2212.
- [31] T. Dierks, B. Schmidt, L. V. Borissenko, J. Peng, A. Preusser, M. Mariappan, K. von Figura, *Cell* **2003**, *113*, 435.
- [32] M. P. Cosma, S. Pepe, I. Annunziata, R. F. Newbold, M. Grompe, G. Parenti, A. Ballabio, *Cell* **2003**, *113*, 445.
- [33] D. A. Brooks, D. A. Robertson, C. Bindloss, T. Litjens, D. S. Anson, C. Peters, C. P. Morris, J. J. Hopwood, *Biochem. J.* **1995**, *307*, 457.
- [34] R. Recksiek, T. Selmer, T. Dierks, B. Schmidt, K. von Figura, *J. Biol. Chem.* **1998**, *273*, 6096.
- [35] C. L. L. Chai, W. A. Loughlin, G. Lowe, *Biochem. J.* **1992**, *287*, 805.
- [36] S. Ahmed, K. James, C. P. Owen, C. K. Patel, L. Sampson, *Bioorg. Med. Chem. Lett.* **2002**, *12*, 1279.
- [37] P. J. O'Brien, D. Herschlag, *Biochemistry* **2002**, *41*, 3207.
- [38] B. T. Burlingham, L. M. Pratt, E. R. Davidson, V. J. Shiner, Jr., J. Fong, T. S. Widlanski, *J. Am. Chem. Soc.* **2003**, *125*, 13036.
- [39] B. Bartholomew, K. S. Dodgson, G. W. J. Matcham, D. J. Shaw, G. F. White, *Biochem. J.* **1977**, *165*, 575.
- [40] J. M. Cloves, K. S. Dodgson, D. E. Games, D. J. Shaw, G. F. White, *Biochem. J.* **1977**, *167*, 843.
- [41] M. Pogorevc, U. T. Strauss, T. Riermeier, K. Faber, *Tetrahedron: Asymmetry* **2002**, *13*, 1443.
- [42] M. Pogorevc, W. Kroutil, S. R. Wallner, K. Faber, *Angew. Chem.* **2002**, *114*, 4230; *Angew. Chem. Int. Ed.* **2002**, *41*, 4052.
- [43] M. Pogorevc, K. Faber, *Appl. Environ. Microbiol.* **2003**, *69*, 2810.
- [44] I. Davies, G. F. White, W. J. Payne, *Biodegradation* **1990**, *1*, 229.
- [45] T. P. Higgins, J. R. Snape, G. F. White, *J. Gen. Microbiol.* **1993**, *139*, 2915.
- [46] A. Kahnert, M. A. Kertesz, *J. Biol. Chem.* **2000**, *275*, 31661.
- [47] Y. Tazuke, K. Matsuda, K. Adachi, Y. Tsukada, *Biosci. Biotechnol. Biochem.* **1994**, *58*, 889.
- [48] J. Davison, F. Brunel, A. Phanopoulos, D. Prozzi, P. Terpstra, *Gene* **1992**, *114*, 19.
- [49] P. J. Matts, G. F. White, W. J. Payne, *Biochem. J.* **1994**, *304*, 937.
- [50] M. A. Kertesz, *FEMS Microbiol. Rev.* **2000**, *24*, 135.
- [51] R. J. Yao, P. Guerry, *J. Bacteriol.* **1996**, *178*, 3335.
- [52] T. Barbeyron, P. Potin, C. Richard, O. Collin, B. Kloareg, *Microbiology* **1995**, *141*, 2897.
- [53] T. Dierks, B. Schmidt, K. von Figura, *Proc. Natl. Acad. Sci. USA* **1997**, *94*, 11963.
- [54] T. Dierks, M. R. Lecca, B. Schmidt, K. von Figura, *FEBS Lett.* **1998**, *423*, 61.
- [55] J. Fey, M. Balleininger, L. V. Borissenko, B. Schmidt, K. von Figura, T. Dierks, *J. Biol. Chem.* **2001**, *276*, 47021.
- [56] T. Yamada, Y. Murooka, T. Harada, *J. Bacteriol.* **1978**, *133*, 536.
- [57] H.-J. Jansen, C. A. Hart, J. M. Rhodes, J. R. Saunders, J. W. Smalley, *J. Med. Microbiol.* **1999**, *48*, 551.
- [58] J. R. Myette, Z. Shriver, C. Claycamp, M. W. McLean, G. Venkataraman, R. Sasisekharan, *J. Biol. Chem.* **2003**, *278*, 12157.
- [59] C. Szameit, C. Miech, M. Balleininger, B. Schmidt, K. von Figura, T. Dierks, *J. Biol. Chem.* **1999**, *274*, 15375.
- [60] D. P. Wright, C. G. Knight, S. G. Parker, D. L. Christie, A. M. Robertson, *J. Bacteriol.* **2000**, *182*, 3002.
- [61] R. Raman, J. R. Myette, Z. Shriver, K. Pojasek, G. Venkataraman, R. Sasisekharan, *J. Biol. Chem.* **2003**, *278*, 12167.
- [62] D. S. Anson, J. Bielicki, *Int. J. Biochem. Cell Biol.* **1999**, *31*, 363.
- [63] Y. Murooka, K. Ishibashi, M. Yasumoto, M. Sasaki, H. Sugino, H. Azakami, M. Yamashita, *J. Bacteriol.* **1990**, *172*, 2131.
- [64] Y. Murooka, H. Azakami, M. Yamashita, *Biosci. Biotechnol. Biochem.* **1996**, *60*, 935.
- [65] Q. Cheng, V. Hwa, A. A. Salyers, *J. Bacteriol.* **1992**, *174*, 7185.
- [66] S. Kornfeld, I. Mellman, *Annu. Rev. Cell Biol.* **1989**, *5*, 483.
- [67] C. Stein, V. Gieselmann, J. Kreysing, B. Schmidt, R. Pohlmann, A. Waheed, H. Meyer, J. O'Brien, K. von Figura, *J. Biol. Chem.* **1989**, *264*, 1252.
- [68] D. S. Anson, J. A. Taylor, J. Bielicki, G. S. Harper, C. Peters, G. J. Gibson, J. J. Hopwood, *Biochem. J.* **1992**, *284*, 789.
- [69] S. Tomatsu, S. Fukuda, M. Masue, K. Sukegawa, T. Fukao, A. Yamagishi, T. Hori, H. Iwata, T. Ogawa, Y. Nakashima, *Biochem. Biophys. Res. Commun.* **1991**, *181*, 677.
- [70] T. Litjens, J. Bielicki, D. S. Anson, K. Friderici, M. Z. Jones, J. J. Hopwood, *Biochem. J.* **1997**, *327*, 89.
- [71] J. Bielicki, J. J. Hopwood, E. L. Melville, D. S. Anson, *Biochem. J.* **1998**, *329*, 145.
- [72] J. Bielicki, J. J. Hopwood, P. J. Wilson, D. S. Anson, *Biochem. J.* **1993**, *289*, 241.
- [73] A. A. Farooqui, P. Mandel, *Biomedicine* **1977**, *26*, 232.
- [74] A. L. Fluharty, R. L. Stevens, E. B. Goldstein, H. Kihara, *Biochim. Biophys. Acta* **1979**, *566*, 321.
- [75] H. Jatzkewi, E. Mehl, *J. Neurochem.* **1969**, *16*, 19.
- [76] E. Mehl, H. Jatzkewitz, *Biochim. Biophys. Acta* **1968**, *151*, 619.
- [77] A. B. Roy, *Biochim. Biophys. Acta* **1975**, *377*, 356.
- [78] A. Vogel, G. Schwarzmann, K. Sandhoff, *Eur. J. Biochem.* **1991**, *200*, 591.
- [79] B. M. Gadella, B. Colenbrander, L. M. G. Vangolde, M. Lopes-cardozo, *Biochim. Biophys. Acta* **1992**, *1128*, 155.
- [80] J. Tantibhedhyangkul, W. Weerachatanukul, E. Carmona, H. Xu, A. Anupriwan, D. Michaud, N. Tanphaichitr, *Biol. Reprod.* **2002**, *67*, 212.
- [81] E. Carmona, W. Weerachatanukul, T. Soboloff, A. L. Fluharty, D. White, L. Promdee, M. Ekker, T. Berger, M. Buhr, N. Tanphaichitr, *Dev. Biol.* **2002**, *247*, 182.
- [82] E. Carmona, W. Weerachatanukul, H. Xu, A. Fluharty, A. Anupriwan, A. Shoushtarian, K. Chakrabandhu, N. Tanphaichitr, *Biol. Reprod.* **2002**, *66*, 1820.
- [83] J. F. Robyt, *Essentials of Carbohydrate Chemistry*, Springer, New York, **1998**.
- [84] T. Islam, R. J. Linhardt in *Carbohydrate-based Drug Discovery, Vol. 1* (Ed.: C. H. Wong), Wiley-VCH, Weinheim, **2003**, p. 407.
- [85] K. S. Dodgson, B. Spencer, *Biochem. J.* **1957**, *65*, 668.
- [86] R. Matalon, B. Arbogast, A. Dorfman, *Biochem. Biophys. Res. Commun.* **1974**, *61*, 1450.

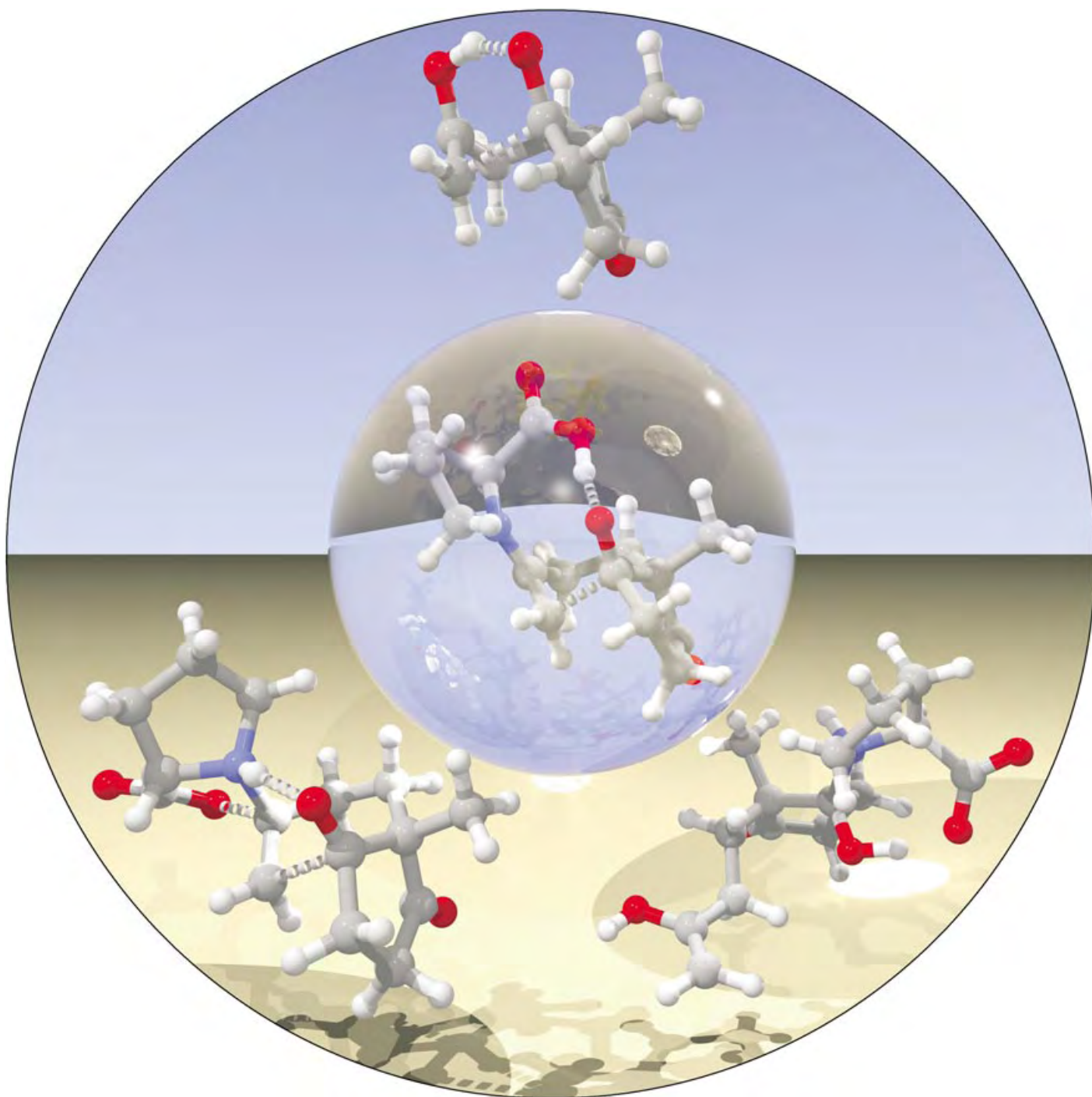
- [87] J. F. O'Brien, M. Cantz, J. Spranger, *Biochem. Biophys. Res. Commun.* **1974**, 60, 1170.
- [88] J. Bielicki, J. J. Hopwood, *Biochem. J.* **1991**, 279, 515.
- [89] J. Bielicki, M. Fuller, X. H. Guo, G. P. Morris, J. J. Hopwood, D. S. Anson, *Biochem. J.* **1995**, 311, 333.
- [90] B. Winchester in *Biology of the Lysosome*, Vol. 27 (Eds.: J. B. Lloyd, R. W. Mason), Plenum, New York, **1996**, p. 191.
- [91] C. Freeman, J. J. Hopwood, *Biochem. J.* **1991**, 279, 399.
- [92] U. Lindahl, G. Backstrom, L. Thunberg, I. G. Leder, *Proc. Natl. Acad. Sci. USA* **1980**, 77, 6551.
- [93] I. G. Leder, *Biochem. Biophys. Res. Commun.* **1980**, 94, 1183.
- [94] G. J. Gibson, G. T. Saccone, D. A. Brooks, P. R. Clements, J. J. Hopwood, *Biochem. J.* **1987**, 248, 755.
- [95] C. Freeman, J. J. Hopwood, *Biochem. J.* **1986**, 234, 83.
- [96] L. C. Ginsberg, D. T. Di Ferrante, N. Di Ferrante, *Carbohydr. Res.* **1978**, 64, 225.
- [97] G. K. Dhoot, M. K. Gustafsson, X. Ai, W. Sun, D. M. Standiford, C. P. Emerson, Jr., *Science* **2001**, 293, 1663.
- [98] J. L. Mullor, A. Ruiz i. Altaba, *BioEssays* **2002**, 24, 22.
- [99] X. Ai, A.-T. Do, O. Lozynska, M. Kusche-Gullberg, U. Lindahl, C. P. Emerson, Jr., *J. Cell Biol.* **2003**, 162, 341.
- [100] J. Lai, J. Chien, J. Staub, R. Avula, E. L. Greene, T. A. Matthews, D. I. Smith, S. H. Kaufmann, L. R. Roberts, V. Shridhar, *J. Biol. Chem.* **2003**, 278, 23107.
- [101] G. H. Baeg, X. H. Lin, N. Khare, S. Baumgartner, N. Perrimon, *Development* **2001**, 128, 87.
- [102] Z. L. Wu, L. Zhang, T. Yabe, B. Kuberan, D. L. Beeler, A. Love, R. D. Rosenberg, *J. Biol. Chem.* **2003**, 278, 17121.
- [103] D. A. Pye, R. R. Vives, J. E. Turnbull, P. Hyde, J. T. Gallagher, *J. Biol. Chem.* **1998**, 273, 22936.
- [104] K. Kamimura, M. Fujise, F. Villa, S. Izumi, H. Habuchi, K. Kimata, H. Nakato, *J. Biol. Chem.* **2001**, 276, 17014.
- [105] X. H. Lin, N. Perrimon, *Nature* **1999**, 400, 281.
- [106] M. Tsuda, K. Kamimura, H. Nakato, M. Archer, W. Staatz, B. Fox, M. Humphrey, S. Olson, T. Futch, V. Kaluza, E. Siegfried, L. Stam, S. B. Selleck, *Nature* **1999**, 400, 276.
- [107] J. D. Esko, S. B. Selleck, *Annu. Rev. Biochem.* **2002**, 71, 435.
- [108] T. Ohto, H. Uchida, H. Yamazaki, K. Keino-Masu, A. Matsui, M. Masu, *Genes Cells* **2002**, 7, 173.
- [109] D. A. Pye, R. R. Vives, P. Hyde, J. T. Gallagher, *Glycobiology* **2000**, 10, 1183.
- [110] J. Schlessinger, A. N. Plotnikov, O. A. Ibrahim, A. V. Eliseenkova, B. K. Yeh, A. Yayon, R. J. Linhardt, M. Mohammadi, *Mol. Cell* **2000**, 6, 743.
- [111] R. Sasisekharan, Z. Shriver, G. Venkataraman, U. Narayanasami, *Nat. Rev. Cancer* **2002**, 2, 521.
- [112] D. F. Liu, Z. Shriver, G. Venkataraman, Y. El Shabrawi, R. Sasisekharan, *Proc. Natl. Acad. Sci. USA* **2002**, 99, 568.
- [113] K. Yamada, K. Akasaka, H. Shimada, *Eur. J. Biochem.* **1989**, 186, 405.
- [114] Q. Yang, L. M. Angerer, R. C. Angerer, *Dev. Biol.* **1989**, 135, 53.
- [115] E. S. Haag, R. A. Raff, *Dev. Genes Evol.* **1998**, 208, 188.
- [116] H. Sasaki, K. Yamada, K. Akasaka, H. Kawasaki, K. Suzuki, A. Saito, M. Sato, H. Shimada, *Eur. J. Biochem.* **1988**, 177, 9.
- [117] S. Kinoshita, H. Saiga, *Exp. Cell Res.* **1979**, 123, 229.
- [118] A. C. Rapraeger, D. Epel, *Dev. Biol.* **1981**, 88, 269.
- [119] C. A. Ettensohn, H. C. Sweet, *Curr. Top. Dev. Biol.* **2000**, 50, 1.
- [120] R. Hobkirk, *Trends Endocrinol. Metab.* **1993**, 4, 69.
- [121] C. Stein, A. Hille, J. Seidel, S. Rijnbout, A. Waheed, B. Schmidt, H. Geuze, K. von Figura, *J. Biol. Chem.* **1989**, 264, 13865.
- [122] L. Dibbelt, E. Kuss, *Biol. Chem. Hoppe-Seyler* **1991**, 372, 173.
- [123] C. T. Noel, M. J. Reed, H. S. Jacobs, V. H. T. James, *J. Steroid Biochem. Mol. Biol.* **1981**, 14, 1101.
- [124] S. Ahmed, C. P. Owen, K. James, L. Sampson, C. K. Patel, *Curr. Med. Chem.* **2002**, 9, 263.
- [125] Y. Miyoshi, A. Ando, S. Hasegawa, M. Ishitobi, T. Taguchi, Y. Tamaki, S. Noguchi, *Clin. Cancer Res.* **2003**, 9, 2288.
- [126] T. Suzuki, T. Nakata, Y. Miki, C. Kaneko, T. Moriya, T. Ishida, S. Akinaga, H. Hirakawa, M. Kimura, H. Sasano, *Cancer Res.* **2003**, 63, 2762.
- [127] A. Billich, P. Nussbaumer, P. Lehr, *J. Steroid Biochem. Mol. Biol.* **2000**, 73, 225.
- [128] D. Poirier, L. C. Ciobanu, R. Maltais, *Expert Opin. Ther. Pat.* **1999**, 9, 1083.
- [129] B. Franco, G. Meroni, G. Parenti, J. Leveilliers, L. Bernard, M. Gebbia, L. Cox, P. Maroteaux, L. Sheffield, G. A. Rappold, G. Andria, C. Petit, A. Ballabio, *Cell* **1995**, 81, 15.
- [130] A. A. Puca, M. Zollo, M. Repetto, G. Andolfi, A. Guffanti, G. Simon, A. Ballabio, B. Franco, *Genomics* **1997**, 42, 192.
- [131] G. Meroni, B. Franco, N. Archidiacono, S. Messali, G. Andolfi, M. Rocchi, A. Ballabio, *Hum. Mol. Genet.* **1996**, 5, 423.
- [132] G. Parenti, G. Meroni, A. Ballabio, *Curr. Opin. Genet. Dev.* **1997**, 7, 386.
- [133] P. Ferrante, S. Messali, G. Meroni, A. Ballabio, *Eur. J. Hum. Genet.* **2002**, 10, 813.
- [134] A. Daniele, G. Parenti, M. d'Addio, G. Andria, A. Ballabio, G. Meroni, *Am. J. Hum. Genet.* **1998**, 62, 562.
- [135] P. Urbitsch, M. J. Salzer, P. Hirschmann, P. H. Vogt, *DNA Cell Biol.* **2000**, 19, 765.
- [136] G. Parenti, P. Buttitta, G. Meroni, B. Franco, L. Bernard, M. G. Rizzolo, N. Brunetti-Pierri, A. Ballabio, G. Andria, *Am. J. Med. Genet.* **1997**, 73, 139.
- [137] J. G. Hall, R. M. Pauli, K. M. Wilson, *Am. J. Med.* **1980**, 68, 122.
- [138] E. Arikava-Hirasawa, H. Watanabe, H. Takami, J. R. Hassell, Y. Yamada, *Nat. Genet.* **1999**, 23, 354.
- [139] M. Bernfield, M. Gotte, P. W. Park, O. Reizes, M. L. Fitzgerald, J. Lincecum, M. Zako, *Annu. Rev. Biochem.* **1999**, 68, 729.
- [140] N. Perrimon, M. Bernfield, *Nature* **2000**, 404, 725.
- [141] M. W. H. Coughtrie, S. Sharp, K. Maxwell, N. P. Innes, *Chem.-Biol. Interact.* **1998**, 109, 3.
- [142] K. Richard, R. Hume, E. Kaptein, E. L. Stanley, T. J. Visser, M. W. H. Coughtrie, *J. Clin. Endocrinol. Metab.* **2001**, 86, 2734.
- [143] C. A. Strott, *Endocr. Rev.* **2002**, 23, 703.
- [144] M. H. A. Kester, E. Kaptein, C. H. Van Dijk, T. J. Roest, D. Tibboel, M. W. H. Coughtrie, T. J. Visser, *Endocrinology* **2002**, 143, 814.
- [145] T. P. Dooley, R. Haldeman-Cahill, J. Joiner, T. W. Wilborn, *Biochem. Biophys. Res. Commun.* **2000**, 277, 236.
- [146] K. S. Dodgson, *Enzymologia* **1959**, 20, 301.
- [147] H. Hatanaka, F. Egami, I. Ishizuka, Y. Nagai, *Biochim. Biophys. Acta* **1976**, 438, 176.
- [148] H. Hatanaka, Y. Ogawa, F. Egami, *Biochem. J.* **1976**, 159, 445.
- [149] M. G. L. Medeiros, T. Ferreira, E. L. Leite, L. Toma, C. P. Dietrich, H. B. Nader, *Comp. Biochem. Physiol. Part A* **1998**, 119, 539.
- [150] T. Moriya, M. Hoshi, *Arch. Biochem. Biophys.* **1980**, 201, 216.
- [151] F. W. Oliveira, S. F. Chavante, E. A. Santos, C. P. Dietrich, H. B. Nader, *Biochim. Biophys. Acta* **1994**, 1200, 241.
- [152] A. Ratzka, H. Vogel, D. J. Kliebenstein, T. Mitchell-Olds, J. Kroymann, *Proc. Natl. Acad. Sci. USA* **2002**, 99, 11223.
- [153] A. B. Roy, *Methods Enzymol.* **1987**, 143, 361.
- [154] K. S. Dodgson, G. M. Powell, *Biochem. J.* **1959**, 73, 666.
- [155] U. Wittstock, M. Fischer, I. Svendsen, B. A. Halkier, *IUBMB Life* **2000**, 49, 71.
- [156] G. R. J. Burns, C. H. Wynn, *Biochem. J.* **1977**, 166, 415.
- [157] W. G. McGuire, G. A. Marzluf, *Arch. Biochem. Biophys.* **1974**, 161, 360.
- [158] J. V. Paietta, *Mol. Cell. Biol.* **1989**, 9, 3630.
- [159] E. L. de Hostos, R. K. Togasaki, A. Grossman, *J. Cell Biol.* **1988**, 106, 29.
- [160] E. L. de Hostos, J. Schilling, A. R. Grossman, *Mol. Gen. Genet.* **1989**, 218, 229.

- [161] A. Hallmann, M. Sumper, *Eur. J. Biochem.* **1994**, 221, 143.
- [162] G. A. Marzluf in *Advances in Genetics*, Vol. 31, Academic Press, San Diego, **1994**, S. 187.
- [163] G. A. Marzluf, *Annu. Rev. Microbiol.* **1997**, 51, 73.
- [164] W. A. Scott, R. Metzenbel, *J. Bacteriol.* **1970**, 104, 1254.
- [165] T. Adachi, Y. Murooka, T. Harada, *J. Bacteriol.* **1975**, 121, 29.
- [166] Y. Murooka, T. Harada, *J. Bacteriol.* **1981**, 145, 796.
- [167] M. J. Henderson, F. H. Milazzo, *J. Bacteriol.* **1979**, 139, 80.
- [168] J. W. Fitzgerald, F. H. Milazzo, *Int. J. Biochem.* **1975**, 6, 769.
- [169] M. A. Kertesz, T. Leisinger, A. M. Cook, *J. Bacteriol.* **1993**, 175, 1187.
- [170] Y. Murooka, M.-H. Yim, T. Harada, *Appl. Environ. Microbiol.* **1980**, 39, 812.
- [171] J. O. Falkinham III, *Int. J. Syst. Bacteriol.* **1990**, 40, 66.
- [172] H. Tomioka, H. Saito, K. Sato, D. J. Dawson, *J. Clin. Microbiol.* **1990**, 28, 2104.
- [173] S. Beil, H. Kehrli, P. James, W. Staudenmann, A. M. Cook, T. Leisinger, M. A. Kertesz, *Eur. J. Biochem.* **1995**, 229, 385.
- [174] J. Hummerjohann, E. Kottel, M. Quadroni, J. Ragaller, T. Leisinger, M. A. Kertesz, *Microbiology* **1998**, 144, 1375.
- [175] S. Mueller, A. Schmidt, *Z. Naturforsch. C* **1986**, 41, 820.
- [176] J. W. Fitzgerald, M. E. Cline, *FEMS Microbiol. Lett.* **1977**, 2, 221.
- [177] M. A. Kertesz, *Res. Microbiol.* **2001**, 152, 279.
- [178] T. Harada, *Biochim. Biophys. Acta* **1964**, 81, 193.
- [179] J. J. Lucas, S. W. Burchiel, I. H. Segel, *Arch. Biochem. Biophys.* **1972**, 153, 664.
- [180] I. Takebe, *J. Biochem.* **1961**, 50, 245.
- [181] M. Osteras, E. Boncompagni, N. Vincent, M. C. Poggi, D. Le Rudulier, *Proc. Natl. Acad. Sci. USA* **1998**, 95, 11394.
- [182] L. T. Smith, J. A. Pocard, T. Bernard, D. Lerudulier, *J. Bacteriol.* **1988**, 170, 3142.
- [183] S. Ernst, R. Langer, C. L. Cooney, R. Sasisekharan, *Crit. Rev. Biochem. Mol. Biol.* **1995**, 30, 387.
- [184] M. J. Hernaiz, R. J. Linhardt in *Proteoglycan Protocols*, Vol. 171 (Ed.: R. V. Iozzo), Humana, Totowa, **2001**, p. 363.
- [185] L. A. LeBrun, R. J. Linhardt in *Proteoglycan Protocols*, Vol. 171 (Ed.: R. V. Iozzo), Humana, Totowa, **2001**, p. 353.
- [186] M. W. McLean, J. S. Bruce, W. F. Long, F. B. Williamson, *Eur. J. Biochem.* **1984**, 145, 607.
- [187] J. S. Bruce, M. W. McLean, W. F. Long, F. B. Williamson, *Eur. J. Biochem.* **1985**, 148, 359.
- [188] J. S. Bruce, M. W. McLean, W. F. Long, F. B. Williamson, *Eur. J. Biochem.* **1987**, 165, 633.
- [189] J. S. Bruce, M. W. McLean, F. B. Williamson, W. F. Long, *Eur. J. Biochem.* **1985**, 152, 75.
- [190] V. Hwa, A. A. Salyers, *J. Bacteriol.* **1992**, 174, 342.
- [191] A. A. Salyers, M. O'Brien, *J. Bacteriol.* **1980**, 143, 772.
- [192] K. Sugahara, T. Kojima, *Eur. J. Biochem.* **1996**, 239, 865.
- [193] K. Sugahara, K. Shigeno, M. Masuda, N. Fujii, A. Kurosaka, K. Takeda, *Carbohydr. Res.* **1994**, 255, 145.
- [194] K. Sugahara, Y. Takemura, M. Sugiura, Y. Kohno, K. Yoshida, K. Takeda, K. H. Khoo, H. R. Morris, A. Dell, *Carbohydr. Res.* **1994**, 255, 165.
- [195] T. Yamagata, H. Saito, O. Habuchi, S. Suzuki, *J. Biol. Chem.* **1968**, 243, 1523.
- [196] G. J. Strous, J. Dekker, *Crit. Rev. Biochem. Mol. Biol.* **1992**, 27, 57.
- [197] A. M. Robertson, S. I. Rosendale, D. P. Wright in *Methods in Molecular Biology*, Vol. 125 (Hrsg.: A. P. Corfield), Humana Press, Totowa, **1999**, S. 417.
- [198] A. V. Nieuw Amerongen, J. G. Bolscher, E. Bloemena, E. C. Veerman, *Biol. Chem.* **1998**, 379, 1.
- [199] A. P. Corfield, D. Carroll, N. Myerscough, C. S. J. Probert, *Front. Biosci.* **2001**, 6, D1321.
- [200] A. M. Robertson, D. P. Wright, *Can. J. Gastroenterol.* **1997**, 11, 361.
- [201] A. M. Robertson, A. P. Corfield, *Mucin Degradation and Its Significance in Inflammatory Conditions of the Gastrointestinal Tract*, Kluwer, Norwell, **1999**.
- [202] H. H. Tsai, C. A. Hart, J. M. Rhodes, *Lett. Appl. Microbiol.* **1991**, 13, 97.
- [203] J. W. Smalley, D. Dwarakanath, J. M. Rhodes, C. A. Hart, *Caries Res.* **1994**, 28, 416.
- [204] A. P. Corfield, S. A. Wagner, J. R. Clamp, M. S. Kriaris, L. C. Hoskins, *Infect. Immun.* **1992**, 60, 3971.
- [205] V. L. N. Murty, J. Piotrowski, M. Morita, A. Slomiany, B. L. Slomiany, *Biochem. Int.* **1992**, 26, 1091.
- [206] H. H. Tsai, D. Sunderland, G. R. Gibson, C. A. Hart, J. M. Rhodes, *Clin. Sci.* **1992**, 82, 447.
- [207] A. M. Robertson, C. G. McKenzie, N. Sharfe, L. B. Stubbs, *Biochem. J.* **1993**, 293, 683.
- [208] K. Clinch, G. B. Evans, R. H. Furneaux, P. M. Rendle, P. L. Rhodes, A. M. Robertson, D. I. Rosendale, P. C. Tyler, D. P. Wright, *Carbohydr. Res.* **2002**, 337, 1095.
- [209] D. P. Wright, D. I. Rosendale, A. M. Robertson, *FEMS Microbiol. Lett.* **2000**, 190, 73.
- [210] H. H. Tsai, A. D. Dwarakanath, C. A. Hart, J. D. Milton, J. M. Rhodes, *Gut* **1995**, 36, 570.
- [211] A. P. Corfield, S. A. Wagner, L. J. D. Odonnell, P. Durdey, R. A. Mountford, J. R. Clamp, *Glycoconjugate J.* **1993**, 10, 72.
- [212] B. L. Slomiany, V. L. Murty, J. Piotrowski, M. Grabska, A. Slomiany, *Am. J. Gastroenterol.* **1992**, 87, 1132.
- [213] J. R. W. Govan, V. Deretic, *Microbiol. Rev.* **1996**, 60, 539.
- [214] R. Ramphal, C. Carnoy, S. Fiebre, J. C. Michalski, N. Houdret, G. Lamblin, G. Strecker, P. Roussel, *Infect. Immun.* **1991**, 59, 700.
- [215] A. Scharfman, E. VanBrussel, N. Houdret, G. Lamblin, P. Roussel, *Am. J. Resp. Crit. Care Med.* **1996**, 154, S163.
- [216] J. Piotrowski, A. Slomiany, V. L. N. Murty, Z. Fekete, B. L. Slomiany, *Biochem. Int.* **1991**, 24, 749.
- [217] J. D. Mougous, R. E. Green, S. J. Williams, S. E. Brenner, C. R. Bertozzi, *Chem. Biol.* **2002**, 9, 767.
- [218] J. Parkhill, B. W. Wren, N. R. Thomson, R. W. Titball, M. T. Holden, M. B. Prentice, M. Sebahia, K. D. James, C. Churcher, K. L. Mungall, S. Baker, D. Basham, S. D. Bentley, K. Brooks, A. M. Cerdeno-Tarraga, T. Chillingworth, A. Cronin, R. M. Davies, P. Davis, G. Dougan, T. Feltwell, N. Hamlin, S. Holroyd, K. Jagels, A. V. Karlyshev, S. Leather, S. Moule, P. C. Oyston, M. Quail, K. Rutherford, M. Simmonds, J. Skelton, K. Stevens, S. Whitehead, B. G. Barrell, *Nature* **2001**, 413, 523.
- [219] J. Parkhill, G. Dougan, K. D. James, N. R. Thomson, D. Pickard, J. Wain, C. Churcher, K. L. Mungall, S. D. Bentley, M. T. Holden, M. Sebahia, S. Baker, D. Basham, K. Brooks, T. Chillingworth, P. Connerton, A. Cronin, P. Davis, R. M. Davies, L. Dowd, N. White, J. Farrar, T. Feltwell, N. Hamlin, A. Haque, T. T. Hien, S. Holroyd, K. Jagels, A. Krogh, T. S. Larsen, S. Leather, S. Moule, P. O'Gaora, C. Parry, M. Quail, K. Rutherford, M. Simmonds, J. Skelton, K. Stevens, S. Whitehead, B. G. Barrell, *Nature* **2001**, 413, 848.
- [220] I. T. Paulsen, L. Banerjee, G. S. Myers, K. E. Nelson, R. Seshadri, T. D. Read, D. E. Fouts, J. A. Eisen, S. R. Gill, J. F. Heidelberg, H. Tettelin, R. J. Dodson, L. Umayam, L. Brinkac, M. Beanan, S. Daugherty, R. T. DeBoy, S. Durkin, J. Kolonay, R. Madupu, W. Nelson, J. Vamathevan, B. Tran, J. Upton, T. Hansen, J. Shetty, H. Khouri, T. Utterback, D. Radune, K. A. Ketchum, B. A. Dougherty, C. M. Fraser, *Science* **2003**, 299, 2071.
- [221] T. D. Read, S. L. Salzberg, M. Pop, M. Shumway, L. Umayam, L. Jiang, E. Holtzapple, J. D. Busch, K. L. Smith, J. M. Schupp, D. Solomon, P. Keim, C. M. Fraser, *Science* **2002**, 296, 2028.
- [222] H. Tettelin, V. Maignani, M. J. Cieslewicz, J. A. Eisen, S. Peterson, M. R. Wessels, I. T. Paulsen, K. E. Nelson, I. Margarit, T. D. Read, L. C. Madoff, A. M. Wolf, M. J. Beanan, L. M.

- Brinkac, S. C. Daugherty, R. T. DeBoy, A. S. Durkin, J. F. Kolonay, R. Madupu, M. R. Lewis, D. Radune, N. B. Fedorova, D. Scanlan, H. Khouri, S. Mulligan, H. A. Carty, R. T. Cline, S. E. Van Aken, J. Gill, M. Scarselli, M. Mora, E. T. Iacobini, C. Brettoni, G. Galli, M. Mariani, F. Vegni, D. Maione, D. Rinaudo, R. Rappuoli, J. L. Telford, D. L. Kasper, G. Grandi, C. M. Fraser, *Proc. Natl. Acad. Sci. USA* **2002**, *99*, 12391.
- [223] J. A. Hoffman, J. L. Badger, Y. Zhang, S.-H. Huang, K. S. Kim, *Infect. Immun.* **2000**, *68*, 5062.
- [224] E. Von Angerer, J. Prekajac, *J. Med. Chem.* **1983**, *26*, 113.
- [225] E. Von Angerer, J. Prekajac, J. Strohmeier, *J. Med. Chem.* **1984**, *27*, 1439.
- [226] H. Birnbock, E. Von Angerer, *Biochem. Pharmacol.* **1990**, *39*, 1709.
- [227] S. J. Santner, R. J. Santen, *J. Steroid Biochem. Mol. Biol.* **1993**, *45*, 383.
- [228] C. K. Wong, W. M. Keung, *Biochem. Biophys. Res. Commun.* **1997**, *233*, 579.
- [229] K. Carlstrom, A. K. Vonuexkull, N. Einhorn, B. Fredricsson, N. O. Lunell, P. Sundelin, *Acta Obstet. Gynecol. Scand.* **1983**, *62*, 519.
- [230] N. Terakawa, H. Ikegami, I. Shimizu, T. Aono, O. Tanizawa, K. Matsumoto, *J. Steroid Biochem. Mol. Biol.* **1987**, *28*, 571.
- [231] N. M. Howarth, G. Cooper, A. Purohit, L. Duncan, M. J. Reed, B. V. L. Potter, *Bioorg. Med. Chem. Lett.* **1993**, *3*, 313.
- [232] L. Duncan, A. Purohit, N. M. Howarth, B. V. L. Potter, M. J. Reed, *Cancer Res.* **1993**, *53*, 298.
- [233] N. M. Howarth, A. Purohit, J. J. Robinson, N. Vicker, M. J. Reed, B. V. L. Potter, *Biochemistry* **2002**, *41*, 14801.
- [234] C. J. Anderson, L. J. H. Lucas, T. S. Widlanski, *J. Am. Chem. Soc.* **1995**, *117*, 3889.
- [235] C. Anderson, J. Freeman, L. H. Lucas, M. Farley, H. Dalhoumi, T. S. Widlanski, *Biochemistry* **1997**, *36*, 2586.
- [236] D. Poirier, R. P. Boivin, *Bioorg. Med. Chem. Lett.* **1998**, *8*, 1891.
- [237] L. C. Ciobanu, R. P. Boivin, V. Luu-The, F. Labrie, D. Poirier, *J. Med. Chem.* **1999**, *42*, 2280.
- [238] L. C. Ciobanu, D. Poirier, *J. Comb. Chem.* **2003**, *5*, 429.
- [239] R. P. Boivin, V. Luu-The, R. Lachance, F. Labrie, D. Poirier, *J. Med. Chem.* **2000**, *43*, 4465.
- [240] L. C. Ciobanu, R. P. Boivin, V. Luu-The, D. Poirier, *Eur. J. Med. Chem.* **2001**, *36*, 659.
- [241] N. M. Howarth, A. Purohit, M. J. Reed, B. V. L. Potter, *J. Med. Chem.* **1994**, *37*, 219.
- [242] A. Purohit, G. J. Williams, N. M. Howarth, B. V. L. Potter, M. J. Reed, *Biochemistry* **1995**, *34*, 11508.
- [243] L. W. L. Woo, A. Purohit, M. J. Reed, B. V. L. Potter, *Bioorg. Med. Chem. Lett.* **1997**, *7*, 3075.
- [244] L. W. L. Woo, A. Purohit, M. J. Reed, B. V. L. Potter, *J. Med. Chem.* **1996**, *39*, 1349.
- [245] A. Purohit, L. W. L. Woo, A. Singh, C. J. Winterborn, B. V. L. Potter, M. J. Reed, *Cancer Res.* **1996**, *56*, 4950.
- [246] L. W. L. Woo, A. Purohit, B. Malini, M. J. Reed, B. V. L. Potter, *Chem. Biol.* **2000**, *7*, 773.
- [247] L. W. L. Woo, N. M. Howarth, A. Purohit, H. A. M. Hejaz, M. J. Reed, B. V. L. Potter, *J. Med. Chem.* **1998**, *41*, 1068.
- [248] L. W. Woo, O. B. Sutcliffe, C. Bubert, A. Grasso, S. K. Chander, A. Purohit, M. J. Reed, B. V. Potter, *J. Med. Chem.* **2003**, *46*, 3193.
- [249] P. Nussbaumer, P. Lehr, A. Billich, *J. Med. Chem.* **2002**, *45*, 4310.
- [250] P. Nussbaumer, P. Lehr, A. Billich, *J. Med. Chem.* **2003**, *46*, 5091.
- [251] P. Nussbaumer, M. Bilban, A. Billich, *Bioorg. Med. Chem. Lett.* **2002**, *12*, 2093.
- [252] P. Jutten, W. Schumann, A. Hartl, L. Heinisch, U. Grafe, W. Werner, H. Ulbricht, *Bioorg. Med. Chem. Lett.* **2002**, *12*, 1339.
- [253] S. Ahmed, K. James, *Bioorg. Med. Chem. Lett.* **1999**, *9*, 1645.
- [254] S. Ahmed, K. James, L. Sampson, C. Matri, *Biochem. Biophys. Res. Commun.* **1999**, *254*, 811.
- [255] S. Ahmed, K. James, C. K. Patel, *Biochem. Biophys. Res. Commun.* **2000**, *272*, 583.
- [256] S. Ahmed, C. P. Owen, K. James, C. K. Patel, M. Patel, *Bioorg. Med. Chem. Lett.* **2001**, *11*, 899.
- [257] S. Ahmed, K. James, C. P. Owen, C. K. Patel, M. Patel, *Bioorg. Med. Chem. Lett.* **2001**, *11*, 841.
- [258] S. Ahmed, K. James, C. P. Owen, C. K. Patel, M. Patel, *Bioorg. Med. Chem. Lett.* **2001**, *11*, 2525.
- [259] S. Ahmed, K. James, C. P. Owen, *Bioorg. Med. Chem. Lett.* **2002**, *12*, 2391.
- [260] C. K. Patel, C. P. Owen, S. Ahmed, *Biochem. Biophys. Res. Commun.* **2003**, *307*, 778.
- [261] S. Ahmed, K. James, C. P. Owen, C. K. Patel, *Bioorg. Med. Chem. Lett.* **2002**, *12*, 1343.
- [262] S. Ahmed, K. James, C. P. Owen, *Biochem. Biophys. Res. Commun.* **2002**, *294*, 180.
- [263] J. M. Trowbridge, R. L. Gallo, *Glycobiology* **2002**, *12*, 117R.
- [264] Z. Shriver, D. F. Liu, R. Sasisekharan, *Trends Cardiovasc. Med.* **2002**, *12*, 71.
- [265] E. M. Selva, N. Perrimon, *Adv. Cancer Res.* **2001**, *83*, 67.
- [266] C. Yuen, K. Bezouska, J. O'Brien, M. Stoll, R. Lemoine, A. Lubineau, M. Kiso, A. Hasegawa, N. Bockovich, K. Nicolaou, *J. Biol. Chem.* **1994**, *269*, 1595.
- [267] P. J. Green, C. T. Yuen, R. A. Childs, W. Chai, M. Miyasaka, R. Lemoine, A. Lubineau, B. Smith, H. Ueno, K. C. Nicolaou, *Glycobiology* **1995**, *5*, 29.
- [268] M. Petitou, J. P. Herault, A. Bernat, P. A. Driguez, P. Duchaussoy, J. C. Lormeau, J. M. Herbert, *Nature* **1999**, *398*, 417.
- [269] T. Toida, R. E. Hileman, A. E. Smith, P. I. Vlahova, R. J. Linhardt, *J. Biol. Chem.* **1996**, *271*, 32040.
- [270] R. V. Iozzo, J. D. San Antonio, *J. Clin. Invest.* **2001**, *108*, 349.
- [271] M. Bomsel, A. Alfsen, *Nat. Rev. Mol. Cell Biol.* **2003**, *4*, 57.
- [272] K. S. Rostand, J. D. Esko, *Infect. Immun.* **1997**, *65*, 1.
- [273] T. Wadstrom, A. Ljungh, *J. Med. Microbiol.* **1999**, *48*, 223.
- [274] R. Sasisekharan, Z. Shriver, S. Mallik, G. Venkataraman in *Carbohydrate-based Drug Discovery*, Vol. 2 (Ed.: C. H. Wong), Wiley-VCH, Weinheim, **2003**, p. 517.
- [275] J. Turnbull, A. Powell, S. Guimond, *Trends Cell Biol.* **2001**, *11*, 75.
- [276] I. Capila, R. J. Linhardt, *Angew. Chem.* **2002**, *114*, 426; *Angew. Chem. Int. Ed.* **2002**, *41*, 39.
- [277] D. L. Rabenstein, *Nat. Prod. Rep.* **2002**, *19*, 312.
- [278] J. E. Turnbull, J. J. Hopwood, J. T. Gallagher, *Proc. Natl. Acad. Sci. USA* **1999**, *96*, 2698.
- [279] G. Venkataraman, Z. Shriver, R. Raman, R. Sasisekharan, *Science* **1999**, *286*, 537.
- [280] R. R. Vives, D. A. Pye, M. Salmivirta, J. J. Hopwood, U. Lindahl, J. T. Gallagher, *Biochem. J.* **1999**, *339*, 767.
- [281] S. E. Stringer, B. S. Kandola, D. A. Pye, J. T. Gallagher, *Glycobiology* **2003**, *13*, 97.
- [282] C. L. R. Merry, M. Lyon, J. A. Deakin, J. J. Hopwood, J. T. Gallagher, *J. Biol. Chem.* **1999**, *274*, 18455.
- [283] P. Jemth, J. Kreuger, M. Kusche-Gullberg, L. Sturiale, G. Gimenez-Gallego, U. Lindahl, *J. Biol. Chem.* **2002**, *277*, 30567.
- [284] S. E. Guimond, J. E. Turnbull, *Curr. Biol.* **1999**, *9*, 1343.
- [285] Z. Shriver, M. Sundaram, G. Venkataraman, J. Fareed, R. Linhardt, K. Biemann, R. Sasisekharan, *Proc. Natl. Acad. Sci. USA* **2000**, *97*, 10365.
- [286] Z. Shriver, R. Raman, G. Venkataraman, K. Drummond, J. Turnbull, T. Toida, R. Linhardt, K. Biemann, R. Sasisekharan, *Proc. Natl. Acad. Sci. USA* **2000**, *97*, 10359.
- [287] N. Keiser, G. Venkataraman, Z. Shriver, R. Sasisekharan, *Nat. Med.* **2001**, *7*, 123.

- [288] J. Liu, Z. Shriver, R. M. Pope, S. C. Thorp, M. B. Duncan, R. J. Copeland, C. S. Raska, K. Yoshida, R. J. Eisenberg, G. Cohen, R. J. Linhardt, R. Sasisekharan, *J. Biol. Chem.* **2002**, 277, 33456.
- [289] R. M. Lauder, T. N. Huckerby, I. A. Nieduszynski, *Glycobiology* **2000**, 10, 393.
- [290] H. O. Yang, N. S. Gunay, T. Toida, B. Kuberan, G. Yu, Y. S. Kim, R. J. Linhardt, *Glycobiology* **2000**, 10, 1033.
- [291] E. E. Simanek, G. J. McGarvey, J. A. Jablonowski, C. H. Wong, *Chem. Rev.* **1998**, 98, 833.
- [292] P. Sears, C.-H. Wong, *Science* **2001**, 291, 2344.
- [293] P. H. Seeberger, *J. Carbohydr. Chem.* **2002**, 21, 613.
- [294] K. M. Koeller, C.-H. Wong, *Glycobiology* **2000**, 10, 1157.
- [295] K. M. Koeller, C.-H. Wong, *Nature* **2001**, 409, 232.
- [296] A. Lubineau, R. Lemoine, *Tetrahedron Lett.* **1994**, 35, 8795.
- [297] K. G. Bowman, B. N. Cook, C. L. de Graffenried, C. R. Bertozzi, *Biochemistry* **2001**, 40, 5382.
- [298] T. Yoshida, *Carbohydr. Res.* **1997**, 304, 249.
- [299] G. V. Reddy, R. K. Jain, R. D. Locke, K. L. Matta, *Carbohydr. Res.* **1996**, 280, 261.
- [300] H. Uzawa, T. Toba, Y. Nishida, K. Kobayashi, N. Minoura, K. Hiratani, *Chem. Commun.* **1998**, 2311.
- [301] H. Uzawa, Y. Nishida, K. Sasaki, N. Minoura, K. Kobayashi, *ChemBioChem* **2003**, 4, 640.
- [302] D. Page, R. Roy, *Glycoconjugate J.* **1997**, 14, 345.
- [303] Z. L. Wu, L. Zhang, D. L. Beeler, B. Kuberan, R. D. Rosenberg, *FASEB J.* **2002**, 16, 539.
- [304] Y. Sawada, T. Ueki, S. Yamamoto, K. Tomita, Y. Fukagawa, T. Oki, *Eur. Pat. Appl.* **1991**, 16.
- [305] J. K. Whalen, P. R. Warman, *Biol. Fertil. Soils* **1996**, 23, 64.
- [306] C. H. L. Shackleton, E. Roitman, A. Phillips, T. Chang, *Steroids* **1997**, 62, 665.
- [307] M. Yegles, F. Mersch, R. Wennig, *Forensic Sci. Int.* **1997**, 84, 211.
- [308] D. Schleheck, M. Lechner, R. Schonenberger, M. J.-F. Suter, A. M. Cook, *Appl. Environ. Microbiol.* **2003**, 69, 938.
- [309] A. J. Ellis, S. G. Hales, N. G. A. Ur-Rehman, G. F. White, *Appl. Environ. Microbiol.* **2002**, 68, 31.
- [310] <http://www.ncbi.nlm.nih.gov/Entrez/>.

Communications



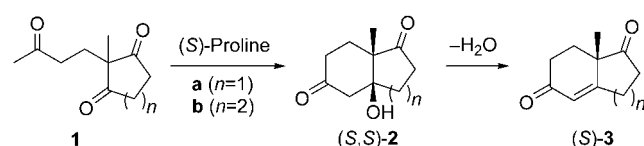
Theoretical evidence now suggests that the mechanism of the long-debated Hajos–Parrish–Eder–Sauer–Wiechert reaction, the prototype for asymmetric organocatalytic reactions, involves a proline enamine intermediate (center) which undergoes a concerted aldol cyclization with proton transfer. For more details see the Communication by K. N. Houk and F. R. Clemente on the following pages.

Density Functional Calculations

Computational Evidence for the Enamine Mechanism of Intramolecular Aldol Reactions Catalyzed by Proline**

Fernando R. Clemente and K. N. Houk*

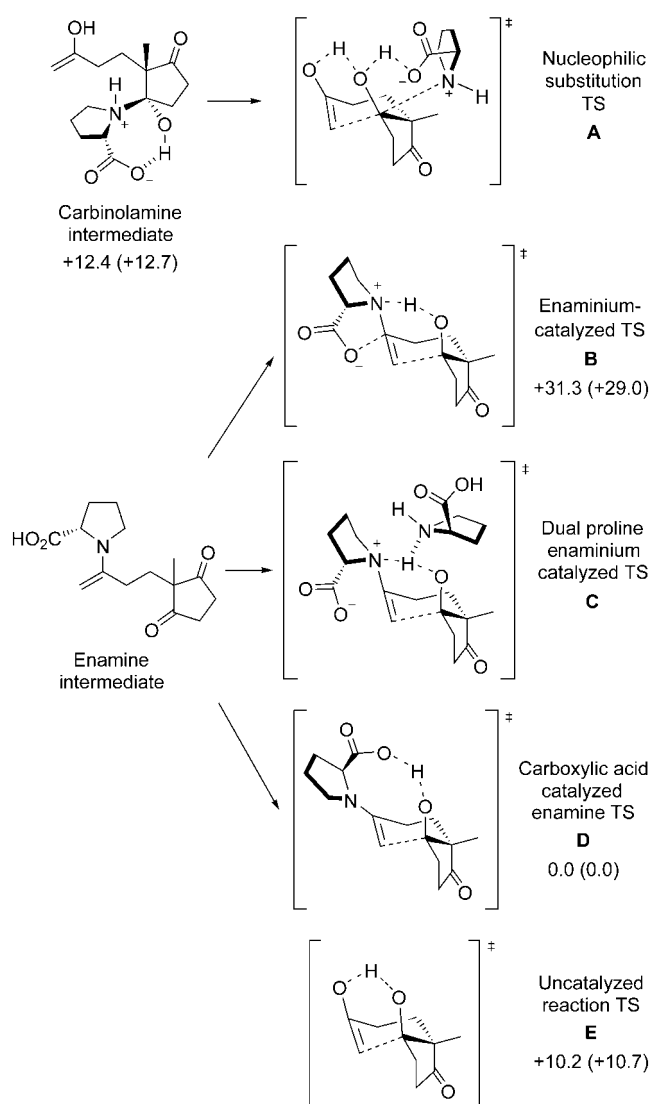
The first examples of enantioselective intramolecular aldol cyclizations catalyzed by proline (Scheme 1) were independently reported by Hajos and Parrish^[1] and by Wiechert and co-workers^[2] in 1971. Useful synthetic intermediates, such as the Wieland–Miescher ketone (**3b**) are easily obtained by this reaction. This reaction constitutes a cornerstone in the emergent field of enantioselective organocatalysis. A variety of C–C bond-forming reactions have been achieved with chiral organocatalysis in recent years.^[3]



Scheme 1. Enantioselective intramolecular aldol cyclization.

In spite of the classic status of this reaction, the mechanism remains controversial. Herein we provide definitive theoretical evaluation of the various mechanisms proposed for the reaction; by computation of all six steps in the reaction we show how the reaction conditions may influence the rate-determining step and the stereoselectivity.

In their original paper,^[1b] Hajos and Parrish proposed two mechanisms (Scheme 2): **A**, which requires the formation of a carbinolamine intermediate followed by nucleophilic substitution at this center by the enol form of the acyclic carbonyl; and **B**, with an enaminium intermediate and C–C bond-formation accompanied by N–H–O hydrogen transfer and nucleophilic assistance by the carboxylate group of proline. Hajos still argues for mechanism **A**,^[1c] on the basis of his experiments with ¹⁸O-labeled water where no incorporation of ¹⁸O in the products was observed.^[1b] However, List et al. have reinvestigated these experiments recently under care-



Scheme 2. Relative energies ($E + \text{ZPE}$, kcal mol⁻¹; ZPE = zero-point energy) of proposed proline-catalyzed aldolization transition states. Values in parentheses include solvation energies in DMSO using the PCM/UAKE model.

fully controlled conditions, and they found efficient (> 90 %) ¹⁸O incorporation.^[4]

In the 1980s, Agami supported the mechanisms involving enamine intermediates^[5] on the basis of accumulated experience in amine catalysis of similar reactions.^[6] Mechanism **B** was criticized, since it involves a protonated enamine that must reduce the nucleophilicity of the C=C bond. They proposed mechanism **C**, which involves a second molecule of proline to assist in the hydrogen transfer.^[5] While model **C** was supported by the observation of a kinetic nonlinear effect, List and co-workers have reported evidence that show the absence of nonlinear effects in these reactions and support a one-proline mechanism.^[7]

Mechanism **D** involves an enamine intermediate with concerted C–C bond formation and proton transfer from the carboxylic acid group to the carbonyl acceptor. This transition state, initially proposed by Jung in a review in 1976,^[8] was

[*] Dr. F. R. Clemente, Prof. Dr. K. N. Houk
Department of Chemistry and Biochemistry
University of California
Los Angeles, CA 90095-1569 (USA)
Fax: (+1) 310-206-1843
E-mail: houk@chem.ucla.edu

[**] We are grateful to the National Institute of General Medical Sciences, National Institutes of Health for financial support of this research, and the National Computational Science Alliance, the National Science Foundation, and UCLA Academic Technology Services for computer resources. F.R.C. thanks Fundación Ramón Areces (Spain) for a postdoctoral fellowship.

Supporting information for this article is available on the WWW under <http://www.angewandte.org> or from the author.

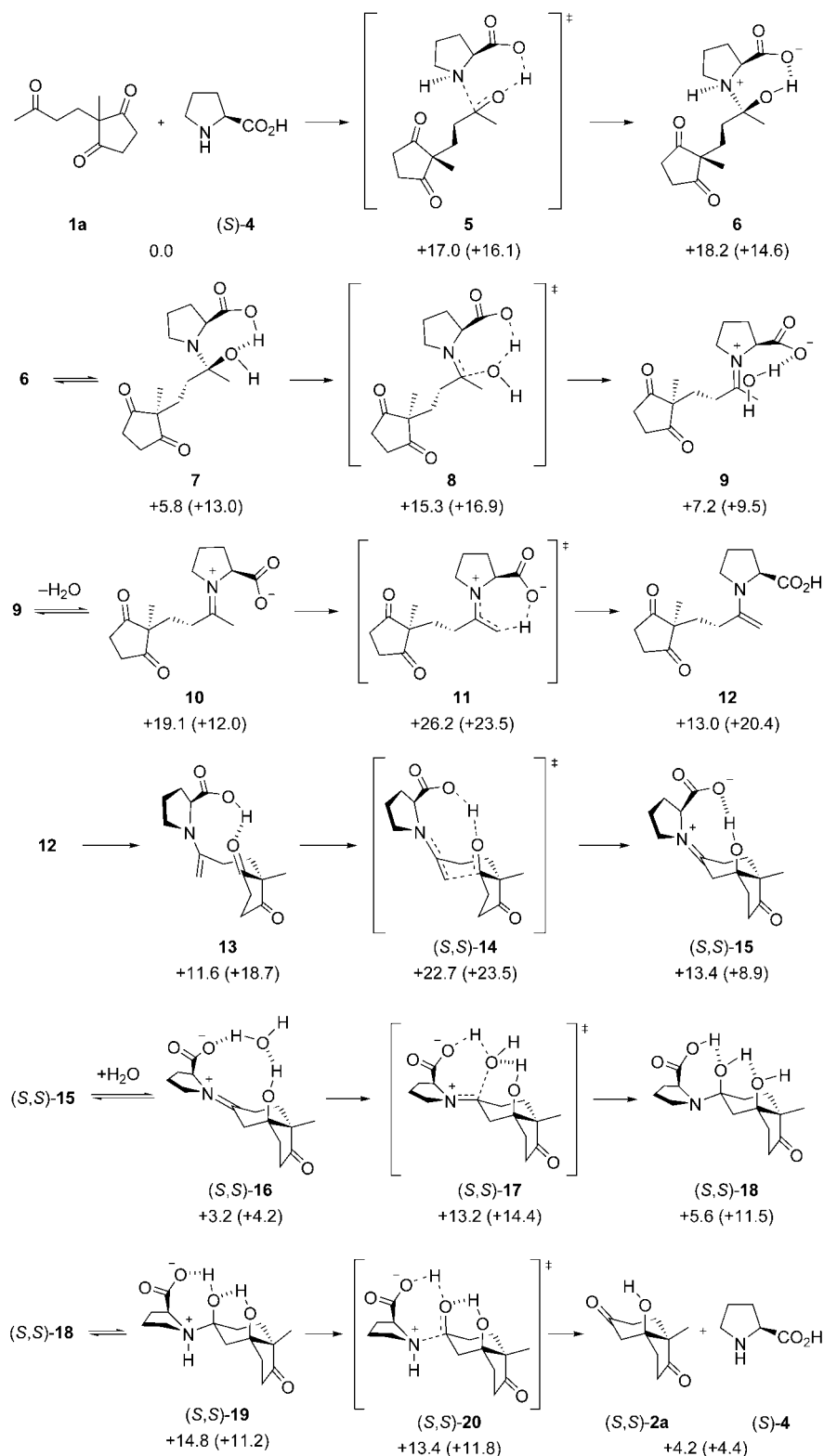
almost abandoned in favor of mechanism **C** until 2000. In their pioneering work on enantioselective proline catalysis of intermolecular aldol reactions, List, Barbas, and co-workers proposed a model similar to **D**.^[9] Our preliminary computational studies on the origins of the stereoselectivity of the intramolecular aldol reactions depicted in Scheme 1 also support mechanism **D**, since transition states computed for this reaction provide a satisfactory explanation of the stereochemical outcome.^[10]

We have located the transition structures for the C–C bond-forming step of the different mechanisms proposed (Scheme 1), which is the presumed rate-determining step for the transformation. All the geometries were fully optimized with GAUSSIAN^[11] at the B3LYP/6-31G(d) level followed by frequency calculations to determine the nature of the stationary points. The reported energies come from B3LYP/6-31+G(d,p) energy calculations on the geometries optimized at the lower level.^[12] Free energies of solvation were computed as the energy difference of HF/6-31+G(d,p) single point energy calculations in DMSO (PCM model^[13] and UAKS radii)^[11b] and in the gas-phase on the DFT gas-phase geometries.

The relative energies of the different transition states or intermediates are given in Scheme 2. The carboxylic acid catalyzed enamine mechanism (**D**) is energetically the most favorable. The transition structure for C–C bond formation by this mechanism is more than 10 kcal mol^{−1} lower in energy than the corresponding one for the uncatalyzed process (**E**). Mechanism **B**, which involves the zwitterionic form of the enamine (enaminium), is disfavored by about 30 kcal mol^{−1} over mechanism **D**. The nucleophilic substitution TS (**A**) could not be located, and all our optimization attempts led to structures similar to **E**, the uncatalyzed process. However, the carbinolamine intermediate preceding this C–C bond-forming TS is more than 12 kcal mol^{−1} higher in energy than TS **D**. It is thus expected that a structure such as TS **A**, if it exists, would be even higher in energy than this intermediate.

The enhanced nucleophilicity of the enamine C=C bond together with the activation of the carbonyl electrophile by the carboxylic acid constitute the basis of the catalytic activity of the amino acid acting through mechanism **D**. Protonation of the enamine nitrogen atom (**B**) drastically reduces the reactivity of the C=C bond. On the other hand, the mechanism originally supported by Hajos (**A**) appears very unlikely since the carbinolamine intermediate is already higher in energy than the transition structure for the uncatalyzed process (**E**).

Scheme 3 depicts the proposed pathway for the enantioselective aldol cyclization of **1a** catalyzed by (*S*)-proline involving the formation of an enamine intermediate (**12**) and



Scheme 3. Proposed pathway for the (*S*)-proline-catalyzed cyclization of **1a** into (*S,S*)-**2a** with the relative gas-phase energies (kcal mol^{−1}). Values in parentheses include solvation energies in DMSO using the PCM/UAKS model.

carboxylic acid catalysis in the C–C bond-forming step ((*S,S*)-**14**). Boyd and co-workers have reported a similar study but for the intermolecular reaction.^[14] The last stage in the formation of enamine intermediate **12** is the intramolecular deprotonation by the carboxylate group (**11**). This process and the subsequent C–C forming step have equal energies in solution and represent the rate-determining steps (Figure 1). The C–C bond forming step ((*S,S*)-**14**) is the stereochemistry-determining step of the reaction. The preferential formation of the *S,S* enantiomer was rationalized in an earlier computational study from our research group.^[10]

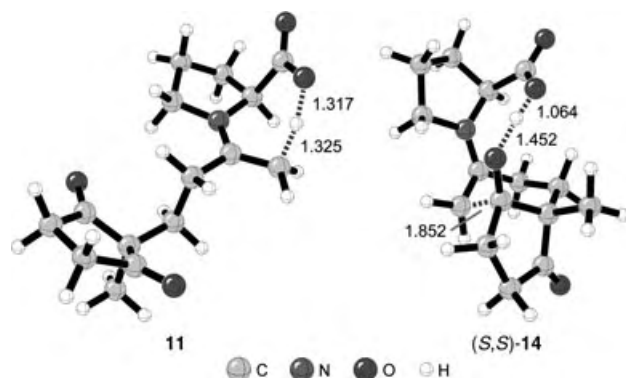


Figure 1. B3LYP/6-31G(d)-optimized transition-state geometries of the rate-determining steps for enamine formation (**11**) and aldol cyclization ((*S,S*)-**14**). Interatomic distances are given in Å.

After the formation of the C–C bond, the hydrolysis of iminium (*S,S*)-**15** is achieved in a series of easy steps that leads to the release of the aldol product (*S,S*)-**2a** and recovery of the catalyst. These steps are analogous, but in reverse order, to those at the beginning corresponding to the formation of iminium intermediate **10**. As expected, the most difficult step in the hydrolysis of (*S,S*)-**15** is the nucleophilic attack of water ((*S,S*)-**17**). This step will compete with the reversal of the C–C bond-forming step ((*S,S*)-**14**) at a low concentration of water. This result has significance on the stereoselectivity.

Recent experimental work,^[4,7] together with these computational studies, have established the previously controversial mechanism of aldol reactions catalyzed by proline.

Received: June 9, 2004

Keywords: aldol reaction · asymmetric catalysis · density functional calculations · proline · reaction mechanisms

[1] a) Z. G. Hajos, D. R. Parrish, German Patent DE 2102623, July 29, 1971; b) Z. G. Hajos, D. R. Parrish, *J. Org. Chem.* **1974**, 39, 1615–1621; c) Z. G. Hajos, <http://preprint.chemweb.com/orgchem/0209001>.

[2] a) U. Eder, G. Sauer, R. Wiechert, German Patent DE 2014757, Oct. 7, 1971; b) U. Eder, G. Sauer, R. Wiechert, *Angew. Chem.* **1971**, 83, 492–493; *Angew. Chem. Int. Ed. Engl.* **1971**, 10, 496–497.

- [3] Reviews: a) P. I. Dalko, L. Moisan, *Angew. Chem.* **2001**, 113, 3840–3864; *Angew. Chem. Int. Ed.* **2001**, 40, 3726–3748; b) E. R. Jarvo, S. J. Miller, *Tetrahedron* **2002**, 58, 2481–2495.
- [4] B. List, L. Hoang, H. J. Martin, *Proc. Natl. Acad. Sci. USA* **2004**, 101, 5839–5842.
- [5] For a review of their work, see C. Agami, *Bull. Soc. Chim. Fr.* **1988**, 3, 499–507.
- [6] a) T. A. Spencer, H. S. Neel, T. W. Flechtner, R. A. Zayle, *Tetrahedron Lett.* **1965**, 3889–3897; b) H. Molines, C. Wakselman, *Tetrahedron* **1976**, 32, 2099–2103; c) K. L. Brown, L. Damm, J. D. Dunitz, A. Eschenmoser, R. Hobi, C. Kratky, *Helv. Chim. Acta* **1978**, 61, 3108–3135.
- [7] L. Hoang, S. Bahmanyar, K. N. Houk, B. List, *J. Am. Chem. Soc.* **2003**, 125, 16–17.
- [8] M. E. Jung, *Tetrahedron* **1976**, 32, 3–31.
- [9] a) B. List, R. A. Lerner, C. F. Barbas III, *J. Am. Chem. Soc.* **2000**, 122, 2395–2396; b) K. Sakthivel, W. Notz, T. Bui, C. F. Barbas III, *J. Am. Chem. Soc.* **2001**, 123, 5260–5267.
- [10] S. Bahmanyar, K. N. Houk, *J. Am. Chem. Soc.* **2001**, 123, 12911–12912.
- [11] a) Gaussian98 (Revision A.9), M. J. Frisch, G. W. Trucks, H. B. Schlegel, G. E. Scuseria, M. A. Robb, J. R. Cheeseman, V. G. Zakrzewski, J. A. Montgomery, Jr., R. E. Stratmann, J. C. Burant, S. Dapprich, J. M. Millam, A. D. Daniels, K. N. Kudin, M. C. Strain, O. Farkas, J. Tomasi, V. Barone, M. Cossi, R. Cammi, B. Mennucci, C. Pomelli, C. Adamo, S. Clifford, J. Ochterski, G. A. Petersson, P. Y. Ayala, Q. Cui, K. Morokuma, D. K. Malick, A. D. Rabuck, K. Raghavachari, J. B. Foresman, J. Cioslowski, J. V. Ortiz, A. G. Baboul, B. B. Stefanov, G. Liu, A. Liashenko, P. Piskorz, I. Komaromi, R. Gomperts, R. L. Martin, D. J. Fox, T. Keith, M. A. Al-Laham, C. Y. Peng, A. Nanayakkara, M. Challacombe, P. M. W. Gill, B. Johnson, W. Chen, M. W. Wong, J. L. Andres, C. Gonzalez, M. Head-Gordon, E. S. Replogle, J. A. Pople, Gaussian, Inc., Pittsburgh, PA, **1998**; b) solvation calculations performed with Gaussian03: Gaussian03 (Revision B.05), M. J. Frisch, G. W. Trucks, H. B. Schlegel, G. E. Scuseria, M. A. Robb, J. R. Cheeseman, J. A. Montgomery, Jr., T. Vreven, K. N. Kudin, J. C. Burant, J. M. Millam, S. S. Iyengar, J. Tomasi, V. Barone, B. Mennucci, M. Cossi, G. Scalmani, N. Rega, G. A. Petersson, H. Nakatsuji, M. Hada, M. Ehara, K. Toyota, R. Fukuda, J. Hasegawa, M. Ishida, T. Nakajima, Y. Honda, O. Kitao, H. Nakai, M. Klene, X. Li, J. E. Knox, H. P. Hratchian, J. B. Cross, C. Adamo, J. Jaramillo, R. Gomperts, R. E. Stratmann, O. Yazyev, A. J. Austin, R. Cammi, C. Pomelli, J. W. Ochterski, P. Y. Ayala, K. Morokuma, G. A. Voth, P. Salvador, J. J. Dannenberg, V. G. Zakrzewski, S. Dapprich, A. D. Daniels, M. C. Strain, O. Farkas, D. K. Malick, A. D. Rabuck, K. Raghavachari, J. B. Foresman, J. V. Ortiz, Q. Cui, A. G. Baboul, S. Clifford, J. Cioslowski, B. B. Stefanov, G. Liu, A. Liashenko, P. Piskorz, I. Komaromi, R. L. Martin, D. J. Fox, T. Keith, M. A. Al-Laham, C. Y. Peng, A. Nanayakkara, M. Challacombe, P. M. W. Gill, B. Johnson, W. Chen, M. W. Wong, C. Gonzalez, J. A. Pople, Gaussian, Inc., Pittsburgh, PA, **2003**.
- [12] Reported energies include zero-point energy corrections at the same level of the geometry (B3LYP/6-31G(d)) scaled by 0.9806: A. P. Scott, L. Radom, *J. Phys. Chem.* **1996**, 100, 16502–16513.
- [13] a) B. Mennucci, R. Cammi, J. Tomasi, *J. Chem. Phys.* **1999**, 110, 6858–6870; b) M. Cossi, G. Scalmani, N. Rega, V. Barone, *J. Chem. Phys.* **2002**, 117, 43–54.
- [14] K. N. Rankin, J. W. Gauld, R. J. Boyd, *J. Phys. Chem. A* **2002**, 106, 5155–5159.

Helical Water Chain

Helix inside a Helix: Encapsulation of Hydrogen-Bonded Water Molecules in a Staircase Coordination Polymer**

Bellam Sreenivasulu and Jagadees J Vittal*

Inspired by the fascinating structural features of helices that exhibit cooperative self-assembly and recognition, as well as remarkable functions such as chemical transport and screening by membrane channels in biological systems, helicity has been successfully introduced into artificial systems by chemists working in the field of metallo-supramolecular chemistry.^[1] As a result, today helical polymers are among the most explored and best investigated supramolecular architectures.^[2] As hydrogen bonds and other noncovalent interactions are the main driving forces behind this self-assembly process, supramolecular chemistry is now in a phase of characterizing and understanding various hydrogen-bonded water clusters in the form of hexamers,^[3,4] octamers,^[5,6] decamers,^[7] (H₂O)₁₅(CH₃OH)₃ clusters^[8] and one-dimensional (1D) infinite water chains^[9,10] in diverse environments of various crystal hosts. Zeolite-like 3D network structures with chiral channels filled with highly ordered water molecules are well known.^[11]

At this juncture, 1D water chains are attracting a great deal of attention because of their vital role in the biological transport of water, protons, and ions.^[12] It was recently found that transport of water or protons across the cell involves the assembly of highly mobile hydrogen-bonded water molecules into a single chain at the positively charged constricted pore of the membrane-channel protein aquaporin-1.^[13] While 1D water chains play crucial roles in stabilizing the native conformation of biopolymers, such helical water chains are extremely rare in synthetic crystal hosts.^[9,10] Here we report an interesting staircaselike helical coordination polymeric architecture of a Ni^{II} complex that hosts a 1D helical chain of lattice water molecules in a helical pore through hydrogen bonding.

The single-crystal X-ray structure of [(H₂O)₂C{Ni(Hsglu)(H₂O)₂}]·H₂O (**1**; H₃sglu = *N*-(2-hydroxybenzyl)-L-glutamic acid) was determined unambiguously.^[14] Compound **1** crystallizes in the monoclinic system with two independent molecules in the asymmetric unit. Each Ni^{II} unit has octahedral geometry (Figure 1), and the Hsglu²⁻ ligand is coordinated through the phenolic oxygen atom (Ni1–O1

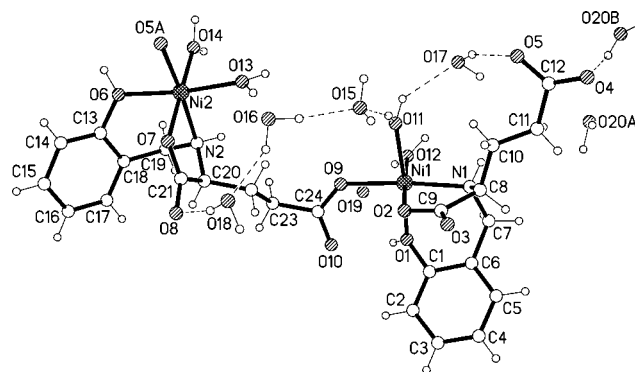
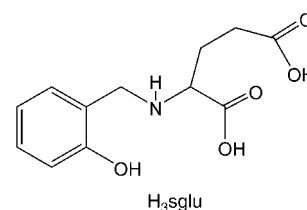


Figure 1. A view of the coordination environments at the two Ni^{II} centers in **1**. Selected bond lengths [Å]: Ni1–O(12) 2.043(4), Ni1–O2 2.047(4), Ni1–O(11) 2.051(4), Ni1–O(9) 2.059(3), Ni1–N1 2.084(4), Ni1–O1 2.089(4), Ni2–O(14) 2.039(4), Ni2–O(7) 2.042(4), Ni2–O(5) (–*x* + 1, *y* – 1/2, –*z* + 1) 2.048(4), Ni2–O(13) 2.070(3), Ni2–N2 2.082(4), Ni2–O6 2.101(3).

2.089(4) Å, Ni2–O6 2.101(3) Å), secondary amine N atom (Ni1–N1 2.084(4) Å, Ni2–N2 2.082(4) Å), and carboxylate α-oxygen atom (Ni1–O2, 2.047(4) Å, Ni2–O7 2.042(4) Å) in a *fac* manner, along with two aqua ligands, and another carboxylate oxygen atom from the neighboring molecule. The intermolecular connectivity via the second carboxylate O atom generates a left-handed staircaselike coordination polymeric architecture with a pseudo-4₁ screw axis. In this helical staircase, the aqua ligands *trans* to phenolic oxygen atoms (i.e., O11 and O13) point into the tube, normal to the helical axis. The NH and OH protons form hydrogen bonds to the carboxylate oxygen atoms along the surface of the helical staircase, as shown in Figure 2; hydrogen-bond parameters are given in Table 1.

The square-shaped chiral channel has dimensions of 7.654 × 7.529 Å (based on Ni···Ni distances; Figure 3). Of the six lattice water molecules present in the asymmetric unit, four are inside the helical pore, and two outside. Two of the former water molecules (O15 and O16, Figure 1) are hydrogen-bonded to produce a 1D helical polymer with a pseudo-4₁ screw axis. This helical water chain, as the pole of the helical staircase, supports and stabilizes its orientation by maintaining hydrogen bonding to aqua ligands. The other two water molecules (O17 and O18) propagate hydrogen bonding with both the helical water chain and the aqua ligands, and their hydrogen bonding tendency appears to have facilitated the positioning and orientation of the water molecules forming the helical chain.

The total solvent volume in the lattice, including that occupied by the helical-chain and lattice water molecules, is 405.1 Å³ (22.7% of the unit cell).^[14] All the tubular coordi-

[*] B. Sreenivasulu, Prof. J. J. Vittal
Department of Chemistry
National University of Singapore
Science Drive 3, Singapore 117543 (Singapore)
Fax: (+65) 6779-1691
E-mail: chmjv@nus.edu.sg

[**] We thank the National University of Singapore for financial support (Grant No. R143-000-153-112).

Supporting information for this article is available on the WWW under <http://www.angewandte.org> or from the author.

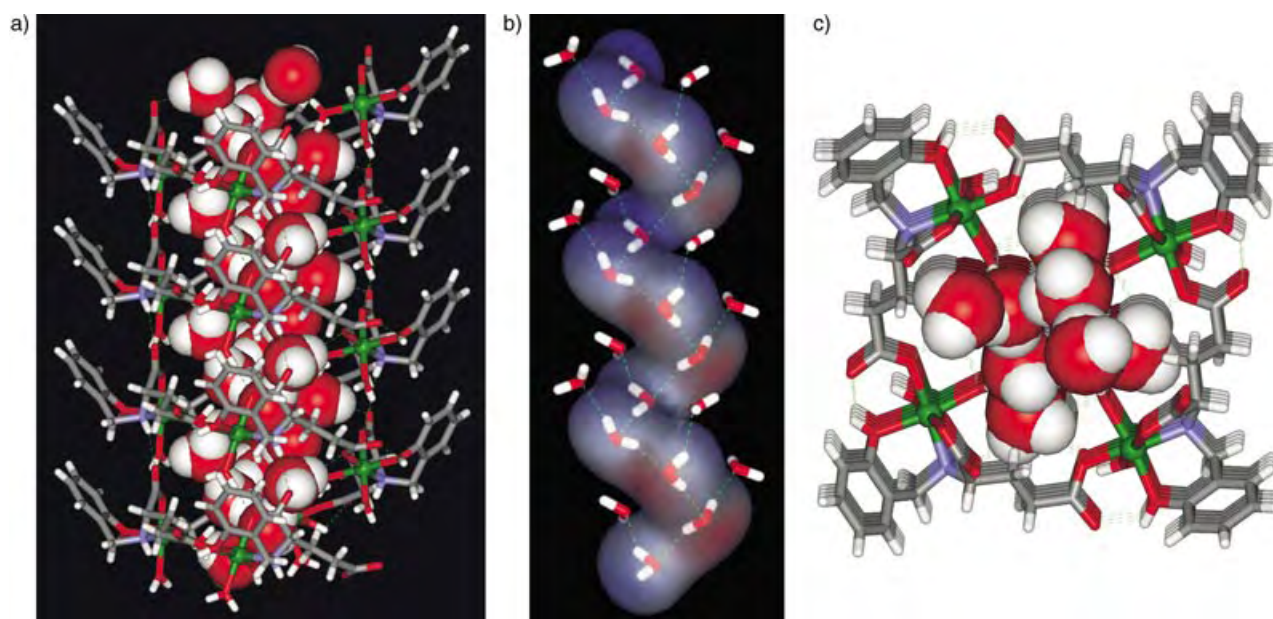


Figure 2. a) Hydrogen-bonded helical water chain inside the staircase coordination polymer in **1**. b) Hydrogen-bonded helical water stream in the channel. c) Top view of the staircase polymer filled with the helical water stream.

nation polymers are aligned along the *b* axis, and two more water molecules (O19 and disordered O20) occupy the empty space in the lattice outside the helical channels. The TG analysis of **1** revealed weight loss in the temperature range 26–232 °C. The total weight loss observed (21.6 %) agrees with the calculated value (22.5 %) for the loss of five water molecules per Ni atom. The single crystal crumbles on removal of water and on cooling to –50 °C.^[15] The structure is not expected to be robust when dehydrated, because these

coordination polymers are not supported by strong non-covalent interactions (Figure 3).

In contrast to **1**, in the crystal structure of [Cu(Hsghu)-(H₂O)]·H₂O (**2**)^[16] the connectivity of the neighboring carboxylate oxygen atoms with Cu^{II} centers results in a 1D zigzag coordination polymer (Figure 4).

As in the majority of the supramolecular syntheses, self-assembly of metal ions and ligands resulted in the formation of single-, double-, triple-, and quadruple-stranded helical

structures.^[2] However, a helical chain inside a helical structure is very rare. Recently a hydrogen-bonded helical supramolecular host was found to be anchored by hydrogen bonding to alternate water molecules in a single-stranded, both right- and left-handed, helical chain of water molecules.^[17] However, the structure of **1** has a hydrogen-bonded helix inside a helical 1D coordination polymer. This highly ordered helical stream of water molecules inside another helical polymer is striking and is a unique structural feature among existing porous helical structures^[2c,18–20] and other patterns of water structures observed in diverse environments of inorganic^[5,7] and organic hosts^[3,4,9] and 2D supramolecular (H₂O)₁₂ rings.^[21] Whereas designing chiral materials from achiral molecular compounds is a promising theme in materials science, using simple and available chiral precursors as an alternative is another practical approach. The structure of **1** exemplifies the feasibility of such an approach.^[22]

In conclusion, the structure of the left-handed helical coordination polymer **1**

Table 1: Relevant hydrogen-bonding parameters in compound **1**.^[a]

D–H...A	D–H [Å]	H...A [Å]	D...A [Å]	∠ D–H...A [°]	Symmetry equivalent operators
O1–H1 ^[b] ...O10	0.93	2.14	2.484(5)	100	
N1–H1A ^[b] ...O3	0.91	2.08	2.953(6)	161	<i>x</i> , <i>y</i> +1, <i>z</i>
N2–H2 ^[b] ...O8	0.91	2.06	2.937(6)	161	<i>x</i> , <i>y</i> +1, <i>z</i>
O6–H6 ^[b] ...O4	0.93	1.98	2.453(9)	109	<i>x</i> –1, <i>y</i> –1/2, <i>z</i> –1
O11–H11C...O15	0.89(3)	1.84(3)	2.713(6)	165(3)	
O11–H11D...O17	0.89(2)	2.10(3)	2.801(6)	135(4)	
O12–H12A...O2	0.89(2)	1.87(2)	2.745(5)	167(3)	<i>x</i> , <i>y</i> +1, <i>z</i>
O12–H12B...O19	0.90(3)	1.83(3)	2.695(9)	160(1)	
O13–H13A...O18	0.89(2)	2.03(3)	2.774(5)	141(4)	<i>x</i> , <i>y</i> +1, <i>z</i>
O13–H13B...O16	0.89(2)	1.84(2)	2.724(6)	172(2)	
O14–H14A...O20B	0.09(3)	2.35(5)	2.803(15)	111(3)	<i>x</i> –1, <i>y</i> –1/2, <i>z</i> –1
O14–H14B...O7	0.90(3)	1.99(4)	2.773(6)	145(5)	<i>x</i> , <i>y</i> +1, <i>z</i>
O15–H15A...O16	0.90(3)	1.92(4)	2.772(7)	158(4)	<i>x</i> –1, <i>y</i> +1/2, <i>z</i> –1
O15–H15B...O17	0.89(4)	1.86(4)	2.727(7)	163(5)	<i>x</i> , <i>y</i> –1, <i>z</i>
O16–H16A...O15	0.90(4)	1.88(4)	2.767(7)	169(4)	
O16–H16B...O18	0.90(5)	1.93(5)	2.732(7)	148(5)	
O17–H17A...O5	0.89(4)	2.26(4)	3.120(6)	162(4)	
O17–H17A...O13	0.89(4)	2.35(3)	2.943(6)	124(3)	<i>x</i> –1, <i>y</i> +1/2, <i>z</i> –1
O17–H17B...O3	0.90(4)	1.99(4)	2.842(6)	157(4)	<i>x</i> , <i>y</i> +1, <i>z</i>
O18–H18A...O8	0.90(3)	1.86(3)	2.729(6)	164(4)	
O18–H18B...O9	0.89(4)	2.11(4)	2.996(6)	161(3)	<i>x</i> , <i>y</i> –1, <i>z</i>
O18–H18B...O11	0.89(4)	2.49(4)	3.011(5)	118(3)	<i>x</i> , <i>y</i> –1, <i>z</i>
O20B–H20C...O4	0.90(4)	2.26(3)	3.035(15)	145(4)	

[a] A = acceptor, D = donor. [b] The hydrogen atoms have been placed in the calculated positions.

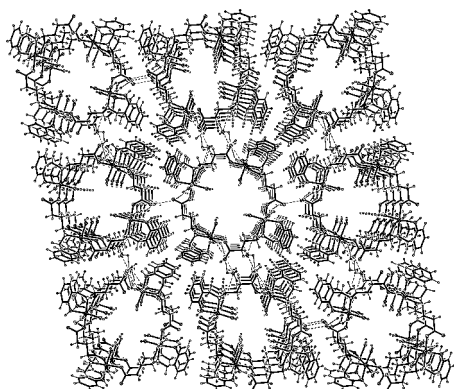


Figure 3. Packing of the staircase polymer viewed along the *b* axis. The water molecules in the channels are omitted for clarity.

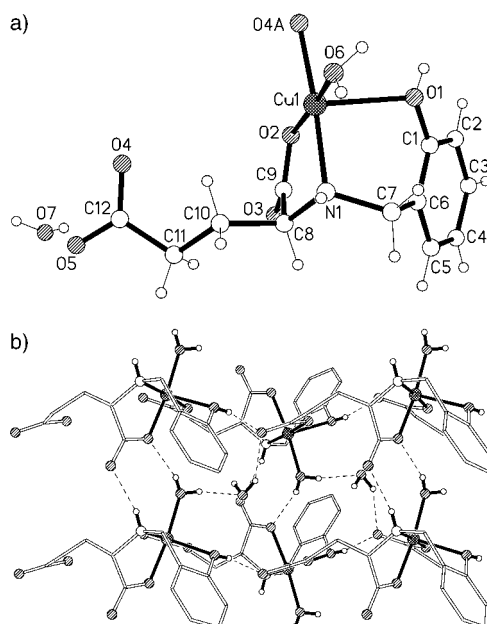


Figure 4. a) A view showing the coordination environment of Cu^{II} in **2**. Selected bond lengths [Å]: Cu1–O4 1.921(1), Cu1–O6 1.964(2), Cu1–O2 1.969(1), Cu1–N1 1.978(2), Cu1–O1 2.345(2). b) A portion of the 2D sheets formed by hydrogen bonding between the zigzag coordination polymer.

encapsulating a hydrogen-bonded helical stream of water molecules exhibits novel cooperative assembly and recognition of water molecules in the inorganic crystal host. These results exemplify the maxim that the structural constraints acting on the orientation of water by its surroundings and vice versa can be very significant. The captivating structure of **1**, in which a helical chain of water molecules supports a helical coordination polymer staircase, suggests another fascinating model for the water chains in membrane aquaporin proteins for the transport of water or protons, and it appears to be extremely rare among metal coordination polymers till now.^[23] The 1D zigzag coordination polymeric structure containing the same ligand in **2** demonstrates that the overall topology depends on the nature of the metal and the coordination geometry at the metal centers.

Experimental Section

H₃sglu: Salicylaldehyde (0.57 g, 4.7 mmol) was added to a solution of L-glutamic acid (0.69 g, 4.7 mmol) and NaOH (0.37 g, 9.4 mmol) in MeOH/H₂O (v/v (1:1), 20 mL), and the resulting yellow solution was stirred for 30 min and cooled in an ice bath prior to reduction with a slight excess of NaBH₄ (0.19 g, 5.1 mmol). The yellow color disappeared immediately, and stirring was continued for a further 20 min. The pH of the mixture was adjusted to 5–6 by adding acetic acid, and it was stirred for a further 45 min. The solvent from the resulting clear solution was completely removed on a rotary evaporator. The sticky mass was treated with EtOH (25 mL). The white product was collected by filtration, washed with EtOH and Et₂O, and dried under vacuum. Yield: 0.85 g (71 %). M.p. 247–248 °C (decomp). Elemental analysis (%) calcd for C₁₂H₁₅NO₅: C 56.9, H 5.9, N 5.5; found: C 56.4, H 5.8, N 5.6. ¹H NMR (300 MHz, D₂O): δ = 6.78–7.27 (m, 4H, ArH), 3.92–4.12 (m, *J*_{AB} = 13.2 Hz, 2H, CH₂), 3.36–3.55 (t, *J* = 6.42 Hz, 1H, CH), 2.24–2.30 (t, *J* = 8.4 Hz, 2H, CH₂), 2.0–2.02 ppm (m, *J* = 6.4 Hz, 2H, CH₂). IR (KBr): $\tilde{\nu}$ = 3460 (OH), 2960 (NH), 1573, 1388 (COO[−]), 1276 cm^{−1} (phenolic CO).

1: A clear solution of H₃sglu (0.25 g, 1 mmol) in water (2.5 mL) was allowed to diffuse slowly into a clear solution of nickel nitrate hexahydrate (0.29 g, 1 mmol) in water (2.5 mL). Greenish rodlike crystals suitable for X-ray diffraction studies were obtained after one week from the solution on slow evaporation. Yield: 0.28 g (70 %). Elemental analysis (%) calcd for C₁₂H₂₃NNiO₁₀: C 36.0, H 5.8, N 3.5; found: C 36.2, H 5.6, N 3.7. IR (KBr): $\tilde{\nu}$ = 3368 (OH), 2746 (NH), 1623, 1348 (COO[−]), 1253 cm^{−1} (phenolic CO). UV/Vis (Nujol): λ_{max} = 385 (CT), 737 nm (d–d). TGA: weight loss (%) calcd for 5H₂O: 22.5; found: 21.6.

2: A clear solution of H₃sglu (0.25 g, 1 mmol) in water (2.5 mL) was allowed to diffuse slowly into a clear solution of copper nitrate trihydrate (0.24 g, 1 mmol) in water (2.5 mL). Dark blue blocks suitable for single-crystal X-ray diffraction studies were obtained after 1 d. Yield: 0.26 g (74 %). Elemental analysis (%) calcd for C₁₂H₁₇CuNO₇: C 41.0, H 4.9, N 4.0; found: C 40.7, H 4.8, N 4.2. IR (KBr): $\tilde{\nu}$ = 3429 (OH); 3118 (NH); 1650, 1429 (COO[−]), 1262 cm^{−1} (phenolic CO). UV/Vis (Nujol): λ_{max} = 285 (CT), 613 nm (d–d). TGA: weight loss calcd for 2H₂O: 10.4; found: 10.8.

Received: April 30, 2004

Revised: July 8, 2004

Keywords: coordination polymers · host–guest systems · hydrogen bonds · nickel · supramolecular chemistry

- [1] a) J. M. Lehn, *Supramolecular Chemistry*, VCH, Weinheim, **1995**; b) M. Albrecht, *Chem. Rev.* **2001**, *101*, 3457; c) C. Piguet, G. Bernardinelli, G. Hopfgartner, *Chem. Rev.* **1997**, *97*, 2005; d) M. J. Hannon, L. J. Childs, *Supramol. Chem.* **2004**, *16*, 7.
- [2] a) O. Mamula, A. von Zelewsky, T. Bark, G. Bernardinelli, *Angew. Chem.* **1999**, *111*, 3129; *Angew. Chem. Int. Ed.* **1999**, *38*, 2945; b) C. Kaes, M. W. Hosseini, C. E. F. Rickard, B. W. Skelton, A. H. White, *Angew. Chem.* **1998**, *110*, 970; *Angew. Chem. Int. Ed.* **1998**, *37*, 920; c) D. A. McMorran, P. J. Steel, *Angew. Chem.* **1998**, *110*, 3295; *Angew. Chem. Int. Ed.* **1998**, *37*, 3295; d) G. Baum, E. C. Constable, D. Fenske, C. E. Housecroft, T. Kulke, *Chem. Eur. J.* **1999**, *5*, 1862; e) M. J. Hannon, C. L. Painting, N. W. Alcock, *Chem. Commun.* **1999**, 2023.
- [3] J. N. Moorthy, R. Natarajan, P. Venugopalan, *Angew. Chem.* **2002**, *114*, 3567; *Angew. Chem. Int. Ed.* **2002**, *41*, 3417.
- [4] R. Custelcean, C. Afloroaei, M. Vlăsa, M. Polverejan, *Angew. Chem.* **2000**, *112*, 3224; *Angew. Chem. Int. Ed.* **2000**, *39*, 3094.
- [5] W. B. Blanton, S. W. Gordon-Wylie, G. R. Clark, K. K. Jordon, J. T. Wood, U. Geiser, T. J. Collins, *J. Am. Chem. Soc.* **1999**, *121*, 3551.

- [6] J. T. Atwood, L. J. Barbour, T. J. Ness, C. L. Ratson, P. L. Ratson, *J. Am. Chem. Soc.* **2001**, *123*, 7192.
- [7] a) L. J. Barbour, W. G. Orr, J. L. Atwood, *Nature* **1998**, *393*, 671; b) L. J. Barbour, W. G. Orr, J. L. Atwood, *Chem. Commun.* **2000**, 859.
- [8] K. Raghuraman, K. K. Katti, L. J. Barbour, N. Pillarsetty, C. L. Barnes, K. V. Katti, *J. Am. Chem. Soc.* **2003**, *125*, 6955.
- [9] a) L. Infantes, J. Chisholm, S. Motherwell, *CrystEngComm* **2003**, *5*, 480; b) L. Infantes, S. Motherwell, *CrystEngComm* **2002**, *4*, 454.
- [10] a) L. E. Cheruzel, M. S. Pometun, M. R. Cecil, M. S. Mashuta, R. J. Wittebort, R. M. Buchanan, *Angew. Chem.* **2003**, *115*, 5610; *Angew. Chem. Int. Ed.* **2003**, *42*, 5452; b) S. Pal, N. B. Sankaran, A. Samanta, *Angew. Chem.* **2003**, *115*, 1783; *Angew. Chem. Int. Ed.* **2003**, *42*, 1741.
- [11] See, for example, a) B. Zhao, P. Cheng, X. Chen, C. Cheng, W. Shi, D. Liao, S. Yan, Z. Jiang, *J. Am. Chem. Soc.* **2004**, *126*, 3012; b) Y. B. Dong, X. Zhao, B. Tang, H. Y. Wang, R. Q. Huang, M. D. Smith, H. C. zur Loye, *Chem. Commun.* **2004**, 220; c) W. Runde, A. C. Bean, B. L. Scott, *Chem. Commun.* **2003**, 1848.
- [12] a) R. Ludwig, *Angew. Chem.* **2001**, *113*, 1856; *Angew. Chem. Int. Ed.* **2001**, *40*, 1808; b) D. Konozo, M. Yasui, L. S. King, P. Agre, *J. Clin. Invest.* **2002**, *109*, 1395; c) B. Roux, R. MacKinnon, *Science* **1999**, *285*, 100; d) U. Buck, F. Huisken, *J. Am. Chem. Soc.* **2000**, *100*, 3863.
- [13] K. Mitsuoka, K. Murata, T. Walz, T. Hirai, P. Agre, J. B. Heymann, A. Engel, Y. Fujiyoshi, *J. Struct. Biol.* **1999**, *128*, 34.
- [14] Crystal data of **1**: $\text{C}_{12}\text{H}_{23}\text{NNiO}_{10}$, monoclinic, space group $P2_1$, $a = 17.135(1)$, $b = 6.1945(4)$, $c = 17.160(1)$ Å, $\beta = 101.220(2)^\circ$, $V = 1786.6(2)$ Å³, $Z = 4$, $\rho_{\text{calcd}} = 1.487$ g cm⁻³. In the final least-squares refinement cycles on $|F|^2$, the model converged at $R_1 = 0.0500$, $wR_2 = 0.1191$, and GOF = 1.050 for 5179 reflections with $F_o > 4\sigma(F_o)$ and 485 parameters. The Flack parameter was refined to $-0.004(16)$; A. L. Spek, *Acta Crystallogr. A* **1990**, *46*, C34.
- [15] Several initial attempts to collect the X-ray data at low temperature failed due to this phenomenon.
- [16] Crystal data of **2**: $\text{C}_{12}\text{H}_{17}\text{CuNO}_7$, monoclinic, space group $P2_1$, $a = 5.9362(2)$, $b = 10.1204(4)$, $c = 11.9417(4)$ Å, $\beta = 94.377(1)^\circ$, $V = 715.33(4)$ Å³, $Z = 4$, $\rho_{\text{calcd}} = 1.629$ g cm⁻³. In the final least-squares refinement cycles on $|F|^2$, the model converged at $R_1 = 0.0288$, $wR_2 = 0.0763$, and GOF = 1.053 for 2844 reflections with $F_o > 4\sigma(F_o)$ and 209 parameters. Data for **1** and **2** were collected on a Bruker APEX diffractometer equipped with a CCD detector and graphite-monochromated $\text{MoK}\alpha$ radiation from a sealed tube (2.4 kW) at 296(2) K. Absorption corrections were made with the program SADABS,^[24] and the crystallographic package SHELXTL^[25] was used for all calculations. CCDC-236742 (**1**) and CCDC-236743 (**2**) contain the supplementary crystallographic data for this paper. These data can be obtained free of charge via www.ccdc.cam.ac.uk/conts/retrieving.html (or from the Cambridge Crystallographic Data Centre, 12 Union Road, Cambridge CB21EZ, UK; fax: (+44)1223-336-033; or deposit@ccdc.cam.ac.uk).
- [17] A. Mukherjee, M. K. Saha, M. Nethaji, A. R. Chakravarty, *Chem. Commun.* **2004**, 716.
- [18] C. D. Wu, C. Z. Lu, X. Lin, D. M. Wu, S. F. Lu, H. H. Zhuang, J. S. Huang, *Chem. Commun.* **2003**, 1284.
- [19] A. L. Pickering, G. Seeber, D. L. Long, L. Cronin, *Chem. Commun.* **2004**, 136.
- [20] C. D. Wu, C. Z. Lu, S. F. Lu, H. H. Zhuang, J. S. Huang, *Dalton Trans.* **2003**, 3192.
- [21] B. Q. Ma, H. L. Sun, S. Gao, *Angew. Chem.* **2004**, *116*, 1398; *Angew. Chem. Int. Ed.* **2004**, *43*, 1374.
- [22] B. Moulton, M. J. Zaworotko in *Crystal Engineering: From Molecules and Crystals to Materials* (Eds.: D. Braga, F. Grepioni, A. G. Orpen), Kluwer, Dordrecht, **1999**, p. 311.
- [23] a) C. Schmuck, *Angew. Chem.* **2003**, *115*, 2552; *Angew. Chem. Int. Ed.* **2003**, *42*, 2448; b) A. E. Rowan, R. J. M. Nolte, *Angew. Chem.* **1998**, *110*, 65; *Angew. Chem. Int. Ed.* **1998**, *37*, 63.
- [24] G. M. Sheldrick, SADABS, Software for empirical absorption corrections, University of Göttingen, Germany, **2000**.
- [25] SHELXTL Reference Manual, Version 5.1, Bruker AXS, Analytical X-Ray Systems, Inc., Madison, WI, USA, **1997**.

Magnetic Properties

Building Molecular Minerals: All Ferric Pieces of Molecular Magnetite**

*Guy W. Powell, Hannah N. Lancashire,
Euan K. Brechin,* David Collison,* Sarah L. Heath,*
Talal Mallah, and Wolfgang Wernsdorfer*

Currently, there is a great deal of interest in the synthesis of transition-metal clusters that can behave as single-molecule magnets (SMMs).^[1] An SMM requires effectively a combination of large spin ground state with a negative zero-field splitting (D value), which leads to magnetic bistability (hysteresis) that is the property of an individual molecule. These clusters may find potential uses in the information storage industry or as qubits in quantum computing.^[2] One logical way to prepare SMMs is by synthesizing fragments of the naturally occurring magnetic oxides. This synthesis can be by either a top-down or bottom-up approach, that is, the breaking down or building up of a mineral lattice. Herein we report the synthesis of two iron oxy hydroxy clusters that represent two related portions of the magnetite lattice,

[*] G. W. Powell, H. N. Lancashire, Dr. E. K. Brechin,⁺ Dr. D. Collison,
Dr. S. L. Heath
Department of Chemistry
University of Manchester
Oxford Road, Manchester, M13 9PL (UK)
Fax: (+44) 161-275-4598
E-mail: euan.k.brechin@man.ac.uk
david.collison@man.ac.uk
sarah.l.heath@man.ac.uk

Prof. T. Mallah
Laboratoire de Chimie Inorganique
Université Paris Sud, UMR CNRS 8613, 91405 Orsay (France)
Dr. W. Wernsdorfer
Laboratoire Louis Néel
CNRS, 25 Avenue des Martyrs BP166
38042 Grenoble Cedex 9 (France)

[†] Current address:
School of Chemistry
The University of Edinburgh
West Mains Road
Edinburgh, EH9 3JJ
E-mail: ebrechin@staffmail.ed.ac.uk

[**] This work was supported by The Royal Society of London, Lloyd's of London Tercentenary Foundation, The Nuffield Foundation, and the EPSRC (UK).

constructed by a bottom-up approach and utilizing ligand-controlled hydrolysis of a metal salt to determine the extent of cluster aggregation.

$[\text{Fe}_9\text{O}_4(\text{OH})_5(\text{heia})_6(\text{Hheia})_2] \cdot 3.5 \text{CH}_3\text{OH} \cdot 8 \text{H}_2\text{O}$ (**1**; $\text{H}_2\text{heia} = \text{HN}[\text{CH}_2\text{COOH}]\text{CH}_2\text{CH}_2\text{OH}$; Figure 1) was synthesized by reaction of iron(III) nitrate nonahydrate with H_2heia and tetramethylammonium hydroxide in methanol. The

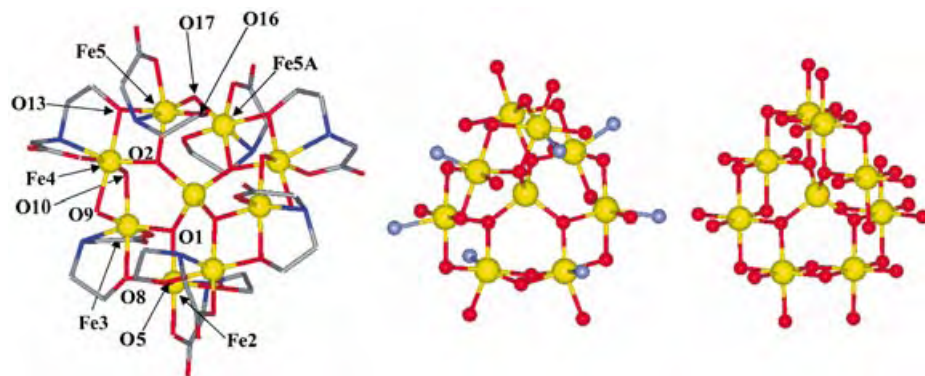


Figure 1. The molecular structure of the cluster in **1** (left), the core of **1** (middle), and its relation to magnetite (right); yellow Fe, red O, blue N, gray C.

hydrolysis was gradually stopped by evaporating the reaction mixture to dryness. Crystals of **1** suitable for single crystal X-ray diffraction were obtained after 2 weeks by crystallization from a MeOH solution of **1** in the presence of liquid drying agent (diethoxymethane) to hinder further hydrolysis.^[3] $\text{Hpy}[\text{Fe}_{17}\text{O}_{16}(\text{OH})_{12}(\text{py})_{12}\text{Cl}_4]\text{Cl}_4 \cdot 4.5 \text{CH}_3\text{OH}$ (**2**; py = pyridine; Figure 2) was prepared by the reaction of anhydrous iron(III) chloride in pyridine in a flask open to the atmosphere at room temperature, and crystals of **2** suitable for single crystal X-ray diffraction were isolated in low yield after diffusion of methanol over 2 weeks.^[3]

The complex in **1** is constructed from a central tetrahedral Fe^{III} ion which links, by four μ_3 -oxo bridges, to the outer eight iron atoms. Each of the outer iron ions is capped by a facially coordinated heia ligand and has distorted octahedral coordination geometry. Six of the heia ligands are fully deprotonated and the alcohol arm of these ligands (O5, O8, O13 and their symmetry equivalents) bridges between pairs of outer

irons: the second bridge between these irons is from the inner μ_3 -oxo ligands. The remaining two Hheia ligands have protonated alcohol arms (O16 and its symmetry equivalent) that coordinate terminally. Two of the outer irons (Fe3 and Fe4) are bridged by two μ_2 -hydroxo ligands (O9 and O10) and two others, Fe5 and Fe5A, are bridged by a single hydroxo ligand (O17). This asymmetry in the mode (and hence angle) of the bridging between the outer iron ions has consequences for the magnetic exchange pathways in **1** (see below). The bromide analogue of **2** can be prepared by a similar route in higher yield and has a cluster that is isostructural with the chloride; this will be reported in detail elsewhere.

The complex in **2** also has at its core a central tetrahedral Fe^{III} ion, but in contrast to **1** this is linked by μ_4 -oxo bridges to twelve outer octahedral Fe^{III} ions, which form a truncated tetrahedron: the octagonal faces of this tetrahedron (Fe2, Fe3, Fe5, Fe7, and symmetry equivalents) are capped by four further iron ions (Fe4, Fe6, and symmetry equivalents), linked by a combination of μ_3 -oxo and μ_2 -hydroxo ligands. The inner Fe^{III} ion and the four outer Fe^{III} ions of **2** sit in the tetrahedral sites of the lattice with the others occupying the octahedral sites. The chloride ions cap the outer tetrahedrally coordinated Fe^{III} ions with the pyridine molecules capping the octahedrally coordinated Fe^{III} ions.

A closer inspection of the cores of **1** and **2** reveals that both are fragments of the iron and oxygen positions defined by the magnetite lattice as shown in the comparison of **1** and **2** to their corresponding fragments of magnetite in Figures 1 and 2. Compound **1** is formally converted into **2** by adding a layer of Fe ions through the conversion of μ_3 -oxo into μ_4 -oxo

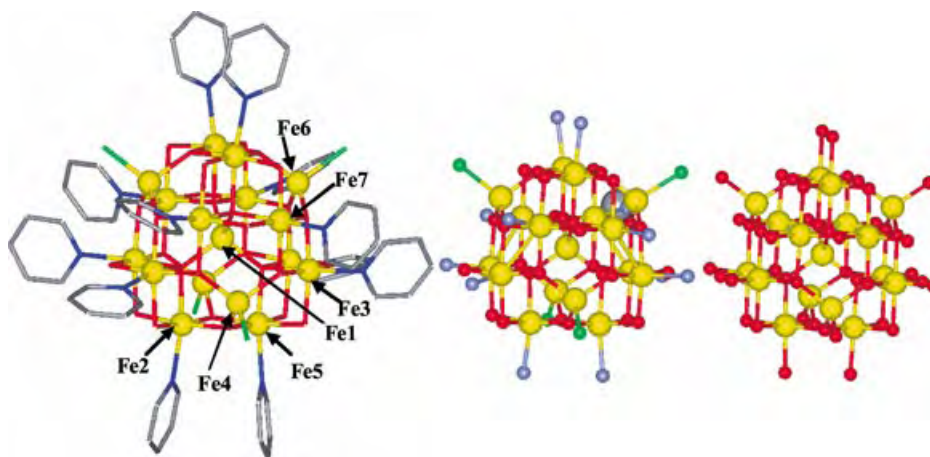


Figure 2. The molecular structure of the cluster in **2** (left), the core of **2** (middle), and its relation to magnetite (right); yellow Fe, red O, blue N, gray C, green Cl.

ligands. Many of the polynuclear transition-metal clusters isolated to date, that resemble mineral units, are fragments of the $M(\text{OH})_2$ brucite lattice.^[4] In our case, **1** is formed by restricting the hydrolysis from a hydrated iron(III) salt using a facially capping tridentate ligand with “arms” of very different $\text{p}K_a$ values. In contrast, **2** is produced by restricting the amount of hydrolytic source in a basic, strongly coordinating medium. The isolation of **2**, in particular, suggests that larger fragments of “molecular magnetite” can be isolated by using coordinating bases of differing strengths.

In both **1** and **2** all the iron centers (both tetrahedral and octahedral) are Fe^{III} ions, this is confirmed by charge-balance considerations and bond valence sum (BVS) calculations.^[5] This result is in contrast to the situation in magnetite where half the octahedral sites in the lattice are occupied by Fe^{II} ions. The assignment of hydroxo versus oxo was achieved on the basis of geometry and BVS calculations.

The magnetic properties of **1** and **2** were examined using variable-temperature magnetic measurements on bulk powdered samples (300–1.8 K, 0.1–5.5 T) and on single crystals to mK temperatures on a micro-SQUID. Susceptibility data for both **1** and **2** indicate the presence of antiferromagnetic interactions, with low-temperature maxima suggesting large spin ground states. To determine the value of the spin ground state for **1** and **2**, magnetization measurements were performed at 2–6 K between 0.1 and 5.5 T. For **1** the best fit (first made for each temperature independently and second by simultaneously fitting the data for the three temperatures for an isolated ground state) was obtained for $S = 25/2$, $g = 1.99$, and $D = -0.07 \text{ cm}^{-1}$ (Figure 3). For **2** the initial best fit was for $S = 35/2$ as the ground state with the following parameters: $g = 1.96$ and $D = +0.33 \text{ cm}^{-1}$ (Figure 4), see below. The occurrence of such large spin ground states for both complexes arises from the presence of competing antiferromagnetic and ferromagnetic exchange-coupling interactions between the octahedral and tetrahedral Fe^{III} ions. Closer

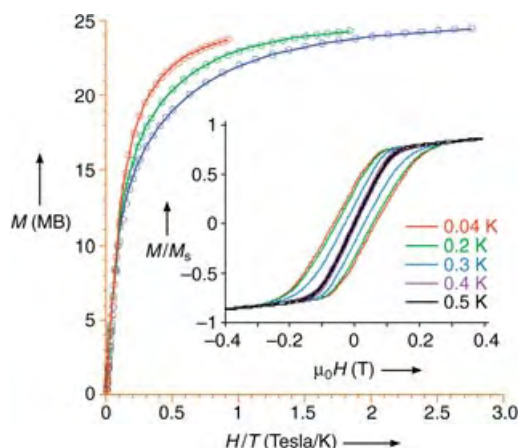


Figure 3. Plot of magnetization (M) versus H/T for **1** in the ranges 0.1–5.5 T and 2 (○), 3 (○), and 6 K (○). The solid lines are fits to $S = 25/2$, $g = 1.99$, $D = -0.07 \text{ cm}^{-1}$. Inset: magnetization of **1** plotted as a fraction of the saturation value M_s versus applied magnetic field ($\mu_0 H$) at sweep rates of 0.007 T s^{-1} and $T = 0.1$ –0.5 K. S = Spin quantum number of the cluster, g = g value of cluster, D = axial zero-field splitting parameter.

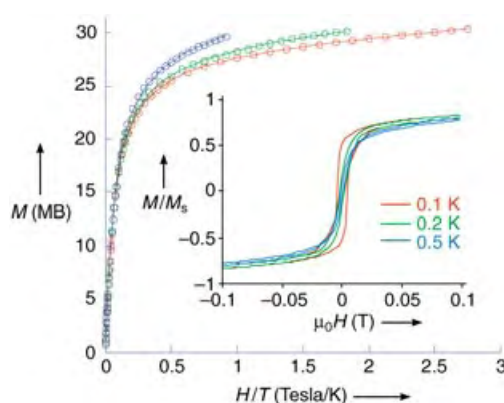


Figure 4. Plot of magnetization (M) versus H/T for **2** in the ranges 0.1–5.5 T and 2 (○), 3 (○), and 6 K (○). The solid lines are fits to $S = 35/2$, $g = 1.96$, $D = +0.33 \text{ cm}^{-1}$. Inset: magnetization of **2** plotted as a fraction of the saturation value M_s versus applied magnetic field ($\mu_0 H$) at sweep rates of 0.001 T s^{-1} and $T = 0.04$ –0.5 K.

examination of the structure of **1** reveals that the Fe–O–Fe bridges fall into two clear categories: those that connect the central tetrahedral Fe^{III} centers to the outer octahedral Fe^{III} centers (by the oxo ligands) are all characterized by angles in the range 125 – 130° , and those that bridge between the Fe^{III} ions in the outer octametallic “twisted ribbon” are characterized by angles in the range 97 – 101° . If we assume that the largest Fe–O–Fe angles promote the strongest antiferromagnetic interaction then we are left with a situation where the central tetrahedral Fe^{III} center is antiferromagnetically coupled to all the octahedrally coordinated Fe^{III} ions, which leads to an $S = 35/2$ spin ground state. However, there is one anomaly in the bridging angles connecting the outer octahedrally coordinated Fe ions: the angle between Fe5 and Fe5A through O17 is 130° . This angle is bigger than the angle connecting either Fe5 or Fe5A to the central metal ion and so we might consider the exchange between the Fe5/Fe5A pair to be dominant, and antiferromagnetic. This situation would lead to a molecule with two “spin up” and seven “spin down” $S = 5/2$ centers and an overall spin ground state of $S = 25/2$, consistent with that obtained from the magnetization measurements.

For complex **2**, the same argument applies: the antiferromagnetic interactions between the tetrahedrally and octahedrally coordinated Fe^{III} ions (through Fe–O–Fe angles of 122 – 126° compared to 94 – 98° between the octahedral Fe centers) dominate, which leads to a situation in which the five tetrahedrally coordinated Fe^{III} ions are “spin up” and the twelve octahedrally coordinated Fe^{III} ions are “spin down” giving an overall $S = 35/2$ ground state.

To examine the low-temperature magnetic behavior of **1** and **2**, single crystal magnetization measurements were performed on them using an array of micro-SQUIDS.^[6] Relaxation data for **1** were determined from direct current (dc) relaxation-decay measurements: a large dc field of 1.4 T was applied to the sample at 5 K to saturate the magnetization in one direction, and the temperature lowered to a specific value between 1.0 and 0.04 K. When the temperature was stable the field was swept from 1.4 T to zero at a rate of

0.14 T s⁻¹ and the magnetization in zero-field measured as a function of time. This method allows the construction of an Arrhenius plot of $\ln \tau$ versus $1/T$, which shows that above approximately 0.15 K the relaxation rate is temperature dependent. The fit to an Arrhenius law yields $\tau_0 = 6 \times 10^{-10}$ s and $U_{\text{eff}} = 7.6$ K. However, below approximately 0.15 K the relaxation rate is temperature independent with a value of 8×10^3 s, indicative of quantum tunneling of the magnetization (QTM) between the lowest energy $M_s = \pm 25/2$ levels of the ground state. Hysteresis loops for **1** (inset, Figure 3) are observed at temperatures below 0.5 K and at sweep rates of 0.001 T s⁻¹, with the field applied in the direction of the easy-axis of the molecules. The hysteresis loops do not show steps at regular intervals of field, indicative of resonant QTM, but are smooth. The steps may be present, but simply broadened out by intermolecular antiferromagnetic interactions between the separate Fe₉ molecules. Indeed, a Curie–Weiss plot suggests antiferromagnetic intermolecular interactions in the order of approximately -0.7 K. Further geometric analysis of **1** shows that the metallic cluster approximates to an oblate spheroid of estimated core dimensions 6.38 × 6.25 Å, and the nearest neighbor intercentroid separations in the lattice are 12.13 and 15.49 Å.

Low-temperature single-crystal magnetic measurements on **2** (inset, Figure 4) using the methods described in the investigation of **1**, show no signs of SMM behavior. The small hysteresis loops observed below approximately 0.5 K result from long-range ferromagnetic ordering between the individual Fe₁₇ molecules and not from the presence of molecular anisotropy. The anomalously large zero-field splitting and low g value (for Fe^{III}, typical parameters are $g \approx 2.00$ and $|D| \leq 0.2$ cm⁻¹) obtained for **2** using a model for magnetization in an isolated spin state (see above) might also suggest the presence of long-range interactions. We would expect the cluster g and D values to be similar to those of the isolated Fe^{III} centers in this case. In **2** the core of the cluster is much more spherical than that in **1** (although it has 12 protruding pyridine rings) with a diameter of the metallic core of approximately 6.96 Å and nearest neighbor intercentroid separations of 14.89 and 16.12 Å. The pyridine rings show no obvious π -stacking interactions between clusters.

For both **1** and **2** the magnetic behavior is comparable to that observed in magnetite, wherein the iron ions in the octahedral and tetrahedral holes are antiferromagnetically coupled, but net magnetization results from the noncompensated spin of the Fe^{II} ions which occupy one quarter of the octahedral sites.

In conclusion, it is possible to construct high-spin molecules, single-molecule magnets, and molecular mineral analogues using a simple bottom-up, controlled hydrolysis approach. That the iron ions in **1** and **2** are all ferric and hence almost electronically isotropic (i.e. $|D|$ is small), probably prevents more exciting magnetic behavior. However, since these clusters form part of a naturally occurring mixed-valence mineral, the reduction of some Fe^{III} ions to form complexes more reminiscent of the parent mineral, remains a possibility, as does incorporation of Fe^{II} during synthesis. Thus, inclusion of some of the much more anisotropic Fe^{II} ions into this new structural family might be

expected to increase substantially the overall zero-field splitting of the clusters.

Experimental Section

1: A solution of heiaH₂ (0.595 g, 5.0 mmol) and N(CH₃)₄(OH)·5H₂O (2.265 g, 12.5 mmol) in MeOH (10 mL) was added slowly to a stirred solution of Fe(NO₃)₃·9H₂O (1.01 g, 2.5 mmol) in MeOH (10 mL). The reaction mixture was allowed to evaporate to dryness over a period of 2 days, before extracting into diethoxymethane (3.1 mL, 25 mmol) and MeOH (6.9 mL). Solids (N(CH₃)₄(NO₃)) were removed by filtration and acetone diffused slowly into the filtrate to yield crystals suitable for single-crystal X-ray diffraction after 2 weeks. Elemental analysis calcd (%) for Fe₉C_{35.5}H₉₃O_{44.5}N₈: C 23.09, H 5.08, N 6.07, Fe 27.22; found: C 23.65, H 5.35, N 6.38, Fe 27.48.

2: FeCl₃ (0.910 g, 3.09 mmol) was added to stirred pyridine (30 mL), the reaction mixture became dark upon dissolution. After stirring for 2 h the reaction mixture was filtered, the filtrate was collected and methanol diffused in slowly to afford single crystals suitable for X-ray diffraction after two weeks. Elemental analysis calcd (%) for Fe₁₇C_{69.5}H₁₀₂O_{35.5}N₁₃Cl₈: C 28.71, H 2.62, N 6.70, Fe 35.03; found: C 28.62, H 2.59, N 6.75, Fe 35.84.

Received: May 12, 2004

Keywords: cluster compounds · hydrolysis · iron · magnetic properties · single-molecule magnets

- [1] a) D. Gatteschi, R. Sessoli, *Angew. Chem.* **2003**, *115*, 278; *Angew. Chem. Int. Ed.* **2003**, *42*, 268; b) R. Sessoli, D. Gatteschi, D. N. Hendrickson, G. Christou, *MRS Bull.* **2000**, *25*, 66; c) W. Wernsdorfer, R. Sessoli, *Science* **1999**, *284*, 133; d) S. Hill, R. S. Edwards, N. Aliaga-Alcalde, G. Christou, *Science* **2003**, *302*, 1015; e) A. J. Tasiopoulos, A. Vinslava, W. Wernsdorfer, K. A. Abboud, G. Christou, *Angew. Chem.* **2004**, *116*, 2169; *Angew. Chem. Int. Ed.* **2004**, *43*, 2117.
- [2] M. N. Leuenberger, D. Loss, *Nature* **2001**, *414*, 789.
- [3] Crystallographic details for **1**: Fe₉C_{35.5}H₉₃O_{44.5}N₈, $M_r = 1846.83$, crystal size $0.05 \times 0.02 \times 0.01$ mm³, trigonal, space group, $P3(2)21$, $a = b = 21.014(10)$, $c = 16.690(11)$ Å, $V = 6383(6)$ Å³, $T = 100(2)$ K, $Z = 3$, $\rho_{\text{calcd}} = 1.441$ g cm⁻³, $\mu(\lambda = 0.71073 \text{ Å}) = 1.574$ mm⁻¹, 28834 reflections collected, 6224 unique ($R_{\text{int}} = 0.1154$), $R(F) = 0.0602$ and $wR2 = 0.1678$ using 5936 reflections with $I > 2\sigma(I)$. **2**: Fe₁₇C_{69.5}H₁₀₂O_{35.5}N₁₃Cl₈, $M_r = 2920.69$, crystal size $0.50 \times 0.50 \times 0.20$ mm³, trigonal, space group, $R3$, $a = b = 16.1170(9)$, $c = 69.928(6)$ Å, $V = 15730.9(19)$ Å³, $T = 100(2)$ K, $Z = 6$, $\rho_{\text{calcd}} = 1.850$ g cm⁻³, $\mu(\lambda = 0.71073 \text{ Å}) = 2.556$ mm⁻¹, 23613 reflections collected, 5023 unique ($R_{\text{int}} = 0.1424$), $R(F) = 0.0529$ and $wR2 = 0.1428$ using 4469 reflections with $I > 2\sigma(I)$. CCDC-238304 (**1**) CCDC-238305 (**2**) contains the supplementary crystallographic data for this paper. These data can be obtained free of charge via www.ccdc.cam.ac.uk/conts/retrieving.html (or from the Cambridge Crystallographic Data Centre, 12 Union Road, Cambridge CB2 1EZ, UK; fax: (+44) 1223-336-033; or deposit@ccdc.cam.ac.uk).
- [4] see for examples a) J. C. Goodwin, R. Sessoli, D. Gatteschi, W. Wernsdorfer, A. K. Powell, S. L. Heath, *J. Chem. Soc. Dalton Trans.* **2000**, 1835; b) R. E. P. Winpenney, *J. Chem. Soc. Dalton Trans.* **2002**, 1; and a recent extension of this observation in J. C. Goodwin, S. J. Teat, S. L. Heath, *Angew. Chem.* **2004**, *116*, 4129; *Angew. Chem. Int. Ed.* **2004**, *43*, 4037.
- [5] a) W. Liu, H. Thorp, *Inorg. Chem.* **1993**, *32*, 4102; b) I. D. Brown, D. Altermatt, *Acta Crystallogr. Sect. B* **1985**, *41*, 244.
- [6] W. Wernsdorfer, *Adv. Chem. Phys.* **2001**, *118*, 99.

Self-Assembly of Interpenetrating Coordination Nets Formed from Interpenetrating Cationic and Anionic Three-Dimensional Diamondoid Cluster Coordination Polymers**

Kai Liang, Hegen Zheng,* Yinglin Song, Michael F. Lappert, Yizhi Li, Xinquan Xin, Zixiang Huang, Jiutong Chen, and Shaofang Lu

The design and synthesis of metal–organic coordination polymers has become an exciting field in the past decade, and numerous interesting coordination polymers based on metal ions and organic bridging ligands have been synthesized by many research groups.^[1] Many of these compounds contain channels or voids that are similar to those in porous materials such as zeolites and clays.^[2] Tetrathiometalate clusters $[\text{MS}_4]^{2-}$ ($\text{M} = \text{W}, \text{Mo}$) have long been explored for their diverse coordination modes and potential applications in catalysis, biological processes, and nonlinear optical (NLO) materials.^[3] Rather few polymeric heterothiometallic cluster coordination polymers based on the thiometalates have been synthesized.^[4] Such coordination polymers have invariably contained polymer aggregates that were: 1) anionic, such as $[\text{NH}_4]_n[\text{AgWS}_4]_n$,^[5] $\{[\text{N}(\text{CH}_2\text{C}_6\text{H}_5)(\text{C}_2\text{H}_5)_3][\text{MoAgS}_4]\}_n$,^[6] $\{[\text{NEt}_4][\text{Mo}_2\text{O}_2\text{S}_6\text{Cu}_6\text{I}_3(4,4'\text{-bipy})_5]\cdot\text{MeOH}\cdot\text{H}_2\text{O}\}_n$ ($4,4'\text{-bipy} = 4,4'\text{-bipyridine}$),^[7] or $\{[\text{Et}_4\text{N}]_2[\text{MoS}_4\text{Cu}_4(\text{CN})_4]\}_n$,^[8] 2) cationic, as in the transition metal coordination polymers, or 3) neutral, as in $[\text{MoS}_4\text{Cu}_6(\text{py})_4]_n$ ($\text{py} = \text{pyridine}$),^[9] $\{[\text{MoOS}_3(\text{CN})(\text{py})_3]\cdot 0.5 \text{C}_6\text{H}_6\}_n$,^[10] or $[\text{Cu}(4,4'\text{-bipy})\text{Cl}]_n$.^[11] Structures containing interpenetrating nets that have different topologies and/or chemical compositions are known,^[1] although no example has previously been reported of a coordination polymer containing both cationic and anionic coordination polymer aggregates.

We report here such an unprecedented cluster coordination polymer, namely compound **1**, which contains interpenetrating cationic and anionic 3D diamondoid cluster coordination polymers.



Compound **1** was obtained from the reaction between $[\text{NH}_4]_2[\text{WS}_4]$, CuI , $[\text{nBu}_4\text{N}]\text{I}$, and $4,4'\text{-bipy}$, in a ratio of 1:2:2:2, in $\text{DMF}/\text{CH}_2\text{Cl}_2$ solution, followed by filtration and slow diffusion of diethyl ether into the filtrate to give single crystals suitable for an X-ray diffraction study. The crystallographic analysis of compound **1**^[12] revealed that the 3D cationic cluster coordination polymer can be considered as comprising square, pentanuclear $[\text{WS}_4\text{Cu}_4]^{2+}$ building blocks, each linked by four pairs of parallel $4,4'\text{-bipy}$ ligands (Figure 1). The W and the four Cu atoms are coplanar in

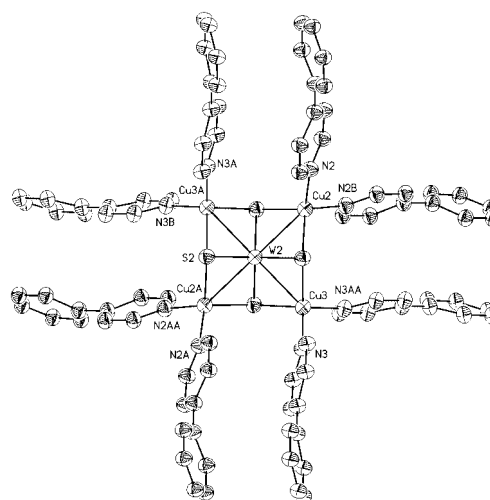


Figure 1. The cationic cluster coordination polymer unit $[\text{WS}_4\text{Cu}_4(4,4'\text{-bipy})_4]^{2+}$.

each $[\text{WS}_4\text{Cu}_4]^{2+}$ building block, and the $[\text{WS}_4]^{2-}$ unit has a tetrahedral structure with $\text{W2}-\text{S2}$ bond lengths of $2.235(2) \text{ \AA}$, and $\text{S2}-\text{W2}-\text{S2}$ angles ranging from $108.60(11)^\circ$ to $110.50(12)^\circ$. Each of the four Cu atoms is also tetrahedrally coordinated by two N atoms from two $4,4'\text{-bipy}$ ligands and two $\mu_3\text{-S}$ atoms, with $\text{Cu2}-\text{N2}$, $\text{Cu3}-\text{N3}$, $\text{Cu2}-\text{S2}$, and $\text{Cu3}-\text{S2}$ bond lengths of $2.023(7) \text{ \AA}$, $2.043(7) \text{ \AA}$, $2.272(2) \text{ \AA}$, and 2.280 \AA , respectively.

The angles $\text{N2}-\text{Cu2}-\text{N2B}$ and $\text{N3}-\text{Cu3}-\text{N3AA}$ are $106.1(4)^\circ$ and $112.3(4)^\circ$, respectively, hence the four $4,4'\text{-bipy}$ molecules are almost tetrahedrally disposed, which results in a diamondoid network with a large channel dimension of $24.482 \text{ \AA} \times 21.009 \text{ \AA}$ (Figure 2a). Each six-membered ring contains six $[\text{WS}_4\text{Cu}_4]^{2+}$ nodes and six pairs of $4,4'\text{-bipy}$ connecting rods. The separation between each pair of $4,4'\text{-bipy}$ units is nearly 3.7 \AA , thus implying weak $\pi-\pi$ interactions.

In fact, there is a twofold interpenetrating 3D network in the cationic coordination polymer (Figure 3a and 3b). Similar interpenetrating diamondoid frameworks have also been

[*] K. Liang, Prof. Dr. H. Zheng, Y. Li, Prof. X. Xin
State Key Laboratory of Coordination Chemistry
Coordination Chemistry Institute, Nanjing University
Nanjing 210093 (P.R. China)
Fax: (+86) 25-83314502
E-mail: hegenz@yahoo.com

Prof. Y. Song
Department of Applied Physics
Harbin Institute of Technology
Harbin 150001 (P.R. China)

Prof. M. F. Lappert
The Chemistry Laboratory
University of Sussex
Brighton, BN1 9QJ (UK)

Dr. Z. Huang, Dr. J. Chen, Prof. S. Lu
State Key Laboratory of Structural Chemistry
Fujian Institute of Research on the Structure of Matter
Chinese Academy of Sciences, Fuzhou 350002 (P.R. China)

[**] This work was supported by the National Natural Science Fund (No. 20171020, 90101028, 10104007)

Supporting information for this article is available on the WWW under <http://www.angewandte.org> or from the author.

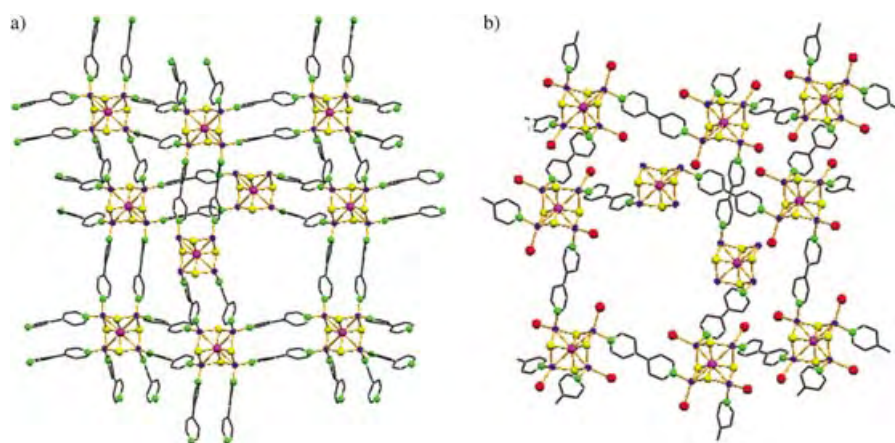


Figure 2. a) The diamondoid structure of the cationic cluster coordination polymer $\{[\text{WS}_4\text{Cu}_4(4,4'\text{-bipy})_4]^{2+}\}_n$. b) The diamondoid structure of the anionic cluster coordination polymer $\{[\text{WS}_4\text{Cu}_4\text{I}_4(4,4'\text{-bipy})_2]^{2-}\}_n$. Hydrogen atoms have been omitted for clarity. W violet, S yellow, Cu blue, N green, C black line.

2.5516(13) Å, respectively, which leads to another diamondoid network with a larger channel dimension of $24.828 \text{ Å} \times 24.217 \text{ Å}$ (Figure 2b). Each six-membered ring contains six $[\text{WS}_4\text{Cu}_4\text{I}_4]^{2-}$ nodes and six 4,4'-bipy connecting rods. The anionic cluster coordination polymer also exists as a twofold interpenetrating framework (Figure 3c and 3d).

It is noteworthy that the two pyridine rings of each 4,4'-bipy ligand are coplanar, except that two C atoms, C₁ and C₂, are disordered and were refined to an occupancy ratio of 0.5 in the anionic cluster coordination polymer; in the cationic cluster coordination polymer the pyridine rings of each 4,4'-bipy

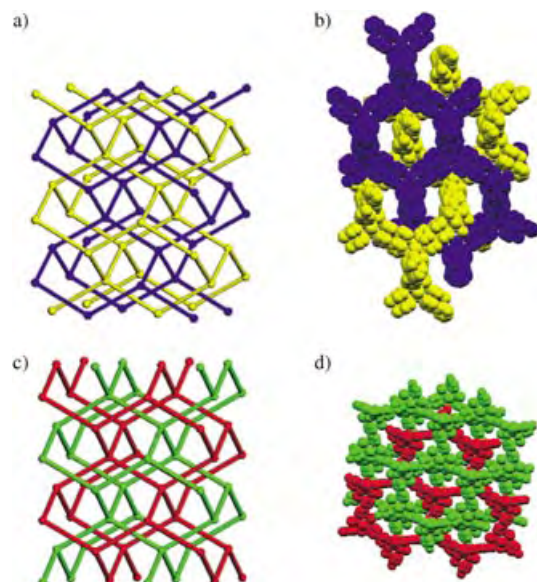


Figure 3. a) View of the cationic cluster coordination polymer. Each node and rod represents a cluster cation $[\text{WS}_4\text{Cu}_4]^{2+}$ and a pair of 4,4'-bipy ligands, respectively; b) space-filling picture showing the twofold interpenetrating cationic cluster coordination polymer $\{[\text{WS}_4\text{Cu}_4(4,4'\text{-bipy})_4]^{2+}\}_n$; c) view of the anionic cluster coordination polymer. Each node and rod represents a cluster anion $[\text{WS}_4\text{Cu}_4\text{I}_4]^{2-}$ and a single 4,4'-bipy ligand, respectively; d) space-filling picture showing the twofold interpenetrating anionic cluster coordination polymer $\{[\text{WS}_4\text{Cu}_4\text{I}_4(4,4'\text{-bipy})_2]^{2-}\}_n$.

found in some other coordination polymers containing transition metal ions.^[13] The 3D anionic cluster coordination polymer is almost exactly analogous to the cationic cluster coordination polymer, except that the building block is the $[\text{WS}_4\text{Cu}_4\text{I}_4]^{2-}$ ion, which is nearly tetrahedrally coordinated by four N atoms of four 4,4'-bipy molecules (Figure 4). Each Cu atom is tetrahedrally coordinated by two μ_3 -S atoms, one I atom, and one N atom from one of the 4,4'-bipy ligands, with Cu1–N1 and Cu1–I1 bond lengths of 2.090(7) Å and

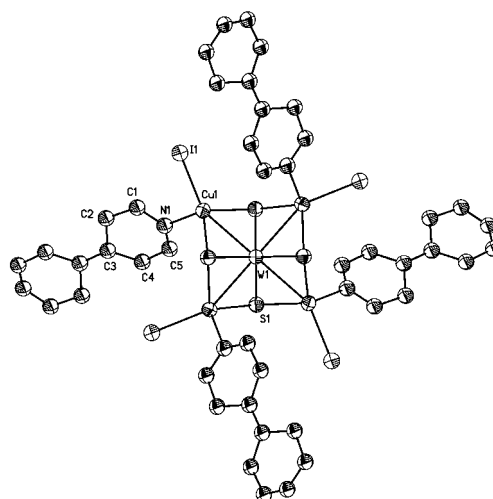


Figure 4. The anionic cluster coordination polymer unit $[\text{WS}_4\text{Cu}_4\text{I}_4(4,4'\text{-bipy})_2]^{2-}$.

ligand are not coplanar, with the pyridine rings twisted by 25.8°, 46.4°, and 63.9°, respectively. The whole molecule has an intricate, fourfold interpenetrating diamondoid structure (Figure 5), containing large $11.124 \text{ Å} \times 11.129 \text{ Å}$ channels; all the solvent water molecules are disordered along the *c* axis (Figure 6). The channel volume is about 293 Å^3 ,^[14] and the water molecules interact with the frameworks through hydrogen bonds.

Thermogravimetric analysis (TGA) of compound **1** under a nitrogen flow showed that the frameworks are rigid, with no weight change observed up to 203 °C. The solvent water and some of the organic ligands were lost between 203 °C and 268 °C (residue 68.1 %), then most of the remaining ligands were gradually removed from 268 °C to 337 °C (residue 54.4 %) and from 337 °C to 571 °C (residue 41.4 %). No further weight change was observed above 700 °C. The unit-cell parameters of a single crystal are nearly identical up to 180 °C, which is consistent with the TGA results. However,

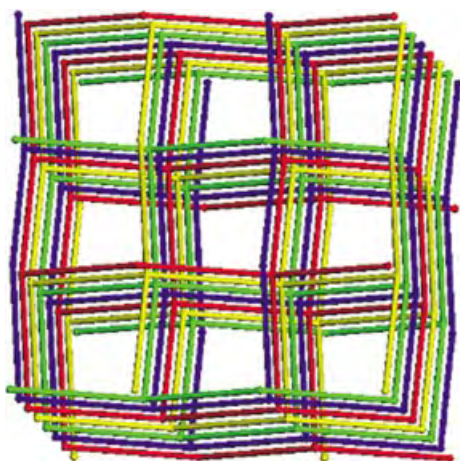


Figure 5. Schematic view of the cluster coordination polymer **1**. The cationic and anionic cluster coordination polymers are shown in blue/yellow and red/green, respectively. (The blue/yellow node and rod represent the cluster cation and the double 4,4'-bipy ligand, respectively; the red/green node and rod represent the cluster anion and the single 4,4'-bipy ligand, respectively.)

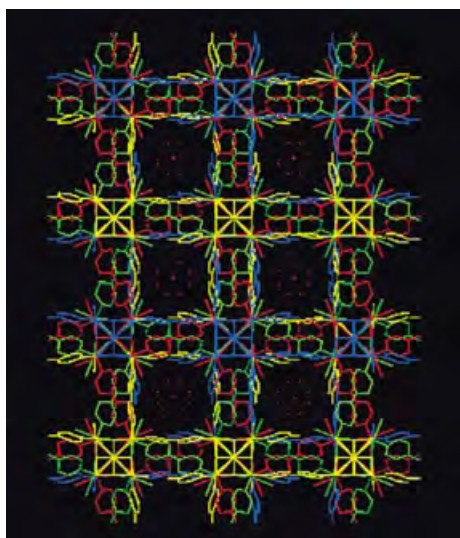


Figure 6. Packing diagram of compound **1**, viewed along the *c* axis. Hydrogen atoms have been omitted for clarity. Blue/yellow and red/green represent the cationic and anionic cluster coordination polymers, respectively. The red balls are the O atoms of the water molecules.

heating compound **1** to 230 °C and then cooling again causes a change in the X-ray powder diffraction (XRPD) pattern compared to that of **1** at room temperature, which indicates that the frameworks are only partially retained.

Two peaks at $\lambda_{\text{max}} = 292$ and 411 nm, observed in the UV/Vis spectrum of **1**, showed that the polymer has a relatively low linear absorption in the visible and near-IR region. We therefore performed a Z-scan experiment to investigate its nonlinear optical properties.^[15] The compound was dissolved in DMSO at a concentration of $5.8 \times 10^{-5} \text{ mol dm}^{-3}$. This solution was then placed in a 2-mm-thick cuvette. The linear transmittance of the sample was 76%. The results of the

open-aperture and the normalized transmittance are shown in Figure 7a.

The open circles are the experimental data, and the solid curves are the fit given by the Z-scan theory described in

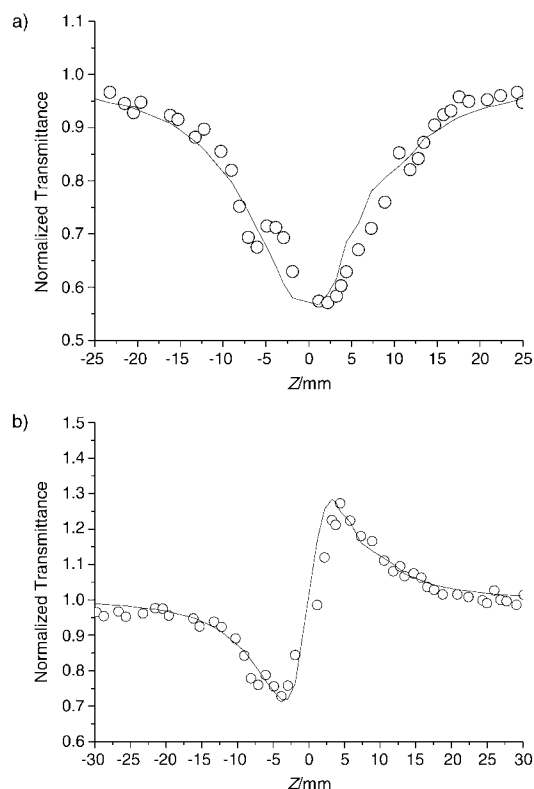


Figure 7. Z-scan data of cluster **1**: a) NLO absorption; b) NLO refraction.

ref. [15]. The open-aperture Z-scan curve of the compound has a deep valley, and the transmittance drops to the lower value of 57%. This result suggests that the compound has a strong nonlinear absorption; it may therefore be a promising candidate for use in optical limiting. It should be pointed out that both the excited-state population (and absorption) and the two-photon absorption could be responsible for the measured NLO effect. It is evident that the theoretical curves qualitatively reproduce the general pattern of the observed experimental data. This suggests an effectively third-order behavior for the experimentally detected NLO effects. The Z-scan data measured with the aperture are depicted in Figure 7b. The normalized curve has a sharp peak and a valley, which identifies compound **1** as a self-focusing material. A reasonably good fit between the experimental data and the theoretical curves, as described in ref. [15], was obtained. The effective third-order NLO absorptive index β and refractive index n_2 value were $1.6 \times 10^{-10} \text{ mW}^{-1}$ and $6.4 \times 10^{-11} \text{ esu}$, respectively; this shows that polymer **1** exhibits optical self-focusing behavior and reverse saturable absorption (RSA) effects.

In summary, a new kind of interpenetrating 3D cluster coordination polymer based on the tetrathiometalates has been obtained. Its NLO properties show that **1** exhibits

optical self-focusing behavior and reverse saturable absorption effects. Further work is in progress.

Experimental Section

A well-ground mixture of $[\text{NH}_4]_2[\text{WS}_4]$ (0.5 mmol), CuI (1.0 mmol), $[n\text{Bu}_4\text{N}]\text{I}$ (1.0 mmol), and 4,4'-bipy (1 mmol) was added to a mixture of DMF and CH_2Cl_2 (15 mL; v/v 2:1) under a purified nitrogen atmosphere. After stirring for 10 h, the filtrate was layered with diethyl ether. A few red crystals were separated several days later. A red prismatic single crystal (0.02 g, 15%) suitable for X-ray diffraction was obtained when the filtrate was allowed to slowly evaporate in air. Elemental analysis calcd (%) for **1**: C 27.20, H 2.13, N 6.34; found: C 27.84, H 1.89, N 6.71. IR (KBr): $\tilde{\nu}$ = 3448 (w), 3043 (w), 1672 (s), 1601 (s), 1530 (m), 1483 (m), 1409 (s), 1213 (m), 1068 (m), 807 (s), 626 (m), 567 (w), 499 (w), 438 cm^{-1} (s).

Received: May 17, 2004

Revised: August 12, 2004

Keywords: clusters · coordination polymers · heterometallic complexes · nonlinear optics · organic–inorganic hybrid composites

- [1] a) S. R. Batten, R. Robson, *Angew. Chem.* **1998**, *110*, 1558; *Angew. Chem. Int. Ed.* **1998**, *37*, 1460; b) S. R. Batten, *CrytEngComm* **2001**, *3*, 67; c) O. M. Yaghi, H. L. Li, C. Davis, D. Richardson, T. L. Groy, *Acc. Chem. Res.* **1998**, *31*, 474; d) A. J. Blake, N. R. Champness, P. Hubberstey, W. S. Li, M. A. Withersby, M. Schröder, *Coord. Chem. Rev.* **1999**, *183*, 117; e) S. Leininger, B. Olenyuk, P. J. Stang, *Chem. Rev.* **2000**, *100*, 853; f) B. Moulton, M. J. Zaworotko, *Chem. Rev.* **2001**, *101*, 1629; g) M. Eddaoudi, D. B. Moler, H. L. Li, B. L. Chen, T. M. Reineke, M. O'Keeffe, O. M. Yaghi, *Acc. Chem. Res.* **2001**, *34*, 319; h) O. R. Evans, W. B. Lin, *Acc. Chem. Res.* **2002**, *35*, 511; i) S. L. James, *Chem. Soc. Rev.* **2003**, *32*, 276; j) M. Oh, G. B. Carpenter, D. A. Sweigart, *Acc. Chem. Res.* **2004**, *37*, 1.
- [2] a) O. M. Yaghi, H. L. Li, *J. Am. Chem. Soc.* **1995**, *117*, 10401; b) N. Takeda, K. Umamoto, K. Yamaguchi, M. Fujita, *Nature* **1999**, *398*, 794; c) B. Olenyuk, J. A. Whiteford, A. Fechtenkötter, P. J. Stang, *Nature* **1999**, *398*, 796; d) K. Biradha, C. Seward, M. J. Zaworotko, *Angew. Chem.* **1999**, *111*, 584; *Angew. Chem. Int. Ed.* **1999**, *38*, 492; e) M. L. Tong, X. M. Chen, B. H. Ye, L. N. Ji, *Angew. Chem.* **1999**, *111*, 2376; *Angew. Chem. Int. Ed.* **1999**, *38*, 2237; f) L. Carlucci, G. Ciani, M. Morel, D. M. Proserpio, S. Rizzato, *Angew. Chem.* **2000**, *112*, 1566; *Angew. Chem. Int. Ed.* **2000**, *39*, 1506; g) K. Biradha, Y. Hongo, M. Fujita, *Angew. Chem.* **2000**, *112*, 4001; *Angew. Chem. Int. Ed.* **2000**, *39*, 3843; h) S. Noro, S. Kitagawa, M. Kondo, K. Seki, *Angew. Chem.* **2000**, *112*, 2162; *Angew. Chem. Int. Ed.* **2000**, *39*, 2082; i) M. C. Hong, Y. J. Zhao, W. P. Su, R. Cao, M. Fujita, Z. Y. Zhou, A. S. C. Chan, *Angew. Chem.* **2000**, *112*, 2586; *Angew. Chem. Int. Ed.* **2000**, *39*, 2468; j) S. M.-F. Lo, S. S.-Y. Chui, L.-Y. Shek, Z. Y. Lin, X. X. Zhang, G. H. Wen, I. D. Williams, *J. Am. Chem. Soc.* **2000**, *122*, 6293; k) M. Eddaoudi, J. Kim, N. Rosi, D. Vodak, J. Wachter, M. O'Keeffe, O. M. Yaghi, *Science* **2002**, *295*, 469; l) K. Biradha, M. Fujita, *Angew. Chem.* **2002**, *114*, 3542; *Angew. Chem. Int. Ed.* **2002**, *41*, 3392; m) N. L. Rosi, J. Eckert, M. Eddaoudi, D. T. Vodak, J. Kim, M. O'Keeffe, O. M. Yaghi, *Science* **2003**, *300*, 1127.
- [3] a) A. Müller, E. Diemann, R. Jostes, H. Bögge, *Angew. Chem.* **1981**, *93*, 957; *Angew. Chem. Int. Ed. Engl.* **1981**, *20*, 934; b) S. Sarkar, S. B. S. Mishra, *Coord. Chem. Rev.* **1984**, *59*, 239; c) S. C. Lee, R. H. Holm, *Chem. Rev.* **2004**, *104*, 1135; d) S. Shi, W. Ji, S. H. Tang, J. P. Lang, X. Q. Xin, *J. Am. Chem. Soc.* **1994**, *116*, 3615.
- [4] Y. Y. Niu, H. G. Zheng, H. W. Hou, X. Q. Xin, *Coord. Chem. Rev.* **2004**, *248*, 169.
- [5] Q. Huang, X. T. Wu, Q. M. Wang, T. L. Sheng, J. X. Lu, *Angew. Chem.* **1996**, *108*, 985; *Angew. Chem. Int. Ed. Engl.* **1996**, *35*, 868.
- [6] H. Yu, W. J. Zhang, X. T. Wu, T. L. Sheng, Q. M. Wang, P. Lin, *Angew. Chem.* **1998**, *110*, 2662; *Angew. Chem. Int. Ed.* **1998**, *37*, 2520.
- [7] Q. F. Zhang, Y. Y. Niu, W. H. Leung, Y. L. Song, I. D. Williams, X. Q. Xin, *Chem. Commun.* **2001**, 1126.
- [8] C. Zhang, Y. L. Song, Y. Xu, H. K. Fun, G. Y. Fang, Y. X. Wang, X. Q. Xin, *J. Chem. Soc. Dalton Trans.* **2000**, 2823.
- [9] H. W. Hou, Y. T. Fan, C. X. Du, Y. Zhu, W. L. Wang, X. Q. Xin, M. K. M. Low, W. Ji, H. G. Ang, *Chem. Commun.* **1999**, 647.
- [10] H. W. Hou, H. G. Zheng, H. G. Ang, Y. T. Fan, M. K. M. Low, Y. Zhu, W. L. Wang, X. Q. Xin, W. Ji, W. T. Wong, *J. Chem. Soc. Dalton Trans.* **1999**, 2953.
- [11] O. M. Yaghi, G. M. Li, *Angew. Chem.* **1995**, *107*, 232; *Angew. Chem. Int. Ed. Engl.* **1995**, *34*, 207.
- [12] Single-crystal X-ray structure determination of **1**: The data were collected at $T = 123$ K on a Rigaku mercury CCD diffractometer with graphite-monochromated $\text{Mo K}\alpha$ radiation ($\lambda = 0.7107$ Å). All calculations were performed by using SHELXTL version 6.10 package on a Dell-4550 computer.^[16] The structure was solved by direct methods and refined by full-matrix least-squares methods. Crystal data: red prism, $0.35 \times 0.30 \times 0.25$ mm, $\text{C}_{60}\text{H}_{56}\text{Cu}_8\text{I}_4\text{N}_{12}\text{O}_4\text{S}_8\text{W}_2$, $M_r = 2649.27$, tetragonal, space group $I4(1)/acd$, $a = b = 24.780(4)$, $c = 28.159(7)$ Å, $V = 17291(6)$ Å³, $Z = 8$, $\mu = 6.242$ mm⁻¹, $\rho_{\text{calcd}} = 2.036$ g cm⁻³, $\text{GOF} = 1.051$, $R1(wR2) = 0.0515$ (0.1369) [4259 observed ($I > 2\sigma(I)$) for 3390 independent reflections (with $R_{\text{int}} = 0.036$)] out of a total of 55837 reflections with 252 parameters]. CCDC-231994 contains the supplementary crystallographic data for this paper. These data can be obtained free of charge at www.ccdc.cam.ac.uk/conts/retrieving.html (or from the Cambridge Crystallographic Data Centre, 12 Union Road, Cambridge CB2 1EZ, UK; fax: (+44) 1223-336-033; or deposit@ccdc.cam.ac.uk).
- [13] a) B. F. Hoskins, R. Robson, *J. Am. Chem. Soc.* **1990**, *112*, 1546; b) K. W. Kim, M. G. Kanatzidis, *J. Am. Chem. Soc.* **1992**, *114*, 4878; c) L. Carlucci, G. Ciani, D. M. Proserpio, A. Sironi, *J. Chem. Soc. Chem. Commun.* **1994**, 2755; d) A. J. Blake, N. R. Champness, S. S. M. Chung, W. S. Li, M. Schröder, *Chem. Commun.* **1997**, 1005.
- [14] A. L. Spek, PLATON, A Multipurpose Crystallographic Tool, Utrecht University, Utrecht, The Netherlands, **2003**.
- [15] M. Sheik-Bahae, A. A. Said, T. H. Wei, D. J. Hagan, E. W. Van Stryland, *IEEE J. Quantum Electron.* **1990**, *26*, 760.
- [16] G. M. Sheldrick, SHELXTL, version 6.10, Bruker AXS Inc., Madison Wisconsin, USA, 2000.

Protein Interactions

Modulation of Compactness and Long-Range Interactions of Unfolded Lysozyme by Single Point Mutations**

Julia Wirmer, Christian Schlörb, Judith Klein-Seetharaman, Ryoma Hirano, Tadashi Ueda, Taiji Imoto, and Harald Schwalbe*

Non-native states of proteins are not only the starting point of protein folding, but they are also implied in misfolding, transport through membranes, protein turnover, and degradation processes. An increasing number of intrinsically unstructured or natively unfolded proteins have been identified, some of which exert their function in this unstructured state.^[1] Unlike the native state of a protein, non-native states cannot be described by a single conformation, but rather they exist as an ensemble of rapidly interconverting conformers. The individual members of this ensemble may differ substantially in their structural and dynamical properties, and different parts of the polypeptide chain may change conformation at different rates.^[2] Previous studies showed that the conformational ensemble samples the preferred regions of the Ramachandran φ, ψ space. This sampling, however, can be restricted by varying degrees of residual structure: Secondary structure elements in unfolded proteins have been identified in a large number of proteins by comparison of local NMR parameters with values expected in a random coil.^[3–9] In contrast, the identification of longer-range interactions is not as straightforward. The conformational averaging in unfolded proteins renders it only possible to detect

short- or medium-range NOE (nuclear Overhauser effect) interactions. Long-range interactions can only be identified by using mutations in combination with NMR spectroscopic techniques such as relaxation rates,^[10] spin labels, residual dipolar couplings, or diffusion rates.

NMR spectroscopic studies of non-native states of hen lysozyme have revealed the existence of clusters of residual secondary structure.^[6,10] The locations of these clusters strongly correlate with clusters of hydrophobic amino acids, a correlation that was also observed for other proteins.^[11–13] These hydrophobic clusters in non-native lysozyme are stabilized by long-range interactions.^[10] However, the extent to which each of these clusters contributes to the stability of the entire conformational ensemble is an important, yet unanswered question. Herein we study the effects of point mutations in the major hydrophobic clusters on the ensemble of structures that are present in unfolded lysozyme. The results show that nonconservative single point mutations in the hydrophobic clusters dramatically change the overall compactness of non-native lysozyme by the modulation of long-range interactions between hydrophobic clusters.

The distribution of hydrophobic amino acids in the lysozyme sequence is shown in Figure 1 a. The hydrophobicity predictions were fitted to six distinct clusters with maximal hydrophobicity around (1) C6, (2) W28, (3) L56, (4) L83, (5) W108, and (6) W123 (C = cysteine, W = tryptophan, and L = leucine) by using Gaussian models. Mapping of the hydrophobic clusters onto the structure of lysozyme^[14] showed that the clusters ultimately result in the hydrophobic cores of the α - and β -domains of the protein. The location of the hydrophobic clusters has an impact on the unfolded states: 1) Experimentally determined folding-core residues map to the central parts of clusters 1–4.^[15–18] 2) Residual non-random secondary structures tend to cluster at similar positions (Figure 2 A). 3) The positions of hydrophobic clusters overlap to a remarkable extent with the average restrictions in conformational space in unfolded ensembles of lysozyme as identified by relaxation rate measurements (Figure 3 a). In contrast to the excellent correlation between the positions of the experimentally determined clusters of residual structure and those of all of the hydrophobic clusters, the intensities of the clusters do not match well for clusters 1 and 4, for which barely elevated relaxation rates were found. Interestingly, these two clusters are the only two regions of predicted increased hydrophobicity (Figure 1 a) that do not contain tryptophan residues.

We investigated the effects of two types of single point mutations on the compactness and interaction of clusters: 1) replacement of tryptophan residues with either tyrosine (Y) or glycine (G) moieties (W62Y/G) and 2) replacement of a central amino acid, with emphasis on tryptophan units, in clusters 1, 3, 5, and 6 with glycine (A9G, W62G, W111G, and W123G (see Figure 1 b). The Trp28 mutant protein was too unstable for sufficient amounts of protein to be obtained and was therefore not investigated. Cluster 4 was not studied because the wild-type (WT) protein already displays very little deviation from the random coil in this region. To obtain a model system for the study of non-native states of lysozyme, WT and mutant lysozyme were denatured, the four native

[*] J. Wirmer, C. Schlörb, J. Klein-Seetharaman, Prof. Dr. H. Schwalbe
Institute for Organic Chemistry and Chemical Biology
Center for Biomolecular Magnetic Resonance
Johann Wolfgang Goethe University Frankfurt
Marie-Curie-Strasse 11, 60439 Frankfurt (Germany)
Fax: (+49) 69-798-29515
E-mail: schwalbe@nmr.uni-frankfurt.de

J. Wirmer
Department of Chemistry
Massachusetts Institute of Technology
Cambridge MA 02139 (USA)

J. Klein-Seetharaman
Department of Pharmacology, University of Pittsburgh
School of Medicine
Pittsburgh PA 15261 (USA)

R. Hirano, T. Ueda
Graduate School of Pharmaceutical Science
Kyushu University
Fukuoka 812-8582 (Japan)

T. Imoto
Department of Applied Microbial Technology
Faculty of Engineering
Sojo University
Ikeda 4-22-1, Kumamoto 860-0082 (Japan)

[**] We thank the Fonds der Chemischen Industrie (Germany) for stipends to J.W. and C.S., and the State of Hessen for financial support.

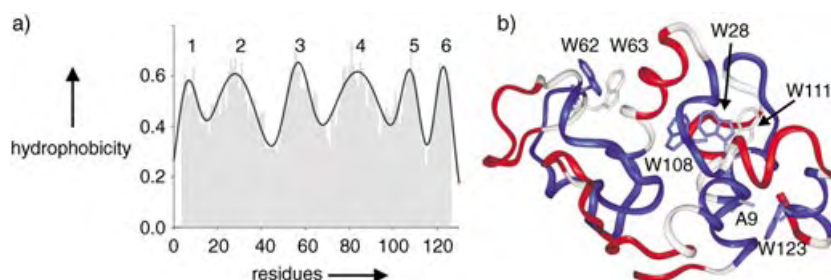


Figure 1. a) Distribution of hydrophobicity in lysozyme: normalized values (0–1) of hydrophobicity according to the scheme of Abraham and Leo.^[32] Gaussian least-squares fitting of hydrophobic clusters is shown as a black line, and the clusters are numbered 1–6. b) Positions of Ala9 (A9) and tryptophans (W) in the native state: the crystal structure of lysozyme (deposited in the Protein Data Bank (193L)^[14]) shown is colored according to the hydrophobicity values that were obtained from the Gaussian fit (red: nonhydrophobic (0–0.46); blue: hydrophobic (0.52–1); for comparison: glycine = 0.49).

disulfide bonds were reduced and methylated (indicated by S^{Me}), and the products were studied in water at pH 2, at which hydrogen exchange is slowed down. This variant of lysozyme remained unfolded in the absence of denaturant even at near-native conditions (pH 6, data not shown), but measurements were carried out at pH 2 owing to the slow rates of amide exchange.

NMR H^N, H^α, and C^α chemical shifts were used for secondary-structure prediction.^[19,20] In WT-S^{Me}, all the chemical shift values were close to those of the random coil which indicates that the reduced protein is unstructured. Remaining

small perturbations in the chemical shift values of H^N and H^α atoms of WT-S^{Me}, relative to chemical shifts measured in small unstructured peptides,^[21,22] are shown in Figure 2 A, parts a and b, respectively. Deviations were found for Gly22 (H^N), for Val29 and Cys-S^{Me} 30 (both H^α), around Trp62/Trp63 (R61 (H^α); W62, W63, and C64 (H^N)), and around Trp108/Trp111 (V109, R112 (H^α); W111, N113, and R114 (H^N); (V = valine, R = arginine)). The degree of helicity was estimated by a comparison of the measured C^α chemical shifts^[23] with those values expected for the random coil^[19] and those derived statistically for α -helices.^[24] High induced helicity was found for residues 8–12 and around Trp108/Trp111. A mean degree of helicity

of 12.3% was calculated (Figure 2 A, part c). This value is in excellent agreement with a global value of 14.4% derived from circular dichroism (CD) spectroscopy measurements (Figure 2 A, part d).

The effect of the replacement of a single amino acid, namely Trp62 in W62G and W62Y in cluster 3, and the mutations A9G, W111G, and W123G, on the H^α chemical shift is shown in Figure 2, B and C, respectively. The data are presented as correlations between the chemical shift values of H^α atoms in the single point mutants with those in WT-S^{Me}. The H^α atoms of the conservative mutations W62Y and A9G

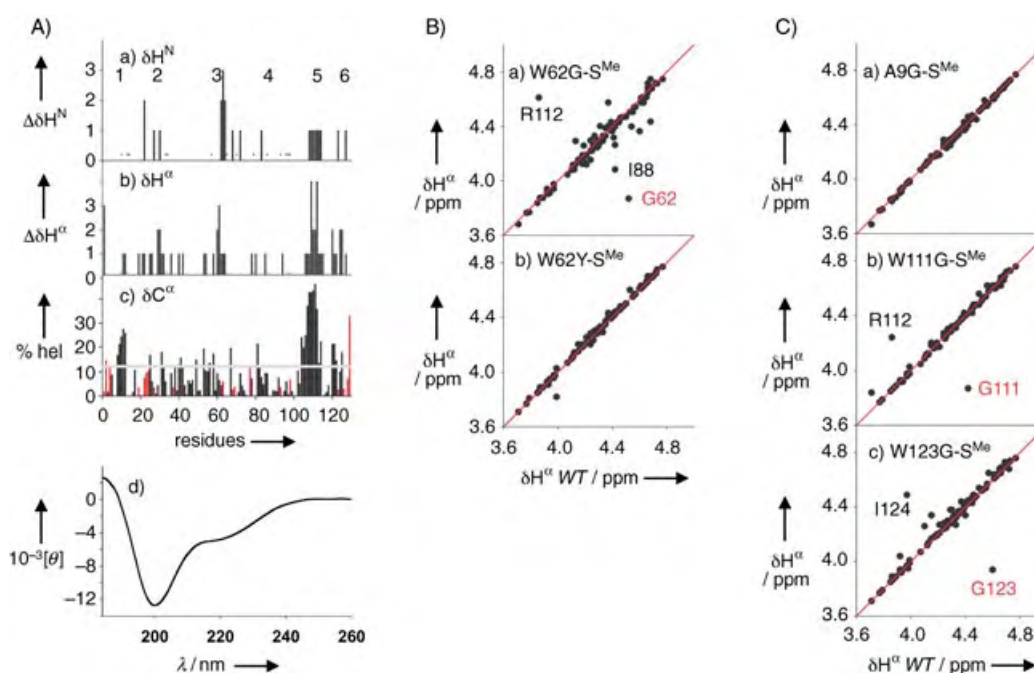


Figure 2. Residual secondary structure in unfolded lysozyme. A) Normalized values of the differences between the chemical shifts of a) H^N and b) H^α centers in WT-S^{Me} relative to those in the random coil ($\Delta\delta = \delta_{\text{exp}} - \delta_{\text{rc}}$).^[6] Residues for which chemical shifts could not be determined are indicated by an asterisk. c) The percentage of residual helicity (% hel) in WT-S^{Me} are shown as black (positive) and red (negative) vertical bars as a function of the number of residues. A mean value of the induced positive helicity of 12.3% is indicated by the horizontal line. d) CD spectrum of WT-S^{Me} ($[\theta]/\text{deg cm}^2 \text{ mol}^{-1}$); a helicity of 14.4% was estimated by using the approach of Rohl and Baldwin.^[36] Correlation between the chemical shift values of H^α in B) W62G-S^{Me} and W62Y-S^{Me}, and C) A9G-S^{Me}, W111G-S^{Me}, and W123G-S^{Me} in WT-S^{Me} with those of the wild-type (WT) protein; strongly deviating residues are indicated (black) as well as the mutated amino acids (red).

display chemical shift values that are virtually identical to those of the WT. The largest deviations in these correlations were found for W62G, which has longer-range effects in particular on R112 and I88 (I = isoleucine), which are distant from the point of mutation at position W62. W111G and W123G show predominantly local deviations, including the mutation site and immediate neighbors in the sequence. However, overall, the deviations of the chemical shifts of the protons from the mutants relative to those of the WT proteins are small for all mutants, even for the regions around the chosen mutation sites which have correlation coefficients that range between 0.996 (A9G) and 0.849 (W62G). We conclude that local regions of residual secondary structure are not disturbed by the mutations.

Because non-native states of proteins are the “averages” of interconverting fluctuating conformations, a single set of tertiary contacts in the unfolded state cannot be determined. However, averaged restrictions in conformational space were measured by the ^{15}N NMR spectroscopic transverse relaxation rates (R_2) and the diffusion-derived hydrodynamic radius (R_h). R_h is determined by the diffusion of the polypeptide chain and is therefore averaged over the ensemble of conformers. R_2 relaxation rates depend on the anisotropic rotational correlation time (τ_c) and are sensitive to motions of the backbone on the subnanosecond timescale and also to slow conformational exchange on the millisecond timescale.^[25–27] Previously, by comparison of R_2 and $R_{1\rho}$, we showed that the effect of slow conformational exchange on R_2 rates in WT-S^{Me} is negligible.^[6] In the fully unfolded state of a protein, the internal motions can be described as arising from segmental motions, and the profile of relaxation rates for the random coil R_2^{rc} can be predicted from polymer theory,^[28] which is independent of the molecular weight. In compact unfolded states, the interactions of some segments lead to deviations from random-coil behavior. Therefore, the extent of deviation from the random-coil model can be used to delineate long-range, tertiary interactions.^[6,10]

Figure 3 shows the heteronuclear ^{15}N transverse relaxation rates (R_2^{exp}) of WT-S^{Me} and the mutants that were studied. For comparison, the rates that were determined previously^[10] for WT-S^{Me} and W62G-S^{Me} are also reproduced. Increased relaxation rates in WT-S^{Me} coincide with the six hydrophobic clusters and the positions of residual secondary structure, which were identified from measurements of the chemical shift values. Replacement of Trp62 by glycine essentially abolishes not only its own cluster 3 (Figure 3b), but also clusters 1–4 and diminishes clusters 5 and 6.^[10] Long-range interactions between Trp62 and the other hydrophobic clusters of lysozyme therefore must be present and stabilized by the tryptophan moiety. To test if this property of Trp62 is unique to tryptophan or whether it may be more generally attributable to aromatic amino acids, the effect of replacing Trp62 by tyrosine on the relaxation behavior of unfolded lysozyme was studied (see Figure 3c). The W62Y mutation

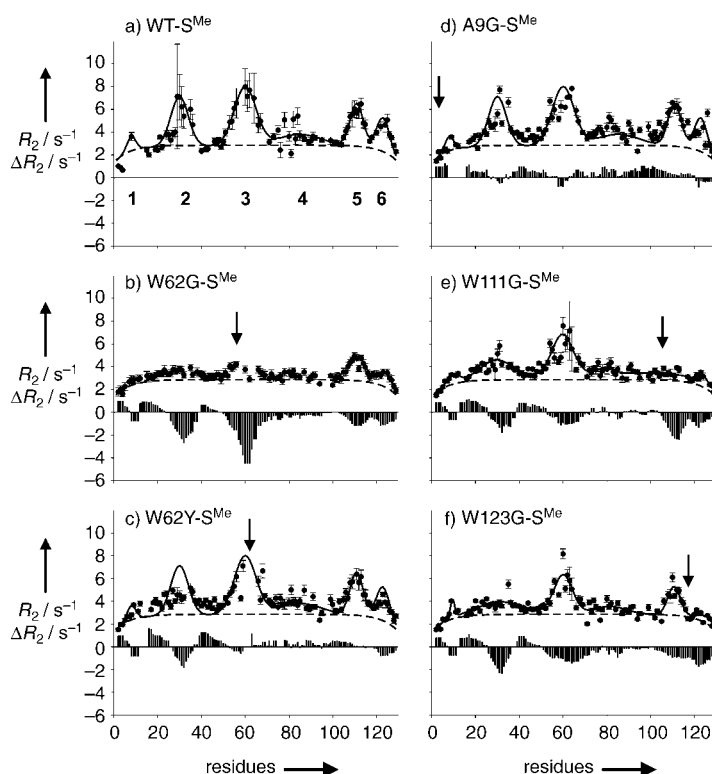


Figure 3. Residual tertiary interactions in unfolded lysozyme (hydrophobic clusters are indicated by numbers 1–6). a–f) ^{15}N R_2 relaxation rates in WT-S^{Me} and W62G-S^{Me}, W62Y-S^{Me}, A9G-S^{Me}, W111G-S^{Me}, and W123G-S^{Me}, respectively. The experimental rates are shown as scatter plots, whereas the rates fitted by a segmental motion model and expected for a random coil with R_2^{rc} ($R_{\text{int}} = 0.2 \text{ s}^{-1}$ and $\lambda_0 = 7$) are shown as dashed lines; black lines show the Gaussian fits for WT-S^{Me} (a, c, and d), W111G-S^{Me} (e), and W123G-S^{Me} (f). Deviations of R_2 relaxation rates of the mutants from relaxation rates of WT-S^{Me} ($\Delta R_2 = R_2(\text{mutant-S}^{\text{Me}}) - R_2(\text{WT-S}^{\text{Me}})$) were averaged over 7 residues and are shown as bars.

has a very minor effect on the relaxation properties of WT-S^{Me} relative to W62G-S^{Me}. This result suggests that aromatic residues play an important role in the stabilization of long-range interactions in unfolded states of lysozyme. A9G-S^{Me} displays even more similar properties to WT-S^{Me}, and there is not even an effect on its own cluster, cluster 1. The size and the position of the hydrophobic clusters remain virtually identical which indicates that Ala9 is not important in the stabilization of the hydrophobic core.

In contrast, the replacement of tryptophan residues at positions 111 and 123 led to significant results. Upon replacement of Trp111 (cluster 5) by glycine, the cluster in which the mutation is located, namely cluster 5, disappeared entirely and cluster 6 also decreased significantly in intensity. A loss in the intensity of cluster 2 (surrounding Trp28) was observed as well as a very small decrease in the intensity of cluster 3 (surrounding Trp62 and Trp63). Similarly, when Trp123 at the C terminus (cluster 6) was changed to glycine, the cluster around the mutation site essentially disappeared, and the intensities of clusters 2, 3, and 5 were lessened. The effect of the replacement in W123G is less significant than that of W111G, as seen by the complete loss of cluster 5 in W111G-S^{Me} but not in W123G-S^{Me}. The largest changes in the

distribution of R_2 relative to WT-S^{Me} were observed with W62G-S^{Me}.

The decrease in the R_2 values upon single point mutations indicates that changes in the conformational ensembles of lysozyme occurred. Thus, it is predicted that those point mutations which cause a change in relaxation profiles can also cause a change in the compactness of the average unfolded state. A loss of conformational restriction in one or more of the hydrophobic clusters would increase the overall propensity for extended states in the ensemble. This hypothesis was tested directly by measuring the averaged hydrodynamic radii R_h from NMR diffusion measurements of the different reduced and methylated proteins. WT-S^{Me} and W123G-S^{Me} diffuse quickly, W111G-S^{Me} diffuses at intermediate velocity, and W62G-S^{Me} diffuses the slowest. Figure 4a shows the

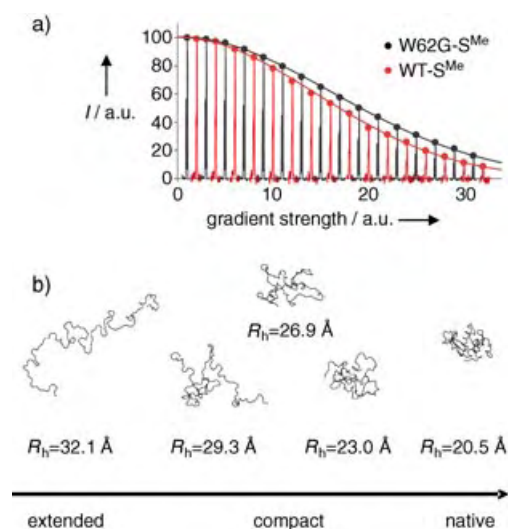


Figure 4. Changes in compactness as a result of point mutations. a) Diffusion experiments that were used to determine the hydrodynamic radii (R_h). The intensity of the NMR signal is shown as a function of gradient strength (g) for WT-S^{Me} (black) and W62G-S^{Me} (red). The decay of the signal was fitted to a function of the form $I = Ae^{-Dg^2}$. R_h values were calculated from decay rates (D , see Experimental Section). b) Randomly chosen conformations with the amino acid sequence of lysozyme in relation to their hydrodynamic radius. Conformations with increasing (experimental) R_h values are shown. The radii of different conformations were calculated using the program Hydropro.^[40]

diffusion measurements for WT-S^{Me} and W62G-S^{Me}. The R_h values that were calculated from the diffusion rates (see the Experimental Section) are 26.9 ± 0.6 , 25.4 ± 1.2 , 29.3 ± 1.3 , and 32.1 ± 0.6 Å for WT-S^{Me}, W123G-S^{Me}, W111G-S^{Me}, and W62G-S^{Me}, respectively (these values are concentration-independent (40–60 μ M)). All R_h values are considerably larger (at least 25 %) than the R_h value of folded lysozyme ($R_h = 20.5$ Å)^[29] which indicates the extended nature of the reduced and methylated states. However, the overall average shape of the ensemble of conformers markedly varies with the position of the single point mutations in the different hydrophobic clusters. Whereas similar hydrodynamic radii were measured for WT-S^{Me} and W123G-S^{Me}, the hydrodynamic radius of W111G-S^{Me} was larger ($R_h = 29.3 \pm 1.3$ Å)

and that of the W62G-S^{Me} mutant was the largest ($R_h = 32.1 \pm 0.6$ Å; see Figure 4b). Conformations were calculated by unbiased molecular dynamics simulations. As one can see, the R_h value of 32.1 Å for W62G-S^{Me} corresponds to a very extended, almost linear conformation, which is consistent with the essentially random-coil behavior observed for the relaxation rates of this mutant (Figure 3b). The radii observed for the other mutants correspond to rather compact states with a clear presence of tertiary contacts. These states are much closer to the native state with a R_h value of 20.5 Å than the very extended conformation that has a R_h value of 32.1 Å.

The comparison between experimental NMR parameters and those expected for a true random coil show that there are six areas that display strong deviations from random-coil behavior in WT-S^{Me}. The observed hydrodynamic radius of 26.9 ± 0.6 Å indicates that the average conformations in WT-S^{Me} are rather compact (Figure 4b) which supports the presence of extensive tertiary contacts in the unfolded state. These contacts are both nativelylike and non-nativelylike. Non-native contacts between cluster 3—around Trp62 and Trp63, which form part of the β -domain in the native structure (see also Figure 1b)—and the clusters 1, 2, and 4, which form the α -domain, must be present because deviations from random-coil relaxation behavior are decreased in the W62G mutant. Breakage of these long-range interactions results in a dramatic increase by 12 % in the measured R_h values from WT-S^{Me} to W62G-S^{Me} which reflects a shift towards very extended conformations (Figure 4b). The presence of native-like contacts is suggested by the effect of the W123G mutation which simultaneously diminishes clusters 6 and 2, indicating nativelylike contacts between Trp123 and sites at or around Trp28. The importance of native-like contacts is consolidated by the central role of the Trp111 interactions in WT-S^{Me}. Disruption of the contacts between Trp111 and the cluster that surrounds Trp28 by the W111G mutation results in a large increase in R_h of $\approx 9\%$. Tryptophan residues or aromatic residues in general apparently play a special role in the stabilization of contacts in compact states of unfolded lysozyme. A comparison of the effects of replacing Trp62 with glycine and with tyrosine shows that there are little changes in the relaxation behavior of W62Y-S^{Me} relative to WT-S^{Me}, in contrast to W62G-S^{Me}, which shows the strongest deviations from WT-S^{Me}. Aromatic residues play a significant role in the organization of nearby residues into arrangements that have restricted motions compared to a completely unfolded polypeptide chain.

Point mutations induce a shift in the distribution of conformers from compact to more-extended states to differing degrees depending on the location of the mutation with respect to the hydrophobic clusters present. Such changes are expected to result in differences in the rates at which folding and misfolding events take place. Extended structures will clearly have different propensities, for example, in the formation of disulfide bonds. Similarly, the time that is needed for an extended stretch of amino acids within the protein sequence to rearrange into another extended or into a more-compact state will be affected by the change in compactness induced by the different mutations.

Experimental Section

Hydrophobicity calculations were performed with the 'protscale' tool from the ExPASy (Expert Protein Analysis System)^[30,31] molecular biology server (<http://us.expasy.org/cgi-bin/protscale.pl>) by using the Abraham and Leo scale.^[32] A window size (i.e., length of the interval used for profile computation) of 7 was used, and the weight at the edge of the window was set to 100%; the degrees of hydrophobicity shown were normalized from 0–1. Centres of elevated regions were identified by the fitting of Gaussian clusters to the data with the program SigmaPlot.

The construction of single point mutants of hen egg-white lysozyme, the expression and purification of ¹⁵N-labelled protein in the yeast *Pichia pastoris*,^[33,34] and the methylation of reduced lysozyme^[35] were performed according to reported methods.

CD spectra were recorded as described,^[23] and the mean helix content was calculated by using the approach of Rohl and Baldwin.^[36] NMR experiments were recorded at 293 K on a four-channel Bruker DRX600 spectrometer, which was equipped with a cryo-probe, with z-gradients. Samples of the proteins (≈ 60–100 μM) were prepared in water (10% D₂O, pH 2). 3D NOESY-HSQC (hetero-nuclear single quantum coherence) experiments were recorded and analyzed as previously reported.^[6] Perturbations of the chemical shifts of H^N and H^α atoms were derived as previously described.^[6] Residual helicity is defined by the percentage of induced helicity (% hel), which is obtained from a comparison of the C^α chemical shifts in WT-S^{Me} (C^α_{exp}) with the C^α chemical shifts in the random coil (C^α_{rc})^[19,20,23] and those derived statistically for α-helices (C^α_{hel}),^[24] according to Equation (1):

$$\% \text{ hel} = 100 \frac{\delta C_{\text{exp}}^{\alpha} - \delta C_{\text{rc}}^{\alpha}}{\delta C_{\text{hel}}^{\alpha} - \delta C_{\text{rc}}^{\alpha}} \quad (1)$$

Diffusion measurements were performed using 40–60 μM protein in D₂O at pH 2 (corrected for D₂O),^[37] with 1,4-dioxane (200–300 μM) as internal standard (hydrodynamic radius: 2.12 Å; it has been shown that dioxane does not interact with proteins^[38]). PFG (pulse field gradient)-NMR diffusion measurements were performed as reported.^[29,38,39] Hydrodynamic radii (*R_h*) were calculated from the decay rates derived from NMR spectra by using Equation (2), in which *D_{diox}* and *D_{prot}* are the decay rates of dioxane and the protein, respectively.

$$R_{\text{h}}^{\text{prot}} = \frac{D_{\text{diox}}}{D_{\text{prot}}} R_{\text{h}}^{\text{diox}} \quad (2)$$

It was reported that the aggregation of methylated lysozyme (WT-S^{Me}), which is in exchange with the unfolded form, is observed as an increase in the apparent *R_h* for concentrations of the protein of 0.2–0.25 mM.^[29] However, here, at concentrations of the protein of 40–60 μM for each mutant, *R_h* remained constant, which excludes aggregation processes. Predicted hydrodynamic radii (Figure 4) were calculated from the structures by using the program Hydropro.^[40]

Transverse relaxation rates *R₂* were measured and analyzed as previously reported.^[6] Relaxation rates in an extended polypeptide can be described by a simple model, which is derived from polymer theory^[28] and is referred to as the segmental motion model. The segmental model assumes that the influence of the neighboring residues decays exponentially as the distance (in terms of the number of peptide bonds) from a given residue increases.^[6] Therefore, *R₂* relaxation rates of unfolded proteins can be fitted to Equation (3), in which *R_{int}* is the intrinsic relaxation rate, which depends also on the temperature and viscosity of the solution, λ₀ is the persistence length of the polypeptide chain (in terms of the numbers of residues), and *N* is the total chain length of the polypeptide:

$$R_2^{\text{rc}}(i) = R_{\text{int}} \sum_{j=1}^N e^{-\frac{|i-j|}{\lambda_0}} \quad (3)$$

Experimental *R₂* rates of lysozyme show that there are regions of positive deviation from the segmental model that can be fitted by Gaussian distributions. Thus, a model is proposed that includes two components: the segmental motion part [Eq. (3)] and a Gaussian term, as shown in Equation (4).

$$R_2^{\text{exp}}(i) = R_{\text{int}} \sum_{j=1}^N e^{-\frac{|i-j|}{\lambda_0}} + \sum_{\text{cluster}} R_{\text{cluster}} e^{-\left(\frac{i-x_{\text{cluster}}}{2\lambda_{\text{cluster}}}\right)^2} \quad (4)$$

These Gaussian clusters are characterized by the position of the cluster in the protein (residue number) *x_{cluster}*, the width of the cluster λ_{cluster}, and a distinct relaxation rate for each cluster *R_{cluster}*.

Received: June 8, 2004

Keywords: biophysics · lysozyme · mutagenesis · NMR spectroscopy · protein folding

- [1] P. Tompa, *Bioessays* **2003**, 25, 847.
- [2] L. J. Smith, K. M. Fiebig, H. Schwalbe, C. M. Dobson, *Folding Des.* **1996**, 1, R95.
- [3] F. J. Blanco, L. Serrano, J. D. Forman-Kay, *J. Mol. Biol.* **1998**, 284, 1153.
- [4] D. Shortle, M. S. Ackerman, *Science* **2001**, 293, 487.
- [5] D. Shortle, C. Abeygunawardana, *Structure* **1993**, 1, 121.
- [6] H. Schwalbe, K. M. Fiebig, M. Buck, J. A. Jones, S. B. Grimshaw, A. Spencer, S. J. Glaser, L. J. Smith, C. M. Dobson, *Biochemistry* **1997**, 36, 8977.
- [7] K. M. Fiebig, H. Schwalbe, M. Buck, L. J. Smith, C. M. Dobson, *J. Phys. Chem.* **1996**, 100, 2661.
- [8] K. B. Wong, S. M. Freund, A. R. Fersht, *J. Mol. Biol.* **1996**, 259, 805.
- [9] M. A. Lietzow, M. Jamin, H. J. Jane Dyson, P. E. Wright, *J. Mol. Biol.* **2002**, 322, 655.
- [10] J. Klein-Seetharaman, M. Oikawa, S. B. Grimshaw, J. Wirmer, E. Duchardt, T. Ueda, T. Imoto, L. J. Smith, C. M. Dobson, H. Schwalbe, *Science* **2002**, 295, 1719.
- [11] D. Neri, M. Billeter, G. Wider, K. Wuthrich, *Science* **1992**, 257, 1559.
- [12] G. Saab-Rincon, P. J. Gualfetti, C. R. Matthews, *Biochemistry* **1996**, 35, 1988.
- [13] I. J. Ropson, C. Frieden, *Proc. Natl. Acad. Sci. USA* **1992**, 89, 7222.
- [14] M. C. Vaney, S. Maignan, M. RiesKautt, A. Ducruix, *Acta Crystallogr. Sect. D* **1996**, 52, 505.
- [15] A. Miranker, S. E. Radford, M. Karplus, C. M. Dobson, *Nature* **1991**, 349, 633.
- [16] M. Buck, S. E. Radford, C. M. Dobson, *J. Mol. Biol.* **1994**, 237, 247.
- [17] S. E. Radford, C. M. Dobson, P. A. Evans, *Nature* **1992**, 358, 302.
- [18] D. P. Nash, J. Jonas, *Biochemistry* **1997**, 36, 14375.
- [19] D. S. Wishart, B. D. Sykes, *J. Biomol. NMR* **1994**, 4, 171.
- [20] D. S. Wishart, B. D. Sykes, F. M. Richards, *Biochemistry* **1992**, 31, 1647.
- [21] D. S. Wishart, C. G. Bigam, A. Holm, R. S. Hodges, B. D. Sykes, *J. Biomol. NMR* **1995**, 5, 67.
- [22] S. Schwarzingier, G. J. Kroon, T. R. Foss, J. Chung, P. E. Wright, H. J. Dyson, *J. Am. Chem. Soc.* **2001**, 123, 2970.
- [23] C. Schlörb, C. Richter, K. Ackermann, J. Wirmer, H. Schwalbe, unpublished results.
- [24] H. Zhang, S. Neal, D. S. Wishart, *J. Biomol. NMR* **2003**, 25, 173.

- [25] G. Wagner, *Curr. Opin. Struct. Biol.* **1993**, 3, 748.
- [26] G. Lipari, A. Szabo, *J. Am. Chem. Soc.* **1982**, 104, 4559.
- [27] G. Lipari, A. Szabo, *J. Am. Chem. Soc.* **1982**, 104, 4546.
- [28] A. Allerhand, R. K. Hailstone, *J. Chem. Phys.* **1972**, 56, 3718.
- [29] D. K. Wilkins, S. B. Grimshaw, V. Receveur, C. M. Dobson, J. A. Jones, L. J. Smith, *Biochemistry* **1999**, 38, 16424.
- [30] R. D. Appel, A. Bairoch, D. F. Hochstrasser, *Trends Biochem. Sci.* **1994**, 19, 258.
- [31] A. Bairoch, R. D. Appel, M. C. Peitsch, *Protein Data Bank Q. Newslett.* **1997**, 81, 5.
- [32] D. J. Abraham, A. J. Leo, *Proteins Struct. Funct. Genet.* **1987**, 2, 130.
- [33] S. Mine, T. Ueda, Y. Hashimoto, Y. Tanaka, T. Imoto, *FEBS Lett.* **1999**, 448, 33.
- [34] S. Mine, S. Tate, T. Ueda, M. Kainosho, T. Imoto, *J. Mol. Biol.* **1999**, 286, 1547.
- [35] R. L. Heinrikson, *J. Biol. Chem.* **1971**, 246, 4090.
- [36] C. A. Rohl, R. L. Baldwin, *Biochemistry* **1997**, 36, 8435.
- [37] P. K. Glasoe, F. A. Long, *J. Phys. Chem.* **1960**, 64, 188.
- [38] D. H. Wu, A. D. Chen, C. S. Johnson, *J. Magn. Reson. Ser. A* **1995**, 115, 260.
- [39] J. A. Jones, D. K. Wilkins, L. J. Smith, C. M. Dobson, *J. Biomol. NMR* **1997**, 10, 199.
- [40] J. Garcia De La Torre, M. L. Huertas, B. Carrasco, *Biophys. J.* **2000**, 78, 719.

Nanoporous Films

Synthesis of a Large-Scale Highly Ordered Porous Carbon Film by Self-Assembly of Block Copolymers**

Chengdu Liang, Kunlun Hong, Georges A. Guiochon, Jimmy W. Mays, and Sheng Dai*

Elemental carbon materials exhibit unique electronic, mechanical, and chemical properties that make them attractive, for example, for nanoelectronic devices,^[1] strength-enhancing materials,^[2] separation media,^[3–6] catalyst supports,^[7] energy storage/conversion systems,^[8] proximal probes,^[9] optical components.^[10] Well-defined nanoporous carbon materials are essential for a number of these

applications. Ordered porous carbon materials have previously been replicated by using colloidal crystals^[10] and presynthesized mesoporous silicas as scaffolds.^[7] These methodologies are extremely difficult to adapt to the fabrication of large-scale ordered nanoporous films with controlled pore orientations. Although numerous methods (e.g., chemical vapor deposition,^[11] ultrasonic deposition,^[3a] silica template synthesis,^[3b,7] hydrothermal decomposition of carbide compounds,^[12] and polymer coating and pyrolysis^[13]) have been developed for the fabrication of carbon films, no ordered nanoporous carbon films have been obtained with such methods. Accordingly, the large-scale alignment of the carbon nanostructural films is still a big challenge. Herein, we demonstrate a stepwise self-assembly approach to the preparation of large-scale, highly ordered nanoporous carbon films. The carbon precursor molecules are spatially arranged into well-defined nanostructures by the self-assembly of block copolymers (BCPs). A hexagonally packed carbon-channel array whose orientation is normal to the carbon film surface has been successfully synthesized. Large-scale crack-free carbon films of up to 6 cm² can be readily fabricated on common substrates such as silica, copper, silicon, and carbon.

The self-assembly of BCPs has proven to be a versatile approach to the selective organization and nanoscale regulation of the concentration distribution of target molecular species for the fabrication of nanoporous materials.^[14–16] The mechanism for such organization involves hydrogen-bonding,^[17] ion-pairing,^[18] and/or dative interactions^[19] between supramolecular assemblies of BCPs and target molecular species. The resulting composites can give rise to various nanostructures according to the structural and phase behaviors of the BCPs. The target molecular species are spatially concentrated in selected microdomains and can eventually serve as nanostructured catalysts,^[20] spacers,^[21] or precursors^[22] for the further fabrication of ordered nanostructures. Highly ordered nanoporous materials, such as polymer,^[22] silica,^[23,24] and organic–inorganic hybrid materials,^[25,26] have been created through polymerization in the presence of the self-assembled BCPs.

Although BCPs contain high atomic carbon concentrations, ordered nanoporous carbon films have not been successfully fabricated through the direct pyrolysis of self-assembled BCPs.^[27] This inability is attributed to the fact that linearly structured BCP compounds have very poor carbon yields in carbonization reactions. Furthermore, the survival of the nanostructures during high-temperature pyrolysis (> 800 °C) is extremely challenging for the self-assembled BCP structures. This deficiency is associated with the linearly structured BCPs, which melt before carbonization reactions occur. The cross-linking of BCPs can significantly stabilize the self-assembled nanostructures. However, it is still difficult for the limited cross-linkage to preserve the preorganized nanostructures, because of the massive loss of carbon in the form of volatile carbon-containing species during pyrolysis.

Highly cross-linked resorcinol–formaldehyde resin (RFR) is a well-known carbonization source.^[6,10] This rigid polymeric carbon precursor can retain the preorganized structures during pyrolysis. However, the low solubility of the highly cross-linked RFR in solvents makes it impossible to directly

[*] C. Liang, Dr. K. Hong, Dr. S. Dai
Chemical Sciences Division, Oak Ridge National Laboratory
Oak Ridge, TN 37831-6201 (USA)
Fax: (+1) 865-576-5235
E-mail: dais@ornl.gov

Prof. G. A. Guiochon, Prof. J. W. Mays
Department of Chemistry, The University of Tennessee
Knoxville, TN 37996-1600 (USA)

[**] This work was performed at the Oak Ridge National Laboratory and supported by the Office of Basic Energy Sciences, U.S. Department of Energy, under contract No. DE-AC05-00OR22725 with UT-Battelle, LLC. We thank Dr. A. C. Buchanan (ORNL) for helpful suggestions, and C.L. thanks TAML for the fellowship.

Supporting information for this article is available on the WWW under <http://www.angewandte.org> or from the author.

blend RFR with BCPs for the formation of nanostructured RFR. To overcome this limitation, we developed a stepwise assembly approach to fabricate highly ordered nanoporous carbon films. The essence of this methodology is to first preorganize the resorcinol monomers into a well-ordered nanostructured film with the assistance of polystyrene-*block*-poly(4-vinylpyridine) (PS-P4VP) self-assembly and solvent-induced structural annealing, which is followed by the in situ polymerization of the resorcinol monomers with formaldehyde vapor to form ordered nanostructured RFR. Upon carbonization, the nanostructured RFR is transformed into a highly ordered nanoporous carbon film with the concomitant decomposition of the PS-P4VP template to gaseous species. Figure 1 schematically illustrates the procedure for the

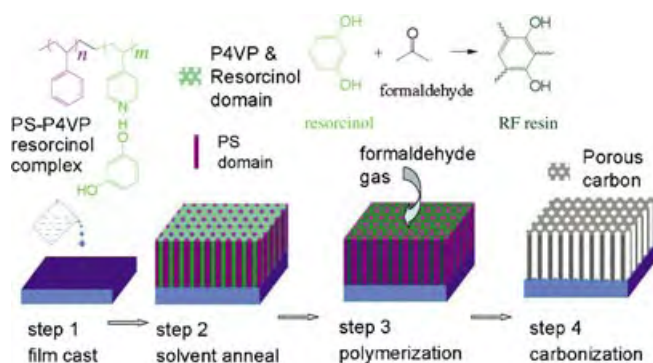


Figure 1. Schematic representation of the synthesis protocol used to prepare well-defined carbon nanostructures. Step 1: film casting of PS-P4VP/resorcinol supramolecular assembly. Step 2: completion of microphase separation by solvent annealing at 80°C in DMF/benzene mixed vapor. The resorcinol is organized in the well-defined P4VP domain. Step 3: in situ polymerization of resorcinol and formaldehyde by exposing the film to formaldehyde gas. Highly cross-linked RFR is formed within the P4VP domain. Step 4: pyrolysis of the polymeric film in N₂. A hexagonal carbon-channel array is formed by sacrificing the block copolymer.

fabrication of ordered porous carbon films. The synthesis protocol involves four basic steps: 1) monomer-BCP film casting, 2) structure refining through solvent annealing, 3) polymerization of the carbon precursor, and 4) carbonization.

In step 1, the precursor films can be cast from a solution containing a mixture of PS-P4VP and resorcinol onto silica, silicon, glassy carbon, or copper, which can withstand the high temperature required by the final carbonization step. Both *N,N'*-dimethylformamide (DMF) and cyclohexanol are good solvents for PS-P4VP and can be used to cast the precursor films. The concentration of PS-P4VP is in the range of 0.5–10 wt %. The final film structures are not dependent on the casting method (dip coating or spin coating). The BCP template used in the synthesis has equal lengths of PS and P4VP blocks. The bulk material of this PS-P4VP copolymer has a lamellar structure.^[15] The self-assembly of the PS-P4VP/resorcinol mixture is essentially driven by the hydrogen-bonding interaction between resorcinol and the P4VP block.^[21,28] This strong hydrogen-bond association between the basic P4VP blocks and the acidic resorcinol monomers enriches the resorcinol molecules selectively in the P4VP

domain. Accordingly, the volume fraction of the P4VP domain is significantly increased relative to that of the PS domain, resulting in a hexagonal structure.^[15,21] The PS block in the PS-P4VP/resorcinol complex is the minor component, which forms cylindrical microdomains in the self-assembled film. Figure 2 compares the Fourier-transform infrared

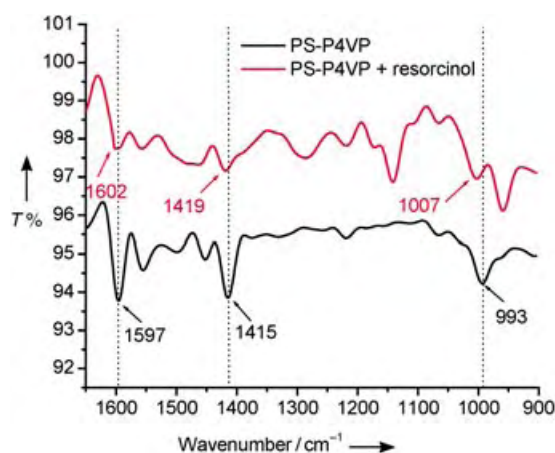


Figure 2. FTIR spectra of PS-P4VP and PS-P4VP/resorcinol mixture in the region from 900 to 1650 cm⁻¹. The characteristic peaks of the pyridine ring in PS-P4VP at 993, 1415, and 1597 cm⁻¹ shift to 1007, 1419, and 1602 cm⁻¹, respectively, as a result of the hydrogen-bonding interaction with resorcinol. T = transmittance.

(FTIR) spectrum of PS-P4VP and that of the PS-P4VP/resorcinol mixture (molar ratio of pyridine groups to resorcinol 1:1). The characteristic stretching modes of the P4VP block at 993, 1415, and 1597 cm⁻¹ shift to 1007, 1419, and 1602 cm⁻¹, respectively, for the PS-P4VP/resorcinol mixture. These vibrational frequency shifts are consistent with a hydrogen-bonding interaction between the pyridine groups and the resorcinol molecules.^[28]

The second step involves solvent annealing,^[21,29] which is the key to the formation of highly ordered and well-oriented nanostructures. Russell and co-workers reported an efficient method based on solvent annealing for refining self-assembled block copolymer nanostructures.^[29] The controlled evaporation of the solvent results in highly ordered nanostructures oriented normal to the substrate. The as-cast film is annealed in DMF/benzene vapor at 80°C through a slow evaporation of the solvents over a period of 24 h, to give a final carbon film having a highly ordered hexagonal structure with all pores oriented perpendicular to the substrate. DMF is a highly miscible solvent for the PS and P4VP blocks, and both blocks have quite good mobility when the film is swollen in DMF vapor. As a result of this mobility, the swollen PS and P4VP blocks repel one another and tend to organize into a well-defined structure.^[29] However, the repulsion of these two blocks is damped by DMF, which is highly miscible with both blocks. We found that the addition of benzene vapor greatly accelerates the self-assembly process and significantly enhances the order of the film.^[29] Benzene is a good solvent only for the PS block, so the absorbed benzene vapor is most likely enriched in the PS block domain. Therefore, the repulsion

between the PS and P4VP domains is enhanced by benzene. A fast microphase separation is thus achieved in the DMF/benzene mixed vapor.

In step 3, the solvent-annealed nanostructured film was exposed to formaldehyde vapor to cross-link the resorcinol molecules into a highly cross-linked phenolic resin located in the P4VP domain. The cross-linking was carried out by vapor/solid reactions with minimum perturbation of the self-assembled nanostructures. The reaction rate can be readily controlled by the vapor pressure of formaldehyde.

The final step involves the decomposition of the BCP template to generate ordered nanopores, and the carbonization of the nanostructured RFR to form the carbon pore walls. This pyrolysis process was studied by using thermogravimetric analysis (TGA) to continuously measure the mass loss upon heating from room temperature to 800 °C under argon at 20 °C min⁻¹. Figure 3 shows the thermograms (TGs)

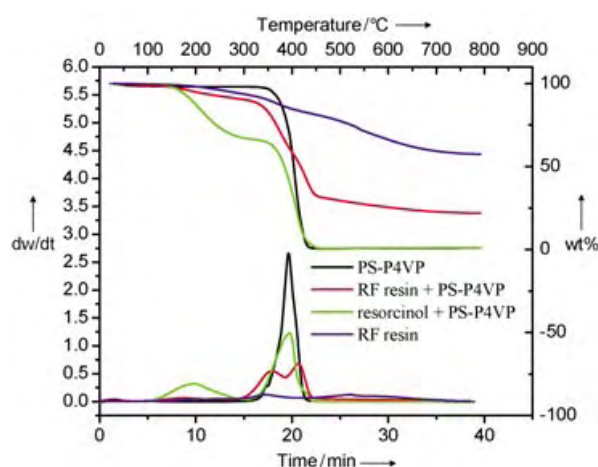


Figure 3. TGA and dTG curves for PS-*block*-P4VP (black), PS-*block*-P4VP/resorcinol mixture (molar ratio of pyridine groups to resorcinol 1:1) (green), resorcinol–formaldehyde resin (RFR) (blue), and PS-*block*-P4VP plus RFR (red). The top and right-hand axes are the temperature and wt% for the thermogram (TG). The left-hand and bottom axes show the weight loss rate and time for the derivative thermogram (dTG).

and the derivative thermograms (dTGs) of four samples: PS-P4VP, PS-P4VP/resorcinol mixture, RFR, and PS-P4VP plus RFR. The pure PS-P4VP sample starts to decompose at 328 °C and finishes at 430 °C with only negligible residue (0.7 wt %). Both the decomposition temperature and the reaction rate of the PS and P4VP blocks are too close to be resolved in the TG and dTG curves. Therefore, the pyrolysis of PS-P4VP exhibits only one peak in the dTG curve of the pure PS-P4VP sample. The TG curve of the PS-P4VP/resorcinol mixture has two weight-loss stages with corresponding dTG peaks at 195 and 392 °C. The weight loss for the first stage starts at 120 °C, which is only 10 °C above the melting point of resorcinol. The first weight-loss stage ends at 284 °C with the loss of about 34 wt %. The mixture of PS-P4VP and resorcinol has 33.87 wt % of resorcinol. Accordingly, this weight loss in the TG curve indicates that all the resorcinol molecules evaporated before the temperature

reached 284 °C. The second weight-loss stage of the PS-P4VP/resorcinol mixture starts at 328 °C and ends at 430 °C. This part of the weight loss is attributed to the decomposition of the PS-P4VP copolymer. The TGA curve of the RFR sample exhibits a continuous weight loss from 200 to 750 °C. The carbonization yield for pyrolysis of RFR is 57.59 wt %. The TGA curve of the PS-*block*-P4VP and RFR sample, prepared by cross-linking the PS-P4VP/resorcinol mixture using formaldehyde vapor, shows a complex pyrolysis behavior. A significant weight loss was found in the range of 200 to 750 °C. The major weight loss occurs from 320 to 430 °C, which is attributed to the decomposition of the PS-P4VP copolymer. The two dTG peaks emerge in this zone, which indicates two different types of decomposition behavior. Comparison of these peaks with the dTG peak of the pure PS-P4VP suggests that the RFR affects the pyrolysis of the PS-P4VP. The decomposition of the PS domain is the least affected, as the RFR is localized in the P4VP domain. The P4VP chain is tangled with the RFR; as a result, the decomposition rate of P4VP may be retarded by RFR because of the interaction between RFR and P4VP. Therefore, the P4VP block may decompose after the PS block. The pyrolysis of the PS-P4VP/RFR mixture yields 22.16 % carbon at 800 °C. After taking into account the weight gain in the polymerization with formaldehyde, the weight percentage of the RFR in the PS-P4VP/RFR mixture rises from 33.87 % (resorcinol wt % in PS-P4VP/resorcinol mixture) to 37.34 %. If one assumes that RFR in the P4VP domain has the same carbon yields as the pure RFR (57.59 %), the PS-P4VP part only accounts for 1.05 wt % carbon in the final product. Clearly, the RFR is the predominant carbon source of the porous carbon film and the BCP is sacrificed as pores.

A crack-free nanoporous carbon film with thickness from several tens of nanometers up to ~1 μm and size up to 6 cm² can be obtained. The nanoporous carbon film strongly adheres to substrates and is homogeneous in thickness. The nanopores are oriented perpendicular to the film surface (Figure 4a,d). An enlarged Z-contrast image of the carbon film is shown in Figure 4b. The Fourier transform of this Z-contrast image of the film shows a pattern of multiple reflections, which confirms that the film has a highly ordered hexagonal-pore array. Based on Figure 4c, the pore diameter is 33.7 ± 2.5 nm and the wall thickness is 9.0 ± 1.1 nm. The volume fraction of the straight channels is about 0.565 (see Supporting Information for details). The pore diameter and thickness can be controlled by the volume fractions of PS in BCP and carbon-forming resin, respectively. The cross section of the film scratched from a film substrate is shown in Figure 4d. All straight channels are across the whole film. The inset in the lower right-hand corner is the Fourier transform of the high-resolution scanning electron microscopy (SEM) image of the film cross section, which reflects parallel periodical channels. No graphitic structure was found in the high-resolution transmission electron microscopy (HRTEM) mode, which suggests that the wall is amorphous carbon. Wide-angle X-ray diffraction (WAXD) shows broad peaks at 23.6, 43.76, and 80.24°, which are characteristic of amorphous carbon. The Raman spectrum shows a broad D band at 1333 cm⁻¹, which overlaps with the G band at 1600 cm⁻¹. Such

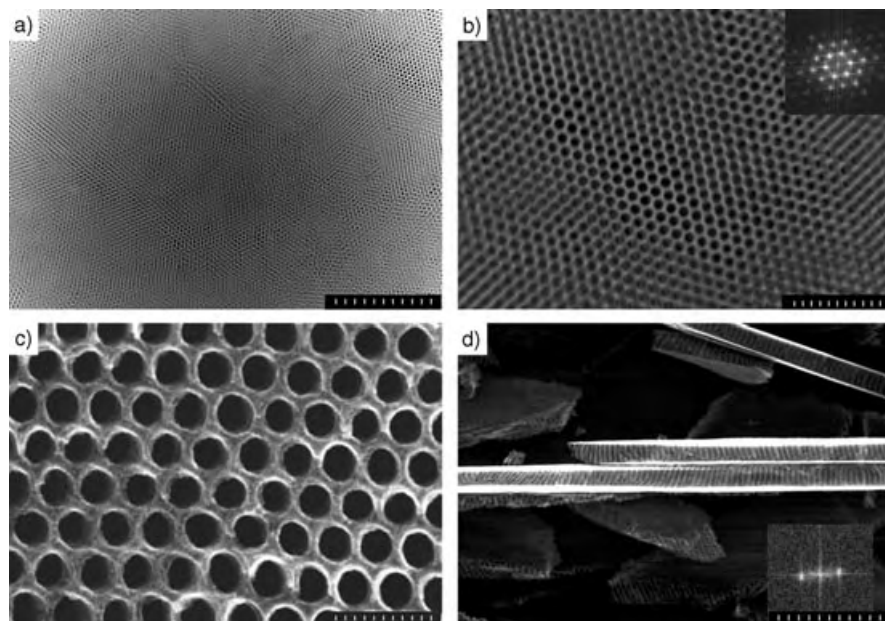


Figure 4. Electron microscopy images of the carbon film. a) Z-contrast image of the large-scale homogeneous carbon film in a $4 \times 3 \mu\text{m}$ area. The scale bar is $1 \mu\text{m}$. b) Z-contrast image showing details of the highly ordered carbon structure. In the inset, a Fourier transform (FT) of the image shows a pattern with multiple reflections, which are characteristic of a highly ordered hexagonal array. The scale bar is 300 nm . c) High-resolution SEM image of the surface of the carbon film with uniform hexagonal-pore array. The pore size is $33.7 \pm 2.5 \text{ nm}$ and the wall thickness is $9.0 \pm 1.1 \text{ nm}$. The scale bar is 100 nm . d) SEM image of the film cross section, which exhibits all parallel straight channels perpendicular to the film surface. The scale bar is 100 nm . The inset is the FT of the cross section image. The FT pattern shows the reflections of the periodic parallel channels.

a broad D band is reminiscent of the glassy carbon texture. The HRTEM image, WAXD pattern, and Raman spectrum are included in the Supporting Information.

In conclusion, a facile methodology based on stepwise self-assembly has been successfully developed to prepare highly ordered and well-oriented mesoporous carbon films through carbonization of a nanostructured phenolic resin and BCP composite. The BCPs play two important roles in the synthesis: 1) directing the formation of the phenolic resin nanostructure and 2) serving as templates for nanopores. The orientation of the ordered carbon nanopores was successfully aligned normal to the substrates using a solvent annealing process. The unique structural feature of this oriented nanoporous carbon film highlights opportunities in areas such as separation membranes, chemical sensors, and catalysts.

Experimental Section

PS-P4VP (0.1 g)—with number average molecular masses (M_n) of $11\,800 \text{ g mol}^{-1}$ for PS and $11\,500 \text{ g mol}^{-1}$ for P4VP, and M_w/M_n of 1.04 for both blocks—and resorcinol (0.0512 g) were dissolved in DMF (2 g). This solution was heated at 100°C for 4 h to ensure the formation of hydrogen bonds. After cooling to room temperature, a drop of solution was cast into a film on a silica plate by spin coating at 1000 rpm for 2 min. The film was dried in a hood, then placed in a preheated chamber at 80°C along with two small vials which contained DMF and benzene. The film was kept in the sealed chamber for 24 h to allow the completion of microphase separation by

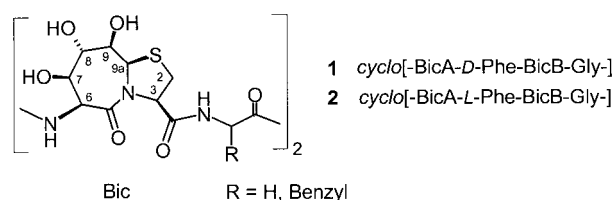
a slow evaporation of the solvents. The microphase-separated film was sequentially cured by exposure to formaldehyde gas at 100°C for 4 h. The cured film was finally carbonized in nitrogen using a temperature ramp of 1°C min^{-1} to 800°C .

Received: June 23, 2004

Keywords: block copolymers · carbon · mesoporous materials · nanostructures · self-assembly

- [1] T. Rueckes, K. Kim, E. Joselevich, G. Y. Tseng, C. L. Cheung, C. M. Lieber, *Science* **2000**, *289*, 94–97.
- [2] L. S. Schadler, S. C. Giannaris, P. M. Ajayan, *Appl. Phys. Lett.* **1998**, *73*, 3842–3844.
- [3] a) M. B. Shiflett, H. C. Foley, *Science* **1999**, *285*, 1902–1905; b) J. Pang, X. Li, D. Wang, Z. Wu, V. T. John, Z. Yang, Y. F. Lu, *Adv. Mater.* **2004**, *16*, 884–886.
- [4] B. J. Hinds, N. Chopra, T. Rantell, R. Andrews, V. Gavalas, L. G. Bachas, *Science* **2004**, *303*, 62–65.
- [5] S. A. Miller, V. Y. Young, C. R. Martin, *J. Am. Chem. Soc.* **2001**, *123*, 12335–12342.
- [6] C. D. Liang, S. Dai, G. A. Guiochon, *Anal. Chem.* **2003**, *75*, 4904–4912.
- [7] S. H. Joo, S. J. Choi, I. Oh, J. Kwak, Z. Liu, O. Terasaki, R. Ryoo, *Nature* **2001**, *412*, 169–172.
- [8] A. C. Dillon, K. M. Jones, T. A. Bekkedahl, C. H. Kiang, D. S. Bethune, M. J. Heben, *Nature* **1997**, *386*, 377–379.
- [9] H. J. Dai, J. H. Hafner, A. G. Rinzier, D. T. Colbert, R. E. Smalley, *Nature* **1996**, *384*, 147–150.
- [10] A. A. Zakhidov, R. H. Baughman, Z. Iqbal, C. X. Cui, I. Khayrullin, S. O. Dantas, I. Marti, V. G. Ralchenko, *Science* **1998**, *282*, 897–901.
- [11] K. H. Kwok, W. K. S. Chiu, *Carbon* **2003**, *41*, 673–680.
- [12] Y. G. Gogotsi, M. Yoshimura, *Nature* **1994**, *367*, 628–630.
- [13] A. Singh, J. Jayaram, M. Madou, S. Akbar, *J. Electrochem. Soc.* **2002**, *149*, E78–E83.
- [14] E. Huang, L. Rockford, T. P. Russell, C. J. Hawker, *Nature* **1998**, *395*, 757–758.
- [15] S. Jain, F. S. Bates, *Science* **2003**, *300*, 460–464.
- [16] M. Park, C. Harrison, P. M. Chaikin, R. A. Register, D. H. Adamson, *Science* **1997**, *276*, 1401–1404.
- [17] J. Ruokolainen, R. Mäkinen, M. Torkkeli, T. Makela, R. Serimaa, G. ten Brinke, O. Ikkala, *Science* **1998**, *280*, 557–560.
- [18] R. T. Clay, R. E. Cohen, *Supramol. Sci.* **1998**, *5*, 41–48.
- [19] M. Antonietti, E. Wenz, L. Bronstein, M. Seregina, *Adv. Mater.* **1995**, *7*, 1000.
- [20] R. A. Pai, R. Humayun, M. T. Schulberg, A. Sengupta, J. N. Sun, J. J. Watkins, *Science* **2004**, *303*, 507–510.
- [21] A. Sidorenko, I. Tokarev, S. Minko, M. Stamm, *J. Am. Chem. Soc.* **2003**, *125*, 12211–12216.
- [22] U. Y. Jeong, D. Y. Ryu, J. K. Kim, D. H. Kim, T. P. Russell, C. J. Hawker, *Adv. Mater.* **2003**, *15*, 1247–1250.
- [23] D. Y. Zhao, J. L. Feng, Q. S. Huo, N. Melosh, G. H. Fredrickson, B. F. Chmelka, G. D. Stucky, *Science* **1998**, *279*, 548–552.
- [24] X. Feng, G. E. Fryxell, L. Q. Wang, A. Y. Kim, J. Liu, K. M. Kemner, *Science* **1997**, *276*, 923–926.
- [25] Z. T. Zhang, S. Dai, *J. Am. Chem. Soc.* **2001**, *123*, 9204–9205.

- [26] Y. F. Lu, Y. Yang, A. Sellinger, M. C. Lu, J. M. Huang, H. Y. Fan, R. Haddad, G. Lopez, A. R. Burns, D. Y. Sasaki, J. Shelnutt, C. J. Brinker, *Nature* **2001**, *410*, 913–917.
- [27] T. Kowalewski, N. V. Tsarevsky, K. Matyjaszewski, *J. Am. Chem. Soc.* **2002**, *124*, 10632–10633.
- [28] O. T. Ikkala, J. Ruokolainen, G. ten Brinke, M. Torkkeli, R. Serimaa, *Macromolecules* **1995**, *28*, 7088–7094.
- [29] S. H. Kim, M. J. Misner, T. Xu, M. Kimura, T. P. Russell, *Adv. Mater.* **2004**, *16*, 226–231.



In a first approximation, cyclic hexapeptides can be regarded as the antiparallel combination of two β turns (Figure 1 a) or two tripeptides (Figure 1 b).^[3] This differentia-

Peptidomimetics



Coupled Hydrogen-Bonding Networks in Polyhydroxylated Peptides**

Peter Tremmel and Armin Geyer*

In memory of Murray Goodman

The active sites of proteins contain networks of hydrogen bonds which are functionally coupled to perform the enzyme function.^[1] The side chains of short peptides cannot align in comparable microenvironments because they are too flexible to form more than transient hydrogen bonds. Dipeptides which are highly decorated with ring-constrained hydrogen-bond donors and acceptors can be assembled to oligocyclic peptidomimetics which are then confined to only a few modes of flexibility. Two such peptides are presented herein which have stable hydrogen-bonding networks involving several side-chain hydroxy groups and backbone amide groups. The side-chain hydroxy groups are pushed against each other to cooperatively align in a chain of hydrogen bonds bridging two backbone amide groups which are 7 Å apart. The inversion of the chirality of a single amino acid results in a flip of the entire hydrogen-bonding network with an exchange of proton donor and acceptor groups. Both peptides are characterized by crystal structures and by NMR spectroscopy. The conformational homogeneity and the existence of a hydrogen-bonding network in solution is corroborated by the dispersion of NMR spectroscopic data.

The synthesis of the bicyclic dipeptide (Bic) starting from D-glucurono-3,6-lactone was described recently.^[2] C-terminal coupling with L-Phe, D-Phe, or Gly yielded three tripeptides which were coupled to hexapeptides and finally cyclized to either **1** or **2**.

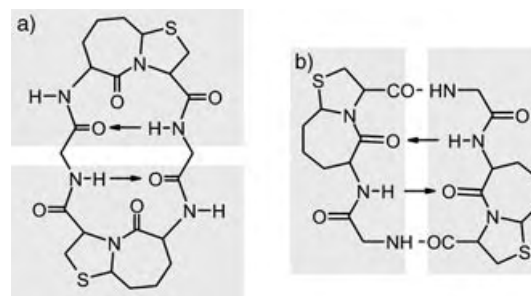


Figure 1. Schematic representations of two possible conformations of C_2 -symmetric cyclic hexapeptides with arrows indicating antiparallel hydrogen bonds of the central mini β sheet. The 7,5-bicyclic dipeptide mimetics can occupy the central $i+1$ and $i+2$ positions of the β turns (a) or occupy the i and $i+1$ positions (b).

tion makes sense when asking for the preferred positions of bicyclic dipeptides in a cyclic hexapeptide. The dipeptide can end up either in the central positions of the β turn as traditionally proposed for so-called β -turn mimics^[4] or in the long side of the antiparallel mini β sheet. Crystal structures of the β -turn dipeptide (BTD)^[4b] or of analogues^[5c] are known but no crystal structures of unprotected oligopeptides containing bicyclic dipeptides are published to date. The concept of β -turn mimics was challenged by detailed experimental analyses^[5] and modeling studies^[6] and therefore the more general label bicyclic dipeptide mimetics is used herein. Oligomers of Bic assume an extended polyproline-II-helical structure^[2c] indicating that Bic will prefer the long side of a cyclic hexapeptide (Figure 1 b) irrespective of the chiralities of the other amino acids.

The crystals of cyclopeptides **1** and of **2** show an overall C_2 -symmetric rectangular backbone structure with Bic occupying the i to $i+1$ positions of β I and β II turns, respectively (Figure 2).^[7] Thus, **1** and **2** fit the general structure of Figure 1 b. In peptide **1**, D-Phe is found in the $i+2$ position of β II turn and Gly in the $i+2$ position of a β I turn. Although only one out of 13 stereocenters was changed in peptide **2**, a mirrored backbone structure is observed with L-Phe occupying the $i+2$ position of a β I turn while Gly is found in the $i+2$ position of β II turn. Four side chain hydroxy groups (7-OH and 9-OH of BicA and BicB) are in close contact in each cyclopeptide. They are aligned in a zipperlike fashion forming a chain of hydrogen bonds connecting the two central amide bonds of the β turns. The inversion of the chirality of the Phe

[*] Dipl.-Chem. P. Tremmel, Prof. Dr. A. Geyer
Fachbereich Chemie
Philipps-Universität Marburg
35032 Marburg (Germany)
Fax: (+49) 6421-2822021
E-mail: geyer@staff.uni-marburg.de

[**] This work was supported by the Deutsche Forschungsgemeinschaft and the Fonds der Chemischen Industrie. The authors thank Dr. Manfred Zabel (Fakultät Chemie, Universität Regensburg) for the X-ray analysis of **1** and **2**.

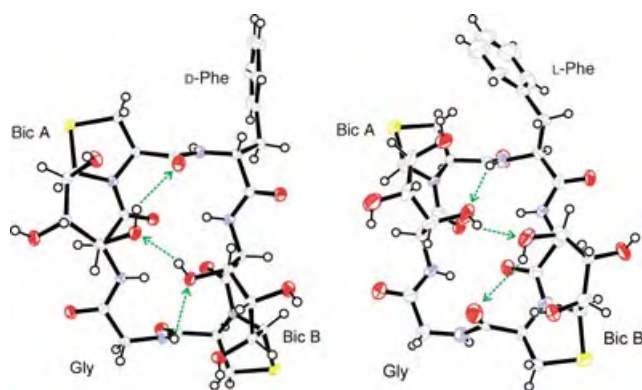


Figure 2. Crystal structures of peptides **1** (left) and **2** (right). Green arrows indicate the chains of intramolecular hydrogen bonds connecting the central amide bonds of the two β turns (red O, blue N, yellow S).^[7,9]

residue is accompanied by an 180° flip of the neighboring amide bond between BicA and L-Phe. As a consequence, the two cyclopeptides exhibit a reversed hydrogen-bonding network with exchanged donor and acceptor groups. Several water molecules and many intermolecular hydrogen bonds are found in both crystals.^[7] To separate potential influences of the crystal environment on the peptide conformations, **1** and **2** were investigated in isotropic solution, too.

In both peptides, the two hydrogen bonds spanning the antiparallel mini β sheet (BicA-6NH-BicB-5CO and BicB-6NH-BicA-5CO) are protected from chemical exchange and therefore no cross-peaks between the two NH protons and the water signal are detectable in the expansion from the ROESY spectrum of **1** (Figure 3).^[8] All residual protons are accessible to water. The mini β sheet is retained in the organic solvent [D₆]DMSO, as shown by the temperature dependence of the ¹H NMR spectroscopy chemical shifts ($\Delta\delta/\Delta T$) of the amide protons. They are close to zero for the amide protons involved in hydrogen bonds 1BicA-6NH (+0.2 ppb/K),

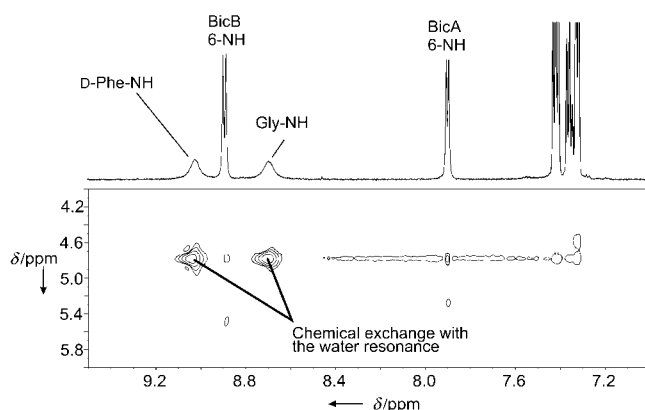


Figure 3. ROESY spectrum (watergate, 600 MHz, 300 K, H₂O/D₂O, 10:1). Expansion of the NH region. All the protons of the hydrogen-bonding network are exchange broadened at room temperature. Both 6NH protons are protected from chemical exchange and therefore no cross-peaks with the solvent signal are observed. D-PheNH and Gly-NH are solvent accessible and show intense cross-signals with water together with chemical exchange broadening.

1BicB-NH (−1.3 ppb/K), 1Gly-NH (−0.6 ppb/K), 2BicA-6NH (−1.0 ppb/K), 2BicB-NH (−0.1 ppb/K), and 2Phe-NH (−0.5 ppb/K). They are significantly larger for the residual amide protons 1Phe-NH (−5.7 ppb/K) and 2Gly-NH (−4.1 ppb/K). Similar to the crystal structures, the exchange of the *i* + 2 amino acid D-Phe against L-Phe is accompanied by a 180° flip of the amide bond preceding this amino acid. Rotating-frame NOEs and ³*J* coupling constants unequivocally identify the main backbone conformations of **1** and of **2** which match the crystal structures. Even the preferred side-chain rotamers of L-Phe and D-Phe in solution are the same as in the crystals, as determined from the ³*J*_{H α ,H β} coupling constants. Hydrophobic stacking between the aromatic side chain and the neighboring thiaproline ring may contribute to stabilize the observed rotamers.

The organic solvent [D₆]DMSO slows down chemical exchange and therefore the ¹H NMR spectroscopy resonance signals of the hydroxy protons are better resolved than in water. As a consequence, even ⁴*J* couplings become observable for **1**: ⁴*J*_{7-OH,6-CH} = 1.4 Hz in BicA and ⁴*J*_{9-OH,9a-CH} = 1.0 Hz in BicB. ⁴*J*_{H,H} long-range couplings are immediately lost upon deviation from the fixed W-arrangement of the four atoms involved and therefore ⁴*J*_{H,H} long-range couplings can be regarded as another indicator of conformational homogeneity. The δ_H chemical shifts, the ³*J* coupling constants, the rotating-frame NOEs, the temperature gradients ($\Delta\delta_H/\Delta T$) of the 7-OH, 9-OH, and NH protons distinguish the network of hydrogen bonds of **1** from that of **2**. Differences between crystal structure and solution structure are detected for the 9-OH moiety of BicA in **1** which forms an intermolecular hydrogen bond in the crystal but finds a different proton acceptor in solution. The ³*J*_{9-CH,OH} coupling constant of 12.4 Hz identifies the inward orientation of BicA 9-OH towards the central carbonyl group of the β II turn. This type of hydrogen bond has been observed in the linear oligomers of Bic.^[2c] Two views of **1** from opposite directions showing all relevant hydrogen-bonding contacts are given in Figure 4. Clearly, all four 7-OH and 9-OH hydroxy groups and two amides are linked by hydrogen bonds and polar contacts in solution. The solution structure of **2** resembles its crystal structure with BicB 7-OH group donating a proton to the carbonyl of the β II-turn and BicA 7-OH accepting a proton from the NH of the β I-turn. Conformational averaging can be excluded for both cyclic hexapeptides in water and in [D₆]DMSO solution, too. Diastereomers **1** and **2** differ in only a single stereocenter but exhibit remarkably stable and significantly different conformations. The overall C₂ symmetry of the cyclic hexapeptides **1** and **2** is broken by the benzyl side chains of the phenylalanines, a minor disturbance which locks the overall conformations through the alignment of all amide and OH groups except for the 8-OH groups which are directed outwards (Figure 2; the numbering of the OH groups corresponds to the numbering of the carbon atoms to which they are bound, see the formula of Bic).

In conclusion, the crystal structures of bicyclic dipeptide analogues within unprotected oligopeptides are described for the first time. The bicyclic dipeptides can occupy the *i* to *i* + 1 position of either β I or β II turns. The rigidified amino acids derived from sugars are able to form stable hydrogen-bonding

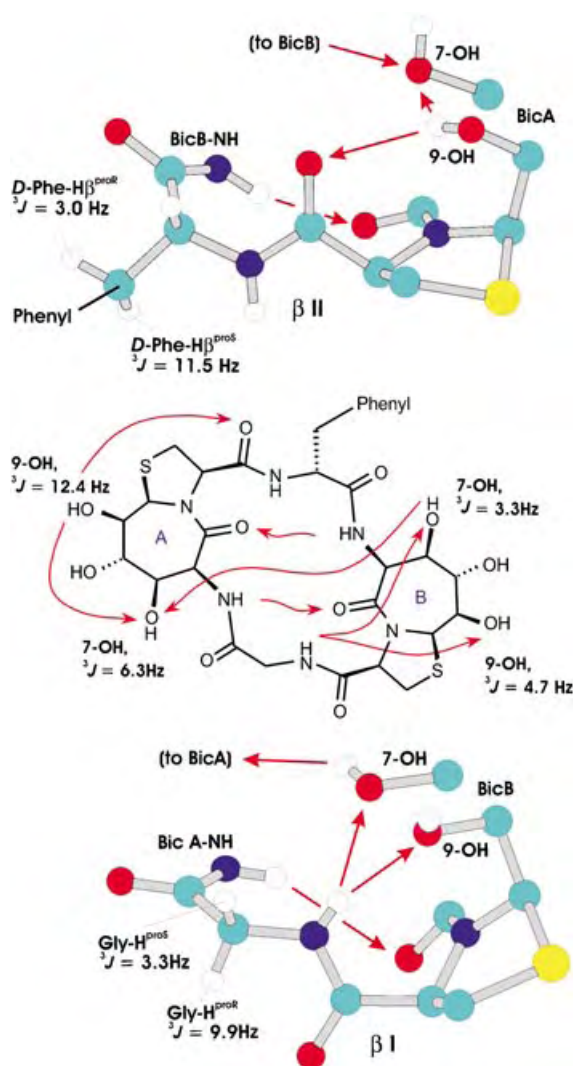


Figure 4. Solution structure of **1** in $[D_6]DMSO$. Two views from opposite directions perpendicular to the central amide bond of each β turn (cyan C, red O, blue N, yellow S). For clarity only selected atom positions are shown. Red arrows indicate hydrogen bonds and polar contacts. The schematic representation in the middle shows the entire hydrogen bonding network. Each of the two bifurcated hydrogen bonds cannot be distinguished from fast averaging between one hydrogen bond together with a polar contact to the second proton acceptor. The model (HyperChem 7.0) is based on NOEs and 3J coupling restraints. The geometry of the two Bic-6NH–Bic-5CO hydrogen bonds was taken from the crystal structure.

networks which can transfer structural information along a chain of ambident proton donors and acceptors over several Å. Extended and functionally coupled hydrogen-bonding networks which can switch between different states play an important role in proteins. The structural diversity of secondary hydroxy groups is characterized by the dispersion of NMR parameters.

Received: June 27, 2004

Published Online: October 25, 2004

Keywords: conformation analysis · hydrogen bonds · NMR spectroscopy · peptides · peptidomimetics

- [1] C. Brandon, J. Tooze, *Introduction to Protein Structure*, Garland Publishing, New York, **1998**.
- [2] a) A. Geyer, D. Bockelmann, K. Weissenbach, H. Fischer, *Tetrahedron Lett.* **1999**, 40, 477–478; b) A. Geyer, F. Moser, *Eur. J. Org. Chem.* **2000**, 1113–1120; c) P. Tremmel, A. Geyer, *J. Am. Chem. Soc.* **2002**, 124, 8548–8549; d) P. Tremmel, J. Brand, V. Knapp, A. Geyer, *Eur. J. Org. Chem.* **2003**, 878–884.
- [3] a) H. Kessler, *Angew. Chem.* **1982**, 94, 509–520; *Angew. Chem. Int. Ed. Engl.* **1982**, 21, 512–523; b) F. Eker, X. Cao, L. Nafie, R. Schweitzer-Stenner, *J. Am. Chem. Soc.* **2002**, 124, 14330–14341.
- [4] a) U. Nagai, K. Sato, *Tetrahedron Lett.* **1985**, 26, 647–650; b) U. Nagai, K. Sato, R. Nakamura, R. Kato, *Tetrahedron* **1993**, 49, 3577–3592; c) J. E. Baldwin, C. Hulme, C. J. Schofield, A. J. Edwards, *J. Chem. Soc. Chem. Commun.* **1993**, 935–936; d) J. A. Robl, C.-Q. Sun, J. Stevenson, D. E. Ryono, L. M. Simpkins, M. P. Cimarusti, *J. Med. Chem.* **1997**, 40, 1570–1577; e) F. Polyak, W. D. Lubell, *J. Org. Chem.* **2001**, 66, 1171–1180.
- [5] a) R. Haubner, W. Schmitt, G. Hoelzemann, S. L. Goodman, A. Jonczyk, H. Kessler, *J. Am. Chem. Soc.* **1996**, 118, 7881–7891; b) L. Belvisi, C. Gennari, A. Mielgo, D. Potenza, C. Scolastico, *Eur. J. Org. Chem.* **1999**, 389–400; c) D. E. Davies, P. M. Doyle, R. D. Farrant, R. D. Hill, P. B. Hitchcock, P. N. Sanderson, D. W. Young, *Tetrahedron Lett.* **2003**, 44, 8887–8891.
- [6] G. Müller, G. Hessler, H. W. Decomez, *Angew. Chem.* **2000**, 112, 926–928; *Angew. Chem. Int. Ed.* **2000**, 39, 894–896.
- [7] CCDC-241421 (**1**) and CCDC-241422 (**2**) contain the supplementary crystallographic data for this paper. These data can be obtained free of charge via www.ccdc.cam.ac.uk/conts/retrieving.html (or from the Cambridge Crystallographic Data Centre, 12 Union Road, Cambridge CB21EZ, UK; fax: (+44) 1223-336-033; or deposit@ccdc.cam.ac.uk).
- [8] A. Bax, D. G. Davis, *J. Magn. Reson.* **1985**, 63, 207–213; b) V. Sklenar, M. Piotto, R. Leppik, V. Saudek, *J. Magn. Reson. Ser. A* **1993**, 102, 241–245.
- [9] The asymmetric unit of **1** contains one cyclopeptide and four water molecules. The asymmetric unit of **2** contains four cyclopeptides and 25 water molecules. The four cyclopeptides of **2** have identical β I, β II arrangements, only one is shown in Figure 2.

Proton Transfer

Asymmetric Double Proton Transfer of Excited 1:1 7-Azaindole/Alcohol Complexes with Anomalously Large and Temperature-Independent Kinetic Isotope Effects**

Oh-Hoon Kwon, Young-Shin Lee, Han Jung Park, Yongho Kim, and Du-Jeon Jang*

Proton transfer has been attracting considerable attention because it plays a key role in a wide variety of biological and chemical processes.^[1–4] Since the discovery of the double-helix structure of DNA by Watson and Crick in 1953, it has been suggested that the tautomerization of DNA base pairs causes inappropriate pairing of bases to result in point mutations. Photo-induced proton transfers are often considered to be useful for understanding the causes of mutagenesis in DNA replication. Thus, proton transfers in the dimers of 7-azaindole (7AI), structurally similar to H-bonded DNA base pairs, have been studied extensively.^[5] 7AI is a chromophoric moiety of 7-azatryptophan, a novel in situ optical probe for the structures and dynamics of proteins.^[6] Metal–7AI complexes are reported to have potential applications in electroluminescent devices.^[7] A number of researchers have shed light on the excited-state double proton transfer (ESDPT) of 7AI, catalyzed by the H-bonded counterpart of a protic solvent molecule or a 7AI molecule in a dimer.^[4–6,8–13]

The mechanism of solvent involvement in the excited-state tautomerization of 7AI in water and alcohols has attracted considerable attention.^[4,6,9–12] In particular, the two-step model described in Scheme 1 has been discussed widely.^[9–11] The first step is solvent reorganization (k_r) about the normal (N) 7AI molecule to form a cyclic H-bonded 1:1 7AI/solvent complex (Nb), and the second step is intrinsic



Scheme 1. The widely discussed ESDPT mechanism of 7AI in alcohols (ROH) and water. In this study Nb is directly photo-generated from the ground state.

[*] Dr. O.-H. Kwon, Y.-S. Lee, H. J. Park, Prof. D.-J. Jang
School of Chemistry, Seoul National University
NS60, Seoul 151-742 (Korea)
Fax: (+82) 2-889-1568
E-mail: djjang@plaza.snu.ac.kr
Prof. Y. Kim
Department of Chemistry, Kyung Hee University
Yongin, Kyunggi 449-701 (Korea)

[**] This work was supported by the Strategic National R&D Program (M1-0214-00-0108). O.H.K. and Y.K. received support from the Brain Korea 21 Program and the Korea Research Foundation (grant 2002-070-C00048), respectively.

proton transfer (k_{pt}) relayed by the complexed protic solvent molecule to give the tautomer (T). Intrinsic proton transfer is often presumed to be very fast and governed by tunneling.^[9c,10] In one limit, solvent reorganization is the rate-limiting step such that the observed rate constant becomes k_r . In the opposite limit when equilibrium (k_r/k_{-r}) between solvent reorganization and solvent randomization (k_{-r}) is rapid relative to k_{pt} , the observed rate constant is independent of solvent dynamics and is expressed as $(k_r/k_{-r})k_{pt}$.^[10] In water and alcohols 7AI has been proposed to undergo ESDPT following the latter scenario.^[9–11] Although 7AI/water complexes formed in aprotic solvents have been suggested to undergo ESDPT as well,^[13a] the intrinsic proton-transfer dynamics of Nb has been rarely studied experimentally and is not well understood.^[12]

Since the unusual catalytic activity of 2-pyridinone in epimerization reactions was found in 1952 by Swain and Brown,^[14] concerted and stepwise motions of protons have been long-standing subjects. Schowen^[4] reviewed this issue to assert that double proton transfer obeys Jencks's principle: if an intermediate along a stepwise route has a very high-energy structure, a transition state with a lower energy can exist for a concerted reaction to occur. The tautomerization of photo-excited 7AI dimers is reported to take place in a stepwise manner in which the zwitterionic intermediate is stabilized by charge delocalization in aromatic rings.^[5b,c] On the other hand, the ESDPT of 7AI in neat water and alcohols was proposed to proceed in a concerted manner.^[16] However, because the ESDPT rates of 7AI in neat protic solvents were revealed later to rely on thermodynamic solvation properties,^[9–11] the harmony and the dissonance of proton motions in Nb deserve revisiting. In this paper, we present the dynamics and the nature of ESDPT initiated by the direct excitation of cyclically H-bonded 1:1 7AI/alcohol complexes at the ground state.

Figure 1 shows that the lowest absorption band of 7AI in *n*-heptane shifts to the red and grows at 310 nm with an increase in the concentration of methanol. The spectral changes imply that 7AI molecules associate with methanol molecules by H-bonding to produce complexes in the non-polar solvent.^[13] The linear Benesi–Hildebrandt plot of the

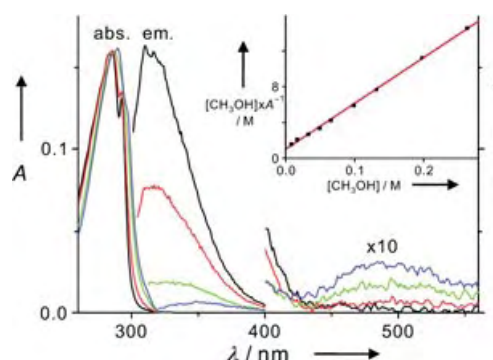


Figure 1. Absorption and emission ($\lambda_{exc}=288$ nm) spectra of 7AI (1.6×10^{-5} M) in *n*-heptane having methanol concentrations of 0 (black), 8.2 (red), 33 (green), and 260 mM (blue). Inset: the Benesi–Hildebrandt plot ($\lambda_{abs}=310$ nm) yields 50 M^{-1} for the association constant of 7AI with methanol to form Nb at 19 °C.

inset in Figure 1 indicates that 7AI and methanol molecules form 1:1 complexes in *n*-heptane with an association constant (K_a) of 50 M^{-1} .^[5a] Compared with the K_a values of 7AI dimers ($2.2 \times 10^3\text{ M}^{-1}$) and 1:1 7AI/acetic acid complexes ($1.8 \times 10^4\text{ M}^{-1}$) in nonpolar media,^[13b] the K_a of 7AI/methanol complexes is quite small, implying that the hydrogen bonds of the complexes at the ground state are not strong owing to the relatively weaker H-bonding ability of methanol. The structures of ground-state H-bonded complexes with single methanol molecules in nonpolar solvents have been simulated to predict that **Nb** is a cyclic 1:1 complex having reasonably loose hydrogen bonds, especially between the pyridinic nitrogen of 7AI and the protic hydrogen of methanol ($\text{N}\cdots\text{H}-\text{O}$).^[9c,11]

Only the UV emission at 315 nm from **N** monomers appears in the absence of methanol. However, with methanol addition, the UV fluorescence shifts to 350 nm and decreases with the concomitantly growing fluorescence at 500 nm from **T**.^[5a,13] Thus, we attribute the UV emission at 350 nm to H-bonded 1:1 complexes. The excitation spectrum of 7AI in *n*-heptane with 260-mm methanol, monitored at 500 nm, is spectrally identical with its lowest absorption band, indicating that both fluorescence bands at 350 and 500 nm originate from the same ground-state species. Therefore, we can infer that excited-state **T** molecules are generated by means of ESDPT from the 1:1 complexes of **Nb**.

The fluorescence at 350 nm of 7AI in *n*-heptane with 67-mm methanol^[17] shows a biexponential decay profile composed of 88 (76 %) and 450 ps (24 %), while the fluorescence at 550 nm rises within 88 ps and decays in 1560 ps (Figure 2).

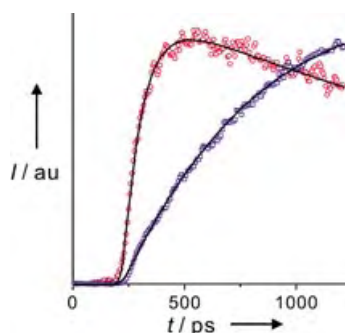


Figure 2. Fluorescence kinetic profiles of 7AI ($1.6 \times 10^{-5}\text{ M}$) in *n*-heptane with $\text{CH}_3\text{O}^1\text{H}$ (red circles) and $\text{CH}_3\text{O}^2\text{H}$ (blue squares) of 67 mm. Samples were excited at 288 nm and kinetic profiles were measured with instrumental response functions (IRF) of 25 ps at 550 nm. The lines fitting the circles and the squares were simulated with the rise time of 88 ps followed by the decay time of 1560 ps and the rise time of 1280 ps followed by the decay time of 1900 ps, respectively.

The rise time is identical with the fast-decay time at 350 nm, indicating that k_{pt} is $(88\text{ ps})^{-1}$.^[18] Quite intriguing is that the k_{pt} of 1:1 complexes isolated in the nonpolar solvent is not as large as the expected values of $\geq (5\text{ ps})^{-1}$.^[9c,10] The slow-decay time at 350 nm is assigned to the fluorescence lifetime of noncomplexed 7AI.^[17]

The ESDPT process of **Nb** occurs by the concerted relay of the two hydrogens through a single transition state or by the stepwise transfer of the two protons by forming a charged

cationic or anionic intermediate. Proton-inventory experiments for the rates of ESDPT by varying the deuteration degree of protic hydrogen atoms in 1:1 7AI/alcohol complexes can give a clue to this issue.^[16] We consider that four possibly different cyclic complexes of $^1\text{H}\cdots\text{N}_7\text{N}_1-^1\text{H}$, $^1\text{H}\cdots\text{N}_7\text{N}_1-^2\text{H}$, $^2\text{H}\cdots\text{N}_7\text{N}_1-^1\text{H}$, and $^2\text{H}\cdots\text{N}_7\text{N}_1-^2\text{H}$ in isotopically mixed systems have the intrinsic rate constants of $k_{\text{pt}}(^1\text{H}^1\text{H})$, $k_{\text{pt}}(^1\text{H}^2\text{H})$, $k_{\text{pt}}(^2\text{H}^1\text{H})$, and $k_{\text{pt}}(^2\text{H}^2\text{H})$, respectively. If $X_D = [\text{protic } ^2\text{H}]/([\text{protic } ^1\text{H}] + [\text{protic } ^2\text{H}])$, then we can deduce Equations (1) and (2).

$$d[^1\text{H}\cdots\text{N}_7]/dt = -\{(1-X_D)k_{\text{pt}}(^1\text{H}^1\text{H}) + X_Dk_{\text{pt}}(^1\text{H}^2\text{H})\}[^1\text{H}\cdots\text{N}_7] \quad (1)$$

$$d[^2\text{H}\cdots\text{N}_7]/dt = -\{(1-X_D)k_{\text{pt}}(^2\text{H}^1\text{H}) + X_Dk_{\text{pt}}(^2\text{H}^2\text{H})\}[^2\text{H}\cdots\text{N}_7] \quad (2)$$

Because the isotope exchange of hydrogen is much slower than ESDPT, we expect that the fluorescence of **T** changes with time following Equation (3).

$$\mathbf{T}(t) = \{1 - A_1 \exp(-k_f t) - A_2 \exp(-k_s t)\} \exp(-t/\tau_d) \quad (3)$$

While the composition of protic-hydrogen isotopes gives the ratio of A_1/A_2 , the fitted parameters of k_f and k_s consist of rate constants as described by Equations (4) and (5), respectively.

$$k_f = k_{\text{pt}}(^1\text{H}^1\text{H}) + \{k_{\text{pt}}(^1\text{H}^2\text{H}) - k_{\text{pt}}(^1\text{H}^1\text{H})\}X_D \quad (4)$$

$$k_s = k_{\text{pt}}(^2\text{H}^1\text{H}) + \{k_{\text{pt}}(^2\text{H}^2\text{H}) - k_{\text{pt}}(^2\text{H}^1\text{H})\}X_D \quad (5)$$

Finally, $k_{\text{pt}}(^1\text{H}^1\text{H})$, $k_{\text{pt}}(^1\text{H}^2\text{H})$, $k_{\text{pt}}(^2\text{H}^1\text{H})$, and $k_{\text{pt}}(^2\text{H}^2\text{H})$ can be extracted from the plots of k_f and k_s with variation of X_D to be $(93\text{ ps})^{-1}$, $(196\text{ ps})^{-1}$, $(700\text{ ps})^{-1}$, and $(1200\text{ ps})^{-1}$, respectively (Figure 3). To assert the concerted mechanism of ESDPT, it is necessary to show that $k_{\text{pt}}(^1\text{H}^2\text{H}) = k_{\text{pt}}(^2\text{H}^1\text{H})$ and that $\{k_{\text{pt}}(^1\text{H}^2\text{H})\}^2 = k_{\text{pt}}(^1\text{H}^1\text{H})k_{\text{pt}}(^2\text{H}^2\text{H})$.^[4,16] However, our data suggest that two hydrogens move in succession. We also infer that one of the two steps, presumably the first step, is rate-limiting, as suggested from the kinetically insignificant formation of cationic or anionic intermediate species (vide infra).

In a nonpolar medium 1:1 7AI/methanol complexes are theoretically shown to possess weakly H-bonded structures, the substantial fraction of which have the H-bond length of $\text{N}\cdots\text{H}-\text{O}$ longer than the nominal H-bond length of 2.5 \AA .^[9c,11] However, 1:1 7AI/acetic acid complexes undergo very facile ESDPT through short and strong hydrogen bonds.^[13c] Thus, we have also obtained k_{pt} and kinetic isotope effect (KIE) values with diverse alcohols having different values of Kamlet–Taft acidity (α) and basicity (β).^[19,20] The magnitudes of α and β provide explicit measures for the respective donating and the accepting abilities of the hydrogen bonds. It is evident from Table 1 that k_{pt} tends to decrease, whereas KIE tends to increase with an increase in α . Even for the complexes with alcohols having $\beta = 0$, ESDPT is very facile and the rate increases profoundly with an increase in α . Thus, the acidity of an alcohol is inferred to control the energetics of

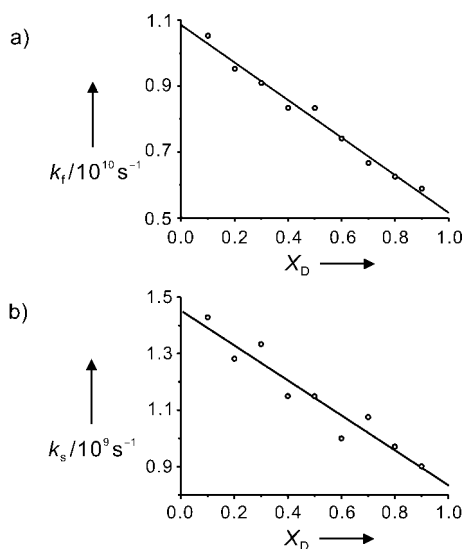


Figure 3. Plots of a) k_f and b) k_s with variation of X_D for 7AI (1.6×10^{-5} M) in *n*-heptane with 67 mm of methanol consisting of $\text{CH}_3\text{O}^1\text{H}$ and $\text{CH}_3\text{O}^2\text{H}$, where k_f and k_s are the fast and the slow components of k_{pt} , respectively, and X_D is $[\text{protic } ^2\text{H}]/([\text{protic } ^1\text{H}] + [\text{protic } ^2\text{H}])$. The obtained values of $k_{\text{pt}}(^1\text{H}^1\text{H})$, $k_{\text{pt}}(^1\text{H}^2\text{H})$, $k_{\text{pt}}(^2\text{H}^1\text{H})$, and $k_{\text{pt}}(^2\text{H}^2\text{H})$ are $(93 \text{ ps})^{-1}$, $(196 \text{ ps})^{-1}$, $(700 \text{ ps})^{-1}$, and $(1200 \text{ ps})^{-1}$, respectively.

Table 1: Alcohol-dependent variation of k_{pt} and KIE.^[a]

Alcohol	α	β	$k_{\text{pt}} [\text{ps}^{-1}]$	KIE
1,1,1,2,2,2-hexafluoroisopropyl alcohol	1.96	0	$\geq 6^{-1}$	^[b]
2,2,2-trifluoroethanol	1.51	0	62^{-1}	5.8
methanol	0.93	0.62	88^{-1}	14.5
ethanol	0.83	0.77	95^{-1}	15.3
2-propanol	0.76	0.95	108^{-1}	17.6
<i>tert</i> -butanol	0.68	1.01	114^{-1}	20.2

[a] Alcohol concentrations and experimental conditions are described in Figure 2, and the values of α and β are taken from ref. [19]. The α and β values measured from bulk alcohols are given here because those from monomeric alcohols, showing similar trends, are not available for all the alcohols employed.^[20] The average deviations of k_{pt} and KIE are $\pm 5\%$ and $\pm 10\%$, respectively. [b] Not measurable due to our limited IRF.

ESDPT. The less acidic alcohol makes ESDPT less exoergic, that is, energetically more symmetric, reducing the overall rate but enhancing the relative contribution of tunneling in the reaction. This suggests that the H-bond donating ability of alcohol in the coordinate of $\text{N} \cdots \text{H}-\text{O}$ plays the key role for the dynamics of ESDPT. Keeping in mind that the decay time of **Nb** and the rise time of **T** coincide and that k_{pt} is dependent on the acidity of alcohol, we propose that the tautomerization of 7AI is initially triggered by the transfer of a proton from the alcohol molecule to the pyridinic nitrogen (N7) of 7AI, forming a cationic 7AI intermediate species, and completed by rapid proton transfer from the pyrrolic nitrogen (N1) of the intermediate to the transient alkoxide moiety. The intermediate complexes are unstable enough to be kinetically insignificant because both the alkoxide moiety and the 7AI cation are energetically unfavorable. Note that our results are consistent with the suggestion that cyclic H-bonded 1:2 7-

hydroxyquinoline/alcohol complexes undergo excited-state tautomerization in a stepwise manner.^[21] Thus, we infer that the observed kinetic results of ESDPT originate mainly from single-proton transfer in the $\text{O}-\text{H} \cdots \text{N7}$ of **Nb**.

The kinetic isotope effect (KIE) of k_{pt} , $k_{\text{pt}}(^1\text{H}^1\text{H})/k_{\text{pt}}(^2\text{H}^2\text{H})$, for a 1:1 7AI/methanol complex is observed to be as great as 14.5 at 19°C (Figure 2). The large KIE and the small k_{pt} of ESDPT imply the existence of an appreciably high barrier and the importance of tunneling through hydrogen bonds. The Arrhenius plots of k_{pt} in Figure 4 clearly show that

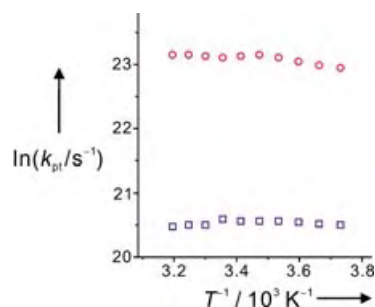


Figure 4. Arrhenius plots for the k_{pt} of 7AI (1.6×10^{-5} M) in *n*-heptane having $\text{CH}_3\text{O}^1\text{H}$ (circles) and $\text{CH}_3\text{O}^2\text{H}$ (squares) of 67 mm.

not only k_{pt} but also KIE is independent of temperature within our experimental errors. This suggests that tunneling is operative certainly in the ESDPT of 7AI.^[22,23] These types of temperature-independent Arrhenius plots have been reported in the enzymatic proton transfer of lipoygenase.^[24] Temperature-independent KIEs have also been observed in the proton transfers of thermophilic alcohol dehydrogenase^[25] and solid-state porphyrin at low temperature.^[26] Temperature-independent and large KIEs in enzymes have been explained with a model employing vibrationally enhanced proton tunneling^[27] originally suggested by Dogonadze et al.^[28,29] When the tunneling contribution is large, the ratio of the Arrhenius preexponential factors, $A(^1\text{H})/A(^2\text{H})$, is much less than unity in general. However, if tunneling becomes large enough to be equally effective for both ^1H and ^2H , then the ratio becomes much greater than unity. We have found $A(^1\text{H})/A(^2\text{H})$ to be 37 from Figure 4, which suggests that the ESDPT of 7AI/methanol complexes takes place with extensive tunneling contribution (vide infra).

The intrinsic double proton transfer, which is governed mostly by tunneling, requires optimized angles and proper H-bond lengths in addition to a cyclic H-bonded structure. The formation of such a precursor configuration for tunneling from the 1:1 7AI/alcohol complex of **Nb** is not sensitive to isotope effects and consists mostly of heavy-atom motions with a little reorganization energy. The precursor-configuration optimization and the intrinsic tunneling are in two orthogonal reaction coordinates of the potential hypersurface, and solvent fluctuations play a crucial role in the formation of such a pretunneling configuration. In the regime that only the motions of hydrogen including tunneling limit the rate, KIE is predicted to be neither dependent on solvent viscosity nor equal to unity. Alternatively, when heavy-atom reorganization assists quantum tunneling, KIE depends on

viscosity. The heavy-atom reorganization that is required to reach the optimal pretunneling configuration becomes slow as viscosity increases. Thus, the tunneling contribution is reduced and KIE tends to be small with increased viscosity.^[30] Table 2 shows that both k_{pt} and KIE tend to decrease as

Table 2: Viscosity-dependent variation of k_{pt} and KIE.^[a]

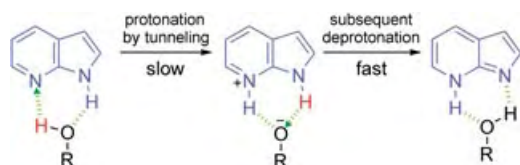
Solvent	Viscosity [cP]	k_{pt} [ps ⁻¹]	KIE
<i>n</i> -heptane	0.41	88 ⁻¹	14.5
<i>n</i> -decane	0.92	93 ⁻¹	13.7
<i>n</i> -dodecane	1.45	97 ⁻¹	12.5

[a] Methanol concentrations and experimental conditions are described in Figure 2, and viscosity values measured at 20°C are taken from ref. [31].

solvent viscosity increases. These trends suggest that the rate of the overall proton-transfer reaction is affected by the configuration-optimization rate of **Nb** more at higher viscosity. If the motions of hydrogen limit the rate, KIE increases in general as k_{pt} becomes smaller. However, our results are opposite to this, supporting the idea that solvent fluctuations assist tunneling in the ESDPT of **Nb**.

Tunneling in our systems is conceptually identical to the vibrationally assisted tunneling suggested in enzymatic reactions.^[25,27–29] The solvent fluctuations replace the low-frequency protein motions. Furthermore, the picture of the proton transfer in **Nb** is in line with that of 7AI dimers in which the heavy-atom motions of N...N coupled to N–H vibrations are crucial for tunneling.^[5b,c] Also in accord with our picture is the acid–base reactions of 1-naphthol/ammonia clusters, which are strongly correlated to acid–base vibrational couplings assisted by solvent fluctuations.^[32] It should be pointed out that proton transfer in the tautomerization of a 1:1 7AI/water complex has not been reported in the gas phase although it is observed in condensed phases.^[13a,33,34] This discrepancy hints at the role of solvent fluctuations on the tautomerization of a 7AI monomer assisted by a protic guest molecule.

The ESDPT of a 1:1 7AI/alcohol complex in nonpolar *n*-alkanes occurs consecutively on a time scale of 100 ps with unusually large, temperature-independent, and viscosity-dependent KIEs near room temperature. The ESDPT is initially triggered by the proton transfer of the alcohol molecule to the pyridinic nitrogen of 7AI, forming a cationic 7AI intermediate species, and completed by rapid proton transfer from the pyrrolic nitrogen of the intermediate to the transient alkoxide moiety (Scheme 2). The H-bond between the pyridinic nitrogen atom of a 7AI molecule and the protic hydrogen atom of an alcohol molecule is suggested to play the



Scheme 2. ESDPT mechanism of a 7AI molecule cyclically H-bonded to an alcohol molecule.

central role for ESDPT. The intrinsic proton transfer of the complex is governed by single-proton tunneling from the alcohol molecule to the pyridinic nitrogen atom, although heavy-atom motions assist the complex to reach the optimized precursor configuration. The detailed dynamics of this process requires multidimensional reaction coordinates to be described properly and thus has great theoretical challenge.

Experimental Section

7-Azaindole ($\geq 99\%$) from Sigma-Aldrich, *n*-alkane (anhydrous), and alcohols were used as purchased. The protic hydrogen atoms of both 7AI and ROH of **Nb** were exchanged with ²H atoms by dissolving 7AI in nonpolar solvents containing RO²H (isotopic purity $\geq 99.5\%$) for the measurements of k_{pt} in proton-inventory experiments. Absorption and emission spectra were obtained by using a UV/Vis spectrometer (Scinco, S-3100) and a fluorimeter consisting of a 75-W Xe lamp (Acton Research, XS432) and two monochromators (Acton Research, Spectrapro), respectively. Fluorescence kinetic profiles, excited with Raman-shifted 288-nm pulses of a mode-locked Nd:YAG laser (Quintel, YG701), were detected using a 10-ps streak camera (Hamamatsu, C2830). Emission wavelengths were selected by combining band-pass filters and cut-off filters. Fluorescence kinetic constants were extracted by fitting profiles to computer-simulated exponential curves convoluted with IRF (fwhm: 25 ps). Sample temperature was controlled using a refrigerated bath circulator (Jeio Tech, RC-10V). Unless specified otherwise, all the measurements were carried out at a temperature of 19°C.

Received: June 28, 2004

Keywords: hydrogen bonds · kinetic isotope effects · N-heterocycles · proton transfer · time-resolved spectroscopy

- [1] C. Tanner, C. Manca, S. Leutwyler, *Science* **2003**, 302, 1736–1739.
- [2] P. L. Geissler, C. Dellago, D. Chandler, J. Hutter, M. Parrinello, *Science* **2001**, 291, 2121–2124.
- [3] O.-H. Kwon, H. Doo, Y.-S. Lee, D.-J. Jang, *ChemPhysChem* **2003**, 4, 1079–1083.
- [4] R. L. Schowen, *Angew. Chem.* **1997**, 109, 1502–1506; *Angew. Chem. Int. Ed. Engl.* **1997**, 36, 1434–1438.
- [5] a) K. C. Ingham, M. A. El-Bayoumi, *J. Am. Chem. Soc.* **1974**, 96, 1674–1682; b) A. Douhal, S. K. Kim, A. H. Zewail, *Nature* **1995**, 378, 260–263; c) T. Fiebig, M. Chachisvilis, M. Manger, A. H. Zewail, A. Douhal, I. Garcia-Ochoa, A. de La Hoz Ayuso, *J. Phys. Chem. A* **1999**, 103, 7419–7431.
- [6] A. V. Smirnov, D. S. English, R. L. Rich, J. Lane, L. Teyton, A. W. Schwabacher, S. Luo, R. W. Thornburg, J. W. Petrich, *J. Phys. Chem. B* **1997**, 101, 2758–2769.
- [7] J. Ashenhurst, G. Wu, S. Wang, *J. Am. Chem. Soc.* **2000**, 122, 2541–2547.
- [8] J. Catalán, P. Pérez, J. C. del Valle, J. L. G. de Paz, M. Kasha, *Proc. Natl. Acad. Sci. USA* **2002**, 99, 5793–5798.
- [9] a) C. F. Chapman, M. Maroncelli, *J. Phys. Chem.* **1992**, 96, 8430–8441; b) R. S. Moog, M. Maroncelli, *J. Phys. Chem.* **1991**, 95, 10359–10369; c) S. Mente, M. Maroncelli, *J. Phys. Chem. A* **1998**, 102, 3860–3876.
- [10] P.-T. Chou, W.-S. Yu, C.-Y. Wei, Y.-M. Cheng, C.-Y. Yang, *J. Am. Chem. Soc.* **2001**, 123, 3599–3600.
- [11] a) J. Waluk, *Acc. Chem. Res.* **2003**, 36, 832–838; b) A. Kyr-ychenko, Y. Stepanenko, J. Waluk, *J. Phys. Chem. A* **2000**, 104, 9542–9555.

- [12] J. Konijnenberg, A. H. Huizer, C. A. G. O. Varma, *J. Chem. Soc. Faraday Trans. 2* **1988**, 84, 1163–1175.
- [13] a) P.-T. Chou, M. L. Martinez, W. C. Cooper, D. McMorro, S. T. Collins, M. Kasha, *J. Phys. Chem.* **1992**, 96, 5203–5205; b) P.-T. Chou, C.-Y. Wei, C.-P. Chang, K. Meng-Shin, *J. Phys. Chem.* **1995**, 99, 11994–12000; c) C.-P. Chang, H. Wen-Chi, K. Meng-Shin, P.-T. Chou, J. H. Clements, *J. Phys. Chem.* **1994**, 98, 8801–8805.
- [14] C. G. Swain, J. F. Brown, Jr., *J. Am. Chem. Soc.* **1952**, 74, 2534–2537, 2538–2543.
- [15] W. P. Jencks, *Acc. Chem. Res.* **1980**, 13, 161–169.
- [16] Y. Chen, F. Gai, J. W. Petrich, *J. Am. Chem. Soc.* **1993**, 115, 10158–10166.
- [17] Of the 7AI molecules 93 % and 77 % are expected to form 1:1 complexes with methanol at methanol concentrations of 260 and 67 mM, respectively. To avoid the possible formation of poly-solvated complexes, we have measured fluorescence kinetics at a concentration of 67 mM.^[13a] The lifetime (450 ps) of noncomplexed 7AI in our system differs from reported values (~1.7 ns) of 7AI monomers in alcohol-free nonpolar solvents.^[9a] However, the Benesi–Hildebrandt plot of **T** fluorescence shows good linearity, yielding $K_a = 45 \text{ M}^{-1}$. This eliminates the possibility of collision-induced ESDPT processes.
- [18] The overall proton-transfer time of 7AI in neat methanol is obtained to be 130 ps, which is very close to the reported value of 124 ps.^[9b]
- [19] M. J. Kamlet, J.-L. M. Abboud, M. H. Abraham, R. W. Taft, *J. Org. Chem.* **1983**, 48, 2877–2887.
- [20] a) J.-L. M. Abboud, K. Sraidi, G. Guiheneuf, A. Negro, M. J. Kamlet, R. W. Taft, *J. Org. Chem.* **1985**, 50, 2870–2873; b) B. Frange, J.-L. M. Abboud, C. Benamou, L. Bellon, *J. Org. Chem.* **1982**, 47, 4553–4557.
- [21] S. Kohtani, A. Tagami, R. Nakagaki, *Chem. Phys. Lett.* **2000**, 316, 88–93.
- [22] We obtained k_{pt} and KIE values by monitoring the fluorescence rise at 550 nm, rather than the fluorescence decay at 350 nm, to avoid the fluorescence interference of noncomplexed 7AI at 350 nm.
- [23] KIE values are reported to be 3.8 and 3.0 for the proton transfer of 7AI in neat water and methanol, respectively.^[9,10]
- [24] T. Jonsson, M. H. Glickman, S. J. Sun, J. P. Klinman, *J. Am. Chem. Soc.* **1996**, 118, 10319–10320.
- [25] A. Kohen, R. Cannio, S. Bartolucci, J. P. Klinman, *Nature* **1999**, 399, 496–499.
- [26] J. Braun, R. Schwesinger, P. G. Williams, H. Morimoto, D. E. Wemmer, H.-H. Limbach, *J. Am. Chem. Soc.* **1996**, 118, 11101–11110.
- [27] A. Kohen, *Prog. Reac. Kinet. Mech.* **2003**, 28, 119–156.
- [28] R. R. Dogonadze, A. M. Kuznetsov, V. G. Levich, *Electrochim. Acta* **1968**, 13, 1025–1044.
- [29] a) A. M. Kuznetsov, J. Ulstrup, *Can. J. Chem.* **1999**, 77, 1085–1096; b) A. A. Kornyshev, A. M. Kuznetsov, U. Stimming, *J. Chem. Phys.* **1997**, 106, 9523–9528.
- [30] J. Basran, M. J. Sutcliffe, N. S. Scrutton, *Biochemistry* **1999**, 38, 3218–3222.
- [31] a) B. Celda, R. Gavara, R. Tejero, J. E. Figueruelo, *J. Chem. Eng. Data* **1987**, 32, 31–33; b) B. Knapstad, P. A. Skjølsvik, H. A. Øye, *J. Chem. Eng. Data* **1989**, 34, 37–43.
- [32] J. A. Syage, *J. Phys. Chem.* **1995**, 99, 5772–5786.
- [33] D. E. Folmer, E. S. Wisniewski, J. R. Stairs, A. W. Castleman, Jr., *J. Phys. Chem. A* **2000**, 104, 10545–10549.
- [34] a) A. Fernández-Ramos, Z. Smedarchina, W. Siebrand, M. Z. Zgierski, *J. Chem. Phys.* **2001**, 114, 7518–7526; b) A. Fernández-Ramos, Z. Smedarchina, W. Siebrand, M. Z. Zgierski, M. A. Rios, *J. Am. Chem. Soc.* **1999**, 121, 6280–6289.

High-Resolution Soft Lithography: Enabling Materials for Nanotechnologies**

Jason P. Rolland, Erik C. Hagberg, Ginger M. Denison, Kenneth R. Carter,* and Joseph M. De Simone*

The availability of commercially viable nanofabrication processes is key to realizing the potential of nanotechnologies, especially in the fields of photonics, electronics, and proteomics. The imprint lithographic (IL) technique is a case in point, an alternative to photolithography for manufacturing integrated circuits, nanofluidic and other devices with sub-100-nm features. However, it is becoming increasingly clear that new materials are needed to advance IL methods to their putative limits.^[1–5] We recently reported the fabrication of organic-solvent resistant, microfluidic devices with features on the order of hundreds of microns made from photocurable perfluoropolyethers (PFPEs).^[6] PFPE-based materials are liquids at room temperature and can be photochemically cross-linked to yield highly fluorinated, solvent resistant, chemically robust, durable, elastomers with a modulus of 4.0 MPa. Herein we report the successful use of PFPE-based materials in high-resolution imprint lithography.

Imprint lithography can be roughly broken into two areas: 1) so-called soft lithographic techniques,^[1] such as solvent-assisted micro-molding (SAMIM), micro-molding in capillaries (MIMIC), and microcontact printing (MCP), and 2) rigid imprint techniques, such as nanocontact molding (NCM),^[7] “step and flash” imprint lithography (S-FIL),^[5] and nanoimprint lithography (NIL).^[8] Polydimethylsiloxane (PDMS)

[*] J. P. Rolland, G. M. Denison, Prof. J. M. De Simone

Department of Chemistry
University of North Carolina at Chapel Hill
Chapel Hill, NC, 27599 (USA)

and

Department of Chemical Engineering
North Carolina State University
Raleigh, NC, 27695 (USA)

Fax: (+1) 919-962-5467

E-mail: DeSimone@email.unc.edu

E. C. Hagberg, Dr. K. R. Carter

IBM Almaden Research Center

Center for Polymeric Interfaces and Macromolecular Assemblies
San Jose, CA, 95120 (USA)

Fax: (+1) 413-545-0082

E-mail: kcarter@almaden.ibm.com

[**] We acknowledge partial support from the Office of Naval Research (N000140210185), partial support from the STC program of the National Science Foundation under Agreement No. CHE-9876674 and the William R. Kenan, Jr. Distinguished Professorship for financial support. We gratefully acknowledge Anthony Brennan at the University of Florida for providing the micron-scale master. We also acknowledge partial support from the MRSEC Program of the NSF Materials Science and Engineering Research Center Grant (9808677) to the Center for Polymer Interfaces and Macromolecular Assemblies (CPIMA) at Stanford University.



Supporting information for this article is available on the WWW under <http://www.angewandte.org> or from the author.

based networks have served as the material of choice for much of the work in soft lithography.^[9,10] The use of soft, elastomeric materials, such as PDMS, offers numerous attractive properties in several lithographic techniques. PDMS is highly UV-transparent and has a very low Young's modulus which gives it the flexibility required for conformal contact, even over surface irregularities, without the risk of cracking.^[11] Furthermore, flexibility in molds facilitates release from masters and replicates without cracking and allows the mold to endure multiple imprinting steps without damaging fragile features. While PDMS offers some advantages, there are a number of properties inherent to PDMS which severely limit its capabilities in soft lithography. First, PDMS-based elastomers swell significantly when exposed to most oil-soluble organic compounds.^[12] With the exception of MCP,^[1] resistance to swelling is critically important in nearly all soft lithographic techniques where a mold is brought into contact with a small amount of curable organic monomer or resin. Second, the surface energy of PDMS ($\approx 22\text{--}25\text{ mN m}^{-1}$) is not low enough for procedures which require high fidelity. Thus, the patterned surface of PDMS-based molds is often fluorinated using a plasma treatment followed by vapor deposition of a fluoroalkyl trichlorosilane.^[1] Third, the most commonly used commercially available form of the material (Dow Corning's Sylgard 184) has a modulus that is too low ($\approx 1.5\text{ MPa}$) for many applications which results in collapse of features. Although elegant solutions to address this last problem have been developed,^[13,14] the materials chosen still exhibit poor solvent resistance and require fluorination steps to allow for mold release.

Rigid materials, such as quartz glass and silicon, have also been utilized in imprint lithography.^[1,3,5,7,8,15–23] Such materials are superior to PDMS in modulus and swelling resistance but lack flexibility and therefore conformal contact with the substrate. Another major drawback of such materials is the direct use of a valuable and difficult to fabricate hard mold which is typically made by using conventional photolithography or e-beam lithography.^[7] Carter and co-workers^[20] and Resnick et al.^[21] have eliminated the requirement to repeatedly use expensive quartz glass or silicon molds in NCM processes by utilizing an acrylate-based mold generated from casting a photopolymerizable monomer mixture against a silicon master.^[7] Despite such advances, there are other

serious disadvantages of rigid materials used as molds which include the necessity to use fluorination steps, or thermoformed rigid fluoropolymers themselves^[24] to lower the surface energy of the mold^[3] and the inherent problem of releasing a rigid mold from a rigid substrate without breaking or damaging it.^[3,10]

The photochemically curable fluoropolymer that we utilize herein is a α,ω -methacryloxy functionalized PFPE (PFPE-DMA) (Figure 1).^[6] We have previously reported the synthesis of novel functionalized PFPEs.^[24] However, herein we treated a commercially available hydroxy-terminated PFPE (Solvay Solexis, $M_n = 3800\text{ g mol}^{-1}$) with isocyanato ethyl methacrylate (Aldrich) to yield a methacryloxy-functionalized polymer which is a pourable liquid of low viscosity (0.36 Pas) at room temperature. A photoinitiator, 1-hydroxy-cyclohexyl phenyl ketone (1 wt %, Aldrich), was dissolved into the PFPE-DMA to make a photocurable liquid resin. A thermally curable polydimethylsiloxane-based material, Sylgard 184, (Dow Corning) was used for comparative controls.

Swelling is a commonplace issue with PDMS based molds since most organic liquids will swell PDMS, and it is organic liquids that are the materials most desirable to mold. To demonstrate the utility of a fluoroelastomer-based material in imprint lithography, we first generated replica molds made from both PDMS as well as from PFPE-DMA and used these to micromold an organic photopolymer resin, trimethylpropane triacrylate (TMPTA).^[26] A patterned silicon-wafer master was used which had features with a width of $2\text{ }\mu\text{m}$, a depth of $5\text{ }\mu\text{m}$, and a spacing of $2\text{ }\mu\text{m}$ (Figure 2A). The fluoroelastomer-based mold was made by pouring an approximately 1 mm thick liquid film of PFPE-DMA, which contained photoinitiator, onto the clean, patterned silicon wafer master. The material was then subjected to UV light ($\lambda = 365\text{ nm}$, 35 mW cm^{-2}) for 1 min under a nitrogen purge. After curing, the approximately 1 mm thick mold was easily peeled from the master without employing a surface fluorination step. In an analogous fashion, PDMS molds were generated by first mixing the Sylgard 184 precursors (10:1 base:curing agent) and degassing under vacuum. An approximately 1 mm thick layer of the PDMS-based material was then poured onto the same clean, patterned silicon wafer master and was placed in a vacuum oven at 80°C for about 15 h . For the PDMS molds, a vapor-deposition pretreatment

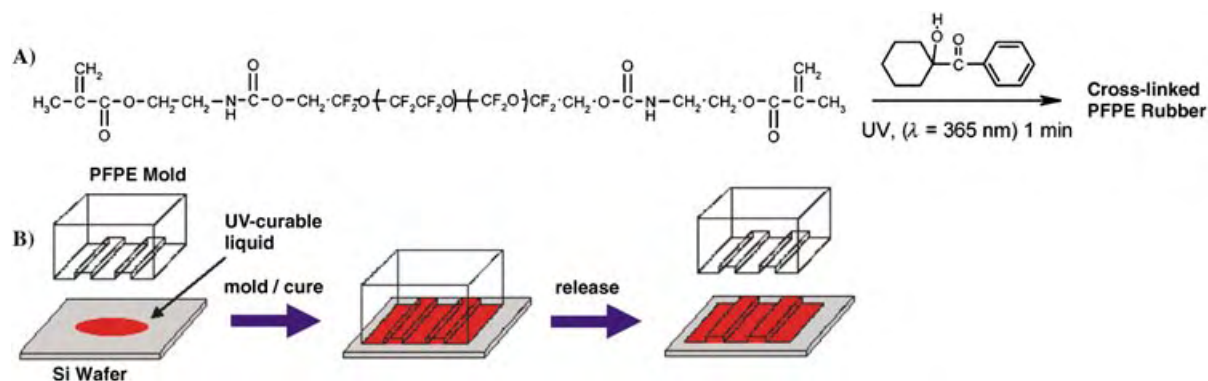


Figure 1. A) Formula of the UV curable PFPE liquid precursor used to generate high resolution stamps. B) Schematic representation of the imprint lithography process. First, a small drop of UV-curable liquid is placed on a silicon wafer. A patterned mold is then brought into contact with the drop and pressure is applied during UV exposure. The mold is then peeled from the wafer leaving the cured resin in the desired pattern.

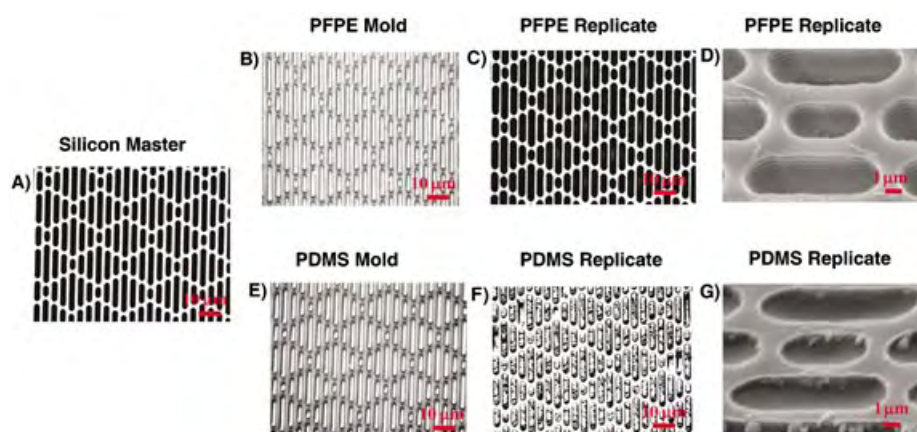


Figure 2. Images of a silicon master with 2- μm features (A), PFPE and PDMS molds made from this master (B, E), and replicate molds of TMPTA using the corresponding stamps (C, D, F, G). While both elastomers produced molds of high quality, the TMPTA replicate made with the PDMS mold contains residual PDMS that was ripped from the mold presumably because of adhesion (F, G). In contrast, the low surface-energy PFPE mold was easily released from the TMPTA replicate (D). The sub-micron striated features on the replicate in (D) are present on the silicon master and are a result of multiple etching steps used during its fabrication.

to the patterned silicon wafer using trichloro(1H,1H,2H,2H-perfluorooctyl) silane was applied to allow release of the mold. Replica molds of high quality with good feature fidelity were generated from both the PFPE-based elastomer (Figure 2B) as well as the PDMS-based elastomer (Figure 2E) when the feature sizes were this large.

Once both of the elastomeric molds were generated, they were each independently brought into contact with a small drop (≈ 2 mm in diameter) of the uncured TMPTA which was first placed on a flat, unpatterned silicon wafer as illustrated in Figure 1B. A fixed pressure was exerted on the mold with a modified Instron to ensure conformal contact. UV light was then passed through the back of each mold for 1 min to fully cure the TMPTA while in contact with the mold. Each mold was then peeled from the wafer revealing the patterned TMPTA replicate.

The TMPTA replicates generated from the PDMS molds were of very poor quality. SEM images (Figure 2F and G) of these replicates reveal pieces of the PDMS mold that were ripped out during the release as a result of swelling of the PDMS mold by the TMPTA prior to curing. In contrast, those replicates made from the PFPE-based mold look identical to the master with no tear out (Figure 2C and G) because it is not swollen by the organic-soluble TMPTA photopolymer resin. Additionally, the PFPE-based mold was extremely easy to peel away from the micromolded TMPTA, presumably because of the extremely low surface energy of the PFPE-based mold^[24] and its elastomeric nature. The intrinsically oleophobic nature of this fluoropolymer-based mold material enables for the first time

imprint lithographic applications of commonplace organics using soft elastomeric mold materials.

In addition to the intrinsic swelling problems illustrated above for PDMS-based materials, previous attempts to perform 1:1 sub 1-micron patterning using PDMS-based elastomers, such as Sylgard 184, does not give replicas of high fidelity. Indeed, accurate replication of patterns using molds of features less than 1-micron in size with PDMS-based elastomers has had only limited success^[1,4,10] even when using elaborate pre-treatment methods to reduce the interfacial adhesion between the object being molded and the PDMS-based replica.

To test the viability of PFPE-based elastomers to perform accurate nanometer-scale molding we chose to fabricate replica molds from a patterned silicon-wafer master with features having a width

of 140 nm, a depth of approximately 50 nm, and a separation of 70 nm (Figure 3A). We found we could cast excellent molds using the PFPE-based fluoroelastomer materials with exact preservation of the nanoscale features of the patterned silicon-wafer master (Figure 3B). The features on the PFPE-based mold had an average height of 51 nm which was in excellent agreement with a measured height of 54 nm for the features in the silicon master. The widths of the features on the PFPE-based molds seem to vary from the top of the

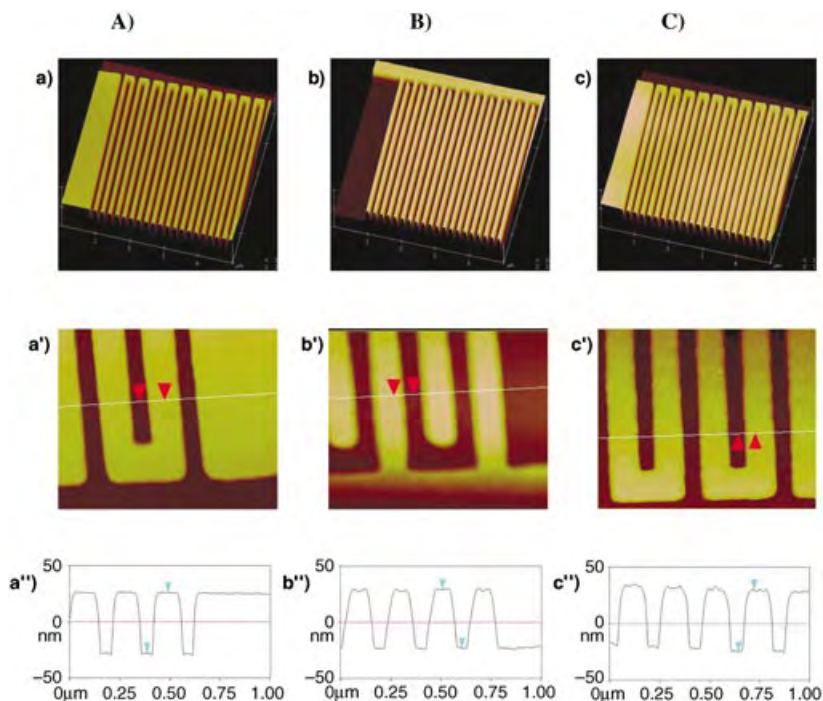


Figure 3. High-resolution AFM images of A) a silicon master with lines of 140 nm width separated by 70 nm (a, a'), B) PFPE mold with 70-nm wide lines separated by 140 nm (b, b'), C) replicate made with PFPE mold with 140-nm wide lines separated by 70 nm (c, c'). Beneath each picture is a representative height profile (a'', b'', c'').

channel through to the bottom (Figure 3B). This is presumably due to some slight relaxation of the polymeric material upon release of its confinement from the patterned silicon wafer master. In contrast, attempts to fabricate PDMS-based molds from the same silicon master failed (Figure 4). The features on the PDMS molds are irregular, rounded, and only 5–10 nm in height.

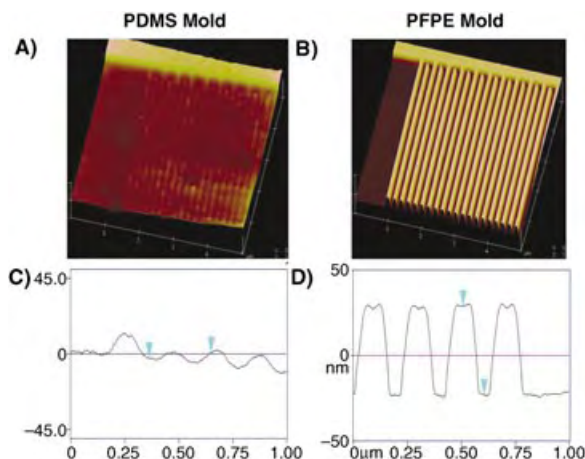


Figure 4. High-resolution AFM image of a PDMS mold (A) and a PFPE mold (B) generated from the silicon master shown in Figure 3. Representative height profiles are shown underneath the respective images (C, D).

The ability of these soft elastomeric replica molds to be useful in the patterning of nanoscale features using NCM imprint lithographic techniques was explored (see Figure 3). The high-fidelity PFPE-based molds having 70-nm wide lines separated by 140-nm spaces (see Figure 3B) were used to contact mold the TMPTA photopolymer resin in a manner identical to that used above for imprinting micron-sized features. Remarkably, when using between 5 and 25 psi of pressure on the PFPE-based mold, we were able to easily imprint a drop of TMPTA photopolymer resin to generate patterns (Figure 3C) having nanometer-sized features that looked identical to the original patterned silicon wafer master (Figure 3A). In addition, the PFPE-based mold was easy to peel off of the nano-molded TMPTA replicates presumably because of the flexibility and low surface-energy of the PFPE-based elastomer and its oleophobic nature which prevented adsorption of the TMPTA into the mold. When using quartz molds, such release processes can take from tens of seconds to minutes and requires large separation forces that often result in delamination failures.

In summary, we have demonstrated the capabilities of PFPE-based elastomers to be used as ideal materials for advanced, high-performance imprint lithographic applications. Such highly fluorinated materials enable both soft lithographic techniques as well as more demanding sub-micron imprint techniques. They are easily fabricated, have the ability to make conformal contact, have a remarkably low surface energy, are resistant to swelling by small organic molecules, and endure multiple printing procedures. We have shown that while replica molds with 2- μ m features can be

generated from both PFPE-based and PDMS-based elastomers, only the PFPE-based materials could be used as molds to imprint and mold desirable organic-soluble materials because of the intrinsically oleophobic nature of such highly fluorinated materials. Furthermore, these PFPE-based materials were able to replicate sub-100-nm sized features with no indications of limits to going to even smaller in size. In addition, the low surface energy of the PFPE-based materials allows for unprecedented ease of release from both silicon masters as well as from patterned replicates-without the need for complex surface functionalization-making it good material to use in the routine fabrication of nanometer-scale structures and devices.

Received: June 29, 2004

Keywords: fluorine · imprinting · lithography · nanostructures · polymers

- [1] Y. Xia, G. M. Whitesides, *Angew. Chem.* **1998**, *110*, 5568; *Angew. Chem. Int. Ed.* **1998**, *37*, 550.
- [2] Y. Xia, J. A. Rogers, K. E. Paul, G. M. Whitesides, *Chem. Rev.* **1999**, *99*, 1823.
- [3] D. J. Resnick, D. P. Mancini, S. V. Sreenivasan, C. G. Willson, *Semicond. Int.* **2002**, *25*, 71.
- [4] K. M. Choi, J. A. Rogers, *J. Am. Chem. Soc.* **2003**, *125*, 4060.
- [5] S. Y. Chou, P. R. Krauss, P. J. Renstrom, *J. Vac. Sci. Technol. B* **1996**, *14*, 4129.
- [6] J. P. Rolland, R. M. Van Dam, D. A. Schorzman, S. R. Quake, J. M. DeSimone, *J. Am. Chem. Soc.* **2004**, *126*, 2322.
- [7] G. M. McClelland, M. W. Hart, C. T. Rettner, M. E. Best, K. R. Carter, B. D. Terris, *Appl. Phys. Lett.* **2002**, *81*, 1483.
- [8] T. Bailey, B. J. Choi, M. Colburn, M. Meissl, S. Shaya, J. G. Ekerdt, S. V. Sreenivasan, C. G. Willson, *J. Vac. Sci. Technol. B* **2000**, *18*, 3572.
- [9] S. R. Quake, A. Scherer, *Science* **2000**, *290*, 1536.
- [10] B. D. Gates, G. M. Whitesides, *J. Am. Chem. Soc.* **2003**, *125*, 14986.
- [11] A. Bietsch, B. Michel, *J. Appl. Phys.* **2000**, *88*, 4310.
- [12] J. N. Lee, C. Park, G. M. Whitesides, *Anal. Chem.* **2003**, *75*, 6544.
- [13] T. W. Odom, V. R. Thalladi, C. J. Love, G. M. Whitesides, *J. Am. Chem. Soc.* **2002**, *124*, 12112.
- [14] T. W. Odom, C. J. Love, D. B. Wolfe, K. E. Paul, G. M. Whitesides, *Langmuir* **2002**, *18*, 5314.
- [15] M. D. Austin, S. Y. Chou, *Appl. Phys. Lett.* **2002**, *81*, 4431.
- [16] M. Austin, S. Y. Chou, *J. Vac. Sci. Technol. B* **2002**, *20*, 665.
- [17] Q. Xia, C. Keimel, H. Ge, Z. Yu, W. Wu, S. Y. Chou, *Appl. Phys. Lett.* **2003**, *83*, 4417.
- [18] W. Zhang, S. Y. Chou, *Appl. Phys. Lett.* **2003**, *83*, 1632.
- [19] S. Y. Chou, P. R. Krauss, P. J. Renstrom, *Science* **1996**, *272*, 85.
- [20] T. A. Von Werne, D. S. Germack, E. C. Hagberg, V. V. Sheares, C. J. Hawker, K. R. Carter, *J. Am. Chem. Soc.* **2003**, *125*, 3831.
- [21] D. J. Resnick, W. J. Dauksher, D. Mancini, K. J. Nordquist, T. C. Bailey, S. Johnson, Stacey, J. G. Ekerdt, C. G. Willson, S. V. Sreenivasan, N. Schumaker, *J. Vac. Sci. Technol. B* **2003**, *21*, 2624.
- [22] M. Otto, M. Bender, B. Hadam, B. Spangenberg, H. Kurz, *Microelectron. Eng.* **2001**, *57*, 361.
- [23] M. D. Austin, H. Ge, W. Wu, M. Li, Z. Yu, D. Wasserman, S. A. Lyon, S. Y. Chou, *Appl. Phys. Lett.* **2004**, *84*, 5299.
- [24] D. Y. Khang, H. H. Lee, *Langmuir* **2004**, *20*, 2445.
- [25] W. C. Bunyard, T. J. Romack, J. M. DeSimone, *Macromolecules* **1999**, *32*, 8224.
- [26] See Supporting Information.

Photocontrol of Smad2, a Multiphosphorylated Cell-Signaling Protein, through Caging of Activating Phosphoserines**

Michael E. Hahn and Tom W. Muir*

The ability to activate proteins with spatial and temporal control inside live cells allows for quantitative kinetic measurements of protein function to be made in a biologically relevant context. Proteins that contain photolabile protecting groups appended to functionalities required for biological activity can be activated by light and provide a means to enable such analyses. Few reports of these reagents, known as caged proteins, have appeared in the literature because of difficulties in the preparation of such complex macromolecules.^[1] Herein, we describe a semisynthetic route to the preparation of caged phosphoproteins. This strategy has been applied to the cellular signaling protein Smad2.

Smad2 is a key element of the intracellular response to cytokines of the transforming growth factor β (TGF- β) superfamily, which are involved in a myriad of normal and disease processes, including development, tissue homeostasis, and cancer.^[2] Binding of TGF- β to its cognate receptor complex results in phosphorylation of the last two serine residues of the C-terminal sequence CSSMS of Smad2 (residues 463–467).^[2] These phosphorylation events activate Smad2, which then disengages from the cytosolic retention factor SARA

(Smad anchor for receptor activation), thus rendering the protein competent to both homotrimerize and interact with Smad4, a binding partner required for downstream functions.^[2,3] Activated Smad2 accumulates in the nucleus, where it regulates transcriptional programs by interacting with a host of other proteins and target promoters.^[2]

These differential protein–protein interactions and the localization of Smad2 provide a basis for understanding how this molecule functions in a cell. However, these descriptions are static and do not adequately describe the dynamics underlying these signaling events. Little is known about where many of these protein–protein interactions are initiated and for how long they exist. The kinetics of nuclear import and export as well as the importance of signal strength, duration, and localization are all poorly understood. We therefore targeted Smad2 for caging because the ability to activate this protein with temporal and spatial control allows one to directly address some of these fundamental issues.

Our caging strategy takes advantage of protein phosphorylation, the post-translational modification most often used to regulate protein activity.^[4] Much recent effort has been directed at the preparation of caged analogues of phosphopeptides and phosphoproteins.^[5,6] We used expressed protein ligation (EPL) as the center point of a semisynthetic scheme for the preparation of Smad2 whose activating phosphorylated residues were caged (Figure 1).^[7] This approach offers several advantages, including the ability to produce caged proteins of any size in quantities sufficient for various biological applications without the need for mutagenesis.^[7] Additionally, EPL readily allows for the installation of

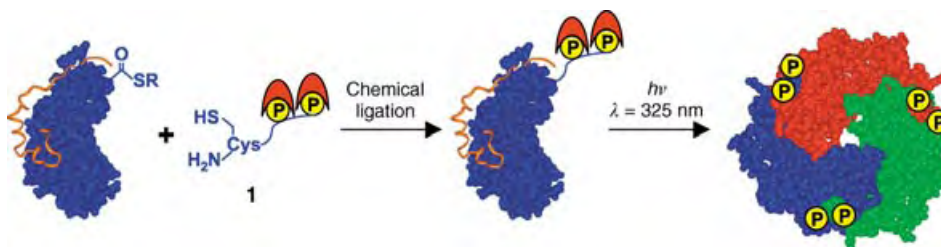


Figure 1. Semisynthesis of caged Smad2-MH2. Expressed protein ligation was used to ligate a recombinant Smad2-MH2- α -thioester/SARA-SBD protein complex to the doubly caged phosphopeptide **1** to give the caged Smad2-MH2/SARA-SBD heterodimer. Caged Smad2-MH2 is activated by exposure to UV light and subsequently releases SARA-SBD and forms a homotrimer. Smad2-MH2 is shown in globular form, SARA-SBD is shown in orange, phosphorylated residues are symbolized by yellow circles, and caging groups are symbolized by red crescents.

[*] M. E. Hahn, Prof. T. W. Muir
The Laboratory of Synthetic Protein Chemistry
The Rockefeller University
Box 223, 1230 York Avenue, New York, NY 10021 (USA)
Fax: (+1) 212-327-7358
E-mail: muir@mail.rockefeller.edu

[**] We gratefully acknowledge Dr. Jean-Philippe Pellois, Dr. Jennifer Ottesen, and Edmund Schwartz for valuable discussions. We thank Claudio Alarcón and Prof. Joan Massagué for help with the nuclear import assay and Dr. Júlio César-Padovan and Prof. Brian Chait for MS/MS measurements. This work was supported by NIH grants CGM55843–07 and EB001991 (to T.W.M.). M.E.H. was supported by the NIH Medical Scientist Training Program grant GM07739.

Supporting information for this article is available on the WWW under <http://www.angewandte.org> or from the author.

multiple caged phosphate groups in a homogenous manner.^[7,8] This characteristic is of significant importance since many proteins, including Smad2, are controlled by multisite phosphorylation.^[9]

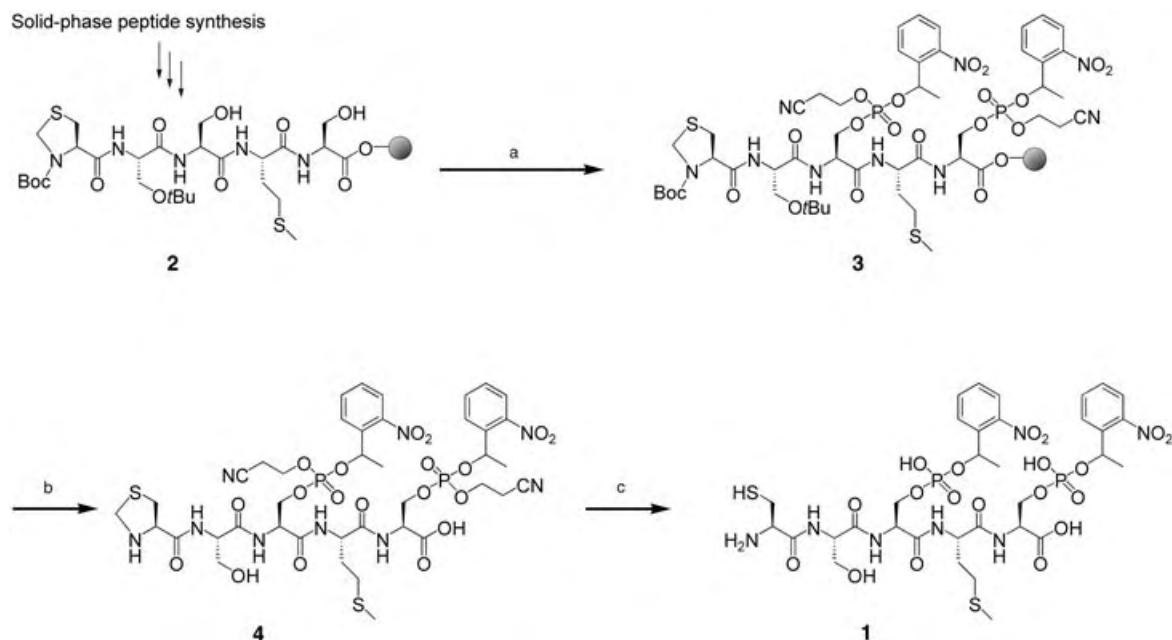
In this study we chose to work with the MH2 domain of Smad2 (residues 241–467, M_w = ca. 25 kDa), since its size enables precise characterization by chromatography and electrospray mass spectrometry (ESMS). The MH2 domain mediates many of the functions of Smad2, including receptor recognition, homo- and hetero-oligomerization, and nuclear import.^[2] Full-length semisynthetic Smad2 has previously been prepared by EPL^[3] and, therefore, we expect that the caging strategy outlined herein will translate effectively to the complete molecule.

Preparation of the caged phosphoprotein commenced with the synthesis of the corresponding doubly caged phosphopeptide **1** by using the 9-fluorenylmethoxycarbonyl (Fmoc) strategy (Scheme 1). Key to the synthesis was 1) orthogonal trityl (Trt) protection of the side chains of the two serine residues to be phosphorylated and 2) incorporation of the N-terminal cysteine (Cys) group required for EPL as *tert*-butoxycarbonyl-1,3-thiazolidine-4-carboxylic acid (Boc-Thz). The latter allowed for the thiol group of Cys to be protected during the critical phosphorylation step and provided a convenient method for deprotection of the Cys residue following cleavage of the peptide from the solid support.^[10] Following chain assembly and selective unmasking of the two serine residues, the resulting peptidyl resin **2** was dried extensively and treated with *O*-1-(2-nitrophenyl)ethyl-*O'*- β -cyanoethyl-*N,N*-diisopropylphosphoramidite,^[5] which contains the 2-nitrophenylethyl (NPE) caging group. *tert*-Butylhydroperoxide was then used to oxidize the intermediate phosphites to the desired phosphates, thus yielding **3**. Notably, the undesired oxidation of the thioether of methionine to the sulfoxide was largely avoided (< 5 %) by limiting the oxidation time to 20 minutes (see the Supporting Information). Attempted on-resin removal of the β -cyanoethyl protecting groups from two juxtaposed phosphates resulted in significant amounts of β -elimination of the protected phosphate moiety.^[11] Interestingly, this side reaction was not found to occur when the deprotection step was carried out in solution following cleavage from the resin. This observation suggests that the elimination was facilitated by the C-terminal ester linkage between the peptide and the solid support. Smooth removal of the β -cyanoethyl groups was therefore carried out under optimized conditions in solution using the hindered amidine 1,8-diazabicyclo[5.4.0]undec-7-ene (DBU).

Methoxylamine was then added in situ to convert Thz into Cys. The crude product contained one major compound (ca. 75 % by reversed-phase high-performance liquid chromatography (RP-HPLC), see the Supporting Information), which was subsequently purified to homogeneity to give the desired peptide that was caged on two phosphorylated serine residues (**1**) in 10 % yield.

The caged peptide **1** was labeled with fluorescein-5-maleimide (thus generating peptide **1-FI**)^[12] and subjected to low-intensity UV irradiation (312 nm, 2 mW cm⁻²) followed by RP-HPLC to determine the kinetics and quantum yield of uncaging. Photolysis followed first-order kinetics with a rate constant of $4.9 \times 10^{-3} \text{ s}^{-1}$, which corresponds to a quantum yield of uncaging of 0.16 per caging group (Figure 2). Interestingly, both possible singly caged peptides were observed in approximately equal amounts after irradiation for an intermediate length of time, thus indicating that the efficiency of photolysis was equivalent for both caging groups (see the Supporting Information). Brief (< 5 s) exposure of the peptide to the output of a He-Cd laser (325 nm, 4.74 W cm⁻²) resulted in near quantitative conversion (> 97 %) into the uncaged peptide (see the Supporting Information).

A recombinantly expressed Smad2-MH2 domain (residues 241–462) bearing a C-terminal thioester was prepared as previously described.^[3] A complex of this protein with the minimal Smad binding domain of SARA (SARA-SBD, residues 665–721) was formed by incubation with excess SARA-SBD and purified by cation-exchange chromatography. The resulting pure protein complex was concentrated to 0.25 mM and a fourfold molar excess of the caged peptide **1** was added to initiate the ligation reaction (Figure 1). The reaction was monitored by RP-HPLC, ESMS, and sodium



Scheme 1. Synthesis of doubly caged phosphopeptide **1**. a) 1. *O*-1-(2-nitrophenyl)ethyl-*O'*- β -cyanoethyl-*N,N*-diisopropylphosphoramidite, 4,5-dicyanoimidazole, DMF (anhydrous); 2. 1 M *t*BuOOH, CH₂Cl₂ (anhydrous); b) 92.5 % TFA, 2.5 % EDT, 2.5 % TIS, 2.5 % H₂O; c) 1 % DBU, DMF then 0.5 M MeONH₂·HCl, H₂O. TFA = trifluoroacetic acid, EDT = 1,2-ethanedithiol, TIS = triisopropylsilane.

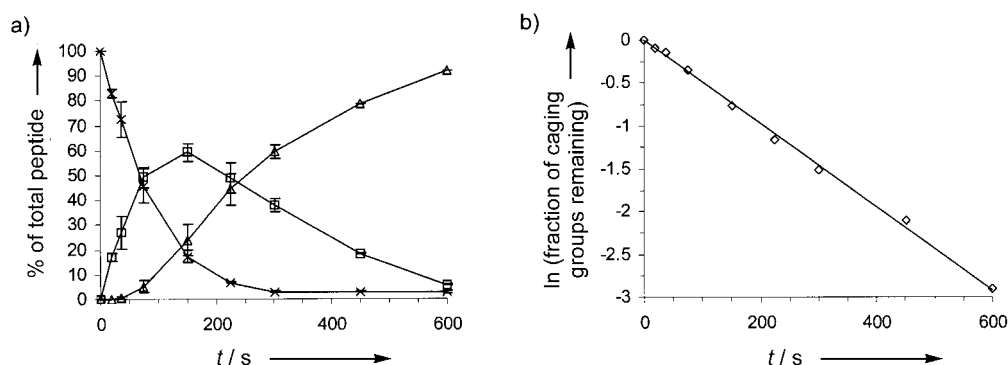


Figure 2. Photolysis kinetics of doubly caged phosphopeptide **1** labeled with fluorescein-5-maleimide (**1-FI**). a) A solution of **1-FI** at $10\ \mu\text{M}$ was irradiated with low-intensity UV light ($312\ \text{nm}$, $2\ \text{mWcm}^{-2}$) for the times indicated and subjected to RP-HPLC for quantitation of the doubly caged (\times), singly caged (\square), and uncaged forms (\triangle). The percentage of each is plotted versus time of irradiation. b) The fraction of caging groups remaining was calculated and the natural logarithm at each time point plotted versus time of irradiation, along with a line of best fit, which yielded a first-order rate constant for photolysis of $4.9 \times 10^{-3}\ \text{s}^{-1}$ and an r^2 value of 0.99. The mean of two experiments is plotted for both (a) and (b), and the standard deviation is represented by error bars in (a).

dodecyl sulfate/polyacrylamide gel electrophoresis (SDS-PAGE) and was complete after 12 h. The caged protein was purified by preparative size-exclusion chromatography (SEC) and its identity was confirmed by ESMS (Figure 3c).

To be deemed effective, the caged protein should behave as if it was nonphosphorylated in the absence of UV light and should display all the properties of the active, doubly phosphorylated Smad2-MH2 when uncaged by UV light. We therefore proceeded with studies designed to determine the oligomerization state of the caged protein before and after UV irradiation. Gratifyingly, the caged protein mimicked nonphosphorylated Smad2-MH2, since it bound SARA-SBD in a 1:1 molar ratio (Figure 3a). This heterodimeric arrangement of Smad2-MH2 and SARA-SBD was verified by SEC coupled with multi-angle laser light scattering (MALLS) detection at a loading concentration of $5\ \mu\text{M}$ (see the Supporting Information).^[13] MALLS analysis indicated that

the caged protein had a slight residual tendency to form homotrimers at higher loading concentrations ($25\text{--}50\ \mu\text{M}$; see the Supporting Information). Indeed, in preliminary studies where only one caging group was installed on either phosphoserine 465 or 467, this tendency to oligomerize was even more pronounced (data not shown). Importantly, the tendency of the doubly caged protein to homo-oligomerize is concentration-dependent, such that at physiologically relevant concentrations ($<5\ \mu\text{M}$)^[14] this behavior is no longer observed. Brief irradiation ($<5\ \text{s}$) of the caged protein with the output of the He-Cd laser followed by SEC, RP-HPLC, and ESMS demonstrated that the caging groups were quantitatively removed from the protein and that SARA-SBD was released from Smad2-MH2 in favor of homotrimerization (Figure 3).

As a step toward our ultimate goal of using caged phosphoproteins in live cells to study the kinetics of biological

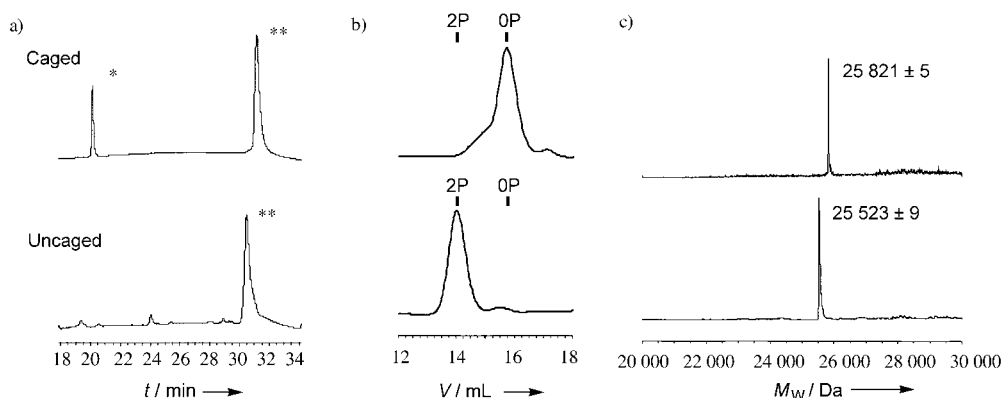


Figure 3. Characterization of caged (top panels) and uncaged (bottom panels) Smad2-MH2. Caged Smad2-MH2 was converted into uncaged Smad2-MH2 by irradiation for 5 s with a He-Cd laser ($325\ \text{nm}$, $4.74\ \text{Wcm}^{-2}$). a) The ratio of caged and uncaged Smad2-MH2 to SARA-SBD was determined by subjecting the caged and uncaged proteins to RP-HPLC with detection at $214\ \text{nm}$ and integrating the peaks corresponding to SARA-SBD (*) and Smad2-MH2 (**). The peak area ratio of caged Smad2-MH2:SARA-SBD is 4:1, which at $214\ \text{nm}$ indicates a 1:1 molar ratio. b) The homo-oligomeric status of caged and uncaged Smad2-MH2 was assessed by SEC with detection at $280\ \text{nm}$. The elution positions of doubly phosphorylated Smad2-MH2 (2P) and nonphosphorylated Smad2-MH2 (0P) controls are indicated. c) The reconstructed molecular weight from ESMS indicates that the caged protein (calcd $M_W = 25\ 818\ \text{Da}$) was assembled successfully. ESMS of the uncaged protein (calcd $M_W = 25\ 519\ \text{Da}$) indicates quantitative removal of the caging groups after laser irradiation. Observed molecular weights are also shown.

signaling and transport processes, we set out to determine the behavior of caged Smad2-MH2 in a nuclear import assay. When incubated with digitonin-permeabilized HeLa cells in the presence of SARA-SBD, nonphosphorylated Smad2-MH2 (OP) is excluded from the nucleus, whereas phosphorylated Smad2-MH2 (2P) accumulates in the nucleus (Figure 4).^[14] UV irradiation had no effect on the localization

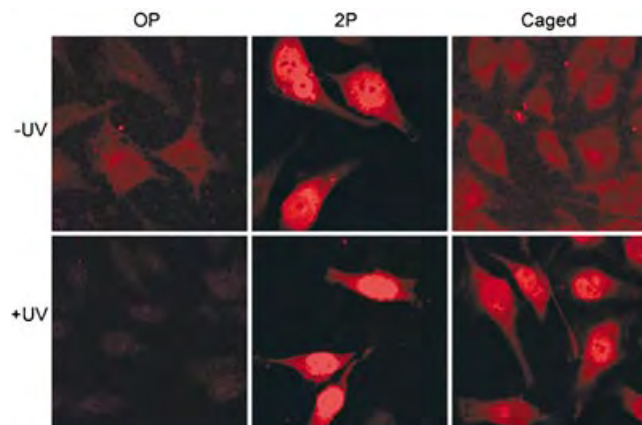


Figure 4. Nuclear import assay of Smad2-MH2 variants labeled with Texas Red C₂-maleimide. Nonphosphorylated (OP), doubly phosphorylated (2P), and caged Smad2-MH2 before (top panels) and after UV (bottom panels) laser irradiation (as in Figure 3) were incubated separately at 1.5 μ M with digitonin-permeabilized HeLa cells for 20 minutes at room temperature in the presence of 4.5 μ M GST-SARA-SBD (GST = glutathione S-transferase), an ATP-regenerating system, and 1 mg mL⁻¹ bovine serum albumen (BSA). After the import reaction, cells were washed, fixed, and analyzed by confocal microscopy for the localization of each Smad2-MH2 variant. A control experiment was performed in which the import reactions were carried out on ice. This treatment prevented nuclear accumulation (data not shown), which is consistent with nuclear import of Smad2 being an energy dependent process, as previously demonstrated.^[14]

pattern of phosphorylated and nonphosphorylated Smad2-MH2 control proteins (Figure 4). In the same assay we found that caged Smad2-MH2 was excluded from the nucleus, whereas uncaging of the protein with UV light led to dramatic nuclear accumulation (Figure 4). This demonstrates that the caged and uncaged proteins behave as desired in a biological context.

In summary, we have prepared Smad2-MH2 caged on two activating phosphate residues by a semisynthetic route. The molecule described represents the first report of a protein caged on a phosphate group. In principle, this approach can be applied to the construction of a caged version of any protein activated by phosphorylation. We are currently investigating this and other strategies of molecular photocontrol over protein function with live cell-imaging techniques.^[15] These studies are expected to yield quantitative insight into the kinetics of Smad2 nuclear import and export. Additionally, we plan to address fundamental questions regarding the importance of signal strength and duration in biological processes.

Received: July 1, 2004

Keywords: bioorganic chemistry · phosphorylation · photochemistry · proteins · semisynthesis

- [1] K. Curley, D. S. Lawrence, *Curr. Opin. Chem. Biol.* **1999**, 3, 84–88.
- [2] a) Y. G. Shi, J. Massague, *Cell* **2003**, 113, 685–700; b) P. M. Siegel, J. Massague, *Nat. Rev. Cancer* **2003**, 3, 807–820.
- [3] J. W. Wu, M. Hu, J. Chai, J. Seoane, M. Huse, C. Li, D. J. Rigotti, S. Kyin, T. W. Muir, R. Fairman, J. Massague, Y. Shi, *Mol. Cell* **2001**, 8, 1277–1289.
- [4] T. Hunter, *Cell* **2000**, 100, 113–127.
- [5] a) D. M. Rothman, M. E. Vazquez, E. M. Vogel, B. Imperiali, *Org. Lett.* **2002**, 4, 2865–2868; b) M. E. Vazquez, M. Nitz, J. Stehn, M. B. Yaffe, B. Imperiali, *J. Am. Chem. Soc.* **2003**, 125, 10150–10151.
- [6] K. Zou, W. T. Miller, R. S. Givens, H. Bayley, *Angew. Chem.* **2001**, 113, 3139–3141; *Angew. Chem. Int. Ed.* **2001**, 40, 3049–3051; b) M. Ghosh, I. Ichetovkin, X. Song, J. S. Condeelis, D. S. Lawrence, *J. Am. Chem. Soc.* **2002**, 124, 2440–2441; c) K. Zou, S. Cheley, R. S. Givens, H. Bayley, *J. Am. Chem. Soc.* **2002**, 124, 8220–8229; d) M. Ghosh, X. Song, G. Mouneimne, M. Sidani, D. S. Lawrence, J. S. Condeelis, *Science* **2004**, 304, 743–746.
- [7] T. W. Muir, *Annu. Rev. Biochem.* **2003**, 72, 249–289.
- [8] M. Huse, M. N. Holford, J. Kuriyan, T. W. Muir, *J. Am. Chem. Soc.* **2000**, 122, 8337–8338.
- [9] P. Cohen, *Trends Biochem. Sci.* **2000**, 25, 596–601.
- [10] M. Villain, J. Vizzavona, H. Gaertner, Proc. Second Int. Seventeenth Am. Peptide Symp. (San Diego, CA, USA), **2001**, 107–108.
- [11] N. Kuder, T. Zelinski, T. Pathak, O. Seitz, H. Waldmann, *Bioorg. Med. Chem.* **2000**, 8, 2433–2439.
- [12] Attachment of fluorescein to **1** allowed the photolysis reaction to be easily monitored by RP-HPLC.
- [13] E. Foltá-Stogniew, K. R. Williams, *J. Biomol. Tech.* **1999**, 10, 51–63.
- [14] L. Xu, Y. G. Chen, J. Massague, *Nat. Cell Biol.* **2000**, 2, 559–562.
- [15] J. P. Pellois, M. E. Hahn, T. W. Muir, *J. Am. Chem. Soc.* **2004**, 126, 7170–7171.

DNA Superstructures

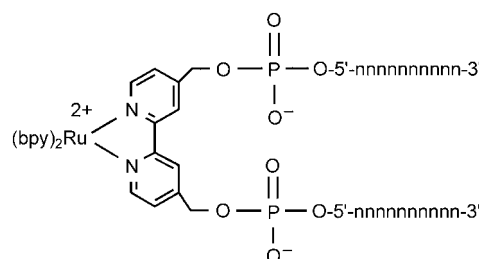
Self-Assembly of Cyclic Metal–DNA Nanostructures using Ruthenium Tris(bipyridine)-Branched Oligonucleotides**

Debbie Mitra, Nicolas Di Cesare, and
Hanadi F. Sleiman*

One of the promises of nanoscience is the creation of ordered structures that contain addressable molecular components, which are designed to accomplish complex operations.^[1] However, whereas many functional molecular components have already been constructed, methods to assemble them in a deliberately designed manner on the nanometer scale have yet to be devised.^[1,2] In this respect, DNA has emerged as a promising template to accomplish this task because of its uniquely selective self-assembly, ready programmability, and facile synthesis.^[3–5] In principle, short (10–30-bases long) strands of DNA can rapidly self-assemble into relatively rigid, programmable, higher-order DNA structures.^[5] Pioneering work by Seeman demonstrated the use of modified Holliday junctions as oligonucleotide-based vertices in the assembly of complex two- and three-dimensional nanostructures.^[3a–c] DNA nanostructures have also been constructed^[3] through the use of oligonucleotide–gold colloidal particles,^[3d–f] biotin–avidin interactions,^[3g] guanine quartets,^[3h,i] and organic vertices.^[3j–l]

We are interested in the creation of cyclic transition-metal–DNA nanostructures that contain short DNA duplexes as arms and transition-metal centers as vertices. In these well-defined supramolecular structures, DNA serves as a nanoscale rigid molecule to spatially position addressable transition metals, which have intrinsic properties such as luminescence and redox activity,^[6] into an ordered array. Whereas transition metals have been used to generate 3D DNA networks,^[4a–c] linear DNA arrays,^[4d] and metalated DNA,^[4g–h] to our knowledge, discrete cyclic metal–DNA structures have not been previously accessed.^[4] Herein, we report the synthesis and properties of a branched ruthenium(II)–DNA complex, in which two parallel DNA strands are linked to a

relatively rigid Ru^{II} tris(bipyridine) center.^[9] Self-assembly of this molecule leads to the formation of a discrete metal–DNA cyclic nanostructure, which contains two DNA duplexes and



1: n=DNA nucleotide

two redox- and photoactive [Ru(bpy)₃]²⁺ centers (bpy = bipyridine). Furthermore, we show that branched oligonucleotides based on the non-metalated ligand undergo less-selective association, which illustrates the role of the transition metal in this self-assembly process.

In a preliminary report,^[10] we described the synthesis of an oligonucleotide-branched transition-metal complex through a convergent, solid-phase approach. In its initial design, a ruthenium(II) center was linked to two d[T₁₀] DNA strands through flexible six-carbon spacers and two monodentate imidazole ligands. To better control the self-assembly of these complexes, we needed to expand this solid-phase strategy to access relatively rigid, branched DNA complexes with mixed DNA sequences.^[11] The vertex used here was based on the complex, *cis*-[Ru(bpy)₂(4,4'-bis(hydroxymethyl)-2,2'-bipyridine)][PF₆]₂ (**2**, see Scheme 1),^[8] which exhibits both luminescence and redox activity. Examination of a number of X-ray crystal structures reported for related complexes indicates that the ruthenium center should orient the 4,4'-carbon centers at an angle of $\approx 70^\circ$ (C...Ru...C), whereas in the free ligand the carbon centers are directed in a transoidal fashion.^[9] Complex **2** was first converted into the bis(phosphoramidite) derivative **3** by reaction with chloro(cyanoethyl)-*N,N*-diisopropylphosphoramidite.^[7] In parallel, a number of DNA sequences were synthesized on a high-density controlled-pore glass (CPG, 56–64 $\mu\text{mol g}^{-1}$) support (Scheme 1). After the removal of the protecting dimethoxytrityl groups from the DNA sequences, the ruthenium complex **3** was added to the oligonucleotide-functionalized CPG support. After oxidation, the DNA-linked Ru complexes were then cleaved from the support.^[7]

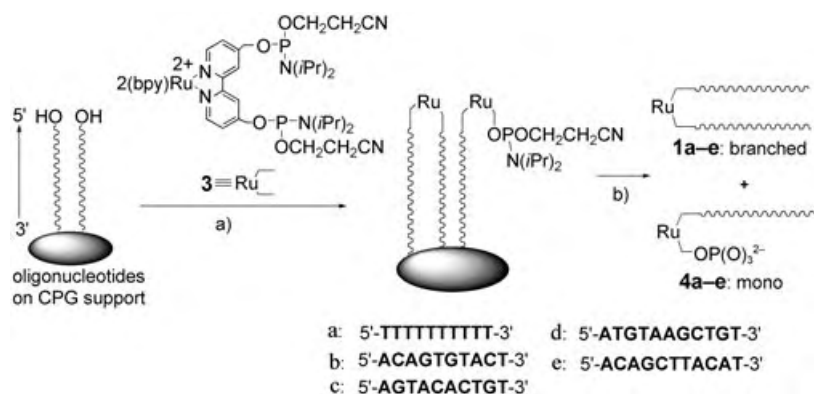
The products of this convergent synthesis were isolated by using denaturing polyacrylamide gel electrophoresis (PAGE), and their structures were analyzed by using PAGE, anion-exchange HPLC, and MALDI-TOF mass spectrometry. The fastest moving band in the gel was identified as unmodified DNA, and the next band was identified as the mono(DNA)-functionalized Ru complex **4** (Scheme 1), which resulted from the coupling of the ruthenium vertex **3** to only one oligonucleotide strand on the solid support. The slowest moving species was confirmed as the desired DNA-branched ruthenium conjugate **1** by MALDI-TOF MS. In parallel to the

[*] D. Mitra, Prof. H. F. Sleiman
Department of Chemistry, McGill University
801 Sherbrooke Street West, Montreal
Quebec H3A2K6 (Canada)
Fax: (+1) 514-398-3797
E-mail: hanadi.sleiman@mcgill.ca

Dr. N. Di Cesare
Cascades Canada Inc.
Boulevard Marie Victorin, Kingsey Falls
Quebec J0A1B0 (Canada)

[**] This work was supported by NSERC (Canada), the Research Corporation (USA), Nanoquebec, CFI (Canada), and the FQRNT Centre for Self-Assembled Chemical Structures. The authors gratefully acknowledge Antisar Hlil for acquiring the MALDI-TOF mass spectra. H.F.S. is a Cottrell Scholar of the Research Corporation.

Supporting information for this article is available on the WWW under <http://www.angewandte.org> or from the author.



Scheme 1. Convergent synthesis of the mono- and branched oligonucleotide-Ru(II) complexes; a) tetrazole, room temperature, 2 h; b) I_2 , pyridine, H_2O , then conc. NH_4OH , 12 h, 55°C .

generation of the ruthenium-DNA conjugates, DNA-branched bipyridine conjugates **5d-e** were also prepared by a similar solid-phase convergent strategy and were isolated and purified by denaturing PAGE (Figure 1).^[7] The UV/Vis absorption spectra of the Ru-DNA conjugates **1** exhibited transitions at $\lambda = 260$ nm which are characteristic of the heterocyclic DNA bases. The bipyridine $\pi-\pi^*$ and metal-to-ligand charge-transfer (MLCT) transitions were observed at $\lambda \approx 280$ and 454 nm, respectively.^[7] Upon irradiation at $\lambda = 454$ nm, the fluorescence spectra of the ruthenium-

oligonucleotide conjugates **1** showed an emission peak at $\lambda = 615$ nm which was identical to that of the unconjugated Ru complex **2** (Figure 2c).^[7] Thus, the fluorescence properties of the ruthenium-bipyridine species are retained in the DNA-branched Ru conjugates.

Because of the branched architecture of the Ru-DNA complexes **1**, it was important to assess the propensity of the DNA arms to form stable duplexes upon hybridization with their complementary partners. Thermal denaturation experiments of complex **1b** in the presence of two equivalents of the complementary oligonucleotide **c** showed the conventional sigmoidal melting-temper-

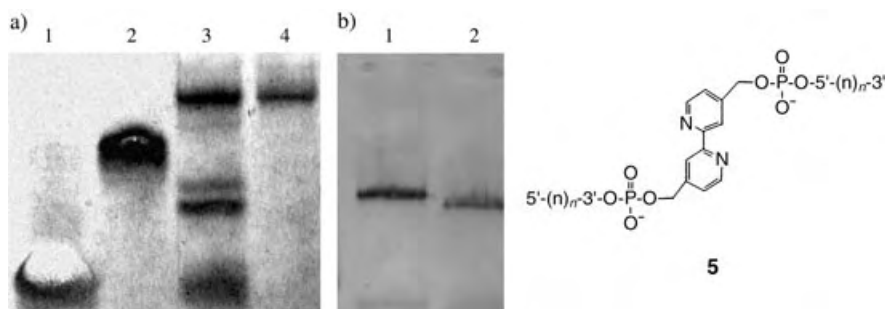


Figure 1. a) Denaturing with 24% PAGE: lane 1) 11-mer control DNA, d; lane 2) 21-mer control DNA; lane 3) crude mixture of **1d**; lane 4) $[\text{Ru}(\text{bpy})_3]^{2+}$ -bis(DNA) **1d**. b) Denaturing with 24% PAGE: lane 1) bpy-bis(DNA) **5d**; lane 2) bpy-bis(DNA) **5e**. n = DNA nucleotide.

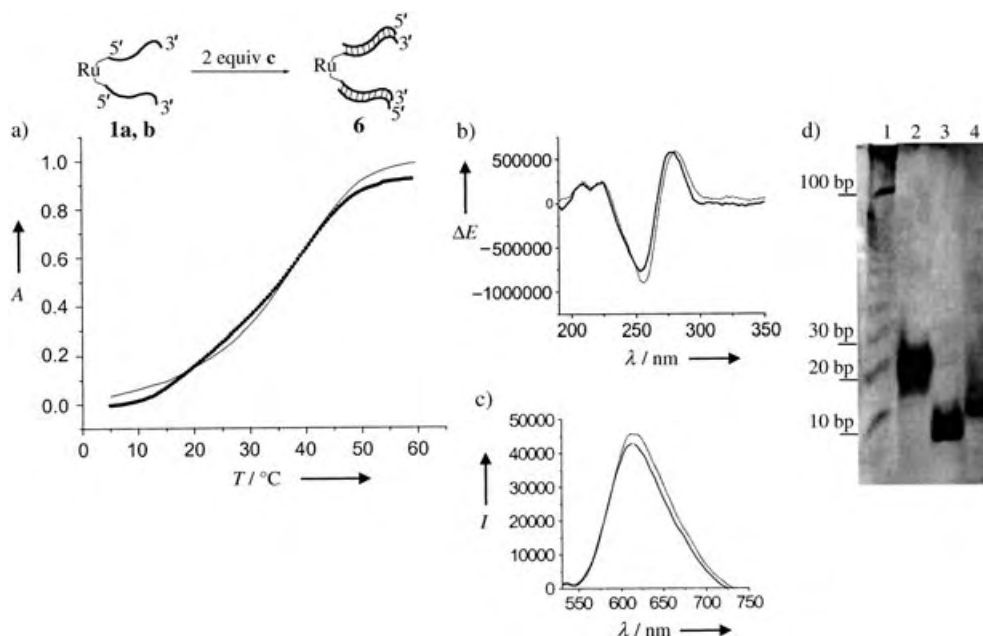
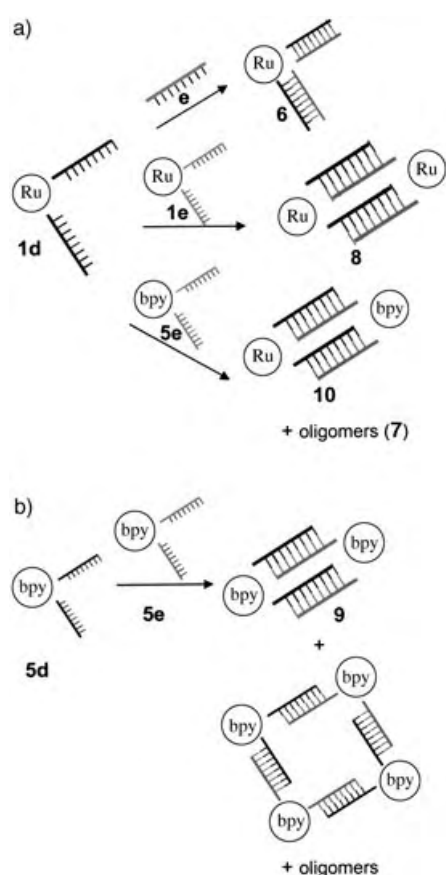


Figure 2. a) Thermal denaturation curves for complex **1**: relative absorbances at $\lambda = 260$ nm of the control duplex **b-c** (—) and the oligonucleotide-branched ruthenium complex **1b** with two equivalents of the single-stranded oligonucleotide **c** (.....). b) CD spectra of the oligonucleotide-branched ruthenium complex **1b** hybridized to 2 equivalents of the complementary oligonucleotide **c** (—) and the control duplex, **b-c** (-----) in TMS (Tris, 50 mM; MgCl_2 , 10 mM; NaCl, 100 mM; pH 8) buffer solutions. c) Steady-state emission spectra of the conjugate **1b** (-----) and **1b** hybridized with 2 equivalents of complement **c** (—) in TMS buffer solutions at 5°C . d) Native PAGE image (TMS buffer): lane 1) 10–330 base-pair ladder; lane 2) Ru-bis(duplex) **6**; lane 3) control duplex **d-e**; lane 4) oligonucleotide-branched ruthenium complex **1d**. bp = base-pair.

ature curves for a DNA duplex (Figure 2a).^[7] Interestingly, a slight increase (1–4 °C) in the melting temperature was observed for the oligonucleotides in the Ru–DNA conjugates **1** relative to the melting temperature of the Watson–Crick control duplex.^[5] Thermal denaturation experiments were also carried out for the mono(DNA)-functionalized Ru complexes **4**, which do not possess a branched architecture. These complexes exhibited a similar enhancement in duplex stability (melting temperatures were increased by 4 °C) which indicates that the positively charged Ru center is likely responsible for this effect in both the mono- and the branched DNA–Ru^{II} complexes.^[7] Further evidence for the formation of a B-DNA duplex was obtained by circular dichroism (CD) spectroscopy (Figure 2b).^[12]

Figure 2d shows an image from the native PAGE analysis of the hybridization product of complex **1d** with two equivalents of a complementary DNA, **e** (Scheme 2). This



Scheme 2. a) Discrete $[\text{Ru}(\text{bpy})_3]^{2+}$ –DNA nanostructures through the self-assembly of **1**, and b) discrete bpy–DNA nanostructures from **5**.

gives rise to a band with electrophoretic mobility similar to that of a duplex that contains 40 nucleotides in the molecular-weight marker ladder. This band can thus be assigned to the Ru–bis(duplex) conjugate **6** (that contains 44 bases, Scheme 2).^[13] Molecular modeling studies of complex **6** show no apparent steric barrier to the formation of two duplex arms at the 4,4'-positions of the bipyridine ligand.^[7] Ru–bis(duplex) **6** was examined by fluorescence spectroscopy;

upon excitation at 454 nm, an emission at $\lambda = 616$ nm was observed which showed a $\approx 6\%$ decrease in its intensity relative to that of the unhybridized DNA–Ru complex **1** (Figure 2c).^[14] Thus, upon hybridization with their complementary partners, the branched Ru^{II} complexes form stable bis(duplex) systems and retain their fluorescence properties.

In light of the ability of complexes **1** to form stable duplexes, we explored the self-assembly of two complementary Ru^{II}-branched oligonucleotides. In principle, this association can result in either discrete cyclic structures or linear oligomeric/polymeric species.^[15] We anticipated that the relative rigidity of the ruthenium vertex in complexes **1** would result in a more efficient formation of cyclic products. Self-assembly was first examined by heating equimolar solutions of the DNA-branched Ru complex **1d** and its complement **1e** to 90 °C, followed by slow cooling of the mixture to 4 °C ($1.8^\circ\text{C min}^{-1}$, 12 h). PAGE analysis revealed the formation of products of extremely slow mobility which correspond to at least 330 base-pairs for the molecular-weight marker (Scheme 2, Figure 3a). This points to the formation of

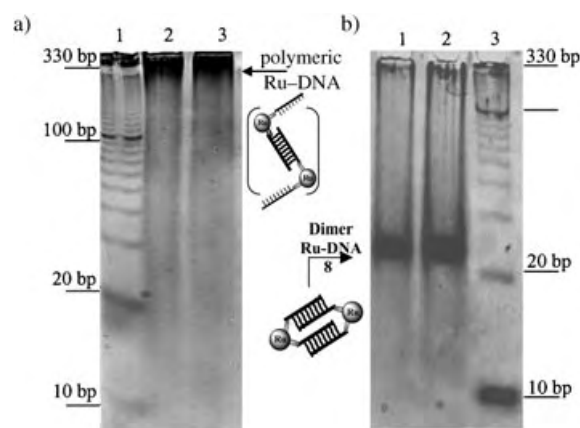


Figure 3. Native PAGE analyses: a) Hybridization from 90 to 4 °C overnight: lane 1) 10–330 base-pair ladder; lane 2) solution of **1d–1e** (20 μM) in TMS; lane 3) solution of **1d–1e** (40 μM) in TMS. b) Hybridization at 4 °C overnight: lane 1) solution of **1d–1e** (40 μM) in TMS; lane 2) solution of **1d–1e** (20 μM) in TMS; lane 3) 10–330 base-pair ladder.

linear polymeric DNA–Ru species **7** (Figure 3a). Interestingly, when the self-assembly of **1d** with **1e** was carried out under milder conditions (4 °C, 12 h), one major discrete product formed along with small amounts of polymeric species. The mobility of this Ru–DNA structure corresponds to a 44-base molecular-weight marker and is consistent with the formation of a dimer, **8**, which contains two DNA duplexes (44 nucleotides) and two $[\text{Ru}(\text{bpy})_3]^{2+}$ vertices (Scheme 2, Figure 3b). To determine whether this dimer was an open, linear product or a cyclic molecule, enzymatic digestion with Mung Bean Nuclease was conducted.^[16] This enzyme is selective to the degradation of single-stranded DNA. It is thus expected to degrade open, oligomeric species that contain single DNA strands, but to leave closed, cyclic species that contain double DNA strands intact. Under conditions that cause the degradation of single-stranded

DNA, the dimer **8** remained unmodified by the enzyme.^[7] Thus, the self-assembly of the DNA-branched Ru complexes **1** generates a discrete metal–DNA cyclic nanostructure.^[17]

To probe the role that the transition-metal ion plays in the self-assembly process, a hybridization experiment was carried out with the unmetalated bipyridine–bis(DNA) conjugates **5**. The DNA-branched bipyridine molecules **5** are expected to show a higher flexibility than the DNA-branched Ru complexes **1** and a twist of the two DNA strands into a transoidal arrangement.^[9] Samples **5d** and **5e** were combined under similar hybridization conditions (4°C, 12 h, Scheme 2, Figure 4). In addition to a band that was assigned to a dimeric

contain a bipyridine ligand as one of their vertices, structures **9** and **10** can potentially be further functionalized with other transition-metal ions (such as Cu⁺, Ag⁺, and Zn²⁺), and thus they have the potential to form hybrid multimetallic DNA nanostructures and networks.^[4]

In conclusion, we have demonstrated the solid-phase, convergent synthesis of DNA-branched Ru^{II} complexes **1** and their self-assembly into the first cyclic metal–DNA nanostructures.^[18] These supramolecular structures contain two DNA duplex arms and two relatively rigid photo- and electroactive [Ru(bpy)₃]²⁺ vertices. We have also shown that branched DNA complexes with unmetalated bipyridine

vertices undergo less-selective self-assembly, which illustrates the role of the transition metal in this process. The transition-metal units in these nanostructures are readily addressable by means of light or electrical energy. Thus, this study represents a new method to use the selective association of DNA to organize functional molecular components on the nanometer scale. Efforts towards understanding the factors that govern the self-assembly process, the isolation of these cyclic structures and the study of their properties, as well as scanning probe microscopy experiments are currently underway.

Received: April 7, 2004

Revised: July 29, 2004

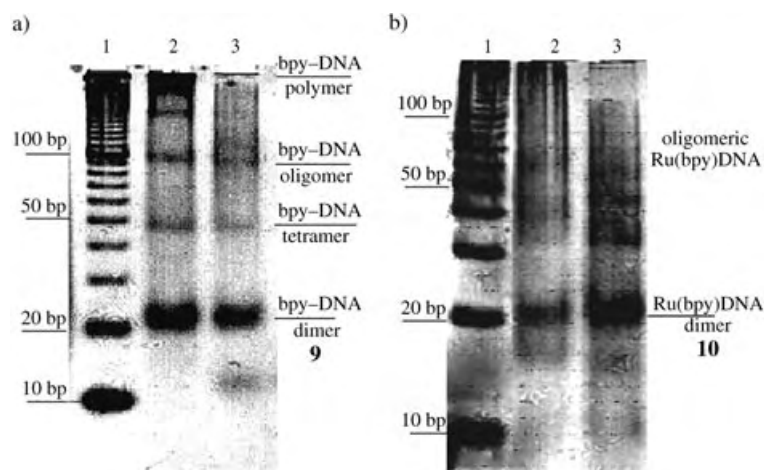


Figure 4. Native PAGE analyses: a) Hybridization with unmetalated-bipyridine–DNA conjugates **5** at 4°C overnight: lane 1) 10–330 base-pair ladder; lane 2) solution of **5d–5e** (20 μM) in TMS; lane 3) solution of **5d–5e** (20 μM) in TMS with added enzyme. b) Hybridization at 4°C overnight of oligonucleotides from the metalated complex **1** with those of the unmetalated conjugates **5**: lane 1) 10–330 base-pair ladder; lane 2) solution of **5d–1e** (20 μM) in TMS; lane 3) solution of **5d–1e** (20 μM) in TMS solution with added enzyme.

species **9**, which contains two bipyridine moieties and two DNA duplexes, several bipyridine assemblies that ranged from tetramers to significant amounts of higher-order oligomers/polymers were observed (Figure 4, Scheme 2). Enzymatic digestion of the hybridized products did not affect the discrete bands that correspond to the dimer and tetramer, which indicates that they therefore correspond to cyclic products. These results are in contrast to the behavior of the DNA-branched Ru complexes **1**, which form the dimer **8** as the sole cyclic product, and illustrate the active role of the transition-metal ion in the self-assembly of these higher-order DNA structures.

Finally, to create hybrid DNA structures that contain both [Ru(bpy)₃]²⁺ units and unfunctionalized bipyridine vertices, the self-assembly of the DNA-branched Ru complex **1d** with the DNA-branched bipyridine **5e** was examined (4°C, 12 h, Scheme 2). This led to the formation of a cyclic dimer **10**, which contains two DNA duplexes and one ruthenium–bipyridine and one bipyridine vertex, along with higher molecular-weight oligomeric species (Figure 4, Scheme 2). The cyclic nature of the dimer **10** was also confirmed by enzymatic digestion with Mung Bean Nuclease. As they

Keywords: bioinorganic chemistry · DNA · nanostructures · ruthenium · self-assembly

- [1] K. E. Drexler, *Nanosystems: Molecular Machinery, Manufacturing and Computation*, Wiley Interscience, New York, **1992**.
- [2] Some representative examples: a) R. Ballardini, V. Balzani, A. Credi, M. T. Gandolfi, M. Venturi, *Acc. Chem. Res.* **2001**, *34*, 445–455; b) J. Tour, *Acc. Chem. Res.* **2000**, *33*, 791–804.
- [3] a) N. C. Seeman, *Nature* **2003**, *421*, 427–431; b) N. C. Seeman, *Biochemistry* **2003**, *42*, 7259–7269; c) N. C. Seeman, *Annu. Rev. Biophys. Biomol. Struct.* **1998**, *27*, 225–248; d) J. J. Storhoff, C. A. Mirkin, *Chem. Rev.* **1999**, *99*, 1849–1862; e) C. A. Mirkin, R. L. Letsinger, R. C. Mucic, J. J. Storhoff, *Nature* **1996**, *382*, 607–609; f) A. P. Alivisatos, K. P. Johnsson, X. Peng, T. E. Wilson, C. J. Loweth, M. P. Bruchez, P. G. Schultz, *Nature* **1996**, *382*, 609–611; g) C. M. Niemeyer, *Curr. Opin. Chem. Biol.* **2000**, *4*, 609–618; h) R. P. Fahlman, M. Hsing, C. S. Sporer-Tuhten, D. Sen, *Nano Lett.* **2003**, *3*, 1073–1078; i) R. P. Fahlman, D. Sen, *J. Am. Chem. Soc.* **1999**, *121*, 11079–11085; j) J. Shi, D. E. Bergstrom, *Angew. Chem.* **1997**, *109*, 70–72; *Angew. Chem. Int. Ed. Engl.* **1997**, *36*, 111–113; k) M. Scheffler, A. Dorenbeck, S. Jordan, M. Wustefeld, G. von Kiedrowski, *Angew. Chem.* **1999**, *111*, 3514–3518; *Angew. Chem. Int. Ed.* **1999**, *38*, 3312–3315; l) M. S. Shchepinov, K. U. Mir, J. K. Elder, M. D. Frank-Kamenetskii, E. Southern, *Nucleic Acids Res.* **1999**, *27*, 3035–3041; m) W. M. Shih, J. D. Quispe, G. F. Joyce, *Nature* **2004**, *427*, 618–621.
- [4] a) K. M. Stewart, L. W. McLaughlin, *J. Am. Chem. Soc.* **2004**, *126*, 2050–2057; b) K. M. Stewart, L. W. McLaughlin, *Chem. Commun.* **2003**, 2934–2935; c) K. V. Gothelf, A. Thomsen, M. Nielsen, E. Clo, R. S. Brown, *J. Am. Chem. Soc.* **2004**, *126*, 1044–

- 1046; d) S. M. Waybright, C. P. Singleton, K. Wachter, C. J. Murphy, U. H. F. Bunz, *J. Am. Chem. Soc.* **2001**, *123*, 1828–1833; e) J. L. Czapinski, T. L. Sheppard, *J. Am. Chem. Soc.* **2001**, *123*, 8618–8619; f) S. Takenaka, Y. Funatsu, H. Kondo, *Chem. Lett.* **1996**, 891–892; g) K. Tanaka, A. Tengeji, T. Kato, N. Toyama, M. Shionoya, *Science* **2003**, *299*, 1212–1213; h) K. Tanaka, Y. Yamada, M. Shionoya, *J. Am. Chem. Soc.* **2002**, *124*, 8802–8803.
- [5] V. A. Bloomfield, D. M. Crothers, I. Tinoco, Jr., *Nucleic Acids: Structures, Properties, and Functions*, University Science Books, Sausalito, USA, **2000**.
- [6] Y. Tor, *Synlett* **2002**, *7*, 1043–1054, and references therein.
- [7] Please refer to the Supporting Information for details.
- [8] J. E. Collins, J. J. S. Lamba, J. C. Love, J. E. McAlvin, C. Ng, B. P. Peters, X. Wu, C. L. Fraser, *Inorg. Chem.* **1999**, *38*, 2020–2024.
- [9] a) D. Heseck, Y. Inoue, S. R. L. Everitt, H. Ishida, M. Kunieda, M. G. B. Drew, *Chem. Commun.* **1999**, 403–404; b) A. C. Benninston, P. R. Mackie, L. J. Farrugia, G. Smith, S. J. Teat, A. J. McLean, *New J. Chem.* **2001**, *25*, 458–464. The ruthenium–bpy linker in **1** is described as “relatively rigid” because it contains only one point of conformational flexibility (one sp³ carbon center attached to its 4- and 4'- positions), and the Ru center inhibits the twist of the two pyridine rings about the 2,2' bond in this ligand.
- [10] I. Vargas-Baca, D. Mitra, H. J. Zolyniak, J. Banerjee, H. F. Sleiman, *Angew. Chem.* **2001**, *113*, 4765–4768; *Angew. Chem. Int. Ed.* **2001**, *40*, 4629–4632.
- [11] M. J. Damha, K. Ganeshan, R. H. E. Hudson, S. V. Zabarylo, *Nucleic Acids Res.* **1992**, *20*, 6565–6573.
- [12] The product from the hybridization of complex **1b** with 2 equivalents of complementary DNA exhibits a characteristic CD spectrum of a B-DNA: a negative band at $\lambda=253$ nm, a crossover point at $\lambda=265$ nm, and a positive band at $\lambda=277$ nm (Figure 2b, solid line). This is very similar to the CD spectrum of the control duplex, **b–c**, which exhibits a negative band at $\lambda=255$ nm, a crossover point at $\lambda=267$ nm, and a positive band at $\lambda=280$ nm (Figure 2b, dashed line); N. Berova, K. Nakanishi, R. W. Woody, *Circular Dichroism: Principles and Applications*, 2nd Ed., Wiley-VCH, Weinheim, **2000**.
- [13] The products of the hybridization of the mono(DNA)-functionalized Ru complexes **4** with their single-stranded DNA complements are observed to have similar electrophoretic mobility to that of a control duplex. Thus, the positive charge of the Ru center does not appear to affect the migration of the Ru–DNA samples.
- [14] Please see the Supporting Information for changes in the fluorescence spectra of the Ru–bis(homopolymeric) sequence, **1a**, upon hybridization to complementary DNA. The results show a 10% decrease in fluorescence intensity upon hybridization.
- [15] a) S. Leininger, B. Olenyuk, P. J. Stang, *Chem. Rev.* **2000**, *100*, 853–908; b) S. R. Seidel, P. J. Stang, *Acc. Chem. Res.* **2002**, *35*, 972–983.
- [16] a) P. H. Johnson, M. Laskowski Sr., *J. Biol. Chem.* **1970**, *245*, 891–898; b) D. Kowalski, W. D. Kroeker, M. Laskowski Sr., *Biochemistry* **1976**, *15*, 4457–4463.
- [17] See Supporting Information for results of molecular modeling studies of **8**. The local energy minimum for **8** was obtained using the AMBER force field method.
- [18] **Note added in Proof:** After acceptance of this manuscript, a communication about the synthesis of DNA triangles with vertices of iron(II) bis(terpyridine) complexes has appeared: J. S. Choi, C. W. Kang, J. W. Yang, Y.-G. Kim, H. Han, *J. Am. Chem. Soc.* **2004**, *126*, 8606–8607.

Ru(II) Tris(bipyridyl) Complexes with Six Oligonucleotide Arms as Precursors for the Generation of Supramolecular Assemblies

Kristen M. Stewart, Javier Rojo, and
Larry W. McLaughlin*

Nucleic acids can assemble into higher-order structures on the basis of complementary Watson–Crick base pairing. This self-assembly process has been exploited by a number of researchers^[1–4] in the “bottom-up” approach to the generation of nonbiological structures of nanoscale dimensions.^[5] In some studies, these assemblies have been based solely upon complementary DNA hybridization in which branch points are created by double-crossover structures^[6,7] (generated as immobile junctions^[8–10]) that are similar to those of DNA recombination intermediates; higher-order DNA networks can be made by this approach.^[11,12] In other cases, DNA sequences have been tethered to multifunctional organic cores^[13,14] or inorganic complexes^[15–19] that are capable of self-assembling into more-complex networks such as dendrimers.^[20,21] Oligonucleotides have been tethered to gold nanoparticles,^[2,22,23] and complementary hydrogen bonding resulted in the formation of large assemblies that were used for diagnostics.^[24,25] Nucleic acids can also be functionalized by conjugation, and this approach has led to the development of nanostructures and devices,^[26,27] DNA–protein conjugates,^[24] and the assembly of two- and three-dimensional networks. DNA-based nanoscale assemblies have been used for the construction of nanowires.^[28,29] Herein we describe the preparation of six-oligonucleotide-armed ruthenium(II) tris-(bipyridyl)-centered complexes as precursors for the generation of supramolecular nanoscale assemblies.

In the present monomer design, we chose $[\text{Ru}(\text{bpy})_3]^{2+}$ with a Ru^{II} ion bound to three bipyridine (bpy) ligands as a core, and the DNA arms were tethered at the 4- and 4'-positions of each bipyridine ligand (Figure 1). Although $[\text{Ru}(\text{bpy})_3]^{2+}$ exists in two enantiomeric forms, substitution at all three 4 and 4' sites results in an octahedral arrangement of the substituents in both enantiomers. First, enantiomerically pure DNA– $[\text{Ru}(\text{bpy})_3]^{2+}$ conjugates should be attainable by appropriate chromatographic resolution of the Ru complexes as has been described for related ruthenium complexes,^[30–32] followed by their incorporation into DNA conjugates. However, such chromatographic separations are not yet routine, and successful isomer resolution still depends in part upon the nature of the complex. The choice of sequences

[*] Dr. K. M. Stewart, Dr. J. Rojo, Prof. L. W. McLaughlin
Department of Chemistry, Merkert Chemistry Center
2609 Beacon St., Boston College
Chestnut Hill, MA 02467 (USA)
Fax: (+1) 617-552-2705
E-mail: larry.mclaughlin@bc.edu



Supporting information for this article is available on the WWW under <http://www.angewandte.org> or from the author.

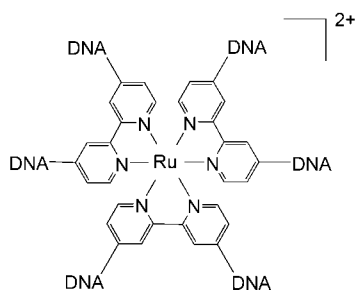


Figure 1. A $[\text{Ru}(\text{bpy})_3]^{2+}$ center with six DNA sequences tethered at the 4 and 4' positions.

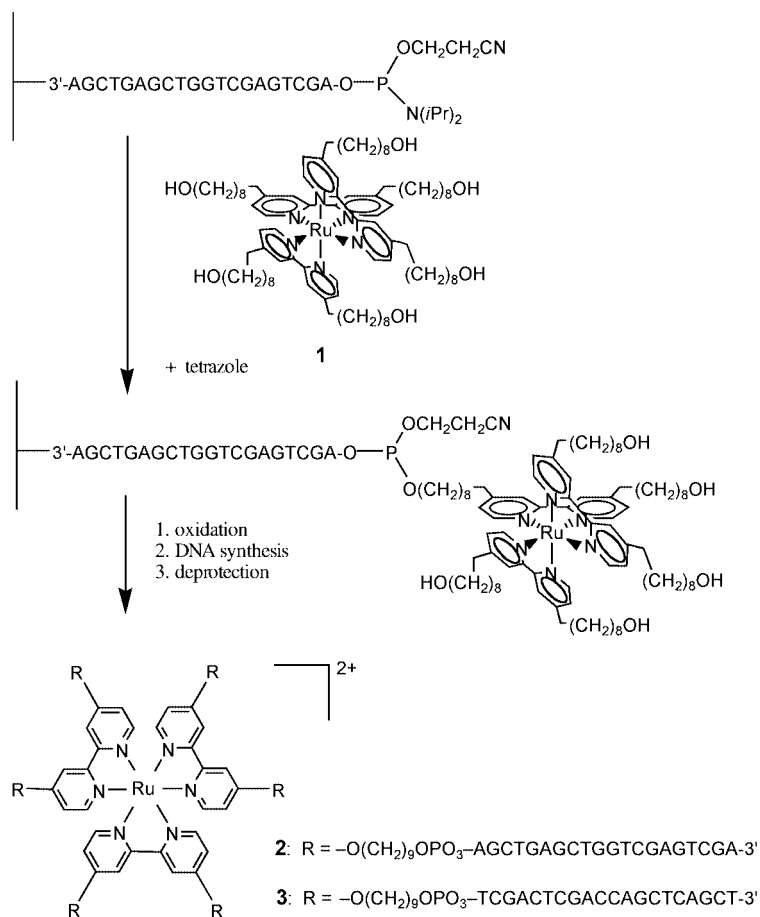
for the present building blocks is quite general, but self-assembly of monomers into higher-order structures requires either monomers that tether self-complementary sequences, or two or more monomers that tether complementary sequences.

Modeling studies suggested that a linker was required between the octahedral core and the DNA duplex to reduce steric crowding between the six termini of the tethered duplexes. A Ru^{II} complex **1** with six nine-carbon-atom linkers was prepared and then incorporated into a single, support-bound DNA sequence (Scheme 1). Subsequent extension of the remaining five linkers by solid-phase DNA synthesis completed the assembly of the monomers (Scheme 1). To generate a complex with six arms of the same sequence and

uniform polarity, we synthesized the initial sequence on a solid support in the conventional 3' to 5'-direction (Scheme 1). The Ru^{II} complex was then incorporated into the support-bound 20-mer by a reverse-coupling protocol.^[33,34] Synthesis of DNA in the unconventional 5' to 3'-direction by using the reverse nucleoside monomers^[35] (3'-dimethoxytrityl, 5'-phosphoramidites) allowed the functionalization of the remaining five linkers at the metal complex. During this latter process, the reaction times for the coupling reactions were extended to 60 min. With six hydroxy-terminated linkers present in **1** (see Scheme 1), it is conceivable that cross-linking of the synthesis support might occur; that is, one Ru^{II} complex could react with two (or more) support-bound DNA sequences. We believe this to be, at most, a minor reaction pathway, but for the described complexes it is also relatively unimportant with respect to the nature of the final product. Because all six sequences attached to the Ru tris(bipyridyl) center are identical both in sequence and polarity, complexes formed by either a single coupling or a cross-linking event to the support-bound sequence are all identical after deprotection. Control reactions with the Ru tris(bipyridyl) complex confirmed that $[\text{Ru}(\text{bpy})_3]^{2+}$ was stable to the basic conditions encountered during the deprotection of the DNA sequences.

The desired six-arm complexes **2** and **3** were purified by a combination of HPLC and PAGE (polyacrylamide gel electrophoresis) techniques. The reversed-phase HPLC traces typically resulted in three peaks (see Supporting Information). The third peak (37.9 min) corresponded to an orange-colored species and contained the product, namely **2** or **3** (see Scheme 1). The first peak (22.7 min) contained DNA without any ruthenium which resulted from the growth of DNA strands that had not coupled with the Ru complex **1**, whereas the second peak (33.1 min) remains unidentified. The desired complexes were isolated by HPLC with a C_{18} fast-flow Poros column, which gave essentially the same peak pattern as the analytical HPLC traces but broader peaks.

Isolation by PAGE was necessary to resolve the 5-arm and 6-arm DNA- $\text{Ru}(\text{bpy})_3$ monomers because the eluted fraction corresponding to the third peak during HPLC isolation comprised both species. The identity of the two conjugates was tentatively assigned from their relative migration in the gel, and this assignment was confirmed by using a hybridization assay (see below). The ratio of the 6-arm to 5-arm complex varied for each synthesis, but it was always at least 2:1. Yields of the 6-arm complex varied typically from 5–10 A_{260} units (absorbance units measured at 260 nm). This relatively low yield is at present largely a result of the need to use wide-pore (2000 Å) supports in the synthesis of the DNA; the initial DNA loading on these supports was generally no more than $8 \mu\text{mol g}^{-1}$. Furthermore, the reverse coupling step used to incorporate the Ru tris(bipyridyl) complex **1** into the DNA strand is not the high yielding reaction typical of phosphoramidite couplings. The six-arm DNA- Ru^{II} complex was characterized by MALDI-



Scheme 1.

TOF mass spectrometry and UV/Vis and fluorescence spectroscopies.

The number of DNA arms present in the isolated Ru-centered monomers was confirmed by stepwise hybridization with the complementary 20-mer (Figure 2). The desired six-arm complex (Figure 2, left panel) exhibited six hybridization products, each leading to a stepwise reduction in the mobility.

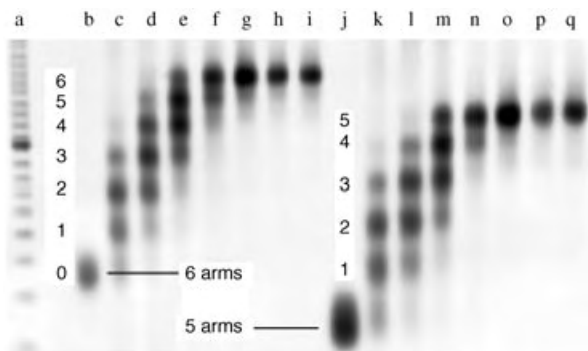


Figure 2. Nondenaturing PAGE analysis of DNA-[Ru(bpy)₃]²⁺ conjugates (≈25 nm) that result from the synthesis of **3**. Left panel, hybridization results for the 6-arm conjugate; right panel, hybridization results for the 5-arm conjugate. Lane a: 20 bp ladder; lane b: isolated 6-arm conjugate; lanes c–i: 6-arm conjugate with increasing amounts of the complementary 20-mer; lane j: isolated 5-arm conjugate; lanes k–q: 5-arm conjugate of lane 10 with increasing amounts of the complementary 20-mer. bp = base-pairs.

The hybridization bands on the gel are thought to correspond to six-arm-monomer complexes that have from one to six arms hybridized to the complementary 20-mer. Besides the identified six-arm complex, a second complex with slightly greater electrophoretic mobility was also isolated. The hybridization assay of this complex with the complementary 20-mer indicated that this material contained only five arms (Figure 2, right panel). These hybridization assays not only confirm the number of arms present, but they also confirm the ability of the arms to participate in hybridization reactions and exist as duplexes. Thermal melting studies were less helpful in the characterization of the hybridization products as a single transition resulted for all six duplexes.

The PAGE analyses of the DNA hybridization products in Figure 2 were complicated by migration anomalies. Migration of the hybridized complexes was only effective upon reduction of the cross-linking in the gels by using a 75:1 acrylamide:bisacrylamide mixture in place of the more conventional 19:1 mixture. However, even with reduced cross-linking, and presumably the presence of larger gel pores, the complexes appeared to migrate anomalously. The complex with six single-stranded arms exhibited a minimal anomaly of 1.13 (Table 1, 0 duplex arms): a moderate effect which suggests that the complex is still relatively flexible and that the geometry of placing six DNA arms about a central core does not significantly alter the nature of the gel migration. That is, the complex appears to be flexible enough to pass through the pores in a similar fashion to single- or double-stranded (ss or ds) DNA even though the geometry of the DNA complex is more starlike rather than linear. The observed small anomaly might be explained by the

Table 1: Migration Anomalies for [Ru(bpy)₃]²⁺ Complexes that Tether up to Six DNA Duplexes.^[a]

DNA Duplex Arms	0	1	2	3	4	5	6
Sequence Size	120	140	160	180	200	220	240
Apparent Size ^[b]	135	190	270	355	453	511	638
Migration Anomaly ^[c]	1.13	1.36	1.69	1.97	2.27	2.32	2.66

[a] Ratio of acrylamide to bisacrylamide 75:1. [b] Apparent size relative to a 20 bp standard ladder. [c] Migration anomaly = apparent size/sequence size.

presence of the ruthenium metal ion and the additional mass of the bipyridine ligands and the six nine-carbon-atom linkers. However, the migration anomaly becomes greater with increasing numbers of hybridized arms; that is, as the single-stranded sequences are converted into duplexes, the complexes migrate more slowly than expected for the lengths of the sequences. One 20-mer hybridization event increases the size of the initial 120-residue complex to 140 residues, but the 140-mer complex migrates as a 190-mer (a migration anomaly of 1.36). With each subsequent hybridization event the sequence size increases by 20 residues, but the apparent size increases by 110, 175, 253, 291, and 398 residues relative to its actual size. The fully hybridized complex is a 240-mer but it migrates as a 638-mer—a migration anomaly of 2.66 (Table 1). This phenomenon may reflect a greater extent of entanglement in the gel fibers by the “starshaped” Ru^{II}-bpy-DNA-duplex complexes relative to the linear shapes of ss and dsDNA or even relative to the more flexible nature of the single-stranded DNA–Ru conjugates. The dramatic migration anomalies observed with an increase in the number of duplexes tethered to the Ru tris(bipyridyl) center suggest that the hybridization events generate a complex that displays a greater rigidity than the unhybridized six-stranded complex; the more rigid the multi-arm complex, then the more entanglement there will be between the complex and the gel, and thus the more difficulty the complex will have in migrating through the matrix. The rigidity of the monomer has been suggested^[4] as an important parameter for the formation of higher-order DNA assemblies.

In this first study of a Ru center that tethers six DNA strands, we employed a nine-carbon-atom linker between the DNA duplexes and the [Ru(bpy)₃]²⁺ center. The linker and the [Ru(bpy)₃]²⁺ moiety taken together have a maximum extension of ≈15 Å from the center of the complex, whereas the diameter of the duplex DNA is ≈20 Å. The length of the linker may introduce some floppiness to the system, but even at this length, rotation of the DNA duplexes about the linker relative to one another can still result in significant restrictive steric or electronic effects with neighboring helices. To examine a more restrictive system, we prepared the [Ru(bpy)₃]²⁺ center with six hydroxyethyl (two-carbon-atom) linkers and attempted to prepare the corresponding complex that tethers six DNA sequences. However, we were unable to obtain any material that contained all six DNA sequences tethered to the Ru-bipyridyl center. The optimal length of the linker for complexes of this type therefore lies between the 9-carbon-atom linker with which the target complex was obtained and the 2-carbon-atom linker that was unsuccessful.

A second hybridization assay (in an agarose gel) was performed with the monomers **2** and **3** (see Scheme 1), each of which contained six identical DNA arms that were complementary to those of the other monomer. As size markers, the respective hybridization products of **2** and **3** with six equivalents of the corresponding complementary 20-mer were used. These samples (Figure 3, lanes a and e, respectively) each provided a species with 240 residues (6×20 bp) that binds ethidium bromide to yield intensely fluorescent

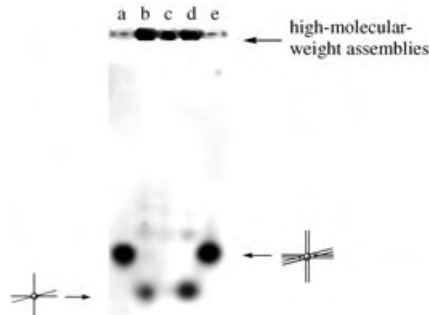


Figure 3. Hybridization of **2** and **3** as visualized by ethidium bromide after agarose gel electrophoresis. Lane a: **2** + excess 20-mer; lane b: **2** + **3** (2:1); lane c, **2** + **3** (1:1); lane d: **2** + **3** (1:2); lane e, **3** + excess 20-mer.

bands in the gel. The hybridization assay was performed with varying ratios of **2:3**. When both **2** and **3** were present, much of the resulting DNA was present as high-molecular-weight assemblies that did not migrate from the gel wells (Figure 3). In the presence of ethidium bromide, the DNA in the gel wells was intensely fluorescent which suggests the presence of conventional duplexes that are capable of intercalative binding. When either of the monomeric complexes was present in excess (Figure 3, lanes b and d), the excess unhybridized monomer was observed at the bottom of the gel with a greater mobility than those of the hybridized standards present in lanes a and e. However, the fluorescence intensity of the starting materials was significantly reduced relative to the standards in lanes a and e because they contain single-stranded arms that do not bind ethidium bromide as effectively. These observations suggest that the high-molecular-weight assemblies in lanes b–d were not simply non-specific aggregates. The absence of any low-molecular-weight species (dimers, trimers, etc.) in lanes b–d (Figure 3) may indicate that the assembly process, which involves multiple hybridization events for each monomer, may mimic crystallization processes in which the monomers readily assemble into a macroscopic system after initiation by a seed structure. We cannot determine at this time whether the assemblies formed by hybridization have an ordered (i.e., cubic) geometry or whether they contain significant amounts of linear hybridization products or other types of nonspecific assemblies such as those resulting from interpenetration.

In conclusion, this study suggests that multi-arm DNA complexes might be useful for the assembly of regular DNA lattices of nanoscale dimensions.

Keywords: bioinorganic chemistry · DNA · nanostructures · ruthenium · self-assembly

- [1] N. C. Seeman, *Angew. Chem.* **1998**, *110*, 3408; *Angew. Chem. Int. Ed.* **1998**, *37*, 3220.
- [2] J. J. Storhoff, C. A. Mirkin, *Chem. Rev.* **1999**, *99*, 1849.
- [3] C. M. Niemeyer, *Angew. Chem.* **2001**, *113*, 4254; *Angew. Chem. Int. Ed.* **2001**, *40*, 4128.
- [4] N. C. Seeman, *Biochemistry* **2003**, *42*, 7259.
- [5] J. Wengel, *Org. Biomol. Chem.* **2004**, *2*, 277.
- [6] J. Chen, N. C. Seeman, *Nature* **1991**, *350*, 631.
- [7] Y. Zhang, N. C. Seeman, *J. Am. Chem. Soc.* **1994**, *116*, 1661.
- [8] N. R. Kallenbach, R.-I. Ma, N. C. Seeman, *Nature* **1983**, *305*, 829.
- [9] R.-I. Ma, N. R. Kallenbach, R. D. Sheardy, M. L. Petrillo, N. C. Seeman, *Nucleic Acids Res.* **1986**, *14*, 9745–9753.
- [10] M. L. Petrillo, C. J. Newton, R. P. Cunningham, R.-I. Ma, N. R. Kallenbach, N. C. Seeman, *Biopolymers* **1988**, *27*, 1337.
- [11] E. Winfree, F. R. Liu, L. A. Wenzler, N. C. Seeman, *Nature* **1998**, *394*, 539.
- [12] D. Liu, M. Wang, Z. Deng, R. Walulu, C. Mao, *J. Am. Chem. Soc.* **2004**, *126*, 2324.
- [13] M. Scheffler, A. Dorenbeck, S. Jordan, M. Wustefeld, G. von Kiedrowski, *Angew. Chem.* **1999**, *111*, 3513; *Angew. Chem. Int. Ed.* **1999**, *38*, 3514.
- [14] K. J. Watson, S.-J. Park, J.-H. Im, S. T. Nguyen, C. A. Mirkin, *J. Am. Chem. Soc.* **2001**, *123*, 5592.
- [15] K. Wiederholt, L. W. McLaughlin, *Nucleic Acids Res.* **1999**, *27*, 2487.
- [16] F. D. Lewis, S. A. Helvoigt, R. L. Letsinger, *Chem. Commun.* **1999**, 327.
- [17] I. Vargas-Baca, D. Mitra, H. J. Zulyniak, J. Banerjee, H. Sleiman, *Angew. Chem.* **2001**, *113*, 4765; *Angew. Chem. Int. Ed.* **2001**, *40*, 4629.
- [18] K. M. Stewart, L. W. McLaughlin, *Chem. Commun.* **2003**, 2934.
- [19] K. M. Stewart, L. W. McLaughlin, *J. Am. Chem. Soc.* **2004**, *126*, 2050.
- [20] M. S. Shchepinov, I. A. Udaloova, A. J. Bridgman, E. M. Southern, *Nucleic Acids Res.* **1997**, *25*, 4447.
- [21] M. S. Shchepinov, K. U. Mir, J. K. Elder, M. D. Frank-Kamenetskii, E. M. Southern, *Nucleic Acids Res.* **1999**, *27*, 3035.
- [22] R. C. Mucic, M. K. Herrlien, C. A. Mirkin, R. L. Letsinger, *Chem. Commun.* **1996**, 555.
- [23] R. Elghanian, J. J. Storhoff, R. C. Mucic, R. L. Letsinger, C. A. Mirkin, *Science* **1997**, *277*, 1078.
- [24] C. M. Niemeyer, *Trends Biotechnol.* **2002**, *20*, 395.
- [25] T. A. Taton, R. C. Mucic, C. A. Mirkin, R. L. Letsinger, *J. Am. Chem. Soc.* **2000**, *122*, 6305.
- [26] N. C. Seeman, *Synlett* **2000**, 1536.
- [27] H. Yan, X. Zhang, Z. Sehn, N. C. Seeman, *Nature* **2002**, *415*, 62.
- [28] E. Braun, Y. Eichen, U. Sivan, G. Ben-Yoseph, *Nature* **1998**, *391*, 775.
- [29] K. Keren, M. Krueger, R. Gilad, G. Ben-Yoseph, U. Sivan, E. Braun, *Science* **2002**, *297*, 72.
- [30] J. K. Barton, *J. Biomol. Struct. Dyn.* **1983**, *1*, 621.
- [31] N. C. Fletcher, M. Nieuwenhuyzen, S. Rainey, *J. Chem. Soc. Dalton Trans.* **2001**, 2641.
- [32] A. Fumiko, K. Heseck, H. Ishida, Y. Inoue, *Chromatography* **2000**, *21*, 133.
- [33] S. B. Rajur, J. Robles, K. Wiederholt, R. W. Kuimelis, L. W. McLaughlin, *J. Org. Chem.* **1997**, *62*, 523.
- [34] D. A. Gianolio, J. M. Segismundo, L. W. McLaughlin, *Nucleic Acids Res.* **2000**, *28*, 2128.
- [35] D. A. Horne, P. B. Dervan, *J. Am. Chem. Soc.* **1990**, *112*, 2435.

Received: April 21, 2004

Revised: July 6, 2004

Heterogeneous Catalysis

The Catalytic Activity of "Naked" Gold Particles**

Massimiliano Comotti, Cristina Della Pina,
Roberto Matarrese, and Michele Rossi*

The metal–support interaction in catalysis is of relevance both for academic studies and for industrial applications, and theoretical concepts have contributed to understanding the basic principles behind this interaction.^[1] In most cases, however, the metal–support interaction is only described in terms of catalytic behavior and its nature often remains debatable. In recent years interest in gold catalysts for various applications in organic and inorganic chemistry^[2] has increased and, our and other research groups have investigated the liquid-phase oxidation of polyol,^[3–7] aminoalcohols,^[8] and glucose^[9] to carboxylates, and the gas-phase oxidation of alcohols to the corresponding carbonyl derivatives^[10] using metal particles supported on different materials.

In liquid-phase applications, carbon was found to be the support of choice, and in the case of ethane-1,2-diol oxidation, by comparing different commercial carbons, a tentative hypothesis of metal–support interactions, connected to the density of phenolic groups at the carbon surface, was formulated.^[11] However, the synergism between gold particles and carbon was not demonstrated and this point remained unresolved.

Although gold colloids have widely been employed to prepare supported gold catalysts, no report of particles derived from colloidal dispersion being used as catalysts has appeared. We have now found that, under controlled conditions, water-dispersed gold sol exhibits a surprising activity when used as "naked particles", that is, in the absence of common protectors as polyvinylalcohol (PVA), polyvinylpyrrolidone (PVP), tetrahydroxymethylphosphonium chloride (THPC). As a model reaction, we have investigated the aerobic oxidation of glucose to gluconate which occurs under mild conditions.

As shown in the conversion–time plot (Figure 1), naked gold particles having a mean diameter of 3.6 nm behave as an active catalyst allowing 21 % glucose conversion in the first 200 s.

These particles are produced as a colloidal sol by reducing HAuCl_4 in the presence of a large excess of glucose acting either as reagent or protector. From the initial rate, a specific molar activity of 18043 mol gluconate $[\text{mol Au}]^{-1} \text{h}^{-1}$ (calcu-

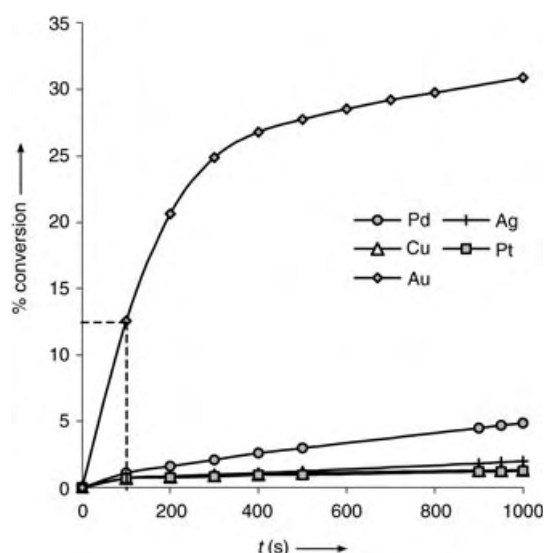


Figure 1. The activity of different metal particles in glucose oxidation. $[\text{Metal}] = 10^{-4} \text{ M}$, $[\text{glucose}] = 0.4 \text{ M}$, $T = 303 \text{ K}$.

lated with respect to the total gold) can be derived. Under similar conditions, Cu, Ag, Pd, and Pt colloidal particles of similar dimension (3–5 nm) were scarcely active. During the catalytic test, gold coagulated into larger particles owing to the formation of sodium gluconate that, as is common with other electrolytes, promoted sol coagulation leaving a colorless, inactive solution after about 400 s. The growth of gold crystallites during the reaction has been followed by X-ray diffraction (XRD) analysis at various time intervals, after sol immobilization on carbon (Figure 2).

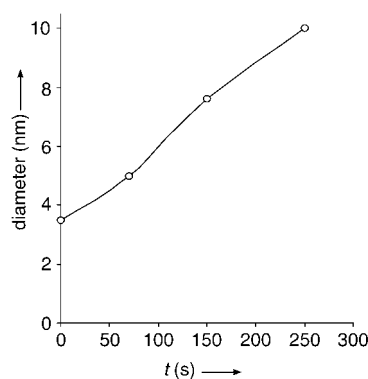


Figure 2. Growth of gold particles during glucose oxidation.

Gold particles are also poisoned by sulfur compounds, such as sulfides and sulfites, and inhibited by protecting molecules, such as polyvinyl alcohol. Although the short life of the gold sol does not allow its use as a practical catalyst, its activity is of relevance both for assigning the catalytic role in the oxidation reaction and for evaluating metal–support interactions. For the latter purpose, a 0.5 % w/w gold-on-carbon catalyst **II** was prepared by contacting the gold sol **I** with carbon powder. The size of gold particles remained unchanged after immobilization on carbon, as derived by

[*] Dr. M. Comotti, Dr. C. Della Pina, Dr. R. Matarrese, Prof. Dr. M. Rossi
Dipartimento di Chimica Inorganica
Metallorganica e Analitica
CIMAIA and ISTM
University of Milano
Via Venezian 21, 20133 Milano (Italy)
Fax: (+39) 02-5031-4424
E-mail: michele.rossi@unimi.it

[**] This work was supported in part by the EC project "AURICAT".

XRD. Under kinetic control, and using the same amount of gold, the curve of glucose oxidation with supported particles is quite similar to that of unsupported particles during the first 100 s (Figure 3a). This result means that both catalytic

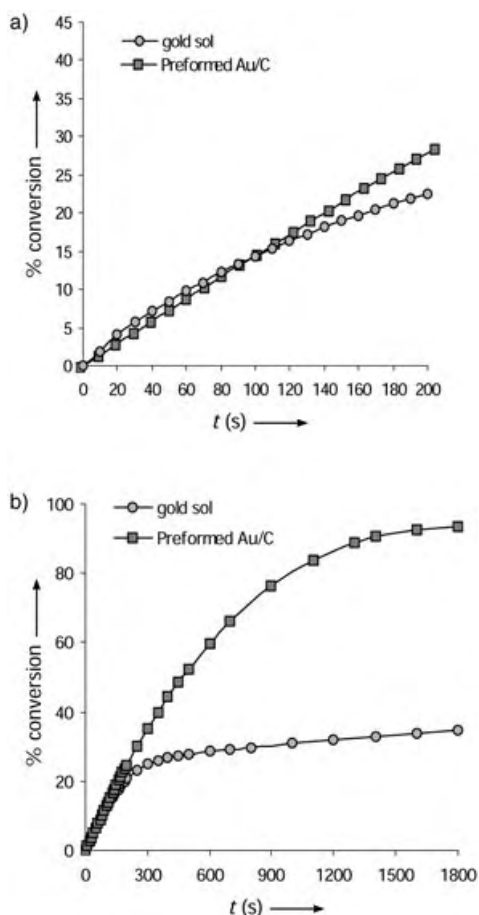


Figure 3. a) Initial rate of glucose oxidation with naked (gold sol) and supported gold particles (preformed Au/C). $[Au] = 10^{-4}$ M, $[glucose] = 0.4$ M, $T = 303$ K. b) Rate of glucose oxidation with naked (gold sol) and supported gold particles (preformed Au/C). $[Metal] = 10^{-4}$ M, $[glucose] = 0.4$ M. $T = 303$ K.

systems are similarly efficient and, therefore, metal-support interactions, if present, are negligible in terms of enhancing gold activity. However, a benefit was obtained by using the supported gold particles as their morphology and activity were preserved for long time allowing the total conversion of glucose (Figure 3b). In particular, the gold dimension resulted unchanged at the end of the first catalytic cycle.

In principle, the knowledge of particle size in the sol allows the calculation of the turnover frequency (TOF) of gold. For this purpose, a series of experiments were undertaken to better characterize the kinetics of glucose oxidation with gold sol. Using colloidal particles having a mean diameter of 3.6 nm, a linear correlation between gold concentration (10^{-5} – 10^{-6} M) and catalytic activity was found (Figure 4), which indicates that the rate is not limited by mass-transport phenomena.

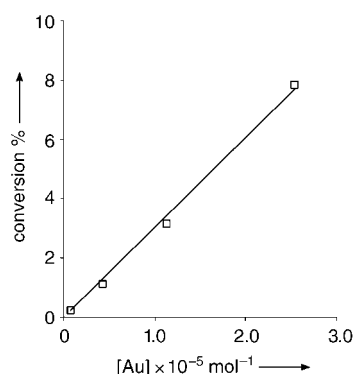


Figure 4. Conversion versus $[Au]$; $t = 100$ s, $[glucose] = 0.1$ M. $T = 303$ K.

Furthermore, colloidal particles of different size have been produced by changing the chlorauric concentration from 50 to 600 mg L^{-1} , and the mean dimension of coherent scattering crystallites was determined by XRD (using the Scherrer equation^[11]) after immobilization on carbon. For comparing activity with size, this technique allows a better correlation than that obtained by TEM where a broad distribution is observed in the case of larger particles (5–10 nm) owing to the formation of aggregates after deposition on carbon. These aggregates, however, retain their XRD identity. The chemical nature of gold particles under reaction conditions has been investigated by X-ray photoemission spectroscopy (XPS) after deposition on carbon. The presence of a sharp peak centered at 83.9 ± 0.2 eV, relative to the Au 4f7/2 signal, suggests the existence of the metallic state only.^[12] By using gold particles of different size in the range 3–6 nm, we observed a catalytic activity inversely proportional to the diameter at the total gold concentration of 3.2×10^{-5} M (Figure 5). Particles larger than 6 nm deviate from linearity and a sharp cut off is observed at approximately 10 nm. We have no arguments that give a satisfactory interpretation for the sudden loss of activity. However, discontinuity at the nanometric scale has been observed in the case of other physicochemical properties of gold, for example, the sharp

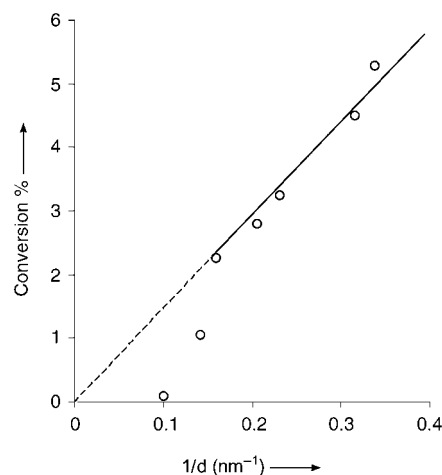


Figure 5. Conversion versus particle dimension; $t = 100$ s, $[glucose] = 0.38$ M; $glucose:Au = 12\,000$.

decrease of the melting point, related to the transition from nonmetallic to metallic bonding, which occurs at a lower sizes, approximately 1–2 nm.^[2] For particles smaller than 6 nm the observed correlation between activity and diameter agrees with the concept that only exposed atoms are catalytically active. By using the simple model of spherical particles, the total surface area, and therefore the number of exposed atoms, at a given metal amount, is in inverse proportion with particle diameter. By assuming in the first instance uniform particles of 3.6 nm present in the gold sol, 0.288 nm being the atomic diameter, the fraction of atoms lying at the surface should be approximately 36%.^[2,13] Therefore, considering the initial specific activity of 18043 mol of gluconate formed per mol of total gold per hour, the initial TOF calculated for gold in the glucose oxidation is 50120 h⁻¹. Further investigation, based on a more appropriate model and using detailed particle size distribution in the liquid matrix, would give a more accurate result. A high activity can be preserved for a long time during the oxidation of glucose with the supported particles (Figure 3b). The estimated TOF value for carbon-supported particles should be similar to the unsupported particles, considering the similar catalytic efficiency (Figure 3a), and observing that dimension and form are in both cases identical (as derived by TEM), whereas diffusion in the carbon-supported catalyst is not a rate-limiting factor. This latter point has been experimentally verified by observing a linear increase of the reaction rate either on increasing the amount of catalyst (0.5% Au on C) or on increasing the loading of gold (0.1–1%) on the carbon.

The catalytic behavior of unsupported gold nanoparticles which interact with dissolved oxygen and glucose under conditions which are at the boundary between homogeneous and heterogeneous conditions, is also of interest for making comparisons with homogeneous catalysis. In fact, homogeneous enzymatic systems, containing the oxidase-catalase proteins derived from *Aspergillus Niger* mould, are the basis of the industrial process for the production of gluconate.^[14] Catalytic tests were carried out, in the same apparatus as for the gold reactions, using a commercial enzymatic system (hyderase, Amano) containing 1.3 × 10⁻⁶ mol g⁻¹ (hydrase) of flavine-adenine dinucleotide (FAD) as the rate-limiting factor. Operating at 303 K and 101.3 kPa, the pH value was fixed at 7 and a glucose/FAD molar ratio of 6.7 × 10⁵ was used for optimizing the activity.

Under these conditions, the enzymatic system was about one order of magnitude more active than gold, its initial TOF value being 7.0 × 10⁵ h⁻¹ referenced to FAD (Figure 6) compared to 5.0 × 10⁴ h⁻¹ for the inorganic catalysis referenced to the exposed gold.

Despite the higher molecular efficiency of the enzymatic catalysis, for practical application gold seems to be a competitive alternative for glucose oxidation owing to the simplicity of catalyst manufacturing, nontoxicity of the metal and possibility of recycling.

In conclusion, the catalytic role and the properties of unsupported gold nanoparticles towards glucose oxidation have been investigated, allowing the evaluation of the specific activity of the metal which resulted comparable to that of enzymatic systems.

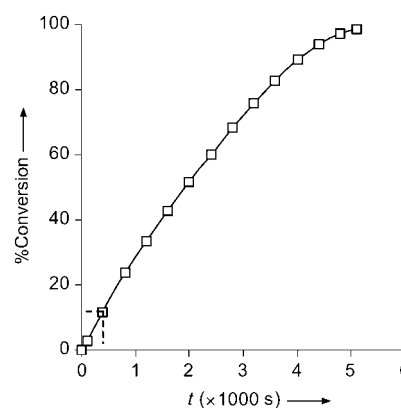


Figure 6. Rate of glucose oxidation with hyderase. [Glucose] = 1 M, [FAD] = 1.5 × 10⁻⁶ M, T = 303 K.

Experimental Section

A colloidal dispersion of gold **I**, was prepared by treating a 1.25 × 10⁻⁴ M aqueous solution of gold (as HAuCl₄) with NaBH₄ (NaBH₄:Au = 5:1) under N₂ atmosphere, in the presence of a large excess of glucose (0.35 M). The resultant brown sol contained metal particles, stable for several hours in the absence of dioxygen, having a mean diameter of 3.6 nm, as determined by TEM performed on a drop of dispersion evaporated on copper grid. In a similar manner Cu, Ag, Pd, and Pt colloidal particles (3–5.5 nm) were prepared. Supported 0.5% (w/w) gold on carbon catalyst, **II**, was prepared by contacting 2 g of carbon powder (X40S, Camel, 1200 m² g⁻¹) with sol **I** containing the appropriate amount of Au. Inductively coupled plasma (ICP) analysis showed total depletion of gold from the solution in a few minutes, and the residue material collected by filtration was used for the catalytic test without washing.

Hyderase: a glucose oxidase preparation produced by *Aspergillus Niger* fermentation (Amano Enzyme Co.) contained 1 mg g⁻¹ of FAD. The oxidation of glucose was carried out in a thermostatted, magnetically stirred reactor (80 mL) purged with dioxygen at atmospheric pressure. The reaction was started by adding the catalyst to the O₂ saturated solution. Gluconic acid was continuously titrated at fixed pH value (9.5 for gold and 7 for hyderase) with NaOH, using a GPD 751 Titrimo apparatus (Metrohm). Catalyst amount, stirring speed (1600 rpm), gas flow (60 L h⁻¹), and temperature (303 K) were chosen to carry out the test under catalyst-controlled kinetics. As the reaction product only gluconate was detected by HPLC as previously reported.^[8]

Received: April 26, 2004

Revised: July 12, 2004

Keywords: colloids · gold · heterogeneous catalysis · oxidation · oxygen

- [1] *Metal-Support Interactions in Catalysis, Sintering and Redispersion* (Eds.: S. A. Stevenson, J. A. Dumesic, R. T. K. Baker, E. Ruckenstein), Van Nostrand Reinhold, New York, **1987**.
- [2] G. C. Bond, D. Thompson, *Catal. Rev. Sci. Eng.* **1999**, *41*, 319–388.
- [3] L. Prati, M. Rossi, *J. Catal.* **1998**, *176*, 552–560.
- [4] C. L. Bianchi, F. Porta, L. Prati, M. Rossi, *Top. Catal.* **2000**, *13*, 231–236.
- [5] F. Porta, L. Prati, M. Rossi, G. Scari, *J. Catal.* **2002**, *211*, 464–469.
- [6] F. Porta, L. Prati, M. Rossi, S. Coluccia, G. Martra, *Catal. Today* **2000**, *61*, 165–172.

- [7] S. Carrettin, P. McMorn, P. Johnston, K. Griffin, G. J. Hutchings, *Chem. Commun.* **2002**, 696–697.
- [8] S. Biella, G. L. Castiglioni, C. Fumagalli, L. Prati, M. Rossi, *Catal. Today* **2002**, 72, 43–49.
- [9] S. Biella, L. Prati, M. Rossi, *J. Catal.* **2002**, 206, 242–247.
- [10] S. Biella, M. Rossi, *Chem. Commun.* **2003**, 378–379.
- [11] C. L. Bianchi, S. Biella, A. Gervasini, L. Prati, M. Rossi, *Catal. Lett.* **2003**, 85, 91–96.
- [12] S. Minicò, S. Scirè, C. Crisafulli, S. Galvagno, *Appl. Catal. B* **2001**, 34, 277–285.
- [13] G. C. Bond, *Surf. Sci.* **1985**, 256, 966–981.
- [14] *Ullmann's Encyclopedia of Industrial Chemistry*, VI ed., Vol. 15, pp. 645–651, Wiley-VCH, Weinheim, **2003**.

Host–Guest Systems

An Aromatic Anion Receptor: Anion– π Interactions do Exist**

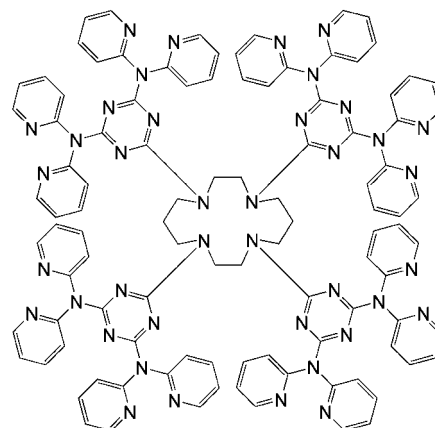
Paul de Hoog, Patrick Gamez,* Ilpo Mutikainen,
Urho Turpeinen, and Jan Reedijk*

Noncovalent supramolecular interactions involving aromatic rings play a significant role in both chemical and biological recognition.^[1] For example, π -stacking interactions between the aryl rings of nucleobase pairs help to stabilize the DNA double helix.^[2,3] It is well known that cation– π interactions are of great importance for many biological systems.^[4,5] Thus, the binding of the agonist acetylcholine to its receptor is very selective and involves cation– π interactions between a quaternary ammonium group and a tryptophan amino acid residue.^[6] Design and preparation of supramolecular host–guest compounds involving neutral or cationic entities have therefore received much attention during the last two decades.^[7] In contrast, the chemistry of noncovalent anion– π interactions is much less developed.^[8,9] This is most likely

due to the electron-donating character of anions, which is expected to lead to repulsive interactions with aromatic π clouds. However, in the last few years, an increasing number of aryl hosts for anionic guests have been studied, probably because of their potential medicinal and biological applications.^[8] Indeed, more than 70 % of enzyme substrates and cofactors are anions.^[10]

Interactions between π -electron-poor aromatic moieties and anions were first demonstrated by NMR studies.^[11–13] Several recent articles have reported theoretical investigations on the binding of halides with electron-deficient π systems such as fluorobenzene derivatives,^[14–16] fluoro-*s*-triazine^[17] and *s*-tetrazine derivatives,^[18] and tetrafluoroethene.^[19] All calculations clearly indicated an energetically favorable noncovalent interaction between halide and π system.^[20] Lately, the first crystallographic evidence was reported for such interactions, between the 1,3,5-triazine group of the ligand 2,4,6-tris(di-2-pyridylamino)-1,3,5-triazine^[21,22] and chloride and tetrachlorocuprate^[23] anions.

In the course of research on the preparation of triazine-based coordination polymers^[24,25] and their physical and catalytic properties,^[26,27] the dendritic octadentate ligand *N,N',N'',N'''*-tetrakis[2,4-bis(di-2-pyridylamino)-1,3,5-triazinyl]-1,4,8,11-tetraazacyclotetradecane (azadendtriz) was synthesized.^[27]



Layering an aqueous solution of CuCl_2 (2 mL, 32 mM) with a solution of azadendtriz in dichloromethane (2 mL, 3.6 mM) gave blue prismatic crystals of $[\text{Cu}_4(\text{azadendtriz})_4](\text{Cl})_4(\text{H}_2\text{O})_{13}$ (**1**) in 54 % yield by slow diffusion of the ligand into the aqueous phase, which gradually turned from colorless to dark blue (see Supporting Information).

The structure of **1** (Figure 1) shows a cationic tetranuclear copper moiety formed by one dendritic ligand, where the four *s*-triazinyl groups stack two by two in a parallel fashion. Consequently, the copper ions are coordinated by two 2,2'-dipyridylamino units belonging to two different *s*-triazine rings. The coordination spheres of the square-pyramidal ($\tau = 0.11, 0.13, 0.11, \text{ and } 0.13$ for Cu1, Cu2, Cu3, and Cu4, respectively)^[28] metal centers are completed by a chloride anion at the apical position at a distance varying from 2.406(6) to 2.431(5) Å. The Cu–N distances of 1.991(9)–2.056(12) Å can be considered normal for square-pyramidal Cu^{II} ions. In

[*] P. de Hoog, Dr. P. Gamez, Prof. Dr. J. Reedijk
Leiden Institute of Chemistry
Gorlaeus Laboratories
University of Leiden
PO Box 9502, 2300 RA Leiden (The Netherlands)
Fax: (+31) 71-527-4671
E-mail: p.gamez@chem.leidenuniv.nl
reedijk@chem.leidenuniv.nl

Dr. I. Mutikainen, Dr. U. Turpeinen
Department of Chemistry
Laboratory of Inorganic Chemistry
University of Helsinki
P.O. Box 55, A. I. Virtasenaukio 1
00014 Helsinki (Finland)

[**] Financial support from COST Action D21/003/2001 and the Dutch National Research School Combination Catalysis (HRSMC and NIOK) are thankfully acknowledged.

Supporting information for this article is available on the WWW under <http://www.angewandte.org> or from the author.

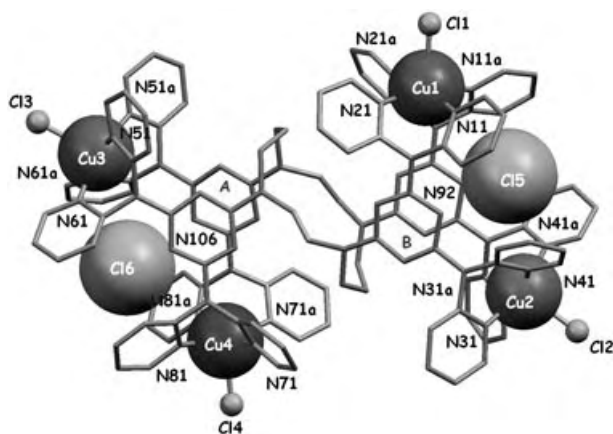


Figure 1. Representation of **1**, showing the four pentacoordinate Cu^{II} ions and the two encapsulated chloride anions Cl5 and Cl6.

addition, four chloride anions and thirteen water molecules are located in the crystal lattice. Some of these noncoordinated entities are disordered, for example, two carbon atoms of the azacrown group. The triazine rings are π - π stacked in pairs with nearly perfect face-to-face alignment (Figure 1), which is quite a rare phenomenon.^[23,29] The distances between the triazine centroids of 3.65 (rings A) and 3.60 Å (rings B) are slightly longer than the usual values for π - π interactions (ca. 3.5 Å). However, such elongation is commonly observed with N-heteroaromatic ligands, especially when the nitrogen atoms of one ring face the nitrogen atoms of the other, which leads to unfavorable electrostatic interactions.^[3] A shorter distance has been observed with a less repulsive N/C face-to-face alignment between two *s*-triazine rings.^[30]

The most fascinating feature of this supramolecular species is its ability to encapsulate two chloride anions. Indeed, Cl5 and Cl6 are the guests of two host cavities formed by four pyridine rings of the ligand (Figure 1). The centroid...Cl⁻ distances vary from 3.521(6) to 3.559(5) Å for Cl5, and from 3.466(5) to 3.697(5) Å for Cl6. These distances are longer than the values calculated for the model *s*-triazine anion.^[17,19] Unfortunately, no theoretical investigations are yet available for the pyridine ring, which is a much less electron deficient aromatic ring, but one would reasonably expect longer ring-anion bonds. The anion- π interactions observed here are favored by the fact that the pyridine rings involved are coordinated to copper ions, which enhances their electron-poor character. In addition to the π interaction, the chloride ions are close to the neighboring triazine rings. Indeed, the Cl5...N92 and Cl6...N106 distances of 3.013(12) and 3.119(13) Å, respectively, suggest some electrostatic interactions between the guest anions and the electron-deficient triazine rings. The combination of both electronic effects confers electrophilic character on the host cavity. The angles of the Cl⁻...centroid axis to the plane of the different pyridine rings are 78 and 80° for Cl5, and 74 and 82° for Cl6. The ideal anion-aromatic plane angle of the extensively studied *s*-triazine moiety is 90°. However, again, no theoretical calculations have been performed on the pyridine ring, and thus the optimal angle has not yet been determined.

In summary, the first coordination compound of the ligand azadendtriz is reported. The supramolecular copper complex **1** shows unusual intramolecular π - π interactions between 1,3,5-triazine rings. Furthermore, this tetranuclear complex exhibits host-guest properties, and the first encapsulation of a chloride anion by four pyridine rings is described, which demonstrates the possible existence of anion- π interactions. The encapsulation of the bromide anion is currently being investigated. A theoretical approach to study this non-hydrogen bonding artificial anionic receptor is also proposed. Understanding how nature can selectively bind, functionalize, and transport anionic species in biological systems would undoubtedly be of great importance for the design of new drugs.

Received: April 28, 2004

Revised: June 30, 2004

Keywords: copper · host–guest systems · N ligands · Pi interactions · supramolecular chemistry

- [1] E. A. Meyer, R. K. Castellano, F. Diederich, *Angew. Chem.* **2003**, *115*, 1244–1287; *Angew. Chem. Int. Ed.* **2003**, *42*, 1210–1250.
- [2] C. A. Hunter, J. K. M. Sanders, *J. Am. Chem. Soc.* **1990**, *112*, 5525–5534.
- [3] C. Janiak, *J. Chem. Soc. Dalton. Trans.* **2000**, 3885–3896.
- [4] J. C. Ma, D. A. Dougherty, *Chem. Rev.* **1997**, *97*, 1303–1324.
- [5] H.-J. Schneider, A. Yatsimirsky, *Principles and Methods in Supramolecular Chemistry*, Wiley, Chichester, **2000**.
- [6] D. A. Dougherty, *J. Phys. Org. Chem.* **1998**, *11*, 334–340.
- [7] J. M. Lehn, *Pure Appl. Chem.* **1994**, *66*, 1961–1966.
- [8] P. D. Beer, P. A. Gale, *Angew. Chem.* **2001**, *113*, 502–532; *Angew. Chem. Int. Ed.* **2001**, *40*, 487–516.
- [9] R. Vilar, *Angew. Chem.* **2003**, *115*, 1498–1516; *Angew. Chem. Int. Ed.* **2003**, *42*, 1460–1477.
- [10] S. Mangani, M. Ferraroni in *Supramolecular Chemistry of Anions* (Eds.: A. Bianchi, K. Bowman-James, E. Garcia-España), Wiley, New York, **1997**, pp. 63–78.
- [11] H. J. Schneider, *Angew. Chem.* **1991**, *103*, 1419; *Angew. Chem. Int. Ed. Engl.* **1991**, *30*, 1417–1436.
- [12] H. J. Schneider, T. Blatter, B. Palm, U. Pfingsttag, V. Ruediger, I. Theis, *J. Am. Chem. Soc.* **1992**, *114*, 7704–7708.
- [13] H. J. Schneider, F. Werner, T. Blatter, *J. Phys. Org. Chem.* **1993**, *6*, 590–594.
- [14] C. Garau, A. Frontera, D. Quinonero, P. Ballester, A. Costa, P. M. Deya, *ChemPhysChem* **2003**, *4*, 1344–1348.
- [15] D. Quinonero, C. Garau, C. Rotger, A. Frontera, P. Ballester, A. Costa, P. M. Deya, *Angew. Chem.* **2002**, *114*, 3539–3542; *Angew. Chem. Int. Ed.* **2002**, *41*, 3389–3392.
- [16] D. Quinonero, C. Garau, A. Frontera, P. Ballester, A. Costa, P. M. Deya, *Chem. Phys. Lett.* **2002**, *359*, 486–492.
- [17] M. Mascal, A. Armstrong, M. D. Bartberger, *J. Am. Chem. Soc.* **2002**, *124*, 6274–6276.
- [18] C. Garau, D. Quinonero, A. Frontera, A. Costa, P. Ballester, P. M. Deya, *Chem. Phys. Lett.* **2003**, *370*, 7–13.
- [19] D. Kim, P. Tarakeshwar, K. S. Kim, *J. Phys. Chem. A* **2004**, *108*, 1250–1258.
- [20] I. Alkorta, I. Rozas, J. Elguero, *J. Org. Chem.* **1997**, *62*, 4687–4691.
- [21] J. Pang, Y. Tao, S. Freiberg, X. P. Yang, M. D'Iorio, S. N. Wang, *J. Mater. Chem.* **2002**, *12*, 206–212.

- [22] P. de Hoog, P. Gamez, W. L. Driessen, J. Reedijk, *Tetrahedron Lett.* **2002**, 43, 6783–6786.
- [23] S. Demeshko, S. Dechert, F. Meyer, *J. Am. Chem. Soc.* **2004**, 126, 4508–4509.
- [24] P. Gamez, P. de Hoog, O. Roubeau, M. Lutz, W. L. Driessen, A. L. Spek, J. Reedijk, *Chem. Commun.* **2002**, 1488–1489.
- [25] P. de Hoog, P. Gamez, O. Roubeau, M. Lutz, W. L. Driessen, A. L. Spek, J. Reedijk, *New J. Chem.* **2003**, 27, 18–21.
- [26] P. Gamez, P. de Hoog, M. Lutz, W. L. Driessen, A. L. Spek, J. Reedijk, *Polyhedron* **2003**, 22, 205–210.
- [27] P. Gamez, P. de Hoog, M. Lutz, A. L. Spek, J. Reedijk, *Inorg. Chim. Acta* **2003**, 351, 319–325.
- [28] A. W. Addison, T. N. Rao, J. Reedijk, J. Vanrijn, G. C. Verschoor, *J. Chem. Soc. Dalton Trans.* **1984**, 1349–1356.
- [29] B. Manimaran, T. Rajendran, Y. L. Lu, G. H. Lee, S. M. Peng, K. L. Lu, *Eur. J. Inorg. Chem.* **2001**, 633–636.
- [30] R. D. Pike, B. D. Borne, J. T. Maeyer, A. L. Rheingold, *Inorg. Chem.* **2002**, 41, 631–633.

Nanostructures

Nanofiber Formation in the Chemical Polymerization of Aniline: A Mechanistic Study**

Jiaxing Huang and Richard B. Kaner*

Polyaniline is unique among conducting polymers because of its simple nonredox doping/dedoping chemistry based on acid/base reactions.^[1,2] The conventional chemical oxidative polymerization of aniline is carried out in an aqueous solution in which aniline is dissolved in a strong acidic solution (for example, 1M HCl) at about 0°C and the polymerization is initiated by adding an oxidant (for example, ammonium peroxydisulfate) into the solution.^[1] Polyaniline nanostructures, such as nanofibers/-wires/-rods/-tubes, can be made by introducing “structural directors” into the chemical polymerization bath. These structural directors include “soft templates” such as surfactants,^[3] organic dopants,^[4,5] or polyelectrolytes^[6] that assist in the self-assembly of polyaniline nanostructures, and “hard templates” such as porous mem-

branes^[7] or zeolites^[8] where the templated polymerization of aniline occurs in the 1-D nanochannels. Films containing polyaniline nanofibers can also be made by using electrospinning^[9] or electrochemical methods to control the polymerization rate.^[10–12] Nanostructures of polyaniline are of great current interest since they combine the properties of low-dimensional organic conductors with high surface area materials. This situation can lead to enhanced properties in applications such as chemical sensors.^[13–16]

Recently we have developed a general chemical route to polyaniline nanofibers by using interfacial polymerization at an aqueous/organic interface.^[15,17] The reactants—*aniline*, ammonium peroxydisulfate, and a doping acid such as HCl—are separated by the interface between an organic solvent containing aniline and an aqueous phase containing the oxidant plus the doping acid. The polyaniline product, polymerized at the interface, contains almost exclusively nanofibers with relatively uniform diameters. The nanofiber diameter is determined by the doping acid used in the polymerization.^[17] This synthesis is very general and does not require any template, special dopant, or specific solvent. Careful analysis of polyaniline made in a conventional single-phase polymerization reaction by microscopy have shown the presence of a small amount of nanofibers.^[17] This observation indicates that the formation of nanofibers is not necessarily determined by the interface but more likely by the nature of the oxidative polymerization of aniline. To more fully understand the formation mechanism of polyaniline nanofibers, several important questions need to be addressed. These include: 1) Why does interfacial polymerization produce “pure” nanofibers while conventional synthesis produces irregularly shaped particles? 2) Why can small amounts of nanofibers be found in polyaniline made by conventional synthesis? 3) Why does polyaniline form such extended, elongated fiberlike nanostructures? Herein we provide answers to these questions by reporting experimental results on the factors affecting the morphology of chemically polymerized polyaniline.

To address the first question we studied the morphological evolution of polyaniline during traditional chemical oxidative polymerization. A solution of the oxidant ammonium peroxydisulfate dissolved in 1M HCl was fed continuously into a solution of aniline dissolved in 1M HCl by using a syringe pump at a preset flow rate. This procedure is analogous to the “drop by drop” titration used in traditional synthesis (Figure 1) but with a precisely controlled feeding rate. The reaction vessel was kept in an ice bath at between –5 and 0°C. Small amounts of product for transmission electron microscopy (TEM) studies were periodically extracted from the reaction bath as soon as the green color of polyaniline was visible. At this point, the samples were immediately diluted with distilled water, cast onto TEM grids, and dried in air to quench the polymerization. Polyaniline nanofibers form at an early stage in the polymerization process (Figure 2a). These nanofibers have average diameters of 30–35 nm, which is consistent with those obtained using interfacial polymerization.^[17] As more ammonium peroxydisulfate is fed into the reaction, the nanofibers become scaffolds for secondary growth of polyaniline (Figure 2b) and finally turn into

[*] J. Huang, Prof. R. B. Kaner
Department of Chemistry & Biochemistry and
California NanoSystems Institute
University of California, Los Angeles
Los Angeles, California 90095-1569 (USA)
Fax: (+1) 310-206-4038
E-mail: kaner@chem.ucla.edu

[**] We thank K. N. Tun, G. J. Tong (UCLA), J. A. Moore, and Prof. H. A. Acquaye (University of Redlands) for technical assistance, T. Kanazawa (JEOL), X. Wang, and Prof. P. Feng (UC-Riverside) for help with SEM experiments, and Prof. M. M. Abu-Omar (UCLA) and Prof. F. Zhou (CSULA) for use of their syringe pumps. This research was supported by the Microelectronics Advanced Research Corporation (MARCO) and the Department of Homeland Security (HSARPA).

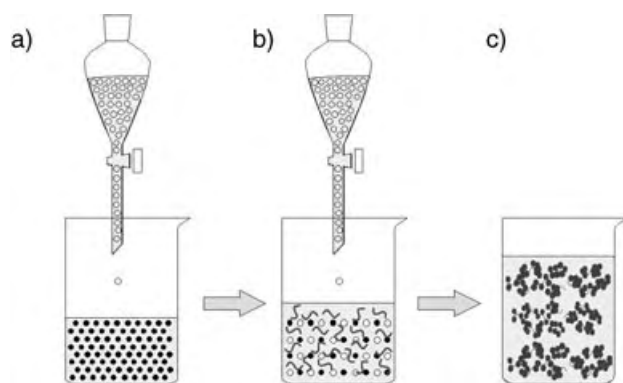


Figure 1. Schematic diagram illustrating the formation of polyaniline agglomerates during conventional chemical synthesis. a) The oxidant (open circles) dopant solution is added slowly to the aniline (solid circles) dopant solution. b) Polyaniline nanofibers form as soon as the polymerization begins. Since the nanofibers are exposed to aniline and oxidant, they are subject to secondary growth. c) Agglomerates of polyaniline particles plus a few nanofibers are found because of severe secondary growth.

irregularly shaped agglomerates containing nanofibers and particulates (Figure 2c). The whole process is illustrated schematically in Figure 1. Therefore, if secondary growth can be suppressed, the yield of nanofibers in the final product could be greatly increased.

Interfacial polymerization represents one effective method to suppress secondary growth (Figure 3).^[17] Since the monomer aniline and the initiator ammonium peroxydisulfate are separated by the boundary between the aqueous and the organic phase, polymerization occurs only at this interface where all the components needed for polymerization come together.^[14,15,17] Polyaniline then forms as nanofibers. Since these newly formed nanofibers are in the doped emeraldine salt form, they are hydrophilic and can rapidly move away from the interface and diffuse into the water layer (Figure 3b). In this way, as the nanofibers form they are continuously withdrawn from the reaction front, thus avoiding secondary growth and allowing new nanofibers to grow at this interface. This effect explains why nanofibers are obtained no matter which solvent is used as the organic phase in interfacial polymerization. Hence, the interface between the immiscible aqueous/organic layers does not contribute directly to the formation of nanofibers; it simply separates nanofiber formation from secondary growth.

With the knowledge that the key to synthesizing polyaniline nanofibers is preventing secondary growth, we have now designed a new, even simpler method to make pure polyaniline nanofibers (Figure 4). The idea is that if all the reactants can be consumed during the formation of nanofibers, secondary growth will be greatly suppressed since no reactants will be available for further reaction. To achieve this goal, the initiator solution (ammonium peroxydisulfate in 1M HCl) was added into the monomer solution (aniline in 1M HCl) all at once (Figure 4a), rather than slowly feeding it in by titration or syringe-pumping. Sufficient mixing can be achieved with a magnetic stirrer or shaker to evenly distribute the initiator and monomer molecules before polymerization

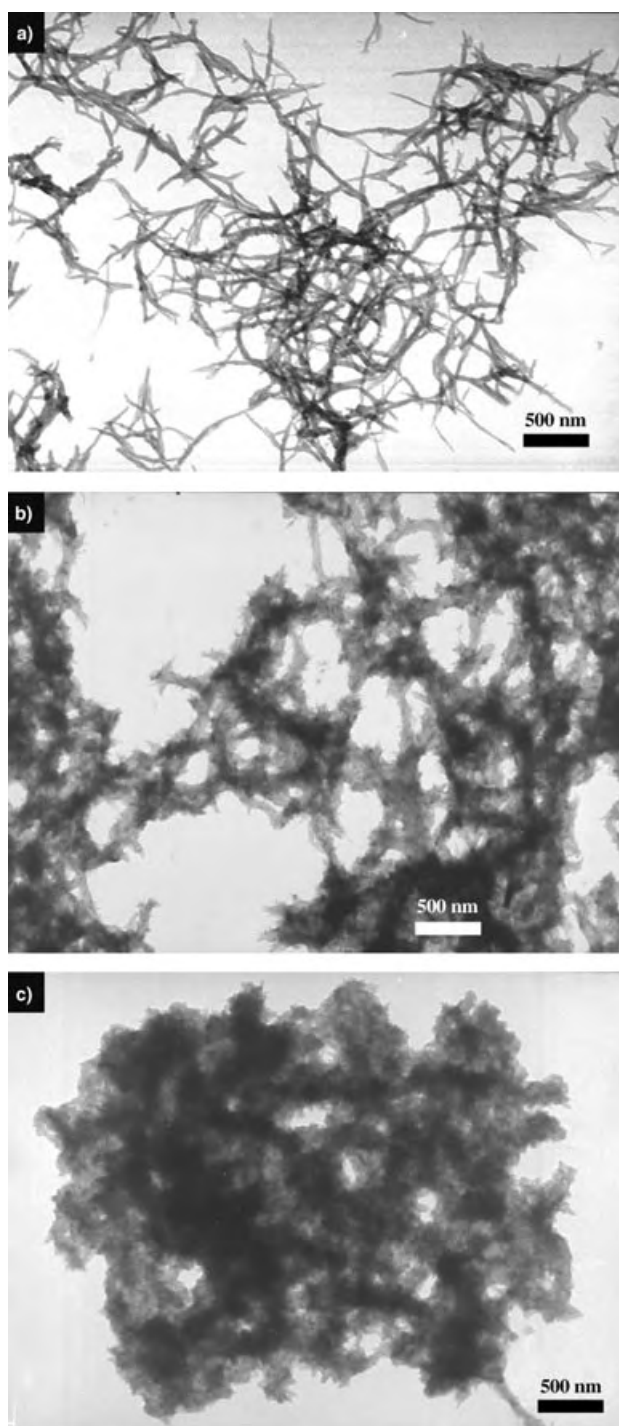


Figure 2. Typical TEM images showing the morphological evolution of polyaniline during chemical oxidative polymerization in 1 M HCl at about 0°C. The samples were extracted: a) as soon as the green color of polyaniline became visible, b) after 25 minutes, and c) after 100 minutes.

(Figure 4b). As the polymerization begins, the initiator molecules induce the formation of nanofibers by rapidly polymerizing aniline monomers in their vicinity. Therefore, all the initiator molecules are consumed to form polyaniline nanofibers, thus suppressing the secondary growth of polyaniline. The product from a fast-mixing reaction in an ice bath is

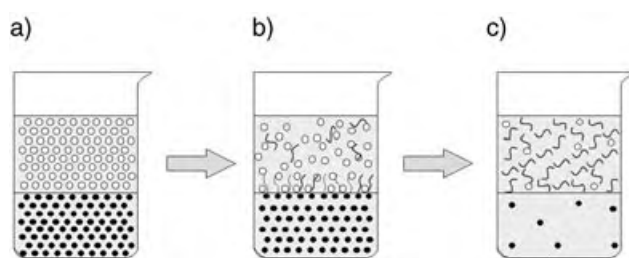


Figure 3. A schematic illustration of the synthesis of polyaniline nanofibers by using interfacial polymerization. a) An interface is set up between an organic phase containing dissolved aniline (solid circles) and an aqueous phase containing the oxidant (open circles). b) Polyaniline nanofibers form at the interface, where aniline meets the oxidant and diffuse into the water phase. Note that this carries the nanofibers away from the reactive interface so they are not subject to further secondary growth. c) As the polymerization proceeds, nanofibers accumulate in the aqueous phase.

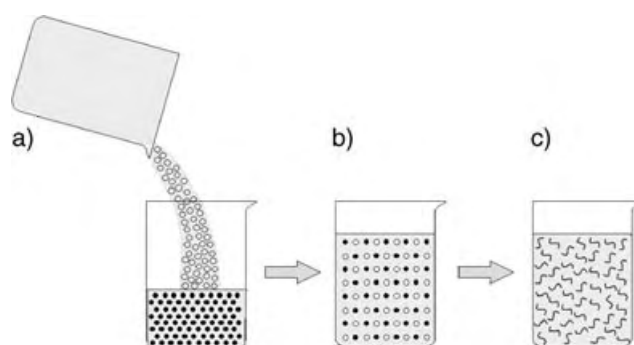


Figure 4. A schematic illustration of the synthesis of polyaniline nanofibers in a rapidly mixed reaction. a) The oxidant (open circles) dopant solution is quickly added into the aniline (solid circles) dopant solution and mixed. b) A homogenous solution is obtained where all the aniline and oxidant molecules are evenly distributed, thus leading to fast polymerization across the entire solution. c) Since all the reactants are consumed in the formation of nanofibers, secondary growth is suppressed.

almost exclusively polyaniline nanofibers of uniform sizes as observed using scanning electron microscopy (SEM; Figure 5a). The nanofibers formed are similar to those obtained by interfacial polymerization. In contrast, agglomerates of nanofibers and irregular particulates are produced by using traditional slow-mixing reactions (Figure 5b). Comparable results are obtained when monomer solution is fed into the initiator solution.

Reactions that are rapidly mixed using other doping acids, including sulfuric, camphorsulfonic, and perchloric acids also produce “pure” nanofibers with comparable shapes and sizes to those made by interfacial polymerization.^[17] Fast-mixing reactions carried out at different temperatures, including in an ice bath (ca. 0°C), at room temperature (ca. 20°C), and at 100°C, all yield high-quality nanofibers. When the reactant concentrations are increased, the induction time of the reaction is reduced, but no apparent difference in the morphology of the product is observed. It is now clear that nanofibers of polyaniline form naturally during chemical oxidative polymerization in aqueous solutions. By suppress-

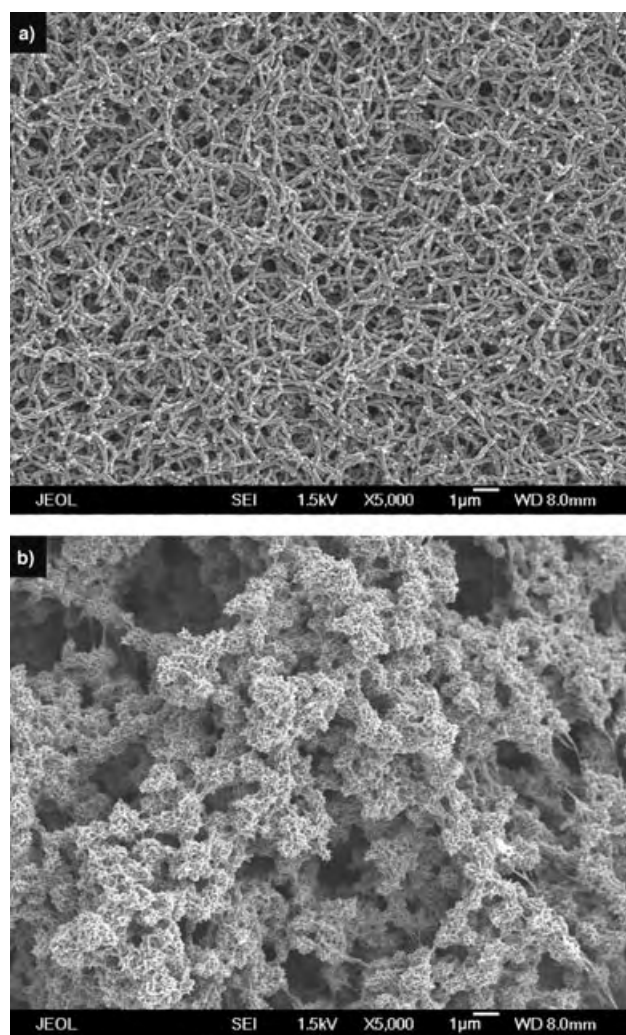


Figure 5. SEM images showing the morphology of polyaniline synthesized from a) a rapidly mixed reaction and b) a slowly mixed reaction. High-quality nanofibers are obtained in the rapidly mixed reaction, while irregular agglomerates form in the slowly mixed reactions.

ing the secondary growth of irregular particles, either through interfacial polymerization or rapid-mixing reactions, essentially pure polyaniline nanofibers can be obtained without the need for any templates or seeds.^[18] Nanofibers appear to be a basic morphological unit for chemically polymerized polyaniline as they are for polyacetylene.^[19]

The next question is why does polyaniline favor an elongated, well-extended 1-D nanofiber morphology in water? The successful rapid-mixing reaction route to making polyaniline nanofibers in water is also applicable to other solvents, which is difficult to do using interfacial polymerization. Figure 6 shows the morphology of polyaniline obtained through rapid-mixing reactions in water, ethanol, and isopropanol at room temperature. Well-defined, relatively long nanofibers are created in water (Figure 6a). The product formed in ethanol is a mixture of short nanofibrils with many irregular particles attached to them (Figure 6b). The reaction in isopropanol produces only agglomerates of 100–300-nm particulates with no discernable nano-

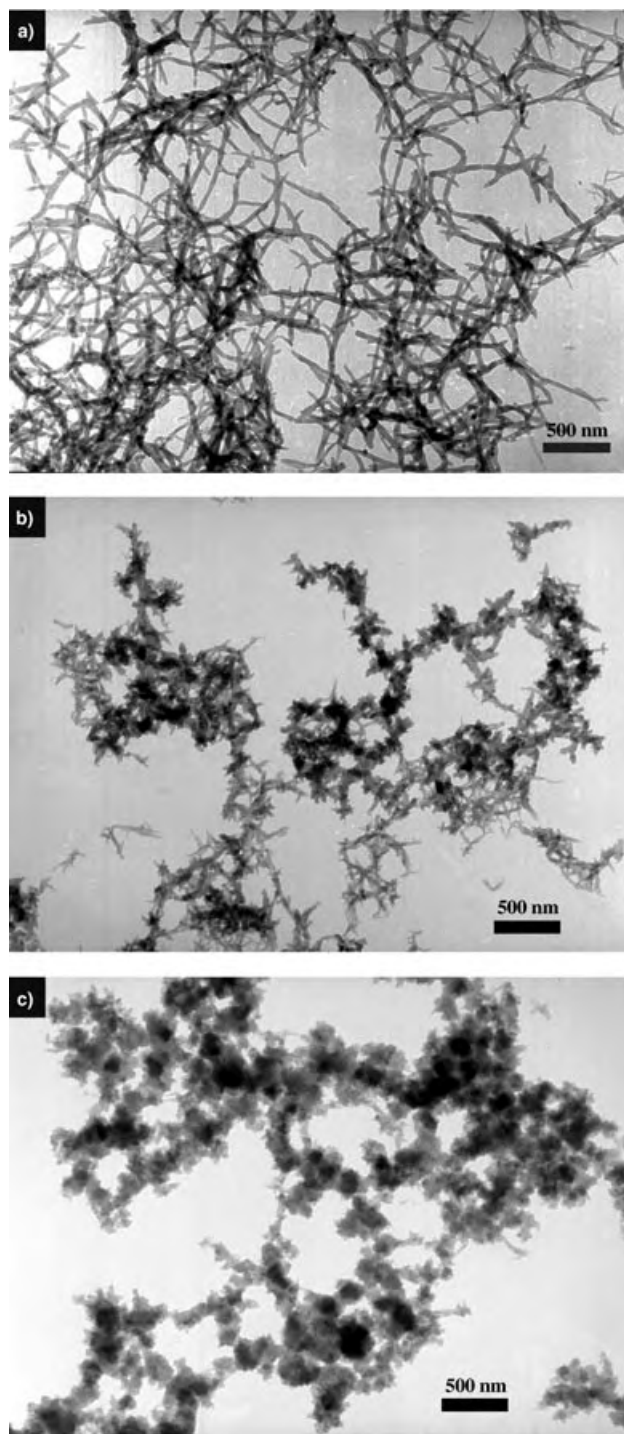


Figure 6. Typical TEM images showing the morphology of polyaniline obtained in different solvents through rapidly mixed reactions in a) water, b) ethanol, and c) isopropanol.

fibers. Note that since the as-prepared polyaniline is in its doped, hydrophilic emeraldine salt form, the affinity of the polyaniline salt for the solvent will decrease from water to ethanol to isopropanol as the polarity decreases. Therefore, it is not surprising that polyaniline favors more compact morphologies in ethanol and isopropanol, while in water elongated 1-D nanofibers form.

In summary, polyaniline preferentially forms as nanofibers in aqueous solution during chemical oxidative polymerization. The nanofibers produced in the early stage of polymerization during slow-feeding reactions are subject to secondary growth, which leads to the large agglomerates containing irregularly shaped particles and nanofibers. Pure nanofibers can be obtained by preventing the secondary growth. In interfacial polymerization secondary growth is suppressed when freshly formed nanofibers diffuse away from the reactive interface. Secondary growth is limited in rapid-mixing reactions by quickly consuming the reactants during the initial polymerization. Rapid-mixing reactions in less-polar solvents produce less-perfect nanofibers, which indicates that water is the best solvent for the synthesis of nanofibers. The rapid mixing reaction route is an even simpler method than interfacial polymerization to make polyaniline nanofibers, especially on a laboratory scale where sufficient mixing can be easily achieved by stirring or shaking before the polymerization starts. This mechanistic study may offer important insights into the synthesis of other conducting polymer nanostructures. It may also help to explain the variation in the properties of polyaniline made in different reactions, since the rate of addition of reactants affects the final morphology, thus resulting in different fractions of nanofibers in the final product.

Experimental Section

Synthesis and purification: All chemicals were of analytical grade and used as received. Reactions were generally carried out in 20-mL vials. Typically, an aqueous solution of aniline (3.2 mmol) in 1M doping acid (10 mL) and another solution of ammonium peroxydisulfate (0.8 mmol) in the same doping acid (10 mL) were prepared and mixed using a syringe pump. HCl was used as the dopant unless otherwise mentioned. The feeding rate of one solution into another was set at 5 mL h^{-1} so that it took 2 h to completely feed into the solution. Reactions were carried out at different temperatures: ca. 0°C (using an ice bath), ca. 20°C (at room temperature), and at ca. 100°C (using boiling water). Sulfuric acid was used as the dopant for reactions at ca. 100°C because of its thermal stability. Rapid-mixing reactions were performed by pouring the two solutions together and immediately stirring or shaking to ensure sufficient mixing before polymerization begins. Polymerization can be observed when the characteristic green color of polyaniline emeraldine salt became visible. More reactions were carried out by increasing or decreasing the reactant concentrations by 10 times; in all cases uniform nanofibers were observed. For reactions in ethanol and isopropanol, the monomer and ammonium peroxydisulfate solutions were prepared in the solvent. Solutions of 1M HCl in ethanol and isopropanol were prepared by diluting a concentrated aqueous solution of HCl (12.1M) with the corresponding alcohols. The products were purified by centrifugation using the reaction solvent until the suspension reached a neutral pH value.

Morphology: The morphologies of the product were examined by TEM (JEOL 100CX) and SEM (JEOL 6700). For the morphological evolution experiments (Figure 2), samples (0.1 mL) were extracted from the reaction at different times and diluted immediately in distilled water (0.5 to 2 mL). An appropriate amount of this suspension was then cast onto copper TEM grids (Formvar coated, 300 mesh, Ted-Pella Inc.). The grids were placed on filter paper to absorb any extra suspension and facilitate rapid drying, therefore quenching the polymerization. Other TEM samples were prepared by diluting the purified products and casting suspensions onto TEM

grids. Samples for SEM experiments were made on conducting stages and observed without gold coatings.

Received: May 11, 2004

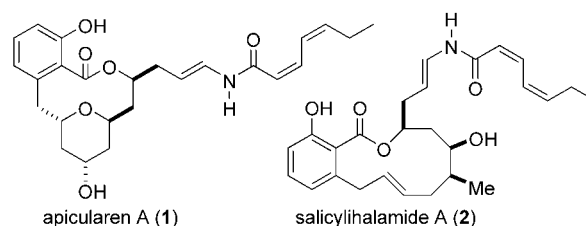
Keywords: nanostructures · polyaniline · polymerization · reaction mechanisms

- [1] W. S. Huang, B. D. Humphrey, A. G. MacDiarmid, *J. Chem. Soc. Faraday Trans.* **1986**, 82, 2385.
- [2] J. C. Chiang, A. G. MacDiarmid, *Synth. Met.* **1986**, 13, 193.
- [3] L. Yu, J. I. Lee, K. W. Shin, C. E. Park, R. Holze, *J. Appl. Polym. Sci.* **2003**, 88, 1550.
- [4] H. J. Qiu, M. X. Wan, B. Matthews, L. M. Dai, *Macromolecules* **2001**, 34, 675.
- [5] J. E. Osterholm, Y. Cao, F. Klavetter, P. Smith, *Polymer* **1994**, 35, 2902.
- [6] J. M. Liu, S. C. Yang, *J. Chem. Soc. Chem. Commun.* **1991**, 1529.
- [7] C. R. Martin, *Acc. Chem. Res.* **1995**, 28, 61.
- [8] C. G. Wu, T. Bein, *Science* **1994**, 264, 1757.
- [9] A. G. MacDiarmid, W. E. Jones, I. D. Norris, J. Gao, A. T. Johnson, N. J. Pinto, J. Hone, B. Han, F. K. Ko, H. Okuzaki, M. Llaguno, *Synth. Met.* **2001**, 119, 27.
- [10] S. J. Choi, S. M. Park, *J. Electrochem. Soc.* **2002**, 149, E26.
- [11] J. Liu, Y. H. Lin, L. Liang, J. A. Voigt, D. L. Huber, Z. R. Tian, E. Coker, B. McKenzie, M. J. Mcdermott, *Chem. Eur. J.* **2003**, 9, 605.
- [12] L. Liang, J. Liu, C. F. Windisch, G. J. Exarhos, Y. H. Lin, *Angew. Chem.* **2002**, 114, 3817; *Angew. Chem. Int. Ed.* **2002**, 41, 3665.
- [13] S. Virji, J. Huang, R. B. Kaner, B. H. Weiller, *Nano Lett.* **2004**, 4, 491.
- [14] J. Huang, S. Virji, B. H. Weiller, R. B. Kaner, *Chem. Eur. J.* **2004**, 10, 1314.
- [15] J. Huang, S. Virji, B. H. Weiller, R. B. Kaner, *J. Am. Chem. Soc.* **2003**, 125, 314.
- [16] H. Liu, J. Kameoka, D. A. Czaplewski, H. G. Craighead, *Nano Lett.* **2004**, 4, 491.
- [17] J. Huang, R. B. Kaner, *J. Am. Chem. Soc.* **2004**, 126, 851.
- [18] X. Zhang, W. J. Goux, S. K. Manohar, *J. Am. Chem. Soc.* **2004**, 126, 4502.
- [19] J. C. W. Chien, Y. Yamashita, J. A. Hirsch, J. L. Fan, M. A. Schen, F. E. Karasz, *Nature* **1982**, 299, 608.

Total Synthesis of Apicularen A through Transannular Pyran Formation**

Andreas F. Petri, Alexander Bayer, and
Martin E. Maier*

Natural products that show cytotoxic effects are important in cancer treatment. As resistance can occur, and not all tumor cells are equally sensitive to a certain drug, there is a need for compounds that have novel modes of action. Such compounds include the benzolactone enamides,^[1] for example, apicularen A (**1**) and salicylihalamide A (**2**). Salicylihalamide A was



isolated from the sponge *Haliclona* sp.,^[2] whereas apicularen A has been found in various myxobacteria strains.^[3] Both compounds were shown to be selective inhibitors of mammalian V-ATPases, which are important as proton pumps for regulating intracellular pH.^[4] Depending on the cell type studied, other downstream effects were observed, such as the phosphorylation of mitogen-activated protein kinases, which results in apoptosis.^[5,6] The structure of apicularen A is characterized by the salicylic acid portion, a *trans* tetrahydropyran embedded in a macrolactone, and an enamide side chain. Several total syntheses of apicularen A,^[7] formal total syntheses,^[8] and synthetic studies^[9,10] have been reported.

Some time ago we proposed that the pyran ring of apicularen A is probably formed by a transannular reaction of a macrolactone precursor through the opening of an epoxide or addition to an enone.^[10a] Herein we describe the application of the transannular etherification strategy for the total synthesis of apicularen A (**1**).

As described previously,^[10b] the dithiane **3**, the epoxides **4** and **5**, and trimethylsilylacetylene (**6**) were combined in a four-component coupling^[11,12] to give the alkyne **7**

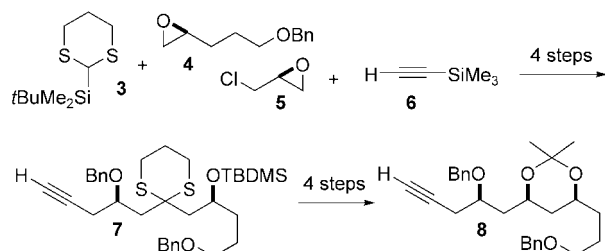
[*] A. F. Petri, A. Bayer, Prof. Dr. M. E. Maier
Institut für Organische Chemie
Universität Tübingen
Auf der Morgenstelle 18, 72076 Tübingen (Germany)
Fax: (+49) 7071-295-137
E-mail: martin.e.maier@uni-tuebingen.de

[**] Financial support by the Deutsche Forschungsgemeinschaft (grant Ma 1012/10-1) and the Fonds der Chemischen Industrie is gratefully acknowledged.



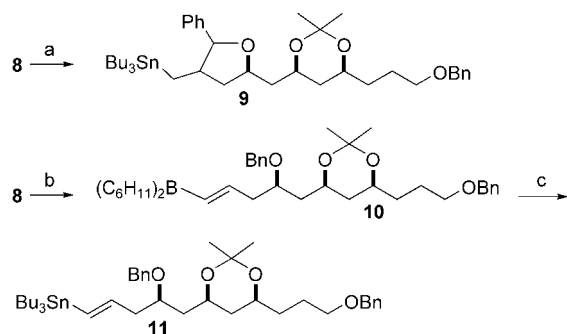
Supporting information for this article is available on the WWW under <http://www.angewandte.org> or from the author.

(Scheme 1). Hydrolysis of the dithiane and desilylation yielded a β -hydroxyketone, which was converted by *syn* reduction and acetalization into the alkyne **8**.



Scheme 1. Synthesis of the alkyne **8** by a four-component coupling strategy. Bn = benzyl, TBDMS = *tert*-butyldimethylsilyl.

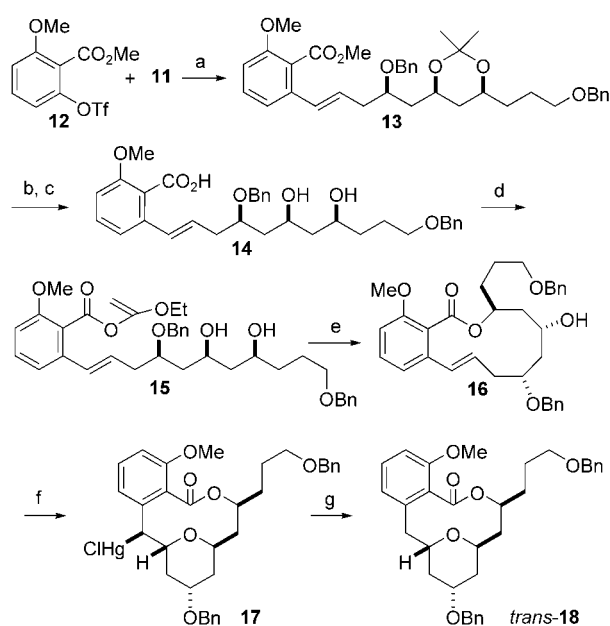
The conversion of the alkyne **8** into a suitable vinyl metal species for cross-coupling turned out to be quite challenging (Scheme 2). For example, the palladium-catalyzed hydro-



Scheme 2. Synthesis of the vinylstannane **11** via an intermediate vinyl borane: a) $n\text{Bu}_3\text{SnH}$, AIBN (cat.), toluene, reflux (56%); b) $(\text{C}_6\text{H}_{11})_2\text{BH}$, THF, 0°C , 1 h; c) NaOH , $[\text{Cu}(\text{acac})_2]$ (cat.), $n\text{Bu}_3\text{SnCl}$, $-15 \rightarrow 23^\circ\text{C}$ (> 93%).

stannylation^[13] of **8** gave an inseparable mixture of the internal and terminal stannane. The hydrostannylation under radical conditions led to the tetrahydrofuran **9** through an atom-transfer and cyclization process. This difficulty was overcome by generation of the vinyl borane **10**^[14] followed by transmetalation to the stannane **11**.^[15] In this way the vinyl stannane was obtained exclusively as the *E* isomer in excellent yield.

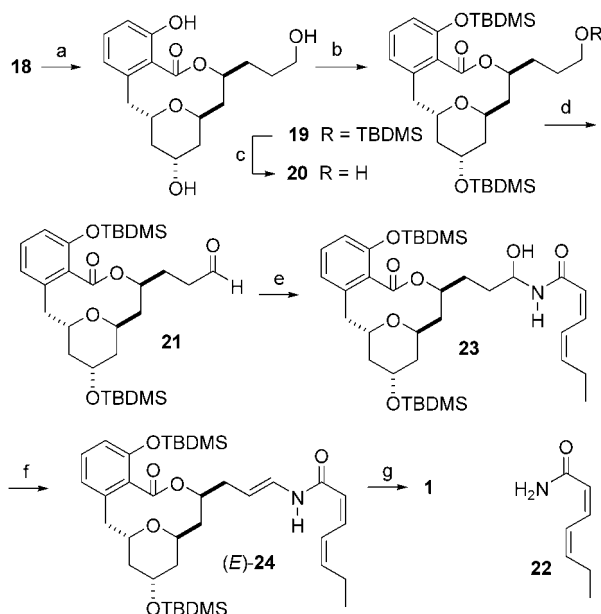
The subsequent cross-coupling reaction of the triflate **12**^[10a] with the stannane **11** proceeded smoothly to furnish the salicylate **13** in excellent yield (Scheme 3). Hydrolysis of the acetal and ester functionalities then gave the dihydroxy acid **14**. As we had observed in this and related cases,^[10] the size-selective macrolactonization under Yamaguchi conditions^[16] gave selectively the larger of the two macrolactones, but the chemical yield was only in the range of 50%. Therefore, the method of Trost and Chisholm was investigated.^[17] In this case, an ethoxyvinyl ester, prepared by the ruthenium-catalyzed addition of the carboxylic acid **14** to ethoxyacetylene, serves as the precursor. The best results for the macrolactonization were obtained at 80°C (5 mM, 63%



Scheme 3. Cross-coupling, size-selective macrolactonization, and transannular etherification to yield the building block *trans*-**18**: a) $\text{P}(\text{furyl})_3$, $[\text{Pd}_2(\text{dba})_3]$, LiCl , NMP, 60°C , 48 h (93% from **8**); b) 80% AcOH , 23°C , 80 min (99%); c) LiOH , $\text{MeOH}/\text{H}_2\text{O}$, 60°C , 72 h (99%); d) $[\{\text{RuCl}_2(p\text{-cymene})\}_2]$, ethoxyacetylene, toluene, 0°C ; e) CSA, toluene, 80°C (63% from **14**); f) $\text{Hg}(\text{O}_2\text{CCF}_3)_2$, CH_2Cl_2 , 23°C , 30 min, then NaCl , 23°C ; g) Et_3B , LiBH_4 , THF, -78°C , 1 h (89% from **16**). CSA = camphorsulfonic acid, NMP = 1-methyl-2-pyrrolidinone, Tf = trifluoromethanesulfonyl.

yield). In contrast to the results of our previous model study,^[10a] the treatment of the macrolactone **16** with *N*-(phenylseleno)phthalimide left the starting material unchanged.^[18] Eventually, it was found that treatment with mercuric trifluoroacetate in dichloromethane gave the cyclized organomercurial intermediate within minutes. To suppress the undesired retrocyclization^[19] of the mercurial intermediate during the reductive demercuration, it was necessary to change the solvent from CH_2Cl_2 to THF and to perform the reduction with LiBH_4 in the presence of Et_3B .^[20] The origin of the high selectivity in the transannular etherification has not yet been clearly ascertained. However, on the basis of previous work, we believe that the transition state of the kinetically controlled reaction is productlike, thus leading to the less strained product.^[8d,10a]

The synthesis continued with the cleavage of all ether protecting groups with 9-iodoborabicyclononane (9-I-9-BBN; Scheme 4).^[21] A sequence of complete silylation and selective desilylation generated the primary alcohol **20**, which was oxidized to the aldehyde **21**^[7c] with tetra-*n*-propylammonium perruthenate (TPAP).^[22] The stage was set for the attachment of the enamide side chain.^[23] The addition of the aluminum carboximidoate derived from the amide **22**^[23b] and diisobutylaluminum hydride^[24] to the aldehyde **21** provided the hemiaminal **23** in 86% yield (1:1 mixture of diastereomers). When a solution of the hemiaminal **23** in THF was heated at reflux in the presence of acetic anhydride and pyridine, the enamide **24** was obtained as a separable *E/Z* mixture (*E/Z* = 75:25). The removal of the silicon protecting groups from (*E*)-**24** with



Scheme 4. Synthesis of apicularen A via the hemiaminal **23**: a) 9-*l*-BBN, CH₂Cl₂, 23 °C, 90 s, MeOH; b) TBDMSCl, imidazole, DMAP (cat.), DMF, 23 °C, 48 h (72% from **18**); c) CSA (cat.), CH₂Cl₂/MeOH, 0 °C, 3 h (85%); d) TPAP, NMO, 0 °C, 1 h (98%); e) **22**, DIBAL, THF, 0 °C, 30 min, add **21**, 0 °C, 18 h (86%); f) THF, pyridine, Ac₂O, reflux, 48 h ((*E*)-**24**: 46%, (*Z*)-**24**: 15%); g) TASF, DMF, 23 °C, 21 h (75%). DIBAL = diisobutylaluminum hydride, DMF = *N,N*-dimethylformamide, NMO = 4-methylmorpholine *N*-oxide, TASF = tris(dimethylamino)sulfonium difluorotrimethylsilicate.

TASF^[25] gave pure apicularen A (**1**). Another method for the conversion of an aldehyde into the corresponding enamide via a bisamide derivative through a base-induced elimination^[26] proved unsuccessful in the case of apicularen.^[7b,c]

In summary, we have developed a concise total synthesis of apicularen A, featuring a number of key transformations: a) a four-component coupling that combines a 1,3-dithiane, a terminal epoxide, an acetylide, and epichlorohydrin, b) a Stille cross-coupling reaction with the vinylstannane generated from a vinylborane, c) a size-selective macrolactonization of an ethoxyvinyl ester, d) a transannular etherification, and e) formation of the enamide from a hemiaminal. This successful strategy underscores the close relationship between salicylilhalamide and apicularen.

Received: May 24, 2004

Keywords: cross-coupling · enamides · macrolactonization · total synthesis · transannulation

- [1] a) J. A. Beutler, T. C. McKee, *Curr. Med. Chem.* **2003**, *10*, 787–796; b) L. Yet, *Chem. Rev.* **2003**, *103*, 4283–4306.
- [2] K. L. Erickson, J. A. Beutler, J. H. Cardellina II, M. R. Boyd, *J. Org. Chem.* **1997**, *62*, 8188–8192.
- [3] a) B. Kunze, R. Jansen, F. Sasse, G. Höfle, H. Reichenbach, *J. Antibiot.* **1998**, *51*, 1075–1080; b) R. Jansen, B. Kunze, H. Reichenbach, G. Höfle, *Eur. J. Org. Chem.* **2000**, 913–919.

- [4] M. R. Boyd, C. Farina, P. Belfiore, S. Gagliardi, J. W. Kim, Y. Hayakawa, J. A. Beutler, T. C. McKee, B. J. Bowman, E. J. Bowman, *J. Pharmacol. Exp. Ther.* **2001**, *291*, 114–120.
- [5] J. Hong, K. Yamaki, K. Ishihara, J. W. Ahn, O. Zee, K. Ohuchi, *J. Pharm. Pharmacol.* **2003**, *55*, 1299–1306.
- [6] H. J. Kwon, D. H. Kim, J. S. Shim, J. W. Ahn, *J. Microbiol. Biotechnol.* **2002**, *12*, 702–705.
- [7] a) A. Bhattacharjee, O. R. Seguil, J. K. De Brabander, *Tetrahedron Lett.* **2001**, *42*, 1217–1220; b) K. C. Nicolaou, D. W. Kim, R. Baati, *Angew. Chem.* **2002**, *114*, 3853–3856; *Angew. Chem. Int. Ed.* **2002**, *41*, 3701–3704; c) K. C. Nicolaou, D. W. Kim, R. Baati, A. O'Brate, P. Giannakakou, *Chem. Eur. J.* **2003**, *9*, 6177–6191; d) Q. Su, J. S. Panek, *J. Am. Chem. Soc.* **2004**, *126*, 2425–2430.
- [8] a) A. Lewis, I. Stefanuti, S. A. Swain, S. A. Smith, R. J. K. Taylor, *Tetrahedron Lett.* **2001**, *42*, 5549–5552; b) A. Lewis, I. Stefanuti, S. A. Swain, S. A. Smith, R. J. K. Taylor, *Org. Biomol. Chem.* **2003**, *1*, 104–116; c) B. R. Graetz, S. D. Rychnovsky, *Org. Lett.* **2003**, *5*, 3357–3360; d) F. Hilli, J. M. White, M. A. Rizzacasa, *Org. Lett.* **2004**, *6*, 1289–1292.
- [9] a) A. Bhattacharjee, J. K. De Brabander, *Tetrahedron Lett.* **2000**, *41*, 8069–8073; b) F. Hilli, J. M. White, M. A. Rizzacasa, *Tetrahedron Lett.* **2002**, *43*, 8507–8510.
- [10] a) S. M. Kühnert, M. E. Maier, *Org. Lett.* **2002**, *4*, 643–646; b) A. F. Petri, S. M. Kühnert, F. Scheufler, M. E. Maier, *Synthesis* **2003**, 940–955.
- [11] For a review, see: A. B. Smith III, C. M. Adams, *Acc. Chem. Res.* **2004**, *37*, 365–377.
- [12] L. F. Tietze, H. Geissler, J. A. Gewert, U. Jakobi, *Synlett* **1994**, 511–512.
- [13] a) M. Lautens, W. Klute, *Angew. Chem.* **1996**, *108*, 472–475; *Angew. Chem. Int. Ed. Engl.* **1996**, *35*, 442–445; b) H. X. Zhang, F. Guibé, G. Balavoine, *J. Org. Chem.* **1990**, *55*, 1857–1867; c) A. N. Cuzzupe, C. A. Hutton, M. J. Lilly, R. K. Mann, K. J. McRae, S. C. Zammit, M. A. Rizzacasa, *J. Org. Chem.* **2001**, *66*, 2382–2393.
- [14] The corresponding vinyl boronic acid (bis(triethylsilyl ether) derivative) obtained in 57% yield did not give the coupling product upon treatment with the triflate **12**.
- [15] M. Hoshi, K. Takahashi, A. Arase, *Tetrahedron Lett.* **1997**, *38*, 8049–8052.
- [16] J. Inanaga, K. Hirata, H. Saeki, T. Katsuki, M. Yamaguchi, *Bull. Chem. Soc. Jpn.* **1979**, *52*, 1989–1993.
- [17] B. M. Trost, J. D. Chisholm, *Org. Lett.* **2002**, *4*, 3743–3745.
- [18] With the more electrophilic phenylselenium triflate (PhSeCl, AgOTf, CH₂Cl₂, 0 °C, 20 min, then –78 °C, add **16**, 1 h (34%)) the cyclization was accompanied by side reactions, such as ether cleavage.
- [19] R. C. Griffith, R. J. Gentile, T. A. Davidson, F. L. Scott, *J. Org. Chem.* **1979**, *44*, 3580–3583.
- [20] S. H. Kang, J. H. Lee, S. B. Lee, *Tetrahedron Lett.* **1998**, *39*, 59–62.
- [21] A. Fürstner, G. Seidel, *J. Org. Chem.* **1997**, *62*, 2332–2336.
- [22] a) W. P. Griffith, S. V. Ley, *Aldrichimica Acta* **1990**, *23*, 13–19; b) S. V. Ley, J. Norman, W. P. Griffith, S. P. Marsden, *Synthesis* **1994**, 639–666.
- [23] a) A. Fürstner, T. Dierkes, O. Thiel, G. Blanda, *Chem. Eur. J.* **2001**, *7*, 5286–5298; b) A. Bayer, M. E. Maier, *Tetrahedron* **2004**, *60*, 6665–6677.
- [24] T. R. Hoye, M. Hu, *J. Am. Chem. Soc.* **2003**, *125*, 9576–9577.
- [25] K. A. Scheidt, H. Chen, B. C. Follows, S. R. Chemler, D. S. Coffey, W. R. Roush, *J. Org. Chem.* **1998**, *63*, 6436–6437.
- [26] D. Labrecque, S. Charron, R. Rej, C. Blais, S. Lamothe, *Tetrahedron Lett.* **2001**, *42*, 2645–2648.

C–N Activation

Unusual Reactivity of a Nickel N-Heterocyclic Carbene Complex: *tert*-Butyl Group Cleavage and Silicone Grease Activation**

Stephen Caddick,* F. Geoffrey N. Cloke,*
Peter B. Hitchcock, and Alexandra K. de K. Lewis

During the past decade there has been considerable interest in N-heterocyclic carbene ligands (NHCs), particularly as alternative to phosphanes for both palladium-[¹] and ruthenium-mediated[²] catalysis of a range of organic transformations. Recently, the use of Ni^{II}/imidazolium salt/base or Ni⁰/NHC combinations for catalytic aminations, in which the active catalyst is believed to be a Ni⁰–NHC complex, has also been described.[³] Our interest in this area to date has focused on the use of isolated, two-coordinate bis(NHC) palladium(0) complexes for catalytic amination[⁴] and mechanistic studies; in the latter context we have recently reported a detailed mechanistic study on the oxidative addition of 4-chlorotoluene to bis(1,3-bis-*tert*-butylimidazol-2-ylidene)palladium.[⁵] Thus we were interested in extending such studies to the nickel analogue, and herein we report the highly unusual reactivity associated with the attempted conventional synthesis of bis(1,3-bis-*tert*-butylimidazol-2-ylidene)nickel.

We have already reported the preparation of [Ni{C(Nt-BuCH)₂}₂] (**1**) by metal vapor synthesis (MVS), although the compound was not structurally characterized at that time.[⁶] We have now determined the structure of **1** (Figure 1).

Ardeungo et al. have reported the molecular structure of an analogue of **1** derived from 1,3-bis-mesitylimidazol-2-ylidene, synthesized by the treatment of [Ni(1,5-cod)₂] (COD = cyclooctadiene) with the free NHC.[⁸] Comparison of **1** with the former shows that both structures display linear geometry around the nickel center, although the nickel–carbene bond length is slightly longer in **1** (1.874(2) Å for **1**, compared to 1.827(6) Å). However, they differ in that the planes of the ligands in **1** are twisted 75° from coplanarity whereas in the Arduengo complex the twist angle is 53°. The bonding in such compounds is predominantly σ in nature, with minimal π bonding,[⁹] so the twist angle is almost certainly

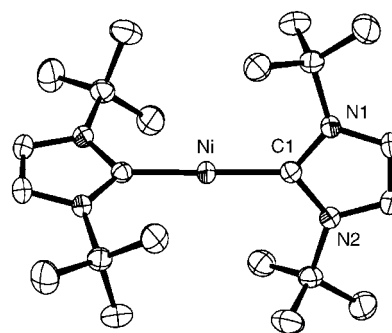


Figure 1. ORTEP diagram of **1** (thermal ellipsoids set at 50% probability). Selected bond lengths [Å] and angles [°]: Ni–C(1) 1.874(2); N(1)–C(1)–N(1) 102.25(15).^[7]

governed by subtle steric interactions and/or crystal packing forces in the solid state. In solution, NMR spectroscopy studies on asymmetrically substituted bis(NHC)-Group 10M⁰ indicate rapid rotation about the metal–carbene bond on the NMR timescale down to –90°.[¹⁰]

Since we wished to develop a conventional, solution-phase route to **1**, [Ni(1,5-cod)₂] was treated with an excess of 1,3-bis-*tert*-butylimidazol-2-ylidene in THF in a Schlenk tube sealed with a greased stopper. After a two-week reaction time, work-up and crystallization from hexane afforded purple crystals of [[Ni{C(Nt-BuCH)₂}][O(Me₂SiOSiMe₂)–μ-O]]₂ (**2**; Figure 2) in low yield.

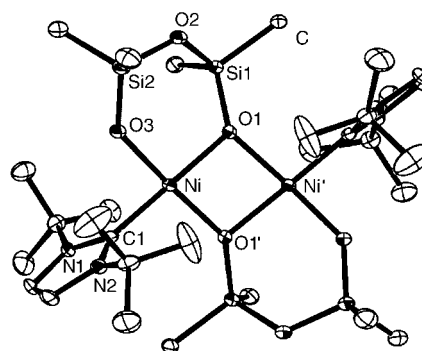


Figure 2. ORTEP diagram of **2** (thermal ellipsoids set at 50% probability). Selected bond lengths [Å] and angles [°]: Ni–C(1) 1.883(6), Ni–O(1) 1.958(4), Ni–O(1') 1.896(4), Ni–O(3) 1.839(4); N(1)–C(1)–N(2) 105.2(15).^[7]

The structure reveals a dinuclear nickel(II) complex, with distorted square-planar geometry about nickel, in which the two metal centers are bridged by disiloxane units derived from silicone grease (see Scheme 1). The central Ni₂(μ-O)₂ core is folded by 21° out-of-plane about the O–O axis, with the bond lengths of the asymmetric μ-O bridges, Ni–O(1) 1.958(4), Ni–O(1') 1.896(4) Å, comparable to those found in the μ-O unit in [[Ni{C(SiMe₃)(2-SiMe₂C₅H₄N)(SiMe₂O)}]]₂ (1.918(4), 1.891(45) Å);^[11] the non-bridging oxygen–nickel bond length in **2** (Ni–O(3) 1.839(4) Å) is very close to that in [Ni(η²-OCHMeCH₂NMe₂)₂] (1.829(3) Å).^[12] The nickel–carbene Ni(1)–C(1) bond length (1.883(6) Å) in **2** is identical to that in **1** (within estimated standard deviations (esds)),

[*] Prof. Dr. F. G. N. Cloke, Dr. P. B. Hitchcock, A. K. de K. Lewis
Department of Chemistry
School of Life Sciences
University of Sussex
Brighton, BN1 9QJ (UK)
Fax: (+44) 1273-677-196
E-mail: f.g.cloke@sussex.ac.uk

Prof. Dr. S. Caddick
Christopher Ingold Laboratories
Department of Chemistry
University College London
20 Gordon Street, London, WC1H 0AJ (UK)
Fax: (+44) 207-679-4694
E-mail: s.caddick@ucl.ac.uk

[**] This work was financially supported by EPSRC and AstraZeneca. We also thank Dr. John Leonard (AstraZeneca) for helpful discussions.

despite the change in nickel oxidation state. Serendipitous activation of silicone grease by lanthanides and early transition metals is not uncommon, but rare for late transition metals and unprecedented for nickel.^[13]

The reaction of $[\text{Ni}(1,5\text{-cod})_2]$ with 1,3-bis-*tert*-butylimidazol-2-ylidene in THF was repeated in greaseless apparatus for two weeks, which resulted in the isolation of deep blue, crystalline **3** (see Scheme 1), whose X-ray structure is shown in Figure 3.

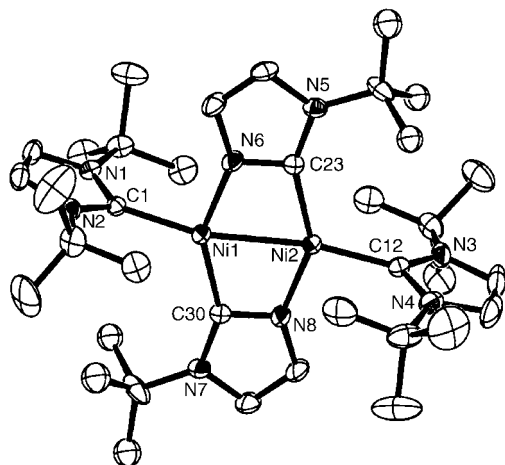


Figure 3. ORTEP diagram of **3** (thermal ellipsoids set at 50% probability). Selected bond lengths [Å] and angles [°]: Ni(1)–C(1) 1.960(5), Ni(2)–C(12) 1.954(5), Ni(2)–C(23) 1.927(5), Ni(1)–C(30) 1.922(5), Ni(1)–N(6) 1.900(5), Ni(2)–N(8) 1.904(5), Ni(1)–Ni(2) 2.4354(9); N(1)–C(1)–N(2) 102.9, N(6)–C(23)–N(5) 105.9; $\Sigma_{\text{angle}} \text{N}(5)$ 360.0, $\Sigma_{\text{angle}} \text{N}(6)$ 359.7, $\Sigma_{\text{angle}} \text{N}(7)$ 359.8, $\Sigma_{\text{angle}} \text{N}(8)$ 359.7.^[7]

Compound **3** is a second binuclear species (the first being **2**), in which the two nickel centers are ligated by terminal NHC ligands and symmetrically bridged by *tert*-butylimidazol-2-ylidene ligands arising from *tert*-butyl group cleavage from the parent NHC (see Scheme 1). The Ni–Ni separation of 2.4354(9) Å is consistent with a Ni–Ni single bond,^[14] and the compound is accordingly diamagnetic by NMR spectroscopy.^[15] The geometry about the nickel centers is square planar with the terminal NHC ligands lying perpendicular to the plane of the $\text{Ni}_2\text{C}_2\text{N}_2$ central core. The terminal NHC–Ni bond lengths (Ni(1)–C(1) 1.960(5), Ni(2)–C(12) 1.954(5) Å) are considerably longer than that in **1**, owing to the increased steric bulk around the metal centers. Within the bridging NHC-derived ligands, the nickel–nitrogen bond lengths (Ni(1)–N(6) 1.900(5), Ni(2)–N(8) 1.904(5) Å) are in the range of other reported Ni–N single bonds (e.g. $[\text{Ni}(t\text{-Bu}_2\text{PC}_2\text{H}_4\text{PrBu}_2)\{\text{N}(\text{Ar})\text{H}\}]$, 1.881(2) Å;^[16] $[\text{NiCp}^*(\text{PET}_3)\{\text{N}(\text{tol})\text{H}\}]$, 1.903(5) Å^[17] ($\text{Cp}^* = \text{C}_5\text{Me}_5$)) whilst the carbene carbon–nickel distances (Ni(1)–C(30) 1.922(5), Ni(2)–C(23) 1.927(5) Å) are comparable to those for the terminal NHC ligands in **3** (within esds). The sum of bond angles around the amido nitrogen atoms N(6) and N(8) are essentially 360°.

The reaction to generate **3** was repeated, but halted after five days; work-up afforded mainly starting materials but also a low yield of a new, yellow compound **4** (see Scheme 1). Crystals suitable for X-ray diffraction were obtained from a hexane solution of **4** (Figure 4).

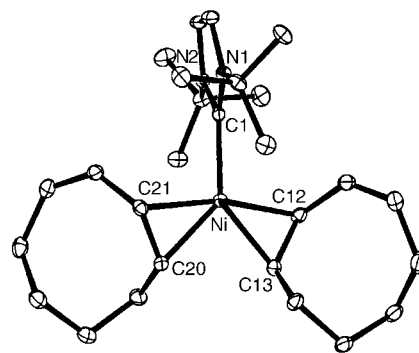
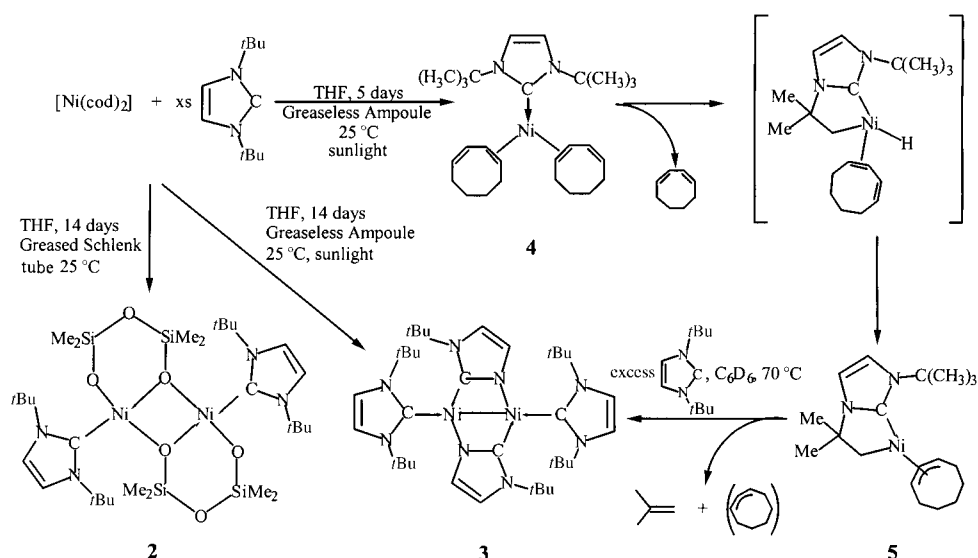


Figure 4. ORTEP diagram of **4** (thermal ellipsoids set at 50% probability). Selected bond lengths [Å] and angles [°]: Ni–C(1) 1.951(4), Ni–C(12) 2.046(5), Ni–C(13) 2.012(5), Ni–C(21) 2.045(5), Ni–C(20) 2.024(4); N(1)–C(1)–N(2) 103.3(3).^[7]

Compound **4** is a 16-electron Ni^0 complex in which the nickel center is ligated by one NHC ligand and two η^2 -cycloocta-1,3-diene ligands in a distorted trigonal-planar arrangement. The nickel–olefin bond lengths range between 2.012(5) and 2.046(5) Å, slightly shorter than those in the $[\text{Ni}(1,5\text{-cod})_2]$ precursor (2.117(5)–2.130(9) Å),^[18] but identical (within esds) to those in $[\text{Ni}(\text{PCy}_3)(\eta^2\text{-C}_2\text{H}_4)_2]$.^[19] As is the case for $[\text{Ni}(\text{PCy}_3)(\eta^2\text{-C}_2\text{H}_4)_2]$, in **3** the coordinated C=C axis and the NHC–Ni axis are coplanar. The NHC–Ni bond length (Ni–C(1) 1.951(4) Å) in **4** is significantly longer than that in **1**, and **4** is highly unstable, particularly in solution. NMR spectroscopy studies show that **4** rapidly converts into a new compound **5**, accompanied by the appearance of free 1,3-COD; nOe experiments and mass spectrometry suggested the structure for **5** shown in Scheme 1, resulting from 1,3-COD loss, C–H activation of a *tert*-butyl substituent on the NHC and subsequent H-atom transfer to the bound 1,3-COD to form a cyclooctenyl ligand (Scheme 1). Isolation of orange crystals of **5**, suitable for X-ray diffraction confirmed the structure (Figure 5).

Compound **5** has a distorted square-planar geometry and is a 16-electron diamagnetic Ni^{II} complex. The Ni–C1 bond length (1.905(4) Å) is slightly shorter than that in the precursor **4** (1.951(4) Å) owing to the change in oxidation state and the metal center being less sterically crowded. The bond between Ni and the central allylic carbon C13 is 1.963(3) Å, which is shorter than those between Ni and C12 and C14 (2.108(3) Å and 2.034(4) Å respectively), as expected. These values are very similar to those of the reported bis(η^3 -methallyl)nickel and the C12–C13–C14 bond angle (123.4(3) Å) is only slightly more obtuse than the idealized value of 120°.^[20] The Ni–C bond in the C–H activated *tert*-butyl group (Ni–C5, 1.958(3) Å) is identical (within esds), to the Ni–CH₃ bond length (1.965(5) Å) in $[\text{Ni}(t\text{-Bu}_2\text{PC}_2\text{H}_4\text{-PrBu}_2)\text{Me}_2]$.^[21]

The successful isolation of complexes **4** and **5** suggests a mechanism for the formation of **3**, summarized in Scheme 1. The reaction to form the intermediate **4** clearly involves isomerization of 1,5-COD to 1,3-COD, presumably initiated by sunlight—this reaction does not work in the dark and [2+2] cycloaddition of 1,5-COD by radical formation readily occurs under UV irradiation).^[22] The conversion of **4** into **5**



Scheme 1. Formation of compounds **2–5**. Proposed mechanism for the formation of **3** via **4** and **5**.

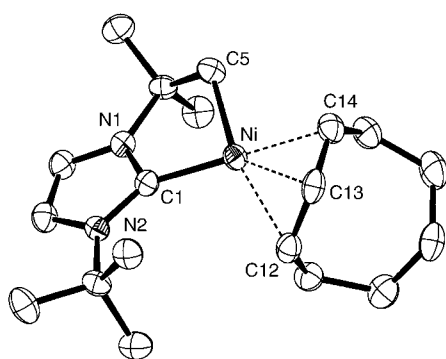


Figure 5. ORTEP diagram of **5** (thermal ellipsoids set at 50% probability). Selected bond lengths [Å] and angles [°]: Ni–C1 1.905(4), Ni–C5 1.958(3), Ni–C13 1.963(3), Ni–C14 2.034(4), Ni–C12 2.108(3); N1–C1–N2 103.5(3).^[7]

proceeds by rapid loss of a 1,3-COD ligand (detected by NMR spectroscopy) and subsequent activation of a *tert*-butyl group, probably by classic C–H activation to generate a Ni–H species (although no resonance signals for Ni–H were detected by NMR spectroscopy during the reaction) followed by hydride migration to the 1,3-COD ligand. The final formation of **3** then requires addition of 1,3-bis-*tert*-butylimidazol-2-ylidene, elimination of isobutene, and loss of the cyclooctenyl ligand. Evidence for this hypothesis was obtained by treating isolated **5** with excess 1,3-bis-*tert*-butylimidazol-2-ylidene. The reaction was monitored by ¹H NMR spectroscopy. Heating the mixture to 70 °C led to the clean formation of **3** and isobutene; however, although the spectrum contained additional peaks in the olefinic and aliphatic regions, the fate of the cyclooctenyl fragment could not be unambiguously deduced.

In conclusion, attempted conventional synthesis of **1** by ligand substitution of [Ni(1,5-cod)₂] with 1,3-bis-*tert*-butylimidazol-2-ylidene leads to *tert*-butyl group cleavage from the NHC via the novel, highly reactive monocarbene bis(olefin) complex **4**; in the presence of vacuum grease, the product is

the disiloxane bridged dimer **2**, an unprecedented example of activation of silicone grease by nickel. Improved synthetic routes to **4** and a study of its reaction chemistry are in progress.

Experimental Section

2: [Ni(1,5-cod)₂] (100 mg, 0.4 mmol), 1,3-bis-*tert*-butylimidazol-2-ylidene (144 mg, 0.8 mmol), THF (35 mL), and a stir bar were added to a Schlenk (100 mL), which was sealed with a stopper coated with silicone vacuum grease. The mixture was left to stir for two weeks at room temperature. The THF was then removed in vacuo; the remaining solid was dissolved in hexane, and the resultant solution collected by filtration, concentrated, and cooled to –25 °C to afford bright, purple crystals of **2**. Yield approximately 5%. ¹H NMR (300 MHz, 20 °C, [D₆]benzene): δ = 6.33 (4H, s, CH), 3.05 (36H, s, *t*Bu), 0.13 (6H, s, SiCH₃), –0.16 ppm (6H, s, SiCH₃); ¹³C NMR (75 MHz, [D₆]benzene): δ = 143.8 (NiC(N*t*BuCH)₂), 118.6 (NiC(N*t*BuCH)₂), 59.4 (CCH₃), 32.8 (CCH₃), 2.4 (SiCH₃), 1.0 ppm (SiCH₃). Elemental analysis (%) calcd for C₃₀H₆₄N₄NiO₆Si₄: C 44.67, H 8.00, N 6.94; found C 44.31, H 7.43, N 7.47.

3: [Ni(1,5-cod)₂] (100 mg, 0.4 mmol) and 1,3-bis-*tert*-butylimidazol-2-ylidene (432 mg, 2.4 mmol) were added to an ampoule (50 mL) equipped with a greaseless stopcock, THF (35 mL) was added through a cannula, and the reaction mixture left to stir for two weeks on the window sill. The THF was removed in vacuo and excess 1,3-bis-*tert*-butylimidazol-2-ylidene removed by sublimation in vacuo onto a liquid nitrogen cooled probe. The remaining solid was dissolved in hexane, and the resultant solution collected by filtration, concentrated, and cooled to –25 °C to afford deep blue crystals of **3**. Yield 55 mg, 38% in two crops. ¹H NMR (300 MHz, 20 °C, [D₆]benzene): δ = 6.72 (4H, s, CH), 6.37 (2H, d, *J* = 1.5 Hz, CH), 5.76 (2H, d, *J* = 1.5 Hz, CH), 2.42 (36H, s, *t*Bu), 1.30 ppm (18H, s, *t*Bu); ¹³C NMR (75 MHz, [D₆]benzene): δ = 193.3 (NiC(N*t*BuCH)₂), 161.9 (NiC(N*t*BuCHCHN)), 127.5 (NiC(N*t*BuCHCHN)), 116.8 (NiC(N*t*BuCH)₂), 111.7 (NiC(N*t*BuCHCHN)), 57.7 (CCH₃), 54.6 (CCH₃), 32.5 (CCH₃), 31.8 ppm (CCH₃). Elemental analysis (%) calcd for C₃₆H₆₂N₈Ni₂: C 59.70, H 8.63, N 15.46; found C 59.55, H 8.73, N 14.87.

4: the synthesis of **3** was repeated, but terminated after 5 days. Extraction with hexane, filtration, concentration, and cooling to –25 °C yielded a mixture of starting materials; further cooling of the mother liquors yielded **4** as a yellow, crystalline solid in small amounts

(ca. 10 mg). The extreme thermal instability of **4** precluded further characterization, other than by low-temperature (173 K) X-ray diffraction studies.

5: concentration and further cooling (-25°C) of the mother liquors from the isolation of **3** (see above) afforded orange crystals of **5** in modest (20%) yield. **5** was also obtained quantitatively from decomposition of a solution of **4** in $[\text{D}_6]\text{benzene}$ at 20°C over 1 h. ^1H NMR (300 MHz, 20°C , $[\text{D}_6]\text{benzene}$): δ = 6.53 (1H, d, J = 1.8 Hz, CH), 6.40 (1H, d, J = 1.8 Hz, CH), 5.15 (1H, t, J = 8.4 Hz, CHCHCH), 3.81–3.72 (1H, q, J = 8.4 Hz, CHCHCH), 3.40–3.34 (1H, q, J = 8.4 Hz, CHCHCH), 2.46–2.24 (10H, br m, CH_2), 2.30 (1H, d, J = 10.7 Hz, $\text{C}(\text{CH}_3)_2\text{CHH}$), 1.76 (1H, d, J = 10.7 Hz, $\text{C}(\text{CH}_3)_2\text{CHH}$), 1.67 (3H, s, $\text{C}(\text{CH}_3)_2\text{CH}_2$), 1.47 (3H, s, $\text{C}(\text{CH}_3)_2\text{CH}_2$), 1.45 ppm (9H, s, *t*Bu); ^{13}C NMR (75 MHz, $[\text{D}_6]\text{benzene}$): δ = 184.4 ($\text{NiC}(\text{NtBuCHCHNC}(\text{CH}_3)_2\text{CH}_2)$), 117.1 ($\text{NiC}(\text{NtBuCHCHNC}(\text{CH}_3)_2\text{CH}_2)$), 114.2 ($\text{NiC}(\text{NtBuCHCHNC}(\text{CH}_3)_2\text{CH}_2)$), 106.8 (NiCHCHCH), 73.9 (NiCHCHCH), 66.1 ($\text{C}(\text{CH}_3)_3$), 59.1 (NiCHCHCH), 56.7 (NiCH_2), 34.6 ($\text{C}(\text{CH}_3)_2\text{CH}_2$), 32.9 (CH_2), 32.4 (CH_2), 32.2 ($\text{C}(\text{CH}_3)_2\text{CH}_2$), 30.9 (CCH_3), 30.4 (CH_2), 29.9 (CH_2), 24.2 ppm (CH_2). MS (EI): 346 [M^+], 238 [M^+ –cyclooctenyl], 182 [M^+ –*t*Bu and cyclooctenyl]. Elemental analysis (%) calcd for $\text{C}_{19}\text{H}_{32}\text{N}_2\text{Ni}$: C 65.73, H 9.29, N 8.07; found C 65.24, H 9.46, N 8.25.

Received: June 14, 2004

Keywords: C–N activation · metal–metal bonds · N-heterocyclic carbenes · nickel · silicone

- [9] J. C. Green, R. G. Scurr, P. L. Arnold, F. G. N. Cloke, *Chem. Commun.* **1997**, 21, 1963.
- [10] R. G. Scurr, Part II Thesis, University of Oxford, **1996**.
- [11] C. Eaborn, M. S. Hill, P. B. Hitchcock, J. D. Smith, *Chem. Commun.* **2000**, 691.
- [12] P. Werndrup, S. Gohil, V. G. Kessler, M. Kritikos and L. G. Hubert-Pfalzgraf, *Polyhedron* **2001**, 20, 2163.
- [13] I. Haiduc, *Organometallics* **2004**, 23, 3, and references therein.
- [14] *Handbook of Chemistry and Physics*, 63rd ed. (Eds.: R. C. Weast, M. J. Astle), CRC, Boca Raton, FL, **1982–1983**, p. F-181.
- [15] IR spectra revealed no bands assignable to a metal hydride, and NMR spectroscopy studies gave no evidence for a Ni–H species over the range δ = +40 to –40 ppm.
- [16] D. J. Mindiola and G. L. Hillhouse, *J. Am. Chem. Soc.* **2001**, 123, 4623.
- [17] P. L. Holland, R. A. Andersen, R. G. Bergman, J. Huang, S. P. Nolan, *J. Am. Chem. Soc.* **1997**, 119, 12800.
- [18] P. Macchi, D. M. Proserpio, A. Sironi, *J. Am. Chem. Soc.* **1998**, 120, 1447.
- [19] C. Krüger, Y.-H. Tsay, *J. Organomet. Chem.* **1972**, 34, 387.
- [20] R. Goddard, C. Kruger, F. Mark, R. Stansfield, X. Zhang, *Organometallics* **1985**, 4, 285.
- [21] I. Bach, R. Goddard, C. Kapiske, K. Seevegol, K.-R. Pörschke, *Organometallics* **1999**, 18, 10.
- [22] R. Gleiter, W. Sander, *Angew. Chem.* **1985**, 97, 575; *Angew. Chem. Int. Ed. Engl.* **1985**, 24, 566.

- [1] W. A. Herrmann, M. Elison, J. Fischer, C. Köcher, G. R. J. Artus, *Angew. Chem.* **1995**, 107, 2602; *Angew. Chem. Int. Ed. Engl.* **1995**, 34, 2371; W. A. Herrmann, C. Köcher, *Angew. Chem.* **1997**, 109, 2256; *Angew. Chem. Int. Ed. Engl.* **1997**, 36, 2162; W. A. Herrmann, C. P. Reisinger, M. Spiegler, *J. Organomet. Chem.* **1998**, 557, 93; W. A. Herrmann, V. P. W. Böhm, C. P. Reisinger, *J. Organomet. Chem.* **1999**, 576, 23; T. Wescamp, V. P. W. Böhm, W. A. Herrmann, *J. Organomet. Chem.* **1999**, 585, 348; D. S. McGuinness, M. J. Green, K. J. Cavell, B. W. Skelton, A. H. White, *J. Organomet. Chem.* **1998**, 565, 165; D. S. McGuinness, K. J. Cavell, B. W. Skelton, A. H. White, *Organometallics* **1999**, 18, 1596.
- [2] A. Furstner, L. Ackermann, B. Gabor, R. Goddard, C. W. Lehmann, R. Mynott, F. Stelzer, O. R. Thiel, *Chem. Eur. J.* **2001**, 15, 3236–3253, and references therein.
- [3] C. Desmarets, R. Schneider, Y. Fort, *J. Org. Chem.* **2002**, 67, 3029; R. Omar-Amrani, A. Thomas, E. Brenner, R. Schneider, Y. Fort, *Org. Lett.* **2003**, 5, 2311.
- [4] S. Caddick, W. Kofie, *Tetrahedron Lett.* **2002**, 43, 9347; S. Caddick, F. G. N. Cloke, P. B. Hitchcock, J. Leonard, A. K. de K. Lewis, D. McKerrecher, L. R. Titcomb, *Organometallics* **2002**, 21, 4318; L. R. Titcomb, S. Caddick, F. G. N. Cloke, D. J. Wilson, D. McKerrecher, *Chem. Commun.* **2001**, 15, 1388; S. Caddick, F. G. N. Cloke, G. K. B. Clentsmith, P. B. Hitchcock, D. McKerrecher, L. R. Titcomb, M. R. V. Williams *J. Organomet. Chem.* **2001**, 617, 635.
- [5] A. K. de K. Lewis, S. Caddick, F. G. N. Cloke, N. C. Billingham, P. B. Hitchcock, J. Leonard, *J. Am. Chem. Soc.* **2003**, 125, 10066.
- [6] P. L. Arnold, F. G. N. Cloke, T. Geldbach, P. B. Hitchcock, *Organometallics* **1999**, 18, 3228.
- [7] CCDC-240908–240912 (compounds **1–5** respectively) contain the supplementary crystallographic data for this paper. These data can be obtained free of charge via www.ccdc.cam.ac.uk/conts/retrieving.html (or from the Cambridge Crystallographic Data Centre, 12 Union Road, Cambridge CB2 1EZ, UK; fax: (+44) 1223-336-033; or deposit@ccdc.cam.ac.uk).
- [8] A. J. Arduengo, S. F. Gamper, J. C. Calabrese, F. Davidson, *J. Am. Chem. Soc.* **1994**, 116, 4391.

Multilayer Assemblies

Surface-Confined Metalloporphyrin Oligomers**

Hal Van Ryswyk, Erin E. Moore, Neel S. Joshi,
Rebecca J. Zeni, Todd A. Eberspacher, and
James P. Collman**

The ability to control charge transfer over long distances is an important aspect of nanometer-scale fabrication. Early work on molecular wires utilized metalloporphyrin oligomers,^[1,2] whereas more recent work with these materials has been

[*] Prof. Dr. H. Van Ryswyk, E. E. Moore, N. S. Joshi, R. J. Zeni
Department of Chemistry
Harvey Mudd College
301 East 12th Street
Claremont, CA 91711-5990 (USA)
Fax: (+1) 909-607-7577
E-mail: Hal_VanRyswyk@hmc.edu
Dr. T. A. Eberspacher, Prof. Dr. J. P. Collman
Department of Chemistry
Stanford University
Stanford, CA 94305-5080 (USA)
Fax: (+1) 650-725-0259
E-mail: collman@stanford.edu

[**] Support from the Petroleum Research Fund of the American Chemical Society (36713-B5) and the U.S. National Science Foundation (CHE-0097262 and CHE-0131206) is gratefully acknowledged. We thank Prof. Patricia D. Sparks, Prof. James C. Eckert, and Prof. Shenda M. Baker (Harvey Mudd College) for the generous use of their equipment.

directed towards the production of supramolecular rods.^[3,4] Metalloporphyrin oligomers in various forms can be used as self-assembling blocks to make discrete, ordered arrays.^[5,6] These are then combined with other molecules to create supramolecular structures,^[7] which have applications as sensors^[8] or as nanoporous materials,^[9,10] or which exhibit electronic properties that are unique to fully π -conjugated systems of this size.^[11,12] We recently developed a modular method for the assembly of metalloporphyrins on surfaces.^[13] Herein we report the preparation of surface-confined, axially-linked metalloporphyrin oligomers and aspects of the electronic coupling along the oligomer backbone.

Our experimental approach is outlined in Figure 1 and is detailed in the Experimental Section. In this modular scheme, we used a monolayer of decanethiol, which contained a low

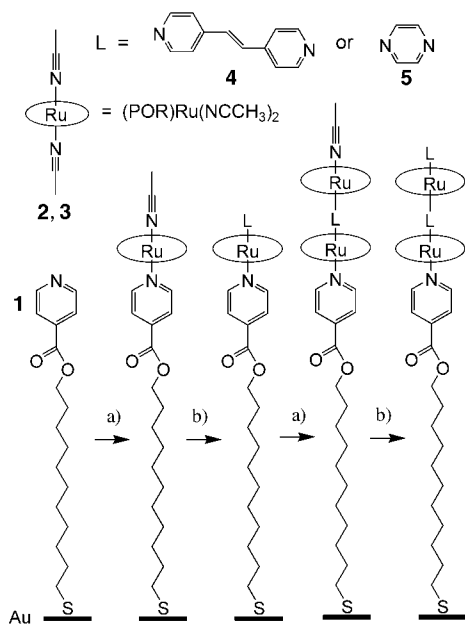


Figure 1. Schematic representation of the modular assembly of ruthenium-porphyrin, (POR)Ru, oligomers onto **1**, which is supported within an alkanethiol monolayer on a Au surface. a) Immersion in a solution of **2** or **3** (1 μ M) in toluene for 20 min; b) immersion in a solution of the linker (L), **4** or **5** (1 mM), in toluene for 5 min; steps a) and b) may be repeated to extend the oligomer.

mole fraction of 11-mercaptoundecylisonicotinate (**1**), as the substrate for the chemisorption of a sub-monolayer of metalloporphyrin. Bis(acetonitrile)-*meso*-tetratolylporphyrinoruthenium(II) (**2**) or bis(acetonitrile)octaethylporphyrinoruthenium(II) (**3**) were anchored to the surface by the exchange of an axial acetonitrile group for the monolayer-bound isonicotinate group. After attachment of the metalloporphyrin, the remaining axial acetonitrile group was exchanged for a linking bidentate ligand such as *trans*-1,2-bis(4-pyridyl)ethylene (**4**) or pyrazine (**5**). The oligomer was extended by repeating the treatment of the surface-bound conjugate with **2** or **3**, followed by linking with **4**; in such a manner, we prepared oligomers that were up to five repeat units long.

The underlying monolayer of the alkanethiolate and the first monolayer of metalloporphyrin have been characterized extensively by a range of techniques, which include optical ellipsometry, contact angle goniometry, X-ray photoelectron spectroscopy, grazing-angle FT-IR spectroscopy, UV/Vis spectroscopy, and scanning tunneling microscopy.^[14] The modular assembly of linkers and metalloporphyrins on top of this substrate was monitored with cyclic voltammetry measurements. Figure 2 shows the cyclic voltammograms of

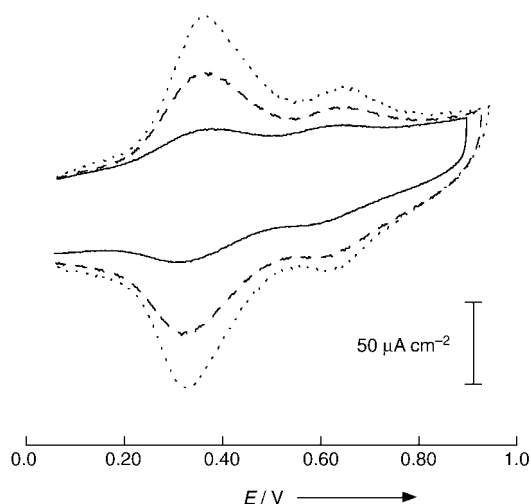


Figure 2. Cyclic voltammograms (E versus SCE) of a) the monomer Au-1-2-4 (—); b) the trimer Au-1-2-4-2-4-2-4 (---); and c) the pentamer Au-1-2-4-2-4-2-4-2-4-2-4 (.....). Scan rate: 0.8 V s⁻¹.

ruthenium-based oxidation and reduction processes in the surface-bound monomer, trimer, and pentamer of **2** linked with **4**. The formal potential of each additional conjugate as another metalloporphyrin is added to the oligomer is similar to that of the original isonicotinate-bound monomer. Integration of the charge under the wave at $E = +0.35$ V allowed the surface coverage of this one-electron couple to be calculated. The surface coverage of **2** in Figure 2a corresponds to 3.4 μ C cm⁻², that is, 50% of a compact, non-overlapping metalloporphyrin monolayer.^[13] The surface coverage of the first layer of chemisorbed metalloporphyrin was controlled by the variation of the mole fraction of **1** in the underlying alkanethiol monolayer. After a further four cycles of the modular assembly process (Figure 2c), five tiers of metalloporphyrin were present on the surface. The resulting coverage, which is based on the total number of immobilized metalloporphyrins in the stacks, corresponded to 225% of the coverage for a single close-packed monolayer.

A control experiment was performed in which an electrode was subjected to five sequential treatments of **2** according to step a in Figure 1 without intervening treatment with the linker (step b). This showed that further added metalloporphyrin units formed oligomer stacks, rather than inserting into unoccupied **1** sites on the underlying monolayer. As illustrated in Figure 3, the final surface coverage of the five-layer control assembly of **2** was identical to that of the monomer. This control experiment shows that further elec-

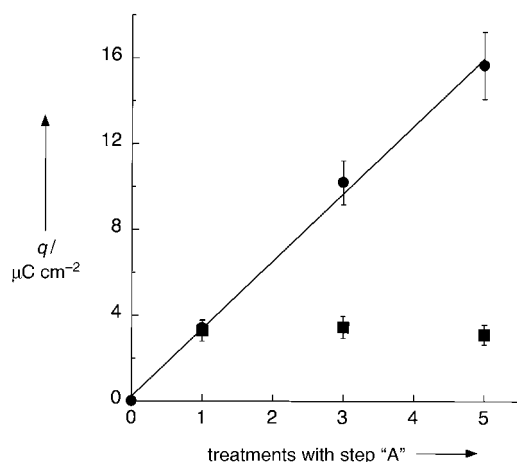


Figure 3. Correlation of the charge under the wave at $E = +0.35$ V with the number of treatments with the metalloporphyrin in Figure 1, step a; ●: metalloporphyrins linked with **4** using steps a) and b); ■: control experiment under the same conditions, but in the absence of a linker—step a) only.

troactive material arising from the elongation of the oligomer, rather than from an increased coverage in the chemisorbed metalloporphyrin monolayer or by the physisorption of the metalloporphyrin onto the original chemisorbed layer.

The electrochemical properties of the oligomer are strongly influenced by the mole fraction of **1** in the underlying alkanethiol monolayer and by the choice of the linking ligand. At higher mole fractions of **1**, a second oxidation wave at $E = +0.65$ V becomes more prominent which eventually yields an integrated area of $\approx 30\%$ of the larger peak observed at $E = +0.35$ V. The increased prominence of this secondary oxidation peak at higher surface coverages of the metalloporphyrin is attributed to the incomplete electrostatic screening of the charge on the oxidized metalloporphyrins in the solvent of low dielectric constant employed here. At higher surface coverages, a greater fraction of unoxidized, neutral metalloporphyrins have a large number of oxidized, cationic nearest-neighbors during the oxidation process; the electrostatic work required to oxidize a neutral metalloporphyrin in an environment of poorly screened positive charge is greater than that required to oxidize an isolated neutral metalloporphyrin.

By the use of a shorter linking ligand such as pyrazine (**5**), a similar effect was observed. Incomplete screening and neutralization of the charge along the backbone of the oxidized metalloporphyrin led to an additional wave of fractional area at more-positive potential. In the case of **5**-linked homogeneous trimers, we observed up to three additional waves. Similar additional waves were observed in the solution-based cyclic voltammetry analysis of axially-linked metalloporphyrin oligomers of undefined length.^[1,2,15,16] Whereas the observation of these waves has been taken as evidence of multivalence effects,^[15] we believe that these additional waves result from electrostatic artifacts.

Heterogeneous surface-confined metalloporphyrin dimers can also be produced with our modular assembly method. Figure 4 shows the near-identical cyclic voltammo-

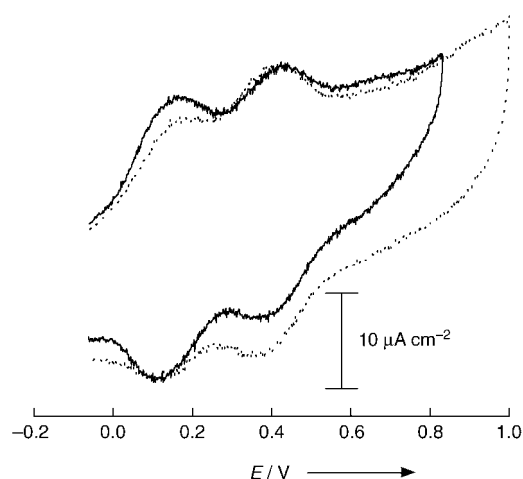


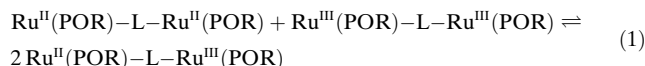
Figure 4. Cyclic voltammograms (E versus SCE) of Au-**1-2-4-3-4** (—) and Au-**1-3-4-2-4** (.....) dimers. Scan rate: 0.4 V s^{-1} .

grams for the Au-**1-2-4-3-4** and Au-**1-3-4-2-4** dimers. The waves at $E = +0.14$ and $+0.36$ V correspond to ruthenium-based redox chemistry at **3** and **2**, respectively. The surface coverage of each of the metalloporphyrins is $\approx 1.9 \mu\text{C cm}^{-2}$, which corresponds to 25% of a compact monolayer. In both cases **3** is oxidized before **2**, regardless of their relative positions in the stack. In a similar fashion, on the return scan **2** is always reduced before **3**. Let us consider the Au-**1-2-4-3-4** dimer under an oxidative scan: The first electron-transfer event corresponds to the tunneling of an electron from the outer metalloporphyrin **3** through the linking ligand, the inner metalloporphyrin, and the backbone of the alkane chain to the underlying Au surface at the formal potential of **3**. This event is independent of the identity or the oxidation state of the inner metalloporphyrin **2**. In other words, neither of these structures exhibits current rectification, which is observed in less-tightly coupled systems;^[17,18] these structures are not viable redox-switched molecular diodes.

Whereas the present solvent system is not ideal for studying the kinetics of the electron-transfer processes, the minimal splitting of the peak at elevated scan rates suggests facile electron-transfer kinetics. Also, it suggests that the electronic coupling along the backbone of the alkanethiolate is at least as strong as that of $[\text{Ru}(\text{NH}_3)_5]^{2+}$ coordinated to pyridine-terminated alkanethiolates of a comparable length to those employed here.^[19–21] Furthermore, the lack of any marked decrease in the rate of transfer of an electron from the outer metalloporphyrin relative to the inner metalloporphyrin argues that the coupling between the two metalloporphyrins by the fully conjugated linker is significantly stronger than that offered by an alkane chain of similar length. For reference, fully conjugated, ferrocene-terminated oligophenylenevinyls display no decrease in their rates of electron-transfer owing to electronic coupling over distances up to 2.8 nm .^[22]

As shown in Figure 2, any differences in the formal potentials for metalloporphyrins within the homogeneous oligomer linked with **4** are smaller than we can resolve with cyclic or square-wave voltammetry. On the basis of the

minimal peak broadening (as measured by the full width at half maximum) that is observed upon moving from the monomer to the pentamer, we estimate the differences in formal potential to be less than 0.06 V, which corresponds to an upper limit of 10 for the conproportionation constant^[23] associated with the reaction (POR represents the porphyrin and L represents the linker):



This means that the electronic coupling contribution between the metal centers in the dimer is small and it falls into the Robin–Day class I or a weak-interaction regime.^[24] However, as the outer metalloporphyrin can be oxidized regardless of the oxidation state of the inner metalloporphyrin (see Figure 4), the electronic communication along the backbone of the oligomer chain from the outer metalloporphyrin, through the inner metalloporphyrin, along the supporting alkane chain, and into the underlying gold substrate can still be considered as substantial.

In conclusion, we have presented a modular method for the assembly of surface-confined metalloporphyrin oligomers. Such structures exhibit electronic communication along their backbone and offer the potential to control charge transfer over long distances. This is of interest for materials or sensing applications, especially when interfacing with a surface is a concern.

Experimental Section

Compounds **1**,^[25] **2**, and **3**^[14] were prepared according to reported methods. Polycrystalline Au electrodes were evaporated onto titanium-coated silicon substrates, and then the conjugates were cleaned by immersion in a solution of H₂SO₄:30 % aqueous H₂O₂ (3:1 v/v) for 10 s and rinsed with deionized water and ethanol, immediately before use. Supported monolayers of **1** were formed by the immersion of the clean Au electrodes into a solution of decanethiol (1.25 mM) and **1** (0.2 equiv) in ethanol. The electrodes were rinsed with ethanol and blown dry with nitrogen prior to transfer to a glove box. The first monolayer of **2** or **3** was chemisorbed to the electrodes in a solution of the metalloporphyrin (1–3 μM) in toluene for 20 min under a nitrogen atmosphere, and the assembly was rinsed with toluene. The distal axial ligand was exchanged in a solution of **4** (1 mM) or pyrazine (**5**, 1 mM) in toluene for 5 min, and the assembly was again rinsed in toluene. Subsequent additions to the oligomer were performed in a similar fashion. Electrochemistry was performed on the benchtop under air with a Princeton Applied Research model 263 potentiostat and model 250 software by using a cell that was formed by pressing a bored-out cone of poly(tetrafluoroethylene) against the electrode. A platinum counter electrode and a silver quasi-reference electrode were used with a solution of tetrabutylammonium hexafluorophosphate (0.1 M) as the supporting electrolyte in CH₂Cl₂. Potentials were checked periodically with a saturated calomel reference electrode (SCE), which was sheathed in the supporting electrolyte and separated from the cell by a cracked-bead junction.

Received: June 17, 2004

Keywords: electron transfer · metal–metal interactions · nanotechnology · porphyrinoids · surface chemistry

- [1] J. P. Collman, J. T. McDevitt, G. T. Yee, C. R. Leidner, L. G. McCullough, W. A. Little, J. B. Torrance, *Proc. Natl. Acad. Sci. USA* **1986**, 83, 4581.
- [2] J. P. Collman, J. T. McDevitt, C. R. Leidner, G. T. Yee, J. B. Torrance, W. A. Little, *J. Am. Chem. Soc.* **1987**, 109, 4606.
- [3] H. L. Anderson, *Chem. Commun.* **1999**, 2323.
- [4] N. Aratani, A. Osuka, Y. H. Kim, D. H. Jeong, D. Kim, *Angew. Chem.* **2000**, 112, 1517–1521; *Angew. Chem. Int. Ed.* **2000**, 39, 1458–1462.
- [5] L. Baldini, C. A. Hunter, *Adv. Inorg. Chem.* **2002**, 53, 213.
- [6] R. A. Haycock, C. A. Hunter, D. A. James, U. Michelsen, L. R. Sutton, *Org. Lett.* **2000**, 2, 2435.
- [7] J. Wojaczynski, L. Latos-Grazynski, *Coord. Chem. Rev.* **2000**, 204, 113.
- [8] G. A. Mines, B. Tzeng, K. J. Stevenson, J. Li, J. T. Hupp, *Angew. Chem.* **2002**, 114, 162–165; *Angew. Chem. Int. Ed.* **2002**, 41, 154–157.
- [9] R. K. Kumar, I. Diskin-Posner, I. Goldberg, *J. Inclusion Phenom. Macrocyclic Chem.* **2000**, 37, 219.
- [10] K. F. Czaplewski, R. Q. Snurr, J. T. Hupp, *Adv. Mater.* **2001**, 13, 1895.
- [11] N. Aratani, A. Osuka, *Bull. Chem. Soc. Jpn.* **2001**, 74, 1361.
- [12] J. J. Piet, P. N. Taylor, B. R. Wegewijs, H. L. Anderson, A. Osuka, J. M. Warman, *J. Phys. Chem. B* **2001**, 105, 97.
- [13] T. A. Eberspacher, J. P. Collman, C. E. D. Chidsey, D. L. Donohue, H. Van Ryswyk, *Langmuir* **2003**, 19, 3814.
- [14] D. A. Offord, S. B. Sachs, M. S. Ennis, T. A. Eberspacher, J. H. Griffin, C. E. D. Chidsey, J. P. Collman, *J. Am. Chem. Soc.* **1998**, 120, 4478.
- [15] M. Saito, A. Endo, K. Shimizu, G. P. Sato, *Chem. Lett.* **1995**, 1079.
- [16] M. Saito, A. Endo, K. Shimizu, G. P. Sato, *Electrochim. Acta* **2000**, 45, 3021.
- [17] K. Uosaki, Y. Sato, K. Shimazu, I. Yagi, *New Funct. Mater.* **1993**, C, 711.
- [18] C. R. Leidner, P. Denisevich, K. W. Willman, R. W. Murray, *J. Electroanal. Chem.* **1984**, 164, 63.
- [19] J. F. Smalley, H. O. Finklea, C. E. D. Chidsey, M. R. Linford, S. E. Creager, J. P. Ferraris, K. Chalfant, T. Zawodzinski, S. W. Feldberg, M. D. Newton, *J. Am. Chem. Soc.* **2003**, 125, 2004.
- [20] D. A. Brevnov, H. O. Finklea, H. Van Ryswyk, *J. Electroanal. Chem.* **2001**, 500, 100.
- [21] H. O. Finklea, D. D. Hanshew, *J. Am. Chem. Soc.* **1992**, 114, 3173.
- [22] H. D. Sikes, J. F. Smalley, S. P. Dudek, A. R. Cook, M. D. Newton, C. E. D. Chidsey, S. W. Feldberg, *Science* **2001**, 291, 1519.
- [23] D. Astruc, *Electron Transfer and Radical Processes in Transition-Metal Chemistry*, Wiley-VCH, Weinheim, **1995**.
- [24] M. B. Robin, P. Day, *Adv. Inorg. Chem. Radiochem.* **1967**, 9, 247.
- [25] H. Van Ryswyk, E. D. Turtle, R. Watson-Clark, T. A. Tanzer, T. K. Herman, P. Y. Chong, P. J. Waller, A. L. Taurog, C. E. Wagner, *Langmuir* **1996**, 12, 6143.

Metallocryptands

Arsenic- π Interactions Stabilize a Self-Assembled As_2L_3 Supramolecular Complex**

W. Jake Vickaryous, Rainer Herges, and
Darren W. Johnson*

The self-assembly of supramolecular coordination compounds has resulted in structures with a diverse range of properties, shapes, sizes, and stoichiometries, including helicates (M_2L_2 , M_2L_3 , etc.), triangles (M_3L_3), squares (M_4L_4), rings (e.g., M_6L_6), and polyhedra (M_4L_4 , M_4L_6 , M_6L_6 , M_8L_{12} , etc.).^[1] These assemblies almost exclusively contain metals with square-planar, tetrahedral or octahedral coordination geometries. Metals that can exhibit more peculiar coordination geometries have typically been avoided as components for a supramolecular design strategy,^[2] most likely because of their variable coordination spheres. Herein we describe a supramolecular design strategy for forming arsenic-based assemblies, which relies on the self-assembly of arsenic(III) with thiol ligands—and hence the reversibility and lability of arsenic-sulfur bonds—and we report the first member of this class, $[\text{As}_2\text{L}_3]$ ($\text{H}_2\text{L} = \alpha, \alpha'$ -dimercapto-*para*-xylene). The design strategy incorporates the unusual, yet predictable trigonal-pyramidal coordination geometry of As^{III} featuring a stereochemically active lone pair when coordinated by sulfur-based ligands (Figure 1 a).^[3–6]

We selected arsenic(III) as a design component because of its unusual coordination geometry and a general lack of specific and powerful chelators for this highly toxic ion.^[7] Arsenic compounds are legendary for their toxicity, and hydrated As^{III} is recognized as a known human carcinogen. Arsenic is abundant in the earth's crust and is all-too-frequently present as an environmental health hazard;^[8–10] however, specific chelators for environmental and in vivo remediation and sensing applications are lacking. Furthermore, the stereochemically active lone pair of As^{III} adds a novel feature to the targeted supramolecular assemblies: for instance, lone pairs directed into the cavity would provide a unique soft, Lewis-basic cavity environment (Figure 1 b).^[11]

Figure 1 illustrates the design strategy for forming C_{3h} -symmetric $[\text{As}_2\text{L}_3]$ assemblies, which is based on rigid, twofold

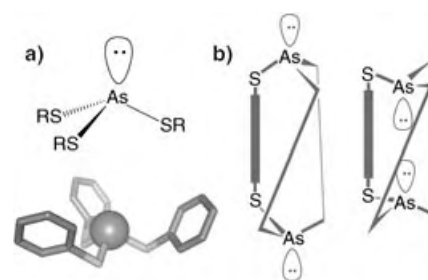
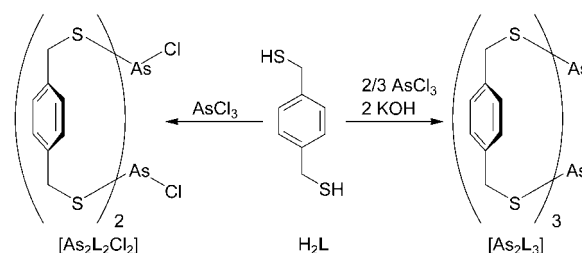


Figure 1. a) Top: Representation of the preferred trigonal coordination geometry of As^{III} with sulfur-based ligands; the stereochemically active lone pair on arsenic is highlighted. Bottom: Structure of $[\text{As}(\text{thiophenol})_3]$ from a single crystal X-ray structure analysis adapted from the Cambridge Structure Database showing an example of this trigonal coordination geometry. b) Two examples of how this As^{III} coordination geometry could be used to form As_2L_3 assemblies with rigid, twofold symmetric dithiolate ligands (solid rods). The arsenic lone pairs can be directed either into or out of the cavity.

symmetric dithiols capable of acting as bridging ligands. Dithiol ligand H_2L ^[12] (Scheme 1) was the initial bridging ligand investigated, because it is easily prepared and thiolates show a well-known affinity for As^{III} .^[12] Using a ligand such as H_2L allows for two possible orientations of the arsenic lone pairs: *into* or *out of* the cavity of the complex. Molecular models (CACH, MM3) indicated that the lone pairs would be directed into the cavity with an As–As distance of about 6 Å.^[13]



Scheme 1. Synthesis of $[\text{As}_2\text{L}_3]$ assemblies.

H_2L , synthesized by a literature procedure,^[12] forms a yellowish white solid in 52 % yield when treated with stoichiometric amounts of AsCl_3 and KOH in THF/methanol mixtures. The product has very simple ^1H and ^{13}C NMR spectra, indicative of formation of the desired high-symmetry C_{3h} complex, and the parent ion peak $[\text{H}\{\text{As}_2\text{L}_3\}]^+$ is present in the electrospray ionization mass spectrum. Interestingly, $[\text{As}_2\text{L}_3]$ also forms in the absence of any base; however, the dominant product under these conditions is a mixture of $[\text{As}_2\text{L}_2\text{Cl}_2]$ macrocycles (Scheme 1), which are presumably kinetically stable intermediates on the self-assembly pathway to forming $[\text{As}_2\text{L}_3]$.^[14]

A single crystal X-ray diffraction study performed on crystals grown by diffusing pentane into a CHCl_3 solution of $[\text{As}_2\text{L}_3]$ at -4°C confirms the solid-state structure of the supramolecular assembly (Figure 2).^[15] $[\text{As}_2\text{L}_3]\cdot\text{CHCl}_3$ crystallizes in space group $\text{C}2/c$ with eight molecules per unit cell. Therefore, one complex makes up the asymmetric unit and the discrete structure has no crystallographic symmetry. However, $[\text{As}_2\text{L}_3]$ has very nearly C_{3h} symmetry. Consistent

[*] W. J. Vickaryous, Prof. Dr. D. W. Johnson
Department of Chemistry
University of Oregon
Eugene, OR 97403-1253 (USA)
Fax: (+1) 541-346-0487
E-mail: dwj@darkwing.uoregon.edu

Prof. Dr. R. Herges
Institut für Organische Chemie
Christian-Albrechts-Universität Kiel
Otto-Hahn-Platz 4, 24098 Kiel (Germany)

[**] The authors thank Prof. Michael M. Haley for helpful discussions. Support from the University of Oregon for funding of this research is gratefully acknowledged. The purchase of the X-ray diffractometer was made possible by a grant from the National Science Foundation (CHE-0234965).

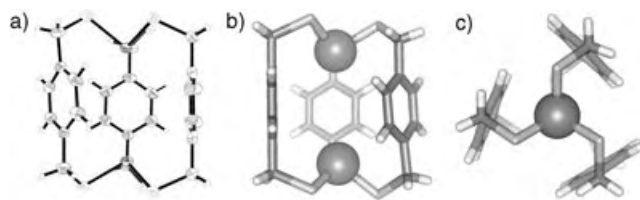


Figure 2. Structure of $[\text{As}_2\text{L}_3]$ in the crystal. a) ORTEP representation with 50% thermal ellipsoids. b) and c) Wireframe representations with arsenic atoms shown as space-filling spheres, the view in (c) is along the pseudo-threefold axis of the assembly showing the twist directions of the methylene groups being of opposite configurations at the two arsenic centers.

with predictions from molecular models, the arsenic lone pairs indeed are directed into the cavity of the complex. The two As^{III} ions are coordinated in a tripodal fashion by the three thiolate ligands, with the stereochemically active lone pairs directed at each other in the cavity.

The arsenic atoms in $[\text{As}_2\text{L}_3]$ are quite a bit closer together than molecular models indicated; they are separated by 5.03 Å (models predicted 6 Å). The average As–S distance is 2.25 Å and the angles between the mean planes of the phenyl rings are 57.3°, 64.2°, and 58.6° showing the complex has very nearly threefold symmetry. Furthermore, the As– C_{Aryl} distances are quite short, with six close contacts between 3.18 and 3.33 Å, suggesting an attractive interaction between the phenyl rings of the ligands and the arsenic ions helps stabilize the assembly.

Previous work by Schmidbaur et al. has shown that As^{III} and other heavier main group elements with stereochemically active lone pairs can form close contacts with arene rings in the solid state.^[16–18] To analyze this attractive interaction, DFT calculations were performed on the AsCl_3 –benzene dimer.^[19] These studies revealed a lower limit for the binding energy of 7.4 kcal mol^{−1} for the arsenic–arene interaction, with C–As distances of 3.2–3.4 Å. Furthermore, although the preferred geometry of the interaction orients the arsenic lone pair at a 68° angle to the phenyl ring, this structure is only 0.5 kcal mol^{−1} more stable than the two C_{3v} -symmetric arrangements. This suggests that, while this interaction is quite strong, its geometry is flexible. Calculations at a higher level of theory to include dispersion energy (Moeller–Plesset and coupled cluster) are currently underway as are efforts to quantify the strength of this interaction in solution.

Figure 2c shows that the orientation of the methylene groups provides a “twisted” arrangement of the sulfur atoms around the arsenic atoms. These twists have opposite directions at the two arsenic centers in one complex, which results in a *meso* static structure with C_{3h} symmetry. The ¹H NMR spectrum (CDCl_3) of $[\text{As}_2\text{L}_3]$ shows one singlet in the aromatic region for the phenyl rings of the ligands and one singlet for the methylene protons, both shifted relative to the signals of the free ligand. That the methylene resonance is a singlet shows that the twisted orientations interconvert quickly on the NMR timescale, otherwise the methylene protons would be inequivalent because they are diastereotopic with one proton closer to the arsenic center than the other. Therefore, the $[\text{As}_2\text{L}_3]$ structure determined in the solid

state is stable in solution on the NMR timescale. Furthermore, the NMR spectrum does not change down to −80 °C, indicating that none of the possible dynamic solution behavior of this assembly is frozen out at this temperature. This is markedly different from the behavior of analogous organic π -prismoids and bicyclopheanes. Gleiter et al. reported that torsional motion in related nitrogen-based systems is frozen out at −20 °C and the rotation of the π systems ceases at −82 °C.^[20]

$[\text{As}_2\text{L}_3]$ is remarkably robust in solution, suggesting this self-assembled compound is indeed the thermodynamic product of the reaction between As^{III} and H_2L . No ligand exchange occurs between $[\text{As}_2\text{L}_3]$ and excess ligand on the NMR timescale, $[\text{As}_2\text{L}_3]$ is air- and water-stable, and it is even stable to a variety of competing metal ions (including Ag^+ , Cu^+ , Pd^{II} , and Zn^{II}). Remarkably, even extended heating in CHCl_3 at reflux in the presence of an excess of trifluoroacetic acid or *p*-toluenesulfonic acid gave neither decomposition nor protonation of $[\text{As}_2\text{L}_3]$ according to ¹H NMR spectroscopy.

The robustness of the $[\text{As}_2\text{L}_3]$ assembly is exciting for several reasons. Firstly, this provides the first proof of principle for the design strategy to form supramolecular assemblies using As^{III} as a building block, and reveals that the coordination chemistry of arsenic–sulfur interactions is sufficiently labile to allow for the self-assembly of discrete species to occur. This is an unusual use of arsenic(III) as a metalloid in coordination chemistry, rather than as a phosphine ligand analogue. Secondly, the intriguing observation that the arsenic lone pairs are oriented into the cavity of the complex hints at exciting host–guest applications. Because guests in encapsulation complexes experience a nonpolar, asymmetric environment, providing functionality to them in a synthetic receptor is challenging. Exposing functional groups to the cavities of synthetic receptors has also been referred to as “endohedral” and “introverted” functionality, and the presence of the arsenic lone pairs inside the cavity is an excellent first step in introducing functionality to a guest from its host shell.^[11b,21]

That $[\text{As}_2\text{L}_3]$ forms in a nonoptimized yield of 52% suggests this reaction indeed occurs by a self-assembly mechanism. It is quite unlikely that six arsenic–sulfur bonds would spontaneously form to yield a discrete species as a kinetic product, and in fact the yields of the stepwise syntheses of related organic π -prismoids are much lower.^[20] The isolation of an intermediate $[\text{As}_2\text{L}_2\text{Cl}_2]$ macrocycle in the absence of base sheds light on the mechanism of this self-assembly reaction. Presumably, this stable macrocycle, which is preorganized for an incoming ligand **L** to bridge the two arsenic ions to form $[\text{As}_2\text{L}_3]$, forms as one of the many possible intermediates. Favorable arsenic– π interactions likely add further stability to the resulting assemblies and suggest that this interaction may help preorganize the arsenic atoms near the sulfur atoms to facilitate formation of the As–S bonds.

We have presented a self-assembled inorganic analogue of the bicyclopheanes and,^[22] specifically, the π -prismoids.^[20,23] The self-assembly strategy allows for increased yields in the macrobicyclization reaction and is a proof of principle of the design strategy to form arsenic-based supramolecular assem-

blies from simple, identical starting compounds. The success of this strategy augurs well for the formation of larger arsenic-based capsules resulting from expanded two- and threefold symmetric ligands. We are pursuing these studies, as well as attempting to prepare host–guest complexes of $[\text{As}_2\text{L}_3]$.

Experimental Section

General: All NMR spectra were measured using a Varian INOVA 300-MHz spectrometer. Single crystal X-ray diffraction studies were performed on a Bruker SMART APEX diffractometer. Mass spectra were recorded on an Agilent 1100 LC/MSD mass spectrometer.

$[\text{As}_2\text{L}_3]$: H_2L (0.763 mmol, 130 mg) was added to a degassed solution of THF (80 mL) and KOH (2.43 mmol, 136 mg) in MeOH (24 mL). This solution was heated to 50°C and AsCl_3 was added dropwise. The reaction was stirred under N_2 for 2.5 h. The resulting white precipitate was removed by filtration and the filtrate was dried in vacuo (yield 87 mg, 52%). Crystals suitable for X-ray diffraction were grown by pentane diffusion into a chloroform solution of AsCl_3 and H_2L at –4°C. ^1H NMR (300 MHz, CDCl_3 , 25°C): δ = 7.09 (s, 12H, CH), 3.81 ppm (s, 12H, CH_2); ^{13}C NMR (75 MHz, CDCl_3 , 25°C): δ = 137.5 (C), 128.9 (CH), 35.0 ppm (CH_2); API-ES MS: m/z (MH $^+$): 655.2 ($[\text{H}\{\text{As}_2\text{L}_3\}]^+$ 654.9 calcd, 23%), 715.2 ($[\text{H}\{\text{As}_2\text{L}_3\} + \text{AcOH}]^+$, 714.9 calcd, 27%).

Received: June 18, 2004

Keywords: arsenic · coordination modes · density functional calculations · self-assembly · supramolecular chemistry

- [1] For examples of these structure types, see: a) C. Piguet, G. Bernardinelli, G. Hopfgartner, *Chem. Rev.* **1997**, 97, 2005; b) S. Leininger, B. Olenyuk, P. J. Stang, *Chem. Rev.* **2000**, 100, 853; c) J.-M. Lehn, *Supramolecular Chemistry: Concepts and Perspectives*, VCH, Weinheim, **1995**; d) M. Fujita, *Chem. Soc. Rev.* **1998**, 27, 417; e) R. W. Saalfrank, B. Demleitner in *Transition Metals in Supramolecular Chemistry, Vol. 5* (Ed.: J.-P. Sauvage), Wiley, Chichester, England, **1999**; f) B. J. Holliday, C. A. Mirkin, *Angew. Chem.* **2001**, 113, 2076; *Angew. Chem. Int. Ed.* **2001**, 40, 2022; g) M. Fujita, K. Umemoto, M. Yoshizawa, N. Fujita, T. Kusakawa, K. Biradha, *Chem. Commun.* **2001**, 509; h) D. W. Johnson, K. N. Raymond, *Supramol. Chem.* **2001**, 13, 639; i) D. L. Caulder, K. N. Raymond, *J. Chem. Soc. Dalton Trans.* **1999**, 1185; j) G. F. Swiegers, T. J. Malefetse, *Chem. Rev.* **2000**, 100, 3483, and references therein.
- [2] A representative list of exceptions includes supramolecular architectures incorporating eight- or nine-coordinate lanthanides, low-coordinate silver(I), hypervalent iodonium, and other main group elements such as Sb: a) G. W. Orr, L. J. Barbour, J. L. Atwood, *Science* **1999**, 285, 1049; b) C. Piguet, C. Edler, S. Rigault, G. Bernardinelli, J. C. G. Bunzli, G. Hopfgartner, *J. Chem. Soc. Dalton Trans.* **2000**, 3999; c) J. Xu, K. N. Raymond, *Angew. Chem.* **2000**, 112, 2857; *Angew. Chem. Int. Ed.* **2000**, 39, 2745; d) P. J. Stang, K. C. Chen, A. M. Arif, *J. Am. Chem. Soc.* **1995**, 117, 8793; e) X. Sun, D. W. Johnson, K. N. Raymond, E. H. Wong, *Inorg. Chem.* **2001**, 40, 4504; f) M. A. Paver, J. S. Joy, M. B. Hursthouse, *Chem. Commun.* **2002**, 2150.
- [3] A search of As^{III} coordination compounds in the Cambridge Structure Database revealed a preference for tripodal coordination geometries featuring a stereochemically active lone pair with sulfur-based ligands: F. H. Allen, O. Kennard, *Chem. Design Autom. News* **1993**, 8, 31.
- [4] O. M. N. Dhubhghaill, P. J. Sadler, *Struct. Bonding (Berlin)* **1991**, 78, 129.
- [5] B. T. Farrer, C. P. McClure, J. E. Penner-Hahn, V. L. Pecoraro, *Inorg. Chem.* **2000**, 39, 5422.
- [6] J. M. Johnson, C. Voegtlin, *J. Biol. Chem.* **1930**, 89, 27.
- [7] The current ligands for treating arsenic poisoning are ethylenediaminetetraacetate (EDTA) and dithiols. None of these ligands are capable of binding arsenic(III) in its preferred coordination geometry, which likely explains their poor selectivity (EDTA) and moderate efficacy (dithiols): M. D. Ford in *Goldfrank's Toxicologic Emergencies*, 6th ed. (Ed.: L. R. Goldfrank), Appleton & Lange, Stamford, CT, **1998**, p. 1261.
- [8] P. Roy, A. Saha, *Curr. Sci.* **2002**, 82, 38.
- [9] P. Bhattacharya, G. Jacks, S. H. Frisbie, E. Smith, R. Naidu, B. Sarkar in *Heavy Metals in the Environment* (Ed.: B. Sarkar), Marcel Dekker, New York, **2002**, p. 147.
- [10] B. K. Mandal, K. T. Suzuki, *Talanta* **2002**, 58, 201.
- [11] a) K. Goto, R. Okazaki, *Liebigs Ann. Chem.* **1997**, 2393; b) A. R. Renslo, J. Rebek, Jr., *Angew. Chem.* **2000**, 112, 3419; *Angew. Chem. Int. Ed.* **2000**, 39, 3281; c) B. W. Purse, P. Ballester, J. Rebek, Jr., *J. Am. Chem. Soc.* **2003**, 125, 14682.
- [12] P. Zhang, D. R. Bundle, *Isr. J. Chem.* **2000**, 40, 189.
- [13] CAChe, Version 5.0, Fujitsu America, Beaverton, USA, **2002**.
- [14] The structures of two $[\text{As}_2\text{L}_2\text{Cl}_2]$ macrocycles have been confirmed by single crystal X-ray diffraction and solution NMR spectroscopy. Further details will be reported in due course: W. J. Vickaryous, D. W. Johnson, **2004**, unpublished results.
- [15] Crystallographic data for $[\text{As}_2\text{L}_3]\cdot\text{CHCl}_3$: crystal size 0.41 × 0.27 × 0.10 mm; $T = -120(2)^\circ\text{C}$; monoclinic, space group $C2/c$ (no. 15), $a = 34.9159(11)$, $b = 8.8957(3)$, $c = 23.0878(7)$ Å; $V = 6152.2(3)$ Å 3 , $Z = 8$, $\mu = 2.857$ mm $^{-1}$, $F(000) = 3104$, $\rho_{\text{calcd}} = 1.67$ g mL $^{-1}$, $2\theta_{\text{max}} = 56.58^\circ$. Of the 15036 reflections which were collected, 6780 were unique ($R_{\text{int}} = 0.014$). Final $R1 = 0.033$ for 6070 data for $I > 2\sigma(I)$ (325 parameters, 0 restraints); for all 6780 data, $wR2 = 0.093$, $GOF = 1.017$; max/min residual electron density +1.680/–0.949 e Å $^{-3}$. CCDC 238936 contains the supplementary crystallographic data for this paper. These data can be obtained free of charge via www.ccdc.cam.ac.uk/conts/retrieving.html (or from the Cambridge Crystallographic Data Centre, 12, Union Road, Cambridge CB21EZ, UK; fax: (+44)1223-336-033; or deposit@ccdc.cam.ac.uk).
- [16] T. Probst, O. Steigelmann, H. Riede, H. Schmidbaur, *Chem. Ber.* **1991**, 124, 1089.
- [17] H. Schmidbaur, W. Bublak, B. Huber, G. Müller, *Angew. Chem.* **1987**, 99, 248; *Angew. Chem. Int. Ed. Engl.* **1987**, 26, 234.
- [18] H. Schmidbaur, R. Nowak, O. Steigelmann, G. Müller, *Chem. Ber.* **1990**, 123, 1221.
- [19] DFT (B3LYP/6-31G*) investigations were performed using the Gaussian 98 software suite: a) A. D. Becke, *J. Chem. Phys.* **1993**, 98, 5648; b) Gaussian 98 (Revision A.7), M. J. Frisch, G. W. Trucks, H. B. Schlegel, G. E. Scuseria, M. A. Robb, J. R. Cheeseman, V. G. Zakrzewski, J. A. Montgomery, R. E. Stratmann, J. C. Burant, S. Dapprich, J. M. Millam, A. D. Daniels, K. N. Kudin, M. C. Strain, O. Farkas, J. Tomasi, V. Barone, M. Cossi, R. Cammi, B. Mennucci, C. Pomelli, C. Adamo, S. Clifford, J. Ochterski, G. A. Petersson, P. Y. Ayala, Q. Cui, K. Morokuma, D. K. Malick, A. D. Rabuck, K. Raghavachari, J. B. Foresman, J. Cioslowski, J. V. Ortiz, B. B. Stefanov, G. Liu, A. Liashenko, P. Piskorz, I. Komaromi, R. Gomperts, R. L. Martin, D. J. Fox, T. Keith, M. A. Al-Laham, C. Y. Peng, A. Nanayakkara, C. Gonzalez, M. Challacombe, P. M. W. Gill, B. G. Johnson, W. Chen, M. W. Wong, J. L. Andres, M. Head-Gordon, E. S. Replogle, J. A. Pople, Gaussian, Inc., Pittsburgh, PA, **1998**.
- [20] A. Kunze, S. Bethke, R. Gleiter, F. Rominger, *Org. Lett.* **2000**, 2, 609.
- [21] K. Goto, R. Okazaki, *Liebigs Ann. Chem.* **1997**, 2393.
- [22] V. J. Catalano, M. A. Malwitz, *J. Am. Chem. Soc.* **2004**, 126, 6560.
- [23] A. Kunze, R. Gleiter, F. Rominger, *Chem. Commun.* **1999**, 171.

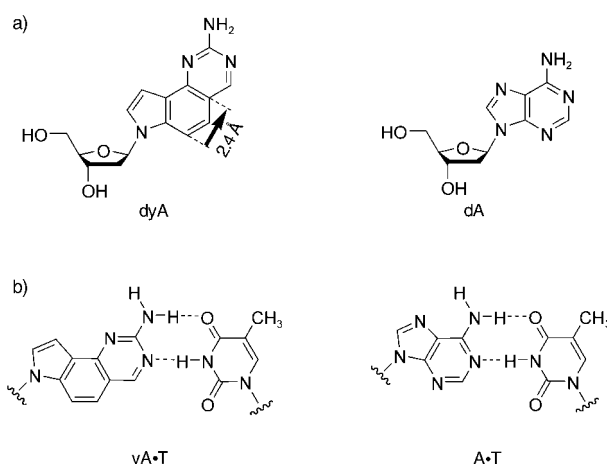
DNA Structures

yDNA: A New Geometry for Size-Expanded Base Pairs**

Haige Lu, Kaizhang He, and Eric T. Kool*

Previous studies have explored whether it is possible to replace the information-encoding part of DNA—the bases and base pairs—with other molecular replacements, and whether such new base pairs might function in recognition and in replication processes, two of the defining characteristics of the natural genetic system.^[1–6] Many of these studies have been aimed at designing base pairs that can function within the content of the natural genetic system, for expansion of nature's genetic alphabet. However, recent studies have moved beyond the purine–pyrimidine framework of the natural system. Examples of this new approach include metal-bridged base pairs,^[4] nonpolar base pairs,^[2,4] and pairs containing more than the three different types of hydrogen bonds found in nature.^[5] We recently adopted a different strategy and described a molecular design in which the dimensions of the natural pairs are stretched by insertion of a benzene ring into the natural heterocycles, thus rendering base pairs 2.4 Å wider than the natural ones.^[6] Such broad alterations of the natural design are not necessarily expected to be compatible with the natural genetic system. Rather, such studies are useful as a test of researchers' understanding of how genetic systems function in general, and they may also lead to useful new applications in biotechnology and in self-assembling nanostructures.

Herein we evaluate whether size-expansion of DNA base pairs can be carried out using a new geometry. Our previous design of expanded DNA-like bases (xDNA) involved a linear extension of pyrimidines and purines by addition of a benzene ring to each of the four DNA base heterocycles.^[6] However, examination of models suggested that at least one other design strategy involving benzohomologation also appeared to allow for reasonable base-pair geometries and stacking with neighboring pairs. This new design, termed “yDNA” (an abbreviated form of “wide DNA”; Scheme 1) involves a different extension vector, but yields a similar degree of perturbation from the framework formed by the natural pair. Analogous designs for the other three nucleobases can be envisioned (not shown). In this initial study we



Scheme 1. a) Structures of the free deoxyribonucleosides yA and natural A; b) proposed base-pair pattern for yA·T (left), compared with the natural A·T base pair (right). The arrow shows the extension vector for the yA base which adds about 2.4 Å to the length of natural adenine base.

tested the concept with one example, that of the expanded adenine base analogue (yA) and the corresponding deoxyriboside (dyA), both of which were previously unknown.

We developed a synthetic route to prepare the phosphoramidite derivative of the new nucleoside analogue dyA in 10 steps (6% overall yield on a gram scale, Scheme 2). Methylation of indole **1** at the 5 position was achieved by addition of three equivalents of methylmagnesium chloride to the unprotected indole **1**, followed by ring oxidation to restore aromaticity.^[7] The transformation of methylindole **3**^[8] to indole-5-carboxaldehyde **4** was a key step; tris(dimethylamino)methane converted **3** into the enamine intermediate which was then oxidized by KMnO₄ in one pot to afford compound **4**.^[9] The protected 2'-deoxyriboside **7** was formed in three subsequent steps from the indole-5-aldehyde **4**. Conventional methods were then used to convert the deoxyriboside **7** into the amidine-protected dyA phosphoramidite **11**.

Studies showed that the yA base is fluorescent, where as its natural congener is not. The yA free nucleoside was found to have absorption maxima at 262 and 355 nm in methanol. A fluorescence spectrum in methanol revealed that the nucleoside emits blue fluorescence ($\lambda_{\text{max}} = 433 \text{ nm}$) with a quantum yield of 0.12 (Figure 1). Thus the yA fluorescence is red-shifted by about 40 nm relative to the xA analogue.^[6]

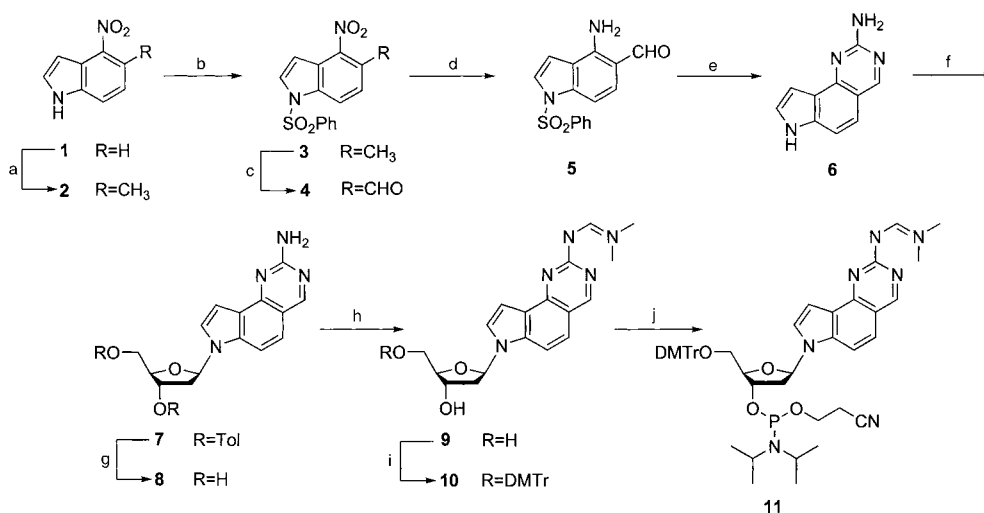
We prepared a short oligomer of sequence 5'-TyAT-3' to confirm that dyA could be incorporated intact into a DNA by automated DNA synthesis. The expected trimer structure was confirmed by ¹H NMR spectroscopy and electron spray ionization (ESI) mass spectrometry after deprotection with concentrated ammonium hydroxide and partial purification by dialysis.

We then investigated the stacking and pairing properties of dyA in the context of natural DNA oligonucleotides. Thermodynamic data from thermal denaturation studies (Table 1) showed that yA (like xA)^[6] stacks more strongly than natural A at the terminus of the duplex formed by 5'-

[*] H. Lu, Dr. K. He, Prof. Dr. E. T. Kool
Department of Chemistry
Stanford University
Stanford, CA 94305-5080 (USA)
Fax: (+1) 650-725-0259
E-mail: kool@leland.stanford.edu

[**] This work was supported by the U.S. National Institutes of Health (GM63587) and by an Abbott Laboratories Graduate Research Fellowship to H.L.

Supporting information for this article (synthesis and structure characterization, thermal denaturation curves, CD spectra) is available on the WWW under <http://www.angewandte.org> or from the author.



Scheme 2. Reagents and conditions: a) 1. CH₃MgCl, THF, −25 °C; 2. Pb(OAc)₄, CH₂Cl₂, 42%; b) 1. NaOH, CH₂Cl₂; 2. ClSO₂Ph, 87%; c) 1. DMF, CH(NMe₂)₃, 105 °C; 2. KMnO₄, THF/H₂O 10:1, 70%; d) Na₂S₂O₄, THF/H₂O = 2:1; e) MeCONMe₂, guanidine carbonate, 150 °C, 61 % over two steps; f) 1. NaH, CH₃CN, RT; 2. Hoffer's chlorosugar, 0 °C, 92 %, β/α > 20:1; g) NaOMe, MeOH, 91%; h) CH(OMe)₂NMe₂, pyridine; i) DMTrCl, pyridine, DIPEA, 62 % over two steps; j) chlorodiisopropyl-cyanoethylphosphoramidite, CH₂Cl₂, DIPEA, 70%. DMTr = 4,4'-dimethoxytriphenylmethyl, DIPEA = *N,N*-diisopropylethylamine, Tol = tolyl.

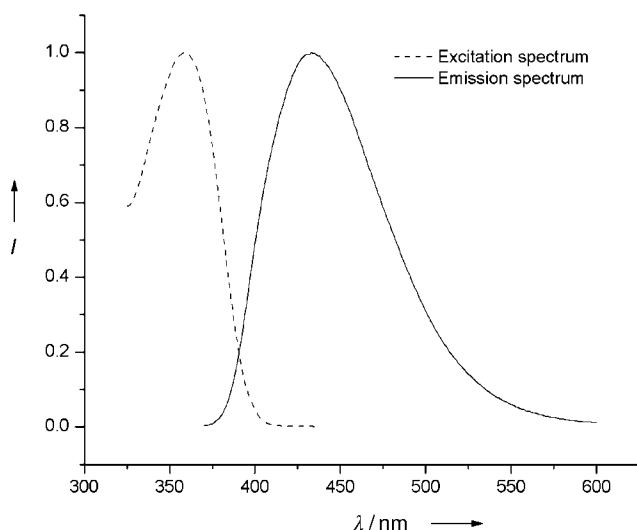


Figure 1. Emission and excitation spectra of the free nucleoside yA in methanol.

CGCGCG-3'. This result may be a consequence of the expanded surface area and higher hydrophobicity of the new analogue. We then tested the pairing properties of yA opposite natural bases in DNA (Table 1, entries 4–15). With a single substitution in DNA, yA was found to be destabilizing to some extent, which may be a result of the distortion of the DNA backbone caused by the increased size of yA relative to A. Interestingly, when yA was paired with T, the duplex was less destabilized by 1.5–2.1 kcal mol^{−1} than when yA was paired opposite A, G, and C. This result suggests that, despite some destabilization, yA may be able to form a selective hydrogen-bonded pair with T in the natural duplex.

Although the yA·T pair was found to be destabilizing in natural DNA, probably because of backbone distortions, we expected that such strain might be avoided if all pairs were expanded in a homologous way. Thus, further studies were performed to test whether it is possible to construct fully expanded helices composed of yA·T and T·yA base pairs. This was tested in two contexts. The first one contained a self-complementary sequence (Table 1, entry 16) and the second one (Table 1, entry 18) contained a non-self-complementary pair of oligonucleotides. Both assays showed distinct cooperative transition curves in thermal denaturation experiments (see Supporting Information). In the first case, the non-natural helix displayed a higher melting temperature (*T*_m, by 25 °C) and more favorable free energy (by 4.1 kcal mol^{−1} at 37 °C) relative to the natural helix of the analogous sequence. Similarly, the helix formed with the second sequence gave a *T*_m value 23 °C higher and a free energy 4.9 kcal mol^{−1} higher than the natural helix. We hypothesize that the added stability of these helical complexes arises from the strong stacking of the larger base pairs; further experiments will be needed to better understand this.

Circular dichroism spectra of the duplex formed in the second case (Table 1, entry 18) suggest an overall helical form resembling that of B-DNA of the analogous sequence (see Supporting Information), but with positive and negative bands red-shifted by 5–20 nm, presumably as a consequence of the extended π system of yA. Interestingly, the single component strands of the putative yDNA duplex also show similar spectra, which is indicative of strong helical stacking in the single-stranded state.

Our study has demonstrated that the new geometric design for benzo-fused bases is successful for at least one such base analogue (yA), and the data show that yA·T and T·yA pairs can self-assemble into cooperative helices that are considerably more stable than natural DNA. Thus, yDNA

Table 1: Melting temperatures and free energies for DNA helices containing yA bases and base pairs.

	Duplex ^[a]	T_m [°C] ^[b]	$-\Delta G_{37}^\circ$ [kcal mol ⁻¹] ^[c]
1	5'- \tilde{A} C G C G C G 3'-G C G C G C \tilde{A}	64.4	13.2 ± 0.5
2	5'-A C G C G C G 3'-G C G C G C A	52.6	10.2 ± 0.1
3	5'-C G C G C G 3'-G C G C G C	43.8	9.2 ± 0.4
4	5'-C T T T T C \tilde{A} T T C T T 3'-G A A A A G T A A G A A	38.7	8.8 ± 0.1
5	5'-C T T T T C \tilde{A} T T C T T 3'-G A A A A G A A A G A A	29.2	6.8 ± 0.1
6	5'-C T T T T C \tilde{A} T T C T T 3'-G A A A A G G A A G A A	31.0	7.1 ± 0.1
7	5'-C T T T T C \tilde{A} T T C T T 3'-G A A A A G C A A G A A	32.2	7.3 ± 0.1
8	5'-C T T T T C \tilde{A} T T C T T 3'-G A A A A G ϕ A A G A A	33.9	7.7 ± 0.1
9	5'-A A G A A \tilde{A} G A A A A G 3'-T T C T T T C T T T T C	35.2	7.9 ± 0.1
10	5'-A A G A A \tilde{A} G A A A A G 3'-T T C T T A C T T T T C	25.9	5.8 ± 0.1
11	5'-A A G A A \tilde{A} G A A A A G 3'-T T C T T G C T T T T C	27.5	6.3 ± 0.1
12	5'-A A G A A \tilde{A} G A A A A G 3'-T T C T T C C T T T T C	28.0	6.4 ± 0.1
13	5'-A A G A A \tilde{A} G A A A A G 3'-T T C T T ϕ C T T T T C	27.5	6.3 ± 0.1
14	5'-A A G A A A G A A A A G 3'-T T C T T T C T T T T C	41.4	9.5 ± 0.1
15	5'-A A G A A \tilde{A} G A A A A G 3'-T T C T T \tilde{A} C T T T T C	35.4	8.0 ± 0.1
16	5'- \tilde{A} T \tilde{A} \tilde{A} T \tilde{A} T T \tilde{A} T 3'-T \tilde{A} T T \tilde{A} T \tilde{A} T \tilde{A}	44.7	8.7 ± 0.1
17	5'-A T A A T A T T A T 3'-T A T T A T A A T A	19.5	4.6 ± 0.2
18	5'- \tilde{A} T \tilde{A} \tilde{A} T T T \tilde{A} \tilde{A} T 3'-T \tilde{A} T T \tilde{A} \tilde{A} T T \tilde{A}	44.1	9.5 ± 0.3
19	5'-A T A A T T T A A T 3'-T A T T A A A T T A	20.9	4.6 ± 0.2

[a] ϕ in entries 8 and 13 denotes an abasic tetrahydrofuran site. [b] Entries 1, 2, 15, 16: the buffer contained 1 M NaCl and 10 mM Na₂HPO₄ at pH 7.0; DNA concentration: 5.0 μ M; error in the T_m value: $\pm 0.5^\circ\text{C}$ or less. Entries 3–14, 17, 18: buffer contained 100 mM NaCl, 10 mM MgCl₂, and 10 mM sodium 1,4-piperazinediethanesulfonate at pH 7.0; DNA concentration: 5.0 μ M. Error in the T_m value: $\pm 0.5^\circ\text{C}$ or less. [c] Data were obtained by averaging free energies from curve fits and a van't Hoff plot. The van't Hoff data were obtained by plotting $1/T_m$ versus $\ln(C/4)$ (where C is the total oligonucleotide concentration) with data from five concentrations. Curve fits data were averaged from fits of five denaturation curves.

may be a candidate for a new genetic system, distinct from the recently described xDNA design.^[6,10] Like xDNA, it appears that the sugar–phosphate backbone in yDNA can tolerate the stretched size of bases and the altered pairing direction, while retaining the structure of the duplex. However, beyond the hypothesized base pairing, the structure of yDNA is unknown and needs to be studied. Also unknown is whether other analogously expanded bases and base pairs could be constructed; studies are underway to test these.

Received: June 22, 2004

Keywords: biomimetic synthesis · DNA structures · hydrogen bonds · nucleosides

- [1] J. A. Piccirilli, T. Krauch, S. E. Moroney, S. A. Benner, *Nature* **1990**, *343*, 33–37.
- [2] a) B. A. Schweitzer, E. T. Kool, *J. Am. Chem. Soc.* **1995**, *117*, 1863–1872; b) T. J. Matray, E. T. Kool, *J. Am. Chem. Soc.* **1998**, *120*, 6191–6192; c) T. J. Matray, E. T. Kool, *Nature* **1999**, *399*, 704–708; d) D. L. McMinn, A. K. Ogawa, Y. Wu, J. Liu, P. G. Schultz, F. E. Romesberg, *J. Am. Chem. Soc.* **1999**, *121*, 11585–11586; e) E. L. Tae, Y. Wu, G. Xia, P. G. Schultz, F. E. Romesberg, *J. Am. Chem. Soc.* **2001**, *123*, 7439–7440; f) T. Mitsui, A. Kitamura, M. Kimoto, T. To, A. Sato, I. Hirao, S. Yokoyama, *J. Am. Chem. Soc.* **2003**, *125*, 5298–5307.
- [3] H. P. Rappaport, *Nucleic Acids Res.* **1988**, *16*, 7253–7267.
- [4] a) E. Meggers, P. L. Holland, W. B. Tolman, F. E. Romesberg, P. G. Schultz, *J. Am. Chem. Soc.* **2000**, *122*, 10714–10715; b) K. Tanaka, A. Tengeiji, T. Kato, N. Toyama, M. Shionoya, *Science* **2003**, *299*, 1212–1213.
- [5] N. Minakawa, N. Kojima, S. Hikishima, T. Sasaki, A. Kiyosue, N. Atsumi, Y. Ueno, A. Matsuda, *J. Am. Chem. Soc.* **2003**, *125*, 9970–9982.
- [6] H. Liu, J. Gao, S. R. Lynch, Y. D. Saito, L. Maynard, E. T. Kool, *Science* **2003**, *302*, 868–871.
- [7] J. Quick, B. Saha, *Tetrahedron Lett.* **1994**, *35*, 8553–8556.
- [8] O. Ottoni, R. Cruz, R. Alves, *Tetrahedron* **1998**, *54*, 13915–13928.
- [9] a) R. D. Clark, D. B. Repke, *Heterocycles* **1984**, *22*, 195–221; b) E. C. Riesgo, X. Jin, R. P. Thummel, *J. Org. Chem.* **1996**, *61*, 3017–3022.
- [10] H. Liu, J. Gao, L. Maynard, Y. D. Saito, E. T. Kool, *J. Am. Chem. Soc.* **2004**, *126*, 1102–1109.

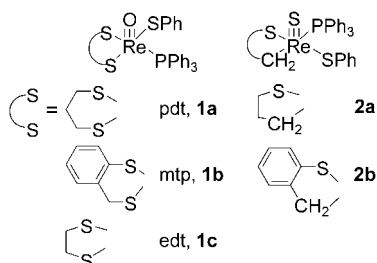
C–S Bond Cleavage

Phosphine-Promoted Conversion of Oxo(dithiolato)rhenium(v) into Thio(thiolatoalkyl)rhenium(v) Compounds**

Ming Li, Arkady Ellern, and James H. Espenson*

The cleavage of C–S bond is the most important step for removing sulfur from petroleum feedstocks.^[1] The common strategies include thermal decomposition,^[2] photolysis,^[3] reduction and/or protonation^[4] of sulfur-containing metal complexes. We have now found that reaction under mild conditions between oxo(dithiolato)rhenium(v) complexes and triphenylphosphine cleaves a C–S bond, giving a thio(thiolatoalkyl)rhenium(v) product. This reaction, to our knowledge, is unprecedented.

Treatment of **1a** or **1b** with triphenylphosphine leads to **2a** or **2b**, as in Equation (1). The reaction follows second-



order kinetics; $k_{1a} = 3.61(2) \times 10^{-3}$ and $k_{1b} = 2.61(5) \times 10^{-4} \text{ L mol}^{-1} \text{ s}^{-1}$ (benzene, 25.0°C). In the reaction in Equation (1) the Re=O bond is cleaved and P=O and Re=S bonds are formed at the expense of a CH₂-S-Re bond, and a new Re–C bond is formed; consequently, the six-membered chelate ring becomes a five-membered one.



On the other hand **1c** does not undergo this reaction, thus avoiding formation of a four-membered chelate ring. Additionally, but incidental to the new chemistry, all three versions of **1** exchange PAR₃ for PPh₃, as do their methyl analogues [MeReO(dithiolato)PPh₃].^[5]

[*] Dr. M. Li, Dr. A. Ellern, Prof. J. H. Espenson
Ames Laboratory and Department of Chemistry
Iowa State University
Ames, Iowa 50011 (USA)
Fax: (+1) 515-294-5233
E-mail: espenson@iastate.edu

[**] This research was supported by the U.S. Department of Energy, Office of Basic Energy Sciences, Division of Chemical Sciences under contract W-7405-Eng-82 with Iowa State University of Science and Technology. Helpful conversations with Professors W. S. Trahanovsky and R. J. Angelici are gratefully acknowledged.

Supporting information for this article is available on the WWW under <http://www.angewandte.org> or from the author.

Both **2a** and **2b** were characterized spectroscopically and analytically (Experimental Section). The methylene resonance signals shift downfield: $\delta = 4.95$ and 3.30 ppm for **1b** as compared to $\delta = 5.89$ and 3.61 ppm for **2b**. Further, the ν_{ReO} frequencies change from the typical values for oxorhenium(v) complexes,^[6] 947 cm⁻¹ (**1b**) to ν_{ReS} 500 (**2a**) and 510 cm⁻¹ (**2b**).^[7] The ³¹P NMR spectrum in C₆D₆ showed the slow disappearance of the resonance signal of **1b** at $\delta = 19.0$ ppm and the growth of new signals for **2b** at $\delta = 34.8$ ppm and for Ph₃PO at $\delta = 26.0$ ppm. Compounds **2a** and **2b** were also characterized by X-ray crystallography.^[8] Their molecular structures are based on a square pyramid with an apical thio ligand (Figure 1). The rhenium–element bond lengths are

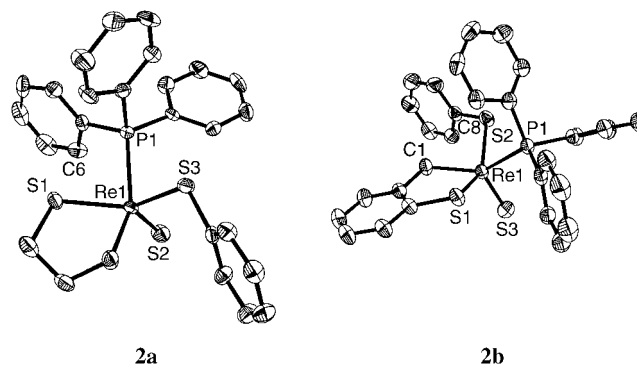
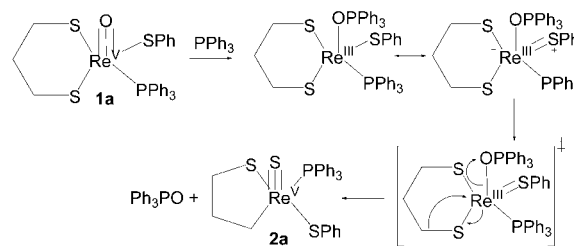


Figure 1. Molecular structures of **2a** and **2b** (thermal ellipsoids set at 50 % probability). Selected bond lengths [pm]: **2a**, Re–S(2) 208.08(15), Re–S(1) 228.49(15), Re–S(3) 228.98(15), Re–C 214.0(6), Re–P 241.56(14); **2b**, Re–S(3) 208.83(9), Re–S(2) 229.50(9), Re–S(1) 229.12(8), Re–C 215.6(3), Re–P 242.02(8).

comparable to those found in related rhenium(v) complexes,^[7,9] save for reported Re=O bonds of 168(3) pm, compared to the Re=S bonds of 208 pm in **2a**, **2b**. Note that in **1b** the phosphorus atom and the phenolic sulfur are in *trans* positions whereas in the product **2b** they lie *cis* to one another (see below).

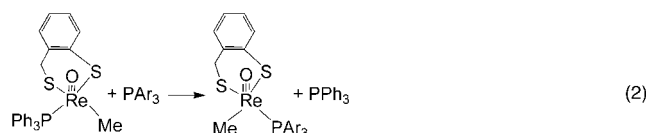
On the basis of the data obtained, we suggest the mechanism shown in Scheme 1. The first step comprises nucleophilic attack on the oxo group of **1a**, a process which is reasonable given the formal charges, Re=O⁺; moreover, attack of phosphine at a terminal oxo group has precedent.^[10] The resulting intermediate is assisted to the product by the Re=S⁺Ph resonance form. The intervention of this resonance form may be the ultimate reason for the failure of [MeReO(dithiolato)PPh₃] complexes to undergo parallel



Scheme 1. Proposed mechanism for the conversion of **1a** into **2a**.

reactions. Reaction of **1a** or **1b** with PAR_3 always leads to PAR_3 products analogous to **2a** or **2b**, because phosphine exchange in **1** occurs more rapidly than the reaction in Equation (1). We have found no precedent for the reaction in Equation (1), although certain features are common to an organic rearrangement.^[11]

Finally, there is an issue for **2b** not accounted for by the mechanism shown in Scheme 1, namely that the crystal structure establishes that the PhS group lies *trans* to the phenolic sulfur atom (S1), opposite to its location in **1b**. Isomerization is not an issue for the reaction of **1a**, of course, because it has equivalent sulfur atoms. It has been shown that geometrical isomerization accompanies the bimolecular, associative ligand substitution reactions between $[\text{MeReO}(\text{mtp})\text{PPh}_3]$ and PAR_3 , Equation (2).^[5] This precedent constitutes the basis for **2b** not being obtained the same isomer as **1b**; it leaves unanswered the question as to whether **2b**, as isolated, is the more stable geometric isomer.



Experimental Section

2a: As a mixture of $[\text{PhSReO}(\text{pdt})_2]$ (the precursor of **1a**)^[12] (165 mg, 0.20 mol) and PPh_3 (484 mg, 1.85 mmol) in toluene (100 mL) was stirred for two days, the solution changed gradually from brown to yellowish. During removal of the solvent a yellowish solid precipitated. This solid was dissolved in the minimum volume of CH_2Cl_2 , loaded onto a silica gel column, and eluted with diethyl ether/hexanes. Yield 71%; ^1H NMR (400 MHz, CD_2Cl_2): δ = 7.77 (b, 6H), 7.56 (dd, J = 7.2 Hz, 2H), 7.52–7.43 (m, 9H), 7.30 (t, J = 7.6 Hz, 2H), 7.23 (t, J = 7.6 Hz, 1H), 5.40 (dd, J = 13.6 Hz, 1H), 3.37–3.33 (m, 1H), 3.24–3.18 (m, 1H), 3.02–2.90 (m, 1H), 2.39–2.31 (m, 1H), 1.74–1.66 ppm (m, 1H), ^{31}P NMR (162 MHz, external reference 85% aq. H_3PO_4 , CD_2Cl_2): δ = 31.2 ppm, IR (KBr pellet) 500 cm^{-1} . Elemental analysis (%) calcd for $\text{C}_{27}\text{H}_{26}\text{S}_3\text{PRe}\cdot 0.5(\text{C}_2\text{H}_5)_2\text{O}:\text{C}$ 49.69, H 4.46, S 13.72; found: C 50.17, H 4.05, S 12.98. Crystals of $\text{C}_{27}\text{H}_{26}\text{S}_3\text{PRe}\cdot 0.5\text{C}_6\text{H}_6$ suitable for diffraction were grown from benzene solutions of **2a**.

2b: The analogous procedure was used to prepare the brown compound **2b** in 61% yield, from **1b**^[12] (50 mg, 0.07 mmol) and PPh_3 (92 mg, 0.35 mmol) in toluene (20 mL). Yield 61%, ^1H NMR (400 MHz, CD_2Cl_2): δ = 7.83 (b, 6H), 7.61–7.56 (m, 3H), 7.52–7.45 (m, 11H), 7.30 (t, 1H), 7.22 (d, 1H), 7.07 (t, 1H), 6.99 (t, 1H), 5.89 (dd, J_1 = 1.2 Hz, J_2 = 17 Hz, 1H), 3.61 ppm (dd, J_1 = 9 Hz, J_2 = 17 Hz, 1H), ^{31}P NMR (162 MHz, external reference 85% aq. H_3PO_4 , CD_2Cl_2): δ = 34.4 ppm (34.8 ppm in C_6D_6). IR (KBr pellet), 510 cm^{-1} (m, $\nu_{\text{Re}=\text{S}}$). Elemental analysis (%) calcd for $\text{C}_{31}\text{H}_{26}\text{S}_3\text{PRe}\cdot 0.5\text{C}_7\text{H}_8$: C 54.73, H 3.99, S 12.69, P 4.09; found: C 55.67, H 3.76, S 11.52, P 3.25. the solvent contained in the powdered sample for analysis was detected by ^1H NMR spectroscopy. The red-brown single crystals of $\text{C}_{31}\text{H}_{26}\text{S}_3\text{PRe}$ that were grown from toluene-hexanes solutions of **2b** contained no solvent of crystallization.

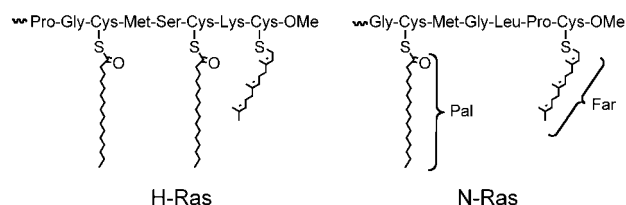
Received: June 23, 2004

Keywords: C–S bond cleavage · P ligands · reaction mechanisms · rhenium · S ligands

- [1] a) C. Bianchini, A. Meli, *Acc. Chem. Res.* **1998**, *31*, 109–116; b) R. J. Angelici, *Polyhedron* **1997**, *16*, 3073–3088; c) H. Topsoe, B. S. Clausen, F. E. Massouth, *Hydrotreating Catalysis*, Springer, Berlin, **1996**.
- [2] a) M. M. Hossain, H.-M. Lin, S.-G. Shyu, *Organometallics* **2003**, *22*, 3262–3270; b) L. Y. Goh, Z. Weng, W. K. Leong, P. H. Leung, *Angew. Chem.* **2001**, *113*, 3336–3339; *Angew. Chem. Int. Ed.* **2001**, *40*, 3236–3239; c) A. V. Firth, E. Witt, D. W. Stephan, *Organometallics* **1998**, *17*, 3716–3722; d) H. Kawaguchi, K. Tatsumi, *Organometallics* **1997**, *16*, 307–309; e) W. E. Piers, L. Koch, D. S. Ridge, L. R. MacGillivray, M. Zaworotko, *Organometallics* **1992**, *11*, 3148–3152; f) D. Coucouvanis, A. Hadjikyracou, R. Lester, M. G. Kanatzidis, *Inorg. Chem.* **1994**, *33*, 3645–3655; g) M. Kamata, T. Yoshida, S. Otsuka, K. Hirotsu, T. Higuchi, *J. Am. Chem. Soc.* **1981**, *103*, 3572–3574.
- [3] a) M. A. Reynolds, R. J. Angelici, I. A. Guzei, *Chem. Commun.* **2000**, 513–514; b) M. A. Reynolds, I. A. Guzei, R. J. Angelici, *Organometallics* **2001**, *20*, 1071–1078; c) M. A. Reynolds, I. A. Guzei, R. J. Angelici, *J. Am. Chem. Soc.* **2002**, *124*, 1689–1697.
- [4] a) K. E. Janak, J. M. Tanski, D. G. Churchill, G. Parkin, *J. Am. Chem. Soc.* **2002**, *124*, 4182–4183; b) T. Arliguie, C. Lescop, L. Ventelon, P. C. Leverd, P. Thuery, M. Nierlich, M. Ephritikhine, *Organometallics* **2001**, *20*, 3698–3703; c) G. E. D. Mullen, P. J. Blower, D. J. Price, A. K. Powell, M. J. Howard, M. J. Went, *Inorg. Chem.* **2000**, *39*, 4093–4098; d) J. Li, D. Miguel, M. D. Morales, V. Riera, S. Garcia-Granda, *Organometallics* **1998**, *17*, 3448–3453; e) L. Ventelon, C. Lescop, T. Arliguie, M. Ephritikhine, P. C. Leverd, M. Lance, M. Nierlich, *Chem. Commun.* **1999**, 659–660; f) G. E. D. Mullen, M. J. Went, S. Wocadlo, A. K. Powell, P. J. Blower, *Angew. Chem.* **1997**, *109*, 1254–1256; *Angew. Chem. Int. Ed. Engl.* **1997**, *36*, 1205–1207; g) A. V. Firth, D. W. Stephan, *Organometallics* **1997**, *16*, 2183–2188; h) K. M. K. Dailey, T. B. Rauchfuss, A. L. Rheingold, G. P. A. Yap, *J. Am. Chem. Soc.* **1995**, *117*, 6396–6397.
- [5] D. W. Lahti, J. H. Espenson, *J. Am. Chem. Soc.* **2001**, *123*, 6014–6024.
- [6] a) X. Shan, A. Ellern, I. A. Guzei, J. H. Espenson, *Inorg. Chem.* **2003**, *42*, 2362–2367; b) X. Shan, A. Ellern, J. H. Espenson, *Inorg. Chem.* **2002**, *41*, 7136–7142; c) J. H. Espenson, X. Shan, Y. Wang, R. Huang, D. W. Lahti, J. Dixon, G. Lente, A. Ellern, I. A. Guzei, *Inorg. Chem.* **2002**, *41*, 2583–2591; d) C. Zhang, I. A. Guzei, J. H. Espenson, *Inorg. Chem.* **2001**, *40*, 2437–2438; e) G. Lente, J. H. Espenson, *Inorg. Chem.* **2000**, *39*, 4809–4814; f) J. Jacob, G. Lente, I. A. Guzei, J. H. Espenson, *Inorg. Chem.* **1999**, *38*, 3762–3763; g) J. Jacob, I. A. Guzei, J. H. Espenson, *Inorg. Chem.* **1999**, *38*, 1040–1041.
- [7] a) F. Tisato, C. Bolzati, A. Duatti, G. Bandoli, F. Refosco, *Inorg. Chem.* **1993**, *32*, 2042–2048; b) P. J. Blower, J. R. Dilworth, J. P. Hutchinson, T. Nicholson, J. Zubietta, *Adv. Chem. Ser.* **1986**, 1339–1345.
- [8] Crystal data for $\text{C}_{27}\text{H}_{26}\text{PReS}_3\cdot 0.5\text{C}_6\text{H}_6$, **2a**, M_r = 702.88, $0.2 \times 0.18 \times 0.08 \text{ mm}^3$, monoclinic, space group $P2_1/n$, a = 9.6367(19), b = 13.743(3), c = 20.877(4) Å, β = 94.338(4)°, V = 2757.0(9) Å³, ρ_{calcd} = 1.693 Mg m^{-3} , Z = 4, $2\theta_{\text{max}}$ = 56.66°, 6614 independent reflections, R_1 = 0.0366 for 4636 reflections with $I > 2\sigma(I)$ and wR_2 = 0.0659, 316 parameters. Crystal data for $\text{C}_{31}\text{H}_{26}\text{PReS}_3$, **2b**, M_r = 711.87, $0.25 \times 0.13 \times 0.10 \text{ mm}^3$, monoclinic, space group $P2_1/n$, a = 11.6792(19), b = 14.108(2), c = 17.107(3) Å, β = 94.460(3)°, V = 2810.2(8) Å³, ρ_{calcd} = 1.683 Mg m^{-3} , Z = 4, $2\theta_{\text{max}}$ = 56.56°, 6554 independent reflections, R_1 = 0.0252 for 5645 reflections with $I > 2\sigma(I)$ and wR_2 = 0.0603, 316 parameters. CCDC-241807 (**2a**) and CCDC-235612 (**2b**) contains the supplementary crystallographic data for this paper. These data can be obtained free of charge via www.ccdc.cam.ac.uk/conts/retrieving.html (or from the Cambridge Crystallographic Data Centre, 12 Union

Road, Cambridge CB21EZ, UK; fax: (+44)1223-336-033; or deposit@ccdc.cam.ac.uk).

- [9] J. Jacob, I. A. Guzei, J. H. Espenson, *Inorg. Chem.* **1999**, *38*, 3266–3267.
- [10] a) S. B. Seymore, S. N. Brown, *Inorg. Chem.* **2000**, *39*, 325–332; b) J. Gangopadhyay, S. Sengupta, S. Bhattacharyya, I. Chakraborty, A. Chakravorty, *Inorg. Chem.* **2002**, *41*, 2616–2622; c) S. Bhattacharyya, I. Chakraborty, B. K. Dirghangi, A. Chakravorty, *Inorg. Chem.* **2001**, *40*, 286–293; d) P. Basu, V. N. Nemykin, R. S. Sengar, *Inorg. Chem.* **2003**, *42*, 7489–7501; e) P. D. Smith, A. J. Millar, C. G. Young, A. Ghosh, P. Basu, *J. Am. Chem. Soc.* **2000**, *122*, 9298–9299.
- [11] W. S. Trahanovsky, A. N. Amah, T. J. Cassady, *J. Am. Chem. Soc.* **1984**, *106*, 2696–2698.
- [12] Compounds **1a–c** with a PhS-Re group are new but will not be described herein as they are the exact analogues of the Me-Re counterparts already reported.^[6]



Scheme 1. Structure of the C-termini of the N-Ras and the H-Ras protein.

Protein Synthesis

Solid-Phase Synthesis of Lipidated Peptides**

Goran Kragol, Maria Lumbierres, Jose M. Palomo, and Herbert Waldmann*

The Ras proteins serve as central molecular switches in biological signal transduction cascades regulating cell growth and differentiation.^[1] They incorporate both acid-labile farnesyl thioethers and base-sensitive palmitic acid thioesters, which are required for biological activity and terminate in a cysteine methyl ester (Scheme 1).

For the efficient and rapid synthesis of tailor-made lipidated peptides representing the characteristic partial

structures of their parent proteins^[2,3] a flexible solid-phase technology is required. Ideally such a technique would:

1. give access to peptides carrying different combinations of acid- and base-labile lipid groups; this requires the application of a set of suitable orthogonally stable protecting groups and a linker to the solid support, all of which can be cleaved under the mildest conditions;^[3]
2. allow for the introduction of additional reporter and/or linking groups required for application of the target peptides in further biological investigations;
3. allow for release of the peptide as a methyl ester, or—if required—equipped with a different functional group, for example, a fluorophore at the C-terminus.^[2d]

The only method currently available for this purpose^[4] requires a large excess of lipidation reagent, is not readily automatable, and is not suitable for the preparation of longer peptides. Thus attempts to prepare peptides with > 10 amino acids by this method failed in our hands.

Here we describe the successful development of a solid-phase synthesis method that meets the demands and overcomes the drawbacks described above. It employs pre-lipidated amino acid building blocks together with the base-labile 9-fluorenylmethoxycarbonyl (Fmoc) group as a blocking function for the N-terminus, and the oxidation-labile hydrazide linker for anchoring to the solid support.

The lipidated building blocks required for the new solid-phase method were synthesized in high overall yields as shown in Scheme 2 employing in part transformations described earlier.^[5] Notably only one equivalent of farnesyl chloride and, in particular, of the *N*-methylantraniloyl (Mant)-functionalized farnesyl analogue GerMantCl were employed.

Building blocks **2** and **4** were then used in the solid-phase synthesis of H- and N-Ras peptides **9** and **10** (Scheme 3). The hydrazide unit^[6] was employed as a linker to the solid support since it can be cleaved under mild oxidative conditions and gives access to lipopeptide esters and acids.^[4] Fmoc-hydrazinobenzoic acid functionalized aminomethyl polystyrene resin is commercially available (NovaBioChem). In order to avoid racemization of cysteines DIC/HOBt or HBTU/HOBt/TMP cocktails in CH₂Cl₂/DMF 1:1 were used for coupling the cysteine building blocks.^[7]

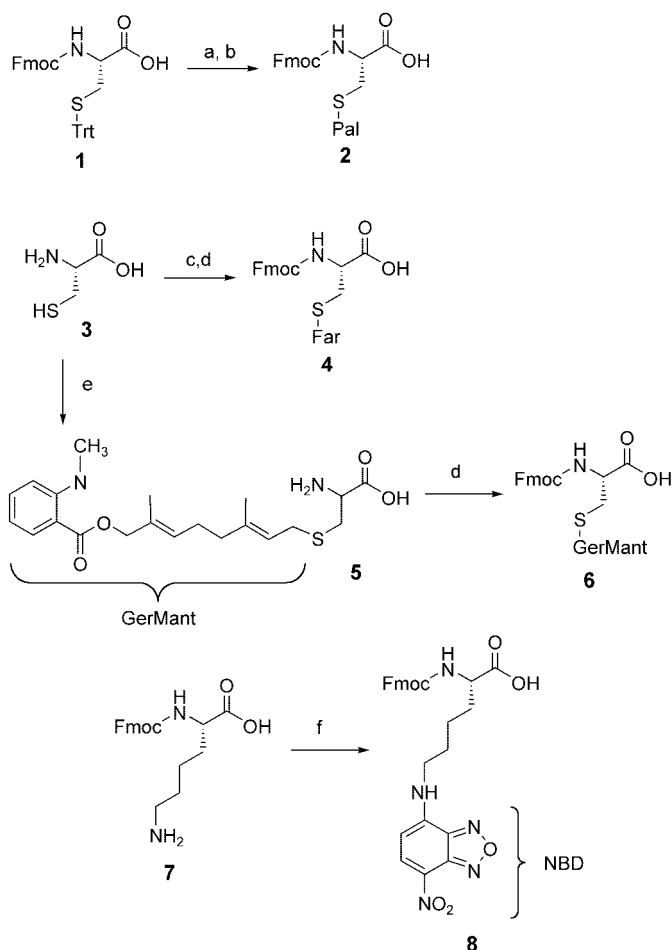
Coupling of Fmoc-Cys(Far)OH and Fmoc-Cys(Pal)OH proceeded with > 90 % efficiency if a coupling time of 4 h was allowed and if for Fmoc-Cys(Pal)OH a double coupling was performed (monitored by Fmoc determination employing the established UV-based method). After oxidative cleavage with Cu(OAc)₂ and release from the resin by treatment with

[*] Dr. G. Kragol,† Dr. M. Lumbierres, Dr. J. M. Palomo, Prof. Dr. H. Waldmann
Max-Planck-Institut für molekulare Physiologie
Abteilung Chemische Biologie
Otto-Hahn-Strasse 11, 44227 Dortmund (Germany)
and
Universität Dortmund
Fachbereich 3, Organische Chemie
Fax: (+49) 231-133-2499
E-mail: herbert.waldmann@mpi-dortmund.mpg.de

[†] Current address:
Department of Organic Chemistry and Biochemistry
Rudjer Boskovic Institute
Bijenicka 54, Zagreb (Croatia)

[**] This research was supported by the Deutsche Forschungsgemeinschaft, the Max-Planck-Gesellschaft, the Fonds der Chemischen Industrie, the Humboldt Foundation (research fellowship to G.K.), and the European Molecular Biology Organization (long-term fellowship to J.M.P.).

Supporting information for this article is available on the WWW under <http://www.angewandte.org> or from the author.



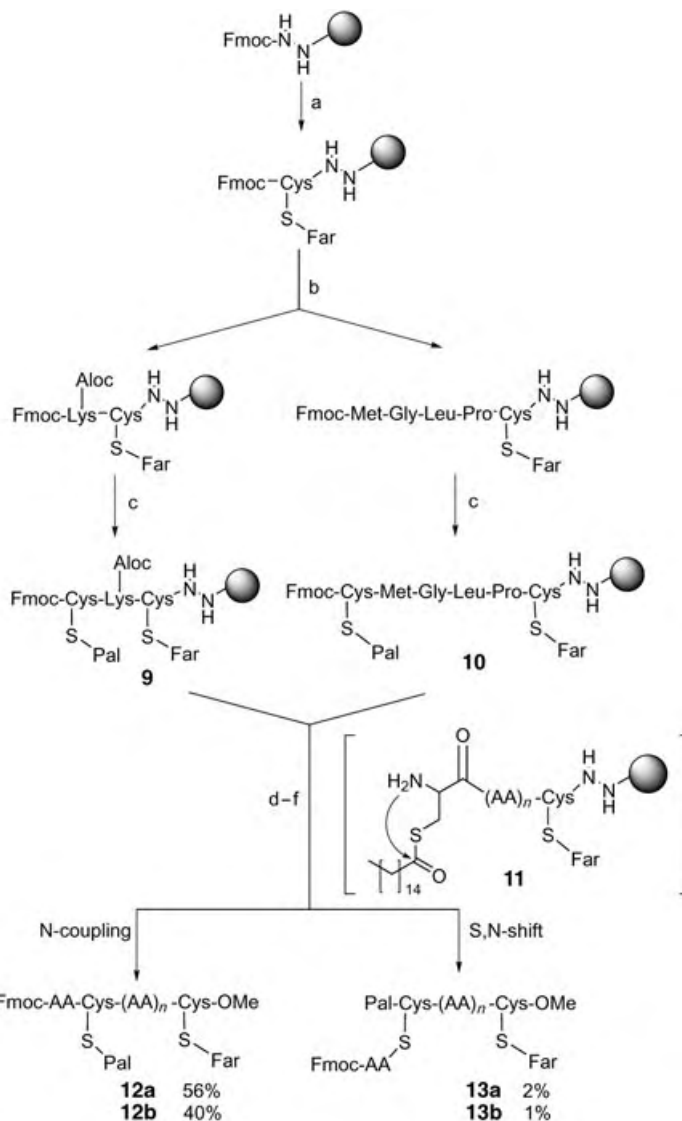
Scheme 2. Synthesis of lipidated building blocks **2**, **4**, **6**, and **8**.

a) 5% TFA, 3% TES, CH_2Cl_2 , 1 h, RT; b) TMSCl (1.1 equiv), 2 h, reflux, CH_2Cl_2 , then PalCl (3 equiv), Et_3N (1.5 equiv) dropwise 3 h, CH_2Cl_2 , RT; c) FarCl (1 equiv), 4 N NH_3 /methanol, 3 h, 0°C, 1 h, RT;^[5a] d) FmocOSu (1.1 equiv), Et_3N (1.1 equiv), CH_2Cl_2 , 2 h, RT; e) GerMantCl (1 equiv), 4 N NH_3 /methanol, 3 h, 0°C, 1 h, RT; f) NBDCl, THF/methanol, 65°C, 2 h.^[5b] Far = farnisyl, Fmoc = 9-fluorenylmethoxycarbonyl, NBD = 4-nitrobenzo-2-oxa-1,3-diazole, Pal = palmitoyl, RT = room temperature, TES = triethylsilane, TFA = trifluoroacetic acid, TMS = trimethylsilyl.

CH_3OH followed by filtration of the crude product through a short silica cartridge, the peptide methyl esters corresponding to immobilized peptides **9** and **10** were obtained in overall yields of 69% and 60%, respectively, and with > 90% purity.

For further elongation of the peptide chain the central problem of the entire method had to be solved. After removal of the Fmoc group from the N-terminal S-palmitoylated cysteine a rapid S→N acyl shift had to be feared,^[8] and, in addition, the base-labile Fmoc group had to be removed under conditions that leave the thioester intact, although this group is very sensitive to nucleophilic attack.^[2]

Substantial experimentation revealed that the desired elongated and S-palmitoylated peptides can be obtained in a very practical and efficient manner if the Fmoc group is cleaved by treatment with a solution of 1% DBU in DMF^[9]



Scheme 3. Solid-phase synthesis of lipidated peptides employing pre-lipidated amino acid building blocks. a) 1. 20% piperidine/DMF, 2. Fmoc-Cys(Far)-OH (4 equiv), DIC/HOBt or HBTU/HOBt/TMP, CH_2Cl_2 /DMF (1:1), 4 h; b) Standard solid-phase synthesis: 1. 20% piperidine/DMF, 2. Fmoc-AA-OH (4 equiv), DIC/HOBt or HBTU/HOBt/DIPEA, CH_2Cl_2 /DMF (1:1) or DMF, 2 h; c) 1. 20% piperidine/DMF, 2. Fmoc-Cys(Pal)-OH (4 equiv), DIC/HOBt or HBTU/HOBt/TMP, CH_2Cl_2 /DMF (1:1), 4 h for **10**, overnight for **9**; d) 1% DBU/DMF, 2 × 30 s; e) Fmoc-AA-OH (5 equiv), HATU (5 equiv), DIPEA (20 equiv), CH_2Cl_2 /DMF (4:1), 2 h; f) $\text{Cu}(\text{OAc})_2$, pyridine, acetic acid, methanol, CH_2Cl_2 , oxygen atmosphere, 3 h. DIC = 1,3-diisopropylcarbodiimide, DIPEA = *N,N*-diisopropylethylamine, DMF = *N,N*-dimethylformamide, HATU = *O*-(7-azabenzotriazol-1-yl)-*N,N,N',N'*-tetramethyluronium hexafluorophosphate, HBTU = *N*-[(1*H*-benzotriazol-1-yl)-(dimethylamino)methylene]-*N*-methylmethanaminium hexafluorophosphate *N*-oxide, HOBt = 1-hydroxybenzotriazole, TMP = tetramethylpiperidine.

for 2 × 30 s followed each time by fast washing with DMF (6 × 5 s) and immediate coupling for 2 h employing five equivalents of preactivated (10 min) amino acid building block, five equivalents of HATU, and twenty equivalents of diisopropyl-

ethylamine in $\text{CH}_2\text{Cl}_2/\text{DMF}$ 4:1 as solvent. Under these conditions the desired elongated peptides **12** and the analogue **13** resulting from S→N acyl shift were formed in a ratio of 95:5.

In order to demonstrate the scope of the method, the lipid-modified peptides shown in Table 1 were prepared. In general, a resin with a loading of 0.35–0.37 mmol g⁻¹ was employed, and the peptides were prepared in 5- to 20-mg amounts. Immediately after release from the resin and filtration through a silica cartridge the peptides were > 80% pure (determined by HPLC analysis; see the Supporting Information).

The peptides shown in Table 1 display different lipidation patterns; in other words, they are mono- or dilipidated and correspond to the C-termini of the H- or N-Ras protein. In addition to the lipid groups they incorporate a fluorescent label (NBD, Mant) or a photoactivatable group (benzophenone) and/or a maleimidocaproyl group (MIC), and a biotin group or an unmasked N-terminal cysteine which can be employed for coupling to expressed proteins by expressed protein ligation.^[2c] Three peptides (**18–20**) incorporating the GerMant analogue of the farnesyl group were synthesized. Due to the laborious preparation of the GerMant residue (see above) in the coupling steps employing Fmoc-Cys(GerMant)OH only 1.5 equivalents of the building block were employed to ensure efficient use.

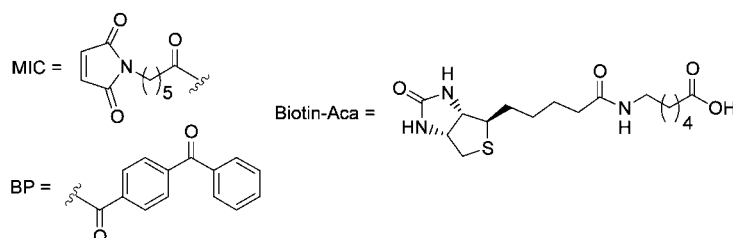
Finally, the applicability of the method to the synthesis of long lipidated peptides was investigated. To this end, decapeptide **27** and tetradecapeptide **28** were prepared, which both mimic the C-terminus of N-Ras. Both were obtained in milligram amounts and characterized by ¹H NMR spectroscopy and mass spectrometry (**27**: ESI-MS: m/z_{calcd} for $[M+H]^+$ = 1887.0, m/z_{found} = 1887.3; **28**: MALDI-MS (DHB): m/z_{calcd} for $[M+Na]^+$ = 2481.3, m/z_{found} = 2481.8; m/z_{calcd} for $[M+K]^+$: 2497.3, m/z_{found} = 2497.9). These peptides represent the longest S-palmitoylated and S-farnesylated peptides synthesized so far. Both were not accessible by the previously reported solid-phase method,^[4] which demonstrates the superiority of the method reported in this article.

In conclusion we have developed an efficient solid-phase method for the synthesis of differently lipidated and additionally modified peptides. This method meets the requirements of a widely applicable

Table 1: Lipidated peptides synthesized by means of the solid-phase method.

Entry	Cmpd.	Structure ^[a]	Yield [%]
1	14		28
2	15		38
3	16		30
4	17		28
5	18		31
6	19		23
7	20		25
8	21		45
9	22		25
10	23		32
11	24		20
12	25		37
13	26		25
14	27		30
15	28		12

[a] Structures to define the abbreviations used:



potentially automatable methodology and overcomes the limitations of earlier procedures. In terms of efficiency and flexibility this solid-phase method is superior to the solution-phase synthesis. It gives pure peptides more quickly and with superior overall yield.

Received: July 1, 2004

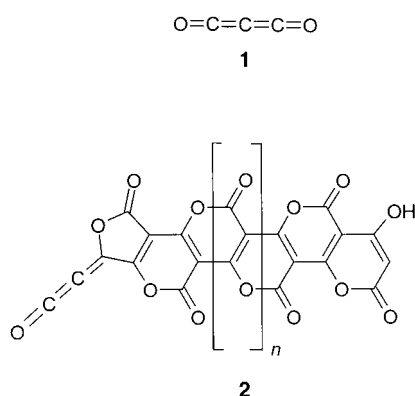
Keywords: lipids · proteins · solid-phase synthesis

-
- [1] a) K. Hinterding, D. Alonso-Diaz, H. Waldmann, *Angew. Chem.* **1998**, *110*, 716–780; *Angew. Chem. Int. Ed.* **1998**, *37*, 688–749; b) A. Wittinghofer, H. Waldmann, *Angew. Chem.* **2000**, *112*, 4360–4383; *Angew. Chem. Int. Ed.* **2000**, *39*, 4193–4214.
- [2] a) B. Bader, K. Kuhn, D. J. Owen, H. Waldmann, A. Wittinghofer, J. Kuhlmann, *Nature* **2000**, *403*, 223–226; b) K. Kuhn, D. J. Owen, B. Bader, A. Wittinghofer, J. Kuhlmann, H. Waldmann, *J. Am. Chem. Soc.* **2001**, *123*, 1023–1035; c) J. Kuhlmann, A. Tebbe, M. Völkert, M. Wagner, K. Uwai, H. Waldmann, *Angew. Chem.* **2002**, *114*, 2655–2658; *Angew. Chem. Int. Ed.* **2002**, *41*, 2546–2550; d) R. Reents, M. Wagner, J. Kuhlmann, H. Waldmann, *Angew. Chem.* **2004**, *116*, 2765–2768; *Angew. Chem. Int. Ed.* **2004**, *43*, 2711–2714; e) A. Rak, O. Pylypenko, T. Durek, A. Watzke, S. Kushnir, L. Brunsfeld, H. Waldmann, R. S. Goody, K. Alexandrov, *Science* **2003**, *302*, 646–650.
- [3] D. Kadereit, J. Kuhlmann, H. Waldmann, *ChemBioChem*, **2000**, *1*, 144–169.
- [4] a) B. Ludolph, F. Eisele, H. Waldmann, *J. Am. Chem. Soc.* **2002**, *124*, 5954–5955; b) B. Ludolph, H. Waldmann, *Chem. Eur. J.* **2003**, *9*, 3683–3691.
- [5] a) M. J. Brown, P. D. Milano, D. C. Lever, W. W. Epstein, C. D. Poulter, *J. Am. Chem. Soc.* **2001**, *123*, 3176–3177; b) C. Peters, PhD thesis University of Dortmund (Germany), **2003**.
- [6] a) C. R. Millington, R. Quarrel, G. Lowe, *Tetrahedron Lett.* **1998**, *39*, 7201–7204; b) C. Rosenbaum, H. Waldmann, *Tetrahedron Lett.* **2001**, *42*, 5677–5680. These investigations demonstrate that cysteinyl-peptide esters are oxidatively released from the solid support without racemization of the C-terminal cysteine.
- [7] Y. M. Angell, J. Alsina, F. Albericio, G. Barany, *J. Pept. Res.* **2002**, *60*, 292–299.
- [8] Y. Trudelle, A. Caille, *Int. J. Pept. Protein Res.* **1977**, *10*, 291–298.
- [9] J. D. Wade, J. Bedford, R. C. Sheppard, G. W. Tregar, *Pept. Res.* **1991**, *4*, 194–199.
-

Analysis of Poly(carbon suboxide) by Small-Angle X-ray Scattering**

Matthias Ballauff,* Sabine Rosenfeldt,
Nico Dingenouts, Johannes Beck,* and
Petra Krieger-Beck

Carbon forms different oxides, of which carbon monoxide and carbon dioxide are among the most widely studied chemical compounds. The most stable oxide with more than two cumulative double bonds, known as carbon suboxide C_3O_2 (**1**; Scheme 1), was synthesized for the first time nearly 100 years



Scheme 1. Structure of monomeric carbon suboxide (**1**) and the poly(α -pyronic) structure of poly(carbon suboxide) (**2**) as postulated by Ziegler.

ago. In 1906, Diels et al. discovered that the dehydration of malonic acid with P_4O_{10} yields a colorless, pungent gas which they later identified as C_3O_2 .^[1] The molecule, whose electronic structure suggests it to be linear, after intensive spectroscopic studies, was found to be quasilinear with a

very small energy barrier of approximately 30 cm^{-1} for the bending vibration of the central carbon atom.^[2–4] Recently the structural analysis has been carried out using crystalline C_3O_2 .^[5]

A specific property of carbon suboxide is its spontaneous polymerization, which results in the formation of a red to black solid, with an unaltered composition of C_3O_2 .^[1] In spite of a number of studies, the structure of poly(carbon suboxide) $(C_3O_2)_n$ is not well understood at the atomic level. Owing to the amorphous nature of the polymer, conventional diffraction methods cannot be employed. The polymerization is highly exothermic (-136 kJ mol^{-1}) and may result in explosions.^[6] The reaction follows first-order kinetics and can be catalyzed by traces of water, acids, bases and γ -rays.^[7] In absence of an initiator, the polymerization depends on the nature of the surface of the reaction vessel.^[8] The polymer is paramagnetic, the susceptibility of which follows the Curie–Weiss law. The spin density reaches a value of 10^{19} g^{-1} , although the polymerization does not follow a radical mechanism.^[9] The IR spectra show identical band patterns independent of the way of preparation. Under highly anhydrous conditions, the IR spectra show a band at 2180 cm^{-1} , which can be assigned to the ketenyl group, $C\equiv C=O$. Exposure of the polymer to small quantities of humid air results in the disappearance of the band along with the paramagnetic moment.^[7]

A number of proposed structures exist. Of which the earlier hypothesis of poly(spirocyclobutanediones)^[10] and of an unordered, planar molecule, whose edges are occupied by carbonyl and ketenyl groups,^[11] were discarded on the basis of spectroscopic findings.^[12] In 1960 Ziegler^[13] postulated for the first time a poly(α -pyronic) structure, (**2**; Scheme 1) which was later confirmed by other studies,^[8,12] and has since found its way into a number of textbooks. This proposed structure has recently been questioned, since the acid–base titration of the polymer shows the presence of two different weakly acidic groups, which are attributed to the coexistence of α - and γ -pyrones.^[14]

The discussion regarding the structure of $(C_3O_2)_n$ is not complete, as the most important parameter in understanding the structure, the degree of polymerization n is not yet well defined. Prepared at temperatures below 100°C poly(carbon suboxide) is soluble in various solvents, such as, water, dimethylsulfoxide (DMSO), or dimethylformamide (DMF). The determination of molecular weight of the polymer $(C_3O_2)_n$ was carried out by Haubenstock and co-workers, who obtained a molecular weight of 311 to 358 g mol^{-1} in DMF solution using vapor-pressure osmometry, and molecular weight of 312 g mol^{-1} in DMSO using cryoscopy.^[7] The degree of polymerization n should therefore be very small, about five units of C_3O_2 . In the sixties, Blake et al. had reported similar results, but with relatively high errors, obtaining a value of $n = 5$ to 10 for amorphous solids by using wide-angle X-ray diffraction.^[12] Recent investigations for the degree of polymerization of polymers treated with NH_3 , by vapor-pressure osmometry in water, gave $n = 6$ – 8 .^[14]

According to the above results, $(C_3O_2)_n$ cannot be represented as a polymeric substance. If the structure of $(C_3O_2)_n$ is indeed as shown Scheme 1, then the polymerization

[*] Prof. Dr. M. Ballauff, L. Li, Dr. S. Rosenfeldt
Physikalische Chemie I
Universität Bayreuth
Universitätsstrasse 30, 95440 Bayreuth (Germany)
Fax: (+49) 921-55-2780
E-mail: matthias.ballauff@uni-bayreuth.de

Prof. Dr. J. Beck, Dr. P. Krieger-Beck
Institut für Anorganische Chemie
Universität Bonn
Gerhard-Domagk-Strasse 1, 53121 Bonn (Germany)
Fax: (+49) 228-73-5660
E-mail: j.beck@uni-bonn.de

Dr. N. Dingenouts
Polymer-Institut, Universität Karlsruhe
Kaiserstrasse 12, 76128 Karlsruhe (Germany)

[**] M.B. would like to thank the Deutsche Forschungsgemeinschaft and Fonds der Chemischen Industrie for financial support. J.B. would like to thank the Deutsche Forschungsgemeinschaft for financial support for this work within the Sonderforschungsbereich 408.

process must result in higher molecular weights and the degree of polymerization must be much greater than $n=5$.

To explain the structure of poly(carbon suboxide) in solution, and to arrive at a comprehensive and meaningful conclusion, we have used small-angle X-ray scattering method, which is suitable for the analysis of dissolved polymers.^[15] It is possible with the help of this method, to determine the degree of polymerization and the shape of the molecule. The details of such an analysis have been discussed recently.^[16] First, the scattering intensity $I(q,c)$ of dilute solutions of poly(carbon suboxide) is measured. The scattering vector q can be described by the scattering angle θ and the wavelength of the incident radiation ($q = (4\pi/\lambda)\sin(\theta/2)$; λ = wavelength, θ = scattering angle).^[15] The weight concentrations are typically 0.5–1 % and the analysis of the data follows according to Equation (1) where K is the optical constant,

$$I(q,c) = kcM_w P(q) S(q,c) = kcI(q) S(q,c) \quad (1)$$

which can be given through the partial molar volume of the dissolved polymer (see *Experimental Section*). M_w is the weight-average molecular weight to be determined and $P(q)$ is the form factor, which describes the intramolecular interactions of the dissolved molecules and provides information about the form of the polymer. The term $S(q,c)$ is the structure factor, which describes the effect of the intermolecular interactions at finite concentrations. By extrapolating $I(q)/c$ to infinite dilution this effect can be eliminated, and the scattering intensity $I_0(q)$ of a single dissolved molecule can be obtained. According to Guinier's law, in the region of small scattering angles, an extrapolation to vanishing scattering angles could be given as Equation (2)^[15], where R_g is the

$$I(q)/c = kM_w \exp\left[-\frac{R_g^2 q^2}{3}\right]; qR_g < 1 \quad (2)$$

radius of gyration, which is a measure of the average extension of the dissolved molecule under consideration.

Figure 1 shows the Guinier plot, where the scattering intensities are extrapolated to infinite dilution. A mixture of 90 % DMF and 10 % water was used as solvent. Along with

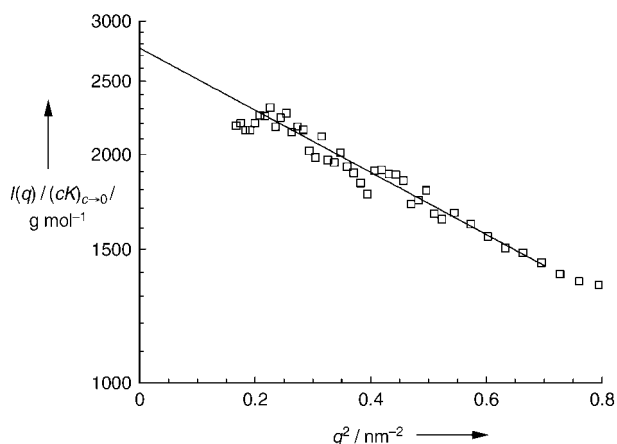


Figure 1. Guinier plot showing the scattering intensities of dissolved poly(carbon suboxide) extrapolated to infinite dilutions.

the optical constant K , determined by the density measurements (see *Experimental Section*), the y-axis intercept gives a molecular weight M_w $2750 \pm 600 \text{ g Mol}^{-1}$. In spite of the relative error in the measurements, as a result of the weak scattering intensities, it can be concluded that the value obtained is approximately higher by one order of magnitude than those obtained by Haubenstock et al. who obtained a value of 311 g mol^{-1} . The radius of gyration R_g , is found to be 1.7 nm, which is indicative of a polymeric structure. These results suggest the polymer structure to be as shown in Scheme 1.

The above analysis is not sufficient to prove the bandlike structure for the poly(carbon suboxide). It is necessary to carry out the analysis of the form factor $P(q)$ at higher scattering angles: first, the form factor must be corrected for the finite diameter of the molecule, as the X-ray scattering interferences, which contribute to the angle dependence of $I_0(q)$, could also result from the finite cross-section of the molecule.^[16] The corrected form factor $P_0(q)$, which then refers to an infinitely thin chain, in which there are only intramolecular interactions along the chains, could then be compared to the theoretical models. The main result of this analysis is the persistence length a , which is a measure of the stiffness of the polymer chain under consideration: if a is smaller than the contour length L_c of the chain, the polymer is a flexible coil, whereas, if a is identical to L_c , then the macromolecule is a rod.

Following Ref. [16] a plot of the scattering intensities $I_0(q)$ measured at higher scattering angles can be carried out according to Equation (3), where M_L is the mass of the

$$\frac{I_0(q)}{kc} \rightarrow \frac{\pi M_L}{q} \exp\left[-\frac{1}{2} R_c^2 q^2\right] \quad (3)$$

polymer chain per unit length and R_c is the radius of gyration across the chain, in which the interferences owing to the finite cross-section are taken into consideration. The mass per unit length M_L can be divided directly by the formula weight of the repeating unit to obtain the length which then provides a good consistence check for the analysis. The form factor $P_0(q)$ corrected for the effect of the finite diameter, could then be given as Equation (4).^[16] This term can be compared directly to the theoretical models.^[16]

$$I_0(q) = kcM_w P_0(q) \exp\left[-\frac{1}{2} R_c^2 q^2\right] \quad (4)$$

Figure 2 shows the plot of the scattering data according to Equation (3). At higher q values a linear relationship was found as expected, this allows a reliable estimation of M_L and R_c . From Figure 2 $M_L = 360 \pm 20 \text{ g Mol}^{-1} \text{ nm}^{-1}$ and $R_c = 0.3 \pm 0.05 \text{ nm}$. For the proposed structure **2** (Scheme 1) $M_L = 340 \text{ g Mol}^{-1} \text{ nm}^{-1}$. The value obtained for R_c is exactly equivalent to the cross-section, derived from the proposed Structure.

The next step of this analysis is demonstrated in Figure 3, which shows the Holtzer plot. Kholodenko's model was used for the theoretical description of $P_0(q)$, which in comparison with simulations^[16] has already been demonstrated to be the

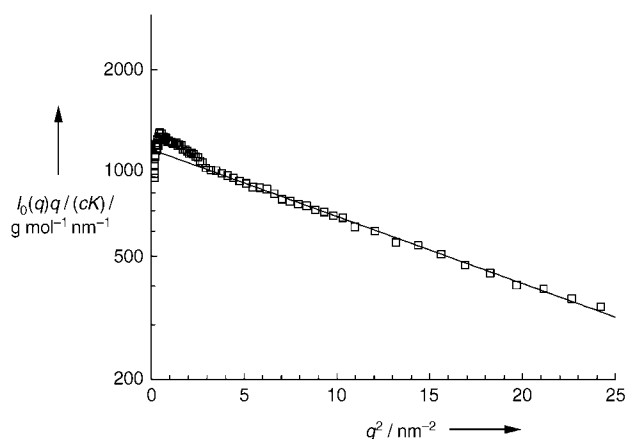


Figure 2. Plot of the scattering intensities corrected according to Equation (3) for the determination of mass per length M_L and the cross-sectional radius of gyration R_c . The y -axis intercept of this plot leads directly to πM_L , and the slope gives the value of R_c according to Equation (3).

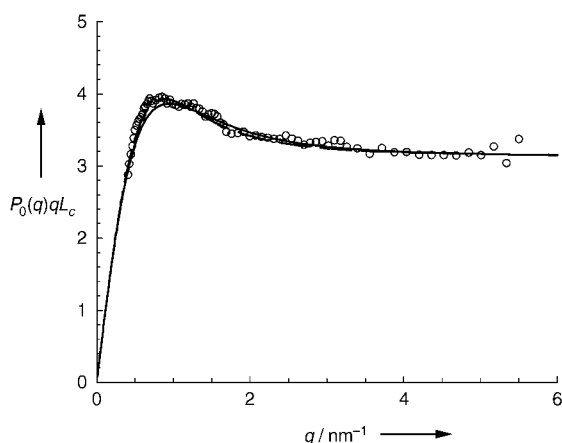


Figure 3. Holtzer plot $P_0(q)qL_c$ of the corrected form factor $P_0(q)$. The points correspond to the experimental data, while the lines show the fits of the experimental data with the form factor from the Kholodenko theory. The dashed line depicts the fit with the dimensionless quantity $L_w/L_n = 1.1$, while the solid line shows the assumption of the dimensionless quantity $L_w/L_n = 1.5$. In both the cases $L_w = 7.7$ nm, the value, which is determined directly from M_w and M_L . The persistence length a is given as 1.5 nm for $L_w/L_n = 1.1$, if $L_w/L_n = 1.5$ then a is 1.3 nm.

optimal theory.^[16] Fit-parameter of this model is the persistence length a , as the contour length used for this model $L_c = 7.7 \pm 1$ nm is given by the molecular weight M_w and the mass per unit length M_L as determined above. The breadth of the molecular-weight distribution must be considered, this is given from the ratio of the weight-average contour length L_w and the number-average contour length L_n . Since no information is available for L_w and L_n , the fit was carried out by assuming $L_w/L_n = 1.1$ (dashed line in Figure 3) and with $L_w/L_n = 1.5$ (solid line in Figure 3). As can be seen in Figure 3, both the assumptions deliver identically good fits, which are within the limits of error. The persistence length $a = 1.5$ nm for $L_w/L_n = 1.1$, if $L_w/L_n = 1.5$ then a slightly smaller value $a = 1.3$ nm is obtained.

In conclusion, small-angle X-ray scattering measurements in solution allow us to fully confirm the suggested polypyronic structure **2** (Scheme 1). The degree of polymerization $n \approx 40$, is in contradiction to the earlier determination of the molecular mass and confirms that $(C_3O_2)_n$ is a one-dimensional bandlike polymer. Hence, a solution to the structure of poly(carbon suboxide) has been obtained.

Experimental Section

1: C_3O_2 was obtained by the thermolysis of malonic acid bis(trimethylsilyl ester) in presence of P_4O_{10} at 160°C .^[17] The gaseous carbon suboxide was collected in a cold-trap thermostated at the temperature of liquid N_2 , which was then purified by distilling two times using two cold-traps in series.

2: For the polymerization, C_3O_2 (1 to 2 mL) was condensed in glass ampules of 15 cm length, with an inner diameter of 1.5 cm and a wall thickness of 2 mm, and dry CCl_4 (3 mL) was added. After freezing with liquid N_2 , the ampule was evacuated and sealed. Storage at room temperature for a few days led to a complete transformation into the brown red polymer.^[18] After opening the ampule under an inert gas, CCl_4 was first evaporated at room temperature for 24 h under vacuum, and then for further 2 h at 50°C . The red brown powder was preserved in an argon filled glove box and weighed there for the preparation of solutions.

Small-angle X-ray scattering: all the scattering intensities shown herein, were obtained using a Kratky compact camera. The measurements were carried out and analyzed analogously to experiments on dissolved polymers reported elsewhere,^[16] as was the extrapolation to infinite dilutions and the desmearing of the scattering intensities, which is necessary owing to the slit geometry of the X-ray beam obtained with a Kratky camera.

The optical constant K could be given as Equation (5).^[16]

$$N_A \Delta z^2 = N_A \left(\frac{n_e}{M_0} - \frac{\bar{v}_2 \rho_{0,e}}{N_A} \right)^2 \quad (5)$$

N_A is the Avogadro number and Δz is the number of excess electrons per mass of the dissolved polymer under consideration. The term n_e is the number of electrons per mass, which can be obtained through the formula weight, and \bar{v}_2 is the partial specific volume, which can be obtained through the density measurements of dilute solutions. For the solutions studied here, in the mixture of 90 % DMF and 10 % water a value of $\bar{v}_2 = 0.61 \pm 0.02 \text{ cm}^3 \text{ g}^{-1}$ and $K = 0.0204 \text{ mol g}^{-2}$ was obtained.

Received: April 8, 2004

Keywords: carbon suboxide · polymers · small-angle X-ray scattering · structure elucidation

- [1] O. Diels, B. Wolf, *Ber. Dtsch. Chem. Ges.* **1906**, 39, 689–697.
- [2] P. Jensen, J. W. C. Johns, *J. Mol. Spectrosc.* **1986**, 118, 248–266.
- [3] Y. Ohshima, S. Yamamoto, K. Satoshi, *Acta Chem. Scand. Ser. A* **1988**, 42, 307–317.
- [4] J. Koput, *Chem. Phys. Lett.* **2000**, 320, 237–244.
- [5] A. Ellern, Th. Drews, K. Seppelt, *Z. Anorg. Allg. Chem.* **2001**, 627, 73–76.
- [6] B. D. Kybett, G. K. Johnson, C. K. Barker, J. L. Margrave, *J. Phys. Chem.* **1965**, 69, 3603–3606.
- [7] A. W. Snow, H. Haubenstock, N.-L. Yang, *Macromolecules* **1978**, 11, 77–86.
- [8] R. N. Smith, D. A. Young, E. N. Smith, C. C. Carter, *Inorg. Chem.* **1963**, 2, 829–838.

- [9] N.-L. Yang, A. Snow, H. Haubenstock, F. Bramwell, *J. Polym. Sci. Polym. Chem. Ed.* **1978**, *16*, 1909–1927.
- [10] O. Diels, R. Beckmann, G. Tönnies, *Liebigs Ann. Chem.* **1924**, *439*, 76–96.
- [11] L. Schmidt, H.-P. Boehm, U. Hofmann, *Z. Anorg. Allg. Chem.* **1958**, *296*, 246–261.
- [12] A. R. Blake, W. T. Eeles, P. R. Jennings, *J. Chem. Soc. Faraday Trans.* **1964**, 691–699.
- [13] E. Ziegler, *Angew. Chem.* **1960**, *72*, 582.
- [14] T. Carofiglio, L. Pandolfo, G. Paiaro, *Eur. Polym. J.* **1986**, *22*, 491–497. The authors indicate their $(C_3O_2)_n$ polymers to be insoluble in DMF and DMSO. This is in contradiction to ours and all the other earlier publications.
- [15] J. S. Higgins, H. C. Benoit, *Polymers and Neutron Scattering*, Clarendon Press, Oxford, **1994**.
- [16] D. Pötschke, P. Hickl, M. Ballauff, P.-O. Astrand, J. S. Pedersen, *Macromol. Theory Simul.* **2000**, *9*, 345–353.
- [17] L. Birkofer, P. Sommer, *Chem. Ber.* **1976**, *109*, 1701–1707.
- [18] The use of an inert solvent for the polymerization reaction was found to be necessary. If the reaction was carried out in glass ampules in the absence of solvent, most of the time our experiments lead to violent, explosive bursts, which could be avoided by the dilution of C_3O_2 with approximately the same volume of CCl_4 . The analysis showed the carbon content to be 2% lower than the expected value, likewise a small hydrogen content of about 1% (elemental analysis calcd (%) for C_3O_2 : C 52.9, O 47.1; found: C 50.9 C, H 1.1). This result is in agreement with the observations by Diels^[19] and Schmidt et al.,^[11] according to which, only the highly purified, gaseous C_3O_2 results in the polymer with exact stoichiometry. The X-ray fluorescence analysis of our samples did not indicate the presence of chlorine from the adsorption of CCl_4 .
- [19] O. Diels, G. Meyerheim, *Chem. Ber.* **1907**, *40*, 355–363.

Cyclophanes

Synthesis of Beltenes by Reactions of 5,6,11,12-Tetradehydrodibenzo[*a,e*]cyclooctene with [CpCo(CO)₂] Derivatives**

Björn Hellbach, Frank Rominger, and Rolf Gleiter*

Paracyclophanes with [1.1] and [0.0] bridges are of considerable interest due to their high strain energy and because the π systems are strongly bent.^[1] Tricyclohexaene **1** can be looked at as either a superphane^[2] with ethylene as the π system or as a [0.0]-paracyclophane (Scheme 1). Hexaene **1**

can be expanded by incorporating the peripheral double bonds into four benzene rings, which leads to tetradehydrodianthracene **2**.^[3] Replacing the central double bond by a cyclic conjugated π system such as a metal-stabilized cyclobutadiene moiety or a benzene ring leads to **3** and the tetrabenzannelated 1,2,4,5-cyclophane (**4**), respectively. The synthesis and structural properties of **4** were reported recently (Scheme 1).^[4] Extending the building units to two *ortho*-substituted benzene rings and one conjugated system leads to conjugated beltenes^[1a,5] as indicated in **5** and **6**. In this communication we report the preparation of four beltenes related to **5** which are the first examples of genuine beltenes^[1a] consisting of annelated conjugated four- and eight-membered rings.

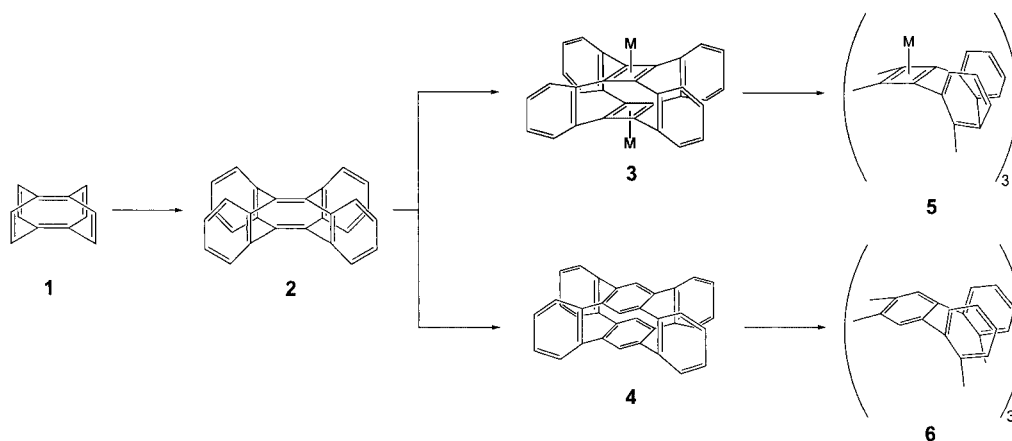
In our previous studies on nonconjugated beltlike macrocycles^[6] we noticed that highly strained cyclic diynes such as **7** react with [CpCo(C₂H₄)₂] preferentially under trimerization to yield **8** (Scheme 2) or the corresponding tetramer.^[6] When the reaction of **7** was carried out with [Cp*Co(C₂H₄)₂] (Cp* = pentamethylcyclopentadienyl) the dimerization to give the corresponding superphane was preferred.^[6] This result was ascribed to the larger size of the Cp* ligand relative to that of Cp. From these experiments we concluded that the reaction of the highly strained cyclodiyne (**9**)^[7] with [CpCoL₂] might lead to a tri- or tetramer. Indeed, the irradiation of **9** at 254 nm in the presence of [CpCo(CO)₂] in decalin for three days gave a yellow colored product in 14 % yield (Scheme 3).

The assignment of the structure to the trimer **10** is based on its spectroscopic data (see the Experimental Section), the molecular weight determined by mass spectrometry, and X-ray structural analysis^[8] (Figure 1). The NMR data (three singlets in the ¹H NMR spectrum, five in the ¹³C NMR spectrum) suggest *D*_{3h} symmetry for **10** in solution. This conclusion is supported by the X-ray diffraction data, which show that substituents at the cyclobutadiene ring are bent by about 11° out of the plane of this ring, away from the {CpCo} unit. The phenyl rings are twisted out of the cyclobutadiene plane around the interconnecting C–C bond by about 60°. This angle is larger than that reported for {CpCo}-stabilized tetraphenylcyclobutadiene, which varies from 32° to 42°.^[9] The strong twisting in **10** indicates a weak interaction between the cyclobutadiene rings through the benzene bridges. The distance of the centers of the cyclobutadiene rings to the center of **10** amounts to 2.1 Å. From this value an inner diameter of 4.2 Å was calculated. To probe possible interactions between the {CpCoCb} units in **10**, we have carried out studies by means of cyclovoltammetry, which indicated an irreversible oxidation.^[10]

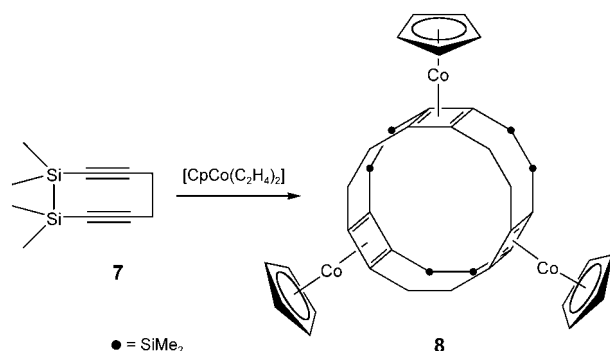
By using [Cp*Co(CO)₂] instead of [CpCo(CO)₂] we hoped to favor the dimerization of the cyclic diyne **9** resulting in superphane **12**. Still the main product remained the trimer **11** besides traces of the dimeric product **12** which have not yet been isolated. The yield of **11** (41 %) in this one-pot trimerization is quite remarkable. We were also able to isolate single crystals of **11** suitable for X-ray structure analysis. The data obtained for **11** resemble very much those of **10**^[11] except the cyclic voltammogram of **11** revealed a reversible redox process at 590 mV and 840 mV (vs. ferrocene/ferricinium in CH₂Cl₂). In further synthetic work, the

[*] Dipl.-Chem. B. Hellbach, Dr. F. Rominger, Prof. Dr. R. Gleiter
Organisch-Chemisches Institut
Universität Heidelberg
Im Neuenheimer Feld 270, 69120 Heidelberg (Germany)
Fax: (+49) 6221-544-205
E-mail: rolf.gleiter@urz.uni-heidelberg.de

[**] We thank the Deutsche Forschungsgemeinschaft, the Fonds der Chemischen Industrie, and Heidelberg University for financial support. B.H. thanks J. Nägele, M. Angelmahr, and A. Kroscky for preparative assistance and C. Bleiholder for calculations.



Scheme 1. Correlations between **1**, phanes **2–4**, and beltenes **5** and **6**.



Scheme 2. Preparation of the beltlike species **8**.

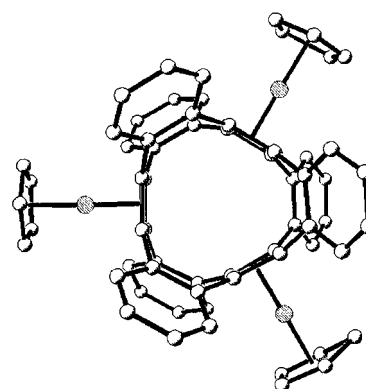
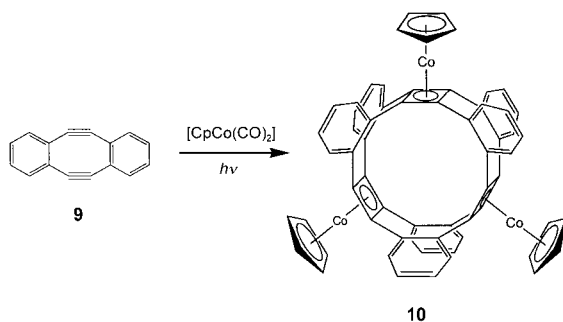


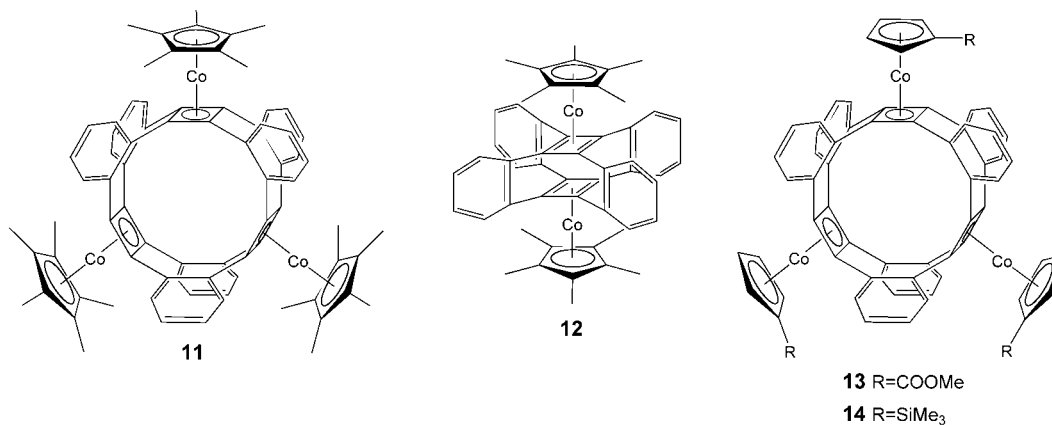
Figure 1. X-ray crystal structure of **10** (ball-and-stick model). Hydrogen atoms are omitted for the sake of clarity.

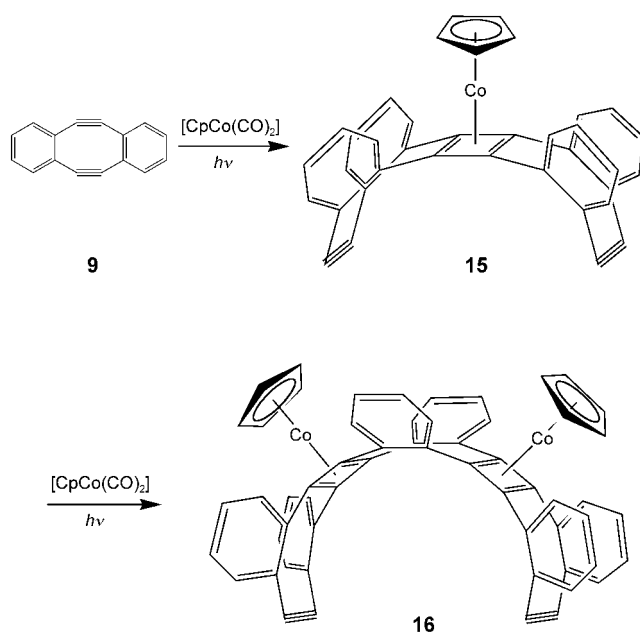


Scheme 3. Preparation of beltene **10**.

trimers **13** and **14** were prepared by using $[(\text{CpCOOMe})\text{Co}(\text{CO})_2]$ and $[(\text{CpSiMe}_3)\text{Co}(\text{CO})_2]$.

To elucidate the mechanism of the one-pot reaction shown in Scheme 3 we investigated the crude reaction products of the synthesis of **11**, **13**, and **14** by means of mass spectrometry. We found evidence for the presence of the Cp^* , CpCO_2Me , and CpSiMe_3 congeners of **15** and **16** based on HRMS data. This let us postulate that first a cobalt-supported dimerization of **9** to **15** takes place. In this intermediate the substituents at the (Scheme 4) cyclobutadiene ring should be bent away from





Scheme 4. Possible intermediates on the way from **9** to **10**.

the CpCo moiety. The reaction of **15** with a third equivalent of **9** in the presence of $\text{CpCo}(\text{CO})_2$ leads to the product **16** which will finally close the ring to **10**. Crucial for the ring closure is the adoption of a boat conformation of the heptacyclic ligand as sketched in **15**. Model calculations at the BP86/STO-3G level^[12,13] on **15** are fully in line with these assumptions. They predict a boat shaped conformation for the $\text{C}_{32}\text{H}_{16}$ ligand.

To sum up, we accomplished the synthesis of four examples of the first conjugated beltenes consisting of annelated rings. This was achieved by a one-pot reaction between the diyne **9** and the corresponding cobalt templates. In case of **10** and **11** we were able to obtain single crystals for X-ray structural analysis. For the mechanism we assume a stepwise annelation of {CpCo}-capped cyclobutadiene rings.

Experimental Section

The reactions were carried out under Ar in predried glassware using Schlenk techniques. Decalin was distilled over Na and was transferred under Ar. $[\text{CpCo}(\text{CO})_2]$ and its derivatives were prepared according to literature procedures.^[14–16]

General procedure: A 250-mL irradiation flask was charged with a solution of **9** (0.72 mmol) in decalin (225 mL). $[\text{CpCo}(\text{CO})_2]$ (1.60 mmol) was then added. The solution was magnetically stirred and cooled to 10°C. After three days of irradiation the solvent was evaporated in vacuo, and the residue was purified by column chromatography (dichloromethane).

10: Thin yellow crystals (plates) in 14% yield. ^1H NMR (500 MHz, CDCl_3): δ = 5.19 (s, 15H, H_{Cp}), 7.08 (t, $^3J(\text{H,H})$ = 4.41 Hz, 12H, H_{arom}), 7.69 ppm (t, $^3J(\text{H,H})$ = 4.23 Hz, 12H, H_{arom}); ^{13}C NMR (125 MHz, CDCl_3): δ = 82.37 (C_{Cb}), 82.58 (C_{Cp}), 126.88 (C_{arom}), 131.70 (C_{arom}), 133.93 ppm (C_{arom}); MS (FAB+): m/z = 973 [M^+ +H], 972 [M^+]; HRMS: m/z calcd for $\text{C}_{63}\text{H}_{39}\text{Co}_3$: 972.1047, found: 972.1094.

11: Yellow-orange crystals in 41% yield. ^1H NMR (500 MHz, CDCl_3): δ = 1.87 (s, 45H, H_{Cp}), 6.94 (m, 12H, H_{arom}), 7.37 ppm (t, 12H, H_{arom}); ^{13}C NMR (125 MHz, CDCl_3): δ = 11.21 (CH_3), 78.70

(C_{Cb}), 90.47 (C_{Cp}), 125.28 (C_{arom}), 129.93 (C_{arom}), 134.52 ppm (C_{arom}); MS (FAB+): m/z = 1183 [M^+ +H], 1182 [M^+]; HRMS: m/z calcd for $\text{C}_{78}\text{H}_{69}\text{Co}_3$: 1182.3395, found: 1182.3379.

13: Yellow solid in 12% yield. ^1H NMR (300 MHz, CDCl_3): δ = 3.48 (s, 9H, H_{methyl}), 5.10 (m, 6H, H_{Cp}), 5.73 (m, 6H, H_{Cp}), 7.91 (m, 12H, H_{arom}), 7.54 ppm (m, 12H, H_{arom}); ^{13}C NMR (75 MHz, CDCl_3): δ = 51.59 (CH_3), 83.65 (C_{Cb}), 83.83 (C_{Cp}), 86.92 (C_{Cp}), 86.94 (C_{Cp}), 127.34 (C_{arom}), 131.38 (C_{arom}), 132.58 (C_{arom}), 168.10 ppm (C_{CO}); MS (FAB+): m/z = 1147 [M^+ +H], 1146 [M^+]; HRMS: m/z calcd for $\text{C}_{69}\text{H}_{45}\text{O}_6\text{Co}_3$: 1146.1212, found: 1146.1274.

14: Yellow solid in 8% yield. ^1H NMR (300 MHz, CDCl_3): δ = -0.23 (s, 27H, H_{TMS}), 4.99 (m, 6H, H_{Cp}), 5.29 (m, 6H, H_{Cp}), 6.94 (m, 12H, H_{arom}), 7.56 ppm (m, 12H, H_{arom}); ^{13}C NMR (75 MHz, CDCl_3): δ = 0.68 (C_{TMS}), 77.36 (C_{Cb}), 82.10 (C_{Cp}), 86.96 (C_{Cp}), 87.18 (C_{Cp}), 126.55 (C_{arom}), 131.89 (C_{arom}), 133.76 ppm (C_{arom}); MS (FAB+): m/z = 1189 [M^+ +H], 1188 [M^+]; HRMS: m/z calcd for $\text{C}_{72}\text{H}_{63}\text{Si}_3\text{Co}_3$: 1188.3033 found: 1188.2197.

Received: May 25, 2004

Keywords: alkynes · beltenes · cobalt · cyclobutadienes · phanes

- [1] Reviews: a) R. Herges in *Modern Cyclophane Chemistry* (Eds.: R. Gleiter, H. Hopf), Wiley-VCH, Weinheim, **2004**, pp. 337–357; b) T. Tsuji in *Modern Cyclophane Chemistry* (Eds.: R. Gleiter, H. Hopf), Wiley-VCH, Weinheim, **2004**, pp. 81–104; c) H. Hopf in *Classics in Hydrocarbon Chemistry*, Wiley-VCH, Weinheim, **2000**.
- [2] Reviews: a) R. Gleiter, D. Kratz, *Acc. Chem. Res.* **1993**, *26*, 311–318; b) R. Gleiter, R. Roers in *Modern Cyclophane Chemistry* (Eds.: R. Gleiter, H. Hopf), Wiley-VCH, Weinheim, **2004**, pp. 159–188.
- [3] R. L. Viavattene, F. D. Greene, L. D. Cheung, R. Majeste, L. M. Trefonas, *J. Am. Chem. Soc.* **1974**, *96*, 4342–4343.
- [4] M. Brettreich, M. Bendikov, S. Chaffins, D. F. Perepichka, O. Dautel, H. Duong, R. Helgeson, F. Wudl, *Angew. Chem.* **2002**, *114*, 3840–3843; *Angew. Chem. Int. Ed.* **2002**, *41*, 3688–3691.
- [5] R. W. Alder, R. B. Sessions, *J. Chem. Soc. Perkin Trans. 2* **1985**, 1849–1854.
- [6] G. Haberhauer, F. Rominger, R. Gleiter, *Angew. Chem.* **1998**, *110*, 3632–3534; *Angew. Chem. Int. Ed.* **1998**, *37*, 3376–3377.
- [7] A. Orita, D. Hasegawa, T. Nakano, J. Otera, *Chem. Eur. J.* **2002**, *8*, 2000–2004.
- [8] Crystal structure of **10**: yellow crystal (plate), dimensions $0.24 \times 0.13 \times 0.03 \text{ mm}^3$, crystal system orthorhombic, space group $Pca2_1$, $Z = 16$, $a = 19.213(2) \text{ \AA}$, $b = 41.880(5) \text{ \AA}$, $c = 24.773(3) \text{ \AA}$, $V = 19933(4) \text{ \AA}^3$, $\rho = 1.535 \text{ g cm}^{-3}$; $T = 100(2) \text{ K}$, $\theta_{\text{max}} = 20.98^\circ$, radiation $\text{MoK}\alpha$, $\lambda = 0.71073 \text{ \AA}$, $0.3^\circ \Omega$ -scans with CCD area detector, covering a whole sphere in reciprocal space; 103 585 reflections measured, 21 169 unique ($R(\text{int}) = 0.2237$), 12 575 observed ($I > 2\sigma(I)$); intensities were corrected for Lorentz and polarization effects; an empirical absorption correction was applied using SADABS^[17] based on the Laue symmetry of the reciprocal space, $\mu = 1.27 \text{ mm}^{-1}$, $T_{\text{min}} = 0.75$, $T_{\text{max}} = 0.96$; structure solved by direct methods and refined against F^2 with a full-matrix least-squares algorithm using the SHELXTL-PLUS (5.10) software package;^[18] 1244 parameters refined, hydrogen atoms were treated using appropriate riding models, Flack absolute structure parameter 0.45(4), goodness of fit 1.01 for observed reflections, final residual values $R1(F) = 0.115$, $wR(F^2) = 0.268$ for observed reflections, residual electron density -1.38 to 2.56 e \AA^{-3} (very close to Co centers, thus with no chemical relevance).
- [9] M. D. Rausch, G. F. Westover, E. Mintz, G. M. Reisner, I. Bernal, A. Clearfield, J. M. Troup, *Inorg. Chem.* **1979**, *18*, 2605–2615.

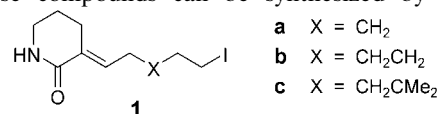
- [10] The CV measurements were carried out in CH_2Cl_2 using a 0.1 M solution of $n\text{Bu}_4\text{PF}_6$ in CH_2Cl_2 as electrolyte. The working electrode was a Metrohm disc electrode (glassy carbon, ~ 0.3 cm radius). The Ag/AgCl reference electrode was separated from the solution by a fine grid and a Luggin capillary. The measurements were recorded at a scan rate varying from 50 to 900 mVs^{-1} at room temperature using a concentration of 0.077 mmol L^{-1} in CH_2Cl_2 . The potential of ferrocene/ferricinium was recorded at 500 ± 10 mV.
- [11] Crystal structure of **11**: yellow crystal (polyhedron), dimensions $0.36 \times 0.18 \times 0.12$ mm^3 , crystal system monoclinic, space group $C2/m$, $Z=4$, $a=18.9214(2)$ Å, $b=21.0375(2)$ Å, $c=16.0400(1)$ Å, $V=6330.45(10)$ Å³, $\rho=1.420$ g cm^{-3} , $T=200(2)$ K, $\theta_{\text{max}}=25.35^\circ$, radiation $\text{Mo K}\alpha$, $\lambda=0.71073$ Å, 0.3° Ω -scans with CCD area detector, covering a whole sphere in reciprocal space; 28319 reflections measured, 5974 unique ($R(\text{int})=0.0400$), 4658 observed ($I>2\sigma(I)$); intensities were corrected for Lorentz and polarization effects; an empirical absorption correction was applied using SADABS^[17] based on the Laue symmetry of the reciprocal space, $\mu=0.99$ mm^{-1} , $T_{\text{min}}=0.72$, $T_{\text{max}}=0.89$; structure solved by direct methods and refined against F^2 with a full-matrix least-squares algorithm using the SHELXTL-PLUS (5.10) software package;^[18] 413 parameters refined, hydrogen atoms were treated using appropriate riding models, goodness of fit 1.03 for observed reflections, final residual values $R1(F)=0.038$, $wR(F^2)=0.096$ for observed reflections, residual electron density -0.72 to 0.41 e Å^{-3} . CCDC 246269 (**10**) and 246377 (**11**) contains the supplementary crystallographic data for this paper. These data can be obtained free of charge via www.ccdc.cam.ac.uk/conts/retrieving.html (or from the Cambridge Crystallographic Data Centre, 12, Union Road, Cambridge CB21EZ, UK; fax: (+44) 1223-336-033; or deposit@ccdc.cam.ac.uk).
- [12] A. D. Becke, *Phys. Rev. A* **1988**, 38, 3098–3100; J. P. Perdew, *Phys. Rev. B* **1986**, 38, 8822–8824.
- [13] W. J. Hehre, R. F. Stewart, J. A. Pople, *J. Chem. Phys.* **1969**, 51, 2657–2664; J. B. Collins, P. v. R. Schleyer, J. S. Binkley, J. A. Pople, *J. Chem. Phys.* **1976**, 64, 5142–5151.
- [14] M. D. Rausch, R. A. Genetti, *J. Org. Chem.* **1970**, 35, 3888–3897.
- [15] T. Dooley, G. Fairhurst, C. D. Chalk, K. Tabatabaian, C. With, *Transition Met. Chem.* **1978**, 3, 299.
- [16] W. P. Hart, D. W. Macomber, M. D. Rausch, *J. Am. Chem. Soc.* **1980**, 102, 1196–1198.
- [17] G. M. Sheldrick, Bruker Analytical X-ray-Division, Madison, WI, **2001**.
- [18] G. M. Sheldrick, Bruker Analytical X-ray-Division, Madison, WI, **1997**.

Hydrogen Bond Mediated Enantioselectivity of Radical Reactions**

Tobias Aechtner, Martina Dressel, and Thorsten Bach*

The renaissance in radical chemistry during the last years and decades can be explained in large part by the improved prediction and control of the important parameters chemo-, regio-, and stereoselectivity.^[1] Recent investigations show that radical reactions can be carried out enantioselectively without an auxiliary being attached covalently to the substrate.^[2] Two different strategies have been reported. On the one hand, it is possible to differentiate the enantiotopic faces of a prochiral radical with chiral reagents (reagent control). For this purpose chiral hydrogen-atom donors have been used most often.^[3] On the other hand, face differentiation is possible by a Lewis acid, which forms a chelate complex with the substrate, and which is in turn coordinated to chiral ligands.^[4] Alternative chiral templates that are based upon noncovalent interactions and are similarly effective have, to the best of our knowledge, not yet been established. In a recent study we were able to show that high enantioselectivity (up to 84% *ee*) in radical reactions can be achieved with the help of a hydrogen-bonding chiral template. Our preliminary results are presented in this communication.

We investigated the enantioselectivity of the reductive radical cyclization of 3-(ω -iodoalkylidene)piperidin-2-ones (**1**). These compounds can be synthesized by the aldol



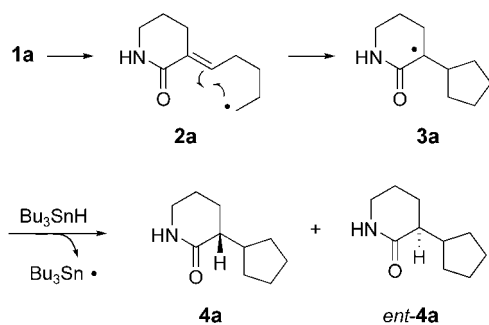
condensation of *N*-*tert*-butoxycarbonyl(Boc)piperidin-2-one with ω -*tert*-butyldimethylsilyl(TBDMS)oxaldehydes followed by conversion of the protected hydroxy group into an iodo group (1. tetrabutylammonium fluoride (TBAF), THF; 2. PPh₃, imidazole, I₂).^[5]

In the presence of an initiator and Bu₃SnH the alkenyl iodides reacted in a 5- or 6-*exo*-trig-cyclization^[1,6] (e.g. **2a** → **3a**, Scheme 1). The intermediate radicals **3** exhibit a prostereogenic center in α -position to the carbonyl function which is transformed by an intermolecular reaction with Bu₃SnH to a stereogenic saturated carbon atom. In the case of the alkenyl iodide **1a** both enantiomeric cyclization products **4a** and *ent*-**4a** are formed during the reaction.

The reaction proceeded smoothly for the three substrates investigated. The appropriate cyclization products were

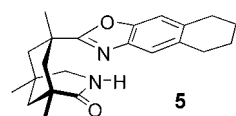
[*] Dr. T. Aechtner, Dipl.-Chem. M. Dressel, Prof. Dr. T. Bach
Lehrstuhl für Organische Chemie I
Technische Universität München
Lichtenbergstrasse 4, 85747 Garching (Germany)
Fax: (+49) 89-28913315
E-mail: thorsten.bach@ch.tum.de

[**] This project was supported by the Deutsche Forschungsgemeinschaft (Ba 1372-4/4) and by the Fonds der Chemischen Industrie.



Scheme 1. Mechanism of the radical cyclization **1a**→**4a/ent-4a**. The hydrogen transfer is the enantioselectivity-determining step.

obtained in good yields (77–83 %) albeit in racemic form. The two enantiotopic faces of the radical center in α -position to the carbonyl function become diastereotopic when linked to a chiral environment. We hoped to achieve such face differentiation by using the chiral complexing reagent **5**,^[7,8] which coordinates to lactams through hydrogen bonds.^[9] For that purpose the radical cyclization of **1a** to give **4a** and **ent-4a** was carried out in a series of experiments in the presence of



compound **5**. BEt_3 was used as the initiator as it allowed the reactions to be carried out at low temperature.

The reaction was indeed enantioselective. The enantiomeric excess of product **4a** in the radical cyclization^[10] of iodide **1a** was dependent on three parameters (Table 1). 1) The temperature should be as low as possible since this leads to a remarkable increase of selectivity (e.g. entries 5 and 9). 2) The amount of initiator BEt_3 must be held to a minimum to achieve optimum enantioselectivity (entries 2 and 3, entries 4–6). 3) The amount of complexing reagent used should preferably be high (entries 7 and 9). These observations are reasonable considering the fact that the enantiomeric excess directly reflects the ratio of bound to unbound substrate.^[9a,d] The association by means of hydrogen

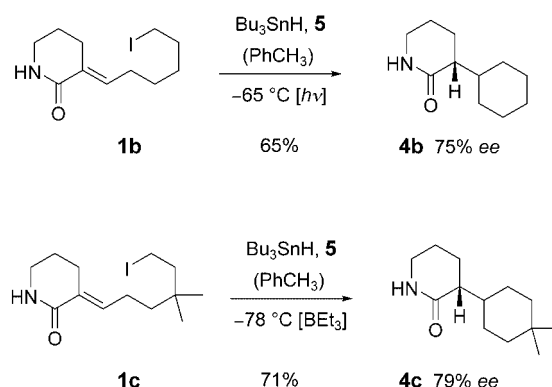
Table 1: Enantioselective radical reaction (cf. Scheme 1) of substrate **1a** to give the products **4a** and **ent-4a** using the chiral complexing reagent **5**.^[10]

Entry	T [°C] ^[a]	Equiv. ^[b]	BEt_3 [mol %]	Yield [%]	ee [%] ^[c]
1	25	—	50	83	—
2	25	2.5	20	84	38
3	25	2.5	10	72	44
4	−10	1.0	50	78	20
5	−10	2.5	20	82	40
6	−10	2.5	10	79	55
7	−78	1.0	20	91	40
8	−78	2.5	50	84	41
9	−78	2.5	20	81	84

[a] Reaction temperature. The reaction was carried out at the cited temperature in toluene with Bu_3SnH (2 equiv). The concentration of substrate was $5 \times 10^{-2} \text{ mol L}^{-1}$. The initiation occurred by addition of the cited amount of BEt_3 .^[10] [b] Equivalents of chiral complexing reagent **5**. The reagent was completely (>90%) recovered. [c] The ee values were calculated from the enantiomeric ratios determined by HPLC analysis (Daicel ChiralCel OD).

bonding is ideal if the reaction is run in nonpolar solvents and at low temperatures. Unfortunately, the reaction did not take place at -78°C with only 10 mol % BEt_3 . Despite good reproducibility the results are not completely coherent. Thus the minimal increase in selectivity upon decreasing the temperature is hard to explain (entries 2 and 5). The interactions of BEt_3 and its decomposition products with the substrate, complexing reagent, and product are apparently complex and must be investigated in further experiments. Selectivity in the reaction **1a**→**4a** did not improve upon photochemical initiation (Original Hanau TQ 150, duran filter, -65°C).

Compounds **1b** and **1c** were also reductively cyclized under optimized conditions (Scheme 2). For the reaction of



Scheme 2. Enantioselective reductive cyclization of substrates **1b** and **1c**.

1b we observed an insignificant increase of enantioselectivity upon photochemical initiation ($c = 5 \times 10^{-2} \text{ mol L}^{-1}$, light source: Original Hanau TQ 150, duran filter). In the reaction of **1c** under the same conditions^[10] as those used for the reaction of **1a**→**4a**, initiation catalyzed by BEt_3 was preferred. In every case we obtained the dextrorotatory 3-cycloalkylpiperin-2-ones as products. The ee values were calculated from HPLC analysis (for **4b**) or chiral shift experiments (for **4c**).^[11]

The comparison with literature data shows that dextrorotatory α -monoalkyl-substituted five to seven membered ring lactams with the priority order $\text{CONH} > \text{alkyl} > \text{CH}_2 > \text{H}$ are *R* configured.^[12] This configuration assignment corroborates the hypothesis that the hydrogen transfer from Bu_3SnH to radical **3**, which is linked to template **5** by means of hydrogen bonding, occurs from the *Si* side. The *Re* side is shielded by the tetrahydronaphthalene residue. This is illustrated in Figure 1 for the enantioselective hydrogen transfer from Bu_3SnH to the prochiral radical **3a**.

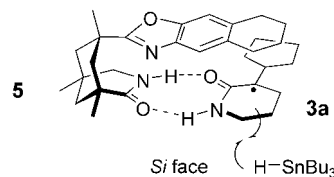


Figure 1. Model to explain the face differentiation in the intermediate radicals **3**.

In ongoing studies we are trying to apply the concept of an enantioselective radical reaction to other model systems and to use it in synthesis.

Received: July 7, 2004

Keywords: asymmetric synthesis · cyclization · enantioselectivity · hydrogen bonds · radical reactions

- [1] General reviews: a) *Radicals in Organic Synthesis* (Eds.: P. Renaud, M. P. Sibi), Wiley-VCH, Weinheim, **2001**; b) T. Linker, M. Schmittel, *Radikale und Radikationen in der Organischen Synthese*, Wiley-VCH, Weinheim, **1998**; c) D. P. Curran, N. A. Porter, B. Giese, *Stereochemistry of Radical Reactions*, VCH, Weinheim, **1996**.
- [2] Reviews on enantioselective radical reactions: a) M. P. Sibi, S. Manyer, J. Zimmerman, *Chem. Rev.* **2003**, *103*, 3263–3295; b) G. Bar, A. Parsons, *Chem. Soc. Rev.* **2003**, *32*, 251–263; c) M. Sibi, N. A. Porter, *Acc. Chem. Res.* **1999**, *32*, 163–171; d) P. Renaud, M. Gerster, *Angew. Chem.* **1998**, *110*, 2704–2722; *Angew. Chem. Int. Ed.* **1998**, *37*, 2562–2579.
- [3] a) D. Nanni, D. P. Curran, *Tetrahedron: Asymmetry* **1996**, *7*, 2417–2422; b) M. Blumenstein, K. Schwarzkopf, J. O. Metzger, *Angew. Chem.* **1997**, *109*, 245–247; *Angew. Chem. Int. Ed. Engl.* **1997**, *36*, 235–236; c) D. Dakternieks, K. Dunn, V. T. Perchyonok, C. H. Schiesser, *Chem. Commun.* **1999**, 1665–1666; d) D. Dakternieks, V. T. Perchyonok, C. H. Schiesser, *Tetrahedron: Asymmetry* **2003**, *14*, 3057–3068; e) M. Blumenstein, M. Lemmler, A. Hayen, J. O. Metzger, *Tetrahedron: Asymmetry* **2003**, *14*, 3069–3077, and references therein.
- [4] First original reports: a) M. Murakata, H. Tsutsui, O. Hoshino, *J. Chem. Soc. Chem. Commun.* **1995**, 481–482; b) H. Urabe, K. Yamashita, K. Suzuki, K. Kobayashi, F. Sato, *J. Org. Chem.* **1995**, *60*, 3576–3577; c) J. H. Wu, R. Radinov, N. A. Porter, *J. Am. Chem. Soc.* **1995**, *117*, 11029–11030; d) M. Nishida, H. Hayashi, A. Nishida, N. Kawahara, *Chem. Commun.* **1996**, 579–580; e) M. P. Sibi, J. Ji, J. H. Wu, S. Gürtler, N. A. Porter, *J. Am. Chem. Soc.* **1996**, *118*, 9200–9201; f) A.-R. Fhal, P. Renaud, *Tetrahedron Lett.* **1997**, *38*, 2661–2664.
- [5] a) J. L. García Ruano, M. M. Cifuentes, A. Lorente, J. H. Rodríguez Ramos, *Tetrahedron: Asymmetry* **1999**, *10*, 4607–4618; b) A. P. Kozikowski, P. W. Shum, A. Basu, J. S. Lazo, *J. Med. Chem.* **1991**, *34*, 2420–2430.
- [6] a) A. L. J. Beckwith, *Tetrahedron* **1981**, *37*, 3073–3100; b) A. L. J. Beckwith, C. H. Schiesser, *Tetrahedron* **1985**, *41*, 3925–3941; c) B. Giese, B. Kopping, T. Göbel, J. Dickhaut, G. Thoma, K. J. Kulicke, F. Trach, *Org. React.* **1996**, *48*, 301–856.
- [7] T. Bach, H. Bergmann, B. Grosch, K. Harms, E. Herdtweck, *Synthesis* **2001**, 1395–1405.
- [8] For the use of similar amides as chiral auxiliaries in radical reactions, see J. G. Stack, D. P. Curran, S. V. Geib, J. Rebek, Jr., P. Ballester, *J. Am. Chem. Soc.* **1992**, *114*, 7007–7018.
- [9] Examples: a) T. Bach, H. Bergmann, K. Harms, *Angew. Chem.* **2000**, *112*, 2391–2393; *Angew. Chem. Int. Ed.* **2000**, *39*, 2302–2304; b) T. Bach, H. Bergmann, B. Grosch, K. Harms, *J. Am. Chem. Soc.* **2002**, *124*, 7982–7990; c) T. Bach, T. Aechtner, B. Neumüller, *Chem. Eur. J.* **2002**, *8*, 2464–2475; d) T. Bach, B. Grosch, T. Strassner, E. Herdtweck, *J. Org. Chem.* **2003**, *68*, 1107–1116; e) B. Grosch, C. N. Orlebar, E. Herdtweck, M. Kaneda, T. Wada, Y. Inoue, T. Bach, *Chem. Eur. J.* **2004**, *10*, 2179–2189.
- [10] Representative experimental procedure: Compound **1a** (15.0 mg, 0.05 mmol) and the chiral complexing reagent **5** (44.1 mg, 0.125 mmol) were dissolved in toluene (1 mL, Merck Uvasol). The solution was cooled to -78°C , and Bu_3SnH (26.9 μL , 29.6 mg, 0.10 mmol) and BEt_3 (10.0 μL , 0.01 mmol, 1 M in hexane) were added. When the reaction was complete (3 h) silica gel was added, the solvent removed on a rotatory evaporator, and the crude product purified by flash chromatography (silica, pentane/ethyl acetate 50:50 \rightarrow ethyl acetate). The cyclization product **4a** was obtained as a colorless solid (6.8 mg, 81 %, 84 % ee). $R_f = 0.16$ (ethyl acetate); $[\alpha]_D^{20} = +45.8$ ($c = 0.6$ in MeOH); IR (KBr): $\tilde{\nu} = 3190\text{ cm}^{-1}$ (m, NH), 1654 (vs, C=O); $^1\text{H NMR}$ (360 MHz, CDCl_3): $\delta = 1.08$ – 1.22 (m, 1H), 1.23– 1.38 (m, 1H), 1.42– 1.90 (m, 10H), 2.22– 2.43 (m, 2H, CH-CH), 3.16– 3.30 (m, 2H, CH_2NH), 6.33 (s, 1H, NH); $^{13}\text{C NMR}$ (90 MHz, CDCl_3): $\delta = 21.3$ (CH_2), 23.3 (CH_2), 25.1 (CH_2), 25.4 (CH_2), 28.7 (CH_2), 30.3 (CH_2), 40.7 (CH), 42.4 (CH_2NH), 44.3 (CH), 175.1 (CO); MS (EI, 70 eV): m/z (%): 167 (6) [M^+], 99 (100) [$M^+ - \text{C}_5\text{H}_8$]; Elemental analysis for $\text{C}_{10}\text{H}_{17}\text{NO}$ (167.248) (%): calcd. C 71.81, H 10.25; found C 71.91, H 10.25.
- [11] H. Bergmann, B. Grosch, S. Sitterberg, T. Bach, *J. Org. Chem.* **2004**, *69*, 970–973.
- [12] a) D. Enders, R. Groebner, G. Raabe, J. Runsink, *Synthesis* **1996**, 941–948; b) M. Brenner, D. Seebach, *Helv. Chim. Acta* **1999**, *82*, 2365–2379; c) Y.-G. Suh, S.-A. Kim, J.-K. Jung, D.-Y. Shin, K.-H. Min, B.-A. Koo, H.-S. Kim, *Angew. Chem.* **1999**, *111*, 3753–3755; *Angew. Chem. Int. Ed.* **1999**, *38*, 3545–3547.

Electron Transfer

Synthesis and Photophysics of a Neutral Organic Mixed-Valence Compound**

Alexander Heckmann, Christoph Lambert,
Mark Goebel, and Rüdiger Wortmann*

*Dedicated to Prof. Jörg Daub
on the occasion of his 65th birthday*

Purely organic mixed-valence (MV) compounds are of great interest for the investigation of intramolecular electron-transfer (ET) processes.^[1–5] Usually these MV compounds are radical ions consisting of two redox centers connected by a saturated or unsaturated bridge. In this communication we present the synthesis and photophysical properties of the first organic MV compound that is neutral rather than charged.

[*] Dipl.-Chem. A. Heckmann, Prof. Dr. C. Lambert
Bayerische Julius-Maximilians-Universität Würzburg
Institut für Organische Chemie
Am Hubland, 97074 Würzburg (Germany)
Fax: (+49) 931-888-4606
E-mail: lambert@chemie.uni-wuerzburg.de
Dipl.-Chem. M. Goebel, Prof. Dr. R. Wortmann
Technische Universität Kaiserslautern
Physikalische Chemie
Erwin-Schrödinger-Strasse, 67663 Kaiserslautern (Germany)

[**] This work was supported by the Deutsche Forschungsgemeinschaft (LA 991/7-3), the Graduiertenkolleg 690 "Electron Density: Theory and Experiment", and Degussa AG.

MV compounds are characterized by a so-called inter-valence charge-transfer (IV-CT) band (usually in the near-IR (NIR) region) which is associated with the optically induced charge transfer from one redox center to the other. The electronic coupling V between the two diabatic (formally noninteracting) states (charge localized on the one and on the other redox center, respectively) is a measure for the electronic communication between these states and can be calculated from the IV-CT band by Equation (1), where μ_{eg}

$$V = \frac{\mu_{eg}}{\Delta\mu_{12}} \tilde{\nu}_{\max} \quad (1)$$

and $\tilde{\nu}_{\max}$ are the transition moment and the energy of the IV-CT band, respectively, and $\Delta\mu_{12}$ is the diabatic dipole moment difference between the two diabatic states mentioned above. The diabatic quantity $\Delta\mu_{12}$ can either be estimated by the effective electron-transfer distance $e \times r$ or can be traced back to purely adiabatic (measurable) quantities by Equation (2)

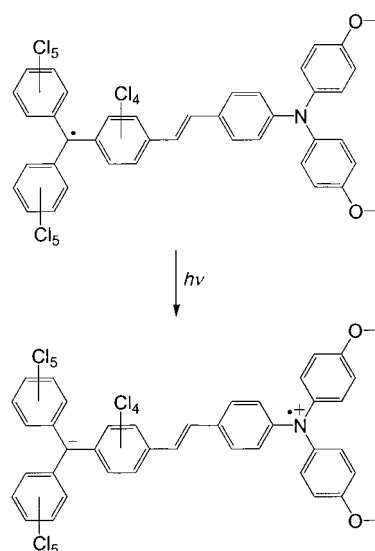
$$er = \Delta\mu_{12} \sqrt{\Delta\mu_{eg}^2 + 4\mu_{eg}^2} \quad (2)$$

(generalized Mulliken–Hush theory, GMH),^[6–8] where $\Delta\mu_{eg}$ is the difference between the adiabatic dipole moments of the ground and excited IV-CT state. However, while both the estimate of $e \times r$ by, for example, the distance of the redox centers r and the determination of $\Delta\mu_{eg}$ by quantum-chemical methods involves major inaccuracies,^[9] the experimental determination of $\Delta\mu_{eg}$ can be achieved by means of electro-optical absorption measurements (EOAM).^[10] Unfortunately, this method is complicated for charged species because of ion migration in the electric field, which can be circumvented by using glass matrices.^[11–13] Further disadvantages of charged MV compounds are the low solubility especially in nonpolar solvents^[14–16] and ion-pair effects.^[17,18] These disadvantages can be avoided by using neutral MV compounds, a class of compounds that has not been described and studied so far to the best of our knowledge,^[19] which is therefore the subject of this communication.

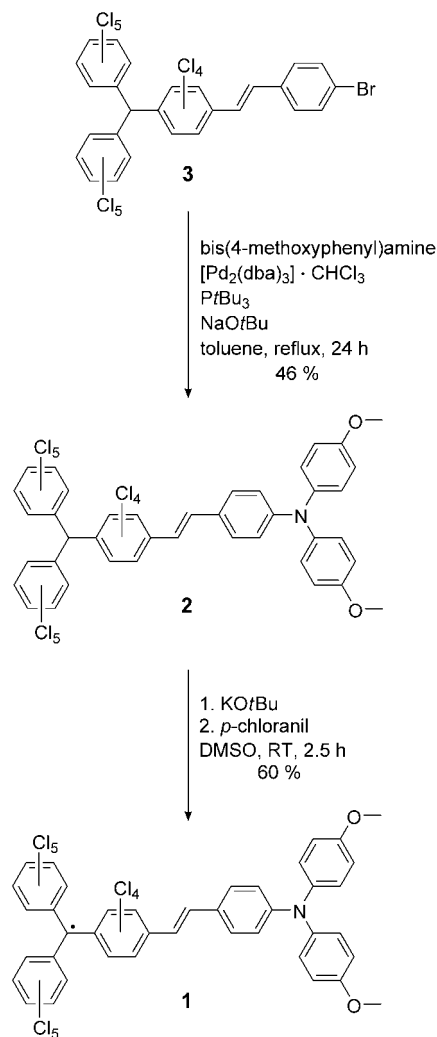
While MV radical cations based on two triarylamine centers^[20–22] and MV radical anions based on perchlorinated triarylmethyl radicals^[23,24] are well known, it was obvious to link the two redox centers by, for example, an ethylene bridge to create a neutral MV system. In the neutral, purely organic MV compound **1** a perchlorinated triarylmethyl radical center acts as the acceptor and a triarylamine redox center as the donor (Scheme 1).

The synthesis of compound **1** is outlined in Scheme 2. Compound **2** was prepared by a Pd-catalyzed Buchwald–Hartwig amination of the stilbene derivative **3**^[24] and bis(4-methoxyphenyl)amine in 46% yield. Because of the low acidity of the α -H atom of **2**, KOtBu in DMSO was required to form the corresponding carbanion salt, which was subsequently oxidized with *p*-chloranil to obtain the air-stable radical **1** in 60% yield.

The cyclic voltammogram of **1** in dichloromethane/tetrabutylammonium hexafluorophosphate (TBAH) solution shows one reversible oxidation process at $E_{1/2} = +240$ mV versus ferrocene (Fc), which is assigned to the oxidation of the



Scheme 1. Optically induced ET process in **1**.



Scheme 2. Synthesis of the neutral radical **1**.

triarylamine center to the radical cation (Figure 1).^[25] Furthermore, a reversible reduction wave at $E_{1/2} = -670$ mV can be observed, which corresponds to the reduction of the carbon radical center to the carbanion.^[24] The large splitting of the two redox processes reflects the pronounced non-degeneracy of the two redox centers in contrast to the degenerate bis(triarylamine) and bis(perchlorotriphenylmethyl) MV compounds mentioned above.

The excellent solubility of neutral **1** gave us the unique chance to investigate the UV/Vis/NIR absorption spectra in thirteen different solvents ranging from totally apolar (*n*-hexane) to strongly polar (acetonitrile). The electronic absorption spectrum of **1** (Figure 2) shows an intense band at $25\,500\text{ cm}^{-1}$, which is typical of perchlorinated benzene derivatives^[26–28] and a weaker band at $24\,900\text{ cm}^{-1}$, which is assigned to methoxy-substituted triarylamine systems.^[29] Furthermore, two weak absorption bands at $19\,000\text{ cm}^{-1}$ and $17\,500\text{ cm}^{-1}$ can be observed which are characteristic for perchlorinated triaryl-methyl radical systems.^[26] Even more interesting is the observation of a weak absorption band in the NIR region at about $12\,000\text{ cm}^{-1}$ which can be assigned to an IV-CT associated with an intramolecular electron transfer from the triarylamine to the radical unit (Scheme 1).

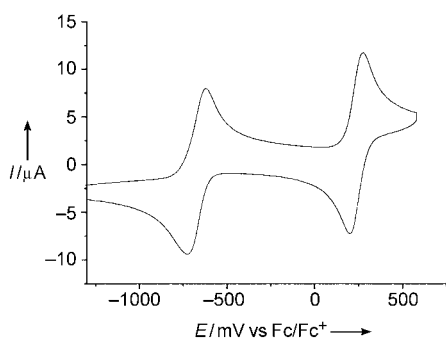


Figure 1. Cyclic voltammogram of radical **1** in $\text{CH}_2\text{Cl}_2/0.1\text{ M TBAH}$. Scan rate $\nu = 250\text{ mVs}^{-1}$.

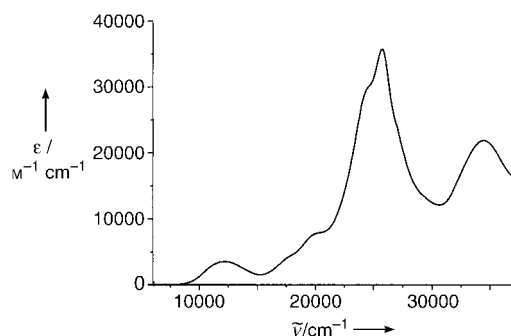


Figure 2. UV/Vis/NIR absorption spectrum of **1** in CH_2Cl_2 .

To our surprise the absorption maximum $\tilde{\nu}_{\text{max}}$ of the IV-CT band of **1** shows a weak and superficially nonsystematical dependence on the solvent polarity (Table 1). The extinction coefficient of the IV-CT band is larger and the band width at half-height is smaller in nonpolar solvents such as *n*-hexane than in polar solvents like acetonitrile (Figure 3). To explain this unexpected behavior we used the Jortner model^[30–32] to simulate the IV-CT band in each solvent. In this calculation an average molecular vibration is treated quantum-mechan-

Table 1: Absorption maxima, extinction coefficients, and other parameters^[a] for **1** in solvents of different polarity.

Solvent	$\tilde{\nu}_{\text{max}} [\text{cm}^{-1}]$	$\epsilon [\text{M}^{-1} \text{cm}^{-1}]$	$\Delta G^{00} [\text{cm}^{-1}]^{\text{[b,c]}}$	$\lambda_0 [\text{cm}^{-1}]^{\text{[b,d]}}$	$\lambda_v [\text{cm}^{-1}]^{\text{[b,e]}}$	$\tilde{\nu}_v [\text{cm}^{-1}]^{\text{[b,f]}}$
<i>n</i> -hexane	12 300	4700	10 400	950	1500	1100
cyclohexane	11 900	4600	10 300	1000	1350	1150
1,4-dioxane	12 200	3900	9450	1850	1650	1400
dibutyl ether	11 900	4200	9400	1700	1500	1400
diethyl ether	11 900	4100	9000	2050	1650	1450
MTBE ^[g]	12 000	3700	8900	2200	1600	1450
ethyl acetate	12 000	3900	8250	2900	1600	1650
THF	11 600	3500	7900	3200	1400	1700
dichloromethane	12 200	3600	8350	3000	1750	1550
benzonitrile	11 700	3600	7500	3550	1400	1800
2-propanol	11 800	3900	8300	2750	1500	1650
acetone	12 100	3600	7450	4000	1550	1850
acetonitrile	12 600	3400	7500	4350	1600	1850

[a] Parameters obtained from the least squares fit of the IV-CT bands. [b] All values were determined with a maximum error of $\pm 50\text{ cm}^{-1}$ except for the λ_0 value of 2-propanol ($\pm 100\text{ cm}^{-1}$). [c] Difference in the free energy between the diabatic ground and excited states. [d] Outer-sphere reorganization energy. [e] Inner-sphere reorganization energy. [f] Mean molecular vibration mode. [g] Methyl *tert*-butyl ether.

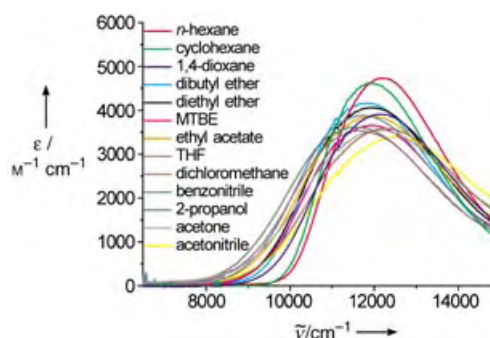


Figure 3. IV-CT bands of **1** measured in solvents of different polarity.

ically, and a classical solvent coordinate is used.^[5] An excellent least squares fit of the IV-CT band of **1** in each solvent was achieved by varying the parameters for the inner-sphere reorganization energy λ_v and the outer-sphere reorganization energy λ_0 as well as the parameters for the difference of the free energy between the diabatic ground and excited state ΔG^{00} and for the average molecular vibrational mode $\tilde{\nu}_v$ in Equation (3). In Figure 4 the fits of

$$\epsilon = \frac{8 N \pi^3}{3000 h \ln 10} n \tilde{\nu}_v^2 \sum_{j=0}^{\infty} \frac{e^{-S} S^j}{j!} \sqrt{\frac{1}{4 \pi \lambda_0 R T}} \exp \left[-\frac{(j \tilde{\nu}_v + \lambda_0 - \tilde{\nu} + \Delta G^{00})^2}{4 \pi \lambda_0 R T} \right] \quad (3)$$

with the Huang-Rhys factor $S = \frac{\lambda_v}{\tilde{\nu}_v}$

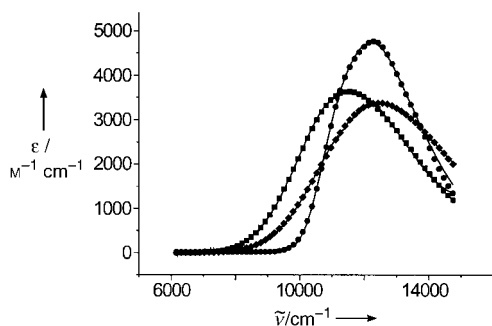


Figure 4. Least squares fit of the IV-CT bands of **1** (experimental data —) in *n*-hexane (●), benzonitrile (■), and acetonitrile (◆) according to the method of Jortner.

the IV-CT band in *n*-hexane, benzonitrile and acetonitrile are shown. The results of all fits are also summarized in Table 1. From these data it becomes apparent that the surprisingly low total reorganization energy is dominated by the solvent part λ_o in all solvents with exception of the hexanes.^[33]

A plot of each parameter against a term describing the solvent polarity $(D-1)/(2D+1)-0.5(n^2-1)/(2n^2+1)$, where D is the permittivity and n is the refractive index, reveals linear correlations for both ΔG^{00} and λ_o (Figure 5a and b).^[34] As initially expected from Marcus' theory,^[35] an increase of the solvent reorganization energy λ_o with solvent polarity is found. The solvent reorganization energy approaches zero for totally apolar environments. Concomitantly, ΔG^{00} decreases due to the fact that the excited state has zwitterionic character while the ground state is apolar (see below). Therefore, the usually observed negative solvatochromism of degenerate ionic compounds is covered (compensated for) by the positive solvatochromism of ΔG^{00} which leads to the weak solvent dependence of the IV-CT band described above. The analysis yields directly ΔG^{00} in CH_2Cl_2 (8350 cm^{-1}) which is in reasonable agreement with the redox potential difference in $\text{CH}_2\text{Cl}_2/0.1\text{M TBAH}$ ($\Delta E = 910\text{ mV} \cong 7340\text{ cm}^{-1}$). As expected, the inner-sphere reorganization energy λ_v is independent on the solvent polarity (Figure 5c). We also recorded a weak but systematic solvent dependence of $\tilde{\nu}_v$ (Figure 5d), which could be due to the varying importance of different molecular modes contributing to the averaged mode $\tilde{\nu}_v$. On the other hand, this shift may also compensate for inaccuracies of the theory in general.

Furthermore, the adiabatic dipole moment of the ground state ($\mu_g = 13 \pm 2 \times 10^{-30}\text{ Cm} = 3.9 \pm 0.6\text{ D}$) and the difference between the adiabatic ground and excited state ($\Delta\mu_{eg} = 64 \pm 4 \times 10^{-30}\text{ Cm} = 19 \pm 1\text{ D}$), and the transition moment ($\mu_{eg} = 11.0 \times 10^{-30}\text{ Cm} = 3.30\text{ D}$) of **1** were determined by EOAM in 1,4-dioxane as previously described.^[10] With these values and Equation (2) the diabatic dipole moment ($\Delta\mu_{12} = 67.8 \times 10^{-30}\text{ Cm} = 20\text{ D}$) was calculated, which corresponds to an effective diabatic ET distance of 4.2 Å ; this is significantly less than the C–N distance between the redox centers (12.3 Å). With these transition moments the electronic coupling V was calculated with Equations (1) and (2). Given the rather short effective ET distance, the transition dipole moment $\mu_{eg} = 11.0 \times 10^{-30}\text{ Cm} = 3.30\text{ D}$ and consequently the electronic

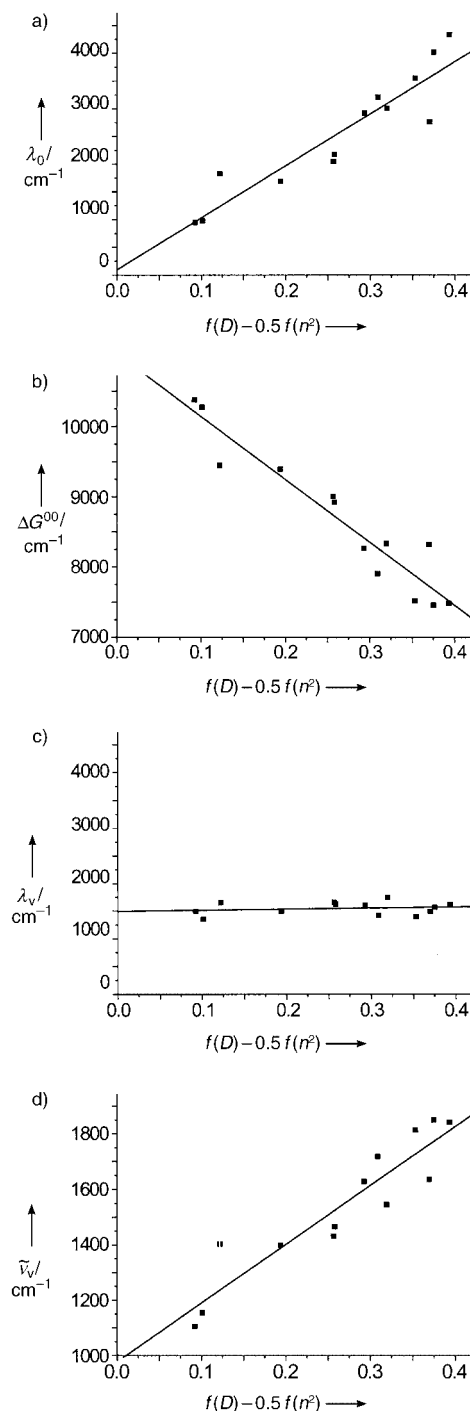


Figure 5. Plots of a) λ_o , b) ΔG^{00} , c) λ_v and d) $\tilde{\nu}_v$ versus the solvent polarity function $f(D)-0.5f(n^2)$ with $f(D) = (D-1)/(2D+1)$ and $f(n^2) = (n^2-1)/(2n^2+1)$.

coupling $V = 2000\text{ cm}^{-1}$ are noticeably small. This implies that the electronic interaction between the two redox centers in **1** is weak compared to that in an analogous MV compound consisting of two triarylamine redox centers.^[33] The AM1-UHF calculation of **1** shows the reason for the weak interaction between the two redox centers: steric interactions among the perchlorinated ring systems cause a twist of the π system.^[36] This effect and the fact that the β -LUMO is largely

concentrated on the central triarylmethyl carbon p orbital while the β -HOMO is delocalized over the triarylamino group results in a weak conjugation of the aromatic redox centers (Figure 6).

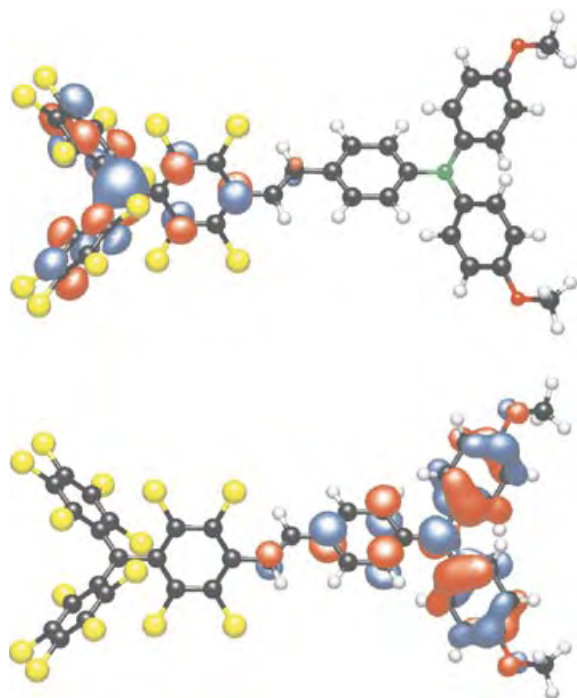


Figure 6. AM1-UHF-optimized structure of radical **1**; β -HOMO (bottom) and β -LUMO (top).

Using the diabatic parameters determined by Jortner's theory as well as the electronic coupling V determined by the GMH theory, we computed the adiabatic potential energy surfaces for *n*-hexane and acetonitrile (Figure 7). It is obvious from these curves that the solvent has a dominating influence on the shape of the potential surfaces and thus also has an impact on the deactivation pathways of the excited state.

In summary we have presented the synthesis and a detailed study of the photophysical properties of the first neutral organic MV compound. Only by using Jortner's one-

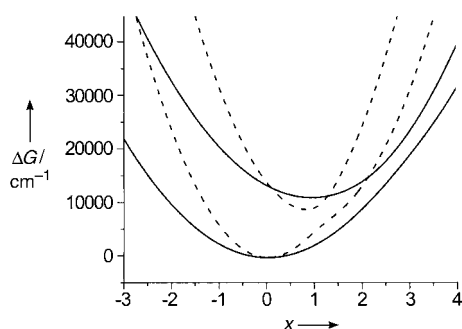


Figure 7. Adiabatic potential energy surfaces of **1** in *n*-hexane (—) and acetonitrile (----) calculated with Equation (3) of ref. [1] with $\mu_{eg} = 11.4 \times 10^{-30}$ Cm = 3.4 D and $V = 2070$ cm $^{-1}$ in *n*-hexane and $\mu_{eg} = 11.4 \times 10^{-30}$ Cm = 3.4 D and $V = 2120$ cm $^{-1}$ in acetonitrile. x = ET coordinate.

mode model were we able to analyze the IV-CT band and to reveal the compensating trends of the solvent reorganization energy λ_0 and the free energy difference ΔG^{00} . Both effects are rather strong due to the highly zwitterionic character of the excited IV-CT state. The analysis demonstrates that a lack of solvatochromism is no indication for a negligible change of dipole moment upon excitation. This large change of dipole moment upon excitation was also directly proved by EOAM. These measurements also revealed that the effective diabatic ET distance is much smaller than the formal separation of the redox centers. The uncharged character of this prototypical neutral MV compound enabled us to perform the presented measurements quite easily. Our findings will be useful for the design of molecular storage and switching devices where a neutral character is of practical advantage.

Experimental Section

2: Pd₂(dba)₃·CHCl₃ (74.0 mg, 71.5 μ mol, 0.05 equiv), P(*t*Bu)₃ (173 μ L, 0.33 mmol, 0.04 equiv), and NaOtBu (344 mg, 3.58 mmol, 2.50 equiv) were added to a solution of stilbene **3**^[24] (1.30 g, 1.43 mmol, 1.00 equiv) and bis(4-methoxyphenyl)amine (361 mg, 1.58 mmol, 1.10 equiv) in absolute toluene. The reaction mixture was stirred for 24 h under reflux in the dark under a nitrogen atmosphere. The solvent was removed in vacuo, and the residue was dissolved in CH₂Cl₂ (50 mL) and washed with water (2 \times 50 mL). The organic layer was dried over MgSO₄, and the solvent was removed under reduced pressure. The residue was purified by flash chromatography on silica gel (petroleum ether/CH₂Cl₂ 1:1). The crude product was precipitated by adding a concentrated solution of **2** in acetone dropwise to methanol which gave 690 mg (0.65 mmol, 46 %) of a yellow solid, m.p. 174 °C. ¹H NMR (400 MHz, [D₆]acetone, 295 K): δ = 7.47 (AA', CH=CHCCHCH, 2H), 7.11 (s, 1H, (C₆Cl₅CH), 7.10 (AA', NCCHCHCO, 4H), 7.08 (d, ³J_{HH} = 16.5 Hz, 1H, C=CH), 7.01 (d, ³J_{HH} = 16.5 Hz, 1H, C=CH), 6.94 (BB', OCCHCH, 4H), 6.85 (BB', CH=CHCCHCHCN, 2H), 3.80 ppm (s, 6H, OCH₃); ¹³C NMR (151 MHz, [D₆]acetone, 295 K): δ = 157.6 (q), 150.7 (q), 141.0 (q), 139.44 (HC=CH), 139.44 (2C, q), 137.79 (q), 137.77 (q), 136.3 (q), 135.9 (2C, q), 135.5 (q), 134.9 (q), 134.8 (q), 134.6 (q), 134.34 (q), 134.29 (q), 134.27 (q), 134.25 (q), 134.1 (q), 133.20 (q), 133.17 (q), 133.0 (q), 128.8 (CH=CHCCHCH), 128.1 (OCCHCH), 120.4 (HC=CH), 120.0 (CH=CHCCHCHCN), 115.7 (NCCHCHCO), 57.6 (C₆Cl₅-CH), 55.7 ppm (OCH₃); IR (KBr): $\tilde{\nu}$ = 3037 (w), 2997 (w), 2929 (w), 2869 (vw), 2832 (w), 1599 (m), 1504 (vs), 1463 (w), 1323 (w), 1294 (w), 1241 (s), 1176 (w), 1105 (w), 1037 (m), 966 (w), 827 (m), 808 (m), 649 (w), 575 (w), 521 cm $^{-1}$ (w); MS (EI, 70 eV) [*m/z*, %]: 1055 (74, *M*⁺), 1040 (8, *M*⁺-Me), 1021 (45, *M*⁺-Cl), 987 (20, *M*⁺-Cl-Me), 807 (36, *M*⁺-C₆Cl₅). Elemental analysis calculated for C₄₁H₂₁Cl₄NO₂: C 46.64, H 2.00, N 1.33; found: C 46.35, H 2.23, N 1.39.

1: Stilbene derivative **2** (50.0 mg, 47.4 μ mol, 1.00 equiv) was dissolved in absolute DMSO (10 mL) under a nitrogen atmosphere. KOtBu (10.6 mg, 94.8 μ mol, 2.00 equiv) was added, and the deep purple solution that formed immediately was stirred for 1.5 h in the dark at room temperature. Then *p*-chloranil (11.7 mg, 47.4 μ mol, 1.00 equiv) was added, and the solution was stirred for further 1.5 h in the dark at room temperature. The deep brown suspension was purified by flash chromatography on silica gel (CH₂Cl₂/petroleum ether 4:1). The crude product was precipitated twice by adding a concentrated solution of **1** in acetone dropwise to methanol to obtain 30.0 mg (28.4 μ mol, 60 %) of a brown solid, m.p. 165 °C (decomp.). IR (KBr): $\tilde{\nu}$ = 3040 (w), 2999 (w), 2945 (w), 2930 (w), 2909 (w), 2832 (w), 1595 (s), 1504 (vs), 1463 (vw), 1440 (vw), 1322 (s), 1242 (vs), 1174 (m), 1105 (w), 1037 (m), 945 (w), 816 (m), 707 (w), 653 (w), 575 (w), 521 cm $^{-1}$ (w); MS (FAB, 70 eV, 2-(octyloxy)nitrobenzene) [*m/z*, %]:

1054 (<1 , M^+); Elemental analysis calculated for $C_{41}H_{20}Cl_{14}NO_2$: C 46.68, H 1.91, N 1.33; found: C 46.53 H 2.11 N 1.27.

Received: April 29, 2004

Revised: July 12, 2004

Keywords: electron transfer · mixed-valent compounds · solvatochromism · triarylamines · vibronic coupling

- [1] B. S. Brunschwig, C. Creutz, N. Sutin, *Chem. Soc. Rev.* **2002**, 31, 168.
- [2] S. F. Nelsen, *Chem. Eur. J.* **2000**, 6, 581.
- [3] J.-P. Launay, *Chem. Soc. Rev.* **2001**, 30, 386.
- [4] S. F. Nelsen, R. F. Ismagilov, D. A. Trieber, *Science* **1997**, 278, 846.
- [5] For a review on solvent effects on CT transitions, see P. Chen, T. J. Meyer, *Chem. Rev.* **1998**, 98, 1439.
- [6] M. D. Newton, *Adv. Chem. Phys.* **1999**, 106, 303.
- [7] R. J. Cave, M. D. Newton, *Chem. Phys. Lett.* **1996**, 249, 15.
- [8] C. Creutz, M. D. Newton, N. Sutin, *J. Photochem. Photobiol. A* **1994**, 82, 47.
- [9] While UHF calculations tend to overemphasize charge localization, DFT calculations yield charge delocalization that is too strong, see ref. [11] in C. S. Lent, B. Isaksen, M. Lieberman, *J. Am. Chem. Soc.* **2003**, 125, 1056. Nelsen et al. recently pointed out that the geometric N–N distance yields much too large effective ET distances in bis(triarylamine) radical cations, see S. F. Nelsen, A. E. Konradsson, M. N. Weaver, J. P. Telo, *J. Am. Chem. Soc.* **2003**, 125, 12493–12501 and S. F. Nelsen, A. E. Konradsson, Y. Luo, K.-Y. Kim, S. C. Blackstock, private communication.
- [10] R. Wortmann, P. Krämer, C. Glania, S. Lebus, N. Detzer, *Chem. Phys.* **1993**, 173, 99.
- [11] B. S. Brunschwig, C. Creutz, N. Sutin, *Coord. Chem. Rev.* **1998**, 177, 61.
- [12] F. W. Vance, R. V. Slone, C. L. Stern, J. T. Hupp, *Chem. Phys.* **2000**, 253, 313.
- [13] G. U. Bublitz, W. M. Laidlaw, R. G. Denning, S. G. Boxer, *J. Am. Chem. Soc.* **1998**, 120, 6068.
- [14] S. F. Nelsen, D. A. Trieber, R. F. Ismagilov, Y. Teki, *J. Am. Chem. Soc.* **2001**, 123, 5684.
- [15] S. F. Nelsen, H. Q. Tran, *J. Phys. Chem. A* **1999**, 103, 8139.
- [16] J. T. Hupp, Y. Dong, R. L. Blackburn, H. Lu, *J. Phys. Chem.* **1993**, 97, 3278.
- [17] S. F. Nelsen, R. F. Ismagilov, *J. Phys. Chem. A* **1999**, 103, 5373.
- [18] R. L. Blackburn, J. T. Hupp, *J. Phys. Chem.* **1990**, 94, 1788.
- [19] Quite recently the synthesis and optical properties of an organometallic neutral MV compound consisting of a perchlorinated triphenylmethyl radical and ferrocene was reported, see O. Elsner, D. Ruiz-Molina, I. Ratera, J. Vidal-Gancedo, C. Rovina, J. Veciana, *J. Organomet. Chem.* **2001**, 637–639, 251. Rassat et al. investigated computationally neutral MV organic monoradicals based on a totally different molecular system, see A. Rassat, G. Del Re, A. Peluso, *Chem. Phys. Lett.* **1999**, 313, 582.
- [20] C. Lambert, G. Nöll, *J. Am. Chem. Soc.* **1999**, 121, 8434.
- [21] P. J. Low, M. A. J. Paterson, H. Puschmann, A. E. Goeta, J. A. K. Howard, C. Lambert, J. C. Cherryman, D. R. Tackley, S. Leeming, B. Brown, *Chem. Eur. J.* **2004**, 10, 83.
- [22] C. Lambert, G. Nöll, J. Schelter, *Nat. Mater.* **2002**, 1, 69.
- [23] J. Bonvoisin, J.-P. Launay, C. Rovira, J. Veciana, *Angew. Chem.* **1994**, 106, 2190; *Angew. Chem. Int. Ed. Engl.* **1994**, 33, 2106.
- [24] C. Rovira, D. Ruiz-Molina, O. Elsner, J. Vidal-Gancedo, J. Bonvoisin, J.-P. Launay, J. Veciana, *Chem. Eur. J.* **2001**, 7, 240.
- [25] C. Lambert, G. Nöll, *J. Chem. Soc. Perkin Trans. 2* **2002**, 2039.
- [26] M. Ballester, J. Castaner, J. Riera, A. Ibanez, J. Pujadas, *J. Org. Chem.* **1982**, 47, 259.
- [27] M. Ballester, J. Riera, J. Castaner, C. Badia, J. M. Monso, *J. Am. Chem. Soc.* **1971**, 93, 2215.
- [28] J. Veciana, O. Armet, C. Rovira, J. Riera, J. Castaner, E. Molins, J. Rius, C. Miravittles, S. Olivella, J. Brichfeus, *J. Phys. Chem.* **1987**, 91, 5608.
- [29] J. Bonvoisin, J.-P. Launay, W. Verbouwe, M. Van der Auweraer, F. C. De Schryver, *J. Phys. Chem.* **1996**, 100, 17079.
- [30] I. R. Gould, D. Noukakis, L. Gomez-Jahn, R. H. Young, J. L. Goodman, S. Farid, *Chem. Phys.* **1993**, 176, 439.
- [31] S. F. Nelsen, M. T. Ramm, J. J. Wolff, D. R. Powell, *J. Am. Chem. Soc.* **1997**, 119, 6863.
- [32] J. Cortes, H. Heitele, J. Jortner, *J. Phys. Chem.* **1994**, 98, 2527.
- [33] The analogous N,N,N',N' -tetraanisylstilbenediamine radical cation has an IV-CT band at $\tilde{\nu}_{\max} = 6150 \text{ cm}^{-1}$ in CH_2Cl_2 , which equals the total reorganization energy and which has a transition dipole moment of $\mu_{\text{eg}} = 43.4 \times 10^{-30} \text{ Cm} = 13.0 \text{ D}$. See also C. Lambert, G. Nöll, *Angew. Chem.* **1998**, 110, 2239; *Angew. Chem. Int. Ed.* **1998**, 37, 2107.
- [34] The usually employed Pekar factor $\gamma = 1/n^2 - 1/D$ from Marcus theory yields a quite similar linear correlation. We refrain from using the Pekar factor as it is negative for very apolar solvents and as it refers to an ion in a spherical cavity. The Onsager model employed here refers to the more realistic situation of a dipole in a spherical cavity, see ref. [32]. If one uses the Marcus theory for calculating the solvent reorganization energy with $\lambda_0 = (\Delta e)^2(r^{-1} - d^{-1})\gamma$, where $\Delta e = 1$ is the charge transferred, $r = 7 \text{ Å}$ is the mean radius of the redox centers, and $d = 12.3 \text{ Å}$ is the distance between the nitrogen of the triarylamine group and the methyl carbon of the triarylmethyl radical (both values estimated from the AM1 computation), a linear correlation with λ_0 from Jortner theory is obtained with a slope of almost unity. However, this good correlation is to some extent fortuitous because the dipole moment differences measured by EOAM indicate a much smaller electron-transfer distance than the geometric distance of the redox centers.
- [35] B. S. Brunschwig, S. Ehrenson, N. Sutin, *J. Phys. Chem.* **1986**, 90, 3657.
- [36] M. Ballester, *Adv. Phys. Org. Chem.* **1989**, 25, 267.

Cover Picture

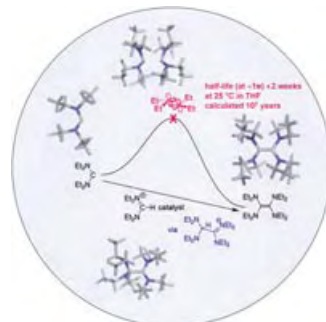
Anna Rencurosi, Edward P. Mitchell, Gianluca Cioci, Serge Pérez, Rogelio Pereda-Miranda,* and Anne Imberty*

In traditional Mexican farming the morning glory “heavenly blue” (*Ipomea tricolor* Cav.) is used as a cover crop. The structure of tricolorin A, one of several phytotoxic resin glycosides present in this plant, has now been determined crystallographically. The lipopolysaccharide contains one macrolactone ring and forms channel structures, which could be responsible for the biological activity of this compound, as reported by R. Pereda-Miranda, A. Imberty, and co-workers in their Communication on page 5918 ff.



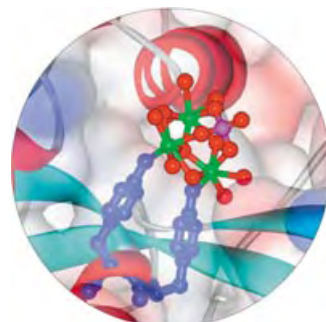
Carbene Dimerization

R. W. Alder et al. give an overview of the thermodynamics, kinetics, and mechanisms of the dimerization of diaminocarbenes in their Review on page 5896 ff., in which they consider both experimental results and those from DFT calculations.



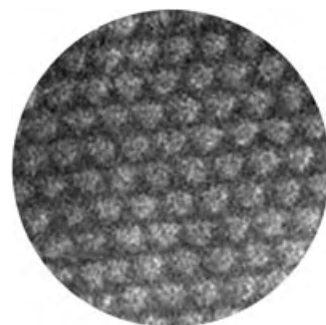
Bioinorganic Chemistry

In their Communication on page 5914 ff., P. J. Sadler and co-workers describe how a trinuclear oxo-zirconium(IV) cluster forms in the binding site of bacterial transferrin.



Mesoporous Materials

The directed synthesis of two- and three-dimensional mesoporous iron oxide structures by varying the aging conditions is presented by F. Jiao and P. G. Bruce in their Communication on page 5958 ff.



Angewandte EarlyView®

The following Communications are available online (in Wiley InterScience). You can find them, as well as forthcoming Reviews, Highlights, and Essays, at www.angewandte.org, under Early View.

Y. K. Hwang, J.-S. Chang,* S.-E. Park,* D. S. Kim, Y.-U. Kwon,
S. H. Jung, J.-S. Hwang, M. S. Park:
**Microwave Fabrication of MFI Zeolite Crystals with a Fibrous
Morphology and Their Applications**
DOI: 10.1002/anie.200461403
Published online: November 2, 2004

B. F. Abrahams, M. G. Haywood, T. A. Hudson, R. Robson*:
**Cubic, Hydrogen-Bonded (10,3)-a Networks in the Family
[C(NH₂)₃]₃[N(CH₃)₄][XO₄] (X = S, Cr, and Mo)**
DOI: 10.1002/anie.200461678
Published online: November 2, 2004

Articles judged by the referees or the editor as being either very important or very urgent are immediately edited, proof-read, and electronically published once the manuscript has arrived in the editorial office in its final form. As long as there is no page number available these articles should be cited in the following manner:

Author(s), *Angew. Chem. Int. Ed.*, online publication date, DOI.

News

J. T. Hynes Receives Hildebrand
Award _____ **5876**

Cope Scholar Award to
R. F. Ismagilov _____ **5876**

P. Knochel Receives Cope Scholar
Award _____ **5876**

Books

Carbon Nanotubes

Stefanie Reich, Christian Thomsen,
Janina Maultzsch

reviewed by D. M. Guldi _____ **5877**

Life Sciences for the 21st Century

Ehud Keinan, Israel Schechter,
Michael Sela

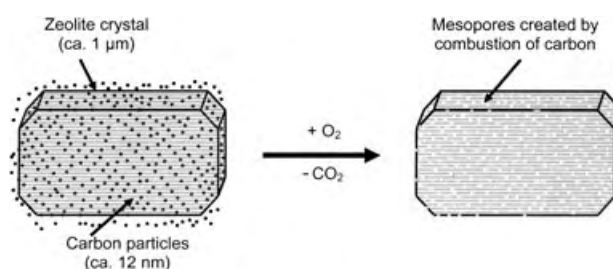
reviewed by U. Schepers _____ **5878**

Highlights

Zeolites

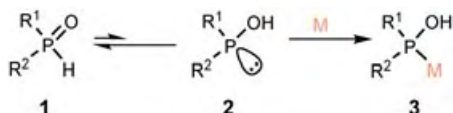
M. Hartmann* _____ **5880–5882**

Hierarchical Zeolites: A Proven Strategy
to Combine Shape Selectivity with
Efficient Mass Transport



Pores for effect: Hierarchical zeolites combine the high activity, shape selectivity, and hydrothermal stability of conventional zeolites with the efficient mass

transport that is typically achieved in mesoporous materials. The mesopores can be templated with carbon during zeolite synthesis (see scheme).



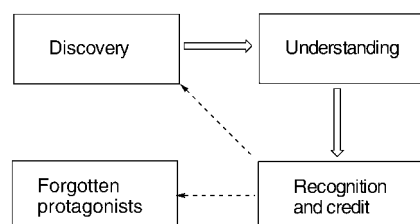
Primed! Secondary phosphine oxides are able to tautomerize in situ to phosphinous acids and then coordinate to soft transition metals through the trivalent phosphorus atom (see scheme). The

presence of a chiral backbone allows this reaction to run stereoselectively and be used for the generation of highly enantioselective homogeneous catalysts.

Ligand Design

N. V. Dubrovina, A. Börner* 5883 – 5886

Enantioselective Catalysis with Chiral Phosphine Oxide Preligands



Discovery is a two-step process—finding and comprehending (see scheme). The history of chemistry contains incorrect attributions, mistakes, and problems created by conflicting interpretations. But retrospective analyses can set matters straight and give credit where credit is due. Language and naming also convey a fascinating human side to research and illustrate that chemical discovery is multifaceted, evolutionary, and very much alive.

Essays

Names in Chemistry

P. Cintas* 5888 – 5894

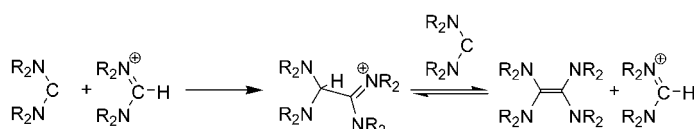
The Road to Chemical Names and Eponyms: Discovery, Priority, and Credit

Reviews

Reaction Mechanisms

R. W. Alder,* M. E. Blake, L. Chaker, J. N. Harvey, F. Paolini, J. Schütz 5896 – 5911

When and How Do Diaminocarbenes Dimerize?



It's amazing what a little help can do: Simple diaminocarbenes, such as $(\text{Et}_2\text{N})_2\text{C}$, do not dimerize at room temperature in THF, even though thermodynamics favor the dimer. Dimerization occurs rapidly in the presence of proton

sources, however (see scheme), and the possibility of catalysis by Li^+ is discussed. DFT calculations give a good account of the thermodynamics and kinetics of dimer formation.

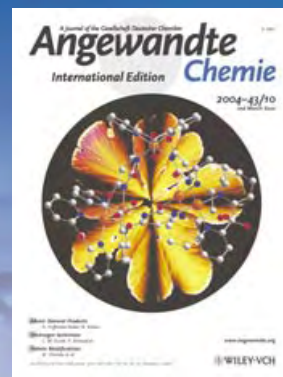
For the USA and Canada:

ANGEWANDTE CHEMIE International Edition (ISSN 1433-7851) is published weekly by Wiley-VCH PO Box 191161, D 69451 Weinheim, Germany. Air freight and mailing in the USA by Publications Expediting Inc. 200 Meacham Ave., Elmont, NY 11003. Periodicals

postage paid at Jamaica NY 11431. US POSTMASTER: send address changes to *Angewandte Chemie*, Wiley-VCH, 111 River Street, Hoboken, NJ 07030. Annual subscription price for institutions: US\$ 4948.00/4498.00 (valid for print and electronic / print or electronic delivery); for individuals who are personal members of a

national chemical society, or whose institution already subscribes, or who are retired or self-employed consultants, print only: US\$ 394.00. Postage and handling charges included. All Wiley-VCH prices are exclusive VAT.

The best in chemistry – for more than a hundred years



A Journal of the Gesellschaft Deutscher Chemiker
Angewandte
International Edition **Chemie**

www.angewandte.org

1888: The beginning
of a success story

Constant Innovations

- 1962:** First issue of the International Edition
- 1976:** Graphical abstracts
- 1979:** Cover pictures
- 1988:** Centenary of Angewandte
- 1989:** Routine use of color
- 1991:** New section: Highlights
- 1992:** Computerized editorial tracking system
- 1995:** Internet service for readers
- 1998:** Regular press service; full-text online
- 2000:** New section: Essays; EarlyView: Communications available online ahead of the printed version
- 2001:** New section: Minireviews
- 2002:** Online submission of manuscripts
- 2003:** Weekly publication; new section: News; new layout
- 2004:** Backfiles (1962-1997); ManuscriptXpress: Online system for authors and referees



**Angewandte's
advisors...**

Richard R. Ernst
ETH Zürich

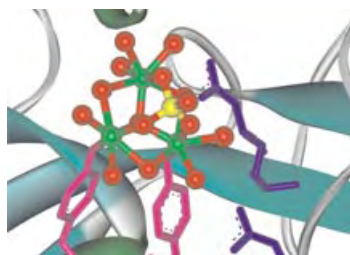
» I support **Angewandte Chemie** because it is a first rank international journal of European origin. More than many other renowned journals, it implements a pioneering spirit, being ready for innovating its form and contents. Its bilingual mode of appearance is another plus. I am looking forward to an equally prosperous future for **Angewandte Chemie**. «

Angewandte Chemie International Edition is
a journal of the German Chemical Society (GDCh)



Communications

Bioinorganic Chemistry

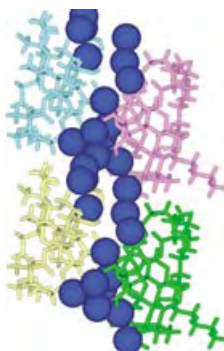


Filling a gap: A trinuclear oxo–zirconium(IV) cluster readily assembles in the “venus fly trap” binding cleft of bacterial transferrin (see picture; cluster: Zr green, O red, P yellow; protein: β sheets cyan, Tyr pink, Arg dark blue). Its structure was determined by EXAFS and X-ray crystallography.

W. Zhong, D. Alexeev, I. Harvey, M. Guo, D. J. B. Hunter, H. Zhu, D. J. Campopiano, P. J. Sadler* ————— **5914–5918**

Assembly of an Oxo–Zirconium(IV) Cluster in a Protein Cleft

A water channel was observed in the first crystallographically determined structure of a natural resin glycoside (see figure). Tricolorin A displays amphipathic features, which have been correlated with its significant mammalian and plant toxicity. The architecture of tricolorin A in the solid state suggests that the cytotoxicity of this class of compounds may be the result of their pore-forming ability.

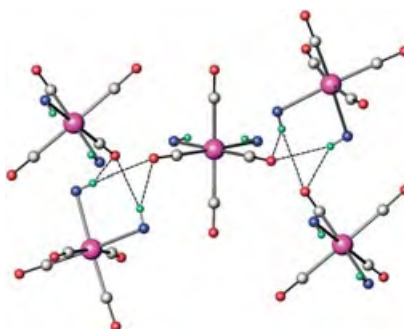


Crystallography of Natural Products

A. Rencurosi, E. P. Mitchell, G. Cioci, S. Pérez, R. Pereda-Miranda,* A. Imberty* ————— **5918–5922**

Crystal Structure of Tricolorin A: Molecular Rationale for the Biological Properties of Resin Glycosides Found in Some Mexican Herbal Remedies

New tricks for an old dog: The solid-state structure of *cis*-[W(CO)₄(piperidine)₂] reveals an intermolecular, bifurcated H-bonding network involving the N–H protons and the two CO ligands *trans* to the piperidine ligands (see X-ray crystal structure; C gray, H green, N blue, O red, W magenta). Such an arrangement accounts for ν_{CO} absorptions as low as 1768 cm^{−1}!

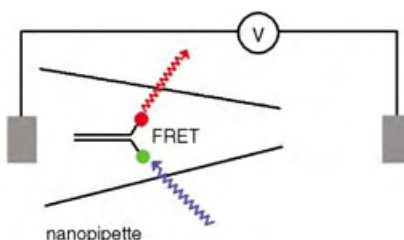


Structure Elucidation

P. Braunstein,* J.-p. Taquet, O. Siri, R. Welter ————— **5922–5925**

Supramolecular, Bifurcated N–H...OC–M Bonding Explains Unusually Low ν_{CO} Frequencies in Metal Carbonyl Compounds: A Case Study

Reversible switching of the fluorescence of an individual dye-labeled DNA molecule is possible by utilizing an electric field applied in the tip of a nanopipette (see picture; FRET = fluorescence resonance energy transfer). The electric field appears to alter the conformation of the acceptor dye only, resulting in a significant change in its quantum yield.



Molecular Devices

S. S. White, L. Ying, S. Balasubramanian, D. Klenerman* ————— **5926–5930**

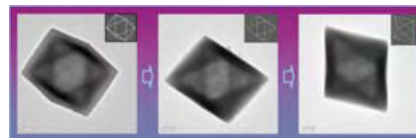
Individual Molecules of Dye-Labeled DNA Act as a Reversible Two-Color Switch upon Application of an Electric Field

Tin Oxide Nanooctahedra

H. G. Yang, H. C. Zeng* — 5930–5933

Self-Construction of Hollow SnO_2 Octahedra Based on Two-Dimensional Aggregation of Nanocrystallites

0D→2D→3D oriented attachment has been exploited to prepare octahedra of rutile-like SnO_2 with a central cavity by a template-free hydrothermal route. The synthesis is based on the two-dimensional attachment of nanocrystallites and stabilization of a family of {111}-like crystal planes in 2-propanol/water in the presence of ethylenediamine. In TEM images

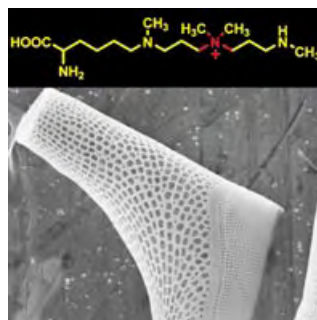


of the octahedron (see picture), the central cavity is evidenced by lighter regions.

Bioinorganic Chemistry

S. Wenzl, R. Deutzmann, R. Hett, E. Hochmuth, M. Sümper* — 5933–5936

Quaternary Ammonium Groups in Silica-Associated Proteins

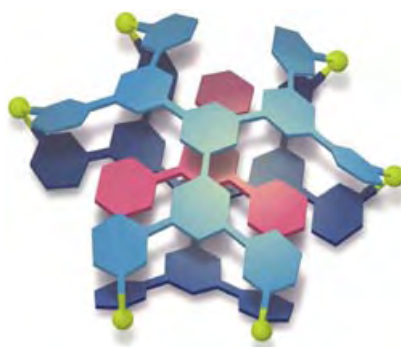


Mother Nature knows best! Silaffins (silica-associated proteins) from the diatom *Eucampia zodiacus* (see picture) were found to contain novel lysine modifications that carry quaternary ammonium groups. It appears that the very special interaction between quaternary ammonium groups and silica is exploited in the natural biomineralization of silica.

Self-Assembly

K. Kumazawa, Y. Yamanoi, M. Yoshizawa, T. Kusakawa, M. Fujita* — 5936–5940

A Palladium(II)-Clipped Aromatic Sandwich



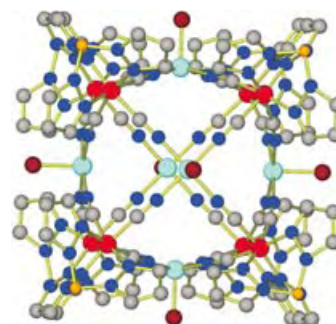
A filling that makes the sandwich: Large aromatic molecules are sandwiched by two π -conjugated ligands (L) that are joined together by six $\{(\text{en})\text{Pd}\}^{2+}$ units (M; en = 1,2-ethanediamine; see picture; guest red, $\{(\text{en})\text{Pd}\}^{2+}$ yellow, ligand blue). This host has an M_6L_2 composition and is distorted by the concave shape of the ligand. Without a guest, it releases the distortion by forming the dimeric M_{12}L_4 in a reversible fashion.

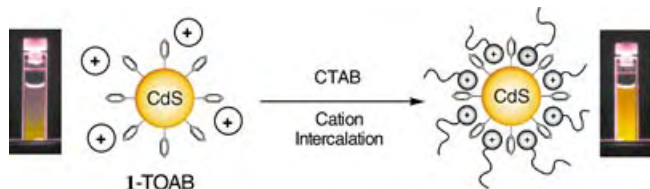
Single-Molecule Magnets

S. Wang, J.-L. Zuo,* H.-C. Zhou,* H. J. Choi, Y. Ke, J. R. Long, X.-Z. You* — 5940–5943

$[(\text{Tp})_8(\text{H}_2\text{O})_6\text{Cu}^{\text{II}}\text{Fe}^{\text{III}}_8(\text{CN})_{24}]^{4+}$: A Cyanide-Bridged Face-Centered-Cubic Cluster with Single-Molecule-Magnet Behavior

A box of magnetic tricks: By using the anionic precursor $[(\text{Tp})\text{Fe}(\text{CN})_3]^-$ (Tp^- = hydrotris(pyrazolyl)borate), the title compound, which is a new face-centered-cubic cluster, has been synthesized (see structure; red Fe, turquoise Cu, orange B, gray C, blue N, dark red O). Magnetic studies show that it exhibits single-molecule-magnet behavior with substantial axial magnetic anisotropy ($D = -0.16 \text{ cm}^{-1}$).





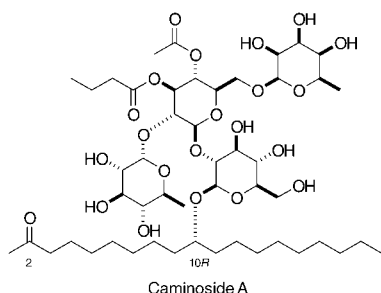
Turning on the light: Remarkable photoluminescence enhancement is observed upon intercalation of cetyltrimethylammonium cations (CTA⁺) among the surface aromatic groups of a complex formed

from the phenyl-capped semiconductor CdS cluster molecule [Cd₁₀S₄(SPh)₁₂] (**1**) and tetraoctylammonium bromide (TOAB) (see scheme).

Luminescent Cluster Compounds

T. Hiratani, K. Konishi* — 5943 – 5946

Surface-Cap-Mediated Host–Guest Chemistry of Semiconductor CdS: Intercalative Cation Accumulation around a Phenyl-Capped CdS Cluster and Its Notable Effects on the Cluster Photoluminescence

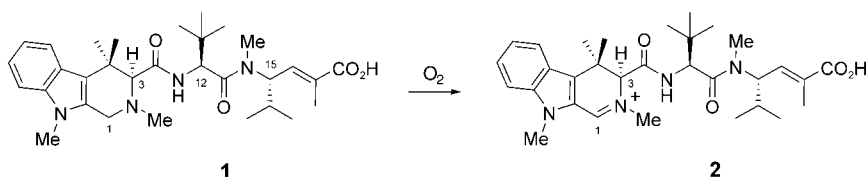


Information technology: The configuration at C10-OH of the caminoside aglycone (see formula) was shown to be *R* by interpretation of exciton coupling in the circular dichroism (CD) spectrum of the tetraphenylporphyrin carboxylate diester of (2*R*,10*R*)-2,10-nonadecanediol. This compound is derived from the title compound and was embedded in highly uniform nanometric liposomes for the CD measurements.

Stereochemistry

J. B. MacMillan, R. G. Linington, R. J. Andersen, T. F. Molinski* — 5946 – 5951

Stereochemical Assignment in Acyclic Lipids Across Long Distance by Circular Dichroism: Absolute Stereochemistry of the Aglycone of Caminoside A



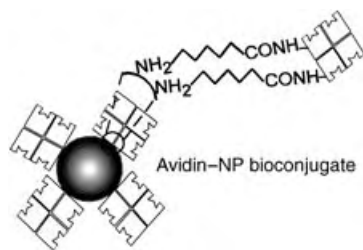
Spontaneous oxidation of the marine-sponge-derived peptide (+)-milnamide A (**1**) to (+)-milnamide D (**2**), which is also a natural product, was observed during

the total synthesis of **1**. The absolute configurations of the structures were determined and are also reported.

Natural Product Synthesis

C. Liu, M. N. Masuno, J. B. MacMillan, T. F. Molinski* — 5951 – 5954

Enantioselective Total Synthesis of (+)-Milnamide A and Evidence of Its Autoxidation to (+)-Milnamide D



Approximately eight avidin molecules are conjugated to each Ce/Tb-doped lanthanum phosphate nanoparticle (NP) through the formation of amide bonds (see scheme). This biofunctionalization process comprises modification of the LaPO₄ NPs with 6-aminohexanoic acid (AHA) to confer colloidal stability, activation of the AHA carboxy groups by 1-ethyl-3-[3-dimethylaminopropyl]carbodiimide, and avidin conjugation.

Biofunctionalization

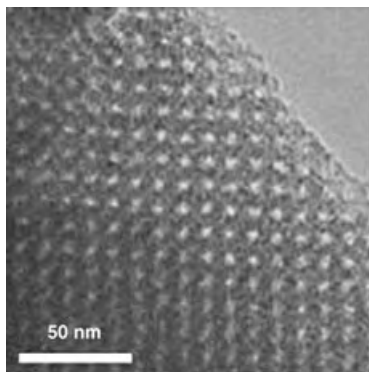
F. Meiser, C. Cortez, F. Caruso* — 5954 – 5957

Biofunctionalization of Fluorescent Rare-Earth-Doped Lanthanum Phosphate Colloidal Nanoparticles



F. Jiao, P. G. Bruce* — 5958 – 5961

Two- and Three-Dimensional Mesoporous Iron Oxides with Microporous Walls

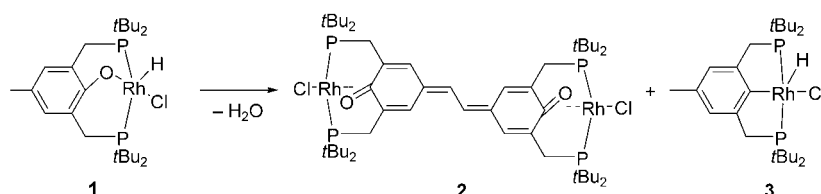


Age concern: Alkyl amine templates act as bifunctional surfactants which can template mesostructures with microporous walls. Ordered two-dimensional hexagonal mesoporous iron oxide with $P6mm$ symmetry and three-dimensional cubic mesoporous iron oxide with $Fm3m$ symmetry (see TEM image) have been prepared by using decylamine as the template, iron(III) ethoxide as the precursor, and different aging conditions.

C–O Activation

M. E. van der Boom,* T. Zubkov, A. D. Shukla, B. Rybtchinski, L. J. W. Shimon, H. Rozenberg, Y. Ben-David, D. Milstein* — 5961 – 5963

Self-Oxidation of a Phenolate Complex to a Bimetallic Stilbene Quinone



Do-it-yourself oxidation: The Rh^{III} complex **1** undergoes a self-oxidative coupling process, in which the phenolate oxygen atom serves as the oxidant, to give **2** and the hydride complex **3** (**2:3** = 1:3). This

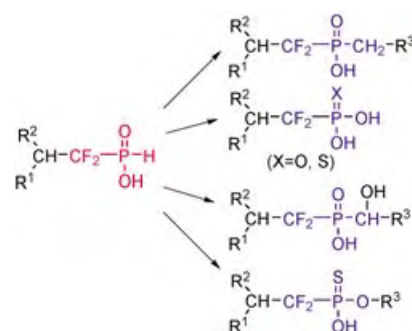
reaction involves cleavage of a strong aryl–oxygen bond. X-ray analysis of **2** reveals that the two quinonoid $C=O$ bonds are η^2 -coordinated to the metal centers.

Radical Reactions

A. Gautier,* G. Garipova, C. Salcedo, S. Balieu, S. R. Piettre* — 5963 – 5967

α,α -Difluoro-*H*-phosphinates: Useful Intermediates for a Variety of Phosphate Isosteres

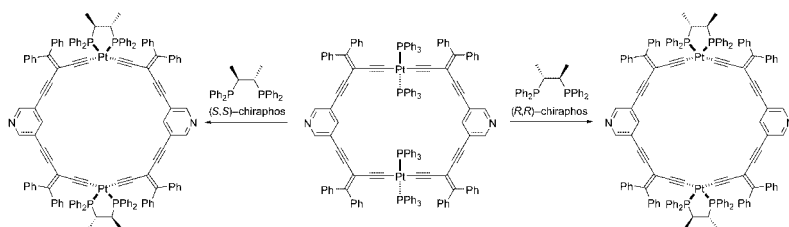
Addition of the radical generated from the sodium salt of hypophosphorous acid to difluoroalkenes results in the formation of α,α -difluoro-*H*-phosphinates. These intermediates can be transformed into different phosphorus-centered isosteres, such as difluorophosphonates, difluorophosphonothioates, and difluorophosphinates (see scheme).



Metallamacrocycles

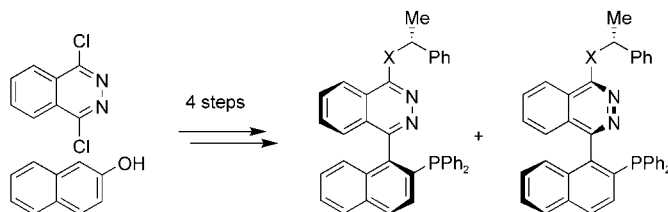
K. Campbell, C. A. Johnson II, R. McDonald, M. J. Ferguson, M. M. Haley, R. R. Tykwinski* — 5967 – 5971

A Simple, One-Step Procedure for the Formation of Chiral Metallamacrocycles



A twist in the final stage: Chiral, conjugated metallamacrocycles can be formed in excellent yield in a single step from achiral precursors by ligand exchange

between (*R,R*)- or (*S,S*)-chiraphos and *trans* platinum acetylide complexes (see scheme).



A short and modular synthesis of novel P,N ligands (pinap; see scheme; X = O or NH) is presented. A covalently bound chiral group allows the separation of the atropisomeric diastereomers, thus avoiding resolution involving chiral Pd–amine

complexes. The utility of the ligands is demonstrated for three reactions catalyzed by different transition metals; in each case products are obtained with high enantiomeric excess (up to 99% *ee*).

Asymmetric Catalysis

T. F. Knöpfel, P. Aschwarden, T. Ichikawa, T. Watanabe, E. M. Carreira* **5971–5973**

Readily Available Biaryl P,N Ligands for Asymmetric Catalysis

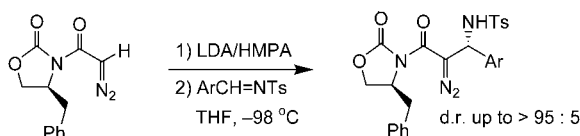
Weighing in: Multiple kinases can be assayed simultaneously by using a method that combines peptide chips and MALDI-TOF mass spectrometry (MS). The method uses self-assembled monolayers that present a set of peptides that are each selective for a kinase. The kinase phosphorylates the peptide, changing its mass. MS analysis of the surface resolves each peptide and gives the activity of each kinase.



Label-Free Assay

D.-H. Min, J. Su, M. Mrksich* **5973–5977**

Profiling Kinase Activities by Using a Peptide Chip and Mass Spectrometry



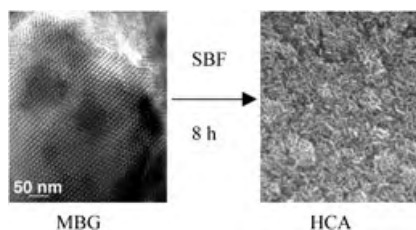
In the presence of an Evans oxazolidinone as the chiral auxiliary, the anion derived from α -diazoacetamide adds to aromatic *N*-tosylimines with high stereoselectivity

(see scheme). The addition products can be used in a concise and stereoselective synthesis of *syn*- and *anti*- α -hydroxy- β -amino acid derivatives.

Asymmetric Synthesis

Y. Zhao, Z. Ma, X. Zhang, Y. Zou, X. Jin, J. Wang* **5977–5980**

A Highly Stereoselective Addition of the Anion Derived from α -Diazoacetamide to Aromatic *N*-Tosylimines



Large pore volumes and highly accessible mesopore surface areas are present in highly ordered mesoporous bioactive glasses (MBGs) prepared by a block copolymer templating approach under non-aqueous conditions. These glasses have a high bone-forming bioactivity in vitro, as shown by immersing them in simulated body fluid (SBF) and monitoring the formation of hydroxycarbonate apatite (HCA) on the surface (see electron micrographs).

Mesoporous Materials

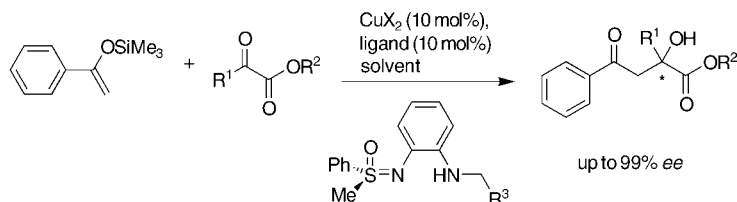
X. Yan, C. Yu,* X. Zhou, J. Tang, D. Zhao* **5980–5984**

Highly Ordered Mesoporous Bioactive Glasses with Superior In Vitro Bone-Forming Bioactivities

Asymmetric Catalysis

M. Langner, C. Bolm* — 5984 – 5987

C_1 -Symmetric Sulfoximines as Ligands in Copper-Catalyzed Asymmetric Mukaiyama-Type Aldol Reactions



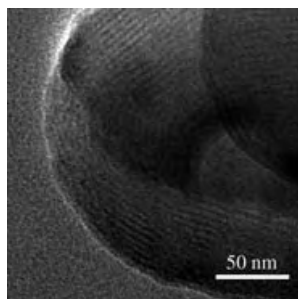
Aldol products with quaternary centers have been obtained with up to 99% *ee* in high yields by using copper(II) catalysts bearing C_1 -symmetric aminosulfoximines as ligands (see scheme). In terms of

ee values and yield the new catalysts compare well with established systems based on metal complexes with bis-(oxazoline) and pyridylbis(oxazoline) ligands.

Electrochemistry

E. Kim, D. Son, T.-G. Kim, J. Cho,*
B. Park,* K.-S. Ryu,
S.-H. Chang — 5987 – 5990

A Mesoporous/Crystalline Composite Material Containing Tin Phosphate for Use as the Anode in Lithium-Ion Batteries

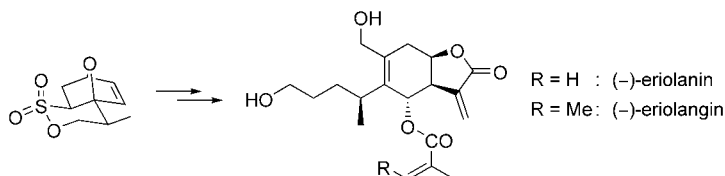


Packed to capacity: The incorporation of mesoporous structures as a buffer layer enhances the structural stability of tin phosphate and alleviates the volume expansion of the tin phosphate anode during Li alloying/dealloying (see TEM image). The mesoporous tin phosphate/ $\text{Sn}_2\text{P}_2\text{O}_7$ composite anode shows a large initial capacity (721 mAh g^{-1}) and excellent cyclability (587 mAh g^{-1} at the 30th cycle).

Sesquiterpene Lactones

J. Merten, R. Fröhlich,
P. Metz* — 5991 – 5994

Enantioselective Total Synthesis of the Highly Oxygenated 1,10-*seco*-Eudesmanolides Eriolanin and Eriolangin



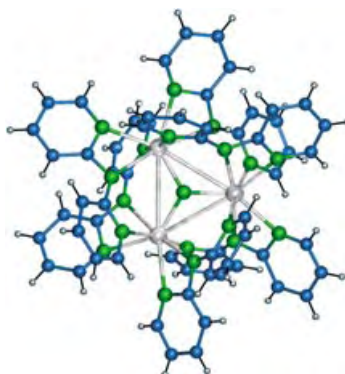
Sultones of swing: A sultone served as the key intermediate in the first enantioselective total syntheses of the bioactive title compounds (see scheme), the absolute configuration of which is now established.

Starting from 2-bromo-1-(2-furyl)ethanone, 24 steps were required to generate the common basic structure, and in each case two additional steps yielded the natural products.

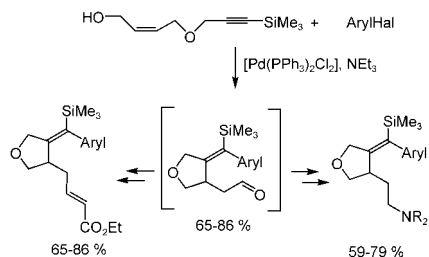
Rare-Earth Metals

C. C. Quitmann,
K. Müller-Buschbaum* — 5994 – 5996

$[\text{Yb}_3\text{N}(\text{dpa})_6][\text{Yb}(\text{dpa})_3]$: A Molecular Nitride of a Rare-Earth Metal with a Yb_3N Unit



Centered by a nitride ion: The oxidation of ytterbium with 2,2'-dipyridylamine in liquid ammonia at low temperatures leads to the novel compound $[\text{Yb}_3\text{N}(\text{dpa})_6][\text{Yb}(\text{dpa})_3]$, which is unique among homoleptic dipyrityldiamides of the rare-earth metals. The complete deprotonation of NH_3 provides the first molecular nitride of a rare-earth metal with a Yb_3N unit (see picture; C blue, N green, Yb silver).



In one fell swoop: the reaction of alkynyl-allyl alcohols with aryl halides in the presence of [Pd(PPh₃)₂Cl₂] under Heck reaction conditions provides cyclic γ,δ-enals (see scheme). This reaction serves as the starting sequence for the one-pot synthesis of diene esters and β-amino-substituted tetrahydrofurans.

One-Pot Syntheses

C. J. Kressierer,
T. J. J. Müller* _____ 5997–6000

Novel Three-Component Reactions Based on a Heck Carbopalladation/Cyclization Domino Reaction



Communications labeled with this symbol have been judged by two referees as being “very important papers”.

WILEY InterScience®
DISCOVER SOMETHING GREAT

“Hot Papers” are chosen by the Editors for their importance in a rapidly evolving field of high current interest. A preview with the graphical abstracts of these articles can be found on the *Angewandte Chemie* homepage in Wiley InterScience at www.angewandte.org.

“VIPs” are Communications which are identified by two referees as being very important. They are published online up to several weeks ahead of print. A preview with short summaries of these articles can also be found on the journal's homepage.

Service

Keywords _____ 6002

Authors _____ 6003

Angewandte's
Sister Journals _____ 6004–6005

Preview _____ 6007



J. T. Hynes Receives Hildebrand Award

James T. (Casey) Hynes is the recipient of the 2005 Joel Henry Hildebrand Award in the Theoretical and Experimental Chemistry of Liquids, administered by the American Chemical Society (ACS). The award recognizes distinguished contributions to the understanding of the chemistry and physics of liquids. Hynes completed his PhD in 1969 at Princeton University (USA). In 1971, following an NIH Postdoctoral Fellowship at the Massachusetts Institute of Technology (MIT), he moved to the University of Colorado, Boulder, where he is currently Professor of Chemistry and Biochemistry. Since 1999 he has also been CNRS Director of Research in the chemistry department of the École Normale Supérieure, Paris (France).



J. T. Hynes

Hynes's research on the theory of chemical reactions in solution, vibrational-energy transfer in solution, and intramolecular energy flow in highly vibrationally excited isolated molecules has had significant impact on the field. Other research interests include chemical reactions in enzymes and other biomolecules, electronic structure in condensed phases, and heterogeneous reactions important in the depletion of atmospheric ozone. One current topic of investigation and the subject of a recent article in *ChemPhysChem*^[1] is the dissociation of aromatic radical anions in solution. Hynes is Co-Chairman of the Editorial Advisory Board of *ChemPhysChem*.

Cope Scholar Award to R. F. Ismagilov

Arthur C. Cope Scholar Awards, administered by the ACS, aim to recognize and encourage excellence in organic chemistry. The highly interdisciplinary research of one recipient for 2005, Rustem F. Ismagilov, includes aspects of chemistry, physics, biology, and engineering. His research group develops new microfluidic technology, which they use to study time-dependent processes in chemistry, biochemistry, and biophysics, as well as the dynamics of complex chemical systems. His most recent Communication in *Angewandte Chemie* about a composite microfluidic system for screening protein crystallization conditions in droplets inside capillaries by on-chip X-ray diffraction was featured on the cover of issue 19/2004.^[2]



R. F. Ismagilov

Ismagilov was born in Ufa (Russia) in 1973 and completed his BSc in chemistry at the Higher Chemical College of the Russian Academy of Sciences in Moscow. He then moved to the USA, where he completed his PhD at the University of Wisconsin, Madison under the guidance of S. F. Nelsen in 1998. After postdoctoral studies at Harvard University with G. M. Whitesides, he became assistant professor in 2001 at the University of Chicago.

P. Knochel Receives Cope Scholar Award

Paul Knochel is also to receive an Arthur C. Cope Scholar Award in 2005. Born in Strasbourg (France) in 1955, Knochel has had a very international career: He completed his studies in chemistry in 1979 at the École Nationale Supérieure de Chimie in Strasbourg, and his PhD in 1982 at the ETH Zürich (Switzerland) under the guidance of D. Seebach. Following several years as a CNRS researcher in the research group of J. F. Normant at the

Université Pierre et Marie Curie in Paris, he moved to the USA to undertake postdoctoral research with M. F. Semmelhack at Princeton University. In 1988 he was appointed assistant professor at the University of Michigan, Ann Arbor (USA), where he became full professor before returning to Europe in 1992 to a position at Philipps-Universität Marburg (Germany). Since 1999 he has been Professor of Organic Chemistry at Ludwig-Maximilians-Universität München.



P. Knochel

Knochel's research interests focus on the development of novel organometallic reagents and methods for organic synthesis and asymmetric catalysis. Main group metals, such as lithium, magnesium, and boron, as well as late transition metals, such as copper and zinc, have been used for the synthesis of complex synthetic building blocks. He recently reported in *Angewandte Chemie* the preparation of polyfunctional arynes via 2-magnesiased diaryl sulfonates.^[3] His Review on highly functionalized Grignard reagents prepared by halogen-metal exchange reactions appeared in 2003.^[4]

- [1] D. Laage, I. Burghardt, T. Sommerfeld, J. T. Hynes, *ChemPhysChem* **2003**, 4, 61.
- [2] B. Zheng, J. D. Tice, L. S. Roach, R. F. Ismagilov, *Angew. Chem.* **2004**, 116, 2562; *Angew. Chem. Int. Ed.* **2004**, 43, 2508.
- [3] I. Sapountzis, W. Lin, M. Fischer, P. Knochel, *Angew. Chem.* **2004**, 116, 4464; *Angew. Chem. Int. Ed.* **2004**, 43, 4364.
- [4] P. Knochel, W. Dohle, N. Gommermann, F. F. Kneisel, F. Kopp, T. Korn, I. Sapountzis, V. A. Vu, *Angew. Chem.* **2003**, 115, 4438; *Angew. Chem. Int. Ed.* **2003**, 42, 4302.

Hierarchical Zeolites: A Proven Strategy to Combine Shape Selectivity with Efficient Mass Transport**

Martin Hartmann*

Keywords:

carbon · ethylbenzene · mesoporous materials · zeolites

Although a variety of chemical reactions of industrial interest are catalyzed by zeolites or zeolite-analogue materials, zeolite-based catalysts have almost exclusively found application in refinery and petrochemical processes where the shape-selective properties of the microporous zeolites are exploited.^[1] One of the reasons that zeolites have not yet found a wider range of industrial applications is the sole presence of micropores which imposes diffusion limitations on the reaction rate. Mass transport to and from the active sites located within the micropores is slow (even compared to Knudsen diffusion) and limits the performance of industrial catalysts. To overcome this limitation, there has been a long-standing drive to either minimize the size of the zeolite crystals or to increase the pore size of zeolites. The latter strategy has led to the discovery of various large-pore zeolites and zeolite analogues (i.e. VPI-5,^[2] UTD-1,^[3] and more recently ECR-34,^[4] SSZ-53, and SSZ-59^[5]) and also to the discovery of mesoporous molecular sieves.^[6] However, the use of these novel materials in industrial applications is rather limited. Another possibility is to decrease the size of the zeolite crystals and several synthesis schemes have been reported which allow the preparation of

very small (< 50 nm) zeolite crystals.^[7] However, none of these attempts has produced an easy means of controlling the crystal size. Moreover, separation of the small zeolite crystals from a reaction mixture by filtration is difficult owing to the colloidal properties of these materials.

Zeolites with hierarchical pore architecture (that is, zeolites containing both micro- and mesopores) have been found to present a solution to this problem. The effect of the presence of mesopores is already used in a number of industrial processes that make use of zeolite catalysts, such as, the cracking of heavy oil fraction over zeolite Y, the isomerization of the C₅/C₆ cut of the light naphtha fraction to increase the octane number, and cumene production over dealuminated mordenite.^[8]

To prepare zeolites with hierarchical pore structure four approaches can be followed: 1) Small zeolite crystals are supported, for example, on latex spheres, carbon fibers, or surfactants, the support is then removed by calcination.^[9] 2) The walls of mesoporous silicates (e.g. MCM-41 or SBA-15) are recrystallized or zeolite precursors are

deposited on the walls of mesoporous supports.^[10] 3) A widely applied method to generate mesopores involves steaming and acid-leaching treatments of zeolite crystals.^[8] These methods generate mesopores by extraction of aluminum from the zeolite lattice. However, the mesopores formed during steaming are predominantly cavities in the zeolite crystals rather than cylindrical pores connecting the external surface with the interior of the crystal.^[8] 4) Mesopores are templated with carbon during zeolite synthesis. This method was recently developed by researchers from Haldor Topsoe.^[11–14] A carbon source, for example, carbon black, carbon nanotubes, or nanofibers,^[15] is impregnated with a zeolite precursor solution after which the material is subject to a hydrothermal treatment to grow the zeolite crystals. In a subsequent calcination step, the carbon and the template are burned away resulting in intracrystalline mesopores in the zeolite (Figure 1). Proper choice of the carbon source and the synthesis conditions allows tuning of size, shape, and connectivity of the mesopores in the system. Furthermore, the mesoporosity and composition of

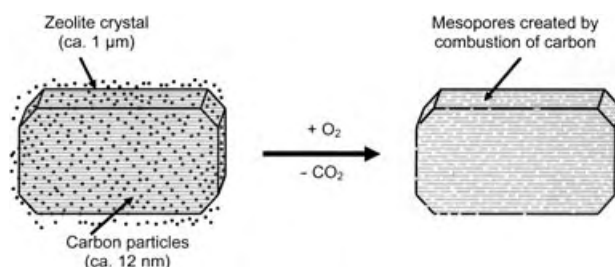


Figure 1. Growth of zeolite crystals around carbon particles. Nucleation of the zeolite occurs between the carbon particles; the crystal growth continues within the pore system of the carbon template.

[*] Priv.-Doz. Dr. M. Hartmann
Fachbereich Chemie, Technische Chemie
Technische Universität Kaiserslautern
Postfach 3049, 67653 Kaiserslautern
(Germany)
Fax: (+49) 631-205-4193
E-mail: hartmann@chemie.uni-kl.de

[**] The author's work in this area has been funded by the Deutsche Forschungsgemeinschaft and the Fonds der Chemischen Industrie.

the material can be varied independently.^[11–14] In this context, the recent publication from the group of Christensen is worth mentioning.^[16] They report the performance of zeolites with a hierarchical pore structure in an industrially relevant reaction, namely the ethylation of benzene to ethylbenzene, and compare the results to a conventional microporous HZSM-5 catalyst. The worldwide demand for ethylbenzene, which is the raw material for styrene production, is roughly 22×10^6 t per year and is almost exclusively produced by this reaction. The alkylation of benzene with ethylene over the HZSM-5 catalyst constitutes the heart of the Mobil-Badger process, which was first brought on stream in 1980. This high-temperature vapor-phase alkylation process offers various advantages over liquid-phase processes (by Monsanto or UOP) based on AlCl_3 or BF_3 catalysts. Compared to these Friedel–Craft catalysts, zeolites have the clear advantages of being noncorrosive and harmless to the environment. With the HZSM-5 catalyst an excellent selectivity for ethylbenzene of more than 98% is obtained at a benzene conversion level of about 20%. The uniform channels (dimensions (d_p) = 0.51×0.55 nm) of zeolite ZSM-5 permit the entrance of the feed molecules as well as departure of the product molecules ethylbenzene and diethylbenzene isomers, while higher alkylated products are restricted from leaving. Any of the higher alkylated products formed within the ZSM-5 channels are forced to undergo transalkylation or dealkylation to facilitate their diffusion back to the bulk. Steric hindrance of the necessary transition states is also believed to inhibit the formation of polyalkylated products. Although these are the clear advantages of using a shape-selective microporous catalyst, the problems of catalyst deactivation by coke formation and low reaction rates owing to mass transport limitations are major obstacles to overcome.

Christensen et al. showed convincingly that the zeolite catalyst with the hierarchical pore architecture is significantly more active than the conventional zeolite catalyst under the reaction conditions employed ($T_R = 583$ to 643 K; $p_R = 0.25$ MPa), which are sufficiently close to the conditions employed

in the industrial process ($T_R \approx 700$ K; $p_R = 2$ to 5 MPa).^[16] Moreover, the selectivity to ethylbenzene increases by 5 to 10% depending on the benzene conversion. The increased activity is ascribed to the improved mass transport in the mesoporous zeolites which is indicated by an increase of the apparent activation energy from 59 to 77 kJ mol^{-1} . Attributing the higher activity to improved mass transport is further substantiated by the differences in selectivities observed for the two catalysts. The higher selectivity to ethylbenzene is explained by Christensen et al. in the following way: Whenever an ethylbenzene molecule is formed, it can either be transported into the product stream or undergo further alkylation. However, in a mesoporous zeolite the diffusion path is significantly shorter than in the conventional zeolite and further alkylation is suppressed.

The hierarchical catalyst used in this study was prepared by impregnating carbon black pearls (particle diameter = 12 nm) to incipient wetness with a clear zeolite synthesis gel. After a hydrothermal treatment at 180°C for 72 h in a stainless steel autoclave, the product was collected by filtration, washed, and the carbon black was removed by controlled combustion in air at 550°C for 8 h. The mesoporous zeolite obtained is characterized by a significantly higher specific pore volume (0.59 versus $0.10 \text{ cm}^3 \text{ g}^{-1}$) and the presence of mesopores with a diameter of approximately 12 nm.^[16] The size of the mesopores is predefined by the primary carbon particles which are encapsulated by the growing zeolite crystal and are later removed by the controlled combustion in air. The shape, size and tortuosity of the mesopores can be controlled by the carbon source used. To produce large zeolite crystals (with a hierarchical pore architecture) rather than nanosized zeolite crystals, it is essential that an excess of sufficiently concentrated gel is used and that the carbon matrix has pores of a size that allows crystal growth to proceed through the pore system. It is still not fully understood which synthesis parameters promote the formation of large mesoporous crystals over nanosized crystals located in the carbon pores. However, it seems reasonable to assume that the ration of the nucleation

rate relative to the growth rate is of primary importance.^[11]

Hierarchical zeolites have also been shown to be superior catalysts in the epoxidation of oct-1-ene and cyclohexene^[12,17] as well as in the isomerization of *n*-hexane and *n*-heptane.^[18] In both cases, the activity as well as the selectivity for the desired products is higher than with the conventional zeolite catalyst.

In conclusion, the primary advantages of these new mesoporous zeolites compared with conventional micron-sized zeolite crystals are related to their higher specific external surface area causing 1) higher reaction rates for diffusion-limited reactions, 2) better transport properties resulting in improved selectivities for the target molecules, 3) better contact between active components in bifunctional catalysts, 4) slower deactivation caused by blocking of the pore mouth, and 5) easier burn-off of coke deposits. Compared with nanocrystal zeolites, the advantages of hierarchical zeolites are related to their larger crystal size, that is, easier processing owing to noncolloidal properties and higher stability in high-temperature processes including catalyst regeneration. While the effect of mesoporosity on the catalytic performance of zeolite catalysts has been known for some time and is already employed in commercial catalysts, the major achievement in the work by Christiansen et al. is that the mesopores can be produced in a more controlled manner. Moreover, the direct connection of the mesopores to the external surface represents a significant improvement compared to the (predominantly internal) mesopores generated by steaming or acid leaching. However, different areas can be identified where further research and development are required, that is, tailoring the properties of the carbon source with respect to particle size and morphology and the use of different zeolites. The effect of a mesoporous secondary pore system on mass transport is expected to be much larger for zeolites with one-dimensional pore systems. In selecting materials used in industrial processes, mordenite or zeolite L might be prime targets. Moreover, synthesis strategies for hierarchical zeolites need to be developed for

zeolites that grow from viscous gels or require seeds to crystallize.

Published Online: October 8, 2004

- [1] P. M. M. Blauwhoff, J. W. Gosselink, E. P. Kieffer, S. T. Sie, W. H. J. Stork in *Catalysis and Zeolites: Fundamentals and Applications* (Eds.: J. Weitkamp, L. Puppe) Springer, Berlin, **1999**, pp. 437–538.
- [2] M. E. Davis, C. Saldarriaga, C. Montes, J. Garces, C. Crowder, *Nature* **1988**, *331*, 698.
- [3] C. C. Freyhard, M. Tsapatsis, R. F. Lobo, K. J. Balkus, *Nature* **1996**, *381*, 295.
- [4] K. G. Strohmaier, D. W. Vaughan, *J. Am. Chem. Soc.* **2003**, *125*, 16035.
- [5] A. Burton, S. Elomari, C.-Y. Chen, R. C. Medrud, I. Y. Chan, L. M. Bull, C. Kibby, T. V. Harris, S. I. Zones, S. E. Vittoratos, *Chem. Eur. J.* **2003**, *9*, 5737.
- [6] C. T. Kresge, M. E. Leonowicz, W. J. Roth, J. C. Vartuli, J. S. Beck, *Nature* **1992**, *359*, 710.
- [7] B. J. Schoeman, J. Sterte, J. E. Ottersted, *Zeolites* **1994**, *14*, 110.
- [8] For a recent review see: S. Van Donk, A. H. Janssen, J. H. Bitter, K. P. de Jong, *Catal. Rev.* **2003**, *45*, 297.
- [9] L. Huang, Z. Wang, J. Sun, L. Miao, Q. Li, Y. Yan, D. Zhao, *J. Am. Chem. Soc.* **2000**, *122*, 3530; b) V. Valtchev, B. J. Schoeman, J. Hedlund, S. Mintova, J. Sterte, *Zeolites* **1996**, *17*, 408; c) A. Karlson, M. Stöcker, R. Schmidt, *Micro-porous Mesoporous Mater.* **1999**, *27*, 181; d) L. Huang, W. Guo, P. Deng, Z. Xue, Q. Li, *J. Phys. Chem. B* **2000**, *104*, 2817.
- [10] K. R. Kloetstra, H. van Bekkum, J. C. Jansen, *Chem. Commun.* **1997**, 2281; b) Y. Liu, W. Zang, T. J. Pinnavia, *Angew. Chem.* **2001**, *113*, 1295; *Angew. Chem. Int. Ed.* **2001**, *40*, 1255; c) Z. T. Zhang, Y. Han, L. Zhu, R. W. Wang, Y. Yu, S. L. Qiu, D. Y. Zhao, F. S. Xiao, *Angew. Chem.* **2001**, *113*, 1298; *Angew. Chem. Int. Ed.* **2001**, *40*, 1258; d) D. T. On, S. Kaliaguine, *Angew. Chem.* **2002**, *114*, 1078; *Angew. Chem. Int. Ed.* **2002**, *41*, 1036.
- [11] C. J. H. Jacobsen, C. Madsen, J. Houzvicka, I. Schmidt, A. Carlson, *J. Am. Chem. Soc.* **2000**, *122*, 7116.
- [12] I. Schmidt, A. Krogh, K. Wienberg, A. Carlsson, M. Brorson, C. J. H. Jacobsen, *Chem. Commun.* **2000**, 2157.
- [13] I. Schmidt, A. Boisen, E. Gustavsson, K. Ståhl, S. Pehrson, S. Dahl, A. Carlsson, C. J. H. Jacobsen, *Chem. Mater.* **2001**, *13*, 4416.
- [14] C. J. H. Jacobsen, J. Houzvicka, A. Carlsson, I. Schmidt, *Stud. Surf. Sci. Catal.* **2001**, *135*, 471.
- [15] A. H. Janssen, I. Schmidt, C. J. H. Jacobsen, A. J. Koster, K. P. de Jong, *Micro-porous Mesoporous Mater.* **2003**, *65*, 59.
- [16] C. H. Christensen, K. Johannsen, I. Schmidt, C. H. Christensen, *J. Am. Chem. Soc.* **2003**, *125*, 13370.
- [17] K. Johannsen, A. Boisen, M. Brorson, I. Schmidt, C. H. Jacobsen, *Stud. Surf. Sci. Catal.* **2002**, *142*, 109.
- [18] J. Houzvicka, C. J. H. Jacobsen, I. Schmidt, *Stud. Surf. Sci. Catal.* **2001**, *135*, 4200.

Enantioselective Catalysis with Chiral Phosphine Oxide Preligands

Natalia V. Dubrovina and Armin Börner*

Keywords:

asymmetric catalysis · iridium · P ligands · palladium · phosphanes

Another new chiral ligand! The search for new construction principles for enantiomerically pure trivalent phosphorus compounds for enantioselective metal catalysis continues unabated. This statement may well give rise to astonishment since the number of chiral P ligands in the literature has in the interim entered the thousands.^[1] Both academic and economic reasons are responsible for this phenomenon. Since the first use of chiral phosphines in Rh hydrogenation catalysts more than 30 years ago^[2] new metal-catalyzed reactions that can be controlled by chiral P ligands have been continuously discovered.^[3,4] Numerous applications of enantioselective syntheses in the pharmaceutical industry as well as in the production of chiral fragrances and agrochemicals also now bear witness to the considerable potential of this methodology in the chemical industry.^[5] Important are a high enantioselectivity and productivity of the catalyst. Unfortunately theory has thus far offered scant help as to which substituents on the trivalent phosphorus atom give rise to the desired catalytic properties. This uncertainty has hitherto challenged the creativity of the catalyst chemist, and as a consequence has thrust many a “treas-

ure” of almost forgotten phosphorus chemistry into the light of day. Meanwhile the palette of phosphorus ligands ranges from electron-rich alkylphosphines^[6], through phosphinites,^[7] and phosphonites,^[8] to electron-deficient phosphites.^[9] The replacement of oxygen substituents in P-OR compounds with amino groups made further electronic and steric variants available.^[10]

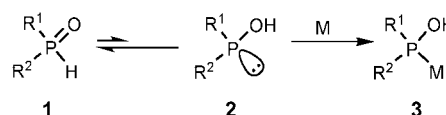
The number of choices is extended by the division into monodentate,^[11] bidentate,^[1] and tridentate^[12] ligands, which in turn can coordinate with the catalytically active metal center with a wide range of bite angles.^[13] Each newly discovered ligand class offers the guarantee of its patenting, an important aspect for an exclusive industrial exploitation in the future.

From a preparative viewpoint many trivalent phosphorus compounds are affected by one problem: they are subject to oxidation. It is therefore frequently necessary to work in an inert gas atmosphere, not exactly an advantage for routine use and scale-up. Repeatedly transient protection of the phosphorus atom is advised. However, only the BH₃ protective group, which when required can be removed in situ shortly before coordination to the metal center, has achieved any significance.^[14] A disadvantage is that the P–BH₃ adduct is unstable towards a series of acids and Lewis bases. Moreover, commonly used deprotecting reagents such as strongly basic amines also attack hydrolyzable P–O bonds.

Significantly more robust is the protection of the phosphorus atom in the form of the P=O bond. Removal of the “oxygen protective group” takes place by reduction, which is normally carried

out with silanes in a separate reaction step prior to catalysis. However, in this way the problem of handling oxidation-sensitive phosphorus compounds is merely postponed, not solved.

One way out is offered by phosphine oxides (**1**; Scheme 1), about which will



Scheme 1. Pre-established tautomerization equilibrium for the generation of a P-ligand-metal complex.

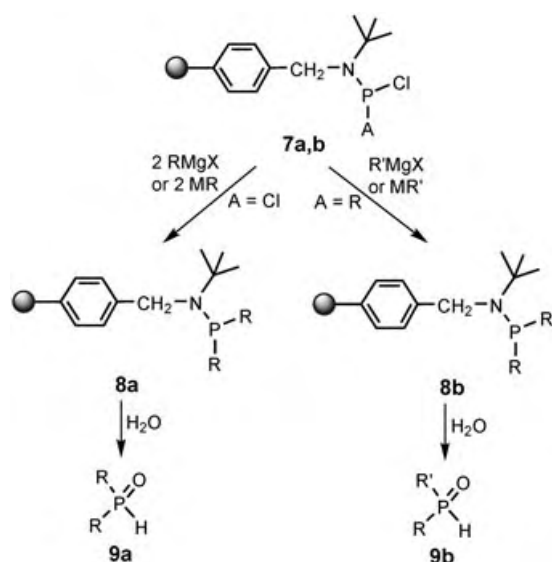
be reported here. These phosphorus derivatives can be synthesized simply by, for example, a P–C coupling reaction with phosphine halides and subsequent hydrolysis of a remaining P–X bond.^[15] They are stable to oxidation and inert to water. Naturally compounds of type **1** are not suitable to coordinate sufficiently strongly to soft transition metals through the hard oxygen atom. Their potential as ligands arises in the first instance through the tautomerism illustrated in Scheme 1 in which the pentavalent phosphine oxides **1** are in chemical equilibrium with the trivalent phosphinous acids **2**. As early as 1968 Chatt and Heaton pointed out that this equilibrium which lies far to the left-hand side can be displaced in favor of **2** by coordination to a suitable metal center.^[16] In catalysis the term precatalyst is used for stable precursors of a catalyst, we therefore logically propose the term “preligand” for compounds of type **1**.

Roundhill and co-workers utilized the displacement of this tautomeric equilibrium (Scheme 1) to construct

[*] Prof. Dr. A. Börner
Fachbereich Chemie
Universität Rostock
Albert-Einstein-Strasse 3a
18059 Rostock (Germany)
E-mail: armin.boerner@ifok.uni-rostock.de
Dr. N. V. Dubrovina, Prof. Dr. A. Börner
Leibniz-Institut für Organische Katalyse
Universität Rostock e.V.
Buchbinderstrasse 5/6
18055 Rostock (Germany)
Fax: (+49) 381-466-9324

the Pt hybrid complex **6** by reaction of the platinum tetrakisphosphine complex **4** with diphenylphosphine oxide (**5**) (Scheme 2).^[17] One interesting detail of the ligand coordination is the intramolecular hydrogen bond in the backbone that leads to the formation of a quasi-chelate which confers additional conformational stability on the complex.^[18]

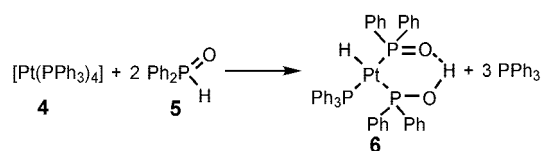
In 1986 van Leeuwen et al. demonstrated for the first time the catalytic potential of preligands, namely in the Pt-catalyzed hydroformylation of olefins with terminal and internal double bonds.^[19] Comparable catalysts were used later by Parkins for the hydrolysis of nitriles.^[20] Although these results already indicated the value of this method for the in situ generation of trivalent P



Scheme 3. Solid-phase synthesis of preligands

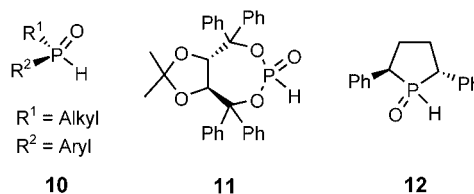
resolution of the racemate. In principle these methods can be used for both tautomeric forms. Of potential for resolution of the racemate are, for example, salt formation or esterification of the phosphinous acid with chiral alcohols.^[26]

The groups of Feringa and de Vries isolated the enantiomerically pure SPOs **10–12** on the 100 mg scale by preparative HPLC on chiral phases.^[27] The new, monodentate preligands were used in the Ir-catalyzed enantioselective hydrogenation of prochiral acetophenone imines, for



Scheme 2. Construction of a Pt complex with a phosphinous acid as ligand by complexation of isomerized phosphine oxides.

The work of Li had already established the ready accessibility of SPOs with a stereogenic phosphorus atom, whose most prominent area of application should be enantioselective catalysis. An old problem of synthetic chemistry could also be a



step closer to a solution: the synthesis of ligands with a stereogenic phosphorus atom is still more difficult than that of P ligands with a chiral carbon backbone,^[25] even though significant improvements have been achieved recently.^[6]

Two possibilities for the synthesis of enantiomerically pure SPOs, which fortunately are highly stable towards epimerization, appear especially promising: the diastereoselective generation of the stereogenic phosphorus atom and

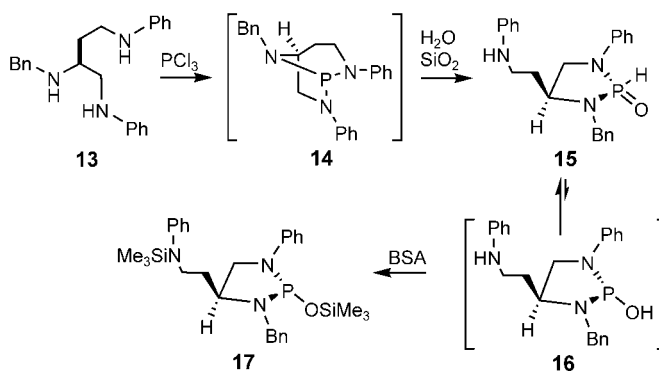
ligands, it is only since 2001 that preligands have been used to a greater extent in homogeneous catalysis. Since this time they have been abbreviated to “SPOs” (secondary phosphine oxides).^[21]

The first highlight point was Li's use of SPOs in Pd-catalyzed cross-coupling reactions with non-activated aryl chlorides.^[22] The syntheses of the preligands received particular impetus through the use of combinatorial methods. An extensive palette of phosphine oxides **9a** was prepared by the addition of Grignard reagents or metal alkyl compounds to the heterogenized dichlorophosphinamines **7a** and hydrolysis of the products **8a** (Scheme 3). Secondary phosphine oxides (**9b**) with four different substituents on the phosphorus center were accessed by the use of monoalkylchlorophosphines (**7b**).

Shortly afterwards Wolf and Lerebours too used SPOs in Pd-catalyzed coupling reactions of arenes.^[23] At the same time they reported the high stability of the catalysts to hydrolysis in Stille couplings in water as solvent.^[24]

which up to 83 % *ee* was obtained with phosphine oxides of type **10**.

Whereas the enantiomerically pure preligands in the above example had to be prepared by tedious HPLC separation, Hamada and co-workers recently succeeded in synthesizing the enantiomerically pure diaminophosphine oxide **15** by highly diastereoselective in situ hydrolysis of the triaminophosphine **14** (Scheme 4).^[28] The starting material for this conversion, the triamine **13**, is accessible in a few steps from L-aspartic acid. The formation of **15**, which was



Scheme 4. In situ synthesis of a diamidophosphorus acid silyl ester ligand. Bn = benzyl.

isolated in 60% yield as the main product of the hydrolysis on moist SiO₂, could be monitored by ³¹P NMR spectroscopy.

The preligand **15** was tested in the Pd-catalyzed enantioselective alkylation of unsymmetrical diketones in the presence of bis(trimethylsilyl)acetamide (BSA).^[29,30] Surprisingly, the best results were obtained with an excess of four equivalents of BSA. Detailed investigations showed that in the presence of Pd^{II}, complete tautomerization with subsequent coordination of the phosphorus acid **16** to the metal ion did not, as expected, take place; the displacement of the equilibrium is first enforced by in situ O,N silylation with BSA. The ligand **17** subsequently coordinates at the palladium center. This compound could also be prepared and isolated in a comparison experiment by silylation of **15**.^[31] Thus, at the end of this new and fascinating reaction sequence a nitrogen analogue of ligand classes recently well established in enantioselective homogeneous catalysis is obtained: that of the chiral, monodentate triesters of phosphorus acid (phosphites)^[9] and diesters of amidophosphorus acid (amidophosphites).^[32,33]

It remains to add that high yields and up to 94% ee were achieved with ligand **17** in the alkylation of cinnamyl acetates with β -substituted cycloalkanones. Kinetic investigations confirmed that two monodentate ligands coordinate at the Pd center. The exocyclic aminoethyl group which was already essential in the diastereoselective formation of the preligand **15** has possibly a directing effect upon the attacking nucleophile within the context of an attractive secondary interaction.^[34]

Published Online: October 21, 2004

[1] Ligand collections are found in: H. Brunner, W. Zettlmeier, *Handbook of Enantioselective Catalysis with Transition Metal Compounds, Vol. II*, VCH, Weinheim, 1993; J. Seyden-Penne, *Chiral Auxiliaries in Asymmetric Synthesis*, Wiley, New York, 1995; D. Laurenti, M. Santelli, *Org. Prep. Proced. Int.* **1999**, 31, 245–294; W. Tang, X. Zhang, *Chem. Rev.* **2003**, 103, 3029–3069; P. J. Guiry, C. P. Saunders, *Adv. Synth. Catal.* **2004**, 346, 497–637.

- [2] L. Horner, H. Büthe, H. Siegel, *Tetrahedron Lett.* **1968**, 9, 4023–4026; W. S. Knowles, M. J. Sabacky, *Chem. Commun.* **1968**, 1445–1446; L. Horner, H. Siegel, H. Büthe, *Angew. Chem.* **1968**, 80, 1034–1035; *Angew. Chem. Int. Ed. Engl.* **1968**, 7, 942–943; T. P. Dang, H. B. Kagan, *Chem. Commun.* **1971**, 481.
- [3] *Comprehensive Asymmetric Catalysis* (Eds.: E. N. Jacobsen, A. Pfaltz, H. Yamamoto), Springer, Berlin, **1999**; *Catalytic Asymmetric Synthesis* (Ed. I. Ojima), Wiley, New York, **2000**.
- [4] Phosphines are increasingly being used not only as ligands but also as organocatalysts in enantioselective syntheses. See, for example: E. Vedejs, O. Daugulis, N. Tuttle, *J. Org. Chem.* **2004**, 69, 1389–1392, and references therein.
- [5] J.-P. Genêt, *Acc. Chem. Res.* **2003**, 36, 908–918; *Asymmetric Catalysis on Industrial Scale* (Eds.: H. U. Blaser, E. Schmidt), Wiley-VCH, Weinheim, **2004**.
- [6] In respect of more recent work see: K. V. L. Crépy, T. Imamoto, *Tetrahedron Lett.* **2002**, 43, 7735–7737; G. Hoge, H.-P. Wu, W. S. Kissel, D. A. Pflum, D. J. Greene, J. Bao, *J. Am. Chem. Soc.* **2004**, 126, 5966–5967.
- [7] See, for example: M. Clochard, E. Mattmann, F. Mercier, L. Ricard, F. Mathey, *Org. Lett.* **2003**, 5, 3093–3094.
- [8] M. T. Reetz, A. Gosberg, R. Goddard, S.-H. Kyung, *Chem. Commun.* **1998**, 2077–2078.
- [9] See, for example: M. Diéguez, A. Ruiz, C. Claver, *Dalton Trans.* **2003**, 2957–2963; Z. Hua, V. C. Vassar, I. Ojima, *Org. Lett.* **2003**, 5, 3831–3834; H. Huang, Z. Zheng, H. Luo, C. Bai, X. Hu, H. Chen, *Org. Lett.* **2003**, 5, 4137–4139; I. Gergely, C. Hegedüs, H. Gulyás, Á. Szöllösy, A. Monsees, T. Riermeier, J. Bakos, *Tetrahedron: Asymmetry* **2003**, 14, 1087–1090; A. Korostylev, A. Monsees, C. Fischer, A. Börner, *Tetrahedron: Asymmetry* **2004**, 15, 1001–1005.
- [10] F. Agbossou-Niedercorn, U. Suisse, *Coord. Chem. Rev.* **2003**, 242, 145–158; N. V. Dubrovina, V. I. Tararov, Z. Kadyrova, A. Monsees, A. Börner, *Synthesis* **2004**, 2047–2051.
- [11] Reviews: F. Lagasse, H. B. Kagan, *Chem. Pharm. Bull.* **2000**, 48, 315–324; I. V. Komarov, A. Börner, *Angew. Chem.* **2001**, 113, 1237–1240; *Angew. Chem. Int. Ed.* **2001**, 40, 1197–1200.
- [12] P. Barbaro, C. Bianchini, G. Giambastiani, A. Togni, *Eur. J. Inorg. Chem.* **2003**, 4166–4172.
- [13] P. W. N. M. van Leeuwen, P. C. J. Kamer, J. N. H. Reek, P. Dierkes, *Chem. Rev.* **2000**, 100, 2741–2769.
- [14] Review: M. Ohff, J. Holz, M. Quirnbach, A. Börner, *Synthesis* **1998**, 1391–1415.
- [15] H.-J. Kleiner, *Phosphorverbindungen in Houben-Weyl, Methoden der Organischen Chemie*, 4. ed. (Ed. M. Regitz), Thieme, Stuttgart, **1982**, p. 240–245.
- [16] J. Chatt, B. T. Heaton, *J. Chem. Soc. A* **1968**, 2745–2757; see also: K. R. Dixon, A. D. Rattray, *Can. J. Chem.* **1971**, 49, 3997–4004; E. Lindner, B. Schilling, *Chem. Ber.* **1977**, 110, 3266–3271.
- [17] W. B. Beaulieu, T. B. Rauchfuss, D. M. Roundhill, *Inorg. Chem.* **1975**, 14, 1732–1734.
- [18] H-bond stabilized quasi chelate ligands were used recently in Rh-catalyzed hydroformylation: B. Breit, W. Seiche, *J. Am. Chem. Soc.* **2003**, 125, 6608–6609.
- [19] P. W. N. M. van Leeuwen, C. F. Roo-beek, R. L. Wife, J. H. G. Frijns, *J. Chem. Soc. Chem. Commun.* **1986**, 31–33; P. W. N. M. van Leeuwen, C. F. Roo-beek, J. H. G. Frijns, A. G. Orpen, *Organometallics* **1990**, 9, 1211–1222.
- [20] Hydrolysis of nitriles: T. Ghaffar, A. W. Parkins, *Tetrahedron Lett.* **1995**, 36, 8557–8660; for a later use in the amidation of nitriles see: C. J. Cobley, M. van den Heuvel, A. Abbadi, J. G. de Vries, *Tetrahedron Lett.* **2000**, 41, 2467–2470.
- [21] Occasionally the abbreviation POP is also used which is intended to describe the tautomeric equilibrium between a P=O and a P compound.
- [22] G. Y. Li, *Angew. Chem.* **2001**, 113, 1561–1564; *Angew. Chem. Int. Ed.* **2001**, 40, 1513–1516.
- [23] C. Wolf, R. Lerebours, *J. Org. Chem.* **2003**, 68, 7077–7084.
- [24] C. Wolf, R. Lerebours, *J. Org. Chem.* **2003**, 68, 7551–7554.
- [25] K. M. Pietrusiewicz, M. Zabłoka, *Chem. Rev.* **1994**, 94, 1375–1411.
- [26] For racemate cleavage of secondary phosphine oxides see: J. Drabowicz, P. Lyzwa, J. Omelanczuk, K. M. Pietrusiewicz, M. Mikołajczyk, *Tetrahedron: Asymmetry* **1999**, 10, 2757–2763; F. Wang, P. L. Polavarapu, J. Drabowicz, M. Mikołajczyk, *J. Org. Chem.* **2000**, 65, 7561–7565.
- [27] X.-b. Jiang, A. J. Minnaard, B. Hessen, B. L. Feringa, A. L. L. Duchateau, J. G. O. Andrien, J. A. F. Boogers, J. G. de Vries, *Org. Lett.* **2003**, 5, 1503–1506.
- [28] T. Nemoto, T. Matsumoto, T. Masuda, T. Hitomi, K. Hatano, Y. Hamada, *J. Am. Chem. Soc.* **2004**, 126, 3690–3691.
- [29] Review: M. T. El Gihani, H. Heaney, *Synthesis* **1998**, 357–375.
- [30] Reviews: E. J. Corey, A. Guzman-Perez, *Angew. Chem.* **1998**, 110, 402–415; *Angew. Chem. Int. Ed.* **1998**, 37, 388–401; J. Christoffers, A. Mann, *Angew. Chem.* **2001**, 113, 4725–4732; *Angew. Chem. Int. Ed.* **2001**, 40, 4591–4597.

- [31] For the preparation of analogous chiral compounds and their reactions see: V. J. Blazis, K. J. Koeller, C. D. Spilling, *J. Org. Chem.* **1995**, *60*, 931–940; A. De la Cruz, K. J. Koeller, N. P. Rath, C. D. Spilling, I. C. F. Vasconcelos, *Tetrahedron* **1998**, *54*, 10513–10524.
- [32] M. van den Berg, A. J. Minnaard, E. P. Schudde, J. van Esch, A. H. M. de Vries, J. G. de Vries, B. L. Feringa, *J. Am. Chem. Soc.* **2000**, *122*, 11 539–11 540; S. Doherty, E. G. Robins, I. Pál, C. R. Newman, C. Hardacre, D. Rooney, D. A. Mooney, *Tetrahedron: Asymmetry* **2003**, *14*, 1517–1527.
- [33] Recently the use of a chiral monodentate diamidophosphite as ligand in Pd-catalyzed enantioselective alkylation was reported: V. N. Tsarev, S. E. Lyubimov, A. A. Shiryaev, S. V. Zheglov, O. G. Bondarev, V. A. Davankov, A. A. Kabro, S. K. Moiseev, V. N. Kalinin, K. N. Gavrilov, *Eur. J. Org. Chem.* **2004**, 2214–2222.
- [34] Reviews: M. Sawamura, Y. Ito, *Chem. Rev.* **1992**, *92*, 857–871; A. Börner, *Eur. J. Inorg. Chem.* **2001**, 327–337.

Why Wait to Make Great Discoveries

When you can make them in an instant with
Wiley InterScience® Pay-Per-View and ArticleSelect™

Now you can have instant, full-text access to an extensive collection of journal articles or book chapters available on Wiley InterScience. With Pay-Per-View and ArticleSelect™, there's no limit to what you can discover...

ArticleSelect™ is a token-based service, providing access to full-text content from non-subscribed journals to existing institutional customers (EAL and BAL)

Pay-Per-View is available to any user, regardless of whether they hold a subscription with Wiley InterScience.

Benefits:

- Access online full-text content from journals and books that are outside your current library holdings
- Use it at home, on the road, from anywhere at any time
- Build an archive of articles and chapters targeted for your unique research needs
- Take advantage of our free profiled alerting service, the perfect companion to help you find specific articles in your field as soon as they're published
- Get what you need instantly, no waiting for document delivery
- Fast, easy, and secure online credit-card processing for Pay-Per-View downloads
- Special, cost-savings for EAL customers: whenever a customer spends tokens on a title equaling 115% of its subscription price, the customer is auto-subscribed for the year
- Access is instant and available for 24 hours

www.interscience.wiley.com



The Road to Chemical Names and Eponyms: Discovery, Priority, and Credit

Pedro Cintas*

Keywords:

discovery · elements · history of chemistry · named reactions

Dedicated to Professor Jerome A. Berson for his “discoveries” of scientific discovery

Introduction

What's in a chemical name? Tracing the origins and significance of such names often requires careful detective work. The naming of a theory, chemical substance, transformation, or unit of measurement dates back at least to the alchemists. The history of science has demonstrated that language is not only the means by which the practitioners communicate, but it also conveys a fascinating and instructive social dimension that enriches our culture. The origins of element names along with the etymology of traditional chemical names (which have been progressively replaced by more systematic ones) constitute representative examples.^[1] In addition, the naming after a scientist reflects a description of the more human side of research and says much about two intertwined issues: discovery and proper recognition. Consider, for instance, a series of 20th century chemists who are credited with discovering some selected and useful organic reactions: Grignard, Robinson, Wittig, Brown, Stille, Heck, and Suzuki. Nowadays, recognition mostly comes naturally because an academic or industrial chemist may use multiple publications to describe the work and because of the present trend of putting value and weight on frequency of citation. But such bibliometric indexes were absent

when the landmark discoveries were made that propelled an obscure branch of natural philosophy into modern chemistry.

In an earlier perspective on discoveries missed and discoveries made, Berson admirably addressed this concern and wrote that the defining property, which is also the immutable precondition of creativity, is the proper conflation of rational and imaginative elements.^[2] In a more recent essay on carbon skeletal rearrangements, he again discussed the act of discovery and disputes over priority.^[3] What is more, Berson formulated a thought-provoking question: why worry about proper attribution of credit?

“A candid response would be that it is good to be first for some easily listed reasons: our grant proposals, our patent applications, and...our egos. ... However, there is another purpose. That is the need to understand the dynamics and temporal course of the process of discovery itself. Only by this kind of analysis is it possible to apprehend the mutual influences of scientific theories and experiments.”

Both premises are likely to be correct. Numerous scientists claimed a particular discovery or invention as their own, while being fully aware of previous (or almost simultaneous) work. In fact, renaming has been a common practice in the history of science. On the other hand, the correct assignment of credit places a discovery within a particular historical context. However, the intriguing question to be addressed is to what extent such an assignment reflects the entire intellectual and imaginative process. Some authors simply describe an isolated, yet remarkable, experimental

observation but overlook its importance entirely.

Even worse, our modern interpretation of a particular phenomenon may often differ from the original statement. This essay is a brief journey through some historical episodes, illustrating that chemical discovery is in fact a domino reaction, in many ways a portrait of the evolution of chemistry through the researchers who claim credit. Here, the philosophy of science, rather than narrative history, can be of further help. It is not my goal to discuss whether discovery is consistent with philosophical theories, an aspect that some chemists will no doubt debate.^[4] Instead we should catch a glimpse of the human side of discovery and credit, which leads to relevant conclusions. Probably the main point is that individual contributions are often overestimated and only a broader perspective contributes to the advancement of science.

Elementary, My Dear Uncle Tungsten^[5]

Many elements have been known since the ancient times and their names have therefore an obscure origin; others with miscellaneous origins were named after a place or a peculiar property; and finally some elements were named after people. These include bohrium, curium, einsteinium, fermium, gadolinium, lawrencium, meitnerium, mendelevium, nobelium, and rutherfordium. None of them were actually discovered by the corresponding scientists, which supports the so-called Stigler's law of eponymy claiming that no scientific discovery is named after its original discoverer.^[6] (It

[*] Prof. Dr. P. Cintas
Departamento de Química Orgánica
Facultad de Ciencias-UEx
06071 Badajoz (Spain)
Fax: (+34) 924-271-149
E-mail: pecintas@unex.es

should be noted, nonetheless, that eponymy holds for names derived from real or mythical figures, not necessarily the discoverer.^[7] Perhaps, there is a notable exception: seaborgium (element 106). It was named after nuclear chemist Glenn Theodore Seaborg (1912–1999). The element was first created by a team led by Albert Ghiorso at the Lawrence Berkeley National Laboratory in 1974. The team also included Glenn Seaborg as co-discoverer. A few months earlier, Russian scientists in Dubna reported to have synthesized the same element. However, credit was given to the Berkeley group in 1993. Dubnium (after Dubna) is now the name of element 105, its production being first reported by Russian scientists in 1967, although in 1970 both the Dubna team and a group from Berkeley confirmed the discovery.^[8]

But if an element is at the heart of disputes on priority, it must surely be oxygen. In their play *Oxygen*,^[9] Carl Djerassi and Roald Hoffmann present their 21st century vision of the act and importance of discovering. As we know, the fictional play recreates an encounter of the three independent discoverers—Scheele, Priestley, and Lavoisier—and their wives in Stockholm in 1777 where they critically discuss their chemical experiments. Then the story launches into the second act with the establishment of a retro-Nobel prize in 2001, on the occasion of the centenary of the prizes. The Nobel committee investigates and analyzes the conflicting claims of the three scientists. At first, this seems to be a story about human psychology, but it is really about human-defined value judgments on science and the sometimes unexpected consequences of their use.

This play is also instrumental in questioning what we call discovery and who deserves proper recognition. Historical records^[8,10] suggest that the discovery should be credited to Joseph Priestley (1733–1804; Figure 1), who isolated oxygen in 1774. It was obtained earlier, in 1771, by Carl Wilhelm Scheele (1742–1786) but published later. Priestley believed that oxygen was “dephlogisticated air” and continued to believe it until his death in 1804, even though Antoine-Laurent Lavoisier (1743–1794) disproved experimentally the phlogiston

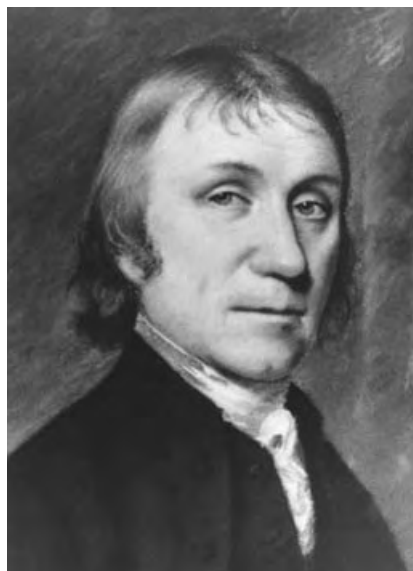


Figure 1. J. Priestley (1733–1804) was a co-discoverer of oxygen. Like Columbus, he died without realizing the importance of his discovery.

theory in 1783. Likewise, Scheele believed that the gas he isolated reacted with phlogiston in combustion reactions. It took several years and a good deal of experimentation before Lavoisier arrived at the conclusion that the gas was a new element, which he called “oxygène”. Only the French chemist truly understood what the discovery meant.^[10] Thus, discovery is really a two-step process: finding and comprehension, although some discoverers should be credited with only the former.

To be honest, it is reasonable to assume that neither Scheele nor Priestley were the first to obtain oxygen. That recognition should go to unknown European or Arabic alchemists who were skilled in thermal reactions. Some scholars have attributed that honor to the Dutch engraver, glassworker, and inventor Cornelius Jacobszoon Drebbel (1572–1633), who reported in 1621 the pyrolysis of saltpeter, a process producing oxygen.^[11] Remarkably, Drebbel also suggested a method of making sulfuric acid by the oxidation of sulfur.

Some scholars hold that chemistry evolved from a metaphysical idea of composition into an empirical idea of composition, which was pioneered by Lavoisier and settled by Dalton’s atomic theory.^[12] The phlogiston theory was one interpretation among others to cope

with such an empirical concept. Neither phlogiston nor combustion itself was a dominating issue before Lavoisier, nevertheless. From the 1770s onwards, investigations on the composition of air boosted combustion as a recurrent theme with theoretical implications, and it was thereby susceptible to refutation. Lavoisier knew that something essential was missing in the phlogiston theory. Unlike the work of Scheele or Priestley, Lavoisier’s discovery was not a matter of experimental skill; he relied on intuition and creative leaps in drawing conclusions.

The story of another gas, radon, equally illustrates this thesis on finding and recognizing phenomena. Radon is a radioactive and hazardous gas, the heaviest of the noble gases. Most noble gases were discovered by Sir William Ramsay (1852–1916) and co-workers between 1895 and 1898. Radon, however, is attributed to the German chemist Friedrich Ernst Dorn (1848–1916), who apparently called it *radium emanation* in 1900. Surprisingly, this erroneous attribution arises from a flawed translation of Dorn’s original paper published in a local journal. This fact was pointed out by Partington almost six decades later^[13] and investigated in detail in a very recent study.^[14]

Dorn certainly noticed a previous observation of Ernest Rutherford (1871–1937) on the emanation from thorium. Dorn also repeated Rutherford’s experiments and found that while uranium and polonium did not show the emanation phenomenon, thorium and radium did. The nature of such an emanation was not investigated by Dorn; it was, however, by Rutherford and Pierre and Marie Curie from 1902 on. Together with Frederick Soddy (1877–1956), Rutherford studied the physico-chemical and nuclear properties of the emanation, noting that it passed unaffected through physical barriers (cotton and water) and chemical substances (phosphorus pentoxide, sulfuric acid, heated magnesium, and even almost-molten platinum). By 1903 they claimed the existence of a new element.^[15] “It will be noticed that the only gases capable of passing in unchanged amount through all the reagents employed are the recently discovered members of the argon family.” Two decades

later, the then International Committee on Chemical Elements replaced the term radium emanation by radon.^[16]

A further story on credit and priority comes from the discovery of vanadium (element 23), first isolated by the Spanish chemist and mineralogist Andrés Manuel del Río in 1801 but officially credited to the Swedish chemist Nils Gabriel Sefström, who rediscovered it in 1831.^[8,17] Del Río (1764–1849) was born in Madrid and after studying chemistry, geology, and mineralogy, he traveled through Germany, France, and England. In 1791 he became an assistant to Lavoisier. By 1794 he moved to Mexico as a teacher at the Real Colegio de Minas en Ciudad de Mexico. In 1801 Del Río analyzed lead ores and, after successive chemical tests, he believed to have discovered a new element, which he called panchromium (from the Greek: all colors) in view of the wide range of colors of its oxides, salts, and solutions. Later, he named it erythronium (from the Greek: red) due to the intense red color of its salts when heated with acids. Del Río gave a sample of the ore containing erythronium to Alexander von Humboldt (1769–1859), who visited the Colegio de Minas in 1803. Humboldt had received instruction in mineral chemistry and convinced Del Río that the new element was presumably chromium, which also forms similar colored derivatives. Del Río withdrew his previous assignment and published a correction in a Spanish journal in 1804.^[18] But Humboldt vacillated, and after returning to Europe, he gave a sample of the lead ores to a French chemist for further analyses, who concluded that no new element was present.^[19] Humboldt finally accepted that erythronium was chromium and forwarded these results to Del Río. It took a long time, however, before this analysis reached Mexico, and Del Río felt frustrated as he had already published the conclusion that the element present in the brown ore was chromium.

The lack of recognition for Del Río adds a critical element of reflection. Chemistry throughout the 19th century was largely influenced and dominated by French and German scientists. Very few Spanish chemists had much contact with other European scientists. The reasons for this lack of contact are not

clear, although at that time cultivated people in Spain often grouped chemistry with astrology and magic. Spaniards turned their attention to practical activities like mineralogy in which they gained reputation.^[20] Del Río's annoyance for the lack of proper credit was expressed in a letter forwarded to Humboldt several years later.^[17] "*We Spaniards should not make any discovery, no matter how small, either in chemistry or mineralogy, these being a foreign monopoly. ... Did I lose all credit for not having known in 1802 all the properties of chromium in a country so lacking in books, where for the same reason the sciences are so little cultivated?*"

Despite this, Del Río and Humboldt professed reciprocal admiration. That Humboldt was not fully convinced that the salt isolated was a chromate is evidenced by the fact that he also gave a sample to Friedrich Wöhler (1800–1882) to reinvestigate its composition. In the meantime Nils Sefström (1787–1845) obtained a new element from an iron mineral and gave it the name of vanadium (after Vanadis, a Scandinavian goddess of love). Sefström gave some vanadium pentoxide to Jöns Jacob Berzelius (1779–1848), who also sent it to Wöhler. The German chemist conclusively demonstrated that vanadium was identical to erythronium, the element isolated by Del Río 30 years earlier.

Renamed Laws

Like elements, some of the most important physico-chemical laws and theories reveal the issues of priority and proper recognition. In most cases incorrect attributions arise from misunderstanding, neglect, and controversy, for which scientists and historians alike are responsible. The forgotten scenarios and actors of physical chemistry have been the subject of scholarly studies by Laidler.^[21] This analysis is reminiscent of that of Nobel prizes, which may certainly be awarded to undeserving scientists whereas deserving ones may be overlooked. In a recent book^[22] Hargittai classes nonwinners into those whose discovery was never honored by a Nobel prize and those who participated in a recognized discovery but who were not

awarded the prize. Similar observations are often made in the history of science.

It might be surprising to state that Robert Boyle (1627–1691) did not discover Boyle's law, but anticipation of the phenomenon should correctly be attributed to Richard Townley (1628–1707) and Henry Power (1623–1668) who, in 1660, established the relationship between pressure and the volume of an expanded gas.^[23] Boyle began his studies on the properties of gases several years earlier with the invaluable help of his assistant Robert Hooke (1635–1701), who helped him to construct a vacuum pump.^[24,25] Boyle described the properties of air and that air is necessary for respiration, combustion, and propagation of sound. Such results were published in 1660 in *New Experiments Physico-Mechanical, Touching the Spring of the Air and its Effects*.^[26] In 1661 Boyle submitted a report to the Royal Society, in which he presented improved experimental results on the relation, now known as Boyle's law, that the pressure of a gas is inversely proportional to its volume at constant temperature. The second edition of his 1660 work containing this result appeared in 1662.

Two of the most salient chemical laws, Le Chatelier's principle and the Arrhenius equation, were not deduced by the scientists who have become recognized by the naming of these laws. In both cases, the proper recognition must go to Dutch chemist and first recipient of the Nobel prize in chemistry, Jacobus Henricus van't Hoff (1852–1911; Figure 2), who suggested these relationships in his pioneering studies on physical chemistry in 1884.^[27]

Henry-Louis Le Chatelier (1850–1936) also published his results the same year stating that if a system in an equilibrium state is disturbed, the system will readjust in such a way as to neutralize the perturbation and restore equilibrium.^[28] In praise of Le Chatelier, it is fair to say that he explicitly mentioned van't Hoff as the pioneer of this conclusion. Some related ideas, yet in a vague form, were anticipated by Josiah Willard Gibbs (1839–1903), whose works Le Chatelier later translated into French.

The equation that correlates the effect of temperature on reaction rates



Figure 2. J. H. van't Hoff (1852–1911) was a key figure in modern stereochemistry and physical chemistry but never claimed priority and recognition.

was also suggested by van't Hoff,^[27] as a consequence of the equation for equilibrium constant. Svante August Arrhenius (1859–1927), quoting van't Hoff, applied this equation to numerous reactions, thereby demonstrating its general value.^[29] Perhaps due to his previous and bitter experience with Kolbe, van't Hoff was always a quiet and modest man. He never claimed priority and shared credit with his contemporaries. This reveals an exceptional and appealing attribute, unusual in most scientists.

Play It Again, Alexander!

The legendary image of scientists as brilliant encyclopedic minds has been progressively replaced by the image of people competent in a narrowly defined domain, at least from the 19th century on. Thus, no one would imagine any modern chemist pursuing chemistry with along with another professional activity. A notable exception, however, was the great Russian composer and chemist Aleksandr Porfirevich Borodin (1833–1887). The author of *Prince Igor* and other operas and symphonies received his doctorate in 1858 from the Medico-Surgical Academy in St. Petersburg. From 1859 to 1862 he studied in western Europe. On returning to Russia

he became adjunct professor of chemistry at the Medico-Surgical Academy and was named full professor in 1864.^[30]

Borodin largely investigated oxygenated compounds, and his most important contribution, which was once called the Borodin reaction, involves the combination of a silver carboxylate with bromine to afford an alkyl bromide, CO₂, and AgBr.^[31] Borodin should be credited with this transformation, even though he did not prove that the product was an alkyl bromide. Most organic chemists have forgotten Borodin and refer to this process as the Hunsdiecker reaction. The Hunsdieckers, husband and wife, reinvented and really developed the Borodin reaction in the 1940s.^[32]

Russian chemists also experienced a lack of recognition as time went on. This is ironic as modern chemistry owes a great debt to Russian chemists ranging from Mendeleev to Arbuzov, and other key figures who are seldom acknowledged. The lack of credit has often been attributed to the insular nature of Russian industry along with unfamiliarity of the West with the Russian language. Recent studies also point to an academic culture in Russia based on theory with little emphasis on the practical uses of basic research.^[33]

Chemists will probably find less compelling those reasons dealing with social, economic, and political factors, which cannot be dismissed anyway.^[34] Thus, in the 20th century the impact of wars, the reaction to the economic depression, and the tragedy of the Jews in the 1930s and 1940s contributed to the oversight and even denial of the role of some scientists. A still controversial factor is the fact that credit and priority are chiefly attributed by a dominant culture.

Consider, for instance, Fritz Georg Arndt (1885–1969), best known for the Arndt–Eistert homologation reaction, who also made significant contributions to the development of resonance theory and the emergence of physical organic chemistry. Christopher Ingold and his associates have been credited as the main protagonists in the field. Arndt was born in Germany in a Jewish family and pursued a significant part of his career in Turkey. He clarified the difference between tautomerism and reso-

nance, and introduced the currently accepted representations of reversible arrows for tautomerism and double-headed arrows for resonance.^[35]

Likewise, olefin formation by means of phosphonate carbanions is often referred to as the Wadsworth–Emmons or Horner–Wadsworth–Emmons modification of the Wittig reaction, although the pioneering studies were carried out by Horner.^[36] Horner's work was subject to another relevant oversight. Homogeneous asymmetric hydrogenation was initiated by Knowles and Horner with their 1968 publications. Subsequent



Figure 3. V. V. Markovnikov (1838–1904). He would hardly recognize the rule now bearing his name.

breakthroughs were made by Kagan and Knowles in the 1970s. This sequence of events has now been acknowledged in modern studies on enantioselective hydrogenation,^[37] though only Knowles has received proper recognition.

Did You Say That?

The assignment of priority and credit to the discoverers in the teaching and learning of the underlying principles of a law or theory, although desirable from a historical point of view, may also be inaccurate. This situation exists when the original statement differs substantially from its subsequent formulation or interpretation, regardless of whether the author deserves recognition. What we

always call the Markovnikov rule is probably a striking example of such an inaccuracy.^[38] Named after a giant of the structural theory and isomerism, Vladimir Vasilyevich Markovnikov (1838–1904; Figure 3), the rule predicts the regiochemistry of addition reactions to unsymmetrical alkenes. Ask any undergraduate student of organic chemistry what the rule says, and the answer will almost certainly be that in the addition of a protic acid to the double bond of an alkene, the proton adds to the less substituted carbon atom of the double bond.

This principle is found in most sophomore and advanced organic chemistry textbooks. Surprisingly, *Markovnikov never wrote this corollary in such a way*. In 1870 Markovnikov published a long paper containing work from his doctoral thesis (1869) at the University of Kazan.^[39] In this paper he described the addition of hypochlorous acid to propene and correctly assigned the structure of the resulting chlorohydrin as 1-chloro-2-propanol. However, he was cautious in formulating a general rule because his PhD mentor Aleksandr Mikhaylovich Butlerov (1828–1886) had previously suggested a structure of a primary alcohol for the addition product of HOCl to isobutene. Markovnikov stated: “While it is impossible at this time ... to detect a clear general rule on the manner of addition of the elements of hypochlorous acid to unsaturated hydrocarbons, for hydrohalic acids such a general rule is available ... the halide adds to the less hydrogenated carbon atom, that is, to the carbon which is more under the influence of other carbons.”^[*]

He continued, on the basis of previous studies with Kolbe,^[40] adding that

“... in the addition of a hydrohalic acid to vinyl chloride, chlorinated propylene, and other analogs, the halide will always add to the carbon atom which is already attached to a halide.”^[**]

It should be emphasized that Markovnikov focuses invariably on the fate of the halide ion in the product. One might argue that our modern citation of the rule, that is, the hydrogen going to the less substituted carbon, is simply an equivalent statement. This change of the perspective is nevertheless especially puzzling within the historical context. In 1874 Henry, without giving credit to Markovnikov, proposed that in the addition of a reagent XY to unsymmetrical substrates, the more negative radical (X) becomes attached to the less hydrogenated carbon and the less negative radical (Y) to the more hydrogenated carbon.^[41] This agrees with the result suggested by Markovnikov for hydrohalic acids; but for HOCl, Henry proposed the polarity $\text{HO}^+ \text{Cl}^-$, and this would add in inverse form to Markovnikov's rule. Markovnikov was forced to reformulate his observations in a more extended way:^[42] “[In the addition of YZ to unsaturated molecules] at low temperature, the more negative element or group (Y) combines with the less hydrogenated carbon atom, or with that which was already attached to some negative element; but at higher temperatures, it is the element Z which becomes attached to the less hydrogenated carbon ... the reaction follows a course entirely opposite from the first case.”^[**]

[*] The original article^[40] reads: “daß bei der Addition der Chlor-, Brom- oder Jodwasserstoffsäuren zu dem Vinylchlorür, gechlorten Propylen und anderen Analogien, sich das Haloïd immer zu dem Kohlenstoffatom addiren werde, welches schon mit einem Haloïd verbunden ist.”

[**] This citation appears as follows in the original article:^[42] “Lorsqu'à une molécule non saturée $\text{C}^m\text{H}^n\text{X}$ s'ajoute un autre système moléculaire YZ à une température basse, l'élément ou le groupe le plus négatif Y se combine avec l'atome de carbone le moins hydrogéné, ou avec celui qui était déjà en liaison directe avec quelque élément négatif; mais, à des températures comparativement plus hautes, c'est l'élément Z qui se fixe sur le carbone le moins hydrogéné, c'est-à-dire que, pour les mêmes substances, la réaction prend une marche tout à fait opposée à la première.”

[*] This citation appears as follows in the original article:^[39] “Wenn es wegen der ungenügenden Zahl der Beobachtungen unmöglich ist, jetzt eine gewisse Gesetzmäßigkeit für die Art der Verbindung der Elemente der unterchlorigen Säure mit ungesättigten Kohlenwasserstoffen auszusuchen, so ist für die Haloïdwasserstoffsäuren eine solche Regelmäßigkeit vorhanden. ... wenn ein unsymmetrisch constituierter Kohlenwasserstoff sich mit einer Haloïdwasserstoffsäure verbindet, so addirt sich das Haloïd an das weniger hydrogenisirte Kohlenstoffatom, d. h. zu dem Kohlenstoff, welcher sich mehr unter dem Einflusse anderer Kohlenstoffe befindet.”

After Markovnikov's death, “his rule” was seldom cited for nearly three decades.^[38a] In the 1930s Kharasch and his associates began their detailed studies on halogen acid addition reactions. Little use was made of the rule, as numerous substrates led to exceptions. On the basis of the peroxide effect in HBr additions, they then referred to “normal” and “abnormal” additions.^[43]

What is especially astonishing throughout this story is the widely used term “anti-Markovnikov”, which is difficult to interpret according to what Markovnikov did say. Anti-Markovnikov additions were popularized after the seminal works on hydroboration by Herbert Brown and his associates.^[44] As strange as it may be, *addition of a borane to an alkene does take place according to Markovnikov's rule of 1875*,^[42] that is, the more negative hydride ion becomes attached to the less hydrogenated carbon in the transition state of this concerted process. It is only after conversion of the borane-addition product into the resulting alcohol that a conflicting result emerges.

We have now learned that a sound interpretation of the regiochemical outcome of addition reactions lies in the principles of physical organic chemistry. The modern rule can thus be extended to electrophiles other than protic acids, by saying that the electrophilic addition to an alkene occurs in such a way as to generate the most stable intermediate, usually a carbocation.^[45]

It comes as a surprise that some scholars question honoring Markovnikov by naming a rule after him.^[38] Markovnikov had great influence on structural chemistry in the 19th century and made important contributions to structure and isomerism for which he should be remembered. But the rule bearing his name draws attention away from the logical principles of modern chemistry. Perhaps Markovnikov himself would have objected to a recognition that misused his words.

What Have We Learned?

In short, a discovery is a complex event. Recognition usually brings a wave of smugness about the superiority of a few scientists. In reality, there is no

such thing. Forgotten geniuses have made huge and often unrecognized contributions to the advancement of science and scientific thought. A discovery is, above all, a domino reaction, in which successive pieces ultimately make up the whole. This metaphor was highlighted in this essay by examples of elements, reactions, and laws which illustrate the distinction between finding and comprehension. The first protagonist may come across an unexpected outcome in the course of a particular topic, while others make efforts to understand and explain the whole phenomenon. Moreover, discoveries (or reformulations) have been the test of many of the theories and techniques of chemistry, which were once accepted. The concluding lesson can be extracted from an insightful Baconian aphorism: “Experiments that yield light are more worth while than experiments that yield fruit.”^[46] As a chemist often turned an apprentice of history, I have nothing more to add.

Published Online: September 16, 2004

- [1] a) W. E. Flood, *The Dictionary of Chemical Names*, Philosophical Library, New York, **1963**; b) D. W. Ball, *J. Chem. Educ.* **1985**, 62, 787–788; c) A. Nickon, E. F. Silversmith, *Organic Chemistry: The Name Game*, Pergamon, Oxford, **1987**.
- [2] J. A. Berson, *Tetrahedron* **1992**, 48, 3–17.
- [3] J. A. Berson, *Angew. Chem.* **2002**, 114, 4849–4854; *Angew. Chem. Int. Ed.* **2002**, 41, 4655–4660.
- [4] Philosophical problems of chemical discovery with examples drawn from organic chemistry have also been analyzed in a recent book: J. A. Berson, *Chemical Discovery and the Logicians’ Program*, Wiley-VCH, Weinheim, **2003**.
- [5] I have deliberately changed the well-known Sherlock Holmes aphorism (“Elementary, my dear Watson”). Uncle Tungsten is a delightful collection of autobiographical memories by an English boy who chronicles his discovery of science in the 1940s and the social atmosphere in which that discovery took place. If you want to uncover the metaphor behind tungsten, you must go, at least, to Chapter 4: O. Sacks, *Uncle Tungsten. Memories of a Chemical Boyhood*, Vintage Books, New York, **2001**.
- [6] a) S. M. Stigler, *Trans. N. Y. Acad. Sci.* **1980**, 39, 147–158; b) S. M. Stigler, *Statistics on the Table. The History of Statistical Concepts and Methods*, Harvard University Press, Cambridge, MA, **1999**.
- [7] The term eponym derives from Greek *eponymos*: giving a significant name. Problems in chronological reconstruction of ancient civilizations have often been solved through eponymy. A salient case is the chronology of Sumerian civilization after about 1450 B.C., which is provided by dated tablets and the so-called lists of eponyms (the names of Assyrian officials who served one-year terms were used to identify each year): *The New Encyclopaedia Britannica*, Vol. 21, 15th ed., Britannica, Chicago, IL, **1990**, pp. 912–913.
- [8] An excellent survey of the elements that compose the Periodic Table, often adorned by personal stories, has been published recently in *Chemical and Engineering News* to celebrate its 80th anniversary: *Chem. Eng. News* **2003**, 81(36), 28–190.
- [9] C. Djerassi, R. Hoffmann, *Oxygen. A Play in Two Acts*, Wiley-VCH, Weinheim, **2001**.
- [10] a) C. S. Quinsey, *J. Chem. Educ.* **2003**, 80, 1124–1128; b) K. R. Williams, *J. Chem. Educ.* **2003**, 80, 1129–1131.
- [11] C. J. Drebbel, *De Natuere der Elementen*, Rotterdam, **1621**, p. 32. A short note can be found in *J. Chem. Educ.* **2003**, 80, 1112.
- [12] R. Siegfried, *From Elements to Atoms: A History of Chemical Composition*, American Philosophical Society, Philadelphia, PA, **2002**.
- [13] J. R. Partington, *Nature* **1957**, 179, 912.
- [14] J. L. Marshall, V. R. Marshall, *Bull. Hist. Chem.* **2003**, 28, 76–83.
- [15] a) E. Rutherford, F. Soddy, *Philos. Mag.* **1902**, 4, 569–585; b) E. Rutherford, F. Soddy, *Philos. Mag.* **1903**, 5, 561–576.
- [16] F. W. Aston, G. P. Baxter, B. Brauner, A. Debierne, A. Leduc, T. W. Richards, F. Soddy, G. Urbain, *J. Am. Chem. Soc.* **1923**, 45, 867–874.
- [17] An excellent account on the Del Río-Humboldt affair and the rediscovery of vanadium has been published recently: L. R. Caswell, *Bull. Hist. Chem.* **2003**, 28, 35–41.
- [18] A. del Río, *Ann. Ciencias Natur.* **1804**, 7, 30–48.
- [19] H.-V. Collet-Descotils, *Ann. Chim.* **1805**, 53, 268–271.
- [20] L. R. Caswell, R. W. S. Daley, *Bull. Hist. Chem.* **1999**, 24, 11–19.
- [21] a) K. J. Laidler, *The World of Physical Chemistry*, Oxford University Press, Oxford, **1993**; b) K. J. Laidler, *Acc. Chem. Res.* **1995**, 28, 187–192.
- [22] I. Hargittai, *The Road to Stockholm*, Oxford University Press, Oxford, **2002**, chap. 12.
- [23] I. B. Cohen, *Nature* **1964**, 204, 618–621.
- [24] J. Bennett, M. Cooper, M. Hunter, L. Jardine, *London’s Leonardo: The Life and Work of Robert Hooke*, Oxford University Press, Oxford, **2003**.
- [25] It has been erroneously claimed that Boyle and Hooke invented the vacuum pump: J. E. McClellan III, H. Dorn, *Science and Technology in World History: An Introduction*, Johns Hopkins University Press, Baltimore, **1999**. They simply improved the pump developed by Otto von Guericke in 1650: G. A. Oravas, *Nature* **2000**, 404, 17–18.
- [26] *The Works of Robert Boyle, Vol. 1* (Eds.: M. Hunter, E. B. Davis), Pickering & Chatto, London, **1999**, pp. 141–301; Vol. 6, pp. 27–188; Vol. 9, pp. 121–264.
- [27] J. H. van’t Hoff, *Études de Dynamique Chimique*, F. Muller, Amsterdam, **1884**.
- [28] H.-L. Le Chatelier, *C. R. Hebd. Seances Acad. Sci.* **1884**, 99, 786–789.
- [29] S. Arrhenius, *Z. Phys. Chem.* **1889**, 4, 226–248.
- [30] a) A. D. White, *J. Chem. Educ.* **1987**, 64, 326–327; b) *The New Encyclopaedia Britannica*, Vol. 2, 15th ed., Britannica, Chicago, **1990**, p. 392.
- [31] A. Borodin, *Justus Liebigs Ann. Chem.* **1861**, 119, 121–123.
- [32] H. Hunsdiecker, C. Hunsdiecker, *Ber. Dtsch. Chem. Ges.* **1942**, 75, 291–297.
- [33] Some critical reviews of some 19th century Russian contributions can be found in: a) R. E. Rice, *Bull. Hist. Chem.* **2002**, 27, 17–25; b) N. M. Brooks, *Bull. Hist. Chem.* **2002**, 27, 26–36; c) see also a detailed analysis in: L. R. Graham, *Science in Russia and the Soviet Union*, Cambridge University Press, Cambridge, **1994**.
- [34] See for instance: *The German Chemical Industry in the Twentieth Century* (Ed.: J. E. Lesch), Kluwer Academic Publishers, Dordrecht, **2000**.
- [35] a) E. Campaigne, *J. Chem. Educ.* **1959**, 36, 336–339; b) M. Saltzman, *J. Chem. Educ.* **1986**, 63, 588–593; c) L. Aka-Burk, *Bull. Hist. Chem.* **2003**, 28, 42–53.
- [36] In his comprehensive treatment of this transformation, Wadsworth recognizes Horner’s preliminary studies with phosphine oxide and phosphinate carbanions and, “in order to avoid misdirecting credit, proper names are omitted and the synthesis termed phosphonate-olefin formation”: W. S. Wadsworth, Jr., *Org. React.* **1977**, 25, 73–253.
- [37] W. Tang, X. Zhang, *Chem. Rev.* **2003**, 103, 3029–3069.
- [38] For excellent scholarly studies from a historical perspective, see: a) G. Jones, *J. Chem. Educ.* **1961**, 38, 297–300; b) T. A. Newton, *J. Chem. Educ.* **1987**, 64, 531–

- 532; c) J. Tierney, *J. Chem. Educ.* **1988**, 65, 1053–1054; d) R. C. Kerber, *Found. Chem.* **2002**, 4, 61–72.
- [39] W. Markownikoff, *Ann. Chem. Pharm.* **1870**, 228–259.
- [40] W. Markownikoff, *Ann. Chem. Pharm.* **1868**, 339–352.
- [41] L. Henry, *C. R. Hebd. Seances Acad. Sci.* **1874**, 79, 1203.
- [42] V. Markovnikoff, *C. R. Hebd. Seances Acad. Sci.* **1875**, 81, 668–671, 728–730, 776–779.
- [43] a) M. S. Kharasch, E. T. Margolis, F. R. Mayo, *J. Org. Chem.* **1936**, 1, 393–404; b) F. R. Mayo, C. Walling, *Chem. Rev.* **1940**, 40, 351–412.
- [44] H. C. Brown, B. C. Subba Rao, *J. Am. Chem. Soc.* **1959**, 81, 6423–6428.
- [45] a) N. Isenberg, M. Grdinic, *J. Chem. Educ.* **1969**, 46, 601–605; b) M. Grdinic, N. Isenberg, *Intra-Sci. Chem. Rep.* **1970**, 4, 145–162.
- [46] F. Bacon, *Novum Organum* (Eds.: P. Urbach, J. Gibson), Open Court, Chicago, **1994**. This is a short version of Aphorism 99, Book I.

Life's Simple Pleasures!



No need to waste precious time looking for the right information – Register now for the free **Wiley-VCH Alerting Service**.

It's simple – and it's fast.

To receive regular news per e-mail tailored precisely to your needs and interests, just fill in the registration form at www.wiley-vch.de/home/pas/

 **WILEY-VCH**

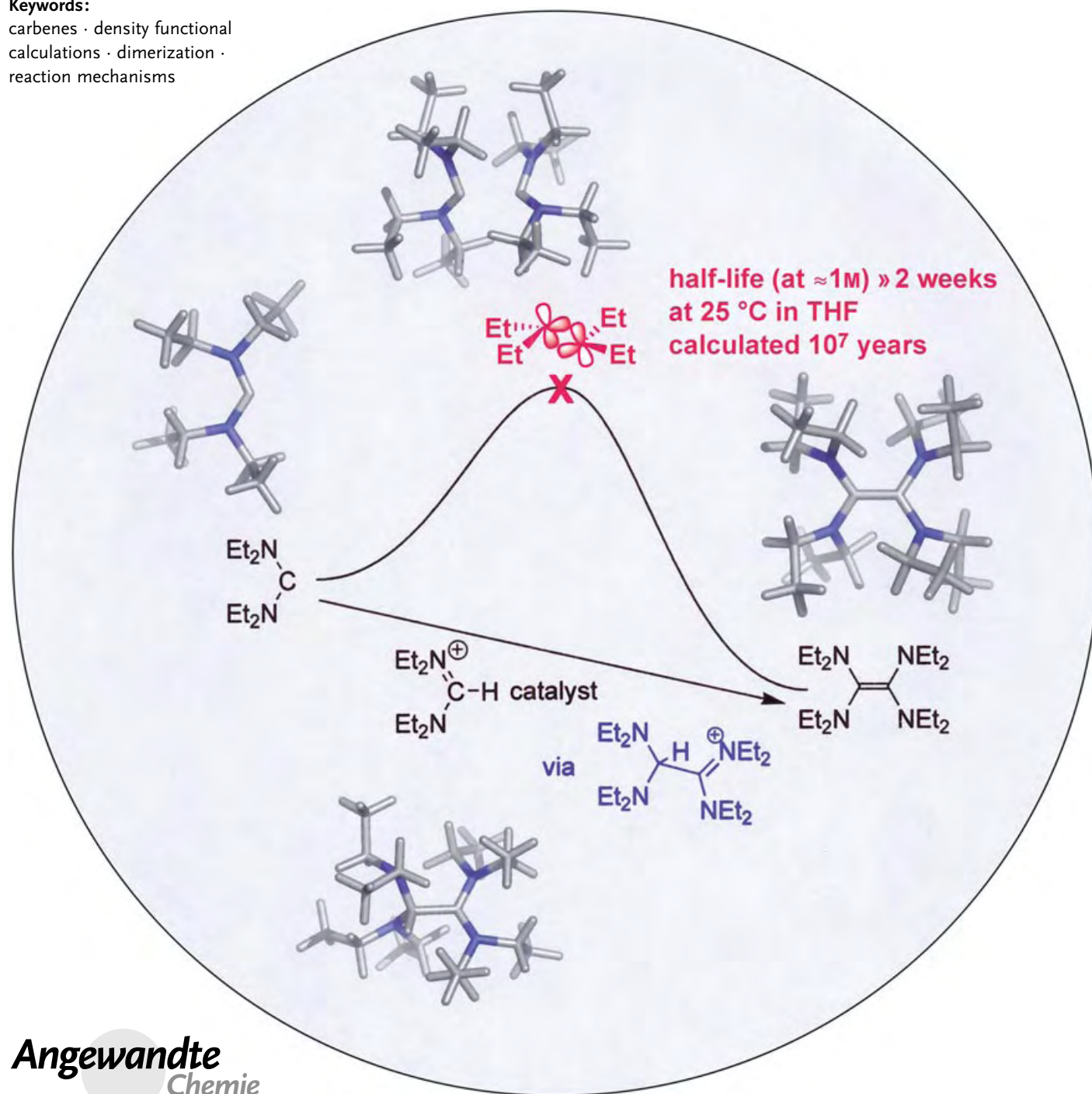
Reaction Mechanisms

When and How Do Diaminocarbenes Dimerize?

Roger W. Alder,* Michael E. Blake, Leila Chaker, Jeremy N. Harvey, François Paolini, and Jan Schütz

Keywords:

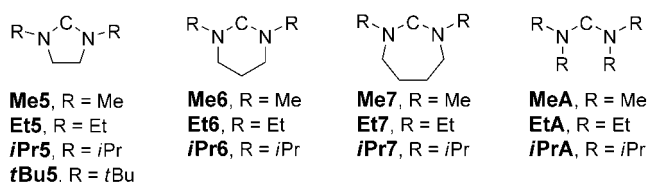
carbenes · density functional calculations · dimerization · reaction mechanisms



No example of a simple uncatalyzed dimerization of a diaminocarbene has been clearly established, so it is timely to ask what factors control the thermodynamics of this reaction, and what mechanisms are responsible for the observed dimerizations? In agreement with qualitative experimental observations, the dimerizations of simple five- and six-membered-ring diaminocarbenes are calculated to be 100 kJ mol^{-1} less favorable than those of acyclic counterparts. This large difference is semiquantitatively accounted for by bond and torsional angle changes around the carbene centers. Carbenes such as $(\text{Et}_2\text{N})_2\text{C}$ are kinetically stable in THF at 25°C in agreement with calculated energy barriers, but they rapidly dimerize in the presence of the corresponding formamidinium ion. This proton-catalyzed process is probably the most common mechanism for dimer formation, and involves formation of C-protonated dimers, which can be observed in suitable cases. The possibility of alkali-metal-promoted dimerization is raised, and circumstantial evidence for this is presented.

1. Introduction

Since the first observation of a stable imidazol-2-ylidene in 1991,^[1] derivatives of diaminocarbene have become the focus of intense study,^[2–4] and have also entered the marketplace as extremely valuable ligands for catalytically active transition-metal complexes.^[5–7] One fundamental aspect of their behavior, their dimerization to derivatives of tetraaminoethene, remains poorly understood however. Herein, we review current knowledge of both equilibria and kinetics for diaminocarbene dimerization; the very limited knowledge about thiazol-2-ylidenes and related species will be mentioned where appropriate. We will use the set of simple diaminocarbenes, **Me5–iPrA** (**5** denotes the ring size, **A**



stands for acyclic) to illuminate the factors which control the answers to two questions:

When do diaminocarbenes dimerize? (Equilibria)

How do they dimerize? (Kinetics and mechanism)

We will show that dimerization is typically 100 kJ mol^{-1} more favorable for acyclic and seven-membered-ring carbenes than for five- and six-membered cyclic carbenes, and discuss the reasons for this unexpected result. With respect to kinetics and mechanism, we will argue that most dimers are formed by proton-catalyzed or possibly metal-ion-catalyzed routes and that the classic dimerization mechanism^[8] for a singlet carbene (Figure 1) in which the filled sp^2 orbital of

each carbene interacts with the formally empty p orbital on the other has yet to be established experimentally and may be extremely uncommon for diaminocarbenes.

We first review the evidence concerning the dimerization of imidazol-2-ylidenes **1**, benzimidazol-2-ylidenes **2**, and dihydroimidazol-2-ylidenes (e.g. **Me5–tBu5** and related derivatives with more complex R substituents).

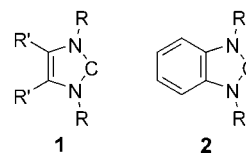


Figure 1. Transition state geometry for the dimerization of singlet carbenes.

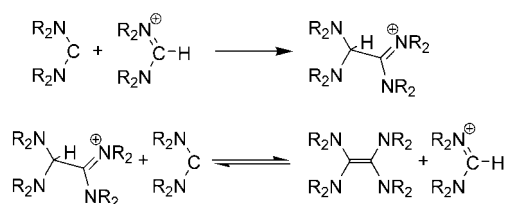
From the Contents

2. Diaminocarbene/Tetraaminoethene Equilibria	5898
3. The Kinetics of the Wanzlick Equilibrium ^[32]	5899
4. Diaminocarbene Preparation	5900
5. Experimental Evidence for Dimer Formation from the Reaction of Diaminocarbenes with Formamidinium Ions	5901
6. Structures for Diaminocarbenes Me5–iPrA, and Their Dimers	5902
7. Dimerization Equilibria for Diaminocarbenes	5904
8. Calculations on the Direct Mechanism for Carbene Dimerization	5905
9. Calculations on Tetraaminoethene Formation from the Reaction of Diaminocarbenes with Formamidinium Ions	5906
10. Possible Mechanisms for Metal-Promoted Dimerization	5907

[*] Prof. Dr. R. W. Alder, Dr. M. E. Blake, Dr. L. Chaker, Dr. J. N. Harvey, F. Paolini, J. Schütz
School of Chemistry
University of Bristol
Cantock's Close, Bristol BS8 1TS (UK)
Fax: (+44) 117-929-8611
E-mail: rog.alder@bristol.ac.uk

Probably well over 90% of all studies of diaminocarbenes concern five-membered-ring compounds, but we will argue that the N-C-N angle (necessarily small in five-membered-ring compounds) is an important parameter in controlling the behavior of diaminocarbenes, and that more attention should be paid to acyclic diaminocarbenes and to other ring sizes.

We then briefly review methods of preparation of diaminocarbenes with particular reference to the generation of **Me5-iPrA**, and provide experimental evidence that proton-catalyzed mechanisms (Scheme 1) are common routes to dimers. The mechanism for dimerization in Scheme 1 has been discussed in other contexts. Thus Arduengo et al.^[9] reported that the dimerization of a relatively stable thiazol-2-ylidene was catalyzed by proton sources, and the elegant labeling experiments of Chen and Jordan^[10] demonstrate dimer formation by nucleophilic thiazol-2-ylidene addition to a thiazolium ion during thiazolium-ion-catalyzed benzoin condensation.



Scheme 1. Proton-catalyzed mechanism for carbene dimerization.

We will then discuss density functional calculations on the thermodynamics for dimerization of carbenes **Me5-iPrA**; these reveal that dimerization is relatively unfavorable for five- and six-membered-ring carbenes, compared to acyclic

and seven-membered-ring species, and we show that unexpected stability trends among the carbenes, rather than the dimers, is responsible for this. An attempt is made to identify the structural factors responsible for these trends. DFT studies of the transition states for the uncatalyzed dimerization of carbenes **Me5**, **Et5**, **Me6**, **MeA**, and **EtA** show that the energy barriers are generally high, but also vary strikingly with carbene structure, so that very few diaminocarbenes are likely to dimerize by the classic mechanism, in agreement with current experimental understanding. Some aspects of the proton-catalyzed mechanism (Scheme 1) will be discussed in the light of the results of DFT calculations which point to the importance of the relative basicity of carbenes and dimers. Finally, we will provide circumstantial evidence that Li species, while stabilizing diaminocarbenes thermodynamically, may also provide metal-catalyzed pathways for dimerization.

2. Diaminocarbene/Tetraaminoethene Equilibria; Previous Experimental and Computational Evidence

Simple unhindered imidazol-2-ylidenes such as **1** ($R = R' = \text{Me}$) are thermodynamically stable towards dimerization to tetraazafulvalenes.^[11] This extraordinary fact should be fully appreciated at the outset of any discussion of diaminocarbene dimerization. Replacing the four hydrogen atoms of ethene with two $\text{RN}-\text{CR}=\text{CR}-\text{NR}$ bridges leads to the complete disappearance of the $> 700 \text{ kJ mol}^{-1}$ bond energy of the $\text{C}=\text{C}$ double bond! This can be seen as the consequence of the enormous stabilization of the singlet state of each imidazol-2-ylidene. Part of this stabilization arises from the



Roger Alder has been at the University of Bristol (UK) since 1965 and is now an Emeritus Professor of Organic Chemistry. His major research interest has been in the physical organic study of novel molecules, including proton sponges, medium-ring bicyclic structures and in/out isomerism, novel types of polymers with strong conformational control and, most recently, stable carbenes.



Leila Chaker was born in Tunisia. She received her Maitrise from the Joseph Fourier University (France) and her PhD from the Claude Bernard University (France). She was a postdoctoral research fellow at the University of Auckland, New Zealand (1996–2000) in the area of supramolecular fullerene-porphyrin chemistry and then at the University of Bristol, (2000–2002). She is currently a research associate at the University of Wollongong (Australia), developing new strategies for regioselective multifunctionalization of the fullerene cage with designed tethers.

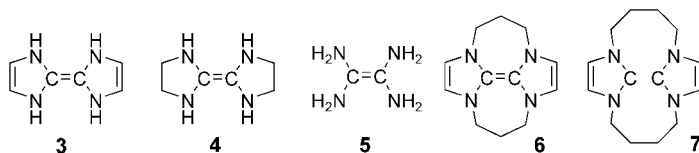


Jeremy Harvey has been a Lecturer in Theoretical Chemistry in Bristol (UK) since 1999, and an EPSRC Advanced Research Fellow since 2003. His research uses computational methods to understand reaction mechanisms, especially in organometallic and bio-inorganic chemistry. As a former organic chemist, he also maintains a strong interest in organic reactivity.



Michael Blake was born in 1973 in Ilseworth (UK). He completed his undergraduate studies at the University of Bristol (UK) where he also obtained his PhD for studies on diaminocarbenes in the group of Prof. R. W. Alder. He held a two-year postdoctoral research position with Prof. M. Jones, Jr. at Princeton University (USA) investigating reactive intermediates. He is currently working at the University of Exeter (UK) within the field of asymmetric catalysis with Dr. R. Bedford.

aromaticity of imidazol-2-ylidenes, and Heinemann and Thiel^[12] calculated the singlet–triplet gap to be 354 for imidazol-2-ylidene, 290 for dihydroimidazol-2-ylidene, and 245 kJ mol^{−1} for diaminocarbene itself. This leads to estimates of the C=C bond strengths of **3**, **4**, and **5** to be 4, 130, and 222 kJ mol^{−1} respectively. Gibbs free energies (at the MP2/6-



311G** and B3LYP/6-311G** levels) for dimerization of a number of carbenes, including those giving **3–5**, have been reported recently.^[13] The most convincing experimental proof of the weakness of the C=C bond in tetraazafulvalenes comes from elegant experiments by Taton and Chen.^[14] The tightly constrained compound **6** exists as the tetraazafulvalene, whereas the homologue with longer tethers dissociates into the dicarbene **7**. Perhaps equally remarkable is the fact that the central C=C bond in **6** is of normal length (1.337 Å), even though the strength of this bond can be only a few kJ mol^{−1}.

Benzoimidazol-2-ylidenes **2** lose less of their aromatic stabilization than imidazol-2-ylidenes when they dimerize, and unhindered examples exist as dimers at ambient temperatures. However, two studies have demonstrated that equilibria between carbene and dimer can be established. Dissociation of (**2**)₂ (R = Et) in [D₁₄]diglyme was observed in the temperature range 313–383 K;^[15] the thermodynamic parameters for dissociation are $\Delta H^\circ = 57.3 \pm 2.5$ kJ mol^{−1} and

$\Delta S^\circ = 127 \pm 7$ J mol^{−1} K^{−1}. The more sterically hindered dimer (**2**)₂ (R = CH₂CHMe₂) dissociates in solution at ambient temperature, reaching an equilibrium of 90 % carbene and 10 % dimer after 24 h.^[16] In non-aromatic five-membered-ring diaminocarbenes, substantial steric hindrance is required for the carbene to be thermodynamically stable to dimerization.

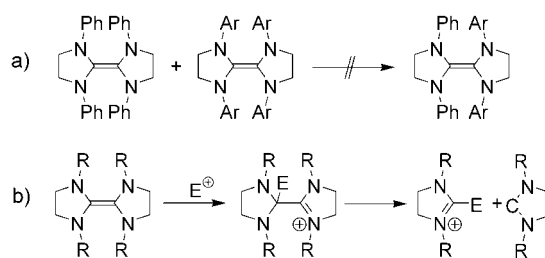
Thus **iBu5** is a stable crystalline solid, but **Me5**, **Et5**, and **iPr5** dimerize.^[17] Cheng and Hu^[18,19] have calculated E_a and ΔE values for the dimerization of some imidazol-2-ylidenes and dihydroimidazol-2-ylidenes at the B3LYP/6-311G(d,p)//B3LYP/6-31G* level of theory. Our results reported in Section 7 agree satisfactorily with theirs.

Six-membered-ring carbenes have received much less attention,^[20,21] but the dimer of carbene **Me6** has been known since 1965,^[22,23] and (**Et6**)₂ is also known.^[24] We found that **iPr6** shows no evidence of dimerization^[25,26] so the boundary line for six-membered-ring diaminocarbenes is clearly established. No seven-membered-ring carbenes such as **Me7–iPr7** have been studied previously.

The boundary line beyond which acyclic carbenes are thermodynamically stable to dimerization has not been clear. Bis(diisopropylamino)carbene (**iPrA**) does not dimerize,^[27] whereas bis(dimethylamino)carbene (**MeA**) is clearly unstable with respect to its well-known dimer tetrakis(dimethylamino)ethene. Dipiperidino-carbene, which may be considered with the acyclic carbenes, has been shown^[28,29] to dimerize slowly to the known tetrakis(piperidino)ethene.^[30,31] The situation with respect to **EtA** will be discussed in Section 4.

3. The Controversy Concerning the Kinetics of the Wanzlick Equilibrium^[32]

In his early papers,^[33–35] Wanzlick proposed that tetraaminoethenes dissociated reversibly to generate diaminocarbenes to account for the reaction of the former with electrophiles to give products apparently derived from the carbene (his examples were all dihydroimidazol-2-ylidenes). However in 1964 Lemal et al.^[36] showed that typical tetraaminoethenes did not dissociate, even under much more drastic conditions than used by Wanzlick et al., by carrying out a negative crossover experiment (Scheme 2a, Ar = *p*-tolyl). Lemal et al. proposed that the reactions with electrophiles proceeded by electrophilic attack on the dimer which then dissociated (Scheme 2b) into one equivalent of product and one of carbene, subsequently also attacked by E⁺.



Scheme 2. Crossover experiment carried out by Lemal et al. and explanation for the reaction of electrophiles with dimers.



François Paoloni was born in 1980, and studied Chemistry at the University of Montpellier (France). He worked under the supervision of Prof. R. W. Alder as part of an Erasmus exchange at Bristol University. He is now doing a PhD in polymer chemistry at the University of Reading under the supervision of Prof. H. Colquhoun.



Jan Schütz was born in 1976 in Langen (Germany) and studied chemistry at the Universities of Darmstadt, Bristol, and Munich. He completed his Diploma studies in Stanford under the supervision of Prof. R. M. Waymouth. Since 2002 he has been working on his PhD thesis with Prof. W. A. Herrmann. His research is focused on new organometallic carbene complexes and their application in catalyses.

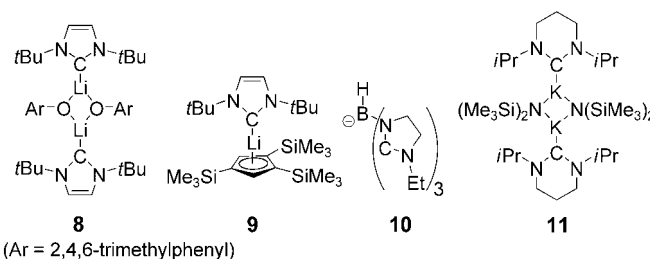
Denk et al.^[37] recently carried out some related crossover experiments and claimed to find crossover under conditions similar to or milder than those used by Lemal et al. This work has been subsequently challenged by Lemal and Liu,^[38] who showed that no crossing over took place when the reactions were run in the presence of potassium hydride to prevent electrophilic catalysis. Lemal and Liu pointed out that a trace impurity “however nefarious” could not prevent the occurrence of unimolecular dissociation, and therefore could not prevent crossover. On the other hand it could catalyze crossing over, for example by the mechanism in Scheme 2 b. It seems therefore that unimolecular tetraaminoethene dissociation has not been convincingly observed so far. In their study of equilibration of benzoimidazol-2-ylidenes with dimers, Hahn et al.^[16] suggested that unimolecular dissociation was involved, but Lemal et al.^[15] were more cautious, suggesting that electrophilic catalysis of equilibration might be occurring. Clearly, the mechanism for proton catalysis of the dimerization of a diaminocarbene (Scheme 1) is simply the reverse of Lemal’s mechanism.

4. Diaminocarbene Preparation; The Example of Bis(diethylamino)carbene

Diaminocarbenes are strong bases,^[39,40] powerful nucleophiles, and complex strongly with most metals in the periodic table.^[5] They are normally rapidly destroyed by moisture,^[41] although they do not react with normal triplet oxygen,^[42] and they can usually only be handled in hydrocarbon or ether solvents. Two general methods for the generation of diaminocarbenes have been reported: a) deprotonation of tetraalkylformamidinium salts with bases, and b) the reaction of potassium metal in THF with the appropriate thiourea.^[43] Bertrand et al.^[44] have recently reported a new general method which involves the reaction of chloroamidinium salts with $\text{Hg}(\text{SiMe}_3)_2$; some important results from this method will be discussed in Section 5. Method (b) above has the advantage that potassium sulfide is insoluble in THF, and so complexation of the carbene with metals should be minimized. However it has the major disadvantage that the reaction is quite slow, even in refluxing THF. For this reason method (a) is usually employed for sensitive diaminocarbenes which may dimerize.

In their original work,^[3] Arduengo and co-workers used NaH or KH in THF, usually in the presence of additives like KO t Bu or DMSO (to generate the soluble dimsyl anion). Herrmann et al.^[45] reported that sodium amide in liquid ammonia/THF at -40°C was also effective for the preparation of imidazol-2-ylidenes. However the amidinium salts that are precursors to carbenes **Me5**–**iPrA** are much more susceptible to nucleophilic attack than the aromatic imidazolium salts used to generate imidazol-2-ylidenes, so that even hexamethyldisilazide bases frequently lead to addition reactions in competition with deprotonation. For the generation of diaminocarbenes **Me5**–**iPrA**, it is generally necessary to use sterically hindered alkali metal amide bases, such as lithium diisopropylamide (LDA) and lithium 2,2,6,6-tetramethylpiperidide (LiTMP). The experimental situation is further

complicated by complexation of the carbenes to the alkali metal counterions of the bases. The first X-ray structural evidence for a carbene–lithium adduct, **8**, obtained by

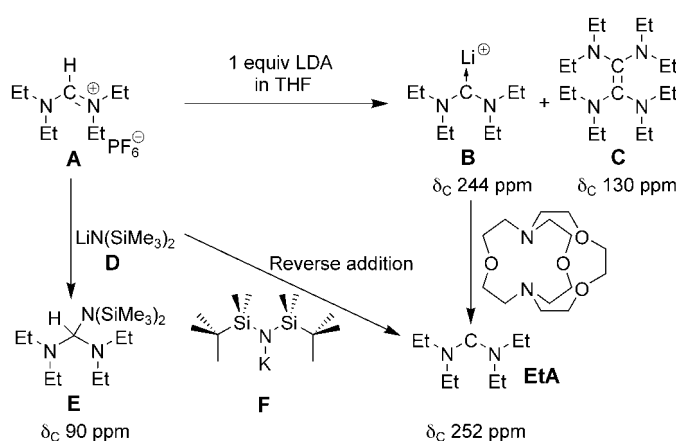


Arduengo, Tamm and co-workers, was reported in a paper by Boche et al.^[46] Other reported lithium complexes include **9**,^[47] and a homoleptic complex containing two of the anionic tripod ligands **10** wrapped around two lithium ions.^[48] We showed that **iPr6** complexed to lithium, sodium, and even potassium species in THF and in toluene and obtained the X-ray structure of the potassium complex **11**.^[25,26]

The preparations of **iPrA**^[27] and **iPr6**^[25] which are stable to dimerization are relatively straightforward, as they can be purified by sublimation or distillation. We have also described the generation of a solution of **MeA** in THF by the addition of a solution of LiTMP in THF to a suspension of tetramethylformamidinium chloride in the same solvent.^[49] A full description of our procedures will be published elsewhere, but the methods and results for the case of bis(diethylamino)carbene, **EtA**, will be described here (Scheme 3), since they are highly relevant to a discussion of diaminocarbene dimerization.

Following our standard procedure, an equivalent of LDA in THF is added to a solution of tetraethylformamidinium hexafluorophosphate (**A**) in THF.^[50] The THF is removed by evaporation and the residue taken up in hexane and filtered to remove as much of the inorganic salts as possible (all operations are carried out under an atmosphere of dry nitrogen). The filtrate is evaporated, and the residue taken up in $[\text{D}_8]\text{THF}$ for the NMR spectroscopic studies. As shown in Scheme 3, this generally results in mixtures of carbene **B** and the known dimer **C**,^[51] each recognized by their distinctive ^{13}C NMR shifts; the ratio of **C** to **D** is typically about 70:30, but is somewhat irreproducible (see below). Addition of one equivalent of [2.1.1]cryptand results in the ^{13}C resonance for the carbene center shifting from 244 to 252 ppm. Addition of more cryptand does not lead to any further shift in the ^{13}C resonance, so free carbene is clearly now present (we have reported^[25] that crown ethers are inadequate for removing lithium complexation). Once formed, the free **EtA** remains essentially unchanged in THF at ambient temperature for at least a week. A small degree of general decomposition is observed, but no dimer beyond that already present is formed. It is clear that **EtA** is kinetically stable to dimerization even though we know equilibrium favors the dimer.

Hexamethyldisilazide bases are too nucleophilic to be used to generate **EtA** (see Scheme 3, E), but we have devised a more hindered base, which yields the free carbene directly.



Scheme 3. Generation of bis(diethylamino)carbene (**EtA**). Reverse addition denotes the addition of **A** to LDA.

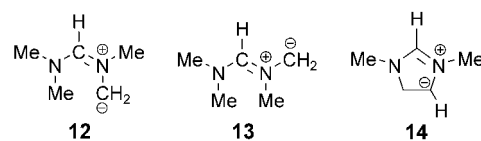
Potassium di-*tert*-butyltetramethyldisilazide (**F**) in THF can be generated by sonicating potassium hydride (freed from oil) with a solution of di-*tert*-butyltetramethyldisilane^[52] in THF overnight (the corresponding lithium derivative is easily generated by using *n*-butyllithium). Unlike potassium diisopropylamide which decomposes THF rapidly, **F** only causes a slow decay over several hours. Moreover, it emerges that **EtA** does not complex significantly to potassium, so we obtain the free carbene directly.

5. Experimental Evidence for Dimer Formation from the Reaction of Diaminocarbenes with Formamidinium Ions

The observation that free carbene does not dimerize, even though the dimer is thermodynamically stable, is not confined to diaminocarbene **EtA**; we see similar behavior with carbenes **Me6** and **Et6**. Once prepared, these carbenes appear to be so stable in THF at room temperature that alternative decomposition pathways intrude before any dimer formation is seen. Bertrand et al.^[44] have recently reported that free **Me6**, generated by reaction of 2-chloro-1,4,5,6-tetrahydro-1,3-dimethylpyrimidinium chloride with $\text{Hg}(\text{SiMe}_3)_2$ is indefinitely stable and can be sublimed at 40 °C. Preliminary studies show that generation of the seven-membered-ring carbene **iPr7** by addition of base to the corresponding amidinium salt does result in the formation of dimer as well as carbene; the dimerization of **iPr7** in the absence of metal ion complexation, and the generation of carbenes **Me7** and **Et7** have not been examined yet. Denk et al.^[17] reported that carbenes **Me5–iPr5** persist in solution (in C_6D_6), but slowly dimerize. It was reported^[17] that these dimerizations obey a second-order rate law, and that pure carbenes dimerize within minutes, but that frozen solutions in benzene at –20 °C can be stored indefinitely. A forthcoming kinetic investigation was mentioned in this work, but has not appeared to our knowledge. We find that when carbene **iPr5** is generated from the formamidinium tetraphenylborate precursor, using a slight excess of **F** in THF, it shows no sign of dimerization after 24 h in ~1 M solution in $[\text{D}_8]\text{THF}$; the

^{13}C NMR peak at $\delta = 235.5$ ppm suggests that the carbene is essentially free of complexation. When prepared by using lithium di-*tert*-butyltetramethyldisilazide in THF, carbenes **Me5** and **Et5** show no sign of dimerization after 24 h in ~1 M solution in $[\text{D}_8]\text{THF}$, but are present as Li complexes (^{13}C NMR peak at $\delta \sim 222$ ppm); we have not yet studied the decomplexation of these carbenes.

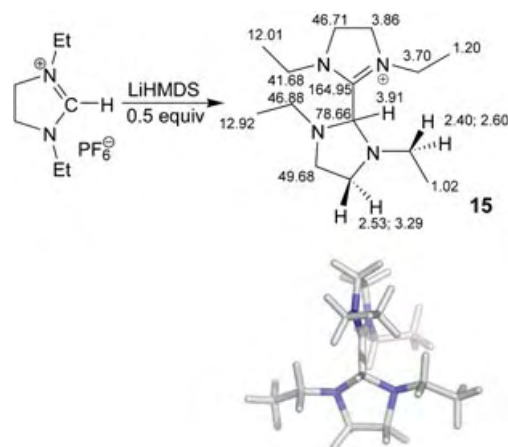
Bis(dimethylamino)carbene, **MeA**, does not survive when [2.1.1]cryptand is added at room temperature to solutions containing its Li complex but the dimer, tetrakis(dimethylamino)ethene, is not formed. Instead a remarkably complex ^{13}C NMR spectrum is seen, with many lines in the 0–100 ppm region, and characterization of the products has proved impossible so far. Bertrand et al.^[44] have recently found that free **MeA**, generated by reaction of 2-chloro-1,1,3,3-tetramethylformamidinium chloride with $\text{Hg}(\text{SiMe}_3)_2$ at low temperatures, does not yield tetrakis(dimethylamino)ethene when warmed to 0 °C, but decomposes over a few hours again producing a complex mixture of products. What alternative pathways might there be for the decomposition of **MeA**? Bertrand's group^[53] have recently described the isomerization of a stable aminoaryl carbene into a transient azomethine ylid, and it is possible that **MeA** is converted by rearrangement or by proton transfer reactions into an azomethine ylid, which then reacts further (the unsymmetrical nature of products expected from the ylid might help explain the numerous ^{13}C NMR resonances). Calculations at the B3LYP/6-31G* level predict that **12** and **13** are 47.8 and 58.3 kJ mol^{–1}, respectively, less stable than **MeA**. While it is hard to assess



how reliable these values might be, they probably do not rule out the involvement of azomethine ylids in the decomposition. Azomethine ylids are less likely to be involved in the reactions of five-membered-ring carbenes; we calculate that **14** is 111.9 kJ mol^{–1} less stable than **Me5**, reflecting the unusual stability of diaminocarbenes in five-membered rings.

Clearly the dimer observed in the earlier experiments does not come from direct carbene plus carbene dimerization. The obvious alternative is reaction of carbene with its precursor formamidinium ion (see Scheme 1 above). By choosing to add the base to the amidinium salt, we are giving this alternative route to dimer the best chance to occur, and it is likely that the rate of addition affects the carbene/dimer ratio. Addition of solutions of the amidinium salt to the base should result in more carbene and less dimer. In practice the procedure described above was normally used because many amidinium salts are more or less insoluble in THF or any other solvent (ethers or hydrocarbons) which is unreactive towards diaminocarbenes. Fortunately tetraethylformamidinium hexafluorophosphate is relatively soluble in THF, and the reverse procedure with slow syringe pump addition of the salt solution to LDA in THF does lead to the formation of nearly pure carbene (< 5% dimer).

A good test of the mechanism in Scheme 1 would be the direct observation of a protonated dimer, and we have indeed found that this is possible in some cases. Addition of 0.5 equivalents of lithium bis(trimethylsilyl)amide to a solution of *N,N'*-diethyl-3,4-dihydroimidazolium hexafluorophosphate in THF, while stirring at 0 °C, followed by removal of the solvent, gave an off-white solid with the ^1H and ^{13}C NMR (in CD_2Cl_2) shifts shown for **15** in Scheme 4. The



Scheme 4. Protonated dimer formation and structure.

chemical shifts are entirely in accord with expectations for the structure shown; Chen and Jordan^[10] report shifts of $\delta = 66$ and 173 ppm for the two conjoined carbon atoms in their protonated dimer derived from a thiazol-2-ylidene. The observation of nonequivalence for the methylene groups associated with the aminal ring in **15** is particularly convincing. As far as we are aware, this is the first observation of a C-protonated tetraaminoethene derivative. The DFT-calculated conformation shown on the right of Scheme 4 is typical of protonated dimers; the two rings are more or less mutually perpendicular.

When the same experiment of adding 0.5 equivalents of base is repeated with tetraethylformamidine hexafluorophosphate, protonated dimer is *not* observed. Instead, the reaction cleanly results in the formation of a 1:1 mixture of the tetrakis(diethylamino)ethene dimer and unchanged amidinium salt. We suggest that in this case there is rapid deprotonation of the protonated dimer intermediate by free carbene. We will provide computational evidence in Section 9 that the different behaviors observed for the experiments associated with carbenes **Et5** and **EtA** are in agreement with the relative basicities of carbene and dimer in the two cases.

6. Structures for Diaminocarbenes **Me5**–**iPrA**, and Their Dimers

We have computed structures for carbenes **Me5**–**iPrA**, the corresponding formamidinium ions, and for the carbene dimers in the gas phase at the B3LYP/6-31G* level.^[54] Many of these species, especially the dimers, can exist in a number of conformations, and this was carefully assessed by carrying out MCOMM conformational searches using the MMFFs force field in MacroModel for dimers and for amidinium ions (used as steric models for the carbenes) to locate low-energy conformations before optimizing these by DFT calculations. Calculated structural data is given in Table 1, together with experimental data, where known, and the structures of the simple methyl-substituted carbenes **Me5**, **Me6**, **Me7**, and **MeA** are illustrated in Figure 2.

B3LYP/6-31G*-calculated structures for the carbenes and formamidinium ions agree well with the limited experimental data. Formamidinium ions have C–N bond lengths of 1.32 ± 0.01 Å, while in the carbenes the C–N bond lengths are 1.35 ± 0.02 Å, and these values are reproduced to within 0.02 Å in the calculations. Denk's group reported the X-ray crystal structure of carbene **tBu5**^[17] and the corresponding formamidinium thiocyanate.^[55] We have reported the X-ray crystal structures of carbene **iPrA** and of the corresponding formamidinium triflate;^[27,50] we also determined the structure of the formamidinium hexafluorophosphate corresponding to **Et6**.^[50] A number of structures contain the tetramethylformamidinium ion; in Table 1 data is shown for the salt $(\text{Me}_2\text{N})_2\text{CH} \cdot [(\text{H}_2\text{C}(\text{NMe}_2)_2)\text{NiCl}_3]$.^[56]

In the complex **11**, comprising **iPr6** and $\text{KN}(\text{SiMe}_3)_2$,^[25] the carbene is coordinated to the potassium ion through a bond 3.00 Å in length that is surely mainly electrostatic in nature. The calculated bond lengths and angles for **iPr6** agree with those for the carbene moieties in the complex. In complex **11**, the isopropyl methyl groups are oriented away from the carbene center, which could reasonably be ascribed

Table 1: Calculated structural data for formamidinium ions and diaminocarbenes (experimental data is given in boldface).

	Formamidinium ion		Diaminocarbene		S–T gap ^[a] [kJ mol ^{−1}]	PA ^[b] [kJ mol ^{−1}]
	N–C–N [°]	C–N–C–N [°]	N–C–N [°]	C–N–C–N [°]		
Me5	114.3	0.0	106.3	0.0	301.2	1112.8
Et5	114.7	0.3	105.5	0.8		1124.6
iPr5	114.8	0.0	106.0	0.0		1135.4
tBu5	115.2	1.1	106.6	6.3		1143.0
	113.6	7.4, 3.8	106.5	6.7, 6.1		
Me6	125.1	0.4	115.1	0.5	258.9	1145.8
Et6	125.4	0.7	115.5	0.6		1156.2
	125.3	2.5, −3.8				
iPr6	125.5	2.2	116.1	0.7		1166.8
			116.3	2.6, −0.6		
Me7	128.0	13.7	117.4	16.3	210.7	1157.4
MeA	130.9	11.0	119.8	14.0	173.0	1149.8
	129.5	10.8				
EtA	133.2	1.3	122.9	6.0		1172.2
iPrA	132.7	18.4	122.9	20.5		1183.7
	133.2	−11.9, −4.6	121.0	−10.6, −13.7		

[a] S–T = singlet–triplet. [b] PA = proton affinity.

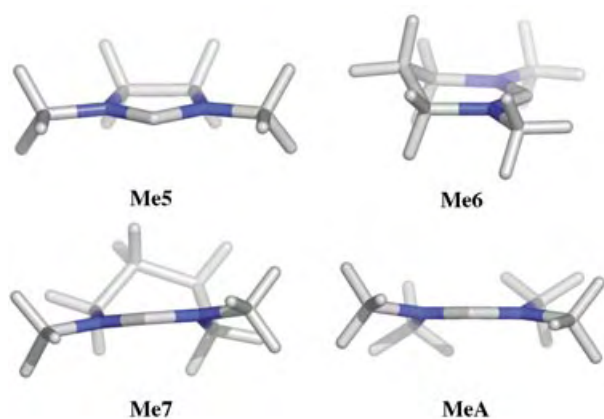
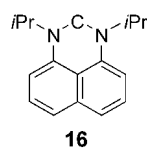


Figure 2. Calculated structures for carbenes **Me5**, **Me6**, **Me7**, and **MeA**.

to steric repulsion from the hexamethyldisilazide anions. Surprisingly however, the isolated carbene **iPr6** is calculated to prefer the same conformation, although the corresponding formamidinium ion prefers the alternative structure with the isopropyl methyl groups clustered around the formamidinium proton according to the calculations. Weak attractive interactions between the isopropyl hydrogen atoms and the carbene sp^2 lone pair might be present in **iPr6**.

Acyclic and seven-membered-ring carbenes and formamidinium ions are somewhat twisted about the C-N-C-N bonds, and this may reduce their stability (see Section 7). One notable trend in Table 1 is that N-C-N angles are typically 10° smaller in the carbenes than in the amidinium ions. The parent diaminocarbene, $(H_2N)_2C$, is calculated to have an N-C-N angle of 112.2° , whereas in $(H_2N)_2CH^+$ this angle is 125.4° according to a B3LYP/6-31G* calculation. These structural differences could have major consequences for the fundamental properties of diaminocarbenes. The singlet-triplet (S-T) gap decreases sharply as the N-C-N angle increases, whereas the proton affinity (PA) increases, as shown in Table 1. Even for acyclic diaminocarbenes such as **MeA** however, the S-T gap is still so large that there is no evidence this has any effect on reactivity. On the other hand,



there is little doubt that the basicity of diaminocarbenes is of major significance. Larger ring and acyclic formamidinium ions are likely to require stronger bases for deprotonation, but be more reactive as bases and nucleophiles once prepared. This is in agreement with qualitative observations. As described above, the generation of acyclic diaminocarbenes generally requires the use of the strongest amide bases, and when competitive deprotonation of five- and six-membered-ring formamidinium ions is attempted, only the five-membered-ring carbene is formed, although this preference may be kinetic rather than thermodynamic. Richeson et al.^[21] have shown that carbene **16** (N-C-N angle 115.3°) is a better donor than dihydroimidazol-2-ylidenes, as judged by the value of ν_{CO} in a $Rh(CO)_2Cl$ complex. By the same criterion however,^[57] it is not as good a donor as the acyclic carbene **iPrA**, which has the largest known N-C-N angle.

Tetraaminoethenes have attracted considerable attention, due to their ease of oxidation and chemiluminescent reactions,^[58] and X-ray crystal structures of a number of these compounds have been reported, although most of these have additional rings and/or aromatic substituents on the nitrogen atoms. Calculated structural data for a number of dimers are given in Table 2 and selected structures are illustrated in Figure 3.

The experimental structures for $(MeA)_2$ ^[59,60] and $(Me5)_2$ ^[17] show conformational differences from the calcu-

Table 2: Calculated structural data for the dimers of diaminocarbenes (experimental data is given in boldface).

Dimer	C=C [Å]	N-C=N [°]	C-N [Å]	$\Sigma(C-N-C)$ [°]	C=C-N-C [°]
Me5	1.35	10.5	1.43	337.7	59.8
	1.35	7.0	1.42	334.7	53.9
Me6	1.36	1.8	1.44,	337.6,	-108.6,
			1.42 ^[a]	351.8 ^[a]	25.6 ^[a]
Et6	1.37	12.5	1.42	353.5	56.0
iPr6	1.37	-15.6	1.43	353.2	-56.5
Me7	1.37	27.7	1.41	360.0	42.0
MeA	1.37	-32.0	1.42	356.4	-35.6
	1.36	-24.1	1.41	351.1	-26.5, -69.1

[a] For axial and equatorial NMe groups.

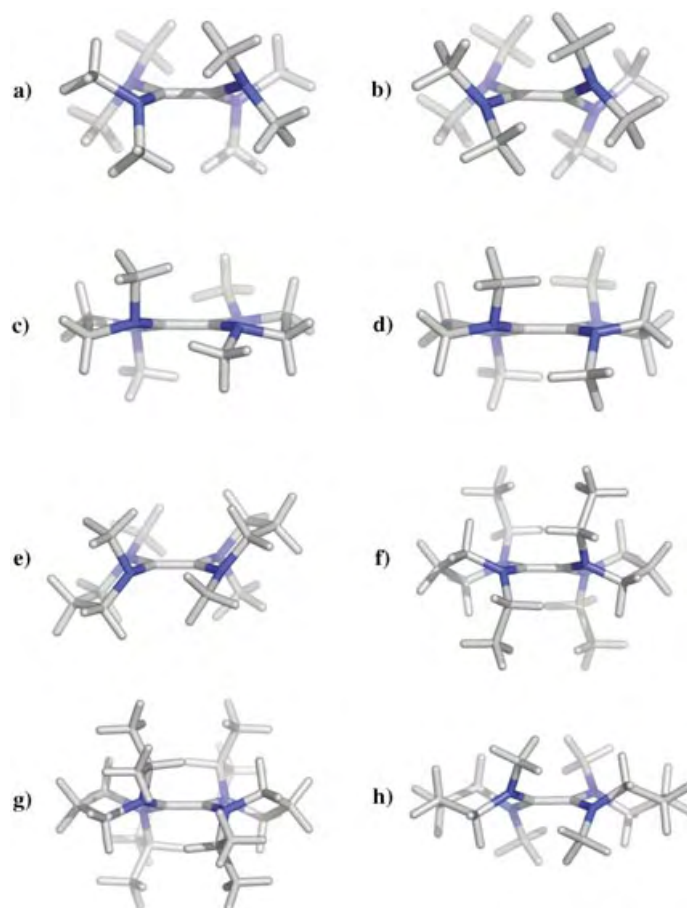


Figure 3. a) Experimental and b) calculated structure of $(MeA)_2$, c) experimental and d) calculated structure of $(Me5)_2$, e)–h) calculated structures of $(Me6)_2$, $(Et6)_2$, $(iPr6)_2$, and $(Me7)_2$, respectively.

lated structures. This may reflect deficiencies in the calculations, but they might also be caused by crystal packing forces, and the calculated structures all seem reasonable. Note that whereas (**Me6**)₂ adopts a double-chair structure with one axial and one equatorial methyl group in each ring, in the preferred structures for (**Et6**)₂ and (**iPr6**)₂ the six-membered rings adopt twist-boat conformations to alleviate the serious interactions between the attached alkyl groups.

7. Dimerization Equilibria for Diaminocarbenes Me5–iPrA; B3LYP/6-31G* Computations

We have used B3LYP calculations to a) study dimerization thermodynamics for all diaminocarbenes **Me5–iPrA** (discussed in this Section), b) find the transition states for the uncatalyzed dimerization (see the Section 8), and c) look at some aspects of the proton-catalyzed mechanism (Scheme 1), particularly in the light of computed proton affinities of carbenes and dimers. The energies (ΔE), enthalpies (ΔH), and free energies (ΔG) for the dimerization of carbenes **Me5–iPrA** from B3LYP/6-31G* calculations in the gas phase are shown in Table 3.

Table 3: ΔE , ΔH , and ΔG values for carbene dimerization at 298 K and 1 atm pressure from B3LYP/6-31G* calculations.

Carbene	ΔE [kJ mol ⁻¹]	ΔH [kJ mol ⁻¹]	ΔG [kJ mol ⁻¹]
Me5	–123.9	–113.0	–42.1
Et5	–116.2	–105.6	–39.6
iPr5	–116.5	–105.7	–43.0
tBu5	36.0	47.0	127.3
Me6	–107.4	–98.8	–36.4
Et6	–88.3	–78.1	–12.0
iPr6	–64.1	–54.7	8.3
Me7	–194.3	–188.1	–132.8
Et7	–172.1	–164.1	–101.8
iPr7	–133.2	–123.2	–52.9
MeA	–209.6	–202.0	–138.5
EtA	–161.1	–154.3	–95.1
iPrA	–54.9	–40.7	40.9

The calculated values for ΔG are in striking agreement with the experimental evidence in THF. Thus **tBu5**, **iPr6**, and **iPrA** are the only carbenes for which ΔG is positive, and these carbenes are indeed the only ones known not to dimerize significantly. Note that **Et6** and **iPr6** are predicted to lie on either side of the borderline, and experimentally we see complete dimerization for the former, but have not observed the dimer of **iPr6**. In spite of this striking agreement of experiment and theory, we recognized that B3LYP/6-31G* calculations represent quite low-level theory, and moreover that we are comparing gas-phase calculations with experimental results from solution. We have therefore sought to calibrate our calculations further from two directions:

There is experimental data for one actual carbene/dimer equilibrium: In the case of **2** (R = Et) Lemal et al.^[15] report $\Delta H = -57.3$, $\Delta G = -19.4$ kJ mol⁻¹ at 298 K in [D₁₄]diglyme. B3LYP/6-31G* calculation of this equilibrium in the gas phase

yields $\Delta H = -62.7$ and $\Delta G = +4.0$ kJ mol⁻¹ in rather satisfactory agreement with the solution data.

For the parent diaminocarbene, we have carried out CCSD(T)/6-311G** calculations, followed by MP2 calculations with a larger basis set and the application of an additional correction (the “G2(B3LYP/MP2/CC)” method^[61]). This method is expected to give a value that is reliable to within 10 kJ mol⁻¹, barring unexpected (and very rare) major problems. The value of ΔE for the dimerization is –198 kJ mol⁻¹, compared with –225.5 kJ mol⁻¹ from the B3LYP/6-31G* calculation; thus the latter appears to favor the dimer by about 30 kJ mol⁻¹. Carbenes should be favored in polar solution relative to their dimers (calculated dipole moments for **MeA** and **Me5** are 2.5 and 2.8 Debye, respectively). We therefore ran B3LYP/6-31G* calculations for carbenes **Me5**, **Me6**, **MeA**, and **EtA** and their dimers in THF, employing the Poisson–Boltzmann continuum solvent model as implemented in the Jaguar program, with the assumption that zero-point energy and thermodynamic parameters can be transferred from the gas-phase calculations. All the ΔE and ΔG values became more positive (favoring the carbenes) by between 20 and 40 kJ mol⁻¹. This error due to the neglect of solvation in the gas-phase computations is rather similar in magnitude to the intrinsic error in the B3LYP/6-31G* calculations suggested by the comparison with the values obtained with the G2(B3LYP/MP2/CC) method, but of opposite sign, so that the two should cancel out. In conclusion, this calibration work suggests that the gas-phase B3LYP/6-31G* computations we have used to assess carbene dimerization thermodynamics fortuitously give rather accurate predictions of the solution behavior.^[49,62]

In any event, it is likely that the *relative* effects of ring size and alkylation on these equilibria can be modeled with useful accuracy at the B3LYP/6-31G* level, and we now return to consider the trends revealed in Table 3. The effects of increasing the size of the alkyl groups on the equilibria in each series are significant but relatively straightforward. As expected, the effects are greatest in the series of acyclic compounds, since four groups are being changed and particularly since larger alkyl groups are being introduced in the hindered “*endo*” positions. Increasing the size of the alkyl group has little effect in the five-membered-ring series, where the group will be most severely tied back from the carbene center, until *t*Bu groups are introduced. Alkyl group effects are roughly equal in the six- and seven-membered-ring series, but the calculations clearly predict that **iPr7** will dimerize, unlike its six-membered-ring counterpart **iPr6**.

Comparison of the five-, six-, seven-membered-ring and acyclic carbenes with methyl substituents reveals that ΔE and ΔG values for carbene dimerization increase in the surprising order **Me6** \approx **Me5** \ll **Me7** \approx **MeA**, and dimerization of **Me6** is 100 kJ mol⁻¹ less favorable than that of **MeA**—a remarkably large difference considering the apparent similarity of these two carbenes.

These striking effects on the dimerization equilibria might be due to unexpected structure and stabilization preferences in either the carbene or the dimers (or in both). As we will show in Section 9, (**Me7**)₂ and (**MeA**)₂ have proton affinities that are about 100 kJ mol⁻¹ lower than those of (**Me5**)₂ and

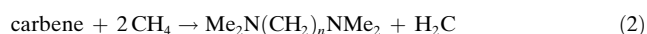
(**Me6**)₂, and so we initially believed that (**Me7**)₂ and (**MeA**)₂ possessed unusual stability and were therefore favored in the respective dimerization equilibrium. In addition, we noticed that these two dimers adopt unusual structures (Figure 3) that involve substantial twisting about both the C=C bond and the C(sp²)-N bonds, whereas the nitrogen atoms remain almost planar. In twisted tetraaminoethenes, the nitrogen lone pairs interact with both σ* and π* orbitals of the C=C bond, as well as with the σ* orbital of the geminal C-N bond, as shown by NBO analysis, and these interactions vary substantially according to the dimer geometry. However careful study of these electronic effects and also the steric interactions failed to reveal any clear reasons for the calculated unusual stability of (**Me7**)₂ and (**MeA**)₂.

To resolve this problem a clear-cut way is needed of dissecting the observed equilibria into relative stabilities associated with the carbenes and with the dimers. This can be achieved by comparing both with a single set of reference compounds that can be confidently assumed to show no unusual electronic effects. In the isodesmic equations described below, the reference compounds are Me₂N(CH₂)_nNMe₂ (*n* = 2, 3, and 4) for cyclic carbenes **Me5**, **Me6**, and **Me7**, and 2(Me₃N) for **MeA**. These strain-free open-chain amines should be well-behaved and have standard bond energies.^[63] In support of this, we find that the energies calculated for the isodesmic reaction given in Equation (1) are negligibly differ-

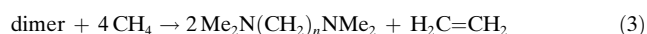


ent: 6.6, 6.9, and 7.9 kJ mol⁻¹ for *n* = 2, 3, and 4, respectively. The slightly unfavorable energy change of these processes is expected given the stronger bond of the electronegative nitrogen atom with the primary alkyl group than with the methyl group.^[64]

The carbenes and dimers are related to the reference compounds by isodesmic reactions given in Equations (2) and



(3) (for acyclic carbene **MeA**, Me₂N(CH₂)_nNMe₂ is replaced



by 2 Me₃N). The energy changes for reactions (2) and (3) in Table 4 clearly demonstrate that it is the relative carbene stability that has the dominant effect on the dimerization equilibria. Carbenes **Me5** and **Me6** are relatively ~50 kJ mol⁻¹ more stable than **Me7** and **MeA** and in particular, this is the only source of difference in the equilibria

Table 4: Energies for isodesmic reactions (2) and (3) (B3LYP/6-31G* energies in kJ mol⁻¹).

Carbene	Me5	Me6	Me7	MeA
ΔE for reaction (2)	424.2	421.6	377.4	371.5
ΔE for reaction (3)	103.4	81.7	80.2	83.7
ΔE for dimer formation	-123.9	-107.4	-194.3	-209.6
E _{(H₂N)₂C} ^[a]	(25.5)	3.4	16.7	22.2

[a] Energy of (H₂N)₂C with the geometry of an alkylated carbene; see text.

for carbenes **Me6** and **MeA**. The energies calculated for reaction (2) are negligibly different for (**Me6**)₂, (**Me7**)₂, and (**MeA**)₂, but dimer (**Me5**)₂ is about 20 kJ mol⁻¹ more stable than the others, probably because of reduced van der Waals interactions between the methyl groups.

The relative stabilities of the carbenes are very different—what are the reasons? The N-C-N angle (see Table 4) surely plays some part, but cannot be the only factor or a clear break might be expected between carbenes **Me5** and **Me6**, whereas it actually comes between **Me6** and **Me7**. Carbenes **Me7** and **MeA** are significantly twisted about the N-C_{carbene} bonds (Table 4), although the nitrogen atoms remain almost planar, and this could destabilize these carbenes. To see what the combined effects of these geometric changes might have on carbene stability, we carried out single-point calculations of (H₂N)₂C at the heavy-atom geometries of carbenes **Me5**, **Me6**, **Me7**, and **MeA** and with a fixed N-H distance of 1.01 Å. For (H₂N)₂C at the geometry of **Me5**, the *endo*-hydrogen atoms are only 1.74 Å apart, and this must destabilize this structure substantially, so no useful conclusions can be drawn in this case. However, for (H₂N)₂C at the geometry of carbene **Me6**, this H...H non-bonded distance is 2.43 Å and non-bonded repulsion should be negligible for this case and for those corresponding to **Me7** and **MeA**. The energies of these structures relative to the equilibrium structure for (H₂N)₂C (N-C-N 112.2°) are listed in Table 4. The combined effects of the N-C-N angle and the C-N-C-N torsion for (H₂N)₂C do indeed show a marked change between carbenes **Me6** and **Me7**, but the size of the effect for the (H₂N)₂C model is only about 40% of that seen for the fully alkylated carbenes. However the increase in N-C-N angle and C-N-C-N torsion for **Me7** and **MeA** is undoubtedly caused by steric effects in these carbenes (e.g. non-bonded repulsion between the *endo*-methyl groups in **MeA**), and the structures adopted by these carbenes is presumably a compromise between steric and electronic requirements. The single-point calculations for (H₂N)₂C should therefore only be expected to account for part of the differences. While there is no simple way of discovering if steric effects can quantitatively account for the remainder of the energy differences, we believe that overall this approach accounts for the dimerization equilibria in a reasonably satisfactory way.

8. Calculations on the Direct Mechanism for Carbene Dimerization

Singlet carbenes cannot dimerize by a least motion, head-to-head, approach, as was first pointed out by Hoffmann, Gleiter, and Mallory in 1970.^[8] The filled sp² lone pair orbital needs to approach the empty p orbital of the other carbene (see Figure 1). This mechanism has been confirmed for methylene itself by calculations of varying sophistication over the years. One thorough study suggested that there might be an energy barrier of 170 kJ mol⁻¹ to the dimerization of singlet H₂C.^[65] On the other hand, it has been known since the 1960s that dimerization of CF₂ to tetrafluoroethene is rapid, with a second-order rate constant of 2.54 ± 0.26 × 10⁷ M⁻¹ s⁻¹ at 298 K,^[66] only about three orders of magnitude below the

diffusion limit. B3LYP/6-31G* calculations for this reaction do not yield a discernable energy barrier along the approach geometry shown in Figure 1. Nevertheless for diaminocarbenes, this approach geometry may lead to extra steric problems in the transition state, and it is also worth noting that it is relatively unfavorable from the point of view of dipole–dipole interactions.

We have reported density functional calculations of the transition states for the dimerization of diaminocarbene itself.^[49] A substantial barrier (36.6 kJ mol^{−1} at BPW91/cc-pVDZ) was found even for this unsubstituted case. The calculated transition state had C₂ symmetry rather than the C_{2h} that might be expected and the nitrogen atoms were pyramidalized in such a way that the lone pairs were *anti* to the forming C–C bond. This brings approaching hydrogen atoms into close proximity and this geometry will be unfavorable once alkyl groups are added. We also reported finding a transition state for the tetramethyl derivative **MeA**.

We now report B3LYP/6-31G* calculations relating to the kinetics of dimerization of several other diaminocarbenes (Table 5). In all cases, the transition states were found to have C₂ symmetry and the length of the forming C–C bond varied from 1.89 to 2.14 Å. The transition state for dimerization of **Me6** is shown in Figure 4.

Table 5: B3LYP/6-31G*-calculated ΔE^\ddagger , ΔH^\ddagger , and ΔG^\ddagger values for carbene dimerization at 298 K (kJ mol^{−1}).

Carbene	ΔE^\ddagger	ΔH^\ddagger	ΔG^\ddagger	C...C [Å]
Me5	39.6	43.5	104.9	1.952
Et5	48.9	53.6	112.5	1.931
Me6	72.3	76.4	137.3	1.893
MeA	53.7	56.4	111.6	2.099
EtA	98.0	101.1	156.5	2.142

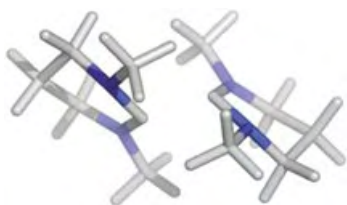
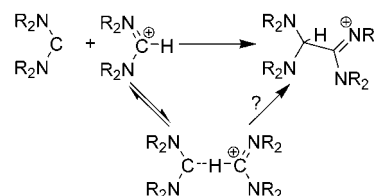


Figure 4. Transition state for the dimerization of **Me6**.

Energies of activation, ΔE^\ddagger , vary over a wide range, but they are all large. Based on the calculated ΔG^\ddagger values, half-lives for carbenes at a concentration of 1M in THF at 298 K would be **Me5**: 100 h; **Me6**: 5000 years; **MeA**: 2 months; **EtA**: 1×10^7 years. If anything, these half-lives may be underestimates, given that solvent stabilization of the transition states is likely to be smaller than that of the dipolar carbenes (see above). While these values are highly speculative, it seems clear that room-temperature dimerization of six-membered ring carbene **Me6** and, especially, **EtA** is unlikely to be observed. This is exactly what we find (See Sections 4 and 5).

9. Calculations on Tetraaminoethene Formation from the Reaction of Diaminocarbenes with Formamidine Ions

In this Section we examine several aspects of the proposed proton-catalyzed dimerization of diaminocarbenes in the light of DFT calculations. In the first step (Scheme 5), the carbene,



Scheme 5. Pathways for reaction of diaminocarbenes with formamidine ions.

a powerful nucleophile, attacks its amidinium ion precursor to generate the C-protonated dimer. We suggest that the formamidine ion/carbene reaction may have a lower energy barrier than direct carbene dimerization, since a) there will be electrostatic attraction even at long distance, as the negative end of the carbene dipole points at the positive charge of the ion, and b) the carbene can approach the formamidine ion more or less perpendicularly and this is always likely to be most favorable sterically.

For five- and six-membered-ring carbenes, B3LYP/6-31G* calculations suggest that, in the gas phase, formation of the protonated dimer is more or less as exothermic as direct dimerization of two carbenes, although this is not the case for acyclic and seven-membered-ring carbenes. Equilibrium will be much less favorable in solution, since the solvation of a cation and a dipolar species (the carbene) is replaced by solvation of one larger cation. Simulation of THF solvation using the Poisson–Boltzmann continuum model as implemented in Jaguar suggests that equilibria are shifted about 50 kJ mol^{−1} towards starting materials (Table 6).

Arduengo et al.^[67] have shown that certain imidazol-2-ylidenes can form hydrogen bonds to the corresponding imidazolium ion, and this offers an alternative trajectory to the C-protonated dimer. We have located a transition state (see Figure 5) for the formation of the protonated dimer from

Table 6: B3LYP/6-31G*-calculated ΔE , ΔH , and ΔG values for protonated dimer formation at 298 K and 1 atm pressure in the gas phase and THF solution (kJ mol^{−1}).

Carbene	Gas phase			THF solution		
	ΔE	ΔH	ΔG	ΔE	ΔH	ΔG
Me5	−125.8	−115.9	−53.0	−70.6	−60.7	−3.5
Et5	−120.9	−111.3	−53.3			
iPr5	−106.5	−96.4	−31.4			
Me6	−96.2	−86.7	−24.0	−47.0	−37.3	23.9
Et6	−77.6	−67.4	1.4			
iPr6	−34.2	−23.1	50.8			
Me7	−95.7	−86.5	−20.7			
MeA	−106.3	−97.9	−34.9	−57.4	−48.5	15.3
EtA	−46.4	−37.6	20.8	−2.8	6.6	67.3

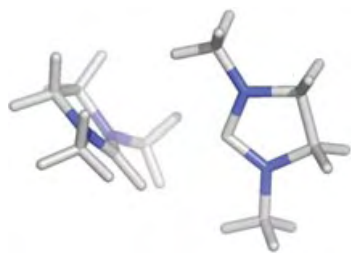


Figure 5. Transition state for the formation of the protonated dimer from **Me5** and the corresponding formamidine ion.

carbene **Me5** and the corresponding formamidine ion which appears to correspond to the latter process. In the two cases we examined, C–C bond formation is only slightly more favorable than hydrogen bonding; thus for hydrogen bonding between carbene **Me5** and the corresponding formamidine ion, $\Delta E = -89.9$, $\Delta H = -84.2$, and $\Delta G = -41.8$ kJ mol⁻¹ at 298 K, while the values for **MeA** are $\Delta E = -84.9$, $\Delta H = -78.0$, and $\Delta G = -31.5$ kJ mol⁻¹.

The second step of the mechanism in Scheme 1 is simply a proton transfer. Imidazol-2-ylidenes have been shown to be strongly basic,^[39,40,68,69] but attempts to measure the basicity of simple diaminocarbenes such as **Me5-iPrA** have failed so far, due to competing addition reactions of the formamidine ions. Tetraaminoethene derivatives should also be strongly basic, but we are not aware of any previous experimental evidence for their conversion to C-protonated cations, and so pK_a values are unknown. We have therefore resorted to comparison of calculated proton affinities (PA, Table 7); it is

Table 7: B3LYP/6-31G*-calculated proton affinities (PA, kJ mol⁻¹) values for carbenes and dimers.

Carbene	PA of carbene	ΔE for reaction (4)	PA of dimer	ΔE for reaction (5)
Me5	1112.8	652.1	1115.8	541.8
Et5	1124.6		1130.4	
iPr5	1135.4		1126.1	
tBu5	1143.0			
Me6	1145.8	683.2	1133.7	540.7
Et6	1156.2		1163.7	
iPr6	1166.8		1135.2	
Me7	1157.4	650.9	1055.8	463.7
MeA	1149.8	637.8	1045.7	455.3
EtA	1171.2		1054.5	
iPrA	1183.7			

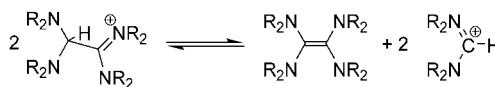
reasonable to expect pK_a values to follow these PA trends. Comparison of the PA values for carbenes and the corresponding dimers shows clear differences between acyclic and five- and six-membered-ring cases. In acyclic and seven-membered-ring cases **Me7**, **MeA**, and **EtA**, the PA for the carbene is approximately 100 kJ mol⁻¹ higher than for the dimer, whereas five- and six-membered-ring dimers have PAs that are almost as high (or higher) than the corresponding carbene. These PA values can be usefully analyzed with the

aid of the reference compounds used earlier and two additional isodesmic reactions according to Equations (4) and (5).



The greater N–C–N angle in (H₂N)₂CH⁺ (125.4°) compared with (H₂N)₂C (112.2°) might lead one to expect that the PA would rise as the N–C–N angle increases. While this is true for carbenes **Me5** and **Me6**, further increases for **Me7** and **MeA** are small, and the failure of a simple correlation is partially explained by reference to the isodesmic reactions. Reaction (4) shows that formamidine ion stability peaks at the six-membered ring, but the fall for larger N–C–N angles almost parallels that for the carbenes (isodesmic reaction (2)). The low PA values for the dimers (**Me7**)₂ and (**MeA**)₂ seem to be mainly due to decreased stabilities for the protonated forms (reaction (5)). We believe that this is largely due to non-bonded interactions in these quite severely crowded ions. It is worth noting that we calculate that for a simple aromatic carbene, 1,3-dimethylimidazol-2-ylidene, the (unstable) dimer has a markedly higher PA (1157) than the carbene (1113 kJ mol⁻¹).

Based on this data, it is simple to calculate the energetics for disproportionation of C-protonated dimers to dimers and formamidine ions (Scheme 6). It is highly favorable in the



Scheme 6. Disproportionation of the C-protonated dimers to the dimers and formamidine ions.

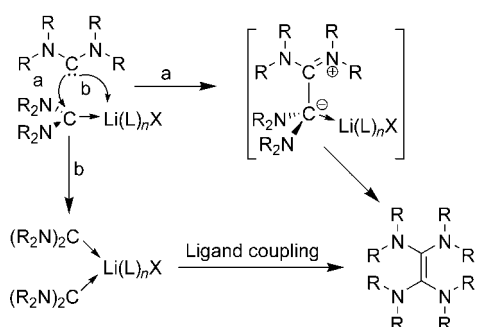
gas phase for the case involving the protonated dimer from **EtA** ($\Delta E = -68$ and $\Delta G = -137$ kJ mol⁻¹), but quite unfavorable for five-membered-ring cases such as **Et5** ($\Delta E = +126$ and $\Delta G = +67$ kJ mol⁻¹), although disproportionation should be favored by solvation. The rate of the actual proton transfer step may be slowed by the need for substantial structural reorganization of the C-protonated dimers to create the favored geometry of the dimers themselves, and by steric constraints in highly crowded examples. Overall, however, our observation that protonated dimer can be observed from **Et5**, but not from **EtA**, seems to be supported by the calculations.

10. Possible Mechanisms for Metal-Promoted Dimerization

A huge variety of metal complexes of diaminocarbenes are now known and decomposition of these to form tetraaminoethene dimers is certainly not generally observed. We have reported^[25] that the rate of dimerization of bis(dimethylamino)carbene was slowed by the addition of extra lithium diisopropylamide, and by changing the solvent from

THF to toluene. Both these observations are in agreement with increased Li complexation stabilizing the carbene.

It may therefore seem perverse to suggest that metals such as lithium may catalyze dimer formation, but we believe that a free diaminocarbene may react more rapidly with a Li-complexed carbene than with another free carbene molecule. Coordination of diaminocarbenes to lithium should increase the reactivity of the p orbital on the carbene center towards nucleophiles such as a free carbene, as in route a in Scheme 7. Alternatively, if two carbenes are transiently coordinated to one lithium center, ligand coupling to form dimer might occur (route b in Scheme 7). These mechanisms require the presence of free carbene, and so rates of dimerization would decrease as all carbenes became complexed.



Scheme 7. Possible mechanisms for metal-promoted dimerization.

One serendipitous observation provides significant support for these ideas. While examining lithium complexation to 2-¹³C-*i*Pr6, we observed the slow conversion of the “normal” complexed carbene signal at $\delta = 216$ –220 ppm to a species showing a remarkable multiplet in the ¹³C NMR spectrum at $\delta = 177$ ppm (Figure 6).

This conversion only happens in the presence of a substantial excess of LiHMDS and when toluene is used as the solvent (it is not observed in THF). Other bases such as LiTMP and LDA do not lead to related species. In the presence of 10 equivalents of LiHMDS, we eventually observe about 80% conversion to the new species. The multiplet is an AB quartet split by a single ⁷Li nucleus (spin 3/2) and it can be simulated with the following parameters:

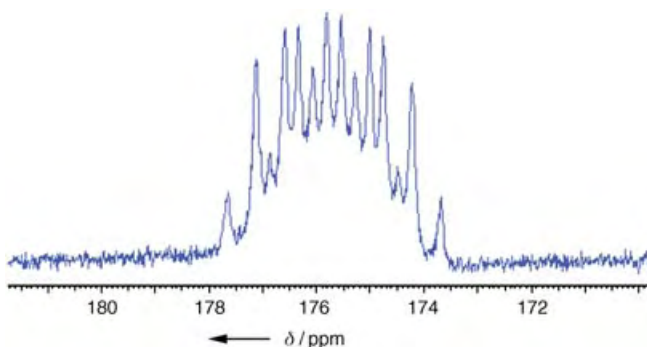
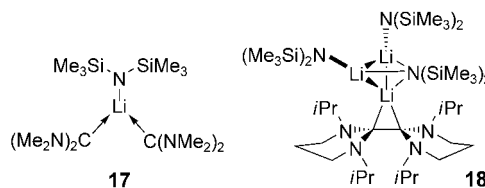


Figure 6. ¹³C NMR multiplet from reaction of 2-¹³C-1,3-diisopropyl-3,4,5,6-tetrahydropyrimidin-2-ylidene with excess LiHMDS.

$\Delta_{C(1)} = 177.84$; $\Delta_{C(2)} = 176.88$; $J_{Li,C(1)} = 79.3$ Hz, $J_{Li,C(2)} = 80.5$ Hz and $J_{C(1),C(2)} = 54.4$ Hz. The size of these coupling constants, especially $J_{C(1),C(2)}$, suggests the presence of a three-membered LiC₂ ring. Calculations^[70] on complex **17** of two



(Me₂N)₂C carbenes coordinating separately to LiN(SiMe₃)₂, led to a predicted $J_{C(1),C(2)}$ value of only 2 Hz. Note that carbene *i*Pr6 has not been observed to form dimer, so it is appealing to assume that this complex represents a foiled dimerization reaction. Unfortunately, all attempts to crystallize the new complex have failed, so further discussion of the structure is speculative. There has to be some lack of symmetry to get the ¹³C–¹³C AB quartet, and at Li/carbene ratio of at least 3:2 to account for the requirement for a large excess of LiHMDS; a cluster such as **18** might provide this.

Returning to tetrakis(dimethylamino)ethene formation, we found this to be cleanly second-order in carbene, and a study over the temperature range 0–40 °C led to a satisfactory Arrhenius plot with $E_{act} = 77.7$ kJ mol^{−1}, and $\log A = 10.6$ M^{−1} s^{−1} at a formal lithium ion concentration of approximately 2 M in THF. When however similar THF solutions are treated with [2.1.1]cryptand to sequester lithium species, the ¹³C NMR signal for the carbene disappears immediately, but formation of dimer is not observed, as described above.

While none of the evidence cited above proves the involvement of Li in the dimerization of simple diaminocarbenes, we do believe that further investigation is warranted.

11. Summary and Outlook

This review set out to answer two questions:

When do diaminocarbenes dimerize?

How do they dimerize?

It is known that dimerization is thermodynamically unfavorable for imidazol-2-ylidenes, and evenly balanced for benzimidazolylidenes, depending on steric effects. We have shown here that for non-aromatic diaminocarbenes, significant steric hindrance is required for dimerization to be unfavorable, and carbenes *i*Pr5, Et6, *i*Pr7, and EtA can all dimerize. However dimerization of MeA is 100 kJ mol^{−1} more favorable than for Me6, even though similar levels of steric hindrance in the dimers are involved. We have proposed, on the basis of DFT calculations, that this is due to the lower stability of acyclic (and seven-membered-ring) carbenes, and that this can be explained in part by increased N–C–N angles and some loss of conjugation through twisting about the N–C_{carbene} bonds.

Several diaminocarbenes (**iPr5**, **Me6**, **Et6**, and **EtA**) do not dimerize within a reasonable timeframe at ambient temperature in THF, and the simplest diaminocarbene **MeA** does not form a dimer when allowed to decompose in the absence of alkali metal species. Calculations show that energy barriers to the uncatalyzed dimerization mechanism may be prohibitively high, in agreement with these observations. We believe it is timely to issue a challenge to find any example of this classic dimerization mechanism, and predict that it is most likely to be found with five-membered-ring diaminocarbenes (dihydroimidazol-2-ylidenes) such as **Me5**.

Diaminocarbenes can dimerize by a proton-catalyzed mechanism. We have observed the protonated dimer intermediate in a favorable case, and we believe that in practice this is by far the most common mechanism for dimer formation. We find that a carbene, which cannot dimerize, **iPr6**, nevertheless forms a complex containing a C₂Li ring in the presence of excess LiHMDS. This raises the possibility that alkali metal species, while thermodynamically stabilizing diaminocarbenes, may nevertheless catalyze dimer formation.

Finally, we have drawn attention in several places to the importance of the N-C-N angle in determining the properties of diaminocarbenes. Larger ring and acyclic diaminocarbenes are likely to require stronger bases for their generation, but be more reactive as bases and nucleophiles once prepared.

12. Addendum

A number of relevant papers have appeared since this review was prepared. The important influence of ring size on carbene reactivity has been mentioned several times in our review, and Grubbs et al. have recently reported the first examples of stable four-membered-ring carbenes, together with some information on their dimerization.^[71] Bertrand et al. have continued to explore novel types of carbenes including stable monoaminocarbenes.^[72–74]

The evidence that **EtA** and several other simple carbenes are kinetically stable to dimerization in THF at ambient temperatures has been published.^[75] The work by Magill, Cavell, and Yates mentioned in reference [69] has now been published;^[76] these authors calculate the pK_a values in DMSO of **Me5**, **Me6**, and **MeA** to be 22.3, 27.1, and 27.9, respectively, using the high-level CBS-QB3 complete basis set method in conjunction with the CPCM solvation model. Further experimental^[77] and computational^[78] evidence that acyclic and six-membered-ring carbenes are better σ donors has appeared.

Roger Alder thanks the Leverhulme Trust for an Emeritus Fellowship, and Jeremy Harvey thanks the EPSRC for an Advanced Research Fellowship. We thank the EPSRC for a postdoctoral research assistantship for L.C. and a studentship for M.E.B, as well as Dr. Mark Oakley for helpful comments and suggestions concerning the calculations.

Received: February 3, 2004

Published Online: September 29, 2004

- [1] A. J. Arduengo, R. L. Harlow, M. Kline, *J. Am. Chem. Soc.* **1991**, *113*, 361.
- [2] A. J. Arduengo, R. Krafczyk, *Chem. Unserer Zeit* **1998**, *32*, 6.
- [3] A. J. Arduengo, *Acc. Chem. Res.* **1999**, *32*, 913.
- [4] R. W. Alder in *Carbene Chemistry: From Fleeting Intermediates to Powerful Reagents* (Ed.: G. Bertrand), FontisMedia/Marcel Dekker, New York, **2002**, p. 153.
- [5] W. A. Herrmann, C. Köcher, *Angew. Chem.* **1997**, *109*, 2256; *Angew. Chem. Int. Ed. Engl.* **1997**, *36*, 2162.
- [6] W. A. Herrmann, *Angew. Chem.* **2002**, *114*, 1342; *Angew. Chem. Int. Ed.* **2002**, *41*, 1290.
- [7] T. M. Trnka, R. H. Grubbs, *Acc. Chem. Res.* **2001**, *34*, 18.
- [8] R. Hoffmann, R. Gleiter, F. B. Mallory, *J. Am. Chem. Soc.* **1970**, *92*, 1460.
- [9] A. J. Arduengo, J. R. Goerlich, W. J. Marshall, *Liebigs Ann.* **1997**, 365.
- [10] Y. T. Chen, F. Jordan, *J. Org. Chem.* **1991**, *56*, 5029.
- [11] A. J. Arduengo, H. V. R. Dias, R. L. Harlow, M. Kline, *J. Am. Chem. Soc.* **1992**, *114*, 5530.
- [12] C. Heinemann, W. Thiel, *Chem. Phys. Lett.* **1994**, *217*, 11.
- [13] L. Nyulaszi, T. Veszpremi, A. Forro, *PCCP Phys. Chem. Chem. Phys.* **2000**, *2*, 3127.
- [14] T. A. Taton, P. Chen, *Angew. Chem.* **1996**, *108*, 1098; *Angew. Chem. Int. Ed. Engl.* **1996**, *35*, 1011.
- [15] Y. F. Liu, P. E. Lindner, D. M. Lemal, *J. Am. Chem. Soc.* **1999**, *121*, 10626.
- [16] F. E. Hahn, L. Wittenbecher, D. Le Van, R. Frohlich, *Angew. Chem.* **2000**, *112*, 551; *Angew. Chem. Int. Ed.* **2000**, *39*, 541.
- [17] M. K. Denk, A. Thadani, K. Hatano, A. J. Lough, *Angew. Chem.* **1997**, *109*, 2719; *Angew. Chem. Int. Ed. Engl.* **1997**, *36*, 2607.
- [18] M. J. Cheng, C. H. Hu, *Chem. Phys. Lett.* **2000**, *322*, 83.
- [19] M. J. Cheng, C. H. Hu, *Chem. Phys. Lett.* **2001**, *349*, 477.
- [20] F. Guillen, C. L. Winn, A. Alexakis, *Tetrahedron: Asymmetry* **2001**, *12*, 2083.
- [21] P. Bazinet, G. P. A. Yap, D. S. Richeson, *J. Am. Chem. Soc.* **2003**, *125*, 13314.
- [22] H. E. Winberg, J. E. Carnahan, D. C. Coffman, M. Brown, *J. Am. Chem. Soc.* **1965**, *87*, 2055.
- [23] B. Alici, E. Cetinkaya, B. Cetinkaya, D. Ulku, M. N. Tahir, *J. Chem. Res. Miniprint* **1996**, *12*, 2953–2962; B. Alici, E. Cetinkaya, B. Cetinkaya, D. Ulku, M. N. Tahir, *J. Chem. Res. Miniprint* **1996**, *12*, 516.
- [24] W. Krasuski, D. Nikolaus, M. Regitz, *Liebigs Ann. Chem.* **1982**, 1451.
- [25] R. W. Alder, M. E. Blake, C. Bortolotti, S. Bufali, C. P. Butts, E. Linehan, J. M. Oliva, A. G. Orpen, M. J. Quayle, *Chem. Commun.* **1999**, 241.
- [26] R. W. Alder, M. E. Blake, C. Bortolotti, S. Bufali, C. P. Butts, E. Linehan, J. M. Oliva, A. G. Orpen, M. J. Quayle, *Chem. Commun.* **1999**, 1049.
- [27] R. W. Alder, P. R. Allen, M. Murray, A. G. Orpen, *Angew. Chem.* **1996**, *108*, 1211; *Angew. Chem. Int. Ed. Engl.* **1996**, *35*, 1121.
- [28] R. W. Alder, M. E. Blake, *Chem. Commun.* **1997**, 1513.
- [29] R. W. Alder, M. E. Blake, *Chem. Commun.* **1998**, 441.
- [30] J. W. Scheeren, R. J. F. Nivard, *Recl. Trav. Chim. Pays-Bas* **1969**, *88*, 289.
- [31] O. Tsuge, K. Yanagi, M. Horie, *Bull. Chem. Soc. Jpn.* **1971**, *44*, 2171.
- [32] V. P. W. Böhm, W. A. Herrmann, *Angew. Chem.* **2000**, *112*, 4200; *Angew. Chem. Int. Ed.* **2000**, *39*, 4036.
- [33] H. W. Wanzlick, E. Schikora, *Angew. Chem.* **1960**, *72*, 494.
- [34] H. W. Wanzlick, E. Schikora, *Chem. Ber.* **1961**, *94*, 2389.
- [35] H. W. Wanzlick, *Angew. Chem.* **1962**, *74*, 129; *Angew. Chem. Int. Ed. Engl.* **1962**, *1*, 75.

- [36] D. M. Lemal, R. A. Lovald, K. I. Kawano, *J. Am. Chem. Soc.* **1964**, *86*, 2518.
- [37] M. K. Denk, K. Hatano, M. Ma, *Tetrahedron Lett.* **1999**, *40*, 2057.
- [38] Y. F. Liu, D. M. Lemal, *Tetrahedron Lett.* **2000**, *41*, 599.
- [39] R. W. Alder, P. R. Allen, S. J. Williams, *J. Chem. Soc. Chem. Commun.* **1995**, 1267.
- [40] Y. J. Kim, A. Streitwieser, *J. Am. Chem. Soc.* **2002**, *124*, 5757.
- [41] A. J. Arduengo, F. Davidson, H. V. R. Dias, J. R. Goerlich, D. Khasnis, W. J. Marshall, T. K. Prakasha, *J. Am. Chem. Soc.* **1997**, *119*, 12742.
- [42] M. K. Denk, J. M. Rodezno, S. Gupta, A. J. Lough, *J. Organomet. Chem.* **2001**, *617*, 242.
- [43] N. Kuhn, T. Kratz, *Synthesis* **1993**, 561.
- [44] M. Otto, S. Conejero, Y. Canac, V. D. Romanenko, V. Rudzevitch, G. Bertrand, *J. Am. Chem. Soc.* **2004**, *126*, 1016.
- [45] W. A. Herrmann, C. Kocher, L. J. Goossen, G. R. J. Artus, *Chem. Eur. J.* **1996**, *2*, 1627.
- [46] G. Boche, C. Hilf, K. Harms, M. Marsch, J. C. W. Lohrenz, *Angew. Chem.* **1995**, *107*, 509; *Angew. Chem. Int. Ed. Engl.* **1995**, *34*, 487.
- [47] A. J. Arduengo, M. Tamm, J. C. Calabrese, F. Davidson, W. J. Marshall, *Chem. Lett.* **1999**, 1021.
- [48] R. Frankel, C. Birg, U. Kernbach, T. Habereeder, H. Noth, W. P. Fehlhammer, *Angew. Chem.* **2001**, *113*, 1961; *Angew. Chem. Int. Ed.* **2001**, *40*, 1907.
- [49] R. W. Alder, M. E. Blake, J. M. Oliva, *J. Phys. Chem. A* **1999**, *103*, 11200.
- [50] R. W. Alder, M. E. Blake, S. Bufali, C. P. Butts, A. G. Orpen, J. Schutz, S. J. Williams, *J. Chem. Soc. Perkin Trans. 1* **2001**, 1586.
- [51] H. Lund, P. Lunde, *Acta Chem. Scand.* **1967**, *21*, 1067.
- [52] R. West, P. Boudjouk, *J. Am. Chem. Soc.* **1973**, *95*, 3983.
- [53] X. Cattoen, S. Sole, C. Pradel, H. Gornitzka, K. Miqueu, D. Bourissou, G. Bertrand, *J. Org. Chem.* **2003**, *68*, 911.
- [54] All calculations were performed with the Jaguar program package, (Jaguar 4.2 ed.; Schrodinger, Inc., Portland, OR, USA, **1991–2002**) using Becke's three-parameter exchange functional (A. D. Becke, *J. Chem. Phys.* **1993**, *98*, 5648) with the correlation functional of Lee, Yang, and Parr (B3LYP). (C. T. Lee, W. T. Yang, R. G. Parr, *Phys. Rev. B* **1988**, *37*, 785) All species were characterized by full-geometry optimization with the standard 6-31G(d) basis set. All stationary points were characterized by analytical frequency calculations. For singlet species, restricted DFT methods were used, whilst unrestricted methods were used for triplets.
- [55] M. K. Denk, S. Gupta, J. Brownie, S. Tajammul, A. J. Lough, *Chem. Eur. J.* **2001**, *7*, 4477.
- [56] P. B. Hitchcock, D. A. Handley, T. H. Lee, G. J. Leigh, *J. Chem. Soc. Dalton Trans.* **2002**, 4720.
- [57] K. Denk, P. Sirsch, W. A. Herrmann, *J. Organomet. Chem.* **2002**, *649*, 219.
- [58] D. M. Lemal in *The Chemistry of Functional Groups, Vol. 4* (Ed.: S. Patai), Wiley, London, **1968**, p. 701.
- [59] H. Bock, H. Borrmann, Z. Havlas, H. Oberhammer, K. Ruppert, A. Simon, *Angew. Chem.* **1991**, *103*, 1733; *Angew. Chem. Int. Ed. Engl.* **1991**, *30*, 1678.
- [60] J. Bruckmann, C. Krueger, H. Borrmann, A. Simon, H. Bock, Z. *Kristallogr.* **1995**, *210*, 521.
- [61] C. W. Bauschlicher, H. Partridge, *J. Chem. Phys.* **1995**, *103*, 1788.
- [62] Single-point B3LYP calculations with the larger 6-311+G(d,p) basis set favor the carbenes relative to the dimers by, typically, 30 kJ mol⁻¹. Thus, increasing the basis set leads to smaller predicted bond energies, and hence actually makes the B3LYP results deviate more from the G2(B3LYP/MP2/CC) results. There is little doubt that these higher level calculations are wrong so far as absolute values for ΔE and ΔG are concerned. This is not an unknown problem with density functional theory calculations (W. Koch, M. C. Holthausen, *A Chemist's Guide to Density Functional Theory*, Wiley-VCH, Weinheim, **2001**); it has been found that B3LYP/6-311+G** calculations lead to an error of similar magnitude for ΔE for the simplest Diels–Alder reaction (butadiene plus ethene). The simpler B3LYP/6-31G* calculation was in better agreement with experiment. Significantly perhaps for our subsequent discussion of energy barriers for carbene dimerization, the calculated activation energy (ΔE^\ddagger) for the Diels–Alder example is in quite good agreement with experiment with both basis sets. We also carried out single point MP2 calculations for several of these species and find that ΔE now shifts in the other direction, thus ΔE for dimerization of carbene MeA in the gas phase becomes a massive 278.3 kJ mol⁻¹. Carried across the series, this would lead to the incorrect prediction that iPr6 would surely dimerize. Our earlier report of dimerization energies for diaminocarbene (–181.5 from B3LYP/cc-pVDZ, and 229.8 from MP2/cc-pVDZ) are incorrect, as a less stable structure with D₂ symmetry was used for the dimer.
- [63] The obvious reference compounds are perhaps the corresponding amins (CH₂ in place of the carbene center), but these were avoided because of potential problems with variable anomeric effects. Note that energies for methane, ethane, singlet methylene, and the methyl and ethyl cations were calculated at the B3LYP/6-31G* level, but are unimportant as far as internal comparison of **Me5**, **Me6**, **Me7**, and **MeA** are concerned. The ethyl cation is actually protonated π -protonated ethene at the B3LYP/6-31G* level.
- [64] J. N. Harvey, *Organometallics* **2001**, *20*, 4887.
- [65] K. Morokuma, K. Ohta, E. R. Davidson, *J. Am. Chem. Soc.* **1985**, *107*, 3466.
- [66] S. Sharpe, B. Hartnett, H. S. Sethi, D. S. Sethi, *J. Photochem.* **1987**, *38*, 1.
- [67] A. J. Arduengo, S. F. Gamper, M. Tamm, J. C. Calabrese, F. Davidson, H. A. Craig, *J. Am. Chem. Soc.* **1995**, *117*, 572.
- [68] T. L. Amyes, S. T. Diver, J. P. Richard, F. M. Rivas, K. Toth, *J. Am. Chem. Soc.* **2004**, *126*, 4366.
- [69] A. M. Magill, K. J. Cavell, B. F. Yates, personal communication.
- [70] This calculation was carried out using the Gaussian 03 program package at the B3LYP/6-31G*-optimized geometry of the corresponding complex, using the B3LYP method, together with the 6-311G* basis on Li and the two carbene atoms, and the 6-31G* basis on all other atoms (Gaussian 03, Revision A.1, M. J. Frisch, G. W. Trucks, H. B. Schlegel, G. E. Scuseria, M. A. Robb, J. R. Cheeseman, J. A. Montgomery, Jr., T. Vreven, K. N. Kudin, J. C. Burant, J. M. Millam, S. S. Iyengar, J. Tomasi, V. Barone, B. Mennucci, M. Cossi, G. Scalmani, N. Rega, G. A. Petersson, H. Nakatsuji, M. Hada, M. Ehara, K. Toyota, R. Fukuda, J. Hasegawa, M. Ishida, T. Nakajima, Y. Honda, O. Kitao, H. Nakai, M. Klene, X. Li, J. E. Knox, H. P. Hratchian, J. B. Cross, C. Adamo, J. Jaramillo, R. Gomperts, R. E. Stratmann, O. Yazyev, A. J. Austin, R. Cammi, C. Pomelli, J. W. Ochterski, P. Y. Ayala, K. Morokuma, G. A. Voth, P. Salvador, J. J. Dannenberg, V. G. Zakrzewski, S. Dapprich, A. D. Daniels, M. C. Strain, O. Farkas, D. K. Malick, A. D. Rabuck, K. Raghavachari, J. B. Foresman, J. V. Ortiz, Q. Cui, A. G. Baboul, S. Clifford, J. Cioslowski, B. B. Stefanov, G. Liu, A. Liashenko, P. Piskorz, I. Komaromi, R. L. Martin, D. J. Fox, T. Keith, M. A. Al-Laham, C. Y. Peng, A. Nanayakkara, M. Challacombe, P. M. W. Gill, B. Johnson, W. Chen, M. W. Wong, C. Gonzalez, and J. A. Pople, Gaussian, Inc., Pittsburgh PA, **2003**).
- [71] E. Despagne-Ayoub, R. H. Grubbs, *J. Am. Chem. Soc.* **2004**, *126*, in press.
- [72] X. Cattoen, H. Gornitzka, D. Bourissou, G. Bertrand, *J. Am. Chem. Soc.* **2004**, *126*, 1342.
- [73] V. Lavallo, J. Mafhouz, Y. Canac, B. Donnadiou, W. W. Schoeller, G. Bertrand, *J. Am. Chem. Soc.* **2004**, *126*, 8670.
- [74] S. Conejero, Y. Canac, F. S. Tham, G. Bertrand, *Angew. Chem.* **2004**, *116*, 4181; *Angew. Chem. Int. Ed.* **2004**, *43*, 4089.

- [75] R. W. Alder, L. Chaker, F. P. V. Paolini, *Chem. Commun. (Cambridge)* **2004**, DOI: 10.1039/b409112d.
- [76] A. M. Magill, K. J. Cavell, B. F. Yates, *J. Am. Chem. Soc.* **2004**, *126*, 8717.
- [77] M. Mayr, K. Wurst, K. Ongania, M. Buchmeiser, *Chem. Eur. J.* **2004**, *10*, 1256.
- [78] M. T. Lee, C. H. Hu, *Organometallics* **2004**, *23*, 976.

Quality counts...

The best of chemistry every week



Wiley-VCH

P.O. Box 10 11 61
69451 Weinheim
Germany
Phone +49 (0) 6201-606-400
Fax +49 (0) 6201-606-184
e-mail: angewandte@wiley-vch.de

www.angewandte.org

Angewandte Chemie International
Edition is a journal of the GDCh,
the German Chemical Society

GDCh

 WILEY-VCH

Assembly of an Oxo-Zirconium(IV) Cluster in a Protein Cleft**

Weiying Zhong, Dmitriy Alexeev, Ian Harvey,
Maolin Guo, Dominic J. B. Hunter, Haizhong Zhu,
Dominic J. Campopiano, and Peter J. Sadler*

There is a wide range of potential uses for small, well-defined oxo-metal clusters, including magnetic devices, optical materials, and catalysts.^[1] The challenge is to discover synthetic methods that allow their size, composition, and, importantly, also the external coating (peripheral ligands) to be controlled. These features determine the chemical and physical properties of the metals in the cluster, including recognition by interacting partners, such as substrates and surfaces. We are exploring the use of flexible protein clefts as templates for assembly of polyoxometalate clusters, in particular that of bacterial transferrin (ferric-ion-binding protein, Fbp). Recently we,^[2,3] and others,^[4] have shown that the “venus fly trap” interdomain cleft of Fbp can accommodate clusters of metal ions, which are effectively small fragments of oxo/

hydroxo minerals. Herein we show that oxo-zirconium clusters are readily assembled on Fbp by reaction with a mononuclear Zr^{IV} complex and nucleated by a dityrosyl (diphenolate) motif in the interdomain binding cleft. We have determined the structures of these multinuclear zirconium-Fbp adducts by EXAFS and X-ray crystallography, and have studied the influence of phosphate and carbonate on the assembly process.

Native, holo-Fbp (34 kDa, 309 amino acids) contains an Fe^{III} center bound to the phenolate oxygen atoms of Tyr195 and Tyr196, a carboxylate oxygen atom of Glu57, and the imidazole nitrogen atom of His9, together with oxygen atoms from phosphate (the “synergistic anion”) and water (Figure 1), in a closed binding cleft.^[5] The cleft is formed by

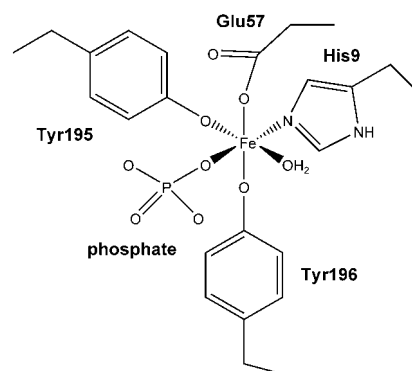


Figure 1. The iron(III)-binding site in holo-Fbp.

two alternating α helix/ β sheet domains hinged by a pair of antiparallel β strands. Serum transferrin and lactoferrin have similar Fe^{III} -binding sites, but use carbonate as the synergistic anion. Carbonate can replace phosphate in holo-Fbp, but binds less strongly.^[6,7]

We prepared Zr-Fbp by treating apo-Fbp with various molar ratios of $[\text{Zr}(\text{NTA})_2]^{2-}$ ($\text{NTA} = N,N$ -bis(carboxymethyl) glycine, ion (3–)) in HEPES (HEPES = 2-(4-(2-hydroxyethyl)-1-piperazinyl)ethanesulfonic acid) buffer pH 7.4 for 24 h followed by extensive ultrafiltration to remove unbound Zr^{IV} . Reaction with 1, 2, and 6 mole equivalents of $[\text{Zr}(\text{NTA})_2]^{2-}$ gave proteins containing an average of 0.8, 1.5, and 3.9 mol Zr, respectively, together with approximately 1 mol of phosphate per mol protein, as determined by inductively coupled plasma atomic emission spectroscopy (ICP-AES; Table 1). Similar results were obtained using Tris (Tris = 2-amino-2-(hydroxymethyl)-1,3-propanediol) buffer at pH 8 (Table 1). Chromatographic studies suggested that the products from these reloading reactions contain both apo and multinuclear forms of Zr-Fbp (see Supporting Information).

The presence of bound clusters was confirmed by Zr K-edge EXAFS studies. The products from 1:1 and 6:1 reactions of $[\text{Zr}(\text{NTA})_2]^{2-}$ with apo-Fbp gave essentially the same EXAFS spectra (Figure 2), and clearly show the presence of Zr–Zr scattering between 3.3–3.6 Å, consistent with the presence of $\{\text{Zr}_3\}$ clusters in both preparations. The apparent slight difference in the distances observed in the Fourier

[*] Dr. W. Zhong, Dr. M. Guo, ** Dr. D. J. B. Hunter, Dr. H. Zhu,
Dr. D. J. Campopiano, Professor Dr. P. J. Sadler
School of Chemistry
King's Buildings
The University of Edinburgh
West Mains Road, Edinburgh EH93JJ (UK)
Fax: (+44) 131-650-6453
E-mail: p.j.sadler@ed.ac.uk

Dr. W. Zhong
School of Pharmacy
Second Military Medical University
Shanghai, 200433 (P. R. China)

Dr. D. Alexeev*
Institute of Cell and Molecular Biology
Michael Swann Building, University of Edinburgh
Mayfield Road, Edinburgh EH93JR (UK)
E-mail: Dmitriy-Alexeev@hotmail.com

Dr. I. Harvey
Synchrotron Radiation Department
CCLRC Daresbury Laboratory, Warrington WA44AD (UK)

[†] X-ray data. Current address:
Millennium Pharmaceuticals Ltd.
45 Sidney Street, Cambridge, MA 02139 (USA)

[††] Current address:
Department of Chemistry and Biochemistry
University of Massachusetts Dartmouth
285 Old Westport Road, North Dartmouth, MA 02747-2300 (USA)

[**] We thank The Wellcome Trust (Travelling Research Fellowship and International Research Development Award for WZ, Sir Henry Wellcome Commemorative Award for DJC and PJS, and Edinburgh Protein Interaction Centre), The Darwin Trust, CCLRC, EPSRC, Royal Society, Wolfson Foundation and the Medical Science Foundation of Chinese PLA (grant No. 01H021 for WZ) for their support for this work, and Dr Lorna Eades and John Wexler for assistance with ICP-MS and graphics, respectively.

Supporting information for this article is available on the WWW under <http://www.angewandte.org> or from the author.

Table 1: Analysis of the products from reactions of apo-Fbp with $[\text{Zr}(\text{NTA})_2]^{2-}$.

Reaction mixture ^[a]	Product ^[b]	
$[\text{Zr}]/[\text{Fbp}]$	$[\text{Zr}]/[\text{Fbp}]$	$[\text{P}]/[\text{Fbp}]$
1:1 ^[c]	0.84	— ^[d]
2:1 ^[e]	1.5	1.4
6:1 ^[e]	3.9	1.1

[a] Reactions carried out for 24 h in 10 mM HEPES buffer containing 5 mM phosphate and 5 mM carbonate, pH 7.4, 298 K. [b] Fbp concentration determined from A_{280} . [c] Similar analyses obtained for reactions in 10 mM phosphate and carbonate. [d] Not determined. [e] Similar analyses obtained for reactions in 10 mM Tris buffer pH 8.0.

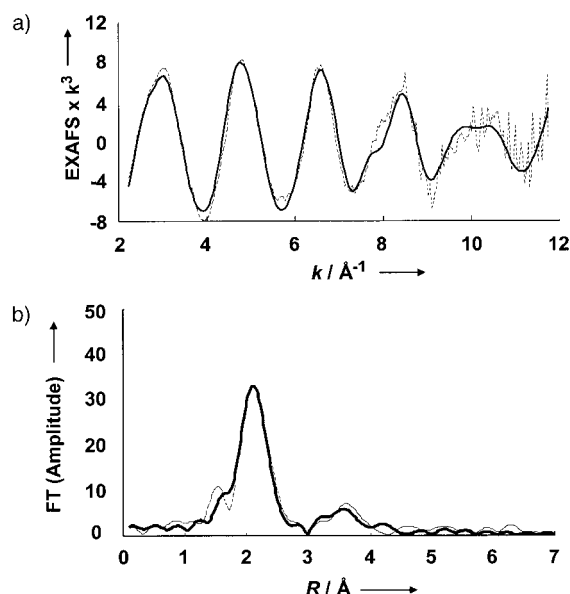


Figure 2. a) EXAFS data, and b) and the Fourier transform data for Zr-Fbp (prepared from 6:1 Zr:apo-Fbp reaction). The data are modeled using the cluster derived from the X-ray data (see Figure 3) but with carbonate as the capping ligand, and full multiple scattering (see Supporting Information for details). Dashed line = experimental data, bold line = model. The peak at approximately 1.5 Å in (b) is an artifact of background subtraction and Fourier truncation (finite EXAFS data range).

transforms for the two samples (see Supporting Information) reflects small differences in the geometry of the clusters (as is also seen in the crystallographic data, see below). The EXAFS data represent an average of the $\{\text{Zr}_3\}$ local environments and could also reflect a higher Zr loading at some centers. The first shell can be fitted with 1 oxygen atom at approximately 2.0 Å, 4 oxygen atoms at approximately 2.15 Å, and a further 2 oxygen atoms at approximately 2.3 Å (see Table 2). However, this leaves an unfilled contribution to the first shell at approximately 2.66 Å. This contribution can be fitted with a carbon atom, which reduces the *R* factor by 6%. A light atom at this distance is consistent with bound carbonate, rather than phosphate. Indeed, inclusion of carbonate rather than phosphate in the final EXAFS model leads to significantly lower *R* factors (29.1% versus 36.5% for 1:1, 25.0% versus 32.2% for the product from the 6:1 reaction) as well as much better matches to the Fourier

Table 2: Refined average EXAFS interatomic distances from the Zr “central atom”, modeled with carbonate as a capping ligand, including multiple scattering.

Atoms/parameter	Sample ^[a]	
	Zr-Fbp (1:1)	Zr-Fbp (6:1)
1 O [Å]	2.03(±0.02)	1.99(±0.02)
4 O [Å]	2.16(±0.02)	2.13(±0.01)
2 O [Å]	2.30(±0.02)	2.27(±0.01)
1 Zr [Å]	3.41(±0.02)	3.38(±0.02)
1 Zr [Å]	3.53(±0.03)	3.50(±0.02)
<i>R</i> factor [%]	29.1	25.0
fit index	0.535	0.437

[a] Ratios refer to the reaction stoichiometry.

transforms (see Figure 2). However, owing to the strength of the Zr–Zr scattering and the averaging of the EXAFS data over three zirconium atoms per cluster, a proportion of clusters with bound phosphate cannot be ruled out. Evidence that carbonate can bind to Zr–Fbp in solution was obtained by NMR spectroscopy. The ^{13}C - $\{^1\text{H}\}$ NMR spectrum of apo-Fbp (0.4 mM) in the presence of 2 mol equivalents of $[\text{Zr}(\text{NTA})_2]^{2-}$ and 20 mM $\text{NaH}^{13}\text{CO}_3$ contained a small resonance signal at $\delta = 168.2$ ppm assignable to zirconium-bound $^{13}\text{CO}_3^{2-}$ (see Supporting Information).^[8]

Crystallization of Zr–Fbp was successful only using a malate/imidazole buffer system and a slightly higher pH value (8–8.2). Crystals were grown at 290 K by the hanging-drop vapor-diffusion technique, using Zr–Fbp obtained by reaction of apo-Fbp with either 1, 4, or 6 mol equivalents of Zr^{IV} , again after ultrafiltration to remove unbound metal. These preparations all gave similar crystals, which contain nine independent molecules in the asymmetric unit. In the 1.5 Å resolution structure (Table 3), all the molecules contain $\{\text{Zr}_3\}$ clusters, with minor differences in bond lengths and angles. The interdomain binding cleft remains open and Zr1 and Zr3 are coordinated directly to Tyr195 and Tyr196, respectively, and to a capping anion which appeared to be best modeled as phosphate, Figure 3 (and Supporting Information). The

Table 3: Crystallographic data and refinement statistics.

Parameter	Zr ₃ -Fbp ^[a]
wavelength [Å]	0.978
resolution [Å]	20–1.5
refined twinning fraction [%]	49.0
completeness [%]	98.5 (94.1)
redundancy	4.9 (2.9)
<i>I</i> / Σ	16.3 (1.3)
<i>R</i> _{sym} ^[b] [%]	9.5 (80.9)
<i>R</i> _{cryst} ^[c] [%]/ <i>R</i> _{free} ^[d] [%]	19.2/27.5
rms deviations	
bonds [Å]	0.01
angles [°]	2.3
average B-factors	
protein [Å ²]	25.5
water [Å ²]	27.6

[a] Numbers in parentheses are for the highest resolution shell. [b] $R_{\text{sym}} = \Sigma |I_h - \langle I_h \rangle| / I_h$, where $\langle I_h \rangle$ is the average intensity over symmetry equivalent reflections. [c] $R_{\text{cryst}} = \Sigma |F_o - F_c| / \Sigma F_o$, where summation is over the data used for refinement. [d] R_{free} was calculated using 5% of data excluded from refinement.

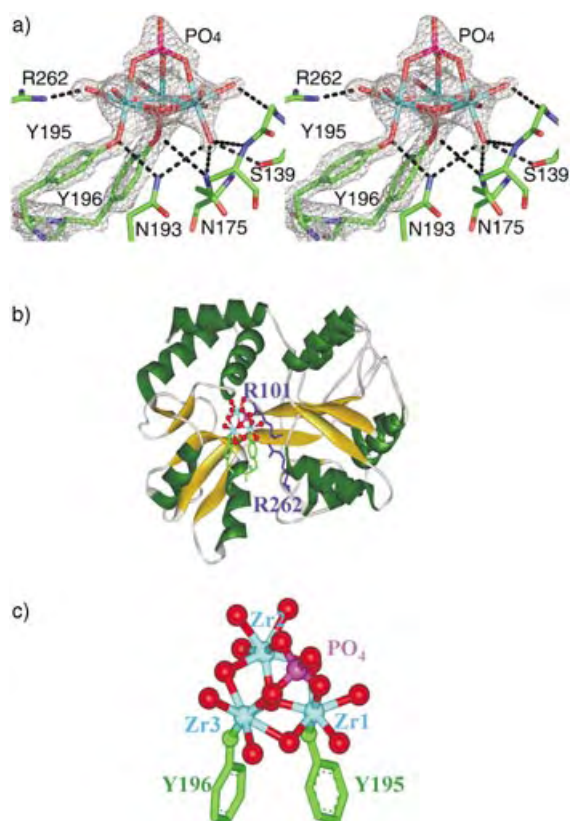


Figure 3. The crystal structure of Zr₃-Fbp. a) Stereo pair of the electron density map (contoured at the 3.5σ level) of the oxo-Zr₃ phosphate cluster (Zr cyan). The map was averaged between all nine molecules in the asymmetric unit. Only the electron density around Tyr195, Tyr196 and the cluster is shown. The only direct coordination to the Zr^{IV} ions in the cluster is by Tyr195 and Tyr196, although the oxygen atoms of the oxo cluster are H-bonded to several amino acids including residues 139–141 on the right side of the cluster in the phosphate-binding loop. b) Ribbon diagram of the protein (molecule D) showing α helices (dark green), β sheets (gold), and the {Zr₃} cluster in the interdomain cleft. Residue and atom colors: Tyr195 and Tyr196 green, Arg101 and Arg262 blue, P (phosphate) pink, oxygen red, Zr cyan. c) The anchoring of the trinuclear cluster by the dityrosyl motif, showing Zr labelling.

cluster structure resembles those found in the oxo-zirconium methacrylate clusters, [Zr₆(OH)₄O₄(OMc)₁₂] and [Zr₄O₂(OMc)₁₂] (OMc = methacrylate),^[9] and in the oxo-zirconium biphenolate cluster [(L₂Zr)₃(OH)₃(O)-Li₅(thf)₈(H₂O)₅] (L = 2,2'-biphenolato dianion),^[10] and is based on a triangular Zr₃O₄ unit with a central bridging μ₃-oxygen atom and three bridging μ₂-oxygen atoms. Each zirconium atom in Zr₃-Fbp is bound to seven oxygen atoms (in agreement with the EXAFS data) in a pentagonal bipyramidal geometry. The five equatorial oxygen atoms are (hydr)oxides, and the axial oxygen atoms are from tyrosinate for Zr1 and Zr3, water for Zr2, and from phosphate (Figure 3c). The Zr...Zr separations range from 3.4 to 3.7 Å, and the Zr–O bond lengths from 2.1–2.4 Å, with the zirconium–tyrosinate bonds being the shortest (1.9–2.1 Å). The positively charged side-chains of Arg101 (which is fully conserved in bacterial transferrins^[3]) and Arg262 are hydro-

gen-bonded to oxygen atoms of the oxo-Zr₃ cluster, as are the side-chains or main chain NH groups of several other amino acids including S139, N175, and N193 (see Figure 3a). The relatively high homogeneity of the zirconium clusters can be contrasted with the heterogeneity of the clusters in Hf-Fbp which were tri- and pentanuclear, either with or without capping phosphate.^[2]

We studied reactions of apo-Fbp (14 μM) with [Zr(NTA)₂]²⁻ in 10 mM HEPES buffer containing 5 mM NaHCO₃, 5 mM phosphate, pH 7.4, 298 K, by UV/Vis spectroscopy. Two new peaks appeared in the difference spectrum at 247 nm and 295 nm (Figure 4a,b). These bands are assignable to π–π transitions of Tyr residues deprotonated by binding to Zr^{IV}. Similar bands are seen when both bacterial and serum transferrins bind to a wide variety of metal ions.^[8,11,12] Titration studies (Figure 4c,d) suggested that a zirconium:protein mol ratio of 1:1 is sufficient to deprotonate both Tyr195 and Tyr196 if phosphate is present as the synergistic anion, but only one Tyr residue when only (bi)carbonate is present (Figure 4b). Phosphate is known to bind in the interdomain cleft of the apo protein and may prepare the cleft for metal entry.^[13] Beyond a 1:1 [Zr(NTA)₂]²⁻:apo-Fbp ratio there was little increase in the absorption at 247 nm (Figure 4d). These data therefore suggest that the initial reaction with apo-Fbp involves Zr^{IV} binding to Tyr195 and Tyr196 followed by subsequent formation of (hydr)oxo-zirconium clusters, and hence little increase in the absorption at 247 nm beyond a 1:1 [Zr(NTA)₂]²⁻:apo-Fbp ratio. Thus the clusters appear to be formed by stepwise insertion of Zr^{IV} ions into the interdomain cleft. ESI-MS studies of K₂[Zr(NTA)₂]²⁻·2H₂O (5 mM) in aqueous solution and HEPES buffer gave a major peak at *m/z* 582.88 (calcd. 582.82 for {K₃Zr(NTA)₂}⁺), with appropriate isotope splitting pattern, showing that the complex is monomeric under the conditions used for MS (50 % CH₃CN/H₂O, 0.1 % formic acid). The mobility of Tyr196 (as observed in crystals of oxo-Fe^{III}-Fbp)^[3] in particular may be important for capturing Zr^{IV} ions at the protein surface and delivering them into the binding cleft. The possibility that the protein can also capture preformed oxo-tri-Zr^{IV} clusters cannot be ruled out.

Low-molecular-weight alkoxide and aryloxide ligands have been used in the synthesis of small organically functionalized oxo-Zr^{IV} clusters.^[1,14–17] The experiments described herein show that oxo-trizirconium clusters anchored by a dityrosyl (diphenolate) motif readily assemble in the hinged cleft of a protein, bacterial transferrin. The provision of a protein coat for a polyoxometalate cluster could have several advantages. For example, the protein can readily be engineered to allow the environment of the cluster to be modified, including the electrostatic potential and hydrophobicity of the outer coordination sphere. Also the amino acids on the protein surface can be mutated to facilitate attachment to other surfaces (e.g. for array experiments), or to promote solubilization in various media. It is apparent that Fbp is a versatile metal-binding scaffold. The remarkable ability of the dityrosyl motif to selectively nucleate the formation of oxo-metal clusters in a positively charged binding cleft is likely to be a useful and widely exploitable property of the protein.

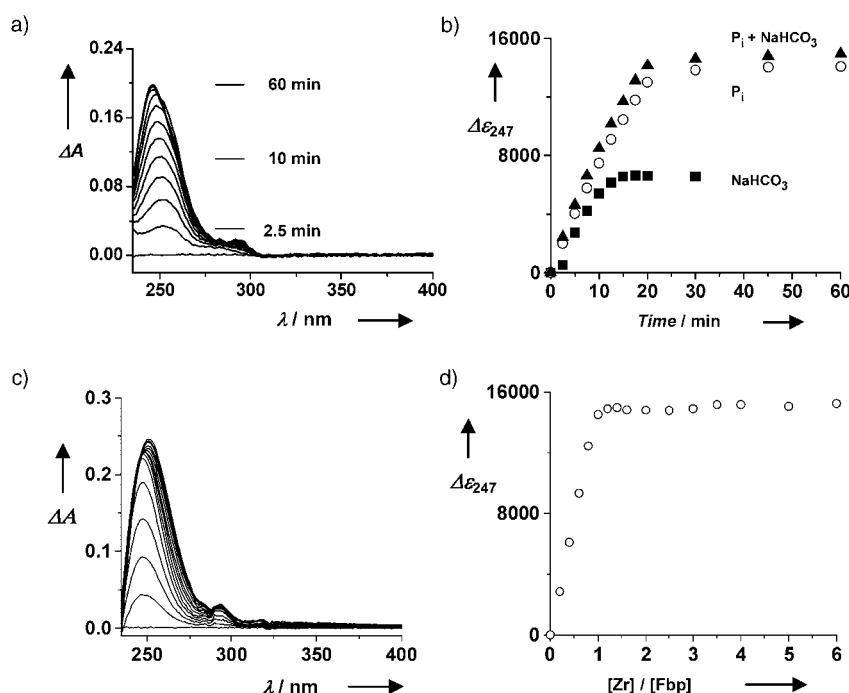


Figure 4. a) Difference UV/Vis spectra recorded at various times during the reaction of apo-Fbp (14 μM) with 2.0 mol equivalents of [Zr(NTA)₂]²⁻ in 10 mM HEPES pH 7.4 in the presence of 5 mM NaHCO₃ and 5 mM KH₂PO₄. b) Plot of molar absorptivity versus time for reaction in the presence of 5 mM NaHCO₃ and 5 mM KH₂PO₄ (▲), and for similar reactions with either 5 mM NaHCO₃ (■) or 5 mM of KH₂PO₄ (○) present. c) Difference UV/Vis spectra for the titration of apo-Fbp (15 μM) with [Zr(NTA)₂]²⁻ in 10 mM HEPES, 5 mM NaHCO₃, pH 7.4, 298 K (1 h equilibration). Mol ratios of [Zr(NTA)₂]²⁻: apo-Fbp from bottom to top: 0–1.6 in 0.2 mol equivalent steps, then 2.0, 2.5, 3.0, 3.5, 4.0, 5.0, 6.0. d) Titration curve for the reaction in (c).

Experimental Section

HEPES, H₃NTA, and Fe and Zr atomic absorption standard solutions were purchased from Aldrich, NaH¹³CO₃ (>99% enriched) from MSD isotopes, and ZrOCl₂ hydrate from Strem Chemicals (Zr content determined by ICP-AES). Crystalline K₂[Zr(NTA)₂·2H₂O] was prepared according to a literature method.^[8,18] Holo- and apo-Fbp were prepared and purified by modifications of described methods.^[6,19]

Zr–Fbp: Typically, microlitre aliquots of NaHCO₃ (0.25 M) and KH₂PO₄ (0.25 M, pH 7.4, final concentrations 5 mM) were added to apo-Fbp (25–100 μM) in 10 mM HEPES buffer pH 7.4 (or Tris buffer pH 8.0), followed by addition of freshly prepared aqueous K₂[Zr(NTA)₂] (10 mM) to give ratios of [Zr]:[Fbp] = 1:1, 2:1, 4:1, or 6:1. The mixture was incubated for 24 h at 310 K, and the buffer was exchanged into 0.1 M KCl by ultrafiltration 8 × (to remove unbound Zr, carbonate, and phosphate) and the solution was concentrated to approximately 8 mg protein mL⁻¹.

Crystals were grown by the hanging-drop vapor-diffusion technique at 290 K by mixing protein solution (5 μL; 3.7–4.0 mg mL⁻¹ in 0.1 M KCl) with an equal amount of a reservoir solution containing approximately 20–22% polyethylene glycol (PEG) 4000, 0.2 M NaCl, 0.4 M imidazole/malate buffer, pH 8.0–8.2.

Crystals were flash-frozen in liquid nitrogen and X-ray data were collected on station 14.2 (SRS, Daresbury Laboratory; λ = 0.978 Å) using an ADSC Quantum4 CCD detector and processed and scaled using HKL2000.^[20] Crystals belong to the space group P3₂ (cell dimensions a = b = 146.2 Å and c = 113.56 Å). The structures were solved using the methods previously described.^[2]

Coordinates have been deposited in the Protein Data Bank (accession code 1XC1).

X-ray spectra were recorded at the Zr K-edge on EXAFS station 9.3 at Daresbury Laboratory Synchrotron Radiation Source (operating at 2 GeV), at 80 K, and in fluorescence mode. Data collection times were 11 h per sample.

A computer-controlled Perkin-Elmer Lambda 16 UV/Vis spectrometer was used together with 1 cm path-length cuvettes maintained at 298 ± 0.1 K or 310 ± 0.1 K with a PTP-1 Peltier temperature programmer. Aliquots (2 or 5 μL) of a [Zr(NTA)₂]²⁻ solution were added to apo-Fbp (10–20 μM) solutions in HEPES buffer (10 mM), and NaHCO₃ (5 mM) and left to equilibrate for 1 h at 298 K or 310 K. The UV/Vis spectra were then recorded. A buffer solution containing the same amounts of NaHCO₃ and [Zr(NTA)₂]²⁻ was used as the reference.

The time courses for the reactions of apo-Fbp with [Zr(NTA)₂]²⁻ were also recorded in HEPES buffer (10 mM). Apo-Fbp (13–15 μM) in HEPES buffer (10 mM, pH 7.4) containing NaHCO₃ (5 mM) and/or KH₂PO₄ was treated with [Zr(NTA)₂]²⁻ (2 mol equivalents) at 298 K and UV/Vis spectra were recorded at 2.5 min intervals against the same buffer solution containing the same amount of [Zr(NTA)₂]²⁻.

The products from reaction of apo-Fbp (180 μM) with 0.5, 1.0 and 6.0 mol equiv of [Zr(NTA)₂]²⁻ at 310 K for 24 h were applied to a Mono S HR5/5 column equilibrated with HEPES buffer (10 mM; pH 7.4, 25 mL), followed by gradient elution with 0–1 M KCl in HEPES (10 mM; pH 7.4) flow

rate 0.5 mL min⁻¹). Fractions of 0.5 mL were collected and analyzed by ICP-AES, and of 0.1 mL by inductively coupled plasma (ICP)-MS.

Zr and P content was determined by ICP-AES (Thermo Jarrell Ash IRIS spectrometer) calibrated with standard solutions using the emission lines at 349.621 nm and 213.618 nm for Zr and P, respectively. For some samples, ⁹⁰Zr was determined on a PlasmaQuad ICP-MS. Samples from reactions of apo-Fbp with [Zr(NTA)₂]²⁻ (Table 1) were purified by ultrafiltration (Centricon MW cut-off 10 kDa), washing 3 × with HEPES or Tris buffer as appropriate before Zr and P analysis.

Details of ESI-MS, NMR, chromatography and pH measurements, and further details of protein preparation, X-ray crystallography and X-ray absorption spectroscopy are given in the Supporting Information.

Received: May 27, 2004

Published Online: October 7, 2004

Keywords: bioinorganic chemistry · cluster compounds · metalloproteins · X-ray diffraction · zirconium

- [1] G. Kickelbick, D. Holzinger, C. Brick, G. Trimmel, E. Moons, *Chem. Mater.* **2002**, *14*, 4382–4389.
- [2] D. Alexeev, H. Zhu, M. Guo, W. Zhong, D. J. B. Hunter, W. Yang, D. J. Campopiano, P. J. Sadler, *Nat. Struct. Biol.* **2003**, *10*, 297–302.

- [3] H. Zhu, D. Alexeev, D. J. B. Hunter, D. J. Campopiano, P. J. Sadler, *Biochem. J.* **2003**, 376, 35–41.
- [4] S. R. Shouldice, R. J. Skene, D. R. Dougan, D. E. McRee, L. W. Tari, A. B. Schryvers, *Biochemistry* **2003**, 42, 11908–11914.
- [5] C. M. Bruns, A. J. Nowalk, A. S. Arvai, M. A. McTigue, K. G. Vaughan, T. A. Mietzner, D. E. McRee, *Nat. Struct. Biol.* **1997**, 4, 919–924.
- [6] M. Guo, I. Harvey, W. Yang, L. Coghill, D. J. Campopiano, J. A. Parkinson, R. T. A. MacGillivray, W. R. Harris, P. J. Sadler, *J. Biol. Chem.* **2003**, 278, 2490–2502.
- [7] S. Dhungana, C. H. Taboy, D. S. Anderson, K. G. Vaughan, P. Aisen, T. A. Mietzner, A. L. Crumbliss, *Proc. Natl. Acad. Sci. USA* **2003**, 100, 3659–3664.
- [8] W. Q. Zhong, J. A. Parkinson, M. L. Guo, P. J. Sadler, *J. Biol. Inorg. Chem.* **2002**, 7, 589–599.
- [9] G. Kickelbick, U. Schubert, *Chem. Ber.* **1997**, 130, 473–477.
- [10] D. Walther, B. Ritter, H. Górls, G. Zahn, *Z. Anorg. Allg. Chem.* **1997**, 623, 1125–1130.
- [11] E. N. Baker, *Adv. Inorg. Chem.* **1994**, 41, 389–463.
- [12] H. Sun, H. Li, P. J. Sadler, *Chem. Rev.* **1999**, 99, 2817–2842.
- [13] C. M. Bruns, D. S. Anderson, K. G. Vaughan, P. A. Williams, A. J. Nowalk, D. E. McRee, T. A. Mietzner, *Biochemistry* **2001**, 40, 15631–15637.
- [14] W. J. Evans, M. A. Ansari, J. W. Ziller, *Polyhedron* **1998**, 17, 869–877.
- [15] Z. A. Starikova, E. P. Turevskaya, N. I. Kozlova, N. Ya. Turova, D. V. Berdyev, A. I. Yanovsky, *Polyhedron* **1999**, 18, 941–947.
- [16] M. A. Walters, K.-C. Lam, S. Damo, R. D. Sommer, A. L. Reingold, *Inorg. Chem. Commun.* **2000**, 3, 316–318.
- [17] P. Sobota, S. Przybylak, J. Utko, L. B. Jerzykiewicz, *Organometallics* **2002**, 21, 3497–3499.
- [18] E. M. Larsen, A. C. Adams, *Inorg. Synth.* **1967**, 10, 7–8.
- [19] S. A. Berish, C. Y. Chen, T. A. Mietzner, S. A. Morse, *Mol. Microbiol.* **1992**, 6, 2607–2615.
- [20] Z. Otwinowski, W. Minor, *Methods Enzymol.* **1997**, 276, 307–326.

Crystal Structure of Tricolorin A: Molecular Rationale for the Biological Properties of Resin Glycosides Found in Some Mexican Herbal Remedies**

Anna Rencurosi, Edward P. Mitchell, Gianluca Cioci, Serge Pérez, Rogelio Pereda-Miranda,* and Anne Imberty*

The traditional uses of several Mexican members of the morning glory family (Convolvulaceae), combined with ecological field observations, have been helpful in the design of an efficient approach for sampling plant materials and the selection of plants for investigation as potential sources of novel biodynamic natural products.^[1] The Mexican variety of the morning glory plant named “heavenly blue” (*Ipomea tricolor* Cav.) has been used for centuries as a cover crop in traditional mesoamerican agriculture because it inhibits the growth of invasive weeds. We now know that the phytotoxins involved are the resin glycosides, collectively called tricolorins.^[2,3] Until recently, the structural complexity of these mixtures seriously hampered the isolation of their individual constituents. The application of recycling high-performance liquid chromatography has allowed no less than 10 lipooligosaccharides to be isolated from the aerial parts of “heavenly blue”.^[2–4] Tricolorin A was the first member of the series to be fully characterized through a combination of NMR and MS methods.^[2,3] This compound consists of the tetrasaccharide L-rhamnopyranosyl-(1→3)-O-α-L-rhamnopyranosyl-(1→2)-O-β-D-glucopyranosyl-(1→2)-O-β-D-fucopyranoside linked to jalapinic acid to form a macrocyclic ester with a 19-membered ring (Scheme 1). Following the elucidation

[*] Dr. R. Pereda-Miranda

Departamento de Farmacia, Facultad de Química
Universidad Nacional Autónoma de México
Ciudad Universitaria, Coyoacán, 04510 D.F. (México)
Fax: (+52) 5-622-5329
E-mail: pereda@servidor.unam.mx

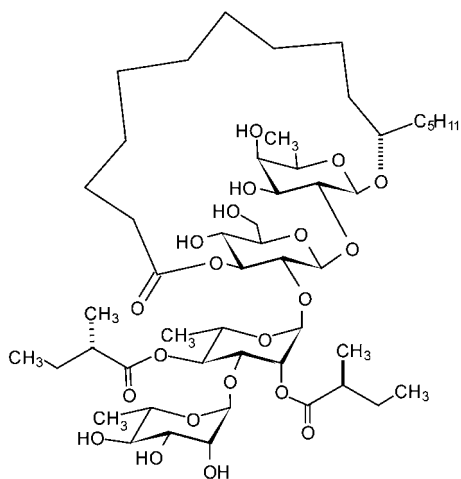
Dr. A. Rencurosi, G. Cioci, Dr. S. Pérez, Dr. A. Imberty
CERMAV-CNRS
(affiliated with Université Joseph Fourier)
601 rue de la Chimie, BP 53, 38041 Grenoble, Cedex 9 (France)
Fax: (+33) 476-54-7203
E-mail: imberty@cermav.cnrs.fr

Dr. E. P. Mitchell
E.S.R.F. Experiments Division
BP 220, 38043 Grenoble, Cedex 9 (France)

[**] G.C. and A.R. are EEC doctoral and postdoctoral fellows, respectively (HPRN-CT2000-00001). R.P.-M. acknowledges financial support from Dirección General de Asuntos del Personal Académico, Universidad Nacional Autónoma de México (Grant nos. IN200902-2 and IX234504-1), and Consejo Nacional de Ciencia y Tecnología (Grant no. 39951-Q). We thank the European Synchrotron Radiation Facility, Grenoble, for access to synchrotron data collection facilities.



Supporting information for this article is available on the WWW under <http://www.angewandte.org> or from the author.



Scheme 1. Structure of tricolorin A.

tion of its chemical structure, total syntheses of tricolorin A in its natural enantiomeric form were developed by Larson and Heathcock, and by Lu and collaborators. Both teams used a macrolactonization approach.^[5,6] Fürstner and Müller later used a ring-closing-metathesis strategy to form the macrolactone moiety and succeeded in synthesizing tricolorin A^[7] and several other resin glycosides.^[8,9]

Tricolorin A demonstrates several biological activities of therapeutic interest, such as mammalian cytotoxicity against cultured P-338 and human breast cancer cells,^[2] antibacterial activity against *Staphylococcus aureus* and *Mycobacterium tuberculosis*,^[1] and antifungal potential correlated to its (1→3)β-D-glucan synthase inhibitory activity.^[10] In the cover crop, tricolorin A acts as a nonprotonophoric uncoupler of photophosphorylation and inhibits electron transport in the photosystem II of chloroplasts.^[11] All the bioactivities of this lipopolysaccharide are associated with its macrocyclic structure; the glycosidic acid derived by saponification of the lactone has been shown to be inactive in all resin glycosides biologically tested.^[1]

The difficulty involved in obtaining a useable pure sample of an individual resin glycoside,^[12] in addition to that related to oligosaccharide crystallization,^[13] represented an enormous challenge for the structural investigation reported herein. Protein crystallization techniques were used to avoid wastage of the isolated tricolorin A (20 mg). The compound is insoluble in water, which was therefore selected as the precipitating agent.^[14] The size of the crystal unit cell indicated the presence of four independent tricolorin A molecules per asymmetric unit.^[15] Each unit contains a total of 284 nonhydrogen atoms and is therefore similar in size to a small protein of about 30 amino acids. The size of the asymmetric unit, together with that of the crystal, demanded the use of intense synchrotron radiation to collect the diffraction data. The SIR2002 method was used to solve the structure. Refinement with the SHELX program indicated the presence of 18 water molecules in the asymmetric unit in addition to the four independent tricolorin molecules (Figure 1). All atoms in the structure were clearly visible in the electron density maps, with the exception of two carbon

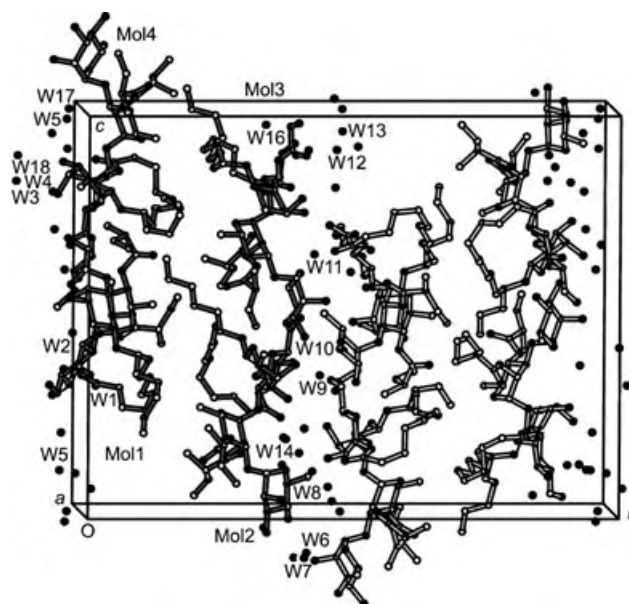


Figure 1. Graphical representation of the unit cell. The contents of the asymmetric unit are shown with gray bonds and the molecules are labeled as Mol1 to Mol4 for tricolorin A and W1 to W18 for water.

atoms in the lipid part of molecule 4. A detailed view of one of the tricolorin A molecules is shown in Figure 2, with ellipsoids representing thermal vibration. The largest temperature

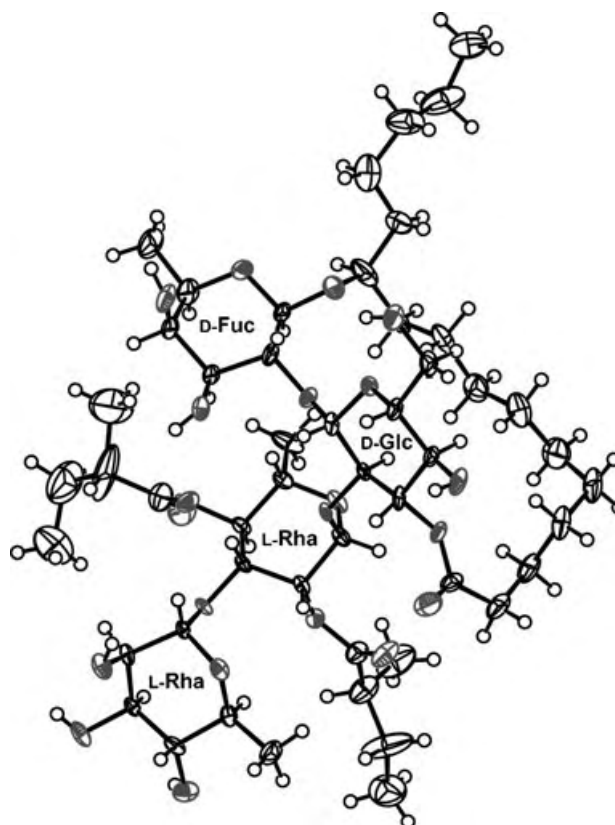


Figure 2. ORTEP representation of one molecule of tricolorin A, drawn with the Platon software.^[28] The ellipsoids of thermal vibration represent a probability of 50%.

factors were measured for the two methylbutyryl groups that form esters with the internal rhamnose unit. The macrocyclic aglycon core of molecule 4 displayed slightly more disorder than those of the other molecules.

Figure 3 shows a superposition of the four tricolorin A independent molecules, all of which share the same global shape, albeit with slightly different conformations of the aglycon moiety stacked under the β -D-glucopyranosyl-(1 \rightarrow 2)-O- β -D-fucopyranoside moiety. The glycosidic linkages are superimposed on the corresponding energy maps^[16] (Figure 3c). Although the energy maps of the three disaccharides differ, all three display low-energy regions centered around a Φ -axis *gauche* conformation, as dictated by the *exo*-anomeric effect. A higher level of conformational freedom is apparent along the Ψ axis: the lowest energy region corresponds to a plateau ranging from $\Psi = -60$ to 180° . While the externally placed L-rhamnopyranosyl-(1 \rightarrow 3)-O- α -L-rhamnopyranoside moiety shows rather different conformations for each of the four molecules in the asymmetric unit, the internal trisaccharide subunit (α -L-rhamnopyranosyl-(1 \rightarrow 2)-O- β -D-glucopyranosyl-(1 \rightarrow 2)-O- β -D-fucopyranoside) has limited conformational freedom. The four molecules each display slightly different sets of torsion angles (see the Supporting Information) but all of these angles yield very similar pseudo-elongated shapes for the macrocyclic aglycon portion of the molecule between the lactone end and the anomeric oxygen atom of the fucose unit. In contrast, the terminal pentyl chain is very flexible. We compared the observed conformations of the tricolorin A molecules to those of the only related molecule that has been crystallized, a synthetic chemical

intermediate of tricolorin A consisting of the β -D-glucopyranosyl-(1 \rightarrow 2)- β -D-fucopyranoside subunit with all its hydroxy groups protected.^[17] The first notable difference is that the lack of the amphipathic properties of the natural sample limits the solubility of the analogue to low-polarity organic solvents. Five independent molecules were refined for the asymmetric unit of the analogue, as opposed to the four molecules found in tricolorin A crystals. This difference resulted in a totally different conformation and molecular packing for the analogue. The lack of water molecules produces a piled parallel arrangement of glycoside residues on one side of the analogue structure, whilst the macrolactone rings stack on the other side with alternating α and β faces. The natural compound structure consists of a succession of hydrophilic and hydrophobic layers.

The most notable feature of tricolorin A in the solid state is the anisotropic repartitioning of the hydrophobic and hydrophilic sections in the crystal packing arrangement (Figure 4). One face of the molecule exhibits an almost flat hydrophobic wall formed by the aglycon unit, the methyl group of the fucose unit, and the three lipophilic inner rhamnose residues (the methyl group and the two esterified methylbutyric acid groups). The other face presents two small hydrophilic areas: one composed of the hydroxy groups of the fucose and glucose residues and the other of those of the external rhamnose unit. The 18 water molecules form a dense network that creates a dividing layer between the hydrophilic faces of the structure (Figure 4). The high water content of the crystal, which is similar to that found in the accepted view of protein crystals, means that the tricolorin A molecular

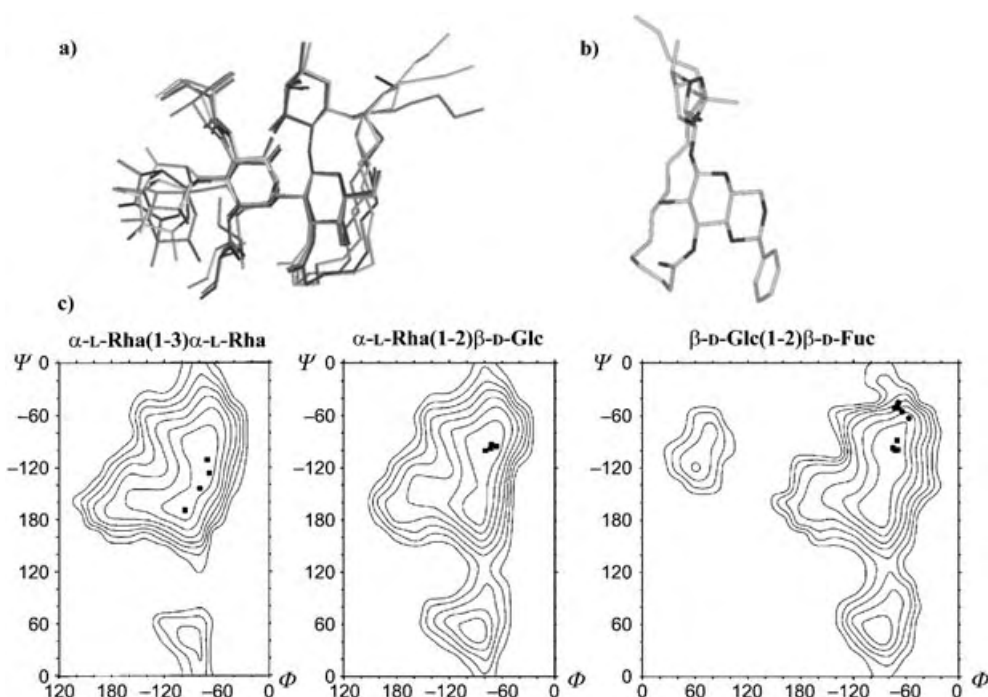


Figure 3. a) Superposition of the four independent molecules of tricolorin A. b) One of the molecules from the crystal structure of the synthetic analogue,^[17] shown with the glucose ring in the same orientation as in (a). c) Glycosidic linkage energy maps for each of the constitutive disaccharide subunits of tricolorin A. The conformations observed in the crystal structure of tricolorin A are indicated by squares and those of the synthetic analogue by circles.

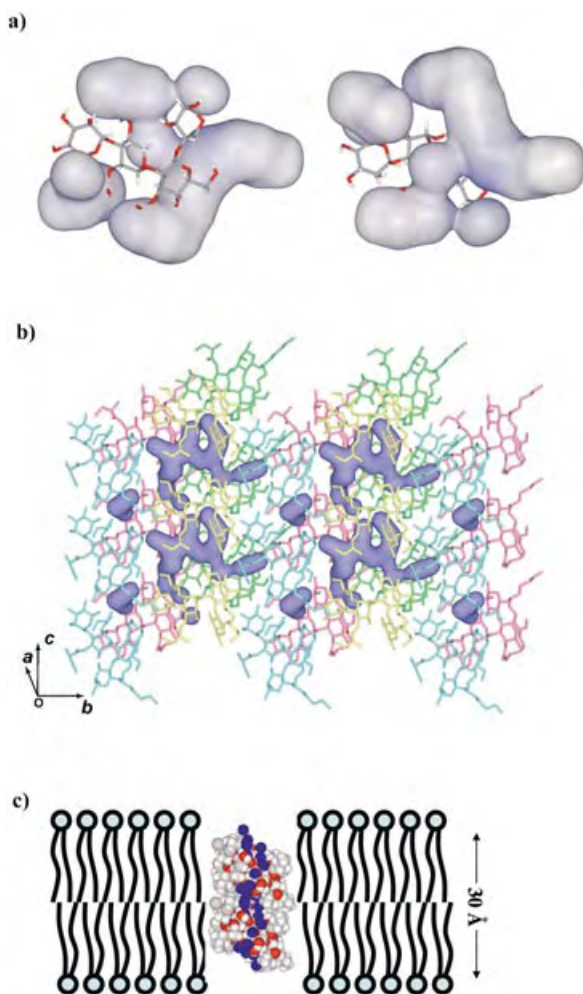


Figure 4. a) Amphiphilic properties of tricolorin A: two orthogonal views of the molecule showing the contours of the accessible surface of the hydrophobic region. b) Graphical representation of packing in the tricolorin A crystal structure: view along the *b* axis with clusters of water molecules represented by their accessible surface (blue). c) Insertion membrane model of the minimal crystal environment made up of four tricolorin A molecules.

conformation in the solid state is not dominated by intermolecular forces and hence might be indicative of the conformation in solution and in supermolecular aggregates.

It has been suggested that the cytotoxic properties of the resin glycosides could be caused by their ability to perturb cell membranes through nonselective pore formation. These compounds have a somewhat peculiar organization in aqueous solution and form micelles or aggregates comparable to those displayed by tricolorin A in the crystalline state. It is therefore of interest to compare the architecture of the water channel formed by the four tricolorin A molecules, which pile up in two pairs along the *c* axis, with the spatial arrangement of a lipid bilayer. The hydrophobic surface exposed externally and elongated along the axis of the water channel is ideally oriented for parallel interaction with the lipids of a biological membrane upon insertion of tricolorin A into the membrane. This hypothesis differs from predictions made by molecular dynamics simulations and NMR studies of micellar solutions

of calonyctin A, another plant-growth-regulating resin glycoside,^[18] which inserts perpendicularly into micelle lipid membranes. The total extension of the channel created by tricolorin A molecules in our study is about 30 Å, which is comparable to the width of a biological membrane such as that of the hydrocarbon core elongation in fluid phospholipid bilayers.^[19] A schematic representation of our insertion model is depicted in Figure 4.

The macrolactone ring is essential to the biological activities of all resin glycosides^[1] since without it the spatial arrangement needed to form aggregates, as well as the above-mentioned channels, probably could not take place. The dried tubers of the medicinal members of the morning glory family yield a purgative remedy of which the main active ingredients are resin glycosides.^[1] All the biological effects displayed by this type of amphipathic oligosaccharide suggest that the activity could be the result of a possible ion flux perturbation in the target cell membrane induced by nonselective pore formation, as illustrated by the insertion model. This model for transmembrane channel formation is based on the crystal structure of tricolorin A and is still speculative in nature. Experimental and theoretical studies are called for to provide substantiation for this hypothesis, as well as to investigate whether other types of architecture could allow better interaction. This first crystallographic analysis of a natural convolvulaceous resin glycoside not only opens avenues for further structural investigations but may also lead to important applications of such compounds in drug design.

Received: April 14, 2004

Keywords: conformation analysis · glycolipids · glycosides · natural products · structure elucidation

- [1] R. Pereda-Miranda, M. Bah, *Curr. Top. Med. Chem.* **2003**, 3, 111.
- [2] R. Pereda-Miranda, R. Mata, A. L. Anaya, D. B. Wickramaratne, J. M. Pezzuto, A. D. Kinghorn, *J. Nat. Prod.* **1993**, 56, 571.
- [3] M. Bah, R. Pereda-Miranda, *Tetrahedron* **1996**, 52, 13063.
- [4] M. Bah, R. Pereda-Miranda, *Tetrahedron* **1997**, 53, 9007.
- [5] D. P. Larson, C. H. Heathcock, *J. Org. Chem.* **1997**, 62, 8406.
- [6] S. F. Lu, Q. O'Yang, Z. W. Guo, B. Yu, Y. Z. Hui, *J. Org. Chem.* **1997**, 62, 8400.
- [7] A. Fürstner, T. Müller, *J. Org. Chem.* **1998**, 63, 424.
- [8] A. Fürstner, T. Müller, *J. Am. Chem. Soc.* **1999**, 121, 7814.
- [9] A. Fürstner, F. Jeanjean, P. Razon, C. Wirtz, R. Mynott, *Chem. Eur. J.* **2003**, 9, 307.
- [10] M. V. Castelli, J. C. Cortes, A. M. Escalante, M. Bah, R. Pereda-Miranda, J. C. Ribas, S. A. Zacchino, *Planta Med.* **2002**, 68, 739.
- [11] L. Achnine, R. Pereda-Miranda, R. Iglesias-Prieto, R. Moreno-Sanchez, B. Lotina-Hennsen, *Physiol. Plant.* **1999**, 106, 246.
- [12] The experimental procedures, including preparative HPLC, handling of the plant material, and extraction of the resin glycosides from the aerial parts of *Ipomoea tricolor*, have been described previously.^[2,3] Preliminary fractionation of the crude resins (100 mg) was achieved by standard column chromatography. The chloroform-soluble pool was subjected to preparative HPLC (Waters column, 150 × 19 mm, μ Bondapak-amino, 10 μ m). This separation was performed to eliminate impurities appearing before and after the selected peak (t_R = 18 min). Isocratic elution was applied, with $\text{CH}_3\text{CN}/\text{H}_2\text{O}$ (92:8) and a flow rate of 6 mL min⁻¹. The tricolorin A peak was collected by

heart-cutting and independently reinjected (40 mg) into the same column. The HPLC system was operated in the recycle mode to achieve the maximal possible purity of the sample.^[3] This process of purification was monitored by using a refractive index detector. The sensitivity setting of the refractometer was increased from $8 \times$ to $64 \times$ to facilitate the detection of all minor impurities. Elution was conducted isocratically with $\text{CH}_3\text{CN}/\text{H}_2\text{O}$ (95:5; flow rate = 8 mL min^{-1}) and complete separation of tricolorin A to homogeneity (20 mg) was achieved after twelve consecutive cycles on the same aminopropyl column.

- [13] S. Pérez, C. Gautier, A. Imberty in *Oligosaccharides in Chemistry and Biology: A Comprehensive Handbook* (Eds.: B. Ernst, G. Hart, P. Sinay), Wiley-VCH, Weinheim, **2000**, pp. 969.
- [14] The first microcrystals were obtained by vapour diffusion with a modified version of the hanging drop method. An ethanolic solution ($3 \mu\text{L}$) of tricolorin A (20 mg mL^{-1}) was mixed with pure poly(ethyleneglycol) 200 (PEG 200; $1 \mu\text{L}$, Sigma) and deposited on a glass coverslide. This drop of solution was covered with a layer of mineral oil (Sigma), then the slide was sealed above a reservoir containing a solution of 10 % PEG 200 in water. Crystals suitable for x-ray analysis were grown by using the same method and a sample solution ($2 \mu\text{L}$, 10 mg mL^{-1} in EtOH) mixed with PEG 200 ($2 \mu\text{L}$) and mineral oil ($2 \mu\text{L}$). The drop was seeded with the microcrystals obtained previously. The reservoir solution was composed of 75 % water, 10 % PEG 200, and 15 % EtOH.
- [15] A needle-shaped crystal ($0.5 \times 0.01 \times 0.01 \text{ mm}^3$) was soaked in a 60 % PEG 6000/water solution for three minutes then cryo-cooled at 100 K. Data were collected from a single crystal on beam line ID29 ($\lambda = 0.8157 \text{ \AA}$) at ESRF (Grenoble) by using an ADSC Q210 CCD detector with a resolution of 0.87 \AA ($\theta_{\text{max}} = 28.3^\circ$). A total of 38162 reflections were measured, of which 18424 were independent, with $R_{\text{int}} = 0.071$. Data were processed with the MOSFLM package.^[20] The structure was solved by direct methods (SIR-2002).^[21] Refinement was performed with the Shelx-97 program.^[22] The nonhydrogen atoms of the sample (four monomers with the formula $\text{C}_{50}\text{H}_{86}\text{O}_{21}$ and $18 \text{ H}_2\text{O}$) were refined with anisotropic displacement parameters, except the water oxygen atoms, for which isotropic refinement parameters were used. A few restraints were included on selected C–C distances. Hydrogen atoms were placed on the model molecules (except the water molecules), which yielded a total of 2770 parameters. All 18424 independent reflections were used in the full matrix least-squares calculations against F^2 . Final refinement cycles yielded factors $R1 = 0.0998$ and $wR = 0.2283$ for 16993 reflections with $I > 2\sigma(I)$. The crystals belong to space group $P2_1$ and have the cell dimensions $a = 14.025(1)$, $b = 33.337(1)$, and $c = 25.512(1) \text{ \AA}$. $\beta = 91.07(1)^\circ$, $V = 11926.1(1) \text{ \AA}^3$, $Z = 8$, $\rho_{\text{calcd}} = 1.211 \text{ g cm}^{-3}$. CCDC 228071 contains the supplementary crystallographic data for this paper. These data can be obtained free of charge via www.ccdc.cam.ac.uk/conts/retrieving.html (or from the Cambridge Crystallographic Data Centre, 12, Union Road, Cambridge CB21EZ, UK; fax: (+44) 1223-336-033; or deposit@ccdc.cam.ac.uk).
- [16] Energy maps were calculated for each constituent disaccharide moiety as a function of two glycosidic linkage torsion angles defined as $\Phi = \theta$ (O5–C1–O1–Cx) and $\Psi = \theta$ (C1–O1–Cx–C(x+1)). Each disaccharide was built with the POLYS software^[23] and energies were calculated by using the MM3 program^[24,25] and employing a previously described procedure^[26] involving full optimization of the structure at each point of the (Φ, Ψ) map except for the two driven angles. To allow consideration of the three possible orientations of the hydroxymethylene group of the glucose unit and the clockwise or anticlockwise possibilities for the hydrogen bonding network around each ring, several starting structures, a step of 20° , and a dielectric constant $\epsilon = 80$ were used for these calculations. The single relaxed maps
- were combined to provide unique adiabatic maps by a procedure designed by our group.^[26] The corresponding plots were generated with the X-Farbe program.^[27]
- [17] C. W. Lehman, A. Fürstner, T. Müller, *Z. Kristallogr.* **2000**, *215*, 114.
- [18] Z. H. Jiang, A. Geyer, R. R. Schmidt, *Angew. Chem.* **1995**, *107*, 2730; *Angew. Chem. Int. Ed. Engl.* **1995**, *34*, 2520.
- [19] M. C. Wiener, S. H. White, *Biophys. J.* **1992**, *61*, 437.
- [20] A. G. W. Leslie, *Joint CCP4 + ESF-EAMCB Newslett. Protein Cryst.* **1992**, *26*.
- [21] M. C. Burla, M. Camalli, B. Carrozzini, G. L. Cascarano, C. Giacovazzo, G. Polidori, R. Spagna, *J. Appl. Crystallogr.* **2003**, *36*, 1103.
- [22] G. M. Sheldrick, University of Gottingen, **1997**.
- [23] S. Perez, M. Kouwijzer, K. Mazeau, S. B. Engelsens, *J. Mol. Graphics* **1996**, *14*, 307.
- [24] N. L. Allinger, Y. H. Yuh, J.-H. Lii, *J. Am. Chem. Soc.* **1989**, *111*, 8551.
- [25] N. L. Allinger, M. Rahman, J.-H. Lii, *J. Am. Chem. Soc.* **1990**, *112*, 8293.
- [26] A. Imberty, S. Pérez, *Chem. Rev.* **2000**, *100*, 4567.
- [27] A. Preusser, *ACM Trans. Math. Software* **1989**, *15*, 79.
- [28] A. L. Spek, *J. Appl. Crystallogr.* **1988**, *21*, 578.

Structure Elucidation

Supramolecular, Bifurcated N-H...OC-M Bonding Explains Unusually Low ν_{CO} Frequencies in Metal Carbonyl Compounds: A Case Study**

Pierre Braunstein, Jean-philippe Taquet, Olivier Siri, and Richard Welter*

*Dedicated to Professor M. Veith
on the occasion of his 60th birthday*

Infrared spectroscopy has played a central part in the identification and elucidation of the structures of metal carbonyl compounds, with the ν_{CO} spectral region being the

[*] Dr. P. Braunstein, J.-p. Taquet, Dr. O. Siri
Laboratoire de Chimie de Coordination, UMR 7513 CNRS
Institut Le Bel, Université Louis Pasteur
4, rue Blaise Pascal, F-67070 Strasbourg Cédex (France)
Fax: (+33) 390-241-322
E-mail: braunst@chimie.u-strasbg.fr
Prof. R. Welter*
Laboratoire DECMET, UMR 7513 CNRS
Institut Le Bel, Université Louis Pasteur
4 rue Blaise Pascal, F-67070 Strasbourg Cedex, (France)

[†] Crystal structure analysis.

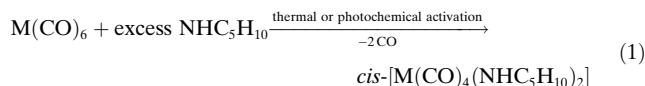
[**] This work was supported by the CNRS and the Ministère de la Recherche (PhD grant to J.-p.T).



Supporting information for this article (including the crystallographic data for *cis*-[W(CO)₄(piperidine)₂], an ORTEP view, a powder X-ray diffraction pattern, and its IR spectrum (KBr pellet and pure solid)) is available on the WWW under <http://www.angewandte.org> or from the author.

most diagnostic. In addition to the relationship derived from group theory between the stereochemistry of a metal carbonyl complex and the number and activity of its ν_{CO} modes, their frequency range correlates with the bonding mode of the CO ligands. In general, terminal CO groups absorb between 2100–1850 cm^{-1} , whereas doubly bridging CO ligands absorb between 1850–1750 cm^{-1} and triply bridging CO ligands absorb below 1730 cm^{-1} . This spectral shift arises as a consequence of the progressive decrease in C–O bond order.^[1] Infrared spectroscopy is far more sensitive than X-ray diffraction to small changes in bond orders, despite the irreplaceable value of the latter for establishing the spatial arrangement of atoms and molecules in the solid state. We show below, in a case study, that an archetypal complex with terminal carbonyl ligands has unusual ν_{CO} frequencies below 1770 cm^{-1} , and that this observation can be rationalized by the presence of a remarkable and unexpected supramolecular, bifurcated N–H \cdots OC–M network in the solid state.

Some metal complexes enjoy the privilege of being ubiquitous precursors to wide ranges of new molecules. This has been the case in metal–carbonyl chemistry with *cis*-[M(CO)₄(piperidine)₂] (M = Mo, W), which have been used for almost 30 years to prepare octahedral metal carbonyl complexes of the type *cis*-[M(CO)₄L₂]; the lability of the piperidine ligands allows the synthesis of the desired products under much milder conditions and in better yields than when starting from the parent hexacarbonyl compounds.^[2,3] It is therefore not surprising that these complexes have been very highly cited and their synthesis has even been published several times—with only minor variations, since it simply results from the thermal or photochemical activation of [M(CO)₆] in the presence of excess piperidine [Eq. (1)].^[4]



The most common characterization methods have been elemental analysis and IR spectroscopy in the ν_{CO} region, where four bands are expected for a C_{2v} local symmetry ($\Gamma_{\text{vib}} = 2A_1 + B_1 + B_2$). To the best of our knowledge, the only IR data available for *cis*-[W(CO)₄(piperidine)₂] are those published by Tripathi et al. who reported values of 2000, 1865, 1844, and 1814 cm^{-1} (in mulls, no intensities given),^[4c] which are different from our own data (see below).

Recent studies on the reaction of *p*-benzoquinonediimine ligands with *cis*-[W(CO)₄(piperidine)₂] revealed an interesting metal-coordination-induced *para*–*ortho*-quinone isomerization and relocation of the π system.^[5] We were surprised to find a solid-state (KBr pellet) IR spectrum (see the Supporting Information) for *cis*-[W(CO)₄(piperidine)₂] with ν_{CO} bands down to 1768(vs) cm^{-1} , that is, at energies much lower than expected for terminal CO ligands in a neutral complex.^[11,6] After performing purity controls and triggered by the lack of any previous report on this most unusual observation,^[7] we grew single crystals of *cis*-[W(CO)₄(piperidine)₂] by slow diffusion of heptane into a THF solution and subjected them to an X-ray diffraction study. The ORTEP view of the crystal structure (see the Supporting Information) confirms that the piperidine ligands are in a *cis* arrangement

and that all the carbonyl groups are of the linear type, with M–C–O angles of 174.1(4) and 179.1(3)°. Figure 1 also reveals the existence of a remarkable network of intermolecular bifurcated H-bonds. Figure 2 shows a projection of the structure in the *a,b* plane, with the channel-like 3D structure evident. Each octahedral complex molecule acts as a bridge between two other molecules: each N–H proton interacts with two carbonyl groups, each belonging to a different molecule. Conversely, each CO ligand *trans* to a piperidine

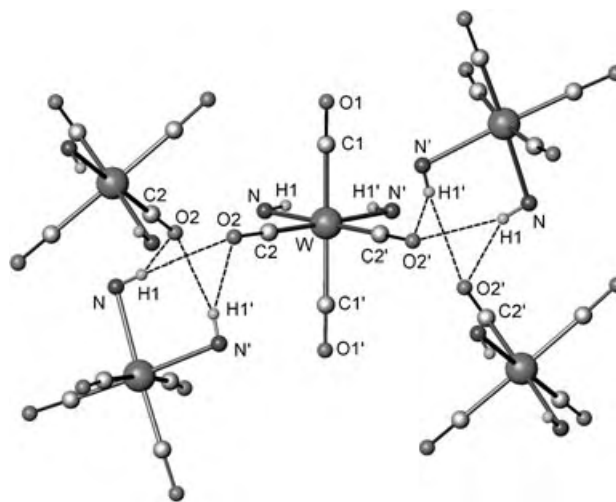


Figure 1. Partial view of the crystal structure of *cis*-[W(CO)₄(piperidine)₂] resulting from a bifurcated H-bonding network involving all the N–H protons and the CO ligands *trans* to the piperidine ligands. The carbon skeleton of the piperidine ligands has been omitted for clarity.

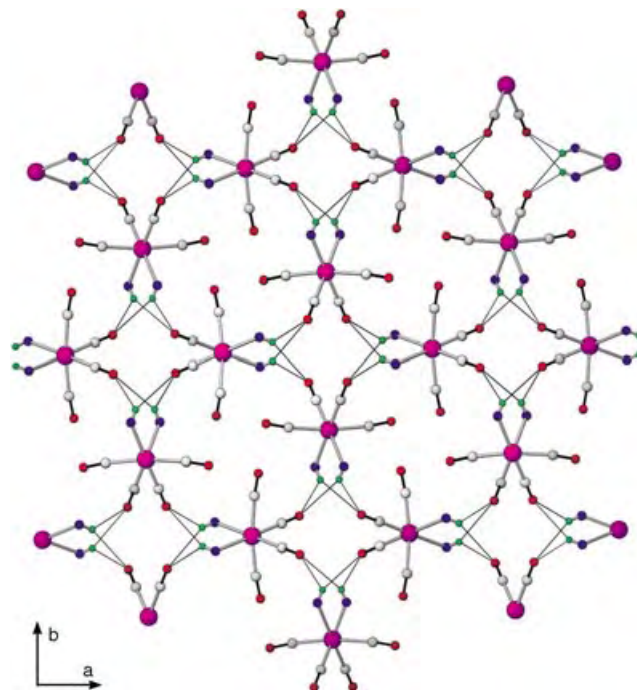


Figure 2. Projection of the crystal structure of *cis*-[W(CO)₄(piperidine)₂] in the *a,b* plane. The carbon skeleton of the piperidine ligands has been omitted for clarity. Color coding: W purple, O red, N blue, N–H green.

moiety on each complex interacts with the two N–H protons from another molecule (Table 1). The observation that these H-bonding interactions selectively involve the two carbonyl ligands which are *trans* to the strong σ -donating/weak π -

Table 1: Selected bond lengths [Å] and angles [°] for *cis*-[W(CO)₄(piperidine)₂].

intramolecular data			
W–C1	2.038(4)	W–C2	1.951(4)
W–N	2.323(3)	C1–O1	1.140(5)
C2–O2	1.168(4)	N–H1	0.77(4)
C1–W–C1'	172.1(2)	C1–W–N'	92.6(1)
C1'–W–N'	93.2(1)	C2'–W–C2	90.7(2)
C2'–W–C1	87.65(15)	C2–W–C1	86.83(15)
C2'–W–N'	91.7(1)	C2–W–N'	177.5(1)
C2'–W–N	177.5(1)	C2–W–N	91.7(1)
N'–W–N	85.90(15)	W–N–H1	97(3)
O1–C1–W	174.1(4)	O2–C2–W	179.1(3)
hydrogen bonds			
O2–N	3.22(1), 3.14(1)	O2–N'	3.14(1), 3.22(1)
O2–H1	2.61(1), 2.50(1)	O2–H1'	2.50(1), 2.61(1)
O2–H1'–N'	141.5(2), 138.7(2)	O2–H1–N	137.7(2), 141.5(2)

accepting piperidine ligands is perfectly consistent with their more electron-rich nature. This results in a) a considerable reduction in the electron density at these oxygen atoms, which leads therefore to ν_{CO} absorptions much more typical of bridging carbonyl groups or isocarbonyl linkages than of terminal CO ligands,^[1] and b) an IR ν_{NH} vibration as low as 3254 cm^{−1} in KBr. The X-ray diffraction pattern of a microcrystalline powder of *cis*-[W(CO)₄(piperidine)₂] was recorded at 300 K and could be completely indexed on the basis of the extinction conditions of the tetragonal system in the space group *P*4₃2₁2 with *a* = 11.864(1) and *c* = 11.058(1) Å. This observation is in complete agreement with the data obtained from the single crystal study (see the Supporting Information). To ensure that no special matrix effect was caused by the KBr pellets, drops of a solution of the complex in THF were evaporated on a single crystal of KBr and the IR spectrum recorded. The ν_{CO} values found were almost identical (see the Supporting Information). These H-bonding interactions also remain in a Nujol mull (ν_{CO} : $\tilde{\nu}$ = 2005(m), 1900(sh), 1874(vs), 1829(s), 1787(sh), 1769(vs) cm^{−1}, and these values are at variance with those reported in the literature,^[4c] but as expected, they disappear in solution, as shown by the IR spectrum showing four ν_{CO} absorptions in the usual range ($\tilde{\nu}$ = 1998(w), 1920(w), 1860(vs), 1823(s) cm^{−1} in THF). The hydrogen-bonding capability of carbonyl ligands versus C–H bond donors is well-documented^[8a,b] and increases with increasing basicity: terminal M–CO < μ_2 -CO < μ_3 -CO.^[8c,d] A search of the Crystallographic Cambridge Data Base for analogous N–H...OC–M (M = Group 6 metal) interactions involving terminal carbonyl groups identified 225 hits with a median value of 2.582 Å (a value which is consistent with our data), but none for *cis*-[M(CO)₄(piperidine)₂] complexes. Interestingly, Kraihanzel and Cotton noted that the “solid-state spectrum of [Mo(CO)₄(ethylenedi-

amine)₂] is strikingly different from the solution spectrum” and suggested that the extreme insolubility of this compound might be a result of NH...OC hydrogen bonding, but this was not (and has never been since) substantiated by X-ray diffraction data.^[9] It was stated on the basis of the X-ray structure of *cis*-(diethylenetriamine)tricarbonylmolybdenum that “clearly, there are no strong intermolecular NH...O bonds”.^[10] Although Shiu et al. noted a low frequency ν_{CO} absorption at 1790 cm^{−1} in the solid-state spectrum of the complex [Mo(CO)₄(N–N)] (N–N = PhCH₂NHCH₂CH₂NMe₂), they concluded from the X-ray data that “an intermolecular H-bond between the N–H atom of one molecule and a carbonyl oxygen atom of another molecule is negligible in this compound”.^[11] However, such an intermolecular bonding interaction was cautiously discussed in [Mo(di-2-pyridylamine)(CO)₄] although it involved only one CO ligand,^[12] whereas no H-bonding was observed in [Mo(bipy)(di-2-pyridylamine)(CO)₃].^[13] An intermolecular N–H...O distance of 2.15 Å has been reported for the pyridine-4(1*H*)-thione complex [W(C₅H₅NS)(CO)₅] but no IR data are available, which precludes any correlation between H-bonding and ν_{CO} shifts.^[14] The IR spectra of *cis*-[W(CO)₄(piperidine)₂] were compared to those of *cis*-[Mo(or W)(CO)₄(pyridine)₂] (in THF solution, KBr pellets, or Nujol mulls).^[15a,b] As expected, the latter display no unusual features, which is consistent with the X-ray structure of the tungsten complex which shows “no particularly short intermolecular contacts”.^[15c] Although ion-pair interactions between an oxygen atom of a carbonylmethylate anion and its associated cation are known to produce significant ν_{CO} shifts to lower energies, this represents a very different situation to that involving a neutral molecule.^[16]

Since the space group in which this molecule crystallizes is chiral, we investigated its nonlinear optical (NLO) properties, but no second order effect was observed.

In conclusion, we have shown that supramolecular H-bonding interactions can dramatically affect the ν_{CO} frequencies of metal–carbonyl compounds, and consequently can make structural assignments based on vibrational spectroscopy alone misleading or incorrect. In a case study, we have established that the long-known and archetypal carbonyl complex *cis*-[W(CO)₄(piperidine)₂] displays most unusual, low-frequency ν_{CO} absorptions in the solid state which are not the result of the strong σ -donor/weak π -acceptor properties of the amine ligands but of supramolecular interactions involving the piperidine N–H proton and the carbonyl oxygen atom of the two CO ligands *trans* to the piperidine ligands. Although the crystal structure of *cis*-[Mo(CO)₄(piperidine)₂] was reported very recently, no mention was made of either intermolecular H-bonding interactions or unusual IR data in the solid state.^[17] We examined a freshly prepared sample of *cis*-[Mo(CO)₄(piperidine)₂] and found that the IR spectra recorded in KBr pellets or Nujol mull were very similar to those of the tungsten derivative (see Experimental section), but at variance with literature values.^[4f] It is therefore most likely that similar intermolecular N–H...O interactions are also present in the Mo derivative. It would not be surprising that other metal–carbonyl complexes containing H-bond donors, even with the less-basic terminal CO ligands, reveal similar features to *cis*-[W(CO)₄(piperidine)₂]. In other cases

where solid-state IR data have been reported for complexes of the type $cis\text{-}[\text{W}(\text{CO})_4(\text{amine})_2]$ and low values found for their ν_{CO} frequencies, no comment was made or explanation offered.^[18] Such questions are of clear relevance to crystal engineering. In a different context, it is interesting to note that the activation of organic carbonyl compounds by double H-bonding is increasingly used in asymmetric catalysis.^[19]

Experimental Section

All reactions were carried out under purified N_2 in freshly distilled solvents by using Schlenk techniques. A solution of $cis\text{-}[\text{W}(\text{CO})_4(\text{piperidine})_2]$, prepared by a slightly modified standard procedure^[4d] (using xylene as a solvent), in THF was layered with heptane and unsolvated, pale yellow crystals were obtained by slow diffusion. $^{13}\text{C}\{^1\text{H}\}$ NMR (125 MHz, CD_3CN , 298 K): $\delta = 211.23$ (s), 210.93 ppm (s, CO). These values are consistent with those reported for similar complexes.^[20]

Crystal data: $\text{C}_{14}\text{H}_{22}\text{N}_2\text{O}_4\text{W}$, $M_r = 466.19$, tetragonal, space group $P4_32_12$, $a = 11.936(1)$, $b = 11.936(1)$, $c = 11.210(1)$ Å, $U = 1597.1(2)$ Å³, $Z = 4$, $\mu(\text{Mo}_{\text{K}\alpha}) = 0.71073$ Å⁻¹ = 7.249 mm⁻¹, $T = 173$ K, 2339 unique reflections collected, $R = 0.0224$ for 2173 reflections with $I > 2\sigma(I)$, $wR2 = 0.0559$. Data collection on a Nonius Kappa-CCD area detector diffractometer using Denzo software. The structure was solved by direct methods (SIR97) with full-matrix least-squares refinement on F^2 using SHELXL97 software. The absorption was corrected empirically.^[21] All non-hydrogen atoms were refined anisotropically. Hydrogen atoms, except H1, which was found by Fourier differences, were generated according to the stereochemistry and refined using a riding model in SHELXL97.^[22] CCDC 234274 contains the supplementary crystallographic data (excluding structure factors). These data can be obtained free of charge via www.ccdc.cam.ac.uk/conts/retrieving.html (or from the Cambridge Crystallographic Data Centre, 12 Union Road, Cambridge CB21EZ, UK; fax: (+44) 1223-336-033; or deposit@ccdc.cam.ac.uk).

The IR spectrum of solid $cis\text{-}[\text{W}(\text{CO})_4(\text{piperidine})_2]$, deposited by evaporation of a THF solution on a single crystal of KBr, contains the expected four ν_{CO} absorptions at $\tilde{\nu} = 2004(\text{m})$, 1875(vs), 1830(s), 1774(vs) cm⁻¹, similar to those found for this complex in a KBr pellet.^[6]

The complex $cis\text{-}[\text{Mo}(\text{CO})_4(\text{piperidine})_2]$ was prepared in a similar manner to the W complex (shorter reaction times) and its IR spectrum was recorded for comparison: ν_{CO} (KBr): $\tilde{\nu} = 2012(\text{mw})$, 1913(sh), 1887(vs), 1838(s), 1792(sh), 1774(vs) cm⁻¹. ν_{CO} (solid deposited by evaporation of a THF solution on a single crystal of KBr): $\tilde{\nu} = 2010(\text{mw})$, 1942(w), 1911(sh), 1882(vs), 1835(s), 1778(vs) cm⁻¹.

Received: July 3, 2004

Keywords: carbonyl ligands · hydrogen bonds · IR spectroscopy · structure elucidation · supramolecular chemistry

- [1] a) K. Nakamoto, *Infrared Spectra of Inorganic and Coordination Compounds*, Wiley, New York, **1963**; b) D. M. Adams, *Metal-Ligand and Related Vibrations* (Ed.: E. Arnold), London, **1967**; c) F. A. Cotton, G. Wilkinson, *Advanced Inorganic Chemistry*, 5th ed., Wiley, New York, **1988**; d) C. Elschenbroich, A. Salzer, *Organometallics*, 2nd ed., Wiley-VCH, Weinheim, **1992**.
- [2] M. S. Wrighton, D. L. Morse, *J. Organomet. Chem.* **1975**, 97, 405.
- [3] See the Supporting Information for a listing of relevant references.
- [4] a) W. Strohmeier, K. Gerlach, D. von Hobe, *Chem. Ber.* **1961**, 94, 164; b) W. Strohmeier, German Patent 498578, **1965**; c) S. C. Tripathi, S. C. Srivastava, G. Prasad, R. P. Mani, *J. Organomet.*

- Chem.* **1975**, 86, 229; d) D. J. Darensbourg, R. L. Kump, *Inorg. Chem.* **1978**, 17, 2680; e) M. A. Beckett, D. P. Cassidy, A. J. Duffin, *Inorg. Chim. Acta* **1991**, 189, 229; f) M. Ardon, P. D. Hayes, G. Hogarth, *J. Chem. Educ.* **2002**, 79, 1249; g) M. A. Beckett, in *Inorganic Experiments*, 2nd ed. (Ed.: J. D. Woollins), Wiley-VCH, Weinheim, **2003**, p. 143; h) M. Ardon, G. Hogarth, D. T. W. Ocroft, *J. Organomet. Chem.* **2004**, 689, 2429.
- [5] P. Braunstein, A. Demessence, O. Siri, J.-p. Taquet, *C. R. Chim.* **2004**, 7, 909.
- [6] See the Supporting Information for the IR spectrum (KBr pellet) in the ν_{CO} region. The two weak bands at $\tilde{\nu} = 1900$ and 1785 cm⁻¹, in addition to the four main absorptions bands at $\tilde{\nu} = 2006(\text{m})$, 1874(vs), 1830(s), 1768(vs) cm⁻¹, have not been assigned.
- [7] See the Supporting information for references from a SCI Finder search on the numerous applications of $cis\text{-}[\text{M}(\text{CO})_4(\text{piperidine})_2]$ but with no mention of such IR data.
- [8] a) D. Braga, F. Grepioni, *Acc. Chem. Res.* **1994**, 27, 51; b) D. Braga, F. Grepioni, *Acc. Chem. Res.* **2000**, 33, 601; c) D. Braga, F. Grepioni, K. Biradha, V. R. Pedireddi, G. R. Desiraju, *J. Am. Chem. Soc.* **1995**, 117, 3156; d) L. Brammer, *Dalton Trans.* **2003**, 3145.
- [9] C. S. Kraihanzel, F. A. Cotton, *Inorg. Chem.* **1963**, 2, 533.
- [10] F. A. Cotton, R. M. Wing, *Inorg. Chem.* **1965**, 4, 314.
- [11] K.-B. Shiu, S.-L. Wang, F.-L. Liao, *J. Organomet. Chem.* **1991**, 420, 207.
- [12] R. A. Howie, G. Izquierdo, G. P. McQuillan, *Inorg. Chim. Acta* **1983**, 72, 165.
- [13] R. A. Howie, G. P. McQuillan, *J. Chem. Soc. Dalton Trans.* **1986**, 759.
- [14] M.-G. Choi, R. J. Angelici, *Acta Crystallogr. Sect. C* **2000**, 56, 808.
- [15] a) S. Chun, E. E. Getty, A. J. Lees, *Inorg. Chem.* **1984**, 23, 2155; b) H.-T. Macholdt, H. Elias, *Inorg. Chem.* **1984**, 23, 4315; c) J. Holzbock, W. Sawodny, E. Grosse, M. Haseidl, L. Walz, *Acta Crystallogr. Sect. C* **1996**, 52, 3039.
- [16] a) M. Y. Darensbourg, P. Jimenez, J. R. Sackett, J. M. Hanckel, R. L. Kump, *J. Am. Chem. Soc.* **1982**, 104, 1521; b) L. Brammer, J. C. Mareque Rivas, C. D. Spilling, *J. Organomet. Chem.* **2000**, 609, 36.
- [17] a) J. Grundy, M. P. Coles, P. B. Hitchcock, *Dalton Trans.* **2003**, 2573; b) the authors of reference [17a] report the X-ray diffraction study of $cis\text{-}[\text{Mo}(\text{CO})_4(\text{piperidine})_2]$ but omitted to include the N-H protons in the empirical formula and consequently did not locate them. It is therefore impossible to draw strict comparisons with our compound. However, using their data we find intermolecular N...O distances of 3.164 and 3.279 Å, similar to the values found in our study. These values, together with the similarity of the unit cell parameters, suggests that a similar H-bonded network is present in both derivatives.
- [18] a) G. W. A. Fowles, D. K. Jenkins, *Inorg. Chem.* **1964**, 3, 257; b) S. C. Tripathi, S. C. Srivastava, *J. Organomet. Chem.* **1970**, 23, 193.
- [19] P. M. Pihko, *Angew. Chem.* **2004**, 116, 2110; *Angew. Chem. Int. Ed.* **2004**, 43, 2062.
- [20] a) B. E. Mann, *J. Chem. Soc. Dalton Trans.* **1973**, 1212; b) G. T. Andrews, I. J. Colquhoun, W. McFarlane, *Polyhedron* **1983**, 2, 783; c) G. M. Gray, *Inorg. Chim. Acta* **1984**, 81, 157.
- [21] R. H. Blessing, *Crystallogr. Rev.* **1987**, 1, 3.
- [22] G. M. Sheldrick, *SHELXL97*, Program for the refinement of crystal structures, University of Göttingen: Germany, **1997**.

Individual Molecules of Dye-Labeled DNA Act as a Reversible Two-Color Switch upon Application of an Electric Field**

Samuel S. White, Liming Ying,
Shankar Balasubramanian, and David Klenerman*

Over the past few years, molecular switches have been heavily researched in the quest for molecular electronic devices. Some switching systems operate by a conformational change in the molecule which is induced by either an electric field,^[1,2] an STM (scanning tunneling microscope) tip,^[3] an electrochemical reaction,^[4] or light.^[5] Alternatively, molecular switches can be operated nonconformationally by redox reactions^[6] or a chemical binding event.^[7] Biomolecules have recently been adapted for new purposes; for example, DNA has been used as part of a conducting wire,^[8] a molecular machine,^[9–12] a crystal template,^[13] a scaffold for nanoscale construction,^[14] and even as a component of a “computing machine”.^[15,16] Herein we show that the fluorescence of individual dye-labeled DNA molecules can be reversibly switched from green to red and vice versa upon application of an electric field.

The use of nucleic acids as molecular switches is a relatively new concept and, so far, has had limited success. The use of an electric field to modulate the fluorescence of labeled DNA adsorbed onto an electrode^[17] and the use of a magnetic field to control the hybridization state of DNA^[18] are known. Conformational switching of DNA by the variation of buffer conditions,^[11,19] the binding of adenosine to an aptamer sequence on DNA,^[20] or the binding of single-stranded DNA (ssDNA) to a DNA quadruplex^[9] have also recently been reported. The main limitation with the current mechanisms for DNA conformational switches is that they require bimolecular hybridization or a change of buffer, thus switching is slow. Furthermore, in some cases switching is not reversible^[20] or the process creates undesirable “waste” DNA.^[9,10] Our DNA switch overcomes these problems by using an electric field to alter the DNA–dye interaction which renders the switching process rapid (< 100 ms) and reversible with no by-products.

Here a controllable electric field and single-molecule fluorescence detection were used to probe the switching of the fluorescent states of individual DNA molecules that were labeled with two different fluorophores at the same end of the DNA duplex. We previously utilized the very high electric-field gradients generated at the tip of a nanopipette to

controllably concentrate and deliver DNA.^[21–23] The pipettes have an inner diameter of 100 nm and the voltage drop occurs in the last few microns of the tip owing to its tapered shape. By application of a potential of 1 V between the electrode in the bath and the electrode in the pipette, a very high electric field of $\approx 8000 \text{ V cm}^{-1}$ is generated at the tip of the pipette.^[22]

The fluorescence of both fluorophores was detected simultaneously with either two-color direct excitation of both fluorophores or single-color excitation of the donor fluorophore only. In the latter experiments, the excited-state energy is transferred nonradiatively from a donor to an acceptor fluorophore by FRET (fluorescence resonance energy transfer). The efficiency of transfer, E , depends on the relative orientation of the fluorophores and the distance that separates them, R , according to Equation (1). R_0 is the Förster distance and this was calculated to be 53 Å for the dye-pair used in these FRET experiments. This inverse-sixth-power separation dependency of energy transfer allows FRET to be used as a sensitive probe of intramolecular distances over the 10–100 Å range.

$$E = R^6 / (R^6 + R_0^6) \quad (1)$$

In FRET, the principle property of interest is not the intensity of fluorescence, but rather the proximity ratio, P . The FRET proximity ratio of each DNA molecule was calculated according to Equation (2), in which I_A and I_D are the intensities of the acceptor and donor fluorescence, respectively. This ratio is strongly dependent on the distance between the fluorophores, whereas it is independent of diffusional motion.^[24] If the excitation power is kept low, photodriven processes such as photobleaching can also be neglected and the proximity ratio becomes independent of the laser intensity.^[25]

$$P = I_A / (I_A + I_D) \quad (2)$$

We studied a 40-base double-stranded DNA (dsDNA) labeled with a donor fluorophore, Rhodamine Green, and an acceptor fluorophore, Alexa 647. Both fluorophores were attached to the bases by C6 linkers that do not constrain the motion of the fluorophore. DNA 1 is a dsDNA with the donor and acceptor fluorophores directly opposite each other on separate strands; it is able to undergo FRET owing to the close proximity of the strands (Figure 1). DNA 2 has the donor and acceptor fluorophores at opposite ends of the duplex and is unable to undergo FRET as their separation is larger than the Förster distance for the dye-pair used (53 Å; Figure 1). A single-molecule study of DNA 1 in solution unexpectedly revealed two peaks in the FRET histogram (Figure 2a), one at $P = 0.05$ and the other at $P = 0.95$, both of which had approximately equal amplitudes. The average single-molecule proximity ratio ($P = 0.40$) gave a value that was almost identical to that of the bulk value ($P = 0.44$). Experiments in which the laser power was varied by two orders of magnitude and in which a radical scavenger (ascorbic acid, 200 μM) was introduced did not lead to any changes in the single-molecule FRET histogram (data not shown). This indicates the absence of photobleaching in this

[*] S. S. White, Dr. L. Ying, Dr. S. Balasubramanian, Dr. D. Klenerman
Department of Chemistry
University of Cambridge
Lensfield Road, Cambridge CB2 1EW (UK)
Fax: (+44) 1223-336-362
E-mail: dk10012@cam.ac.uk

[**] This work was supported by the Biotechnology and Biological Sciences Research Council (UK).

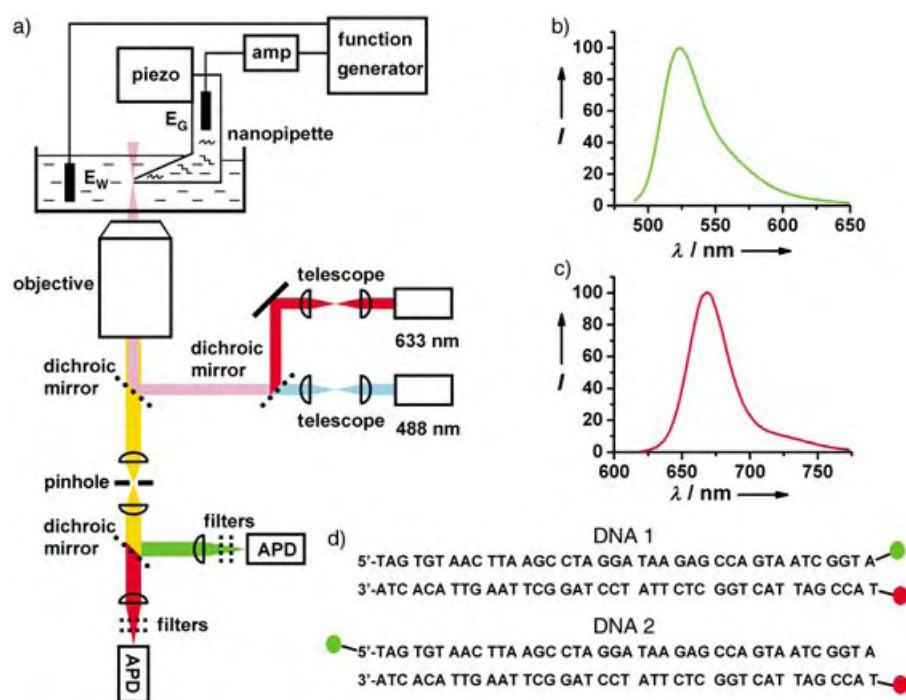


Figure 1. a) A schematic of the experimental setup used (E_G = ground electrode, E_W = working electrode, APD = Avalanche Photo Diode detector); b) and c) the fluorescence emission spectra of the fluorophores Rhodamine Green (donor) and Alexa 647 (acceptor), respectively; d) the two DNA samples labeled with the donor (green circle) and the acceptor (red circle) dyes.

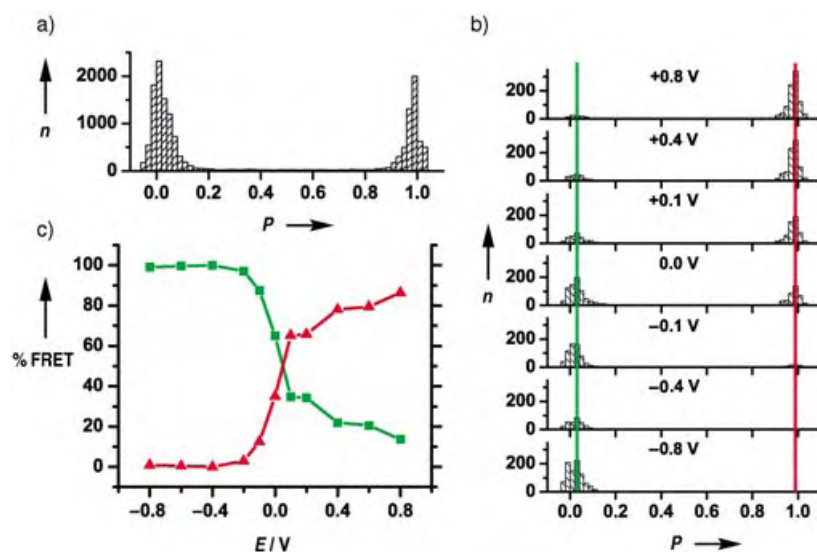


Figure 2. a) Single-molecule FRET histogram of DNA 1 (50 pM) in solution; b) single-molecule FRET histogram of DNA 1 (1 nM) in a nanopipette upon excitation at $\lambda = 488$ nm (on the tip); P = FRET proximity ratio, n = number of molecules. c) Variation of the percentages of the low-FRET peak (green; donor emission) and the high-FRET (red; acceptor emission) with the applied dc potential, E .

experiment. A temperature-dependent study over the range 12–38 °C also revealed no variation in the two FRET peaks (data not shown). These results indicated that two equally occupied conformational states are present in solution: one low-FRET state that is green-fluorescent and one high-FRET state that is red-fluorescent.

The possibility of altering the populations of these two fluorescent states through the generation of an electric field in the nanopipette was then explored. Indeed, the amplitudes of the two FRET peaks were dramatically altered by the application of different potentials (Figure 2b). No additional states were observed. The pipette in these experiments was earthed, and a potential was applied to the electrode in the bath. At a negative potential below -0.2 V only the low-FRET peak was observed, whereas a positive potential above 0.4 V favored almost entirely the high-FRET peak. This implies that the low-FRET peak is not due to the presence of DNA labeled only with the donor, but that it is a true FRET state because its population can be altered by an applied voltage. The absolute values in Figure 2b cannot be compared because of the slight differences in the alignment of the pipette, thus the percentage of each FRET population at a given voltage is displayed in Figure 2c. This shows a clear switching between the two states with the applied voltage. To determine if the change was reversible, the laser was then focused outside the pipette at approximately $20 \mu\text{m}$ from the tip, and a positive voltage was applied so that the DNA flowed out of the pipette. The DNA is in a high-FRET state in the pipette tip, however, the measured single-molecule FRET histogram and the mean proximity ratio value were identical to those in free solution which indicates no irreversible processes (e.g. redox reactions) had taken place in the tip. Switching was determined to be rapid (< 100 ms) from the application of a square wave (± 0.8 V, 0.25 Hz) and from measurement of the time taken for the FRET to change from low to high and vice versa.

Fluorophore excimers,^[26,27] exciplexes,^[28] and excitonic interactions^[29,30] have previously been observed in DNA or RNA. The main characteristic of an excitonic interaction is a change in the UV/Vis absorption spectrum, whereas the main characteristic of an excimer or exciplex is a change in the fluorescence spectrum. No changes in the UV/Vis absorption or fluorescence spectra were

observed for DNA 1 compared to the control sample, DNA 2, which indicates that neither a fluorophore exciplex nor an exciton interaction between the two fluorophores is likely to be present in solution. No perturbation of the electronic state of the Alexa 647 dye attached to the DNA could be detected in the absorption or fluorescence spectra relative to the free dye. The melting temperatures for DNA 1 and 2 were $68 \pm 0.2^\circ\text{C}$ and $67 \pm 0.3^\circ\text{C}$, respectively. This also suggests that there is no significant dye–dye interaction in solution.

Each fluorophore was then excited directly by using a two-color setup. When a negative potential was applied to DNA 1 in a nanopipette and upon excitation at $\lambda = 488\text{ nm}$, fluorescence from Rhodamine Green was observed. However, emission from Alexa 647 was not detected even upon direct excitation at $\lambda = 633\text{ nm}$. The same behavior was observed with DNA 2. In contrast, it was possible to excite directly the Alexa 647 moieties in both DNA 1 and 2 upon application of a positive potential. An experiment was then performed to determine if dsDNA was required to observe this effect. A 5'-Alexa 647-labeled ss40-mer and a Rhodamine Green-labeled noncomplementary ss65-mer (used as a control to check the presence of DNA at the tip) were excited at $\lambda = 488$ and 633 nm in the nanopipette. A square-wave waveform was applied, and the fluorescence was monitored. Many bursts of Alexa 647 emission were observed during the positive half-cycle because of the electrophoretic flow to the pipette tip, and fewer bursts were detected during the negative half-cycle. However, when the fluorescence counts per burst were individually analyzed, no differences were observed in the fluorescence amplitude histogram (Figure 3a). Double-stranded DNA would therefore seem to be a prerequisite for the switching process. These experiments suggest that dye–dye interactions are not the reason for the observed switching, but rather switching occurs upon a change in the interaction between the Alexa 647 moiety and the duplex DNA upon application of an electric field.

Quenching of the donor was ruled out by analysis of the individual fluorescence counts from the donor per burst of DNA 1 (upon selection of only the low-FRET bursts) and DNA 2 in free solution. No differences in the fluorescence amplitude histogram were seen (Figure 3, b and c), and mean amplitudes of 46 and 50 counts were obtained for DNA 1 and DNA 2, respectively, which indicate that the donor is not quenched.

We postulate that there are two states for the Alexa 647 dye: 1) Under a positive potential, the dye is free to move such that the Rhodamine Green donor can transfer energy to Alexa 647 through FRET with nearly 100% efficiency owing to the proximity of the fluorophores. 2) Under a negative potential, the Alexa 647 dye interacts with the duplex DNA, possibly by base-stacking on the end of the DNA duplex, whereupon it is quenched by the DNA. Base-stacking of the Alexa dye that results in restricted movement of the dye is suggested by the high bulk fluorescence anisotropy value (0.204 ± 0.004). Rhodamine Green has a low bulk fluorescence anisotropy value (0.090 ± 0.008) which implies that it is

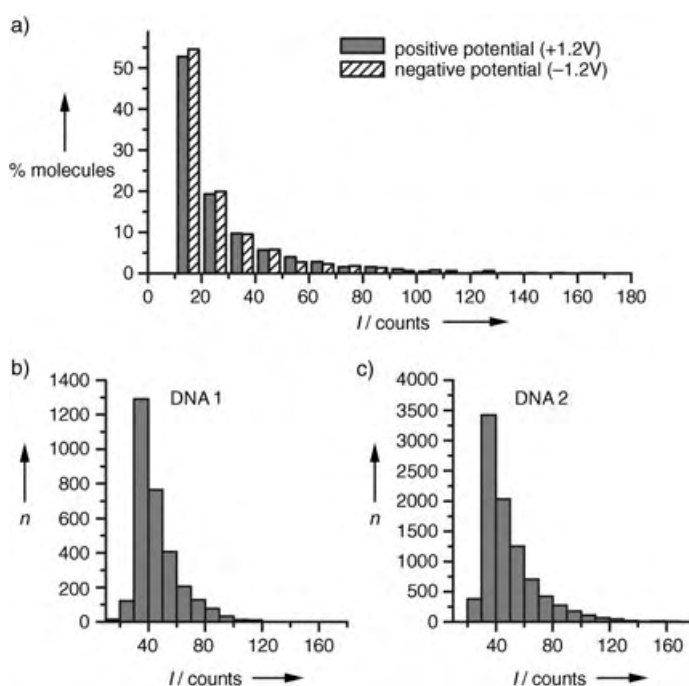


Figure 3. a) Fluorescence amplitude histogram of 5'-Alexa 647-labeled ss40-mer DNA; excited at $\lambda = 633\text{ nm}$ with a $\pm 1.2\text{-V}$ square-wave (0.125 Hz) applied. b) and c) Donor fluorescence amplitude histograms of DNA 1 (only the low-FRET population is selected, that is, $P < 0.5$; mean fluorescence burst amplitude = 46) and DNA 2 (mean fluorescence burst amplitude = 50), respectively, in free solution.

relatively mobile. The fluorophore Cy3, a cyanine dye like Alexa 647, is known to stack onto the end of DNA helices in a similar manner to that of an additional base pair.^[31] Base-stacking has been observed for other dyes, with millisecond-range rates of conversion between the stacked and unstacked states observed at room temperature.^[32,33] In this case, the Alexa dye is closer to the Rhodamine Green moiety and is not free to rotate. Only Rhodamine Green emission is observed in this state for two possible reasons: First, the weak coupling assumed in the Förster transfer process breaks down, and an excitonic state is formed whose fluorescence originates entirely from the Rhodamine fluorophore. This excitonic state was not observed in solution so the interactions, separation, or orientation of the fluorophore must be altered in the presence of the high electric field. Alternatively, weak coupling between the dyes may still occur, but Rhodamine Green cannot transfer energy to the Alexa dye owing to the relative orientation of the two dyes, and thus Rhodamine Green fluorescence is observed.

In conclusion, we have shown that duplex DNA with donor and acceptor fluorophores at the same end can be reversibly switched between a donor-emitting green state and an acceptor-emitting red state on the application of an electric field. The electric field appears to alter the conformation of the acceptor dye only which results in a significant change in its fluorescence quantum yield presumably owing to interactions with the DNA strand. This is important for applications as a two-state switch in single-molecule optoelectronic devices and indicates that the conformations of other

biological molecules as well as voltage-gated ion channels may be switched by the application of an electric field.

Experimental Section

HPLC-purified 40-base oligonucleotide 5'-TAG TGT AAC TTA AGC CTA GGA TAA GAG CCA GTA ATC GGT A-3' (MWG-Biotech, Ebersberg, Germany) was labeled at the 3' terminus with the fluorophore Rhodamine Green; a 5'-labeled and unlabeled versions were also purchased. Its 40-base complementary oligonucleotide, modified at the 5' terminus with a C6 linker chain (IBA, Göttingen, Germany), was desalted (NAP 5 column; Amersham, U.K.) and labeled by using an Alexa Fluor 647 Oligonucleotide Amine Labeling Kit (Molecular Probes, Eugene, USA). Dimethylsulfoxide was removed from the labeled DNA solution by using a NAP 5 column. The labeled oligonucleotide was separated from excess dye by precipitation in ethanol and further purified by HPLC to remove unlabelled DNA and any remaining dye. Acetonitrile (from the HPLC fractions) was removed with a NAP 10 column (Amersham, U.K.). All oligonucleotides were prepared in a buffer solution containing Tris-HCl (10 mM; Amersham, U.K.), EDTA (1 mM; Amersham, U.K.), and NaCl (100 mM; Acros Organics, Fairlawn, USA) at pH 7.4. The concentration of the dye-labeled DNA was determined by the absorbance at $\lambda = 260$ nm; the absorbances at $\lambda = 505$ (Rhodamine Green) or 650 nm (Alexa 647) were used as internal references. Double-stranded DNA (dsDNA) samples were prepared by mixing two complementary single-stranded oligonucleotides, heating the mixture to 90 °C and then slowly cooling this to room temperature. Melting temperatures of 68 °C and 67 °C (in NaCl-Tris-EDTA buffer) for DNA 1 and DNA 2, respectively, were observed by the evolution of UV/Vis spectra with temperature.

The nanopipettes were made by using a laser-based pipette puller (Model P-2000, Sutter Instrument Co.). A two-line program was used to pull borosilicate glass capillaries (0.58- and 1-mm inside and outside diameters, respectively) with the following parameters: Heat = 350, Fil = 3, Vel = 30, Del = 220, Pull = ; Heat = 330, Fil = 2, Vel = 27, Del = 180, Pull = 250. For the pipette experiments, a solution of DNA (1 nM) was back-filled into the bent nanopipette by a microfiller (Microfil 34, World Precision Instruments, Sarasota, USA). A coverglass-bottomed dish (Willco Wells GWST-1000) that contained buffer solution (2–3 mL) was used as the bath. The pipette tip was placed 5 to 10 μ m above the surface of the dish. Two Ag/AgCl electrodes, one placed in the bath and the other placed inside the pipette, served as the working and reference electrodes, respectively. The ion current flowing through the pipette was the same in the presence and absence of DNA because the ion current is dominated by the flow of sodium and chloride ions. Furthermore, no reduction in the ion current could be detected with DNA present in the pipette (from partial blocking). The same buffer solutions (Tris-HCl, 10 mM; EDTA, 1 mM; NaCl, 100 mM) were used both in the pipette and in the bath. EDTA served to remove multivalent cations in the solution. For experiments in solution, DNA was diluted to 50 pM in the NaCl-Tris-EDTA buffer solution (pH 7.4) and Tween 20 (0.01 %) was added to prevent surface adhesion of the DNA molecules.

The two-color setup and apparatus for the experiments performed in the pipette were described previously.^[34] The potential waveforms applied to the electrodes were created by using a function generator (Model DS345, Stanford Research Systems, Sunnyvale, USA). This function generator was also used to provide a trigger for the MCS (Multi Channel Scalar) cards. Solution experiments were performed on the same setup, except that the laser beams were focused 5 μ m into a 1-mL aliquot of the solution of the sample supported in a Lab-Tek chambered coverglass (Scientific Laboratory Suppliers Ltd, U.K.). All experiments were performed at room temperature with a 1-ms bin time (data-acquisition time) used on both MCS cards. A threshold of 35 counts per millisecond bin for the sum of the donor and acceptor fluorescence signals was used to differ-

entiate between the signal bursts of the background and the single-molecules. A background of 1–2 counts per millisecond, obtained from independent measurements of buffer solution that did not contain labeled DNA, was subtracted from each burst. The emission spectra of the two fluorophores are very well separated (see Figure 1 which reduces the cross-talk to a negligible level.^[34]

Steady-state fluorescence measurements were recorded on an Aminco-Bowman Series 2 fluorimeter, which was equipped with a water bath set to 20 °C. A 50-nM concentration of DNA was used. Fluorescence anisotropies, r , for Rhodamine Green and Alexa 647 were calculated from the polarization of the emission components $I_{||}$, I_{\perp} , $I_{||\perp}$, and $I_{\perp\perp}$ ($||$ and \perp denote the parallel and perpendicular orientations, respectively, of the excitation and emission polarisers) according to Equation (3), with $G = I_{\perp}/I_{\perp\perp}$.

$$r = (I_{||} - GI_{\perp}) / (I_{||} + 2GI_{\perp}) \quad (3)$$

For the fluorescence anisotropy of Rhodamine Green, excitation was carried out at $\lambda = 505$ nm and the emission was monitored at $\lambda = 530$ nm. For Alexa 647, excitation was carried out at $\lambda = 649$ nm and the emission was monitored at $\lambda = 666$ nm.

Received: April 14, 2004

Revised: June 14, 2004

Keywords: DNA · FRET (fluorescence resonance energy transfer) · molecular devices · nanotechnology · single-molecule studies

- [1] Z. J. Donhauser, B. A. Mantooth, K. F. Kelly, L. A. Bumm, J. D. Monnell, J. J. Stapleton, D. W. Price, A. M. Rawlett, D. L. Allara, J. M. Tour, P. S. Weiss, *Science* **2001**, 292, 2303.
- [2] V. Bermudez, N. Capron, T. Gase, F. G. Gatti, F. Kajzar, D. A. Leigh, F. Zerbetto, S. W. Zhang, *Nature* **2000**, 406, 608.
- [3] F. Moresco, G. Meyer, K. H. Rieder, H. Tang, A. Gourdon, C. Joachim, *Phys. Rev. Lett.* **2001**, 86, 672.
- [4] R. A. Bissell, E. Cordova, A. E. Kaifer, J. F. Stoddart, *Nature* **1994**, 369, 133.
- [5] L. Giordano, T. M. Jovin, M. Irie, E. A. Jares-Erijman, *J. Am. Chem. Soc.* **2002**, 124, 7481.
- [6] D. I. Gittins, D. Bethell, D. J. Schiffrin, R. J. Nichols, *Nature* **2000**, 408, 67.
- [7] B. S. T. Kasibhatla, A. P. Labonte, F. Zahid, R. G. Reifengerger, S. Datta, C. P. Kubiak, *J. Phys. Chem. B* **2003**, 107, 12378.
- [8] E. Braun, Y. Eichen, U. Sivan, G. Ben-Yoseph, *Nature* **1998**, 391, 775.
- [9] P. Alberti, J. L. Mergny, *Proc. Natl. Acad. Sci. USA* **2003**, 100, 1569.
- [10] B. Yurke, A. J. Turberfield, A. P. Mills, F. C. Simmel, J. L. Neumann, *Nature* **2000**, 406, 605.
- [11] C. D. Mao, W. Q. Sun, Z. Y. Shen, N. C. Seeman, *Nature* **1999**, 397, 144.
- [12] H. Yan, X. P. Zhang, Z. Y. Shen, N. C. Seeman, *Nature* **2002**, 415, 62.
- [13] E. Winfree, F. R. Liu, L. A. Wenzler, N. C. Seeman, *Nature* **1998**, 394, 539.
- [14] J. H. Chen, N. C. Seeman, *Nature* **1991**, 350, 631.
- [15] Y. Benenson, R. Adar, T. Paz-Elizur, Z. Livneh, E. Shapiro, *Proc. Natl. Acad. Sci. USA* **2003**, 100, 2191.
- [16] M. N. Stojanovic, D. Stefanovic, *Nat. Biotechnol.* **2003**, 21, 1069.
- [17] M. Ueda, M. Takai, K. Taniguchi, Y. Takamura, Y. Horiike, Y. Baba, *Appl. Phys. Lett.* **2003**, 83, 5086.
- [18] K. Hamad-Schifferli, J. J. Schwartz, A. T. Santos, S. G. Zhang, J. M. Jacobson, *Nature* **2002**, 415, 152.
- [19] D. S. Liu, S. Balasubramanian, *Angew. Chem.* **2003**, 115, 5912; *Angew. Chem. Int. Ed.* **2003**, 42, 5734.

- [20] R. P. Fahlman, D. Sen, *J. Am. Chem. Soc.* **2002**, *124*, 4610.
- [21] L. M. Ying, A. Bruckbauer, A. M. Rothery, Y. E. Korchey, D. Klenerman, *Anal. Chem.* **2002**, *74*, 1380.
- [22] L. M. Ying, S. S. White, A. Bruckbauer, L. Meadows, Y. E. Korchey, D. Klenerman, *Biophys. J.* **2004**, *86*, 1018.
- [23] A. Bruckbauer, L. M. Ying, A. M. Rothery, D. J. Zhou, A. I. Shevchuk, C. Abell, Y. E. Korchey, D. Klenerman, *J. Am. Chem. Soc.* **2002**, *124*, 8810.
- [24] A. A. Deniz, M. Dahan, J. R. Grunwell, T. J. Ha, A. E. Faulhaber, D. S. Chemla, S. Weiss, P. G. Schultz, *Proc. Natl. Acad. Sci. USA* **1999**, *96*, 3670.
- [25] M. I. Wallace, L. M. Ying, S. Balasubramanian, D. Klenerman, *J. Phys. Chem. B* **2000**, *104*, 11 551.
- [26] M. Masuko, H. Ohtani, K. Ebata, A. Shimadzu, *Nucleic Acids Res.* **1998**, *26*, 5409.
- [27] E. Kostenko, M. Dobrikov, D. Pyshnyi, V. Petyuk, N. Komarova, V. Vlassov, M. Zenkova, *Nucleic Acids Res.* **2001**, *29*, 3611.
- [28] S. G. Kruglik, P. Mojzes, Y. Mizutani, T. Kitagawa, P. Y. Turpin, *J. Phys. Chem. B* **2001**, *105*, 5018.
- [29] S. Bernacchi, Y. Mely, *Nucleic Acids Res.* **2001**, *29*, e62.
- [30] S. Bernacchi, E. Piemont, N. Potier, A. van Dorsselaer, Y. Mely, *Biophys. J.* **2003**, *84*, 643.
- [31] D. G. Norman, R. J. Grainger, D. Uhrin, D. M. J. Lilley, *Biochemistry* **2000**, *39*, 6317.
- [32] C. Eggeling, J. R. Fries, L. Brand, R. Gunther, C. A. M. Seidel, *Proc. Natl. Acad. Sci. USA* **1998**, *95*, 1556.
- [33] L. Edman, U. Mets, R. Rigler, *Proc. Natl. Acad. Sci. USA* **1996**, *93*, 6710.
- [34] H. T. Li, L. M. Ying, J. J. Green, S. Balasubramanian, D. Klenerman, *Anal. Chem.* **2003**, *75*, 1664.

Tin Oxide Nanooctahedra

Self-Construction of Hollow SnO₂ Octahedra Based on Two-Dimensional Aggregation of Nanocrystallites**

Hua Gui Yang and Hua Chun Zeng*

The past few years have witnessed an increasing trend toward synthetic fabrication of micro- and nanostructures with hollow interiors, owing to their potential applications as photonic crystals, host materials for intercalants, drug-delivery carriers, sensors, and chemical reactors.^[1–14] These hollow structures, which normally consist of inorganic materials such as metals or metal oxides, provide both chemical functionality

and designable inner space for meeting new technological challenges. Among many preparative methods,^[1–14] template-assisted synthesis is an effective approach in which hard templates, such as polymeric core supports or sacrificial metal substrates, and soft templates, such as micelles in emulsions or ionic liquids, have been utilized.^[1–11] Recent developments in this area show that hollow structures can also be created via direct solid evacuation with Ostwald ripening,^[12] and the Kirkendall effect,^[13] or formed from self-assembly of building blocks through hydrophobic interactions.^[14] It would also be desirable to search for one-pot syntheses, preferably by template-free routes.

“Oriented attachment” has attracted increasing interest in recent years as a new means for fabrication and self-organization of nanocrystalline materials under one-pot conditions.^[15–19] As summarized in Figure 1, recent examples

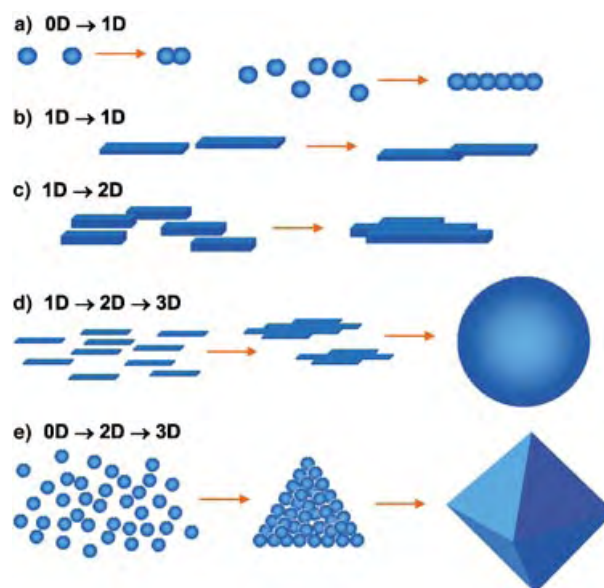


Figure 1. Various organizing schemes for self-construction of nanostructures by oriented attachment.

include formation of one-dimensional (1D) nanorods (e.g., TiO₂ and ZnO) from their respective 0D nanocrystallites (Figure 1a).^[15,16] The formed 1D nanorods or nanoribbons can also further self-attach through stacking by planar van der Waals interaction (for layered compounds, e.g., α -MoO₃; Figure 1b)^[17] or lateral “lattice fusion” (for ionic compounds, e.g., ZnO; Figure 1c)^[16,18] to generate either length-multiplied 1D nanostructures or 2D crystal sheets and walls. Recently, this size-amplifying mechanism was extended to 3D architectures of 2D crystal strips (formed from 1D nanoribbons; Figure 1d),^[19] in which rhomb-shaped 2D building blocks can self-aggregate into “dandelion”-like hollow spheres. Here we report another novel organizing principle (Figure 1e) with an underlying oriented-attachment mechanism in which complex geometrical structures (e.g., polyhedra) can be built by the assembly route 0D→2D→3D. Using the wide-band-gap semiconductor tin dioxide as an example,^[11,20,21] we demonstrate that hollow geometrical

[*] H. G. Yang, Prof. Dr. H. C. Zeng
Department of Chemical and Biomolecular Engineering
Faculty of Engineering
National University of Singapore
10 Kent Ridge Crescent, Singapore 119260 (Singapore)
Fax: (+65) 6779-1936
E-mail: chezhc@nus.edu.sg

[**] The authors gratefully acknowledge the financial support of the Ministry of Education, Singapore.

Supporting information for this article is available on the WWW under <http://www.angewandte.org> or from the author.

objects of micro- and nanoscales can be prepared by one-pot solution routes without using templates. This strategy is based on the ability to stabilize certain crystallographic planes while the 0D nanocrystallites form and undergo 2D self-aggregation.

The crystallographic structure and chemical composition of the SnO_2 octahedra were determined by powder XRD and energy-dispersive X-ray spectroscopy (EDX; Supporting Information). These data show that the prepared SnO_2 has a rutile-like tetragonal symmetry and a strictly stoichiometric atomic ratio (space group $P4_2/mnm$, $a_o = 4.738$, $c_o = 3.188$ Å; JCPDS file no. 21-1250;^[11,20,21] $\text{Sn}/\text{O} = 1:2$). In particular, the broad XRD peaks of (110), (101), (200), (211), and (112) reflect the nanocrystalline nature of samples, but no lattice relaxation was detected.

The field-emission scanning electron microscopy (FESEM) images in Figure 2a show the general morphology of the hollow SnO_2 octahedra synthesized in this work. A high yield (> 95 %) of this polyhedral form can be easily achieved after only one sedimentation run (Figure 2e). Interestingly,

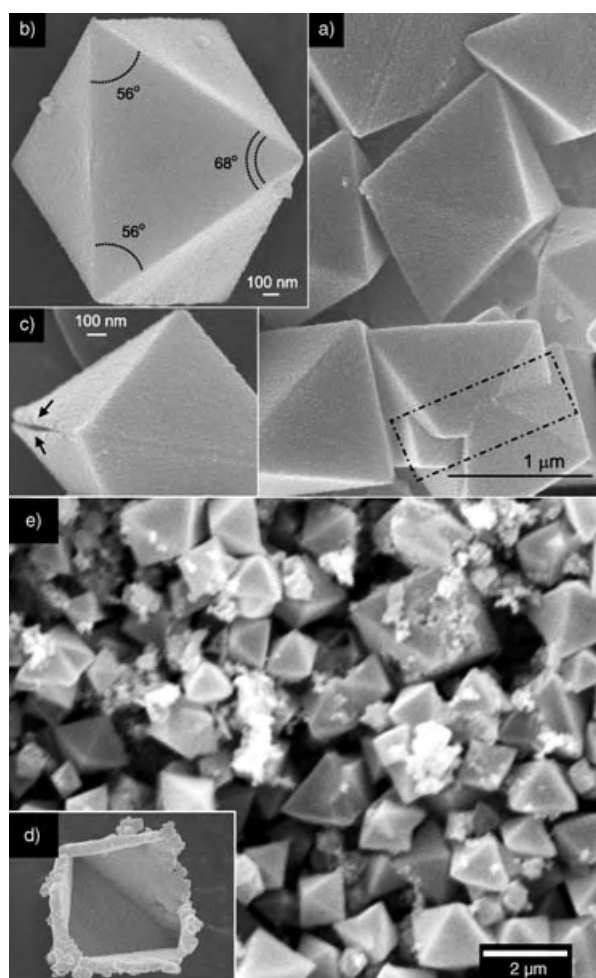


Figure 2. FESEM images of hollow SnO_2 crystal octahedra. a) General sample morphology (the framed area indicates the joined part of two intersecting octahedra). b) A tilted SnO_2 octahedron. c) Ridge opening (indicated by arrows) on a SnO_2 octahedron. d) Interior morphology. e) Overall product morphology after only one sedimentation run (SEM image).

geometrical parameters of the bipyramidal octahedra, such as interplanar angles and edge-length ratios, are essentially identical regardless of the actual sizes of the hollow structures (Supporting Information). This observation indicates that an overall crystallographic relationship exists among the nanocrystallites that constitute the octahedra. The isosceles-triangular crystal planes (Figure 2b) have angles of $56 \pm 1^\circ$ and $68 \pm 1^\circ$,^[22] that is, the crystallographic planes of each octahedral surface are similar to the {111} family (Figure 3d). There is a total of 16 {111}-like planes per octahedron: eight for inner surfaces, and eight for outer ones. The interior space of the hollow SnO_2 octahedra was examined directly by FESEM for incomplete or cracked SnO_2 crystal octahedra (Figure 2d). The size of these hollow octahedra can be as small as 150 nm to as large as several micrometers (Figure 2e), and the thickness of the shell walls is in the range of 20–200 nm, depending on synthetic conditions (see also Supporting Information). In general, higher initial concentrations of SnF_2 and longer reaction times lead to the formation of larger octahedra.

The hollow interior and geometrical symmetry of the as-synthesized octahedra were further elucidated by TEM (Figure 3). In agreement with the above FESEM findings, a

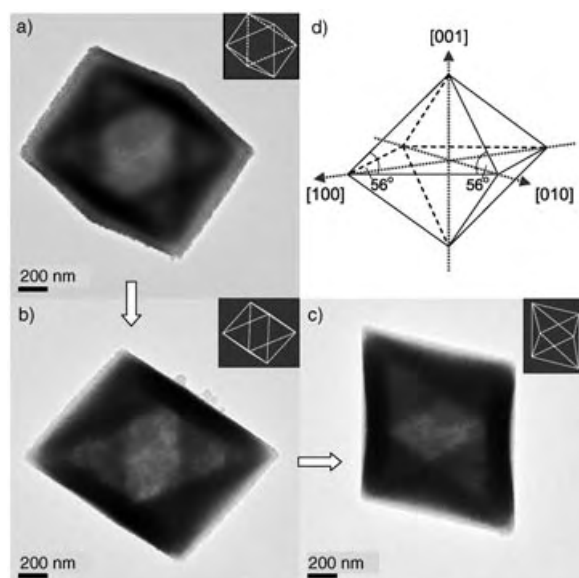


Figure 3. Sequential TEM images (a–c) for a hollow SnO_2 octahedron taken with different tilt angles (a) was viewed perpendicular to the top crystal plane), and a schematic illustration of crystal orientation of an SnO_2 octahedron (d). Edge outlines of the octahedra are depicted in the insets.

high geometric symmetry of the examined octahedron can be seen from the image evolution, while the inner cavity is clearly revealed by the changes in contrast on tilting the sample.

Individual crystal sheets that formed the SnO_2 octahedra can be obtained by sonication (5–10 min in an ultrasonic water bath; Supporting Information). High-resolution TEM (HRTEM; Figure 4a) indicates that triangular SnO_2 sheets are composed of fine crystallites in a size range of only

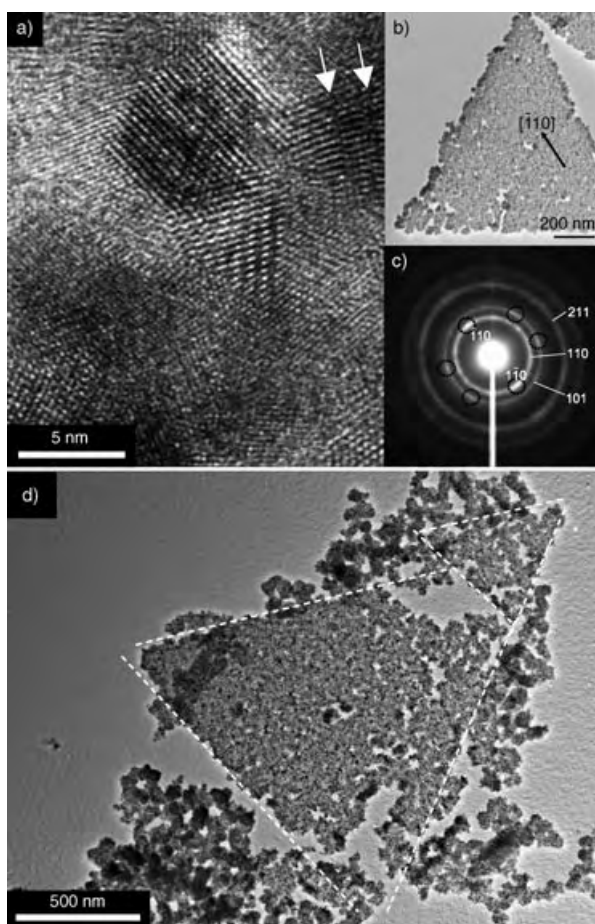


Figure 4. a) Representative HRTEM image of triangular SnO_2 crystallite aggregates (white arrows indicate twin boundaries within a crystallite; spacing = d_{110}). b) TEM image of a detached SnO_2 nanocrystalline triangle. c) SAED pattern of the SnO_2 sheet in b). d) Formation of triangles (framed with white dashed lines) from SnO_2 nanocrystallites. Brighter spots (circled) in c) belong to the same set of $[111]$ zone spots.

3–5 nm. These particles were well crystallized, as shown by clear lattice fringes ($d_{110} = 3.3 \pm 0.1$, $d_{101} = 2.6 \pm 0.1$, $d_{200} = 2.4 \pm 0.1$ Å, etc.) and relatively sharp selected-area electron-diffraction (SAED) rings. Although individual crystallites within a local area seem to be random, the overall crystalline aggregates still exhibit global features of $\{111\}$ vicinal surfaces that suggest long-range ordering of nanocrystallites owing to oriented attachment.^[15–19] As can be seen in Figure 4b and c, for example, diffraction spots of (-110) and $(1-10)$ of the $[111]$ zone are visible on the 110 diffraction ring, and they are aligned parallel to the baseline of the triangle, that is, a clear crystalline relationship exists among these $[111]$ -oriented crystallites. Indeed, the lattice fringe of d_{110} is also prominent among the observed nanocrystallites (Figure 4a).

To understand the formation mechanism of the octahedral hollow structures, time-dependent experiments were carried out, which revealed that the hollow octahedra were grown by a plane-by-plane process. As shown in Figure 4d, growth starts with the formation of triangular crystallite aggregates. With appropriate changes in direction at the edges of the triangle (i.e., interplanar angle of 95.2 or 117.1°), further

planar coalescence leads to three-dimensional construction of octahedra (Figure 1e and Supporting Information). When two or more such initial sheets are close to each other under low-fluidity conditions, the chance of joining exists (Figure 2a and Figure 4d), that is, the octahedra grow into each other, a process which can be utilized as a means for fabricating even more complex hollow polyhedra. About 5–10% of the octahedra are in this type of joined configuration. It is believed that the addition of ethylenediamine, in combination with the present solvent system, is crucial for stabilizing the $\{111\}$ -like sheets of SnO_2 while maintaining the small crystallite size. With longer reaction times, smoother crystal facets can be attained for the hollow octahedra, because of continuous surface flattening. Liplike slits arising from accumulated crystal imperfections (twins, disoriented crystallites, etc.), are often found on the edges of the octahedra (e.g., Figure 2c) as a result of mismatched closure. This type of opening may serve as a gateway for materials/chemicals exchange between the interior cavity and exterior space, which is of interest for potential applications of the hollow structures.

In summary, octahedra of rutile-like SnO_2 with a central cavity have been prepared by a template-free hydrothermal route. The synthesis is based on the two-dimensional attachment of nanocrystallites giving an overall $\{111\}$ -like termination for each octahedral surface in the presence of ethylenediamine and 2-propanol/water. In principle, other hollow polyhedra could also be prepared by stabilizing selected crystal orientations.

Experimental Section

In a typical experiment, SnF_2 (0.24 g) was added to deionized water (50 mL) with vigorous stirring; the pH value was 2.83. The fresh solution (1–2 mL, 0.03 M), deionized water (3–6 g), 2-propanol (13–15 g), and ethylenediamine (1–2 g) were added to a Teflon-lined stainless steel autoclave. The autoclave was kept at 180°C for 6–50 h in an electric oven. After reaction, white octahedral products were harvested by sedimentation (to separate them from smaller irregular SnO_2 aggregates), washed three times with deionized water, and dried under vacuum overnight. The crystallographic phase of the SnO_2 products was determined by powder XRD (Shimadzu XRD-6000, $\text{Cu}_{\text{K}\alpha}$ radiation). The products were further investigated by scanning electron microscopy and energy dispersive X-ray spectroscopy (SEM/EDX, JSM-5600LV), field-emission SEM (FESEM/EDX, JSM-6700F), transmission electron microscopy and selected area electron diffraction (TEM/SAED, JEM-2010F, 200 kV), and high-resolution transmission electron microscopy (HRTEM/SAED/EDX, Tecnai-G², FEI).

Received: June 30, 2004

Keywords: hydrothermal synthesis · nanostructures · oriented attachment · self-assembly · tin oxide

[1] F. Caruso, R. A. Caruso, H. Möhwald, *Science* **1998**, 282, 1111.

[2] C. G. Göltner, *Angew. Chem.* **1999**, 111, 3347; *Angew. Chem. Int. Ed.* **1999**, 38, 3155.

[3] F. Caruso, *Adv. Mater.* **2001**, 13, 11.

[4] A. D. Dinsmore, M. F. Hsu, M. G. Nikolaides, M. Marquez, A. R. Bausch, D. A. Weitz, *Science* **2002**, 298, 1006.

- [5] Y. Sun, Y. Xia, *Science* **2002**, 298, 2176.
- [6] Y. Sun, B. Mayers, Y. Xia, *Adv. Mater.* **2003**, 15, 641.
- [7] T. Nakashima, N. Kimizuka, *J. Am. Chem. Soc.* **2003**, 125, 6386.
- [8] C.-W. Guo, Y. Cao, S.-H. Xie, W.-L. Dai, K.-N. Fan, *Chem. Commun.* **2003**, 700.
- [9] H. G. Yang, H. C. Zeng, *Angew. Chem.* **2004**, 116, 5318; *Angew. Chem. Int. Ed.* **2004**, 43, 5206.
- [10] J. Goldberger, R. He, Y. Zhang, S. Lee, H. Yan, H.-J. Choi, P. Yang, *Nature* **2003**, 422, 599.
- [11] B. Liu, H. C. Zeng, *J. Phys. Chem. B* **2004**, 108, 5867.
- [12] H. G. Yang, H. C. Zeng, *J. Phys. Chem. B* **2004**, 108, 3492.
- [13] Y. Yin, R. M. Rioux, C. K. Erdonmez, S. Hughes, G. A. Somorjai, A. P. Alivisatos, *Science* **2004**, 304, 711.
- [14] S. Park, J.-H. Lim, S.-W. Chung, C. A. Mirkin, *Science* **2004**, 303, 348.
- [15] R. L. Penn, J. F. Banfield, *Science* **1998**, 281, 969.
- [16] C. Pacholski, A. Kornowski, H. Weller, *Angew. Chem.* **2002**, 114, 1234; *Angew. Chem. Int. Ed.* **2002**, 41, 1188.
- [17] X. W. Lou, H. C. Zeng, *J. Am. Chem. Soc.* **2003**, 125, 2697.
- [18] B. Liu, H. C. Zeng, *J. Am. Chem. Soc.* **2003**, 125, 4430.
- [19] B. Liu, H. C. Zeng, *J. Am. Chem. Soc.* **2004**, 126, 8124.
- [20] Z. R. Dai, J. L. Gole, J. D. Stout, Z. L. Wang, *J. Phys. Chem. B* **2002**, 106, 1274.
- [21] Z. R. Dai, Z. W. Pan, Z. L. Wang, *J. Am. Chem. Soc.* **2002**, 124, 8673.
- [22] Theoretical values are 54.1 and 71.8°, respectively; the observed deviation is probably due to the presence of disoriented crystallites and crystal defects in the triangular sheets that result in mismatched planes.

a diatom, genetic control of this process is evident. Cell-wall formation in diatoms has been regarded as an example for the controlled production of nanostructured silica. Therefore, understanding the underlying mechanism of silica fabrication may inspire synthetic routes to produce novel silica-based materials under mild reaction conditions.^[2,3] Diatom biosilica is mainly composed of amorphous, hydrated SiO₂ (silica) that contains a small proportion of proteins, which have long been speculated to be involved in silica deposition.^[4,5] Remarkably, more than three decades ago, Volcani's group recognized the existence of unusual amino acid derivatives such as ϵ -N,N,N-trimethyl- δ -hydroxylysine in diatom biosilica.^[6,7] However, proteins associated with biosilica from *C. fusiformis* have only recently been purified to homogeneity and found to be the source of a number of unusual amino acid modifications. Typically, these proteins (denoted as silaffins) contain a high percentage of lysine and serine groups and all of these residues are modified.^[8–10] The serine residues are phosphorylated, whereas the lysines are converted into three different derivatives: ϵ -N,N-dimethyllysine, ϵ -N,N,N-trimethyl- δ -hydroxylysine, and lysines that are covalently linked to long-chain polyamines (N-methylated polypropyleneamines). As well as silaffins, many cell walls in diatoms contain the same type of long-chain polyamines that are bound to putrescine.^[11] Silaffins as well as long-chain polyamines have been shown to promote the formation of silica nanospheres from silicic acid in vitro.^[8,11,12] A model which is based on phase-separation processes of polyamines explains the formation of patterns during silica formation.^[13] Recently hexagonal silica structures were produced in vitro under the influence of polyamines.^[14] Polyamines are known to affect silica formation in several ways: they catalyze the formation of siloxane bonds and act as flocculating agents.^[15,16]

More than 40 years ago, quaternary ammonium ions were recognized as structure-directing agents in the synthesis of zeolites.^[17] The tetramethylammonium cation favors the formation of symmetric oligosilicate anions, such as the cubic octamer Si₈O₂₀^{8–}, and this control of silicate speciation influences the nucleation phase of silica formation.^[18] Furthermore, these organic cations exhibit a high affinity to silica surfaces. The existence of the ϵ -N,N,N-trimethyl- δ -hydroxylysine residue in silaffins from *C. fusiformis* indicates that nature exploits this very special interaction in the biomineralization of silica.

Herein we demonstrate that quaternary ammonium cations are indeed a characteristic feature of silica-associated proteins. Three novel lysine derivatives, which contain quaternary ammonium groups, were identified in silaffins that were purified from silica shells of the diatom *Eucampia zodiacus* (Figure 1A). Silica was removed from the purified shells by treatment with anhydrous hydrogen fluoride, and the remaining silica-associated proteins were analyzed by sodium dodecyl sulphate polyacrylamide gel electrophoresis (SDS-PAGE). The protein extract from *Eucampia* shells exhibited one major protein band with an apparent molecular mass of 22 kDa and three or four additional minor components (Figure 1B). These proteins were then analyzed for the presence of unusually modified amino acids. After acid hydrolysis, the resulting amino acid mixture was directly

Bioinorganic Chemistry

Quaternary Ammonium Groups in Silica-Associated Proteins**

Stephan Wenzl, Rainer Deutzmann, Robert Hett, Eduard Hochmuth, and Manfred Sumper*

The formation of inorganic minerals under the control of an organism (biomineralization) is a widespread phenomenon in nature. Silica biomineralization on earth is dominated by simple aquatic life-forms, which include unicellular organisms such as diatoms, radiolarians, and synurophytes as well as multicellular sponges.^[1] These organisms produce silica based exo- and endoskeletons. In diatoms, the silica-based cell walls exhibit intricate patterns in the nano- to micrometer range. As these patterns are precisely reproduced in each generation of

[*] Dr. S. Wenzl, Prof. Dr. R. Deutzmann, R. Hett, E. Hochmuth, Prof. Dr. M. Sumper
Lehrstuhl Biochemie I
Universität Regensburg
93040 Regensburg (Germany)
Fax: (+49) 941-943-2936
E-mail: manfred.sumper@vkl.uni-regensburg.de

[**] The present work was supported by the Deutsche Forschungsgemeinschaft (grant SFB 521A2) and the Fonds der Chemischen Industrie.

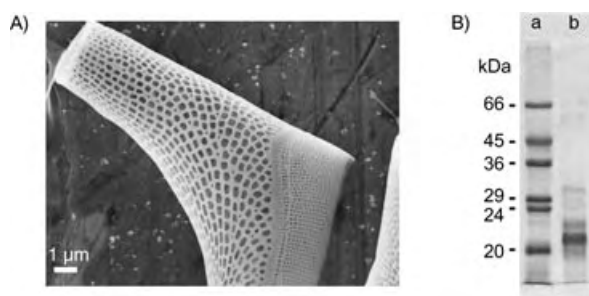


Figure 1. The silica cell wall of the diatom *Eucampia zodiacus* and its protein components: A) SEM image of the cell wall. B) Silaffin proteins extracted from purified cell walls with anhydrous HF—the extracted proteins were subjected to 12-% SDS-PAGE and were stained with Coomassie blue (lane a); molecular-weight standards were applied in lane b.

subjected to high performance anion-exchange chromatography (Figure 2A). Remarkably, a significant fraction of the amino acid mixture (Figure 2A,

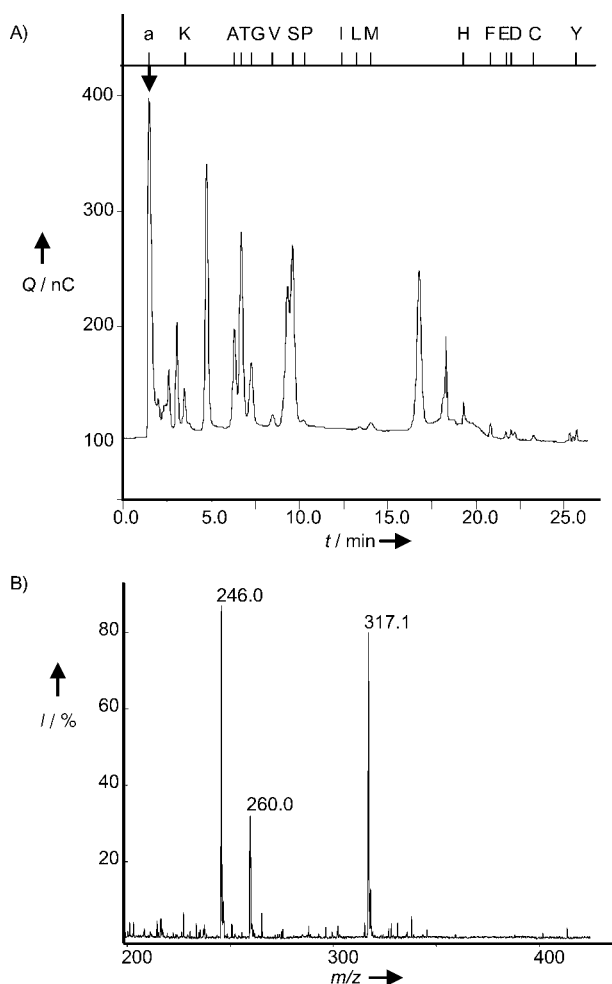


Figure 2. Amino acid analysis of silaffins: A) High performance anion-exchange chromatography of amino acids obtained by acidic hydrolysis of silaffins; the elution times of amino acid standards are indicated on the upper bar; peak a represents amino acids that contain a cationic modification. B) ESI-MS analysis (I = relative intensity) of the fraction that contains cationic amino acids (part A, peak a).

peak a) did not bind to the anion-exchange matrix even under the extremely alkaline conditions (NaOH, 60 mM) which indicates the existence of amino acid derivatives with a permanently cationic modification that compensates the charge of the carboxylate anion. Electrospray ionization mass spectrometry (ESI-MS) of this fraction revealed the presence of two main components at m/z 246 and 317 as well as a further component at m/z 260 (Figure 2B). The chemical structures of these derivatives were analyzed by MS/MS analysis. The resulting fragmentations of all three species are documented in Figure 3A, Figure 4A, and Figure 5A. Each

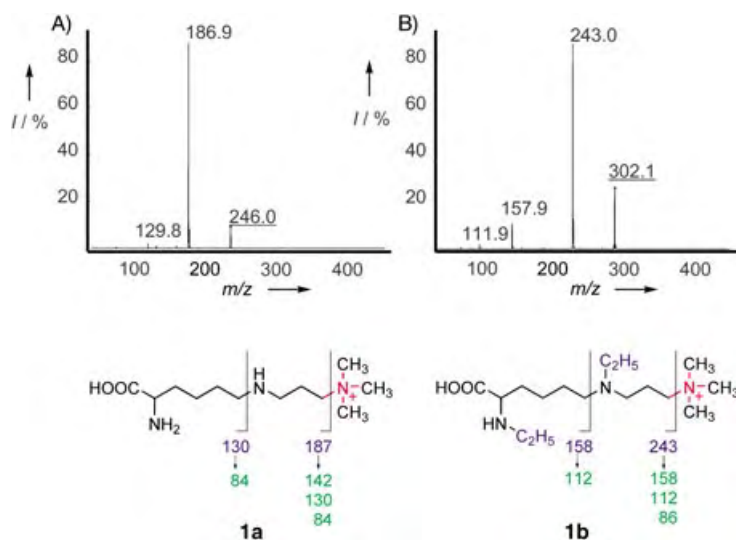


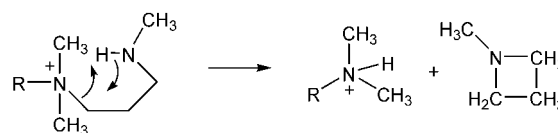
Figure 3. Structural analysis by mass spectrometry of the fragment with m/z 246. Ions were isolated by the ion-trap mode and were subjected to collision-induced fragmentation. Fragmentation patterns obtained A) before and B) after reductive ethylation (m/z after ethylation was 302 which indicates the introduction of two ethyl groups). m/z values shown in green indicate the results of (MS)³ fragmentations of selected ions.

of the spectra displays a fragment at m/z 130 that subsequently (MS/MS/MS) decays into a species of m/z 84 (elimination of 46 mass units, which corresponds to the loss of H₂O and CO). This indicates the presence of a lysine moiety. Aminopropylations as well as methylations of the ϵ -amino groups of lysine residues were previously found to take place in silaffins isolated from the diatom *C. fusiformis*.^[8] Aminopropylation followed by exhaustive methylation of the terminal amino group would create a lysine derivative of m/z 246 that contains a quaternary ammonium group as depicted (1a; Figure 3). Further methylation of the ϵ -amino group of the lysine moiety would create a derivative with m/z 260 (2a; Figure 4). These proposed structures are able to account for all of the remaining mass fragments observed in MS/MS analysis (Figure 3A and Figure 4A).

To prove the correctness of this interpretation, both of the components at m/z 246 and m/z 260 were converted into their fully methylated derivatives by reductive alkylation. As expected, reductive methylation converted both species into a derivative with m/z 288, which corresponds to the introduction of three and two methyl groups, respectively (data not

shown). Reductive ethylation is known to be less efficient and converted the α -amino group of the lysine moiety only into the secondary amine.^[19] Under the conditions employed, only two ethyl residues were introduced into the component at m/z 246 and only one ethyl residue was introduced into the component at m/z 260. The resulting fragmentation patterns of the partially ethylated derivatives (Figure 3B and Figure 4B) confirm the proposed structures (**1b**; **2b**).

Introduction of a second aminopropyl residue into the species at m/z 260 would create a homologous structure with m/z 317 (**3a**; Figure 5). The fragmentation pattern of the component at m/z 317 supported this interpretation (Figure 5A). As expected, reductive methylation introduced



Scheme 1. Proposed mechanism of internal proton transfer to explain the production of a fragment with m/z 246 (see also Figure 5A) in the collision-induced fragmentation of **3a**.

three methyl groups into the compound and reductive ethylation introduced two ethyl groups. The fragmentation spectra of the partially ethylated derivative again confirmed the proposed structure (**3b**). Remarkably, the compound with m/z 317 produced an unexpected fragment (m/z 246) that appears to result from N–C bond cleavage at the quaternary ammonium site. In the partially ethylated derivative, the corresponding fragment (calculated m/z : 274) was no longer observed in the fragmentation pattern. This behavior is likely to be caused by a favored internal proton transfer from the terminal secondary amino group as depicted in Scheme 1. This proton transfer would no longer be possible after ethylation, and this observation strongly supports the proposed structure. Furthermore, ^1H NMR analysis of the compound with m/z 317 at pH 11.8 gave rise to a signal at $\delta = 3.14$ ppm (methyl) whose position did not shift upon lowering the pH (pH 5). This is characteristic of methyl groups attached to a quaternary ammonium group (data not shown) and confirms the conclusion drawn from mass spectrometry.

The characterization of novel lysine derivatives with quaternary ammonium groups indicates that this cationic modification represents a special structural feature of silica-associated proteins from diatoms. It is well documented that quaternary ammonium ions exhibit very unusual behavior in silica systems which is probably owed to the high affinity of the ions to silica surfaces and their inability to form coordinate bonds with the oxygen of SiOH groups as sodium does.^[16] Nature probably uses these special properties to design proteins with high affinities for silica surfaces.

Experimental Section

Culture Conditions: *Eucampia zodiacus* was isolated from the North Sea and cultivated in an artificial seawater medium according to the protocol from the North East Pacific Culture Collection (www.ocgy.ubc.ca/projects/nepcc/media.htm).

Purification of Silaffins: A 20-L culture of silaffins was harvested by filtration through a nylon screen (40 μm). The diatom colonies were suspended in 10-mL lysis buffer (EDTA (100 mM), SDS (2 %)), and the suspensions were incubated at 95 °C for 10 min. The resulting silica shells were collected by

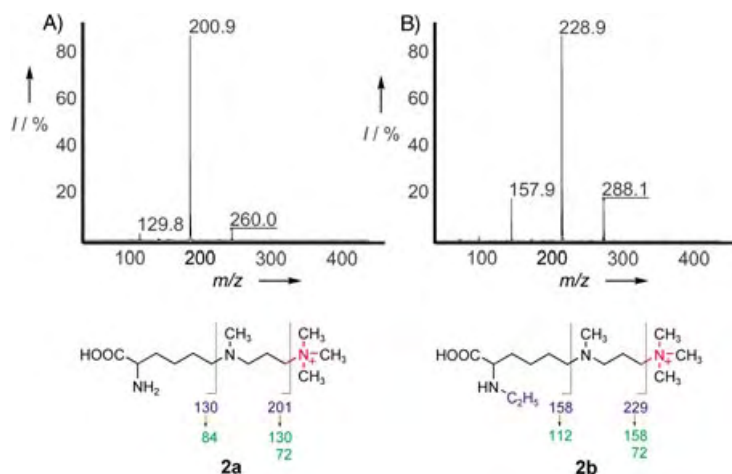


Figure 4. Structural analysis by mass spectrometry of the fragment with m/z 260. Ions were isolated by the ion-trap mode and subjected to collision-induced fragmentation. Fragmentation patterns obtained A) before and B) after reductive ethylation (m/z after ethylation was 288 which indicates the introduction of one ethyl group). m/z values shown in green indicate the results of $(\text{MS})^3$ fragmentations of selected ions.

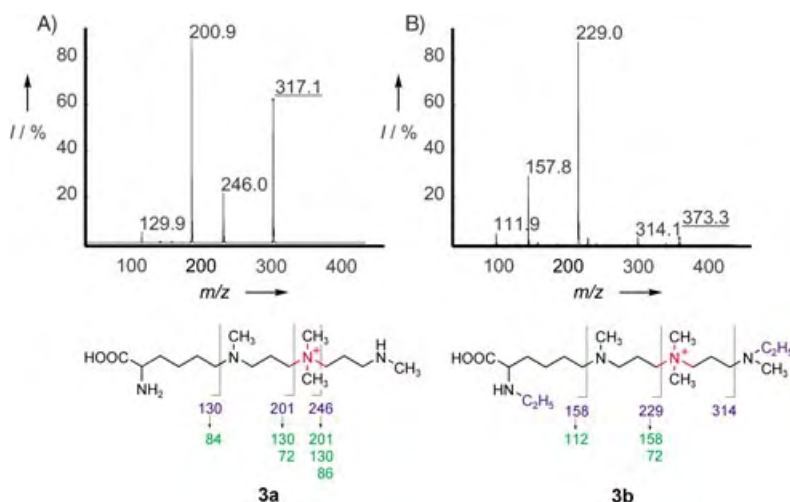


Figure 5. Structural analysis by mass spectrometry of the fragment with m/z 317. Ions were isolated by the ion-trap mode and subjected to collision-induced fragmentation. Fragmentation patterns obtained A) before and B) after reductive ethylation (m/z after ethylation was 373 which indicates the introduction of two ethyl groups). m/z values shown in green indicate the results of $(\text{MS})^3$ fragmentations of selected ions.

centrifugation ($2500 \times g$; 10 min), washed extensively with water, and dried in vacuo. Silica shells (100 mg) were dissolved in anhydrous hydrogen fluoride and the solution was incubated at 0°C for 30 min. Hydrogen fluoride was evaporated, and the remaining material was neutralized with Tris-HCl (250 mM, pH 7.5; 2 mL). HighS cation-exchange resin (NH_4^+ form; Bio-Rad; 100 μL) was added to this extract, and the mixture was incubated at 4°C for 1 h. The resin was washed with H_2O , followed by NH_4OH (4 N), and again with H_2O . The silaffins were then eluted with NaCl (2 M)/ Na_2CO_3 (20 mM). After dialysis against H_2O (Spectra/Por CE dialysis tubing; molecular-mass cutoff: 500 Da), the eluted proteins were size-fractionated on a Superdex-Peptide HR 10/30 column (Amersham Pharmacia; running buffer ammonium acetate (250 mM); flow rate: 0.3 mL min^{-1}). Fractions were analyzed for silaffins by 12-% SDS PAGE with subsequent staining with Coomassie blue. Silaffin-containing fractions were pooled and dried by lyophilization.

Purification of Basic Amino Acids: Purified silaffins were hydrolyzed in HCl (6 N; Pierce; Sequanal Grade; 1 mL) at 110°C for 24 h. After evaporation, the material was dissolved in H_2O (300 μL), filtered (Millipore; Millex PV 0.22 μm), and loaded onto an Amino-Pac PA10 4/250 mm anion-exchange column (Dionex; elution gradient: NaOH/NaOAc). Amino acids were detected electrochemically (Dionex ED40). Basic amino acids modified with a quaternary ammonium group eluted with NaOH (60 mM). To eliminate Na^+ ions, this fraction was loaded onto a Biorex 70 cation-exchange column (H^+ -form; Bio-Rad; 0.6 mL), washed with H_2O (1.0 mL) and NH_4OH (0.15 N; 3.4 mL), and eluted with NH_4OH (0.5 N; 0.7 mL). After filtration and drying, the residue was dissolved in H_2O (200 μL).

Alkylation of Modified Lysine Residues: A dried sample, which contained lysine residues modified with a quaternary ammonium group, was dissolved in sodium phosphate (50 mM, pH 7.0), and the solution was treated with sodium cyanoborohydride and acetaldehyde (reductive ethylation) according to a previously described protocol.^[19] Reductive methylation was similarly carried out with sodium cyanoborohydride and formaldehyde.^[19]

Mass Spectrometry of Basic Amino Acids: Electrospray ionization MS and fragmentation were performed by using an Ion Trap ESQUIRE LC instrument (Bruker, Billerica, MA). Samples were infused by a nanospray source in MeOH (50 %)/AcOH (0.5 %).

Received: July 8, 2004

Keywords: bioinorganic chemistry · diatoms · mass spectrometry · proteins · silicates

- [14] M. Sumper, *Angew. Chem.* **2004**, *116*, 2301–2304; *Angew. Chem. Int. Ed.* **2004**, *43*, 2251–2254.
- [15] T. Mizutani, H. Nagase, N. Fujiwara, H. Ogoishi, *Bull. Chem. Soc. Jpn.* **1998**, *71*, 2017–2022.
- [16] R. K. Iler, *The Chemistry of Silica*, Wiley, New York, **1979**.
- [17] R. M. Barrer, P. J. Denny, *J. Chem. Soc.* **1961**, 971–982.
- [18] D. Hoebbel, G. Garzo, G. Engelhardt, R. Ebert, E. Lippmaa, M. Alla, *Z. Anorg. Allg. Chem.* **1980**, *465*, 15–33.
- [19] N. Jentoft, D. G. Dearborn, *Methods Enzymol.* **1983**, *91*, 570–579.

- [1] H. A. Lowenstam, S. Weiner, *On Biomineralization*, Oxford University Press, Oxford, **1989**.
- [2] S. Mann, G. Ozin, *Nature* **1996**, *382*, 313–318.
- [3] J. Parkinson, R. Gordon, *Trends Biotechnol.* **1999**, *17*, 190–196.
- [4] R. Hecky, K. Mopper, P. Kilham, T. Degens, *Mar. Biol.* **1973**, *19*, 323–331.
- [5] D. Swift, A. Wheeler, *J. Phycol.* **1992**, *28*, 202–209.
- [6] T. Nakajima, B. E. Volcani, *Science* **1969**, *164*, 1400–1406.
- [7] T. Nakajima, B. E. Volcani, *Biochem. Biophys. Res. Commun.* **1970**, *39*, 28–33.
- [8] N. Kröger, R. Deutzmann, M. Sumper, *Science* **1999**, *286*, 1129–1132.
- [9] N. Kröger, R. Deutzmann, M. Sumper, *J. Biol. Chem.* **2001**, *276*, 26066–26070.
- [10] N. Kröger, S. Lorenz, E. Brunner, M. Sumper, *Science* **2002**, *298*, 584–586.
- [11] N. Kröger, R. Deutzmann, C. Bergsdorf, M. Sumper, *Proc. Natl. Acad. Sci. USA* **2000**, *97*, 14133–14138.
- [12] M. Sumper, S. Lorenz, E. Brunner, *Angew. Chem.* **2003**, *115*, 5350–5353; *Angew. Chem. Int. Ed.* **2003**, *42*, 5192–5195.
- [13] M. Sumper, *Science* **2002**, *295*, 2430–2433.

Self-Assembly

A Palladium(II)-Clipped Aromatic Sandwich**

Kazuhiisa Kumazawa, Yoshinori Yamanoi,
Michito Yoshizawa, Takahiro Kusakawa, and
Makoto Fujita*

Enclathration of large π -conjugated molecules by a synthetic receptor is an interesting task because the properties of these molecules, such as stability, reactivity, solubility, and photo- and electroresponse, can be controlled.^[1] To enclathrate large π -conjugated molecules, however, a synthetic receptor with a cavity is required, whose dimensions should be larger than that of the π -conjugated guests. While there are many examples of three-dimensional receptors,^[2] large two-dimensional receptors have been less explored.^[3] Herein we describe the self-assembly of a π -stacked host–guest system in which large aromatic guests are sandwiched by metal-clipped π -conjugated ligands. The ligand **1** is a roughly 2-nm-sized hexagonal planar molecule that consists of ten aromatic rings with six pyridyl donor sites at the periphery. Upon complexation with [(en)Pd(NO₃)₂] (en = 1,2-ethanediamine) this ligand is assembled to give large two-dimensional receptors. In the presence of D_{3h} -symmetric guests (**2**), sandwich complexes [**2**⊂**3**]¹²⁺, where **3**¹²⁺ has a composition of [(en)Pd]₆(**1**)₂¹²⁺, are quantitatively assembled. The guest molecule is wrapped by two ligands whose pyridyl donor sites

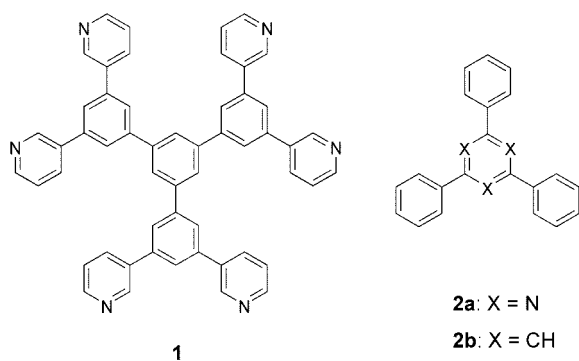
[*] K. Kumazawa, Dr. Y. Yamanoi, Dr. M. Yoshizawa, Dr. T. Kusakawa,⁺ Prof. M. Fujita
Department of Applied Chemistry, School of Engineering
The University of Tokyo
7-3-1 Hongo, Bunkyo-ku, Tokyo 113-8656 (Japan)
Fax: (+81) 3-5841-7257
E-mail: mfujita@appchem.t.u-tokyo.ac.jp

[⁺] Present address:
Department of Chemistry and Materials Technology
Kyoto Institute of Technology
Sakyo-ku, Kyoto 606-8585 (Japan)

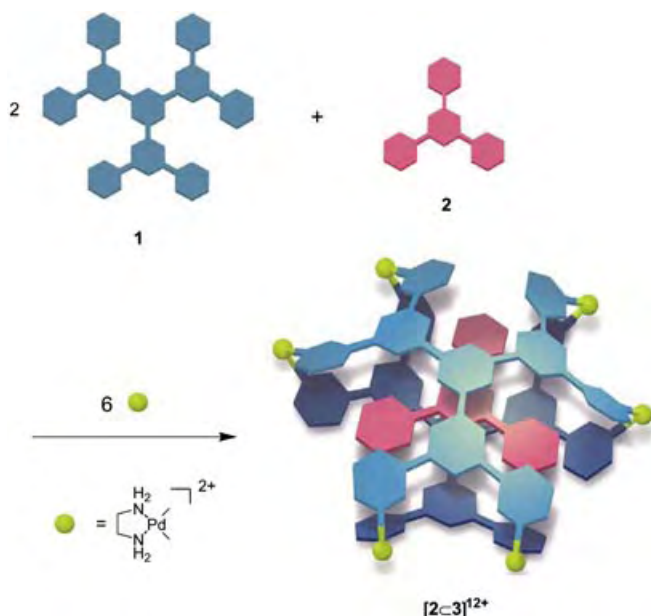
[**] This work was supported by the CREST (Core Research for Evolutional Science and Technology) project of Japan Science and Technology Agency. K.K. thanks the JSPS fellowship for Japanese Young Scientists.



Supporting information for this article is available on the WWW under <http://www.angewandte.org> or from the author.



are fully clipped by six $\{(en)Pd\}^{2+}$ units at the rim of the structure (Scheme 1).



Scheme 1. The self-assembly of $[2C3]^{12+}$ complex.

An excess of **2a** (suspension) was treated with **1** (3.5 μmol) and $[(en)Pd(NO_3)_2]$ (15 μmol) in $D_2O:CD_3CN$ (2:1; 0.7 mL) for 2 h at 60 °C. After filtration of non-encapsulated **2a**, a simple 1H NMR spectrum was obtained from the clear solution, which indicated the formation of a single product (Figure 1). The seven signals observed in the aromatic region (H_{a-g}) agree with the D_{3h} structure of **3**¹²⁺. Highly upfield-shifted signals (H_{h-i}), showing a typical phenyl splitting pattern, were assigned to guest **2a** accommodated within the cavity of **3**¹²⁺. The $[2aC3]^{12+}$ structure was strongly supported by NOESY experiment, which showed correlation between H_f of **3**¹²⁺ and H_j of **2a**.^[4]

Cold spray ionization mass spectroscopy (CSI-MS) clearly suggested the formation of $[2aC3]^{12+}$, it showed a series of prominent peaks corresponding to $[2aC3+(NO_3^-)_m+(dmf)_n]^{12-m+}$ ($m=5-9$, $n=0-14$). For example, in 4⁺ and 5⁺ regions, two intense peaks at m/z 872.3 and 729.4 were assigned to $[2aC3+(NO_3^-)_8+(dmf)_2]^{4+}$ and $[2aC3+(NO_3^-)_7+(dmf)_5]^{5+}$, respectively (Figure 2).^[5] Note that,

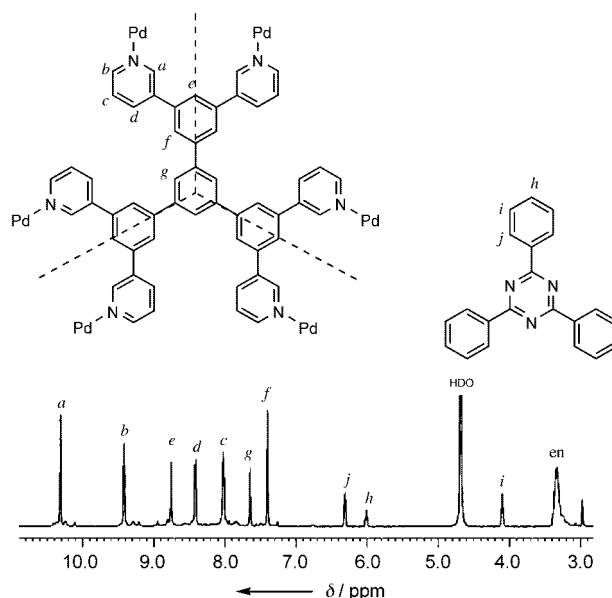


Figure 1. 1H NMR spectrum of $[2aC3]^{12+}$. Assignments of H_a-H_j are given.

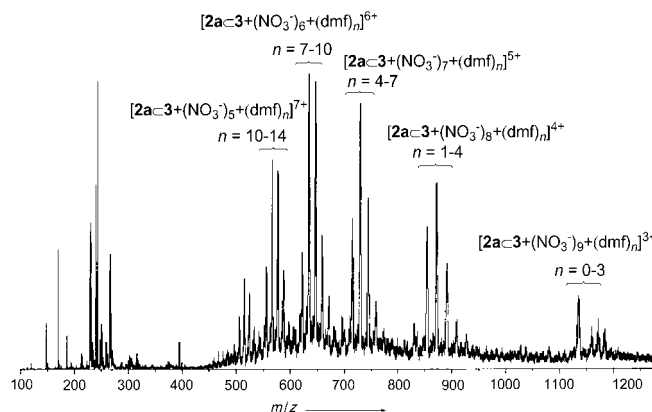


Figure 2. CSI-MS spectrum of $[2aC3]^{12+}$ ($H_2O:CH_3CN:DMF = 12:6:1$, RT).

under CSI-MS conditions, there was little indication for the presence of either guest-free species or fragmented species, which shows the remarkable stability of the $[2aC3]^{12+}$ complex in solution.

When guest **2a** was replaced by 1,3,5-triphenylbenzene (**2b**), single crystals suitable for X-ray analysis were obtained by slow diffusion of THF into an aqueous solution of the complex.^[6] The X-ray analysis revealed the expected structure where two molecules of **1** are clipped by six $\{(en)Pd\}^{2+}$ units allowing the complete wrapping of the large planar guest (Figure 3). The conformation of **1** is not planar but slightly concave. The pyridine ring centers are situated above the face of the core benzene ring at an average separation of 1.2 Å. The 3-pyridyl groups are tilted by 31–42° with respect to adjacent phenyl groups so that they coordinate to Pd^{II} centers with ideal bite angles (89–91°). Thus, host distortion exists not around the Pd^{II} centers but along the large framework of **1**, which suggests that close host–guest packing generates a

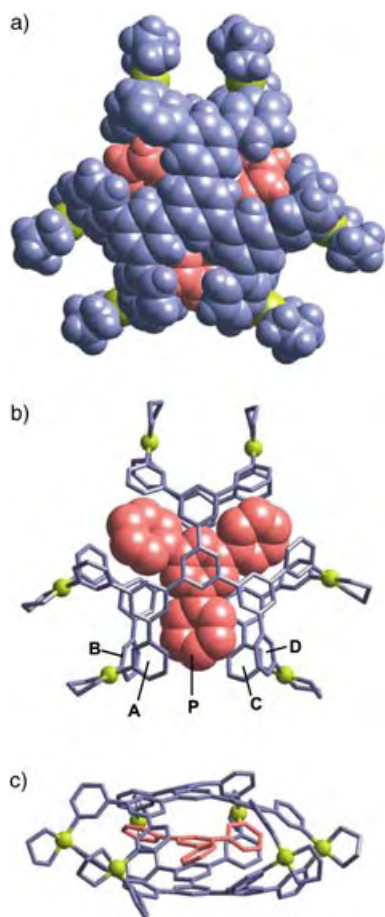
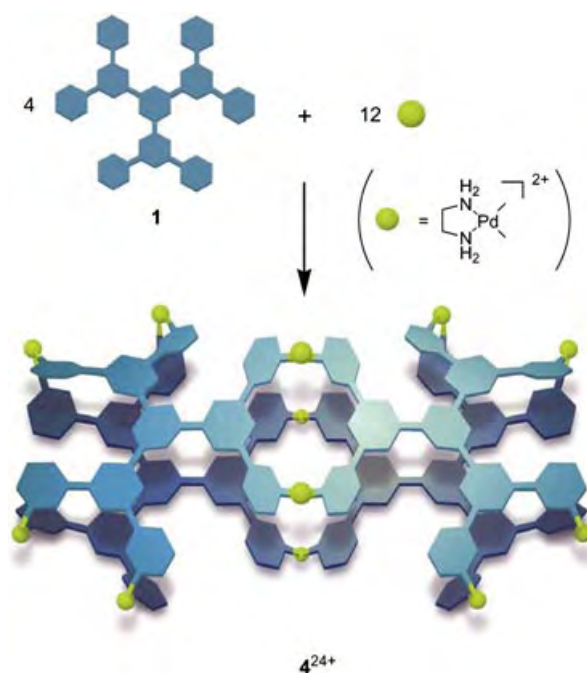


Figure 3. X-ray crystallographic structure of $[2bC3]^{12+}$. a) Space-filling representation (top view), b) top view showing the D_3 orientation of guest **2b**. Around the phenyl group **P**, π - π stacking with pyridine rings **A** and **C**, and CH- π contact with pyridine rings **B** and **D** are observed; c) A side view.

greater distortion. The core benzene ring of **2b** is tightly stacked with the two ligands (3.5 Å van der Waals contact). In the crystal, D_3 symmetry is observed (not D_{3h}), each phenyl group of the guest being tilted by 30–36° allowing efficient π - π and CH- π interactions with four surrounding pyridine rings (Figure 3b). As a result, **2b** is fully wrapped by 3^{12+} .

While $[2C3]^{12+}$ complexes are stabilized by sufficient host-guest interactions, the host framework itself is considerably distorted. In the absence of a guest, therefore, less distorted structure 4^{24+} is formed (Scheme 2). Compound 4^{24+} is a dimer of 3^{12+} generated through the breaking of two Pd-N bonds. The high-yield formation of 4^{24+} was confirmed by NMR spectroscopy and CSI-MS spectrometry. When **1** and $[(en)Pd(NO_3)_2]$ were mixed in a 1:3 ratio without guest molecules, 19 resonance signals, corresponding to half the framework of **1**, appeared in the aromatic region indicating the reduction, after complexation, of the inherent D_{3h} symmetry of **1** into D_{2h} symmetry (Figure 4a). CSI-MS measurement showed the molecular weight of 6562 Da, which is exactly twice as much as $3^{12+}[NO_3^-]_{12}$, supporting the proposed $M_{12}L_4$ dimeric structure 4^{24+} .



Scheme 2. Self-assembly of the dimeric structure, 4^{24+} .

A smaller aromatic guest, triphenylene (**5**), is included in the cavity of 4^{24+} (which is expanded compared to that of 3^{12+}) in a 1:2 ratio upon treating it with a solution of 4^{24+} for 2 h at 60°C. The formation of the $[(5)_2C4]^{24+}$ complex was revealed by NMR spectroscopy with the highly upfield-shifted signals of **5** ($\delta = 6.9$ and 6.0 ppm) and the slightly shifted 19 signals in the aromatic region of the host (Figure 4b). Some minor signals in Figure 4b may be assigned to other host-guest complexes, such as 1:1 complex $[5C4]^{24+}$ or monomer complex $[5C3]^{12+}$. CSI-MS also indicated the required stoichiometry for the $[(5)_2C4]^{24+}$ complex (see Supporting Information).

When guest **2a** was suspended in the solution of the $[(5)_2C4]^{24+}$ complex, guest exchange took place at 60°C within 24 h concomitant with host monomerization.^[7] That is, $[(5)_2C4]^{24+}$ was converted into $[2aC3]^{12+}$, as shown by NMR spectroscopy (Figure 4b–e). Clearly, the self-assembly of hosts 3^{12+} and 4^{24+} is dynamic owing to the labile nature of the Pd-N bond. The host-guest stabilization in $[2aC3]^{12+}$ dominates over the distortion of the host framework, whereas less distorted 4^{24+} is favored when a guest is absent or less efficiently trapped by the host.

In summary we have constructed a large π -conjugated, expanded two-dimensional receptor by self-assembly. Extension of this study could ease the handling of very large π -molecules, such as molecular graphites, which are in general tedious to treat in solution because of their very poor solubility. The chemical and physical properties of such large π -molecules may be restricted within large two-dimensional cavities.

Received: June 4, 2004

Keywords: molecular recognition · palladium · pi interactions · receptors · self-assembly

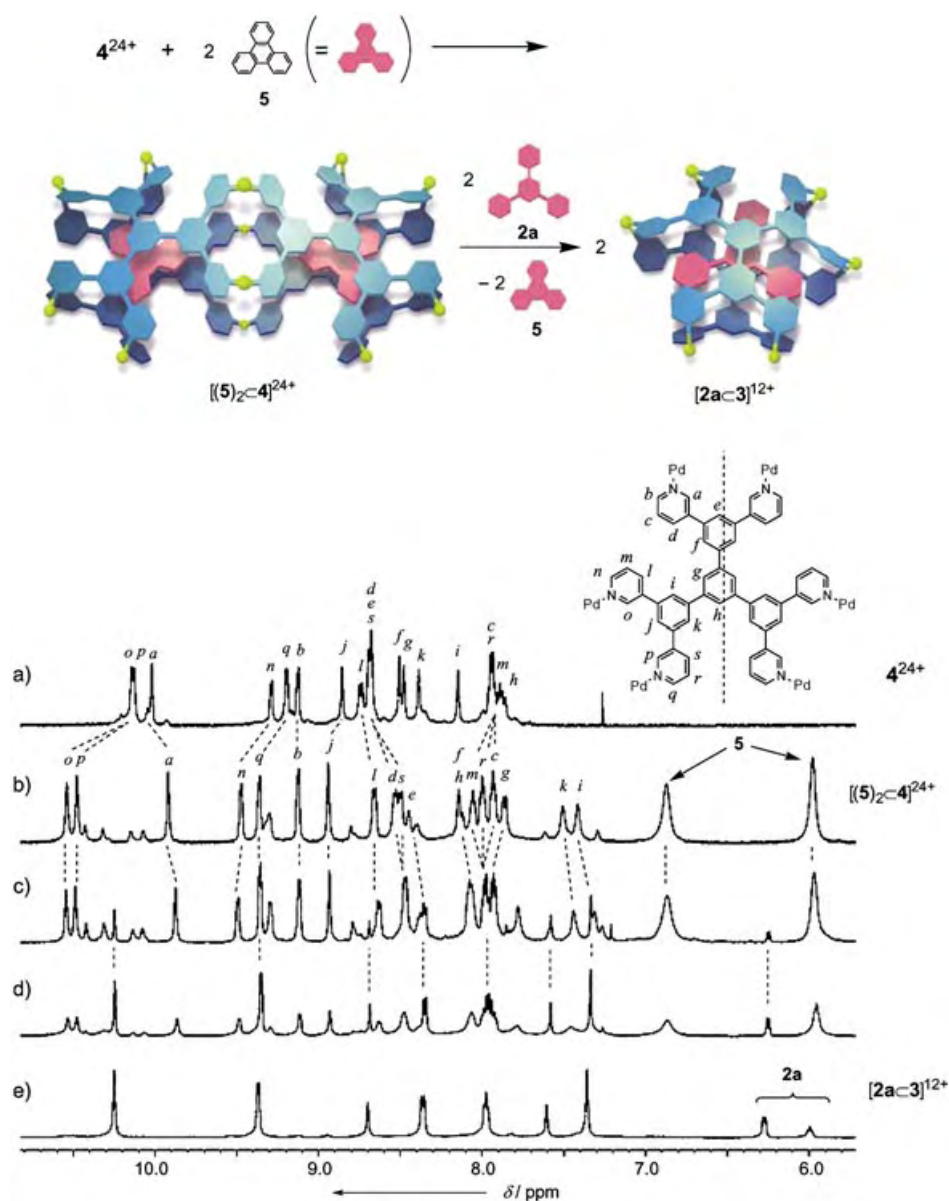


Figure 4. ^1H NMR spectroscopic monitoring of the conversion of $[(5)_2\text{C}4]^{24+}$ into $[2\text{aC}3]^{12+}$. The spectrum of a) dimeric host 4^{24+} , b) $[(5)_2\text{C}4]^{24+}$, c) the spectra upon the addition of **2** (1 equiv) to the $[(5)_2\text{C}4]^{24+}$ solution after 1 h, d) after 24 h, e) The spectrum after filtration, further addition of **2** (1 equiv) to the solution, and stirring the mixture for an additional 2 h.

- [1] For specific guest behaviors in noncovalent receptors see; a) F. Hof, S. L. Craig, C. Nuckolls, J. Rebek, Jr., *Angew. Chem.* **2002**, *114*, 1556–1578; *Angew. Chem. Int. Ed.* **2002**, *41*, 1488–1508; b) M. Yoshizawa, Y. Takeyama, T. Okano, M. Fujita, *J. Am. Chem. Soc.* **2003**, *125*, 3243–3247; c) M. Ziegler, J. L. Brumaghim, K. N. Raymond, *Angew. Chem.* **2000**, *112*, 4285–4287; *Angew. Chem. Int. Ed.* **2000**, *39*, 4119–4121; d) J. M. C. A. Kerckhoffs, F. W. B. van Leeuwen, A. L. Spek, H. Kooijman, M. Crego-Calama, D. N. Reinhoudt, *Angew. Chem.* **2003**, *115*, 5895–5900; *Angew. Chem. Int. Ed.* **2003**, *42*, 5717–5722.
- [2] a) M. Fujita, K. Umemoto, M. Yoshizawa, N. Fujita, T. Kusukawa, K. Biradha, *Chem. Commun.* **2001**, 509–518; b) M. M. Conn, J. Rebek, Jr., *Chem. Rev.* **1997**, *97*, 1647–1668; c) R. W. Saalfrank, E. Uller, B. Demleitner, I. Bernt, *Struct. Bonding (Berlin)* **2000**, *96*, 149–175; d) R. W. Saalfrank, H. Glaser, B. Demleitner, F. Hampel, M. M. Chowdhry, V. Schünemann, A. X. Trautwein, G. B. M. Vaughan, R. Yeh, A. V. Davis, K. N. Raymond, *Chem. Eur. J.* **2002**, *8*, 493–497; e) R. L. Paul, Z. R. Bell, J. C. Jeffery, J. A. McCleverty, M. D. Ward, *Proc. Natl. Acad. Sci. USA* **2002**, *99*, 4883–4888.
- [3] a) K. Kumazawa, K. Biradha, T. Kusukawa, T. Okano, M. Fujita, *Angew. Chem.* **2003**, *115*, 4039–4043; *Angew. Chem. Int. Ed.* **2003**, *42*, 3909–3913; b) R. D. Sommer, A. L. Rheingold, A. J. Goshe, B. Bosnich, *J. Am. Chem. Soc.* **2001**, *123*, 3940–3952; c) S.-S. Sun, A. Lees, *Chem. Commun.* **2001**, 103–104.
- [4] In the NOESY spectrum, not only host–guest correlation but also the orientation of the ligand **1** (between H_a and H_e) were assigned, see the Supporting Information.
- [5] K. Yamaguchi, *J. Mass Spectrom.* **2003**, *38*, 473–490.
- [6] Crystal data for $[2\text{bC}3]^{12+}$: $\text{C}_{144}\text{H}_{138}\text{N}_{36}\text{O}_{57}\text{Pd}_6$, $M_r = 3927.85$, crystal dimensions $0.40 \times 0.20 \times 0.20 \text{ mm}^3$, monoclinic, $P2(1)/n$, $a = 20.5995(11)$, $b = 26.3842(15)$, $c = 30.3963(16) \text{ \AA}$, $V = 16340.8(15) \text{ \AA}^3$, $Z = 4$, $\rho_{\text{calcd}} = 1.597 \text{ g cm}^{-3}$, $F(000) = 7951$,

$\lambda(\text{Mo}_{\text{K}\alpha}) = 0.71073 \text{ \AA}$, $T = 173(2) \text{ K}$, 104 788 reflections collected, 37 340 independent reflections observed; 2079 number of parameters; $R_1 = 0.0556$; $wR_2 = 0.1403$. CCDC-238928 (**2b** \subset **3**¹²⁺) contains the supplementary crystallographic data for this paper. These data can be obtained free of charge via www.ccdc.cam.ac.uk/conts/retrieving.html (or from the Cambridge Crystallographic Data Centre, 12, Union Road Cambridge CB2 1EZ, UK; fax: (+44) 1223-336-033; or deposit@ccdc.cam.ac.uk).

- [7] Conformational change in self-assembled frameworks: a) S. Hiraoka, T. Yi, M. Shiro, M. Shionoya, *J. Am. Chem. Soc.* **2002**, *124*, 14 510–14 511; b) S. Tashiro, M. Tominaga, T. Kusukawa, M. Kawano, S. Sakamoto, K. Yamaguchi, M. Fujita, *Angew. Chem.* **2003**, *115*, 3389–3992; *Angew. Chem. Int. Ed.* **2003**, *42*, 3267–3270; c) S. Hiraoka, M. Fujita, *J. Am. Chem. Soc.* **1999**, *121*, 10 239–10 240; d) P. N. W. Baxter, J.-M. Lehn, G. Baum, D. Fenske, *Chem. Eur. J.* **2000**, *6*, 4510–4517; e) D. P. Funeriu, J.-M. Lehn, K. M. Fromm, D. Fenske, *Chem. Eur. J.* **2000**, *6*, 2103–2111.

Single-Molecule Magnets

 $[(\text{Tp})_8(\text{H}_2\text{O})_6\text{Cu}^{\text{II}}_6\text{Fe}^{\text{III}}_8(\text{CN})_{24}]^{4+}$: A Cyanide-Bridged Face-Centered-Cubic Cluster with Single-Molecule-Magnet Behavior**

Shi Wang, Jing-Lin Zuo,* Hong-Cai Zhou,*
Hye Jin Choi, Yanxiong Ke, Jeffrey R. Long, and Xiao-Zeng You*

In the past decade, an increasing number of molecular clusters have been shown to exhibit magnetic bistability. These

species, called single-molecule magnets (SMMs), have gained considerable attention because they retain information in a single molecule rather than in a magnetic particle or array of particles^[1] and can potentially be used in quantum computers.^[2] Furthermore, understanding the magnetic properties of these molecules is important to help bridge the gap between the quantum and classical understanding of magnetism.^[3] The most thoroughly studied SMMs are $[\text{Mn}_{12}\text{O}_{12}(\text{CH}_3\text{CO}_2)_{16}(\text{H}_2\text{O})_4]$ and its derivatives,^[4] but there are a number of other clusters containing Fe^{III} ,^[5] V^{III} ,^[6] Co^{II} ,^[7] or Ni^{II} ^[8] ions that have been reported to be SMMs. These species are all homometallic systems in which magnetic exchange interactions occur through bridging oxygen atoms.

Important to the future of the field of SMMs is the development of new synthetic schemes that can yield clusters with a large spin and/or anisotropy. Metal–cyanide cluster systems offer an advantage for achieving such control, through the substitution of various metal ions into a given structure type. Moreover, the nature of the magnetic exchange coupling between different metal ions in the resulting cluster is readily predicted.^[9] One approach to synthesizing high-nuclearity metal–cyanide clusters employs multidentate capping ligands to inhibit growth of an extended solid and direct the structure of the product. Many clusters have been prepared by this method,^[10–12] including the face-centered-cubic species $[(\text{Me}_3\text{tacn})_8\text{Cr}_8\text{Ni}_6(\text{CN})_{24}]^{12+}$ ($\text{Me}_3\text{tacn} = N,N,N'$ -trimethyl-1,4,7-triazacyclononane)^[11b] and $[(\text{tach})_8(\text{H}_2\text{O})_6\text{Cu}_6\text{Co}_8(\text{CN})_{24}\cdot\text{THF}]^{12+}$ ($\text{tach} = 1,3,5$ -triaminocyclohexane).^[11d] However, as far as we know, there are only a very few cyanide-bridged SMMs,^[13] and none of the established SMMs exhibit cubic symmetry.

In an effort to extend this chemistry, we have chosen to employ the precursor compound $(\text{Bu}_4\text{N})[(\text{Tp})\text{Fe}(\text{CN})_3]$ (**1**; $\text{Tp}^- = \text{hydrotris}(\text{pyrazolyl})\text{borate}$), featuring a low-spin Fe^{III} center octahedrally coordinated by three CN^- groups and the tridentate ligand Tp^- . This monoanionic complex has also been utilized by Julve and co-workers as the tetraphenylphosphonium salt.^[14] Tp^- is a classical scorptonate ligand with a C_3 axis, and in contrast to neutral capping ligands, such as Me_3tacn and tach , is negatively charged which should help alleviate the build-up of excessive positive charge in clusters. Thus, $[(\text{Tp})\text{Fe}(\text{CN})_3]^-$ is anticipated to direct the formation of new cyanide-bridged compounds with interesting structures and magnetic properties. Indeed, we have recently reported its use in the preparation of $[(\text{Tp})_2\text{Fe}_2(\text{CN})_6\text{Cu}(\text{CH}_3\text{OH})\cdot 2\text{CH}_3\text{OH}]_n$, a single-chain magnet with a blocking temperature of approximately 6 K.^[15] Herein, we disclose its use in the synthesis of $[(\text{Tp})_8(\text{H}_2\text{O})_6\text{Cu}^{\text{II}}_6\text{Fe}^{\text{III}}_8(\text{CN})_{24}]^{4+}$, a face-centered-cubic cluster exhibiting SMM-type behavior.

The compound $[(\text{Tp})_8(\text{H}_2\text{O})_6\text{Cu}_6\text{Fe}_8(\text{CN})_{24}](\text{ClO}_4)_4\cdot 12\text{H}_2\text{O}\cdot 2\text{Et}_2\text{O}$ (**2**) crystallizes in space group *Immm*,^[16] with the well-isolated $[(\text{Tp})_8(\text{H}_2\text{O})_6\text{Cu}_6\text{Fe}_8(\text{CN})_{24}]^{4+}$ molecules residing on special positions of *mmm* site symmetry. As shown in Figure 1, the clusters adopt a face-centered-cubic geometry, in which eight Tp^- -capped Fe^{III} ions are arranged in a cube and linked through cyanide to six Cu^{II} ions located just above the center of each cube face. Here, each octahedral $[(\text{Tp})\text{Fe}(\text{CN})_3]^-$ unit uses the three cyanide groups to connect with three Cu^{II} ions, which are further ligated by water to give

[*] Dr. S. Wang, Prof. Dr. J.-L. Zuo, Prof. X.-Z. You
Coordination Chemistry Institute
State Key Laboratory of Coordination Chemistry
Nanjing University
Nanjing 210093 (China)
Fax: (+86) 25-8331-7761
E-mail: zuojl@nju.edu.cn
xyz@nju.edu.cn

Prof. Dr. H.-C. Zhou, Dr. Y. Ke
Department of Chemistry and Biochemistry
Miami University
Oxford, Ohio 45056-1465 (USA)
Fax: (+1) 513-529-8091
E-mail: zhohu@muohio.edu

Dr. H. J. Choi, Prof. Dr. J. R. Long
Department of Chemistry
University of California
Berkeley, CA 94720-1460 (USA)

[**] This work was supported by The Major State Basic Research Development Program (Grant No. G2000077500), the National Natural Science Foundation of China, and the US National Science Foundation (Grant No. CHE-0072691). H.C.Z. thanks the Research Corporation for a Research Innovation Award. The X-ray diffractometer was supported by NSF grant EAR-0003201. We thank Prof. Yi-Zhi Li and Dr. You Song for useful discussions and experimental assistance. $\text{Tp}^- = \text{hydrotris}(\text{pyrazolyl})\text{borate}$.

Supporting information for this article is available on the WWW under <http://www.angewandte.org> or from the author.

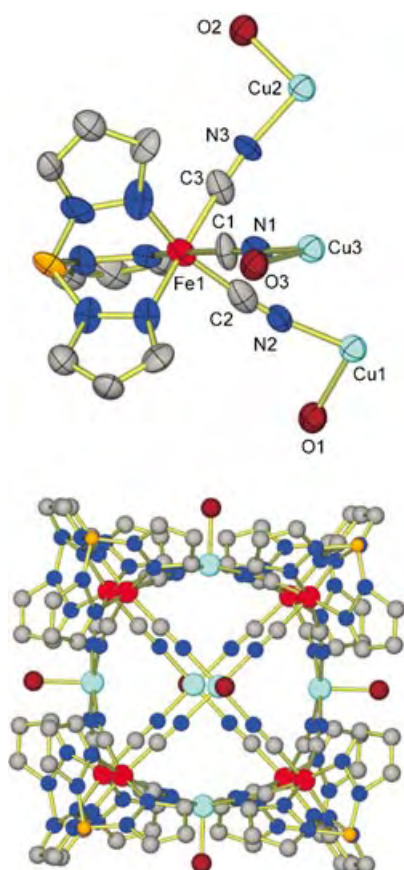


Figure 1. Structure of the face-centered-cubic cationic cluster in **2**. Top: repeat unit, thermal ellipsoids are set at 50% probability. Bottom: red Fe, turquoise Cu, orange B, gray C, blue N, dark red O; hydrogen atoms have been omitted for clarity. Selected bond lengths [Å] and angles [°]: Fe1–C1 1.879(7), Fe1–C2 1.925(7), Fe1–C3 1.937(10), Cu1–N2 1.955(6), Cu2–N3 1.971(6), Cu3–N1 1.972(5), Cu1–O1 2.146(9), Cu2–O2 2.224(10), Cu3–O3 2.108(9); Fe1–C1–N1 173.6(6), Fe1–C2–N2 174.2(6), Fe1–C3–N3 174.6(7), Cu1–N2–C2 177.6(6), Cu2–N3–C3 171.3(6), Cu3–N1–C1 172.6(6), O1–Cu1–N2 99.59(17), O2–Cu2–N3 92.74(17), O3–Cu3–N1 97.68(15).

a square pyramidal $\{\text{Cu}(\text{NC})_4(\text{H}_2\text{O})\}$ coordination sphere. The Fe–C bond lengths (1.879(7)–1.937(10) Å) are in good agreement with those observed previously in related compounds.^[14,15] The Cu–N bonds range from 1.955(6) to 1.972(5) Å, and the Cu–O bonds vary from 2.108(9) to 2.224(10) Å. The O–Cu–N bond angles are 92.7(2)–99.6(2)°. All of the cyanide bridges deviate slightly from strict linearity, as reflected in the Fe–C–N and Cu–N–C angles, which are distributed within the range 171.3(6)–177.6(6)°. The $\text{C}\equiv\text{N}$ stretching region in the IR spectrum of **2** is consistent with the presence of only bridging cyanide ligands (a peak of medium intensity at 2176 cm^{-1}) and the high symmetry of the structure. In all, the cluster closely approaches cubic (O_h) symmetry, with Fe···Fe cube edge distances in the range 6.827–6.938 Å and crystallographically imposed Fe···Fe angles of 90°.

Importantly, the Cu_6Fe_8 cluster represents the first structurally characterized example of a face-centered-cubic cluster in which both metal sites are occupied by paramagnetic ions. Magnetic measurements were therefore per-

formed on a sample of pulverized single crystals of **2** in the temperature range of 1.8–300 K. The variation of $\chi_M T$ with temperature is plotted in Figure 2. At room temperature its value is 5.77 emu K mol^{-1} , somewhat above the spin-only

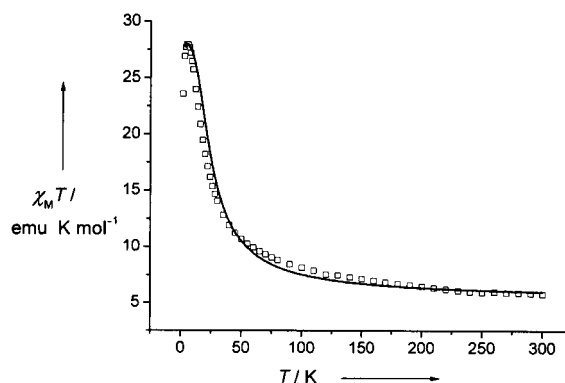


Figure 2. Temperature dependence of $\chi_M T$ for compound **2**, as measured in an applied DC field of 2000 G. The solid line corresponds to a simulation of the data with $J = 15 \text{ cm}^{-1}$, $g = 2.00$, and temperature-independent paramagnetism (TIP) = 0.00070 emu mol^{-1} .

value of 5.25 emu K mol^{-1} expected for eight low-spin Fe^{III} ($S = 1/2$) and six Cu^{II} ($S = 1/2$) ions in the absence of any exchange coupling. With decreasing temperature, $\chi_M T$ increases, reaching a maximum of 27.94 emu K mol^{-1} at approximately 5 K, after which point it decreases to 23.57 emu K mol^{-1} at 1.8 K. This magnetic behavior is indicative of the expected ferromagnetic interactions between the orthogonal spin orbitals of the Fe^{III} and Cu^{II} ions,^[9] resulting in an $S = 7$ ground state. This conclusion is confirmed by the field dependence of the magnetization of **2** at 1.8 K, which saturates at a value of $M_S = 13.78 N\mu_B$ (see the Supporting Information). The sudden decrease in $\chi_M T$ below 5 K is attributed to the presence of zero-field splitting, the effects of which are also discernible in the magnetization data shown in Figure 3. The $\chi_M T$ data above 5 K were simulated employing

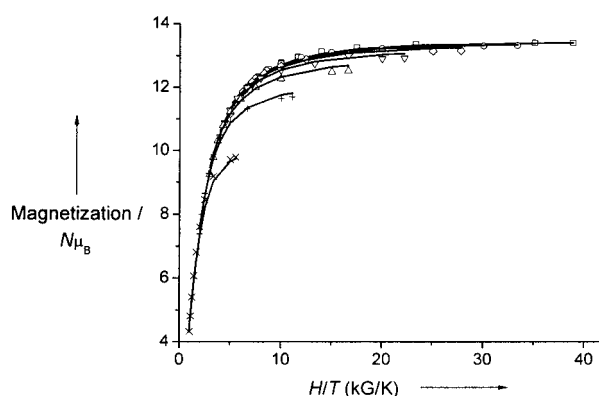


Figure 3. Plot of reduced magnetization, $M/N\mu_B$ (N is Avogadro's number and μ_B is Bohr magneton) versus H/T for **2**. Data were measured in the 1.8–10 K range and at seven magnetic fields: (x) 10.0, (+) 20.0, (Δ) 30.0, (∇) 40.0, (\diamond) 50.0, (\circ) 60.0, and (\square) 70.0 kG. The solid lines resulted from least-squares fitting of the data in the 1.8–10 K range; see text for fitting parameters.

MAGPAK^[17] and an exchange Hamiltonian of the form given in Equation (1).

$$\begin{aligned} \hat{H} = & -2J[\hat{S}_{\text{Fe1}} \cdot (\hat{S}_{\text{Cu1}} + \hat{S}_{\text{Cu2}} + \hat{S}_{\text{Cu3}}) + \hat{S}_{\text{Fe2}} \cdot (\hat{S}_{\text{Cu1}} + \hat{S}_{\text{Cu3}} + \hat{S}_{\text{Cu4}}) + \\ & \hat{S}_{\text{Fe3}} \cdot (\hat{S}_{\text{Cu1}} + \hat{S}_{\text{Cu4}} + \hat{S}_{\text{Cu5}}) + \hat{S}_{\text{Fe4}} \cdot (\hat{S}_{\text{Cu1}} + \hat{S}_{\text{Cu2}} + \hat{S}_{\text{Cu5}}) + \\ & \hat{S}_{\text{Fe5}} \cdot (\hat{S}_{\text{Cu6}} + \hat{S}_{\text{Cu2}} + \hat{S}_{\text{Cu3}}) + \hat{S}_{\text{Fe6}} \cdot (\hat{S}_{\text{Cu6}} + \hat{S}_{\text{Cu3}} + \hat{S}_{\text{Cu4}}) + \\ & \hat{S}_{\text{Fe7}} \cdot (\hat{S}_{\text{Cu6}} + \hat{S}_{\text{Cu4}} + \hat{S}_{\text{Cu5}}) + \hat{S}_{\text{Fe8}} \cdot (\hat{S}_{\text{Cu6}} + \hat{S}_{\text{Cu2}} + \hat{S}_{\text{Cu5}})] \end{aligned} \quad (1)$$

The best simulation was obtained with $J = +15 \text{ cm}^{-1}$, which indicates significantly stronger coupling than previously observed for complexes containing more bent Fe^{III} -CN- Cu^{II} bridges.^[18]

To assess the zero-field splitting associated with the $S = 7$ ground state, magnetization data were collected on compound **2** at a variety of fields in the temperature range 1.8–10 K (see Figure 3). The seven isofield data sets were fitted using ANISOFIT^[11c] to give zero-field splitting parameters of $D = -0.16 \text{ cm}^{-1}$ and $E = 0.0055 \text{ cm}^{-1}$ with $g = 1.93$. Thus, despite the near cubic symmetry of the cluster, the presence of orbitally degenerate low-spin Fe^{III} centers enables the development of significant axial magnetic anisotropy. Indeed, if the sign and magnitude of D obtained from the fit are correct, then the Cu_6Fe_8 cluster should behave as an SMM with a spin reversal barrier of $U = S^2 |D| = 7.8 \text{ cm}^{-1}$.

One of the defining characteristics of an SMM is the observation of a frequency-dependent out-of-phase AC magnetic susceptibility (χ_M'') signal. To determine whether the slow magnetization relaxation behavior occurs in **2**, AC magnetic measurements were performed in the temperature range of 1.8–6 K (Figure 4). Although no maximum was

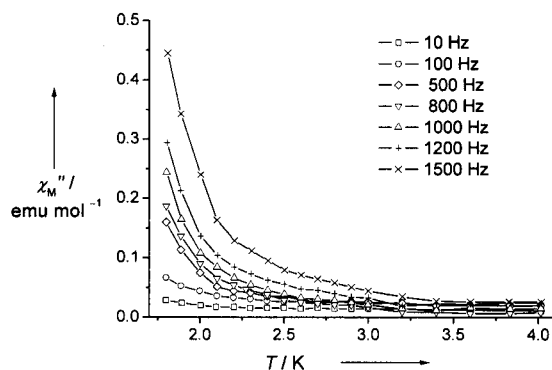


Figure 4. Temperature dependence of the out-of-phase component of the AC susceptibility for **2** in zero applied static field and with a 5 G field oscillating at frequencies between of 10 and 1500 Hz. The lines are to guide the eye.

observed down to 1.8 K, frequency-dependent χ_M'' signals were observed below 3 K, which indicates the superparamagnet-like slow relaxation of an SMM. The results are similar to those observed for $[(\text{tmphen})\text{Mn}_5(\text{CN})_{12}]$ (tmphen = 3,4,7,8-tetramethyl-1,10-phenanthroline),^[13b] and place an upper bound of 20 cm^{-1} (assuming an attempt frequency of $1/\tau_0 < 10^{10} \text{ Hz}$) on the effective spin-reversal barrier for the Cu_6Fe_8 cluster.

In summary, the use of Tp^- as a capping ligand has permitted isolation of a face-centered-cubic cluster, with a

well-isolated $S = 7$ ground state. Despite its cubic symmetry, the molecule possesses substantial axial magnetic anisotropy ($D = -0.16 \text{ cm}^{-1}$), which leads to single-molecule-magnet behavior.

Experimental Section

1: Prepared by a modified literature method.^[14] **2:** Solid $\text{Cu}(\text{ClO}_4)_2 \cdot 6\text{H}_2\text{O}$ (37 mg, 0.13 mmol) was added to a solution of $(\text{Bu}_4\text{N})[(\text{Tp})\text{Fe}(\text{CN})_3]$ (59 mg, 0.10 mmol) in acetonitrile and ethanol (5 mL; mole ratio = 2:1). The solution was filtered. Brown block-shaped crystals of **2** were obtained in 85% yield by diffusing diethyl ether vapor into the filtrate. IR: $\nu = 2176 \text{ cm}^{-1} (\nu_{\text{CN}})$; elemental analysis (%) calcd for $\text{C}_{96}\text{H}_{116}\text{B}_8\text{Cl}_4\text{Cu}_6\text{Fe}_8\text{N}_{72}\text{O}_{34}$: C 29.73, H 3.01, N 26.00; found: C 30.02, H 2.73, N 26.24.

Received: August 3, 2004

Keywords: cluster compounds · cyanides · iron · magnetic properties · single-molecule magnets

- [1] E. D. Dahlberg, J.-G. Zhu, *Phys. Today* **1995**, 48, 34.
- [2] a) G. P. Berman, G. D. Doolen, D. D. Holm, V. I. Tsifrinovich, *Phys. Lett. A* **1994**, 193, 444; b) D. A. Garanin, E. M. Chudnovsky, *Phys. Rev. B* **1997**, 56, 11 102.
- [3] a) J. R. Friedman, M. P. Sarachik, J. Tejada, R. Ziolo, *Phys. Rev. Lett.* **1996**, 76, 3830; b) W. Wernsdorfer, R. Sessoli, *Science* **1999**, 284, 133.
- [4] a) G. Christou, D. Gatteschi, D. N. Hendrickson, R. Sessoli, *MRS Bull.* **2000**, 25, 66; b) D. Gatteschi, R. Sessoli, *Angew. Chem.* **2003**, 115, 278; *Angew. Chem. Int. Ed.* **2003**, 42, 268.
- [5] a) A. L. Barra, P. Debrunner, D. Gatteschi, C. E. Schultz, R. Sessoli, *Europhys. Lett.* **1996**, 35, 133; b) A. L. Barra, P. Debrunner, R. Sessoli, *Chem. Eur. J.* **2000**, 6, 1608.
- [6] S. L. Castro, Z. M. Sun, C. M. Grant, J. C. Bollinger, D. N. Hendrickson, G. Christou, *J. Am. Chem. Soc.* **1998**, 120, 2365.
- [7] a) E. C. Yang, D. N. Hendrickson, W. Wernsdorfer, M. Nakano, L. N. Zakharov, R. D. Sommer, A. L. Rheingold, M. Ledezma-gairaud, G. Christou, *J. Appl. Phys.* **2002**, 91, 7382; b) M. Murrie, S. J. Teat, H. Stöckli-Evans, H. U. Güdel, *Angew. Chem.* **2003**, 115, 4801; *Angew. Chem. Int. Ed.* **2003**, 42, 4653.
- [8] a) S. T. Ochsenbein, M. Murrie, E. Rusanov, H. Stöckli-Evans, C. Sekine, H. U. Güdel, *Inorg. Chem.* **2002**, 41, 5133; b) H. Andres, R. Basler, A. J. Blake, C. Cadiou, G. Chaboussant, C. M. Grant, H. U. Güdel, M. Murrie, S. Parsons, C. Paulsen, F. Semadini, V. Villar, W. Wernsdorfer, R. E. P. Winpenny, *Chem. Eur. J.* **2002**, 8, 4867.
- [9] H. Weihe, H. U. Güdel, *Comments Inorg. Chem.* **2000**, 22, 75.
- [10] a) T. Mallah, C. Auberger, M. Verdager, P. Veillet, *J. Chem. Soc. Chem. Commun.* **1995**, 61; b) V. Marvaud, C. Decroix, A. Scullier, C. Guyard-Duhayon, J. Vaissermann, F. Gonnet, M. Verdager, *Chem. Eur. J.* **2003**, 9, 1677.
- [11] a) J. L. Heinrich, P. A. Berseth, J. R. Long, *Chem. Commun.* **1998**, 1231; b) P. A. Berseth, J. J. Sokol, M. P. Shores, J. L. Heinrich, J. R. Long, *J. Am. Chem. Soc.* **2000**, 122, 9655; c) M. P. Shores, J. J. Sokol, J. R. Long, *J. Am. Chem. Soc.* **2002**, 124, 2279; d) J. Y. Yang, M. P. Shores, J. J. Sokol, J. R. Long, *Inorg. Chem.* **2003**, 42, 1403.
- [12] a) K. K. Klausmeyer, T. B. Rauchfuss, S. R. Wilson, *Angew. Chem.* **1998**, 110, 1808; *Angew. Chem. Int. Ed.* **1998**, 37, 1694; b) E. J. Schelter, A. V. Provirin, W. M. Reiff, K. R. Dunbar, *Angew. Chem.* **2004**, 116, 5020; *Angew. Chem. Int. Ed.* **2004**, 43, 4912.
- [13] a) J. J. Sokol, A. G. Hee, J. R. Long, *J. Am. Chem. Soc.* **2002**, 124, 7656; b) C. P. Berlinguette, D. Vaughn, C. Cañada-Vilalta, J. R.

- Galán-Mascarós, K. R. Dunbar, *Angew. Chem.* **2003**, *115*, 1561; *Angew. Chem. Int. Ed.* **2003**, *42*, 1523; c) H. J. Choi, J. J. Sokol, J. R. Long, *Inorg. Chem.* **2004**, *43*, 1606.
- [14] R. Lescouëzec, J. Vaissermann, F. Lloret, M. Julve, M. Verdaguer, *Inorg. Chem.* **2002**, *41*, 5943.
- [15] S. Wang, J.-L. Zuo, S. Gao, Y. Song, H.-C. Zhou, Y.-Z. Zhang, X.-Z. You, *J. Am. Chem. Soc.* **2004**, *126*, 8900.
- [16] Crystallographic analysis: **2** ($\text{C}_{104}\text{H}_{136}\text{B}_8\text{Cl}_4\text{Cu}_6\text{Fe}_8\text{N}_{72}\text{O}_{36}$): $M_r = 4027.17$, $T = 213$ K, orthorhombic, space group *Immm*, $a = 16.2010(16)$, $b = 35.317(4)$, $c = 17.1566(17)$ Å, $V = 9816.5(18)$ Å³, $Z = 2$, $\rho_{\text{calcd}} = 1.362$ g cm⁻³, $R_1 = 0.0621$, $wR_2 = 0.1363$ ($I > 2\sigma(I)$) for 23 664 data (3882 independent), 470 parameters, and 15 restraints. Data were collected on a Bruker Apex CCD diffractometer. Absorption corrections were applied for **2** using SADABS supplied by Bruker. The structure was solved by direct methods and refined by full-matrix least-squares methods using SHELXTL-97. In the structure of **2**, all the atoms of the Tp ligands and some hydrogen atoms are disordered. CCDC-246475 (**2**) contains the supplementary crystallographic data for this paper. These data can be obtained free of charge via www.ccdc.cam.ac.uk/conts/retrieving.html (or from the Cambridge Crystallographic Data Centre, 12 Union Road, Cambridge CB2 1EZ, UK; fax: (+44)1223-336-033; or deposit@ccdc.cam.ac.uk).
- [17] J. J. Borrás-Almenar, J. M. Clemente-Juan, E. Coronado, B. S. Tsukerblat, *J. Comput. Chem.* **2001**, *22*, 985.
- [18] a) H.-Z. Kou, D.-Z. Liao, P. Cheng, Z.-H. Jiang, S.-P. Yan, G.-L. Wang, X.-K. Yao, H.-G. Wang, *J. Chem. Soc. Dalton Trans.* **1997**, 1503; b) M. Salah El Fallah, J. Ribas, X. Solans, M. Font-Bardia, *J. Chem. Soc. Dalton Trans.* **2001**, 247; c) H. Oshio, M. Yamamoto, T. Ito, *Inorg. Chem.* **2002**, *41*, 5817; d) M. K. Saha, F. Lloret, I. Bernal, *Inorg. Chem.* **2004**, *43*, 1969.

usually bear multiple surface organic ligands, which are utilized not only for stabilizing the cluster core but also for the construction of conjugates with chemical and biochemical reagents.^[2,3] Although a variety of ligands with covalently appended functionalities have been designed to date,^[3] there have been few examples of the host–guest-type conjugation involving guest penetration into the surface organic shell. Herein we show that simple aromatic groups at the cluster surface are capable of trapping organic cations in an intercalative fashion, allowing guest penetration close to the cluster core without direct bonding interactions. We also report the notable effects of this guest penetration on the cluster photoluminescence.

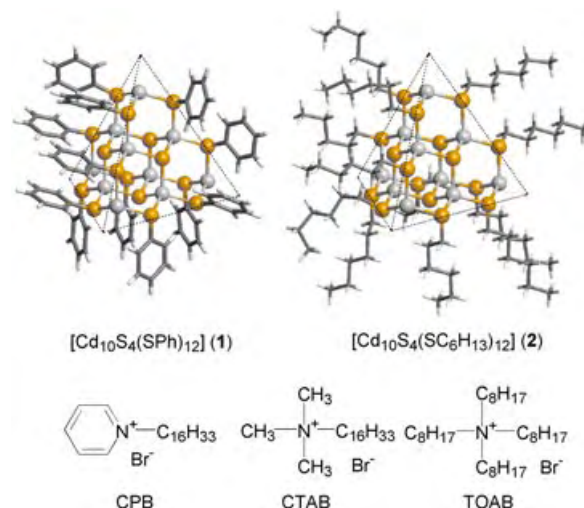
Aryl- and alkyl-capped molecular clusters of cadmium chalcogenides have been of interest as models and precursors of colloidal particles.^[4,5] The clusters we use in this case are neutral $[\text{Cd}_{10}\text{S}_4(\text{SPh})_{12}]$ (**1**) and $[\text{Cd}_{10}\text{S}_4(\text{SC}_6\text{H}_{13})_{12}]$ (**2**) bearing a truncated tetrahedral $[\text{Cd}_{10}\text{S}_{16}]$ core and twelve surface substituents.^[5] The four unsaturated cadmium atoms at the apexes serve as coordination sites for donating ligands. Accordingly, these clusters easily formed ionic complexes with organic bromide salts by coordination of bromide anions to the apex cadmium atoms.^[5b] When the cation moiety has a long alkyl chain, such as cetyltrimethylammonium (CTA⁺), 1-cetylpyridinium (CP⁺), or tetraoctylammonium (TOA⁺), the

Luminescent Cluster Compounds

Surface-Cap-Mediated Host–Guest Chemistry of Semiconductor CdS: Intercalative Cation Accumulation around a Phenyl-Capped CdS Cluster and Its Notable Effects on the Cluster Photoluminescence**

Takayuki Hiratani and Katsuaki Konishi*

Semiconductor nanoclusters of cadmium chalcogenides have attracted continuing attention in relation to their unique optical and electronic properties.^[1] These small clusters



resulting complexes were very soluble in chloroform, in contrast to the original clusters (**1**, **2**).

¹H NMR spectroscopic studies of the phenyl-capped cluster **1** upon complexation with the bromide salts of CTA⁺ and CP⁺ (CTAB and CPB, respectively) indicated the close cation proximity to the surface phenyl groups. For example, when CTAB (9.2 mM) was mixed with **1** (2.3 mM) in CDCl₃, clear upfield shifts were observed for the signals arising from the *N*-CH₃ ($\delta = 3.48 \rightarrow \delta = 3.04$ ppm) and *N*-CH₂ ($\delta = 3.57 \rightarrow \delta = 3.17$ ppm) of the cation (Figure 1a: 1, 3). Similar upfield shifts were observed when CPB was used in place of CTAB. These upfield shifts indicate that the cations are bound to **1** in an intercalative fashion (Figure 2), where the cationic center is located in close proximity to the SPh

[*] T. Hiratani, Prof. Dr. K. Konishi
PRESTO
Japan Science and Technology Agency (JST) and
Creative Research Initiative "Sosei" (CRIS) and
Division of Material Science
Graduate School of Environmental Earth Science
Hokkaido University
North 21 West 10, Sapporo 001-0021 (Japan)
Fax: (+81) 11-706-9290
E-mail: konishi@ees.hokudai.ac.jp

[**] This work was partly supported by Nagase Science and Technology Foundation.

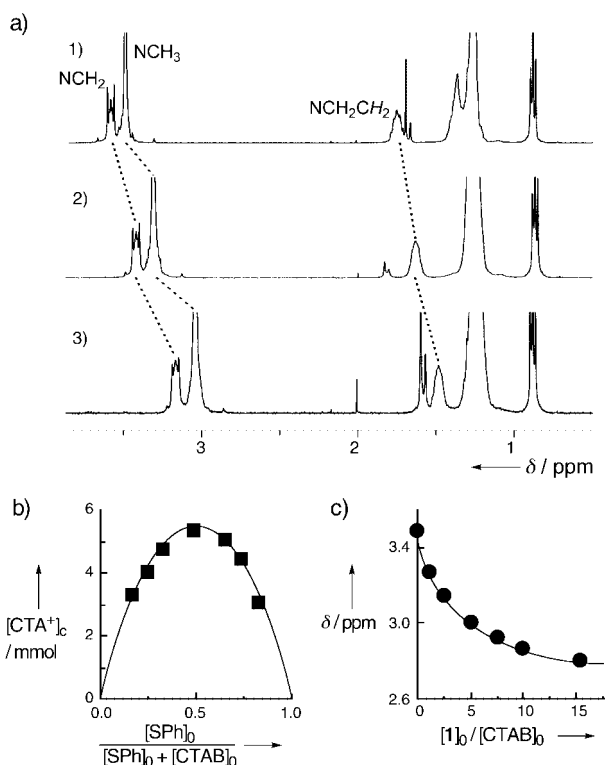


Figure 1. a) ^1H NMR spectra of 1) CTAB (9.2 mM), 2) **1**/CTAB (2.3/46.0 mM), and 3) **1**/CTAB (2.3/9.2 mM) in CDCl_3 at 25 °C; b) Job plots for the intercalative complexation between SPh of **1** and CTAB. Plots of $[\text{complexed CTA}^+]$ versus $[\text{SPh}]_0/([\text{SPh}]_0 + [\text{CTAB}]_0)$ with $[\text{SPh}]_0 + [\text{CTAB}]_0$ kept constant (38 mM); c) ^1H NMR titration of CTAB (4.3 mM) with **1**/TOAB (1:4 molar ratio) in CDCl_3 at 25 °C. Plots of δ values for N- CH_3 protons versus $[\text{1}]_0/[\text{CTAB}]_0$.

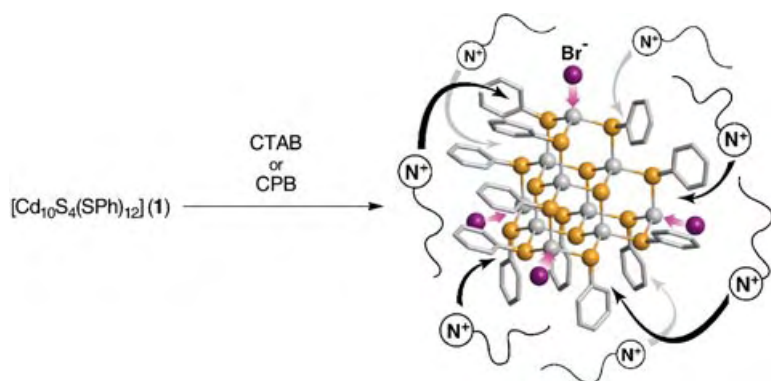


Figure 2. Schematic illustration of the complexation between **1** and CTAB or CPB showing cation intercalation among the surface phenyl groups.

groups and thus near the cluster core, while the C_{16} chain is extended away from the cluster surface.

On the other hand, when sterically hindered TOAB was used for the complexation with **1**, only very small shifts of the signals arising from the cation were observed. Owing to the severe steric bulk around the cationic center, TOA^+ seems reluctant to intercalate into the interstitial space and is therefore located outside the cluster periphery. This “outside-cation” complex still has vacant intercalation sites that can

accommodate small cations. The intercalative binding of CTA^+ and CP^+ towards the preformed **1**/TOAB complex occurred similarly to that towards **1** alone. Job plots for the complexation with CTAB in the presence of TOAB,^[6] where the sum of $[\text{SPh}]_0 (= 12 \times [\text{1}]_0)$ and $[\text{CTAB}]_0$ was kept constant, exhibited a maximum at a $[\text{SPh}]_0:[\text{CTAB}]_0$ ratio of unity (Figure 1 b), indicating the 1:1 stoichiometry of SPh and CTA^+ ions. Likewise, CPB gave a similar Job diagram to show a 1:1 complexation with SPh. Thus, considering twelve SPh groups at the surface of **1**, multiple, up to twelve, cations participate in the complexation with a single cluster molecule. From the NMR spectroscopy titration data (Figure 1 c),^[6] the association constants for the 1:1 complexation were estimated to be 94 M^{-1} for CPB and 70 M^{-1} for CTAB.^[7]

The cation accumulation near the CdS core of **1**, thus observed, is considered to be the results of cation- π interaction with the surface phenyl groups and/or direct cation adsorption on the polar sites of the anionic cluster $[\text{Cd}_{10}\text{Br}_4\text{S}_4(\text{SPh})_{12}]^{4-}$ (e.g., the Br, S sites). The latter has been claimed as a possible driving force in surfactant-stabilized colloid systems,^[8] but seems not dominant in the present case. This assumption was supported from the photoluminescence quenching profiles of **1** and the alkyl-substituted control **2** by using CP^+ ion as the electron acceptor: Upon excitation of the cluster moieties at 360 nm, **1** and **2**, in the presence of TOAB in CHCl_3 , showed trap emissions at 560 and 530 nm, respectively. Both emissions were quenched by the addition of CPB, but the Stern–Volmer plots of the two systems were different. As expected from the intercalative binding of the quencher CP^+ near the cluster core, **1** gave a clear saturation behavior (Figure 3). On the other hand, **2**

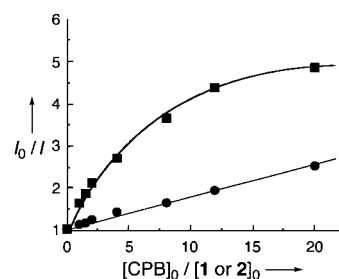


Figure 3. Stern–Volmer plots for the photoluminescence quenching of CdS clusters (**1** (■), **2** (●); $6.7 \mu\text{M}$) by CPB in the presence of TOAB (3.3 mM) in CHCl_3 at 25 °C. The fluorescence intensities (I , $\lambda_{\text{exc}} = 360 \text{ nm}$) were monitored at 560 nm for **1** and 530 nm for **2**.

showed a less efficient luminescence quenching with a linear Stern–Volmer correlation ($r = 0.996$; Figure 3) characteristic of a dynamic process. This situation indicates there exists no particular static interaction leading to the close proximity of the quencher to the cluster-anion moiety of **2**.^[9] Therefore, a π -mediated force associated with the surface phenyl groups is most likely to be responsible for the cation intercalation towards the phenyl-capped cluster **1**.

The photoluminescence changes upon complexation with CTAB were also investigated. In colloidal systems, the addition of tetraalkylammonium salts induces some degree of dynamic quenching.^[10] In contrast, the intercalative binding

of CTA⁺ ions with **1** caused notable luminescence enhancement. For example, when CTAB (2.0 mM) was added to a mixture of **1** and TOAB in CHCl₃ under Ar, the emission intensity was drastically increased with a shift to a longer wavelength (570 nm; Figure 4(b)),^[11] whereas the absorption

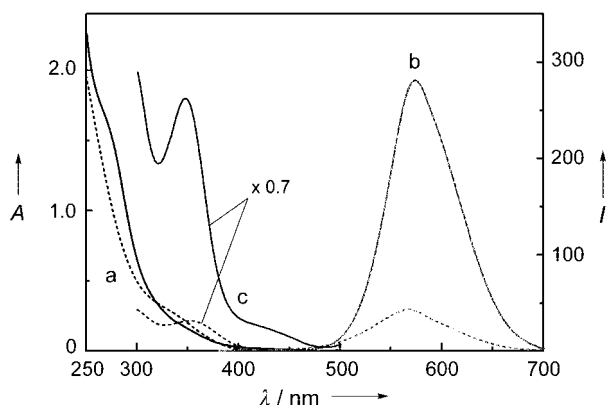


Figure 4. Absorption (a), photoluminescence ($\lambda_{\text{em}} = 360$ nm; (b)), and excitation ($\lambda_{\text{ex}} = 570$ nm (c)) spectra of **1**/TOAB (6.7/26.8 μm) before (dotted line) and after (solid line) the addition of CTAB (2.0 mM) in degassed CHCl₃ at 25 °C.

spectrum showed a small change (Figure 4a). Excitation spectra before and after the addition of CTAB were similar in shape with a maximum at approximately 360 nm (Figure 4c), which indicates that the strong luminescence of the CTAB complex arises from the cluster core. On the other hand, alkyl-substituted **2** under similar conditions showed a small decrease of the luminescence intensity, which is similar to that reported for colloidal system.^[10] Thus, the large luminescence enhancement with **1** is not due to simple salt effects, but is caused by the intercalative cation binding near the cluster core.

The luminescence enhancement reported above appears to be correlated to the structural changes of the phenyl-group shell surrounding the cluster core upon intercalation. In connection with this, in the ¹H NMR spectrum the SPh signals showed a significant change upon cation intercalation: The nonintercalative complex **1**/TOAB showed broad and complicated pattern of signals at $\delta = 6.0$ –7.8 ppm (Figure 5a), which reflects the disordered orientation of the SPh groups arising from S–C bond rotation. On the other hand, upon

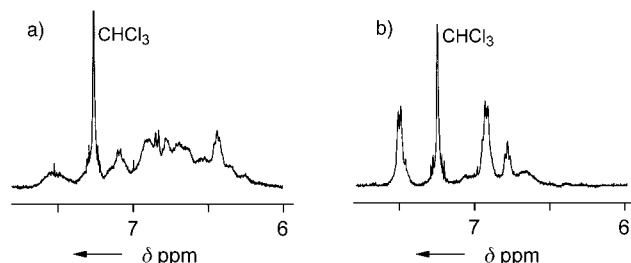


Figure 5. Aromatic region of the ¹H NMR spectra of a) **1** (2.3 mM) and b) **1**/CTAB (2.3/46 mM) in the presence of TOAB (9.2 mM) in CDCl₃ at 25 °C.

addition of 20 equivalents of CTAB to this solution, the SPh signals converged into three major signals assignable to the *ortho*, *meta*, and *para* protons (Figure 5b), which suggests that the cation intercalation restricts the phenyl-ring rotation and so induces a uniform arrangement. Such ordered orientation and/or enhanced conformational rigidity of the surface substituents may suppress the quenching path to the medium by effective core protection and thus increase the luminescence intensity.^[11,12]

In conclusion, we have demonstrated π -interaction mediated cation accumulation around a phenyl-capped CdS cluster and the guest-responsive photoluminescence properties of this cluster. Application to sensing systems by rational tuning of the π -functionalities as well as the sizes and structures of the clusters is worthy of further investigations.

Experimental Section

1: [Cd₁₀S₄(SPh)₁₆](NMe₄)₄^[4b] (1.16 g, 0.35 mmol) was heated under vacuum at 180 °C for 6 h, and the resulting solid was washed with hexane and chloroform to give **1** as a pale-yellow solid (0.87 g, 97 %), which gave satisfactory IR and ¹H NMR spectra. Elemental analysis calcd (%) for C₇₂H₆₀Cd₁₀S₁₆: C 33.75, H 2.36, S 20.02; found: C 33.56, H 2.37, S 19.87; no nitrogen was found.

2: Compound **2** was prepared by the thiolate-exchange reaction of **1** with C₆H₁₃SH in the presence of TOAB. 1-hexanethiol (21 mmol) was added to an MeCN solution of **1** (100 mg, 0.039 mmol/5 mL) containing TOAB (0.16 mmol), and the mixture was stirred at RT for 12 h. The mixture was evaporated to dryness and the residue was washed copiously with MeOH to give **2** as a white solid (81 mg, 78 %), which gave satisfactory IR and ¹H NMR spectra. Elemental analysis calcd (%) for C₇₂H₁₅₆Cd₁₀S₁₆: C 32.52, H 5.91, S 19.29; found C 32.27, H 5.47, S 18.89; no nitrogen was found.

Received: July 5, 2004

Keywords: cadmium · cluster compounds · luminescence · π interactions · semiconductors · supramolecular chemistry

- [1] a) M. Nirmal, L. Brus, *Acc. Chem. Res.* **1999**, 32, 407; b) H. Weller, *Curr. Opin. Colloid Interface Sci.* **1998**, 3, 194; c) A. P. Alivisatos, *Science* **1996**, 271, 933; d) H. Weller, *Angew. Chem.* **1993**, 105, 43; *Angew. Chem. Int. Ed. Engl.* **1993**, 32, 41; e) A. Henglein, *Chem. Rev.* **1989**, 89, 1861.
- [2] a) C. B. Murray, D. J. Norris, M. G. Bawendi, *J. Am. Chem. Soc.* **1993**, 115, 8706; b) A. L. Rogach, A. Kornowski, M. Gao, A. Eychmüller, H. Weller, *J. Phys. Chem. B* **1999**, 103, 3065; c) W. W. Yu, X. Peng, *Angew. Chem.* **2002**, 114, 2474; *Angew. Chem. Int. Ed.* **2002**, 41, 2368; d) O. Schmelz, A. Mews, T. Basche, A. Herrmann, K. Müllen, *Langmuir* **2001**, 17, 2861; e) N. Pradhan, S. Efrima, *J. Am. Chem. Soc.* **2003**, 125, 2050.
- [3] a) W. C. W. Chan, S. Nie, *Science*, **1998**, 281, 2016; c) J. G. C. Veinot, M. Ginzburg, W. J. Pietro, *Chem. Mater.* **1997**, 9, 2117; J. Aldana, Y. A. Wang, X. Peng, *J. Am. Chem. Soc.* **2001**, 123, 8844; d) H. Skaff, M. F. Ilker, E. B. Coughlin, T. Emrick, *J. Am. Chem. Soc.* **2002**, 124, 5729; e) C. Zhang, S. O'Brien, L. Balogh, *J. Phys. Chem. B* **2002**, 106, 10316.
- [4] a) I. G. Dance, A. Choy, M. L. Scudder, *J. Am. Chem. Soc.* **1984**, 106, 6285; b) W. E. Farneth, N. Herron, Y. Wang, *Chem. Mater.* **1992**, 4, 916; c) T. Türk, U. Resch, M. A. Fox, A. Vogler, *J. Phys. Chem.* **1992**, 96, 3818; d) N. Herron, J. C. Calabrese, W. E. Farneth, Y. Wang, *Science* **1993**, 259, 1426; e) T. Vossmeier, G. Reck, L. Katsikas, E. T. K. Haupt, B. Schulz, H. Weller, *Science*

- 1995, 267, 1476; f) V. Soloviev, A. Eichofer, D. Fenske, U. Banin, *J. Am. Chem. Soc.* **2000**, 122, 2673; g) S. L. Cumberland, K. M. Hanif, A. Javier, G. A. Khitrov, F. Strouse, M. W. S. M. Stephen, C. S. Yun, *Chem. Mater.* **2002**, 14, 1576.
- [5] a) W. E. Farneth, N. Herron, Y. Wang, *Chem. Mater.* **1992**, 4, 916; b) R. D. Adams, B. Zhang, C. J. Murphy, L. K. Yeung, *Chem. Commun.* **1999**, 383; c) F. E. Osterloh, D. P. Hewitt, *Chem. Commun.* **2003**, 1700.
- [6] The cluster/CTAB (CPB) mixtures at a low salt concentration gave emulsion-like suspensions in CDCl_3 , so that the titration experiments were carried out in the presence of TOAB since this combination gave a homogeneous mixture at a wide range of concentration ratios.
- [7] The association constants were determined by using a nonlinear curve-fitting method, assuming that each binding site works independently.
- [8] a) J. Kuczynski, J. K. Thomas, *Langmuir* **1985**, 1, 158; b) R. R. Chandler, J. L. Coffey, *J. Phys. Chem.* **1993**, 97, 9767.
- [9] Other weak interactions, such as van der Waals forces also seem not to be dominant. No signs of guest (cation)–cluster close proximity were detected in the ^1H NMR spectra of the **2**/CTAB(CPB) and **1**/dimethylhexadecylamine systems in the presence of TOAB.
- [10] M. Hamity, R. H. Lema, C. A. Suchetti, *J. Photochem. Photobiol. A* **1998**, 115, 163.
- [11] Titration of **1** with CTAB under the conditions given in Figure 4 showed saturation of the emission intensities at $[\text{CTAB}]_0/[\text{1}]_0 \approx 400$. At this molar ratio, it is estimated that, from the NMR-spectroscopy-determined association constant, at most, two of twelve intercalation sites were occupied by the CTA^+ ions, which suggests that steric isolation of the core by the intercalated cations is not a critical factor for the photoluminescence enhancement. When the $[\text{CTAB}]_0/[\text{1}]_0$ ratio was increased over 600, the intensity was inversely decreased probably a result of the reverse-micelle formation of CTAB.
- [12] For an analogous phenyl-capped CdS cluster, increase of the luminescence intensities upon lowering temperature has been reported: N. Herron, A. Suna, Y. Wang, *J. Chem. Soc. Dalton Trans.* **1992**, 2329.

Stereochemical Assignment in Acyclic Lipids Across Long Distance by Circular Dichroism: Absolute Stereochemistry of the Aglycone of Caminoside A**

John B. MacMillan, Roger G. Linington,
Raymond J. Andersen, and Tadeusz F. Molinski*

In memory of D. John Faulkner

The glycolipid caminoside A (**1**, Figure 1), isolated from the marine sponge *Caminus sphareoconia* from Dominica, was shown to be an inhibitor of a type III bacterial secretory system.^[1] The components of type III secretory pathways mediate insertion of virulence factors into host cells by pathogenic bacteria including *Bordetella pertussis*, *Chlamydia trachomatis*, *Salmonella typhi*, and enterohemorrhagic *Escherichia coli* (EHEC); the latter being responsible for “hamburger” disease. Caminoside A is an unusual marine glycolipid^[2] with a non-glycerol aglycone (the C₁₉ hydroxyketone **2**) that is glycosylated at the C10 hydroxy group by a tetrasaccharide consisting of D-deoxytalose, two D-glucose units, and L-quinovose that are linked through 1,2' and 1,6'-O-glycosidic bonds. The secondary C10 OH group of **2** is separated from the chain termini by at least seven CH₂ groups, consequently, the configuration could not be assigned by conventional NMR spectroscopic methods. This situation typifies a well-recognized problem in natural products structure elucidation—assignment of stereochemistry at remote stereocenters in acyclic molecules.^[3]

The problem can be described in terms of the logical order of analysis employed by natural products chemists when addressing absolute configuration by NMR spectroscopy. Assignment of configuration at stereogenic centers along an acyclic carbon chain requires reliable chemical shift assignments to reduce the problem to one of defining the stereotopicity of groups flanking the left and right sides of each substituted carbon in the chain (Figure 2). For example, the configurations of many secondary alcohols are conveniently assigned from their derived Mosher^[4] or mandelate esters^[5]

[*] J. B. MacMillan, Prof. T. F. Molinski

Department of Chemistry
University of California
Davis, CA 95616 (USA)
Fax: (+1) 530-752-8995
E-mail: tfmolinski@ucdavis.edu

R. G. Linington, Prof. R. J. Andersen
Department of Chemistry, Earth and Ocean Sciences
University of British Columbia, Vancouver, B.C. Canada, V6T 1Z3
(Canada)

[**] We gratefully acknowledge Novozymes Biotech, Inc. (Davis, CA) for a sample of Novozyme 435. The NMR spectrometers used in this study were funded in part by NSF CHE-9808183 (400 MHz NMR spectrometer) and NIH RR11973 (600 MHz NMR spectrometer). This work was supported by the NIH (AI 39987, CA85602) to T.F.M. and NSERC to R.J.A.

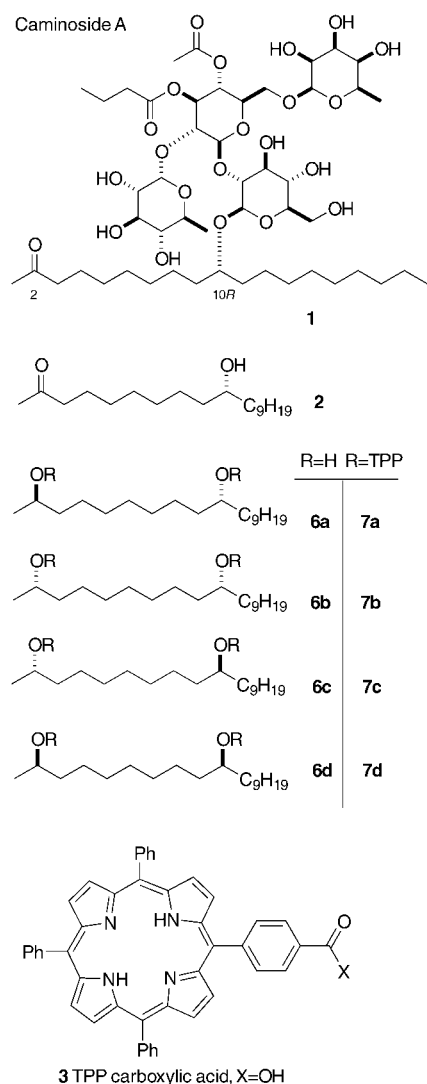


Figure 1. Caminoside A (1), the aglycone 2, and the four possible stereoisomers of reduced aglycone (6a–d) and 5-(4'-carboxy)-5,10,15,20-tetraphenylporphyrin (TPP, X = OH, 3).

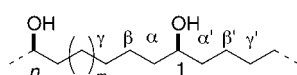


Figure 2. Acyclic 1,n-glycol. The configuration of C1 can be deduced from NMR spectroscopic assignments of the stereotopicity of the two families of chemical shifts [α , β , γ ...] and [α' , β' , γ' ...]. To obtain the relative configuration of the 1,n-glycol, similar conditions must be satisfied for Cn, or the C1 and Cn configurations must be cross-correlated.

by interpretation of anisotropic shifts ($\Delta\delta$) of the families of chemical shifts [α , β , γ ...] and [α' , β' , γ' ...]. Data are fitted to an empirical model which orders the diastereotopic groups located to the left and right of the CH(OH) group by the sign of their $\Delta\delta$ values. The use of integrated ^1H - ^1H and ^1H - ^{13}C coupling constant analysis (Karplus-like analysis) provides assignments of stereochemistry from defined dihedral angle dependencies (J -based methods).^[6] J -based analysis can relay stereochemical information along the chain (α to β to γ ...) to

reveal relative stereochemistry at contiguous carbon atoms (1,2-disubstituted) or even alternating substituted carbon atoms (1,3-disubstituted). The requirement (and limitation) of these methods is that stereotopicity of the signals of intervening CH_2 groups must be made by measurements of J coupling constants under favorable conditions of NMR spectroscopy signal dispersion and dihedral angles that conform to all-staggered molecular conformations. These methods, although usually successful for polyketides bearing contiguous 1,2 or 1,3-disubstituted stereoelements, become less reliable for molecules containing two or more stereocenters separated by three or more methylene bridges because the two diastereotopic chain segments subtended at each stereocenter cannot always be differentiated by NMR spectroscopy.^[7]

We describe, herein, the configurational assignment of the aglycone of caminoside A (2) in which these limitations are overcome by exploiting long-range exciton-coupling circular dichroism (ECCD) of 1,n-glycol diesters in acyclic lipid chains that are formulated in highly uniform liposomes prepared from 1,2-distearoyl-*sn*-glycero-3-phosphocholine (DPC). The success of the method (defined here as liposomal exciton-coupling circular dichroism, LECCD) relies on the structural order imposed on the long-chain lipid by the hydrophobic alignment of the 1,n-glycol diesters of *O*-tetraphenylporphyrin-carboxylic acid (TPP, X = OH 3) upon being constrained by the fatty acyl chains in small diameter, uniform DPC liposomes (average $\varnothing \approx 30$ nm, Figure 3). Partial ordering of the

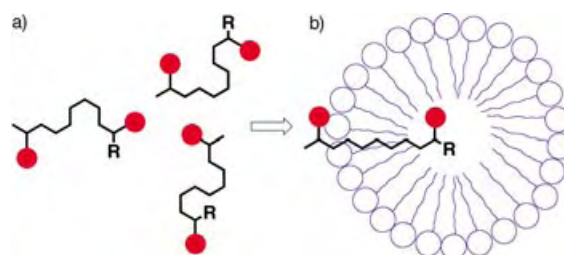


Figure 3. Imposing order upon random coiled, long-chain 1,n-diol TPP-carboxylate esters (a) by chain alignment within liposomes (b). Red circles TPP chromophores, blue DPC, R = alkyl

lipid chain limits conformational averaging and allows detection of ECCD that would not be observable in isotropic solution. The TPP chromophore was chosen from the many chromophores useful in ECCD^[8] because of its exceptionally strong charge-transfer band and successful applications across long distances in conformationally rigid diols and amino-alcohols.^[9] Since the TPP ester chromophore dipole moments are aligned predominantly along the C–O bond vectors of the ester groups at defined angular orientations, the sign of the resulting bisignate CD bands reveals the sign of the absolute helicity or “screw” angle subtended by the C–O bonds and the stereochemistry at the OH substituted carbon atoms.^[10] Herein, we demonstrate an application to an otherwise intractable problem of natural product stereochemical assignment: the relative and absolute configurations of a natural product containing an OH group isolated within an acyclic

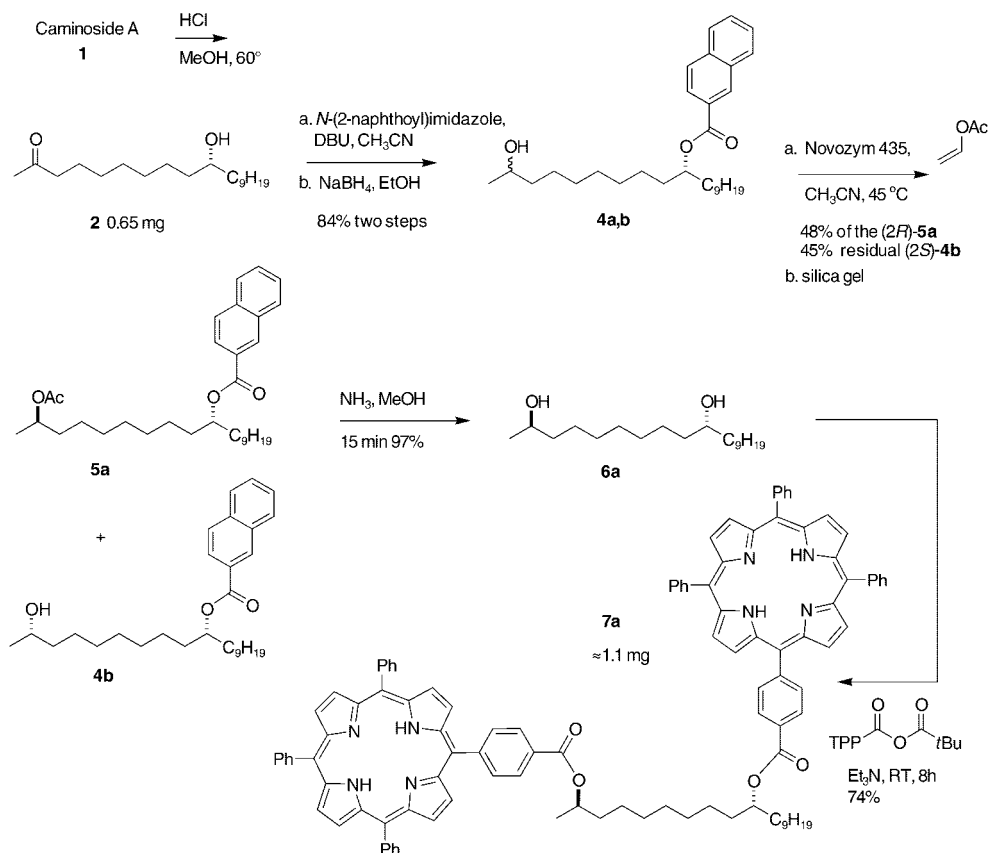
lipid chain. The LECCD achieves exceptional sensitivity (limit of detection ≈ 40 pmol) through two factors: the use of liposomes with uniform, small diameters ($< \lambda_{\text{max}}$) that reduce CD signal loss from non-Rayleigh scattering and the colossal charge-transfer dipole moment of the TPP chromophore ($\lambda = 418$ nm, ϵ 350000^[9b]) which allows propagation of relative stereochemical information in substituted acyclic lipids over distances of at least 10 Å.

We recently showed that the stereochemistry of *meso* and C_{2v} symmetric 1,5-glycols can be assigned based on the LECCD spectra of their derived TPP esters and that the method can be extended to 1,7- and 1,9-glycols.^[10] To apply the bis(TPP glycol) method to **2**, the C2 carbonyl group was asymmetrically transformed to introduce a stereodefined C2 OH group that would be used to “interrogate” the remote C10 OH configuration. A sample of **1** was methanolized under acidic conditions (Scheme 1, MeOH, HCl, reflux) and the resulting mixture of aglycone and *O*-methyl glycosides separated by silica gel chromatography (7:3 hexanes/EtOAc) to afford pure **2**.^[11] A convenient UV chromophore (2-naphthoic acid: $\lambda = 234$ nm, ϵ 58000 M⁻¹ cm⁻¹) was first attached at the C10 hydroxy group to assist detection of intermediates during each of the following conversions. Esterification of **2** (≈ 0.6 mg, *N*-2-naphthoylimidazole, 1,8-diazabicyclo[5.4.0]undec-7-ene (DBU), CH₃CN) gave **4** that was reduced (NaBH₄, EtOH) to a mixture of C2 epimeric glycol mononaphthoates (**4a,b**). The mixture was resolved by enzyme-catalyzed acetylation (Novozym 435, vinyl acetate, CH₃CN, 45°C) to give the product (*2R*)-*O*-acetate ester **5a**

(48%) and residual (*2S*)-alcohol **4b** (45%), which were easily separated by silica chromatography. The configurations at C2 of **5a** and **4b** followed from the enantiopreference of Novozyme 435 for (*2R*)-methyl carbinols^[12] and were supported by Mosher ester analysis of synthetic homologues (see below).^[13]

The configuration of the natural product-derived glycol diester **5a** corresponds to one of the family of stereoisomers **6a–d** depicted in Figure 1. As expected, the relative stereo relationship of the known C2 center to C10 in **5a** or **4b** could not be determined at this stage owing to the large distance between the two OH groups, however, the correct natural product configuration was successfully elucidated as follows: The ester groups in **5a** were removed (NH₃, MeOH, 15 min, 97%) to give the 1,9-glycol **6a**. Glycol **6a** was converted into the purple TPP ester **7a** (Scheme 1; λ_{max} 416 nm, ϵ 428000, HRFABMS *m/z* 1582.9874, [MH]⁺) via the mixed TPP anhydride (*O*-pivaloyl TPP, CH₂Cl₂, 8 h, Et₃N) followed by HPLC purification (74%). CD measurement of a sample of **7a** that had been constituted into liposomes (DPC 2 mg mL⁻¹, average diameter $\varnothing \approx 30$ nm, $c = 0.65$ μ M based on the extinction of TPP, ϵ 428000) showed strong exciton coupling (Figure 4) characterized by a high intensity positive bisignate CD signal ($A = +22$), however, the CD of **7a** in MeOH showed only baseline as expected from conformational averaging of the lipid chains of **7a** in isotropic solution.

We propose that the lipid chains are partially oriented in the extended conformation by hydrophobic packing with the fatty acyl chains of DPC. Assuming that the liposomal bilayer



Scheme 1. Conversion of **1** into nonadecane-1,10-diol TPP-carboxylate diester (**7a**).

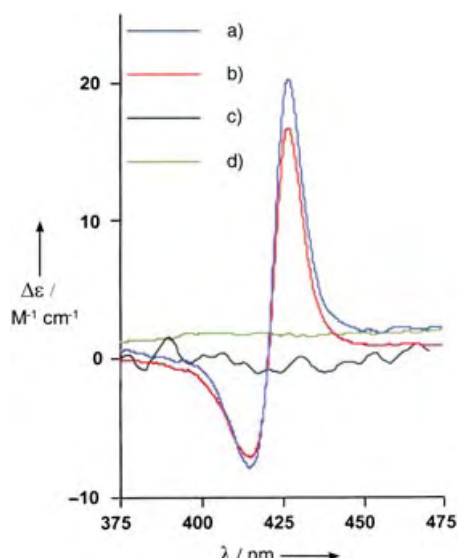


Figure 4. CD spectra of TPP esters formulated in MeOH or DPC liposomes (2 mg mL⁻¹, 1,2-distearoyl-*sn*-glycero-3-phosphocholine), *T* = 22 °C. a) “pseudo-*C*₂” **9a** in liposomes. b) **7a** in liposomes. c) “pseudo-*meso*” **9b** in liposomes. d) **7a** in MeOH.

orients the long-chain bis(TPP ester) **7a** in an extended conformation and that the *O*-TPP groups subtend torsional angles as shown in Figure 5, the observed positive bisignate

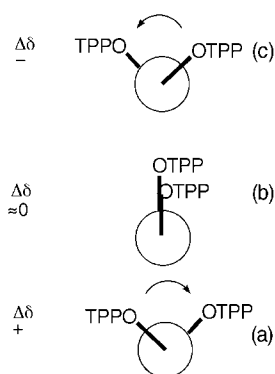
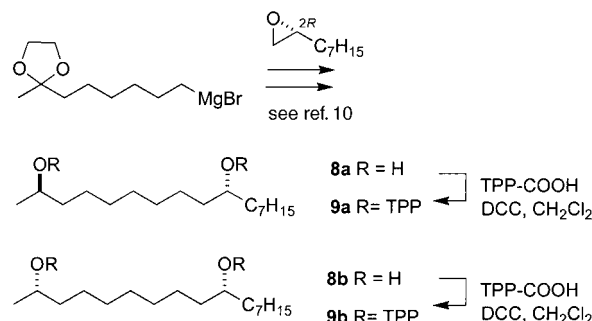


Figure 5. Predicted sign of exciton coupling CD for extended conformation of long-chain 1,*n*-glycol TPP diesters (*n* = 7, 9). a) *anti* conformation, positive helicity (“pseudo-*C*₂” symmetric) → positive split CD. b) synperiplanar (“pseudo-*meso*”) → zero signal; c) *anti* conformation, negative helicity (“pseudo-*C*₂” symmetric) → negative split CD.

signal would be expected for the (2*R*,10*R*)-**7a** where the two TPP groups are oriented *anti* with respect to the plane of the extended chain conformation (Figure 5a). Conversely, a negative signal would be expected for the *anti*-oriented TPP groups of the enantiomeric (2*S*,10*S*)-**7c** (Figure 5c) and a weak or baseline signal would be observed for the synperiplanar TPP groups of the remaining “pseudo-*meso*” stereoisomers, (2*S*,10*R*)-**7b** and (2*R*,10*S*)-**7d** (Figure 5b). Indeed, the configurational assignment of **7a** was entirely supported by measurements of the corresponding TPP esters of synthetic

homologues **8a** and **8b**, each prepared from (*R*)-1,2-epoxynonane (Scheme 2).^[10,13] The CD spectrum of liposomal formulations of the corresponding TPP ester (2*R*,10*R*)-**9a** (Scheme 2) was virtually identical to that of the natural product derived **7a**, but the synthetic epimer, (2*S*,10*R*)-**9b**, gave only baseline signal.



Scheme 2. Synthesis of model 1,9-diols.

In conclusion, the C10 configuration of caminoside A is assigned as *R*, which completes the entire configurational assignment of **1**.^[14] The advantage of LECCD lies in partial ordering of the lipid chains that induces a non-averaged net ECCD signal in 1,9-glycol TPP diesters that communicates the relative configuration of the 1,9-glycol, derived from aglycone **2** in a stereodefined manner. Since the C2 configuration of **6a** is securely established, the absolute configuration at C10 is communicated by the relative stereochemistry revealed from LECCD measurements of the corresponding 1,9-glycol TPP diesters **7a** and **7b**. In principle, the method may be extended to other suitably derivatized acyclic hydroxy-substituted long-chain lipids that defy conventional methods for stereochemical interrogation because they contain remotely located stereocenters, such as the antiviral glycolipids, fattiviracin^[15] from *Streptomyces microflavus* No. 2445 and cycloviracins from *Kibdelosporangium albatum* so. nov. (R761-7).^[16] We have estimated, by extrapolation of the A magnitudes from LECCD spectra of 1,*n*-glycol TPP esters (*n* = 7, 9), that a measurable LECCD signal should be observed up to *n* = 13,^[10] however, refinements of methods for ordering of long-chain esters in liposomes may extend transmission of stereochemical information beyond this limit.

Experimental Section

All the new compounds were purified by HPLC and gave satisfactory high-resolution mass spectra (HRMS) and ¹H NMR spectra.

LECCD: General procedures for liposome preparation and characterization of the materials by TEM are described in detail, elsewhere.^[10] Briefly, measured aliquots of DPC and TPP ester **7a** were dissolved in CHCl₃ and “shell-evaporated” in a round bottom flask. Water (2 mL) was added and the mixture sonicated (ultrasound bath). The crude liposomes were annealed by thermal cycling (60 → 25 °C → 60 °C, × 3) before repeated passage through a porous nylon membrane (100 nm pore, Liposofast, Avestin). CD spectra were on purified material were measured at room temperature (23 °C) in a 1-

mm path-length cell (Jasco 810 spectropolarimeter). No smoothing or noise reduction algorithms were applied to the spectral data.

4a and **4b**: A solution of **2** (0.6 mg, 2 μ mol), *N*-2-naphthoylimidazole (1.0 mg, 4.48 μ mol), and DBU (0.5 mg, 3.3 μ mol) in CH_3CN (0.5 mL) was heated to 65 °C. After 8 h the mixture was cooled to room temperature and the volatiles were removed under a stream of N_2 . The residue was purified on a short SiO_2 column (pipette, 5:95 EtOAc/*n*-hexane) to obtain a yellow oil of crude naphthoate esters (0.78 mg, 87 %). The ester mixture was dissolved in EtOH and treated with NaBH_4 (1 mg, 26 μ mol) at 0 °C. After stirring for 20 minutes, the mixture was quenched with NH_4Cl (sat. aq) and extracted with CH_2Cl_2 (2 \times 2 mL). The volatiles were removed, and the residue purified through a short plug of silica (1:4 EtOAc/*n*-hexane) to provide an inseparable mixture of **4a** and **4b** (0.71 mg, 84 % yield over 2 steps) that was used immediately in the next step. ^1H NMR (CDCl_3): δ = 7.28–7.51 (m, 7H), 4.02 (m, 1H), 3.34 (m, 1H), 1.57 (m, 4H), 1.19–1.47 (m, 26H), 0.90 (t, J = 6.8 Hz, 3H).

5a: Novozym 435 (1 mg) was added to a solution of **4a** and **4b** (0.7 mg, 1.6 μ mol) in CH_3CN (1 mL) followed by the addition of a solution of vinyl acetate (2.7 μ mol) in CH_3CN (100 μ L). The mixture was heated to 45 °C with vigorous stirring for 17 h, cooled to room temperature and filtered through a plug of cotton. Purification of the product on a short SiO_2 column (4 \times 10 mm, 1:99 EtOAc/*n*-hexane) gave acetate **5a** (0.36 mg, 48 %). FAB HRMS m/z [$M+\text{H}$] $^+$ found 497.3634; calcd for $\text{C}_{32}\text{H}_{49}\text{O}_4$, 497.3631.

6a: A methanol solution of acetate **5a** (0.34 mg, 0.7 μ mol) was treated with saturated solution of NH_3 in MeOH (0.5 mL), and the mixture allowed to stir at 0 °C for 15 minutes before neutralization with 1M HCl (aq). The mixture was concentrated, extracted with CH_2Cl_2 (2 \times 1 mL) and the volatiles removed to provide **6a** (0.2 mg, 97 %). Desorption chemical ionization (DCI) HRMS m/z [$M+\text{H}$] $^+$ found 301.3015; calcd for $\text{C}_{19}\text{H}_{41}\text{O}_2$, 301.3017.

7a: The mixed anhydride (4 mg, 6.1 μ mol), prepared from 5-(4'-carboxyphenyl)-5,10,15,20-tetraphenylporphyrin and pivalic acid, in a solution of **6a** (0.19 mg, 0.7 μ mol) in CH_2Cl_2 (1 mL) was treated with Et_3N (4 μ L). After stirring for 8 h, the mixture was washed with H_2O , dried over Na_2SO_4 , and concentrated to give a purple film. Purification of the product by normal phase HPLC (SiO_2 , 5 μ , 4.6 \times 250, 2:98 *i*PrOH:*n*-hexane) gave **7a** (0.92 mg, 74 %). FAB HRMS m/z [$M+\text{H}$] $^+$ found: 1582.9874; calcd for $\text{C}_{109}\text{H}_{97}\text{N}_8\text{O}_4$: 1582.9877. UV (MeOH) λ 645 (ϵ 4700), 511 (16300), 416 nm (428000).

Received: July 1, 2004

Keywords: circular dichroism · glycolipids · liposomes · natural products · stereochemistry

- [1] R. G. Linington, M. Robertson, A. Gauthier, B. B. Finlay, R. van Soest, R. J. Andersen, *Org. Lett.* **2003**, *5*, 4089–4092.
- [2] V. Costantino, E. Fattorusso, A. Mangoni in *Bioactive Compounds from Natural Sources*, Taylor and Francis, New York, **2001**.
- [3] A similar difficulty was evident in the structure elucidation of cycloviracin B₁ where the stereochemical issue was addressed by total synthesis of the natural product, together with stereo-isomeric models, followed by critical evaluation of ^{13}C NMR shifts. a) A. Fürstner, M. Albert, J. Mlynarski, M. Matheu, *J. Am. Chem. Soc.* **2002**, *124*, 1168–1169; b) A. Fürstner, M. Albert, J. Mlynarski, M. Matheu, E. DeClercq, *J. Am. Chem. Soc.* **2003**, *125*, 13132–13142; c) A. Fürstner, J. Mlynarski, M. Albert, *J. Am. Chem. Soc.* **2002**, *124*, 10274–10275.
- [4] a) I. Ohtani, T. Kusumi, Y. Kashman, H. Kakisawa, *J. Am. Chem. Soc.* **1991**, *113*, 4092; b) T. Kusumi, T. Hamada, M. O. Ishitsuka, I. Ohtani, H. Kakisawa, *J. Org. Chem.* **1992**, *57*, 1033–1035.
- [5] a) B. M. Trost, J. L. Belletire, S. Godleski, P. G. McDougal, J. M. Balkovec, J. J. Baldwin, M. Christy, G. S. Ponticello, S. L. Varga,

- J. P. Springer, *J. Org. Chem.* **1986**, *51*, 2370–2374; b) J. M. Seco, E. Quiñoá, R. Riguera, *Tetrahedron: Asymmetry* **2001**, *12*, 2915–2925.
- [6] a) N. Matsumori, D. Kaneno, M. Murata, H. Nakamura, K. Tachibana, *J. Org. Chem.* **1999**, *64*, 866–876; b) M. Murata, S. Matsuoka, N. Matsumori, K. P. Gopal, K. Tachibana, *J. Am. Chem. Soc.* **1999**, *121*, 870; c) R. T. Williamson, A. Boulanger, A. Vulpanovici, M. A. Roberts, W. H. Gerwick, *J. Org. Chem.* **2002**, *67*, 7927–7936.
- [7] Stereochemistry in contiguous polyols has also been addressed using the “universal database” approach involving “least difference” analysis of $\Delta\delta$ values in ^{13}C NMR spectra of model compounds. S. Higashibayashi, W. Czechtizky, Y. Kobayashi, Y. Kishi, *J. Am. Chem. Soc.* **2003**, *125*, 14379–14393, and references therein. This powerful approach also has limitations. From experience in ^{13}C NMR stereochemical analysis of maitoxin and compounds in the AAL toxin (AAL = *Alternaria alternata* F.sp. *lycopersi*) /fumonis class, Kishi states, “stereoelectronic interactions ... between stereoclusters connected with a two or more methylene bridge are negligible”, which recapitulates the familiar notion that such stereoelements in long-chain molecules are effectively insulated from one another.
- [8] a) J. Gawroński, P. Skowronek, *Curr. Org. Chem.* **2004**, *8*, 65–82; b) N. Harada, K. Nakanishi, *Circular Dichroic Spectroscopy: Exciton Coupling in Organic Stereochemistry*, University Science Books, Mill Valley, **1983**.
- [9] a) S. Matile, N. Berova, K. Nakanishi, J. Fleischhauer, R. W. Woody, *J. Am. Chem. Soc.* **1996**, *118*, 5198–5206; b) S. Matile, N. Berova, K. Nakanishi, S. Novkova, I. Philipova, B. Blagoev, *J. Am. Chem. Soc.* **1995**, *117*, 7021–7022; c) X. F. Huang, K. Nakanishi, N. Berova, *Chirality* **2000**, *12*, 237–255.
- [10] J. B. MacMillan, T. F. Molinski, *J. Am. Chem. Soc.* **2004**, *126*, 9944–9945.
- [11] R. G. Linington, Ph.D. thesis, **2004**, University of British Columbia, Canada.
- [12] a) C. Orrenius, N. Öhrner, D. Rotticci, A. Mattson, K. Hult, T. Norin, *Tetrahedron: Asymmetry* **1995**, *6*, 1217–1220; b) H. Frykman, N. Öhrner, T. Norin, K. Hult, *Tetrahedron Lett.* **1993**, *34*, 1367.
- [13] Synthetic 10-*O*-acetyl-10-hydroxyheptadecan-2-one was prepared as described in detail, elsewhere.^[10] Briefly, addition of 6-(2-methyl-1,3-dioxolan-2-yl)hexyl magnesium bromide to (*R*)-1,2-epoxynonane (> 95 % *ee*, prepared from 1-nonene and Jacobsen’s catalyst, S. E. Schaus, B. D. Brandes, J. F. Larrow, M. Tokunaga, K. B. Hansen, A. E. Gould, M. E. Furrow, E. N. Jacobsen, *J. Am. Chem. Soc.* **2002**, *124*, 1307–1315) followed by acetylation (Ac_2O , pyridine), transketalization (4-methyl benzenesulfonic acid (*p*-PTS), acetone) and reduction (NaBH_4 , EtOH) of the resultant ketone provided synthetic (2 ξ ,10*R*)-heptadecan-2,10-diol. Sequential acetylation (Novozym 435, vinyl acetate), separation of the products by SiO_2 chromatography and ammoniolysis of the esters, using a procedure similar to that described in the text, gave samples of (2*R*,10*R*)-**8a** and (2*S*,10*R*)-**8b**. The diastereomeric ratios at C2 were measured as 99 % and 98 %, respectively, from their corresponding Mosher diester (*R* or *S* α -trifluoromethyl- α -methoxyphenylacetic acid, *N,N'*-dicyclohexyl methanediimine (DCC), CH_2Cl_2 , *N,N'*-dimethyl-4-pyridinamine (DMAP), yields 63–73 %). Note that although a Mosher *O*-ester group acylated on the C10 OH of either **8a** or **8b** induced differential anisotropic $\Delta\delta$ shifts for the ^1H NMR signals of H9 and H11, these signals could not be assigned and, thus, were considered interchangeable. Consequently, the $\Delta\delta$ values are not informative for the configuration at C10.
- [14] Three other analogues from *C. sphaeroconia* (caminosides B–D) are homologues of **1** that differ only by replacement or interchange of *O*-acetyl or butanoyl groups at C3 and C4 of

the second glucose residue.^[11] Since the constitution of the aglycone is the same in each of the caminosides A–D, we assume that the configuration is also the same (10*R*).

- [15] a) M. Uyeda, K. Yokomizu, Y. Miyamoto, E.-S. E. Habib, *J. Antibiot.* **1998**, *51*, 823–828; b) K. Yokomizo, Y. Miyamoto, K. Nagao, E. Kumagae, E.-S. E. Habib, K. Suzuki, S. Harada, M. Uyeda, *J. Antibiot.* **1998**, *51*, 1035–1039; c) E.-S. E. Habib, K. Yokomizo, K. Murata, M. Uyeda, *J. Antibiot.* **2000**, *53*, 1420–1423; d) E.-S. E. Habib, K. Yokomizo, K. Suzuki, M. Uyeda, *Biosci. Biotechnol. Biochem.* **2001**, *65*, 861–864.
- [16] a) M. Tsunakawa, N. Komiyama, O. Tenmyo, K. Tomita, K. Kawano, C. Kotake, M. Konishi, T. Oki, *J. Antibiot.* **1992**, *45*, 1467–1471; b) M. Tsunakawa, C. Kotake, T. Yamasaki, T. Moriyama, M. Konishi, T. Oki, *J. Antibiot.* **1992**, *45*, 1472–1480; c) M. Tsunakawa, T. Yamasaki, K. Tomita, T. Osamu, EP 0472005A1, **1991**.

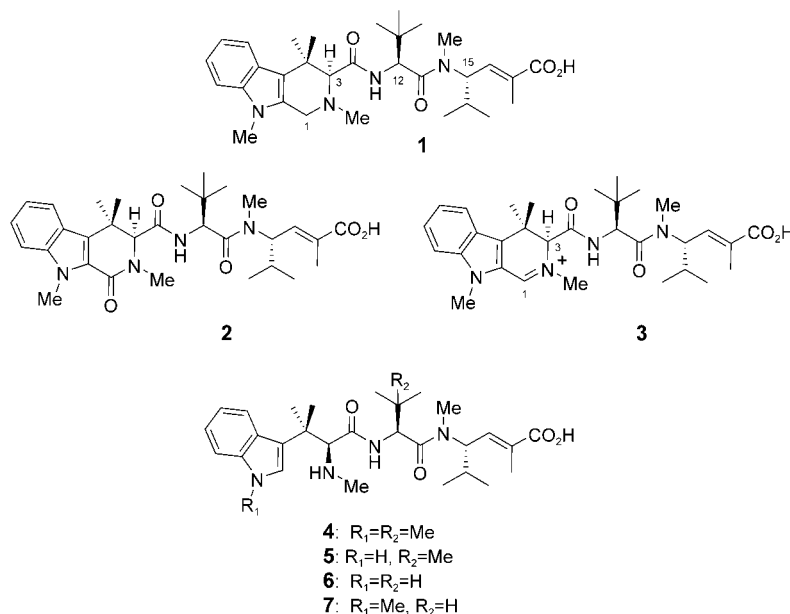


Figure 1. Milnamides A, C, and D (**1–3**), hemiasterlin (**4**), and hemiasterlins A–C (**5–7**). Numbering is taken from Reference [1a].

Natural Product Synthesis

Enantioselective Total Synthesis of (+)-Milnamide A and Evidence of Its Autoxidation to (+)-Milnamide D**

Chaomin Liu, Makoto N. Masuno, John B. MacMillan, and Tadeusz F. Molinski*

Milnamides A,^[1a] C,^[1b] and D^[1c] (**1–3**), (–)-hemiasterlin (**4**),^[2a–d] and hemiasterlins A–C (**5–7**)^[2b,d] (Figure 1) comprise a small family of exceptionally cytotoxic tripeptides that were isolated from marine sponges *Auletta* sp., *Hemiasterella minor*, *Cymbastella* sp. and *Siphonochalina* sp. Compounds **1–7** are powerful antimitotics that disrupt microtubule assembly during cell division and inhibit growth of cultured tumor cells (e.g. **4**, IC₅₀ < 1 nM, MCF-7 breast tumor cells).^[4] Hemiasterlin is a more potent cytotoxin in vitro than paclitaxel (Taxol) and is comparable to dolastatin 10.^[2c] As a consequence of this exceptional activity, a synthetic analogue of **4**, SPA110, has entered advanced phase I clinical trials for the treatment of solid tumors.^[4] X-ray crystallographic analyses confirmed the relative stereochemistries of **2** and (–)-**4**, and by the total synthesis of (–)-**4**, the *S* configurations at each α -amino acid residue were verified.^[3,4] Very

recently, the X-ray crystal structure of **2** was reported,^[1c] however, the absolute stereochemical configurations of **1–3** were not defined. Comparison of the ¹H NMR spectroscopic data of **1–3** suggests that the differences from (–)-**4** are located solely within the region of the heterocyclic amino acid. Because the highly methylated β -carboline amino acid **8**, which is found in **1–3**, has no precedent in other natural products, the preparation of both *3R* and *3S* (β -carboline numbering) stereoisomers of **1** would inform stereochemical determinations of the milnamide family. Herein, we report the first enantioselective total syntheses of (*3S*)-**1** and (*3R*)-**1** that employs an expedient synthesis of the requisite **8** through an oxazoline–dihydrooxazinone rearrangement. The synthesis confirms the absolute configuration of natural (+)-**1** as (*3S*,*12S*,*15S*) and demonstrates the first use of the aforementioned rearrangement in natural peptide synthesis. Furthermore, we show that **1** undergoes facile autoxidation to milnamide D (**3**) which thus correlates the absolute configurations of both natural product peptides and suggests a nonbiogenic origin for the iminium salt **3**.

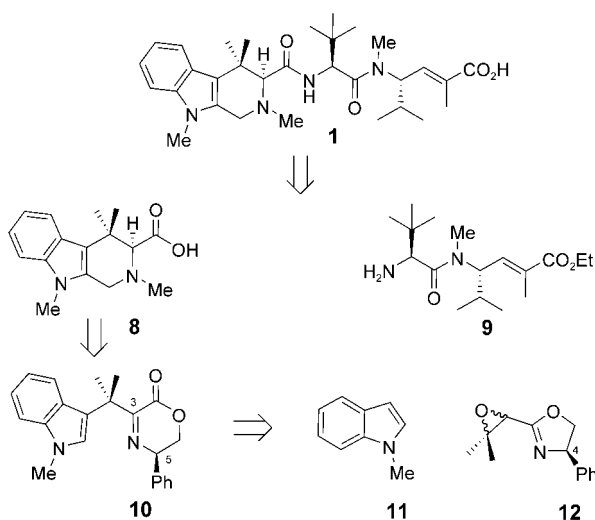
Retrosynthetic analysis of **1** (Scheme 1) suggests disconnections to a pivotal intermediate, namely the β -carboline amino acid (**8**), and the known dipeptide **9**.^[3a] The precursor **10** to the heterocyclic amino acid arises from aromatic electrophilic substitution of *N*-methylindole (**11**) by an epoxide **12**, which itself is obtained by a Darzen's-type condensation of (4*R*)-2-chloromethyl-4-phenyloxazoline and acetone.

The synthesis of **1** is outlined in Scheme 2. The pivotal step relies upon our SeO₂-promoted oxidative rearrangement of 2-alkyl- or 2-(arylmethyl)oxazolines to 3,5-disubstituted dihydro-2*H*-oxazinones.^[5] The required oxazinone **10** was synthesized in two steps as follows. *N*-methylindole and the epoxide **12**^[6] were coupled under Lewis acid conditions (SnCl₄, CH₂Cl₂, –78 °C, 56 %)^[7] to provide the requisite oxazoline

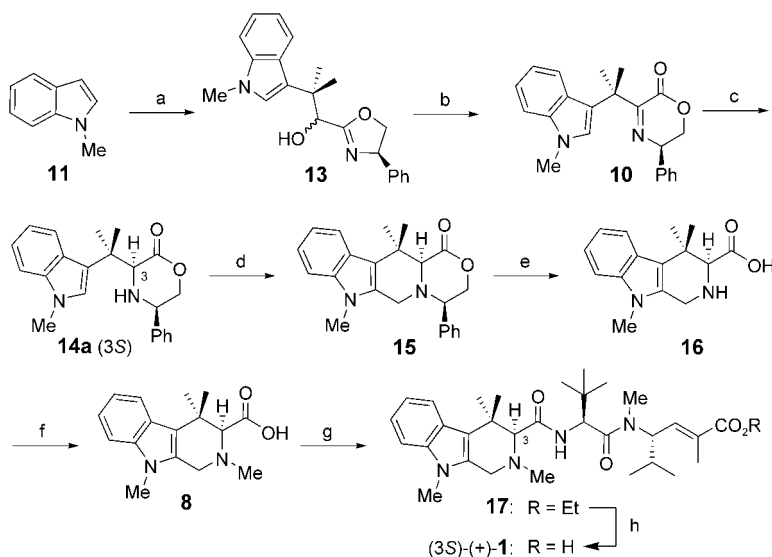
[*] C. Liu, M. N. Masuno, J. B. MacMillan, Prof. T. F. Molinski
Department of Chemistry
University of California
Davis, CA 95616 (USA)
Fax: (+1) 530-752-8995
E-mail: tfmolinski@ucdavis.edu

[**] We thank Professor Chris Ireland (University of Utah) for generous gifts of natural (+)-**1** and (+)-**3**. The Bruker Avance 600 MHz and Varian Inova 400 MHz spectrometers were purchased with funds provided by NIH RR11973 and NSF CHE-9808183, respectively. This work was funded by the NIH (RO1 CA 85602).

Supporting information for this article is available on the WWW under <http://www.angewandte.org> or from the author.



Scheme 1. Retrosynthetic analysis of **1**.



Scheme 2. Synthesis of (+)-milnamide **A** (**1**): a) **12**,^[6] SnCl₄, CH₂Cl₂, –78 °C (56%); b) SeO₂, CHCl₃, reflux (90%); c) PtO₂, H₂, MeOH, room temperature (90%); d) paraformaldehyde, MgSO₄, benzene, 75 °C (100%); e) Pd(OH)₂/C, H₂, 4 atm, TFA, H₂O room temperature (89%); f) paraformaldehyde, Pd/C (10%), H₂, MeOH, 50 °C (78%); g) **9**,^[3a] pivaloyl chloride, *i*Pr₂EtN, THF, 0 °C (10%); h) LiOH, MeOH, H₂O, degassed, room temperature (92%). TFA = trifluoroacetic acid.

13 as a mixture of epimers.^[8] Attempted oxidative rearrangement of **13** to the required 5,6-dihydro-2*H*-1,4-oxazin-3-one **10** with SeO₂ under standard conditions (dioxane, reflux) was disappointing ($\leq 23\%$ yield), probably owing to decomposition of the indole ring.^[9] A survey of varying conditions (Table 1) identified that SeO₂ in CHCl₃ or ethyl acetate at reflux provided rapid reactions and the highest yields. Accordingly, oxazoline **13** was smoothly converted (SeO₂, CHCl₃, reflux) into **10** in 90% yield.

Control of the correct configuration at the C3 center in **8** was anticipated from the diastereofacial hydrogenation of the C=N bond directed by the Ph substituent at the C5 center of the dihydrooxazinone **10**. The synthesis of either enantiomer of **8** is possible by the choice of the configuration of the

Table 1: Oxidative rearrangement of **13** to **10** with SeO₂ (2.6 equiv).

Entry	Solvent	<i>T</i> [°C]	<i>t</i> [h]	Yield of 13 [%]
1	dioxane	100	2	– ^[a]
2	dioxane	30	72	87
3	dioxane	40	72	23
4	CH ₂ Cl ₂	40	72	53
5	EtOAc	77	2 ^[b]	90
6	CHCl ₃	61	4	90

[a] Trace. [b] Stirred at 24 °C for an additional 14 h.

phenylglycinol that is used in the preparation of the oxazoline **12**. Thus, reduction of (5*R*)-**10** or (5*S*)-**10** would provide (3*S*)-**1** or (3*R*)-**1**, respectively. After experimentation under different conditions (Table 2), we found that **10** underwent hydrogenation (PtO₂, H₂, 4 atm, MeOH, RT, 90%) to give **14** with excellent diastereoselectivity ($\approx 70:1$). The major isomer, **14a**, which was separated from the mixture by column chromatography (silica gel), was shown to have the expected *cis* configuration by NOE studies; irradiation of the H3 center (CDCl₃, $\delta = 4.39$, s) resulted in an NOE enhancement of the benzylic proton H5 (oxazinone numbering). Condensation of **14a** with H₂C=O under optimized Pictet–Spengler^[10] conditions (paraformaldehyde, MgSO₄, benzene, 75 °C) gave **15** in quantitative yield. Removal of the chiral auxiliary from **15** by hydrogenolysis–hydrolysis (Pd(OH)₂/C, H₂, 4 atm, TFA/H₂O, 89%),^[11] followed by reductive methylation (paraformaldehyde, Pd/C, H₂, MeOH, 50 °C, 78%)^[12] provided the key amino acid **8**.

The amide coupling of **8** and **9**^[3a] was far more troublesome than expected. Attempted amide bond formation with a variety of coupling reagents (dicyclohexyl carbodiimide (DCC), 1-ethyl-3-(3-dimethylaminopropyl)carbodiimide) hydrochloride (EDC), *O*-(7-azabenzotriazol-1-yl)-*N,N,N',N'*-tetramethyluronium hexafluorophosphate (HATU), bromotripyrrolidinophosphonium hexafluorophosphate (PyBrOP)) all failed to produce the expected tripeptide. Clearly, the highly hindered molecule **8** precluded the formation of the amide bond with the sterically crowded *tert*-leucyl amino terminus of **8** under conditions

that were similar to those employed by Andersen et al in the synthesis of **4** from the less hindered (2*S*)-*N*-Boc-*N',N',C*-tetramethyltryptophan (52%).^[3a] Eventually, amide coupling was possible under mixed anhydride conditions (pivaloyl chloride, *i*Pr₂EtN, THF, 0 °C, 10%) to give the ethyl ester **17**.^[13] Saponification of **17** (LiOH, MeOH, H₂O, degassed, N₂,

Table 2: Hydrogenation of **10** in the presence of PtO₂ (20 mol%).

Entry	Solvent	<i>P</i> _{H₂} [atm]	<i>t</i> [h]	d.r. ^[b] (14a : 14b)	Yield of 14a,b [%]
1	CH ₂ Cl ₂	2	48	17:1	90
2	EtOAc	4	52	39:1	96
3	CH ₃ OH	4	72	72:1	90 ^[a]

[a] Isolated yield of **14a**. [b] From integration of ¹H NMR spectra.

RT, 92 %) completed the synthesis of (3*S*)-**1**. Its counterpart (3*R*)-**1**^[14] was synthesized by the same route starting with the (4*S*)-oxazoline **12**. Synthetic (3*S*)-**1** was identical to natural (+)-**1** from ¹H NMR and circular dichroism (CD; see Figure 2) spectroscopic analysis, ESI-MS measurements, and LC-MS retention times.^[15] However, the CD spectrum of epimilnamide A ((3*R*)-**1**) differed significantly from that of natural (+)-**1**.

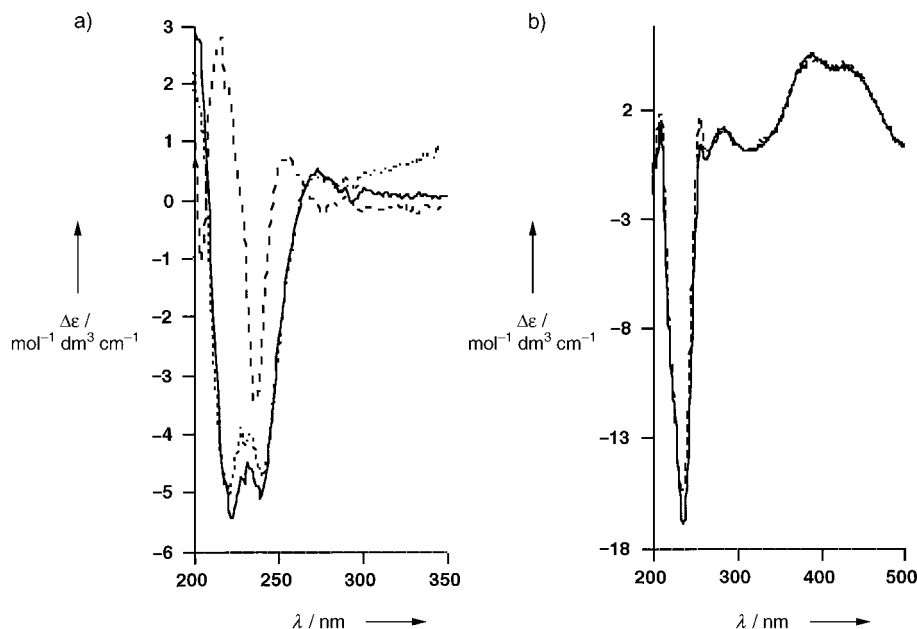


Figure 2. CD spectra of milnamides: a) synthetic milnamide A [(3*S*)-**1**] (—), synthetic epimilnamide A [(3*R*)-**1**] (---), and natural milnamide A [(3*S*)-**1**] (....); b) synthetic milnamide D [(3*S*)-**3**] (---) and natural (+)-milnamide D [(3*S*)-**3**] (—).

Over time, **1** slowly autooxidized to **3** upon standing in solvent. Both (3*S*)-**1** and (3*R*)-**1** were oxidized at similar rates, but the apparent rate of autooxidation was greatly accelerated when samples were stored in aged CDCl₃ or CHCl₃.^[16] As the analyses of this autooxidation product **3** were identical to those of natural milnamide D by CD (Figure 2) and ¹H NMR spectroscopy and LCMS, we conclude that the latter also has the 3*S* configuration. Given the ease of this oxidation, it is plausible that **3**, which is obtained from natural sources, originates from the autooxidation of **1** during its isolation–purification process, although we cannot exclude **3** as a “true” natural product or an intermediate precursor in the biosynthesis of **1**.

The key feature of this synthesis of (+)-milnamide A (**1**) is the high-yielding preparation of the highly methylated β-carboline amino acid **8**, which is made possible through the facile oxidative rearrangement of oxazoline **12** to the corresponding substituted dihydrooxazinone. This rearrangement reaction was exploited for the first time in natural product synthesis for the preparation of amino acid **8** and should find application in the synthesis of other marine-derived peptides that containing rare *tert*-alkyl amino acids.^[17]

Received: July 9, 2004

Keywords: carboline · enantioselectivity · natural products · peptides · total synthesis

- [1] a) P. Crews, J. J. Farias, R. Emrich, P. A. Keifer, *J. Org. Chem.* **1994**, 59, 2932; b) R. N. Sonnenschein, J. J. Farias, K. Tenney, S. L. Mooberry, E. Lobkovsky, J. Clardy, P. Crews, *Org. Lett.* **2004**, 6, 779; c) C. Chevallier, A. D. Richardson, M. C. Edler, E. Hamel, M. K. Harper, C. M. Ireland, *Org. Lett.* **2003**, 5, 3737.
- [2] a) R. Talpir, Y. Benayahu, Y. Kashman, L. Pannell, M. Schleyer, *Tetrahedron Lett.* **1994**, 35, 4453; b) J. E. Coleman, E. D. de Silva, F. Kong, R. J. Anderson, T. M. Allen, *Tetrahedron* **1995**, 51, 10653; c) H. J. Anderson, J. E. Coleman, R. J. Andersen, M. Roberge, *Cancer Chemother. Pharmacol.* **1997**, 39, 223; d) Y. Kashman, D. G. Gravalos, US Patent 5661175, **1997**; e) W. R. Gamble, N. A. Durso, R. W. Fuller, C. K. Westergaard, T. R. Johnson, D. L. Sackett, E. Hamel, J. H. Cardellina II, M. R. Boyd, *Bioorg. Med. Chem.* **1999**, 7, 1611.
- [3] a) R. J. Andersen, J. E. Coleman, E. Piers, D. J. Wallace, *Tetrahedron Lett.* **1997**, 38, 317; b) E. Vedejs, C. Kongkittigam, *J. Org. Chem.* **2001**, 66, 7355.
- [4] J. A. Nieman, J. E. Coleman, D. J. Wallace, E. Piers, L. Y. Lim, M. Roberge, R. J. Anderson, *J. Nat. Prod.* **2003**, 66, 183.
- [5] C. M. Shafer, T. F. Molinski, *J. Org. Chem.* **1996**, 61, 2044.
- [6] a) K. Kamato, H. Sato, E. Takagi, I. Agata, A. I. Meyers, *Heterocycles* **1999**, 51, 373; b) S. Flori, V. Capriati, R. Luisi, *Tetrahedron Lett.* **1996**, 37, 4781.
- [7] R. Reddy, J. B. Jaquith, V. R. Neelagiri, S. Saleh-Hanna, T. Durst, *Org. Lett.* **2002**, 4, 695.
- [8] All new compounds gave satisfactory HRMS and ¹H and ¹³C NMR spectroscopic data. The resulting 1:1 epimeric mixture of **13** was inconsequential as both epimers were converted into **10** in the subsequent reaction.
- [9] We assume from the slower rate of the SeO₂ oxidation reaction under the original conditions (reference [5]; anhydrous 1,4-dioxane, reflux) that oxidative degradation of the indole ring is competitive with the oxazoline→oxazinone rearrangement.
- [10] Addition of stoichiometric or catalytic quantities of Brønsted acid (*p*-toluenesulfonic acid or CF₃COOH) to the reaction led to decomposition of the substrate.
- [11] L. M. Harwood, S. N. G. Tyler, A. S. Anslow, I. D. MacGlip, M. G. B. Drew, *Tetrahedron: Asymmetry* **1997**, 8, 4007.
- [12] P. L. Ornstein, D. D. Schoepp, M. B. Arnold, N. K. Augenstein, D. Lodge, J. D. Millar, J. Chambers, J. Campbell, J. W. Paschal, D. M. Zimmerman, J. D. Leander, *J. Med. Chem.* **1992**, 35, 3547.
- [13] Ester **17** was purified by HPLC (C₁₈ column; gradient, CH₃CN/H₂O with HCOOH (0.01 %)). A by-product, *N*-pivaloyl-**9**, which was observed during the coupling reaction, attests to the presence of the highly congested carboxy group in the mixed pivalic anhydride of **8**.
- [14] Significant differences between the (3*R*)-**1** epimer and (3*S*)-(+)-**1** were seen in both the ¹H NMR and the CD spectra (see Experimental and Supporting Information).

- [15] CD, UV, LCMS, and ^1H NMR spectroscopic data for synthetic (3*S*)-**1** and natural (+)-**1** were identical. The HPLC retention time (co-injection) were also identical.
- [16] The ethyl ester, **17**, was also sensitive to autoxidation. Handling of NMR samples of **1** in 100% CDCl_3 from freshly opened ampoules did not induce autoxidation. Traces of chlorine or phosgene, which are present in aged CHCl_3 , are possible initiators of the autoxidation of **1**. The iminium salt **3** is easily reduced back to **1** (NaBH_4 , MeOH, 100%).
- [17] T. Hamada, T. Sugawara, S. Matsunaga, N. Fusetani, *Tetrahedron Lett.* **1994**, 35, 609.

Biofunctionalization

Biofunctionalization of Fluorescent Rare-Earth-Doped Lanthanum Phosphate Colloidal Nanoparticles**

Felix Meiser, Christina Cortez, and Frank Caruso*

In recent years, the utilization of nanoparticles (NPs) for conjugation with biomolecules has attracted widespread interest.^[1–7] In particular, fluorescent semiconductor colloidal nanoparticles, or quantum dots (QDs), have played an important role in the application of NPs in biomedical applications.^[1–3] Compared with their organic fluorophore counterparts, QDs can be prepared with high chemical stability, high quantum yield, and can exhibit high resistance to photobleaching. In addition, the optical properties of QDs can be tuned by controlling their size through synthesis. A range of biomolecules, such as deoxyribonucleic acid (DNA) and proteins, have been conjugated to QDs and used in labeling studies.^[1] For example, QD bioconjugates have been used in the fluorescent labeling of cells,^[2,3] agglutination assays,^[3] *in vitro* detection assays,^[8] and most recently, in selective and generalized imaging of live cells.^[9–11] Despite the wide and successful use of QDs in diverse biomedical studies,

commercial preparations of QDs face challenges associated with reproducible QD preparation, suitable surface coatings, and, in certain cases, cytotoxicity issues, particularly *in vivo*.^[12,13]

An alternative class of colloidal NPs that are potentially promising for biolabeling studies are those based on rare-earth-doped lanthanum phosphates (LaPO₄). Recent work by Haase and co-workers reported the synthesis of monodisperse fluorescent LaPO₄ NPs.^[14–16] These NPs, approximately 7 nm in size, have fluorescence that originates from their bulk properties—transitions between d and f electron states and their local symmetry—and is independent of their size.^[14–16] The optical properties of the LaPO₄ NPs can also be tuned by the rare-earth dopant used—different colors are available by varying the dopants used in their synthesis (e.g., Ce, Tb, Eu, Dy).^[14–17] The high chemical stability, high quantum yield (up to 61 %),^[16] and expected low toxicity^[18] of these NPs make them potentially suitable for biological labeling applications. In addition, the application of rare-earth-doped LaPO₄ thin films (from micron-sized powders) as coatings for luminescent lamps points to a high photostability of such materials.^[19,20] Herein, we report the first demonstration of the biofunctionalization of nanometer-sized colloidal LaPO₄ NPs. Green (Ce/Tb-doped) LaPO₄ NPs^[17] were conjugated to the model protein avidin, a tetrameric protein that can bind with high affinity to four biotin molecules. NP functionalization was examined by using a suite of techniques, including analytical ultracentrifugation (AUC), microelectrophoresis, absorption and fluorescence spectroscopy, dynamic light scattering (DLS), and transmission electron microscopy (TEM).

Figure 1 illustrates the conjugation of LaPO₄ NPs with avidin. A primary requirement was to first obtain stable, aqueous colloidal dispersions of the NPs. This was achieved by dispersing the LaPO₄ NPs in an aqueous solution contain-

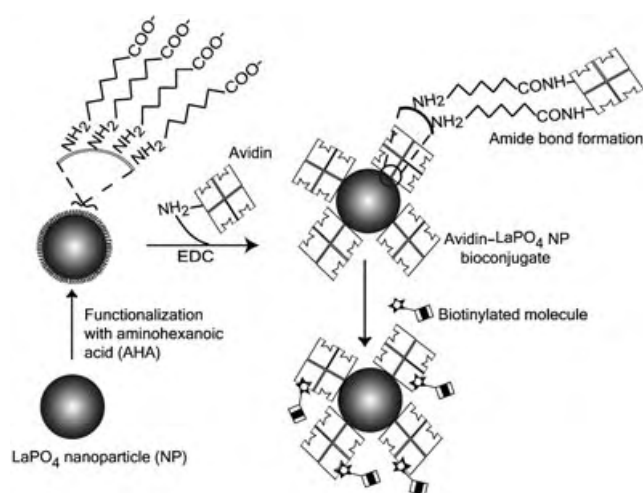


Figure 1. Schematic illustration showing the biofunctionalization of fluorescent Ce/Tb-doped LaPO₄ NPs with avidin. The NPs were first modified with AHA, and the carboxy groups of AHA were then activated by EDC to conjugate avidin through the formation of amide bonds. The binding of avidin–NP bioconjugates with biotinylated molecules is also shown.

[*] F. Meiser, C. Cortez, Prof. F. Caruso
Centre for Nanoscience and Nanotechnology
Department of Chemical and Biomolecular Engineering
The University of Melbourne
Victoria, 3010 (Australia)
Fax: (+61) 3-8344-4153
E-mail: fcaruso@unimelb.edu.au

[**] This work was supported by the Australian Research Council, the Victorian State Government Science, Technology, and Innovation initiative, and the BMBF. The Particulate Fluids Processing Centre is acknowledged for infrastructure support. S. Haubold and C. Meyer from Nanosolutions GmbH, Hamburg (Germany) are thanked for providing the nanoparticles. We thank H. Zastrow, A. Völkel, and C. Pilz (MPI Potsdam (Germany)) for technical assistance, and S. Crawford (The University of Melbourne) for assistance with the TEM measurements.

Supporting information for this article is available on the WWW under <http://www.angewandte.org> or from the author.

ing the bifunctional spacer 6-aminohexanoic acid (AHA). AHA imparts a negative charge on the surface of the NPs, as confirmed by the strongly negative ζ -potential at basic pH values (Figure 2). The isoelectric point (pI) of 4.5 obtained for

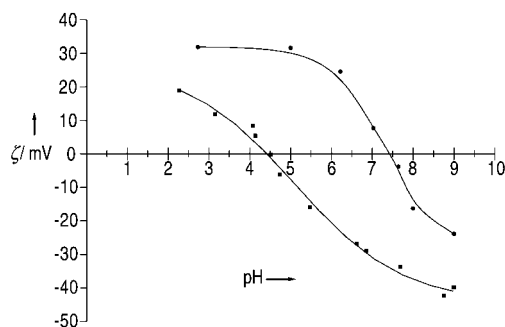


Figure 2. ζ -potential of the functionalized Ce/Tb-doped LaPO_4 NPs as a function of pH: after modification with AHA (■); and after AHA-modification and avidin bioconjugation (●). The plot shows the shift in isoelectric point upon AHA modification and avidin coating. The curves drawn are to guide the eye.

the AHA-modified LaPO_4 NPs is close to values reported for particles bearing carboxy groups,^[21,22] which suggests that the amine group of AHA is attached to the particle surface, whereas the carboxy group is directed into the surrounding solution. Modification of the LaPO_4 NPs with AHA serves two important purposes. First, it confers sufficient colloidal stability to the nanoparticles where subsequent biofunctionalization is to be performed (pH 7). Support for this is also provided by examination of the AHA-coated LaPO_4 NPs by TEM, which reveals no signs of significant NP aggregation (Figure 3). Second, the terminal carboxy group at the particle surface allows the immobilization of amine-containing ligands, such as proteins. The protein avidin was chosen in this study to make use of the highly specific interaction between avidin and biotin ($K_d = 10^{-15} \text{ M}$),^[23] since a wide variety of biotinylated molecules are commercially available. Avidin is composed of four identical subunits with each subunit folded in the form of a barrel (β -barrel).^[24] The biotin-binding site is positioned near one end of the avidin barrel, hence two biotin-binding sites are present on each end of the protein.

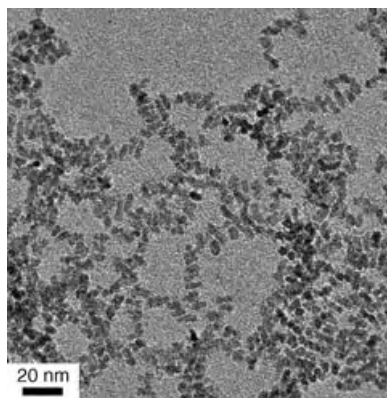


Figure 3. TEM image of AHA-modified Ce/Tb-doped LaPO_4 NPs.

The covalent coupling of avidin to the NP surface was facilitated by the crosslinker 1-ethyl-3-[3-dimethylaminopropyl]carbodiimide (EDC), which activates the carboxy groups on the NPs and leads to the formation of amide bonds with avidin. The avidin-coated AHA-modified LaPO_4 NPs showed a pI of 7.5, with a positive ζ -potential (30 mV) at pH 4.75 (Figure 2). The shift in ζ -potential after exposure to avidin (pI of 10–10.5)^[25] indicates the successful conjugation of avidin to the NP surface.

Figure 4 shows the absorption and fluorescence spectra of the LaPO_4 NPs before and after conjugation with avidin. Three washing steps after the reaction ensured the removal of

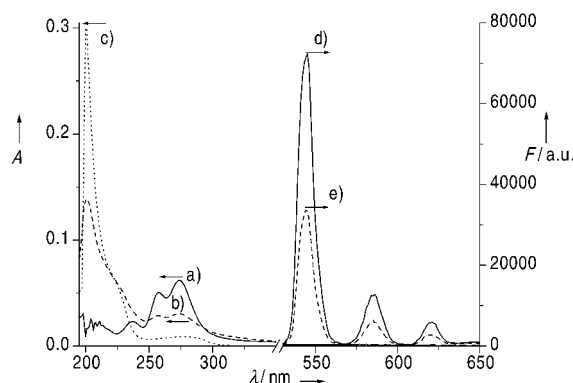


Figure 4. Absorption (A; a, b, c) and fluorescence (F; d, e) spectra of AHA-modified Ce/Tb-doped LaPO_4 NPs before (—) and after (---) avidin functionalization. The absorption peaks of the NPs at 257 and 274 nm are evident. The absorption spectrum of pure avidin (c,) is also shown.

unconjugated avidin in solution. The absorption spectrum of the AHA-modified Ce/Tb-doped LaPO_4 NPs (Figure 4, spectrum a) shows intense peaks at 257 and 274 nm, which are due to the absorption of the cerium dopant.^[16] As expected, the avidin/AHA- LaPO_4 NP bioconjugates (Figure 4, spectrum b) show absorption features characteristic of both the AHA-functionalized NPs (peaks at 257 and 274 nm) and of pure avidin (major peak at ~200 nm, Figure 4, spectrum c). These results support the microelectrophoresis data for avidin conjugation to the NP surface. For the AHA-modified NPs three distinct fluorescence peaks are observed at 545, 585, and 622 nm (Figure 4, spectrum d). These fluorescence peaks are due to the d–f orbital transitions of the dopants.^[14–16] An additional peak was also observed at 490 nm (not shown).^[26] The same characteristic fluorescence peaks can also be observed after avidin biofunctionalization (Figure 4, spectrum e). These data are in agreement with our previous work where the characteristic fluorescence peaks of LaPO_4 NPs interacting with polyelectrolytes in multilayer thin films appear at the same spectral positions as those for the corresponding NPs in solution.^[17]

To verify the increase in diameter as a result of bioconjugation, AUC was used to measure the size distribution of the NPs before and after avidin coating (Figure 5 a). Assuming a density of 5.0 g cm^{-3} for the LaPO_4 NPs,^[27] we determined an average diameter of 7.6 nm for the AHA-

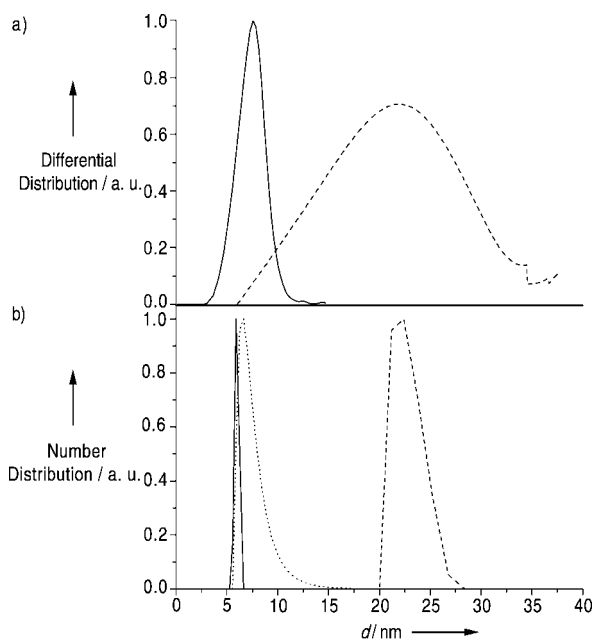


Figure 5. Diameter distribution of AHA-modified Ce/Tb-doped LaPO₄ NPs before (—) and after (---) avidin functionalization, as determined by a) AUC and b) DLS methods. In the AUC measurements (a), a particle density of 5.0 g cm⁻³ was used. In (b), the diameter distribution of avidin is also shown (.....).

modified NPs. This value is close to that derived from TEM (mean size 6–8 nm; see Figure 3 and ref. [17]).^[28] After bioconjugation, if the same density is assumed, the diameter increases to 21.8 nm, which is consistent with having a monolayer of avidin molecules, approximately 7 nm in size. This value is slightly higher than the size of avidin (dimensions 6.0 × 5.5 × 4.0 nm^[29]). Since the exact density of avidin-coated NPs is not known, the method of DLS was also employed to yield information on the hydrodynamic radius of the NPs. Figure 5b shows the DLS diameters of the individual AHA-modified LaPO₄ NPs and avidin, as well as the avidin–LaPO₄ NP bioconjugate. The measured diameter for the AHA-modified NPs (~7 nm) is in good agreement with that determined from TEM and AUC, while the measured diameter of avidin (~7 nm) is similar to that determined from AUC experiments. The DLS diameter of about 22 nm for the bioconjugate closely agrees with the AUC data when assuming a density of 5.0 g cm⁻³ for the AUC experiments (Figure 5b). Both the AUC and DLS data further support avidin functionalization of the LaPO₄ NPs.

We also performed an assay utilizing biotin covalently linked to the organic dye fluorescein (biotin-FITC) to test the binding capacity of the avidin-functionalized NPs to biotin. The bioconjugates were mixed with biotin-FITC in the presence of 2-[*N*-morpholino]ethanesulfonic acid (MES) buffer (pH 4.75) and phosphate buffer (PB, pH 9) in a 9:1 volume ratio, and then centrifuged to sediment the particles, leading to the formation of a pellet. The supernatant fluorescence was measured and compared against a standard of known biotin-FITC concentration. A decrease in the amount of biotin-FITC in the supernatant (i.e., decrease in fluorescence intensity) was observed after incubation with the

bioconjugates, indicating biotin-FITC binding to the avidin-functionalized LaPO₄ NPs. The decrease in fluorescence intensity is directly correlated to the amount of biotin-FITC bound, and the point at which the fluorescence begins to appear in the supernatant corresponds to saturation binding of the avidin-coated LaPO₄ NPs. From these experiments, we calculated that 29 biotin molecules are bound per particle (see Supporting Information). Assuming that each avidin can bind four biotin molecules, the number of avidin molecules conjugated to each NP is calculated as about seven.

A second approach, the micro BCA protein assay, was performed to determine the amount of avidin conjugated to the NPs. This method is based on a colorimetric measurement and involved the comparison of the amount of avidin per NP with a standard concentration series of avidin (see Supporting Information). Approximately 6.2×10^{17} avidin molecules were calculated to be present in a sample of 7.7×10^{16} avidin-functionalized NPs, which equates to approximately eight avidin molecules per NP. This value is in good agreement with that determined from the fluorescence assay. The protein-to-nanoparticle ratio obtained is similar to that reported for bioconjugation of a maltose binding protein, which is slightly smaller than avidin (size 3 × 4 × 6.5 nm), with 6-nm diameter QDs, where it was found that about ten proteins were coupled to each QD NP.^[30]

In conclusion, fluorescent Ce/Tb-doped LaPO₄ NPs with a diameter of about 7 nm have been prepared as stable colloidal dispersions by modification with AHA, and subsequently biofunctionalized with the model protein avidin. Assays show that approximately eight avidin molecules are conjugated to each LaPO₄ NP. The avidin molecules on the NP surface remain active, as demonstrated by the ability of these avidin–NP conjugates to bind biotin. Since biotinylated molecules are easily obtained, we envisage the applicability of these bioconjugates in biosensing and biolabeling applications where their photostability and fluorescent properties should prove useful. Binding to biotinylated antibodies would demonstrate their use in immunofluorescence assays, particularly in ELISA-type applications. The successful bioconjugation of the AHA-functionalized LaPO₄ NPs with avidin suggests that, in principle, coupling of other biomolecules (such as protein A, antibodies, and DNA) to the rare-earth-doped LaPO₄ NPs through the same protocol is possible. Other features, such as dopant-tunable emission,^[14–17] photon-upconversion properties,^[31] and the possibility to detect multiple labels using a single excitation wavelength with no spectral overlap,^[17] offer considerable promise for the use of biofunctionalized rare-earth-doped lanthanide phosphate NPs in various biotechnological applications.

Experimental Section

Ce/Tb-doped LaPO₄ NPs, as a powder, were kindly provided by Nanosolutions GmbH, Hamburg, Germany. The NPs were synthesized according to the method of Haase and co-workers.^[16] Modification of the NPs was achieved by dispersing them with AHA in 0.1 M NaOH. The NPs were washed several times in 0.1 M tris(hydroxymethyl)aminomethane hydrochloride (Tris) buffer (pH 9) and ethanol, and then redispersed in 0.1 M Tris buffer (pH 9). For details see Supporting Information. This dispersion was colloiddally stable for at

least two months when stored at 4°C. The AHA-modified NPs were functionalized with avidin in a reaction mixture containing EDC dissolved in *N*-methyl-imidazole buffer (0.05 M, pH 7), and then redispersed in 0.05 M MES buffer, pH 4.75. For details see Supporting Information.

ζ-potentials of the NPs in aqueous solution were measured by using a ZetaSizer 2000, Malvern Instruments. DLS data were obtained with a High Performance Particle Sizer from Malvern Instruments. AUC measurements were performed on a Beckman-Coulter Optima XL-1 ultracentrifuge. UV/Vis spectra were obtained with a 8453 spectrophotometer from Agilent Technologies. The LaPO₄ NP molar extinction coefficient at a wavelength of 274 nm was calculated as $9.0 \times 10^5 \text{ M}^{-1} \text{ cm}^{-1}$, using a density of 5.0 g cm^{-3} and a radius of 3.8 nm. Fluorescence spectral measurements were performed by using a Cary Eclipse fluorescence spectrophotometer. The excitation wavelength for the LaPO₄ NPs was set at 254 nm. Excitation of biotinylated fluorescein was at 494 nm. TEM experiments were carried out on a Philips CM120 BioTWIN TEM operated at an acceleration voltage of 120 kV. Samples for TEM experiments were prepared by placing 3 μL of the NPs diluted 1/100 in 0.01 M Tris buffer (pH 9) on a TEM copper grid and allowing them to air dry overnight.

Binding of biotinylated fluorescein (biotin-FITC) to the avidin-functionalized NPs was tested by mixing the two components in the presence of buffer and centrifuging at 15000 g for 15 min to sediment the NPs containing bound biotin-FITC. The fluorescence of the supernatant was measured and compared against a standard containing the same initial amount of biotin-FITC. The concentration at which the avidin-coated NPs were saturated with biotin was determined by performing the assay with final concentrations of biotin-FITC ranging from 0.05 μM to 2.5 μM. An adsorption isotherm was plotted and the amount of biotin bound to the avidin-coated NPs was determined, and hence the amount of avidin per NP (see Supporting Information). The Micro BCA Protein Assay Reagent Kit was obtained from Pierce (Rockford, IL) and used as described in the protocol (see Supporting Information).

Received: June 3, 2004

Keywords: biolabeling · colloids · lanthanides · luminescence · nanoparticles

- [13] A. M. Derfus, W. C. W. Chan, S. N. Bhatia, *Nano. Lett.* **2004**, *4*, 11.
- [14] H. Meyssamy, K. Riwotzki, A. Kornowski, S. Naused, M. Haase, *Adv. Mater.* **1999**, *11*, 840.
- [15] K. Riwotzki, H. Meyssamy, A. Kornowski, M. Haase, *J. Phys. Chem. B* **2000**, *104*, 2824.
- [16] K. Riwotzki, H. Meyssamy, H. Schnablegger, A. Kornowski, M. Haase, *Angew. Chem.* **2001**, *113*, 574; *Angew. Chem. Int. Ed.* **2001**, *40*, 573.
- [17] P. Schuetz, F. Caruso, *Chem. Mater.* **2002**, *14*, 4509.
- [18] A. J. Hutchison, *Peritoneal Dial. Int.* **1999**, *19*, S408. Based on this and other studies using lanthanum ions for medical applications.
- [19] J. C. Bourcet, F. K. Fong, *J. Chem. Phys.* **1974**, *60*, 34.
- [20] N. Hashimoto, Y. Takada, K. Sato, S. Ibuki, *J. Lumin.* **1991**, *22*, 893.
- [21] N. Kato, P. Schuetz, A. Fery, F. Caruso, *Macromolecules* **2002**, *35*, 9780.
- [22] S. E. Burke, C. J. Barrett, *Langmuir* **2003**, *19*, 3297.
- [23] M. Wilchek, E. A. Bayer, *Methods Enzymol.* **1990**, *184*, 14.
- [24] O. Livnah, E. A. Bayer, M. Wilchek, J. L. Sussman, *Proc. Natl. Acad. Sci. USA* **1993**, *90*, 5076.
- [25] A. L. Lehninger, *Biochemistry*, 2nd ed., Worth Publishers, New York, **1975**.
- [26] The spectral range from 480 to 520 nm is not shown, as the use of a filter was required to eliminate excitation light.
- [27] For calculation, a density of 5.0 g cm^{-3} was used, as this is the mean value for the mineral monazite, which has the same constituents as the LaPO₄ NPs. *Encyclopedia of Minerals* (Eds.: W. L. Roberts, G. R. Rapp, Jr., J. Weber), Van Nostrand Reinhold, New York, **1974**, p. 143.
- [28] Both spherical and ellipsoidal nanoparticle shapes are observed by TEM, in agreement with previous work.^[16]
- [29] N. M. Green, M. A. Joynson, *Biochem. J.* **1970**, *118*, 71.
- [30] I. G. Medintz, A. R. Clapp, H. Matoussi, E. R. Goldman, B. Fischer, J. M. Mauro, *Nat. Mater.* **2003**, *2*, 630.
- [31] S. Heer, O. Lehmann, M. Haase, H.-U. Güdel, *Angew. Chem.* **2003**, *115*, 3288; *Angew. Chem. Int. Ed.* **2003**, *42*, 3179.

- [1] W. J. Parak, D. Gerion, T. Pellegrino, D. Zanchet, C. Micheel, S. C. Williams, R. Boudreau, M. A. Le Gros, C. A. Larabell, A. P. Alivisatos, *Nanotechnology* **2003**, *14*, R15.
- [2] M. Bruchez, M. Moronne, P. Gin, S. Weiss, A. P. Alivisatos, *Science* **1998**, *281*, 2013.
- [3] W. C. W. Chan, S. Nie, *Science* **1998**, *281*, 2016.
- [4] H. Weller, *Adv. Mater.* **1993**, *5*, 88.
- [5] A. P. Alivisatos, *Science* **1996**, *271*, 933.
- [6] Y. Xiao, F. Patolsky, E. Katz, J. F. Hainfeld, I. Willner, *Science* **2003**, *299*, 1877.
- [7] C. M. Niemeyer, *Angew. Chem.* **2001**, *113*, 4254; *Angew. Chem. Int. Ed.* **2001**, *40*, 4128.
- [8] E. R. Goldman, E. D. Balighian, H. Matoussi, M. K. Kuno, J. M. Mauro, P. T. Tran, G. P. Anderson, *J. Am. Chem. Soc.* **2002**, *124*, 6378.
- [9] X. Y. Wu, H. J. Liu, J. Q. Liu, K. N. Haley, J. A. Treadway, J. P. Larson, N. F. Ge, F. Peale, M. P. Bruchez, *Nat. Biotechnol.* **2003**, *21*, 41.
- [10] B. Dubertret, P. Skourides, D. J. Norris, V. Noireaux, A. H. Brivanlou, A. Libchaber, *Science* **2002**, *298*, 1759.
- [11] J. K. Jaiswal, H. Matoussi, J. M. Mauro, S. M. Simon, *Nat. Biotechnol.* **2003**, *21*, 47.
- [12] B. Ballou, B. C. Lagerholm, L. A. Ernst, M. C. Bruchez, A. S. Waggoner, *Bioconjugate Chem.* **2004**, *15*, 79.

Two- and Three-Dimensional Mesoporous Iron Oxides with Microporous Walls**

Feng Jiao and Peter G. Bruce*

There is intense interest in preparing mesoporous transition-metal oxides—in part because of their potential applications, including for catalysis, electron transfer, energy conversion and storage, and as magnetic materials.^[1,2] Several mesoporous transition-metal oxides have been prepared, such as TiO_2 , ZrO_2 , Nb_2O_5 , WO_3 , and MnO_x ,^[3,4] however, mesoporous iron oxides are of particular interest. Reversible intercalation of Li can occur for nanoparticulate Fe_2O_3 , but it is much more difficult to carry out such intercalation with Fe_2O_3 of normal particle size. Similar behavior may be possible with mesoporous iron oxides since the walls are of nanodimensions. The limited dimensions of the walls will also alter the magnetic behavior from that of bulk Fe_2O_3 . Although disordered iron oxides with high surface areas (ca. $270\text{ m}^2\text{ g}^{-1}$) have been prepared, to the best of our knowledge no ordered mesoporous iron oxides have been synthesized directly.^[5] Herein, we report the synthesis of ordered mesoporous Fe_2O_3 with controllable pore structures. Ordered two-dimensional (2D) hexagonal mesoporous iron oxide (2DMIO) with $P6mm$ symmetry and three-dimensional (3D) cubic mesoporous iron oxide (3DMIO) with $Fm3m$ symmetry have been prepared by using decylamine as the template and Fe^{III} ethoxide as the precursor. Different aging conditions were used for 2DMIO and 3DMIO, and in both cases, the walls exhibit a microporous structure.

We first confirmed successful removal of the template from 2DMIO and 3DMIO by elemental analysis. As-prepared 2DMIO contained C 44.0%, H 9.69%, and N 4.82% by weight, while the 2DMIO after ethanol extraction contained C 6.48%, H 2.17%, and N 0.28%. As-prepared 3DMIO contained C 37.9%, H 8.80%, and N 4.14%, while the values for 3DMIO after ethanol extraction were C 7.08%, H 1.71%, and N 0.35%. Based on the elemental analysis for nitrogen, about 94% and 92% of the template had been removed from 2DMIO and 3DMIO, respectively. Slightly high C and H contents were observed after removal of the template, which may correspond to a small amount of ethanol remaining in the pores (<7% by weight in both cases).

A transmission electron microscopy (TEM) image of ordered 2DMIO was recorded along the (001) direction (Figure 1a) and the corresponding electron diffraction pat-

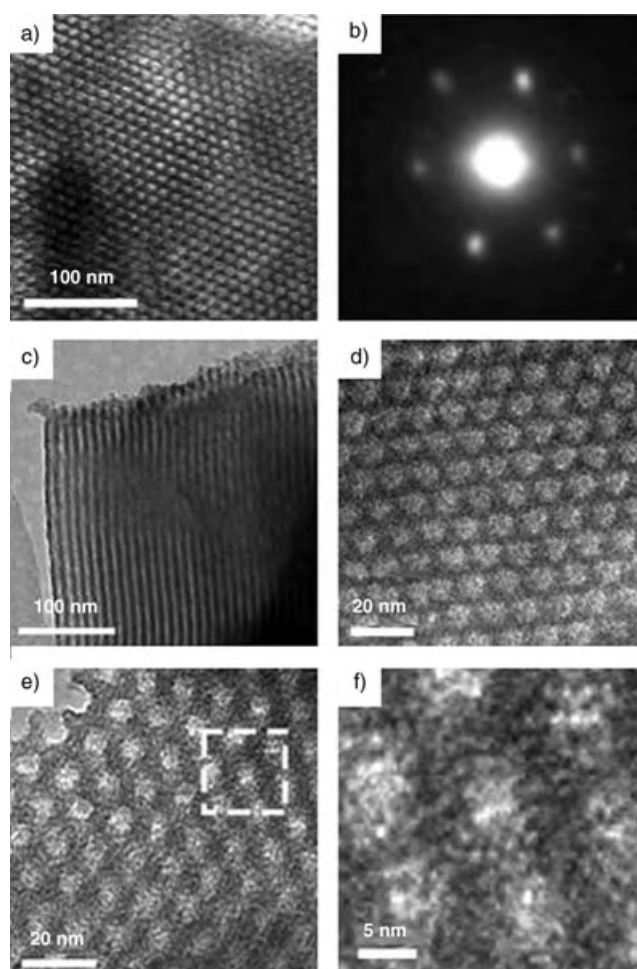


Figure 1. a) TEM image of as-prepared 2DMIO recorded along the (001) direction, b) the corresponding electron diffraction pattern, c) TEM image recorded along the (110) direction. The HRTEM images recorded along the (001) direction of d) as-prepared 2DMIO and e) after ethanol extraction. f) Enlarged HRTEM image of a selected area of (e).

tern (Figure 1b) confirmed a hexagonal structure over a large area. Examination of a wide range of particles demonstrated that they all had similar structures. Combining these results with the TEM result recorded along the (110) direction (Figure 1c) led to the conclusion that our 2DMIO has a large-scale well-ordered 2D hexagonal array of mesopores, similar to those typically observed in 2D hexagonal mesoporous silica materials, such as MCM-41 and SBA-15.^[6] The TEM results recorded along the (110) direction confirmed that the mesoporosity exists throughout the particles, not just near surface regions. An average pore size of 70 Å and wall thickness of 40 Å , with a cell parameter a_0 of 110 Å , were estimated from the high-resolution transmission electron microscopy (HRTEM) image recorded along the (001) direction of as-prepared 2DMIO (Figure 1d). The low-angle powder X-ray diffraction (PXRD) pattern (Figure 2a) of as-prepared 2DMIO exhibits a diffraction peak at $2\theta = 1.14^\circ$, which translates to a d spacing of 97.6 Å ($\text{Fe}_{K\alpha_1}$, $\lambda = 1.936\text{ Å}$). The peak may be indexed as the (100) reflection, based on the hexagonal space group $P6mm$ identified by TEM/electron

[*] F. Jiao, Prof. Dr. P. G. Bruce
School of Chemistry
University of St. Andrews
The Purdie Building, North Haugh, St Andrews KY16 9ST (UK)
Fax: (+44) 1334-463-808
E-mail: p.g.bruce@st-and.ac.uk

[**] P.G.B. is indebted to the EPSRC, the Royal Society, and the EU for financial support. The authors are grateful to J.-C. Jumas, Montpellier, for carrying out the Moessbauer measurements.

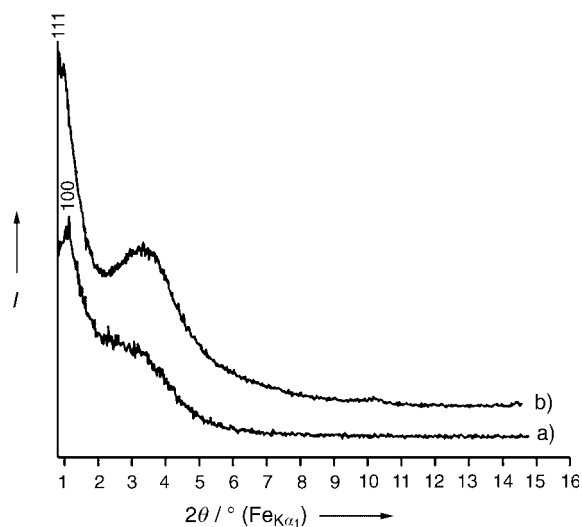


Figure 2. Low-angle PXRD patterns: a) as-prepared 2DMIO; b) as-prepared 3DMIO.

diffraction analysis. The (100) reflection corresponds to a unit cell parameter a_0 of 113 Å, which is in good agreement with the TEM data. From the well-ordered hexagonal arrangement of mesopores revealed in Figure 1 a–c, peaks might also be expected in the PXRD pattern at $2\theta = 1.97$ and 2.29° , which corresponds to d spacings of 56.4 and 48.4 Å for the (110) and (200) reflections, respectively. These peaks are not evident. This appears to result, at least in part, from the existence of a broad peak in the range of 2θ from 2.2 to 4° , which corresponds to d spacings between 25 and 45 Å. Such a broad peak is consistent with disordered microporous regions within the walls as observed by HRTEM (Figure 1 f) and discussed later. After removing the template by ethanol extraction, the HRTEM image of 2DMIO (Figure 1 e) shows a smaller average pore size of 54 Å and a wall thickness of 51 Å; the reduced pore diameter is a consequence of shrinkage accompanying removal of the decylamine. Such a pore size is larger than those previously reported for mesoporous transition-metal oxides templated by alkyl amines of comparable size, such as TiO_2 and Nb_2O_5 ,^[1,4,7] which indicates the formation mechanism may be different in the present case. Samples of 2DMIO were calcined at various temperatures to investigate the thermal stability. TEM analysis confirmed that the mesostructure was thermally stable up to 250 °C. Moessbauer measurements indicate that the Fe oxidation state is +3 (high spin) and that the iron is in an octahedral environment of oxygen atoms. More details concerning the Moessbauer studies will be published subsequently, along with magnetic measurements; however, the Moessbauer data suggest superparamagnetic behavior consistent with the small (approximately 51 Å) dimensions of the walls.

A detailed examination of the HRTEM image (Figure 1 f) for as-prepared 2DMIO shows a large quantity of disordered micropores within the walls and with pore sizes of around 10 Å. This observation suggests that the mechanism for the formation of 2DMIO mesopores may involve self-assembly of microporous structures. Further extensive studies will be

required to understand the exact nature of the formation mechanism for this micro-/mesoporous solid, including the role of the template and self-assembly of microporous structures into the micro-/mesoporous solid; this is beyond the scope of the present study. The microporosity of 2DMIO is further confirmed by nitrogen adsorption/desorption analysis. The N_2 adsorption/desorption isotherms (Figure 3 a) for

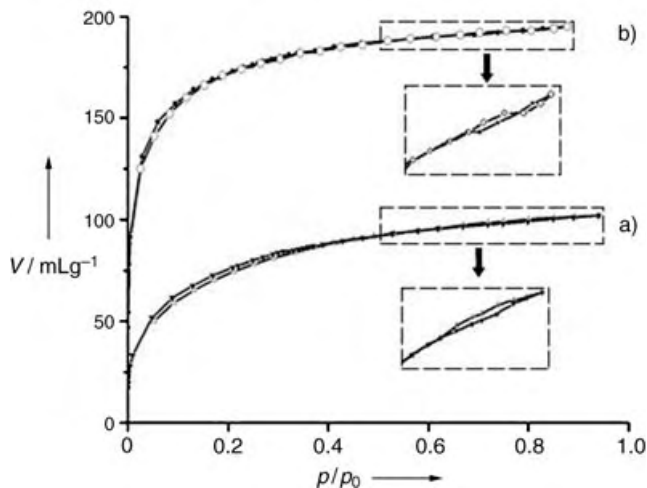


Figure 3. Nitrogen adsorption/desorption isotherms: a) 2DMIO and b) 3DMIO after ethanol extraction. The inset shows an enlarged region of the curves between relative pressures of 0.6 and 0.8.

2DMIO after removal of the template show predominantly a type I curve, thus indicating that the dominant surface area is in fact the micropores. There is a small step at a relative pressure of 0.7–0.8, which corresponds to mesoporous adsorption in 2DMIO. The identification of microporosity in the walls of mesoporous materials has only occasionally been observed before, particularly in SBA-15, MAS-7, and MTS-9.^[8] There is an important and unique difference between SBA-15, MAS-7, and MTS-9 and our materials: The ratio of micropores to mesopores is much higher in the transition-metal oxides, as is evident from the small mesopore adsorption at relative pressures of 0.7 and 0.8. As the TEM image clearly indicates significant mesoporosity, we propose that the surfaces of the mesoporous walls may themselves be highly microporous so that N_2 “sees” a mainly microporous material during adsorption. The Brunauer–Emmett–Teller (BET) surface area of 2DMIO is 340 $\text{m}^2 \text{g}^{-1}$.

Our approach can also be used to prepare three-dimensional mesoporous iron oxides by adjusting the aging temperature. Ordered 3D cubic mesoporous iron oxide (3DMIO) with $Fm\bar{3}m$ symmetry is obtained when the Fe^{III} ethoxide/decylamine mixture is further aged at 150 °C. TEM images recorded from different directions (Figure 4 a–c) confirmed the large area of ordered cubic $Fm\bar{3}m$ mesoporous iron oxides, and Moessbauer measurements confirmed that the oxidation state is +3. The low-angle PXRD spectra (Figure 2 b) show a main diffraction peak at $2\theta = 1.06^\circ$, which corresponds to a d spacing of 104.6 Å. The unit cell parameter a_0 calculated from the PXRD pattern is 182 Å, which is in reasonable agreement with the value of 192 Å determined

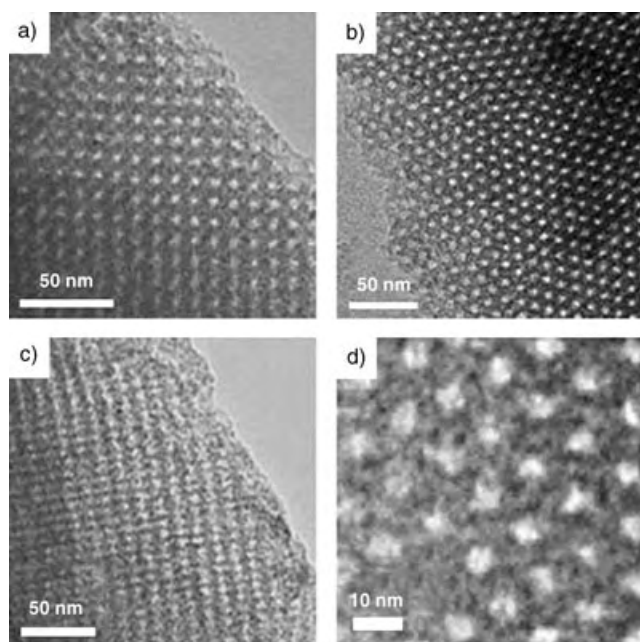


Figure 4. TEM images of 3DMIO recorded along the: a) (100) direction; b) (110) direction; c) (211) direction. d) Enlarged region of (b).

from the TEM analysis. Microporosity similar to that observed in 2DMIO is seen in 3DMIO by HRTEM (Figure 4d) and in the N_2 adsorption/desorption analysis (Figure 3b). The BET surface area calculated from the desorption isotherm is approximately $610 \text{ m}^2 \text{ g}^{-1}$, which is about twice that for 2DMIO, perhaps because of the higher accessible pore surface in the three-dimensional structure.

The simultaneous presence of micro- and mesoporous structures is not common. This is the first time alkyl amine templates have been used as bifunctional surfactants which can template micro- as well as mesostructures.

Experimental Section

The synthesis procedure was adapted from that employed for Nb_2O_5 .^[4] In a typical synthesis of 2D hexagonal ordered mesoporous Fe_2O_3 , Fe^{III} ethoxide (0.573 g, 3 mmol; 99%, ABCR) was dissolved in ethanol (35 mL), with stirring for 5 minutes, followed by addition of decylamine (0.472 g, 3 mmol; 95%, Aldrich). After stirring the mixture at 40°C for 2 h, it was maintained at 40°C for 24 h, and further aged at 80°C for 6 h. In the case of 3DMIO, additional aging at 150°C was carried out. The products were then filtered and washed with ethanol. The template may be removed by extraction with excess ethanol. As-prepared material (0.1 g) was added to ethanol (100 mL) with stirring at RT for 30 min, followed by filtration and drying at 70°C under vacuum for 1 h. The materials before and after template removal were characterized by elemental analysis (Carlo Erba CHNS analyzer), TEM (Jeol JEM-2011), PXRD (Stoe STADI/P diffractometer operating in transmission mode with $\text{Fe}_{K\alpha_1}$ radiation, $\lambda = 1.936 \text{ \AA}$), N_2 adsorption (Hiden IGA porosimeter), and Moessbauer spectroscopy (^{57}Fe Moessbauer spectra, collected at RT on a EG&G constant accelerator spectrometer in transmission mode).

Received: May 28, 2004

Published Online: August 20, 2004

Keywords: materials science · mesoporous materials · microporous materials · transition metals

- [1] D. M. Antonelli, J. Y. Ying, *Angew. Chem.* **1995**, *107*, 2202; *Angew. Chem. Int. Ed. Engl.* **1995**, *34*, 2014.
- [2] a) F. Schüth, *Chem. Mater.* **2001**, *13*, 3184; b) P. Yang, T. Deng, D. Zhao, P. Feng, D. Pine, B. F. Chmelka, G. M. Whitesides, G. D. Stucky, *Science* **1998**, *282*, 2244; c) X. He, D. Antonelli, *Angew. Chem.* **2002**, *114*, 222; *Angew. Chem. Int. Ed.* **2002**, *41*, 214; d) P. Behrens, *Angew. Chem.* **1996**, *108*, 561; *Angew. Chem. Int. Ed. Engl.* **1996**, *35*, 515; e) Q. S. Huo, D. I. Margolese, U. Ciesla, D. G. Demuth, P. Y. Feng, T. E. Gier, P. Sieger, A. Firouzi, B. F. Chmelka, F. Schuth, G. D. Stucky, *Chem. Mater.* **1994**, *6*, 1176.
- [3] a) P. Yang, D. Zhao, D. I. Margolese, B. F. Chmelka, G. D. Stucky, *Nature* **1998**, *396*, 152; b) Z. Tian, W. Tong, J. Wang, N. Duan, V. V. Krishnan, S. L. Suib, *Science* **1997**, *276*, 926; c) B. Tian, H. Yang, X. Liu, S. Xie, C. Yu, J. Fan, B. Tu, D. Zhao, *Chem. Commun.* **2002**, 1824; d) E. L. Crepaldi, G. J. de A. A. Soler-Illia, D. Grosso, F. Cagnol, F. Ribot, C. Sanchez, *J. Am. Chem. Soc.* **2003**, *125*, 9770; e) N. Ulagappan, C. N. R. Rao, *Chem. Commun.* **1996**, 1685; f) X. Xu, B. Tian, J. Kong, S. Zhang, B. Liu, D. Zhao, *Adv. Mater.* **2003**, *15*, 1932.
- [4] D. M. Antonelli, A. Nakahira, J. Y. Ying, *Inorg. Chem.* **1996**, *35*, 3126.
- [5] a) D. N. Srivastava, N. Perkas, A. Gedanken, I. Felner, *J. Phys. Chem. B* **2002**, *106*, 1878; b) A. S. Malik, M. J. Duncan, P. G. Bruce, *J. Mater. Chem.* **2003**, *13*, 2123.
- [6] a) C. T. Kresge, M. E. Leonowicz, W. J. Roth, J. C. Vartulli, J. S. Beck, *Nature* **1992**, *357*, 710; b) D. Y. Zhao, J. L. Feng, Q. S. Huo, N. Melosh, G. H. Fredrickson, B. F. Chmelka, G. D. Stucky, *Science* **1998**, *279*, 548.
- [7] T. Sun, J. Y. Ying, *Nature* **1997**, *389*, 704.
- [8] a) M. Kruk, M. Jaroniec, C. H. Ko, R. Ryoo, *Chem. Mater.* **2000**, *12*, 1961; b) P. I. Ravikovitch, A. V. Neimark, *J. Phys. Chem. B* **2001**, *105*, 6817; c) J. Liu, X. Zhang, Y. Han, F. S. Xiao, *Chem. Mater.* **2002**, *14*, 2536.
- [9] Note after publication of this manuscript online on August 20, 2004 in the Early View mode: The TEM data shown in Figures 1 and 4 indicate an ordered mesostructure prior to template removal and suggest the presence of mesopores in the material after template removal, yet the N_2 isotherms do not show the typical behavior expected for large mesopores of around 5 nm. It

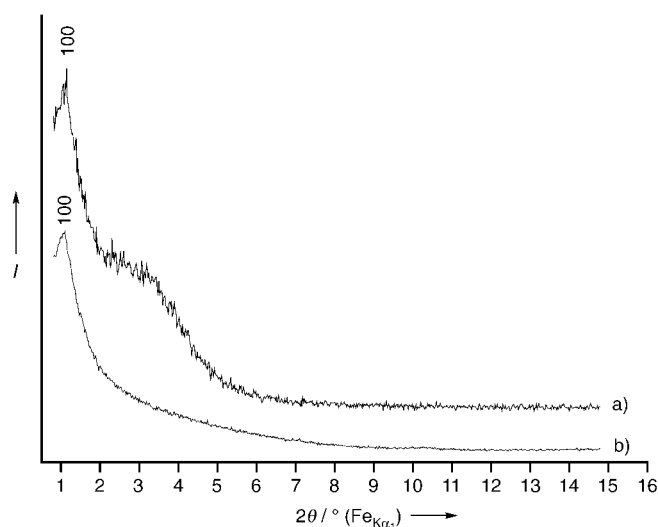


Figure 5. Low-angle PXRD patterns: a) as-prepared 2DMIO and b) 2DMIO after removal of the template.

should, however, be noted that pore dimensions are not well-determined by TEM. The N_2 isotherms are consistent with smaller mesopores (M. Kruk and M. Jaroniec, *Chem. Mater.* **2001**, *13*, 3169), as observed in mesoporous TiO_2 (D. M. Antonelli, *Micropor. Mesopor. Mater.* **1999**, *30*, 315), and the presence of microporosity; they also indicate that the pores are distributed in size. Further work is required to rationalize the isotherms and TEM data in detail. One possible explanation is that the pores shrink unevenly on removal of the template, thus leading to distortion of the pores and rough walls; some material may even detach from the walls and locate within the pores. As a result the pores cannot be described as regular cylinders and exhibit a smaller effective diameter than suggested by TEM. The TEM data after template removal (for example, Figure 1e) are consistent with pores that are more distorted than prior to removal of the template. An X-ray diffraction pattern after removal of the template shows one low-angle peak (see Figure 5) indicating that the pore order is not sufficient to generate higher angle peaks.

tive oxidative C–C coupling of alkylated phenols to stilbenequinones is rare^[3] and this process often requires strong oxidants.^[4] To our knowledge, self-oxidation of phenols or phenol derivatives, in the absence of external oxidant, has not been reported. Herein we report an unprecedented oxidative-coupling process in which a phenolate oxygen atom serves as the oxidant, which results in cleavage of the aryl–oxygen bond. This process involves a phenolate metal complex and results in the synthesis and crystallographic characterization of a new bimetallic stilbenequinone complex having two quinonoid C=O bonds η^2 -coordinated to the metal centers.^[5] The metal oxidation state in the C–O cleaved product is retained. Oxidative coupling of the metal complex, can also be affected by an external oxidant, and, significantly, it is metal selective.

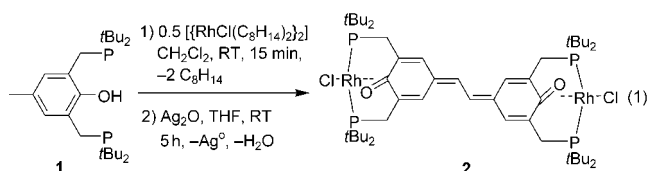
Treatment of the 4-methylphenol bisphosphine ligand **1**^[6] with 0.5 equivalents of $[\{\text{RhCl}(\text{cyclooctene})_2\}_2]$ in CH_2Cl_2 at room temperature for 15 min followed by addition of Ag_2O (2–3 equiv) and continuous stirring for 5 h resulted in the selective formation of the bimetallic stilbenequinone complex **2** [Eq. (1)]. Formation of **2** was indicated by a change of the green reaction mixture to deep blue.

C–O Activation

Self-Oxidation of a Phenolate Complex to a Bimetallic Stilbene Quinone**

Milko E. van der Boom,* Tatiana Zubkov, Atindra D. Shukla, Boris Rybtchinski, Linda J. W. Shimon, Haim Rozenberg, Yehoshua Ben-David, and David Milstein*

Oxidation chemistry of phenol derivatives is of interest,^[1–4] mainly since it affords convenient routes to a variety of basic chemicals.^[1] Widely used phenolic food antioxidants, such as 4-methyl-2,6-di-*tert*-butylphenol (butylated hydroxy toluene, BHT) are known to form a diversity of compounds upon oxidation, including colored stilbenequinone systems.^[2] Selec-



The diamagnetic complex **2** was formed quantitatively as judged by $^{31}\text{P}\{^1\text{H}\}$ NMR spectroscopy, isolated as a blue solid in 50% yield, and fully characterized by a combination of ^1H and $^{31}\text{P}\{^1\text{H}\}$ NMR spectroscopy techniques, UV/Vis spectroscopy, FAB mass spectrometry, and by single-crystal X-ray crystallography. The $^{31}\text{P}\{^1\text{H}\}$ NMR spectrum showed a doublet at $\delta = 44.18$ ppm ($J_{\text{Rh,P}} = 117.7$ Hz), which indicates that the phosphorus atoms are chemically equivalent and coordinated to a metal center. FAB-MS measurements showed the signal for the molecular ion (m/z 1118.307) and a correct isotope pattern. The UV/Vis spectrum of **2** exhibited one broad charge-transfer band at $\lambda_{\text{max}} = 576$ nm ($\omega_{1/2} = 77$ nm, $\epsilon = 29 \times 10^3$ in acetone).

Dark blue crystals of complex **2** were obtained upon slow evaporation of a CH_2Cl_2 solution under a nitrogen atmosphere at room temperature. The X-ray structure of **2** reveals the formation of the bimetallic stilbenequinone structure and the rare η^2 coordination mode of the metal centers to the quinonoid C=O double bonds (Figure 1).^[17]

The fourteen carbon atoms of the stilbenequinone backbone are located in the same plane with the two metal-coordinated oxygen atoms out of the plane by about 0.3 Å. The relatively short C(14)–C(14A) bond length of 1.404(5) Å may indicate a contribution of other resonance structures.^[3] The phosphine groups are mutually *trans* with a significantly distorted P–Rh–P angle of 167.84(2)°. Distorted P–M–P angles are common for pincer complexes.^[7] The C–O, Rh–O, and Rh–C bonds of 1.325(3), 2.0562(16), and 2.186(2) Å, respec-

[*] Dr. M. E. van der Boom, T. Zubkov, Dr. A. D. Shukla, Dr. B. Rybtchinski, Y. Ben-David, Prof. D. Milstein
Department of Organic Chemistry
Weizmann Institute of Science
76100 Rehovot (Israel)
Fax: (+972) 8-934-4142
E-mail: milko.vanderboom@weizmann.ac.il
david.milstein@weizmann.ac.il

Dr. L. J. W. Shimon, Dr. H. Rozenberg
Chemical Research Support
Weizmann Institute of Science, 76100 Rehovot (Israel)

[**] This research was supported by the Israel Science Foundation, Helen and Martin Kimmel Center for Molecular Design, and the Minerva Foundation (Munich). A.S. is the recipient of The Reva G. Stone Postdoctoral Fellowship. D.M. holds the Israel Matz Professorial Chair of Organic Chemistry. M.E.vd.B. is the incumbent of the Dewey David Stone and Harry Levine Career Development Chair and thanks the Israeli Council for Higher Education for an Alon Fellowship.

Supporting information for this article is available on the WWW under <http://www.angewandte.org> or from the author.

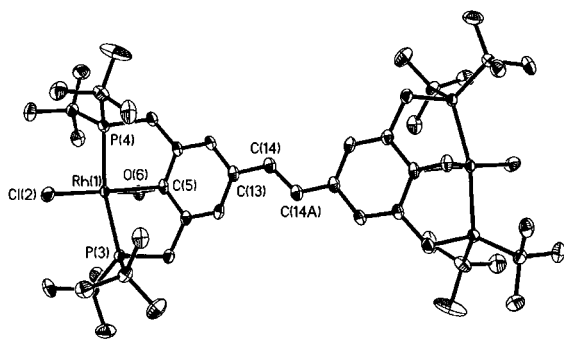
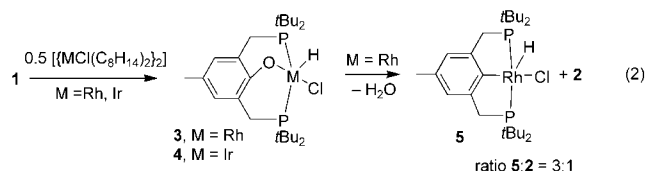


Figure 1. Ortep diagram of complex **2** (thermal ellipsoids set at 50 % probability). Selected bond lengths [Å] and angles [°]: Rh(1)–O(6) 2.0562(16), Rh(1)–C(5) 2.186(2), Rh(1)–Cl(2) 2.3156(8), Rh(1)–P(3) 2.3290(7), Rh(1)–P(4) 2.3457(7), C(5)–O(6) 1.325(3), C(13)–C(14) 1.395(3), C(14)–C(14A) 1.404(5); P(3)–Rh(1)–P(4) 167.84(2).

tively, compare well with those observed for a monomeric Ir^I phenoxonium cation.^[8] Other coordination modes in quinonoid systems are much more common.^[9–12]

¹H, ³¹P{¹H}, and ¹³C{¹H} NMR spectroscopy measurements of a sample of the reaction mixture before addition of the oxidation reagent indicated the initial formation of the unstable Rh^{III} hydride complex **3** as the only detectable phosphorus-containing product [Eq. (2)]. Remarkably, continuous stirring of the reaction mixture for three days without Ag₂O in a sealed vessel with rigorous exclusion of air resulted in the disappearance of intermediate **3** with formation of the stilbenequinone **2** and complex **5** in a 1:3 molar ratio as judged by ³¹P{¹H} NMR spectroscopy.



Complex **5** shows very similar spectroscopic properties to an analogous complex lacking the *p*-methyl group on the aromatic ring.^[13] The ¹H NMR spectrum clearly shows a characteristic rhodium-hydride double triplets at $\delta = -27.53$ ppm (¹J_{Rh,H} = 52.8 Hz, ²J_{P,H} = 12.0 Hz), which collapse into a doublet in the ¹H{³¹P} NMR spectrum, whereas the ³¹P{¹H} spectrum shows a doublet at $\delta = 74.9$ ppm (¹J_{Rh,P} = 115.1 Hz). The product distribution does not change after consumption of intermediate **3**, and the stoichiometry is consistent with the formation of water. Water has been detected by GC-MS. Performing this reaction at 60 °C for three days resulted in the same outcome. Formation of complex **5** by activation of the strong aryl C–O bond at room temperature is unexpected. Only a few cases of aryl–O bond cleavage of ethers or phenols under mild homogeneous reaction conditions have been reported.^[6,14,15]

Formation of complex **2** is a clear example of transition-metal-based selectivity. Treatment of compound **1** with 0.5 equivalent of [[IrCl(cyclooctene)]₂] resulted in O–H

activation and quantitative formation of the fully characterized Ir^{III} phenoxy hydride complex **4** [Eq. (2)]. Orange crystals of **4** were obtained from a benzene solution by slow evaporation of the solvent under N₂ at room temperature (Figure 2).^[17] The C–O, Ir–O, Ir...C separations of 1.334(9), 2.083(5), and 2.363(8) Å are in agreement with a phenoxy type structure.^[16]

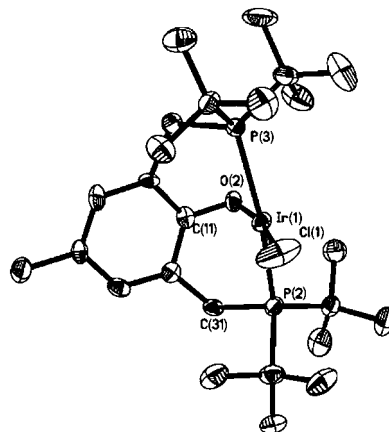


Figure 2. Ortep diagram of complex **4** (thermal ellipsoids set at 50 % probability). Selected interatomic distances [Å] and angles [°]: Ir(1)–O(2) 2.083(5), Ir(1)···C(1) 2.363(8), Ir(1)–Cl(1) 2.349(3), Ir(1)–P(2) 2.354(1), Ir(1)–P(3) 2.363(72), C(1)–O(2) 1.334(9); P(2)–Ir(1)–P(3) 163.97(8).

In sharp contrast to the aforementioned reactivity of the analogous Rh^{III} hydride complex **3**, no formation of bimetallic compounds or other iridium complexes was detected even after three days of heating at 60 °C in THF in a sealed pressure tube. Attempts to oxidize complex **4** with Ag₂O, O₂, ferrocenium hexafluorophosphate, and cyclic voltammetry resulted in an indicative color change from red to purple but ³¹P{¹H} NMR spectroscopy measurements showed mixtures of unidentifiable compounds. Apparently the metal center plays an important role in the stilbenequinone complex formation. Although in both cases (**3**, **4**) a d⁶ metal center is used, the second-row metal hydride complex **3** is less stable and readily undergoes stilbenequinone formation whereas the third-row metal hydride complex **4** is far more thermally robust but exhibits an unselective reactivity pattern.

Mechanistically, it is likely that the room-temperature dearomatization and dimerization of complex **3** at the methyl group to form **2** proceeds via a *p*-quinonemethide intermediate. An unusual series of monomeric phosphorus–carbon–phosphorus(PCP)-type Rh^I and Ir^I quinone methide complexes (C=C bond bound to the metal center) have been isolated.^[11] Formation of a strong metal–olefin bond may contribute to the stability of these compounds, whereas the Rh^I intermediate proposed herein (C=O bond bound to the metal center) undergoes oxidative coupling to afford **2**. However, other mechanistic pathways are also possible. The steric hindrance provided by the two bulky CH₂PtBu₂ groups and stabilization of the *p*-quinonemethide structure by η²-C=O bond coordination to the low-valent rhodium center may allow this postulated intermediate sufficient lifetime to

interact with a second intermediate. No coupling products with complex **5** or solvents were detected. It is remarkable that quantitative formation of the stilbenequinone complex **2** occurs even in the absence of an added oxidant. The Rh^{III} hydride intermediate **3** plays a dual role—as precursor for formation of stilbenequinone complex **2** and as an oxygen-transfer agent. Examples of chemical processes wherein one metal complex fulfills two or more distinctly different tasks are not common.

In summary, a unique oxidative dimerization process of a phenolic compound has been observed with a pincer model system, in which the phenolic oxygen atom itself serves as an oxidant by aryl–oxygen and C–H cleavage, leading to a new metal complex. The oxidative dimerization process can also be affected by an external oxidant. The process is metal selective.

Received: April 19, 2004

Revised: July 11, 2004

Keywords: C–O activation · iridium · quinones · rhodium

- [13] C. J. Moulton, B. L. Shaw, *J. Chem. Soc. Dalton Trans.* **1976**, 1020.
 - [14] a) F. Kakiuchi, M. Usui, S. Ueno, N. Chatani, S. Murai, *J. Am. Chem. Soc.* **2004**, *126*, 2706; b) H. Kawaguchi, T. Matsuo, *J. Am. Chem. Soc.* **2003**, *125*, 14254; c) R. Baumann, R. Stumpf, W. M. Davis, L.-C. Liang, R. R. Schrock, *J. Am. Chem. Soc.* **1999**, *121*, 7822; d) J. B. Bonanno, T. P. Henry, D. R. Neithamer, P. T. Wolczanski, E. B. Lobkovsky, *J. Am. Chem. Soc.* **1996**, *118*, 5132.
 - [15] Analogous benzylic complexes undergo sp²–sp³ C–C bond activation, for a review see: B. Rybtchinski, D. Milstein, *Angew. Chem.* **1999**, *111*, 918; *Angew. Chem. Int. Ed.* **1999**, *38*, 870.
 - [16] The M–C_{aryl} σ-bond length in cyclometalated pincer complexes is approximately 2.1 Å.^[7,15] X-ray characterized Pd^{II} and Rh^I phenoxy pincer complexes are reported in ref. [6].
 - [17] CCDC-236289 (**2**), CCDC-236290 (**4**) contain the supplementary crystallographic data for this paper. These data can be obtained free of charge via www.ccdc.cam.ac.uk/conts/retrieving.html (or from the Cambridge Crystallographic Data Centre, 12 Union Road, Cambridge CB2 1EZ, UK; fax: (+44) 1223-336-033; or deposit@ccdc.cam.ac.uk).
-
- [1] a) Y. Feng, L. Liu, Y. Fang, Q.-X. Guo, *J. Phys. Chem. A* **2002**, *106*, 11518; b) C. J. Davis, C. J. Moody, *Synlett* **2002**, *11*, 1874; c) J. S. Wright, E. R. Johnson, G. A. Dilabio, *J. Am. Chem. Soc.* **2001**, *123*, 1173; d) L. Forni, C. Oliva, A. V. Vishniakov, A. M. Ezerets, I. E. Mukovozov, F. P. Vatti, V. N. Zubkovskaja, *J. Catal.* **1994**, *145*, 194; e) M. Shimizu, Y. Watanabe, H. Orita, T. Hayakawa, K. Takehira, *Bull. Chem. Soc. Jpn.* **1993**, *66*, 251; f) J. Pilar, J. Rotschova, J. Pospisil, *Angew. Makromol. Chem.* **1992**, *200*, 147; g) A. S. Hay, *J. Polym. Sci. Part A* **1998**, *36*, 505.
 - [2] a) K. J. Omura, *J. Org. Chem.* **1992**, *57*, 306; b) B. M. Benjamin, V. F. Raaen, E. W. Hagaman, L. L. Brown, *J. Org. Chem.* **1978**, *43*, 2986.
 - [3] K. Oyaizu, K. Saito, E. Tsuchida, *Chem. Lett.* **2000**, 1318.
 - [4] a) D. E. Katsoulis, M. T. Pope, *J. Chem. Soc. Dalton Trans.* **1989**, *8*, 1483; b) K. Omura, *J. Org. Chem.* **1984**, *49*, 3046; c) V. Balogh, M. Fétizon, M. Golfier, *J. Org. Chem.* **1971**, *36*, 1339.
 - [5] For recent examples of bimetallic pincer complexes, see: a) G. Rodríguez, M. Albrecht, J. Schoenmaker, A. Ford, M. Lutz, A. L. Spek, G. van Koten, *J. Am. Chem. Soc.* **2002**, *124*, 5127; b) S. Back, M. Lutz, A. L. Spek, H. Lang, G. van Koten, *J. Organomet. Chem.* **2001**, *620*, 227; c) P. Steenwinkel, D. M. Grove, N. Veldman, A. L. Spek, G. van Koten, *Organometallics* **1998**, *17*, 5647.
 - [6] a) M. E. van der Boom, S.-Y. Liou, Y. Ben-David, L. J. W. Shimon, D. Milstein, *J. Am. Chem. Soc.* **1998**, *120*, 6531; b) M. E. van der Boom, S.-Y. Liou, Y. Ben-David, A. Vigalok, D. Milstein, *Angew. Chem.* **1997**, *109*, 636; *Angew. Chem. Int. Ed. Engl.* **1997**, *36*, 625.
 - [7] a) M. E. van der Boom, D. Milstein, *Chem. Rev.* **2003**, *103*, 1759; b) M. Albrecht, G. van Koten, *Angew. Chem.* **2001**, *113*, 3866; *Angew. Chem. Int. Ed.* **2001**, *40*, 3750.
 - [8] A. Vigalok, B. Rybtchinski, Y. Gozin, T. Koblenz, Y. Ben-David, H. Rozenberg, D. Milstein, *J. Am. Chem. Soc.* **2003**, *125*, 15692.
 - [9] A. Vigalok, D. Milstein, *J. Am. Chem. Soc.* **1997**, *119*, 7873.
 - [10] M. E. van der Boom, Y. Ben-David, D. Milstein, *J. Am. Chem. Soc.* **1999**, *121*, 6652.
 - [11] A. Vigalok, D. Milstein, *Acc. Chem. Res.* **2001**, *34*, 798.
 - [12] a) G. Pierpont, *Coord. Chem. Rev.* **2001**, *219–221*, 415; b) T. Hirao, *Coord. Chem. Rev.* **2002**, *226*, 81; c) D. L. Boger, S. E. Wolkenberg, C. W. Boyce, *J. Am. Chem. Soc.* **2000**, *122*, 6325.

Radical Reactions

α,α -Difluoro-*H*-phosphinates: Useful Intermediates for a Variety of Phosphate Isosteres

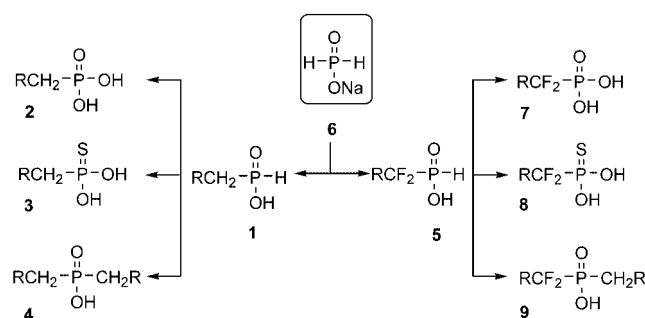
Arnaud Gautier,* Goulnara Garipova, Carmen Salcedo, Sébastien Balieu, and Serge R. Piettre*

Dedicated to Professor Clayton Heathcock

Research efforts have long since established *H*-phosphinates **1** as important and valuable intermediates for the preparation of bioactive analogues of natural phosphates (Scheme 1).^[1] Despite various methodologies for their easy preparation, the synthesis of phosphonate **2**, phosphonothioates **3**, and phosphinates **4** remains an area of intense activity.^[2]

Moreover, major progress has been made in the chemistry of α,α -difluorophosphonates **7** since their introduction slightly more than two decades ago.^[3] Indeed, physicochemical studies have provided some rationale for the isosteric behavior of the above functional group to the phosphate group, and numerous applications have flourished.^[4] Among these, analogues targeting phospholipase C (PLC), purine nucleoside phosphorylase (PNP), and protein phosphotyrosine, phosphoserine, or phosphothreonine phosphatases have been reported.^[5] This functional group has also been success-

[*] Dr. A. Gautier, G. Garipova, C. Salcedo, S. Balieu, Prof. Dr. S. R. Piettre
Laboratoire des Fonctions Azotées et Oxygénées Complexes
UMR 6014 CNRS, IRCOF, Université de Rouen
76821 Mont Saint Aignan (France)
Fax: (+33) 2-3552-2971
E-mail: Arnaud.Gautier@univ-rouen.fr
Serge.Piettre@univ-rouen.fr



Scheme 1. General structure of *H*-phosphinates **1**, related structures **2–4** obtained therefrom, and target compounds **5–9**.

fully used to mimic the phosphate group in nucleotide monophosphates and triphosphates: analogues of adenosine monophosphate, cyclic adenosine monophosphate, adenosine triphosphate, and adenosyl adenosine triphosphate, as well as structurally related potent inhibitors of the reverse transcriptase of human immunodeficiency virus (HIV), have been described in the literature.^[6]

Despite their potential both as a new class of isosteres of natural phosphates and as important intermediates in the synthesis of numerous α,α -difluorinated organophosphorus compounds, reports on fluorinated *H*-phosphinates **5** are scarce.^[7] The main reasons behind this situation are the synthetic problems underlying their preparation. Indeed, processes such as nucleophilic substitution of halodifluorinated centers (including the Arbuzov reaction) have long been known to be disfavored,^[8] and we and others have confirmed the sluggishness of phosphorus-centered radicals with respect to addition onto difluoroalkenes, when compared to their nonfluorinated analogues.^[9] In this context, we found that the sodium salt **6** of hypophosphorous acid behaves in a unique way, and have developed an efficient and practical preparation of α,α -difluoro-*H*-phosphinates. As shown below, these compounds can be easily transformed into difluorophosphonates **7**, difluorophosphonothioates **8**, and difluorophosphinates **9** (Scheme 1).

When a solution of **6** (0.2 M, 1.3 equiv) in methanol was refluxed for four hours with difluoroalkene **10–13** in the presence of *tert*-butyl peroxyphosphate (TBPP) or *tert*-butyl 2-ethylhexyl peroxydicarbonate (TBEC)^[10] as a radical initiator, complete consumption of the substrate occurred and led to the formation of a single product in each case. A simple workup led to the isolation of products **14–17** in 75, 85, 83, and 80% yield, respectively, in the case of TBPP (Table 1). Later, we found that the $\text{Et}_3\text{B}/\text{O}_2$ system also allows a smooth conversion to take place.^[11] The α,α -difluoro-*H*-phosphinates are stable for weeks under standard conditions (room temperature and air). As expected, the ^{31}P NMR spectra of compounds **14–17** displayed signals around 20 ppm with a P,H coupling constant of 590 Hz and P,F coupling constants of about 120 Hz. Similarly, the ^{19}F NMR spectra were characterized by signals with two-bond F,P and three-bond F,H couplings, in accordance with the depicted structures. Additionally, FTIR signals were detected at 1250(s) and around 2370(m) cm^{-1} , which correspond to the P=O and P–H bonds, respectively.^[7]

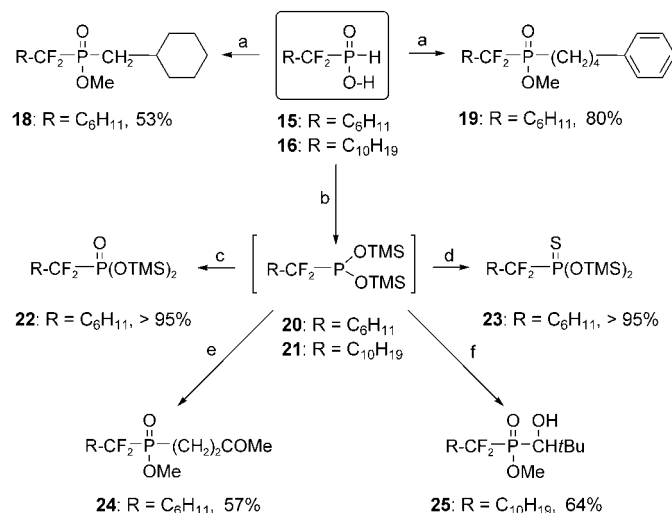
Table 1: Structures of *gem*-difluoroalkenes and α,α -difluoro-*H*-phosphinates, and yields of the latter.

Entry	Substrate	Product	Yield [%]
1			14 75 ^[a]
2			15 85 ^[a,b]
3			16 83 ^[a,c]
4			17 80 ^[a]

[a] Using TBPP. [b] A complete conversion also occurred with $\text{B}(\text{Et})_3/\text{O}_2$. [c] Isolated as a 4:1 mixture of diastereoisomers.

The weak phosphorus–hydrogen bond present in adducts **14–17** renders it prone to homolytic cleavage and highlights the possibility of generating yet another phosphorus-centered radical by treating these compounds with a radical initiator, and of a second radical addition on an alkene. Thus, interaction of a 1.6 M methanolic solution of **15** with methylenecyclohexane in the presence of a catalytic amount of radical initiator (TBPP) led to the formation of the expected α,α -difluorophosphinic acid, which was isolated in the form of its methyl ester **18** (diazomethane) in 53% yield (Scheme 2). A similar two-step process involving sequential addition of 4-phenylbut-1-ene and diazomethane gave methyl difluorophosphinate **19** in 80% yield.

The documented tautomeric equilibrium between an *H*-phosphinate and the corresponding phosphite led us to envision the possible transformation of α,α -difluoro-*H*-phosphinates into the corresponding bis-*O,O*-silylated difluoroal-



Scheme 2. Transformation of α,α -difluoro-*H*-phosphinates into difluorophosphonates, difluorophosphonothioates, and difluorophosphinates.

a) 1. Alkene, **6** (0.3 equiv), C_6H_6 , 55 °C, 18 h; 2. CH_2N_2 , Et_2O , 12 h; b) bis(trimethylsilyl)acetamide (BSA, 3 equiv), CH_2Cl_2 , 25 °C, 1 h; c) O_2 , CH_2Cl_2 , 25 °C, 0.5 h; d) S_8 , CH_2Cl_2 , 25 °C, 0.5 h; e) 1. but-3-en-2-one, BSA (3 equiv), CH_2Cl_2 , 25 °C, 18 h, 2. CH_2N_2 , Et_2O , 12 h; f) 1. pivalaldehyde, BSA (5.5 equiv), CH_2Cl_2 , 25 °C, 3 h, 2. CH_2N_2 , Et_2O , 12 h.

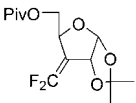
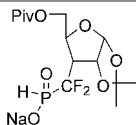
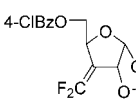
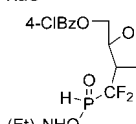
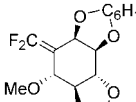
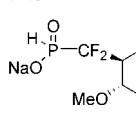
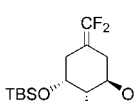
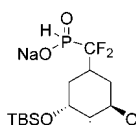
kylphosphites, and the use of the nucleophilic P^{III} species.^[12] Accordingly, treatment of **16** with a threefold excess of trimethylsilyl chloride (TMSCl) and pyridine led to quantitative formation of the corresponding air-sensitive phosphites **20** and **21**, as demonstrated by a shift of the ^{31}P NMR signals to about 130 ppm, and the lack of any one-bond P,H coupling. Exposure of the bis-*O,O*-trimethylsilyl phosphites to oxygen or elemental sulfur quickly transformed these products into difluorophosphonates **22** or difluorophosphonothioates **23**.

Interactions between bisilylated difluoroalkylphosphites and electrophilic carbon atoms were exemplified through the 1,2- and 1,4-addition reactions (Abramov and Pudovic reactions, respectively).^[13] Thus, a degassed solution of **15**, methyl vinyl ketone, BSA, and TMSCl in dichloromethane was stirred at room temperature, and the crude sample was sequentially subjected to a classical workup and treatment with diazomethane, which delivered difluorophosphinate **24** in 57% yield. Similarly, trimethylacetaldehyde (pivalaldehyde) reacted with **21** to furnish α,α -difluoro- α' -hydroxyphosphinate **25** (64% yield). Few examples of difluorophosphinates have so far been reported,^[2b,9a,14] and the present methodology constitutes the first general preparation of these compounds. It was particularly gratifying to note that the presence of the fluorine atoms did not prevent the P^{III} species from interacting with electrophiles.

The scope of the methodology was investigated by developing an application in the field of ribofuranosyl and cyclitol phosphates. Thus, reaction between **6** and ribofuranose derivatives **26** or **27** resulted in complete conversions, and the desired adducts **30** and **31** could be isolated in yields of 78 and 63%, respectively (Table 2). Similarly, cyclitol derivatives **28** and **29** reacted smoothly with **6** to deliver compounds **32** and **33** in good yields. These results are significant in light of the complete lack of reactivity of both diethyl phosphite and diethyl thiophosphite under similar conditions.^[15]

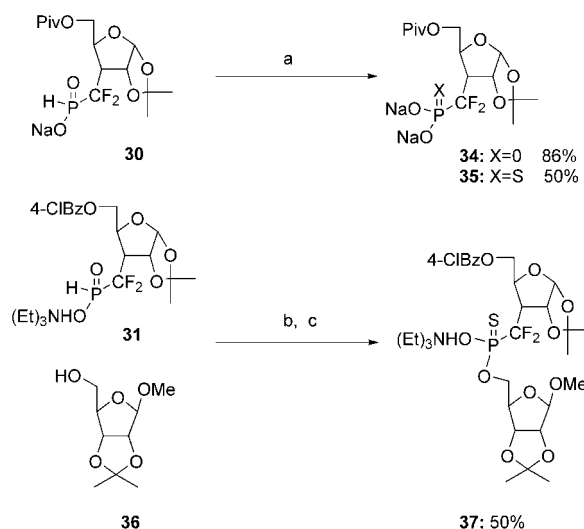
Table 2 clearly indicates the complete failure of any addition process in the case of phosphoryl and phosphonothioyl radicals, despite the demonstrated higher reactivity of the latter.^[9a-b,16] The involvement of a tautomeric P^{III} species of the radical generated from **6** has been ruled out by Beckwith,^[17] and the nature of this radical and those generated from phosphites and thiophosphites should therefore be similar. Additional physicochemical studies will be needed to explain the peculiar, but synthetically useful, behavior of **6** and shed light on the steric and electronic factors at play in this reaction.^[18] α,α -Difluoro-*H*-phosphinates **30** and **31** are useful intermediates to various compounds with potential applications in the fields of modified nucleotides and oligonucleotides (hence the antisense and

Table 2: Addition of hypophosphorous acid sodium salt, diethyl phosphite, and diethyl thiophosphite to difluoroalkenes **26–29**.

Entry	Substrate	Product	Phosphorus precursor	Conversion [%] (yield [%])
1			30 $NaOP(O)H_2$ $(EtO)_2P(O)H$ $(EtO)_2P(S)H$	100 (78 ^[a,b])
2				0
3				0
4			31 $NaOP(O)H_2$ $(EtO)_2P(O)H$ $(EtO)_2P(S)H$	100 (63 ^[b,c])
5				0
6				0
7			32 $NaOP(O)H_2$ $(EtO)_2P(O)H$ $(EtO)_2P(S)H$	100 (76 ^[a])
8				0
9				0
10			33 $NaOP(O)H_2$ $(EtO)_2P(O)H$ $(EtO)_2P(S)H$	100 (70 ^[a,d])
11				0
12				0

[a] Using TBPP. [b] The addition proceeded with a diastereoselectivity greater than 95%. [c] Using $B(Et)_3/O_2$. [d] Isolated as a 3:7 mixture of diastereoisomers.

antigene strategies). For example, *H*-phosphinate **30** was easily transformed into difluorophosphonate **34** and difluorophosphonothioate **35** by treatment with TMSCl, pyridine, and the requisite O_2 or S_8 (Scheme 3).^[2a,15,19] In addition, *H*-phosphinate **31** could easily be esterified by reaction with ribofuranose **36** in the presence of dicyclohexylcarbodiimide (DCC) and trifluoroacetic acid (TFA). The resultant *H*-phosphinate was treated with sulfur and TMSCl in pyridine to



Scheme 3. Transformation of α,α -difluoro-*H*-phosphinates **30** and **31** into difluorophosphonate **34** and difluorophosphonothioates **35** and **37**. a) Pyridine/TMSCl/ O_2 or pyridine/TMSCl/ S_8 ; b) DCC/TFA; c) pyridine/TMSCl/ S_8 . Bz = benzoyl, Piv = pivaloyl.

afford difluorophosphonothioic acid monoester **37** in 50% yield (a 1:1 mixture of two diastereoisomers at the phosphorus center).^[2a] This last result demonstrated the efficacy of the methodology in providing precursors of modified dinucleotides with new phosphorus-centered linkers.

In summary, radical addition of **6** on *gem*-difluoroalkenes constitutes a powerful method of constructing the previously unreported α,α -difluoro-*H*-phosphinates. This new functional group is easily and efficiently transformed into difluorophosphonates, difluorophosphonothioates, and difluorophosphinates. The methodology can be expected to have a major impact on the preparation of difluorophosphonyl, difluorophosphonothioyl, and difluorophosphinyl analogues of natural phosphates.

Experimental Section

General procedure for the synthesis of α,α -difluoro-*H*-phosphinates using *tert*-butyl peroxyphosphate or *tert*-butyl 2-ethylhexyl peroxyphosphate as initiator: The requisite 1,1-difluoroalkene^[20–22] (1.0 equiv) and initiator (0.3 equiv) were added to a solution of hypophosphorous acid sodium salt monohydrate (0.2M, 1.3 equiv) in degassed methanol. The solution was refluxed for 4 h under a nitrogen atmosphere and cooled to room temperature. The solution was poured into water and the aqueous phase was extracted with diethyl ether and lyophilized after separation of the layers. The solid was dissolved in aqueous NaHSO₄ (2.0M) and extracted with dichloromethane. The organic layer was dried and evaporated to give a viscous oil.

Gram-scale synthesis of **31**: Hypophosphorous acid sodium salt monohydrate (1.24 g, 1.7 mmol, 4.0 equiv) was added to a solution of **27** (1.0 g, 2.8 mmol, 1.0 equiv) in nondegassed methanol (25 mL) at room temperature in an open flask. Triethylborane (5 mL, 1M solution in hexane, 5.0 mmol, 5.0 equiv) was added under vigorous stirring, and the solution was stirred for 10 min. This operation was repeated twice. The fast addition of Et₃B solution was crucial. After the third addition of Et₃B, the solution was stirred for 1 h and then the solvent removed by evaporation. Water (50 mL) was added and the aqueous layer was extracted with ethyl acetate (20 mL). The aqueous layer was lyophilized and the crude solid was dissolved in aqueous triethylammonium carbonate (1.0M, 30 mL). The solution was extracted twice with dichloromethane (30 mL); the organic layer was dried and evaporated to give a viscous oil (930 mg, 63%). $[\alpha]_{25}^D = +33.9$ ($c = 1.08$ in CHCl₃); ¹H NMR (200 MHz, CDCl₃): $\delta = 7.10$ (dd, $J = 5.56$ Hz, $J = 6$ Hz, 1H), 7.92 (d, $J = 8.7$ Hz, 2H), 7.33 (d, $J = 8.7$ Hz, 2H), 5.80 (d, $J = 3.9$ Hz, 1H), 5.04 (t, $J = 3.9$ Hz, 1H), 4.8 (m, 1H), 4.73 (d, $J = 12$ Hz, 1H), 4.32 (dd, $J = 12$ Hz, $J = 5.5$ Hz, 1H), 3.00 (q, $J = 7.3$ Hz, 6H), 2.70 (m, 1H), 1.50 (s, 3H), 1.26 (s, 3H), 1.26 ppm (t, $J = 7.3$ Hz, 9H); ¹³C NMR (50 MHz, CDCl₃): $\delta = 165.1$, 139.1, 130.9, 128.4, 128.1, 120.2 (td, $J = 257$ Hz, $J = 121$ Hz, CF₂), 112.5, 104.7, 79.4 (d, $J = 7.6$ Hz), 74.4, 64.6, 49.0 (td, $J = 22.7$ Hz, $J = 13.6$ Hz), 45.3, 26.3 (d, $J = 6.1$ Hz), 8.26 ppm; ³¹P NMR (81 MHz, CDCl₃): $\delta = 9.7$ ppm (dd, $J = 92$ Hz, $J = 86$ Hz); ¹⁹F NMR (188 MHz, CDCl₃, C₆F₆): $\delta = 51.5$ (ddt, $J = 301$ Hz, $J = 85$ Hz, $J = 10$ Hz), 47.4 ppm (ddd, $J = 301$ Hz, $J = 92$ Hz, $J = 23$ Hz); IR (NaCl): $\tilde{\nu} = 2986$, 1721, 1455, 1275, 1091 cm⁻¹. MS (MALDI, matrix: 2,4,6-trihydroxyacetophenone) $m/z = 425.1$ [$M - 102.1$].

37: Compound **24** (58 mg, 0.28 mmol, 1.5 equiv), DCC (118 mg, 0.76 mmol, 4.0 equiv), and trifluoroacetic acid (72 μ L, 0.95 mmol, 5.0 equiv) were added to a solution of **31** (100 mg, 0.19 mmol, 1.0 equiv) in degassed dichloromethane (3 mL). A white precipitate immediately formed and the slurry was stirred for 10 min. Powdered S₈ (200 mg, 6.2 mmol, 32.6 equiv), pyridine (1 mL, 12.2 mmol, 43.8 mmol), and TMSCl (1 mL, 7.9 mmol, 28.1 equiv) were then added sequentially. The reaction was stirred for an additional 15 min, then water (1 mL) was added, and the solution was filtered. The

filtrate was extracted with ice-cold aqueous HCl (0.1M, 10 mL), washed with aqueous triethylammonium carbonate (1.0M), and evaporated. The residue was purified by flash chromatography over silica gel (AcOEt/MeOH/triethylamine 90:8:2) to give a viscous oil (70 mg, 50%) as a 1:1 mixture of two diastereoisomers (stereogenic phosphorus atom). A second chromatography procedure was performed which allowed partial separation of one of the diastereoisomers from the mixture. $[\alpha]_{25}^D = +17.2$ ($c = 0.5$ in CHCl₃); ¹H NMR (200 MHz, CDCl₃): $\delta = 8.00$ (d, $J = 8.4$ Hz, 2H), 7.30 (d, $J = 8.4$ Hz, 2H), 5.80 (d, $J = 3.7$ Hz, 1H), 5.10 (t, $J = 3.7$ Hz, 1H), 4.90 (s, 1H), 4.82 (d, $J = 5.8$ Hz, 1H), 4.70 (dd, $J = 10.2$ Hz, $J = 3.6$ Hz, 1H), 4.54 (d, $J = 5.8$ Hz, 1H), 4.40–3.90 (m, 4H), 3.30 (s, 3H), 3.10 (q, $J = 7.3$ Hz, 6H), 1.50 (s, 3H), 1.4 (s, 3H), 1.3–1.2 ppm (m, 16H); ¹³C NMR (50 MHz, CDCl₃): $\delta = 165.4$, 139.2, 131.0, 128.6, 128.4, 112.5, 111.9, 109.0, 104.5, 85.4, 84.9, 81.6, 80.4 (m), 75.0, 66.7, 65.1, 54.6, 47.4 (m), 45.4, 26.8, 26.3, 26.3, 24.8, 8.3 ppm (CF₂ not observed); ³¹P NMR (81 MHz, CDCl₃): $\delta = 61.5$ ppm (dd, $J = 93$ Hz, $J = 90$ Hz); ¹⁹F NMR (188 MHz, CDCl₃, C₆F₆): $\delta = 56.4$ (ddd, $J = 306$ Hz, $J = 97$ Hz, $J = 14$ Hz), 50.0 ppm (ddd, $J = 306$ Hz, $J = 97$ Hz, $J = 17$ Hz); IR (NaCl): $\tilde{\nu} = 2987$, 2935, 1722, 1274, 1108, 1093, 1013 cm⁻¹; MS (MALDI, matrix: 2,4,6-trihydroxyacetophenone) $m/z = 643.1$ [$M - 103.1$].

Received: April 30, 2004

Keywords: phosphinates · phosphorus · radical reactions · synthesis design

- [1] a) W. H. Parsons, A. A. Patchett, H. G. Bull, W. R. Schoen, D. Taub, J. Davidson, P. L. Combs, J. P. Springer, H. Gadebusch, B. Weissberger, M. E. Valiant, T. N. Mellin, R. D. Busch, *J. Med. Chem.* **1988**, *31*, 1772–1778; b) D. S. Karanewsky, M. C. Badia, D. W. Cushman, J. M. DeForrest, T. Dejneka, M. J. Loots, M. G. Perri, E. W. Petrillo, Jr., J. R. Powell, *J. Med. Chem.* **1988**, *31*, 204–212; c) N. S. Sampson, P. A. Bartlett, *J. Org. Chem.* **1988**, *53*, 4500–4503; d) M. T. Martin, T. S. Angeles, R. Sugawara, N. I. Aman, A. D. Napper, M. J. Darsley, R. I. Sanchez, P. Booth, R. C. Titmas, *J. Am. Chem. Soc.* **1994**, *116*, 6508–6512; e) F. Tian, J.-L. Montchamp, J. W. Frost, *J. Org. Chem.* **1996**, *61*, 7373–7381.
- [2] a) J. Stawinski, A. Kraszewski, *Acc. Chem. Res.* **2002**, *35*, 952–960; b) W. Froestl, S. J. Mickel, G. Sprecher, P. J. Diel, R. G. Hall, L. Maier, S. Dietrich, V. Melillo, P. A. Baumann, R. Bernasconi, C. Gentsch, K. Hauser, J. Jaekel, G. Karlsson, K. Klebs, L. Maitre, C. Marescaux, M. F. Pozza, M. Schmutz, M. W. Steinmann, H. Riesen, A. Vassout, C. Mondadori, H. R. Olpe, P. C. Waldmeier, H. Bittiger, *J. Med. Chem.* **1995**, *38*, 3313–3331.
- [3] a) C. E. McKenna, P.-D. Shen, *J. Org. Chem.* **1981**, *46*, 4773–4776; b) G. M. Blackburn, D. A. England, F. Kolmann, *J. Chem. Soc. Chem. Commun.* **1981**, 930–932; c) G. M. Blackburn, D. E. Kent, F. Kolmann, *J. Chem. Soc. Chem. Commun.* **1981**, 1188–1190.
- [4] a) R. D. Chambers, R. Jaouhari, D. O'Hagan, *Tetrahedron* **1989**, *45*, 5101–5108; b) R. D. Chambers, D. O'Hagan, R. B. Lamont, S. C. Jain, *J. Chem. Soc. Chem. Commun.* **1990**, 1053–1054.
- [5] a) T. R. Burke, Jr., M. S. Smyth, M. Nomizu, A. Otaka, P. P. Roller, *J. Org. Chem.* **1993**, *58*, 1336–1340; b) S. F. Martin, Y.-L. Wong, A. S. Wagman, *J. Org. Chem.* **1994**, *59*, 4821–4831; c) D. B. Berkowitz, Q. Shen, J.-H. Maeng, *Tetrahedron Lett.* **1994**, *35*, 6445–6448; d) T. R. Burke, Jr., B. Ye, M. Akamatsu, H. Ford, Jr., X. Yan, H. K. Kole, G. Wolf, S. E. Shoelson, P. P. Roller, *J. Med. Chem.* **1996**, *39*, 1021–1027; e) D. B. Berkowitz, M. Eggen, Q. Shen, R. K. Shoemaker, *J. Org. Chem.* **1996**, *61*, 4666–4675; f) B. Ye, T. R. Burke, Jr., *Tetrahedron* **1996**, *52*, 9963–9970; g) M. N. Qabar, J. Urban, M. Khan, *Tetrahedron* **1997**, *53*, 11171–11178; h) T. Yokomatsu, H. Abe, T. Yamagishi,

- K. Suemune, S. Shibuya, *J. Org. Chem.* **1999**, *64*, 8413–8418; i) T. R. Burke, Jr., K. Lee, *Acc. Chem. Res.* **2003**, *36*, 426–433.
- [6] a) G. M. Blackburn, D. E. Kent, *J. Chem. Soc. Chem. Commun.* **1981**, 511–513; b) G. M. Blackburn, D. E. Kent, F. Kolkman, *J. Chem. Soc. Perkin Trans. 1* **1984**, 1119–1125; c) G. M. Blackburn, M.-J. Guo, S. P. Langston, G. E. Taylor *Tetrahedron Lett.* **1990**, *31*, 5637–5640; d) G. M. Blackburn, S. P. Langston, *Tetrahedron Lett.* **1991**, *32*, 6425–6428; e) J. Matulic-Adamic, N. Usman, *Tetrahedron Lett.* **1994**, *35*, 3227–3230; f) J. Matulic-Adamic, P. Haeberli, N. Usman, *J. Org. Chem.* **1995**, *60*, 2563–2569; g) S. G. Levvy, B. Wasson, D. A. Carson, H. B. Cottam, *Synthesis* **1996**, 843–846; h) C. J. Hamilton, S. M. Roberts, A. Shipitsin, *Chem. Commun.* **1998**, 1087–1088; i) C. J. Hamilton, S. M. Roberts, *J. Chem. Soc. Perkin Trans. 1* **1999**, 1051–1056.
- [7] a) H. J. Emeleus, R. N. Haszeldinze, R. C. Paul, *J. Chem. Soc.* **1955**, 563–574; b) A. B. Burg, J. E. Griffiths, *J. Am. Chem. Soc.* **1961**, *83*, 4333–4337; c) A. Golovanov, I. G. Maslennikov, A. N. Lavrent'ev, *Zh. Obshch. Khim.* **1988**, *58*, 1525–1529.
- [8] a) L. Z. Soborovskii, N. F. Baina, *Zh. Obshch. Khim.* **1959**, *29*, 1142–1143; b) D. J. Burton, R. M. Flynn, *J. Fluorine Chem.* **1977**, *10*, 329–332; c) D. J. Burton, R. M. Flynn, *Synthesis* **1979**, 615.
- [9] a) S. R. Piettre, *Tetrahedron Lett.* **1996**, *37*, 2233–2236; b) T. F. Herpin, W. B. Motherwell, B. P. Roberts, S. Roland, J.-M. Weibel, *Tetrahedron* **1997**, *53*, 15085–15100; c) J. Kovensky, M. McNeil, P. Sinay, *J. Org. Chem.* **1999**, *64*, 6202–6205.
- [10] For the synthesis of *tert*-butyl peroxyvalate (TBPP), see: P. D. Bartlett, E. P. Benzing, R. E. Pincock, *J. Am. Chem. Soc.* **1960**, *82*, 1762–1768; TBPP has a half-life of 5 h at 60 °C. *Tert*-butyl 2-ethylhexyl peroxy carbonate (TBEC) is commercially available and has a half-life of 10 h at 77 °C and 1 h at 95 °C.
- [11] a) S. Deprele, J.-L. Montchamps, *J. Org. Chem.* **2001**, *66*, 6745–6755; b) A. Gautier, G. Garipova, O. Dubert, H. Oulyadi, S. R. Piettre, *Tetrahedron Lett.* **2001**, *42*, 5673–5676.
- [12] a) J. Jankowska, A. Sobkowska, J. Cieslak, M. Sobkowski, A. Kraszewski, J. Stawinski, D. Shugar, *J. Org. Chem.* **1998**, *63*, 8150–8156; b) M. A. Maier, A. P. Guzaev, M. Manoharan, *Org. Lett.* **2000**, *2*, 1819–1822.
- [13] a) A. N. Pudovik, I. V. Konovalova, *Zh. Obshch. Khim.* **1959**, *29*, 3342–3346; b) V. S. Abramov, *Dokl. Akad. Nauk SSSR* **1950**, *73*, 487–489; c) R. Engel, *Handbook of Organophosphorus Chemistry*, Marcel Dekker, New York, **1992**.
- [14] J. Ong, D. I. B. Kerr, W. Froestl, *Eur. J. Pharmacol.* **1999**, *374*, 351–354.
- [15] A considerable amount of time and effort was spent attempting the addition of phosphonyl and phosphonothioyl radicals onto difluoroalkenes related to **26** and **27**, without any success; see: C. Lopin, A. Gautier, G. Gouhier, S. Piettre, *J. Am. Chem. Soc.* **2002**, *124*, 14668–14675.
- [16] A. N. Pudovik, I. V. Konovalova, *Zh. Obshch. Khim.* **1959**, *29*, 3342–3346.
- [17] A. L. Beckwith, *Aust. J. Chem.* **1972**, *25*, 1887–1905.
- [18] J. M. Tedder, J. C. Walton, *Acc. Chem. Res.* **1976**, *9*, 183–191, and references therein.
- [19] This type of furanose derivative has recently been investigated: a) A. H. Butt, J. M. Percy, N. S. Spencer, *Chem. Commun.* **2000**, 1691–1692; b) T. Murano, S. Muroyama, T. Yokomatsu, S. Shibuya, *Synlett* **2002**, 1657–1660; c) T. Murano, Y. Yuasa, S. Muroyama, T. Yokomatsu, S. Shibuya, *Tetrahedron* **2003**, *59*, 9059–9073.
- [20] The 1,1-difluoroalkenes **10–13**, **26**, **27**, and **29** described in this paper were obtained from the corresponding ketone in yields ranging from 55 to 65 % by either the method of Wheaton and Burton or the modification of the Motherwell procedure by Serafinowski and Barnes.^[21] For instance, a 6.0-g batch of compound **27** was prepared according to reference 21a. Substrate **28** was synthesized by the three-step procedure published by McCarthy.^[22]
- [21] a) G. A. Wheaton, D. J. Burton, *J. Org. Chem.* **1983**, *48*, 917–927; b) P. J. Serafinowski, C. L. Barnes, *Tetrahedron* **1996**, *52*, 7929–7938.
- [22] J. S. Sabol, J. R. McCarthy, *Tetrahedron Lett.* **1992**, *33*, 3101–3104.

Metallamacrocycles

A Simple, One-Step Procedure for the Formation of Chiral Metallamacrocycles**

Katie Campbell, Charles A. Johnson II,
Robert McDonald, Michael J. Ferguson,
Michael M. Haley, and Rik R. Tykwinski*

*Dedicated to Professor Larry Scott
on the occasion of his 60th birthday*

Metal-directed self-assembly reactions have become a powerful method used for the construction of supramolecular architectures including molecular squares, cages, and other polygons, as well as numerous polymeric and dendrimeric species.^[1] In the last decade, scientists have become particularly intrigued with the effect of incorporating chiral ligands/groups into metallosupramolecular systems. These materials have demonstrated potential in numerous enantioselective processes including asymmetric catalysis,^[2] chemical sensing,^[3] and selective guest inclusion.^[4]

[*] K. Campbell, Prof. Dr. R. R. Tykwinski

Department of Chemistry
University of Alberta
Edmonton, AB, T6G 2G2 (Canada)
Fax: (+1) 780-492-8231
E-mail: rik.tykwinski@ualberta.ca

C. A. Johnson II, Dr. R. McDonald, Dr. M. J. Ferguson
X-Ray Crystallography Laboratory
Department of Chemistry
University of Alberta
Edmonton, AB, T6G 2G2 (Canada)

Prof. Dr. M. M. Haley
Department of Chemistry
University of Oregon
Eugene, OR 97403-1253 (USA)

[**] Financial support as provided by the University of Alberta, the Natural Sciences and Engineering Research Council of Canada (NSERC), and the National Science Foundation (NSF) is gratefully acknowledged. C.A.J. acknowledges the NSF for an IGERT fellowship. K.C. thanks NSERC for a graduate scholarship. We thank M. Miskolzie and G. Bigam for assistance with NMR analyses, A. Morales-Izquierdo for ESI-MS analyses, and Dr. W. Moffat for assistance with the CD spectroscopic analysis.



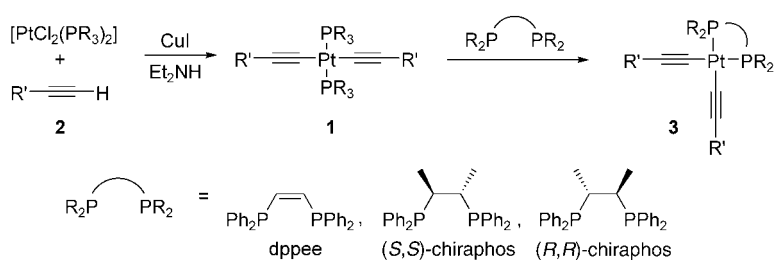
Supporting information for this article is available on the WWW under <http://www.angewandte.org> or from the author.

In most cases, the synthesis of metal-containing chiral supramolecules involves derivatization of an enantiopure building block, as in the numerous chiral binaphthyl-based molecules. Using a typically step-wise process, these chiral segments are elaborated with functionality capable of binding to a metal or metal ion, such as pyridyl and alkynyl moieties.^[5] These larger segments are then assembled into the desired supramolecule, and this ultimately provides a chiral metal-containing architecture of predictable size, shape, and function.

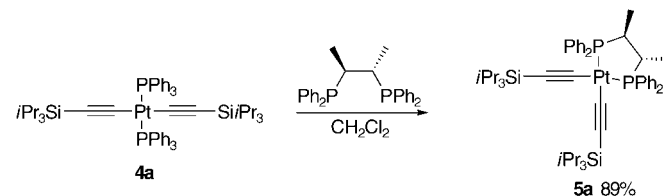
The most costly component of a chiral framework is nearly always the optically pure building block. Thus, a synthetic sequence that initiates from a chiral building block will inherently suffer from losses due to subsequent synthetic and purification steps.^[2,3] A more attractive approach would be a method that introduced chirality after construction of the desired supramolecular assembly. This approach would not only circumvent waste of the chiral building block prior to the ultimate synthetic step, but would also facilitate the divergent preparation of both enantiomers of a given target from a common precursor. Described herein is a simple and general protocol that provides economical access to chiral metal-containing molecules by ligand exchange between *trans* platinum acetylide complexes (**1**) and the chiral diphosphine ligands (*R,R*- and (*S,S*)-chiraphos (Scheme 1).

Metal-organic frameworks can be expediently accessed by the conversion of terminal acetylenes (**2**) into *trans* platinum acetylide complexes (**1**) by reaction with [PtCl₂(PR₃)₂].^[6] It has been established that transformation of *trans* complexes **1** into their *cis* counterparts **3** can be readily accomplished by ligand exchange with a chelating diphosphine ligand,^[7] provided the lability of the exiting phosphine ligand is carefully controlled. In the case of *trans* acetylides with PEt₃ ligands (e.g., **1**, R = Et), ligand exchange to give the *cis* derivatives **3** is either extremely slow or completely retarded in reactions with dppee.^[7] The *trans* complexes **1** with pendant PPh₃ ligands, on the other hand, are readily converted to their *cis* counterparts **3** in good to excellent yield, when using dppee to effect ligand exchange.

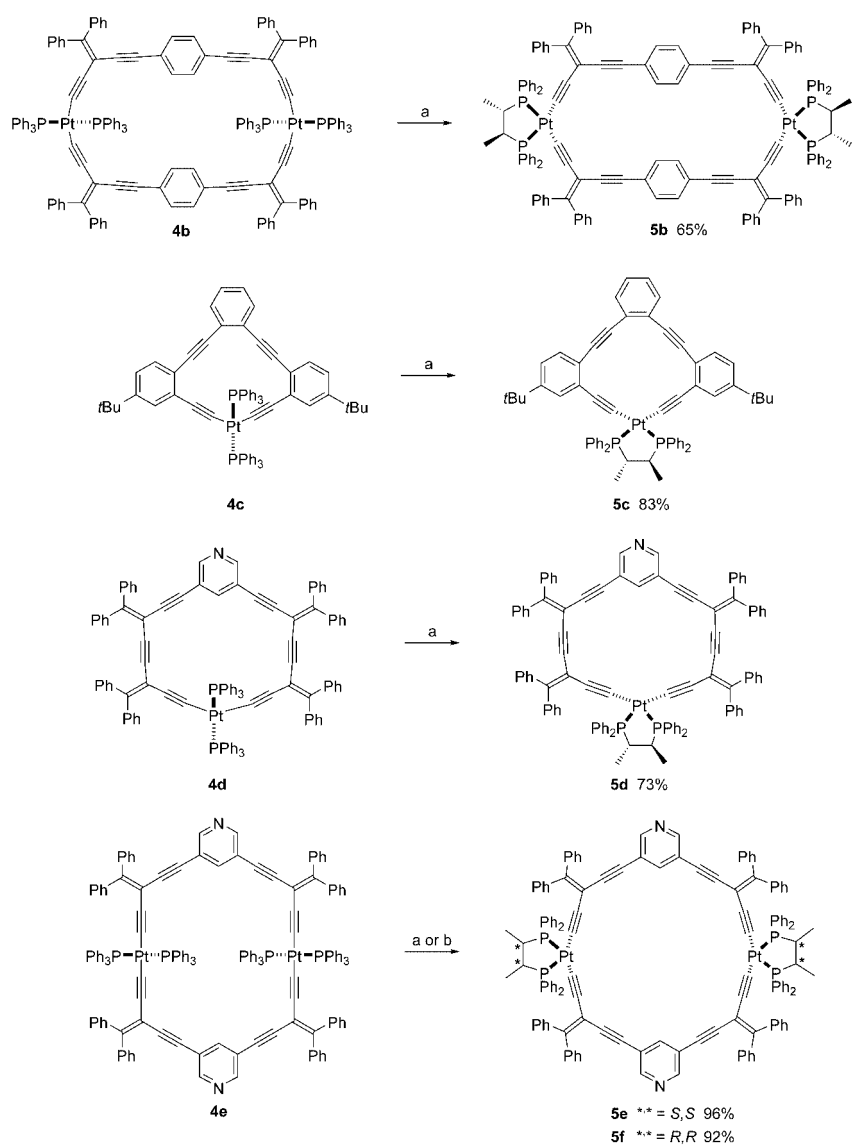
For the current study, formation of requisite *trans* platinum complexes **4a–e** (Schemes 2 and 3) was effected by treating the appropriate terminal acetylene with [PtCl₂(PPh₃)₂] in degassed Et₂NH with a catalytic amount of CuI.^[8] In the case of cyclic derivatives such as **4b–e**,



Scheme 1. Construction of achiral and chiral *cis* platinum acetylide complexes by ligand exchange.



Scheme 2. Synthesis of chiral *cis* acetylide complex **5a**.



Scheme 3. Synthesis of chiral macrocycles **5b–f**. a) (*S,S*)-chiraphos, CH₂Cl₂, RT; b) (*R,R*)-chiraphos, CH₂Cl₂, RT.

high dilution was used to facilitate closure of the macrocyclic skeleton. All *trans* complexes were readily purified by either selective precipitation or flash chromatography on silica gel.

To probe the transformation of the achiral complexes into chiral supramolecules, the acyclic system **4a** was used as a model system. Treatment of **4a** with (*S,S*)-chiraphos in CH₂Cl₂ at RT for 14 h cleanly formed the chiral *cis* complex **5a** in 89 % yield (Scheme 2). This protocol was next applied to a structurally diverse selection of metallamacrocycles **4b–e**.^[9] Gratifyingly, the reaction of these *trans* acetylide complexes with (*S,S*)-chiraphos under analogous conditions led to the *cis* acetylide macrocyclic complexes **5b–e** in good to excellent yields. The reaction of **4e** with the ligand (*R,R*)-chiraphos to give **5f** was equally successful, highlighting the economy of our methodology which allows for the divergent generation of both enantiomeric macrocycles, **5e** and **5f**, from **4e** by simply changing the ligand system in the final step of the synthesis. Thus, this one-step transformation is equally effective for carbocyclic systems such as **5b,c** and complexes with pyridine rings containing one (**5d**) or two metal centers (**5e,f**). The successful formation of **5d–f** is noteworthy as they are excellent candidates for use as chiral building blocks in self-assembly reactions, through coordination through the pyridine unit(s).^[10]

The formation of **5a–f** is easily monitored by ¹H and ³¹P NMR spectroscopy. The alkyl protons of the free ligand, (*S,S*)-chiraphos, appear as a multiplet (methine) and quartet (methyl) at δ = 2.50–2.43 and 1.17 ppm, respectively. Upon binding to the metal center, these protons are shifted upfield and appear as broad multiplets centered at δ = 2.49–2.16 and 0.95–0.84 ppm, respectively. Even more diagnostic are the ³¹P NMR spectra. The free chiraphos ligand gives rise to a singlet at δ = –8.7 ppm that diminishes in intensity as ligand exchange proceeds, while the resonance of uncoordinated PPh₃ emerges at δ = –4.4 ppm. Concurrently, the intensity of the ³¹P NMR resonance from the ligated PPh₃ of the *trans* acetylide complex **4**, observed at δ = 18–21 ppm, disappears as the reaction proceeds. It is replaced by a new resonance at δ = 42–47 ppm from the chiraphos ligand bound to platinum in complex **5**. As the coordination geometry about the platinum center changes from *trans* to *cis*, a diagnostic change in the coupling constant J_{P-Pt} is also observed (2600–2720 Hz for **4a–e**, 2190–2250 Hz for **5a–f**).

It is well known that five-membered chelate rings can adopt two puckered, chiral conformations (Figure 1).^[11] In the presence of stereogenic centers (as is the case with chiraphos), these two conformations become diastereomeric, and one conformation is therefore energetically more favorable. For (*S,S*)-chiraphos, the most stable conformation is the one in

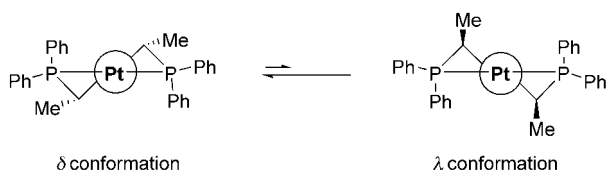


Figure 1. δ and λ conformations resulting from bonding of (*S,S*)-chiraphos to platinum.

which the substituents of the chelate ring are equatorially disposed (the δ conformation). As a result of this conformational preference, the phenyl groups on the phosphorus centers are locked into a chiral arrangement. It is through this arrangement that the chiraphos ligand can convey chirality to the entire molecular framework by the steric influence of the phenyl groups of the phosphine, which is relayed to other ligands bonded to platinum.

Conclusive structural proof of the chiral structures of **5a** and **5d** as a result of the chiraphos ligand has been provided by single crystal X-ray crystallographic analysis. The ORTEP drawing of **5a** (Figure 2) shows that the complex is in the

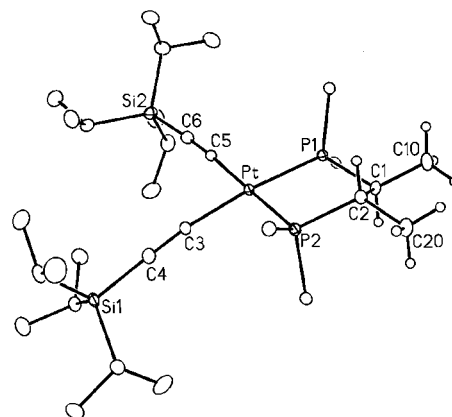


Figure 2. ORTEP drawing of **5a** (20 % probability level; solvent molecules and all but the *ipso* carbon atoms of the phenyl rings have been removed).

expected δ conformation in which the two methyl groups of the chiraphos ligand are pseudoequatorial.^[12] The coordination geometry about the platinum center is square planar with angles of 86.29(2)° (P1–Pt–P2) and 87.93(9)° (C3–Pt–C5) which are comparable to other Pt^{II}–chiraphos complexes.^[13] All other angles and bond lengths are unremarkable.

The solid-state structure of **5d**, by contrast, shows several unexpected features. Complex **5d** crystallizes with two independent molecules in the unit cell (molecule A is shown in Figure 3).^[14] While much of the macrocyclic core is nearly planar, the structure pivots dramatically at the alkylidene carbons C17 and C23 to accommodate the *cis* acetylide linkage to platinum. In spite of the inherent strain, the coordination geometry about the platinum center remains unchanged with bond angles about the metal of 87.5(6)° (C20–Pt1–C21) and 86.04(16)° (P1–Pt1–P2). The strain imparted by the *cis* conformation is therefore borne almost exclusively by the enyne core of the macrocycle, as evidenced by the alkylidene and alkyne bond angles, which have mean values of 112.2° and 172.3°, respectively.

The most remarkable feature of the solid-state structure of **5d** is that the Chiraphos ligand has adopted a λ conformation, which places the two methyl groups in pseudodaxial positions with a dihedral angle C43–C41–C42–C44 between the methyl groups of 166.2° (molecule B is similar, with C43–C41–C42–C44 = 167.4°). This is only the second example of Chiraphos adopting this conformation (in

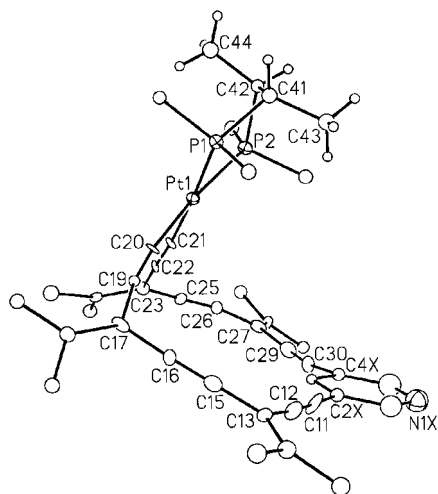


Figure 3. ORTEP drawing of molecule A of **5d** (20% probability level; solvent molecules and all but the *ipso* carbon atoms of the phenyl rings have been removed).

the solid-state) that could be found in the Cambridge structural database.^[15] It is speculated that this unusual result is directed by steric interactions between the phenyl groups on the diphosphine ligand and the pendant diphenylalkylidene groups of the macrocycle.

The CD spectra for chiral *cis* complexes **5a–f** are shown in Figure 4. The CD curve for complex **5b** shows the strongest

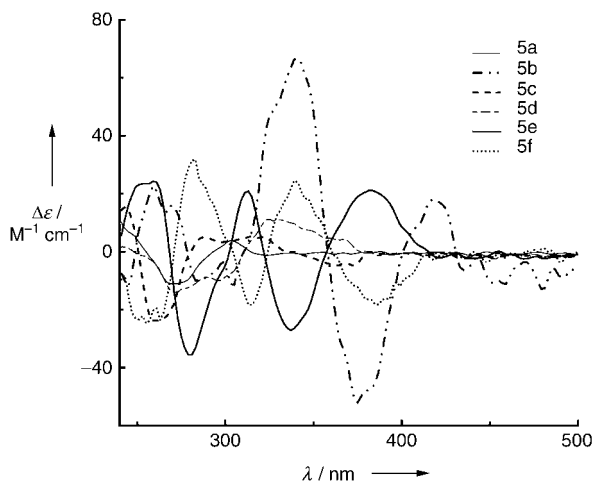


Figure 4. CD spectra for **5a–f** in CH_2Cl_2 .

response and is dominated by two intense Cotton effects that form a negative couplet centered at $\lambda = 358$ nm, attributable to the $\pi \rightarrow \pi^*$ transition.^[16,17] A third, positive Cotton effect is observed at high energy ($\lambda \approx 260$ nm). The CD curves for complexes **5e** and **5f** demonstrate several moderately strong signals, and the two spectra mirror each other in both form and intensity, consistent with an enantiomeric relationship. More specifically, these spectra show two bisignate signals, centered at $\lambda \approx 360$ and 305 nm. The lower energy couplet likely arises from the MLCT absorption band, whereas the high-energy band is associated with an unassigned transition

in the UV/Vis absorption spectrum at $\lambda = 305$ nm. Unlike complexes **5b** and **5e,f**, the remaining complexes, acyclic **5a** and the more strained macrocycles **5c** and **5d**, show only weaker, high-energy signals in the lower energy region of the CD spectra.

The solid-state and CD spectroscopic data for **5a–f** unambiguously demonstrate the ability of the chiraphos ligand to efficiently transfer chirality to the conjugated molecular framework of platinum acetylide complexes. There are, however, several important design considerations that appear to govern this process. As demonstrated by CD spectroscopy, the chiral influence from chiraphos is strongest when the acetylenic chromophore attached to the platinum metal center is large and sufficiently rigid to interact with the chiral array of phenyl groups on the diphosphine ligand, as observed for macrocycles **5b** and **5e–f**. The macrocycle must also, however, maintain sufficient conformational mobility to be biased by this interaction, that is, when the macrocycle is too strained or rigid, the chiral influence is minimal, as observed for **5c** and **5d**. Optimization of this process and the formation of chiral, conjugated frameworks using ligand-exchange methodology with other chiral phosphine ligands are currently underway.

Received: June 30, 2004

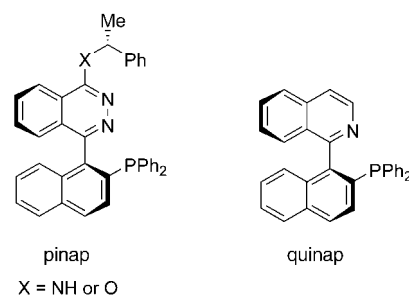
Revised: August 12, 2004

Keywords: chirality · macrocycles · P ligands · platinum · supramolecular chemistry

- [1] a) S. Leininger, B. Olenyuk, P. J. Stang, *Chem. Rev.* **2000**, *100*, 853–908; b) M. Fujita, *Chem. Soc. Rev.* **1998**, *27*, 417–425; c) G. Fuhrmann, T. Debaerdemaeker, P. Bäuerle, *Chem. Commun.* **2003**, 948–949; d) K. Onitsuka, A. Iuchi, M. Fujimoto, S. Takahashi, *Chem. Commun.* **2001**, 741–741; e) K. Onitsuka, Y. Hurada, F. Takei, S. Takahashi, *Chem. Commun.* **1998**, 643–644.
- [2] S. J. Lee, A. Hu, W. Lin, *J. Am. Chem. Soc.* **2003**, *125*, 12948–12949.
- [3] S. J. Lee, W. Lin, *J. Am. Chem. Soc.* **2002**, *124*, 4554–4555.
- [4] E. Barea, J. A. R. Navarro, J. M. Salas, M. Quirós, M. Willermann, B. Leppert, *Chem. Eur. J.* **2003**, *9*, 4414–4421.
- [5] a) S. G. Telfer, R. Kuroda, *Coord. Chem. Rev.* **2003**, *242*, 33–46; b) O. Mamula, A. von Zelewsky, *Coord. Chem. Rev.* **2003**, *242*, 87–95.
- [6] K. Sonogashira, K. Ohga, S. Takahashi, N. Hagihara, *J. Organomet. Chem.* **1980**, *188*, 237–243.
- [7] K. Campbell, R. McDonald, M. J. Ferguson, R. R. Tykwinski, *J. Organomet. Chem.* **2003**, *683*, 379–387.
- [8] For a general synthetic procedure for the synthesis of cyclic and acyclic *trans* platinum acetylide complexes, please see ref. [7].
- [9] Full experimental details are provided in the Supporting Information.
- [10] a) K. Campbell, R. McDonald, R. R. Tykwinski, *J. Org. Chem.* **2002**, *67*, 1133–1140; b) K. Campbell, C. J. Kuehl, M. J. Ferguson, P. J. Stang, R. R. Tykwinski, *J. Am. Chem. Soc.* **2002**, *124*, 7266–7267.
- [11] a) M. D. Fryzuk, B. Bosnich, *J. Am. Chem. Soc.* **1977**, *99*, 6262–6267; b) N. M. Brunkan, P. S. White, M. R. Gagné, *Angew. Chem.* **1998**, *110*, 1615–1618; *Angew. Chem. Int. Ed.* **1998**, *37*, 1579–1582.
- [12] Crystallographic data for **5a**: $\text{C}_{50}\text{H}_{70}\text{P}_2\text{PtSi}_2\text{CH}_2\text{Cl}_2$, $M_r = 1069.20$, orthorhombic, space group $P2_12_1$ (No. 19); $a =$

- 14.1414(6), $b = 14.6660(6)$, $c = 25.5887(11)$ Å; $V = 5307.0(4)$ Å³; $Z = 4$; $\rho_{\text{calcd}} = 1.338$ g cm⁻³; $\mu(\text{MoK}\alpha) = 2.881$ mm⁻¹; $T = -80^\circ\text{C}$; $R_1(F) = 0.0208$ (10217 reflections $F_o^2 \geq 2\sigma(F_o^2)$) and $wR_2(F^2) = 0.0457$ for all 10797 unique data.
- [13] M. H. Johansson, T. Malmström, O. F. West, *Inorg. Chim. Acta* **2001**, 316, 149–152.
- [14] Crystallographic data for **5d**: C₁₀₁H₇₁NP₂Pt·1.75 C₂H₄Cl₂·H₂O, $M_r = 1746.80$, triclinic, space group $P1$ (No. 1); $a = 10.2491(6)$, $b = 15.5943(10)$, $c = 27.6134(17)$ Å; $\alpha = 77.4626(12)$, $\beta = 84.5413(13)$, $\gamma = 79.1701(11)^\circ$; $V = 4224.6(4)$ Å³; $Z = 2$; $\rho_{\text{calcd}} = 1.373$ g cm⁻³; $\mu(\text{MoK}\alpha) = 1.860$ mm⁻¹; $T = -80^\circ\text{C}$; $R_1(F) = 0.0622$ (20815 reflections $F_o^2 \geq 2\sigma(F_o^2)$) and $wR_2(F^2) = 0.1389$ for all 28700 unique data. CCDC-243208 (**5d**) and CCDC-243209 (**5a**) contain the supplementary crystallographic data for this paper. These data can be obtained free of charge via www.ccdc.cam.ac.uk/conts/retrieving.html (or from the Cambridge Crystallographic Data Centre, 12, Union Road, Cambridge CB21EZ, UK; fax: (+44)1223-336-033; or deposit@ccdc.cam.ac.uk).
- [15] D. K. Wicht, M. A. Zhuravel, R. V. Gregush, D. S. Glueck, I. A. Guzei, L. M. Liable-Sands, A. L. Rheingold, *Organometallics* **1998**, 17, 1412–1419.
- [16] The MLCT band for **5b** is likely combined or masked with the $\pi \rightarrow \pi^*$ transition. UV/Vis spectra and a brief discussion are provided as Supporting Information.
- [17] a) V. W.-W. Yam, *Acc. Chem. Res.* **2002**, 35, 555–563; b) R. Faust, F. Diederich, V. Gramlich, P. Seiler, *Chem. Eur. J.* **1995**, 1, 111–117.

available atropisomeric P,N ligands (pinap)^[5] that are structurally similar to quinap and have parallel reactivity. They



have the additional advantage, however, that, unlike quinap, they are conveniently prepared and resolved as well as easily amenable to structural and electronic modifications. We describe their synthesis, as well as applications in reactions involving Rh, Ag, and Cu catalysts, which demonstrate their utility. In the Cu-catalyzed coupling of acetylenes and imines they are superior to quinap and afford products with the highest enantioselectivity reported to date.

Quinap was developed by Brown and co-workers in 1993.^[6] The six-step sequence for its synthesis includes a Pd-catalyzed coupling of 2-methoxy-1-naphthylboronic acid and 1-chloroisoquinoline to generate the biaryl scaffold. After introduction of the phosphinyl group, the resolution of the enantiomeric atropisomers is carried out as the final step by treatment of (±)-quinap with a preformed chiral Pd complex prepared from (*R*)- or (*S*)-*N,N*-dimethyl-1-naphthalen-1-ylethylamine.^[7] Quinap is commercially available, but it is rather expensive.^[8] The design and synthesis of related biaryl P,N ligands has been the focus of numerous research groups.^[2a,c] However, resolution of the ligands has proven difficult and has inevitably involved fractional crystallization of diastereomeric Pd complexes. This has limited the extent of structural and electronic modification that can be examined with this scaffold.

Key to our ligand design is the use of a covalently bound chiral group, which facilitates resolution at any of the various steps of the ligand synthesis. As shown in Scheme 1, the core of the ligand is easily accessed by coupling 1,4-dichlorophthalazine with 2-naphthol to give **1** in 77% yield.^[9] Importantly, the use of the dichlorophthalazine allows both convenient construction of the biaryl unit and subsequent introduction of a chiral amine or an alcohol.

Treatment of **1** with (*R*)-phenylethanol afforded the diastereomeric aryl ethers (82% yield, d.r. = 1:1), which were subsequently converted into triflates **2** (91% yield). Ni-catalyzed coupling of **2** with HPPH₂ furnished ligands **3a** and **3b** in 70% combined yield. The two atropisomeric diastereomers were separated at this stage either by chromatography on silica gel or, alternatively, by crystallization.^[10] The absolute configuration of **3a** was shown to be *R,M* by X-ray structure analysis.^[11]

The synthesis of a related structure incorporating (*R*)-(+)- α -phenethylamine was carried out similarly (Scheme 1). Ligands **5a** and **5b** were isolated in 69% yield over three

Asymmetric Catalysis

Readily Available Biaryl P,N Ligands for Asymmetric Catalysis**

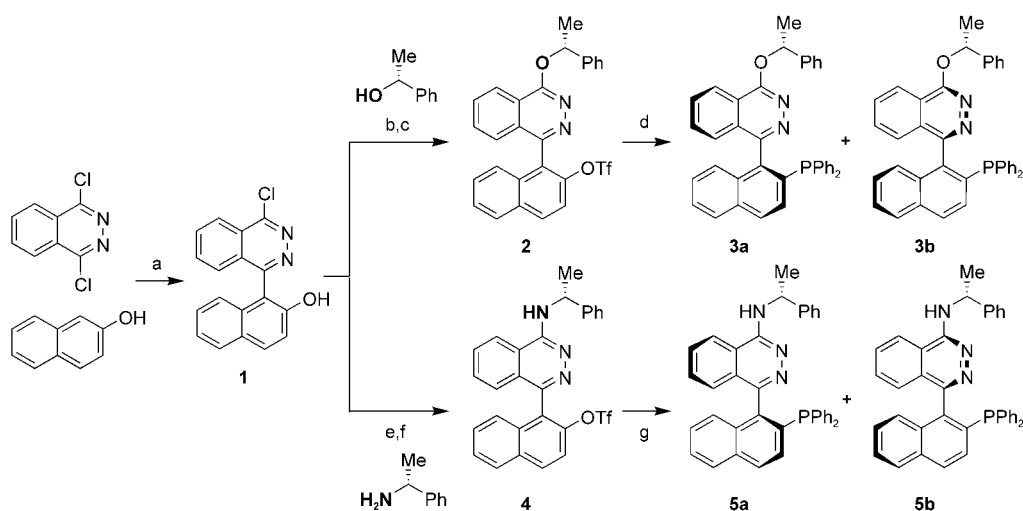
Thomas F. Knöpfel, Patrick Aschwanden,
Takashi Ichikawa, Takumi Watanabe, and
Erick M. Carreira*

The discovery and development of new chiral ligands for transition-metal complexes is critical for expanding the scope of catalytic asymmetric synthesis.^[1] The P,N ligands are a highly successful class,^[2] in which quinap^[3] holds a special place because it displays unique reactivity and selectivity^[4] (e.g. in hydroboration,^[4a] alkyne addition,^[4c] diboration^[4d] and azomethine cycloaddition).^[4e] Herein, we present new, readily

[*] T. F. Knöpfel, P. Aschwanden, Dr. T. Ichikawa, Dr. T. Watanabe, Prof. Dr. E. M. Carreira
Laboratorium für Organische Chemie
ETH Hönggerberg, HCI H335
8093 Zürich (Switzerland)
Fax: (+41) 1-632-1328
E-mail: carreira@org.chem.ethz.ch

[**] This work was generously supported by Sumika Fine Chemicals (now Sumitomo Chemical Co., Ltd.).

Supporting information for this article is available on the WWW under <http://www.angewandte.org> or from the author.

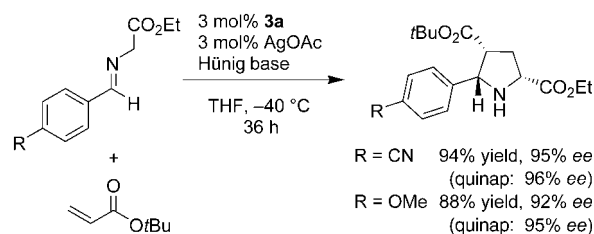


Scheme 1. a) AlCl_3 , DCE, 80°C , 77%; b) (*R*)-phenylethanol, NaH (2 equiv), THF, 23°C , 82%; c) Tf_2O , pyridine, CH_2Cl_2 , 0°C , 91%; d) $[\text{NiCl}_2(\text{dppe})]$ (10 mol %), HPPH_2 , DABCO, DMF, 100°C , 70%; e) Tf_2O , pyridine, CH_2Cl_2 , 0°C , 93%; f) (*R*)-phenylethylamine (5 equiv), neat, 120°C , 93%, g) $[\text{NiCl}_2(\text{dppe})]$ (10 mol %), HPPH_2 , DABCO, DMF, 130°C , 80%. DABCO = 1,4-diazabicyclo[2.2.2]octane, DCE = 1,2-dichloroethane, Tf = trifluoromethanesulfonyl.

steps (d.r. = 1:1.2). These ligands are conveniently separated by crystallization or chromatography on silica gel.^[10] The stereochemistry of **5a** was assigned unambiguously by X-ray structure analysis.^[11]

We tested these ligands in three different reactions. In the Rh-catalyzed hydroboration^[12] the cationic Rh^I complex formed with **3a** proved to be optimal,^[13] leading to optically active alcohols in 2 h using 1 mol % catalyst (room temperature). The regio- (86:14 to >99:1) and enantioselectivity (84–92% ee; Table 1) are comparable to those reported for

that 3 mol % of the putative Ag^I complex of **3a** catalyzes the reaction, affording adducts with high yields and enantioselectivities (Scheme 2).^[15]



Scheme 2. Ag-catalyzed azomethine cycloaddition reaction with acrylates.

Table 1: Rh-catalyzed hydroboration.

1) 1 mol % $[\text{Rh}(\mathbf{3a})(\text{cod})]\text{BF}_4$ catecholborane toluene, RT, 2 h				
2) H_2O_2 , NaOH, H_2O				
Entry	R	Yield [%]	ee [%]	Quinap [% ee] ^[4a]
1	Ph	73	92	92
2	<i>p</i> -Tol	94	92	89
3	<i>m</i> -Tol	85	84	86
4	<i>o</i> -Tol	81	91	92
5	<i>p</i> -MeO-C ₆ H ₄	80	90	94
6	<i>p</i> -Cl-C ₆ H ₄	87	87	78

quinap, which is the ligand that demonstrates the broadest scope for this reaction.^[4a] Interestingly, an important difference in reactivity was observed for the Rh^I complex of **3a** when compared to previous work. Thus, in contrast to reactions with quinap, the electronics of the aryl substrate exerted little influence on the ee value of the product (Table 1, entries 5 and 6), indicating an unanticipated advantage of the complex derived from **3a**.

The asymmetric, Ag-catalyzed azomethine cycloaddition reaction with acrylates first reported by Zhang et al.^[14] was examined next. Its substrate scope has been recently expanded by using a Ag–quinap catalyst.^[4e] We have observed

Our interest in the chemistry of terminal acetylenes^[16] compelled us to examine the ligands in the Cu-catalyzed reaction of alkynes and imines. First reported in 1963,^[17] these additions have been recently investigated by Knochel et al. with the complex formed by quinap and CuBr .^[4c] We have observed that the Cu^I complexes of **5a** and **5b** catalyze the formation of the propargylic amines in 90–99% ee,^[18] which are the best values obtained to date (Table 2).

Table 2: Cu-catalyzed addition of alkynes to imines.

5.5 mol % 5a or 5b 5 mol % CuBr toluene, RT					
R	R'	Ligand	Yield [%]	ee [%]	Quinap [% ee] ^[4c]
<i>i</i> Pr	Me_3Si	5a	84	98 (<i>R</i>)	92
		5b	82	99 (<i>S</i>)	
<i>i</i> Pr	Ph	5a	88	90 (<i>R</i>)	84
		5b	82	95 (<i>S</i>)	
<i>i</i> Bu	<i>n</i> Bu	5a	74	91 (<i>R</i>)	82
		5b	72	94 (<i>S</i>)	

In the examined reactions, the configuration of the biaryl moiety dictates stereoselection. It is noteworthy that in this process subtle remote effects are observed with respect to the stereogenic center in the phenethyl group. Thus, when compared to **5a**, the use of the diastereomeric ligand **5b** can lead to a measurable and consistent increase (up to 5%) in the *ee* value of the product (Table 2). Interestingly, in these additions it is the *R,P*-configured ligand that affords the higher selectivities, whereas in the hydroboration and cycloaddition reactions the *R,M*-configured ligands proved superior.

In conclusion, we have presented a new class of P,N ligands and demonstrated their utility in three different asymmetric reactions with three different metals. The efficiency (four steps from commercially available material) and modular nature of the synthesis should permit fine tuning of the ligand to accommodate a broad scope of asymmetric transformations. Further studies aimed at diversifying the structure of the ligands and their application in new reactions are underway in our laboratories.

Received: July 13, 2004

Keywords: asymmetric catalysis · atropisomerism · heterocycles · hydroboration · P,N ligands

ving.html (or from the Cambridge Crystallographic Data Centre, 12, Union Road, Cambridge CB2 1EZ, UK; fax: (+44) 1223-336-033; or deposit@ccdc.cam.ac.uk).

- [1] *Comprehensive Asymmetric Catalysis*, Vol. 1–3 (Eds.: E. N. Jacobsen, A. Pfaltz, H. Yamamoto), Springer, Berlin, **1999**.
- [2] a) P. J. Guiry, C. P. Saunders, *Adv. Synth. Catal.* **2004**, *346*, 497–537; b) G. Helmchen, A. Pfaltz, *Acc. Chem. Res.* **2000**, *33*, 336–345; c) For an extensive review on P,N Ligands with pyridine donors, see: G. Chelucci, G. Orru, G. A. Pinna, *Tetrahedron* **2003**, *59*, 9471–9515.
- [3] Quinap: 1-(2-diphenylphosphino-1-naphthyl)isoquinoline.
- [4] a) H. Doucet, E. Fernandez, T. P. Layzell, J. M. Brown, *Chem. Eur. J.* **1999**, *5*, 1320–1330; b) J. W. Faller, B. J. Grimmond, *Organometallics* **2001**, *20*, 2454–2458; c) N. Gommermann, C. Koradin, K. Polborn, P. Knochel, *Angew. Chem.* **2003**, *115*, 5941–5944; *Angew. Chem. Int. Ed.* **2003**, *42*, 5763–5766; d) J. B. Morgan, S. P. Miller, J. P. Morken, *J. Am. Chem. Soc.* **2003**, *125*, 8702–8703; e) C. Chen, X. Li, S. L. Schreiber, *J. Am. Chem. Soc.* **2003**, *125*, 10174–10175.
- [5] We suggest the acronym pinap in analogy to quinap, where “pi” refers to phthalazine.
- [6] N. W. Alock, J. M. Brown, D. I. Hulmes, *Tetrahedron: Asymmetry* **1993**, *4*, 743–756.
- [7] C. W. Lim, O. Tissot, A. Mattison, M. W. Hooper, J. M. Brown, A. R. Cowley, D. I. Hulmes, A. J. Blacker, *Org. Process Res. Dev.* **2003**, *7*, 379–384.
- [8] 50 mg (*P*)- or (*M*)-quinap costs € 143 at STREM.
- [9] M. Pal, V. R. Batchu, K. Parasuraman, K. Yeleswarapu, *J. Org. Chem.* **2003**, *68*, 6806–6809.
- [10] Depending on the scale, different separation procedures were applied. Typically on > 2 g scale either **3a** or **5a** was selectively crystallized from the mixture (see Supporting Information for details), and the residue was purified by flash chromatography. On a smaller scale the diastereomers were separated by flash chromatography; for example, 1.21 g of a mixture of **3a/3b** was separated by flash chromatography to give **3a** (595 mg) and **3b** (501 mg; 91% mass recovery).
- [11] CCDC-243850 (**3a**) and CCDC-243851 (**5a**) contain the supplementary crystallographic data for this paper. These data can be obtained free of charge via www.ccdc.cam.ac.uk/conts/retrieving.html (or from the Cambridge Crystallographic Data Centre, 12, Union Road, Cambridge CB2 1EZ, UK; fax: (+44) 1223-336-033; or deposit@ccdc.cam.ac.uk).
- [12] a) T. Hayashi, Y. Matsumoto, Y. Ito, *J. Am. Chem. Soc.* **1989**, *111*, 3426–3428; b) J. M. Brown, D. I. Hulmes, T. P. Layzell, *J. Chem. Soc. Chem. Commun.* **1993**, 1673–1674; c) A. Schnyder, L. Hintermann, A. Togni, *Angew. Chem.* **1995**, *107*, 628–630; *Angew. Chem. Int. Ed. Engl.* **1995**, *34*, 931–933.
- [13] Ligand **3b** gave slightly lower enantioselectivities (89% *ee* in the hydroboration of styrene). The complexes with ligands **5a** and **5b** gave lower enantioselectivities and yields.
- [14] J. M. Longmire, B. Wang, X. Zhang, *J. Am. Chem. Soc.* **2002**, *124*, 13400–13401.
- [15] Ligand **3b** gave slightly lower enantioselectivities (93% *ee* for R = CN). The complexes with ligands **5a** and **5b** gave lower enantioselectivities and yields.
- [16] a) D. E. Frantz, R. Fässler, E. M. Carreira, *J. Am. Chem. Soc.* **2000**, *122*, 1806–1807; b) N. K. Anand, E. M. Carreira, *J. Am. Chem. Soc.* **2001**, *123*, 9687–9688; c) D. E. Frantz, R. Fässler, E. M. Carreira, *J. Am. Chem. Soc.* **1999**, *121*, 11245–11246; d) C. Fischer, E. M. Carreira, *Org. Lett.* **2001**, *3*, 4319–4321; e) T. F. Knöpfel, E. M. Carreira, *J. Am. Chem. Soc.* **2003**, *125*, 6054–6055.
- [17] K. C. Brannock, R. D. Burpitt, J. G. Thweatt, *J. Org. Chem.* **1963**, *28*, 1462–1464.
- [18] Ligands **3a** and **3b** gave comparable results (for R = *i*Pr and R' = Ph; **3a**: 92% *ee* (*R*) and **3b**: 94% *ee* (*S*)).

Label-Free Assay

Profiling Kinase Activities by Using a Peptide Chip and Mass Spectrometry***Dal-Hee Min, Jing Su, and Milan Mrksich**

Herein we describe a strategy that combines peptide chips with matrix-assisted laser desorption/ionization time-of-flight (MALDI-TOF) mass spectrometry (MS) to evaluate kinase activities rapidly and semi-quantitatively. We have already shown that monolayers of alkanethiolates on gold are well-suited as substrates for MALDI-TOF MS, and could be used to measure enzyme activities and to perform high-throughput screenings.^[1,2] A significant aspect of this approach—which we term SAMDI (*self-assembled monolayers for MALDI*) MS—is that it avoids the use of labels, greatly simplifying the formatting of assays. Herein we establish two important

[*] D.-H. Min, J. Su, Prof. M. Mrksich
Department of Chemistry
Institute for Biophysical Dynamics
The University of Chicago
5735 South Ellis Avenue
Chicago, IL 60637 (USA)
Fax: (+1) 773-702-0805
E-mail: mmmrksich@uchicago.edu

[**] This work was supported by the National Science Foundation. D.-H.M. was supported by the Burroughs Wellcome Fund Interfaces Program.

benefits that make this method well-suited to profiling multiple enzyme activities. First, SAMDI allows different classes of analytes, which may normally each require separate labeling strategies, to be evaluated by using a single method. Second, by using peptide substrates that are mass-resolved, the substrates can be immobilized on a single surface as mixtures, and do not need to be patterned into arrays.

Protein kinases are enzymes that catalyze the transfer of a phosphate group to tyrosine, serine, or threonine residues of substrate proteins. Protein kinases serve important regulatory functions in essentially all cellular processes including cell growth, migration, differentiation, and death.^[3] Hence, assays that measure kinase activities are important in research and in the identification of lead compounds in drug discovery. Traditional kinase-activity assays follow one of two formats. In the first, a radioactive ³²P atom is used to label the phosphorylated substrates. Separation of the phosphorylated products using gel electrophoresis, phosphocellulose binding, or liquid chromatography then allows quantitation of the extent of phosphorylation and therefore of the kinase activity.^[4] In the second format, the phosphorylated peptides are detected with antibodies that recognize the phosphopeptide. The assays can employ many strategies to analyze the binding of the antibody, including enzyme linked immuno sorbent assay (ELISA) formats and fluorescence polarization.^[5] These techniques provide reliable methods for measuring kinase activities, but they do require substantial manipulation and are not readily extended to multikinase formats. Recent efforts have recognized that mass-spectrometric techniques could prove useful for measuring the activities because these techniques avoid labels, which leads to simpler assay formats.^[6] A remaining challenge with these methods is to ease the requirement for sample enrichment, including by HPLC and affinity chromatography, prior to MS analysis.

We illustrate the SAMDI assay with the c-Src kinase.^[7] We prepared mixed self-assembled monolayers (SAMs) presenting maleimide groups among a background of tri(ethylene glycol) groups.^[8] A peptide substrate for c-Src (Pep1, 1 mM) was immobilized by the reaction of the terminal cysteine residue with the maleimide groups. Analysis of the monolayer by MALDI-TOF MS showed a single major peak at *m/z* 2079 ([P1+H]⁺) corresponding to the mixed disulfide derived from the peptide-terminated alkanethiol and a glycol-terminated alkanethiol (termed P1 (from Pep1)). An identical monolayer was treated with c-Src kinase (0.4 U μL⁻¹ *N*-(2-hydroxyethyl)-*N'*-(2-ethanesulphonyl)piperazine (HEPES)

buffer (pH 7.5) containing 80 μM adenosine-5'-triphosphate (ATP), 15 mM MgCl₂) for 1 h at 30 °C. The monolayer was then rinsed, treated with matrix (2,4,6-trihydroxyacetophenone (THAP), 2 μL, 5 mg mL⁻¹ in methanol) and analyzed by MALDI-TOF MS.^[9] The original peak arising from the substrate peptide was absent and a new peak resulting from phosphorylation of the peptide was observed at *m/z* 2159 ([PP1+H]⁺; Figure 1a). Importantly, all of the original peptide underwent phosphorylation, which shows that the ligands, when immobilized to the structurally well-defined monolayers, retain full activity towards the enzyme.

We assayed the catalytic subunits of protein kinase A (PKA), protein kinase G (PKG), calmodulin-dependent protein kinase II (CaMKII), casein kinase I (CKI), and Abl

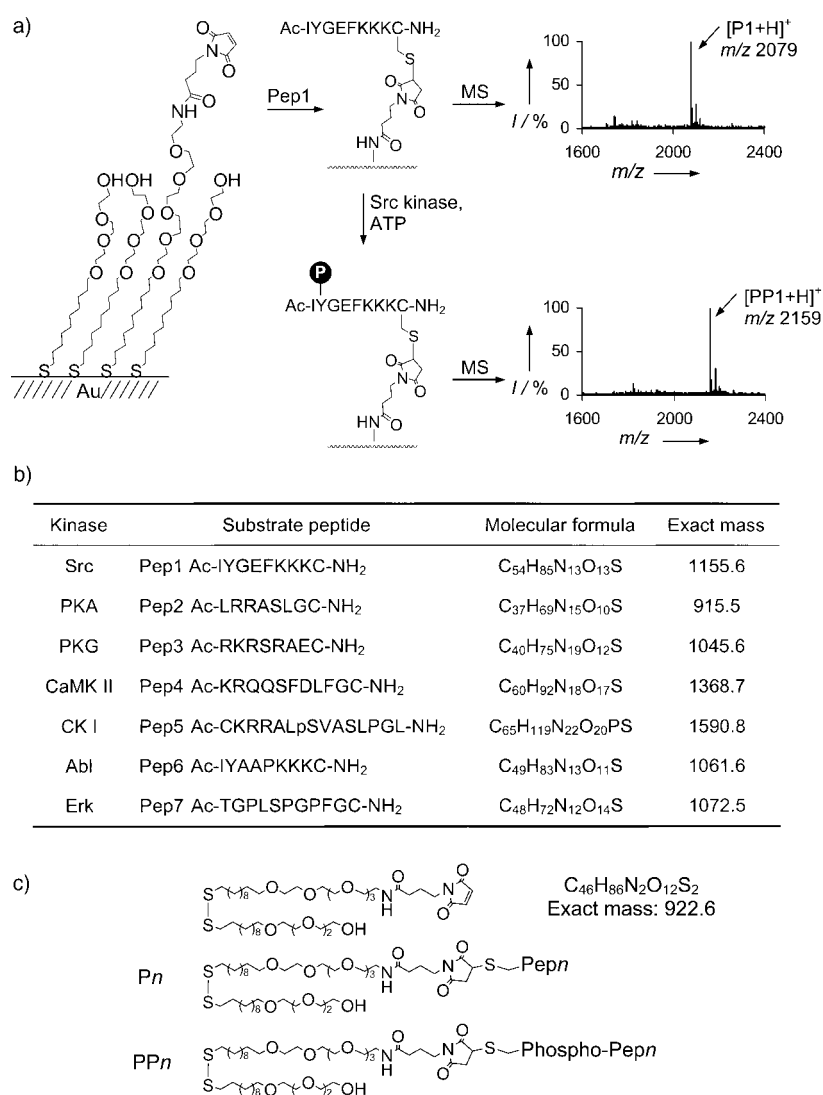


Figure 1. Design of monolayers for characterizing enzyme activities by MALDI-TOF MS. a) A peptide substrate for c-Src kinase (Pep1) was immobilized on a SAM presenting maleimide groups. The monolayer was treated with c-Src kinase. Both monolayers before and after the kinase treatment were analyzed by MS, which showed one major peak corresponding to the mixed disulfide containing the peptide ([P1+H]⁺) and phosphorylated product ([PP1+H]⁺), respectively. b) Sequences and masses of substrate peptides used in this work are listed. c) Molecular structures corresponding to mass peaks observed in this study are shown.

kinase by using the set of selective substrate peptides in Figure 1b.^[10] The enzymatic reaction conditions were chosen to give complete phosphorylation by each kinase. Representative mass spectra are shown in Figure 2. We found that in each case, the kinase reactions resulted in the expected mass change of 80, which confirms the addition of phosphate groups to each of the peptide substrates.

Multiple kinase activities can be measured simultaneously by using monolayers that present mixtures of kinase-specific peptide substrates. We treated a maleimide-terminated monolayer with a mixture of four peptides (Pep2, Pep4, Pep5, and Pep7). The ratio of the peptides in the mixture was adjusted to give monolayers that displayed the four peptides at similar intensities in MALDI-TOF spectra.^[11] Indeed, a mass spectrum of the monolayer showed four well resolved peaks corresponding to disulfides derived from each peptide-terminated alkanethiolates ($[P2+H]^+$ m/z 1839, $[P4+H]^+$ m/z 2292, $[P5+H]^+$ m/z 2514, $[P7+Na]^+$ m/z 2018; Figure 3a). An identical monolayer was treated with the CK I kinase, which is expected to phosphorylate only Pep5. Mass analysis revealed that the original mass peak for the CK I substrate peptide ($[P5+H]^+$) was absent and gave rise to a new peak corresponding to phosphorylation of this peptide ($[PP5+H]^+$ m/z 2594), while the other peptides remained unmodified by the kinase (Figure 3b). In an additional example, we treated the same chip with PKA and found that the peptide substrate for this kinase was phosphorylated ($[PP2+H]^+$ m/z 1919), but the other peptides were not modified (Figure 3c). These examples show that the SAMDI approach can be applied to peptide chips for rapid and easily interpretable characterization of enzymatic reactions in a multi-analyte format.

The SAMDI assay can be used to quantitatively characterize the inhibition of kinases by known inhibitors. We prepared several solutions containing CKI (1 U μL^{-1}) and the inhibitor *N*-[2-((*p*-bromocinnamyl)amino)ethyl]-5-isoquinolinesulfonamide (H-89) at concentrations ranging from 0.001 to 1 mM in assay buffer (pH 7.5 2-amino-2-(hydroxymethyl)-1,3-propanediol (Tris) buffer containing 10 mM MgCl_2 and 0.2 mM ATP). A portion of each reaction mixture (1 μL) was applied onto a circular region (2 mm in diameter)

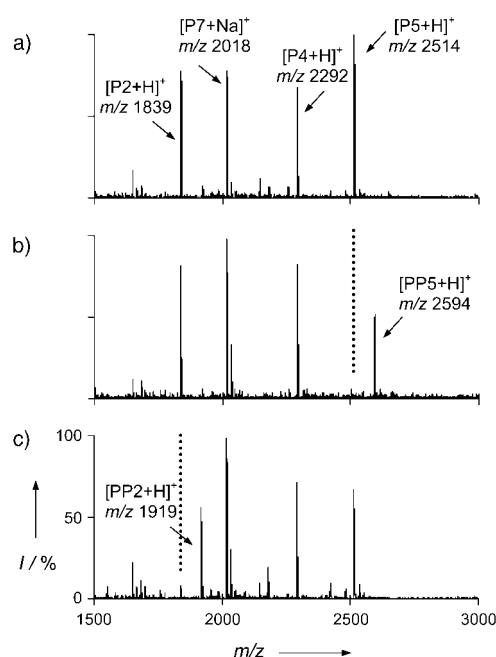


Figure 3. Enzymatic reactions on monolayers presenting multiple peptide substrates. a) The monolayer was prepared by applying a mixed solution of the four peptides (Pep2, Pep4, Pep5, and Pep7) to monolayers presenting maleimide groups. Molecular ion peaks corresponding to disulfides containing each substrate peptide were well resolved. b) Treatment of the monolayer with CK I resulted in phosphorylation of only the CK I substrate peptide Pep5 ($[P5+H]^+$). c) Treatment of the monolayer with PKA resulted in phosphorylation of only Pep2 ($[PP2+H]^+$). Dotted vertical line indicates the position of the peak for the substrate peptide.

of a monolayer presenting CKI selective substrate peptide, Pep5. The array was incubated for 30 min at 25 °C to allow the kinase reactions to proceed and then each spot was characterized by SAMDI to determine the extent of reaction. Figure 4a shows the relationship between the concentration of H-89 and the extent of the phosphorylation reaction. The data are fit well by a 1:1 inhibition model and give an IC_{50} value of 93 μM .^[12] We followed the same procedure to

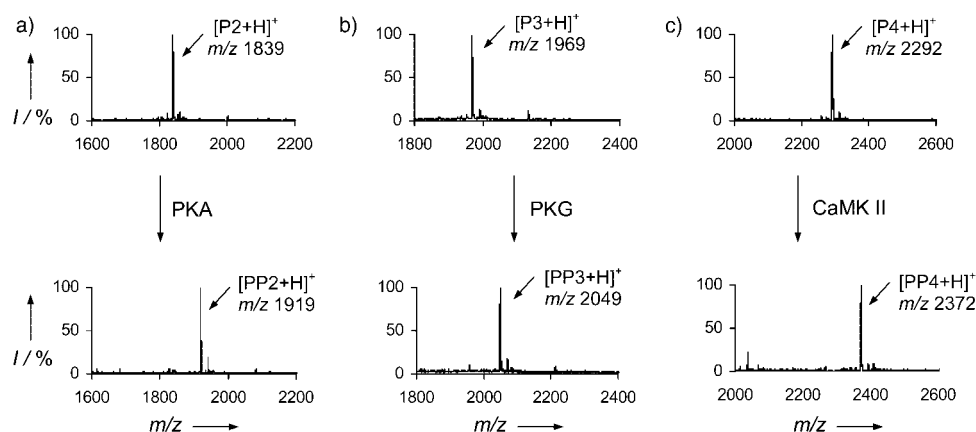


Figure 2. Characterization of three different kinase reactions with MALDI-TOF MS. MS spectra of the monolayers presenting substrate peptides are shown before (top) and after (bottom) treatment with a) PKA onto Pep2-immobilized SAMs, b) PKG onto Pep3-immobilized SAMs, and c) CaMKII onto Pep4-immobilized SAMs. After treatment with kinases, the original peaks ($[Pn+H]^+$) were absent and gave rise to new peaks corresponding to the phosphorylated product peptides ($[PPn+H]^+$).

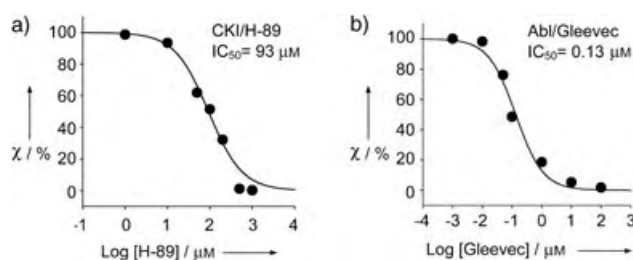


Figure 4. Dose-dependent inhibition curves of kinase reactions determined by SAMDI MS. a) Solutions of CKI and H-89, ranging in concentrations from 0.001 to 1 mM, were applied to the SAMs presenting substrate peptide (Pep5). The relative amount of phosphorylated peptide χ , is plotted versus H-89 concentrations. b) Abl kinase and Gleevec also show dose-dependent inhibition.

characterize inhibition of Abl kinase by the approved drug Gleevec (also known as STI571, a 2-phenylaminopyrimidine derivative) on a monolayer presenting a selective substrate peptide of Abl kinase, Pep6.^[13] A dose-dependent inhibition curve showed an IC_{50} value of 0.13 μM (Figure 4b).^[14] These data show that the SAMDI approach enables quantitative analysis of kinase activities to evaluate inhibition kinetics.

The method reported herein advances a significant body of work in which MS was employed to analyze enzyme activities. Siuzdak and co-workers, for example, have characterized enzymatic glycosylation by β -1,4-galactosyltransferase and showed that enzyme inhibitors could be quantitatively characterized with electrospray ionization (ESI) MS.^[15] Leary and co-workers have evaluated enzyme kinetics of the carbohydrate sulfotransferase and hexokinase, and screened a mock library to identify possible inhibitors of hexokinase by using ESI MS.^[16] Henion and co-workers have quantitatively evaluated the hydrolysis of dinucleotides by ribonuclease A and the hydrolysis of lactose by β -galactosidase using HPLC MS.^[17] Additionally, phosphorylated proteins and peptides have been characterized by MS after enriching samples by affinity chromatography or liquid chromatography before MS analysis.^[6] The features that distinguish our method is that the peptide substrate is immobilized on an inert surface. The immobilization simplifies the preparation of the sample for MS analysis, since the spectator molecules can be removed by rinsing. The use of an inert surface permits quantitative enzyme reactions in a solid-phase format.^[18]

The high sensitivity for detecting analytes and the avoidance of labels have led many researchers to apply MS to biochemical studies, including enzyme assays, protein-ligand interactions, and biomarker characterization from biological samples.^[6, 15–17, 19–21] One limitation with these practices is that the preparation of samples for MS analysis is not straightforward. Our goal is to develop relatively simple processes that can be routinely used in biological research. The use of immobilized substrates together with surfaces that provide for specific interactions, is an advance in this direction. We believe that the ability to conduct multiple assays on a single surface will prove useful in chemical biology and signal transduction research.

Received: June 23, 2004

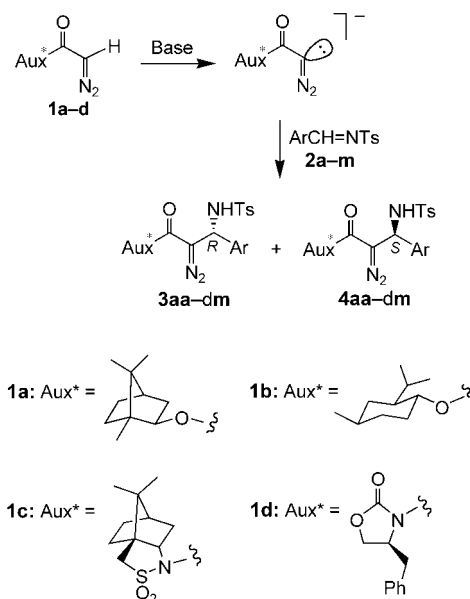
Keywords: assays · enzymes · mass spectrometry · monolayers · peptides

- [1] a) J. Su, M. Mrksich, *Angew. Chem.* **2002**, *114*, 4909; *Angew. Chem. Int. Ed.* **2002**, *41*, 4715; b) W.-S. Yeo, M. Mrksich, *Angew. Chem.* **2003**, *115*, 3229; *Angew. Chem. Int. Ed.* **2003**, *42*, 3121; c) D.-H. Min, W.-S. Yeo, M. Mrksich, *Anal. Chem.* **2004**, *76*, 3923.
- [2] D.-H. Min, W.-J. Tang, M. Mrksich, *Nat. Biotechnol.* **2004**, *22*, 717.
- [3] T. Hunter, *Cell* **2000**, *100*, 113.
- [4] a) J. E. Casnellie, *Methods Enzymol.* **1991**, *200*, 115; b) J. X. Yan, N. H. Packer, A. A. Gooley, K. L. Williams, *J. Chromatogr. A* **1998**, *808*, 23; c) T. Obata, M. B. Yaffe, G. G. Leparc, E. T. Piro, H. Maegawa, A. Kashiwagi, R. Kikkawa, L. C. Cantley, *J. Biol. Chem.* **2000**, *275*, 36108; d) H. Zhu, J. F. Klemic, S. Chang, P. Bertone, A. Casamayor, K. G. Klemic, D. Smith, M. Gerstein, M. A. Reed, M. Snyder, *Nat. Genet.* **2000**, *26*, 283; e) A. C. Bishop, O. Buzko, K. M. Shokat, *Trends Cell Biol.* **2001**, *11*, 167; f) N. Gotoh, S. Laks, M. Nakashima, I. Lax, J. Schlessinger, *FEBS Lett.* **2004**, *564*, 14.
- [5] a) A. Simeonov, X. Bi, T. T. Nikiforov, *Anal. Biochem.* **2002**, *304*, 193; b) G. Rijksen, B. A. Van Oirschot, G. E. Staal, *Methods Enzymol.* **1991**, *200*, 98; c) L. E. DeForge, A. G. Cochran, S. H. Yeh, B. S. Robinson, K. L. Billeci, W. L. Wong, *Assay Drug Dev. Technol.* **2004**, *2*, 131.
- [6] a) D. T. McLachlin, B. T. Chait, *Curr. Opin. Chem. Biol.* **2001**, *5*, 591; b) N. Ibarrola, D. E. Kalume, M. Gronborg, A. Iwahori, A. Pandey, *Anal. Chem.* **2003**, *75*, 6043.
- [7] B. T. Houseman, J. H. Huh, S. J. Kron, M. Mrksich, *Nat. Biotechnol.* **2002**, *20*, 270.
- [8] B. T. Houseman, E. S. Gawalt, M. Mrksich, *Langmuir* **2003**, *19*, 1522.
- [9] For kinase reactions, 1 μL of the enzyme solutions was applied to the substrates (4 mm²). Mass analysis was performed using a Voyager DE-PRO Biospectrometry mass spectrometer (Applied Biosystems, Framingham, MA) operating in the delayed extraction mode with a 337 nm nitrogen laser for desorption and ionization with an accelerating voltage of 20 kV.
- [10] a) Z. Songyang, K. L. Carraway III, M. J. Eck, S. C. Harrison, R. A. Feldman, M. Mohammadi, J. Schlessinger, S. R. Hubbard, D. P. Smith, C. Eng, M. J. Lorenzo, B. A. J. Ponder, B. J. Mayer, L. C. Cantley, *Nature* **1995**, *373*, 536; b) Z. Songyang, K. P. Lu, Y. T. Kwon, L. H. Tsai, O. Filhol, C. Cochet, D. A. Brickey, T. R. Soderling, C. Bartleson, D. J. Graves, A. J. DeMaggio, M. F. Hoekstra, J. Blenis, T. Hunter, L. C. Cantley, *Mol. Cell. Biol.* **1996**, *16*, 6486; c) B. E. Kemp, D. J. Graves, E. Benjamini, E. G. Krebs, *J. Biol. Chem.* **1977**, *252*, 4888; d) J. P. Huggins, A. J. Ganzhorn, V. Saudek, J. T. Pelton, R. A. Atkinson, *Eur. J. Biochem.* **1994**, *221*, 581.
- [11] Total peptide concentration was 1 mM and the ratio of four peptides was Pep2:Pep4:Pep7 = 5:1:5:15.
- [12] A previous study reported an IC_{50} value of 38 μM : see T. Chijiwa, A. Mishima, M. Hagiwara, M. Sano, K. Hayashi, T. Inoue, K. Naito, T. Toshioka, H. Hidaka, *J. Biol. Chem.* **1990**, *265*, 5267.
- [13] We prepared mixtures of Abl (1 μM) and Gleevec at concentrations ranging from 0.001 to 100 μM in the assay buffer containing 0.1 mM ATP. Other reaction conditions are as described in the text for the CKI inhibition assay.
- [14] Reported IC_{50} values of Gleevec with Abl kinase are 0.025 μM , 0.038 μM , and 0.44 μM . Differences in the values may reflect differences in Abl concentrations and the use of different substrates: see a) B. J. Druker, S. Tamura, E. Buchdunger, S. Ohno, G. M. Segal, S. Fanning, J. Zimmermann, N. B. Lydon, *Nat. Med.* **1996**, *2*, 561; b) E. Buchdunger, J. Zimmermann, H. Mett, T. Meyer, M. Muller, B. J. Druker, N. B. Lydon, *Cancer*

- Res.* **1996**, 56, 100; c) B. B. Brasher, R. A. Van Etten, *J. Biol. Chem.* **2000**, 275, 35631.
- [15] J. Wu, S. Takayama, C. H. Wong, G. Siuzdak, *Chem. Biol.* **1997**, 4, 653.
- [16] a) N. Pi, J. I. Armstrong, C. R. Bertozzi, J. A. Leary, *Biochemistry* **2002**, 41, 13283; b) H. Gao, J. A. Leary, *J. Am. Soc. Mass Spectrom.* **2003**, 14, 173.
- [17] F. Y. Hsieh, X. Tong, T. Wachs, B. Ganem, J. Henion, *Anal. Biochem.* **1995**, 229, 20.
- [18] B. T. Houseman, M. Mrksich, *Trends Biotechnol.* **2002**, 20, 279.
- [19] a) C. J. Zea, N. L. Pohl, *Anal. Biochem.* **2004**, 327, 107; b) A. R. de Boer, T. Letzel, D. A. van Elswijk, H. Lingeman, W. M. Niessen, H. Irth, *Anal. Chem.* **2004**, 76, 3155.
- [20] a) J. Gao, Q. Wu, J. Carbeck, Q. P. Lei, R. D. Smith, G. M. Whitesides, *Biophys. J.* **1999**, 76, 3253; b) T. Lee, A. N. Hoofnagle, Y. Kabuyama, J. Stroud, X. Min, E. J. Goldsmith, L. Chen, K. A. Resing, N. G. Ahn, *Mol. Cell* **2004**, 14, 43; c) R. W. Nelson, D. Nedelkov, K. A. Tubbs, *Electrophoresis* **2000**, 21, 1155; d) W. H. Gong, G. G. Polkowski, I. Fritsch, C. L. Wilkins, *Int. J. Mass Spectrom.* **2003**, 222, 397.
- [21] B. Ye, D. W. Cramer, S. J. Skates, S. P. Gygi, V. Pratomo, L. Fu, N. K. Horick, L. J. Licklider, J. O. Schorge, R. S. Berkowitz, S. C. Mok, *Clin. Cancer Res.* **2003**, 9, 2904.

base-promoted, aldol-type nucleophilic addition of acyldiazomethane to aldehydes or ketones to afford diazoketols.^[3] A similar addition to *N*-tosylimines gives α -diazocarbonyl compounds bearing a β -(*N*-tosyl)amino substituent, which demonstrate a novel reactivity in various transition-metal-catalyzed reactions.^[4] To further explore the chemistry of this type of nucleophilic addition, we decided to study the stereocontrol of the reaction. Herein, we report a highly diastereoselective base-promoted condensation of an α -diazocarbonyl compound and *N*-tosylimines in the presence of Evans' chiral oxazolidinone auxiliary.^[5] The condensation products can be further converted into *syn*- and *anti*- α -hydroxy- β -amino esters.^[6]

Our investigation began with the reaction of *N*-tosylbenzaldehyde (2a) with the α -diazocarbonyl compounds 1a–d^[7] that contain chiral auxiliaries (Scheme 1, Table 1). The



Scheme 1. Base-promoted reaction of chiral diazo compounds 1a–d with *N*-tosylimines 2a–m.

Table 1: Base-promoted reaction of 1a–d with *N*-tosylbenzaldehyde 2a.

Entry	Diazo compound	Base	T [°C]	Additive ^[a]	d.r. ^[b]	Yield [%] ^[c]
1	1a	LDA	–78–RT	– ^[d]	51:49	50
2	1b	LDA	–78–RT	–	55:45	52
3	1c	LDA	–78	–	17:83	46
4	1d	LDA	–78	–	88:12	87
5	1d	LDA	–23	–	84:16	14
6	1d	LDA	–98	–	90:10	90
7	1d	NaHMDS	–98	–	76:24	95
8	1d	DBU	–98–RT	–	–	– ^[e]
9	1d	Et ₂ Zn	–98–RT	–	–	–
10	1d	LDA	–98	LiCl	88:12	81
11	1d	LDA	–98	MgBr ₂	75:25	97
12	1d	LDA	–98	HMPA	95:5	84

[a] Five equivalents of additive were employed. [b] Diastereomeric ratio was determined from the ¹H NMR (400 MHz) spectrum of the crude product, or by HPLC analysis. [c] Yield of the inseparable diastereomeric mixture after silica gel column chromatography. [d] No additive was used. [e] No reaction.

Asymmetric Synthesis

A Highly Stereoselective Addition of the Anion Derived from α -Diazoacetamide to Aromatic *N*-Tosylimines**

Yonghua Zhao, Zhihua Ma, Xiaomei Zhang, Yaping Zou, Xianglin Jin, and Jianbo Wang*

α -Diazocarbonyl compounds have found wide application in organic synthesis as a result of their diverse reactivities.^[1] The previous research activities in this area have mostly concentrated on the transition metal complex catalyzed diazo decompositions, which generate metal–carbene intermediates. In addition to serving as metal–carbene precursors, however, the relatively stable α -diazocarbonyl compounds can tolerate a variety of transformations with retention of the diazo functionality, thus allowing the chemical modification of α -diazo compounds.^[1c,2] One such transformation is the

[*] Y. Zhao, Dr. Z. Ma, Dr. X. Zhang, Y. Zou, Prof. X. Jin, Prof. Dr. J. Wang
Key Laboratory of Bioorganic Chemistry and Molecular Engineering
of the Ministry of Education
College of Chemistry, Peking University
Beijing 100871 (P.R. China)
Fax: (+86) 10-6275-1708
E-mail: wangjb@pku.edu.cn

[**] Thanks are due to Cheng Peng, Shufeng Chen, and Wei Qian for their valuable experimental contributions. Y.Z. and Z.M. contributed equally to this work. The project was generously supported by the Natural Science Foundation of China (grant nos. 20225205, 20172002, and 20390050).

Supporting information for this article is available on the WWW under <http://www.angewandte.org> or from the author.

reaction with diazo esters **1a** and **1b** gave the addition products in moderate yields, although with essentially no stereoselectivity (Table 1, entries 1 and 2). The reaction with diazoamides **1c** and **1d**, on the other hand, gave good diastereomeric ratios of 17:83 and 88:12, respectively (Table 1, entries 3 and 4). Further improvement of the reaction was then focused on *N*-(diazoacetyl)oxazolidinone (**1d**). The reaction temperature was found to have an influence—reaction at higher temperature (−23 °C) resulted in a lower yield (Table 1, entry 5), presumably because of the instability of the diazo compounds. A slightly higher selectivity can be achieved at −98 °C without affecting the yield or the reaction time (Table 1, entry 6). Changing the base from lithium diisopropylamide (LDA) to sodium hexamethyldisilazide (NaHMDS) gave an improved yield, but with lower stereoselectivity (Table 1, entry 7). Both 1,8-diazabicyclo[5.4.0]undec-7-ene (DBU) and Et₂Zn, which are known to promote condensation of acyldiazomethane with aldehydes and imines,^[3i,8] failed to promote the reaction of **1d** with **2a** (Table 1, entries 8 and 9). Commonly used additives, such as LiCl or MgBr₂, were found to have no effect on the stereoselectivity. However, we quite unexpectedly found that HMPA, which binds strongly to lithium ions,^[9] significantly improved the stereoselectivity (Table 1, entry 12).^[10] It is likely that HMPA disrupts the ion pairing by coordinating to lithium, thus allowing the α-diazocarbonyl anion to react more efficiently at low temperature.

Table 2 illustrates the scope and limitation of the optimized reaction conditions for the reaction of **1d** with a series of aryl *N*-tosylimines **2a–m**. The reaction of most imine

Table 2: Base-promoted reaction of **1d** with aryl *N*-tosylimines **2a–m**.^[a]

Entry	Ar group of imine 2	Product	d.r. ^[b]	Yield [%] ^[c]
1	C ₆ H ₅	3da	95:5	84
2	<i>p</i> -PhC ₆ H ₄	3db	> 95:5	90
3	<i>p</i> -ClC ₆ H ₄	3dc	> 95:5	82
4	<i>p</i> -FC ₆ H ₄	3dd	> 95:5	84
5	<i>p</i> -MeOC ₆ H ₄	3de	93:7	79
6	<i>m</i> -CNC ₆ H ₄	3df	> 95:5	83
7	<i>m</i> -BrC ₆ H ₄	3dg	95:5	73
8	<i>o</i> -MeC ₆ H ₄	3dh	76:24	76
9	2,4-Cl ₂ C ₆ H ₃	3di	90:10	94
10	2,6-Cl ₂ C ₆ H ₃	3dj	56:44	85
11	C ₆ H ₅ CH=CH–	3dk	91:9	76
12	2-(5-bromo)thienyl	3dl	94:6	73
13	2-furyl	3dm	> 95:5	78

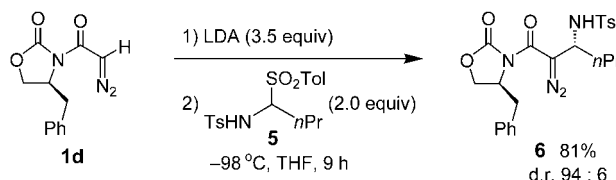
[a] Reaction was carried out with LDA (1.2 equiv), **1d** (1.0 equiv), and HMPA (5.0 equiv), followed by slow addition of a solution of **2** (1.5 equiv) in THF at −98 °C. [b] The diastereomeric ratio was determined from the ¹H NMR (400 MHz) spectrum of the crude product. [c] Yield after purification by silica gel column chromatography.

substrates gave high diastereoselectivities and yields, although the stereoselectivities were lower with *N*-tosylimines bearing *ortho* substituents (Table 2, entries 8–10). In the case of *N*-tosyl-2,6-dichlorobenzaldimine, the reaction was essentially nonselective (Table 2, entry 10).

Although most of the addition products were isolated as amorphous solids, one of them (**3dm**) yielded crystals that

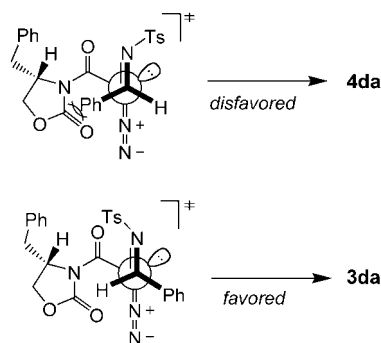
allowed us to determine the stereochemistry of the newly created chiral center. A single-crystal X-ray diffraction study of this product indicated that the new chiral center has an *R* configuration.^[11]

Preliminary experiments also indicated that the LDA-promoted diastereoselective reaction of **1d** with imines can be further extended to aliphatic *N*-tosylimines. Thus, *N*-tosyl-*n*-butylimine, which was generated in situ from the sulfonamide sulfone **5**,^[12] was treated with **1d** under similar reaction conditions, but without HMPA additive, to give the addition product **6** in 81% yield and a diastereomeric ratio of 94:6 (Scheme 2).



Scheme 2. LDA-promoted reaction of **1d** with sulfonamide sulfone **5**.

The stereochemical outcome of the reaction can be rationalized by the transition states depicted in Scheme 3.



Scheme 3. Plausible stereochemical pathway for the addition of deprotonated **1d** to **2a**.

Initial deprotonation of **1d** generates the diazocarbonyl anion or enolate.^[13] Since the HMPA additive coordinates strongly to the lithium ion, the diazocarbonyl anion becomes less associated.^[14] Moreover, the *N*-tosylamino group coordinates only weakly to lithium because of the strongly electron-withdrawing tosyl group. Consequently, the nucleophilic addition proceeds through a nonchelated open transition state in which the *N*-tosylimine approaches from the less sterically hindered side of the anion with an orientation that avoids steric repulsion between the aryl group and the oxazolidinone auxiliary. The anions derived from diazo amides **1c** and **1d** are conformationally more rigid than the corresponding anions derived from diazo esters **1a** and **1b** because of the rotational restriction of the amide C–N bond. The rigid structure of the anion might be responsible for the high diastereoselectivities observed for the reactions of **1c** or **1d** in the absence of chelation,^[15] while the reaction with

diazo esters **1a** or **1b** is nonselective because of the flexibility of the anion conformation. This stereochemical process is in contrast with the addition of the enolates of acyl oxazolidinones to C=O or C=N bonds,^[5,16] where complexation is usually responsible for the high stereoselectivities. Interestingly, the reaction of aromatic aldehydes with **1d** under similar conditions gave rather poor diastereoselectivities and low yields.

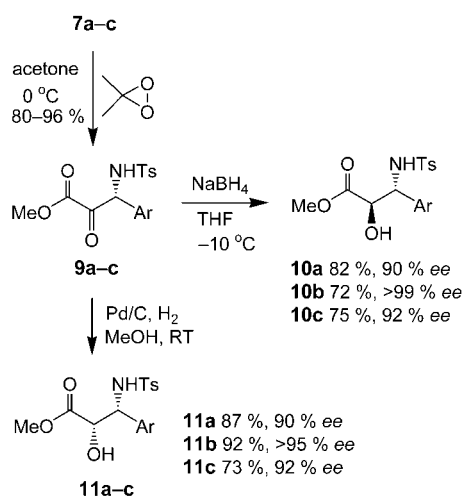
The utility of the addition products **3** was demonstrated by the concise synthesis of *syn*- and *anti*- α -hydroxy- β -amino acid derivatives. Thus, the chiral oxazolidinone auxiliary was removed by addition of lithium methoxide in THF to give the chiral methyl α -diazoesters **7a–g,k–m**, and **8** (Table 3).^[17]

Table 3: Removal of the chiral oxazolidinone auxiliary.

3da-dg,dk-dm, 6		7a-g,k-m, 8		
Entry	R	Product	ee [%] ^[a]	Yield [%] ^[b]
1	C ₆ H ₅	7a	90	65
2	<i>p</i> -PhC ₆ H ₄	7b	> 99	67
3	<i>p</i> -ClC ₆ H ₄	7c	92	58
4	<i>p</i> -FC ₆ H ₄	7d	95	83
5	<i>p</i> -MeOC ₆ H ₄	7e	85	66
7	<i>m</i> -CNC ₆ H ₄	7f	91	78
8	<i>m</i> -BrC ₆ H ₄	7g	90	69
9	C ₆ H ₅ CH=CH–	7k	83	73
10	2-(5-bromo)thienyl	7l	88	77
11	2-furyl	7m	> 99	56
12	<i>n</i> Pr	8	87	60

[a] ee value determined by chiral HPLC (see Supporting Information for details). [b] Total yield.

The diazo groups of **7a–c** were subsequently oxidized with dimethyldioxirane (DMD) to give α -ketoesters **9a–c**, respectively (Scheme 4). Reduction of the oxo group with NaBH₄ in



Scheme 4. Synthesis of both *anti*- and *syn*- α -hydroxy- β -amino acid derivatives from chiral methyl α -diazoesters **7a–c**.

THF at -10°C was highly efficient and stereoselective to afford the *anti*- α -hydroxy- β -amino esters **10a–c**.^[18,19] Pd/C-catalyzed hydrogenation of the α -ketoesters **9a–c**, on the other hand, gave the *syn*- α -hydroxy- β -amino esters **11a–c**,^[20] respectively, also with high yields and selectivities (Scheme 4).^[18,19b]

In summary, this study is the first example of the highly diastereoselective nucleophilic addition of the anion derived from α -diazocarbonyl compounds to a C=N bond. This reaction can be successfully applied to the synthesis of both *anti*- and *syn*- α -hydroxy- β -amino acid derivatives. Since the diazo group has diverse reactivity, it should be possible to apply the addition products obtained by this reaction to other organic syntheses.

Received: May 20, 2004

Revised: July 27, 2004

Keywords: amino acids · chiral auxiliaries · diastereoselectivity · diazo compounds · nucleophilic addition

- [1] For recent reviews, see: a) T. Ye, M. A. McKerver, *Chem. Rev.* **1994**, 94, 1091; b) A. Padwa, D. J. Austin, *Angew. Chem.* **1994**, 106, 1881; *Angew. Chem. Int. Ed. Engl.* **1994**, 33, 1797; c) M. P. Doyle, M. A. McKerver, T. Ye, *Modern Catalytic Methods for Organic Synthesis with Diazo Compounds*, Wiley, New York, **1998**; d) A. Padwa, *J. Organomet. Chem.* **2001**, 617–618, 3; e) M. P. Doyle, D. C. Forbes, *Chem. Rev.* **1998**, 98, 911; f) H. M. L. Davies, E. G. Antoulinakis, *J. Organomet. Chem.* **2001**, 617–618, 47; g) D. J. Timmons, M. P. Doyle, *J. Organomet. Chem.* **2001**, 617–618, 98; h) D. M. Hodgson, F. Y. T. M. Pierard, P. A. Stupp, *Chem. Soc. Rev.* **2001**, 30, 50.
- [2] For a review, see: M. Regitz, *Synthesis* **1972**, 351.
- [3] a) U. Schöllkopf, H. Frasnelli, D. Hoppe, *Angew. Chem.* **1970**, 82, 291; *Angew. Chem. Int. Ed. Engl.* **1970**, 9, 300; b) U. Schöllkopf, B. Bánhidai, H. Frasnelli, R. Meyer, H. Beckhaus, *Liebigs Ann. Chem.* **1974**, 1767; c) R. Pellicciari, B. Natalini, *J. Chem. Soc. Perkin Trans. 1* **1977**, 1822; d) R. Pellicciari, B. Natalini, B. M. Sadeghpour, M. Marinozzi, J. P. Snyder, B. L. Williamson, J. T. Kuethe, A. Padwa, *J. Am. Chem. Soc.* **1996**, 118, 1; e) C. J. Moody, R. J. Taylor, *Tetrahedron Lett.* **1987**, 28, 5351; f) E. Wenkert, C. A. McPherson, *J. Am. Chem. Soc.* **1972**, 94, 8084; g) T. L. Burkoth, *Tetrahedron Lett.* **1969**, 10, 5049; h) N. F. Woolsey, M. H. Khalil, *J. Org. Chem.* **1972**, 37, 2405; i) N. Jiang, J. Wang, *Tetrahedron Lett.* **2002**, 43, 1285; j) W. Yao, J. Wang, *Org. Lett.* **2003**, 5, 1527.
- [4] a) N. Jiang, Z. Qu, J. Wang, *Org. Lett.* **2001**, 3, 2989; b) N. Jiang, Z. Ma, Z. Qu, X. Xing, L. Xie, J. Wang, *J. Org. Chem.* **2003**, 68, 893.
- [5] a) D. A. Evans, J. Bartoli, T. L. Shih, *J. Am. Chem. Soc.* **1981**, 103, 2127; b) for a review, see: D. J. Ager, I. Prakash, D. R. Schaad, *Chem. Rev.* **1996**, 96, 835.
- [6] For recent reviews on the synthesis of β -amino acid derivatives, see: a) S. Abele, D. Seebach, *Eur. J. Org. Chem.* **2000**, 1; b) M. Liu, M. P. Sibi, *Tetrahedron* **2002**, 58, 7991; c) J.-A. Ma, *Angew. Chem.* **2003**, 115, 4426; *Angew. Chem. Int. Ed.* **2003**, 42, 4290.
- [7] a) N. Haddad, N. Galili, *Tetrahedron: Asymmetry* **1997**, 8, 3367; b) Y. Landais, D. Planchenault, *Tetrahedron* **1997**, 53, 2855; c) M. P. Doyle, R. L. Dorow, J. W. Terpstra, R. A. Rodenhouse, *J. Org. Chem.* **1985**, 50, 1663; d) *N*-(diazoacetyl)oxazolidinone **1d** can be easily prepared from the reaction of (*S*)-(–)-4-benzyl-2-oxazolidinone with triphosgene, followed by treatment with diazomethane, or by deprotonation of (*S*)-(–)-4-benzyl-2-oxa-

zolidinone acetamide with LDA and diazo transfer from *o*-nitrophenylsulfonyl azide. See the Supporting Information for details.

- [8] a) F. Sarabia, F. J. López-Herrera, *Tetrahedron Lett.* **2001**, 42, 8801; b) C. J. Moody, C. N. Morfitt, *Synthesis* **1998**, 1039.
- [9] a) H. J. Reich, W. H. Sikorski, *J. Org. Chem.* **1999**, 64, 14; b) W. H. Sikorski, H. J. Reich, *J. Am. Chem. Soc.* **2001**, 123, 6527.
- [10] The use of HMPA for improving the diastereoselectivity in lithium enolate reactions has been reported; see: E. Juaristi, J. L. León-Romo, Y. Ramírez-Quirós, *J. Org. Chem.* **1999**, 64, 2914, and references therein.
- [11] a) CCDC-239004 contains the supplementary crystallographic data for this paper. These data can be obtained free of charge via www.ccdc.cam.ac.uk/conts/retrieving.html (or from the Cambridge Crystallographic Data Centre, 12 Union Road, Cambridge CB21EZ, UK; fax: (+44)1223-336-033; or deposit@ccdc.cam.ac.uk); b) the *R* configuration was also confirmed by correlating the product **3da** with the known compound (2*R*,3*S*)-**11a**. See the Supporting Information.
- [12] a) C. Palomo, M. Oiarbide, M. C. González-Rego, A. K. Sharma, J. M. García, A. González, C. Landa, A. Linden, *Angew. Chem.* **2000**, 112, 1105; *Angew. Chem. Int. Ed.* **2000**, 39, 1063; b) F. Chemla, V. Hebbe, J.-F. Normant, *Synthesis* **2000**, 1, 75.
- [13] Although the exact structure of the deprotonated diazoacetyl compound is not known, it should be more reasonable to consider it as a carbanion, in which the negative charge is localized on the diazo-bound carbon atom.
- [14] HMPA has been known to dramatically alter the regio- and/or stereoselectivity in the reaction of lithium enolates with electrophiles; see a) ref. [9, 10]; b) D. A. Hunt, *Org. Prep. Proceed. Int.* **1989**, 21, 705; c) L. M. Jackman, B. C. Lange, *J. Am. Chem. Soc.* **1981**, 103, 4494; d) T. Cohen, W. D. Abraham, M. Myers, *J. Am. Chem. Soc.* **1987**, 109, 7923.
- [15] Chelated and nonchelated enolates derived from Evans' reagents have been reported to give opposite stereoselectivities in aldol reactions, see: M. A. Walker, C. H. Heathcock, *J. Org. Chem.* **1991**, 56, 5747.
- [16] a) M. T. Crimmins, B. W. King, E. A. Tabet, *J. Am. Chem. Soc.* **1997**, 119, 7883; b) N. B. Ambhaikar, J. P. Snyder, D. C. Liotta, *J. Am. Chem. Soc.* **2003**, 125, 3690; c) T. Kawakami, H. Ohtake, H. Arakawa, T. Okachi, Y. Imada, S.-I. Murahashi, *Bull. Chem. Soc. Jpn.* **2000**, 73, 2423.
- [17] The reaction of **3a** with MeOMgBr in MeOH gave low yields of **7a**. Other methods for removing the oxazolidinone auxiliary, such as addition of LiOH/H₂O₂ in THF/H₂O, were also examined, but the diazo compound **3a** decomposes to give a complex mixture of products.
- [18] Only one diastereoisomer could be identified in the ¹H NMR (400 MHz) spectrum of the crude product of each reaction.
- [19] a) A similar diastereoselective reduction of β-amino-α-keto esters with NaBH₄ has been reported: J.-M. Lee, H.-S. Lim, K.-C. Seo, S.-K. Chung, *Tetrahedron: Asymmetry* **2003**, 14, 3639; b) the assignment of the relative stereochemistry is based on the correlation of the product **11a** with the known compound (2*R*,3*S*)-**11a**, and an X-ray crystal structure of the reduction product of the racemic α-keto β-amino ester: Y. Zhao, N. Jiang, S. Zhang, J. Wang, unpublished results.
- [20] a) G. Li, K. B. Sharpless, *Acta Chem. Scand.* **1996**, 50, 649; b) G. Li, H.-T. Chang, K. B. Sharpless, *Angew. Chem.* **1996**, 108, 449; *Angew. Chem. Int. Ed. Engl.* **1996**, 35, 451.

Highly Ordered Mesoporous Bioactive Glasses with Superior In Vitro Bone-Forming Bioactivities**

Xiaoxia Yan, Chengzhong Yu,* Xufeng Zhou, Jiawei Tang, and Dongyuan Zhao*

Bioactive glasses (BGs) have attracted much attention since the pioneering work by Hench et al. in 1971.^[1] Glass ceramics with $\text{CaO-P}_2\text{O}_5\text{-SiO}_2\text{-MO}$ ($\text{M} = \text{Na, Mg, etc}$) compositions have been widely studied and used in clinical applications because such materials can chemically bond with living bone.^[2,3] The inorganic part of the human bone is hydroxy-carbonate apatite (HCA), and when BGs are implanted in the human body an HCA layer with the ability to bond with living bone is formed on the surface of the bioactive material. For the sol-gel-derived BGs^[4,5] to exhibit in vitro behaviour, it has been shown that both the composition and structure are important,^[6-9] while melt-derived glasses show a direct dependence on composition. Increasing the specific surface area and pore volume of BGs may greatly accelerate the kinetic deposition process of HCA and therefore enhance the bone-forming bioactivity of BGs.^[6] More importantly, precise control over porosity, pore size, and internal pore architecture of BGs on different length scales is essential for the understanding of the structure-bioactivity relationship and the rational design of better bone-forming biomaterials. However, a multicomponent glass system is quite complex and consists of mainly amorphous oxides, and thus the synthesis of ordered mesoporous BGs by using a well-studied surfactant-templating route^[10] has not been reported. Herein we demonstrate that highly ordered mesoporous bioactive glasses (MBGs) have been successfully synthesized by templating with a block copolymer.^[11] MBGs lead to superior bone-forming bioactivities in vitro compared to normal BGs derived from sol-gels. Moreover, the mesostructure of MBGs is also shown to be important with regard to their bioactivities. Such MBGs are important in both mesoporous material and biomaterial research and may open up new opportunities

[*] X. Yan, Prof. Dr. C. Yu, X. Zhou, J. Tang, Prof. Dr. D. Zhao
Department of Chemistry and
Shanghai Key Laboratory of Molecular Catalysis and
Innovative Materials
Fudan University
Shanghai 200433 (P. R. China)
Fax: (+86) 21-6564-1740
E-mail: czyu@fudan.edu.cn
dyzhao@fudan.edu.cn

[**] This work was financially supported by the National Science Foundations of China (20301004, 20233030, and 20173012), State Key Research Program (2002AA321010 and 001CB510202), and Shanghai Science Committee (0212 nm043, 0352 nrm108, 03DJ14004, and 03QF14002).



Supporting information for this article is available on the WWW under <http://www.angewandte.org> or from the author.

in implanting, drug delivery, and as coating-materials in tissue engineering.^[12–16]

Highly ordered MBGs were synthesized by using nonionic block copolymers as structure-directing agents^[11] through an evaporation-induced self-assembly (EISA) process.^[17] The powder X-ray diffraction (XRD) pattern of the calcined MBG 80S15C (80S and 15C represents the molar fraction of Si and Ca, respectively) shows three diffraction peaks in the small-angle regime ($2\theta = 1.19, 2.11, 2.41^\circ$), which can be indexed to the (100), (110), and (200) diffractions of a two-dimensional hexagonal ($p6mm$) lattice with a cell parameter a of 8.50 nm (Figure 1 a). Transmission electron microscope

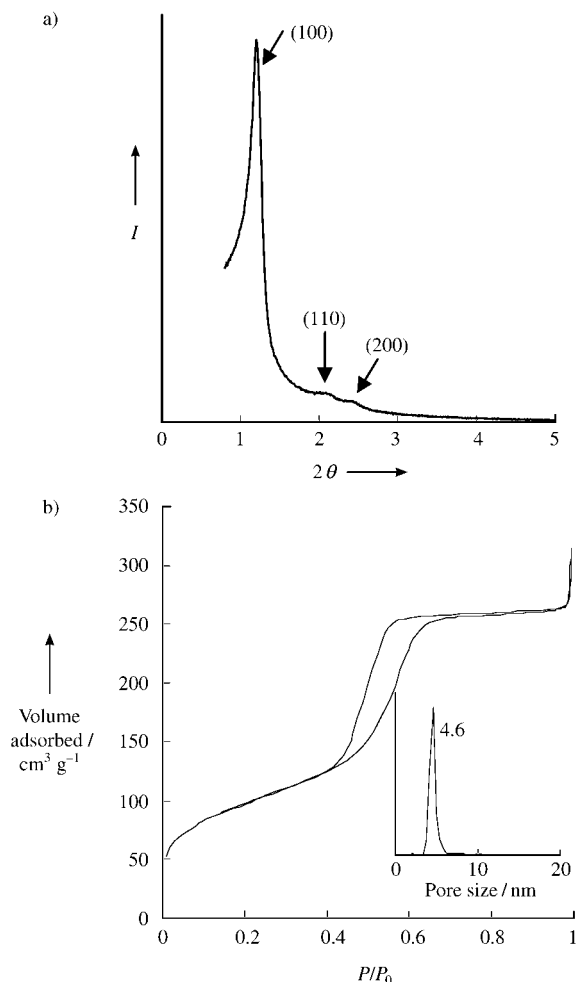


Figure 1. a) XRD pattern and b) N_2 sorption isotherm of calcined MBG 80S15C synthesized in the presence of P123 template. The inset shows a plot of the pore size distribution (calculated by BdB method).

(TEM) images along the [001] and [100] directions also reveal a highly ordered hexagonal arrangement of one-dimensional channels (Figure 2 a and b, respectively). Nitrogen sorption isotherms further confirm the existence of uniform mesopores (Figure 1 b). The BET surface area, pore volume, and pore size is calculated to be $351 \text{ m}^2 \text{ g}^{-1}$, $0.49 \text{ cm}^3 \text{ g}^{-1}$, and 4.60 nm, respectively. For comparison, calcined BG 80S15C synthesized without surfactants has a relatively lower pore volume of $0.067 \text{ cm}^3 \text{ g}^{-1}$. MBGs synthesized in a range of compositions

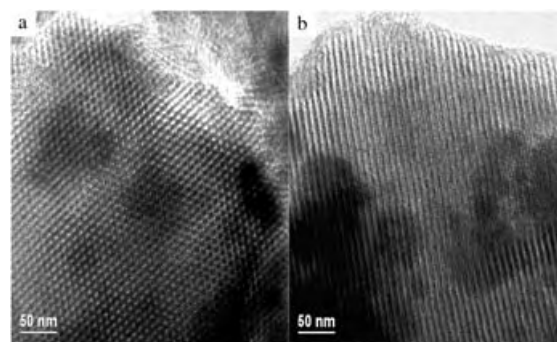


Figure 2. TEM images of calcined hexagonal MBG 80S15C recorded along the a) [001] and b) [100] directions.

by using P123 as the template in an EISA process possess ordered hexagonal structures. Furthermore, the pore sizes of MBGs can be tuned in the range of 4–7 nm by varying the structure-directing agent, for example, F127 or B50-6600. The physicochemical properties of the MBGs studied are summarized in Table 1.

Table 1: Physicochemical properties of MBGs and BGs.

	Structure	d (100) [nm]	BET surface area [$\text{m}^2 \text{ g}^{-1}$]	Pore volume [$\text{cm}^3 \text{ g}^{-1}$]	Pore size [nm]
100S-P123	$p6mm$	6.9	300	0.40	4.4
80S15C-P123	$p6mm$	7.4	351	0.49	4.6
70S25C-P123	$p6mm$	7.4	319	0.49	4.6
60S35C-P123	$p6mm$	6.9	310	0.43	4.3
70S25C-F127	wormlike	9.2	300	0.36	5.0
60S35C-B50-6600	wormlike	10.5	228	0.42	7.1
80S15C	—	—	9.8	0.07	—

Thermogravimetric analysis (TGA) and differential TGA (DTGA) curves for MBG 80S15C and BG 80S15C are shown in Figure 3. As the heating process proceeds, four clear mass losses are observed for BG samples between 18 and 150°C , 150 and 300°C , 300 and 430°C , and 440 and 560°C . For the MBG samples, two mass losses are observed between 25 and 125°C as well as between 140 and 270°C ; a steep weight loss stage occurs between 300 and 325°C . Larger mass losses (70%, between 25 and 700°C) are observed in the case of MBG compared to BG (55%) as a result of the extra weight loss of the surfactants. A comparison of the TGA and DTGA profiles of two samples suggests that MBG samples are more homogenous in composition than BG samples.^[18] The peak appearing around $300\text{--}325^\circ\text{C}$ most likely arises from the simultaneous decomposition of inorganic precursors and block copolymers.

Most of the previous syntheses of sol-gel-derived BGs were carried out under aqueous conditions, and a high-temperature ($>100^\circ\text{C}$) drying process was required to remove the solvents; therefore, ordered MBGs were not

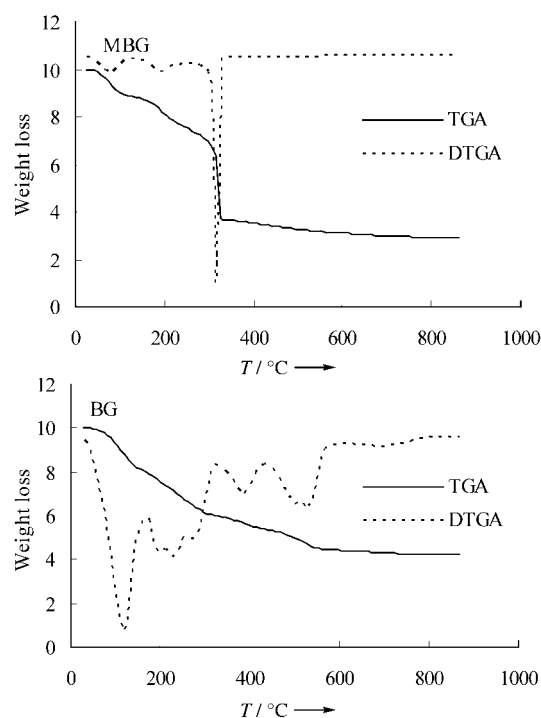


Figure 3. TGA and DTGA curves of MBG 80S15C obtained with a P123 template and BG 80S15C synthesized in the absence of surfactant.

obtained, even in the presence of surfactants. Performing the EISA process in near non-aqueous conditions in the current strategy is essential for the assembly of highly ordered MBGs. It is important to note that the MBGs fabricated in our study are unique compared to conventional BGs for the following two reasons. Firstly, the mechanism for the generation of the mesopore is different: Conventional BGs also possess mesopores which arise from the random distribution of CaO within the network of SiO₂.^[6] The self-assembly of surfactants in MBGs gives rise to uniform mesopores as well as ordered mesostructures. To support this point, MBG 60S35C and 80S15C show similar N₂ adsorption isotherms and pore diameters (5.0 and 4.6 nm, respectively; see Table 1), while BG 60S35C and 80S15C synthesized by Vallet-Regi et al. have a mean pore size of 12 and 5 nm, respectively.^[6] Accordingly, BG 80S15C shows H₂-type hysteresis loops associated with ink-bottle-like pores^[6] while MBG 80S15C shows H₁-type hysteresis loops typical of one-dimensional channels (Figure 1b). Secondly, the compositional homogeneity of the framework is different. The microphase separation and heterogeneity is common in normal sol-gel-derived BGs,^[18] and is also observed in our BGs obtained by the EISA process. The TGA, energy dispersive spectroscopy (EDS), and scanning electron microscopy (SEM) results (see below) indicate that all the components are homogeneously distributed in the network in the case of MBGs. Since ordered mesostructured materials are formed by the regular packing of composite micelles on the nanometer scale, it is suggested that the homogeneous dispersion of inorganic species on this length scale may lead to a more homogeneous material (MBG) than conventional BGs. Inorganic salts have also been

employed in the EISA process to produce macro- and mesoporous materials^[19] as well as metal oxide nanowire arrays within mesostructured frameworks^[20] where the crystallization of the salt/metal oxide and phase separation of a crystalline phase from amorphous sol-gel materials is unavoidable. In our case, the utilization of calcium nitrate in the synthesis gives rise to transparent monoliths and films before calcination (see Supporting Information), and a homogeneous glassy state is obtained after thermal treatment at 700 °C, as evidenced by wide-angle XRD measurements. It is important to note that the use of a nitrate salt and its subsequent decomposition during calcination is another essential factor in the fabrication of homogeneous MBGs.^[21]

MBGs with high specific surface area and pore volume should have a greatly enhanced bone-forming bioactivity than conventional BGs.^[6] It is believed that the prerequisite for glasses and glass ceramics to bond to living bone is the formation of a biologically active HCA layer on the surface of the BGs in the body. Therefore, the bone-forming activity of MBGs (and BG for comparison) *in vitro* was tested in simulated body fluid (SBF)^[22] to monitor the formation of HCA on the surface of MBGs over time. SEM images of MBG 80S15C before soaking shows a smooth and homogeneous surface (Figure 4a), which is in accordance with the results suggested by EDS and TGA analysis. The growth of nanoparticles (<100 nm in diameter) is observed after soaking the sample for 4 h (Figure 4b). It is surprising to note that a rodlike morphology (ca. 100 nm in length) which is similar to the morphology of HCA in human bones is exclusively observed after 8 h (Figure 4c). TEM examination reveals that such rods consist of even smaller nanorods about 5 nm in diameter (Figure 4g). EDS analysis shows that the molar ratio of Ca/P is 1.53:1 within such rods (Figure 4g, inset). Fourier transform infrared spectroscopy (FTIR) analysis of MBG 80S15C after immersing in SBF for 8 h shows the absorption bands of the phosphate group at 1040, 962, 603, and 562 cm⁻¹, together with the absorption bands of the carbonate group at 1488, 1432, and 870 cm⁻¹, which is in accordance with the IR spectra of HCA (see Supporting Information).^[6] High-resolution TEM studies further confirms the existence of crystalline HCA nanorods (Figure 4h); however, some amorphous rodlike morphology is still observed, which is in agreement with the diffraction rings in the electron diffraction (ED) pattern (Figure 4h, inset). The rodlike morphology is maintained with increasing immersion time and the crystallinity of HCA increases as reflected by FTIR results (data not shown). EDS analysis shows a molar ratio of Ca/P = 1.66:1 in the rodlike HCA materials after seven days, a ratio almost equal to that of perfect HCA materials. The surface of BG 80S15C synthesized in the absence of surfactant and before soaking is heterogeneous (Figure 4d), which is very different from the MBG samples. The induction time for the formation of amorphous HCA and the subsequent deposition rate of HCA on the surface of BG is much slower than for MBG (Figure 4e, f), a result which is in accordance with the inductively coupled plasma (ICP) atomic emission spectroscopy results (see Supporting Information).^[6,23] The rodlike HCA materials cannot be observed even after three days in the case of BG samples. It is

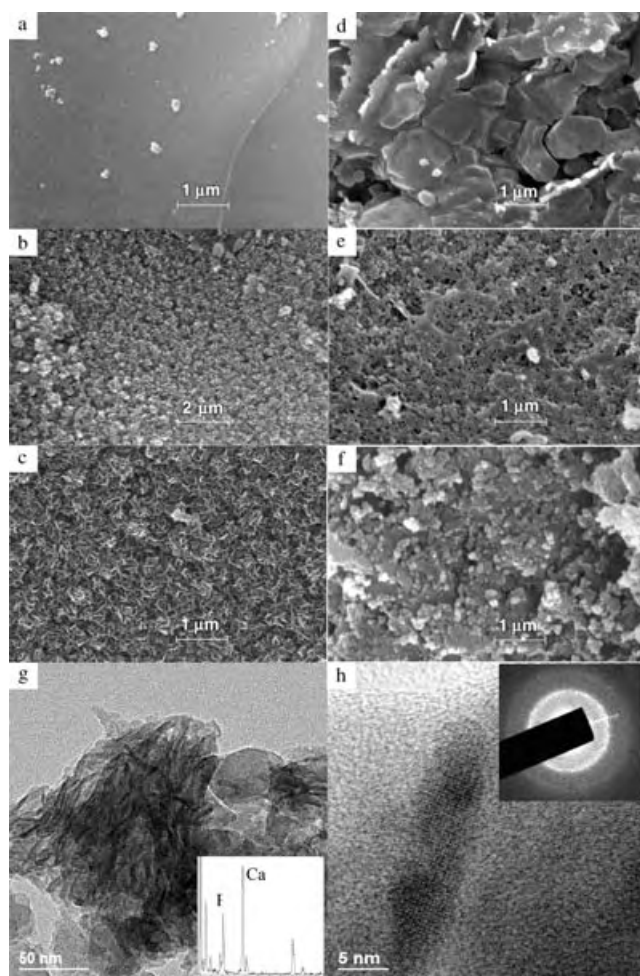


Figure 4. SEM images of MBG 80S15C (P123 template) after immersing in SBF for 0, 4, and 8 h (a)–(c). SEM images of BG 80S15C after soaking in SBF for 0, 8 and 48 h (d)–(f). TEM images of MBG 80S15C after soaking in SBF for 8 h at different magnifications (g) and (h). The EDS result (inset of g) and ED pattern (inset of h) of HCA deposited on MBG samples are also shown.

concluded that MBG with its larger pore volume and more accessible mesopore surface area has a much better bone-forming bioactivity in vitro than BG materials. The fast (ca. 8 h) and biomimetic HCA formation behavior (morphology of HCA similar to that in human body formed in simulated biological conditions) of MBGs means that the MBGs synthesized by the current strategy possess an outstanding bone-forming activity in vitro compared to other reported BGs.

The composition of MBGs is another important factor for their bioactivity. SEM results (see the Supporting Information) reveal that the bioactivity of MBGs in vitro follows the following sequence: 80S15C > 70S25C > 60S35C > 100S. The type of mesostructure in MBGs of the same composition is also important to the in vitro bioactivity. MBGs with the same composition (70S25C) have been synthesized in the presence of F127 and P123 (denoted MBG-F127 and MBG-P123, respectively) and their in vitro bioactivity compared. The dominant morphology of HCA deposited on MBG-P123 after immersing the MBG in SBF for 4 h is nanoparticles (see the

Supporting Information), but a rodlike morphology is already observed in the case of MBG-F127 (see the Supporting Information). Since the composition, the pore volume, and pore size of both MBG materials are similar, the observed difference in bioactivity is most likely attributed to their pore structures (Table 1): MBG-F127 with 3-dimensional pore structures may facilitate the transportation of dissolved Ca^{2+} and O-Si-O species as well as the subsequent deposition of HCA materials. More importantly, since the pore size and pore structure is important in the protein-adsorption behavior for mesoporous materials,^[24] it is believed that MBGs with a tunable pore size and pore structure may greatly influence the protein adsorption and nutrient delivery behavior for better in vivo bioactivity.

In conclusion, highly ordered mesoporous bioactive glasses have been synthesized with superior bone-forming bioactivity in vitro. Successful control of the mesostructure of MBGs adds a new dimension to the art of designed synthesis of bioactive glass materials. By carefully tuning the pore size, pore structure, and composition of MBGs, it is anticipated that MBGs with better in vivo bioactivity may be synthesized. MBGs with controllable morphologies may also be used for drug delivery, implant coating materials, and tissue engineering.

Experimental Section

MBGs were synthesized by using nonionic block copolymers such as $\text{EO}_{20}\text{PO}_{70}\text{EO}_{20}$ (P123), $\text{EO}_{106}\text{PO}_{70}\text{EO}_{106}$ (F127), and $\text{EO}_{39}\text{BO}_{47}\text{EO}_{39}$ (B50–6600) as structure-directing agents (EO is poly(ethylene oxide), PO is poly(propylene oxide), and BO is poly(butylene oxide)). In a typical synthesis of MBG, P123 (4.0 g), tetraethyl orthosilicate (TEOS, 6.7 g), $\text{Ca}(\text{NO}_3)_2 \cdot 4\text{H}_2\text{O}$ (1.4 g), triethyl phosphate (TEP, 0.73 g; Si/Ca/P = 80:15:5, molar ratio), and 0.5 M HCl (1.0 g) were dissolved in ethanol (60 g) and stirred at room temperature for 1 day. The resulting sol was introduced into a Petri dish to undergo an evaporation-induced self-assembly (EISA) process.^[17] The dried gel was calcined at 700 °C for 5 h to obtain the final MBG products (denoted 80S15C according to the molar fraction of Si and Ca). For comparison, BG 80S15C was synthesized by an identical process but without surfactants.

MBG and BG materials were ground and sieved. Granules with sizes in 76–38 μm fractions were selected. The bone-forming activity of MBGs (and BGs) in vitro was tested by immersing selected granules (100 mg) in simulated body fluid (SBF, 100 mL)^[22] to monitor the formation of HCA on the surface of MBGs over time. The solids were separated by filtration, washed three times with acetone, and dried in air.

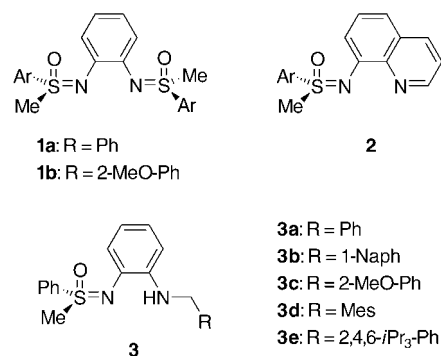
Received: May 8, 2004

Keywords: bioinorganic chemistry · block copolymers · glasses · mesoporous materials · template synthesis

- [1] L. L. Hench, R. J. Splinter, W. C. Allen, T. K. Greenlee, *J. Biomed. Mater. Res.* **1971**, 2, 117.
- [2] L. L. Hench, *J. Am. Ceram. Soc.* **1998**, 81, 1705.
- [3] L. L. Hench, J. M. Polak, *Science* **2002**, 295, 1014.
- [4] R. Li, A. E. Clark, L. L. Hench, *J. Appl. Biomater.* **1991**, 2, 231.
- [5] T. Peltola, M. Jokinen, H. Rahiala, E. Levanen, J. B. Rosenholm, I. Kangasniemi, A. Yli-Urpo, *J. Biomed. Mater. Res.* **1999**, 44, 12.
- [6] M. Vallet-Regi, C. V. Ragel, A. J. Salinas, *Eur. J. Inorg. Chem.* **2003**, 1029.

- [7] M. M. Pereira, A. E. Clark, L. L. Hench, *J. Am. Ceram. Soc.* **1995**, 78, 2463.
- [8] M. Vallet-Regi, A. Ramila, *Chem. Mater.* **2000**, 12, 961.
- [9] M. Vallet-Regi, D. Arcos, J. Perez-Pariente, *J. Biomed. Mater. Res.* **2000**, 51, 23.
- [10] C. T. Kresge, M. E. Leonowicz, W. J. Roth, J. C. Vartuli, J. S. Beck, *Nature* **1992**, 359, 710.
- [11] D. Y. Zhao, J. L. Feng, Q. S. Huo, N. Melosh, G. H. Fredrickson, B. F. Chmelka, G. D. Stucky, *Science* **1998**, 279, 548.
- [12] L. L. Hench, *J. Biomed. Mater. Res.* **1998**, 41, 511.
- [13] P. Sepulveda, J. R. Jones, L. L. Hench, *J. Biomed. Mater. Res.* **2002**, 59, 340.
- [14] E. M. Santos, S. Radin, P. Ducheyne, *Biomaterials* **1999**, 20, 1695.
- [15] T. Kokubo, *Biomaterials* **1991**, 12, 155.
- [16] J. M. Gomez-Vega, A. Hozumi, H. Sugimura, O. Takai, *Adv. Mater.* **2001**, 13, 822.
- [17] C. J. Brinker, Y. F. Lu, A. Sellinger, H. Y. Fan, *Adv. Mater.* **1999**, 11, 579.
- [18] M. Jokinen, H. Rahiala, J. B. Rosenholm, T. Peltola, I. Kangasniemi, *J. Sol-Gel Sci. Technol.* **1998**, 12, 159.
- [19] D. Y. Zhao, P. D. Yang, B. F. Chmelka, G. D. Stucky, *Chem. Mater.* **1999**, 11, 1174.
- [20] H. F. Yang, Q. H. Shi, B. Z. Tian, Q. Y. Lu, F. Gao, S. H. Xie, J. Fan, C. Z. Yu, B. Tu, D. Y. Zhao, *J. Am. Chem. Soc.* **2003**, 125, 4724.
- [21] C. J. Brinker, G. W. Scherer, *Sol-gel science: the physics and chemistry of sol-gel processing*, Academic Press, New York, **1990**.
- [22] T. Kokubo, H. Kushitani, S. Sakka, T. Kitsugi, T. Yamamuro, *J. Biomed. Mater. Res.* **1990**, 24, 721.
- [23] M. M. Pereira, L. L. Hench, *J. Sol-Gel Sci. Technol.* **1996**, 7, 59.
- [24] J. Fan, C. Z. Yu, T. Gao, J. Lei, B. Z. Tian, L. M. Wang, Q. Luo, B. Tu, W. Z. Zhou, D. Y. Zhao, *Angew. Chem.* **2003**, 115, 3254; *Angew. Chem. Int. Ed.* **2003**, 42, 3146.

bioactive molecules^[3] and pseudopeptides,^[4] chiral auxiliaries for asymmetric synthesis,^[5] and ligands for enantioselective metal catalysis.^[6] In the latter context we and others have prepared sulfoximines, such as **1** and **2**, which lead to products with up to 99% *ee* by palladium and copper catalysis.^[7,8]



Relevant intermediates in copper-catalyzed cycloaddition reactions were recently identified by spectroscopic means.^[9] We have now investigated the use of sulfoximines in Mukaiyama-type aldol reactions and found novel benzene-bridged aminobenzyl-substituted sulfoximines **3** (Mes = mesityl) to be excellent ligands for this synthetically important C–C bond-forming reaction.

We chose the reaction between 1-phenyl-1-(trimethylsiloxy)ethene (**4**) and methyl pyruvate (**5a**, Scheme 1) as a model reaction to allow meaningful comparisons to be made with well-established systems such as [Cu(*t*Bubox)]²⁺ or [Sn(pybox)]²⁺ (box = bis(oxazoline), pybox = pyridylbis(oxazoline)) catalysts.^[10] The initial experiments were performed in THF with copper(II) triflate as the metal source.

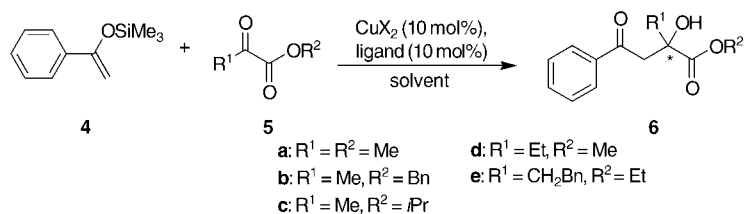
To our disappointment complexes based on C₂-symmetric bis-sulfoximines **1** and *N*-quinolyl-substituted sulfoximine **2**,

Asymmetric Catalysis

C₁-Symmetric Sulfoximines as Ligands in Copper-Catalyzed Asymmetric Mukaiyama-Type Aldol Reactions**

Martin Langner and Carsten Bolm*

Since the report of the discovery of sulfoximines by Whitehead and Bentley in 1952,^[1] they have found numerous applications in organic synthesis.^[2] For example, they have been used as building blocks in



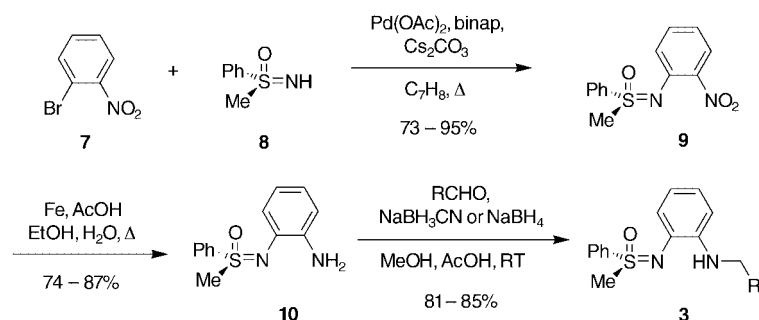
Scheme 1. Mukaiyama-type aldol reaction. Bn = benzyl.

which previously had been successfully applied in copper-catalyzed cycloaddition reactions,^[8] led to rather unsatisfying results and gave products with low or moderate enantioselectivities.^[11] On the basis of the hypothesis that an amino group would improve the metal-binding properties of the ligands, novel C₁-symmetric benzene-bridged benzylamino-sulfoximines **3** were designed. Their syntheses are summarized in Scheme 2. Starting from 2-bromonitrobenzene (**7**) and enantiopure (*S*)-*S*-methyl-*S*-phenylsulfoximine (**8**),^[12] the desired sulfoximines **3** were readily available by a three-step reaction sequence involving first a Buchwald–Hartwig-type

[*] Dipl.-Chem. M. Langner, Prof. Dr. C. Bolm
 Institut für Organische Chemie der Rheinisch-Westfälischen
 Technischen Hochschule Aachen
 Professor-Pirlet-Strasse 1, 52056 Aachen (Germany)
 Fax: (+49) 241-8092391
 E-mail: carsten.bolm@oc.rwth-aachen.de

[**] We are grateful to the Fonds der Chemischen Industrie and to the Deutsche Forschungsgemeinschaft (DFG, within SFB 380 "Asymmetric Synthesis by Chemical and Biological Methods") for financial support.

Supporting information for this article is available on the WWW under <http://www.angewandte.org> or from the author.



Scheme 2. Synthesis of benzene-bridged aminosulfoximines **3**. Binap = 2,2'-bis(diphenylphosphanyl)-1,1'-binaphthyl.

coupling reaction,^[13] followed by reduction of the nitro group and a reductive amination. Aniline **10** reacted readily with a wide variety of aldehydes, and thus a library of sulfoximine analogues became easily accessible. The high modularity of this synthetic approach becomes apparent when it is considered that other aromatic core units, various sulfoximines, and a number of aldehydes could be combined in the synthetic scheme.

In the test reaction shown in Scheme 1, the use of aminosulfoximine **3a**, which was prepared by reductive amination of **10** and benzaldehyde in 81 % yield, yielded aldol product **6a** with a promising *ee* value of 70 % (Table 1,

Table 1: Influence of the ligand structure on the Mukaiyama-aldol reaction shown in Scheme 1.^[a]

Entry	Aminosulfoximine	R of 3	Yield [%] ^[b]	<i>ee</i> [%] ^[c]
1	3a	Ph	64	70
2	3b	1-Naph	77	83
3	3c	2-MeO-Ph	72	86
4	3d	Mes	88	93
5	3e	2,4,6- <i>i</i> Pr ₃ -Ph	> 99	93

[a] Reaction conditions: **4** (0.6 mmol), **5a** (0.5 mmol), Cu(OTf)₂ (0.05 mmol), aminosulfoximine (0.05 mmol), THF, RT, 24 h. [b] After column chromatography. [c] Determined by HPLC on a column with a chiral stationary phase (Chiralcel OD).

entry 1). Aminosulfoximines **3b** and **3c** were prepared (in 85 and 81 % yield, respectively) for the conversion of **10**, with the expectation that the introduction of an electron-donating substituent on the *N*-benzyl arene group would provide a sterically more demanding environment at the metal center and further increase the metal–ligand interaction.^[14] Confirmation of this hypothesis was obtained when **6a** was generated with higher enantioselectivities in both cases (83 % and 86 % *ee* for catalysis with **3b** and **3c**, respectively; Table 1, entries 2 and 3) than when **3a** was used. The introduction of a substituent with two *ortho* groups improved the enantioselectivity even further, and the use of mesitylene derivative **3d** (prepared in 81 % yield) led to aldol product **6a** with 93 % *ee*. Finally, the best result in terms of both enantioselectivity and yield was obtained with triisopropyl-substituted analogue **3e** (prepared in 82 % yield), which gave **6a** with 93 % *ee* in > 99 % yield (Table 1, entry 5).

Next, we focused our attention on the optimization of the reaction conditions. First the effect of the solvent was investigated. It was deduced from studies with **3d** in various solvents (such as THF, diethyl ether, dioxane, toluene, dichloromethane, and chloroform) that weakly coordinating or aromatic solvents were important for achieving high enantioselectivity. THF proved to be the most suitable solvent in terms of catalytic activity.^[15]

Additional optimizations (with **3d**) in regard to the copper(II) salt and the reaction temperature were also performed. In general, the application of counterions other than triflate (for example, PF₆, BF₄, SbF₆, or ClO₄) resulted in a significant decrease in the *ee* value of the product.^[15] In terms of product yield, Cu(ClO₄)₂ was superior to all other metal sources (> 99 %). With this copper salt, however, the enantioselectivity (81 % *ee* for **6a**) was always lower than that obtained with the catalyst based on copper(II) triflate (93 % *ee*). The enantioselectivity of the reaction was improved to 98 % *ee* by performing the reaction at –55 °C instead of ambient temperature. However, long reaction times (> 9 days) were necessary under those reaction conditions to obtain the product in acceptable yields. Since 2,2,2-trifluoroethanol had been reported to facilitate the turnover in catalytic Mukaiyama-type reactions,^[16] its capability to accelerate the copper(II)–sulfoximine catalysis at low temperature was studied. To our delight we found that in the presence of this additive (1.2 equiv) the catalysis proceeded smoothly even at –30 °C to afford **6a** with 98 % *ee* in 89 % yield after only 15 h (Table 2, entry 1). This result clearly confirmed the accel-

Table 2: Effect of the substrate in reactions between **4** and **5** to give **6** (Scheme 1).^[a]

Entry	Product	<i>T</i> [°C]	<i>t</i> [h]	Yield [%] ^[b]	<i>ee</i> [%] ^[c]
1	6a	–30	15	89	98
2	6b	–50	47	86	98
3	6c	–40	28	90	99
4	6d	RT	24	78	89
5	6e	–20	40	86	96

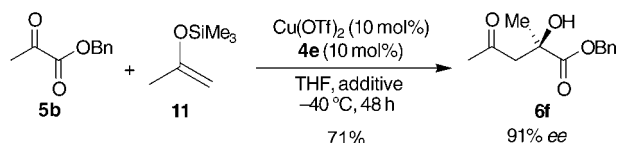
[a] Reaction conditions: **4** (0.6 mmol), **5a–e** (0.5 mmol), CF₃CH₂OH (0.6 mmol), Cu(OTf)₂ (0.05 mmol), aminosulfoximine **3e** (0.05 mmol). [b] After column chromatography. [c] Determined by HPLC.

ation effect, which occurred without affecting the enantioselectivity.

The substrate scope was evaluated under the conditions optimized for the reaction between **4** and **5a** (use of **3e** as the ligand, THF as the solvent, Cu(OTf)₂ as the copper source, and 2,2,2-trifluoroethanol as the additive at low temperature). Gratifyingly, we found that other α -keto esters also reacted well with enolsilyl ether **4**. Thus, the reaction between benzyl pyruvate (**5b**) and **4** at –50 °C yielded the corresponding aldol product **6b** with 98 % *ee*, and use of isopropyl pyruvate (**5c**) furnished **6c** with 99 % *ee* (Table 2, entries 2 and 3, respectively). These results showed that the efficiency of the catalyst was independent of the size of the ester moiety. Substrates

bearing more bulky acyl substituents were also investigated. The reaction between methyl α -keto butyrate (**5d**) and **4** gave **6d** with 89% *ee* at room temperature (Table 2, entry 4). No conversion was observed at lower temperatures. The sterically more-demanding ethyl 2-oxo-4-phenyl butyrate (**5e**) yielded **6e** with 96% *ee* at -20°C (Table 2, entry 5). Apparently, the catalyst tolerates an enlarged alkyl chain adjacent to the acyl function, although in some cases higher temperatures are required.

To test the applicability of another enolsilane, benzyl pyruvate (**5b**) was treated with 1-methyl-1-(trimethylsilyl)oxy)ethane (**11**) to afford the corresponding product **6f** with 91% *ee* in 71% yield (Scheme 3).



Scheme 3. Synthesis of **6f**. Tf = trifluoromethanesulfonyl.

In summary, we have described the synthesis of new C_1 -symmetric benzene-bridged aminosulfoximines, which are capable of serving as efficient ligands in copper-catalyzed enantioselective Mukaiyama-type aldol reactions. Aldol products with quarternary centers, which are commonly difficult to prepare in enantiomerically enriched form,^[17] have been obtained with up to 99% *ee* in high yields. In terms of *ee* values and yield, the new catalysts compare well with the established $[\text{Cu}(\text{tBubox})]^{2+}$ or $[\text{Sn}(\text{pybox})]^{2+}$ systems.^[10,18] Ongoing studies are directed to further expand the substrate scope and to demonstrate the applicability of the novel aminosulfoximines in other enantioselective catalyses.

Experimental Section

Representative example for the syntheses of aminosulfoximines **3a–e**: Preparation of **3e**: Glacial acetic acid (172 μL , 3.00 mmol) was added to a solution of aniline **10** (3.00 mmol, 739 mg) and 2,4,6-triisopropylbenzaldehyde (3.60 mmol, 837 mg) in MeOH (20 mL) at RT. The solution was stirred for 3 h and then cooled to 0°C . Subsequently, NaBH_4 (7.50 mmol, 284 mg) was added over 20 min, and the mixture was stirred at RT overnight. The solution was partitioned between 10% aqueous K_2CO_3 (20 mL) and CH_2Cl_2 (20 mL), and the aqueous layer was extracted with CH_2Cl_2 (3×20 mL). The combined organic layers were dried over MgSO_4 , and the solvent was evaporated. The product was purified by flash chromatography on silica gel (pentane/EtOAc 10:1) to afford 1.14 g (2.46 mmol, 82%) of **3e** as a colorless solid. For analytical data see the Supporting Information.

General procedure for the Mukaiyama-type aldol reaction: A flame-dried Schlenk flask under Ar atmosphere was charged with $\text{Cu}(\text{OTf})_2$ (18.1 mg, 0.05 mmol) and the aminosulfoximine **3a–e** (0.05 mmol). Dry THF (2 mL) was then added and the resulting deep green solution was stirred for 30 min at RT. The mixture was subsequently cooled to the selected temperature, and the α -keto ester **5a–e** (0.5 mmol), silylenol ether **4** (0.6 mmol, 123 μL), and 2,2,2-trifluoroethanol (0.6 mmol, 44 μL) were added. After stirring the reaction mixture for the indicated period of time, it was warmed to RT, diluted with diethyl ether (50 mL) and filtered through a plug of silica gel. The solvent was evaporated, and the product was purified

by flash chromatography. For analytical data and determinations of the *ee* values see the Supporting Information.

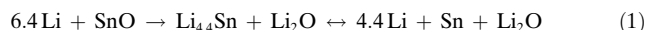
Received: June 14, 2004

Keywords: aldol reaction · asymmetric catalysis · copper · N ligands · sulfoximines

- [1] J. K. Whitehead, H. R. Bentley, *J. Chem. Soc.* **1952**, 1572–1574.
- [2] Reviews: a) C. R. Johnson, *Acc. Chem. Res.* **1973**, 6, 341–347; b) S. G. Pyne, *Sulfur Rep.* **1992**, 12, 57–59; c) M. Reggelin, C. Zur, *Synthesis* **2000**, 1–64.
- [3] Selected reviews: a) A. Meister, *Biochim. Biophys. Acta* **1995**, 1271, 35–42; b) M. E. Anderson, *Chem.-Biol. Interact.* **1998**, 111, 1–14; h) L. L. Muldoon, L. S. L. Walker-Rosenfeld, C. Hale, S. E. Purcell, L. C. Bennett, E. A. Neuwelt, *J. Pharmacol. Exp. Ther.* **2001**, 296, 797–805.
- [4] a) W. L. Mock, J.-T. Tsay, *J. Am. Chem. Soc.* **1989**, 111, 4467–4472; b) W. L. Mock, J. Z. Zhang, *J. Biol. Chem.* **1991**, 266, 6393–6400; c) C. Bolm, G. Moll, J. D. Kahmann, *Chem. Eur. J.* **2001**, 7, 1118–1128; d) C. Bolm, D. Müller, C. P. R. Hackenberger, *Org. Lett.* **2002**, 4, 893–896; e) C. Bolm, D. Müller, C. Dalhoff, C. P. R. Hackenberger, E. Weinhold, *Bioorg. Med. Chem. Lett.* **2003**, 13, 3207–3211.
- [5] For selected contributions, see: a) M. Reggelin, T. Heinrich, *Angew. Chem.* **1998**, 110, 3005–3008; *Angew. Chem. Int. Ed.* **1998**, 37, 2883–2886; ; b) M. Harmata, X. Hong, C. L. Barnes, *Tetrahedron Lett.* **2003**, 44, 7261–7264; c) S. Koep, H.-J. Gais, G. Raabe, *J. Am. Chem. Soc.* **2003**, 125, 9653–9667.
- [6] Reviews: a) M. Harmata, *Chemtracts* **2003**, 16, 660–666; b) H. Okamura, C. Bolm, *Chem. Lett.* **2004**, 33, 482–487, and references therein.
- [7] For Pd-catalyzed allylic alkylations, see: a) C. Bolm, O. Simic, M. Martin, *Synlett* **2001**, 12, 1878–1880; b) M. Harmata, S. K. Ghosh, *Org. Lett.* **2001**, 3, 3321–3323.
- [8] For Cu-catalyzed cycloadditions reactions, see: a) C. Bolm, O. Simic, *J. Am. Chem. Soc.* **2001**, 123, 3830–3831; b) C. Bolm, M. Martin, O. Simic, M. Verrucci, *Org. Lett.* **2003**, 5, 427–429; c) C. Bolm, M. Verrucci, O. Simic, P. G. Cozzi, G. Raabe, H. Okamura, *Chem. Commun.* **2003**, 2826–2827.
- [9] C. Bolm, M. Martin, G. Gescheidt, C. Palivan, D. Neshchadin, H. Bertagnolli, M. P. Feth, A. Schweiger, G. Mitrikas, J. Harmer, *J. Am. Chem. Soc.* **2003**, 125, 6222–6227.
- [10] For examples of highly enantioselective addition reactions of enolsilyl ethers and pyruvate esters or glyoxalates, see: a) K. Mikami, S. Matsukawa, *J. Am. Chem. Soc.* **1994**, 116, 4077–4078; b) D. A. Evans, J. A. Murry, M. C. Kozlowski, *J. Am. Chem. Soc.* **1996**, 118, 5814–5815; c) D. A. Evans, M. C. Kozlowski, C. S. Burgey, D. W. C. MacMillan, *J. Am. Chem. Soc.* **1997**, 119, 7893–7894; d) D. A. Evans, D. W. C. MacMillan, K. R. Campos, *J. Am. Chem. Soc.* **1997**, 119, 10859–10860; e) D. A. Evans, M. C. Kozlowski, J. A. Murry, C. S. Burgey, K. R. Campos, B. T. Connel, R. J. Staples, *J. Am. Chem. Soc.* **1999**, 121, 669–685; f) D. A. Evans, C. S. Burgey, M. C. Kozlowski, S. W. Tregay, *J. Am. Chem. Soc.* **1999**, 121, 686–699; g) D. A. Evans, C. E. Masse, J. Wu, *Org. Lett.* **2002**, 4, 3375–3378.
- [11] For example, copper(II) complexes of **1a** and **1b** gave **6a** with only 35 and 58% *ee*, respectively. For the results obtained with metal complexes bearing *N*-quinolyl-substituted sulfoximine **2**, see: M. Verrucci, dissertation RWTH Aachen, **2004**.
- [12] a) R. Fusco, F. Tericoni, *Chem. Ind. (Milan)* **1965**, 47, 61–62; b) C. R. Johnson, C. W. Schroeck, *J. Am. Chem. Soc.* **1973**, 95, 7418–7423; c) J. Brandt, H. J. Gais, *Tetrahedron: Asymmetry* **1997**, 8, 909–912.
- [13] a) C. Bolm, J. P. Hildebrand, *Tetrahedron Lett.* **1998**, 39, 5731–5734; b) C. Bolm, J. P. Hildebrand, *J. Org. Chem.* **2000**, 65, 169–

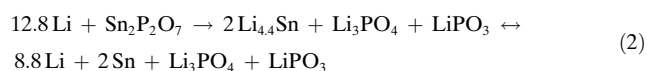
- 175; b) C. Bolm, J. P. Hildebrand, J. Rudolph, *Synthesis* **2000**, 911–913.
- [14] The effect of *ortho*-alkoxy groups is particularly pronounced in hetero-Diels–Alder reactions catalyzed by copper complexes bearing *N*-quinolylsulfoximines **2**; for details, see ref. [8c].
- [15] For details see the Supporting Information.
- [16] For applications of fluorinated alcohols in Mukaiyama-type reactions, see: a) D. A. Evans, D. S. Johnson, *Org. Lett.* **1999**, *1*, 595–598; b) D. A. Evans, M. C. Willis, J. N. Johnston, *Org. Lett.* **1999**, *1*, 865–868; c) D. A. Evans, T. Rovis, M. C. Kozlowski, J. S. Tedrow, *J. Am. Chem. Soc.* **1999**, *121*, 1994–1996.
- [17] a) I. Denissova, L. Barriault, *Tetrahedron*, **2003**, *59*, 10105–10146; b) J. Christoffers, A. Mann, *Angew. Chem.* **2001**, *113*, 4725–4732; *Angew. Chem. Int. Ed.* **2001**, *40*, 4591–4597; c) E. J. Corey, A. Guzman-Perez, *Angew. Chem.* **1998**, *110*, 402–415; *Angew. Chem. Int. Ed.* **1998**, *37*, 388–401; d) K. Fuji, *Chem. Rev.* **1993**, *93*, 2037–2066; e) S. F. Martin, *Tetrahedron* **1980**, *36*, 419–460.
- [18] Compound **6a** was obtained with a comparable *ee* value (98 versus 99%) but in higher yield (89 versus 77%) with respect to the previously reported results obtained with [M(box)] complexes. In the case of **6f**, the *ee* value and the yield were similar with both systems (91 versus 93% *ee* and 71 versus 76% yield). To the best of our knowledge, **6b–e** have not yet been prepared.

graphite,^[1] many studies on Sn-based materials for use as anode materials have been performed.^[2–4] Courtney et al. have reported the overall reaction of Sn-containing anode materials using SnO as Equation (1).^[2]



The tin atoms aggregate during cycling, and the Li–Sn alloys embedded in the Li_2O matrix exhibit rapid loss of capacity.

The presence of substantial amounts of other “spectator atoms”, such as the B and P atoms in Sn_2BPO_6 , apparently prevents Sn aggregation.^[2] However, these materials show an initial capacity of about 500 mA h g^{-1} , with a relatively high irreversible capacity of about 500 mA h g^{-1} during the first cycle. Xiao et al. prepared a crystalline $\text{Sn}_2\text{P}_2\text{O}_7$ phase, and proposed the decomposition reaction [Eq. (2)].^[3]



However, the irreversible capacity of this material is high (523 mA h g^{-1}), and the initial capacity of 544 mA h g^{-1} decreases quickly even at a low current (C) rate (20 mA g^{-1}). Behm and Irvine have reported that crystalline $\text{Sn}_2\text{P}_2\text{O}_7$ (obtained by heating SnHPO_4 to 550°C) exhibits an initial charge capacity of 519 mA h g^{-1} , which decreases rapidly to 148 mA h g^{-1} after 30 cycles.^[4] They proposed that lithium phosphates (Li_3PO_4 and LiPO_3), as reaction products, could not play a similar role as Li_2O in the SnO system, which is as a “glue” that keeps the Li–Sn particles mechanically connected during the large volume changes during alloying/dealloying. The mesoporous $\text{SiO}_2/\text{SnO}_2$ composite reported by Chen et al.^[5] has a good cycling stability, as evident from the cyclic voltammogram recorded with a single-powder microelectrode.

Herein we report the synthesis of a mesoporous tin phosphate/crystalline $\text{Sn}_2\text{P}_2\text{O}_7$ composite as a novel anode material. This material has the highest initial charge capacity (721 mA h g^{-1}) of the known tin-based anode materials, and shows an excellent cycling stability. The mesoporous structure was incorporated to improve the structural/electrochemical properties by alleviating the volume change of the tin during the alloying/dealloying process.

Figure 1 shows small-angle X-ray scattering (SAXS) patterns of the mesoporous tin phosphates prepared in the presence of cetyltrimethylammonium bromide (CTAB, $\text{CH}_3(\text{CH}_2)_{15}\text{N}(\text{CH}_3)_3\text{Br}$) as a structure-directing agent, before and after annealing at 400°C for 8 h. The three resolved peaks indexed as (100), (110), and (200) confirm a well-ordered hexagonal mesoporous structure.^[6,7] The intense (100) peak at $2\theta = 2.18^\circ \pm 0.09^\circ$ of the as-synthesized mesoporous tin phosphate corresponds to a d spacing of $4.0 \pm 0.2\text{ nm}$ (from $2d \sin \theta = \lambda$), with a nearest-neighbor distance of $4.7 \pm 0.2\text{ nm}$. The high-angle XRD pattern shown in the inset of Figure 1a indicates the formation of crystalline SnHPO_4 with a space group $P2_1/c$ (monoclinic).^[8]

The appearance of small-angle diffraction peaks corresponding to a hexagonal structure for the annealed meso-

Electrochemistry

A Mesoporous/Crystalline Composite Material Containing Tin Phosphate for Use as the Anode in Lithium-Ion Batteries**

Eunjin Kim, Dongyeon Son, Tae-Gon Kim, Jaephil Cho,* Byungwoo Park,* Kwang-Sun Ryu, and Soon-Ho Chang

Since Idota et al. first discovered in 1997 that Sn anodes containing amorphous $\text{SnB}_{0.56}\text{P}_{0.4}\text{Al}_{0.42}\text{O}_{3.46}$ have a capacity of about 600 mA h g^{-1} , compared to a value of 372 mA h g^{-1} for

[*] E. Kim, Prof. Dr. J. Cho
Department of Applied Chemistry
Kumoh National Institute of Technology
Gumi 730-701 (South Korea)
Fax: (+82) 54-467-4477
E-mail: jpcho@kumoh.ac.kr

D. Son, T.-G. Kim, Prof. Dr. B. Park
School of Materials Science and Engineering
and Research Center for Energy Conversion and Storage
Seoul National University, Seoul 151-744 (South Korea)
Fax: (+82) 2-883-8197
E-mail: byungwoo@snu.ac.kr

Dr. K.-S. Ryu, Dr. S.-H. Chang
Power Source Device Team, Electronics & Telecommunications
Research Institute (ETRI), Daejeon 305-350 (Korea)

[**] This work was supported by the Ministry of Information and Communication (MIC) in Korea, and the Korea Science and Engineering Foundation (KOSEF) through the Research Center for Energy Conversion and Storage at Seoul National University.

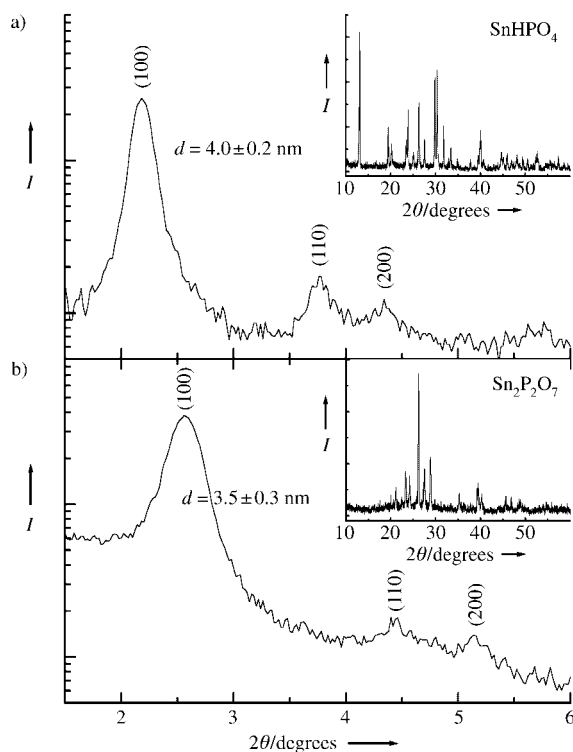


Figure 1. Small-angle X-ray scattering patterns of: a) as-prepared mesoporous tin phosphate/SnHPO₄ composite, and b) mesoporous tin phosphate/Sn₂P₂O₇ composite after annealing at 400 °C for 8 h. The high-angle XRD diffraction patterns of (a) and (b) are shown in the insets (*I*: intensity).

porous sample indicates that the mesostructure is preserved upon removal of the CTAB surfactant after annealing. However, the meso periodicity is contracted; the corresponding *d* spacing of the annealed mesoporous tin phosphate is 3.5 ± 0.3 nm.^[6,9,10] The high-angle XRD pattern of the annealed sample clearly shows the presence of Sn₂P₂O₇ (inset of Figure 1b).^[4] The crystal size of the sample both before and after annealing, calculated using the Scherrer formula, was estimated to be approximately 100 nm,^[11] which is two orders of magnitude larger than the wall thickness of the pure mesoporous phase (ca. 1 nm). These results indicate the formation of a mesoporous tin phosphate mixed with a crystalline phase.

Figure 2 shows the TEM micrographs of the samples before and after annealing, and clearly shows the presence of hexagonal mesoporous materials. The corresponding *d* spacings (by TEM) are approximately 3.8 nm before annealing and about 3.3 nm after annealing; these values are consistent with the SAXS data. The TEM image of the annealed tin phosphate clearly shows that the hexagonal mesostructure is preserved after heating to 400 °C.^[12,13] The light stripes in Figure 2 can be considered as projections of the mesopore channels, whereas the dark lines are from the tin phosphate walls.^[14]

The nitrogen-adsorption isotherm of the annealed sample, which has a Brunauer–Emmett–Teller (BET) surface area of 75.6 m² g^{−1}, is shown in Figure 3. The measured surface area is smaller than that of other mesoporous metal oxides reported

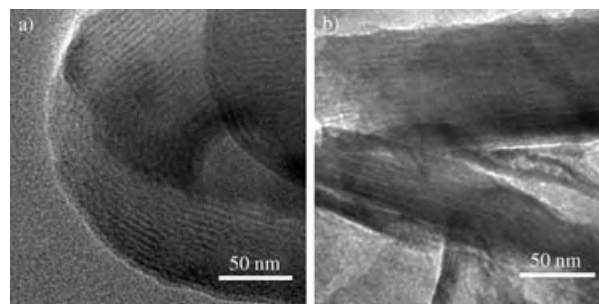


Figure 2. TEM images of: a) as-synthesized mesoporous tin phosphate, and b) mesoporous tin phosphate after annealing at 400 °C for 8 h.

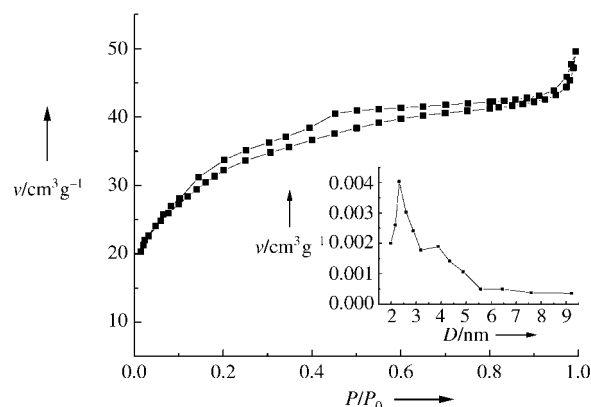


Figure 3. Representative nitrogen adsorption and desorption isotherms for the mesoporous tin phosphate/Sn₂P₂O₇ composite. The corresponding BJH distribution is shown in the inset (*v*: adsorbed volume; *D*: pore diameter; *P*/*P*₀: relative pressure).

in the literature because of the coexistence of a crystalline phase. The nitrogen isotherm curve of the mesoporous tin phosphate/Sn₂P₂O₇ composite has a well-defined step, which is characteristic of framework-confined mesopores.^[15–17] A rough estimation of the mass ratio for mesoporous tin phosphate versus crystalline Sn₂P₂O₇ is approximately 1:3. (This ratio was estimated from the BET surface areas of both the mesoporous tin phosphate and crystalline Sn₂P₂O₇ by considering the pore diameter and wall thickness.) As shown in the inset of Figure 3, the average pore size in the annealed sample is approximately 2.3 nm (Barrett–Joyner–Halenda (BJH) analysis), which is consistent with the SAXS and TEM data (Figures 1 and 2, respectively).

Figure 4 compares the voltage profiles of pure crystalline Sn₂P₂O₇ and mesoporous tin phosphate/Sn₂P₂O₇ composite anodes, which were cycled up to the 30th cycle at a rate of 144 mA g^{−1} (first cycle at 72 mA g^{−1}) between 2.5 and 0 V. The crystalline Sn₂P₂O₇ anode shows a large initial irreversible capacity (389 mA h g^{−1}) and poor retention property after 30 cycles (from 704 to 146 mA h g^{−1}). On the other hand, the mesoporous tin phosphate/Sn₂P₂O₇ composite anode shows an initial charge capacity of 721 mA h g^{−1}, which is much larger than the tin phosphate anodes reported previously.^[1–4] Moreover, the irreversible capacity of the sample during the first cycle is 297 mA h g^{−1}, which is far superior to the previous

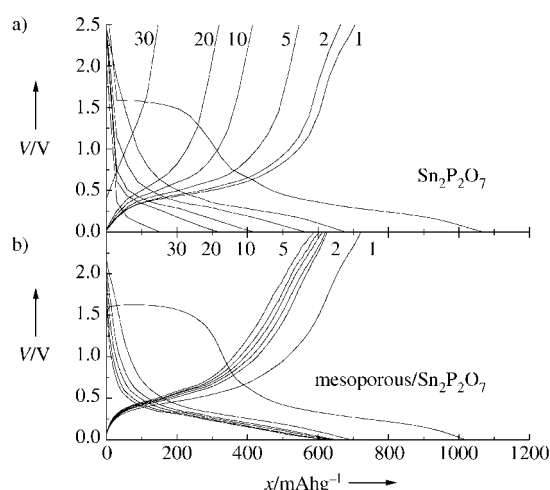


Figure 4. Voltage profiles of a) a crystalline $\text{Sn}_2\text{P}_2\text{O}_7$ anode and b) a mesoporous tin phosphate/ $\text{Sn}_2\text{P}_2\text{O}_7$ composite anode in coin-type half-cells during the 1st, 2nd, 5th, 10th, 20th, and 30th cycles between 2.5 and 0 V. The C rate was maintained at 144 mA h g^{-1} (first cycle at 72 mA h g^{-1} ; V: cell potential).

studies on Sn-based oxides or alloys.^[1–4] In addition, the mesoporous tin phosphate/ $\text{Sn}_2\text{P}_2\text{O}_7$ composite exhibits excellent cyclability: the retentive capacity up to 30 cycles is 587 mA h g^{-1} . This result indicates that the mesoporous tin phosphate plays a significant role in retaining the capacity. The XRD patterns of the cycled electrodes show that the crystalline $\text{Sn}_2\text{P}_2\text{O}_7$ peaks disappear during the first discharge (at ca. 1.1 V) and give only weak and broad diffraction patterns. The amorphous or nanocrystalline electrode in the phosphate matrix may prevent formation of large Sn clusters.^[18,19] The measured discharge and charge capacities are higher than the theoretical values (834 mA h g^{-1} and 572 mA h g^{-1} , respectively).^[3] The formation of a solid-electrolyte interface layer^[20] and a reversible lithium phosphate matrix^[18] may induce these higher values, although the exact mechanisms need to be identified.

Figure 5 shows the cell potential of the mesoporous tin phosphate/ $\text{Sn}_2\text{P}_2\text{O}_7$ composite anodes during the first discharging/charging together with the corresponding changes of the mesopore periodicity. Surprisingly, the d spacing expands and shrinks with Li alloying/dealloying. We believe that the lithium-tin phosphates form a flexible, three-dimensional mesoporous framework such that the mesopores do not collapse during discharge and charge. The cutoff voltage in Sn-based oxides has been typically limited to 1.2 V as a consequence of rapid tin aggregation above 1.2 V. The mesopores play an important role in reducing possible aggregation of Sn particles, and act as a “buffer zone” which accommodates the volume change of the Sn phase during Li alloying/dealloying. More detailed experiments with the optimum microstructures are currently underway to improve the electrochemical properties shown in Figure 4.

In conclusion, our mesoporous tin phosphate/ $\text{Sn}_2\text{P}_2\text{O}_7$ composite anode shows superior electrochemical properties, such as a large initial capacity (ca. 721 mA h g^{-1}) and excellent cyclability (ca. 587 mA h g^{-1} at the 30th cycle). Our approach

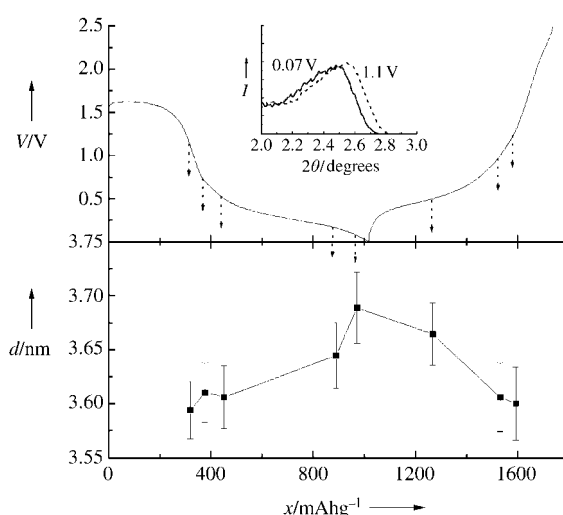


Figure 5. Plots of: a) cell potential of the mesoporous tin phosphate/ $\text{Sn}_2\text{P}_2\text{O}_7$ composite anode in coin-type half-cells during the first discharging and charging, and b) the corresponding d spacing of the composite electrode at the cell potential indicated by the arrow. The inset shows small-angle X-ray diffraction patterns of the electrode at 1.1 V and 0.07 V (V: cell potential; d : d spacing; I : intensity).

for enhancing the structural stability of tin phosphate is to incorporate mesoporous structures as a buffer layer to alleviate the volume expansion of the tin phosphate anode during lithiation/delithiation. We believe that this novel mesoporous tin phosphate/ $\text{Sn}_2\text{P}_2\text{O}_7$ composite has an enormous potential for use in Li-battery anode materials.

Experimental Section

The mesoporous tin phosphate/ SnHPO_4 composite was prepared by mixing SnF_2 (6.0 g) and H_3PO_4 (13.8 g) and dissolving this mixture in distilled-deionized water (DDW, 40 mL). CTAB (5.5 g) was then dissolved in DDW (20 mL), and this solution was added to the first solution. The mixture was stirred at 40°C for 1 h and then loaded into an autoclave and heated to 90°C for 12 h. After cooling the mixture to room temperature, the precipitate was recovered by filtration, washed with distilled water and ethanol, and vacuum-dried at 100°C for 10 h. The as-prepared powders (mesoporous tin phosphate/ SnHPO_4 composite) were then annealed at 400°C for 8 h to give the mesoporous tin phosphate/ $\text{Sn}_2\text{P}_2\text{O}_7$ composite.

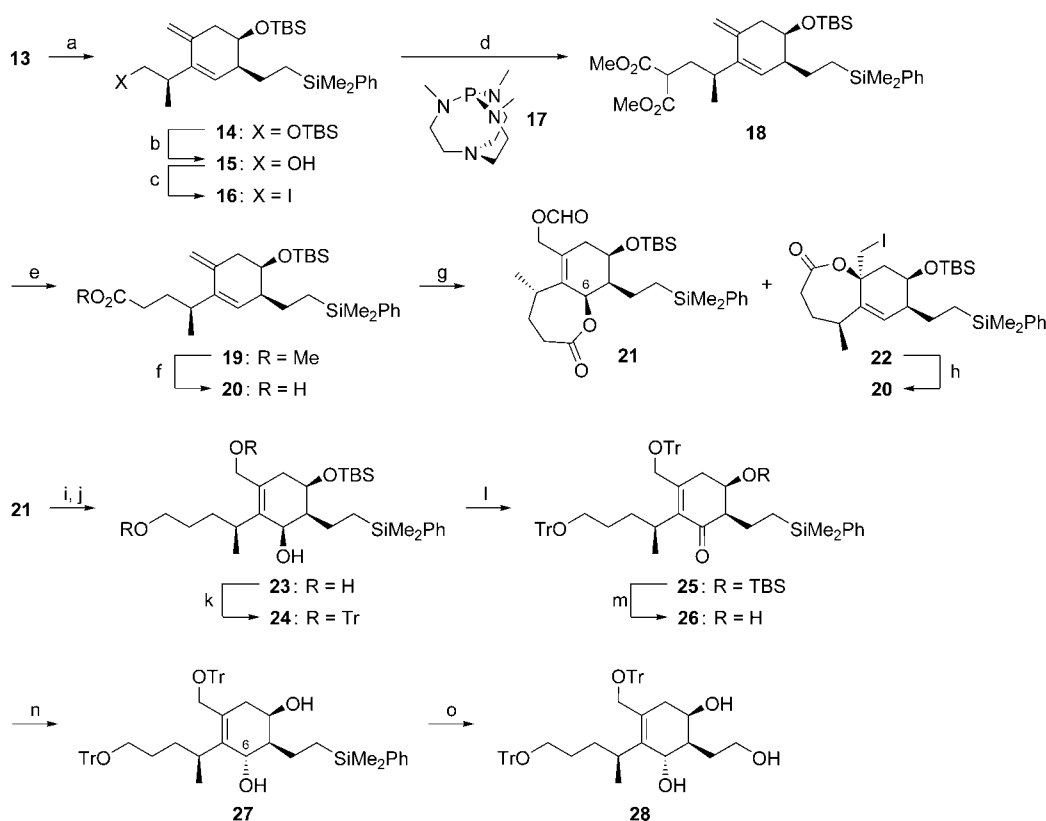
The procedure for assembling a coin-type half-cell with Li as an anode has been described in detail elsewhere.^[21–24] The electrode consisted of 60 wt-% active materials, 20 wt-% Super P carbon black, and 20 wt-% poly(vinylidene fluoride). A mixture of ethylene carbonate/diethylene carbonate and 1 M LiPF_6 salt was used as the electrolyte. The SAXS patterns were measured using $\text{Cu K}\alpha$ radiation (40 kV, 35 mA) on a Bruker Nanostar instrument. The nitrogen-adsorption isotherm was measured at 77 K with a Micromeritics ASAP 2010 analyzer.

Received: February 23, 2004

Revised: July 16, 2004 [Z54080]

Keywords: battery materials · electrochemistry · lithium · mesoporous materials · tin

- [1] Y. Idota, T. Kubota, A. Matsufuji, Y. Maekawa, T. Miyasaka, *Science* **1997**, 276, 1395.
- [2] I. A. Courtney, W. R. Mckinnon, J. R. Dahn, *J. Electrochem. Soc.* **1999**, 146, 59.
- [3] Y. W. Xiao, J. Y. Lee, A. S. Yu, Z. L. Liu, *J. Electrochem. Soc.* **1999**, 146, 3623.
- [4] M. Behm, J. T. S. Irvine, *Electrochim. Acta* **2002**, 47, 1727.
- [5] F. Chen, Z. Shi, M. Liu, *Chem. Commun.* **2000**, 2095.
- [6] G. Li, S. Bhosale, T. Wang, Y. Zhang, H. Zhu, J.-H. Fuhrhop, *Angew. Chem.* **2003**, 115, 3948; *Angew. Chem. Int. Ed.* **2003**, 42, 3818.
- [7] T. Katou, B. Lee, D. Lu, J. N. Kondo, M. Hara, K. Domen, *Angew. Chem.* **2003**, 115, 2484; *Angew. Chem. Int. Ed.* **2003**, 42, 2382.
- [8] M. L. E. Moubtassim, J. I. Corredor, J. M. Lloris, C. P. Vicente, J. L. Tirado, *J. Electrochem. Soc.* **2002**, 149, A1030.
- [9] C. Serre, A. Auroux, A. Gervassini, M. Hervieu, G. Ferey, *Angew. Chem.* **2002**, 114, 1664; *Angew. Chem. Int. Ed.* **2002**, 41, 1594.
- [10] N. K. Mal, S. Ichikawa, M. Fujiwara, *Chem. Commun.* **2002**, 112.
- [11] Y. Kim, J. Oh, T.-G. Kim, B. Park, *Appl. Phys. Lett.* **2001**, 78, 2363.
- [12] M. Tiemann, M. Fröba, *Chem. Mater.* **2001**, 13, 321, and references therein.
- [13] K. G. Severin, T. M. Abdel-Fattah, T. J. Pinnavia, *Chem. Commun.* **1998**, 1471.
- [14] M. Kruk, M. Jaroniec, T.-W. Kim, R. Ryong, *Chem. Mater.* **2003**, 15, 2815.
- [15] F. Schüth, W. Schmidt, *Adv. Mater.* **2002**, 14, 629.
- [16] S.-H. Baeck, K.-S. Choi, T. F. Jaramillo, G. D. Stucky, E. W. McFarland, *Adv. Mater.* **2001**, 13, 11.
- [17] F. Chen, Z. Shi, M. Liu, *Chem. Commun.* **2000**, 2095.
- [18] P. Poizot, S. Laruelle, S. Grugeon, L. Dupont, J.-M. Tarascon, *Nature* **2000**, 407, 496.
- [19] N. Zheng, X. Bu, P. Feng, *Nature* **2003**, 426, 428.
- [20] D. Aurbach, A. Nimberger, B. Markovsky, E. Levi, E. Sominski, A. Gedanken, *Chem. Mater.* **2002**, 14, 4155.
- [21] J. Cho, Y. J. Kim, B. Park, *Chem. Mater.* **2000**, 12, 3788.
- [22] Y. J. Kim, H. Kim, B. Kim, D. Ahn, J.-G. Lee, T.-J. Kim, D. Son, J. Cho, Y.-W. Kim, B. Park, *Chem. Mater.* **2003**, 15, 1505.
- [23] J. Cho, Y. J. Kim, T.-J. Kim, B. Park, *Angew. Chem.* **2001**, 113, 3471; *Angew. Chem. Int. Ed.* **2001**, 40, 3367.
- [24] J. Cho, Y.-W. Kim, B. Kim, J.-G. Lee, B. Park, *Angew. Chem.* **2003**, 115, 1656; *Angew. Chem. Int. Ed.* **2003**, 42, 1618.



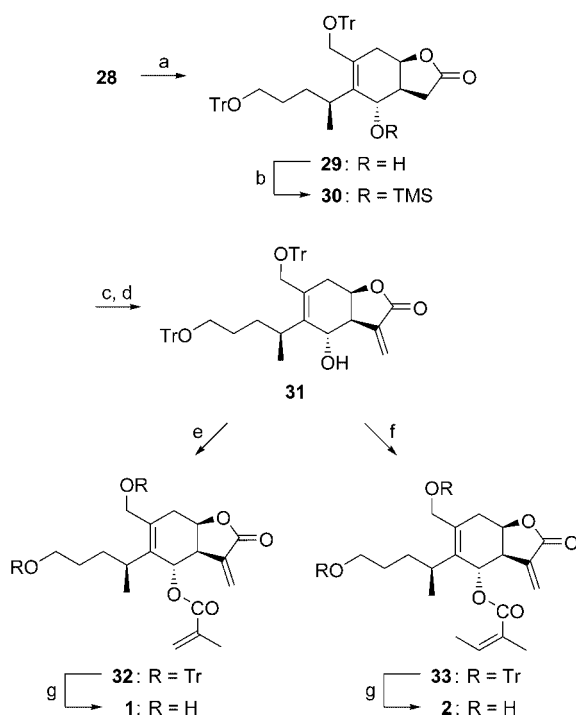
Scheme 3. Synthesis of the completely oxygenated basic skeleton **28**. a) TBSCl, imidazole, DMAP, DMF, RT, 99%; b) TBAF, THF, 0°C, 81% **15** + 17% **13**; c) I₂, Ph₃P, imidazole, THF, MeCN, −20°C→RT, 84%; d) **17**, dimethyl malonate, MeCN, RT, 91%; e) PhSH, K₂CO₃, DMF, 90°C, 89%; f) KOH, MeOH, H₂O, reflux, 100%; g) 1. I(col)₂PF₆, PhMe, 0°C, 2. AgOAc, DMF, PhMe, RT, 67% **21** + 15% **22**; h) zinc dust, HOAc, H₂O, THF, 0°C→RT, 86%; i) LiAlH₄, Et₂O, 0°C; j) LiBH₄, Et₂O, −10°C, 91% over two steps; k) TrCl, DMAP, pyridine, CH₂Cl₂, RT, 91%; l) Dess–Martin periodinane, pyridine, CH₂Cl₂, RT, 99%; m) TBAF, HOAc, THF, RT, 96%; n) Red-Al, CH₂Cl₂, PhMe, −20°C→RT, 90%; o) 1. TBAF, MS 4 Å, THF, reflux, 2. KF, H₂O₂, NaHCO₃, THF, MeOH, reflux, 99%. col = *sym*-collidine, DMAP = 4-(*N,N*-dimethylamino)pyridine, MS = molecular sieves, Red-Al = sodium bis(2-methoxyethoxy)aluminum hydride, TBAF = tetrabutylammonium fluoride, TBS = *tert*-butyldimethylsilyl, Tr = triphenylmethyl.

britannilactones **3** and **4**. Iodolactone **22**, which was formed in small amounts next to **21**, can be reductively eliminated^[26] to return **20**. The undesired configuration at C6 (eudesmane numbering) in **21** set up in a completely stereoselective fashion during the sequential iodolactonization/allyl formate generation from **20** was subsequently corrected by an oxidation/reduction strategy.^[27] Reduction of diester **21** with lithium aluminum hydride to give a hydroxy lactol^[28] and further reduction with lithium borohydride afforded triol **23**. Chemoselective tritylation of the two primary hydroxy groups (→**24**), Dess–Martin oxidation^[29] (→**25**), and mild desilylation^[30] led to β-hydroxy ketone **26**. Hydroxy-directed^[31] reduction of the latter with the sodium aluminum dihydride Red-Al furnished the desired 6α allyl alcohol **27** with excellent diastereoselectivity.^[32] After Tamao–Fleming oxidation,^[33,34] the completely oxygenated skeleton of the target molecules with correct configuration at all stereogenic centers was finally available in the form of triol **28**.

The final stage of the synthesis was initiated with a chemoselective oxidation^[35] of triol **28** to give hydroxy γ-lactone **29** (Scheme 4). After protection of the secondary hydroxy group, a one-step α-methylenation of lactone **30** succeeded with sodium hydride and paraformaldehyde,^[36] and

following desilylation, lactone **31** was isolated in good overall yield. Preparation^[2] of methacrylate **32** as well as detritylation to give **1** proceeded uneventfully and delivered (−)-eriolanin, which proved to be identical to the natural product by comparison of optical rotation data.^[37] Thus, our synthesis of **1** also clarifies the previously unknown absolute configuration of this sesquiterpene lactone, since the absolute configuration of **9** was unambiguously established.^[9] In addition, an X-ray diffraction analysis of our synthetic product **1** provided a further independent proof of the absolute configuration by anomalous X-ray scattering.^[38] Using a modified Yamaguchi esterification,^[39] **31** could also be transformed smoothly to angelate **33** without *Z/E* isomerization. Deblocking to give **2** delivered (−)-eriolanin, which also turned out to be identical to the natural product by comparison of optical rotation data.^[40]

Due to the sultone strategy applied, our enantioselective route to the 1,10-*seco*-eudesmanolides **1** and **2** requires only 26 steps from 2-bromo-1-(2-furyl)ethanone (**6**). Average yields of 87% for **1** and 86% for **2** highlight the efficacy of the route reported. Moreover, the selective manipulation of the diverse hydroxy groups on the 1,10-*seco*-eudesmanolide framework possible here offers great flexibility with respect



Scheme 4. Final steps of the synthesis of (–)-eriolanin (**1**) and (–)-eriolangin (**2**). a) BAIB, cat. TEMPO, CH₂Cl₂, RT, 75%; b) TMSCl, imidazole, CH₂Cl₂, RT, 96%; c) NaH, paraformaldehyde, THF, 100 °C (sealed tube); d) TBAF, THF, 0 °C, 61% over two steps; e) methacrylic acid anhydride, Et₃N, DMAP, THF, 0 °C→RT, 85%; f) 1. angelic acid, 2,4,6-trichlorobenzoyl chloride, Et₃N, PhMe, RT, 2. **31**, 100 °C, 60%; g) cat. *p*-TsOH, MeOH, RT, 97% **1** from **32**, 85% **2** from **33**. BAIB = bisacetoxiodobenzene, TEMPO = 2,2,6,6-tetramethylpiperidin-1-oxyl (free radical), TMS = trimethylsilyl, *p*-TsOH = *p*-toluenesulfonic acid.

to the assembly of synthetic analogues. A synthesis of the britannilactone derivatives **3** and **4** is in preparation.

Received: June 11, 2004

Keywords: domino reactions · natural products · sulfur heterocycles · terpenoids · total synthesis

- [1] S. M. Kupchan, R. L. Baxter, C.-K. Chiang, C. J. Gilmore, R. F. Bryan, *J. Chem. Soc. Chem. Commun.* **1973**, 842–843.
- [2] P. A. Grieco, T. Oguri, S. Gilman, *J. Am. Chem. Soc.* **1980**, *102*, 5886–5891.
- [3] a) M. R. Roberts, R. H. Schlessinger, *J. Am. Chem. Soc.* **1981**, *103*, 724–725; b) T. Wakamatsu, N. Miyachi, F. Ozaki, M. Shibasaki, Y. Ban, *Tetrahedron Lett.* **1988**, *29*, 3829–3832.
- [4] Review on sultone chemistry: P. Metz, *J. Prakt. Chem.* **1998**, *340*, 1–10.
- [5] Isolation: a) B.-N. Zhou, N.-S. Bai, L.-Z. Ling, G. A. Cordell, *Phytochemistry* **1993**, *34*, 249–252; b) F. Jeske, S. Huneck, J. Jakupovic, *Phytochemistry* **1993**, *34*, 1647–1649.
- [6] Compounds **3** and **4** effect phosphorylation of the antiapoptosis protein Bcl-2 and induce apoptosis in several cancer cell lines; for **4** cell-cycle arrest at the G2/M phase as well as polymerization of microtubules was proven: C.-T. Ho, M. Rafi, R. S. Dipaola, G. Ghai, R. T. Rosen, N. Bai, *US 6,627,623 B2*, **2003**.
- [7] For the relative configuration of **3** and **4** shown in Scheme 1, see ref. [5b] as well as the crystal structures of **3** depicted in: a) A.-R. Han, W. Mar, E.-K. Seo, *Nat. Prod. Sci.* **2003**, *9*, 28–30; b) S. Liu, H. Liu, W. Yan, L. Zhang, N. Bai, C.-T. Ho, *Bioorg. Med. Chem. Lett.* **2004**, *14*, 1101–1104.
- [8] P. Metz, J. Stölting, M. Läge, B. Krebs, *Angew. Chem.* **1994**, *106*, 2275–2276; *Angew. Chem. Int. Ed. Engl.* **1994**, *33*, 2195–2197.
- [9] A. Bierstedt, J. Stölting, R. Fröhlich, P. Metz, *Tetrahedron: Asymmetry* **2001**, *12*, 3399–3407.
- [10] T. Hamada, T. Torii, K. Izawa, R. Noyori, T. Ikariya, *Org. Lett.* **2002**, *4*, 4373–4376.
- [11] J. Dubac, A. Gaset, M. Maraval, *Synth. Commun.* **1991**, *21*, 11–16.
- [12] This unusual regioselectivity of epoxide opening was already reported for racemic **8**: B. Alcaide, P. Areces, E. Borredon, C. Biurrun, J. P. Castells, J. Plumet, *Heterocycles* **1990**, *31*, 1997–2002. We found that the stereochemical course is strongly dependent on the nature of the methyl nucleophile. With methylmagnesium bromide, again regioisomer **9** is preferentially formed; however, the reaction proceeds with extensive racemization.
- [13] A. A. Goldberg, *J. Chem. Soc.* **1945**, 464–467.
- [14] Thioether **11** was prepared by radical addition of PhSH to Me₂PhSiCH=CH₂ at 100 °C (87%); see also: C.-N. Hsiao, H. Shechter, *Tetrahedron Lett.* **1982**, *23*, 1963–1966.
- [15] T. Cohen, M. Bhupathy, *Acc. Chem. Res.* **1989**, *22*, 152–161.
- [16] B. Plietker, D. Seng, R. Fröhlich, P. Metz, *Eur. J. Org. Chem.* **2001**, 3669–3676.
- [17] P. J. Garegg, B. Samuelsson, *J. Chem. Soc. Chem. Commun.* **1979**, 978–980.
- [18] Review: J. G. Verkade, P. B. Kisanga, *Tetrahedron* **2003**, *59*, 7819–7858.
- [19] S. Arumugam, D. McLeod, J. G. Verkade, *J. Org. Chem.* **1998**, *63*, 3677–3679.
- [20] E. Keinan, D. Eren, *J. Org. Chem.* **1986**, *51*, 3165–3169.
- [21] B. Simonot, G. Rousseau, *J. Org. Chem.* **1994**, *59*, 5912–5919.
- [22] A. G. Martinez, A. C. Villalobos, M. O. Ruiz, *Synthesis* **1988**, 58–60.
- [23] Apparently the intermediate allylcarbenium ion is trapped by the solvent DMF as the nucleophile to generate an immonium ion, which is converted to the formate during aqueous workup.
- [24] F. Homsí, G. Rousseau, *J. Org. Chem.* **1998**, *63*, 5255–5258.
- [25] W. P. Neumann, *Synthesis* **1987**, 665–683.
- [26] B. Deguin, J.-C. Florent, C. Monneret, *J. Org. Chem.* **1991**, *56*, 405–411.
- [27] Experiments toward Mitsunobu inversion at C6 in **24** were not successful.
- [28] Increasing the reaction temperature in order to achieve complete reduction caused desilylation of the secondary silyl ether.
- [29] D. B. Dess, J. C. Martin, *J. Am. Chem. Soc.* **1991**, *113*, 7277–7287.
- [30] a) J. S. Debenham, R. Rodebaugh, B. Fraser-Reid, *J. Org. Chem.* **1997**, *62*, 4591–4600; b) D. L. Boger, R. M. Borzilleri, S. Nukui, R. T. Beres, *J. Org. Chem.* **1997**, *62*, 4721–4736.
- [31] A. H. Hoveyda, D. A. Evans, G. C. Fu, *Chem. Rev.* **1993**, *93*, 1307–1370.
- [32] In addition to **27** the C6-epimeric alcohol was isolated in 6% yield.
- [33] Review: I. Fleming, *Chemtracts: Org. Chem.* **1996**, *9*, 1–64.
- [34] a) H.-J. Knölker, G. Wanzl, *Synlett* **1995**, 378–382; b) Addition of molecular sieves 4 Å in the first step caused a significant increase in yield.
- [35] T. M. Hansen, G. J. Florence, P. Lugo-Mas, J. Chen, J. N. Abrams, C. J. Forsyth, *Tetrahedron Lett.* **2003**, *44*, 57–59.
- [36] B. Noya, M. D. Paredes, L. Ozores, R. Alonso, *J. Org. Chem.* **2000**, *65*, 5960–5968.
- [37] Synthetic **1**: [α]_D²⁵ = –88.6 (*c* = 1.0 in CHCl₃); natural **1**:^[1] [α]_D²⁵ = –93 (CHCl₃).

- [38] Crystal dimensions $0.25 \times 0.20 \times 0.20 \text{ mm}^3$, orthorhombic, space group $P2_12_12_1$ (No. 19), $a = 8.251(1)$, $b = 10.895(1)$, $c = 20.845(2) \text{ \AA}$, $V = 1873.9(3) \text{ \AA}^3$, $\rho_{\text{calcd}} = 1.242 \text{ g cm}^{-3}$, $\text{Cu}_{\text{K}\alpha}$ radiation, $\lambda = 1.54178 \text{ \AA}$, $\omega/2\theta$ scans, $T = 233 \text{ K}$, 4186 reflections measured, 3823 independent ($R_{\text{int}} = 0.031$), of which 3369 were observed [$I \geq 2\sigma(I)$], $\mu = 7.58 \text{ cm}^{-1}$, empirical absorption correction ($0.833 \leq T \leq 0.863$), $Z = 4$, 230 refined parameters, hydrogen atoms calculated and refined as riding atoms, $R = 0.041$, $wR^2 = 0.106$, largest difference peak and hole $0.15/-0.20 \text{ e \AA}^{-3}$, Flack parameter $0.04(19)$. Programs used: EXPRESS, MolEN, SHELXS-97, SHELXL-97, SCHAKAL. CCDC-239240 contains the supplementary crystallographic data for this paper. These data can be obtained free of charge via www.ccdc.cam.ac.uk/conts/retrieving.html (or from the Cambridge Crystallographic Data Centre, 12, Union Road, Cambridge CB21EZ, UK; fax: (+44) 1223-336-033; or deposit@ccdc.cam.ac.uk).
- [39] B. Hartmann, A. M. Kanazawa, J. P. Deprés, A. E. Greene, *Tetrahedron Lett.* **1991**, 32, 5077–5080.
- [40] Synthetic **2**: $[\alpha]_{\text{D}}^{25} = -87.5$ ($c = 1.05$ in CHCl_3); natural **2**: $^{[1]}$ $[\alpha]_{\text{D}}^{25} = -91$ (CHCl_3).

Rare-Earth Metals

[Yb₃N(dpa)₆][Yb(dpa)₃]: A Molecular Nitride of a Rare-Earth Metal with a Yb₃N Unit**

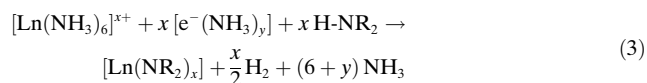
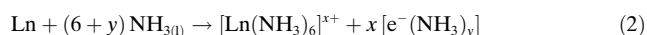
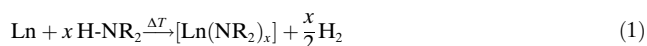
Catharina C. Quitmann and Klaus Müller-Buschbaum*

Rare-earth compounds containing a nitrogen center have so far only been known in solid-state chemistry, for example, in the nitrides of metal-rich rare-earth halides.^[1] In these compounds the nitride ions are surrounded in a tetrahedral manner by rare-earth ions,^[2a,b] with a few exceptions showing an octahedral environment.^[2c] Nitride ions with a triangular coordination are only found in Ce₁₅N₇I₂₄.^[3] In coordination chemistry neither molecular nitrides nor equivalent Ln₃N species were known.

Although liquid ammonia was used in the synthesis of divalent ytterbium and europium metallocenes in the early days of organometallic chemistry,^[4] it no longer plays an important role as a reaction medium or as a reactant for obtaining new coordination compounds of these elements. The significance of liquid ammonia is, however, evident in the synthesis and stabilization of many Zintl anions.^[5] Nonetheless,

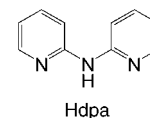
syntheses in standard solvents dominate all preparative approaches to organometallic rare-earth compounds,^[6] including rare-earth amido compounds.^[6d]

Similar to the alkaline metals,^[7] europium and ytterbium can be dissolved in liquid ammonia under normal pressure.^[8] Because of the formation of an electride solution, these metals can be oxidized by amines at −50 °C.^[9] Thus, the solvent-free melt and solvothermal syntheses that are employed for the preparation of homoleptic amides of rare-earth elements^[10] [Eq. (1), Ln = lanthanoid] can be extended to two consecutive steps in a different temperature range [Eq. (2), (3)].



The formation of homoleptic ammine complexes^[11] [Eq. (2)] offers the possibility of inserting NH₃ and its deprotonation products into the coordination sphere of the rare-earth metals. This approach supplements the high-temperature synthetic routes commonly used in solid-state chemistry^[10] and also renders redox chemistry feasible at low temperatures.

Here we report the reaction of ytterbium with 2,2'-dipyridylamine (Hdpa, (C₅H₄N)₂NH) in liquid ammonia and demonstrate how the oxidation of rare-earth metals with amines at low temperatures leads to rare-earth metal compounds with unusual nitrogen coordination. The product of this reaction is [Yb₃N(dpa)₆][Yb(dpa)₃] (**1**), a novel dipyriddyamide of ytterbium that consists of two different neutral molecular building units.



Centered by a nitride ion, the three Yb³⁺ atoms in the [Yb₃N(dpa)₆] unit of **1** form an approximate equilateral triangle with no metal–metal bonds (Yb⋯Yb 359 pm). Because the nitride ion is almost in the plane of the Yb³⁺ ions, the Yb–N distances are particularly short, ranging from 207(1) to 209(1) pm. Taking into consideration the different radius of Ce³⁺, these values are in good agreement with the Ce–N(nitride) distances of 217–220 pm observed for Ce₁₅N₇I₂₄.^[3] Owing to the voluminous dipyriddyamide ligands surrounding the Yb₃N unit the nitride ion shows only a slight deviation from the triangular plane (4 pm). In comparison, tetrahedrally coordinated nitride ions exhibit longer Ln–N distances, for example, 226–229 pm in Gd₂NCl₃, in which the nitride ion is in the center of the tetrahedron.^[2b] The very short Yb–N distances within the Yb₃N unit indicate that a π-bonding component may be possible.

The Yb₃N triangle is surrounded by six dipyriddyamide anions that employ all nitrogen atoms for coordination: Each ligand is coordinated to one Yb atom in a 1,3-chelating mode and to another Yb atom through a single bond (Figure 1). This results in a distorted pentagonal-bipyramidal coordina-

[*] C. C. Quitmann, Dr. K. Müller-Buschbaum
Institut für Anorganische Chemie
Universität zu Köln
Greinstrasse 6, 50939 Köln (Germany)
Fax: (+49) 221-470-5083
E-mail: klaus.mueller-buschbaum@uni-koeln.de

[**] This work was supported by the Fonds der Chemischen Industrie with a Ph.D. scholarship. We thank Prof. Dr. W. Jung for the EDX analysis and Prof. Dr. G. Meyer for financial support. dpa[−] = dipyriddyamide, (C₅H₄N)₂N[−].

Supporting information for this article is available on the WWW under <http://www.angewandte.org> or from the author.

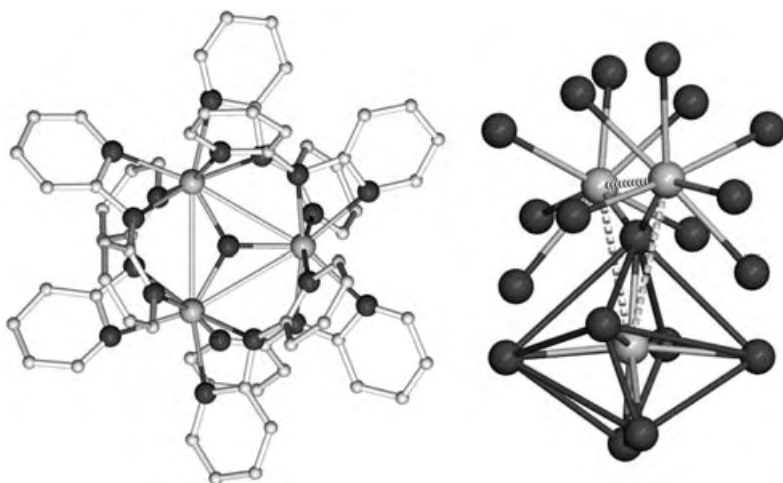


Figure 1. The triangular nitrido unit $[\text{Yb}_3\text{N}(\text{dpa})_6]$ (left) and the distorted pentagonal-bipyramidal coordination sphere of the Yb atoms in the $[\text{Yb}_3\text{N}(\text{dpa})_6]$ unit in **1** (right). The nitride ion lies in the plane of the three Yb atoms. Lines connecting Yb–Yb and N–N are meant to highlight the triangular unit and a coordination polyhedron and do not represent bonds. Selected distances [pm] and angles $^\circ$: Yb1–N1 207(1), Yb2–N1 207(1), Yb3–N1 209(1), Yb1–Yb2 359.4(1), Yb1–Yb3 359.0(1), Yb2–Yb3 359.4(1), Yb1–N18 240(2), Yb1–N15 241(2), Yb1–N19 243(2), Yb1–N14 244(2), Yb1–N4 245(2), Yb1–N2 250(2), Yb2–N3 240(2), Yb2–N8 249(2), Yb3–N11 241(2), Yb3–N17 250(2); Yb2–Yb1–Yb3 60.04(2), Yb1–Yb2–Yb3 59.93(2), Yb1–N1–Yb2 120.5(5), Yb1–N1–Yb3 119.2(5), N2–Yb1–N19 55.9(7), N14–Yb1–N15 54.4(6), N5–Yb2–N6 54.8(5), N7–Yb2–N8 55.7(6), N11–Yb3–N12 54.7(5), N16–Yb3–N17 55.2(7), N4–Yb1–N18 169.8(6). C white, N dark gray, Yb light gray.

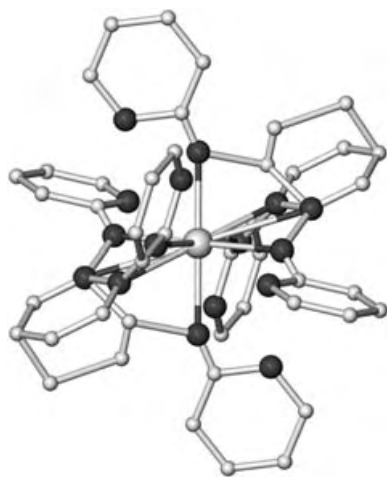


Figure 2. Structure of the homoleptic $[\text{Yb}(\text{dpa})_3]$ unit of **1** in the solid state. The metal/amide ratio of 1:3 results in a disorder of the ligands, because the Yb5 atom is positioned on a center of symmetry. The positions of the ligand atoms are occupied to 50%. Selected distances [pm] and angles $^\circ$: Yb5–N29 223(2), Yb5–N32 229(3), Yb5–N35 237(3), Yb5–N33 242(2), Yb5–N/C30 260(2); N32–Yb5–N33 62(1), N35–Yb5–N/C30 65(1). N dark gray, Yb light gray.

tion sphere of seven nitrogen atoms around the Yb atoms. Therefore, with regard to coordination mode as well as coordination number, $[\text{Yb}_3\text{N}(\text{dpa})_6]$ is not equivalent to the homoleptic rare-earth dipyriddydamides,^[12] dipyriddydamides of transition metals,^[13] or related aminopyridinato complexes.^[14] The coordination number of seven as in $[\text{Yb}_3\text{N}(\text{dpa})_6]$ is also

found in the Ce_3N units of $\text{Ce}_{15}\text{N}_7\text{I}_{24}$,^[3] here each Ce^{3+} ion is coordinated by six additional iodide ions.

The second molecular unit in **1**, the homoleptic monomer $[\text{Yb}(\text{dpa})_3]$, does not coincide with the dimeric structure of the homoleptic rare-earth dipyriddydamides^[12] either. The Yb atoms are coordinated by 1,3-chelating dpa ligands (coordination number six) and positioned on symmetry centers. Because of the Yb:N ratio of 1:3 the atoms of the dpa ligands are disordered (Figure 2).^[15,16]

To verify that **1** is indeed a molecular nitride of a rare-earth metal and to exclude the participation of oxygen in the coordination sphere—as is seen in units containing oxygen, such as $\{\text{Eu}_4\text{O}\}$ in Eu_4OCl_6 ^[17] or $\{\text{Yb}_4\text{O}\}$ in Yb_4OCl_6 ^[17] and $[\text{K}(\text{thf})_3][\text{Yb}_4\text{O}\{\text{Ph}_2\text{C}(\text{C}_4\text{H}_3\text{N})_2\}_4]\cdot 2\text{THF}$ ^[18]—the compound was investigated by IR spectroscopy and EDX analysis. There was no indication for the presence of oxygen in **1** (see the Supporting Information). Furthermore, the absence of oxygen is supported by the electron neutrality as well as the oxygen-free synthesis in liquid ammonia,^[19] and this therefore renders the identification of the center ion as a nitride ion plausible.

The deprotonation of ammonia proceeds more readily with cations of higher charge than alkaline metal ions,^[20] but had not yet been observed for the nitride ion. With compound **1** it was shown that with low-temperature oxidation of ytterbium in liquid ammonia, completely different products can be obtained and stabilized than with the direct high-temperature oxidation of a melt synthesis.^[12]

In conclusion the approach presented here offers possibilities for obtaining molecular nitrides of the rare-earth metals. Enclosure by amide ligands results in different nitrido amides.

Experimental Section

1: Ytterbium metal chips (173 mg, 1 mmol, ChemPur, 99.9%) and 2,2'-dipyriddydamine (Hdpa; 514 mg, 3 mmol, Aldrich, 99%) were filled in a glass ampoule, and then NH_3 (6 mL) was condensed into the ampoule with liquid nitrogen. Upon warming to approximately -50°C the solution turned dark blue. The color changed from dark blue to green and then yellow upon dissolution of 2,2'-dipyriddydamine and further warming of the reaction mixture (red streaks appeared which also turned yellow). Evaporation of excess NH_3 gave a green-yellow solid. The ampoule was sealed under vacuum. The reaction mixture was heated to 150°C in 5 h and then to 190°C in 4 h, and then held at this temperature for 168 h. It was then cooled to 120°C in 270 h and then room temperature within 30 h. When the reaction was complete (based on Yb), **1** was obtained as a yellow crystalline solid; small amounts of a red, X-ray amorphous material were also observed. Yield (Yb): 515 mg (92%); elemental analysis calcd (%) for $\text{C}_{90}\text{H}_{72}\text{N}_{28}\text{Yb}_4$: C 48.30, H 3.24, N 17.52; found: C 47.8, H 3.5, N 18.0; IR (MIR: KBr, 99.9%, dried; FarIR: PE, 99.9%): $\tilde{\nu} = 3019\text{ m}$, 2823 m , 1600 vssh , 1593 vs , 1555 m , 1475 vssh , 1462 vs , 1429 vs , 1376 s , 1342 m , 1299 s , 1285 m , 1235 s , 1153 s , 1148 ssh , 1107 m , 1052 w , 1001 s ,

990 ssh, 938 w, 912 m, 828 m, 769 s, 733 s, 692 m, 623 m, 594 w, 541 m, 531 m, 514 w, 503 w, 409 m, 353 w, 339 w, 268 m, 258 msh, 229 m, 194 m, 162 w, 148 wsh, 73 w cm⁻¹.

Received: April 28, 2004

Keywords: coordination chemistry · lanthanoids · N ligands · nitrides · ytterbium

- [1] A. Simon, H. Mattausch, G. J. Miller, W. Bauhofer, R. K. Kremer in *Handbook on the Physics and Chemistry of Rare Earth*, Vol. 15 (Eds.: K. A. Gschneider, L. Eyring), Elsevier, Amsterdam, **1991**.
- [2] a) A. Simon, T. Koehler, *J. Less-Common Met.* **1986**, *116*, 279; b) U. Schwanitz-Schueller, A. Simon, *Z. Naturforsch. B* **1985**, *40*, 705–709; c) H.-J. Meyer, N. L. Jones, J. D. Corbett, *Inorg. Chem.* **1989**, *28*, 2635–2637.
- [3] H. Mattausch, R. K. Kremer, A. Simon, *Z. Anorg. Allg. Chem.* **1996**, *622*, 649–654.
- [4] a) E. O. Fischer, H. Fischer, *Angew. Chem.* **1964**, *76*, 52; *Angew. Chem. Int. Ed. Engl.* **1964**, *3*, 132; b) R. G. Hayes, J. L. Thomas, *J. Am. Chem. Soc.* **1969**, *91*, 6876; c) W. J. Evans, *Coord. Chem. Rev.* **2000**, *263*–283.
- [5] a) N. Korber, F. Richter, *Angew. Chem.* **1997**, *109*, 1575–1577; *Angew. Chem. Int. Ed. Engl.* **1997**, *36*, 1512–1514; b) M. Grothe, N. Korber, *Z. Anorg. Allg. Chem.* **2003**, *629*, 399–402.
- [6] a) H. Schumann, *Angew. Chem.* **1984**, *96*, 475–493; *Angew. Chem. Int. Ed. Engl.* **1984**, *23*, 474–492; b) W. J. Evans, B. L. Davis, *Chem. Rev.* **2002**, *102*, 2119–2136; c) H. Schumann, J. A. Meese-Marktscheffel, L. Esser, *Chem. Rev.* **1995**, *95*, 865–986; d) Cambridge Crystallographic Data Centre, 12 Union Road, Cambridge CB21EZ; Fax: (+44)1223-336-033; or deposit@ccdc.cam.ac.uk.
- [7] a) W. Weyl, *Pogg. Ann.* **1864**, *121*, 601; b) M. C. R. Symons, *Chem. Soc. Rev.* **1976**, *5*, 337–358.
- [8] a) D. S. Thompson, E. E. Hazen, J. S. Waugh, *J. Chem. Phys.* **1966**, *44*, 2954–2958; b) R. Navaneethakrishnan, J. C. Warf, *Inorg. Chem.* **1976**, *15*, 2849–2852.
- [9] K. Müller-Buschbaum, *Z. Anorg. Allg. Chem.* **2004**, *630*, 895–899.
- [10] a) G. B. Deacon, A. Gitlits, P. W. Roesky, M. R. Bürgstein, K. C. Lim, B. W. Skelton, A. H. White, *Chem. Eur. J.* **2001**, *7*, 127–138; b) K. Müller-Buschbaum, *Z. Anorg. Allg. Chem.* **2002**, *628*, 2731–2737; c) K. Müller-Buschbaum, C. C. Quitmann, *Inorg. Chem.* **2003**, *42*, 2742–2751; d) K. Müller-Buschbaum, C. C. Quitmann, *Z. Anorg. Allg. Chem.* **2003**, *629*, 1610–1616.
- [11] a) D. S. Thompson, M. J. Stone, J. S. Waugh, *J. Phys. Chem.* **1966**, *70*, 934–935; b) H. Oesterreicher, M. Mammano, M. J. Sienko, *J. Solid State Chem.* **1969**, *1*, 10–18.
- [12] a) K. Müller-Buschbaum, *Z. Anorg. Allg. Chem.* **2003**, *629*, 2127–2132; b) C. C. Quitmann, K. Müller-Buschbaum, unpublished results.
- [13] a) N. Ray, B. Hathaway, *J. Chem. Soc. Dalton Trans.* **1980**, 1105–1111; b) M.-W. Suen, Y.-Y. Wu, J.-D. Chen, T.-C. Keng, J.-C. Wang, *Inorg. Chim. Acta* **1999**, *288*, 82–89; c) S. Youngme, K. Poopasit, K. Chinnakali, S. Chantrapromma, H.-K. Fun, *Inorg. Chim. Acta* **1999**, *292*, 57–63; d) F. A. Cotton, L. M. Daniels, C. A. Murillo, H.-C. Zhou, *Inorg. Chim. Acta* **2000**, *305*, 69–74.
- [14] a) R. Kempe, H. Noss, T. Irrgang, *J. Organomet. Chem.* **2002**, *647*, 12–20; b) A. Spangenberg, P. Arndt, R. Kempe, *Angew. Chem.* **1998**, *110*, 824–827; *Angew. Chem. Int. Ed. Engl.* **1998**, *37*, 832–835.
- [15] a) T. Araki, *Z. Kristallogr.* **1991**, *194*, 161–191; b) A. L. Spek, PLATON-99, *A Multipurpose Crystallographic Tool*, Utrecht, **1999**.
- [16] Crystal structure analysis of **1**: (C₉₀H₇₂N₂₈Yb₄, *M_r* = 2237.9 g mol⁻¹): crystal size 0.2 × 0.1 × 0.1 mm³; space group *P* $\bar{1}$ (no. 2), *a* = 1858.0(3), *b* = 1860.7(3), *c* = 1877.9(3) pm, α = 90.04(1), β = 119.65(2), γ = 119.91(1)°, *T* = 170 K, *Z* = 2, *V* = 4619.6(3) × 10⁶ pm³, ρ_{calcd} = 1.857 g cm⁻³, $2\theta_{\text{max}}$ = 54.68°, STOE IPDS II diffractometer, φ scan with $\Delta\varphi$ = 2° and Ω = 0.90°, MoK α radiation, λ = 0.71073 Å; of 18795 measured reflections, 18767 were unique and 5701 with *I* > 2 σ (*I*); 1168 refined parameters. The structure was solved with direct methods (SHELXS-97^[21a]) and refined with the least-squares method (SHELXL-97^[21b]) for all unique reflections against $|F^2|$, *R*₁ = 0.0614 for 5701 reflections with *I* > 2 σ (*I*), *wR*₂ = 0.1520 for all 18767 unique reflections; max./min. residual electron density +1.82/−1.47 e Å⁻³. The hydrogen atoms were placed in preset positions with adjustment of the thermal parameters by a factor of 1.2 with respect to those of the neighboring carbon atoms (AFIX 43). The atoms of the ligands in the [Yb(dpa)₃] units were disordered, with each occupying two positions, which made the use of “rigid bond” models necessary to refine the ligand positions.^[21b] All non-hydrogen atoms were anisotropically refined by least-square techniques. There was no indication of a possible non-centrosymmetry of the structure or hemihedral twinning.^[15] Because **1** exhibits a pseudo-hexagonal metric, powder diffraction was used to exclude the possibility that the metrics was falsely determined due to twinning. CCDC-232899 contains the supplementary crystallographic data for this paper. These data can be obtained free of charge via www.ccdc.cam.ac.uk/conts/retrieving.html (or from the Cambridge Crystallographic Data Centre, 12, Union Road, Cambridge CB21EZ, UK; fax: (+44)1223-336-033; or deposit@ccdc.cam.ac.uk).
- [17] G. Meyer, M. S. Wickleder in *Handbook on the Physics and Chemistry of Rare Earth*, Vol. 28 (Eds.: K. A. Gschneider, L. Eyring), Elsevier, Amsterdam, **2000**, chap. 177.
- [18] D. M. M. Freckmann, T. Dube, C. D. Berube, S. Gambarotta, G. P. A. Yap, *Organometallics* **2002**, *21*, 1240–1246.
- [19] Although it is difficult to distinguish a nitride ion from an oxide anion in the crystal structure analysis, the presence of the latter can be largely excluded: The formation of the electride in liquid ammonia allows no oxygen contamination and therefore forces an oxygen-free synthesis, and the assumption of an O²⁻ ion in place of the N³⁻ ion would not result in a neutral charge for this trivalent ytterbium compound (see also the Supporting Information).
- [20] N. Korber, personal communication.
- [21] a) G. M. Sheldrick, SHELXS-97, program for the determination of crystal structures, Universität Göttingen, **1997**; b) G. M. Sheldrick, SHELXL-97, program for the refinement of crystal structures, Universität Göttingen, **1997**.

One-Pot Syntheses

Novel Three-Component Reactions Based on a Heck Carbopalladation/Cyclization Domino Reaction**

Christoph J. Kressierer and Thomas J. J. Müller*

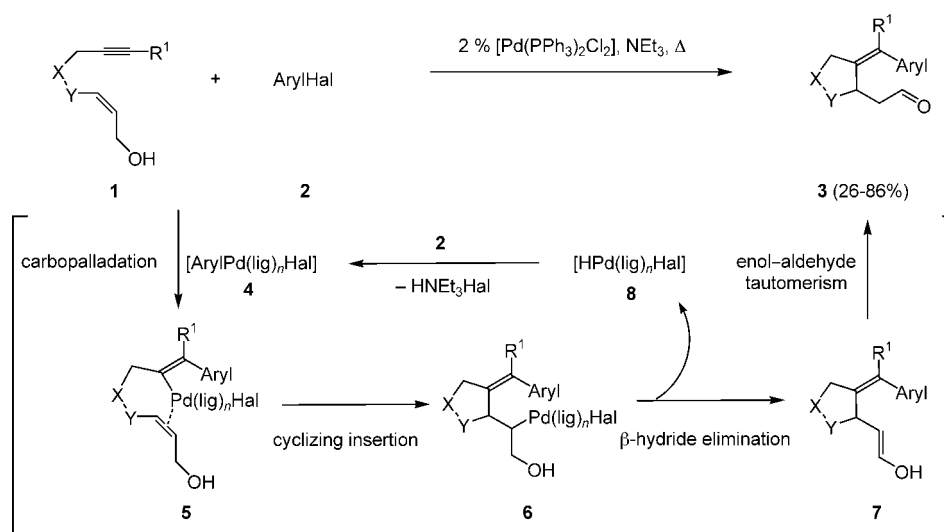
Dedicated to Professor Armin de Meijere on the occasion of his 65th birthday

Palladium-catalyzed domino reactions based on sequences of insertions of organopalladium species into multiple bonds (carbopalladation) have fundamentally revolutionized synthetic concepts for the formation of carbo- and heterocyclic systems.^[1,2] These transformations proceed under exceptionally mild reaction conditions and are highly compatible with polar functional groups. Conceptually, multicomponent reactions^[3] initiated by palladium-catalyzed carbon–carbon bond-forming reactions^[2,4] address very fundamental principles of synthetic efficiency and reaction design and, therefore, they have recently attracted considerable and steadily increasing academic, economic, and ecological interest. Besides, the prospect of extending one-pot reactions for combinatorial and solid-phase applications^[3c,5] promises manifold opportunities for developing novel lead structures for pharmaceut-

icals, catalysts, and even novel molecule-based materials. Therefore, mastering unusual combinations of elementary organic reactions is a major conceptual challenge in engineering novel types of sequences. As part of our program directed toward developing new one-pot sequences and domino processes based upon transition-metal-catalyzed in situ activation of alkynes by cross coupling^[6] or cycloisomerization,^[7] we report herein on the first Heck carbopalladation/cyclization sequence of ynallyl alcohols and aryl halides to give γ,δ -enals. Two novel consecutive three-component reactions initiated by this new domino reaction serve as illustrations.

Although intramolecular Heck reactions^[8] have a broad range of applications culminating in domino sequences like the impressive Negishi zipper reactions,^[1a] and since the use of enynes as relays for Heck carbopalladation/cyclization sequences has been thoroughly studied,^[9,10] the transformation of ynallyl alcohols that could furnish γ,δ -enals has remained unexplored to date. However, the generation of an aldehyde functionality en route could enormously enhance the degree of molecular diversity possible in multicomponent reactions.

The reaction of alkynylallyl alcohols **1**^[11] and aryl halides **2** in the presence of 2 mol % of $[\text{Pd}(\text{PPh}_3)_2\text{Cl}_2]$ in boiling triethylamine under Heck reaction conditions furnished the cyclized γ,δ -enals **3** (the tetrahydrofuran derivatives **3a–i** and chromane derivatives **3k–m**) in moderate to good yields (Scheme 1, Table 1).^[12]



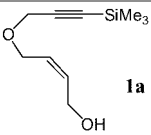
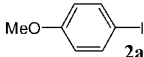
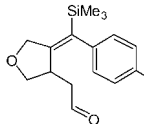
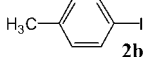
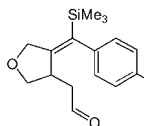
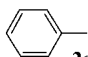
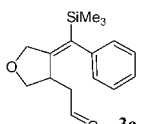
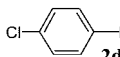
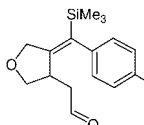
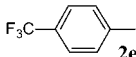
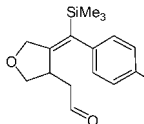
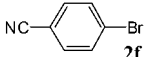
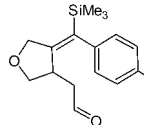
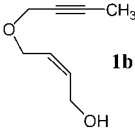
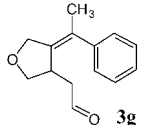
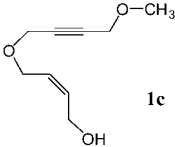
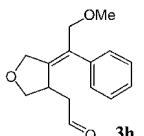
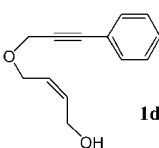
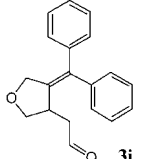
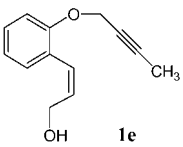
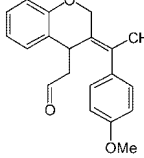
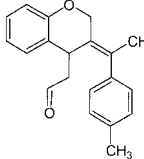
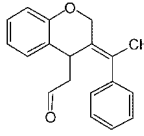
Scheme 1. The palladium-catalyzed Heck carbopalladation/cyclization sequence for the conversion of ynallyl alcohols **1** into γ,δ -enals **3**.

[*] Dipl.-Chem. C. J. Kressierer, Prof. Dr. T. J. J. Müller
Organisch-Chemisches Institut
Ruprecht-Karls-Universität Heidelberg
Im Neuenheimer Feld 270, 69120 Heidelberg (Germany)
Fax: (+49) 6221-546-579
E-mail: thomas_j.j.mueller@urz.uni-heidelberg.de

[**] This work was supported by the Deutsche Forschungsgemeinschaft (SFB 623), the Fonds der Chemischen Industrie, and the Dr.-Otto-Röhm Gedächtnisstiftung is gratefully acknowledged. The authors also cordially thank the BASF AG for the generous donation of chemicals.

The structures of the ethylidenetetrahydrofuranyl and ethylidenechromanyl acetaldehydes **3** were supported unambiguously by spectroscopic analyses (¹H, ¹³C and DEPT, COSY, NOESY, HETCOR, and HMBC NMR experiments, IR, UV/Vis, mass spectrometry). The configuration of the tetrasubstituted double bonds can be deduced unequivocally from the appearance of significant cross peaks (between the signals of the exocyclic trimethylsilyl, methyl, and methylene substituents and endocyclic methylene proton resonances in α -position to the ether bridge) in the NOESY spectra.

Table 1: Palladium-catalyzed Heck carbopalladation/cyclization of ynallyl alcohols **1** to give γ,δ -enals **3**.^[a]

Entry	Ynallyl alcohol 1	Aryl halide 2	<i>t</i> [h]	γ,δ -Enal 3	Yield [%] ^[b]
1	 1a	 2a	5	 3a	65
2	1a	 2b	2.5	 3b	85
3	1a	 2c	5	 3c	86
4	1a	 2d	2	 3d	76
5	1a	 2e	15	 3e	66
6 ^[c]	1a	 2f	0.5	 3f	85
7	 1b	2c	4.5	 3g	47
8 ^[d]	 1c	2c	24	 3h	29
9 ^[d]	 1d	2c	28	 3i	26
10	 1e	2a	6	 3j	58
11	1e	2b	5	 3k	60
12	1e	2c	6	 3l	65

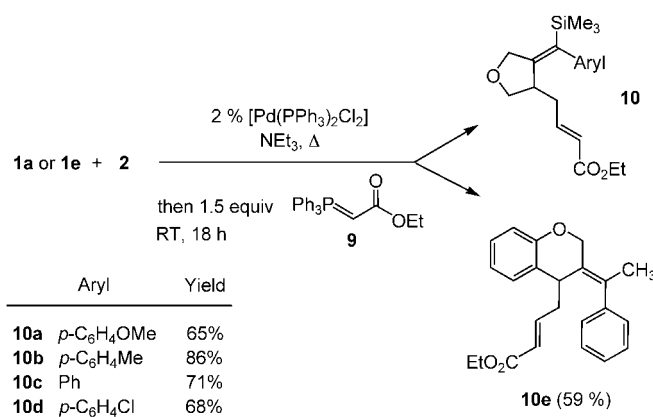
For footnotes, see next page.

This new palladium-catalyzed domino reaction has precedence in its elementary steps, such as intramolecular insertion of tethered alkynes and alkenes,^[1a] and the Heck reaction of allyl alcohols to furnish 3-arylpropanals,^[13] and can therefore be rationalized as follows (Scheme 1): After the oxidative addition of the aryl halide **2** to the in situ generated Pd⁰ species, the arylpalladium halide **4** coordinates and the triple bond of the ynallyl alcohol **1** is inserted by means of a *syn* carbopalladation to furnish the vinylpalladium species **5** in a stereospecific fashion. Coordination and cyclizing insertion of the allyl alcohol fragment generates the alkylpalladium species **6** which then undergoes a β -hydride elimination to give the dienol **7**. Instantaneously tautomerization of **7** gives the enal product **3**, and the hydridopalladium halide species **8**, which reductively eliminates hydrogen halide with base assistance to regenerate the Pd⁰ species. After the oxidative addition of **2** the catalytic cycle starts again. Interestingly, the reaction with the trimethylsilyl-substituted alkynylallyl alcohol **1a** gives considerably higher yields (Table 1, entries 1–6 and entries 7–9). The rigidified phenylene-bridged ynallyl alcohol **1e** readily participates in the sequence furnishing chromanylacetaldehyde derivatives in reasonable yields (entries 10–12). Since the Heck carbopalladation/cyclization sequence is considerably hampered with electron-deficient aryl halides—as reflected by either the longer reaction times or, alternatively, microwave irradiation to achieve complete conversion (entries 5 and 6)—the arylpalladium species exerts a strong electronic effect in the carbopalladation step.

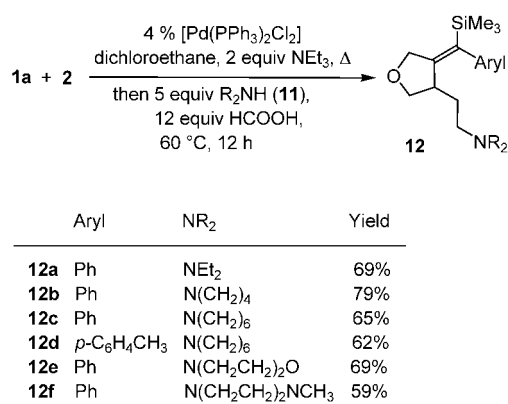
This new Heck carbopalladation/cyclization domino sequence of alkynylallyl alcohols to give γ,δ -enals forms the basis for sequential one-pot three-component reactions that are compatible with the mild reaction conditions of the initial Pd-catalyzed process. The newly formed aldehyde functionality is perfectly suited for a subsequent Wittig olefination. Thus, the reaction of alkynylallyl alcohols **1a** and **1e** with the aryl halides **2** in the presence of a catalytic amount of [Pd(PPh₃)₂Cl₂] in boiling triethylamine followed by addition of a stabilized phosphorus ylide of type **9** at room temperature furnishes the 2,3,6,7-diene esters **10** in moderate to good yields (Scheme 2).^[12]

Additionally, upon reducing the amount of triethylamine to only two equivalents, the new Heck carbopalladation/cyclization sequence can serve as an entry for a subsequent reductive amination under Leuckart–Wallach conditions^[14] in a sequential one-pot reaction. Thus, the reaction of alkynylallyl alcohol **1a** in the presence of a catalytic amount of [Pd(PPh₃)₂Cl₂] and 2 equiv of triethylamine in boiling 1,2-dichloroethane followed by addition of various secondary amines **11** and formic acid at 60 °C results in the formation of β -aminoethylalkylidenetetrahydrofurans **12** in moderate to excellent yields (Scheme 3).^[12]

In conclusion, we have developed a Heck carbopalladation/cyclization domino reaction starting from ynallyl alcohols **1** and aryl halides to give γ,δ -enals **3**. This new domino



Scheme 2. The palladium-catalyzed Heck carbopalladation/cyclization/Wittig sequence giving 2,3,6,7-diene carbonyl compounds **10**.



Scheme 3. The palladium-catalyzed Heck carbopalladation/cyclization/reductive amination sequence yielding β -ethylaminobenzylidene tetrahydrofurans **12**.

process was readily elaborated into two consecutive one-pot three-component sequences in which a Heck carbopalladation/cyclization/Wittig sequence and a Heck carbopalladation/cyclization/reductive amination sequence give rise to heterocyclic 2,3,6,7-diene esters and β -aminoethylalkylidenetetrahydrofurans, respectively. Studies addressing the scope of these novel sequences and related sequential transformations to enhance molecular diversity in pharmaceutically interesting targets are currently under investigation.

Experimental Section

Heck carbopalladation/cyclization sequence (3b): In a 50-mL screw-top pressure vessel [Pd(PPh₃)₂Cl₂] (15 mg, 0.02 mmol) was dissolved in degassed triethylamine (10 mL). Then, **1a** (198 mg, 1.00 mmol) and **2b** (240 mg, 1.10 mmol) were added successively to the solution. The

Table 1: [a] Reaction conditions: 1.0 equiv ynallyl alcohol **1**, 1.1 equiv aryl halide **2** (0.1 M in triethylamine), and 0.02 equiv [Pd(PPh₃)₂Cl₂] were heated at reflux for 2–28 h. [b] Yields refer to yields of isolated compounds **3** after flash chromatography on silica gel; purity was estimated to be $\geq 95\%$ by NMR spectroscopy and elemental analysis and/or HRMS. [c] The reaction was performed in a microwave oven (0.50 mmol **1a**, 0.55 mmol **2f**, 2 mol % [Pd(PPh₃)₂Cl₂]; heating rate: 160 s with 300 W to 150 °C, 30 min of reaction time at 150 °C, cooling rate: 240 s to 45 °C. [d] [Pd(PPh₃)₃] as a catalyst.

reaction mixture was heated at reflux for 2.5 h then allowed to cool to room temperature before diethyl ether (150 mL) was added, and the resulting precipitate was filtered. The solvents were removed from the filtrate in vacuo, and the residue was flash chromatographed on silica gel to give analytically pure **3b** (239 mg, 85% yield) as a pale yellow oil, $R_f = 0.59$ (hexane/diethyl ether 1:1). ^1H NMR (CDCl_3 , 500 MHz): $\delta = -0.17$ (s, 9H), 2.34 (s, 3H), 2.50–2.55 (m, 1H), 2.76–2.81 (m, 1H), 2.93 (ddd, $J = 1.6, 9.7, 17.8$ Hz, 1H), 3.68–3.72 (m, 1H), 3.81 (dd, $J = 1.6, 11.3$ Hz, 1H), 4.08 (d, $J = 17.1$ Hz, 1H), 4.20 (dd, $J = 2.3, 17.2$ Hz, 1H), 6.97–7.01 (m, 2H), 7.10–7.14 (m, 2H), 9.86–9.87 ppm (m, 1H); ^{13}C NMR (CDCl_3 , 125.8 MHz): $\delta = 0.2$ (CH_3), 21.1 (CH_3), 31.2 (CH), 46.8 (CH_2), 67.3 (CH_2), 70.6 (CH_2), 128.5 (CH), 128.7 (CH), 133.8 (C_{quat}), 137.2 (C_{quat}), 137.4 (C_{quat}), 149.5 (C_{quat}), 201.5 ppm (CH); HRMS calcd for $\text{C}_{17}\text{H}_{24}\text{O}_2\text{Si}$: 288.1546, found: 288.1543; Elemental analysis calcd for $\text{C}_{17}\text{H}_{24}\text{O}_2\text{Si}$ (288.5): C 70.78, H 8.39; found: C 70.61, H 8.43.

Heck carbopalladation/cyclization/Wittig sequence (**10b**): In a 50-mL screw-top pressure vessel [$\text{Pd}(\text{PPh}_3)_2\text{Cl}_2$] (14 mg, 0.02 mmol) was dissolved in degassed triethylamine (10 mL). Then, **1a** (198 mg, 1.00 mmol) and **2b** (241 mg, 1.10 mmol) were added successively to the solution. The reaction mixture was heated at reflux for 2.5 h then allowed to cool to room temperature before THF (5 mL) and **9** (523 mg, 1.50 mmol) were added successively, and the reaction mixture was stirred at room temperature for 18 h. The precipitates were removed by filtration, the solvents were removed from the filtrate in vacuo, and the residue was flash chromatographed on silica gel to give the analytically pure **10b** (301 mg, 86%) as a yellow oil, $R_f = 0.72$ (hexane/diethyl ether 1:1). ^1H NMR (CDCl_3 , 250 MHz): $\delta = -0.16$ (s, 9H), 1.30 (t, $J = 7.1$ Hz, 3H), 2.23–2.61 (m, 6H), 3.58–3.66 (m, 1H), 3.81 (dd, $J = 1.9, 11.2$ Hz, 1H), 4.02–4.26 (m, 4H), 5.92 (dt, $J = 1.4, 15.6$ Hz, 1H), 6.91–7.15 ppm (m, 5H); ^{13}C NMR (CDCl_3 , 75.5 MHz): $\delta = 0.4$ (CH_3), 14.2 (CH_3), 21.1 (CH_3), 35.2 (CH_2), 36.0 (CH), 60.1 (CH_2), 66.0 (CH_2), 70.5 (CH_2), 122.8 (CH), 128.6 (CH), 128.7 (CH), 134.5 (C_{quat}), 137.1 (C_{quat}), 137.6 (C_{quat}), 147.1 (CH), 149.2 (C_{quat}), 166.4 ppm (C_{quat}); HRMS calcd for $\text{C}_{21}\text{H}_{30}\text{O}_3\text{Si}$: 358.1964, found: 358.1950; Elemental analysis calcd for $\text{C}_{21}\text{H}_{30}\text{O}_3\text{Si}$ (358.6): C 70.35, H 8.43; found: C 70.31, H 8.42.

Heck carbopalladation/cyclization/reductive amination sequence (**12b**): In a 50-mL screw-top pressure vessel [$\text{Pd}(\text{PPh}_3)_2\text{Cl}_2$] (28 mg, 0.04 mmol) was dissolved in a mixture of degassed 1,2-dichloroethane (10 mL) and triethylamine (202 mg, 2.00 mmol). Then, **1a** (198 mg, 1.00 mmol) and **2c** (240 mg, 1.10 mmol) were added successively to the solution. The reaction mixture was heated at reflux for 3 h then allowed to cool to room temperature before formic acid (552 mg, 12.0 mmol) and pyrrolidine (**11b**) (356 mg, 5.00 mmol) were added successively, and the reaction mixture was heated to 60°C for 12 h. The reaction mixture was allowed to cool to room temperature, diethyl ether (150 mL) and anhydrous potassium carbonate were added, and the precipitates were removed by filtration. The solvents were removed from the filtrate in vacuo, and the residue was flash chromatographed on basic alumina (Brockmann activity IV) to give the analytically pure **12b** (261 mg, 79%) as a yellow-red oil, $R_f = 0.31$ (hexane/diethyl ether 1:2). ^1H NMR (CDCl_3 , 500 MHz): $\delta = -0.22$ (s, 9H), 1.67–1.85 (m, 6H), 2.09–2.18 (m, 1H), 2.42–2.60 (m, 6H), 3.60–3.67 (m, 1H), 3.83 (dd, $J = 2.2, 11.0$ Hz, 1H), 4.04 (d, $J = 16.9$ Hz, 1H), 4.20 (dd, $J = 2.2, 16.9$ Hz, 1H), 7.04–7.11 (m, 2H), 7.20–7.30 ppm (m, 3H); ^{13}C NMR (CDCl_3 , 125.8 MHz): $\delta = 0.4$ (CH_3), 23.4 (CH_2), 31.5 (CH_2), 35.3 (CH), 54.3 (CH_2), 54.9 (CH_2), 66.8 (CH_2), 70.4 (CH_2), 127.2 (CH), 127.9 (CH), 128.8 (CH), 135.8 (C_{quat}), 141.0 (C_{quat}), 148.2 ppm (C_{quat}); HRMS calcd for $\text{C}_{20}\text{H}_{31}\text{NOSi}$: 329.2175, found:

329.2167; Elemental analysis calcd for $\text{C}_{20}\text{H}_{31}\text{NOSi}$ (329.56): C 72.89, H 9.48, N 4.25; found: C 73.36, H 9.71, N 3.91.

Received: June 30, 2004

Keywords: amination · C–C coupling · domino reactions · multicomponent reactions · olefination

- [1] For excellent reviews, see for example, a) E.-I. Negishi, C. Copéret, S. Ma, S.-Y. Liou, F. Liu, *Chem. Rev.* **1996**, *96*, 365; b) M. Malacria, *Chem. Rev.* **1996**, *96*, 289; c) S. Bräse, A. de Meijere in *Metal-Catalyzed Cross-Coupling Reactions*, Wiley-VCH, Weinheim, **1998**, p. 99.
- [2] For recent reviews on transition-metal-catalyzed reactions in heterocyclic synthesis, see for example, a) G. Kirsch, S. Hesse, A. Comel, *Curr. Org. Synth.* **2004**, *1*, 47; b) I. Nakamura, Y. Yamamoto, *Chem. Rev.* **2004**, *104*, 2127, and references therein; c) For a monograph on heterocycle synthesis by means of palladium-catalyzed reactions, see for example, J. J. Lie, G. W. Gribble, *Palladium in Heterocyclic Chemistry*, Pergamon, Oxford, **2000**.
- [3] a) H. Bienaymé, C. Hulme, G. Oddon, P. Schmitt, *Chem. Eur. J.* **2000**, *6*, 3321; b) I. Ugi, A. Dömling, B. Werner, *J. Heterocycl. Chem.* **2000**, *37*, 647; c) L. Weber, K. Illgen, M. Almstetter, *Synlett* **1999**, 366; d) G. H. Posner, *Chem. Rev.* **1986**, *86*, 831.
- [4] For recent excellent reviews on transition-metal-assisted sequential transformations and domino processes, see for example, a) G. Balme, E. Bossharth, N. Monteiro, *Eur. J. Org. Chem.* **2003**, 4101; b) G. Battistuzzi, S. Cacchi, G. Fabrizi, *Eur. J. Org. Chem.* **2002**, 2671; c) L. F. Tietze, *Chem. Rev.* **1996**, *96*, 115.
- [5] S. Kobayashi, *Chem. Soc. Rev.* **1999**, *28*, 1.
- [6] a) A. S. Karpov, T. Oeser, T. J. J. Müller, *Chem. Commun.* **2004**, 1502; b) A. S. Karpov, F. Rominger, T. J. J. Müller, *J. Org. Chem.* **2003**, *68*, 1503; c) N. A. M. Yehia, K. Polborn, T. J. J. Müller, *Tetrahedron Lett.* **2002**, *43*, 6907; d) R. U. Braun, K. Zeitler, T. J. J. Müller, *Org. Lett.* **2001**, *3*, 3297; e) T. J. J. Müller, J. P. Robert, E. Schmäzlin, C. Bräuchle, K. Meerholz, *Org. Lett.* **2000**, *2*, 2419; f) T. J. J. Müller, M. Ansorge, D. Aktah, *Angew. Chem.* **2000**, *112*, 1323; *Angew. Chem. Int. Ed.* **2000**, *39*, 1253.
- [7] a) C. J. Kressierer, T. J. J. Müller, *Tetrahedron Lett.* **2004**, *45*, 2155; b) C. J. Kressierer, T. J. J. Müller, *Synlett* **2004**, 655.
- [8] J. T. Link, L. E. Overman in *Metal-Catalyzed Cross-Coupling Reactions*, Wiley-VCH, Weinheim, **1998**, p. 231.
- [9] For a review, see for example, a) B. M. Trost, *Acc. Chem. Res.* **1990**, *23*, 34; b) B. M. Trost, J. Dumas, M. Villa, *J. Am. Chem. Soc.* **1992**, *114*, 9836; c) B. M. Trost, J. Dumas, *J. Am. Chem. Soc.* **1992**, *114*, 1924; d) S. Brown, S. Clarkson, R. Grigg, V. Sridharan, *Tetrahedron Lett.* **1993**, *34*, 157.
- [10] X. Xie, X. Lu, *Tetrahedron Lett.* **1999**, *40*, 8415.
- [11] The syntheses of alkynylallyl alcohol substrates were performed according to H. Sajiki, K. Hirota, *Tetrahedron* **1998**, *54*, 13981. The detailed protocols will be described elsewhere.
- [12] All compounds were fully characterized spectroscopically and provided either correct elemental analysis or HRMS.
- [13] a) T. Jeffery, *Tetrahedron Lett.* **1990**, *31*, 6641; b) S. A. Buntin, R. F. Heck, *Org. Synth. Coll. Vol.* **1990**, *7*, 361.
- [14] For reviews, see for example, a) M. L. Moore, *Org. React.* **1949**, *5*, 301; b) A. Lukaszewicz, *Tetrahedron* **1963**, *19*, 1789.

Cover Picture

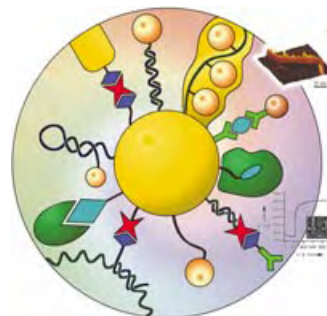
Ariel Ismach, Lior Segev, Ellen Wachtel, and Ernesto Joselevich*

The assembly of nanowire arrays is a critical prerequisite for the large-scale fabrication of nanocircuitry. In their Communication on pp. 6140 ff., E. Joselevich and co-workers show how single-wall carbon nanotubes are formed along the atomic steps of vicinal surfaces, to give highly aligned, dense arrays of discrete, nanometer-wide wires. The cover picture shows how the nanotubes (blue AFM image) reproduce the atomic features of the surface (red model).



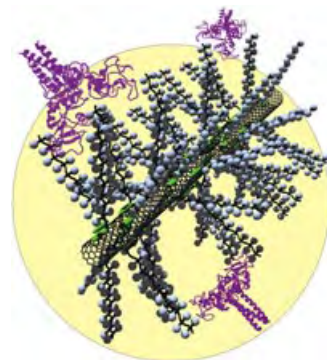
Nanobiotechnology

The recent advances in the preparation of biomaterial–nanoparticle conjugates, as well as the organization of these systems as functional devices, are presented by E. Katz and I. Willner in their Review on page 6042 ff.



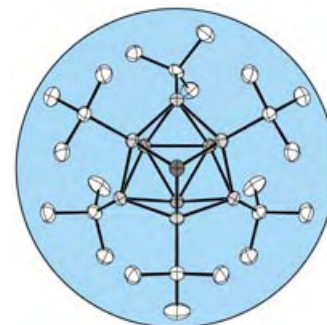
Biomimetic Synthesis

The assembly of water-soluble carbohydrate-functionalized polymers designed to mimic the structures of mucin glycoproteins on carbon nanotubes is described by A. Zettl, C. R. Bertozzi et al. in their Communication on page 6111 ff.



Cluster Compounds

In their Communication on page 6202 ff Klinkhammer et al. report the formation of two neutral lead clusters bearing σ -bonded substituents from the reaction of a plumbylene with a hydride source.



Angewandte EarlyView®

The following Communications are available online (in Wiley InterScience). You can find them, as well as forthcoming Reviews, Highlights, and Essays, at www.angewandte.org, under Early View.

A. Glättli, W. F. van Gunsteren*:

Are NMR-Derived Model Structures for β -Peptides Representative for the Ensemble of Structures Adopted in Solution?

DOI: 10.1002/anie.200460384

Published online: November 2, 2004

T. Yamaguchi, T. Kimura, H. Matsuda, T. Aida*:

Macroscopic Spinning Chirality Memorized in Spin-Coated Films of Spatially Designed Dendritic Zinc Porphyrin J-Aggregates

DOI: 10.1002/anie.200461431

Published online: November 11, 2004

Articles judged by the referees or the editor as being either very important or very urgent are immediately edited, proof-read, and electronically published once the manuscript has arrived in the editorial office in its final form. As long as there is no page number available these articles should be cited in the following manner:

Author(s), *Angew. Chem. Int. Ed.*, online publication date, DOI.

Web Sites

<http://www.geo.arizona.edu/AMS/>

A Crystallographic Database for Minerals

D. Hoppe and M. Ruck _____ 6024

Books

Hydrocarbon Thermal Isomerizations

Joseph J. Gajewski

reviewed by H. Hopf _____ 6025

The Molecular World—Alkenes and Aromatics

Peter Taylor, Michael Gagan

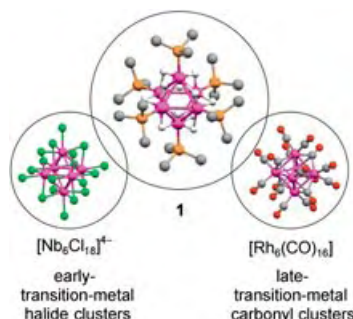
reviewed by H. Hopf _____ 6025

Highlights

Cluster Chemistry

P. J. Dyson,* J. S. McIndoe* 6028 – 6030

An Octahedral Rhodium Cluster with Six Phosphine and 12 Hydride Ligands and 10 Too Few Electrons



Six of one and half a dozen of the other: A late-transition-metal octahedral cluster $[\text{Rh}_6(\text{PiPr}_3)_6(\mu\text{-H})_{12}]^{2+}$ (**1**) with six phosphine ligands has been reported with a structure and electron count akin to that of early-transition-metal halide clusters, and provides a unique link between the two classes of cluster (see scheme). Cluster **1** is also decorated with 12 hydride ligands.

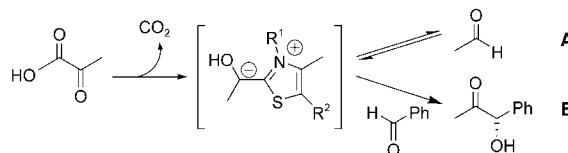
Minireviews

Reaction Specificity of Enzymes

U. T. Bornscheuer,*

R. J. Kazlauskas* _____ 6032 – 6040

Catalytic Promiscuity in Biocatalysis: Using Old Enzymes to Form New Bonds and Follow New Pathways



Unfaithful enzymes, that is, enzymes that catalyze alternative reactions, play a natural role in evolution and occasionally in the biosynthesis of secondary metabolites. In one example pyruvate decarboxy-

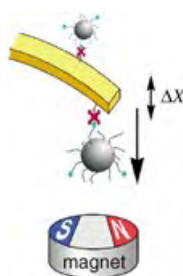
lase catalyzes not only the natural reaction (**A**) but also the enantioselective acyloin condensation of acetaldehyde and benzaldehyde (**B**).

Reviews

Nanobiotechnology

E. Katz, I. Willner* 6042–6108

Integrated Nanoparticle–Biomolecule Hybrid Systems: Synthesis, Properties, and Applications



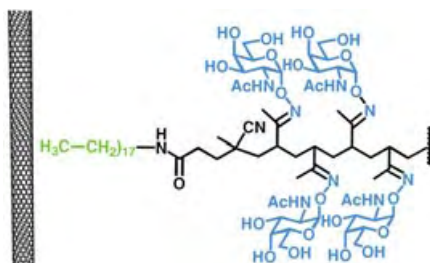
Blue-sky research bears down-to-earth applications: this describes the integration of biological materials with nanomaterials to yield systems that can be applied as biosensors or as building blocks for electronic circuitry. This review describes recent advances in the preparation and the applications of biomolecule–nanoparticle conjugates. The picture shows one such example with the magneto-mechanical analysis of DNA.

Communications

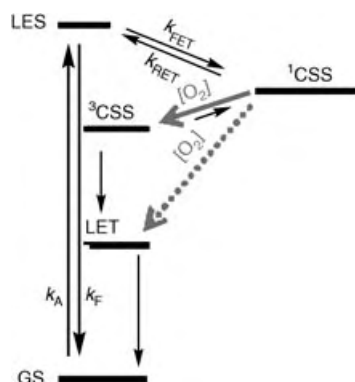
Biomimetic Synthesis

X. Chen, G. S. Lee, A. Zettl,*
C. R. Bertozzi* 6111–6116

Biomimetic Engineering of Carbon Nanotubes by Using Cell Surface Mucin Mimics



Biocompatible nanotubes: Glycosylated polymers designed to mimic natural mucins were assembled on carbon nanotubes (see picture). Carbon nanotubes coated with mucin mimics were soluble in water, resisted nonspecific protein binding, and bound specifically to biomolecules through receptor–ligand interactions.



The dynamics of reversible photoinduced electron transfer in individual perylene-diimide–triphenylamine-based donor–acceptor dendrimers immobilized in polystyrene were investigated by single-molecule spectroscopy. By changing the local concentration of oxygen, it was possible to influence the transition of the charge-separation state (CSS) either to the locally excited state (LES) or to the ground state (GS, see graphic).

Single-Molecule Studies

M. Cotlet, S. Masuo, M. Lor, E. Fron,
M. Van der Auweraer, K. Müllen,
J. Hofkens,* F. De Schryver* 6116–6120

Probing the Influence of O₂ on Photo-induced Reversible Electron Transfer in Perylenediimide–Triphenylamine-Based Dendrimers by Single-Molecule Spectroscopy

For the USA and Canada:
ANGEWANDTE CHEMIE International Edition (ISSN 1433-7851) is published weekly by Wiley-VCH PO Box 191161, D 69451 Weinheim, Germany. Air freight and mailing in the USA by Publications Expediting Inc. 200 Meacham Ave., Elmont, NY 11003. Periodicals

postage paid at Jamaica NY 11431. US POSTMASTER: send address changes to *Angewandte Chemie*, Wiley-VCH, 111 River Street, Hoboken, NJ 07030. Annual subscription price for institutions: US\$ 4948.00/4498.00 (valid for print and electronic / print or electronic delivery); for individuals who are personal members of a

national chemical society, or whose institution already subscribes, or who are retired or self-employed consultants, print only: US\$ 394.00. Postage and handling charges included. All Wiley-VCH prices are exclusive VAT.

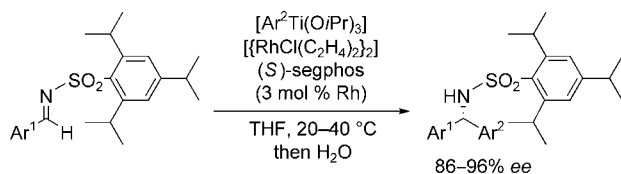
A subtle electronic balance between covalent and dative interactions involving coordinated phosphanyl iminolate ligands results in the formation of an oriented, 1D coordination/organometallic heterodimetallic polymer with Pd–Ag interactions (shown as purple and green, respectively). In the solid-state, the lipophilic aromatic rings of the infinite zigzag chains are all on one side of the planes of metal ions, which results in an unusual layered structure.



Coordination Polymers

P. Braunstein,* C. Frison, N. Oberbeckmann-Winter, X. Morise, A. Messaoudi, M. Bénard, M.-M. Rohmer, R. Welter — 6120–6125

An Oriented 1D Coordination/Organometallic Dimetallic Molecular Wire with Ag–Pd Metal–Metal Bonds



A rational tuning of the arene sulfonamide moiety (by introducing isopropyl groups onto the phenyl ring) brought about high enantioselectivity in the asymmetric synthesis of diarylmethyl amines by the

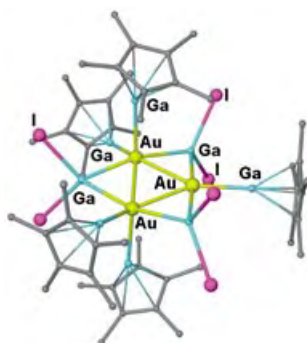
title reaction (see scheme). $\text{Ar}^1 = 4\text{-CF}_3\text{C}_6\text{H}_4$, $4\text{-ClC}_6\text{H}_4$, $4\text{-FC}_6\text{H}_4$, $3\text{-MeOC}_6\text{H}_4$, $4\text{-MeOC}_6\text{H}_4$, $2\text{-MeOC}_6\text{H}_4$, 1-naphthyl , Ph ; $\text{Ar}^2 = \text{Ph}$, $4\text{-FC}_6\text{H}_4$, $3\text{-MeOC}_6\text{H}_4$, $4\text{-MeOC}_6\text{H}_4$.

Amine Synthesis

T. Hayashi,* M. Kawai, N. Tokunaga — 6125–6128

Asymmetric Synthesis of Diarylmethyl Amines by Rhodium-Catalyzed Asymmetric Addition of Aryl Titanium Reagents to Imines

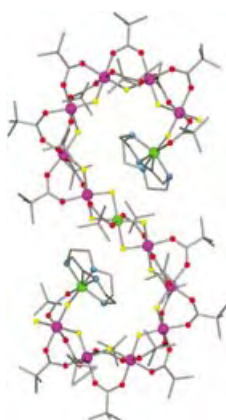
A triangular arrangement of gold atoms is observed in the complex $[\text{Au}_3(\mu\text{-GaI}_2)_3(\text{Cp}^*\text{Ga})_5]$, which results when a mixture of Cp^*Ga and GaI_3 capture the reduced Au fragments from $[\text{LAuX}]$ ($\text{L} = \text{ligand}$, $\text{X} = \text{halide}$). The Au atoms are bonded only to Ga atoms and each other: two Au atoms are coordinated by two Cp^*Ga units and one Au atom is coordinated by a single Cp^*Ga unit.



Heterometallic Clusters

U. Anandhi, P. R. Sharp* — 6128–6131

A Gallium-Coated Gold Cluster



Ring the changes: Complexes of azamacrocycles were used for the template synthesis of extraordinary new cyclic and acyclic chromium–nickel chains, which include the “S”-shaped cluster shown (see picture) obtained when a cyclen-based template is used. The results suggest a new method for making sophisticated polymetallic architectures.

Heterometallic Complexes

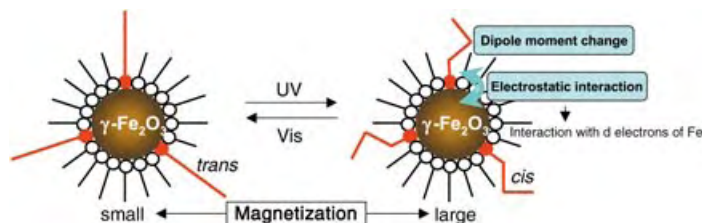
S. L. Heath, R. H. Laye, C. A. Muryn, N. Lima, R. Sessoli,* R. Shaw, S. J. Teat, G. A. Timco,* R. E. P. Winpenny* — 6132–6135

Templating Open- and Closed-Chain Structures around Metal Complexes of Macrocycles

Photo-Switching

R. Mikami, M. Taguchi, K. Yamada,
K. Suzuki, O. Sato,
Y. Einaga* _____ 6135–6139

Reversible Photo-Switching of the
Magnetization of Iron Oxide
Nanoparticles at Room Temperature



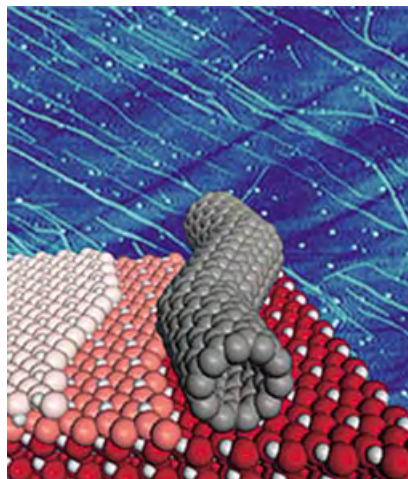
In the solid state at room temperature, reversible control of magnetic properties was achieved with photo-illumination of a composite material made up of $\gamma\text{-Fe}_2\text{O}_3$

nanoparticles encapsulated with *n*-octylamine and an azobenzene-containing amphiphilic compound (see picture).

Carbon Nanotubes

A. Ismach, L. Segev, E. Wachtel,
E. Joselevich* _____ 6140–6143

Atomic-Step-Templated Formation of
Single Wall Carbon Nanotube Patterns

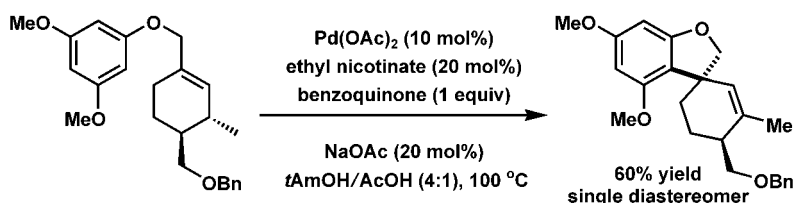


Mind the step! Single-wall carbon nanotubes grow along the atomic steps of vicinal $\alpha\text{-Al}_2\text{O}_3$ surfaces to give highly aligned arrays of nanometer-wide wires on a dielectric material. The nanotubes (see blue background image) reproduce the atomic features of the surface including steps, facets, and kinks (see model). The direction and morphology of the atomic steps can be controlled by the crystal miscut.

Pd-Catalyzed Cyclizations

H. Zhang, E. M. Ferreira,
B. M. Stoltz* _____ 6144–6148

Direct Oxidative Heck Cyclizations: Intra-
molecular Fujiwara–Moritani Arylations
for the Synthesis of Functionalized
Benzofurans and Dihydrobenzofurans



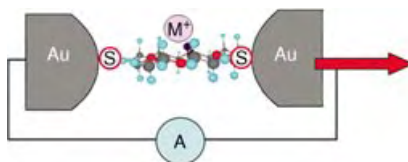
No extra functionalization step is required for palladium(II)-catalyzed oxidative carbocyclizations like that shown, which provide highly substituted benzofuran and dihydrobenzofuran derivatives by net

dehydrogenation. The mechanism is similar to that of Heck cyclizations. Products containing quaternary carbon stereocenters can be obtained in diastereomerically pure form.

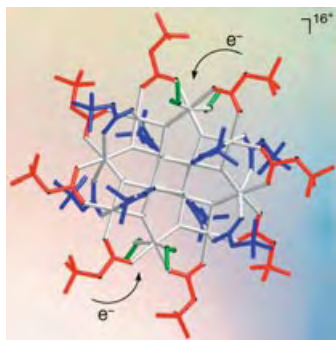
Single-Molecule Conductance

X. Y. Xiao, B. Q. Xu,
N. J. Tao* _____ 6148–6152

Changes in the Conductance of Single
Peptide Molecules upon Metal-Ion
Binding



The binding of a guest (metal ion, M^+) to a single host molecule (peptide) was studied by the measurement of the conductance of the peptide (see picture). The conductance of the peptide in the metal–peptide complexes increases by an amount that is dependent on the sequence and the length of the host.

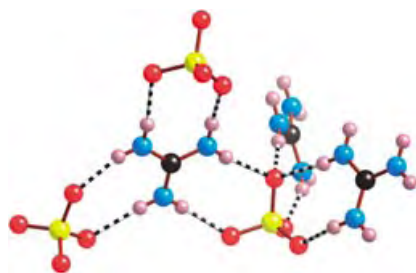


Manganese magnets: Trimethylammonio groups appended to the surface of a Mn_{12} single-molecule magnet lead to a highly charged magnetic cluster that behaves as an electron reservoir. This cluster spontaneously forms its two-electron reduced species which has a ground spin state $S=11$. The cluster is a precursor for the synthesis of network materials containing Mn_{12} and for their deposition onto metal and metal oxide surfaces.

Magnetic Clusters

E. Coronado,* A. Forment-Aliaga, A. Gaita-Ariño, C. Giménez-Saiz, F. M. Romero,*
W. Wernsdorfer ————— **6152–6156**

Polycationic Mn_{12} Single-Molecule Magnets as Electron Reservoirs with $S > 10$ Ground States

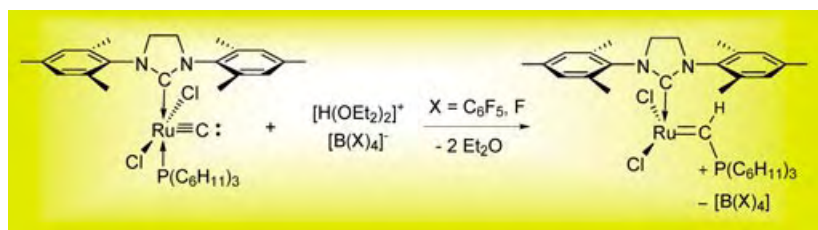


It takes two: The complementary sulfate and guanidinium ions in $[\text{C}(\text{NH}_2)_3][\text{N}(\text{CH}_3)_4][\text{SO}_4]$ both act as 3-connecting nodes to give a 3D hydrogen-bonded network with the chiral (10,3)- α topology (see X-ray crystal structure; O red, S yellow, H pink, N blue, C black). In contrast, the 3-connected hydrogen-bonded network in the much-studied guanidinium sulfonates is 2D.

Crystal Engineering

B. F. Abrahams, M. G. Haywood, T. A. Hudson, R. Robson* — **6157–6160**

Cubic, Hydrogen-Bonded (10,3)- α Networks in the Family $[\text{C}(\text{NH}_2)_3][\text{N}(\text{CH}_3)_4][\text{XO}_4]$ ($\text{X} = \text{S}, \text{Cr}, \text{and Mo}$)



Olefin Metathesis

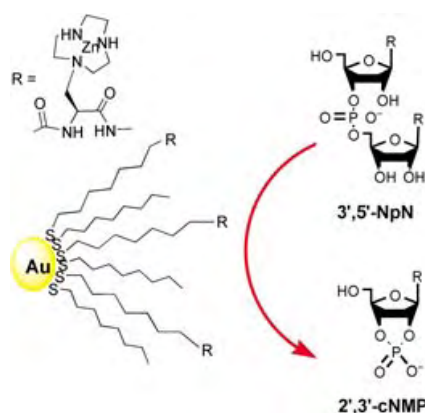
P. E. Romero, W. E. Piers,*
R. McDonald ————— **6161–6165**

Rapidly Initiating Ruthenium Olefin-Metathesis Catalysts

Vacancies: Protonation of the ruthenium carbide compounds $[\text{Cl}_2(\text{L})(\text{PR}_3)_2\text{Ru}=\text{C}]$ gives the 14-electron four-coordinate ruthenium phosphonium alkylidenes $[\text{Cl}_2(\text{L})\text{Ru}=\text{CH}(\text{PR}_3)]^+[\text{B}(\text{X})_4]^-$ (see

scheme). These compounds which already have a vacant coordination site provide direct access to the active species in olefin metathesis catalysis and thus very fast initiation.

Particularly effective: The self-assembly of triazacyclonane-functionalized thiols on the surface of nanosize gold particles provides a facile entry to functional gold nanoparticles that, upon complexation with Zn^{II} , turn into powerful catalysts for the cleavage of phosphate esters (see scheme). Because of their RNase-like behavior they are dubbed nanozymes.



Nanoparticles and Catalysis

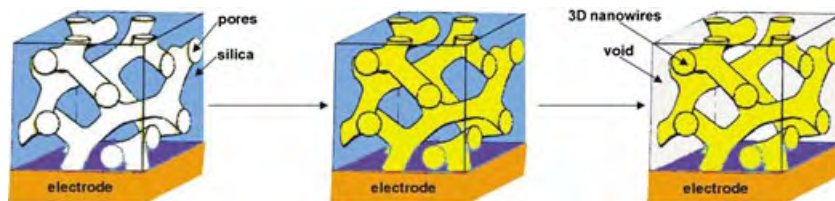
F. Manea, F. B. Houillon, L. Pasquato,*
P. Scrimin* ————— **6165–6169**

Nanozymes: Gold-Nanoparticle-Based Transphosphorylation Catalysts

Nanostructures

D. Wang, H. Luo, R. Kou, M. P. Gil, S. Xiao,
V. O. Golub, Z. Yang,* C. J. Brinker,
Y. Lu* **6169–6173**

A General Route to Macroscopic
Hierarchical 3D Nanowire Networks



Pulling the rug out! A templated electro-deposition technique has been applied to prepare stable 3D, organized networks of metal or semiconductor nanowires (see scheme). The process involves a) the

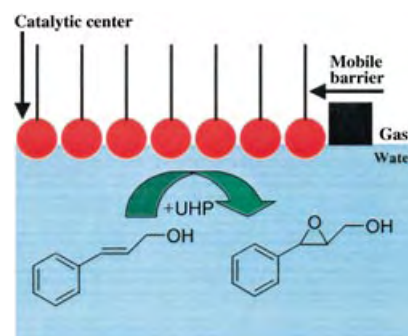
deposition of mesoporous silica onto an electrode, b) the introduction of metals or semiconductors into the pore channels, and c) removal of the silica template to yield the nanowire network.

Catalysis Methods

A. Pasc-Banu, C. Sugisaki, T. Gharsa,
J.-D. Marty, I. Gascon, G. Pozzi,
S. Quici, I. Rico-Lattes,
C. Mingotaud* **6174–6177**

A Catalytic Langmuir Film as a Model
for Heterogeneous and Homogeneous
Catalytic Processes

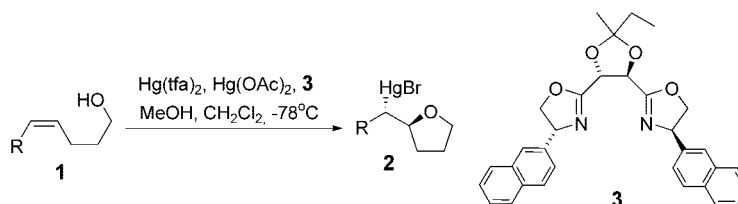
An amphiphilic manganese salen complex forms Langmuir films that catalyze the epoxidation of cinnamyl alcohol with the urea/hydrogen peroxide complex (UHP) dissolved in the subphase (see picture). Compression of the monolayer changes the organization of the film and thus strongly modifies the rate of the reaction, which is enhanced for molecular areas of about 140–160 Å².



Oxygen Heterocycles

S. H. Kang,* M. Kim,
S. Y. Kang **6177–6180**

Catalytic Asymmetric Mercuriocyclization
of γ -Hydroxy-*cis*-Alkenes



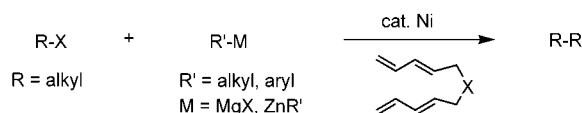
2-Monosubstituted tetrahydrofurans 2 are obtained with 73–95% *ee* through the catalytic enantioselective mercuriocyclization of γ -hydroxy-*(Z)*-alkenes **1** by using $\text{Hg}(\text{OAc})_2$ in the presence of Hg^{II} com-

plexed with tartrate-derived 4-(2-naphthyl)bisoaxazoline **3**. The chiral complex was prepared from $\text{Hg}(\text{tfa})_2$ (0.2 equiv) and **3** (0.3 equiv). The amount of MeOH greatly influences the enantioselectivity.

Synthetic Methods

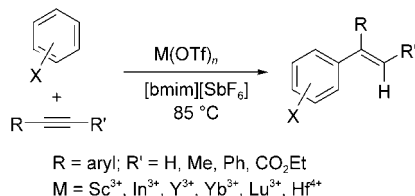
J. Terao, H. Todo, H. Watanabe, A. Ikumi,
N. Kambe* **6180–6182**

Nickel-Catalyzed Cross-Coupling Reaction
of Alkyl Halides with Organozinc and
Grignard Reagents with 1,3,8,10-Tetraenes
as Additives



Essential additives: The addition of bis(1,3-butadienyl) compounds (tetraenes) was essential in the efficient Ni-catalyzed cross-coupling of organozinc reagents with alkyl bromides and a tosy-

late (see scheme, $\text{X} = \text{C}(\text{CO}_2\text{Me})_2$ or NCH_2Ph). The efficiency of the Ni-catalyzed cross-coupling of an alkyl fluoride with a Grignard reagent was also improved by using these tetraenes.



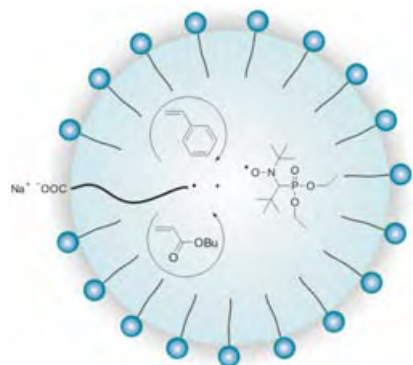
A simple and highly efficient method for the Friedel–Crafts alkenylation of aromatic

compounds has been developed by using a metal triflate (OTf) catalyst in an ionic liquid (see scheme, bmim = 1-butyl-3-methylimidazolium). Not only is the catalytic activity significantly enhanced in the ionic liquid and by-product formation decreased, but some reactions that were not possible in conventional organic solvents were shown to proceed smoothly.

Synthetic Methods

C. E. Song,* D.-u. Jung, S. Y. Choung, E. J. Roh, S.-g. Lee* — 6183–6185

Dramatic Enhancement of Catalytic Activity in an Ionic Liquid: Highly Practical Friedel–Crafts Alkenylation of Arenes with Alkynes Catalyzed by Metal Triflates



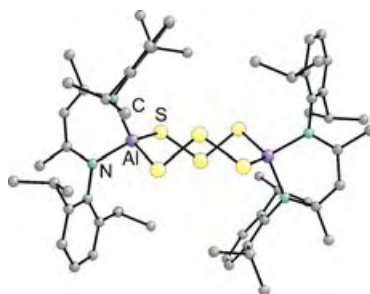
Latex: Nitroxide-mediated emulsion polymerizations of *n*-butyl acrylate and styrene were successfully carried out in a multi-step process, with a novel water-soluble SG1-based alkoxyamine as initiator. Fast reactions lead to stable latex particles containing polymers with controlled molar masses.

Polymerizations

J. Nicolas, B. Charleux,* O. Guerret, S. Magnet — 6186–6189

Nitroxide-Mediated Controlled Free-Radical Emulsion Polymerization of Styrene and *n*-Butyl Acrylate with a Water-Soluble Alkoxyamine as Initiator

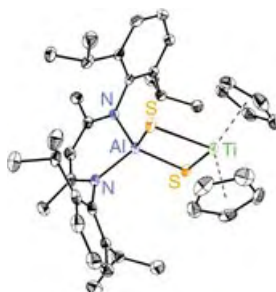
Pieces of eight: The reaction of [LAl] with elemental sulfur yields the crown shaped complex [LAl(μ-S₃)₂AlL] (L = HC(CMe-NAr)₂, Ar = 2,6-*i*Pr₂C₆H₃) containing an Al₂S₆ eight-membered ring, in which two (μ-S₃) chains are bridging two aluminum atoms (see structure). The relative stabilities of the possible [L₂Al₂S_n] (*n* = 2–8) species are estimated by theoretical calculation.



Metal Polysulfides

Y. Peng, H. Fan, V. Jancik, H. W. Roesky,* R. Herbst-Irmer — 6190–6192

[LAl(μ-S₃)₂AlL]: A Homobimetallic Derivative of the Sulfur Crown S₈



Sulfur bridges: The reactions of [LAl(SH)₂] (L = HC(CMeNAr)₂, Ar = 2,6-*i*Pr₂C₆H₃) with LiN(SiMe₃)₂ in molar ratio 1:2 and 1:1, respectively, lead to species with the formula [{LAl[(SLi)(thf)₃]}₂]·2 THF and [{LAl(SH)[SLi(thf)₂]}₂] in high yields. These lithium salts react further with [Cp₂MCl₂] (M = Ti, Zr; Cp = C₅H₅) to give unique heterobimetallic sulfides of composition [LAl(μ-S)₂MCP₂] (see structure; M = Ti).

Mixed-Metal Compounds

V. Jancik, H. W. Roesky,* D. Neculai, A. M. Neculai, R. Herbst-Irmer — 6192–6196

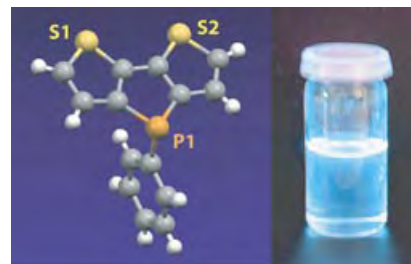
Preparation of [LAl(μ-S)₂MCP₂] (M = Ti, Zr) from the Structurally Characterized Lithium Complexes [{LAl(SH)[SLi(thf)₂]}₂] and [{LAl[(SLi)₂(thf)₃]}₂]·2 THF

Phospholes

T. Baumgartner,* T. Neumann,
B. Wirges ————— **6197 – 6201**

The Dithieno[3,2-*b*:2',3'-*d*]phosphole
System: A Novel Building Block for Highly
Luminescent π -Conjugated Materials

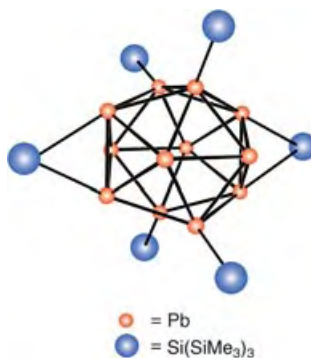
Like a bolt from the blue, the blue photoluminescence of novel phosphole-based materials is extraordinarily intense. The optoelectronic properties show great stability and broad flexibility with respect to wavelength, intensity, and tuneability. The special features of the dithienophosphole system were incorporated in a high-molecular-weight smart polymer potentially suitable for optoelectronic applications.



Cluster Compounds

K. W. Klinkhammer,* Y. Xiong,
S. Yao ————— **6202 – 6204**

Molecular Lead Clusters—From Unexpected Discovery to Rational Synthesis

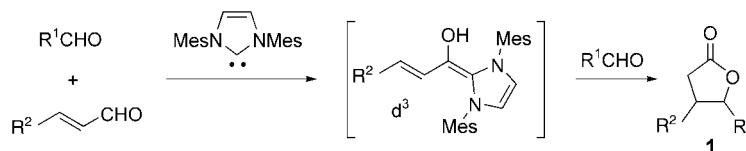


Feats of lead: The cluster compounds $[\text{Pb}_{12}\text{Hyp}_6]$ (**1**; see structure) and $[\text{Pb}_{10}\text{Hyp}_6]$ (**2**) result from the reaction of the plumbylene $[\text{Pb}\{\text{Si}(\text{SiMe}_3)_3\}_2]$ ($[\text{PbHyp}_2]$) with hydride sources, such as PH_3 or $[(\text{Ph}_3\text{P})\text{CuH}]_6$. They are the first examples of neutral lead clusters bearing σ -bonded substituents. Whereas **2** is isolated from the reaction mixture on a multigram scale, **1** is only obtained in traces.

Organocatalysis

C. Burstein, F. Glorius* — **6205 – 6208**

Organocatalyzed Conjugate Umpolung of α,β -Unsaturated Aldehydes for the Synthesis of γ -Butyrolactones



Advantage organocatalysis: N-heterocyclic carbenes can generate homoenolate equivalents under mild conditions by conjugate umpolung of α,β -unsaturated

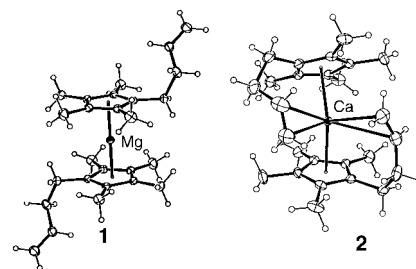
aldehydes. This organocatalytic reaction allows an efficient one-step synthesis of substituted γ -butyrolactones **1** (see scheme, Mes = mesityl).

Metalloenes

H. Schumann,* S. Schutte, H.-J. Kroth,
D. Lentz* ————— **6208 – 6211**

Butenyl-Substituted Alkaline-Earth
Metallocenes: A First Step towards Olefin
Complexes of the Alkaline-Earth Metals

Sandwich any one? The bis(butenyltetramethylcyclopentadienyl) complexes of calcium (**2**), strontium and barium exhibit an interaction of the alkaline-earth metals with olefin double bonds. Whereas the magnesium derivative (**1**) crystallizes as a sandwich complex with coplanar cyclopentadienyl ligands and free butenyl side chains, these coordinate to the metal in the analogous but open sandwich complexes of the larger metals calcium, strontium, and barium.



Communications labeled with this symbol have been judged by two referees as being “very important papers”.

The issues for November 2004 appeared online on the following dates
Issue 41: October 13. • Issue 42: October 20. • Issue 43: November 2. • Issue 44: November 11

WILEY InterScience®
DISCOVER SOMETHING GREAT

"Hot Papers" are chosen by the Editors for their importance in a rapidly evolving field of high current interest. A preview with the graphical abstracts of these articles can be found on the *Angewandte Chemie* homepage in Wiley InterScience at www.angewandte.org.

"VIPs" are Communications which are identified by two referees as being very important. They are published online up to several weeks ahead of print. A preview with short summaries of these articles can also be found on the journal's homepage.

Service

Keywords 6212

Authors 6213

Angewandte's
Sister Journals 6214–6215

Preview 6217



ISBN 3-527-30542-4

Prices per volume:

€ 259.– / £ 200.– / US\$ 370.–

Publication dates:

volumes 1–5	Feb 2004
volumes 6–10	Aug 2004
volumes 11–16	May 2005

The Nucleus of Knowledge

Robert A. Meyers (Ed.), Ramtech Ltd., Tarzana, CA, USA

Encyclopedia of Molecular Cell Biology and Molecular Medicine

2nd Edition, 16 Volume Set

Highly acclaimed and referenced by the scientific community, the *Encyclopedia of Molecular Biology and Molecular Medicine* is now entering its second edition. The new edition features extensive new material on the molecular aspects of cell biology, which is reflected in its new title: *Encyclopedia of Molecular Cell Biology and Molecular Medicine*. With new articles on functional genomics, proteomics, and bioinformatics, there is no better, cutting-edge reference in the field.

"This series is a classic..."

Molecular Medicine Today/Trends in Molecular Medicine

<http://meyers-emcbmm.de>

John Wiley & Sons, Inc., Customer Care,
Fax: +1 800-597-3299, e-mail: custserv@wiley.com, www.wiley.com
Wiley-VCH, Customer Service Department,
Fax: +49 (0) 6201-606-184, e-mail: service@wiley-vch.de, www.wiley-vch.de
John Wiley & Sons, Ltd, Customer Services Department,
Fax: +44 (0) 1243-843-296, e-mail: cs-books@wiley.co.uk, www.wiley-europe.com

 **WILEY**

 **WILEY-VCH**

6839072_Ba

An Octahedral Rhodium Cluster with Six Phosphine and 12 Hydride Ligands and 10 Too Few Electrons

Paul J. Dyson* and J. Scott McIndoe*

Keywords:

cluster compounds · electron counting · hydride ligands · P ligands · rhodium

Late-transition-metal (low-oxidation state) clusters, with π -acceptor ligands and early-transition-metal (high-oxidation state) clusters, with π -donor ligands, have been intensively studied for several decades.^[1] Apart from the fascinating structural aspects of cluster compounds and rationalization of their bonding, much motivation for their study has been driven by potential applications. It was suggested that transition-metal clusters might prove to be effective catalysts, filling the void between mononuclear species and colloidal (or heterogeneous) catalysts and open up new possibilities in catalysis and organic synthesis.^[2]

Research at the interface of late- and early-transition-metal cluster chemistry has not been forthcoming although polyoxometalates have been combined with organometallic fragments^[3] and late-early-transition-metal bonds are well known.^[4] However, in a recent communication by Weller et al., a late-transition-metal cluster based on an octahedral rhodium core was reported that has a structure and an electron count similar to that of an early-transition-metal cluster, and thus bridges the two largely separate and distinct re-

gimes.^[5] The cluster was isolated after a remarkably simple synthesis involving reduction under hydrogen of the complex, $[\text{RhL}_2(\text{nbd})]^+$, where L is a phosphine and nbd is norbornadiene. The rhodium precursor represents a widely used class of hydrogenation catalyst, especially for asymmetric reductions where L_2 is a chiral bisphosphine.^[6] Therefore, apart from the absence of any substrate, what is so different about the synthesis which leads to such an intriguing cluster? The answer to this question remains to be confirmed, but three factors appear to be important. First, commencing with a rhodium salt comprising a weakly coordinating anion, that is, $[\text{1-H-closo-CB}_{11}\text{Me}_{11}]^-$ or $[\text{B}(\text{Ar}_F)_4]^-$ ($\text{Ar}_F = 3,5\text{-bis(trifluoromethyl)phenyl}$). Second, the use of relatively weakly coordinating solvents, that is, $\text{C}_6\text{H}_5\text{F}$ or CH_2Cl_2 . Third, the utilization of a phosphine which appears to have the ideal topology to form a protective sheath over the cluster (see below). The cluster in question, $[\text{Rh}_6(\text{P}i\text{Pr}_3)_6(\mu\text{-H})_{12}]^{2+}$, is prepared according to Scheme 1, and accounts for about 20 % of the starting material—the other compounds formed in the reaction remain uncharacterized.

each edge bridged by a hydride (Figure 1). It resembles the early-transition-metal cluster $[\text{Zr}_6(\mu\text{-Cl})_{12}(\text{PMe}_2\text{Ph})_6(\text{H})_x]$ in the arrangement of ligands.^[7]

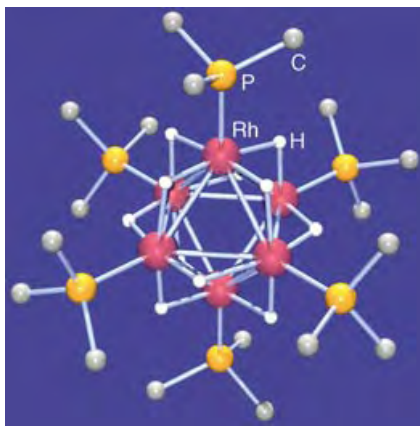
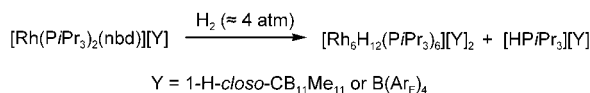


Figure 1. Ball-and-stick representation of the structure of $[\text{Rh}_6(\text{P}i\text{Pr}_3)_6(\mu\text{-H})_{12}]^{2+}$. For clarity the *iso*-propyl groups are represented by a single carbon atom. POV-RAY diagram drawn using ORTEP-3.8.^[8]

What is perhaps most interesting, and could indicate why the cluster is stable, is that the *iso*-propyl groups attached to the phosphine ligand appear to cloak the metal core almost completely as can be appreciated from the space filling representation shown in Figure 2. While there are approximately 90 structurally characterized examples of $[\text{M}_6(\text{PR}_3)_6\text{L}_x]$ clusters known, the vast majority have sterically undemanding ligands (typically PEt_3) and only one, $[\text{W}_6(\mu_3\text{-S})_8(\text{PCy}_3)_6]$ ($\text{Cy} = \text{cyclohexyl}$)^[9] has a



Scheme 1. The preparation of $[\text{Rh}_6(\text{P}i\text{Pr}_3)_6(\mu\text{-H})_{12}]^{2+}$.

The structure of the $[\text{Rh}_6(\text{P}i\text{Pr}_3)_6(\mu\text{-H})_{12}]^{2+}$ dication comprises an essentially regular octahedron in which each vertex is capped by a phosphine ligand and

[*] Prof. Dr. P. J. Dyson
Institut des Sciences et
Ingénierie Chimiques
Ecole Polytechnique Fédérale de Lausanne
EPFL-BCH, 1015 Lausanne (Switzerland)
Fax: (+41) 21-693-98-85
E-mail: paul.dyson@epfl.ch
Prof. Dr. J. S. McIndoe
Department of Chemistry
University of Victoria
P.O. Box 3065, Victoria BC V8W 3V6
(Canada)
Fax: (+1) 250-721-7147
E-mail: mcindoe@uvic.ca.

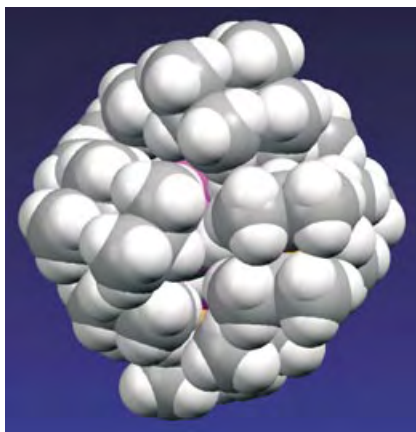


Figure 2. Space-filling representation of the structure of $[\text{Rh}_6(\text{PiPr}_3)_6(\mu\text{-H})_{12}]^{2+}$.

ligand more bulky than PiPr_3 . Packing six bulky phosphines around the cluster core does have a distorting effect on the geometry of the octahedral core, but the efficient packing probably helps considerably to stabilize the numerous labile hydride ligands.

The electronic structure of the cluster bears closer resemblance to early-transition-metal clusters with π -donor ligands than to late-transition-metal clusters with π -acceptor ligands. Most octahedral clusters with π -acceptor ligands have 86 electrons, and deviations from this rule for late-transition-metals are rare and usually involve clusters with unusual ligand assemblies, or Group 10 or 11 metals, or both, such as the 90 electron $[\text{Ni}_6(\eta^5\text{-C}_5\text{H}_5)_6]$.^[10] There are many clusters known of the type $[\text{M}_6(\mu_3\text{-E})_8(\text{PR}_3)_6]$ (M = Group 6, 7, 8, or 9 metal; E = S, Se, or Te)^[11] that span the early–late-transition-metal divide, and these have electron counts^[12] ranging from 79 for $[\text{W}_6(\mu_3\text{-S})_8(\text{PET}_3)_6]^{+13}$ to 98 for $[\text{Co}_6(\mu_3\text{-S})_8(\text{PET}_3)_6]$.^[14] However, $[\text{Rh}_6(\text{PiPr}_3)_6(\mu\text{-H})_{12}]^{2+}$ has an electron count of just 76 electrons, a value entirely without precedent for the late-transition-metals and comparable only to early-transition-metal halide clusters, such as $[\text{M}_6(\mu\text{-Cl})_{12}\text{Cl}_6]^{4-}$ (M = Nb, Ta; also 76 electrons).

In addition, the ratio of hydrides to rhodium is remarkably high, and represents one of the highest ratios observed to date. High hydride to metal ratios are important with respect to hydrogen (hydride) storage and also have implications in hydrogenation catalysis where

hydrogen spillage could account for accelerated reductions.^[15]

It is probably not unfair to say that cluster chemistry has been in decline since its peak in popularity in the late 1980s. However, without the high expectations that once dominated the field it remains healthy and some of the best work has since been carried out. High-nuclearity clusters, such as $[\text{Os}_{20}(\text{CO})_{40}]^{2-}$,^[16] $[\text{Ni}_{35}\text{Pt}_9(\text{CO})_{48}]^{6-}$,^[17] $[\text{Pd}_{145}(\text{CO})_x(\text{PET}_3)_{30}]^{18}$ and $[\text{Cu}_{146}\text{Se}_{73}(\text{PPh}_3)_{30}]$,^[19] the larger ones exceeding the size of many colloids, have been prepared and characterized by X-ray crystallography. A fascinating series of ruthenium–palladium and ruthenium–platinum clusters prepared by condensation of preformed ruthenium clusters with the $\{\text{M}(\text{P}t\text{Bu}_3)_2\}$ unit (also an active catalyst precursor—but for carbon–carbon coupling reactions) have been reported,^[20] and related compounds have been used as precursors to highly active supported naked nanoparticle catalysts.^[21] Also, the on-going question of whether intact clusters can act as catalysts has finally been resolved, at least for hydrogenation reactions. The answer is yes, demonstrated directly by para-hydrogen NMR spectroscopy, but the process is highly solvent dependent and this might explain why there has been so much controversy in the literature surrounding this topic.^[22] However, the isolation of $[\text{Rh}_6(\text{PiPr}_3)_6(\mu\text{-H})_{12}]^{2+}$ from $[\text{Rh}(\text{PiPr}_3)_2(\text{nbd})]^+$ under a hydrogen atmosphere raises another question. Could clusters, especially one so electronically unsaturated and presumably as reactive as $[\text{Rh}_6(\text{PiPr}_3)_6(\mu\text{-H})_{12}]^{2+}$, be the active catalysts in hydrogenation reactions commencing with the widely used $[\text{Rh}(\text{PiPr}_3)_2(\text{nbd})]^+$ precursors, that operate under similar conditions to those in which the cluster was isolated, merely in the presence of a suitable substrate? It is already well established that homogeneous (mononuclear) pre-catalysts often decompose to nanoparticles which are the active catalysts,^[23] but little attention has been paid to the mechanism and whether molecular cluster intermediates play an influential role. The distinctive spectroscopic properties of $[\text{Rh}_6(\text{PiPr}_3)_6(\mu\text{-H})_{12}]^{2+}$ may well facilitate such investigations.

Further development of the unique cluster chemistry introduced by Weller

et al. could take many paths. The X-ray data notwithstanding, a neutron diffraction study to pinpoint the exact hydride locations is clearly desirable. Similarly, extension of the structural motif to other late-transition-metals, other bulky two-electron donor ligands, and perhaps other hydride ligand counts, will all provide interesting insights into what represents a new frontier for cluster chemistry.

Published Online: November 10, 2004

- [1] For example, see: a) *Metal Clusters in Chemistry* (Eds.: P. Braunstein, L. A. Oro, P. R. Raithby), Wiley-VCH, New York, **1999**; b) *Early Transition Metal Clusters with π -Donor Ligands* (Ed.: M. H. Chisholm), Wiley-VCH, New York, **1995**.
- [2] E. L. Muetterties, T. N. Rhodin, E. Band, C. Brucker, H. Pretzer, *Chem. Rev.* **1979**, 79, 91.
- [3] D. Laurencin, E. G. Fidalgo, R. Villaneau, F. Villain, P. Herson, J. Pacifico, H. Stoeckli-Evans, M. Benard, M. M. Rohmer, G. Süß-Fink, A. Proust, *Chem. Eur. J.* **2004**, 10, 208.
- [4] L. H. Gade, *Angew. Chem.* **2001**, 113, 2768; *Angew. Chem. Int. Ed.* **2001**, 40, 2659.
- [5] M. J. Ingleson, M. F. Mahon, P. R. Raithby, A. S. Weller, *J. Am. Chem. Soc.* **2004**, 126, 4784.
- [6] H. U. Blaser, C. Malan, B. Pugin, F. Spindler, H. Steiner, M. Studer, *Adv. Synth. Catal.* **2003**, 345, 103.
- [7] F. A. Cotton, P. A. Kibala, W. J. Roth, *J. Am. Chem. Soc.* **1988**, 110, 298; L. Chen, F. A. Cotton, W. A. Wojtczak, *Angew. Chem.* **1995**, 107, 2050; *Angew. Chem. Int. Ed. Engl.* **1995**, 34, 1877.
- [8] L. J. Farrugia, *J. Appl. Crystallogr.* **1997**, 30, 565.
- [9] S. Jin, D. Venkataraman, F. J. DiSalvo, *Inorg. Chem.* **2000**, 39, 2747.
- [10] M. S. Paquette, L. F. Dahl, *J. Am. Chem. Soc.* **1980**, 102, 6621.
- [11] I. Dance, K. Fisher, *Prog. Inorg. Chem.* **1994**, 41, 637.
- [12] P.-D. Fan, P. Deglmann, R. Ahlrichs, *Chem. Eur. J.* **2002**, 8, 1059.
- [13] L. I. Hill, S. Jin, R. Zhou, D. Venkataraman, F. J. DiSalvo, *Inorg. Chem.* **2001**, 40, 2660.
- [14] F. Cecconi, C. A. Ghilardi, S. Midollini, A. Orlandini, *Inorg. Chim. Acta* **1983**, 76, L183.
- [15] H. Gao, R. J. Angelici, *Organometallics* **1999**, 18, 989.
- [16] A. J. Amoroso, L. H. Gade, B. F. G. Johnson, J. Lewis, P. R. Raithby, W.-T. Wong, *Angew. Chem.* **1991**, 103, 102;

- Angew. Chem. Int. Ed. Engl.* **1991**, *30*, 107.
- [17] C. Femoni, M. C. Iapalucci, G. Longoni, P. H. Svensson, P. Zanello, F. F. De Biani, *Chem. Eur. J.* **2004**, *10*, 2318.
- [18] N. T. Tran, D. R. Powell, L. F. Dahl, *Angew. Chem.* **2000**, *112*, 4287; *Angew. Chem. Int. Ed.* **2000**, *39*, 4121.
- [19] H. Krautscheid, D. Fenske, G. Baum, M. Semmelmann, *Angew. Chem.* **1993**, *105*, 1303; *Angew. Chem. Int. Ed. Engl.* **1993**, *32*, 1303.
- [20] R. D. Adams, B. Captain, W. Fu, M. B. Hall, J. Manson, M. D. Smith, C. E. Webster, *J. Am. Chem. Soc.* **2004**, *126*, 5253.
- [21] J. M. Thomas, B. F. G. Johnson, R. Raja, G. Sankar, M. A. Midgley, *Acc. Chem. Res.* **2003**, *36*, 20.
- [22] D. Blazina, S. B. Duckett, P. J. Dyson, J. A. B. Lohman, *Angew. Chem.* **2001**, *113*, 3992; *Angew. Chem. Int. Ed.* **2001**, *40*, 3874.
- [23] P. J. Dyson, *Dalton Trans.* **2003**, 2964.

Quality counts...

The best of chemistry every week



Wiley-VCH

P.O. Box 10 11 61
69451 Weinheim
Germany

Phone +49 (0) 6201-606-400

Fax +49 (0) 6201-606-184

e-mail: angewandte@wiley-vch.de

www.angewandte.org

Angewandte Chemie International Edition is a journal of the GDCh, the German Chemical Society

GDCh



WILEY-VCH

Reaction Specificity of Enzymes

Catalytic Promiscuity in Biocatalysis: Using Old Enzymes to Form New Bonds and Follow New Pathways

Uwe T. Bornscheuer* and Romas J. Kazlauskas*

Keywords:

biosynthesis · biotransformations · enzyme catalysis · molecular modeling · proteins

Biocatalysis has expanded rapidly in the last decades with the discoveries of highly stereoselective enzymes with broad substrate specificity. A new frontier for biocatalysis is broad reaction specificity, where enzymes catalyze alternate reactions. Although often underappreciated, catalytic promiscuity has a natural role in evolution and occasionally in the biosynthesis of secondary metabolites. Examples of catalytic promiscuity with current or potential applications in synthesis are reviewed here. Combined with protein engineering, the catalytic promiscuity of enzymes may broadly extend their usefulness in organic synthesis.

1. Introduction

The realization that many enzymes have broad substrate specificity fueled much of the growth in biocatalysis over the last twenty years, especially in organic synthesis. Identifying a few enzymes that show high stereoselectivity toward a broad range of synthetically useful molecules enabled organic chemists to rapidly develop new synthetic applications for these enzymes.

One current frontier for biocatalysis is reaction specificity. Can a single active site catalyze more than one distinct chemical transformation? Can small changes in the active site enable new chemistry in that active site? Over the last few years evidence has mounted that such catalytic promiscuity exists not just among a few enzymes but is rather common.^[1] This Minireview will focus on catalytic promiscuity related to biocatalysis—enzyme-catalyzed reactions that are or might be

useful in organic synthesis. We will give examples of individual proteins with several catalytic abilities and also examples in which small changes (typically metal-ion substitutions or site-

directed mutagenesis) introduce new catalytic activity. The most successful examples are carbon–carbon bond-forming reactions, oxidations catalyzed by hydrolytic enzymes, and glycosyl transfer reactions.

2. Classifying Catalytic Promiscuity

Catalytic promiscuity in enzymes is the ability of enzyme active sites to catalyze distinctly different chemical transformations. The chemical transformations may differ in the functional group involved, that is, the type of bond formed or cleaved during the reaction and/or may differ in the catalytic mechanism or path of bond making and breaking. Most examples of catalytic promiscuity include both changes. For example, adding a vanadium ion to a phosphatase converts it into an oxidase capable of the enantioselective oxidation of sulfides (this is discussed in more detail in Section 4.2). These two reactions involve different functional groups—breaking the O–O bond in hydrogen peroxide instead of the P–O bond in a phosphate ester. In addition, the reaction mechanism differs significantly because one reaction is a hydrolysis while the other is an oxidation.

In Figure 1 catalytic promiscuity is organized according to differences in the functional groups involved and differences in the mechanisms of catalysis (for selected examples see Table 1). The placement of a reaction on this graph is subjective because the degree of similarity of functional groups and reaction pathways, whose details are likely unknown, is a subjective judgment. Nevertheless, this classi-

[*] Prof. Dr. U. T. Bornscheuer
Institute of Chemistry and Biochemistry
Department of Technical Chemistry and Biotechnology
Greifswald University
Soldmannstrasse 16, 17487 Greifswald (Germany)
Fax: (+49) 3834-86-80066
E-mail: uwe.bornscheuer@uni-greifswald.de
Prof. Dr. R. J. Kazlauskas
University of Minnesota
Department of Biochemistry, Molecular Biology and Biophysics
1479 Gortner Avenue, 174 Gortner Lab, St. Paul, MN 55108 (USA)
Fax: (+1) 612-625-5780
E-mail: rjk@umn.edu

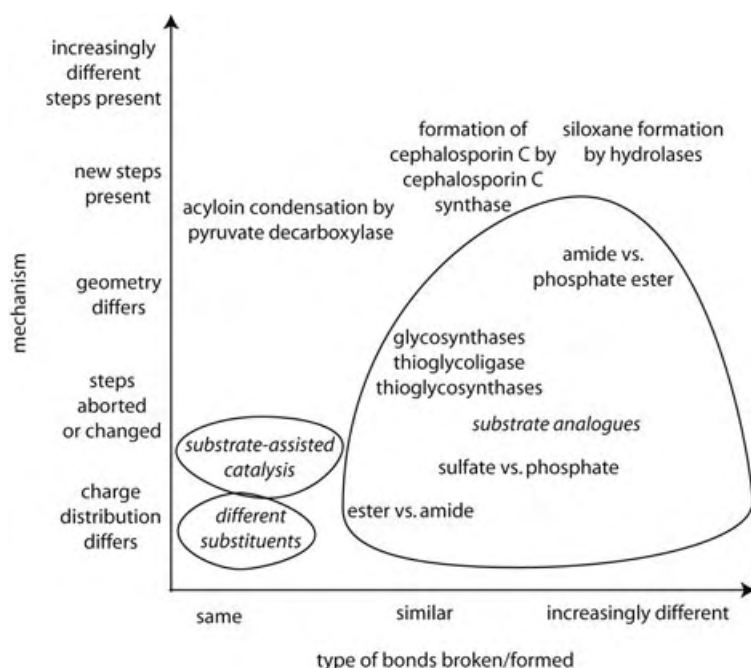


Figure 1. Classifying catalytic promiscuity. Catalytic promiscuity may involve reaction of a different functional group, a change in the catalytic mechanism, or both. The balloons indicate the types of catalytic promiscuity labeled in *italics*. Table 1 lists selected examples, a few of which are also included in this figure.

fication helps distinguish different types of catalytic promiscuity.

The largest group of reactions involves functional group analogues. For example, many proteases also catalyze ester hydrolysis. The bonds broken in the two cases (C–N vs. C–O) differ, but the catalytic mechanism is likely very similar. Several metalloproteases also catalyze the hydrolysis of P–O^[2] or P–F^[3] bonds. Conversely, several esterases cleave the C–N bond in β -lactams,^[4] and proteases can cleave the S–O^[5] in sulfites or the S–N bond in sulfinamides.^[6] On a commercial scale, BASF uses a lipase, which normally cleaves C–O bonds in triglycerides, to resolve amines by enantioselective acylation, which forms a C–N bond.^[7] Asparaginase, which cleaves the primary amide in the side chain of asparagine, also cleaves a nitrile in an analogous substrate, β -cyanoalanine.^[8]

Pyruvate kinase, which catalyzes phosphoryl group transfer, can also catalyze sulfonyl group transfer.^[9] Some phosphatases also catalyze sulfate ester hydrolysis.^[10] Enzyme inhibitors such as phosphonate inhibitors of serine hydrolases will not be included because they rarely involve a complete catalytic turnover.

Other reaction classes must involve changes in mechanism. For example, removal of a catalytically essential amino acid residue dramatically slows the reaction but does not eliminate it. The remaining, less efficient reaction must follow a different path. For example, a Cys-to-Asp mutation in a phosphatase retains some activity.^[11] Another group of reactions involve substrate-assisted catalysis, where the only substrates converted are those that restore the missing functional group so that it can actively participate in catalysis.^[12] In some reactions stereochemistry reveals alternate paths. For example, epoxide hydrolase converts one enantiomer by inversion of the stereocenter, while the other reacts by retention.^[13] These pathways must differ, even though the details are not clear.

Binding proteins can sometimes catalyze reactions, which is clearly a change in mechanism—from no bond breaking to some bond breaking. For example, bovine serum albumin catalyzes Kemp elimination, β -elimination of 3-ketobutyl umbelliferyl ethers (a useful reaction in enzyme assays),^[14] and moderately enantioselective oxidation of amines to amine oxides with sodium periodate.^[15] Myoglobin (an oxygen-carrying iron heme protein) catalyzes slow oxidation in the presence of hydrogen peroxide.^[16] Site-directed mutagenesis to shift the position of the distal histidine (Leu29His/His64Leu) increased the rate of reaction more than 20-fold and enantioselectivity significantly. Oxidation of thioanisole yielded the sulfoxide with 97% *ee*, and oxidation of *cis*- β -methylstyrene gave the epoxide in 99% *ee*.^[17]

All catalytic antibodies are examples of binding molecules that can catalyze a reaction. Interestingly, a catalytic antibody that catalyzes an aldol addition by nucleophilic catalysis (formation of an imine between the substrate carbonyl and a lysine residue) also catalyzes the Kemp elimination, which



Romas Kazlauskas was born in 1956 and studied chemistry at the Massachusetts Institute of Technology (PhD) and Harvard University (postdoc with George Whitesides). He worked at General Electric Company (1985–1988) and McGill University, Montreal, Canada (1988–2003) and is currently an associate professor in Biochemistry, Molecular Biology, and Biophysics at the University of Minnesota, Twin Cities. He is an expert in enantioselective organic synthesis using enzymes.



Uwe Bornscheuer was born in 1964 and studied chemistry at the University of Hannover, Germany, where he graduated with his Diploma in 1990. After receiving his PhD in Chemistry in 1993 at the Institute of Technical Chemistry at the same university, he spent a postdoctoral year at the University of Nagoya, Japan. He then returned to Germany and joined the Institute of Technical Biochemistry at the University of Stuttgart, where he finished his Habilitation in 1998. Since 1999 he has been Professor for Technical Chemistry and Biotechnology at the University of Greifswald. His main research interest is the application of biocatalysts in the synthesis of optically active compounds and in lipid modification.

Table 1: Selected examples of catalytic promiscuity in a single enzyme.

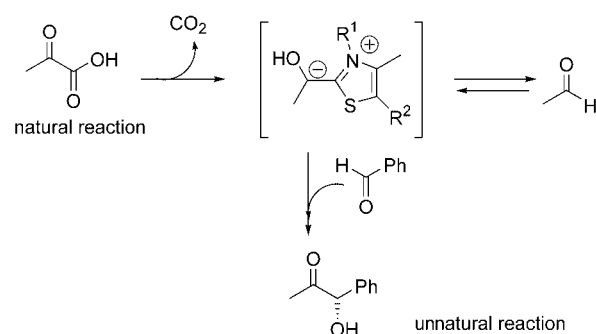
Enzyme	Enzyme class	Normal activity	Promiscuous activity	Ref.
proline aminopeptidase	metallohydrolase (two Mn^{2+} centers)	C–N hydrolysis in proline amides	P–F hydrolysis in diisopropyl fluorophosphate	[3]
aminopeptidase	metallohydrolase (two Zn^{2+} centers)	C–N hydrolysis in amides	P–O hydrolysis in bis- <i>p</i> -nitrophenylphosphate	[2]
pyruvate kinase	metalloenzyme (Mn^{2+} , K^+ , Mg^{2+} centers)	phosphoryl transfer from phosphoenolpyruvate	sulfonyl transfer from sulfoenolpyruvate; also phosphoryl transfer to fluoride, hydroxylamine, or α -hydroxycarboxylic acids	[10]
<i>o</i> -succinylbenzoate synthase	metalloenzyme (Mn^{2+} center)	dehydration of 2-hydroxy-6-succinyl-2,4-cyclohexadiene carboxylate	racemization of <i>N</i> -acylamino acids	[36]
methane monooxygenase	non-heme diiron	hydroxylation of methane	epoxidation, <i>N</i> -oxide formation, dehalogenation, desaturation of benzylic substrates	[48]
plant steroyl acyl carrier protein Δ^9 desaturase	non-heme diiron	desaturation of the C9–C10 link in stearic acid to give oleic acid	sulfoxidation of 9-thia or 10-thia analogues of stearate and the hydroxylation of 9-fluoro analogues	[46, 47]
cephalosporin C synthase	metalloenzyme (non-heme Fe center, 2-oxoglutarate-dependant)	oxidative ring expansion of the five-membered ring to a six-membered, hydroxylation of a methyl group	one of the two normal activities	[43]
lipase, esterase	serine hydrolase	ester hydrolysis	β -lactam hydrolysis	[5]
lipase, chymotrypsin	serine hydrolase	triglyceride or peptide hydrolysis	aldol addition or Michael addition	[27, 30]
subtilisin	serine hydrolase	peptide hydrolysis	sulfinamide hydrolysis	[7]
lipase, trypsin	serine esterase	triglyceride or peptide hydrolysis	oligomerization of $(Si(CH_3)_2(OEt)_2)_n$, dimerization of $Si(CH_3)_3OCH_3$	[32, 33]
pepsin	aspartate hydrolase	amide hydrolysis	sulfite hydrolysis	[4]
asparaginase	Thr-Lys-Asp triad	C–N hydrolysis in asparagine to give aspartate	C≡N hydrolysis in β -cyanoalanine to give aspartate	[9]
epoxide hydrolase	Asp-His-Asp triad	hydrolysis of epoxides with inversion of configuration	hydrolysis of epoxides with retention of configuration	[14]
oxynitrilase	Ser-His-Asp triad	addition of cyanide to aldehydes	addition of cyanide to imines	[35]
aldolase catalytic antibody	Lys	aldol reaction	Kemp elimination	[19]
serine hydroxymethyltransferase	pyridoxal-dependent	transfer of C_β of serine to tetrahydropteroylglutamate	threonine retroaldol reaction, decarboxylation of aminomalonate, racemization of alanine, transamination of alanine and pyruvate	[26]
pyruvate decarboxylase	thiamine-dependent	decarboxylation of pyruvate	acyloin condensation of acetaldehyde and benzaldehyde	[22–24]

requires the lysine to act as a base.^[18] Another catalytic antibody that catalyzes decarboxylation also catalyzes ester hydrolysis.^[19]

In principle, changes in substrate specificity cause subtle changes in the electron distribution in the transition state and could be considered as examples of catalytic promiscuity. However, these differences are usually much smaller than the examples considered here.

3. Catalytic Promiscuity within the Same Protein

A classic example of catalytic promiscuity is yeast pyruvate decarboxylase, which not only decarboxylates pyruvate but also links acetaldehyde and benzaldehyde (a lyase activity) to form (*R*)-phenylacetylcarbinol, a precursor for ephedrine manufacture (Scheme 1).^[20] This acyloin condensation involves an additional step—formation of a carbon–carbon bond—that does not occur in the natural reaction. Although Neuberg and Hirsch discovered this reaction in whole yeast cells in 1921,^[21] researchers more recently identified pyruvate decarboxylase as the responsible enzyme.^[22] This reaction also demonstrates that the alternate



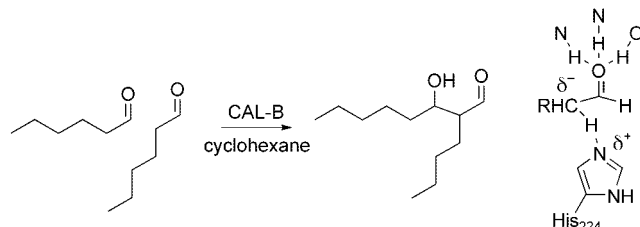
Scheme 1. Pyruvate decarboxylase, a thiamine-dependent enzyme, also catalyzes the enantioselective acyloin condensation of acetaldehyde and benzaldehyde.

substrates (acetaldehyde plus benzaldehyde) can be much larger than the natural substrate (pyruvate only). More recently, a single amino acid substitution in the more stable pyruvate decarboxylase from *Xymomonas mobilis*, which does not catalyze the lyase reaction, added this lyase ability.^[23]

The pyridoxal-dependent enzymes are another classic example of catalytic promiscuity. In most pyridoxal-dependent enzymes the additional functional groups in the active site

direct the aldimine intermediate toward a single pathway.^[24] But in some cases, the aldimine can react by multiple paths. For example, serine hydroxymethyltransferase also catalyzes threonine retroaldol reaction, decarboxylation of aminomalate, and racemization of alanine.^[25] Site-directed mutagenesis of alanine racemase decreased its racemase activity and enhanced its minor transamination activity.^[26]

Another carbon–carbon bond-forming reaction is an aldol addition of hexanal catalyzed by lipase B from *Candida antarctica* (Scheme 2).^[27] Although the reaction was not enan-

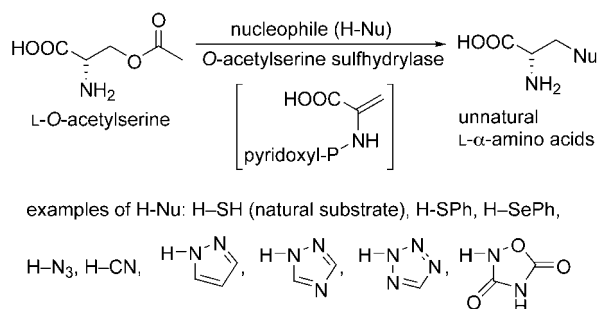


Scheme 2. Lipase B from *Candida antarctica* (CAL-B) catalyzes an aldol addition of hexanal. Although this side reaction is $> 10^5$ times slower than the normal reaction (hydrolysis of triglycerides), it is at least ten times faster than aldol additions catalyzed by a catalytic antibody with aldolase activity. The calculated transition-state structure for enolate formation is on the right.

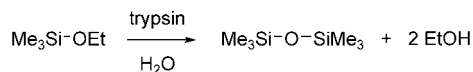
tioselective, the diastereoselectivity differed from that of the spontaneous reaction. The authors hypothesized that the aldol addition did not require the active site serine, and indeed, replacement with alanine (Ser105Ala) increased the aldol addition approximately twofold.

One reaction that forms several new types of bonds is a Michael addition with alternate nucleophiles catalyzed by *O*-acetylserine sulphydrylase (Scheme 3). The normal role of this pyridoxal-containing enzyme is cysteine biosynthesis from *O*-acetylserine by the elimination of acetate to give an amino acrylate intermediate. Michael addition of the nucleophile sulfide to this intermediate yields cysteine. However, other nucleophiles also react including thiols, selenols, azide, cyanide, and some aromatic *N*-heterocycles yielding unnatural amino acids. Thus, besides catalyzing formation of a C–S bond, this enzyme can also catalyze formation of C–Se, C–C, and C–N bonds using a similar mechanism.^[28] Recently, Maier engineered an *E. coli* strain for these unnatural reactions. Normal fermentation produced the starting material *O*-acetylserine and the enzyme; addition of nucleophile yielded the unnatural amino acids in 45–91 % yield.^[29] Lipases also catalyze Michael addition of various nucleophiles to 2-(trifluoromethyl)-propenoic acid.^[30]

Lipase^[31] and trypsin^[32] catalyze the condensation of silanols and alkoxy silanes, respectively, which involves formation of Si–O–Si bonds. Trypsin catalyzed the hydrolysis and condensation of trimethylethoxysilane to hexamethylsiloxane in water (Scheme 4). Al-



Scheme 3. Michael addition of alternate nucleophiles by *O*-acetylserine sulphydrylase to give an amino acrylate intermediate yields unnatural amino acids.

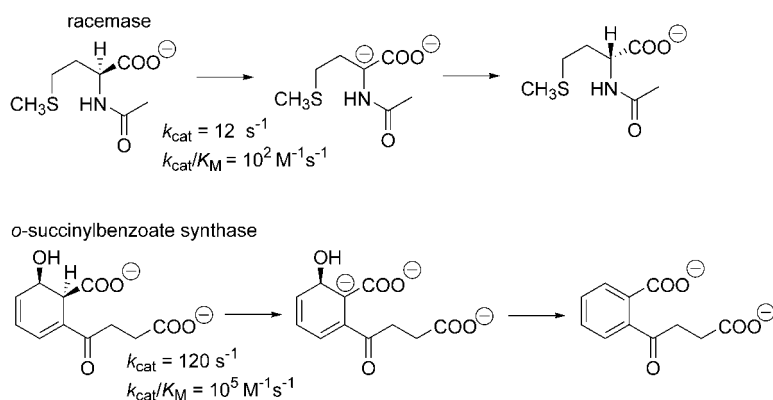


Scheme 4. Trypsin-catalyzed hydrolysis and condensation of trimethylethoxysilane to give hexamethyldisiloxane in water.

though silanols and alkoxy silanes are inherently reactive and can undergo spontaneous condensation or peptide-promoted condensation,^[33] the trypsin-catalyzed reaction was at least ten times faster than the spontaneous reaction. The condensation involves the trypsin active site because addition of trypsin-specific inhibitors eliminated catalysis and because not all trypsins catalyze this reaction: porcine trypsin was effective, but trypsin from Atlantic cod was not.

Oxynitrilase, which catalyzes addition of cyanide to aldehydes, also catalyzes the addition of cyanide to imines with moderate stereoselectivity (3:1–4:1).^[34]

A case of mistaken identity due to catalytic promiscuity is an enzyme originally identified as a *N*-acyl amino acid racemase.^[35] Gerlt and co-workers recently discovered that this enzyme is 1000 times more efficient as a catalyst for a dehydration to form *o*-succinylbenzoate, suggesting that succinylbenzoate formation is its true role (Scheme 5). By changing the *N*-acyl amino acid from *N*-acetyl methionine (the previous best substrate for racemase activity) to *N*-succinyl phenylglycine, which better resembles the succinyl-

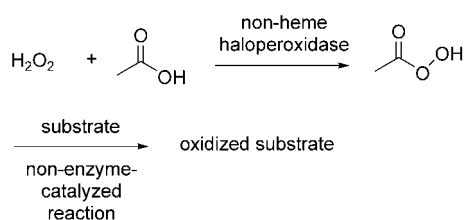


Scheme 5. An enzyme discovered as an *N*-acyl amino acid racemase is 1000-fold more efficient in the dehydration to form *o*-succinylbenzoate. Both reaction mechanisms involve a similar anionic intermediate.

benzoate precursor, the efficiency of the racemization reaction increased 1000-fold, making it similar to the succinylbenzoate reaction.

Esterases and lipases, which catalyze hydrolysis of esters, have overlapping catalytic activities with non-heme haloperoxidases, which catalyze oxidations by hydrogen peroxide via a peroxycarboxylic acid (Scheme 6). For example, esterase from *Pseudomonas fluorescens*,^[36] a lactonase,^[37] and many lipases,^[38] show low peroxidase activity in the presence of a carboxylic acid and hydrogen peroxide. Conversely, at least one haloperoxidase shows low esterase activity.^[39]

The overlapping catalytic activity of these enzymes stems from common transition states and acyl enzyme intermediates in both reactions (Scheme 7). In esterases, the acyl enzyme

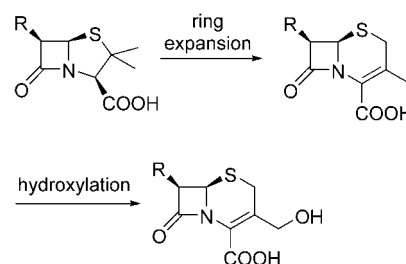


Scheme 6. Non-heme haloperoxidases catalyze the formation of a peroxycarboxylic acid by means of an esterase-like mechanism. The subsequent oxidation of substrates with the peracid may not be enzyme catalyzed.

intermediate undergoes hydrolysis, while in haloperoxidases, it undergoes perhydrolysis to yield a peroxycarboxylic acid. The subsequent oxidation of halide to hypohalous acid by this peroxycarboxylic acid may not be enzyme catalyzed. In spite of this overlap, esterases and lipases are more efficient at ester hydrolysis, while haloperoxidases are more efficient at generating peroxycarboxylic acids. Detailed structural analysis of a related haloperoxidase^[40] and an esterase^[41] showed only

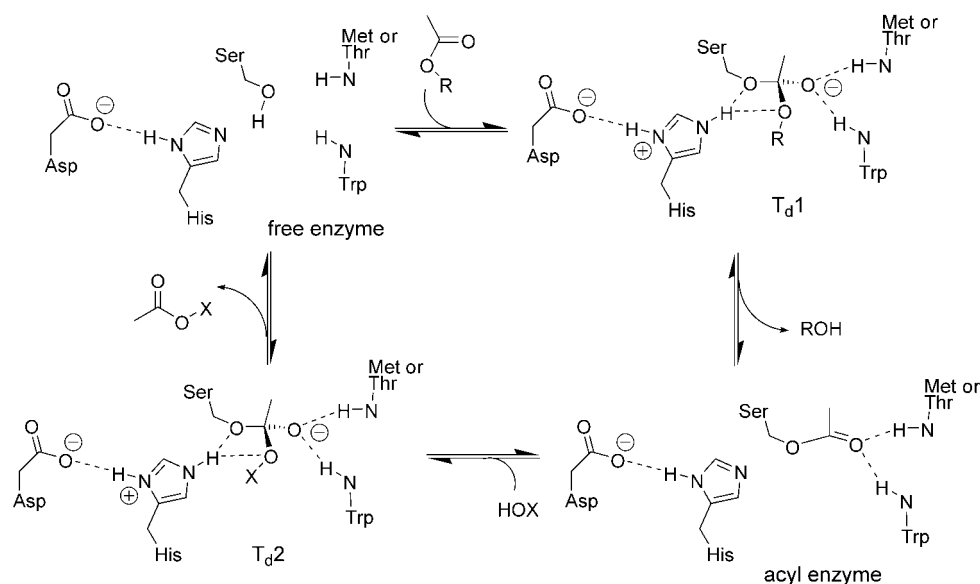
subtle differences in the two active sites and did not reveal why one is a better haloperoxidase and the other a better esterase.

Catalytic promiscuity has a natural role in the biosynthesis of several secondary metabolites. For example, the synthesis of the antibiotic cephalosporin C in eukaryotes uses a single enzyme with a single active site to catalyze two different oxidative reactions—an oxidative ring expansion of the five-membered ring to a six-membered and a hydroxylation of a methyl group (Scheme 8). Single amino acid substitutions can inactivate either activity.^[42] In contrast cephalosporin synthesis in prokaryotes uses separate enzymes for the two steps, but both of these enzymes are closely related to the bifunctional one in eukaryotes.



Scheme 8. A non-heme iron(II) and 2-oxoglutarate-dependent cephalosporin C synthase in eukaryotes catalyzes two different catalytic steps with the same active site.

These non-heme iron(II) and 2-oxoglutarate-dependent oxidative enzymes can even have trifunctional roles. Gibberellin 20-oxidase catalyzes three successive oxidations of the C20 methyl group to the alcohol, aldehyde and finally to the carboxylate.^[43] Clavaminate synthase catalyzes a hydroxylation, an oxidative cyclization, and desaturation.^[44]



Scheme 7. Mechanisms for ester hydrolysis and peroxidation by non-heme haloperoxidases both involve an acyl enzyme intermediate. In esterases (X=H), the H_2O attacks this intermediate to complete a hydrolysis. In haloperoxidases (X=OH), the acyl enzyme intermediate comes from acetate added to the reaction mixture. Hydrogen peroxide attacks this intermediate to form a peracid. R=Ph for esterase, H for haloperoxidase.

Other non-heme diiron oxidative enzymes also catalyze a wide range of oxidations. For example, the plant steroyl acyl carrier protein Δ^9 desaturase normally catalyzes the desaturation of stearic acid to oleic acid but also catalyzes sulfoxidation of 9-thia or 10-thia stearate analogues^[45] and the hydroxylation of 9-fluoro analogues.^[46] Methane monooxygenase, another non-heme diiron enzyme, catalyzes methane hydroxylation as well as a wide range of other oxidations including epoxidation, N-oxide formation, dehalogenation, and desaturation of benzylic substrates.^[47] Degradation enzymes, such as cytochrome P450 enzymes, which contain a heme iron, also catalyze a wide range of oxidations.

4. Catalytic Promiscuity within Modified Proteins

4.1. Natural Evolution of New Catalytic Activity

Divergent evolution is a natural process that creates different species from a common ancestor. This process also works on a molecular scale to create enzymes with new catalytic activities. New enzymatic activities arise by gene duplication followed by evolution of new activity for the copy.^[48] Two examples of divergent evolution are the α/β -hydrolase-fold superfamily^[49] and the enolase superfamily.^[50] The α/β -hydrolase-fold enzymes all involve nucleophilic catalysis but include a wide range of substrates and reaction types including ester or peptide hydrolysis (serine nucleophile), dehalogenase, and epoxide hydrolase (aspartate nucleophile). The enolase enzymes have similar active sites and catalyze divalent-metal-assisted general-base-catalyzed removal of a proton α to a carboxylic acid to form an enolic intermediate. Examples of different reactions catalyzed by the enolase superfamily include racemization (mandelate, *N*-acyl amino acids) and β -eliminations (*o*-succinyl benzoate synthase). An example of a “misassigned” enolase enzyme was mentioned in Section 3.

One example of a surprisingly rapid natural evolution of new catalytic activity is an atrazine chlorohydrolase (Scheme 9).^[51] Researchers initially found that atrazine, an herbicide widely used since the late 1950s, did not readily degrade in soils, but since 1993 a number of groups have reported rapid degradation. The key enzyme in this biodegradation—atrazine chlorohydrolase, which cleaves the C–Cl bond—differs by only eight amino acid substitutions from melamine hydrolase, which catalyzes the hydrolysis of a C–N bond in melamine. Melamine hydrolase has low atrazine

chlorohydrolase activity, but the new enzyme has no detectable melamine hydrolase activity. Directed evolution further expanded the substrate range of this atrazine chlorohydrolases to include C–S and C–O bond cleavage.^[52] Another example of rapid natural evolution is the evolution of a phosphotriesterase that degrades the insecticide paraoxon.^[53]

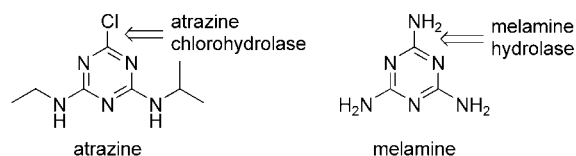
4.2. Changing the Metal Ion

Metal substitutions can also change catalytic activity. One of the earliest examples from 1976 shows that replacement of the Zn^{2+} ion in the active site of a carboxypeptidase with a Cu^{2+} ion converted this peptidase into a slow oxidase.^[54] Replacement of the Zn^{2+} ion in the active site of thermolysin with much larger ions such as tungstate, molybdate, and selenate created enzymes that catalyze oxidation of thioethers to sulfoxides with hydrogen peroxide.^[55] Replacing the active-site serine in subtilisin with selenomethionine resulted in peroxidase activity.^[56]

Other examples of overlapping catalytic activity are acid phosphatases and vanadate-dependent haloperoxidases.^[57,58] The amino acid sequence, three-dimensional structure, and active site are similar in both classes of enzymes. Vanadate binds to the same site as a phosphate ester presumably because it readily adopts a five-coordinate structure that resembles the transition state for phosphate ester hydrolysis. The vanadate ion catalyzes peroxidation by binding peroxide to the vanadium center, thereby increasing its electrophilicity. Further support for the similarity of the two active sites is the ability of vanadate to inhibit phosphatases and the ability of phosphate to inactivate vanadate-dependent haloperoxidases by displacing the vanadate. This exchange of active sites also exchanges the catalytic activity of these two classes of enzymes. Several acid phosphatases show low haloperoxidase activity upon addition of vanadate,^[59] and conversely, apohaloperoxidases show low phosphatase activity.^[60] Sheldon and co-workers reported an enantioselective oxidation of sulfides to sulfoxides using a vanadate-substituted phytase.^[61] However, the altered enzymes were much less effective catalysts than the true enzyme: the turnover numbers were 10^3 – 10^4 times lower for the haloperoxidase activity of a vanadate-containing phosphatase than for a true haloperoxidase, or for the phosphatase activity of apo-haloperoxidase as compared to that of a true phosphatase. This large difference shows that each enzyme is optimized for the reaction it catalyzes. However, like the esterase/non-heme haloperoxidase case mentioned above, even with the available X-ray crystal structures, it is not clear which structural features are responsible for the different optimized activity.

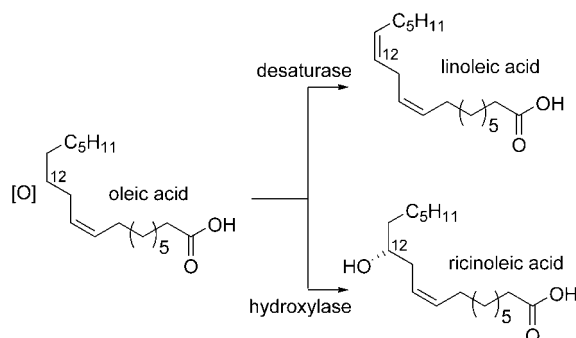
4.3. Engineering of Enzymes

A number of groups mimicked divergent evolution by using site-directed mutagenesis. By comparing related enzymes with different catalytic activity, they identified substitutions that change the catalytic activity. Making these changes in one of the enzymes altered the catalytic activity.



Scheme 9. An atrazine chlorohydrolase recently evolved naturally from a melamine hydrolase. The starting melamine hydrolase (C–N bond cleavage) has low atrazine chlorohydrolase activity (C–Cl bond cleavage), but the new atrazine chlorohydrolase has lost its melamine hydrolase activity.

For example, four amino acid substitutions in a fatty acid desaturase by their equivalents in a fatty acid hydroxylase yielded an efficient hydroxylase (Scheme 10).^[62] In another

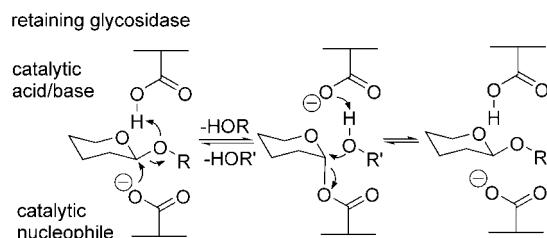


Scheme 10. Both desaturases and hydroxylases have a diiron center and oxidize C12 of oleic acid. Mutating four amino acids in a desaturase turned it into a hydroxylase.

example, single amino acid changes in L-Ala-D/L-Glu epimerase introduced *ortho*-succinoyl benzoate synthase activity or muconate-lactonizing enzyme activity.^[63] Within the family of glutathione transferases, mutations changed a transferase that catalyzes a Michael addition into one that catalyzes a nucleophilic aromatic substitution.^[64] Similarly, a glutathione transferase with peroxidase activity gained steroid isomerase activity after five mutations to mimic the active site in a related steroid isomerase.^[65] Mutations within an oxidosqualene cyclase changed the site of proton loss, thereby yielding different steroids.^[66] A much more challenging task is converting a noncatalytic protein into a dehydratase with low activity.^[67]

4.4. Glycosynthases, Thioglycoligases, and Thioglycosynthases

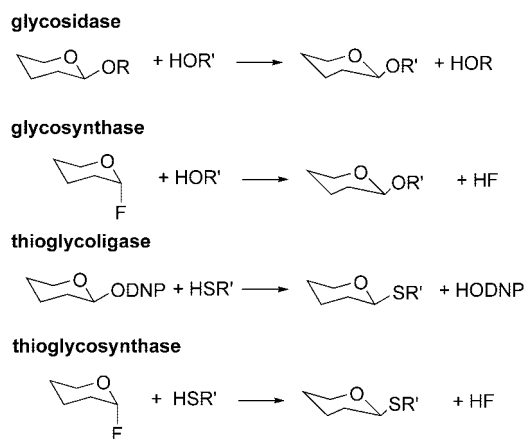
Retaining β -glycosidases normally catalyze the hydrolysis of β -glycosidic links, but they also catalyze glycoside exchange under conditions of low water concentration. The reaction involves a starting β -glycoside (sugar-OR) reacting with an incoming nucleophile (HOR', Scheme 11). The incoming nucleophile is water in the case of hydrolysis and a second glycoside in the case of glycoside exchange. Retaining



Scheme 11. Glycoside exchange using retaining β -glycosidases involves a double displacement. A glycosyl donor (β -sugar-OR) forms an α -linked glycosyl enzyme, which then reacts with an incoming nucleophile or acceptor (HOR') to make a new β -glycosidic link (sugar-OR').

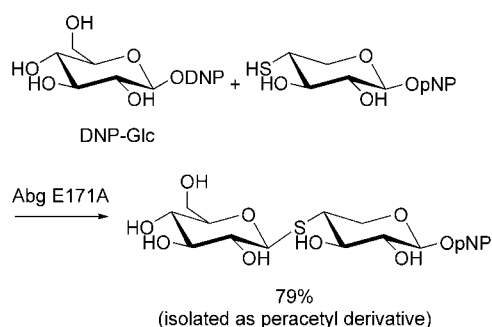
glycosidases use a double displacement mechanism with a catalytic acid/base and a catalytic nucleophile. In the initial step an α -linked covalent intermediate is formed by attack of the catalytic nucleophile on the starting β -glycoside. The catalytic acid assists this step by protonating the leaving group. In the second step this covalent intermediate is released by the catalytic-base-assisted attack of the incoming nucleophile—water or a new glycoside.

By disabling key steps in the mechanism, Withers and colleagues made three new catalysts (Scheme 12). The first,



Scheme 12. Disabling key mechanistic steps in a retaining β -glycosidase creates new catalytic activities. Removal of the catalytic nucleophile creates a glycosynthase where only α -glycosyl fluorides react presumably by a single displacement mechanism. Removal of the catalytic acid/base creates a thioglycoligase (only strong incoming nucleophiles such as thiols react), and removal of both catalytic nucleophile and catalytic acid/base creates a thioglycosynthase (only α -glycosyl fluorides and strong incoming nucleophiles react). DNP = 2,4-dinitrophenyl.

glycosynthase, results upon removing the catalytic nucleophile (e.g., a Glu-to-Ala mutation).^[68] This removal prevents formation of the key covalent intermediate, dramatically altering the mechanism. Normal glycosides no longer react, but α -glycosyl fluorides do react, likely by a direct displacement mechanism. Glycosynthases, like the starting enzyme, form β -glycoside links. However, glycosynthases no longer catalyze hydrolysis of product, which is a nonactivated glycoside, and thus give higher yields. Five different glycosynthases have been reported with differing glycosyl fluoride specificity and differing regioselectivity (formation of β -1,3 vs. β -1,4 links). The second type of new catalyst, thioglycoligase, results upon removing the catalytic acid/base.^[69] One role of this catalytic acid/base is activation of the incoming nucleophile. Absence of this activator precludes reaction with normal incoming nucleophiles and requires strong nucleophiles such as thiols. Introducing single amino acid mutations into β -glycosidases from *Agrobacterium* sp. Abg (mutation: E171A) created a variant that formed S-glycosidic linkages in high yield (Scheme 13). The wild-type enzyme gave no product, possibly due to steric hindrance caused by the larger sulfur atom. Finally, removing both the catalytic nucleophile



Scheme 13. A thioglycosylase lacking the catalytic acid/base no longer catalyzes hydrolysis. However, using an activated glycosyl donor overcomes the lack of a proton donor for the leaving group, and using a nucleophilic thiol overcomes the lack of base to activate the incoming nucleophile. Thus, the mutant now catalyzes formation of an S-glycosidic link.

and the catalytic acid/base creates a thioglycosynthase, which requires both an α -glycosyl fluoride and a thiol acceptor.^[70]

5. Summary and Outlook

Catalytic promiscuity in enzymes is more common than generally appreciated. The dense collection of catalytic groups in an active site can accept alternate functional groups in the substrate and follow alternate reaction pathways. Small modifications in an active site can further dramatically expand the range of alternative pathways. In most, but not all, cases these alternate reactions are slower than the natural reactions. We hope that this review will encourage others to both search more extensively for catalytic promiscuity in existing enzymes and to use the current tools of protein engineering and directed evolution to extend the useful applications of enzymes.

We thank Bernhard Hauer (BASF, Ludwigshafen, Germany) for helpful suggestions and discussion. U.T.B. thanks the Fonds der Chemischen Industrie (Frankfurt, Germany) for financial support.

Received: April 22, 2004

Published Online: November 2, 2004

- [1] Reviews: a) S. D. Copley, *Curr. Opin. Chem. Biol.* **2003**, 7, 265–272; b) A. Yarnell, *Chem. Eng. News* **2003**, 81, 33–35; c) P. J. O'Brien, D. Herschlag, *Chem. Biol.* **1999**, 6, 91–105.
- [2] a) H. I. Park, L.-J. Ming, *Angew. Chem.* **1999**, 111, 3097–3100; *Angew. Chem. Int. Ed.* **1999**, 38, 2914–2916; b) A. Ercan, H. I. Park, L.-J. Ming, *Chem. Commun.* **2000**, 2501–2502.
- [3] T. C. Cheng, S. P. Harvey, G. L. Chen, *Appl. Environ. Microbiol.* **1996**, 62, 1636–1641.
- [4] PLE: M. Jones, M. I. Page, *J. Chem. Soc. Chem. Commun.* **1991**, 316–317; PFL: R. Brieva, J. Z. Crich, C. J. Sih, *J. Org. Chem.* **1993**, 58, 1068–1075; CAL-B: a) W. Adam, P. Groer, H.-U. Humpf, C. R. Saha-Möller, *J. Org. Chem.* **2000**, 65, 4919–4922; b) E. Forró, F. Fülöp, *Org. Lett.* **2003**, 5, 1209–1212; c) S. Park, E. Forró, H. Grewal, F. Fülöp, R. J. Kazlauskas, *Adv. Synth. Catal.* **2003**, 345, 986–995.
- [5] T. W. Reid, D. Fahrney, *J. Am. Chem. Soc.* **1967**, 89, 3941–3943.
- [6] P. F. Mugford, V. P. Magloire, R. J. Kazlauskas, unpublished results.
- [7] Review: M. Breuer, K. Dittrich, T. Habicher, B. Hauer, M. Kessler, R. Stuermer, T. Zelinski, *Angew. Chem.* **2004**, 116, 806–843; *Angew. Chem. Int. Ed.* **2004**, 43, 788–824.
- [8] R. C. Jackson, R. E. Handschumacher, *Biochemistry* **1970**, 9, 3585–3590.
- [9] J. A. Peliska, M. H. O'Leary, *Biochemistry* **1989**, 28, 1604–1611.
- [10] P. J. O'Brien, D. Herschlag, *J. Am. Chem. Soc.* **1998**, 120, 12369–12370.
- [11] Y. Romsicki, G. Scapin, V. Beaulieu-Audy, S. Patel, J. W. Becker, B. P. Kennedy, E. Asante-Appiah, *J. Biol. Chem.* **2003**, 278, 29009–29015.
- [12] A recent example in biocatalysis: A. Magnusson, K. Hult, M. Holmquist, *J. Am. Chem. Soc.* **2001**, 123, 4354–4355.
- [13] a) W. Kroutil, M. Mischitz, K. Faber, *J. Chem. Soc. Perkin Trans. 1* **1997**, 3629–3636; b) K. Faber, W. Kroutil, *Tetrahedron: Asymmetry* **2002**, 13, 377–382.
- [14] a) F. Hoffelder, A. J. Kirby, D. S. Tawfik, *Nature* **1996**, 383, 60–62; b) G. Klein, J.-L. Reymond, *Bioorg. Med. Chem. Lett.* **1998**, 8, 1113–1116.
- [15] S. Colonna, N. Gaggero, J. Drabowicz, P. Lyzwa, M. Mikolajczyk, *Chem. Commun.* **1999**, 1787–1788.
- [16] D. C. Levinger, J.-A. Stevenson, L.-L. Wong, *J. Chem. Soc. Chem. Commun.* **1995**, 2305–2306.
- [17] S. Ozaki, T. Matsui, Y. Watanabe, *J. Am. Chem. Soc.* **1996**, 118, 9784–9785; S. Ozaki, H.-J. Yang, T. Matsui, Y. Goto, Y. Watanabe, *Tetrahedron: Asymmetry* **1999**, 10, 183–192.
- [18] L. C. James, D. S. Tawfik, *Protein Sci.* **2001**, 10, 2600–2607.
- [19] A. C. Backes, K. Hotta, D. Hilvert, *Helv. Chim. Acta* **2003**, 86, 1167–1174.
- [20] Review: O. P. Ward, A. Singh, *Curr. Opin. Biotechnol.* **2000**, 11, 520–526.
- [21] C. Neuberger, J. Hirsch, *Biochem. Z.* **1921**, 115, 282–310.
- [22] a) S. Bringer-Meyer, H. Sahm, *Biocatalysis* **1988**, 1, 321–331; b) D. H. G. Crout, H. Dalton, D. W. Hutchinson, M. Miyagoshi, *J. Chem. Soc. Perkin Trans. 1* **1991**, 1329–1334.
- [23] G. Goetz, P. Iwan, B. Hauer, M. Breuer, M. Pohl, *Biotechnol. Bioeng.* **2001**, 74, 317–325.
- [24] Review: H. Hayashi, *J. Biochem.* **1995**, 118, 463–473.
- [25] R. Contestabile, A. Paiardini, S. Pascarella, M. L. di Salvo, S. D'Aguzzo, F. Bossa, *Eur. J. Biochem.* **2001**, 268, 6508–6525.
- [26] G.-Y. Yow, A. Watanabe, T. Yoshimura, N. Esaki, *J. Mol. Catal. B: Enzym.* **2003**, 23, 311–319.
- [27] C. Branneby, P. Carlqvist, A. Magnusson, K. Hult, T. Brinck, P. Berglund, *J. Am. Chem. Soc.* **2003**, 125, 874–875.
- [28] a) F. Ikegami, I. Murakoshi, *Phytochemistry* **1994**, 35, 1089–1104; b) D. H. Flint, J. F. Tuminello, T. J. Miller, *J. Biol. Chem.* **1996**, 271, 16053–16067.
- [29] T. H. P. Maier, *Nat. Biotechnol.* **2003**, 21, 422–427.
- [30] T. Kitazume, T. Ikeya, K. Murata, *J. Chem. Soc. Chem. Commun.* **1986**, 1331–1333.
- [31] H. Nishino, T. Mori, Y. Okahata, *Chem. Commun.* **2002**, 2684–2685.
- [32] A. R. Bassindale, K. F. Brandstadt, T. H. Lane, P. G. Taylor, *J. Inorg. Biochem.* **2003**, 96, 401–406.
- [33] N. Kröger, S. Lorenz, E. Brunner, M. Sumper, *Science* **2002**, 298, 584–586.
- [34] T. Lee, Y. Ahn, *Bull. Korean Chem. Soc.* **2002**, 23, 1490–1492.
- [35] a) D. R. J. Palmer, J. B. Garrett, V. Sharma, R. Meganathan, P. C. Babbitt, J. A. Gerlt, *Biochemistry* **1999**, 38, 4252–4258; b) E. A. Taylor Ringia, J. B. Garrett, J. B. Thoden, H. M. Holden, I. Rayment, J. A. Gerlt, *Biochemistry* **2004**, 43, 224–229.
- [36] I. Pelletier, J. Altenbuchner, *Microbiology* **1995**, 141, 459–468.
- [37] M. Kataoka, K. Honda, S. Shimizu, *Eur. J. Biochem.* **2000**, 267, 3–10.

- [38] a) F. Björkling, H. Frykman, S. E. Godtfredsen, O. Kirk, *Tetrahedron* **1992**, 48, 4587–4592; b) O. Kirk, L. S. Conrad, *Angew. Chem.* **1999**, 111, 1031–1033; *Angew. Chem. Int. Ed.* **1999**, 38, 977–979.
- [39] I. Pelletier, J. Altenbuchner, *Microbiology* **1995**, 141, 459–468.
- [40] B. Hofmann, S. Tölzer, S. I. Pelletier, J. Altenbuchner, K.-H. van Pée, H. J. Hecht, *J. Mol. Biol.* **1998**, 279, 889–900.
- [41] J. D. Cheeseman, A. Tocilj, S. Park, J. D. Schrag, R. J. Kazlauskas, *Acta Crystallogr. D* **2004**, 60(7), 1237–1243.
- [42] M. D. Lloyd, S. J. Lipscomb, K. S. Hewitson, C. M. H. Hensgens, J. E. Baldwin, C. J. Schofield, *J. Biol. Chem.* **2004**, 279, 15420–15426.
- [43] T. Lange, P. Hedden, J. E. Graebe, *Proc. Natl. Acad. Sci. USA* **1994**, 91, 8552–8556.
- [44] M. D. Lloyd, K. D. Merritt, V. Lee, T. J. Sewell, B. Wha-Son, J. E. Baldwin, C. J. Schofield, S. W. Elson, K. H. Baggaley, N. H. Nicholson, *Tetrahedron* **1999**, 55, 10201–10220.
- [45] B. Behrouzian, P. H. Buist, J. Shanklin, *Chem. Commun.* **2001**, 401–402.
- [46] a) B. Behrouzian, B. Dawson, P. H. Buist, J. Shanklin, *Chem. Commun.* **2001**, 765–766; b) B. Behrouzian, C. K. Savile, B. Dawson, P. H. Buist, J. Shanklin, *J. Am. Chem. Soc.* **2002**, 124, 3277–3283.
- [47] Y. Jin, J. D. Lipscomb, *J. Biol. Inorg. Chem.* **2001**, 6, 717–725.
- [48] J. A. Gerlt, P. C. Babbitt, *Annu. Rev. Biochem.* **2001**, 70, 209–246.
- [49] a) D. L. Ollis, E. Cheah, M. Cygler, B. Dijkstra, F. Frolow, S. M. Franken, M. Harel, S. J. Remington, I. Silman, J. Schrag, J. L. Sussman, K. H. G. Verschuere, A. Goldman, *Protein Eng.* **1992**, 5, 197–211; b) M. Holmquist, *Curr. Protein Pept. Sci.* **2000**, 1, 209–235.
- [50] P. C. Babbitt, M. S. Hasson, J. E. Wedekind, D. R. J. Palmer, W. C. Barrett, G. H. Reed, I. Rayment, D. Ringe, G. L. Kenyon, J. A. Gerlt, *Biochemistry* **1996**, 35, 16489–16501.
- [51] J. L. Seffernick, L. P. Wackett, *Biochemistry* **2001**, 40, 12747–12750.
- [52] S. Raillard, A. Krebber, Y. Chen, J. E. Ness, E. Bermudez, R. Trinidad, R. Fullem, C. Davis, M. Welch, J. Seffernick, L. P. Wackett, W. P. C. Stemmer, J. Minshull, *Chem. Biol.* **2001**, 8, 891–898.
- [53] T. S. Scanlan, R. C. Reid, *Chem. Biol.* **1995**, 2, 71–75.
- [54] K. Yamamura, E. T. Kaiser, *J. Chem. Soc. Chem. Commun.* **1976**, 830–831.
- [55] M. Bakker, F. van Rantwijk, R. A. Sheldon, *Can. J. Chem.* **2002**, 80, 622–625.
- [56] I. M. Bell, M. L. Fisher, Z. P. Wu, D. Hilvert, *Biochemistry* **1993**, 32, 3754–3762.
- [57] a) A. F. Neuwald, *Protein Sci.* **1997**, 6, 469–472; b) J. Littlechild, E. Garcia-Rodriguez, A. Dalby, M. Isupov, *J. Mol. Recognit.* **2002**, 15, 291–296.
- [58] W. Hemrika, R. Renirie, H. L. Dekker, P. Barnett, R. Wever, *Proc. Natl. Acad. Sci. USA* **1997**, 94, 2145–2149.
- [59] N. Tanaka, V. Dumay, Q. Liao, A. J. Lange, R. Wever, *Eur. J. Biochem.* **2002**, 269, 2162–2167.
- [60] R. Renirie, W. Hemrika, R. Wever, *J. Biol. Chem.* **2000**, 275, 11650–11657.
- [61] a) F. van de Velde, L. Könemann, F. van Rantwijk, R. A. Sheldon, *Chem. Commun.* **1998**, 1891–1892; b) F. van de Velde, L. Könemann, F. van Rantwijk, R. A. Sheldon, *Biotechnol. Bioeng.* **2000**, 67, 87–96.
- [62] a) P. Broun, J. Shanklin, E. Whittle, C. Somerville, *Science* **1998**, 282, 1315–1317; b) J. A. Broadwater, E. Whittle, J. Shanklin, *J. Biol. Chem.* **2002**, 277, 15613–15620.
- [63] D. M. Z. Schmidt, E. C. Mundorff, M. Dojka, E. Bermudez, J. E. Ness, S. Govindarajan, P. C. Babbitt, J. Minshull, J. A. Gerlt, *Biochemistry* **2003**, 42, 8387–8393.
- [64] L. O. Nilsson, A. Gustafsson, B. Mannervik, *Proc. Natl. Acad. Sci. USA* **2000**, 97, 9408–9412.
- [65] P. L. Pettersson, A.-S. Johansson, B. Mannervik, *J. Biol. Chem.* **2002**, 277, 30019–30022.
- [66] a) E. A. Hart, L. Hua, L. B. Darr, W. K. Wilson, J. Pang, S. P. T. Matsuda, *J. Am. Chem. Soc.* **1999**, 121, 9887–9888; b) M. M. Meyer, R. Xu, S. P. T. Matsuda, *Org. Lett.* **2002**, 4, 1395–1398.
- [67] A. E. Nixon, S. M. Firestone, F. G. Salinas, S. J. Benkovic, *Proc. Natl. Acad. Sci. USA* **1999**, 96, 3568–3571.
- [68] S. J. Williams, S. G. Withers, *Aust. J. Chem.* **2002**, 55, 3–12; for earlier work on converting an inverting enzyme to a retaining enzyme see: R. Kuroki, L. H. Weaver, B. M. Matthews, *Nat. Struct. Biol.* **1995**, 2, 1007–1011.
- [69] M. Jahn, J. Marles, R. A. J. Warren, S. G. Withers, *Angew. Chem.* **2003**, 115, 366–368; *Angew. Chem. Int. Ed.* **2003**, 42, 352–354.
- [70] M. Jahn, H. Chen, J. Muellegger, J. Marles, R. A. J. Warren, S. G. Withers, *Chem. Commun.* **2004**, 274–275.

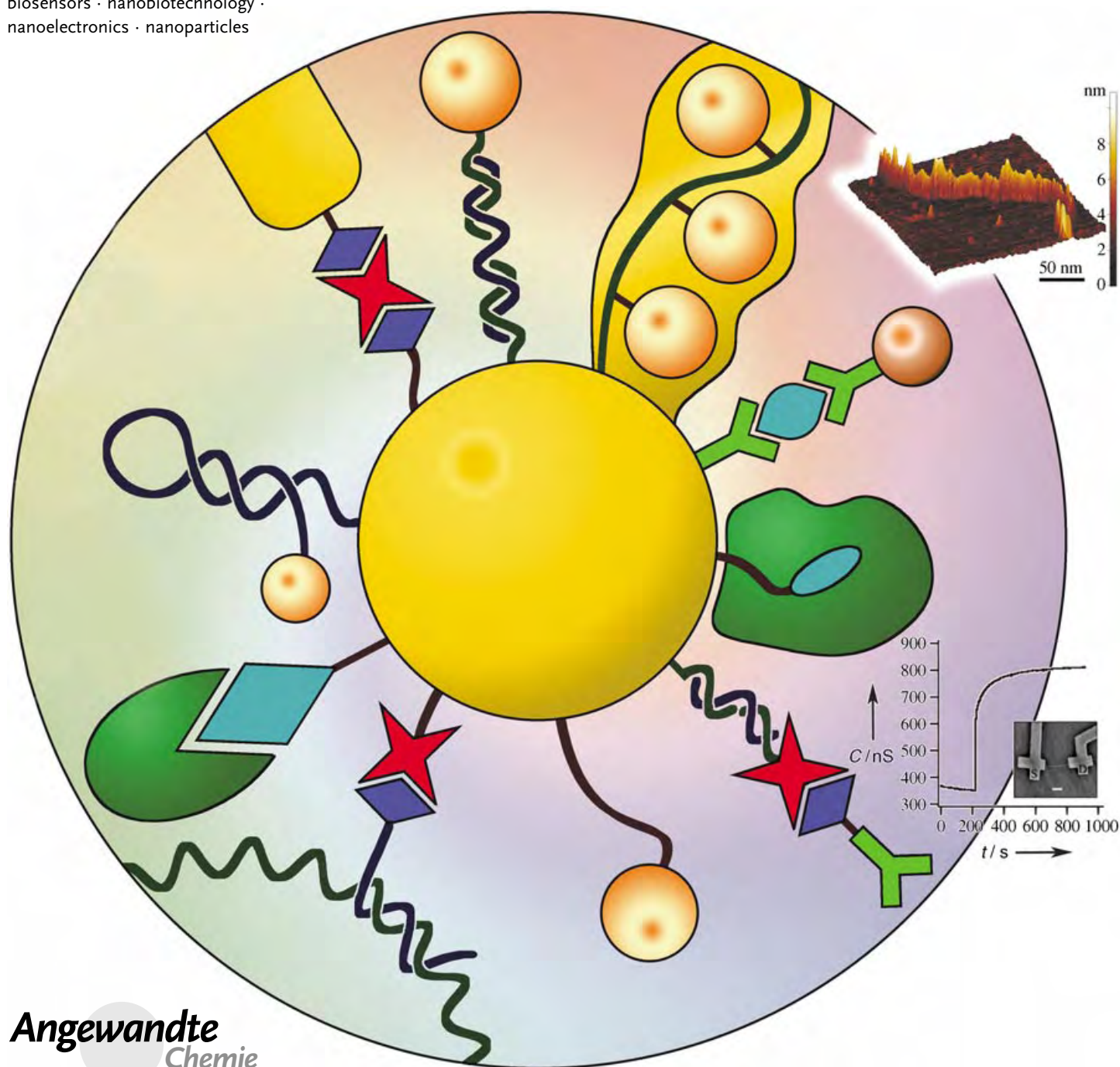
Nanobiotechnology

Integrated Nanoparticle–Biomolecule Hybrid Systems: Synthesis, Properties, and Applications

Eugenii Katz and Itamar Willner*

Keywords:

biosensors · nanobiotechnology ·
nanoelectronics · nanoparticles



Angewandte
Chemie

Nanomaterials, such as metal or semiconductor nanoparticles and nanorods, exhibit similar dimensions to those of biomolecules, such as proteins (enzymes, antigens, antibodies) or DNA. The integration of nanoparticles, which exhibit unique electronic, photonic, and catalytic properties, with biomaterials, which display unique recognition, catalytic, and inhibition properties, yields novel hybrid nanobiomaterials of synergetic properties and functions. This review describes recent advances in the synthesis of biomolecule–nanoparticle/nanorod hybrid systems and the application of such assemblies in the generation of 2D and 3D ordered structures in solutions and on surfaces. Particular emphasis is directed to the use of biomolecule–nanoparticle (metallic or semiconductive) assemblies for bioanalytical applications and for the fabrication of bioelectronic devices.

1. Introduction

The unique electronic, optical, and catalytic properties of metal and semiconductor nanoparticles (1–200 nm), together with the different methods available for the preparation of nanoparticles of controlled shape and size, provide exciting building blocks for nanoscale assemblies, structures, and devices. Nobel Laureate Richard Feynman in his visionary lecture “*There is plenty of room at the bottom*”^[1] inspired the concepts for the rapidly exploding research topic of nanotechnology. Although the term “nanotechnology” had not appeared on the horizon, Feynman said: “What I want to talk about is the problem of manipulating and controlling things on a small scale... What I have demonstrated is that there is room—that you can decrease the size of things in a practical way... I will not discuss how we are going to do it, but only what is possible in principle... We are not doing it simply because we haven’t yet gotten around to it.” Four decades later, scientists have learnt that the manipulation of atoms, molecules, and clusters on surfaces is feasible and that new fundamental physics governs the properties of nanoobjects.

The miniaturization of structures by conventional^[2] and electron-beam lithography^[3] is reaching the theoretical limits of about 50 nm. For the further miniaturization of chemical objects, alternative approaches must be developed. Following Feynman’s vision, one may employ atoms and molecules as building units for the “bottom-up” assembly and construction of architectures with nanometer dimensions. Nanoparticles (NPs) that consist of metals^[4] (e.g. Au, Ag, Pt, and Cu) or semiconductors^[5] (e.g. PbS, Ag₂S, CdS, CdSe, and TiO₂) seem to be attractive units for the engineering of such structures. The unique electrical properties of these particles^[6] as well as their optical and photophysical features,^[7] such as size-controlled plasmon absorbance, photonic electron–hole pair generation, and fluorescence, allow the particles to be addressed by means of electronic and photonic signals.

A variety of synthetic methodologies for the preparation of NPs within a narrow size distribution are available.^[4] Often,

the NPs are prepared by “wet chemistry” procedures, in which clusters of metal atoms or semiconductor molecules are formed in the presence of a surface-capping ligand. This capping ligand binds to the metal/semiconductor clusters, prevents aggregation of the particles into bulk material, and controls the final dimensions of the NPs. Many capping systems are available: hydrophobic monolayers,^[8] positively or negatively charged hydrophilic monolayers,^[9] and polymer layers.^[10] Association of molecular units to the NPs introduces chemical functionalities that can provide recognition or affinity interactions between different appropriately modified particles and thereby dictate the structure when aggregation occurs.^[11] New collective properties of aggregated NPs,^[7] such as coupled-plasmon absorbance, interparticle energy transfer, and electron transfer or conductivity, may be observed in the clustered assemblies.

The chemical functionalities associated with nanoparticles enable the assembly of 2D and 3D NP architectures on surfaces.^[7] On the basis of the tremendous success in supramolecular chemistry,^[12] NPs functionalized with various molecular and biomolecular units were assembled into complex hybrid systems. Composite layered or aggregated structures of (macro)molecule-cross-linked NPs on surfaces

From the Contents

1. Introduction	6043
2. Synthesis and Properties of Biomolecule-Functionalized Nanoparticles	6045
3. Biomolecule-Functionalized Nanoparticles for Controlled Chemical Reactivity	6050
4. The Aggregation of Biomolecule-Functionalized Nanoparticles	6052
5. Assembly of Biomolecule–Nanoparticle Architectures on Surfaces	6060
6. Functional Biomolecule–Nanoparticle Structures on Surfaces for Application as Sensors	6063
7. Biomolecule-Functionalized Magnetic Particles	6078
8. Biomolecule-Based Nanocircuitry	6087
9. Conclusions	6098

[*] Dr. E. Katz, Prof. I. Willner
Institute of Chemistry
The Hebrew University of Jerusalem
Jerusalem 91904 (Israel)
Fax: (+972) 2-6527-715
E-mail: willner@vms.huji.ac.il

have been prepared,^[13] and specific sensing of substrates,^[13a] tunable electroluminescence,^[13b] and enhanced photoelectrochemistry^[14] have been observed. The assembly of NP architectures on surfaces has also led to the fabrication of nanoscale devices such as single-electron transistors,^[15] NP-based molecular switches,^[16] and metal–insulator–nanoparticle–insulator–metal (MINIM) capacitors.^[17] Several reviews have addressed the recent advances in the synthesis and properties of nanoparticles^[7,18] and the progress made in the integration of composite nanoparticle systems with surfaces.^[7,19]

The convergence of biotechnology and nanotechnology has led to the development of hybrid nanomaterials that incorporate the highly selective catalytic and recognition properties of biomaterials, such as proteins/enzymes and DNA, with the unique electronic, photonic, and catalytic features of nanoparticles. The conjugation of NPs and other nanoobjects (e.g. nanorods and carbon nanotubes) with biomolecules is an attractive area of research within nanobiotechnology.^[20,21] Biomolecules are fascinating macromolecular structures in terms of their unique recognition, transport, and catalytic properties. The conjugation of NPs with biomolecules could provide electronic or optical transduction of biological phenomena in the development of novel biosensors.^[22] Enzymes, antigens and antibodies, and biomolecular receptors have dimensions in the range of 2–20 nm, similar to those of NPs, thus the two classes of materials are structurally compatible.

Because of several fundamental features, biomaterials are important future building blocks for NP architectures: 1) Biomaterials display specific and strong complementary recognition interactions, for example, antigen–antibody, nucleic acid–DNA, and hormone–receptor interactions. The functionalization of nanoparticles with biomolecules could lead to biomolecule–nanoparticle recognition interactions and thus to self-assembly. 2) Various biomolecules contain several binding sites, for example, antibodies exhibit two Fab (antigen-binding fragment) sites, whereas streptavidin or concanavalin A each display four binding domains. This allows the multidirectional growth of NP structures. 3) Proteins may be genetically engineered and modified with specific anchoring groups. This facilitates their aligned binding to NPs or the site-specific linkage of the biomaterial to

surfaces. Consequently, the directional growth of NP structures may be dictated. Furthermore, other biomaterials, such as double-stranded DNA, may be synthetically prepared in complex rigidified structures that act as templates for the assembly of nanoparticles by intercalation, electrostatic binding to phosphate groups, or association to functionalities tethered to the DNA. 4) Enzymes are catalytic tools for the manipulation of biomaterials. For example, the ligation or the endonuclease scission processes of nucleic acids provide effective tools for controlling the shape and structure of biomolecule–NP hybrid systems. In this context, it is important to note that Mother Nature has developed unique biocatalytic replication processes. The use of biocatalysts for the replication of biomolecule–NP conjugates may provide an effective system for the formation of nanostructures of predesigned shapes and compositions.

Modern efforts in biotechnology involve the application of combinatorial methods for the synthesis of new biocatalysts or drugs. The simultaneous analysis of many pathogens, mutants, or therapeutic drugs is a major challenge in bioanalytical chemistry. Thus, the unique optical or electronic properties of metal or semiconductor NPs are of key interest for the development of high-throughput techniques for the parallel analysis of numerous components in samples. The possibility to control and tune these unique optical and electronic properties of metal or semiconductor NPs through their dimensions paves the way to the application of NPs as versatile analytical probes. That is, the application of size-controlled metal or semiconductor nanoparticles as libraries of probes for different analytes promises a great potential in future biosensing assays.

The importance of functionalized nanoparticles for biomedical applications cannot be overestimated. For instance, targeted entry into cells is an increasingly important area of research.^[23] The nucleus is a desirable target because the genetic information of the cell and transcription machinery resides there. Targeted nuclear delivery is a challenging task because a nuclear probe must, at least, satisfy the following requirements: 1) it should enter the cell (e.g. through receptor-mediated endocytosis), 2) it should escape endosomal/lysosomal pathways, 3) it should possess a nucleus localization signal to interact with the nuclear-core complex, and 4) the probe should be small enough (< 30 nm) to cross



Itamar Willner, born in 1947, completed his PhD in Chemistry in 1978 at The Hebrew University of Jerusalem. After a postdoctoral stay with M. Calvin at the University of California, Berkeley, he joined the Institute of Chemistry at The Hebrew University of Jerusalem in 1982 and was appointed Professor in 1986. He is a member of several editorial boards, the Israel Academy of Sciences, and the European Academy of Sciences. He is the recipient of the Kolthoff Award, the Max Planck Research Award for International Cooperation, the Israel Chemical Society Award (2001), and the Israel Prize in Chemistry (2002).



Eugenii Katz, born in 1952 in Moscow, completed his PhD in 1983 at the Frumkin Institute of Electrochemistry, Moscow, and then worked as a senior scientist at the Institute of Photosynthesis, Pushchino. In 1991 he joined the The Hebrew University of Jerusalem as a postdoctoral researcher and in 1993, as a recipient of the Humboldt scholarship, he moved to the Technische Universität, München. He returned to the Hebrew University in 1994 as a senior research associate in the group of Professor I. Willner. His research interests include electroanalytical chemistry and functionalized nanoparticles.

the nuclear membrane. The most-efficient nuclear targets in biology are viruses, which commonly utilize different peptides for crossing each cell-membrane barrier. Artificial systems that model viral behavior could be designed on derivatives of functionalized nanoparticles. In a biologically inspired model system, Au NPs (20 nm) were modified with shells of bovine serum albumin (BSA) which were conjugated to various cellular targeting peptides to provide functional nanoparticles that penetrate the biological membrane and target the nuclei.^[23b] Various NPs are applied as targeted biomarkers and drug-delivery agents to tumors in the analysis and medical treatment of cancers.^[24] Hybrids of silver NPs with amphiphilic hyperbranched macromolecules exhibit antimicrobial properties and are used as drugs.^[25]

One-dimensional nanostructures, wires, rods, belts, and tubes with lateral dimensions in the range of 1 to 100 nm, have recently received attention as potential components for nanotechnology and particularly nanoelectronic devices.^[26] 1D structures of various compositions can be produced in copious quantities by chemical and physical methods. A range of unique properties (thermal, mechanical, electronic, optoelectronic, optical, nonlinear optical, and field emission) associated with different types of 1D nanostructures have been discovered. Some of the unique properties have already been applied in novel nanodevices, whereas others are still awaiting practical applications. The combination of 1D nanostructures with biomolecules paves the way to novel nanobioelectronic elements that could, for example, transport bioelectronic signals along 1D nanowires.

The combination of nanoobjects, nanotools, and nanotemplates^[27–29] with biomolecules yields new facets of bioelectronics^[30] to open new horizons of nanobioelectronics. Herein, we aim to review the synthesis and properties of biomolecule–nanoparticle/nanorod hybrid systems as well as the organization of these systems as functional devices (Figure 1). We discuss their properties and the methods to assemble two-dimensional and three-dimensional nanoparticle structures on surfaces, and we describe the operation of these biomolecule–nanoparticle structures as functional devices. Specifically, we discuss the use of the systems as sensors, as building blocks for electronic circuitry, and as electronic and optoelectronic elements. We highlight the findings of the past few years that have already established the core elements of the new research area—nanobiotechnology.

2. Synthesis and Properties of Biomolecule-Functionalized Nanoparticles

Biological molecules have been immobilized on polymer matrices and inorganic supports through a variety of techniques that includes physical adsorption, electrostatic binding, specific recognition, and covalent coupling.^[31,32] These supports, which are modified with biological molecules such as proteins/enzymes, antigens/antibodies, and DNA/oligonucleotides, have been used for numerous biotechnological applications: affinity separations, biosensing, bioreactors, and the construction of biofuel cells. Recently, these immobilization techniques—developed for the functionalization of

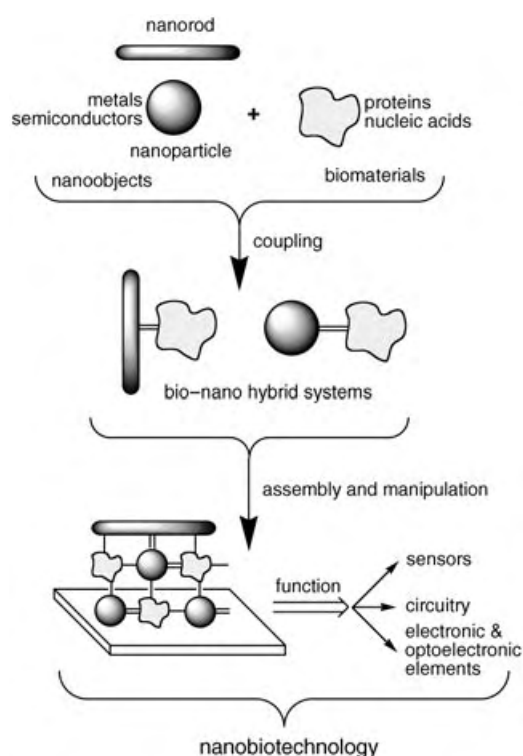


Figure 1. The conceptual generation of biomolecule–nanoparticle/nanorod conjugates to yield functional devices.

macrosized supports—have been applied to bring together biomolecules and nanoparticles.

2.1. Functionalization of Nanoparticles with Biomolecules Through Electrostatic Adsorption

The simple adsorption of biomolecules on NPs has frequently been performed and studied for biomolecules, which range from low-molecular-weight organic substances (e.g. vitamin C)^[33] to large protein/enzyme molecules.^[34–37] In the case of NPs that are stabilized by anionic ligands such as carboxylic acid derivatives (citrate, tartrate, lipoic acid), the adsorption of positively charged proteins originates from electrostatic interactions (Figure 2A).^[38–43] Gold and silver NPs produced by citrate reduction were functionalized with immunoglobulin G (IgG) molecules at pH values that lie slightly above the isoelectric point of the citrate ligand.^[38] This allowed effective binding between the positively charged amino acid side chains of the protein and the negatively charged citrate groups of the colloids. Other examples of protein coating through electrostatic interactions include the direct adsorption of heme-containing redox enzymes at citrate-stabilized Ag NPs^[34,39] and the binding of basic leucine zipper proteins to lipoic acid stabilized semiconductor CdSe_{core}/ZnS_{shell} particles.^[40] Au NPs coated with a negatively charged phospholipid were prepared by the photoreduction of NaAuCl₄ in the presence of dimyristoyl-L- α -phosphatidyl-DL-glycerol,^[41] which could provide further electrostatic

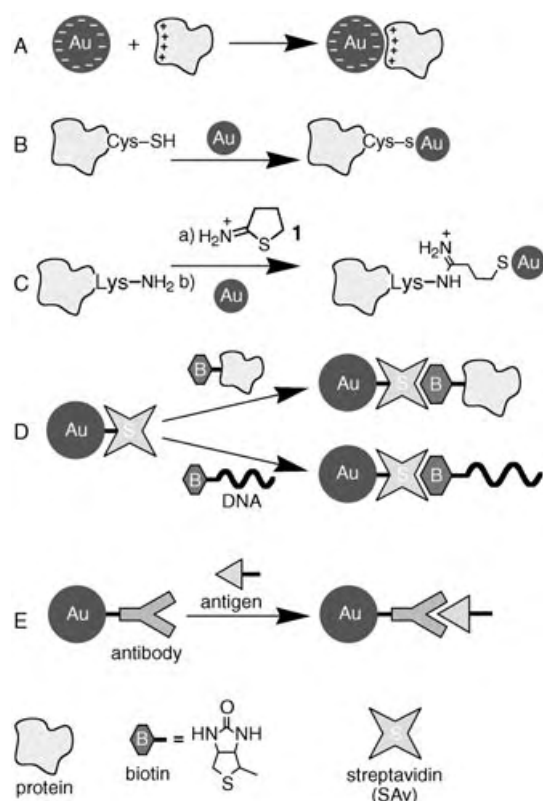


Figure 2. Formation of the biomolecule–nanoparticle (NP) hybrids: A) The assembly of NP–protein conjugates by electrostatic interactions. B), C) The formation of NP–protein conjugates by adsorption of NPs on natural (B) and synthetic (C) thiol groups of the protein. D), E) The assembly of biomolecule–nanoparticle conjugates by the use of bioaffinity interactions upon streptavidin–biotin binding (D) and antibody–antigen associations (E).

binding of positively charged proteins, to yield a nanosized model of a biomembrane. Differential scanning calorimetry (DSC) was used to demonstrate the electrostatic nature of the bond of the adsorbed proteins on silica particles, and these measurements allowed the calculation of the thermodynamic binding parameters.^[42] A theoretical model was developed to correlate the structure of metal_{core}/protein_{shell} NPs with the experimental data obtained from the light-scattering spectra.^[37] The method of rapid expansion of a supercritical solution into a liquid solvent was applied for the preparation of BSA protein-conjugated Ag or Ag₂S NPs.^[43] Monodispersed BSA-functionalized nanoparticles were produced. As the protein underwent pH-dependent association and dissociation, the BSA–nanoparticle hybrids also assembled and disassembled with changes in pH of the solution in a reversible fashion. Ethylene glycol monolayer-protected NPs were used for the elimination of nonspecific binding to biological molecules.^[44] Also, Au NPs were used as templates for the assembly of peptides to yield *de novo* proteins connected to the nanoparticle support.^[45]

The electrostatic deposition of biomolecules, particularly proteins or enzymes, can also be extended to multilayer-level assemblies.^[46] Proteins that are electrostatically attracted to the charged nanoparticles can provide an interface for the

further deposition of an oppositely charged polyelectrolyte polymer, which again allows the deposition of a secondary protein layer. Multilayer films of BSA,^[47] IgG,^[47] β -glucosidase,^[48] glucose oxidase (GOx),^[49,50] urease,^[51] and horseradish peroxidase (HRP)^[50] have been assembled on polystyrene NPs by the alternate deposition of the proteins and an oppositely charged synthetic polyelectrolyte as a linker (e.g. poly(diallyldimethylammonium chloride) or poly(sodium 4-styrenesulfonate) were used as positively or negatively charged polyelectrolytes, respectively). The protein/polymer multilayer shell could be varied from several to hundreds of nanometers in thickness. This strategy permits the preparation of functional films on nanoparticles with a high density of enzyme molecules. An increase in the loading of NPs by organic materials upon layer-by-layer deposition enhances the sensitivity of the analytical protocol to which the NPs are applied. For example, polystyrene particles were functionalized with a multilayer assembly of polyelectrolytes functionalized with a fluorescent dye. The assembly was terminated with a layer of IgG, which allowed the use of the modified particles as labels in fluorescence immunoanalyses.^[52] The increase in the loading of the particles with the dye owing to the multilayer deposition resulted in a higher fluorescence output and thus in a higher sensitivity of the analysis.

The electrostatically driven adsorption of negatively charged DNA on positively charged Cd²⁺-rich CdS NPs has been studied in detail.^[53–57] The photoluminescence of semiconductor quantum dots was used to probe the effect of DNA structure on its binding to the nanoparticles.^[53–55,58] It was found that “kinked” oligonucleotides, which exhibit a curvature of ≈ 3 nm from crystallographic and biochemical experiments, bind more tightly and faster to NPs that display curvatures of similar dimensions relative to straight or bent DNA.^[53,54] The understanding of the binding modes and their separation into static and dynamic components is still a topic of investigation.^[59] Negatively charged DNA was found to substitute citrate ions around Au NPs to form a DNA shell.^[60]

2.2. Functionalization of Nanoparticles with Biomolecules by Chemisorption of Thiol Derivatives and by Covalent Binding through Bifunctional Linkers

The primary binding of functionalized thiolated molecules, such as oligopeptides, to Au NPs could provide a means for the covalent tethering of biomolecules to nanoparticles. Gold NPs were functionalized with L-cysteine through the thiol groups. Subsequent oligomerization of the cysteine moieties in an aqueous solution resulted in the binding of oligopeptides to the Au NPs.^[61] Elsewhere, CdS NPs were capped with glutathione through the strong binding of its thiol groups to Cd²⁺ ionic sites on the surface of the nanoparticles.^[62]

In some cases, tight chemisorption of proteins on Au NPs can originate from the binding of thiol groups from cysteine residues that exist in the proteins (e.g. serum albumin)^[63] to the Au surface (Figure 2B). If no thiolated residues are available in the native proteins, thiol groups can be incorporated by chemical means, for example, with 2-iminothiolane

(Traut's reagent, **1**; see Figure 2C)^[64] or through genetic engineering.^[65] Some proteins and enzymes preserve their native structures and activities when they are directly adsorbed on nanoparticles. A surface-enhanced resonance Raman (SERR) study of native hemoglobin adsorbed on citrate-stabilized Ag colloids was reported^[36] in which reversible dioxygen and carbon monoxide binding to the R hemoglobin conformation resulted in a transition to the T conformation. A non-heme iron enzyme, chlorocatechol dioxygenase, physically adsorbed on citrate-reduced Ag colloids also showed its native structure and biocatalytic activity through SERR spectroscopy.^[34] However, physically adsorbed biomolecules can be readily lost from the surface, and adsorbed proteins are often prone to denaturation and thereby lose their biocatalytic or biorecognition activities. Some proteins and enzymes that were directly adsorbed on NPs showed conformational changes and loss of biological activity. Studies on bovine fibrinogen, which was adsorbed on TiO₂ nanoparticles, by circular dichroism (CD) spectroscopy, DSC, and fluorescence spectroscopy indicated that the α -helical content of the protein decreased markedly upon its adsorption.^[35]

Reversible binding with specific alignment was observed with pepsin as a model enzyme on alumina NPs through the interaction of the phosphoryl group and the alumina surface.^[66] One phosphoryl group is attached to the Ser68 residue in the native porcine pepsin. The crystal structure of the enzyme indicates that this modified residue is positioned at the protein surface, far away from the active site that comprises Asp32 and Asp215. This feature enabled the oriented coupling of the phosphoryl group on Ser68 to alumina. Furthermore, phosphate ions in aqueous solution were found to compete with the phosphorylated protein–alumina bonds to induce the release of the enzyme. Thus, protein–alumina nanoparticle hybrids that exhibit a similar controlled-release behavior open an interesting possibility in the design of new drug-delivery methods. That is, the immobilization of functionalized therapeutic proteins on alumina nanoparticles may generate vehicles for delivery in vivo and allow the targeted release of the drug by added phosphate ions.

By covalent attachment of proteins to nanoparticle surfaces, problems of instability and inactivation can be overcome.^[46] Low-molecular bifunctional linkers, which have anchor groups for their attachment to NP surfaces and functional groups for their further covalent coupling to the target biomolecules, were extensively used in the generation of covalent-tethered conjugates of biomolecules with various NPs.^[21a] Anchor groups such as thiols, disulfides, or phosphine ligands are often used for the binding of the bifunctional linkers to Au, Ag, CdS, and CdSe NPs. These anchor groups may readily substitute weakly adsorbed molecules to stabilize the NPs or may be incorporated in the synthesis of the NP to yield a nanoparticle surface that is functionalized for further reactions. Alkoxy- or halosilane groups are used for the covalent attachment of bifunctional linkers to the surfaces of NPs coated with SiO₂ and other oxides. Au NPs that are covered with polysiloxane shells and functionalized with a variety of functional groups for covalent binding to biomolecules have been synthesized.^[67]

A wide variety of terminal functional groups are available in different bifunctional linkers. The most common amine, active ester, and maleimide groups are used to couple biological compounds covalently by means of carbodiimide-mediated esterification and amidation reactions or through reactions with thiol groups.^[21a] Single functional groups (e.g. active ester or amine units) on Au NPs are available either by a statistical approach or by the modification of chemically defined clusters.^[68] These structures provide unique synthetic routes for the covalent binding of a single target biomolecule per nanoparticle. A versatile method for the monofunctionalization of Au NPs (≈ 2 nm) with L-lysine residues through solid-phase reactions was reported recently.^[68d] The Au NPs, which were functionalized with a single L-lysine residue, were suggested as building blocks for 1D nanoparticle–peptide chains.

Nucleic acids can be synthesized with tethered alkanethiol groups by using appropriate phosphoramidate precursors in a solid-phase synthesis. The *n*-alkylthiolated nucleic acids have been extensively used in the preparation of DNA-functionalized gold NPs^[69] and CdSe_{core}/ZnS_{shell}^[70] or CdS^[56] semiconductor NPs. DNA functionalized with a steroid–disulfide derivative can readily bind to Au NPs and demonstrates a high adsorption stability because two sulfur atoms of the disulfide anchor group are involved in the attachment process.^[71] Phosphorothiolate anchor groups were also utilized to bind oligonucleotides to CdS NPs.^[72] The conformation of single-stranded DNA (ss-DNA) attached to Au NPs through thiol anchor groups was reported to be dependent on the length of the DNA and the loading. Thiolated single-stranded nucleic acids of different lengths (8 to 135 bases) were attached to 10-nm-diameter Au nanoparticles at different ratios of nucleic acid/Au NPs (1, 2, ..., saturation).^[73] The effective diameter and electrophoretic mobility of the conjugates were followed on 2% agarose gels and were found to be controlled by the conformation of the nucleic acids associated with the Au NPs. At low surface coverages of the nucleic acids, they were found to wrap around the nanoparticles. At high surface coverages of short nucleic acids, stretched, perpendicularly oriented DNA configurations were observed. At high surface coverages of long oligonucleotides, a dense, stretched structure with the inner part of the DNA oriented perpendicular to the nanoparticles was suggested, whereas the outer region of the chains revealed random, flexible coil-shaped orientations.

2.3. Functionalization of Nanoparticles with Biomolecules by Specific Affinity Interactions

Nanoparticles functionalized with groups that provide affinity sites for the binding of biomolecules have been used for the specific attachment of proteins and oligonucleotides. For example, streptavidin (SAv)-functionalized Au NPs have been used for the affinity binding of biotinylated proteins (e.g. immunoglobulins and serum albumins) or biotinylated oligonucleotides (Figure 2D).^[21a,74] Likewise, biotinylated CdSe_{core}/CdS_{shell} NPs can be bound to SAv.^[75] Protein A conjugate bound to Ag NPs was used as a versatile linker to Fc

fragments of various immunoglobulins.^[76] Also, NP–antibody conjugates were used for affinity binding of their respective antigens (Figure 2E).^[77] This may be advantageous because upon association with their respective antigens, nanoparticle-conjugated antibodies can demonstrate association constants that are even higher than those of the free antibody.^[77b]

Recently, metal NPs have been used to tether a variety of carbohydrate ligands.^[78–81] Such 3D multivalent ligands provide a globular structure on which clustering and orientation effects may be studied.^[79] Furthermore, the properties of the metal core can be applied for the development of methods to study molecular recognition between carbohydrates and their respective binding proteins. For example, mannose-stabilized Au NPs have been used to visualize FimH proteins on type 1 pili of *Escherichia coli* by using electron microscopy.^[80a] The further development of stabilized colloidal systems for the colorimetric detection of carbohydrate binding proteins was reported.^[82] A mannose derivative was self-assembled onto preformed citrate-capped, water-soluble gold nanoparticles. Through the use of a short (C_2) hydrocarbon tether between the gold surface and the mannose recognition center, a selective, quantitative, and, importantly, rapid colorimetric detection method for the carbohydrate-binding protein concanavalin A has been developed. Surface plasmon resonance (SPR) spectroscopy was also used to follow the recognition process between carbohydrate-functionalized Au NPs and concanavalin A.^[80b] Multivalent interactions between Au NPs, which were modified by galactosyl and glucosyl headgroups, with HIV-associated glycoprotein gp120 were also studied.^[83] These particles were prepared from disulfides, which contained C-glycosides linked to triethylene glycol through an amide bond, by using a modification of the Brust method.^[8b] Gold NPs capped with a monolayer of the synthetic drug vancomycin demonstrated multivalent affinity binding to membranes of Gram-negative bacteria that resulted in antimicrobial activity.^[84]

Nanoparticles could be encapsulated by some natural proteins to provide their affinity binding. The chaperonin proteins GroEL (from *Escherichia coli*) and *T.th* cpn (from *Thermus thermophilus* HB8) encapsulate denatured proteins inside cylindrical cavities and later release them upon addition of ATP, which stimulates conformational changes of the cavities. It was also demonstrated that GroEL and *T.th* cpn encapsulate CdS semiconductor NPs to provide them with high thermal and chemical stability in aqueous media.^[85] In a similar fashion to the ATP-induced release of proteins from the chaperonin proteins, ATP stimulates the release of the CdS NPs from the cavities. The integration of such biological mechanisms into materials science-based applications could open the door to new bioresponsive devices. The chaperonin protein GroEL comprises a double-decker architecture formed from two stacked rings, which consist of seven 60-kDa protein subunits each (Figure 3A, part a), to yield a cylindrical cavity that has a diameter of 4.5 nm and a wall thickness of 4.6 nm. The chaperonin protein *T.th* cpn comprises a tetradecamer protein subunit (840 kDa), which is end-capped by a [cpn10]₇ (70 kDa) protein unit on one side of the supramolecular cylindrical cavity (internal diameter ≈ 5 nm; Figure 3A, part a). These cavities may also act as containers for the controlled release of semiconductor nanoparticles (Figure 3B). The release of the CdS NPs in the presence of ATP, Mg^{2+} , and K^+ (Figure 3A, part b) activates their photoelectrochemical function (e.g. photoinduced electron transfer).

2.4. Synthesis of Nanoparticles by Biochemical and Microbial Systems

The use of bacteria as a novel biotechnology to facilitate the production of NPs is in its infancy. In contrast to purely chemical procedures for the manufacture of NPs, biological

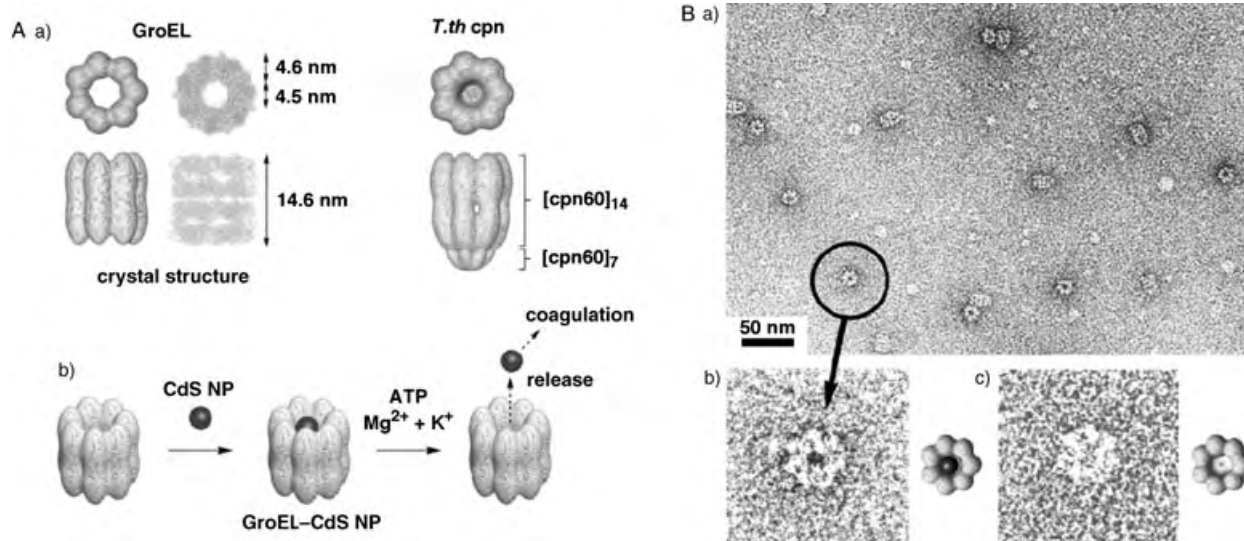


Figure 3. A) Chaperonin proteins as ATP-responsive barrels for the inclusion of nanoparticles: a) Top and side views of GroEL and *T.th* cpn; b) The formation of GroEL–CdS NP complexes by inclusion of CdS NPs into the cylindrical cavity of GroEL, and the ATP-triggered release of the guest. B) Transmission electron micrographs: a) *T.th* cpn–CdS NP complexes and intact *T.th* cpn; b) Enlarged image and model of complex; c) Enlarged image and model of *T.th* cpn. (Adapted from Ref. [85], with permission).

and, particularly, microbial reactions that are characterized by their selectivity and precision for NP formation^[86] provide environmentally friendly “green” technological processes.^[86f] In most bioprocesses, it is assumed that highly specific structures such as enzymes and proteins exist on the bacterial membrane which, in turn, drive highly specific interactions with the culture medium. These biological processes could rapidly produce copious amounts of nanoparticles. Many details of the underlying biology remain unanswered, but from an electrochemical viewpoint, bacteria may be thought of as electrodes that operate at a relatively fixed potential. The range of inorganic nanosized products that are observed is consistent with this model. The NPs produced by bacteria could be isolated with the parent biomaterial shells to demonstrate the use of bacteria as living reactors for the preparation of nanomaterials.

Microorganisms, particularly prokaryotic bacteria, are often exposed to extreme environmental conditions that force them to resort to specific defense mechanisms to quell such stresses as the toxicity of foreign metal ions or metals. The toxicity of metal ions is reduced or eliminated by a change in the redox state of the metal ions and/or precipitation of the metals intracellularly. This forms the basis of many important applications of microorganisms such as bioleaching, bioremediation, microbial corrosion, as well as the synthesis of nanoparticles. A number of biological systems have developed highly orchestrated detoxification mechanisms towards the bioreduction and mineralization of noble metals. These systems incorporate small peptides and proteins as nucleation sites to bind metals and stabilize NPs. For example, silver nanoparticles in the 2–5-nm range were synthesized extracellularly by a silver-tolerant yeast strain MKY3 when challenged with Ag^+ ions (1 mM) in the log phase of growth.^[86d] Live fungus and plants could also be used to generate metallic and semiconductive NPs.^[87] It was found that the fungus *Fusarium oxysporum* is able to synthesize CdS semiconductor NPs extracellularly by a purely enzymatic process.^[87a] Similarly, the formation and growth of Au NPs inside Alfalfa plants has been reported.^[87b] Also, semiconductive nanoparticles (e.g. CdSe and $\text{CdSe}_{\text{core}}/\text{ZnS}_{\text{shell}}$) of controllable sizes and unique shapes were generated with the use of genetically engineered predesigned proteins.^[88] Bio-mineralization, particularly with the use of ferritin, is widely used for the preparation of magnetic nanoparticles (see Section 7.1.).

2.5. Properties of Nanoparticle–Biomolecule Hybrid Systems

The functionalization of NPs with biomolecules results in changes in the properties of the NPs and their interactions with the environment. Upon adsorption of vitamin C on TiO_2 NPs, the optical properties of the particles were red-shifted by 1.6 eV as a result of charge transfer that originates from the specific binding of the electron-donating modifier to corner defects on the surface of the nanoparticles.^[33] The solubility of NPs in water can be greatly improved by the functionalization of their surfaces with highly hydrophilic biomolecules.^[9] Whereas Au NPs modified with long chain alkanethiols are

only soluble in low-polarity organic solvents, Au NPs with ω -carboxylic acid functionalized alkanethiolate ligand shells are soluble in polar organic solvents such as ethanol and acetone. Furthermore, Au NPs that are modified with biomolecules such as tiopronin or coenzyme A demonstrate excellent solubility in water.^[9c]

Intrinsic properties of biomolecules can be changed upon their association with metal nanoparticles. For example, vibrations of the biologically active prosthetic heme groups of myoglobin or hemoglobin are selectively enhanced by adsorption of the proteins on metal NPs relative to the vibrational modes characteristic of the protein backbone as recently shown in a SERR spectroscopic studies.^[89]

Alteration by external signals (e.g. electrical, optical) of the chemical properties of the biomolecules or the biomaterial analogues that modify nanoparticles can be used to control the interactions of the modified nanoparticles with the environment. Thereby, the binding properties of the modifier or the aggregation of the nanoparticles can be controlled. For example, the formation of a complex between a diamino-pyridine derivative and a flavin derivative was studied at the surface of a Au NP.^[90] It was shown that more-stable hydrogen bonding occurred when the flavin derivative was electrochemically reduced (Figure 4). This allowed the electrochemically controlled switching of the binding of the bioorganic molecules to the organic-functionalized shell of the nanoparticle.

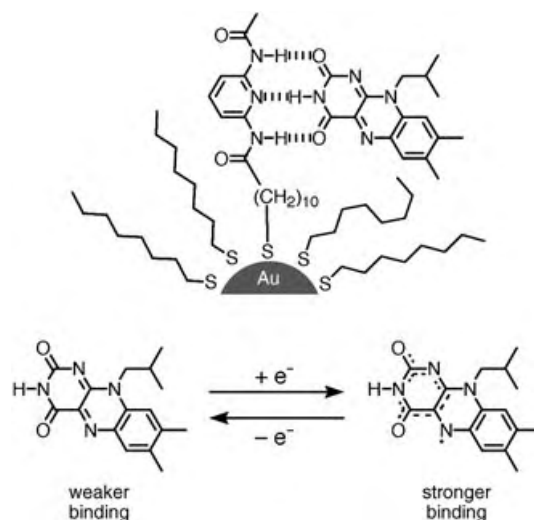


Figure 4. The electrochemically controlled recognition of flavin by a pyridinediamide-functionalized nanoparticle.

Energy and/or electron transfer processes between NPs and coupled biomolecules may proceed upon photoexcitation of one of the hybrid components so affecting the properties of the biomolecule–NP hybrid systems. Efficient photoinduced electron transfer between a carotenoid shell and the TiO_2 NP core has been demonstrated.^[91] In another system, photoexcitation of TiO_2 NPs resulted in the oxidation of hemin molecules that were bound to the semiconductive core which induced further heme-catalyzed oxidation of organic hal-

ides.^[92] Efficient resonance energy transfer from tryptophan moieties of proteins to the semiconductor NP core (e.g. in a BSA–CdTe conjugate)^[93] resulted in a significant increase in the fluorescence of the nanoparticle upon photoexcitation of the protein shell.

3. Biomolecule-Functionalized Nanoparticles for Controlled Chemical Reactivity

The interactions of functionalized nanoparticles with biomaterials or within biomaterial structures can control the chemical reactivity of the biomolecules. Alternatively, they can report on the state of the reaction or reactants and allow the reactivity to be controlled externally. It is well known that small molecules and polymers can affect the chemical reactivity of biomolecules. If there are several possible parallel reactions, the effect produced by a promoter/inhibitor on a specific chemical reaction can change the effective chemical path of the whole process to result in the regulation of the biochemical system. Molecular labels such as fluorescent dyes incorporated into biomolecules can report on the state of the biomolecule through transduction of the molecular transformations into an output signal: this is used, for example, in biomaterial-based diagnostics. Functionalized NPs can operate in the same way, demonstrating properties of a biopromoter/bioinhibitor or a reporter with some advantages over their molecular-sized counterparts owing to the unique photophysical and electronic properties of the NPs. Nanomechanical devices based on NPs functionalized by biomolecules (particularly DNA) are also feasible.^[94]

3.1. Biomolecule-Functionalized Nanoparticles for Controlling DNA Reactivity

Enzymatic manipulations of DNA bound to metal NPs, such as the enzymatic extension of the DNA chain, present some challenges. The extension reaction requires not only the efficient hybridization of a template to the particle-bound primer, but also accessibility to the DNA polymerase enzyme (the 68-kDa Klenow fragment). Thus, the extension reaction might be expected to show greater sensitivity to steric effects than hybridization alone. Extension efficiencies as high as 100 % were observed for DNA primers bound to Au NPs by a HSC₆H₁₂ linker.^[95]

Biocatalytic reactions that occur on DNA, such as transcription or translation, require the association of enzymes with the DNA chain. The competitive association of other molecules to the DNA chain may decrease the binding of the enzyme and thus inhibit the process which finally results in gene regulation. It has been shown that small molecules,^[96] dendrimers,^[97] and polymers^[98] efficiently bind to DNA and, in some cases, lead to the inhibition of the transcription machinery. In these systems, however, the creation of suitably preorganized scaffolds for controlled binding to DNA presents a significant design challenge. For small molecules, this challenge arises from the detailed synthesis required for a rigid scaffold that contains several functional groups. For

polymer systems, the precise placement of substituents along the backbone as well as the macroconformation of the polymer in solution are difficult to control. An excellent solution to these problems is the application of “mixed monolayer-protected (Au) clusters” (MMPCs).^[99] The self-assembled monolayer coating of the Au NPs presents a highly organized surface for the recognition of DNA which is of a similar size (6–10 nm) to that of DNA-binding proteins. The central metal core rigidifies the particle to limit the organic components to a much smaller subset of structures than a similarly sized polymer. The mobility of thiols on the surface of the NP also allows the formation of recognition elements to be controlled in subsequent steps.^[100] NPs for the recognition of double-stranded DNA (ds-DNA) were prepared by the partial displacement of octanethiol on the Au surface with 11-mercaptoundecyltrimethylammonium.^[101] The mixed monolayer of this MMPC system is designed to electrostatically attract the negatively charged DNA to the surface-confined positively charged ammonium groups. These MMPCs bind to the ds-DNA and inhibit the binding of the enzymes involved in gene regulation, thus resulting in effective inhibition of the biocatalytic transcription process.

A simple method to protect DNA from cleavage was developed by using bioconjugated amine-modified silica NPs (45 ± 4 nm).^[102] Negatively charged DNA molecules could be easily concentrated onto the positively charged surface of the NPs for further manipulation. The DNA strands were protected from enzymatic cleavage and had the same properties as the free DNA strands when released from the NPs.

A gold NP–DNA molecular beacon conjugate, **2**, has recently been exploited for the remote electronic control of DNA hybridization.^[103] By the inductive coupling of a radio-frequency (1-GHz) electromagnetic field to the 1.4-nm Au NP, which functions as an antenna in the DNA conjugate, the local temperature of the bound DNA is increased and thereby induces denaturation whilst leaving surrounding molecules relatively unaffected. Figure 5 A, curve a, shows the absorbance of a solution of the Au NP–DNA molecular beacon conjugate **2** at 260 nm as a function of the time in which the electromagnetic field is switched on and off. The increase in the absorbance reflects the denaturation of the DNA double-helix upon local heating, whereas the decrease in the absorbance corresponds to the DNA rehybridization when the electromagnetic field is switched off. The switching between two distinct states is fully reversible. A control experiment revealed that the DNA molecular beacon, **3**, which lacks the Au nanoparticle, is not affected by the electromagnetic field (Figure 5 A, curve b). Although inductive heating has already been applied to macroscopic samples as well as to the treatment of cancer cells with electromagnetic field-induced excitation of biocompatible superparamagnetic nanoparticles,^[104] the use of Au NP–DNA conjugates should allow extension of this concept. Complex operations, such as gene regulation, biomolecular assembly, and enzymatic activity, of distinct portions of nucleic acids or proteins might be controlled, whereas the rest of the molecule and neighboring species would remain unaffected. Moreover, since the addressing method is not optical, this technology could even be applicable in highly scattering media.

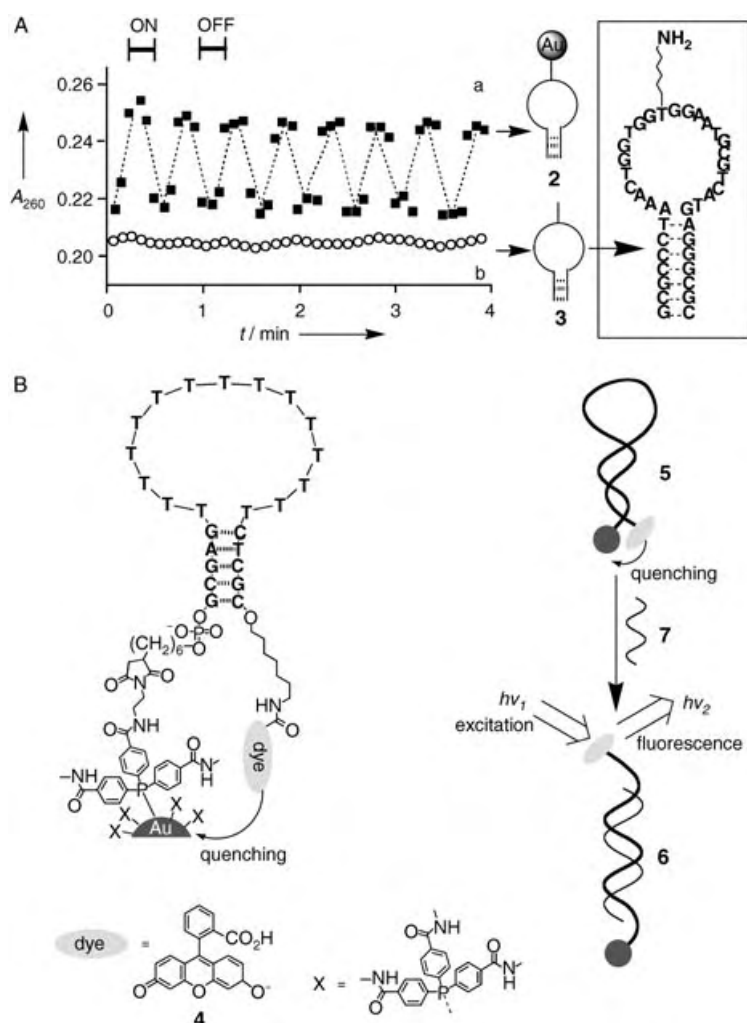


Figure 5. A) a) The reversible change of the Au NP–DNA molecular beacon conjugate **2** between denaturated and hybridized conformations upon switching “ON” and “OFF”, respectively, the radiofrequency electromagnetic field; b) The DNA hairpin molecule **3**, which lacks the Au nanoparticle, is not affected by the electromagnetic field. B) Fluorescence emission controlled by the transformation from the hairpin conformation **5** to the extended state **6** of a DNA chain upon hybridization with the complementary oligonucleotide **7**. (Part A is adapted from Ref. [103], with permission).

3.2. Biomolecule-Functionalized Nanoparticles for Reporting DNA Reactivity

DNA molecules that are functionalized at specific positions with a fluorescence dye and a quencher can produce a fluorescence output, which is controlled by the distance that separates the two, to act as a reporter of the conformation of the DNA chain. Au nanoparticles can quench the fluorescence of chromophores 100-fold better than molecular quenchers and they also exhibit higher quenching efficiencies for dyes that emit in the near-infrared region. A gold NP, which was functionalized with a single maleimide group, was covalently linked to a $(\text{CH}_2)_6\text{SH}$ group that was tethered to the 5' end of a DNA oligonucleotide, which was functionalized with a fluorescent dye (e.g. fluorescein (**4**) or rhodamine 6G) at the 3' end.^[105] The molecule could adopt two

conformations (Figure 5B): a stem-loop structure with the fluorophore and the Au nanoparticle held in close proximity (hairpin state) and a rodlike structure with them far apart (open state). The hairpin state, **5**, is self-generated by the intramolecular complementarity of the terminal parts of the DNA chain that induces a double-stranded structure within the same molecule. On the other hand, the open state, **6**, is produced upon the interaction and hybridization with an analyte DNA molecule **7**, which exhibits complementarity to the central part of the DNA chain. This target DNA hybridizes with the modified DNA and results in the formation of ds-DNA, thereby opening the hairpin and increasing the distance between the fluorophore and the NP and therefore enhancing the fluorescence. The process and the reporting signal only occur in the case of complementarity between the analyte DNA and the central part of the sensing DNA. The system was successfully applied for the detection of single-base mismatches in DNA sequences.^[105] Competitive hybridization assays revealed that the ability to detect single-base mutations is about 8-fold greater than that with conventional molecular beacons, which use a molecular quencher instead of a Au NP, whereas the sensitivity of detection is enhanced up to 100-fold.

Au NPs have been used to develop a new class of nanobiosensors that are able to recognize and detect specific DNA sequences and single-base mutations in a homogeneous assay.^[106] The Au NPs were used as nanoscaffolds to tether ss-DNA that were functionalized with an organic dye at the opposite end of the nucleic acid chain. The flexible DNA chain yields a short distance between the dye and the Au NP which leads to the efficient quenching of the fluorescence of the dye by the metal NP. Hybridization of the ss-DNA with the complementary DNA analyte resulted in a rigidified spacer between the dye and the Au NP thus inhibiting the quenching process and restoring the fluorescence. Unlike conventional molecular beacons with a stem-and-loop structure, the NP probes do not require a stem and their background fluorescence increases little with temperature.

3.3. Biomolecule-Functionalized Nanoparticles for Controlling Enzyme Reactivity

Functionalized nanoparticles may affect the activities of enzymes: for example, they could effectively inhibit some enzymatic reactions. It has been shown that anion-functionalized NPs are highly effective surface-based inhibitors of chymotrypsin (ChT) by a two-step inactivation mechanism.^[107] This inhibition occurs through electrostatic complementarity between the negatively charged carboxylate end-

groups of the shell and the positively charged cationic residues located around the periphery of the enzyme active site. The primary reversible inhibition step yields a complex between the enzyme and the NPs. The secondary step results in the irreversible denaturation of the enzyme associated with the functionalized NPs. Complete inhibition of the enzyme activity was observed at a ratio of 1:5 of the nanoparticle/ChT and arises from the large surface area of the anion-functionalized NP ($\approx 110 \text{ nm}^2$). However, this irreversible inhibition of chymotrypsin could be reversed through modification of the surface of the NP in situ by using cationic surfactants.^[107b] Up to 50 % of the original chymotrypsin activity was retained upon the addition of a long-chain surfactant, and dynamic light-scattering studies demonstrated that chymotrypsin was released from the NP surface.

The controlled release of inhibitors, promoters, or cofactors into a reaction medium may be employed as a general strategy to deactivate or activate enzymes, respectively. Also, controlled delivery of drugs or neurotransmitters is essential for the regulation of complex physiological biocatalytic processes. Functionalized CdS NPs were used to entrap drugs or neurotransmitters in the channels (average diameter $\approx 2.3 \text{ nm}$) of MCM-41-type mesoporous silica nanospheres (MSNs) in a configuration that enabled the controlled release of the entrapped substances (Figure 6).^[108] Vancomycin or adenosine triphosphate (ATP) were loaded in the channels of the MSN. The MSN matrix was functionalized with an amine-terminated tether that contained a disulfide group and was linked to the matrix by a siloxane anchoring site, **8**. The MSN matrix loaded with the respective substrate was then treated with carboxylic acid modified CdS NPs **9** ($\approx 2.0 \text{ nm}$). The covalent coupling of the CdS NPs to the amine functions of the matrix **10** and the steric fit between the CdS NPs and the channels in the matrix resulted in the entrapment of the substrates in the channels. The chemical splitting of the disulfide bonds that bridge the NPs to the MSN matrix by dithiothreitol (DTT; **11**) removed the CdS NP stoppers and released the substrates stored within the MSN channels. This new MSN system could play a significant role in the development of new generations of site-selective, controlled-release delivery nanodevices.

4. The Aggregation of Biomolecule-Functionalized Nanoparticles

The organization and patterning of inorganic nanoparticles into 2D and 3D functional structures is a fundamental prerequisite for the assembly of chemical, optical, magnetic, and electronic devices.^[7] Many approaches have been described for the formation of 2D and 3D arrays of metal and semiconductor NPs: 1) by evaporation of the solvent of hydrophobic colloids,^[109] 2) by random inclusion of the nanoparticles into gel and glassy matrices,^[110] 3) by template-directed synthesis at structured surfaces^[111] in porous protein crystals^[112,113] or in bacterial superstructures,^[114] and 4) through chemical coupling in solution by means of bifunctional cross-linkers.^[115,116] An example of the latter is the alkanedithiol-directed aggregation of Au NPs.^[115,116] The

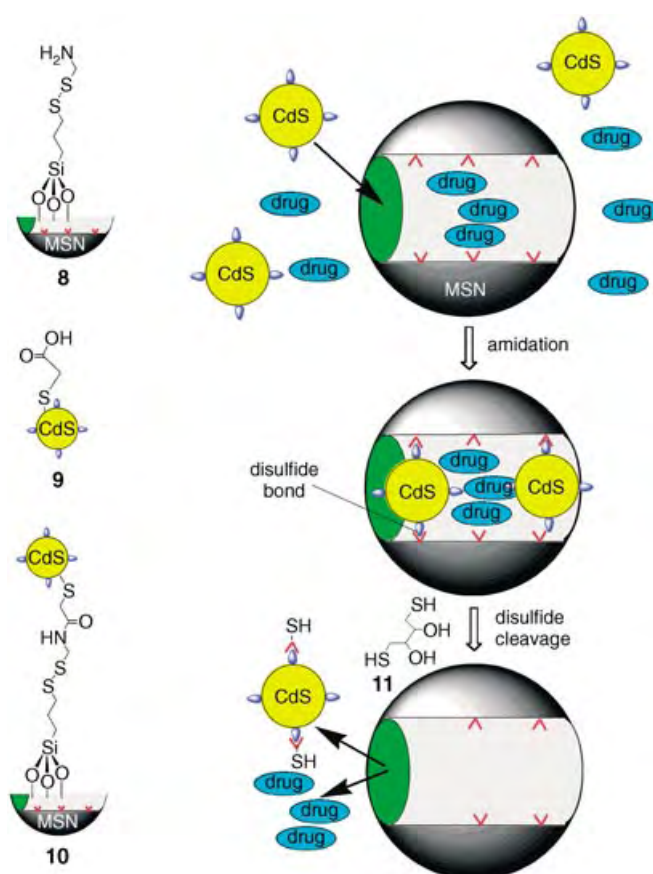


Figure 6. CdS NP-capped mesoporous silica nanosphere (MSN)-based system for the controlled delivery of drugs and neurotransmitters. (Adapted from Ref. [108], with permission; Copyright American Chemical Society, 2003).

aggregation of NPs induced by specific biological interactions attracts interest as a self-assembly process for the construction of complex nanostructures that exhibit new collective properties.

Several reasons support the concept of utilizing biomolecules as building blocks of NP structures: 1) The diversity of biomolecules enables the selection of building units of predesigned size, shape, and functionality. 2) The availability of chemical and biological means to modify and synthesize biomolecules. For example, the synthesis of nucleic acids of predesigned composition and shape, the elicitation of monoclonal antibodies, or the modification of proteins by genetic engineering to allow the construction of biomaterials for the directed assembly of nanoparticles. 3) Enzymes may act as biocatalytic tools for the manipulation of the biomaterials. The hydrolysis of proteins, the scission or ligation of DNA, or the replication of nucleic acids may be employed as tools for the assembly of NP architectures through manipulation of the biomaterial. 4) Mother Nature has developed routes for the repair of biomolecules that may be applied to stabilize the biomolecule–NP structures. 5) Nanoparticles that are cross-linked with enzyme units may generate biocatalytic assemblies of predesigned functionality. These different features of the biomolecule cross-linking units provide a flexible means

of generation of NP structures of tunable physical, chemical, and functional properties. For the generation of biomolecule-cross-linked NPs, two types of biomolecule-functionalized NPs with complementary units should participate in the assembly process. Biomaterials utilized in the fabrication of such biomolecule–NP aggregates include biological protein host–guest pairs such as biotin–streptavidin,^[117] antigen–antibody,^[118] and complementary oligonucleotide pairs.^[117,119,120] A large variety of methods including optical methods, such as differential light-scattering spectroscopy,^[121] has been used to study the biospecific assembly of NPs with proteins and oligonucleotides. Electrophoretic and structural studies of the DNA-directed aggregation of Au NPs have been published recently.^[122]

4.1. Receptor-Induced Aggregation of Guest-Functionalized Nanoparticles

Protein-based recognition systems can be used to organize inorganic NPs into network aggregates. For instance, the interaction between D-biotin and the biotin-binding protein streptavidin (SAv) was utilized to induce the aggregation of NPs.^[117] The recognition between water-soluble biotin and the homotetrameric protein SAv is characterized by an extraordinary affinity constant, $K_a > 10^{14} \text{ M}^{-1}$, that makes it the strongest ligand–receptor binding interaction presently known.^[123] Another great advantage of SAv is its extremely high chemical and thermal stability. The applicability of the biotin–SAv system to generate supramolecular aggregates is enhanced by the availability of various avidin analogues^[124] and recombinant SAv mutants.^[125] A wide range of rate and equilibrium constants ($10^0 \leq K_a \leq 10^{15} \text{ M}^{-1}$) are available that allow the construction of carefully designed NP aggregates. Many biotinylated materials are commercially available or can be prepared under mild conditions. Two routes to the aggregation of NPs by biotin–SAv interactions are possible: 1) NPs functionalized with biotin groups can be cross-linked with the tetraivalent SAv receptor (Figure 7 A), and 2) NPs functionalized with SAv can be cross-linked with the dibiotin derivative **12** (Figure 7 B). Metal and semiconductor NPs can be functionalized with biotin derivatives by one of several synthetic routes. In the simplest method, thiol or disulfide derivatives of biotin are directly adsorbed onto metal NPs (e.g. Au, Ag). Alternatively, NPs can first be coated with an organic “shell” (e.g. by the polymerization of a trialkoxysilyl derivative or by polymer adsorption) and then covalently modified with biotin, for example, by carbodiimide coupling.

Au NPs functionalized with adsorbed biotin units and then cross-linked with SAv units have been shown to yield aggregates of Au NPs with the biotin–SAv recognition pairs between the individual NPs (Figure 7 A).^[117,126] A similar architecture can be built by reversing the steps: SAv was interacted with the biotin disulfide derivative **13** to produce a complex, which was then treated with Au NPs (Figure 7 C).^[126a] In both cases, fast, spontaneous aggregation of the Au NPs was observed which resulted in a nonordered network of particles. Dynamic light-scattering spectroscopy, small-angle X-ray scattering studies, and TEM were used to

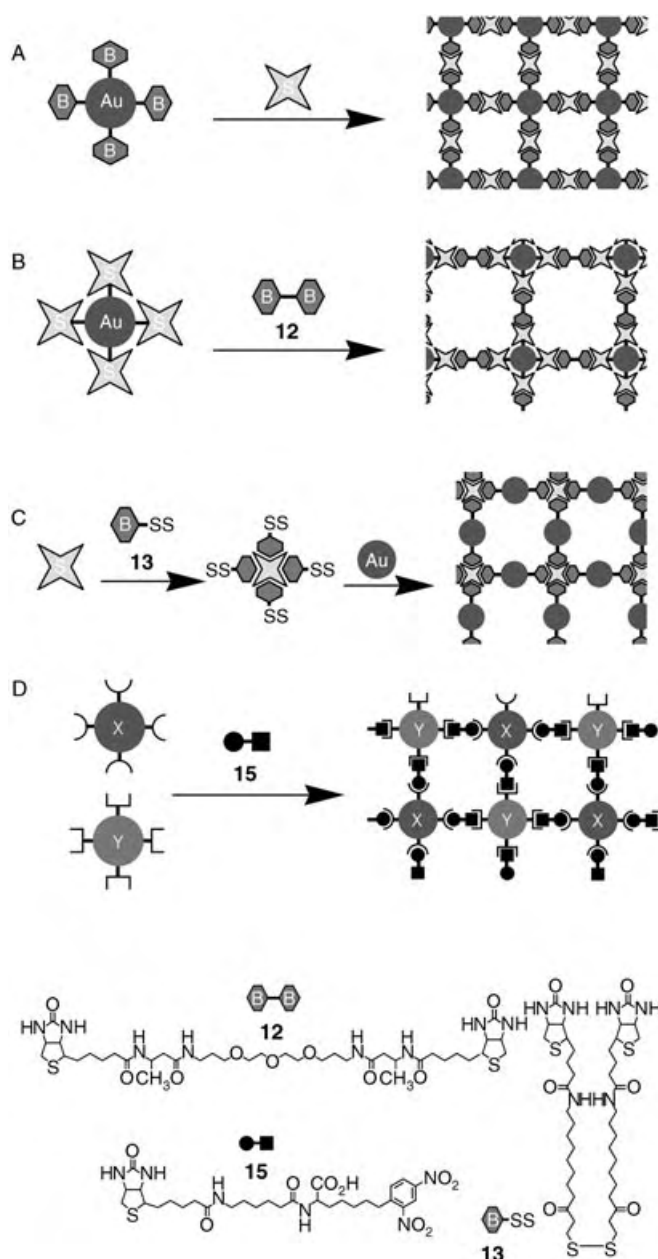


Figure 7. The use of biotin–streptavidin (SAv) interactions to build nanoparticle networks: A) Streptavidin as a linker between biotin-functionalized Au NPs; B) A biotin dimer used to link streptavidin-functionalized Au NPs; C) Streptavidin-linked thiolated biotin used to build NP networks; D) The formation of a network from two types of NPs that are functionalized with different recognition units and cross-linked with a bifunctional linker, **15**, which is composed of a biotin unit and a dinitrophenyl-antigen unit.

follow the aggregation process and to characterize the product. The kinetics of this process was fitted to the theoretical Smoluchowski model of aggregation, which was modified for nanoparticles.^[126b] This kinetic analysis allows the control of the aggregate structure by the optimization of the conditions, that is, the molar ratio of the biotin-functionalized NPs and the SAv cross-linker.

A related SAv-induced aggregation of Au nanorods was reported recently.^[127] Gold nanorods (aspect ratio = 18) were

prepared in water in the presence of a shape-directing surfactant, cetyltrimethylammonium bromide (CTAB), and were further functionalized with a biotin disulfide derivative. The addition of a streptavidin linker to the biotin-modified Au nanorods produced an unexpectedly high proportion of end-to-end-linked Au nanorods that were separated by 4–5 nm spacing, which corresponds to the size of a streptavidin molecule ($\approx 4.5 \times 4.5 \times 5.8 \text{ nm}^3$), and were at angles expected for the four biotin binding sites on the streptavidin projected into two dimensions (Figure 8A). The mechanism behind the

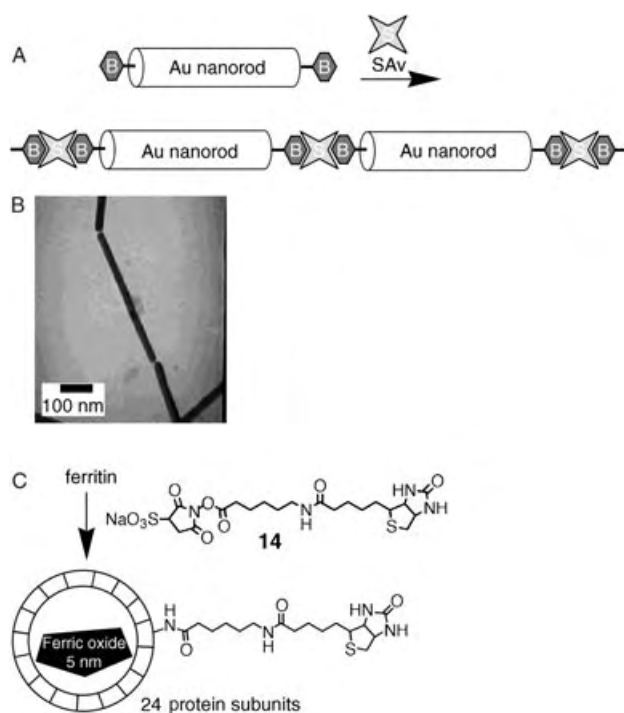


Figure 8. A) End-to-end assembly of biotin-functionalized Au nanorods that are cross-linked by streptavidin (SAv). B) Transmission electron micrograph of the SAv-interconnected Au nanorods. C) Biotin-functionalized ferritin. (Part B is adapted from Ref. [127], with permission; Copyright American Chemical Society, 2003).

higher-than-expected proportion of end-to-end linkages of the Au nanorods is not understood yet. However, there are two possible explanations of the phenomenon: 1) The biotin disulfide was unsuccessful at displacing the CTAB bound to the length of the gold nanorods. Thus, the biotin preferentially binds to the {111} ends of the Au rods which results in preferential end-to-end linkages upon the addition of streptavidin. The bilayer structure of CTAB on the nanorod surface may make the surfactant less easy to displace than at the end defects. 2) The biotin indeed binds all over the rods, but streptavidin is sterically constrained to bind only to the sides of the rods. Nevertheless, the generated nanostructures (Figure 8B) provide evidence that chemical linkages can organize nanorods in a nonrandom fashion, which may be exploited for the assembly of higher-order arrays of nanomaterials. By the future use of metal NP-modified SAv,

catalytic protein cross-linkers may be envisaged, and Au nanorods may be connected by other metals, such as Ag^0 , to continuous wires.

Another example of biotin–SAv cross-linked NPs involves the native protein ferritin, which consists of a hollow polypeptide shell (8- and 12-nm internal and external diameters, respectively) and a 5-nm-diameter ferric oxide core ($5\text{Fe}_2\text{O}_3 \cdot 9\text{H}_2\text{O}$).^[128] The ferric oxide NP can be easily removed from the protein shell by reductive dissolution, and the empty cage of apo-ferritin can be remineralized in vitro with a range of inorganic oxides, sulfides, and selenides (e.g. MnO , FeS , CdS , CdSe)^[129,130] or more-complex compounds (e.g. Prussian Blue).^[131] A succinimidyl active ester derivative of biotin, **14**, was covalently linked to the amine groups of lysine residues of the polypeptide shell of ferritin to yield a biotin-functionalized protein shell that contained the ferric oxide core (Figure 8C). Addition of SAv resulted in the cross-linking and therefore the aggregation of the functionalized ferric oxide NPs.^[132] Considering the library of core NPs possible, this ferritin-based aggregate is a very promising material for the production of electronic, magnetoelectronic, and optoelectronic devices.

Nanoparticle aggregates have also been produced by means of the interaction between antigens and antibodies.^[38,118] In the simplest approach, anti-DNP IgE antibodies (DNP = dinitrophenyl) were adsorbed onto 12-nm Au NPs, and these conjugates were then cross-linked with a synthetic antigen (*N*-2,4-bis(dinitrophenyl)octamethylenediamine), which comprised two hapten DNP head groups that were separated by a spacer. A more sophisticated approach allows the association of two different types of NPs. For this purpose, two different NPs that are functionalized with different kinds of bioreceptors (e.g. different antibodies, or an antibody and SAv) are cross-linked with a ligand, which contains two different head groups to provide affinity binding to the two respective receptors. As an example, two types of Au NPs were functionalized, one with anti-DNP IgE and the other with SAv.^[38,118] They were cross-linked with the linker **15**, which contains a biotin unit at one end and a DNP group at the other end of a spacer (Figure 7D). Each ligand recognizes its respective receptor—biotin binds to SAv; DNP binds to anti-DNP IgE—to create a network composed of both nanoparticles.

The aggregation of NPs by antigen–antibody interactions in solution was applied to develop immunoassay procedures with optical detection of the association process. A laser-based double-beam absorption detection system for aggregation immunoassays has been developed.^[133,134] The assay was based on the aggregation of gold NPs, which were coated with protein antigens, in the presence of the corresponding antibodies. The aggregation of the gold NPs resulted in a change in the absorption bands which enabled the assay to be monitored at 635 nm with a detection limit for an antibody of $3 \times 10^{-8} \text{ M}$. A rapid immunoassay for the detection of an analyte within complex biological media without any sample preparation was demonstrated with gold nanoshells, namely, layered dielectric-metal NPs, whose optical resonance is a function of the relative size of their constituent layers.^[135] The aggregation of antibody–nanoshell conjugates, which exhibit

absorption spectra in the near-infrared region, was monitored spectroscopically in the presence of the analyte. Immunoglobulins were successfully detected from saline, serum, and whole blood media.

Complementary bioconjugates that consist of an antibody–antigen pair were immobilized on luminescent CdTe NPs (quantum dots) of variable sizes, and these were used for the examination of interparticle energy-transfer processes.^[136] The antigen bovine serum albumin (BSA) was conjugated to red-emitting CdTe NPs, whereas the corresponding anti-BSA antibody (IgG) was linked to green-emitting CdTe NPs. The formation of the BSA–IgG immunocomplex resulted in fluorescence resonance energy transfer (FRET) between the two different nanoparticles. The luminescence of the green-emitting nanoparticles was quenched, whereas the emission of the red-emitting nanoparticles was enhanced. The luminescence of the green-emitting quantum dots could be recovered upon exposure of the complex to unlabeled antigen. The antigen–antibody–CdTe-NP aggregate may, thus, be considered as a functional superstructure for the competitive optical detection of antigens or antibodies.

A novel approach to induce the cross-linking of NPs involves the application of predesigned de novo proteins that display specific affinities to inorganic crystal surfaces.^[21a] These structures can specifically and directly bind to unmodified surfaces of various semiconductive nanoparticles to act as bridges and result in the aggregation of the NPs. From a combinatorial library of $\approx 10^9$ random 12-mer peptides, de novo proteins that exhibit specific binding capabilities to single-crystal semiconductors including GaAs(100), GaAs(111), InP(100), and Si(100) have been discovered.^[137]

4.2. Nucleic Acid Functionalized Nanoparticles for Controlled Aggregation

DNA molecules are very powerful and versatile linkers for the controlled aggregation of nanoparticles.^[119, 120, 138] DNA chains are of a controllable length and composition and provide predictable properties and enormous control over complementarity. Double-stranded DNA provides rigid spacers that allow control over the distances between nanoparticles. Long DNA chains can act as templates, ready to accommodate complementary DNA-functionalized nanoparticles in a controlled order and with controlled distances between the nanoparticles.

To demonstrate the DNA-mediated binding of NPs, two batches of 13-nm-diameter Au NPs were separately functionalized with two thiol-derivatized noncomplementary DNA oligonucleotides: 3'-thiol-TACCGTTG-5' and 5'-AGTCGTTT-3'-thiol (**16** and **17**, respectively; Figure 9A).^[69a] A DNA linker, **18**, composed of ds-DNA in the center and two single-stranded fragments on the ends was constructed. The two single-stranded sections were complementary to the oligonucleotides connected to the two different NPs. The addition of the linker to a mixed solution of the two DNA-functionalized Au NPs resulted in the cross-linking and aggregation of the nanoparticles. The resulting NP aggregate should theoretically have some degree of regularity, but this

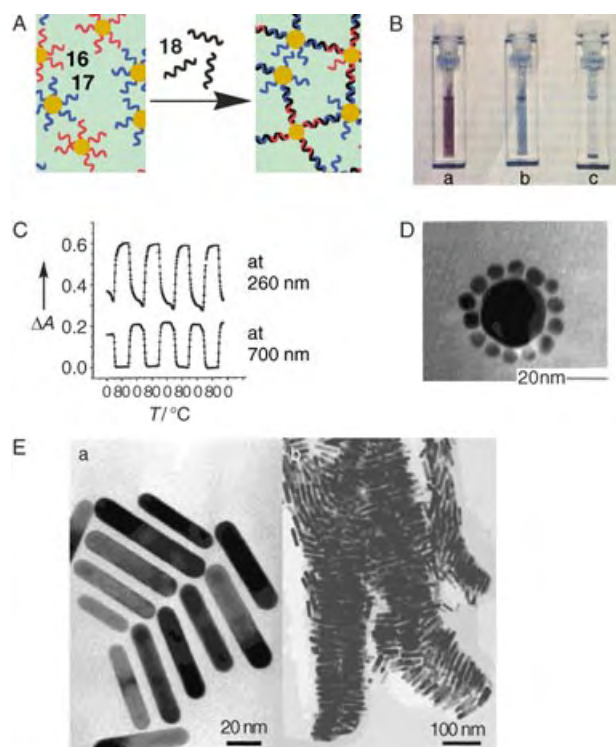


Figure 9. A) The aggregation of oligonucleotide-functionalized Au NPs by the addition of a DNA strand **18** which has sections that are complementary to the DNA strands **16** and **17**. B) Cuvettes with a mixture of the Au NPs and the added DNA strand responsible for the assembly process: a) at 80 °C, the DNA-functionalized NPs are in the unhybridized state; b) soon after cooling to room temperature, the NPs undergo association, but the precipitate has not yet settled; c) after the associated NPs have settled to the bottom of the cuvette. C) Variations in the absorption spectrum of the DNA-linked NP networks as a function of temperature. D) A “satellite” system that consists of two different sizes of nanoparticles. E) Transmission electron micrographs of gold nanorods that are organized by DNA hybridization. (Parts A–C are adapted from Ref. [69a]; Part D is adapted from Ref. [142]; Part E is adapted from Ref. [144]; Reproduced with permission of the Royal Society of Chemistry).

could not be observed as both NPs had identical cores. Aggregation changed the color of the solution owing to a collective phenomenon originating from the short distance of the interparticle separation. Separate Au NPs have a red color as a consequence of their plasmon absorbance, but upon aggregation, another absorbance arises at lower energies because of interparticle plasmon coupling (Figure 9B). The association process is temperature-dependent, and the aggregated Au NPs can reversibly dissociate upon elevation of the temperature through melting of the double-strands and associate again upon a decrease in the temperature through the rehybridization process which results in the reversible changes of the spectrum (Figure 9C). In a control experiment, a noncomplementary linker was added to the solution of the mixed particles and no color changes were observed.

Changes in the optical and electronic properties of NPs upon their aggregation provide a way to detect the association process and thus allows the design of optical DNA biosensors.^[139–141] The color change lies in the background of the

simplest and most powerful analytical tool to monitor the aggregation of Au NPs, namely, the “Northwestern” spot test, developed by Mirkin and co-workers.^[139] This is an extremely sensitive method to discriminate between aggregated and nonaggregated gold NPs in aqueous solution and it relies on a perceptible color change from red to blue upon aggregation. The test consists of the evaporation of a droplet of an aqueous solution of particles on a reverse-phase thin-layer chromatography plate. A blue spot indicates aggregation, whereas a red spot indicates the presence of freely dispersed particles.

In a more sophisticated investigation, a mixture of DNA-functionalized Au NPs of 40-nm (A) and 5-nm (B) diameters were cross-linked with a DNA linker.^[142] The larger NP A accommodates many small NPs B around it to produce a so-called “satellite” AB_n system (Figure 9D). Interconnections between these “satellite” aggregates yield a 3D network $(AB_n)_m$. An important factor that controls the optical properties of the network is the length of the cross-linking DNA oligonucleotide bridge—it controls not only the interparticle distances, but also the rate of aggregation and thus, the number of NPs per aggregate.^[143] In a similar approach, DNA-functionalized CdSe/ZnS NPs and Au NPs were cross-linked with a complementary linker to yield a binary network.^[70] Fluorescence and absorption spectroscopy indicated cooperative optical and electronic phenomena within the resulting material. The application of DNA-functionalized Au nanorods instead of spherical nanoparticles resulted in micro-sized rods, which were composed of many cross-linked nanounits (Figure 9E),^[144] that exhibited unusual anisotropic properties.

Au NPs were applied as colorimetric reporter groups that show distinctive color changes upon different aggregation states for DNA sensing.^[139–141] The sensitivity and selectivity of this method rivals other methods, such as those based on fluorescence spectroscopy. Whereas this method plays an increasingly important role in genomic research, the nanoparticle aggregation methodology has expanded beyond the detection of DNA to the analysis of other analytes such as heavy metal ions,^[145] potassium ions,^[146] and protein A.^[134] Interesting recent examples have demonstrated the controlled aggregation of nucleic acid functional-

ized Au NPs as optical labels for the detection of Pb^{2+} ions or adenosine by DNAzymes.^[147] Catalytic deoxyribonucleic acids (catalytic DNAs or DNAzymes) attract substantial recent research efforts, and specific DNAzymes that bind Pb^{2+} , Cu^{2+} , or Zn^{2+} ions were elicited by the combinatorial in vitro selection method.^[148] Particularly, “8–17” DNAzyme has demonstrated high activity and specificity towards Pb^{2+} ions.^[149] The nucleic acid sequence **17E** was found to exhibit high affinity for Pb^{2+} ions, and the resulting complex revealed catalytic activity towards the specific scission of the complementary nucleic acid **17DS** that includes mostly deoxyribonucleosides as bases as well as one adenosine ribonucleoside (rA) entity at the cleavage site (Figure 10A a).^[147a] Upon the

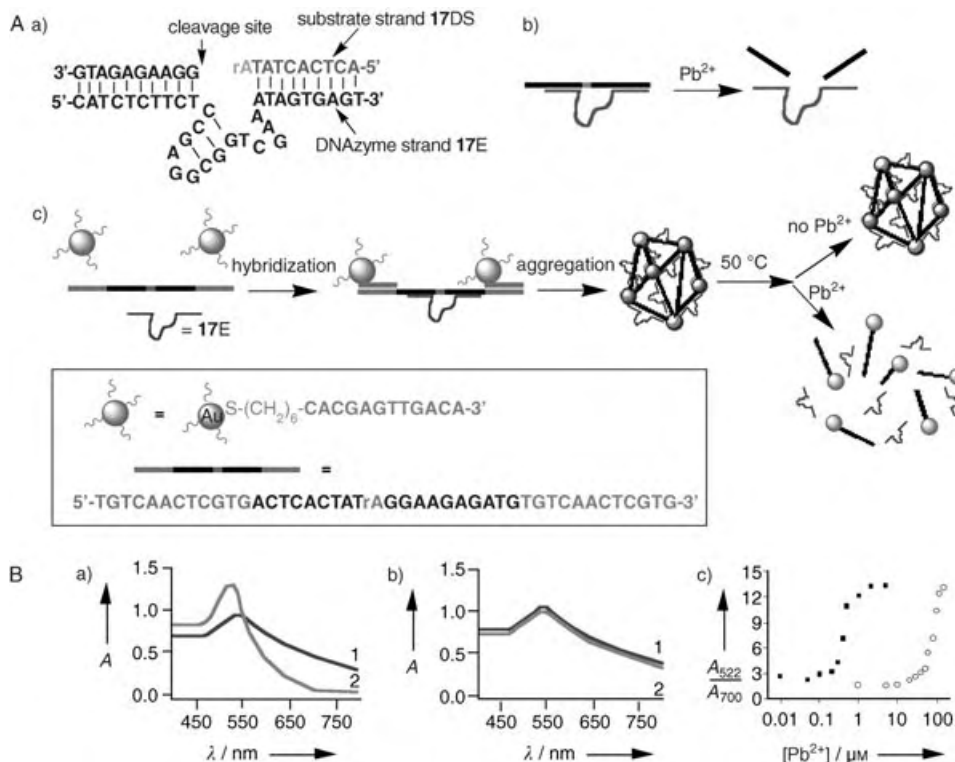


Figure 10. A) DNAzyme system for the analysis of metal ions. a) Secondary structure of the “8–17” DNAzyme system that consists of the enzyme strand **17E** and a substrate strand **17DS**. Except for a ribonucleoside adenosine (rA) at the cleavage site, all other nucleosides are deoxyribonucleosides; b) Cleavage of **17DS** by **17E** in the presence of Pb^{2+} ions; c) DNAzyme-directed assembly of the oligonucleotide-functionalized Au NPs, and the application of the assemblies for Pb^{2+} sensing. B) UV/Vis absorbance spectra of a) the active **17E** DNAzyme–NP sensor and b) an inactive **17Ec** DNAzyme–NP sensor. The spectra were recorded in the absence (1) or in the presence (2) of Pb^{2+} ions ($5 \mu M$); c) Calibration plots for the analysis of Pb^{2+} ions, in which the enzyme strand is the active **17E** only (■) and when the ratio of **17E**/**17Ec** is 1:20 (○). (Adapted from Ref. [147], with permission; Copyright American Chemical Society, 2003).

cleavage of the double-stranded nucleic acid, the melting point of the cleaved duplex is lowered, and the single strands are easily separated (Figure 10A b). Accordingly, the complementary substrate of the DNAzyme, **17DS**, was elongated with nucleic acids that are complementary to secondary nucleic acid labeled Au NPs. Mixing of all three components—the DNAzyme **17E**, the complementary nucleic acid substrate **17DS**, and the nucleic acid labeled Au NPs—resulted in the hybridization of the respective components, and the aggregation of the hybrid system into clusters

(Figure 10A c). In the aggregate, the characteristic interparticle-coupled plasmon absorbance was observed (Figure 10B a, curve 1). The addition of Pb^{2+} ions resulted in the DNAzyme-assisted cleavage of the complementary nucleic acid, which led to the separation of the Au NP aggregates and the formation of the localized plasmon absorbance of the nonaggregated Au NPs (Figure 10B a, curve 2). With this approach, Pb^{2+} ions could be detected in the concentration range of 0.1–4 μM (Figure 10B c, ■). In a control experiment, the function of the DNAzyme as the active component for the detection of Pb^{2+} ions was nicely demonstrated. The T base at the tenth position in the sequence was exchanged by a C base which led to complementarity in the loop region of the DNAzyme (17Ec). This resulted in a very poor scission activity of the duplex structure in the presence of Pb^{2+} ions (Figure 10B b, curves 1 and 2) and in a substantial decrease in the sensitivity of the system (Figure 10B c, ○).

To expand the methodology to a broader range of analytes, a colorimetric biosensor for adenosine was tailored on the basis of the aptazyme-directed assembly of gold NPs.^[147b] The aptazyme was bound on a 8–17 DNAzyme that is allosterically activated by the adenosine aptamer. In the absence of adenosine, an inactive aptazyme is formed, and the DNA strand operates as a linker for the assembly of a blue-colored aggregate of 13-nm Au NPs. In the presence of adenosine, however, the aptazyme is activated, and the DNA strand is cleaved. This prevents the aggregation of the Au NPs which results in a red-colored system characteristic of the discrete individual nanoparticles. Concentrations of up to 1 mM of adenosine could be semiquantitatively measured by the extent of blue-to-red color changes, or quantitatively measured by the ratios of the absorbances at 520 and 700 nm. The addition of guanosine, cytidine, or uridine (all 5 mM) in place of adenosine did not affect the aggregation of the DNA-bound Au NPs which indicates the specificity of the system towards adenosine. Because aptamers may be developed for different analytes, the rational design of aptazymes through the incorporation of aptamer units and upon coupling to Au NPs may lead to versatile colorimetric biosensors.

Biocatalyzed transformations of functionalized oligonucleotide assemblies were used to perform controlled association of NPs and to provide stabilization of the particulate aggregates.^[150] Au NPs (15 nm) were functionalized with thiolated single-stranded DNA of 45 bases, **19** (Figure 11 A). The Au NP-bound DNA was then converted into the double-stranded form through hybridization with the complementary ss-DNA, **20**. The DNA sequence was chosen so that the double strands that were formed on the particles would contain recognition sites for a number of restriction endonucleases. After DNA hybridization, the system did not contain any single-stranded DNA capable of further hybridization with complementary linker strands. To create reactive sites by deprotection, the restriction enzyme *EcoRI* was used to cleave the double strands on the particles at specific recognition sites to leave a cohesive end for further hybridization (Figure 11 A, step a). After this first enzymatic step, hybridization between the newly created cohesive ends through the relatively labile overlap of only four complementary base pairs resulted in the formation of weakly

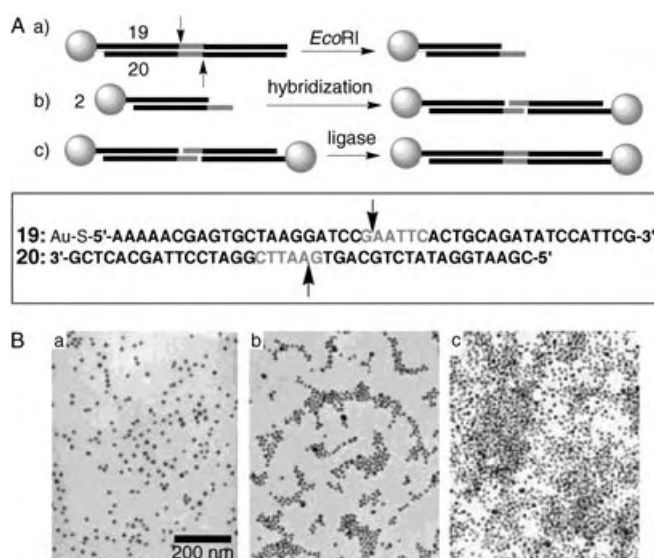


Figure 11. A) Controlled association of Au NPs based on biocatalytic transformations of oligonucleotides. a) Au NPs that are derivatized with ds-DNA are treated with the restriction enzyme *EcoRI*, which cleaves the DNA to yield cohesive ends (the gray color represents the recognition site of the enzyme, and the arrows indicate the sites of cleavage on each strand); b) Two cohesive ends hybridize, which leads to a weak association of particles; c) The DNA backbones are covalently joined at the hybridized site by DNA ligase to yield a stable 40-base-pair double-stranded link between the particles. B) TEM analysis of the DNA–NP complexes before (a) and after (b) treatment with *EcoRI* and after subsequent treatment with DNA ligase (c). (Adapted from Ref. [150], with permission).

associated aggregates of particles (Figure 11 A, step b). This process was investigated by TEM as shown in Figure 11 B, images a and b. The formation of small aggregates is clearly seen in comparison to the randomly distributed individual particles prior to enzyme treatment. To stabilize the system at this stage, the DNA backbones at the hybridized cohesive ends were covalently joined in a second enzymatic step by using T-4 DNA ligase (Figure 11 A, step c). The resulting TEM image shows the presence of significantly larger aggregates that are formed as a consequence of much stronger interparticle binding by the newly formed 40-base-pair double-stranded linker (Figure 11 B, image c). In this sequence of biocatalytic reactions, randomly dispersed DNA-coated Au NPs were converted first into weakly associated structures and subsequently into an aggregated system through simple and predictable manipulation with DNA-processing enzymes.

Proteins such as bacterial DNA methyltransferases (*M.EcoRI* and *M.HhaI*) or restriction endonuclease (*R.EcoRI*) are known to bind and produce specific conformational changes in DNA. *M.EcoRI* recognizes the GAATTC sequence and methylates the second adenine by bending the DNA strand by approximately 55–59° and flipping the target adenine out of the DNA duplex. This process could affect significantly the distance between nanoparticles bridged by the ds-DNA. For example, a 40-mer duplex DNA with an incorporated base-pair target site (GAATTC) was used as a rigid spacer between two 1.4-nm Au NPs to separate them by

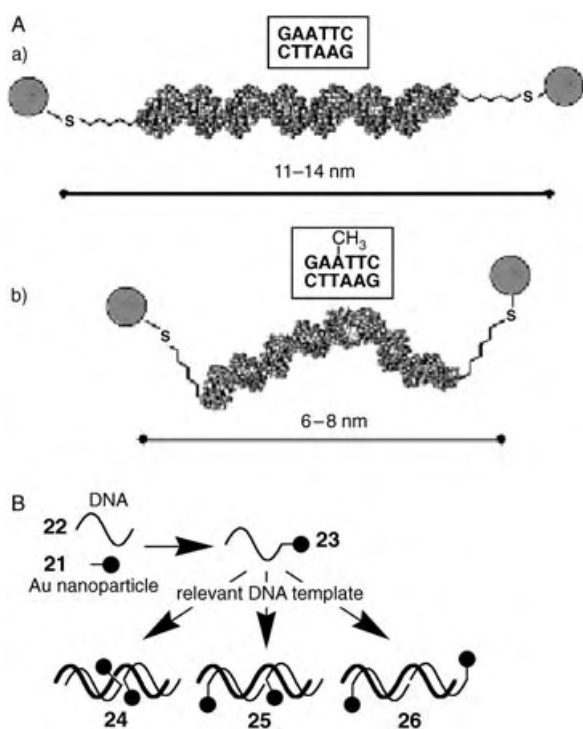


Figure 12. A) Enzyme-controlled distance between DNA-bridged Au NPs. a) ds-DNA–Au NP hybrid with the *M.EcoRI* recognition site; b) The hybrid with a 59° bend following the binding of the *M.EcoRI* enzyme. B) The assembly of controlled multiparticle composites upon hybridization on a DNA template. (Part A is adapted from Ref. [151], with permission; Copyright American Chemical Society, 2002).

11–14 nm (Figure 12 A a).^[151] Upon addition of *M.EcoRI* to a solution of the ds-DNA–Au NP hybrid, the binding of the protein and the biocatalytic methylation of the adenine base produces a drastic decrease in the Au–Au separation distance to 6–8 nm (Figure 12 A b). The measured distances correlate with the expected topological changes that are induced by the binding of *M.EcoRI* to the DNA chain.

Long DNA molecules that are capable of accommodating several complementary DNA fragments in different domains on the strand can serve as templates for the construction of specific linear assemblies.^[152,153] To prevent the microscopic cross-linking of nanoparticles which results in a network, Au NPs functionalized with a single maleimide group, **21**, were reacted with thiol-derivatized DNA oligonucleotides **22**. The resulting mono-DNA-functionalized Au NPs, **23**, were associated with the respective complementary domains on the DNA template molecule (Figure 12 B). Individual placement of the nanoparticles at specific complementary domains of the template allows control of the distances between them as well as controlled placement of different types of NPs (different sizes and materials) on the template to result in a variety of properties of the NPs assemblies. For example, two DNA-functionalized Au NPs can be placed on the DNA template in three different orientations, “head-to-head” (**24**), “head-to-tail” (**25**), and “tail-to-tail” (**26**), thus providing different distances between the nanoparticles.

Recently, a newly discovered aggregation phenomenon of DNA-functionalized gold nanoparticles induced by the

hybridization of a DNA target was reported in which the NPs are not cross-linked.^[154] The Au NPs (15 nm) were functionalized with a single-stranded DNA (≈ 200 DNA probes per particle). Whereas bare Au NPs without the probe DNA immediately aggregated in NaCl solution (0.1 M), the DNA-functionalized NPs did not exhibit any visible change in solutions of NaCl (concentrations up to 2.5 M). Thus, the surface-immobilized probe DNA stabilizes the nanoparticle dispersion. An equivalent amount of a complementary target DNA was added to the system and resulted in the hybridization of the DNA probe that was associated with the Au NPs. The subsequent addition of aqueous NaCl at concentrations higher than 0.5 M resulted in a fast (< 3 min) color change to purple that represents an aggregation of the particles. Although the mechanism of this phenomenon is not fully understood at present, the conformational transition of the immobilized DNA probably plays an essential role—formation of the probe-target duplex makes the conformation more tight and more rigid. This conformational transition may decrease two contributions of the repulsive interactions between the nanoparticles. First, electrostatic repulsion may be decreased by the screening effect because the tight conformation raises the binding constant with counterions. Second, steric repulsion may be decreased by the stiffening of the DNA which lowers the entropic effect. In this non-cross-linking system, the aggregation is driven by London–van der Waals attractive forces between the nanoparticles in which the repulsive interaction is greatly reduced by the formation of duplexes on the surfaces of the NPs. The attractive force works from a distance and leads to the rapid aggregation.

The use of peptide nucleic acids (PNAs), which are DNA analogues in which the entire sugar-phosphate backbone is replaced by a polypeptide backbone, as a means to control the aggregation of nanoparticles was reported recently.^[155] Au NPs (13 ± 1.2 nm) were functionalized with various PNA primers, and these were used for the self-assembled aggregation of the particles upon hybridization of the complementary PNA sequences. PNA complexes offer two important advantages for biomaterials-based nanofabrication: 1) PNA complexes exhibit enhanced stability relative to their respective DNA analogues and 2) the amino acid unit may be easily altered in the PNA backbone to enable a higher degree of complexity in the strands. For example, by the substitution of glycine with other amino acids in the PNA, the structural and electrostatic properties of the PNA complex may be regulated and the dynamics of assembly may be controlled. Besides the possible applications of PNA complexes for nanofabrication, PNA–NP conjugates may offer advantages over DNA–NP conjugates for biosensing. The enhanced base-pair mismatch selectivity of PNA may improve the specificity of the sensors in the analysis of sequence-specific nucleic acids.

4.3. Composite Assemblies of Nucleic Acids, Proteins, and Nanoparticles

A combination of the synthetic methods to prepare biomolecule-functionalized nanoparticles (See Sections 2.1–

2.3) and the application of proteins, which have affinity properties (e.g. SAV, antibodies), oligonucleotides, and nanoparticles as building blocks allows the construction of very sophisticated biomolecule–NP hybrid clusters (Figure 13 A).^[21a] To functionalize Au NPs with antibodies, a

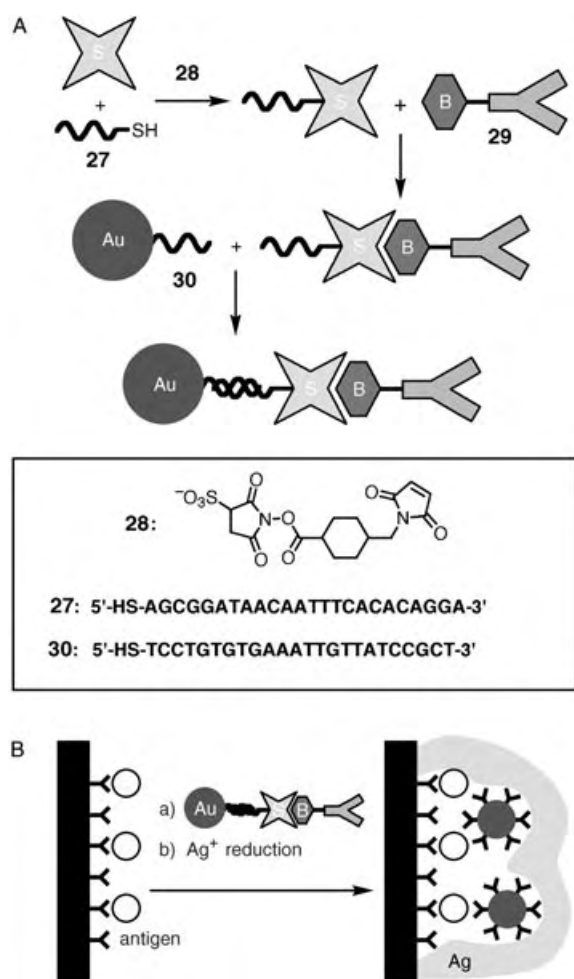


Figure 13. A) The formation of a Au nanoparticle–IgG–antibody conjugate. B) The use of the conjugate for the sensing of antigens.

multistep procedure was developed.^[156] The 5'-thiol-modified oligonucleotide, 27, was covalently bound to SAV through the heterobifunctional cross-linker sulfo succinimidyl-4-(maleimido methyl)cyclohexane-1-carboxylate (28). The resulting conjugate had four binding sites for biotin ligands and one nucleic acid function. The SAV receptor sites were treated with biotinylated antibodies, 29, which were directed against mouse IgG (αM -IgG) or rabbit IgG (αR -IgG), to yield DNA-tagged antibody conjugates that could bind to a complementary DNA strand from one side and to the respective antigens from the other. This architecture was treated with Au NPs that were functionalized with oligonucleotides 30, which were complementary to the DNA tag, to yield Au NPs that were modified with the antibody molecules. The resulting conjugate was then applied as a label for the immunoassay of the respective antigens, which were bound to

a surface. The linkage of the Au NPs to the antigen–antibody complex was further amplified by the electroless deposition of Ag on the Au NPs (Figure 13 B).^[156]

A combination of receptor proteins and oligonucleotides as bridging units for the directed aggregation of nanoparticles allows the complex structuring of the assemblies.^[157] As an example, SAV was interacted with biotinylated DNA to result in a four-DNA–SAV conjugate.^[157a] Application of this conjugate as a building block for the aggregation of DNA-functionalized Au NPs yielded a network with a motif that was different from that which resulted upon the direct aggregation of DNA-functionalized NPs bound by the complementary oligonucleotide. Even more fascinating aggregation resulted when Au NPs were primarily associated with SAV to yield nanoclusters, which were then placed on a DNA template (Figure 14 A).^[158] 1.4-nm Au NPs with a single

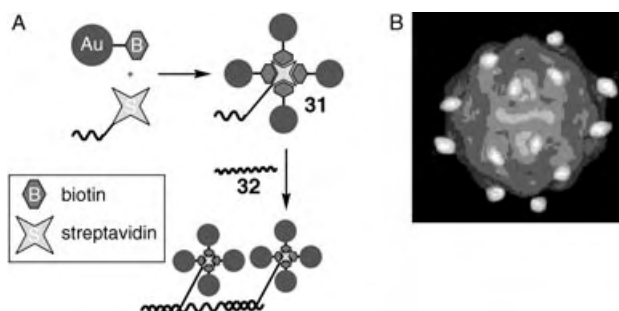


Figure 14. A) The construction of four-nanoparticle clusters, and their assembly into linear composites along a DNA template. B) A computer-generated electron-density map derived from the X-ray crystal structure of cowpea mosaic virus (CPMV) that is labeled with 1.4-nm Au clusters. (Part B is adapted from Ref. [159], with permission).

amine substituent were derivatized with a biotin group, and the biotin moiety was used to organize the nanoclusters into a tetrahedral superstructure defined by the geometry of the biotin-binding sites of the SAV. Prior to cluster formation, SAV was derivatized with a single DNA molecule. The resulting tetrahedral four-Au NP clusters, 31, each with a single DNA tail, were assembled on a DNA template molecule, 32, which dictated the positions and distances. This approach could allow the formation of almost any imaginable structure from nanoparticles of different sizes and various materials. NPs were also applied for the site-specific labeling of complex biological species such as viruses; for instance, a 30-nm-diameter sphere of the cowpea mosaic virus (CPMV) was labeled with 1.4-nm Au NPs (Figure 14 B).^[159]

Inorganic nanostructures were crystallographically controlled by using synthetic biomolecular templates that consisted of anionic DNA and cationic lipid membranes. These membranes self-assembled into a multilamellar structure in which a periodic 1D lattice of parallel DNA chains was confined between stacked 2D lipid sheets.^[160] Positively charged Cd^{2+} ions were electrostatically bound within the interhelical pores between the DNA strands and they were subsequently treated with H_2S to form CdS nanorods of controlled widths and crystallographic orientation. The strong

electrostatic interactions align the templated CdS (002) polar planes parallel to the negatively charged sugar-phosphate DNA backbone to ensure that the inorganic nanostructures are imprinted into the biomolecular matrix.

5. Assembly of Biomolecule–Nanoparticle Architectures on Surfaces

The immobilization of biomolecules on transducers such as electrodes, piezoelectric crystals, or field-effect transistors is attractive in the development of biosensors and bioelectronic devices.^[161–165] Several methods for the surface functionalization of electronic elements have been developed, and the means to couple the active sites or recognition processes of biomaterials with the electronic elements to yield the electronic transduction of the biological events have been demonstrated. Biosensors,^[166] biofuel-cell elements,^[167] and optobioelectronic systems^[168] have been constructed. Also, the deposition of biomaterials on nonconductive surfaces (e.g. plastics, glasses), and especially the patterning of such surfaces with biomaterials,^[165,169] is of great interest in tailoring protein and DNA chips for proteomic and genomic analyses, respectively. Diverse methods for the assembly of 2D and 3D nanoparticle structures on surfaces have been developed. Various applications of these systems, such as in the fabrication of photoelectrochemical cells (e.g. solar cells), light-emitting diodes, electrochromic systems, and computing devices, as well as the organization of different nanometric single-electron devices have been discussed.^[7a]

The integration of biomolecule–nanoparticle hybrid systems with surfaces paves the way for the generation of ordered architectures with new functionalities. The unique photonic properties of NPs may be employed to detect and probe biological recognition events on surfaces. Biomaterial structures adsorbed on the surfaces of nanoparticles may be probed by means of surface plasmon resonance (SPR), surface-enhanced Raman spectroscopy (SERS), and surface-enhanced fluorescence spectroscopic techniques. Also, the unique electronic (conductive) and catalytic properties of NPs may be used to provide electron transfer from or to redox centers of enzymes or to enhance the chemical reactivities of biomaterial structures.

Biomaterial constituents on surfaces also provide unique features for the formation of hybrid biomolecule–NP structures. Biomaterials, such as nucleic acids, and streptavidin–biotin or antigen–antibody complexes assembled on surfaces can provide templates for the immobilization of nanoparticles. Enzymes may be used as catalytic tools for the manipulation of biomaterials on surfaces; the ligation, scission, or polymerization of nucleic acids may be used to tailor nucleic acids of specific lengths and compositions. Thus,

complex biomaterial-based structures on surfaces may be engineered by the genetic manipulation of biomaterials, the synthesis of nucleic acids, and the biocatalytic manipulation of the biomaterial on the surface. The incorporation and integration of NPs in surface-confined biological templates can then yield new functional materials; as an example, the catalytic deposition of metals on NP seeds can generate circuitry with the shape of the biomaterial. Thus, hybrid biomolecule–NP composites on surfaces provide functional interfaces that could be important as materials for bioelectronic, electronic, optobioelectronic, and photonic applications.

The association of functionalized NPs and biomaterials with solid supports and liquid/liquid or liquid/air interfaces can be driven by charge interactions^[170] or by specific bioaffinity binding.^[21a] The subsequent sections address the methods to organize these composite biomolecule–NP systems on surfaces and discuss recent activities that utilize these systems for sensory, photoelectrochemical, and electronic circuitry applications.

5.1. Assembly of Layered Nanoparticle–Protein Arrays on Surfaces

Multilayer systems, which are composed of proteins and nanoparticles and assembled on solid supports,^[171] have been fabricated by the layer-by-layer deposition of the biological and inorganic components. Cytochrome c (cyt c)–TiO₂ NP layers were reported^[171a] in which the TiO₂ NP layers were deposited by boric acid promoted hydrolysis of hexafluorotitanate ions from aqueous solution (liquid-phase deposition process, LPD; Figure 15 A).^[172] The LPD technique enables the preparation of anatase TiO₂ without the need for organic

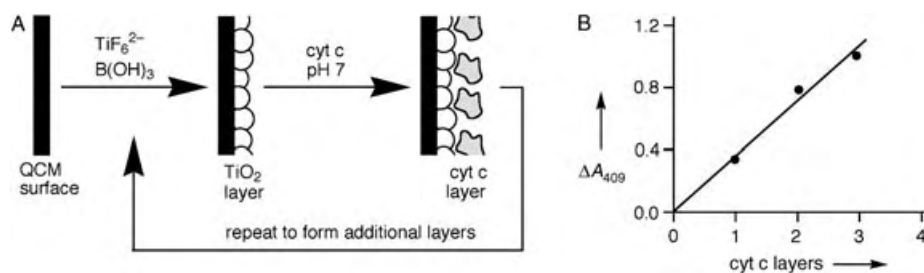


Figure 15. A) Method for the construction of TiO₂/cyt c multilayers on a QCM electrode. B) Optical absorbance at $\lambda = 409$ nm of assemblies of different thicknesses: the buildup of layers of cyt c is shown. (Part B is adapted from Ref. [171a], with permission).

solvents: this is essential for the codeposition of the biomaterial. The TiO₂ NPs on the surface produced by this technique are negatively charged. The subsequent deposition of the positively charged protein cyt c (isoelectric point, $pI = 10.1$) results in electrostatic attraction between the TiO₂ NPs and the protein which leads to the formation of multilayers. The deposition of the multilayers was followed by quartz crystal microbalance (QCM) microgravimetric measurements, which demonstrated a linear increase of the mass upon deposition of each double layer of TiO₂/cyt c. This

observation was also verified by absorbance spectroscopy (Figure 15B). This method could be widely extended to the preparation of other protein/metal-oxide multilayers that would facilitate the creation of photofunctional protein–inorganic superlattices. In another approach, assemblies of polyurethane_{core}/Au_{shell} NPs were used as permeable high-surface supports for the immobilization of enzymes such as pepsin to provide easy access of the substrate molecules to the enzyme active centers in the multilayer enzyme assembly.^[173]

Scanning electron microscopy (SEM) was applied for the quantitative analysis of protein chips.^[174] Interactions between biotin and streptavidin, and between an antibody with its cognate hapten, were used as model systems. The number of target-coated gold NPs that interact specifically with proteins arrayed on a derivative microscope glass slide were counted by utilizing backscattering electron detection. This approach facilitated the determination of the absolute, rather than relative, number of biomolecules bound to the chip.

5.2. Nucleic Acid–Nanoparticle Architectures on Surfaces

As discussed in Section 4.2, nucleic acids can serve as templates that bind DNA-functionalized nanoparticles at complementary segments. When DNA templates are fixed at a surface of a solid support, the resulting assemblies of NPs can yield a pattern that is dependent on either the shape produced by the DNA template itself or on the pattern produced upon its immobilization.

A natural single-stranded long-chain viral DNA, M13mp18 phage vector, **33**, which contains 7249 bases, was hybridized with a biotinylated short-chain target oligonucleotide, **34**, which was complementary to a specific segment of

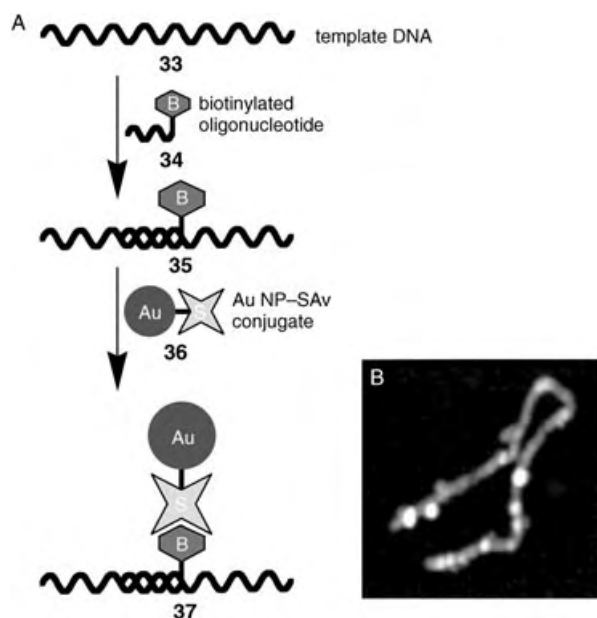


Figure 16. A) The controlled association of a SAu-coated Au NP with a ss-DNA template by means of the hybridization of a biotinylated ss-DNA with the template DNA. B) AFM image of a DNA strand with Au NPs that are specifically bound to the template through biotin–SAu interactions. (Part B is adapted from Ref. [175], with permission).

the viral DNA (Figure 16A).^[175] It should be noted that the template viral DNA **33** can have more than one complementary domain, thus it is capable of accommodating more than one biotinylated DNA chain. The hybridized DNA-holding biotin units **35** were then treated with SAu-coated Au NPs **36** (5 nm). The resulting negatively charged Au NP-labeled DNA template **37** was adsorbed on a surface of positively charged Mg²⁺-coated mica substrate and was subjected to atomic force microscopy (AFM) measurements (Figure 16B). The images obtained clearly show Au NPs associated with the DNA template, yet the number of Au NPs per DNA chain was not perfectly defined; this reflects either incomplete hybridization of the template with the biotinylated target DNA or incomplete association of the SAu-functionalized Au NPs with the biotinylated domains. As different biotinylated nucleic acid segments may be hybridized with the M13mp18 DNA, the entire viral DNA may be decorated with SAu–Au NPs. Indeed, such experiments revealed that the Au NP-functionalized viral DNA was formed on the solid support.

The electrostatic association of CdS NPs with DNA was applied as the driving force for the formation of a semiconductor NP–DNA wire on the surface.^[176] Negatively charged ds-DNA molecules associated with the water/air interface of a solution that contained cationic surfactant molecules (dioleoyltrimethylammonium propane, **38**; Figure 17). The layer at the interface was compressed by

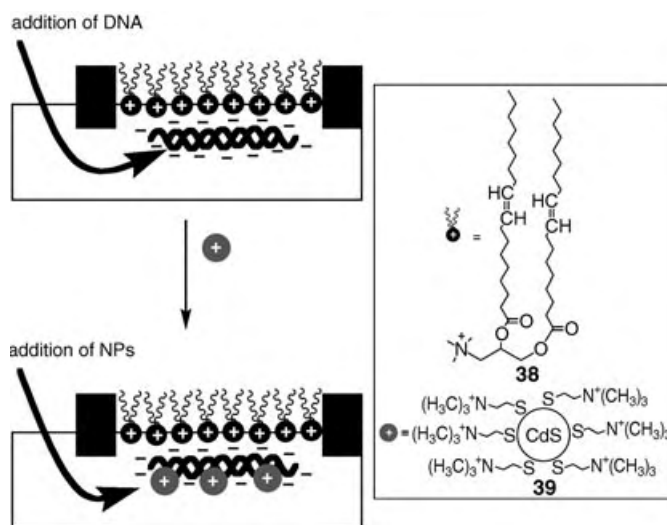


Figure 17. Electrostatic deposition of CdS NPs on a DNA chain at the air/water interface by using the Langmuir–Blodgett technique.

using the Langmuir–Blodgett technique to provide a high-density packing of the DNA molecules. Positively charged CdS NPs (3 nm) capped with thiocholine, **39**, were then added to the aqueous phase which resulted in their aggregation with the DNA. The formed DNA–CdS aggregates were transferred to a solid support, and electron microscopy images revealed the formation of densely packed CdS NPs along the DNA template. These generated chains were composed of semiconductor NPs with a diameter of ≈ 3 nm and an average separation of ≈ 3.5 nm.

Several other methods were reported to generate DNA–semiconductor (or metal) hybrid nanostructures on surfaces. The circular plasmid ds-DNA pUCLeu4 (3455 base pairs) was treated with Cd^{2+} ions, and the resulting Cd^{2+} /DNA complex was adsorbed by spin-coating onto a polylysine-coated glass slide. The complexed Cd^{2+} ions were treated with S^{2-} ions to yield CdS, and electron microscopy images revealed the formation of CdS NPs that followed the circular shape of the DNA template.^[177] In another example, Au NPs capped with positively charged lysine were deposited onto a surface that was coated with a thick, negatively charged DNA film.^[178,179] Electrostatic interaction between the positive charges associated with the Au NPs and the negatively charged phosphate groups of the DNA template led to the assembly of the nanoparticles into linear superstructures. The DNA, which are locked into a fairly rigid structure prior to the addition of the lysine-capped Au NPs, are rendered mobile owing to solvation during the addition of the solution of NPs to the surface of the DNA film. This process facilitates reorganization into highly regular linear NP superstructures during electrostatic complexation. Visualization by means of AFM and STM of the surface-confined DNA can be greatly improved through the addition of complementary-DNA-functionalized Au NPs. These latter particles introduce not only clearly visible Au clusters associated with the DNA that lies on the surface, but can also change the orientation of the long DNA molecules at the surface to produce tethered, rather than flat-lying, DNA chains.^[180] Both of these effects can ease the visualization of DNA molecules at surfaces.

Negatively charged DNA molecules can form complexes with positively charged metal ions that are later reduced to the metallic state to produce a metal wire across the DNA template. For example, upon reduction of Pd^{2+} cations loaded on a DNA template, nanoscale Pd clusters formed on the DNA.^[181] Depending on the duration of the reduction process, either well-separated Pd clusters or a quasi-continuous Pd wire with a grainlike structure could be produced.

A system which utilizes DNA that cross-links into a continuous network has been investigated in an attempt to improve structural control over a longer distance (Fig-

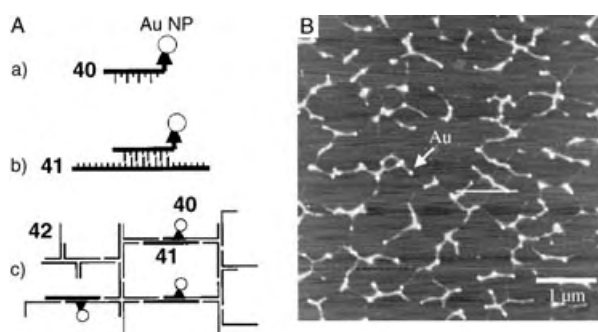


Figure 18. A) The 2D assembly of Au NPs by using a DNA-based method: a) A gold NP is attached to oligonucleotide **40** through a Au–thiol interaction; b) The oligonucleotide **40** is hybridized with oligonucleotide **41**, which possesses a complementary base sequence; c) The components are incorporated into a DNA network that consists of oligonucleotide **42**. B) AFM image of the resulting 2D Au NP–DNA network. (Adapted from Ref. [182], with permission).

ure 18A).^[182] Three types of oligonucleotides were used: **40**, **41**, and **42**. Oligonucleotide **40** had a sequence of 17 bases, and its 3' end was modified with a thiol group (5'-GTAAAC-GACGACGCCAGT-SH-3'). The 57-base oligonucleotide **41** included a central sequence complementary to **40** and side sequences of alternating A and T bases. Oligonucleotide **42** was a 50-base poly(dA-dT) (poly(deoxyadenylic acid–deoxythymidylic acid)) that forms a network structure and is hybridized upon contact with **41**. All three oligonucleotides were mixed with 5-nm Au NPs. The resulting network was adsorbed onto a mica surface, and the surface was probed by AFM (Figure 18B). These images resembled a nanocircuit that lacked organization and direct contact between the Au NPs. To construct real micro-sized DNA-templated wires, microwires prepared by electrochemical metal deposition in a porous alumina membrane were bound to thiolated DNA molecules and were treated with a solid support functionalized with a complementary DNA oligonucleotide.^[183] The hybridization process between the surface-confined DNA and the DNA linked to the microwires yielded ds-DNA bridges that bound the microwires to the surface. It should be noted that in this case, the DNA molecules were used as “molecular glue” to bind micro-sized predesigned wires to the surface instead of individual nanoparticles which provides a significant advance to microscale circuitry.

Another approach to the directed placement of nanoparticles on solid supports by means of DNA is based on the micropatterning of a surface with DNA molecules. This approach provides the specific binding of complementary-DNA-functionalized NPs at specific domains of the pattern. An amine derivative of an oligonucleotide was deposited in a pattern onto a chemically modified glass surface by a nanoliter dispensing device and was then covalently bound to the surface.^[184] Au NPs (34 nm) functionalized with a complementary oligonucleotide were then treated with the DNA-patterned surface to yield a Au NP pattern that followed the shape of the DNA pattern. Even more precise placement of Au NPs was demonstrated by the “dip-pen nanolithography” method, which was applied for the patterning of the addressable primary DNA on a surface.^[185] Two types of amine-functionalized DNA oligonucleotides TCTCAACTCGTAA₁₀ (**43**) and A₁₀CGCATTCAGGAT (**44**) were deposited and then covalently bound to a gold surface that was functionalized with 1,16-mercaptohexadecanoic acid (Figure 19A). The deposition was performed in two sequential steps to yield a pattern that was composed of spots of both oligonucleotides. This primary pattern was treated with an oligonucleotide of sequence TACGAGTTGA-GAATCCTGAATGCG (**45**), which was composed of two domains—one was complementary to **43** and the other was complementary to **44**. The resulting DNA-functionalized surface provided addressable complementary DNA chains for two kinds of DNA-functionalized Au NPs: **43**–Au (13 nm) and **44**–Au (31 nm) particles. A pattern was observed on the DNA-functionalized surface by AFM: **43**–Au NPs were specifically bound to the spots of **44/45**, and **44**–Au NPs were bound to the spots of **43/45** that were periodically located on the solid support (Figure 19B). A similar procedure was used to pattern a surface with functionalized Au NPs

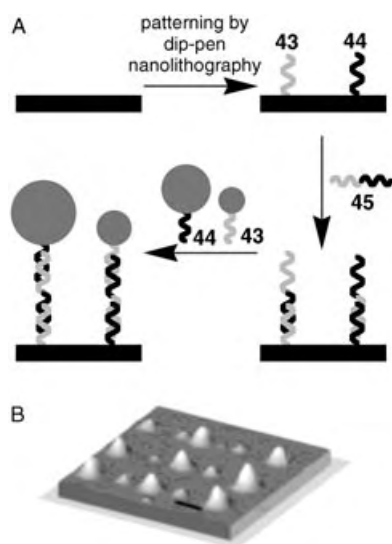


Figure 19. A) The use of dip-pen lithography and DNA to produce a predefined multinanoparticle pattern. B) AFM image of the assembly, which consists of large and small nanoparticles (scale bar = 1 μm). (Part B is adapted from Ref. [185], with permission).

by direct-write dip-pen nanolithography based on antigen–antibody specific recognition.^[186]

Multilayers of nanoparticles can be assembled on solid supports by utilizing DNA complementarity.^[187] For this purpose, a glass surface was functionalized with a monolayer of an oligonucleotide, **46**, and then the surface was treated with an oligonucleotide, **47**, which was composed of two domains—one domain was complementary to **46**, whereas the second provided complementarity for **48**. Au nanoparticles (13 nm) that were functionalized with oligonucleotide **48** were then added to yield a monolayer of ds-DNA (ds-**47/48**) attached to the Au NPs (Figure 20A). As many of the DNA chains (**48**) around the Au NP are not treated with the surface-confined DNA **47**, they can be reacted with further complementary domains of oligonucleotide **47** to provide binding sites for **46**. A second type of Au NP modified with the oligonucleotide **46** was treated with this first layer assembly to result in a second layer of Au NPs. The repetitive stepwise deposition of Au NPs functionalized with the oligonucleotides **46** and **48** resulted in a multilayer assembly of Au NPs. Each hybridized Au NP layer imparted a deeper red color onto the substrate. This method could allow the layer-by-layer deposition of different (sizewise or in chemical nature; e.g. Ag, CdS, CdSe) types of nanoparticles.

A similar approach was applied to construct a multilayer of CdS NPs (2.6 nm) on a glass support (Figure 20A).^[188] The absorbance and the intensity of the fluorescence emission of the multilayer structure of the NPs increased as the number of layers of the nanoparticles increased (Figure 20B and C). Gold NPs functionalized with several different thiolated oligonucleotides provided complementarity for more than one DNA sequence.^[189] These multioligonucleotide-functionalized Au NPs were applied to address DNA arrays, which were modified with oligonucleotide libraries to allow the simultaneous sensing of many DNA analytes and to construct

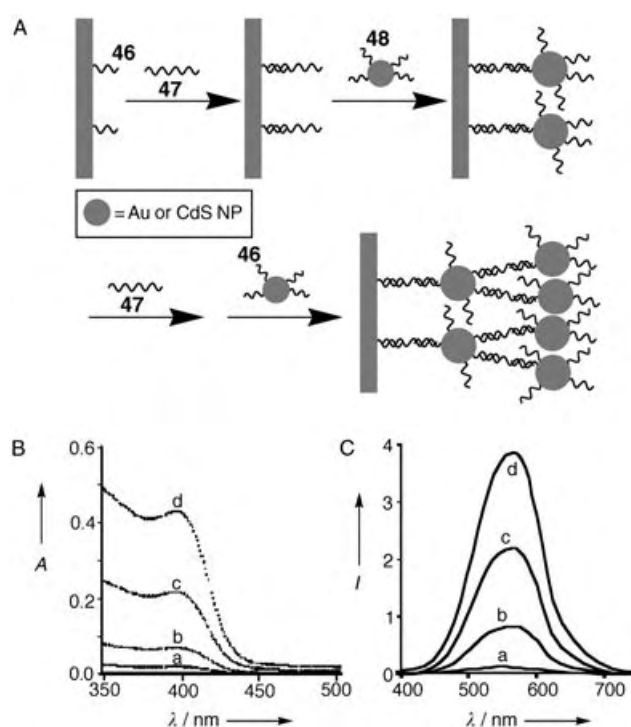


Figure 20. A) The use of DNA as a linker to construct nanoparticle multilayers on surfaces. B), C) The absorbance and the fluorescence spectrum, respectively, of the CdS NP multilayer assemblies: a)–d) 1 to 4 layers. (Parts B and C are adapted from Ref. [188], with permission).

nanoparticle multilayers that were bound to a solid support and cross-linked by various oligonucleotides.^[189a] Also, Au NPs which were functionalized with two different oligonucleotides were used as building blocks that contained two independently addressable DNA sequences: one of the sequences was utilized for attaching the Au NPs at the solid support, whereas the other sequence was used to establish lateral cross-links between the adjacently immobilized NPs.^[189b] AFM analyses proved the functionality of the interparticle cross-links that led to the enhanced surface coverage of the monolayered DNA–Au NP assembly attached to the solid support. The methods for the assembly of nanoparticle layers on surfaces may be expanded to other nanoparticles and have important implications in the design of active electronic, photonic, and photoelectrochemical sensors (see Sections 6.2 and 6.3).

6. Functional Biomolecule–Nanoparticle Structures on Surfaces for Application as Sensors

The unique properties of nanoparticles render biomolecule–nanoparticle conjugates attractive labels for applications as sensors. The optical and electronic sensing of biomaterials on surfaces is a common practice in analytical biochemistry. Thus, the immobilization of biomolecule–NP conjugates on surfaces provides a general route for the development of optical or electronic biosensors. Metal NPs such as Au or Ag NPs exhibit plasmon absorbance bands in the visible spectral

region that are controlled by the size of the respective particles. Numerous studies on the labeling of bioassays and the staining of biological tissues by metal particles as a means to image and visualize biological processes have been reported.^[190] The spectral shifts which originate from adjacent or aggregated metal nanoparticles, such as Au NPs,^[139–141] are of increasing interest in the development of optical biosensors based on biomolecule–NP hybrid systems. As an example, NPs that were functionalized with two kinds of nucleic acid, which were complementary to two segments of an analyzed DNA, were hybridized with the analyzed DNA. This led to the aggregation of the NPs and to the detection of a red-shifted interparticle plasmon absorbance of the nanoparticle aggregate.^[69a]

An alternative approach for the optical detection of biorecognition processes that involved the use of metallic NPs as local quenchers of the fluorescence of dyes was reported. In a DNA molecular beacon, which was terminated at its ends with a Au NP and a dye, intramolecular quenching of the dye fluorescence persists. Opening of the DNA molecular beacon by hybridization with an analyte DNA molecule led to the regeneration of the fluorescence of the dye because of the spatial separation of the nanoparticle and dye units.^[105] Similarly, semiconductor NPs exhibit size-dependent tunable fluorescence. Their favorable properties—high fluorescence quantum yields, their photostability, and their tunable fluorescence bands—evoked substantial research efforts for the application of semiconductor NPs as fluorescence labels for biorecognition processes.^[75]

The extensive use of metal and semiconductor NPs in biosensing applications suggests that the unique catalytic or photoelectrochemical properties of the NPs could be used to develop electronic biosensors.^[191] The catalytic electroless deposition of metals on biomolecule–NP hybrid labels could be used to generate conductive domains and surfaces, and the conductivity properties of the systems may then transduce the biosensing processes.^[156] Functionalized NPs are extensively used in bioelectroanalytical chemistry.^[192] Also, the localized plasmon of metal NPs, which act as bioconjugate labels, may interact with the surface plasmon of a gold support^[193] to result in the amplification of the biorecognition events that occur on the surface. Furthermore, charging of the NPs through biological transformations may lead to a perturbation of the surface plasmon resonance (SPR) spectra. These effects may then be utilized to develop new transduction methods for the signals that originate from the biotransformations at interfaces. The following sections address the recent advances in the application of biomolecule–nanoparticle conjugates as active components in bioelectronic and biosensing systems.

6.1. Bioelectronic Systems Based on Nanoparticle–Enzyme Hybrids as Sensors

The electrical contacting of redox enzymes with electrodes is a key process in the design of enzyme electrodes for bioelectronic applications such as biosensors^[162,165,194] or biofuel-cell elements.^[167] Redox enzymes usually lack direct

electrical communication with electrodes,^[165] but the electrical contacting of redox proteins with electrodes has been reported by the application of diffusional electron mediators,^[195] the tethering of redox-relay groups to the protein,^[196] or the immobilization of the enzymes in redox-active polymers.^[163,197] Relatively inefficient electrical contacting of the enzymes with the electrode is observed because of the nonoptimal modification of the enzymes by the redox units,^[196f] or the lack of appropriate alignment of the enzymes with respect to the electrode. On the other hand, very efficient electrical communication between redox proteins and electrodes was observed upon the reconstitution of apo-enzymes on relay cofactor monolayers associated with electrodes.^[198–200] Apo-glucose oxidase was reconstituted on a relay FAD (flavin adenine dinucleotide) layer,^[198,199a] and apo-glucose dehydrogenase was reconstituted on a pyrrolo-quinoline quinone (PQQ)-modified polyaniline film that was associated with an electrode.^[199b] Effective electrical communication between the redox centers of the biocatalysts and the different electrodes was observed, and high-turnover electron-transfer rates from the redox sites to the electrodes were noted. The effective electrical contacting of these redox enzymes was attributed to the alignment of the proteins on the electrodes and to optimal positioning of the intermediary electron-relay units between the redox centers of the enzyme and the electrode.

Biocatalytic electrodes for biosensor applications have been prepared by the codeposition of redox enzymes/proteins and Au nanoparticles on electrode supports.^[201,202] In one example, direct electron transfer between hemoglobin and a glassy carbon electrode was facilitated by lipid-protected Au NPs.^[202] The biocatalytic electrodes were reported to operate without electron-transfer mediators. However, the random and nonoptimized positioning of the redox proteins on the conductive NPs did not allow efficient electron transfer between the active sites of the enzyme and the electrode support. Highly efficient electrical contacting of the redox enzyme glucose oxidase (GOx) through a single Au NP was demonstrated by the reconstitution of the apo-flavoenzyme, apo-glucose oxidase (apo-GOx), on a 1.4-nm Au₅₅ nanoparticle that was functionalized with *N*⁶-(2-aminoethyl)flavin adenine dinucleotide (FAD cofactor, amine derivative; **49**). The resultant conjugate was assembled on a thiolated monolayer by using different dithiols as linkers (**50–52**, Figure 21 A).^[203] Alternatively, the FAD-functionalized Au NP could be assembled on a thiolated monolayer associated with an electrode, and apo-GOx could be subsequently reconstituted on the functional NPs (Figure 21 B). The enzyme electrodes prepared by these two routes reveal similar surface coverages of about 1×10^{-12} mol cm⁻² of the protein. The nanoparticle-reconstituted glucose oxidase layer was found to be electrically contacted with the electrode without any additional mediators, and the enzyme assembly stimulated the bioelectrocatalyzed oxidation of glucose (Figure 21 C). The resulting nanoparticle-reconstituted enzyme electrodes revealed unprecedented efficient electrical communication with the electrode (electron-transfer turnover rate ≈ 5000 s⁻¹). This electrical contacting renders the enzyme electrode insensitive to oxygen or to common

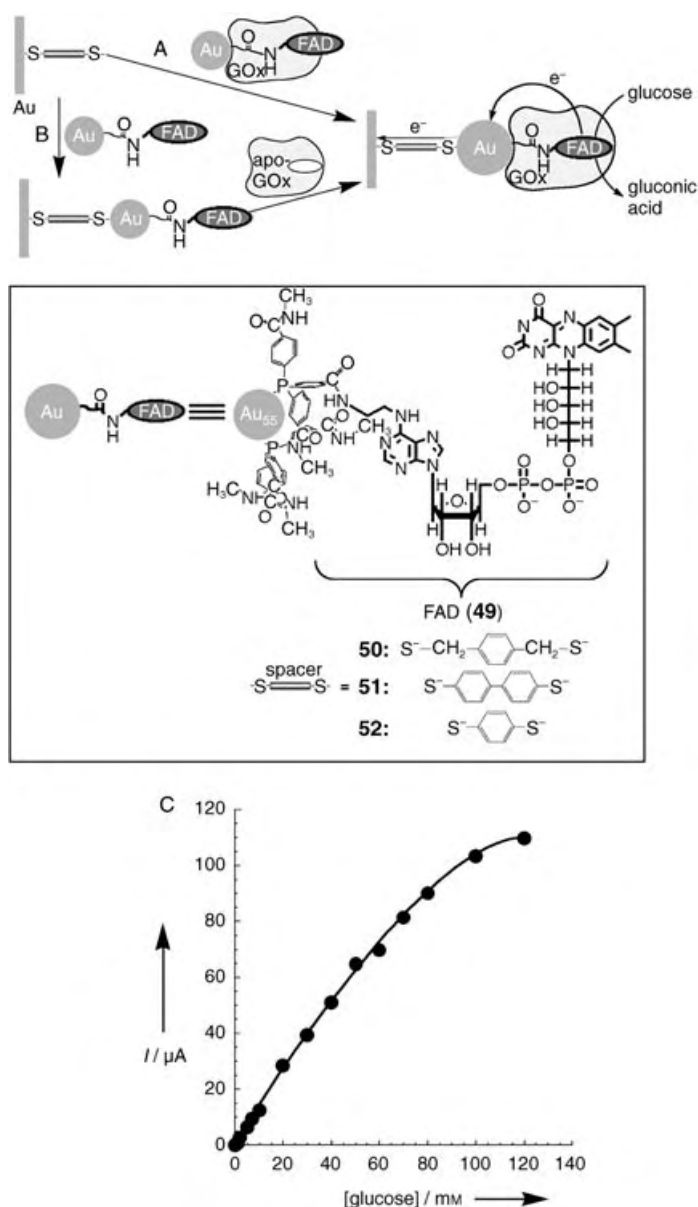


Figure 21. The electrical “wiring” of glucose oxidase (GOx) by apo-enzyme reconstitution with a gold nanoparticle that is functionalized with a single FAD cofactor unit. A) Reconstitution of apo-GOx performed prior to the adsorption of the assembly onto a dithiol-modified Au electrode. B) Adsorption of the Au–FAD conjugate onto a dithiol-modified Au electrode followed by the reconstitution of apo-GOx at the interface. C) Calibration plot of the electrocatalytic current developed by the reconstituted GOx electrode in the presence of different concentrations of glucose.

oxidizable agents such as ascorbic acid. The rate of electron transfer from the enzyme active center through the Au NP is limited by the structure of the dithiol molecular linker that bridges the particle to the electrode. The conjugated benzene dithiol **52** was found to be the most efficient electron-transport unit among the linkers **50–52**. The application of effective molecular wires such as oligophenylacetylene units could further improve the efficiency of electrical contacting processes.

Whereas the previous system employed the metal nanoparticle as a nanoelectrode to electronically link the enzyme

redox site to the macroscopic electrode, one may also use enzyme–nanoparticle hybrid systems, in which the product generated by the biocatalytic process activates the functions of the NP. This has recently been demonstrated by tailoring an acetylcholine esterase (AChE)–CdS NP hybrid monolayer on a Au electrode, and activation of the photoelectrochemical functions of the NPs by the biocatalytic process.^[204] The CdS–AChE hybrid interface was assembled on a gold electrode by the stepwise coupling of cystamine-functionalized CdS to the electrode, and the secondary covalent linkage of the enzyme AChE to the particles (Figure 22 A). In the presence of acetylthiocholine (**53**) as the substrate, the enzyme catalyzes the hydrolysis of **53** to thiocholine (**54**) and acetate. Photoexcitation of the CdS semiconductor yields an electron–hole pair in the conduction band and the valence band, respectively. The enzyme-generated thiocholine (**54**) acts as an electron donor for valence-band holes. The scavenging of the valence-band holes results in the accumulation of the electrons in the conduction band and their transfer to the electrode with the generation of a photocurrent, which is controlled by the concentration of the substrate (Figure 22, B and C). The addition of enzyme inhibitors such as 1,5-bis(4-allyldimethylammoniumphenyl)pentan-3-one dibromide (**55**) blocks the biocatalytic functions of the enzyme and, as a result, inhibits the photocurrent formation in the system (Figure 22 D). Thus, the hybrid CdS–AChE system provides a functional interface for the sensing of the AChE inhibitors by means of photocurrent measurements and is thus applicable to the analysis of chemical warfare. A similar system that was composed of photoactivated CdS NPs and coimmobilized formaldehyde dehydrogenase, which utilizes formaldehyde as an electron donor, has been reported.^[205] In this hybrid system, the direct electron transfer from the active center of the enzyme to the photogenerated holes of the CdS was possible, and the steady-state photocurrent signal in the system was reported to be directly related to the substrate concentration.

6.2. Bioelectronic Systems Based on Nanoparticles as Sensors of Biorecognition Events

The unique optical,^[206] photophysical,^[7a] electronic,^[6,207] and catalytic^[208] properties of metal and semiconductor nanoparticles render them ideal labels for biorecognition and biosensing processes. For example, the unique plasmon absorbance features of Au NPs and, specifically, the interparticle-coupled plasmon absorbance of conjugated particles have been widely used for DNA^[209] and antibody–antigen^[210] analyses. Similarly, the tunable fluorescence properties of semiconductor NPs were used for the photonic detection of biorecognition processes.^[21a,75] Also, electrochemical methods were used to monitor NP labels bound to biomolecules. Differential pulse voltammetry signals (≈ 1.2 V), which correspond to the oxidation of Au NP

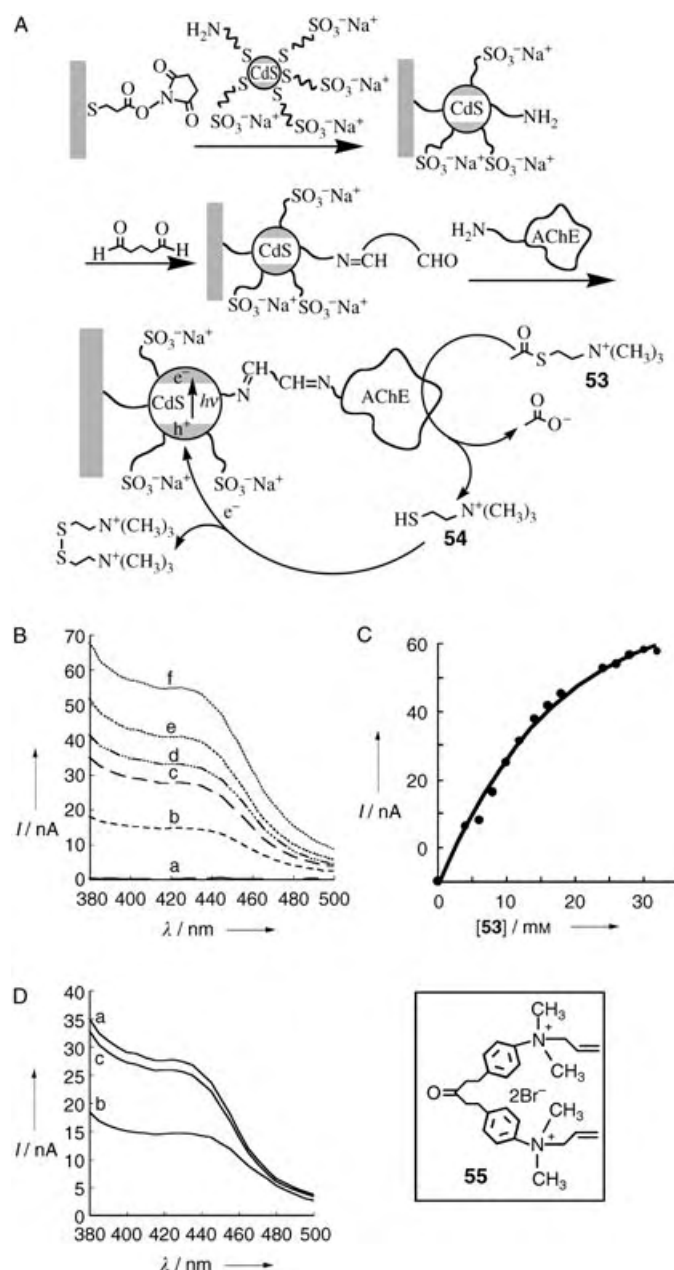


Figure 22. A) Assembly of the CdS NP-AChE hybrid system for the photoelectrochemical detection of enzyme activity (h = hole). B) Photocurrent action spectra observed in the presence of acetylthiocholine (53): a) 0 mM, b) 6 mM, c) 10 mM, d) 12 mM, e) 16 mM, and f) 30 mM. C) Calibration curve of the photocurrent at $\lambda = 380$ nm at variable concentrations of 53. D) Photocurrent spectra for the CdS-AChE system in the presence of 53 (10 mM): a) in the absence of inhibitor 55, b) upon addition of the inhibitor 55 (1×10^{-6} M), and c) after rinsing the system, exclusion of the inhibitor, and addition of 53 (10 mM).

labels that are connected to the target DNA molecules, were applied for the electrochemical analysis of DNA.^[211]

Metal and semiconductor NPs coupled to biomaterials generate solubilized entities. The solubility of the biomolecule-NP structures allows washing procedures to be performed on surfaces that contain a sensing interface, and thus nonspecific adsorption processes can be eliminated. Also, even nanoscale particulate clustered systems include many

atoms/molecules in the clusters. The specific capturing of biomolecule-nanoparticles on the respective sensing interfaces allows the secondary dissolution of the captured nanoparticles and thus enables the amplified detection of the respective analyte by the release of many ions/molecules as a result of a single recognition event.

Most of the detection schemes employed until now have commonly relied on a highly sensitive electrochemical stripping transduction/measurement of the metal tracer. Stripping voltammetry is a powerful electroanalytical technique for trace-metal measurements.^[212] Its remarkable sensitivity is attributed to the "built-in" preconcentration step, during which the target metals are accumulated (plated) onto the working electrode. The detection limits are thus lowered by 3–4 orders of magnitude compared to pulse-voltammetric techniques, which were used earlier to monitor DNA hybridization. Such ultrasensitive electrical detection of metal tags has been observed with a variety of novel DNA-linked particle nanostructure networks. The clustered systems could be loaded with additional markers, including redox-active moieties. Silica nanoparticles loaded with tris(2,2'-bipyridyl)-cobalt(III)^[213] or Au NPs functionalized with tethered ferrocene units^[214] were applied for the labeling of DNA and for the further electrochemical detection of DNA on the basis of redox processes of the redox-active complex units.

Powerful nanoparticle-based electrochemical DNA-hybridization assays were developed using Au, Ag, Cu, or In metal tracers.^[215–219] Such protocols have relied on capturing the gold,^[215,216] silver,^[217] or Cu_{core}/Au_{shell} NPs, or In nanorods^[219] on the hybridized target followed by anodic stripping electrochemical measurement of the metal tracer. Immobilization of the probe or the target has been performed directly on carbon or indium-tin oxide (ITO) electrodes.^[220,221] Alternatively, the DNA probe was linked to streptavidin-coated magnetic beads^[215] or adsorbed onto the walls of polystyrene microwells.^[216] The DNA-functionalized beads were collected on an electrode surface, and picomolar levels of the DNA target were electrochemically detected. An electrochemical method was employed for the Au NP-based quantitative detection of the 406-base human cytomegalovirus DNA sequence (HCMV DNA).^[216] The HCMV DNA was immobilized on a microwell surface and hybridized with the complementary oligonucleotide-modified Au NP. The resulting surface-immobilized Au NP-ds-DNA assembly was treated with HBr/Br₂ which resulted in the oxidative dissolution of the gold particles. The solubilized Au³⁺ ions were then electrochemically reduced and accumulated on the electrode, and the Au was subsequently determined by anodic stripping voltammetry by means of a sandwich-type screen-printed microband electrode (SPMBE). The combination of the sensitive detection of Au³⁺ ions at the SPMBE (owing to nonlinear mass transport of the ions) and the release of a large number of Au³⁺ ions upon the dissolution of the particles associated with a single recognition event provides an amplification path: the HCMV DNA was detected at a concentration of 5×10^{-12} M. The sensitivity was further enhanced by the catalytic growth of the gold tracer, which was associated with the double-stranded DNA assembly, by the deposition of gold^[215] or silver.^[222] Combining

such growth of the metal-particle tags with the effective “built-in” amplification of electrochemical stripping analysis paved the way to subpicomolar detection limits.

An electrochemical protocol for the detection of DNA hybridization that is based on the deposition of metal clusters along the DNA backbone rather than attaching them at the end of the duplex was described recently.^[223] This protocol relies on the DNA-template-induced generation of conducting nanowires as a result of DNA hybridization. The use of DNA as a metallization template^[224] has evoked substantial research activity directed towards the generation of conductive nanowires and the construction of functional circuits.^[181, 225–227] Such an approach was applied to grow silver,^[225, 226] palladium,^[181] or platinum^[227] clusters on DNA templates. Aspects of the methods used to generate metal nanocircuitry from DNA templates were adapted to develop DNA detection schemes as outlined in Figure 23. The short DNA primer **56** which is attached to the electrode hybridizes with the target DNA **57** (step a). The phosphate groups associated with the long target DNA **57** collect Ag^+ ions from the solution by electrostatic interaction (step b). The bound Ag^+ ions are then reduced by hydroquinone which results in the formation of metallic silver aggregates along the DNA (step c). The subsequent dissolution and stripping electrochemical detection of the nanoscale silver clusters (step d) thus allows detection of the hybridized DNA. It should be noted, however, that the short DNA primer might also bind some Ag^+ ions which would yield a background response. The background signal could be avoided and the sensitivity provided by this method could be improved upon application of peptide nucleic acids (PNA), which lack phosphate groups and thus do not bind Ag^+ ions, as the primer for the hybridization of the target DNA.

The catalytic features of metal NPs that enable the electroless deposition of metals on the NP clusters allows the enlargement of the particles to conductive interparticle-connected entities. The formation of conductive domains as a result of biorecognition events provides then an alternative path for the electrical transduction of biorecognition events. This was exemplified by the design of a miniaturized immunosensor based on Au NPs and their catalytic properties (Figure 24 A).^[228] Latex particles which were stabilized by an anionic protective layer were attracted to a gap between micron-sized Au electrodes upon the application of a nonuniform alternating electric field between the electrodes (dielectrophoresis). Removal of the protective layer from the latex particles by an oppositely charged polyelectrolyte resulted in the aggregation of the latex particles and their fixation in the gap domain. Adsorption of protein A on the latex surface yielded a sensing interface for the specific association of the human immunoglobulin (IgG) antigen. The association of human IgG on the surface was probed by the binding of the secondary Au NP-labeled antihuman IgG antibodies to the surface, followed by the catalytic deposition of a layer of silver on the Au NPs. The silver layer bridged the gap between the two microelectrodes to result in a conductive “wire”. Typical resistances between the microelectrodes were 50–70 Ω , whereas control experiments conducted without the specific catalytic enlargement of the domain by the Au NP–antibody

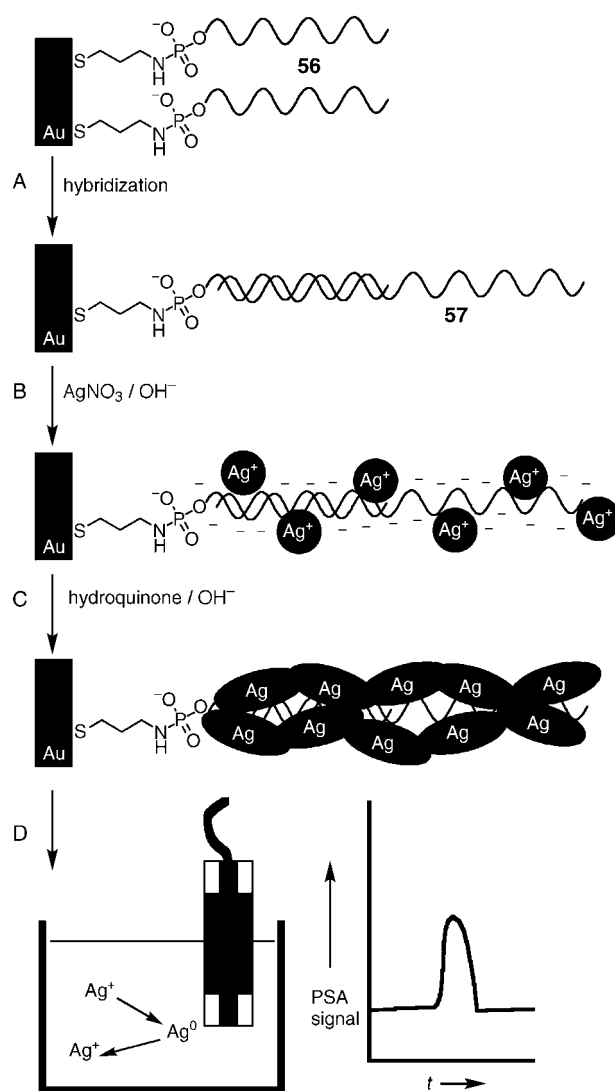


Figure 23. Outline of the steps involved in the amplified electrochemical detection of DNA by the deposition of catalytic silver clusters on the DNA strand: A) Hybridization of the complementary target DNA **57** with the DNA probe **56**, which is covalently linked to the electrode surface through a cystamine monolayer; B) Loading of the Ag^+ ions onto the immobilized DNA; C) Reduction of Ag^+ ions by hydroquinone to form silver aggregates on the DNA backbone; D) Dissolution of the silver aggregates in acidic solution, and transfer of the solution to the detection cell for stripping potentiometric measurement (PSA = potentiometric stripping analysis).

conjugate yielded resistances $> 10^3 \Omega$. The method enabled the analysis of human IgG with a detection limit of $\approx 2 \times 10^{-13} \text{ M}$.

A related DNA detection scheme was developed by using microelectrodes fabricated on a silicon chip (Figure 24 B).^[229] A probe nucleic acid, **58**, was immobilized on the SiO_2 interface in the gap that separates the microelectrodes.^[229a] The target 27-mer nucleotide **59** was then hybridized with the probe interface, and Au NPs that were functionalized with a nucleic acid **60** were subsequently hybridized with the free 3' end of the target DNA. The Au NPs catalyzed the reduction of Ag^+ ions by hydroquinone which resulted in the deposition

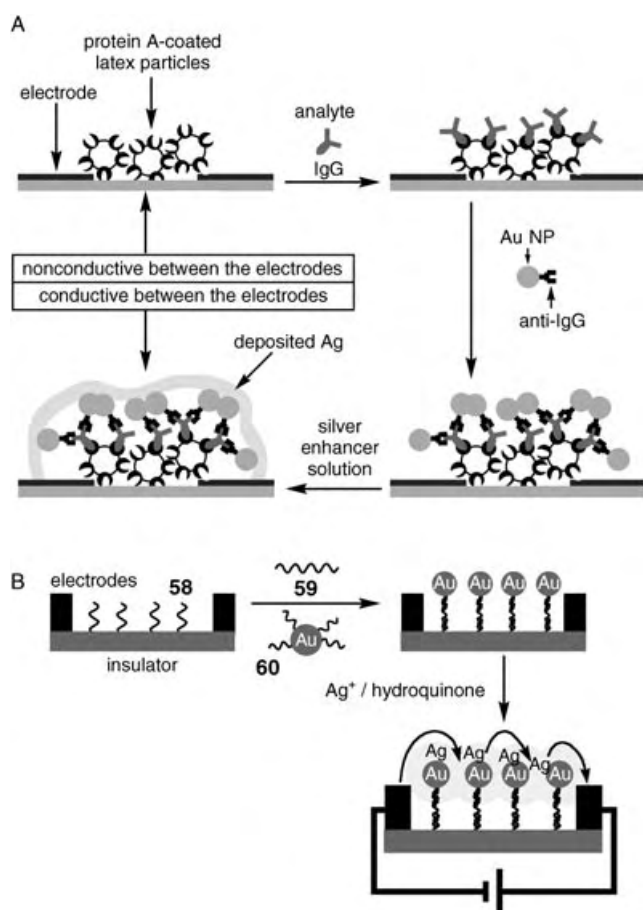


Figure 24. A) Immunosensing at micro-sized Au electrodes by the change of conductivity between the Au strips upon the binding of Au NPs and the deposition of silver. B) The use of a DNA–NP conjugate and the deposition of silver to connect two microelectrodes and sense a DNA analyte. (Part A is adapted from Ref. [7a], with permission).

of silver on the Au NP assembly and the decrease of the resistance between the electrodes. Single-base mutants of the analyte oligonucleotide **59** were washed away from the probe nucleic acid **58** with a buffer of appropriate ionic strength. A difference of 10^6 in the gap resistance was observed upon analysis of the target DNA and its mutant by this method. The low resistances between the microelectrodes were found to be controlled by the concentration of the target DNA, and the detection limit for the analysis was estimated to be $\approx 5 \times 10^{-13}$ M. This sensitivity translates to $\approx 1 \mu\text{g mL}^{-1}$ of human genomic DNA or $\approx 0.3 \text{ ng mL}^{-1}$ of DNA from a small bacterium. The sensitivity suggests that the DNA extracted from pathogens may be analyzed with no pre-PCR (polymerase chain reaction) amplification. Elsewhere, the hybridization of DNA was analyzed by capacitance measurements on a chip.^[229b] A collection of DNA targets was simultaneously analyzed with a chip socket that included 42 electrode gaps and appropriate different nucleic acid sensing probes between the electrode gaps.^[230]

The immobilization of nanoparticles on surfaces may also be used to yield high-surface-area electrodes^[231] and hence to increase the hybridization capacity of the surface.^[232] Such use of NP supporting films relied on the self-assembly of 16-nm-

diameter Au NPs on a cystamine-modified gold electrode and resulted in surface densities of oligonucleotides as high as 4×10^{14} molecules per cm^{-2} . The detection of the ferrocenecarboxaldehyde tag (conjugated to the target DNA) resulted in a detection limit of 500 pM. The roughening of a Au–quartz crystal with a monolayer of Au NPs was employed for the enhanced microgravimetric analysis of DNA.^[233] Similarly, electrode surfaces roughened by the deposition of Au or SiO_2 NPs were employed as platforms for enhanced immunoassays that used microgravimetric, impedimetric, or amperometric readout signals.^[234]

Efficient methods for the preparation of semiconductor NPs (e.g. CdS, CdSe, PbS, ZnS) and their functionalization with biomolecules were recently developed.^[235] These NPs were applied as labels of biomaterials in biorecognition processes such as DNA sensing. For instance, CdS semiconductor NPs that were modified with nucleic acids were employed as tags for the detection of hybridization events of DNA.^[236] Dissolution of the CdS NPs (in the presence of 1 M HNO_3), followed by the electrochemical reduction of the Cd^{2+} to Cd^0 , which accumulates on the electrode, and the removal of the generated Cd^0 (as Cd^{2+}) provided the electrical signal for the DNA analysis. Figure 25 A shows the chrono-

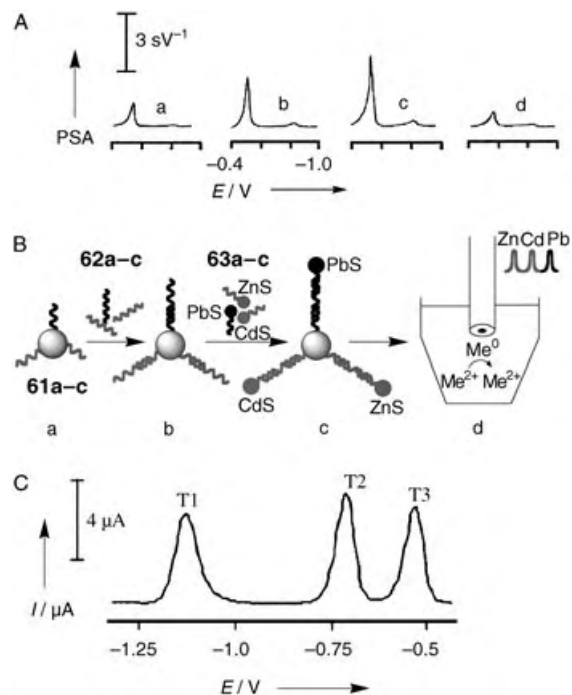


Figure 25. A) Stripping potentiograms measured upon the sensing of different concentrations of DNA that are bound to magnetic particles and labeled with CdS NPs: a) 0.2, b) 0.4, and c) 0.6 mg L^{-1} ; d) Control experiment with noncomplementary DNA (0.6 mg L^{-1}). B) Multitarget electrochemical DNA detection with different nanocrystal labels: a) Introduction of probe-modified magnetic beads; b) Hybridization with the DNA targets; c) Second hybridization with the NP-labeled probes; d) Dissolution of the NPs and the electrochemical detection. C) Stripping voltammogram recorded upon the simultaneous analysis of three different 60-mer DNA targets (T1–3; 54 nm each), which are related to the BRCA1 breast cancer gene. The DNA molecules are labeled with ZnS NPs (T1), CdS NPs (T2), and PbS NPs (T3). (Part A is adapted from Ref. [236]; Parts B and C are adapted from Ref. [237], with permission; Copyright American Chemical Society, 2003).

potentiograms that result from the analysis of different concentrations of the complementary target DNA by using the CdS NPs as tags. A further development has been the use of magnetic particles, which are functionalized with the sensing nucleic acid, and CdS NPs, which are functionalized with the complementary oligonucleotide, as labels. The hybridization of the complementary nucleic acids allowed the separation of the duplex from the reaction mixture and the determination of its concentration on the electrode surface followed by the electrochemical detection. Electroless deposition of Cd^0 onto CdS NPs allowed their enlargement and, thus, a further amplification of the electrochemical signal to result in a sensitivity level as low as 100 fmol of the analyte DNA.

An interesting aspect of these systems is, however, the future possibility of a combination of different metal or semiconductor tags, which are linked to different nucleic acids, for the simultaneous high-throughput analysis of different DNA targets that are linked to different magnetic beads. By this approach,^[237] different nucleic acid probes that are complementary to a series of DNA targets are linked to different magnetic particles. Similarly, different semiconductor- or metal-NP tags, which were complementary to segments of the series of the target DNAs, were used as amplifying detection units for the primary hybridization process. The hybridization of the nucleic acid functionalized semiconductor or metal particle to the specific DNA targets followed by the dissolution of the NPs and the electrochemical accumulation and removal (stripping off) of the metals enables the determination of the specific DNA targets that are present in the sample. That is, the characteristic potentials needed to strip off the metal provide electrochemical indicators for the nature of the analyzed DNA. A model system that follows this principle was developed^[237] in which three kinds of magnetic particles modified with three different nucleic acids, **61a–c**, were hybridized with the complementary analyte nucleic acids, **62a–c**. The particles were subsequently hybridized with three different kinds of semiconductor NPs, ZnS, CdS, and PbS, that were functionalized with nucleic acids, **63a–c**, which were complementary to the free ends of the analyte DNA molecules (Figure 25B). The magnetic particles allow easy transportation and purification of the analyte sample, whereas the semiconductor particles provide nonoverlapping electrochemical signals that transduce the specific kind of hybridized DNA. Stripping voltammetry measurements of the metals that originated from the semiconductor NPs yielded well-defined and well-resolved stripping peaks at -1.12 V (Zn), -0.68 V (Cd), and -0.53 V (Pb; all versus Ag/AgCl reference electrode) that allow the simultaneous electrochemical analysis of several DNA analytes that are tagged with the semiconductor NP labels. Figure 25C depicts the stripping voltammograms for a solution that contains three DNA samples that are labeled with the ZnS, CdS, and PbS NP tracers, respectively. The functionalization of the nanocrystal tags with thiolated oligonucleotide probes offered the voltammetric signature with distinct electrical hybridization signals for the corresponding DNA targets. The position and size of the resulting stripping peaks provided the desired identification and

quantitative information, respectively, of a given target DNA molecule. The multitarget DNA detection was combined with the amplification feature of stripping voltammetry to yield femtomolar detection limits and an efficient magnetic removal of nonhybridized nucleic acids to offer high sensitivities and selectivities. Up to 5–6 targets can thus be measured simultaneously in a single run in connection with ZnS, PbS, CdS, InAs, and GaAs semiconductor particles. The performance of parallel assays in microwells of microtiter plates or by using multichannel microchips in which each microwell or channel carries out multiple measurements could thus lead to a high-throughput analysis of DNA.

The amplification paths for the electrochemical analysis of DNA that were discussed in the previous sections have employed a single reporter unit, such as a metal or semiconductor NP, per hybridization event. To further enhance the sensitivity of DNA detection, it is possible to load multiple tags per binding event^[238,239] by linking the biorecognition units to polymeric microbeads, which carry multiple redox tracers in external positions (on their surface) or internal positions (through encapsulation). A triple-amplification bioassay that couples the carrier-sphere amplifying units (loaded with numerous gold NP tags) with the “built-in” preconcentration feature of the electrochemical stripping detection and the catalytic enlargement of the multiple gold particle tags was demonstrated (Figure 26A).^[238a] The gold-tagged beads were prepared by binding biotinylated Au NPs to streptavidin-coated polystyrene spheres. These beads were functionalized with a single-stranded oligonucleotide, which

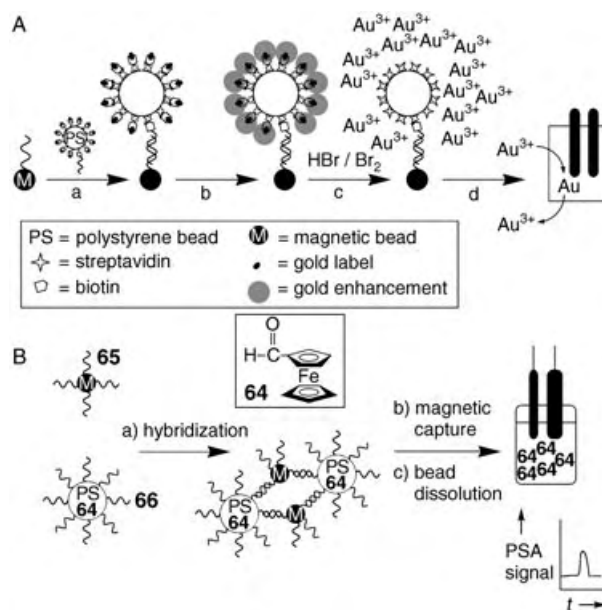


Figure 26. A) The amplified detection of DNA by using nucleic acid–Au NP-functionalized beads as labels and electroless catalytic deposition of gold on the NPs as a means of amplification: a) Hybridization of the nucleic acid–Au NP-functionalized beads with the target DNA, which is associated with a magnetic bead; b) The enhanced catalytic deposition of gold on the NPs; c) Dissolution of the gold clusters; d) The detection of the Au^{3+} ions by stripping voltammetry. B) The amplified detection of DNA with polystyrene beads, which are loaded with a ferrocene redox marker **64**.

was further hybridized with a complementary oligonucleotide that was linked to a magnetic particle (Figure 26 A, step a). The numerous Au NP labels associated with one ds-oligonucleotide pair were enlarged by the electroless deposition of gold (Figure 26 A, step b) and transported to the electrode array with the use of the magnetic particle. Then, the Au assembly was dissolved upon treatment with HBr/Br₂ and electrochemically analyzed by using the electrochemical deposition/stripping procedure (Figure 26 A, steps c and d). Such a triple-amplification route offered a dramatic enhancement of the sensitivity. In another approach, carbon nanotubes that were loaded with many CdS NPs were employed as labels for DNA hybridization.^[238b] Dissolution of the bound CdS NPs in 1 M HNO₃ solution followed by the electrochemical detection of the released Cd²⁺ ions provided an amplified signal for the hybridization event.

The internal encapsulation of electroactive tags within carrier beads offers an alternative means to label the probes and it might offer some advantages relative to the external labeling of the probes by nanoparticles. Ultrasensitive electrical DNA detection based on polystyrene beads impregnated with ferrocenecarboxaldehyde (**64**) as a redox marker (Figure 26 B) was recently reported.^[239a] The probe DNA **65** was linked to magnetic particles, whilst the polystyrene beads were functionalized with the complementary nucleic acid **66**, and the conjugates were then hybridized with the nucleic acid modified magnetic particles. Collection of the hybridized system and dissolution of the beads in an organic solvent released the immobilized redox label **64**. This allowed the chronopotentiometric detection of the target DNA with a sensitivity of 5.1×10^{-21} mol ($\sim 31\,000$ molecules) under experimental conditions that involved hybridization during 20 minutes and dissolution of the modified beads in an organic medium to “release” the marker. The amplified electrochemical readout signal was observed with the remarkable discrimination of a large excess (10^7 -fold) of noncomplementary nucleic acids to highlight the analytical advantages of this sensing process. Further efforts were directed to encapsulate different redox-active NPs (ZnS, GaAs, CdS, InAs, and PbS) in polystyrene host beads to provide libraries with electrochemically readable encoding to allow parallel multitarget DNA detection.^[239b] Other marker-encapsulation routes hold great promise for electrical DNA detection. Particularly attractive are the recently developed nanoencapsulated microcrystalline particles prepared by the layer-by-layer technique which offer large marker/biomolecule ratios and superamplified bioassays.^[240] Related analytical procedures that combined multiple amplification pathways based on enzyme-functionalized liposomes and the accumulation of the biocatalytic reaction product were reported as ultrasensitive DNA assays.^[241] Such bioassays relied on the large surface area of the liposomes that carry a large number of enzyme molecules; the accumulated product was detected by means of chronopotentiometry.

The photoelectrochemical transduction of DNA recognition processes has been demonstrated by using semiconductor (CdS) nanoparticles modified with nucleic acids.^[188] Semiconductor CdS NPs (2.6 ± 0.4 nm) were functionalized with one of the two thiolated nucleic acids **67** or **68** that are

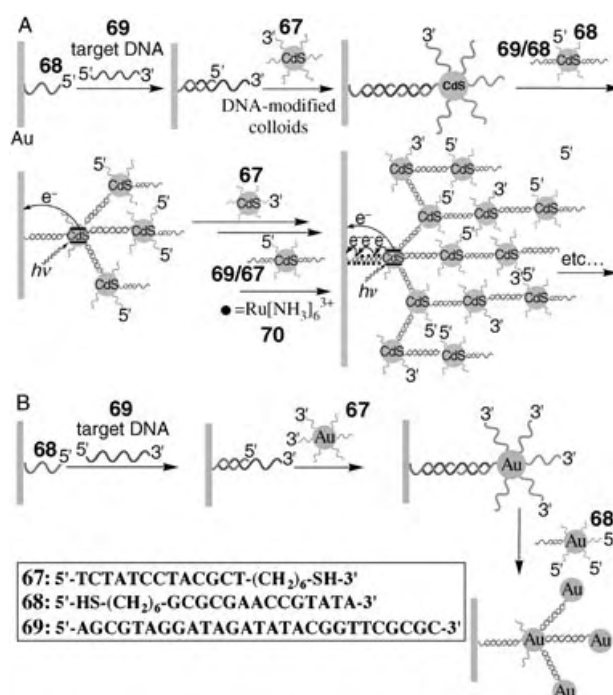


Figure 27. A) The construction of CdS NP–DNA superstructures and their use for the generation of photocurrents. B) Dendritic amplified DNA sensing by the use of oligonucleotide-functionalized Au NPs, which are assembled on a quartz crystal microbalance (QCM) electrode.

complementary to the 5′ and 3′ ends of a target DNA molecule, **69**. An array of CdS NP layers was then constructed on a Au electrode by a layer-by-layer hybridization process (Figure 27 A). A primary thiolated DNA monolayer of **68** was assembled on a Au electrode, and the target DNA **69** was used as a cross-linking unit for the association of the **67**–CdS NPs to the electrode. The subsequent association of the CdS nanoparticles that were functionalized with **68** and hybridized with **69** resulted in the second generation of CdS particles. By the stepwise association of the two different kinds of nucleic acid functionalized CdS NPs with **69**, an array with a controlled number of nanoparticle generations could be assembled on the electrode. This array was characterized by absorbance and fluorescence spectroscopy upon the assembly of the array on glass supports (as in Figure 20, parts B and C), and by microgravimetric quartz crystal microbalance analyses on Au–quartz piezoelectric crystals. Illumination of the array resulted in the generation of a photocurrent. The photocurrents increased with the number of generations of CdS NPs associated with the electrode, and the photocurrent action spectra followed the absorbance features of the CdS NPs which implies that the photocurrents originated from the photoexcitation of the CdS nanoparticles. That is, photoexcitation of the semiconductor induced the transfer of electrons to the conduction band and led to the formation of an electron–hole pair. Transfer of the conduction-band electrons to the bulk electrode and the concomitant transfer of electrons from a sacrificial electron donor to the valence-band holes yielded the steady-state photocurrent in the system. The ejection of the conduction-band electrons into

the electrode occurred from the NPs that were in intimate contact with the electrode support. This was supported by the fact that $\text{Ru}(\text{NH}_3)_3^{6+}$ units **70** ($E^0 = -0.16$ V versus saturated calomel electrode, SCE), which were electrostatically bound to the DNA, enhanced the photocurrent from the DNA–CdS array. In other words, the $\text{Ru}(\text{NH}_3)_6^{3+}$ units acted as electron-wiring elements that facilitate the hopping of conduction-band electrons from CdS particles, which lack contact with the electrode, through the DNA tether. The system is important not only because it demonstrates the use of photoelectrochemistry as a transduction method for DNA sensing but also as the system reveals the nanoengineering of organized DNA-tethered semiconductor NPs on conductive supports. These latter nanoengineered structures comprise the first step towards electronic nanocircuitry (see Section 8.2).

Nanoparticles as components of metal NP–nucleic acid hybrids represent high-molecular-weight units that render these conjugates ideal labels for the analyses of biorecognition processes on the surfaces of piezoelectric crystals by quartz crystal microgravimetry (QCM). Furthermore, as NPs act as catalysts for the deposition of metals, even higher mass changes may be stimulated and thus the microgravimetric detection of biorecognition processes may be amplified. For a quartz piezoelectric crystal (AT-cut), the crystal resonance frequency changes by Δf when a mass change Δm occurs on the crystal according to the Sauerbrey equation, Equation (1),^[242] in which f_0 is the fundamental frequency of the quartz crystal, Δm is the mass change, A is the piezoelectrically active area, ρ_q is the density of quartz (2.648 g cm^{-3}), and μ_q is the shear modulus ($2.947 \times 10^{11} \text{ dyn cm}^{-2}$ for AT-cut quartz).

$$\Delta f = -2f_0^2 \frac{\Delta m}{A (\mu_q \rho_q)^{1/2}} \quad (1)$$

The microgravimetric (QCM) detection of DNA was possible by using nucleic acid functionalized Au NPs as “nanoweights”. A target DNA molecule **69** was hybridized to a Au–quartz crystal that was modified with a probe oligonucleotide **68**. This was followed by the hybridization of the interface with Au NPs that were functionalized with the DNA **67**, which is complementary to the free 3' segment of the target DNA, **69** (Figure 27B).^[243] Further amplification of the response was reported by the use of a secondary Au NP that was functionalized with the nucleic acid **68**, which is complementary to the 5' segment of the target DNA **69** and which enabled a layer-by-layer deposition of the Au NPs. The hybridization of the **68**–Au NPs with the analyzed DNA **69** followed by hybridization of the complex to the primary nanoparticle layer yielded a “second generation” of Au NPs—a process that is reminiscent of the growth of dendrimers.^[243b,244] Concentrations of DNA as low as $1 \times 10^{-10} \text{ M}$ could be detected by the amplification of the target DNA by the nucleic acid functionalized Au NP labels. It has been shown that the increase in the size of the Au NP labels from 10 nm up to ≈ 40 –50 nm results in an enhanced Δf signal, which increases the amplification factor of the DNA analysis.^[245] Further increase in the size of the Au NPs, however, resulted in smaller changes in the microgravimetric signal

because of the incomplete hybridization of the DNA analyte as a result of the labeling particles being too large.

A further method for the amplified microgravimetric QCM analysis of DNA utilized catalytic metal deposition on the NP labels.^[246] Figure 28 A depicts the amplified detection

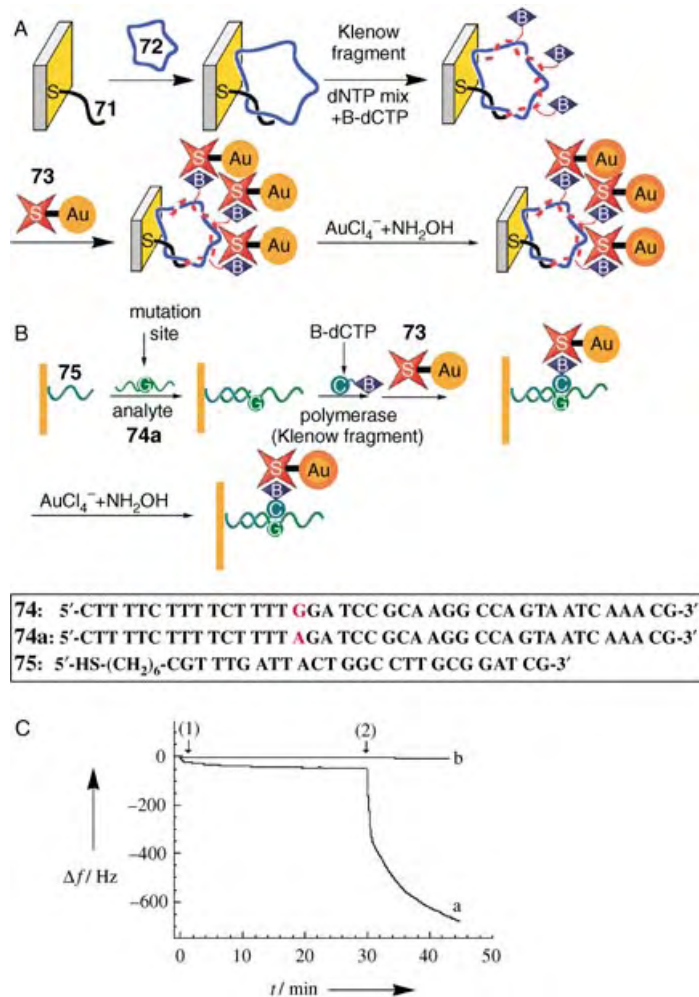


Figure 28. The catalytic deposition of gold on a Au NP conjugate for A) the amplified detection of the 7249-base M13mp18 DNA, B) the analysis of a single-base mismatch in DNA, and C) the microgravimetric detection of a single-base mutant. The frequency responses in C) were observed with a mutant DNA sequence (a) and with a normal DNA sequence (b). Arrows indicate (1) the attachment of the SAV–Au conjugate and (2) the catalytic deposition of gold on the Au NPs. (Adapted from Ref. [247]; Reproduced with permission of the Royal Society of Chemistry).

of the 7249-base M13mp18 DNA by using the catalytic deposition of gold on a Au NP conjugate.^[247] The DNA primer **71** was assembled on a Au–quartz crystal. After hybridization with M13mp18 DNA **72**, the double-stranded assembly was replicated in the presence of a mixture of nucleotides (deoxynucleotide triphosphates, dNTP mix) that included dATP, dGTP, dUTP, biotinylated dCTP (B-dCTP), and polymerase (Klenow fragment). The resulting biotin-labeled replica was then treated with a streptavidin–Au NP conjugate **73**, and the resulting Au-labeled replica was subjected to the Au NP-catalyzed deposition of gold by the NH_2OH -stimu-

lated reduction of AuCl_4^- . The replication process represents the primary amplification step as it increases the mass associated with the crystal and simultaneously generates a high number of biotin labels for the association of the streptavidin–Au NP conjugate. The binding of the conjugate represents the secondary amplification step for the analysis of M13mp18 DNA. The third step, which involves the catalyzed precipitation of the metal, led to the greatest amplification in the sensing process as a result of the increase in the mass of the Au NPs. The M13mp18 DNA could be sensed by this method with a lower detection limit of $\approx 1 \times 10^{-15}$ M.

This means of amplification was also applied to the analysis of a single-base mismatch in DNA as depicted in Figure 28B. This was exemplified with the analysis of the DNA mutant **74a**, which differs from the normal gene **74** by the substitution of a G base with an A base. The analysis of the mutant was performed by the immobilization of the probe DNA **75**, which is complementary to the normal gene **74** as well as to the mutant **74a** (up to one base prior to the mutation site), on the Au–quartz crystal. Hybridization of the normal gene or the mutant with this probe interface, followed by the reaction of the hybridized surfaces with biotinylated dCTP (B-dCTP) in the presence of polymerase (Klenow fragment) led to the incorporation of the biotin-labeled base only into the assembly that included the mutant **74a**. The subsequent association of the SAV–Au conjugate **73** followed by the catalyzed deposition of gold on the Au NPs amplified the analysis of the single-base mismatch in **74a**. Figure 28C, curve a, shows the microgravimetric detection of the mutant **74a** by this method, whereas the normal gene **74** does not alter the frequency of the crystal (Figure 28C, curve b). With this method, the mutant could be detected with a detection limit of 5×10^{-13} M.

6.3. Nanoparticle–Biomolecule Conjugates for Optical Sensing and Analysis

Metal or semiconductor nanoparticles that are linked to bioreceptors provide labeled conjugates that can be used to optically follow the biorecognition events at biosensor surfaces. Various optical methods have been employed to detect the association of NPs on biochips, including the scanometric detection of light scattering, surface plasmon resonance spectroscopy, resonance-enhanced absorption by NPs, nanoparticle fluorescence, and enhanced Raman scattering. Although not limited, most of these detection schemes have been applied in the detection of DNA.

In a typical setup for scanometric detection, a modified glass slide was mounted on a microscope stage and was illuminated in the plane of the slide with white light. In this configuration, the slide served as a planar waveguide to prevent any light from reaching the microscope objective by total internal reflectance. Wherever NP probes were attached to the surface, evanescently coupled light was scattered from the slide and was observed as bright, colored spots. This approach was used for the detection of Au NP-labeled DNA molecules that were specifically bound to a DNA-functionalized surface.^[248] Enlargement of the Au NPs by the catalytic

reduction of silver ions and the deposition of silver metal on the Au NPs resulted in a 100-fold amplification of the signal and thus increased the sensitivity.^[248a,d] Two different DNA sequences could be detected at once when two Au NPs of different sizes were used to label different oligonucleotides.^[248c] Spots with different colors, corresponding to the primary association of two kinds of Au NPs, were detected on the glass support when domains functionalized with different DNA probes were treated with the corresponding complementary DNA labeled with Au nanoparticles of 50- and 100-nm diameter. This method was used to detect single-base mismatches in oligonucleotides, which were hybridized to DNA probes that were immobilized at different domains of a glass support.^[248a] High analytical sensitivity was provided by the deposition of silver, whereas the selectivity was demonstrated by examination of the “melting” profiles of the spots: the mismatched spot reveals a lower “melt” temperature owing to its lower association constant. The melting properties of DNA-linked nanoparticle aggregates are affected by a number of factors, which includes DNA surface density, nanoparticle size, interparticle distance, and salt concentration.^[249] A theoretical model that describes this process was recently developed.^[249a] The sharpness of the melting profile is highly dependent on the size of the nanoparticle; with 50-nm Au NPs, a melting transition of one degree was observed.^[249b] As the sharpness of the melting transition correlates directly with the selectivity of the respective assay, this latter observation points a way for greatly improving the selectivity of DNA detection systems based on nanoparticles.

Ag NPs have similarly been used as antibody labels for the detection of antigens. This setup provided high-enough sensitivity to perform immunoassays based on single-target detection.^[250] A simple desktop flatbed scanner was used to read out signals from the immunosensing surface upon pesticide immunoassay with Au NP-labeled antibodies.^[251] Also, a low-cost image analyzer was used for a genomic analysis to capture evanescent wave-induced light scatter from silver-amplified Au nanolabels.^[248d]

A real-time DNA detection method that utilizes single-strand DNA-modified Au NP probes and micropatterned chemoresponsive diffraction gratings interrogated simultaneously at multiple laser wavelengths was recently reported.^[252] The surface-bound NP-probe-based assay with the chemoresponsive diffraction grating signal transduction scheme resulted in a simple DNA detection protocol that combines the high sensitivity and selectivity afforded by NP probes with the experimental simplicity, wavelength-dependent resonant enhancement features, and miniaturization potential of the diffraction-based sensing technology.

Resonance enhancement of the optical absorptive properties of metal NPs upon biorecognition interactions was also used as an effective means for biosensing.^[253] Ag NPs were used as a support for further biorecognition binding,^[253b] or metal NPs (Ag, Au, Pt) were employed as labels bound to the sensing interface upon the biorecognition events.^[253a] A good agreement between the experimental observations and the extended Mie theory provided a theoretical approach to the quantitative estimation of the amount of bound biomolecules.^[253c] The unique optical properties of gold NPs were

applied to the development of a reagent-dry strip-type biosensor that enables visual detection of double-stranded DNA within minutes.^[254] Sensitive naked-eye detection of immunoglobulin G by the enlargement of Au NPs has been reported.^[255] Au NPs were also used as spectroscopic enhancers for *in vitro* studies on single viruses.^[256] Extrinsic parameters, such as the dielectric properties of the immediate environment (nanoenvironment) of the particle or charge distributions, decisively influence the position of the nanoparticle plasmon resonance.^[257] Protein or DNA binding events cause a change in the refractive index of the nanoenvironment of a gold NP that results in a shift of the position of the NP plasmon resonance. This shift was used as a reporter signal of biorecognition events on a single NP.^[258]

An interesting application of submicrometer metallic “barcodes”^[259] for the analysis of biomaterials such as DNA or antigens has recently been reported.^[259b] “Barcodes” that are a few hundred nanometers in diameter, several microns long, and composed of many different metals (Pt, Pd, Ni, Co, Ag, Cu, and Au) were prepared by the electrochemical deposition of the metals in a porous Al_2O_3 membrane. The length of the respective metal segments in the strips was controlled by the charge applied in the electrochemical process (Figure 29A). The structure of the “barcode” could be identified by optical reflectivity or field emission SEM. Figure 29B shows an optical image of a Au–Ag multistripe barcode that consists of 240-, 170-, 110-, and 60-nm Ag stripes that are separated by ≈ 550 -nm Au stripes. It was suggested that with the available optical resolution, the number of possible readable “barcodes” that comprise two metals with a coding length of $6.5\ \mu\text{m}$ is 4160, whereas for three-metal barcodes, 8.0×10^5 distinctive striping patterns are possible. The use of a mixture of “barcodes”, each used to identify a

specific biomaterial adsorbed on it, could enable the simultaneous analysis of numerous components in biological mixtures. Thus, the “barcode” concept introduces a NP-based analysis method that competes with chip arrays and encoded microbeads.

As the identification of the label can be performed optically, fluorescence spectroscopy can be used to characterize a biorecognition event.^[259b] Figure 30A outlines the fluorescence detection of an analyte DNA, **76**, by a primer

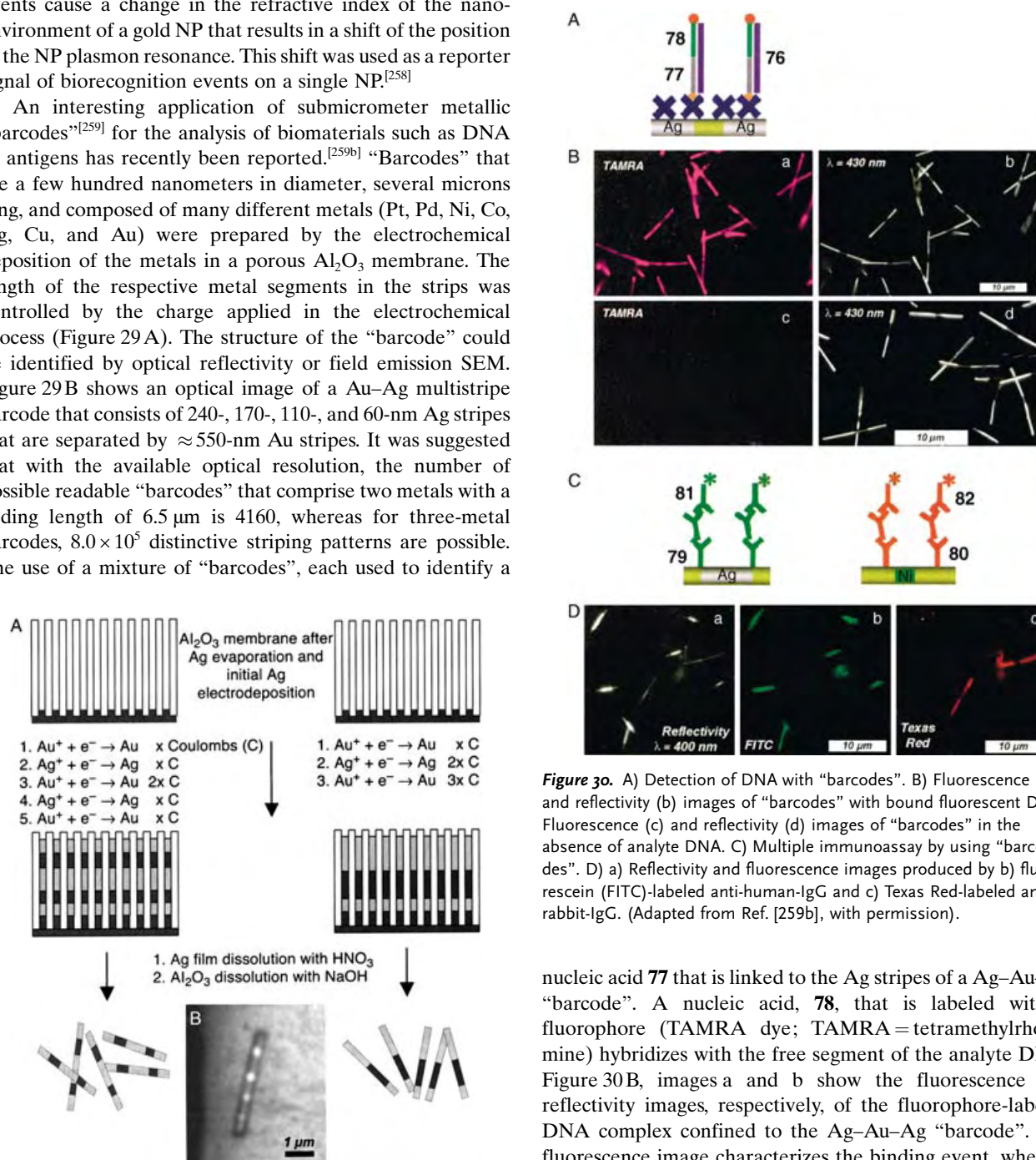


Figure 29. A) The construction of mixed-metal “barcodes” in an alumina membrane. B) An optical image of a Au–Ag multistripe “barcode” nanorod. (Adapted from Ref. [259b], with permission).

Figure 30. A) Detection of DNA with “barcodes”. B) Fluorescence (a) and reflectivity (b) images of “barcodes” with bound fluorescent DNA; fluorescence (c) and reflectivity (d) images of “barcodes” in the absence of analyte DNA. C) Multiple immunoassay by using “barcodes”. D) a) Reflectivity and fluorescence images produced by b) fluorescein (FITC)-labeled anti-human-IgG and c) Texas Red-labeled anti-rabbit-IgG. (Adapted from Ref. [259b], with permission).

nucleic acid **77** that is linked to the Ag stripes of a Ag–Au–Ag “barcode”. A nucleic acid, **78**, that is labeled with a fluorophore (TAMRA dye; TAMRA = tetramethylrhodamine) hybridizes with the free segment of the analyte DNA. Figure 30B, images a and b show the fluorescence and reflectivity images, respectively, of the fluorophore-labeled DNA complex confined to the Ag–Au–Ag “barcode”. The fluorescence image characterizes the binding event, whereas the reflectivity image identifies the “barcode” and thus the attached DNA probe. When the analyte DNA **76** is omitted, a very low fluorescence background is observed and the

particles are visible only in the reflectivity image (Figure 30B, images c and d).

The simultaneous analysis of different biological analytes was exemplified with the immunoassay of human immunoglobulin G (IgG) and rabbit IgG.^[259b] Two different “barcodes”, namely, a Au–Ag–Au (4- μm length) and a Au–Ni–Au (8- μm length), were employed. The Ag stripes of the Au–Ag–Au “barcode” were modified with the anti-human IgG antibody **79**, and the Au stripes of the Au–Ni–Au “barcodes” were derivatized with the anti-rabbit IgG antibody **80** (Figure 30C). Challenging the mixture of “barcodes” with the mixture of antigens followed by the labeling of the antibodies with fluorescein-labeled anti-human IgG **81** and Texas Red-labeled anti-rabbit IgG **82** allows the optical detection of the respective “barcodes” and the fluorescence detection of the two antigens. Figure 30D, image a, shows the image of the two kinds of “barcodes” by optical reflectance, whereas Figure 30D, images b and c, show the specific fluorescence from the fluorescein-labeled antibodies that are bound to the Au–Ag–Au “barcodes” and the Texas-Red-labeled antibodies that are linked to the Au–Ni–Au “barcodes”, respectively.

Selective noncovalent binding of proteins to specific domains of bimetallic Ni–Au nanorods was demonstrated.^[259c] Gold surfaces of the bimetallic nanorods were functionalized with alkanethiols that were terminated with hexa(ethylene glycol) groups, which prevent the adsorption of proteins, whereas nickel domains were functionalized with palmitic acid, a 16-carbon fatty acid that, on the other hand, allows the effective adsorption of proteins. Thus, “solution arrays” of highly encodable and chemically diverse nanorods provide an interesting approach for the future analysis of complex biological samples (e.g. genomics, proteomics).

The label encoding for the analysis of multiple biospecies can be performed in a different way. Nanoparticle labels encoded with DNA molecules were used for ultrasensitive multianalyte immunosensing.^[260] This has been demonstrated for the analysis of a prostate-specific antigen (PSA; Figure 31). An antibody which is complementary to PSA was linked to magnetic beads to give **83** as the primary sensing interface. After the association of PSA to the sensing interface, a gold nanoparticle that was functionalized with a second antibody, which was complementary to another domain of PSA, and with the double-stranded nucleic acids

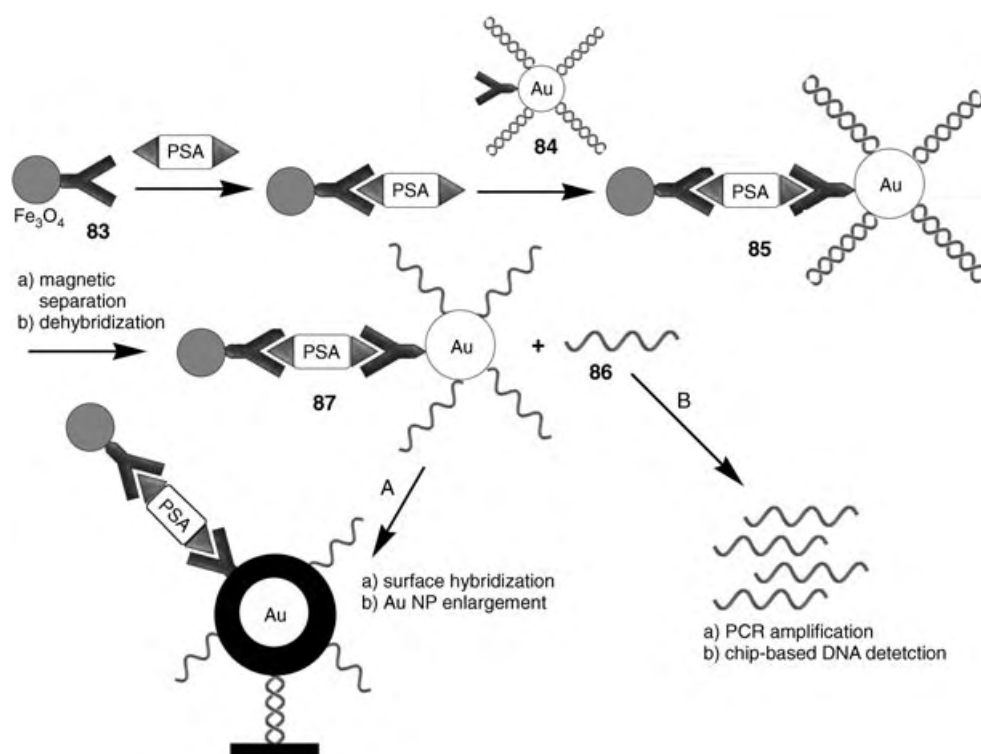


Figure 31. Application of Au nanoparticle labels that are encoded with DNA for the amplified immunosensing of prostate-specific antigen (PSA).

84 was linked to the magnetic bead–antibody–PSA complex to form a triple-component sandwich assay configuration, **85**. The assembly was separated by an external magnet and was washed free from any nonspecific adsorbates. The subsequent thermal dissociation of the nucleic acid duplex yielded the free nucleic acid, **86**, and the single-stranded-oligonucleotide-functionalized Au NPs, **87**. Two different routes were then employed to analyze the assay sample: a) The Au NPs, **87**, which held the assay components, were hybridized on a chip surface that was functionalized with the complementary oligonucleotides. Then the Au NPs were enlarged by the electroless deposition of Ag and were further analyzed by optical means (Figure 31, route A). b) The free oligonucleotides **86** were multiplied by the PCR procedure and then analyzed upon their deposition on a chip surface. The sequence analysis of the dissociated nucleic acid then provided a specific signal for the analyzed antigen (Figure 31, route B). This analytical protocol includes an intrinsic amplification feature as numerous nucleic acid barcodes are released in the thermal dehybridization step as a result of a single PSA recognition event. Furthermore, the subsequent PCR amplification of the released nucleic acid provides an invaluable tool to further amplify the PSA detection, and the antigen can be detected with an unprecedented sensitivity of 3 attomolar by this approach. A multi-analyte immunoassay could therefore be performed when each specific antigen analyte is encoded with a different oligonucleotide sequence.

Au NPs have been extensively used for the detection of bioaffinity binding by virtue of nanoparticle-enhanced sur-

face plasmon resonance (SPR) spectroscopy.^[261] The SPR signals were dramatically enhanced when Au nanoparticles were used as labels in immunosensing^[210b,c] and DNA sensing applications.^[209] A sensing interface that was modified with antibody units was employed to bind the complementary antigen component, and the resulting affinity complex was treated with a secondary antibody labeled with a Au NP. Whereas the association of the antigen to the antibody-functionalized surface yielded a small shift in the SPR spectrum, a substantial shift in the SPR spectrum was detected upon the binding of the secondary Au NP-labeled antibody. As the secondary antibody associates with the modified surface only if the antigen is bound to the sensing interface, the Au NP-labeled antibody provides a means of amplification of the primary recognition event. The binding of Au NPs to the immunosensing interface led to a large shift in the plasmon angle, a broadening of the plasmon resonance, and an increase in the minimum reflectance, all of which thereby allowed picomolar detection of the antigen. Similarly, the sensitivity of DNA analysis was enhanced by ≈ 3 orders of magnitude when Au NP-functionalized DNA molecules were used as probes (Figure 32).^[209] Au NPs have been used to

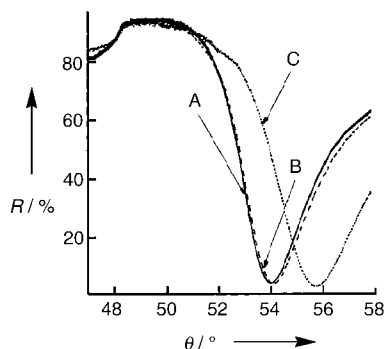


Figure 32. Surface plasmon resonance (SPR) spectroscopy enhanced by Au NPs for DNA analysis (R = reflectance). A) SPR spectrum of the DNA primer-functionalized surface, B) SPR spectrum after hybridization with the target DNA molecules, and C) SPR spectrum after hybridization with the target DNA molecules conjugated with Au NPs. (Adapted from Ref. [209], with permission; Copyright American Chemical Society, 2000).

label polypeptides, and the assembly of a de novo protein from the labeled polypeptide fragments has been followed by the SPR technique. Changes in the SPR spectrum are also observed upon the chemically directed association of the Au NP labels in the de novo protein structure.^[262]

A novel class of fiber-optic evanescent-wave sensor was constructed by the modification of the unclad part of an optical fiber with self-assembled gold NPs that were functionalized with biomolecules to provide selectivity for the substrate molecules that bind to the sensing interface.^[263] The optical properties and, hence, the attenuated total reflection (ATR) spectrum of self-assembled Au NPs on the optical fiber change upon alteration of the refractive index of the local environment of the Au NPs. Accordingly, biorecognition events that take place on the NPs change the refractive index of the interface and result in a change in the total reflection

spectrum of the system. In a model system, the modification of the Au NP interface with biotin enabled the detection of streptavidin with a detection limit of 9.8×10^{-11} M.

A DNA sensor was based on enhanced transmission surface plasmon resonance (ET-SPR) spectroscopy.^[264] ET-SPR spectroscopy is based on the high sensitivity of the surface plasmon absorption band of gold NPs to their environment. Indeed, advantage has been taken of gold “nanoislands” that are deposited onto glass slides to provide an inexpensive and simple method for sensing medium changes (such as air versus water) and for quantifying adsorbed or chemically bound molecules or both. Changes in the ET-SPR spectra were observed upon hybridization of Au NP-labeled DNA with the complementary DNA primer immobilized on Au nanoislands thus allowing spectral detection of the hybridization process.

Triangular silver nanoparticles, ≈ 100 -nm wide and 50-nm high, are formed (Figure 33 A) and these show very unique

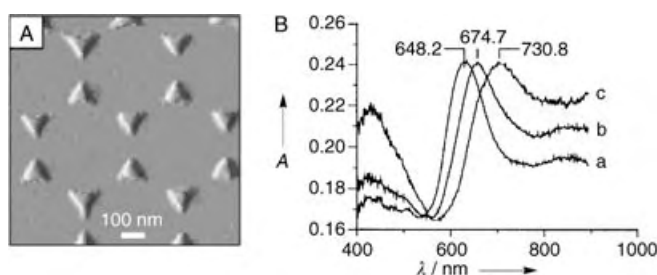


Figure 33. Localized surface plasmon resonance (LSPR) nanobiosensor that uses triangular silver NPs for the labeling of biomaterials. A) AFM image of the triangular Ag NPs. B) Amplified LSPR analysis of streptavidin (SAv) with the triangular Ag NPs: a) Ag NPs after modification with biotin (1 mM); b) Biotinylated Ag NPs after reaction with SAv (100 nM); c) SAv-loaded Ag NPs after reaction with biotinylated Au NPs. (Adapted from Ref. [265a], with permission; Copyright American Chemical Society, 2002).

optical properties (Figure 33 B).^[265] In particular, the maximum absorbance wavelength, λ_{\max} , of their localized surface plasmon resonance (LSPR) spectrum is unexpectedly sensitive to the size, shape, and local (≈ 10 – 30 nm) external dielectric environment of the nanoparticle. The sensitivity of λ_{\max} (LSPR) to the nanoenvironment has allowed the development a new class of nanoscale affinity biosensors^[265] that operate in a totally analogous manner to their SPR counterparts by transducing small changes in the refractive index near the noble-metal surface into a measurable wavelength-shift response. The novel affinity biosensor based on the LSPR wavelength shift was tested using the streptavidin–biotin recognition system.^[265a] Triangular silver NPs were functionalized with biotin units, and the changes in the LSPR spectra were followed upon the binding of streptavidin molecules (Figure 33 B). The detection by LSPR was further amplified by the secondary coupling of biotinylated Au NPs to the streptavidin-saturated interface. A similar method was applied to design an immunosensor.^[265b]

SPR spectroscopy was used to follow biocatalytic reactions with amplification of the signal by Au nanoparticles. Au NPs that were functionalized by the covalent binding of N,N' -

bipyridinium (viologen) units to the tiopronin shell were coupled to the redox processes of NAD^+/NADH cofactors.^[266] The viologen-shell units were biocatalytically reduced by the NADH cofactor in the presence of diaphorase. The reduced viologen units were adsorbed onto a SPR plate which brought the Au cores closer to the sensing interface. Plasmon coupling between the Au SPR plate and the Au NPs resulted in an amplified change in the SPR spectrum that depended on the concentration of NADH. In the opposite setup, the viologen-shell units were electrochemically reduced and precipitated onto the surface of the SPR electrode. In the presence of NAD^+ cofactor and diaphorase, the reduced viologen units were reoxidized by NAD^+ and redissolved. The decrease of the loading of the Au NPs on the SPR electrode again resulted in the NAD^+ concentration-dependent amplified change in the SPR spectrum. It should be noted that application of molecular viologen unbound to Au NPs under the same conditions results in only minute changes to the SPR spectrum which do not allow the detection of the NAD^+/NADH cofactors.

The electrical charging of Au nanoparticles that are associated with a SPR interface results in changes in the SPR spectra which depend on the extent of the electrical charge on the Au NPs. Therefore, coupling biocatalytic reactions, which involve an electron-transfer process, to Au NPs which results in their charging allows the analysis of the processes by SPR spectroscopy.^[267] Au NPs (1.4 nm) that were functionalized with N^6 -(2-aminoethyl)flavin adenine dinucleotide (FAD cofactor, amine derivative; **49**) were reconstituted with apo-glucose oxidase (apo-GOx). The nanoparticles were then self-assembled on a gold thin-film (SPR electrode) by using a long-chain dithiol, $\text{HS}(\text{CH}_2)_9\text{SH}$, monolayer as a linker. This yielded the biocatalytically active glucose oxidase (GOx) bound to the Au NPs in an aligned configuration (Figure 34A).^[267a] The biocatalyzed oxidation of glucose resulted in the formation of the reduced form of the cofactor, FADH_2 . In the absence of O_2 , which is a natural electron acceptor for GOx, electron transfer proceeds from the reduced cofactor to the Au NPs to result in their charging. The long-chain dithiol monolayer provided a barrier for the electron tunneling from the Au NPs to the bulk Au support to preserve the electrical charge that was produced on the Au NPs. The plasmon coupling between the charged Au NPs and the Au support resulted in a shift of the SPR spectrum which was dependent on the charge generated on the NPs (Figure 34B). As the

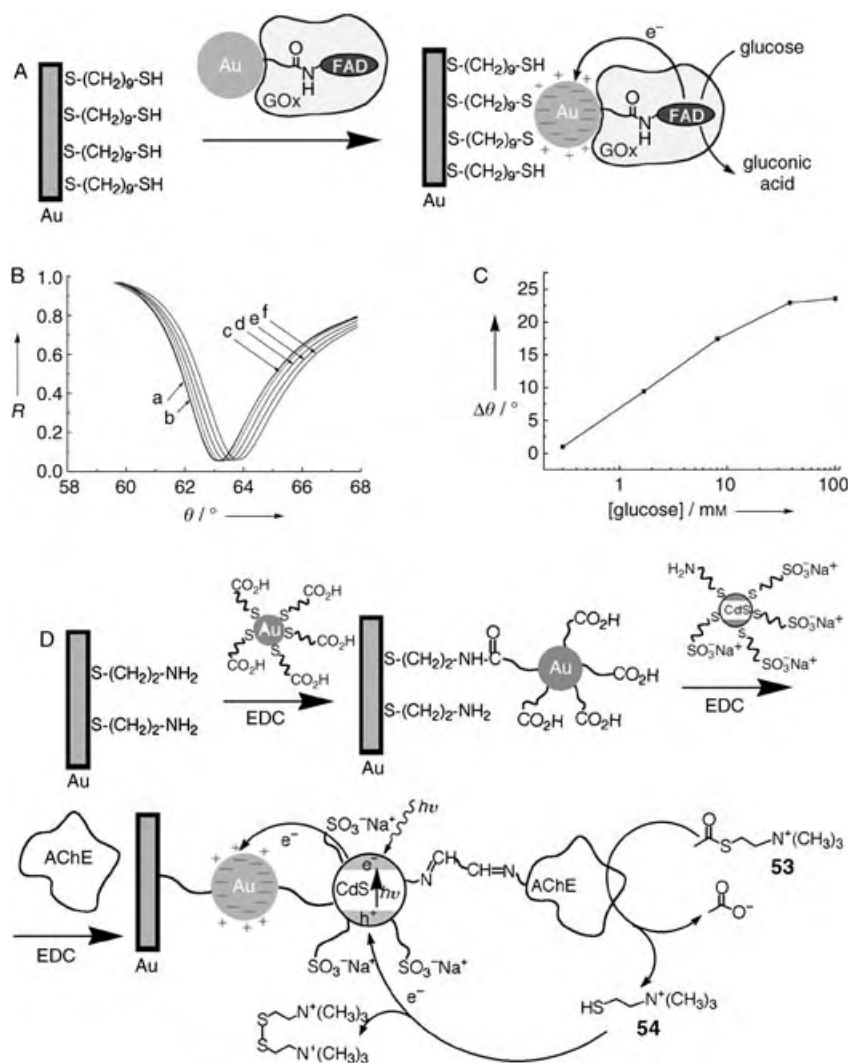


Figure 34. A) Assembly of Au NP-bound reconstituted glucose oxidase (GOx) on a dithiol monolayer that is associated with a SPR-active surface, and biocatalytic charging of the Au NPs in the presence of glucose. B) SPR spectra of the Au NP-GOx hybrid system upon the addition of various concentrations of glucose: a) 0, b) 0.3, c) 1.6, d) 8, e) 40, and f) 100 mM. C) Calibration plot of the SPR spectra minimum shift as a function of glucose concentration. D) Assembly of the Au NP-CdS NP-acetylcholine hybrid system on a SPR-active surface, and photochemical charging of the Au NPs controlled by the biocatalytic reaction. EDC = 1-ethyl-3-(3-dimethylaminopropyl)carbodiimide.

charge value was controlled by the rate of the biocatalytic reaction, the shift in the SPR spectrum was enhanced upon elevation of the glucose concentration (Figure 34C). This optical transduction of the glucose concentrations upon the “biopumping” of electrons into the Au NPs is a new concept in biosensing.

A related system has employed the photoelectrochemical charging of Au nanoparticles by CdS nanoparticles as a method to detect acetylcholine esterase inhibitors.^[267b] A bilayer that consists of Au NPs covalently bound to CdS NPs was assembled on a SPR-active Au surface by using a cystamine monolayer as a linker (Figure 34D). The enzyme acetylcholine esterase (AChE) was covalently coupled to the CdS NPs to yield the Au/CdS nanoparticles-AChE enzyme biocatalytic assembly. Hydrolysis of acetylthiocholine (**53**) by

the enzyme yields thiocholine (**54**), which acts as an electron donor. Photoexcitation of the CdS nanoparticles results in the generation of electron–hole pairs in the conduction band and valence band, respectively. The electron donor **54**, which is generated by the enzyme in situ, scavenges the valence-band holes to enable the transport of the conduction-band electrons to the Au NPs. As the cystamine linker provides a tunneling barrier against further electron transfer to the bulk Au support, the charge is preserved on the Au NPs and thus results in changes in the SPR spectrum of the system. The changes in the SPR spectra are controlled by the extent of the NP charging, which itself is dominated by the concentration of the electron donor **54** generated in situ. In the presence of AChE inhibitors, such as 1,5-bis(4-allyldimethylammonium-phenyl)pentan-3-one dibromide (**55**), the biocatalyzed generation of the electron donor declined as the concentration of the inhibitor increased which altered the electrical charging of the Au NPs and the resulting SPR spectrum of the system. Therefore, this system allowed the optical assay of AChE activity and quantitative analysis of the enzyme inhibitors.

Surface-enhanced Raman (SER) scattering of nanoparticle-bound substrates allows the amplification of molecular vibrational spectra by up to 10^5 -fold.^[21a,268] Some early studies demonstrated the enhanced Raman scattering spectra of cytochrome c that was coupled to Au NPs, which were associated with aggregated Ag clusters.^[269] Also, SER spectra were observed for hemoglobins bound to Ag NPs.^[36] Modification of metal NPs with different Raman dyes could generate multiply coded NPs^[270] that allow thousands of codes to be written and read by means of surface-enhanced resonance Raman (SERR) scattering without the need for spatial resolution of components of the code.^[270a] The use of surface enhanced Raman spectroscopy (SERS) for the analysis of biorecognition events was demonstrated with the application of Au NPs that were functionalized with Raman dyes and recognition elements.^[270b,c] Formation of the complementary recognition complex on surfaces followed by the electroless deposition of Ag⁰ islands on the Au NPs enabled the readout of the biorecognition events by SERS. The concept was applied for the parallel detection of various analytes on surfaces in an array configuration. For example, three different thiol-functionalized Raman-active dyes, Cy3, Cy3.5, and Cy5, were linked through a spacer, which comprised twenty adenine bases (A₂₀), to the three small molecules, biotin, digoxigenin, and dinitrophenyl, respectively.^[270b] These functional units were then coupled to Au NPs (13 nm) to yield three different Raman dye-labeled Au NPs (Figure 35 A). These labeled nanoparticles were then employed to detect the specific interactions with the complementary mouse monoclonal antibodies for biotin, digoxigenin, and dinitrophenyl, respectively, by SERS. The different kinds of antibodies were spotted on a surface and the specific binding of Au NPs was followed by the electroless deposition of Ag⁰ on the Au NPs and analysis by SERS (Figure 35 B). The selective analysis of the three different Au NP labels by the pre patterning of the surface with the antibodies is depicted in Figure 35 C. A similar concept was also used to identify protein–protein interactions by using Au NPs that were functionalized with specific antibodies and encoded with

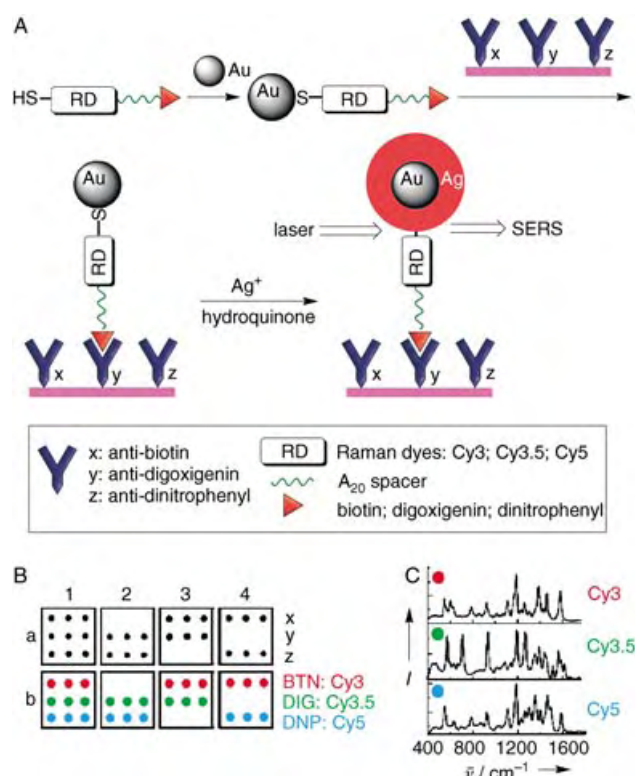


Figure 35. A) Application of Raman dye-functionalized Au NPs for amplified multitarget immunosensing. B) Flatbed scanner images of silver-enhanced microarrays upon the immunosensing of different antibodies by Au NPs that are functionalized with the respective antigens and various Raman dyes. C) Typical Raman spectra that correspond to the colored dots in the immunosensing array. (Parts B and C are adapted from Ref. [270b], with permission; Copyright American Chemical Society, 2003).

specific Raman dyes.^[270b] Further development of the SERS technique allowed highly sensitive immunoassay procedures^[271] such as femtomolar detection of a prostate-specific antigen (PSA) by using Au NPs labeled with the respective antibody.^[271a]

Semiconductor nanoparticles (e.g. CdS, CdSe, ZnS) can be used as fluorescent labels for immunosensing and DNA sensing as they provide tunable wavelengths, narrow emission peaks, and 100-fold higher stability relative to molecular fluorescent dyes.^[21a,75,272] CdSe_{core}/ZnS_{shell} NPs were functionalized with avidin and these were used as fluorescent labels for biotinylated antibodies. Fluoroimmunoassays utilizing these antibody-conjugated NPs were successfully used in the detection of protein toxins (staphylococcal enterotoxin B and cholera toxin).^[272f]

Four different-sized CdSe_{core}/ZnS_{shell} NPs that exhibit nonoverlapping emission wavelengths in the region 530–640 nm were used to modify four different nucleic acids.^[272g] The NP-labeled nucleic acids were selectively collected by specific hybridization with a spotted array of the complementary DNA and were analyzed by fluorescence imaging of the array. Another approach for DNA hybridization assays that uses metal-enhanced fluorescence was reported recently.^[273] For this, thiolated oligonucleotides were bound to silver NPs that were associated with a glass substrate.

Addition of the complementary fluorescein-labeled oligonucleotide in the presence of the Ag NPs resulted in a 12-fold increase in the fluorescence intensity. The enhanced steady-state fluorescence was attributed to the shortening in the lifetime of the dye as it entered into proximity of the Ag NPs. Thus, hybridization could be followed by the analysis of the decay kinetics of the emission of the dye. These results suggest that silver particles could be used as a versatile label for the amplified detection of DNA hybridization. Similarly, Ag nanoparticle-enhanced fluorescence was applied in the immunoassay of insulin in serum.^[274]

CdSe_{core}/ZnS_{shell} NPs were also applied as photochemical centers for lighting-up the dynamics of DNA replication or telomerization processes that occur on the nanoparticles. Dye units were incorporated into the newly synthesized DNA replica or telomer to act as energy acceptors for fluorescence resonance energy-transfer (FRET) processes.^[275] CdSe_{core}/ZnS_{shell} NPs were functionalized with the primer **88**, which is complementary to a section of M13mp18 DNA. Hybridization of the M13mp18 DNA with the nanoparticle interface followed by the replication of the assembly in the presence of polymerase enzyme (Klenow fragment) and the nucleotide (dNTP) mixture that included Texas Red-functionalized dUTP (**89**) resulted in the concomitant incorporation of the dye labels into the DNA replica (Figure 36A, route a). A FRET process from the semiconductor NPs to the incorporated dye units resulted in emission from the dye with concomitant quenching of the fluorescence of the NPs (Figure 36B).

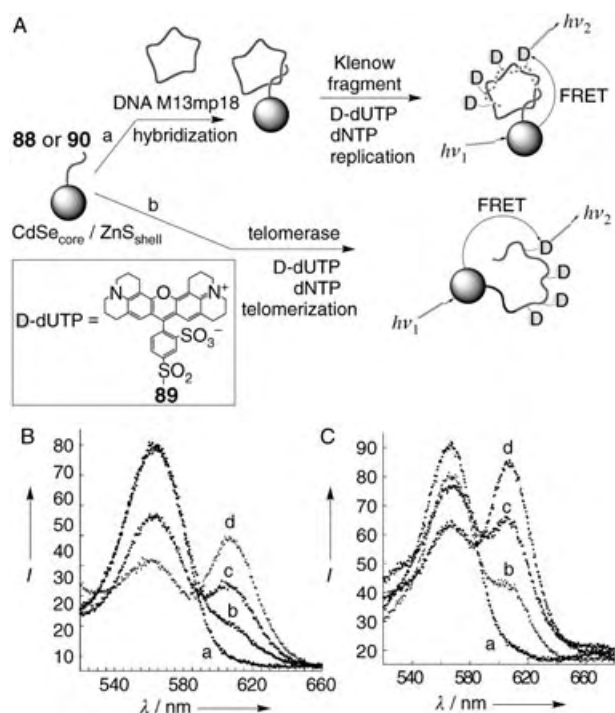


Figure 36. A) Replication (path a) and telomerization (path b) of nucleic acid functionalized CdSe_{core}/ZnS_{shell} NPs with incorporated Texas Red-labeled dUTP followed by FRET from the photoexcited quantum dots to the incorporated dye molecules. B) Emission spectra upon the time-dependent DNA replication: a) 0, b) 10, c) 30, and d) 60 min. C) Emission spectra upon the time-dependent DNA telomerization: a) 0, b) 10, c) 30, and d) 60 min.

Telomerase activity in cancer cells was monitored by an identical method.^[275] The CdSe_{core}/ZnS_{shell} NPs were functionalized with the nucleic acid **90**, which is recognized by telomerase. Treatment of the NPs with a HeLa cancer-cell extract in the presence of the dNTP mixture that contained the Texas Red-functionalized dUTP (**89**) resulted in the telomerization of the primer with incorporation of the dye labels (Figure 36A, route b). The incorporation of the dye units into the telomer enabled FRET from the excited semiconductor NPs to the dye units. The time-dependent increase in the dye emission was used to follow the dynamics of telomerization and to probe the telomerase activity in the cancer cells (Figure 36C). Similarly, the FRET process was applied to follow the binding of dye-functionalized proteins to the CdSe_{core}/ZnS_{shell} NPs,^[276] thus opening the way to FRET-based immunosensing. Functionalization of a protein backbone with photoisomerizable photochromic units yielded a hybrid system, in which the FRET efficiency was controlled by the isomeric state of the photochrome to allow modulation of the fluorescence intensity from the bound nanoparticle.^[277]

Recently, dye-doped silica NPs were developed as labels for bioanalytical applications.^[278] The SiO₂ NPs, sized between 2 and 100 nm, provide a versatile matrix for the immobilization of biomaterials, such as proteins or DNA, and the entrapped fluorophores reveal an enhanced stability towards photodegradation. Also, the accumulation of numerous entrapped fluorescence labels in a single SiO₂ NP provides a means of signal amplification path in biosensing because a single biorecognition event is imaged by the emission of numerous fluorophore units.

7. Biomolecule-Functionalized Magnetic Particles

Magnetic particles (microspheres, nanospheres, and ferrofluids) are widely studied and applied in various fields of biology and medicine such as magnetic targeting (of drugs, genes, and radiopharmaceuticals), magnetic resonance imaging, diagnostics, immunoassays, RNA and DNA purification, gene cloning, and cell separation and purification.^[279] These magnetic particles generally exist in a “core/shell” configuration in which biological species, such as cells, nucleic acids, and proteins, are bound to the magnetic “core” through organic linkers, which are often organized as a polymeric “shell” around the core.^[280] The efficiency of the binding of a biomaterial to the primary organic shell that surrounds the magnetic core was analyzed by various techniques including capillary electrophoresis with laser-induced fluorescence detection.^[280a] Most of the applications of biomaterial–magnetic-particle hybrid conjugates involve the concentration, separation, regeneration, mechanical translocation, and targeting of biomaterials. Phospholipid-coated magnetic NPs with a mean magnetite core size of 8 nm were used for the recovery and separation of proteins from protein mixtures.^[280b] Antibodies were adsorbed on synthetic Fe₃O₄ magnetic particles, and these particles were then used for specific binding to cells and the separation of the cells by an external magnetic field.^[281] Magnetic NPs (FePt, ≈4-nm diameter) that were functionalized with vancomycin (Van) were used to

capture selectively Gram-positive bacteria cells through molecular recognition between Van and the terminal peptide, D-Ala-D-Ala, on the surface of the cells.^[282] Unexpectedly, the Van-modified magnetic particles were also found to associate to Gram-negative bacteria such as *E. coli*.

A magnetic nanocapturer has been developed for the separation and collection of trace amounts of DNA/mRNA from mixtures and cancer cells. The nanocapturer was fabricated by using a magnetic NP as a magnetic carrier that was then functionalized with a molecular beacon as a DNA probe for gene recognition and collection.^[283] High sensitivity detection of molecular recognition was observed by using magnetically labeled biomolecules and magneto-resistive sensors.^[284] The layer-by-layer deposition of enzymes and magnetic particles was applied to prepare a bioreactor and allowed the biocatalytic layer to be stripped out with an external magnet when it was deactivated so that the surface could be reloaded with a new active biocatalyst layer.^[285]

Magnetic NPs could be applied to design magnetoelectronic materials and devices with improved properties. In this context, biomaterials can be used as a template for the synthesis of the magnetic NPs. As an example, monodisperse Co/Pt magnetic NPs were produced inside the apo-ferritin cavity. These assemblies were subsequently self-organized as a thin-film array on a glass support to yield a magnetic recording media with the potential to support Terabit inch⁻² recording densities.^[286]

Some recent research, however, has been directed to the coupling of functional magnetic particles with biomaterials to yield magnetically controlled functions of the biomaterial–magnetic particle hybrids. The results of these studies are outlined in the following chapters.

7.1. Synthesis of Biomolecule-Functionalized Magnetic Particles

The core of magnetic particles is usually composed of Fe₃O₄ or γ -Fe₂O₃, and its primary modification with an organic shell can include the adsorption of an organic polymer or the covalent attachment of a functionalized organosilane film. Convenient syntheses of magnetic particles with controlled size and magnetization have been developed.^[287,288] The size-controlled synthesis of magnetite (Fe₃O₄) NPs was reported in organic solvents.^[289] Gold-coated iron NPs with a specific magnetic moment of 145 emu g⁻¹ and a coercivity of 1664 Oe were prepared and tested for biomedical applications.^[290] The gold shell allows the further modification of the magnetic NPs with biomolecules by using the self-assembly method. Elsewhere, silica particles that carry encapsulated magnetic NPs were used to bind proteins to the outer sphere of the inorganic beads for biocatalysis.^[291]

Organic functional groups introduced by these techniques allow the coupling of biomolecules to the organic shell.^[292] Several synthetic approaches to couple biomolecules to magnetic particles and to use the hybrid assemblies for various bioanalytical applications have been reported. The preparation and characterization of magnetic NPs that are coated by organic shells for the covalent immobilization of enzymes (e.g. HRP or lipase) was described recently.^[293] The

immobilization of enzymes on magnetic particles yields biocatalytically active particles. In one example, alcohol dehydrogenase was covalently bound to Fe₃O₄ magnetic particles, and the immobilized enzyme demonstrated high biocatalytic activity.^[294] Enzyme-modified magnetic particles could also demonstrate bioelectrocatalytic activities while being in contact with an electrode surface.^[293d] The reversible association of proteins with negatively charged polyacrylic_{shell}/Fe₃O₄_{core} magnetic particles was demonstrated.^[295] The binding of proteins was controlled by electrostatic interactions between the proteins and the negatively charged shells. The protein molecules, which were positively charged at low pH values (pH < pI; pI = isoelectric point), were electrostatically attracted to the negatively charged shells, whereas at higher pH values (pH > pI), the negatively charged protein molecules were repelled from the functionalized magnetic particles. The reversible association/dissociation of the proteins to and from the magnetic particles, respectively, was used to collect, purify, and transport proteins. DNA molecules were treated with a mixture of Fe²⁺/Fe³⁺ ions, which were electrostatically associated with DNA chains.^[296] The Fe²⁺/Fe³⁺ ions were then reacted to give Fe₃O₄ magnetic particles associated with the DNA molecules. The labeled DNA could hybridize with complementary oligonucleotides, and the magnetic particles linked to the DNA molecules allowed the separation of the labeled DNA from nonlabeled strands.

The cooperative assembly of magnetic NPs in the presence of amino acid based polymers was studied, and it was demonstrated that electrostatic interactions between block copolypeptides and NPs could control the organization of these components.^[297] The presence of polyaspartic acid initiated the aggregation of maghemite NPs into clusters without the formation of a precipitate. The addition of the block copolypeptide poly(EG₂-Lys)₁₀₀-*b*-poly(Asp)₃₀ induced a controlled organization of the magnetic NPs (possibly through the formation of micelles) with cores that consisted of the NPs electrostatically bound to the polyaspartic acid end of the block copolypeptide. In this case, the poly(EG₂-Lys) ends of the copolymers formed the micelle shell, and the micelles both stabilized the clusters and controlled their size. By altering the composition of the block copolypeptide, it should be possible to control both the size and the stability of the resulting dispersed NP clusters to thereby greatly expand the potential applications and usefulness of these cooperatively assembled nanocomposite materials.

Inorganic nano- and micro-sized particles including magnetic particles could be generated by biochemical means. The field of biomineralization has highlighted the possibility to synthesize materials based on the molecular interactions between supramolecular organic or bioorganic assemblies and inorganic materials.^[21a,298] Protein cages,^[299] and particularly viral protein cages,^[299d-f] provide structurally constrained reaction nanoenvironments that act as templates for the generation of inorganic nanomaterials. Viral protein cages exist in a wide variety of sizes and shapes and have structural transitions that allow controlled access to the interior of the protein cage.^[299f] Genetic and chemical modifications of protein templates provide a further flexibility to the syntheses of nanomaterials.^[299g] The natural

protein ferritin provides a structurally constrained reaction medium for the syntheses of both natural and synthetic inorganic nanomaterials.^[129,299a–c,300] In particular, ferritin can be used to generate precisely sized and shaped magnetic particles in the protein cavity.^[301] For this purpose, the nonmagnetic natural core that was composed of $5\text{Fe}_2\text{O}_3 \cdot 9\text{H}_2\text{O}$ was chemically removed from the protein cavity, and an artificial magnetic core that was composed of magnetite (Fe_3O_4)^[129c] or magnetite/maghemite ($\text{Fe}_3\text{O}_4/\gamma\text{-Fe}_2\text{O}_3$)^[302] was generated inside apo-ferritin. The direct electrochemistry of ferritin adsorbed on an ITO electrode was studied.^[303] It was shown that the iron-oxide core of ferritin is electrically contacted with the electrode and its reductive dissolution yielded the apo-ferritin. Genetic engineering was employed to tune the size of the cavity to provide monodisperse ferric oxide magnetic NPs of variable size.^[304]

The unusual ferritin-like protein from the bacteria *Listeria innocua* has been shown to form a twelve-subunit cage structure around a 5-nm-diameter interior cavity.^[305] This small cage structure has the capacity to hold only 500 Fe atoms in the form of a ferric oxyhydroxide NP.^[306] This cage provides a new size regime and holds promise for tuning size-dependent material properties. The natural protein shell that surrounds the NPs provides binding groups for the covalent attachment of biomolecules. The well-characterized cowpea chlorotic mottle virus (CCMV), which is devoid of nucleic acid, was used as the starting material to create a new cage with specific chemical functionality that mimics the iron-storage protein ferritin.^[307] The CCMV protein cages are composed of 180 identical 20-kDa subunits that self-assemble into an empty virion that has icosahedral symmetry (Figure 37A). Structural analysis indicated that the viral protein cage should allow access to small molecules through pores that are created at the interfaces of the protein subunits. This empty protein cage has an outer diameter of 28 nm and an inner diameter ranging from 18–24 nm (Figure 37B). Thus, CCMV has a cavity of approximately twice the diameter of ferritin. The CCMV coat protein was genetically modified by replacing 9 basic residues at the N terminus with glutamic acid. The mutant assembled readily into a cagelike architecture similar to the wild-type protein. This electrostatically altered viral protein cage catalyzed the rapid oxidation of Fe^{2+} which led to the formation of a spatially constrained iron oxide NP, 24.0 ± 3.5 nm, within the cage.

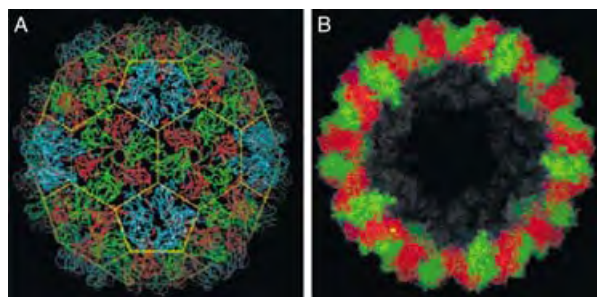


Figure 37. A) Ribbon diagram of the 180-subunit protein cage of the cowpea chlorotic mottle virus (CCMV). B) Cut-away view that shows the central cavity of the protein cage. (Adapted from Ref. [307], with permission).

Biominingeralization which is performed by many microorganisms yields various micro- and nanostructured magnetic materials that are included into biological structures.^[308] For example, some bacteria (e.g. *Magnetospirillum magnetotacticum* MS-1,^[309] *Magnetospirillum* sp. MGT-1,^[310] *Magnetospirillum* sp. AMB-1,^[311] and *Magnetospirillum gryphiswaldense*^[312]) produce natural magnetic particles (Fe_3O_4 , 50–100 μm in size) that are aligned in chains and enveloped by a lipid membrane.^[313] These naturally produced lipid-coated magnetic particles could be isolated from the parent bacteria^[314] and modified with biomolecules by the use of bifunctional coupling reagents (e.g. glutaric dialdehyde). These magnetic particles have been applied as active components in fluoroimmunoassays,^[315] chemiluminescence immunoassays,^[316] mRNA recovery,^[317] and as DNA carriers.^[318]

7.2. Antigen- or Antibody-Functionalized Magnetic Particles Applied as Immunosensors

Magnetic particles functionalized with antigens or antibodies have been applied in various immunoassay schemes.^[319] In most of these applications, the functionalized magnetic particles were used for the isolation and concentration of the sensing materials as well as for the exchange of the sensing interface at the end of the analysis. As an example, magnetic NPs were functionalized with antigens or antibodies and these were then attracted to a quartz crystal microbalance by the use of an external magnet and used for immuno-sensing.^[319a] The method allowed the rapid regeneration of the sensing interface by simple exchange of the modified magnetic particles. In another application, Au NPs were coated with dinitrophenyl-functionalized mercaptodextrans, which bind specifically to magnetic beads that are modified with the corresponding DNP-antibody.^[320] The hybrid system allowed the spectral detection of immunorecognition reactions by following the absorbance spectra of the Au NP labels. The magnetic beads provided an easy means of purification and concentration of the analyte samples. Magnetic particles with an encoding symbol introduced by functionalization were applied to a parallel multianalyte immunoassay that used a self-assembled addressable microparticle array on a chip.^[321]

The intrinsic magnetic properties of the particles were also used as a means of detection in biosensing. For example, adenovirus (ADV) species were cross-linked by anti-ADV-functionalized magnetic NPs to yield an aggregated system.^[322] The formation of the ADV–magnetic NP assembly was detected by measurement of the changes of the T_2 relaxation times of water. The method allowed the detection of as few as five viral particles in 10 μL of 25 % protein solution.

7.3. DNA Analysis by Oligonucleotide-Functionalized Magnetic Particles

The separation and purification steps that are performed prior to the electrochemical analysis of DNA were simplified

by the attachment of the DNA analyte to magnetic particles.^[323] The reversible, magnetically controlled oxidation of DNA was accomplished in the presence of nucleic acid-modified magnetic particles.^[324] Avidin-modified magnetic particles were functionalized with the biotinylated probe nucleic acid, and these were subsequently hybridized with the complementary DNA. Two carbon-paste electrodes were patterned on a surface and applied as working electrodes. Spatial deposition of the functionalized magnetic particles on the left or right electrode enabled the magneto-controlled oxidation of the DNA by chronopotentiometric experiments (potential pulse from 0.6 to 1.2 V; Figure 38). Changing the

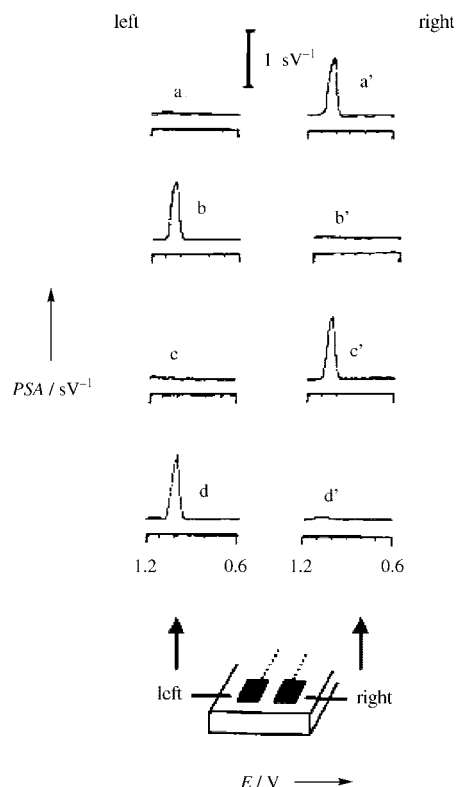


Figure 38. Chronopotentiometric (PSA=potentiometric stripping analysis) signals for the DNA-oligomer-functionalized magnetic particles by the dual carbon-paste electrode assembly: a–d) Potentiograms obtained at the left electrode; a'–d') Potentiograms obtained at the right electrode. Potentiograms a), b'), c), and d') were obtained in the absence of the magnet, whereas potentiograms a'), b), c'), and d) were recorded in the presence of the magnet. (Adapted from Ref. [324], with permission).

position of the magnet (to below the planar printed electrodes) allowed “ON” and “OFF” switching of the oxidation of the DNA (through attraction and removal of DNA-functionalized magnetic particles). Such magnetic triggering of the DNA oxidation holds great promise for the analysis of DNA on arrays.

Several protocols for the detection of DNA have combined the inherent signal amplification of stripping analysis with an effective discrimination against nonhybridized

DNA.^[215,239a] Besides the efficient isolation of the duplex, magnetic spheres can open the door to elegant ways to trigger and control electrical DNA detection.^[324,325] An interesting magnetic triggering of the electrical DNA detection was demonstrated by the “magnetic” collection of the magnetic bead–DNA hybrid metal tracer assembly onto a thick-film electrode transducer that allowed the direct electrical contact of the silver precipitate.^[325] By this approach, a biotinylated nucleic acid is linked to avidin-modified magnetic particles that act as the capturing particles. Hybridization of the analyzed DNA with the capturing nucleic acid is followed by the secondary association of metal or semiconductor NPs, which are functionalized with a nucleic acid that is complementary to a free segment of the analyzed DNA. The binding of the NP labels to the biorecognition assay provides amplifying cluster tags that enable the release of numerous ions upon dissolution. Furthermore, the metal NPs associated with the sensing interface may act as catalytic sites for the electroless deposition of other metals. This leads to the amplified detection of DNA by the intermediary accumulation of metals that are stripped off or by the generation of an enhanced amount of dissolved product that can be electrochemically analyzed.^[223,326]

Figure 39A depicts the amplified detection of DNA by the application of nucleic acid functionalized magnetic beads and Au NPs as catalytic seeds for the deposition of silver.^[325] A biotin-labeled nucleic acid, **91**, was immobilized on avidin-functionalized magnetic particles, and these conjugations were then hybridized with the complementary biotinylated nucleic acid **92**. The hybridized assembly was then treated with a Au NP–avidin conjugate. The magnetic separation of the particles by an external magnet concentrated the hybridized assembly from the analyzed sample. Treatment of the magnetic particles–DNA–Au NP conjugate with silver ions (Ag^+) in the presence of hydroquinone resulted in the electroless catalytic deposition of silver on the Au NPs, with the latter acting as the catalyst. The deposition process provided amplification because the catalytic accumulation of silver on the Au NPs originated from a single DNA-recognition event. The current which resulted from the accumulated silver being stripped off then provided the electronic signal for the detection of the target DNA.

In a related system (Figure 39B),^[215] DNA was electrochemically detected by the use of Au NPs as electroactive and catalytic tags. The primer biotinylated nucleic acid **93** was linked to magnetic beads through an avidin bridge, and the conjugate was hybridized with the nucleic acid **94** functionalized with Au NPs. The hybridization was detected after the dissolution of the Au NPs in a solution of HBr/Br_2 , followed by the electrochemical reduction of the generated Au^{3+} ions onto the electrode, and the subsequent electrochemical “stripping” of the surface-generated gold (Figure 39B, route a). This analytical procedure was further amplified by the intermediary deposition of gold on the Au NPs (Figure 39B, route b). The higher gold content after the catalytic deposition led to a higher chronopotentiometric signal. Figure 39C, a and b, respectively, show the potentiograms that correspond to route a) the stripping of the gold generated on the electrode upon the analysis of the nucleic acid that is

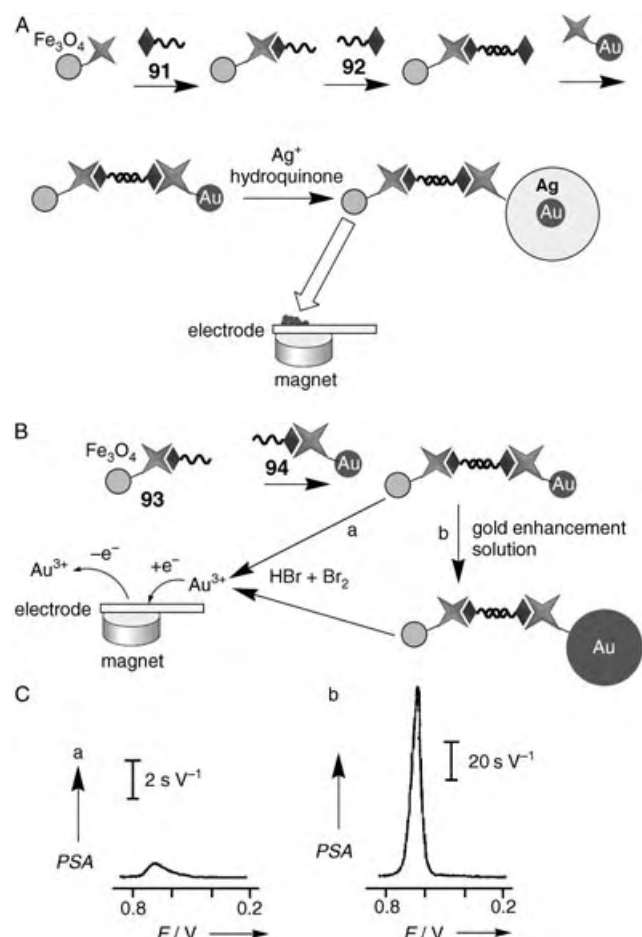


Figure 39. Electrochemical analysis of DNA upon the assembly of DNA molecules at magnetic particles followed by their association with Au NPs. A) Au NPs are used for the deposition of silver, and the DNA analysis is performed by the electrochemical stripping of Ag. B) The Au NPs are chemically dissolved, then the resulting Au^{3+} ions are electrochemically reduced, and the deposited gold is electrochemically stripped (path a); The intermediate enlargement of the Au NPs results in the further amplification of the signal (path b). C) The effect of gold enhancement upon the stripping response for the DNA analyte: PSA signals prior to treatment of the system with gold enhancement solution (a) and after 10 minutes of reaction (b). (Part C is adapted from Ref. [215], with permission; Copyright American Chemical Society, 2001).

associated with 5-nm Au NPs, and route b) after the deposition of gold on the Au NPs for 10 minutes.

It is also possible to use the magnetic beads as reporters (tags) in association with stripping voltammetry measurements of the iron content for the detection of DNA hybridization.^[327] A related protocol, which was developed in the same study, involved probes that were labeled with gold-coated iron core/shell NPs. In both cases, the captured iron-containing particles were dissolved after hybridization, and the released iron was quantified by cathodic stripping voltammetry in the presence of a 1-nitroso-2-naphthol ligand and a bromate catalyst. The application of functionalized magnetic particles as carriers for DNA

samples provided convenient analytical schemes for complicated purposes. Single nucleotide polymorphism genotyping of the aldehyde dehydrogenase 2 gene was studied by using a single bacterial magnetic particle.^[328]

7.4 Application of Redox-Functionalized Magnetic Particles for the Triggering and Enhancement of Electrocatalytic and Bioelectrocatalytic Processes

Micro- and nanosized magnetic particles that are functionalized with redox-active units were used to control biocatalytic reactions that are particularly important for bioelectroanalysis. A series of electroactive relay units, which consist of 2,3-dichloro-1,4-naphthoquinone (**95**), *N*-(ferrocenylmethyl)aminohexanoic acid (**96**), *N*-methyl-*N'*-(dodecanoic acid)-4,4'-bipyridinium (**97**), pyrroloquinoline quinone (PQQ, **98**), or microperoxidase-11 (MP-11, **99**), were covalently linked to magnetite (Fe_3O_4) particles (Figure 40).^[329,330] The electrochemical activities of the func-

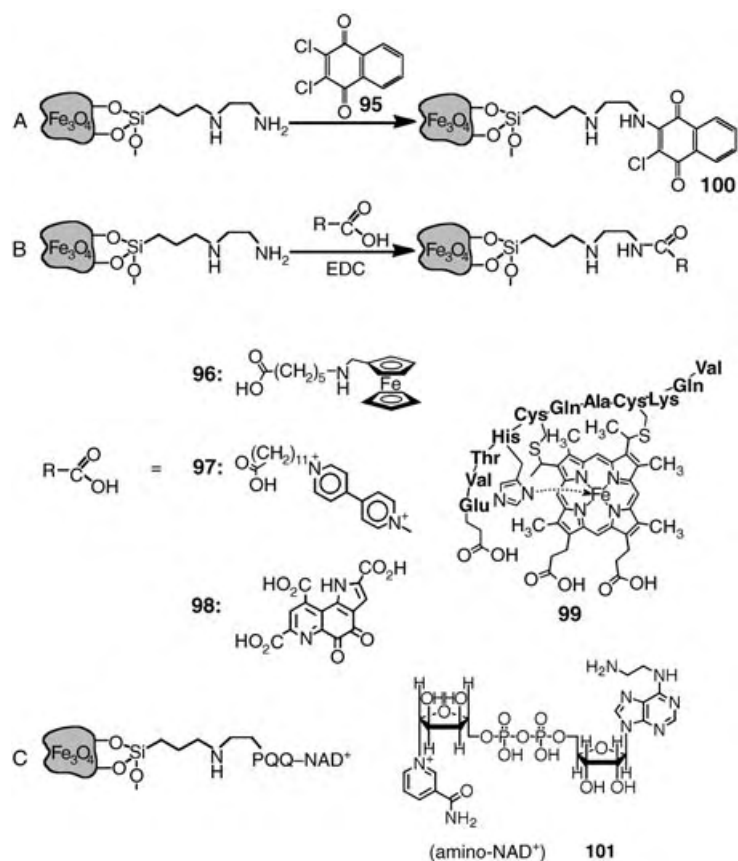


Figure 40. Synthesis of redox-relay-functionalized magnetic particles through the covalent linkage of redox-active units to magnetic particles that are functionalized with a [3-(2-aminoethyl)aminopropyl]siloxane film. A) Linkage of 2,3-dichloro-1,4-naphthoquinone (**95**) to the functionalized particles to yield the aminonaphthoquinone (**100**)-functionalized magnetic particles. B) Carbodiimide coupling of the electron-relay carboxylic derivatives **96–99** to the amino groups of the siloxane layer. C) Functionalization of magnetic particles with the PQQ– NAD^+ dyad for the electrochemical activation of NAD^+ -dependent enzymes. (Adapted from Ref. [329b], with permission).

tional magnetic particles were triggered by means of an external magnet as schematically outlined in Figure 41 A. Attraction of the magnetic particles to the electrode surface by means of the external magnet activates the electrical contact between the redox units, R, and the electrode that switches on the redox features of the redox components. Positioning of the magnet above the electrochemical cell retracts the magnetic particles from the electrode, and the electrochemical activity of the functional magnetic particles is switched off. Figure 41 B exemplifies the reversible activation and deactivation of the redox features of magnetic particles that are functionalized with the ferrocene derivative **96** ($E^0 = 0.32$ V vs SCE), upon the attraction of the magnetic particles to the electrode support or their retraction from the electrode surface, respectively, by means of the external magnetic field. Similarly, reversible “ON” and “OFF” switching was observed for the electrochemical response of magnetic particles that were functionalized with aminonaphthoquinone (**100**, $E^0 = -0.39$ V vs SCE at pH 7.0).

The electrochemical activation of redox units that are associated with magnetic particles enables the secondary magneto-controlled switchable activation and deactivation of bioelectrocatalytic processes. PQQ (**98**; $E^0 = -0.16$ V at pH 8.0 vs SCE) acts as an electrocatalyst in the oxidation of 1,4-dihydro- β -nicotinamide adenine dinucleotide (NADH).^[331] Accordingly, the magnetic particles functionalized with **98** (average surface coverage of 7.5×10^3 PQQ units per particle) were employed to control the electrocatalyzed oxidation of NADH by means of an external magnet.^[329b] In a similar way, magnetic particles functionalized with microperoxidase-11, **99**, were employed for the magnetically switched electrocatalytic reduction of hydrogen peroxide.^[329b]

Electron-relay units act as electron-transfer mediators that electrically communicate the active sites of redox enzymes with electrode supports. Ferrocene or bipyridinium redox-relay units were reported to electrically contact oxidative redox enzymes, such as glucose oxidase, or reductive biocatalysts, such as nitrate reductase, respectively.^[195] The

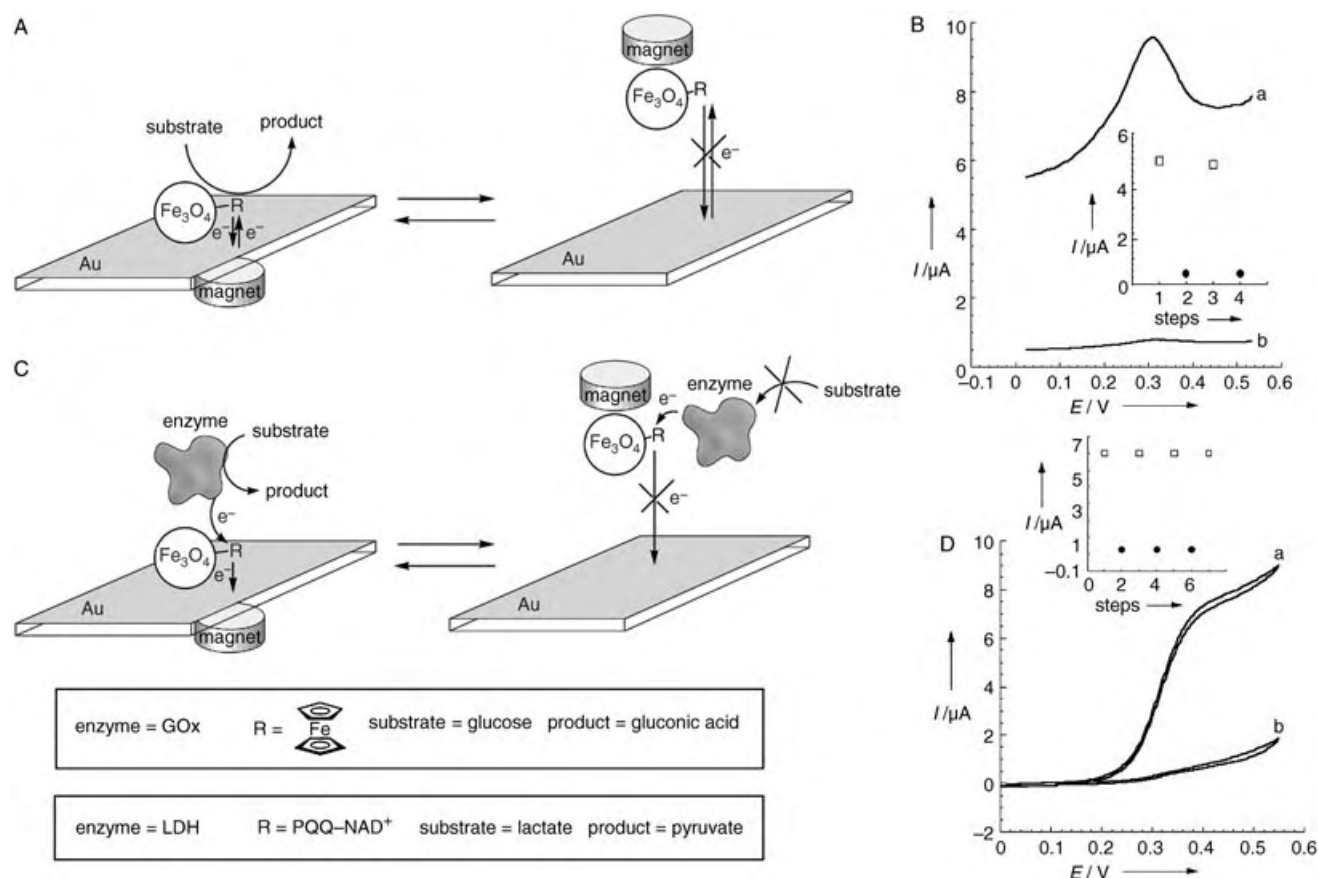


Figure 41. The electrochemical, electrocatalytic and bioelectrocatalytic reactions of functional magnetic particles which are controlled by means of an external magnet. A) Switching “ON” and “OFF” the electrochemical reaction of the redox-relay groups (R) that are covalently bound to the magnetic particles and the electrocatalytic function that is provided by the redox groups. B) Differential pulse voltammograms of a Au electrode in the presence of the ferrocene (**96**)-functionalized magnetic particles. The particles are magnetically attracted to (a) or retracted from (b) the electrode surface. Inset: Reversible changes of the peak current upon magnetic activation (□) and deactivation (●) of the electrochemical process. C) Switching “ON” and “OFF” either the bioelectrocatalytic oxidation of glucose in the presence of glucose oxidase (GOx) and ferrocene (**96**)-functionalized magnetic particles or the oxidation of lactate in the presence of lactate dehydrogenase (LDH) and PQQ-NAD⁺-functionalized magnetic particles. D) Cyclic voltammograms at a Au electrode in the presence of ferrocene (**96**)-functionalized magnetic particles (10 mg), glucose (10 mM), and GOx (1 mg mL⁻¹). The redox functions of the particles are switched “ON” by their attraction to the electrode (a) and “OFF” by their retraction from the electrode (b). Inset: Reversible changes of the electrocatalytic current (measured at *E* = 0.45 V vs SCE) upon attraction (□) or retraction (●) of the magnetic particles to/from the electrode. (Adapted from Ref. [329b], with permission).

activation of the redox functionalities of the relay-modified magnetic particles enabled the subsequent switchable activation and deactivation of enzyme bioelectrocatalytic transformations by means of an external magnet.^[329] Figure 41 C shows the schematic magnetoswitchable activation of redox enzymes in the presence of electron-relay-functionalized magnetic particles, such as the bioelectrocatalyzed oxidation of glucose by glucose oxidase in the presence of ferrocene (**96**)-functionalized magnetic particles. The magnetic attraction of the ferrocene-functionalized magnetic particles to the electrode results in the oxidation of the ferrocene units to ferrocenyl cations. The ferrocenyl cation relay units oxidize the redox center of glucose oxidase and activate the bioelectrocatalyzed oxidation of glucose. Figure 41 D shows the magnetic activation of the bioelectrocatalyzed oxidation of glucose which is reflected by the electrocatalytic anodic current upon attraction of the functional magnetic particles to the electrode. Retraction of the magnetic particles from the electrode support by means of an external magnet blocks the electrical communication between the electrode and the ferrocene units which inhibits the secondary bioelectrocatalyzed oxidation of glucose. The reversible attraction and removal of the magnetic particles to and from the electrode, respectively, allowed cyclic “ON” and “OFF” activation and deactivation of the bioelectrocatalytic process.

A similar approach was applied to the magnetic switching of the bioelectrocatalyzed reduction of nitrate to nitrite by using nitrate reductase as a biocatalyst and magnetic particles that were functionalized with bipyridinium **97** ($E^0 = -0.57$ V vs SCE) as mediator units.^[329b] Upon attraction of the **97**-functionalized magnetic particles to the electrode and application of a potential of $E = -0.7$ V to the electrode, the bipyridinium radical-cation-mediated bioelectrocatalyzed reduction of nitrate to nitrite occurred at a rate of $6.5 \times 10^{-3} \text{ mm min}^{-1}$, whereas retraction of the particles from the electrode by positioning the magnet above the electrochemical cell blocked the bioelectrocatalytic process. By switching the position of the external magnet from below to above the electrode surface, the electrocatalyzed reduction of NO_3^- was reversibly switched between “ON” and “OFF” states, respectively.

Functional magnetic particles were also employed for the cyclic activation and deactivation of NAD^+ -dependent enzymes by means of an external magnet. It was reported that a covalently linked monolayer of pyrroloquinoline quinone (PQQ)– NAD^+ units associated with an electrode provides an active interface for the activation of NAD^+ -dependent enzymes such as lactate dehydrogenase.^[332] The biocatalyzed oxidation of the substrate yields NADH, which is oxidized to NAD^+ by PQQ. The resulting PQQH_2 is electrooxidized to PQQ, which thus stimulates the electrochemically driven biocatalyzed oxidation of the substrate (e.g. lactate). As an example, PQQ (**98**)-functionalized magnetic particles were treated with N^6 -(2-aminoethyl)- β -nicotinamide dinucleotide (**101**)^[333] to yield PQQ– NAD^+ -modified particles (Figure 40 C).^[329b] The resulting particles were then applied to the magnetoswitching of the bioelectrocatalytic functions of the NAD^+ -dependent enzyme lactate dehydrogenase (LDH) by means of an external magnet Figure 41 C.

Attraction of the PQQ– NAD^+ -functionalized magnetic particles to the electrode in the presence of lactate dehydrogenase (LDH) activated the bioelectrocatalyzed oxidation of lactate to pyruvate. The biocatalyzed reduction of the NAD^+ cofactor unit by lactate was followed by the oxidation of the resulting NADH by the PQQ electrocatalyst. An appropriate potential ($E = 0.05$ V vs SCE) was then applied to oxidize the resulting PQQH_2 and to regenerate the electrocatalyst. This enabled the continuous bioelectrocatalyzed oxidation of lactate to pyruvate in the presence of LDH. The electrocatalytic anodic current developed by the system increased as the lactate concentration was elevated, and it leveled off to a saturation value of the current density of $i_{\text{max}} = 1.8 \mu\text{A cm}^{-2}$ at a lactate concentration of 50 mM. Analysis of the electrocatalyzed oxidation of lactate to pyruvate by LDH under steady-state electrolysis indicated that pyruvate is generated at a rate of 0.13 mm min^{-1} . Retraction of the functionalized magnetic particles from the electrode by an external magnet prohibited the bioelectrocatalyzed oxidation of lactate. By the cyclic positioning of an external magnet below and above the cell, the process was reversibly switched between “ON” and “OFF” states, respectively.

The concept of controlling bioelectrocatalytic transformations by an external magnet was utilized to develop selective dual biosensing systems.^[334] The specific simultaneous electrochemical sensing of two substrates in an overlapping redox-potential region is a challenging topic in bioelectronics. The bioelectrochemical dual sensing of lactate and glucose in the presence of the two oxidative enzymes, lactate dehydrogenase (LDH) and glucose oxidase (GOx), was performed by using an electrode that was functionalized with a monolayer of ferrocene, NAD^+ –PQQ-functionalized magnetic particles, and an external magnet. Application of a potential on the electrode ($E > 0.32$ V vs SCE) while retracting the magnetic particles from the electrode resulted in the ferrocene-mediated bioelectrocatalyzed oxidation of glucose, whereas the bioelectrocatalyzed oxidation of lactate was prohibited. Magnetic attraction of the NAD^+ –PQQ-functionalized magnetic particles to the electrode followed by sweeping the potential on the electrode in the range $-0.13 \text{ V} < E < 0.32 \text{ V}$ (vs SCE) allowed the PQQ– NAD^+ -mediated oxidation of lactate in the presence of the NAD^+ -dependent lactate dehydrogenase. As the ferrocene units are not oxidized in this potential range, the bioelectrocatalyzed oxidation of glucose was prohibited.

An important advance in the magnetic control of electrocatalytic and bioelectrocatalytic transformations involves the attraction of magnetic particles to an electrode support, followed by the rotation of the magnetic particles on the electrode by means of an external rotating magnet.^[335] The rotation of the magnetic particles turns the redox-functionalized magnetic particles into circular-rotating microelectrodes. As a result, redox-activated electrocatalytic or bioelectrocatalytic processes mediated by the functional particles are controlled by convection rather than by the diffusion of the respective substrates onto the microelectrodes. Accordingly, enhanced amperometric responses of the particle-mediated electrocatalytic processes are anticipated, and the resulting currents should be controlled by the rotation speed of the

particles. Figure 42 A depicts schematically the amplified amperometric analysis of glucose by the rotation of magnetic particles, which are functionalized with ferrocene (**96**), on the electrode support. As the interaction of glucose oxidase (GOx) with the electron-transfer mediator, which is associ-

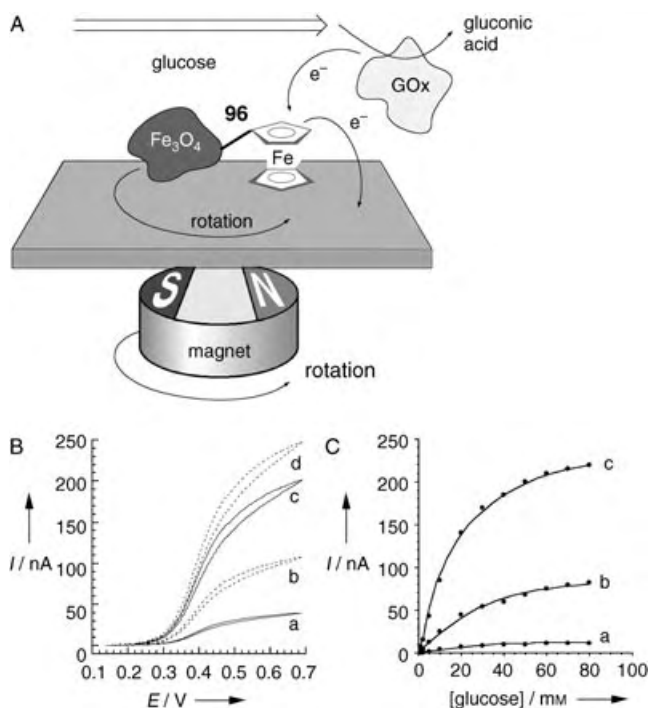


Figure 42. A) Enhanced bioelectrocatalytic oxidation of glucose in the presence of glucose oxidase (GOx) and ferrocene-functionalized magnetic particles; enhancement occurs upon circular rotation of the particles by means of an external rotating magnet. B) Cyclic voltammograms of a Au electrode with the magnetically attracted **96**-functionalized magnetic particles (6 mg) in the presence of GOx (1×10^{-5} M) and glucose (50 mM) and upon rotation of the magnet: a) 0, b) 10, c) 100, and d) 400 rpm (potential scan rate: 5 mVs^{-1}). C) Calibration plots for the amperometric detection of glucose ($E = 0.5 \text{ V}$ vs SCE) upon rotation of the magnet: a) 0, b) 100, and c) 400 rpm. (Adapted from Ref. [335], with permission; Copyright American Chemical Society, 2002).

ated with the rotating magnetic particles, is convection-controlled, the resultant electrocatalytic currents relate to the square root of the rotation speed ($I_{\text{cat}} \propto \omega^{1/2}$). Figure 42 B shows the bioelectrocatalytic currents observed in the system at different rotation speeds of the external magnet. Clearly, the amperometric responses increased as the rotation speed was elevated. Figure 42 C shows the amperometric responses of the system at different concentrations of glucose with the rotation of particles at speeds of 400 and 100 rpm (curves c and b, respectively) relative to when the particles are in a steel, nonrotating configuration (curve a). The rotation of the particles (400 rpm) resulted in a ≈ 15 -fold increase in the amperometric responses of the bioelectrocatalytic process. The responses of the bioelectrocatalytic transformations were analyzed with the conventional rotating-disc electrode (RDE) theory.^[336] Analysis using Levich theory of the experimental currents that were obtained at different rotation

speeds of the redox-functionalized magnetic particles allowed the interfacial electron-transfer rate constant to be estimated.

The enhanced electrocatalysis and bioelectrocatalysis in the presence of rotating magnetic particles can be used to amplify biosensing events. This is schematically depicted in Figure 43 A in which an analyte, **a**, is sensed by magnetic particles functionalized with the complementary unit **b**. Binding of a second recognition element **c** for **a**, which is conjugated to horseradish peroxidase (HRP), yields the biocatalytic sandwich structure for analyzing **a**. The magnetic attraction between a mixture of magnetic particles, which comprises magnetic particles that are functionalized with aminonaphthoquinone (**100**), with the sandwich structure that is generated between the magnetic particles that contain the components **b/a/c**–HRP“ enables the amplified detection of the analyte by electrogenerated chemiluminescence. Electroreduction of the aminonaphthoquinone (**100**) units leads to the electrocatalyzed reduction of O_2 to H_2O_2 , which, in the presence of luminol (**102**) and HRP, yields the biocatalyzed generation of light. Upon the rotation of the magnetic particles, O_2 and luminol interact with the functionalized magnetic particles by convection which leads to the amplified generation of chemiluminescence (Figure 43 B). The biosensing affinity interactions that occur on the magnetic particles may be antigen–antibody, nucleic acid–DNA, or any other host–guest intermolecular binding process. The amplified detection of immunological interactions, such as the analysis of the dinitrophenyl (DNP) antibody in the presence of magnetic particles that are functionalized with the DNP antigen **103**, and the ultrasensitive detection of DNA have been demonstrated in the presence of rotating functionalized magnetic particles.^[337]

A modified scheme for the amplified detection of viral DNA by functional magnetic particles is exemplified in Figure 44 A with the analysis of the 7249-base M13mp18 DNA.^[338] The 27-base DNA primer **104**, which is complementary to a segment of the analyte DNA, was associated with the magnetic particles. The hybridization of **104** with the M13mp18 DNA **105** was followed by a polymerization process in the presence of the dNTP mixture, which included biotin-labeled dUTP (deoxyuridine triphosphate). The replication process introduced biotin labels into the replicated nucleic acid on the magnetic particles. This replication process was followed by a sequence of thermal cycles by which the M13mp18 DNA was dissociated, rehybridized with another primer on the particle, and further replicated to incorporate the biotin labels. The resulting particles were then interacted with the avidin–HRP bioconjugate, and the resulting functionalized magnetic particles were collected by means of an external magnet on the electrode surface and then mixed with the aminonaphthoquinone (**100**)-labeled particles. The electrocatalyzed reduction of O_2 by the quinone units yielded H_2O_2 , which, in the presence of luminol and HRP, led to the generation of chemiluminescence. Furthermore, rotation of the magnetic particles led to amplified light emission. Figure 44 B shows the intensity of the emitted light upon the analysis of the M13mp18 DNA ($8 \times 10^{-9} \text{ M}$) at different rotation speeds of the particles. With this method, the target DNA was analyzed with a detection limit of $8 \times 10^{-18} \text{ M}$

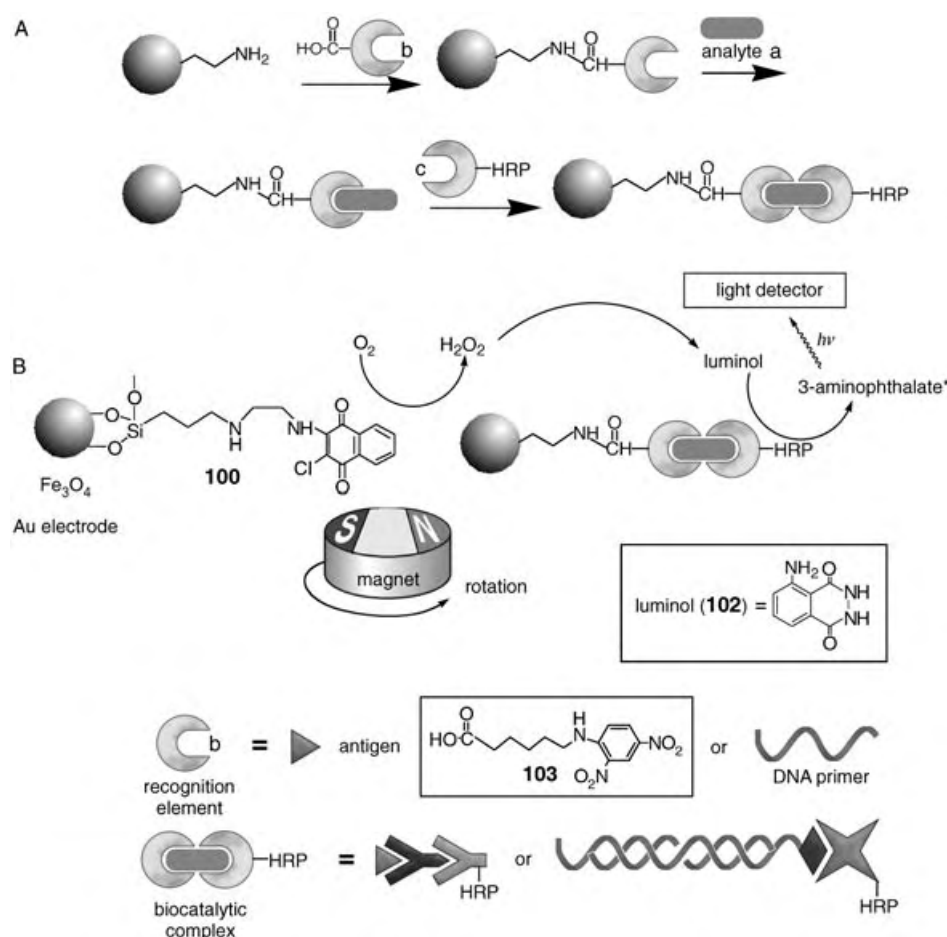


Figure 43. Amplified detection of bioaffinity recognition processes by multilabeled rotating magnetic particles. A) Synthesis of the functionalized magnetic particles for the biorecognition assay. B) Amplified biorecognition assay upon the rotation of the functionalized magnetic particles. HRP=horseradish peroxidase, * denotes an excited state.

(Figure 44 C). The intensity of the chemiluminescence light, which was generated in the system, correlated linearly with the square root of the rotation speed ($\omega^{1/2}$) and is consistent with the fact that the luminescence intensity was controlled by the convection of the substrates to the rotating particles. A similar approach has been applied to detect single-base mismatches in DNA^[338] and to follow telomerase activity in cancer cells.^[339]

7.5. Magnetomechanical Detection of Biorecognition Events

The possibility of chemically modifying cantilevers and optically monitoring their nanometric deflections render these microelements ideal mechanical sensors.^[340] Indeed, stress interactions that occur on the surface of the cantilevers were reported to induce their mechanical deflection. For instance, a thin polyaniline film associated with a lever was reported to act as a reversible electrochemically driven mechanical device.^[341] Oxidation of the polymer film led to the electrostatic repulsion of the polymer chains which resulted in stress on the cantilever and its deflection. The

reduction of the oxidized polymer removed the surface stress, and the lever was retracted to its original position. Biorecognition events such as antibody–antigen^[342] or nucleic acid–DNA^[343] binding processes were similarly reported to stimulate the mechanical deflection of cantilevers. The electrostatic repulsions between surface-hybridized DNA were reported to induce a surface stress that resulted in the mechanical deflection of the lever.^[343] The use of a cantilever array for the parallel micromechanical detection of different target DNAs or different mutants was also suggested. The force exerted on a lever that is modified with magnetic particles and subjected to an external magnetic field could drive the deflection of the cantilever. Indeed, upon mounting magnetic particles on a cantilever, a highly sensitive magnetic-field sensor was developed.^[342] The deflection of the cantilever could monitor changes in the magnetic field as low as 10 nT. The extensive use of magnetic particles as supports for biosensing processes^[344] suggests that the amplified magnetomechanical detection of biorecognition processes is feasible.

The ultrasensitive magnetomechanical detection of DNA and single-base-mismatches in nucleic acids and the assay of telomerase activity were performed by monitoring the magnetically induced deflection of a cantilever, which was functionalized with magnetic beads that were associated with the biosensing interfaces.^[345] The analyzed M13mp18 DNA was hybridized with nucleic acid functionalized magnetic beads and then subsequently replicated in a similar process to that shown in Figure 44 A in the presence of dNTPs (including biotin-labeled dUTP, B-dUTP). The DNA primer-functionalized magnetic particles were interacted with the M13mp18 DNA and subjected to 90 cycles of replication with the incorporation of biotin labels. By this, the particles were hybridized with M13mp18 DNA, which was then replicated in the presence of Taq polymerase and the dNTPs mixture and then melted to dissociate the double-stranded DNA assembly before repeating the cycle (90 times). This procedure resulted in a linear amplification of the biotin-labeled chains that were associated with the magnetic particles. The resulting beads were then attached to an avidin-coated cantilever, and the modified cantilever was deflected by an external magnetic field (Figure 45 A). Figure 45 B shows the reversible magne-

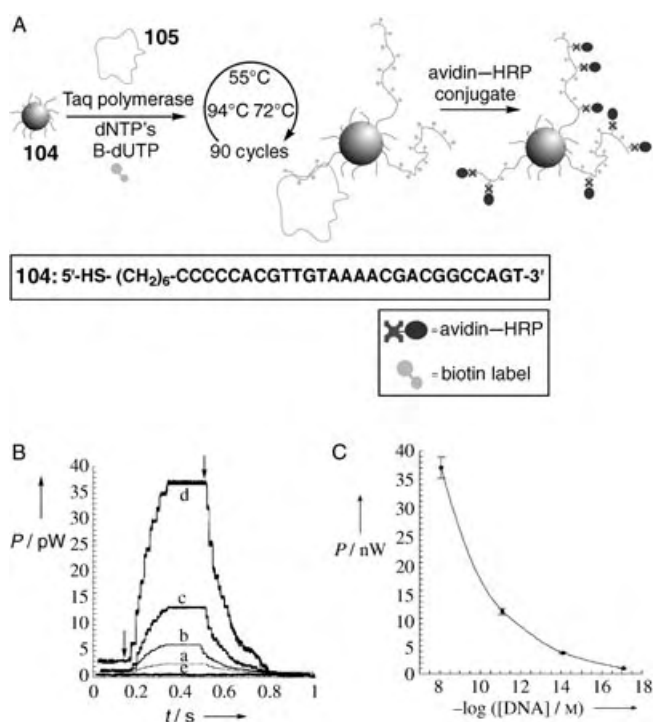


Figure 44. A) Labeling of the nucleic acid replica with biotin units by thermal cycles for the amplified detection of viral DNA by multilabeled rotating magnetic particles. B) Chemiluminescence intensities upon the analysis of M13mp18 DNA (8×10^{-9} M) at different rotation speeds: a) 0, b) 60, c) 400, and d) 2000 rpm.; e) Chemiluminescence signal observed by applying the protocol in the absence of M13mp18 DNA and with a rotation speed of 2000 rpm. C) Calibration curve for the chemiluminescence intensities upon the analysis of different concentrations of M13mp18 DNA at 2000 rpm. In all experiments, the chemiluminescence was generated by the application of a potential step from $E=0.0$ V to -0.5 V and back under air. Arrows indicate the times for switching the potential to -0.5 V and to 0.0 V. (Parts B and C are adapted from Ref. [338], with permission).

tomechanical deflection and retraction of the avidin-modified cantilever, which was interacted with the preamplified biotin-labeled magnetic particles. Placement of the external magnet below the lever led to the attraction of the lever to the magnet and resulted in its mechanical deflection, whereas the removal of the external magnet retracted the lever to its original position. The extent of the magneto-induced deflection of the cantilever depended on the amount of the functionalized magnetic particles bound to its surface which, in turn, was dependent on the concentration of the analyzed M13mp18 DNA. Thus, this allowed the magnetomechanical biosensing of DNA with a sensitivity limit of 7.1×10^{-20} M (Figure 45C).

Similarly, a magnetomechanical process for the detection of single-base mismatches in nucleic acids was developed.^[345] The concept was also applied to the magnetomechanical detection of telomerase activity that originates from cancer cells.^[345] A nucleic acid primer that is recognized by telomerase was linked to the magnetic particles, and the telomerization of the primer was performed in the presence of the HeLa-cell extract and the dNTPs mixture, which included the biotin-

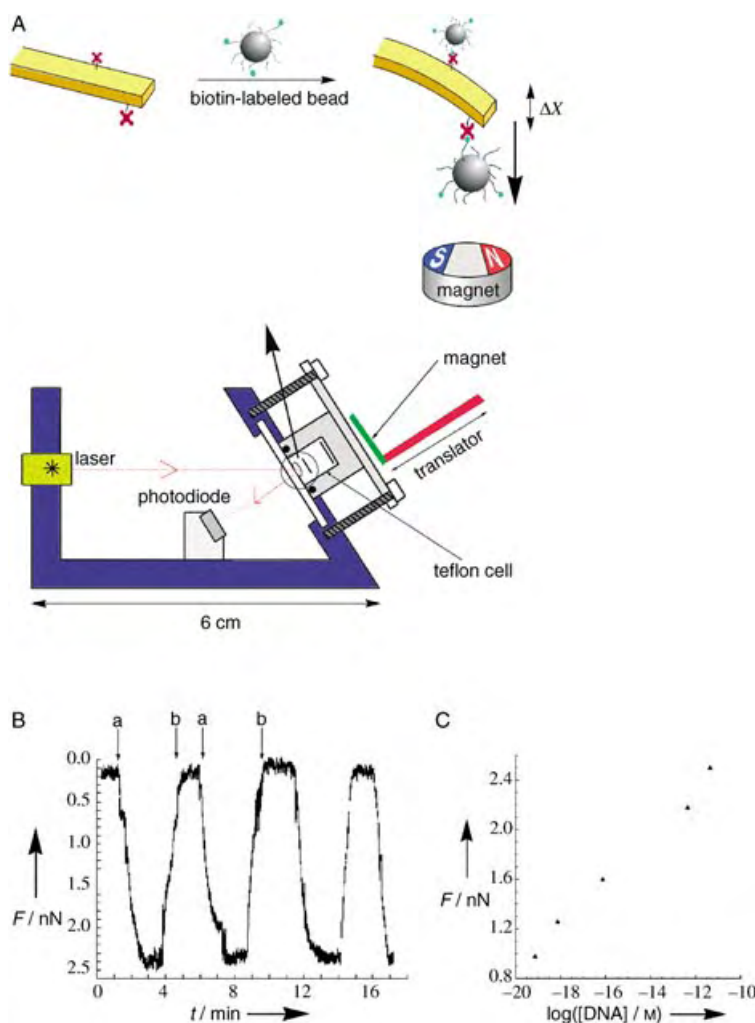


Figure 45. A) Schematic configuration of the instrumental setup and concept for the magnetomechanical analysis of biorecognition processes on functionalized cantilevers (X = deflection). B) Magnetomechanical deflection or retraction of the cantilever in the analysis of M13mp18 DNA (7.1×10^{-12} M) by using Taq polymerase and thermal cycles for replication and labeling processes. a) The cantilever is subjected to the external magnet; b) The external magnet is removed. C) Dependence of the deflection signal on the concentration of the M13mp18 DNA. (Adapted from Ref. [345], with permission; Copyright American Chemical Society, 2004).

labeled dUTP. The process led to the incorporation of the biotin labels into the telomers and the association of the resulting magnetic particles to the avidin-modified cantilever. This enabled the magnetomechanical detection of the telomerase activity. The telomerase activity that originates from approximately 100 cancer cells could be detected by this method.

8. Biomolecule-Based Nanocircuitry

The miniaturization of objects by lithographic methods has reached its theoretical limits, and it is generally accepted that the development of different miniaturization methodologies is necessary to overcome this barrier. Whereas lithographic methods use a “top-down” miniaturization of

patterns, the alternative approach of the “bottom-up” construction of objects has been suggested as a means to overcome the limitations of lithography. That is, the construction of objects at the molecular or supramolecular level could be used to generate templates or “seeds” for nanometer-size features. Nanowires are considered as building blocks for the self-assembly of logic and memory circuits in future nanoelectronic devices.^[346] Thus, the development of methods to assemble metal or semiconductor nanowires is a basic prerequisite for the construction of nanocircuits and nanodevices. Furthermore, the nanowires should include functional sites that allow their incorporation into structures of higher complexity and hierarchical functionality. The use of biomaterials as templates for the generation of nanowires and nanocircuitry is particularly attractive. Besides the ingenious structures that Mother Nature provides us which may act as templates for the generation of nanoobjects, the unique recognition features of biomaterials may act as driving forces for self-assembly and for the generation of complex functional structures.

Biological templates such as DNA,^[182,225,347] viruses,^[299d,e,348] antibodies,^[38] S-layers (surface layers),^[112,349] protein cages,^[130] bacterial rhabdosomes,^[350] and microtubules^[351] have been used to direct the nucleation, deposition, and assembly of inorganic micro- and nanostructures. Besides microtubules, a variety of other polymorphic tubulin assemblies such as sheets, macrotubules, and S-ribbons are also known.^[352]

Biomolecules exhibit dimensions that are comparable to those of the envisaged nanoobjects. Besides the fascinating structures of biomaterials that may lead to new inorganic or organic materials, templates of biological origin may act as “factories” for the production of “molds” for nanotechnology. The proliferation of cells, the replication of DNA, the synthesis of proteins, and the association of protein monomers into sheets, tubules, or ribbons all represent biological processes for the high-throughput synthesis of potential biomaterial templates for nanotechnology. The further application of genetic engineering to manipulate proteins and the application of chemical methods to synthesize new de novo proteins, modify proteins by synthetic amino acids, or modify DNA by synthetic nucleotides provides us with a flexible arsenal of means to tailor the templates for the desired nanostructures. Although this topic is in its infancy, it attracts substantial research efforts, and the already visible results promise exciting future developments.

8.1. Protein-Based Nanocircuitry

Natural protein structures such as microtubules^[351] were applied as templates for the deposition of metal nanoparticles. Microtubules are cylindrical proteins that consist of characteristically arranged $\alpha\beta$ -heterodimeric tubulin subunits. The length of the tubulin dimer is about 8 nm and its diameter is 4–5 nm. Depending on the conditions of the in vitro assembly, thirteen or fourteen protofilaments are aligned in an almost parallel configuration to form hollow cylinders, which exhibit outer diameters of 25 nm and lengths of several micrometers.

These assemblies were used as biotemplates for the generation of metal nanowires by the deposition and catalytic enlargement of NPs (Figure 46).^[353]

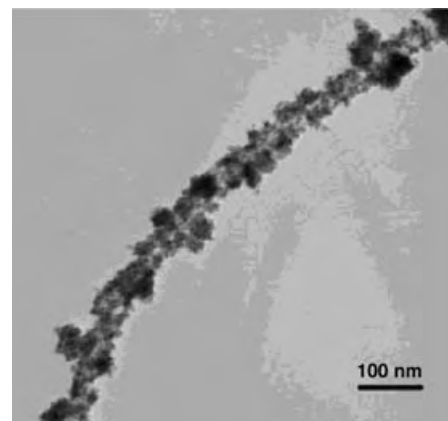


Figure 46. TEM image which shows the quasi-continuous coverage of a microtubule surface with Pt NP aggregates. (Adapted from Ref. [353], with permission).

Many proteins comprise well-defined channels or cavities (e.g. ferritin)^[128] or are organized in the form of pore-containing layers on surfaces (e.g. S-layers).^[354] These channel- or pore-containing materials may act as templates for the generation of nanostructures, nanorods, and even circuitry. Ferritin, for example, consists of a hollow polypeptide shell that is 8 and 12 nm in its internal and external diameters, respectively, and a 5-nm-diameter ferric oxide ($5\text{Fe}_2\text{O}_3 \cdot 9\text{H}_2\text{O}$) core.^[128] After the reduction of the ferric oxide core, the reduced material can be washed away from the protein and the apo-ferritin channel can be remineralized with different inorganic oxides, sulfides, or selenides that form nanorods (e.g. MnO, FeS, CdS, or CdSe).^[129,130]

Aromatic short-chain peptides, such as Alzheimer's diphenylalanine β -amyloid (**106**), form well-ordered nanotubes that have been used as templates for growing Ag nanowires (Figure 47A).^[355] The peptide nanotubes were loaded with Ag^+ ions, which were reduced with citrate to yield metallic silver nanowires inside the peptide nanotubes (Figure 47B). The peptide coating was then removed by enzymatic degradation in the presence of proteinase K to yield micrometer-long Ag nanowires with a diameter of ≈ 20 nm (Figure 47C). Upon the application of D-phenylalanine-based peptide fibrils, which are resistant to proteinase K, the peptide coating of the Ag nanowires was preserved. Various kinds of biomaterial nanotubes have been applied to generate metallic nanowires that are protected by a biomolecule “skin”. For example, Au NPs of 3–10-nm width were organized in a glycolipid hollow cylinder nanotube by filling the internal channel of the lipid nanotube with an aqueous solution of HAuCl_4 by capillary force and subsequently photochemically reducing the $[\text{AuCl}_4]^-$ to give metal–lipid nanotube wires.^[356]

Crystalline bacterial-cell surface layers (S-layers)^[354] have exhibited a broad potential for applications owing to the following features: 1) Pores passing through S-layers show identical size and morphology and are in the range of

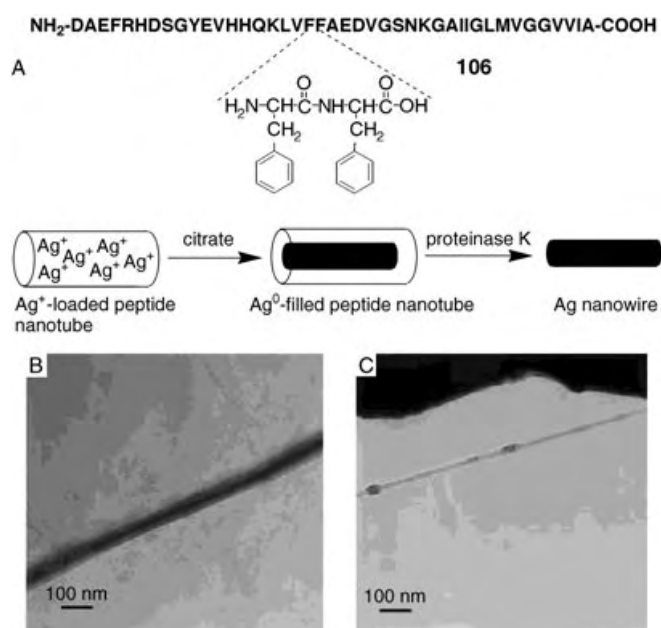


Figure 47. A) Formation of a silver nanowire inside a channel of a short-chain diphenylalanine-peptide tube. B) TEM image of the peptide template, which is filled with a metallic silver nanowire. C) TEM image of the silver nanowire after the degradation of the peptide template in the presence of proteinase K. (Adapted from Ref. [355], with permission).

ultrafiltration membranes. 2) Functional groups on the surface and in the pores are aligned in well-defined positions and orientations and are accessible for chemical modifications and binding of functional molecules in a very precise fashion. 3) Isolated S-layer subunits from a variety of organisms are capable of recrystallizing as closed monolayers onto solid supports such as metals, polymers, and silicon wafers. 4) Functional domains can be incorporated in S-layer proteins by genetic engineering. Thus, S-layer technologies particularly provide new approaches for biotechnology, biomimetics, molecular nanotechnology, the nanopatterning of surfaces, and the formation of ordered arrays of metal clusters or NPs as required for nanoelectronics. S-layers have been patterned by deep ultraviolet radiation or by the application of a soft lithography technique:^[357] micromolding in capillaries (MIMIC; Figure 48A).^[354c] The patterned S-layers were used as matrices for the immobilization of functional biomaterials or as templates for the formation of ordered arrays of NPs that are important for nanoelectronics and nonlinear optics. Monodisperse gold particles, 4–5 nm, were formed in the pore region of the S-layer, and the interparticle spacing of the gold superlattice resembled the S-layer lattice (Figure 48B). MIMIC technology was applied to pattern the S-layers to produce nanocircuits of high complexity. Following recrystallization of the S-layer and removal of the mold, human IgG was covalently attached to active carboxylate groups on the S-layer track surface. Subsequent binding of fluorescein isothiocyanate-labeled anti-human IgG enabled fluorescence imaging of the pattern that was produced by the modified S-layer (Figure 48C).

Alternatively, metallization could be performed on the exterior sides of peptide-based templates.^[358] Bis(*N*-α-amido-

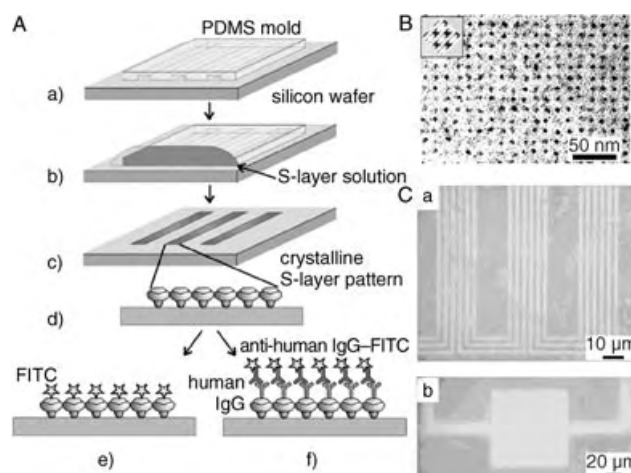


Figure 48. Nanocircuitry produced upon biospecific interactions on surfaces. A) Schematic representation of S-layer protein patterning and assembly by MIMIC (micromolding in capillaries): a) Channels are formed upon contact of a poly(dimethylsiloxane) (PDMS) mold with a silicon-wafer support; b) Channels are filled with a solution of protein by capillary forces; c) The mold is removed; d) Crystalline protein patterns are observed on the support surface; e) S-layer patterns are either labeled with a fluorescent marker (FITC = fluorescein isothiocyanate) or f) they are used as substrates for an antibody–antigen (IgG = immunoglobulin) immunoassay. B) Electron micrograph of a nanometer-scale gold superlattice on an S-layer that exhibits square-lattice symmetry. The inset shows a scanning force microscopy image of the native S-layer on the same scale. C) Fluorescence images at different magnifications (a and b) of an S-layer pattern that was generated from a circuit-like PDMS mold. (Parts A and C are adapted from Ref. [354c]; part B is adapted from Ref. [354e], with permission).

glycylglycine)-1,7-heptane dicarboxylate molecular units were self-assembled into nanotube templates through intermolecular hydrogen bonds between the amide and carboxylic acid groups.^[359] The sequenced histidine-rich peptide **107** was then assembled on the nanotubes, where it selectively trapped Au ions (chlorotrimethylphosphinegold salt, ClAuPMe₃; Figure 49A).^[358a,b] After the Au ions were reduced, highly monodisperse Au nanocrystals were grown on the nanotubes. The conformations and the charge distributions of the histidine-rich peptide were determined by pH measurements, and the concentration of the Au ions in the growth solution was responsible for the size and the packing density of the Au nanocrystals. The diameter of the Au nanocrystals was limited by the spacing between the neighboring histidine-rich peptides on the nanotubes. This simple metal–nanotube fabrication by the biomineralization method could be applied to various metals and semiconductors by using peptides with sequence-specific groups for the association of metal ions.

Similarly, a histidine-rich epitope (HRE) AHHAH-HAAD from HRP II was used as a peptide that was suitable to mediate the synthesis of a variety of metal sulfide, metal oxide, and zerovalent metal clusters in aqueous solutions.^[360] Screening of the resulting clusters against a monoclonal antibody for HRP II revealed molecular recognition of the ligand epitope along the nanocluster surfaces by some of the peptide-encapsulated nanoclusters. The peptide, Asn-Pro-Ser-Ser-Leu-Phe-Arg-Tyr-Leu-Pro-Ser-Asp, recognized and

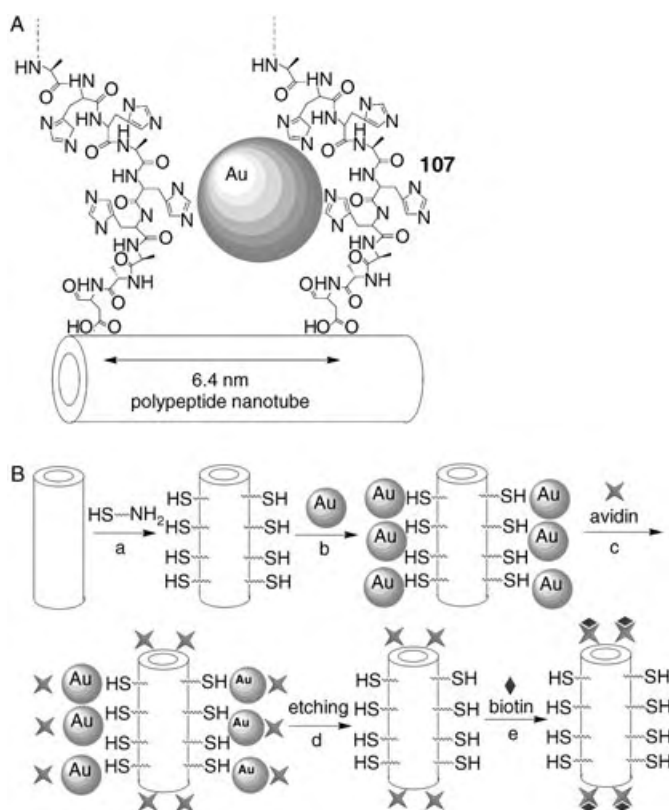


Figure 49. A) Structure of the Au NP–peptide complex on the histidine-rich polypeptide nanotube template. B) Immobilization of avidin units at the ends of peptide nanotubes by using Au NPs as protective masks to yield only end-to-end interconnected peptide nanotubes.

effected the growth of hexagonal Ag nanocrystals on the (111) face.^[358c] Upon the sequencing and the incorporation of the peptide onto the surface of the nanotube template, the biomineralization of Ag⁺ ions on the polypeptide nanotubes led to an isotropic coating of hexagonal Ag nanocrystals.

Peptide nanotubes^[359] incorporate many free amide and carboxylic groups on the surfaces as binding sites to anchor biological molecules and metal ions in order to produce various other functional nanotubes. Also, thiol groups could be introduced into the protein backbone to anchor Au NPs. Usually these binding sites are distributed on the entire surface of the nanotube to provide a uniform attachment of modifying units along the entire length of the nanotube. As an example, amyloid protein fibers (10-nm wide) were generated by the self-assembly of the prion determinant from *Saccharomyces cerevisiae* (the N-terminal and middle (NM) regions of Sup35p), which was genetically engineered to include thiol groups on the protein surface. Gold NPs were associated to the activated surface of the protein fibers, and by the subsequent catalytic deposition of silver on the Au NPs, micrometer-long wires with a diameter of about 100 nm and with good electrical conductivity were generated.^[361]

A novel method has been developed for the directional functionalization of peptide nanotubes at their ends, whilst the sidewalls remain untouched.^[362] The approach involved, first, the thiolation of the nanotube sidewalls by the carbo-

diimide coupling of 2-mercaptoethylamine to carboxylic groups of the polypeptide nanotubes (Figure 49B, step a). Then, Au nanoparticles were coated as a mask on the sidewalls of the nanotube (Figure 49B, step b), and the assembly was incubated in a solution of sulforhodamine-labeled avidin (Figure 49B, step c). After avidin was immobilized at the ends (not masked by Au nanocrystals) and the sidewalls (masked by Au NPs) of the nanotubes, the Au NPs on the sidewalls were chemically etched (Figure 49B, step d). The chemical etching of the Au nanocrystal masks on the sidewalls of the nanotubes led to the removal of avidin from the sidewalls, whereas avidin at the ends of the nanotube remained bound. The chemical etching process did not denature avidin, and the nanotube ends could recognize and immobilize the complementary biotin units (Figure 49B, step e). This fabrication method is useful to guide each individual nanotube to each corresponding location on complementary protein-patterned surfaces. End-to-end specific coupling of peptide nanotubes, such as through biotin–avidin interactions, could allow the formation of a template that could yield a conductive nanocircuit upon further metallization.

The specific assembly of protein subunits into template structures could provide a means of patterning the generated metal nanowires. An f-actin filament provides specific binding of the biomolecular motor protein, myosin, which forms a mobile complex with the filament and whose motility along the filament is driven by ATP.^[363] The f-actin filament is formed by the reversible association of g-actin subunits in the presence of ATP, Mg²⁺, and Na⁺ ions. Recently, the f-actin filament was used as a template for the formation of Au nanowires,^[364] whereby the filament was covalently modified with Au NPs (1.4 nm) that were functionalized with single *N*-hydroxysuccinimidyl ester groups **108**. Removal by dialysis of the ATP, Mg²⁺, and Na⁺ ions that were used to assemble the g-actin monomer units into the filament resulted in the separation of the filament and the formation of Au NP-functionalized g-actin subunits. The association of Au NPs to the polymeric form of the actin followed by its dissociation was essential to protect the binding sites of the monomeric actin subunits. The Au NP-functionalized g-actin subunits were then used as versatile building blocks for the Mg²⁺/Na⁺/ATP-induced polymerization of the functionalized monomers to yield the Au NP-functionalized filaments of a predesigned pattern (Figure 50A). Electroless catalytic gold deposition on the Au NP-functionalized f-actin filament yielded 1–3-μm-long gold wires of 80–150-nm-heights, which depended on the time elapsed during the gold deposition. By sequential polymerization of the naked actin filament on the preformed Au–NP–actin wire and the subsequent electroless catalytic deposition of gold on the Au NPs, patterned actin/Au wire/actin filaments were generated (Figure 50C). A related approach was applied to yield the inverse Au wire/actin/Au wire patterned filaments (Figure 50B). The latter configuration suggests that the two Au wires may act as contacts for the deposition of a semiconductor nanotube and the fabrication of a transistor element. The gold deposited on the actin filament exhibited metallic conductivity with a resistance similar to the value obtained for bulk gold.

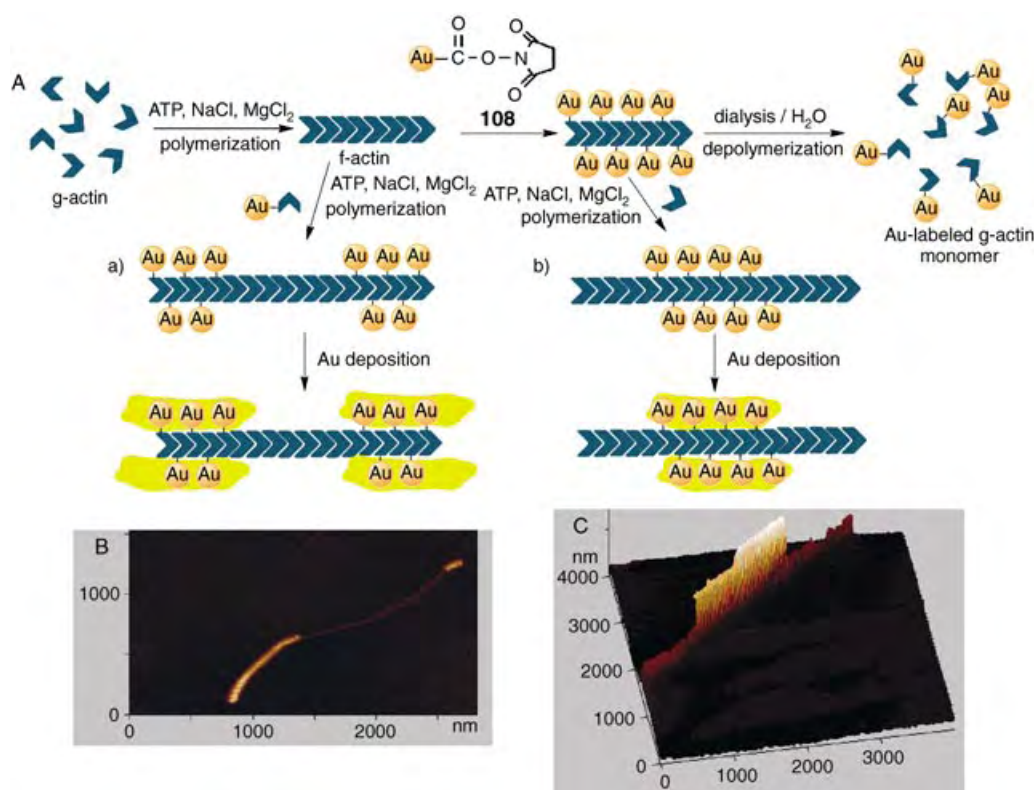


Figure 50. A) The assembly of patterned actin-based Au nanowires: Left: a Au wire/actin/Au wire filament; Right: an actin/Au wire/actin filament. B) AFM image of the Au wire/actin/Au wire filament. C) AFM image of the actin/Au wire/actin filament.

The specific binding interactions of proteins can provide specific cross-linking or bridging properties for the generation of nanoparticle circuits. The homotetrameric protein streptavidin (SAv) is characterized by four high-affinity ($K_a > 10^{14} \text{ M}^{-1}$) binding sites for biotin. By the appropriate functionalization of Au NPs^[126] (or ferritin particles)^[132] with biotin units, 3D NP aggregates were generated. Nanoparticle aggregates that exhibit 3D ordering were also generated by the use of complementary antigen–antibody binding interactions.^[38,118] The simplest antigen–antibody–metal NP-ordered aggregate involved the cross-linking of Au NPs (12 nm), which were functionalized with the anti-dinitrophenyl antibody (anti-DNP), with a bifunctional bis(dinitrophenyl) antigen (bis-(*N*-2,4-dinitrophenyloctamethylenediamine)). Circuits of greater complexity were generated by the application of different protein receptors and different metals for the ordered organization of the NP systems.^[38,118] A nanoparticle aggregate was formed from two NPs that were differently functionalized, namely with streptavidin (SAv) and anti-DNP groups. The oligomeric aggregates generated from bioorganic SAv particles and bisbiotinylated ds-DNA spacers were used as model

systems to study the properties of complex particle networks. SAv functioned as a 5-nm model particle that could undergo a limited number of interconnections to other particles within the network. Either one, two, three, or four biotinylated DNA fragments were conjugated with SAv by means of the high-affinity SAv–biotin interaction to result in dimers, trimers, and oligomers that were interconnected in a network as observed by scanning force microscopy (SFM; Figure 51).^[21a]

8.2. DNA as a Functional Template for Nanocircuitry

Among the different biomaterials, DNA is of specific interest as a template for the construction of nanocircuits.

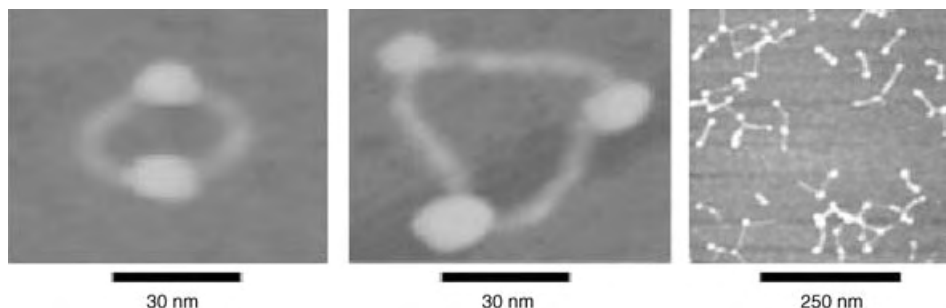


Figure 51. SFM images of nanoparticle networks that were prepared with ds-DNA as spacer groups. The ds-DNA fragments contain two biotin-binding sites at the two 5' ends of the ds-DNA which allow the cross-linking of the biotin-binding protein SAv as a model nanoobject. (Adapted from Ref. [21a], with permission).

Several arguments support the use of DNA as a future building block of nanostructures: 1) Nucleic acids of pre-designed lengths, base-orderings, and shapes can be synthesized, and complex structures have been generated by self-assembly methods.^[365] Whereas the variable DNA shapes may be used as pre-designed templates for the nanocircuits, the base-sequence may be used as specific addressable domains for the binding of the reactants that form the nanowires. As a result, patterned nanocircuits may be envisaged. 2) Nature provides us with numerous biocatalysts that can manipulate DNA. These enzymes may be considered as tools for shaping the desired DNA and eventually for the generation of nanocircuits. For example, the enzyme ligase ligates nucleic acids, endonucleases affect the specific scission of nucleic acids, telomerase elongates single-stranded nucleic acids by telomer units, and polymerase replicates DNA. These biocatalysts represent “cut and paste” tools for the formation of DNA templates. By the application of the replication biocatalyst, the design of future factories of nanowires may be envisaged. 3) The intercalation of molecular components into DNA and the binding of cationic species such as metal ions to the phosphate units of nucleic acids allows the assembly of chemically active functional complexes. These linked molecular components may be used as precursors for the formation of the nanowires. Specifically, intercalators that selectively bind to appropriate base pairs may be used as directing units for the selective deposition of chemicals on the nucleic acids. Such directed assembly of reactive sites may then lead to patterned nanocircuits. 4) Different proteins bind specifically to certain nucleic acid sequences. This allows the addressable assembly of complex DNA–protein structures. Such protein–DNA complexes may act either as addressable domains for the selective deposition of metals or semiconductors, or alternatively as temporary shielding domains that protect the DNA from metal deposition. These insulated domains may then be used for the deposition of other metals or semiconductors to enable the fabrication of patterned complex structures.

The interaction of metal NPs with DNA is a well-known phenomenon,^[179,181,347,366] and the microscopic mechanism of the nucleation of metal nanoclusters on DNA templates has been studied.^[227] Usually, single or double-stranded DNA is decorated by the metal particles, which can easily be imaged by TEM or AFM.^[367] Upon the interaction of DNA with Au NPs that are stabilized with phosphane ligands ($\text{Au}_{55}(\text{Ph}_2\text{PC}_6\text{H}_4\text{SO}_3\text{H})_{12}\text{Cl}_6$), the formation of Au-decorated wirelike DNA structures was demonstrated by AFM (Figure 52A).^[367a] Molecular-modeling studies of the interactions between the DNA and Au_{55} and Au_{13} NPs showed that the NPs could be arranged inside the grooves of DNA (Figure 52B). Some of the phosphane ligands could be substituted by the DNA phosphate groups which provided strong binding of the Au NPs to the DNA. Au NPs capped with other phosphane ligands such as tris(hydroxymethyl)phosphine-capped Au NPs^[368] were also used to decorate DNA templates that yielded nanowires. 1D chains of Au NPs (4.4 nm) coated with cationic trimethyl(mercaptopoundecyl)ammonium monolayers were electrostatically assembled along DNA molecules in solution by the careful control of the relative molar

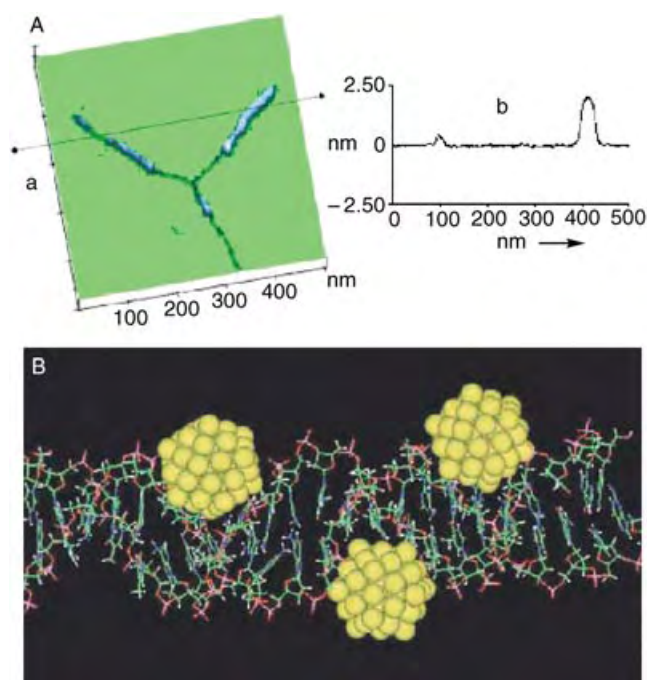


Figure 52. A) a) AFM image of λ -DNA, which is partially linked with Au_{55} clusters; b) Height profile of both the bare DNA and a decorated part. B) Energy-minimized structure of the DNA fragment with Au_{55} clusters arranged along the phosphate backbone of the DNA major grooves. (Adapted from Ref. [367a], with permission).

quantities of NPs and DNA base pairs.^[367b] TEM images of the dried droplets of solutions of the DNA–base-pair/MPC (monolayer-protected cluster) in a molar ratio of 20:1 displayed chains of NPs that were a few microns long in which the Au cores were lined up with nearly contacting cationic monolayer edges along the anionic DNA template.

With the vision that DNA can act as a template for the generation of nanocircuits, attempts were made to explore the possibility to organize DNA-cross-linked semiconductor NPs and DNA-based metal NP nanowires on surfaces. As nanoparticles are loaded on the DNA template with gaps between the adjacent particles, the issue of electrical conductivity of the DNA matrix itself is important. Electron transport through DNA has been one of the most intensively debated subjects in chemistry over the past ten years,^[224,369] and the subject is still under extensive theoretical^[370] and experimental^[371] investigation. Despite some optimistic observations that show highly conductive properties of the entire DNA backbone,^[372] most of the studies report poorly conductive^[373] or insulator^[374] properties of the DNA. To examine the electrical conductivity of DNA, the conductivity of double-stranded DNA that connects Au NPs was analyzed. Thiol-derivatized oligonucleotides were linked to Au NPs, and then the DNA-functionalized Au NPs were bridged with DNA chains that were composed of double-stranded helices of various lengths (24, 48, or 72 bases). These helices were terminated on both sides with single-stranded domains, which were complementary to the oligonucleotides bound to the Au NPs.^[69b] The resulting Au NP aggregates, which were linked

with ds-DNA spacers, were deposited on an electrically nonconductive solid support, and their conductivity was measured by the four-probe method. Surprisingly, the conductivities of the aggregates generated by all three linkers ranged from 10^{-5} to 10^{-4} S cm^{-1} at room temperature, and the linkers all showed similar temperature-dependent behavior. The similarity of the electrical properties of the aggregates originates from the fact that the DNA spacers are compressed and thus yield small and similar distances between the Au NPs. Accordingly, the measured conductivity parameters reflect the electrical properties of the metallic NPs separated by small gaps.

The conductivity of metallic NP aggregates on a DNA template can be enhanced by the chemical deposition of another metal, such as the deposition of Ag on Au aggregates, to fill the gaps and to form a continuous conductive nanowire. DNA metallization is based on the association of metal complexes or metallic NPs with the DNA template and the further growth of the metal seeds with either the same or a different metal upon chemical reduction of the respective metal ions in the presence of strong reductants, such as dimethylaminoborane, hydroquinone, or sodium borohydride.^[224] When metal ions or metal complexes, such as silver or copper ions,^[375] or platinum or palladium complexes,^[227] which are electrostatically associated with a DNA template, are used as the active sites for the metallization of the DNA, the formation of the continuous nanowire proceeds over a period of time which ranges from several hours up to one day.^[181,347] Application of pre-prepared metal NPs that are associated with the DNA template makes this process significantly shorter.^[368] The binding of the primary metallic clusters to the template DNA for the subsequent catalytic deposition of wires on the DNA frame may be performed by several means: 1) By the reduction of metal ions that are linked to the phosphate groups to metallic seeds that are linked to the DNA. 2) By the use of metal or semiconductor NPs that are functionalized with intercalator units—intercalation of the molecular components into ds-DNA leads to the association of the NPs with the DNA template. 3) By the synthesis of DNA that have functional tethers, which enable the covalent attachment of the metal or semiconductor NPs to the DNA. 4) By the synthesis of ss-DNA that includes constant repeat units (e.g. telomers) and the hybridization of metal or semiconductor NPs that are functionalized with short nucleic acids, which are complementary to the ss-DNA repeat units.

Figure 53A exemplifies the method for the assembly of Au NPs on a DNA template by using Au nanoparticles that are functionalized with an intercalator.^[376] The psoralen-amine derivative **109** was treated with the Au₅₅ nanocluster (1.4 nm-diameter), which includes a single *N*-hydroxysuccinimide ester group **108**, to yield the psoralen-functionalized Au₅₅ nanoparticle **110**. As psoralen acts as a specific intercalator for A–T base pairs, the functionalized Au₅₅ nanoparticles were treated with the pA–pT–ds-DNA **111** (pA–pT = polyadenylic acid–polythymidylic acid). Subsequently, the assembly was irradiated with UV light to induce the $2\pi+2\pi$ cycloaddition reaction between the psoralen units and the thymine base sites of DNA. This latter

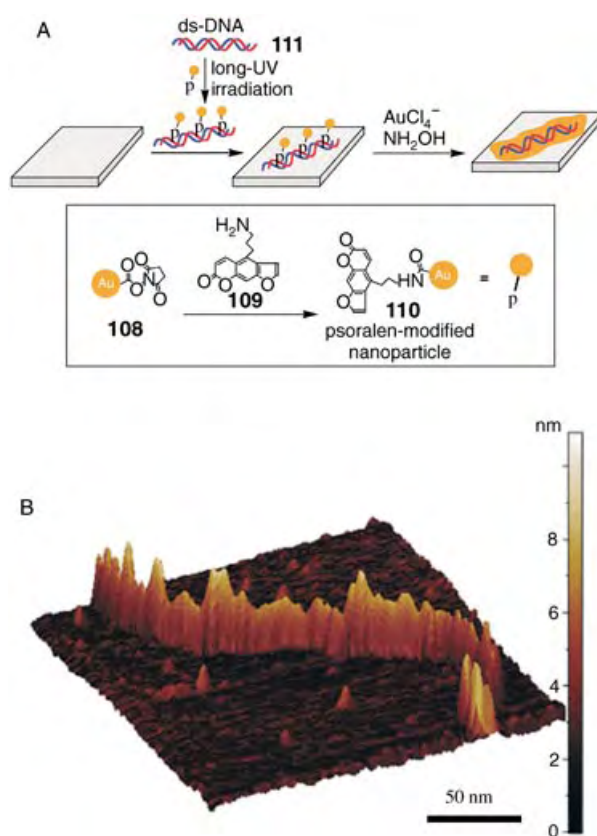


Figure 53. A) Assembly of a Au NP wire in the pA/pT template by using Au NPs that are functionalized with intercalator (psoralen) molecules. B) AFM image of the Au NP wire in the pA/pT template. pA/pT = polyadenylic acid/polythymidylic acid.

process covalently fixed the Au₅₅ NPs to the DNA matrix. Figure 53B depicts the AFM image of the resulting NP wire. A NP wire that was approximately 600–700-nm-long was formed. Its width corresponds to around 3.5–8 nm and is controlled by the width of the DNA template. The height of the wire was about 3–4 nm, which is consistent with the fact that the Au NPs intercalate into the DNA on opposite sides of the double-stranded DNA template. The continuous appearance of the Au NP wire is owed to the dimensions of the scanning AFM tip, and in reality, most of the particles are not in intimate contact with one another. The possibility to arrange the Au NPs on the DNA template allows the further catalytic enlargement of the particles by an electroless deposition process (e.g. reaction of AuCl₄[−] with NH₂OH) to yield continuous conductive nanowires.

Another approach involved the electrostatic association of metastable Au NPs with a DNA template to yield a conductive wire along the DNA matrix.^[377] Gold NPs were capped with thiocholine, HS(CH₂)₂N⁺(CH₃)₃ (**54**), as a cationic stabilizer to provide the electrostatic association of the nanoparticles with the negatively charged DNA template. Then, the unstable Au NPs underwent self-fusion into the conductive wire structures. Au_{core}/aniline_{shell} NPs were self-assembled onto a DNA template, which was stretched on a surface, to yield aligned assemblies that were ordered over a

long range.^[378] The aniline shell provided a positive charge on the NPs which resulted in their electrostatic binding to the negatively charged phosphate backbone of the DNA template. Linear arrays of the aniline-coated Au NPs with interparticle spacing were organized on DNA to form a necklacelike nanostructure. By the deposition of different metals or NPs in the interparticle spacings, it should be possible to tune the electrical or optical properties of linear arrays.

A high-throughput synthesis of DNA templates for the generation of metallic nanowires was demonstrated by the use of HeLa cancer cell generated telomerase. Telomers are nucleic acids of constant repeat units (5'-TTAGGG-3') that protect the chromosome ends from erosion.^[379] Their stepwise degradation during the normal cell life cycle results in a cellular signal for the termination of the cell life-cycle and proliferation.^[380] In certain cells, the ribonucleoprotein telomerase can be accumulated, and this enzyme elongates the telomer ends with the constant repeat units which results in the production of immortal malignant or cancer cells. Thus, telomerase is a characteristic biomarker for cancer cells.^[381] The constant repeat units that exist in the telomers provided addressable domains for the application of the telomers, which were generated from HeLa cells, as templates for the

formation of metallic nanowires.^[382] In one approach, the primer **112** was telomerized in the presence of the dNTPs nucleotide mixture, which contained (aminoallyl)dUTP **113** (Figure 54A). The resulting amine-containing telomers were treated with Au NPs (1.4 nm; **108**), which were functionalized with single *N*-hydroxysuccinimidyl ester groups, to yield Au NP-modified telomers. The Au nanoparticle-decorated DNA wires were then enlarged by electroless gold deposition to generate a metallic nanowire (Figure 54, C and D). In a different approach, the telomer was hybridized with the complementary nucleic acid segments **114** that were functionalized with Au NPs (Figure 54B). The resulting Au NP-modified DNA duplex was enlarged by the electroless deposition of gold on the nanoparticles to generate a metallic nanowire (Figure 54E).

Practical applications of the nanowires require their electrical contacting with macro- or microelectrodes. Towards this goal, a single nanowire, which was produced on a DNA template that bridges two microsize electrodes, was constructed.^[225,226] Two microelectrodes, which were positioned opposite each other with 12–16- μm separation, were functionalized with 12-base oligonucleotides that were then bridged with a 16- μm -long λ -DNA (Figure 55A). The resulting phosphate units of the DNA bridge were loaded with Ag^+

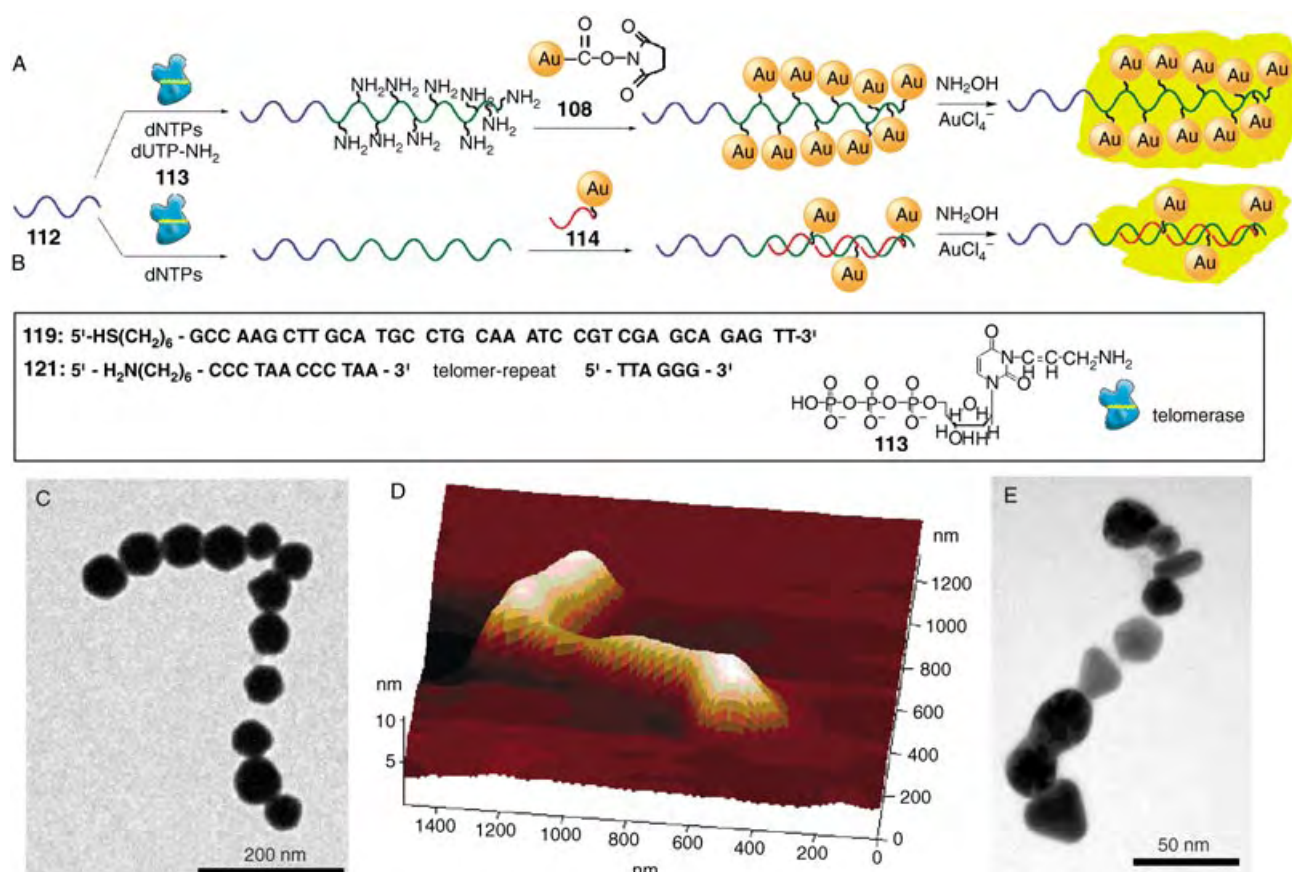


Figure 54. The assembly of Au nanowires on a telomer template. A) Covalent attachment of Au NPs to amine groups, which were introduced into the telomer structure during the telomerization step, followed by catalytic enlargement of the NPs. B) Binding of oligonucleotide-functionalized Au NPs to the complementary domains of the telomer followed by the catalytic enlargement of the NPs. C), D) TEM and AFM images, respectively, of a Au nanowire that was generated according to the procedure outlined in (A). E) TEM image of a Au nanowire that was generated according to the procedure outlined in (B). (Adapted from Ref. [382], with permission; Copyright American Chemical Society, 2004).

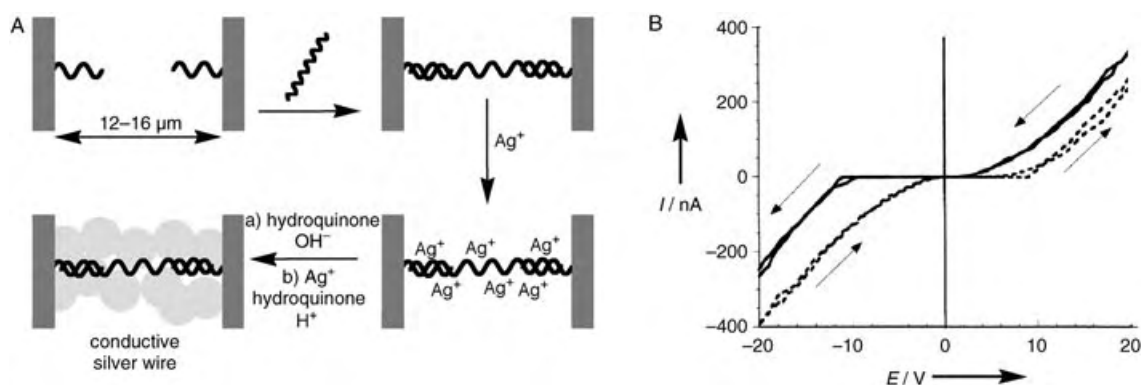


Figure 55. A) The construction of a nanowire that bridges two microelectrodes by the deposition of Ag^+ ions on a bridging DNA strand followed by the chemical reduction of the Ag^+ ions to the metallic agglomerate. B) Current versus voltage (I/V) curves obtained with the structures produced. (Part B adapted from Ref. [225], with permission).

ions by ion-exchange, and the bound Ag^+ ions were reduced to Ag metal with hydroquinone. The small Ag aggregates which were produced along the DNA backbone were then used as catalysts for the further reductive deposition of silver, which eventually led to the formation of a Ag nanowire. This micrometer-sized element had a typical width of 100 nm and a granular morphology (determined by AFM). Electrical measurements revealed nonlinear graphs of I versus V (Figure 55B). The nonlinear current–voltage graphs and the observed hysteresis are not understood at present. This behavior may originate from quantum effects of the nanoscale wire. Alternatively, local defects in the generated wire morphology may introduce a tunneling barrier for the transport of electrons through the wire.

A similar approach was used to generate highly conductive DNA-templated nanowires that bridged macroscopic Au interdigitated electrodes.^[383] DNA molecules were positioned between macroscopic Au electrodes and were loaded with Pd^{2+} ions,^[383a] which were then chemically reduced into continuous metallic wires. The Pd wires provided specific conductivity that was only one order of magnitude lower than that of bulk palladium. Also, the vectorial immobilization of linear M13mp18 ds-DNA ($\approx 2.5\text{-}\mu\text{m}$ -length) between interdigitated electrodes with $2.0\text{-}\mu\text{m}$ spacings was performed by the nonsymmetrical modification of the opposite electrode surfaces.^[383b] One side of the interdigitated electrodes was selectively modified with a coating of streptavidin, whereas the second side was coated with Au NPs. An asymmetric double-stranded M13mp18 DNA strand that carries a 5'-thiol group at one end and a 5'-biotin at the other end was obtained through polymerase chain reaction (PCR) by using two differently labeled primers. The DNA interaction with the electrode system resulted in the selective bridging of the electrode surfaces owing to the biotin–streptavidin coupling at one side and the adsorption of thiol on the Au NPs at the other side. Further metallization of the DNA bridges yielded electrical contacting between the interdigitated electrodes.

Molecular electronics, however, requires more elaborate manipulations that include the formation of richer geometries, wire patterning with nanometer resolutions, and molecularly accurate device localization. The binding of

proteins such as RecA to DNA has been used as a means for the patterning of nanoscale DNA-based metal wires with nonconductive or semiconductive gaps.^[384] The biomolecular lithography used for this process is based on homologous recombination processes carried out by the RecA protein, which operates on ds-DNA substrate molecules. The information that guides the lithography is encoded in the 48502-base-pair ds-DNA substrate **115** and in the auxiliary 2027-base ss-DNA probe **116**. The RecA proteins were polymerized on the ss-DNA probe **116** to form a nucleoprotein filament **117**. This filament was then mixed with the ds-DNA substrate **115** (Figure 56A, steps a and b). The polymerization of RecA on the ss-DNA probe **116** is not sequence-specific. However, the binding specificity of the nucleoprotein filament **117** to the ds-DNA substrate **115** is dictated by the base-sequence and its homology to the substrate molecule. Subsequently, Ag^+ ions were bound to the protein-deficient DNA domains of the nucleoprotein filament, and these were reduced into Ag clusters that were associated with free domains of the DNA assembly (Figure 56A, step c). The ds-DNA **115** was modified with aldehyde groups prior to this process to allow the chemical reduction of the electrostatically bound Ag^+ ions to Ag clusters. The localized RecA proteins, which served as a resistance, prevented the deposition of Ag on the nucleoprotein filament **117** domain and created a gap of predefined sequence length between the Ag-loaded segments of the substrate molecule. The Ag clusters served as catalysts for the subsequent electroless deposition of Au (Figure 56A, step d), and this process produced two continuous gold wires separated by the predesigned gap (Figure 56B). The domain of the nucleoprotein filament **117** could be further functionalized by using various protein-recognition reactions (based on biotin–streptavidin or antigen–antibody affinity) which led to the formation of complex metal (or semiconductor)–biomaterial hybrid nanowire structures. In a similar approach, the nucleoprotein filament **117** was used to protect the DNA from the aldehyde derivatization process rather than the metallization process.^[385] The binding of RecA to the DNA prohibited its reaction with glutaraldehyde which created an underivatized region on the DNA. After the removal of excess glutaraldehyde, the RecA

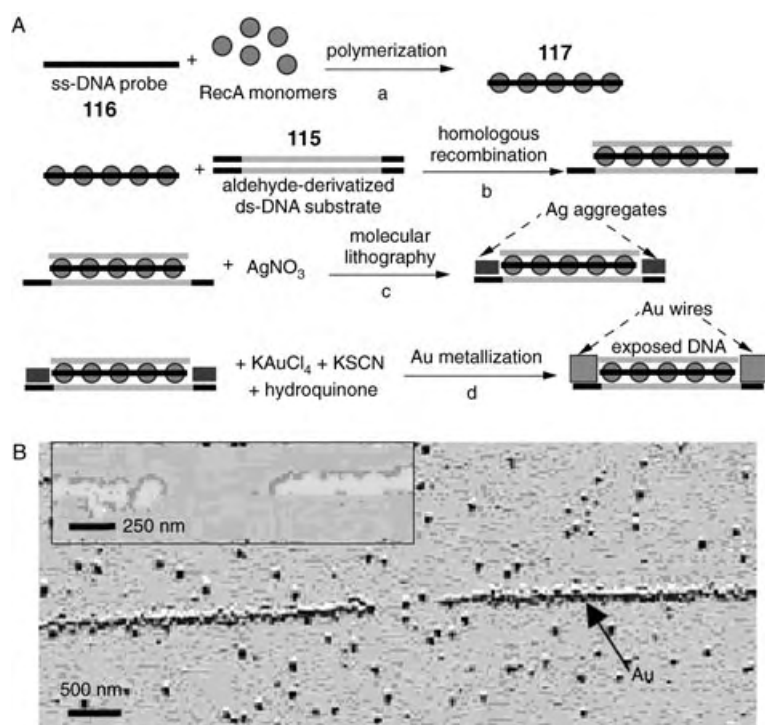


Figure 56. A) Molecular lithography based on homologous recombination processes carried out by the RecA protein, which operates on ds-DNA substrate molecules. B) AFM image of the patterned DNA template after gold metallization; Inset: Close-up image of the gap. The height of the metallized sections is approximately 50 nm. (Adapted from Ref. [384], with permission).

protein was disassembled and the DNA was purified. The resulting DNA molecules, which possessed a predesigned aldehyde-derivatization pattern, were combed onto a passivated silicon wafer and these were incubated in a silver solution. The patterned aldehyde derivatization served as a blueprint for the creation of an insulating gap in the DNA metallization process.

Recently, 1D and 2D metallic nanowire arrays have been obtained by the combination of molecular combing and DNA metallization.^[386] The method involved three steps: 1) A fluid flow was used to prepare parallel unidirectional DNA arrays of controlled density (Figure 57A); to create 2D arrays of DNA, a second alignment was made along another direction. 2) Pd^{2+} ions were absorbed onto the negatively charged DNA backbones. 3) Chemical reduction of the absorbed Pd^{2+} ions produced palladium nanowires. The resulting Pd nanowires followed the patterns defined by the DNA array to produce either parallel or crossed networks of Pd nanowires on a mica substrate. The resulting nanowires were composed of NPs with an average diameter of about 30 nm. It should be noted that the actual diameter may be even smaller because of the limited lateral resolution of the AFM tip. A section analysis (Figure 57B) showed that these nanowires are about 5 nm in height. Figure 57C also presents an AFM image at high magnification that shows a well-defined meshlike 2D Pd nanowire array. This method could be especially useful for the parallel assembly of nanosized building blocks into functional

networks. Further complexity was introduced into the generated 2D arrays of DNA by means of a molecular “cut and paste” technique by using an AFM tip as an instrument for molecular manipulation.^[387] A DNA strand was cut at a certain point (Figure 57D) and a part of the DNA was swept away by an AFM tip. The residual DNA structure was manipulated with the AFM tip to yield various patterns (Figure 57E and F). Metallization of the generated DNA patterns yielded nanocircuit junctions of different structures and high complexity.

The possible variability and complexity in DNA design establishes unique opportunities for programming the shape and structure of the DNA templates.^[365] A cross structure of eight ds-DNA units that exhibits four wings with appropriate “sticky” ends was used as a tile for the self-assembly of a 2D lattice of nanogrid morphology or a nanoribbon morphology of uniform width.^[388] Both morphologies displayed periodic square cavities. The resulting nanoribbons acted as scaffolds for the metallization and formation of highly conductive silver wires. Also, DNA lattices were generated by using a linear array of DNA triple crossover molecules to yield templates for the formation of Au NP arrays.^[389]

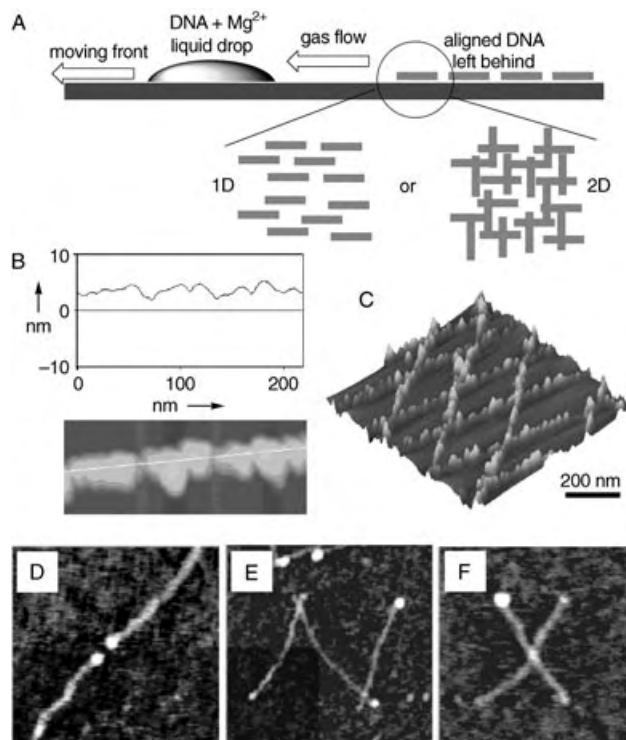


Figure 57. A) The fluid-flow-assisted molecular combing of DNA molecules on a surface to yield 1D or 2D arrays. B) AFM image of a Pd nanowire, a section analysis of which shows an average particle height of approximately 5 nm. C) AFM image of a meshlike 2D array of Pd nanowires that is formed by the metallization of a 2D aligned DNA sample. D) A DNA strand cut by an AFM tip. E), F) The patterns generated upon the manipulation of DNA with an AFM tip on the nanometer scale. (Parts A–C were adapted from Ref. [386]; parts D–F were adapted from Ref. [387], with permission; Copyright American Chemical Society, 2002).

8.3. Viral Matrices as Functional Templates for Nanocircuitry

It has been shown that several types of rodshape viruses form well-controlled liquid-crystalline phases.^[390] Recently, a method of fabrication of a self-assembled, ordered nanocrystal film that used a nanocrystal-functionalized M13 virus was reported.^[391] Through genetic-engineering techniques, one end of the M13 virus was functionalized to nucleate or bind to a desired semiconductor material (specifically II–VI semiconductor nanoparticles).^[392] These semiconductor nanocrystal-functionalized viral liquid-crystalline building blocks were grown into ordered hybrid self-supporting films. The resulting nanocrystal-hybrid film was ordered at the nano- and microscale into 72- μm periodically striped domains. To align other materials, such as metallic and magnetic nanoparticles, another general approach has been suggested which includes the genetic-engineered formation of a virus that specifically binds streptavidin, SAv. The anti-SAv M13 viruses, which have specific binding moieties for SAv, were prepared by genetic engineering and were further treated with Au NP–SAv hybrids. Smectic-ordered self-supporting Au NP/virus films were obtained and were characterized by AFM. Because the modification of the DNA insert allows the controlled modification of the virus length, the spacing in the smectic layer can be genetically controlled.

Viruses were also used as templates to assemble NPs with precise placement of the clusters.^[393] For example, Pt, Au, or Ag metal NPs were organized into nanowires by using Tobacco Mosaic Virus (TMV) as templates.^[393a,b] The respective precursor ions, PtCl_6^{2-} , AuCl_4^- , or Ag^+ , were associated with the virus surface and were chemically reduced to yield the specific decoration of the external surface of wild-type TMV rods with metallic NPs that were less than 10 nm in size. Similarly, Ni and Co nanowires that were only a few atoms in diameter and up to the micrometer range in length, were generated by using the central channel of TMV as a template.^[394] Elsewhere, different mutants of Cowpea Mosaic Virus (CPMV) have been used as scaffolds to bind 2- and 5-nm Au NPs through gold–sulfur bonds at specific locations on the virus to produce 3D patterns of specific interparticle distances.^[393c]

8.4. The Integration of Nanowires into Nanodevices

The ultimate goal of nanobioelectronics is the integration of nanowires into operating electronic systems or functional devices. Until now, most of the studies have addressed the structural features of nanocircuitry and the conductivity properties of the nanostructures. The fabrication of functional devices is still in its infancy, although recent developments suggest potential advances in this area.

Nanoscale biosensors that are based on functionalized nanowires^[395] and nanotubes^[396] have recently received considerable attention. Functionalized silicon nanowires were used for DNA analysis on the basis of conductance measurements.^[397] Silicon nanowires (p-type) were synthesized by using gold nanocluster-catalyzed chemical vapor deposition, and then the wires were assembled into sensor devices that

consisted of electrically addressable nanowires (Figure 58 A, inset).^[397a] A PNA (peptide nucleic acid) probe with the sequence 5'-ATCATCTTTG-3', which is fully complementary to the wild-type cystic fibrosis transmembrane receptor (CFTR) sequence, was bound to a nanowire surface and

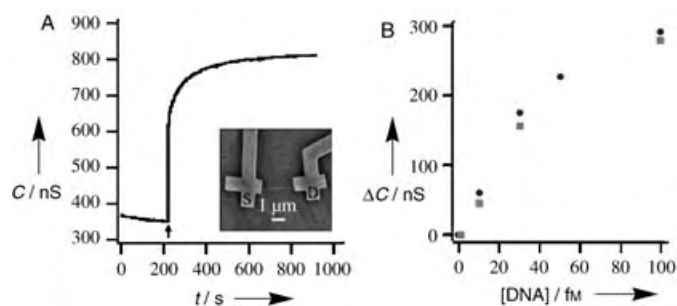


Figure 58. A) Real-time conductance response from a Si nanowire device that is functionalized with a PNA (peptide nucleic acid) receptor. The arrow marks the point in time when the sample of the analyte DNA (wild-type CFTR; 60 fM) was added; Inset: SEM image of a typical Si nanowire device with source (S) and drain (D) indicated. B) Conductance of the device as a function of the concentration of the analyte DNA. The data points shown ■ and ● were obtained from two independent Si nanowire devices. (Adapted from Ref. [397a], with permission; Copyright American Chemical Society, 2004).

was used as the receptor for the analysis of the wild-type and mutant oligonucleotide sequences that spanned the ΔF508 region of the CFTR (5'-CATAGGAAACACCAAGATGATATTTTCTTT-3' and 5'-CATAGGAAACACCAATGATATTTTCTTT-3', respectively). Formation of the negatively charged double-stranded complex between the surface-confined PNA receptor units and the complementary analyte DNA resulted in a change in the conductance of the nanowire (Figure 58 A). On the other hand, the noncomplementary mutant DNA did not yield any conductance change, which suggests that the electronic signal originated from the specific, rather than nonspecific, binding of the analyte DNA. Concentration-dependent measurements show that the detection limit is in the femtomolar range (Figure 58 B). This analytical method with nanowires represents an important advance towards a direct, label-free, selective, and highly sensitive means of analyzing DNA. The method could thus provide a route to the high-throughput, multiplexed analysis of DNA; a process that will be important for genetic sensing, clinical diagnostics, and for the detection of biothreats.

An actin/Au nanowire/actin filament that was generated by the stepwise polymerization of Au nanoparticle-functionalized g-actin, followed by the polymerization of naked g-actin at the nanoparticle–filament ends, and the subsequent enlargement of the Au NPs to a continuous Au bar (see Section 8.1) was used as a nanotransport system.^[364] Towards this goal, the actin/Au nanowire/actin filament was rigidified with phalloidin and deposited on a myosin interface that was linked to a glass support. Upon addition of ATP to the system, the actin-linked Au nanorods moved on the surface, and the motility of the nanoobjects was followed by reflectance

microscopy (Figure 59). The Au nanorods were found to move at a speed of 250 nm s^{-1} . In a related approach, CdSe NPs were assembled on microtubules and the generated filaments were driven in the presence of kinesin.^[398] In the future, such systems may be employed as nanotransporters.

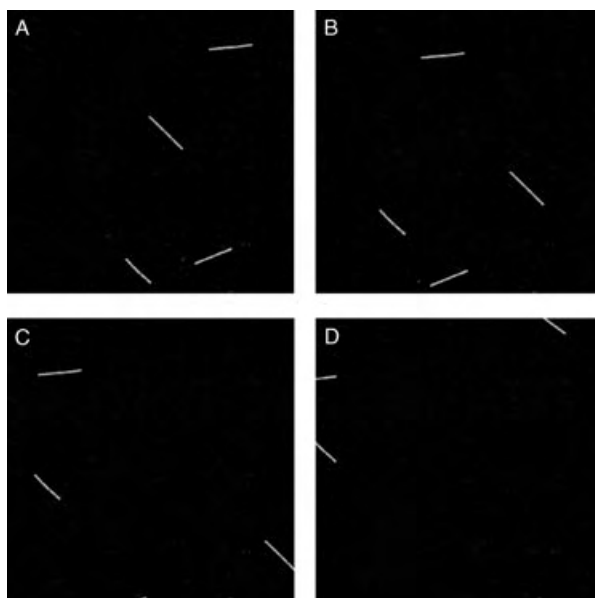


Figure 59. Images of the motility of actin/Au wire/actin filaments on a glass surface, which was modified with myosin, upon the addition of ATP. Images were recorded by reflectance microscopy: A–D) The same frame imaged at 5-s time intervals.

9. Conclusions

This review has summarized recent advances in the rapidly developing area of functional biomolecule–nanoparticle/nanorod hybrid systems. This topic represents an interdisciplinary effort to combine the unique optical, electronic, and catalytic properties of nanoobjects with the naturally optimized recognition and reactivity functions of biomaterials. The fact that NPs and biomaterials such as enzymes, antibodies, or nucleic acids are of similar dimensions makes the hybrid systems attractive nanoelements or building blocks of nanostructures and devices.

Several functions and applications of biomolecule–NP hybrid systems have been discussed, including analytical applications, signal-triggered electronic functions, nanostructures for circuitry, and the assembly of devices. Some of these functions represent viable technologies, whereas others are still in an embryonic phase and require additional fundamental research. The analytical applications of biomolecule–NP systems have advanced tremendously in the last decade. The understanding of the unique optical properties of NPs and the photophysics of coupled interparticle interactions has enabled the use of these particles as optical labels for recognition events. Similarly, the catalytic properties of nanomaterials have enabled the amplification of biorecognition events.

Upon the assembly of biomolecule–NP hybrid systems on surfaces, the electronic detection of biorecognition events can become feasible by means of electrical conductivity or piezoelectric or photoelectrochemical transduction. Alternatively, the unique size-controlled optical properties of semiconductor NPs imply that the organization of combinatorial libraries of biomolecule–semiconductor NP hybrid systems or the assembly of different biomolecule–NP hybrids in array configurations may lead to the high-throughput parallel analysis of numerous analytes.

Novel uses of biomaterial–magnetic particle conjugates for analytical applications were also discussed. Whereas the concentration and separation of substances by magnetic particles is a common practice, novel concepts such as the amplification of electronic sensing through the rotation of the magnetic particles by an external magnetic motor represents a new analytical concept. Many future applications of rotating magnetic particles are envisaged in the detection of antigen–antibody, nucleic acid–DNA, protein–DNA, or receptor–cell interactions. Also, enhanced reactivity at rotating magnetic particles (e.g. accelerated hybridization or polymerization) may facilitate analytical processes. Future analytical perspectives of hybrid NP systems may involve the mechanical actuation of microelements. The detection of biomaterials, such as antibodies^[399] or DNA,^[400] by the mechanical movement of microlevers owing to surface-stress interactions is well established. The integration of charged NPs or magnetic particles as labels for such biorecognition events may enhance the surface stress and provide mechanical activation of microobjects.

The electronic triggering of redox proteins by the incorporation of nanoparticles represents a novel strategy for the electrical contacting of redox enzymes with their macroscopic environment. The use of other nanoobjects, such as metal or semiconductor nanorods and carbon nanotubes, for the electrical contacting of redox enzymes may be envisaged. Also, the magnetic triggering of redox proteins will certainly find applications in tailoring complex sensor systems and the development of new surface-patterning methods.

The use of biomaterials as templates for the generation of nanostructures and nanocircuitry in the presence of NPs is in an early phase of development. The viability of the concept has been proven, and nanowires of controlled shapes and electronic functions have been generated by the incorporation of nanoparticles on template biomaterials. However, the biggest challenges are ahead of us, and exciting systems are envisaged for the future. Besides the interesting nanoarchitectures that may be generated, fundamental problems, such as probing charge-transport phenomena in such biomolecule–NP systems, may be highlighted. Nonetheless, the organization of NP architectures on biomaterial templates involves relatively simple motifs that do not make full use of the catalytic functions of the biomaterial. The replication of NP-labeled DNA, and specifically, the tailoring of PCR for the formation of NP wires, represents a novel approach to design biological machines for the synthesis of nanoparticle wires and circuitry. Finally, the use of biomolecule–NP composite systems for the fabrication of nanodevices is at a very early

stage. Nevertheless, it is already clear that fascinating new phenomena may be discovered.

For the future development of biomolecule–NP systems, it is mandatory to develop new synthetic methodologies. At present, most NPs are capped with a stabilizing layer. The synthesis of NPs that have a single functionality is a challenging goal, yet the successful synthesis of monofunctionalized Au₅₅ clusters implies that the preparation of such particles is feasible. Once particles are modified with a controlled number of chemical functionalities, the programmed vectorial growth of biomolecule–nanoparticle structures should be possible. In this context, the specific chemical functionalization of the edges of nanorods with biomaterials could be a means to grow nanostructures of controlled shape and composition.

Biomolecule-functionalized NPs and nanorods could be exploited for numerous applications in biomolecular electronics,^[401] biosensors,^[402,403] bioactuators,^[345,364] and medicine, namely in photodynamic anticancer therapy,^[404] targeted delivery of radioisotopes,^[405] drug delivery,^[406] electronic DNA sequencing, nanotechnology of gene-delivery systems,^[407] and gene therapy.^[408] Novel fascinating areas of technologies are feasible with the use of bionanomaterials. For example, nanorobotics, which is still at an embryonic stage, encompasses the design, fabrication, and programming of robots with overall dimensions below a few micrometers and the programmable assembly of nanoscale objects.^[409] Nanorobots are quintessential nanoelectromechanical systems and raise all the important issues of sensing, actuation, control, communications, power, and interfacing across spatial scales and between the organic/inorganic and biological/mechanical systems. Nanorobots are expected to have revolutionary applications in such areas as environmental monitoring and health care. The novel field of nanoelectronics and nanoelectromechanical quantum circuits and systems is also emerging.^[410] The field exploits progress in techniques for the fabrication (of down to nanometer-length scales) of freestanding device structures, which incorporate mechanical motion and which may be designed to perform a variety of functions (such as optical, electrical, and, in particular, mechanical). To fully exploit the potential of this technology in sensing, computation, and signal processing applications, the use of bionanohybrid systems is essential.

A combination of the unique properties of nanoobjects (such as nanoparticles and nanorods) and biomaterials provides a unique opportunity for physicists, chemists, biologists, and material scientists to mold the new area of nanobiotechnology.^[411] Based on recent advances in the field, exciting new science and novel systems can be anticipated from this interdisciplinary effort.

Our research on biomolecule–nanoparticle hybrid systems is supported by the German–Israeli Foundation (GIF). The cover picture for this review was designed by Dr. Andrew N. Shipway.

Received: January 20, 2004

Published Online: November 10, 2004

- [1] *There is Plenty of Room at the Bottom*, R. Feynman in *The Pleasure of Finding Things Out*, (Ed.: J. Robbins), Perseus Books, 1999.
- [2] D. Qin, Y. N. Xia, J. A. Rogers, R. J. Jackman, X.-M. Zhao, G. M. Whitesides, *Top. Curr. Chem.* **1997**, *194*, 1–20.
- [3] D. M. Tennant, K. Feder, K. F. Dreyer, R. P. Gnall, T. L. Koch, U. Koren, B. I. Miller, M. G. Young, *Microelectron. Eng.* **1995**, *27*, 427–434.
- [4] *Metal Nanoparticles: Synthesis, Characterization, and Application*, (Eds.: D. L. Feldheim, C. A. Foss Jr), Marcel Dekker, New York, 2002.
- [5] a) F. C. Meldrum, J. Flath, W. Knoll, *Langmuir* **1997**, *13*, 2033–2049; b) L. Spanhel, H. Weller, A. Fojtik, A. Henglein, *Ber. Bunsen-Ges.* **1987**, *91*, 88–94; c) E. Stathatos, P. Lianos, F. Del Monte, D. Levy, D. Tsiourvas, *Langmuir* **1997**, *13*, 4295–4300; d) R. Rizza, D. Fitzmaurice, S. Hearne, G. Hughes, G. Spoto, E. Ciliberto, H. Kerp, R. Schropp, *Chem. Mater.* **1997**, *9*, 2969–2982; e) D. L. Klein, R. Roth, A. K. L. Lim, A. P. Alivisatos, P. L. McEuen, *Nature* **1997**, *389*, 699–701.
- [6] a) J. F. Hicks, D. T. Miles, R. W. Murray, *J. Am. Chem. Soc.* **2002**, *124*, 13322–13328; b) J. F. Hicks, F. P. Zamborini, A. J. Osisek, R. W. Murray, *J. Am. Chem. Soc.* **2001**, *123*, 7048–7053; c) S. Chen, R. W. Murray, *J. Phys. Chem. B* **1999**, *103*, 9996–10000; d) J. F. Hicks, F. P. Zamborini, R. W. Murray, *J. Phys. Chem. B* **2002**, *106*, 7751–7757; e) S. Chen, R. W. Murray, S. W. Feldberg, *J. Phys. Chem. B* **1998**, *102*, 9898–9907.
- [7] a) A. N. Shipway, E. Katz, I. Willner, *ChemPhysChem* **2000**, *1*, 18–52; b) M.-C. Daniel, D. Astruc, *Chem. Rev.* **2004**, *104*, 293–346.
- [8] a) A. Badia, S. Singh, L. Demers, L. Cuccia, G. R. Brown, R. B. Lennox, *Chem. Eur. J.* **1996**, *2*, 359–363; b) M. Brust, J. Fink, D. Bethell, D. J. Schiffrin, C. Kiely, *J. Chem. Soc. Chem. Commun.* **1995**, 1655–1666.
- [9] a) H. Yao, O. Momozawa, T. Hamatani, K. Kimura, *Chem. Mater.* **2001**, *13*, 4692–4697; b) N. Hussain, B. Singh, T. Sakthivel, A. T. Florence, *Int. J. Pharm.* **2003**, *254*, 27–31; c) A. C. Templeton, S. Chen, S. M. Gross, R. W. Murray, *Langmuir* **1999**, *15*, 66–76.
- [10] a) A. Miyazaki, Y. Nakano, *Langmuir* **2000**, *16*, 7109–7111; b) W. P. Wuelfing, S. M. Gross, D. T. Miles, R. W. Murray, *J. Am. Chem. Soc.* **1998**, *120*, 12696–12697; c) T. Teranishi, I. Kiyokawa, M. Miyake, *Adv. Mater.* **1998**, *10*, 596–599.
- [11] M. Valina-Saba, G. Bauer, N. Stich, F. Pittner, T. Schalkhammer, *Mater. Sci. Eng. C* **1999**, *8–9*, 205–209.
- [12] J.-M. Lehn, *Supramolecular Chemistry: Concepts and Perspectives*, Wiley-VCH, Weinheim, 1995.
- [13] a) M. Lahav, A. N. Shipway, I. Willner, *J. Chem. Soc. Perkin Trans. 2* **1999**, 1925–1931; b) W. Chen, D. Grouquist, J. Roark, *J. Nanosci. Nanotechnol.* **2002**, *2*, 47–53.
- [14] A. N. Shipway, I. Willner, *Chem. Commun.* **2001**, 2035–2045.
- [15] a) D. L. Feldheim, C. D. Keating, *Chem. Soc. Rev.* **1998**, *27*, 1–12; b) T. W. Kim, D. C. Choo, J. H. Shim, S. O. Kang, *Appl. Phys. Lett.* **2002**, *80*, 2168–2170.
- [16] J. Liu, M. Gomez-Kaifer, A. E. Kaifer in *Structure and Bonding*, Vol. 99 (Ed.: J.-P. Sauvage), Springer, New York, **2001**, pp. 141–162.
- [17] D. L. Feldheim, K. C. Grabar, M. J. Natan, T. E. Mallouk, *J. Am. Chem. Soc.* **1996**, *118*, 7640–7641.
- [18] a) T. Trindade, P. O'Brien, N. L. Pickett, *Chem. Mater.* **2001**, *13*, 3843–3858; b) J.-T. Lue, *J. Phys. Chem. Solids* **2001**, *62*, 1599–1612; c) K. Grieve, P. Mulvaney, F. Grieser, *Curr. Opin. Colloid Interface Sci.* **2000**, *5*, 168–172; d) P. Schwerdtfeger, *Angew. Chem.* **2003**, *115*, 1936–1939; *Angew. Chem. Int. Ed.* **2003**, *42*, 1892–1895.
- [19] a) M. Brust, C. J. Kiely, *Colloids Surf. A* **2002**, *202*, 175–186; b) W. P. McConnell, J. P. Novak, L. C. Brousseau III, R. R.

- Fuierer, R. C. Tenent, D. L. Feldheim, *J. Phys. Chem. B* **2000**, *104*, 8925–8930; c) R. Gangopadhyay, A. De, *Chem. Mater.* **2000**, *12*, 608–622.
- [20] E. Katz, A. N. Shipway, I. Willner, in *Nanoparticles – From Theory to Applications*, (Ed.: G. Schmid), Wiley-VCH, Weinheim, **2003**, pp. 368–421.
- [21] a) C. M. Niemeyer, *Angew. Chem.* **2001**, *113*, 4254–4287; *Angew. Chem. Int. Ed.* **2001**, *40*, 4128–4158; b) C. M. Niemeyer, *Angew. Chem.* **2003**, *115*, 5974–5978; *Angew. Chem. Int. Ed.* **2003**, *42*, 5796–5800; c) W. J. Parak, D. Gerion, T. Pellegrino, D. Zanchet, C. Micheel, S. C. Williams, R. Boudreau, M. A. Le Gros, C. A. Larabell, A. P. Alivisatos, *Nanotechnology* **2003**, *14*, R15–R27; d) A. Csaki, G. Maubach, D. Born, J. Reichert, W. Fritzsche, *Single Mol.* **2002**, *3*, 275–280.
- [22] a) S. G. Penn, L. Hey, M. J. Natan, *Curr. Opin. Chem. Biol.* **2003**, *7*, 609–615; b) J. L. West, N. J. Halas, *Annu. Rev. Biomed. Eng.* **2003**, *5*, 285–292; c) P. Alivisatos, *Nat. Biotechnol.* **2004**, *22*, 47–52.
- [23] a) V. Escrivi, M. Carrière, D. Scherman, P. Wils, *Adv. Drug Delivery Rev.* **2003**, *55*, 295–306; b) A. G. Tkachenko, H. Xie, D. Coleman, W. Glomm, J. Ryan, M. F. Anderson, S. Franzen, D. L. Feldheim, *J. Am. Chem. Soc.* **2003**, *125*, 4700–4701.
- [24] I. Brigger, C. Dubernet, P. Couvreur, *Adv. Drug Delivery Rev.* **2002**, *54*, 631–651.
- [25] C. Aymonier, U. Schlotterbeck, L. Antonietti, P. Zacharias, R. Thomann, J. C. Tiller, S. Mecking, *Chem. Commun.* **2002**, 3018–3019.
- [26] Y. Xia, P. Yang, Y. Sun, Y. Wu, B. Mayers, B. Gates, Y. Yin, F. Kim, H. Yan, *Adv. Mater.* **2003**, *15*, 353–389.
- [27] I. W. Hamley, *Angew. Chem.* **2003**, *115*, 1730–1752; *Angew. Chem. Int. Ed.* **2003**, *42*, 1692–1712.
- [28] H. Cölfen, S. Mann, *Angew. Chem.* **2003**, *115*, 2452–2468; *Angew. Chem. Int. Ed.* **2003**, *42*, 2350–2365.
- [29] K. J. C. van Bommel, A. Friggeri, S. Shinkai, *Angew. Chem.* **2003**, *115*, 1010–1030; *Angew. Chem. Int. Ed.* **2003**, *42*, 980–999.
- [30] *Bioelectronics: From Theory to Applications*, (Eds.: I. Willner, E. Katz), Wiley-VCH, Weinheim, **2005**, in press.
- [31] a) G. T. Hermanson, A. K. Mallia, P. K. Smith, *Immobilized Affinity Ligand Techniques*, Academic Press, London, **1992**; b) R. F. Taylor, *Protein Immobilization*, Dekker, New York, **1990**; c) A. F. Collings, F. Caruso, *Rep. Prog. Phys.* **1997**, *60*, 1397–1445.
- [32] a) S. V. Rao, K. W. Anderson, L. G. Bachas, *Microchim. Acta* **1998**, *128*, 127–143; b) W. H. Scouten, J. H. T. Luong, R. S. Brown, *Trends Biotechnol.* **1995**, *13*, 178–185.
- [33] T. Rajh, J. M. Nedeljkovic, L. X. Chen, O. Poluektov, M. C. Thurnauer, *J. Phys. Chem. B* **1999**, *103*, 3515–3519.
- [34] J. B. Broderick, M. J. Natan, T. V. O'Halloran, R. P. Van Duyne, *Biochemistry* **1993**, *32*, 13771–13776.
- [35] C. Yongli, Z. Xiufang, G. Yandao, Z. Nanming, Z. Tingying, S. Xinqi, *J. Colloid Interface Sci.* **1999**, *214*, 38–45.
- [36] J. De Groot, R. E. Hester, S. Kaminaka, T. Kitagawa, *J. Phys. Chem.* **1988**, *92*, 2044–2048.
- [37] N. G. Khlebtsov, V. A. Bogatyrev, B. N. Khlebtsov, L. A. Dykman, P. Englebiegne, *Colloid J.* **2003**, *65*, 622–635.
- [38] W. Shenton, S. A. Davis, S. Mann, *Adv. Mater.* **1999**, *11*, 449–452.
- [39] a) I. D. G. MacDonald, W. E. Smith, *Langmuir* **1996**, *12*, 706–713; b) B. N. Rospadowski, K. Kelly, C. R. Wolf, W. E. Smith, *J. Am. Chem. Soc.* **1991**, *113*, 1217–1225.
- [40] H. Mattoussi, J. M. Mauro, E. R. Goldman, G. P. Anderson, V. C. Sundar, F. V. Mikulec, M. G. Bawendi, *J. Am. Chem. Soc.* **2000**, *122*, 12142–12150.
- [41] D. Ibano, Y. Yokota, T. Tominaga, *Chem. Lett.* **2003**, *32*, 574–575.
- [42] H. Larsericsdotter, S. Oscarsson, J. Buijs, *J. Colloid Interface Sci.* **2001**, *237*, 98–103.
- [43] a) M. J. Meziani, H. W. Rollins, L. F. Allard, Y.-P. Sun, *J. Phys. Chem. B* **2002**, *106*, 11178–11182; b) M. J. Meziani, Y.-P. Sun, *J. Am. Chem. Soc.* **2003**, *125*, 8015–8018.
- [44] M. Zheng, F. Davidson, X. Huang, *J. Am. Chem. Soc.* **2003**, *125*, 7790–7791.
- [45] P. Pengo, Q. B. Broxterman, B. Kaptein, L. Pasquato, P. Scrimin, *Langmuir* **2003**, *19*, 2521–2524.
- [46] F. Caruso, *Adv. Mater.* **2001**, *13*, 11–22.
- [47] F. Caruso, H. Möhwald, *J. Am. Chem. Soc.* **1999**, *121*, 6039–6046.
- [48] F. Caruso, H. Fiedler, K. Haage, *Colloids Surf. A* **2000**, *169*, 287–293.
- [49] C. Schüller, F. Caruso, *Macromol. Rapid Commun.* **2000**, *21*, 750–753.
- [50] F. Caruso, C. Schüller, *Langmuir* **2000**, *16*, 9595–9603.
- [51] Y. Lvov, F. Caruso, *Anal. Chem.* **2001**, *73*, 4212–4217.
- [52] W. Yang, D. Trau, R. Renneberg, N. T. Yu, F. Caruso, *J. Colloid Interface Sci.* **2001**, *234*, 356–362.
- [53] R. Mahtab, J. P. Rogers, C. J. Murphy, *J. Am. Chem. Soc.* **1995**, *117*, 9099–9100.
- [54] R. Mahtab, J. P. Rogers, C. P. Singleton, C. J. Murphy, *J. Am. Chem. Soc.* **1996**, *118*, 7028–7032.
- [55] R. Mahtab, H. H. Harden, C. J. Murphy, *J. Am. Chem. Soc.* **2000**, *122*, 14–17.
- [56] J. R. Lakowicz, I. Gryczynski, Z. Gryczynski, K. Nowaczyk, C. J. Murphy, *Anal. Biochem.* **2000**, *280*, 128–136.
- [57] S. R. Bigham, J. L. Coffer, *J. Cluster Sci.* **2000**, *11*, 359–372.
- [58] C. J. Murphy, E. B. Brauns, L. Gearheart, *Mater. Res. Soc. Symp. Proc.* **1997**, *452*, 597–601.
- [59] a) E. B. Brauns, C. J. Murphy, M. A. Berg, *J. Am. Chem. Soc.* **1998**, *120*, 2449–2456; b) E. B. Brauns, M. L. Madaras, R. S. Coleman, C. J. Murphy, M. A. Berg, *J. Am. Chem. Soc.* **1999**, *121*, 11644–11649; c) J. Wildeson, C. J. Murphy, *Anal. Biochem.* **2000**, *284*, 99–106.
- [60] L. A. Gearheart, H. J. Ploehn, C. J. Murphy, *J. Phys. Chem. B* **2001**, *105*, 12609–12615.
- [61] K. Naka, H. Itoh, Y. Tampo, Y. Chujo, *Langmuir* **2003**, *19*, 5546–5549.
- [62] V. I. Korsounski, R. B. Neder, K. Hradil, C. Barglik-Chory, G. Muller, J. Neufeind, *J. Appl. Crystallogr.* **2003**, *36*, 1389–1396.
- [63] M. A. Hayat, *Colloidal Gold: Principles, Methods, and Applications*, Academic Press, New York, **1989**.
- [64] a) S. S. Ghosh, P. M. Kao, A. W. McCue, H. L. Chappelle, *Bioconjugate Chem.* **1990**, *1*, 71–76; b) E. Droz, M. Taborrelli, P. Descouts, T. N. C. Wells, R. C. Werlen, *J. Vac. Sci. Technol. B* **1996**, *14*, 1422–1426.
- [65] a) H.-G. Hong, P. W. Bohn, S. G. Sligar, *Anal. Chem.* **1993**, *65*, 1635–1638; b) H.-G. Hong, M. Jiang, S. G. Sligar, P. W. Bohn, *Langmuir* **1994**, *10*, 153–158; c) M. A. Firestone, M. L. Shank, S. G. Sligar, P. W. Bohn, *J. Am. Chem. Soc.* **1996**, *118*, 9033–9041; d) S. Kanno, Y. Yanagida, T. Haruyama, E. Kobatake, M. Aizawa, *J. Biotechnol.* **2000**, *76*, 207–214.
- [66] J. Li, J. Wang, V. G. Gavalas, D. A. Atwood, L. G. Bachas, *Nano Lett.* **2003**, *3*, 55–58.
- [67] A. Schroedter, H. Weller, *Angew. Chem.* **2002**, *114*, 3346–3350; *Angew. Chem. Int. Ed.* **2002**, *41*, 3218–3221.
- [68] a) H. Jeon, G. G. Shipley, *J. Biol. Chem.* **2000**, *275*, 30465–30470; b) M. Malecki, A. Hsu, L. Truong, S. Sanchez, *Proc. Natl. Acad. Sci. USA* **2002**, *99*, 213–218; c) O. Medalia, M. Heim, R. Guckenberger, R. Sperling, J. Sperling, *J. Struct. Biol.* **1999**, *127*, 113–119; d) K.-M. Sung, D. W. Mosley, B. R. Peelle, S. Zhang, J. M. Jacobson, *J. Am. Chem. Soc.* **2004**, *126*, 5064–5065.
- [69] a) C. A. Mirkin, R. L. Letsinger, R. C. Mucic, J. J. Storhoff, *Nature* **1996**, *382*, 607–609; b) S.-J. Park, A. A. Lazarides, C. A.

- Mirkin, P. W. Brazis, C. R. Kannewurf, R. L. Letsinger, *Angew. Chem.* **2000**, *112*, 4003–4006; *Angew. Chem. Int. Ed.* **2000**, *39*, 3845–3848; c) L. M. Demers, C. A. Mirkin, R. C. Mucic, R. A. Reynolds III, R. L. Letsinger, R. Elghanian, G. Viswanadham, *Anal. Chem.* **2000**, *72*, 5535–5541.
- [70] G. P. Mitchell, C. A. Mirkin, R. L. Letsinger, *J. Am. Chem. Soc.* **1999**, *121*, 8122–8123.
- [71] R. L. Letsinger, R. Elghanian, G. Viswanadham, C. A. Mirkin, *Bioconjugate Chem.* **2000**, *11*, 289–291.
- [72] L. Jiang, B. Q. Yang, Y. D. Ma, Y. C. Liu, W. S. Yang, T. J. Li, C. C. Sun, *Chem. Phys. Lett.* **2003**, *380*, 29–33.
- [73] W. J. Parak, T. Pellegrino, C. M. Micheel, D. Gerion, S. C. Williams, A. P. Alivisatos, *Nano Lett.* **2003**, *3*, 33–36.
- [74] J. E. Gestwicki, L. E. Strong, L. L. Kisseling, *Angew. Chem.* **2000**, *112*, 4741–4744; *Angew. Chem. Int. Ed.* **2000**, *39*, 4567–4570.
- [75] M. Bruchez, Jr., M. Moronne, P. Gin, S. Weiss, A. P. Alivisatos, *Science* **1998**, *281*, 2013–2015.
- [76] B. M. Sergeev, M. V. Kiryukhin, M. Y. Rubtsova, A. N. Prusov, *Colloid J.* **2003**, *65*, 636–638.
- [77] a) K. Okano, S. Takahashi, K. Yasuda, D. Tokinaga, K. Imai, M. Koga, *Anal. Biochem.* **1992**, *202*, 120–125; b) T. Soukka, H. Härmä, J. Paukkunen, T. Lövgren, *Anal. Chem.* **2001**, *73*, 2254–2260; c) I. Sonodi, O. Siiman, S. Koester, E. Matijevic, *Langmuir* **2000**, *16*, 3107–3118.
- [78] a) A. Yoshizumi, N. Kanayama, Y. Maehara, M. Ide, H. Kitano, *Langmuir* **1999**, *15*, 482–488; b) M. J. Hernáiz, J. M. de la Fuente, A. G. Barrientos, S. Penadés, *Angew. Chem.* **2002**, *114*, 1624–1627; *Angew. Chem. Int. Ed.* **2002**, *41*, 1554–1557.
- [79] J. M. de la Fuente, A. G. Barrientos, T. C. Rojas, J. Rojo, J. Cañada, A. Fernández, S. Penadés, *Angew. Chem.* **2001**, *113*, 2317–2321; *Angew. Chem. Int. Ed.* **2001**, *40*, 2258–2261.
- [80] a) C.-C. Lin, Y.-C. Yeh, C.-Y. Yang, C.-L. Chen, G.-F. Chen, C.-C. Chen, Y.-C. Wu, *J. Am. Chem. Soc.* **2002**, *124*, 3508–3509; b) C.-C. Lin, Y.-C. Yeh, C.-Y. Yang, G.-F. Chen, Y.-C. Chen, Y.-C. Wu, C.-C. Chen, *Chem. Commun.* **2003**, 2920–2921.
- [81] H. Otsuka, Y. Akiyama, Y. Nagasaki, K. Kataoka, *J. Am. Chem. Soc.* **2001**, *123*, 8226–8230.
- [82] D. C. Hone, A. H. Haines, D. A. Russell, *Langmuir* **2003**, *19*, 7141–7144.
- [83] B. Nolting, J.-J. Yu, G.-Y. Liu, S.-J. Cho, S. Kauzlarich, J. Gervay-Hague, *Langmuir* **2003**, *19*, 6465–6473.
- [84] H. Gu, P. L. Ho, E. Tong, L. Wang, B. Xu, *Nano Lett.* **2003**, *3*, 1261–1263.
- [85] D. Ishii, K. Kinbara, Y. Ishida, N. Ishii, M. Okochi, M. Yohda, T. Aida, *Nature* **2003**, *423*, 628–632.
- [86] a) M. Kowshik, N. Deshmukh, W. Vogel, J. Urban, S. K. Kulkarni, K. M. Paknikar, *Biotechnol. Bioeng.* **2002**, *78*, 583–588; b) Y. Roh, R. J. Lauf, A. D. McMillan, C. Zhang, C. J. Rawn, J. Bai, T. J. Phelps, *Solid State Commun.* **2001**, *118*, 529–534; c) J. M. Sloicik, D. W. Wright, *Biomacromolecules* **2003**, *4*, 1135–1141; d) M. Kowshik, S. Ashtaputre, S. Kharrazi, W. Vogel, J. Urban, S. K. Kulkarni, K. M. Paknikar, *Nanotechnol. Sci.* **1998**, *5*, 391–394; f) P. Raveendran, J. Fu, S. L. Wallen, *J. Am. Chem. Soc.* **2003**, *125*, 13940–13941; g) S. S. Shankar, A. Ahmad, M. Sastry, *Biotechnol. Prog.* **2003**, *13*, 1627–1631; h) A. Ahmad, S. Senapati, M. Khan, R. Kumar, R. Ramani, V. Srinivas, M. Sastry, *Nanotechnology* **2003**, *14*, 824–828.
- [87] a) A. Ahmad, P. Mukherjee, D. Mandal, S. Senapati, M. I. Khan, R. Kumar, M. Sastry, *J. Am. Chem. Soc.* **2002**, *124*, 12108–12109; b) J. L. Gardea-Torresdey, J. G. Parsons, E. Gomez, J. Peralta-Videa, H. E. Troiani, P. Santiago, M. J. Yacamán, *Nano Lett.* **2002**, *2*, 397–401.
- [88] S.-Y. Ding, M. Jones, M. P. Tucker, J. M. Nedeljkovic, J. Wall, M. N. Simon, G. Rumbles, M. E. Himmel, *Nano Lett.* **2003**, *3*, 1581–1585.
- [89] a) A. R. Bizzarri, S. Cannistraro, *Appl. Spectrosc.* **2002**, *56*, 1531–1537; b) H. Xu, E. J. Bjerneld, M. Käll, L. Börjesson, *Phys. Rev. Lett.* **1999**, *83*, 4357–4360.
- [90] A. K. Boal, V. M. Rotello, *J. Am. Chem. Soc.* **1999**, *121*, 4914–4915.
- [91] J. Pan, G. Benkö, Y. Xu, T. Pascher, L. Sun, V. Sundström, T. Polivka, *J. Am. Chem. Soc.* **2002**, *124*, 13949–13957.
- [92] S. O. Obare, T. Ito, M. H. Balfour, G. J. Meyer, *Nano Lett.* **2003**, *3*, 1151–1153.
- [93] N. N. Mamedova, N. A. Kotov, A. L. Rogach, J. Studer, *Nano Lett.* **2001**, *1*, 281–286.
- [94] C. M. Niemeyer, M. Adler, *Angew. Chem.* **2002**, *114*, 3933–3937; *Angew. Chem. Int. Ed.* **2002**, *41*, 3779–3783.
- [95] S. R. N. Peña, S. Raina, G. P. Goodrich, N. V. Fedoroff, C. D. Keating, *J. Am. Chem. Soc.* **2002**, *124*, 7314–7323.
- [96] M. J. Hannon, V. Moreno, M. J. Prieto, E. Moldrheim, E. Sletten, I. Meistermann, C. J. Isaac, K. J. Sanders, A. Rodger, *Angew. Chem.* **2001**, *113*, 903–908; *Angew. Chem. Int. Ed.* **2001**, *40*, 880–884.
- [97] A. U. Bielinska, C. Chen, J. Johnson, J. R. Baker Jr., *Bioconjugate Chem.* **1999**, *10*, 843–850.
- [98] K. Iijima, M. Yoshizumi, M. Hashimoto, S. Kim, M. Eto, J. Ako, Y. Q. Kiang, N. Sudoh, K. Hosoda, K. Nakahara, K. Toda, Y. Ouchi, *Circulation* **2000**, *101*, 805–811.
- [99] M. J. Hostetler, A. C. Templeton, R. W. Murray, *Langmuir* **1999**, *15*, 3782–3789.
- [100] A. K. Boal, V. M. Rotello, *J. Am. Chem. Soc.* **2000**, *122*, 734–735.
- [101] C. M. McIntosh, E. A. Esposito III, A. K. Boal, J. M. Simard, C. T. Martin, V. M. Rotello, *J. Am. Chem. Soc.* **2001**, *123*, 7626–7629.
- [102] X. He, K. Wang, W. Tan, B. Liu, X. Lin, C. He, D. Li, S. Huang, J. Li, *J. Am. Chem. Soc.* **2003**, *125*, 7168–7169.
- [103] K. Hamad-Schifferli, J. J. Schwartz, A. T. Santos, S. Zhang, J. M. Jacobson, *Nature* **2002**, *415*, 152–155.
- [104] A. Jordan, R. Scholz, P. Wust, H. Fähring, R. Felix, *J. Magn. Magn. Mater.* **1999**, *201*, 413–419.
- [105] B. Dubertret, M. Calame, A. J. Libchaber, *Nat. Biotechnol.* **2001**, *19*, 365–370.
- [106] D. J. Maxwell, J. R. Taylor, S. Nie, *J. Am. Chem. Soc.* **2002**, *124*, 9606–9612.
- [107] a) N. O. Fischer, C. M. McIntosh, J. M. Simard, V. M. Rotello, *Proc. Natl. Acad. Sci. USA* **2002**, *99*, 5018–5023; b) N. O. Fischer, A. Verma, C. M. Goodman, J. M. Simard, V. M. Rotello, *J. Am. Chem. Soc.* **2003**, *125*, 13387–13391; c) R. Hong, N. O. Fischer, A. Verma, C. M. Goodman, T. Emrick, V. M. Rotello, *J. Am. Chem. Soc.* **2004**, *126*, 739–743.
- [108] C.-Y. Lai, B. G. Trewyn, D. M. Jeftinija, K. Jeftinija, S. Xu, S. Jeftinija, V. S.-Y. Lin, *J. Am. Chem. Soc.* **2003**, *125*, 4451–4459.
- [109] a) C. Petit, A. Taleb, M.-P. Pileni, *Adv. Mater.* **1998**, *10*, 259–261; b) C. B. Murray, C. R. Kagan, M. G. Bawendi, *Science* **1995**, *270*, 1335–1338; c) T. Vossmeier, G. Reck, L. Katsikas, E. T. K. Haupt, B. Schulz, H. Weller, *Science* **1995**, *267*, 1476–1479; d) B. A. Korgel, D. Fitzmaurice, *Adv. Mater.* **1998**, *10*, 661–665.
- [110] A. Sashchiuk, E. Lifshitz, R. Reisfeld, T. Saraidarov, M. Zelner, A. Willenz, *J. Sol-Gel Sci. Technol.* **2002**, *24*, 31–38.
- [111] S. A. Davis, M. Breulmann, K. H. Rhodes, B. Zhang, S. Mann, *Chem. Mater.* **2001**, *13*, 3218–3226.
- [112] W. Shenton, D. Pum, U. B. Sleytr, S. Mann, *Nature* **1997**, *389*, 585–587.
- [113] S. Dieluwit, D. Pum, U. B. Sleytr, *Supramol. Sci.* **1998**, *5*, 15–19.
- [114] S. A. Davis, H. M. Patel, E. L. Mayers, N. H. Mendelson, G. Franco, S. Mann, *Chem. Mater.* **1998**, *10*, 2516–2524.

- [115] R. P. Andres, J. D. Bielefeld, J. I. Henderson, D. B. Janes, V. R. Kolagunta, C. P. Kubiak, W. J. Mahoney, R. G. Osifchin, *Science* **1996**, 273, 1690–1693.
- [116] M. Brust, D. Bethell, D. J. Schiffrin, C. J. Kiely, *Adv. Mater.* **1995**, 7, 795–797.
- [117] S. Cobbe, S. Connolly, D. Ryan, L. Nagle, R. Eritja, D. Fitzmaurice, *J. Phys. Chem. B* **2003**, 107, 470–477.
- [118] S. Mann, W. Shenton, M. Li, S. Connolly, D. Fitzmaurice, *Adv. Mater.* **2000**, 12, 147–150.
- [119] R. Bashir, *Superlattices Microstruct.* **2001**, 29, 1–16.
- [120] C. M. Niemeyer, *Appl. Phys. A* **1999**, 68, 119–124.
- [121] V. A. Bogatyrev, L. A. Dykman, Y. M. Krasnov, V. K. Plotnikov, N. G. Khlebtsov, *Colloid J.* **2002**, 64, 671–680.
- [122] D. Zanchet, C. M. Micheel, W. J. Parak, D. Gerion, S. C. Williams, A. P. Alivisatos, *J. Phys. Chem. B* **2002**, 106, 11758–11763.
- [123] P. C. Weber, D. H. Ohlendorf, J. J. Wendoloski, F. R. Salemme, *Science* **1989**, 243, 85–88.
- [124] a) B. K. Sinha, C. F. Chingell, *Methods Enzymol.* **1979**, 62, 295–308; b) U. Piran, W. J. Riordan, *J. Immunol. Methods* **1990**, 133, 141–143.
- [125] a) T. Sano, M. W. Pandori, X. M. Chen, C. L. Smith, C. R. Cantor, *J. Biol. Chem.* **1995**, 270, 28204–28209; b) T. Sano, C. R. Cantor, *Proc. Natl. Acad. Sci. USA* **1995**, 92, 3180–3184.
- [126] a) S. Connolly, D. Fitzmaurice, *Adv. Mater.* **1999**, 11, 1202–1205; b) S. Connolly, S. Cobbe, D. Fitzmaurice, *J. Phys. Chem. B* **2001**, 105, 2222–2226.
- [127] K. K. Caswell, J. N. Wilson, U. H. F. Bunz, C. J. Murphy, *J. Am. Chem. Soc.* **2003**, 125, 13914–13915.
- [128] P. M. Harrison, P. Arosio, *Biochim. Biophys. Acta* **1996**, 1275, 161–203.
- [129] a) T. Douglas, D. P. E. Dickson, S. Betteridge, J. Charnock, C. D. Garner, S. Mann, *Science* **1995**, 269, 54–57; b) F. C. Meldrum, T. Douglas, S. Levi, P. Arosio, S. Mann, *J. Inorg. Biochem.* **1995**, 58, 59–68; c) F. C. Meldrum, B. R. Heywood, S. Mann, *Science* **1992**, 257, 522–523.
- [130] K. K. W. Wong, S. Mann, *Adv. Mater.* **1996**, 8, 928–931.
- [131] J. M. Dominguez-Vera, E. Colacio, *Inorg. Chem.* **2003**, 42, 6983–6985.
- [132] M. Li, K. K. W. Wong, S. Mann, *Chem. Mater.* **1999**, 11, 23–26.
- [133] N. T. K. Thanh, J. H. Rees, Z. Rosenzweig, *Anal. Bioanal. Chem.* **2002**, 374, 1174–1178.
- [134] N. T. K. Thanh, Z. Rosenzweig, *Anal. Chem.* **2002**, 74, 1624–1628.
- [135] L. R. Hirsch, J. B. Jackson, A. Lee, N. J. Halas, J. L. West, *Anal. Chem.* **2003**, 75, 2377–2381.
- [136] S. Wang, N. Mamedova, N. A. Kotov, W. Chen, J. Studer, *Nano Lett.* **2002**, 2, 817–822.
- [137] S. R. Whaley, D. S. English, E. L. Hu, P. F. Barbara, A. M. Belcher, *Nature* **2000**, 405, 665–668.
- [138] a) C. A. Mirkin, *Inorg. Chem.* **2000**, 39, 2258–2272; b) J. J. Storhoff, C. A. Mirkin, *Chem. Rev.* **1999**, 99, 1849–1862.
- [139] R. Elghanian, J. J. Storhoff, R. C. Mucic, R. L. Letsinger, C. A. Mirkin, *Science* **1997**, 277, 1078–1081.
- [140] J. J. Storhoff, R. Elghanian, R. C. Mucic, C. A. Mirkin, R. L. Letsinger, *J. Am. Chem. Soc.* **1998**, 120, 1959–1964.
- [141] a) R. A. Reynolds III, C. A. Mirkin, R. L. Letsinger, *J. Am. Chem. Soc.* **2000**, 122, 3795–3796; b) G. R. Souza, J. H. Miller, *J. Am. Chem. Soc.* **2001**, 123, 6734–6735.
- [142] R. C. Mucic, J. J. Storhoff, C. A. Mirkin, R. L. Letsinger, *J. Am. Chem. Soc.* **1998**, 120, 12674–12675.
- [143] J. J. Storhoff, A. A. Lazarides, R. C. Mucic, C. A. Mirkin, R. L. Letsinger, G. C. Schatz, *J. Am. Chem. Soc.* **2000**, 122, 4640–4650.
- [144] E. Dujardin, L.-B. Hsin, C. R. C. Wang, S. Mann, *Chem. Commun.* **2001**, 1264–1265.
- [145] Y. J. Kim, R. C. Johnson, J. T. Hupp, *Nano Lett.* **2001**, 1, 165–167.
- [146] S. Y. Lin, S. W. Liu, C. M. Lin, C. H. Chen, *Anal. Chem.* **2002**, 74, 330–335.
- [147] a) J. Liu, Y. Lu, *J. Am. Chem. Soc.* **2003**, 125, 6642–6643; b) J. Liu, Y. Lu, *Anal. Chem.* **2004**, 76, 1627–1632.
- [148] a) R. R. Breaker, *Curr. Opin. Biotechnol.* **2002**, 13, 31–39; b) R. R. Breaker, *Chem. Rev.* **1997**, 97, 371–390; c) G. F. Joyce in *The RNA World*, Vol. 37 (Eds.: R. F. Gesteland, T. R. Cech, J. F. Atkins), Cold Spring Harbor Laboratory Press, New York, **1999**, pp. 687–689.
- [149] a) J. Li, W. Zheng, A. H. Kwon, Y. Lu, *Nucleic Acids Res.* **2000**, 28, 481–488; b) S. W. Santoro, G. F. Joyce, *Proc. Natl. Acad. Sci. USA* **1997**, 94, 4262–4266; c) D. Faulhammer, M. Famulok, *Angew. Chem.* **1996**, 108, 2984–2988; *Angew. Chem. Int. Ed. Engl.* **1996**, 35, 2837–2841.
- [150] A. G. Kanaras, Z. Wang, A. D. Bates, R. Cosstick, M. Brust, *Angew. Chem.* **2003**, 115, 201–204; *Angew. Chem. Int. Ed.* **2003**, 42, 191–194.
- [151] C. S. Yun, G. A. Khitrov, D. E. Vergona, N. O. Reich, G. F. Strouse, *J. Am. Chem. Soc.* **2002**, 124, 7644–7645.
- [152] A. P. Alivisatos, K. P. Johnsson, X. Peng, T. E. Wilson, C. J. Loweth, M. P. Bruchez Jr., P. G. Schultz, *Nature* **1996**, 382, 609–611.
- [153] C. J. Loweth, W. B. Caldwell, X. Peng, A. P. Alivisatos, P. G. Schultz, *Angew. Chem.* **1999**, 111, 1925–1929; *Angew. Chem. Int. Ed.* **1999**, 38, 1808–1812.
- [154] K. Sato, K. Hosokawa, M. Maeda, *J. Am. Chem. Soc.* **2003**, 125, 8102–8103.
- [155] R. Chakrabarti, A. M. Klibanov, *J. Am. Chem. Soc.* **2003**, 125, 12531–12540.
- [156] C. M. Niemeyer, B. Ceyhan, *Angew. Chem.* **2001**, 113, 3798–3801; *Angew. Chem. Int. Ed.* **2001**, 40, 3685–3688.
- [157] a) S.-J. Park, A. A. Lazarides, C. A. Mirkin, R. L. Letsinger, *Angew. Chem.* **2001**, 113, 2993–2996; *Angew. Chem. Int. Ed.* **2001**, 40, 2909–2912; b) C. M. Niemeyer, *Biochem. Soc. Trans.* **2004**, 32, 51–53.
- [158] C. M. Niemeyer, W. Bürger, J. Peplies, *Angew. Chem.* **1998**, 110, 2391–2395; *Angew. Chem. Int. Ed.* **1998**, 37, 2265–2268.
- [159] Q. Wang, T. Lin, L. Tang, J. E. Johnson, M. G. Finn, *Angew. Chem.* **2002**, 114, 477–480; *Angew. Chem. Int. Ed.* **2002**, 41, 459–462.
- [160] H. Liang, T. E. Angelini, J. Ho, P. V. Braun, G. C. L. Wong, *J. Am. Chem. Soc.* **2003**, 125, 11786–11787.
- [161] I. Willner, *Science* **2002**, 298, 2407–2408.
- [162] F. A. Armstrong, G. S. Wilson, *Electrochim. Acta* **2000**, 45, 2623–2645.
- [163] A. Heller, *Acc. Chem. Res.* **1990**, 23, 128–134.
- [164] A. Heller, *J. Phys. Chem.* **1992**, 96, 3579–3587.
- [165] I. Willner, E. Katz, *Angew. Chem.* **2000**, 112, 1230–1269; *Angew. Chem. Int. Ed.* **2000**, 39, 1180–1218.
- [166] a) J. Wang, *J. Pharm. Biomed. Anal.* **1999**, 18, 47–53; b) H.-L. Schmidt, W. Schuhmann, *Biosens. Bioelectron.* **1996**, 11, 127–135; c) I. Willner, E. Katz, B. Willner, *Electroanalysis* **1997**, 9, 965–977.
- [167] a) I. Willner, G. Arad, E. Katz, *Bioelectrochem. Bioenerg.* **1998**, 44, 209–214; b) I. Willner, E. Katz, F. Patolsky, A. F. Bückmann, *J. Chem. Soc. Perkin Trans. 2* **1998**, 1817–1822; c) E. Katz, B. Filanovsky, I. Willner, *New J. Chem.* **1999**, 23, 481–487; d) E. Katz, I. Willner, A. B. Kotlyar, *J. Electroanal. Chem.* **1999**, 479, 64–68; e) S. C. Barton, H.-H. Kim, G. Binyamin, Y. Zhang, A. Heller, *J. Am. Chem. Soc.* **2001**, 123, 5802–5803; f) T. Chen, S. C. Barton, G. Binyamin, Z. Gao, Y. Zhang, H.-H. Kim, A. Heller, *J. Am. Chem. Soc.* **2001**, 123, 8630–8631; g) E. Katz, A. N. Shipway, I. Willner in *Handbook of Fuel Cells—Fundamentals, Technology, Applications*, Vol. 1 (Eds.: W. Vielstich, H. Gasteiger, A. Lamm), Wiley, **2003**, pp. 355–381.

- [168] a) I. Willner, A. Doron, E. Katz, *J. Phys. Org. Chem.* **1998**, *11*, 546–560; b) R. Blonder, E. Katz, I. Willner, V. Wray, A. F. Bückmann, *J. Am. Chem. Soc.* **1997**, *119*, 11747–11757.
- [169] a) G. Sundarababu, H. Gao, H. Sigris, *Photochem. Photobiol.* **1995**, *61*, 540–544; b) S. K. Bhatia, J. L. Teixeira, M. Anderson, L. Shriver-Lake, J. M. Calvert, J. H. Georger, J. J. Hickman, C. S. Dulcey, P. E. Schoen, F. S. Ligler, *Anal. Biochem.* **1993**, *208*, 197–205.
- [170] M. Sastry, M. Rao, K. N. Ganesh, *Acc. Chem. Res.* **2002**, *35*, 847–855.
- [171] a) N. Kimizuka, M. Tanaka, T. Kunitake, *Chem. Lett.* **1999**, 1333–1334; b) P. He, N. Hu, J. F. Rusling, *Langmuir* **2004**, *20*, 722–729.
- [172] S. Deki, Y. Aoi, O. Hiroi, A. Kajinami, *Chem. Lett.* **1996**, 433–434.
- [173] S. Phadtare, A. Kumar, V. P. Vinod, C. Dash, D. V. Palaskar, M. Rao, P. G. Shukla, S. Sivaram, M. Sastry, *Chem. Mater.* **2003**, *15*, 1944–1949.
- [174] N. Levit-Binnun, A. B. Lindner, O. Zik, Z. Eshhar, E. Moses, *Anal. Chem.* **2003**, *75*, 1436–1441.
- [175] Y. Maeda, T. Nakamura, K. Uchimura, T. Matsumoto, H. Tabata, T. Kawai, *J. Vac. Sci. Technol. B* **1999**, *17*, 494–496.
- [176] T. Torimoto, M. Yamashita, S. Kuwabata, T. Sakata, H. Mori, H. Yoneyama, *J. Phys. Chem. B* **1999**, *103*, 8799–8803.
- [177] J. L. Coffey, S. R. Bigham, X. Li, R. F. Pinizzotto, Y. G. Rho, R. M. Pirtle, I. L. Pirtle, *Appl. Phys. Lett.* **1996**, *69*, 3851–3853.
- [178] M. Sastry, A. Kumar, S. Datar, C. V. Dharmadhikari, K. N. Ganesh, *Appl. Phys. Lett.* **2001**, *78*, 2943–2945.
- [179] A. Kumar, M. Pattarkine, M. Bhadhade, A. B. Mandale, K. N. Ganesh, S. S. Datar, C. V. Dharmadhikari, M. Sastry, *Adv. Mater.* **2001**, *13*, 341–344.
- [180] a) S. Han, J. Lin, F. Zhou, R. L. Vellanoweth, *Biochem. Biophys. Res. Commun.* **2000**, *279*, 265–269; b) E. Huang, M. Satjapipat, S. Han, F. Zhou, *Langmuir* **2001**, *17*, 1215–1224.
- [181] J. Richter, R. Seidel, R. Kirsch, M. Mertig, W. Pompe, J. Plaschke, H. K. Schackert, *Adv. Mater.* **2000**, *12*, 507–510.
- [182] Y. Maeda, H. Tabata, T. Kawai, *Appl. Phys. Lett.* **2001**, *79*, 1181–1183.
- [183] J. K. N. Mbindyo, B. D. Reiss, B. R. Martin, C. D. Keating, M. J. Natan, T. E. Mallouk, *Adv. Mater.* **2001**, *13*, 249–254.
- [184] C. M. Niemeyer, B. Ceyhan, S. Gao, L. Chi, S. Peschel, U. Simon, *Colloid Polym. Sci.* **2001**, *279*, 68–72.
- [185] L. M. Demers, S.-J. Park, T. A. Taton, Z. Li, C. A. Mirkin, *Angew. Chem.* **2001**, *113*, 3161–3163; *Angew. Chem. Int. Ed.* **2001**, *40*, 3071–3073.
- [186] a) K.-B. Lee, J.-H. Lim, C. A. Mirkin, *J. Am. Chem. Soc.* **2003**, *125*, 5588–5589; b) H. Zhang, K. B. Lee, Z. Li, C. A. Mirkin, *Nanotechnology* **2003**, *14*, 1113–1117.
- [187] T. A. Taton, R. C. Mucic, C. A. Mirkin, R. L. Letsinger, *J. Am. Chem. Soc.* **2000**, *122*, 6305–6306.
- [188] I. Willner, F. Patolsky, J. Wasserman, *Angew. Chem.* **2001**, *113*, 1913–1916; *Angew. Chem. Int. Ed.* **2001**, *40*, 1861–1864.
- [189] a) C. M. Niemeyer, B. Ceyhan, P. Hazarika, *Angew. Chem.* **2003**, *115*, 5944–5948; *Angew. Chem. Int. Ed.* **2003**, *42*, 5766–5770; b) C. M. Niemeyer, B. Ceyhan, M. Noyong, U. Simon, *Biochem. Biophys. Res. Commun.* **2003**, *301*, 995–999.
- [190] a) L. Cognet, C. Tardin, D. Boyer, D. Choquet, P. Tamarat, B. Lounis, *Proc. Natl. Acad. Sci. USA* **2003**, *100*, 11350–11355; b) Y. F. Wang, D. W. Pang, Z. L. Zhang, H. Z. Zheng, J. P. Cao, J. T. Shen, *J. Med. Virol.* **2003**, *70*, 205–211; c) K. Sokolov, M. Follen, J. Aaron, I. Pavlova, A. Malpica, R. Lotan, R. Richards-Kortum, *Cancer Res.* **2003**, *63*, 1999–2004.
- [191] a) D. M. Willard, *Anal. Bioanal. Chem.* **2003**, *376*, 284–286; b) J. Wang, *Anal. Chim. Acta* **2003**, *500*, 247–257.
- [192] D. Hernández-Santos, M. B. González-García, A. C. García, *Electroanalysis* **2002**, *14*, 1225–1235.
- [193] a) W. R. Holland, D. G. Hall, *Phys. Rev. B* **1983**, *27*, 7765–7768; b) T. Kume, N. Nakagawa, S. Hayashi, K. Yamamoto, *Solid State Commun.* **1995**, *93*, 171–175; c) G. S. Agarwal, S. D. Gupta, *Phys. Rev. B* **1985**, *32*, 3607–3611.
- [194] a) I. Willner, E. Katz, B. Willner in *Biosensors and Their Applications*, (Eds.: V. C. Yang, T. T. Ngo), Kluwer, New York, **2000**, pp. 47–98; b) I. Willner, B. Willner, E. Katz, *Rev. Mol. Biotechnol.* **2002**, *82*, 325–355; c) L. Habermüller, M. Mosbach, W. Schuhmann, *Fresenius J. Anal. Chem.* **2000**, *366*, 560–568; d) I. Willner, B. Willner, *Trends Biotechnol.* **2001**, *19*, 222–230; e) F. A. Armstrong, H. A. Heering, J. Hirst, *Chem. Soc. Rev.* **1997**, *26*, 169–179.
- [195] P. N. Bartlett, P. Tebbutt, R. G. Whitaker, *Prog. React. Kinet.* **1991**, *16*, 55–155.
- [196] a) Y. Degani, A. Heller, *J. Phys. Chem.* **1987**, *91*, 1285–1289; b) W. Schuhmann, T. J. Ohara, H.-L. Schmidt, A. Heller, *J. Am. Chem. Soc.* **1991**, *113*, 1394–1397; c) Y. Degani, A. Heller, *J. Am. Chem. Soc.* **1988**, *110*, 2615–2620; d) I. Willner, A. Riklin, B. Shoham, D. Rivenzon, E. Katz, *Adv. Mater.* **1993**, *5*, 912–915; e) I. Willner, E. Katz, A. Riklin, R. Kasher, *J. Am. Chem. Soc.* **1992**, *114*, 10965–10966; f) A. Badia, R. Carlini, A. Fernandez, F. Battaglini, S. R. Mikkelsen, A. M. English, *J. Am. Chem. Soc.* **1993**, *115*, 7053–7060.
- [197] S. A. Emr, A. M. Yacynych, *Electroanalysis* **1995**, *6*, 913–923.
- [198] a) I. Willner, V. Heleg-Shabtai, R. Blonder, E. Katz, G. Tao, A. F. Bückmann, A. Heller, *J. Am. Chem. Soc.* **1996**, *118*, 10321–10322; b) E. Katz, A. Riklin, V. Heleg-Shabtai, I. Willner, A. F. Bückmann, *Anal. Chim. Acta* **1999**, *385*, 45–58.
- [199] a) O. A. Raitman, E. Katz, A. F. Bückmann, I. Willner, *J. Am. Chem. Soc.* **2002**, *124*, 6487–6496; b) O. A. Raitman, F. Patolsky, E. Katz, I. Willner, *Chem. Commun.* **2002**, 1936–1937.
- [200] a) L.-H. Guo, G. McLendon, H. Razafitrimo, Y. Gao, *J. Mater. Chem.* **1996**, *6*, 369–374; b) H. Zimmermann, A. Lindgren, W. Schuhmann, L. Gorton, *Chem. Eur. J.* **2000**, *6*, 592–599.
- [201] a) J. Zhao, R. W. Henkens, J. Stonehurner, J. P. O'Daly, A. L. Crumbliss, *J. Electroanal. Chem.* **1992**, *327*, 109–119; b) A. L. Crumbliss, S. C. Perine, J. Stonehurner, K. R. Tubergen, J. Zhao, R. W. Henkens, J. P. O'Daly, *Biotechnol. Bioeng.* **1992**, *40*, 483–490; c) J. Zhao, J. P. O'Daly, R. W. Henkens, J. Stonehurner, A. L. Crumbliss, *Biosens. Bioelectron.* **1996**, *11*, 493–502; d) S. Bharathi, M. Nogami, *Analyst* **2001**, *126*, 1919–1922; e) S. Liu, H. Ju, *Electroanalysis* **2003**, *15*, 1488–1493; f) X.-Y. Wang, H. Zhong, Y. Lv, H.-Y. Chen, *Chem. Lett.* **2003**, *32*, 1054–1055; g) S. Liu, H. Ju, *Biosens. Bioelectron.* **2003**, *19*, 177–183; h) S. Liu, H. Ju, *Analyst*, **2003**, *128*, 1420–1424; i) H.-Y. Gu, R.-X. Sa, S.-S. Yuan, H.-Y. Chen, A.-M. Yu, *Chem. Lett.* **2003**, *32*, 934–935; j) T. Liu, J. Zhong, X. Gan, C. Fan, G. Li, N. Matsuda, *ChemPhysChem* **2003**, *4*, 1364–1366; k) L. Wang, E. Wang, *Electrochem. Commun.* **2004**, *6*, 225–229; l) S. Liu, Z. Dai, H. Chen, H. Ju, *Biosens. Bioelectron.* **2004**, *19*, 963–969; m) Y. Zhang, P. He, N. Hu, *Electrochim. Acta* **2004**, *49*, 1981–1988; n) S. Xu, X. Han, *Biosens. Bioelectron.* **2004**, *19*, 1117–1120.
- [202] X. Han, W. Cheng, Z. Zhang, S. Dong, E. Wang, *Biochim. Biophys. Acta* **2002**, *1556*, 273–277.
- [203] Y. Xiao, F. Patolsky, E. Katz, J. F. Hainfeld, I. Willner, *Science* **2003**, *299*, 1877–1881.
- [204] V. Pardo-Yissar, E. Katz, J. Wasserman, I. Willner, *J. Am. Chem. Soc.* **2003**, *125*, 622–623.
- [205] M. L. Curri, A. Agostiano, G. Leo, A. Mallardi, P. Cosma, M. D. Monica, *Mater. Sci. Eng. C* **2002**, *22*, 449–452.
- [206] a) P. Mulvaney, *Langmuir* **1996**, *12*, 788–800; b) M. M. Alvarez, J. T. Khoury, T. G. Schaaff, M. N. Shafigullin, I. Vezmar, R. L. Whetten, *J. Phys. Chem. B* **1997**, *101*, 3706–3712; c) A. P. Alivisatos, *J. Phys. Chem.* **1996**, *100*, 13226–13329; d) L. Brus, *Appl. Phys. A* **1991**, *53*, 465–474.

- [207] a) R. F. Khairutdinov, *Colloid J.* **1997**, 59, 535–548; b) *Single Charge Tunneling: Coulomb Blockade Phenomena in Nanostructures*: NATO ASI Ser. B, Vol. 294, (Eds.: H. Grabert, M. H. Devoret), Plenum Press, New York, **1992**.
- [208] a) L. N. Lewis, *Chem. Rev.* **1993**, 93, 2693–2730; b) V. Kesavan, P. S. Sivanand, S. Chandrasekaran, Y. Kolytyn, A. Gedanken, *Angew. Chem.* **1999**, 111, 3729–3730; *Angew. Chem. Int. Ed.* **1999**, 38, 3521–3523; c) R. Schlögl, S. B. A. Hamid, *Angew. Chem.* **2004**, 116, 1656–1667; *Angew. Chem. Int. Ed.* **2004**, 43, 1628–1637.
- [209] L. He, M. D. Musick, S. R. Nicewarner, F. G. Salinas, S. J. Benkovic, M. J. Natan, C. D. Keating, *J. Am. Chem. Soc.* **2000**, 122, 9071–9077.
- [210] a) S. Kubitschko, J. Spinke, T. Brückner, S. Pohl, N. Oranth, *Anal. Biochem.* **1997**, 253, 112–122; b) L. A. Lyon, M. D. Musick, M. J. Natan, *Anal. Chem.* **1998**, 70, 5177–5183; c) P. Englebienne, A. V. Hoonacker, M. Verhas, *Analyst* **2001**, 126, 1645–1651.
- [211] M. Ozsoz, A. Erdem, K. Kerman, D. Ozkan, B. Tugrul, N. Topcuoglu, H. Ekren, M. Taylan, *Anal. Chem.* **2003**, 75, 2181–2187.
- [212] J. Wang, *Stripping Analysis*, VCH, Weinheim, **1985**.
- [213] N. Zhu, H. Cai, P. He, Y. Fang, *Anal. Chim. Acta* **2003**, 481, 181–189.
- [214] J. Wang, J. Li, A. J. Baca, J. Hu, F. Zhou, W. Yan, D.-W. Pang, *Anal. Chem.* **2003**, 75, 3941–3945.
- [215] J. Wang, D. Xu, A.-N. Kawde, R. Polsky, *Anal. Chem.* **2001**, 73, 5576–5581.
- [216] L. Authier, C. Grossiord, P. Brossier, B. Limoges, *Anal. Chem.* **2001**, 73, 4450–4456.
- [217] H. Cai, Y. Xu, N. Zhu, P. He, Y. Fang, *Analyst* **2002**, 127, 803–808.
- [218] H. Cai, N. Zhu, Y. Jiang, P. He, Y. Fang, *Biosens. Bioelectron.* **2003**, 18, 1311–1319.
- [219] J. Wang, G. Liu, Q. Zhu, *Anal. Chem.* **2003**, 75, 6218–6222.
- [220] T. G. Drummond, M. G. Hill, J. K. Barton, *Nat. Biotechnol.* **2003**, 21, 1192–1199.
- [221] T. M.-H. Lee, L.-L. Li, I.-M. Hsing, *Langmuir* **2003**, 19, 4338–4343.
- [222] J. Wang, R. Polsky, D. Xu, *Langmuir* **2001**, 17, 5739–5741.
- [223] J. Wang, O. Rincón, R. Polsky, E. Dominguez, *Electrochem. Commun.* **2003**, 5, 83–86.
- [224] J. Richter, *Physica E* **2003**, 16, 157–173.
- [225] E. Braun, Y. Eichen, U. Sivan, G. Ben-Yoseph, *Nature* **1998**, 391, 775–778.
- [226] Y. Eichen, E. Braun, U. Sivan, G. Ben-Yoseph, *Acta Polym.* **1998**, 49, 663–670.
- [227] M. Mertig, L. C. Ciacchi, R. Seidel, W. Pompe, A. De Vita, *Nano Lett.* **2002**, 2, 841–844.
- [228] O. D. Velev, E. W. Kaler, *Langmuir* **1999**, 15, 3693–3698.
- [229] a) S.-J. Park, T. A. Taton, C. A. Mirkin, *Science* **2002**, 295, 1503–1506; b) L. Moreno-Hagelsieb, P. E. Lobert, R. Pampin, D. Bourgeois, J. Remacle, D. Flandre, *Sens. Actuators B* **2004**, 98, 269–274.
- [230] M. Urban, R. Möller, W. Fritzsche, *Rev. Sci. Instrum.* **2003**, 74, 1077–1081.
- [231] A. Doron, E. Katz, I. Willner, *Langmuir* **1995**, 11, 1313–1317.
- [232] H. Cai, C. Xu, P. He, Y. Fang, *J. Electroanal. Chem.* **2001**, 510, 78–85.
- [233] H. Lin, H. Zhao, J. Li, J. Tang, M. Duan, L. Jiang, *Biochem. Biophys. Res. Commun.* **2000**, 274, 817–820.
- [234] a) M. Wang, L. Wang, G. Wang, X. Ji, Y. Bai, T. Li, S. Gongb, J. Li, *Biosens. Bioelectron.* **2004**, 19, 575–582; b) C.-X. Lei, F.-C. Gong, G.-L. Shen, R.-Q. Yu, *Sens. Actuators B* **2003**, 96, 582–588; c) S.-Q. Hua, J.-W. Xie, Q.-H. Xu, K.-T. Rong, G.-L. Shen, R.-Q. Yu, *Talanta* **2003**, 61, 769–777; d) H. Wang, J. Li, Y. Ding, C. Lei, G. Shen, R. Yu, *Anal. Chim. Acta* **2004**, 501, 37–43; e) C.-X. Lei, F.-C. Gong, G.-L. Shen, R.-Q. Yu, *Sens. Actuators B* **2003**, 96, 582–588; f) M. Wang, C. Sun, L. Wang, X. Ji, Y. Bai, T. Li, J. Li, *J. Pharm. Biomed. Anal.* **2003**, 33, 1117–1125.
- [235] E. Katz, A. N. Shipway, I. Willner in *Nanoscale Materials*, (Eds.: L. M. Liz-Marzan, P. Kamat), Kluwer, **2003**, pp. 5–78.
- [236] J. Wang, G. Liu, R. Polsky, A. Merkoçi, *Electrochem. Commun.* **2002**, 4, 722–726.
- [237] J. Wang, G. Liu, A. Merkoçi, *J. Am. Chem. Soc.* **2003**, 125, 3214–3215.
- [238] a) A. Kawde, J. Wang, *Electroanalysis* **2004**, 16, 101–107; b) J. Wang, G. Liu, M. R. Jan, Q. Zhu, *Electrochem. Commun.* **2003**, 5, 1000–1004.
- [239] a) J. Wang, R. Polsky, A. Merkoçi, K. Turner, *Langmuir* **2003**, 19, 989–991; b) J. Wang, G. Liu, G. Rivas, *Anal. Chem.* **2003**, 75, 4667–4671.
- [240] D. Trau, W. J. Yang, M. Seydack, F. Caruso, N.-T. Yu, R. Renneberg, *Anal. Chem.* **2002**, 74, 5480–5486.
- [241] L. Alfonta, A. Singh, I. Willner, *Anal. Chem.* **2001**, 73, 91–102.
- [242] D. A. Buttry, M. D. Ward, *Chem. Rev.* **1992**, 92, 1355–1379.
- [243] a) X. C. Zhou, S. J. O'Shea, S. F. Y. Li, *Chem. Commun.* **2000**, 953–954; b) F. Patolsky, K. T. Ranjit, A. Lichtenstein, I. Willner, *Chem. Commun.* **2000**, 1025–1026; c) T. Liu, J. Tang, L. Jiang, *Biochem. Biophys. Res. Commun.* **2004**, 313, 3–7.
- [244] S. Han, J. Lin, M. Satjapipat, A. J. Baca, F. Zhou, *Chem. Commun.* **2001**, 609–610.
- [245] T. Liu, J. Tang, H. Zhao, Y. Deng, L. Jiang, *Langmuir* **2002**, 18, 5624–5626.
- [246] I. Willner, F. Patolsky, Y. Weizmann, B. Willner, *Talanta* **2002**, 56, 847–856.
- [247] Y. Weizmann, F. Patolsky, I. Willner, *Analyst* **2001**, 126, 1502–1504.
- [248] a) T. A. Taton, C. A. Mirkin, R. L. Letsinger, *Science* **2000**, 289, 1757–1760; b) J. Reichert, A. Csáki, J. M. Köhler, W. Fritzsche, *Anal. Chem.* **2000**, 72, 6025–6029; c) T. A. Taton, G. L. Lu, C. A. Mirkin, *J. Am. Chem. Soc.* **2001**, 123, 5164–5165; d) J. J. Storhoff, S. S. Marla, P. Bao, S. Hagenow, H. Mehta, A. Lucas, V. Garimella, T. Patno, W. Buckingham, W. Cork, U. R. Müller, *Biosens. Bioelectron.* **2004**, 19, 875–883.
- [249] a) S. Y. Park, D. Stroud, *Physica B* **2003**, 338, 353–356; b) R. Jin, G. Wu, Z. Li, C. A. Mirkin, G. C. Schatz, *J. Am. Chem. Soc.* **2003**, 125, 1643–1654.
- [250] S. Schultz, D. R. Smith, J. J. Mock, D. A. Schultz, *Proc. Natl. Acad. Sci. USA* **2000**, 97, 996–1001.
- [251] A. P. Han, M. Dufva, E. Belleville, C. B. V. Christensen, *Lab on a Chip* **2003**, 3, 329–332.
- [252] R. C. Bailey, J.-M. Nam, C. A. Mirkin, J. T. Hupp, *J. Am. Chem. Soc.* **2003**, 125, 13541–13547.
- [253] a) G. Bauer, F. Pittner, T. Schalkhammer, *Microchim. Acta* **1999**, 131, 107–114; b) F. Frederix, J.-M. Friedt, K.-H. Choi, W. Laureyn, A. Campitelli, D. Mondelaers, G. Maes, G. Borghs, *Anal. Chem.* **2003**, 75, 6894–6900; c) L. Olofsson, T. Rindzevicius, I. Pfeiffer, M. Käll, F. Höök, *Langmuir* **2003**, 19, 10414–10419.
- [254] K. Glynnou, P. C. Ioannou, T. K. Christopoulos, V. Syriopoulou, *Anal. Chem.* **2003**, 75, 4155–4160.
- [255] Z. Ma, S.-F. Sui, *Angew. Chem.* **2002**, 114, 2280–2283; *Angew. Chem. Int. Ed.* **2002**, 41, 2176–2179.
- [256] B. Dragnea, C. Chen, E.-S. Kwak, B. Stein, C. C. Kao, *J. Am. Chem. Soc.* **2003**, 125, 6374–6375.
- [257] C. Bohren, D. Huffman, *Absorption and Scattering of Light by Small Particles*, Wiley, New York, **1983**.
- [258] G. Raschke, S. Kowarik, T. Franzl, C. Sönnichsen, T. A. Klar, J. Feldmann, *Nano Lett.* **2003**, 3, 935–938.
- [259] a) S. R. Nicewarner-Peña, A. J. Carado, K. E. Shale, C. D. Keating, *J. Phys. Chem. B* **2003**, 107, 7360–7367; b) S. R. Nicewarner-Peña, R. G. Freeman, B. D. Reiss, L. He, D. J. Pena, I. D. Walton, R. Cromer, C. D. Keating, M. J. Natan,

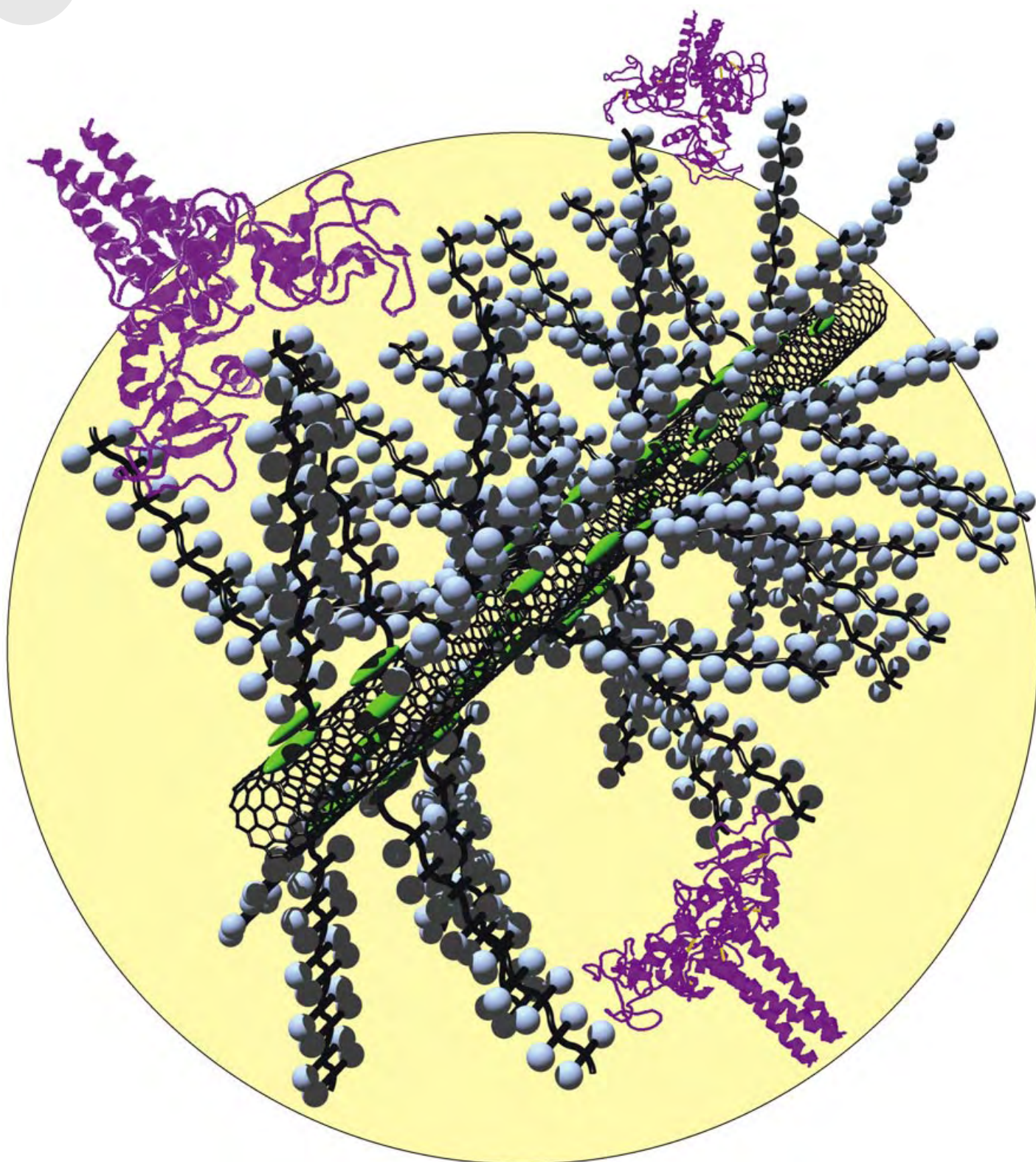
- Science* **2001**, 294, 137–141; c) N. S. Birenbaum, B. T. Lai, C. S. Chen, D. H. Reich, G. J. Meyer, *Langmuir* **2003**, 19, 9580–9582.
- [260] J.-M. Nam, C. S. Thaxton, C. A. Mirkin, *Science* **2003**, 301, 1884–1886.
- [261] D. A. Schultz, *Curr. Opin. Biotechnol.* **2003**, 14, 13–22.
- [262] M. G. Ryadnov, B. Ceyhan, C. M. Niemeyer, D. N. Woolfson, *J. Am. Chem. Soc.* **2003**, 125, 9388–9394.
- [263] S.-F. Cheng, L.-K. Chau, *Anal. Chem.* **2003**, 75, 16–21.
- [264] E. Hutter, M.-P. Pileni, *J. Phys. Chem. B* **2003**, 107, 6497–6499.
- [265] a) A. J. Haes, R. P. Van Duyne, *J. Am. Chem. Soc.* **2002**, 124, 10596–10604; b) J. C. Riboh, A. J. Haes, A. D. McFarland, C. R. Yonzon, R. P. Van Duyne, *J. Phys. Chem. B* **2003**, 107, 1772–1780; c) A. J. Haes, S. Zou, G. C. Schatz, R. P. Van Duyne, *J. Phys. Chem. B* **2004**, 108, 109–116.
- [266] M. Zayats, S. P. Pogorelova, A. B. Kharitonov, O. Lioubashevski, E. Katz, I. Willner, *Chem. Eur. J.* **2003**, 9, 6108–6114.
- [267] a) O. Lioubashevski, V. Chegel, F. Patolsky, E. Katz, I. Willner, *J. Am. Chem. Soc.* **2004**, 126, 7133–7143; b) M. Zayats, A. B. Kharitonov, S. P. Pogorelova, O. Lioubashevski, E. Katz, I. Willner, *J. Am. Chem. Soc.* **2003**, 125, 16006–16014.
- [268] a) H. Kneipp, I. Itzkan, R. R. Dasari, M. S. Feld, *Chem. Rev.* **1999**, 99, 2957–2975; b) A. Campion, P. Kambhampati, *Chem. Soc. Rev.* **1998**, 27, 241–250.
- [269] a) C. D. Keating, K. M. Kovalski, M. J. Natan, *J. Phys. Chem. B* **1998**, 102, 9404–9413. b) C. D. Keating, K. M. Kovalski, M. J. Natan, *J. Phys. Chem. B* **1998**, 102, 9414–9425.
- [270] a) F. T. Docherty, M. Clark, G. McNay, D. Graham, W. E. Smith, *Faraday Discuss.* **2004**, 126, 281–288; b) Y. C. Cao, R. Jin, J.-M. Nam, C. S. Thaxton, C. A. Mirkin, *J. Am. Chem. Soc.* **2003**, 125, 14676–14677; c) K. Faulds, W. E. Smith, D. Graham, *Anal. Chem.* **2004**, 76, 412–417.
- [271] a) D. S. Grubisha, R. J. Lipert, H.-Y. Park, J. Driskell, M. D. Porter, *Anal. Chem.* **2003**, 75, 5936–5943; b) S. Xu, X. Ji, W. Xu, X. Li, L. Wang, Y. Bai, B. Zhao, Y. Ozaki, *Analyst* **2004**, 129, 63–68.
- [272] a) B. M. Lingerfelt, H. Mattoussi, E. R. Goldman, M. Mauro, G. P. Anderson, *Anal. Chem.* **2003**, 75, 4043–4049; b) L.-Y. Wang, L. Wang, F. Gao, Z.-Y. Yu, Z.-M. Wu, *Analyst* **2002**, 127, 977–980; c) L.-Y. Wang, X.-W. Kan, M.-C. Zhang, C.-Q. Zhu, L. Wang, *Analyst* **2002**, 127, 1531–1534; d) L. Wang, L. Wang, C. Zhu, X. W. Wei, X. Kan, *Anal. Chim. Acta* **2002**, 468, 35–41; e) L.-Y. Wang, Y.-Y. Zhou, L. Wang, C.-Q. Zhu, Y.-X. Li, F. Gao, *Anal. Chim. Acta* **2002**, 466, 87–92; f) E. R. Goldman, E. D. Balighian, H. Mattoussi, M. K. Kuno, J. M. Mauro, P. T. Tran, G. P. Anderson, *J. Am. Chem. Soc.* **2002**, 124, 6378–6382; g) D. Gerion, W. J. Parak, S. C. Williams, D. Zanchet, C. M. Micheel, A. P. Alivisatos, *J. Am. Chem. Soc.* **2002**, 124, 7070–7074; h) S. Kim, M. G. Bawendi, *J. Am. Chem. Soc.* **2003**, 125, 14652–14653; i) W. C. W. Chan, S. Nie, *Science* **1998**, 281, 2016–2018.
- [273] J. Malicka, I. Gryczynski, J. R. Lakowicz, *Biochem. Biophys. Res. Commun.* **2003**, 306, 213–218.
- [274] N. Lochner, C. Lobmaier, M. Wirth, A. Leitner, F. Pittner, F. Gabor, *Eur. J. Pharm. Biopharm.* **2003**, 56, 469–477.
- [275] F. Patolsky, R. Gill, Y. Weizmann, T. Mokari, U. Banin, I. Willner, *J. Am. Chem. Soc.* **2003**, 125, 13918–13919.
- [276] A. R. Clapp, I. L. Medintz, J. M. Mauro, B. R. Fisher, M. G. Bawendi, H. Mattoussi, *J. Am. Chem. Soc.* **2004**, 126, 301–310.
- [277] I. L. Medintz, S. A. Trammell, H. Mattoussi, J. M. Mauro, *J. Am. Chem. Soc.* **2004**, 126, 30–31.
- [278] a) X. Zhao, R. Tapeç-Dytioco, W. Tan, *J. Am. Chem. Soc.* **2003**, 125, 11474–11475; b) W. Yang, C. G. Zhang, H. Y. Qu, H. H. Yang, J. G. Xua, *Anal. Chim. Acta* **2004**, 503, 163–169.
- [279] a) *Scientific and Clinical Applications of Magnetic Carriers*, (Eds.: U. Häfeli, W. Schütt, J. Teller, M. Zborowski), Plenum Press, New York, **1997**; b) K. Nishimura, M. Hasegawa, Y. Ogura, T. Nishi, K. Kataoka, H. Handa, M. Abe, *J. Appl. Phys.* **2002**, 91, 8555–8556; c) C. Grüttner, J. Teller, *J. Magn. Magn. Mater.* **1999**, 194, 8–15; d) R. V. Mehta, R. V. Upadhyay, S. W. Charles, C. N. Ramchand, *Biotechnol. Tech.* **1997**, 11, 493–496; e) D. C. F. Chan, D. B. Kirpotin, P. A. Bunn Jr., *J. Magn. Magn. Mater.* **1993**, 122, 374–378; f) R. F. Borch, M. D. Bernstein, H. D. Durst, *J. Am. Chem. Soc.* **1971**, 93, 2897–2898; g) P. M. Dey, *Eur. J. Biochem.* **1984**, 140, 385–390; h) B. A. Schwartz, G. R. Gray, *Arch. Biochem. Biophys.* **1977**, 181, 542–548; i) Q. A. Pankhurst, J. Connolly, S. K. Jones, J. Dobson, *J. Phys. D* **2003**, 36, R167–R181; j) C. C. Berry, A. S. G. Curtis, *J. Phys. D* **2003**, 36, R198–R206; k) J. Ugelstad, P. Stenstad, L. Kilaas, W. S. Prestvik, R. Herje, A. Berge, E. Hornes, *Blood Purif.* **1993**, 11, 349–369; l) M. Uhlén, *Nature* **1989**, 340, 733–744; m) *Advances in Biomagnetic Separation*, (Eds.: M. Uhlén, E. Hornes, O. Olsvik), Eaton, Natick, **1994**; n) M. Shinkai, *J. Biosci. Bioeng.* **2002**, 94, 606–613; o) A. S. Arbab, L. A. Bashaw, B. R. Miller, E. K. Jordan, B. K. Lewis, H. Kalish, J. A. Frank, *Radiology* **2003**, 229, 838–846; p) Y. H. Zhu, X. L. Yang, P. L. Li, H. Ying, *Progr. Chem.* **2003**, 15, 512–517; q) A. M. Koch, F. Reynolds, M. F. Kircher, H. P. Merkle, R. Weissleder, L. Josephson, *Bioconjugate Chem.* **2003**, 14, 1115–1121; r) A. K. Gupta, A. S. G. Curtis, *Biomaterials* **2004**, 25, 3029–3040; s) D. Wang, J. He, N. Rosenzweig, Z. Rosenzweig, *Nano Lett.* **2004**, 4, 409–413; t) A. K. Gupta, C. Berry, M. Gupta, A. Curtis, *IEEE Trans. Nanobioscience* **2003**, 2, 255–261.
- [280] a) F.-H. Wang, T. Yoshitake, D.-K. Kim, M. Muhammed, B. Bjelke, Jan Kehr, *J. Nanopart. Res.* **2003**, 5, 137–146; b) S. Bucak, D. A. Jones, P. E. Laibinis, T. A. Hatton, *Biotechnol. Prog.* **2003**, 19, 477–484.
- [281] a) S. V. Sonti, A. Bose, *J. Colloid Interface Sci.* **1995**, 170, 575–585; b) J. Roger, J. N. Pons, R. Massart, A. Halbreich, J. C. Bacri, *Eur. Phys. J. Appl. Phys.* **1999**, 5, 321–325.
- [282] a) H. Gu, P.-L. Ho, K. W. T. Tsang, C.-W. Yu, B. Xu, *Chem. Commun.* **2003**, 1966–1967; b) H. Gu, P.-L. Ho, K. W. T. Tsang, L. Wang, B. Xu, *J. Am. Chem. Soc.* **2003**, 125, 15702–15703.
- [283] X. Zhao, R. Tapeç-Dytioco, K. Wang, W. Tan, *Anal. Chem.* **2003**, 75, 3476–3483.
- [284] D. L. Graham, H. A. Ferreira, P. P. Freitas, J. M. S. Cabral, *Biosens. Bioelectron.* **2003**, 18, 483–488.
- [285] M. Fang, P. S. Grant, M. J. McShane, G. B. Sukhorukov, V. O. Golub, Y. M. Lvov, *Langmuir* **2002**, 18, 6338–6344.
- [286] J. Hoinville, A. Bewick, D. Gleeson, R. Jones, O. Kasyutich, E. Mayes, A. Nartowski, B. Warne, J. Wiggins, K. Wong, *J. Appl. Phys.* **2003**, 93, 7187–7189.
- [287] L. Shen, P. E. Laibinis, T. A. Hatton, *Langmuir* **1999**, 15, 447–453.
- [288] T. Hyeon, *Chem. Commun.* **2003**, 927–934.
- [289] S. Sun, H. Zeng, *J. Am. Chem. Soc.* **2002**, 124, 8204–8205.
- [290] M. Chen, S. Yamamuro, D. Farrell, S. A. Majetich, *J. Appl. Phys.* **2003**, 93, 7551–7553.
- [291] a) X. Gao, K. M. K. Yu, K. Y. Tam, S. C. Tsang, *Chem. Commun.* **2003**, 2998–2999; b) H.-H. Yang, S.-Q. Zhang, X.-L. Chen, Z.-X. Zhuang, J.-G. Xu, X.-R. Wang, *Anal. Chem.* **2004**, 76, 1316–1321.
- [292] a) T. Tanaka, T. Matsunaga, *Anal. Chem.* **2000**, 72, 3518–3522; b) C. R. Martin, D. T. Mitchell, *Anal. Chem.* **1998**, 70, 322A–327A.
- [293] a) A. Dyal, K. Loos, M. Noto, S. W. Chang, C. Spagnoli, K. V. P. M. Shafi, A. Ulman, M. Cowman, R. A. Gross, *J. Am. Chem. Soc.* **2003**, 125, 1684–1685; b) M. Ma, Y. Zhang, W. Yu, H. Shen, H. Zhang, N. Gu, *Colloids Surf. A* **2003**, 212, 219–226; c) S.-H. Huang, M.-H. Liao, D.-H. Chen, *Biotechnol. Prog.* **2003**, 19, 1095–1100; d) D. Cao, P. He, N. Hu, *Analyst* **2003**, 128, 1268–1274.

- [294] a) M. Shinkai, H. Honda, T. Kobayashi, *Biocatalysis* **1991**, 5, 61–69; b) M.-H. Liao, D.-H. Chen, *Biotechnol. Lett.* **2001**, 23, 1723–1727.
- [295] M.-H. Liao, D.-H. Chen, *Biotechnol. Lett.* **2002**, 24, 1913–1917.
- [296] S. Mornet, A. Vekris, J. Bonnet, E. Duguet, F. Grasset, J.-H. Choy, J. Portier, *Mater. Lett.* **2000**, 42, 183–188.
- [297] L. E. Euliss, S. G. Grancharov, S. O'Brien, T. J. Deming, G. D. Stucky, C. B. Murray, G. A. Held, *Nano Lett.* **2003**, 3, 1489–1493.
- [298] a) *Biomimetic Materials Chemistry* (Ed.: S. Mann), VCH Publishers, New York, **1996**; b) Focus article, *Chem. Commun.* **2004**, 1–4.
- [299] a) F. C. Meldrum, V. J. Wade, D. L. Nimmo, B. R. Heywood, S. Mann, *Nature* **1991**, 349, 684–687; b) F. C. Meldrum, B. R. Heywood, S. Mann, *Science* **1992**, 257, 522–523; c) T. Douglas, V. T. Stark, *Inorg. Chem.* **2000**, 39, 1828–1830; d) T. Douglas, M. Young, *Nature* **1998**, 393, 152–155; e) T. Douglas, M. Young, *Adv. Mater.* **1999**, 11, 679–681; f) C. E. Flynn, S.-W. Lee, B. R. Peelle, A. M. Belcher, *Acta Mater.* **2003**, 51, 5867–5880; g) M. L. Flenniken, D. A. Willits, S. Brumfield, M. J. Young, T. Douglas, *Nano Lett.* **2003**, 3, 1573–1576.
- [300] S. Mann, F. C. Meldrum, *Adv. Mater.* **1991**, 3, 316–318.
- [301] D. P. E. Dickson, S. A. Walton, S. Mann, K. Wong, *Nanostruct. Mater.* **1997**, 9, 595–598.
- [302] K. K. W. Wong, T. Douglas, S. Gider, D. D. Awschalom, S. Mann, *Chem. Mater.* **1998**, 10, 279–285.
- [303] a) K. C. Martin, S. M. Villano, P. R. McCurdy, D. C. Zapien, *Langmuir* **2003**, 19, 5808–5812; b) M. Tominaga, I. Taniguchi, *Chem. Lett.* **2003**, 954–955; c) F. Marken, D. Patel, C. E. Madden, R. C. Millward, S. Fletcher, *New J. Chem.* **2002**, 26, 259–263.
- [304] M. Allen, D. Willits, J. Mosolf, M. Young, T. Douglas, *Adv. Mater.* **2002**, 14, 1562–1565.
- [305] a) M. Bozzi, G. Mignogna, S. Stefanini, D. Barra, C. Longhi, P. Valenti, E. Chiancone, *J. Biol. Chem.* **1997**, 272, 3259–3265; b) A. Ilari, S. Stefanini, E. Chiancone, D. Tsernoglou, *Nat. Struct. Biochem. J.* **2000**, 7, 38–43.
- [306] a) S. Stefanini, S. Cavallo, B. Montagnini, E. Chiancone, *Biochem. J.* **1999**, 338, 71–75; b) X. Yang, E. Chiancone, S. Stefanini, A. Ilari, N. D. Chasteen, *Biochem. J.* **2000**, 349, 783–786.
- [307] T. Douglas, E. Strable, D. Willits, A. Aitouchen, M. Libera, M. Young, *Adv. Mater.* **2002**, 14, 415–418.
- [308] E. Bäuerlein, *Angew. Chem.* **2003**, 115, 636–664; *Angew. Chem. Int. Ed.* **2003**, 42, 614–641.
- [309] R. P. Blakemore, D. Maratea, R. S. Wolfe, *J. Bacteriol.* **1979**, 140, 720–729.
- [310] T. Matsunaga, F. Tadokoro, N. Nakamura, *IEEE Trans. Magn.* **1990**, 26, 1557–1559.
- [311] T. Matsunaga, T. Sakaguchi, F. Tadokoro, *Appl. Microbiol. Biotechnol.* **1991**, 35, 651–655.
- [312] K. H. Scheifer, D. Schuler, S. Spring, M. Weizenegger, R. Amann, W. Ludwig, M. Kohler, *Syst. Appl. Microbiol.* **1991**, 14, 379–385.
- [313] a) Y. A. Gorby, T. J. Beveridge, R. P. Blakemore, *J. Bacteriol.* **1988**, 170, 834–841; b) T. Matsunaga, *Trends Biotechnol.* **1991**, 9, 91–95.
- [314] T. Matsunaga, H. Takeyama, *Supramol. Sci.* **1998**, 5, 391–394.
- [315] a) N. Nakamura, K. Hashimoto, T. Matsunaga, *Anal. Chem.* **1991**, 63, 268–272; b) N. Nakamura, J. G. Burgess, K. Yagiuda, S. Kudo, T. Sakaguchi, T. Matsunaga, *Anal. Chem.* **1993**, 65, 2036–2039; c) N. Nakamura, T. Matsunaga, *Anal. Chim. Acta* **1993**, 281, 585–589.
- [316] T. Matsunaga, M. Kawasaki, X. Yu, N. Tsujimura, N. Nakamura, *Anal. Chem.* **1996**, 68, 3551–3554.
- [317] K. Sode, S. Kudo, T. Sakaguchi, N. Nakamura, T. Matsunaga, *Biotechnol. Tech.* **1993**, 7, 688–694.
- [318] H. Takeyama, A. Yamazawa, N. Nakamura, T. Matsunaga, *Biotechnol. Tech.* **1995**, 9, 355–360.
- [319] a) J. Li, X. He, Z. Wu, K. Wang, G. Shen, R. Yu, *Anal. Chim. Acta* **2003**, 481, 191–198; b) V. Kourilov, M. Steinitz, *Anal. Biochem.* **2002**, 311, 166–170; c) Tadashi Matsunaga, F. Ueki, K. Obata, H. Tajima, T. Tanaka, H. Takeyama, Y. Goda, S. Fujimoto, *Anal. Chim. Acta* **2003**, 475, 75–83; d) H. Furukawa, R. Shimojyo, N. Ohnishi, H. Fukuda, A. Kondo, *Appl. Microbiol. Biotechnol.* **2003**, 62, 478–483.
- [320] R. Wilson, *Chem. Commun.* **2003**, 108–109.
- [321] Z.-L. Zhi, Y. Murakami, Y. Morita, Q. Hasan, E. Tamiya, *Anal. Biochem.* **2003**, 318, 236–243.
- [322] J. M. Perez, F. J. Simeone, Y. Saeki, L. Josephson, R. Weisleder, *J. Am. Chem. Soc.* **2003**, 125, 10192–10193.
- [323] J. Wang, A.-N. Kawde, A. Erdem, M. Salazar, *Analyst* **2001**, 126, 2020–2024.
- [324] J. Wang, A.-N. Kawde, *Electrochem. Commun.* **2002**, 4, 349–352.
- [325] J. Wang, D. Xu, R. Polsky, *J. Am. Chem. Soc.* **2002**, 124, 4208–4209.
- [326] H. Cai, Y. Wang, P. He, Y. Fang, *Anal. Chim. Acta* **2002**, 469, 165–172.
- [327] J. Wang, G. Liu, A. Merkoçi, *Anal. Chim. Acta* **2003**, 482, 149–155.
- [328] T. Yoshino, T. Tanaka, H. Takeyama, T. Matsunaga, *Biosens. Bioelectron.* **2003**, 18, 661–666.
- [329] a) R. Hirsch, E. Katz, I. Willner, *J. Am. Chem. Soc.* **2000**, 122, 12053–12054; b) E. Katz, L. Sheeney-Haj-ichia, I. Willner, *Chem. Eur. J.* **2002**, 8, 4138–4148.
- [330] I. Willner, E. Katz, *Angew. Chem.* **2003**, 115, 4724–4737; *Angew. Chem. Int. Ed.* **2003**, 42, 4576–4588.
- [331] a) E. Katz, T. Lötzbeyer, D. D. Schlereth, W. Schuhmann, H.-L. Schmidt, *J. Electroanal. Chem.* **1994**, 373, 189–200; b) I. Willner, A. Riklin, *Anal. Chem.* **1994**, 66, 1535–1539.
- [332] a) A. Bardea, E. Katz, A. F. Bückmann, I. Willner, *J. Am. Chem. Soc.* **1997**, 119, 9114–9119; b) M. Zayats, E. Katz, I. Willner, *J. Am. Chem. Soc.* **2002**, 124, 14724–14735.
- [333] A. F. Bückmann, V. Wray, *Biotechnol. Appl. Biochem.* **1992**, 15, 303–310.
- [334] E. Katz, L. Sheeney-Haj Ichia, A. F. Bückmann, I. Willner, *Angew. Chem.* **2002**, 114, 1399–1402; *Angew. Chem. Int. Ed.* **2002**, 41, 1343–1346.
- [335] E. Katz, I. Willner, *J. Am. Chem. Soc.* **2002**, 124, 10290–10291.
- [336] A. J. Bard, L. R. Faulkner, *Electrochemical Methods: Fundamentals and Applications*, Wiley, New York, **1980**.
- [337] Y. Weizmann, F. Patolsky, E. Katz, I. Willner, *J. Am. Chem. Soc.* **2003**, 125, 3452–3454.
- [338] F. Patolsky, Y. Weizmann, E. Katz, I. Willner, *Angew. Chem.* **2003**, 115, 2474–2478; *Angew. Chem. Int. Ed.* **2003**, 42, 2372–2376.
- [339] F. Patolsky, Y. Weizmann, E. Katz, I. Willner, *ChemBioChem* **2004**, 5, 943–948.
- [340] a) R. Raiteri, M. Grattarola, H. J. Butt, P. Skládal, *Sens. Actuators B* **2001**, 79, 115–126; b) M. Sepaniak, P. Datskos, N. Lavrik, C. Tipple, *Anal. Chem.* **2002**, 74, 568A–575A.
- [341] M. Lahav, C. Durkan, R. Gabai, E. Katz, I. Willner, M. E. Welland, *Angew. Chem.* **2001**, 113, 4219–4221; *Angew. Chem. Int. Ed.* **2001**, 40, 4095–4098.
- [342] J. Fritz, M. K. Baller, H. P. Lang, H. Rothuizen, P. Vettinger, E. Meyer, H.-J. Güntherodt, C. Gerber, J. K. Gimzewski, *Science* **2000**, 288, 316–318.
- [343] R. P. Cowburn, A. M. Moulin, M. E. Welland, *Appl. Phys. Lett.* **1997**, 71, 2202–2204.
- [344] E. Paleček, S. Billová, L. Havran, R. Kizwek, A. Mičulková, F. Jelen, *Talanta* **2002**, 56, 919–930.
- [345] Y. Weizmann, F. Patolsky, O. Lioubashevski, I. Willner, *J. Am. Chem. Soc.* **2004**, 126, 1073–1080.

- [346] N. I. Kovtyukhova, T. E. Mallouk, *Chem. Eur. J.* **2002**, *8*, 4354–4363.
- [347] W. E. Ford, O. Harnack, A. Yasuda, J. M. Wessels, *Adv. Mater.* **2001**, *13*, 1793–1797.
- [348] W. Shenton, T. Douglas, M. Young, G. Stubbs, S. Mann, *Adv. Mater.* **1999**, *11*, 253–256.
- [349] S. R. Hall, W. Shenton, H. Engelhardt, S. Mann, *ChemPhys-Chem* **2001**, *2*, 184–186.
- [350] M. Pazirandeh, S. Baral, J. Cambell, *Biomimetics* **1992**, *1*, 41–47.
- [351] a) R. Kirsch, M. Mertig, W. Pompe, R. Wahl, G. Sadowski, K. J. Böhm, E. Unger, *Thin Solid Films* **1997**, *305*, 248–253; b) M. Mertig, R. Kirsch, W. Pompe, *Appl. Phys. A* **1998**, *66*, S723–S727; c) W. Fritzsche, K. J. Böhm, E. Unger, J. M. Köhler, *Appl. Phys. Lett.* **1999**, *75*, 2854–2856.
- [352] E. Unger, K.-J. Böhm, W. Vater, *Electron Microsc. Rev.* **1990**, *3*, 355–395.
- [353] S. Behrens, K. Rahn, W. Habicht, K.-J. Böhm, H. Rösner, E. Dinjus, E. Unger, *Adv. Mater.* **2002**, *14*, 1621–1625.
- [354] a) M. Sára, U. B. Sleytr, *J. Bacteriol.* **2000**, *182*, 859–868; b) U. B. Sleytr, P. Messner, D. Pum, M. Sára, *Angew. Chem.* **1999**, *111*, 1098–1120; *Angew. Chem. Int. Ed.* **1999**, *38*, 1034–1054; c) E. S. Györfvay, A. O’Riordan, A. J. Quinn, G. Redmond, D. Pum, U. B. Sleytr, *Nano Lett.* **2003**, *3*, 315–319; d) U. B. Sleytr, M. Sára, D. Pum, B. Schuster, *Prog. Surf. Sci.* **2001**, *68*, 231–278; e) D. Pum, U. B. Sleytr, *Trends Biotechnol.* **1999**, *17*, 8–12.
- [355] M. Rechtes, E. Gazit, *Science* **2003**, *300*, 625–627.
- [356] B. Yang, S. Kamiya, K. Yoshida, T. Shimizu, *Chem. Commun.* **2004**, 500–501.
- [357] Y. Xia, G. M. Whitesides, *Angew. Chem.* **1998**, *110*, 568–594; *Angew. Chem. Int. Ed.* **1998**, *37*, 550–575.
- [358] a) R. Djalali, Y. Chen, H. Matsui, *J. Am. Chem. Soc.* **2002**, *124*, 13660–13661; b) R. Djalali, Y. Chen, H. Matsui, *J. Am. Chem. Soc.* **2003**, *125*, 5873–5879; c) L. Yu, I. A. Banerjee, H. Matsui, *J. Am. Chem. Soc.* **2003**, *125*, 14837–14840.
- [359] a) H. Matsui, B. Gologan, *J. Phys. Chem. B* **2000**, *104*, 3383–3386; b) T. Shimizu, M. Kogiso, M. Masuda, *Nature* **1996**, *383*, 487–488; c) M. Kogiso, S. Ohnishi, K. Yase, M. Masuda, T. Shimizu, *Langmuir* **1998**, *14*, 4978–4986; d) T. Shimizu, M. Kogiso, M. Masuda, *J. Am. Chem. Soc.* **1997**, *119*, 6209–6210.
- [360] J. M. Slocik, J. T. Moore, D. W. Wright, *Nano Lett.* **2002**, *2*, 169–173.
- [361] T. Scheibel, R. Parthasarathy, G. Sawicki, X.-M. Lin, H. Jaeger, S. L. Lindquist, *Proc. Natl. Acad. Sci. USA* **2003**, *100*, 4527–4532.
- [362] I. A. Banerjee, L. Yu, H. Matsui, *Nano Lett.* **2003**, *3*, 283–287.
- [363] a) R. D. Vale, *J. Cell Biol.* **2003**, *163*, 445–450; b) C. G. dos Remedios, P. D. J. Moens, *Biochim. Biophys. Acta* **1995**, *1228*, 99–124.
- [364] F. Patolsky, Y. Weizmann, I. Willner, *Nat. Mater.* **2004**, *3*, 692–695.
- [365] a) N. C. Seeman, *Acc. Chem. Res.* **1997**, *30*, 357–363; b) N. C. Seeman, *Angew. Chem.* **1998**, *110*, 3408–3428; *Angew. Chem. Int. Ed.* **1998**, *37*, 3220–3238; c) X. Yang, L. A. Wenzler, J. Qi, X. Li, N. C. Seeman, *J. Am. Chem. Soc.* **1998**, *120*, 9779–9786; d) J. Wengel, *Org. Biomol. Chem.* **2004**, *2*, 277–280; e) D. Liu, M. Wang, Z. Deng, R. Walulu, C. Mao, *J. Am. Chem. Soc.* **2004**, *126*, 2324–2325.
- [366] D. Zanchet, C. M. Micheel, W. J. Parak, D. Gerion, A. P. Alivisatos, *Nano Lett.* **2001**, *1*, 32–35.
- [367] a) Y. Liu, W. Meyer-Zaika, S. Franzka, G. Schmid, M. Tsoli, H. Kuhn, *Angew. Chem.* **2003**, *115*, 2959–2963; *Angew. Chem. Int. Ed.* **2003**, *42*, 2853–2857; b) G. Wang, R. W. Murray, *Nano Lett.* **2004**, *4*, 95–101.
- [368] O. Harnack, W. E. Ford, A. Yasuda, J. M. Wessels, *Nano Lett.* **2002**, *2*, 919–923.
- [369] a) S. O. Kelley, J. K. Barton, *Science* **1999**, *283*, 375–381; b) M. Ratner, *Nature* **1999**, *397*, 480–481.
- [370] Y. Asai, *J. Phys. Chem. B* **2003**, *107*, 4647–4652.
- [371] a) T. Carell, C. Behrens, J. Gierlich, *Org. Biomol. Chem.* **2003**, *1*, 2221–2228; b) D. Hennig, J. F. R. Archilla, J. Agarwal, *Physica D* **2003**, *180*, 256–272; c) M. A. O’Neill, H.-C. Becker, C. Wan, J. K. Barton, A. H. Zewail, *Angew. Chem.* **2003**, *115*, 6076–6080; *Angew. Chem. Int. Ed.* **2003**, *42*, 5896–5900.
- [372] a) D. D. Eley, R. B. Leslie, *Nature* **1963**, *197*, 898–899; b) H.-W. Fink, C. Schönenberger, *Nature* **1999**, *398*, 407–410.
- [373] a) P. Tran, B. Alavi, G. Gruner, *Phys. Rev. Lett.* **2000**, *85*, 1564–1567; b) L. T. Cai, H. Tabata, T. Kawai, *Appl. Phys. Lett.* **2000**, *77*, 3105–3106; c) Y. Okahata, T. Kobayashi, K. Tanaka, M. Shimomura, *J. Am. Chem. Soc.* **1998**, *120*, 6165–6166.
- [374] a) P. J. de Pablo, F. Moreno-Herrero, J. Colchero, J. Gómez-Herrero, P. Herrero, A. M. Baró, P. Ordejón, J. M. Soler, E. Artacho, *Phys. Rev. Lett.* **2000**, *85*, 4992–4995; b) M. Bockrath, N. Markovic, A. Shepard, M. Tinkham, L. Gurevich, L. P. Kouwenhoven, M. W. Wu, L. L. Sohn, *Nano Lett.* **2002**, *2*, 187–190; c) A. J. Storm, J. van Noort, S. de Vries, C. Dekker, *Appl. Phys. Lett.* **2001**, *79*, 3881–3883.
- [375] C. F. Monson, A. T. Woolley, *Nano Lett.* **2003**, *3*, 359–363.
- [376] F. Patolsky, Y. Weizmann, O. Lioubashevski, I. Willner, *Angew. Chem.* **2002**, *114*, 2429–2433; *Angew. Chem. Int. Ed.* **2002**, *41*, 2323–2327.
- [377] T. Yonezawa, S. Onoue, N. Kimizuka, *Chem. Lett.* **2002**, 1172–1173.
- [378] H. Nakao, H. Shiigi, Y. Yamamoto, S. Tokonami, T. Nagaoka, S. Sugiyama, T. Ohtani, *Nano Lett.* **2003**, *3*, 1391–1394.
- [379] R. J. Preston, *Radiat. Res.* **1997**, *147*, 529–534.
- [380] a) M. A. Blasco, *Eur. J. Cell Biol.* **2003**, *82*, 441–446; b) P. J. Perry, J. R. P. Arnold, T. C. Jenkins, *Expert Opin. Invest. Drugs* **2001**, *10*, 2141–2156.
- [381] C. Testorelli, *J. Exp. Clin. Cancer Res.* **2003**, *22*, 165–169.
- [382] Y. Weizmann, F. Patolsky, I. Popov, I. Willner, *Nano Lett.* **2004**, *4*, 787–792.
- [383] a) J. Richter, M. Mertig, W. Pompe, I. Mönch, H. K. Schackert, *Appl. Phys. Lett.* **2001**, *78*, 536–538; b) R. Hölzel, N. Gajovic-Eichelmann, F. F. Bier, *Biosens. Bioelectron.* **2003**, *18*, 555–564.
- [384] K. Keren, M. Krueger, R. Gilad, G. Ben-Yoseph, U. Sivan, E. Braun, *Science* **2002**, *297*, 72–75.
- [385] K. Keren, R. S. Berman, E. Braun, *Nano Lett.* **2004**, *4*, 323–326.
- [386] Z. Deng, C. Mao, *Nano Lett.* **2003**, *3*, 1545–1548.
- [387] J. Hu, Y. Zhang, H. Gao, M. Li, U. Hartmann, *Nano Lett.* **2002**, *2*, 55–57.
- [388] H. Yan, S. H. Park, G. Finkelstein, J. H. Reif, T. H. LaBean, *Science* **2003**, *301*, 1882–1884.
- [389] H. Li, S. H. Park, J. H. Reif, T. H. LaBean, H. Yan, *J. Am. Chem. Soc.* **2004**, *126*, 418–419.
- [390] a) Z. Dogic, S. Fraden, *Phys. Rev. Lett.* **1997**, *78*, 2417–2420; b) Z. Dogic, S. Fraden, *Langmuir* **2000**, *16*, 7820–7824.
- [391] S.-W. Lee, C. Mao, C. E. Flynn, A. M. Belcher, *Science* **2002**, *296*, 892–895.
- [392] a) S.-W. Lee, S. Kwan, A. M. Belcher, *Adv. Mater.* **2003**, *15*, 689–692; b) C. Mao, D. J. Solis, B. D. Reiss, S. T. Kottmann, R. Y. Sweeney, A. Hayhurst, G. Georgiou, B. Iverson, A. M. Belcher, *Science* **2004**, *303*, 213–217.
- [393] a) E. Dujardin, C. Peet, G. Stubbs, J. N. Culver, S. Mann, *Nano Lett.* **2003**, *3*, 413–417; b) M. Knez, M. Sumser, A. M. Bittner, C. Wege, H. Jeske, T. P. Martin, K. Kern, *Adv. Funct. Mater.* **2004**, *14*, 116–124; c) A. S. Blum, C. M. Soto, C. D. Wilson, J. D. Cole, M. Kim, B. Gnade, A. Chatterji, W. F. Ochoa, T. Lin, J. E. Johnson, B. R. Ratna, *Nano Lett.* **2004**, *4*, 867–870.
- [394] M. Knez, A. M. Bittner, F. Boes, C. Wege, H. Jeske, E. Mai, K. Kern, *Nano Lett.* **2003**, *3*, 1079–1082.
- [395] Y. Cui, Q. Wei, H. Park, C. M. Lieber, *Science* **2001**, *293*, 1289–1292.

- [396] a) R. J. Chen, S. Bangsaruntip, K. A. Drouvalakis, N. W. S. Kam, M. Shim, Y. Li, W. Kim, P. J. Utz, H. Dai, *Proc. Natl. Acad. Sci. USA* **2003**, *100*, 4984–4989; b) A. Star, J.-C. P. Gabriel, K. Bradley, G. Gruner, *Nano Lett.* **2003**, *3*, 459–463.
- [397] a) J. Hahn, C. M. Lieber, *Nano Lett.* **2004**, *4*, 51–54; b) Z. Li, Y. Chen, X. Li, T. I. Kamins, K. Nauka, R. S. Williams, *Nano Lett.* **2004**, *4*, 245–247.
- [398] G. D. Bachand, S. B. Rivera, A. K. Boal, J. Gaudioso, J. Liu, B. C. Bunker, *Nano Lett.* **2004**, *4*, 817–821.
- [399] a) C. Grogan, R. Raiteri, G. M. O'Connor, T. J. Glynn, V. Cunningham, M. Kane, M. Charlton, D. Leech, *Biosens. Bioelectron.* **2002**, *17*, 201–207; b) D. P. Allison, P. Hinterdorfer, W. H. Han, *Curr. Opin. Biotechnol.* **2002**, *13*, 47–51; c) G. H. Wu, R. H. Datar, K. M. Hansen, T. Thundat, R. J. Cote, A. Majumdar, *Nat. Biotechnol.* **2001**, *19*, 856–860.
- [400] a) H. Clausen-Schaumann, M. Rief, M. Seitz, *ChemPhysChem* **2000**, *1*, 89–92; b) K. M. Hansen, H.-F. Ji, G. H. Wu, R. Datar, R. Cote, A. Majumdar, T. Thundat, *Anal. Chem.* **2001**, *73*, 1567–1571.
- [401] A. M. Rawlett, T. J. Hopson, I. Amlani, R. Zhang, J. Tresek, L. A. Nagahara, R. K. Tsui, H. Goronkin, *Nanotechnology* **2003**, *14*, 377–384.
- [402] W. Fritzsche, T. A. Taton, *Nanotechnology* **2003**, *14*, R63–R73.
- [403] R. Möller, A. Csaki, W. Fritzsche, *Tech. Mess.* **2003**, *70*, 582–584.
- [404] A. C. S. Samia, X. Chen, C. Burda, *J. Am. Chem. Soc.* **2003**, *125*, 15736–15737.
- [405] P. R. Lockman, M. O. Oyewumi, J. M. Koziara, K. E. Roder, R. J. Mumper, D. D. Allen, *J. Controlled Release* **2003**, *93*, 271–282.
- [406] T. M. Allen, P. R. Cullis, *Science* **2004**, *303*, 1818–1822.
- [407] a) A. K. Salem, P. C. Searson, K. W. Leong, *Nat. Mater.* **2003**, *2*, 668–671; b) Z. R. Cui, R. J. Mumper, *Crit. Rev. Ther. Drug Carrier Syst.* **2003**, *20*, 103–137; c) D. Luo, E. Han, N. Belcheva, W. M. Saltzman, *J. Controlled Release* **2004**, *95*, 333–341.
- [408] A. D. Miller, *ChemBioChem* **2004**, *5*, 53–54.
- [409] A. A. G. Requicha, *Proc. IEEE* **2003**, *91*, 1922–1933.
- [410] a) H. J. De los Santos, *Proc. IEEE* **2003**, *91*, 1907–1921; b) M. Forshaw, R. Stadler, D. Crawley, K. Nikolic, *Nanotechnology* **2004**, *15*, S220–S223.
- [411] M. Sarikaya, C. Tamerler, A. K. Y. Jen, K. Schulten, F. Baneyx, *Nat. Mater.* **2003**, *2*, 577–585.

Communications



Carbohydrate-functionalized polymers designed to mimic the structures of mucin glycoproteins assembled on carbon nanotubes are water soluble and can be functionalized with ligands for specific receptor binding. For more information see the Communication by A. Zettl, C. R. Bertozzi et al. on the following pages.

Biomimetic Synthesis

Biomimetic Engineering of Carbon Nanotubes by Using Cell Surface Mucin Mimics**

Xing Chen, Goo Soo Lee, A. Zettl,* and Carolyn R. Bertozzi*

One of the most exciting applications of nanoscale science and technology is in the exploration of biological systems.^[1] Carbon nanotubes (CNTs) have unique structural, mechanical, and electrical properties, and consequently numerous potential applications in biology, including sensing,^[2] imaging,^[3] and scaffolding for cell growth.^[4] Few of these applications have yet been realized, however, because of the incompatibility of the CNT surface, which is hydrophobic and prone to nonspecific bioadsorption, with biological components such as cells and proteins. In addition, the aqueous environment required for biological materials are not suitable for unfunctionalized CNTs.^[5] In nature, cells are faced with a similar challenge of resisting nonspecific biomolecule interactions while engaging in specific molecular recognition. These functions can be simultaneously fulfilled by mucin glycoproteins, defined by their dense clusters of O-linked glycans. Here we describe a biomimetic surface modification of CNTs using glycosylated polymers designed to mimic natural cell-surface mucins. CNTs modified with mucin mimics were soluble in water, resisted nonspecific protein binding, and bound specifically to biomolecules through receptor–ligand interactions. This strategy for biomimetic surface engineering provides a means to bridge nanomaterials and biological systems.

Mucins coat the surfaces of numerous cell types^[6] and present epitopes for receptor-mediated cell–cell recogni-

tion.^[7] Their dense glycosylation confers rigidity to the polypeptide backbone and thereby extends the mucin polymer well above the cell surface.^[8] In addition, the glycans provide for strong hydration and passivation against biofouling. We have recently developed glycosylated polymers that share many properties with natural mucins (Figure 1 a).^[9] In native mucins, the clustered α -N-acetylgalactosamine (α -GalNAc) residues proximal to the peptide are the major contributors to the rigidification of peptide backbones. Although the core α -GalNAc residue is usually elaborated with additional sugars, removal of those sugars does not affect the mucin architecture.^[10] The importance of the α -GalNAc residue for mucin structure has also been suggested by NMR analysis of synthetic glycopeptides.^[11] Accordingly, we designed a synthetically tractable mucin mimic in which α -GalNAc residues were linked through an oxime bond to a poly(methyl vinyl ketone) [poly(MVK)] backbone (Figure 1 a). The synthesis involved chemoselective ligation of poly(MVK) with an aminoxy-functionalized GalNAc analogue.^[12] Light-scattering analysis indicated that the α -GalNAc-conjugated polymers adopt a rigid extended structure in water, similar to native mucin, whereas the unconjugated polymers adopt a more conventional globular structure.^[9]

We introduced a C_{18} lipid at one end of a mucin mimic polymer with a molecular weight of about 75000 g mol^{-1} to enable surface modification of CNTs (Figure 1 b; see Supporting Information for synthetic details). The hydrated diameter of the lipid-terminated mucin mimic was determined by light-scattering analysis to be about 54 nm. Lipids are known to self-assemble on the surface of CNTs through hydrophobic interactions in the presence of water^[13] and lipid-functionalized glycopolymers have been shown to form ordered arrays on graphite surfaces.^[14] We envisioned that lipid-functionalized mucin mimics could assemble on CNTs in a similar manner as the organization of native mucins in the cell membrane, with the glycosylated polymers projecting into the aqueous medium (Figure 1 c).

We first subjected single-walled carbon nanotubes (SWNTs) to ultrasonication in the presence of an aqueous solution of the C_{18} -functionalized mucin mimic bearing α -GalNAc residues (C_{18} - α -MM, Figure 1 b). The SWNTs were fully solubilized during the procedure (Figure 2 a), which suggests the formation of a hydrophilic surface coating. A similar procedure was applied to multiwalled carbon nanotubes (MWNTs) with the same outcome (Figure 2 c). The suspensions of C_{18} - α -MM-functionalized CNTs were stable for more than three months, while unfunctionalized CNTs precipitated very quickly (within hours) in aqueous solutions (Figure 2 b and d). The C_{18} lipid on the mucin mimic polymer was essential to solubilize the CNTs: they rapidly precipitated from solutions of polymers identical to the above mucin mimics but lacking the lipid tail (not shown). These observations are consistent with a model in which C_{18} - α -MMs coat the CNTs as shown in Figure 1 c.

The CNTs coated with mucin mimics (C_{18} - α -MM-SWNTs, for example) were directly characterized by atomic force microscopy (AFM), scanning electron microscopy (SEM), and transmission electron microscopy (TEM). As produced,

[*] Prof. A. Zettl

Department of Physics
University of California and Materials Sciences Division
Lawrence Berkeley National Laboratory
Berkeley, CA 94720 (USA)
Fax: (+1) 510-643-8497
E-mail: azettl@socrates.berkeley.edu

Prof. C. R. Bertozzi

Departments of Chemistry and Molecular and Cell Biology, and
Howard Hughes Medical Institute
University of California, and
Materials Sciences Division, Lawrence Berkeley National Laboratory
Berkeley, CA 94720 (USA)
Fax: (+1) 510-643-2628
E-mail: crb@berkeley.edu

X. Chen, Dr. G. S. Lee

Department of Chemistry, University of California and Materials
Sciences Division, Lawrence Berkeley National Laboratory
Berkeley, CA 94720 (USA)

[**] The authors thank N. Bodzin for assistance with graphics as well as W. Han and R. Zalpuri for help with TEM experiments. This work was supported by the Director, Office of Energy Research, Office of Basic Energy Sciences, Division of Materials Sciences, of the US Department of Energy under Contract No. DE-AC03-76SF00098, within the Interfacing Nanostructures Initiative.

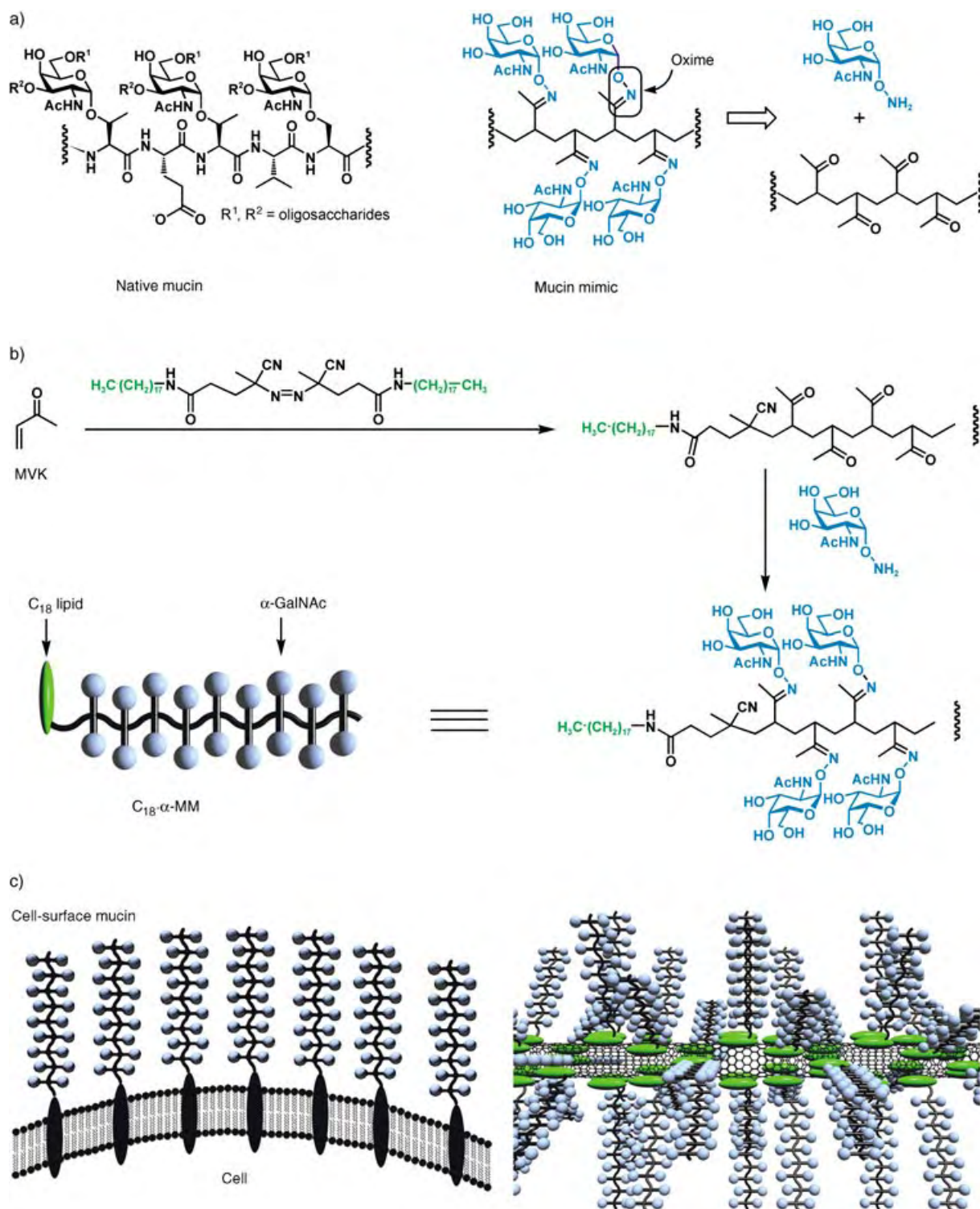


Figure 1. a) The structural features of native mucin (left) as well as the designed and synthesized mucin mimic (right). Natural mucins are characterized by dense clusters of O-linked glycans bound to Ser/Thr residues of the polypeptide. The α -GalNAc residues attached to the Ser/Thr residues are elaborated with additional sugars but only the initial GalNAc residues are required for the mucin structure. b) Synthesis of C_{18} - α -MM. The C_{18} lipid was conjugated to 4,4'-azobis(4-cyanopentanoic acid) (ACPA) and the amide-linked product was used to initiate radical polymerization of MVK to produce C_{18} -poly(MVK). C_{18} - α -MM was obtained by chemoselective ligation of C_{18} -poly(MVK) with aminoxy-GalNAc. c) A model for the self-assembly of C_{18} -MMs on the surface of carbon nanotubes (right), which is similar to the proposed arrangement of cell-surface mucins (left).

SWNTs usually exist as bundles that are heavily entangled with one another to form three-dimensional (3D) networks.

After functionalization with C₁₈- α -MM, the entangled SWNT bundles dissociate to form much finer bundles and even

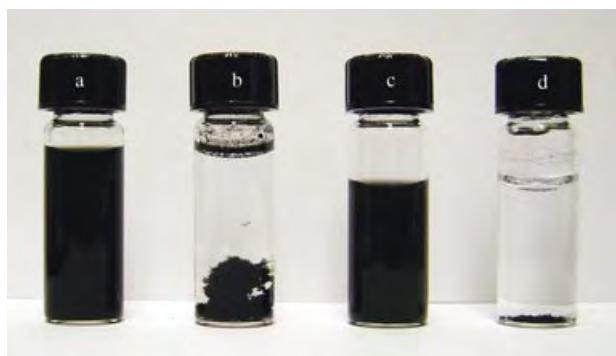


Figure 2. Photographs of vials containing a) a stable suspension of C_{18} - α -MM-SWNTs in H_2O after more than three months, b) as-produced SWNTs in H_2O , which precipitate in several hours, c) stable suspension of C_{18} - α -MM-MWNTs in H_2O after more than three months, d) as-produced MWNTs in H_2O , which precipitate over several hours.

individual nanotubes, as observed by all three imaging techniques. AFM permitted analysis of the modified tubes at ambient pressure and in an hydrated form, which is important for maintaining the structure of the mucin coating. As shown in Figure 3a, tapping mode AFM images on a silicon substrate revealed C_{18} - α -MM-SWNTs with fairly uniform diameters of 65–70 nm. The idealized model shown in Figure 1c would predict a diameter on the order of 100 nm,

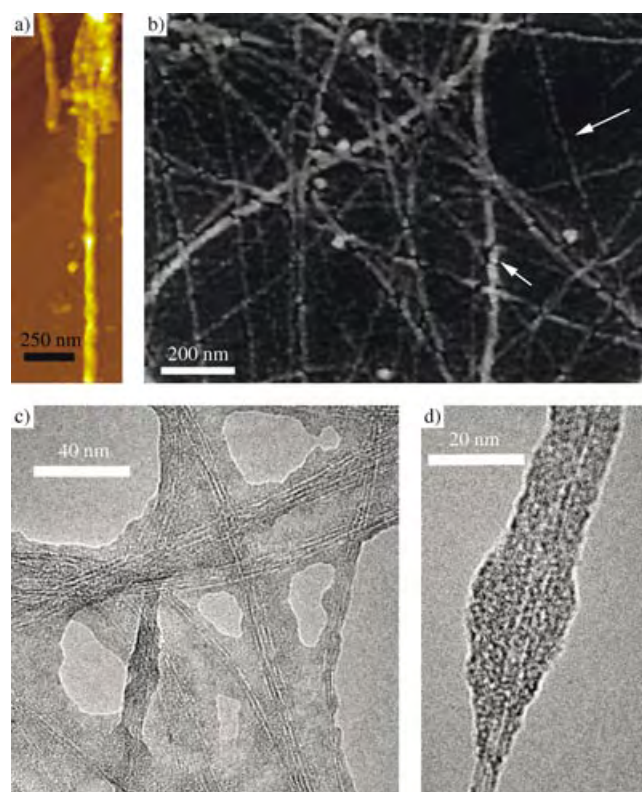


Figure 3. a) Tapping mode AFM image of C_{18} - α -MM-SWNTs on a silicon substrate. b) SEM image of C_{18} - α -MM-SWNTs. The arrows indicate damaged regions of the mucin mimic coating caused by the electron beam. c), d) TEM images of C_{18} - α -MM-SWNTs stained with 0.5 % methylamine vanadate.

roughly twice that of the polymer mimicking the mucin (the SWNT itself is only ca. 2 nm in diameter). However, distortions to the soft mucin coating imposed by the AFM tip or substrate, or a nonperpendicular angle of projection of the mucin polymer from the SWNT surface could account for the discrepancy.

SEM analysis of C_{18} - α -MM-SWNTs also provided evidence of the mucin coating. Exposure of the sample to the 5-keV electron beam led to visible sites of damage along the SWNT surface, as indicated by the arrows in Figure 3b. This result was expected based on the sensitivity of organic species to decomposition induced by an electron beam. The damage induced by the electron beam increased with longer exposure times, and culminated in near-complete destruction of the coating after 15 minutes (see the Supporting Information). By contrast, unmodified CNTs are fairly stable under the electron beam, and showed no visible change in surface morphology after prolonged exposure.

TEM analysis of C_{18} - α -MM-SWNTs provided a direct visualization of the mucin coating (Figure 3c and d). The thickness of the coating varied from 10 to 25 nm under these conditions, in which the sample is dehydrated under high vacuum. The coating was associated with the CNT surface (Figure 3c), and was not observed in regions of the image lacking CNTs. A single tube (or small bundle) coated with C_{18} - α -MM is shown in Figure 3d. The coating was not entirely uniform along the length of this SWNT, perhaps the result of damage induced by the electron beam (100 keV) or collapse of the mucin polymers under high vacuum. In this regard, AFM imaging is a superior technique for visualizing mucin-coated SWNTs as they would exist in a functionally relevant aqueous environment.

On cells, mucins serve the dual role of molecular recognition and resistance to biofouling. We sought to determine if these same functions could be realized in the context of the nanotube surface. The C_{18} - α -MM coating introduces α -GalNAc residues onto the CNT surface, which could be recognized by an α -GalNAc-specific receptor such as the lectin *Helix pomatia* agglutinin (HPA).^[15] To test this we incubated C_{18} - α -MM-SWNTs with a solution of HPA conjugated with fluorescein isothiocyanate (HPA-FITC; shown schematically in Figure 4a I). The C_{18} - α -MM-SWNTs were dialyzed to remove excess HPA-FITC and then analyzed for bound lectin by fluorescence spectroscopy. The C_{18} - α -MM-SWNTs showed significant fluorescence, which was attributed to bound fluorescein (trace I of Figure 4b). HPA-FITC labeling of the C_{18} - α -MM-SWNTs was inhibited when 0.2 M free GalNAc was present in solution (Figure 4a III and trace III of Figure 4b), thus confirming that fluorescent labeling was dependent on the receptor–ligand interaction.

In addition, we prepared a similar mucin mimic in which the GalNAc residues were conjugated to the polymer backbone through a β -anomeric linkage (C_{18} - β -MM; see Supporting Information for synthetic details). This mucin mimic was physically identical to its α -linked counterpart but should not be capable of binding HPA.^[16] We coated SWNTs with C_{18} - β -MM and incubated them with HPA-FITC (shown schematically in Figure 4a II). No significant fluorescence labeling was observed (trace II in Figure 4b), thus indicating that the lectin

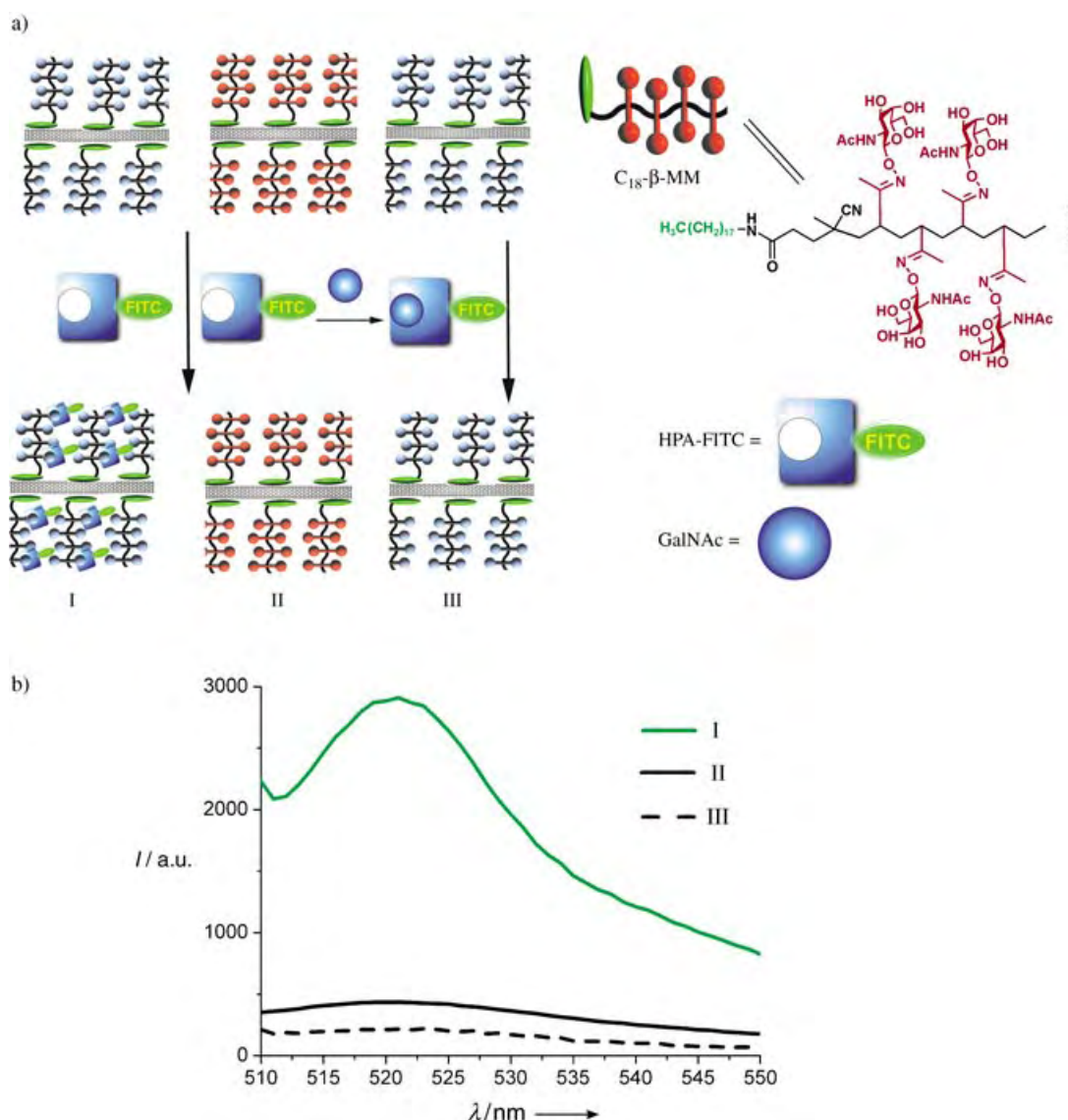


Figure 4. Specific binding of HPA to C₁₈-α-MM-coated nanotubes. a) Scheme for: I) specific binding of HPA to the surface of C₁₈-α-MM-SWNTs, II) lack of binding of HPA to C₁₈-β-MM-SWNTs, III) inhibition of HPA binding by soluble GalNAc. b) Fluorescence spectra (510–550 nm) showing the specific binding of HPA to the surface of C₁₈-α-MM-SWNTs. Trace I: spectrum showing bound HPA-FITC on the surface of C₁₈-α-MM-SWNTs; trace II: spectrum showing the lack of bound HPA to C₁₈-β-MM-SWNTs; trace III: spectrum showing fluorescence associated with HPA-FITC binding in the presence of soluble GalNAc. The excitation wavelength was 492 nm. Spectra were corrected for background fluorescence by subtracting the fluorescence spectrum of C₁₈-α-MM-SWNTs or C₁₈-β-MM-SWNTs alone. These data are representative of results observed in triplicate experiments.

does not interact with the tubes coated with the mucin mimic in the absence of its preferred ligand. These results demonstrate that CNTs coated with a mucin mimic can engage in specific molecular recognition with protein receptors and resist nonspecific protein binding.

In summary, we have developed a practical and general approach to engineering biomimetic surfaces on CNTs. The mucin mimics used in this study endowed the CNT surfaces with properties shared by cell surfaces, including the display of carbohydrates capable of molecular recognition. The synthetic process leading to the mucin mimic allows for the introduction of myriad functional epitopes, in addition to sugars, that could encode interactions with numerous receptor

types. This work should facilitate the integration of CNTs into aqueous biological systems that include proteins and cells.

Received: May 11, 2004

Keywords: biomimetic synthesis · bioorganic chemistry · glycoproteins · nanotubes

- [1] a) M. Sarikaya, C. Tamerler, A. K. Y. Jen, K. Schulten, F. Baneyx, *Nat. Mater.* **2003**, 2, 577; b) G. M. Whitesides, *Nat. Biotechnol.* **2003**, 21, 1161; c) P. Alivisatos, *Nat. Biotechnol.* **2004**,

- 22, 47; d) D. H. Reich, M. Tanase, A. Hultgren, L. A. Bauer, C. S. Chen, G. J. Meyer, *J. Appl. Phys.* **2003**, 93, 7275.
 - [2] R. J. Chen, S. Bangsaruntip, L. A. Drouvalakis, N. Wong, S. Kam, M. Shim, Y. Li, W. Kim, P. J. Utz, H. Dai, *Proc. Natl. Acad. Sci. USA* **2003**, 100, 4984.
 - [3] S. S. Wong, E. Joselevich, A. T. Woolley, C. L. Cheung, C. M. Lieber, *Nature* **1998**, 394, 52.
 - [4] M. P. Mattson, R. C. Haddon, A. M. Rao, *J. Mol. Neurosci.* **2000**, 14, 175.
 - [5] Y. Lin, S. Taylor, H. P. Li, K. A. S. Fernando, L. W. Qu, W. Wang, L. R. Gu, B. Zhou, Y. P. Sun, *J. Mater. Chem.* **2004**, 14, 527.
 - [6] G. J. Strous, J. Dekker, *Crit. Rev. Biochem. Mol. Biol.* **1992**, 27, 57.
 - [7] Y. Shimizu, S. Shaw, *Nature* **1993**, 366, 630.
 - [8] J. Hikens, M. J. L. Ligtenberg, H. L. Vos, S. V. Litvinov, *Trends Biochem. Sci.* **1992**, 17, 359.
 - [9] G. S. Lee, Y. Shin, I. Choi, H. Hahn, C. R. Bertozzi, *J. Am. Chem. Soc.*, submitted.
 - [10] a) R. Shogren, T. A. Gerken, N. Jentoft, *Biochemistry* **1989**, 28, 5525; b) T. A. Gerken, K. J. Butenhof, R. Shogren, *Biochemistry* **1989**, 28, 5536.
 - [11] D. H. Live, L. J. Williams, S. D. Kuduk, J. B. Schwarz, P. W. Glunz, X. T. Chen, D. Sames, R. A. Kumar, S. J. Danishefsky, *Proc. Natl. Acad. Sci. USA* **1999**, 96, 3489.
 - [12] L. A. Marcaurelle, Y. Shin, S. Goon, C. R. Bertozzi, *Org. Lett.* **2001**, 3, 3691.
 - [13] C. Richard, F. Balavoine, P. Schultz, T. W. Ebbesen, C. Mioskowski, *Science* **2003**, 300, 775.
 - [14] N. B. Holland, Y. Qiu, M. Ruegsegger, R. E. Marchant, *Nature* **1998**, 392, 799.
 - [15] N. Sharon, *Adv. Immunol.* **1983**, 34, 213.
 - [16] V. Piller, F. Piller, J. Cartron, *Eur. J. Biochem.* **1990**, 191, 461.
-

Probing the Influence of O₂ on Photoinduced Reversible Electron Transfer in Perylenediimide–Triphenylamine-Based Dendrimers by Single-Molecule Spectroscopy**

Mircea Cotlet, Sadahiro Masuo, Marc Lor, Eduard Fron, Mark Van der Auweraer, Klaus Müllen, Johan Hofkens, and Frans De Schryver**

Room temperature single-molecule fluorescence detection has evolved as a powerful tool to monitor dynamic processes in individual molecules.^[1] Probing single molecules through their spectroscopic properties removes the inherent averaging factor that is present in ensemble experiments to render single-molecule detection as the method of choice to yield information at the most detailed level. Phenomena which are not necessarily predictable by ensemble experiments, such as fluctuations in the fluorescence intensity, lifetimes, or emission maxima, can be obtained by single-molecule detection. Here we use single-molecule detection to probe the influence of molecular oxygen (O₂) on the dynamics of photoinduced electron transfer (PET) in a dendrimer. PET is usually an efficient mechanism for fluorescence quenching, which renders single-molecule detection difficult, if not impossible. Therefore reports on PET in single molecules are rather limited.^[2,3a,b]

A particular aspect of the electron-transfer (ET) process occurs in the case where the locally excited singlet (LES) state and the charge-separated state (CSS) lie close in energetic terms to each other (Figure 1a, with the CSS at level 2). Normally, upon excitation, the LES is deactivated mainly through forward electron transfer (FET) to the CSS. If the radiationless deactivation of the CSS to the ground state (GS) is slow and inefficient, the CSS decays mainly through the LES by a reverse electron-transfer (RET) process. If so, fluorescence is delayed but it is still characterized by a high quantum yield. This allows the electron-transfer process to be

[*] M. Cotlet, S. Masuo, M. Lor, E. Fron, M. Van der Auweraer, J. Hofkens, F. De Schryver
Laboratory of Photochemistry and Spectroscopy
Katholieke Universiteit Leuven
3001 Heverlee (Belgium)
Fax: (+32) 16-327-990
E-mail: johan.hofkens@chem.kuleuven.ac.be
frans.deschryver@chem.kuleuven.ac.be

K. Müllen
Max Planck Institut für Polymerforschung
Ackermannweg 10
55128 Mainz (Germany)

[**] M.C. acknowledges K. U. Leuven for a fellowship. Support from FWO, K. U. Leuven (GOA 2001/2), the Federal Science Policy of Belgium (IUAP-V-03), and a Max Planck Research Award are acknowledged. J. W. Verhoeven (University of Amsterdam) is acknowledged for useful discussions.



Supporting information for this article is available on the WWW under <http://www.angewandte.org> or from the author.

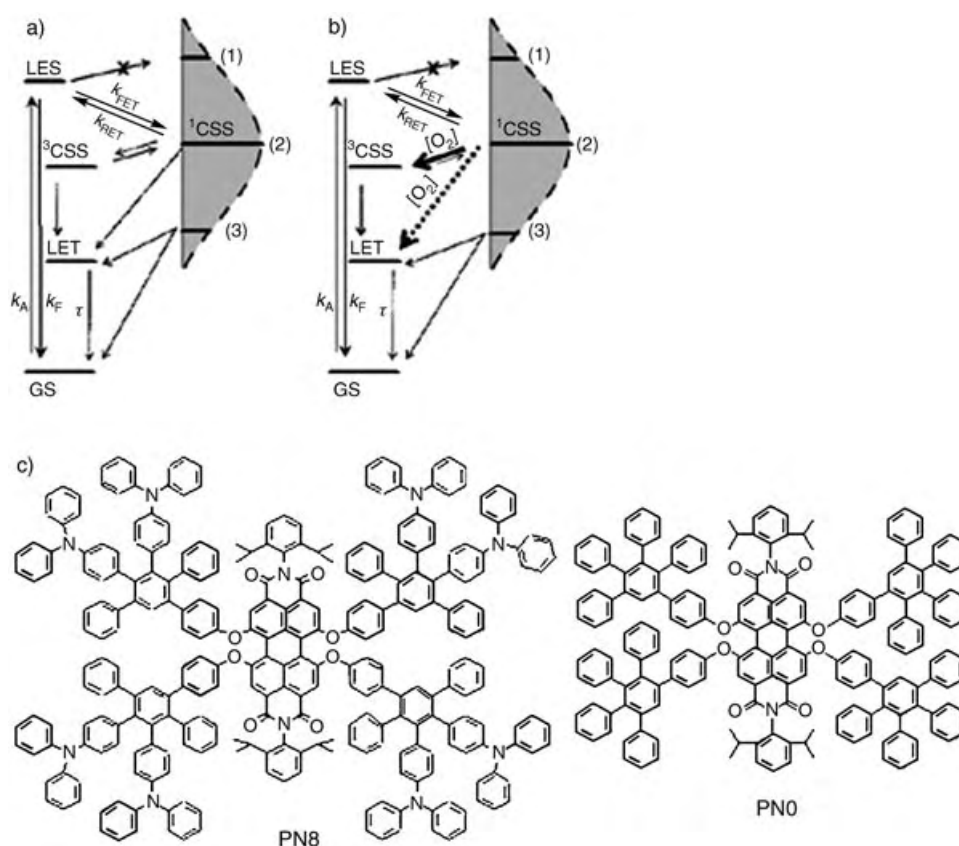


Figure 1. Scheme accounting for photoinduced reversible electron transfer in PN8 under a) deaerated (N_2 ; $\tau \approx 40 \mu s$) and b) aerated (O_2 ; $\tau < 1 \mu s$) atmospheric conditions; thick arrows indicate the pathways enhanced by the presence of O_2 ; τ represents the decay time; LES = locally excited singlet state; LET = locally excited triplet state; GS = ground state; 1CSS = singlet charge-separation states; 3CSS = triplet charge-separation states; k_A , k_F , k_{FET} , k_{RET} are the rate constants for absorption, fluorescence, forward-, and reverse-ET, respectively. 1CSS is drawn at different levels within a Gauss-type density of states induced by polymer chain motion (see text); for simplicity, the 3CSS in both schemes is shown together with 1CSS at level 2. c) Structures of PN8 and PNO.

probed at the single-molecule level if the excited chromophore shows both a high quantum yield of fluorescence and long-term photostability. We have shown previously that single molecules of a perylenediimide–triphenylamine (PDI–TPA)-based dendrimer, which are embedded in polystyrene, undergo photoinduced reversible electron transfer upon excitation at $\lambda = 543 \text{ nm}$.^[3a,b] Herein we focus on a first generation rigid polyphenylene dendrimer, PN8, which contains a PDI core as an electron acceptor and eight TPA electron donor moieties at the rim (Figure 1c)—a system we have shown previously to be capable of undergoing photoinduced reversible electron transfer.^[3b]

In an apolar solvent (methylcyclohexane), PN8 shows a quantum yield of fluorescence that approaches unity, and the fluorescence ($\lambda_{exc} = 543 \text{ nm}$, $\lambda_{em} = 600 \text{ nm}$) decays monoexponentially with a lifetime of 6.5 ns (see Supporting Information): a value that is characteristic for unquenched PDI. In this case, the CSS lies at a higher energy than the LES and no ET occurs (Figure 1a, with the CSS at level 1). In aerated toluene, the fluorescence quantum yield of PN8 drops to 0.14 and the fluorescence decay becomes multiexponential with

decay times of 0.07 (70% amplitude), 1.2 (12%), 6.5 (11%), and 14 ns (7%). Upon deaeration of the solution of PN8 in toluene, the fluorescence quantum yield increases to 0.38. The fluorescence decay of the deaerated solution of PN8 is also multiexponential, with decay times of 0.07 (62% amplitude), 1.2 (10%), 6.5 (9%), and 22.2 ns (19%) (see Supporting Information). For PN8 as well as for similar electron-donor–acceptor compounds, short decay times—that is, relative to the lifetime of unquenched PDI (6.5 ns)—reflect FET from the LES to the CSS, whereas longer decay times are associated with RET from the CSS to the LES.^[3a–c] For such compounds, delayed fluorescence (long decay times) is a characteristic of RET (Figure 1a, with the CSS at level 2). Upon deaeration of the solution of PN8 in toluene, the long decay time related to delayed fluorescence increases both in value and in contribution (see Supporting Information) as does the fluorescence quantum yield. This suggests that O_2 influences the deactivation of the CSS and therefore plays a

role in the dynamics of RET in PN8. Nanosecond-transient absorption data of the deaerated and aerated solutions of PN8 in toluene strongly support the previous assumption (see Supporting Information).

For PN8, because of a rather large edge-to-edge donor–acceptor distance,^[3b] the singlet (1CSS) and the triplet (3CSS) charge-separated states lie close in energy, which allows intersystem crossing (ISC) to occur through hyperfine coupling interactions.^[4,5] Moving from the unsubstituted PDI to PN8, the quantum yield of fluorescence in toluene drops from 1 to 0.38, which suggests that charge recombination in PN8 does not take place only through the LES state. From 1CSS , charge recombination can also occur through ISC to the locally excited triplet (LET) state, either directly or, more likely, via 3CSS (Figure 1a).^[3c,4] Nanosecond-transient absorption data (see Supporting Information) strongly suggest that the triplet and the charge separation states are interconnected in PN8. O_2 enhances ISC from the 1CSS to the 3CSS and LET states (Figure 1b, pathways indicated by thick arrows) which leads to enhanced charge recombination and a decrease in the fluorescence quantum yield of PN8.^[4,5]

According to time-correlated single-photon counting (TCSPC) data from the entire ensemble of PN8 molecules in solution in deaerated toluene, 9% of the molecules do not undergo ET processes—they have a fluorescence lifetime that is characteristic of that of unquenched PDI. By single-molecule detection, we can selectively identify molecules that do undergo RET because this phenomenon relates to the observation of delayed fluorescence.

Observation of single molecules on a longer timescale requires their immobilization. Here we immobilized single molecules of PN8 in polystyrene (PS) as this polymer is comparable to toluene in terms of polarity and polarizability.^[3a,b] Figure 2 shows a fluorescence lifetime image of single PN8 molecules in PS ($\lambda_{\text{exc}} = 543 \text{ nm}$, $20 \times 20 \mu\text{m}^2$, see Supporting Information). In the image, single PN8 molecules that undergo RET can be easily identified by their decay times, which are longer than the lifetime of unquenched PDI ($\tau \approx 6 \text{ ns}$). This allows the dynamics of RET in PN8 as well as the role of O_2 on the radiationless deactivation of the CSS to be probed at the single-molecule level.

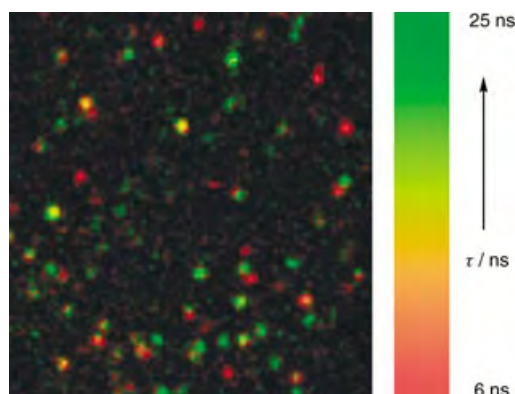


Figure 2. Fluorescence lifetime image ($\lambda_{\text{exc}} = 543 \text{ nm}$; $20 \times 20 \mu\text{m}^2$, $100 \times 100 \text{ pixels}^2$, 10 ms pixel^{-1}) of a polystyrene (PS) film that contains single molecules of PN8.

Figure 3, A and B, show the fluorescence intensity and decay time trajectories, respectively, of a single molecule of PN8 (immobilized in PS) undergoing reversible photoinduced electron transfer. The data were recorded by alternating a stream of either nitrogen (N_2) or air over the sample of the single molecule. Initially, under N_2 atmosphere (Figure 3 A and B, a), an average photon count rate of 30 counts per 10 ms and a decay time of 22 ns were detected. After switching to an air atmosphere (Figure 3 A and B, b), decreases in both the count rate, to 10 counts per 10 ms, and the decay time, to 10 ns, were observed. Switching back to a N_2 atmosphere (Figure 3 A and B, c) resulted in a partial increase in both the count rate, to 20 counts per 10 ms, and the decay time, to 16 ns.^[6] Typical single-molecule fluorescence decay profiles (1000 photons) that correspond to the regions a, b, and c are shown in Figure 3 C–E, parts b, respectively. Data for a single PN8 molecule that undergoes RET in an alternating atmosphere prove that O_2 influences the decay of the CSS by enhancing ISC, which leads to radiationless deactivation of

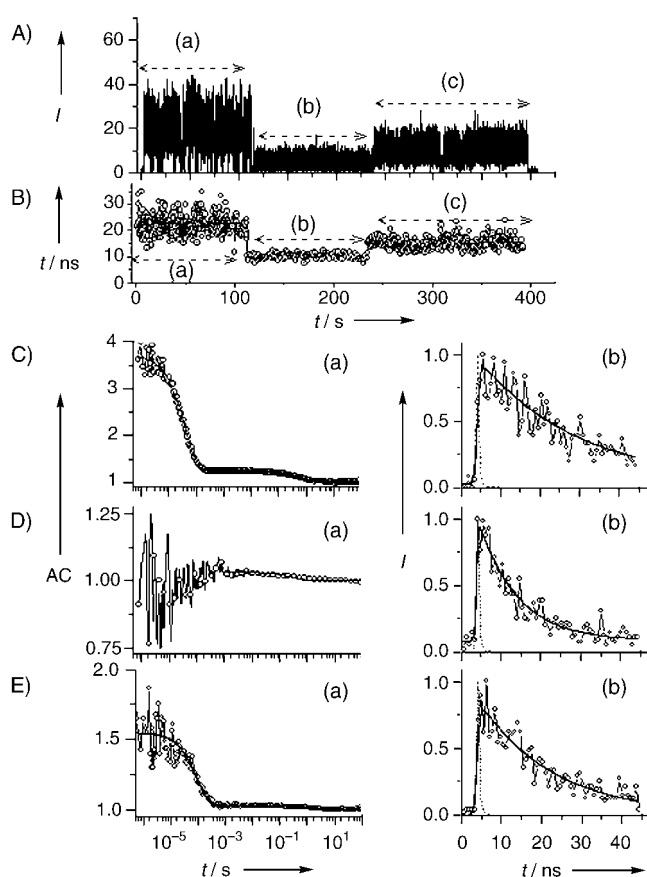


Figure 3. A) Fluorescence intensity (I represents the number of counts per 10 ms) and B) decay time (τ) trajectories recorded from a single molecule of PN8 in PS by alternating the atmosphere from (a) N_2 to (b) air and (c) back to N_2 . C), D), and E) show the autocorrelations (AC) of the fluorescence intensity (parts (a), \circ) and the fluorescence decays (I_f (a.u.), parts (b), \circ , 1000 photons) that correspond to part A) (a), (b), and (c), respectively. Exponential fits (—) are also shown.

the CSS to the ground state. Indeed, both the fluorescence intensity (Figure 3 A) and the decay times of RET decrease (or increase) when the concentration of O_2 is increased (or decreased).

For the single molecule of PN8 under an alternating atmosphere, on/off dynamics can be seen in the fluorescence intensity trajectory, especially under a N_2 atmosphere (Figure 4a). To capture the timescale of such dynamics, we computed the autocorrelation (AC) of the fluorescence intensity $AC = \langle I(t)I(t + \Delta t) \rangle / \langle I \rangle^2$ with the intensities $I(t)$ and $I(t + \Delta t)$ at times t and $t + \Delta t$, respectively (see Supporting Information). Figure 3 C–E, parts a, show the autocorrelation of the fluorescence intensity (AC) for the regions a, b, and c, respectively. For region a, the AC decays biexponentially with offtimes of 0.4 ms (90% weight) and 700 ms (10%). When O_2 is present (b), the AC shows only a slow and low contributing component of 900 ms. Restoring the N_2 atmosphere (c), we again detect fast on/off dynamics with an offtime of 0.35 ms (90% weight), together with slow on/off dynamics with an offtime of 1000 ms (10%).

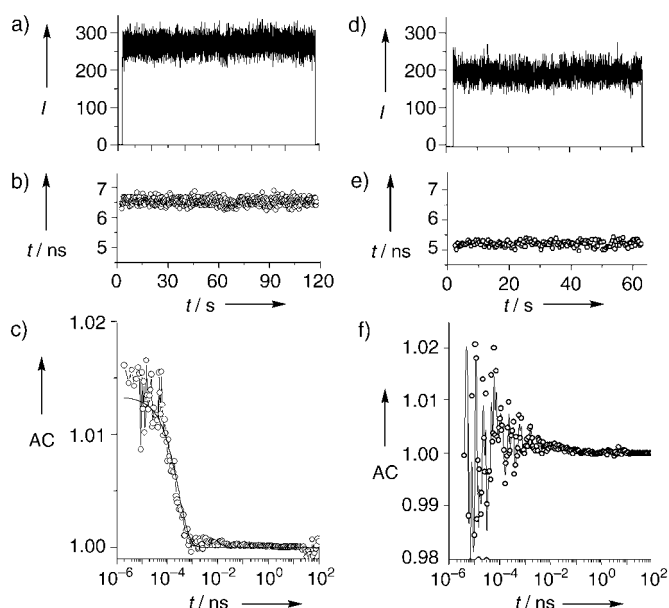


Figure 4. a) Fluorescence intensity (I =counts per 10 ms) and b) lifetime (1000 photons per decay) trajectories from a single molecule of PN0 in polystyrene under a N₂ atmosphere; c) the autocorrelation (AC) of the single molecule which corresponds to parts a–b); d) fluorescence intensity and e) lifetime (1000 photons per decay) trajectories from a single molecule of unsubstituted PDI in polystyrene under an O₂ atmosphere; f) the AC of the single molecule that corresponds to panels d–e.

The fast on/off dynamics that were detected in the fluorescence intensity of single PN8 molecules that undergo RET, which is only observed under a N₂ atmosphere, relates to the population of the LET state (Figure 1a). Similar fast on/off dynamics were detected in the fluorescence intensity of single molecules of a model compound, which did not have rim-substituted amine groups (PN0) and which was embedded in PS, again only under N₂ atmosphere (Figure 4a–c). Under N₂ atmosphere, a single molecule of PN0 emits fluorescence with one stable intensity level (Figure 4a, average count rate: 280 counts per 10 ms) and a lifetime of ≈ 6.5 ns (Figure 4b), and the AC from such a single molecule of PN0 decays monoexponentially with an off-time of 0.3 ms, which relates to the population of the triplet state (Figure 4c). In the presence of O₂, a small decrease in both the fluorescence intensity and lifetime of a single PN0 molecule was detected (Figure 4, d and e) as well as the disappearance of the fast on/off dynamics in the related AC (Figure 4f). The decay of the triplet was faster than the time resolution of the experiment (μ s). However, the contribution of the off-events was significantly smaller in single molecules of PN0 (Figure 4c) relative to single molecules of PN8 (Figure 3C, a), which suggests that triplet formation in PN8 (in PS) is strongly enhanced through the formation of a radical-ion-pair that can recombine through ISC to the LET state (Figure 1a). In an aerated atmosphere, because O₂ is an efficient triplet quencher, the off-events become shorter than the experimental bin time (μ s) and do not contribute to the decay of the AC (Figure 3D, a) for PN8; Figure 4f for PN0). On/off dynamics on the timescale of 0.1–1 ms with off-times that are sensitive to

the concentration of O₂ were reported previously for single dye molecules, which were embedded in polymers, and these were related to the population of the triplet.^[7] The data reported here demonstrate, on a single-molecule level, that 1) O₂ influences the dichotomy between the return from the CSS to the LES or to the GS and 2) owing to the formation of a radical anion, the population of the triplet state and hence the quantum yield for ISC are strongly enhanced. From the data for single molecules under a N₂ atmosphere, we estimate quantum yields for the ISC process of 10^{-4} and 10^{-2} for PN0 and PN8, respectively.^[8]

Single molecules of PN0 in PS do not show slow on/off dynamics (Figure 4, c and f). Therefore, the slow on/off process present in the fluorescence emission of single molecules of PN8 that undergo reversible photoinduced electron transfer must be related to the interaction between the PDI acceptor and the rim-substituted TPA donors—that is, to the presence of the radical anion. RET occurs in a single molecule of PN8 only if the local environment—that is, the polymer—has a polarity such that the CSS and the LES lie close in energy (Figure 1a, with the CSS at level 2). We have shown previously in a single-molecule study on RET that motion of the polystyrene chain can induce fluctuations on the second timescale in the RET-related decay times of single molecules of PN8.^[3b] The polymer can therefore modulate the local polarity of the rim-substituted donors through its chain motion to influence the feasibility of charge separation. This can be regarded as a density of states in which the energy of the CSS of the single molecule fluctuates with the motion of the polymer (Figure 1a, with the density of states for the CSS drawn as a Gauss envelope). If the CSS becomes more stabilized than the LES owing to polymer chain motion (Figure 1a, with the CSS at level 3), charge recombination from the CSS will take place only to the ground state (GS) either directly or via the LET state; that is, only through a nonradiative pathway. If so, the fluorescence of a single molecule of PN8 will be interrupted as long as the CSS lies at lower energy than the LES, with a time interval in which the molecule can undergo many optical excitation cycles. If the polymer chain reorients such that the CSS and the LES state become close again in energy, the pathway for charge recombination through the LES state becomes available again and fluorescence is restored. Polymer chain motion will impose, with its own timescale,^[9] the length of the dark periods in the fluorescence emission of a single molecule of PN8 that undergoes reversible photoinduced electron transfer. Indeed, the timescale of the slow dynamics is independent of the presence/absence of O₂, within experimental error (Figure 3C–E, a), as it is dictated by the polymer motion. Only the frequency of such off-events will be influenced by O₂ whose presence enhances ISC from the ¹CSS to the ³CSS and LET states. Slow on/off dynamics were observed in the fluorescence intensity of single perylenediimide dimers, and this observation was suggested to be connected to the population of a nonfluorescent ion-pair state.^[2e]

In summary, we have shown that the deactivation of the CSS either to the LES state or to the GS for a single molecule can be influenced in a reversible fashion^[6] by the modification of the local O₂ concentration. Furthermore, we have shown

that polymer chain motion can induce “off” periods in the emission of a single molecule that undergoes ET; the length of such periods reflects the timescale of the polymer motion. This suggests that electron donor–acceptor systems such as PN8 can be used as single-molecule probes for polymer dynamics. To our knowledge, this is the first report, which involves single molecules, that demonstrates the influence of molecular oxygen on the radiationless deactivation of the CSS to the GS for an electron donor–acceptor system as well as of the role of polymer motion on the dynamics of fluorescence of a single molecule that undergoes electron transfer.

Experimental Section

PN8 and PN0 were prepared according to reported methods.^[10] Ensemble experiments were performed on aerated and degassed (freeze–pump–thaw cycles) of solutions (10^{-5} M) in toluene. Details on bulk-phase stationary and time-resolved experiments are provided in the Supporting Information. For single-molecule detection, a solution of either PN8 or PN0 (10^{-10} M) in chloroform was mixed with the polymer (PS), and the mixture was spin-coated onto a cover glass. Single-molecule experiments were performed upon 543-nm pulsed (laser) excitation on a scanning stage confocal microscope.^[11] Experimental details and data analysis are provided in the Supporting Information.

Received: May 5, 2004

Revised: July 15, 2004

Keywords: dendrimers · electron transfer · fluorescence spectroscopy · oxygen · single-molecule studies

local O₂ concentration, mainly because not all of the O₂ was removed, or long-lived fluctuations of the polymer that lead to an energetically different CSS of the single molecule.

- [7] a) J. A. Veerman, M. F. Garcia-Parajo, L. Kuipers, N. F. van Hulst, *Phys. Rev. Lett.* **1999**, 83, 2155–2158; b) W. T. Yip, D. H. Hu, J. Yu, D. A. Van den Bout, P. F. Barbara, *J. Phys. Chem. A* **1998**, 102, 7564–7575; c) R. Zondervan, F. Kulzer, S. B. Orlinskii, M. Orrit, *J. Phys. Chem. A* **2003**, 107, 6670–6677.
- [8] T. Vosch, M. Cotlet, J. Hofkens, K. Van der Biest, M. Lor, K. Weston, P. Tinnefeld, M. Sauer, L. Latterini, K. Müllen, F. De Schryver, *J. Phys. Chem. A* **2003**, 107, 6920–6931.
- [9] M. D. Ediger, *Annu. Rev. Phys. Chem.* **2000**, 51, 99–128.
- [10] J. Qu, N. G. Pschirer, D. J. Liu, A. Stefan, F. De Schryver, K. Müllen, *Chem. Eur. J.* **2004**, 10, 528–537.
- [11] M. Cotlet, J. Hofkens, S. Habuchi, G. Dirix, J. Van der Leyden, F. De Schryver, *Proc. Natl. Acad. Sci. USA* **2001**, 98, 14398–14404.

- [1] a) X. S. Xie, J. K. Trautman, *Annu. Rev. Phys. Chem.* **1998**, 49, 441–480; b) S. Weiss, *Science* **1999**, 283, 1676–1683.
- [2] a) H. P. Lu, X. S. Xie, *J. Phys. Chem. B* **1997**, 101, 2753–2757; b) L. Edman, U. Mets, R. Rigler, *Proc. Natl. Acad. Sci. USA* **1996**, 93, 6710–6715; c) J. P. Knemeyer, N. Marme, M. Sauer, *Anal. Chem.* **2000**, 72, 3717–3724; d) C. Eggeling, J. R. Fries, R. Gunther, C. A. M. Seidel, *Proc. Natl. Acad. Sci. USA* **1998**, 95, 1556–1561; e) H. Yang, G. Luo, P. Karnchanaphanurach, T. Louie, I. Rech, S. Cova, L. Xun, X. S. Xie, *Science* **2003**, 302, 262–266; f) L. Zang, R. C. Liu, M. W. Holman, K. T. Nguyen, D. M. Adams, *J. Am. Chem. Soc.* **2002**, 124, 12640–12641; g) R. Liu, M. W. Holman, L. Zang, D. M. Adams, *J. Phys. Chem. A* **2003**, 107, 6522–6526.
- [3] a) R. Gronheid, A. Stefan, M. Cotlet, J. Hofkens, J. Qu, K. Müllen, M. Van der Auweraer, J. Verhoeven, F. De Schryver, *Angew. Chem.* **2003**, 115, 4341–4346; *Angew. Chem. Int. Ed.* **2003**, 42, 4209–4214; b) M. Cotlet, S. Masuo, G. Luo, J. Hofkens, K. Müllen, M. Van der Auweraer, J. W. Verhoeven, X. S. Xie, F. De Schryver, *Proc. Natl. Acad. Sci. USA* **2004**, 101, 14343–14348; c) M. Lor, J. Thielemans, L. Viaene, M. Cotlet, J. Hofkens, T. Weil, C. Hampel, K. Müllen, J. W. Verhoeven, M. Van der Auweraer, F. C. De Schryver, *J. Am. Chem. Soc.* **2002**, 124, 9918–9925.
- [4] U. Steiner, W. Haas, *J. Phys. Chem.* **1991**, 95, 1880–1888.
- [5] S. P. McGlynn, T. Azumi, M. Kinoashita, *Molecular Spectroscopy of the Triplet State*, Prentice-Hall, New Jersey, **1969**, pp. 289–307.
- [6] For the single molecule of PN8 in an alternating air/N₂ atmosphere, the fluorescence intensity and decay times from (c) do not recover completely to the original values from (a). Possible reasons for this observation are either differences in the

Coordination Polymers

An Oriented 1D Coordination/Organometallic Dimetallic Molecular Wire with Ag–Pd Metal–Metal Bonds**

Pierre Braunstein, Céline Frison,
Nicola Oberbeckmann-Winter, Xavier Morise,
Abdelatif Messaoudi, Marc Bénard, Marie-
Madeleine Rohmer, and Richard Welter*

*Dedicated to Professor Jean-Marie Lehn
on the occasion of his 65th birthday*

In addition to conferring unique catalytic properties to their metal complexes when they behave as spectator ligands,

[*] Dr. P. Braunstein, C. Frison, Dr. N. Oberbeckmann-Winter,
Dr. X. Morise, A. Messaoudi
Laboratoire de Chimie de Coordination, UMR 7513 CNRS
Institut Le Bel, Université Louis Pasteur
4, rue Blaise Pascal, 67070 Strasbourg Cédex (France)
E-mail: braunst@chimie.u-strasbg.fr
Dr. M. Bénard, Dr. M.-M. Rohmer
Laboratoire de Chimie Quantique, UMR 7551 CNRS
Institut Le Bel, Université Louis Pasteur
4, rue Blaise Pascal, 67070 Strasbourg Cédex (France)
Prof. R. Welter⁺
Laboratoire DECMET, UMR 7513 CNRS
Institut Le Bel, Université Louis Pasteur
4, rue Blaise Pascal, 67070 Strasbourg Cedex (France)

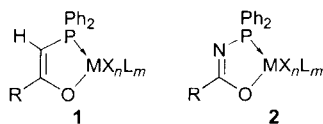
[[†]] Crystal structure analysis.

[**] This work was supported by the CNRS and the Ministère de la Recherche and the European Commission. N.O.-W. is grateful for a Marie Curie fellowship (HPMF-CT-2002-01659) and also to the French Embassy in Berlin and the Ministère des Affaires Etrangères (Paris) for a grant. M.B. and M.-M.R. thank the IDRIS computer center (Orsay, France) and the “GdR DFT” action from the CNRS.



Supporting information for this article (including crystallographic data for **4**-SO₃CF₃·0.5 CH₂Cl₂, **5**-SO₃CF₃·2 CH₂Cl₂ and **6**-SO₃CF₃, and all the experimental and computational details) is available on the WWW under <http://www.angewandte.org> or from the author.

coordinated P,O-phosphanyl enolates in a moiety such as **1** also display a very rich reactivity based on their intrinsic ambident behavior.^[1–3] Harder electrophiles, such as chlorophosphanes, generally react at the oxygen atom,^[4] whereas softer electrophiles, for example, activated alkynes,^[5] CO₂, or RNCO,^[6] bind to the prochiral carbon center.

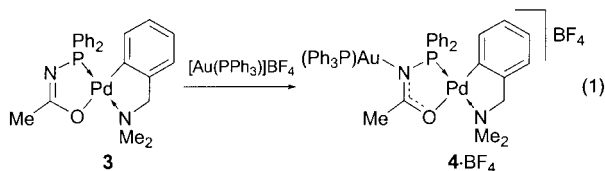


The latter selectivity also applies to late-transition metals and opens an interesting route to (hetero)dimetallic complexes in which the PC carbon atom has become sp³ hybridized.^[7] Although control of the stereochemistry at the PC carbon atom is possible,^[8] the generation of both the *R* and *S*-configured stereogenic P-C centers is generally expected.

We thus considered that replacing the PCH functionality with the isoelectronic PN group of phosphanyl iminolates (**2**) might simplify this issue, since the nitrogen atom could retain a planar coordination geometry. Furthermore, the simple exchange of a CH group by an N atom can bring about interesting electronic and geometric differences in molecular complexes, as shown with the phosphanes Ph₂PNHC(O)R and Ph₂PCH₂C(O)R,^[9] or induce unexpectedly large effects in supramolecular chemistry.^[10]

We have now found that metal coordination at the nitrogen atom of the P,O chelate in a complex of type **2**: 1) readily leads to (μ-P,N)-bridged heterodimetallic complexes, 2) occurs with retention of the planar coordination geometry at the nitrogen atom, and rather unexpectedly 3) opens an unprecedented route to ordered structures containing alternating metals in heterodimetallic units to form oriented, 1D coordination/organometallic polymers.

The new, air-stable complex **3**^[11] was treated with one equivalent of [Au(PPh₃)]BF₄ in THF to afford **4**·BF₄ [Eq. (1)] and the structure of the analogous complex **4**·SO₃CF₃ was determined by X-ray diffraction analysis (Figure 1 and see the Supporting Information).^[11]



N-metalation leads to an Au⋯N distance of 2.085(6) Å, similar to those found in complexes with a covalent Au–N bond in an Au–NPPH₂ moiety.^[12] The coordination geometry around the nitrogen atom is planar, with the sum of the three bond angles around N(2) being 360.0(3)° (max deviation out of the mean plane containing the atoms Pd, P1, N2, C10, O1,

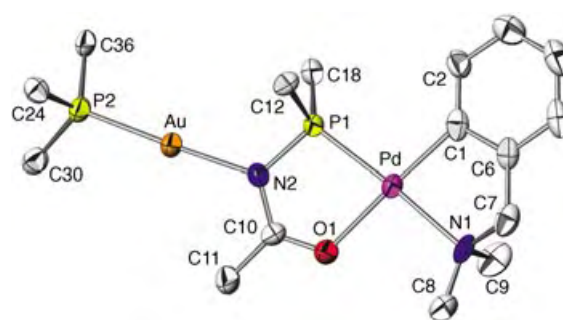
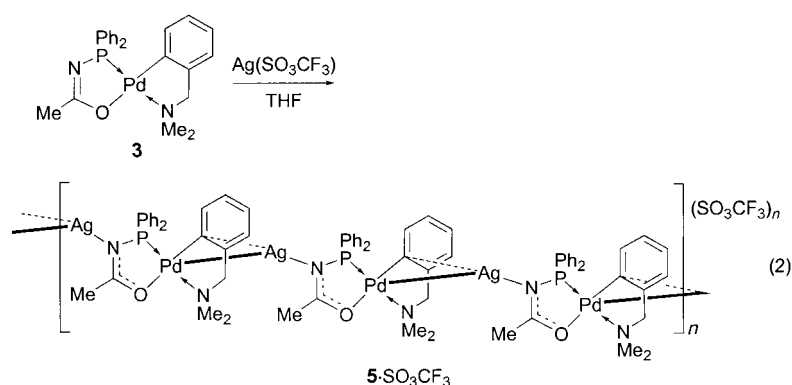


Figure 1. ORTEP view of the structure of complex **4** in **4**·SO₃CF₃·0.5CH₂Cl₂. Only the *ipso* aryl carbon atoms on P1 and P2 are shown for clarity. Thermal ellipsoids enclose 50% of the electron density.

and Au: 0.01 Å).^[13] Accordingly, the NCH₂ protons only show a doublet in the ¹H NMR spectrum as a result of coupling to the P atom. The O1–C10 and N2–C10 bond lengths of 1.273(9) and 1.353(9) Å, respectively, are consistent with C=O and N=C bond orders intermediate between single and double bonds.^[7,9,14]

A solution of **3** in THF was then treated with pure, acid-free AgSO₃CF₃ in a 1:1 stoichiometry, and slow crystallization afforded high yields of a beige product **5**·SO₃CF₃ [Eq. (2)], which was shown by X-ray diffraction studies to be an unprecedented Ag–Pd coordination polymer (Figure 2 and see the Supporting Information).^[11]



The Ag⁺ ion is, as anticipated, linked to the iminolate nitrogen atom, which retains its planar coordination geometry (sum of the three bond angles around N2 = 359.5(3)°; Ag⋯N = 2.133(3) Å; see the Supporting Information). If only a covalent Ag–N interaction was present, the silver center would remain, with 12 electrons, coordinatively unsaturated. It was therefore expected to interact with the triflate oxygen atom(s),^[15] as observed in other cases,^[16] but it prefers to find the required additional electron density in the Pd–C1 σ bond involving the cyclometalated ligand of another complex molecule (Figure 2). This situation is best described as a multicentered interaction resulting in the donation of σ- and π-electron density from the Pd–C1 (*p_z* orbital) and Pd-bound aryl regions to the coordinatively unsaturated silver center.

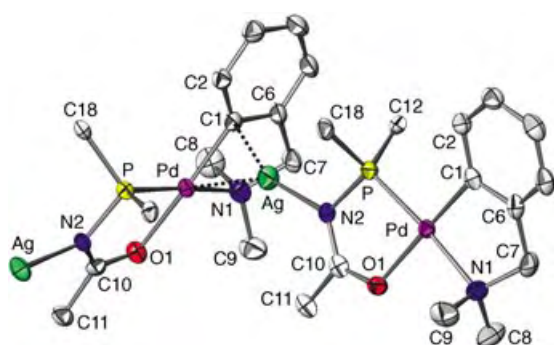


Figure 2. ORTEP view of the structure of the “repeat unit” Ag_2Pd_2 of the polymeric complex **5** in $5\text{-SO}_3\text{CF}_3\cdot 2\text{CH}_2\text{Cl}_2$. Only the *ipso* aryl carbon atoms on P are shown for clarity. Thermal ellipsoids enclose 50% of the electron density.

The electronic transfer occurs from the d^8 Pd^{II} center to the d^{10} Ag^{I} center and results in a relatively short $\text{Ag}-\text{C1}$ bonding distance of $2.263(4)$ Å,^[17] and in one of the shortest $\text{Pd}-\text{Ag}$ bonds ($2.884(1)$ Å) reported in the literature.^[17a,18] Since two consecutive square-planar Pd^{II} units are almost orthogonal to each other (see the Supporting Information), the structural repeating unit in the extended structure is Ag_2Pd_2 (Figure 2), which results in a novel, oriented, 1D coordination/organometallic wire structure in which the metal centers are situated in the *ab* plane (Figure 3). A view along the *a* axis (see the Supporting Information) shows the adjacent rows of silver atoms flanked by two rows of palladium atoms and illustrates another remarkable feature resulting from the arrangement of these infinite zigzag chains in the solid state: the lipophilic aromatic rings are all on one side of the metal planes and this results in an unusual layered structure (see Figure 4). Attempts to obtain an analogous $\text{Ag}-\text{Pd}$ extended structure from the isovalent phosphanyl enolate/ Pd^{II} complex have remained unsuccessful, which emphasizes the differences that may result from the replacement of the CH group in **1** by an N atom in **2**.

The mass spectrum (MALDI-TOF) of $5\text{-SO}_3\text{CF}_3$ contains two main peaks at m/z 483 for $[\mathbf{3} + \text{H}]^+$ and 1073, whose characteristic isotopic pattern indicates the composition $[\text{Ag}(\mathbf{3})_2]^+$. The structure of $[\text{Ag}(\mathbf{3})_2]^+$ cannot be predicted

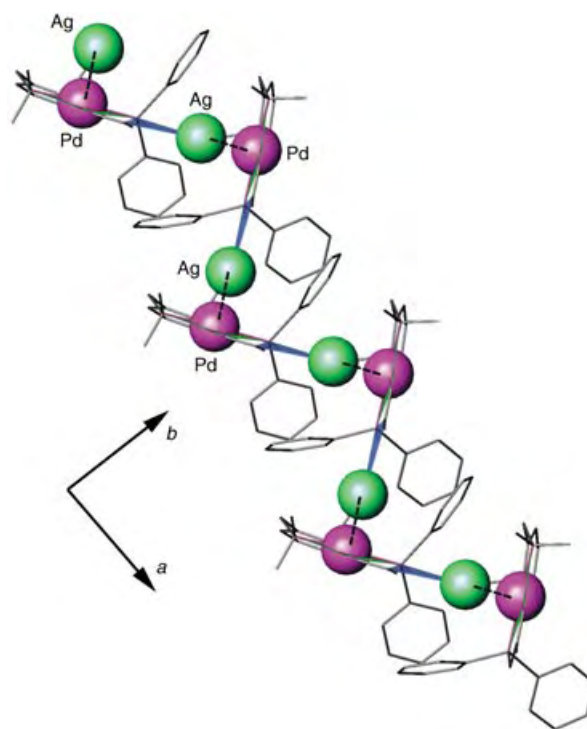
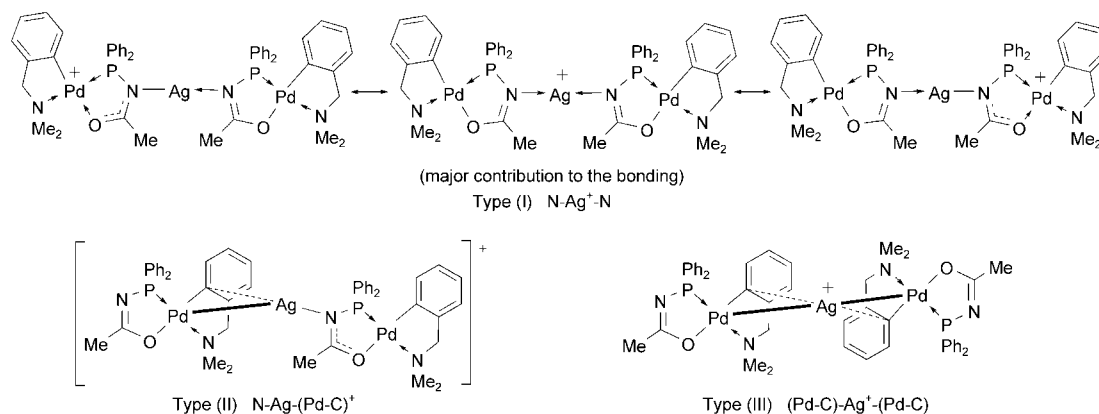


Figure 3. View in the *ab* plane of the zigzag wire structure of the polymeric complex structure of **5** in $5\text{-SO}_3\text{CF}_3\cdot 2\text{CH}_2\text{Cl}_2$.

with certainty to reproduce the alternate bonding pattern observed for **5** and is referred as the type II structure in Scheme 1.

Indeed, two bonding modes in which an Ag^+ ion is coordinated to the same site of two molecules of **3** should also be considered. In a type I structure, the donation pattern can be viewed as intermediate between two limiting forms in which one nitrogen atom acts as a two-electron donor and the other as a two-electron or one-electron donor ligand, respectively. In such a model, part of the electron density from the nitrogen lone pair of electrons is transferred to the π system, thus increasing the covalent character of the $\text{Ag}-\text{N}$ bond and affecting in return the geometry of the phosphanyl iminolate ligands. A further possibility to be considered is the



Scheme 1. Hypothetical discrete structures formed from **3** and Ag^+ ions in a 2:1 ratio. Type (I) corresponds to the actual structures of complex **6**.

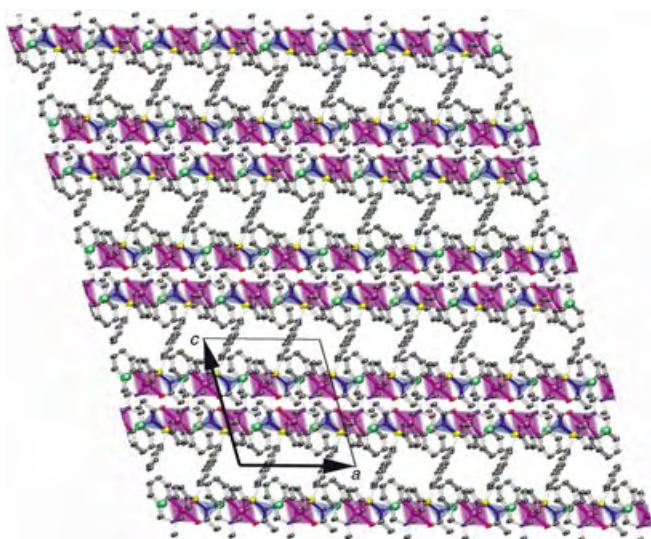


Figure 4. Projection in the a,c plane of the layered structure of **5** in $5\text{-SO}_3\text{CF}_3 \cdot 2\text{CH}_2\text{Cl}_2$. The space between the pairs of metal-rich layers contains the phenyl rings, the triflate anions, and solvent molecules (Ag green, Pd pink, N blue, P yellow, O orange).

formation of a complex of type (III), in which each neutral molecule of **3** behaves as an electron donor through its Pd–C σ bond and its extended Pd–aryl π system (only the transoid structure is depicted in Scheme 1).

Extended Hückel (EHT) and density functional theory (DFT) calculations have been carried out on a series of discrete structures featuring the various types of attachment that can be expected between the Ag^+ ion and one or two molecules of **3'**, a model of **3** in which the methyl and phenyl substituents have been replaced with hydrogen atoms. A model (**4'**) of the gold complex was also investigated. Technical details of the calculations, Cartesian coordinates of the optimized structures with selected interatomic distances, and an extensive discussion of the results are available in the Supporting Information. The most important conclusions of the theoretical study are as follows:

- The amount of electron transfer to the Ag^+ ion is equivalent in the two bonding modes symbolized as Ag^+-N and $\text{Ag}^+-\text{(Pd-C)}$. However, the nature of the two donation processes is quite different: concentrated, directional, and originating from a single source (the in-plane p orbital of N) for $\text{N} \rightarrow \text{Ag}^+$; soft, diffuse, multicentered, and long-range for $\text{(Pd-C)} \rightarrow \text{Ag}^+$. In the latter case, a variety of donor centers could interact with the Ag^+ ion, with the most important being the Pd–C1 σ bond (20%); the d shell of Pd (17%) and the π orbitals of C1 (20%), C2 and C6 (27%), and C4 (10%). Both types of calculations predict that the Ag^+-N and the $\text{Ag}^+-\text{(Pd-C)}$ bonding modes are competitive in terms of electron-transfer and bonding energy. This description confirms the dual bonding ability of **3'** and **3**, which was substantiated by the synthesis of $(5\text{-SO}_3\text{CF}_3)_n$, and suggests that the production of monocationic, trinuclear Pd/Ag/Pd complexes could be achieved by a careful tuning of the

Ag^+ supply. Such a discrete complex was indeed obtained subsequently (see below).

- The complexation of an Ag^+ ion to one molecule of **3'** is computed to be exothermic by 2.88 eV and 2.79 eV for the Ag^+-N and $\text{Ag}^+-\text{(Pd-C)}$ forms, respectively, compared to 1.82 eV calculated for the η^1 coordination of an Ag^+ ion to benzene. The complexation energies calculated for the three forms of $[\text{Ag}(\text{3}')_2]^+$ are -5.15 eV for N– Ag^+ –N (type I in Scheme 1), -4.71 eV for type II, and -4.36 eV for type III. The energy associated with the coordination of a second molecule of **3'** is just slightly reduced with respect to the first complexation for the type I system, but somewhat more for type III. At variance with the polymer, it was clear from these results that a type I structure should be predicted for $[\text{Ag}(\text{3}')_2]^+$.

This theoretical prediction was actually verified by the reaction between AgSO_3CF_3 and two equivalents of **3** affording the AgPd_2 complex **6**· SO_3CF_3 in 92% yield. The crystal-structure analysis of this complex established indeed that the coordination of both molecules of **3** to Ag^+ occurred through their nitrogen atoms (type I in Scheme 1; see Figure 5

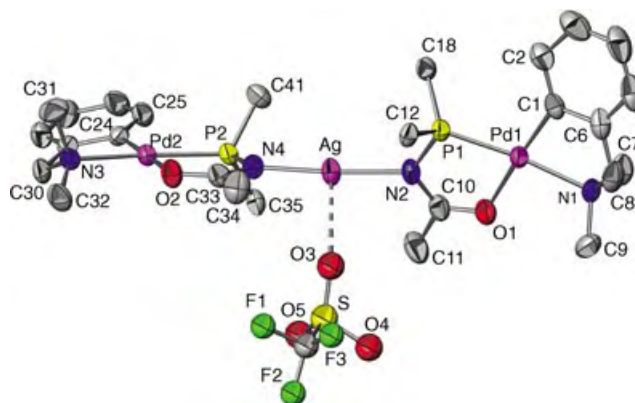


Figure 5. ORTEP view of the structure of **6**· SO_3CF_3 . Only the *ipso* aryl carbon atoms on P1 and P2 are shown for clarity. Thermal ellipsoids enclose 50% of the electron density.

and the Supporting Information).^[11] The N2–Ag–N4 angle of $175.4(2)^\circ$ allows a coordination number of two to be formally assigned to the silver ion, a situation which occurs in less than 25% of the structures of Ag^+ complexes.^[19] However, a weak electrostatic interaction probably exists between the triflate anion and the Ag^+ ion, with the $\text{Ag} \cdots \text{O3}$ distance of $2.82(1)$ Å being nevertheless in the upper range of those found on the CSD (version 5.25) which are in most cases between 2.38 and 2.55 Å (for comparison, the nearest triflate oxygen atom is at $3.86(2)$ Å from Ag^+ in $5\text{-SO}_3\text{CF}_3 \cdot 2\text{CH}_2\text{Cl}_2$). The dihedral angle between the two best Pd^{II} square planes is $75(2)^\circ$.

Although the term “coordination polymers” was first coined 40 years ago,^[20] the corresponding research area continues to gain increasing importance.^[21] Furthermore, the considerable current interest in extended metal atom chains (EMACs)^[22] is partly a consequence of their expected unique and challenging physical properties.^[17c,23–27] While the linking

of homodinuclear units through (weak) metal–metal bonding or suitable ligands allows the formation of exciting coordination polymers,^[24,25,27] we believe that the structure of **5**-SO₃CF₃ is not only an unprecedented example of perfectly alternating and ordered 1D heterodimetallic polymeric structure, and the first molecular wire containing Ag–Pd bonds, but that its synthesis reaches beyond the realm of extended structures in purely inorganic chemistry^[28] and opens up new perspectives in coordination/organometallic supramolecular chemistry.

Received: July 13, 2004

Keywords: coordination polymers · density functional calculations · heterometallic complexes · ligand reactivity · metal–metal interactions

- [1] For Ni^{II} complexes used in the catalytic oligomerization of ethylene, see, for example, P. Braunstein, Y. Chauvin, S. Mercier, L. Saussine, A. De Cian, J. Fischer, *J. Chem. Soc. Chem. Commun.* **1994**, 2203.
- [2] For Pd^{II} complexes used in the reversible coordination of CO₂ and telomerization with butadiene, see P. Braunstein, D. Matt, D. Nobel, *J. Am. Chem. Soc.* **1988**, *110*, 3207.
- [3] For Rh^I complexes in alkane activation, see P. Braunstein, Y. Chauvin, J. Nähring, A. DeCian, J. Fischer, A. Tiripicchio, F. Uguzzoli, *Organometallics* **1996**, *15*, 5551.
- [4] a) F. Balegroune, P. Braunstein, D. Grandjean, D. Matt, D. Nobel, *Inorg. Chem.* **1988**, *27*, 3320; b) J. Andrieu, P. Braunstein, A. Tiripicchio, F. Uguzzoli, *Inorg. Chem.* **1996**, *35*, 5975.
- [5] a) P. Braunstein, T. M. Gomes Carneiro, D. Matt, F. Balegroune, D. Grandjean, *Organometallics* **1989**, *8*, 1737; b) F. Balegroune, P. Braunstein, T. M. Gomes Carneiro, D. Grandjean, D. Matt, *J. Chem. Soc. Chem. Commun.* **1989**, 582.
- [6] a) P. Braunstein, D. Matt, D. Nobel, *Chem. Rev.* **1988**, *88*, 747; b) P. Braunstein, D. Nobel, *Chem. Rev.* **1989**, *89*, 1927.
- [7] J. Andrieu, P. Braunstein, M. Drillon, Y. Dusauroy, F. Ingold, P. Rabu, A. Tiripicchio, F. Uguzzoli, *Inorg. Chem.* **1996**, *35*, 5986.
- [8] A. Apfelbacher, P. Braunstein, L. Brissieux, R. Welter, *Dalton Trans.* **2003**, 1669.
- [9] P. Braunstein, C. Frison, X. Morise, R. D. Adams, *J. Chem. Soc. Dalton Trans.* **2000**, 2205.
- [10] A. Affeld, G. M. Hübner, C. Steel, C. A. Schalley, *Eur. J. Org. Chem.* **2001**, 2877.
- [11] For full experimental data on the synthesis, spectroscopy, and elemental analysis of the complexes see the Supporting Information. X-ray structure analysis of **4**-SO₃CF₃·0.5CH₂Cl₂, **5**-SO₃CF₃·2CH₂Cl₂, and **6**-SO₃CF₃: Selected crystals were mounted on a Nonius Kappa-CCD area detector diffractometer (MoK α , λ = 0.71073 Å). The complete conditions of data collection (Denzo software) and structure refinements are given below. The cell parameters were determined from reflections taken from one set of ten frames (1.0° steps in phi angle), each at 20 s exposure. The structures were solved by direct methods (SHELXS97) and refined against F^2 using the SHELXL97 software. The absorption was corrected empirically (with Sortav). All non-hydrogen atoms were refined anisotropically. Hydrogen atoms were generated according to the stereochemistry and refined using a riding model in SHELXL97. **4**-SO₃CF₃·0.5CH₂Cl₂: C₄₂H₄₀AuF₃N₂O₄P₂S₂·0.5CH₂Cl₂; M_r = 1133.59, monoclinic, space group $P2_1/c$, a = 9.379(3), b = 41.299(5), c = 12.061(3) Å, β = 99.46(5)°, V = 4608(2) Å³, Z = 4, ρ_{calcd} = 1.634 g cm⁻³, μ = 3.796 mm⁻¹, $F(000)$ = 2228, T = 173 K. Colorless crystal, dimensions 0.04 × 0.05 × 0.06 mm³. A total of 10051 reflections were collected on a Kappa CCD diffractometer (phi scans), 1.78° < θ < 27.50°, 10051 independent reflections with 6631 having $I > 2\sigma(I)$; 532 parameters; $R1$ = 0.0482; $wR2$ = 0.1586, GOF = 0.982, maximum residual electronic density = 1.442 e Å⁻³. **5**-SO₃CF₃·2CH₂Cl₂: C₂₄H₂₅AgF₃N₂O₄P₂S₂·2CH₂Cl₂; M_r = 909.61, monoclinic, space group $P2_1/a$, a = 12.437(5), b = 20.109(6), c = 14.107(4) Å, β = 106.52(5)°, V = 3383(2) Å³, Z = 4, ρ_{calcd} = 1.786 g cm⁻³, μ = 1.586 mm⁻¹, $F(000)$ = 1800. Colorless crystal, dimensions 0.08 × 0.10 × 0.13 mm³. A total of 14300 reflections were collected on a Kappa CCD diffractometer (phi scans), 1.51° < θ < 27.48°, 7719 independent reflections with 5826 having $I > 2\sigma(I)$; 395 parameters; $R1$ = 0.0397; $wR2$ = 0.1388, GOF = 1.135, maximum residual electronic density = 1.253 e Å⁻³. The figure shown in the Supporting Information was produced using the UCSF Chimera package from the Computer Graphics Laboratory, University of California, San Francisco: “Chimera: An Extensible Molecular Modeling Application Constructed Using Standard Components”: C. C. Huang, G. S. Couch, E. F. Pettersen, T. E. Ferrin, *Pacific Symposium on Biocomputing* **1996**, *1*, 724. **6**-SO₃CF₃: C₄₇H₅₀AgF₃N₄O₅P₂S₂; M_r = 1222.58, triclinic, space group $P\bar{1}$, a = 13.169(1), b = 14.722(1), c = 14.769(1) Å, α = 61.42(5)°, β = 81.93(5)°, γ = 87.04(5)°, V = 2489.2(3) Å³, Z = 2, ρ_{calcd} = 1.631 g cm⁻³, μ = 1.269 mm⁻¹, $F(000)$ = 1224. Colorless crystal, dimensions 0.08 × 0.10 × 0.12 mm³. A total of 14969 reflections were collected on a Kappa CCD diffractometer (phi scans), 1.56° < θ < 30.33°, 14471 independent reflections with 8498 having $I > 2\sigma(I)$; 586 parameters; $R1$ = 0.0545; $wR2$ = 0.1751, GOF = 1.023, maximum residual electronic density = 1.420 e Å⁻³. CCDC-240188–240190 contain the supplementary crystallographic data for this paper. These data can be obtained free of charge via www.ccdc.cam.ac.uk/conts/retrieving.html (or from the Cambridge Crystallographic Data Centre, 12 Union Road, Cambridge CB2 1EZ, UK; fax: (+44) 1223-336-033; or deposit@ccdc.cam.ac.uk).
- [12] a) R. Uson, A. Laguna, M. Laguna, B. R. Manzano, P. G. Jones, G. M. Sheldrick, *J. Chem. Soc. Dalton Trans.* **1985**, 2417; b) P. A. Bella, O. Crespo, E. J. Fernandez, A. K. Fischer, P. G. Jones, A. Laguna, J. M. Lopez-de-Luzuriaga, M. Monge, *J. Chem. Soc. Dalton Trans.* **1999**, 4009.
- [13] The closest interactions between the triflate anion and the metal complex in **4**-SO₃CF₃·0.5CH₂Cl₂ involve atoms F3 and O2 of the former and H27 and H28 of an aryl group bound to P2 at 2.84(1) and 2.59(1) Å, respectively.
- [14] P. Braunstein, C. Frison, X. Morise, *C. R. Chim.* **2002**, *5*, 131.
- [15] In the crystal structure of (**5**-SO₃CF₃·2CH₂Cl₂)_n the triflate anion is positioned in the vicinity of the Ag⁺ ion but does not act as a ligand. The shortest intermolecular contacts are found between the triflate oxygen atom O3 and H7A and H13 (2.42(1) and 2.59(1) Å, respectively), and the fluorine atoms F1 and F3 and the methyl protons H11C and H11A (2.50(1) and 2.77(1) Å, respectively).
- [16] P. Braunstein, T. M. Gomes Carneiro, D. Matt, A. Tiripicchio, M. Tiripicchio Camellini, *Angew. Chem.* **1986**, *98*, 721; *Angew. Chem. Int. Ed. Engl.* **1986**, *25*, 748.
- [17] a) J. E. Kickham, S. J. Loeb, *Organometallics* **1995**, *14*, 3584; b) W. Xu, R. J. Puddephatt, K. W. Muir, A. A. Torabi, *Organometallics* **1994**, *13*, 3054; c) T. Yamaguchi, F. Yamazaki, T. Ito, *J. Am. Chem. Soc.* **2001**, *123*, 743.
- [18] a) For reviews, see I. D. Salter, in *Comprehensive Organometallic Chemistry II*, Vol. 10 (Eds.: E. W. Abel, F. G. A. Stone, G. Wilkinson), Elsevier, Oxford, **1995**, p. 255; S.-M. Lee, W.-T. Wong, *J. Cluster Sci.* **1998**, *9*, 417; b) Y. Liu, K. H. Lee, J. J. Vittal, T. S. A. Hor, *J. Chem. Soc. Dalton Trans.* **2002**, 2747; c) E. Alonso, J. Fornies, C. Fortuño, A. Martin, A. G. Orpen, *Organometallics* **2003**, *22*, 5011.

- [19] M. A. Carvajal, J. J. Novoa, S. Alvarez, *J. Am. Chem. Soc.* **2004**, *126*, 1465.
- [20] J. C. Bailar in *Preparative Inorganic Reactions, Vol. 1* (Ed.: W. L. Jolly), Interscience, New York, **1964**, pp. 1.
- [21] For recent reviews, see C. Janiak, *Dalton Trans.* **2003**, 2781; S. Kitagawa, R. Kitaura, S.-i. Noro, *Angew. Chem.* **2004**, *116*, 2388; *Angew. Chem. Int. Ed.* **2004**, *43*, 2334; and for Ag^I-based coordination polymers: A. N. Khlobystov, A. J. Blake, N. R. Champness, D. A. Lemenovskii, A. G. Majouga, N. V. Zyk, M. Schröder, *Coord. Chem. Rev.* **2001**, *222*, 155.
- [22] a) J. F. Berry, F. A. Cotton, L. M. Daniels, C. A. Murillo, X. Wang, *Inorg. Chem.* **2003**, *42*, 2418; b) J. F. Berry, F. A. Cotton, P. Lei, T. Lu, C. A. Murillo, *Inorg. Chem.* **2003**, *42*, 3534; c) J. F. Berry, F. A. Cotton, C. A. Murillo, *Organometallics* **2004**, *23*, 2503, and references therein.
- [23] R. Clérac, F. A. Cotton, L. M. Daniels, K. R. Dunbar, K. Kirschbaum, C. A. Murillo, A. A. Pinkerton, A. J. Schultz, X. Wang, *J. Am. Chem. Soc.* **2000**, *122*, 6226.
- [24] J. K. Bera, K. R. Dunbar, *Angew. Chem.* **2002**, *114*, 4633; *Angew. Chem. Int. Ed.* **2002**, *41*, 4453, and references therein.
- [25] a) I. P. Y. Shek, W.-Y. Wong, T.-C. Lau, *New J. Chem.* **2000**, *24*, 733; b) S.-M. Peng, C.-C. Wang, Y.-L. Jang, Y.-H. Chen, F.-Y. Li, C.-Y. Mou, M.-K. Leung, *J. Magn. Magn. Mater.* **2000**, *209*, 80; c) T. Nakajima, A. Ishiguro, Y. Wakatsuki, *Angew. Chem.* **2001**, *113*, 1096; *Angew. Chem. Int. Ed.* **2001**, *40*, 1066; d) F. Jalilehvand, L. Eriksson, J. Glaser, M. Maliarik, J. Mink, M. Sandström, I. Toth, J. Toth, *Chem. Eur. J.* **2001**, *7*, 2167; e) A. F. Heyduk, D. J. Krodel, E. E. Meyer, D. G. Nocera, *Inorg. Chem.* **2002**, *41*, 634; f) C.-Y. Yeh, C.-H. Chou, K.-C. Pan, C.-C. Wang, G.-H. Lee, Y. O. Su, S.-M. Peng, *J. Chem. Soc. Dalton Trans.* **2002**, 2670; g) C. Tejel, M. A. Ciriano, B. E. Villarroja, J. A. Lopez, F. J. Lahoz, L. A. Oro, *Angew. Chem.* **2003**, *115*, 547; *Angew. Chem. Int. Ed.* **2003**, *42*, 530; h) T. Sheng, R. Appelt, V. Comte, H. Vahrenkamp, *Eur. J. Inorg. Chem.* **2003**, 3731; i) E. J. Fernandez, J. M. Lopez-de-Luzuriaga, M. Monge, M. Montiel, M. E. Olmos, J. Pérez, A. Laguna, F. Mendizabal, A. A. Mohamed, J. P. Fackler, Jr., *Inorg. Chem.* **2004**, *43*, 3573.
- [26] a) M.-M. Rohmer, M. Bénard, *Chem. Soc. Rev.* **2001**, *30*, 340; b) M.-M. Rohmer, A. Strich, M. Bénard, J.-P. Malrieu, *J. Am. Chem. Soc.* **2001**, *123*, 9126; c) N. Benbellat, M.-M. Rohmer, M. Bénard, *Chem. Commun.* **2001**, 2368; d) F.-Y. Li, L. Chen, C.-Y. Mou, S.-M. Peng, Y. Wang, *Int. J. Mol. Sci.* **2002**, *3*, 38; e) P. Kiehl, M.-M. Rohmer, M. Bénard, *Inorg. Chem.* **2004**, *43*, 3151.
- [27] a) F. A. Cotton, C. A. Murillo, D. J. Timmons, *Chem. Commun.* **1999**, 1427; b) F. A. Cotton, E. V. Dikarev, M. A. Petrukhina, *J. Chem. Soc. Dalton Trans.* **2000**, 4241; c) K.-T. Wong, J.-M. Lehn, S.-M. Peng, G.-H. Lee, *Chem. Commun.* **2000**, 2259; d) F. P. Pruchnik, P. Jakimowicz, Z. Ciunik, K. Stanislawek, L. A. Oro, C. Tejel, M. A. Ciriano, *Inorg. Chem. Commun.* **2001**, *4*, 19; e) F. A. Cotton, C. Lin, C. A. Murillo, *Chem. Commun.* **2001**, 11.
- [28] J.-P. Lang, S.-J. Ji, Q.-F. Xu, Q. Shen, K. Tatsumi, *Coord. Chem. Rev.* **2003**, *241*, 47.

Asymmetric Synthesis of Diarylmethyl Amines by Rhodium-Catalyzed Asymmetric Addition of Aryl Titanium Reagents to Imines**

Tamio Hayashi,* Masahiro Kawai, and Norihito Tokunaga

Asymmetric synthesis of diarylmethyl amines has attracted growing attention owing to their importance in biological activity.^[1] Among several methods for performing the asymmetric synthesis,^[2,3] catalytic asymmetric addition of aryl metal reagents to imine derivatives seems to be most promising, provided that both high enantioselectivity and high catalytic activity are realized.^[4] After our publication on the rhodium-catalyzed asymmetric addition of aryl stannanes to *N*-sulfonylimines,^[5] two reports appeared on catalytic asymmetric arylation: 1) Bräse, Bolm, and co-workers described the addition of a phenylzinc reagent to masked *N*-formylimines in the presence of a chiral ketimine catalyst,^[6] and 2) Tomioka illustrated the rhodium-catalyzed addition of aryl boroxines to *N*-tosylimines in which high enantioselectivity was observed for sterically tuned aryl imines.^[7] Herein we report another rhodium-catalyzed asymmetric arylation in which the addition of aryl titanium reagents to sulfonylimines proceeds with high enantioselectivity under mild conditions (20 °C, 1 h) to give diarylmethyl amines with up to 96 % *ee*.

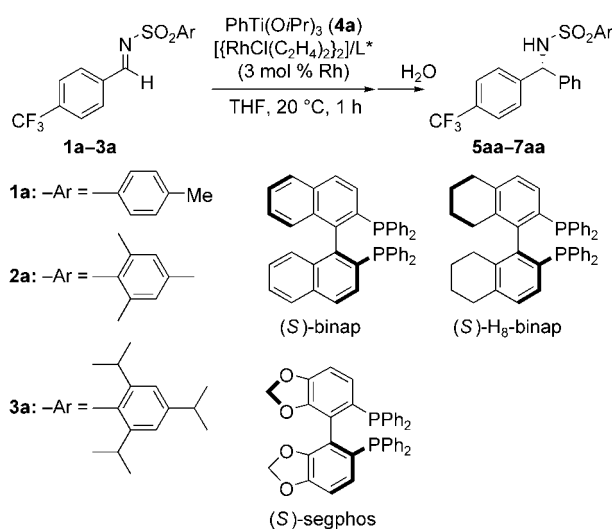
During our studies on rhodium-catalyzed asymmetric 1,4-additions to α,β -unsaturated ketones,^[8] we found that the phenyltitanium reagent $\text{PhTi}(\text{O}i\text{Pr})_3$ is highly reactive toward transmetalation and forms a phenyl–rhodium bond. In the presence of a rhodium/(*S*)-binap catalyst in THF at 20 °C, the catalytic 1,4-addition gives titanium enolates as 1,4-addition products with high enantioselectivity.^[9] Under similar reaction conditions (Scheme 1), the addition of $\text{PhTi}(\text{O}i\text{Pr})_3$ ^[10] (**4a**) to *N*-tosylarylimine **1a**, which was prepared from 4-trifluoromethylbenzaldehyde and 4-toluenesulfonamide,^[11] took place rapidly to give the tosylamide of diarylmethyl amine **5aa** after aqueous workup, unfortunately with only 28 % *ee* (Table 1, entry 1). The use of (*S*)- H_8 -binap^[12] and (*S*)-segphos^[13] in place of (*S*)-binap^[14] improved the enantioselectivity up to 43 % and 76 % *ee*, respectively (Table 1, entries 4 and 6). The relatively narrow dihedral angle of the biaryl bisphosphine ligand segphos^[14] is considered to exert a positive influence on the enantioselectivity in the present

[*] Prof. T. Hayashi, M. Kawai, N. Tokunaga
Department of Chemistry, Graduate School of Science
Kyoto University
Sakyo, Kyoto 606-8502 (Japan)
Fax: (+81) 75-753-3988
E-mail: thayashi@kuchem.kyoto-u.ac.jp

[**] This work was supported by a Grant-in-Aid for Scientific Research, the Ministry of Education, Culture, Sports, Science, and Technology, Japan. N.T. thanks the Japan Society for the Promotion of Science for the award of a fellowship for graduate students.



Supporting information for this article is available on the WWW under <http://www.angewandte.org> or from the author.



Scheme 1. Rhodium-catalyzed asymmetric arylation of imines **1a-3a** with $\text{PhTi}(\text{OiPr})_3$ (**4a**).

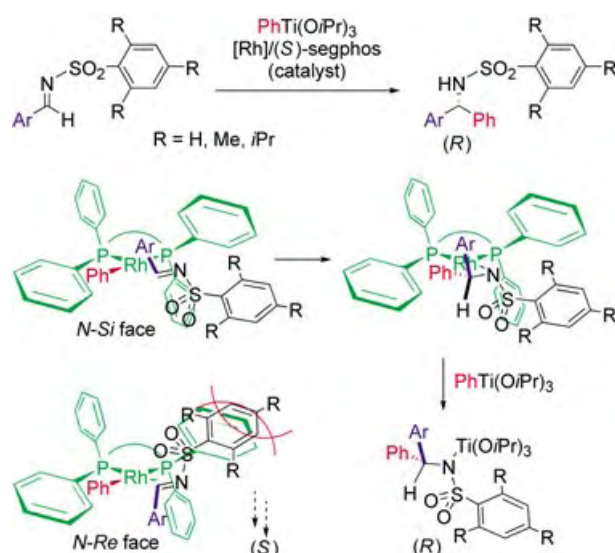
Table 1: Rhodium-catalyzed asymmetric arylation of imines **1a-3a** with $\text{PhTi}(\text{OiPr})_3$ (**4a**).^[a]

Entry	Imine	Ligand	Yield [%] ^[b]	ee [%] ^[c,d]
1	1a	(S)-binap	97 (5aa)	28 (R)
2	2a	(S)-binap	71 (6aa)	49 (R)
3	3a	(S)-binap	58 (7aa)	71 (R)
4	1a	(S)-H ₈ -binap	96 (5aa)	43 (R)
5	3a	(S)-H ₈ -binap	86 (7aa)	82 (R)
6	1a	(S)-segphos	99 (5aa)	76 (R)
7	2a	(S)-segphos	97 (6aa)	88 (R)
8	3a	(S)-segphos	98 (7aa)	93 (R)

[a] The reaction was carried out in THF at 20 °C for 1 h with **4a** (2 equiv) in the presence of the catalyst generated from $[\{\text{RhCl}(\text{C}_2\text{H}_4)_2\}_2]$ and a chiral phosphine ligand. [b] Yields of isolated amines (column chromatography: silica gel, hexane/EtOAc (2:1)). [c] Determined by HPLC analysis with a chiral stationary phase column (Chiralcel OD-H: hexane/2-propanol=80:20 for **5aa** and **6aa**; hexane/2-propanol=98:2 for **7aa**). [d] The configurations of the amines were assigned by consideration of the stereochemical reaction pathway (see text).

asymmetric phenylation, although the enantioselectivity is still not satisfactory.

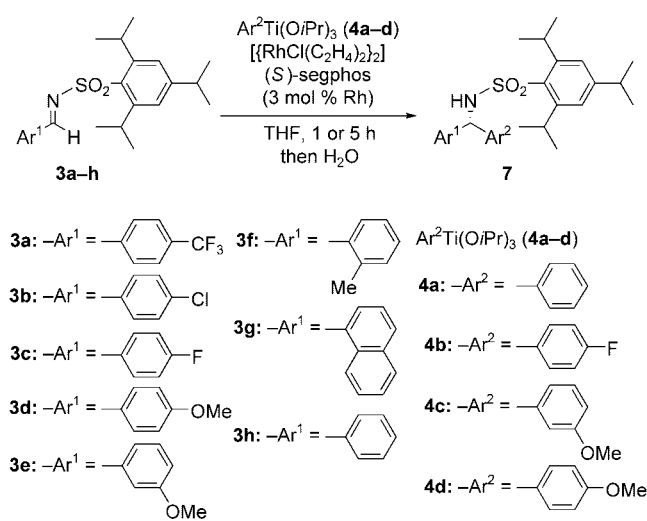
For the asymmetric 1,4-addition to α,β -unsaturated ketones,^[15] esters,^[16] and alkenylphosphonates^[17] catalyzed by a rhodium complex coordinated with (S)-binap, we have proposed stereorecognition models that successfully rationalize the absolute configuration of the products. By applying this type of model to the present reaction of N-alkylidene sulfonamides,^[18] it is evident that the enantioface of the imine is recognized by steric repulsions between one of the phenyl rings on the diphenylphosphino group and the aromatic ring on the arene sulfonamide (Scheme 2). Steric tuning of the arene sulfonamide moiety by introduction of sterically bulky groups onto the aromatic ring actually brought about enhancement of the enantioselectivity to an acceptable level. Thus, the asymmetric addition of phenyltitanium **4a** to mesitylenesulfonamide **2a** and triisopropylbenzenesulfonamide **3a** catalyzed by rhodium/(S)-binap gave the corre-



Scheme 2. Stereochemical pathway in the catalytic asymmetric arylation of imines.

sponding phenylation products **6aa** and **7aa** with 49 and 71 % ee, respectively (Table 1, entries 2 and 3). The higher enantioselectivity in the asymmetric addition to triisopropylbenzenesulfonamide (**3a**) was also observed in the reaction catalyzed by the rhodium complexes of (S)-H₈-binap and (S)-segphos (Table 1, entries 5 and 8). The combination of (S)-segphos and triisopropylbenzenesulfonamide **3a** gave the diarylmethylamine (R)-**7aa** with 93 % ee (Table 1, entry 8).

The present asymmetric phenylation with phenyltitanium **4a** catalyzed by rhodium/(S)-segphos was also successful for triisopropylbenzenesulfonamides of other aromatic imines **3**. The aromatic imines substituted with chloro (**3b**), fluoro (**3c**), and methoxy (**3d**) at the 4-position of the phenyl and the imines **3e-g** derived from 2-MeC₆H₄CHO, 3-MeOC₆H₄CHO, and 1-naphthaldehyde, respectively, gave the corresponding sulfonamides of diarylmethyl amines (R)-**7** in high yields (Scheme 3). The enantioselectivity ranged from 86 to 96 % ee



Scheme 3. Asymmetric arylation of imines **3** with $\text{Ar}^2\text{Ti}(\text{OiPr})_3$ (**4**) catalyzed by rhodium/(S)-segphos.

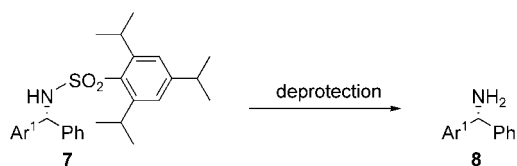
(Table 2, entries 2–7). The reaction of aryl titanium reagents **4b–d** (with the fluoro or methoxy group at the 3- or 4-position on the phenyl ring) also proceeded with high enantioselectivity (Table 2, entries 8–11). The reaction of imine **3h** with 4-fluorophenyltitanium **4b**, which is a reverse combination of the reaction of **3c** with **4a**, gave the *S* isomer of (4-fluorophenyl)(phenyl)methylamine **7ca** (93% *ee*) in quantitative yield (Table 2, entry 8). The reaction of 4-methoxyphenyltitanium **4d** with imines **3a** and **3b** proceeded as well to give diarylmethyl amines in which both aryl groups are substituted phenyls (Table 2, entries 10 and 11).

Table 2: Asymmetric arylation of imines **3** with $\text{ArTi}(\text{OiPr})_3$ (**4**) catalyzed by rhodium/(*S*)-segphos.^[a]

Entry	3	4	<i>T</i> [°C]	Yield [%] ^[b]	<i>ee</i> [%] ^[c,d]
1	3a	4a	20	98 (7aa)	93 (<i>R</i>)
2	3b	4a	20	95 ^[e] (7ba)	94 (<i>R</i>)
3	3c	4a	30	99 (7ca)	92 (<i>R</i>)
4	3d	4a	40	98 (7da)	92 (<i>R</i>)
5	3e	4a	40	99 (7ea)	86 (<i>R</i>)
6 ^[f]	3f	4a	20	99 (7fa)	89 (<i>R</i>)
7	3g	4a	30	99 (7ga)	96 (<i>R</i>)
8	3h	4b	20	96 (7hb) ^[g]	93 (<i>S</i>)
9 ^[f]	3h	4c	40	86 (7hc) ^[h]	90 (<i>S</i>)
10	3a	4d	40	97 (7ad)	88 (<i>S</i>)
11	3b	4d	40	94 (7bd)	88 (<i>R</i>)

[a] The reaction was carried out in THF at the given temperature for 1 h with **4** (2 equiv) in the presence of the catalyst (3 mol%) generated from $[\{\text{RhCl}(\text{C}_2\text{H}_5)_2\}_2]$ and (*S*)-segphos. [b] Yields of isolated amines (column chromatography: silica gel, hexane/EtOAc (2:1)). [c] Determined by HPLC analysis with a chiral stationary phase column (Chiralcel OD-H: hexane/2-propanol=98:2 for **7aa**, **7ba**, **7ca**, **7da**, **7hb**; hexane/2-propanol=100:1 for **7ga**, **7ad**, **7bd**. Chiralcel AD-H: hexane/2-propanol=98:2 for **7ea**, **7fa**). [d] The absolute configurations of **7ba**, **7da**, **7ga** were determined by comparison of the specific rotations of free amines **8** or their derivatives (see text). For other products, the configurations were assigned by consideration of the stereochemical reaction pathway. [e] The sulfonamide of (phenyl)(4-biphenyl)methylamine was formed in 3% yield. [f] For 5 h. [g] Enantiomer of **7ca**. [h] Enantiomer of **7ea**.

The 2,4,6-triisopropylbenzenesulfonyl group^[19] was removed from the diarylmethyl amines by standard methods for the deprotection of *p*-toluenesulfonamides (Scheme 4).^[20] Treatment of **7da** ($\text{Ar}^1 = 4\text{-MeOC}_6\text{H}_4$) with lithium in liquid ammonia at -78°C gave free amine **8da** in quantitative yield without loss of its enantiomeric purity. For **7ba** ($\text{Ar}^1 = 4\text{-ClC}_6\text{H}_4$) and **7ga** ($\text{Ar}^1 = 1\text{-naphthyl}$), the deprotection with



For **7ba** ($\text{Ar}^1 = 4\text{-ClC}_6\text{H}_4$): SmI_2 , HMPA, THF, reflux, 1 h: 53%
 For **7da** ($\text{Ar}^1 = 4\text{-MeOC}_6\text{H}_4$): Li/NH_3 (liq), THF, -78°C , 20 min: 100%
 For **7ga** ($\text{Ar}^1 = 1\text{-naphthyl}$): RedAl, toluene, 80°C , 5 h: 76%

Scheme 4. Deprotection of the sulfonamide.

lithium in ammonia was accompanied by reduction of the aryl groups to a considerable extent: $4\text{-ClC}_6\text{H}_4$ and 1-naphthyl gave phenyl and tetrahydronaphthyl, respectively. The deprotection was more selective with samarium iodide in HMPA/THF and RedAl in toluene for **7ba** and **7ga**, respectively.

In summary, the asymmetric synthesis of diarylmethyl amines was realized by rhodium-catalyzed asymmetric addition of aryl titanium reagents to *N*-alkylidene sulfonamides. A rational tuning of the arene sulfonamide moiety by introducing isopropyl groups onto the phenyl ring brought about high enantioselectivity (86–96% *ee*).

Received: July 16, 2004

Keywords: amines · arylation · asymmetric catalysis · rhodium · titanium

- [1] For examples, see: a) M. J. Bishop, R. W. McNutt, *Bioorg. Med. Chem. Lett.* **1995**, 5, 1311; b) C. M. Spencer, D. Foulds, D. H. Peters, *Drugs* **1993**, 46, 1055; c) S. Sakurai, N. Ogawa, T. Suzuki, K. Kato, T. Ohashi, S. Yasuda, H. Kato, Y. Ito, *Chem. Pharm. Bull.* **1996**, 44, 765.
- [2] For examples of asymmetric synthesis of diarylmethyl amines, see: a) K. Tomioka, I. Inoue, M. Shindo, K. Koga, *Tetrahedron Lett.* **1990**, 31, 6681; b) L. N. Pridgen, M. K. Mokhallalati, M. J. Wu, *J. Org. Chem.* **1992**, 57, 1237; c) E. J. Corey, C. J. Helal, *Tetrahedron Lett.* **1996**, 37, 4837; d) D. Delorme, C. Berthelette, R. Lavoie, E. Roberts, *Tetrahedron: Asymmetry* **1998**, 9, 3963; e) D. Taniyama, M. Hasegawa, K. Tomioka, *Tetrahedron Lett.* **2000**, 41, 5533; f) D. A. Pflum, D. Krishnamurthy, Z. Han, S. A. Wald, C. H. Senanayake, *Tetrahedron Lett.* **2002**, 43, 923; g) N. Plobeck, D. Powell, *Tetrahedron: Asymmetry* **2002**, 13, 303; h) Z. Han, D. Krishnamurthy, P. Grover, Q. K. Fang, D. A. Pflum, C. H. Senanayake, *Tetrahedron Lett.* **2003**, 44, 4195; i) N. Cabello, J.-C. Kizirian, A. Alexakis, *Tetrahedron Lett.* **2004**, 45, 4639.
- [3] For a recent pertinent review on catalytic enantioselective addition to imines, see: S. Kobayashi, H. Ishitani, *Chem. Rev.* **1999**, 99, 1069.
- [4] For a Review on catalytic asymmetric arylations, see: C. Bolm, J. P. Hildebrand, K. Muniz, N. Hermanns, *Angew. Chem.* **2001**, 113, 3382; *Angew. Chem. Int. Ed.* **2001**, 40, 3284.
- [5] T. Hayashi, M. Ishigedani, *J. Am. Chem. Soc.* **2000**, 122, 976.
- [6] N. Hermanns, S. Dahmen, C. Bolm, S. Bräse, *Angew. Chem.* **2002**, 114, 3844; *Angew. Chem. Int. Ed.* **2002**, 41, 3692.
- [7] M. Kuriyama, T. Soeta, X. Hao, Q. Chen, K. Tomioka, *J. Am. Chem. Soc.* **2004**, 126, 8128.
- [8] For reviews, see: a) T. Hayashi, K. Yamasaki, *Chem. Rev.* **2003**, 103, 2829; b) K. Fagnou, M. Lautens, *Chem. Rev.* **2003**, 103, 169.
- [9] a) T. Hayashi, N. Tokunaga, K. Yoshida, J. W. Han, *J. Am. Chem. Soc.* **2002**, 124, 12102; see also: b) K. Yoshida, T. Hayashi, *J. Am. Chem. Soc.* **2003**, 125, 2872; c) N. Tokunaga, K. Yoshida, T. Hayashi, *Proc. Natl. Acad. Sci. USA* **2004**, 101, 5445.
- [10] B. Weidmann, L. Widler, A. G. Olivero, C. D. Maycock, D. Seebach, *Helv. Chim. Acta* **1981**, 64, 357.
- [11] B. E. Love, P. S. Raje, T. C. Williams II, *Synlett* **1994**, 493.
- [12] X. Zhang, K. Mashima, K. Koyano, N. Sayo, H. Kumobayashi, S. Akutagawa, H. Takaya, *Tetrahedron Lett.* **1991**, 32, 7283.
- [13] T. Saito, T. Yokozawa, T. Ishizaki, T. Moroi, N. Sayo, T. Miura, H. Kumobayashi, *Adv. Synth. Catal.* **2001**, 343, 264.
- [14] H. Takaya, S. Mashima, K. Koyano, M. Yagi, H. Kumobayashi, T. Taketomi, S. Akutagawa, R. Noyori, *J. Org. Chem.* **1986**, 51, 629.
- [15] Y. Takaya, M. Ogasawara, T. Hayashi, M. Sakai, N. Miyaura, *J. Am. Chem. Soc.* **1998**, 120, 5579.

- [16] Y. Takaya, T. Senda, H. Kurushima, M. Ogasawara, T. Hayashi, *Tetrahedron: Asymmetry* **1999**, *10*, 4047.
- [17] T. Hayashi, T. Senda, Y. Takaya, M. Ogasawara, *J. Am. Chem. Soc.* **1999**, *121*, 11 591.
- [18] For the insertion of an imine into an aryl–rhodium bond to form an amido complex, see: C. Krug, J. F. Hartwig, *J. Am. Chem. Soc.* **2004**, *126*, 2694.
- [19] For the deprotection of a 2,4,6-triisopropylbenzenesulfonamide with lithium and DBB in THF, see: C. E. Neipp, J. M. Humphrey, S. F. Martin, *J. Org. Chem.* **2001**, *66*, 531.
- [20] T. W. Greene, P. G. M. Wuts, *Protective Groups in Organic Synthesis*, 3rd ed., Wiley, New York, **1999**, p. 604.

Heterometallic Clusters

A Gallium-Coated Gold Cluster**

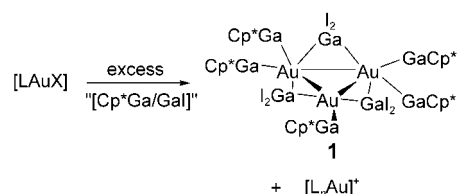
U. Anandhi and Paul R. Sharp*

There is much interest in the properties of gold in heterogeneous catalysis,^[1–3] supramolecular chemistry,^[4] nanochemistry,^[1] cluster-complex chemistry,^[5] luminescent complexes,^[6] and intermetallic compounds and alloys.^[7–12] Much of this interest centers on gold–gold and gold–other metal interactions. For applications in catalysis and intermetallic chemistry, the combination of gold—the most electronegative metal—with electropositive metals yields gold in formal negative oxidation states (aurides) or materials with strongly polarized gold–electropositive metal bonds.^[2,9–13] In this report, we describe the first complex that contains a Au–Ga bond which is also the first gold cluster complex in which the gold atoms are bonded only to an electropositive main-group metal.^[14]

Recent advances in group 13 chemistry have provided reagents of low-valent electropositive group 13 metals that can function as ligands and as reducing agents.^[15–19] With these properties in mind, we investigated reactions of gold(I) complexes with Cp*M (Cp* = pentamethylcyclopentadienyl;

M = Ga, Al) reagents to prepare gold cluster complexes of gold–electropositive metals.

First, “[Cp*Ga/GaI]”, which was prepared by the addition of Cp*K·DME (DME = 1,2-dimethoxyethane) to GaI^[20] in a ratio of ≈ 1:2, was added to a solution of [(Ph₃P)AuCl] in dichloromethane. The resulting orange solution contained the known^[21,22] gold cluster [(Ph₃P)₆Au₆]²⁺, which indicated that the gallium reagent had reduced the gold(I) centers but failed to coordinate the resulting reduced Au species. In contrast, reversing the order of addition of the components such that [(Ph₃P)AuCl] was added to excess “[Cp*Ga/GaI]” instead yielded a yellow solution from which air-sensitive orange-yellow crystals of the phosphine-free gold–gallium cluster complex [Au₃(μ-GaI₂)₃(Cp*Ga)₅] (**1**, see Scheme 1) were isolated.^[23]



Scheme 1. Isolation of the gold–gallium cluster complex [Au₃(μ-GaI₂)₃(Cp*Ga)₅] (**1**).

A yellow solid **2** was also isolated which spectroscopic data suggested was [(Ph₃P)_nAu]⁺ (*n* = 2–3)^[24–26] The addition of PCy₃ (Cy = cyclohexyl) to solutions of **2** gave rise to peaks in the ³¹P NMR spectrum which were associated with free PPh₃ and [(Cy₃P)₂Au]⁺; PCy₃ does not form *tris* adducts.^[27] The nature of the anion in **2** in solution was more difficult to define. The data obtained indicated the presence of several different Cp*Ga-containing ions at ambient temperatures that were exchanging rapidly on the ¹H and ¹³C NMR timescale. At ambient temperature, ¹H and ¹³C NMR spectra showed a single peak for Cp*, whereas ¹H NMR spectra at low temperature showed several peaks for Cp*, and ⁷¹Ga NMR measurements at ambient temperature displayed several peaks for Ga. To eliminate the possibility of a contribution from chloride ion to this mixture, [(Ph₃P)AuI] was used instead of [(Ph₃P)AuCl] in the preparation of **1**. The yield of **1** was improved, but the properties of the side product **2** were not significantly altered. Finally, the use of [(Cy₃P)AuI] in the preparation yielded a mixture of crystals of **1** and [(Cy₃P)₂Au]⁺[Cp*GaI₃][–] (**3**) from NMR spectroscopic and X-ray crystal structural analysis.^[23] These results point to the presence of several different [(Cp*)_xGa_yI_z][–] anions (*x*, *y*, *z* = integers) in solutions of **2**. Although anions that comprise polynuclear Ga complexes with Cp* have not been reported, anions which consist of polynuclear Ga complexes with Si(SiMe₃)₃ have been isolated.^[28] Cluster **1** was also prepared in a similar yield from [(Ph₃P)AuI] and a mixture of Cp*Ga and GaI₃, but in this case, **2** was not formed and the co-products were not isolated or identified.^[29]

The molecular structure of cluster **1** in the solid-state^[23] is shown in Figure 1. The structure consists of a triangle of gold atoms which is bridged by GaI₂ units on its edges. A two-fold

[*] Dr. U. Anandhi, Prof. P. R. Sharp
125 Chemistry
University of Missouri
Columbia, MO 65211 (USA)
Fax: (+1) 573-882-2754
E-mail: sharp@missouri.edu

[**] Support from the Chemical Sciences, Geosciences, and Biosciences Division, Office of Basic Energy Sciences, Office of Science, and the U.S. Department of Energy (DE-FG02-88ER13880) is gratefully acknowledged. We thank the National Science Foundation (Grant No. 9221835) for a contribution towards the purchase of NMR equipment. We also thank Dr. C. Barnes for assistance with the X-ray experiments and Dr. R. Glaser for helpful discussions on the DFT calculations.



Supporting information for this article is available on the WWW under <http://www.angewandte.org> or from the author.

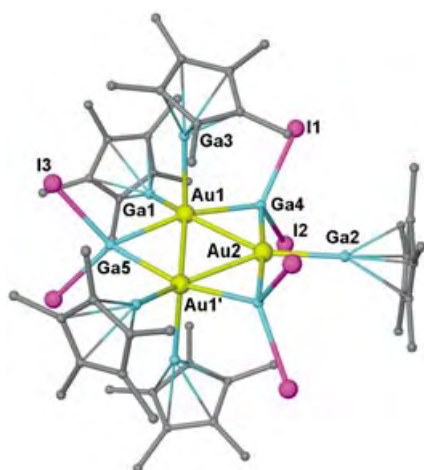


Figure 1. Drawing of $[\text{Au}_3(\mu\text{-GaI}_2)_3(\text{Cp}^*\text{Ga})_5]$ **1**. Hydrogen atoms are omitted for clarity. Only one orientation of the twofold disordered Cp^* of Ga2 is shown. Selected distances [Å] and angles [°]: Au1–Au2 2.7256(6), Au1–Au1' 2.8045(8), Au1–Ga1 2.3840(12), Au1–Ga3 2.6199(13), Au2–Ga2 2.3773(17), Au1–Ga5 2.5325(13), Au1–Ga4 2.5322(12), Au2–Ga4 2.5280(12); Au2–Au1–Au1' 59.04(1), Au1–Au2–Au1' 61.93(2), Ga1–Au1–Ga3 101.93(5), Au2–Ga4–Au1 65.18(3), Au1–Ga5–Au1' 67.24(4).

axis along the Ga2–Au2–Ga5 vector relates the two halves of the molecule. The two symmetry-related Au atoms (Au1 and Au1') are each coordinated by two Cp^*Ga units, whereas the third unique gold atom (Au2), which lies on the two-fold axis, is coordinated by only one Cp^*Ga unit (Ga2). This Cp^*Ga unit also lies on the two-fold axis and results in the disorder of the Cp^* group over two positions. The Cp^*Ga units are arranged around the Au_3 triangle in approximately axial and equatorial positions. The unique Cp^*Ga unit (Ga2) and the Cp^*Ga units of Ga1 and Ga1' occupy axial positions in, or nearly in, the Au_3 plane. The other two Cp^*Ga units (Ga3 and Ga3') are nearly perpendicular to the plane in opposite axial positions to Au1 and Au1'. The absence of an axial Cp^*Ga unit on Au2 may result from steric crowding because with three axial ligands, two must be on the same side of the Au_3 plane. The axial Cp^*Ga groups lie at a greater distance (Au1–Ga3 = 2.6199(13) Å) from the gold atoms than the equatorial Cp^*Ga groups (Au1–Ga1 = 2.3840(12) Å, Au2–Ga2 = 2.3773(17) Å) which suggests a weaker interaction with the former. The axial distance is close to the sum of the single-bond covalent radii of 2.58 Å for Au–Ga.^[30] The shorter equatorial distances are comparable to the Pt–Ga bond lengths (average = 2.335 Å) in $[\text{Pt}(\text{Cp}^*\text{Ga})_4]$ after correction for the slightly larger (0.04 Å) covalent radius of Au.^[31]

The $\text{Cp}^*(\text{centroid})\text{--Ga}$ distance in Cp^*Ga –metal complexes is thought to correlate with the degree of charge transfer from the Ga center to the metal atom.^[32] Greater charge transfer results in a smaller radius for gallium and a smaller $\text{Cp}^*(\text{centroid})\text{--Ga}$ distance. The axial $\text{Cp}^*(\text{centroid})\text{--Ga}$ distance of 2.01(1) Å is somewhat smaller than those of Cp^*Ga in the solid state (2.081 Å)^[33] or in the gas phase (2.081(5) Å)^[34] and is similar to $[(\text{Cp}^*\text{Ga})_4\text{Ni}]$ (2.003(4) Å)^[32]—a complex which is thought to involve relatively little charge transfer from the Cp^*Ga ligand. The

corresponding equatorial distances of 1.89(1) and 1.88(1) Å indicate a greater degree of charge transfer to the gold centers and are similar to that found in $[\text{Cp}^*\text{GaFe}(\text{CO})_4]$ (1.863(4) Å).^[35] The two Au–Au distances in **1** (2.7256(6) and 2.8045(8) Å) are shorter than those found in metallic gold (2.884 Å) and are well within the range associated with Au–Au cluster bonds.^[5] DFT (density functional theory) calculations also support the presence of Au–Au bonds (see below). The three other known Au_3 clusters have, on average, similar Au–Au distances, although $[(\text{dppe})_2\text{Au}_3\text{In}_3\text{Br}_7(\text{thf})]^-$ and $[(\text{dppe})_2\text{Au}_3\text{In}_3\text{Cl}_6(\text{thf})_6]$ (dppe = 1,2-bis(diphenylphosphino)ethane) show much greater variation with one very short distance (2.575(1) and 2.562(1) Å, respectively) and two longer distances (2.860(1) and 2.858(1), and 2.939(1) and 2.931(1) Å, respectively).^[36,37] The Au–Au distances (2.764(2), 2.780(3), and 2.757(2) Å) for the symmetric Au_3 cluster $[(\text{Cp}'\text{Nb})_3\text{Au}_3(\mu\text{-H})_6]$ ($\text{Cp}' = \text{C}_5\text{H}_4\text{SiMe}_3$) are very regular and lie between the two values for **1**.^[38]

In contrast to the results obtained for **1** in the solid state that indicate three different types of Cp^*Ga groups, ^1H and ^{13}C NMR spectra of **1** in CD_2Cl_2 show only one signal for the Cp^*Ga ligands at 25 °C. Lowering the temperature down to –90 °C leads to increased broadening of the peak without the resolution of the 1:2:2 pattern expected for the three different Cp^* groups. This most likely indicates rapid exchange of the different Cp^*Ga groups. No signals were detected in the ^{71}Ga NMR spectrum at 25 °C or at –70 °C; the absence of signals in the ^{71}Ga NMR spectra for several Cp^*Ga –Pt complexes has also been reported.^[39] Addition of free Cp^*Ga to a solution of **1** at 25 °C yielded a single peak in the ^1H NMR spectrum which lies between the values for **1** and Cp^*Ga . This indicates exchange of free and coordinated Cp^*Ga groups. Fluxional behavior and exchange with free Cp^*M units has been observed with the linear Pd_3 cluster $[\text{Pd}_3(\text{Cp}^*\text{In})_4(\mu\text{-Cp}^*\text{In})_4]$,^[40] but not with dinuclear $[\text{Pt}_2(\text{Cp}^*\text{Ga})_2(\mu\text{-Cp}^*\text{Ga})_3]$ complexes.^[31,41]

The above data show the presence of a Au_3 triangular cluster with neutral electron-donor Cp^*Ga ligands. However, the presence of the bridging GaI_2 units allows an alternative interpretation of the structure as a six-membered Au–Ga ring without Au–Au bonds.^[42] Furthermore, there is ambiguity in the assignment of the oxidation states of the Au centers. With neutral Cp^*Ga ligands, the GaI_2 units may be assigned a positive, neutral, or negative charge which corresponds to the oxidation states +3, +2, or +1 of gallium. Corresponding oxidation states for the Au centers would then be –1, 0, or +1. To assist in the resolution of these ambiguities, DFT calculations with the LAN2DZ basis set, which has been shown to be effective for Au clusters,^[43] were performed on an analogue of **1** with Cp ligands (Cp = cyclopentadienyl).^[29] The optimized structure (no symmetry constraints) corresponded closely to the structure for **1** showing the same axial–equatorial distribution of the CpGa ligands. Isodensity surfaces of the electron-density distribution show the topological features expected for Au_3 and Au_2Ga rings (see Figure 2). Ring critical points in the centers and bond paths^[44a] along the Au–Au and Au–Ga bonds are clearly visible and support the view of **1** as a Au_3 cluster ligated by Ga centers. Natural population analysis^[44b] atom charges are

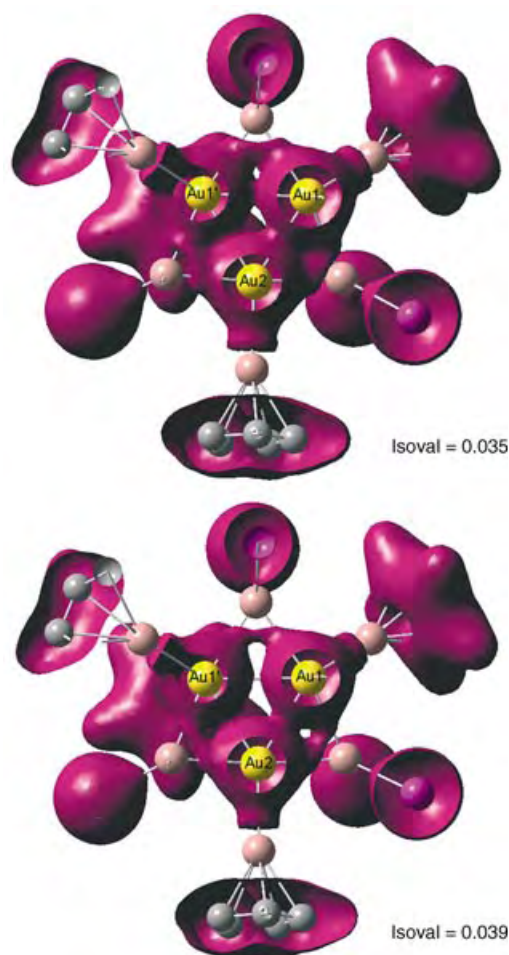


Figure 2. Isodensity surfaces of the electron-density distribution (0.035 e.a.u.³ (top) and 0.039 e.a.u.³). Hydrogen atoms are not shown. Atoms and density from slightly above the Au₃ plane have been removed for clarity.

provided in Table 1. A small positive charge is assigned to the gold atoms. This charge is nearly equal to those of the bridging gallium atoms (Ga4 and Ga5) which indicates an essentially nonpolar covalent bond and suggests the oxidation assignment of +2 for the Ga centers of the GaI₂ units and 0 for the Au atoms. Large positive charges are assigned to the Ga atoms of the CpGa ligands (Ga1, Ga2, Ga3) and indicate substantial bond polarization for these Ga–Au bonds. Negative charges reside on the Cp groups and the iodine centers.^[29] The polarity of the axial CpGa–Au bond is somewhat less than those of the equatorial bonds; this

Table 1: Calculated atom charges in the Cp analogue of **1**.

Atom	Charge	Atom	Charge
Au1	0.12	Ga1	0.86
Au2	0.16	Ga2	0.90
		Ga3	0.78
		Ga4	0.11
		Ga5	0.11

observation is consistent with the Cp*(centroid)–Ga distances discussed above.

In conclusion, low-valent Ga species are effective reducing reagents for [LAuX] (L = ligand, X = anion) and, when present in excess, they effectively trap the reduced gold centers by ligation. Given the large number of phosphine–gold cluster complexes reported,^[22,45] this bodes well for the synthesis of a new family of group 13 ligated gold cluster complexes. DFT calculations on the Cp analogue of **1** show a Au₃ cluster with Au–Au bonds with near-charge-neutral gold atoms and strongly polarized CpGa–Au bonds. Efforts are now underway to prepare the aluminum analogue of **1** and other Au–electropositive metal cluster complexes through a similar approach.

Experimental Section

All manipulations were performed under N₂ atmosphere in a dry box (Vacuum Atmospheres Co.) with anhydrous, dioxygen-free solvents.

[Cp*Ga/GaI].^[46] A mixture of Ga metal particles (0.50 g, 7.17 mmol) and I₂ (0.91 g, 3.58 mmol) in benzene (10 mL) was sonicated for 12 h at 50°C. KCp*·DME (0.983 g, 3.71 mmol) was added to the resulting pale green suspension of GaI,^[20] and the mixture was stirred for 48 h to give a yellow solution and a light gray precipitate. After filtration, the solid was washed with benzene (20 mL), and the combined yellow filtrates were concentrated to yield the title compound as a green-yellow solid, which was used without any further purification (Cp*Ga was not obtained on attempted sublimation of the solid). ¹H NMR (C₆D₆, 250 MHz, 25°C): δ = 1.93 (s, Cp*), 3.01 (s, DME), 3.10 ppm (s, DME); integration ratio of 10:3:2, respectively; ⁷¹Ga NMR (C₆D₆, 91.5 MHz, –70°C): δ = –645.6 ppm (br s, ω_{1/2} = 9800 Hz); no signal was observed at 25°C.

1: [(Ph₃P)AuI] (12.5 mg, 21.3 mmol) in CH₂Cl₂ (4 mL) was added dropwise to [Cp*Ga/GaI] (35.2 mg) in CH₂Cl₂ (2 mL). Small amounts of gray solid formed and the initial yellow color faded. The reaction mixture was stirred for 5 h and was then passed through diatomaceous earth. The volatiles were removed in vacuo. Addition of diethyl ether to the resulting oily residue gave a pale yellow solid, **2**, and a dark yellow-colored solution, which were separated by filtration. Solid **2** was washed several times with ether until the washings were colorless, and then dried (20.6 mg). The dark yellow filtrate and the ether washings were combined; on standing overnight at room temperature, orange-yellow crystals of **1**, which were suitable for X-ray crystal structure analysis, formed (8.5 mg, 47% based on Au). (The same procedure repeated with [(Ph₃P)AuCl] gave similar results.)

Data for **1**: ¹H NMR (CD₂Cl₂, 250 MHz, 25°C): δ = 1.15 (t, 6H, (CH₃CH₂)₂O), 2.12 (s, 75H, Cp*), 3.45 ppm (q, 4H, (CH₃CH₂)₂O); ¹³C NMR (CD₂Cl₂, 75.47 MHz, 25°C): δ = 10.17 (Cp*–CH₃), 14.98 ((CH₃CH₂)₂O), 65.54 ((CH₃CH₂)₂O), 114.79 ppm (Cp*–ring); at –70°C, the peaks broaden slightly; Far-IR (Nujol mull, polyethylene plates): ν̄ = 468 cm^{–1} (br, Au–GaCp*); elemental analysis: calcd for C₅₀H₇₅Au₃Ga₈I₆·C₄H₁₀O: C 24.38, H 3.22; found: C 24.65, H 3.22.

Data for **2**: ¹H NMR (CD₂Cl₂, 250 MHz, 25°C): δ = 1.79 (s), 7.53–7.22 ppm (m); relative integrations 1.7:1.0; ¹H NMR (CD₂Cl₂, 250 MHz, –70°C): δ = 1.74 & 1.71 (s), 1.63 (s), 7.50–7.06 ppm (m); relative integrations 0.8:0.9:1.0; ¹³C NMR (CD₂Cl₂, 62.9 MHz, 25°C): δ = 9.16 (Cp*–CH₃), 113.93 (Cp*–ring), 128.88 (t, J_{C-P} = 15 Hz), 130.08 (s), 133.17 ppm (d, J_{C-P} = 50 Hz); ³¹P NMR (CD₂Cl₂, 101.25 MHz, –70°C): δ = 19.45 ppm (s); no signal is observed at 25°C. ⁷¹Ga NMR (CH₂Cl₂, 91.5 MHz, 25°C): δ = –457.74 (s, ω_{1/2} = 164 Hz), –236.53 (s, ν_{1/2} = 401 Hz), –40.81 (s, ω_{1/2} = 328 Hz), 123.15 ppm (s, ω_{1/2} = 255 Hz).

Received: July 13, 2004

Revised: August 18, 2004

Keywords: cluster compounds · cyclopentadienyl ligands · gallium · gold · heterometallic complexes

- [1] P. Schwerdtfeger, *Angew. Chem.* **2003**, *115*, 1936; *Angew. Chem. Int. Ed.* **2003**, *42*, 1892.
- [2] A. Cho, *Science* **2003**, *299*, 1684.
- [3] M. Haruta, *Catal. Today* **1997**, *36*, 153.
- [4] H. Schmidbaur, *Gold Bull.* **2000**, *33*, 3.
- [5] D. M. P. Mingos, *J. Chem. Soc. Dalton Trans.* **1996**, 561.
- [6] Leading reference: A. A. Mohamed, I. Kani, A. O. Ramirez, J. John, P. Fackler, *Inorg. Chem.* **2004**, *43*, 3833.
- [7] R. B. King, *Inorg. Chim. Acta* **1998**, *277*, 202.
- [8] W. S. Rapson, *Gold Bull.* **1996**, *29*, 141.
- [9] U. Zachweija in *Gold: Progress in Chemistry, Biochemistry, and Technology* (Ed.: H. Schmidbaur), Wiley, New York, **1999**, p. 495.
- [10] M. Jansen, A.-V. Mudring in *Gold: Progress in Chemistry, Biochemistry, and Technology* (Ed.: H. Schmidbaur), Wiley, New York, **1999**, p. 747.
- [11] P. Pyykkö, *Angew. Chem.* **2002**, *114*, 3723; *Angew. Chem. Int. Ed.* **2002**, *41*, 3573.
- [12] A.-V. Mudring, M. Jansen, J. Daniels, S. Krämer, M. Mehrling, J. P. P. Ramalho, M. P. A. H. Romero, *Angew. Chem.* **2002**, *114*, 128; *Angew. Chem. Int. Ed.* **2002**, *41*, 120.
- [13] A. Vittadini, A. Selloni, *J. Chem. Phys.* **2002**, *117*, 353.
- [14] For a gold cluster in which the gold atoms are bonded only to a transition metal see: A. J. Whoolery, L. F. Dahl, *J. Am. Chem. Soc.* **1991**, *113*, 6683.
- [15] N. J. Hardman, R. J. Wright, A. D. Phillips, P. P. Power, *J. Am. Chem. Soc.* **2003**, *125*, 2667.
- [16] a) G. Linti, H. Schnöckel, *Coord. Chem. Rev.* **2000**, *206–207*, 285; b) A. Schnepf, H. Schnöckel, *Angew. Chem.* **2002**, *114*, 3682; *Angew. Chem. Int. Ed.* **2002**, *41*, 3532; c) J. Vollet, J. R. Hartig, H. Schnöckel, *Angew. Chem.* **2004**, *116*, 3248; *Angew. Chem. Int. Ed.* **2004**, *43*, 3186.
- [17] R. A. Fischer, J. Weiß, *Angew. Chem.* **1999**, *111*, 3002; *Angew. Chem. Int. Ed.* **1999**, *38*, 2830.
- [18] W. Uhl, *Rev. Inorg. Chem.* **1998**, *18*, 239.
- [19] R. Murugavel, V. Chandrasekhar, *Angew. Chem.* **1999**, *111*, 1287; *Angew. Chem. Int. Ed.* **1999**, *38*, 1211.
- [20] M. L. H. Green, P. Mountford, G. J. Smout, R. S. Speel, *Polyhedron* **1990**, *9*, 2763.
- [21] B. W. Flint, Y. Yang, P. R. Sharp, *Inorg. Chem.* **2000**, *39*, 602.
- [22] K. P. Hall, D. M. P. Mingos, *Prog. Inorg. Chem.* **1984**, *32*, 237.
- [23] X-ray diffraction data for **1**: $M_f = C_{50}H_{75}Au_3Ga_8I_6 \cdot C_4H_{10}O$, $T = 173$ K, $\lambda = 0.71073$ Å, monoclinic, $C2/c$, $a = 24.5902(13)$ Å, $b = 14.3255(7)$ Å, $c = 23.9938(13)$ Å, $\beta = 119.3630(10)^\circ$, $Z = 4$, no. refl = 8167 ($5062 > 2\sigma(I)$), refinement on F^2 , $R_f(> 2\sigma(I)) = 0.0528$, $R_w(\text{all data}) = 0.1215$, $GOF = 1.003$. Data for **3**: $M_f = C_{46}H_{81}AuGaI_3P_2$, $T = 173$ K, $\lambda = 0.71073$ Å, triclinic, $P\bar{1}$, $a = 11.2723(4)$ Å, $b = 11.7563(4)$ Å, $c = 19.9135(7)$ Å, $\alpha = 83.9070(10)$, $\beta = 89.1700(10)$, $\gamma = 77.3550(10)^\circ$, $Z = 4$, no. refl = 11 107 ($8862 > 2\sigma(I)$), refinement on F^2 , $R_f(> 2\sigma(I)) = 0.0652$, $R_w(\text{all data}) = 0.1946$, $GOF = 1.038$. A drawing of the structure is available in the Supporting Information. 1H NMR (CD_2Cl_2 , 250 MHz, 25 °C): $\delta = 1.78$ (s, 15H, Cp*), 1.94 (m, 24H, PCy₃), 1.79 (m, 6H, PCy₃), 1.38 ppm (m, 36H, PCy₃); ^{31}P NMR (CD_2Cl_2 , 101 MHz, 25 °C): $\delta = 64.4$ (s). CCDC 244293 (**1**) and 244294 (**3**) contain the supplementary crystallographic data for this paper. These data can be obtained free of charge via www.ccdc.cam.ac.uk/conts/retrieving.html (or from the Cambridge Crystallographic Data Centre, 12, Union Road, Cambridge CB21EZ, UK; fax: (+44)1223-336-033; or deposit@ccdc.cam.ac.uk).
- [24] G. A. Bowmaker, J. C. Dyson, P. C. Healy, L. M. Engelhardt, C. Pakawatchai, A. H. White, *J. Chem. Soc. Dalton Trans.* **1987**, 1089.
- [25] R. V. Parish, O. Parry, C. A. McAuliffe, *J. Chem. Soc. Dalton Trans.* **1981**, 2098.
- [26] C. B. Colburn, W. E. Hill, C. A. McAuliffe, R. V. Parish, *J. Chem. Soc. Chem. Commun.* **1979**, 218.
- [27] G. A. Bowmaker, C. L. Brown, R. D. Hart, P. C. Healy, C. E. F. Rickard, A. H. White, *J. Chem. Soc. Dalton Trans.* **1999**, 881.
- [28] a) W. Kostler, G. Linti, *Angew. Chem.* **1997**, *109*, 2758; *Angew. Chem. Int. Ed. Engl.* **1997**, *36*, 2644; b) M. Kehrwald, W. Köstler, A. Rodig, G. Linti, T. Blank, N. Wiberg, *Organometallics* **2001**, *20*, 860.
- [29] See Supporting Information.
- [30] L. Pauling, *The Nature of the Chemical Bond and the Structure of Molecules and Crystals*, Cornell University Press, **1960**.
- [31] G. Christian, T. Steinke, D. Weiss, M. Cokoja, M. Winter, R. A. Fischer, *Organometallics* **2003**, *22*, 2705.
- [32] P. Jutzi, B. Neumann, L. O. Schebaum, A. Stämmler, H.-G. Stämmler, *Organometallics* **1999**, *18*, 4462.
- [33] D. Loos, E. Baum, A. Ecker, H. Schnöckel, A. J. Downs, *Angew. Chem.* **1997**, *109*, 894; *Angew. Chem. Int. Ed. Engl.* **1997**, *36*, 860.
- [34] A. Haaland, K. G. Martinsen, H. V. Volden, D. Loos, H. Schnöckel, *Acta Chem. Scand.* **1994**, *48*, 172.
- [35] P. Jutzi, B. Neumann, G. Reumann, H.-G. Stämmler, *Organometallics* **1998**, *17*, 1305.
- [36] F. P. Gabbai, S.-C. Chung, A. Schier, S. Krueger, N. Roesch, H. Schmidbaur, *Inorg. Chem.* **1997**, *36*, 5699.
- [37] F. P. Gabbai, A. Schier, J. Riede, H. Schmidbaur, *Inorg. Chem.* **1995**, *34*, 3855.
- [38] A. Antinolo, F. A. Jalon, A. Otero, M. Fajardo, B. Chaudret, F. Lahoz, J. A. Lopez, *J. Chem. Soc. Dalton Trans.* **1991**, 1861.
- [39] D. Weiss, PhD thesis, Ruhr Universität Bochum (Bochum), **2001**.
- [40] T. Steinke, C. Gemel, M. Winter, R. A. Fischer, *Angew. Chem.* **2002**, *114*, 4955; *Angew. Chem. Int. Ed.* **2002**, *41*, 4761.
- [41] D. Weiss, M. Winter, R. A. Fischer, C. Yu, K. Wichmann, G. Frenking, *Chem. Commun.* **2002**, 2495.
- [42] We thank a referee for this observation.
- [43] J. J. BelBruno, *Heteroat. Chem.* **1998**, *9*, 651.
- [44] a) R. F. W. Bader, *Atoms in Molecules: A Quantum Theory*, Oxford University Press, New York, **1994**; b) E. D. Glendening, A. E. Reed, J. E. Carpenter, F. Weinhold, NBO, version 3.1.
- [45] J. J. Steggerda, J. J. Bour, J. W. A. Van der Velden, *Recl. J. R. Neth. Chem. Soc.* **1982**, *101*, 164.
- [46] Based on the preparation of Cp*Ga: P. Jutzi, L. O. Schebaum, *J. Organomet. Chem.* **2002**, *654*, 176.

Heterometallic Complexes

Templating Open- and Closed-Chain Structures around Metal Complexes of Macrocycles**

Sarah L. Heath, Rebecca H. Laye,
Christopher A. Muryn, Nicola Lima, Roberta Sessoli,*
Rachel Shaw, Simon J. Teat, Grigore A. Timco,* and
Richard E. P. Winpenny*

The ability to control the structures of polymetallic complexes is a key concern if we are ever to exploit their properties. A lot of beautiful science has emerged with this challenge, as shown by the grid structures created by Lehn^[1] and Thompson,^[2] or the panel structures created by Fujita.^[3] A particularly attractive idea is to template the structure about an otherwise innocent ion to modify the structure without changing electronic properties. The work of Saalfrank et al. in which different sized metallocryptands were templated is particularly relevant here,^[4] as is the work of Raymond and co-workers in which the geometry of the molecule is varied from a dimetallic helix to a tetrahedron depending on the presence of a tetrahedral counterion.^[5] Our work has concerned new methods to influence structure, and, in the case of cyclic chromium fluoride cages, we have shown that the size of metal rings can be influenced by the choice of secondary ammonium cations.^[6,7] Here we use metal complexes of macrocycles as templates to show that further unusual structures can be formed.

Previously we reported the first heterometallic rings of the type $[\text{NH}_2\text{R}_2][\text{Cr}_7\text{MF}_8(\text{O}_2\text{CCMe}_3)_{16}]$ (R = alkyl sidechain; $\text{M} = \text{Ni}^{2+}$, Co^{2+} , Fe^{2+} , Mn^{2+} , or Cd^{2+}).^[6] The facile synthesis of these compounds led us to look more widely at a reaction matrix that contains chromium fluoride, pivalate ion, a second metal ion, and templates that contain NH groups. When the second metal is nickel and the template is a simple azacrown ether, either 1,4,7-triazacyclonane (tacn) or 1,4,7,10-tetraaza-

cyclododecane (cyclen), the macrocycle binds the nickel ion and the resultant complex then acts as the template.

Initially, chromium fluoride, nickel carbonate, and tacn were treated in pivalic acid to give $[\text{Ni}(\text{tacn})_2][\text{Cr}_8\text{Ni}_2\text{F}_{10}(\text{O}_2\text{CCMe}_3)_{20}]$ (**1**).^[8] In which the dicationic mononuclear nickel complex was found within a dianionic ring (Figure 1).

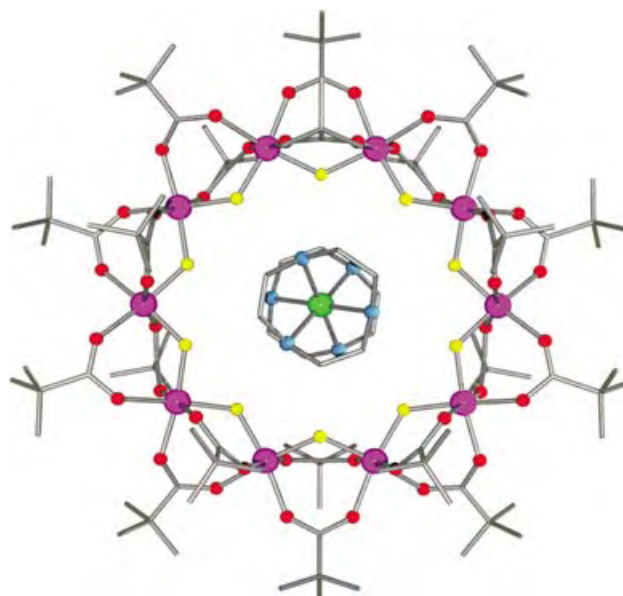


Figure 1. The crystal structure of **1**: the M_{10} wheel contains two disordered Ni atoms (see text for details). Hydrogen atoms have been omitted for clarity. Selected bond-length ranges: $\text{M}-\text{F}$ 1.930–1.949, $\text{M}-\text{O}$ 1.874–2.111, $\text{Ni}-\text{N}$ 2.115–2.135 Å (average estimated standard deviation: 0.009 Å). Colors: Cr, purple; Ni, green; F, yellow; O, red; N, blue; C, grey lines.

A better route to **1** involved the prior preparation of $[\text{Ni}(\text{tacn})_2](\text{O}_2\text{CCMe}_3)_2$ and addition of this complex to the reaction mixture (CrF_3 , NiCO_3 , and pivalic acid). The metal sites within the dianion are disordered: two Ni^{2+} ions are present according to microanalytical measurement and charge-balance considerations. The structure of the mononuclear dication is very similar to that of $[\text{Ni}(\text{tacn})_2]^{2+}$ crystallized with simpler anions,^[10] however, disorder in the structure renders a meaningful comparison of bond lengths difficult. Each of the $\text{M}\cdots\text{M}$ edges of the ten-metal ring, which is almost planar, is bridged by one fluoride and two pivalate ions in a similar manner to $[\text{Cr}_7\text{NiF}_8(\text{O}_2\text{CCMe}_3)_{16}]^-$. Each of the NH groups of the two tacn ligands are involved in hydrogen bonds; these bonds are longer than the hydrogen bonds found when simpler amines are used ($\text{N}\cdots\text{F}$ contacts range from 2.98 to 3.30 Å rather than 2.7–2.9 Å).^[6]

With the $\text{Cr}-\text{F}$ -pivalate system, octa-,^[6] nona-,^[7] and decanuclear metal rings could be synthesized by variation of the template. If 1,4,7,10-tetrazacyclododecane (cyclen) or [12]-ane- N_4) is used as a template in this chemistry, $[[\text{Ni}(\text{cyclen})_2]\text{Cr}_{12}\text{NiF}_{20}(\text{O}_2\text{CCMe}_3)_{22}]$ (**2**, see Figure 2)^[8] results. The fifteen metal sites define an “S”, in which a Ni^{2+} ion is located at the center of the “S” and two Ni^{2+} -[12]-ane- N_4 complexes lie at the termini. The cyclen macrocycles bind in the usual

[*] Dr. S. L. Heath, Dr. R. H. Laye, Dr. C. A. Muryn, R. Shaw,
Dr. G. A. Timco, Prof. R. E. P. Winpenny
Department of Chemistry
The University of Manchester
Oxford Road, Manchester, M13 9PL (UK).
Fax: (+44) 161-275-4616;
E-mail: grigore.timco@man.ac.uk
richard.winpenny@man.ac.uk

N. Lima, Prof. R. Sessoli
Laboratorio di Magnetismo Molecolare Dipartimento di Chimica
Università degli Studi di Firenze & INSTM
Via della Lastruccia, 3
50019 Sesto Fiorentino (Italy).
Fax: (+39) 055-457-3372;
E-mail: roberta.sessoli@unifi.it

S. J. Teat
CCLRC Daresbury Laboratory
Warrington, Cheshire, WA4 4AD (UK).

[**] This work was supported by the EPSRC(UK), the EC-TMR Network “QuEMolNa” (MRTN-CT-2003–504880), the University of Manchester, and the Italian MIUR (for FIRB and PRIN funding).

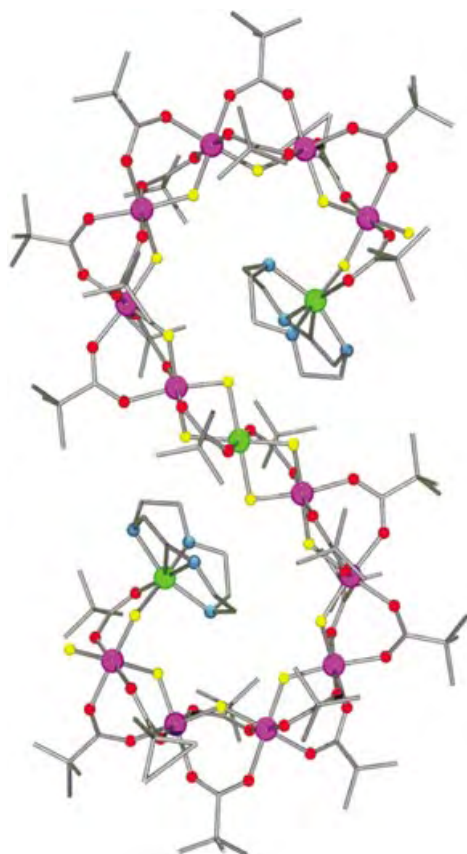


Figure 2. The crystal structure of **2**. Hydrogen atoms have been omitted for clarity. Bond-length ranges: Cr–O 1.824–2.003, Cr–F 1.893–1.966, Ni–O 1.995–2.073, Ni–F 2.015–2.093, Ni–N 2.063–2.116 (average estimated standard deviation: 0.005 Å). Colors: Cr, purple; Ni, green; F, yellow; O, red; N, blue; C, gray lines.

manner to leave *cis* vacancies on the coordinated Ni^{2+} ions, and it is the two atoms that occupy these *cis* sites which link the $[\text{Ni}([12]\text{-ane-N}_4)]^{2+}$ fragments to the termini of the metal chain. An analogous molecule with 2,2-dimethylbutyrate as the carboxylate moiety was also prepared.

The twelve Cr^{3+} ions form two hexametallac chains, which are very similar to the anionic Cr_6 horseshoes we have previously reported.^[11] However, in the previous structures, the horseshoes were linked by hydrogen bonds to secondary ammonium cations, whereas here fluoride ions directly bridge to a nickel site to create the “S” shape. The $\text{Cr}\cdots\text{Cr}$ vectors in the structure are all bridged by two pivalate ions and one fluoride ion, whereas the two $\text{Cr}\cdots\text{Ni}$ contacts at the center of the “S” are each bridged by two fluoride ions and one pivalate ion. The terminal $[\text{Ni}(\text{cyclen})]^{2+}$ units are each attached by one $\mu\text{-F}$ bridge and the oxygen atom of a pivalate ion, which chelates the final Cr^{3+} ion of the chain and also bridges to the Ni site. The metal core is almost planar with a mean deviation from planarity of 0.25 Å. There is a single $\text{N}\cdots\text{H}\cdots\text{F}$ hydrogen bond ($\text{N}\cdots\text{F}$ contact of 2.94 Å) between the cyclen unit and the bridging fluoride ion.

Preliminary magnetic studies of **1** and **2** were performed. A χT value of 16.2 emu K mol^{-1} was obtained for **1** at room temperature which is slightly smaller than the uncorrelated

value for three $S=1$ ($g_{\text{Ni}} \approx 2.2$) and eight $S=3/2$ ($g_{\text{Cr}} \approx 2.0$) centers (18.6 emu K mol^{-1}) and suggests that an antiferromagnetic interaction is present as often found in fluoro-bridged Cr^{3+} rings.^[13] Whereas χT decreases, the χ value reaches a plateau around 30 K and undergoes a steep increase below 10 K (Figure 3). The χT value levels off at low

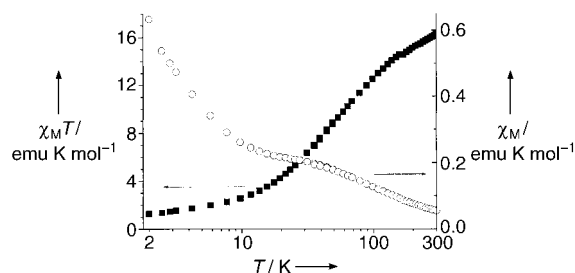


Figure 3. Temperature dependence of the magnetic susceptibility, χ (○), and its product, χT (■), for **1**.

temperature and the lowest measured value, 1.27 emu K mol^{-1} , is compatible with an uncoupled spin for Ni^{2+} (1.21 emu K mol^{-1} for $g=2.2$). This behavior can be rationalized if we assume that the antiferromagnetic-coupled ring has a $S=0$ ground state, and its contribution is superimposed on the paramagnetic ground state of the isolated $[\text{Ni}(\text{tacn})_2]^{2+}$ cation. The ring is expected to have a diamagnetic ground state only if the two Ni^{2+} ions occupy an even and an odd site of the ring. In a random distribution, the ions have a significant probability (4/9 versus 5/9) to occupy sites of the same parity to give an uncompensated $S=1$ ground state, which is not observed. Impurities, such as rings with $\text{Cr}:\text{Ni}$ stoichiometries of 9:1 or 7:3, would also influence the value of χT at low temperature, but the presence of such impurities is not compatible with the observed behavior. The most likely explanation for the $S=0$ ground state of the ring is that the Ni^{2+} ions, even if they are disordered, are always located next to each other within the rings as observed in $[(\text{VO})_2\text{Cr}_6]^{11}$ and $[(\text{VO})_2\text{Cr}_7]$ ring systems.^[7]

To our knowledge, **2** is the longest open-chain structure prepared (except for infinite 1D chains)—the longest finite acyclic chain previously reported contained seven metal ions.^[14] The magnetic behavior of **2** was measured from 1.8 to 300 K (Figure 4). The χT value at room temperature of 23.0 emu K mol^{-1} , which is smaller than the uncorrelated value (27.3 emu K mol^{-1}), is consistent with moderate antiferromagnetic exchange between the metal centers within the chain. The curve for χ versus T (Figure 4) is qualitatively similar to that of **1**, with a plateau at ≈ 30 K and a rapid increase at lower temperature. At low temperature, the curve tends to a constant value of ≈ 1 emu K mol^{-1} , which is consistent with a ground state of $S=1$.

The odd-member open-chain structure of **2** should stabilize a ferrimagnetic structure with a resultant spin of $S=1$. To confirm this, the magnetic data were fitted by employing a classical Monte Carlo simulation together with the MINUIT^[15] minimization routine. A full quantum mechanical treatment was hampered by the large number of spins in the cluster. However, a quantum correction was used on spin values, and a combination of Metropolis^[16] and

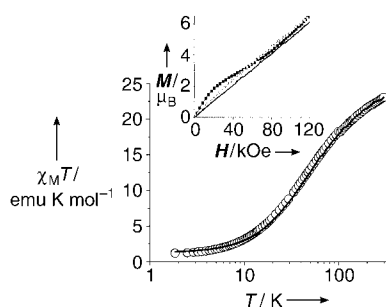


Figure 4. Temperature dependence of the product χT for **2** (1 kOe = 0.1 T). The solid line represents the fitting performed with a classical Monte Carlo simulation. Inset: magnetization (M) versus applied field (H) curves recorded at three different temperatures: 2 K ■, 5 K ○, 10 K —.

overrelaxed algorithms^[17] were applied to reduce the correlation time. The Hamiltonian (\mathcal{H}) that was used for the calculation is shown in Equation (1), in which $S_i = [S_i(S_i + 1)]^{1/2}$ ($i = \text{Ni}^{2+}, \text{Cr}^{3+}$) is the scaled classical spin and J is the exchange interaction:

$$\mathcal{H} = -J_{\text{Ni-Cr}}(S_{\text{Ni}} \cdot S_{\text{Cr}}) - J_{\text{Cr-Cr}}(S_{\text{Cr}} \cdot S_{\text{Cr}}) \quad (1)$$

Values of $S_{\text{Ni}} = 1$, $g_{\text{Ni}} = 2.2$, $S_{\text{Cr}} = 3/2$, and $g_{\text{Cr}} = 2.0$ were used. The best-fit values obtained were $J_{\text{Ni-Cr}} = -20.8$ and $J_{\text{Cr-Cr}} = -20.3 \text{ cm}^{-1}$, with an agreement factor of $R = 1.03 \times 10^{-3}$. Despite there being two distinct Cr···Ni interactions, no significant improvement in the fitting was observed upon including two Cr···Ni exchanges. The classical Monte Carlo simulation did not provide information about the energy spectrum of the spin levels. However, the curves of magnetization (M) versus field strength (H) recorded at different temperatures (Figure 4, inset) show some features typical of level crossings, which are induced by the field, that stabilize states with larger spins.^[13,18] The magnetization at 2 K, relative to that at 5 K, rapidly reaches $2\mu_B$ and then begins to level off. Above 80 kOe, the slope of the curve slightly increases, as expected for a level crossing occurring in this field range. As the energy spacing is not expected to follow a regular trend like the Landé rule,^[18] fitting of the data was not attempted. Nevertheless, the data from M versus H confirm that the ground spin state has $S = 1$, and this state is well separated, by $5\text{--}10 \text{ cm}^{-1}$, from the first excited state as expected for the ferrimagnetic structure of this unusual open-chain cluster.

Experimental Section

All reagents were used as received from Aldrich, except cyclen, which was obtained from Strem Chemicals. 1,4,7-triazacyclononane^[19] and $[\text{Ni}_2(\mu\text{-OH})_2(\text{O}_2\text{CCMe}_3)_4(\text{HO}_2\text{CCMe}_3)_4]$ ^[20] were prepared according to reported methods. Complexes **1** and **2** were prepared in teflon flasks supplied by Fisher.

$[\text{Ni}(\text{tacn})_2][(\text{O}_2\text{CCMe}_3)_2] \cdot 2\text{Me}_3\text{CCO}_2\text{H} \cdot \text{H}_2\text{O}$ (complex **A**): $[\text{Ni}_2(\mu\text{-OH})_2(\text{O}_2\text{CCMe}_3)_4(\text{HO}_2\text{CCMe}_3)_4]$ (0.70 g, 0.74 mmol) in toluene (5 mL) was added to a solution of tacn (0.35 g, 2.7 mmol) in toluene (5 mL), and the resultant blue solution was stirred for 5 min. Pink crystals of **A** began to form during this time. The solution was allowed to stand at room temperature for one day, then the crystals were collected by filtration, washed with toluene, and dried in air

(0.44 g, 40%). Elemental analysis: calcd for $\text{C}_{32}\text{H}_{70}\text{N}_6\text{NiO}_9$: Ni 7.91, C 51.82, H 9.51, N 11.33; found: Ni 7.81, C 51.96, H 9.73, N 11.33 %.

1: Complex **A** (0.25 g, 0.34 mmol), $\text{Me}_3\text{CCO}_2\text{H}$ (10.0 g, 98 mmol), $\text{CrF}_3 \cdot 4\text{H}_2\text{O}$ (0.8 g, 4.4 mmol), and basic nickel carbonate $[\text{2NiCO}_3 \cdot 3\text{Ni}(\text{OH})_2 \cdot 4\text{H}_2\text{O}]$ (0.07 g, 0.12 mmol) were heated with stirring at 140°C for 0.5 h, then the temperature was increased to 160°C and the mixture was heated for 5 h. The mixture was cooled to room temperature, acetone (30 mL) was added and the contents were stirred for 15 min. The product was filtered, washed with a large quantity of acetone, and dried in air. The solid (0.5 g) was then added to a solution of $\text{Me}_3\text{CCO}_2\text{H}$ (0.5 g) in THF (50 mL) and the solution was heated at reflux for 15–20 min with stirring. The green mixture was filtered hot, and the filtrate was diluted at room temperature with CH_3CN (1–2 mL) until it became cloudy and then reheated to obtain a clear solution. Slow cooling and then partial evaporation of the solvent at ambient temperature produced light green crystals. After 1 week, the crystals were collected by filtration, washed with THF/ CH_3CN (10:1), and dried in air (0.18 g, 17.5%). Elemental analysis calcd (%) for $\text{C}_{112}\text{H}_{210}\text{Cr}_8\text{F}_{10}\text{N}_6\text{Ni}_3\text{O}_{40}$: Cr 13.58, Ni 5.75, C 43.92, H 6.91, N 2.74, F 6.20; found: Cr 13.61, Ni 5.74, C 43.84, H 7.00, N 2.60, F 6.20.

2: Basic nickel carbonate (1.0 g, 1.7 mmol) was dissolved in pivalic acid (15 g, 147 mmol) at 100°C , and the solution was stirred for 15 min to produce a lime-green solution. The temperature was then raised to 120°C and cyclen (0.7 g, 4.0 mmol) was added to produce a blue solution, which indicates the production of $\text{Ni}(\text{cyclen})(\text{piv})_2$. The temperature was then maintained at 140°C for 10 min before $\text{CrF}_3 \cdot 4\text{H}_2\text{O}$ (5.0 g, 28 mmol) was added. The temperature was increased to 160°C for 5 h and the mixture was then left to cool overnight. The product was collected by filtration, washed with acetone, dried, and then recrystallized from hot THF/ MeCN (4.2 g, 53%). Elemental analysis calcd (%) for $\text{C}_{136}\text{H}_{256}\text{Cr}_{12}\text{F}_{18}\text{N}_8\text{Ni}_3\text{O}_{48}$: Cr 15.94, Ni 4.50, C 41.74, H 6.59, N 2.86, F 8.74; found: Cr 15.89, Ni 4.51, C 41.39, H 6.74, N 2.74, F 8.64.

The byproducts of the syntheses of **1** and **2** have very high solubility in acetone and have not yet been fully characterized. The magnetic properties of polycrystalline samples of **1** and **2** were investigated by using a Cryogenic M600 SQUID magnetometer and a VSM magnetometer based on the Oxford Instruments MAGLAB platform.

Received: June 18, 2004

Revised: July 19, 2004

Keywords: chromium · heterometallic complexes · nickel · supramolecular chemistry · template synthesis

- [1] M. Ruben, E. Breuning, J.-M. Lehn, V. Ksenofontov, F. Renz, P. Güthlich, G. B. M. Vaughan, *Chem. Eur. J.* **2003**, *9*, 4422–4429.
- [2] a) L. K. Thompson, *Coord. Chem. Rev.* **2002**, *233–234*, 193–206; b) L. Zhao, Z. Xu, L. K. Thompson, S. L. Heath, D. O. Miller, M. Ohba, *Angew. Chem.* **2000**, *112*, 3244–3247; *Angew. Chem. Int. Ed.* **2000**, *39*, 3114–3117.
- [3] M. Fujita, K. Umemoto, M. Yoshizawa, N. Fujita, T. Kusakawa, K. Biradha, *Chem. Commun.* **2001**, 509–518.
- [4] R. W. Saalfrank, I. Bernt, E. Uller, F. Hampel, *Angew. Chem.* **1997**, *109*, 2596–2599; *Angew. Chem. Int. Ed. Engl.* **1997**, *36*, 2482–2485.
- [5] R. M. Yeh, A. V. Davis, K. N. Raymond in *Comprehensive Coordination Chemistry II*, Vol. 7 (Eds.: J. A. McCleverty, T. J. Meyer), Elsevier, Amsterdam, **2004**, *7*, pp. 327–355.
- [6] F. K. Larsen, E. J. L. McInnes, H. El Mkami, J. Overgaard, S. Piligkos, G. Rajaraman, E. Rentschler, A. A. Smith, G. M. Smith, V. Boote, M. Jennings, G. A. Timco, R. E. P. Winpenny, *Angew. Chem.* **2003**, *115*, 105–109; *Angew. Chem. Int. Ed.* **2003**, *42*, 101–105.

- [7] O. Cador, D. Gatteschi, R. Sessoli, F. K. Larsen, J. Overgaard, A.-L. Barra, S. J. Teat, G. A. Timco, R. E. P. Winpenny, *Angew. Chem.* **2004**, *116*, 5308–5312; *Angew. Chem. Int. Ed.* **2004**, *43*, 5196–5200.
- [8] Crystal data for **1**·H₂O: C₁₁₂H₂₀₆Cr₈F₁₀N₆Ni₃O_{40.5}; $M_r = 3066.96 \text{ g mol}^{-1}$; green prisms, orthorhombic, space group *Cmca*, $a = 33.586(4)$, $b = 21.249(3)$, $c = 22.741(3) \text{ Å}$, $V = 16230(4) \text{ Å}^3$, $Z = 4$, $T = 150(2) \text{ K}$, $\rho = 1.255 \text{ g cm}^{-3}$, $F(000) = 6440$, $\mu(\text{MoK}\alpha) = 0.930 \text{ mm}^{-1}$. Crystal data for **2**·5.5 THF·1.5 MeCN: C₁₆₁H_{298.5}Cr₁₂F₁₈N_{9.5}Ni₃O_{53.5}; $M_r = 4365.7 \text{ g mol}^{-1}$; green blocks, triclinic, space group *P*–1, $a = 15.978(3)$, $b = 16.249(2)$, $c = 23.260(4) \text{ Å}$, $\alpha = 79.721(13)$, $\beta = 72.172(15)$, $\gamma = 84.778(13)^\circ$, $V = 5652.6(16) \text{ Å}^3$, $Z = 1$ (the molecule lies on an inversion center), $T = 100(2) \text{ K}$, $\rho = 1.281 \text{ g cm}^{-3}$, $F(000) = 2293$, $\mu(\text{MoK}\alpha) = 0.877 \text{ mm}^{-1}$. Data were collected on Bruker SMART CCD diffractometer (Mo–K α , $\lambda = 0.6892 \text{ Å}$ for **1** and 0.71073 Å for **2**). In all cases the selected crystals were mounted on the tip of a glass pin by using Paratone-N oil and placed in the cold flow produced by an Oxford Cryocooling device. Complete hemispheres of data were collected using ω -scans (0.3° , 30 seconds/frame). Integrated intensities were obtained with SAINT+ and were corrected for absorption by using SADABS; structure solution and refinement were performed with the SHELX-package (reference [9]). The structures were solved by direct methods and completed by iterative cycles of ΔF syntheses and full-matrix least-squares refinement against F^2 to give for **1**: using 431 parameters and 430 restraints, $wR_2 = 0.3106$ (8450 unique reflections), $R_1 = 0.1079$ (6865 reflections with $I > 2\sigma(I)$); for **2**: using 1297 parameters and 611 restraints, $wR_2 = 0.3248$ (19910 unique reflections), $R_1 = 0.1105$ (12282 reflections with $I > 3\sigma(I)$). CCDC 242096 and CCDC 231875 contains the supplementary crystallographic data for this paper. These data can be obtained free of charge via www.ccdc.cam.ac.uk/conts/retrieving.html (or from the Cambridge Crystallographic Data Centre, 12, Union Road, Cambridge CB2 1EZ, UK; fax: (+44) 1223-336-033; or deposit@ccdc.cam.ac.uk).
- [9] SHELX-PC Package. Bruker Analytical X-ray Systems: Madison, WI, **1998**.
- [10] For example, in **A** the average Ni–N bond length is $2.105(5) \text{ Å}$, compared with $2.125(9) \text{ Å}$ in **1**.
- [11] F. K. Larsen, J. Overgaard, S. Parsons, E. Rentschler, G. A. Timco, A. A. Smith and R. E. P. Winpenny, *Angew. Chem.* **2003**, *115*, 6160–6163; *Angew. Chem. Int. Ed.* **2003**, *42*, 5978–5981.
- [12] K. Wieghardt, W. Schmidt, W. Herrmann, H.-J. Küppers, *Inorg. Chem.* **1983**, *22*, 2953–2956.
- [13] J. Van Slageren, R. Sessoli, D. Gatteschi, A. A. Smith, M. Helliwell, R. E. P. Winpenny, A. Cornia, A. L. Barra, A. G. M. Jansen, E. Rentschler, G. A. Timco, *Chem. Eur. J.* **2002**, *8*, 277–285.
- [14] S.-Y. Lai, T.-W. Lin, Y.-H. Chen, C.-C. Wang, G.-H. Lee, M.-H. Yang, M.-K. Leung, S.-M. Peng, *J. Am. Chem. Soc.* **1999**, *121*, 250–251.
- [15] MINUIT Function Minimization and Error Analysis, CERN Program Library entry D506, CERN, Geneva 1994–1998.
- [16] N. Metropolis, A. W. Rosenbluth, M. N. Rosenbluth, A. Teller, W. Teller, *J. Chem. Phys.* **1953**, *21*, 1087–1092.
- [17] R. Gupta, J. DeLapp, G. G. Batrouni, G. C. Fox, C. F. Baillie, J. Apostolakis, *Phys. Rev. Lett.* **1988**, *61*, 1996–1999.
- [18] A. Cornia, D. Gatteschi, R. Sessoli in *Comprehensive Coordination Chemistry II*, Vol. 7 (Eds.: J. A. McCleverty, T. J. Meyer) **2004**, Elsevier, Amsterdam, **2004**, pp. 779–813.
- [19] R. Yang, L. J. Zompa, *Inorg. Chem.* **1976**, *15*, 1499–1502.
- [20] G. Chaboussant, R. Basler, H.-U. Güdel, S. Ochsenein, A. Parkin, S. Parsons, G. Rajaraman, A. Sieber, A. A. Smith, G. A. Timco, R. E. P. Winpenny, *J. Chem. Soc. Dalton Trans* **2004**, 2757–2765.

Photo-Switching

Reversible Photo-Switching of the Magnetization of Iron Oxide Nanoparticles at Room Temperature**

Rie Mikami, Minori Taguchi, Koji Yamada, Koji Suzuki, Osamu Sato, and Yasuaki Einaga*

Optically switchable magnetic materials are becoming increasingly important in the field of high-density information storage media.^[1–3] We have been trying to prepare new types of magnets in which the magnetic properties can be controlled by photo-illumination. Our previous work has shown that cobalt–iron cyanide exhibits photoinduced magnetization effects due to an internal electron transfer.^[4] However, practical examples of such photo-magnetic systems are limited in number^[5] because the strategies that are necessary to achieve photoinduced switching in the solid state are yet to be clarified.

The use of organized organic assemblies to direct the formation of mesoscopic inorganic structures under mild conditions and the attempts to intercalate inorganic materials into functional organic molecules are also of topical interest.^[6] We have focused our attention on composite materials as a novel strategy for realizing such photo-functional magnetic systems. These include the incorporation of organic photochromes into magnetic systems, for example, photo-controllable magnetic vesicles and Langmuir–Blodgett films containing Prussian blue (a ferromagnet at low temperature) and azobenzene.^[7]

Although the examples described above show interesting photo-responsive phenomena, the results were only achieved at low temperature. It is evident that the temperature at which photo-switching occurs needs to be increased to room temperature in order to realize devices for practical applications. In the present work we have focused on iron oxide

[*] R. Mikami, M. Taguchi, Prof. Y. Einaga
Department of Chemistry
Faculty of Science and Technology
Keio University
3-14-1 Hiyoshi, Yokohama 223-8522 (Japan)
Fax: (+81) 45-566-1697
E-mail: einaga@chem.keio.ac.jp
Dr. K. Yamada, Prof. K. Suzuki
Department of Applied Chemistry
Faculty of Science and Technology
Keio University
3-14-1 Hiyoshi, Yokohama 223-8522 (Japan)
Dr. O. Sato
Kanagawa Academy of Science and Technology
KSP, 3-2-1 Sakado, Kawasaki 213-0012 (Japan)

[**] This work was supported by a Grant-in-Aid for Scientific Research on Priority Areas (417) and the 21st Century COE program “KEIO Life Conjugate Chemistry” from the Ministry of Education, Culture, Sports, Science, and Technology (MEXT) of the Japanese Government.

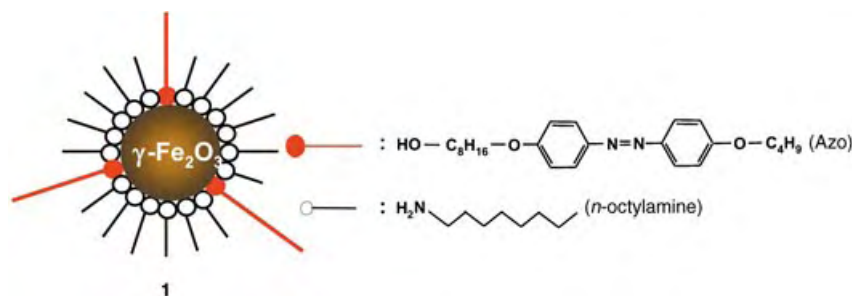


Supporting information for this article is available on the WWW under <http://www.angewandte.org> or from the author.

nanoparticles as magnetic materials that can function at room temperature. We recently reported our results for photo-responsive spiropyran vesicles containing iron oxide particles.^[8] Although we were able to increase the magnetization values of these materials by carrying out photo-illumination at room temperature, the reversible photo-switching of their magnetic properties was far below our expectations. This was because the photoinduced increase in the magnetization was due to aggregation of the iron oxide particles, and we guess that it is difficult for aggregated particles to be separated.

To realize reversible photo-switching of magnetization at room temperature, we have now focused on a surface modification of nano-scale iron oxide particles and a combination of azobenzene-containing amphiphilic compounds and γ -Fe₂O₃ magnetic nanoparticles. Surface modification of nanoparticles is a useful technique for functionalizing the material properties.^[9] For example, Rotello et al. reported that alkylamines in a monolayer could be displaced by harder Lewis base ligands such as alcohols.^[9b]

Our strategy was to synthesize an appropriate azobenzene derivative for preparing the target photo-responsive nanomagnetic materials. In addition to encapsulating the surface of the γ -Fe₂O₃ nanoparticles with the azo moiety, we incorporated *n*-octylamine. The amphiphilic azo compound 8-[4-{4-butoxy-phenyl(azo)-phenoxy}octan-1-ol] (Azo) was synthesized according to literature methods^[10] and then used to prepare the photo-responsive composite magnetic nanoparticles **1** (see the Experimental Section).



The transmission electron microscope (TEM) image of **1** indicates the global presence of γ -Fe₂O₃ nanoparticles with almost homogeneous diameters (5 nm, Figure 1). We estimated the diameter of **1**, including the encapsulating agent, to be 9 nm by means of a dynamic light-scattering method.

The photoisomerization of **1** on the quartz substrates was monitored by UV/Vis absorption spectroscopy at room temperature (Figure 2a). Before illumination, **1** exhibited two absorption peaks at about $\lambda = 360$ nm and a weak band at about 480 nm, which correlate to the π - π^* and the n - π^* transitions, respectively, in the *trans* form of the azo compound. The spectra demonstrate that the π - π^* absorption at 360 nm remains invariant with respect to passivation of the nanoparticles, which proves that the azo components are protected during the synthesis of the γ -Fe₂O₃ nanoparticles. The absence of any shift in the absorption bands also indicates that there was no π stacking between the azo molecules (black

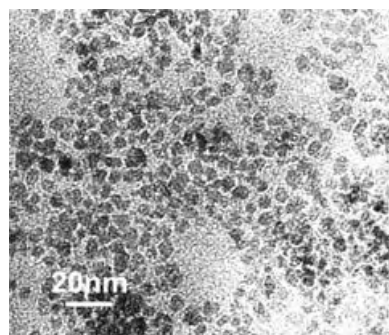


Figure 1. The TEM image of **1**.

line). After 5 min of UV illumination, the intensity of the band at 360 nm decreased and the intensity of the band at 480 nm increased, indicating the *trans*-to-*cis* photoisomerization (blue line). A photostationary state was obtained after 5 min of illumination, that is, the photoisomerization had saturated. Following subsequent illumination with visible light for 5 min, the reverse process, the *cis*-to-*trans* isomerization, proceeded to completion (red line). The *trans*-to-*cis* photoisomerization cycles were repeated several times by alternately illuminating with UV and visible light (Figure 2b).

Because the photoisomerization of azobenzene derivatives (in particular the *trans*-to-*cis* isomerization) is normally accompanied by an increase in molecular volume, the solid-state reaction is greatly inhibited due to the close packing of the chromophores. In practical terms, when the solid-state compound contains only Azo, it does not exhibit any photoisomerization behavior. In the case of **1**, sufficient free volume is guaranteed by the dilution of the azo moieties with *n*-octylamine to allow photoisomerization to take place. Another important point is the Lewis basicity of the capping ligands. *n*-Octylamine, which functions as an encapsulating agent for the γ -Fe₂O₃ nanoparticles,^[11] contains an amino group, while Azo contains a harder Lewis basic hydroxy group. This means that Azo takes precedence over *n*-octylamine, resulting in the successful preparation of composite nanoparticles **1**.

The magnetic properties of **1** on a glass substrate were studied by SQUID measurements. The temperature dependence of the magnetization of **1** exhibits a cusp around 12 K in the zero field cooled (ZFC) susceptibility as well as a blocking temperature T_B determined from the branching of the ZFC and field-cooled (FC) data (Figure 3); thus, **1** exhibits superparamagnetic behavior. According to Néel's superparamagnetic model^[12] at high temperatures, the magnetic moments of spin clusters are free to respond to an external field but freeze when the temperature is low enough. This freezing of the spin clusters over a wide temperature range can be visualized in terms of the progressive blocking of the cluster moments, depending on their size and magnetocrystalline anisotropy. Below the freezing temperature, the clusters freeze in random orientations dictated by the magnetocrystalline anisotropy.

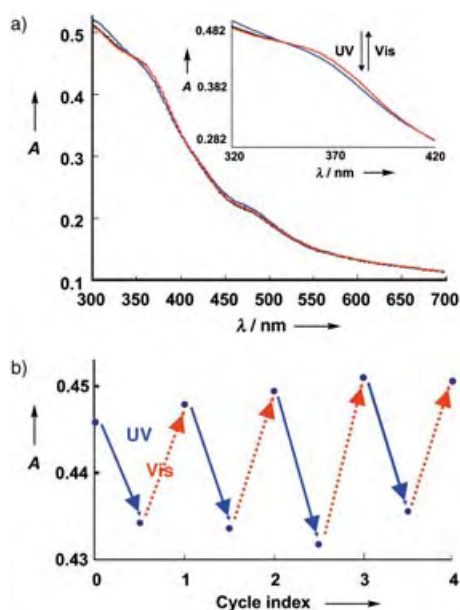


Figure 2. a) Changes in the optical absorption spectra due to photoisomerization for **1** cast on quartz substrates at room temperature: before illumination (black line), after illumination with UV light for 5 min (blue line), after subsequent illumination with visible light for 5 min (red line). The inset shows a magnified region. b) Changes in the absorbance *A* at 360 nm by alternating illumination with UV and visible light (5 min each).

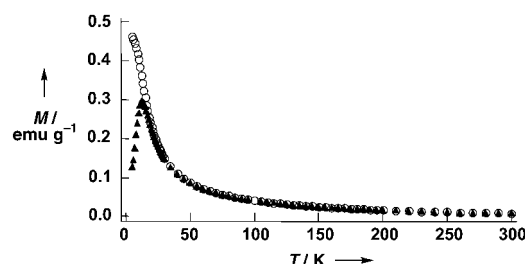


Figure 3. The plot of magnetization *M* versus temperature *T* for **1** at 5 G: \blacktriangle : zero-field cooled (ZFC), \circ : field cooled (FC).

Since the magnetic moments of the spin clusters are frozen in a direction where magnetization occurs easily at low temperatures, this gives rise to a low value of magnetization. In contrast, the magnetization decreases (as T^{-1}) at high temperatures due to thermal fluctuations of the magnetic moments. Therefore, a peak occurs in ZFC susceptibility between these two regions.^[13] The ⁵⁷Fe Mössbauer spectra for **1** at room temperature and at 8 K revealed the presence of γ -Fe₂O₃ nanoparticles (see the Supporting Information).

Based on these data, **1** exhibits typical superparamagnetic behavior of magnetic particles, with a particle size that is consistent with that observed by TEM (5 nm).^[14] Generally speaking, iron oxide nanoparticles exhibit superparamagnetic behavior because of the infinitely small coercivity arising from the negligible energy barrier in the hysteresis of the magnetization loop of the particles.^[12,15]

The magnetization curve of **1** was measured at 5 K (Figure 4a) in the field-cooled (FC) state. A small hysteresis

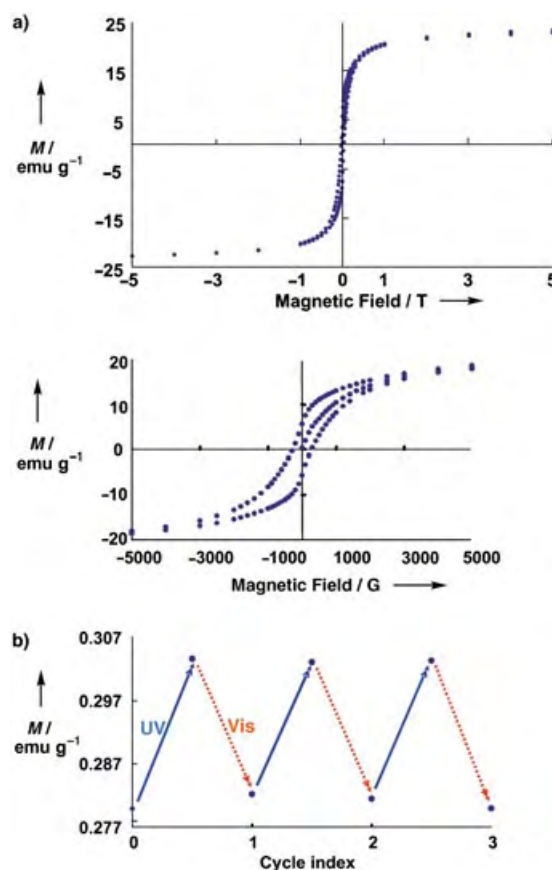


Figure 4. a) The plot of magnetization *M* versus applied magnetic field for **1** at 5 K and a magnified region ($1 \text{ G} = 10^{-4} \text{ T}$). b) Change in the magnetization for **1** induced by alternating illumination with UV and visible light (10 min each) at 5 K with an external magnetic field of 10 G.

loop with remanence (5.67 emu g⁻¹) and coercivity (300 G) was observed. Below *T_B* the superparamagnetic transition is blocked, that is, the magnetization cannot relax during the time frame of the measurement and therefore cannot appear on the plot of magnetization as a function of the magnetic field.

We next investigated the influence of photo-illumination on the magnetic properties of **1** at 5 K (Figure 4b). Compound **1** was cooled from room temperature to 5 K in an external magnetic field of 10 G. The initial magnetization value of **1** at 10 G increased from 0.279 to 0.305 emu g⁻¹ upon UV illumination. The sample was exposed to UV light until saturation, that is, until the change in magnetization was complete (10 min). Even after the illumination was stopped, this increased magnetization was maintained for several hours. Compound **1** was then illuminated with visible light for a further 10 min. The magnetization value decreased from 0.305 to 0.280 emu g⁻¹. This UV light induced increase and visible light induced decrease in the level of magnetization was repeated several times. The total change of the magnetization value resulting from photoinduced switching was about 9.3%, which is larger than that achieved by our first photo-functional magnetic vesicles system.^[7a]

To investigate the feasibility of using **1** for practical applications, corresponding measurements were performed at

room temperature (300 K). No saturation of the magnetization was found at 300 K with a field of 50 000 G. Characteristics that are typical of superparamagnetic behavior were observed, such as almost immeasurable coercivity and remanence (Figure 5a). This was consistent with the notion that, above T_B , the magnetization should be free to align with the field during the measurement time.

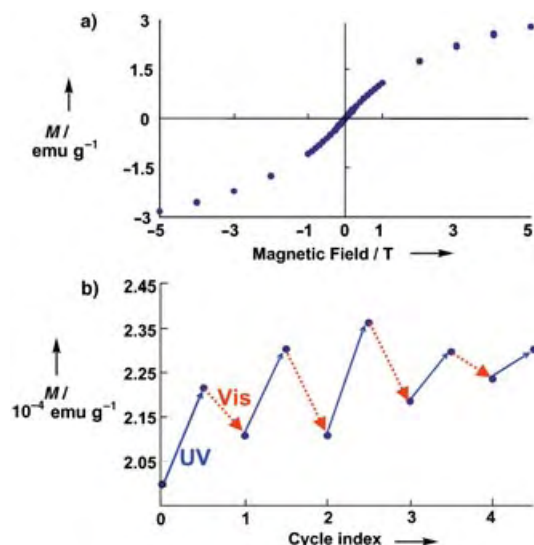


Figure 5. a) The plot of magnetization M versus applied magnetic field for **1** at 300 K. b) Change in the magnetization for **1** induced by alternating illumination with UV and visible light (30 min each) at 300 K with an external magnetic field of 10 G.

Next, the influence of photo-illumination on the magnetic properties of **1** at 300 K was examined. The same changes in magnetization upon photo-illumination were noted, that is, the magnetization increased upon illumination with UV light and decreased upon illumination by visible light (Figure 5b). The changes in the magnetization values do not give rise to a distinct trace because of the superparamagnetic properties. These changes in magnetization are consistent with the changes in the UV/Vis spectra and can be explained in the same fashion. The reversible control of the magnetic properties of **1** at room temperature was also confirmed by EPR and ^{57}Fe Mössbauer spectroscopy (see the Supporting Information).

To confirm the effect of the azo moiety, $\gamma\text{-Fe}_2\text{O}_3$ nanoparticles that were only encapsulated with *n*-octylamine were prepared (**2**). The TEM image of **2** also showed the presence of global $\gamma\text{-Fe}_2\text{O}_3$ nanoparticles with almost homogeneous diameters (5 nm), and **2** exhibited almost the same magnetic properties as **1** (not shown). However, when **2** was illuminated with UV or visible light, no changes were observed in the total magnetization. This result suggests that the azo moiety in **1** plays an important role in the photocontrol of the magnetization.

It appears that photoinduced changes in the electrostatic field around the $\gamma\text{-Fe}_2\text{O}_3$ magnetic nanoparticles affect the magnetization. Examples from our previous work could also be explained by similar interactions.^[7] Changes in the dipole

moments induced by the photoisomerization of the Azo moieties resulted in magnetic fields and moments in the materials. We have previously observed that the change in the dipole moments of the azo compounds did not affect the magnetization value in the paramagnetic region.^[7] Those results were consistent with the present results in terms of the temperature dependence (at 5 K and room temperature): The stronger the magnetic exchange interactions between spins are, the greater the effect the dipole moment has on the magnetization values.

The relationship between the electronic polarization (including the charge or the dipole moments) and the magnetization has been discussed by several physicists.^[16,17] The origins of the behavior of magneto-electric materials are the electric field induced g shift, the spin-orbit interactions, the exchange energies, and the electric field induced shift in the single-ion anisotropy energy. The underlying electrodynamics are complicated by induced fields interacting with electric and magnetic moments. That is, the spin orientation is coupled to the electric multi-pole through the lattice. Morup et al. also discussed the existence of significant collective effects in a magnetic nanoparticle system and made several speculations regarding a spin-glass-like phase at low temperatures on dipole–dipole interacting systems.^[17b] Moreover, the surface magnetic phase diagram of the tetragonal manganites depends on the electrostatic interactions caused by the surface environment, such as surface termination.^[15]

In 1999 Alivisatos et al. described the preparation of soluble crystalline $\gamma\text{-Fe}_2\text{O}_3$ nanoparticles by high-temperature organic-phase decomposition of an iron precursor.^[18] The process was then extended to the synthesis of monodisperse MFe_2O_4 ($\text{M} = \text{Fe}, \text{Co}, \text{Mn}$) nanoparticles by Sun et al.^[19] through the use of oleic acid and oleylamine. They studied the stability of the nanoparticles by varying the ratio of the capping agents and described how $\gamma\text{-Fe}_2\text{O}_3$ nanoparticles can be stabilized by alkylamine surfactants,^[9b,11] suggesting that NH_2 coordinates with Fe^{III} on the surface of the particles. Furthermore, Zhang et al. studied the effects of surface coordination chemistry on the magnetic properties of MnFe_2O_4 nanoparticles.^[20a,b] They observed that the coercivity of magnetic nanoparticles decreased upon coordination of the ligands on the nanoparticle surface, whereas the saturation magnetization increased. They concluded that the magnetic properties of the nanoparticles change with the functional group bound onto the nanoparticle surface. The correlation suggests a decrease in the spin-orbital coupling and surface anisotropy of magnetic nanoparticles due to surface coordination.

Gedanken et al. also studied the magnetic properties, especially the blocking temperature T_B , of iron nanoparticles coated by various surfactants.^[20c] They observed large variations in T_B for various functional groups attached to the iron nanoparticles. For example, the magnetization values for alcohols and carboxylic acids were different from those for sulfonic and phosphonic acid. These differences could be explained by the variation in particle size as well as the effect of the iron-bound functional group on the d electrons of iron. The functional groups interact strongly with the d electrons and cause a large splitting of the doubly and triply degenerate

d levels. This affects the spin state and the magnetization values as a result of exchange interactions between the spins of the iron center.

The above discussion also suggests that photoinduced changes in the electrostatic field around the γ -Fe₂O₃ magnetic nanoparticles affect the magnetization. Photo-switchable magnetic films—Prussian blue intercalated in Langmuir–Blodgett films consisting of an amphiphilic azobenzene and a clay mineral,^[7c] which was one of our previous photo-functional systems—supplied data that support these mechanisms. A band corresponding to intervalence charge transfer (IVCT) between Fe^{II} to Fe^{III} in the Prussian blue layer was changed reversibly by alternate UV and visible illumination, accompanied by photoisomerization of the azo compound. That is, changes in the electrostatic field driven by the photoisomerization of the azobenzene chromophore led to changes in the Coulomb energy (which is necessary to transfer an electron) and this might affect the superexchange interaction between the spins in the Prussian blue magnet.

In conclusion, we have designed novel photoresponsive γ -Fe₂O₃ nanoparticles that are encapsulated by an azo compound and *n*-octylamine. To photo-control the magnetization, the design of the interfaces between the photoresponsive materials and the magnetic materials is important. The advantage of the current system is that nano-scale particles, from which much larger areas of photoresponsive interfaces might be expected, were used as the magnetic materials. Another important aspect was the dilution of the azo moieties with *n*-octylamine. The free volume gained is responsible for the ideal photoreaction. Use of azo compounds with appropriate end groups and alkyl chain length for direct interaction with the metal oxide surface was also important. Finally, we have succeeded in switching the magnetization value of composite magnetic nanoparticles by photo-illumination in the solid state at room temperature.

Experimental Section

The amphiphilic compound Azo^[10] and the γ -Fe₂O₃ nanoparticles^[11] were synthesized according to literature methods.

1: FeCl₃·6H₂O (0.47 g), sodium acetate (0.43 g, used as a hydrolyzing agent), H₂O (0.35 mL), *n*-octylamine (0.61 mL), and Azo (0.01 g) in 1,2-propanediol (6 mL) were heated under reflux at 150°C for 5 h. The materials were then precipitated by the addition of a large volume of 2-propanol (ca. 20 mL). After being washed with 2-propanol, the solids were collected by centrifugation, washed with Et₂O, and dried in air. The crude product was re-dissolved in toluene (5 mL) containing a small amount of the encapsulating agents *n*-octylamine and Azo (0.3 mL, 100:1). Most of the crude product went into solution within 13 h. A solution of **1** in toluene was then cast onto the substrates for further study.

The UV/Vis spectra were recorded on a V-560 spectrophotometer (JASCO). UV illumination (filtered light, $\lambda_{\text{max}} = 360$ nm, 1.0 mW cm⁻²) was applied with an ultra-high pressure mercury lamp (HYPERCURE 200, Yamashita Denso). Visible light (400–700 nm, 1.0 mW cm⁻²) was provided by a xenon lamp (XFL-300, Yamashita Denso). The magnetic properties were investigated with a SQUID magnetometer (model MPMS-5S Quantum Design). The lamps were guided into the SQUID magnetometer by an optical fiber to study the photomagnetic effects. The ⁵⁷Fe Mössbauer spectra were measured at room temperature and at low temperature with a Topologic Systems Model 222 constant-acceleration spectrometer with a ⁵⁷Co/Rh source

in transmission mode. A closed-cycle helium refrigerator (Nagase Electronic Equipments Service Co., Ltd.) was used for measuring the spectra at low temperature.

Received: June 15, 2004

Keywords: azo compounds · iron · magnetic properties · nanoparticles · photochromism

- [1] W. Kuch, *Nat. Mater.* **2003**, 2, 505.
- [2] C. Thirion, W. Wernsdorfer, D. Mailly, *Nat. Mater.* **2003**, 2, 524.
- [3] P. Gülich, Y. Garcia, T. Woike, *Coord. Chem. Rev.* **2001**, 219–221, 839.
- [4] a) O. Sato, T. Iyoda, A. Fujishima, K. Hashimoto, *Science* **1996**, 272, 704; b) O. Sato, Y. Einaga, T. Iyoda, A. Fujishima, K. Hashimoto, *J. Electrochem. Soc.* **1997**, 144, L11.
- [5] S. Hayami, Z.-Z. Gu, M. Shiro, Y. Einaga, A. Fujishima, O. Sato, *J. Am. Chem. Soc.* **2000**, 122, 7126.
- [6] a) J. H. Fendler, *Chem. Rev.* **1987**, 87, 877; b) S. Mann, D. D. Archibald, J. M. Didymus, T. Douglas, B. R. Heywood, F. C. Meldrum, N. J. Reeves, *Science* **1993**, 261, 1286; c) K. Nakatani, P. Yu, *Adv. Mater.* **2001**, 13, 1411; d) N. Kimizuka, *Adv. Mater.* **2000**, 12, 1461.
- [7] a) Y. Einaga, O. Sato, T. Iyoda, A. Fujishima, K. Hashimoto, *J. Am. Chem. Soc.* **1999**, 121, 3745; b) Y. Einaga, T. Yamamoto, T. Sugai, O. Sato, *Chem. Mater.* **2002**, 14, 4846; c) T. Yamamoto, Y. Umemura, O. Sato, Y. Einaga, *Chem. Mater.* **2004**, 16, 1195.
- [8] a) Y. Einaga, M. Taguchi, G. Li, T. Akitsu, Z.-Z. Gu, T. Sugai, O. Sato, *Chem. Mater.* **2003**, 15, 8; b) M. Taguchi, G. Li, Z.-Z. Gu, O. Sato, Y. Einaga, *Chem. Mater.* **2003**, 15, 4756.
- [9] a) A. Manna, P.-L. Chen, H. Akiyama, T.-X. Wei, K. Tamada, W. Knoll, *Chem. Mater.* **2003**, 15, 20; b) A. K. Boal, K. Das, M. Gray, V. M. Retello, *Chem. Mater.* **2002**, 14, 2628; c) S. Thimmaiah, M. Rajamathi, N. Singh, P. Bera, F. Meldrum, N. Chandrasekhar, R. A. Seshadri, *J. Mater. Chem.* **2001**, 11, 3215.
- [10] W.-H. Wei, T. Tomohiro, M. Kodaka, H. Okuno, *J. Org. Chem.* **2000**, 65, 8979.
- [11] M. Rajamathi, M. Ghosh, R. Seshadri, *Chem. Commun.* **2002**, 1152.
- [12] L. Neel, *Ann. Geophys.* **1949**, 5, 99.
- [13] M. D. Mukadam, S. M. Yusuf, P. Sharma, S. K. Kulshreshtha, *J. Magn. Magn. Mater.* **2004**, 269, 317.
- [14] A. B. Bourlino, A. Simopoulos, C. Petridis, *Chem. Mater.* **2002**, 14, 899.
- [15] J. C. Mallinson, *The Foundations of Magnetic Recording*, Academic Press, Berkeley, **1987**, ch. 3.
- [16] V. K. Sharma, F. Waldner, *J. Appl. Phys.* **1977**, 48, 4298.
- [17] a) J. Baker-Jarvis, P. Kabos, *Phys. Rev. E* **2001**, 64, 056127-1; b) S. Morup, E. Tronc, *Phys. Rev. Lett.* **1994**, 72, 3278.
- [18] J. Rockenberger, E. C. Scher, P. A. Alivasatos, *J. Am. Chem. Soc.* **1999**, 121, 11595.
- [19] a) S. Sun, H. Zeng, *J. Am. Chem. Soc.* **2002**, 124, 8204; b) S. Sun, H. Zeng, D. B. Robinson, S. Raoux, P. M. Rice, S. X. Wang, G. Li, *J. Am. Chem. Soc.* **2004**, 126, 273.
- [20] a) C. R. Vestal, Z. J. Zhang, *J. Am. Chem. Soc.* **2003**, 125, 9828; b) C. Liu, B. Zou, A. J. Rondinone, Z. J. Zhang, *J. Am. Chem. Soc.* **2000**, 122, 6263; c) G. Kataby, Y. Koltypin, A. Ulman, I. Felner, A. Gedanken, *Appl. Surf. Sci.* **2002**, 201, 191.

Carbon Nanotubes

Atomic-Step-Templated Formation of Single Wall Carbon Nanotube Patterns**

Ariel Ismach, Lior Segev, Ellen Wachtel, and Ernesto Joselevich*

Following recent advances in the control of the electronic properties of nanowires,^[1–4] nonlithographic organization of nanowire arrays on surfaces remains a critical prerequisite for the large-scale fabrication of nanoscale circuitry.^[5,6] Current strategies^[7] include the application of physical means, such as electric fields,^[4,8,9] gas^[10] and liquid^[11,12] flows, and superlattices,^[13] as well as chemical means including self-assembly^[14,15] and biotemplated assembly.^[16] Step decoration^[15,17] is another attractive chemical approach that exploits the selective deposition of atoms, ions, or molecules at the oriented, periodic steps present on high-index crystalline surfaces. However, the general scheme, in which nanowire growth propagates transversely from the steps, is not compatible with nanowire materials that form by axial growth mechanisms, such as carbon nanotubes.^[18–20] Here we demonstrate and characterize the longitudinally propagating decoration of atomic steps by a nanowire material. Single-wall carbon nanotubes that are catalytically produced on miscut C-plane sapphire wafers, grow along the 2-Å-high atomic steps of the vicinal α -Al₂O₃ (0001) surfaces to yield highly aligned, dense arrays of discrete, nanometer-wide, conducting or semiconducting wires on a dielectric material. The nanotubes reproduce the atomic features of the surface, such as steps, facets, and kinks. These findings open up the possibility of assembling nanotube architectures by atomic-scale surface engineering.

The phenomenon of atomic step decoration by single-wall carbon nanotubes (SWNTs) was first observed while investigating the effects of electric field and gas flow on the catalytic growth of SWNTs on different materials. Surprisingly, nanotubes grown on C-plane sapphire wafers, that is, α -Al₂O₃ (0001) surfaces, showed the highest degree of alignment

(Figures 1 a, 2 a, 3 a–c, and 4 a), but not in the directions of the field or the flow. When the same surface was precoated with a thin layer (20 nm) of amorphous SiO₂, the nanotubes were

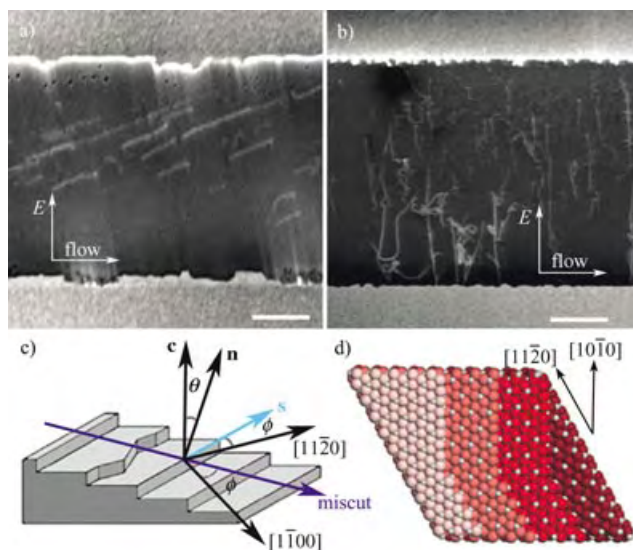


Figure 1. Alignment of SWNTs grown under an electric field ($2 \times 10^6 \text{ V m}^{-1}$) on sapphire (a) and on SiO₂-coated sapphire (b). The low-voltage field-emission SEM micrographs (scale bar: 5 μm) show the SWNTs (light) lying on the dielectric surfaces (dark), and the Pt electrodes (light, top and bottom). Arrows indicate the directions of the field *E* and flow. The alignment of the SWNTs on sapphire is unrelated to the electric field, whereas on the same sapphire that was precoated with 20 nm of amorphous SiO₂, the alignment is parallel to the electric field. c) Schematic representation of the atomic steps on vicinal α -Al₂O₃ (0001), and definition of the step vector *s* = (*c*/*c*) × *n*, miscut inclination θ , and miscut azimuth ϕ . d) Idealized structure of atomic steps in different low-index directions, based on the bulk crystal structure, that is, without relaxation and reconstruction. Oxygen atoms (red) are colored darker at lower atomic layers.

aligned with the electric field (Figure 1b), as previously observed on SiO₂-coated silicon.^[8] This result indicated that the nanotubes grow in contact with the Al₂O₃ surface, which dictates their alignment. On the other hand, the nanotubes were not aligned along a particular crystallographic direction. Moreover, α -Al₂O₃ is a trigonal crystal of the *R*3c space group and an ideal α -Al₂O₃ (0001) surface has *C*₃ symmetry, from which one would expect alignment in at least three directions, not one. These facts ruled out the possibility of lattice-oriented SWNT growth.^[21] However, commercial “C-plane” sapphire wafers are often cut and polished in a plane that slightly deviates from the actual C plane. The resulting vicinal α -Al₂O₃ (0001) surfaces are terminated with parallel, regularly spaced atomic steps.^[22] The atomic steps of most materials are generally more reactive than atomically flat areas.^[23] We then hypothesized that SWNTs could have grown along such atomic steps. This is proven below for the case where no electric field was applied. Application of an electric field was shown to have no effect.

The morphology and dynamics of vicinal α -Al₂O₃ (0001) surfaces have been investigated by several research groups.^[22,24] The atomic steps, with a height equal to one

[*] A. Ismach, L. Segev, Dr. E. Joselevich
Department of Materials and Interfaces
Weizmann Institute of Science, Rehovot 76100 (Israel)
Fax: (+972) 8-934-4138
E-mail: ernesto.joselevich@weizmann.ac.il
Dr. E. Wachtel
Chemical Research Infrastructure
Weizmann Institute of Science, Rehovot 76100 (Israel)

[**] We acknowledge A. Jorio, G. Dresselhaus, and M. S. Dresselhaus for Raman measurements. We thank L. Leiserowitz and M. Lahav for helpful discussions. This research was funded by the Israel Science Foundation, the U.S.–Israel Binational Science Foundation, and the Djanogly Center for New Scientists. E.J. holds the Dr. Victor Erlich Career Development Chair.

Supporting information (experimental methods, XRD data, statistical histograms, and a table of comprehensive results) for this article is available on the WWW under <http://www.angewandte.org> or from the author.

sixth of the hexagonal unit cell, that is, $h = c/6 = 0.219$ nm, follow a general direction perpendicular to the miscut direction (Figure 1c). Their average spacing is $d = h/\sin\theta$ where θ is the miscut inclination. For convenience, we define a step vector $\mathbf{s} = (\mathbf{c}/c) \times \mathbf{n}$, where \mathbf{c} is the principal lattice vector and \mathbf{n} is a unit vector normal to the surface. Then, \mathbf{s} points along the general step direction so that steps descend to the right, and its modulus equals the slope of the steps ($s = h/d$). We define the miscut azimuth ϕ ($-60^\circ < \phi < +60^\circ$) as the angle of \mathbf{s} relative to the $[11\bar{2}0]$ direction, which is perpendicular to the $(11\bar{2}0)$ c -glide plane, so that the sign of ϕ expresses the handedness of chiral miscuts. The atomic step structure depends on the miscut azimuth ϕ . This is illustrated by Figure 1d, which represents different unreconstructed steps based on the bulk structure. The actual structure of the atomic steps is still unknown,^[22] although the high-temperature reconstruction of $\alpha\text{-Al}_2\text{O}_3(0001)$ surfaces was recently characterized.^[25]

The characterization of a typical sample of aligned SWNTs on sapphire is shown in Figure 2. Figure 2a displays an AFM topographic image of the highly aligned SWNTs. The apparent diameter distribution of the SWNTs is 1.0 ± 0.4 nm, which is 0.2 nm smaller than the value determined from Raman spectra (1.2 ± 0.5 nm). An asymmetric double-exposure back-reflection X-ray diffraction (XRD) method was used to determine the orientations of both the lattice and the miscut of the $\alpha\text{-Al}_2\text{O}_3(0001)$ substrate (Figure 2b), in which a long and a short exposure were taken before and after 180° rotation of the sample, respectively. The miscut inclination and azimuth are $\theta = 2.1 \pm 0.2^\circ$ and $\phi = 0 \pm 5^\circ$, respectively, and the general step direction, expressed by \mathbf{s} , matches the direction of the nanotube alignment. In addition, a destructive characterization by thermal annealing at 1100°C in air (Figure 2c) was performed. Then, the thermodynamically unstable $c/6$ atomic steps, which could not be resolved by AFM, bunch into visible macrosteps with heights of $c\text{--}3c$.^[22,24] The step orientation and miscut inclination are independently determined from these images, thus yielding results ($\theta = 1.9 \pm 0.2^\circ$) similar to those obtained from XRD studies. The angular distribution of the nanotubes and macrosteps with respect to reference marks are $108 \pm 4^\circ$ and $109 \pm 2^\circ$, respectively (see Supporting Information for histograms). This precise coincidence is a clear indication of step decoration. The apparent reduction in SWNT height is consistent with the size of $c/6$ atomic steps.

Similar experiments were performed on about twenty samples of SWNTs grown on either side of seven different C -plane sapphire wafers of random miscut inclinations (up to $\theta = 4^\circ$). Some representative results are displayed in Figure 3 (see Supporting Information for comprehensive data). In all cases, except for $\theta < 0.5^\circ$, SWNTs grow parallel to the atomic steps and not to a particular lattice direction. The degree of alignment correlates with the miscut inclination. However, SWNTs grown on substrates having similar miscut inclinations show better alignment when the atomic steps run along low-index directions, such as $[11\bar{2}0]$ (Figure 3c) or $[10\bar{1}0]$ (Figure 3b), than along high-index directions (Figure 3d). This phenomenon may be attributed to the fact that straighter steps can have a closer interaction with the SWNTs. The

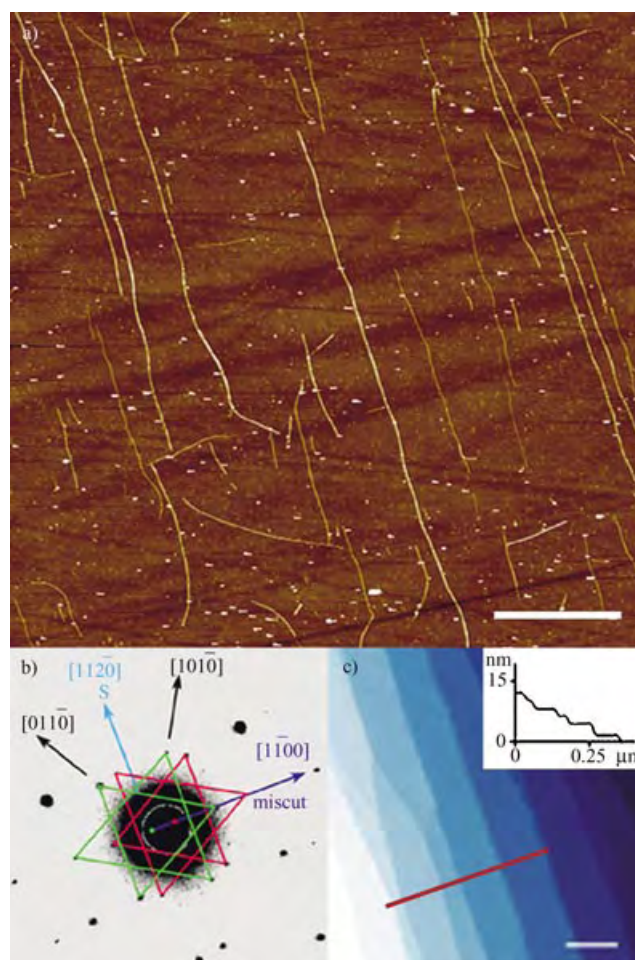


Figure 2. Comprehensive characterization of a typical sample of aligned SWNTs on miscut sapphire. a) AFM topographic image of the SWNTs (scale bar: 1 μm). Note the high degree of alignment and the straight conformation of most SWNTs, beyond the persistence length (ca. 1 μm). Polishing scratches (randomly oriented dark lines) of approximately 1-nm depth do not affect SWNT alignment. b) Asymmetric double-exposure back-reflection XRD indicating relevant low-index directions and the resulting step vector (\mathbf{s}). The green and red triangles indicate the reference reflections arising from the first exposure (2 h) and second exposure (1 h, after 180° sample rotation), respectively (see Supporting Information for reference XRD). The \mathbf{s} vector is $+90^\circ$ from the vector connecting the green-to-red pattern centers. c) AFM topographic image of a piece of sample after annealing at 1100°C (scale bar: 100 nm). The darker blue indicates lower terraces, whose edges correspond to the $c\text{--}3c$ macrosteps. The inset shows a section analysis along the red line. Note that both the \mathbf{s} vector from (b) and the macrosteps from (c) are parallel to the SWNTs in (a) (all the images are displayed in the same orientation with respect to reference marks).

density of the SWNT arrays also correlates with the value of θ . The samples with the lowest miscut inclination (Figure 3f) have visible atomic steps decorated by nanoparticles, but no nanotubes. The steps could play a role in stabilizing the catalyst nanoparticles, so that a higher density of steps leads to a higher yield of SWNTs.

Interestingly, certain samples show kinked nanotubes running in zigzags along two different low-index directions. In Figure 4a, alternating long and short segments of the same

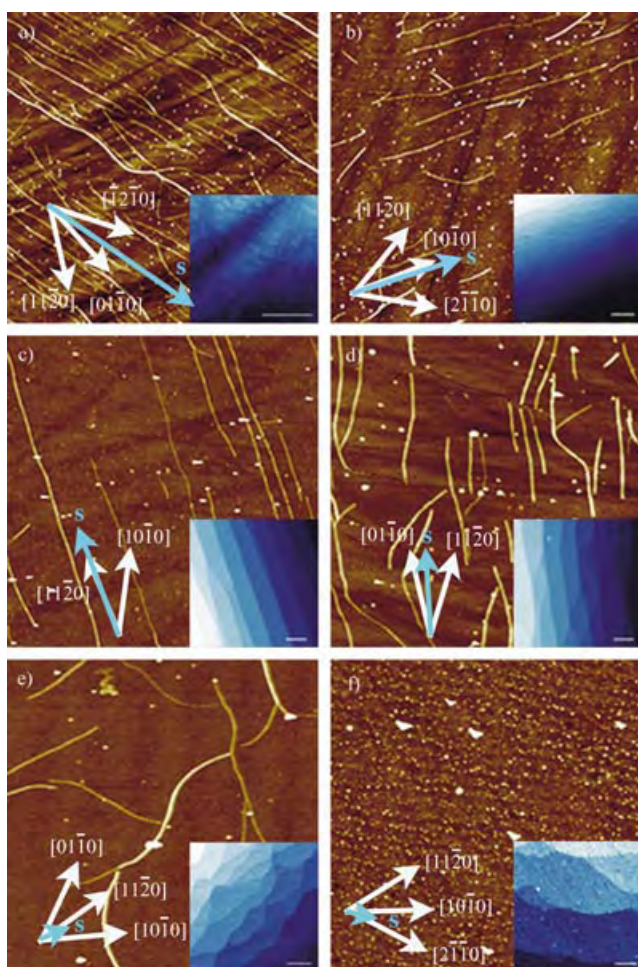


Figure 3. SWNTs on miscut sapphire. Comparative analysis of representative samples with different miscut inclination and azimuth angles (see Supporting Information for XRD and full data table): a) $\theta = 3.4 \pm 0.3^\circ$, $\phi = 42 \pm 5^\circ$; b) $\theta = 2.3 \pm 0.2^\circ$, $\phi = -33 \pm 5^\circ$; c) $\theta = 2.1 \pm 0.2^\circ$, $\phi = 0 \pm 5^\circ$; d) $\theta = 1.7 \pm 0.1^\circ$, $\phi = 18 \pm 5^\circ$; e) $\theta = 0.4 \pm 0.2^\circ$, $\phi = -5 \pm 5^\circ$; and f) $\theta = 0.3 \pm 0.2^\circ$, $\phi = -50 \pm 5^\circ$ (image sizes are 2.5 μm , except (e), 5 μm). The vectors indicate the relevant lattice directions and the step vector s (blue) obtained from XRD (except in (e) and (f), where s is from AFM). Insets show AFM topographic images of the respective annealed samples (inset scale bars 100 nm) with macrosteps. In (f), the atomic steps are spaced enough to be observed, and are decorated with inactive catalyst nanoparticles.

SWNTs run along the $[11\bar{2}0]$ and $[10\bar{1}0]$ directions, respectively, in accordance with their proximity to the general step direction (a few segments along the $[01\bar{1}0]$ and $[2\bar{1}\bar{1}0]$ directions are occasionally seen too). This result can be attributed to SWNT growth along faceted atomic steps (Figure 4b). Since the sharp 30° kinks presumably occur during growth, they could involve pentagon–heptagon defects, which are an energetically favored alternative to bending or buckling. The energy associated with pentagon–heptagon defects was calculated to be about 7 eV,^[26] whereas the minimum strain energy required to produce a 30° buckle in a 1-nm-diameter SWNT was estimated to be about 13 eV.^[27] Single-nanotube Raman spectra from these samples exhibit a high intensity of D-band peaks, which indicates a significant

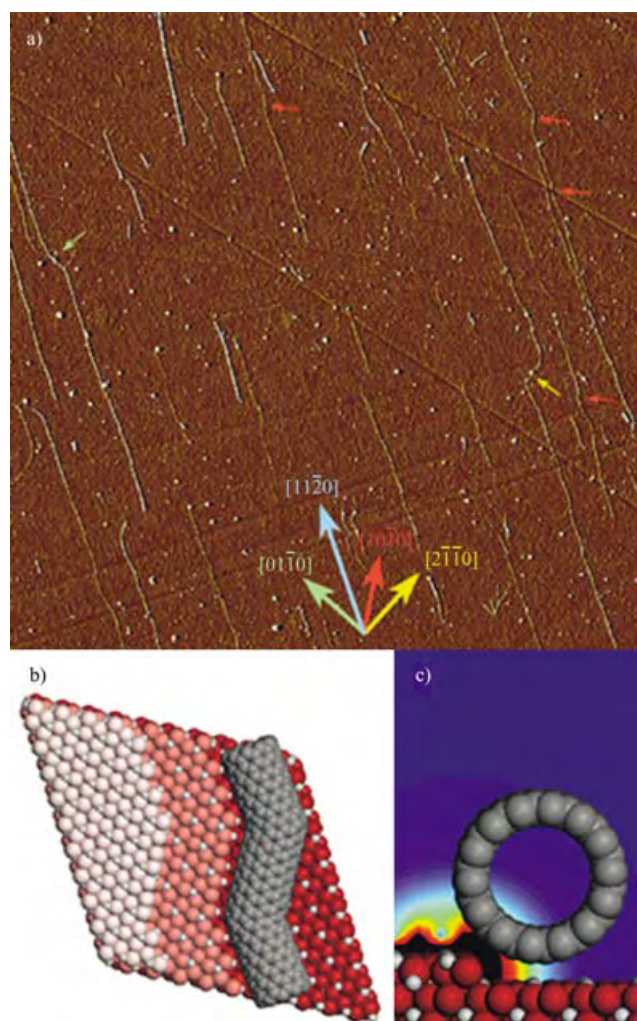


Figure 4. SWNT growth along atomic steps. a) AFM amplitude image of kinked SWNTs growing along the $[11\bar{2}0]$ direction (blue) with short segments along the $[10\bar{1}0]$ direction (red), and occasionally $[2\bar{1}\bar{1}0]$ (yellow) and $[01\bar{1}0]$ (green; image size 5 μm). The short arrows in the respective color point to a few such segments. b) Illustration of a $(10,0)$ – $(6,6)$ – $(10,0)$ kinked nanotube along $[11\bar{2}0]$ – $[10\bar{1}0]$ – $[11\bar{2}0]$. c) Model of a 1-nm-diameter SWNT along a $[11\bar{2}0]$ atomic step. The color gradient represents an estimated SWNT–step electrostatic interaction energy per unit of nanotube length as a function of SWNT axis position, $U(x,z)$. This was calculated from the force exerted on a polarizable body by an inhomogeneous field, $\mathbf{F} = (\alpha \mathbf{E} \cdot \nabla) \mathbf{E}$. Averaging the potential along the direction of the step and the SWNT (y) gives $U(x,z) = -\frac{1}{2} \alpha_{xx} E^2(x,z)$, where α_{xx} is the transverse polarizability of the SWNT per length^[31] and $E(x,z)$ is the local field. The latter was derived from the unreconstructed atomic step, by summation of Coulomb potentials from bulk Mulliken charges, averaged along the y axis and corrected for slab edge effects by subtracting a similar potential without the step. (The blue-to-red scale is 0–750 eV nm^{−1}.)

loss of translational symmetry, that is consistent with this picture. Pentagon–heptagon defects are known to cause structural changes along the SWNTs,^[28] thus producing interesting metal–semiconductor heterojunctions.^[29] In addition, the right-handedness of the kinked nanotubes reveals the chirality of the miscut substrate, which could in principle distinguish between enantiomorphic SWNTs. A different intriguing aspect is that faceting of vicinal $\alpha\text{-Al}_2\text{O}_3(0001)$

atomic steps has not yet been observed,^[22] because of their relatively low anisotropy energy below $\theta = 1^\circ$. The anisotropy is expected to increase at higher miscut inclinations as a result of step–step interactions, but could not be resolved by AFM. Here, the decoration by SWNTs reveals a faceting that would otherwise remain unseen.

We propose a “wake-growth” mechanism to describe the atomic-step-templated formation of SWNTs, in which the catalyst nanoparticle slides along the atomic step and leaves the growing SWNT behind as a wake. This would involve three main factors: 1) higher nanotube-surface van der Waals (vdW) interactions near the step that result from increased contact area; 2) electrostatic interaction between the local electric fields created by uncompensated dipoles at the atomic steps and the induced dipoles across the SWNTs; and 3) better wetting of the atomic steps by the Fe metal catalyst nanoparticles, because of capillarity and higher coordination. The vdW contribution to the interaction energy per unit of nanotube length can be theoretically extrapolated from previous calculations on Si surfaces (2.2 eV nm^{-1}),^[30] by assuming proportionality with the substrate polarizability^[31] and a Clausius–Mossotti relation,^[31] which yields 1.4 eV nm^{-1} on SiO_2 and 2.2 eV nm^{-1} on $\alpha\text{-Al}_2\text{O}_3$ surfaces. This small difference cannot account for the results in Figures 1 a and b. Moreover, the lack of alignment by the approximately 1-nm-deep polishing scratches (Figure 2 a) suggests that vdW interactions may not be the only aligning factor. On the other hand, electrostatic interactions may be especially high as a result of the ionic character of $\alpha\text{-Al}_2\text{O}_3$. The electrostatic nanotube–step interaction was modeled, as a first approximation, by applying theoretical SWNT polarizabilities^[32] and a Coulomb potential near an unreconstructed step (Figure 4 c). This electrostatic interaction is about 50 eV nm^{-1} at a reasonable vdW distance (0.34 nm) from the step. Although this remarkable value should be diminished by surface relaxation and reconstruction, it may still significantly account, along with vdW forces, for the strong SWNT– Al_2O_3 interaction compared to that of SWNT– SiO_2 (Figure 1 a,b), as well as for the high degree of nanotube alignment along the atomic steps.

The present study shows that atomic-scale surface features can direct the orientation and conformation, and possibly also the structure, of single-wall carbon nanotubes. The direction and morphology of the atomic steps can be macroscopically controlled in the crystal cutting process by two degrees of freedom, namely the miscut inclination θ and azimuth ϕ . Although the nanotubes are not yet regularly spaced, the atomic steps are. Therefore, an improved catalyst should in principle be able to yield periodic arrays of SWNTs with controllable spacing. Lastly, step-templated assembly may not be limited to carbon nanotubes and vicinal surfaces, but could be generally applicable to other axial-growth nanowires as well as to other controllable surface defects, such as etch pits, grain boundaries, and screw dislocations. This will enable new strategies for the large-scale fabrication of nanoscale devices from the bottom up.

Keywords: crystal engineering · nanostructures · nanotechnology · nanotubes · surface chemistry

- [1] M. S. Strano, C. A. Dyke, M. L. Usrey, P. W. Barone, M. J. Allen, H. W. Shan, C. Kittrell, R. H. Hauge, J. M. Tour, R. E. Smalley, *Science* **2003**, *301*, 1519–1522.
- [2] R. Krupke, F. Hennrich, H. von Lohneysen, M. M. Kappes, *Science* **2003**, *301*, 344–347.
- [3] E. Joselevich, *Angew. Chem.* **2004**, *116*, 3052–3054; *Angew. Chem. Int. Ed.* **2004**, *43*, 2992–2994.
- [4] X. F. Duan, Y. Huang, Y. Cui, J. F. Wang, C. M. Lieber, *Nature* **2001**, *409*, 66–69.
- [5] P. Avouris, *Acc. Chem. Res.* **2002**, *35*, 1026–1034.
- [6] *Nanoelectronics and Information Technology* (Ed.: R. Waser), Wiley-VCH, Weinheim, **2003**.
- [7] Y. N. Xia, P. D. Yang, Y. G. Sun, Y. Y. Wu, B. Mayers, B. Gates, Y. D. Yin, F. Kim, Y. Q. Yan, *Adv. Mater.* **2003**, *15*, 353–389.
- [8] E. Joselevich, C. M. Lieber, *Nano Lett.* **2002**, *2*, 1137–1141.
- [9] A. Ural, Y. M. Li, H. J. Dai, *Appl. Phys. Lett.* **2002**, *81*, 3464–3466.
- [10] S. M. Huang, B. Maynor, X. Y. Cai, J. Liu, *Adv. Mater.* **2003**, *15*, 1651–1655.
- [11] Y. Huang, X. F. Duan, Q. Q. Wei, C. M. Lieber, *Science* **2001**, *291*, 630–633.
- [12] M. R. Diehl, S. N. Yaliraki, R. A. Beckman, M. Barahona, J. R. Heath, *Angew. Chem.* **2002**, *114*, 363–366; *Angew. Chem. Int. Ed.* **2001**, *41*, 353–356.
- [13] N. A. Melosh, A. Boukai, F. Diana, B. Gerardot, A. Badolato, P. M. Petroff, J. R. Heath, *Science* **2003**, *300*, 112–115.
- [14] W. A. Lopes, H. M. Jaeger, *Nature* **2001**, *414*, 735–738.
- [15] M. P. Zach, K. H. Ng, R. M. Penner, *Science* **2000**, *290*, 2120–2123.
- [16] H. Yan, S. H. Park, G. Finkelstein, J. H. Reif, T. H. LaBean, *Science* **2003**, *301*, 1882–1884.
- [17] P. Gambardella, M. Blanc, H. Brune, K. Kuhnke, K. Kern, *Phys. Rev. B* **2000**, *61*, 2254–2262.
- [18] S. Iijima, *Nature* **1991**, *354*, 56–58.
- [19] D. G. Dresselhaus, A. P. Dresselhaus, *Carbon Nanotubes: Synthesis, Properties, and Applications*, Springer, Heidelberg, **2004**.
- [20] S. Helveg, C. Lopez-Cartes, J. Sehested, P. L. Hansen, B. S. Clausen, J. R. Rostrup-Nielsen, F. Abild-Pedersen, J. K. Nørskov, *Nature* **2004**, *427*, 426–429.
- [21] M. Su, Y. Li, B. Maynor, A. Buldum, J. P. Lu, J. Liu, *J. Phys. Chem. B* **2000**, *104*, 6505–6508.
- [22] O. Kurnosikov, L. P. Van, J. Cousty, *Surf. Sci.* **2000**, *459*, 256–264.
- [23] G. A. Somorjai, *Chem. Rev.* **1996**, *96*, 1223–1235.
- [24] J. R. Heffelfinger, M. W. Bench, C. B. Carter, *Surf. Sci.* **1997**, *370*, L168–L172.
- [25] C. Barth, M. Reichling, *Nature* **2001**, *414*, 54–57.
- [26] J. Han, M. P. Anantram, R. L. Jaffe, J. Kong, H. Dai, *Phys. Rev. B* **1998**, *57*, 14983–14989.
- [27] B. I. Yakobson, C. J. Brabec, J. Bernholc, *Phys. Rev. Lett.* **1996**, *76*, 2511–2514.
- [28] M. Ouyang, J. L. Huang, C. L. Cheung, C. M. Lieber, *Science* **2001**, *291*, 97–100.
- [29] Z. Yao, H. W. C. Postma, L. Balents, C. Dekker, *Nature* **1999**, *402*, 273–276.
- [30] T. Hertel, R. E. Walkup, P. Avouris, *Phys. Rev. B* **1998**, *58*, 13870–13873.
- [31] J. Israelachvili, *Intermolecular and Surface Forces*, Harcourt Brace & Company, San Diego, **1997**.
- [32] L. X. Benedict, S. G. Louie, M. L. Cohen, *Phys. Rev. B* **1995**, *52*, 8541–8549.

Received: April 18, 2004

Pd-Catalyzed Cyclizations

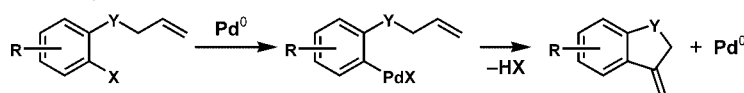
Direct Oxidative Heck Cyclizations: Intramolecular Fujiwara–Moritani Arylations for the Synthesis of Functionalized Benzofurans and Dihydrobenzofurans**

Haiming Zhang, Eric M. Ferreira, and Brian M. Stoltz*

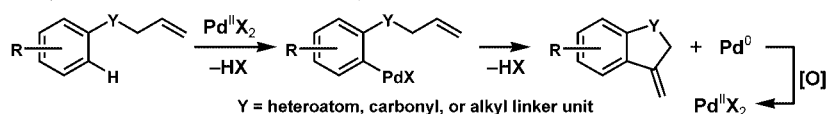
Over the past two and a half decades, the intramolecular Heck reaction has proven to be an integral process for the formation of C–C linkages in the synthesis of complex molecules.^[1] While the reaction provides desirable products by the coupling of an aryl or vinyl halide with an olefin by extrusion of the hydrohalic acid, the overall process involves two discrete functionalization events: 1) halogenation of an aryl or vinyl precursor and 2) palladium(0)-catalyzed C–C bond formation (Scheme 1a). A potentially more efficient process would involve oxidative coupling of an unfunctionalized arene directly with an olefin, thus obviating the necessity for prehalogenation of the substrate (Scheme 1b). Although the intermolecular version of this reaction was discovered in 1967 by Fujiwara and Moritani,^[2] subsequent studies have largely focused on couplings of benzene with activated olefins (e.g., acrylate esters).^[3] In fact, the direct intramolecular oxidative arene/olefin coupling (i.e., oxidative Heck cyclization^[4]) has not been studied thoroughly.^[5]

In the course of our efforts to develop palladium(II)-catalyzed dehydrogenation as a general oxidation method,^[6,7] we recently described the catalytic oxidative cyclization of unsaturated indoles to give annulated derivatives (Scheme 1c).^[8] Our studies determined that the indole cyclization

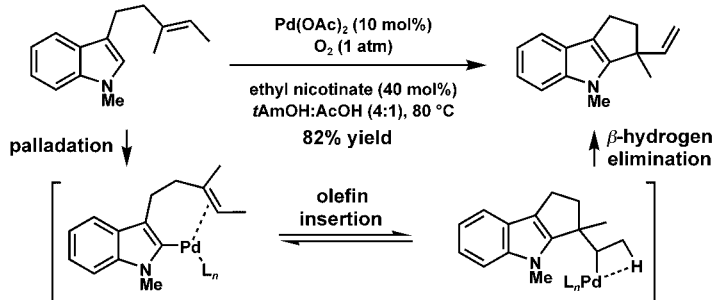
a) Heck Cyclization



b) Fujiwara–Moritani/Oxidative Heck Cyclization



c) Indole Annulation



Scheme 1. a) A generalized Heck cyclization (note that the halide must be installed in a discrete step). b) A generalized Fujiwara–Moritani/oxidative Heck cyclization. c) An example of an indole annulation by oxidative arene–olefin cyclization.^[8]

Table 1: Screening of oxidants for the intramolecular oxidative Heck cyclization.^[a]

Entry	Oxidant [1 equiv]	Yield [%] ^[b]	Entry	Oxidant [1 equiv]	Yield [%] ^[b]
1	O ₂ (1 atm)	56	5	Tl(OCOCF ₃) ₃	< 10
2	benzoquinone	62	6	K ₂ S ₂ O ₈	30
3	Cu(OAc) ₂	31	7	H ₂ NC(S)NH ₂	< 10
4	AgOAc	29	8	PhCO ₃ tBu	42

[a] All reactions were carried out with 0.10 mmol **1**, 10 mol % Pd(OAc)₂ (0.01 mmol), 40 mol % ethyl nicotinate (0.04 mmol), and 0.10 mmol or 1 atm oxidant in 1.0 mL 4:1 tAmOH:AcOH (0.1 M in substrate). [b] Yield determined by gas chromatography.

mechanism most likely involves initial arene palladation with subsequent olefin insertion and β -hydrogen elimination.^[9] Importantly, this mechanism is analogous to that of the Heck cyclization, since a similar aryl–Pd^{II} species is believed to be the key intermediate in both processes; however, the new process is oxidative due to the initial C–H bond functionalization event and net dehydrogenation of the substrate. Furthermore, since Pd⁰-mediated oxidative addition to electron-rich aryl halides is typically slower than that to electron-poor arenes,^[10] this direct oxidative process (initiated by electrophilic palladation by Pd^{II}) is complementary to the Heck technology. We envisioned that electron-rich arenes other than indoles could participate in such oxidative cyclizations with unactivated olefins under similar catalysis.

[*] Dr. H. Zhang, E. M. Ferreira, Prof. B. M. Stoltz
The Arnold and Mabel Beckman Laboratories of Chemical Synthesis
Division of Chemistry and Chemical Engineering
California Institute of Technology
1200 East California Boulevard, MC 164-30
Pasadena, CA 91125 (USA)
Fax: (+1) 626-564-9297
E-mail: stoltz@caltech.edu

[**] The authors wish to thank the NIH-NIGMS (R01 GM65961-01), the NSF (predoctoral fellowship to E.M.F.), Johnson and Johnson, Pfizer, Merck, Amgen, Research Corporation, Roche, GlaxoSmith-Kline, and Eli Lilly for generous funding.

Supporting information for this article is available on the WWW under <http://www.angewandte.org> or from the author.

Herein, we report a direct method for the synthesis of benzofurans and dihydrobenzofurans by palladium-catalyzed intramolecular Fujiwara–Moritani/oxidative Heck reactions.^[11,12]

In order to test the viability of applying the intramolecular oxidative Heck cyclization to a nonindolic system, we prepared allyl phenyl ether **1** by alkylation of the corresponding phenol. Ether **1** was subjected to our optimized conditions for the aforementioned indole cyclization in the presence of a variety of stoichiometric oxidants (Table 1). We were gratified to observe that in the presence of a range of oxidants, ether **1** cyclized to give benzofuran **2** at 80 °C, presumably by palladium-catalyzed C–C bond formation and β -hydride elimination, followed by isomerization of the olefinic product to the thermodynamically more stable benzofuran. As we observed for indole cyclization, it was found that molecular oxygen was a competent stoichiometric oxidant for the cyclization **1**→**2**. However, in the case at hand, benzoquinone provided the highest yield of **2** (62 % yield by GC) and thus was used for further optimization.

Having found benzoquinone to be the optimal oxidant in the cyclization **1**→**2**, we examined the other parameters in the process (Table 2).^[13] It was found that a 1:2 ratio of Pd:ethyl nicotinate was ideal (entries 1–4) and that inclusion of a substoichiometric amount of NaOAc (20 mol %) provided increased yields (entries 5 and 6). Finally, increasing the

Table 2: Optimization studies for the intramolecular oxidative Heck cyclization.^[a]

Entry	Ethyl nicotinate [mol %]	NaOAc [mol %]	T [°C]	t [h]	Yield [%] ^[b]
1	40	–	80	24	62
2	20	–	80	24	66
3	10	–	80	24	59
4	0	–	80	24	55
5	20	100	80	24	70
6	20	20	80	24	74
7	20	20	100	12	80 (77) ^[c]
8	20	20	120	12	67

[a] All reactions were carried out with 0.10 mmol **1**, 10 mol % Pd(OAc)₂ (0.01 mmol), 0–40 mol % ethyl nicotinate (0–0.04 mmol), 0–0.10 mmol NaOAc, and 0.10 mmol benzoquinone in 1.0 mL 4:1 tAmOH:AcOH (0.1 M in substrate). [b] Yield determined by gas chromatography. [c] Yield of isolated product in parentheses.

temperature to 100 °C led to optimal results, providing benzofuran **2** in 77 % yield after 12 h (entry 7).

Table 3: Oxidative benzofuran synthesis.^[a]

Entry	Substrate	Product	t [h]	Yield [%] ^[b]
1			12	77
2			12	74
3			13	72
4			12	62
5			14	54
6			12	61
7			14	75
8			12	79
9			12	61
10			16	56 ^[c]
11			16	52 ^[c]

[a] All reactions were carried out with 0.50 mmol substrate, 10 mol % Pd(OAc)₂ (0.05 mmol), 20 mol % ethyl nicotinate (0.10 mmol), 0.10 mmol NaOAc, and 0.50 mmol benzoquinone in 5.0 mL 4:1 tAmOH:AcOH (0.1 M in substrate) at 100 °C. [b] Yield of isolated product. [c] Produced as a single regioisomer.

With a viable oxidative cyclization to produce benzofuran **2** in hand, we set out to explore the generality of the transformation. As shown in Table 3, the scope of the oxidative benzofuran synthesis is quite broad, leading to highly substituted products by selective *ortho* reactivity. The methodology is currently limited to the use of electron-rich arenes; however, the aryl subunit tolerates several alkoxy and alkyl groups and substitution patterns. Likewise, the allylic portion may be functionalized at both the proximal and distal positions relative to the ether linkage with a variety of groups (e.g. alkyl, aryl, functionalized alkyl).

We next investigated the feasibility of synthesizing quaternary carbon-containing dihydrobenzofurans by employing tri- and tetrasubstituted olefins in the process to avoid olefin isomerization after the cyclization step. As shown in Table 4, an array of highly functionalized dihydrobenzofuran derivatives can be synthesized in good yields with as little as 5 mol % Pd(OAc)₂ (Table 4, entry 2).^[14]

In order to probe the mechanism of these carbocyclizations, we prepared substrate **3** and subjected it to the oxidative cyclization conditions (Scheme 2). Cyclization of this substrate can distinguish between two mechanistically distinct pathways (Scheme 2, A and B) by formation of diastereomeric products (i.e., either **4** or **5**). Specifically, a mechanism

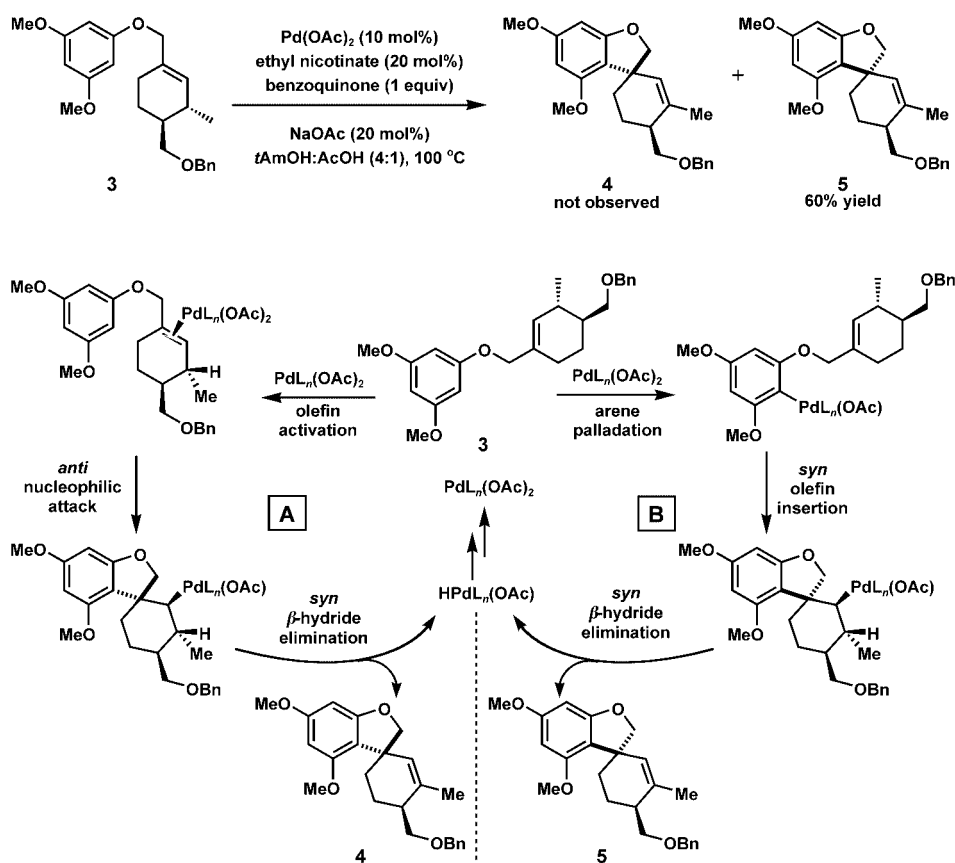
proceeding by means of olefin activation, *anti* nucleophilic attack of the arene on the Pd π complex, and *syn* β -hydride elimination (Scheme 2, pathway A) can be differentiated from one involving aryl-palladation, *syn* olefin insertion, and *syn* β -hydride elimination (Scheme 2, pathway B). Under our standard reaction conditions, ether **3** cyclized to produce a diastereomerically pure product in 60% yield, which was determined to be dihydrobenzofuran **5** by ¹H NMR NOE experiments.^[15] The outcome of this mechanistic study suggests that pathway B is operative and that C–H bond functionalization precedes olefin insertion and β -hydride elimination.^[16] Additionally, this reaction demonstrates that quaternary carbon stereocenters can be generated diastereoselectively, by chirality transfer, from a tertiary carbon center.

In summary, we have developed a method for intramolecular oxidative C–C bond formation that relies on Pd^{II} catalysis to access electron-rich, highly substituted benzofuran and dihydrobenzofuran derivatives. These oxidations produce important heterocyclic ring systems^[11] by direct C–H bond functionalization of the aromatic ring and cyclization with unactivated olefins. Based on mechanistic insight (i.e. the proposed intermediacy of an aryl Pd^{II} species), we have illustrated the analogy of such oxidative carbocyclizations to the corresponding intramolecular Heck reaction, and we thus

Table 4: Oxidative dihydrobenzofuran synthesis.^[a]

Entry	Substrate	Product	<i>t</i> [h]	Yield [%] ^[b]
1			16	74
2 ^[c]			12	71
3			30	58 ^[d]
4			28	55
5			15	74 ^[e]
6			24	80
7			18	78
8			15	50
9			15	63
10			15	60
11			15	66

[a] All reactions were carried out with 0.50 mmol substrate, 10 mol % Pd(OAc)₂ (0.05 mmol), 20 mol % ethyl nicotinate (0.10 mmol), 0.10 mmol NaOAc, and 0.50 mmol benzoquinone in 5.0 mL 4:1 *t*-AmOH:AcOH (0.1 M in substrate) at 100 °C. [b] Yield of isolated product. [c] Performed with 5 mol % Pd(OAc)₂ and 10 mol % ethyl nicotinate. [d] An inseparable mixture of roughly 66% product (*E/Z* = 3:1) and 10% starting material was isolated after 18 h. This mixture was subjected to another reaction with 5 mol % Pd(OAc)₂, 10 mol % ethyl nicotinate, 20 mol % NaOAc, and 50 mol % benzoquinone in 4:1 *t*-AmOH:AcOH (0.1 M) for 12 h after which only the *E* isomer was observed. The yield presented is the overall yield of isolated product. [e] A 2.3:1 mixture of diastereomers was isolated with the major isomer shown.



Scheme 2. Mechanistic probe for the oxidative cyclization.

classify these transformations as Fujiwara–Moritani/oxidative Heck cyclizations. Furthermore, this methodology may be considered orthogonal to the traditional Heck reaction in that highly electron-rich arenes may be employed directly. In certain cases, halogenated derivatives of such arenes may be difficult to access selectively or may have undesirably low reactivity toward Pd^0 catalysts. While the method is currently limited to the synthesis of five-membered ring ethers, the utilization of the oxidative Heck cyclization for the synthesis of complex molecules and the demonstration of its orthogonality to the Heck reaction should help to further elucidate the scope; these remain primary goals of our laboratory.^[17]

Received: July 13, 2004

Keywords: benzofurans · homogeneous catalysis · oxidation · palladium

- [1] For outstanding reviews on Pd-catalyzed intramolecular Heck reactions, see: a) S. Braese, A. de Meijere, in *Handbook of Organopalladium Chemistry for Organic Synthesis*, Vol. 1 (Ed.: E.-I. Negishi), Wiley, Hoboken, New Jersey, **2002**, pp. 1223–1254; b) J. Tsuji, *Palladium Reagents and Catalysts*, Wiley, Chichester, UK, **1995**, chap. 4; c) J. T. Link, *Org. React.* **2002**, *60*, 157–534.

- [2] a) I. Moritani, Y. Fujiwara, *Tetrahedron Lett.* **1967**, 1119–1122; b) Y. Fujiwara, I. Moritani, S. Danno, R. Asano, S. Teranishi, *J. Am. Chem. Soc.* **1969**, *91*, 7166–7169; c) Y. Fujiwara, R. Asano, I. Moritani, S. Teranishi, *J. Org. Chem.* **1976**, *41*, 1681–1683; d) Y. Fujiwara, O. Maruyama, M. Yoshidomi, H. Taniguchi, *J. Org. Chem.* **1981**, *46*, 851–855; e) C. Jia, W. Lu, T. Kitamura, Y. Fujiwara, *Org. Lett.* **1999**, *1*, 2097–2100; f) C. Jia, T. Kitamura, Y. Fujiwara, *Acc. Chem. Res.* **2001**, *34*, 633–639.
- [3] For additional examples of Pd-catalyzed intermolecular Fujiwara–Moritani arylations, see: a) T. Yokota, M. Tani, S. Sakaguchi, Y. Ishii, *J. Am. Chem. Soc.* **2003**, *125*, 1476–1477; b) M. Dams, D. E. De Vos, S. Celen, P. A. Jacobs, *Angew. Chem.* **2003**, *115*, 3636–3639; *Angew. Chem. Int. Ed.* **2003**, *42*, 3512–3515; c) M. D. K. Boele, G. P. F. van Strijdonck, A. H. M. de Vries, P. C. J. Kamer, J. G. de Vries, P. W. N. M. van Leeuwen, *J. Am. Chem. Soc.* **2002**, *124*, 1586–1587; d) K. Mikami, M. Hatano, M. Terada, *Chem. Lett.* **1999**, 55–56; e) K. Hirota, H. Kuki, Y. Maki, *Heterocycles* **1994**, *37*, 563–570; f) K. Hirota, Y. Isobe, Y. Kitade, Y. Maki, *Synthesis* **1987**, 495–496; g) J. Tsuji, H. Nagashima, *Tetrahedron* **1984**, *40*, 2699–2702.
- [4] Recently, a number of catalytic intermolecular oxidative Heck arylations have been reported. These protocols typically employ main-group organometallic arenes with a range of olefinic coupling partners and Pd^{II} catalysis. As in the typical Heck cases, these also require the prefunctionalization of the arene substrate. For examples, see: a) M. M. S. Andappan, P. Nilsson, H. von Schenck, M. Larhed, *J. Org. Chem.* **2004**, *69*, 5212–5218; b) E. J. Farrington, J. M. Brown, C. F. J. Barnard, E. Rowsell, *Angew. Chem.* **2002**, *114*, 177–179; *Angew. Chem. Int. Ed.* **2002**, *41*, 169–171, and references therein.
- [5] For a stoichiometric Pd-mediated intramolecular oxidative arene–olefin cyclization with an unactivated olefin, see: a) P. S. Baran, C. A. Guerrero, E. J. Corey, *J. Am. Chem. Soc.* **2003**, *125*, 5628–5629. For Pd-catalyzed intramolecular oxidative arene–olefin cyclizations with activated olefins, see: b) H.-J. Knölker, W. Fröhner, K. R. Reddy, *Synthesis* **2002**, 557–564; c) H. Hagelin, J. D. Oslob, B. Åkermarck, *Chem. Eur. J.* **1999**, *5*, 2413–2416; d) H.-J. Knölker, K. R. Reddy, A. Wagner, *Tetrahedron Lett.* **1998**, *39*, 8267–8270.
- [6] a) D. D. Caspi, D. C. Ebner, J. T. Bagdanoff, B. M. Stoltz, *Adv. Synth. Catal.* **2004**, *346*, 185–189; b) R. M. Trend, B. M. Stoltz, *J. Am. Chem. Soc.* **2004**, *126*, 4482–4483; c) J. T. Bagdanoff, B. M. Stoltz, *Angew. Chem.* **2004**, *116*, 357–361; *Angew. Chem. Int. Ed.* **2004**, *43*, 353–357; d) R. M. Trend, Y. K. Ramtohul, E. M. Ferreira, B. M. Stoltz, *Angew. Chem.* **2003**, *115*, 2998–3001; *Angew. Chem. Int. Ed.* **2003**, *42*, 2892–2895; e) J. T. Bagdanoff,

- E. M. Ferreira, B. M. Stoltz, *Org. Lett.* **2003**, *5*, 835–837; f) E. M. Ferreira, B. M. Stoltz, *J. Am. Chem. Soc.* **2001**, *123*, 7725–7726.
- [7] a) B. M. Stoltz, *Chem. Lett.* **2004**, *33*, 362–367; b) S. S. Stahl, *Angew. Chem.* **2004**, *116*, 3480–3501; *Angew. Chem. Int. Ed.* **2004**, *43*, 3400–3420.
- [8] E. M. Ferreira, B. M. Stoltz, *J. Am. Chem. Soc.* **2003**, *125*, 9578–9579.
- [9] For recent reviews on Pd-catalyzed C–H bond functionalization, see: a) ref. [2f]; b) Y. Fujiwara, in *Handbook of Organopalladium Chemistry for Organic Synthesis*, Vol. 2 (Ed.: E.-I. Negishi), Wiley, Hoboken, New Jersey, **2002**, pp. 2863–2871; c) V. Ritleng, C. Sirlin, M. Pfeffer, *Chem. Rev.* **2002**, *102*, 1731–1769.
- [10] a) A. Jutand, A. Mosleh, *Organometallics* **1995**, *14*, 1810–1817; b) M. Portnoy, D. Milstein, *Organometallics* **1993**, *12*, 1665–1673; c) C. Amatore, F. Pflüger, *Organometallics* **1990**, *9*, 2276–2282; d) R. Benhaddou, S. Czernecki, G. Ville, A. Zegar, *Organometallics* **1988**, *7*, 2435–2439; e) J.-F. Fauvarque, F. Pflüger, M. Troupel, *J. Organomet. Chem.* **1981**, *208*, 419–427.
- [11] For recent examples of biologically active benzofuran derivatives, see: Antifungal agents: a) M. Masubuchi, H. Ebike, K.-i. Kawasaki, S. Sogabe, K. Morikami, Y. Shiratori, S. Tsuji, T. Fujii, K. Sakata, M. Hayase, H. Shindoh, Y. Aoki, T. Ohtsuka, N. Shimma, *Bioorg. Med. Chem.* **2003**, *11*, 4463–4478; Oxytocin antagonists: b) P. G. Wyatt, M. J. Allen, J. Chilcott, C. J. Gardner, D. G. Livermore, J. E. Mordaunt, F. Nerozzi, M. Patel, M. J. Perren, G. G. Weingarten, S. Shabbir, P. M. Woollard, P. Zhou, *Bioorg. Med. Chem. Lett.* **2002**, *12*, 1405–1411; Serotonin release enhancer: c) F. Yoneda, T. Moto, M. Sakae, H. Ohde, B. Knoll, I. Miklya, J. Knoll, *Bioorg. Med. Chem.* **2001**, *9*, 1197–1212. For references on the biological activity of dihydrobenzofuran derivatives, see: Tubulin polymerization inhibitors: d) L. Pieters, S. Van Dyck, M. Gao, R. Bai, E. Hamel, A. Vlietinck, G. Lemiére, *J. Med. Chem.* **1999**, *42*, 5475–5481; Anti-inflammatory and analgesic agents: e) J. M. Janusz, P. A. Young, M. W. Scherz, K. Enzweiler, L. I. Wu, L. Gan, S. Pikul, K. L. McDowdunham, C. R. Johnson, C. B. Senanayake, D. E. Kellstein, S. A. Green, J. L. Tulich, T. Rosario-Jansen, I. J. Magrisso, K. R. Wehmeyer, D. L. Kühlenbeck, T. H. Eichhold, R. L. M. Dobson, *J. Med. Chem.* **1998**, *41*, 1124–1137; Acyl-CoA:cholesterol acyltransferase inhibitors: f) K.-i. Kataoka, T. Shiota, T. Takeyasu, T. Minoshima, K. Watanabe, H. Tanaka, T. Mochizuki, K. Taneda, M. Ota, H. Tanabe, H. Yamaguchi *J. Med. Chem.* **1996**, *39*, 1262–1270.
- [12] The Pd-mediated construction of benzofuran ring systems from acyclic precursors has been an active area of research in recent years. For a review, see: S. Cacchi, G. Fabrizi, A. Goggiani, *Heterocycles* **2002**, *56*, 613–632.
- [13] A screen of solvents and ligands was also conducted, but provided no improvements. These parameters were investigated extensively in our indole system.^[8]
- [14] Pd-promoted aryl Claisen rearrangements appear not to be generally competitive, and no such products were isolated in any of the reactions in Tables 3 and 4. Only one such case, involving the reaction of a 1-allyloxynaphthalene derivative, has been observed under our conditions.
- [15] In addition to **5**, a small amount of starting ether **3** was isolated. No other isomeric products were observed in the reaction.
- [16] A similar observation was made in our studies directed toward the oxidative annulation of indoles.^[8]
- [17] We recently utilized an oxidative C–C bond-forming reaction as a key step for the total synthesis of the marine alkaloid drarmacidin F, see: N. K. Garg, D. D. Caspi, B. M. Stoltz, *J. Am. Chem. Soc.* **2004**, *126*, 9552–9553.

Changes in the Conductance of Single Peptide Molecules upon Metal-Ion Binding***Xiaoyin Xiao, Bingqian Xu, and Nongjian Tao**

As the field of silicon-based microelectronics attempts, with difficulty, to head towards the nanoscale, the construction of electronic devices with individual molecules becomes an attractive alternative^[1] and has stimulated a recent surge of interest in the study of the electronic properties of single molecules.^[2,3] As well as displaying excellent electronic properties, single molecules can also recognize other molecules through specific binding interactions, which is something that current silicon-based technology is unable to offer. This capability of molecular recognition is used with astonishing accuracy and efficiency in biological systems and serves as an important design principle for chemical and biological sensors. Various molecular recognition processes have been studied and applied to sensor applications, but most methods to date measure an optical, electrochemical, or mechanical signal that arises from a large number of molecules.^[4–8] Herein we demonstrate that the binding of a guest species onto a single host molecule can be studied electrically by wiring the host molecule to two electrodes. The measurement of electron-transport processes through a single molecule also allows the rectification properties of asymmetric host molecules and host–guest complexes to be studied.

Peptides were chosen as the host molecules because of the unlimited choice of different sequences that can be tuned to obtain optimal binding strength and specificity for a metal ion—our chosen guest.^[7] Four peptides were studied, cysteamine-Cys, cysteamine-Gly-Cys, Cys-Gly-Cys, and cysteamine-Gly-Gly-Cys (Cys = cysteine, Gly = glycine), which each have two thiol termini that can form reproducible contact to Au electrodes for electrical measurement. These peptides were expected to bind transition-metal ions, such as Cu^{2+} and Ni^{2+} , specifically through deprotonated peptide bonds.^[9] The binding configuration and the binding constant are sensitive to the pH of the peptide local environment. To form the most stable metal–peptide complexes and also to avoid the precipitation of metal hydroxides on the Au electrodes, the pH of the solution was maintained at 8 and 9 for Cu^{2+} and Ni^{2+} , respectively. Under the experimental conditions, the metal ions and the peptides were expected to form mainly 1:1 metal-to-ligand complexes. For cysteamine-Cys, cysteamine-Gly-Cys, and Cys-Gly-Cys, the peptide bonds are completely deprotonated so the number of deprotonated

[*] Dr. X. Y. Xiao, B. Q. Xu, Prof. Dr. N. J. Tao
The Center for Solid State Electronics Research
Arizona State University
Tempe, AZ85287 (USA).
Fax: (+1) 480-965-8118
E-mail: nongjian.tao@asu.edu

[**] We thank the NSF (CHE-0243423) and the DOE (DE-FG03-01ER45943) for financial support to B.Q.X. and X.Y.X., respectively.

peptide bonds is 1, 2, and 3, respectively, whereas for cysteamine-Gly-Gly-Cys, the number of deprotonated bonds is 2 or 3.^[10]

To reliably measure the conductance of a single molecule,^[11–15] we used two complementary approaches. The first was a statistical approach, which has been described in detail elsewhere.^[16,17] Briefly, individual molecular junctions were created by repeatedly moving an Au scanning tunneling microscope (STM) tip into and out of contact with an Au substrate in a solution that contained the sample molecules (1 mM, pH \approx 8, Figure 1a). The process was controlled by a feedback loop that started by driving the electrode into contact with the substrate by using a piezoelectric transducer (PZT). Once the contact was established, the feedback loop activated the PZT to pull the electrode out of contact. After breaking the contact, a series of steps appeared in the conductance that signaled the formation of the molecular junctions (Figure 1b for cysteamine-Gly-Cys). The conductance steps correspond to the breakdown of the contact of individual molecules to the electrodes.^[18] When the last molecule was broken, we then repeated the above process to

quickly obtain a large number of conductance curves. The histogram of the conductance curves exhibit well-defined peaks that are located at integer multiples of a fundamental conductance value, which is identified as the conductance of a single molecule (Figure 1c). The first peak for cysteamine-Gly-Cys is located at $4.2 \times 10^{-6} G_0$ ($G_0 = 2e^2 h^{-1} \approx 77 \mu S$), which gives a conductance of ≈ 0.3 nS or a resistance of ≈ 3 G Ω . This statistical approach has allowed us to determine the single-molecule conductivity values for a variety of systems,^[16,17,19] but important features associated with the individual molecular junctions may be lost. For example, the current–voltage (*I*–*V*) curve in the statistical approach is assembled from the positions of the peaks in the conductance histograms, which are obtained at different bias voltages and which smears out possible rectification behavior of asymmetric peptides. To overcome this difficulty, we used a second approach, which is similar to the break-junction method,^[11] to measure the *I*–*V* characteristics of the peptides in this work. First, the Au tip was brought into contact with the substrate and then the tip was gently pulled out of contact by controlling the PZT whilst the conductance was measured continuously. Once the conductance dropped to the last step, which corresponds to the formation of a single molecule bridged between the electrodes, the position of the tip was fixed and *I*–*V* curves were measured.

Figure 2, a–c, shows the *I*–*V* curves obtained for three of the peptide sequences. The slopes of the *I*–*V* curves near zero bias voltage give the conductance values of these peptides, which agree with the conductance values extracted from the conductance histograms. The most striking feature shared by all the peptides is asymmetry in the *I*–*V* curves. For clarity, only the *I*–*V* curves with the same polarity (i.e. the current at negative bias is greater than the current at positive bias) are shown in Figure 2. In reality, the polarity of the asymmetric *I*–*V* curves varies from one junction to another owing to the random orientation of the molecules in these individual molecular junctions. Rectification behavior in peptides is expected because of the asymmetry and the electric dipoles of the molecules. In a control experiment, *I*–*V* curves were measured for 1,8-octanedithiol, which gave rather symmetric curves (Figure 2d). Rectification is one of the most actively pursued goals in molecular electronics because of its potential application in molecular diodes.^[1] Reichert et al. reported asymmetric *I*–*V* curves for asymmetric molecules by using a break-junction method.^[11] Early observation of rectification behavior in a molecular system was observed on a Langmuir–Blodgett film of molecules that contained donor and acceptor groups.^[20] More recently, Whitesides and co-workers demonstrated rectification behavior in a molecular junction, which involved two molecular layers sandwiched between silver and mercury electrodes.^[21] In general, the observation of rectification requires asymmetric molecular junctions.^[22–24]

The binding of Cu²⁺ to each of the peptides, which were self-assembled on the gold substrate, was studied by the introduction of Cu²⁺ (2 mM) into NaClO₄ (0.1 M) and adjustment of the pH to 8 with NaOH at which value Cu²⁺ is expected to bind to the peptides.^[10,25] Figure 3 shows the conductance curves of cysteamine-Gly-Gly-Cys during the formation of individual molecular junctions in the absence

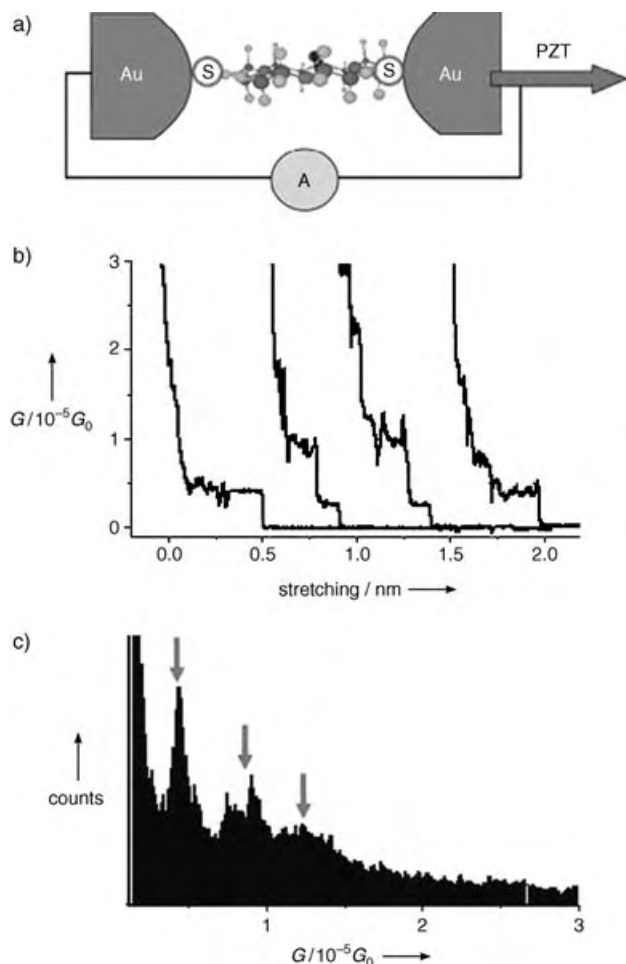


Figure 1. a) Schematic illustration of a molecular junction formed by the separation of two electrodes (PZT = piezoelectric transducer); b) several typical conductance curves of cysteamine-Gly-Cys during the stretching of the molecular junctions; c) conductance histogram constructed from over 500 individual conductance curves.

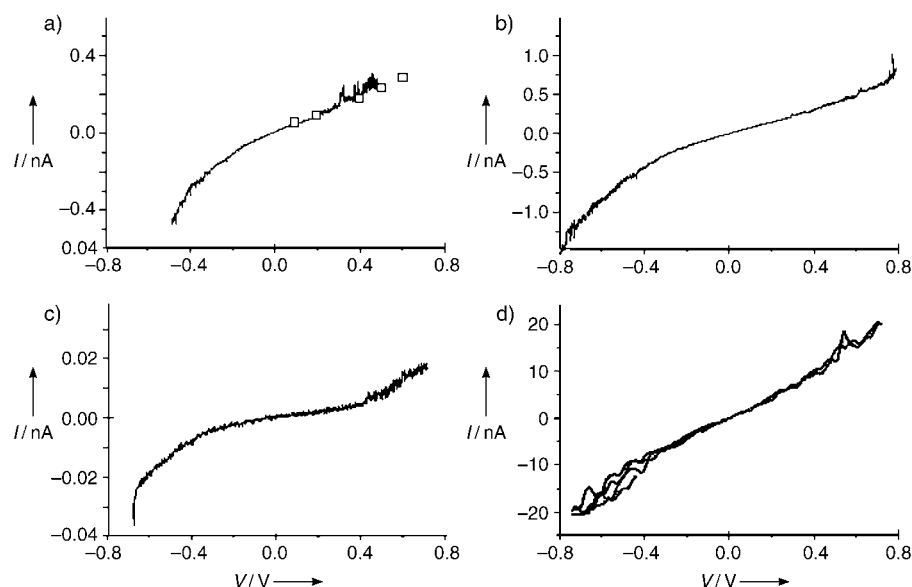


Figure 2. Asymmetric I - V curves of a) cysteamine-Gly-Cys, b) Cys-Gly-Cys, and c) cysteamine-Gly-Gly-Cys; I - V data which were determined from conductance histograms for cysteamine-Gly-Cys are also shown (\square); d) symmetric I - V curves of symmetric 1,8-octanedithiol.

(Figure 3a) and presence (Figure 3b) of Cu^{2+} . The last conductance steps in these curves correspond to the formation of single molecule junctions. The conductance steps of the peptide occur at values that are two orders of magnitude higher in the presence of Cu^{2+} ion than those in the absence of Cu^{2+} ion which shows that the Cu^{2+} binding event drastically changes the conductance of the peptide. From the corresponding conductance histograms (Figure 3, a and b, insets), conductance values of the peptide and the peptide- Cu^{2+} complex are 5×10^{-7} and $1.6 \times 10^{-4} G_0$, respectively. A typical I - V curve of the peptide complex is shown in Figure 3d which is also asymmetric, but its slope (conductance) near zero bias voltage is much greater than that of the peptide itself (Figure 3c).

Cyclic voltammetry measurements were also made on an Au substrate, which was coated with monolayers of the peptides, before and after exposure of the substrate to Cu^{2+} . Pronounced redox peaks

after exposure to Cu^{2+} were observed. As shown in Figure 4, the quasi-reversible peaks around 160 mV (half of the sum of the potentials of the anodic and cathodic peaks) correspond to $\text{Cu}^{2+}/\text{Cu}^+$ redox processes, which is in agreement with a similar Cu-peptide complex,^[26] and confirms the formation of the Cu-peptide (deprotonated) complex. Previous cyclic voltammetry studies also reported such redox process for Cu^{2+} -diglycine and Cu^{2+} -triglycine complexes, but at potentials below -200 mV.^[27,28] The positive shift of the redox potential may arise from surface adsorption.^[26,29] No other redox features were observed which indicates the absence of Cu^{2+} ions that are simply coordinated with carboxyl or amine groups.^[30,31] This is reasonable because all of the peptides studied here are flexible so they can fully use their binding sites. As a result, the complexes have high binding constants at pH 8. In a further control experiment, after conductance measurements of solutions of the free peptide and Cu^{2+} -peptide complex, respec-

tively, we acidified the solutions with HClO_4 (10 mM) to $\text{pH} \approx 2$ and again measured the conductance values of the substrates. As expected, the conductance of the single

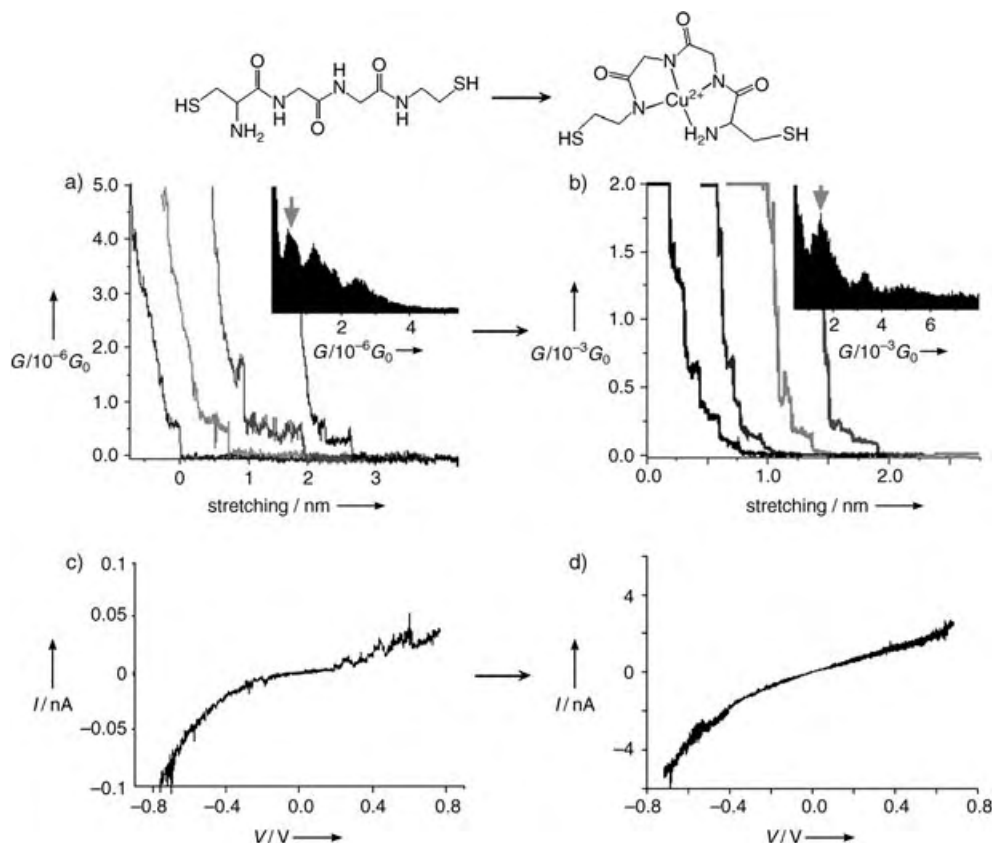


Figure 3. Individual conductance curves of cysteamine-Gly-Gly-Cys a) before and b) after binding to Cu^{2+} ; the insets show the conductance histograms. I - V curves of cysteamine-Gly-Gly-Cys c) before and d) after binding to Cu^{2+} .

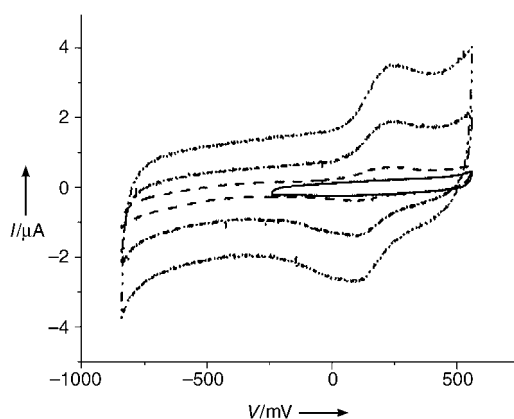


Figure 4. Cyclic voltammogram (vs. Ag/AgCl) of a (Cys-Gly-Cys)-modified electrode before (—) and after (---- and) exposure to copper(II) solution recorded in Cu^{2+} -free buffer solution ($\text{pH} \approx 8$). Cu^{2+} was accumulated at the (Cys-Gly-Cys)-modified electrode at open circuit for 10 min and then removed. Sweep rates: — and ----: 100 mVs^{-1} ;: 500 and 1000 mVs^{-1} .

molecule complex returned to the value found for the free peptide, an indication of the dissociation of Cu^{2+} -peptide complex in acidic solution.

The binding of different metal ions, such as Na^+ , K^+ , Cu^{2+} , Ni^{2+} , and Zn^{2+} to the different peptides in similar ways were also investigated. For Na^+ and K^+ ions, no changes in the conductance of the peptide were observed, which is expected because these ions do not bind to peptides. In the case of Zn^{2+} , a small increase in the conductance of the longest peptide was observed, which may be due to the weak Zn-peptide binding. However, the peaks in the conductance histograms for the Zn^{2+} -peptide complex are not well-defined and prevented further more-quantitative studies. The changes in the conductance upon the binding of Cu^{2+} and Ni^{2+} ions are rather dramatic, and the results are summarized in Table 1. The binding of the metal ions to the peptides increases the conductance, but the magnitude of the increase depends on the length and the sequence of the peptides as well as on the nature of the metal ions. For example, the change in the conductance is only $\approx 10\%$ for the shortest peptide, cysteamine-Cys, and ≈ 300 times for cysteamine-Gly-Gly-Cys. The change in the metal-ion-binding-induced conductance also depends on the sequence of the peptides. Cysteamine-Gly-Cys and Cys-Gly-Cys have the same length, but the binding of Cu^{2+} changes the conductance of the two peptides by 2 and 4 times, respectively. This dependence on the sequence may be attributed to the difference in the number of Cu^{2+} ion binding sites in the two peptides (2 in cysteamine-Gly-Cys and 3 in Cys-Gly-Cys). The binding of Ni^{2+} ions to the peptides also increases the conductance of the peptide but by a smaller amount than Cu^{2+} ions. This difference between the binding of Cu^{2+} and Ni^{2+} ions shows that the measurement of conductance can be used to distinguish different metal ions with similar binding configurations to a host molecule.

The binding of a metal ion to a peptide changes the conductance of a peptide in several ways. First, it affects the charge distribution of the peptide owing to the presence of the metal ion and the associated deprotonation of the peptide bonds. We recently observed that a change in the charge distribution of peptides can indeed change the conductance through a change in the tunneling barrier for the electrons, but the effect alone is usually small.^[19] Furthermore, the effect of charge distribution cannot easily explain the sensitive dependence of the conductance of the metal-ion-peptide complex on the length of the peptide. Second, the presence of metal ions introduces new energy levels along the electron-transport pathway which may dramatically enhance the electron transport through a resonant tunneling effect.^[32–36] Cyclic voltammograms indicate that the redox levels of Cu^{2+} -peptide complexes are closer to the Fermi energy levels of the electrode than those of corresponding Ni^{2+} -peptide complexes. This seems to explain the different changes induced by Cu^{2+} and Ni^{2+} in the conductance of the peptides. However,

Table 1: Effects of the binding of metal ions (Cu^{2+} and Ni^{2+}) on the conductance of peptides of various lengths and sequences.

Peptide	No. of binding sites	Conductance of peptide [G_0]	Conductance of peptide-ion complex [G_0]	Conductance ratio
Cysteamine-Cys	2	1.8×10^{-4}	1.9×10^{-4} (Cu^{2+})	≈ 1
Cysteamine-Gly-Cys	3	4.2×10^{-6}	9.1×10^{-6} (Cu^{2+}) 6.5×10^{-6} (Ni^{2+})	2.2 1.5
Cys-Gly-Cys	4	5.3×10^{-6}	2.3×10^{-5} (Cu^{2+})	4.3
Cysteamine-Gly-Gly-Cys	4	5.0×10^{-7}	1.6×10^{-4} (Cu^{2+}) 6.0×10^{-5} (Ni^{2+})	320 120

like the charge distribution model, this metal-ion-induced resonant tunneling mechanism alone cannot easily explain the sensitive dependence of the conductance of the metal-ion-peptide complex on the length of the peptide. Finally, the binding of a metal ion to a peptide can significantly change the conformation of the peptide. As we discussed in the previous sections, metal ions, under the experimental conditions, have a tendency to coordinate to all of the peptide binding sites which thus forces the peptide to adapt a new conformation (illustrated in Figure 3). This has been observed by X-ray crystallographic measurements and supported by other experimental data.^[37,38] As the binding process does not significantly change the bond lengths and angles of the peptide bonds, one may argue that the conformational change should not change the conductance if electron transport through the peptide backbone is considered as the dominant conduction pathway.^[39] However, the electrons may be transported through the chelate bonds, mediated by the metal ion, and thus provide a new pathway for electron transport. As the amount of conformational change increases with the peptide length, the metal-ion-mediated transport pathway is more efficient than the peptide backbone pathway for long peptides. On the basis of these considerations, we believe that the dominant mechanism for the observed changes in the conductance arises from conformational change together with

metal-ion-mediated tunneling, although effects such as changes in charge distribution may also play a role.

In conclusion, the conductance and I - V characteristics of single peptide molecules covalently bound to two Au electrodes have been measured. The I - V curves are highly asymmetric, which reflects the asymmetric structures and electric dipoles of the peptides. Upon binding of metal ions, the conductance of the peptides increases by an amount that depends on the sequence and length of the peptides. This work demonstrates a method to study molecular recognition on a single-molecule level.

Received: June 7, 2004

Revised: July 21, 2004

Keywords: electron transport · molecular recognition · peptides · single-molecule studies · transition metals

- [1] A. Aviram, M. Ratner, *Chem. Phys. Lett.* **1974**, 29, 277.
- [2] J. K. Gimzewski, C. Joachim, *Science* **1999**, 283, 1683.
- [3] A. Nitzan, M. A. Ratner, *Science* **2003**, 300, 1384.
- [4] T. Thundat, E. Finot, Z. Hu, R. H. Ritchie, G. Wu, A. Majumdar, *Appl. Phys. Lett.* **2000**, 77, 4061.
- [5] A. J. Ricco, R. M. Crooks, G. C. Osbourn, *Acc. Chem. Res.* **1998**, 31, 289.
- [6] D. T. McQuade, A. E. Pullen, T. M. Swager, *Chem. Rev.* **2000**, 100, 2537.
- [7] W. Yang, D. Jaramillo, J. J. Gooding, D. B. Hibbert, R. Zhang, G. D. Willet, K. J. Fisher, *Chem. Commun.* **2001**, 1982.
- [8] H. Zhang, S. Boussaad, N. Ly, N. J. Tao, *Appl. Phys. Lett.* **2004**, 84, 133.
- [9] H. Sigel, R. B. Martin, *Chem. Rev.* **1982**, 82, 385.
- [10] N. V. Nagy, T. Szabo-Planka, A. Rockenbauer, G. Peintler, I. Nagypal, L. Korecz, *J. Am. Chem. Soc.* **2003**, 125, 5227.
- [11] J. Reichert, R. Ochs, D. Beckmann, H. B. Weber, M. Mayor, H. von Löhneysen, *Phys. Rev. Lett.* **2002**, 88, 176804.
- [12] J. Park, A. N. Pasupathy, J. L. Goldsmith, C. Chang, Y. Yaish, J. R. Petta, M. Rinkoski, J. P. Sethna, H. D. Abruña, P. L. McEuen, D. C. Ralph, *Nature* **2002**, 417, 722.
- [13] W. J. Liang, M. Shores, M. Bockrath, J. R. Long, H. Park, *Nature* **2002**, 417, 725.
- [14] H. B. Weber, J. J. Reichert, F. Weigend, R. Ochs, D. Beckmann, M. Mayor, R. Ahlrichs, H. von Löhneysen, *Chem. Phys.* **2002**, 281, 113.
- [15] X. D. Cui, X. Zarate, J. Tomfohr, A. Primak, A. L. Moore, T. A. Moore, D. Gust, G. Harris, O. F. Sankey, S. M. Lindsay, *Nanotechnology* **2002**, 13, 5.
- [16] B. Q. Xu, N. J. Tao, *Science* **2003**, 301, 1221.
- [17] X. Y. Xiao, B. Q. Xu, N. J. Tao, *Nano Lett.* **2004**, 4, 267.
- [18] B. Q. Xu, X. Y. Xiao, N. J. Tao, *J. Am. Chem. Soc.* **2004**, 126, 16164.
- [19] X. Xiao, B. Xu, N. Tao, *J. Am. Chem. Soc.* **2004**, 126, 5370.
- [20] R. M. Metzger, *Chem. Rev.* **2003**, 103, 3803.
- [21] M. L. Chabinyc, X. X. Chen, R. E. Holmlin, H. Jacobs, H. Skulason, C. D. Frisbie, V. Mujica, M. A. Ratner, M. A. Rampi, G. M. Whitesides, *J. Am. Chem. Soc.* **2002**, 124, 11730.
- [22] R. McCreery, J. Dieringer, A. O. Solak, B. Snyder, A. M. Nowak, W. R. McGovern, S. DuVall, *J. Am. Chem. Soc.* **2003**, 125, 10748.
- [23] A. Troisi, M. A. Ratner, *J. Am. Chem. Soc.* **2002**, 124, 14528.
- [24] P. E. Kornilovitch, A. M. Bratkovsky, R. S. Williams, *Phys. Rev. B* **2002**, 66.
- [25] H. Kozłowski, W. Bal, M. Dyba, T. Kowalik-Jankowska, *Coord. Chem. Rev.* **1999**, 184, 319.
- [26] W. R. Yang, E. Chow, G. D. Willett, D. B. Hibbert, J. J. Gooding, *Analyst* **2003**, 128, 712.
- [27] G. Thomas, P. S. Zacharias, *Polyhedron* **1984**, 3, 861.
- [28] M. P. Youngblood, D. W. Margerum, *J. Coord. Chem.* **1981**, 11, 103.
- [29] R. P. Bonomo, G. Impellizzeri, G. Pappalardo, E. Rizzarelli, G. Tabbi, *Chem. Eur. J.* **2000**, 6, 4195.
- [30] G. Facchin, M. H. Torre, E. Kremer, E. J. Baran, A. Mombru, H. Pardo, M. P. Araujo, A. A. Batista, A. J. Costa, *Inorg. Chim. Acta* **2003**, 355, 408.
- [31] D. W. M. Arrigan, L. Le Bihan, *Analyst* **1999**, 124, 1645.
- [32] R. A. Wassel, G. M. Credo, R. R. Fuierer, D. L. Feldheim, C. B. Gorman, *J. Am. Chem. Soc.* **2004**, 126, 295.
- [33] N. J. Tao, *Phys. Rev. Lett.* **1996**, 76, 4066.
- [34] X. Lu, K. W. Hipps, X. D. Wang, U. Mazur, *J. Am. Chem. Soc.* **1996**, 118, 7197.
- [35] M. Mayor, C. von Hanisch, H. B. Weber, J. Reichert, D. Beckmann, *Angew. Chem. Int. Ed.* **2002**, 41, 1183; *Angew. Chem.* **2002**, 114, 1228.
- [36] H. B. Weber, J. Reichert, R. Ochs, D. Beckmann, M. Mayor, H. von Löhneysen, *Phys. E* **2003**, 18, 231.
- [37] H. C. Freeman, J. M. Guss, R. L. Sinclair, *Acta Crystallogr. Sect. B Struct. Sc.* **1978**, 34, 2459.
- [38] H. C. Freeman, M. R. Taylor, *Acta Crystallogr.* **1965**, 21, 939.
- [39] K. Slowinski, R. V. Chamberlain, C. J. Miller, M. Majda, *J. Am. Chem. Soc.* **1997**, 119, 11910.

Magnetic Clusters

Polycationic Mn₁₂ Single-Molecule Magnets as Electron Reservoirs with $S > 10$ Ground States**

Eugenio Coronado, Alicia Forment-Aliaga,
Alejandro Gaita-Ariño, Carlos Giménez-Saiz,
Francisco M. Romero,* and Wolfgang Wernsdorfer*

Magnetic clusters with a large-spin ground state and a significant magnetic anisotropy may develop a potential-

[*] Prof. E. Coronado, A. Forment-Aliaga, A. Gaita-Ariño,
Dr. C. Giménez-Saiz, Dr. F. M. Romero
Institut de Ciència Molecular
Universitat de València
Dr. Moliner 50, 46100 Burjassot (Spain)
Fax: (+34) 963-544-859
E-mail: eugenio.coronado@uv.es
fmrm@uv.es

Dr. W. Wernsdorfer
Laboratoire Louis Néel-CNRS
25, Avenue des Martyrs BP 166
38042 Grenoble Cedex 9 (France)

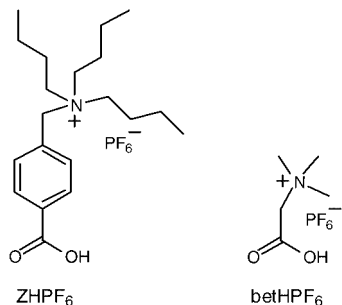
[**] This work was supported by the European Union (TMR HPRN-CT-1999-00012) and the Spanish Ministerio de Ciencia y Tecnología (MCT; Project No. MAT2001-5408-E). F.M.R. and C.G.S. thank the MCT for research contracts (Programa Ramón y Cajal). A.F.A. and A.G.A. thank, respectively, the Universitat de València and the Generalitat Valenciana for a predoctoral fellowship.



Supporting information for this article is available on the WWW under <http://www.angewandte.org> or from the author.

energy barrier for reversal of the direction of magnetization. At low temperatures, the spin of a single cluster can be permanently magnetized in the direction of the applied field.^[1] Switching off the field leads to typical magnetic relaxation phenomena and hysteresis loops are observed. Magnetic clusters of this kind are called single-molecule magnets (SMM). These systems provide a remarkable example of macroscopic quantum tunneling,^[2] but their interest lies also in their possible application as nanomagnetic devices.

A well-known type of SMM is the family of dodecanuclear manganese complexes (Mn_{12}) of formula $[Mn_{12}O_{12}(O_2CR)_{16}(H_2O)_4]$.^[3,4] These mixed-valence compounds contain four Mn^{IV} centers and eight Mn^{III} centers that are exchange-coupled to give a large-spin ground state ($S=10$). The axially distorted Mn^{III} centers provide the source for magnetic anisotropy and are also involved in the redox activity of the system. They can easily undergo reduction to Mn^{II} , so that the neutral Mn_{12} species can be transformed into the corresponding SMM Mn_{12}^- and Mn_{12}^{2-} ions with spin ground states $S=19/2$, $21/2$ and $S=10$, respectively.^[5,6] A modification of the magnetic behavior of the system is observed when these anions are combined with appropriate cations (paramagnetic and/or redox-active).^[7,8] In this context, we have recently developed a strategy to synthesize and characterize polycationic Mn_{12} SMMs bearing 16 quaternary ammonium substituents in the periphery^[9] by a carboxylate-exchange reaction between the acetate precursor $[Mn_{12}O_{12}(O_2CCH_3)_{16}(H_2O)_4]$ ($Mn_{12}Ac$) and tributylammonium salt ZHPF₆.



The redox behavior of Mn_{12} derivatives is strongly correlated to the electron-withdrawing ability of the carboxylate ligands located in the periphery.^[5b] A shorter separation between the cations and the $Mn_{12}O_{12}$ core should result in more stable reduced forms, as a result of the strong inductive effect caused by the cationic shell. We thus turned our attention to betaine hexafluorophosphate salt (betHFPF₆) as the incoming carboxylic acid in the synthesis of $[Mn_{12}O_{12}^{2-}(bet)_{16}(EtOH)_4](PF_6)_{14} \cdot 4CH_3CN \cdot H_2O$ (**1**), a two-electron reduced polycationic single-molecule magnet.

Complex **1** crystallizes in the centrosymmetric $P2_1/c$ space group.^[10] The structure of the $Mn_{12}O_{12}$ core (Figure 1) is similar to that found in all Mn_{12} derivatives and comprises a central Mn_4O_4 cubane core surrounded by a nonplanar Mn_8O_8 ring held together with μ_3 -oxo bridges. Peripheral bridging is

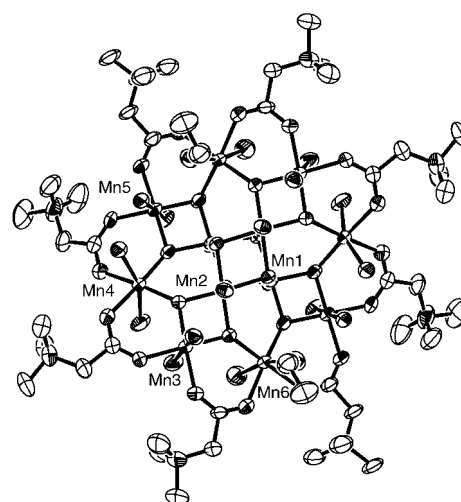


Figure 1. View along the b axis (ORTEP, ellipsoids are set at the 50% probability level) of the Mn_{12} polycation of **1** showing the propeller-like arrangement of the equatorial ligands (axial betaines and disordered EtOH molecules are omitted for clarity).

ensured by sixteen η^2 - μ -carboxylate anions which provide a positive charge of $z=+16$ per cluster. The high charge is partially compensated by the presence of 14 hexafluorophosphate anions in the crystal lattice. Electroneutrality can thus be achieved if the Mn_{12} molecules are considered as two-electron reduced species. Bond valence sum (BVS) calculations^[11] (see Supporting Information) were performed to confirm this hypothesis. The structures of the central cubane units compare well with previous results and are characteristic of Mn^{IV} centers. Half of the manganese ions located in the Mn_8 rings ($Mn3$ and $Mn5$) are clearly Mn^{III} centers and exhibit Jahn–Teller distortion, with the anisotropy axes lying almost perpendicular to the mean plane of the cluster.^[12] The four remaining coordination sites ($Mn4$, $Mn6$, and their symmetry equivalents) do not show axial distortion and exhibit longer Mn–O bonds, which indicates partial reduction to Mn^{II} . These four Mn atoms are in a +2.5 oxidation state according to BVS analysis. Interestingly, one of these Mn atoms ($Mn6$) is coordinated to two ethanol molecules located in axial positions. This arrangement yields four ethanol molecules per Mn_{12} species distributed in a “trans” (0:2:0:2) arrangement as a result of the local C_2 symmetry of the cluster. The polycations exhibit a propeller-like arrangement of the equatorial betaine ligands around the Mn_8 ring. All the magnetic clusters have the same orientation in the crystal lattice, with their symmetry axis situated parallel to the crystallographic y axis. Hexafluorophosphate anions and solvent molecules fill the intercluster space.

AC magnetic susceptibility measurements of **1** were performed at different frequencies on crystals dried under vacuum and dispersed in oil. Figure 2a shows the temperature dependence of $\chi' T$, where χ' is the real part of the AC molar magnetic susceptibility. The plateau observed in the 5–8 K range ($68\text{--}69\text{ emu K mol}^{-1}$) lies considerably above the typical values ($45\text{--}50\text{ emu K mol}^{-1}$) found for other Mn_{12} compounds and is close to the expected value for an $S=11$ ground state (66 emu K mol^{-1}). Frequency-dependent out-of-phase signals

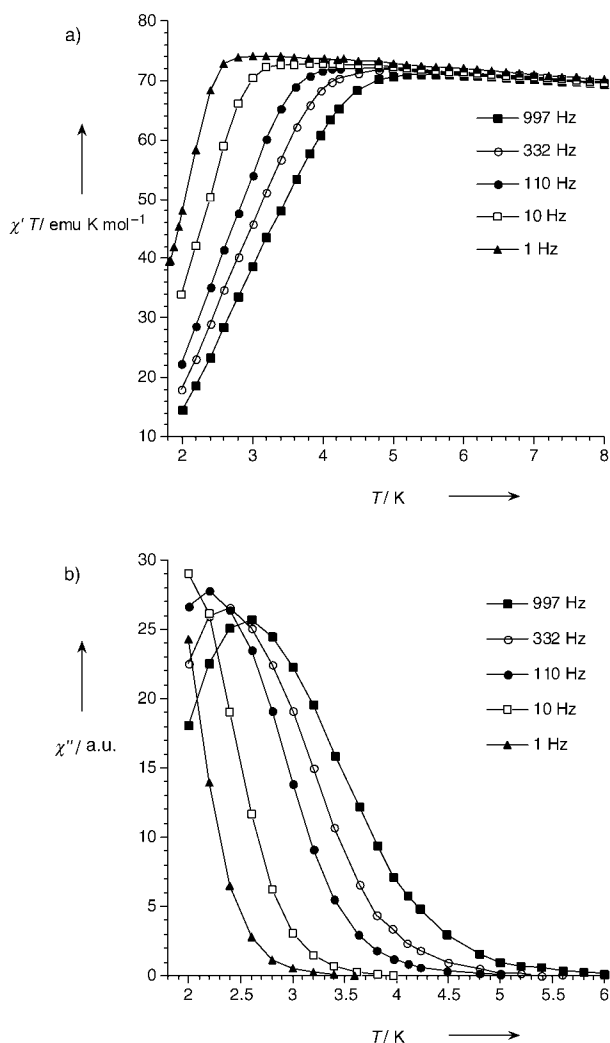


Figure 2. a) Thermal variation of the product of $\chi' T$ of **1** with temperature (in-phase component) at different frequencies. b) Temperature dependence of the out-of-phase χ'' component. a.u. = arbitrary units.

with very broad maxima in the 2–4 K range were observed (see Supporting Information), which indicates partial desolvation of the sample. Measurements on wet samples (Figure 2b) afforded better results, and the presence of well-defined maxima in the 2–3 K range was confirmed. An effective energy barrier $U_{\text{eff}} = 34$ K for reversal of the magnetization was determined from the frequency dependence of these maxima. The out-of-phase AC results are similar to those obtained for $(\text{PPh}_4)_2[\text{Mn}_{12}\text{O}_{12}(\text{O}_2\text{CCHCl}_2)_{16}(\text{H}_2\text{O})_4]$ (**2**), the only two-electron reduced Mn_{12} species reported to date,^[6b] and clearly support a reduced state for **1**. Upon reduction, some of the anisotropic Mn^{III} ions become Mn^{II} , and the intrinsic energy barrier for reversal of the spins is lowered compared to neutral Mn_{12} molecules. The $\chi''(T)$ maxima are then shifted to lower temperatures. A novel aspect of this work is that, whereas **2** seems to have the same $S = 10$ ground state as its neutral analogue, two-electron reduction results in a higher-spin ground state $S = 11$. This result is consistent with the usual spin topology of the cluster (spins of the Mn_4O_4 cubane core oriented antiparallel to the

spins of the Mn_8 ring) determined by the strong $\text{Mn}^{\text{IV}}\text{--Mn}^{\text{III}}$ antiferromagnetic coupling mediated by the double μ -oxo bridge.

To verify this hypothesis, DC magnetization data were collected at $H = 0.1\text{--}5$ T at different temperatures between 2 and 5 K (Figure 3). A spin Hamiltonian including a Zeeman

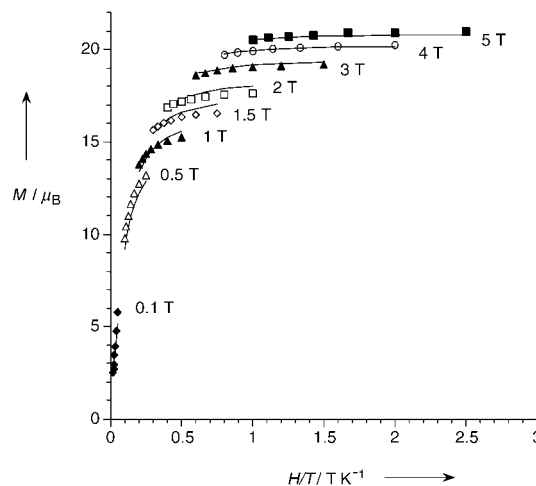


Figure 3. Plots of reduced magnetization M versus H/T for **1** at different field strengths H . The isofield lines are least-squares fits to the data according to ref. [13]. The best-fit values for the different parameters are $S = 11$, $g = 2.05$, $D = -0.22\text{ cm}^{-1}$, $B_4^0 = 0.41 \times 10^{-4}\text{ cm}^{-1}$.

term and axial and quartic zero-field splitting was used to fit the isofield data.^[13] The value of the zero-field splitting parameter ($D = -0.22\text{ cm}^{-1}$), obtained by assuming an $S = 11$ ground state, compares well with the existing data for doubly reduced species.^[6b] This value gives an activation energy $E = M_S^2 D = 38$ K, which is higher than the effective energy barrier obtained from the AC data ($U_{\text{eff}} = 34$ K). This difference points to the presence of quantum tunneling through the barrier.

Low-temperature magnetization measurements were performed on single crystals of **1** down to 0.04 K. The applied field was set parallel to the experimentally observed easy axis of magnetization. The SMM character of the sample was confirmed by the observation of hysteresis loops in the 1.6–0.25 K range that are strongly temperature dependent (Figure 4) and field sweep rate dependent (not shown). In contrast to the situation found in most Mn_{12} derivatives, hysteresis was only observed below 2 K, a fact that correlates with the decrease of the energy barrier that occurs upon reduction. The magnetization is saturated down to zero field, which indicates a well-defined spin ground state. Quantum tunneling of the magnetization is evidenced by the observation of temperature-independent loops below 0.25 K that remain strongly dependent on the field-sweep rate. Quantum steps are observed with regular spacings of 0.24 T magnetic field. This yields a $|D|$ parameter of 0.23 cm^{-1} that matches the value obtained from magnetization measurements. The smearing of the quantum steps at high temperatures and/or low magnetic fields can be interpreted in terms of a distribution of energy barriers. This has been confirmed by

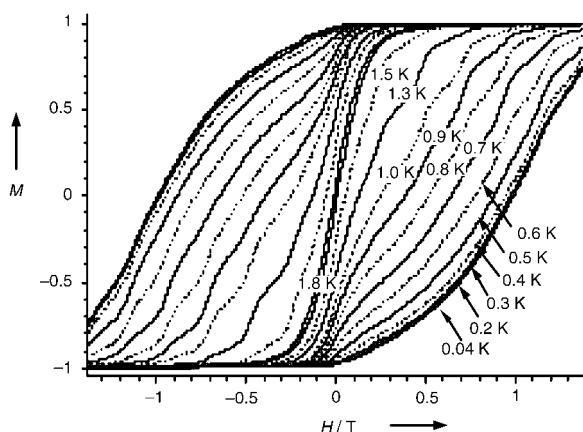


Figure 4. Single crystal measurement of magnetization M (normalized to its saturation value) versus the field H applied in the direction of the easy axis of magnetization. The sweep rate was 0.035 T s^{-1} .

relaxation measurements and is another indication of possible crystal defects subsequent to solvent losses.

The unusual oxidation state of this polycationic Mn_{12} compound is related to the strong electron-withdrawing ability of the trimethylammonium groups. Note that betaine hydrochloride has a very low $\text{p}K_{\text{a}}$ value of 1.8, compared with the value for acetic acid (4.76). This electron-accepting character pushes the first and second reduction potentials of **1** to more positive values relative to most Mn_{12} compounds, as has been observed for the dichloroacetic acid derivative **2** with $\text{p}K_{\text{a}} = 1.29$. The differential pulse voltammogram (DPV) of **1** exhibits first and second reduction waves at $E = +0.49$ and $+0.21 \text{ V}$ (versus ferricinium/ferrocene couple), respectively. A third quasi-reversible reduction signal appears at -0.72 V (see Supporting Information). Thus, the stability range of the two-electron reduced species is extremely wide (ca. 1 V !) as compared with previous examples.

An interesting feature is that all of the reported syntheses of Mn_{12} reduced species employ iodide as reductant. It is possible that ethanol plays this role in the present example as manganese oxides are common reagents for the oxidation of alcohols.^[14] Also, coordination of ethanol to the Mn_{12} core is unprecedented, and suggests further studies in which the nature of the ligands that occupy the four “water sites” is changed. Finally, preliminary results show that the polycationic compound **1** with an $S = 11$ ground state opens the way to the preparation of a variety of crystalline SMM salts by simple metathesis reactions, and that it is a useful precursor for the deposition of these magnetically active entities onto metal and metal oxide surfaces.

Experimental Section

All chemicals and solvents were used as received. $[\text{Mn}_{12}\text{O}_{12}(\text{O}_2\text{CCH}_3)_{16}(\text{H}_2\text{O})_4]$ ($\text{Mn}_{12}\text{Ac}_{16}$) was prepared as previously described.^[15]

betHPF₆: A solution of potassium hexafluorophosphate (5.4 g, 2.93 mmol) in hot water (33 mL) was slowly added to a stirred solution of betaine hydrochloride (4.5 g, 2.93 mmol) in hot water

(18 mL). As the mixture cooled, betHPF₆ precipitated as a white crystalline powder. The product was filtered, washed with cold water, and dried under vacuum. Yield: 50%. ¹H NMR (300.1 MHz, CD_3CN): $\delta = 3.95$ (s, 2H), 3.20 ppm (s, 9H); ¹³C NMR (75.5 MHz, CD_3CN): $\delta = 166.90$ (COOH), 64.84 (CH_2), 54.53 ppm (CH_3); IR (KBr): $\tilde{\nu} = 1739$ (s), 1479 (s), 1420 (m), 1266 (m), 1223 (m), 841 (s), 558 cm^{-1} (s); elemental analysis calcd (%) for $\text{C}_5\text{H}_{12}\text{F}_6\text{NO}_2\text{P}$ (263.1): C 22.82, H 4.60, N 5.32; found: C 22.28, H 4.07, N 5.10.

1: $\text{Mn}_{12}\text{Ac}_{16}$ (0.25 g, 0.125 mmol) was added to a solution of betHPF₆ (0.60 g, 2.3 mmol) in $\text{C}_6\text{H}_5\text{CN}$ (35 mL) and CH_3CN (20 mL). The mixture was stirred overnight, filtered, and the solvent was evaporated under reduced pressure to complete precipitation. The solid was collected by filtration and dissolved in a small amount of CH_3CN . After addition of toluene, the solution was evaporated to dryness to remove the acetic acid as the toluene azeotrope. This stage was repeated twice. The product was then dissolved in $\text{C}_6\text{H}_5\text{CN}$ (35 mL) and CH_3CN (20 mL) and treated again with excess betHPF₆. The entire process was repeated. Finally, the product was dissolved in CH_3CN (35 mL). The resulting solution was then filtered and layered with EtOH. Black plates suitable for X-ray crystallography formed after a few days at room temperature. ¹H NMR (300.1 MHz, CD_3CN): $\delta = 42\text{--}39$ (CH_2), $39\text{--}33$ (CH_2), $30\text{--}25$ (CH_2), $16.9\text{--}15.5$ (CH_2), $15.5\text{--}14.2$ (CH_2), $6.3\text{--}4.6$ (CH_3), 4.0 (CH_3), 3.01 (CH_3), 2.12 (CH_3), 2.03 (CH_3), 0.80 ppm (CH_3); ¹⁹F NMR (282.4 MHz, CD_3CN): $\delta = 68.52$ ppm (d, $J_{\text{FP}} = 709 \text{ Hz}$); ³¹P NMR (121.5 MHz, CD_3CN): $\delta = -142.20$ ppm (m, $J_{\text{PF}} = 709 \text{ Hz}$); IR (KBr): $\tilde{\nu} = 3065$ (w), 2967 (w), 1626 (s), 1495 (w), 1436 (m), 1410 (m), 1341 (m), 1240 (w), 967 (w), 910 (w), 837 (s), 725 (w), 619 (w), 558 (m), 461 cm^{-1} (w); ESI-MS (CH_3CN , 30 V): m/z : 2159 $[[\text{Mn}_{12}\text{O}_{12}(\text{bet})_{16}](\text{PF}_6)_{11} + 1 \text{ e}^{-1}]^{2+}$; 2086 $[[\text{Mn}_{12}\text{O}_{12}(\text{bet})_{16}](\text{PF}_6)_{10} + 2 \text{ e}^{-1}]^{2+}$; 2028 $[[\text{Mn}_{12}\text{O}_{12}(\text{bet})_{15}](\text{PF}_6)_{10} + 2 \text{ e}^{-1}]^{2+}$; 1956 $[[\text{Mn}_{12}\text{O}_{12}(\text{bet})_{15}](\text{PF}_6)_9 + 3 \text{ e}^{-1}]^{2+}$; 1007 $[[\text{Mn}_{12}\text{O}_{12}(\text{bet})_{16}](\text{PF}_6)_9 + 1 \text{ e}^{-1}]^{4+}$; 777 $[[\text{Mn}_{12}\text{O}_{12}(\text{bet})_{16}](\text{PF}_6)_8 + 1 \text{ e}^{-1}]^{5+}$; elemental analysis calcd (%) for $[\text{Mn}_{12}\text{O}_{12}(\text{bet})_{16}](\text{PF}_6)_{14}$ (4755.1): C 20.21, H 3.73, N 4.71; found: C 19.86, H 4.26, N 4.46.

Physical measurements: NMR spectra were recorded on a Bruker Avance DRX 300-MHz spectrometer. ESI mass spectra were recorded on a Waters ZQ mass spectrometer using nitrogen as the drying and nebulizing gas. The equipment was calibrated with appropriate standard samples. All the magnetic measurements were carried out on polycrystalline samples with a magnetometer (Quantum Design MPMS-XL-5) equipped with a SQUID sensor. The samples were dispersed in oil to avoid torquing of the crystals. Variable-temperature susceptibility measurements were carried out at 2–300 K in a 0.1 T magnetic field. The susceptibility data were corrected for the diamagnetic contributions of the salts, as deduced by using a Pascal constants table. The AC measurements were performed in the temperature range 2–8 K at different frequencies with an oscillating magnetic field of $H = 0.395 \text{ mT}$. The magnetization data were collected in the $H = 0\text{--}5 \text{ T}$ field range at different temperatures between 2 and 5 K. The hysteresis studies were performed at $T = 2 \text{ K}$ with H between 5 and -5 T , at, with sample cooling at zero field. Low-temperature magnetization measurements were performed on single crystals of **1** at $0.04\text{--}7 \text{ K}$ using a micro-SQUID apparatus at different sweep rates between 0.1 and 0.001 T s^{-1} .^[16] The applied field was parallel to the experimentally observed easy axis of magnetization. IR transmission measurements of pressed KBr pellets were recorded at room temperature with a Nicolet Avatar 320 FTIR spectrophotometer ($\tilde{\nu} = 4000\text{--}400 \text{ cm}^{-1}$). C,H,N elemental analysis was carried out on samples dried under vacuum in a CE instruments EA 1110 CHNS analyzer.

Received: April 9, 2004

Revised: July 21, 2004

Keywords: carboxylate ligands · magnetic properties · manganese · mixed-valent compounds · single-molecule studies

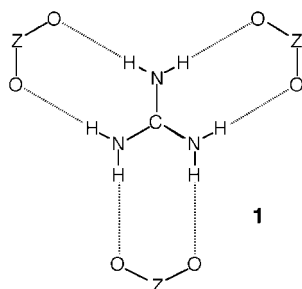
- [1] R. Sessoli, D. Gatteschi, A. Caneschi, M. A. Novak, *Nature* **1993**, 365, 141.
- [2] a) J. Friedman, M. Sarachik, J. Tejada, R. Ziolo, *Phys. Rev. Lett.* **1996**, 76, 3830; b) J. Hernández, X. Zhang, F. Louis, J. Bartolomé, J. Tejada, R. Ziolo, *Europhys. Lett.* **1996**, 35, 301; c) L. Thomas, F. Lionti, R. Ballou, D. Gatteschi, R. Sessoli, B. Barbara, *Nature* **1996**, 383, 145.
- [3] a) A. Caneschi, D. Gatteschi, R. Sessoli, A. L. Barra, L. C. Brunel, M. Guillot, *J. Am. Chem. Soc.* **1991**, 113, 5873; b) R. Sessoli, H.-L. Tsai, A. R. Schake, S. Wang, J. B. Vincent, K. Folting, D. Gatteschi, G. Christou, D. N. Hendrickson, *J. Am. Chem. Soc.* **1993**, 115, 1804; c) G. Christou, D. Gatteschi, D. N. Hendrickson, R. Sessoli, *Mater. Res. Bull.* **2000**, 35, 66.
- [4] D. Gatteschi, A. Caneschi, L. Pardi, R. Sessoli, *Science* **1994**, 265, 1054.
- [5] a) A. R. Schake, H.-L. Tsai, N. de Vries, R. J. Webb, K. Folting, D. N. Hendrickson, G. Christou, *J. Chem. Soc. Chem. Commun.* **1992**, 181; b) H. J. Eppley, H.-L. Tsai, N. de Vries, K. Folting, G. Christou, D. N. Hendrickson, *J. Am. Chem. Soc.* **1995**, 117, 301; c) S. M. J. Aubin, Z. Sun, L. Pardi, J. Krzystek, K. Folting, L. C. Brunel, A. L. Rheingold, G. Christou, D. N. Hendrickson, *Inorg. Chem.* **1999**, 38, 5329.
- [6] a) M. Soler, S. K. Chandra, D. Ruiz, E. R. Davidson, D. N. Hendrickson, G. Christou, *Chem. Commun.* **2000**, 2417; b) M. Soler, W. Wernsdorfer, K. A. Abboud, J. C. Huffman, E. R. Davidson, D. N. Hendrickson, G. Christou, *J. Am. Chem. Soc.* **2003**, 125, 3576.
- [7] K. Takeda, K. Awaga, *Phys. Rev. B* **1997**, 56, 14560.
- [8] T. Kuroda-Sowa, M. Lam, A. L. Rheingold, C. Frommen, W. M. Reiff, M. Nakano, J. Yoo, A. L. Maniero, L. C. Brunel, G. Christou, D. N. Hendrickson, *Inorg. Chem.* **2001**, 40, 6469.
- [9] a) E. Coronado, M. Feliz, A. Forment-Aliaga, C. J. Gómez-García, R. Llugar, F. M. Romero, *Inorg. Chem.* **2001**, 40, 6084; b) A. Forment-Aliaga, E. Coronado, M. Feliz, A. Gaita-Ariño, R. Llugar, F. M. Romero, *Inorg. Chem.* **2003**, 42, 8019.
- [10] Crystal data for **1**: $C_{96}H_{214}F_{84}Mn_{12}N_{20}O_{49}P_{14}$, $M_r = 5121.73$, monoclinic, space group $P2_1/c$, $a = 20.7870(4)$, $b = 18.3190(4)$, $c = 31.1280(7)$ Å, $\beta = 117.0730(10)^\circ$, $V = 10554.6(4)$ Å³, $Z = 2$, $\rho_{\text{calcd}} = 1.612$ Mg m⁻³, $\mu(\text{MoK}\alpha) = 0.939$ mm⁻¹. A dark brown platelike single crystal of **1** of dimensions $0.25 \times 0.10 \times 0.04$ mm³ was used for data collection on a Nonius Kappa CCD diffractometer ($3.54^\circ < 2\theta < 50.74^\circ$) equipped with a graphite monochromated MoK α radiation source ($\lambda = 0.71073$ Å). Data collection was performed at 180(2) K. Of 112612 measured reflections, 19136 were independent ($R_{\text{int}} = 0.0868$) and used to refine 1278 parameters and 89 restraints. A multiscan absorption correction, based on equivalent reflections, was applied to the data using the program SORTAV^[17] ($T_{\text{max}}/T_{\text{min}} = 0.9626/0.7613$). The structure was solved by direct methods (SIR97)^[18] and refined against F^2 with a full-matrix least-squares algorithm using SHELX-97^[19] and the WinGX (1.64) software package.^[20] One ethanol molecule shows orientational disorder that was modeled with a set of two positions for each carbon atom having refined occupancies close to 0.5. These occupancies were fixed to 0.5 in the last cycles of refinement and refined isotropically. The disordered C atoms were presumed to have the same isotropic displacement parameters. Furthermore, C–C and C–O distances were restrained so that they were the same for both orientations within the same molecule. This kind of disorder in the coordinated ethanol molecule has also been observed in several Mn^{III}–Schiff base complexes.^[21] A water molecule with an occupancy of 0.5 was located near this disordered ethanol molecule. The other ethanol molecule coordinated to Mn6 is not disordered and was refined anisotropically. Nine different hexafluorophosphate anions were located, three of them on special positions and one (on a general position) with a refined occupancy of 0.5, thus accounting for the +14 charge of the Mn₁₂ complex. Four acetonitrile solvent molecules were also located, which had refined occupancies of 0.5 that were fixed to this value in the last cycles of refinement. Geometrical restraints were applied to some of the hexafluorophosphate anions and solvent molecules which had high anisotropic displacement parameters. All the remaining non-hydrogen atoms were refined anisotropically. The positions of the H atoms on the C atoms were added into the calculated positions and refined on the corresponding atoms. H atoms on the O atoms of ethanol molecules were refined using the AFIX 147 instruction of SHELX-97. The H atoms of the water molecule were placed in theoretical positions using Nardelli's method. These H atoms were included in structure-factor calculations with fixed positional parameters and isotropic displacement parameters of 0.05 Å². Final R ($I > 2\sigma(I)$), $R_1 = 0.0853$, $wR_2 = 0.2284$; final R (all data), $R_1 = 0.1304$, $wR_2 = 0.2723$. Max./min. residual electron density $1.135/-1.378$ e Å⁻³. CCDC-235825 contains the supplementary crystallographic data for this paper. These data can be obtained free of charge via www.ccdc.cam.ac.uk/contents/retrieving.html (or from the Cambridge Crystallographic Data Centre, 12 Union Road, Cambridge CB21EZ, UK; fax: (+44) 1223-336-033; or deposit@ccdc.cam.ac.uk).
- [11] I. D. Brown, D. Altermatt, *Acta Crystallogr. Sect. B* **1985**, 41, 244.
- [12] S. M. J. Aubin, Z. Sun, H. J. Eppley, E. M. Rumberger, I. A. Guzei, K. Folting, P. K. Gantzel, A. L. Rheingold, G. Christou, D. N. Hendrickson, *Inorg. Chem.* **2001**, 40, 2127.
- [13] The complete spin Hamiltonian is given by the following expression:^[22]

$$\hat{H} = -g\mu_B H \hat{S} + D[\hat{S}_z^2 - \frac{1}{3}S(S+1)] + B_4^0 \hat{O}_4^0$$
 The best-fit values for the different parameters are $g = 2.05$, $D = -0.22$ cm⁻¹, $B_4^0 = 0.41 \times 10^{-4}$ cm⁻¹. The g value obtained is slightly higher than expected for a Mn₁₂ cluster ($g < 2$). A scaling factor of 3% can solve this problem, which lies within experimental uncertainty.
- [14] E. P. Papadopoulos, A. Jarrar, C. H. Issidorides, *J. Org. Chem.* **1966**, 31, 615.
- [15] T. Lis, *Acta Crystallogr. Sect. B* **1980**, 36, 2042.
- [16] W. Wernsdorfer, *Adv. Chem. Phys.* **2001**, 118, 99.
- [17] R. H. Blessing, *J. Appl. Crystallogr.* **1997**, 30, 421.
- [18] A. Altomare, M. C. Burla, M. Camalli, G. Cascarano, C. Giacovazzo, A. Guagliardi, A. G. G. Moliterni, G. Polidori, R. Spagna, *J. Appl. Crystallogr.* **1999**, 32, 115.
- [19] G. M. Sheldrick, SHELX-97, an integrated system for solving and refining crystal structures from diffraction data, University of Göttingen, Germany, **1997**.
- [20] L. J. Farrugia, *J. Appl. Crystallogr.* **1999**, 32, 837.
- [21] I. V. Korendovych, E. V. Rybak-Akimova, *Acta Crystallogr. Sect. C* **2004**, 60, m82.
- [22] P. Artus, C. Boskovic, J. Yoo, W. E. Streib, L. C. Brunel, D. N. Hendrickson, G. Christou, *Inorg. Chem.* **2001**, 40, 4199.

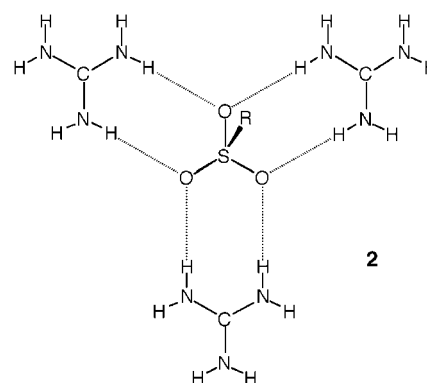
Cubic, Hydrogen-Bonded (10,3)-a Networks in the Family $[C(NH_2)_3][N(CH_3)_4][XO_4]$ ($X = S, Cr$, and Mo)**

Brendan F. Abrahams, Marissa G. Haywood,
Timothy A. Hudson, and Richard Robson*

The guanidinium cation $C(NH_2)_3^+$ serves as a powerful structure-determining component in a number of networks, both metal/ligand-bonded and hydrogen-bonded. The six hydrogen atoms of the cation are nicely disposed to form a pair of hydrogen bonds to each of three oxyanions, as shown in the generalized representation **1**. In an extensive family of



carbonate-bridged coordination polymers reported recently, the guanidinium cation plays the crucial structural role represented in **1** ($Z = C$), thus promoting the formation of highly symmetrical metal/carbonate networks with cubic symmetry and sodalite-like topology.^[1] The arrangement seen in **1** ($Z = B$) is present in some highly symmetrical cubic guanidinium borate derivatives we discovered recently which have the boracite topology.^[2] A closely related hydrogen-bonding mode, again as in **1** ($Z = S$), is seen in a range of guanidinium sulfonates in which the sulfonate units, as well as the guanidinium components, act as 3-connecting nodes, each being attached to three guanidinium units as in **2**. In some of the nicest examples of true crystal engineering, Ward and co-workers have elegantly exploited this complementarity between the guanidinium cation and various sulfonate anions to generate an extensive family of solids having a common, predictable, yet pliable, underlying hydrogen-bonded 3-connected sheet structure with the (6,3) topology or hexagonal grid topology.^[3] We report here a new family of



hydrogen-bonded frameworks related to these guanidinium sulfonates in which the guanidinium cation again acts as in **1** ($Z = S$) and a sulfur oxyanion (in this case SO_4^{2-}) again acts as a second type of 3-connecting node; however, the network generated is the most symmetrical 3-connected 3D network possible, namely the (10,3)-a net,^[4] rather than the most symmetrical 3-connected 2D network possible that was seen by Ward and co-workers.

Solvent-free crystalline products of composition $[C(NH_2)_3][N(CH_3)_4][XO_4]$, ($X = S, Cr$ and Mo) suitable for single-crystal X-ray diffraction studies were obtained directly from mixtures containing the component ions in the following solvents or solvent mixtures: $X = S$, from methanol; $X = Cr$, from aqueous DMSO; $X = Mo$, from methanol/DMF.^[5] All our attempts to generate the analogous tungsten derivative $[C(NH_2)_3][N(CH_3)_4][WO_4]$ have failed. In all cases, the crystals appear almost exclusively as well-formed tetrahedra, space group $P2_13$, $a = 10.5828(6)$ Å ($X = S$), $10.7589(5)$ Å ($X = Cr$), or $10.8802(4)$ Å ($X = Mo$).^[6] The three compounds are isostructural and the following observations pertaining to the sulfate apply equally well to the chromate and molybdate, except for minor differences in some distances and angles. All the guanidinium cations in $[C(NH_2)_3][N(CH_3)_4][SO_4]$ are equivalent and act as 3-connecting nodes, each being attached to three sulfate anions by hydrogen-bond pairs as represented in **1** ($Z = S$). Each sulfate unit is attached by hydrogen-bond pairs to three guanidinium cations (Figure 1), and therefore acts as a second type of 3-connecting node. Figure 2a shows the extended 3D network and Figure 2b shows the net generated by linking together the carbon centers of the

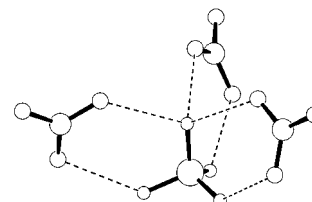


Figure 1. Three guanidinium cations each provide a pair of hydrogen bonds to a sulfate ion in the structure of $[C(NH_2)_3][N(CH_3)_4][SO_4]$. The three equivalent hydrogen bonds to the oxygen atom at the apex of the SO_4 tetrahedron are slightly longer ($N-H\cdots O$, 2.899 Å) than the other three (2.792 Å); this expands the C-S-C angle to 97.5°.

[*] B. F. Abrahams, M. G. Haywood, T. A. Hudson, Prof. R. Robson
School of Chemistry
University of Melbourne
Victoria 3010 (Australia)
Fax: (+61) 3-9347-5180
E-mail: r.robson@unimelb.edu.au

[**] The authors gratefully acknowledge support from the Australian Research Council.

Supporting information for this article is available on the WWW under <http://www.angewandte.org> or from the author.

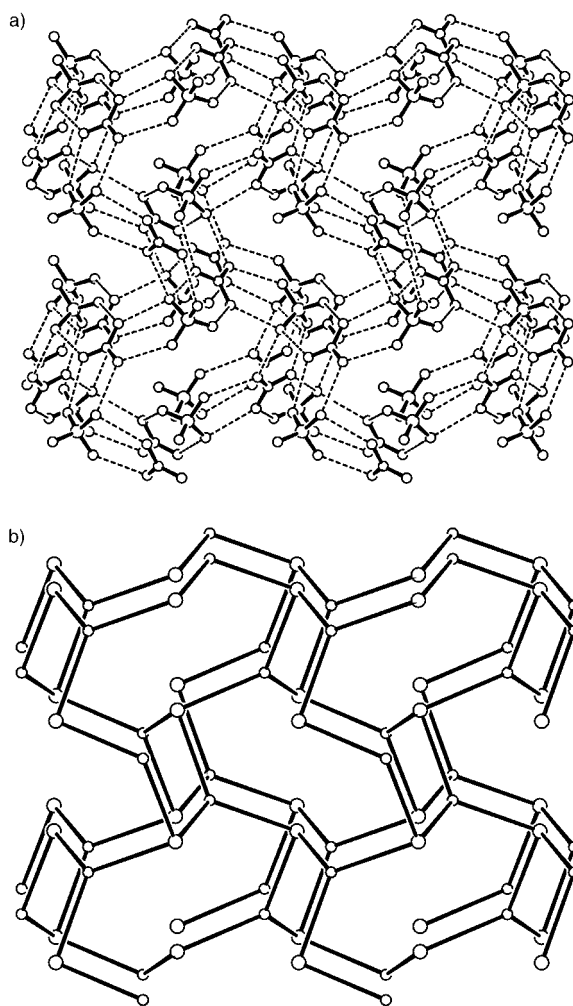


Figure 2. a) The extended 3D hydrogen-bonded $[\text{C}(\text{NH}_2)_3]/[\text{SO}_4]$ network in $[\text{C}(\text{NH}_2)_3][\text{N}(\text{CH}_3)_4][\text{SO}_4]$. b) The underlying (10,3)-a connectivity of the network showing only the sulfur atoms and the carbon atoms of the guanidinium units.

guanidinium units and the sulfur centers of the sulfate units that are hydrogen-bonded to them. The net has the intrinsically chiral (10,3)-a topology.^[4] The guanidinium nodes are slightly pyramidal (S-C-S angle 118.6°) but the sulfur nodes are much more so (C-S-C angle 97.5°). We have noted previously that it is possible to construct strain-free (10,3)-a nets and still retain the cubic symmetry not only when all the nodes are trigonal planar but also when all the nodes are trigonal pyramidal;^[7] the present case brought to our attention the fact, previously unrecognized we believe, that it is also possible to construct strain-free (10,3)-a nets, again conserving cubic symmetry, in which half the nodes are trigonal planar and the other half are pyramidal, provided the latter retain a threefold axis of symmetry. These variants on the (10,3)-a net highlight the distinction that should be drawn (in considerations of networks in general) between geometry and topology: from the geometrical point of view, the three variants—1) all nodes trigonal planar, 2) all nodes trigonal pyramidal, and 3) alternate nodes trigonal planar and trigonal

pyramidal—appear to be very different, but from a topological point of view they are of course identical.

The tetramethylammonium cations, all of which are equivalent, are snugly accommodated in cavities within the framework (Figure 3). In the imaginary transition from a (10,3)-a net in which all the nodes are trigonal planar (Figure 4a) to one in which every other node is made trigonal pyramidal (Figure 4b), half the cavities centered on the

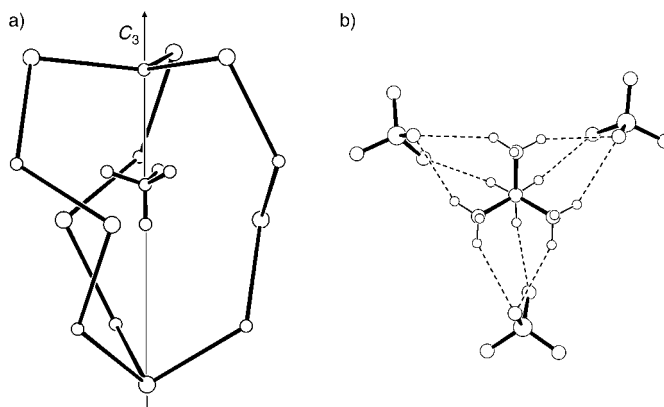


Figure 3. a) The environment of the tetramethylammonium ion showing only the guanidinium carbon atoms and the sulfur atoms of the surrounding hydrogen-bonded (10,3)-a net. b) View down the threefold axis showing the nine C-H...O interactions in which each $[\text{N}(\text{CH}_3)_4]^+$ ion participates.

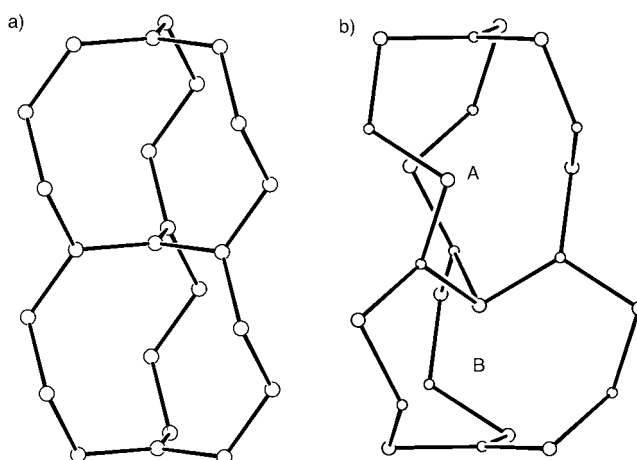
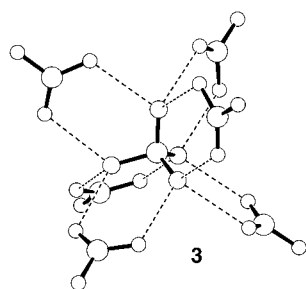


Figure 4. The imaginary transformation of a (10,3)-a net in which all nodes are trigonal planar (a) to one in which alternate nodes are trigonal planar and trigonal pyramidal (b). In the latter net, which retains cubic symmetry, half the cavities centered on the threefold axes are expanded (site A) and the others (site B) are contracted.

threefold axes are increased in size (A in Figure 4b) and the others (B) are contracted: the $[\text{N}(\text{CH}_3)_4]^+$ units are found in the expanded cavities of type A and the sites on the threefold axes at the centers of the contracted cavities are empty. One C-N bond of the tetramethylammonium cation is oriented along one of the threefold axes with its carbon atom very

close to the center of an equilateral triangle of sulfur atoms (Figure 3a). Each of the C–H bonds of this methyl group located on the threefold axis is directed towards a sulfate oxygen atom (C⋯O 3.324 Å; angle at hydrogen atom ca. 168°; Figure 3b), thus indicating significant directional C–H⋯O hydrogen-bonding interactions in addition to the electrostatic attraction. Desiraju has drawn attention to the significance of C–H⋯O hydrogen bonding as a supramolecular motif in a variety of crystalline solids and to its importance in crystal engineering.^[8] As can be seen in Figure 3b, two hydrogen atoms on each of the other three methyl groups are also directed towards a sulfate oxygen atom (C⋯O, 3.447 and 3.455 Å), thus providing additional C–H⋯O hydrogen-bonding interactions. All but three of the twelve C–H atoms of the $\text{N}(\text{CH}_3)_4^+$ ion are therefore involved in this hydrogen-bonding arrangement. Every sulfate ion is associated in this way with three tetramethylammonium ions by three trios of C–H⋯O hydrogen bonds and every tetramethylammonium ion is likewise associated with three sulfate ions. A 3-connected, 3D network of C–H⋯O interactions can therefore be envisaged in which the sulfur atoms and the nitrogen centers of the tetramethylammonium ions provide the nodes. This net also has the chiral (10,3)-*a* topology, but it is of the opposite sense to that of the primary (10,3)-*a* net composed of guanidinium and sulfate nodes. The C–H⋯O interactions between the tetramethylammonium cation and the sulfate anion are very likely much weaker than the N–H⋯O interactions that support the primary (10,3)-*a* network. In discussions of many networks it is convenient for simplicity to focus on certain selected interactions as constituting “the net” and to set aside other weaker interactions, whilst recognizing that these may nevertheless be structurally important. Such is the case here—the (10,3)-*a* net involving the stronger $[\text{C}(\text{NH}_2)_3]^+ / [\text{SO}_4]^{2-}$ interactions is conveniently regarded as the primary net, but the secondary $[\text{N}(\text{CH}_3)_4]^+ / [\text{SO}_4]^{2-}$ (10,3)-*a* net of the opposite chirality is of undoubted, possibly crucial, structural importance.^[9]

In guanidinium sulfate itself,^[10] every cation is attached by pairs of hydrogen bonds, again as in **1** ($Z = \text{S}$), to three sulfate anions. However, since in this case there are twice as many guanidinium cations as sulfate anions, each anion is connected to six guanidinium cations in the manner represented in the idealized form shown in **3**. The environment of the sulfate ion in guanidinium sulphate, as seen in **3**, can be envisaged in terms of guanidinium cations associated by a pair of hydrogen bonds at each of the six edges of the sulfate O_4 tetrahedron. In the guanidinium sulfonates, as represented in **2**, a cation



provides a pair of hydrogen bonds at each of the three edges of an O_3 triangle, thus disposing the system to form a 2D network, since the CN_3 planes of the three guanidinium cations surrounding any sulfonate are close to coplanar with the plane that includes all three guanidinium carbon centers. In the case of $[\text{C}(\text{NH}_2)_3][\text{N}(\text{CH}_3)_4][\text{SO}_4]$ reported here the $[\text{C}(\text{NH}_2)_3]^+$ and $[\text{SO}_4]^{2-}$ ions are present in equal numbers and only three of the six edges of the O_4 tetrahedron are required to participate in the hydrogen-bonding network and, as can be seen in Figure 1, the particular edges used are those that share an apex of the O_4 tetrahedron. This arrangement disposes the system to form a 3D network, rather than the 2D network seen in the sulfonates because, as can be seen in Figure 1, the CN_3 planes of the three guanidinium units are now close to perpendicular to the plane containing the three carbon atoms. If the two N–H⋯O hydrogen bonds in any particular $[\text{C}(\text{NH}_2)_3]^+ / [\text{SO}_4]^{2-}$ association had been equal in length the C–S–C angles would have been 90°. The observed C–S–C angle of 97.5° is achieved by slightly stretching the three equivalent hydrogen bonds to the apex oxygen atom (to N–H⋯O = 2.899 Å) relative to the other three hydrogen bonds (2.792 Å). The C–S–C angle dictates the size of the cavity where the tetramethylammonium cation is located and presumably the inequality in the two hydrogen-bond lengths is such as to optimize the fit of the tetramethylammonium cation therein. It is significant in our view that guanidinium sulfate, itself a relatively stable, multiple hydrogen-bonded crystal lattice and therefore relatively insoluble, can be converted in the presence of $[\text{N}(\text{CH}_3)_4]^+$ into $[\text{C}(\text{NH}_2)_3][\text{N}(\text{CH}_3)_4][\text{SO}_4]$; this presumably reflects the snug fit of the $[\text{N}(\text{CH}_3)_4]^+$ ion into the expanded cavities within the $[\text{C}(\text{NH}_2)_3]^+ / [\text{SO}_4]^{2-}$ (10,3)-*a* framework, with the formation of nine C–H⋯O interactions.

Only very minor differences are seen between the sulfate, chromate, and molybdate structures, consequences presumably of the different bond lengths within the anion (S–O, 1.449(2) and 1.486(4) Å; Cr–O, 1.631(4) and 1.657(7); Mo–O, 1.752(3) and 1.780(4) Å). For each of the structures, the longer Z–O bond corresponds to the unique bond lying on the threefold axis. Given the fact that this oxygen atom is involved in three hydrogen bonds to guanidinium ions this is not surprising. Differences in hydrogen-bonded N⋯O separations are very minor (sulfate: 2.792(3), 2.899(4) Å; chromate: 2.790(6), 2.887(5) Å; molybdate: 2.790(5), 2.914(4) Å).

The (10,3)-*a* net, being the most symmetrical of all possible 3-connected 3D nets, should occupy a position comparable in importance and significance to that of its better known 4-connected counterpart, the (6,4) diamond net; both are cubic in their undistorted forms and Wells long ago drew attention to their close relationship.^[4] No doubt the (10,3)-*a* net has been accorded less significance by chemists than its topology warrants simply because the number of examples known is not large, but, with the current burgeoning interest in the generation of new 3D networks, this situation is likely to change. Although numbers of metal/ligand-bonded frameworks with the (10,3)-*a* topology are now increasing, hydrogen-bonded examples such as the ones reported here remain rare.^[11] The results presented here, together with others,^[1,2] indicate the potential of the guanidinium cation as a

structure-directing ion for the generation of new networks of high symmetry. These are possibilities we are actively pursuing.

Received: August 17, 2004

Keywords: coordination modes · crystal engineering · hydrogen bonds · structure elucidation · supramolecular chemistry

- [1] B. F. Abrahams, M. G. Haywood, R. Robson, D. A. Slizys, *Angew. Chem.* **2003**, *115*, 1144; *Angew. Chem. Int. Ed.* **2003**, *42*, 1112; B. F. Abrahams, A. Hawley, M. G. Haywood, T. A. Hudson, R. Robson, D. A. Slizys, *J. Am. Chem. Soc.* **2004**, *126*, 2894.
- [2] B. F. Abrahams, M. G. Haywood, R. Robson, unpublished results.
- [3] K. T. Holman, A. M. Pivovar, M. D. Ward, *Science* **2001**, *294*, 1907; K. T. Holman, S. M. Martin, D. P. Parker, M. D. Ward, *J. Am. Chem. Soc.* **2001**, *123*, 4421; V. A. Russell, M. D. Ward, *Chem. Mater.* **1996**, *8*, 1654.
- [4] A. F. Wells, *Three-Dimensional Nets and Polyhedra*, Wiley-Interscience, New York, **1977**, p. 35.
- [5] $[\text{C}(\text{NH}_2)_3][\text{N}(\text{CH}_3)_4][\text{SO}_4]$: A solution of guanidinium chloride (110 mg, 1.15 mmol) in hot methanol (10 mL) was added to a solution of tetramethylammonium chloride (1.52 g, 13.9 mmol) and tetramethylammonium sulfate (225 mg, 0.93 mmol) in hot methanol (40 mL) on the steambath. The crystals of $[\text{C}(\text{NH}_2)_3][\text{N}(\text{CH}_3)_4][\text{SO}_4]$ that separated on cooling were collected after 3 h and washed with methanol. Yield: 80 mg, 38%. The X-ray powder pattern of the bulk solid was in good agreement with that calculated on the basis of the single-crystal data. Elemental analysis calcd for $\text{C}_5\text{H}_{18}\text{N}_4\text{O}_4\text{S}$ (%): C 26.1, H 7.9, N 24.4; found: C 26.1, H 7.9, N 24.3. $[\text{C}(\text{NH}_2)_3][\text{N}(\text{CH}_3)_4][\text{CrO}_4]$: Na_2CrO_4 (150 mg, 0.925 mmol) together with excess guanidinium chloride and tetramethylammonium chloride were dissolved in hot water (2 mL) on the steambath. Hot dimethylsulfoxide (4.5 mL) was added on the steambath. The yellow crystals of $[\text{C}(\text{NH}_2)_3][\text{N}(\text{CH}_3)_4][\text{CrO}_4]$ which formed upon cooling were collected after 5 h and washed with a minimal amount of water. Yield: 70 mg, 30%. The X-ray powder pattern of the bulk solid was in good agreement with that calculated on the basis of the single crystal data. Elemental analysis calcd $\text{C}_5\text{H}_{18}\text{N}_4\text{O}_4\text{Cr}$ (%): C 24.0, H 7.2, N 22.3; found: C 23.9, H 7.3, N 22.2. $[\text{C}(\text{NH}_2)_3][\text{N}(\text{CH}_3)_4][\text{MoO}_4]$: MoO_3 (130 mg, 0.925 mmol) and guanidinium chloride (160 mg, 1.85 mmol) were dissolved in a hot solution of tetramethylammonium hydroxide (1 mL of 25% w/w in methanol, 2.4 mmol) and water (1 mL). Hot dimethylformamide (4 mL) was added and colorless crystals, which were deliquescent, separated after one day at room temperature. A single crystal was removed, immersed in oil and cooled as quickly as possible prior to collecting X-ray diffraction data.
- [6] Crystal data for $[\text{C}(\text{NH}_2)_3][\text{N}(\text{CH}_3)_4][\text{SO}_4]$: $0.50 \times 0.50 \times 0.50$ mm, cubic, space group $P2_13$, $a = 10.5828(6)$ Å, $V = 1185.2(1)$ Å³, $\rho_{\text{calcd}} = 1.291$ g cm⁻³, $2\theta_{\text{max}} = 49.9^\circ$, $\lambda = 0.71073$ Å, $T = 293$ K, no. of measured (and independent) reflections: 6294 (708), $\mu = 0.273$ mm⁻¹, min./max. apparent transmission ratio: 0.867, no. of parameters: 50, $R1 [I > 2\sigma(I)] = 0.0476$, $wR2$ (all data) = 0.0899, max./min. residual electron density: 0.198/−0.159 e Å⁻³. Crystal data for $[\text{C}(\text{NH}_2)_3][\text{N}(\text{CH}_3)_4][\text{CrO}_4]$: $0.08 \times 0.08 \times 0.08$ mm, cubic, space group $P2_13$, $a = 10.7589(5)$ Å, $V = 1245.4(1)$ Å³, $\rho_{\text{calcd}} = 1.335$ g cm⁻³, $2\theta_{\text{max}} = 49.9^\circ$, $\lambda = 0.71073$ Å, $T = 293$ K, no. of measured (and independent) reflections: 6547 (737), $\mu = 0.918$ mm⁻¹, min./max. apparent transmission ratio: 0.837, no. of parameters: 49, $R1 [I > 2\sigma(I)] = 0.0673$, $wR2$ (all data) = 0.1399, max./min. residual electron density: 0.325/−0.19 e Å⁻³. Crystal data for $[\text{C}(\text{NH}_2)_3][\text{N}(\text{CH}_3)_4][\text{MoO}_4]$: $0.10 \times 0.10 \times 0.10$ mm, cubic, space group $P2_13$, $a = 10.8802(4)$ Å, $V = 1287.98(8)$ Å³, $\rho_{\text{calcd}} = 1.517$ g cm⁻³, $2\theta_{\text{max}} = 55.0^\circ$, $\lambda = 0.71073$ Å, $T = 130$ K, no. of measured (and independent) reflections: 8159 (996), $\mu = 1.018$ mm⁻¹, min./max. apparent transmission ratio: 0.925, no. of parameters: 49, $R1 [I > 2\sigma(I)] = 0.0398$, $wR2$ (all data) = 0.0668, max./min. residual electron density: 0.591/−0.370 e Å⁻³. In all cases all independent reflections were included in the refinement; multiscan absorption corrections were applied, all structures were solved by using direct methods and refined against F^2 using a full-matrix least-squares refinement;^[12] hydrogen atoms were included at geometrically estimated positions. CCDC-247060–247062 contain the supplementary crystallographic data for this paper. These data can be obtained free of charge via www.ccdc.cam.ac.uk/conts/retrieving.html (or from the Cambridge Crystallographic Data Centre, 12 Union Road, Cambridge CB21EZ, UK; fax: (+44) 1223-336-033; or deposit@ccdc.cam.ac.uk).
- [7] S. R. Batten, R. Robson, *Angew. Chem.* **1998**, *110*, 1558; *Angew. Chem. Int. Ed.* **1998**, *37*, 1475.
- [8] G. R. Desiraju, *Acc. Chem. Res.* **1996**, *29*, 441.
- [9] If the tetramethylammonium centers along with the sulfate and guanidinium centers are all considered as nodes in a single network, then the result is a 3,6-connected net (S of sulfate being a 6-connecting node and C of guanidinium and N of tetramethylammonium being 3-connecting nodes). This 3,6-connected net has the same topology as cubic PdF_2 . The relationship between the (10,3)-*a* net and the cubic PdF_2 net is considered in the Supporting Information.
- [10] P. Dera, A. Katrusiak, M. Szafranski, *Pol. J. Chem.* **2000**, *74*, 1637.
- [11] I. Boldog, E. B. Rusanov, J. Sieler, S. Blaurock, K. V. Domasevitch, *Chem. Commun.* **2003**, 740; L. Carlucci, G. Ciani, D. M. Proserpio, A. Sironi, *J. Am. Chem. Soc.* **1995**, *117*, 12861; S. C. Abrahams, R. L. Collin, W. N. Lipscomb, *Acta Crystallogr.* **1951**, *4*, 15; M. Tadokoro, T. Shiomi, K. Isobe, K. Nakasuji, *Inorg. Chem.* **2001**, *40*, 5476; L. Denner, P. Luger, J. Buschmann, *Acta Crystallogr. Sect. C* **1988**, *44*, 1979. (The structure of cyanamide reported in the latter reference was recognised as two interpenetrating (10,3)-*a* nets in ref. [6].)
- [12] G. M. Sheldrick, SHELX-97, Program for Crystal Structure Analysis, University of Gottingen, Gottingen (Germany), **1997**.

Olefin Metathesis

Rapidly Initiating Ruthenium Olefin-Metathesis Catalysts**

Patricio E. Romero, Warren E. Piers,* and Robert McDonald

Olefin metathesis is arguably the most powerful carbon-carbon bond breaking and making reaction in chemical synthesis.^[1] Depending on the nature of the reacting partners, olefin metathesis can be used for ring-opening polymerization (ROMP),^[2] to create advanced polymeric materials,^[3] transformation of acyclic diene substrates into complex cyclic organic molecules (in ring-closing metathesis (RCM))^[4] or polymers (in acyclic diene metathesis (ADMET))^[5] or in cross metathesis (CM) to generate unsymmetrical olefins.^[6,7] Although olefin metathesis is fully reversible, RCM, ADMET, and CM rely on the elimination of ethylene, the simplest olefin, as a thermodynamic driving force. Used by itself or in tandem with other synthetic transformations,^[8,9] olefin metathesis is a versatile method for the modern synthetic chemist.

It is generally acknowledged that a metal carbene species, $[L_nM=CRR']$, is required and that interaction with an olefin substrate leads to four-membered metallacyclobutane intermediates or transition states, $[L_nM(CRR')_3]$, by a 2+2 cycloaddition; cleavage of this intermediate in the opposite sense by which it was formed leads to olefin metathesis, creating a new carbon-carbon double bond and regenerating an active metal carbene. Metal carbenes are generally classified as being nucleophilic (electron rich) or electrophilic (electron poor) in character at the carbene carbon atom, but an effective olefin-metathesis catalyst exhibits behavior between these two extremes. Two carefully tuned classes of mediator have evolved into the catalysts of choice for olefin metathesis. Schrock catalysts^[10,11] are molybdenum- or tungsten-based alkylidenes with a fairly specific ligand set designed to modulate the properties of the carbene (Figure 1). These catalysts display high activities and stabilities, but are sensitive to ambient air and moisture and are relatively intolerant of polar functionalities. The Grubbs-catalyst portfolio^[12] consists of a variety of ruthenium-based systems of

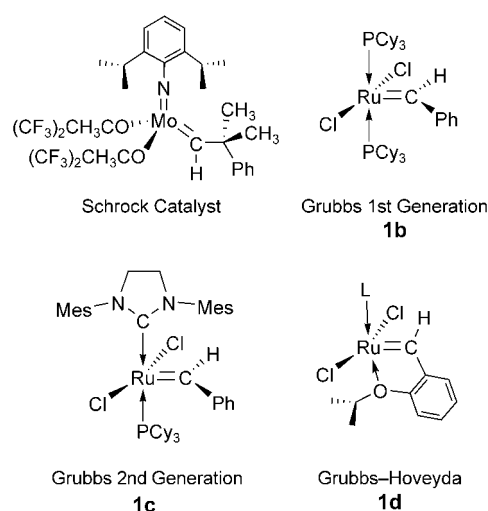


Figure 1. Commercially available olefin-metathesis catalysts. Cy = cyclohexyl, Mes = 2,4,6-trimethylphenyl.

general formula $[Cl_2(L)(L')Ru=C(H)R]$ (compounds **1**) which are significantly more functional-group tolerant, but do not exhibit the same levels of activity or longevity as the Schrock catalysts.

The root of the lower activities of the Grubbs systems lies in their mode of initiation and the accessibility of the reactive species, which has been shown experimentally^[13,14] and computationally^[15,16] to be the 14-electron alkylidene $[Cl_2(L)Ru=C(H)R]$ formed upon reversible dissociation of L' . The reaction temperatures required to overcome this initiation step can lead to decreased catalyst lifetimes. Successful improvements to the "Grubbs first-generation" catalyst $[Cl_2(PCy_3)_2Ru=C(H)Ph]$ (**1b**) are modifications that either encourage loss of L' ^[17] or reduce the tendency of $[Cl_2(L)Ru=C(H)R]$ to re-capture the liberated L' ,^[18] which competes with the olefin substrate for the unsaturated metal center in $[Cl_2(L)Ru=C(H)R]$. Alternatively, Hoveyda and co-workers have developed catalysts **1d**, in which L' is incorporated into a loosely chelating group associated with the carbene ligand that is removed upon the first metathesis event.^[19,20] Fast-initiating improvements on this motif have been devised by Blechert and Wakamatsu.^[21]

Herein we report a surprising twist on the Grubbs-catalyst motif that improves the kinetics of initiation dramatically by circumventing the initiation step in commercially available Grubbs catalysts completely, thus providing direct access to the reactive 14-electron catalyst species with no free L' present to interfere with the operation of the catalyst. This new generation catalyst precursor is easily prepared from existing Grubbs catalysts and brings their activity into the realm of the Schrock family, while retaining the favorable functional-group tolerance associated with the ruthenium systems.

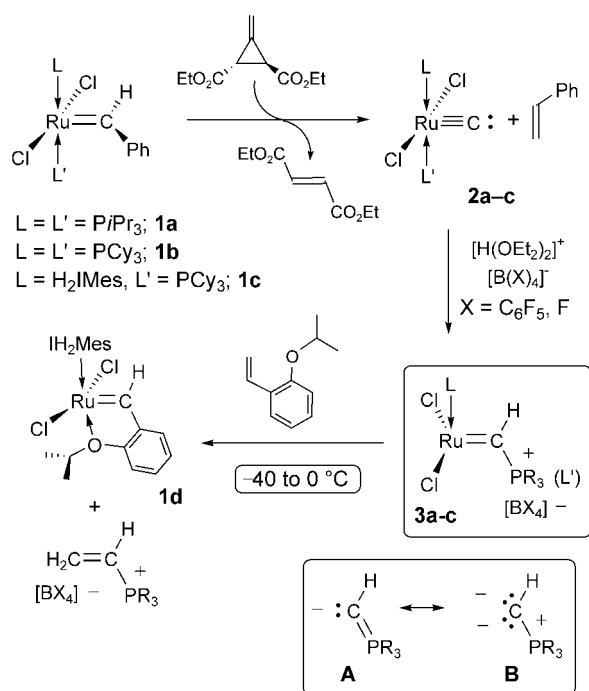
Recently, Heppert and co-workers reported a stoichiometric metathesis reaction between catalyst precursors **1b** and **1c** and a methylene cyclopropane olefin known as Feist's ester.^[22] Metathesis and elimination of diethyl fumarate provides the unusual ruthenium carbides **2a-c** (Scheme 1).

[*] P. E. Romero, Prof. Dr. W. E. Piers
Department of Chemistry
University of Calgary
2500 University Drive N. W., Calgary, Alberta T2N 1N4 (Canada)
Fax: (+1) 403-289-9488
E-mail: wpiers@ucalgary.ca

Dr. R. McDonald
X-Ray Structure Laboratory, Department of Chemistry
University of Alberta, Edmonton, Alberta T6G 2G2 (Canada)

[**] Financial support for this work was provided by the Natural Sciences and Engineering Research Council of Canada through a discovery grant to W.E.P. Materia Inc. is acknowledged for generous donations of catalysts shown in Figure 1.

Supporting information for this article is available on the WWW under <http://www.angewandte.org> or from the author.



Scheme 1. Synthesis of rapidly initiating metathesis catalysts **3**; $\text{H}_2\text{IMes} = \text{N-heterocyclic carbene ligand}$.

Heppert and co-workers reported the preparation of carbides **2b** and **2c** in low yields; we have found this to be fairly a general reaction and a variety of carbides containing other combinations of L and L' can be prepared in improved yields (90–96%) from **2b** and **2c**. We became interested in the reactivity of these carbides with electrophiles and discovered that protonation with $[\text{H}(\text{OEt}_2)_2]^+[\text{B}(\text{C}_6\text{F}_5)_4]^-$, Jutzi's acid,^[23] leads to the cationic four-coordinate, 14-electron phosphonium alkylidenes **3a–c** by transfer of a trialkylphosphine ligand (that is, L' , Scheme 1) to the protonated carbide carbon atom in high yields (87–95%).^[24]

Evidently, protonation of the carbide carbon atom switches it from being electron rich to electron poor; the electrophilicity of the protonated carbide carbon atom is quenched by transfer of the phosphine (L') from the metal center, generating the observed phosphonium alkylidenes. For **3a** and **3b** ($L = \text{PR}_3$, $R = i\text{Pr}$ or Cy), the signal for the alkylidene proton appears as a distinctive doublet of doublets in the proton NMR spectrum at $\delta = 17.35$ ppm for **3a** and 17.46 ppm for **3b** ($^2J_{\text{H,P}} = 36$ Hz; $^3J_{\text{H,P}} = 1.5 \pm 3$ Hz). In **3c**, where $L = \text{H}_2\text{IMes}$, the three-bond hydrogen–phosphorus coupling is lost and the alkylidene hydrogen resonance signal appears as a doublet at $\delta = 17.70$ ($^2J_{\text{H,P}} = 36$ Hz). In the $^{31}\text{P}\{^1\text{H}\}$ NMR spectra, the signals for the phosphonium phosphorus atoms appear in the region around $\delta = 54$ –58 ppm, while those of the phosphorus nuclei bonded to ruthenium appear at $\delta = 97.6$ (**3a**) and 88.7 ppm (**3b**). These latter resonance signals, while shifted about 60 ppm downfield relative to those found for **1b** and **1c**, are similar to that observed for the four coordinate complex $[(t\text{BuO})_2(\text{PCy}_3)\text{Ru}=\text{C}(\text{H})\text{Ph}]$ prepared by Grubbs and co-workers.^[25] In **3c**, rotation of the IH_2Mes ligand about the $\text{Ru}-\text{C}2$ bond (see

Figure 2) is fast on the NMR timescale, with a free energy barrier of $11.5(5)$ kcal mol $^{-1}$ at 236 K calculated from the coalescence behavior of the NMR signals arising from the inequivalent mesityl groups at low temperature. This contrasts with the behavior for the parent compound **1c**, which exhibits slow rotation with a barrier of 21.8 kcal mol $^{-1}$.^[26] Remarkably, when solutions of **3c** are exposed to the atmosphere, the NMR spectra remain unchanged for several hours, which indicates that the compound is stable to oxygen and ambient moisture. Indeed, introduction of water into these samples results only in minor perturbations to the spectra, owing to reversible coordination of H_2O to the ruthenium center. The compounds are thermally stable indefinitely in the solid state at room temperature and can be heated under refluxing CD_2Cl_2 (45 °C, sealed tube) for several hours with no evidence of decomposition. Heating at 75 °C in $\text{C}_6\text{D}_5\text{Br}$ results in clean decomposition to an unidentified species ($^{31}\text{P}\{^1\text{H}\}$ NMR $\delta = 37$ ppm) with a half-life of approximately 5 h; the nature of this process is under investigation.^[27] Preliminary studies show that the carbides can be converted into more economically viable BF_4 salts of cations **3a–c** by protonation with $[\text{H}(\text{Et}_2\text{O})_x]^+[\text{BF}_4]^-$ with little change in the behavior of the compounds.

The precise structure of **3c** was determined by X-ray crystallography (Figure 2).^[28] Compounds **3** represent the closest structural models for the proposed four-coordinate,

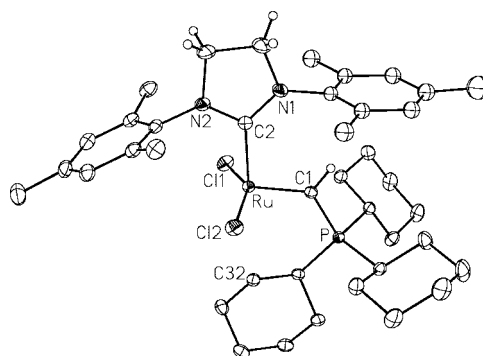


Figure 2. ORTEP diagram of **3c** (thermal ellipsoids set at 50% probability; counteranion and hydrogen atoms omitted for clarity). Selected bond lengths [Å] and angles [°]: $\text{Ru}-\text{C}1$ 1.817(2), $\text{Ru}-\text{C}2$ 1.988(2), $\text{Ru}-\text{Cl}1$ 2.2951(5), $\text{Ru}-\text{Cl}2$ 2.2809(5), $\text{P}-\text{C}1$ 1.805(2); $\text{C}1-\text{Ru}-\text{C}2$ 100.07(7), $\text{Cl}1-\text{Ru}-\text{Cl}2$ 150.51(2), $\text{Cl}1-\text{Ru}-\text{C}1$ 103.15(6), $\text{Cl}2-\text{Ru}-\text{C}1$ 102.79(6), $\text{Cl}1-\text{Ru}-\text{C}2$ 96.14(5), $\text{Cl}2-\text{Ru}-\text{C}2$ 92.90(5). Selected torsion angle [°]: $\text{C}2-\text{Ru}-\text{C}1-\text{P}$, $-175.06(11)$.

14-electron active species in the Grubbs-catalyst family; the only other structurally characterized example, the *bis-tert*-butoxide derivative $[(t\text{BuO})_2(\text{PCy}_3)\text{Ru}=\text{C}(\text{H})\text{Ph}]$,^[25] relies on the replacement of the chloride ligands with sterically bulky groups for kinetic stabilization, but is essentially inactive as an olefin metathesis catalyst. As in the *bis-tert*-butoxide complex, the geometry about the ruthenium center in **3c** is a distorted trigonal pyramid with the H_2IMes ligand occupying the apex; however, the $\text{Cl}1-\text{Ru}-\text{Cl}2$ angle is at $150.51(2)^\circ$ substantially larger than the $\text{O}1-\text{Ru}-\text{O}2$ angle of $133.19(6)^\circ$ in

$[(t\text{BuO})_2(\text{PCy}_3)\text{Ru}=\text{C}(\text{H})\text{Ph}]$. The Ru-C1 and Ru-C2 bonds of 1.817(2) and 1.988(2) Å, are slightly shorter than those in **1c**,^[17] a difference accounted for by the reduced coordination number in **3c**. The phosphonium alkylidene unit is oriented such that the PCy_3 group is pointing away from the IH_2Mes ligand. Angles and separations are normal within this part of the molecule and although C32 is positioned near a vacant ruthenium coordination site, any stabilization of the ruthenium center from the C–H sigma bonds of C32 is weak (Ru...C32 3.001 Å). No evidence for a C–H agostic interaction is observed in the proton NMR spectra, nor are low-frequency C–H vibrations apparent in the IR spectra of compounds **3**, which would be expected if any of the C–H bonds were donating electron density to the unsaturated ruthenium center.^[29] Four-coordinate ruthenium complexes not stabilized by C–H agostic interactions are rare;^[30] thus, apart from being models for the 14-electron active species in olefin metathesis, compounds **3** are unusual coordination compounds.

Metal carbenes are classified according to the donor qualities of the atoms directly bonded to the carbene carbon atom. Fischer carbenes incorporate π -donating groups (OR, NR_2), while the nucleophilic Schrock carbenes have π -neutral groups, such as H or alkyl substituents.^[1] The phosphonium substituted carbenes of compounds **3** are a less common third class since the $[\text{PR}_3]^+$ group is a π acceptor.^[31] Formally, this CHPR_3 ligand can be viewed as a deprotonated phosphorus ylid species (ylide resonance structure **A**, inset Scheme 1), but according to experimental^[32] and computational^[33] studies and the parameters for **3c** discussed above, a more realistic depiction is the dicarbanionic ylid resonance structure **B**. The ruthenium centers in compounds **3** may thus be viewed as formally Ru^{IV} with the carbene ligand functioning as a four-electron donor.

The electron-withdrawing nature of the phosphonium substituent in the carbene ligands of compounds **3** does not impede their ability to conduct olefin metathesis; they are exceptionally active RCM catalysts in comparison to catalyst precursors **1**. Using the RCM of diallyldiethylmalonate as a benchmark reaction, catalysts **1c** (Grubbs 2nd Generation), Schrock's molybdenum-based catalyst (Figure 1), the fast-initiating Grubbs catalyst $[(\text{IH}_2\text{Mes})\text{Cl}_2(3\text{-Br-py})_2\text{Ru}=\text{CHPh}]$,^[34] and compounds **3b** and **3c** were compared at 0°C by monitoring reaction progress to the cyclized product (Figure 3). At 0°C **1c** is a poor initiator^[18] and only reaches approximately 25% conversion after 4 h. Compound **3b** fares somewhat better, providing about 90% conversion after 4 h, while Schrock's catalyst mediates the reaction to a similar point in this time. The sigmoidal shape of the curve for **3b** is reflective of the different activities of initiating versus propagating species at 0°C for this catalyst.^[13] The transformation is very rapid for compound **3c**, however, which brings the reaction to >90% conversion after only 2 h at 0°C, twice as fast as the Schrock catalyst under these conditions and, significantly, it out-performs the fast-initiating Grubbs catalyst incorporating more labile 3-bromopyridine ligands. Furthermore, the rate of RCM for **3c** is qualitatively similar to the best Blechert catalyst,^[21b] a less conveniently available metathesis catalyst.

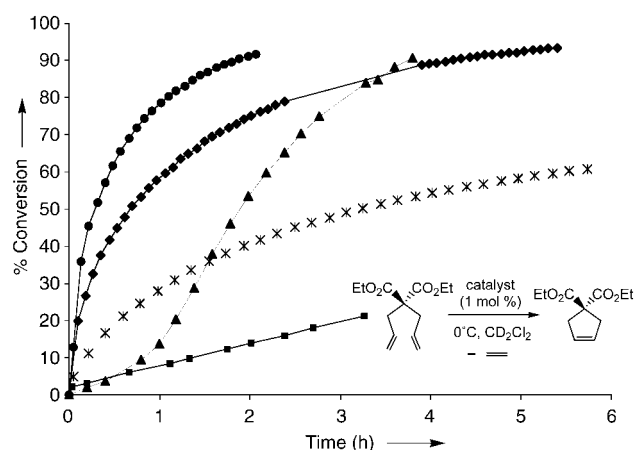


Figure 3. Relative rates of conversion for RCM of diethyldiallylmalonate at 273 K by (■) **1c**, (◆) Schrock's molybdenum alkylidene, (★) the Grubbs fast-initiating catalyst $[(\text{IH}_2\text{Mes})\text{Cl}_2(3\text{-Br-py})_2\text{Ru}=\text{CHPh}]$, (▲) **3b**, and (●) **3c**.

We have also explored additional substrates for the RCM process with catalyst **3c** and initial results are summarized in Table 1. The reactions are completed within 2–60 min at room temperature (1% mol catalyst loading, except entry 2 and 6). Diethyldiallylmalonate (entry 1) is ring-closed in under 2 min, this is determined as an upper limit since the reaction time is too fast to be accurately measured at room temperature. Using 0.1% mol catalyst loading, a 100% conversion is reached within 30 min (entry 2). Similar results are found in the formation of a six-membered ring (entry 4 and 5), while higher catalyst loadings are required to push the closing of a seven-membered ring to acceptable conversions (entry 6). Notably, the closing of trisubstituted olefins proceeds to high conversion, under very mild conditions (entries 3 and 5). In particular, formation of the trisubstituted cyclopentene is complete in less than 10 min (entry 3); this particular substrate allows a more direct comparison with Blechert's catalyst, which accomplished this conversion in 40 min, under otherwise identical conditions.^[21]

The reason **3c** is so active is that the need to dissociate a ligand for the ruthenium complex to enter the catalytic cycle^[13,18] has been completely obviated and initiation is now the much more energetically favorable binding of the substrate C=C bond to the ruthenium center. Rate constants for this process have been measured by monitoring the reaction of **3c** with varying excesses of *ortho*-isopropoxy styrene (10–40 equiv) at –30 to 0°C by proton NMR spectroscopy. This substrate was chosen since it produces the Grubbs–Hoveyda catalyst **1d** (Figure 1), which is inactive towards further metathesis reactions at the temperatures used; the other product is $[(\text{CH}_2=\text{CH})\text{PCy}_3][\text{B}(\text{C}_6\text{F}_5)_4]$, which was identified by separate synthesis and comparison of ^1H and ^{31}P NMR spectroscopy data. Use of this less-active substrate slows the reaction down, but also avoids complications in the kinetics arising from the presence of multiple active species in the reaction.^[35] These studies indicate that the reaction is second order, first order in each of **3c** and [styrene]

Table 1: Ring-closing metathesis using **3c**^[a] at room temperature.

Entry	Substrate	Product	R	CL ^[b]	t [min]	Conversion [%] ^[c]
1			H	1.0	< 2	100
2			H	0.1	30	100
3			Me	1.0	< 10	100
4			H	1.0	< 10	100
5			Me	1.0	60	98
6			—	5.0	< 10	85

[a] Conditions: room temperature, toluene, [diene] = 0.23 M. [b] Catalyst loading. [c] Conversions determined by ¹H NMR spectroscopy.

substrate, with a second order rate constant of $5.9 \pm 0.3 \times 10^{-4} \text{ M}^{-1} \text{ s}^{-1}$ at -10°C .^[36] By evaluating this rate constant as a function of temperature (30 equiv of styrene), the thermodynamic activation parameters of the reaction were measured as $\Delta H^\ddagger = 8.6(4) \text{ kcal mol}^{-1}$ and $\Delta S^\ddagger = -55(6) \text{ eu}$. The large, negative activation entropy is consistent with a bimolecular initiation step, which supports the notion that the measured barrier corresponds to rate-limiting olefin binding. Nevertheless, even for this very unreactive substrate,^[20] the magnitude of the second-order rate constant at -10°C is comparable to the initiation rate of $4.6 \pm 0.4 \times 10^{-4} \text{ s}^{-1}$ measured at 35°C for the widely used Grubbs second-generation catalyst **1c**.^[18]

These results are an advance in the evolution of ruthenium-based olefin-metathesis catalysis. Slow initiation has been a limiting factor for the existing Grubbs-catalyst portfolio and the phosphonium alkylidene compounds disclosed herein circumvent this problem by effectively eliminating the phosphine-dissociation initiation step altogether. In essence, all of the ruthenium added is actually operating as a catalyst in these reactions as compared to the traditional Grubbs catalysts, where the majority of ruthenium is tied up as the non-active **1c**. In compounds **3**, initiation consists of the much lower barrier olefin-binding event; subsequent metathesis to liberate $[(\text{CH}_2=\text{CH})\text{PR}_3][\text{B}(\text{C}_6\text{F}_5)_4]$ provides rapid and direct access to the propagating 14-electron ruthenium alkylidene complexes without any free phosphine present to drain the catalyst pool of active ruthenium.

The benefits of fast-initiating catalysts for a variety of metathesis applications are many. Lower catalyst loadings can be achieved which improves the economics and the environmental impact associated with use of these catalysts. Reactions can be performed at much lower temperatures, potentially providing greater enantioselectivity in asymmetric RCM reactions^[37] and better chemoselectivity in commercially important CM processes.^[38] In ROMP applications, rapid initiation leads to polymer products with narrower molecular-weight distributions.^[39] Finally, the new compounds

provide an opportunity to probe the mechanism of the propagating steps in the olefin metathesis reaction without the problem of excess phosphine in the reaction medium, as well as catalyst decomposition processes that do not involve the dissociated phosphine ligand of catalysts **1**.^[40]

Experimental Section

Complete experimental details, including synthesis and characterization of all the new compounds, can be found in the Supporting Information.

Received: July 21, 2004

Revised: August 27, 2004

Keywords: carbene ligands · homogeneous catalysis · metathesis · ruthenium

- [1] *Handbook of Metathesis*, Vol. 1–3 (Ed.: R. H. Grubbs), Wiley-VCH, Weinheim, 2003.
- [2] U. Frenzel, O. Nuyken, *J. Polym. Sci. Part A* **2002**, 40, 2895.
- [3] C. W. Bielawski, D. Benitez, R. H. Grubbs, *Science* **2002**, 297, 2041.
- [4] A. Fürstner, *Angew. Chem.* **2000**, 112, 3140; *Angew. Chem. Int. Ed.* **2000**, 39, 3012.
- [5] T. E. Hopkins, K. B. Wagener, *Adv. Mater.* **2002**, 14, 1703.
- [6] S. J. Connon, S. Blechert, *Angew. Chem.* **2003**, 115, 1944; *Angew. Chem. Int. Ed.* **2003**, 42, 1900.
- [7] A. K. Chatterjee, T.-L. Choi, D. P. Sanders, R. H. Grubbs, *J. Am. Chem. Soc.* **2003**, 125, 11360.
- [8] S. D. Drouin, F. Zamaian, D. E. Fogg, *Organometallics* **2001**, 20, 5495.
- [9] J. Louie, C. W. Bielawski, R. H. Grubbs, *J. Am. Chem. Soc.* **2001**, 123, 11312.
- [10] R. R. Schrock, J. S. Murzdek, G. C. Bazan, M. Robbins, M. Dimare, M. O'Regan, *J. Am. Chem. Soc.* **1990**, 112, 3875.
- [11] R. R. Schrock, A. H. Hoveyda, *Angew. Chem.* **2003**, 115, 4740; *Angew. Chem. Int. Ed.* **2003**, 42, 4592.
- [12] T. M. Trnka, R. H. Grubbs, *Acc. Chem. Res.* **2001**, 34, 18.
- [13] E. L. Dias, S. T. Nguyen, R. H. Grubbs, *J. Am. Chem. Soc.* **1997**, 119, 3887.
- [14] C. Adlhart, C. Hinderling, H. Baumann, P. Chen, *J. Am. Chem. Soc.* **2000**, 122, 8204.
- [15] C. Adlhart, P. Chen, *J. Am. Chem. Soc.* **2004**, 126, 3496.
- [16] L. Cavallo, *J. Am. Chem. Soc.* **2002**, 124, 8965.
- [17] J. A. Love, M. S. Sanford, M. W. Day, R. H. Grubbs, *J. Am. Chem. Soc.* **2003**, 125, 10103.
- [18] M. S. Sanford, J. A. Love, R. H. Grubbs, *J. Am. Chem. Soc.* **2001**, 123, 6543.
- [19] J. S. Kingsbury, J. P. A. Harrity, P. J. Bonitatebus, Jr., A. H. Hoveyda, *J. Am. Chem. Soc.* **1999**, 121, 791.
- [20] S. B. Garber, J. S. Kingsbury, B. L. Gray, A. H. Hoveyda, *J. Am. Chem. Soc.* **2000**, 122, 8168.
- [21] a) H. Wakamatsu, S. Blechert, *Angew. Chem.* **2002**, 114, 832; *Angew. Chem. Int. Ed.* **2002**, 41, 794; b) H. Wakamatsu, S. Blechert, *Angew. Chem.* **2002**, 114, 2509; *Angew. Chem. Int. Ed.* **2002**, 41, 2403.

- [22] R. G. Carlson, M. A. Gile, J. A. Heppert, M. H. Mason, D. R. Powell, D. Vander Velde, J. M. Vilain, *J. Am. Chem. Soc.* **2002**, *124*, 1580.
- [23] P. Jutzi, C. Muller, A. Stammer, H.-G. Stammer, *Organometallics* **2000**, *19*, 1442.
- [24] Other cationic ruthenium olefin metathesis catalysts: a) S. M. Hansen, M. A. O. Volland, F. Rominger, F. Eisenträger, P. Hofmann, *Angew. Chem.* **1999**, *111*, 1360; *Angew. Chem. Int. Ed.* **1999**, *38*, 1273; b) A. Fürstner, M. Liebl, C. W. Lehmann, M. Picquet, R. Kunz, C. Bruneau, D. Touchard, P. H. Dixneuf, *Chem. Eur. J.* **2000**, *6*, 1847.
- [25] M. S. Sanford, L. M. Henling, M. W. Day, R. H. Grubbs, *Angew. Chem.* **2000**, *112*, 3593; *Angew. Chem. Int. Ed.* **2000**, *39*, 3451. See also: J. N. Coalter III, J. C. Bollinger, O. Eisenstein, K. G. Caulton, *New J. Chem.* **2000**, *24*, 925.
- [26] M. S. Sanford, Ph.D. Thesis, California Institute of Technology (2001).
- [27] Decomposition processes involving the active species in Grubbs catalysts are largely a mystery: S. H. Hong, M. W. Day, R. H. Grubbs, *J. Am. Chem. Soc.* **2004**, *126*, 7414.
- [28] Crystal data for **3c**: $C_{64}H_{60}BCl_2F_{20}N_2PRu$, $M_r = 1450.89$, triclinic, $P\bar{1}$, $a = 12.0671(6)$ Å, $b = 16.4448(9)$ Å, $c = 17.6951(9)$ Å, $\alpha = 102.1701(8)^\circ$, $\beta = 108.1299(8)^\circ$, $\gamma = 102.6938(9)^\circ$, $V = 3104.4(3)$ Å³, $Z = 2$, $\rho_{\text{calcd}} = 1.552$ g cm⁻³, $MoK\alpha$ radiation, $\lambda = 0.71073$ Å, $T = -80^\circ\text{C}$, 23973 measured reflections, 12683 unique ($R_{\text{int}} = 0.0168$), 11455 reflections with $I_{\text{net}} > 2.0(I_{\text{net}})$, $\mu = 0.467$ mm⁻¹, min/max transmission = 0.7732 and 0.8803, $R1$ ($I > 2\sigma$) = 0.0310, $wR2$ 0.0822, GoF = 1.037, No. of parameters = 820, final difference map within +0.686 and -0.392 e Å⁻³. CCDC-243766 (**3c**) contains the supplementary crystallographic data for this paper. These data can be obtained free of charge via www.ccdc.cam.ac.uk/conts/retrieving.html (or from the Cambridge Crystallographic Data Centre, 12 Union Road, Cambridge CB21EZ, UK; fax: (+44)1223-336-033; or deposit@ccdc.cam.ac.uk).
- [29] W. Scherer, G. S. McGrady, *Angew. Chem.* **2004**, *116*, 1816; *Angew. Chem. Int. Ed.* **2004**, *43*, 1782.
- [30] L. A. Watson, O. V. Ozerov, M. Pink, K. G. Caulton, *J. Am. Chem. Soc.* **2003**, *125*, 8426.
- [31] X. Li, M. Schopf, J. Stephan, K. Harms, J. Sundermeyer, *Organometallics* **2002**, *21*, 2356.
- [32] J. W. Gilje, R. E. Cramer, M. A. Bruck, K. T. Higa, K. Panchantheswaran, *Inorg. Chim. Acta* **1985**, *110*, 139.
- [33] R. S. McDowell, A. Streitwieser, Jr., *J. Am. Chem. Soc.* **1984**, *106*, 4047.
- [34] J. A. Love, J. P. Morgan, T. M. Trnka, R. H. Grubbs, *Angew. Chem.* **2002**, *114*, 4207; *Angew. Chem. Int. Ed.* **2002**, *41*, 4035.
- [35] Attempts to determine rate constants by monitoring the ring closing of diallyldiethylmalonate gave nonlinear plots because, even at -60°C , the alkylidene product of initiation was active for turning the reaction over, as evidenced by the slow build-up of ethylene in the sample over time.
- [36] The pseudo first-order plots from which the rate constants were obtained are linear for the duration of the reaction after a region of curvature at the beginning of the reaction (see Supporting Information). The origins of this kinetic behavior are not currently understood; further investigations are underway.
- [37] T. J. Seiders, D. W. Ward, R. H. Grubbs, *Org. Lett.* **2001**, *3*, 3225.
- [38] R. L. Pederson, I. M. Fellows, T. A. Ung, H. Ishihara, S. P. Hajela, *Adv. Synth. Catal.* **2002**, *344*, 728.
- [39] T.-L. Choi, R. H. Grubbs, *Angew. Chem.* **2003**, *115*, 1785; *Angew. Chem. Int. Ed.* **2003**, *42*, 1743.
- [40] S. H. Hong, M. W. Day, R. H. Grubbs, *J. Am. Chem. Soc.* **2004**, *126*, 7414.

**Nanozymes: Gold-Nanoparticle-Based
Transphosphorylation Catalysts****

Flavio Manea, Florence Bodar Houillon,
Lucia Pasquato,* and Paolo Scrimin*

In his review on catalysis by colloid aggregates that appeared in this journal more than ten years ago, Menger wrote:^[1] "...groups of molecules, properly assembled, can obviously accomplish much more than an equal number of molecules functioning separately". This observation is becoming more and more important as evidence is mounting that many biological systems interact and function through multiple simultaneous interactions.^[2] On these bases a number of multivalent synthetic systems have been designed and studied for the recognition of simple molecules or more challenging biological targets. However, multivalent catalysts in which real cooperativity between the components is observed remain elusive, particularly in the case of self-assembling systems. For instance, most of the relevant rate accelerations often observed with aggregation colloids (such as, micelles and vesicles) appear to be related to concentration effects in the reaction loci (which include effects on the local pH value as well as on reactants and catalytic units) rather than to cooperativity.^[3] Nevertheless, cooperativity is a rule in biological systems, such as enzymes. The reason for this lack of cooperativity in colloidal systems is largely entropic, and is related to the mobility of the constituent units (lipids/surfactants) that does not allow a catalytic site to last the time required for the catalyzed process to occur. Synthetic, functional polymers (synzymes)^[4] allowed this problem to be solved, at least in part. Indeed cooperative catalysts based on these systems have been described.^[5] However, a polymer presents other problems related to the difficulty in controlling its composition and conformation in solution.^[6] Note that, as in the natural systems, not only the sequence of the building blocks (amino acids or any other) but also the conformation of the polymer are key requisites for catalysis. Alternatively,

[*] F. Manea, Dr. F. B. Houillon, Prof. Dr. P. Scrimin
University of Padova
Department of Chemical Sciences and ITM-CNR, Padova Section
Via Marzolo, 1-35131 Padova (Italy)
Fax: (+39) 049-8275239
E-mail: paolo.scrimin@unipd.it
Prof. Dr. L. Pasquato
University of Trieste
Department of Chemical Sciences
Via Giorgieri, 1-34127 Trieste (Italy)
Fax: (+39) 040-5583903
E-mail: pasquato@dsch.univ.trieste.it

[**] This work was supported by the European Community's Human Potential Programme under contract HPRN-CT1999-00008, ENDEVAN (fellowship to F.B.H.) and by the Ministry of Education, University, and Research of Italy (MIUR, contract 2002031238).



Supporting information for this article is available on the WWW under <http://www.angewandte.org> or from the author.

dendrimers functionalized on the periphery may constitute a suitable alternative for which, contrasting results have been reported.^[7]

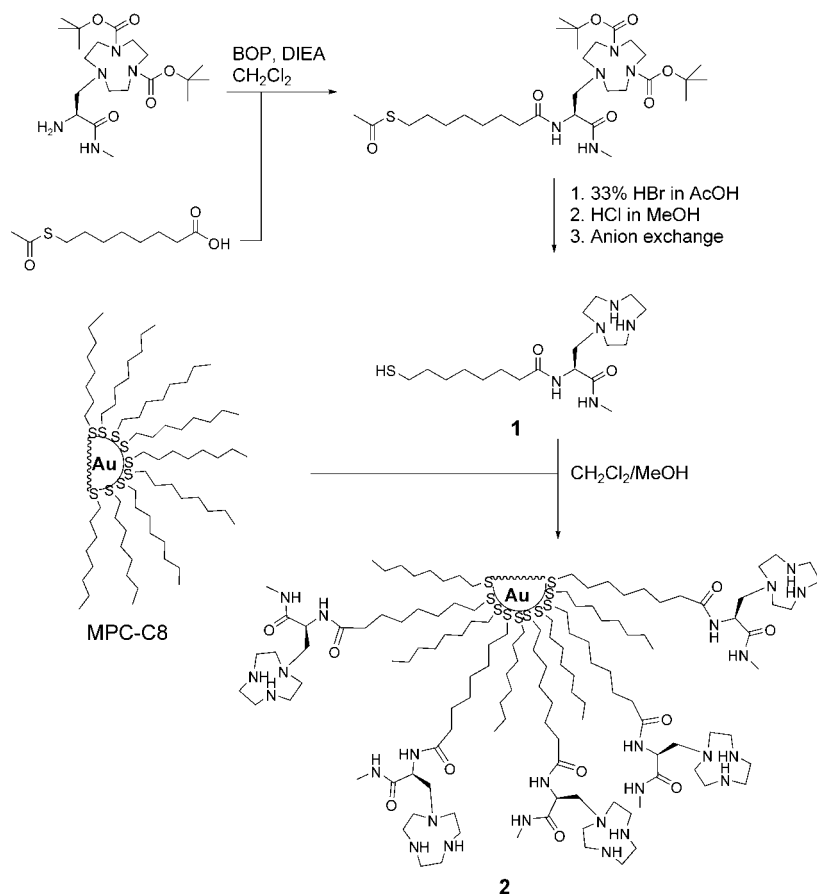
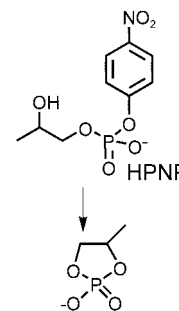
It occurred to us that by exploiting the well known ability of thiols to bind to gold nanoparticles we could have facile access to multivalent, functional systems^[8,9] anchored on a support, and yet fully soluble, with limited mobility and conformationally constrained and, hence, suitable to act cooperatively in a catalytic process. To test this hypothesis we have chosen one of the most challenging reactions: the cleavage of the phosphate bond of phosphodiester as a model of a RNase. Most of these enzymes require for their activity at least two metal ions that act cooperatively.^[10]

Gold nanoparticles (MPC) protected by a monolayer of 1-sulfanyloctane (MPC-C8) were prepared by the procedure reported by Brust and co-workers^[11] and optimized by Murray and co-workers.^[12] They were subsequently subjected to site exchange^[13] with the azacrown-functionalized thiol **1** to yield functional nanoparticles **2** (Scheme 1).^[14] Proton NMR spectroscopic analysis of the monolayer composition of **2** revealed a 1:1.2 ratio of 1-sulfanyloctane and **1**, respectively. The core size of these ligand-functionalized MPC was 2.5 ± 0.7 nm as determined by transmission electron microscopy (TEM), see Supporting Information. Because of the presence of the triazacyclononane units, gold MPC **2** are expected to be

able to bind transition-metal ions (such as, Cu^{II} , Zn^{II}) with high binding constants.^[15] In the case of Cu^{II} the binding process can be followed spectrophotometrically at 648 nm, the maximum of the absorption band of the triazacyclononane– Cu^{II} complex. This property was used to determine the concentration of the ligand units (**1**) in stock solutions of **2**.

Transphosphorylation activity of **2** was tested with Zn^{II} ions because of the relevance of these ions in biological phosphate-cleavage catalysis.^[10] A thorough analysis of the system was carried out by using 2-hydroxypropyl *p*-nitrophenyl phosphate (HPNP) as the substrate, an activated phosphate diester frequently used as a model of RNA.

With HPNP the release of *p*-nitrophenol (or *p*-nitrophenolate, depending on pH) is accompanied by the formation of a cyclic phosphate^[16] and can be easily followed spectrophotometrically. Figure 1 shows the reactivity profile obtained by progressively adding Zn^{II} ions to a solution of **2** up to the saturation of the metal-ion binding subunits. This kinetic analysis reveals that a) the most active system is the one fully loaded with Zn^{II} ions, b) the sigmoidal profile of the curve supports cooperativity^[18] between the metal centers



Scheme 1. Reaction scheme for the synthesis of ligand thiol **1**, and ligand-functionalized gold nanoparticles **2**; BOP = (1*H*-benzotriazol-1-yl)-*O*-(*N*-methylmethanaminato)-phosphorus hexafluorophosphate, DIEA = *N*,*N*-diisopropylethylamine.

because the catalytic efficiency becomes much higher after the first 30 % of Zn^{II} ions is added. The plot also indicates that possible cooperativity between a metal ion and an ammonium ion^[19] (owing to the presence of the uncomplexed and hence protonated azacrown) is less important than the cooperativity between Zn^{II} ions. The presence of such a contribution to the catalysis would have resulted in a bell-shaped profile, the maximum corresponding to a nanoparticle where Zn^{II} complexes and ammonium ions coexist in close proximity.

The real catalytic nature of the process was assessed by carrying out experiments with excess substrate. No formation of an intermediate was detected and first-order kinetics were observed up to the complete cleavage of all the substrate present. By varying the initial substrate concentration a kinetic profile of the reaction towards saturation was observed. These kinetics allowed the determination of the apparent Michaelis–Menten parameters $K_{\text{M}} = 0.93$ mM and $k_{\text{cat}} = 4.2 \times 10^{-3} \text{ s}^{-1}$. Zinc(II)-nanoclusters **2** (Zn^{II} -**2**)^[20] are, however, not selective in the binding of anions and, in fact, they also bind zwitterionic HEPES used as buffer for the experiments, which acts as an inhibitor of the catalytic process (see Supporting Information).^[21]

The formal second-order rate constant for HPNP cleavage ($k_{\text{cat}}/K_{\text{M}}$) by Zn^{II} -**2** is $4.4 \text{ s}^{-1} \text{ M}^{-1}$ which is more than 600-times

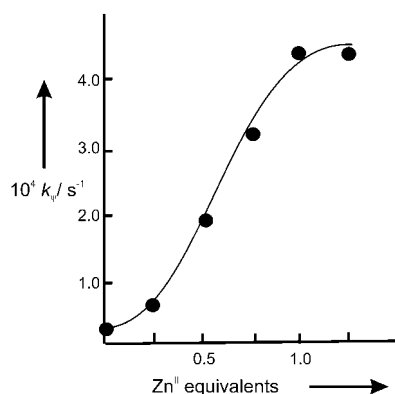


Figure 1. Dependence of the rate constant for the cleavage of HPNP by **2** on the amount of Zn^{II} ions. Conditions: 40 °C, pH 7.5 (5 mM *N*-(2-hydroxyethyl)-*N'*-(2-ethanesulphonyl)piperazine (HEPES) buffer), $[\text{1}] = 0.1 \text{ mM}$.^[17]

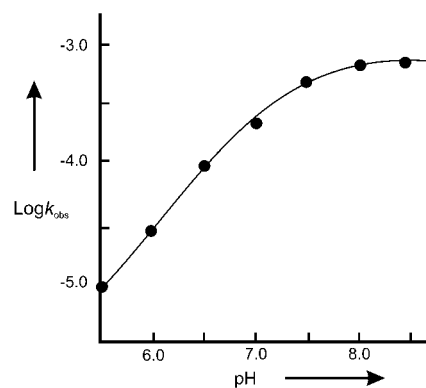


Figure 2. Dependence of the rate of cleavage of HPNP by 2-Zn^{II} as a function of pH value. Conditions: 40 °C, [buffer] = 5 mM, $[\text{1-Zn}^{\text{II}}] = 0.1 \text{ mM}$.

higher (see Table 1) than that determined under identical conditions for the mononuclear catalyst $\text{Zn}^{\text{II}}\text{-3}$, which corresponds to the “active unit” on the surface of MPC **2**.

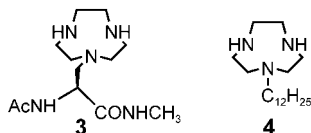


Table 1: Rate constants for the cleavage of HPNP by different Zn^{II} -based catalysts.

Catalyst	$k_{\text{cat}} [10^{-4} \text{ s}^{-1}]$	$k_2 [\text{M}^{-1} \text{ s}^{-1}]$	Relative rate ^[a]
$\text{Zn-3}^{\text{[b]}}$	—	0.007	1
$\text{Zn-2}^{\text{[b,c]}}$	42	4.4	629
$\text{Zn-4}^{\text{[b]}}$	—	0.028	4
Calix[4]arene- $2\text{Zn}^{\text{[d,e]}}$	7.7	43	3071
Calix[4]arene- $3\text{Zn}^{\text{[d,f]}}$	24	2.9	138

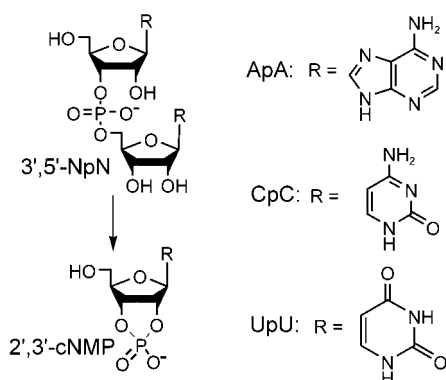
[a] Relative second-order rate constant normalized for the number of metal centers present in the catalyst; [b] At pH 7.4 and 40 °C; [c] The activity of MPC-C8 (if any) could not be tested because of the insolubility of these nanoparticles in the aqueous environment; [d] At pH 7.0, 25 °C, and 50% aqueous CH_3CN ; [e] Dinuclear Zn^{II} complex of 2,6-diaminomethylpyridine-functionalized calix[4]arene reported in ref. [25]; [f] Trinuclear Zn^{II} complex of 2,6-diaminomethylpyridine-functionalized calix[4]arene reported in ref. [25].

Micellar $\text{Zn}^{\text{II}}\text{-4}$ scores slightly better than $\text{Zn}^{\text{II}}\text{-3}$ but still the second-order rate constant determined for this catalytic system is approximately 160-fold lower than that of the nanoparticle-based catalyst. To study the origin of this impressive rate acceleration we have run kinetics at different pH values to assess the pK_{a} of the active nucleophile in the process (Figure 2). Available data from our^[22] as well as from other^[23] laboratories indicate that the close proximity of several metal centers induces the decrease of the pK_{a} of metal-ion-bound protic species with respect to monomeric complexes. The apparent pK_{a} value for the active nucleophilic

species is 7.4 which is 0.4 units lower than that reported^[24] for the Zn^{II} complex of triazacyclononane.

Thus part of the reactivity gain is due to a decrease of the pK_{a} value of the nucleophile. Allowing for this difference in pK_{a} value, catalyst $\text{Zn}^{\text{II}}\text{-2}$ is still 380 times more effective than $\text{Zn}^{\text{II}}\text{-3}$. Indeed the k_{cat} of $\text{Zn}^{\text{II}}\text{-2}$ is comparable to that of the best multinuclear Zn^{II} catalysts for HPNP cleavage reported so far (see Table 1).^[25] These systems are based on calyx[4]arene functionalized with two or three 2,6-diaminomethylpyridine units and are thus able to bind up to three Zn^{II} ions. They show a rate versus pH-value profile that goes through a maximum at approximately pH 7. This behavior indicates that cooperativity between the metal centers may be due to the occurrence of general-acid/general-base catalysis or nucleophilic catalysis and substrate binding.^[26] In our case, on the contrary, the plot indicates that the role of the metal ions is in stabilizing the complexed substrate towards the transition state where a further negative charge develops and in facilitating deprotonation of the nucleophilic species.^[22] Note that the efficiency of catalyst **2** was estimated on the basis of the total concentration of the active monomers, **1**, and not on that of the nanoparticles, in analogy to what is conventionally carried out with aggregation colloids. We do not know the number of Zn^{II} ions that actually take part in the catalytic process and that would define the catalytic site of the system (we estimate, on the basis of elemental analysis and particle size, the presence of about 45 thiol units **1** per nanoparticle). Accordingly, the reactivity reported is per single Zn^{II} complex and clearly underestimates the intrinsic reactivity of the active catalytic cluster. For comparison it is as if the reactivity of the calyx[4]arene systems were divided by two or three, that is, the number of metal centers present in the systems. In contrast with the nanoparticles, these latter systems are more efficient in the binding of the substrate because of the presence of the calyx[4]arene cavity.

With such an outstanding catalyst in hands we turned to more appealing substrates such as RNA dinucleotides (3',5'-NpN), namely ApA, CpC, and UpU. Their uncatalyzed cleavage is extremely slow with rate constants (at pH 7) ranging from $9.8 \times 10^{-9} \text{ s}^{-1}$ (UpU)^[27] to $1.7 \times 10^{-9} \text{ s}^{-1}$ (ApA),^[28] that is, about two orders of magnitude less reactive



than HPNP. The cleavage process was followed by HPLC monitoring the disappearance of the substrates and the formation of cyclic ribonucleoside monophosphate (2',3'-cNMP) and the corresponding nucleoside. As in the case of HPNP, the process is an intramolecular transesterification, in this case by the hydroxy group at the 2'-position of the ribose. At pH 7.5 (5 mM HEPES buffer) and 40 °C, Zn^{II}-2 cleaves ApA, CpC, and UpU with second-order rate constants of $3.0 \times 10^{-4} \text{ s}^{-1} \text{ M}^{-1}$ (ApA), $3.6 \times 10^{-4} \text{ s}^{-1} \text{ M}^{-1}$ (CpC), $1.2 \times 10^{-2} \text{ s}^{-1} \text{ M}^{-1}$ (UpU).^[29] Thus catalyst Zn^{II}-2 is fairly active in the cleavage of RNA dinucleotides. The activity of Zn^{II}-2 is, in this case too, subjected to inhibition by anions. We also observed relevant inhibition by the internal standard used for the HPLC analysis (sodium 3-nitrophenylsulphonate, see Supporting Information). The much higher activity observed with UpU may be related to a tighter binding of this substrate to the catalyst as suggested in the case of the above mentioned calyx[4]arene-based catalysts.^[30] However, for UpU, Zn^{II}-2 is less active than the best calyx[4]arene-based catalyst.^[31] Since UpU binding probably occurs by coordination to a Zn^{II} ion of the unprotonated amide of the base^[32] it is possible that the geometry of binding of the substrate to the nanocluster is less appropriate than that obtained with the calyx[4]arene-based systems. These are just speculations and a more detailed analysis of the system is necessary.

In conclusion, we have shown that the self-assembly of ligand-functionalized thiols on gold nanoclusters provides a straightforward entry to a Zn^{II}-based catalyst that is extremely effective in the cleavage of phosphate diesters, such as HPNP and 3',5'-NpN. In the case of HPNP, gold nanoclusters Zn^{II}-2, constitute one of the best Zn^{II}-based catalyst described to date. The facile synthesis of these systems and their outstanding catalytic properties induce us to call them "nanozymes" in analogy to the nomenclature of catalytic polymers (synzymes). Changing the nature of the functional units present on the gold-protecting monolayer may afford easy access to a variety of powerful, self-assembled catalysts (nanozymes) of which Zn^{II}-2 is just a prototype.^[33]

Experimental Section

1: 1,1-Dimethylethoxycarbonyl (Boc) diprotected ATANP methylamide^[34] (152 mg, 0.35 mmol; ATAMP = (S)-2-amino-3-[1-(1,4,7-tri-

azacyclononane]propionic acid) was treated with 8-acetylsulfanyloctanoic acid (91 mg, 0.36 mmol) under coupling conditions (BOP) in CH₂CH₂ to yield 97 mg of a oily product (43 %) after column chromatography (SiO₂, ethyl acetate:light petroleum 7:3). This material was treated with 33 % HBr in acetic acid (6 h, amine deprotection) and the precipitate obtained by addition of ethyl ether was treated with a solution of acetylchloride in methanol (24 h, thiol deprotection). The solid obtained was passed through an IRA-410 Amberlite resin (acetate) to give the diacetate salt of **1** in quantitative yield. ¹H NMR (250 MHz, D₂O): δ = 1.30 (bm), 1.55 (bm), 2.17–2.31 (m), 2.76–2.98 (m), 4.65 ppm (m). ESI-MS, *m/z*: [M+H]⁺, 387 [M⁺].

2: In a thermostated reactor kept at 28 °C MPC-C8 (26 mg), prepared according to Murray's procedure,^[12] was dissolved in CH₂CH₂ (15 mL). Compound **1** (13 mg) dissolved in methanol (15 mL) was added to the solution which was then stirred for five days. Removal of the solvent and triturating the waxy solid with water gave a dark solution that was passed through a Sephadex G-50 resin eluting with water. Liophilization of the appropriate fractions gave 19 mg of MPC **2** whose authenticity was ascertained by ¹H NMR (300 MHz, D₂O) and IR (KBr) spectroscopy (see Supporting Information).

Kinetics: For the cleavage of HPNP, kinetic experiments were recorded by monitoring the absorbance of released *p*-nitrophenol (317 nm) or *p*-nitrophenate (400 nm) against the pH value of the solution with a Perkin-Elmer Lambda 16 instrument equipped with a thermostated cell holder. Rate constants were determined by interpolation of the absorbance versus time data using MicroMath Scientist version 2.01 software whenever the kinetics were followed to completion. For kinetics in the presence of excess substrate the initial-rate method was used monitoring at least 20 % product formation. Reproducibility within ± 15 % was observed in repeated runs. For the cleavage of ApA, CpC, and UpU the reaction was followed by HPLC by withdrawing 10 µL of the reaction solution which was mixed with 40 µL of a 10 mM solution of ethylenediaminetetraacetic acid (EDTA). Reaction vessels were carefully sterilized before use at 130 °C for 1 h. Separation conditions: column Alltech LiChrospher RP-18 (150 mm × 4.6 mm); eluent gradient (0–20 % of B in A; A = H₂O 0.075 % trifluoroacetic acid (TFA); B = 1:1 CH₃CN/H₂O 0.075 % TFA). For a typical chromatogram see the Supporting Information.

Received: May 13, 2004

Keywords: enzyme models · homogeneous catalysis · nanoparticles · phosphates · zinc

- [1] F. M. Menger, *Angew. Chem.* **1991**, *103*, 1104–1118; *Angew. Chem. Int. Ed. Engl.* **1991**, *30*, 1086–1099.
- [2] M. Mammen, S.-K. Choi, G. M. Whitesides, *Angew. Chem.* **1998**, *110*, 2908–2953; *Angew. Chem. Int. Ed.* **1998**, *37*, 2754–2794.
- [3] P. Scrimin, P. Tecilla, U. Tonellato, C. A. Bunton, *Colloids Surf. A* **1998**, *144*, 71–79.
- [4] a) I. M. Klotz in *Enzyme Mechanisms* (Eds.: M. I. Page, A. Williams), Royal Society of Chemistry, London, **1987**, chap. 2; b) J. Suh, *Acc. Chem. Res.* **2003**, *36*, 562–570.
- [5] J. Liu, G. Wulff, *Angew. Chem.* **2004**, *116*, 1307–1311; *Angew. Chem. Int. Ed.* **2004**, *43*, 1287–1290.
- [6] J. E. Gestwicki, C. W. Cairo, L. E. Strong, K. A. Oetjen, L. L. Kiessling, *J. Am. Chem. Soc.* **2002**, *124*, 14922–14933.
- [7] a) R. Breinbauer, E. N. Jacobsen, *Angew. Chem.* **2000**, *112*, 3750–3753; *Angew. Chem. Int. Ed.* **2000**, *39*, 3604–3607; b) A. V. Kleij, R. A. Gossage, J. T. B. H. Jastrzebski, J. Boersa, G. van Koten, *Angew. Chem.* **2000**, *112*, 179–181; *Angew. Chem. Int. Ed.* **2000**, *39*, 176–178; c) C. Francavilla, M. D. Drake, F. V. Bright, M. R. Detty, *J. Am. Chem. Soc.* **2001**, *123*, 57–67; d) L. Ropartz, R. E. Morris, D. F. Foster, D. J. Cole-Hamilton, *Chem.*

- Commun.* **2001**, 361–362; e) Y. Ribourdouille, G. D. Engel, M. Richard-Plouet, L. H. Gade, *Chem. Commun.* **2003**, 1228–1229.
- [8] a) M.-C. Daniel, D. Astruc, *Chem. Rev.* **2004**, 104, 293–346; b) R. Shenhar, V. M. Rotello, *Acc. Chem. Res.* **2003**, 36, 549–561; c) A. C. Templeton, W. P. Wuelfing, R. W. Murray, *Acc. Chem. Res.* **2000**, 33, 27–36.
- [9] a) G. Fantuzzi, P. Pengo, R. Gomila, P. Ballester, C. A. Hunter, L. Pasquato, P. Scrimin, *Chem. Commun.* **2003**, 1004–1005; b) P. Pengo, Q. B. Broxterman, B. Kaptein, L. Pasquato, P. Scrimin, *Langmuir* **2003**, 19, 2521–2525.
- [10] a) N. Sträter, W. N. Lipscomb, T. Klabunde, B. Krebs, *Angew. Chem.* **1996**, 108, 2158–2191; *Angew. Chem. Int. Ed. Engl.* **1996**, 35, 2024–2055; b) D. E. Wilcox, *Chem. Rev.* **1996**, 96, 2435–2458.
- [11] M. Brust, M. Walker, D. Bethell, D. Schiffrin, R. Whyman, *J. Chem. Soc. Chem. Commun.* **1994**, 801–802.
- [12] M. J. Hostetler, J. E. Wingate, C.-J. Zhong, J. E. Harris, R. W. Vachet, M. R. Clark, J. D. Londono, S. J. Green, J. J. Stokes, G. D. Wignall, G. L. Glish, M. D. Porter, N. D. Evans, R. W. Murray, *Langmuir* **1998**, 14, 17–30.
- [13] M. J. Hostetler, S. J. Green, J. J. Stokes, R. W. Murray, *J. Am. Chem. Soc.* **1996**, 118, 4212–4213.
- [14] Heterogeneous, silica-supported catalysts for the hydrolysis of phosphates have been reported: B. R. Bodsgard, J. N. Burstyn, *Chem. Commun.* **2001**, 647–648.
- [15] R. M. Smith, A. E. Martell, *Critical Stability Constants*, Vol. 6, Plenum, New York, **1989**.
- [16] L. Bonfà, M. Gatos, F. Mancin, P. Tecilla, U. Tonellato, *Inorg. Chem.* **2003**, 42, 3943–3949.
- [17] It is convenient to report the concentration in terms of the active component, that is, **1**. This concentration was determined by spectrophotometric titration as mentioned in the text.
- [18] We do not know if a higher concentration of **1** on the surface of **2** would produce more active nanoparticles because the 1:1.2 ratio between 1-sulfanyloctane and **1** was the highest ratio we could obtain; furthermore the sorting of the components (that is, an uneven distribution of **1**), if it occurs, cannot be assessed.
- [19] a) H. Ait-Haddou, J. Sumaoka, S. L. Wiskur, J. F. Folmer-Andersen, E. V. Anslyn, *Angew. Chem.* **2002**, 114, 4185–4188; *Angew. Chem. Int. Ed.* **2002**, 41, 4014–4016; b) E. Kövəri, J. Heitker, R. Krämer, *J. Chem. Soc. Chem. Commun.* **1995**, 1205–1206.
- [20] Zn^{II} -**2** denotes nanoclusters **2** to which a stoichiometric amount of Zn^{II} has been added with respect to the concentration of **1** present in the monolayer.
- [21] Product inhibition was also observed at very high substrate loadings; nevertheless the turnover number (TON) is ≥ 100 for Zn^{II} -**2** and HPNP.
- [22] A. Scarso, F. Bodar-Houillon, P. Scrimin, unpublished results.
- [23] O. Iranzo, A. Y. Kovalevsky, J. R. Morrow, J. P. Richard, *J. Am. Chem. Soc.* **2003**, 125, 1988–1993.
- [24] P. Rossi, F. Felluga, P. Tecilla, F. Formaggio, M. Crisma, C. Toniolo, P. Scrimin, *J. Am. Chem. Soc.* **1999**, 121, 6948–6949.
- [25] P. Molenveld, W. M. G. Stikvoort, H. Kooijman, A. L. Spek, J. F. J. Engbersen, D. N. Reinhoudt, *J. Org. Chem.* **1999**, 64, 3896–3906.
- [26] K. Worm, F. Chu, K. Matsumoto, M. D. Best, V. Lynch, E. V. Anslyn, *Chem. Eur. J.* **2003**, 9, 741–747.
- [27] W. H. Chapman, Jr., R. Breslow, *J. Am. Chem. Soc.* **1995**, 117, 5462–5469.
- [28] M. Komiyama, K. Yoshinari, *J. Org. Chem.* **1997**, 62, 2155–2160.
- [29] These rates were obtained by extrapolating the experimental values to zero internal standard concentration.
- [30] P. Molenveld, J. F. J. Engbersen, D. N. Reinhoudt, *Angew. Chem.* **1999**, 111, 3387–3390; *Angew. Chem. Int. Ed.* **1999**, 38, 3189–3192.
- [31] The trinuclear Zn^{II} calix[4]arene-based catalyst gives $k_2 = 0.32 \text{ M}^{-1} \text{ s}^{-1}$ at 50 °C, pH 8, 35 % aqueous ethanol.
- [32] S. Aoki, Y. Honda, E. Kimura, *J. Am. Chem. Soc.* **1998**, 120, 10018–10026.
- [33] L. Pasquato, F. Rancan, P. Scrimin, F. Mancin, C. Frigeri, *Chem. Commun.* **2000**, 2253–2254.
- [34] a) A. Scarso, U. Scheffer, M. Göbel, Q. B. Broxterman, B. Kaptein, F. Formaggio, C. Toniolo, P. Scrimin, *Proc. Natl. Acad. Sci. USA* **2002**, 99, 5144–5149; b) P. Rossi, F. Felluga, P. Scrimin, *Tetrahedron Lett.* **1998**, 39, 7159–7162.

Nanostructures

A General Route to Macroscopic Hierarchical 3D Nanowire Networks**

Donghai Wang, Hongmei Luo, Rong Kou, Maria P. Gil, Shuaigang Xiao, Vladimir O. Golub, Zhenzhong Yang, C. Jeffrey Brinker, and Yunfeng Lu**

Nanoscale building blocks, such as equiaxial nanocrystals, one-dimensional nanotubes, wires, and rods, and 3D nano-

[*] D. Wang, H. Luo, R. Kou, M. P. Gil, Prof. Y. Lu
Department of Chemical and Biomolecular Engineering
Tulane University
New Orleans, LA 70118 (USA)
Fax: (+1) 504-865-6744
E-mail: ylu@tulane.edu

S. Xiao
Department of Chemical and Biological Engineering
University of Wisconsin
Madison, Wisconsin 53706 (USA)

Dr. V. O. Golub
Advanced Materials Research Institute
University of New Orleans
New Orleans, LA 70118 (USA)

Prof. Z. Yang
State Key Laboratory of Polymer Physics and
Chemistry Joint Laboratory of Polymer Science and Materials
Institute of Chemistry
Chinese Academy of Science
Beijing, 100080 (P. R. China)
Fax: (+86) 10-6255-9373
E-mail: yangzz@iccas.ac.cn

Prof. C. J. Brinker
Sandia National Laboratories and
The University of New Mexico
1001 University Blvd. SE
Albuquerque, NM 87106 (USA)

[**] The work was partially funded by NASA (Grants NAG-1-02070 and NCC-3-946), the Office of Naval Research, Louisiana Board of Regents (Grant LEQSF(2001-04)-RD-B-09), the National Science Foundation (Grant NSF-DMR-0124765 and CAREER Award), and the National Science Foundation of China (Grants 50325313 and 20128004). We thank Dr. Jibao He for help with TEM imaging measurements.



Supporting information for this article is available on the WWW under <http://www.angewandte.org> or from the author.

structures, such as nanomesh and superlattices, have been studied intensively not only because of their interesting intrinsic properties, which arise from low dimensionality and quantum effects, but also their capability for direct nano-system integration. To date, nanoscale building-block assemblies for applications such as nanocomputing and nanophotonics have been developed by using microfluidic,^[1] Langmuir–Blodgett,^[2] and other techniques.^[3] These 2D structures that are assembled through weak noncovalent interactions^[4,5] or external fields (e.g. shearing^[6] and electric fields^[3]) are unsuitable for devices that require intensive interwire communications (e.g. efficient charge transport), high surface areas, excellent accessibility, and mechanical robustness. Fabrication of 3D nanowire networks with controlled diameters and arrangements of the wire, tailored pore structures, and effective interwire connectivity is therefore paramount for new device applications. Current inverse opal networks^[7] are limited by the large diameters of the wire that may preclude quantum effects, and recent biomimetic approaches have also resulted in networks of large, randomly connected wires.^[8]

We report here a general synthetic route to stable, 3D continuous, hierarchically organized networks of metals or semiconductors that are composed of nanowire-like elements which uses a templated electrodeposition technique. Although reverse surfactant liquid-crystalline^[9] and 2D hexagonal mesoporous silica templates^[10] have been used to electrochemically deposit 2D nanowires, removal of the templates has resulted in aggregated nanowires with poor structural control. Here we have electrochemically replicated the bicontinuous surfactant liquid-crystalline (LC) phases to obtain a robust nanowire network. Figure 1 outlines the approach: first, a film of mesoporous silica is coated onto a conductive substrate through the co-assembly of the silicate and surfactant molecules followed by removal of the surfactant,^[11] then, the pore channels are filled with metals or semiconductors by electrodeposition, and lastly, the silica template is removed to create a replicated mesoporous nanowire network. Besides the excellent control over the composition, this approach enables precise structural tuning by replication of the complicated but well-studied silicate/surfactant LC mesophases. For example, the diameter of the nanowire can be tuned from 2 to 20 nm depending on the pore sizes of the template, and 3D networks of nanowires can be controlled by the 3D cubic mesostructure. Pore sizes of the

nanowire networks can be tuned from 1 to 4 nm depending on the thickness of the pore walls of the templates.^[12,13] Hierarchical pore structures can be readily obtained by the incorporation of colloidal silica porogens, which range in size from a few to several hundred nanometers, or by the incorporation of templates with various shapes, such as particles, rods, and plates, into the self-assembled surfactant/silicate mesophases followed by their removal.

The replication of ordered 3D crystalline nanowire networks can be analyzed by transmission electron microscopy (TEM) and X-ray diffraction (XRD) measurements. Figure 2, a–c show TEM images of cubic mesoporous templates, which were prepared by using Brij 58 surfactant (unit cell parameter of 8.4 nm), along the [111], [211], and [100] orientations. The diameter and wall thickness of the pores of the templates were estimated from nitrogen sorption, XRD, and TEM studies to have values of around 4–6 nm and 2–3 nm, respectively. Small angle XRD shows the presence of a (211) reflection, which corresponds to a d-spacing of 34.6 Å, for both the nanowire networks and the template and indicates good fidelity of the replication process. The broadening of the (211) reflection and the absence of the (210) reflection from the nanowire networks are due to a partial destruction of long-range mesostructural order upon removal of the template (see Supporting Information). Figure 2, d–f show TEM images of the replicated Pd (parts d and e) and Pt (part f) 3D nanowire networks. The average diameters of the nanowire (5 nm) and the pore (2–3 nm) agree well with the pore sizes (4–6 nm) and pore-wall thickness (2–3 nm), respectively, of the templates. The crystalline lattice of the Pt nanowire networks is clearly revealed in the high-resolution TEM (HRTEM) image (Figure 2g). The ring patterns from selected area electron diffraction (SAED) studies of the Pd and Pt nanowire networks (insets of Figure 2d and f, respectively) indicate that these nanowire networks possess randomly oriented *fcc* crystalline domains. The crystallite sizes estimated from XRD and TEM are ≈ 5 nm, which is similar to the pore size of the template.

Macroscopic connectedness of the networks was confirmed by field emission scanning electron microscopy (FESEM) studies as shown in Figure 3. The Pt nanowire network shows a continuous, homogeneous surface morphology (Figure 3a) with an ordered mesostructure (Figure 3b). Electronic continuity was demonstrated by cyclic voltammetry measurements performed upon an acidic aqueous solution

in which hydrogen adsorption–desorption occurred at the surface of the Pt nanowire (Figure 4a). The charge associated with hydrogen adsorption and oxidation is proportional to the active surface area of the Pt nanowire network. By this approach, an average active surface area of $27 \pm 2 \text{ m}^2 \text{ g}^{-1}$ was determined, which is comparable to that of mesoporous Pt.^[14] Three anodic hydrogen oxidation peaks were present at relative potentials of 0.03, –0.03, and –0.08 V (vs.

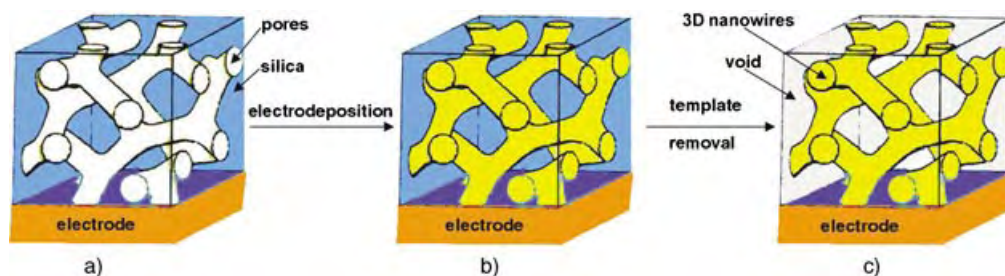


Figure 1. Schematic showing the formation of 3D continuous macroscopic metal or semiconductor nanowire networks by a templated electrodeposition technique. a) 3D cubic mesoporous template, b) 3D nanowire/silica nanocomposites, c) 3D nanowire network.

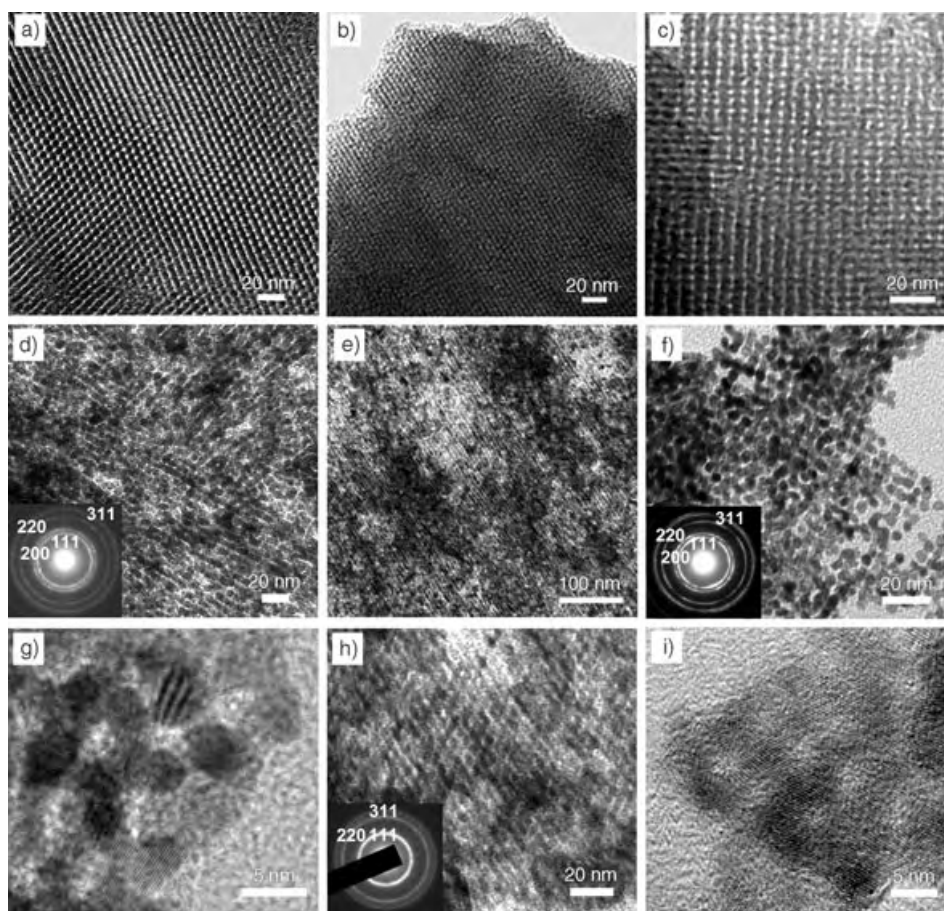


Figure 2. TEM images of the 3D cubic mesoporous silica templates prepared using Brij 58 surfactant, and the replicated metal or semiconductor nanowire networks. a), b), and c) TEM images of the cubic structured template along the [111], [211], and [100] directions, respectively. The pore-to-pore distances measured from the TEM images are ≈ 4.8 , 3.4, and 8.2 nm, respectively, and agree well with the results of XRD studies ($a = 8.4$ nm). d) and e) TEM images of the Pd nanowire network replicas along the [111] and [211] directions, respectively, which indicate the formation of a highly ordered Pd nanowire network; the inset in (d) shows a SAED pattern of the Pd nanowire network with a typical Pd *fcc* crystal structure. f) TEM image of a Pt nanowire network replica along the [100] direction; the inset in (f) shows the SAED pattern of the Pt nanowire network with a typical Pt *fcc* crystal structure. g) HRTEM image of a Pt nanowire network. h) TEM image of a [111]-oriented CdSe nanowire network; the inset of (h) shows the SAED pattern of a polycrystalline CdSe network with a randomly oriented crystalline structure. i) HRTEM image of a CdSe nanowire network showing crystalline lattice fringes.

SCE, saturated calomel electrode), which is consistent with the isotropic polycrystalline nature of the nanowire network. The cyclic voltammetry studies demonstrate catalytic activity, pore accessibility, and electrical continuity of the nanowire networks.

Device applications often require hierarchical pore structures that may provide higher surface areas and more-efficient mass transport. The strategy presented here has particular advantages in the preparation of such hierarchical nanowire networks because silica templates with hierarchical structures can easily be made through the surfactant-assembly process.^[15] For example, hierarchical templates used in this research were prepared by the introduction of colloidal silica spheres (20–100-nm diameters) into the surfactant/silicate thin-film assemblies, followed by calcination. Electrodeposition and template removal resulted in the hierarchical

nanowire networks shown in Figure 3, c–e. FESEM and TEM images (Figure 3, d and e, respectively) of the hierarchical Pt nanowire networks clearly indicate the formation of secondary pores (20–100 nm). Highly porous nanowire networks with spongelike (Figure 3 c) and grasslike (Figure 3 e) morphologies are clearly revealed. As the silica particles which are added may significantly affect the nucleation and growth of the silicate/surfactant assemblies, more-complicated structures were created by varying the size and shape of the silica additives.

Besides the precise structural control over relatively large distances, this method can be extended to synthesize nanowire networks with various chemical compositions such as other metals (e.g. Co), alloys (e.g. PtNi), and semiconductors (CdSe, CdS, and Bi₂Te₃). An example of CdSe nanowire networks is shown in Figure 2, h and i. The images suggest an ordered (Figure 2 h) and crystalline (Figure 2 i) replicated mesostructure in the semiconductor nanowire networks. The SAED pattern (Figure 2 h, inset) indicates a randomly oriented zinc blende crystalline structure. Crystalline CdSe networks composed of ≈ 11 -, 5-, and 3-nm diameter nanowires were synthesized by using cubic templates which offered the corresponding pore

diameters. The ability to control the nanowire diameter in turn allows continuously tuned optical absorption owing to quantum confinement. The first excitonic peaks in the absorption spectra of the CdSe nanowire network shift from $\lambda = 640$ to 470 nm upon decreasing the diameters of the nanowire from 11 to 3 nm (Figure 4 b). As the nanowires are arranged in a stable network through strong metallic or covalent bonds, as-synthesized networks are stable in organic solvents and remain unaffected after thermal treatments. Crystallized semiconductor nanowire networks with 3D interconnected hierarchical structures and tunable optical properties are great candidates for optical hosts, photovoltaics, and other applications.

Figure 4 c shows magnetization hysteresis loops measured at room temperature of a Co 3D nanowire network by using a field applied either parallel or perpendicular to the substrate.

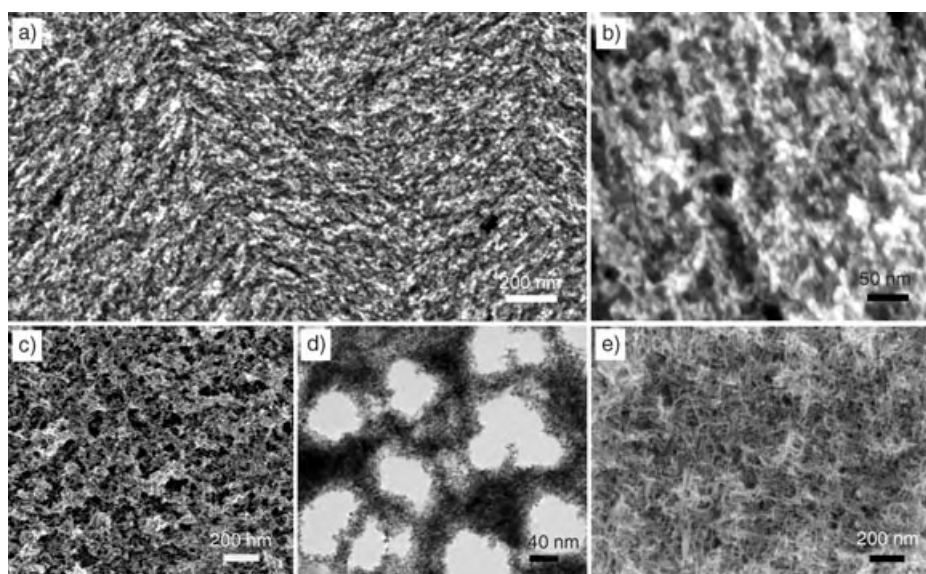


Figure 3. Top-view FESEM and TEM images of Pt nanowire networks of controlled macroscopic morphologies. a) and b) Low- and high-magnification FESEM images of 3D Pt nanowire networks, prepared by using the Brij 58-directed mesoporous silica template, which show homogeneous surface morphology and the ordered mesostructure, respectively. c) and d) FESEM and TEM images of a hierarchically porous Pt nanowire network cotedemplated by Brij 58-directed mesoporous silica and dense colloidal silica particles with an average diameter of 20–70 nm. e) FESEM image of a Pt nanowire sponge cotedemplated by P123-directed mesoporous silica and dense colloidal silica (70–100 nm). This sponge structure consists of intertwined 3D nanowires that form an interconnected hierarchical pore network.

The presence of the hysteresis loop in both directions indicates that the Co nanowire network is ferromagnetic at room temperature. A higher coercivity (255 Oe) than that of Co thin films (≈ 10 Oe)^[16] is observed. Furthermore, the 3D nanowire network, different from Co thin films or 2D wire arrays with uniaxial anisotropic magnetization,^[16,17] gives isotropic magnetism as indicated by its similar coercivity and remanent magnetization behaviors shown in the inset of Figure 4c. In comparison, diluted Co nanoparticles of 2–11-nm diameter and 2D Co nanoparticle superlattices show superparamagnetic behavior at room temperature.^[18,19] Such

superparamagnetic behavior is due to the randomized particle magnetic polarizations at a temperature higher than the blocking temperature.^[18] The unique continuous 3D nanowire network structure may enhance the dipolar interactions between magnetic domains or the intercoupling along nanowire chains, which may result in increased blocking temperatures and room temperature ferromagnetic behavior.^[20,21] A 3D Co nanowire network with a smaller diameter of the nanowire (3–4 nm) also shows ferromagnetic behavior at room temperature.^[22] Detailed studies are underway to understand fundamentally the magnetic behaviors. Nevertheless, such room temperature ferromagnetic nanowire networks with small nanowire dimensions and enhanced coercivities show potential for high-density information storage applications.

In conclusion, we have developed a rapid and effective

approach to fabricate stable macroscopic nanowire networks with controllable composition, tunable hierarchical structure, and unique properties. The dimensions of the nanowire and the network structure are tunable by the precise replication of the self-assembled silica/surfactant liquid-crystalline structure. Hierarchical pore morphology can be obtained by using secondary silica porogens that have desired shapes and sizes. This versatile approach is applicable to a variety of materials such as polymers, metals, and semiconductors. Robust 3D nanowire networks fabricated with this low-cost templated electrodeposition technique are of great interest for photo-

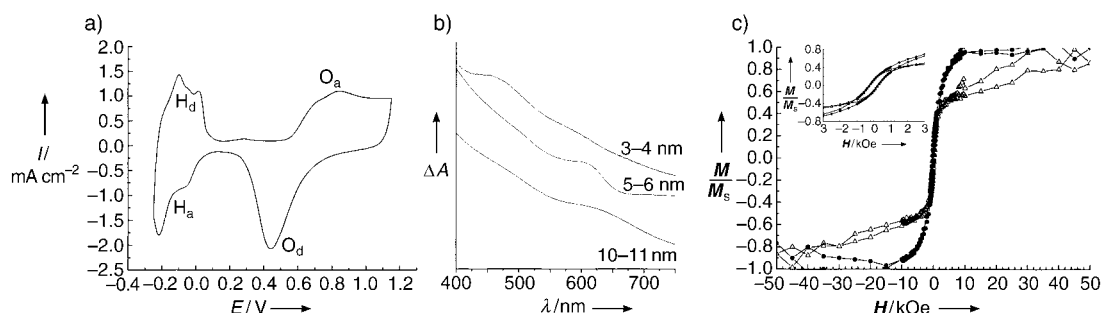


Figure 4. a) Cyclic voltammogram of 3D Pt nanowire networks in sulfuric acid (0.5 M). H_a: hydrogen adsorption, H_d: hydrogen desorption, O_a: adsorption of oxygen, O_d: reduction of oxygen layer. b) UV/Vis spectra of CdSe nanowire networks with various nanowire diameters, which were controlled by the pore diameters of the mesoporous silica templates. Surfactants F127, Brij 58, and CTAB were used to prepare cubic mesoporous templates with pore diameters of 10–11, 5–6, and 3–4 nm, respectively. c) Room temperature magnetization hysteresis loops of 3D Co nanowire networks with a wire diameter of 5–6 nm in an applied field which is either parallel (Δ) or perpendicular (●) to the substrate. Each curve was normalized to full saturation. The inset shows a hysteresis loop curve indicating near-equal coercivity and remanent magnetization of the Co nanowire network.

voltaic and thermoelectric devices, fuel cells, hydrogen separation membranes, sensors, high-density information storage media, and other device applications.

Experimental Section

Mesoporous silica films were spin- or dip-coated onto conductive glass substrates (ITO (indium tin oxide) or F-doped SnO₂) by using surfactant/silicate sols that were prepared by mixing tetraethoxysilane (TEOS), H₂O, surfactant, HCl, and ethanol in a molar ratio of 1:5:0.02–0.05:0.028:22 at room temperature for 2 h. As-deposited films were calcined in air at 400 °C for 1 h to remove the surfactants and to create mesoporous networks. The nonionic surfactant, Brij 58 (C₁₆H₃₃(OCH₂CH₂)₂₀OH), was used as the pore-structure directing agent to synthesize 3D mesoporous templates with pore diameters of 5 nm. Triblock copolymer Pluronic F127 (EO₁₀₆PO₇₀EO₁₀₆; EO = ethylene oxide, PO = propylene oxide), P123 (EO₂₀PO₇₀EO₂₀), and cationic surfactant cetyltrimethylammonium bromide (CTAB) were used to synthesize 3D mesoporous templates with different pore diameters. Commercial solutions (adjusted to pH 1) of dense silica particles with controllable diameters of 20–100 nm were added to the precursor sols to synthesize templates with hierarchical pore structures.

Electrodeposition was conducted in aqueous precursor solutions by using a galvanostatic or potentiostatic electroplating circuit in a conventional three-electrode cell. Electrodeposition of Pd was carried out with a periodic galvanostatic pulse current (0.5 mA cm⁻² for 100 ms and 1 s at 0 mA cm⁻²) by using an aqueous solution of PdCl₂–HCl (0.5 wt. %). Pt deposition was conducted under similar conditions by using a 2-wt. % H₂PtCl₆ precursor solution. Deposition of Co was conducted at –1.2 V vs. SCE by using aqueous solutions containing methanol (20 vol. %), CoSO₄ (1.3 M), and H₃BO₃ (0.7 M). Typical CdSe deposition was conducted at 85 °C at –0.65 V vs. SCE by using a deposition solution (pH 2.5) that contained CdSO₄ (0.2 M) and SeO₂ (1.0 mM).^[23] The electrodeposited films of the metal nanowire networks were annealed at 400 °C in forming gas (N₂ with 10 % H₂) for 30 min. The silica templates were removed with HF (1 %) or NaOH solution (2 M) at 80 °C, and the networks were rinsed with distilled water. Nanowire networks were characterized by XRD, TEM, SEM, UV/Vis, cyclic voltammetry, and SQUID techniques (see Supporting Information).

Received: May 1, 2004

Revised: July 27, 2004

Keywords: electrochemistry · magnetic properties · mesoporous materials · nanostructures · template synthesis

- [10] D. Wang, W. L. Zhou, B. F. McCaughy, J. E. Hampsey, X. Ji, Y.-B. Jiang, H. Xu, J. Tang, R. H. Schmehl, C. O'Connor, C. J. Brinker, Y. Lu, *Adv. Mater.* **2003**, *15*, 130.
- [11] Y. Lu, R. Ganguli, C. A. Drewien, M. T. Anderson, C. J. Brinker, W. Gong, Y. Guo, H. Soye, B. Dunn, M. H. Huang, J. I. Zink, *Nature* **1997**, *389*, 364.
- [12] M. Choi, R. Ryoo, *Nat. Mater.* **2003**, *2*, 473.
- [13] S. H. Joo, S. J. Choi, I. Oh, J. Kwak, Z. Liu, O. Terasaki, R. Ryoo, *Nature* **2001**, *412*, 169.
- [14] G. S. Attard, P. N. Bartlett, N. R. B. Coleman, J. M. Elliott, J. R. Owen, J. H. Wang, *Science* **1997**, *278*, 838.
- [15] J. Lee, J. Kim, T. Hyeon, *Chem. Commun.* **2003**, 1138.
- [16] T. Thurn-Albrecht, J. Schotter, G. A. Kastle, N. Emley, T. Shibauchi, L. Krusin-Elbaum, K. Guarini, C. T. Black, M. T. Tuominen, T. P. Russell, *Science* **2000**, *290*, 2126.
- [17] T. M. Whitney, J. S. Jiang, P. C. Searson, C. L. Chien, *Science* **1993**, *261*, 1316.
- [18] S. Sun, C. B. Murray, *J. Appl. Phys.* **1999**, *85*, 4325.
- [19] C. T. Black, C. B. Murray, R. L. Sandstrom, S. Sun, *Science* **2000**, *290*, 1131.
- [20] J. Garcia-Otero, M. Porto, J. Rivas, A. Bunde, *Phys. Rev. Lett.* **2000**, *84*, 167.
- [21] A. F. Gross, M. R. Diehl, K. C. Beverly, E. K. Richman, S. H. Tolbert, *J. Phys. Chem. B* **2003**, *107*, 5475.
- [22] H. Luo, D. Wang, V. O. Golub, J. He, Y. Lu, **2004**, unpublished results.
- [23] L. Beaunier, H. Cachet, R. Cortes, M. Froment, A. Etcheberry, *Thin Solid Films* **2001**, *387*, 108.

- [1] B. Messer, J. H. Song, P. Yang, *J. Am. Chem. Soc.* **2000**, *122*, 10232.
- [2] P. Yang, *Nature* **2003**, *425*, 243.
- [3] X. Duan, Y. Huang, Y. Cui, J. Wang, C. M. Lieber, *Nature* **2001**, *409*, 66.
- [4] F. X. Redl, K. S. Cho, C. B. Murray, S. O'Brien, *Nature* **2003**, *424*, 968.
- [5] S. Sun, C. B. Murray, D. Weller, L. Folks, A. Moser, *Science* **2000**, *287*, 1989.
- [6] Y. Huang, X. Duan, Q. Wei, C. M. Lieber, *Science* **2001**, *291*, 630.
- [7] O. D. Velev, P. M. Tessier, A. M. Lenhoff, E. W. Kaler, *Nature* **1999**, *401*, 548.
- [8] D. Walsh, L. Arcelli, T. Ikoma, J. Tanaka, S. Mann, *Nat. Mater.* **2003**, *2*, 386.
- [9] L. Huang, H. Wang, Z. Wang, A. Mitra, K. N. Bozhilov, Y. Yan, *Adv. Mater.* **2002**, *14*, 61.

Catalysis Methods

A Catalytic Langmuir Film as a Model for Heterogeneous and Homogeneous Catalytic Processes**

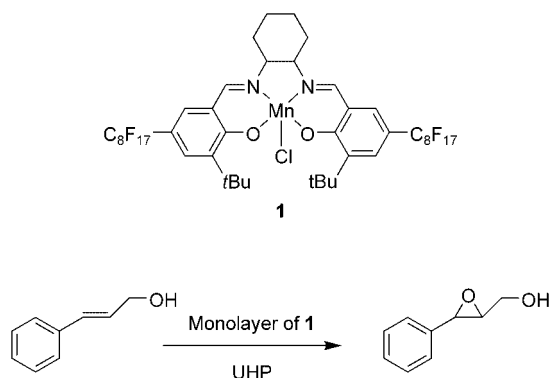
Andrea Pasc-Banu, Claudia Sugisaki, Thierry Gharsa, Jean-Daniel Marty, Ignacio Gascon, Gianluca Pozzi, Silvio Quici, Isabelle Rico-Lattes, and Christophe Mingotaud*

The design and optimization of new catalytic systems continue to inspire a tremendous amount of work due to the importance of catalysis in many scientific fields and especially in industry. In particular, development of recoverable catalysts,^[1] for example, by immobilization of a homogeneous catalyst on a solid surface^[2] or by means of surface organometallic chemistry,^[3] offers interesting perspectives. Pseudohomogeneous systems such as dendritic catalysts have also been recently developed.^[4] They exhibit many of the advantages of homogeneous catalysts, but also some of the benefits of heterogeneous catalysts (e.g., easy recovery after the reaction). Their well-controlled synthesis allows one to tune their chemical properties by adjusting their core and peripheral structure. In several cases, the dendrimer generation also has a strong influence on the reaction catalyzed by the dendrimer.^[5,6] This is supposedly related to an increased density of external groups or to lesser accessibility to reactants.

Regardless of the type of catalytic system, it is difficult to perfectly control or characterize the density and orientation of the catalytic centers, as well as the accessibility of these centers to reactants. Yet the influence of these structural parameters on the catalytic properties is paramount. Therefore, there is a clear lack of a chemical system in which the orientation and density of the catalytic sites can be easily modified, so that the effect of those parameters on catalysis efficiency can be measured. We propose using the gas/water interface as a model for such catalytic processes. Indeed, the

organization and molecular density in a monolayer at this interface are readily adjustable through compression of the layer and choice of amphiphilic compound. Chemical reactions (e.g., hydrolysis, polymerization) have indeed been performed in Langmuir films,^[7–10] but in all cases the surfactants forming the monolayer were themselves the reactants. Langmuir films have also been used to organize molecular catalysts on a solid substrate to generate well-defined supported catalytic systems.^[11–13] However, to our knowledge, no attempt has been made heretofore to form monolayers at the gas/water interface in which the Langmuir film is the catalyst.

We chose to study olefin epoxidation as a model reaction considering the scientific and industrial importance of this class of reaction. For this purpose, we selected a salen complex **1** bearing two fluorinated chains (Scheme 1) as a



Scheme 1. Salen complex **1** and the chemical reaction studied in this work.

potential catalyst. Metal salen complexes are chemically robust, and their catalytic activity in epoxidation reactions is well documented for various substrates in many solvents.^[14] Furthermore, fluorinated tails are well known for their ability to facilitate the formation of stable Langmuir films.^[15] Finally, compound **1** is an efficient catalyst for the epoxidation of alkenes in bulk solution.^[16] To assess the catalytic properties of a Langmuir film of **1** in such a reaction (Scheme 1), we chose as reactants a vinylic compound which is slightly soluble in water, namely, cinnamyl alcohol, and the urea/hydrogen peroxide complex (UHP) as an oxygen source for the oxidation, because of its stability and ease of handling.^[17]

When spread at the gas/water interface, salen complex **1** formed stable monolayers up to its collapse at about 24 mN m⁻¹ (Figure 1 and Table 1). Before the onset of the surface pressure (at about 183 Å² molecule⁻¹), Brewster-angle microscopy (BAM) demonstrated that the monolayer is in a biphasic state (inset of Figure 1) in which gaseous domains are in equilibrium with liquid domains. After the onset, the monolayer appeared quite homogeneous. The molecular area at collapse was around 115 Å², which is comparable to the average area of a salen complex with a conformation in which the average MnN₂O₂ plane is more or less perpendicular to the surface.^[18] The monolayer of **1** was also transferred onto a calcium fluoride substrate in order to check its chemical

[*] Dr. A. Pasc-Banu, Dr. C. Sugisaki, T. Gharsa, Dr. J.-D. Marty, Dr. I. Gascon, Dr. I. Rico-Lattes, Dr. C. Mingotaud
Laboratoire des Interactions Moléculaires et Réactivités Chimique et Photochimique
CNRS UMR 5623, Université Paul Sabatier
118 route de Narbonne, 31062 Toulouse Cedex 4 (France)
Fax: (+33) 5-6155-8155
E-mail: cmingo@chimie.ups-tlse.fr
Dr. G. Pozzi, Dr. S. Quici
CNR-Istituto di Scienze e Tecnologie Molecolari
c/o Dipartimento di Chimica Organica e Industriale
Università degli Studi di Milano
via Camillo Golgi, 19, 20133 Milano (Italy)

[**] The authors acknowledge the financial support of the CNRS, the French Ministry for Research and Technology (ACI Nanosciences and postdoctoral fellowships), the European Commission (HPRN CT 2000-00002, "Development of fluorine phase technology for oxidation processes") and the Ministerio de Educacion y Ciencia of Spain for a postdoctoral fellowship. They also thank Prof. A. Lattes for useful discussions.

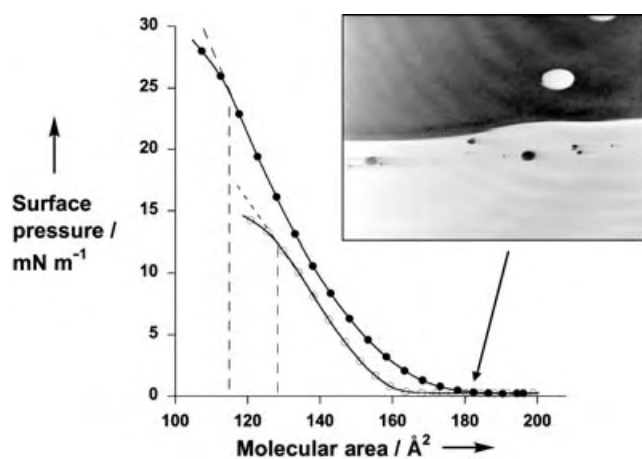


Figure 1. Compression isotherm of **1** at room temperature on pure water (●) and on a solution of UHP ($5 \times 10^{-5} \text{ mol L}^{-1}$) and cinnamyl alcohol ($10^{-5} \text{ mol L}^{-1}$) (○). Inset: Typical morphology of the film observed by BAM at low surface pressure (dark domains: gaseous phase; light domains: liquid phase; real size: $430 \times 536 \mu\text{m}^2$).

Table 1: Analysis of the compression isotherms of **1** on various subphases at 20°C .

Subphase solution	Surface pressure onset [\AA^2]	Collapse area [\AA^2]	Collapse surface pressure [mN m^{-1}]
pure water	183	115	24.4
cinnamyl alcohol ^[a]	189	119	22.5
UHP solution ^[b]	165	123	15.7
UHP and cinnamyl alcohol ^[c]	163	129	12.3

[a] Concentration: $10^{-5} \text{ mol L}^{-1}$. [b] Concentration: $5 \times 10^{-5} \text{ mol L}^{-1}$. [c] Concentrations: $5 \times 10^{-5} \text{ mol L}^{-1}$ and $10^{-5} \text{ mol L}^{-1}$, respectively.

stability at the gas/water interface: the equivalence of the IR spectra of **1** in a KBr pellet and in the LB film proved the chemical integrity of the catalyst at the interface.

When cinnamyl alcohol was added to the subphase in a concentration of $10^{-5} \text{ mol L}^{-1}$ (molar ratio catalyst/alkene close to 1/50), the isotherm was slightly shifted towards larger areas per molecule (Table 1). This may be related to some interaction or adsorption of cinnamyl alcohol molecules at the interface due to their partial lipophilic character. The effect of UHP ($5 \times 10^{-5} \text{ mol L}^{-1}$) was clearly stronger: the collapse pressure decreased to about 16 mN m^{-1} , and the monolayer was more dense at a given surface pressure. These changes suggest strong interactions between salen **1** and the oxidant and could be an indication of the formation of oxidized forms of **1**. Adding cinnamyl alcohol to this UHP solution did not induce any further important modification of the isotherm (Table 1).

When a solution of cinnamyl alcohol and UHP (10^{-5} and $5 \times 10^{-5} \text{ mol L}^{-1}$, respectively) was kept for 18 h in the Langmuir trough without any monolayer spread at its interface, no oxidation of the cinnamyl alcohol could be detected by GC after extraction of the subphase with dichloromethane (see Experimental Section). To assess the effect of a mono-

layer of **1**, a shorter reaction time was used (typically 6 h) to limit any (undetected) bulk oxidation. After spreading and compression of the monolayer (if necessary), GC analysis demonstrated that some epoxide of the cinnamyl alcohol had formed in the subphase. The area of the epoxide peak (a few tenths of a per cent to a few per cent of the peak for unconverted cinnamyl alcohol) varied with compression of the monolayer (see below) and the reaction time. Preliminary experiments suggested a linear dependence of this peak area on time in the range 6–24 h. Thus, this oxidation was not an artefact due to the extraction/analysis process but was directly related to the Langmuir film.

Consequently, it can be stated that the monolayer of **1** plays the role of a catalytic surface for the epoxidation of cinnamyl alcohol dissolved in the subphase. Direct comparison of the kinetics in this system (without stirring) and in bulk solution is clearly difficult. Therefore, we concentrated on the relative effect of the compression of the Langmuir film on the reaction by measuring the area of the epoxide peak relative to the alkene peak (%A) in the GC chromatogram for different molecular areas of the catalyst at the interface. When the monolayer was compressed, the Langmuir film did not cover the whole surface of the subphase (which was, however, entirely recovered for the GC analysis). To take this experimental limitation into account, we assumed that the quantity of formed epoxide is proportional to the surface area S of the catalytic monolayer, and therefore we defined an apparent rate of reaction ρ [Eq. (1)], where τ is the reaction time. Figure 2 shows the experimental variation of the apparent rate with the molecular area of **1** in the monolayer.

$$\rho = \%A (S\tau)^{-1} \quad (1)$$

For low surface pressures and large molecular areas (greater than ca. $155\text{--}160 \text{ \AA}^2$), the apparent rate increased slowly with compression of the film. For such low surface pressures, the monolayer was in a biphasic state. Compression of the Langmuir film leads only to changes in the proportions

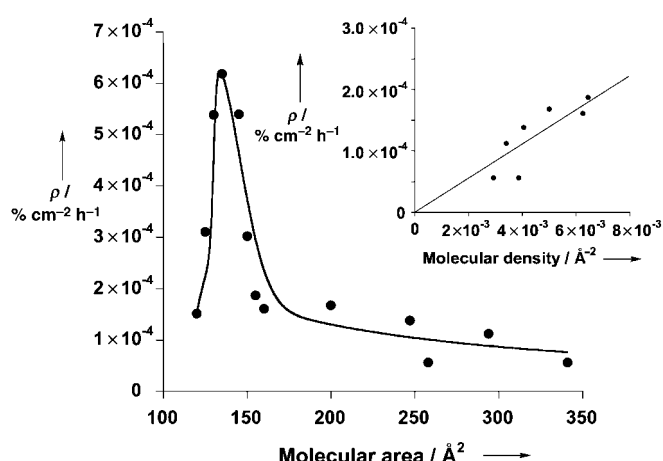


Figure 2. Apparent rate ρ of the catalyzed reaction (see text) versus the molecular area of catalyst **1** spread at the gas/water interface (the line is a guide to the eye). The inset plots ρ versus the molecular density for molecular areas larger than 155 \AA^2 (linear fit).

of the liquid phase and the gaseous phase, but should not modify the organization within the liquid domains. Thus, the small increase in reactivity can not be ascribed to a change in the molecular orientation in the Langmuir film, but should be simply related to the variation of the average molecular density. Because the epoxidation of cinnamyl alcohol should be roughly first order in catalyst concentration, as was demonstrated in the bulk for indene,^[19] we can assume that the reaction along the monolayer is also first-order in the average catalyst surface density. Therefore, the apparent rate of reaction should be proportional to the surface molecular density of **1**. Experimentally, this rate is indeed found to be reasonably proportional to the surface molecular density (i.e., the reciprocal molecular area) of **1** at the interface (inset in Figure 2).

When the monolayer was in a monophasic state (i.e., for molecular areas below ca. 160 Å²), the apparent rate deviated strongly from the previous simple law, and the formation of epoxide was clearly enhanced. Contrary to the previous case, such a change can not be only related to the increase in the molecular density. Even if a definitive explanation of this higher catalytic activity can not be given at this stage of the study, one can propose a simple hypothesis. The increase in molecular density when the monolayer is compressed in its liquid phase can be achieved only by a reorientation of various chemical groups of **1**. In particular, the manganese salen complex should be less and less tilted versus the normal to the interface with increasing compression. Therefore, the access (ease and main relative orientation) of hydrogen peroxide or cinnamyl alcohol to the manganese center should depend on the mean molecular area of **1**. This effect alone may explain the observed change in the catalytic activity.^[20]

For molecular areas below about 135 Å², the apparent rate ρ of the reaction was strongly decreased. Again, this may be due to changes in the orientation of the catalytic center. However, most probably, this is simply related to the slow collapse of the monolayer. Indeed, the collapse area at constant compression rate was found to be around 129 Å² molecule⁻¹ (Table 1). Given that this value depends on the exact compression mode and that the collapse process is not abrupt (Figure 1), the observed change in reaction rate was more or less simultaneous with collapse of the monolayer. Such a process, which should lead to multilayer formation, decreases the number of catalyst molecules in close contact with the subphase, and this explains the experimental drop in catalytic activity.

These results demonstrate that the monolayer of **1** catalyzes the epoxidation of cinnamyl alcohol dissolved in the subphase with a rate strongly related to the molecular density and organization within the Langmuir film. For this particular catalyst/substrate pair, the highest efficiency is obtained for an average molecular area of about 140–145 Å². Further experiments will try to determine the molecular orientation within the monolayer and relate this to the molecular structure of the catalyst and the apparent rate of reaction. Finally, similar experiments will be performed with chiral salen complexes to check whether the architecture of the Langmuir film has any effect on the stereoselectivity of the epoxidation.

More generally, the present study proves that a soft and controllable interface like a Langmuir film is a powerful model of reactive surfaces and may help understand the reactivity in various heterogeneous and homogeneous catalytic systems.

Experimental Section

Amphiphilic complex **1** was prepared by metalation of the corresponding racemic salen ligand derived from *trans*-1,2-diaminocyclohexane by following a procedure previously described for the chiral analogue.^[16] The crude compound was recrystallized from EtOH to give a brownish solid in 85 % yield. UV/Vis (10⁻⁵ mol L⁻¹, CH₃OH): λ_{max} (lg ϵ) = 235 (4.72), 405 nm (3.71). Elemental analysis (%) calcd for C₄₄H₃₄ClF₃₄MnN₂O₂ (1359.1): C 38.88, H 2.52, N 2.06; found: C 39.02, H 2.44, N 2.36.

All other compounds were obtained from Aldrich and used without further purification. The water of the subphase, purified by a Purite Select apparatus, had a resistivity higher than 16 M Ω cm. Chloroform (HPLC-grade from SDS) was the spreading solvent, and the solutions of the amphiphilic complex were kept at -18 °C between experiments to limit solvent evaporation.

Isotherms were obtained with a NIMA trough (type 601BAM) equipped with a Wilhelmy plate and maintained at 20 °C. The compression rate of the monolayer was close to 3 Å² molecule⁻¹ min⁻¹. A BAM2plus from NFT was used for the Brewster-angle microscopy experiments.

The reactions were performed on a laboratory-made Langmuir–Blodgett trough (maximum available surface area ca. 1100 cm², volume of the subphase ca. 340 ± 40 mL including a ca. 30 mL dipping well) working at room temperature and under partial nitrogen atmosphere.^[21] For the catalysis experiments, the subphase was an aqueous solution containing 5 × 10⁻⁵ mol L⁻¹ of UHP and 10⁻⁵ mol L⁻¹ of cinnamyl alcohol. Shortly after spreading, the monolayer was compressed (if necessary) at a rate of ca. 35 Å² molecule⁻¹ min⁻¹, and the area per molecule was kept constant during the experiment. After 6 h, the whole subphase was recovered and extracted with ca. 20 mL of HPLC-grade dichloromethane. The solvent of the organic solution was evaporated under reduced pressure, and the residue was kept at -18 °C until GC analysis.

Built-up films were obtained by the vertical lifting method with a dipping speed set to 1 cm min⁻¹. Films (19 layers) were transferred from the gas/pure water interface onto optically polished calcium fluoride substrate (Y-type transfer with a transfer ratio of ca. 0.7 for a transfer pressure of 10 mN m⁻¹).

GC analysis was performed with a Varian Chrompack (CP-3800) apparatus equipped with an SGE nonpolar capillary column (BPX5 30 m × 0.25 mm) (injector temperature: 250 °C; splitless injection mode; carrier gas: helium at 1 mL min⁻¹; initial oven temperature: 30 °C, 2 min; rate 1: 15 °C min⁻¹; final temperature 1: 150 °C, 15 min; rate 2: 20 °C min⁻¹; final temperature 2: 250 °C, 2 min; detector temperature: 300 °C). The retention times were found to be ca. 12.5 min for the cinnamyl alcohol, and 13.6 min for the corresponding epoxide.

Infrared spectra were recorded on a Perkin Elmer FT 1760-X spectrometer. For spectra of the pristine powder of **1**, KBr pellets (containing ca 0.5 wt % of **1**) were used.

Received: June 18, 2004

Keywords: epoxidation · heterogeneous catalysis · manganese · monolayers · N,O ligands

- [1] "Recoverable Catalysts and Reagents": *Chem. Rev.* **2002**, *102*, 3215–3892 (special issue).
- [2] J. M. Thomas, R. G. Bell, C. R. Catlow in *Handbook of Heterogeneous Catalysis, Vol. 1* (Eds.: G. Ertl, H. Knözinger, J. Weitkamp), Wiley-VCH, Weinheim, **1997**, p. 286.
- [3] C. Copéret, M. Chabanas, R. P. Saint-Arroman, J.-M. Basset, *Angew. Chem.* **2003**, *115*, 164; *Angew. Chem. Int. Ed.* **2003**, *42*, 156.
- [4] G. E. Oosterom, J. N. H. Reek, P. C. J. Kamer, P. W. N. M. van Leeuwen, *Angew. Chem.* **2001**, *113*, 1878; *Angew. Chem. Int. Ed.* **2001**, *40*, 1828.
- [5] C. Bolm, N. Derrien, A. Seger, *Chem. Commun.* **1999**, 2087.
- [6] A. Schmitzer, S. Francheschi, E. Perez, I. Rico-Lattes, A. Lattes, L. Thion, M. Erard, C. Vidal, *J. Am. Chem. Soc.* **2001**, *123*, 5956.
- [7] G. L. Gaines, Jr., *Insoluble Monolayers at Liquid-Gas Interfaces*, Interscience, New York, **1966**.
- [8] L. J. Kleppner, J. H. Batten, R. S. Duran, *Macromolecules* **2000**, *33*, 8006.
- [9] M. Bardosova, P. Hodge, H. Matsuda, F. Nakanishi, R. H. Tredgold, *Langmuir* **1999**, *15*, 631.
- [10] M.-H. Ropers, G. Brezesinski, H. Möhwald, *Stud. Interface Sci.* **2002**, *16*, 207.
- [11] I. O. Benitez, B. Bujoli, L. J. Camus, C. M. Lee, F. Odobel, D. R. Talham, *J. Am. Chem. Soc.* **2002**, *124*, 4363.
- [12] K. Töllner, R. Popovitz-Biro, M. Lahav, D. Milstein, *Science* **1997**, *278*, 2100.
- [13] D. Abatti, M. E. D. Zaniquelli, Y. Iamamoto, Y. M. Idemori, *Thin Solid Films* **1997**, *310*, 296.
- [14] Y. N. Ito, T. Katsuki, *Bull. Chem. Soc. Jpn.* **1999**, *72*, 603.
- [15] A.-F. Mingotaud, C. Mingotaud, L. K. Patterson, *Handbook of Monolayers*, Academic Press, **1993**.
- [16] M. Cavazzini, A. Manfredi, F. Montanari, S. Quici, G. Pozzi, *Eur. J. Org. Chem.* **2001**, 4639.
- [17] R. I. Kureshy, N.-u. H. Khan, S. H. Abdi, S. T. Patel, R. V. Jasra, *Tetrahedron: Asymmetry* **2001**, *12*, 433.
- [18] T. Fujii, K. Miyamura, *Bull. Chem. Soc. Jpn.* **2000**, *73*, 365.
- [19] D. L. Hughes, G. B. Smith, J. Liu, G. C. Dezeny, C. H. Senanayake, R. D. Larsen, T. R. Verhoeven, P. J. Reider, *J. Org. Chem.* **1997**, *62*, 2222.
- [20] H. Jacobsen, L. Cavallo, *Chem. Eur. J.* **2001**, *7*, 800.
- [21] M. Clemente-Leon, B. Agricole, C. Mingotaud, C. J. Gomez-Garcia, E. Coronado, P. Delhaes, *Langmuir* **1997**, *13*, 2340.

Catalytic Asymmetric Mercuriocyclization of γ -Hydroxy-*cis*-Alkenes**

Sung Ho Kang,* Mihyong Kim, and Suk Youn Kang

Conversion of prochiral olefinic double bonds into the corresponding chiral functional groups is one of the most influential fields of study in modern synthetic organic chemistry, which has been realized preeminently through asymmetric epoxidation,^[1] dihydroxylation,^[2] aminohydroxylation,^[3] hydrogenation,^[4] and hydroboration.^[5] Another versatile process can be evolved from electrophile-promoted additions.^[6] Whereas few studies into intermolecular asymmetric additions have been carried out, the intramolecular version has been explored to some extent. The latter asymmetric cyclizations have been achieved by substrate-controlled means, but rarely through reagent-controlled methods. Although the reagent-controlled approach has been recognized as more challenging and beneficial, progress has lagged behind owing to lack of lucid strategic clues. Examples include organoselenylation with chiral selenium reagents,^[7] iodocyclization with iodonium ion/dihydroquinine complexes,^[8] iodocyclization with Co^{II}–salen complexes,^[9] and mercuriocyclization with Hg^{II}–bisoxazoline complexes.^[10] Most of the aforementioned methods have some limitations such as poor enantioselectivity, multistep synthesis of the involved reagent, and excessive use of the expensive reagent. Since our reported intramolecular mercurioetherification also requires 1.2 equivalents of chiral Hg^{II} complexes, even though the reaction itself is highly enantioselective,^[10] development of the corresponding catalytic version would no doubt have a significant impact. Herein we describe asymmetric mercuriocyclization by using catalytic amounts of chiral bisoxazoline to prepare highly enantiopure 2-substituted tetrahydrofurans.

To develop a catalytic version of asymmetric mercuriocyclization, we proposed the use of catalytic amounts of a chiral bisoxazoline together with excess amounts of readily available achiral ligand, which can hold all the existing Hg^{II} ions tightly enough to transfer preferentially not to the olefinic substrate but to the chiral ligand. After assaying several kinds of additives, amine bases were found to retard the cyclization significantly. Based on the observation, structural tuning led us to choose oxazoline as the prospective achiral ligand. Since our proposed relaying process was shown experimentally to work with a complex between Hg^{II} and oxazoline **2** (1:2), mercuriocyclization of the model substrate **1** was implemented with this complex composition in the

[*] Prof. Dr. S. H. Kang, Dr. M. Kim, Dr. S. Y. Kang
Center for Molecular Design and Synthesis
Department of Chemistry, School of Molecular Science (BK21)
Korea Advanced Institute of Science and Technology
Daejeon 305-701 (Korea)
Fax: (+82) 42-869-2810
E-mail: shkang@kaist.ac.kr

[**] This work was supported by CMDS and the Brain Korea 21 Project.

presence of various oxazolines to evaluate which one would be effective. Some of the results are presented in Table 1. Although **4** and **5** promoted the cyclization to a greater extent (Table 1, entries 3 and 4), the use of **2**, **3**, **6**, and **7** seemed to induce more-encouraging progress (Table 1, entries 1, 2, 5, and 6).

Table 1: Mercuriocyclization of **1** in the presence of oxazoline–Hg^{II} complexes (L₂Hg^{II}; 1.2 equiv).

Entry	L	Yield [%]	Recovered starting material [%]
1	2	22	74
2	3	23	72
3	4	44	48
4	5	55	41
5	6	8	90
6	7	11	83

2: R = Ph **5:** R = 2,4,6-Cl₃C₆H₂

3: R = Me **6:** R = 3,4,5-(MeO)₃C₆H₂

4: R = *t*Bu **7:** R = 4-MeOC₆H₄

With the promising relay ligands in hand, catalytic asymmetric mercuriocyclization of **1** was attempted with the corresponding Hg^{II} complexes in the presence of bisoxazoline **9**. The outcomes are summarized in Table 2. As reported

Table 2: Mercuriocyclization of **1** by using oxazoline L–Hg^{II} complexes (L₂Hg^{II}; 1.2 equiv) in the presence of bisoxazoline **9** (0.3 equiv) and MeOH (2.5 equiv).

Entry	L	Yield (sm) [%] ^[a]	ee [%] ^[b,c,d]
1 ^[e]	2	70 (26)	89
2	2	72 (24)	90
3	3	47 (52)	89
4	6	72 (26)	91
5	7	39 (54)	72

[a] Values in parentheses refer to the recovery of starting material. [b] Measured for the reductively demercurated product (LiBH₄ and Et₃B in THF at –78 °C). [c] Determined by HPLC analysis using Regis Welk-O1 (R,R). [d] For the determination of the absolute configuration, see reference [10]. [e] MeOH (10 equiv) and K₂CO₃ (5 equiv) were added.

before, MeOH (10 equiv) and K₂CO₃ (5 equiv) were employed as additives and resulted in good chemical conversion and remarkable stereoselectivity (Table 2, entry 1). Later, it was found that the addition of 2.5 equivalents of MeOH was sufficient to give comparable results (Table 2, entry 2). The best cyclization was attained with oxazolines **2**

and **6** (Table 2, entries 2 and 4). The reaction conditions in Table 2, entry 2 were applied to substrates **10–12**. The experimental data in Table 3 reveal that the enantioselectivity

Table 3: Mercuriocyclization with **2**–Hg^{II} (1.2 equiv) in the presence of bisoxazoline **9** (0.3 equiv) and MeOH (2.5 equiv).

Entry	Substrate	Product	Yield (sm) [%]	ee [%] ^[a]
1	1	8	72 (24)	90
2	10	13	51 (46)	82 ^[b,c]
3	11	14	63 (35)	91 ^[b,c]
4	12	15	42 (56)	75 ^[d,e]

10 R = (CH₂)₂OTBDPS **13** R = (CH₂)₂OTBDPS

11 R = (CH₂)₃OTBDPS **14** R = (CH₂)₃OTBDPS

12 R = *i*Pr **15** R = *i*Pr

[a] For the determination of the absolute configuration, see reference [10]. [b] Measured for the reductively demercurated product (LiBH₄ and Et₃B in THF at –78 °C). [c] Determined by HPLC analysis using DAICEL OD-H. [d] Measured for the iodinated product (I₂ in THF at 0 °C). [e] Determined by GC analysis using CHIRALDEX B-DM. The absolute configuration was not determined.

reached a more satisfactory level than the chemical conversion. When the cyclization proceeded further, it became slower, probably as a result of the gradually increasing oxazoline concentration. All attempts to suppress the ligating power of the generated excess oxazoline with acidic additives proved futile.

To ameliorate the incomplete conversion, a different protocol was elicited. In the second approach, **1** was treated with the complex between **9** and Hg^{II} (1:1; 0.2 equiv) in the presence of Hg(OAc)₂ (1.0 equiv) and additive(s). The use of MeOH (10 equiv) with or without K₂CO₃ resulted in moderate enantioselectivity (Table 4, entries 1 and 2). The use of allyl alcohol instead of MeOH led to improved stereoselectivity, notably with poorer chemical yield (Table 4, entry 3). The best cyclization resulted when the amount of MeOH was adjusted to 1.5 equivalents (Table 4, entry 5).

Table 4: Mercuriocyclization of **1** with **9**–Hg^{II} (0.2 equiv) in the presence of Hg(OAc)₂ (1.0 equiv) and additive(s).

Entry	Additive (equiv)	Yield (sm) [%]	ee [%]
1	MeOH (10), K ₂ CO ₃ (5)	84 (10)	54
2	MeOH (10)	92 (5)	43
3	allyl alcohol (10)	61 (25)	74
4	<i>i</i> PrOH	77 (19)	37
5	MeOH (1.5)	87 (11)	91

A variety of *Z* olefinic hydroxyalkenes **10–12** and **16–22** were subjected to the developed cyclization conditions. Under conditions A (Table 5), most of the substrates delivered good to excellent stereoselectivity; however, **10** and **12**

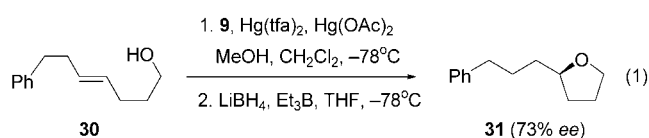
Table 5: Mercuriocyclization with **9**-Hg^{II} in the presence of Hg(OAc)₂ and MeOH.

Entry	Substrate	Product	Conditions A ^[a]		Conditions B ^[b]	
			Yield (sm) [%]	ee [%]	Yield (sm) [%]	ee [%] ^[b,c]
1	1	8	87 (11)	91	93 (6)	94
2	10	13	71 (25)	48	80 (17)	84
3	11	14	81 (17)	91	87 (11)	95
4	16	23	79 (15)	78	72 (15)	82 ^[d,e]
5	17	24	84 (9)	79	83 (10)	87 ^[d,e]
6	18	25	72 (13)	88	68 (20)	90 ^[d,e]
7	12	15	83 (10)	22	70 (13)	73
8	19	26	83 (11)	75	80 (12)	84 ^[d,e]
9	20	27	83 (10)	88	79 (11)	93 ^[e,f]
10	21	28	87 (11)	71	80 (15)	82 ^[g]
11	22	29	75 (14)	83	72 (19)	92 ^[g]

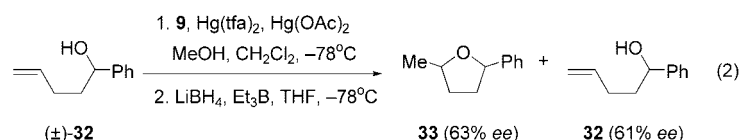
[a] Conditions A: 0.2 equiv of **9**, 0.2 equiv of Hg(tfa)₂, 1.5 equiv of MeOH and 1.0 equiv of Hg(OAc)₂ were used. Conditions B: 0.3 equiv of **9**, 0.2 equiv of Hg(tfa)₂, 2.0 equiv of MeOH and 1.0 equiv of Hg(OAc)₂ were used. [b] For the determination of the absolute configuration, see reference [10]. [c] Determined by GC analysis using CHIRALDEX B-DM. [d] Measured for the iodinated product (I₂ in THF at 0°C). [e] The absolute configuration was not determined. [f] Measured for the reductively demercurated product (LiBH₄ and Et₃B in THF at -78°C). [g] Measured for the reductively demercurated alcohol, which was produced by concomitant reductive demercuration and ester reduction using LiBH₄ and Et₃B in THF at -78°C.

resulted in poor enantioselectivity (Table 5, entries 2 and 7). To overcome the inferior asymmetric induction, it was necessary to maintain the concentration of the free Hg^{II} ion as low as possible. As a consequence, the cyclization conditions were optimized by increasing the amount of **9** to 0.3 equivalents with 2.0 equivalents of MeOH (Table 5, conditions B). The enantioselectivity under the established conditions was improved considerably from 48 to 84% ee for **13** and from 22 to 73% ee for **15** (Table 5, entries 2 and 7). Most of the remaining substrates also underwent cyclization with significant enantiomeric enhancement.^[11] Scrutiny of the data suggests that not only the steric bulk of the substituent but also the distance of the bulky region from the olefinic double bond seem to be greatly influential. It is possible that the two factors are involved in forming the tight coordination bond between the substrate and **9**-Hg^{II} complex, which is thought to be crucial for high facial selectivity.

Finally, the newly developed cyclization conditions were employed for the asymmetric mercurioetherification of the *trans* alkene **30** (isomeric to **1**) and the racemic terminal alkene (±)-**32** as a kinetic resolution experiment. The former proceeded somewhat more sluggishly to afford the expected tetrahydrofuran **31** in 74% yield with 73% ee (15% of recovered **30**) [Eq. (1), tfa = trifluoroacetate].



On the other hand, the latter produced 43% of the *trans*-2,5-disubstituted tetrahydrofuran **33** with 63% ee, and 47% of starting alcohol **32** with 61% ee [Eq. (2)].



In conclusion, we have established a highly enantioselective catalytic mercuriocyclization of γ -hydroxy-*cis*-alkenes employing Hg(OAc)₂ in the presence of catalytic amounts of the 4-(2-naphthyl)bisoaxazoline-Hg^{II} (**9**-Hg^{II}) complex to obtain 2-monosubstituted tetrahydrofurans with up to 95% ee.

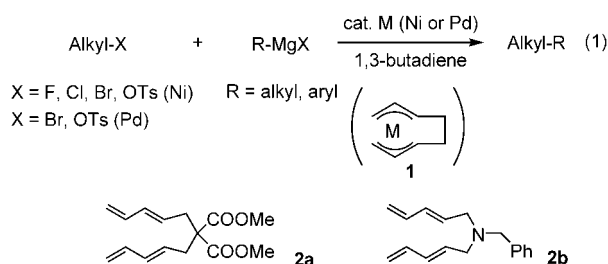
Received: July 13, 2004

Keywords: asymmetric synthesis · cyclization · homogeneous catalysis · mercury · tetrahydrofurans

- [1] a) T. Katsuki in *Comprehensive Asymmetric Catalysis*; Vol. 2 (Eds.: E. N. Jacobsen, A. Pfaltz, H. Yamamoto), Springer, Heidelberg, **1999**, chap. 18.1; b) E. N. Jacobsen, M. F. Wu in *Comprehensive Asymmetric Catalysis*, Vol. 2 (Eds.: E. N. Jacobsen, A. Pfaltz, H. Yamamoto), Springer, Heidelberg, **1999**, chap. 18.2; c) R. W. Murray, *Chem. Rev.* **1989**, 89, 1187.
- [2] a) I. E. Marko, J. S. Svendsen in *Comprehensive Asymmetric Catalysis*, Vol. 2 (Eds.: E. N. Jacobsen, A. Pfaltz, H. Yamamoto), Springer, Heidelberg, **1999**, chap. 20; b) H. C. Kolb, M. S. Van Nieuwenhze, K. B. Sharpless, *Chem. Rev.* **1994**, 94, 2483.
- [3] a) G. Li, H.-T. Chang, K. B. Sharpless, *Angew. Chem.* **1996**, 108, 449; *Angew. Chem. Int. Ed. Engl.* **1996**, 35, 451; b) G. Li, H. H. Angert, K. B. Sharpless, *Angew. Chem.* **1996**, 108, 2991; *Angew. Chem. Int. Ed. Engl.* **1996**, 35, 2813.
- [4] a) R. Noyori, *Angew. Chem.* **2002**, 114, 2108; *Angew. Chem. Int. Ed.* **2002**, 41, 2008; b) W. S. Knowles *Angew. Chem.* **2002**, 114, 2096; *Angew. Chem. Int. Ed.* **2002**, 41, 1998.
- [5] a) F. Y. Kwong, Q. Yong, T. C. W. Mak, A. S. C. Chan, K. S. Chan, *J. Org. Chem.* **2002**, 67, 2769, and references therein; b) K. Burgess, W. A. Van der Donk in *Advanced Asymmetric Synthesis* (Ed.: G. R. Stephenson), Chapman & Hall, London, **1996**, p. 181.
- [6] a) G. Rousseau, S. Robin, *Tetrahedron* **1998**, 54, 13681; b) K. E. Harding, T. H. Tinger in *Comprehensive Organic Synthesis*, Vol. 4 (Eds.: B. M. Trost, I. Fleming), Pergamon, Oxford, **1991**, p. 463; c) J. Mulzer in *Organic Synthesis Highlights* (Eds.: J. Mulzer, H. J. Altenbach, M. Braun, K. Krohn, H. U. Reissig), Wiley-VCH, Weinheim, **1991**, p. 157.
- [7] a) T. G. Back, B. P. Dyck, S. Nan, *Tetrahedron* **1999**, 55, 3191; b) Y. Nishibayashi, S. K. Srivastava, H. Takada, S.-I. Fukuzawa, S. Uemura, *J. Chem. Soc. Chem. Commun.* **1995**, 2321; c) T. Wirth, *Angew. Chem.* **1995**, 107, 1872; *Angew. Chem. Int. Ed.*

- Engl.* **1995**, 34, 1726; d) R. Déziel, S. Goulet, L. Grenier, J. Bordeleau, J. Nernier, *J. Org. Chem.* **1993**, 58, 3619; e) K.-I. Fujita, M. Iwaoka, S. Tomoda, *Chem. Lett.* **1992**, 1123.
- [8] a) R. B. Grossman, R. J. Trupp, *Can. J. Chem.* **1998**, 76, 1233; b) H. B. Vardhan, R. D. Bach, *J. Org. Chem.* **1992**, 57, 4948.
- [9] S. H. Kang, S. B. Lee, C. M. Park, *J. Am. Chem. Soc.* **2003**, 125, 15748.
- [10] S. H. Kang, M. Kim, *J. Am. Chem. Soc.* **2003**, 125, 4684.
- [11] When the cyclization of **1** was scaled up from 0.2 to 2.0 mmol, the enantioselectivity decreased to 90% *ee*. However, the addition of **1** by a syringe pump over 8 h instead of in one portion restored it to the initial level (93% *ee*).

cross-coupling reaction of alkyl halides with organozinc reagents^[4-6] in a THF/*N*-methylpyrrolidone (NMP) mixed solvent containing magnesium bromide. It was also found that these tetraenes (**2**) were effective also for the nickel-catalyzed cross-coupling of alkyl fluorides with Grignard reagents.



Synthetic Methods

Nickel-Catalyzed Cross-Coupling Reaction of Alkyl Halides with Organozinc and Grignard Reagents with 1,3,8,10-Tetraenes as Additives**

Jun Terao, Hirohisa Todo, Hideyuki Watanabe, Aki Ikumi, and Nobuaki Kambe*

Transition-metal-catalyzed cross-coupling reactions between organic halides and organometallic reagents is a powerful tool for constructing carbon skeletons.^[1] Significant advances have been achieved in this field over the last decade that have enabled cross-coupling reactions to be effected between alkyl groups by using either a nickel or palladium catalyst.^[2] We have contributed to this progress by developing a unique catalytic system that proceeds efficiently under mild conditions by using 1,3-butadiene as an additive in the absence of phosphane ligands, where bis- π -allylnickel or -palladium intermediates (**1**) are proposed to be involved [Eq. (1)].^[3] This system facilitates the cross-coupling of a wide variety of alkyl tosylates and halides, such as fluorides, chlorides, and bromides, with Grignard reagents. However, a drawback of this methodology is the range of functional groups that are tolerant to this system because of the high reactivity of the Grignard reagents. Herein, we reveal a solution to this problem by employing 1,3,8,10-tetraenes (**2**) that serve as extremely efficient ligands to promote the nickel-catalyzed

First we examined a cross-coupling reaction of alkyl halides with organozinc reagents that used 1,3-butadiene as the additive. For example, *n*-decyl bromide (1 mmol), diethylzinc (2 equivalents, 1M in hexane), NiCl₂ (0.03 equiv), and 1,3-butadiene (1 equivalent) were added sequentially to a solution of THF (8 mL) and NMP (4 mL) at -78°C and the mixture stirred at 25°C for 48 hours. However, this reaction gave only a trace amount of the cross-coupling product, *n*-dodecane (< 1%), as shown in Table 1 (entry 1). Addition of magnesium bromide increased the yield of *n*-dodecane to 45%, but side reactions (reduction and HBr elimination) could not be suppressed (entry 2). Only a trace amount of dodecane was obtained without 1,3-butadiene even in the presence of magnesium bromide (entries 3 and 4). The salts Bu₄NBr, Bu₄NI,^[5] and LiBr were also shown to be not effective as additives (entries 5–7). The yield of dodecane was increased up to 73% by adding four equivalents of 1,3-butadiene; however, formation of by-products, *n*-decane and decenes, could not completely be suppressed (entries 8 and 9). Under similar conditions, [Ni(acac)₂] (acac = acetylacetonate) afforded a slightly better yield of the product (entry 10), while nickel catalysts bearing phosphane ligands were less efficient (entries 11 and 12). PdCl₂ did not show a high catalytic activity (entry 13). The coupling products were obtained in yields of only 37 and 7%, respectively (entries 14 and 15), when isoprene and *p*-fluorostyrene^[5] were employed as additives under the same conditions as entry 10.

It is noteworthy that this cross-coupling reaction proceeded very rapidly and quantitatively when 2,2-bis(penta-2,4-dienyl)malonic acid dimethyl ester (**2a**) was employed as an additive in place of 1,3-butadiene, with complete suppression of the formation of decane and decenes (entry 16). The NiCl₂ catalyst also gave a satisfactory result under identical conditions (entry 17). The excellent performance of tetraene **2a** is demonstrated readily as the reaction was completed within 1 h at 25°C with only 9 mol % of **2a** and 1.3 equivalents of diethylzinc (entry 18). *N,N*-Bis(penta-2,4-dienyl)benzylamine (**2b**) also showed high activity (entry 19). The yield of dodecane decreased when the amount of magnesium bromide was decreased (entry 18).

Reactions of various alkyl halides and a tosylate with organozinc reagents were examined with **2a** as an additive

[*] Dr. J. Terao, H. Todo, H. Watanabe, A. Ikumi, Prof. Dr. N. Kambe
Department of Molecular Chemistry and Science and
Technology Center for Atoms, Molecules, and Ions Control
Graduate School of Engineering, Osaka University
Yamadaoka 2-1, Suita, Osaka 565-0871 (Japan)
Fax: (+81) 6-6879-7390
E-mail: kambe@chem.eng.osaka-u.ac.jp

[**] This research was supported financially in part by a Grant-in-Aid for Scientific Research. We thank the Instrumental Analysis Center, Faculty of Engineering, Osaka University, for high-resolution mass-spectrometric measurements and elemental analysis.

Supporting information for this article is available on the WWW under <http://www.angewandte.org> or from the author.

Table 1: Nickel-catalyzed cross-coupling reaction of $n\text{C}_{10}\text{H}_{21}\text{-Br}$ with diethylzinc.^[a]

Entry	Catalyst	Additive (equiv)	<i>t</i> [h]	Product yield [%] ^[b]		
				Dodecane	Decane	Decenes ^[c]
1	NiCl ₂	C ₄ H ₆ (1)	48	< 1	23	< 1
2	NiCl ₂	C ₄ H ₆ (1), MgBr ₂ (3)	48	45	20	11
3	NiCl ₂	none	48	0	5	< 1
4	NiCl ₂	MgBr ₂ (3)	48	2	49	46
5	NiCl ₂	C ₄ H ₆ (1), Bu ₄ NBr (3)	48	< 1	45	3
6	NiCl ₂	C ₄ H ₆ (1), Bu ₄ NI (3)	48	3	69	23
7	NiCl ₂	C ₄ H ₆ (1), LiBr (3)	48	16	7	0
8	NiCl ₂	C ₄ H ₆ (2), MgBr ₂ (3)	48	69	14	9
9	NiCl ₂	C ₄ H ₆ (4), MgBr ₂ (3)	48	73	2	2
10	[Ni(acac) ₂]	C ₄ H ₆ (4), MgBr ₂ (3)	48	84	3	3
11	[NiCl ₂ (PPh ₃) ₂]	C ₄ H ₆ (4), MgBr ₂ (3)	48	40	2	< 1
12	[NiCl ₂ (dppp)]	C ₄ H ₆ (4), MgBr ₂ (3)	48	31	3	0
13	PdCl ₂	C ₄ H ₆ (4), MgBr ₂ (3)	48	5	55	3
14	[Ni(acac) ₂]	isoprene (4), MgBr ₂ (3)	48	37	5	3
15	[Ni(acac) ₂]	<i>p</i> -fluorostyrene (4), MgBr ₂ (3)	48	7	< 1	23
16	[Ni(acac) ₂]	2a (2), MgBr ₂ (3)	48	> 99	0	0
17	NiCl ₂	2a (2), MgBr ₂ (3)	48	> 99	0	0
18 ^[d,e]	[Ni(acac) ₂]	2a (0.09), MgBr ₂ (3)	1	> 99	0	0
19 ^[d]	[Ni(acac) ₂]	2b (0.09), MgBr ₂ (3)	1	> 99	0	0

[a] Conditions unless otherwise stated: *n*-Decyl bromide (1 mmol), catalyst (3 mol%), additive (equivalents based on the substrate), diethylzinc (2 equiv, 1 M in hexane), mixed solution of THF (8 mL) and NMP (4 mL), 25 °C, 48 h. [b] Determined by GC analysis. [c] A mixture of 1-decene and 2-decenes. [d] *n*-Decyl bromide (1 mmol), diethylzinc (1.3 equiv, 1 M in hexane), mixed solution of THF (8.4 mL) and NMP (4.2 mL), 25 °C, 1 h. [e] The yields were decreased to 41 and 11 % when the amount of MgBr₂ was decreased to 1.3 and 0.65 equivalents, respectively.

(Table 2). This catalytic system tolerates unsaturated heteroatom functional groups, such as nitriles, ketones, amides, and esters (entries 1–4). The use of the secondary alkyl zinc reagent *i*Pr₂Zn (entry 5) or an aryl zinc reagent (entry 6) also afforded the corresponding products in good yields. An alkyl tosylate was also shown to undergo this cross-coupling reaction under the same conditions (entry 7). Secondary alkyl halides and tosylates were found to react sluggishly. For example, treatment of 2-octyl bromide with diethylzinc afforded decane in a yield of only 3 %, along with octane (6 %) and octenes (3 %), and 82 % of 2-octyl bromide was

Table 2: Nickel-catalyzed cross-coupling reaction of alkyl halides and a tosylate with organozinc reagents using tetraene **2a**.^[a]

Entry	RX	R' ₂ Zn	Product	Yield [%] ^[b]
1		<i>n</i> Oct ₂ Zn		96
2		<i>n</i> Oct ₂ Zn		87
3		(PhCH ₂) ₂ Zn		91
4		<i>n</i> Pr ₂ Zn		87
5		<i>i</i> Pr ₂ Zn		79 ^[c]
6	<i>n</i> PrBr	Ph ₂ Zn		86 ^[c]
7		Et ₂ Zn		83 ^[c]

[a] Conditions: RX (1 mmol), R'₂Zn (1.3 equiv), NiCl₂ (3 mol%), **2a** (9 mol%), MgBr₂ (3 mmol), mixed solution of THF (8.4 mL) and NMP (4.2 mL), 25 °C, 1 h. [b] Yield of isolated product. [c] GC yield.

recovered. Cyclohexyl tosylate also gave butylcyclohexane in a yield of only 5 % after treatment with dibutylzinc.

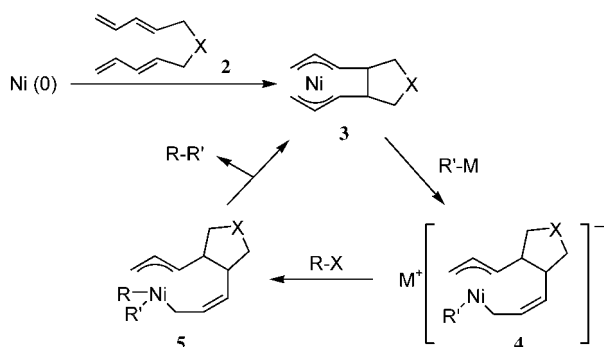
We have shown that nickel catalyzes cross-coupling reactions of alkyl fluorides with Grignard reagents in the presence of 1,3-butadiene. However, this reaction is less efficient than those of the alkyl bromides, as they afford only moderate yields of the coupling products.^[3b] For example, treatment of *n*-nonyl fluoride with 1.5 equivalents of *n*PrMgBr in the presence of 3 mol % of [Ni(acac)₂] and 30 mol % of 1,3-butadiene gave dodecane in a yield of only 11 % (Table 3, entry 1). Increasing the amount of 1,3-butadiene improved the yield moderately; however, satisfactory yields could not be attained (Table 3, entries 2–4). These poor yields were probably because the Ni⁰ center will react with more than two equivalents of

Table 3: Affect of the additive on the cross-coupling of alkyl fluorides.

$n\text{C}_9\text{H}_{19}\text{-F} + n\text{C}_3\text{H}_7\text{-MgBr} \xrightarrow[\text{THF (1.5 mL), RT, 6 h}]{3 \text{ mol \% [Ni(acac)}_2\text{]}}$ Dodecane			
Entry	[Ni(acac) ₂] [mol %]	Additive (mol %)	Yield [%]
1	3	1,3-butadiene (30)	11
2	3	1,3-butadiene (100)	58
3	3	1,3-butadiene (200)	65
4	3	1,3-butadiene (30)	67
5	0.6	2b (15)	94

1,3-butadiene in the presence of a high concentration of 1,3-butadiene and will form complexes composed of C₁₂-butadiene-oligomer units. The formation of these units will then predominantly result in a low concentration of **1**.^[7] To prepare the bis- π -allylnickel complex structure exclusively, we applied tetraene **2b** as an additive and found that the yield was dramatically improved by the use of only 0.6 mol % of nickel catalyst and 15 mol % of **2b** (entry 5).

A plausible reaction pathway is shown in Scheme 1. A bis- π -allylnickel structure **3** is constructed by the oxidative cycloaddition of Ni⁰ with two butadiene moieties of a



Scheme 1. A plausible reaction pathway.

1,3,8,10-tetraene.^[8] An organomagnesium or -zinc reagent attacks the bis- π -allyl complex **3** to generate the η^1, η^3 -octadienediynickelate complex **4**, which then reacts with alkyl halides to give a complex **5**. Subsequent reductive elimination affords the coupling product along with **3** to complete the catalytic cycle. Selective and efficient formation of **3** from Ni^0 and **2** would, in comparison to 1,3-butadiene,^[7] facilitate the generation of complex **4** and so accelerate the subsequent oxidative addition process that leads to **5**.

In conclusion, it was found that tetraenes **2** exerted dramatic effects that improved the cross-coupling reactions of organozinc reagents with alkyl halides catalyzed by nickel. This reaction proceeds efficiently by the use of primary and secondary alkyl or aryl zinc reagents under mild conditions. The use of tetraene **2b** as an additive also resulted in high yields of products in the cross-coupling of an alkyl fluoride with a Grignard reagent.

Experimental Section

Heptadecan-5-one: A solution of $n\text{Oct}_2\text{Zn}$ (0.33 M in THF, 3.9 mL, 1.3 mmol) was added to a solution of 1-bromononan-5-one (221 mg, 1.0 mmol), MgBr_2 (552 mg, 3.0 mmol), NiCl_2 (4 mg, 0.03 mmol), **2a** (24 mg, 0.09 mmol), and NMP (4.2 mL) in THF (4.6 mL) at 25 °C under nitrogen. After stirring the mixture for 1 h, 1 M HCl (ca. 2 mL) was added to the solution at 0 °C and the mixture was warmed to 25 °C. Saturated aqueous NaHCO_3 solution (20 mL) was then added, and the product was extracted with diethyl ether (20 mL), dried over MgSO_4 , and evaporated to give the crude product. Purification by silica gel column chromatography with hexane/diethyl ether (15:1) as an eluent afforded 233 mg (87 %) of octadecan-5-one. ^1H NMR (400 MHz, CDCl_3): δ = 2.39 (t, J = 7.6 Hz, 2H), 2.38 (t, J = 7.4 Hz, 2H), 1.59–1.51 (m, 4H), 1.34–1.21 (m, 22H), 0.90 (t, J = 8.4 Hz, 3H), 0.88 ppm (t, J = 8.8 Hz, 3H); ^{13}C NMR (100 MHz, CDCl_3): δ = 211.1, 42.7, 42.4, 31.8, 29.60, 29.57, 29.56, 29.54, 29.40, 29.35, 29.28, 29.20, 25.9, 23.8, 22.6, 22.3, 14.1, 13.8 ppm; MS (EI) m/z (relative intensity, %) 268 (M^+ , 0.4), 211 (25), 113 (20), 101 (33), 85 (74), 71 (39), 58 (100); HR-MS: calcd for $\text{C}_{18}\text{H}_{36}\text{O}$: 268.2766, found 268.2758; elemental analysis (%): calcd for $\text{C}_{18}\text{H}_{36}\text{O}$: C 80.53, H 13.52; found: C 80.46, H 13.40.

Received: April 7, 2004

Keywords: alkyl halides · cross-coupling · Grignard reagents · nickel · organozinc reagents

- [1] a) For the history and recent development of transition-metal-catalyzed cross-coupling reactions, see: International Symposium on 30 years of the Cross-coupling Reaction, *J. Organomet. Chem.* **2002**, 653, 1–291; b) *Metal-catalyzed Cross-coupling Reactions* (Eds.: F. Diederich, P. J. Stang), Wiley-VCH, New York, **1998**.
- [2] For a recent study and a review of transition-metal-catalyzed cross-coupling reactions of alkyl halides with organometallic reagents, see: a) D. J. Cárdenas, *Angew. Chem.* **2003**, 115, 398–401; *Angew. Chem. Int. Ed.* **2003**, 42, 384–387; b) T.-Y. Luh, M. Leung, K.-T. Wong, *Chem. Rev.* **2000**, 100, 3187–3204. Several important papers concerning cross-coupling reactions using alkyl halides were subsequently reported; see, for example: c) J. H. Kirchhoff, M. R. Netherton, I. D. Hills, G. C. Fu, *J. Am. Chem. Soc.* **2002**, 124, 13662–13663; d) A. C. Frisch, N. Shaikh, A. Zapf, M. Beller, *Angew. Chem.* **2002**, 114, 4218–4221; *Angew. Chem. Int. Ed.* **2002**, 41, 4056–4059; e) T. Tsuji, H. Yorimitsu, K. Oshima, *Angew. Chem.* **2002**, 114, 4311–4313; *Angew. Chem. Int. Ed.* **2002**, 41, 4137–4139; f) K. Menzel, G. C. Fu, *J. Am. Chem. Soc.* **2003**, 125, 3718–3719; g) J.-Y. Lee, G. C. Fu, *J. Am. Chem. Soc.* **2003**, 125, 5616–5617; h) J. Zhou, G. C. Fu, *J. Am. Chem. Soc.* **2003**, 125, 12527–12530; i) M. Eckhardt, G. C. Fu, *J. Am. Chem. Soc.* **2003**, 125, 13642–13643; j) J. Zhou, G. C. Fu, *J. Am. Chem. Soc.* **2003**, 125, 14726–14727; k) S. L. Wiskur, A. Korte, G. C. Fu, *J. Am. Chem. Soc.* **2004**, 126, 82–83; l) J. Zhou, G. C. Fu, *J. Am. Chem. Soc.*, **2004**, 126, 1340–1341; m) M. Nakamura, K. Matsuo, S. Ito, E. Nakamura, *J. Am. Chem. Soc.* **2004**, 126, 3686–3687; n) T. Nagano, T. Hayashi, *Org. Lett.* **2004**, 6, 1297–1299; o) R. Martin, A. Fürstner, *Angew. Chem.* **2004**, 116, 4045–4047; *Angew. Chem. Int. Ed.* **2004**, 43, 3955–3957.
- [3] a) J. Terao, H. Watanabe, A. Ikumi, H. Kuniyasu, N. Kambe, *J. Am. Chem. Soc.* **2002**, 124, 4222–4223; b) J. Terao, A. Ikumi, H. Kuniyasu, N. Kambe, *J. Am. Chem. Soc.* **2003**, 125, 5646–5647; c) J. Terao, Y. Naitoh, H. Kuniyasu, N. Kambe, *Chem. Lett.* **2003**, 32, 890–891.
- [4] For Ni-catalyzed cross-coupling reactions of alkyl halides with alkyl zinc reagents, see: a) A. Devasagayaram, T. Stüdemann, P. Knochel, *Angew. Chem.* **1995**, 107, 2723–2725; *Angew. Chem. Int. Ed. Engl.* **1995**, 34, 2723–2725; b) R. Giovannini, T. Stüdemann, G. Dussin, P. Knochel, *Angew. Chem.* **1998**, 110, 2512–2515; *Angew. Chem. Int. Ed.* **1998**, 37, 2387–2390; c) R. Giovannini, P. Knochel, *J. Am. Chem. Soc.* **1998**, 120, 11186–11187; d) M. Piber, A. E. Jensen, M. Rottländer, P. Knochel, *Org. Lett.* **1999**, 1, 1323–1326; e) R. Giovannini, T. Stüdemann, A. Devasagayaram, G. Dussin, P. Knochel, *J. Org. Chem.* **1999**, 64, 3544–3553; f) A. E. Jensen, P. Knochel, *J. Org. Chem.* **2002**, 67, 79–85; g) ref. [2j].
- [5] It is reported that alkyl zinc reagents undergo Ni-catalyzed cross-coupling with alkyl bromides by the combined use of Bu_4NI and *p*-fluorostyrene as additives; see: ref. [4f].
- [6] For Pd-catalyzed cross-coupling reaction of alkyl halides with alkyl zinc reagents, see: ref. [2h].
- [7] For structures and stabilities of nickel complexes involved in cyclo-oligomerization of 1,3-butadiene, see: S. Tobisch, *Adv. Organomet. Chem.* **2003**, 49, 167–224, and references therein.
- [8] For Ni-mediated cyclization of 1,3,8,10-tetraenes, see: a) P. A. Wender, M. J. Tebbe, *Synthesis* **1991**, 1089–1094, and references therein; b) M. Takimoto, M. Mori, *J. Am. Chem. Soc.* **2002**, 124, 10008–10009.

Synthetic Methods

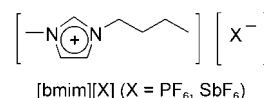
Dramatic Enhancement of Catalytic Activity in an Ionic Liquid: Highly Practical Friedel–Crafts Alkenylation of Arenes with Alkynes Catalyzed by Metal Triflates**

Choong Eui Song,* Da-un Jung, Su Yhen Choung, Eun Joo Roh, and Sang-gi Lee*

The Friedel–Crafts alkylation of aromatic compounds with alkenes is one of the fundamental methods for incorporating carbon skeletons into aromatic systems and, thus, has been extensively studied and is well established.^[1] In contrast, the corresponding alkenylation process with alkynes still remains to be solved. One major drawback from the direct Friedel–Crafts alkenylation of arenes is alkyne polymerization, which results in the formation of a variety of undesirable side products.^[2] Well-known Lewis acidic metal chlorides, such as ZrCl_4 and AlCl_3 , produce the desired alkenylated products but in extremely low yields (for example, 1 and 6 % yields of 1-phenyl-1-(*p*-xylyl)ethene for the reaction of *p*-xylene with phenylacetylene at 85 °C, respectively).^[3] Recently, a number of catalysts, such as the solid acid zeolite HSZ-360,^[4] phenoxy-magnesium bromide,^[5] and $\text{SnCl}_4/\text{NBu}_3$,^[6] were found to be active for the *ortho* selective alkenylation of phenols with a limited range of alkynes (only aryl-substituted terminal alkynes underwent this reaction). It has been also found that GaCl_3 can promote the alkenylation of arenes with silylthyne, but excessive amounts of this Lewis acid (3 equiv) are required.^[7] Recently, Tsuchimoto et al. made a breakthrough on this important reaction by finding that some metal triflates $[\text{M}(\text{OTf})_n; \text{M} = \text{Sc}, \text{Zr}, \text{In}]$ catalyze the alkenylation of arenes with internal alkynes as well as terminal alkynes through an alkenyl cation intermediate.^[3] However, the catalytic activity of these metal triflates is far too low for preparative use. For example, the reaction of benzene and phenylacetylene in the presence of 10 mol % of $\text{Sc}(\text{OTf})_3$ at 85 °C requires 186 hours to give 1,1-diphenylethene in 73 % yield.^[3] Moreover, $\text{Sc}(\text{OTf})_3$ was totally inactive for electron-

deficient alkynes, such as *p*-trifluoromethylphenylacetylene and *p*-chlorophenylacetylene. Therefore, a more efficient and practical catalytic system for Friedel–Crafts alkenylation is still highly desirable. Herein, we report that the use of ionic liquids in Friedel–Crafts alkenylations of aromatic compounds by alkynes catalyzed by metal triflates not only enhanced catalytic activity markedly but also decreased by-product formation, which resulted in higher yields of the monoalkenylated arenes. Moreover, in some cases, reactions that do not usually occur in conventional organic solvents were found to proceed smoothly in ionic liquids.

Room-temperature ionic liquids (RTILs) are now regarded as eco-friendly alternatives to volatile organic solvents in chemical processes.^[8] During the course of our extensive efforts on the utilization of RTILs in various catalytic reactions, we found that switching from an organic solvent to an ionic liquid often resulted in significant improvements in catalytic performance (for example, increased reaction rates, improved selectivities, etc.) as well as catalyst recycling.^[9] Recently, we found that the $\text{Sc}(\text{OTf})_3$ -catalyzed Friedel–Crafts alkylation of aromatic compounds with alkenes is dramatically accelerated in the presence of hydrophobic ionic liquids, such as $[\text{bmim}][\text{PF}_6]$ or $[\text{bmim}][\text{SbF}_6]$ ($\text{bmim} = 1\text{-butyl-3-methylimidazolium}$).^[9a] This result encouraged us to investigate the metal triflate catalyzed Friedel–Crafts alkenylation of aromatics with alkynes in ionic liquids.



To investigate the effect of ionic liquids on the catalytic activity of metal triflates in Friedel–Crafts alkenylation we first examined the reaction between benzene and 1-phenyl-1-propyne under various conditions (Table 1).

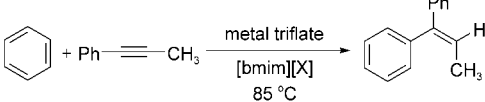
As observed by Tsuchimoto et al.,^[3] the alkenylation of benzene with 1-phenyl-1-propyne in the presence of 10 mol % of $\text{Sc}(\text{OTf})_3$ without an ionic liquid proceeded very slowly with a yield of only 27 % after 96 hours (entry 1). Moreover, this long reaction time resulted in increased the formation of undesired side products. On the other hand, when the reaction was carried out in hydrophobic ionic liquids, such as $[\text{bmim}][\text{PF}_6]$ or $[\text{bmim}][\text{SbF}_6]$, the catalytic activity of $\text{Sc}(\text{OTf})_3$ was dramatically enhanced: the reaction was completed within 4 hours to afford the desired product (1,1-diphenyl-1-propene) in excellent yields (91 or 90 %, respectively; entries 2 and 3).^[10,11] Among the various metal triflates investigated for catalytic activity, indium triflate, hafnium triflate, and yttrium triflate in particular were found to exhibit higher activity than scandium triflate, with the reaction completed within 2.5, 1, and 2 hours, respectively (entries 4, 7, and 10). The reactions proceeded smoothly with excellent yields even in the presence of smaller amounts of these metal triflates (5 and 2.5 mol %; entries 5, 6, 8, and 9). Ytterbium triflate and lutetium triflate also exhibited similar catalytic activities to that of scandium triflate (entries 11 and 12). This

[*] Prof. C. E. Song, S. Y. Choung
Institute of Basic Science
Department of Chemistry, Sungkyunkwan University
300 Chunchun, Jangsan, Suwon, Kyunggi, 440-746 (Korea)
Fax: (+82) 31-290-7075
E-mail: s1673@skku.edu
D.-u. Jung, Dr. E. J. Roh, Dr. S.-g. Lee
Life Sciences Division
Korea Institute of Science and Technology
PO Box 131, Cheongryang, Seoul 130-650 (Korea)
Fax: (+82) 2-958-5189
E-mail: sanggi@kist.re.kr

[**] This work was supported by the BK21 project of the Ministry of Education in Sungkyunkwan University (SKKU) and the National Research Laboratory Program in Korea Institute of Science and Technology (KIST).

Supporting information for this article is available on the WWW under <http://www.angewandte.org> or from the author.

Table 1: Friedel–Crafts alkenylation of benzene by 1-phenyl-1-propyne.^[a]



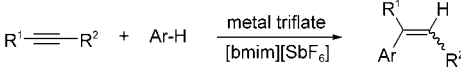
Entry	Catalyst (equiv)	Ionic liquid	t [h]	Yield [%] ^[b]
1	Sc(OTf) ₃ (0.1)	none	96	27
2	Sc(OTf) ₃ (0.1)	[bmim][SbF ₆]	4	91
3	Sc(OTf) ₃ (0.1)	[bmim][PF ₆]	4	90
4	In(OTf) ₃ (0.1)	[bmim][SbF ₆]	2.5	81
5	In(OTf) ₃ (0.05)	[bmim][SbF ₆]	6	94
6	In(OTf) ₃ (0.025)	[bmim][SbF ₆]	24	91
7	Hf(OTf) ₄ (0.1)	[bmim][SbF ₆]	1	90
8	Hf(OTf) ₄ (0.05)	[bmim][SbF ₆]	5	91
9	Hf(OTf) ₄ (0.025)	[bmim][SbF ₆]	9	85
10	Y(OTf) ₃ (0.1)	[bmim][SbF ₆]	2	80
11	Yb(OTf) ₃ (0.1)	[bmim][SbF ₆]	4	81
12	Lu(OTf) ₃ (0.1)	[bmim][SbF ₆]	4	94

[a] All reactions were carried out at 85 °C using 1-phenyl-1-propyne (1 mmol), benzene (6 mL), and the ionic liquid (1 mL) in the presence of the metal triflate as a catalyst. [b] Yield of isolated product based on 1-phenyl-1-propyne.

significant rate acceleration may be ascribed to the stabilization of the unstable vinyl cationic intermediate in a highly polar ionic liquid, in which the polar vinyl cation may gain a longer lifetime. The catalytic activities of other metal triflates were also investigated, for example (yields are given in parentheses), Ag(OTf) (4 %), Cu(OTf)₂ (27 %), Mg(OTf)₂ (21 %), Zn(OTf)₂ (2 %), Sn(OTf)₂ (69 %), La(OTf)₃ (62 %), Pr(OTf)₃ (19 %), Nd(OTf)₃ (37 %), Sm(OTf)₃ (15 %), Eu(OTf)₃ (16 %), Gd(OTf)₃ (23 %), Tb(OTf)₃ (34 %), Dy(OTf)₃ (28 %), Ho(OTf)₃ (30 %), Er(OTf)₃ (40 %), and Tm(OTf)₃ (22 %). However, their catalytic activities were much lower than those of Sc(OTf)₃, In(OTf)₃, Hf(OTf)₄, Y(OTf)₃, Yb(OTf)₃, and Lu(OTf)₃.

To study the scope of this reaction a series of Friedel–Crafts alkenylations of arenes with various types of alkynes were carried out in [bmim][SbF₆] (Table 2). In all cases, the reactions proceeded successfully within a few hours to afford the corresponding alkenylated products in good to excellent yields. In particular, Sc(OTf)₃, In(OTf)₃, and Hf(OTf)₄ effectively catalyzed the alkenylation of the electron-deficient alkynes, such as *p*-trifluoromethylphenylacetylene and *p*-chlorophenylacetylene, which were totally inactive without the presence of an ionic liquid (entries 14–18).^[3] Similarly, the reaction of arenes with ethyl phenylpropiolate in the presence of Hf(OTf)₄ proceeded smoothly in [bmim][SbF₆] (entries 19 and 20), whereas without [bmim][SbF₆] a conversion of only < 5 % was observed. It should also be noted that the ionic liquid phase containing the metal triflate could be readily recovered by simple decantation of the organic layer (the upper phase) after reaction. The recovered ionic liquid phase containing the metal triflate was reused without further addition of metal triflate. However, a decrease in catalytic activity over successive reactions was observed and, thus, the reaction time became longer upon reuse (compare entries 6 and 7 in Table 2).

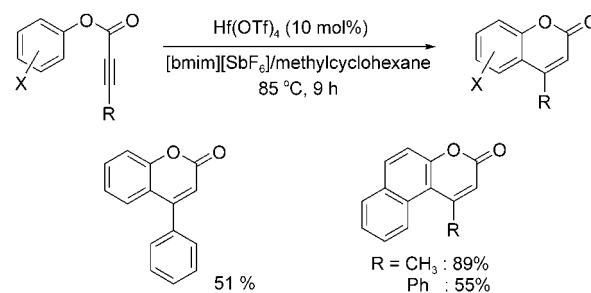
Table 2: Friedel–Crafts alkenylation of various arenes with various alkynes.^[a]



Entry	R ¹	R ²	Arene	Catalyst	t [h]	Yield [%] ^[b]
1	Ph	Me	<i>p</i> -xylene	Sc(OTf) ₃	4	96 ^[c]
2	Ph	H	benzene	Sc(OTf) ₃	4	68
3	Ph	H	<i>p</i> -xylene	Sc(OTf) ₃	4	60
4	Ph	H	<i>p</i> -xylene	In(OTf) ₃	3	80
5	Ph	H	<i>p</i> -xylene	Hf(OTf) ₄	3	85
6	Ph	Ph	benzene	Sc(OTf) ₃	2	59
7 ^[d]	Ph	Ph	benzene	Sc(OTf) ₃	4	62
8	Ph	Ph	benzene	In(OTf) ₃	2	72
9	Ph	Ph	benzene	Hf(OTf) ₄	1	92
10	Ph	Ph	<i>p</i> -xylene	Sc(OTf) ₃	4	80 ^[c]
11	Ph	Ph	toluene	Sc(OTf) ₃	2	83 ^[e]
12	Ph	Ph	chlorobenzene	Sc(OTf) ₃	6	44 ^[e]
13	Ph	Ph	anisole	Sc(OTf) ₃	2	73 ^[e]
14	<i>p</i> -CF ₃ Ph	H	<i>p</i> -xylene	Sc(OTf) ₃	22	73
15	<i>p</i> -CF ₃ Ph	H	<i>p</i> -xylene	In(OTf) ₃	5	78
16	<i>p</i> -CF ₃ Ph	H	<i>p</i> -xylene	Hf(OTf) ₄	5	58
17	<i>p</i> -ClPh	H	<i>p</i> -xylene	Sc(OTf) ₃	12	63
18	<i>p</i> -ClPh	H	<i>p</i> -xylene	Hf(OTf) ₄	4	70
19	Ph	CO ₂ Et	benzene	Hf(OTf) ₄	22	89
20	Ph	CO ₂ Et	<i>p</i> -xylene	Hf(OTf) ₄	10	70 ^[c]

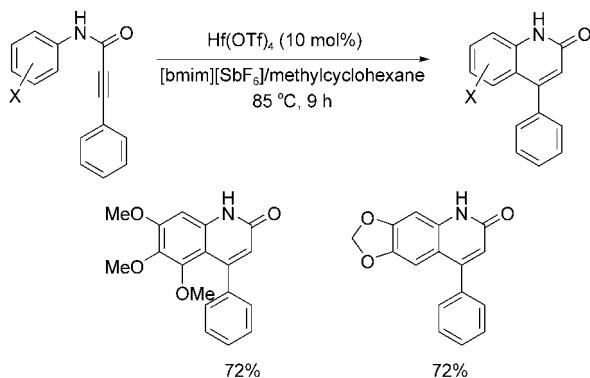
[a] All reactions were carried out with an alkyne (1 mmol), an arene (6 mL), and [bmim][SbF₆] (1 mL) in the presence of the metal triflate catalyst (10 mol %) at 85 °C. [b] Yield of isolated product based on the alkyne. [c] *cis/trans* ratios were determined by ¹H NMR spectroscopy as follows: 96/4 (entry 1), 88/12 (entry 10), and 87/13 (entry 20). [d] Reaction was carried out with the recovered ionic liquid phase from entry 6 without further addition of Sc(OTf)₃. [e] The reaction gave an inseparable mixture of four isomers of *ortho* and *para* regioisomers, including the corresponding *cis/trans* isomers. The isomer ratios determined by GC-MS analysis are as follows; 2/33/32/32 (entry 11); 2/35/31/32 (entry 12); 8/18/34/40 (entry 13).

Finally, our protocol has been further extended to intramolecular Friedel–Crafts alkenylations. The intramolecular reaction of aryl phenyl propiolates catalyzed by Hf(OTf)₄ (10 mol %) in a mixture of [bmim][SbF₆] and methylcyclohexane at 85 °C for 9–10 hours resulted in the formation of the 4-phenylcoumarins in moderate yields (Scheme 1). Surprisingly, the reaction of aryl-2-butynoates also was successfully performed to afford the corresponding coumarin in an excellent yield (89 %; Scheme 1). The smaller stabilizing influence of the alkyl group on the vinyl cation intermediate



Scheme 1. Synthesis of 4-phenylcoumarins by intramolecular Friedel–Crafts alkenylations.

resulted in the alkyl-substituted alkynes usually undergoing self-oligomerization rather than the desired alkenylation reaction. Intramolecular alkenylation allowed us to synthesize 2(1*H*)-quinolinones from the corresponding aryl amides of phenylpropionic acid in good yields (Scheme 2).



Scheme 2. Synthesis of 2(1*H*)-quinolinones by intramolecular Friedel–Crafts alkenylations.

In conclusion, we have found that the employment of hydrophobic ionic liquids dramatically enhanced the catalytic activities of metal triflates in Friedel–Crafts alkenylations, and thus allowed the development of a simple and highly efficient method for coupling aromatic compounds with various alkyl- and aryl-substituted alkynes. In some cases, reactions that were not possible in conventional organic solvents also proceeded smoothly in the presence of ionic liquids. To our knowledge, the described protocol could be the most efficient preparative Friedel–Crafts alkenylation method published to date for the synthesis of a range of alkenylated arenes,^[12] such as styrenes, *cis*-aryl- α,β -unsaturated carbonyl compounds, coumarines, and 2(1*H*)-quinolinones. Studies into the origin of the effects of ionic liquids on catalytic activity are in progress.

Experimental Section

Typical procedure for intermolecular Friedel–Crafts alkenylations in an ionic liquid: 1-Phenyl-1-propyne (178.2 mg, 1 mmol) was added to a mixture of $\text{Sc}(\text{OTf})_3$ (49.2 mg, 0.1 mmol), benzene (6 mL), and $[\text{bmim}][\text{SbF}_6]$ (1 mL) under a nitrogen atmosphere. Two phases formed and the mixture was heated to reflux for 4 h. After completion of the reaction, the reaction mixture was cooled to room temperature. The organic layer (upper phase) was separated by extraction with benzene to leave the ionic liquid phase containing the catalyst, which could be reused. All the volatile organic compounds were then removed under reduced pressure and the residue was purified by flash column chromatography on silica gel (hexane) to give 177 mg (91 %) of pure 1,1-diphenyl-1-propene as a pale yellow solid.

Typical procedure for intramolecular Friedel–Crafts alkenylations in an ionic liquid: A mixture of $\text{Hf}(\text{OTf})_4$ (77.4 mg, 0.1 mmol), phenyl 3-phenylpropionate (222.1 mg, 1 mmol), methylcyclohexane (6 mL), and $[\text{bmim}][\text{SbF}_6]$ (1 mL) was heated to reflux for 9 h under a nitrogen atmosphere. The reaction mixture was then cooled to room temperature. All the volatile organic compounds were then removed under reduced pressure and the residue was purified by flash column

chromatography on silica gel (hexane/diethyl ether) to give 113 mg (51 %) of pure 4-phenylcoumarin as a pale yellow solid.

Received: April 12, 2004

Keywords: alkenylation · C–C bond formation · homogeneous catalysis · ionic liquids · Lewis acids

- [1] For reviews of Friedel–Crafts alkylation reactions, see: a) *Friedel–Crafts and Related Reactions, Vol. II*, part 1 (Ed.: G. A. Olah), Wiley-Interscience, New York, **1964**; b) *Friedel–Crafts Alkylation Chemistry. A Century of Discovery* (Eds.: R. M. Roberts, A. A. Khalaf), Marcel Dekker, New York, **1984**; c) G. A. Olah, R. Krishnamurthi, G. K. S. Prakash, in *Friedel–Crafts Alkylations in Comprehensive Organic Synthesis* (Eds.: B. M. Trost, I. Fleming), Pergamon, Oxford, **1991**.
- [2] O. W. Cook, V. J. Chabert, *J. Am. Chem. Soc.* **1921**, *43*, 334; J. S. Reichert, J. A. Nieuwland, *J. Am. Chem. Soc.* **1923**, *45*, 3090; J. A. Reilly, J. A. Nieuwland, *J. Am. Chem. Soc.* **1928**, *50*, 2564.
- [3] T. Tsuchimoto, T. Maeda, E. Shirakawa, Y. Kawakami, *Chem. Commun.* **2000**, 1573.
- [4] G. Sartori, F. Bigi, A. Pastorio, C. Porta, A. Arienti, R. Maggi, N. Moretti, G. Gnappi, *Tetrahedron Lett.* **1995**, *36*, 9177.
- [5] G. Casiraghi, G. Casnati, G. Puglia, G. Sartori, G. Terenghi, *Synthesis* **1977**, 122.
- [6] M. Yamaguchi, Y. Kido, A. Hayashi, M. Hirama, *Angew. Chem.* **1997**, *109*, 1370; *Angew. Chem. Int. Ed. Engl.* **1997**, *36*, 1313; Y. Kido, S. Yoshimura, M. Yamaguchi, T. Uchimaru, *Bull. Chem. Soc. Jpn.* **1999**, *72*, 1445.
- [7] M. Yamaguchi, A. Hayashi, M. Hirama, *J. Am. Chem. Soc.* **1995**, *117*, 1151.
- [8] For recent reviews on ionic liquids, see: a) C. E. Song, *Chem. Commun.* **2004**, 1033; b) R. Sheldon, *Chem. Commun.* **2001**, 2399; c) P. Wasserscheid, W. Keim, *Angew. Chem.* **2000**, *112*, 3926; *Angew. Chem. Int. Ed.* **2000**, *39*, 3772; d) T. Welton, *Chem. Rev.* **1999**, *99*, 2071.
- [9] Our recent examples: a) C. E. Song, W. H. Shim, E. J. Roh, J. H. Choi, *Chem. Commun.* **2000**, 1695; b) C. E. Song, E. J. Roh, *Chem. Commun.* **2000**, 837; c) C. E. Song, W. H. Shim, E. J. Roh, S.-g. Lee, J. H. Choi, *Chem. Commun.* **2001**, 1122; d) S.-g. Lee, J. W. Park, J. Kang, J. K. Lee, *Chem. Commun.* **2001**, 1698; e) D. W. Kim, C. E. Song, D. Y. Chi, *J. Am. Chem. Soc.* **2002**, *124*, 10278; f) S.-g. Lee, J. W. Park, *Bull. Korean Chem. Soc.* **2002**, *23*, 1367; g) D. W. Kim, C. E. Song, D. Y. Chi, *J. Org. Chem.* **2003**, *68*, 4281; h) E. J. Kim, S. Y. Ko, C. E. Song, *Helv. Chim. Acta* **2003**, *86*, 894; i) S.-g. Lee, Y. J. Zhang, P. Z. Yu, H. Yoon, C. E. Song, J. H. Choi, J. Hong, *Chem. Commun.* **2003**, 2624; j) S.-g. Lee, J. W. Park, *J. Mol. Catal. A* **2003**, *194*, 49.
- [10] In sharp contrast to these results, only very small amounts of the alkenylated product was obtained (<2 % yield) in the hydrophilic ionic liquids, $[\text{bmim}][\text{BF}_4]$ or $[\text{bmim}][\text{OTf}]$.
- [11] Recently, Rogers and co-workers reported the instability of the ionic liquids' counterion PF_6^- towards moisture, which resulted in hydrolysis and the formation of HF (R. P. Swatloski, J. D. Holbrey, R. D. Rogers, *Green Chem.* **2003**, *5*, 361). Therefore, to examine the possible catalytic effect of HF on this reaction, we also carried out the reaction only in $[\text{bmim}][\text{SbF}_6]$ or in a mixture of $[\text{bmim}][\text{SbF}_6]$ and water (1:1, v/v) without any metal triflate catalyst. However, the reaction did not occur at all.
- [12] A new synthetic route to alkenylated arenes involving Pd- and Pt-catalyzed addition of arenes to alkynes in the presence of trifluoroacetic acid was recently reported: a) C. Jia, D. Piao, J. Oyamada, W. Lu, T. Kitamura, Y. Fujiwara, *Science* **2000**, *287*, 1992; b) C. Jia, W. Lu, J. Oyamada, T. Kitamura, K. Matsuda, M. Irie, Y. Fujiwara, *J. Am. Chem. Soc.* **2000**, *122*, 7252.

Polymerizations

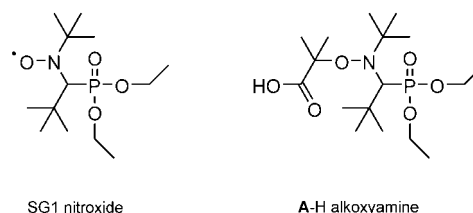
Nitroxide-Mediated Controlled Free-Radical Emulsion Polymerization of Styrene and *n*-Butyl Acrylate with a Water-Soluble Alkoxyamine as Initiator

Julien Nicolas, Bernadette Charleux,* Olivier Guerret, and Stéphanie Magnet

Controlled free-radical polymerization (CRP) in water-based systems has been studied intensely during the last ten years as it combines the environmental and technical advantages of polymerization in aqueous dispersed media with the ability to synthesize tailor-made macromolecular architectures.^[1–4] Most CRP methods, however, have not been applied in traditional macroemulsion polymerization processes (usually called simply emulsion polymerization),^[5] but in miniemulsion polymerization,^[1–4,6] as the latter process offers benefits from the mechanistic viewpoint and can be regarded as a simplified model of emulsion polymerization. Indeed, nucleation takes place directly in the monomer droplets, which become polymer particles upon initiation with either a hydrophobic or a hydrophilic initiator, and subsequent propagation. However, the formation of small, stable monomer droplets requires the application of high shear to the initial monomer-in-water emulsion and the addition of a highly hydrophobic molecule to the monomer phase.^[6] Many authors have demonstrated the great success of this method for all CRP techniques.^[1–4] However, industrial applications usually demand an easier process; in particular, the use of a high shear device in large-volume reactors is usually avoided, and furthermore, the introduction of a hydrophobic additive, which is sometimes a volatile organic compound, is not encouraged. Consequently, true emulsion polymerization is usually the technique of choice owing to its simplicity: this process does not require any special manipulation of the initial monomer-in-water emulsion, only the use of a water-soluble initiator,^[5] and particles are generated in the aqueous phase, independently from the oil droplets, which only act as a monomer reservoir. Mainly due to the sensitivity of the nucleation step, CRP in emulsion systems often leads to unstable latexes, and is therefore still a challenge.^[1–4] The formation of these unstable latexes has been explained by the very specific features of the chain growth in CRP with respect

to a classical free-radical polymerization—a large number of oligomers undergo slow and simultaneous growth in the early stage of the polymerization, which completely modifies the particle-formation mechanism.

The goal of this work was to apply nitroxide-mediated polymerization in an emulsion process. This CRP method^[7] takes advantage of the reversible deactivation of the propagating radicals by nitroxide, which gives alkoxyamine-terminated dormant chains and induces a controlled chain-growth. This method has recently been improved significantly with the discovery of very efficient acyclic nitroxides, such as SG1 (Scheme 1),^[8] which can control the polymerization of a



Scheme 1. Structure of the nitroxide SG1 and of the SG1-based water-soluble alkoxyamine initiator (A-H for the displayed acidic form; A-Na for the corresponding sodium salt).

much broader range of monomers than cyclic nitroxides like TEMPO (2,2,6,6-tetramethylpiperidinyl-1-oxy).^[7] To perfectly control the chain growth and polymerization kinetics, a monocomponent alkoxyamine initiator should be selected rather than a normal bicomponent initiator system (classical radical initiator along with free nitroxide), because the latter suffers from poorly controlled initiator efficiency.^[7] Consequently, the real challenge in nitroxide-mediated emulsion polymerization is first to select an appropriate water-soluble alkoxyamine initiator, and second to find the appropriate conditions to form a stable latex with sufficiently high solids content.^[9] The very few reports on nitroxide-mediated ab initio emulsion polymerization have mainly concerned the application of a water-soluble radical initiator in conjunction with free nitroxide, either TEMPO^[9–11] or SG1.^[12] Marestin et al.^[10] are the only group to report the use of a TEMPO-based water-soluble alkoxyamine in a diluted emulsion polymerization of styrene. However, the polymerization was rather slow and the use of TEMPO restricted its use to styrene.

In this paper we present a new and simple way to perform nitroxide-mediated emulsion polymerization of both *n*-butyl acrylate (BA) and styrene (S), as well as the synthesis of a block copolymer, using a novel, water-soluble, SG1-based alkoxyamine (Scheme 1),^[13] which can also be successfully applied in a miniemulsion.^[14] The solubility in water is imparted by the sodium carboxylate group, providing the pH remains above about 6 ($pK_a = 4.98$),^[15] at least during the nucleation step. Due to the hydrophobicity of the SG1 capping agent, A-Na exhibits surface activity in aqueous solution^[14] but undergoes homolytic dissociation to the highly water-soluble 2-(hydroxycarbonyl)prop-2-yl sodium salt radical, which initiates the polymerization in the water phase.

[*] J. Nicolas, Prof. B. Charleux
Laboratoire de Chimie des Polymères
UMR 7610 Associée au CNRS
Université Pierre et Marie Curie, T44, E1
4, Place Jussieu, 75252 Paris, Cedex 05 (France)
Fax: (+33) -1-4427-7089
E-mail: charleux@ccr.jussieu.fr
Dr. O. Guerret, Dr. S. Magnet
ATOFINA
Groupement de Recherches de Lacq
B.P. no 34, 64170 Lacq (France)



Supporting information for this article is available on the WWW under <http://www.angewandte.org> or from the author.

In a preliminary study, emulsion polymerizations initiated with the water-soluble **A**-Na alkoxyamine were performed in a single-batch step with 20 wt % monomer content and 2.2 wt % of various surfactants (see Supporting Information). In all cases the latexes underwent destabilization after about 50 % monomer conversion, most probably due to the partition of the initially formed oligomeric alkoxyamines between the water phase and the oil phase, leading to unwanted droplet nucleation. Nevertheless, all polymers were well controlled, demonstrating the efficiency of the selected initiator. Consequently, improvement of the colloidal characteristics of the latexes was the main issue to address. This was done by making the process a multi-step polymerization.

The first polymerization step was the preparation of a living poly(*n*-butyl acrylate) seed latex, from a very dilute monomer-in-water emulsion (0.7 wt %; apparent concentration of 0.055 mol L⁻¹), with two different surfactant concentrations above the critical micelle concentration (experiments **1** and **2** in Table 1). The pH of the water phase was 7.4 and 6.9 for experiments **1** and **2**, respectively, that is, above the lower limit of 6 needed for a high ionization degree of the initiator. The majority of the *n*-butyl acrylate monomer was located either in the water solution^[16] or in the swollen micelles. If present, the monomer droplets should therefore remain in only very small quantities. Indeed, with both the selected surfactant concentrations a clear solution was obtained at the polymerization temperature before the start of the reaction. The main purpose was to favor micellar nucleation over droplet nucleation. In both experiments the oligomers were obtained reproducibly with controlled molar masses in almost perfect agreement with the theoretical value (conversion at 8 h was close to 60 % and theoretical $M_n = 1100 \text{ g mol}^{-1}$; experimental $M_n = 1060 \text{ g mol}^{-1}$ for experiment **1** with $M_w/M_n = 1.14$; experimental $M_n = 1080 \text{ g mol}^{-1}$

for experiment **1'**, with $M_w/M_n = 1.17$; experimental $M_n = 1120 \text{ g mol}^{-1}$ for experiment **2**, with $M_w/M_n = 1.20$; experimental $M_n = 1110 \text{ g mol}^{-1}$ for experiment **2'**, with $M_w/M_n = 1.17$). The molar masses indicate a high initiator efficiency, meaning that all **A**-Na molecules are consumed and turned into the hydrophobic polymer chains that form the particles.

Both seed latexes are stable, with an average particle diameter, given by dynamic light scattering (DLS), of 210 nm for the lowest amount of surfactant used (experiment **1**) and 150 nm when the amount of surfactant was multiplied by a factor of 2.3 (experiment **2**). As shown in Table 1, both experiments are also reproducible from the particle-size viewpoint, although the diameters are rather large and the particle-size distribution broad, in contrast to what is expected in a classical emulsion polymerization. Nucleation might lead to a change in the thermodynamic properties of the system, in close analogy with the theory of "super-swelling" proposed for miniemulsions by Luo et al.^[17] The presence of a large concentration of oligomers in the growing particles during the early stages of the reaction would lead to a lower chemical potential than in the non-nucleated micelles or droplets, which would enhance swelling of the former by the monomer. This would favor the formation of large particles with a broad particle-size distribution. The low amount of monomer, however, allowed us to limit the effects of this unwanted trend.

The low-solids-content poly(*n*-butyl acrylate) latexes produced in the first step were further used as a seed for the batch emulsion polymerization of *n*-butyl acrylate and styrene (Table 1). As illustrated by the conversion versus time plots in Figure 1 and Figure 2, the dispersed oligomeric alkoxyamines initiate the polymerization and lead to fast and nearly complete polymerizations (85 to 95 % conversion within 8 h), with very good reproducibility (see Table 1 and

Table 1: Experimental conditions for the living seed latex preparation and the seeded batch emulsion polymerization.^[a]

Exp.	Seed Latex	Monomer(s)	Monomer content [wt %]	[Surfactant] ^[b] [mol L ⁻¹ _{aq}] ([wt %]) ^[c]	T [°C]	[A-Na] ₀ [mol L ⁻¹ _{aq}]	Overall theoretical DP _n at 100 % conv. ^[d]	Overall conversion after 8 h ^[e] [%]	Final average diameter from DLS [nm]
1	–	BA	0.7	6.89×10^{-3}	112	5.82×10^{-3}	10	55	210
1'	–	BA	0.7	6.89×10^{-3}	112	5.82×10^{-3}	10	60	230
2	–	BA	0.7	1.54×10^{-2}	112	5.71×10^{-3}	10	60	150
2'	–	BA	0.7	1.54×10^{-2}	112	5.71×10^{-3}	10	60	155
3	1	BA + BA	16.5	6.89×10^{-3} (2.2)	112	5.82×10^{-3}	267	95	660
3'	1	BA + BA	16.5	6.89×10^{-3} (2.2)	112	5.82×10^{-3}	267	95	650
4	1	BA + S	16.5	6.89×10^{-3} (2.2)	120	5.82×10^{-3}	327	87	530
									(TEM: $D_n = 450$; $D_w = 830$) ^[f]
5	2	BA + BA	16.3	1.54×10^{-2} (5.1)	112	5.71×10^{-3}	266	92	270
6	2	BA + S	16.1	1.55×10^{-2} (5.1)	120	5.71×10^{-3}	328	85	260
									(TEM: $D_n = 90$; $D_w = 350$) ^[f]
7 ^[g]	2	BA + BA + S	26.4	1.55×10^{-2} (2.9)	112	5.71×10^{-3}	532	80	330
7' ^[g]	2	BA + BA + S	26.4	1.55×10^{-2} (2.9)	112	5.71×10^{-3}	532	85	310

[a] $[\text{NaHCO}_3] = 0.012 \text{ mol L}^{-1}$; $p = 3 \text{ bar N}_2$; **A**-H was dissolved in a 0.4 M sodium hydroxide solution (1.6 equiv.) to give **A**-Na, and was then added into the reactor at 90 °C, triggering the reaction. The experiments **1**, **2**, **3**, and **7** were duplicated, with the same experimental conditions. [b] Dowfax 8390; critical micelle concentration = 0.05 wt % at 25 °C, approximately 0.5–1 mM. [c] Based on the overall weight of monomer. [d] Theoretical $\text{DP}_n = [\text{monomer}]_0 / [\text{alkoxyamine}]_0$. [e] Determined by gravimetry. [f] Determined by TEM, using $D_n = \sum n_i D_i / \sum n_i$ and $D_w = \sum n_i D_i^4 / \sum n_i D_i^3$ (see the full distribution in the supporting information). [g] Same initial molar amount of *n*-butyl acrylate and styrene (55 wt % of BA); composition of copolymer **7** at 80 % conversion determined by ¹H NMR spectroscopy (200 MHz, CDCl₃) to be 47 mol % of BA.

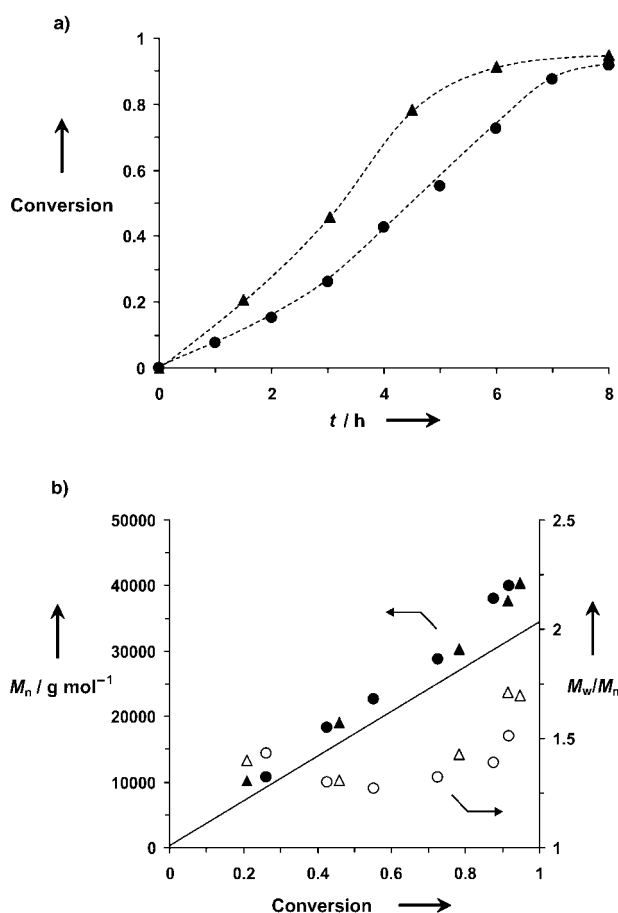


Figure 1. Seeded emulsion polymerizations of *n*-butyl acrylate (experiment 3: \blacktriangle , \triangle ; experiment 5: \bullet , \circ): a) monomer conversion versus time; b) number-average molar mass and polydispersity index versus conversion. Straight line: theoretical evolution of M_n versus conversion.

the Supporting Information for the comparison of experiments 3 and 3'). Moreover, controlled molar masses and narrow molar-mass distributions were observed (Figure 1 and 2): the M_n values were close to the predicted ones, indicating a good reinitiation efficiency. For *n*-butyl acrylate polymerization, broadening of the molar-mass distribution was observed at the end of the reaction, possibly due to irreversible termination and/or to intermolecular chain transfer to the polymer, which are not unexpected at such large conversions.^[18]

From the colloidal viewpoint, the important result is that the latexes are all stable for months. The final average diameters are given in Table 1. They are strongly dependent on the seed used (i.e. to the initial concentration of surfactant) and on the amount of polymer, but do not depend much on the type of monomer polymerized in the second step. DLS gave an average diameter of 660 nm for the poly(*n*-butyl acrylate) latex 3 and 530 nm for the polystyrene latex 4, both extended from seed 1 (the calculated final diameter is 600 nm, on the basis of the DLS seed diameter and the amount of polymerized monomer). Moreover, the diameter increases with conversion in such a way that the total number of latex

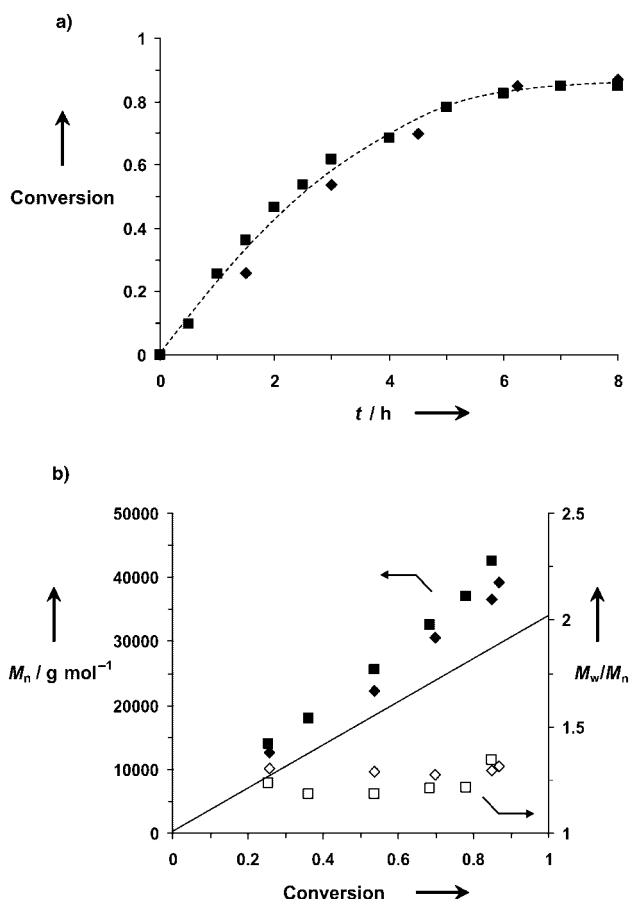


Figure 2. Seeded emulsion polymerizations of styrene (experiment 4: \blacklozenge , \diamond ; experiment 6: \blacksquare , \square): a) monomer conversion versus time; b) number-average molar mass and polydispersity index versus conversion. Straight line: theoretical evolution of M_n versus conversion.

particles remains fairly constant throughout the polymerization. For latex 4, transmission electron microscopy (TEM) was performed: $D_n = 450$ nm and $D_w = 830$ nm, indicating a broad particle-size distribution. For the latexes extended from seed 2, DLS gave an average diameter of 270 nm for the poly(*n*-butyl acrylate) latex 5 and 260 nm for the polystyrene latex 6, whereas the calculated diameter is 400 nm (TEM measurements on the latter gave $D_n = 90$ nm and $D_w = 350$ nm). The large discrepancy between DLS and TEM in those experiments comes from the existence of very small particles that are barely detectable by DLS. Although these results do not indicate a perfect control over the particle size and particle-size distribution, they are essentially the same as those currently obtained in analogous miniemulsion polymerizations.^[1–4]

The process was also applied to the three-step synthesis of a block copolymer with a 1:1 molar composition. The first two steps were identical to those for the poly(*n*-butyl acrylate) latex 5. Before the end of the second step (5.5 h, 55% *n*-butyl acrylate conversion), the polymerization was stopped by cooling the reaction medium. The unreacted BA monomer was not removed, part of the styrene was added, and the mixture was stirred gently overnight at room temperature.

After addition of the remaining styrene, the temperature was raised again to 112°C. All the features of a controlled polymerization were maintained, with the continuous increase of the average molar masses with monomer conversion, the low polydispersity indexes (Figure 3), and the

field of controlled free-radical polymerization, is of high academic and industrial relevance.

Received: May 18, 2004

Revised: August 26, 2004

Keywords: alkoxyamines · emulsions · living polymerization · nitroxides · polymerization

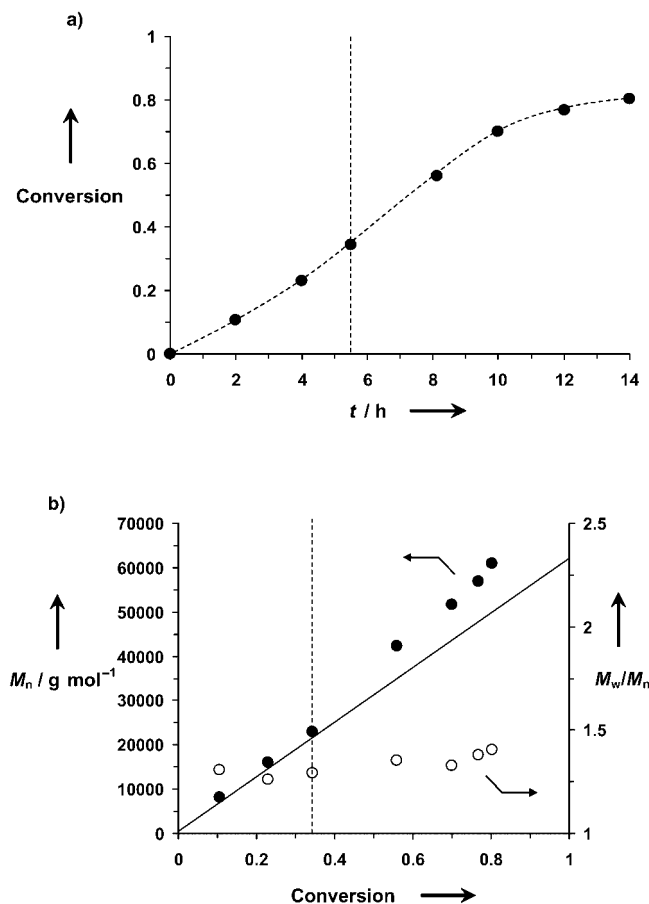


Figure 3. Synthesis of a poly(*n*-butyl acrylate)-*b*-poly(*n*-butyl acrylate-co-styrene) block copolymer in a three-step emulsion polymerization (experiment 7): a) monomer conversion versus time; b) number-average molar mass and polydispersity index versus conversion. Vertical dotted line: time when styrene was added. Straight line: theoretical evolution of M_n versus conversion.

shift of the size-exclusion chromatography (SEC) peaks toward larger molar masses (see Supporting Information). Again, a stable latex was recovered, with 26% solids content.

Nitroxide-mediated emulsion polymerization of *n*-butyl acrylate and styrene was successfully carried out in a multi-step process in the presence of a novel water-soluble alkoxyamine initiator based on the nitroxide SG1. Fast reactions were observed, leading to polymers with controlled molar mass and narrow molar-mass distribution, which could be further extended by monomer addition. The process allowed us to form stable latexes with a solids content as high as 26 wt%. Such a true emulsion polymerization process in living conditions, which was previously a real challenge in the

- [1] J. Qiu, B. Charleux, K. Matyjaszewski, *Prog. Polym. Sci.* **2001**, 26, 2083–2134.
- [2] M. F. Cunningham, *Prog. Polym. Sci.* **2002**, 27, 1039–1067.
- [3] B. Charleux, *ACS Symp. Ser.* **2003**, 854, 438–451.
- [4] M. F. Cunningham, *C. R. Chim.* **2003**, 6, 1351–1374.
- [5] R. G. Gilbert, *Emulsion Polymerization. A Mechanistic Approach*, Academic Press, London, **1995**.
- [6] K. Landfester, *Macromol. Rapid Commun.* **2001**, 22, 896–936.
- [7] C. J. Hawker, A. W. Bosman, E. Harth, *Chem. Rev.* **2001**, 101, 3661–3688.
- [8] S. Grimaldi, J. P. Finet, F. Le Moigne, A. Zeghdaoui, P. Tordo, D. Benoit, M. Fontanille, Y. Gnanou, *Macromolecules* **2000**, 33, 1141–1147.
- [9] A. R. Szkurhan, M. K. Georges, *Macromolecules* **2004**, 37, 4776–4782.
- [10] C. Marestin, C. Noël, A. Guyot, J. Claverie, *Macromolecules* **1998**, 31, 4041–4044.
- [11] J. Cao, J. He, C. Li, Y. Yang, *Polym. J.* **2001**, 33, 75–80.
- [12] M. Lansalot, C. Farcet, B. Charleux, J. P. Vairon, R. Pirri, P. Tordo, *ACS Symp. Ser.* **2000**, 768, 138–151.
- [13] J. L. Couturier, O. Guerret, D. Bertin, D. Gigmes, S. Marque, P. Tordo, F. Chauvin, P. E. Dufils, WO 2004/014926.
- [14] J. Nicolas, B. Charleux, O. Guerret, S. Magnet, *Macromolecules* **2004**, 37, 4453–4463.
- [15] The pK_a of the acidic A-H alkoxyamine initiator was determined by titration in anhydrous ethanol against a 0.1M sodium hydroxide solution. The conversion between aqueous and alcoholic acidic scales was performed as described in the following reference: R. B. Bates, *Determination of pH, Theory and Practice*, Wiley, **1964**, Ch. 7.
- [16] The saturated solution of *n*-butyl acrylate in water has concentration of $6.4 \times 10^{-3} \text{ mol L}^{-1}$ at 50°C, according to ref. [5] and I. Capek, J. Barton, E. Orolinova, *Chem. Zvesti* **1984**, 38, 803–822.
- [17] Y. Luo, J. G. Tsavalas, F. J. Schork, *Macromolecules* **2001**, 34, 5501–5507.
- [18] C. Farcet, J. Belleney, B. Charleux, R. Pirri, *Macromolecules* **2002**, 35, 4912–4918.

Metal Polysulfides

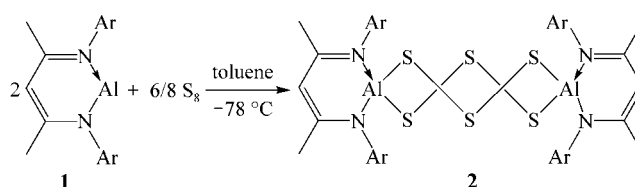
[LAl(μ -S₃)₂AlL]: A Homobimetallic Derivative of the Sulfur Crown S₈**

Ying Peng, Hongjun Fan, Vojtech Jancik, Herbert W. Roesky,* and Regine Herbst-Irmer

Dedicated to Professor Tobin J. Marks on the occasion of his 60th birthday

Metal polysulfides, synthesized by a variety of methods using various reagents as sulfur source, such as S₈, M₂S_n (M = alkali metal), P₄S₁₀, H₂S, and organic polysulfanes, have attracted much attention not only regarding their structure and reactivity but also owing to their potential uses.^[1] Metal polysulfide complexes^[1b] may be viewed as derivatives of the S_x²⁻ (x ≥ 2) ion. Transition-metal polysulfides have attracted interest as catalysts and intermediates in enzymatic processes and in catalytic reactions of industrial importance, such as the hydrodesulfurization (HDS) of fossil fuels.^[2] Furthermore, the metal polysulfides can be used as precursor for metal-sulfur clusters. In contrast, such complexes containing heavier main-group elements, such as the Group 13, 14, and 15 metals have been much less explored.^[1a,d] Among the numerous investigations of the metal polysulfides, complexes with the (μ-S₃) chain are rarely reported. The most common examples are those of transition-metal complexes [(η⁵-RC₅H₄)₂Ti(μ-S₃)₂] (R = H, Me)^[3] and [(η⁵-MeC₅H₄)Ru(PPh₃)(μ-S₃)₂]^[4] which were obtained by treatment of [(η⁵-RC₅H₄)₂TiS₃] (R = H, Me) with PPh₃, and [(η⁵-MeC₅H₄)Ru(PPh₃)₂S₃]^[5] [SbF₆]₂ with (NBu₄)₂S₆, respectively. [LAl^I] (**1**) (L = HC(CMeNAr)₂, Ar = 2,6-*i*Pr₂C₆H₃)^[5] with its nonbonding lone pair of electrons at aluminum has a singlet carbene-like character and may show unprecedented chemical reaction behavior.^[6] Herein, we describe the synthesis and structural characterization of [LAl(μ-S₃)₂AlL] (**2**) containing two (μ-S₃) chains.

Compound **2** was synthesized by the reaction of **1** with sulfur in a molar ratio of 2:6^[7] (Scheme 1). Cold toluene was added to the mixture of **1** and sulfur at -78 °C. After several minutes a suspension was obtained which was kept at -78 °C for 2 h. Subsequently the suspension was slowly warmed to room temperature under formation of more precipitate. The compound [LAl(μ-S)₂AlL]^[8] was isolated from the precipitate



Scheme 1. Synthesis of **2**.

and characterized by its characteristic melting point and EI mass spectrum. Pale yellow crystals of **2** were obtained from the concentrated filtrate at 4 °C, as well as at room temperature. It is noted that even when the above reaction was employed in a molar ratio of 2:3,^[7] the isolated product is also **2** however in lower yield (about 10%). Compound **2** was characterized by ¹H and ¹³C NMR spectroscopy, EI mass spectrometry, and elemental analysis. The most intense peak in the EI mass spectrum of **2** appears at *m/z* 508 [M⁺-LAlS₄]. The signals at 540 (38%) and 572 (15%) are assigned to the [M⁺-LAlS₃] and [M⁺-LAlS₂] fragments, respectively. Compound **2** is sparingly soluble in [D₆]benzene, and the solubility does not improve even when heated. **2** does not dissolve in hexane and pentane. When the reaction mixture or the isolated compound is exposed to traces of moisture, the free ligand LH can be detected by ¹H NMR spectroscopy.

Single crystals of **2**^[9] suitable for X-ray structural analysis were obtained in toluene at 4 °C. Compound **2** crystallizes in the monoclinic space group *P*2₁/*n* with two co-crystallized molecules of toluene per molecule of **2** (Figure 1). Two (μ-S₃) chains connect two aluminum atoms to form an aluminum polysulfide with an Al₂S₆ eight-membered ring. The two L ligands are almost coplanar. The symmetry of the structure is *C*₂. In the S₈ structure,^[10] the two S₃ units are eclipsed, whereas in **2** they are staggered, thus we cannot simply argue that the two aluminum atoms are replacing the corresponding sulfur atoms in S₈. The S-S bond length (av 2.08 Å) in **2** is

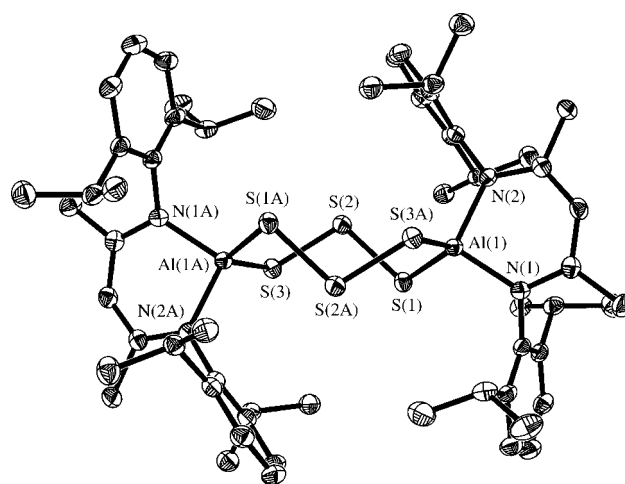


Figure 1. Thermal ellipsoids plot of **2** (thermal ellipsoids set at 50% probability). Hydrogen atoms and solvent molecules are omitted for clarity. Selected bond lengths [Å] and angles [°]: Al(1)-N(1) 1.882(2), Al(1)-N(2) 1.904(2), Al(1)-S(1) 2.223(1), Al(1)-S(3A) 2.248(1), S(1)-S(2) 2.095(1), S(2)-S(3) 2.073(1); N(1)-Al(1)-N(2) 97.7(1), S(2)-S(1)-Al(1) 98.0(1), S(1)-Al(1)-S(3A) 116.9(1), S(3)-S(2)-S(1) 104.7(1).

[*] Dipl.-Chem. Y. Peng, V. Jancik, Prof. Dr. H. W. Roesky, Dr. R. Herbst-Irmer
Institut für Anorganische Chemie der Universität Göttingen
Tammannstrasse 4
37077 Göttingen (Germany)
Fax: (+49) 551-39-3373
E-mail: hroesky@gwdg.de

Dr. H. Fan
Labor für Physikalische und Theoretische Chemie
Universität Siegen, 57068 Siegen (Germany)

[**] L = HC(CMeNAr)₂, Ar = 2,6-*i*Pr₂C₆H₃. This work was supported by the Deutsche Forschungsgemeinschaft, the Göttinger Akademie der Wissenschaften and the Fonds der Chemischen Industrie.

Table 1: The reaction energy of $[L_2Al_2S_n]$ ($n=2-8$).^[a]

	2	3	4	5	6	7	8
reaction energy [kJ mol ⁻¹]	-648 (S1 S1)	-641 (S1 S2)	-644 (S1 S3) -571 (S2 S2)	-602 (S1 S4) -581 (S2 S3)	-621 (S1 S5) -608 (S3 S3)	-594 (S1 S6) -570 (S3 S4)	-609 (S1 S7) -524 (S4 S4)

[a] The reaction energy is obtained from $E([L_2Al_2S_n]) - 2E([LAl]) - n/8E(S_8)$. The notes next to the energies show the conformations. For example, S3 S4 means one bridge has three S atoms, while the other one has four S atoms

slightly longer than that in S_8 ^[10] (av 2.05 Å), $[(\eta^5\text{-MeC}_5\text{H}_4)_2\text{-Ti}(\mu\text{-S}_3)]_2$ ^[3] (av 2.06 Å), and $[(\eta^5\text{-MeC}_5\text{H}_4)\text{Ru}(\text{PPh}_3)(\mu\text{-S}_3)]_2$ ^[4] (av 2.05 Å). The Al–S bond lengths (av 2.24 Å) are comparable with those in the dimer $[LAl(\mu\text{-S})_2AlL]$ (av 2.24 Å)^[8] and in $[LAl(\text{SH})_2]$ (av 2.22 Å).^[11] The Al–N bond length (av 1.89 Å) falls within the range of those in aluminum derivatives bearing the L ligand.^[12] The S–S–S angle (104.7°) is close to those found in $[(\eta^5\text{-MeC}_5\text{H}_4)_2\text{Ti}(\mu\text{-S}_3)]_2$ ^[3] (109.1°) and $[(\eta^5\text{-MeC}_5\text{H}_4)\text{Ru}(\text{PPh}_3)(\mu\text{-S}_3)]_2$ ^[4] (105.2°).

The S_8 ring can have different cleavage patterns and thus forms various types of structures.^[1a] For $[L_2Al_2S_n]$ species the product with $n=2$ is known,^[8] and herein compound **2** has $n=6$. Theoretical calculations were carried out to estimate the relative stability of the compounds with $n=2-8$. The method used is RI-BP86/TZVP within the TURBOMOLE^[13] program. The optimized structure of $[L_2Al_2S_6]$ is in good agreement with the X-ray values for **2** (mean deviation < 0.04 Å), which shows the reliability of the selected theoretical method. In the calculation the CHMe_2 groups in the ligand L were replaced by H atoms. The relative stability of $[L_2Al_2S_n]$ was estimated by the reaction energy of $2[LAl] + n/8S_8 \rightarrow [L_2Al_2S_n]$. The calculated reaction energies are listed in Table 1. All the reactions are exothermic. Compound $[L_2Al_2S_6]$ ^[8] is the most stable. However, there are quite a few conformations with only a slightly smaller reaction energy, and thus thermodynamically they are all possible. Most $[L_2Al_2S_n]$ species prefer only one bridging S atom, while all the other S atoms are arranged in the second bridge (Table 1). We could isolate **2** but not the (theoretically favored) S1 S5 isomer, this might be due to the very low solubility of the latter species.

Therefore, the theoretical work shows that all $[L_2Al_2S_n]$ ($n=2-8$) species have rather stable conformations (and that there can be more than one).^[14] These compounds may coexist in the product, and under different reaction conditions another species may be preferentially formed. To obtain a single crystal out of such a mixture is difficult except for $n=2$ where one can use excess of **1** to react with sulfur.

In summary, we report herein the first compound of Group 13 with two $(\mu\text{-S}_3)$ chains connecting two aluminum atoms under formation of an eight-membered Al_2S_6 ring. Studies of the other possible conformations of $[L_2Al_2S_n]$ estimated by calculation are underway.

Experimental Section

All manipulations were performed under a dry and oxygen-free nitrogen atmosphere using Schlenk-line and glovebox techniques.

2: Toluene (30 mL) was added to a mixture of **1** (0.580 g, 1.3 mmol) and S_8 (0.125 g, 3.9 mmol) at -78°C . The resulting

suspension was stirred at this temperature for 2 h and slowly warmed to room temperature. The mixture was stirred for additional 15 h. After removal of the precipitate by filtration, the concentrated solution was kept at room temperature for 3 days to afford pale yellow crystals of **2**. (0.150 g, 22 %). M.p. 185°C (decomp); EI-MS: m/z (%) 508 (100) $[M^+ - \text{LAIS}_4]$, 540 (38) $[M^+ - \text{LAIS}_3]$, 572 (15) $[M^+ - \text{LAIS}_2]$. ^1H NMR (500.13 MHz, C_6D_6): δ = 7.20–6.90 (m, 12 H, Ar-H), 4.72 (s, 2 H, $\gamma\text{-H}$), 3.30 (sept, 8 H, J = 6.8 Hz, CHMe_2), 1.50 (s, 12 H, Me), 1.37 (d, 24 H, J = 6.8 Hz, CHMe_2), 1.00 ppm (d, 24 H, J = 6.8 Hz, CHMe_2); ^{13}C NMR (125.77 MHz, C_6D_6): δ = 171.78 (CN), 145.74, 143.69, 128.20, 123.83 (Ar), 97.74 ($\gamma\text{-C}$), 28.92 (CHMe_2), 25.45 (CHMe_2), 23.93 (CHMe_2), 23.55 ppm (Me); ^{27}Al NMR: resonance is silent. Elemental analysis (%) calcd for $\text{C}_{58}\text{H}_{82}\text{Al}_2\text{N}_4\text{S}_6$ (1081.66): C 64.40, H 7.64, N 5.18; found C 64.65, H 7.88, N 4.76 %.

Received: July 6, 2004

Keywords: aluminum · bridging ligands · density functional calculations · structure elucidation · sulfur

- [1] a) N. Takeda, N. Tokitoh, R. Okazaki, *Top. Curr. Chem.* **2003**, 231, 153–202, and references therein; b) M. Draganjac, T. B. Rauchfuss, *Angew. Chem.* **1985**, 97, 745–760; *Angew. Chem. Int. Ed. Engl.* **1985**, 24, 742–757; c) D. Coucouvanis, *Adv. Inorg. Chem.* **1998**, 45, 1–73; d) R. Okazaki, *Phosphorus Sulfur Silicon* **2001**, 168, 41–50; e) M. R. Dubois, *Chem. Rev.* **1989**, 89, 1–9; f) C. Sinonnet-Jégat, F. Sécheresse, *Chem. Rev.* **2001**, 101, 2601–2611; g) A. Müller, W. Jaegermann, J. H. Enemark, *Coord. Chem. Rev.* **1982**, 46, 245–280; h) J. W. Kolis, *Coord. Chem. Rev.* **1990**, 105, 195–219; i) A. Müller, *Polyhedron* **1986**, 5, 323–340; j) A. Müller, E. Diemann, R. Jostes, H. Bögge, *Angew. Chem.* **1981**, 93, 957–977; *Angew. Chem. Int. Ed. Engl.* **1981**, 20, 934–954; k) D. Coucouvanis, A. Hadjikyriacou, M. Draganjac, M. G. Kanatzidis, O. Ileperuma, *Polyhedron* **1986**, 5, 349–356; l) V. Jancik, H. W. Roesky, D. Neculai, A. M. Neculai, R. Herbst-Irmer, *Angew. Chem.* **2004**, 116, 6318–6322; *Angew. Chem. Int. Ed.* **2004**, 43, 6192–6196.
- [2] T. B. Rauchfuss, *Inorg. Chem.* **2004**, 43, 14–26.
- [3] C. M. Bolinger, T. B. Rauchfuss, S. R. Wilson, *J. Am. Chem. Soc.* **1981**, 103, 5620–5621.
- [4] J. Amarasekera, T. B. Rauchfuss, A. L. Rheingold, *Inorg. Chem.* **1987**, 26, 2017–2018.
- [5] C. Cui, H. W. Roesky, H.-G. Schmidt, M. Noltemeyer, H. Hao, F. Cimpoesu, *Angew. Chem.* **2000**, 112, 4444–4446; *Angew. Chem. Int. Ed.* **2000**, 39, 4274–4276.
- [6] a) C. Cui, S. Köpke, R. Herbst-Irmer, H. W. Roesky, M. Noltemeyer, H.-G. Schmidt, B. Wrackmeyer, *J. Am. Chem. Soc.* **2001**, 123, 9091–9098; b) C. Cui, H. W. Roesky, H. G. Schmidt, M. Noltemeyer, *Angew. Chem.* **2000**, 112, 4705–4707; *Angew. Chem. Int. Ed.* **2000**, 39, 4531–4534; c) H. Zhu, J. Chai, V. Chandrasekhar, H. W. Roesky, J. Magull, D. Vidovic, H.-G. Schmidt, M. Noltemeyer, P. P. Power, W. A. Merrill, *J. Am. Chem. Soc.* **2004**, 126, 9472–9473; d) H. Zhu, J. Chai, A. Stasch, H. W. Roesky, T. Blunck, D. Vidovic, J. Magull, H.-G. Schmidt, M. Noltemeyer, *Eur. J. Inorg. Chem.*, in press; e) Y. Peng, H.

- Fan, H. Zhu, H. W. Roesky, J. Magull, C. E. Hughes, *Angew. Chem.* **2004**, *116*, 3525–3527; *Angew. Chem. Int. Ed.* **2004**, *43*, 3443–3445.
- [7] The ratio corresponds to the stoichiometry of S.
- [8] V. Jancik, M. M. Moya Cabrera, H. W. Roesky, R. Herbst-Irmer, D. Neculai, A. M. Neculai, M. Noltemeyer, H.-G. Schmidt, *Eur. J. Inorg. Chem.* **2004**, 3508–3512.
- [9] Crystal data for **2**·2 toluene: $C_{72}H_{98}Al_2N_4S_6$, $M_r = 1265.86$, monoclinic, space group $P2_1/n$, $a = 14.277(1)$, $b = 16.387(1)$, $c = 15.786(1)$ Å, $\beta = 109.66(1)^\circ$, $V = 3478(1)$ Å³, $Z = 2$, $\rho_{\text{calcd}} = 1.209$ Mg m⁻³, $F(000) = 1360$, $\lambda = 1.54178$ Å, $T = 100(2)$ K, $\mu(\text{Cu}_{K\alpha}) = 2.386$ mm⁻¹. Data for the structure were collected on a Bruker three-circle diffractometer equipped with a SMART 6000 CCD detector. Intensity measurements were performed on a rapidly cooled crystal (dimensions $0.30 \times 0.20 \times 0.10$ mm³) in the range of $7.24 \leq 2\theta \leq 117.84^\circ$. Of the 15352 measured reflections, 4907 were independent ($R(\text{int}) = 0.0363$). The structure was solved by direct methods (SHELXS-97)^[15] and refined with all data by full-matrix least-squares methods on F^2 .^[16] The hydrogen atoms of C–H bonds were placed in idealized positions. The final refinements converged at $R1 = 0.0328$ for $I > 2\sigma(I)$, $wR2 = 0.0868$ for all data. The final difference Fourier synthesis gave a min/max residual electron density $-0.263/+0.619$ e Å⁻³.^[14] CCDC-241840 (**2**) contains the supplementary crystallographic data for this paper. These data can be obtained free of charge via www.ccdc.cam.ac.uk/conts/retrieving.html (or from the Cambridge Crystallographic Data Centre, 12 Union Road, Cambridge CB21EZ, UK; fax: (+44) 1223-336-033; or deposit@ccdc.cam.ac.uk).
- [10] A. C. Gallacher, A. A. Pinkerton, *Acta. Cryst.* **1993**, *C49*, 125–126.
- [11] V. Jancik, Y. Peng, H. W. Roesky, J. Li, D. Neculai, A. M. Neculai, R. Herbst-Irmer, *J. Am. Chem. Soc.* **2003**, *125*, 1452–1453.
- [12] C. Cui, H. W. Roesky, H. Hao, H.-G. Schmidt, M. Noltemeyer, *Angew. Chem.* **2000**, *112*, 1885–1887; *Angew. Chem. Int. Ed.* **2000**, *39*, 1815–1817.
- [13] R. Ahlrichs, M. Bär, H.-P. Baron, R. Bauernschmitt, S. Böcker, P. Deglmann, M. Ehrig, K. Eichkorn, S. Elliott, F. Furche, F. Haase, M. Häser, H. Horn, C. Hättig, C. Huber, U. Huniar, M. Katanek, A. Köhn, C. Kölmel, M. Kollwitz, K. May, C. Ochsenfeld, H. Öhm, A. Schäfer, U. Schneider, M. Sie, *TURBOMOLE 5.5*, University of Karlsruhe, Germany, **2002**.
- [14] The residual electron density 0.619 e Å⁻³ can be explained by the presence of a higher homologue in the crystal (ca. 3 %). It can be refined as either $[L_2Al_2S_7]$ or $[L_2Al_2S_8]$. Owing to the inversion center it is not possible to distinguish between these two homologues. Although this disordered model shows good geometry and leads to a lower R value, the ordered model for **2** was used for the discussion and theoretical calculations.
- [15] SHELXS-97, Program for Structure Solution: G. M. Sheldrick, *Acta Crystallogr. Sect. A* **1990**, *46*, 467–473.
- [16] G. M. Sheldrick, SHELXL-97, *Program for Crystal Structure Refinement*, University of Göttingen, Göttingen (Germany), **1997**.

Preparation of $[\text{LAl}(\mu\text{-S})_2\text{MCp}_2]$ ($\text{M} = \text{Ti}, \text{Zr}$) from the Structurally Characterized Lithium Complexes $[\{\text{LAl}(\text{SH})[\text{SLi}(\text{thf})_2]\}_2]$ and $[\{\text{LAl}[(\text{SLi})_2(\text{thf})_3]\}_2] \cdot 2\text{THF}$ **

Vojtech Jancik, Herbert W. Roesky,* Dante Neculai, Ana M. Neculai, and Regine Herbst-Irmer

Dedicated to Professor Hubert Schmidbaur on the occasion of his 70th birthday

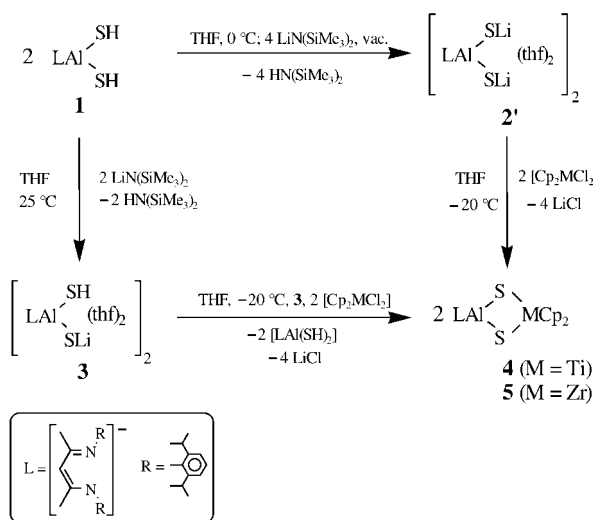
Recently, we reported the preparation of the unique monomeric $[\text{LAl}(\text{SH})_2]$ (**1**) ($\text{L} = \text{HC}(\text{CMeNAr})_2$; $\text{Ar} = 2,6\text{-iPr}_2\text{C}_6\text{H}_3$) comprising two terminal SH moieties.^[1] This unusual species led us to explore the substitution pattern of the SH protons, their exchange with transition metals would open a new route for the preparation of heterobimetallic sulfides containing aluminum. To date very few examples with aluminum bridging sulfide are known. Such species include $[(t\text{BuAl})(t\text{BuAlMe})_2(\mu_3\text{-S})_3\text{ZrCp}_2]$ ($\text{Cp} = \text{C}_5\text{H}_5$), prepared by degradation of the $[\{t\text{BuAl}(\mu_3\text{-S})\}_4]$ cage with two equivalents of $[\text{Cp}_2\text{ZrMe}_2]$.^[2] Moreover, there are known aluminum sulfides with $[\text{AlS}]_n$ core, which can be either planar ($n = 2$), cubic ($n = 4$), drum ($n = 6$), or possess more complex structures with an Al:S molar ratio different from 1:1.^[3]

Attempts to prepare heterobimetallic sulfides with **1** and ZnMe_2 or CdMe_2 through alkane elimination failed, in spite of the high affinity of these elements towards chalcogens.^[4] We observed even at low temperature only the formation of an inseparable mixture of products and the free ligand. This situation is in contrast to the successful preparation of $[\text{LAl}(\mu\text{-S})_2\text{AlL}]$ from **1** and $[\text{LAlH}_2]$.^[3] Following the protocol of Nöth et al. on the preparation of aluminum–lithium salts from LiAlH_4 and thiols,^[5] we chose the lithiation of **1** with MeLi and $n\text{BuLi}$ in diethyl ether or THF as an alternative route to the desired compounds. Unfortunately, under the given conditions the decomposition of **1** was observed. However, the difficulties encountered in the preparation of the dilithium salt $[\{\text{LAl}[(\text{SLi})_2(\text{thf})_3]\}_2] \cdot 2\text{THF}$ (**2**) were overcome by direct reaction of **1** with two equivalents of $\text{LiN}(\text{SiMe}_3)_2$ in THF at 0°C . The extremely sensitive pale yellow product **2** is a dimer solvated by eight molecules of THF as demonstrated by X-ray structural analysis. It has low solubility in THF and forms a microcrystalline precipitate within a few seconds of starting materials being mixed. The recovery of the crystals

[*] Dipl.-Chem. V. Jancik, Prof. Dr. H. W. Roesky, Dr. D. Neculai, Dr. A. M. Neculai, Dr. R. Herbst-Irmer
Institut für Anorganische Chemie
Georg-August Universität
Tammannstrasse 4, 37077 Göttingen (Germany)
Fax: (+49) 551-39-3373
E-mail: hroesky@gwdg.de

[**] This work was supported by the Deutsche Forschungsgemeinschaft and the Göttinger Akademie der Wissenschaften. V.J. thanks the Fonds der Chemischen Industrie for the predoctoral fellowship.
 $\text{L} = \text{HC}(\text{CMeNAr})_2$, $\text{Ar} = 2,6\text{-iPr}_2\text{C}_6\text{H}_3$; $\text{Cp} = \text{C}_5\text{H}_5$.

was performed within 15 min of the addition of the solvent to avoid decomposition caused by free $\text{HN}(\text{SiMe}_3)_2$. However, compound **2** loses THF upon drying in vacuo, leading to a dimeric product $[\{\text{LAl}[(\text{SLi})_2(\text{thf})_2]\}_2]$ (**2'**) containing only four molecules of THF as determined by ^1H NMR spectroscopy. This final product proved to be stable upon storage for several months under an inert atmosphere. After the successful isolation of **2'**, we became interested in the preparation of the monolithium salt $[\{\text{LAl}(\text{SH})[\text{SLi}(\text{thf})_2]\}_2]$ (**3**). To our knowledge such systems are not known for any kind of metal and, could be precursors for substitution reactions. For the preparation of **3** a similar method was used as for **2'**. After removal of all volatiles in vacuo compound **3** was isolated in 84 % yield. Moreover, no decomposition was detected in the presence of $\text{HN}(\text{SiMe}_3)_2$ or during the removal of the solvent, thus demonstrating a higher stability of **3** compared to that of **2**. As expected, **3** has a dimeric arrangement in the solid state, with each lithium coordinated to two molecules of THF and two sulfur atoms. The amount of THF in **3** remains unchanged even after keeping **3** for several hours in vacuo (Scheme 1).



Scheme 1. Synthesis of compounds **2'**–**5**.

We focused on reactivity studies of **2'** and **3** towards the transition-metal halides, namely $[\text{Cp}_2\text{TiCl}_2]$ and $[\text{Cp}_2\text{ZrCl}_2]$. When a solution of $[\text{Cp}_2\text{MCl}_2]$ ($\text{M} = \text{Ti}, \text{Zr}$) in THF was added dropwise to the solution of **2'** in THF at -20°C , the color of the resulting mixture became brownish-green, $\text{M} = \text{Ti}$, and deep yellow for $\text{M} = \text{Zr}$. After removal of the THF, extraction of the crude product with toluene and several purification steps, compounds $[\text{LAl}(\mu\text{-S})_2\text{MCp}_2]$ ($\text{M} = \text{Ti}$ (**4**), $\text{M} = \text{Zr}$ (**5**)) were isolated in 89 % and 85 % yield, respectively.

Surprisingly the reaction of **3** with $[\text{Cp}_2\text{TiCl}_2]$ or $[\text{Cp}_2\text{ZrCl}_2]$ in a molar ratio 2:1 does not yield the expected $[\{\text{LAl}(\text{SH})\text{S}\}_2\text{MCp}_2]$ but rather a mixture of **1** and **4** (or **5**) is formed. This result suggests that the formation of the four-membered ring $[\text{LAl}(\mu\text{-S})_2\text{MCp}_2]$ is preferred over a $\text{LAl}(\text{SH})\text{-S-M}(\text{Cp})_2\text{-S-Al}(\text{SH})\text{L}$ chain arrangement containing free SH groups. One pathway for the formation of **1** and **4** (or **5**) in the above reaction may involve the intermediate

$[\text{LAl}(\text{SH})(\mu\text{-S})\text{M}(\text{Cl})\text{Cp}_2]$, followed by a translithiation with a second molecule of **3**, yielding **1** and $[\text{LAl}(\text{SLi})(\mu\text{-S})\text{M}(\text{Cl})\text{Cp}_2]$. Subsequently, $[\text{LAl}(\text{SLi})(\mu\text{-S})\text{M}(\text{Cl})\text{Cp}_2]$ undergoes an intramolecular elimination of LiCl to yield $[\text{LAl}(\mu\text{-S})_2\text{MCp}_2]$. A second possible mechanism is an in situ formation of $[\{\text{LAl}(\text{SH})(\mu\text{-S})\}_2\text{MCp}_2]$ followed by its rapid rearrangement to yield **1** and **4** (or **5**) (Scheme 1).

X-ray quality crystals of **2** and **3** were obtained by slow cooling their THF solutions.^[6] Both derivatives crystallize in the monoclinic space group $P2_1/n$ as pale yellow crystals. Compound **3** shows a simple coordination environment for the Li atoms $[\text{LAl}(\text{SH})(\mu_3\text{-S})(\mu\text{-Li-2 THF})_2(\mu_3\text{-S})\text{Al}(\text{SH})\text{L}]$, while the structure of **2** is more complex and none of the four lithium atoms are equivalent. As depicted in Figure 1, the lithium atoms Li(1), Li(2) and Li(4) are coordinated by two, one, and three THF molecules, respectively, whereas Li(3) is not coordinated to THF. This diversity is due to the steric bulk of the ligand L.

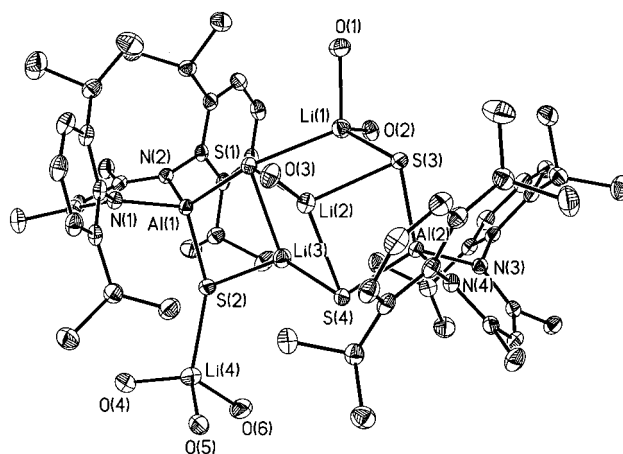


Figure 1. Molecular structure of $[\{\text{LAl}[(\text{SLi})_2(\text{thf})_3]\}_2] \cdot 2\text{THF}$ (**2**); thermal ellipsoids set at 50% probability. All hydrogen atoms, noncoordinated THF molecules and carbon atoms of the coordinating THF molecules are omitted for clarity. Selected bond lengths [Å] and angles [°]: Al(1)–S(1) 2.186(1), Al(1)–S(2) 2.182(1), Al(2)–S(3) 2.173(1), Al(2)–S(4) 2.181(1), Li(1)–S(1) 2.482(2), Li(1)–S(3) 2.414(2), Li(2)–S(1) 2.544(2), Li(2)–S(3) 2.449(2), Li(2)–S(4) 2.565(2), Li(3)–S(1) 2.502(2), Li(3)–S(2) 2.345(2), Li(3)–S(4) 2.323(2), Li(4)–S(2) 2.343(3); S(1)–Al(1)–S(2) 111.6(1), S(3)–Al(2)–S(4) 113.0(1), Al(1)–S(1)–Li(1) 149.6(1), Al(1)–S(1)–Li(2) 126.3(1), Al(1)–S(1)–Li(3) 74.3(1), Al(1)–S(2)–Li(3) 77.7(1), Al(1)–S(2)–Li(4) 152.1(1), Al(2)–S(3)–Li(1) 114.8(1), Al(2)–S(3)–Li(2) 76.3(1), Al(2)–S(4)–Li(2) 73.7(1), Al(2)–S(4)–Li(3) 118.0(1), Li(1)–S(1)–Li(2) 68.2(1), Li(1)–S(1)–Li(3) 92.5(1), Li(1)–S(3)–Li(2) 70.8(1), Li(2)–S(1)–Li(3) 66.0(1), Li(2)–S(4)–Li(3) 68.2(1), Li(3)–S(2)–Li(4) 116.8(1), S(1)–Li(1)–S(3) 112.1(1), S(1)–Li(2)–S(3) 108.9(1), S(1)–Li(2)–S(4) 107.8(1), S(1)–Li(3)–S(2) 96.4(1), S(1)–Li(3)–S(4) 117.6(1), S(2)–Li(3)–S(4) 134.6(1), S(3)–Li(2)–S(4) 92.8(1).

The two THF molecules coordinated to Li(1) require there to be more space between the 2,6-*i*-Pr₂C₆H₃ moieties of L and thus force the substituents on the opposite side closer together. This steric pressure results in Li(4) being pushed out of the central area of the dimer. Subsequently the coordination of three THF molecules covers the unsaturated sites on Li(4). For the two remaining Li atoms, the situation is similar.

Li(2) can still be coordinated by one THF molecule whereas Li(3) is coordinated only to three sulfur atoms. These different coordination sites of lithium atoms are compensated by the variation of the Li–S bond lengths (2.323–2.565 Å). The $\text{Al}_2\text{S}_4\text{Li}_4$ core can also be described as being a six-membered AlS_3Li_2 ring with alternating sulphur and metal atoms, which is capped by another lithium atom and a bent Al–S–Li unit is joined to one of the S–Li edges of this hexagonal pyramid to form a condensed four-membered AlS_2Li ring. The shortness of the S(4)–Li(3) bond (2.323 Å) is caused by the unsaturated coordination sphere of Li(3) which contains only three sulfur atoms and is one of the shortest S–Li bonds observed to date.^[7a–c] All the other S–Li bonds of **2** (2.343–2.565 Å) and **3** (2.424 and 2.478 Å) are in the range observed for similar species (2.327–2.964 Å).^[5,7] Figure 2 shows the molecular structure of **3** in which the S_2Li_2 core is essentially planar owing to the crystal symmetry.

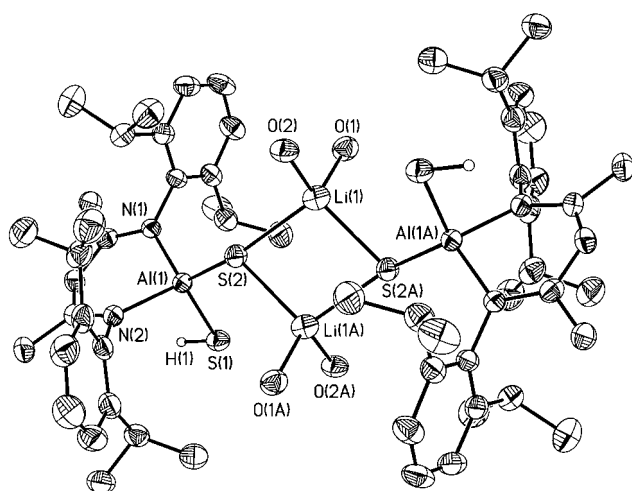


Figure 2. Molecular structure of $[\{\text{LAL}(\text{SH})[\text{SLi}(\text{thf})_2]\}_2]$ (**3**); thermal ellipsoids set at 50% probability. All hydrogen atoms (except those of the S–H moieties), and the carbon atoms of the THF molecules are omitted for clarity. Selected bond lengths [Å] and angles [°]: Al(1)–N(1) 1.928(2), Al(1)–N(2) 1.935(2), Al(1)–S(1) 2.268(1), Al(1)–S(2) 2.123(1), H(1)–S(1) 1.28(5), Li(1)–S(2) 2.478(5), Li(1)–S(2A) 2.424(5); S(1)–Al(1)–S(2) 115.7(1), Al(1)–S(2)–Li(1) 151.6(1), Al(1)–S(2)–Li(1A) 111.7(1), Li(1)–S(2)–Li(1A) 78.0(2), S(2)–Li(1)–S(2A) 102.0(2).

This S_2Li_2 motif can be found in many substances containing these two elements including **2**.^[5,7] The free SH groups are not involved in any kind of hydrogen bonding and are orientated *trans* to each other.

Crystals of **4** were obtained by slow cooling of its toluene/hexane solution.^[6] **4** crystallizes in the monoclinic space group $P2_1$ and its molecular structure is shown in Figure 3.

The AlS_2Ti ring is essentially planar with the sum of inner angles of 360°. The widest angle (102.5°) corresponds to that at the aluminum center, while the one at the titanium center is almost a right angle (89.3°). The Ti– X_{Cp} separations (X_{Cp} is the centroid of the Cp group) are 2.091 and 2.090 Å and the $\text{X}_{\text{Cp1}}\text{–Ti–X}_{\text{Cp2}}$ angle is 130°. All these data are in good agreement with those reported for $[\text{Cp}_2\text{Ti}(\mu\text{-S})\text{ML}'\text{L}']$ (e.g. M = Si, Ti, Ru, L' = Cp, L'' = Cl) species (2.425–2.458 Å for

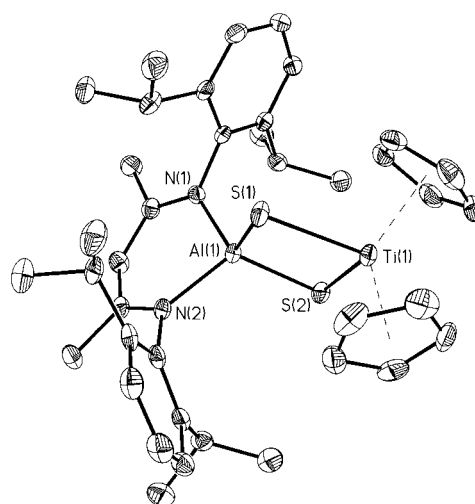


Figure 3. Molecular structure of $[\text{LAL}(\mu\text{-S})_2\text{TiCp}_2]$ (**4**); thermal ellipsoids set at 50% probability. All hydrogen atoms are omitted for clarity. Selected bond lengths [Å] and angles [°]: Al(1)–N(1) 1.918(2), Al(1)–N(2) 1.921(2), Al(1)–S(1) 2.208(1), Al(1)–S(2) 2.197(1), Ti(1)–S(1) 2.416(1), Ti(1)–S(2) 2.473(1), Ti(1)– X_{Cp1} 2.091(3), Ti(1)– X_{Cp2} 2.090(3); S(1)–Al(1)–S(2) 102.5(1), Al(1)–S(1)–Ti(1) 84.7(1), Al(1)–S(2)–Ti(1) 83.6(1), S(1)–Ti(1)–S(2) 89.3(1), $\text{X}_{\text{Cp1}}\text{–Ti(1)–X}_{\text{Cp2}}$ 130.0(2); X = centroid of Cp ring.

Ti–S, 2.059–2.093 Å for $\text{X}_{\text{Cp}}\text{–Ti}$, 129.6–131.6° for $\text{X}_{\text{Cp1}}\text{–Ti–X}_{\text{Cp2}}$ and 86.5–95.9° for S–Ti–S).^[8] The substitution of the SH protons by Li or Ti has a significant influence on the Al–S bond length. The Al–S bond lengths decrease in the series from **1** (2.223 Å and 2.217 Å)^[1] to **4** (2.208 and 2.197 Å), to **2** (2.173–2.186 Å) and finally to **3** (2.123 Å). The partial negative charge on the substituted S atom in **3** causes a shortening of the Al–S bond and thus, increases the electron density on the aluminum center resulting in an elongation of the Al–S(H) bond (2.268 Å).

In summary, we have developed a new strategy for the preparation of heterobimetallic sulfides containing aluminum and isolated four new species. Furthermore, the lithium salts $[\{\text{LAL}[(\text{SLi})_2(\text{thf})_2]\}_2]$ and $[\{\text{LAL}(\text{SH})[\text{SLi}(\text{thf})_2]\}_2]$ are promising precursors for further reactions.

Experimental Section

All manipulations were performed under a dry and oxygen-free atmosphere (N_2 or Ar) using Schlenk-line and glovebox techniques. **2**: Compound **1** (2.000 g, 3.916 mmol) and $\text{LiN}(\text{SiMe}_3)_2$ (1.311 g, 7.832 mmol) were mixed as solids in a flask and subsequently cold THF (70 mL, 0°C) was added. Within a few seconds pale yellow crystals of **2** started to precipitate from the reaction mixture. After 5 min of stirring at 0°C, the reaction mixture was cooled to –20°C and maintained at this temperature for 5–10 min under vigorous stirring to support the crystallization. The time allowed for the crystallization is determined by the color of the solution. The original pale yellow color of the solution turned slowly into a dark brown, which indicates decomposition of the product. Thus, the filtration of the microcrystalline product should occur within the first significant color change of the mother liquor. After washing the crude product with cold THF (5 mL) and drying in vacuo, **2** was obtained as a pale yellow powder. Yield 2.19 g (84%). M.p. 320°C (decomp). ^1H NMR (500 MHz, $[\text{D}_8]\text{THF}$, 25°C, TMS): δ = 1.07 (d, $^3J(\text{H,H})$ = 6.8 Hz, 24H,

CH(CH₃)₂), 1.25 (d, ³J(H,H) = 6.8 Hz, 24H, CH(CH₃)₂), 1.51 (s, 12H, CH₃), 1.77 (m, 16H, O(CH₂CH₂)₂), 3.62 (m, 16H, O(CH₂CH₂)₂), 4.00 (sept, ³J(H,H) = 6.8 Hz, 8H, CH(CH₃)₂), 5.01 (s, 2H, CH), 7.00–7.01 ppm (m, 12H, *m*-, *p*-Ar(H)); ¹³C NMR (125.8 MHz, [D₈]THF, 25 °C, TMS): δ = 24.7 (CH(CH₃)₂), 24.8 (CH(CH₃)₂), 26.4 (O(CH₂CH₂)₂), 27.4 (CH(CH₃)₂), 28.7 (CH₃), 68.2 (O(CH₂CH₂)₂), 98.1 (γ-CH), 124.2, 126.2, 145.1, 146.1 (*i*-, *o*-, *m*-, *p*-C of Ar), 168.1 ppm (C=N); ⁷Li NMR (116.6 MHz, [D₈]THF, 25 °C, LiCl, 1M in D₂O): δ = 1.26 (SLI). Elemental analysis calcd (%) for C₇₄H₁₁₄Al₂Li₄N₄O₈S₄ (1333.71): C 66.64, H 8.62, N 4.20; found: C 65.70, H 8.57, N 4.27.

3: Compound **1** (1.000 g, 1.958 mmol) and LiN(SiMe₃)₂ (0.328 g, 1.958 mmol) were mixed as solids in a flask and subsequently THF (30 mL) was added at ambient temperature. The mixture was stirred for 5 min, all the volatiles were removed in vacuo. The crude product was washed with cold hexane (5 mL) to remove the remaining HN(SiMe₃)₂, yielding **3** as a pale yellow powder. Yield 1.11 g (85 %). M.p. 230 °C (decomp). ¹H NMR (500 MHz, [D₈]THF, 25 °C, TMS): δ = -1.00 (s, 2H, SH), 1.04 (d, ³J(H,H) = 6.8 Hz, 12H, CH(CH₃)₂), 1.21 (d, ³J(H,H) = 6.8 Hz, 12H, CH(CH₃)₂), 1.25 (d, ³J(H,H) = 6.8 Hz, 12H, CH(CH₃)₂), 1.40 (d, ³J(H,H) = 6.8 Hz, 12H, CH(CH₃)₂), 1.69 (s, 12H, CH₃), 1.77 (m, 16H, O(CH₂CH₂)₂), 3.62 (m, 16H, O(CH₂CH₂)₂), 3.77 (sept, ³J(H,H) = 6.8 Hz, 4H, CH(CH₃)₂), 3.85 (sept, ³J(H,H) = 6.8 Hz, 4H, CH(CH₃)₂), 5.13 (s, 2H, CH), 7.06–7.16 ppm (m, 12H, *m*-, *p*-Ar-H); ¹³C NMR (125.8 MHz, [D₈]THF, 25 °C, TMS): δ = 24.3 (CH(CH₃)₂), 24.4 (CH(CH₃)₂), 25.1 (CH(CH₃)₂), 25.1 (CH(CH₃)₂), 26.4 (O(CH₂CH₂)₂), 28.0 (CH(CH₃)₂), 28.5 (CH(CH₃)₂), 29.6 (CH₃), 68.2 (O(CH₂CH₂)₂), 97.6 (γ-CH), 124.1, 134.3, 126.4, 143.6, 145.7, 146.0 (*i*-, *o*-, *m*-, *p*-C of Ar), 169.0 ppm (C=N); ⁷Li NMR (116.6 MHz, [D₈]THF, 25 °C, LiCl, 1M in D₂O) δ = 0.32 (SLI). IR(KBr pellet): 2552 vw (SH) cm⁻¹. Elemental analysis calcd (%) for C₇₄H₁₁₆Al₂Li₂N₄O₈S₄ (1321.84): C 67.24, H 8.85, N 4.24; found: C 66.45, H 8.45, N 4.52.

4: A solution of [Cp₂TiCl₂] (0.224 g, 0.900 mmol) in THF (20 mL) was added dropwise to a solution of **2** (0.600 g, 0.450 mmol) in THF (40 mL) at -20 °C. During the addition, the color of the solution changed to deep brown-green. After the addition was complete, the reaction mixture was stirred for additional 5 min at -20 °C and then allowed to warm to ambient temperature. The solvent was removed in vacuo and the crude product was extracted twice with cold toluene (15 mL, 5 °C). After filtration, removing of the toluene from the filtrate, washing of the product with a cold toluene:pentane (5 mL, 1:4) mixture and drying in vacuo, **4** was obtained as a brown-green powder. Yield 0.55 g (89 %). Decomposition without melting at 270 °C. ¹H NMR (500 MHz, C₆D₆, 25 °C, TMS): δ = 1.06 (d, ³J(H,H) = 6.8 Hz, 12H, CH(CH₃)₂), 1.64 (s, 6H, CH₃), 1.88 (d, ³J(H,H) = 6.8 Hz, 12H, CH(CH₃)₂), 3.57 (sept, ³J(H,H) = 6.8 Hz, 4H, CH(CH₃)₂), 4.84 (s, 1H, CH), 5.71 (s, 10H, C₅H₅), 7.30(-7.37 ppm (m, 6H, *m*-, *p*-Ar(H)); ¹³C NMR (125.8 MHz, C₆D₆, 25 °C, TMS): δ = 24.0 (CH(CH₃)₂), 25.7 (CH(CH₃)₂), 25.7 (CH(CH₃)₂), 29.1 (CH₃), 94.9 (γ-CH), 118.3 (C₅H₅), 125.0, 128.0, 140.6, 146.0 (*i*-, *o*-, *m*-, *p*-C of Ar), 170.2 ppm (C=N); ²⁷Al NMR (78.2 MHz, C₆D₆, 25 °C, [Al(H₂O)₆]³⁺) δ = 94 ppm. MS (70 eV): *m/z* (%): 686 (8) [*M*⁺], 621 (100) [*M*⁺(Cp)]. Elemental analysis calcd (%) for C₃₉H₅₁AlN₂S₂Ti (686.83): C 68.20, H 7.48, N 4.08; found: C 67.61, H 7.46, N 4.02.

5: preparation like that of **4** from [Cp₂ZrCl₂] (0.263 g, 0.900 mmol) and **2** (0.600 g, 0.450 mmol). The product was isolated as a deep yellow powder. Yield 0.56 g (85 %). Decomposition without melting at 180 °C. ¹H NMR (500 MHz, C₆D₆, 25 °C, TMS): δ = 1.06 (d, ³J(H,H) = 6.8 Hz, 12H, CH(CH₃)₂), 1.65 (s, 6H, CH₃), 1.82 (d, ³J(H,H) = 6.8 Hz, 12H, CH(CH₃)₂), 3.59 (sept, ³J(H,H) = 6.8 Hz, 4H, CH(CH₃)₂), 4.87 (s, 1H, CH), 5.65 (s, 10H, C₅H₅), 7.22–7.32 ppm (m, 6H, *m*-, *p*-Ar(H)); ¹³C NMR (125.8 MHz, C₆D₆, 25 °C, TMS): δ = 24.4 (CH(CH₃)₂), 25.7 (CH(CH₃)₂), 25.7 (CH(CH₃)₂), 29.0 (CH₃), 95.1 (γ-CH), 114.4 (C₅H₅), 124.9, 128.0, 140.1, 146.1 (*i*-, *o*-, *m*-, *p*-C of Ar), 170.6 ppm (C=N); ²⁷Al NMR (78.2 MHz, C₆D₆, 25 °C, [Al(H₂O)₆]³⁺) δ = 101 ppm. MS (70 eV): *m/z* (%): 728 (58) [*M*⁺], 663 (100) [*M*⁺(Cp)].

Elemental analysis calcd (%) for C₃₉H₅₁AlN₂S₂Zr (730.17): C 64.15, H 7.04, N 3.84; found: C 63.09, H 7.30, N 3.83.

Received: July 9, 2004

Keywords: aluminum · bridging ligands · sulfur · titanium · zirconium

- [1] V. Jancik, Y. Peng, H. W. Roesky, J. Li, D. Neculai, A. M. Neculai, R. Herbst-Irmer, *J. Am. Chem. Soc.* **2003**, *125*, 1452–1453.
- [2] C. J. Harlan, A. R. Barron, *J. Cluster Sci.* **1996**, *7*, 455–467.
- [3] a) V. Jancik, M. M. Moya Cabrera, H. W. Roesky, R. Herbst-Irmer, D. Neculai, A. M. Neculai, M. Noltemeyer, H.-G. Schmidt, *Eur. J. Inorg. Chem.* **2004**, 3508–3512, and references therein; b) Y. Peng, H. Fan, V. Jancik, H. W. Roesky, R. Herbst-Irmer, *Angew. Chem.* **2004**, *116*, 6316–6318; *Angew. Chem. Int. Ed.* **2004**, *43*, 6190–6192.
- [4] N. N. Greenwood, A. Earnshaw, *Chemistry of the Elements*; Butterworth-Heinemann, Oxford, U.K., **2002**, pp. 1205–1210.
- [5] J. Knizek, H. Nöth, A. Schlegel, *Eur. J. Inorg. Chem.* **2001**, 181–187.
- [6] Crystal data for **2**: C₉₀H₁₄₆Al₂Li₄N₄O₈S₄, *M*_r = 1622.07, monoclinic, space group *P*₂₁/*n*, *a* = 22.746(1), *b* = 16.414(1), *c* = 26.111(1) Å, β = 106.45(1)°, *V* = 9350(1) Å³, *Z* = 4, ρ_{calcd} = 1.152 Mg m⁻³, *F*(000) = 3520, λ = 1.54178 Å, *T* = 100(2) K, μ(Cu_{Kα}) = 1.525 mm⁻¹. Of the 50723 measured reflections, 13679 were independent (*R*_{int} = 0.0214). The final refinements converged at *R*1 = 0.0288 for *I* > 2σ(*I*), *wR*2 = 0.0747 for all data. The final difference Fourier synthesis gave a min/max residual electron density of -0.187/+0.250 eÅ⁻³; crystal data for **3**: C₇₄H₁₁₆Al₂Li₂N₄O₈S₄, *M*_r = 1321.78, monoclinic, space group *P*₂₁/*n*, *a* = 12.558(1), *b* = 19.423(1), *c* = 16.862(1) Å, β = 111.29(1)°, *V* = 3832(1) Å³, *Z* = 2, ρ_{calcd} = 1.145 Mg m⁻³, *F*(000) = 1432, λ = 1.54178 Å, *T* = 100(2) K, μ(Cu_{Kα}) = 1.721 mm⁻¹. Of the 14831 measured reflections, 5403 were independent (*R*_{int} = 0.0567). The final refinements converged at *R*1 = 0.0441 for *I* > 2σ(*I*), *wR*2 = 0.1219 for all data. The final difference Fourier synthesis gave a min/max residual electron density of -0.238/+0.277 eÅ⁻³; crystal data for **4**: C₃₉H₅₁AlN₂S₂Ti, *M*_r = 686.82, monoclinic, space group *P*₂₁, *a* = 11.831(1), *b* = 8.727(1), *c* = 17.776(1) Å, β = 99.10(1)°, *V* = 1812(1) Å³, *Z* = 2, ρ_{calcd} = 1.259 Mg m⁻³, *F*(000) = 732, λ = 1.54178 Å, *T* = 100(2) K, μ(Cu_{Kα}) = 3.525 mm⁻¹. Of the 6417 measured reflections, 3178 were independent (*R*_{int} = 0.0189). The final refinements converged at *R*1 = 0.0235 for *I* > 2σ(*I*), *wR*2 = 0.0591 for all data and the absolute structure parameter was refined to 0.013(5). The final difference Fourier synthesis gave a min/max residual electron density of -0.199/+0.250 eÅ⁻³. Data for the structures were collected on a Bruker three-circle diffractometer equipped with a SMART 6000 CCD detector. Intensity measurements were performed on a rapidly cooled crystal (0.3 × 0.2 × 0.1 mm³) in the range 4.56 ≤ 2θ ≤ 120.08° (**2**), (0.2 × 0.1 × 0.1 mm³) in the range 7.24 ≤ 2θ ≤ 118.02° (**3**), and (0.5 × 0.2 × 0.2 mm³) in the range 8.40 ≤ 2θ ≤ 113.68° (**4**). The structures were solved by direct methods (SHELXS-97^[9]) and refined against all data by full-matrix least-squares on *F*²^[10]. The hydrogen atoms of C–H bonds were placed in idealized positions, whereas the hydrogen atom from the SH moiety in **3** was localized from the difference electron-density map and refined isotropically. Disordered THF molecules (**2**, **3**) were refined with distance restraints and restraints for the anisotropic displacement parameters. CCDC-244078 (**2**), CCDC-244079 (**3**), and CCDC-244080 (**4**) contain the supplementary crystallographic data for this paper. These data can be obtained free of charge via www.ccdc.cam.ac.uk/conts/retrieving.html (or from the Cambridge Cry-

tallographic Data Centre, 12 Union Road, Cambridge CB2 1EZ, UK; fax: (+44) 1223-336-033; or deposit@ccdc.cam.ac.uk).

- [7] a) M. Aslam, R. A. Bartlett, E. Block, M. M. Olmstead, P. P. Power, G. E. Sigel, *J. Chem. Soc. Chem. Commun.* **1985**, 1674–1675; b) M. Niemeyer, P. P. Power, *Inorg. Chem.* **1996**, *35*, 7264–7272; c) A. Gebauer, J. A. R. Schmidt, J. Arnold, *Inorg. Chem.* **2000**, *39*, 3424–3427; d) F. Pauer, P. P. Power, *Lithium Chemistry: A Theoretical and Experimental Overview*, (Eds.: A. M. Sapse, P. v. R. Schleyer), Wiley, New York, **1995**, ch. 9, pp. 295–392; e) S. Chadwick, U. Englich, K. Ruhlandt-Senge, *Organometallics* **1997**, *16*, 5792–5803; f) W.-Y. Chen, C. Eaborn, I. B. Gorrell, P. B. Hitchcock, J. D. Smith, *J. Chem. Soc. Dalton Trans.* **2000**, 2313–2317; g) S. C. Lee, J. Li, J. C. Mitchell, R. H. Holm, *Inorg. Chem.* **1992**, *31*, 4333–4338; h) K. Tatsumi, Y. Inoue, H. Kawaguchi, M. Kohsaka, A. Nakamura, R. E. Cramer, W. VanDoorne, G. J. Taogoshi, P. N. Richmann, *Organometallics* **1993**, *12*, 352–364; i) H. Kawaguchi, K. Tatsumi, R. E. Cramer, *Inorg. Chem.* **1996**, *35*, 4391–4395; j) J. Knizek, H. Nöth, *J. Organomet. Chem.* **2000**, 593-613, 168–187; k) J. Francis, S. G. Bott, A. R. Barron *J. Organomet. Chem.* **2000**, 597, 29–37, and references therein.
- [8] a) F. Bottomley, R. W. Day, *Can. J. Chem.* **1992**, *70*, 1250–1259; b) P. G. Maué, D. Fenske, *Z. Naturforsch.* **1988**, *43b*, 1213–1218; c) S. Kabashima, S. Kuwata, M. Hidai, *J. Am. Chem. Soc.* **1999**, *121*, 7837–7845; d) D. M. Giolando, T. B. Rauchfuss, G. M. Clark, *Inorg. Chem.* **1987**, *26*, 3080–3082.
- [9] SHELXS-97, *Program for Structure Solution*: G. M. Sheldrick, *Acta Crystallogr. Sect. A* **1990**, *46*, 467–473.
- [10] G. M. Sheldrick, SHELXL-97, *Program for Crystal Structure Refinement*, University of Göttingen, Göttingen (Germany), **1997**.

Phospholes

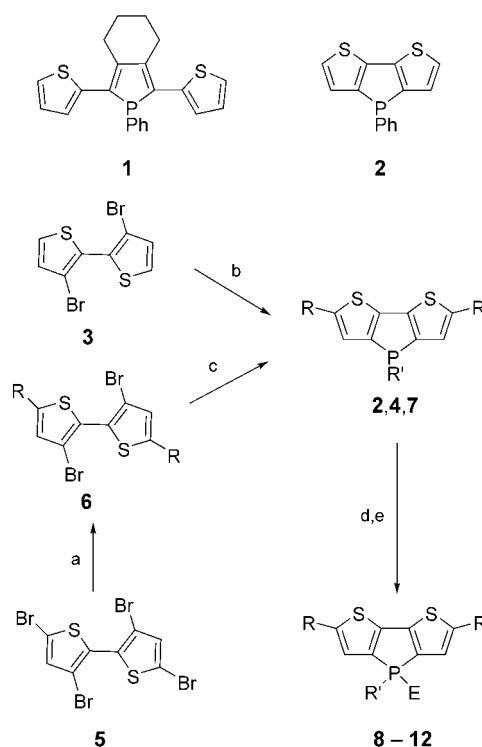
The Dithieno[3,2-*b*:2',3'-*d*]phosphole System: A Novel Building Block for Highly Luminescent π -Conjugated Materials**

Thomas Baumgartner,* Toni Neumann, and
Bastian Wirges

The incorporation of phosphorus centers into polymeric materials has recently attracted a great deal of attention.^[1] The versatile reactivity and electronic properties of phosphorus offer considerable promise for the development of new functional materials with novel properties. Exploring the use of phosphole in this context should be of particular interest, as materials possessing the structurally related pyrrole and thiophene moieties are already well-established in the field of molecular electronics.^[2] For example, thiophene-based materials show significant potential for application in electronic devices such as photovoltaic cells, organic and polymer light-emitting diodes (OLEDs, PLEDs), polymeric sensors, and TFT-based flat-panel displays.^[3]

Careful consideration of the HOMO–LUMO gap, which strongly influences the optical and electronic properties of these materials, is essential for their utility.^[4] The ability to fine-tune the electronic structure of the π -conjugated system is therefore highly desirable in order to achieve the required material properties. Recent work by Réau and co-workers incorporating the phosphole moiety into extended thiophene-containing π -conjugated systems (**1**, see Scheme 1), has demonstrated the advantageous electronic features of the phosphorus situated in this system.^[1e,5] Due to the pyramidalization of the phosphorus center, orbital interaction with the conjugated π system is reduced. As a result, the lone pair at the phosphorus atom only functions as an n-dopant for the π system. Conveniently, the doping mode can be inverted easily from n- (electron donor) to p-type (electron acceptor) by simple chemical modifications such as oxidation or complexation at the phosphorus center.^[1e,5] Although these intriguing features as well as theoretical calculations^[6] strongly support the advantages of incorporating phosphole moieties into polymeric systems, only three examples of phosphole-containing macromolecules have been reported to date.^[1e,7]

We now report on the synthesis and optoelectronic properties of novel dithieno[3,2-*b*:2',3'-*d*]phospholes^[8] and the preparation of a well-defined dithienophosphole-containing polymer built on a polystyrene backbone. The dithieno[3,2-*b*:2',3'-*d*]phosphole **2** (Scheme 1) was chosen as



Scheme 1. Synthesis of dithienophosphole derivatives and precursors: a) 2 *n*BuLi, 2 *t*BuMe₂SiCl, THF, –78 °C (**6**: R = Si*t*BuMe₂); b) 2 *n*BuLi, R'PCl₂, Et₂O, –78 °C → RT (**2**: R = H, R' = Ph, **4**: R = H, R' = 4-*t*BuC₆H₄); c) 2 *n*-BuLi, (4-vinylphenyl)PCl₂, TMEDA, Et₂O, –78 °C → RT (**7**: R = Si*t*-BuMe₂, R' = 4-vinylphenyl); d) BH₃·SMe₂ (1 M in CH₂Cl₂), CH₂Cl₂, RT (E = BH₃; **8**: R = H, R' = Ph, **9**: R = H, R' = 4-*t*BuC₆H₄); e) H₂O₂ (30 % in H₂O), pentane, RT (E = O; **10**: R = H, R' = Ph, **11**: R = H, R' = 4-*t*BuC₆H₄, **12**: R = Si*t*BuMe₂, R' = 4-vinylphenyl).

a synthetic target since the annelation of aromatic rings has been found to be a powerful approach for tuning the band gap of conjugated materials.^[4,9] This is further supported by a recent theoretical investigation in which thiophene-based, fused tricyclic polymers were found to have a much more favorable band gap than the related polythiophenes.^[10] The incorporation of the phosphole moiety into a rigid, tricyclic dithieno system should therefore lead to a significantly higher degree of π conjugation than that reported for comparable systems.^[11]

To verify the synthetic accessibility of the dithienophosphole system as well as to explore its optoelectronic properties, we initiated our studies on model compounds and functionalized monomers. Dithienophospholes **2** and **4** are accessible by reaction of 3,3'-dibromo-2,2'-dithiophene (**3**) with *n*BuLi, then subsequent addition of the corresponding dichlorophosphine at low temperatures, followed by purification by filtration over neutral alumina (yields: **2**: 70 %, **4**: 72 %). Both compounds exhibit signals in the ³¹P NMR spectrum (**2**: δ = –21.5 ppm; **4**: δ = –22.5 ppm) that are shifted significantly upfield from those of related phospholes, for example, those reported by Réau et al. (δ ³¹P = 11–45 ppm).^[1e] The ¹H and ¹³C NMR data, on the other hand, are not significantly different than data previously reported for related dithieno systems.^[12] To our satisfaction, both **2** and **4** display strong,

[*] Dr. T. Baumgartner, T. Neumann, B. Wirges
Institut für Anorganische Chemie, RWTH-Aachen
Professor-Pirlet-Strasse 1, 52074 Aachen (Germany)
Fax: (+49) 241-8096244
E-mail: thomas.baumgartner@ac.rwth-aachen.de

[**] We thank Prof. Dr. J. Okuda for his generous support of this work. Financial support from the Fonds der Chemischen Industrie and BMBF is gratefully acknowledged. We also thank Prof. Dr. U. Englert for the X-ray data collection, Dr. K. Beckerle for analytical assistance, and both for helpful discussions.

blue photoluminescence, and should thus have the desired optoelectronic properties (vide infra). We were able to obtain light-yellow crystals of **2** suitable for X-ray structure analysis^[13] from a concentrated pentane/toluene (1:1) solution cooled to -30°C . As expected, the rigid tricyclic dithienophosphole is planar and displays an *anti* configuration of the two thiophene moieties and the phosphole unit (see Figure 1). The high degree of π conjugation is apparent in the

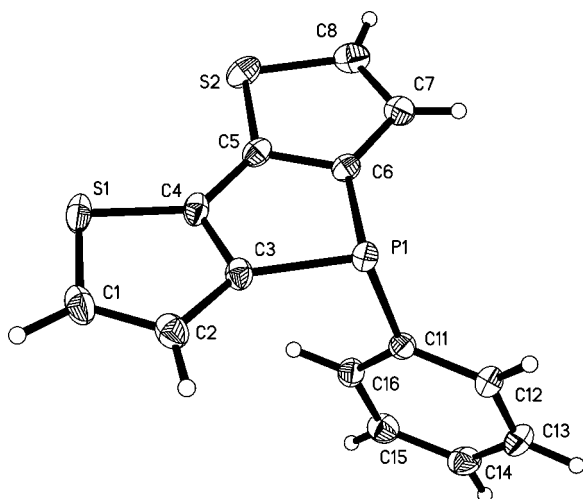


Figure 1. Molecular structure of **2** (50% probability level) in the solid state. Selected bond lengths [Å] and angles [°]: P1–C3 1.8193(14), P1–C6 1.8218(14), P1–C11 1.8367(13), C3–C4 1.3842(19), C5–C6 1.3817(18), C4–C5 1.4397(19); C6–C7 1.4228(18), C7–C8 1.364(2); C3–P1–C6 89.25(6), C3–P1–C11 103.82(6), C6–P1–C11 99.92(6).

shortened single bonds {C2–C3 1.427(2), C4–C5 1.440(2), C6–C7 1.423(2) Å} as well as the elongated double bonds (C1–C2 1.365(2), C3–C4 1.384(2), C5–C6 1.382(2), C7–C8 1.364(2) Å) of the fused ring system. It is interesting to note that the bond shortening/elongation is significantly more pronounced in **2** than in the thienyl-substituted phosphole **1**,^[5a] supporting the positive effects of the rigid ring system on the π conjugation. The endocyclic P–C bonds P1–C3 (1.8193(14) Å) and P1–C6 (1.8218(14) Å) are only slightly shorter than the exocyclic P1–C11 bond (1.8367(13) Å) due to minimal hyperconjugation of the phosphorus lone pair with the π system, which affords a reduced aromatic phosphole unit. This structural feature strongly supports the role of the phosphorus center as a dopant for the π -conjugated system, which is potentially interesting for the optoelectronic properties of the material.

To gain access to polymeric systems we functionalized the phosphorus center of the dithienophosphole with a vinylphenyl group. We also investigated silyl functionalization of the dithienophosphole ring to provide increased solubility for the targeted polymer. An additional benefit with respect to the optoelectronic properties was anticipated, as the silyl center provides an acceptor component expected to further extend the delocalized π system, thus optimizing the electronic structure of the dithienophosphole.^[11]

The vinylphenyl-functionalized monomer **7** is accessible in a two-step reaction starting from 3,3',5,5'-tetrabromo-2,2'-bithiophene (**5**). In the first step, the silyl functionalities were introduced by treating **5** with two equivalents of *n*BuLi and then adding *tert*-butyl(dimethyl)silyl chloride in THF at -78°C to provide **6** in almost quantitative yield. The silyl-functionalized dithiophene **6** was then treated with another two equivalents of *n*BuLi in Et₂O at -78°C , and dichloro(4-vinylphenyl)phosphane^[14] was then added in the presence of an excess of TMEDA to afford the vinylphenyl-functionalized dithienophosphole **7** in good yields (ca. 80%) after filtration over neutral alumina. The dithienophosphole monomer **7** exhibits a resonance in the ^{31}P NMR spectrum of $\delta = -26.4$ ppm that is shifted slightly upfield from those observed for **2** and **4**. The ^1H and ^{13}C NMR data confirm the expected structure and are very similar to those recorded for **2** and **4**.

As previously noted, it should be possible to alter the electronic structure, thus inverting the doping mode of the phosphole, by either oxidation or complexation of the phosphorus atom. We therefore investigated the reaction of the dithienophospholes **2** and **4** with borane (applied as $\text{BH}_3\cdot\text{SMe}_2$) to afford the phosphole–borane adducts **8** and **9**, and hydrogen peroxide to give the phosphole oxides **10** and **11**, all in almost quantitative yields.^[15] The NMR data for the borane adducts show downfield resonances in the ^{31}P NMR spectrum ($\delta(^{31}\text{P}) = 13.5$ (**8**), 14.6 ppm (**9**)) in correlation with the electron-withdrawing effect of the BH_3 group. This is even more pronounced in the case of the oxide functionality ($\delta(^{31}\text{P}) = 18.8$ ppm (**10**), 19.1 (**11**)). The same effect was observed for the silyl-functionalized phosphole oxide **12** ($\delta(^{31}\text{P}) = 14.7$ ppm) that was synthesized in an analogous manner.^[15] The ^1H and ^{13}C NMR data for all compounds show a similar trend, and fall within the range of values previously reported for related phospholes.^[1e,5]

As indicated earlier, the dithienophosphole derivatives exhibit a strong blue photoluminescence. Fluorescence spectroscopy reveals the dependence of the optical properties on the electronic structure of the phosphorus center (Table 1). All compounds show a maximum excitation wavelength in the UV region, whereas the emission spectra show a maximum wavelength in the visible blue region. The dithienophosphole derivatives exhibit Stokes shifts of 70–80 nm similar to the related systems reported by Réau et al. (70–90 nm).^[1e] It is interesting to note that the silyl-functionalized dithienophosphole monomer **7** shows a significant red shift of about

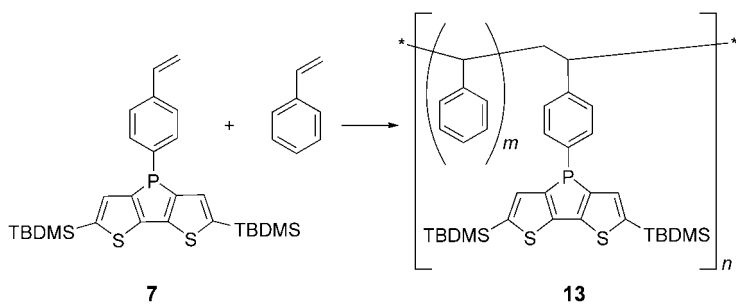
Table 1: Optical spectroscopy data for **2**, **4**, and **7–14**.

Cmpd.	λ_{ex} [nm] ^[a]	λ_{em} [nm] ^[b]	lg ϵ	$\phi^{\text{[c]}}$
2 (4)	338 (336)	415 (408)	4.38 (4.50)	0.779 (0.881)
8 (9)	346 (346)	424 (423)	4.35 (4.47)	0.690 (0.753)
10 (11)	366 (363)	453 (450)	4.33 (4.45)	0.565 (0.590)
7	352	422	4.57	0.687
12	379	461	4.48	0.579
13 ^[d]	352 (374)	424 (452)	4.87 (–)	0.743 (–)
14 ^[d]	374 (352)	458 (456)	4.92 (–)	0.572 (–)

[a] λ_{max} for excitation in CH_2Cl_2 . [b] λ_{max} for emission in CH_2Cl_2 . [c] Relative to quinine sulfate (0.1 M H_2SO_4 solution); excitation at 365 nm. [d] Values for thin film in brackets.

10–15 nm for the maximum excitation and emission wavelengths ($\lambda_{\text{ex}}=352$, $\lambda_{\text{em}}=422$ nm) compared to the model compounds **2** ($\lambda_{\text{ex}}=338$, $\lambda_{\text{em}}=415$ nm) and **4** ($\lambda_{\text{ex}}=336$, $\lambda_{\text{em}}=408$ nm), supporting the electron-accepting character of the silyl center. The same trend is observed when the doping mode of the phosphorus center is inverted to p-type in the borane adducts **8** and **9** and the phosphole oxides **10–12**. In correlation with the low-field shift of the ^{31}P NMR resonances, the maximum wavelengths for excitation and emission experience a red shift of about 10 nm for the borane adducts and an even stronger red shift of about 30 nm (excitation) and 40 nm (emission) for the phosphole oxides. In the case of the silyl-functionalized phosphole oxide **12**, a cumulative effect of both electron-accepting centers (Si and P) is observed (see Table 1). It should be mentioned that the observed photoluminescence is very intense, particularly for the borane adducts and the phosphole oxides. More importantly, the quantum yields for all compounds range between 55 and almost 90 %, which is unprecedented for phospholes^[1e] and dithieno systems.^[12a,16] Therefore, the optoelectronic data strongly emphasize the potential of the dithienophosphole system for applications in optoelectronic devices such as blue-light-emitters and sensory materials.

The favorable properties of macromolecules in terms of processability (e.g. as thin films) would be an added benefit for future materials applications. We therefore investigated the possibility of generating a polymer that would display the extraordinary blue photoluminescence of the model compounds by incorporating the dithienophosphole system as side-chain functionalities. Radical polymerization of functionalized styrene seemed to be the method of choice since it is usually not affected by the presence of phosphine centers.^[14b] To reduce the steric bulk in the polymeric material caused by the dithienophosphole ring system, which could potentially terminate the polymerization process at an early stage, we targeted the copolymer **13** by using styrene as solvent for the reactions (**7**/styrene ca. 1:30, Scheme 2). The resulting “dilution” of the dithienophosphole centers in the polymeric material was expected to also enhance the optoelectronic properties, due to the great distance between the emitting centers, reducing the potential for quenching processes that could occur at higher densities.^[17] The polymerization was performed in a sealed ampule under vacuum at 110 °C for 16 h using a catalytic amount of 2,2,6,6-tetramethylpiperidiny-1-oxy (TEMPO)^[18] as the initiator



Scheme 2. Synthesis of the dithienophosphole-containing polymer **13**: cat. TEMPO, 110 °C, 16 h. TBDMS = *tert*-butyl(dimethyl)silyl.

(Scheme 2). The material obtained after precipitation into degassed pentane was a white amorphous solid. Analysis by gel permeation chromatography (GPC) revealed a high molecular weight of $M_n=147\,650\text{ g mol}^{-1}$ with a relatively narrow polydispersity (PDI) of 2.46. Analysis of the smart polystyrene **13** by differential scanning calorimetry (DSC) showed a glass transition temperature of $T_g=114.2^\circ\text{C}$ (cf. native polystyrene: $<100^\circ\text{C}$ ^[19]) and a thermal decomposition temperature of 428.2 °C. The ^{31}P NMR spectrum for **13** shows a broad signal at $\delta(^{31}\text{P})=-25.0$ ppm (cf.: $\delta=-26.4$ ppm for **7**), confirming the existence of dithienophosphole units within the polymeric material. ^1H and ^{13}C NMR data revealed a ratio of ca. 1:30 for dithienophosphole/styrene as was expected from the reaction conditions.

The smart polymer **13** exhibits a very strong blue photoluminescence upon irradiation with UV light. The maximum of the excitation and emission wavelengths of **13** ($\lambda_{\text{ex}}=352$ nm; $\lambda_{\text{em}}=424$ nm; dissolved in CH_2Cl_2) nicely match the values observed for the vinylphenyl-functionalized monomer **7** (Figure 2), supporting the expected side-chain functional-

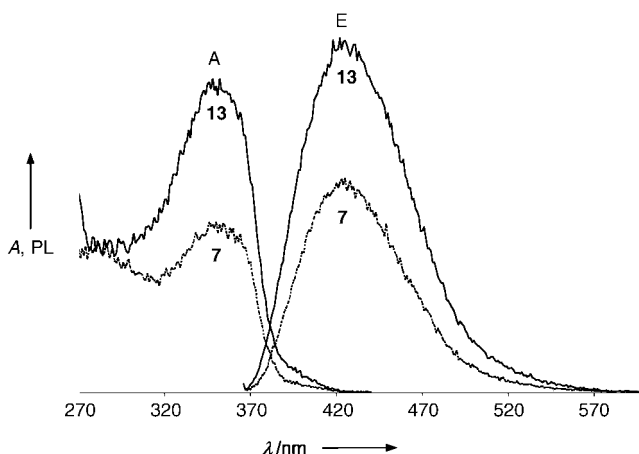


Figure 2. Excitation (A) and emission (E) spectra of **7** and **13** in CH_2Cl_2 .

ization. The dithienophosphole-containing polymer **13** can be oxidized conveniently with hydrogen peroxide (in analogy to the model compounds) to afford the phosphole oxide containing polymer **14**. It should be mentioned that the same oxidation process is observed within a day when a solution of **13** is exposed to air, whereas the solid material does not show any significant signs of oxidation—even after several weeks.

We were also interested in the optoelectronic properties of a thin film of **13** with regards to applications as a PLED material. A thin film was obtained from a concentrated solution of **13** in CH_2Cl_2 by slow evaporation of the solvent. Relative to the properties of the CH_2Cl_2 solution, the very intense blue photoluminescence of the thin film of **13** is red-shifted approximately 20 nm for excitation and roughly 30 nm for emission ($\lambda_{\text{ex}}=374$ nm; $\lambda_{\text{em}}=452$ nm). Surprisingly, the emission wavelength for a

thin film of the oxidized polymer (**14**, $\lambda_{\text{em}} = 456 \text{ nm}$) almost matches that observed for the nonoxidized material **13**, whereas the value for the excitation wavelength is blue-shifted to 352 nm in **14** (cf. 374 nm for **13**; Figure 3). With

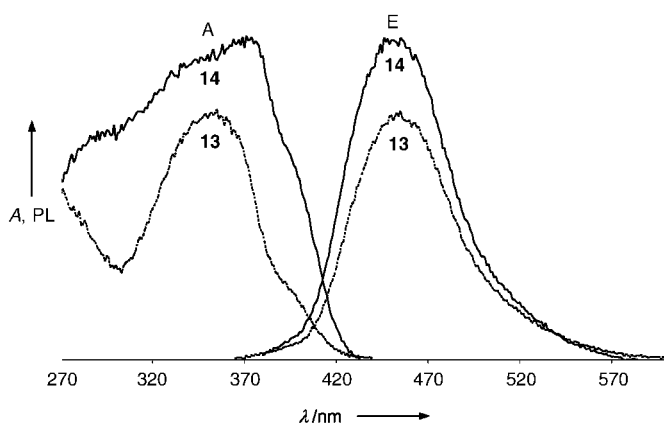


Figure 3. Excitation (A) and emission (E) spectra of **13** and **14** as thin films.

respect to resistance to light, **13** was found to exhibit fairly good stability; this is intrinsically important for the lifetime of optoelectronic devices. Irradiation of a solution of **13** in CH_2Cl_2 at 352 nm for 2 h results in a stable emission (intensity detected at 424 nm) within a loss of at most 3 %, suggesting a potential use in optoelectronic devices. The same is true for a thin film of the oxidized polymer (**14**) with a margin of 5 %.

In conclusion, we have synthesized novel dithieno[3,2-*b*:2',3'-*d'*]phosphole derivatives in a convenient one- or two-step synthesis, demonstrating that a broad variety of functionalized systems are accessible by this method. The optoelectronic properties of the dithienophospholes are extraordinary with respect to wavelength, intensity, and tuneability, allowing for the possibility of fine-tuning the electronic structure by simple chemical modifications. Additionally, we have shown that it is possible to incorporate the dithienophosphole moiety into polymeric systems, opening up potential applications in optoelectronic devices such as blue-light-emitting PLEDs and polymeric sensors. We are currently probing the range of dithienophosphole-based sensory materials by tuning the optoelectronic properties with different functionalities and modifications of the phosphorus center. Furthermore, the incorporation of polymers **13** and **14** into optoelectronic devices is currently under investigation.

Experimental Section

Dithienophospholes: To a solution of **3** (1.62 g, 5 mmol) in Et_2O (100 mL) was added *n*BuLi (4 mL, 10 mmol) dropwise at -78°C . Subsequently, RPhCl_2 ($\text{R} = \text{Ph}$: 0.90 g, 5 mmol; $\text{R} = 4\text{-}t\text{Bu-C}_6\text{H}_4$, 1.18 g, 5 mmol) dissolved in Et_2O (10 mL), was added slowly to the reaction mixture, and the resulting suspension was allowed to warm quickly to room temperature. The solvent was then removed under vacuum, the residue taken up in pentane (ca. 60 mL) and filtered over neutral alumina to remove LiCl and a small amount of brown impurities. The

filtrate was evaporated to dryness, and **2** and **4** were obtained as light-yellow solids (**2**: 1.1 g, 70 % yield; **4**: 1.2 g, 72 % yield).

2: $^{31}\text{P}\{^1\text{H}\}$ NMR (162.0 MHz, 25°C , CDCl_3): $\delta = -21.5 \text{ ppm}$; ^1H NMR (400 MHz, 25°C , CDCl_3): $\delta = 7.31$ (br, 2H; *o*-Ph), 7.26–7.23 (m, 5H; Ar-H), 7.14 ppm (d, $^3J(\text{H,H}) = 5.0 \text{ Hz}$, 2H; Ar-H); $^{13}\text{C}\{^1\text{H}\}$ NMR (100.6 MHz, 25°C , CDCl_3): $\delta = 146.6$ (d, $J(\text{C,P}) = 8.0 \text{ Hz}$; Ar), 141.7 (d, $J(\text{C,P}) = 2.3 \text{ Hz}$; Ar), 133.5 (d, $J(\text{C,P}) = 15.3 \text{ Hz}$; Ar), 132.2 (d, $^2J(\text{C,P}) = 20.5 \text{ Hz}$; *o*-Ar), 129.1 (s; *p*-Ph), 128.5 (d, $^3J(\text{C,P}) = 7.6 \text{ Hz}$; *m*-Ar), 126.4 (d, $^2J(\text{C,P}) = 19.6 \text{ Hz}$; *o*-Ar), 126.0 ppm (d, $^3J(\text{C,P}) = 6.2 \text{ Hz}$; *m*-Ar); MS (70 eV): m/z (%): 272 (100) [M^+], 239 (90) [$M-\text{S}\}^+$, 195 (40) [$M-\text{Ph}\}^+$; elemental analysis calcd (%) for $\text{C}_{14}\text{H}_9\text{PS}_2$: C 61.75, H 3.33, S 23.55; found: C 61.77, H 3.45, S 23.38.

4: $^{31}\text{P}\{^1\text{H}\}$ NMR (162.0 MHz, 25°C , CDCl_3): $\delta = -22.5 \text{ ppm}$; ^1H NMR (400 MHz, 25°C , CDCl_3): $\delta = 7.28$ –7.23 (m, 6H; Ar-H), 7.13 (d, $^3J(\text{H,H}) = 4.9 \text{ Hz}$, 2H; Ar-H), 1.24 ppm (s, 9H; *t*Bu); $^{13}\text{C}\{^1\text{H}\}$ NMR (100.6 MHz, 25°C , CDCl_3): $\delta = 152.4$ (s; *p*-Ar), 147.0 (d, $J(\text{C,P}) = 8.7 \text{ Hz}$; Ar), 141.6 (d, $J(\text{C,P}) = 2.1 \text{ Hz}$; Ar), 132.1 (d, $J(\text{C,P}) = 20.5 \text{ Hz}$; *o*-Ar), 129.7 (d, $^1J(\text{C,P}) = 11.4 \text{ Hz}$; Ar), 126.5 (d, $^2J(\text{C,P}) = 16.9 \text{ Hz}$; *o*-Ar), 125.9 (d, $^3J(\text{C,P}) = 5.7 \text{ Hz}$; *m*-Ar), 125.7 (d, $^3J(\text{C,P}) = 8.5 \text{ Hz}$; *m*-Ar), 34.5 (s; CMe_3), 31.0 ppm (s; $\text{C}(\text{CH}_3)_3$). MS (70 eV): m/z (%): 328 (100) [M^+], 271 (50) [$M-\text{tBu}\}^+$, 195 (90) [$M-\text{C}_{10}\text{H}_{13}\}^+$, 57 (25) [$\text{tBu}\}^+$; elemental analysis calcd (%) for $\text{C}_{18}\text{H}_{17}\text{PS}_2$: C 65.83, H 5.22, S 19.53; found: C 65.42, H 5.39, S 19.46.

7: To a solution of 3,3'-dibromo-5,5'-bis(*tert*-butyldimethylsilyl)-2,2'-bithiophene (1.11 g, 2 mmol) and TMEDA (1.51 mL, 10 mmol) in Et_2O (50 mL) was added *n*BuLi (1.6 mL, 4 mmol) dropwise at -78°C . Subsequently, (4-vinylphenyl) PCl_2 (0.41 g, 2 mmol), dissolved in Et_2O (10 mL), was added slowly to the reaction mixture, and the resulting mixture was allowed to warm quickly to room temperature. The solvent was then removed under vacuum, and the residue taken up in pentane (ca. 60 mL) and filtered to remove LiCl. The filtrate was concentrated and left for crystallization at -30°C . **7** was obtained as white amorphous powder in 80 % yield (0.84 g).

$^{31}\text{P}\{^1\text{H}\}$ NMR (162.0 MHz, 25°C , CDCl_3): $\delta = -26.4 \text{ ppm}$; ^1H NMR (500 MHz, 25°C , CDCl_3): $\delta = 7.32$ (br, 2H; Ar-H), 7.31 (s, 2H; Ar-H), 7.26 (s, 2H; Ar-H), 6.65 (dd, $^3J(\text{H,H}) = 17.7 \text{ Hz}$, $^3J(\text{H,H}) = 11.3 \text{ Hz}$, 1H; $\text{CH}=\text{CH}_2$), 5.73 (d, $^3J(\text{H,H}) = 17.7 \text{ Hz}$, 1H; $\text{CH}=\text{CHH}$), 5.73 (d, $^3J(\text{H,H}) = 11.3 \text{ Hz}$, 1H; $\text{CH}=\text{CHH}$), 0.93 (s, 18H; *Si*tBu), 0.31 (s, 6H; *Si*Me₂), 0.30 ppm (s, 6H; *Si*Me₂); $^{13}\text{C}\{^1\text{H}\}$ NMR (125.7 MHz, 25°C , CDCl_3): $\delta = 148.7$ (d, $^1J(\text{C,P}) = 10.3 \text{ Hz}$; *ipso*-Ar), 147.0 (s; Ar), 139.8 (d, $^2J(\text{C,P}) = 6.2 \text{ Hz}$; Ar), 139.5 (d, $^1J(\text{C,P}) = 19.6 \text{ Hz}$; Ar), 138.4 (s; *p*-Ar), 136.3 (s; $\text{CH}=\text{CH}_2$), 134.3 (d, $^2J(\text{C,P}) = 16.6 \text{ Hz}$; *o*-Ar), 132.8 (d, $^2J(\text{C,P}) = 21.7 \text{ Hz}$; *o*-Ar), 126.4 (d, $^3J(\text{C,P}) = 8.3 \text{ Hz}$; *m*-Ar), 114.7 (s; $\text{CH}=\text{CH}_2$), 26.4 (s; $\text{SiC}(\text{CH}_3)_3$), 17.0 (s; $\text{SiC}(\text{CH}_3)_3$), -4.9 ppm (s; *Si*Me₂); elemental analysis calcd (%) for $\text{C}_{26}\text{H}_{37}\text{PS}_2\text{Si}_2$: C 63.83, H 7.46, S 12.17; found: C 63.66, H 7.68, S 12.14.

Polymerization: To a solution of **7** (0.26 g, 0.5 mmol) dissolved in styrene (2 mL, 17.5 mmol) in an ampule was added a catalytic amount of TEMPO. The ampule was then evacuated, sealed, and kept overnight at 110°C . The resulting yellowish solid obtained after the reaction mixture had cooled to room temperature was then dissolved in ca. 10 mL of dichloromethane and precipitated into degassed pentane. After the solvent had been decanted off and the residue dried under vacuum, polymer **13** was obtained as a white solid (1.76 g, ca. 85 %). GPC: $M_n = 147650 \text{ g mol}^{-1}$, PDI = 2.46; DSC: $T_g = 114.2^\circ\text{C}$, $T_{\text{decomp}} = 428.2^\circ\text{C}$; $^{31}\text{P}\{^1\text{H}\}$ NMR (162.0 MHz, 25°C , CD_2Cl_2): $\delta = -25.0 \text{ ppm}$; ^1H NMR (500 MHz, 25°C , CD_2Cl_2): $\delta = 7.09$ (m br, ca. 132H; Ar-H), 6.53 (m br, ca. 88H; Ar-H); 1.84 (m br, ca. 48H; CHCHH); 1.48 (m br, ca. 96H; CHCHH), 0.98 (br, 18H; *Si*tBu), 0.35 ppm (br, 12H; *Si*Me₂); $^{13}\text{C}\{^1\text{H}\}$ NMR (125.7 MHz, 25°C , CD_2Cl_2): $\delta = 149.3$ (br; Ar), 145.0 (br; Ar), 140.2 (br; Ar), 134.9 (br; Ar), 132.2 (br; Ar), 128.4 (br; Ar), 128.0 (br; Ar), 126.0 (br; Ar), 45.0 (m br; CHCH_2), 40.8 (m br; CHCH_2), 26.6 (br; $\text{SiC}(\text{CH}_3)_3$), 17.2 (br; $\text{SiC}(\text{CH}_3)_3$), -4.7 ppm (br; *Si*Me₂).

Received: July 14, 2004

Keywords: luminescence · optical properties · phosphorus heterocycles · polymers · thiophene

- [1] a) F. Mathey, *Angew. Chem.* **2003**, *115*, 1616; *Angew. Chem. Int. Ed.* **2003**, *42*, 1578; b) Z. Jin, B. L. Lucht, *J. Organomet. Chem.* **2002**, *653*, 167; c) C.-W. Tsang, M. Yam, D. P. Gates, *J. Am. Chem. Soc.* **2003**, *125*, 1480; d) R. C. Smith, J. D. Protasiewicz, *J. Am. Chem. Soc.* **2004**, *126*, 2268; e) C. Hay, M. Hissler, C. Fischmeister, J. Rault-Berthelot, L. Toupet, L. Nyulászi, R. Réau, *Chem. Eur. J.* **2001**, *7*, 4222.
- [2] See e.g.: a) *Handbook of Oligo- and Polythiophenes* (Ed.: D. Fichou), Wiley-VCH, Weinheim, **1999**; b) *Conjugated Conducting Polymers, Vol. 102* (Ed.: H. Kiess), Springer, New York, **1992**.
- [3] G. Tourillon, *Handbook of Conducting Polymers* (Ed.: T. A. Skotheim), Marcel Dekker, New York, **1986**, pp. 293–350.
- [4] J. Roncali, *Chem. Rev.* **1997**, *97*, 173.
- [5] a) C. Hay, C. Fischmeister, M. Hissler, L. Toupet, R. Réau, *Angew. Chem.* **2000**, *112*, 1882; *Angew. Chem. Int. Ed.* **2000**, *39*, 1812; b) C. Hay, D. Le Vilain, V. Deborde, L. Toupet, R. Réau, *Chem. Commun.* **1999**, 345; c) C. Fave, T.-Y. Cho, M. Hissler, C.-W. Chen, T.-Y. Luh, C.-C. Wu, R. Réau, *J. Am. Chem. Soc.* **2003**, *125*, 9254.
- [6] a) D. Delaere, M. T. Nguyen, L. G. Vanquickenborne, *Phys. Chem. Chem. Phys.* **2002**, *4*, 1522; b) D. Delaere, M. T. Nguyen, L. G. Vanquickenborne, *J. Phys. Chem. A* **2003**, *107*, 838; c) J. Ma, S. Li, Y. Jiang, *Macromolecules* **2002**, *35*, 1109.
- [7] a) S. S. H. Mao, T. D. Tilley, *Macromolecules* **1997**, *30*, 5566; b) Y. Morisaki, Y. Aiki, Y. Chujo, *Macromolecules* **2003**, *36*, 2594.
- [8] Dithieno[3,2-*b*:2',3'-*d'*]-1-(phenyl)phosphole oxide has been reported before, see: J.-P. Lampin, F. Mathey, *J. Organomet. Chem.* **1974**, *71*, 239.
- [9] a) M. Pomerantz, *Handbook of Conducting Polymers*, 2nd ed. (Eds.: T. A. Skotheim, R. L. Elsenbaumer, J. R. Reynolds), Marcel Dekker, New York, **1998**, pp. 277–309; b) X. Zhang, A. J. Matzger, *J. Org. Chem.* **2003**, *68*, 9813.
- [10] S. Y. Hong, J. M. Song, *J. Chem. Phys.* **1997**, *107*, 10607.
- [11] T. Baumgartner, *Macromol. Symp.* **2003**, *196*, 279.
- [12] a) K. Ogawa, S. C. Rasmussen, *J. Org. Chem.* **2003**, *68*, 2921; b) J. Ohshita, M. Nodono, H. Kai, T. Watanabe, A. Kunai, K. Komaguchi, M. Shiotani, A. Adachi, K. Okita, Y. Harima, K. Yamashita, M. Ishikawa, *Organometallics* **1999**, *18*, 1453.
- [13] Crystal data for **2**: (C₁₄H₉PS₂): *M*_r = 272.30, *T* = 153(2) K, monoclinic, space group *P*2(1)/*c*, *a* = 12.740(3), *b* = 8.2365(16), *c* = 11.729(2) Å, *α* = 90°, *β* = 92.62(3)°, *γ* = 90°, *V* = 1229.5(4) Å³, *Z* = 4, *ρ*_{calcd} = 1.471 Mg m⁻³, *μ* = 0.534 mm⁻¹, *λ* = 0.71073 Å, *2θ*_{max} = 56.62°, 12358 measured reflections, 3046 [*R*(int) = 0.0227] independent reflections, GOF on *F*² = 1.080, *R*₁ = 0.0317, *wR*₂ = 0.0857 (*I* > 2σ(*I*)), *R*₁ = 0.0332, *wR*₂ = 0.0868 (for all data), largest difference peak and hole 0.429 and -0.248 e Å⁻³. The intensity data were collected on a Bruker SMART D8 goniometer with an APEX CCD detector. The structure was solved by direct methods (SHELXTL) and refined on *F*² by full-matrix least-squares techniques. Hydrogen atoms were included by using a riding model. CCDC-244042 contains the supplementary crystallographic data for this paper. These data can be obtained free of charge via www.ccdc.cam.ac.uk/conts/retrieving.html (or from the Cambridge Crystallographic Data Centre, 12, Union Road, Cambridge CB2 1EZ, UK; fax: (+44) 1223-336-033; or deposit@ccdc.cam.ac.uk).
- [14] a) K. Diemert, B. Kottwitz, W. Kuchen, *Phosphorus Sulfur Relat. Elem.* **1986**, *26*, 307; b) M. K. W. Choi, H. S. He, P. H. Toy, *J. Org. Chem.* **2003**, *68*, 9831.
- [15] Selected physical data: **9**: ³¹P{¹H} NMR (80.9 MHz, 25°C, CDCl₃): δ = 14.6 ppm; ¹H NMR (500 MHz, 25°C, CDCl₃): δ = 7.54 (dd, ³*J*(H,P) = 11.6 Hz, ³*J*(H,H) = 8.4 Hz, 2H; *o*-Ph), 7.40 (dd, ³*J*(H,H) = 8.4 Hz, ³*J*(H,P) = 2.1 Hz, 2H; *m*-Ph), 7.34 (dd, ³*J*(H,H) = 4.9 Hz, ³*J*(H,P) = 3.1 Hz, 2H; Ar-H), 7.16 (dd, ³*J*(H,H) = 4.9 Hz, ⁴*J*(H,P) = 1.2 Hz, 2H; Ar-H), 1.29 (s, 9H; *t*Bu); ¹³C{¹H} NMR (125.6 MHz, 25°C, CDCl₃): δ = 150.5 (d, ²*J*(C,P) = 2.9 Hz; Ar-Ar), 144.9 (d, ⁴*J*(C,P) = 10.5 Hz; *p*-Ph), 139.3 (d, ¹*J*(C,P) = 63.3 Hz; *ipso*-Ar), 131.8 (d, *J*(C,P) = 10.5 Hz; Ar-H), 128.1 (d, *J*(C,P) = 12.5 Hz; Ar-H), 126.1 (d, *J*(C,P) = 16.3 Hz; Ar-H), 126.1 (d, *J*(C,P) = 11.5 Hz; Ar-H), 122.3 (d, ¹*J*(C,P) = 54.7 Hz; *ipso*-Ph), 35.0 (s; CMe₃), 31.0 ppm (s; CH₃); ¹¹B NMR (160.3 MHz, 25°C, CDCl₃): δ = -39.2 ppm. **11**: ³¹P{¹H} NMR (126.0 MHz, 25°C, CDCl₃): δ = 19.1 ppm; ¹H NMR (400 MHz, 25°C, CDCl₃): δ = 7.62 (dd br, ³*J*(H,P) = 13.2 Hz, ³*J*(H,H) = 8.5 Hz, 2H; *o*-Ph), 7.40 (dd br, ³*J*(H,H) = 8.5 Hz, ⁴*J*(H,P) = 3.0 Hz, 2H; *m*-Ph), 7.26 (dd, ³*J*(H,H) = 5.0 Hz, ³*J*(H,P) = 3.4 Hz, 2H; Ar-H), 7.12 (dd, ²*J*(H,H) = 5.0 Hz, ⁴*J*(H,P) = 2.5 Hz, 2H; Ar-H), 1.26 ppm (s, 9H; *t*Bu); ¹³C{¹H} NMR (100.6 MHz, 25°C, CDCl₃): δ = 155.9 (s; *p*-Ar), 145.4 (d, ²*J*(C,P) = 24.0 Hz; Ar), 139.0 (d, ¹*J*(C,P) = 111.9 Hz; Ar), 130.6 (d, ²*J*(C,P) = 11.8 Hz; *o*-Ar), 128.0 (d, ²*J*(C,P) = 14.7 Hz; *o*-Ar), 126.0 (d, ¹*J*(C,P) = 111.1 Hz; Ar), 125.9 (d, ³*J*(C,P) = 13.2 Hz; *m*-Ar), 125.8 (d, ³*J*(C,P) = 12.8 Hz; *m*-Ar), 34.9 (s; CMe₃), 30.8 ppm (s; C(CH₃)₃). **12**: ³¹P{¹H} NMR (162.0 MHz, 25°C, CDCl₃): δ = 14.7 ppm; ¹H NMR (500 MHz, 25°C, CDCl₃): δ = 7.70 (dd, ³*J*(H,P) = 12.8 Hz, ³*J*(H,H) = 8.2 Hz, 2H; Ar-H), 7.46 (dd, ³*J*(H,H) = 8.2 Hz, ⁴*J*(H,P) = 2.8 Hz, 2H; Ar-H), 7.19 (d, ³*J*(H,P) = 2.4 Hz, 2H; Ar-H), 6.71 (dd, ³*J*(H,H) = 17.4 Hz, ³*J*(H,H) = 10.7 Hz, 1H; CH=CH₂), 5.83 (d, ³*J*(H,H) = 17.4 Hz, 1H; CH=CHH), 5.35 (d, ³*J*(H,H) = 10.7 Hz, 1H; CH=CHH), 0.91 (s, 18H; Si^{*t*}Bu), 0.28 (s, 6H; SiMe₂), 0.27 ppm (s, 6H; SiMe₂); ¹³C{¹H} NMR (125.7 MHz, 25°C, CDCl₃): δ = 150.8 (d, ¹*J*(C,P) = 23.9 Hz; *ipso*-Ar), 142.8 (d, *J*(C,P) = 14.3 Hz; Ar), 141.4 (d, *J*(C,P) = 18.2 Hz; Ar), 140.4 (s; *p*-Ar), 135.9 (s; CH=CH₂), 133.3 (d, ²*J*(C,P) = 15.3 Hz; *o*-Ar), 131.3 (d, ²*J*(C,P) = 12.4 Hz; *o*-Ar), 129.0 (d, ¹*J*(C,P) = 110.2 Hz; *ipso*-Ar), 126.6 (d, ³*J*(C,P) = 12.4 Hz; *m*-Ar), 116.5 (s; CH=CH₂), 26.2 (s; SiC(CH₃)₃), 16.8 (s; SiC(CH₃)₃), -5.0 (s; SiMe), -5.1 ppm (s; SiMe).
- [16] G. Barbarella, L. Favaretto, G. Sotgiu, L. Antolini, G. Gigli, R. Cingolani, A. Bongini, *Chem. Mater.* **2001**, *13*, 4112.
- [17] B. Valeur, *Molecular Fluorescence, Principles and Applications*, Wiley-VCH, Weinheim, **2002**.
- [18] M. Georges, R. P. N. Veregin, P. M. Kazmaier, G. K. Hamer, *Macromolecules* **1993**, *26*, 2987.
- [19] *Encyclopedia of Polymer Science and Engineering*, Rev. Ed., Wiley, New York, **1998**.

Molecular Lead Clusters—From Unexpected Discovery to Rational Synthesis

Karl W. Klinkhammer,* Yun Xiong, and Shenglai Yao

In memory of Peter Böttcher

Anionic cluster compounds of lead have been known for more than one century.^[1] The first species, NaPb₄ and KPb₂, were obtained as early as 1891 by Joannis from the reaction of alkali metals with lead in liquid ammonia.^[2] Extensive exploration of this chemistry was done by Kraus, Zintl, and others during the first decades of the 20th century.^[3] Addition of cryptands finally allowed for the isolation of macrocrystalline material and the structural characterization of several species, such as [Pb₅]²⁻, [Pb₉]⁴⁻, and [Pb₉]³⁻.^[4] The structures observed may all be understood using Wade's electron-counting rules. Molecular lead clusters bearing hydrocarbon or related substituents are unknown to date. There are some reports, however, about transition-metal carbonyl complexes of anionic lead clusters.^[5] Only for the lighter congeners germanium and tin, are organic- or organoelement-substituted species available.^[6] For most of these compounds the synthesis was not by derivatization of anionic clusters, but proceeded through cluster formation from smaller units.^[7] Wade's rules are usually, but not generally obeyed for such compounds or for the related clusters of the neighboring elements of Group 13.^[8]

We have investigated the reaction of dihypersilylplumbylene [(Me₃Si)₃Si]₂Pb ([Hyp₂Pb]) with phosphine in inert solvents, such as toluene or *n*-pentane. As main product the heterocubane [(HypPPb)₄] (Hyp = hypersilyl, Si(SiMe₃)₃) was isolated.^[9] At short reaction times and low temperature several intermediates could be detected by NMR spectroscopy. In attempts to isolate one of these species, the initial reaction mixture was stored at -60 °C for several days. Indeed a few dark brown well formed crystals were found in a matrix of unconsumed blue Hyp₂Pb. To our surprise, the structure analysis revealed that the compound contains no phosphorus, but is the molecular lead cluster [Pb₁₂Hyp₆] (**1**).^[10] Despite of disordering of the lead core about the crystallographic threefold axis, it can be shown that the model in Figure 1 is the only one having sensible Pb–Pb separations that is consistent with the diffraction data. The hypersilyl groups are well ordered, however, and clearly determine the arrangement of the molecules within the crystal. The enveloped twelve lead atoms constitute a distorted icosahedron. Six atoms (Pb_A) bear no substituent and form a puckered ring with chair conformation (the belt). Each of the remaining six

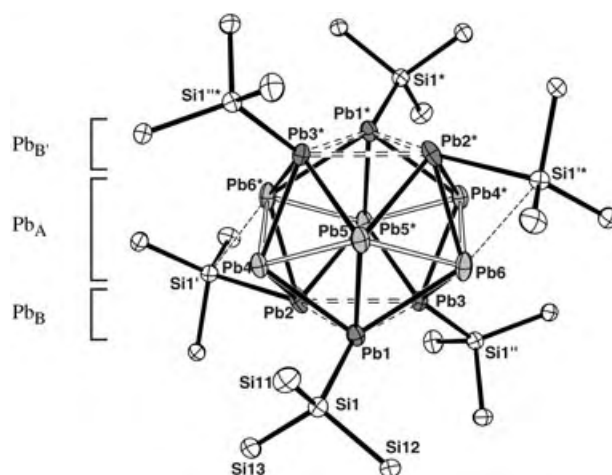
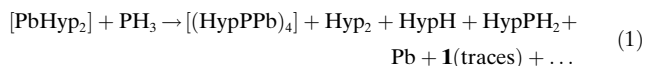


Figure 1. Structure of **1** (C and H atoms omitted for clarity). Selected bond lengths [pm]: Pb1–Pb2 336.83(10), Pb1–Pb3 332.39(9), Pb1–Pb4 311.33(13), Pb1–Pb5 310.7(5), Pb1–Pb6 334.81(12), Pb2–Pb3 338.87(11), Pb2–Pb4 319.99(10), Pb2–Pb5* 321.6(2), Pb2–Pb6* 305.61(13), Pb3–Pb6 323.21(12), Pb3–Pb4* 310.21(12), Pb3–Pb5* 311.4(9), Pb4–Pb5 326.9(6), Pb4–Pb6* 324.49(10), Pb5–Pb6 322.9(9), Pb1–Si1 269.5(2), Pb2–Si1' 308.5(2), Pb3–Si1'' 263.7(2), Pb6–Si1' 328.3(2).

atoms (Pb_B, Pb_{B'}) bears a hypersilyl group. Together they form two three-membered rings above and below the central Pb₆ belt. The Pb–Pb separations between neighboring lead atoms range from 305.6(1) to 339.0(1) pm. The largest distances are found between the lead atoms of type Pb_B (av. 336.1 pm), shorter ones between the lead atoms of the belt (Pb_A) (av. 324.8 pm), and the shortest between Pb_A and Pb_B (av. 316.5 pm). Although there is some overlap between these ranges, the description of the polyhedron as an icosahedron with two opposite open faces would be in line with Wade's rules, since with 30 electrons for the Pb₁₂ skeleton a *arachno*-type cluster is expected. A further structural detail of compound **1** is noteworthy. Whereas four hypersilyl groups are bonded in the expected terminal fashion, the other two substituents each bridge two lead atoms. As a consequence the bridged edge (Pb2–Pb6*) is the shortest within the cluster.

Unfortunately, compound **1** can only be obtained in traces and no spectroscopic data may be provided to date. The question arises how this cluster is formed in the reaction of PbHyp₂ and PH₃ and if there are alternative routes giving access to larger quantities.

NMR spectroscopy data of the reaction mixture as well as the composition of the isolated intermediates, such as the cyclic dimer [(Hyp(H)PPbHyp)₂] and of the main products [Eq. (1)] indicate that after the initial addition step, ligand

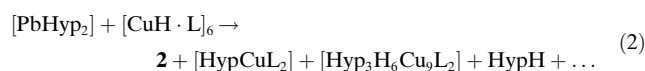


exchange between the lead and phosphorus centers occurs, which leads to the adduct [Hyp(H)Pb←PH₂Hyp]. After elimination of HypH and/or H₂ this adduct may either give the Pb–P heterocycles or on dissociation may yield HypPH₂ and the elusive hydridoplumbylene [Pb(H)Hyp]. Recently a

[*] Prof. Dr. K. W. Klinkhammer, MSc Y. Xiong, MSc S. Yao
Institut für Anorganische Chemie
Johannes-Gutenberg-Universität Mainz
Duesbergweg 10–14, 55128 Mainz (Germany)
Fax: (+49) 6131-39-25419
E-mail: klink@uni-mainz.de

related hydridoplumbylene with an extremely bulky *meta*-terphenyl substituent was postulated by Power et al. as the key intermediate in the formation of the first diplumbyne.^[11] In contrast to this particular kinetically stabilized diplumbyne, we expect that the analogous but less-shielded [Pb₂Hyp₂], which would form from dimerization and hydrogen loss of [Pb(H)Hyp], would not be stable under ambient conditions, but owing to its bis(plumbylene) nature would undergo addition and insertion reactions, thus possibly resulting in the formation of stable or less stable lead cluster compounds.

To support our assumption we looked for a rational synthesis of [Pb(H)Hyp]. At first we investigated the reaction of the [PbHyp₂] with several hydride sources, such as B₂H₆, [BH₄][−] and [AlH₄][−] under various conditions, but only found the formation of lead and HypH (with B₂H₆) or the reversible formation of adducts (with NaBH₄ and LiAlH₄). Finally we succeeded by treating [PbHyp₂] with the triphenylphosphine adduct of copper hydride [Eq. (2); L = PPh₃].^[12] During the reaction at −20 °C almost no lead precipitated, and from the resulting dark brown solution appreciable amounts of dark brown crystals were isolated. The structural analysis reveals that indeed a lead cluster had been formed, not the expected [Pb₁₂Hyp₆] (**1**), however, but the novel cluster [Pb₁₀Hyp₆] (**2**).



The NMR spectroscopic data from the crude reaction mixture shows that ligand exchange has taken place, since the main products, beside cluster compound **2** are HypH and the new hypersilyl copper(i) derivatives [HypCu(PPh₃)₂] and [Hyp₃H₆Cu₉(PPh₃)₂]. Small amounts of further products are present, however, which give rise to lowfield shifted ¹H NMR signals (δ = 0.6–0.8 ppm) as does compound **2** (δ = 0.64 ppm). We therefore assume that a mixture of several cluster compounds is produced, from which only the predominant and less-soluble species crystallizes easily. The best structural parameters were derived from specimens with cocrystallized benzene.^[10] The whole molecule has crystallographic C_s symmetry and the Pb₁₀ core approximately C_{3v} symmetry (Figure 2). The Pb₁₀ polyhedron is best derived from a Pb₁₂ icosahedron by replacing one trigonal face by a single lead atom. This picture would match the prediction made by Wade's rules which only hold for cluster compound **2** if it is formally composed from a [Hyp₆Pb₉]hypho-type cluster dianion (26 skeletal electrons) and a Pb²⁺ counteranion (Figure 3). The Pb–Pb separations within the hypho-Pb₉ fragment (Pb1 to Pb6) of **2** differ only slightly (312.36(4)–320.99(5) pm) and are all within the same range found for compound **1** and lead cluster anions, whereas the three bonds to the capping atom Pb7 are significantly shorter (299.80(4)–300.58(6) pm) indicating higher bond orders, that is, less delocalized bonds. In contrast to **1**, all six hypersilyl groups are located at the puckered six-membered ring (Pb_A), whereas the capping Pb₃ triangle (Pb_B) only consists of “naked” Pb atoms. The hypersilyl groups are all bonded in a terminal fashion. The three Pb–Si bonds to the silicon atoms (Si4, Si4', Si6) that lie more or less in the plane the

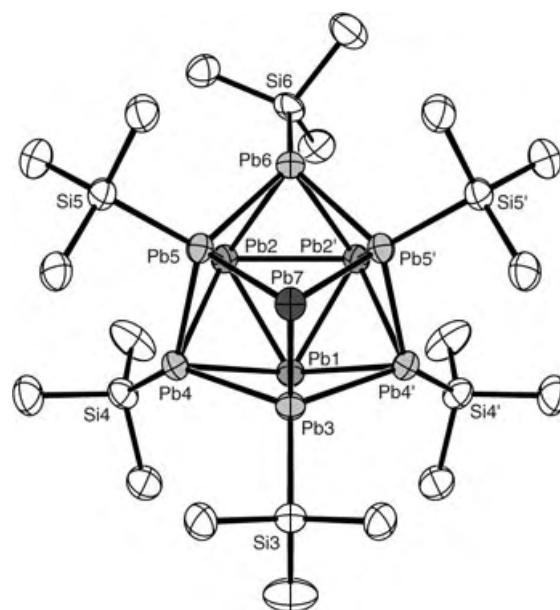


Figure 2. Structure of **2** (C and H atoms omitted for clarity). Selected bond lengths [pm] and angles [°]: Pb1–Pb2 320.11(5), Pb2–Pb2' 320.99(5), Pb1–Pb3 314.00(6), Pb1–Pb4 320.45(4), Pb2–Pb4 319.39(4), Pb2–Pb5 312.36(4), Pb2–Pb6 319.44(5), Pb3–Pb4 314.98(3), Pb3–Pb7 300.58(6), Pb4–Pb5 315.38(4), Pb5–Pb6 316.05(4), Pb5–Pb7 299.80(4), Pb3–Si3 270.0(3), Pb4–Si4 276.4(2), Pb5–Si5 268.8(2), Pb–Si6 277.8(4); Pb3–Pb7–Pb5 86.94(1), Pb5–Pb7–Pb5' 86.46(1).

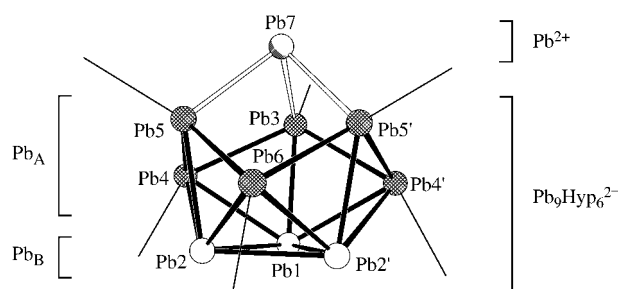


Figure 3. The Pb₁₀Si₆ skeleton of **2** illustrating the applicability of Wade's rules.

unsubstituted lead triangle (Pb1, Pb2, and Pb2'), perhaps for steric reasons, are significantly longer (276.4(2)–277.8(4) pm) than the remaining ones (268.8(2)–270.0(3) pm).

The ¹H NMR spectrum of **2** in [D₈]toluene at room temperature has only one signal at δ = 0.59 ppm for all the hypersilyl groups indicating a dynamic behavior of the Pb₁₀Si₆ core. On cooling, the resonance signal splits into two signals of equal intensity (δν = 18 Hz; T_c = 243–248 K) giving an approximate activation barrier of 50 kJ mol^{−1} for the scrambling process. By ESI mass spectroscopy of compound **2** the molecular ion [Pb₁₀Hyp₆] was not found, instead the ion [Pb₁₀Hyp₅]⁺ could be detected as particle of highest mass (*m/z* 3311). The UV/Vis spectra of **2** show strong absorptions across the whole visible spectral range with only two weakly pronounced maxima at 656 and 770 nm (both: ε = 49 000).

At ambient temperature and if light is excluded, solid **2** is indefinitely stable under argon. In solution at room temperature **2** quickly decomposes, yielding elementary lead and initially nearly equal amounts of the octasilane Hyp-Hyp and the plumbylene [PbHyp₂].^[13] Since the reaction rate is first order in **2**, the initial formation of “naked” lead clusters can be postulated. To get more information on this species we are currently studying the decomposition of **2** in inert polymer matrices.

Experimental Section

1: In a typical experiment LiPH₂·0.86DME (1.0 g, 8.53 mmol) was treated with 2,6-di-*tert*-butylphenol (1.76 g, 8.53 mmol) at -70°C in DME (25 mL). The solution was warmed slowly to room temperature, and the produced gaseous PH₃ fed into a Schlenk tube containing a dark blue solution of [PbHyp₂] (1.60 g, 0.89 mmol) in *n*-pentane (25 mL) at -60°C . After warming it to -30°C for 30 min the solution turned deep red and dark red solid material precipitated. The solution was decanted to another Schlenk tube and concentrated to about 3 mL. After storage of the solution at -60°C for two weeks several dark brown rod-shaped crystals of **1** were found among large amounts of dark blue crystals of unconsumed [PbHyp₂].

2: A solution of [PbHyp₂] (3.01 g, 4.28 mmol) in toluene (20 mL) was added to a suspension of [HCuPPh₃]₆ (1.40 g, 4.28 mmol) in toluene (30 mL) at -25°C under intense stirring. After 25 min the reaction mixture was warmed to room temperature and stirred for another 20 min. The suspension turned from deep violet to brown. After the filtration and washing with toluene the filtrate was concentrated to 9 mL and cooled to -60°C for 24 h. Dark brown rhombus-shaped crystals of **2** are obtained (0.73 g, 0.20 mmol, 47.0%). ¹H NMR (400.13 MHz, [D₆]benzene, 25°C): δ = 0.63 ppm; ¹³C NMR (100.62 MHz, [D₆]benzene, 25°C): δ = 9.1 ppm. MS (ESI; Et₂O/MeCN (4:1)): *m/z* (%): 3311 (100, *M*⁺-Hyp), 2816 (8, [Pb₁₀Hyp₃]⁺), 2113 (25, [Pb₉Hyp]⁺), 2099 (43, [Pb₉Hyp-H-CH₃]⁺), 717 (51, [Hyp₂MePb]⁺).

Received: August 16, 2004

Keywords: cluster compounds · lead · ligand exchange · silicon

- [1] Reviews: a) J. D. Corbett, *Struct. Bonding (Berlin)* **1997**, 87, 157; b) T. F. Fässler in *Metal Clusters in Chemistry* (Eds.: P. Braunstein, L. A. Oro, P. R. Raithby), Wiley-VCH, Weinheim, **1998**, 1610–1642.
- [2] C. R. Joannis, *C. R. Hebd. Seances Acad. Sci.* **1891**, 113, 795; C. R. Joannis, *C. R. Hebd. Seances Acad. Sci.* **1892**, 114, 587.
- [3] See for example: C. A. Kraus, *J. Am. Chem. Soc.* **1907**, 29, 1571; E. Zintl, J. Goubeau, W. Z. Dullenkopf, *Z. Phys. Chem. Abt. B* **1932**, 16, 183.
- [4] First reports: D. Kummer, L. Diehl, *Angew. Chem.* **1970**, 82, 881; *Angew. Chem. Int. Ed. Engl.* **1970**, 9, 895; P. A. Edwards, J. D. Corbett, *Inorg. Chem.* **1976**, 15, 903.
- [5] See for example: B. W. Eichhorn, R. C. Haushalter, *J. Chem. Soc. Chem. Commun.* **1990**, 937.
- [6] For a recent review see: A. Schnepf, *Angew. Chem.* **2004**, 116, 680; *Angew. Chem. Int. Ed.* **2004**, 43, 664.
- [7] Very recently Sevov and Ugrinov reported some examples of nucleophilic addition reactions to anionic germanium clusters resulting in organoelement substituted cluster anions: A. Ugrinov, S. C. Sevov, *Chem. Eur. J.* **2004**, 10, 3727 and literature cited herein.
- [8] See: A. Schnepf, H. Schnöckel, *Angew. Chem.* **2002**, 114, 4344; *Angew. Chem. Int. Ed.* **2002**, 41, 3532.

- [9] S. L. Yao, Y. Xiong, K. W. Klinkhammer, unpublished results.
- [10] Structural Analyses: Bruker AXS CCD SMART, MoK α (λ = 0.71073 Å); computer programs: SHELXS-97, PLATON, Siemens diffractometer software. Crystal data for **1** (Pb₁₂Si₂₄C₅₄H₁₆₂·C₅H₁₂): crystal size: 0.6 × 0.5 × 0.3 mm³, rhombohedral (hex. setting), space group *R* $\bar{3}$, *a* = 16.1051(3), *c* = 41.6827(10) Å, *V* = 9363.0(3) Å³, *Z* = 3, ρ_{calcd} = 2.152 g cm⁻³, *F*(000) = 5544, $\mu(\text{MoK}\alpha)$ = 16.374 mm⁻¹, *T* = 173 K, 23469 reflections, 5159 unique (*R*_{int} = 0.1139), structure solution by direct methods, refinement on *F*²(2 θ_{max} = 56.6°), 3637 unique (2 σ), 192 parameters, 13 restraints, *R*₁ (*I* > 2 σ) = 0.0452, *wR*₂ (all data) = 0.1137, GOF = 1.009, $\rho(e)(\text{min/max})$ = -0.930/1.630 e Å⁻³ (near Pb); absorption correction with MULABS (*T*_{min}/*T*_{max} = 0.01649/0.05882). Although the Pb₁₂ core is disordered about the threefold axis, only one model can be derived having meaningful Pb–Pb separations. All non-hydrogen atoms were refined anisotropically, H atoms riding with fixed thermal parameters. Crystal data for **2** (Pb₁₀Si₂₄C₅₄H₁₆₂·(C₆H₆)₃): crystal size: 0.3 × 0.3 × 0.2 mm³, monoclinic, space group *P*2₁/*m*, *a* = 15.6703(3), *b* = 25.1007(5), *c* = 18.6999(4) Å, *V* = 6685.2(2) Å³, *Z* = 2, ρ_{calcd} = 1.884 g cm⁻³, *F*(000) = 3536, $\mu(\text{MoK}\alpha)$ = 12.786 mm⁻¹, *T* = 193 K, 36258 reflections, 9966 unique (*R*_{int} = 0.0610), structure solution by direct methods, refinement on *F*²(2 θ_{max} = 50.2°), 7175 unique (2 σ), 224 parameters, 609 restraints, *R*₁ (*I* > 2 σ) = 0.0275, *wR*₂ (all data) = 0.0523, GOF = 0.906, $\rho(e)(\text{min/max})$ = -1.138/0.884 e Å⁻³ (near Pb); absorption correction by equivalent reflections with MULABS (*T*_{min}/*T*_{max} = 0.01320/0.04077). All non-hydrogen atoms could be refined anisotropically, H atoms riding with fixed thermal parameters. CCDC-247552 (**1**) and CCDC-247553 (**2**) contain the supplementary crystallographic data for this paper. These data can be obtained free of charge via www.ccdc.cam.ac.uk/conts/retrieving.html (or from the Cambridge Crystallographic Data Centre, 12 Union Road, Cambridge CB21EZ, UK; fax: (+44)1223-336-033; or deposit@ccdc.cam.ac.uk).
- [11] L. Pu, B. Twamley, P. P. Power, *J. Am. Chem. Soc.* **2000**, 122, 3524.
- [12] An analogous ligand exchange between [Hyp₂Pb] and aryl copper complexes has been successfully used in the synthesis of other heteroleptic plumbylens: J. Klett, K. W. Klinkhammer, M. Niemeyer, *Chem. Eur. J.* **1999**, 5, 2531.
- [13] [PbHyp₂] decomposes within several hours also giving lead and Hyp-Hyp as the only products. Both decomposition reactions—of **2** and of [PbHyp₂]⁺—are first order in starting material. The half-life periods were determined by ¹H NMR spectroscopic monitoring to be 4 (**2**) and 47 h ([PbHyp₂]⁺).

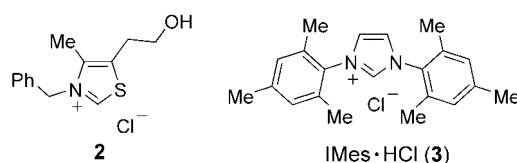
Organocatalysis

Organocatalyzed Conjugate Umpolung of α,β -Unsaturated Aldehydes for the Synthesis of γ -Butyrolactones**

Christian Burstein and Frank Glorius*

Most reactions in organic synthesis are polar and can be described as the reaction of a nucleophile (donor d) with an electrophile (acceptor a).^[1] The umpolung^[2] of the “natural” reactivity of a functional group opens up an avenue to a new set of reactions. It has been known for a long time that the umpolung of electrophilic aldehydes is possible by using catalysts such as cyanide or thiazolium carbenes.^[3] The resulting d¹-nucleophiles can react with aromatic aldehydes (benzoin condensation^[4]) or with electron-poor, polarized olefins (Stetter reaction^[5]).^[6] In contrast to this a¹-to-d¹-umpolung, the term “conjugate” umpolung describes the transformation of α,β -unsaturated aldehydes into d³-nucleophiles (homoenolate equivalents^[7]) by attack of nucleophilic catalysts on the aldehyde function (Scheme 1). Herein we report the organocatalyzed, chemo- and stereoselective reaction of conjugate “umpoled” α,β -unsaturated aldehydes with aromatic aldehydes and ketones to give γ -butyrolactones **1** and **4** (see Schemes 1 and 4).

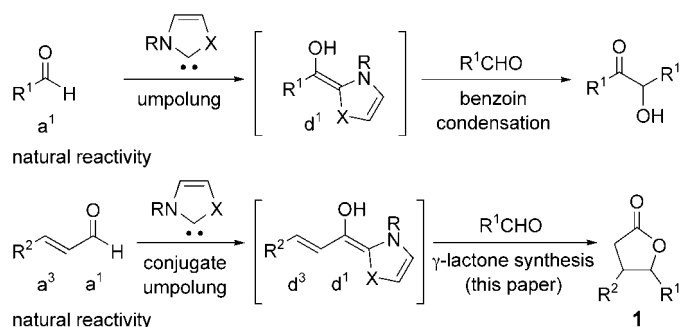
We started our investigation with the reaction of cinnamaldehyde and 4-chlorobenzaldehyde. As a result of the organocatalyzed umpolung of both aldehydes, numerous products can be formed (Scheme 2, R¹ = 4-ClC₆H₄, R² = Ph). The use of the commercially available thiazolium salt **2**^[8] as a catalyst does not provide lactone **1a**, but results in the formation of several benzoin products in low yield (Table 1, entry 1). Recently, imidazolium derived N-heterocyclic carbenes (NHCs) have been very successfully used as ligands in transition-metal catalysis^[9] and as organocatalysts of transesterification reactions.^[10] We were pleased to find that the



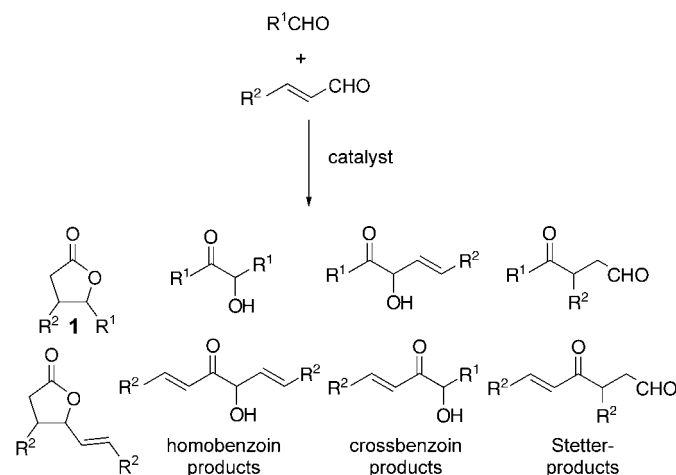
[*] C. Burstein, Dr. F. Glorius
Max-Planck-Institut für Kohlenforschung
Kaiser-Wilhelm-Platz 1, 45 470 Mülheim an der Ruhr (Germany)
Fax: (+49) 208-306-2994
E-mail: glorius@mpi-muelheim.mpg.de

[**] We thank Prof. A. Fürstner for generous support and the Deutsche Forschungsgemeinschaft, the BMBF and the Fonds der Chemischen Industrie (Liebig scholarship to F.G.) for financial support. We also thank Dr. C. W. Lehmann for the X-ray analyses, Dr. D. Belder, A. Deege, and H. Hinrichs for separations by HPLC, Dr. R. J. Mynott for help with the NMR spectroscopy analysis, and S. Holle, F. Schroer, and M. Rusek for experimental contributions.

Supporting information for this article is available on the WWW under <http://www.angewandte.org> or from the author.



Scheme 1. Comparison of umpolung and conjugate umpolung.



Scheme 2. Expected products of the organocatalyzed reaction of an α,β -unsaturated aldehyde with another aldehyde.

use of 1,3-di(2,4,6-trimethylphenyl)imidazolin-2-ylidene (IMes), derived from **3** by deprotonation, results in the selective formation of γ -butyrolactone **1a**. Under optimized conditions, IMes (5 mol%) was added dropwise to a 1:1 mixture of the aldehydes, and the reaction was stirred at ambient temperature for 16 h, allowing the isolation of the *cis* and *trans* diastereomers of **1a** in 44% and 9% yield, respectively (Table 1, entry 2). Larger amounts of potassium cyanide also catalyze this transformation. A combination of KCN (30 mol%) and [18]crown-6^[11] (10 mol%) leads to the formation of lactone **1a** in 33% yield (Table 1, entry 3). A variety of differently substituted lactones can be synthesized through this method. With the exception of 2-chlorobenzaldehyde (Table 1, entry 10), the *cis* diastereomer^[12] was formed predominantly in all cases (Table 1, Figure 1).

Currently, the scope of reactions that involve the umpolung of aldehydes, for example, the benzoin condensation or the Stetter reaction, is generally^[13] limited, as self-condensation or intramolecular reactions are required for good chemoselectivity. In stark contrast, the reaction of aromatic aldehydes with conjugate umpoled α,β -unsaturated aldehydes allows the selective linking of two different aldehydes in an intermolecular manner, representing a one-step formation of γ -butyrolactones with two new stereocenters.^[14]

Table 1: Reaction of cinnamaldehyde ($R^2 = \text{Ph}$) with aromatic aldehydes according to Scheme 2.^[a]

Entry	R^1	1	Yield [%]	<i>cis/trans</i> ^[b]
1 ^[c]	4-ClC ₆ H ₄	a	0	—
2	4-ClC ₆ H ₄	a	53	80:20
3 ^[d,e]	4-ClC ₆ H ₄	a	33	81:19
4	4-BrC ₆ H ₄	b	49	80:20
5	4-MeO(CO)C ₆ H ₄	c	70	79:21
6	4-F ₃ CC ₆ H ₄	d	44	77:23
7	3-FC ₆ H ₄	e	52	78:22
8	3-ClC ₆ H ₄	f	61	79:21
9	3-BrC ₆ H ₄	g	60	79:21
10 ^[e]	2-ClC ₆ H ₄	h	32	23:77

[a] General reaction conditions: **3** (0.05 mmol), KO^tBu (0.1 mmol), THF (3 mL); cinnamaldehyde (1.0 mmol), substituted benzaldehyde (1.0 mmol), 16 h, room temperature. Yields of the isolated products given as the sum of separately isolated *cis* and *trans* isomers.

[b] Determined by GC–MS. [c] **2** was used as catalyst instead of **3**.

[d] KCN (0.3 mmol) and [18]crown-6 (0.1 mmol) were used as catalyst instead of **3**. [e] Isolated as mixture of diastereomers.

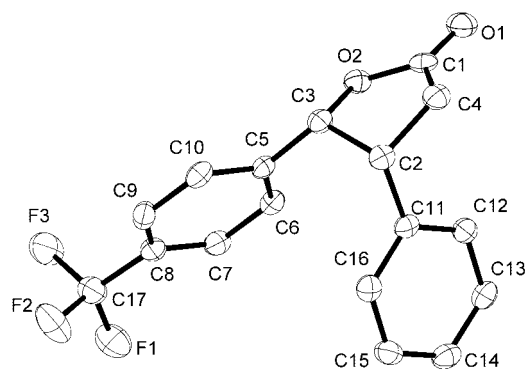
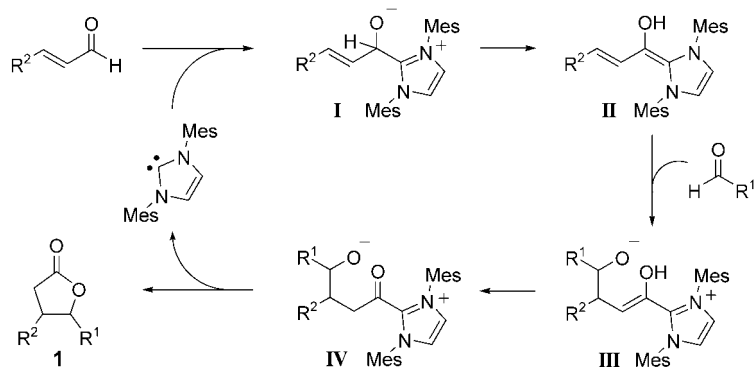


Figure 1. X-ray crystal structure of *cis*-**1d**.^[17]

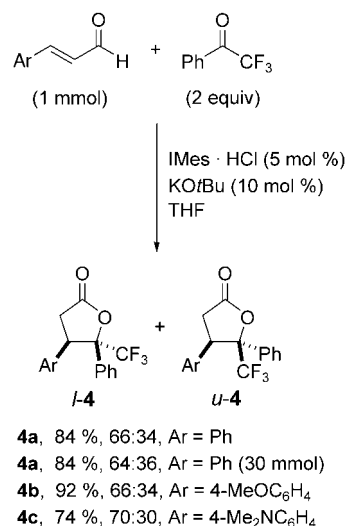
A plausible mechanism is depicted in Scheme 3. Reaction of the NHC with the α,β -unsaturated aldehyde gives rise to a zwitterionic structure **I**, which isomerizes by protonation/deprotonation to the conjugated dienamine **II**. Nucleophilic attack of **II** or its zwitterionic homoenolate tautomer at the aromatic aldehyde results in the formation of alcoholate **III**,



Scheme 3. Plausible mechanism of the NHC-catalyzed γ -butyrolactone formation. Mes = mesityl.

followed by isomerisation to the corresponding tautomer **IV**. These activated carboxylates are thought to be intermediates in NHC-catalyzed transesterification reactions, leading to ester formation when attacked by alcohol nucleophiles.^[10] Analogously, intramolecular attack of the alkoxide of **IV** or its protonated form at the carbonyl group leads to the closing of the lactone ring and the regeneration of the nucleophilic catalyst.

Fortunately, ketones^[15] also react as electrophiles with α,β -unsaturated aldehydes in good yield, thereby significantly increasing the scope of this reaction (Scheme 4).^[16] The



Scheme 4. NHC-catalyzed reaction of the conjugate umpoled unsaturated aldehyde with a ketone.^[16]

reaction of cinnamaldehyde and α,α,α -trifluoroacetophenone (1 equiv) results in the formation of γ -butyrolactone **4a** in 70 % yield, with the generation of one quaternary stereocenter. *L*- and *U*-diastereomers^[12] (Figure 2) can be separated by column chromatography. By using 2 equivalents of ketone, the yield can be increased to 84 % (Scheme 4); the reaction can also be run on a 30-mmol scale.^[17] Furthermore, substituted cinnamaldehyde derivatives such as 4-methoxy- and 4-dimethylaminocinnamaldehyde react equally well.^[17]

Recently, chiral triazolium salt derived NHCs were successfully used in the highly enantioselective benzoin

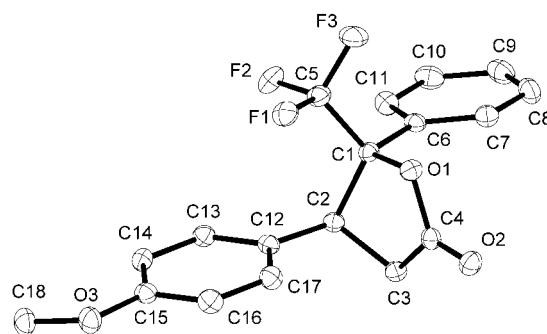
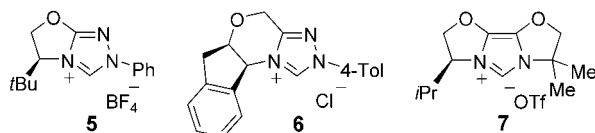


Figure 2. X-ray crystal structure of *U*-**4b** (minor diastereomer).^[12]

condensation^[18] and Stetter reaction.^[19] Interestingly, triazolium salts **5**^[18] and **6**^[19] are not suitable catalysts for the synthesis of **4a** under standard conditions (0% and 10% yield, respectively). In contrast, the NHC derived from imidazolium salt **7** (Tf = trifluoromethanesulfonyl)^[20] is a competent catalyst for this transformation. In the presence of **7** (5 mol %), **4a** is formed in 70% yield^[17] with an improved *l/u* ratio of 74:26 and with 12 and 25% *ee*, respectively.



In summary, the organocatalyzed conjugate umpolung of α,β -unsaturated aldehydes allows the direct, intermolecular, and crossed linking of an α,β -unsaturated aldehyde with another aldehyde or ketone, resulting in a flexible one-step synthesis of substituted γ -butyrolactones.^[21]

Experimental Section

Typical procedure: Generation of the catalyst solution (for multiple reactions): Under an atmosphere of argon, IMes-HCl (85.1 mg, 0.25 mmol) and potassium *tert*-butoxide (56.1 mg, 0.5 mmol) were dissolved in THF (5 mL) and stirred for 45 min at room temperature.

A part of the preformed catalyst solution (1 mL, 0.05 mmol IMes) was added over a period of 1 min to a solution of 4-formylbenzoic acid methyl ester (164 mg, 1 mmol) and *trans*-cinnamaldehyde (126 μ L, 1 mmol) in THF (5 mL). The solution was stirred for 16 h at ambient temperature, after which MeOH (2 mL) was added and the solution was stirred for a further 15 min. The solvent was evaporated in vacuo, and the residue was distilled in a Kugelrohr apparatus (5×10^{-2} mbar, 150–200°C). Purification of the distillate by column chromatography (SiO₂, 2.5 cm \times 12 cm, MTBE/hexane 1:3) yielded *cis*-**1c** (164 mg, 56%) and *trans*-**1c** (41 mg, 14% after crystallization from CH₂Cl₂/hexane) as colorless solids.

Received: August 6, 2004

Keywords: aldehydes · carbene · heterocycles · organocatalysis · umpolung

- [1] a) K. C. Nicolaou, E. J. Sorensen, *Classics in Total Synthesis*, VCH, Weinheim, 1996; b) K. C. Nicolaou, S. A. Snyder, *Classics in Total Synthesis II*, Wiley-VCH, Weinheim, 2003.
- [2] D. Seebach, *Angew. Chem.* **1979**, 91, 259; *Angew. Chem. Int. Ed. Engl.* **1979**, 18, 239.
- [3] For recent reviews on nucleophilic organocatalysis, see: a) D. Enders, T. Balensiefer, *Acc. Chem. Res.* **2004**, 37, 534; b) J. S. Johnson, *Angew. Chem.* **2004**, 116, 1348; *Angew. Chem. Int. Ed.* **2004**, 43, 1326.
- [4] a) F. Wöhler, J. Liebig, *Ann. Pharm.* **1832**, 3, 249; b) A. Lapworth, *J. Chem. Soc.* **1903**, 83, 995; c) R. Breslow, *J. Am. Chem. Soc.* **1958**, 80, 3719.
- [5] a) H. Stetter, H. Kuhlmann in *Organic Reactions*, Vol. 40 (Ed.: L. A. Paquette), Wiley, New York, 1991, pp. 407–496; b) H. Stetter, H. Kuhlmann, *Chem. Ber.* **1976**, 109, 2890.
- [6] For new approaches in the organocatalyzed umpolung of aldehydes, see: opening of epoxyaldehydes: a) K. Y.-K. Chow,

- J. W. Bode, *J. Am. Chem. Soc.* **2004**, 126, 8126; redox reactions of α -haloaldehydes: b) N. T. Reynolds, J. Read de Alaniz, T. Rovis, *J. Am. Chem. Soc.* **2004**, 126, 9518; conversion of α,β -unsaturated aldehydes into saturated carboxylic acid derivatives by using stoichiometric amounts of trimethylsilyl cyanide: c) H. Kawabata, M. Hayashi, *Tetrahedron Lett.* **2002**, 43, 5645.
- [7] a) H. Ahlbrecht, U. Beyer, *Synthesis* **1999**, 365; b) D. Hoppe, *Angew. Chem.* **1984**, 96, 930; *Angew. Chem. Int. Ed. Engl.* **1984**, 23, 932; c) N. Westiuk, *Tetrahedron* **1983**, 39, 205.
- [8] T. Ukai, R. Tanaka, T. Dokawa, *J. Pharm. Soc. Jpn.* **1943**, 63, 296 [*Chem. Abstr.* **1951**, 45, 5148].
- [9] For reviews on NHCs, see: a) W. A. Herrmann, *Angew. Chem.* **2002**, 114, 1342; *Angew. Chem. Int. Ed.* **2002**, 41, 1291; b) W. A. Herrmann, C. Köcher, *Angew. Chem.* **1997**, 109, 2256; *Angew. Chem. Int. Ed. Engl.* **1997**, 36, 2162; c) A. J. Arduengo III, R. Krafczyk, *Chem. Unserer Zeit* **1998**, 32, 6; d) D. Bourissou, O. Guerret, F. P. Gabbaï, G. Bertrand, *Chem. Rev.* **2000**, 100, 39.
- [10] For a review, see: a) G. A. Grasa, R. Singh, S. P. Nolan, *Synthesis* **2004**, 971; for carbene-catalyzed transesterifications, see: b) G. A. Grasa, R. M. Kissling, S. P. Nolan, *Org. Lett.* **2002**, 4, 3583; c) G. W. Nyce, J. A. Lamboy, E. F. Connor, R. M. Waymouth, J. L. Hedrick, *Org. Lett.* **2002**, 4, 3587; d) G. A. Grasa, T. Güveli, R. Singh, S. P. Nolan, *J. Org. Chem.* **2003**, 68, 2812; e) G. W. Nyce, T. Glauser, E. F. Connor, A. Möck, R. M. Waymouth, J. L. Hedrick, *J. Am. Chem. Soc.* **2003**, 125, 3046; f) R. Singh, R. M. Kissling, M.-A. Letellier, S. P. Nolan, *J. Org. Chem.* **2004**, 69, 209.
- [11] D. A. Evans, L. K. Truesdale, *Tetrahedron Lett.* **1973**, 14, 4929.
- [12] The stereochemistry of the lactones **1** and **4** was assigned by X-ray crystal-structure and NMR spectroscopy analysis. The ¹H NMR data for the lactone ring hydrogen atoms of **1a–h** is very similar within the *cis* and *trans* series. The stereochemistry of the products **1** was therefore assigned by comparison of the NMR data for these compounds with that of *cis*-**1d**, whose structure was unequivocally established by X-ray crystal-structure analysis. The stereochemistry of lactones **4** was assigned in an analogous manner (see Supporting Information). Crystal data for *cis*-**1d**: C₁₇H₁₃F₃O₂, from CH₂Cl₂/hexane, *M_r* = 306.27 g mol^{−1}, crystal size: 0.07 \times 0.05 \times 0.02 mm³; orthorhombic, space group *P*2₁2₁2₁, *a* = 5.6377(2), *b* = 15.4285(5), *c* = 16.3106(5) Å, *V* = 1418.72(8) Å³, ρ_{calcd} = 1.434 g cm^{−3}, *Z* = 4, *T* = 100 K, $\mu(\text{MoK}\alpha)$ = 0.119 mm^{−1}, 21 653 measured and 4520 independent reflections, 3217 with *I* > 2 σ (*I*), θ_{max} = 30.99°, (*R*_{int} = 0.0674), 199 parameters, H atoms placed on ideal positions, *R*₁ (*I* > 2 σ (*I*)) = 0.0536, *wR*² (all data) = 0.1049, *S* = 0.988, $\Delta\rho_{\text{max/min}}$ = 0.222/−0.226 e Å^{−3}, structure determination by direct methods (G. M. Sheldrick, SHELXS-97, Program for the Solution of Crystal Structures, Universität Göttingen, Göttingen, 1997) and by least-squares refinement on *F*_o² (G. M. Sheldrick, SHELXL-97, Program for Crystal Structure Refinement, Universität Göttingen, Göttingen, 1997). Crystal data for *u*-**4b**: C₁₈H₁₅F₃O₃, from CH₂Cl₂/hexane, *M_r* = 336.30 g mol^{−1}, crystal size: 0.18 \times 0.03 \times 0.03 mm³; monoclinic, space group *P*2₁, *a* = 5.7766(2), *b* = 7.6268(3), *c* = 17.3771(5) Å, β = 93.745(2)°, *V* = 763.95(5) Å³, ρ_{calcd} = 1.462 g cm^{−3}, *Z* = 2, *T* = 100 K, $\mu(\text{MoK}\alpha)$ = 0.123 mm^{−1}, 14 383 measured and 4102 independent reflections, 3618 with *I* > 2 σ (*I*), θ_{max} = 29.16°, (*R*_{int} = 0.0488), 218 parameters, H atoms placed on ideal positions, *R*₁ (*I* > 2 σ (*I*)) = 0.0379, *wR*² (all data) = 0.0852, *S* = 1.018, $\Delta\rho_{\text{max/min}}$ = 0.208/−0.288 e Å^{−3}, structure determination by direct methods (SHELXS-97), least-squares refinement on *F*_o² (SHELXL-97). CCDC-246 600 (*cis*-**1d**) and CCDC-250 238 (*u*-**4b**) contain the supplementary crystallographic data for this paper. These data can be obtained free of charge via www.ccdc.cam.ac.uk/conts/retrieving.html (or from the Cambridge Crystallographic Data Centre, 12, Union Road, Cambridge CB2 1EZ, UK; fax: (+44) 1223-336-033; or deposit@ccdc.cam.ac.uk).

- [13] Some enzymes are intriguingly selective catalysts and enable the crossed and asymmetric benzoin condensation: a) P. Dunkelmann, D. Kolter-Jung, A. Nitsche, A. S. Demir, P. Siegert, B. Lingen, M. Baumann, M. Pohl, M. Müller, *J. Am. Chem. Soc.* **2002**, *124*, 12084; or an intermolecular Stetter reaction: b) T. Kitazume, N. Ishikawa, *Chem. Lett.* **1984**, 1815.
- [14] For comparison: similar γ -butyrolactones can be formed highly diastereoselectively in six steps from cinnamaldehyde by using stoichiometric amounts of a zirconium complex: a) D. Enders, M. Kroll, G. Raabe, J. Runsink, *Angew. Chem.* **1998**, *110*, 1770; *Angew. Chem. Int. Ed.* **1998**, *37*, 1673; for some recent, less stereoselective syntheses of related γ -butyrolactones, see: b) M. C. Whisler, L. Vaillancourt, P. Beak, *Org. Lett.* **2000**, *2*, 2655; c) N. Kise, Y. Hirata, T. Hamaguchi, N. Ueda, *Tetrahedron Lett.* **1999**, *40*, 8125; d) D. J. Pippel, M. D. Curtis, H. Du, P. Beak, *J. Org. Chem.* **1998**, *63*, 2.
- [15] The intermolecular addition of umpoled aldehydes to ketones is a challenging problem. The intramolecular benzoin condensation of an aldehyde and a ketone was recently reported: Y. Hachisu, J. W. Bode, K. Suzuki, *J. Am. Chem. Soc.* **2003**, *125*, 8432.
- [16] Preliminary experiments show that other ketones can be used as electrophiles and alkyl-substituted α,β -unsaturated aldehydes can be used as nucleophiles after conjugate umpolung; we will report on these results in due course.
- [17] Isolated as a mixture of diastereomers.
- [18] a) D. Enders, U. Kallfass, *Angew. Chem.* **2002**, *114*, 1822; *Angew. Chem. Int. Ed.* **2002**, *41*, 1743; b) T. Dudding, K. N. Houk, *Proc. Natl. Acad. Sci. USA*, **2004**, *101*, 5770.
- [19] a) M. S. Kerr, J. Read de Alaniz, T. Rovis, *J. Am. Chem. Soc.* **2002**, *124*, 10298; b) M. S. Kerr, T. Rovis, *Synlett* **2003**, 1934; enantioselective formation of quaternary stereocenters: c) M. S. Kerr, T. Rovis, *J. Am. Chem. Soc.* **2004**, *126*, 8876; see also: d) D. Enders, K. Breuer, J. Runsink, J. H. Teles, *Helv. Chim. Acta* **1996**, *79*, 1899.
- [20] a) F. Glorius, G. Altenhoff, R. Goddard, C. Lehmann, *Chem. Commun.* **2002**, 2704; for the successful application of these ligands in the Suzuki cross-coupling of sterically hindered aryl chlorides, see: b) G. Altenhoff, R. Goddard, C. W. Lehmann, F. Glorius, *Angew. Chem.* **2003**, *115*, 3818; *Angew. Chem. Int. Ed.* **2003**, *42*, 3690; c) G. Altenhoff, R. Goddard, C. W. Lehmann, F. Glorius, *J. Am. Chem. Soc.* **2004**, in press.
- [21] In parallel to this work, a manuscript describing a similar transformation was published: S. S. Sohn, E. L. Rosen, J. W. Bode, *J. Am. Chem. Soc.*, 13.10.2004, doi 10.1021/ja044714b.

Butenyl-Substituted Alkaline-Earth Metallocenes: A First Step towards Olefin Complexes of the Alkaline-Earth Metals**

Herbert Schumann,* Stefan Schutte, Heinz-Jürgen Kroth, and Dieter Lentz*

The coordination of an α -olefin to the metal center of a 14-electron metallocene alkyl complex,^[1] for example to zirconium complexes of the type $[\text{Cp}_2\text{ZrR}]^+$ is assumed to be the primary reaction step in the polymerization of olefins catalyzed by such metallocenes.^[2] In the case of zirconium, however, thus far only the isolation and X-ray characterization of complexes with chelating η^1, η^2 or η^5, η^2 olefin ligands have been successful.^[3–5] The formation of vanadium,^[6] niobium,^[7] and the yttrium complexes investigated by Casey et al.^[8–10] with non-chelating olefins have until now only been detectable by NMR spectroscopy. Both ourselves and Evans et al. have been able to show recently that chelating η^5, η^2 -cyclopentadienyl ligands such as $\text{C}_5\text{Me}_4\text{CH}_2\text{CH}_2\text{CH}=\text{CH}_2$ ^[11] or $\text{C}_5\text{Me}_4\text{SiMe}_2\text{CH}_2\text{CH}=\text{CH}_2$ ^[12] in the form of their alkali metal salts form metallocenes with the diiodides of Eu, Sm, and Yb in which the terminal olefin groups of the side chains coordinate to the metal center.

No olefin complexes of Ba^{II} , which is isoelectronic with these lanthanoids at the oxidation level Ln^{II} (apart from the occupation of the 4f shell), and the other alkaline-earth metals are thus far known. An interaction between the alkyne ligand and the magnesium could be detected only with $[\text{TiCp}][\text{MgCp}][\mu\text{-}\eta^2\text{-}\eta^2\text{-C}_2(\text{SiMe}_3)_2]$ ^[13] and $[(\text{C}_5\text{HMe}_4)_2\text{Ti}(\eta^1\text{-C}\equiv\text{CSiMe}_3)_2][\text{Mg}(\text{thf})\text{Cl}]$ ^[14] from X-ray structural data, and for $[(\text{C}_5\text{Me}_5)_2\text{Ca}(\text{Me}_3\text{SiC}\equiv\text{C-C}\equiv\text{CSiMe}_3)]$ ^[15] a coordination of the diyne to calcium. Alkaline-earth metallocenes such as $[(\text{C}_5\text{HMe}_4)_2\text{Mg}(\text{Me-carb})]$ or $[(\text{C}_5\text{HMe}_4)_2\text{Sr}(\text{Pr-carb})]$ (Me-carb and Pr-carb = 1,3,4,5-tetramethylimidazol-2-ylidene and 1,3-di(isopropyl)-4,5-dimethylimidazol-2-ylidene, respectively) are highly active catalysts for the polymerization of acrylates;^[16] therefore it appeared obvious to assume that the solvent-free alkaline-earth metallocenes as 12-electron complexes could also seek to compensate their electron deficiency

[*] Prof. Dr. H. Schumann, S. Schutte, Dr. H.-J. Kroth
Institut für Chemie
Technische Universität Berlin
Strasse des 17. Juni 135, 10623 Berlin (Germany)
Fax: (+49) 30-3142-2168
E-mail: schumann@chem.tu-berlin.de
Priv.-Doz. Dr. D. Lentz
Institut für Chemie
Freie Universität Berlin
Fabeckstrasse 34–36, 14195 Berlin (Germany)
Fax: (+49) 30-838-52424
E-mail: lentz@chemie.fu-berlin.de

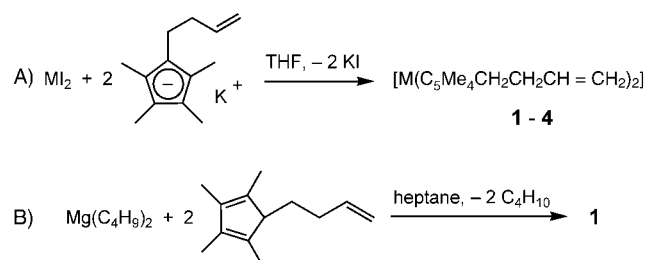
[**] This work was supported by the Deutsche Forschungsgemeinschaft and the Fonds der Chemischen Industrie.



Supporting information for this article is available on the WWW under <http://www.angewandte.de> or from the author.

by coordination to olefinic π systems. Herein we confirm this assumption with the synthesis of the first alkaline-earth metal complexes with alkenyl-substituted chelating η^5, η^2 -cyclopentadienyl ligands.

$C_5Me_4HCH_2CH_2CH=CH_2$ may be readily deprotonated with KH in THF at room temperature with the formation of $K[C_5Me_4CH_2CH_2CH=CH_2]$, a pyrophoric, beige-colored powder.^[11a] This reacts with alkaline-earth diiodides (MI_2) in THF suspension with loss of KI and formation of the corresponding metallocenes $[M(C_5Me_4CH_2CH_2CH=CH_2)_2]$, $M = Mg$ (**1**), Ca (**2**), Sr (**3**), Ba (**4**) (Scheme 1, A). The latter



Scheme 1. A) Synthesis of the metallocenes **1–4** from alkaline-earth diiodides and $K[C_5Me_4CH_2CH_2CH=CH_2]$; $M = Mg$ (**1**), Ca (**2**), Sr (**3**), Ba (**4**). B) Synthesis of **1** from dibutylmagnesium and 5-but-3-en-1-yl-1,2,3,4-tetramethylcyclopenta-1,3-diene.

are isolated as colorless, solvent-free crystals after precipitation from hexane and subsequent crystallization from hexane (**1–3**) or toluene (**4**) at $-78^\circ C$. Compound **1** may also be obtained by the reaction of dibutylmagnesium with 5-but-3-en-1-yl-1,2,3,4-tetramethylcyclopenta-1,3-diene in heptane after heating for 12 h under reflux (Scheme 1, B). Compound **1** melts at $37^\circ C$ with the formation of a colorless liquid that rapidly turns yellow. Compounds **2**, **3**, and **4** decompose above 138 (**2**), 208 (**3**), and $157^\circ C$ (**4**) with yellow coloration without previously melting.

The isolation single crystals was very difficult and required special care since all four metallocenes are highly sensitive and decompose immediately with yellow coloration on contact with very small amounts of moisture and oxygen. The structural investigations show that only the magnesium complex **1** satisfies the strict arrangement of a sandwich structure with a parallel arrangement of the cyclopentadienyl ring planes above and below the central metal atom, an arrangement that was also found for $[Mg(C_5H_5)_2]$ ^[17] and $[Mg(C_5Me_5)_2]$.^[18] Two independent molecules are located in the unit cell that differ only slightly in the angles $Cp1_{cen}-Mg1-Cp2_{cen}$ (175.84°) and $Cp1_{cen}-Mg2-Cp2_{cen}$ (180°) and in the torsion angles: $C1r-Cp1_{cen}-Cp2_{cen}-C6r = -32.1(1)^\circ$ and $C1r-Cp1_{cen}-Cp1'_{cen}-C1r' = -180^\circ$ (Figure 1, cen = ring centroid). The respective distance between the centers of the two cyclopentadienyl ligands (3.930 and 3.926 Å, respectively, Table 1) corresponds to the value determined for $[Mg(C_5Me_5)_2]$ (3.94 Å).^[18] The two butenyl

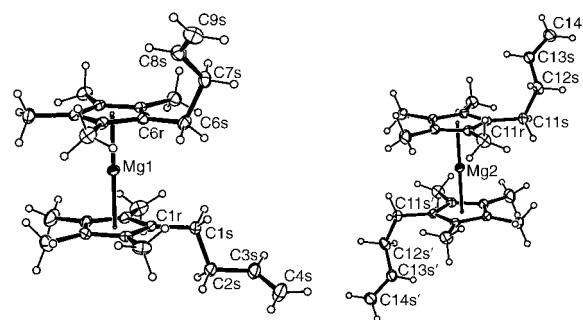


Figure 1. Molecular structure of **1** (ORTEP,^[19] ellipsoids at 30% probability).

side chains are directed away from the magnesium center above and below, respectively.

The compounds with the heavy alkaline-earth metals, **2–4**, have in principal the same molecular structure with C_2 symmetry (**3**) or approximate C_2 symmetry (**2**, **4**; see Figure 2). Unlike in **1**, but in agreement with the structures of $[Ca(C_5Me_5)_2]$,^[20] $[Sr(C_5Me_5)_2]$,^[21] and $[Ba(C_5Me_5)_2]$,^[20,21] the cyclopentadienyl rings in **2–4** are inclined towards each other; furthermore, the butenyl side chains of the cyclopentadienyl ligands are directed towards the metal center. This bent structure, which all metallocenes of the heavy alkaline-earth metals and also metallocenes of Eu^{II} ,^[22] Sm^{II} ,^[22] and Yb^{II} ^[23] exhibit, cannot be attributed here to a lone pair of electrons at the metal center as in the likewise bent metallocenes of Ge, Sn, and Pb. On the contrary, it is accounted for by a slight polarizability of the original spherically symmetrical distribution of the positive charge of the large metal cations caused by the negatively charged Cp ligands, which reduces their mutual repulsion.^[22] Further explanations for the bent arrangement of the Cp ligands are their Van der Waals attractions^[24,25] or the $(n-1)d$ orbital involvement of the metal centers in the sense of an $(n-1)dns$ hybridization.^[26]

The centers of the Cp ligands and the double bonds in **2–4** form a strongly distorted tetrahedral coordination sphere around the metals. The centers of the cyclopentadienyl ligands form an angle of almost exactly 140° with the metal center in all three compounds (Table 1): 140.9° (**2**), $139.3/140.4^\circ$ (**3**), and 139.1° (**4**). In contrast very different $Cp_{cen}-M-$

Table 1: Selected bond lengths [Å] and angles [$^\circ$] of **1–4**.

	1 (1) ^[a]	1 (2) ^[b]	2	3 (1) ^[a]	3 (2) ^[b]	4
M–C _{cen}	1.962(2)	1.963(2)	2.382(2)	2.55(1)	2.55(1)	2.721(3)
	1.968(2)	1.963(2)	2.412(2)			2.715(3)
M–C4s	6.882(2)	6.620(2)	3.045(2)	3.04(2)		3.179(3)
M–C9s	6.589(2)	6.620(2)	2.941(2)		2.99(2)	3.212(3)
M–C3s	5.928(2)	5.389(2)	3.230(2)	3.25(2)		3.435(3)
M–C8s	5.381(2)	5.389(2)	3.078(2)		3.20(2)	3.375(3)
C3s–C4s	1.306(2)	1.319(2)	1.267(2)	1.32(2)		1.316(3)
C8s–C9s	1.314(2)	1.319(2)	1.361(2)	1.33(2)		1.316(3)
Cp–M–Cp	175.84(5)	180	140.92(6)	139.3(4)	140.4(4)	139.1(1)
C4s–M–C9s			81.30(6)	88.9(4)	85.3(4)	98.55(7)
C3s–M–C8s			105.52(6)	93.8(4)	92.2(4)	102.17(7)

[a] Molecule 1. [b] Molecule 2.

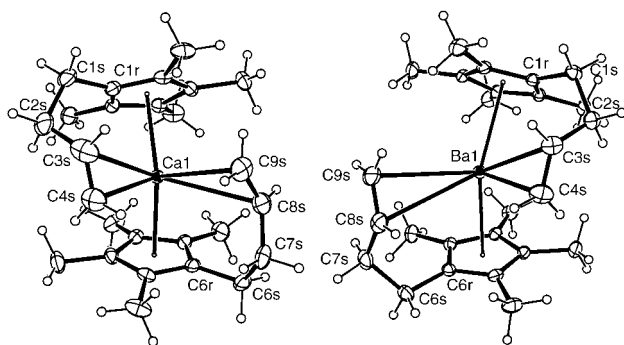


Figure 2. Molecular structure of **2** (left) and **4** (right; ORTEP,^[19] ellipsoids at 30% probability).

Cp_{cen} angles, dependent upon the size of the central metal atom are found for both the solvent-free alkaline-earth compounds $[M(C_5Me_5)_2]$ and the alkaline-earth carbene complexes $[(C_5Me_5)_2ML]$ ($L = 1,3,4,5$ -tetramethylimidazol-2-ylidene): 147.7° for $[Ca(C_5Me_5)_2]$ and 131° for $[Ba(C_5Me_5)_2]$ at 116 and 118 K, respectively, in the crystal,^[20] 149° for $[Sr(C_5Me_5)_2]$ and 148° for $[Ba(C_5Me_5)_2]$ in the gas phase,^[21] and 143.9° for $[(C_5Me_5)_2CaL]$ and 137.0° for $[(C_5Me_5)_2BaL]$ at $-70^\circ C$ in the crystal.^[27]

This difference and, with consideration of the metal radius, the almost identical M–C distances of the olefin-carbon atoms coordinated unsymmetrically to the metal center (M–C3s and M–C8s = 3.23/3.08 (**2**), 3.25/3.20 (**3**), 3.44/3.38 (**4**) and M–C4s and M–C9s = 3.05/2.94 (**2**), 3.04/2.99 (**3**), 3.18/3.21 Å (**4**)) are a clear confirmation that this orientation of the butenyl side chains directed towards the metal center is caused by a coordination of the olefin to the alkaline-earth metal center and not perhaps by crystal packing effects. The distances to the terminal carbon atoms C4s and C9s are generally shorter than to C3s and C8s, but significantly longer than to the cyclopentadienyl carbon atoms. The range of the distances, which is moreover relatively large, and the constant C=C lengths in the open magnesium derivative **1** and in **2–4** suggest, however, a very labile coordination of the olefin ligands. Crystallization of the complexes from THF is not possible because they are too soluble. No crystals suitable for X-ray structure analysis could be isolated even by the addition of small amounts of THF to hexane or toluene solutions of **2–4**. Therefore it was not possible in this way to determine whether the olefin side chains are displaced from the coordination sphere of the metals by the Lewis basic THF and whether THF complexes with non-coordinated olefin side chains are formed.

The 1H NMR spectra of **1–4** recorded in $[D_6]$ benzene (selected data in Table 2) show almost identical chemical shifts for the C_5Me_4 , α - CH_2 , β - CH_2 , and γ -CH protons of the ligands. The respective chemical shifts of the signals of the *cis*-

and *trans*- δ - $CH_2=CH$ protons of **3** and **4** are also practically identical, although they are shifted by up to 0.3 ppm to higher field compared to the corresponding signals of **1** (with the butenyl groups orientated away from the magnesium center). With the addition of $[D_8]THF$, which as σ -donor ligand should displace the olefin from the coordination sphere of the metal, the chemical shifts of all signal groups of **1** change only marginally, in the case of **4**, however, the signal of the *cis*- $CH_2=CH$ protons shifts by 0.11, and that of the *trans*- $CH_2=CH$ proton by 0.17 ppm to lower field and thus in the direction of the signals of **1**. With $[Yb(C_5Me_4SiMe_2CH_2CH=CH_2)_2]$ too a low field shift of the same order of magnitude for the $CH_2=CH$ protons was observed with the change from benzene to THF as solvent, although with a simultaneous high field shift of the $CH_2=CH$ protons.^[12] These small signal shifts do not allow any prediction about whether the olefin coordinates to the alkaline-earth metal or ytterbium center, since unlike the transition-metal–olefin complexes no electron density modifying backbonding is possible. In low-temperature 1H NMR spectra of **4** in $[D_8]THF$ the position of the $CH_2=CH$ and $CH_2=CH$ signals remain constant to $-83^\circ C$. Over the same temperature range in $[D_8]$ toluene, however, they are shifted successively to higher fields by up to 0.16 ppm. Compound **3** also shows high-field shifts of up to 0.2 ppm for these signals in $[D_8]$ toluene at $-83^\circ C$.

Table 2: 1H and ^{13}C NMR data [ppm] of **1–4**.

	Solvent	1H NMR			^{13}C NMR	
		$\delta=CH$	$\delta CH=CHH$ (<i>trans</i>)	$\delta CH=CHH$ (<i>cis</i>)	$\delta CH=$	$\delta CH_2=$
1	$[D_6]$ benzene	5.83 (ddt)	5.07 (ddt)	4.97 (ddt)	138.93	114.64
1	$[D_8]THF$	5.78 (ddt)	4.98 (ddt)	4.89 (ddt)	139.56	114.57
2	$[D_6]$ benzene	5.82 (ddt)	4.81 (m)		147.63	115.03
3	$[D_6]$ benzene	5.83 (ddt)	4.73 (ddt)	4.70 (ddt)	149.82	115.20
4	$[D_6]$ benzene	5.89 (ddt)	4.79 (ddt)	4.73 (ddt)	148.80	115.92
4	$[D_8]THF$	5.83 (ddt)	4.96 (ddt)	4.84 (ddt)	142.17	113.78

The ^{13}C NMR spectra of **1–4** recorded in both $[D_6]$ benzene and $[D_8]$ toluene as well as in $[D_8]THF$ show the expected nine signals, which depending upon the metal and the solvent show no substantial shifts apart from the inner olefin-carbon atom. The γ -C signal in the spectra measured in $[D_6]$ benzene shifts from $\delta = 138.93$ (**1**) through 147.63 (**2**) and 149.82 (**3**) to 148.80 ppm (**4**). In contrast in the ^{13}C NMR spectrum of a solution of **4** in $[D_8]THF$ the signal for the γ -C atom shows a chemical shift of $\delta = 142.17$ ppm, a value that is close to the value for **1**. In the coordinating solvent THF the olefin is clearly displaced from the coordination sphere of the barium center. This effect also corresponds to that for the high-field shift found for the inner olefin-carbon atom in $[Yb(C_5Me_4SiMe_2CH_2CH=CH_2)_2]$ on comparison of the spectrum in $[D_6]$ benzene ($\delta = 147.6$ ppm) with that in $[D_8]THF$ ($\delta = 140.5$ ppm).^[12]

The X-ray structure analyses of these olefin complexes of the alkaline-earth metals (**2–4**) synthesized for the first time show an orientation of the terminal olefin double bonds of both ligands in the direction of the Ca, Sr, and Ba ions. Owing to the lack of $(n-1)d$ electrons of the alkaline-earth metal

ions, this weak coordination cannot be interpreted as a σ -donor– π -acceptor interaction as in classical olefin complexes of transition metals. The NMR spectra measured in $[D_6]$ benzene and $[D_8]$ toluene show, however, a weak high-field shift of the signals of the δ -CH₂ protons; this may be interpreted by the influence exerted upon the double bond attracted towards the alkaline-earth metal center by the electron shell of the metal negatively polarized in the direction of the olefin, as is suggested by the electrostatic model for the explanation of the bent structure of the metallocenes of the heavy alkaline-earth metals.^[22] A reduction in the Cp–M–Cp angle to 140.92(6)° in **2** and 140.4(4)° in **3** compared with 147.7 and 149°, respectively, for the non-olefin-coordinated analogues $[Ca(C_5Me_5)_2]$ and $[Sr(C_5Me_5)_2]$ is in agreement with this. The widening of this angle of 131° in the case of $[Ba(C_5Me_5)_2]$ to 139.1(1)° in **4** is attributable to the enlarged ionic radius of Ba^{II}. σ -Donor ligands such as THF displace the weakly coordinated olefin from the alkaline-earth metal ion, which is demonstrated for the barium derivative **4** by its ¹H and ¹³C NMR spectra in $[D_8]$ THF. Analogous structural and bonding relationships are found in the corresponding Yb^{II} derivative $[Yb(C_5Me_4CH_2CH_2CH=CH_2)_2]$ ^[11a] and in $[Ln(C_5Me_4SiMe_2CH_2CH=CH_2)_2]$,^[12] which suggests a remarkable similarity between the organyls of the heavy alkaline-earth metals and the lanthanoids in the oxidation state Ln^{II}. This was discussed in detail recently for the chemistry and catalytic behavior of Ca^{II} and Yb^{II} compounds.^[28]

Experimental Section

The synthesis and the comprehensive spectroscopic characterization of the alkaline-earth complexes **1–4** and their crystal data are available in the Supporting Information.

CCDC-240854–240857 contain the supplementary crystallographic data for this paper. These data can be obtained free of charge via www.ccdc.cam.ac.uk/conts/retrieving.html (or from the Cambridge Crystallographic Data Centre, 12, Union Road, Cambridge CB2 1EZ, UK; fax: (+44) 1223-336-033; or deposit@ccdc.cam.ac.uk).

Received: June 10, 2004

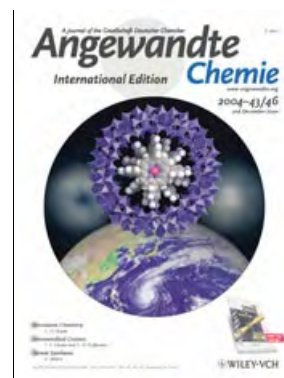
Keywords: alkaline-earth metals · metallocenes · olefin complexes

- [1] M. Brookhart, A. F. Volpe, Jr., D. M. Lincoln, *J. Am. Chem. Soc.* **1990**, *112*, 5634–5636.
- [2] H. H. Brintzinger, D. Fischer, R. Mühlhaupt, B. Rieger, R. Waymouth, *Angew. Chem.* **1995**, *107*, 1255–1283; *Angew. Chem. Int. Ed. Engl.* **1995**, *34*, 1143–1170.
- [3] Z. Wu, R. F. Jordan, J. L. Petersen, *J. Am. Chem. Soc.* **1995**, *117*, 5867–5868.
- [4] C. P. Casey, D. W. Carpenetti II, *Organometallics* **2000**, *19*, 3970–3977.
- [5] M. G. Galakhov, G. Heinz, P. Royo, *Chem. Commun.* **1998**, 17–18.
- [6] P. T. Witte, A. Meetsma, B. Hessen, P. J. M. Budzelaar, *J. Am. Chem. Soc.* **1997**, *119*, 10561–10562.
- [7] M. J. Humphries, R. E. Douthwaite, M. L. H. Green, *J. Chem. Soc. Dalton Trans.* **2000**, 2952–2959.
- [8] a) C. P. Casey, T. Y. Lee, J. A. Tunge, D. W. Carpenetti II, *J. Am. Chem. Soc.* **2001**, *123*, 10762–10763; b) C. P. Casey, J. A. Tunge, T. Y. Lee, D. W. Carpenetti II, *Organometallics* **2002**, *21*, 389–396.
- [9] a) C. P. Casey, S. L. Hallenbeck, D. W. Pollock, C. R. Landis, *J. Am. Chem. Soc.* **1995**, *117*, 9770–9771; b) C. P. Casey, S. L. Hallenbeck, J. M. Wright, C. R. Landis, *J. Am. Chem. Soc.* **1997**, *119*, 9680–9690; c) C. P. Casey, M. A. Fagan, S. L. Hallenbeck, *Organometallics* **1998**, *17*, 287–289; d) C. P. Casey, J. F. Klein, M. A. Fagan, *J. Am. Chem. Soc.* **2000**, *122*, 4320–4330.
- [10] C. P. Casey, J. A. Tunge, M. A. Fagan, *J. Organomet. Chem.* **2002**, *663*, 91–97.
- [11] a) H. Schumann, A. Heim, D. Karasiak, J. Demtschuk, S. Mühle, Canadian Society of Chemistry 2002 National Meeting, Vancouver, BC, Juni **2002**, S. 510; b) H. Schumann, A. Heim, J. Demtschuk, S. H. Mühle, *Organometallics* **2002**, *21*, 3323–3334.
- [12] W. J. Evans, J. M. Perotti, J. C. Brady, J. W. Ziller, *J. Am. Chem. Soc.* **2003**, *125*, 5204–5212.
- [13] V. Varga, K. Mach, G. Schmid, U. Thewald, *J. Organomet. Chem.* **1993**, *454*, C1–C4.
- [14] S. I. Troyanov, V. Varga, K. Mach, *Organometallics* **1993**, *12*, 2820–2824.
- [15] R. A. Williams, T. P. Hanusa, J. C. Huffman, *J. Am. Chem. Soc.* **1990**, *112*, 2454–2455.
- [16] H. Schumann, M. Glanz, J. Gottfriedsen, S. Dechert, D. Wolff, *Pure Appl. Chem.* **2001**, *73*, 279–282.
- [17] a) E. Weiss, E. O. Fischer, *Z. Anorg. Allg. Chem.* **1955**, *278*, 219–224; b) W. Bünder, E. Weiss, *J. Organomet. Chem.* **1975**, *92*, 1–6.
- [18] J. Vollet, E. Baum, H. Schnöckel, *Organometallics* **2003**, *22*, 2525–2527.
- [19] ORTEP3 for Windows, L. J. Farrugia, *J. Appl. Crystallogr.* **1997**, *30*, 565.
- [20] a) R. A. Williams, T. P. Hanusa, J. C. Huffman, *J. Chem. Soc. Chem. Commun.* **1988**, 1045–1046; b) R. A. Williams, T. P. Hanusa, J. C. Huffman, *Organometallics* **1990**, *9*, 1128–1134.
- [21] R. A. Andersen, R. Blom, C. J. Burns, H. V. Volden, *J. Chem. Soc. Chem. Commun.* **1987**, 768–769.
- [22] W. J. Evans, L. A. Hughes, T. P. Hanusa, *Organometallics* **1986**, *5*, 1285–1291.
- [23] R. A. Andersen, J. M. Boncella, C. J. Burns, R. Blom, A. Haaland, H. V. Volden, *J. Organomet. Chem.* **1986**, *312*, C49–C52.
- [24] T. K. Hollis, J. K. Burdett, B. Bosnich, *Organometallics* **1993**, *12*, 3385–3386.
- [25] T. V. Timofeeva, Jenn-Huei Lii, N. L. Allinger, *J. Am. Chem. Soc.* **1995**, *117*, 7452–7459.
- [26] T. P. Hanusa, *Chem. Rev.* **1993**, *93*, 1023–1036.
- [27] A. J. Arduengo III, F. Davidson, R. Krafczyk, W. J. Marshall, M. Tamm, *Organometallics* **1998**, *17*, 3375–3382.
- [28] S. Harder, *Angew. Chem.* **2004**, *116*, 2768–2773; *Angew. Chem. Int. Ed.* **2004**, *43*, 2714–2718.

Cover Picture

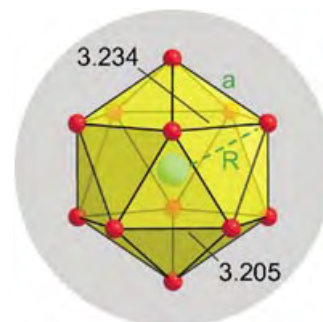
Akihiko Tsuda,* Eri Hirahara, Yeong-Sang Kim, Hiroyuki Tanaka, Tomoji Kawai,* and Takuzo Aida*

A generous host describes the fully inorganic doughnut-shaped polyoxometalate crown cluster illustrated in the cover picture which has a 2.3-nm-wide and 1.3-nm-deep nanoscopic cavity and serves as a novel host for three metalloporphyrin molecules that contain 3- or 4-aminophenyl groups. A. Tsuda, T. Kawai, T. Aida, and co-workers describe in their Communication on page 6327 ff. how this new organic/inorganic hybrid complex forms through multiple hydrogen-bonding interactions.



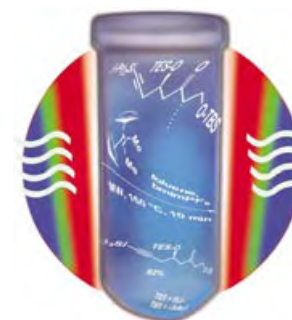
Intermetalloid Clusters

T. F. Fässler and S. D. Hoffmann describe in their Minireview on page 6242 ff. the formation of large, endohedral clusters (e.g. $[\text{Pt}@\text{Pb}_{12}]^{2-}$) in the context of fullerenes and fullerides.



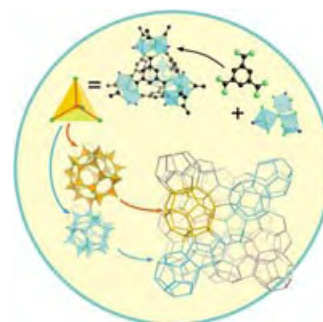
Microwave Chemistry

Heating reactions with microwaves offers a noteworthy alternative to conventional heating methods. In his Review on page 6250 ff., C. O. Kappe highlights recent applications of this procedure in organic synthesis.



Nanoporous Materials

In their Communications on pages 6285, 6290, and 6296 ff., C. Serre, C. Mellot-Draznieks, G. Férey, and co-workers demonstrate a solvothermal route involving metal(III) trimeric secondary building units and how the crystal structures of hybrid organic-inorganic structures can be predicted.



Angewandte EarlyView®

The following Communications are available online (in Wiley InterScience). You can find them, as well as forthcoming Reviews, Highlights, and Essays, at www.angewandte.org, under Early View.

A. I. Jiménez,* G. Ballano, C. Cativiela:

First Observation of Two Consecutive γ Turns in a Crystalline Linear Dipeptide

DOI: 10.1002/anie.200461230

Published online: November 11, 2004

A. Côté, A. A. Boezio, A. B. Charette*:

Evidence for the Structure of the Enantioactive Ligand in the Phosphine–Copper-Catalyzed Addition of Diorganozinc Reagents to Imines

DOI: 10.1002/anie.200461920

Published online: November 11, 2004

Articles judged by the referees or the editor as being either very important or very urgent are immediately edited, proof-read, and electronically published once the manuscript has arrived in the editorial office in its final form. As long as there is no page number available these articles should be cited in the following manner:

Author(s), *Angew. Chem. Int. Ed.*, online publication date, DOI.

News

Creativity Rewarded:

J. M. DeSimone _____ 6234

Creative Synthesis:

C.-H. Wong _____ 6234

S. I. Stupp Receives Polymer

Award _____ 6234

Books

Handbook of Proteomic Methods

P. Michael Conn

reviewed by E. W. Wang

and M. S. Bogoy _____ 6235

Polymeric Materials in Organic Synthesis and Catalysis

Michael R. Buchmeiser

reviewed by Q.-H. Fan _____ 6236

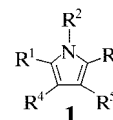
Highlights

Heterocycle Synthesis

G. Balme* _____ 6238–6241

Pyrrole Syntheses by Multicomponent Coupling Reactions

Versatile strategies of multicomponent coupling reactions to synthesize variously substituted pyrroles **1** are summarized. These heterocycles are important targets as molecules in their own right, for their pharmacological properties, as well as intermediates for more elaborate syntheses.



Minireviews

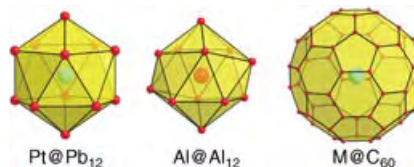
Endohedral Clusters

T. F. Fässler,*

S. D. Hoffmann _____ 6242–6247

Endohedral Zintl Ions: Intermetallic Clusters

The close race between Zintl ions and fullerides has gone into the second round, initialized by the synthesis of the soluble endohedral cluster $[\text{Pt}@\text{Pb}_{12}]^{2-}$ (see picture, left). The structural characterization of an anion with almost ideal icosahedral symmetry illustrates that many heteroatomic clusters observed in the gas phase can, indeed, be regarded as endohedral clusters.



Reviews

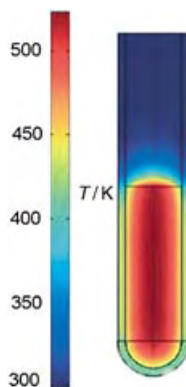
Synthetic Methods

C. O. Kappe* ————— 6250 – 6284

Controlled Microwave Heating in Modern Organic Synthesis

Out of the kitchen into the laboratory:

Direct heating by microwave irradiation (see picture) in many cases enables synthesis to be carried out in a fraction of the time required with conventional heating techniques. The use of microwave heating in organic synthesis is growing rapidly and the advantages not only include faster reaction times, but also higher product yields, cleaner reactions, better controllability, and reproducibility.

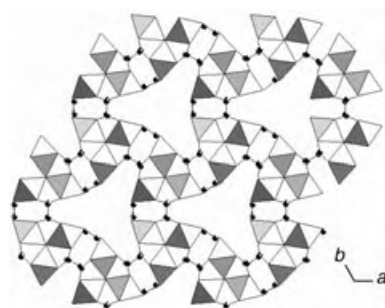


Communications

Nanoporous Materials

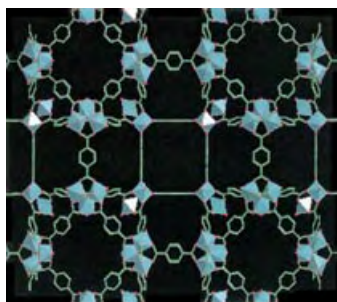
C. Serre,* F. Millange, S. Surblé,
G. Férey ————— 6285 – 6289

A Route to the Synthesis of Trivalent Transition-Metal Porous Carboxylates with Trimeric Secondary Building Units



Prefabricated construction techniques: A solvothermal route involving iron(III) trimeric secondary building units has been developed. Two new open-framework iron(III) dicarboxylates have been characterized from X-ray powder diffraction studies. Their 3D structures are built up from trimers of iron polyhedra related through dicarboxylates, thus creating cationic frameworks with 1D pore systems filled with solvent molecules and anions (see example).

Structure prediction of hybrid organic–inorganic frameworks is now computationally possible. The employed method embraces the concept of hybrid framework through the automated assembly of predefined organic and inorganic building units in 3D space. Crystal structures of hybrid candidates are predicted (space group, cell parameters, atomic positions; see picture), together with an estimate of their lattice energies.



Molecular Modeling

C. Mellot-Draznieks,* J. Dutour,
G. Férey ————— 6290 – 6296

Hybrid Organic–Inorganic Frameworks: Routes for Computational Design and Structure Prediction

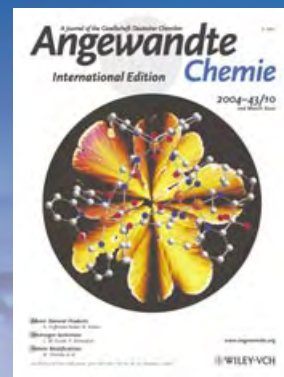
For the USA and Canada:

ANGEWANDTE CHEMIE International Edition (ISSN 1433-7851) is published weekly by Wiley-VCH PO Box 191161, D 69451 Weinheim, Germany. Air freight and mailing in the USA by Publications Expediting Inc. 200 Meacham Ave., Elmont, NY 11003. Periodicals

postage paid at Jamaica NY 11431. US POSTMASTER: send address changes to *Angewandte Chemie*, Wiley-VCH, 111 River Street, Hoboken, NJ 07030. Annual subscription price for institutions: US\$ 4948.00/4498.00 (valid for print and electronic / print or electronic delivery); for individuals who are personal members of a

national chemical society, or whose institution already subscribes, or who are retired or self-employed consultants, print only: US\$ 394.00. Postage and handling charges included. All Wiley-VCH prices are exclusive VAT.

The best in chemistry – for more than a hundred years



A Journal of the Gesellschaft Deutscher Chemiker
Angewandte
International Edition **Chemie**

www.angewandte.org

1888: The beginning
of a success story

Constant Innovations

- 1962:** First issue of the International Edition
- 1976:** Graphical abstracts
- 1979:** Cover pictures
- 1988:** Centenary of Angewandte
- 1989:** Routine use of color
- 1991:** New section: Highlights
- 1992:** Computerized editorial tracking system
- 1995:** Internet service for readers
- 1998:** Regular press service; full-text online
- 2000:** New section: Essays; EarlyView: Communications available online ahead of the printed version
- 2001:** New section: Minireviews
- 2002:** Online submission of manuscripts
- 2003:** Weekly publication; new section: News; new layout
- 2004:** Backfiles (1962-1997); ManuscriptXpress: Online system for authors and referees



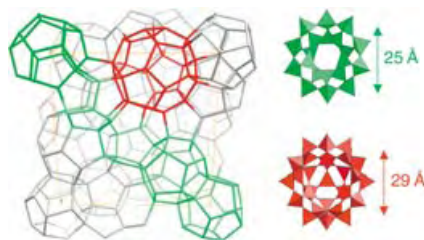
Angewandte's advisors...

Rolf Thauer
MPI für terrestrische
Mikrobiologie, Marburg

» In 1970 Karl Decker, Kurt Jungermann, and I published a review on "Energy Production in Anaerobic Organisms" in **Angewandte Chemie**. We were soon surprised how many scientists from all over the world had read the article. Ever since then I have admired the broad scope, the high impact, and internationality of this Journal and I am therefore very proud, as a "chemical microbiologist", to be a member of its Editorial Board. «

Angewandte Chemie International Edition is
a journal of the German Chemical Society (GDCh)



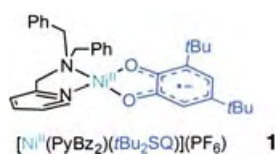


A perfect combination: The association of a chromium(III) trimeric building unit and 1,3,5-benzenetricarboxylate led to the powdered solid MIL-100. Simulations provided a crystal structure solution, which matched the experimental powder XRD pattern. This unique simulation/diffraction combination allowed the structure determination of a giant-pore solid with a zeotype architecture, built up from hybrid supertetrahedra (see picture).

Molecular Modeling

G. Férey,* C. Serré, C. Mellot-Draznieks, F. Millange, S. Surblé, J. Dutour, I. Margiolaki ——— 6296 – 6301

A Hybrid Solid with Giant Pores Prepared by a Combination of Targeted Chemistry, Simulation, and Powder Diffraction



Fine-tuning the N-donor ability of a bidentate aminopyridyl ligand facilitated the selective synthesis of complexes **1** (no methyl substituent) and **2** (with a methyl

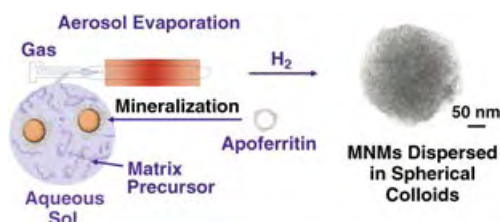


substituent) which possess valence tautomeric nickel(II) semiquinonato and nickel(III) catecholato frameworks, respectively.

Valence Tautomerism

H. Ohtsu, K. Tanaka* ——— 6301 – 6303

Chemical Control of Valence Tautomerism of Nickel(II) Semiquinone and Nickel(III) Catecholate States



Small world: Metallic nanomagnets (MNMs) dispersed in spherical colloids can be prepared by the aerosol evaporation of an aqueous sol containing miner-

alized ferritin and a colloidal matrix precursor (see picture). Essential to the success of the method is the template effect provided by ferritin.

Nanotechnology

P. Tartaj,* T. González-Carreño, M. L. Ferrer,* C. J. Serna — 6304 – 6307

Metallic Nanomagnets Randomly Dispersed in Spherical Colloids: Toward a Universal Route for the Preparation of Colloidal Composites Containing Nanoparticles



Robust porous frameworks are formed by the dipeptides L-Ala-L-Ala (see structure) and L-Val-L-Ala that have a high capacity and selectivity for gas sorption. The dipeptides assemble through hydrogen bonds as a 6_1 helix to form channels with average diameters of 5.13 and 4.90 Å, respectively.

Organic Zeolites

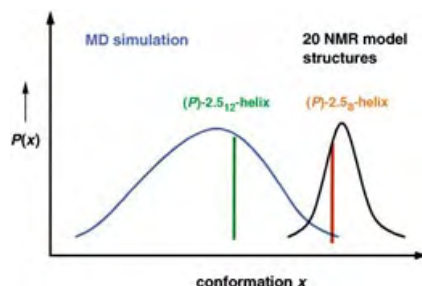
D. V. Soldatov,* I. L. Moudrakovski, J. A. Ripmeester* ——— 6308 – 6311

Dipeptides as Microporous Materials

Peptide Solution Structures

A. Glättli,
W. F. van Gunsteren* — 6312–6316

Are NMR-Derived Model Structures for β -Peptides Representative for the Ensemble of Structures Adopted in Solution?



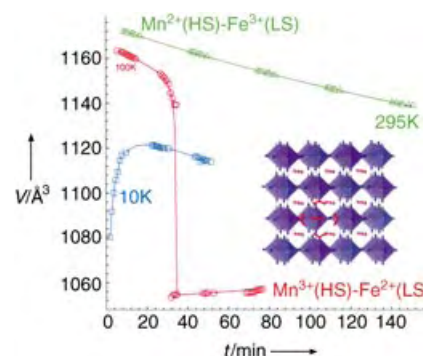
The data fit, but the structures are different. Two methods for the interpretation of NMR data of a β -hexapeptide are compared. While the simulated annealing procedure suggests the formation of a (P)-2₈-helix, unrestrained molecular dynamics simulations indicate that the NMR data can also be described by a much broader ensemble of conformations, in which (P)-2.5₁₂-helical structures are prominent (see diagram).

Mixed-Valence Compounds

S. Margadonna,* K. Prassides,
A. N. Fitch — 6316–6319

Large Lattice Responses in a Mixed-Valence Prussian Blue Analogue Owing to Electronic and Spin Transitions Induced by X-ray Irradiation

Illuminating phase changes: Absorption of X-ray photons induces reversible internal charge-transfer processes in the mixed-valence Mn/Fe cyanide $\text{Rb}_{0.7}\text{Mn}^{\text{II}}[\text{Fe}^{\text{III}}(\text{CN})_6] \cdot 2\text{H}_2\text{O}$ over a broad temperature range. Both continuous and abrupt phase transformations can be triggered (see scheme; HS = high spin, LS = low spin) and because the X-rays simultaneously probe the structural properties of the material, the resulting phase diagram can be elucidated in detail.

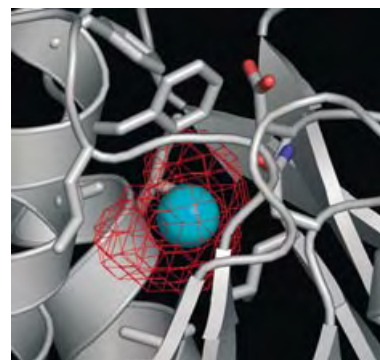


Protein Conformation

T. J. Lowery, S. M. Rubin, E. J. Ruiz,
A. Pines, D. E. Wemmer* — 6320–6322

Design of a Conformation-Sensitive Xenon-Binding Cavity in the Ribose-Binding Protein

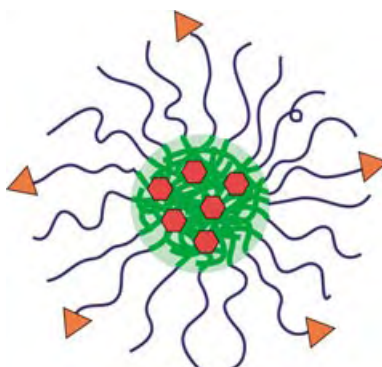
^{129}Xe NMR spectroscopy meets protein engineering: NMR spectroscopy with laser-polarized ^{129}Xe can be used to report protein conformations only if a protein has a conformationally sensitive xenon-binding cavity. However, many proteins lack such reporter sites. A straightforward design process is used to engineer a xenon-binding cavity into the ribose-binding protein (see picture) that allows the ^{129}Xe NMR spectroscopic report of protein conformation and ligand binding.



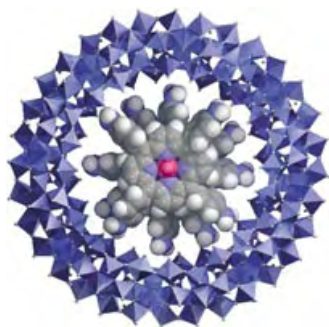
Bioorganic Chemistry

N. Nasongkla, X. Shuai, H. Ai,
B. D. Weinberg, J. Pink, D. A. Boothman,
J. Gao* — 6323–6327

cRGD-Functionalized Polymer Micelles for Targeted Doxorubicin Delivery



Targeting micelles: Cyclic pentapeptide cRGDfK (red triangles), which targets integrin $\alpha_v\beta_3$, was conjugated to the outer shell of doxorubicin-loaded (red hexagons) polymeric micelles by using a post-micelle modification method. The modified micelles significantly enhanced their internalization (up to 30-fold) by receptor-mediated endocytosis in tumor endothelial cells overexpressing the $\alpha_v\beta_3$ receptor.

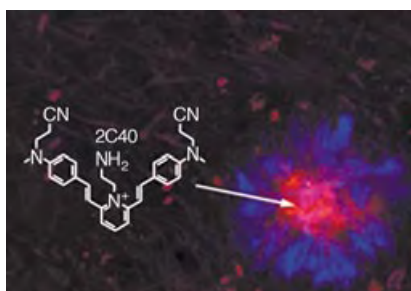


Filled doughnuts: Molybdenum crown cluster MC accommodates up to three molecules of aminophenyl-substituted metalloporphyrins through hydrogen-bonding interactions, to form discrete inorganic–organic nanocomposite materials (see picture; blue polyhedra = MC, space-filling model = metalloporphyrin). Ultrahigh-vacuum scanning tunneling microscopy, in conjunction with scanning tunneling spectroscopy, at 80 K confirms the formation of the inclusion complex.

Polyoxomolybdates

A. Tsuda,* E. Hirahara, Y.-S. Kim,
H. Tanaka, T. Kawai,*
T. Aida* ————— 6327 – 6331

A Molybdenum Crown Cluster Forms Discrete Inorganic–Organic Nanocomposites with Metalloporphyrins

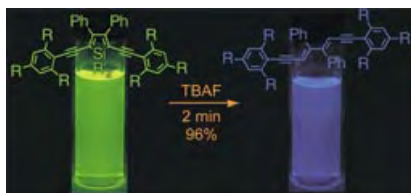


The combinatorial approach: A library of fluorescent styryl dyes (320 compounds) was prepared by solid-phase chemistry. The dyes were screened for their detection of amyloid aggregates, which are associated with diseases such as Alzheimer's, and two of the 320 compounds screened, 2C40 and 2E10, showed promise as brain-imaging agents (see microscopy image).

Fluorescent Probes

Q. Li, J.-S. Lee, C. Ha, C. B. Park, G. Yang,
W. B. Gan, Y.-T. Chang* — 6331 – 6335

Solid-Phase Synthesis of Styryl Dyes and their Application as Amyloid Sensors



A brighter future for siloles. Luminescent silole chromophores with the highest

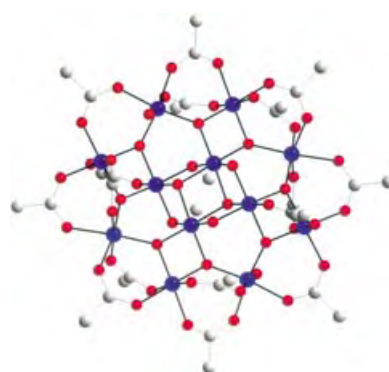
quantum efficiencies reported for a fully substituted monomeric silole are generated by altering the steric properties of the substituent groups. Treatment of 1,1-dimethylsiloles with Bu_4NF (TBAF) in THF rapidly gives stereospecific desilylation at room temperature (see scheme). Intense solid-state photoluminescence is observed in thin films of the silole fluorophores.

Luminescent Materials

A. J. Boydston,
B. L. Pagenkopf* ————— 6336 – 6338

Improving Quantum Efficiencies of Siloles and Silole-Derived Butadiene Chromophores through Structural Tuning

Axes of power: Jahn–Teller isomerism (that is, Jahn–Teller distortion along different axes) accounts for the presence of both faster and slower relaxing magnetization dynamics of the title compound (see core structure; blue Mn, red O, gray C), which is a single-molecule magnet (SMM). The new compound is a structural variant of the $[\text{Mn}_{12}]$ family of SMMs and is prepared by a reductive aggregation of $[\text{MnO}_4]^-$ in a mixture of MeOH/ PhCO_2H .



Magnetic Properties

A. J. Tasiopoulos, W. Wernsdorfer,
K. A. Abboud, G. Christou* 6338 – 6342

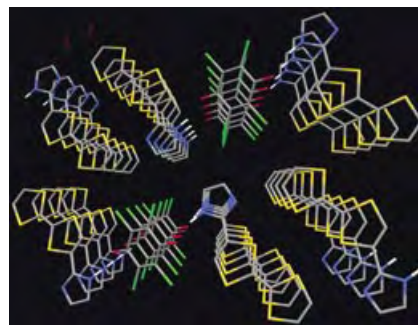
A Reductive-Aggregation Route to $[\text{Mn}_{12}\text{O}_{12}(\text{OMe})_2(\text{O}_2\text{CPh})_{16}(\text{H}_2\text{O})_2]^{2-}$ Single-Molecule Magnets Related to the $[\text{Mn}_{12}]$ Family

Charge-Transfer Organic Metal

T. Murata, Y. Morita,* K. Fukui, K. Sato,
D. Shiomi, T. Takui, M. Maesato,
H. Yamochi, G. Saito,*
K. Nakasuji* ————— **6343–6346**

A Purely Organic Molecular Metal Based
on a Hydrogen-Bonded Charge-Transfer
Complex: Crystal Structure and Electronic
Properties of TTF-Imidazole-*p*-Chloranil

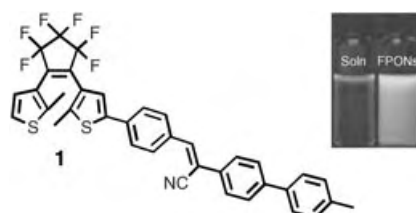
Modification of tetrathiafulvalene with an
imidazolyl substituent as a hydrogen-
bond donor allows the generation of a
hydrogen-bonded 2:1 charge-transfer
complex with chloranil. This complex
forms a three-dimensional network with
columnar stacking of each component
and multiple S...S interactions (see pic-
ture). This strongly hydrogen-bonded
purely organic conducting material is the
first to display metallic behavior.



Photochromism

S.-J. Lim, B.-K. An, S. D. Jung, M.-A. Chung,
S. Y. Park* ————— **6346–6350**

Photoswitchable Organic Nanoparticles
and a Polymer Film Employing Multi-
functional Molecules with Enhanced
Fluorescence Emission and Bistable
Photochromism



Get turned on: Fluorescent photochromic
organic nanoparticles (FPONs) of **1** (see
picture) show a strongly enhanced fluo-
rescence emission with increasing con-
centration and bistable photochromism.
High-contrast on/off fluorescence switch-
ing has been successfully implemented in
size-tuned FPONs of **1** and also in a
photo-rewritable polymer film highly
loaded with **1**.

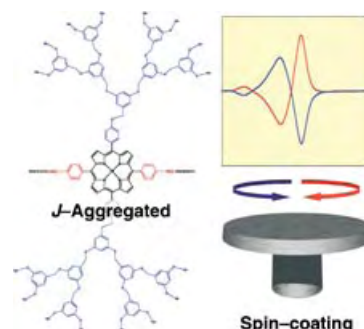


Chirality

T. Yamaguchi, T. Kimura, H. Matsuda,
T. Aida* ————— **6350–6355**

Macroscopic Spinning Chirality
Memorized in Spin-Coated Films of
Spatially Designed Dendritic Zinc
Porphyrin *J*-Aggregates

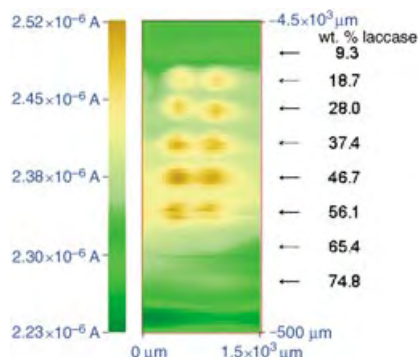
Supramolecular polymerization of dendri-
tic zinc porphyrins with two carboxylic
acid functionalities leads to the formation
of *J*-aggregates through multipoint π -
stacking interactions. Spin-coating of the
J-aggregate solutions gives optically active
films, whose sense of chirality can be
selected by the spinning direction (see
picture). The chiroptical memory is ther-
mally stable up to the melting tempera-
tures of the spin-coated films.



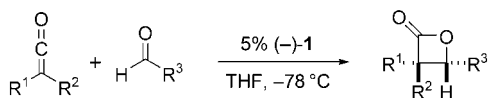
Analytical Methods

J. L. Fernández, N. Mano,* A. Heller,
A. J. Bard* ————— **6355–6357**

Optimization Of “Wired” Enzyme O₂-
Electroreduction Catalyst Compositions
by Scanning Electrochemical Microscopy

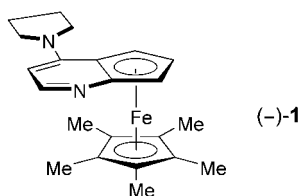


Rapid screening: For optimizing the
weight fraction of enzyme in enzyme
electrodes, the scanning electrochemical
microscopy (SECM) screening method
described gives results (see picture) in
good agreement with those obtained by
the traditional rotating-disk-electrode
method but in one tenth of the time and
with a reduction in the amount of polymer
and enzyme required by a factor of
100 000.



α,α -Disubstituted β -lactones can be obtained by the cycloaddition of the corresponding ketenes with aldehydes (see scheme). For the first time, a chiral PPY derivative, **1**, serves as an efficient catalyst for the asymmetric synthesis of β -

lactones (PPY = 4-pyrrolidin-1-ylpyridine). To date, this is the only catalyst that is effective for enantioselective cycloadditions of disubstituted ketenes with aldehydes.

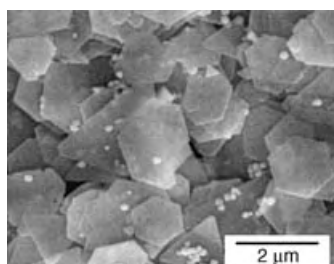


Lactone Synthesis

J. E. Wilson, G. C. Fu* — 6358 – 6360

Asymmetric Synthesis of Highly Substituted β -Lactones by Nucleophile-Catalyzed [2+2] Cycloadditions of Disubstituted Ketenes with Aldehydes

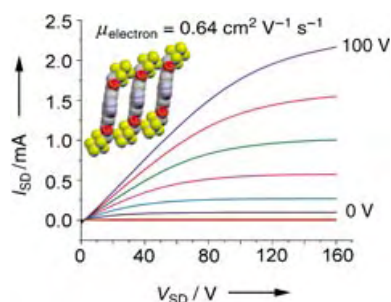
The chemical reduction of $\text{H}[\text{AuCl}_4]$ with *ortho*-phenylenediamine in aqueous media at room temperature and ambient pressure allows the synthesis of Au nanoplates with lengths of several micrometers (see SEM image). The as-prepared nanoplates are single crystals with a preferential growth direction along the Au (111) plane and mainly hexagonal in shape.



Nanostructures

X. Sun, S. Dong,* E. Wang* — 6360 – 6363

Large-Scale Synthesis of Micrometer-Scale Single-Crystalline Au Plates of Nanometer Thickness by a Wet-Chemical Route



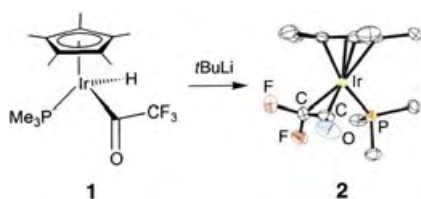
Taking up the semiconducting baton:

Organic field-effect transistors fabricated with a new class of extremely electron-deficient cyanated perylene diimides are air-stable and exhibit n-type mobilities as high as $0.64 \text{ cm}^2 \text{ V}^{-1} \text{ s}^{-1}$ (see scheme). Devices can be fabricated from vapor-deposited and solution-cast films as well as top- and bottom-contact electrode configurations.

Electron Transport

B. A. Jones, M. J. Ahrens, M.-H. Yoon, A. Facchetti, T. J. Marks,*
M. R. Wasielewski* — 6363 – 6366

High-Mobility Air-Stable n-Type Semiconductors with Processing Versatility: Dicyanoperylene-3,4:9,10-bis(dicarboximides)



Deprotonation of the trifluoroacetyl hydride complex **1** with *tert*-butyllithium leads to difluoroketene adduct **2**. Coordination of the difluoroketene to iridium through the C–C bond is confirmed by X-ray diffraction (see scheme). This complex is the first isolated and characterized dihaloketene complex and provides the only structural data for difluoroketene.

Iridium Complexes

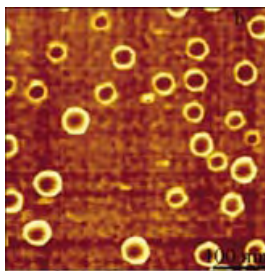
J. G. Cordaro, H. van Halbeek, R. G. Bergman* — 6366 – 6369

An Iridium Difluoroketene Complex: Synthesis and Isolation

Nanostructures

Y. Ding, Y. Hu, X. Jiang,* L. Zhang,
C. Yang ————— 6369–6372

Polymer–Monomer Pairs as a Reaction
System for the Synthesis of Magnetic
Fe₃O₄–Polymer Hybrid Hollow
Nanospheres



Magnetic hollow Fe₃O₄–polymer hybrid nanospheres (see figure) were prepared by adding Fe₃O₄ nanoparticles to an aqueous solution of polymer–monomer pairs composed of a cationic polymer (chitosan) and an anionic monomer (acrylic acid), followed by polymerization of acrylic acid and selective crosslinking of chitosan at the end of the polymerization.

Organic Synthesis

P. Gunda, L. M. Russon,
M. K. Lakshman* ————— 6372–6377

Pd-Catalyzed Amination of
Nucleoside Arylsulfonates to yield
N⁶-Aryl-2,6-Diaminopurine Nucleosides



Substituents on both the nucleoside aryl-sulfonate as well as the aryl amine component have a significant impact on their coupling to form 2,6-diaminopurine-2'-deoxyribonucleosides (see scheme). A

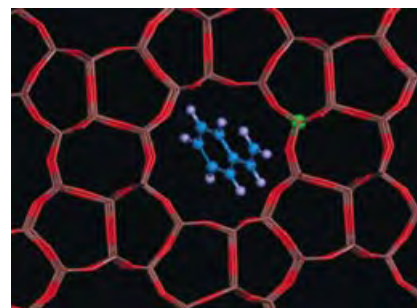
systematic study of ligands for the Pd catalysts in amination and C–C cross-coupling reactions gives insight into the structural elements that lead to effective catalysis.

Heterogeneous Catalysis

J. Zhuang, G. Yang, D. Ma,* X. Lan, X. Liu,
X. Han, X. Bao,* U. Mueller — 6377–6381

In Situ Magnetic Resonance Investigation
of Styrene Oxidation over TS-1 Zeolites

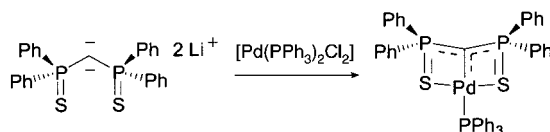
Competing reactions, not consecutive processes, are the oxidation of styrene to styrene epoxide and the formation of phenylacetaldehyde (PADH). In situ NMR and EPR spectroscopic analysis of styrene oxidation on TS-1 zeolite (see picture) demonstrated that Brønsted acid sites provide the active centers needed to transform an intermediate hemiacetal species into PADH.



Carbene Complexes

T. Cantat, N. Mézailles, L. Ricard, Y. Jean,*
P. Le Floch* ————— 6382–6385

A Bis(thiophosphinoyl)methanediide
Palladium Complex: Coordinated Dianion
or Nucleophilic Carbene Complex?



A question of identity: A palladium complex featuring a carbenic S,C,S-based pincer ligand is reported (see scheme). DFT calculations show that, unlike classical carbene complexes, coordination occurs through donation from a d orbital

at the metal into the empty n_p orbital of the carbene fragment, with the n_s orbital essentially acting as a nonbonding orbital. The complex is shown to have nucleophilic character.



Communications labeled with this symbol have been judged by two referees as being “very important papers”.

Deadline for recruitment adverts

47/2004	November 18	Publication date: December 3
48/2004	November 25	Publication date: December 10

Angewandte Chemie International Edition

Advertising Sales Department:

Marion Schulz

Phone: 0 62 01 – 60 65 65

Fax: 0 62 01 – 60 65 50

E-Mail: MSchulz@wiley-vch.de

Place an advert in the printed version
and have it made available online for 1 month, free of charge!

Service

Vacancies _____ 6249

Keywords _____ 6386

Authors _____ 6387

Preview _____ 6389

Why Wait to Make Great Discoveries

When you can make them in an instant with Wiley InterScience® Pay-Per-View and ArticleSelect™

Now you can have instant, full-text access to an extensive collection of journal articles or book chapters available on Wiley InterScience. With Pay-Per-View and ArticleSelect™, there's no limit to what you can discover...

ArticleSelect™ is a token-based service, providing access to full-text content from non-subscribed journals to existing institutional customers (EAL and BAL)

Pay-Per-View is available to any user, regardless of whether they hold a subscription with Wiley InterScience.

Benefits:

- Access online full-text content from journals and books that are outside your current library holdings
- Use it at home, on the road, from anywhere at any time
- Build an archive of articles and chapters targeted for your unique research needs
- Take advantage of our free profiled alerting service, the perfect companion to help you find specific articles in your field as soon as they're published
- Get what you need instantly, no waiting for document delivery
- Fast, easy, and secure online credit-card processing for Pay-Per-View downloads
- Special, cost-savings for EAL customers: whenever a customer spends tokens on a title equaling 115% of its subscription price, the customer is auto-subscribed for the year
- Access is instant and available for 24 hours

www.interscience.wiley.com





Creativity Rewarded: J. M. DeSimone

Joseph M. DeSimone is to receive the ACS (American Chemical Society) Award for Creative Invention in 2005. The award, worth US\$5000, is sponsored by the chemical industry and awarded annually to an inventor in recognition of the application of research in chemistry or chemical engineering that "... contributes to the material prosperity and happiness of people". For a recipient to qualify for the award, a patent must have been granted for the work.



J. M. DeSimone

DeSimone studied chemistry at Ursinus College in Collegeville, PA (USA). Upon completion of his PhD in 1990 under the guidance of J.E. McGrath at Virginia Polytechnic Institute and State University in Blacksburg (USA), he became assistant professor at the University of North Carolina in Chapel Hill (USA). He is currently William R. Kenan, Jr. Distinguished Professor of Chemistry and Chemical Engineering and Director of the Institute for Advanced Materials, Nanoscience and Technology there. His research focuses on polymer synthesis, green chemistry, and methods based on liquid and supercritical carbon dioxide. He reported on this last topic in a Review in *Angewandte Chemie* and an article in the *Encyclopedia of Polymer Science and Technology*.^[1] DeSimone is a member of the Editorial Board of the *Journal of Polymer Science A*.

Creative Synthesis: C.-H. Wong

Chi-Huey Wong, Professor at The Scripps Research Institute in La Jolla, CA (USA), will receive the ACS Award for Creative Work in Synthetic Organic Chemistry for his "... pioneering contributions to preparative biocatalysis and programmable one-pot organic synthesis." Wong studied chemistry at the Taiwan National University and completed his PhD in 1982 at Massachusetts Institute of Technology (Cambridge, MA, USA) in the research group of George M. Whitesides. As a postdoctoral fellow he moved, together with his PhD supervisor, within Cambridge to Harvard University. In 1983 he began his independent career as assistant professor at the Texas A&M University. There he moved up through the ranks to become full professor, and transferred to The Scripps Research Institute in 1989 to take up his current position as Ernest W. Hahn Professor of Chemistry.



C.-H. Wong

Wong's research interests encompass a broad spectrum of bioorganic and synthetic chemistry, from the interactions of small molecules with RNA and other biologically important molecules, and the design and synthesis of inhibitors of receptors and enzymes, to the development of synthetic methods, including programmable one-pot reactions for the synthesis of oligosaccharides and glycoarrays. His research on biocatalysis has a special focus on carbohydrate-mediated biological recognition. He recently contributed a comprehensive Review on sulfotransferases^[2a] to *Angewandte Chemie*, followed by a related Review on sulfatases.^[2b] Wong is a member of the Editorial Board of *Advanced Synthesis & Catalysis* and the Editorial Advisory Board of *ChemBioChem*.

S. I. Stupp Receives Polymer Award

Samuel I. Stupp is the recipient for 2005 of the ACS Award in Polymer Chemistry, sponsored by ExxonMobil. Stupp studied chemistry at the University of California in Los Angeles and completed his PhD in materials science and engineering in 1977 under the guidance of Stephen H. Carr at Northwestern University in Evanston, IL (USA). He remained there as Professor of Biological Materials until 1980, when he moved to the University of Illinois, Urbana-Champaign as Professor of Materials Science. In 1999, he returned to Northwestern University as Professor of Materials Science, Chemistry, and Medicine, and since 2000 he has directed the Institute for Bioengineering and Nanoscience in Advanced Medicine there.



S. I. Stupp

Stupp's research has four main focuses: the self-assembly of inorganic structures on organic templates, biomaterials for regenerative medicine (interactions of cells with ordered structures), devices and properties of materials (e.g. liquid-crystal templates for conducting polymers,^[3] lithography), and the synthesis of novel self-assembling molecules. He is a member of the Editorial Advisory Board of *Small*.

- [1] a) S. L. Wells, J. DeSimone, *Angew. Chem.* **2001**, *113*, 534; *Angew. Chem. Int. Ed.* **2001**, *40*, 518. b) J. I. Kroschwitz, *Encyclopedia of Polymer Science and Technology*, Wiley, Hoboken, **2004**; <http://interscience.wiley.com/mrw/epst>; DOI: 10.1002/0471440264.pst086.
- [2] a) E. Chapman, M. D. Best, S. R. Hanson, C.-H. Wong, *Angew. Chem.* **2004**, *116*, 3610; *Angew. Chem. Int. Ed.* **2004**, *43*, 3526; b) S. R. Hanson, M. D. Best, C.-H. Wong, *Angew. Chem.* **2004**, *116*, 5858; *Angew. Chem. Int. Ed.* **2004**, *43*, 5736.
- [3] a) J. F. Hulvat, S. I. Stupp, *Angew. Chem.* **2003**, *115*, 802; *Angew. Chem. Int. Ed.* **2003**, *42*, 778; b) J. F. Hulvat, S. I. Stupp, *Adv. Mater.* **2004**, *16*, 589.

Pyrrole Syntheses by Multicomponent Coupling Reactions

Geneviève Balme*

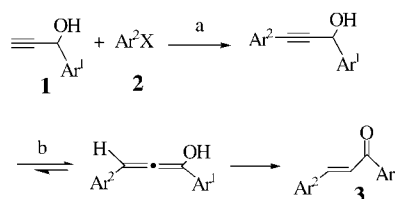
Keywords:

cyclization · multicomponent reactions · nitrogen heterocycles · pyrroles · synthetic methods

Pyrroles represent an important class of heterocycles that display remarkable pharmacological—antibacterial, antiviral, anti-inflammatory, antitumoral, and antioxidant—activities.^[1] Furthermore, they are useful intermediates in the synthesis of natural products as well as in heterocyclic chemistry^[2] and they are widely used in materials science.^[3] As a consequence, many synthetic methods are known for the construction of the pyrrole structure.^[4] The most frequently used methods include the classical Hantzsch procedure,^[5] the cyclocondensation of primary amines with 1,4-dicarbonyl compounds (Paal–Knorr synthesis),^[6] and various cycloaddition strategies.^[7] Whereas these methods have proven very useful for the synthesis of pyrrole derivatives, they generally involve multistep synthetic operations that limit the scope of these reactions. Multicomponent strategies offer significant advantages over classical linear syntheses by combining a series of reactions from easily available and simple precursors without the need for isolation of the intermediates^[8] to allow the construction of complex molecules. Such reactions are thus economically and environmentally attractive and have become an important area of research in organic chemistry.

Within this context, an elegant four-component reaction for the construction

of substituted pyrroles was recently reported by Müller and co-workers.^[9] This new multicomponent approach developed on from their earlier discovery that the Sonogashira coupling reaction of 1-arylprop-2-yn-1-ols **1** with electron-deficient aryl or heteroaryl halides **2** followed by a base-catalyzed isomerization reaction of the coupled products **3** (Scheme 1).^[10] Building on the results of

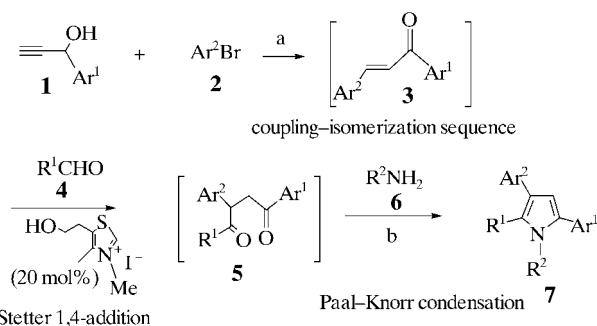


Scheme 1. Coupling–isomerization sequence that leads to chalcones: a) $[\text{PdCl}_2(\text{PPh}_3)_2]$ (2 mol %), CuI (1 mol %), Et_3N , THF, reflux; b) Et_3N .

these pioneering studies, Müller and collaborators developed an integrated procedure for the synthesis of pyrroles based on the reactivity of the newly formed enone functionality. To this end, the palladium-catalyzed enone synthesis was combined with a Stetter reaction to give 1,4-diketone intermediates,^[11] which were treated with primary amines in a subsequent Paal–Knorr cyclocondensation reaction. These three reactions were efficient-

ly integrated in a one-pot domino sequence to yield highly substituted pyrrole derivatives in rather good yields (Scheme 2). Thus, after the reaction of various 1-arylprop-2-yn-1-ols **1** with electron-deficient aryl bromides **2** under the reaction conditions of the Sonogashira coupling–isomerization sequence in boiling triethylamine, the newly formed enones **3** were treated with an aldehyde **4** in the presence of a catalytic amount of a thiazolium salt. After the complete conversion of **3** into the corresponding diketone **5**, the subsequent addition of primary amines **6** and acetic acid to the reaction mixture yielded the expected tri- or tetrasubstituted pyrroles **7**. Three or four diverse functionalities (one from each of the components **1**, **2**, and **4**, as well as **6** when $\text{R}^2 \neq \text{H}$) were introduced into the products.

One of the limitation of the Paal–Knorr reaction for the construction of the pyrrole ring is the accessibility of the 1,4-dicarbonyl precursors. As illustrated in the previous example, the classical Stetter addition of aldehydes to unsaturated carbonyl electrophiles is often

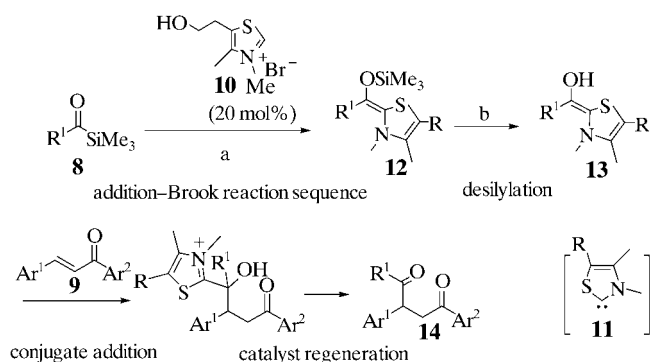


Scheme 2. Palladium-catalyzed four-component assembly of pyrroles starting from 1-arylprop-2-yn-1-ols: a) $[\text{PdCl}_2(\text{PPh}_3)_2]$ (2 mol %), CuI (1 mol %), Et_3N , reflux; b) AcOH , Δ . $\text{R}^1 = \text{aryl}$, heteroaryl; $\text{R}^2 = \text{H}$, Bn (benzyl), $(\text{CH}_2)_2\text{OH}$, $\text{CH}_2\text{C}(\text{O})\text{NH}_2$.

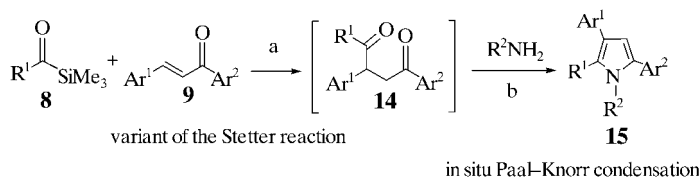
[*] Dr. G. Balme
Laboratoire de Chimie Organique 1
CNRS UMR 5622
Université Claude Bernard, Lyon 1, CPE
43, Bd. du 11 Novembre 1918, 69622
Villeurbanne (France)
Fax: (+33) 472-431-214
E-mail: balme@univ-lyon1.fr

used for this purpose. However, during the condensation reaction, a self-condensation of aldehydes (benzoin condensation) often occurs. Recently, Scheidt and co-workers demonstrated that the reaction of acylsilanes **8** with unsaturated conjugate acceptors **9** promoted by a thiazolium salt **10** in the presence of DBU (1,8-diazabicyclo[5.4.0]undec-7-ene) provides an attractive alternative to the classical Stetter addition of aldehydes (Scheme 3).^[12] This reaction is thought to proceed through the addition of the carbene catalyst **11** to **8** followed by a 1,2-silyl group shift (Brook rearrangement) to give the silylated intermediate **12**. The alcohol (*i*PrOH) then generates the acyl anion nucleophile **13**, which undergoes selective addition to the conjugate acceptor **9** that then, after elimination of the heterocyclic catalyst, leads to the corresponding diketones **14**. During this process, the formation of benzoin products is not observed owing to the lower electrophilicity of the acylsilanes **8** relative to aldehydes.

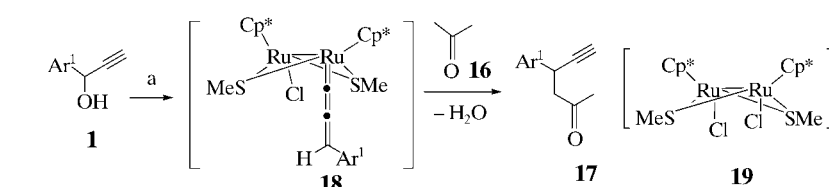
Based on this concept, a novel three-component approach to the synthesis of pyrrole derivatives was developed by the same group by the combination of



Scheme 3. Thiazolium-catalyzed addition of acylsilane to unsaturated carbonyl electrophiles to yield 1,4-dicarbonyl products: a) DBU, THF; b) *i*PrOH. DBU = 1,8-diazabicyclo[5.4.0]undec-7-ene; R = (CH₂)₂OH.



Scheme 4. A sequential three-component synthesis of pyrrole derivatives by using a Sila-Stetter/Paal-Knorr strategy: a) **10** (10 mol%), DBU (30 mol%), THF, *i*PrOH (4 equiv), 70°C; b) TsOH, molecular sieves (4 Å), 70°C. Ts = *p*-toluenesulfonyl; R¹ = aryl, alkyl; R² = H, aryl, alkyl.



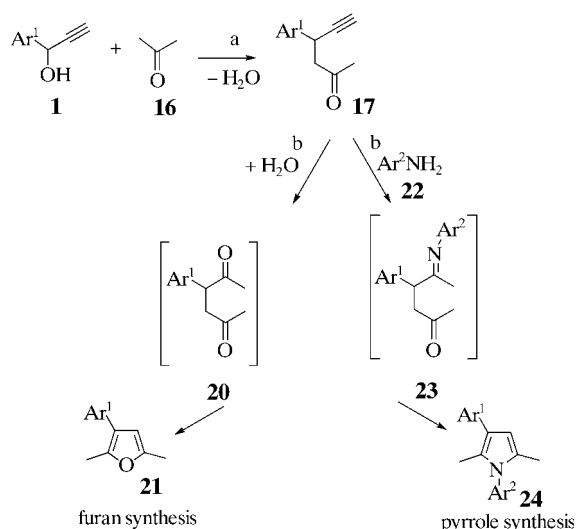
Scheme 5. Ruthenium-catalyzed propargyl alkylation of 1-arylprop-2-yn-1-ols with ketones: a) **19** (10%), NH₄BF₄ (20%). Cp* = pentamethylcyclopentadienyl.

this new variant of the Stetter reaction with a Paal-Knorr condensation.^[13] To this end, the thiazolium-catalyzed coupling reaction of an aryl or alkyl acylsilane with a chalcone was monitored to completion by TLC (thin-layer chromatography) analysis. Treatment of the resulting 1,4-dicarbonyl compound in situ with a primary amine in the presence of *p*-toluenesulfonic acid and molecular sieves produces the corresponding trisubstituted pyrrole derivative **15** (Scheme 4). Remarkably, in this process, various electron-donating or electron-withdrawing aryl substituents may be incorporated on either side of the unsaturated ketone.

Another creative convergent approach to pyrrole derivatives that starts from 1-arylprop-2-yn-1-ols **1** was recently developed by Uemura, Hidai, and co-

workers.^[14] In an early example, this group reported a ruthenium-catalyzed substitution of the propargyl group in the 1-aryl-substituted propargyl alcohol of type **1** with a dialkyl ketone such as acetone (**16**) in the presence of NH₄BF₄ which leads to the corresponding γ -ketoacetylene **17** (Scheme 5).^[15] The proposed mechanism involves the formation of the allenylidene complex **18** from the reaction of propargyl alcohol **1** with the thiolate-bridged diruthenium complex **19**. This is followed by a nucleophilic attack of the enolate carbon of the ketone on the electrophilic γ C atom of the reactive intermediate **18**. Taking advantage of the formation of water during this process, Uemura, Hidai, and co-workers further developed an ingenious strategy for the one-pot synthesis of substituted furans **21** by a combination of the above Ru-catalyzed reaction with the hydration of the alkyne moiety of **17** which was promoted by a second catalyst in the medium (Scheme 6). Under the reaction conditions, an intramolecular cyclization of the newly formed 1,4 diketone **20** results in the formation of the expected furans. The success of this domino reaction is highly dependent on the ability of the two catalysts to promote *sequentially* the three specific reactions: the ruthenium catalyst **19** and PtCl₂ give the best results.

The authors have extended these elegant studies to the one-pot synthesis of pyrroles **24** by carrying out this novel ruthenium/platinum-catalyzed multi-component reaction in the presence of various aniline derivatives **22**. The reaction is considered to proceed through the platinum-catalyzed nucleophilic attack of anilines on the carbon-carbon triple bond of the γ -ketoalkyne intermediate that leads to **23**, followed by an intramolecular cyclization to yield the pyrroles **24**.^[16]



Scheme 6. Sequential ruthenium/platinum-catalyzed three-component assembly reactions of furans and pyrroles starting from 1-arylprop-2-yn-1-ols: a) **19** (10 mol %), NH_4BF_4 (20 mol %); b) PtCl_2 (20 mol %).

More recently, a convergent four-component assembly of substituted pyrroles was developed by Dhawan and Arndtsen.^[17] The strategy is based on the ability of münchnones (1,3-oxazolium-5-oxides) to react with acetylenic dipolarophiles to produce bicyclic intermediates that undergo a cycloreversion reaction to yield pyrroles.^[18] A recent paper from this laboratory^[19] described the first catalytic synthesis of münchnones from a palladium-mediated three-component coupling of an imine, an acid chloride, and carbon monoxide (Scheme 7). A new synthesis of diprotected α -amino acid derivatives **30** was developed by the addition of methanol in the reaction mixture to trap these reactive intermediates. In this process, oxidative addition of imine **25** and acid chloride **26** to palladium(0) gives the Pd-chelated amide complex **27**. Then, insertion of carbon monoxide into the Pd–C bond followed by a β -hydride elimination via the metalloketene complex **28** produces a metal-free münchnone **29**.

The combination of the three-component assembly of münchnones **29** with a cycloaddition process with acetylenic dipolarophiles **31** present in the reaction mixture leads to a remarkably concise and efficient synthesis of pyrrole derivatives (Scheme 8). It was found that the success of this methodology depends on the nature of the Pd–phosphine com-

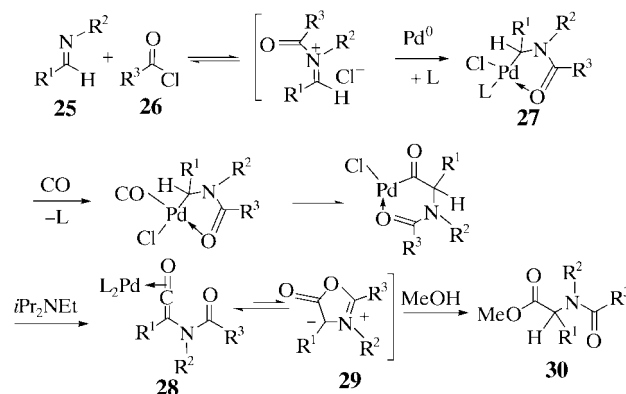
plex. Strong ligands such as triphenylphosphine were ineffective for the preparation of münchnones. A more labile ligand such as the bulky tri(*o*-tolyl)phosphine played a significant role in sufficiently stabilizing intermediate **27** while still allowing subsequent catalysis steps (Scheme 5). In a typical procedure, a mixture of imine **25**, acid chloride **26**, alkyne **31**, EtNiPr_2 , $\text{P}(o\text{-tolyl})_3$ (15 mol %), and the palladium catalyst **32** (generated by the pretreatment of $\text{Pd}_2(\text{dba})_3 \cdot \text{CHCl}_3$ (5 mol %) with the imine and the acid chloride) in acetonitrile/THF was stirred under CO (4 atm) at

65 °C during 16 h. This optimized protocol produced substituted pyrrole derivatives **33** in good yields. This strategy tolerates the presence of many func-

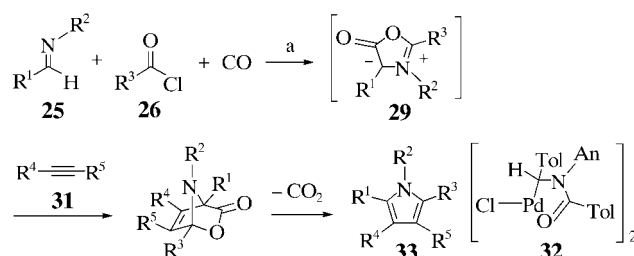
tional groups: Most combinations of aliphatic/aromatic imines, acid chlorides, and electron-rich or electron-poor alkynes are compatible with the mild reaction conditions and give access to a variety of densely substituted pyrroles. Interestingly, the reaction was found to proceed with complete regioselectivity with unsymmetrical alkynes and even acetylene participated efficiently in this process.

The four creative metal-catalyzed multicomponent one-pot assemblies of pyrroles highlighted herein elegantly demonstrate that multicomponent reactions are a powerful tool for the introduction of molecular diversity in an efficient, economic, and environmentally friendly way. Without doubt many innovative methodologies for the synthesis of this important structure will continue to emerge from this very stimulating research area.

[1] a) P. A. Jacobi, L. D. Coult, J. S. Guo, S. I. Leung, *J. Org. Chem.* **2000**, *65*, 205–213; b) A. Fürstner, *Angew. Chem.* **2003**,



Scheme 7. Proposed mechanism for the palladium-catalyzed three-component assembly of münchnones—synthesis of α -amino acid derivatives.



Scheme 8. The four-component assembly of pyrroles which involves an intermolecular 1,3-cycloaddition of münchnones with alkynes: a) **32** (5 mol %), $\text{P}(o\text{-tolyl})_3$ (15 mol %), $i\text{Pr}_2\text{NEt}$, CH_3CN /THF. Tol = *p*-tolyl; An = *p*- $\text{C}_6\text{H}_4\text{OCH}_3$; R^1 , R^2 , R^3 = aryl, alkyl; R^4 , R^5 = H, aryl, electron-withdrawing groups.

- 115, 3706–3728; *Angew. Chem. Int. Ed.* **2003**, 42, 3528–3603.
- [2] D. L. Boger, C. W. Boyce, M. A. Labrili, C. A. Sehon, Q. Jin, *J. Am. Chem. Soc.* **1999**, 121, 54–62.
- [3] a) L. Groenendaal, E.-W. Meijer, J. A. J. M. Vekemans in *Electronic Materials: The Oligomer Approach* (Eds.: K. Müllen, G. Wegner), Wiley-VCH, Weinheim, **1997**; b) V. M. Domingo, C. Aleman, E. Brillas, L. Julia, *J. Org. Chem.* **2001**, 66, 4058–4061.
- [4] For reviews on pyrrole synthesis, see: R. J. Sundberg in *Comprehensive Heterocyclic Chemistry*, Vol. 2 (Eds.: A. R. Katritzky, C. W. Rees, E. F. V. Scriven), Pergamon, Oxford, **1996**, pp. 119–206; V. F. Ferreira, M. C. B. V. De Souza, A. C. Cunha, L. O. R. Pereira, M. L. G. Ferreira, *Org. Prep. Proced. Int.* **2001**, 33, 411–454.
- [5] For recent examples of the Hantzsch synthesis, see: a) F. Palacios, D. Aparico, J. M. de los Santos, J. Vicario, *Tetrahedron* **2001**, 57, 1961–1972; b) A. W. Trautwein, R. D. Süßmuth, G. Jung, *Bioorg. Med. Chem. Lett.* **1998**, 8, 2381–2384.
- [6] For recent examples of the Paal–Knorr synthesis, see: a) B. M. Trost, G. A. Doherty, *J. Am. Chem. Soc.* **2000**, 122, 3801–3810; b) B. Quiclet-Sire, L. Quintero, G. Sanchez-Jimenez, S. Z. Zard, *Synlett* **2003**, 75–78; c) M. R. Tracey, R. P. Hsung, R. H. Lambeth, *Synthesis* **2004**, 918–922.
- [7] a) A. R. Katritzky, S. Zhang, M. Wang, H. C. Kolb, P. J. Steel, *J. Heterocycl. Chem.* **2002**, 39, 759–765; b) J. L. Bunting, R. R. Wolff, P. F. Jackson, *J. Org. Chem.* **2002**, 67, 9439–9442; c) K.-I. Washizuka, S. Minakata, I. Ryu, M. Komatsu, *Tetrahedron* **1999**, 55, 12969.
- [8] For recent reviews, see: a) G. Balme, E. Bossharth, N. Monteiro, *Eur. J. Org. Chem.* **2003**, 4101–4111; b) C. Hulme, V. Gore, *Curr. Med. Chem.* **2003**, 10, 51–80; c) R. V. A. Orru, M. de Greef, *Synthesis* **2003**, 1471–1499; d) J. Zhu, *Eur. J. Org. Chem.* **2003**, 1133–1144; e) H. Bienaymé, C. Hulme, G. Oddon, P. Schmitt, *Chem. Eur. J.* **2000**, 6, 3321–3329; f) A. Dömling, I. Ugi, *Angew. Chem.* **2000**, 112, 3300–3344; *Angew. Chem. Int. Ed.* **2000**, 39, 3168–3210; g) L. F. Tietze, A. Modi, *Med. Res. Rev.* **2000**, 20, 304–322; h) L. Weber, K. Illgen, M. Almstetter, *Synlett* **1999**, 366–374; i) S. L. Dax, J. J. McNally, M. A. Youngman, *Curr. Med. Chem.* **1999**, 6, 255–270.
- [9] R. Braun, K. Zeitter, T. J. J. Müller, *Org. Lett.* **2001**, 3, 3297–3300.
- [10] T. J. J. Müller, M. Ansorge, D. Aktah, *Angew. Chem.* **2000**, 112, 1323–1326; *Angew. Chem. Int. Ed.* **2000**, 39, 1253–1256.
- [11] J. S. Johnson, *Angew. Chem.* **2004**, 116, 1348–1350; *Angew. Chem. Int. Ed.* **2004**, 43, 1326–1328.
- [12] A. E. Mattson, A. R. Bharadwaj, K. A. Scheidt, *J. Am. Chem. Soc.* **2004**, 126, 2314–2315.
- [13] A. R. Bharadwaj, K. A. Scheidt, *Org. Lett.* **2004**, 6, 2465–2468.
- [14] Y. Nishibayashi, M. Yoshikawa, Y. Inada, M. D. Milton, M. Hidai, S. Uemura, *Angew. Chem.* **2003**, 115, 2785–2788; *Angew. Chem. Int. Ed.* **2003**, 42, 2681–2684.
- [15] Y. Nishibayashi, I. Wakiji, Y. Ishii, S. Uemura, M. Hidai, *J. Am. Chem. Soc.* **2001**, 123, 3393–3394.
- [16] This reaction could also be considered as a formal Paal–Knorr reaction. Indeed, another possible mechanistic hypothesis is that the formation of imines, by the reaction of anilines on the carbonyl of intermediate **17** to generate water, occurs first. This would be followed by hydration of the alkyne moiety to lead to the corresponding ketoimine, which is closely related to intermediate **23**.
- [17] R. Dhawan, B. A. Arndtsen, *J. Am. Chem. Soc.* **2004**, 126, 468–469.
- [18] B. Santiago, C. R. Dalton, E. W. Huber, J. M. Kane, *J. Org. Chem.* **1995**, 60, 4947–4950.
- [19] R. D. Dghaym, R. Dhawan, B. A. Arndtsen, *Angew. Chem.* **2001**, 113, 3328–3330; *Angew. Chem. Int. Ed.* **2001**, 40, 3228–3230.

Endohedral Clusters

Endohedral Zintl Ions: Intermetalloid Clusters

Thomas F. Fässler* and Stephan D. Hoffmann

Keywords:

cluster compounds · endohedral compounds · fullerenes · polyhedra · Zintl anions

Dedicated to Professor Hans-Jörg Deiseroth on the occasion of his 60th birthday

Tetrels can be regarded as most promising candidates for the construction of larger clusters. Recent examples have shown that larger clusters are particularly stable if they contain interstitial atoms (e.g. $[\text{Pt}@\text{Pb}_{12}]^{2-}$). Many salts of the polyhedral anions are soluble, but a number of examples—usually those with higher charges—occur only as quasi-discrete units in saltlike crystals (Zintl phases) or as building blocks in intermetallic phases. In this Minireview, the chemistry of intermetalloid clusters is reviewed with reference to the endohedral Zintl ions, Zintl phases, and polyhedral building blocks of intermetallic compounds, including heteroatomic species in the gas phase. We focus on selected examples and discuss the new findings in the context of recent advances in the field of metalloid clusters and (endohedral) fullerenes and fullerides.

Soluble Main-Group-Element Deltahedra

According to Wade's rules, closed polyhedra with triangular faces (deltahedra) and n vertices are particularly stable whenever $2n+2$ valence electrons are available for the formation of the cluster framework.^[1] Starting from the corresponding boranes, ligand-free homoatomic main-group-element polyhedra can readily be described by replacing the B–H units by a lone pair of electrons localized at each vertex atom. With N referring to their group number, each of these atoms contributes $N-2$ electrons to the framework formation of the polyhedron. The charge of the cluster q acts as a variable, which adjusts the number of electrons of the neutral cluster to the optimum configuration. Consequently, the resulting number of electrons provided by these atoms for the formation of the framework is given by $n(N-2)-q$. According to Wade's rules, *closo*, *nido*, *arachno*, and *hypho* clusters with n vertices and $2n+m$ electrons are particularly stable for $m=2, 4, 6$, and 8 , and from $2n+m=n(N-2)-q$ the resulting overall charge of the cluster is given by $q=-(n(N-4)+m)$. As a direct consequence, the charge q for $N=4$ (Group 14

elements) is independent of n and hence of the size of the cluster (Figure 1),^[2] whereas clusters that contain Group 13 and Group 15 elements exhibit increasingly negative and positive charge, respectively.^[2]

Despite the constant and relatively low charge, the number of examples of larger homoatomic clusters that contain Group 14 elements (tetrels) is rather limited. One reason may be the growing size of the cavity inside the cluster as a consequence of the increase in cluster size. In contrast to the larger fullerenes, the deltahedra of the heavier Group 14 element congeners (Si to

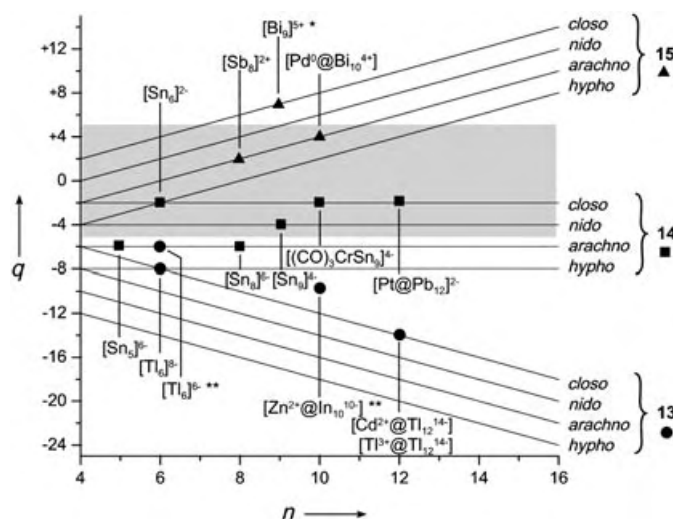


Figure 1. Graphical representation of the relation between cluster size n and charge q in homoatomic polyhedra $[\text{E}_n]^{+q}$ (E = vertex atom). Examples of structurally characterized clusters of Group 13, 14, 15 are indicated. *Deviation from the expected structure according to Wade's rules; ***closo* clusters with $2n$ electrons.

[*] Prof. T. F. Fässler, S. D. Hoffmann
Department of Chemistry
Technische Universität München
Lichtenbergstrasse 4, 85747 Garching (Germany)
Fax: (+49) 89-289-13186
E-mail: thomas.faessler@lrz.tum.de

Pb) do not have a rigid stable σ -bonding framework, and the bonding of the atoms is delocalized over the whole polyhedron. This fluctuational bonding allows a rapid exchange of atomic positions, as shown by NMR spectroscopy experiments for the anions $[\text{Sn}_9]^{4-}$ and $[\text{Pb}_9]^{4-}$.^[3] Although the so-called Zintl ions and the fullerenes show some parallel properties concerning the delocalized framework bonds and π electrons,^[4] respectively, the stability of the fullerenes is based to a major extent on the energy of the σ bonds.

As a consequence of weaker framework bonding, larger cavities inside the clusters become less stable and the deficit must be compensated by the incorporation of atoms or small molecules into the cluster, as demonstrated, for example, in the synthesis of a number of nanoporous materials. Recently, this type of stabilization was realized for the first time through the synthesis of “filled” main-group-element clusters.

The largest soluble clusters described to date are based on the well-established Zintl ions $[\text{Sn}_9]^{4-}$ and $[\text{Pb}_9]^{4-}$,^[5,6] which—with their singly capped square-antiprismatic structure—represent a *nido*-type cluster (Figure 2a).^[7–9] Addition of a transition-metal fragment $\text{M}(\text{CO})_3$ —which according to the isolobal principle does not contribute any electrons to the framework and therefore simply acts as a vertex atom—to the open square face of this cluster leads to closed polyhedra with 10 vertices (Figure 2b). In the latter case, isomeric structures (Figure 2c) as well as exchange of the vertex atoms, which is rapid on the NMR timescale, are possible.^[10]

The soluble clusters described herein are stable up to a size of 10 atoms, without a central host; the first filled examples are also observed for $n = 10$. It therefore appears that the stability limit for empty clusters of the heavier Group 13–15 elements is attained for species with $n = 10$. The incorporation of a Ni atom into the Sn_9 framework, as in the case of the anion $[\text{Ni}@\text{Sn}_9\text{Ni}(\text{CO})]^{3-}$, leads to only a much smaller expansion of the polyhedron (Figure 2d) than in the Sn_9Cr cluster.^[11] Since the $\text{Ni}(\text{CO})$ fragment carries two electrons that can contribute to the framework bonding, it corresponds—according to the isolobal concept—to a Sn vertex atom, and the cluster can be assumed to have the charge distribution $[\text{Ni}^0@\text{Sn}_9\text{Ni}(\text{CO})]^{3-}$. The odd number of electrons implies that we are dealing with a $(2n + 1)$ -electron, *closo*-type cluster, which is analogous to the well-established oxidized form of the *nido* clusters $[\text{E}_9]^{3-}$ ($\text{E} = \text{Ge}, \text{Sn}, \text{Pb}$) with $2n + 3$ electrons.^[6]

The anion $[\text{Pt}@\text{Pb}_{12}]^{2-}$ represents the first isolated (soluble) ligand-free cluster of a Group 14 element with $n > 10$ (Figure 2e).^[12] The 12 Pb atoms are arranged around a central Pt atom in the form of a highly symmetrical icosahedron. An orbital analysis reveals only weak interactions between the cluster orbitals and the orbitals of the central atom, thereby suggesting the formulation of the cluster as $[\text{Pt}^0@\text{Pb}_{12}^{2-}]$. The central Pt atom acts as a template for the electron-precise (according to the Wade rules) Pb_{12}^{2-} cluster and not as an electron donor or acceptor, as observed in other types of filled clusters, such as $[\text{C}@\text{Au}_6\text{L}_6]^{2+}$ and $[\text{Pt}@\text{Sn}_9\text{Pt}]^{2+}$ (Figure 2p and q).^[13]

The Icosahedron

Due to its uniform surface built of equilateral triangles, the icosahedron (Figure 2, I) belongs to the so-called platonic bodies. Truncation of the vertices can lead to new polyhedra in which the symmetry is retained. If the truncation results in the formation of equilateral six-membered rings, the polyhedron of C_{60} -fullerene with 60 vertices is generated (Figure 2, II). The dual of a polyhedron is formed when the centers of the faces are connected to generate edges. In the case of the icosahedron, this procedure leads to a pentagonal dodecahedron, and vice versa (Figure 2, III). The 12 edge-sharing five-membered rings in III show a different relative orientation to that of the 12 five-membered rings of the 60-vertex polyhedron in II. In an icosahedral cage molecule, the 30 interatomic distances a between the vertex atoms on the surface of the polyhedron are of equal length (Figure 2e). In contrast, the distances R between these atoms and the center of the polyhedron are $\approx 5\%$ shorter ($R/a = 0.951$).^[14] As point groups of icosahedral symmetry do not represent crystallographic point groups, real clusters with 12 vertices present in crystals deviate more or less from the ideal icosahedral symmetry. For an estimation of the volume of distorted polyhedra we propose the deviation from the ideal ratio of the radii $R/a = 0.951$ as a simple criterion (Table 1). The corresponding value, for example, for a polyhedron with cuboctahedral symmetry is $R/a = 1$. In the case of filled icosahedra, the average distances between the central atom and the 12 vertex atoms can be used for R . With the average



Thomas F. Fässler was born in Bad Waldsee/Reute (Germany) in 1959. He studied chemistry and mathematics at the University of Konstanz. In 1988 he received his PhD with Prof. G. Huttner (Heidelberg). After a period of research at the University of Chicago with Prof. J. Burdett, he moved to the ETH Zürich in 1991, where he completed his habilitation in 1997. In 2000 he became Professor at Darmstadt University of Technology, where he also directed the Institute of Inorganic Chemistry in 2001/2002. In 2003 he was appointed Chair of Inorganic Chemistry with Focus on New Materials at the TU München.



Stephan D. Hoffmann was born in 1972 in Königstein (Germany). He studied chemistry (1992–1997) at the Darmstadt University of Technology, where he also received his Ph.D. under the supervision of Professor Johann W. Buchler (2001). He pursued postdoctoral work with Professor Thomas F. Fässler in Darmstadt and since 2003 at the Technische Universität München.

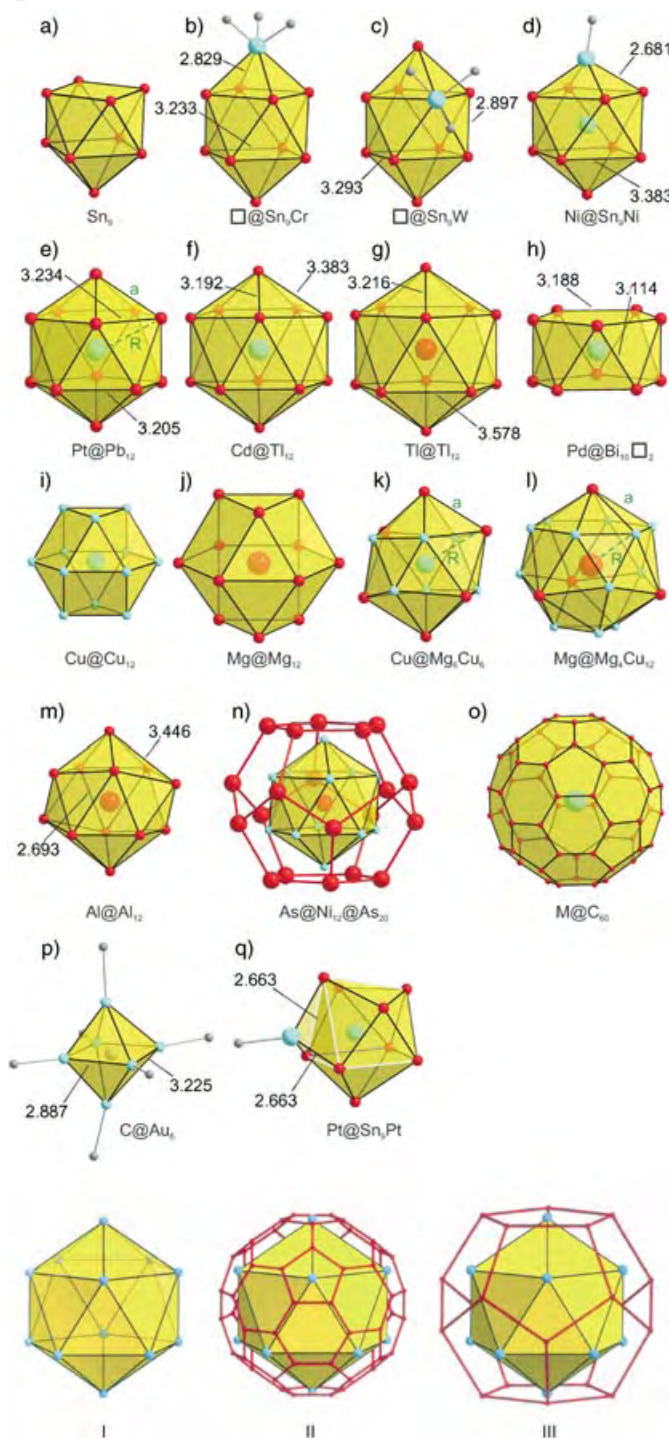


Figure 2. a–q) Structures of known clusters and coordination polyhedra (to scale). The shortest and longest edges of the polyhedra are given in Å. a) Sn_5^{4+} ; b) $[\text{Sn}_9\text{Cr}(\text{CO})_3]^{4-}$; c) $[\text{Sn}_9\text{W}(\text{CO})_3]^{4-}$; d) $[\text{NiSn}_9\text{Ni}(\text{CO})_3]^{3-}$ (in b)–d), the C atoms of the CO ligands are drawn in gray; e) $[\text{Pt@Pb}_{12}]^{2-}$; f) $[\text{Cd@Ti}_{12}]^{12-}$ in $\text{Na}_{14}\text{K}_6\text{Ti}_{18}\text{Cd}$; g) $[\text{Ti}_{13}]^{11-}$ in $\text{Na}_3\text{K}_8\text{Ti}_{13}$; h) $[\text{Pd@Bi}_{10}]^{4+}$ in $\text{Bi}_{14}\text{PdBr}_{16}$; i) part of the structure of elemental Cu; j) part of the structure of elemental Mg; k) and l) coordination polyhedra of Cu and Mg, respectively, in the Laves phase MgCu_2 ; m) coordination sphere of the central Al atom in $[\text{Al}_7\{\text{N}(\text{SiMe}_2)_2\}_{20}]^{2-}$; n) $[\text{As-Ni}_{12}\text{As}_{20}]^{2-}$; o) endohedral fullerene; p) $[\text{CAu}_6(\text{PPh}_3)_6]^{2+}$; q) $[\text{PtSn}_9\text{Pt}(\text{PPh}_3)_2]^{2-}$ (in p) and q), the P atoms of the PPh_3 ligands are drawn in gray).

I–III: Polyhedra with icosahedral symmetry; I icosahedron, II truncation of the vertices leads to C_{60} fullerene (red), III the pentagonal dodecahedron (red) represents the dual of the icosahedron.

distances of 3.215 Å for $d(\text{Pb-Pb})$ and 3.058 Å for $d(\text{Pb-Pt})$, the ideal value of 0.951 is obtained for the $[\text{Pt@Pb}_{12}]^{2-}$ anion.

Main-Group-Element Deltahedra in Salt-like Crystals

In solid phases, more compounds that contain deltahedral main-group-element clusters are known than soluble species. In cases in which cluster units exist exclusively in solid phases, it first has to be ascertained that they can be regarded as isolated units. This is of importance not only for a consideration of the binding within the cluster framework but also with respect to the overall distribution and localization of the electrons. For Zintl phases, an ionic charge distribution is assumed according to the Zintl–Klemm–Busmann concept,^[15,16] and the anionic substructures are interpreted by following the $(8-N)$ rule or the Wade rules. The solubility in polar solvents of several Zintl phases that contain Group 14 elements (e.g. K_4Sn_9) supports the concept of ionic character. Sr_3Sn_5 contains *arachno*-type Sn_5^{6-} units, which are not known in solution, however, and the solid exhibits metallic behavior.^[17] The charge distribution in many Group 13 element clusters with higher charges cannot be determined unambiguously solely on the basis of structural data. In general, it is not known whether these phases are soluble, and deviations from the expected number of electrons or structures as well as the appearance of different clusters within one compound are quite common. An example is the electron-precise cluster $[\text{Ti}_6]^{8-}$, which is found with filled, larger clusters as part of $\text{Na}_{14}\text{K}_6\text{Ti}_{18}\text{Cd}$. On the other hand, KTI contains $[\text{Ti}_6]^{6-}$ clusters with a smaller number of framework electrons ($2n$ instead of $2n+2$) and features a tetragonally compressed O_h symmetry.^[18] In both compounds, direct contacts between the cluster atoms and the alkaline metals have to be taken into consideration, and it is not very likely that these highly charged cages are stable in solution.

It has also been demonstrated for solid phases that polyhedra with triangular faces can be filled as soon as they comprise 10 or more atoms. As shown for the corresponding empty Group 13 element clusters, deviations from the expected number of electrons are quite common. Thus, $\text{K}_8\text{In}_{10}\text{Zn}$ contains the electron-poor cluster unit $[\text{Zn}^{2+}@\text{In}_{10}]^{10-}$ ($2n$ electrons). The phase $\text{Na}_{14}\text{K}_6\text{Ti}_{18}\text{Cd}$ mentioned above contains $[\text{Cd@Ti}_{12}]^{12-}$ units (Figure 2 f) and, according to the formula $[\text{Cd}^{2+}@\text{Ti}_{12}]^{14-}$, can be regarded as an electron-precise centered cluster with an almost ideal icosahedral symmetry. The unit $[\text{Ti}^{3+}@\text{Ti}_{12}]^{14-}$ observed in $\text{Na}_3\text{K}_8\text{Ti}_{13}$ (Figure 2 g) can be described as an electron-precise cluster only if a formal charge separation is assumed.^[18,19] In both cases, the edges of the polyhedra are about 5% longer than the distances between the vertices and the central atoms (Table 1).

Interestingly, a recent publication described a centered *arachno*-type cluster whose structure can be derived from the icosahedral $[\text{Pt@Pb}_{12}]^{2-}$ unit by removing two opposite vertices. To date, however, this cluster $[\text{Pd@Bi}_{10}]^{4+}$ has been observed only as a component of the solid-phase $\text{Bi}_{14}\text{PdBr}_{16}$.^[19] In the cation $[\text{Pd@Bi}_{10}]^{4+}$, there appears to be virtually no interactions between the central Pd atom and the

Table 1: Minimum, maximum, and average distances R and a [Å] within the closed polyhedra shown in Figure 2.

	Figure 2	R_{\min}	R_{\max}	R_{av}	a_{\min}	a_{\max}	a_{av}	$R_{\text{av}}/a_{\text{av}}^{[b]}$
Sn_9Cr	b	2.480	3.130	2.645	2.829	3.233	3.004	0.880
Sn_9W	c	2.460	3.189	2.673	2.897	3.293	3.034	0.881
$\text{Ni}@ \text{Sn}_9\text{Ni}$	d	2.619	2.827	2.658	2.681	3.383	3.042	0.874
$\text{Pt}@ \text{Pb}_{12}$	e	3.056	3.059	3.058	3.205	3.234	3.215	0.951
$\text{Cd}@ \text{Ti}_{12}$	f	3.180	3.180	3.180	3.192	3.383	3.345	0.951
$\text{Ti}@ \text{Ti}_{12}$	g	3.204	3.273	3.239	3.216	3.578	3.401	0.952
$\text{Pd}@ \text{Bi}_{10}$	h	2.969	3.019	3.000	3.114	3.188	3.153	0.951
$\text{Cu}@ \text{Cu}_{12}$	i	2.556	2.556	2.556	2.556	2.556	2.556	1.000
$\text{Mg}@ \text{Mg}_{12}$	j	3.209	3.209	3.209	3.209	3.209	3.209	1.000
$\text{Mg}@ \text{Mg}_6\text{Cu}_6$	k	2.487	2.916	2.702	2.487	3.046	2.856	0.946
$\text{Cu}@ \text{Cu}_4\text{Mg}_{12}$	l	2.916	3.046	2.949	2.487	2.916	2.702	1.091
$\text{Al}@ \text{Al}_{12}$	m	2.675	2.868	2.760	2.693	3.446	2.914	0.947
$\text{As}@ \text{Ni}_{12}$	n	2.541	2.580	2.557	2.667	2.709	2.689	0.951
$\text{N}@ \text{C}_{60}$	o	3.535	3.535	3.535	1.399	1.441	1.416	2.497
$\text{C}@ \text{Au}_6$	p	2.090	2.153	2.124	2.887	3.225	3.005	0.707
$\text{Pt}@ \text{Sn}_9\text{Pt}$	q	2.683	2.762	2.737	2.663	4.104	3.188	0.859

[a] R is the distance between the vertex atom and the center of the polyhedron; a is the distance between the vertex atoms on the surface of the polyhedra. [b] The ideal value in the icosahedron is 0.951.

skeletal Bi atoms, which are arranged in the shape of a pentagonal antiprism (Figure 2 h). Again the orbital analysis is in agreement with the formula $[\text{Pd}^0@ \text{Bi}_{10}^{4+}]$, and the skeletal cation $[\text{Bi}_{10}]^{4+}$ can be regarded as an electron-precise *arachno*-type cluster with a Pd atom in the center. Even when a few vertices are removed, the average Pd–Bi distances remain about 5 % shorter than the peripheral Bi–Bi distances ($R/a = 0.951$). In this ionic description, the one-dimensional polymeric string $^1[\text{Bi}_{14}\text{Br}_{16}]^{4-}$ acts as a counterion. This charge partition is supported by significantly longer Bi–Br distances *between* the two units than the corresponding distances *within* the anionic unit. A similar situation is found in the well-established *nido* cluster $[\text{Bi}_9]^{5+}$.^[5] However, the $(2n + 4)$ electron cluster has a *closo*-type structure.

Deltahedra in Intermetallic Phases

The preferred coordination number in packing modes made up by atoms of approximately equal size is 12. This is realized in an ideal way in the variants of close packing of metallic elements, which preferably adopt the cubic (Cu type) and hexagonal (Mg type) close packing. The resulting coordination polyhedra are the cuboctahedron (Figure 2 i) and the anti-cuboctahedron (Figure 2 j), respectively. In these entities, the distances between the central atom and the atoms of the surrounding polyhedron are equal to those within the framework of the polyhedron ($R/a = 1$). However, these polyhedra do not belong to the class of deltahedra, as they also contain square planes. According to the notation introduced above, the corresponding structure units can be described as $\text{Cu}@ \text{Cu}_{12}$ and $\text{Mg}@ \text{Mg}_{12}$, respectively.

For binary alloys in which the atoms have different sizes and the components tend to approach close packing, a coordination geometry derived from an icosahedron is generally observed.^[20] The cubic Laves phase MgCu_2 is an example in which the smaller Cu atom is located in the center

of the heteroatomic deltahedron $\text{Cu}@ \text{Mg}_6\text{Cu}_6$, whose structure is shown in Figure 2 k. As a consequence of this arrangement the Mg atom is accommodated inside a heteroatomic deltahedron with 16 vertices of T_d symmetry (Figure 2 l). If a model is applied in which the Mg as well as the Cu atoms touch each other, an ideal ratio $r(\text{Mg})/r(\text{Cu}) = 1.225$ is obtained. The resulting space filling for this arrangement still reaches a remarkable 71 % (compare closest packing: 74 %).^[21]

The coordination polyhedra with 12 vertices described above are found for intermetallic compounds with the ratios of the radii in the range between 1.05 and 1.67. The corresponding value for $r(\text{Pb})/r(\text{Pt})$ in $[\text{Pt}@ \text{Pb}_{12}]^{2-}$ (calculated by using the metallic radii $r(\text{Pt}) = 1.373$ and $r(\text{Pb}) = 1.750$ Å)

was found to be 1.274 and is very close to the value of 1.225 calculated by Laves.

If a model of touching spheres with the metallic radii $r(\text{Pt}) = 1.373$ and $r(\text{Pb}) = 1.750$ Å is also applied for $[\text{Pt}@ \text{Pb}_{12}]^{2-}$, the distances on the polyhedral surface are calculated as $d(\text{Pb}–\text{Pb}) = 3.500$ Å and the distances between the Pb atoms and the central Pt atom as 3.123 Å. With the conventional radii as a reference, the Pb–Pt distance is shortened by ≈ 11 %, with the central Pt atoms slightly too small (5 % relative to the standard value). In the isolated dianions $[\text{Pt}@ \text{Pb}_{12}]^{2-}$, the atomic radii appear to be smaller than the metallic radii, owing to a better localization of the electrons than in the metal, and the average distances $d(\text{Pb}–\text{Pb})$ and $d(\text{Pb}–\text{Pt})$ are 3.215 and 3.058 Å, respectively ($R/a = 0.95$).

Another series of heteroatomic deltahedra that allow close packing of atoms of different sizes has been investigated systematically by Frank and Kasper: In addition to the deltahedra with 12 and 16 vertices (above), the so-called Frank–Kasper polyhedra comprise another two deltahedra with 14 and 15 vertices,^[21] and it is therefore conceivable that besides $[\text{M}@ \text{E}_{12}]^{2-}$ there may be many larger, soluble, filled, and ligand-free main-group-element clusters of compositions $[\text{M}@ \text{E}_{14}]^{2-}$, $[\text{M}@ \text{E}_{15}]^{2-}$, and $[\text{M}@ \text{E}_{16}]^{2-}$ that are stable.

Soluble Metalloid and Intermetalloid Clusters

The structure of $[\text{Pt}@ \text{Pb}_{12}]^{2-}$ also shows interesting parallels to the metalloid clusters described by Schnöckel: The central Al atom of the anion $[\text{Al}_{77}\{\text{N}(\text{SiMe}_2)_2\}_{20}]^{2-}$ again has 12 close neighbors in a strongly distorted icosahedral environment,^[22] and, as is the case for $[\text{Pt}@ \text{Pb}_{12}]^{2-}$, the central atom has a coordination sphere that neither corresponds to a section of a close packing with a cuboctahedral nor to an anticuboctahedral structure. The distortion of the observed icosahedron can be recognized from the deviation of the two

parallel five-membered rings from planarity (Figure 2m). As a consequence of this deviation, very long Al–Al distances of 3.446 Å appear on the surface of the polyhedron which are more than 25% longer than the shortest ones (2.693 Å). However, the average of the distances on the surface is again about 5.3% longer than the average of those to the interstitial atom. Referring to the term *metalloid* clusters of Group 13 elements,^[23] it appears to be appropriate to suggest the term *intermetalloid* clusters for the growing class of metal-centered heteroatomic clusters.^[24]

In the meantime, the formation of big clusters could also be demonstrated for As.^[25] In the anion $[\text{As}@\text{Ni}_{12}@\text{As}_{20}]^{2-}$ there are, however, strong interactions between the fascinating pentagonal dodecahedron of 20 As atoms and the central $\text{As}@\text{Ni}_{12}$ cluster (Figure 2n). In this case the As-centered Ni_{12} icosahedron can be regarded as a template for the formation of the As_{20} polyhedron. In contrast to the observations in $[\text{Pt}@\text{Pb}_{12}]^{2-}$, relatively strong Ni–As interactions contribute to the stabilization of the As framework.

Together with the large cations $[\text{K}([2.2.2]\text{crypt})]^+$,^[26] the anion $[\text{Pt}@\text{Pb}_{12}]^{2-}$ forms a packing in which the anions are arranged in layers analogous to a closest packing of atoms. These layers are separated by the cations and are aligned congruently along the *c* axis, thereby forming a primitive hexagonal arrangement that is compressed along this axis (Figure 3a and b). This packing mode corresponds to that observed for $[\text{Al}_{77}\{\text{Ni}(\text{SiMe}_2)_2\}_{20}]^{2-}$, which crystallizes with $[\text{Li-I-Li}]^+$ counterions (Figure 3c and d), and that present in C_{60}^{2-} anions, which in combination with $[\text{K}(2.2.2\text{-crypt})]^+$ cations also form a layer-type aggregation (Figure 3e and f).^[27] The observed similarity in the packing modes of large anions of different sizes together with different counterions suggests that the packing can be predominantly explained by repulsive forces between the dianions.

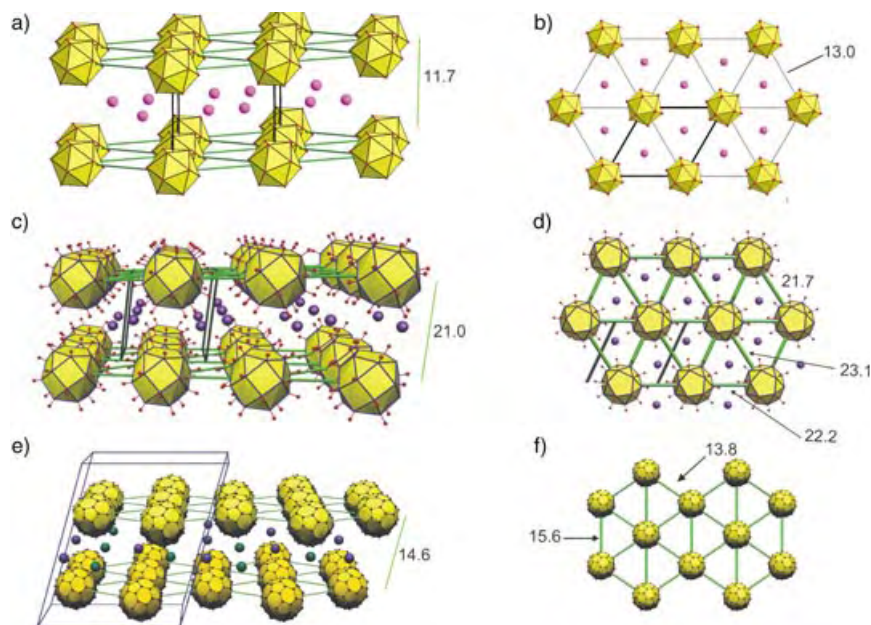


Figure 3. The packing of large dianions in the crystal (unit cells in black, distances between the centers of gravity of the clusters in Å). a) and b) $[\text{Pt}@\text{Pb}_{12}]^{2-}$ with $[\text{K}(2.2.2)\text{crypt}]^+$ counterions (only K atoms shown); c) and d) $[\text{Al}_{77}\{\text{N}(\text{SiMe}_2)_2\}_{20}]^{2-}$ with $[\text{Li-I-Li}]^+$ counterions (only the N atoms of the ligand and the I atom of the counterion are shown); e) and f) C_{60}^{2-} with $[\text{K}(2.2.2)\text{crypt}]^+$ counterions (only K atoms shown).

Intermetalloid Clusters in the Gas Phase

Although the structures of a large number of filled main-group-element clusters detected by mass spectrometry have been deduced on the basis of theoretical calculations, there is still a lack of experimental proof.^[28] In contrast to gas-phase experiments on bimetallic species, the structures of the clusters discussed above have been proven unambiguously. The experimental structure determination is especially important, as the minor component does not necessarily reside in the center of the cluster, but can—as observed in the anions $[(\text{CO})_3\text{CrSn}_9]^{2-}$ and $[(\text{CO})_3\text{WSn}_9]^{2-}$ —occupy a vertex of the polyhedron. Structure determinations of these electron-precise clusters have proven the presence of isomers in which the transition-metal atoms occupy different vertices of the polyhedra, and NMR spectroscopy experiments have indicated a rapid exchange between these positions in solution.^[11] Accordingly, the presence of two transition-metal atoms increases the number of possible isomers. For these cases, the structure of the endohedral Zintl anion $[\text{Ni}@\text{Sn}_9\text{Ni}(\text{CO})]^{3-}$ can serve as an important reference for theoretical predictions of the structures of species with two transition-metal atoms already detected in the gas phase. Although the transition metals in the examples mentioned above bear ligands, it is a safe assumption that the framework of the polyhedron is retained upon the loss of the carbonyl ligands in the gas phase.

Whereas heteroatomic clusters that contain Group 14 elements and alkaline metals have been known in the gas phase for quite some time,^[29,30] the corresponding species with main-group/transition-metal atoms are less well investigated.^[31] According to theoretical investigations, the bimetallic clusters $[\text{AlPb}_{10}]^+$ and $[\text{AlPb}_{12}]^+$, which are very stable in the gas phase, have structures with D_{4d} and I_h symmetry, respectively (Figure 2d and e). Analogously to the endohedral Zintl ions, they can be described as filled, electron-precise *closo* clusters $[\text{Al}^{3+}@\text{Pb}_{10}^{2-}]$ and $[\text{Al}^{3+}@\text{Pb}_{12}^{2-}]$.^[32]

Endohedral Clusters and Fullerenes

Recently we pointed out the exciting analogy between Zintl ions and fullerenes.^[33] By including endohedral compounds into this concept, the anion $[\text{Pt}@\text{Pb}_{12}]^{2-}$ can be taken as further evidence for its validity. Although a larger number of endohedral compounds have been detected in the case of the fullerenes, structural proof is rather limited.^[34,35] The comparable size of C_{60} and Pb_{12} allows the incorporation of a metal atom in both cases. The interactions between the central atom and the framework atoms are expected to be small in both cases, but with

significant contributions in the case of the endohedral anions. The structural analogy mentioned above can be readily rationalized in Figure 2e and o, which have been drawn to scale.

Summary

According to Wade's rules larger clusters that contain Group 14 elements are expected to exist and to be stable. In many cases, these counting rules can also be applied successfully to naked endohedral Zintl ions. For the electron count of these systems, a formal charge separation between the polyhedral framework and the central atom is helpful. Owing to the relatively small charge, the synthesis of larger endohedral intermetallic clusters built from Group 14 elements should generally be possible, as already demonstrated for the first time by the characterization of the anion $[\text{Pt}@\text{Pb}_{12}]^{2-}$. The formation of larger clusters starting from the well-established and readily available nine-atom Zintl ions of Group 14 elements seems to be favored if a central atom can be incorporated. The choice of appropriate "template atoms" for the formation of larger clusters may be guided by the species detected in the gas phase, or by the structural features observed in Laves phases or in Frank–Kasper polyhedra. The centered polyanion $[\text{Pt}@\text{Pb}_{12}]^{2-}$ again illustrates the amazing parallel between deltahedral Zintl ions and fullerenes.

We thank Prof. B. Eichhorn and Prof. M. Ruck for supplying structural data, Dr. A. Schier for revision of the manuscript, and the Deutsche Forschungsgemeinschaft for financial support (SPP 1072).

Received: April 23, 2004

Published Online: October 26, 2004

- [1] K. Wade, *Adv. Inorg. Chem. Radiochem.* **1976**, 18, 1.
- [2] T. F. Fässler in *Metal Clusters in Chemistry* (Eds.: P. Braunstein, L. A. Oro, P. R. Raithby), Wiley-VCH, Weinheim, **1999**, p. 1612.
- [3] W. L. Wilson, R. W. Rudolph, L. L. Lohr, F. Parker, R. C. Taylor, D. C. Pyykkö, *Inorg. Chem.* **1986**, 25, 1535.
- [4] A. Hirsch, Z. Chen, H. Jiao, *Angew. Chem.* **2001**, 113, 2916; *Angew. Chem. Int. Ed.* **2001**, 40, 2834.
- [5] J. D. Corbett, *Chem. Rev.* **1985**, 85, 383.
- [6] T. F. Fässler, *Coord. Chem. Rev.* **2001**, 215, 347.
- [7] Some evidence for the existence of a heavily disordered Ge_{10}^{2-} cluster^[8,9] could not be affirmed. Compounds with very similar lattice parameters and the same symmetry did not allow a decision between a Ge_9^{2-} or a Ge_{10}^{2-} species.^[36]
- [8] C. Belin, H. Mercier, V. Angilella, *New J. Chem.* **1991**, 15, 931.
- [9] R. C. Burns, J. D. Corbett, *J. Am. Chem. Soc.* **1982**, 104, 2804.
- [10] B. Kesanli, J. Fetting, B. Eichhorn, *Chem. Eur. J.* **2001**, 7, 5277.
- [11] B. Kesanli, J. Fetting, D. R. Gardner, B. Eichhorn, *J. Am. Chem. Soc.* **2002**, 124, 4779.
- [12] E. N. Esenturk, J. Fetting, Y.-F. Lam, B. Eichhorn, *Angew. Chem.* **2004**, 116, 2184; *Angew. Chem. Int. Ed.* **2004**, 43, 2132.
- [13] H. Schmidbaur, F. Scherbaum, B. Huber, G. Müller, *Angew. Chem.* **1988**, 100, 441; *Angew. Chem. Int. Ed.* **1998**, 37, 417.
- [14] For an ideal icosahedron: $R = \frac{a}{4}\sqrt{10 + 2\sqrt{5}} = 0.951$.
- [15] W. Klemm, *Proc. Chem. Soc. London* **1959**, 329.
- [16] E. Zintl, *Angew. Chem.* **1939**, 52, 1.
- [17] F. Zürcher, R. Nesper, S. Hoffmann, T. F. Fässler, *Z. Anorg. Allg. Chem.* **2001**, 627, 2211.
- [18] J. D. Corbett, *Angew. Chem.* **2000**, 112, 682; *Angew. Chem. Int. Ed.* **2000**, 39, 670; J. D. Corbett, *Struct. Bonding (Berlin)* **1997**, 87, 158.
- [19] M. Ruck, V. Dubenskyy, T. Söhnel, *Angew. Chem.* **2003**, 115, 3086; *Angew. Chem. Int. Ed.* **2003**, 42, 2978.
- [20] For a Review on packing modes of intermetallic compounds see: R. Nesper, *Angew. Chem.* **1994**, 106, 891; *Angew. Chem. Int. Ed. Engl.* **1994**, 33, 843.
- [21] W. Hume-Rothery, R. E. Smallman, C. W. Haworth, *The Structure of Metals and Alloys*, 5th ed., Antony Rowe, Chippenham, Wilts, **1969**.
- [22] A. Ecker, E. Weckert, H. Schnöckel, *Nature* **1997**, 387, 379.
- [23] A. Schnepf, H. Schnöckel, *Angew. Chem.* **2002**, 114, 3683; *Angew. Chem. Int. Ed.* **2002**, 41, 3533.
- [24] More clusters of the composition $\text{Pt}_2\text{Sn}_{18}$ are known: B. Eichhorn, personal communication.
- [25] M. J. Moses, J. C. Fetting, B. W. Eichhorn, *Science* **2003**, 300, 778.
- [26] 2.2.2-crypt = 4,7,13,16,21,24-hexaoxa-1,10-diazabicyclo-[8.8.8]hexacosane.
- [27] T. F. Fässler, A. Spiekermann, M. Spahr, R. Nesper, *Angew. Chem.* **1997**, 109, 502; *Angew. Chem. Int. Ed. Engl.* **1997**, 36, 486.
- [28] Despite the existence of experimental structural data for a variety of clusters, they are neglected quite often in the discussion of the results of theoretical calculations; for example, see: D. E. Bergeron, A. W. Castleman, Jr., T. Morisato, S. N. Khanna, *Science* **2004**, 304, 84.
- [29] T. P. Martin, *Angew. Chem.* **1986**, 98, 197; *Angew. Chem. Int. Ed. Engl.* **1986**, 25, 197.
- [30] T. F. Fässler, H.-J. Muhr, M. Hunziker, *Eur. J. Inorg. Chem.* **1998**, 1433.
- [31] X. Zhang, G. Li, X. Xing, X. Zhao, Z. Tang, Z. Gao, *Rapid Commun. Mass Spectrom.* **2001**, 15, 2399.
- [32] S. Neukermans, E. Janssens, Z. F. Chen, R. E. Silverans, P. v. R. Schleyer, P. Lievens, *Phys. Rev. Lett.* **2004**, 92, 163401.
- [33] T. F. Fässler, *Angew. Chem.* **2001**, 113, 4289; *Angew. Chem. Int. Ed.* **2001**, 40, 4161.
- [34] For a review on metallafullerenes, see: H. Shinohara, *Rep. Prog. Phys.* **2000**, 63, 843.
- [35] M. M. Olmstead, A. d. Bettencourt-Dias, J. C. Duchamp, S. Stevenson, H. C. Dorn, A. L. Balch, *J. Am. Chem. Soc.* **2000**, 122, 12220; T. Wägberg, P. Launois, R. Moret, H. J. Huang, S. H. Yang, I. L. Li, Z. K. Tang, *Eur. Phys. J. B* **2003**, 35, 371.
- [36] T. F. Fässler, M. Hunziker, M. Spahr, H. Lueken, *Z. Anorg. Allg. Chem.* **2000**, 626, 692.

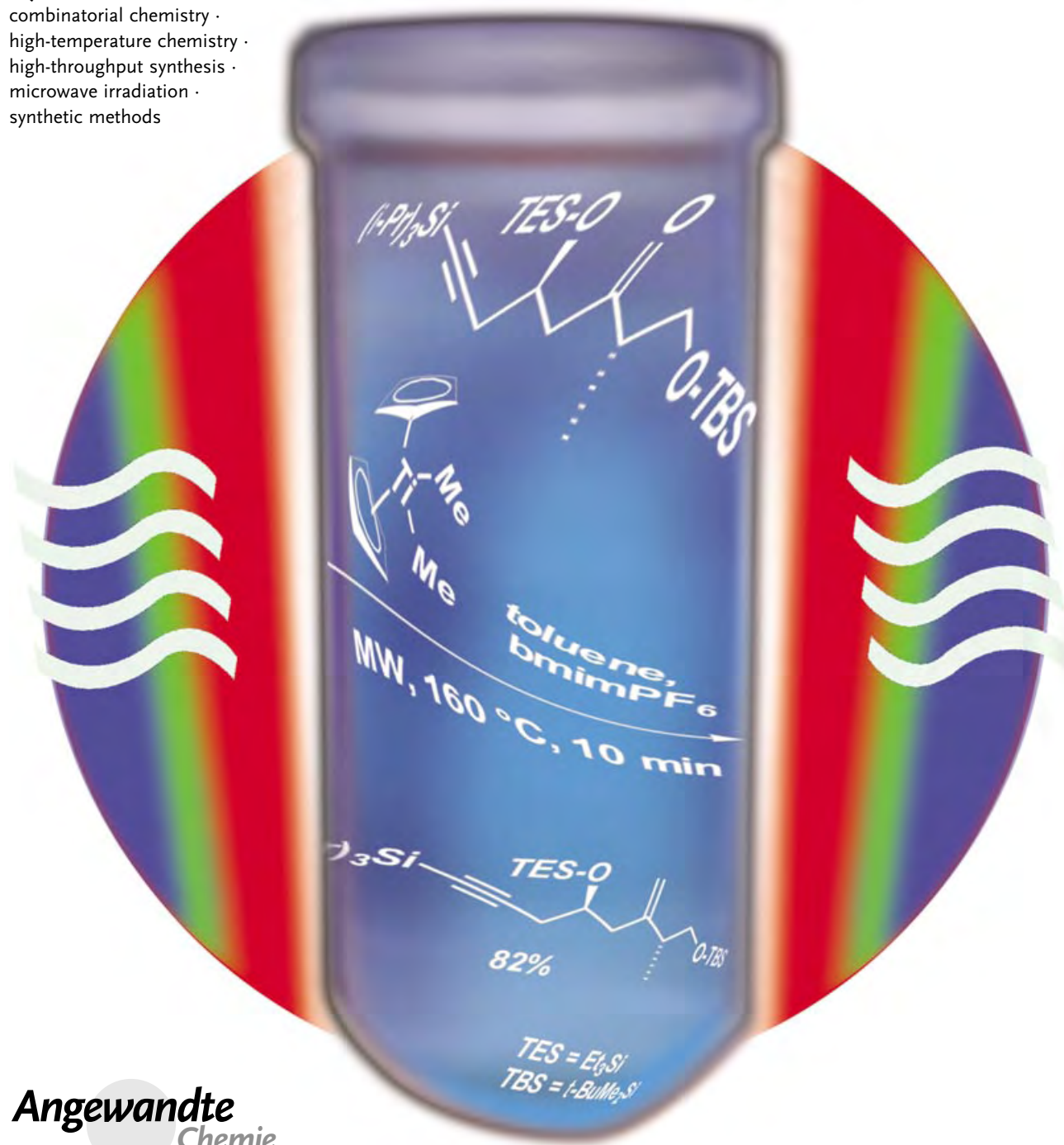
Synthetic Methods

Controlled Microwave Heating in Modern Organic Synthesis

C. Oliver Kappe*

Keywords:

combinatorial chemistry ·
high-temperature chemistry ·
high-throughput synthesis ·
microwave irradiation ·
synthetic methods



Angewandte
Chemie

Although fire is now rarely used in synthetic chemistry, it was not until Robert Bunsen invented the burner in 1855 that the energy from this heat source could be applied to a reaction vessel in a focused manner. The Bunsen burner was later superseded by the isomantle, oil bath, or hot plate as a source for applying heat to a chemical reaction. In the past few years, heating and driving chemical reactions by microwave energy has been an increasingly popular theme in the scientific community. This nonclassical heating technique is slowly moving from a laboratory curiosity to an established technique that is heavily used in both academia and industry. The efficiency of “microwave flash heating” in dramatically reducing reaction times (from days and hours to minutes and seconds) is just one of the many advantages. This Review highlights recent applications of controlled microwave heating in modern organic synthesis, and discusses some of the underlying phenomena and issues involved.

1. Introduction

High-speed synthesis with microwaves has attracted a considerable amount of attention in recent years.^[1] More than 2000 articles have been published in the area of microwave-assisted organic synthesis (MAOS) since the first reports on the use of microwave heating to accelerate organic chemical transformations by the groups of Gedye and Giguere/Majetich in 1986.^[2,3] The initial slow uptake of the technology in the late 1980s and early 1990s has been attributed to its lack of controllability and reproducibility, coupled with a general lack of understanding of the basics of microwave dielectric heating. The risks associated with the flammability of organic solvents in a microwave field and the lack of available systems for adequate temperature and pressure controls were major concerns.

Although most of the early pioneering experiments in MAOS were performed in domestic, sometimes modified, kitchen microwave ovens, the current trend is to use dedicated instruments which have only become available in the last few years for chemical synthesis. The number of publications related to MAOS has therefore increased dramatically since the late 1990s to a point where it might be assumed that, in a few years, most chemists will probably use microwave energy to heat chemical reactions on a laboratory scale. Not only is direct microwave heating able to reduce chemical reaction times from hours to minutes, but it is also known to reduce side reactions, increase yields, and improve reproducibility. Therefore, many academic and industrial research groups are already using MAOS as a forefront technology for rapid optimization of reactions, for the efficient synthesis of new chemical entities, and for discovering and probing new chemical reactivity. A large number of review articles^[4–13] and several books^[14–16] provide extensive coverage of the subject. The aim of this Review is to highlight some of the most recent applications and trends in microwave synthesis, and to discuss the impact and future potential of this technology.

From the Contents

1. Introduction	6251
2. Literature Survey	
● Transition-Metal-Catalyzed Reactions	
● Heterocycle Synthesis	
● Combinatorial Synthesis and High-Throughput Techniques	6254
3. Summary and Outlook	6275

1.1. Microwave Theory

Microwave irradiation is electromagnetic irradiation in the frequency range of 0.3 to 300 GHz. All domestic “kitchen” microwave ovens and all dedicated microwave reactors for chemical synthesis operate at a frequency of 2.45 GHz (which corresponds to a wavelength of 12.24 cm) to avoid interference with telecommunication and cellular phone frequencies. The energy of the microwave photon in this frequency region (0.0016 eV) is too low to break chemical bonds and is also lower than the energy of Brownian motion. It is therefore clear that microwaves cannot induce chemical reactions.^[17–19]

Microwave-enhanced chemistry is based on the efficient heating of materials by “microwave dielectric heating” effects. This phenomenon is dependent on the ability of a specific material (solvent or reagent) to absorb microwave energy and convert it into heat. The electric component^[20] of an electromagnetic field causes heating by two main mechanisms: dipolar polarization and ionic conduction. Irradiation of the sample at microwave frequencies results in the dipoles or ions aligning in the applied electric field. As the applied field oscillates, the dipole or ion field attempts to realign itself with the alternating electric field and, in the process, energy is lost in the form of heat through molecular friction and dielectric loss. The amount of heat generated by this process is directly related to the ability of the matrix to align itself with the frequency of the applied field. If the dipole does not have enough time to realign, or reorients too quickly with the applied field, no heating occurs. The allocated frequency of 2.45 GHz used in all commercial systems lies between these two extremes and gives the molecular dipole time to align in the field, but not to follow the alternating field precisely.^[18,19]

The heating characteristics of a particular material (for example, a solvent) under microwave irradiation conditions

[*] Prof. Dr. C. O. Kappe
Institute of Chemistry, Organic and Bioorganic Chemistry
Karl-Franzens University Graz
Heinrichstrasse 28, A-8010 Graz (Austria)
Fax: (+43)316-380-9840
E-mail: oliver.kappe@uni-graz.at

are dependent on its dielectric properties. The ability of a specific substance to convert electromagnetic energy into heat at a given frequency and temperature is determined by the so-called loss factor $\tan\delta$. This loss factor is expressed as the quotient $\tan\delta = \epsilon''/\epsilon'$, where ϵ'' is the dielectric loss, which is indicative of the efficiency with which electromagnetic radiation is converted into heat, and ϵ' is the dielectric constant describing the ability of molecules to be polarized by the electric field. A reaction medium with a high $\tan\delta$ value is required for efficient absorption and, consequently, for rapid heating. The loss factors for some common organic solvents are summarized in Table 1. In general, solvents can be classified as high ($\tan\delta > 0.5$), medium ($\tan\delta$ 0.1–0.5), and low microwave absorbing ($\tan\delta < 0.1$).

Table 1: Loss factors ($\tan\delta$) of different solvents.^[a]

Solvent	$\tan\delta$	Solvent	$\tan\delta$
ethylene glycol	1.350	DMF	0.161
ethanol	0.941	1,2-dichloroethane	0.127
DMSO	0.825	water	0.123
2-propanol	0.799	chlorobenzene	0.101
formic acid	0.722	chloroform	0.091
methanol	0.659	acetonitrile	0.062
nitrobenzene	0.589	ethyl acetate	0.059
1-butanol	0.571	acetone	0.054
2-butanol	0.447	tetrahydrofuran	0.047
1,2-dichlorobenzene	0.280	dichloromethane	0.042
NMP	0.275	toluene	0.040
acetic acid	0.174	hexane	0.020

[a] Data from ref. [15]; 2.45 GHz, 20 °C.

Other common solvents without a permanent dipole moment such as carbon tetrachloride, benzene, and dioxane are more or less microwave transparent. It has to be emphasized that a low $\tan\delta$ value does not preclude a particular solvent from being used in a microwave-heated reaction. Since either the substrates or some of the reagents/catalysts are likely to be polar, the overall dielectric properties of the reaction medium will in most cases allow sufficient heating by microwaves (see Section 1.2). Furthermore, polar additives such as ionic liquids, for example, can be added to otherwise low-absorbing reaction mixtures to increase the absorbance level of the medium (see Section 2.2.1).



C. Oliver Kappe received his doctoral degree from the Karl-Franzens-University in Graz (Austria), where he worked with Prof. G. Kollenz on cycloaddition and rearrangements of acylketenes. After postdoctoral research work with Prof. C. Wentrup at the University of Queensland (Australia) and Prof. A. Padwa at Emory University (US), he moved back to the University of Graz where he obtained his Habilitation (1998) and is currently associate Professor. In 2003 he spent a sabbatical period at the Scripps Research Institute in La Jolla (US) with Prof.

K. B. Sharpless. His research interests include microwave-enhanced synthesis, combinatorial chemistry, and multicomponent reactions.

Traditionally, organic synthesis is carried out by conductive heating with an external heat source (for example, an oil bath). This is a comparatively slow and inefficient method for transferring energy into the system, since it depends on the thermal conductivity of the various materials that must be penetrated, and results in the temperature of the reaction vessel being higher than that of the reaction mixture. In contrast, microwave irradiation produces efficient internal heating (in-core volumetric heating) by direct coupling of microwave energy with the molecules (solvents, reagents, catalysts) that are present in the reaction mixture. Since the reaction vessels employed are typically made out of (nearly) microwave-transparent materials, such as borosilicate glass, quartz, or teflon, an inverted temperature gradient results compared to conventional thermal heating (Figure 1). The very efficient internal heat transfer results in minimized wall effects (no hot vessel surface) which may lead to the observation of so-called specific microwave effects (see Section 1.2), for example, in the context of diminished catalyst deactivation.

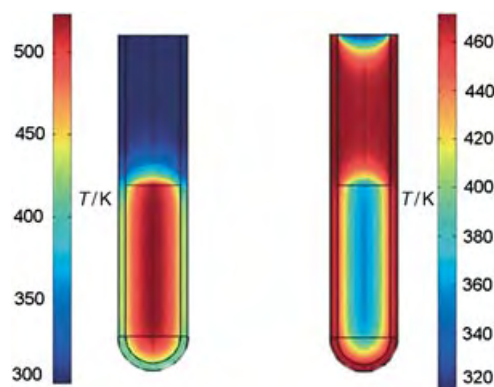


Figure 1. Inverted temperature gradients in microwave versus oil-bath heating: Difference in the temperature profiles (finite element modeling) after 1 min of microwave irradiation (left) and treatment in an oil-bath (right). Microwave irradiation raises the temperature of the whole volume simultaneously (bulk heating) whereas in the oil-heated tube, the reaction mixture in contact with the vessel wall is heated first.^[38]

1.2. Microwave Effects

Since the early days of microwave synthesis, the observed rate accelerations and sometimes altered product distributions compared to oil-bath experiments have led to speculation on the existence of so-called “specific” or “non-thermal” microwave effects.^[21–23] Historically, such effects were claimed when the outcome of a synthesis performed under microwave conditions was different from the conventionally heated counterpart carried out at the same apparent temperature. Today most scientists agree that in the majority of cases the reason for the observed rate enhancements is a purely thermal/kinetic effect, that is, a consequence of the high reaction temperatures that can rapidly be attained when irradiating polar materials in a microwave field. As shown in Figure 2, a high microwave absorbing solvent such as methanol ($\tan\delta = 0.659$) can be rapidly superheated to

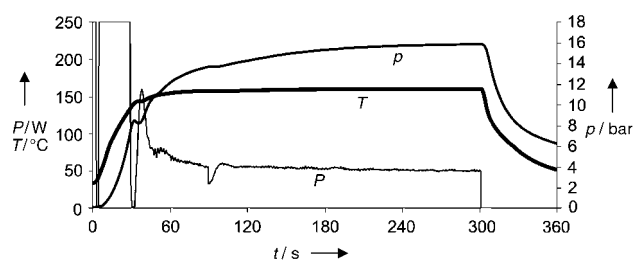


Figure 2. Temperature (T), pressure (p), and power (P) profile for a sample of methanol (3 mL) heated under sealed-vessel microwave irradiation conditions (single-mode heating, 250 W, 0–30 s), temperature control using the feedback from IR thermography (40–300 s), and active gas-jet cooling (300–360 s). The maximum pressure in the reaction vessel was ca. 16 bar. After the set temperature of 160 °C is reached, the power regulates itself down to ca. 50 W.

temperatures > 100 °C above its boiling point when irradiated under microwave conditions in a sealed vessel. The rapid increase in temperature can be even more pronounced for media with extreme loss factors, such as ionic liquids (see Section 2.2.1), where temperature jumps of 200 °C within a few seconds are not uncommon. Naturally, such temperature profiles are very difficult if not impossible to reproduce by standard thermal heating. Therefore, comparisons with conventionally heated processes are inherently troublesome.

Dramatic rate enhancements between reactions performed at room temperature or under standard oil-bath conditions (heating under reflux) and high-temperature microwave-heated processes have frequently been observed. As Baghurst and Mingos have pointed out on the basis of simply applying the Arrhenius law [$k = A \exp(-E_a/RT)$], a transformation that requires 68 days to reach 90 % conversion at 27 °C, will show the same degree of conversion within 1.61 seconds (!) when performed at 227 °C (Table 2).^[18] The very

Table 2: Relationship between temperature and time for a typical first-order reaction.^[a]

T [°C]	k [s ⁻¹]	t (90 % conversion)
27	1.55×10^{-7}	68 days
77	4.76×10^{-5}	13.4 h
127	3.49×10^{-3}	11.4 min
177	9.86×10^{-2}	23.4 s
227	1.43	1.61 s

[a] Data from ref. [18]; $A = 4 \times 10^{10} \text{ mol}^{-1} \text{ s}^{-1}$, $E_a = 100 \text{ kJ mol}^{-1}$.

rapid heating and extreme temperatures observable in microwave chemistry means that many of the reported rate enhancements can be rationalized by simple thermal/kinetic effects.

In addition to the above mentioned thermal/kinetic effects, microwave effects that are caused by the uniqueness of the microwave dielectric heating mechanisms (see Section 1.1) must also be considered. These effects should be termed “specific microwave effects” and shall be defined as accelerations that can not be achieved or duplicated by conventional heating, but essentially are still thermal effects. In this category fall, for example 1) the superheating effect of

solvents at atmospheric pressure,^[24] 2) the selective heating of, for example, strongly microwave absorbing heterogeneous catalysts or reagents in a less polar reaction medium,^[25–27] 3) the formation of “molecular radiators” by direct coupling of microwave energy to specific reagents in homogeneous solution (microscopic hotspots),^[26] and 4) the elimination of wall effects caused by inverted temperature gradients (Figure 1).^[28] It should be emphasized that rate enhancements falling under this category are essentially still a result of a thermal effect (that is, a change in temperature compared to heating by standard convection methods), although it may be difficult to experimentally determine the exact reaction temperature.

Some authors have suggested the possibility of “non-thermal microwave effects” (also referred to as athermal effects). These should be classified as accelerations that can not be rationalized by either purely thermal/kinetic or specific microwave effects. Nonthermal effects essentially result from a direct interaction of the electric field with specific molecules in the reaction medium. It has been argued that the presence of an electric field leads to orientation effects of dipolar molecules and hence changes the pre-exponential factor A or the activation energy (entropy term) in the Arrhenius equation.^[21,22] A similar effect should be observed for polar reaction mechanisms, where the polarity is increased going from the ground state to the transition state, thus resulting in an enhancement of reactivity by lowering the activation energy.^[22] Microwave effects are the subject of considerable current debate and controversy,^[21–23] and it is evident that extensive research efforts will be necessary to truly understand these and related phenomena.^[29] Since the issue of microwave effects is not the primary focus of this Review, the interested reader is referred to more detailed surveys and essays covering this topic.^[21–23]

1.3. Processing Techniques

Frequently used processing techniques employed in microwave-assisted organic synthesis involve solventless (“dry-media”) procedures where the reagents are preadsorbed onto either a more or less microwave transparent (silica, alumina, or clay)^[32] or strongly absorbing (graphite)^[33] inorganic support, which can additionally be doped with a catalyst or reagent. The solvent-free approach was very popular particularly in the early days of MAOS since it allowed the safe use of domestic household microwave ovens and standard open-vessel technology. Although a large number of interesting transformations with “dry-media” reactions have been published in the literature,^[32] technical difficulties relating to non-uniform heating, mixing, and the precise determination of the reaction temperature remain unsolved, in particular when scale-up issues need to be addressed. In addition, phase-transfer catalysis (PTC) has also been widely employed as a processing technique in MAOS.^[34]

Alternatively, microwave-assisted synthesis can be carried out in standard organic solvents either under open- or sealed-vessel conditions. If solvents are heated by microwave

irradiation at atmospheric pressure in an open vessel, the boiling point of the solvent (as in an oil-bath experiment) typically limits the reaction temperature that can be achieved. In the absence of any specific or nonthermal microwave effects (such as the superheating effect at atmospheric pressure which has been reported to be up to 40 °C)^[24] the expected rate enhancements would be comparatively small. To nonetheless achieve high reaction rates, high-boiling microwave-absorbing solvents such as DMSO, *N*-methyl-2-pyrrolidone (NMP), 1,2-dichlorobenzene (DCB), or ethylene glycol (see Table 1) have been frequently used in open-vessel microwave synthesis.^[6] However, the use of these solvents presents serious challenges during product isolation. The recent availability of modern microwave reactors with on-line monitoring of both temperature and pressure has meant that MAOS in sealed vessels—a technique pioneered by Strauss in the mid 1990s^[35]—has been celebrating a comeback in recent years. This is clearly evident from surveying the recently published literature in the area of MAOS (see Section 2), and it appears that the combination of rapid dielectric heating by microwaves with sealed-vessel technology (autoclaves) will most likely be the method of choice for performing MAOS in the future.

1.4. Equipment

Although many of the early pioneering experiments in microwave-assisted organic synthesis were carried out in domestic microwave ovens, the current trend is undoubtedly to use dedicated instruments for chemical synthesis. In a domestic microwave oven the irradiation power is generally controlled by on/off cycles of the magnetron (pulsed irradiation), and it is typically not possible to monitor the reaction temperature in a reliable way. This disadvantage, combined with the inhomogeneous field produced by the low-cost magnetrons and the lack of safety controls, means that the use of such equipment can not be recommended. In contrast, all of today's commercially available dedicated microwave reactors for synthesis^[36–38] feature built-in magnetic stirrers, direct temperature control of the reaction mixture with the aid of fiber-optic probes or IR sensors, and software that enables on-line temperature/pressure control by regulation of microwave power output (Figure 2).

Two different philosophies with respect to microwave reactor design are currently emerging: multimode and monomode (also referred to as single-mode) reactors.^[17] In the so-called multimode instruments (conceptually similar to a domestic oven), the microwaves that enter the cavity are reflected by the walls and the load over the typically large cavity. In most instruments a mode stirrer ensures that the field distribution is as homogeneous as possible. In the much smaller monomode cavities, the electromagnetic irradiation is directed through an accurately designed rectangular or circular wave guide onto the reaction vessel mounted at a fixed distance from the radiation source, thus creating a standing wave. The key difference between the two types of reactor systems is that whereas in multimode cavities several reaction vessels can be irradiated simultaneously in multi-

vessel rotors (parallel synthesis), in monomode systems only one vessel can be irradiated at the time. In the latter case high throughput can be achieved by integrated robotics that move individual reaction vessels in and out of the microwave cavity. Most instrument companies offer a variety of diverse reactor platforms with different degrees of sophistication with respect to automation, database capabilities, safety features, temperature and pressure monitoring, and vessel design. Importantly, single-mode reactors processing comparatively small volumes also have a built-in cooling feature that allows for rapid cooling of the reaction mixture with compressed air after completion of the irradiation period (see Figure 2). The dedicated single-mode instruments available today can process volumes ranging from 0.2 to about 50 mL under sealed-vessel conditions (250 °C, ca. 20 bar), and somewhat higher volumes (ca. 150 mL) under open-vessel reflux conditions. In the much larger multimode instruments several liters can be processed under both open- and closed-vessel conditions. Continuous-flow reactors are nowadays available for both single- and multimode cavities that allow the preparation of kilograms of materials by using microwave technology (see Section 2.10).^[36–38]

2. Literature Survey

2.1. Scope and Organization of the Review

This Review highlights recent applications of controlled microwave heating technology in organic synthesis. The term “controlled” here refers to the use of a dedicated microwave reactor for synthetic chemistry purposes (single- or multimode). Therefore, the exact reaction temperature during the irradiation process has been adequately determined in the original literature source. Although the aim of this Review is not primarily to speculate about the existence or non-existence of microwave effects (see Section 1.2), the results of adequate control experiments or comparison studies with conventionally heated transformations will sometimes be presented. The reader should not draw any definitive conclusions about the involvement or non-involvement of “microwave effects” from those experimental results, because of the inherent difficulties in conducting such experiments (see above). In terms of processing techniques (Section 1.3), preference is given to transformations in solution under sealed-vessel conditions, since this reflects the recent trend in the literature, and these transformations are in principle scalable in either batch or continuous-flow modes. Sealed-vessel microwave technology was employed unless otherwise specifically noted. Most of the examples have been taken between 2002 and 2003. Earlier examples of controlled MAOS are limited and can be found in previous review articles and books.^[4–16]

2.2. Transition-Metal-Catalyzed C–C Bond Formations

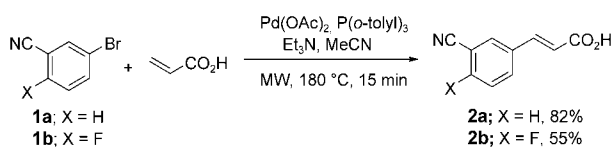
Homogeneous transition-metal-catalyzed reactions represent one of the most important and best studied reaction

types in MAOS. Transition-metal-catalyzed carbon–carbon and carbon–heteroatom bond-forming reactions typically need hours or days to reach completion with traditional heating under reflux conditions and often require an inert atmosphere. The research groups of Hallberg, Larhed, and others have demonstrated over the past few years that the rate of many of those transformations can be enhanced significantly by employing microwave heating under sealed-vessel conditions (“microwave flash heating”), in most cases without an inert atmosphere.^[10] The use of metal catalysts in conjunction with microwaves may have significant advantages over traditional heating methods, since the inverted temperature gradients under microwave conditions (Figure 1) may lead to an increased lifetime of the catalyst through elimination of wall effects.^[28,39]

2.2.1. Heck Reactions

The Heck reaction, a palladium-catalyzed vinylic substitution, is typically conducted with alkenes and organohalides or pseudohalides as reactants. Numerous elegant synthetic transformations based on C–C bond-forming Heck reactions have been developed both in classical organic synthesis and natural product chemistry.^[40] Solution-phase Heck reactions were carried out successfully by MAOS as early as 1996, thereby reducing reaction times from several hours under conventional reflux conditions to sometimes less than five minutes.^[41] These early examples of microwave-assisted Heck reactions have been extensively reviewed by Larhed and will not be discussed herein.^[10]

Scheme 1 shows a recent example of a standard Heck reaction involving aryl bromides **1** and acrylic acid to furnish

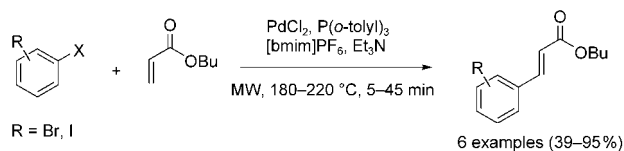


Scheme 1. Examples of Heck Reactions carried out on a 2 and 80 mmol scale.

the corresponding cinnamic acids **2**.^[42] Optimization of the reaction conditions under small-scale (2 mmol) single-mode microwave conditions led to a protocol that employed MeCN as the solvent, 1 mol% $\text{Pd}(\text{OAc})_2/\text{P}(\text{o-tolyl})_3$ as the catalyst system, and triethylamine as the base. The reaction time was 15 minutes at a reaction temperature of 180°C . Interestingly, the authors have discovered that the rather expensive homogeneous catalyst system can be replaced by 5% Pd/C (<0.1 mol% concentration of Pd catalyst) without the need to change any of the other reaction parameters.^[42] The yields for cinnamic acid derivative **2a** were very similar when either homogeneous or heterogeneous Pd catalysts were used in the Heck reaction. In the same article^[42] the authors also demonstrate that it is possible to directly scale-up the 2-mmol Heck reaction to 80 mmol (ca. 120 mL total reaction volume) by switching from a single-mode to a larger multi-mode microwave cavity (see also Section 2.10). Importantly,

the optimized small-scale reaction conditions could be directly used for the larger scale reaction, thus giving rise to very similar product yields.

In 2002 Larhed and co-workers reported microwave-promoted Heck arylations in the ionic liquid 1-butyl-3-methylimidazolium hexafluorophosphate ($[\text{bmim}]\text{PF}_6$; Scheme 2).^[43] Among the variety of possible “green” solvent

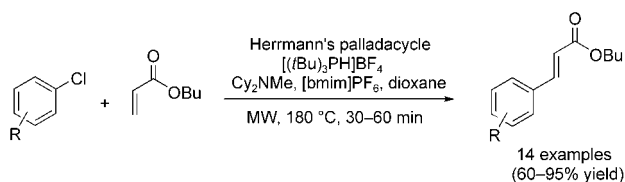


Scheme 2. Heck reactions in ionic liquids.

alternatives for catalytic and other reactions, nonvolatile room-temperature ionic liquids have attracted a considerable amount of attention in recent years.^[44] Ionic liquids interact very efficiently with microwaves through the ionic conduction mechanism (see Section 1.1) and are rapidly heated at rates easily exceeding 10°C s^{-1} without any significant pressure build-up. Therefore, safety problems arising from over-pressurization of heated sealed reaction vessels can be minimized.^[45,46] In the Heck reactions shown in Scheme 2, 4 mol% of $\text{PdCl}_2/\text{P}(\text{o-tolyl})_3$ was used. Full conversions were achieved within 5 (X = I) and 20 minutes (X = Br). Transformations that were performed without the phosphane ligand required 45 minutes. A key feature of this catalyst/ionic liquid system is the recyclability: the phosphane-free system $\text{PdCl}_2/[\text{bmim}]\text{PF}_6$ was recyclable at least five times. After each cycle, the volatile product was directly isolated in high yield by rapid distillation under reduced pressure.^[43]

The concept of performing microwave synthesis in room-temperature ionic liquids has been applied to 1,3-dipolar cycloaddition reactions,^[47] catalytic transfer hydrogenations,^[48] ring-closing metathesis,^[49] and the conversion of alcohols into alkyl halides.^[50] As an alternative to the use of the rather expensive ionic liquids as solvents, several research groups have used ionic liquids as “doping agents” for microwave heating of otherwise nonpolar solvents such as hexane, toluene, THF, or dioxane. This technique, first introduced by Ley et al. in 2001 (see Section 2.9.4),^[51] is becoming increasingly popular, as demonstrated by the many recently published examples.^[52–60] Systematic studies on temperature profiles and the thermal stability of ionic liquids under microwave irradiation conditions by Leadbeater and Torenus^[52,53] have shown that addition of a small amount of an ionic liquid (0.1 mmol mL^{-1} solvent) suffices to obtain dramatic changes in the heating profiles by changing the overall dielectric properties (namely, $\tan\delta$) of the reaction medium.

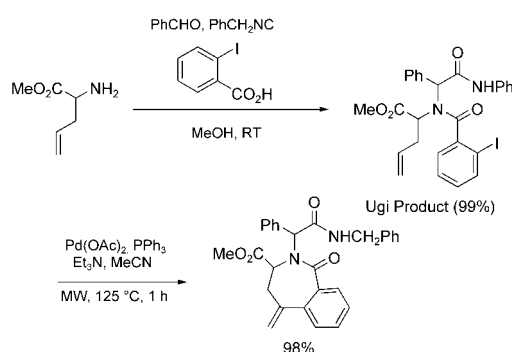
Larhed and co-workers have exploited the combination of $[\text{bmim}]\text{PF}_6$ and dioxane in the Heck coupling of both electron-rich and electron-poor aryl chlorides with butyl acrylate (Scheme 3).^[56] Transition-metal-catalyzed carbon–carbon bond-forming reactions involving unreactive aryl chlorides have represented a synthetic challenge for a long time. Only recently, as a result of advances in the develop-



Scheme 3. Heck reactions of aryl chlorides with air-stable phosphonium salts as ligand precursors. Electron-rich and electron-poor aryl chlorides are equally suitable substrates.

ment of highly active catalyst/ligand systems, have those transformations been accessible.^[61] For the Heck coupling shown in Scheme 3, the air-stable but highly reactive $[(t\text{Bu})_3\text{PH}]\text{BF}_4$ phosphonium salt described by Netherton and Fu^[62] was employed as a ligand precursor using the palladacycle *trans*-di(μ -acetato)bis[*o*-di-*o*-tolylphosphanyl]-benzyl]dipalladium(II)^[63] developed by Herrmann et al. as the palladium precatalyst. Depending on the reactivity of the aryl chloride, 1.5–10 mol % of Pd catalyst (3–20 % of ligand), 1.5 equivalents of Cy_2NMe as a base, and 1.0 equivalent of $[\text{bmim}]\text{PF}_6$ in dioxane were irradiated at 180 °C under sealed-vessel conditions (no inert gas atmosphere) with the aryl chloride and butyl acrylate for 30–60 min. The desired cinnamic esters were obtained in moderate to excellent yields under these optimized conditions (Scheme 3).^[56]

A synthetically useful application of an intramolecular microwave-assisted Heck reaction was described by Gracias et al. (Scheme 4).^[64] In their approach toward the synthesis of



Scheme 4. Sequential Ugi reactions and Heck cyclizations for the synthesis of seven-membered N-heterocycles.

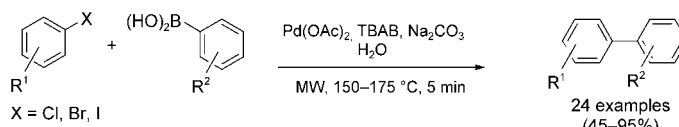
seven-membered N-heterocycles, the initial product of an Ugi four-component reaction was subjected to an intramolecular Heck cyclization using 5 mol % $\text{Pd}(\text{OAc})_2/\text{PPh}_3$ as the catalytic system. Microwave irradiation at 125 °C in acetonitrile for 1 h provided 98 % yield of the product shown in Scheme 4. A number of related sequential Ugi reaction/Heck cyclizations were reported in the original publication, also involving aryl bromides instead of iodides.

A very recent addition to the already powerful spectrum of microwave Heck chemistry is the development of a general procedure for carrying out oxidative Heck couplings, that is, the Pd^{II} -catalyzed carbon–carbon coupling of aryl boronic acids with alkenes using $\text{Cu}(\text{OAc})_2$ as a reoxidant (100–170 °C, 5–30 min).^[65]

2.2.2. Suzuki Reactions

The Suzuki reaction (the palladium-catalyzed cross-coupling of aryl halides with boronic acids) is arguably one of the most versatile and at the same time also one of the most often used cross-coupling reactions in modern organic synthesis.^[66,67] Carrying out high-speed Suzuki reactions under controlled microwave conditions can be considered almost a routine synthetic procedure today, given the enormous literature precedent for this transformation.^[10] Recent examples include the use of the Suzuki protocol for the high-speed modification of various heterocyclic scaffolds of pharmacological or biological interest.^[68–74]

A significant advance in Suzuki chemistry has been the observation that Suzuki couplings can be readily carried out using water as the solvent in conjunction with microwave heating.^[75–79] Water, being cheap, readily available, nontoxic, and nonflammable, has clear advantages as a solvent for use in organic synthesis. With its comparatively high loss factor ($\tan\delta$) of 0.123 (see Table 1), water is also a potentially very useful solvent for microwave-mediated synthesis, especially in the high-temperature region accessible by using sealed vessel technology. Leadbeater and Marco have recently described very rapid, ligand-free palladium-catalyzed aqueous Suzuki couplings of aryl halides with aryl boronic acids (Scheme 5).^[75] Key to the success of this method was the



Scheme 5. Ligand-free Suzuki reactions with TBAB as an additive.

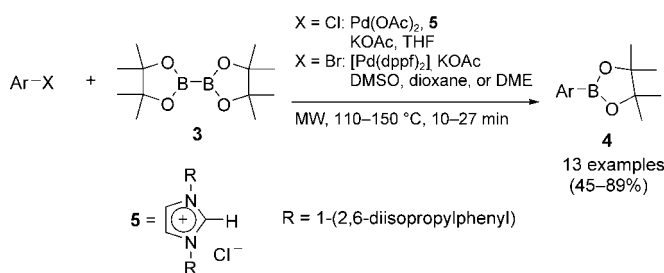
use of 1.0 equivalents of tetrabutylammonium bromide (TBAB) as a phase-transfer catalyst. The role of the ammonium salt is to facilitate the solubility of the organic substrates and to activate the boronic acid by formation of $[\text{R}_4\text{N}]^+[\text{ArB}(\text{OH})_3]^-$. A wide variety of aryl bromides and iodides were successfully coupled with aryl boronic acids by using controlled microwave heating at 150 °C for 5 minutes with only 0.4 mol % of $\text{Pd}(\text{OAc})_2$ as catalyst (Scheme 5).^[75] Aryl chlorides also reacted but required higher temperatures (175 °C).

The same Suzuki couplings could also be performed under microwave-heated open-vessel reflux conditions (110 °C, 10 min) on a tenfold scale and gave nearly identical yields to the closed-vessel reactions.^[76,77] Importantly, nearly the same yields were also obtained when the Suzuki reactions were carried out in a preheated oil bath (150 °C) instead of using microwave heating, clearly indicating the absence of any specific or nonthermal microwave effects (see Section 1.2).^[76]

The same authors have reported another modification in which, surprisingly, it was also possible to carry out the Suzuki reactions depicted in Scheme 5 in the absence of the palladium catalyst!^[78,79] These transition-metal-free aqueous Suzuki-type couplings again utilized 1.0 equivalent of TBAB

as an additive, 3.8 equivalents of Na_2CO_3 as a base, and 1.3 equivalents of the corresponding boronic acid (150 °C, 5 min). High yields were obtained with aryl bromides and iodides whereas aryl chlorides proved unreactive under the conditions used. The reaction is also limited to electron-poor or electron-neutral boronic acids. While the exact mechanism of this unusual transformation remains unknown, one possibility would be a radical pathway where the reaction medium, water, provides an enhanced π -stacking interaction as a result of the hydrophobic effect.^[67]

The large number of boronic acids that are commercially available makes the Suzuki reaction and related types of coupling chemistry highly attractive in the context of high-throughput synthesis and derivatization. In addition, boronic acids are air and moisture stable, of relatively low toxicity, and the boron-derived by-products can easily be removed from the reaction mixture. Therefore, it is not surprising that efficient and rapid microwave-assisted protocols have been developed for their preparation. In 2002 Fürstner and Seidel outlined the synthesis of pinacol aryl boronates from aryl chlorides bearing electron-withdrawing groups and commercially available bis(pinacol)borane (**3**), using a palladium catalyst formed in situ from $\text{Pd}(\text{OAc})_2$ and imidazolium chloride **5** (Scheme 6, $\text{X} = \text{Cl}$).^[80] The very reactive N-



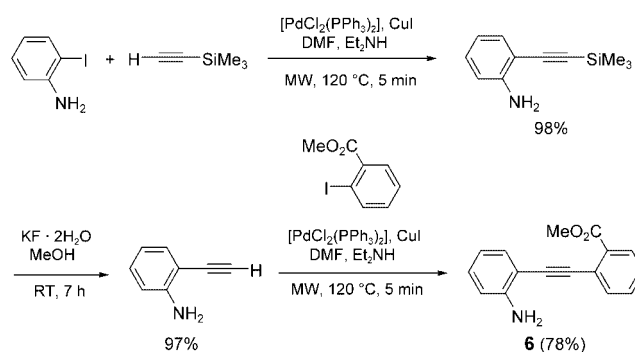
Scheme 6. Palladium-catalyzed formation of aryl boronates from electron-rich and electron-poor (hetero)aryl halides.

heterocyclic carbene (NHC) ligand (6–12 mol%) allowed this transformation to proceed to completion within 10–20 minutes at 110 °C in THF by using microwave irradiation in sealed vessels. The conventionally heated process (reflux THF (ca. 65 °C), argon atmosphere) gave comparable yields, but required 4–6 h to reach completion. Dehaen and co-workers subsequently disclosed a complementary approach in which electron-rich aryl bromides were used as substrates (Scheme 6, $\text{X} = \text{Br}$) and 3 mol% $[\text{Pd}(\text{dppf})\text{Cl}_2]$ ($\text{dppf} = 1,1'$ -bis(diphenylphosphanyl)ferrocene) was used as the catalyst.^[81] A somewhat higher reaction temperature (125–150 °C) was employed to produce a variety of different aryl boronates in good to excellent yields.^[81] High-speed microwave-assisted trifluoromethanesulfonation (triflation) reactions of phenols with *N*-phenyltrifluorosulfonimide (120 °C, 6 min) have also been reported in the literature.^[82]

2.2.3. Sonogashira Reactions

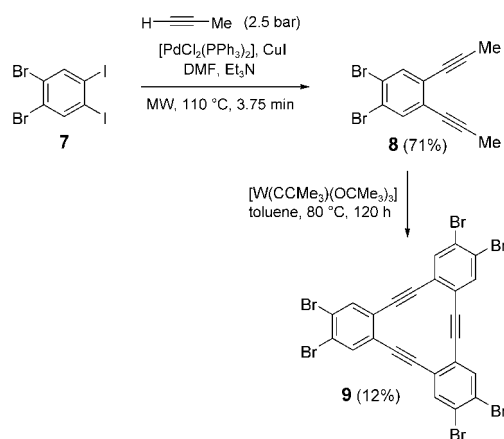
The Sonogashira reaction (palladium/copper-catalyzed coupling of terminal acetylenes with aryl and vinyl halides)

enjoys considerable popularity as a reliable and general method for the preparation of unsymmetrical alkynes.^[83] General protocols for microwave-assisted Sonogashira reactions under controlled conditions were first reported in 2001 by Erdélyi and Gogoll.^[84] Typical reaction conditions for the coupling of aryl iodides, bromides, chlorides, and triflates involve DMF as the solvent, diethylamine as the base, and $[\text{PdCl}_2(\text{PPh}_3)_2]$ (2–5 mol%) as the catalyst with CuI (5 mol%) as an additive.^[84] Gogoll and co-workers later utilized these protocols in a rapid domino Sonogashira sequence to synthesize amino ester **6** (Scheme 7).^[85]



Scheme 7. Domino Sonogashira sequence for the synthesis of bis(aryl)acetylenes.

Essentially the same experimental protocol was employed by Vollhardt and co-workers to synthesize *o*-dipropynylated arene **8**, which served as the precursor to tribenzocyclone **9** through an alkyne metathesis reaction (Scheme 8).^[86] In this



Scheme 8. Double Sonogashira reactions under propyne pressure.

case the Sonogashira reaction was carried out in a prepressurized (ca. 2.5 atm of propyne) sealed microwave vessel. Double Sonogashira coupling of the dibromodiiodobenzene **7** was completed within 3.75 minutes at 110 °C. It is worth mentioning that the authors have not carried out the corresponding tungsten-mediated alkyne metathesis chemistry under microwave conditions to shorten the exceedingly long reaction times and perhaps to improve the low yield (see

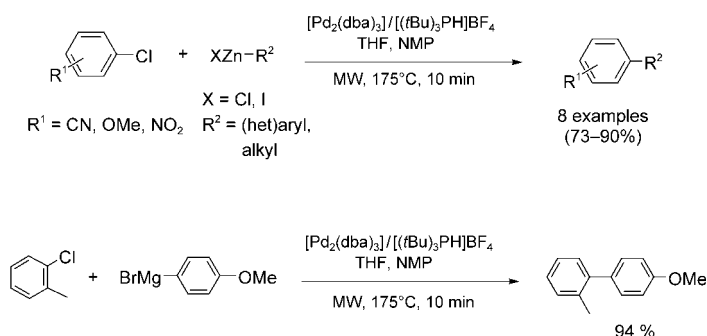
Scheme 16 for a microwave-assisted alkyne metathesis reaction). Additional examples of microwave-assisted Sonogashira couplings in the derivatization of pyrazinones^[70] and pyrimidine^[87] scaffolds have been reported.

As with the Suzuki reaction, there have been two recent independent reports by the groups of Leadbeater and Van der Eycken^[88] that have shown that it is also possible to perform transition-metal-free Sonogashira couplings. Again, these methods rely on the use of microwave-heated water as the solvent, a phase-transfer catalyst (TBAB or polyethylene glycol), and a base (NaOH or Na₂CO₃). So far these metal-free procedures have been successful for aryl bromides and iodides, and typical reaction conditions involve heating to about 170 °C for 5–25 minutes. A recent report by He and Wu describes a copper-catalyzed (palladium-free) Sonogashira-type cross-coupling reaction.^[89]

2.2.4. Stille, Negishi, and Kumada Reactions

Microwave-assisted Stille reactions involving organotin reagents as coupling partners were reviewed in 2002.^[10] Until recently, very little work was published on Negishi (organozinc reagents) and Kumada (organomagnesium reagents) cross-coupling reactions under microwave conditions. There are two examples in the peer-reviewed literature describing Negishi cross-coupling reactions of activated aryl bromides^[90] and heteroaryl chlorides^[91] with organozinc halides.

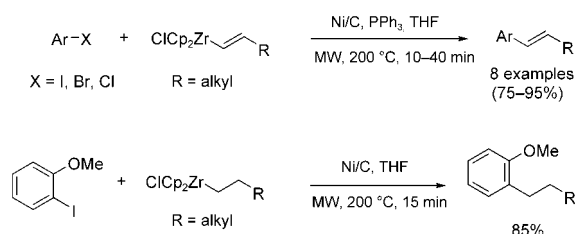
A general procedure describing high-speed microwave-assisted Negishi and Kumada couplings of unactivated aryl chlorides was recently reported (Scheme 9).^[92] This procedure



Scheme 9. Negishi and Kumada cross-coupling reactions.

uses 0.015–2.5 mol % of [Pd₂(dba)₃] as a palladium source and the air-stable [(tBu)₃PH]BF₄ phosphonium salt (see Scheme 3) as ligand precursor. Successful couplings were observed for both aryl organozinc chlorides and iodides. By using this methodology it was also possible to successfully couple aryl chlorides with alkyl zinc reagents such as *n*-butylzinc chloride very rapidly without the need for an inert atmosphere. The optimized conditions involved the use of sealed-vessel microwave irradiation at 175 °C for 10 minutes. Grignard reactions were also carried out successfully by applying the same reaction conditions (Scheme 9). In the same article the authors also describe microwave-assisted methods for the preparation of the corresponding organozinc and magnesium compounds.^[92]

In addition to the classical Negishi cross-coupling in which organozinc reagents are utilized, the “zirconium version” involving the coupling of zirconocenes with aryl halides has also been described by using sealed-vessel microwave technology. Lipshutz and Frieman have reported the rapid coupling of both vinyl and alkyl zirconocenes (prepared in situ by hydrosilylation of alkynes or alkenes, respectively), with aryl iodides, bromides, and chlorides (Scheme 10).^[93] While aryl iodides required only 5 mol %



Scheme 10. Nickel-catalyzed cross-coupling of alkenyl and alkyl zirconocenes with aryl halides.

Ni/C as a ligand-free heterogeneous catalytic system, the presence of triphenylphosphane as a ligand was necessary to successfully couple aryl bromides (10 mol %) and chlorides (20 mol % ligand). Full conversion was achieved under those conditions within 10–40 min at 200 °C using THF as the solvent.

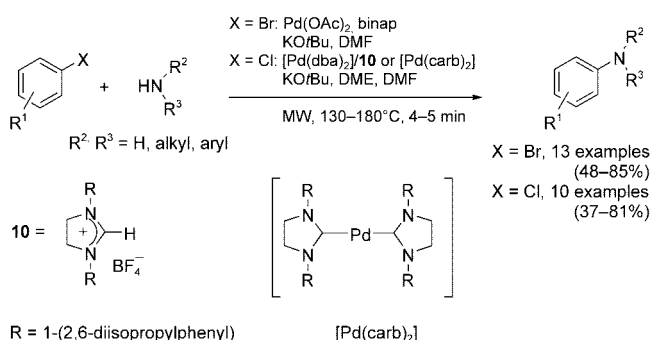
2.3. Transition-Metal-Catalyzed Carbon–Heteroatom Bond Formation

2.3.1. Buchwald–Hartwig Reactions

The research groups of Buchwald^[94] and Hartwig^[95] have developed a large variety of useful palladium-mediated methods for C–O and C–N bond formation. These arylations have been enormously popular in recent years. A vast amount of published material is available describing a wide range of palladium-catalyzed methods, ligands, solvents, temperatures, and substrates which has led to a broad spectrum of tunable reaction conditions that allows access to most target molecules that incorporate an aryl amine motif.

In 2002 Alterman and co-workers described the first high-speed Buchwald–Hartwig aminations by controlled microwave heating (Scheme 11).^[96] The best results were obtained in DMF as the solvent without an inert atmosphere by employing 5 mol % of Pd(OAc)₂ as precatalyst and 2,2'-bis(diphenylphosphanyl)-1,1'-binaphthyl (binap) as the ligand. The procedure proved to be quite general and provided moderate to high yields for both electron-rich and electron-poor aryl bromides. Caddick and co-workers were also able to extend this rapid amination protocol to electron-rich aryl chlorides by utilizing more reactive discrete Pd–N-heterocyclic carbene (NHC) complexes or in situ generated palladium/imidazolium salt complexes (1 mol %, Scheme 11).^[97]

Independent investigations by Maes and co-workers have described the use of 2-(dicyclohexylphosphanyl)biphenyl as a



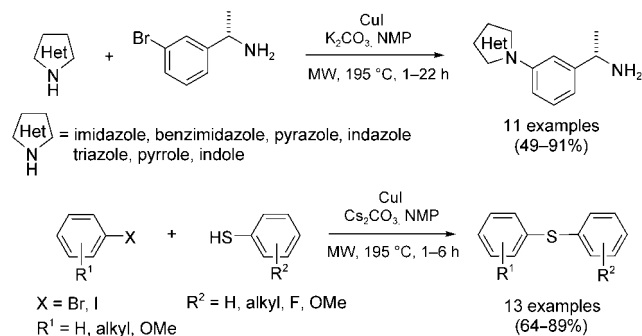
Scheme 11. Buchwald–Hartwig amination reactions.

ligand for the successful and rapid Buchwald–Hartwig coupling of (hetero)aryl chlorides with amines under microwave conditions (0.5–2 mol % Pd catalyst).^[98] Microwave-assisted palladium-catalyzed aminations have been reported on a number of different substrates, including bromoquinolines,^[99] aryl triflates,^[100] intramolecular aminations for the synthesis of benzimidazoles,^[101] and the coupling of aryl chlorides with sulfonamides.^[102]

Direct palladium- or nickel-catalyzed carbon–phosphorous couplings of aryl iodides, bromides, and triflates with diphenylphosphane in the presence of a base such as KOAc or diazobicyclo[2.2.2]octane (DABCO) are also reported to result in the rapid formation of triarylphosphanes.^[103]

2.3.2. Ullmann Condensation Reactions

A recent survey of the literature on the Ullmann and related condensation reactions has highlighted the growing importance and popularity of copper-mediated C–N, C–O, and C–S bond-forming protocols.^[104] Scheme 12 shows two



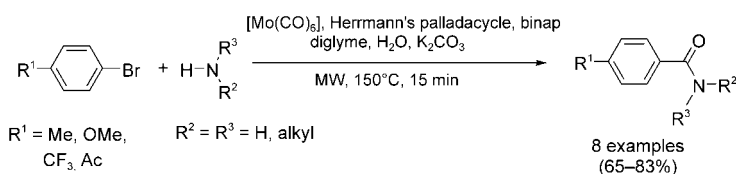
Scheme 12. Ullmann-type carbon–nitrogen and carbon–sulfur bond formations.

examples of microwave-assisted Ullmann-type condensations from researchers at Bristol–Myers Squibb. In the first example, (*S*)-1-(3-bromophenyl)ethylamine was coupled with eleven heteroarenes containing N–H groups in the presence of 10 mol % CuI and 2.0 equivalents of K₂CO₃ base.^[105,106] The comparatively high reaction temperature (195°C) and the long reaction times are noteworthy. For the coupling of 3,5-dimethylpyrazole, for example, microwave heating for 22 h was required to afford a 49 % yield of the

isolated product! The average reaction times were 2–3 h. In the second example, similar conditions were chosen to react mainly aromatic thiols with aryl bromides and iodides to afford aryl sulfides.^[107] The same authors have also described the synthesis of diaryl ethers by copper-catalyzed arylation of phenols with aryl halides.^[108]

2.4. Transition-Metal-Catalyzed Carbonylation Reactions

Larhed and co-workers took advantage of the rapid and controlled heating made possible by microwave irradiation of solvents under sealed-vessel conditions and reported a number of valuable palladium-catalyzed carbonylation reactions (Scheme 13).^[109–113] The key feature of all those proto-

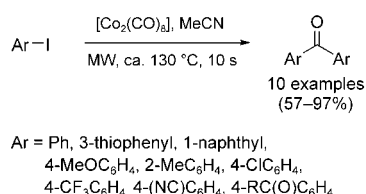


Scheme 13. Palladium-catalyzed aminocarbonylations. Diglyme = diethyleneglycol dimethylether.

cols is the use of molybdenum hexacarbonyl as a solid precursor of carbon monoxide, which is required in carbonylation chemistry. [Mo(CO)₆] liberates enough CO in situ at 150°C, for example, that rapid aminocarbonylation reactions take place (at 210°C, CO is liberated instantaneously). The initially reported conditions used a combination of the palladacycle developed by Herrmann and co-workers (7.4 mol % Pd) and binap as the catalytic system in a diglyme/water mixture and provided the desired secondary and tertiary amides in high yield (Scheme 13).^[109] As in many other cases, an inert atmosphere was not required.

Subsequent improvements in the experimental protocol allowed the use of sterically and electronically more-demanding amines (for example, anilines, unprotected amino acids), whereby DBU was used as the base and THF as the solvent for both aryl bromides and iodides.^[110] Simple modifications of the general strategy outlined in Scheme 13 enabled the corresponding carboxylic acids^[109] and esters^[111] to be obtained instead of the amides. Further modifications by Alterman and co-workers have resulted in the use of DMF as a source of CO^[112] and the use of formamide as a combined source of NH₃ and CO.^[113] The latter method is useful for the preparation of primary aromatic amides from aryl bromides. In both cases, strong bases and temperatures around 180°C (7–20 min) have to be used to mediate the reaction.

A somewhat related process is the cobalt-mediated synthesis of symmetrical benzophenones from aryl iodides and [Co₂(CO)₈] (Scheme 14).^[114] Here, [Co₂(CO)₈] is used as a combined activator of the aryl iodide and as CO source. A variety of aryl iodides with different steric and electronic properties underwent the carbonylative coupling in excellent yields when acetonitrile was employed as the solvent. Remarkably, six seconds of microwave irradiation were in



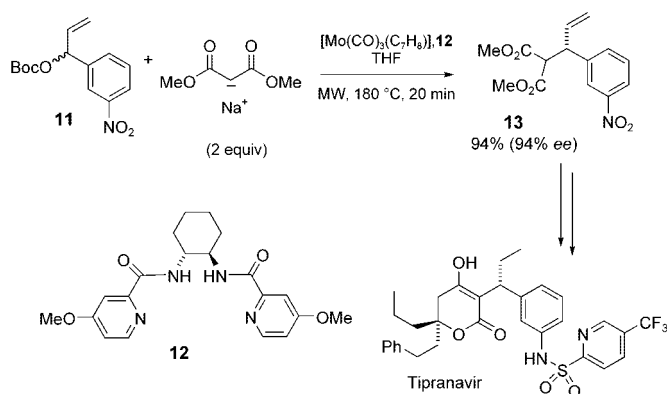
Scheme 14. [Co₂(CO)₈]-mediated synthesis of symmetric diaryl ketones.

several cases sufficient to achieve full conversion! The use of an inert atmosphere, bases, or other additives were unnecessary. No conversion occurred in the absence of heating, regardless of the reaction time. However, equally high yields could also be achieved by heating the reaction mixture in an oil bath for two minutes.

2.5. Asymmetric Allylic Alkylations

A frequent criticism of microwave synthesis has been that the typically high reaction temperatures will invariably lead to reduced selectivities. This is perhaps the reason why comparatively few enantioselective processes driven by microwave heating have been reported in the literature. For a reaction to occur with high enantioselectivity there must be a large enough difference in the activation energy for the processes leading to the two enantiomers. The higher the reaction temperature, the larger the difference in energy required to achieve high selectivity. Despite these limitations, a number of very impressive enantioselective reactions involving chiral transition-metal complexes have been described. The research groups of Moberg, Hallberg, and Larhed reported on microwave-mediated palladium-^[115,116] and molybdenum-catalyzed^[117–119] asymmetric allylic alkylation reactions involving neutral carbon, nitrogen, and oxygen nucleophiles in 2000. Both processes were carried out under non-inert conditions and yielded the desired products in high chemical yield and with typical *ee* values of > 98 %.

More recently, Trost and Andersen have applied this concept in their approach to the orally bioavailable HIV inhibitor tipranavir (Scheme 15).^[120] Synthesis of the key



Scheme 15. Molybdenum-catalyzed asymmetric allylic alkylation in the total synthesis of the HIV inhibitor tipranavir. Boc = *tert*-butoxycarbonyl.

chiral intermediate **13** was achieved by asymmetric allylic alkylation starting from carbonate **11**. A 94 % yield of the product was achieved by employing 10 mol % of the molybdenum precatalyst and 15 mol % of the chiral ligand **12** with 2.0 equivalents of sodium dimethylmalonate as the additive. The reaction was carried out under sealed-vessel microwave heating at 180 °C for 20 minutes. Thermal heating under reflux conditions (67 °C) required 24 h and produced the same chemical yield of intermediate **13**, albeit in slightly higher enantiomeric purity (96 % *ee*).

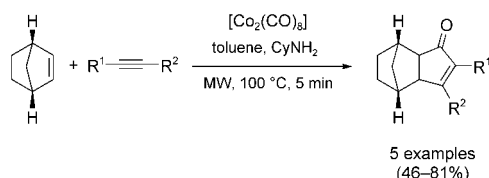
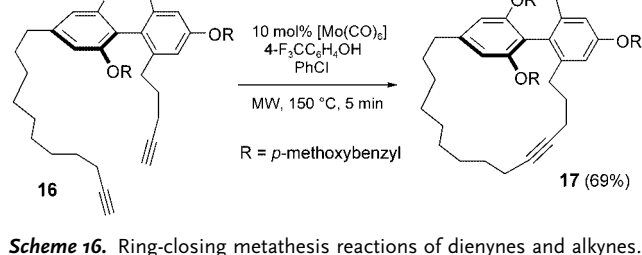
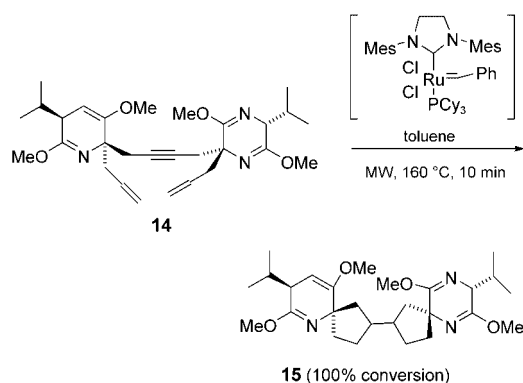
A similar pathway involving a microwave-driven molybdenum-catalyzed asymmetric allylic alkylation (160 °C, 6 min, THF) as the key step was elaborated by Moberg and co-workers for the preparation of the muscle relaxant (*R*)-baclofen.^[121] Other enantioselective reactions performed by microwave heating include asymmetric Heck reactions^[122] and ruthenium-catalyzed asymmetric hydrogen transfer processes.^[123]

2.6. Other Transition-Metal-Mediated Processes

In recent years the olefin metathesis reaction has attracted widespread attention as a versatile carbon–carbon bond-forming method.^[124] Among the numerous different metathesis methods, ring-closing metathesis (RCM) has emerged as a very powerful method for the construction of small, medium, and macrocyclic ring systems.^[124] In general, metathesis reactions are carried out at room or at slightly elevated temperatures (for example, at 40 °C in refluxing CH₂Cl₂), sometimes requiring several hours of reaction time to achieve full conversion. With microwaves, otherwise sluggish RCM protocols have been reported to be completed within minutes or even seconds.^[49,55,71,125–128] In 2003, for example, Efskind and Undheim reported the domino RCM of dienyne **14** with a Grubbs type II catalyst (Scheme 16).^[127] While the thermal process (toluene, 85 °C) required multiple addition of fresh catalyst (3 × 10 mol %) over a period of 9 h to furnish a 92 % yield of product **15**, microwave irradiation for 10 min at 160 °C (5 mol % catalyst, toluene) led to full conversion. The authors ascribe the dramatic rate enhancement to the rapid and uniform heating of the reaction mixture and increased catalyst lifetime by the elimination of wall effects.^[127]

An interesting ring-closing alkyne metathesis reaction (RCAM) was recently reported by Fürstner et al. (Scheme 16).^[128] Treatment of diyne **16** with 10 mol % of the catalyst prepared in situ from [Mo(CO)₆] and 4-trifluoromethylphenol at 150 °C for 5 minutes led to a 69 % yield of cycloalkyne **17**, which was further manipulated into a naturally occurring DNA cleaving agent of the turriane family. Conventional heating under reflux conditions in chlorobenzene for 4 h produced a 83 % yield of product under otherwise identical conditions.

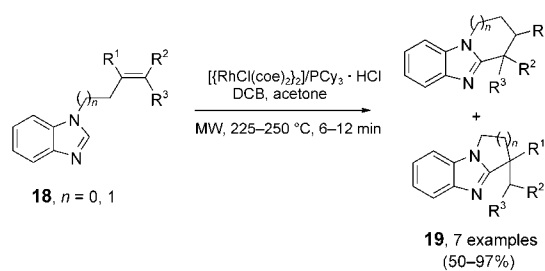
The [2+2+1] cycloaddition of an alkene, an alkyne, and carbon monoxide is often the method of choice for the preparation of complex cyclopentenones.^[129] Groth and co-workers have demonstrated that such Pauson–Khand reactions can be carried out very efficiently with microwave heating (Scheme 17);^[130] 20 mol % of [Co₂(CO)₈] was suffi-



Scheme 17. Pauson–Khand [2 + 2 + 1] cycloadditions.

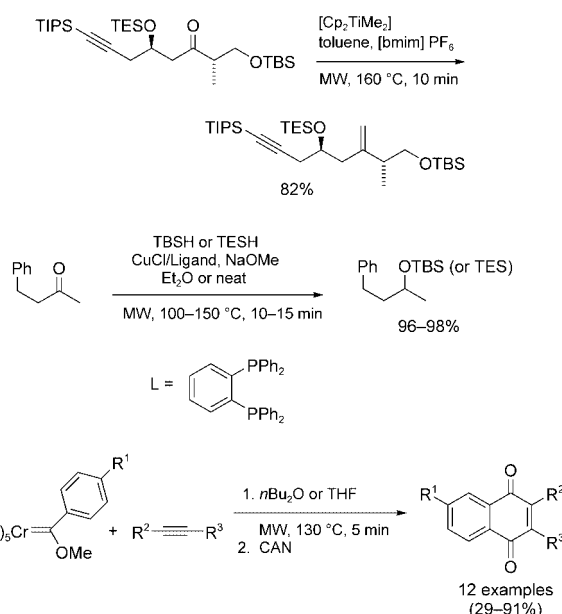
cient to drive all of the studied Pauson–Khand reactions to completion under sealed-vessel conditions, without the need for additional carbon monoxide. Under the carefully optimized reaction conditions utilizing 1.2 equivalents of cyclohexylamine as an additive in toluene, microwave heating for 5 minutes at 100 °C provided good yields of the desired cycloadducts.^[130] Similar results were published independently by Evans and co-workers.^[131]

Another important reaction principle in modern organic synthesis is C–H bond activation.^[132] Bergman, Ellman, and co-workers have introduced a protocol that allows otherwise extremely sluggish inter- and intramolecular rhodium-catalyzed C–H bond activation to occur efficiently under microwave heating conditions. In their investigations, they found that heating the olefin-tethered benzimidazoles **18** in a mixture of 1,2-dichlorobenzene and acetone in the presence of 2.5–5 mol % $[(\text{RhCl}(\text{coe})_2)_2]$ (coe = cyclooctene) and 5–10 mol % $\text{PCy}_3 \cdot \text{HCl}$ provided the desired tricyclic heterocycles **19** in moderate to excellent yields (Scheme 18).^[133] Microwave heating to 225–250 °C for 6–12 min proved to be the optimum conditions. The solvents were not degassed or dried before use, but air was excluded by purging the reaction vessel with nitrogen.



Scheme 18. Intramolecular coupling of a benzimidazole ring with an alkene group under C–H activation.

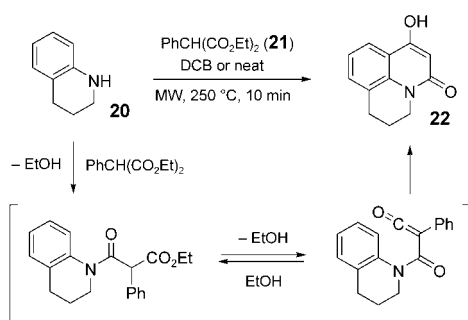
Other microwave-assisted reactions involving metal catalysts or metal-based reagents are shown in Scheme 19.^[60,134,135]



Scheme 19. Petasis olefination,^[60] hydrosilylation of ketones,^[134] and Dötz benzannulation.^[135] CAN = cerium ammonium nitrate, TBS = *tert*-butyldimethylsilyl, TES = triethylsilyl, TIPS = triisopropylsilyl.

2.7. Heterocycle Synthesis

The formation of heterocyclic rings by cyclocondensation reactions is typically a process well-suited for microwave technology. Many of these condensation reactions require high temperatures and conventional reaction conditions very often involve heating the reactants in an oil, metal, or sand bath for many hours or even days. One representative example is the formation of 4-hydroxy-1*H*-quinolin-2-ones of type **22** from anilines and malonic esters (Scheme 20). The corresponding conventional, thermal protocol involves heating the two components in equimolar amounts in an oil bath at 220–300 °C for several hours (without solvent),^[136] whereas similar high yields can be obtained by microwave heating at 250 °C for 10 minutes.^[137] Here it was essential to use open-vessel technology, since the two equivalents of the volatile by-product ethanol that formed under normal (atmospheric pressure) conditions were simply distilled off and therefore



Scheme 20. Formation of 4-hydroxy-1*H*-quinolin-2-one **22** from aniline **20** and malonic ester **21**.

removed from the equilibrium (Scheme 20).^[136] Preventing removal of ethanol from the reaction mixture, by using a standard closed-vessel microwave system, leads to significantly lower yields (Table 3). These experiments highlight the

Table 3: Yields for **22** on microwave heating under closed- and open-vessel conditions (Scheme 20).^[a,b]

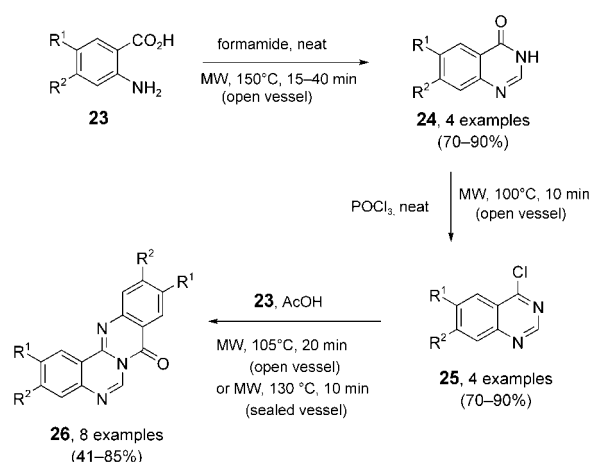
<i>x</i> [mmol] ^[c]	Solvent [mL]	Yield [%]	<i>p</i> [bar]
1	2	76	3.6
2	2	67	5.3
4	2	60	7.4
1	0.5	91	2.0
2	–	92	[d]
4	–	90	[d]

[a] Data from ref. [137]. [b] Microwave heating (250 °C, 10 min) in dichlorobenzene or without solvent. [c] Reaction quantity. [d] Open vessel.

importance of choosing appropriate experimental conditions when using microwave heating technology. In the present example, scale-up of the synthesis shown in Scheme 20 would clearly only be feasible by using open-vessel technology.^[138]

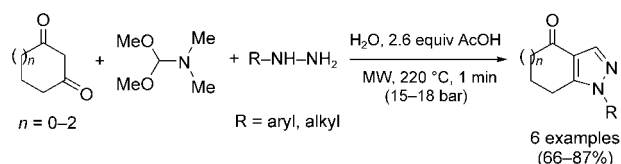
A related cyclocondensation was recently described by Besson and co-workers in the context of synthesizing 8*H*-quinazolino[4,3-*b*]quinazolin-8-ones by Niementowski condensation reactions (Scheme 21).^[139] In the first step of this multistep sequence, anthranilic acid derivatives **23** were condensed with formamide (5.0 equiv) under open-vessel microwave conditions (Niementowski condensation).^[140] Subsequent chlorination with excess POCl₃, again using open-vessel conditions, produced the anticipated 4-chloroquinazoline derivatives **25**, which were subsequently condensed with **23** in acetic acid to produce the tetracyclic target structures **26**. The final condensation reactions were completed within 20 minutes at reflux (ca. 105 °C) under open-vessel conditions, but not surprisingly could also be performed more rapidly by using sealed-vessel heating at 130 °C. The reaction depicted in Scheme 21 is one of the growing number of examples where not only one, often conventionally difficult to execute transformation has been carried out by microwave synthesis, but several steps in a sequence have been performed by microwave dielectric heating.

Molteni et al. have described the three-component, one-pot synthesis of fused pyrazoles by treating cyclic 1,3-



Scheme 21. Formation of 8*H*-quinazolino[4,3-*b*]quinazolin-8-ones **26** by Niementowski condensation.

diketones with dimethylformamide dimethylacetal (DMFDMA) and a suitable bidentate nucleophile such as a hydrazine derivative (Scheme 22).^[141] The reaction proceeds

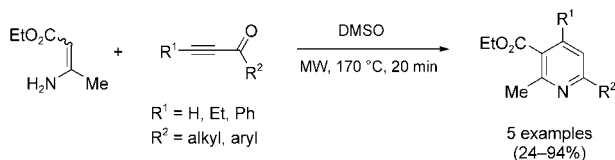


Scheme 22. Three-component condensation of fused pyrazoles in water.

with initial formation of an enaminoketone as the key intermediate from the 1,3-diketone and DMFDMA precursors, followed by a tandem addition-elimination/cyclodehydration step. Remarkably, the authors were able to perform the multicomponent condensation by heating all three building blocks together with a small amount of acetic acid (2.6 equiv) in water at 220 °C for 1 minute! Upon cooling the reaction, the desired products crystallized directly and were isolated in high purity by simple filtration. Although most of the starting materials are actually insoluble in water at room temperature, at 220 °C water behaves similar to an organic solvent and is therefore able to dissolve many organic materials that are otherwise not soluble in such a polar solvent. It should be emphasized that high-temperature water chemistry at near-critical conditions (ca. 275 °C, 60 bar) has received considerable attention in recent years,^[142] and that sealed-vessel microwave heating technology appears to be an ideal tool to rapidly attain this environment.^[5,143] Molteni et al. have successfully used other bidentate nucleophiles such as amidines and hydroxylamine for the synthesis of related heterocycles.^[141] Numerous reports of the use of DMFDMA as a building block for the rapid synthesis of a large variety of heterocyclic ring systems by MAOS have also appeared.^[144–147]

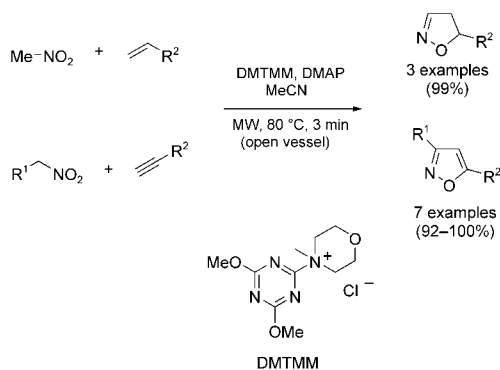
The Bohlmann–Rahtz synthesis of trisubstituted pyridines from β -aminocrotonates and an ethynyl ketone has found application in the preparation of a variety of heterocycles

containing this structural motif.^[148] Bagley et al. have developed a microwave-assisted modification of this heteroannulation method, which is best conducted in DMSO at 170 °C for 20 minutes, and provides the desired pyridine derivatives in 24–94 % yield (Scheme 23).^[149] A related protocol involving a tandem oxidation/heteroannulation of propargylic alcohols was described by the same authors.^[150]



Scheme 23. Bohlmann–Rahtz synthesis of trisubstituted pyridines.

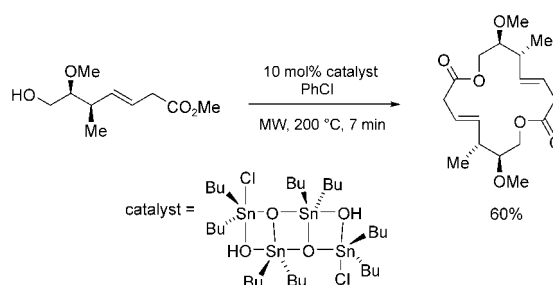
Cycloaddition reactions are clearly very important for the construction of heterocycles, and numerous examples of heterocycle synthesis by controlled microwave heating have been described. For example, nitro alkenes are converted in situ into nitrile oxides by 4-(4,6-dimethoxy[1,3,5]triazin-2-yl)-4-methylmorpholinium chloride (DMTMM) and 4-dimethylaminopyridine (DMAP, Scheme 24).^[151] The generated



Scheme 24. Nitrile oxide cycloaddition reactions.

1,3-dipoles undergo cycloaddition with the double or triple bond of an alkene or acetylene dipolarophile (5.0 equiv), respectively, to furnish 4,5-dihydroisoxazoles or isoxazoles. Open-vessel conditions were used and full conversion with very high yields of products was achieved within 3 minutes at 80 °C.

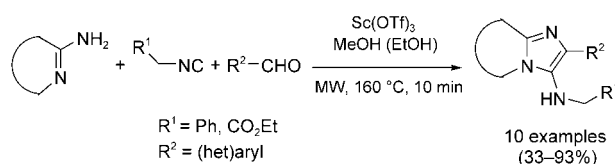
An unusual class of heterocycles are polyketide-derived macrodiolide natural products. The research groups of Porco and Panek have recently shown that stereochemically well-defined macrodiolides can be obtained by cyclodimerization of nonracemic chiral hydroxy esters (Scheme 25).^[152] Preliminary experiments involving microwave irradiation demonstrated that exposing dilute solutions of the hydroxy ester (0.02 M) in chlorobenzene to sealed-vessel microwave irradiation conditions (200 °C, 7 min) in the presence of a distannoxane transesterification catalyst led to a 60 % yield of the 16-membered macrodiolide heterocycle. Conventional



Scheme 25. Formation of macrodiolides by cyclodimerization with a distannoxane catalyst.

reflux conditions (ca. 135 °C) in the same solvent (0.01 M of hydroxy ester) provided a 75 % yield after 48 h.

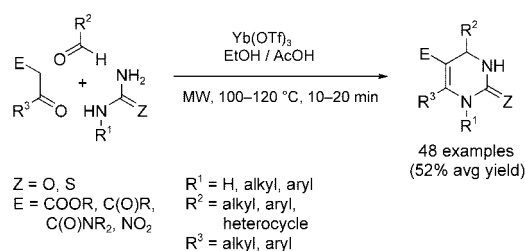
Multicomponent reactions (MCRs) are of increasing importance in organic and medicinal chemistry. In times where a premium is put on speed, diversity, and efficiency in the drug discovery process, MCR strategies offer significant advantages over conventional linear-type syntheses.^[153] The Ugi four-component condensation in which an amine, an aldehyde or ketone, a carboxylic acid, and an isocyanide combine to yield an α -acylaminoamide is particularly interesting because of the wide range of products obtainable through variation of the starting materials.^[154] The reaction of heterocyclic amidines with aldehydes and isocyanides in the presence of 5 mol % $\text{Sc}(\text{OTf})_3$ as a catalyst in an Ugi-type three-component condensation (Scheme 26) generally



Scheme 26. Ugi-type three-component condensation.

requires extended reaction times of up to 72 h at room temperature for the generation of the desired fused 3-aminoimidazoles.^[155] Tye and co-workers have demonstrated that this process can be speeded up significantly by performing the reaction under sealed-vessel microwave conditions.^[156] A reaction time of 10 min at 160 °C in methanol (in some cases ethanol was employed) produced similar yields of products than the same process at room temperature, but at a fraction of the time.

Another important MCR is the Biginelli synthesis of dihydropyrimidines by the acid-catalyzed condensation of aldehydes, CH-acidic carbonyl components, and urea-type building blocks (Scheme 27).^[157] Under conventional conditions this MCR typically requires several hours of heating under reflux conditions (ca. 80 °C) in a solvent such as ethanol. The ideal microwave heating conditions with respect to solvent, catalyst type/concentration, irradiation time, and temperature were rapidly optimized by using the condensation of benzaldehyde, ethyl acetoacetate, and urea as a model reaction.^[158] Figure 3 shows the time/temperature optimization profile for the standard Biginelli reaction using 10 mol %



Scheme 27. Biginelli synthesis of dihydropyrimidines through a three-component reaction. Tf = trifluoromethanesulfonyl.

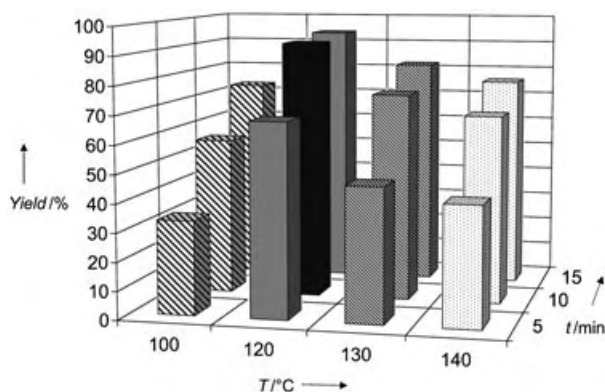


Figure 3. Rapid optimization of reaction time and temperature for the Biginelli condensation of ethyl acetoacetate, benzaldehyde, and urea (Scheme 27) in AcOH/EtOH (3:1) with 10 mol% $Yb(OTf)_3$ as a catalyst. The optimal conditions (marked in black: 120 °C, 10 min) affords the product in 92 % yield.

ytterbium triflate in a acetic acid/ethanol (3:1). An optimum yield of 92 % of isolated dihydropyrimidine ($R^1 = H$, $Z = O$, $R^2 = Ph$, $E = CO_2Et$, $R^3 = Me$) was obtained by heating the mixture of reactants at 120 °C for 10 minutes. The fact that a temperature only marginally higher than the optimal reaction temperature leads to a significantly decreased yield for this transformation^[159] underscores the importance of using controlled microwave irradiation conditions with adequate temperature control.

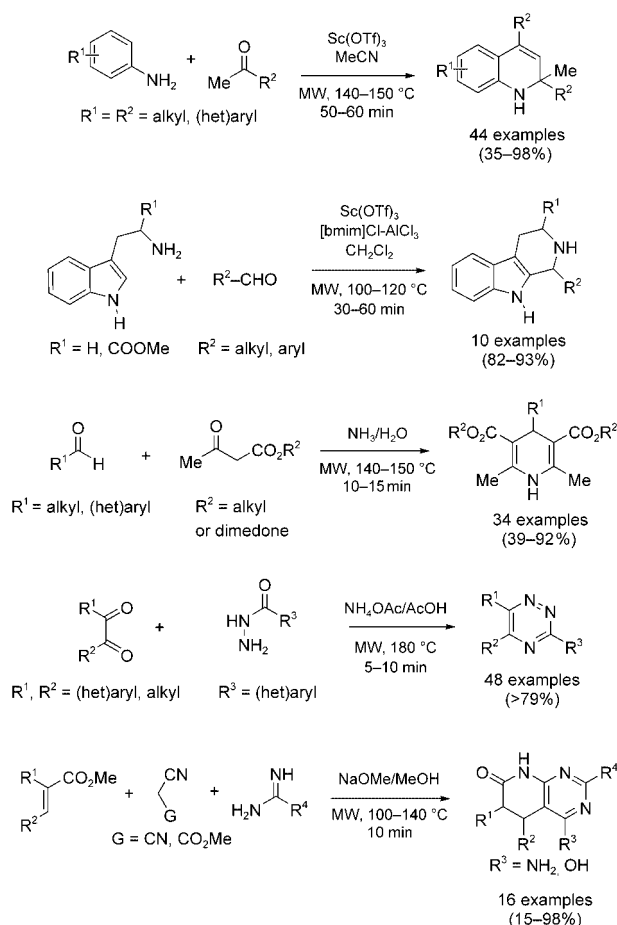
Figure 3 illustrates one of the key advantages of high-speed microwave synthesis, namely the rapid optimization capabilities that are particularly useful if microwave heating is coupled with automation.^[158] Recent work by researchers from Arqule and Pfizer has demonstrated how the overall process can be further improved if rapid testing and tuning of reaction conditions involving microwave heating is coupled with statistical experimental design.^[160] This is a particularly valuable method if a large number of reaction parameters needs to be considered.

The above-mentioned robotics are also useful for preparing compound libraries through automated sequential microwave synthesis. A diverse set of 17 CH-acidic carbonyl compounds, 25 aldehydes, and 8 urea/thioureas was used for the preparation of a dihydropyrimidine library under the optimized conditions for the Biginelli reaction displayed in Scheme 27. Out of the full set of 3400 possible dihydropyr-

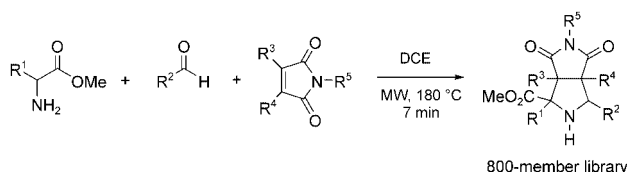
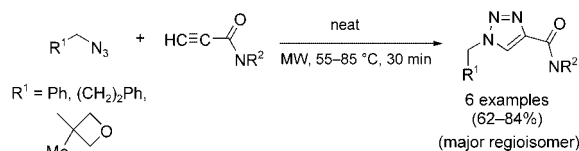
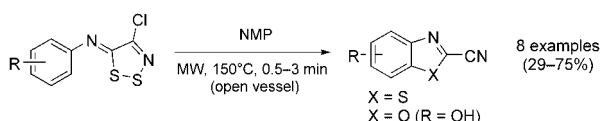
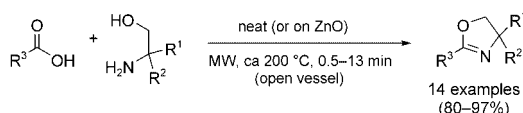
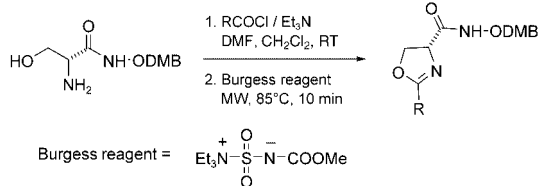
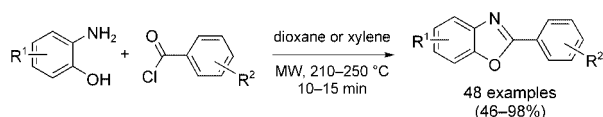
imidine derivatives, a representative subset of 48 analogues was prepared within 12 h by automated addition of building blocks and subsequent sequential microwave irradiation of each reaction vessel in a single-mode microwave reactor equipped with suitable robotics.^[158]

In a conceptually different approach, Nüchter, Ondruschka et al. presented the parallel generation of a 36-member library of Biginelli dihydropyrimidines in a suitable multivessel rotor placed inside a dedicated multimode microwave reactor.^[161,162] Given the fact that modern multimode microwave reactors can operate with specifically designed 96-well plates under sealed-vessel conditions, the parallel approach offers a considerable higher throughput than the automated sequential technique, albeit at the cost of having less control over the reaction parameters for each individual vessel/well. One additional limitation of the parallel approach is that all reaction vessels during library production are exposed to the same irradiation conditions in terms of reaction time and microwave power, thus not allowing specific needs of individual building blocks to be addressed by varying the time or temperature.

A range of other heterocyclic ring systems synthesized by microwave-assisted cyclocondensation or cycloaddition protocols is shown in Schemes 28 and 29.



Scheme 28. Skraup synthesis of dihydroquinolines,^[163] Pictet–Spengler reaction,^[57] Hantzsch–MCR synthesis of dihydropyridines,^[164] triazine synthesis,^[165] and Victory reaction.^[166]



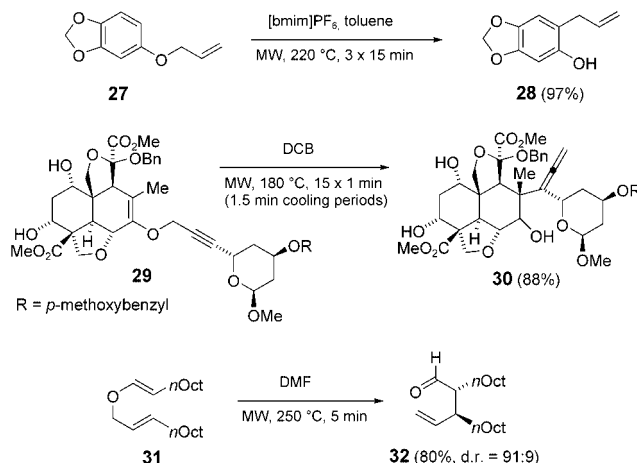
Scheme 29. Synthesis of benzoxazoles,^[167] oxazolines,^[168,169] and benzothiazoles,^[170] 1,3-dipolar cycloaddition reaction to form triazoles,^[171] and [3 + 2] cycloadditions of azomethine ylides and maleimide.^[172] DCE = 1,2-dichloroethane, DMB = 2,4-dimethoxybenzyl.

2.8. Miscellaneous Solution-Phase Organic Transformations

Since MAOS is becoming an increasingly popular tool for a steadily growing number of researchers, both in academia and industry, it becomes evident that, in principle, all chemical transformations requiring heat can be carried out under microwave conditions. The following literature survey of organic chemical transformations carried out in the solution phase by microwave heating is therefore limited to selected examples that highlight particularly interesting reactions or applications.

2.8.1. Rearrangements

Ley and co-workers have described the microwave-assisted Claisen rearrangement of allyl ether **27** in their synthesis of the natural product carpanone (Scheme 30).^[173] A 97 % yield of the rearranged product **28** could be obtained by three successive 15-minute irradiations at 220 °C using



Scheme 30. Examples of Claisen rearrangements. Bn = benzyl.

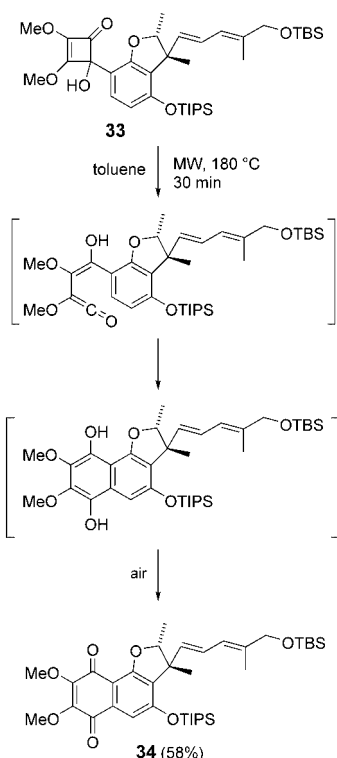
toluene doped with the ionic liquid [bmim]PF₆ as the solvent. Interestingly, one single irradiation of 45 minutes at the same temperature gave a somewhat lower yield (86 %).

A related Claisen rearrangement, albeit on a much more complex substrate was reported by the same research group, again under “pulsed” microwave irradiation conditions. Heating a solution of the propargylic enol ether **29** in dichlorobenzene at 180 °C for 15 minutes resulted in a 71 % yield of the desired allene **30** as a single diastereomer, which was further elaborated into the skeleton of the triterpenoid natural product azadirachtin.^[174] An 88 % yield of product was obtained by applying 15 pulses irradiation of 1 minute duration. No rationalization for the increased yields in these “pulsed versus continuous irradiation” experiments can be given at present. Nordmann and Buchwald recently reported the diastereoselective Claisen rearrangement of allyl vinyl ether **31** to aldehyde **32**.^[175] The product was obtained in 80 % yield with a diastereomeric ratio of 91:9 by microwave heating at 250 °C for 5 minutes in DMF. Conventional heating at 120 °C for 24 hours provided somewhat higher yields and selectivities (90 % yield, d.r. = 94:6).

In their search for synthetic routes to analogues of the furaquinocin antibiotics, Trost et al. have utilized a microwave-assisted squaric acid/vinylketene rearrangement to synthesize dimethoxynaphthoquinone **34**, a protected analogue of furaquinocin E (Scheme 31).^[176] Since the conventional rearrangement conditions successfully applied in a closely related series of transformations (toluene, 110 °C) led to incomplete conversion, the reaction was attempted by microwave heating at 180 °C; this afforded an acceptable yield of **34** (58 %) after oxidation to the naphthoquinone.

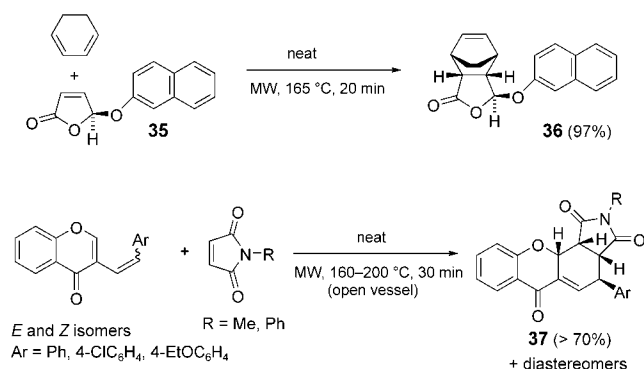
2.8.2. Cycloaddition Reactions

Cycloaddition reactions were among the first transformations to be studied by using microwave heating technology,^[3,7] and numerous examples have been summarized in previous review articles and book chapters.^[4–16] Conventional cycloaddition reactions require, in many cases, the use of harsh conditions such as high temperatures and long reaction times, but they can be performed with great success with the aid of



Scheme 31. Rearrangement of a squaric acid derivative to a vinylketene, which further reacts to form the tricyclic product **34**.

microwave heating. Scheme 32 shows two recent examples of Diels–Alder cycloadditions performed by microwave dielectric heating. In both cases the diene and dienophile were

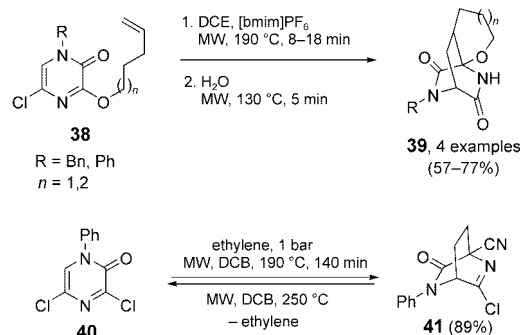


Scheme 32. Examples of Diels–Alder cycloadditions.

reacted neat without the addition of solvent. For the transformation **35**→**36** described by Trost and Crawley, irradiation for 20 minutes at 165 °C (or for 60 min at 150 °C) gave the cycloadduct **36** in near quantitative yield.^[177] In the process reported by de la Hoz and co-workers, open-vessel irradiation of 3-(2-arylethenyl)chromones with maleimides at 160–200 °C for 30 minutes furnished the tetracyclic adducts of type **37** along with minor amounts of other diastereoisomers.^[178]

Inter- and intramolecular hetero-Diels–Alder cycloaddition reactions of a series of functionalized 2(1*H*)-pyrazinones

have been studied in detail by the research group of Van der Eycken (Scheme 33).^[54,179,180] In the intramolecular series, cycloaddition of alkenyl-tethered 2(1*H*)-pyrazinones **38** requires 1–2 days under conventional thermal conditions



Scheme 33. Hetero-Diels–Alder cycloaddition reactions of 1*H*-pyrazin-2-ones.

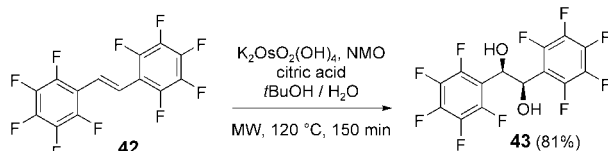
(chlorobenzene, reflux, 132 °C). The use of 1,2-dichloroethane doped with the ionic liquid [bmim]PF₆ and sealed-vessel microwave technology at 190 °C enabled the same transformations to be completed within 8–18 minutes.^[54] The primary imidoyl chloride cycloadducts were not isolated, but rapidly hydrolyzed by addition of small amounts of water and microwave irradiation (130 °C, 5 min). The overall yields of **39** were in the same range as reported for the conventional thermal protocols.^[54]

In the intermolecular series, the Diels–Alder cycloaddition reaction of the pyrazinone heterodiene **40** with ethylene led to the bicyclic cycloadduct **41** (Scheme 33).^[54] Under conventional conditions, these cycloaddition reactions have to be carried out in an autoclave at an ethylene pressure of 25 bar before the setup is heated to 110 °C for 12 hours. In contrast, the Diels–Alder addition of pyrazinone precursor **40** with ethylene in a sealed vessel that had been flushed with ethylene before sealing was completed after irradiation for 140 minutes at 190 °C. It was however not possible to further increase the reaction rate by raising the temperature. At temperatures above 200 °C an equilibrium between the cycloaddition **40**→**41** and the competing retro-Diels–Alder fragmentation process was observed (Scheme 33).^[54] Only by using a microwave reactor that allowed pre-pressurization of the reaction vessel with 10 bar of ethylene could the Diels–Alder addition **40**→**41** be carried out much more efficiently at 220 °C within 10 minutes.^[179]

2.8.3. Oxidations

The osmium-catalyzed dihydroxylation reaction, the addition of osmium tetroxide to olefins to produce a vicinal diol, is one of the most selective and reliable organic transformations. Recent work by Sharpless, Fokin, and co-workers has uncovered that electron-deficient olefins can be converted into the corresponding diols much more efficiently when the reaction medium is kept acidic.^[181] One of the most useful additives in this context is citric acid (2.0 equiv), which

in combination with 4-methylmorpholine *N*-oxide (NMO) as the reoxidant for Os^{VI} and K₂OsO₂(OH)₄ (0.2 mol %) as a stable, nonvolatile substitute for OsO₄, allows the conversion of many olefinic substrates into their corresponding diols at ambient temperatures. In specific cases, such as for the extremely electron-deficient olefin **42** (Scheme 34), the reaction had to be carried out under microwave irradiation at 120 °C to produce the pure diol **43** in 81 % yield.^[181]



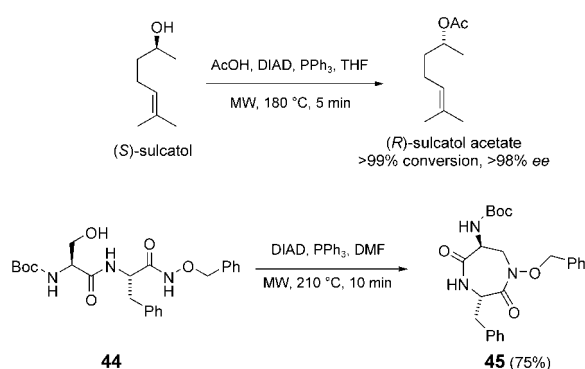
Scheme 34. Osmium-catalyzed dihydroxylation of electron-deficient alkenes.

Another industrially important oxidation reaction is the conversion of cyclohexene into adipic acid. The well-known Noyori method uses hydrogen peroxide, a catalytic amount of tungstate, and a phase-transfer catalyst to afford the clean oxidation of cyclohexene to adipic acid. Ondruschka and co-workers have demonstrated that a modified protocol employing microwave heating without solvent gave comparable yields of the desired product, but in a much shorter time.^[182] Rhodium and ruthenium-catalyzed hydrogen transfer type oxidations of primary and secondary alcohols have also been reported recently.^[183]

2.8.4. Mitsunobu Reactions

The Mitsunobu reaction is a powerful stereochemical transformation. This reaction is very efficient for inverting the configuration of chiral secondary alcohols since a clean S_N2 process is generally observed ("Mitsunobu inversion"). The fact that the Mitsunobu reaction is typically carried out at or below room temperature would suggest that high-temperature Mitsunobu reactions performed under microwave conditions would have little chance of success. It was established in 2001 that Mitsunobu reactions can indeed be carried out at high-temperatures to effect an enantioconvergent approach to the aggregation pheromones (*R*)- and (*S*)-sulcatol (Scheme 35).^[184] While the conventional Mitsunobu protocol carried out at room temperature proved to be extremely sluggish, complete conversion of (*S*)-sulcatol to the *R* acetate (S_N2 inversion) using essentially the standard Mitsunobu conditions (1.9 equiv DIAD, 2.3 equiv Ph₃P) was achieved within 5 minutes at 180 °C under sealed-vessel microwave conditions. Despite the high reaction temperatures, no by-products could be identified in these Mitsunobu experiments, and the *R* acetate was formed in > 98 % *ee*.

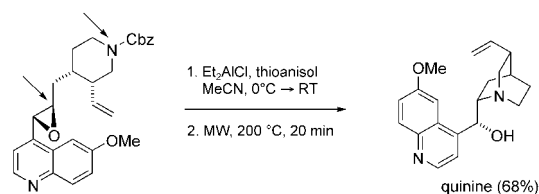
An application of these rather unusual high-temperature Mitsunobu conditions for the preparation of conformationally constrained peptidomimetics based on the 1,4-diazepan-2,5-dione core was recently disclosed by the group of Taddei and co-workers.^[185] Cyclization of the dipeptide hydroxyhydroxamate **44** under the DIAD/Ph₃P microwave conditions



Scheme 35. Mitsunobu reactions. DIAD = diisopropylazodicarboxylate.

(210 °C, 10 min) provided the desired 1,4-diazepan-2,5-dione **45** in 75 % yield. Standard room-temperature conditions (DMF, 12 h) were significantly less efficient and gave only 46 % of the desired compound.

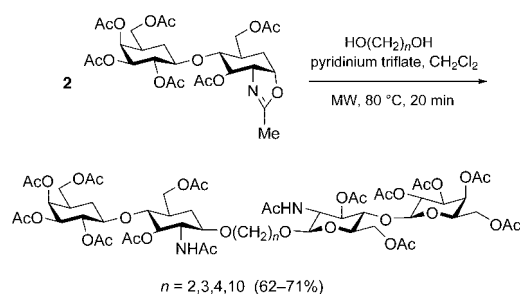
Another microwave-mediated intramolecular S_N2 reaction results in the formation of one of the key steps in a recent catalytic asymmetric synthesis of the cinchona alkaloid quinine by Jacobsen and co-workers.^[186] The strategy to construct the crucial quinuclidine core of the natural product relies on an intramolecular S_N2 reaction/epoxide ring opening (Scheme 36). After removal of the benzyl carbamate (Cbz) protecting group with Et₃AlCl/thioanisole, microwave heating of the acetonitrile solution to 200 °C for 20 minutes provided a 68 % yield of the natural product as the final transformation in a 16-step total synthesis.



Scheme 36. Intramolecular S_N2 reaction in the total synthesis of quinine.

2.8.5. Glycosylation Reactions

Glycosylation reactions involving oxazoline donors are generally rather slow and require prolonged reaction times because of the low reactivity of the donors. Oscarson and co-workers have reported the preparation of dimers of *N*-acetyllactosamine linked by alkyl spacers by microwave-assisted glycosylations with oxazoline donors in the presence of pyridinium triflate as a promoter (Scheme 37).^[187] Rapid and efficient coupling was achieved in dichloromethane with four different diols using 2.2 equivalents each of the oxazoline donor and pyridinium triflate promoter. Microwave irradiation at 80 °C for 20 minutes led to moderate to high yields of the dimers, with yields increased by 12–15 % over the conventional process. Fraser-Reid and co-workers recently described related saccharide couplings by employing *n*-pentenyglycosyl donors and *N*-iodosuccinimide (NIS) as

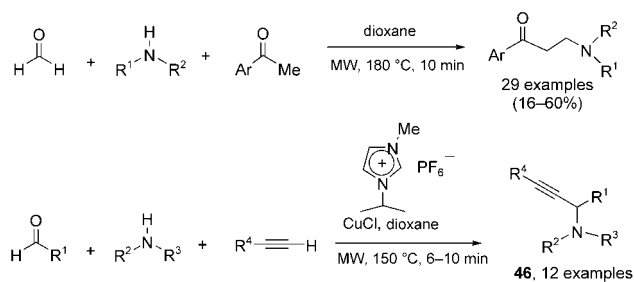


Scheme 37. Microwave-assisted glycosylation reactions.

the promotor in acetonitrile.^[31] Various rapid microwave-assisted protection and deprotection methods are also known in the area of carbohydrate chemistry.^[188]

2.8.6. Multicomponent Reactions

The Mannich reaction has been known since the early 1900s and has since then been one of the most important transformations to produce β -amino ketones. Although the reaction is powerful, it suffers from some disadvantages, such as the need for drastic reaction conditions, long reaction times, and sometimes low yields of products. Luthman and co-workers have reported microwave-assisted Mannich reactions that employed paraformaldehyde as a source of formaldehyde, a secondary amine in the form of its hydrochloride salt, and a substituted acetophenone (Scheme 38).^[189] Optimized



Scheme 38. Examples of Mannich condensations and related reactions.

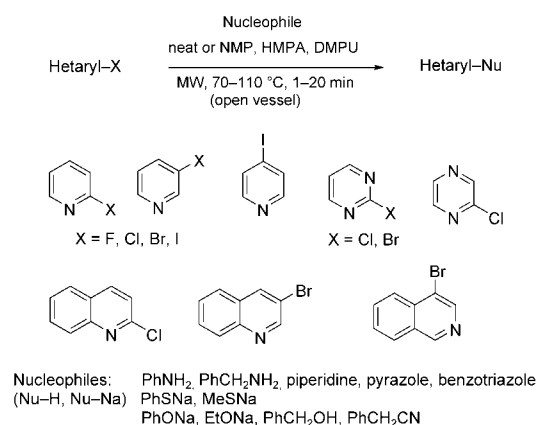
reaction conditions utilized equimolar amounts of reactants, dioxane as solvent, and microwave irradiation at 180 °C for 8–10 minutes to produce the desired β -amino ketones in moderate to good yields. Importantly, in several examples the reaction was performed both on a 2-mmol scale using a single-mode microwave reactor and also on a 40-mmol scale using a dedicated multimode instrument. As seen with other transformations described earlier (Scheme 1), all the microwave-assisted Mannich reactions studied proved to be “directly scalable”: nearly identical yields were obtained on a 2-mmol and 40-mmol scale without the need for reoptimization of the reaction conditions.^[189]

The research group of Leadbeater reported a different type of Mannich reaction, which involved condensation of an aldehyde (1.5 equiv) with a secondary amine and a terminal

acetylene in the presence of CuCl (10 mol %) to activate the terminal acetylene (Scheme 38).^[58] Optimum yields of propargylamines **46** were obtained by microwave irradiation of the three building blocks with the catalyst in dioxane doped with an ionic liquid at 150 °C for 6–10 minutes. A high-speed microwave approach also exists for the Petasis multicomponent reaction (boronic-Mannich reaction)^[190] and for the Kindler thioamide synthesis (the condensation of an aldehyde, amine, and sulfur).^[191]

2.8.7. Nucleophilic Aromatic Substitution

An alternative to the palladium-catalyzed Buchwald–Hartwig reactions and the related copper-catalyzed methods for C(aryl)–N, C(aryl)–O, and C(aryl)–S bond formations (Section 2.3) are nucleophilic aromatic substitution reactions. A benzene derivative substituted by a leaving group may be treated, for example, with an amine, but here the benzene derivative must generally also contain an electron-withdrawing group. Such nucleophilic aromatic substitution reactions are notoriously difficult to perform and often require high temperatures and long reaction times. A number of publications report efficient nucleophilic aromatic substitutions driven by microwave heating involving either halogen-substituted aromatic^[192,193] or heteroaromatic systems.^[72,73,194–196] Scheme 39 summarizes some heteroaromatic

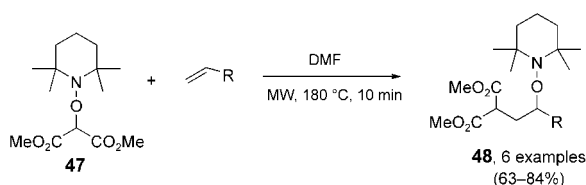


Scheme 39. Nucleophilic aromatic substitution reactions involving halo-substituted N-heterocycles. DMPU = *N,N'*-dimethyl-*N,N'*-propylene urea, HMPA = hexamethyl phosphoramide.

systems and nucleophiles along with the reaction conditions that have been developed by Cherng for microwave-assisted nucleophilic substitution reactions.^[194–196] In general, the microwave-driven processes provide significantly higher yields of the desired products in much shorter reaction times.

2.8.8. Radical Reactions

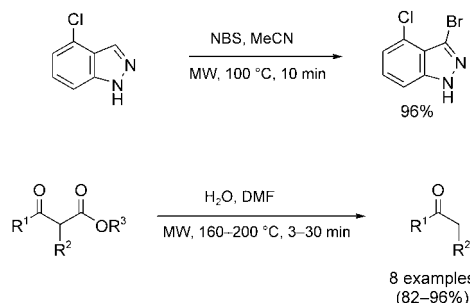
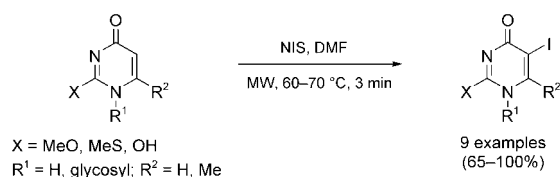
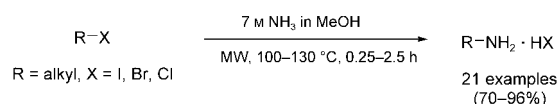
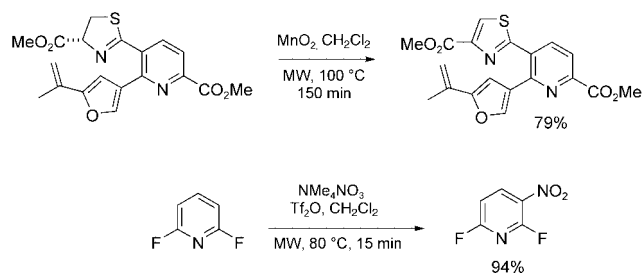
There are only a limited number of examples in the literature that involve radical reactions under controlled microwave heating conditions.^[197] Wetter and Studer have described radical carboaminoxylations of various nonactivated olefins and difficult radical cyclizations (Scheme 40).^[198]



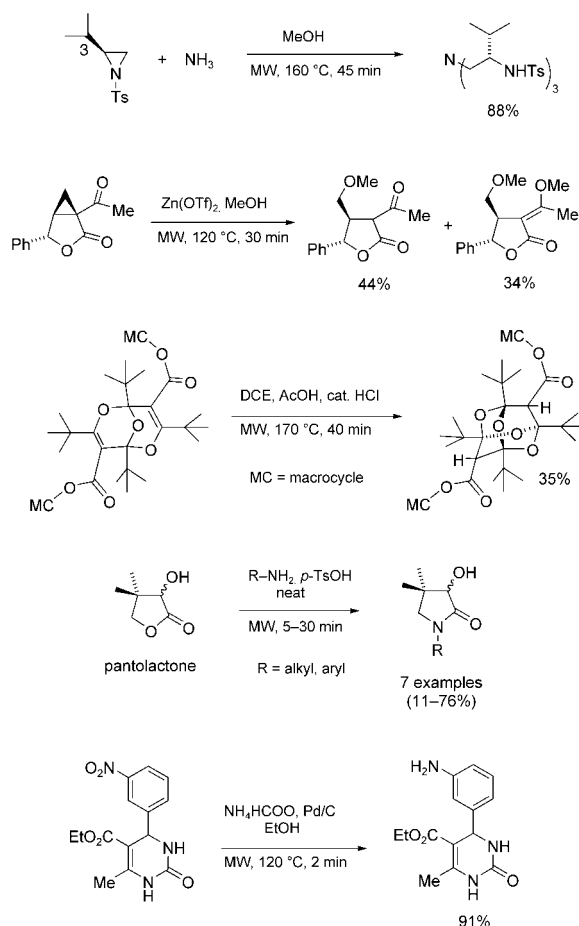
Scheme 40. Radical carboxaminations with malonyl radicals.

The thermally reversible homolysis of alkoxyamine **47** generates the stable radical 2,2,6,6-tetramethylpiperidinyl-1-ol (TEMPO) and a stabilized transient malonyl radical, which subsequently reacts with an alkene to afford the carboaminoxylation product **48**. These radical addition processes take up to three days under conventional conditions (DMF, sealed tube, 135 °C), while the same transformation was complete after microwave heating at 180 °C for 10 minutes in a sealed vessel; higher yields were also obtained in all but one example.

Several other selected examples of microwave-assisted organic transformations are summarized in Schemes 41 and 42.



Scheme 41. Oxidation of thiazolidines,^[199] electrophilic nitration,^[200] amination,^[201] iodination,^[87] bromination,^[73] and dealkoxycarbonylation reactions.^[202] NBS = *N*-bromosuccinimide.



Scheme 42. Aziridine^[203] and cyclopropane ring-opening,^[204] double Michael addition,^[205] lactam formation,^[206] and reduction of a nitro group by catalytic transfer hydrogenation.^[207] Ts = toluenesulfonyl.

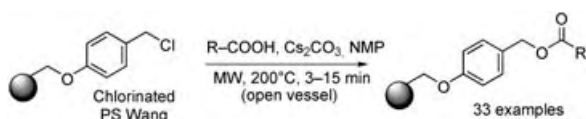
2.9. Combinatorial and High-Throughput Methodologies

2.9.1. Solid-Phase Organic Synthesis

Solid-phase organic synthesis (SPOS) exhibits several advantages compared with classical protocols in solution. Reactions can be accelerated and driven to completion by using a large excess of reagents, as these can easily be removed by filtration and subsequent washing of the solid support. In addition, SPOS can easily be automated by using appropriate robotics and applied to “split-and-mix” strategies, useful for the synthesis of large combinatorial libraries.^[208] However, SPOS also exhibits several shortcomings, as a result of the inherent nature of the heterogeneous reaction conditions; nonlinear kinetic behavior, slow reactions, solvation problems, and degradation of the polymer support, because of the long reaction times, are some of the problems typically experienced in SPOS. A technique such as microwave-assisted synthesis which is able to address some of these issues is therefore of considerable interest, particularly for research laboratories involved in high-throughput synthesis. As far as the polymer supports for microwave-assisted SPOS are concerned, the use of cross-linked macroporous or microporous polystyrene resins has been most prevalent. In contrast to the common belief that the use of polystyrene

resins limits the reaction conditions to temperatures below 130°C, it has recently been amply demonstrated, both in microwave-assisted SPOS and in the use of polymer-supported reagents and catalysts (see Section 2.9.4), that these resins can withstand microwave irradiation for short periods of time even at temperatures above 200°C.

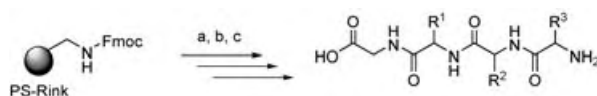
Early examples of SPOS under controlled microwave conditions^[12] typically involved the use of microwaves in one single step to either attach or cleave material onto or off the resin. A study published in 2001 demonstrated that high-temperature microwave heating (200°C) can be effectively employed to attach aromatic carboxylic acids to chloromethylated polystyrene resins (Merrifield and Wang) by the cesium carbonate method (Scheme 43).^[209] Significant rate



Scheme 43. Attachment of aromatic carboxylic acids to chlorinated polystyrene Wang resin.

accelerations and higher loadings were observed when the microwave-assisted protocol was compared to the conventional thermal method. Reaction times were reduced from 12–48 hours with conventional heating at 80°C to 3–15 minutes with microwave heating at 200°C in NMP in open glass vessels. A comparison of the kinetics of the thermal coupling of benzoic acid to the chlorinated Wang resin at 80°C with the microwave-assisted coupling at the same temperature demonstrated the absence of any microwave effects.

Peptide synthesis has long been one of the cornerstones of solid-phase organic synthesis, and attempts to speed up the rather time-consuming process by microwave heating were made as early as 1992.^[210] Erdélyi and Gogoll recently applied controlled microwave irradiation to the synthesis of a small tripeptide containing three of the most hindered natural amino acids (Thr, Val, Ile; Scheme 44).^[211]



Scheme 44. Synthesis of a tripeptide. a) deprotection with piperidine at RT; b) coupling reagent, Fmoc-protected amino acid, $i\text{Pr}_2\text{NEt}$, DMF, MW, 110°C, 20 min; c) TFA, RT, 2 h. Fmoc = 9-fluorenylmethoxycarbonyl, TFA = trifluoroacetic acid.

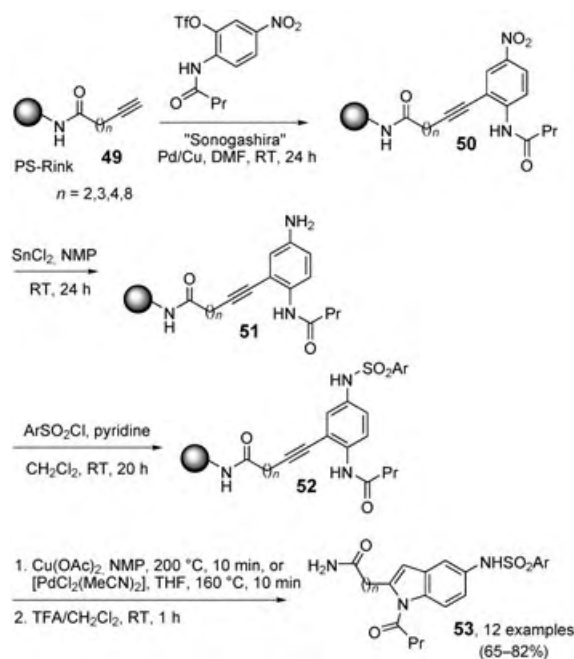
A variety of common coupling reagents have been investigated for the synthesis of this rather difficult peptide sequence on standard Rink polystyrene resin. The coupling of the activated amino acids under microwave conditions was completed in a few minutes (1.5–20 min) without the need for double or triple coupling steps as in conventional protocols. Most of the coupling reagents used showed increased coupling efficiency up to 110°C, with *O*-(7-azabenzotriazol-1-yl)-*N,N,N',N'*-tetramethyluronium hexafluorophosphate

(HATU) being the most effective, and allowed complete coupling within 1.5 minutes at 110°C. Decomposition of the reagents was indicated by a color change of the reaction mixtures above this temperature. However, no degradation of the solid support was observed. Furthermore, both LC-MS and ^1H NMR spectroscopic analysis confirmed the absence of racemization during the high-temperature treatment, despite the presence of the diisopropylethylamine base.

The formation of a number of related peptide bonds have been reported under optimized microwave conditions.^[212] In fact, specialized equipment dedicated specifically to microwave-assisted solid-phase peptide synthesis is commercially available.^[36]

As in solution-phase chemistry (see Sections 2.2 and 2.3), many transition-metal-catalyzed transformations have been conducted successfully on a solid phase by using microwave-assisted techniques. Examples include solid-phase Suzuki-,^[213] Stille-,^[213] and Sonogashira couplings,^[214] Negishi reactions,^[92] Mo-catalyzed allylic alkylations,^[117] aminocarbonylations,^[110] cyanation reactions,^[215] trifluoromethanesulfonations,^[82] Buchwald–Hartwig aminations,^[216] and Cu-catalyzed Ullmann-type C–N arylations.^[217]

An interesting example of a transition-metal-mediated microwave-assisted SPOS involving either Cu^{II} - or Pd^{II} -mediated cyclizations of 2-alkynylanilides to indoles has been studied by Dai et al. (Scheme 45).^[218] The required alkynylanilide precursor **52** was constructed on Rink resin following standard SPOS procedures. The desired cyclization step **52**→**53** was extremely sluggish under conventional thermal conditions and only partial ring closure was observed (80°C, 4–5 h). In contrast, dielectric heating with microwaves for 10 minutes at 160°C in THF in the presence of 20 mol % of $[\text{PdCl}_2(\text{MeCN})_2]$ afforded indole **53** ($\text{Ar} = p\text{-CF}_3\text{C}_6\text{H}_4$, $n =$

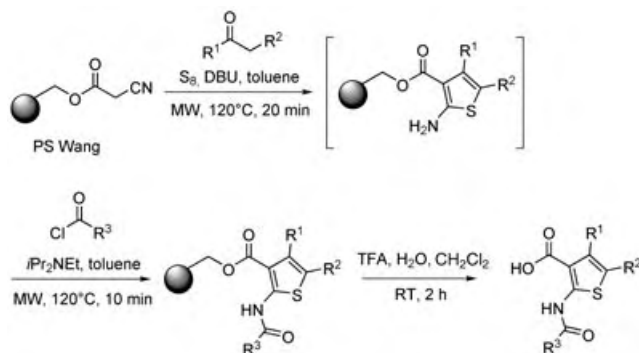


Scheme 45. Pd- or Cu-mediated ring closure of resin-bound 2-alkynylanilides to indoles.

8) in 75% yield and 94% purity after cleavage. Alternatively, the equivalent Cu^{II} -mediated process (1 equiv of $\text{Cu}(\text{OAc})_2$, NMP, 200°C, 10 min) also provided the desired indoles in similar yields and purities. The authors specifically note that no decomposition of the resin was observed even at 200°C.

A related indole synthesis on Rink resin based on the Pd-catalyzed cyclization of propargylamines to iodoanilines was published by Berteina-Raboin and co-workers.^[219] In this case, open-vessel microwave technology was used for all the three steps of the synthesis (< 15 min, < 140°C) as well as for the final cleavage reaction, which was carried out at room temperature. Higher yields of final products were achieved in much shorter reaction times by using the microwave protocol as compared to conventional heating.

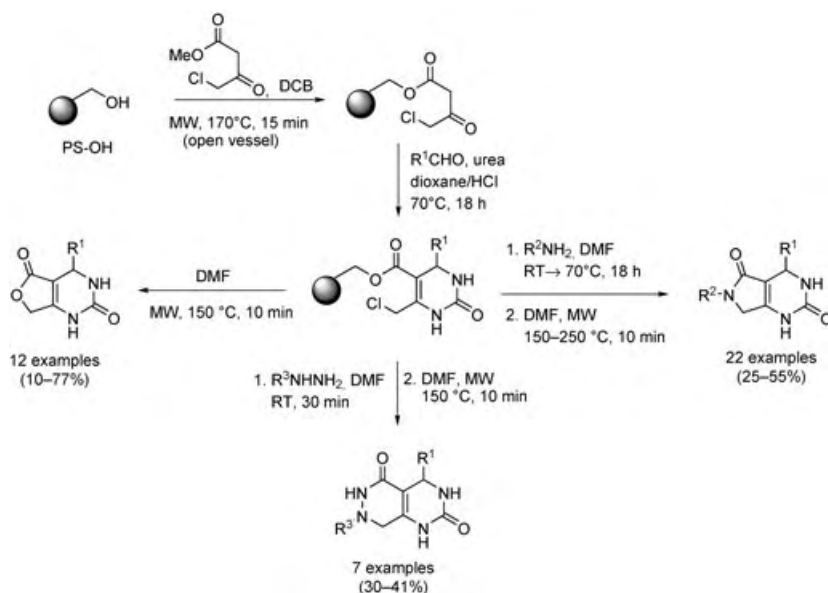
An interesting multicomponent reaction is the Gewald synthesis of 2-amino-3-acylthiophenes. Earlier reports of the classical Gewald synthesis had described the rather long reaction times required by conventional heating and the laborious purification of the resulting thiophenes. In view of these issues, researchers from Morphochem investigated a “one-pot” microwave-assisted Gewald synthesis on a commercially available cyanoacetylated Wang resin as the solid support (Scheme 46).^[220] The overall two-step reaction procedure,



Scheme 46. Gewald synthesis of 2-acylaminothiophenes through a three-component reaction.

including the acylation of the initially formed 2-aminothiophenes, could be performed in less than one hour. This process is an efficient route to 2-acylaminothiophenes which requires no filtration between the two reaction steps. Various aldehydes, ketones, and acylating agents have been employed to generate the desired thiophene products in high yields (81–99%) and in generally good purities.

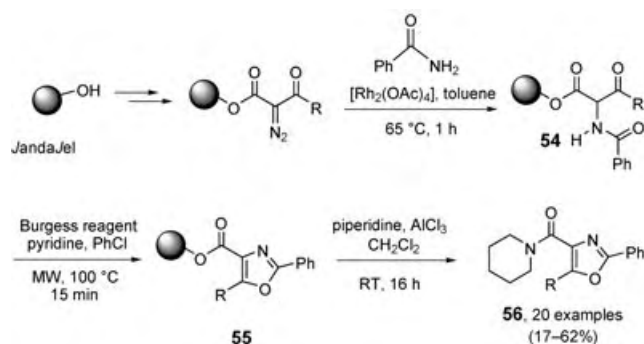
Kappe and co-workers have reported a multistep solid-phase synthesis of bicyclic pyrimidine derivatives by a Biginelli multicomponent reaction combined with multidirectional cyclative cleavage reactions (Scheme 47).^[221] This approach required the synthesis of the 4-chloroacetoacetate resin as the key starting material, which was prepared by microwave-assisted acetoacetylation of hydroxymethyl poly-



Scheme 47. Preparation of various bicyclic dihydropyrimidinones by cyclative cleavage.

styrene resin. In analogy to earlier work,^[222] this transesterification was best carried out under open-vessel conditions in 1,2-dichlorobenzene (170°C) to allow the formed methanol to be removed from the equilibrium (see also Scheme 20). This resin precursor was subsequently treated with urea and various aldehydes in an acid-catalyzed Biginelli multicomponent reaction (dioxane, 70°C) to afford the corresponding resin-bound dihydropyrimidinones. The desired furo[3,4-*d*]pyrimidine-2,5-diones were obtained by cyclative release in DMF at 150°C. Pyrrolo[3,4-*d*]pyrimidine-2,5-diones were also synthesized using the same pyrimidine resin precursor, which was first treated with a representative set of primary amines to substitute the chlorine atom. Subsequent cyclative cleavage was carried out at temperatures between 150 and 250°C and led to the corresponding pyrrolopyrimidine-2,5-dione products in high purity. The synthesis of pyrimido[4,5-*d*]pyridazine-2,5-diones was carried out in a similar manner, by employing hydrazines for the nucleophilic substitution prior to cyclative cleavage. A number of related microwave-assisted cyclative-release protocols have been reported.^[223,224]

Apart from traditional cross-linked polystyrene resins a number of different supports and formats have been used in microwave-assisted SPOS. These include tentagel resins,^[117,213,214,225] cellulose membranes (SPOT synthesis),^[226,227] cellulose beads,^[228] and glass surfaces.^[229] Janda and co-workers have described the use of JandaJel as the support in the solid-phase synthesis of oxazoles (Scheme 48).^[230] In this case, resin-bound α -acylamino- β -ketoesters **54** were treated with Burgess reagent to form oxazoles **55**, which were then cleaved from the resin by using a diversity-building amidation reaction. The conditions for the key cyclization step **54**→**55** were carefully optimized with microwave dielectric heating and by monitoring the reaction by on-bead IR spectroscopy. The best conditions utilized 3.0 equivalents of the Burgess reagent and 20 equivalents of pyridine in chlorobenzene (100°C, 15 min). Interestingly,



Scheme 48. Preparation of oxazoles by cyclization of α -acetylamino- β -ketoesters.

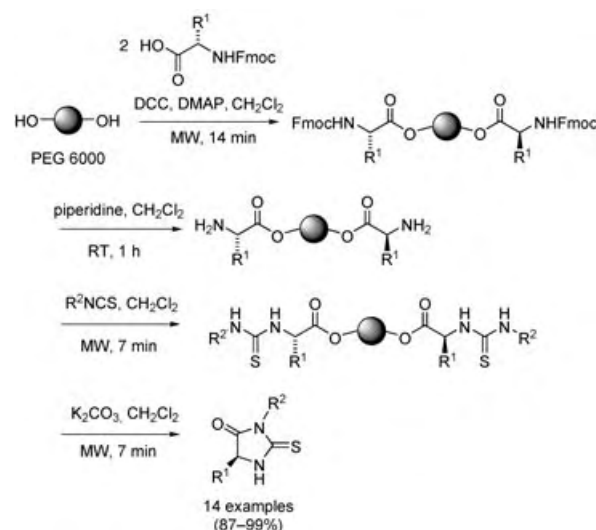
conventional thermal heating at 80 °C for 4 hours was used for the production of the final library since it provided conversions as high as the 15 minutes microwave run.

One reason why microwave-assisted SPOS has not been as powerful a technique as it perhaps could be is the lack of suitable technology that would allow the combination of sealed-vessel microwave heating and bottom filtration (or related) methods for automated removal of excess reagents or solvents and for performing the required washing steps.^[231] Currently such vessel equipment is not generally available, and therefore the advantages of SPOS in conjunction with microwave technology can not be fully exploited. Additional examples of SPOS with controlled microwave heating are found in ref. [232].

2.9.2. Liquid-Phase Synthesis on Soluble Polymer Supports

Besides solid-phase organic synthesis (SPOS) involving insoluble cross-linked polymer supports, chemistry on soluble polymer matrices, sometimes called liquid-phase organic synthesis, has emerged as a viable alternative.^[233] Problems associated with the heterogeneous nature of the ensuing chemistry and on-bead spectroscopic characterization in SPOS have led to the development of soluble polymers as alternative matrices for the production of combinatorial libraries. Synthetic approaches that utilize soluble polymers couple the advantages of homogeneous solution chemistry (high reactivity, lack of diffusion phenomena, and ease of analysis) with those of solid-phase methods (use of excess reagents and easy isolation and purification of products). Separation of the functionalized matrix is achieved by either solvent or heat precipitation, membrane filtration, or size-exclusion chromatography.^[233]

A variety of successful microwave-assisted transformations involving soluble polymers such as polyethylene glycol (PEG) have been reported since 1999,^[234] and most recently by Sun and co-workers using controlled open-vessel microwave conditions.^[235,236] In the example shown in Scheme 49 polyethylene glycol of molecular weight 6000 (PEG 6000) was used as a support for the synthesis of a small library of thiohydantoin.^[235] In the first step Fmoc-protected amino acids (3.0 equiv) were loaded onto the support by standard peptide coupling with classical DCC/DMAP activation. The coupling was carried out in dichloromethane and required



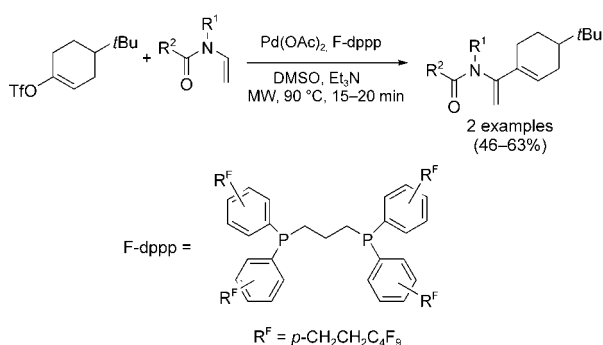
Scheme 49. Preparation of thiohydantoin on a PEG support. All microwave-assisted steps were carried out under open-vessel conditions.

14 minutes of microwave irradiation under open-vessel reflux conditions. Following deprotection with 10% piperidine in dichloromethane at room temperature, various isothiocyanates (3.0 equiv) were introduced by heating under reflux conditions (7 min), again in the same solvent. The cyclization/traceless cleavage step was completed under mildly basic conditions (K_2CO_3) within 7 minutes and provided the desired thiohydantoin in high overall yield and purity. Although the authors did not report any reaction temperatures apart from “reflux conditions” they noted that control experiments under conventional reflux conditions required significantly longer reaction times, which would indicate the presence of a specific microwave effect (namely, a superheating effect at atmospheric pressure).

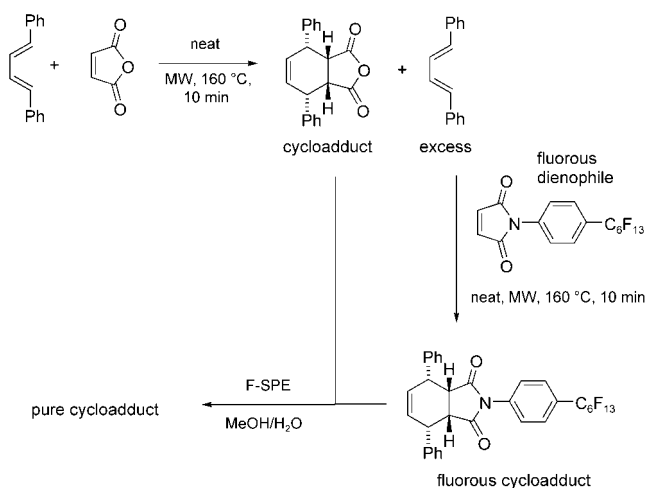
2.9.3. Reactions in Fluorous Phases

Tagged fluorous substrates, reagents, catalysts, and scavengers are becoming increasingly popular in organic synthesis, particularly since the advent of high-speed purification techniques such as fluorous solid-phase extraction (F-SPE).^[237] The first reports on fluorous synthesis under microwave conditions date back to 1997 and involved Stille coupling reactions with fluorous tin reagents.^[238] This was later followed by examples of radical reactions initiated by fluorous tin hydrides.^[197] More recently there have been reports on very efficient Pd-catalyzed cross-coupling reactions of perfluoroalkylsulfonates with thiols,^[239] and on the use of fluorous-tagged bidentate ligands in microwave-assisted Heck reactions of vinyl triflates with enamides (Scheme 50).^[240] F-SPE was used to remove excess reagents or ligands, respectively, in the two cases.

An interesting application of the use of fluorous scavenging in conjunction with microwave synthesis and F-SPE purification was recently illustrated by Werner and Curran^[241] in their investigation of the Diels–Alder cycloaddition of maleic anhydride with diphenylbutadiene (Scheme 51). After



Scheme 50. Heck vinylation of enamides in the presence of fluorinated ligands.



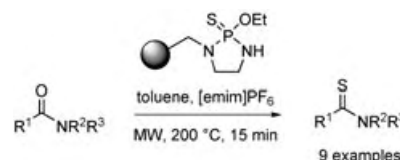
Scheme 51. Fluorous dienophiles as diene scavengers in Diels–Alder cycloadditions.

performing a microwave-assisted cycloaddition (160 °C, 10 min) with a 50% excess of the diene, the excess diene reagent was rapidly scavenged by a structurally related fluorinated dienophile under the same reaction conditions. Elution of the product mixture through a F-SPE column with MeOH/H₂O provided the desired cycloadduct in 79% yield and 90% purity. Subsequent elution with diethyl ether furnished the fluorinated Diels–Alder cycloadduct.

2.9.4. Polymer-Supported Reagents, Catalysts, and Scavengers

Apart from traditional solid-phase organic synthesis (SPOS), the use of polymer-supported reagents (PSR) has gained increasing attention from practitioners in the field of combinatorial chemistry.^[242] The use of PSRs combines the benefits of SPOS with many advantages of traditional solution-phase synthesis. The most important advantages of these reagents are the simplification of reaction work-up and product isolation, with the former being reduced to simple filtrations. In addition, PSRs can be used in excess without affecting the purification step. Reactions can be driven to completion more easily by using this technique than in conventional solution-phase chemistry.

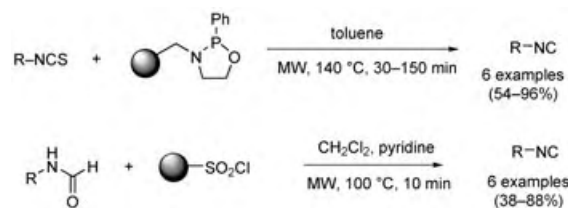
The combination of MAOS and PSR technology is a rapidly growing field.^[243] An early example of microwave-assisted PSR chemistry published by Ley et al. involves the rapid conversion of amides into thioamides by employing a polystyrene-supported Lawesson-type thionating reagent.^[51] A range of secondary and tertiary amides was converted within 15 min with 3–20 equivalents of the PSR into the corresponding thioamides in high yield and purity by using microwave irradiation at 200 °C (Scheme 52). These thiona-



Scheme 52. Thionation of amides using a polymer-supported thionating reagent.

tion reactions showed a marked acceleration in the reaction rate compared to classical reflux conditions, with reaction times being reduced from 30 hours to 10–15 minutes. Interestingly, heating at these elevated temperatures caused no damage to the polymeric support. As toluene itself is a less than optimum solvent for absorption and dissipation of microwave energy (see Table 1), a small amount of ionic liquid (1-ethyl-3-methyl-1*H*-imidazolium hexafluorophosphate) was added to the reaction mixture to ensure an even and efficient distribution of heat.

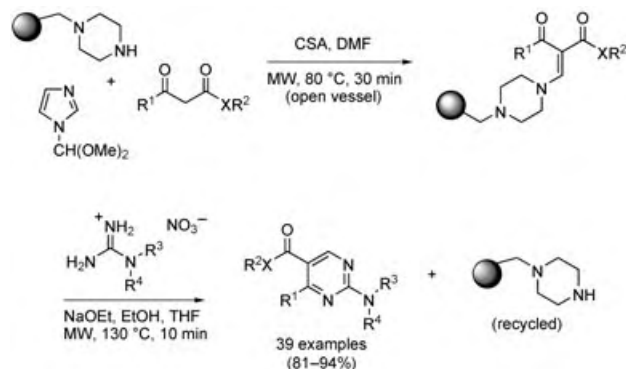
Isonitriles represent an important class of monomers, and their unique reactivity in MCRs (see for, example, Scheme 26) have made them ideal targets for synthesis. Since the preparation and subsequent purification of the sometimes unstable isonitriles prepared by solution-phase methods is not trivial, a process allowing the rapid generation of isonitriles “on demand” is highly desirable. Two independent routes to isonitriles involving microwave-assisted PSR chemistry were reported in 2002 (Scheme 53).^[244–246] In the approach described by Ley and Taylor, a suspension of an isothiocyanate and a polymer-supported 1,3,2-oxazaphosphoridine reagent (1.5–3.0 equiv) in toluene was heated under sealed-vessel microwave irradiation conditions at 140 °C. This method enabled the preparation of primary, secondary, tertiary and aromatic isocyanides in high yields and purities.^[244] In an alternative method presented by Bradley and co-workers,^[245] formamides (which themselves can be efficiently prepared by MAOS)^[246] were treated with a sulfonyl



Scheme 53. Preparation of isonitriles by using polymer-bound reagents.

chloride resin (3.0 equiv) and pyridine (50 equiv) in dichloromethane. The optimum conditions involved heating the mixture at 100 °C for 10 minutes and provided the desired isonitriles in moderate to high yields.^[245,246]

Very recently, Porcheddu et al. described an attractive “resin capture and release” strategy for the preparation of libraries of 2,4,5-trisubstituted pyrimidines (Scheme 54).^[247]

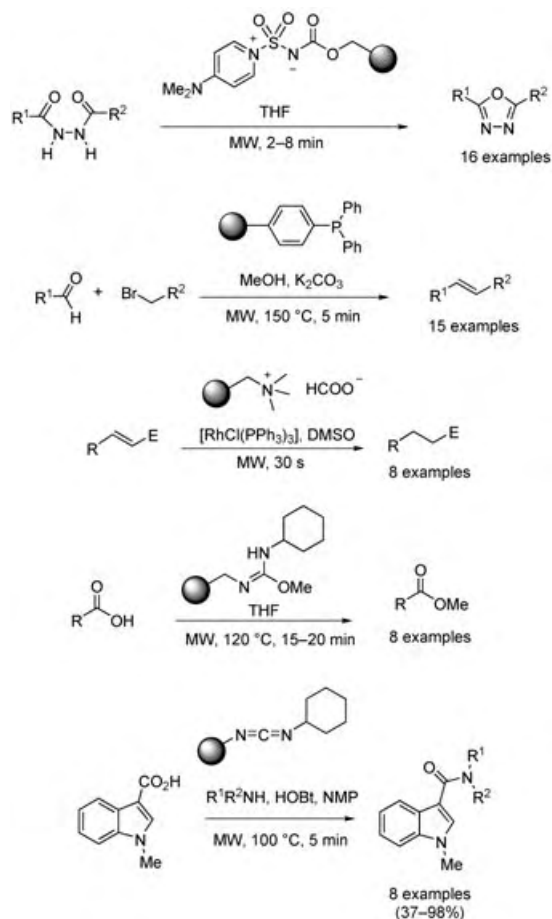


Scheme 54. Resin capture and release strategy for the solid-phase synthesis of pyrimidine libraries.

The key to the success of the “traceless” synthesis of the pyrimidines is the capturing of β -ketoesters or β -ketoamides on a solid-supported piperazine. Heating a mixture of the piperazine resin, *N*-formylimidazole dimethyl acetal, and the 1,3-dicarbonyl compound in DMF in the presence of 10 mol % camphersulfonic acid (CSA) at 80 °C for 30 minutes provided resin-bound enaminones in high yields. As in earlier examples described in this Review (see Schemes 20 and 47), it was found to be advantageous to work under open-vessel conditions to allow the removal of the formed methanol from the equilibrium. The desired pyrimidines were then released from the resin by heating the resin-bound enaminones in the presence of 1.0 equivalent of guanidinium nitrates (prepared by a MAOS method) at 130 °C for 10 minutes. A 39-member library of pyrimidines was prepared in excellent overall yields and purities. Related microwave-assisted capture and release strategies have been reported by Turner and co-workers.^[248] Some other applications of microwave-assisted PSR chemistry are summarized in Scheme 55.

A truly remarkable combination of polymer-bound reagents, catalysts, and scavengers was used by Ley and co-workers in their total synthesis of the natural product (+)-plicamine (Scheme 56).^[254] Microwave dielectric heating was used as the primary means of accelerating a number of slow reactions to maximize the quantities of intermediates that could be progressed through the synthetic sequence. The rapid optimization and screening of reaction conditions permitted by the adoption of automated microwave synthesis was crucial to the successful completion of this synthesis. Further details are found in the original references.^[254]

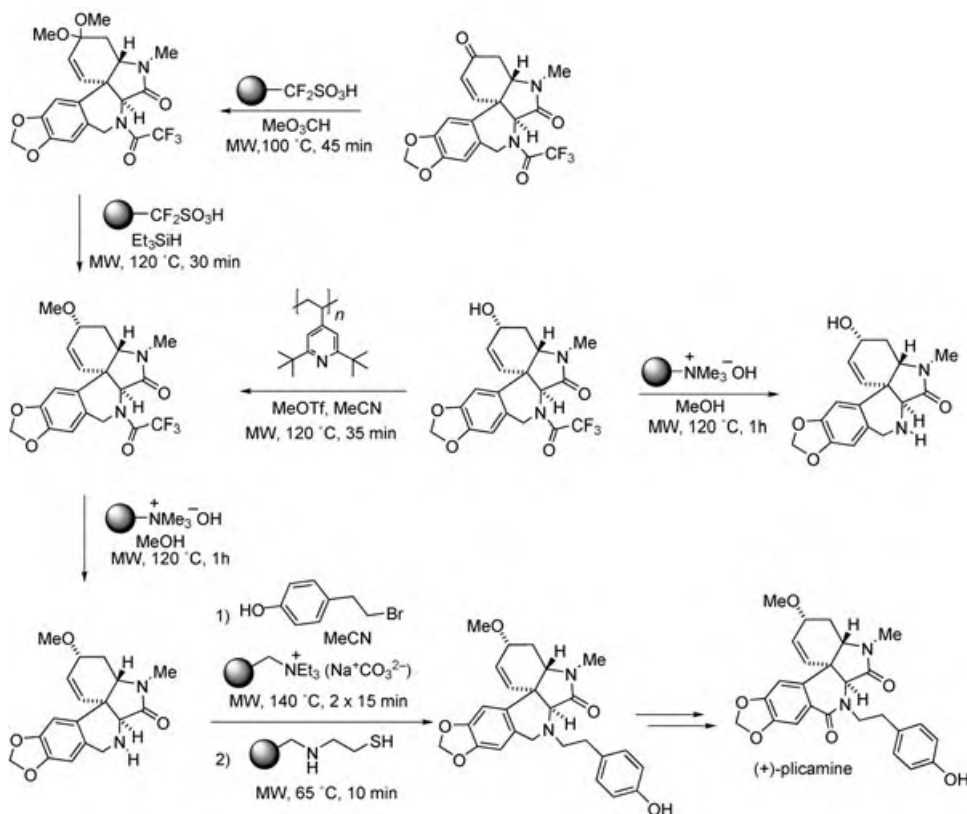
The methodical examination of microwave-assisted scavenging techniques has only been explored recently. An appealing sequence of microwave-assisted synthesis and scavenging was reported by Ellman and co-workers



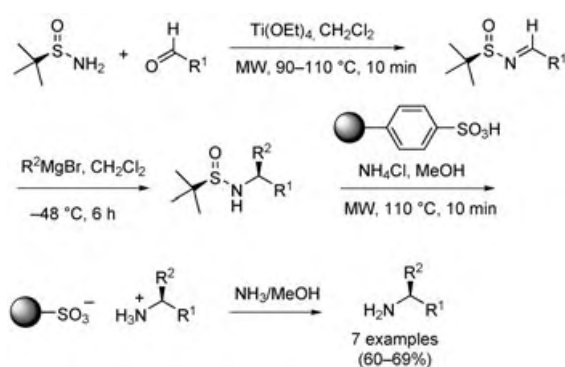
Scheme 55. Examples of resin-bound reactions: synthesis of 1,3,4-oxadiazoles using Burgess reagent,^[249] Wittig reactions with triarylphosphanes,^[250] catalytic transfer reaction involving formate,^[251] O-alkylation with O-alkyl isoureas,^[252] and formation of amide bonds with carbodiimide.^[253] HOBt = 1-hydroxybenzotriazole.

(Scheme 57).^[255] The authors used microwave heating in the first step of their asymmetric synthesis of α -substituted amines to facilitate the formation of an imine intermediate from chiral 2-methylpropan-2-sulfinamide and an aldehyde precursor. Optimized conditions involved heating the sulfinamide with the aldehyde (1.2 equiv) in the presence of the Lewis acid and water scavenger $\text{Ti}(\text{OEt})_4$ (2.2 equiv) in dichloromethane at 90–110 °C for 10 minutes. Excess titanium reagent was removed by treatment of the crude mixture with water-saturated diatomaceous earth and subsequent filtration through silica gel. The nucleophilic addition of organomagnesium reagents to sulfinylimines proceeded with high diastereoselectivity at –48 °C. Finally, cleavage of the sulfinyl group with concomitant capture using a macroporous sulfonic acid resin in the presence of catalytic amounts of ammonium chloride (110 °C, 10 min) provided the desired amine tightly bound to the acidic ion-exchange resin. After washing the resin with methanol and dichloromethane, elution with ammonia furnished the chiral amines in high overall yield and purity.

A related, microwave-assisted scavenging process involving the rapid sequestration of amines by a high-loading Wang



Scheme 56. Total synthesis of (+)-plicamine.^[243]



Scheme 57. Preparation of chiral amines from sulfinylimines.

aldehyde resin was reported by Messeguer and co-workers,^[256] and a systematic kinetic study on microwave-assisted scavenging techniques involving various types of supports was published in 2003.^[257]

A recent review has highlighted the growing importance of utilizing immobilized catalysts (namely, nanopalladium species) in conjunction with microwave dielectric heating.^[258]

2.10. Scale-Up Problems

It has to be noted that, with very few exceptions, most examples of microwave-assisted synthesis discussed in this

Review were performed on a less than 1 g scale (typically 1–5 mL reaction volume). This is in part a consequence of the recent availability of single-mode microwave reactors that allow the safe processing of small reaction volumes under sealed-vessel conditions by microwave irradiation (see Section 1.3).^[36, 38]

While these instruments have been very successful for small-scale organic synthesis, it is clear that for microwave-assisted synthesis to become a fully accepted technology in the future there is a need to develop larger scale MAOS techniques that can ultimately provide products routinely on a multikilogram scale (or even higher).

Two different approaches to closed-vessel microwave synthesis on a larger scale (> 100 mL processing volume) have emerged that have taken into consideration the physical limitations of micro-

wave dielectric heating.^[259] While some research groups have employed larger batch-type multimode^[35, 42, 46, 137, 189, 200, 260] or monomode reactors,^[261] others have used continuous-flow techniques (multi- and monomode)^[59, 262] to overcome the inherent problems associated with scaling-up MAOS.

Modern single-mode microwave technology allows the performance of MAOS in very small reaction volumes (0.2 mL).^[263] Several authors have reported independently the feasibility of directly scaling reaction conditions from small-scale single-mode (typically 0.5–5 mL) to larger scale multimode batch microwave reactors (10–500 mL) without reoptimization of the reaction conditions.^[42, 131, 137, 189, 200] In particular, volumes of up to 1000 mL have been reported to be processed successfully in open-vessel environments under microwave conditions.^[46] The preferable option for processing volumes of > 1 L seems to be a continuous-flow technique, although here the number of published examples using dedicated microwave reactors is limited.^[59, 262] At the present time there are no documented published examples of the use of microwave technology for organic synthesis on a production-scale level (> 1000 kg), which is a clear limitation of this otherwise so successful technology.^[26]

3. Summary and Outlook

The examples provided in Section 2 of this Review should make it clear that many types of chemical transformations can be carried out successfully under microwave conditions. This

does not necessarily imply that dramatic rate enhancements compared to a classical, thermal process will be observed in all cases,^[264] but the simple convenience of using microwave technology will make this nonclassical heating method a standard tool in the laboratory within a few years. In the past, microwaves were often used only when all other options for performing a particular reaction have failed, or when exceedingly long reaction times or high temperatures were required to complete a reaction. This practice is now slowly changing and, as a result of the growing availability of microwave reactors in many laboratories, routine synthetic transformations are also now being carried out by microwave heating.

The benefits of controlled microwave heating, in particular in conjunction with using sealed-vessel systems, are manifold:

- Most importantly, microwave processing frequently leads to dramatically reduced reaction times, higher yields, and cleaner reaction profiles. In many cases the observed rate enhancements may be simply a consequence of the high reaction temperatures that can rapidly be obtained by using this nonclassical heating method, or may result from the involvement of so-called specific or nonthermal microwave effects (Section 1.2).
- The choice of solvent for a given reaction is not governed by the boiling point (as in a conventional reflux setup) but rather by the dielectric properties of the reaction medium which can be easily tuned by, for example, addition of highly polar materials such as ionic liquids.
- The monitoring mechanisms for temperature and pressure in modern microwave reactors allow for an excellent control of reaction parameters (Figure 2), which generally leads to more reproducible reaction conditions.
- The overall process is more energy efficient than classical oil-bath heating, since direct “in-core” heating of the medium occurs (Figure 1).
- Microwave heating can rapidly be adapted to a parallel or automatic sequential processing format. In particular, the latter technique allows for the rapid testing of new ideas and high-speed optimization of reaction conditions (see Figure 3). The fact that a “yes or no answer” for a particular chemical transformation can often be obtained within 5 to 10 minutes (as opposed to several hours in a conventional protocol) has contributed significantly to the acceptance of microwave chemistry both in industry and academia. The recently reported incorporation of real-time, in situ monitoring of microwave-assisted reactions by Raman spectroscopy will allow a further increase in efficiency and speed in microwave chemistry.^[265]

Apart from traditional organic and combinatorial synthesis protocols covered in this Review (see Section 2), more recent applications of microwave chemistry include biochemical processes such as a high-speed polymerase chain reaction (PCR),^[266] rapid enzyme-mediated protein mapping,^[267] and general enzyme-mediated organic transformations (biocatalysis).^[268] Furthermore, microwaves have been used in conjunction with electrochemical^[269] and photochemical processes,^[270] and are also employed in polymer chemistry^[271] and material science applications,^[272] such as the fabrication and modification of carbon nanotubes or nanowires.^[273]

So why isn't everybody using microwaves? One of the major drawbacks of this relatively new technology is equipment cost. While prices for dedicated microwave reactors for organic synthesis have come down considerably since their first introduction in the late 1990s, the current price range for microwave reactors is still many times higher than that of conventional heating equipment.^[36–38] As with any new technology, the current situation is bound to change over the next several years, and less expensive equipment should become available. Microwave reactors will then truly have become the “Bunsen burners of the 21st century”^[274] and will be standard equipment in every chemical laboratory.

Addendum

Many additional applications of controlled microwave-assisted organic synthesis have appeared in the literature since the submission of the original manuscript. A selection is described below.

A series of air- and moisture-stable [Pd(allyl)Cl(NHC)] complexes with N-heterocyclic carbene ligands has been shown by Nolan and co-workers to catalyze Suzuki–Miyaura cross-coupling reactions of aryl chlorides with boronic acids.^[275] This catalytic system is compatible with microwave conditions and rapid couplings were observed within 1.5 minutes at 120 °C. The conventionally heated reactions (60 °C) required several hours to reach completion. The same article also reports on microwave-assisted dehalogenations of aryl chlorides by using the same catalytic system.

Alterman and co-workers have employed a tandem carbonylation/lactonization sequence for the synthesis of phthalides.^[276] Optimum conditions involved the use of [Mo(CO)₆] as a solid source of CO, and Pd(OAc)₂/dpfp as a catalyst (5 mol %) at 180 °C. The microwave-assisted carbonylation/cyclization method was also applied for the synthesis of other scaffolds, such as dihydroisocoumarins, dihydroisindones, and phthalimides.

Harmata et al. have disclosed an efficient protocol for the Pd-catalyzed N-arylation of enantiopure sulfoximines with aryl chlorides.^[277] Optimal results were achieved by using Pd(OAc)₂ as the Pd source in combination with *rac*-binap or PtBu₃ as ligands under microwave irradiation conditions. The corresponding benzothiazines were obtained with aryl chlorides bearing *ortho*-carbonyl substituents.

Hydrozirconation is a mild method for the selective preparation of functionalized organometallic compounds, and its compatibility with a range of common protecting groups represents a considerable advantage of these species over traditional organometallic reagents. Wipf et al. recently reported that the hydrozirconation of alkynes with [Cp₂Zr(H)Cl] can be greatly accelerated by microwave irradiation.^[278] A synthetically useful one-pot method for the preparation of allylic amides was elaborated where an alkyne was first hydrozirconated by microwave irradiation, followed by rapid addition of imines in the presence of dimethylzinc.

Several research groups have reported other high-speed microwave-assisted transition-metal-catalyzed transforma-

tions, such as Suzuki,^[279] Heck,^[280] Sonogashira,^[281] Negishi,^[282] and Liebeskind–Srogl reactions,^[283] Buchwald–Hartwig aminations,^[284] and related reactions.^[285]

Bahn and Adolffson have demonstrated that functionalized 2,5-dihydropyrroles can be obtained by microwave-mediated ruthenium-catalyzed ring-closing metathesis (RCM).^[286] The required olefin precursors were conveniently obtained from aza-Baylis–Hillman adducts. Microwave irradiation for 1–2 minutes at 100 °C of a dilute solution of the diene with 5 mol% Grubbs II catalyst in dichloromethane produces the desired dihydropyrroles in high yield. Microwave-assisted enyne-RCM chemistry has been reported by Brown and co-workers.^[287]

A simple, high-yielding synthesis of 2,4,5-trisubstituted imidazoles from 1,2-diketones and aldehydes in the presence of ammonium acetate was recently reported by Wolkenberg et al.^[288] Alkyl-, aryl-, and heteroaryl-substituted imidazoles were formed in very high yields ranging from 76–99% by utilizing microwave irradiation. Further microwave-assisted alkylation of 2,4,5-trimethylimidazole with benzyl chloride in the presence of base led to the alkaloid lepidiline B in 43% overall yield.

Wellner and co-workers have made extensive use of microwave chemistry in the preparation of cyclic thioureas and guanidines.^[289] It was possible to assemble all intermediates and target molecules by MAOS without any need for activation or protecting groups, thus reducing reaction and workup times to a minimum. A variety of other heterocycle syntheses based on microwave protocols have also been published.^[290]

A recent publication by the research group of Baran reports the total synthesis of ageliferin, an antiviral agent with interesting molecular architecture.^[291] Just one minute (!) of microwave irradiation of sceptrin, another natural product, at 195 °C in water under sealed-vessel conditions provides ageliferin in 40% yield, along with 52% of recovered starting material. Remarkably, if the reaction is performed without microwaves at the same temperature only starting material and decomposition products are observed.

Moody and co-workers have employed a “biomimetic” hetero-Diels–Alder/aromatization sequence for the construction of the pyridine ring in amythiamicin D.^[292] The key cycloaddition reaction between the azadiene and enamine component was carried out by microwave irradiation at 120 °C for 12 hours and gave the required 2,3,6-tris(thiazolyl)pyridine intermediate in moderate yield. Coupling of the remaining building blocks then completed the first total synthesis of the thiopeptide antibiotic amythiamicin D.

The synthesis of fully N-differentiated heparin oligosaccharides has been demonstrated by Lohman and Seeberger. One of the many synthetic steps involves the simultaneous installment of an *N,N*-diacetate and *O*-acetyl functionality in a trisaccharide building block.^[293] Microwave irradiation of a solution in isopropenyl acetate in the presence of *p*-TsOH at 90 °C for 5 hours led to the desired product in 86% yield. This transformation could not be achieved under a variety of thermal conditions, with only poor yields achieved even after several days.

Vasudevan and Verzal have found that terminal alkynes can be hydrated under neutral conditions in the absence of metal compounds (such as AuBr₃) in distilled water.^[294] Extension of this methodology led to a one-pot conversion of alkynes into imines (hydroamination).

A recent report by Takvorian and Combs discloses the rapid synthesis of 2-amino-substituted purines by rapid, microwave-assisted nucleophilic aromatic substitution (S_N2Ar).^[295] Importantly, the authors also describe the use of small-scale reaction vessels (0.2 mL) for optimization of reaction conditions under optimal reaction concentrations.

Fukase and co-workers have reported the solid-phase synthesis of indol-2-ones (four diversity centers) by a radical cyclization pathway.^[296] The key cyclization step was carried out by using Bu₃SnH and azodiisobutyronitrile (AIBN) in DMF under microwave irradiation conditions and provided a small library of 40 compounds. Interestingly, the related radical cyclization in the solution phase was considerably less effective.

A recent publication by Blackwell and co-workers reports the multistep synthesis of a spatially addressed pyrimidine library on planar membrane supports (SPOT synthesis).^[297] Microwave irradiation was used to speed up all three steps of the synthesis on the planar support. Importantly, microwave irradiation did not affect the integrity of the cellulose support and the reaction could be easily scaled up by employing other (nonplanar) types of cellulose supports.

A study by Zhang and co-workers describes a new strategy for improving the efficiency of Suzuki coupling reactions by combining rapid microwave synthesis with fluororous separation techniques (F-SPE).^[298] The aryl perfluorooctylsulfonate precursors for Suzuki-type couplings were readily prepared from phenols and commercially available perfluorooctylsulfonyl fluoride. Subsequent Suzuki reaction with aryl boronic acids in the presence of a suitable Pd catalyst provided the desired biaryls in high yield. Work-up simply involved filtration of the reaction mixture through a F-SPE cartridge. The same authors have also recently reported on the deoxygenation reactions of aryl perfluorooctylsulfonates.^[299]

Lei and Porco have demonstrated the usefulness of a thermally stable polymer-supported anthracene derivative for scavenging dienophiles under microwave conditions.^[300] This strategy was used successfully to rapidly sequester reactive dienophiles from reaction mixtures containing Diels–Alder cycloadducts prepared by microwave-assisted Diels–Alder reaction of flavonoid dienes. Diels–Alder reactions under microwave conditions have also been used to modify single-wall carbon nanotubes (SWNT).^[301]

Two recent review articles highlight the importance of microwave chemistry for carbohydrate chemistry.^[302]

The authors work in the area of microwave chemistry has been generously supported by the Austrian Science Fund (FWF, P15582, and I18-N07), the “Jubiläumsfonds der Österreichischen Nationalbank” (ÖNB, Project 7904), and various industrial contributors. I wish to thank all my former and

present co-workers for their dedication, enthusiasm, and for their essential contributions to microwave chemistry.

Received: February 12, 2004

- [1] D. Adam, *Nature* **2003**, 421, 571–572.
- [2] R. Gedye, F. Smith, K. Westaway, H. Ali, L. Baldisera, L. Laberge, J. Rousell, *Tetrahedron Lett.* **1986**, 27, 279–282.
- [3] R. J. Giguere, T. L. Bray, S. M. Duncan, G. Majetich, *Tetrahedron Lett.* **1986**, 27, 4945–4958.
- [4] General organic synthesis: a) R. A. Abramovitch, *Org. Prep. Proced. Int.* **1991**, 23, 685–711; b) S. Caddick, *Tetrahedron* **1995**, 51, 10403–10432; c) Lidström, J. Tierney, B. Wathey, J. Westman, *Tetrahedron* **2001**, 57, 9225–9283; for more technical reviews, see: d) M. Nüchter, B. Ondruschka, W. Bonrath, A. Gum, *Green Chem.* **2004**, 6, 128–141; e) M. Nüchter, U. Müller, B. Ondruschka, A. Tied, W. Lautenschläger, *Chem. Eng. Technol.* **2003**, 26, 1207–1216.
- [5] a) C. R. Strauss, R. W. Trainor, *Aust. J. Chem.* **1995**, 48, 1665–1692; b) C. R. Strauss, *Aust. J. Chem.* **1999**, 52, 83–96.
- [6] Open-vessel technology (MORE): a) A. K. Bose, B. K. Banik, N. Lavlinskaia, M. Jayaraman, M. S. Manhas, *Chemtech* **1997**, 27, 18–24; b) A. K. Bose, M. S. Manhas, S. N. Ganguly, A. H. Sharma, B. K. Banik, *Synthesis* **2002**, 1578–1591.
- [7] Cycloaddition reactions: A. de la Hoz, A. Díaz-Ortiz, A. Moreno, F. Langa, *Eur. J. Org. Chem.* **2000**, 3659–3673.
- [8] Heterocycle synthesis: a) J. Hamelin, J.-P. Bazureau, F. Texier-Boullet in *Microwaves in Organic Synthesis* (Ed.: A. Loupy), Wiley-VCH, Weinheim, **2002**, pp. 253–294; b) T. Besson, C. T. Brain in *Microwave-Assisted Organic Synthesis* (Eds.: P. Lidström, J. P. Tierney), Blackwell, Oxford, **2004**, Chap. 3; c) Y. Xu, Q.-X. Guo, *Heterocycles* **2004**, 63, 903–974.
- [9] Radiochemistry: a) N. Elander, J. R. Jones, S.-Y. Lu, S. Stone-Elander, *Chem. Soc. Rev.* **2000**, 29, 239–250; b) S. Stone-Elander, N. Elander, *J. Labelled Compd. Radiopharm.* **2002**, 45, 715–746.
- [10] Homogeneous transition-metal-catalysis: a) M. Larhed, C. Moberg, A. Hallberg, *Acc. Chem. Res.* **2002**, 35, 717–727; b) K. Olofsson, M. Larhed, in *Microwave-Assisted Organic Synthesis* (Eds.: P. Lidström, J. P. Tierney), Blackwell, Oxford, **2004**, Chap. 2.
- [11] Medicinal chemistry: a) J. L. Krstenansky, I. Cotterill, *Curr. Opin. Drug Discovery Dev.* **2000**, 3, 454–461; b) M. Larhed, A. Hallberg, *Drug Discovery Today* **2001**, 6, 406–416; c) B. Wathey, J. Tierney, P. Lidström, J. Westman, *Drug Discovery Today* **2002**, 7, 373–380; d) N. S. Wilson, G. P. Roth, *Curr. Opin. Drug Discovery Dev.* **2002**, 5, 620–629; e) C. D. Dzierba, A. P. Combs in *Ann. Rep. Med. Chem.*, Vol. 37 (Ed.: A. M. Doherty), Academic Press, **2002**, pp. 247–256.
- [12] Combinatorial chemistry: a) A. Lew, P. O. Krutznik, M. E. Hart, A. R. Chamberlin, *J. Comb. Chem.* **2002**, 4, 95–105; b) C. O. Kappe, *Curr. Opin. Chem. Biol.* **2002**, 6, 314–320; c) P. Lidström, J. Westman, A. Lewis, *Comb. Chem. High Throughput Screening* **2002**, 5, 441–458; d) H. E. Blackwell, *Org. Biomol. Chem.* **2003**, 1, 1251–1255; e) F. Al-Obeidi, R. E. Austin, J. F. Okonya, D. R. S. Bond, *Mini-Rev. Med. Chem.* **2003**, 3, 449–460; f) K. M. K. Swamy, W.-B. Yeh, M.-J. Lin, C.-M. Sun, *Curr. Med. Chem.* **2003**, 10, 2403–2423; g) *Microwaves in Combinatorial and High-Throughput Synthesis* (Ed.: C. O. Kappe), Kluwer, Dordrecht, **2003** (a special issue of *Mol. Diversity* **2003**, 7, pp. 95–307); h) A. Stadler, C. O. Kappe in *Microwave-Assisted Organic Synthesis* (Eds.: P. Lidström, J. P. Tierney), Blackwell, Oxford, **2004**, Chapter 7.
- [13] For online resources on microwave-assisted organic synthesis (MAOS), see: www.maos.net.
- [14] *Microwaves in Organic Synthesis* (Ed.: A. Loupy), Wiley-VCH, Weinheim, **2002**.
- [15] B. L. Hayes, *Microwave Synthesis: Chemistry at the Speed of Light*, CEM Publishing, Matthews NC, **2002**.
- [16] *Microwave-Assisted Organic Synthesis* (Eds.: P. Lidström, J. P. Tierney), Blackwell, Oxford, **2004**.
- [17] a) D. Stuerge, M. Delmotte in *Microwaves in Organic Synthesis* (Ed.: A. Loupy), Wiley-VCH, Weinheim, **2002**, pp. 1–34; b) M. D. P. Mingos in *Microwave-Assisted Organic Synthesis* (Eds.: P. Lidström, J. P. Tierney), Blackwell, Oxford, **2004**, Chap. 1.
- [18] D. R. Baghurst, D. M. P. Mingos, *Chem. Soc. Rev.* **1991**, 20, 1–47.
- [19] C. Gabriel, S. Gabriel, E. H. Grant, B. S. Halstead, D. M. P. Mingos, *Chem. Soc. Rev.* **1998**, 27, 213–223.
- [20] In specific cases, magnetic field interactions have also been observed, see: a) D. V. Stass, J. R. Woodward, C. R. Timmel, P. J. Hore, K. A. McLauchlan, *Chem. Phys. Lett.* **2000**, 329, 15–22; b) C. R. Timmel, P. J. Hore, *Chem. Phys. Lett.* **1996**, 257, 401–408; c) J. R. Woodward, R. J. Jackson, C. R. Timmel, P. J. Hore, K. A. McLauchlan, *Chem. Phys. Lett.* **1997**, 272, 376–382.
- [21] a) K. C. Westaway, R. Gedye, *J. Microwave Power* **1995**, 30, 219–230; b) F. Langa, P. de la Cruz, A. de la Hoz, A. Díaz-Ortiz, E. Díez-Barra, *Contemp. Org. Synth.* **1997**, 4, 373–386.
- [22] L. Perreux, A. Loupy, *Tetrahedron* **2001**, 57, 9199–9223.
- [23] a) N. Kuhnert, *Angew. Chem.* **2002**, 114, 1943–1946; *Angew. Chem. Int. Ed.* **2002**, 41, 1863–1866; b) C. R. Strauss, *Angew. Chem.* **2002**, 114, 3741–3743; *Angew. Chem. Int. Ed.* **2002**, 41, 3589–3590.
- [24] a) D. R. Baghurst, D. M. P. Mingos, *J. Chem. Soc. Chem. Commun.* **1992**, 674–677; b) R. Saillard, M. Poux, J. Berlan, M. Audhuy-Peaudercerf, *Tetrahedron* **1995**, 51, 4033–4042; c) F. Chemat, E. Esveld, *Chem. Eng. Technol.* **2001**, 24, 735–744.
- [25] a) D. Bogdal, M. Lukasiewicz, J. Pielichowski, A. Miciak, Sz. Bednarz, *Tetrahedron* **2003**, 59, 649–653; b) M. Lukasiewicz, D. Bogdal, J. Pielichowski, *Adv. Synth. Catal.* **2003**, 345, 1269–1272.
- [26] M. Hajek in *Microwaves in Organic Synthesis* (Ed.: A. Loupy), Wiley-VCH, Weinheim, **2002**, pp. 345–378.
- [27] a) H. Will, P. Scholz, B. Ondruschka, *Chem. Ing. Tech.* **2002**, 74, 1057–1067; b) X. Zhang, C. S.-M. Lee, D. M. P. Mingos, D. O. Hayward, *Catal. Lett.* **2003**, 88, 129–139; c) X. Zhang, D. O. Hayward, D. M. P. Mingos, *Catal. Lett.* **2003**, 88, 33–38.
- [28] The elimination of wall effects and low thermal gradients (bulk heating) in microwave heated reactions has frequently been suggested to rationalize the outcome of microwave-assisted reactions; for examples, see refs. [5a], [41], [127], [143a], [197].
- [29] Related to the issue of microwave effects is the recent concept that simultaneous external cooling of the reaction mixture (or maintaining subambient reaction temperatures) while heating by microwaves leads to an enhancement of the overall process. For published examples, see refs. [30], [31], and [15] (in particular pp. 22–23).
- [30] J. J. Chen, S. V. Deshpande, *Tetrahedron Lett.* **2003**, 44, 8873–8876.
- [31] F. Mathew, K. N. Jayaprakash, B. Fraser-Reid, J. Mathew, J. Scicinski, *Tetrahedron Lett.* **2003**, 44, 9051–9054.
- [32] a) A. Loupy, A. Petit, J. Hamelin, F. Texier-Boullet, P. Jacquault, D. Mathé, *Synthesis* **1998**, 1213–1234; b) R. S. Varma, *Green Chem.* **1999**, 1, 43–55; c) M. Kidawi, *Pure Appl. Chem.* **2001**, 73, 147–151; d) R. S. Varma, *Pure Appl. Chem.* **2001**, 73, 193–198; e) R. S. Varma, *Tetrahedron* **2002**, 58, 1235–1255; f) R. S. Varma, *Advances in Green Chemistry: Chemical Syntheses Using Microwave Irradiation*, Kavitha, Bangalore, **2002**; see also refs. [14] and [15].

- [33] A. Laporterie, J. Marquié, J. Dubac in *Microwaves in Organic Synthesis* (Ed.: A. Loupy), Wiley-VCH, Weinheim, **2002**, pp. 219–252.
- [34] S. Deshayes, M. Liagre, A. Loupy, J.-L. Luche, A. Petit, *Tetrahedron* **1999**, *55*, 10851–10870.
- [35] C. R. Strauss in *Microwaves in Organic Synthesis* (Ed.: A. Loupy), Wiley-VCH, Weinheim, **2002**, pp. 35–60.
- [36] J. D. Ferguson, *Mol. Diversity* **2003**, *7*, 281–286; CEM Corporation, www.cemsynthesis.com.
- [37] L. Favretto, *Mol. Diversity* **2003**, *7*, 287–291; Milestone Inc., www.milestonesci.com.
- [38] J.-S. Schanche, *Mol. Diversity* **2003**, *7*, 293–300; Biotage AB (formerly Personal Chemistry AB), www.personalchemistry.com; www.biotage.com.
- [39] On the other hand, the sometimes extreme reaction temperatures may eventually lead to the decomposition of the metal catalyst and to the deposition of metal black on the inner surface of the reaction vessel. This may lead to arcing phenomena which potentially can lead to the destruction of the reaction vessel. For details on arcing phenomena under microwave conditions, see: A. G. Whittaker, D. M. P. Mingos, *J. Chem. Soc. Dalton Trans.* **2000**, 1521–1526.
- [40] I. P. Beletskaya, A. V. Cheprakov, *Chem. Rev.* **2000**, *100*, 3009–3066.
- [41] M. Larhed, A. Hallberg, *J. Org. Chem.* **1996**, *61*, 9582–9584.
- [42] A. Stadler, B. H. Yousefi, D. Dallinger, P. Walla, E. Van der Eycken, N. Kaval, C. O. Kappe, *Org. Process Res. Dev.* **2003**, *7*, 707–716.
- [43] K. S. A. Vallin, P. Emilsson, M. Larhed, A. Hallberg, *J. Org. Chem.* **2002**, *67*, 6243–6246.
- [44] *Ionic liquids in Synthesis* (Eds.: P. Wasserscheid, T. Welton), Wiley-VCH, Weinheim, **2002**.
- [45] For the preparation of ionic liquids under microwave conditions, see: a) R. S. Varma, V. V. Namboodiri, *Chem. Commun.* **2001**, 643–644; b) B. M. Khadilkar, G. L. Rebeiro, *Org. Process Res. Dev.* **2002**, *6*, 826–828; c) R. S. Varma, V. V. Namboodiri, *Tetrahedron Lett.* **2002**, *43*, 5381–5383; d) V. V. Namboodiri, R. S. Varma, *Chem. Commun.* **2002**, 342–343; e) J. F. Dubreuil, M.-H. Famelart, J. P. Bazureau, *Org. Process Res. Dev.* **2002**, *6*, 374–378; f) G. V. Thanh, B. Pegot, A. Loupy, *Eur. J. Org. Chem.* **2004**, 1112–1116.
- [46] M. Deetlefs, K. R. Seddon, *Green Chem.* **2003**, *5*, 181–186.
- [47] J. F. Dubreuil, J. P. Bazureau, *Tetrahedron Lett.* **2000**, *41*, 7351–7355.
- [48] H. Berthold, T. Schotten, H. Hönig, *Synthesis* **2002**, 1607–1610.
- [49] K. G. Mayo, E. H. Nearhoof, J. J. Kiddle, *Org. Lett.* **2002**, *4*, 1567–1570.
- [50] N. E. Leadbeater, H. M. Torenus, H. Tye, *Tetrahedron* **2003**, *59*, 2253–2258.
- [51] S. V. Ley, A. G. Leach, R. I. Storer, *J. Chem. Soc.* **2001**, 358–361.
- [52] N. E. Leadbeater, H. M. Torenus, *J. Org. Chem.* **2002**, *67*, 3145–3148.
- [53] For a further investigation, see: J. Hoffmann, M. Nüchter, B. Ondruschka, P. Wasserscheid, *Green Chem.* **2003**, *5*, 296–299.
- [54] E. Van der Eycken, P. Appukkuttan, W. De Borggraeve, W. Dehaen, D. Dallinger, C. O. Kappe, *J. Org. Chem.* **2002**, *67*, 7904–7909.
- [55] S. Garbacia, B. Desai, O. Lavastre, C. O. Kappe, *J. Org. Chem.* **2003**, *68*, 9136–9139.
- [56] G. K. Datta, K. S. A. Vallin, M. Larhed, *Mol. Diversity* **2003**, *7*, 107–114.
- [57] N. Srinivasan, A. Ganesan, *Chem. Commun.* **2003**, 916–917.
- [58] N. E. Leadbeater, H. M. Torenus, H. Tye, *Mol. Diversity* **2003**, *7*, 135–144.
- [59] W.-C. Shieh, M. Lozanov, O. Repic, *Tetrahedron Lett.* **2003**, *44*, 6943–6945.
- [60] M. J. Gaunt, A. S. Jessiman, P. Orsini, H. R. Tanner, D. F. Hook, S. V. Ley, *Org. Lett.* **2003**, *5*, 4819–4822.
- [61] For a recent review, see: A. F. Littke, G. C. Fu, *Angew. Chem.* **2002**, *114*, 4350–4386; *Angew. Chem. Int. Ed.* **2002**, *41*, 4176–4211.
- [62] M. R. Netherton, G. C. Fu, *Org. Lett.* **2001**, *3*, 4295–4298.
- [63] W. A. Herrmann, V. P. H. Böhm, C. P. Reisinger, *J. Organomet. Chem.* **1999**, *576*, 23–41.
- [64] a) V. Gracías, J. D. Moore, S. W. Djuric, *Tetrahedron Lett.* **2004**, *45*, 417–420; for intramolecular Heck reactions in the steroid series, see: b) L. F. Tietze, J. M. Wiegand, C. Vock, *J. Organomet. Chem.* **2003**, *687*, 346–352.
- [65] M. M. S. Andappan, P. Nilsson, M. Larhed, *Mol. Diversity* **2003**, *7*, 97–106.
- [66] N. Miyaoura, A. Suzuki, *Chem. Rev.* **1995**, *95*, 2457–2483.
- [67] C.-J. Li, *Angew. Chem.* **2003**, *115*, 5004–5006; *Angew. Chem. Int. Ed.* **2003**, *42*, 4856–4858.
- [68] Y. Gong, W. He, *Org. Lett.* **2002**, *4*, 3803–3805.
- [69] a) D. Nöteberg, W. Schaal, E. Hamelink, L. Vrang, M. Larhed, *J. Comb. Chem.* **2003**, *5*, 456–464; b) S. P. Miller, J. B. Morgan, F. J. Nepveux, J. P. Morken, *Org. Lett.* **2004**, *6*, 131–133.
- [70] a) N. Kaval, K. Bisztray, W. Dehaen, C. O. Kappe, E. Van der Eycken, *Mol. Diversity* **2003**, *7*, 125–134; b) Y. Gong, W. He, *Heterocycles* **2004**, *62*, 851–856.
- [71] M. G. Organ, S. Mayer, F. Lepifre, B. N'Zemba, J. Khatri, *Mol. Diversity* **2003**, *7*, 211–227.
- [72] G. Luo, L. Chen, G. S. Pointdexter, *Tetrahedron Lett.* **2002**, *43*, 5739–5742.
- [73] T. Y. H. Wu, P. G. Schultz, S. Ding, *Org. Lett.* **2003**, *5*, 3587–3590.
- [74] J. W. Han, J. C. Castro, K. Burgess, *Tetrahedron Lett.* **2003**, *44*, 9359–9362.
- [75] N. E. Leadbeater, M. Marco, *Org. Lett.* **2002**, *4*, 2973–2976.
- [76] N. E. Leadbeater, M. Marco, *J. Org. Chem.* **2003**, *68*, 888–892.
- [77] See also, L. Bai, J.-X. Wang, Y. Zhang, *Green Chem.* **2003**, *5*, 615–617.
- [78] N. E. Leadbeater, M. Marco, *Angew. Chem.* **2003**, *115*, 1445–1447; *Angew. Chem. Int. Ed.* **2003**, *42*, 1407–1409.
- [79] N. E. Leadbeater, M. Marco, *J. Org. Chem.* **2003**, *68*, 5660–5667.
- [80] A. Fürstner, G. Seidel, *Org. Lett.* **2002**, *4*, 541–543.
- [81] P. Appukkuttan, E. Van der Eycken, W. Dehaen, *Synlett* **2003**, 1204–1206.
- [82] A. Bengtson, A. Hallberg, M. Larhed, *Org. Lett.* **2002**, *4*, 1231–1233.
- [83] K. Sonogashira, *J. Organomet. Chem.* **2002**, *653*, 46–49.
- [84] M. Erdélyi, A. Gogoll, *J. Org. Chem.* **2001**, *66*, 4165–4169.
- [85] M. Erdélyi, V. Langer, A. Karlén, A. Gogoll, *New J. Chem.* **2002**, *26*, 834–843.
- [86] O. Š. Miljanić, K. P. C. Vollhardt, G. D. Whitener, *Synlett* **2003**, 29–34.
- [87] E. Petricci, M. Radi, F. Corelli, M. Botta, *Tetrahedron Lett.* **2003**, *44*, 9181–9184.
- [88] a) N. E. Leadbeater, M. Marc, B. J. Tominack, *Org. Lett.* **2003**, *5*, 3919–3922; b) P. Appukkuttan, W. Dehaen, E. Van der Eycken, *Eur. J. Org. Chem.* **2003**, 4713–4716.
- [89] H. He, Y.-J. Wu, *Tetrahedron Lett.* **2004**, *45*, 3237–3239.
- [90] L. Öhberg, J. Westman, *Synlett* **2001**, 1893–1896.
- [91] P. Stanetty, M. Schnürch, M. D. Mihovilovic, *Synlett* **2003**, 1862–1864.
- [92] P. Walla, C. O. Kappe, *Chem. Commun.* **2004**, 564–565.
- [93] B. H. Lipshutz, B. Frieman, *Tetrahedron* **2004**, *60*, 1309–1316.
- [94] a) A. R. Muci, S. L. Buchwald, *Top. Curr. Chem.* **2002**, *219*, 131–209; b) J. P. Wolfe, S. Wagaw, J. F. Marcoux, S. L. Buchwald, *Acc. Chem. Res.* **1998**, *31*, 805–818.
- [95] J. F. Hartwig, *Angew. Chem.* **1998**, *110*, 2154–2177; *Angew. Chem. Int. Ed.* **1998**, *37*, 2046–2067.

- [96] Y. Wan, M. Alterman, A. Hallberg, *Synthesis* **2002**, 1597–1600.
- [97] A. J. McCarroll, D. A. Sandham, L. R. Titcomb, A. K. de K. Lewis, F. G. N. Cloke, B. P. Davies, A. P. de Santana, W. Hiller, S. Caddick, *Mol. Diversity* **2003**, 7, 115–123.
- [98] B. U. W. Maes, K. T. J. Loones, G. L. F. Lemi  re, R. A. Dom-misse, *Synlett* **2003**, 1822–1825.
- [99] T. Wang, D. R. Magnin, L. G. Hamann, *Org. Lett.* **2003**, 5, 897–900.
- [100] T. Ulrich, F. Giraud, *Tetrahedron Lett.* **2003**, 44, 4207–4211.
- [101] C. T. Brain, J. T. Steer, *J. Org. Chem.* **2003**, 68, 6814–6816.
- [102] G. Burton, P. Cao, G. Li, R. Rivero, *Org. Lett.* **2003**, 5, 4373–4376.
- [103] A. Stadler, C. O. Kappe, *Org. Lett.* **2002**, 4, 3541–3544.
- [104] A. W. Thomas, S. V. Ley, *Angew. Chem.* **2003**, 115, 5558–5607; *Angew. Chem. Int. Ed.* **2003**, 42, 5400–5449.
- [105] Y.-J. Wu, H. He, A. L'Heureux, *Tetrahedron Lett.* **2003**, 44, 4217–4218.
- [106] For a microwave-assisted Goldberg reaction, see: J. H. M. Lange, L. J. F. Hofmeyer, F. A. S. Hout, S. J. M. Osnabrug, P. C. Verveer, C. G. Kruse, R. W. Feenstra, *Tetrahedron Lett.* **2002**, 43, 1101–1104.
- [107] Y.-J. Wu, H. He, *Synlett* **2003**, 1789–1790.
- [108] H. He, Y.-J. Wu, *Tetrahedron Lett.* **2003**, 44, 3445–3446.
- [109] N.-F. K. Kaiser, A. Hallberg, M. Larhed, *J. Comb. Chem.* **2002**, 4, 109–111.
- [110] J. Wannberg, M. Larhed, *J. Org. Chem.* **2003**, 68, 5750–5753.
- [111] J. Georgsson, A. Hallberg, M. Larhed, *J. Comb. Chem.* **2003**, 5, 456–458.
- [112] Y. Wan, M. Alterman, M. Larhed, A. Hallberg, *J. Org. Chem.* **2002**, 67, 6232–6235.
- [113] Y. Wan, M. Alterman, M. Larhed, A. Hallberg, *J. Comb. Chem.* **2003**, 5, 82–84.
- [114] P.-A. Enquist, P. Nilsson, M. Larhed, *Org. Lett.* **2003**, 5, 4875–4878.
- [115] N.-F. K. Kaiser, U. Bremberg, M. Larhed, C. Moberg, A. Hallberg, *J. Organomet. Chem.* **2000**, 603, 2–5.
- [116] U. Bremberg, S. Lutsenko, N.-F. K. Kaiser, M. Larhed, A. Hallberg, C. Moberg, *Synthesis* **2000**, 1004–1008.
- [117] N.-F. K. Kaiser, U. Bremberg, M. Larhed, C. Moberg, A. Hallberg, *Angew. Chem.* **2000**, 112, 3741–3744; *Angew. Chem. Int. Ed.* **2000**, 39, 3596–3598.
- [118] O. Belda, N.-F. Kaiser, U. Bremberg, M. Larhed, A. Hallberg, C. Moberg, *J. Org. Chem.* **2000**, 65, 5868–5870.
- [119] O. Belda, C. Moberg, *Synthesis* **2002**, 1601–1606.
- [120] B. M. Trost, N. G. Andersen, *J. Am. Chem. Soc.* **2002**, 124, 14320–14321.
- [121] O. Belda, S. Lundgren, C. Moberg, *Org. Lett.* **2003**, 5, 2275–2278.
- [122] P. Nilsson, H. Gold, M. Larhed, A. Hallberg, *Synthesis* **2002**, 1611–1614.
- [123] S. Lutsenko, C. Moberg, *Tetrahedron: Asymmetry* **2001**, 12, 2529–2532.
- [124] a) R. H. Grubbs, S. Chang, *Tetrahedron* **1998**, 54, 4413–4450; b) A. F  rstner, *Angew. Chem.* **2000**, 112, 3140–3172; *Angew. Chem. Int. Ed.* **2000**, 39, 3012–3043.
- [125] C. Yang, W. V. Murray, L. J. Wilson, *Tetrahedron Lett.* **2003**, 44, 1783–1786.
- [126] a) R. Grigg, W. Martin, J. Morris, V. Sridharan, *Tetrahedron Lett.* **2003**, 44, 4899–4901; b) D. Balan, H. Adolfsson, *Tetrahe-dron Lett.* **2004**, 45, 3089–3092.
- [127] J. Efskind, K. Undheim, *Tetrahedron Lett.* **2003**, 44, 2837–2839.
- [128] A. F  rstner, F. Stelzer, A. Rumbo, H. Krause, *Chem. Eur. J.* **2002**, 8, 1856–1871.
- [129] P. L. Pauson, *Tetrahedron* **1985**, 41, 5855–5860.
- [130] S. Fischer, U. Groth, M. Jung, A. Schneider, *Synlett* **2002**, 2023–2026.
- [131] M. Iqbal, N. Vyse, J. Dauvergne, P. Evans, *Tetrahedron Lett.* **2002**, 43, 7859–7862.
- [132] For reviews, see: a) G. Dyker, *Angew. Chem.* **1999**, 111, 1808–1822; *Angew. Chem. Int. Ed.* **1999**, 38, 1699–1712; b) F. Kakiuchi, S. Murai, *Acc. Chem. Res.* **2002**, 35, 826–834; c) V. Ritleng, C. Sirlin, M. Pfeffer, *Chem. Rev.* **2002**, 102, 1731–1769.
- [133] K. L. Tan, A. Vasudevan, R. G. Bergman, J. A. Ellman, A. J. Souers, *Org. Lett.* **2003**, 5, 2131–2134.
- [134] B. H. Lipshutz, C. C. Caires, P. Kuipers, W. Chrisman, *Org. Lett.* **2003**, 5, 3085–3088.
- [135] E. J. Hutchinson, W. J. Kerr, E. J. Magennis, *Chem. Commun.* **2002**, 2262–2263.
- [136] W. Stadlbauer, O. Schmut, T. Kappe, *Monatsh. Chem.* **1980**, 111, 1005–1013.
- [137] A. Stadler, S. Pichler, G. Horeis, C. O. Kappe, *Tetrahedron* **2002**, 58, 3177–3183.
- [138] J. H. M. Lange, P. C. Verveer, S. J. M. Osnabrug, G. M. Visser, *Tetrahedron Lett.* **2001**, 42, 1367–1369.
- [139] F.-R. Alexandre, A. Berecibar, R. Wrigglesworth, T. Besson, *Tetrahedron* **2003**, 59, 1413–1419.
- [140] F.-R. Alexandre, A. Berecibar, T. Besson, *Tetrahedron Lett.* **2002**, 43, 3911–3913.
- [141] V. Molteni, M. M. Hamilton, L. Mao, C. M. Crane, A. P. Termin, D. M. Wilson, *Synthesis* **2002**, 1669–1674.
- [142] For references on performing chemistry in near-critical and supercritical water, see: a) D. Br  ll, C. Kaul, A. Kr  mer, P. Krammer, T. Richter, M. Jung, H. Vogel, P. Zehner, *Angew. Chem.* **1999**, 111, 3180–3196; *Angew. Chem. Int. Ed.* **1999**, 38, 2999–3018; b) P. E. Savage, *Chem. Rev.* **1999**, 99, 603–621; c) N. Akiya, P. E. Savage, *Chem. Rev.* **2002**, 102, 2725–2750; d) M. Siskin, A. R. Katritzky, *Chem. Rev.* **2001**, 101, 825–835; e) Katritzky, D. A. Nichols, M. Siskin, R. Murugan, M. Balasubramanian, *Chem. Rev.* **2001**, 101, 837–892; f) A. Nolen, C. L. Liotta, C. E. Eckert, R. Gl  aser, *Green Chem.* **2003**, 5, 663–669.
- [143] For references on MAOS in near-critical water, see: a) L. Bagnell, T. Cablewski, C. R. Strauss, R. W. Trainor, *J. Org. Chem.* **1996**, 61, 7355–7359; b) J. An, L. Bagnell, T. Cablewski, C. R. Strauss, R. W. Trainor, *J. Org. Chem.* **1997**, 62, 2505–2511; c) T. A. Bryson, J. J. Stewart, J. M. Gibson, P. S. Thomas, J. K. Berch, *Green Chem.* **2003**, 5, 174–176; d) T. A. Bryson, J. M. Gibson, J. J. Stewart, H. Voegtle, A. Tiwari, J. H. Dawson, W. Marley, B. Harmon, *Green Chem.* **2003**, 5, 177–180; e) A. Vasudevan, M. K. Verzal, *Synlett* **2004**, 631–634.
- [144] J. Westman, R. Lundin, J. Stalberg, M. Ostbye, A. Franzen, A. Hurynowicz, *Comb. Chem. High Throughput Screening* **2002**, 5, 565–570.
- [145] G. Giacomelli, A. Porcheddu, M. Salaris, M. Taddei, *Eur. J. Org. Chem.* **2003**, 537–541.
- [146] N. Yu. Gorobets, B. Yousefi, C. O. Kappe, *Tetrahedron* **2004**, 60, 8633–8644.
- [147] J. Siu, I. R. Baxendale, S. V. Ley, *Org. Biomol. Chem.* **2004**, 2, 160–167.
- [148] F. Bohlmann, D. Rahtz, *Chem. Ber.* **1957**, 90, 2265–2273.
- [149] M. C. Bagley, R. Lunn, X. Xiong, *Tetrahedron Lett.* **2002**, 43, 8331–8334.
- [150] M. C. Bagley, D. D. Hughes, H. M. Sabo, P. H. Taylor, X. Xiong, *Synlett* **2003**, 1443–1446.
- [151] G. Giacomelli, L. De Luca, A. Porcheddu, *Tetrahedron* **2003**, 59, 5437–5440.
- [152] Q. Su, A. B. Beeler, E. Lobkovsky, J. A. Porco, J. S. Panek, *Org. Lett.* **2003**, 5, 2149–2152.
- [153] *Multicomponent Reactions* (Eds.: J. Zhu, H. Bienaym  ), Wiley-VCH, Weinheim, **2004**.
- [154] I. Ugi, *Pure Appl. Chem.* **2001**, 73, 187–191.
- [155] C. Blackburn, B. Guan, P. Fleming, K. Shiosaki, S. Tsai, *Tetrahedron Lett.* **1998**, 39, 3635–3638.

- [156] S. M. Ireland, H. Tye, M. Whittaker, *Tetrahedron Lett.* **2003**, *44*, 4369–4371.
- [157] a) C. O. Kappe, *Acc. Chem. Res.* **2000**, *33*, 879–888; b) C. O. Kappe, *QSAR Comb. Sci.* **2003**, *22*, 630–645.
- [158] a) A. Stadler, C. O. Kappe, *J. Comb. Chem.* **2001**, *3*, 624–630; b) C. O. Kappe, A. Stadler in *Combinatorial Chemistry Part B* (Eds.: B. B. Bunin, G. Morales), Elsevier, Amsterdam, **2003**, pp. 197–223.
- [159] A. Stadler, C. O. Kappe, *J. Chem. Soc. Perkin Trans. 1* **2000**, 1363–1368.
- [160] a) M. D. Evans, J. Ring, A. Schoen, A. Bell, P. Edwards, D. Berthelot, R. Nicewonger, C. M. Baldino, *Tetrahedron Lett.* **2003**, *44*, 9337–9341; see also: b) H. Tye, M. Whittaker, *Org. Biomol. Chem.* **2004**, *2*, 813–815.
- [161] M. Nüchter, B. Ondruschka, *Mol. Diversity* **2003**, *7*, 253–264.
- [162] M. Nüchter, B. Ondruschka, A. Tied, W. Lautenschläger, K. J. Borowski, *Am. Genomic/Proteomic Technol.* **2001**, *1*, 34–39.
- [163] M.-E. Theoclitou, L. A. Robinson, *Tetrahedron Lett.* **2002**, *43*, 3907–3910.
- [164] L. Öhberg, J. Westman, *Synlett* **2001**, 1296–1298.
- [165] a) Z. Zhao, W. H. Leister, K. A. Strauss, D. D. Wisnoski, C. W. Lindsley, *Tetrahedron Lett.* **2003**, *44*, 1123–1128; b) C. W. Lindsley, D. D. Wisnoski, Y. Wang, W. H. Leister, Z. Zhao, *Tetrahedron Lett.* **2003**, *44*, 4495–4498.
- [166] a) N. Mont, J. Teixidó, J. I. Borrell, C. O. Kappe, *Tetrahedron Lett.* **2003**, *44*, 5385–5388; b) N. Mont, J. Teixidó, J. I. Borrell, C. O. Kappe, *Mol. Diversity* **2003**, *7*, 153–159.
- [167] R. S. Pottorf, N. K. Chadha, M. Katkevics, V. Ozola, E. Suna, H. Ghane, T. Roberg, M. R. Player, *Tetrahedron Lett.* **2003**, *44*, 175–178.
- [168] M. C. Pirrung, L. N. Tumey, A. L. McClerren, C. R. H. Raetz, *J. Am. Chem. Soc.* **2003**, *125*, 1575–1586.
- [169] F. García-Tellado, A. Loupy, A. Petit, A. L. Marrero-Terrero, *Eur. J. Org. Chem.* **2003**, 4387–4391.
- [170] S. Frère, V. Thiéry, C. Bailly, T. Besson, *Tetrahedron* **2003**, *59*, 773–779.
- [171] A. R. Katritzky, S. K. Singh, *J. Org. Chem.* **2002**, *67*, 9077–9079.
- [172] N. S. Wilson, C. R. Sarko, G. P. Roth, *Tetrahedron Lett.* **2001**, *42*, 8939–8942.
- [173] I. R. Baxendale, A.-I. Lee, S. V. Ley, *J. Chem. Soc. Perkin Trans.* **2002**, 1850–1857.
- [174] T. Durand-Reville, L. B. Gobbi, B. L. Gray, S. V. Ley, J. S. Scott, *Org. Lett.* **2002**, *4*, 3847–3850.
- [175] G. Nordmann, S. L. Buchwald, *J. Am. Chem. Soc.* **2003**, *125*, 4978–4979.
- [176] B. M. Trost, O. R. Thiel, H.-C. Tsui, *J. Am. Chem. Soc.* **2003**, *125*, 13155–13164.
- [177] B. M. Trost, M. L. Crawley, *J. Am. Chem. Soc.* **2002**, *124*, 9328–9329.
- [178] D. C. G. A. Pinto, A. M. S. Silva, L. M. P. M. Almeida, J. R. Carrillo, A. Díaz-Ortiz, A. de la Hoz, J. A. S. Cavaleiro, *Synlett* **2003**, 1415–1418.
- [179] N. Kaval, W. Dehaen, C. O. Kappe, E. Van der Eycken, *Org. Biomol. Chem.* **2004**, *2*, 154–156.
- [180] N. Kaval, J. Van der Eycken, J. Caroen, W. Dehaen, G. A. Strohmeier, C. O. Kappe, E. Van der Eycken, *J. Comb. Chem.* **2003**, *5*, 560–568.
- [181] P. Dupau, R. Epple, A. A. Thomas, V. V. Fokin, K. B. Sharpless, *Adv. Synth. Catal.* **2002**, *344*, 421–433.
- [182] J. Freitag, M. Nüchter, B. Ondruschka, *Green Chem.* **2003**, *5*, 291–295.
- [183] M. Takahashi, K. Oshima, S. Matsubara, *Tetrahedron Lett.* **2003**, *44*, 9201–9203.
- [184] A. Steinreiber, A. Stadler, S. F. Mayer, K. Faber, C. O. Kappe, *Tetrahedron Lett.* **2001**, *42*, 6283–6286.
- [185] L. R. Lampariello, D. Piras, M. Rodriguez, M. Taddei, *J. Org. Chem.* **2003**, *68*, 7893–7895.
- [186] I. T. Raheem, S. N. Goodman, E. N. Jacobsen, *J. Am. Chem. Soc.* **2004**, *126*, 706–707.
- [187] H. Mohan, E. Gemma, K. Ruda, S. Oscarson, *Synlett* **2003**, 1255–1256.
- [188] E. Söderberg, J. Westman, S. Oscarson, *J. Carbohydr. Chem.* **2001**, *20*, 397–410.
- [189] F. Lehmann, Å. Pilotti, K. Luthman, *Mol. Diversity* **2003**, *7*, 145–152.
- [190] N. J. McLean, H. Tye, M. Whittaker, *Tetrahedron Lett.* **2004**, *45*, 993–995.
- [191] O. I. Zbruyev, N. Stiasni, C. O. Kappe, *J. Comb. Chem.* **2003**, *5*, 145–148.
- [192] Y.-J. Cherg, *Tetrahedron* **2000**, *56*, 8287–8289.
- [193] G. R. Brown, A. J. Foubister, C. A. Roberts, S. L. Wells, R. Wood, *Tetrahedron Lett.* **2001**, *42*, 3917–3919.
- [194] Y.-J. Cherg, *Tetrahedron* **2002**, *58*, 887–890.
- [195] Y.-J. Cherg, *Tetrahedron* **2002**, *58*, 1125–1129.
- [196] Y.-J. Cherg, *Tetrahedron* **2002**, *58*, 4931–4935.
- [197] K. Olofsson, S.-Y. Kim, M. Larhed, D. P. Curran, A. Hallberg, *J. Org. Chem.* **1999**, *64*, 4539–4541.
- [198] C. Wetter, A. Studer, *Chem. Commun.* **2004**, 174–175.
- [199] M. C. Bagley, J. W. Dale, X. Xiong, J. Bower, *Org. Lett.* **2003**, *5*, 4421–4424.
- [200] S. A. Shackelford, M. B. Anderson, L. C. Christie, T. Goetzen, M. C. Guzman, M. A. Hananel, W. D. Kornreich, H. Li, V. P. Pathak, A. K. Rabinovich, R. J. Rajapakse, L. K. Truesdale, S. M. Tsank, H. N. Vazir, *J. Org. Chem.* **2003**, *68*, 267–275.
- [201] M. G. Saulnier, K. Zimmermann, C. P. Struzynski, X. Sang, U. Velaparthi, M. Wittman, D. B. Frennesson, *Tetrahedron Lett.* **2004**, *45*, 397–399.
- [202] D. P. Curran, O. Zhang, *Adv. Synth. Catal.* **2003**, *345*, 329–332.
- [203] F. Lake, C. Moberg, *Eur. J. Org. Chem.* **2002**, 3179–3188.
- [204] N. A. Swain, R. C. D. Brown, G. Bruton, *Chem. Commun.* **2002**, 2042–2043.
- [205] V. A. Chebanov, C. Reidlinger, H. Kanaani, C. Wentrup, C. O. Kappe, G. Kollenz, *Supramol. Chem.* **2004**, *16*, 121–127.
- [206] I. Barrios, P. Camps, M. Comes-Franchini, D. Muñoz-Torrero, A. Ricci, L. Sánchez, *Tetrahedron* **2003**, *59*, 1971–1979.
- [207] N. Stiasni, C. O. Kappe, *ARKIVOC* **2002**, *8*, 71–79.
- [208] a) F. Zaragoza Dörwald, *Organic Synthesis on Solid Phase*, Wiley-VCH, Weinheim, **2002**; b) *Handbook of Combinatorial Chemistry* (Eds.: K. C. Nicolaou, R. H. Hanco, W. Hartwig), Wiley-VCH, Weinheim, **2002**.
- [209] a) A. Stadler, C. O. Kappe, *Eur. J. Org. Chem.* **2001**, 919–925; b) A. Stadler, C. O. Kappe, *Tetrahedron* **2001**, *57*, 3915–3920.
- [210] H.-M. Yu, S.-T. Chen, K.-T. Wang, *J. Org. Chem.* **1992**, *57*, 4781–4784.
- [211] M. Erdélyi, A. Gogoll, *Synthesis* **2002**, 1592–1596.
- [212] C. Lindquist, U. Tedebark, O. Ersoy, P. Somfai, *Synth. Commun.* **2003**, *33*, 2257–2262.
- [213] M. Larhed, G. Lindeberg, A. Hallberg, *Tetrahedron Lett.* **1996**, *37*, 8219–8222.
- [214] M. Erdélyi, A. Gogoll, *J. Org. Chem.* **2003**, *68*, 6431–6434.
- [215] M. Alterman, A. Hallberg, *J. Org. Chem.* **2000**, *65*, 7984–7989.
- [216] K. Weigand, S. Pelka, *Mol. Diversity* **2003**, *7*, 181–184.
- [217] A. Combs, S. Saubern, M. Rafalski, P. Y. S. Lam, *Tetrahedron Lett.* **1999**, *40*, 1623–1626.
- [218] W.-M. Dai, D.-S. Guo, L.-P. Sun, X.-H. Huang, *Org. Lett.* **2003**, *5*, 2919–2922.
- [219] A. Finaru, A. Berthault, T. Besson, G. Guillaumet, S. Berteina-Raboin, *Org. Lett.* **2002**, *4*, 2613–2615.
- [220] A. P. Frutos Hoener, B. Henkel, J.-C. Gauvin, *Synlett* **2003**, 63–66.
- [221] R. Pérez, T. Beryozkina, O. I. Zbruyev, W. Haas, C. O. Kappe, *J. Comb. Chem.* **2002**, *4*, 501–510.
- [222] G. A. Strohmeier, C. O. Kappe, *J. Comb. Chem.* **2002**, *4*, 154–161.

- [223] Y.-D. Gong, H.-Y. Sohn, M. J. Kurth, *J. Org. Chem.* **1998**, *63*, 4854–4856.
- [224] B. Martin, H. Sekljic, C. Chassaing, *Org. Lett.* **2003**, *5*, 1851–1853.
- [225] A. M. L. Hoel, J. Nielsen, *Tetrahedron Lett.* **1999**, *40*, 3941–3944.
- [226] D. Scharn, H. Wenschuh, U. Reineke, J. Schneider-Mergener, L. Germeroth, *J. Comb. Chem.* **2000**, *2*, 361–369.
- [227] D. Scharn, L. Germeroth, J. Schneider-Mergener, H. Wenschuh, *J. Org. Chem.* **2001**, *66*, 507–513.
- [228] L. De Luca, G. Giacomelli, A. Porcheddu, M. Salaris, M. Taddei, *J. Comb. Chem.* **2003**, *5*, 465–471.
- [229] A. A. Yates, M. O. Jones, C. E. Clarke, A. K. Powell, S. R. Johnson, A. Porch, P. P. Edwards, J. E. Turnbull, *J. Mater. Chem.* **2003**, *13*, 2061–2063.
- [230] B. Clapham, S.-H. Lee, G. Koch, J. Zimmermann, K. D. Janda, *Tetrahedron Lett.* **2002**, *43*, 5407–5410.
- [231] For prototype bottom filtration vessels suitable for controlled microwave-assisted SPOS, see: a) C. M. Coleman, J. M. D. MacElroy, J. F. Gallagher, D. F. O'Shea, *J. Comb. Chem.* **2002**, *4*, 87–93; b) see also ref. [186a]; the use of bottom-filtration 96-well plates in microwave-assisted SPOS has been described in: c) B. M. Glass, A. P. Combs in *High-Throughput Synthesis. Principles and Practices* (Ed.: I. Sucholeiki), Marcel Dekker, New York, **2001**, pp. 123–128.
- [232] a) J. Westman, R. Lundin, *Synthesis* **2003**, *7*, 1025–1030; b) R. E. Austin, J. F. Okonya, D. R. S. Bond, F. Al-Obeidi, *Tetrahedron Lett.* **2002**, *43*, 6169–6171; c) V. A. Yaylayan, M. Siu, J. M. R. Bélanger, J. R. J. Paré, *Tetrahedron Lett.* **2002**, *43*, 9023–9025; d) P. Grieco, P. Campiglia, I. Gomez-Monterrey, T. Lama, E. Novellino, *Synlett* **2003**, 2216–2218; e) R. Schobert, C. Jagusch, *Tetrahedron Lett.* **2003**, *44*, 6449–6451; f) S. Weik, J. Rademann, *Angew. Chem.* **2003**, *115*, 2595–2598; *Angew. Chem. Int. Ed.* **2003**, *42*, 2491–2494; g) S. M. Miles, R. J. Leatherbarrow, S. P. Marsden, W. J. Coates, *Org. Biomol. Chem.* **2004**, *2*, 281–283; h) P. Campiglia, I. Gomez-Monterrey, L. Langobardo, T. Lama, E. Novellino, P. Grieco, *Tetrahedron Lett.* **2004**, *45*, 1453–1456; i) B. Henkel, *Tetrahedron Lett.* **2004**, *45*, 2219–2221.
- [233] a) D. J. Gravert, K. D. Janda, *Chem. Rev.* **1997**, *97*, 489–509; b) P. Wentworth, K. D. Janda, *Chem. Commun.* **1999**, 1917–1924; c) C. M. Sun, *Comb. Chem. High Throughput Screening* **1999**, *2*, 299–318; d) P. H. Toy, K. D. Janda, *Acc. Chem. Res.* **2000**, *33*, 546–554.
- [234] a) C. G. Blettner, W. A. König, W. Stenzel, T. Schotten, *J. Org. Chem.* **1999**, *64*, 3885–3890; b) B. Sauvagnat, F. Lamaty, R. Lazaro, J. Martinez, *Tetrahedron Lett.* **2000**, *41*, 6371–6375; c) J. J. Vanden Eynde, D. Rutot, *Tetrahedron* **1999**, *55*, 2687–2694; d) A. Porcheddu, G. F. Ruda, A. Sega, M. Taddei, *Eur. J. Org. Chem.* **2003**, 907–910; e) M. Xia, Y.-G. Wang, *J. Chem. Res. Synop.* **2002**, 173–175; f) M. Xia, Y.-G. Wang, *Tetrahedron Lett.* **2002**, *43*, 7703–7705; g) M. Xia, Y.-G. Wang, *Synthesis* **2003**, 262–266.
- [235] a) M.-J. Lin, C.-M. Sun, *Tetrahedron Lett.* **2003**, *44*, 8739–8742; b) W.-B. Yeh, M.-J. Lin, M.-J. Lee, C.-M. Sun, *Mol. Diversity* **2003**, *7*, 185–198.
- [236] a) P. M. Bendale, C.-M. Sun, *J. Comb. Chem.* **2002**, *4*, 359–361; b) C.-Y. Wu, C.-M. Sun, *Synlett* **2002**, 1709–1711; c) W.-J. Chang, W.-B. Yeh, C.-M. Sun, *Synlett* **2003**, 1688–1692; d) W.-B. Yeh, C.-M. Sun, *J. Comb. Chem.* **2004**, *6*, 279–282; e) M.-J. Lee, C.-M. Sun, *Tetrahedron Lett.* **2004**, *45*, 437–440; f) C.-L. Tung, C.-M. Sun, *Tetrahedron Lett.* **2004**, *45*, 1159–1162.
- [237] W. Zhang, *Tetrahedron* **2003**, *59*, 4475–4489.
- [238] M. Larhed, M. Hoshino, S. Hadida, D. P. Curran, A. Hallberg, *J. Org. Chem.* **1997**, *62*, 5583–5587.
- [239] a) W. Zhang, Y. Lu, C. H.-T. Chen, *Mol. Diversity* **2003**, *7*, 199–202; b) W. Zhang, C. H.-T. Chen, Y. Lu, T. Nagashima, *Org. Lett.* **2004**, *6*, 1473–1476.
- [240] K. S. A. Vallin, Q. Zhang, M. Larhed, D. P. Curran, A. Hallberg, *J. Org. Chem.* **2003**, *68*, 6639–6645.
- [241] a) S. Werner, D. P. Curran, *Org. Lett.* **2003**, *5*, 3293–3296; b) a complimentary strategy involving a polymer-bound anthracene as a dienophile scavenger has recently been described: X. Lei, J. A. Porco, *Org. Lett.* **2004**, *6*, 795–798.
- [242] a) S. V. Ley, I. R. Baxendale, R. N. Bream, P. S. Jackson, A. G. Leach, D. A. Longbottom, M. Nesi, J. S. Scott, R. I. Storer, S. J. Taylor, *J. Chem. Soc. Perkin Trans. 1* **2000**, 3815–4196; b) S. V. Ley, I. R. Baxendale, *Nature Rev. Drug Discovery* **2002**, *1*, 573–586; c) A. Kirschning, H. Monenschein, R. Wittenberg, *Angew. Chem.* **2001**, *113*, 670–701; *Angew. Chem. Int. Ed.* **2001**, *40*, 650–679; d) A. Kirschning, H. Monenschein, R. Wittenberg, *Chem. Eur. J.* **2000**, *6*, 4445–4450; e) C. C. Tzschucke, C. Markert, W. Bannwarth, S. Roller, A. Hebel, R. Haag, *Angew. Chem.* **2002**, *114*, 4136–4173; *Angew. Chem. Int. Ed.* **2002**, *41*, 3964–4000.
- [243] I. R. Baxendale, A.-L. Lee, S. V. Ley in *Microwave-Assisted Organic Synthesis* (Eds.: P. Lidström, J. P. Tierney), Blackwell, Oxford, **2004**, Chap. 6.
- [244] S. V. Ley, S. J. Taylor, *Bioorg. Med. Chem. Lett.* **2002**, *12*, 1813–1816.
- [245] D. Launay, S. Booth, I. Clemens, A. Merritt, M. Bradley, *Tetrahedron Lett.* **2002**, *43*, 7201–7203.
- [246] S. Crosignani, D. Launay, B. Linclau, M. Bradley, *Mol. Diversity* **2003**, *7*, 203–210.
- [247] A. Porcheddu, G. Giacomelli, L. De Luca, A. M. Ruda, *J. Comb. Chem.* **2004**, *6*, 105–111.
- [248] C. E. Humphrey, M. A. M. Easson, J. P. Tierney, N. J. Turner, *Org. Lett.* **2003**, *5*, 849–852.
- [249] a) C. T. Brain, J. M. Paul, Y. Loong, P. J. Oakley, *Tetrahedron Lett.* **1999**, *40*, 3275–3276; C. T. Brain, S. A. Brunton, *Synlett* **2001**, 382–384.
- [250] J. Westman, *Org. Lett.* **2001**, *3*, 3745–3747.
- [251] B. Desai, T. N. Danks, *Tetrahedron Lett.* **2001**, *42*, 5963–5965.
- [252] S. Crosignani, P. D. White, B. Linclau, *Org. Lett.* **2002**, *4*, 2961–2963.
- [253] D. R. Sauer, D. Kalvin, K. M. Phelan, *Org. Lett.* **2003**, *5*, 4721–4724.
- [254] a) I. R. Baxendale, S. V. Ley, C. Piutti, *Angew. Chem.* **2002**, *114*, 2298–2301; *Angew. Chem. Int. Ed.* **2002**, *41*, 2194–2197; b) I. R. Baxendale, S. V. Ley, M. Nessi, C. Piutti, *Tetrahedron* **2002**, *58*, 6285–6304; c) see also ref. [243].
- [255] T. Mukade, D. R. Dragoli, J. A. Ellman, *J. Comb. Chem.* **2003**, *5*, 590–596.
- [256] I. Masip, C. Ferrándiz-Huertas, C. García-Martínez, J. A. Ferragut, A. Ferrer-Montiel, A. Messegue, *J. Comb. Chem.* **2004**, *6*, 135–141.
- [257] a) D. Dallinger, N. Yu. Gorobets, C. O. Kappe, *Org. Lett.* **2003**, *5*, 1205–1208; b) D. Dallinger, N. Yu. Gorobets, C. O. Kappe, *Mol. Diversity* **2003**, *7*, 229–245.
- [258] a) B. Desai, C. O. Kappe, *Top. Curr. Chem.* **2004**, *242*, in press, and references therein; see also: b) Y. Liu, C. Khemtong, J. Hu, *Chem. Commun.* **2004**, 398–399; c) M. D. Smith, A. F. Stepan, C. Ramarao, P. E. Brennan, S. V. Ley, *Chem. Commun.* **2003**, 2652–2653; see also reference [262].
- [259] One of the main limitations of scaling-up microwave technology is the restricted depth of penetration of microwave irradiation into absorbing materials (solvents or reaction mixtures). At the typical operating frequency of most microwave reactors of 2.45 GHz, the penetration depth depends on the dielectric properties of the medium but is generally of the order of a few centimeters. This means that the microwave energy density inside a large batch reactor (> 1 L volume) may

only be a small fraction of the density on the surface. Therefore, solvents or reagents in the center of the reaction vessel are heated by convection and not by direct microwave dielectric heating. This physical limitation is one of the main reasons for the development of continuous-flow reactors, where the reaction mixture is passed through a relatively small microwave-heated flow cell, thus avoiding problems of penetration depth. On the other hand, continuous-flow reactors with pumping systems may not be appropriate for processing solids, highly viscous liquids, or heterogeneous reaction mixtures.

- [260] a) K. D. Raner, C. R. Strauss, R. W. Trainor, J. S. Thorn, *J. Org. Chem.* **1995**, *60*, 2456–2460; b) B. A. Roberts, C. R. Strauss in *Microwave-Assisted Organic Synthesis* (Eds.: P. Lidström, J. P. Tierney), Blackwell, Oxford, **2004**, Chap. 9.
- [261] a) B. Perio, M.-J. Dozias, J. Hamelin, *Org. Process Res. Dev.* **1998**, *2*, 428–430; b) J. Cléophas, M. Liagre, A. Loupy, A. Petit, *Org. Process Res. Dev.* **2000**, *4*, 498–504.
- [262] a) T. Cablewski, A. F. Faux, C. R. Strauss, *J. Org. Chem.* **1994**, *59*, 3408–3412; b) K. Kazba, B. R. Chapados, J. E. Gestwicki, J. L. McGrath, *J. Org. Chem.* **2000**, *65*, 1210–1214; c) B. M. Khadlikar, V. R. Madyar, *Org. Process Res. Dev.* **2001**, *5*, 452–453; d) E. Esveld, F. Chemat, J. van Haveren, *Chem. Eng. Technol.* **2000**, *23*, 279–283; e) E. Esveld, F. Chemat, J. van Haveren, *Chem. Eng. Technol.* **2000**, *23*, 429–435; f) W.-C. Shieh, S. Dell, O. Repiè, *Tetrahedron Lett.* **2002**, *43*, 5607–5609; g) W.-C. Shieh, S. Dell, O. Repiè, *Org. Lett.* **2001**, *3*, 4279–4281; h) K. A. Savin, M. Robertson, D. Gernert, S. Green, E. J. Hembre, J. Bishop, *Mol. Diversity* **2003**, *7*, 171–174; i) N. S. Wilson, C. R. Sarko, G. Roth, *Org. Process Res. Dev.* **2004**, *8*, 535–538; j) P. He, S. J. Haswell, P. D. Fletcher, *Lab Chip* **2004**, *4*, 38–41.
- [263] A. G. Takvorian, A. P. Combs, *J. Comb. Chem.* **2004**, *6*, 171–174.
- [264] It should be emphasized that despite the large number of examples presented in Section 2, clearly not all chemical processes are amenable to a high-temperature microwave approach, in particular in those cases where a kinetically controlled pathway leads to the desired product. Also, there may be cases where one of the reagents or substrates is too temperature-sensitive to allow heating to higher than ambient temperatures. The reader should keep in mind that, naturally, the failed examples do not appear in the literature, which distorts the success rate of microwave synthesis.
- [265] a) D. E. Pivonka, J. R. Empfield, *Appl. Spectrosc.* **2004**, *58*, 41–46; b) for online UV monitoring, see: G. S. Getvoldsen, N. Elander, S. A. Stone-Elander, *Chem. Eur. J.* **2002**, *8*, 2255–2260.
- [266] a) C. Fermér, P. Nilsson, M. Larhed, *Eur. J. Pharm. Sci.* **2003**, *18*, 129–132; b) K. Orrling, P. Nilsson, M. Gullberg, M. Larhed, *Chem. Commun.* **2004**, 790–791.
- [267] a) B. N. Pramanik, U. A. Mirza, Y. H. Ing, Y.-H. Liu, P. L. Bartner, P. C. Weber, A. K. Bose, *Protein Sci.* **2002**, *11*, 2676–2687; b) B. N. Pramanik, Y. H. Ing, A. K. Bose, L.-K. Zhang, Y.-H. Liu, S. N. Ganguly, P. Bartner, *Tetrahedron Lett.* **2003**, *44*, 2565–2568; c) A. J. Bose, Y. H. Ing, N. Lavlinskaia, C. Sareen, B. N. Pramanik, P. L. Bartner, Y.-H. Liu, L. Heimark, *J. Am. Soc. Mass Spectrom.* **2002**, *13*, 839–850.
- [268] a) B. Réjasse, S. Lamare, M.-D. Legoy, T. Besson, *Org. Biomol. Chem.* **2004**, *2*, 1086–1089; b) T. Maugard, D. Gaunt, M. D. Legoy, T. Besson, *Biotechnol. Lett.* **2003**, *25*, 623–629; c) B. K. Pchelka, A. Loupy, J. Pleniewicz, L. Blanco, *Tetrahedron: Asymmetry* **2000**, *11*, 2719–2732; d) G. Lin, W.-Y. Lin, *Tetrahedron Lett.* **1998**, *39*, 4333–4336; e) M.-C. Parker, T. Besson, S. Lamare, M.-D. Legoy, *Tetrahedron Lett.* **1996**, *37*, 8383–8386; f) M. Gelo-Pujic, E. Guibé-Pujic, E. Guibé-Jampel, A. Loupy, *Tetrahedron* **1997**, *53*, 17247–17252; g) M. Gelo-Pujic, E. Guibé-Jampel, A. Loupy, S. A. Galema, D. Mathé, *J. Chem. Soc. Perkin Trans.* **1996**, 2777–2780; h) J.-R. Carrillo-Munoz, D. Bouvet, E. Guibé-Jampel, A. Loupy, A. Petit, *J. Org. Chem.* **1996**, *61*, 7746–7749.
- [269] Y.-C. Tsai, B. A. Coles, R. G. Compton, F. Marken, *J. Am. Chem. Soc.* **2002**, *124*, 9784–9788.
- [270] P. Klan, V. Cvrka, in *Microwaves in Organic Synthesis* (Ed.: A. Loupy), Wiley-VCH, Weinheim, **2002**, pp. 463–486.
- [271] a) D. Bogdal, P. Penczek, J. Pielichowski, A. Prociak, *Adv. Polym. Sci.* **2003**, *163*, 193–263; b) K. R. Carter, *Macromolecules* **2002**, *35*, 6757–6759; c) A. Khan, S. Hecht, *Chem. Commun.* **2004**, 300–301.
- [272] a) S. Barlow, S. R. Marder, *Adv. Funct. Mater.* **2003**, *13*, 517–518; b) R. G. Blair, E. G. Gillan, N. K. B. Nguyen, D. Daurio, R. B. Kaner, *Chem. Mater.* **2003**, *15*, 3286–3293; c) M. Melucci, M. Gazzano, G. Barbarella, M. Cavallini, F. Biscarini, P. Maccagnani, P. Ostojia, *J. Am. Chem. Soc.* **2003**, *125*, 10266–10274.
- [273] a) E. H. Hong, K.-H. Lee, S. H. Oh, C.-G. Park, *Adv. Funct. Mater.* **2003**, *13*, 961–966; b) T. J. Imholt, C. A. Dyke, B. Hasslacher, J. M. Perez, D. W. Price, J. A. Roberts, J. B. Scott, A. Wadhawan, Z. Ye, J. M. Tour, *Chem. Mater.* **2003**, *15*, 3969–3970; c) F. Della Negra, M. Meneghetti, E. Menna, *Fullerenes Nanotubes Carbon Nanostruct.* **2003**, *11*, 25–34; d) Y.-J. Zhu, W.-W. Wang, R.-J. Qi, X.-L. Hu, *Angew. Chem.* **2004**, *116*, 1434–1438; *Angew. Chem. Int. Ed.* **2004**, *43*, 1410–1424.
- [274] The term “Bunsen burner of the 21st century” was originally coined by A. K. Bose (ref [6a]), one of the pioneers of applying microwave heating to organic synthesis.
- [275] O. Navarro, H. Kaur, P. Mahjoor, S. P. Nolan, *J. Org. Chem.* **2004**, *69*, 3173–3180.
- [276] X. Wu, A. K. Mahalingam, Y. Wan, M. Alterman, *Tetrahedron Lett.* **2004**, *45*, 4635–4638.
- [277] M. Harmata, X. Hong, S. K. Ghosh, *Tetrahedron Lett.* **2004**, *45*, 5233–5236.
- [278] P. Wipf, J. Janjic, C. R. J. Stephenson, *Org. Biomol. Chem.* **2004**, *2*, 443–445.
- [279] a) M. Melucci, G. Barbarella, M. Zambianchi, P. Di Pietro, A. Bongini, *J. Org. Chem.* **2004**, *69*, 4821–4828; b) Y. Wang, D. R. Sauer, *Org. Lett.* **2004**, *6*, 2793–2796.
- [280] a) L. Botella, C. Najera, *Tetrahedron Lett.* **2004**, *45*, 1833–1836; b) L. Botella, C. Najera, *Tetrahedron* **2004**, *60*, 5563–5570; c) A. Svennebring, P. Nilsson, M. Larhed, *J. Org. Chem.* **2004**, *69*, 3345–3349.
- [281] a) H. He, Y.-J. Wu, *Tetrahedron Lett.* **2004**, *45*, 3237–3239; b) P. H. Kwan, M. J. MacLachlan, T. M. Swager, *J. Am. Chem. Soc.* **2004**, *126*, 8638–8639.
- [282] I. Mutule, E. Suna, *Tetrahedron Lett.* **2004**, *45*, 3909–3912.
- [283] A. Lengar, C. O. Kappe, *Org. Lett.* **2004**, *6*, 771–774.
- [284] T. A. Jensen, X. Liang, D. Tanner, N. Skjaerbaek, *J. Org. Chem.* **2004**, *69*, 4936–4947.
- [285] a) D. A. Alonso, C. Najera, M. C. Pacheco, *J. Org. Chem.* **2004**, *69*, 1615–1619; b) G. Vo-Tanh, H. Lahrache, A. Loupy, I.-J. Kim, D. H. Chang, C.-H. Jun, *Tetrahedron* **2004**, *60*, 5539–5543.
- [286] D. Balan, H. Adolfsson, *Tetrahedron Lett.* **2004**, *45*, 3089–3092.
- [287] S. S. Salim, R. K. Bellingham, R. C. D. Brown, *Eur. J. Org. Chem.* **2004**, 800–806.
- [288] S. E. Wolkenberg, D. D. Wisnoski, W. H. Leister, Y. Wang, Z. Zhao, C. W. Lindsley, *Org. Lett.* **2004**, *6*, 1453–1456.
- [289] H. Sandin, M.-L. Swanstein, E. Wellner, *J. Org. Chem.* **2004**, *69*, 1571–1580.
- [290] a) G. Minetto, L. F. Raveglia, M. Taddei, *Org. Lett.* **2004**, *6*, 389–392; b) A. R. Bharadwaj, K. A. Scheidt, *Org. Lett.* **2004**, *6*, 2465–2468; c) C. D. Cox, M. J. Breslin, B. J. Mariano, *Tetrahedron Lett.* **2004**, *45*, 1489–1493; d) R. B. Sparks, A. P. Combs, *Org. Lett.* **2004**, *6*, 2473–2475; e) H.-K. Lee, T. M. Rana, *J. Comb. Chem.* **2004**, *6*, 504–508; f) Y. Peng, G. Song, *Tetrahe-*

- dron *Lett.* **2004**, 45, 5313–5316; g) Z. Zhao, D. D. Wisnoski, S. E. Wolkenberg, W. H. Leister, Y. Wang, C. W. Lindsley, *Tetrahedron Lett.* **2004**, 45, 4873–4876; h) D. Tejedor, D. González-Cruz, F. García-Tellado, J. J. Marrero-Tellado, M. López Rodríguez, *J. Am. Chem. Soc.* **2004**, 126, 8390–8391.
- [291] P. S. Baran, D. P. O'Malley, A. L. Zografos, *Angew. Chem.* **2004**, 116, 2728–2731; *Angew. Chem. Int. Ed.* **2004**, 43, 2674–2677.
- [292] R. A. Hughes, S. P. Thompson, L. Alcaraz, C. J. Moody, *Chem. Commun.* **2004**, 946–948.
- [293] G. J. S. Lohman, P. H. Seeberger, *J. Org. Chem.* **2004**, 69, 4081–4093.
- [294] A. Vasudevan, M. K. Verzal, *Synlett* **2004**, 631–634.
- [295] A. G. Takvorian, A. P. Combs, *J. Comb. Chem.* **2004**, 6, 171–174.
- [296] H. Akamatsu, K. Fukase, S. Kusumoto, *Synlett* **2004**, 1049–1053.
- [297] M. D. Bowman, R. C. Jeske, H. E. Blackwell, *Org. Lett.* **2004**, 6, 2019–2022.
- [298] W. Zhang, C. H.-T. Chen, Y. Lu, T. Nagashima, *Org. Lett.* **2004**, 6, 1473–1476.
- [299] W. Zhang, T. Nagashima, Y. Lu, C. H.-T. Chen, *Tetrahedron Lett.* **2004**, 45, 4611–4613.
- [300] X. Lei, J. A. Porco, Jr., *Org. Lett.* **2004**, 6, 795–798.
- [301] J. L. Delgado, P. de la Cruz, F. Langa, A. Urbina, J. Casado, J. T. López Navarrete, *Chem. Commun.* **2004**, 1734–1735.
- [302] a) S. K. Das, *Synlett* **2004**, 915–932; b) A. Corsaro, U. Chiacchio, V. Pistara, G. Romeo, *Curr. Org. Chem.* **2004**, 8, 511–538.

Time to invest in batch synthesis for up to 1 liter volume!

The Synthos 3000 opens new dimensions in scaling up the microwave-assisted synthesis of chemical targets under enhanced pressure and temperature conditions.

Your benefits:

- Direct scalability – no reoptimization
- Excellent reproducibility for batch synthesis
- Homogeneous microwave field for large-scale parallel reactions
- Comprehensive safety measures, designed for extreme conditions

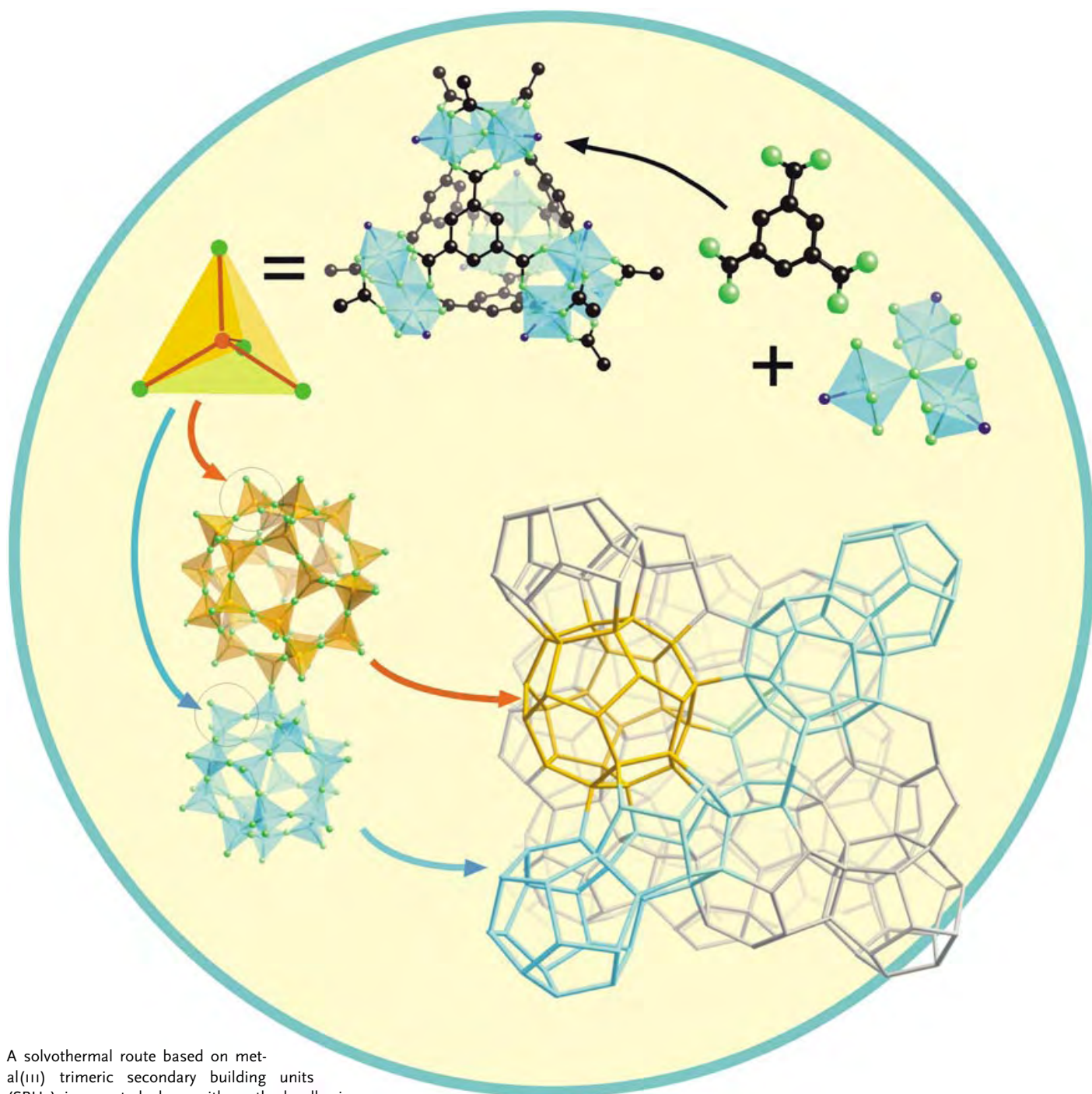


Anton Paar

Ask your local Anton Paar representative for a quotation or contact us directly:

Tel: +43 (0)316 257-0
E-mail: info@anton-paar.com
Web: www.anton-paar.com

Communications



A solvothermal route based on metal(III) trimeric secondary building units (SBUs) is reported along with methods allowing the crystal structures of hybrid organic-inorganic structures to be predicted. The association of a chromium(III) trimeric SBU and 1,3,5-benzenetricarboxylate gives a micro- and mesoporous solid. The simulated crystal-structure solution matches the experimental X-ray pattern. For more information see the Communications by C. Serre, C. Mellot-Draznieks, G. Férey, and co-workers on the following pages.

A Route to the Synthesis of Trivalent Transition-Metal Porous Carboxylates with Trimeric Secondary Building Units**

Christian Serre,* Franck Millange, Suzy Surblé, and Gérard Férey

Porous solids with either purely inorganic^[1] or organic–inorganic hybrid skeletons^[2] are currently very topical,^[3–7] owing to their applications in ion exchange, gas separation, catalysis, and more recently in hydrogen storage.^[8–10] The recent introduction of transition metals in the framework has increased the range of possible applications by exploiting their electronic and magnetic properties.^[11–13] However, most hydrothermal or solvothermal syntheses are based on “trial and error” but with some successes with divalent (e.g., Co, Ni, Cu) or trivalent cations (V, Cr),^[11,13,14] The most important goal in the field is always to reach a real “design” of hybrid porous solids, that is, the way to obtain tailor-made solids with the required structures and properties starting from well-characterized inorganic and organic species. From this point of view, the number of synthetic routes that use a controlled approach based on secondary building units (SBUs) is still scarce. If some relative successes have been achieved in the past decade with the use of porphyrin building blocks^[15] or by the combination of zinc, bipyridine, and SiF_6^{2-} ions,^[16,17] then the most efficient synthetic route was developed by Yaghi and co-workers with the use of tetrameric Zn_4O zinc clusters.^[18] A few solids were also obtained recently with dimeric^[19] or trimeric zinc SBUs.^[20–22] Thus, a large number of hybrid solids with pore sizes up to 27 Å and very high surface areas ($\approx 4500 \text{ m}^2 \text{ g}^{-1}$) have been prepared. However, in the cases mentioned above their synthesis conditions are not a complete SBU approach. Soluble monomeric zinc precursors and defined synthesis conditions are used either to allow

the formation, with reasonable stability, of these building units in solution prior to the reaction with carboxylate moieties, or to allow the cooperative formation of the building unit in the presence of the carboxylate moieties.

We report herein a new and “controlled SBU” approach for trimeric inorganic species (three metallic octahedra shared by $\mu_3\text{-O}$), which keeps the integrity of the inorganic precursor during the formation of the solid. The approach involves acetates of trivalent transition metals (e.g., Fe, Cr, V, Ru, Mn, Co),^[23,24] as precursors, which are trimeric. The trimeric acetate building unit is first prepared, then introduced into the reaction media in the presence of the dicarboxylic acid and finally, by increasing the temperature and in the presence of base, a direct exchange between the monocarboxylate (acetate) and the dicarboxylate moieties occurs to produce a 3D solid in which the trimeric SBU remains intact. We also report the successful use of these SBUs in the rational synthesis of two new open-framework iron(III) dicarboxylates. This paper deals with the synthesis, characterization and the structure determination from X-ray powder data of two new 3D open-framework iron(III) dicarboxylates: $\text{Fe}^{\text{III}}_3\text{O}(\text{CH}_3\text{OH})_3\{\text{O}_2\text{C}(\text{CH}_2)_n\text{CO}_2\}_3 \cdot X \cdot (\text{CH}_3\text{OH})_m$; $X^- = \text{CH}_3\text{CO}_2^-$, $n = 2$, $m \approx 4.5$ (**MIL-88**; see Figure 1) or $X = \text{Cl}^-$, $n = 4$, $m \approx 6$ (**MIL-89**).

MIL-88 exhibits a 3D structure built up from trimers of iron(III) octahedra linked to fumarate dianions to create a 3D framework (Figure 2). This structure delimits both a 1D pore-

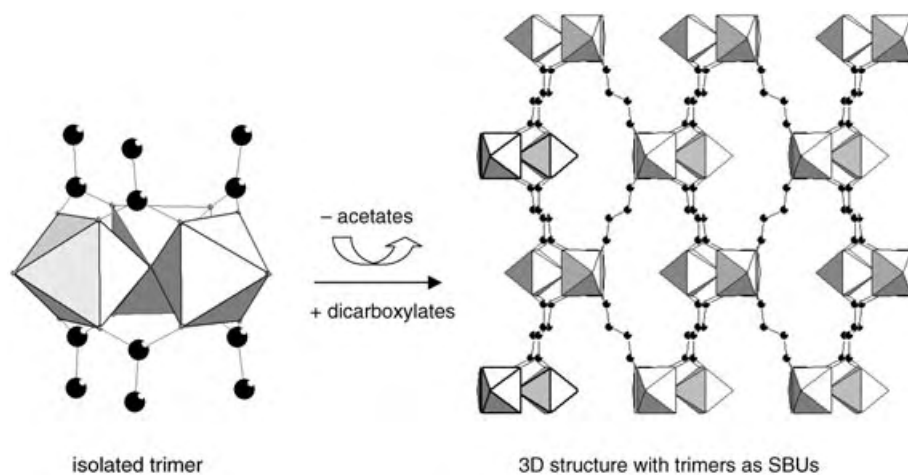


Figure 1. Schematic representation of the synthetic route involving trimeric SBUs with **MIL-88** given as an example.

[*] C. Serre, F. Millange, S. Surblé, G. Férey
Institut Lavoisier
UMR CNRS 8637
Université de Versailles St-Quentin en Yvelines
45 Avenue des Etats-Unis, 78035 Versailles Cedex (France)
Fax: (+33) 1-3925-4358
E-mail: serre@chimie.uvsq.fr

[**] Authors are indebted to Daniel Loüer and Gérard Marsolier from Rennes (France) for collecting the X-ray data of **MIL-89ht** and Dr C. Mellot-Draznieks for helpful discussions.

Supporting information for this article is available on the WWW under <http://www.angewandte.org> or from the author.

channel system along the *c* axis (Figure 2a), which is filled with solvent molecules, and cages, which are filled with acetate groups (Figure 2b). The free methanol molecules that are present within the pores interact both through hydrogen bonds with oxygen atoms of the inorganic trimers and through Van der Waals interactions with the $-\text{CH}_3$ groups of both the free and bound methanol molecules. It should be noticed that during the determination of the structure, a partial-site occupancy was applied (see Supporting Information) for the disordered free methanol (C(4)-O(6) and C(7)-O(5)) and acetate groups (C(5), C(6) and O(7)).

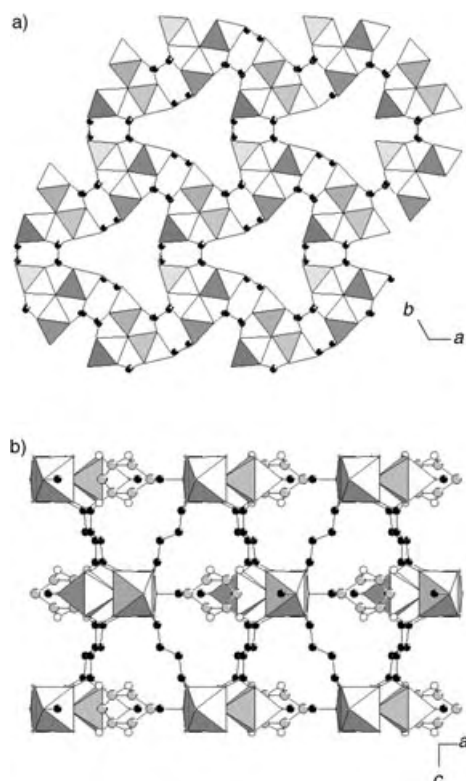


Figure 2. View of the structure of **MIL-88**: a) along the *c* axis; b) along the *b* axis. Iron octahedra, oxygen and carbon atoms are represented in white, white and black respectively. For a better understanding, free methanol molecules and acetate groups have been removed from (a) whereas carbon atoms from the acetate are in gray in (b).

In the case of **MIL-89**, only the structure of the high-temperature form of **MIL-89** labeled **MIL-89 ht** (ht signifies high temperature) or $\text{Fe}^{\text{III}}_3\text{O}(\text{CH}_3\text{OH})_3\{\text{O}_2\text{C}-\text{C}_4\text{H}_4-\text{CO}_2\}_3\cdot\text{Cl}^-$ has been determined (see Experimental Section). **MIL-89 ht** also exhibits a 3D structure built up from trimers of iron(III) octahedra. The trimers are related together by *trans*, *trans* muconate moieties, which ensures the three-dimensionality of the framework (Figure 3); small channels are also present along the *c* axis and are filled with terminal methanol groups and chloride ions. As previously observed for **MIL-88**, a partial occupancy was found for a carbon atom (C(11)) of one terminal methanol molecule (C(11)-O(7)).

In both structures, iron atoms are situated within an octahedral environment of four oxygen atoms from the bidentate dicarboxylates, one $\mu_3\text{O}$ atom, and one oxygen atom from the terminal methanol group. Octahedra are related through the $\mu_3\text{O}$ oxygen atom to form the trimeric building units. Interatomic distances and angles are generally well defined with Fe–O, C–O, and C–C bond lengths within 1.83–2.04, 1.26–1.50, and 1.37–1.40 Å, respectively, for **MIL-88** and 1.88–2.23, 1.27–1.50 Å, 1.37–1.48 Å, respectively, for **MIL-89 ht**. Bond-valence calculations indicate that iron atoms in both structures are in a trivalent state. Mössbauer experiments indicate that both solids have only octahedral iron(III) centers in a high-spin state; these results will be reported soon in a full paper with a detailed study of the thermal behavior and the sorption capacities of these solids.^[25]

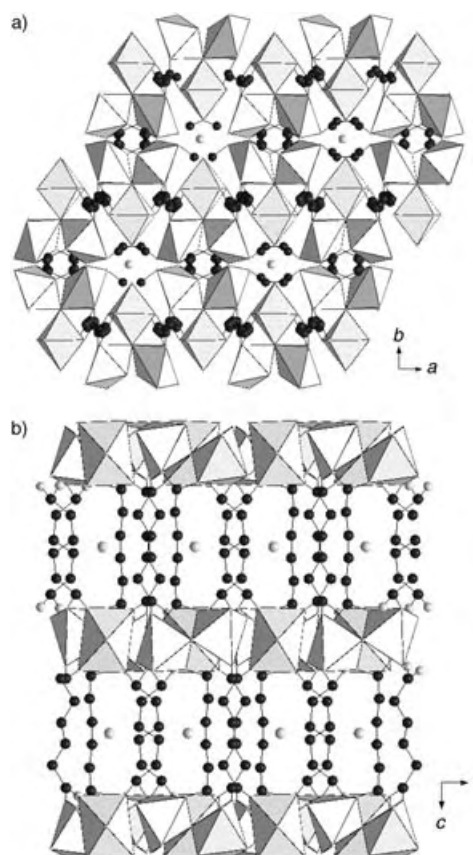


Figure 3. View of the structure of **MIL-89 ht**: a) along the *c* axis; b) along the *b* axis. Key: Fe octahedra white; O atoms white; C atoms black; Cl atoms gray.

Despite the presence of the same SBUs in both **MIL-88** and **MIL-89 ht**, their structures have significant differences. First, the position of the counteranion (Figure 4): in **MIL-88**, the counterions are disordered acetate groups located at the centre of cages and surrounded by five trimers and six organic chains. **MIL-88** can thus be considered as being built up from successive layers of trimers alternating with acetate groups in the (010) plane; the three-dimensionality is ensured by the fumarate moieties along the *c* axis. In **MIL-89 ht**, the packing of trimers in the (010) plane is much denser and thus the chloride counterion is now located between the layers within the small channels along the *c* axis, delimited by six different alkenes chains and six iron trimers. These differences could come from the presence of free solvent in **MIL-88**, whereas solvent from **MIL-89 ht** has been removed; it is likely that **MIL-89** increases its cell volume when filled with methanol as this phenomenon occurs with **MIL-88** (cell volume increase >50%) when filled with methanol. This “breathing” is probably accompanied by a displacement of the anions in both cases; these results will be reported soon.^[25]

As described above, two new open-framework iron(III) dicarboxylates have been obtained through the “controlled SBU” approach with retention of the initial trimeric SBU. However, it cannot be proven experimentally whether the trimeric SBU precursor remains intact throughout the synthesis or whether it breaks up and reforms. In the presence of

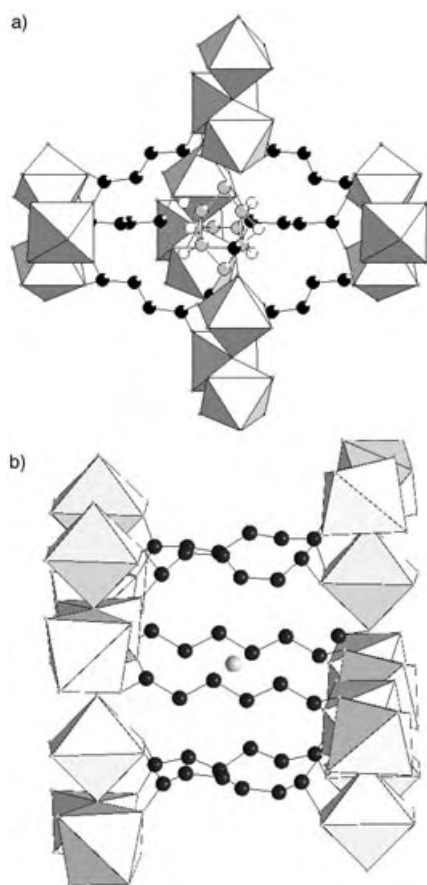


Figure 4. View of the cages delimiting the anionic moieties in **MIL-88** (a) and **MIL-89ht** (b). Key: same as that Figure 3 except C atoms from the acetate and Cl atoms are in gray.

terephthalic acid and with the same trimeric SBU precursor under similar solvothermal conditions, a partial destruction of the SBU occurred during the synthesis. The resulting solid, **MIL-85**, was built up from both trimeric SBUs and monomers and even some of the acetate ligands present in the initial precursor were retained.^[26] The presence of both trimers and acetate moieties within **MIL-85** indicates that part of the trimeric precursor is probably kept during the synthesis.

Trivalent metal dicarboxylate (**MIL-59**) built up from trimers of octahedra has been reported recently by our group by using a vanadium(III) complex and isophthalic acid under hydrothermal conditions following the “trial and error” method. In this case, a cubic structure with cuboidal cages filled with solvent and chloride ions was observed.^[14] This is the only case of trimeric transition-metal carboxylate obtained to date under hydrothermal conditions that exhibit trimeric SBU.

Finally, our method is a new synthetic route that favors the synthesis of open framework transition-metal carboxylates with the trimeric SBUs.

These results show also that despite the presence of identical trimeric SBUs, the structural type in the final solids strongly depends on the nature of the organic linker, thus demonstrating the structural richness of this synthetic route. This successful use of predetermined SBUs in the synthesis of

metal carboxylates also opens the way for the “design” of hybrid solids by using the simulation tool.^[27–29] This is also the first SBU route that involves trivalent cations; the number of hybrid solids based on trivalent transition or p-block metals is still scarce.^[11–14,30–32]

In addition, as clusters of trimeric metal acetates with various physical properties can be obtained with a large number of transition metals, such as chromium, iron, vanadium, ruthenium, manganese, or cobalt,^[23,24] there is a the potential to synthesize open-framework trivalent metal polycarboxylates with different pore shapes and sizes as well as unique physical properties. Several other porous hybrid solids based on these trimeric SBUs with various trivalent cations have been synthesized and will be soon reported, thus enlarging the field of hybrid phases based on trimeric transition-metals SBU.

Experimental Section

Synthesis: The trimeric iron(III) acetate SBU was first prepared according to Dziobkowski et al.^[33] Subsequently, iron(III) acetate, fumaric acid ($\text{HO}_2\text{C}-\text{C}_2\text{H}_2-\text{CO}_2\text{H}$; Acros, 99%) or *trans,trans*-muconic acid ($\text{HO}_2\text{C}-\text{C}_4\text{H}_4-\text{CO}_2\text{H}$; Aldrich, 98%), sodium hydroxide (Aldrich, 97%), deionized water, and methanol (Prolabo, 99%) were mixed in the following ratios: 1:3:1.5:50:1000 (based on one trimer). The resulting orange gels were aged at 100°C for 3 days in a teflon-lined Parr bomb and cooled down to room temperature. The light-orange solids are filtered, washed with methanol and acetone, and dried at room temperature.

General analysis: Structure determination of **MIL-89** was carried out only on the high-temperature form **MIL-89ht**; general analysis was carried out on the room-temperature form that contains free solvent molecules.

Thermal gravimetric analysis (TGA): TGA were performed in air on both solids (**MIL-88** and **MIL-89**) by using a TA-Instrument type 2050 analyzer. The results from both samples showed several weight losses in the range from 273 to 873 K (see the Supporting Information). The residual solid was identified as Fe_2O_3 . **MIL-88** exhibits two weight losses of ≈ 19.5 and 49%, the first within the range of 373–423 K, which corresponds to the departure of the free methanol groups followed by the departure of bound methanol; the second within the range of 673–773 K, which corresponds to the loss of the dicarboxylate and the anionic group. The same behavior is observed for **MIL-89** with two losses of $\approx 20\%$ and 56%. In the analysis of both samples, Fe_2O_3 crystallizes at higher temperatures. The losses generally agree with the theoretical values (**MIL-88**: free solvent: 17.3%, bound solvent plus organic fraction plus anion: 53.8%; **MIL-89**: free solvent: 20.7%, bound solvent plus organic fraction plus anion: 53.7%). In the case of **MIL-89**, the best matching between observed and calculated TGA losses has been reached for a content of six free methanol groups per trimer of iron octahedra.

Elemental analysis: Iron, carbon, and chlorine contents were determined at the C.N.R.S. Central Laboratory of Analysis of Vernaison (France). Elemental analysis (%) calcd for **MIL-88**: C 31.04, Fe 20.2; found: C 24.0, Fe 21.8, Cl trace. Elemental analysis (%) calcd for **MIL-89**: C 34.9, Fe 18.1, Cl 3.83; found: C 28.12, Fe 20.22, Cl 3.92. The deficit in observed carbon content comes in both cases from the rapid loss of free methanol at room temperature (**MIL-88**: ≈ 3 –4 days; **MIL-89**: < 1 day), which automatically decreases the carbon content observed by quantitative analysis.

Density measurements: To avoid problems of free methanol desorption at room temperature, an experiment performed on a fresh sample of **MIL-88** by using a Micromeritics apparatus, Accupyc 1330.

A volumic density of 1.55 g cm^{-3} corresponds reasonably well with the calculated one (1.73 g cm^{-3}).

Infrared spectroscopy: The infrared spectra of the title compounds clearly shows in both cases the presence of the vibrational bands characteristic of the $-(\text{O}-\text{C}-\text{O})-$ groups around 1550 and 1430 cm^{-1} , thus confirming the presence of the dicarboxylate within the solids. Large bands around 3500 cm^{-1} also confirmed the presence of OH groups in both solids.

Structure determination: All attempts at obtaining single crystals failed in both cases. The powder X-ray diffraction pattern of **MIL-88** was collected on a D5000 (θ - 2θ mode) Siemens diffractometer with $\lambda(\text{Cu}_{\text{K}\alpha 1+\text{K}\alpha 2}) = 1.54059, 1.54439 \text{ \AA}$. In the case of **MIL-89**, due to the rapid evolution of the pattern at room temperature as well as a decrease in the crystallinity (see Supporting Information), a temperature in situ data collection was performed at 373 K by using a D5000 (θ - 2θ mode) Siemens diffractometer equipped with an Anton Paar HTK1200 oven. The pattern of **MIL-88** was indexed in the hexagonal space group $P6_2c$ (no. 196) by using the Dicvol program.^[34] with the following cell parameters $a = 11.04(1) \text{ \AA}$, $c = 14.80(1) \text{ \AA}$. The pattern of **MIL-89ht** was indexed in the orthorhombic space group $Pbnn$ (no. 52) with $a = 9.135(1) \text{ \AA}$, $b = 16.137(1) \text{ \AA}$, $c = 19.968(1) \text{ \AA}$. Then, direct methods were realized by using the Expo program to localize the iron atoms and some of the oxygen atoms.^[35] Due to poor quality of the data in the case of **MIL-89ht**, a combination of the Expo and the Cerius programs was used,^[36] which allows the manipulation of the whole trimeric building block and based on the position of the iron atoms found by Expo, Cerius allowed us to place the whole inorganic SBU and the first carbon atoms of the muconate moieties at a position compatible with the direct-method findings and the experimental X-Ray diffraction pattern. Finally, free and bound methanol molecules and the anionic counterions were located by successive Fourier difference by using Shelxtl.^[37] In the case of **MIL-88**, disorder was present for the methanol groups and for the acetate anion and half occupancies were applied during the refinement. For **MIL-89ht**, the carbon atom of one of the terminal methanol groups was also placed with a half occupancy. Finally, both structures were refined by using Fullprof^[38] and its Winplotr program.^[39] Full details of the structure determination are reported in the Supporting Information.

The formula deduced from the structure determinations for **MIL-88** and **MIL-89ht** are: $\text{Fe}^{\text{III}}_3\text{O}(\text{CH}_3\text{OH})_3\{\text{O}_2\text{C}-\text{C}_2\text{H}_2-\text{CO}_2\}_3 \cdot (\text{CH}_3\text{CO}_2)_n \cdot n \text{ CH}_3\text{OH}$ ($n = 4.5$) and $\text{Fe}^{\text{III}}_3\text{O}(\text{CH}_3\text{OH})_3\{\text{O}_2\text{C}-\text{C}_4\text{H}_4-\text{CO}_2\}_3 \cdot \text{Cl}$. The final agreement factors^[40] were satisfactory for **MIL-88**: $R_p = 11.9\%$, $R_{\text{Bragg}} = 8.3\%$ and $R_F = 7.7\%$. In the case of **MIL-89ht**, factors are higher because of the poor quality of the X-ray data ($R_p = 13.7\%$; $R_{\text{Bragg}} = 15.6\%$, $R_F = 9.7\%$) and only an approached structure of **MIL-89ht** is proposed for the moment; better X-ray data will be collected soon on the wet phase by using capillaries to determine more precisely the structure of **MIL-89**. Final Rietveld plots, atomic coordinates, and principal interatomic distances are given in the Supporting Information.

Received: March 12, 2004 [Z54250]

Keywords: carboxylates · host–guest systems · iron · nanoporous materials · organic–inorganic hybrid composites

[1] M. E. Davis, *Nature* **2002**, *417*, 813.

[2] O. M. Yaghi, M. O'Keeffe, H. K. Ockwig, M. Chae, M. Eddaoudi, J. Kim, *Nature* **2003**, *423*, 705.

[3] C. Robl, *Mater. Res. Bull.* **1992**, *27*, 99.

[4] A. Clearfield, *Curr. Opin. Solid State Mater. Sci.* **1996**, *1*, 268.

[5] A. K. Cheetham, G. Férey, T. Loiseau, *Angew. Chem.* **1999**, *111*, 3466; *Angew. Chem. Int. Ed.* **1999**, *38*, 3269.

[6] G. Férey, *Chem. Mater.* **2001**, *13*, 3084.

[7] S. Feng, R. Xu, *Acc. Chem. Res.* **2001**, *34*, 239.

[8] G. Férey, M. Latroche, C. Serre, F. Millange, T. Loiseau, A. Percheron-Guégan, *Chem. Commun.* **2003**, 2976.

[9] P. M. Forster, J. S. Chang, S. E. Park, G. Férey, A. K. Cheetham, *J. Am. Chem. Soc.* **2003**, *125*, 125.

[10] N. L. Rosi, J. Eckert, M. Eddaoudi, D. T. Vodak, J. Kim, M. O'Keeffe, O. M. Yaghi, *Science* **2003**, *300*, 1127.

[11] K. Barthelet, J. Marrot, D. Riou, G. Férey, *Angew. Chem.* **2002**, *41*, 291; *Angew. Chem. Int. Ed.* **2002**, *41*, 281.

[12] F. Millange, C. Serre, G. Férey, *Chem. Commun.* **2002**, 822.

[13] C. Serre, F. Millange, C. Thouvenot, M. Nogues, G. Marsolier, D. Louër, G. Férey, *J. Am. Chem. Soc.* **2002**, *124*, 13519.

[14] K. Barthelet, D. Riou, G. Férey, *Chem. Commun.* **2002**, 1492.

[15] B. F. Abrahams, B. F. Hoskins, D. M. Michail, R. Robson, *Nature* **1994**, *369*, 727.

[16] S. Subramanian, M. J. Zaworotko, *Angew. Chem.* **1995**, *107*, 2295; *Angew. Chem. Int. Ed. Engl.* **1995**, *34*, 2127.

[17] S. Noro, S. Kitagawa, M. Kondo, K. Seki, *Angew. Chem.* **2000**, *39*, 2161; *Angew. Chem. Int. Ed.* **2000**, *39*, 2082.

[18] M. Eddaoudi, D. B. Moler, H. Li, B. Chen, T. Reineke, M. O'Keeffe, O. M. Yaghi, *Acc. Chem. Res.* **2001**, *34*, 319.

[19] O. M. Yaghi, C. E. Davies, G. Li, H. Li, *J. Am. Chem. Soc.* **1997**, *119*, 2861.

[20] O. M. Yaghi, R. Jernigan, H. Li, C. E. Davies, T. L. Groy, *J. Chem. Soc. Dalton Trans.* **1997**, 2383.

[21] H. Li, C. E. Davies, T. L. Groy, D. G. Kelley, O. M. Yaghi, *J. Am. Chem. Soc.* **1998**, *120*, 2186.

[22] J. S. Seo, D. Whang, H. Lee, S. I. Jun, J. Oh, Y. J. Jeon, K. Kim, *Nature* **2000**, *404*, 982.

[23] R. D. Cannon, R. P. White, *Chemical and Physical Properties of Trinuclear Bridged Metal Complexes*, Vol. 36, London, **1987**.

[24] B. J. Hataway, Vol. 2 (Ed.: G. Wilkinson), Pergamon, Oxford, **1987**, pp. 439.

[25] S. Surblé, C. Serre, F. Millange, C. Mellot-Draznieks, G. Férey, unpublished results.

[26] C. Serre, F. Millange, S. Surblé, J. M. Greneche, G. Férey, *Chem. Mater.*, in press.

[27] C. Mellot-Draznieks, J. M. Newsam, A. M. Gorman, C. M. Freeman, G. Férey, *Angew. Chem.* **2000**, *39*, 2358; *Angew. Chem. Int. Ed.* **2000**, *39*, 2270.

[28] C. Mellot-Draznieks, G. Férey, C. Schön, Z. Cancarevic, M. Jansen, *Chem. Eur. J.* **2002**, *8*, 4102.

[29] C. Mellot-Draznieks, J. Dutour, G. Férey, *Angew. Chem. Int. Ed.* **2004**, submitted.

[30] B. Gomez-Lor, E. Gutierrez-Puebla, M. Iglesias, M. A. Monge, C. Ruiz-Valero, N. Snejko, *Inorg. Chem.* **2002**, *41*, 2429.

[31] T. Loiseau, C. Serre, C. Huguenard, G. Fink, F. Taulelle, M. Henry, T. Bataille, G. Férey, *Chemistry, Chem. Eur. J.* **2004**, *10*, 1.

[32] K. Barthelet, J. Marrot, G. Férey, D. Riou, *Chem. Commun.* **2004**, 520.

[33] C. T. Dziobkowski, T. J. Wroblewski, D. B. Brown, *Inorg. Chem.* **1982**, *21*, 671.

[34] A. Boulitf, D. Louër, *J. Appl. Crystallogr.* **1991**, *24*, 987.

[35] A. Altomare, M. C. Burla, M. Camalli, B. Carrozzini, G. L. Casciarano, C. Giacovazzo, A. Guagliardi, A. G. G. Moliterni, G. Polidori, R. Rizzi, *J. Appl. Crystallogr.* **1999**, *32*, 339.

[36] Cerius Software Suite, Version 3.9, Accelrys Inc., USA.

[37] SHELXL97, University of Göttingen, Germany, **1997**.

[38] J. Rodriguez-Carvajal in *Collected Abstracts of Powder Diffraction Meeting* (Toulouse, France), **1990**, p. 127.

[39] T. Roisnel, J. Rodriguez-Carvajal in *Abstracts of the 7th European Powder Diffraction Conference* (Barcelona, Spain), **2000**, p. 71.

[40] R. A. Young, D. B. Wiles, *J. Appl. Crystallogr.* **1982**, *15*, 430.

Hybrid Organic–Inorganic Frameworks: Routes for Computational Design and Structure Prediction**

Caroline Mellot-Draznieks,* Julien Dutour, and Gérard Férey

The controlled synthesis of materials with very large pores is an ongoing challenge in the area of materials science. Research into large-pore materials is fueled by their use in catalysis, gas storage, and separation.^[1] After intense development of inorganic frameworks in the early 1990s,^[2] the subsequent discovery of hybrid porous solids, in which the connection of inorganic moieties is ensured by organic functionalized N-donor or O-donor molecules, paved the way for the rational design of hybrid frameworks.^[3–11] A new class of materials has emerged at the crossroads of inorganic materials science and coordination chemistry. Among the most illustrative examples of open frameworks are the zinc carboxylate series by Yaghi, O’Keeffe, and co-workers, and the transition-metal terephthalates that have remarkable methane- and hydrogen-storage properties,^[12] together with, for example, a recent series of 3d transition-metal^[13a,14] and rare-earth^[15]-based hybrids that exhibit interesting magnetic properties.^[13a] The richness of this area lies in the diversity of topologies (from molecular to 3D) and properties, which is conveyed in the wide choice of metal atoms that are available, combined with a virtually infinite choice of organic counterparts (e.g., carboxylates, phosphonates, polyamines).

In the current search for new and interesting hybrid open frameworks, the predictability of the framework architecture and the control of its dimensionality are essential, even if one is confronted with the underlying issue of polymorphism.^[6] The possibility of rational design with these types of solids has rapidly emerged through the use of topological and chemical considerations on existing networks.^[7] The concept of rational design is rooted in the fact that topochemically selected reactions govern the construction process of the hybrid framework under hydrothermal conditions. Although metal-containing secondary building units (SBUs) may not be

isolated, their recurrence in a large number of structures suggests that the targeted inorganic subunit already exists in solution before their condensation into the framework structure and thus may be obtained under appropriate synthetic conditions. For example, this aspect is apparent through the *iso*-reticular synthesis of IRMOFs1–16^[12b] derived from the prototypic MOF-5 structure.^[12a]

In this context, structural prediction is an important issue. It is crucial to consider how systematic approaches might be computationally developed for producing new hybrid frameworks, with the desire of developing virtual libraries that might be accessible by rational synthesis.

It is worth underscoring here that crystal-structure prediction is now routinely explored in organic chemistry and polymer science,^[16,17] in which candidate structures may be predicted by assembling molecular entities through hydrogen-bond intermolecular interactions. In contrast, such developments have only been recently reported for inorganic crystal structures, which are extremely difficult to predict due to their infinite lattices. Pioneered by Newsam et al. in the field of zeolites,^[18] crystal-structure prediction^[18–28] and rational design^[29–31] are now at work in the field of open frameworks. Due to their ability to cross hypersurface energy barriers and search for low-energy regions, global optimization techniques are intensively used to predict atomic-scale arrangements of infinite lattices and are able to handle the assembly of atoms, ions,^[20,22–25] or predefined building units in three dimensions.^[21,27,28]

We have introduced the concept of building units for the computational prediction of crystal structures with the AASBU method (automated assembly of secondary building units).^[21,27,28] This method explores the possible ways of assembling predefined inorganic building units, and focuses on the topology of network-based structures.

Inspired by these recent developments, we present herein the extension of the AASBU method to the realm of hybrid organic–inorganic frameworks and demonstrate its capacity to produce hybrid candidate crystal structures that are built from predefined organic and inorganic counterparts. To our knowledge, no systematic computational strategy has been reported in this field so far.

Indeed, hybrid frameworks offer ideal features for computational developments: although the isolated metal ion, taken alone, lacks directional information, the inorganic unit derived from the metal atom and the organic ligand does (Figure 1). Once the inorganic and organic units are defined, one may assume that there are a limited number of arrangements that are compatible with periodicity and symmetry. With predefined organic and inorganic building units, AASBU simulations are used here to perform their automated assembly in three dimensions, thus exploring the possibilities of connection. The simulations yield a virtual library of candidate hybrid frameworks that are assorted by their space group, cell parameters, and atomic positions.

Our initial efforts were aimed at validating the AASBU approach in the field of hybrid frameworks by simulating existing architectures. In the second instance, we aimed at predicting structures that have not yet been synthesized, both to tackle the issue of polymorphism by limiting the domain of

[*] Dr. C. Mellot-Draznieks, J. Dutour
Institut Lavoisier–UMR CNRS 8637
Université de Versailles St. Quentin
45 Avenue des Etats-Unis, 78035 Versailles Cedex (France)
Fax: (+33) 1-3925-4358
E-mail: mellot@chimie.uvsq.fr
Prof. G. Férey
Institut Universitaire de France
Institut Lavoisier
Université de Versailles St. Quentin
45 Avenue des Etats-Unis, 78035 Versailles Cedex (France)

[**] This work was supported by Centre National de la Recherche Scientifique. We thank C. Serre and F. Millange for useful assistance and discussions.

Supporting information for this article is available on the WWW under <http://www.angewandte.org> or from the author.

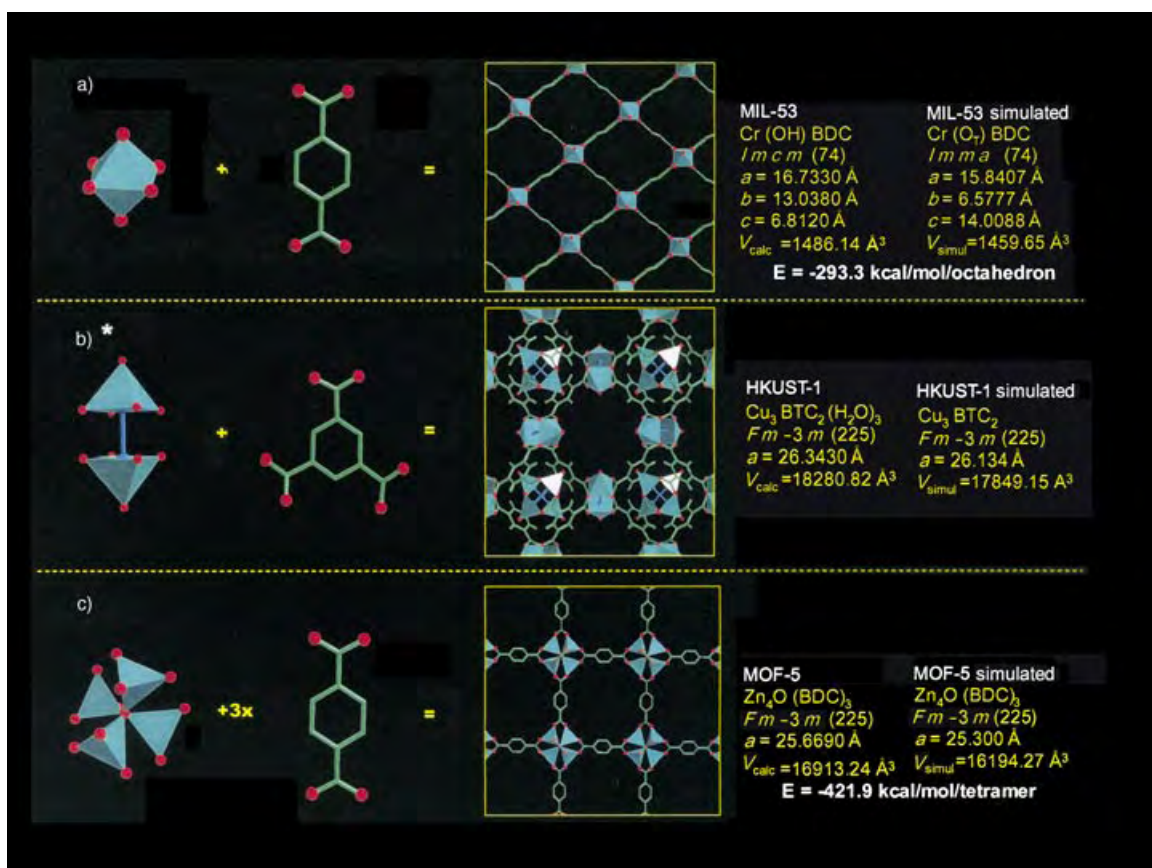


Figure 1. Left: Examples of mono-(a), di-(b), and tetrameric (c) metal clusters and organic carboxylate ligands commonly found in hybrid frameworks. Right: For each organic/inorganic combination, an example of existing very open framework is shown. (*) The lattice energy of HKUST-1 could not be easily estimated due to the Cu–Cu metal bond and therefore the difficulty of estimating partial charges on Cu atoms.

structures that are possible for a given metal–organic–ligand pair, and to aid the often-difficult task of crystal-structure determination.

In the computational approach that we have developed, the inorganic and organic counterparts may be treated as two different building units, or encapsulated in a single hybrid building block. Both approaches were explored. The preliminary step consists of the elaboration of a suitable library of SBUs, which we directly extracted from known and typical hybrid frameworks (Figure 1). The inorganic unit is modeled by a rigid body, ($\{M_x L_y^{\text{inorg}}\}$; *M*: metal centers; *L*^{inorg}: ligand atoms of the inorganic units). The organic unit is treated as a flexible body, ($C_n L_m^{\text{org}}$; *C*: carbon skeleton, *L*^{org}: ligand atoms of the organic units such as oxygen atoms of carboxylate functions). The computational assembly is further controlled through the use of predefined “sticky-atoms”: all ligand atoms on both the organic and inorganic units, *L*^{inorg} and *L*^{org}, are defined as equally possible linkage points.

The rules that control the possible assembly of the organic and inorganic building units during the subsequent simulation steps are encapsulated in a forcefield that includes “sticky-atom” pairs. They are parameterized on an atom–atom basis by a simple Lennard–Jones expression for the energy of interaction between pairs of atoms *i* and *j*, as defined in Equation (1):

$$E_{ij} = \varepsilon_{ij} [(r_{ij}^*/r_{ij})^{12} - 2(r_{ij}^*/r_{ij})^6] \quad (1)$$

The *L*^{org}...*L*^{inorg} sticky-atom pairs are those that form the organic–inorganic linkages, parameterized as a highly attractive potential well with a minimum at very short *L*^{org}...*L*^{inorg} separations. Similarly, *L*^{inorg}...*L*^{inorg} sticky-atom pairs are those that form inorganic–inorganic clusters. A repulsive potential between *L*^{org}...*L*^{org} pairs avoids overlapping or connections of organic molecules to one another (Table 1). This potential serves simply to “glue” together organic and inorganic units according to general criteria. The total cost or energy of a given arrangement of organic and inorganic building units in a unit cell, *E*_{total}, is calculated as the sum over the set of building units of the Lennard–Jones terms [Eq. (1)] that involve

Table 1: Lennard–Jones (L–J) parameters used in the AASBU simulations for assembling BDC and octahedral metal centres {ML₆}.^[a]

Atom pairs	L–J. potential	ε_{ij} [kcal mol ^{−1}]	<i>r</i> _{<i>ij</i>} [Å]
<i>L</i> ^{inorg} ... <i>L</i> ^{org}	attractive	1000	0.2
<i>L</i> ^{inorg} ... <i>L</i> ^{inorg}	attractive	1000	0.2
<i>L</i> ^{org} ... <i>L</i> ^{org}	repulsive	1	2.2

[a] The potential parameters that ensure the intramolecular flexibility (bond, angle, torsions) of the organic ligand during the AASBU simulations are given in the Supporting Information.

dissimilar pairs of atoms, plus a term relating to the intramolecular energy of the flexible organic unit, as defined in Equation (2):

$$E_{\text{organic}} = \sum_{\text{atoms}} (E_{\text{bond}} + E_{\text{angle}} + E_{\text{torsion}}) \text{ with}$$

$$E_{\text{bond}} = \frac{1}{2} k_{ij} (r_{ij} - r_o)^2, E_{\text{angle}} = \frac{1}{2} k_{ijk} (\theta_{ijk} - \theta_o)^2, E_{\text{torsion}} = \frac{1}{2} \sum_n B (1 - \cos(n \varphi_{ijkl})) \quad (2)$$

The cost function used here is not an expression of the internal energy of the system, but simply evaluates its degree of connectivity.

Minimal amount of input data is required for a given simulation: the number of organic units per asymmetric unit, the number of inorganic units per asymmetric unit (alternatively the number of hybrid building blocks), and optionally the space group, as in the most general case simulations may be performed in *P1*. The simulations are not constrained by the cell dimensions. The number of independent entities (organic versus inorganic) is the key input parameter restricting the subsequent search within structures that have the desired metal:organic ratio. This method is therefore adequate for searching polymorphs of hybrid frameworks.

The computational steps for generating candidate periodic hybrid structures are performed by using the AASBU method.^[27] The main steps are summarized below, further details may be found in reference [27]: 1) periodic trial arrangements of organic and inorganic units are generated by using a simulated annealing Monte Carlo procedure within the imposed space group and the imposed number of organic and inorganic units per asymmetric unit. At this stage, the stored configurations correspond to unconnected organic and inorganic units in 3D space. 2) Each unique arrangement is minimized with respect to the total cost function [Eqs. (1) and (2)]. This is a key step at which the assembly of inorganic and organic units (or alternatively hybrid building blocks) through the predefined linkage points is performed, which possibly leads to periodic connected hybrid arrangements. At this step, the flexibility of the organic unit is crucial to make adequate connections to the inorganic units. 4) Sticky-atom pairs, $L^{\text{org}} \dots L^{\text{inorg}}$ and $L^{\text{inorg}} \dots L^{\text{org}}$, are reduced to a single atom. Realistic predictions of crystal structures are thus produced. The symmetry of each candidate hybrid structure is redetermined by using the Find_Symmetry algorithm.^[32]

The AASBU simulation steps were performed by using the Polymorph Predictor of the Cerius2 program.^[33] The simulations are left with a list of candidate hybrid structures (space group, cell, atomic positions). A typical calculation requires from around 2 h for “mixing” one simple inorganic unit and one organic molecule per asymmetric unit up to more than 16 h for assembling a more-complex hybrid building block on an Octane SGI R12000 workstation operating at 300 MHz.

As a final step to estimate the stabilities of the hybrid candidates, lattice-energy minimizations were performed on each candidate crystal structure. Short-range interactions were calculated by using the UFF forcefield.^[34] The electrostatic contribution was calculated with an Ewald summation

by using partial charges obtained from the charge-equilibration method.^[35]

With the purpose of demonstrating the viability of our approach in the area of hybrid frameworks, we first focused our efforts on the simulation of existing and well-characterized hybrid frameworks. A limited number of very-large-pore hybrids were chosen as prototypic structures, such as **MIL-53** ($M(\text{OH})(\text{BDC})$, BDC = benzene-1,4-dicarboxylate, $M = \text{V}^{3+}$,^[36a] Cr^{3+} ,^[36b] or Al^{3+} ,^[36c]), **HKUST-1** ($\text{Cu}_3(\text{BTC})_2(\text{H}_2\text{O})_3$; BTC = benzene, 1,3,5 tricarboxylate),^[37] and **MOF-5** ($\text{Zn}_4\text{O}(\text{BDC})_3$)^[12a] (Figure 1), that is, with the specific aim of predicting their full crystal structure by using the related inorganic unit (monomer, dimer, tetrameric respectively) and organic ligand.

A first possible approach consists in computationally assembling independent organic and inorganic units. This mixture approach was explored in the case of the monomeric, trimeric, and tetrameric metal clusters. In the case of the dimeric metal cluster an approach with a hybrid building block is presented below. For example, a series of AASBU simulations were performed with one single octahedron per asymmetric unit, in which the six ligand atoms were possible linkage points, together with one BDC molecule per asymmetric unit in which the four oxygen atoms were defined as possible linkage points thus ensuring a 1:1 metal:organic ratio. Various space groups were sampled: *P1*, $\bar{P}1$, *Cc*, *Pna*2₁, *P3*, $\bar{P}3$, *P4*, $\bar{P}4$, *P6*, and $\bar{P}6$. The **MIL-53** topology was produced in space group *Cc* among a list of 54 candidates, with the final high symmetry, *Imma*, in excellent agreement with that of the experimental structure, (*Imcm*)^[36c] (See Figure 1a). Interestingly, **MIL-53** belongs to the class of flexible networks that exhibit a very large breathing effect upon water adsorption/removal, which results in important changes in the symmetry and cell size (hydrated:*C2/c*; calcined:*Imcm*).^[36c] Interestingly, the simulations performed here in the absence of extraframework species (i.e., water) yield the **MIL-53** topology in its high symmetry form, which is indeed the symmetry of the experimental calcined (water-free) structure.

When this method was adopted for each inorganic and organic units in the required ratio, the expected metal-organic frameworks were generated (Table 2, Figure 1, and Figure 2). An illustrative example was tackled with the tetrameric units found in the prototypic **MOF-5** (Figure 1b).^[12a] AASBU simulations were performed by mixing one single tetrameric unit, $\{M_4(\mu_3\text{-O})(L_3)_4\}$, defined with 12 possible linkage points, and 3 BDC molecules per asymmetric unit, defined with 3×4 possible linkage points. During the simulations steps, only connections between the inorganic unit and the BDC molecules were allowed, while preventing inorganic-inorganic connections with repulsive parameters. The **MOF-5** topology was predicted successfully and appeared in space group *Aba*2, which was ranked the lowest-energy structure among a list of 115 candidates. Indeed, only the first two candidates corresponded to plausible inorganic-organic frameworks: the framework adopts the topology in which $\{M_4(\mu_3\text{-O})(L_3)_4\}$ tetramers are connected through twelve $L^{\text{inorg}} \dots L^{\text{org}}$ interactions to six carboxylates in the octahedral directions to form the expected

Table 2: AASBU simulations of experimentally known hybrid frameworks.

Organic and inorganic units	Organic/inorganic ratio imposed	Initial space group ^[a]	Predicted structure	Final space group ^[a]	Ref.
BDC + {ML ₆ }	1:1	<i>Cc</i>	MIL-53	<i>Imma</i>	[36]
BDC + {M ₄ (μ ₃ -O)L ₁₂ }	3:1	<i>Ab2</i>	MOF-5	<i>Fm3m</i>	[12a]
Hybrid building-block	Organic/inorganic ratio imposed	Initial space group ^[a]	Predicted structure	Final space group ^[a]	Ref.
{M ₆ (BTC) ₄ } ^[b]	3:2	<i>C2</i>	HKUST-1	<i>Fm3m</i>	[37]
{M ₆ (BTC) ₄ } ^[b]	3:2	<i>Fd3m</i>	MIL-100	<i>Fd3m</i>	[41]

[a] We make a distinction between the space group as imposed during the AASBU simulations themselves (initial space group) and the space group as obtained from the final symmetry analysis of the simulated structures (final space group). They may be different as arrangements of higher symmetry than that imposed may be produced. [b] The building blocks are built with 12 metal centers (4 trimeric clusters or 6 dimers). However, each dimeric (or trimeric) metal cluster is parameterized to be half-shared with another building block, hence the reported composition of 6 metal centers per building block.

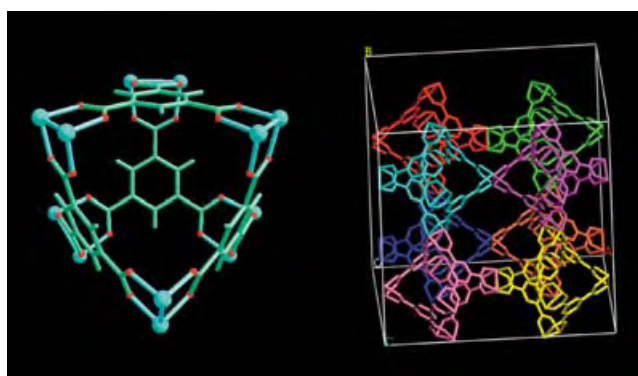


Figure 2. Left: Hybrid building blocks derived from $[\{Cu_3(BTC)_2(H_2O)_3\}_n]$.^[37] This is an octahedral unit where $\{Cu_2\}$ dimers are placed at the six vertices. The four BTC molecules are placed at four of the eight triangular faces of the octahedron. Right: The expected **HKUST-1** structure was computationally generated by self-assembling the hybrid building block (different colors are used for each building block).

porous cubic structure. The lattice energy minimizations, the simulated cell parameter, and symmetry (25.3 Å, *Fm3m*) of the first candidate are in excellent agreement with the experimental findings (25.67 Å, *Fm3m*).

An interesting alternative to the computational mixture of independent organic and inorganic units (see above) is to consider a single hybrid building block and to allow its self-assembly during the subsequent simulation steps. This approach, which has the advantage of being directly inspired by the concept of secondary building blocks used by synthesis chemists for the design of targeted networks, was explored with a paddle-wheel cluster that is known in many complexes^[38] and was involved in the synthesis of hybrid frameworks.^[7a,37] We started from the SBU proposed by Williams and co-workers in the description of the 3D hybrid framework, **HKUST-1**.^[37] As illustrated in Figure 2, the $\{Cu_2\}$ dimers were placed at the vertices of an octahedral unit while being interconnected through BTC molecules placed at four of the eight triangular faces of the octahedron. During

the AASBU simulations, this hybrid building block was allowed to self-assembly by direct edge sharing at the Cu–Cu metal bond. By using two building blocks per asymmetric-unit, we successfully simulated and energy minimized the expected **HKUST-1** structure in the initial space group *C2*, which lead to a crystal structure with the expected symmetry *Fd3m* and cell parameters ($a_{sim} = 26.134$ Å/ $a_{exp} = 26.343$ Å).

When compared to the first approach, which mixes independent organic and inorganic units, the hybrid building block inherently contains additional structural information on organic–inorganic

connections. While obviously requiring an advanced knowledge of the system under study, this approach should in principle allow a more restricted (i.e., more rapid) production of viable hybrid candidates.

An attractive feature of the simulations is indeed the generation of new topologies. Typically, while assembling one $\{MO_6\}$ octahedron and one BDC molecule (section above), not only the experimentally known **MIL-53** structure was predicted but also a series of not-yet-synthesized topologies ranging from lamellar to 3D extended structures. Figure 3 shows a selection of three hypothetical structures chosen for their serendipitous topological relationships. The three structures derive from the same layer (Figure 3a) and differ only by the degree of “condensation” of the sheets: the stacking of unconnected sheets builds the first structure (Figure 3b), while the second (Figure 3c) shows stacking of dimerized-planes. The third structure has a 3D network (Figure 3d) that results from the infinite stacking of the planes. Another interesting 3D hexagonal structure was produced (Figure 4a), which exhibits large tunnels ($\varnothing = 15.6$ Å). These candidates illustrate how simulations may be a valuable tool for highlighting topological relationships.

On the other hand, the number of hybrid structures that contain trimeric metal clusters formed by the assembly of three vertex-sharing octahedra is very scarce.^[7b,39] For this reason, our group has recently focused on their chemical condition of existence in hydrothermal synthesis.^[40] By using our computational approach to encapsulate the trimeric metal cluster and BDC (or BTC) molecules in a hybrid building block, we simulated a whole series of plausible and very open frameworks.

Figure 4b–c show two hypothetical topologies generated by using a building block that contains BDC and trimeric metal clusters. These topologies represent cubic polymorphs with large cell volumes, 23579 Å³ and 64524 Å³, and have central cages with an internal diameter of 25 Å, accessible through “four rings” of trimers. A detailed study on this new family of polymorphs will be published elsewhere.^[41]

Most interestingly, one of the trimeric BTC-based hybrid polymorph (Table 2) has a giant unit cell and exhibits a

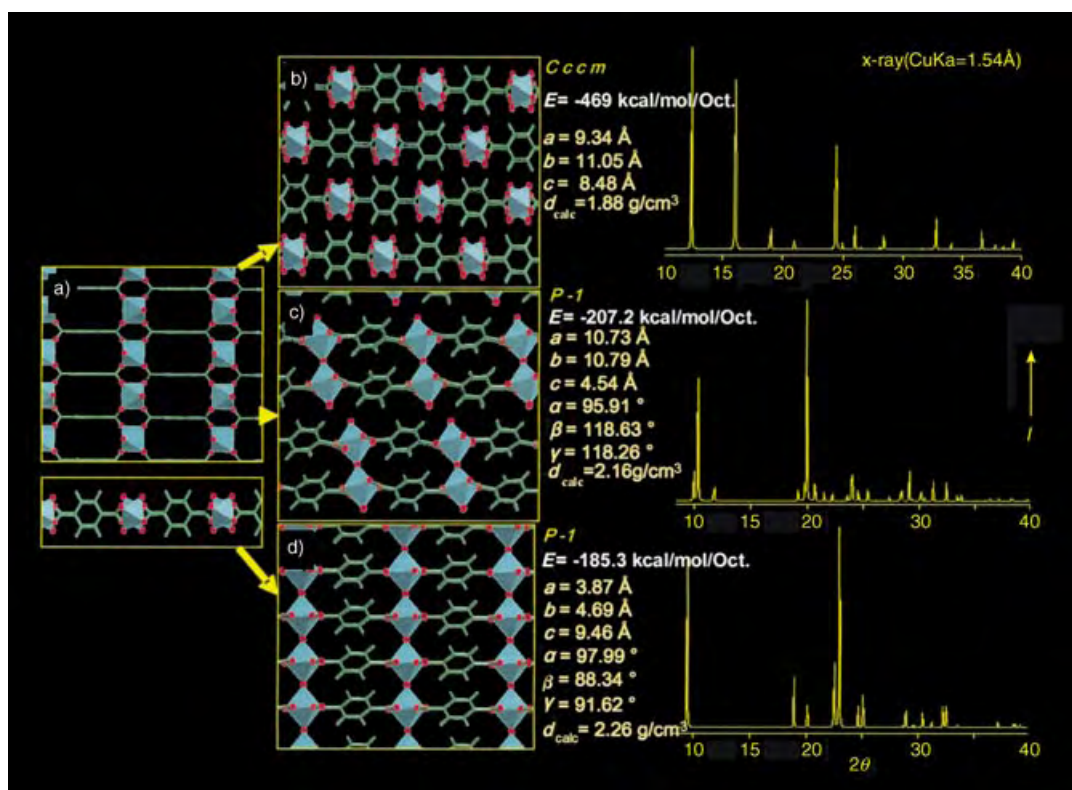


Figure 3. Topological relationships between three simulated hybrids that were obtained by assembling one BDC molecule and one octahedron per asymmetric unit. The three structures are built from the same plane (top and side view in a), which range from lamellar (b and c) to 3D networks (d). *I*: intensity (arbitrary units).

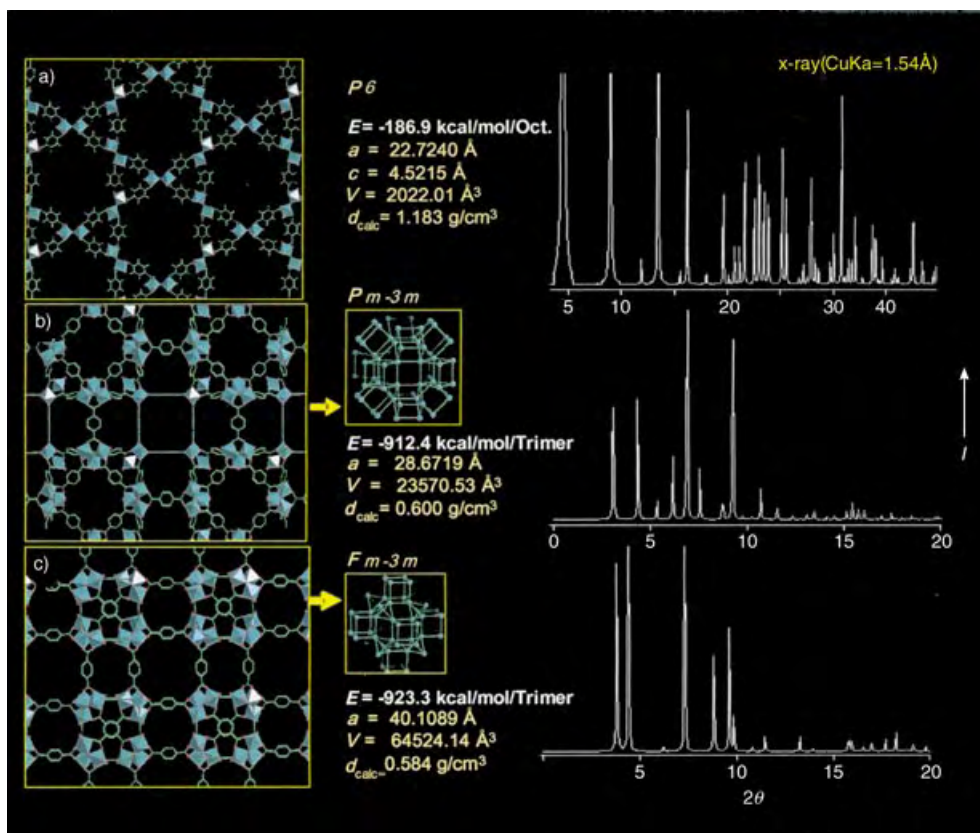


Figure 4. Hypothetical very-open hybrid frameworks, simulated by assembling BDC with a single octahedron (a), and with trimeric metal clusters (b) and (c).

simulated diffraction pattern that exactly matched the experimental pattern of a new phase synthesized in our group, MIL-100. Thus we obtained the solution of its direct-space structure and ensured a valid model for subsequent structure refinement.^[42]

In conclusion, this work addresses the computational prediction of hybrid organic–inorganic extended lattices. The production of candidates of crystal structures was successfully performed by direct-space assembly of building units by the AASBU method, either through mixing independent organic and inorganic units or by assembling predefined hybrid building blocks. Hybrid candidates that are compatible with the imposed metal:organic ratios were generated with their cell parameters, space group, atomic positions, along with their simulated diffraction pattern and an estimate of their lattice energies. Since no explicit limit regarding the nature, number, and size of the inorganic and organic units, or hybrid building block is involved, the method offers boundless potential for exploring hybrid frameworks in terms of the topological diversity.

The most appealing development arises from the computer-assisted design of hybrid frameworks. Indeed, in a significant number of systems, it is well-known that controlled synthesis conditions can promote the occurrence of specific building units, which serve to “propagate” the infinite crystal structure. We believe that the computational approach presented herein is valuable to create virtual libraries of viable hybrid polymorphs. Furthermore, AASBU simulations have proven to be, for the first time in the realm of hybrids, a tangible route towards structure solution in direct space.^[42] This challenging area is of crucial interest when high quality diffraction data are not available or when very large cell sizes are involved. The development of a structural model in direct space, starting with minimal knowledge such as the metal:organic ratio, is shown to be possible. With such a method in hand, formerly intractable structural problems when using methods based on conventional reciprocal space become feasible in direct space.

We believe this approach serves a step forward in the computational anticipation and structure solution of hybrid frameworks. It should allow one to tackle the issue of polymorphism, while opening up the field of synthesis of new hybrid frameworks and structure solution for compounds that have not yet been characterized.

Received: March 12, 2004 [Z54251]

Keywords: carboxylate ligands · molecular modeling · nanoporous materials · organic–inorganic hybrid composites · structure elucidation

- [1] a) G. Férey, A. K. Cheetham, *Science* **1999**, 283, 1125–1126; b) G. Férey, *Science* **2000**, 289, 994–995.
- [2] A. K. Cheetham, G. Férey, T. Loiseau, *Angew. Chem.* **1999**, 111, 3466; *Angew. Chem. Int. Ed.* **1999**, 38, 3268–3292.
- [3] a) C. Janiak, *Angew. Chem.* **1997**, 109, 1499; *Angew. Chem. Int. Ed. Engl.* **1997**, 36, 1431; b) C. Janiak, *Dalton Trans.* **2003**, 2781–2804.
- [4] S. R. Batten, R. Robson, *Angew. Chem.* **1998**, 110, 1558; *Angew. Chem. Int. Ed.* **1998**, 37, 1460–1494.
- [5] P. L. Hargman, D. Hargman, J. Zubieta, *Angew. Chem.* **1999**, 111, 2798; *Angew. Chem. Int. Ed.* **1999**, 38, 2638.
- [6] B. Moulton, M. Zavorotko, *Chem. Rev.* **2001**, 101, 1629–1658.
- [7] a) M. Eddaoudi, D. B. Moler, H. Li, B. Chen, T. M. Reineke, M. O’Keeffe, O. M. Yaghi, *Acc. Chem. Res.* **2001**, 34, 319–330; b) O. M. Yaghi, M. O’Keeffe, N. W. Ockwig, H. K. Chae, M. Eddaoudi, J. Kim, *Nature* **2003**, 423, 705; c) O. M. Yaghi, M. O’Keeffe, Kanatzidis, *J. Solid State Chem.* **2000**, 152, 1–321. (Special Issue.)
- [8] G. Férey, *Chem. Mater.* **2001**, 13, 3084.
- [9] S. L. James, *Chem. Soc. Rev.* **2003**, 32, 276–288.
- [10] H. Eckert, M. Ward, *Chem. Mater.* **2001**, 13, 3061–3809. (Special issue: Organic–Inorganic Nanocomposite Materials.)
- [11] C. N. R. Rao, S. Natarajan, R. Vaidyanathan, *Angew. Chem.* **2004**, 116, 1490–1521; *Angew. Chem. Int. Ed.* **2004**, 43, 1466.
- [12] a) H. Li, M. Eddaoudi, M. O’Keeffe, O. M. Yaghi, *Nature* **1999**, 402, 276–279; b) M. Eddaoudi, J. Kim, N. Rosi, D. Vodak, J. Wachter, M. O’Keeffe, O. M. Yaghi, *Science* **2002**, 295, 469; c) N. L. Rosi, J. Eckert, M. Eddaoudi, D. T. Vodak, J. Kim, M. O’Keeffe, O. M. Yaghi, *Science* **2003**, 300, 1127; d) H. K. Chae, D. Y. Siberio-Pérez, J. Kim, Y. Go, M. Eddaoudi, A. J. Matzger, M. O’Keeffe, O. M. Yaghi, *Nature* **2004**, 427, 523–527.
- [13] a) C. Serre, F. Millange, C. Thouvenot, M. Noguères, G. Marsolier, D. Louër G. Férey, *J. Am. Chem. Soc.* **2002**, 124, 13519–13526; b) G. Férey, M. Latoche, C. Serre, F. Millange, T. Loiseau, A. Percheron-Guégan, *Chem. Commun.* **2003**, 2976–2977.
- [14] a) C. Livage, C. Egger, G. Férey, *Chem. Mater.* **1999**, 11, 1546–1550; b) T. M. Reineke, M. Eddaoudi, M. O’Keeffe, O. M. Yaghi, *Angew. Chem.* **1999**, 111, 2712; *Angew. Chem. Int. Ed.* **1999**, 38, 2590; c) C. Livage, C. Egger, G. Férey, *Chem. Mater.* **2001**, 13, 410; d) M. Sanselme, J. M. Grenèche, M. Riou-Cavellec, G. Férey, *Chem. Commun.* **2002**, 2172.
- [15] a) G. Férey, C. Serre, *J. Mater. Chem.* **2002**, 12, 3053; b) G. Férey, C. Serre, *Chem. Mater.* **2002**, 14, 2409; c) F. Millange, C. Serre, J. Marrot, N. Gardant, F. Pellé, G. Férey, *Mater. Chem.* **2004**, 14, 642–645.
- [16] a) R. J. Gdanitz, *Curr. Opin. Solid. State Mater. Sci.* **1998**, 3, 414–418; b) R. J. Gdanitz in *Theoretical Aspects and Computer Modeling* (Ed.: A. Gavezzotti) Wiley, New York, **1997**, p. 185.
- [17] a) P. Veuwer, F. J. J. Leusen in *Reviews of Computational Chemistry, Vol. 12* (Eds: K. B. Lipkowitz, D. B. Boyd) Wiley, New-York, **1998**, pp. 327–365; b) J. P. M. Lommerse, W. D. S. Motherwell, H. L. Ammon, J. D. Dunitz, A. Dzyabchenko, P. Erk, A. Gavezzotti, D. W. M. Hofmann, F. J. J. Leusen, J. P. M. Lommerse, W. T. M. Mooij, S. L. Price, H. Scheraga, B. Schweizer, M. U. Schmidt, B. P. van Eijck, P. Verwer, D. E. Williams, *Acta Cryst. Sect. B* **2000**, 56, 697.
- [18] a) M. W. Deem, J. Newsam, *Nature* **1989**, 342, 260; b) M. W. Deem, *J. Am. Chem. Soc.* **1992**, 114, 7189; c) M. Falcioni, M. W. Deem, *J. Chem. Phys.* **1999**, 110, 1754.
- [19] *Computer Modeling in Inorganic Chemistry* (Ed: C. R. A. Catlow), Academic Press, San Diego, **1997**.
- [20] J. C. Schön, M. Jansen, *Angew. Chem.* **1996**, 108, 1358; *Angew. Chem. Int. Ed. Engl.* **1996**, 35, 1286.
- [21] C. Mellot-Draznieks, G. Férey, C. Schön, Z. Cancarevic, M. Jansen, *Chem. Eur. J.* **2002**, 8, 184102.
- [22] J. Pannetier, J. Bassas-Alsina, J. Rodriguez-Carvajal, V. Caignaert, *Nature* **1990**, 346, 343.
- [23] C. M. Freeman, J. M. Newsam, S. M. Levine, C. R. A. Catlow, *J. Mater. Chem.* **1993**, 3, 531.
- [24] a) S. M. Woodley, P. D. Battle, J. D. Gale, C. R. A. Catlow, *Phys. Chem. Chem. Phys.* **1999**, 1, 2535; b) S. M. Woodley, C. R. A. Catlow, P. D. Battle, J. D. Gale, *Chem. Commun.* **2004**, 22–23.

- [25] a) J. C. Schön, M. Jansen, *Comput. Mater. Sci.* **1998**, *11*, 309; b) M. A. C. Wevers, J. C. Schön, M. Jansen, *J. Solid State Chem.* **1998**, *136*, 223; c) J. C. Schön, M. A. C. Wevers, M. Jansen, *J. Mater. Chem.* **2001**, *11*, 69.
- [26] M. D. Foster, O. Delgado-Friedrichs, R. G. Bell, F. A. Almeida - Paz, J. Klinowski, *Angew. Chem.* **2003**, *115*, 4026–4029; *Angew. Chem. Int. Ed.* **2003**, *42*, 3896–3999.
- [27] C. Mellot-Draznieks, J. M. Newsam, A. M. Gorman, C. M. Freeman, G. Férey, *Angew. Chem.* **2000**, *112*, 2353–2353; *Angew. Chem. Int. Ed.* **2000**, *39*, 2270–2275.
- [28] a) C. Mellot-Draznieks, S. Girard, G. Férey, *J. Am. Chem. Soc.* **2002**, *124*, 15326–15335; b) S. Girard, P. Pullumbi, C. Mellot-Draznieks, G. Férey, *Stud. Surf. Sci. Catal.* **2001**, *135*, 254.
- [29] D. W. Lewis, D. J. Willock, C. R. A. Catlow, J. M. Thomas, G. J. Hutchings, *Nature* **1996**, *382*, 604.
- [30] a) M. O'Keeffe, *J. Solid State Chem.* **2000**, *152*, 3; b) G. Férey, *J. Solid State Chem.* **2000**, *152*, 37; See also: *J. Solid. State Chem.* **2000**, *152*(1). (Special Issue.)
- [31] M. Jansen, *Angew. Chem.* **2002**, *114*, 3896–3917; *Angew. Chem. Int. Ed.* **2002**, *41*, 3746–3766.
- [32] *Biosym Catalysis 2.0 Software Manual 1993*, Accelrys Inc. USA; See also: *Accuracy in Powder Diffraction II (NIST Specila Publication No 846)* (Eds.: J. M. Newsam, M. W. Deem, C. M. Freeman, E. Prince, J. K. Stalick), National Institute of Standards and Technology, Bethesda, MD, USA, **1992**, p. 80.
- [33] Polymorph Predictor is available in the *Cerius2* Program suite from Accelrys, San Diego, USA and Cambridge, UK.
- [34] A. K. Rappé, C. J. Casewit, K. S. Colwell, W. A. Goddard III, W. M. Skiff, *J. Am. Chem. Soc.* **1992**, *114*, 10024.
- [35] A. K. Rappé, W. A. Goddard III, *J. Phys. Chem. B* **1991**, *95*, 3358.
- [36] a) K. Barthelet, J. Marrot, D. Riou, G. Férey, *Angew. Chem.* **2002**, *114*, 291–294; *Angew. Chem. Int. Ed.* **2002**, *41*, 281; b) C. Serre, F. Millange, C. Thouvenot, M. Noguès, G. Marsolier, D. Louër, G. Férey, *J. Am. Chem. Soc.* **2002**, *124*, 13519–13526; c) T. Loiseau, C. Serre, C. Huguenard, G. Fink, F. Taulelle, M. Henry, T. Bataille, G. Férey, *Chem. Eur. J.* **2004**, *10*, 1–11.
- [37] B. Chen, S. S.-Y. Chui, S. M. F. Lo, J. P. H. Charmant, A. G. Orpen, I. D. Williams, *Science* **1999**, *283*, 1148–1150.
- [38] W. Clegg, I. R. Little, B. P. Straughan, *J. Chem. Soc. Trans.* **1986**, 1283–1288.
- [39] a) J. S. Seo, D. Whang, H. Lee, S. I. Jun, J. Oh, Y. J. Jeon, K. Kim, *Nature* **2000**, *404*, 982–986; b) K. Barthelet, D. Riou, G. Férey, *Chem. Commun.* **2002**, 1492.
- [40] C. Serre, F. Millange, S. Surblé, G. Férey, *Angew. Chem.* **2004**, *116*, 6445–6449; *Angew. Chem. Int. Ed.* **2004**, *43*, 6285–6289.
- [41] C. Mellot-Draznieks, J. Dutour, G. Férey, *Z. Anorg. Allg. Chem.*, in press.
- [42] G. Férey, C. Serre, C. Mellot-Draznieks, F. Millange, S. Surblé, J. Dutour, I. Margiolaki, *Angew. Chem.* **2004**, *116*, 6456–6461; *Angew. Chem. Int. Ed.* **2004**, *43*, 6296–6301.

A Hybrid Solid with Giant Pores Prepared by a Combination of Targeted Chemistry, Simulation, and Powder Diffraction

G rard F rey, Christian Serre, Caroline Mellot-Draznieks, Franck Millange, Suzy Surbl , Julien Dutour, and Ir ne Margiolaki*

Molecular gigantism is very topical in inorganic chemistry.^[1–5] Inorganic and hybrid nanoporous solids, and keplerates^[5] provide illustrations of this trend. Beside its academic interest, this research is motivated by the numerous applications related to this gigantism, such as their use as possible nanoreactors, or in catalysis,^[6] gas separation,^[7] and gas storage.^[8] Besides the systematic chemical search of new systems, two main topological concepts were applied to reach a possible design of porous solids: “scale chemistry”^[9] for inorganics and “reticular synthesis from augmented nets”^[3,10,11] for metal–organic frameworks (MOFs). These two concepts have however limitations: they cannot always provide polymorphs; their topological predictions rapidly lead to complex structures that are almost impossible to solve in the absence of single crystals. We shall prove in the following that, in the domain of MOFs, the introduction of computer simulation beside targeted chemistry of the inorganic moiety push forward these limits. It leads to a new crystalline MOF (**MIL-100**) with a giant cubic cell, the volume of which is close to 380 000 Å³. It exhibits a hierarchy of micro- ($\varnothing \approx 6.5$ Å) and mesopores ($\varnothing \approx 25$ – 30 Å) and a large sorption capacity (3100 m² g^{−1}).

The dream of the solid-state chemist is the synthesis of “tailor-made” compounds with predicted structures and properties. Forbidden in the case of high-temperature synthesis, which is governed by diffusion processes, the synthesis of tailor-made solids is indeed on the way to being realized in the ever growing domain of MOFs, the synthesis of which gives solids by precipitation of the species from solution. In three main seminal articles,^[3,11,12] Yaghi, O’Keeffe, and co-workers progressively defined the concept of reticular chemistry with the chemical and topological rules that govern this possible design. This concept starts from the existence in solution of well defined and rigid inorganic and

[*] G. Férey

Institut universitaire de France

Fax: (+33) 1-3925-4358

E-mail: ferey@chimie.uvsq.fr

G. Férey, C. Serre, C. Mellot-Draznieks, F. Millange, S. Surblé,
J. Dutour

Institut Lavoisier

UMR CNRS 8637

Université de Versailles St-Quentin en Yvelines

45 Avenue des Etats-Unis, 78035 Versailles Cedex (France)

I. Margiolaki

ESRF, Grenoble (France)

Supporting information for this article is available on the WWW under <http://www.angewandte.org> or from the author.

organic building blocks, which must maintain their structural integrity throughout the construction process of the solid. The proper choice of these inorganic and organic building blocks and their assembly by strong bonding must lead to predetermined ordered structures, reminiscent of the topology of dense structures. Numerous examples in the literature illustrate this concept.^[9,12]

However, one of the limitations of this approach concerns the enumeration of the possible predetermined frameworks accessible from predefined building blocks. So far, what is usually called “design” is the realization of a reasonable expectation of a given structural arrangement. Indeed, the idea of a framework resulting from the connection of building blocks refers only to the most probable organization, based on an initial intuition strengthened by topological symmetry rules.^[12] Keeping in mind the principles of reticular chemistry, we applied our new concept to crystal structures of MOFs with the aim of exploring all possible combinations of connections between inorganic and organic building blocks in the system experimentally under study by using original global optimization simulations.^[13] This computational approach takes advantage of our previous AASBU method,^[14] based on the concept of secondary building units (SBU), to assemble organic and inorganic units. It explores the whole space of configurations with the corresponding cell parameters, space groups, and theoretical atomic coordinates; it classifies the different solutions by their relative energies and therefore gives the most likely arrangements. The validity of the method was first proved by finding hybrid structures that are already known, built from different types of inorganic and organic building units. Moreover, unknown topologies with reasonable relative “energies” appeared during the calculations for all the inorganic and organic building units considered. Finally, the calculated X-ray powder-diffraction pattern for each candidate topology may be directly compared to patterns obtained experimentally, thus allowing the rapid identification of new phases. The efficiency of this method relates to the way that it is carried out, but requires that the inorganic building block be present at an early stage of the reaction.

We recently developed separately the computational^[13] and experimental^[15] aspects of our concept. Among the best identified inorganic building blocks, our attention focused on the determination of the chemical conditions leading to trimers that are formed by the assembly of three octahedra sharing a common vertex $\mu_3\text{-O}$,^[15] because known examples are scarce.^[3,16] The conditions used to synthesize the inorganic building units depend on the nature of the cation. Although we initially focused on complexes of Fe^{3+} ions,^[15] the search was extended to complexes of Cr^{3+} ions. The combination of Cr^{3+} ions with trimesic acid (benzene-1,3,5-tricarboxylate; BTC) under hydrothermal conditions leads to a new powdered chromium hybrid solid (**MIL-100**).

MIL-100 is a highly crystalline and pure green solid, a chromium trimesate of chemical composition $\text{Cr}_3\text{F}(\text{H}_2\text{O})_3\text{O}[\text{C}_6\text{H}_3(\text{CO}_2)_3]_2 \cdot n\text{H}_2\text{O}$ ($n \sim 28$). Its resulting pattern is so complicated (Figure 1) that, in the absence of single crystals, the knowledge of the related structure is ruled out. Consequently, our new simulation method^[13] dedicated to the

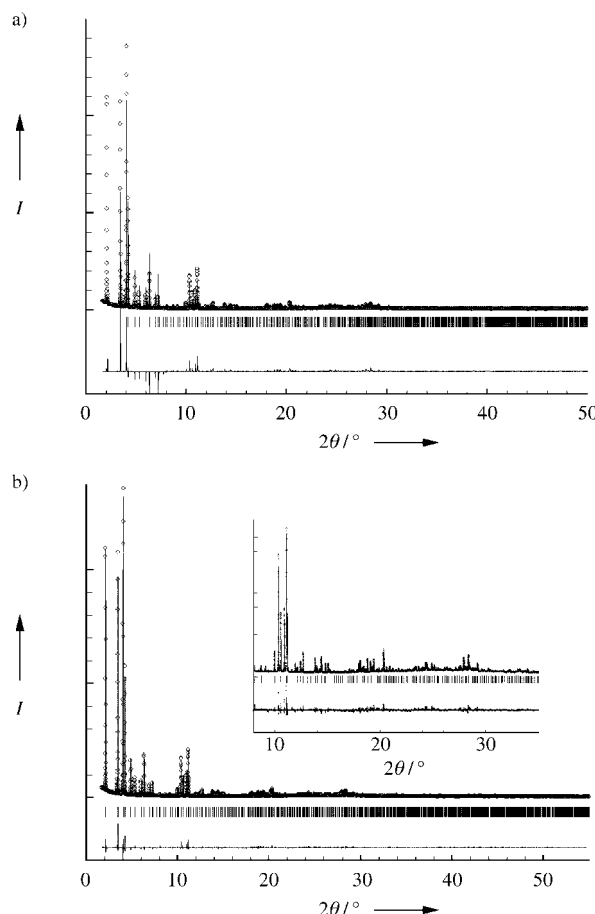


Figure 1. a) Comparison of the simulated X-ray pattern predicted for **MIL-100** (full lines) with that of the experimental (circles). b) Final Rietveld plot of the as-synthesized **MIL-100**. In both figures, the difference spectrum appears at the bottom. I = intensity.

prediction of MOFs is used to predict candidate crystal structures of **MIL-100**. Candidates polymorphs for the [Cr–BTC] system are simulated as follows. Based on the assumption that there are inorganic trimers (Figure 2a) in the new hybrid **MIL-100**, as highly suggested by our previous results,^[15] and that these trimers are linked to the constitutive organic ligand (BTC), possible hybrid building blocks are computationally designed and auto-assembled. Indeed, the arrangement of BTC and inorganic trimers into a large super tetrahedron (ST) was considered as a possible hybrid building block (Figure 2b) and was selected for its compatibility with the chemical composition (metal:organic ratio) of **MIL-100**. The ST is built in such a way that the four vertices of the ST are occupied by the trimers while the organic linker is located at the four faces of the ST. The connection of the ST is established through vertices to ensure a 3D network of “corner-sharing” super tetrahedra. At this stage, three interesting candidates of likely crystal structures were identified and assorted with their full crystallographic parameters together with their simulated X-ray powder patterns. Strikingly, all three candidates are upper homologues of zeotype architectures,^[19] that is, MEP, MTN and a new hexagonal type, referred to hereafter as HEX, in which each tetrahedral

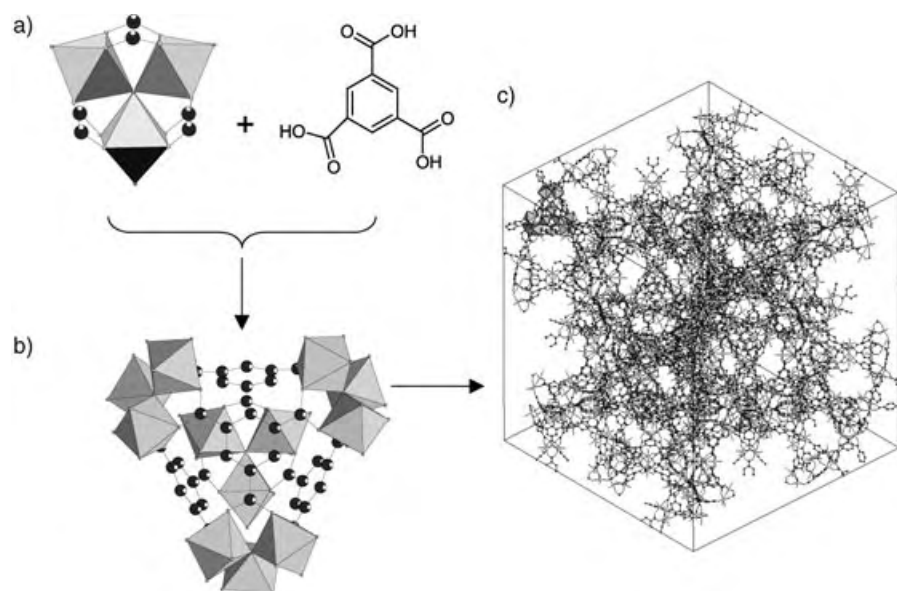


Figure 2. a) The original building block with a trimer of metal octahedra chelated by three carboxylic functions. b) The ST formed by using trimesic acid, which occupies the faces of ST. c) Ball-and-stick view of a unit cell of **MIL-100**; one supertetrahedron is represented by using octahedra for a better understanding. Free water molecules have been omitted for clarity.

center (TO_4), typical of zeolites, is occupied by one super tetrahedron. The corresponding structures, described with more details below (Table 1) illustrate the concept of “scale chemistry”.^[9] They represent polymorphs with cell volumes in the range 120 000–360 000 Å³. Two of them are cubic (MEP,

challenge was then to consider the possibility of a Rietveld refinement of the structure, which required first a very good collection of powder data by using synchrotron radiation (see Experimental Section). Finally, the atomic coordinates and cell parameters of MTN-type model predicted from the simulations were used to perform the Rietveld refinement of the synchrotron diffraction pattern of **MIL-100**. Surprisingly,

Table 1: Simulation of Cr–BTC hybrid frameworks: Selected structural features of three candidate polymorphs.

^[a] MTN		
cubic $Fd\bar{3}m$	BTC	
a [Å]	71.26	
V [Å ³]	361 774	
No. of independent positions per asymmetric unit	68	
Density _{calcd} [g cm ⁻³] ^[b]	0.7843	
Supertetrahedron		
Edge length [Å] (between $\mu_3\text{O}$)	9.40	
No. of atoms of the wall	24 $\text{O}_{\text{carboxy}}$ + 36 C_{BTC} + 12 M	
Internal diameter [Å]	6.64	
(Recall for C_{84} : $18.96 - 2.80 = 16.16$ Å)		
Pentagonododecahedral cages (20 vertices)		
Coordinates of the centroid	0,0,0 (16c positions of $Fd\bar{3}m$ with origin at 0,0,0)	
Accessible diameter [Å]	24.6	with R_c^{vdw} : 1.40 Å
Large cages (28 vertices)		
Coordinates of the centroid	1/8, 1/8, 1/8 (8a positions of $Fd\bar{3}m$ with origin at 0,0,0)	
Accessible diameter [Å]	31.0	with R_c^{vdw} : 1.40 Å
^[a] MEP		
cubic $Pm\bar{3}n$	BTC	
a [Å]	49.27	
V [Å ³]	119 635	
No. of independent positions per asymmetric unit	82	
Density _{calcd} [g cm ⁻³] ^[b]	0.8022	

MTN; space group $Fd\bar{3}m$, $Pm\bar{3}n$, respectively), the third is hexagonal (HEX, space group $P6_3/mmc$). From this point of view, our computational approach is able to create the potential upper homologues of numerous silicates and zeolites with ST instead of small tetrahedra.

Interestingly, the simulated pattern of the MTN-type hybrid structure matches the targeted experimental pattern of **MIL-100** (Figure 1a), thus yielding the solution of the direct-space structure of the new phase and ensuring a valid model for subsequent structure refinement. The diffraction pattern calculated from the MTN-type computed model corresponds exactly to the position of the Bragg peaks of the new structure. The only difference (Figure 1a) concerns the discrepancy between simulated and experimental intensities; the simulated pattern obtained from the computed model corresponds only to the skeleton whereas the experimental pattern also takes into account the contribution of the occluded species.

Owing to the large cell volumes involved, the challenge was then to consider the possibility of a Rietveld refinement of the structure, which required first a very good collection of powder data by using synchrotron radiation (see Experimental Section). Finally, the atomic coordinates and cell parameters of MTN-type model predicted from the simulations were used to perform the Rietveld refinement of the synchrotron diffraction pattern of **MIL-100**. Surprisingly, despite the large number of parameters (67 independent framework atoms, ≈ 170 parameters, in a cell volume of 387 000 Å³), the refinement converges toward good R values and improves the prediction by locating the position of inserted species, which are free water molecules in the case of **MIL-100**. The final Rietveld plot is represented on Figure 1b. The refinement correctly converged towards the general formula $\text{Cr}_3\text{F}(\text{H}_2\text{O})_3\text{O}[\text{C}_6\text{H}_3(\text{CO}_2)_3]_2 \cdot n\text{H}_2\text{O}$ ($n \approx 28$), which is in agreement with the chemical analysis. Extra framework water molecules were localized by using Fourier-difference maps (45 independent water molecules). Full details are given in the Supporting Information.

This is the first time, in the field of hybrid solids, that a rational simulation approach provides a solution of the crystal structure constructed only from topological criteria, which matches the experimental X-ray diffraction pattern of the solid (Figure 1). It is a new method in which conventional direct- or reciprocal-space methods cannot be used in the structure-solution process. The very-

Table 1: (Continued)

Supertetrahedron		
Edge length [Å] (between $\mu_3\text{O}$)	9.40	
No. of atoms of the wall	$24 \text{ O}_{\text{carboxy}} + 36 \text{ C}_{\text{BTC}} + 12 \text{ M}$	
Internal diameter [Å]	6.64	with $R_{\text{c}}^{\text{vdw}}: 1.40 \text{ Å}$
Pentagonododecahedral cages (20 vertices)		
Coordinates of the centroid	0,0,0 (2a positions of $Pm\bar{3}n$ with origin at 0,0,0)	
Accessible diameter [Å]	24.5	with $R_{\text{c}}^{\text{vdw}}: 1.40 \text{ Å}$
Large cages (24 vertices; ovoidal)		
Coordinates of the centroid	$1/2, 0, 3/4$ (12f positions of $Pm\bar{3}n$ with origin at 0,0,0)	
Accessible diameter [Å]	29.2–20.2	with $R_{\text{c}}^{\text{vdw}}: 1.40 \text{ Å}$
^[a] NEW HEX		
hexagonal $P6_3/mmc$	BTC	
a [Å]	50.17	
c [Å]	82.12	
V [Å ³]	179 179	
No. of independent positions per asymmetric unit	245	
Density _{calcd} [g cm ⁻³] ^[b]	0.7918	
Supertetrahedron		
Edge length [Å] (between $\mu_3\text{O}$)	9.40	
No. of atoms of the wall	$24 \text{ O}_{\text{carboxy}} + 36 \text{ C}_{\text{BTC}} + 12 \text{ M}$	
Internal diameter [Å]	6.64	with $R_{\text{c}}^{\text{vdw}}: 1.40 \text{ Å}$
Pentagonododecahedral cages (20 vertices)		
Coordinates of the centroid	0.8495, 0.1701, 0.2439 (24l positions of $P6_3/mmc$ (194) with origin at 0,0,0)	
Accessible diameter [Å]	25	with $R_{\text{c}}^{\text{vdw}}: 1.40 \text{ Å}$
Large cages (28 vertices)		
Coordinates of the centroid	$1/3, 2/3, 0.40$ (4f positions of $P6_3/mmc$ (194) with origin at 0,0,0)	
Accessible diameter [Å]	29.7	with $R_{\text{c}}^{\text{vdw}}: 1.40 \text{ Å}$

[a] MTN, MEP refer to a zeolitic structure type (see Atlas of Zeolites, <http://www.iza-structure.org/>); NEW HEX does not correspond to any known structural type. [b] Densities are estimated by using the Cr form of the simulated topologies.

large cell volume involved in our results opens the window to the discovery of numerous new solids with huge potential applications. In the absence of single crystals, such solids could never be tackled before owing to the extreme complexity of the corresponding structures. They now become accessible.

In the supertetrahedra (see Supporting Information), all the bond lengths are in the usual range (1.81–2.18 Å for Cr–O, 1.37–1.64 Å for C–C; 1.23–1.37 Å for C–O). Moreover, valence-bond calculations show that in the trimer the terminal oxygen atom is from a water molecule. The aromatic ring of BTC occupies the center of the faces of the ST. Within the ST, the cage, which has 24 oxygen atoms and carbon 36 atoms and an internal diameter of 6.6 Å. This dimension corresponds to the domain of micropores, in the same range as zeolites.

More interestingly, the corner sharing of the ST delimits a framework with two types of cages (Figure 3), whose dimensions are now typically in the range of mesopores. The smallest cage, which has 20 ST, has an internal diameter of

$\approx 25 \text{ Å}$. The polyhedron obtained by joining the centers of the ST is a pentagon dodecahedron (the free opening of the pentagonal windows: ($\approx 4.8 \times 5.8 \text{ Å}$) being rather small because the terminal water molecules of the trimer point toward the center of the window). The centers of the dodecahedra, are in the (0,0,0) 16c positions of the space group $Fd\bar{3}m$ (origin choice 2). The sub-network that joins these centers forms corner-linked tetrahedra as in the pyrochlore structure.^[17] The dodecahedra share faces and form (see the Supporting Information) infinite linear rodlike chains,^[18] which cross orthogonally to each other through common faces to ensure the 3D network. This connection creates larger cavities, which have 28 ST. These cages are centered on the (1/8,1/8,1/8) 8a sites of the space group $Fd\bar{3}m$. The polyhedron determined by the centers of the ST has now 12 pentagonal and 4 hexagonal faces. The aperture of the large hexagonal windows is $\approx 8.6 \times 8.6 \text{ Å}^2$ and the internal diameter becomes close to $\approx 29 \text{ Å}$. In the as-prepared materials, the cavities are occupied only by water molecules. The location of the fluoride counterions within **MIL-100** could not be determined due to the similar diffusion factors of oxygen and fluorine atoms; thus, these anions may be either located

in terminal position bound to chromium atoms or within cages as they are in previous structures based on iron trimers.^[15]

In inorganic chemistry, such dimensions of pores are mostly reached with mesoporous solids, which, in contrast to the compounds presented herein, have amorphous walls. Thus, **MIL-100** provides the first example of a porous solid with crystalline walls, with a unique hierarchical system of three types of cages of different dimensions. Indeed, this solid may have applications in the domain of adsorption/separation of species.

The two other polymorphs found by our computer simulations have the same relative “energy” cost as **MIL-100** (see Table 1). Both of them have infinite chains of face sharing pentagon dodecahedral cages, already described for **MIL-100**. In the cubic structure ($Pm\bar{3}n$), the corresponding rods cross in three directions of space, thus creating larger cages, this time with 24 vertices instead of 28 and the resulting framework is an upper homologue of zeolite MEP.^[19] The topology of the hexagonal polymorph ($P6_3/mmc$), hitherto

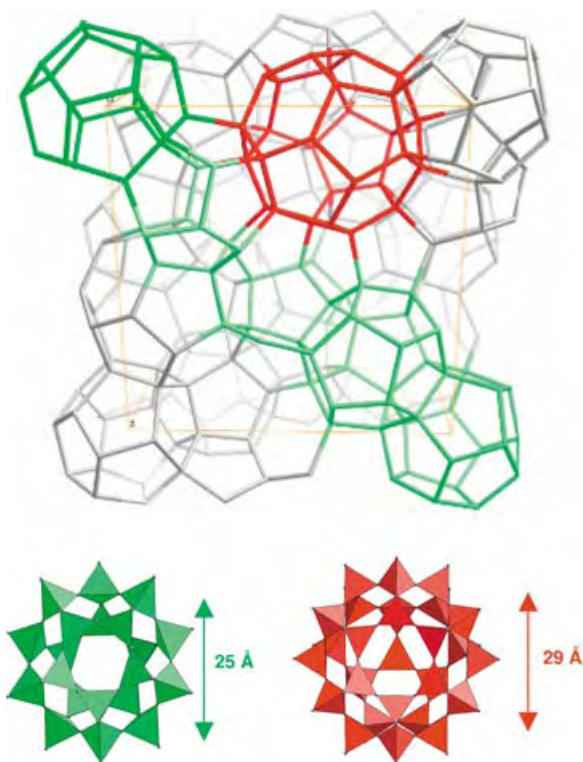


Figure 3. Top: Schematic view of the 3D organization of the structure of MIL-100 with the medium (green) and large (red) cages delimited by the vertex sharing of the ST (the vertices represent the centers of each ST). Bottom: View and dimensions of the two different cages (green, 20 tetrahedra; red, 28 tetrahedra). The medium cages share faces and form interconnected rods (in green) in the interstices of which are located the large cages.

unknown, corresponds to intersecting rods at 60° to each other, and the larger cages are the same as those in MIL-100.

The thermal behavior and the sorption properties of MIL-100 were investigated. First, the thermal gravimetric analysis carried out in air (see Supporting Information) reveals an interesting stability of the title phase up to 275 °C. X-ray thermogravimetry shows that the evacuation of the guests does not affect the topology of the skeleton; only the intensity of some Bragg peaks change, otherwise the pattern fits with that predicted. Second, the title material takes up gases readily. The gaseous N₂ sorption isotherm on the fully evacuated samples (Figure 4) is between type I and IV with

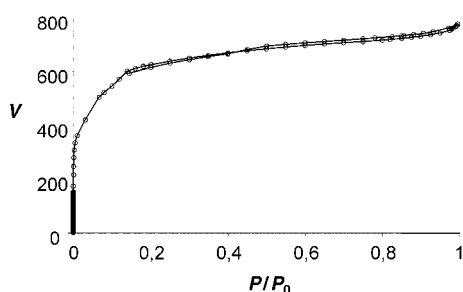


Figure 4. Nitrogen gas sorption isotherm at 78 K for MIL-100 degassed overnight at 100 °C. P/P_0 is the ratio of gas pressure (P) to saturation pressure ($P_0 = 750$ torr). V is the adsorbed volume ($\text{cm}^3 \text{g}^{-1}$).

a slight secondary uptake, which is indicative of the presence of both micro- and mesopores. No hysteresis is observed. Using the Dubinin-Radushkevich equation, we found a pore volume of around $1.16 \text{ cm}^3 \text{g}^{-1}$ for MIL-100. For a monolayer coverage of N₂ (which may not be strictly correct with such large cavities), we estimate the apparent Langmuir surface area to be $3100(40) \text{ m}^2 \text{g}^{-1}$, which is close to the highest values known.^[20]

In conclusion, we have shown from a straightforward example the strength of the combined chemistry–simulation approach for obtaining new materials. The resulting hybrid chromium carboxylate, MIL-100, has an eye-catching structure that has a hierarchical pore system (micro: $\approx 5\text{--}9 \text{ \AA}$; mesoporous: $\approx 25\text{--}30 \text{ \AA}$) with a very-high surface area ($\approx 3100 \text{ m}^2 \text{g}^{-1}$). While tackling the polymorphism of MOFs by limiting the domain of structures that are possible for a given metal–organic ligand pair, we found that simulations applied to hybrids is a tangible route towards structure solution in direct space. This new approach has the advantage that single crystals are not required for the resolution of the structures, which can be done from Rietveld refinements of powder-diffraction data. This represents a useful tool to bridge a gap because many solids, previously isolated by several groups, were abandoned owing to the lack of single crystals and the complexity of the powder patterns. Incidentally, the results obtained here open a window of opportunity to search for new porous solids with giant pores, which represent the upper homologues of numerous well-known zeolites. This work provides a new example of the possibilities of the concept of “scale chemistry”: the increase of the size of the ST generates larger pores, which open the way to new applications for MOF porous solids. Finally, the question may be posed as to whether structures such as MIL-100 arise from design. The answer is clearly no because in design, one must first imagine something then realize it afterwards. In our approach, the first step does not involve imagination (which is a creative act), but is the result of a computational prediction. For this reason, we prefer to suggest that the label of “simulation assisted chemical structures” (SACS) is the best description for solids obtained by using our method.

Experimental Section

Syntheses and chemical analyses: Metallic chromium (52 mg, 1 mmol; Aldrich, 99 %) was dispersed into an aqueous solution of 5 M hydrofluoric acid (0.4 mL, 2 mmol). After the addition of 1,3,5-benzene tricarboxylic acid H₃BTC (150 mg, 0.67 mmol; Aldrich, 99 %) and H₂O (4.8 mL, $265 \times 10^{-3} \text{ mol}$), the mixture was heated in a hydrothermal bomb at a rate of $20.0^\circ \text{C h}^{-1}$ to 220 °C, kept at this temperature during 96 h, then cooled at a rate of $10.0^\circ \text{C h}^{-1}$ to room temperature. The resulting green powder was washed with deionized water and acetone and dried in air. The yield of the reaction was $\approx 45\%$ based on chromium.

Chemical analyses: These were performed at the National Center of Analysis of the CNRS in Vernaion (France). As the amount of water present in the samples is very sensitive to the temperature (see TGA), only the C:Cr and F:Cr ratios are significant. They agree well with the formula deduced from the structure (C:Cr_{exp} calcd 6.0, found 6.75; F:Cr calcd 0.33, found 0.31).

TGA measurements: A crystalline sample was heated from 25 to 600 °C in air at a constant rate of $2^\circ \text{C min}^{-1}$. Two weight-loss steps

were observed: the first (35% of initial weight) occurred between 25 and 250 °C and is attributed to the loss of guest water molecules (calcd 40%); the second (44% of initial weight) is due to the removal of fluoride ions and the decomposition of the framework and occurred between 275 and 400 °C.

Sorption measurements: Experiments were performed on a Micromeritics ASAP 2010 with nitrogen as the adsorbed gas. MIL-100 was dehydrated under vacuum overnight at 150 °C.

Crystallographic study: Powder X-ray diffraction data were collected at the high resolution beamline ID31 of the European Synchrotron radiation Source (ESRF), Grenoble (France), from a sample contained in a 1 mm diameter capillary. ID31 beamline receives X-rays from the synchrotron source (which operates with an average energy of 6 GeV and a current beam of typically 200 mA) from an undulator device. The incident X-ray wavelength was 1.55075 Å. Data collection was performed over the angular range 1–97° 2 θ , with a step 0.005° at 80 K by using a cryostream (cold nitrogen gas blower). Cubic cell, $a = 72.906$ Å (MIL-100) with adequate figures of merit was found. Systematic absences were consistent with the space group $Fd\bar{3}m$ (no. 227). After the pattern had been matched, the structure refinement was initiated by using the atomic positions obtained from the simulations. The final agreement factors (Figure 1b) were satisfactory: $R_p = 5.48\%$, $R_{wp} = 7.61\%$, and $R_{Bragg} = 9.28\%$. For details see the Supporting Information.

The Supporting Information accompanying this paper contains crystallographic and TGA data.

Received: May 7, 2004

Keywords: microporous materials · molecular modeling · nanoporous materials · organic–inorganic hybrid composites · powder diffraction

- [10] O. M. Yaghi, M. O’Keeffe, M. Kanatzidis, *J. Solid State Chem.* **2000**, *152*, 1–321.
- [11] M. Eddaoudi, D. B. Moler, H. Li, B. Chen, T. M. Reineke, M. O’Keeffe, O. M. Yaghi, *Acc. Chem. Res.* **2001**, *34*, 319–330.
- [12] O. Delgado-Friedrichs, M. O’Keeffe, O. M. Yaghi, *Acta Crystallogr. Sect. A* **2003**, *59*, 22–27.
- [13] C. Mellot-Draznieks, J. Dutour, G. Férey, *Angew. Chem.* **2004**, *116*, 6450–6456; *Angew. Chem. Int. Ed.* **2004**, *43*, 6290–6296.
- [14] C. Mellot-Draznieks, J. M. Newsam, A. M. Gorman, C. M. Freeman, G. Férey, *Angew. Chem.* **2000**, *112*, 2258–2363; *Angew. Chem. Int. Ed.* **2000**, *39*, 2270–2275; C. Mellot-Draznieks, S. Girard, G. Férey, C. Schön, Z. Cancarevic, M. Jansen, *Chem. Eur. J.* **2002**, *8*, 4103–4113; C. Mellot-Draznieks, S. Girard, G. Férey, *J. Am. Chem. Soc.* **2002**, *124*, 15326–15335.
- [15] C. Serre, F. Millange, S. Surblé, G. Férey, *Angew. Chem.* **2004**, *116*, 6445–6449; *Angew. Chem. Int. Ed.* **2004**, *43*, 6285–6289.
- [16] J. S. Seo, D. Wang, H. Lee, S. I. Jun, J. Oh, Y. J. Jeon, K. Kim, *Nature* **2000**, *404*, 982–986.
- [17] R. De Pape, G. Férey, *Mater. Res. Bull.* **1986**, *21*, 971–978.
- [18] M. O’Keeffe, S. Andersson, *Acta Crystallogr. Sect. A* **1977**, *33*, 914–923; S. Lidin, M. Jacob, S. Andersson, *J. Solid State Chem.* **1995**, *114*, 36–41.
- [19] M. M. J. Treacy, J. B. Higgins in *Collection of Simulated XRD Powder Patterns for Zeolites*, 4th ed., Elsevier **2001**, and <http://www.iza-structure.org/databases/>.
- [20] H. K. Chae, D. Y. Siberio-Perez, J. Kim, Y.-B. Go, M. Eddaoudi, A. J. Matzger, M. O’Keeffe, O. M. Yaghi, *Nature* **2004**, *427*, 523–527.

- [1] G. Férey, A. K. Cheetham, *Science* **1999**, *283*, 1125–1126; G. Férey, *Science* **2000**, *289*, 994–995.
- [2] H. Li, M. Eddaoudi, M. O’Keeffe, O. M. Yaghi, *Nature* **1999**, *402*, 276–279.
- [3] O. M. Yaghi, M. O’Keeffe, N. W. Ockwig, H. K. Chae, M. Eddaoudi, J. Kim, *Nature* **2003**, *423*, 705–714; M. Eddaoudi, J. Kim, N. Rosi, D. Vodak, J. Wachter, M. O’Keeffe, O. M. Yaghi, *Science* **2002**, *295*, 469–472.
- [4] L. Beitone, C. Huguenard, M. Henry, F. Taulelle, T. Loiseau, G. Férey, *J. Am. Chem. Soc.* **2003**, *125*, 9102–9110.
- [5] A. Müller, E. Krickemeyer, H. Bögge, M. Schmidtman, S. Roy, A. Berkle, *Angew. Chem.* **2002**, *114*, 3756–3761; *Angew. Chem. Int. Ed.* **2002**, *41*, 3604–3609; A. Müller, S. K. Das, S. Talismanov, S. Roy, E. Beckmann, H. Bögge, M. Schmidtman, A. Merca, A. Berkle, L. Allouche, Y. Zhou, L. Zhang, *Angew. Chem.* **2003**, *115*, 5193–5198; *Angew. Chem. Int. Ed.* **2003**, *42*, 5039–5044.
- [6] N. Guillou, P. M. Forster, Q. Gao, J. S. Chang, M. Nogues, S.-E. Park, A. K. Cheetham, G. Férey, *Angew. Chem.* **2001**, *113*, 2913–2916; *Angew. Chem. Int. Ed.* **2001**, *40*, 2831–2834.
- [7] F. Schüth, K. S. W. Sing in *Handbook of Porous Solids* (Eds.: J. Weitkamp), Wiley-VCH, Weinheim, **2002**.
- [8] S. Kitagawa, M. Kondo, *Bull. Chem. Soc. Jpn.* **1998**, *71*, 1739–1753; P. M. Forster, J. Eckert, J.-S. Chang, S.-E. Park, G. Férey, A. K. Cheetham, *J. Am. Chem. Soc.* **2003**, *125*, 1309–1312; N. Rosi, J. Eckert, M. Eddaoudi, D. Vodak, J. Kim, M. O’Keeffe, O. M. Yaghi, *Science* **2003**, *300*, 1127–1129; G. Férey, M. Latroche, C. Serre, F. Millange, T. Loiseau, A. Percheron-Guégan, *Chem. Commun.* **2003**, 2276.
- [9] G. Férey, *J. Solid State Chem.* **2000**, *152*, 37–48; G. Férey, *J. Solid State Sci.* **2003**, *5*, 79–94.

Valence Tautomerism

Chemical Control of Valence Tautomerism of Nickel(II) Semiquinone and Nickel(III) Catecholate States**

*Hideki Ohtsu and Koji Tanaka**

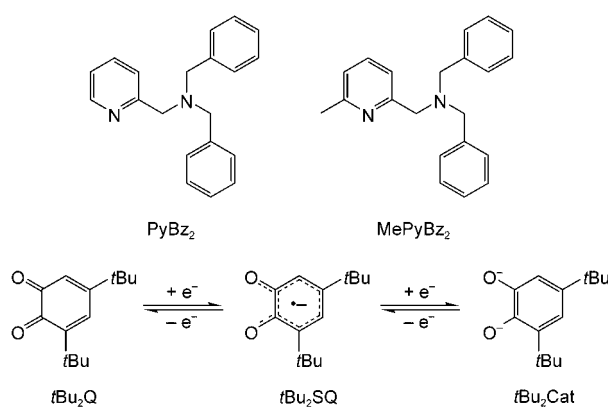
Transition-metal complexes with dioxolene ligands have been attracting much attention because of their characteristic ligand-localized redox reactions among the three redox states of quinone (Q), semiquinone (SQ), and catecholate (Cat) in addition to metal-centered redox reactions.^[1] Interest has especially been paid to interconversion of valence tautomers in the metal–dioxolene framework.^[1] Valence tautomers are characterized by displacement of electron density to one redox center or the other, for example, M^{II}-SQ

[*] Dr. H. Ohtsu, Prof. K. Tanaka
Institute for Molecular Science, CREST
Japan Science and Technology Agency (JST)
38 Nishigonaka, Myodaiji, Okazaki, Aichi, 444-8585 (Japan)
Fax: (+81) 564-55-5245
E-mail: ktanaka@ims.ac.jp

[**] We are grateful to Prof. Toshihiko Yokoyama and Dr. Takeshi Nakagawa, Institute for Molecular Science, for measuring X-ray photoelectron spectra.

and M^{III} -Cat compounds, which interconvert by intramolecular electron transfer between the two redox centers. Knowledge gathered for a number of metal complexes with dioxolene^[2] and other redox-active ligands^[3–5] showing valence-tautomeric behavior greatly aids in exploiting this phenomenon for molecular switching devices.^[6] However, neither nickel dioxolene complexes exhibiting interconversion of valence tautomers nor control of valence tautomerism by modification of electron-donor ability of ligands to central metal atoms has been reported so far.

We report herein the synthesis and characterization of nickel(II) semiquinonato and nickel(III) catecholato complexes containing bidentate ligands with modulated nitrogen-donor ability,^[7] namely, $[Ni^{II}(PyBz_2)(tBu_2SQ)]PF_6$ (**1**) and $[Ni^{III}(MePyBz_2)(tBu_2Cat)]PF_6$ (**2**) as the first example for successful control of valence tautomerism between the Ni^{II} -SQ and Ni^{III} -Cat frameworks by fine-tuning of the donor ability of the bidentate ligands to the nickel ion (Scheme 1).

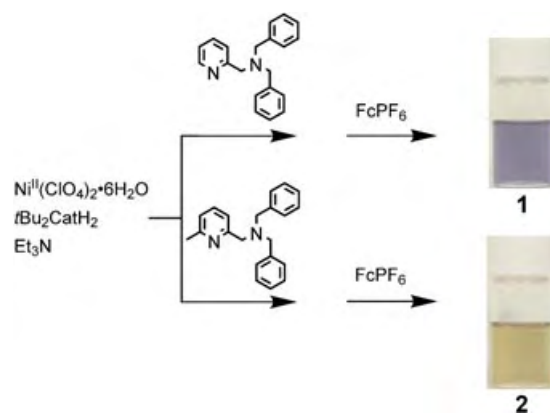


Scheme 1. Structures of bidentate ligands and dioxolene redox forms.

The Ni^{II} semiquinonato complex of $PyBz_2$, **1**, was obtained by mixing $PyBz_2$, tBu_2CatH_2 , and $Ni^{II}(ClO_4)_2 \cdot 6H_2O$ in a 1:1:1 ratio in acetonitrile and subsequent addition of 2 equivalents of Et_3N and 1 equivalents of ferrocenium hexafluorophosphate ($FcPF_6$). The Ni^{III} catecholato complex, **2**, was prepared in a similar manner to **1** by using $MePyBz_2$ in place of $PyBz_2$. Solutions of **1** in CH_2Cl_2 are blue, whereas those of **2** are brown (see Scheme 2).

The X-ray molecular structure of **1**^[8] is shown in Figure 1. The nickel ion in **1** has a tetracoordinate square-planar environment formed by the pyridine N atom, tertiary amine N atom, and the two O atoms of the dioxolene ligand. The C(1)–O(1) and C(2)–O(2) bond lengths of the dioxolene ligand in **1** are 1.305(5) and 1.294(5) Å, respectively. These C–O bond lengths are consistent with those of nickel(II) semiquinonato complexes reported so far.^[9] Although many attempts to prepare single crystals of **2** suitable for X-ray structure determination failed, its coordination geometry is safely concluded to be distorted square-planar on the basis of EPR measurements.

The EPR spectrum of **1** in CH_2Cl_2 at 77 K (Figure 2a) exhibits a sharp isotropic signal with a g value of 2.0066,^[10] close to the free-spin value ($g = 2.0023$), which can safely be



Scheme 2. Synthesis of **1** and **2**.

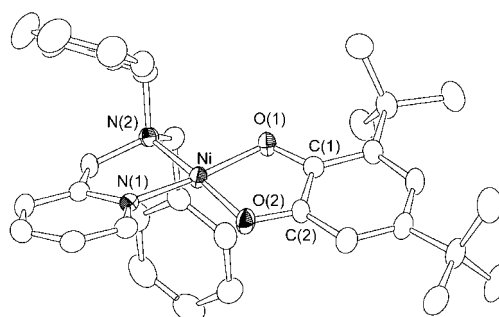


Figure 1. ORTEP view of **1**. Hydrogen atoms and counteranion are omitted for clarity. Thermal ellipsoids are drawn at the 50% probability level. Selected bond lengths [Å] and angles [°]: Ni–N(1) 1.858(3), Ni–N(2) 1.918(3), Ni–O(1) 1.860(3), Ni–O(2) 1.843(3), C(1)–O(1) 1.305(5), C(2)–O(2) 1.294(5); N(1)–Ni–N(2) 86.7(1), N(1)–Ni–O(1) 172.8(1), N(1)–Ni–O(2) 93.6(1), N(2)–Ni–O(1) 93.9(1), N(2)–Ni–O(2) 175.1(1), O(1)–Ni–O(2) 86.5(1).

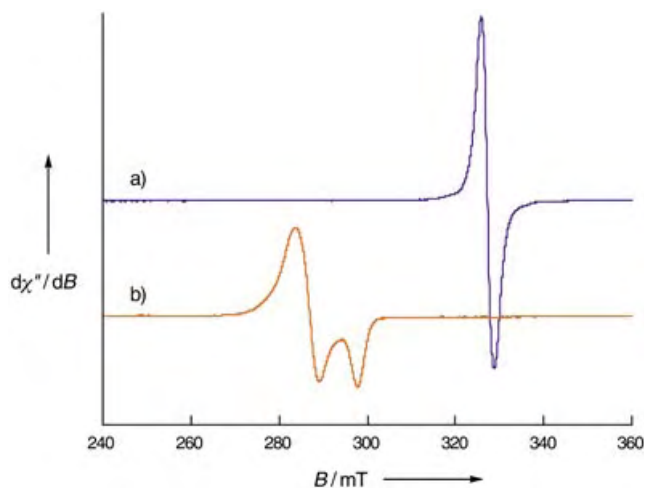


Figure 2. EPR spectra of a) **1** (10^{-3} M) and b) **2** (10^{-3} M) in CH_2Cl_2 at 77 K.

assigned to a ligand-centered radical species composed of low-spin $d^8 Ni^{II}$ ($S = 0$) and the semiquinone ($S = 1/2$) framework. Indeed, the C–O bond lengths of **1** determined by X-ray analysis agree well with those of semiquinone radicals (see

above). In contrast to **1**, an anisotropic signal ($g_{\perp} = 2.29$, $g_{\parallel} = 2.20$, $g_{\text{iso}} = 2.26$) is observed in the EPR spectra of **2** (Figure 2b).^[10] The significantly larger g value of **2** ($g_{\text{iso}} = 2.26$) compared with that of **1** ($g = 2.0066$) apparently results from an unpaired electron localized on the metal center. Thus, the electronic structure of **2** is explained by a combination of low-spin d^7 Ni^{III} ($S = 1/2$) and catecholate ($S = 0$). Furthermore, the EPR parameters ($g_{\perp} = 2.29$, $g_{\parallel} = 2.20$) provide valuable information about the coordination environment of the nickel(III) ion, which is a distorted square-planar structure with a d_{z^2} ground state.^[11] The oxidation states of nickel in **1** and **2** were further confirmed by X-ray photoelectron spectra. The observed binding energy of the Ni $2p_{3/2}$ signals at 854.9 (**1**) and 856.1 eV (**2**) is consistent with oxidation states of Ni^{II} and Ni^{III} , respectively.^[12]

Such a drastic difference in the electronic states of **1** and **2** can be ascribed to the steric effect induced by the *o*-methyl group^[13–15] in the MePyBz₂ ligand. This group weakens the coordination of the pyridine moiety to the nickel ion compared with the unsubstituted PyBz₂ ligand. As a result, the dioxolene ligand of **2** binds to the nickel ion more strongly than that of **1**, and this results in the displacement of electron density to form the Ni^{II} -SQ and Ni^{III} -Cat frameworks in **1** and **2**, respectively.

Experimental Section

The complexes were synthesized under nitrogen atmosphere.

1: $\text{Ni}(\text{ClO}_4)_2 \cdot 6\text{H}_2\text{O}$ (0.366 g, 1.0 mmol) was added to a solution of PyBz₂ (0.288 g, 1.0 mmol) and $t\text{Bu}_2\text{CatH}_2$ (0.222 g, 1.0 mmol) in acetonitrile (20 mL), and triethylamine (0.202 g, 2.0 mmol) was then added to the resulting solution. FcPF_6 (0.331 g, 1.0 mmol) was added to the mixture, and the solution was stirred for 2 h at room temperature. After removal of the solvent under reduced pressure, the resulting residue was dissolved in dichloromethane, and ammonium hexafluorophosphate (0.326 g, 2.0 mmol) was added to the solution. The mixture was stirred overnight at room temperature, and insoluble material was removed by filtration. Addition of pentane to the filtrate gradually gave a blue powder that was collected by filtration and recrystallized from dichloromethane/pentane. Yield: 0.380 g (53.4%). Elemental analysis (%) calcd for $\text{C}_{34}\text{H}_{40}\text{F}_6\text{N}_2\text{O}_2\text{-Ni}_1\text{P}_1$: C 57.33, H 5.66, N 3.93; found: C 57.14, H 5.62, N 3.90. ESI-MS: m/z : 566 $[\text{M-PF}_6]^+$.

Complex **2** was prepared in the same manner as **1** by using MePyBz₂ instead of PyBz₂. Yield: 0.259 g (35.7%). Elemental analysis (%) calcd for $\text{C}_{35}\text{H}_{42}\text{F}_6\text{N}_2\text{O}_2\text{-Ni}_1\text{P}_1 \cdot 0.5\text{CH}_3\text{CN}$: C 57.89, H 5.87, N 4.69; found: C 57.63, H 6.04, N 4.51. ESI-MS: m/z : 580 $[\text{M-PF}_6]^+$.

Received: March 17, 2004

Keywords: N ligands · nickel · O ligands · substituent effects · tautomerism

- 1179; d) P. Gütllich, A. Dei, *Angew. Chem.* **1997**, *109*, 2852–2855; *Angew. Chem. Int. Ed. Engl.* **1997**, *36*, 2734–2736; e) C. W. Lange, C. G. Pierpont, *Inorg. Chim. Acta* **1997**, *263*, 219–224.
- [3] F. V. Lovecchio, E. S. Gore, D. H. Busch, *J. Am. Chem. Soc.* **1974**, *96*, 3109–3118.
- [4] J. Seth, V. Palaniappan, D. F. Bocian, *Inorg. Chem.* **1995**, *34*, 2201–2206.
- [5] Y. Shimazaki, F. Tani, K. Fukui, Y. Naruta, O. Yamauchi, *J. Am. Chem. Soc.* **2003**, *125*, 10512–10513.
- [6] a) O. Kahn, J. P. Launay, *Chemtronics* **1988**, *3*, 140–151; b) O. Kahn, J. Kröber, C. Jay, *Adv. Mater.* **1992**, *4*, 718–728.
- [7] Y. Shimazaki, T. Nogami, F. Tani, A. Odani, O. Yamauchi, *Angew. Chem.* **2001**, *113*, 3977–3980; *Angew. Chem. Int. Ed.* **2001**, *40*, 3859–3862.
- [8] X-ray crystal structure determination was carried out on a Rigaku/MSU Mercury CCD diffractometer equipped with a Rigaku GUNN low-temperature device. Data were collected at 173 K under cold nitrogen gas with graphite-monochromated $\text{MoK}\alpha$ radiation ($\lambda = 0.71070 \text{ \AA}$). Crystallographic data for **1**: $\text{C}_{34}\text{H}_{40}\text{F}_6\text{N}_2\text{O}_2\text{-Ni}_1\text{P}_1$, $M_r = 712.37$, blue crystals, monoclinic, $P2_1/c$, $a = 11.496(4)$, $b = 29.01(1)$, $c = 11.271(4) \text{ \AA}$, $\beta = 114.390(4)^\circ$, $V = 3423(2) \text{ \AA}^3$, $Z = 4$, $\rho_{\text{calcd}} = 1.382 \text{ g cm}^{-3}$, $\mu = 6.79 \text{ cm}^{-1}$, $R = 0.058$ ($I > 2.0\sigma(I)$), $R_w = 0.059$ ($I > 2.0\sigma(I)$), 7760 measured reflections, 7627 independent reflections, 415 parameters. CCDC-233975 contains the supplementary crystallographic data for this paper. These data can be obtained free of charge via www.ccdc.cam.ac.uk/conts/retrieving.html (or from the Cambridge Crystallographic Data Centre, 12, Union Road, Cambridge CB21EZ, UK; fax: (+44) 1223-336-033; or deposit@ccdc.cam.ac.uk).
- [9] a) C. Benelli, A. Dei, D. Gatteschi, L. Pardi, *Inorg. Chem.* **1988**, *27*, 2831–2836; b) D. A. Shultz, K. E. Vostrikova, S. H. Bodnar, H.-J. Koo, M.-H. Whangbo, M. L. Kirk, E. C. Depperman, J. W. Kampf, *J. Am. Chem. Soc.* **2003**, *125*, 1607–1617.
- [10] The EPR spectrum is practically independent of temperature down to 4.2 K.
- [11] T. J. Collins, T. R. Nichols, E. S. Uffelman, *J. Am. Chem. Soc.* **1991**, *113*, 4708–4709.
- [12] A. Davidson, J. F. Tempere, M. Che, *J. Phys. Chem.* **1996**, *100*, 4919–4929.
- [13] H. Nagao, N. Komeda, M. Mukaida, M. Suzuki, K. Tanaka, *Inorg. Chem.* **1996**, *35*, 6809–6815.
- [14] Y. Shimazaki, S. Huth, S. Hirota, O. Yamauchi, *Bull. Chem. Soc. Jpn.* **2000**, *73*, 1187–1195.
- [15] a) H. Ohtsu, Y. Shimazaki, A. Odani, O. Yamauchi, S. Itoh, S. Fukuzumi, *J. Am. Chem. Soc.* **2000**, *122*, 5733–5741; b) H. Ohtsu, S. Itoh, S. Nagatomo, T. Kitagawa, S. Ogo, Y. Watanabe, S. Fukuzumi, *Inorg. Chem.* **2001**, *40*, 3200–3207; c) H. Ohtsu, S. Fukuzumi, *Chem. Lett.* **2001**, *30*, 920–921; d) H. Ohtsu, K. Tanaka, *Inorg. Chem.* **2004**, *43*, 3024–3030.

- [1] a) C. G. Pierpont, R. M. Buchanan, *Coord. Chem. Rev.* **1981**, *38*, 45–87; b) C. G. Pierpont, C. W. Lange, *Prog. Inorg. Chem.* **1994**, *41*, 331–442; c) C. G. Pierpont, *Coord. Chem. Rev.* **2001**, *216–217*, 99–125.
- [2] a) R. M. Buchanan, C. G. Pierpont, *J. Am. Chem. Soc.* **1980**, *102*, 4951–4957; b) G. A. Abakumov, G. A. Razuvaev, V. I. Nevodchikov, V. K. Cherkasov, *J. Organomet. Chem.* **1988**, *341*, 485–494; c) A. S. Attia, C. G. Pierpont, *Inorg. Chem.* **1995**, *34*, 1172–

Metallic Nanomagnets Randomly Dispersed in Spherical Colloids: Toward a Universal Route for the Preparation of Colloidal Composites Containing Nanoparticles**

Pedro Tartaj,* Teresa González-Carreño, María L. Ferrer,* and Carlos J. Serna

The fabrication of colloids with desired properties has been the aim of many recent investigations.^[1] Their modification with metallic nanoparticles is a particularly suitable tool to modulate their optical, catalytic, and mechanical properties.^[2] Of special interest for biotechnology and data storage applications, as well as for fundamental studies in the areas of physics and physical chemistry, is the modification of colloids with metallic nanomagnets (MNMs).^[3] The properties of these composites in particular, and magnetic composites in general, strongly depend on the size of the nanoparticles, the distance between them, and the nature of the nanoparticle–colloidal matrix interaction.^[4] Thus, the development of methods able to fine-tune the size of MNMs, their interparticle distance, and their particle composition (e.g., preparation of multicomponent alloys), while readily modifying the composition of the colloidal matrixes, could help us to produce materials with a highly predictable magnetic response and/or showing unusual magnetic phenomena of interest, for example, in recording applications.^[4c] Herein, we report a synthetic route for the preparation of MNMs randomly dispersed in inorganic spherical colloids, which have potential interest in biotechnology.^[5] Random distribution, instead of the typical confined distribution obtained in the widely used surface template methods, helps to screen magnetic dipolar interactions.^[6] Even though we have focused on the preparation of MNMs randomly dispersed in spherical colloids, the adaptability of the synthetic strategy reported here could allow its use in the fabrication of spherical colloids containing nanoparticles of very different nature and properties.

Aerosol-based processes are convenient routes to prepare nanoparticles randomly dispersed in spherical colloidal matrixes.^[7] In fact, we recently reported that α -Fe MNMs dispersed in spherical silica colloids can be produced by heating, in air and H_2 , a powder obtained by aerosol pyrolysis of a methanol solution of iron(III) nitrate and tetraethoxysi-

lane.^[7c] However, the method fails when trying to obtain MNMs made up of more than one component (alloys) dispersed in colloidal matrixes, because of differences in the solubility of the metallic precursors. Compositional homogeneity at the particle level in aerosol methods is strongly dependent on the solubility of the precursors.^[7,8] Specifically, the different solubilities of the metallic precursors during thermal drying (especially at low-volume-packing fractions) result in their sequential precipitation within the colloidal matrix. Thus, at the end of the process, the chemical composition of each individual MNM is not necessarily equal to the average of the alloy (compositional inhomogeneity at the nanoparticle level).

The approach we used to overcome the problem of compositional inhomogeneity, and simultaneously to better control the size of MNMs, was to generate an aerosol from an aqueous sol of ferritin and a matrix precursor (Figure 1). Our

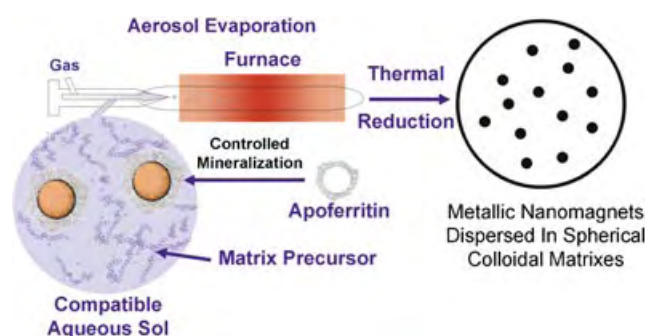


Figure 1. Stepwise fabrication of MNMs randomly dispersed in spherical colloids.

synthetic route is similar to that used for the preparation of mesoporous silica (undoped and doped with gold nanoparticles) and titania materials by aerosol evaporation of sols containing surfactant micelles,^[7a,9] though logically we need to produce nanoparticles not “holes”. In this sense, ferritin seems an ideal template for reaching our final goal and, more importantly, ferritin could serve as an ideal model to extend the synthetic strategy to other ferritin-like systems. For example, one can easily deduce that the ability of dendrimers to encapsulate metallic nanoparticles of very different composition (Au, Pt, Pd, Cu, Ag, Ni)^[10] could be used for the direct fabrication of colloidal composites containing nanoparticles of very different nature and properties.

Nature has developed a variety of proteins that function as carriers or storage devices for metal components. Of these systems, the iron-storage protein ferritin is one of the most intensively studied.^[11] Ferritin consists of a spherical polypeptide shell surrounding a ferrihydrite core. Ferritin can easily be demineralized (apoferritin), to leave an approximately 8-nm internal cavity that can be used as a template for the production of nanomaterials containing elements such as Fe, Mn, U, Co, Ni, and Cr.^[11,12] The biological template of ferritin has also been used to prepare CoPt nanometallic alloys of interest in data-storage technology, nanoparticles of Prussian blue ferritin, and very recently to prepare metallic Pd nanoparticles of interest in catalysis.^[13] In addition, Lan

[*] Dr. P. Tartaj, Dr. T. González-Carreño, Dr. M. L. Ferrer, Prof. C. J. Serna
Instituto de Ciencia de Materiales de Madrid
CSIC, Cantoblanco, 28049 Madrid (Spain)
Fax: (+34) 9-137-20-623
E-mail: ptartaj@icmm.csic.es
mferrer@icmm.csic.es

[**] Financial support from CICYT (MAT2002-04001-C02) is gratefully acknowledged. P.T. and M.L.F. thank the Ramon y Cajal program for financial support.

Supporting information for this article is available on the WWW under <http://www.angewandte.org> or from the author.

et al. demonstrated that it is possible to prepare a sol containing a silica inorganic component and the protein ferritin.^[14] However, their final goal was to encapsulate ferritin in a sol–gel-derived silica glass, and not to prepare metallic nanoparticles dispersed in colloidal matrixes with a spherical shape.

Therefore, based on previous work carried out with ferritin, we expected that the internal cavity of ferritin would allow us to confine the various metallic precursors (in the form of inorganic nanoparticles), thus avoiding the problems associated with compositional inhomogeneity in aerosol processes. Besides, if the right matrix is chosen, the particle size can easily be controlled by the particle size of the inorganic component of ferritin. A necessary requirement for the success of the method is the preparation of an aqueous sol of ferritin and the matrix precursor. Simple arguments based on colloid science dictate that both ferritin and the matrix precursor must be equally charged to avoid heterocoagulation. An additional advantage of using ferritin is that its protein cage is remarkably stable, and able to withstand extremes of pH (2–10) and temperature (up to 70 °C).^[12] Thus, the high stability of ferritin allows the use of a wide range of experimental conditions to prepare stable sols (that is, compatibility with different matrix precursors).

To probe the reliability of the method in obtaining MNMs of different size and composition dispersed in spherical colloids we used ferritin with its internal cavity fully or partially filled with Fe- and FeCo-containing species. An amorphous silica sol and a crystalline boehmite (AlOOH) sol were selected to probe the versatility of the method in changing the nature of the colloidal matrix. An amorphous silica sol was selected in the first instance because of the several benefits that amorphous colloidal silica matrixes with spherical shape impart to MNMs for applications in biotechnology (colloidal stability, functionality, biocompatibility, and corrosion resistance).^[15] The criteria we followed to select a crystalline boehmite sol were based on the different colloidal behavior of boehmite and silica (isoelectric points of ca. 9 and 3, respectively) and the different nature of the initial sol (crystalline versus amorphous).

The aerosol evaporation of a stable aqueous sol containing commercial ferritin^[16] and silica (see Experimental Section) led to powders that were heated in air (500 °C, 2 h) to eliminate residual organic matter and hydroxy groups, and finally reduced in H₂ atmosphere (700 °C, 10 h) to produce α -Fe MNMs randomly dispersed in silica colloids (Figure 2a). The presence of this phase was confirmed by X-ray diffraction (XRD, see the Supporting Information).^[17] The crystallite size estimated from the width of the (110) α -Fe reflection was 5.3 nm, which is similar to the diameter obtained by transmission electron microscopy (TEM; 4–6 nm, Figure 2a). This value is consistent with the expected shrinkage when going from the ferrihydrite (average size of the ferrihydrite core of ferritin is about 7 nm)^[11] to the α -Fe phase, by considering the amount of iron in a unit volume of these two phases (that is, no significant interparticle sintering between MNMs on heating).

A similar methodology was used for the preparation of spherical composites with α -Fe MNMs of smaller size (3–

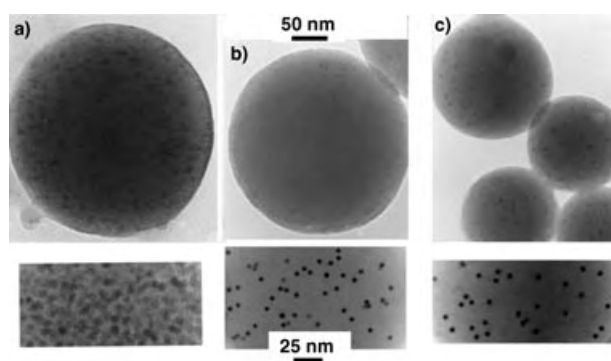


Figure 2. TEM pictures of powders showing random distributions of MNMs in spherical silica colloids: a) from ferritin; b) from Fe-reconstituted apoferritin; c) from FeCo-reconstituted apoferritin. The lower pictures are magnified to enhance the visual resolution of the MNMs (dark spots). The higher concentration of MNMs in (a) reflects the higher number of Fe atoms in commercial ferritin with respect to the reconstituted apoferritin. The pictures were computer-enhanced to improve the MNM contrast.

4 nm, Figure 2b), though in this case we started from an apoferritin reconstituted only with 1000 Fe atoms (for details of reconstitution, see the Experimental Section). The decrease in the size of the α -Fe MNMs was also detected by XRD (see the Supporting Information). Specifically, a decrease from 5.3 to 3.4 nm was estimated from the width of the (110) α -Fe reflection. The volume estimated from the experimental data for a spherical shape (10–35 nm³, 3–4 nm diameter) is within the margins of experimental error expected for a cubic cluster of 1000 Fe atoms in the α -Fe phase (ca. 12 nm³). However, the fact that the 1000-atom cluster volume is at the lower limit does not allow us to ignore the possible growth of some nanocrystallites. Finally, FeCo MNMs (Co content ca. 30 mol %; 3–4 nm) dispersed in silica colloids (Figure 2c) were also prepared by using a similar methodology. This particular Co/Fe composition was selected because it has the highest magnetic moment.^[18] In this case, apoferritin was reconstituted with 670 Fe atoms and 330 Co atoms (see Experimental Section). Energy-dispersive X-ray (EDX) analyses carried out on the MNMs clearly indicated that the composition of individual nanomagnets was the expected one (Co content of ca. 30 mol % in the FeCo alloy).^[19] Thus, we showed the versatility of the method in preparing spherical composites containing randomly distributed MNMs of controlled composition and size. An important point is that the colloids are polydisperse in size (70–400 nm); however, monodispersity can be achieved with aerosol techniques by using differential mobility analyzers.^[20]

We also used a crystalline boehmite sol (see Experimental Section) to probe the versatility of the method in changing the nature of the colloidal matrix. Specifically, the use of a boehmite sol (no ferritin added) resulted in a porous matrix (Figure 3a), which was not ideal for stabilizing small MNMs (< 5–6 nm) against corrosion. Thus, the results for boehmite probe the benefit of the confinement effect of ferritin in controlling chemical composition at the nanoparticle level (that is, preparation of multicomponent MNMs) even in porous matrixes. The aerosol evaporation of an aqueous sol of

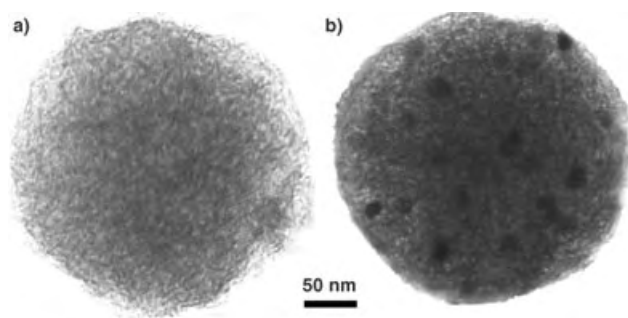


Figure 3. TEM pictures of powders obtained after aerosol evaporation of an aqueous sol of a) boehmite and b) FeCo-reconstituted apoferritin and boehmite with further heating in air (500°C, 2 h) and H₂ (800°C, 10 h).

apoferritin (after reconstitution with 670 Fe atoms and 330 Co atoms) and boehmite, followed by thermal annealing first in air and then in H₂, produced powders made up of FeCo MNMs dispersed in γ -Al₂O₃ colloids (Figure 3b). After the thermal treatment boehmite transformed to γ -Al₂O₃, as evident by XRD analysis. EDX analyses clearly indicate that we were successful in controlling the chemical composition at the nanomagnet level even in a porous matrix. An increase in MNM size was produced when silica was replaced by alumina (ca. 15 nm versus ca. 3–4 nm, Figure 3b and 2c). Thus, no temperature was found that reduced the porosity of the alumina matrix while avoiding sintering between MNMs (small MNMs cannot be stabilized against oxidation). Finally, similar results were obtained in the case of MNMs made up of Fe atoms, which additionally confirmed the benefit of the silica matrixes in providing protection against corrosion.

In summary, metallic nanomagnets (MNMs) of different size and composition randomly dispersed in spherical colloids have been prepared by the aerosol evaporation of an aqueous sol containing mineralized ferritin and a colloidal matrix precursor. Essential to the success of the method is the template effect provided by ferritin. Its internal cavity offers the ideal environment for the encapsulation of multicomponent MNM precursors with the simultaneous control of size. Moreover, the high stability of the ferritin cage allows compatibility with different matrix precursor sols (that is, the nature of the colloidal matrix can be changed). Our results indicate that this synthetic strategy could be extended to other ferritin-like systems, for example, metals encapsulated in dendrimers.

Experimental Section

Aerosol generation: The aerosol device used for the preparation of the spherical composites containing nanoparticles is described elsewhere.^[8b] It essentially consists of two furnaces that could be set at different temperatures for drying (first furnace) and thermal decomposition (second furnace). In our experiments we set the temperature of the two furnaces at 400°C (aerosol evaporation). The aqueous sol containing the ferritin and matrix precursor was atomized at 1.6 mL min⁻¹ with an air pressure of 1.7 kg cm⁻² to give different spherical colloidal composites. The particles obtained were collected with an electrostatic filter (8 kV). Experiments carried out with a freshly prepared sol and a sol aged for 6 h led to similar results, which

confirms the reproducibility during the aerosol experiment (typically 2 h).

Ferritin reconstitution: A dispersion of apoferritin (Sigma; 75 mL, 1.46 μ M) in NaCl (0.1M) and 3-(*N*-morpholine)propanesulfonic acid (MOPS) buffer (50 mM, pH 6.5) was reconstituted by the controlled addition of a deaerated FeSO₄ solution (25 mM, pH 2) at a rate of 0.1 μ mol min⁻¹ until completion of the calculated loading of 1000 Fe atoms per unit of protein. The method is similar to that described by Chasteen and co-workers.^[11c,d] In our case the rate of addition was slower and reconstitution was restricted to 1000 atoms to assure complete mineralization inside the protein. No iron(III) hydroxide sediment or deposit was found after centrifuging at 4000 rpm (r_{max} = 12 cm, rotor angle = 30°) for 5 minutes and then filtering through a 0.1- μ m Millipore filter, which further suggests that the formation of iron(III) hydroxide did not take place outside the protein.

To prepare the FeCo-reconstituted apoferritin, an apoferritin dispersion (75 mL, 1.46 μ M) in NaCl (0.1M) and MOPS buffer (50 mM, pH 6.5) was reconstituted by the controlled addition of a deaerated FeSO₄ solution (25 mM, pH 2) at a rate of 0.1 μ mol min⁻¹ until completion of the calculated loading of 670 Fe atoms per molecule of protein. Again following this protocol, we did not find any evidence of the formation of iron(III) hydroxide outside the protein. The dispersion was dialyzed (12-kDa cutoff membrane) against aqueous NaCl solution (0.1M) to eliminate unwanted ions and then 330 Co atoms per protein unit were added by controlled addition of Co(NO₃)₂ (25 mM, 0.125 μ mol min⁻¹) and H₂O₂ (25 mM, 0.125 μ mol min⁻¹) to the partially filled apoferritin dispersion (75 mL, 50 mM 3-[(1,1-dimethyl-2-hydroxyethyl)amino]-2-hydroxypropanesulfonic acid (AMPSO) buffer, pH 8.5). The method is a combination of the one reported by Chasteen and co-workers for iron mineralization^[11c,d] and that reported by Douglas and co-workers for cobalt mineralization.^[12d,e] Since ferritin has more affinity for iron than for cobalt, we added the iron atoms first. In this way, nucleation of cobalt atoms inside the ferritin core was favored by the presence of the Fe-containing nuclei. The high compositional homogeneity of the nanoparticles dispersed in the colloidal matrixes suggests that cobalt was indeed mineralized in the ferritin cores containing iron atoms. To avoid mineralization outside the protein, we only filled the apoferritin with a total of 1000 Fe atoms.

Before mixing with the matrix precursor sol both the Fe- and FeCo-reconstituted apoferritin dispersions were dialyzed against water to avoid excess electrolyte, which can induce coagulation.

Preparation of aqueous sol containing ferritin and silica: Horse spleen ferritin dispersion (2 mL, Sigma Aldrich, type I, 102 mg mL⁻¹) in NaCl (0.15M) was diluted with water to 96 mL and mixed with a silica sol (2 mL). The clear silica sol stock dispersion was prepared by mixing tetramethoxysilane (2.95 mL, Aldrich, 99%), water (1.4 mL), and HCl (0.04 mL, 0.04M) at 4°C with strong agitation for 15 minutes. Use of this procedure to prepare the silica sol allows the amount of alcohol present in the system to be reduced as much as possible, thus avoiding the possible denaturation of the protein ferritin.^[14] When reconstituted apoferritin was used instead ferritin, silica sol (2 mL, pH 5.5) was added to reconstituted apoferritin dispersion (75 mL). At this pH value both ferritin (isoelectric point 4–5) and silica (isoelectric point ca. 3) are negatively charged, so heterocoagulation is avoided. The order of addition of the protein, water of dilution, and silica sol was important for the stability of the system. Coagulation of the protein was observed if the silica sol (2 mL) was added to water (96 mL) and followed by ferritin (2 mL).

Preparation of aqueous sol containing ferritin and boehmite: A stable boehmite sol was prepared by following a standard methodology.^[21] HCl (final concentration 0.02M) was added to an aqueous suspension of aluminum isopropoxide (0.25M, Aldrich) which had been previously heated at 80°C for 1 h. The vessel was opened at 90°C for 2 h to allow evaporation of the isopropanol generated from the alkoxide hydrolysis. Finally, the suspension was refluxed at 90°C

for 16 h to produce a stable sol. For the preparation of the aqueous sol containing apoferritin and boehmite, the reconstituted apoferritin sol (60 mL) was added to boehmite sol (40 mL, 0.25 M). The pH value of the resulting sol was 3.5, which assures compatibility between apoferritin and boehmite. In this case both colloids are below their isoelectric points (that is, positively charged).

The morphology of the powders was examined by TEM (2000 FX2, Jeol). Chemical analyses at the particle level were carried out with an EDX spectrometry analyzer (QX 2000, Oxford Link) integrated in the transmission electron microscope. The different phases present in the solids were detected by X-ray diffraction (XRD, PW1710, Philips).

Received: May 30, 2004

Revised: August 5, 2004

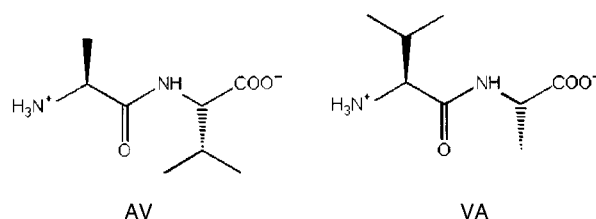
Keywords: aerosols · colloids · iron · magnetic properties · nanotechnology

- [1] a) D. Zhang, L. Qi, J. Ma, H. Cheng, *Adv. Mater.* **2002**, *14*, 1499; b) Z. Yang, Z. Niu, Y. Lu, Z. Hu, C. C. Han, *Angew. Chem.* **2003**, *115*, 1987; *Angew. Chem. Int. Ed.* **2003**, *42*, 1943; c) G. A. Ozin, *Chem. Commun.* **2003**, 2639; d) C. López, *Adv. Mater.* **2003**, *15*, 1679.
- [2] a) F. Caruso, *Adv. Mater.* **2001**, *13*, 11; b) L. M. Liz-Marzán, P. Mulvaney, *J. Phys. Chem. B* **2003**, *107*, 7312; c) T. Li, J. Moon, A. A. Morrone, J. J. Mecholsky, D. R. Talhalm, J. H. Adair, *Langmuir* **1999**, *15*, 4328; d) A. A. Antipov, G. B. Sukhorukov, Y. A. Fedutik, J. Hartmann, M. Giersig, H. Möhwald, *Langmuir* **2002**, *18*, 6687.
- [3] a) C. Niemeyer, *Angew. Chem.* **2001**, *113*, 4254; *Angew. Chem. Int. Ed.* **2001**, *40*, 128; b) M. Zhao, L. Josephson, Y. Tang, R. Weissleder, *Angew. Chem.* **2003**, *115*, 1413; *Angew. Chem. Int. Ed.* **2003**, *42*, 1375; c) S. Sun, S. Anders, T. Thomson, J. E. E. Baglin, M. F. Toney, H. F. Hamann, C. B. Murray, B. D. Terris, *J. Phys. Colloid Chem.* **2003**, *107*, 5419; d) F. X. Redl, K.-S. Cho, C. B. Murray, S. O. O'Brien, *Nature* **2003**, *423*, 968.
- [4] a) S. Mørup, F. Bødker, P. V. Hendriksen, S. Linderroth, **1995**, *52*, 287; b) P. Allia, M. Coisson, P. Tiberto, F. Vinai, M. Knobel, M. A. Novak, W. C. Nunes, *Phys. Rev. B* **2001**, *64*, 144420; c) V. Skumryev, S. Stoyanov, Y. Zhang, G. Hadjipanayis, D. Givord, J. Nogués, *Nature* **2003**, *423*, 850; d) P. Tartaj, T. González-Carreño, C. J. Serna, *J. Phys. Chem. B* **2003**, *107*, 20.
- [5] a) Q. A. Pankhurst, J. Connolly, S. K. Jones, J. Dobson, *J. Phys. D: Appl. Phys.* **2003**, *36*, R137; b) P. Tartaj, M. P. Morales, S. Veintemillas-Verdaguer, T. González-Carreño, C. J. Serna, *J. Phys. D: Appl. Phys.* **2003**, *36*, R182.
- [6] P. Tartaj, *ChemPhysChem* **2003**, *4*, 1371.
- [7] a) Y. Lu, H. Fan, A. Stump, T. L. Ward, C. Rieker, C. J. Brinker, *Nature* **1999**, *398*, 223; b) P. Tartaj, T. González-Carreño, C. J. Serna, *Langmuir* **2002**, *18*, 4556; c) P. Tartaj, T. González-Carreño, O. Bomati-Miguel, P. Bonville, C. J. Serna, *Phys. Rev. B* **2004**, *69*, 94401.
- [8] a) G. L. Messing, S. Zhang, G. V. Jayanthi, *J. Am. Ceram. Soc.* **1993**, *76*, 2707; b) P. Tartaj, T. González-Carreño, C. J. Serna, *Adv. Mater.* **2001**, *13*, 1620; c) P. Tartaj, T. González-Carreño, C. J. Serna, *Adv. Mater.* **2004**, *16*, 529.
- [9] a) C. Boissiere, D. Grosso, H. Amenitsch, A. Gibaud, A. Coupé, N. Baccile, C. Sanchez, *Chem. Commun.* **2003**, 2798; b) N. Baccile, D. Grosso, C. Sanchez, *J. Mater. Chem.* **2003**, *13*, 3011; c) D. Grosso, F. Cagnol, G. J. Soler-Illa, E. L. Crepaldi, H. Amenitsch, A. Brunet-Bruneau, A. Burgeouis, C. Sanchez, *Adv. Funct. Mater.* **2004**, *14*, 309.
- [10] a) R. M. Crooks, M. Zhao, L. Sun, V. Chechik, L. K. Yeung, *Acc. Chem. Res.* **2001**, *34*, 181; b) Y. Niu, R. M. Crooks, *Chem. Mater.* **2003**, *15*, 3463; c) K. Inoue, *Prog. Polym. Sci.* **2000**, *25*, 453; d) F. Vögtle, S. Gestermann, R. Hesse, H. Schwier, B. Windisch, *Prog. Polym. Sci.* **2000**, *25*, 987.
- [11] a) S. Mann in *Biomaterialization: Principles and Concepts in Bioinorganic Materials Chemistry* (Eds.: R. G. Compton, S. G. Davies, J. Evans), Oxford University Press, Oxford, **2001**; b) H. Heqing, R. K. Watt, R. B. Frankel, G. D. Watt, *Biochemistry* **1993**, *32*, 1687; c) G. Zhao, F. Bou-Abdallah, X. Yang, P. Arosio, N. D. Chasteen, *Biochemistry* **2001**, *40*, 10832; d) G. Zhao, F. Bou-Abdallah, P. Arosio, S. Levi, C. Janus-Chandler, N. D. Chasteen, *Biochemistry* **2003**, *42*, 3142.
- [12] a) F. C. Meldrum, V. J. Wade, D. L. Nimmo, B. R. Heywood, S. Mann, *Nature* **1991**, *349*, 684; b) F. C. Meldrum, B. R. Heywood, S. Mann, *Science* **1992**, *257*, 522; c) F. C. Meldrum, T. Douglas, S. Levi, P. Arosio, S. Mann, *J. Inorg. Biochem.* **1995**, *58*, 59; d) T. Douglas, V. T. Stark, *Inorg. Chem.* **2000**, *39*, 1828; e) M. Allen, D. Willits, M. Young, T. Douglas, *Inorg. Chem.* **2003**, *42*, 6300; f) M. Okuda, K. Iwahori, I. Yamashita, H. Yoshimura, *Biotechnol. Bioeng.* **2003**, *84*, 187.
- [13] a) B. Warne, O. Kasyutich, E. Mayes, J. Wiggins, K. Wong, *IEEE Trans. Magn.* **2000**, *36*, 3009; b) J. Hoinville, A. Bewick, D. Gleeson, R. Jones, O. Kasyutich, E. Mayes, A. Nartowski, B. Warne, J. Wiggins, K. Wong, *J. Appl. Phys.* **2003**, *93*, 7187; c) J. M. Dominguez-Vera, E. Colacio, *Inorg. Chem.* **2003**, *42*, 6983; d) T. Ueno, M. Suzuki, T. Goto, T. Matsumoto, K. Nagayama, Y. Watanabe, *Angew. Chem.* **2004**, *116*, 2581; *Angew. Chem. Int. Ed.* **2004**, *43*, 2527.
- [14] E. H. Lan, B. Dunn, J. Selverston-Valentine, J. I. Zink, *J. Sol-Gel Sci. Technol.* **1996**, *7*, 109.
- [15] a) P. Mulvaney, L. M. Liz-Marzan, M. Giersig, T. Ung, *J. Mater. Chem.* **2000**, *10*, 1259; b) A. Ulman, *Chem. Rev.* **1996**, *96*, 533; c) I. Roy, T. Y. Ohulchanskyy, H. E. Pudavar, E. J. Bergey, A. R. Oseroff, J. Morgan, T. J. Dougherty, P. N. Prasad, *J. Am. Chem. Soc.* **2003**, *125*, 7860; d) P. Tartaj, C. J. Serna, *J. Am. Chem. Soc.* **2003**, *125*, 15754.
- [16] We did not try to eliminate the inorganic phosphate, because of the small amount of phosphate with respect to iron in native horse spleen ferritin (usually about 5 mol% of the Fe content, Ref. [11a]) and the fact that its presence could even help to stabilize the metallic phase against corrosion (phosphates are routinely used in metallurgy as anticorrosive agents). When the reduction, elimination, or even addition of inorganic phosphate is needed for other systems, protocols can be found in the literature (see for example reference [11b]).
- [17] Apart from α -Fe, we expect the formation of a low-crystallinity Fe_2SiO_4 shell (not observable by XRD) surrounding the α -Fe MNMs, as happens in Fe/silica systems obtained in a similar way (see references [7c] and [15d]). This protective layer imparts stability against corrosion of the metallic component.
- [18] R. H. Victora, L. M. Falikov, *Phys. Rev. B* **1984**, *30*, 259.
- [19] The Fe and Co atoms form a metallic alloy throughout the range of compositions and we expect, at the end of thermal treatment, the diffusion of Co atoms within the Fe metallic core. In fact, the formation of $\text{Fe}_{1-x}\text{Co}_x$ metallic alloys is reported in the literature by using methods such as ball milling (see for example M. Sorescu, A. Grabias, *Intermetallics* **2002**, *10*, 317 and E. C. Passamani, C. Larica, V. P. Nascimento, *J. Mater. Sci.* **2002**, *37*, 809).
- [20] J. H. Kim, T. Germer, G. W. Mulholland, S. H. Ehrman, *Adv. Mater.* **2002**, *14*, 518.
- [21] X. H. Chen, Y. B. Hu, G. S. Wilson, *Biosens. Bioelectron.* **2002**, *17*, 1005.

Dipeptides as Microporous Materials**

Dmitriy V. Soldatov,* Igor L. Moudrakovski, and John A. Ripmeester*

The synthesis and characterization of hydrophobic porous frameworks designed for a variety of applications has attracted significant research efforts over the last few years.^[1] The key idea in such studies is to design building elements which allow for controllable assembly and disassembly, and which may be extensively replaced and modified to give porous frameworks with various topologies and functions. The natural world often provides excellent examples of how to proceed with the design of materials; for example, the initial experiences with natural zeolites has led to very successful efforts to produce a wide variety of industrially relevant synthetic materials.^[2] Recently, supramolecular architectures based upon weaker interactions have motivated a number of studies;^[3] polypeptides that can build tubular and helical structures, frequently referred as nanotubes, have attracted considerable attention because of their biological relevancy as ion channels, membrane pores, etc.^[4] These naturally occurring and artificially created materials reveal a sophisticated complexity and are often difficult to characterize in detail. Thus, the lower oligomeric peptides, being both simpler model systems and cheaper, would appear to be useful as practical porous materials, especially since some dipeptides demonstrate the ability to host small organic molecules.^[5] Moreover, the ability of single crystals of the dipeptides to sustain guest solvent exchange and removal was reported.^[5d] Herein we examine the structure and sorption properties of the two closely related dipeptides L-alanyl-L-valine (AV) and L-valyl-L-alanine (VA; Scheme 1), and show that these lower oligomers have considerable promise as novel porous materials. Moreover, the wide variety of amino acids available should allow the assembly of materials with quite diverse structural motifs containing significant void space.



Scheme 1. Dipeptides studied.

The two dipeptides AV and VA are microporous crystalline materials. Hexagonal prisms of the dipeptides were grown from water and characterized by single-crystal X-ray diffraction (XRD) analysis at room temperature (Table 1).^[6–8]

Table 1: Single-crystal XRD analysis of guest-free AV and VA.

Compound	AV	VA
temperature [K]	293	293
empirical formula	C ₈ H ₁₆ N ₂ O ₃	C ₈ H ₁₆ N ₂ O ₃
formula weight	188.2	188.2
crystal system, space group	hexagonal, <i>P</i> 6 ₁	hexagonal, <i>P</i> 6 ₁
<i>a</i> [Å]	14.462(2)	14.461(2)
<i>c</i> [Å]	10.027(1)	10.083(1)
<i>V</i> [Å ³]	1816.2(4)	1826.1(4)
<i>Z</i>	6	6
total data collected	21480	15948
data unique (<i>I</i> > 2σ(<i>I</i>))	2189	1954
refined parameters	142	122
calculated density [g cm ⁻³]	1.033	1.027
final <i>R</i> 1 (<i>I</i> > 2σ(<i>I</i>))	0.048	0.057
<i>wR</i> 2 (<i>I</i> > 2σ(<i>I</i>))	0.103	0.116
max peak and hole [e Å ⁻³]	+0.17, -0.15	+0.15, -0.14

Both crystals are hexagonal with a *P*6₁ space group and lattice parameters that are nearly identical. Each dipeptide assembles through hydrogen bonds as a 6₁ spiral to form a channel (Figure 1). Mapping out the channel diameter along the *z* axis (Figure 2) shows that the channels have a smooth, constant-diameter shape similar to that of urea^[10] (a well-known and extremely versatile host material) with an average diameter of 5.13 and 4.90 Å for AV and VA, respectively. A feature that distinguishes AV and VA from most other tubulates, however, is that their channels are essentially chiral.^[11] The center of the channel is displaced from the 6₁ axis by 0.60 and 1.05 Å for AV and VA, respectively, and rotates around the axis in a right-handed fashion (Figure 3). It should be noted that chiral sorbents are important and challenging targets in crystal engineering. While researchers resort to subtle strategies to induce chirality into novel, artificially created porous materials,^[12] the peptides form an endless source of naturally chiral building blocks ideally suited to this task.

Another distinction of the materials studied is the remarkable stability of their porous frameworks. The majority of hosts known to date collapse into a dense form once the stabilizing guest template is removed; only a few may exist in a porous form as a result of their kinetic stability with respect to the dense, thermodynamically stable polymorph.^[13] To check for possible polymorphism, AV and VA samples were obtained from different commercial sources, and were

[*] Dr. D. V. Soldatov
Institute of Inorganic Chemistry
Siberian Branch of the Russian Academy of Sciences
Ac. Lavrentiev Av. 3, 630090, Novosibirsk (Russia)
Fax: (+7) 3832-344489
E-mail: Dmitriy.Soldatov@nrc.ca
E-mail: soldatov@che.nsk.su

Dr. I. L. Moudrakovski, Dr. J. A. Ripmeester
Stearns Institute for Molecular Sciences
National Research Council of Canada
100 Sussex Drive, K1A0R6, Ottawa (Canada)
Fax: (+1) 613-998-7833
E-mail: John.Ripmeester@nrc.ca

[**] We thank E. V. Grachev (Institute of Inorganic Chemistry, Novosibirsk) for the SHADEWIN software package. D.V.S. acknowledges the support received for this research during his work at the Stearns Institute.

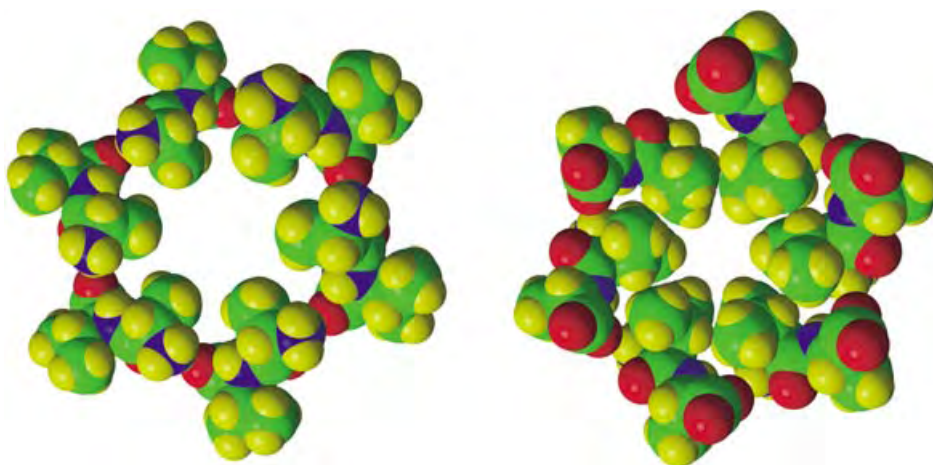


Figure 1. Spiral assembly of AV (left) and VA (right) dipeptide molecules that form a channel (van der Waals dimensions).

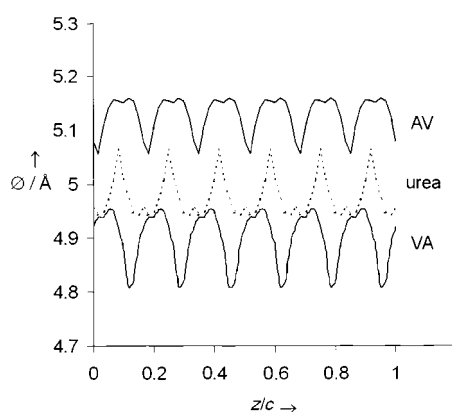


Figure 2. Channel diameter (\varnothing) along the z axis in AV ($c = 10.027$ Å), VA ($c = 10.083$ Å), and urea ($c = 11.017$ Å).

examined both as received and after recrystallization under a variety of conditions.^[6] Only the porous forms of the materials were obtained in every case, as determined by powder XRD (PXRD). This observation reflects the fact that the structural motifs are governed by strongly directional H-bonding interactions rather than close packing. Therefore, dense forms of the materials are not easily obtained, or may not exist at all.

As materials that have permanent void space, it is worthwhile comparing AV and VA with the many varieties of zeolites—a large family of covalently bonded aluminosilicates assembled from a limited number of basic structural units.^[14] Zeolites are kinetically stable with respect to the thermodynamically stable dense form, and they are widely used as sorbents, with porosities varying from about 18% ($8\text{ cm}^3\text{ g}^{-1}$) for analcime to about 53% ($28\text{ cm}^3\text{ g}^{-1}$) for faujasite.^[2a] The porosity of the dipeptide materials was determined by comparing the density measured by He pycnometry with the density calculated from XRD unit cell measurements.^[15] According to these determinations the volume fractions in the materials accessible to He gas were 11.7(3)% and 11.3(2)% for AV and VA, respectively. Similar values (11.4% and 10.4%) were calculated from the XRD

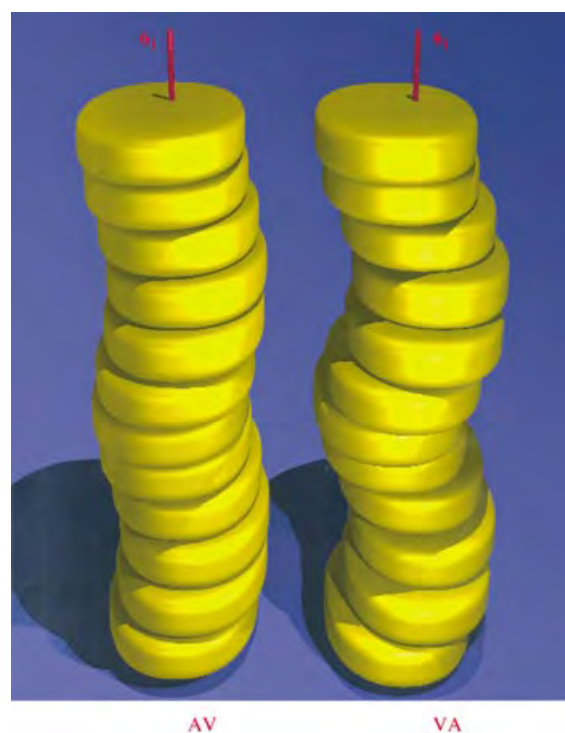


Figure 3. The channel shape in AV (left) and VA (right) shown as a set of inscribed disks threaded on a sixfold screw axis. Two c -translation periods are shown for each dipeptide.

results.^[16] Taking into account the much lower density of the dipeptides, the capacity of the materials of about $11\text{ cm}^3\text{ g}^{-1}$ falls into the range of values observed in practically useful zeolite materials.

A well-utilized property of zeolites is their ability to behave as molecular sieves, that is, they can distinguish between sorbate molecules differing in size as a result of the characteristic apertures that define the access to the internal void space. The channels in AV and VA, with average diameters of 5.13 and 4.90 Å, possess rather minor surface irregularities and are essentially hydrophobic, and therefore may exhibit a molecular-sieving effect. Since the materials

displayed a high affinity towards Xe gas, we used it as the sorbate species to investigate the sorption behavior of the dipeptide materials.

The Xe adsorption isotherms were measured at room temperature for both AV and VA by using a combination of standard volumetric techniques and ^{129}Xe NMR spectroscopy.^[17] It is quite remarkable that the two materials with such similar channel sizes show markedly different behavior towards Xe gas (Figure 4). Although the calculated sorption

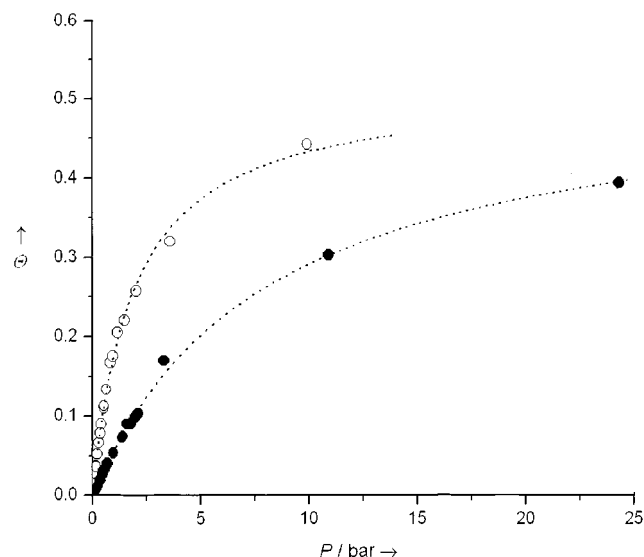


Figure 4. The sorption isotherms (298 K) of Xe in AV (solid circles) and VA (open circles) crystalline materials. θ is the Xe/dipeptide molar ratio. The best-fit curves are drawn using a Langmuir equation.

capacities are very similar (0.525(9) and 0.525(8) mol Xe per mol dipeptide for AV and VA, respectively), the sorption constants differ by a factor greater than four (0.120(5) and 0.52(2) bar^{-1} for AV and VA, respectively). The difference, in this case, should be attributable to a tighter binding between the host channel and the guest atom. With a van der Waals diameter of 4.4 Å, a Xe atom can interact more efficiently with the smaller channel in VA (4.90 Å) than with the larger channel of AV (5.13 Å). Although this size difference seems rather minor, it clearly has major consequences, and represents an example of molecular recognition based primarily on size-matching between the host and guest.

The observed sorption capacity implies ideal compositions of $\text{AV} \cdot 0.5\text{Xe}$ and $\text{VA} \cdot 0.5\text{Xe}$, that is, three Xe atoms per unit cell, or three Xe atoms per one *c*-translation. Taking the volume of a Xe atom to be 44.6 Å³, the packing efficiency of the Xe atoms in the channels are 64.6 and 70.4 % for AV and VA, respectively. The total gas storage capacity of the materials is about 60 mL g⁻¹. For comparison, the gas storage capacity of a variety of recently designed metal-organic and organic sorbents is 9–52 mL g⁻¹.^[18]

The studied materials showed significant thermal stability, as demonstrated by differential scanning calorimetry (DSC) and thermogravimetric analysis (TGA) experiments.^[19] The dipeptides showed no decomposition, phase transitions, or

mass loss up to their melting points of 238°C (AV) and 213°C (VA), followed by quantitative evaporation up to 270°C.

Other potential applications of the current and related materials assembled from lower peptides are connected to their relevance to biological materials. Surprisingly, very few molecules, such as urea, gossypol, and deoxycholic acid, amongst the vast number of compounds utilized as hosts are known to arise from living organisms.^[20] Dipeptides may be generated to form the entire family of bioorganic hosts and microporous solids.^[5,21] The peptide materials are nontoxic and may be used in biological and medical contexts, such as in chiral recognition/separation or preservation/storage of drugs. Also, they may be extensively utilized to model, for example, transmembrane pores and ion channels,^[4d] or the NMR spectroscopic signals of laser-polarized noble gases in proteins and living tissues.^[22]

In conclusion, the dipeptides studied in this work have robust porous frameworks with a high capacity and the capability of preferential sorption, even towards chemically inert species such as Xe. Moreover, the new sorbents studied are constructed from natural organic materials and pose no environmental problems. This study suggests that a diverse variety of lower peptides with a propensity for forming frameworks with voids of different geometry should be considered as a promising new class of materials for potential applications where selective sorption/release or gas storage is important.

Received: June 14, 2004

Keywords: chirality · inclusion compounds · microporosity · peptides · zeolites

- [1] a) J. Lipkowski in *Inclusion Compounds, Vol. 1* (Eds. J. L. Atwood, J. E. D. Davies, D. D. MacNicol), Academic, London, **1984**, pp. 59–103; b) B. T. Ibragimov, S. A. Talipov, T. F. Aripov, *J. Inclusion Phenom. Mol. Recognit. Chem.* **1994**, *17*, 317–324; c) A. T. Ung, D. Gizachew, R. Bishop, M. L. Scudder, I. G. Dance, D. C. Craig, *J. Am. Chem. Soc.* **1995**, *117*, 8745–8756; d) D. V. Soldatov, J. A. Ripmeester, S. I. Shergina, I. E. Sokolov, A. S. Zanina, S. A. Gromilov, Yu. A. Dyadin, *J. Am. Chem. Soc.* **1999**, *121*, 4179–4188; e) D. V. Soldatov, J. A. Ripmeester, *Chem. Mater.* **2000**, *12*, 1827–1839; f) P. Sozzani, A. Comotti, R. Simonutti, T. Meersmann, J. W. Logan, A. Pines, *Angew. Chem.* **2000**, *112*, 2807–2810; *Angew. Chem. Int. Ed.* **2000**, *39*, 2695–2698; g) O. Kristiansson, L.-E. Tergenius, *J. Chem. Soc. Dalton Trans.* **2001**, 1415–1420; h) A. V. Nossov, D. V. Soldatov, J. A. Ripmeester, *J. Am. Chem. Soc.* **2001**, *123*, 3563–3568; i) G. J. Halder, C. J. Kepert, B. Moubaraki, K. S. Murray, J. D. Cashion, *Science* **2002**, *298*, 1762–1765; j) K. Uemura, S. Kitagawa, M. Kondo, K. Fukui, R. Kitaura, H.-C. Chang, T. Mizutani, *Chem. Eur. J.* **2002**, *8*, 3586–3600; k) K. Seki, *Phys. Chem. Chem. Phys.* **2002**, *4*, 1968–1971; l) T. Ueda, T. Eguchi, N. Nakamura, R. E. Wasylshen, *J. Phys. Chem. B* **2003**, *107*, 180–185; m) R. Kitaura, K. Seki, G. Akiyama, S. Kitagawa, *Angew. Chem.* **2003**, *115*, 381; *Angew. Chem. Int. Ed.* **2003**, *42*, 428–431; n) E. B. Rusanov, V. V. Ponomareva, V. V. Komarchuk, H. Stoeckli-Evans, E. Fernandez-Ibañez, F. Stoeckli, J. Sieler, K. V. Domasevitch, *Angew. Chem.* **2003**, *115*, 2603–2605; *Angew. Chem. Int. Ed.* **2003**, *42*, 2499–2501; o) L. Pan, M. B. Sander, X. Huang, J. Li, M. Smith, E. Bittner, B. Bockrath, J. K. Johnson, *J. Am. Chem. Soc.* **2004**, *126*, 1308–1309.

- [2] a) R. M. Barrer in *Inclusion Compounds, Vol. 1* (Eds.: J. L. Atwood, J. E. D. Davies, D. D. MacNicol), Academic Press, London, **1984**, pp. 191–248; b) *Nanoporous Materials III, Studies in Surface Science and Catalysis, Vol. 141* (Eds.: A. Sayari, M. Jaroniec), Elsevier, Amsterdam, **2002**.
- [3] a) D. V. Soldatov, *J. Inclusion Phenom. Mol. Recognit. Chem.* **2004**, *48*, 3–9, and references therein; b) D. V. Soldatov in *Encyclopedia of Supramolecular Chemistry* (Eds. J. L. Atwood, J. W. Steed), Marcel Dekker, New York, **2004**, pp. 1302–1306, and references therein.
- [4] a) M. R. Ghadiri, J. R. Granja, R. A. Milligan, D. E. McRee, N. Khazanovich, *Nature* **1993**, *366*, 324–327; b) S. McKim, J. F. Hinton, *Biochim. Biophys. Acta* **1994**, *1193*, 186–198; c) D. Seebach, P. E. Ciceri, M. Overhand, B. Jaun, D. Rigo, L. Oberer, U. Hommel, R. Amstutz, H. Widmer, *Helv. Chim. Acta* **1996**, *79*, 2043–2067; d) J. D. Hartgerink, T. D. Clark, M. R. Ghadiri, *Chem. Eur. J.* **1998**, *4*, 1367–1372; e) M. Rechez, E. Gazit, *Science* **2003**, *300*, 625–627; f) T.-L. Lau, K. J. Barnham, C. C. Curtain, C. L. Masters, F. Separovic, *Aust. J. Chem.* **2003**, *56*, 349–356.
- [5] a) K. Ogura, *Yukagaku* **1994**, *43*, 779–786 (in Japanese); b) S. N. Mitra, E. Subramanian, *Biopolymers* **1994**, *34*, 1139–1143; c) C. H. Görbitz, *Acta Chem. Scand.* **1998**, *52*, 1343–1349; d) C. H. Görbitz, *Acta Crystallogr.* **2002**, *B58*, 849–854.
- [6] Crystallizations of AV and VA were performed from distilled water without using a template. Crystals suitable for single-crystal XRD analyses were obtained by evaporation of 0.3 M solutions at 60 °C. PXRD analyses indicated a total correspondence between the bulk products and the samples studied. The same single-crystal phase for each dipeptide, as confirmed by PXRD, was observed for the as-received samples (Sigma and ICN), solid products of fast crystallizations (evaporation in seconds at RT; evaporation over 2 h at 60 °C), very slow crystallizations (evaporation over 2 months at RT), and for crystals exhaustively equilibrated with their supernatant aqueous solutions (8 months at RT).
- [7] Single-crystal XRD analyses: Bruker SMART CCD diffractometer, Mo_{Kα} radiation ($\lambda = 0.7107$ Å), crystal size $0.5 \times 0.07 \times 0.07$ mm (similar for AV and VA). The structures were solved with the SHELXTL programs (direct methods) and refined with full-matrix least-squares on F^2 . CCDC-238397 (AV) and CCDC 238398 (VA) contain the supplementary crystallographic data for this paper. These data can be obtained free of charge via www.ccdc.cam.ac.uk/conts/retrieving.html (or from the Cambridge Crystallographic Data Centre, 12 Union Road, Cambridge CB21EZ, UK; fax: (+44)1223-336-033; or deposit@ccdc.cam.ac.uk).
- [8] Low-temperature crystal structures of the compounds were reported: AV at 150 K (ref. [5d]) and VA at 120 K (ref. [9]).
- [9] C. H. Görbitz, E. Gundersen, *Acta Crystallogr.* **1996**, *C52*, 1764–1767.
- [10] A. R. George, K. M. D. Harris, *J. Mol. Graphics* **1995**, *13*, 138–141.
- [11] Although the crystal structure of urea shows a chiral hexagonal structure, the channel is almost an ideal cylinder, with its center not deviating significantly from the sixfold crystallographic axis.
- [12] a) W. Yue, R. Bishop, M. L. Scudder, D. C. Craig, *Chem. Lett.* **1998**, 803–804; b) T. E. Gier, X. Bu, P. Feng, G. D. Stucky, *Nature* **1998**, *395*, 154–157; c) J. S. Seo, D. Whang, H. Lee, S. I. Jun, J. Oh, Y. J. Jeon, K. Kim, *Nature* **2000**, *404*, 982–986; d) C. J. Kepert, T. J. Prior, M. J. Rosseinsky, *J. Am. Chem. Soc.* **2000**, *122*, 5158–5168; e) H.-Z. Shi, Y.-K. Shan, M.-Y. He, L.-Y. Dai, Y.-Y. Liu, L.-H. Weng, *Acta Chim. Sin.* **2003**, *61*, 711–714 (in Chinese); f) P. Grosshans, A. Jouaiti, V. Bulach, J.-M. Planeix, M. W. Hosseini, J.-F. Nicoud, *CrystEngComm* **2003**, *5*, 414–416; g) Y. V. Mironov, N. G. Naumov, K. A. Brylev, O. A. Efremova, V. E. Fedorov, K. Hegetschweiler, *Angew. Chem.* **2004**, *116*, 1317–1321; *Angew. Chem. Int. Ed.* **2004**, *43*, 1297–1300.
- [13] S. Kitagawa, M. Kondo, *Bull. Chem. Soc. Jpn.* **1998**, *71*, 1739–1753.
- [14] The diversity of zeolite structures results from the 16 identified “secondary structural units” which must be fitted together to give the combinations of channels and cavities which yield the repeat unit of the zeolite structures; see W. Meier, D. H. Olson, *Atlas of Zeolite Structure Types 2nd ed.*, University Press, Cambridge, **1987**; (the list of the units is given on p 5 therein).
- [15] He pycnometry experiments were performed on an AccuPyc 1330 gas pycnometer (Micromeritics). Three samples (from different sources) of each dipeptide were measured several times (10 runs for each) till the results became stable. Typically, the first two measurements gave lower densities presumably because of blockage of the isolated channels by impurities (likely water in trace quantities; from TGA, the mass of possible adsorbed sorbates was lower 0.5 %). Average densities found for the “peptide framework body” were $1.169(4) \text{ g cm}^{-3}$ and $1.157(3) \text{ g cm}^{-3}$ for AV and VA, respectively (27 °C). Calculations performed as described in Ref. [1d] gave the following values (AV/VA): pore volume per unit cell, $212(6)/206(4) \text{ Å}^3$; pore volume fraction, $11.7(3)/11.3(2) \%$; average cross-section area of the channel, $21.2(5)/20.4(4) \text{ Å}^2$; average diameter of the channel, $5.2(1)/5.1(1) \text{ Å}$.
- [16] The channel volumes were calculated from single-crystal XRD results by integration of the spatial figure composed of discs having diameters corresponding to the maximum-sized sphere that could be inscribed in the channel and centered on a given level along the crystallographic z axis.
- [17] The intensity of the ^{129}Xe NMR signal in a known amount of material was monitored as a function of gas pressure and compared with that of a standard xenon sample to give the absolute amount of adsorbed xenon. The T_1 relaxation times of adsorbed xenon in the materials studied were found to be in the range of 50 to 80 s and care was taken to set the delays in the NMR experiments sufficiently long to ensure quantitative results. Equilibrium was reached typically in 2 h and the data were highly reproducible both when approaching equilibrium in the sorption or desorption modes. The sorption isotherms were approximated by a Langmuir equation, and the maximum sorption capacity and sorption constants were calculated as described in Ref. [1h].
- [18] D. V. Soldatov, I. L. Moudrakovski, C. I. Ratcliffe, R. Dutrisac, J. A. Ripmeester, *Chem. Mater.* **2003**, *15*, 4810–4818; (the sorption capacities of various sorbents are compared on p 4818 therein).
- [19] DSC experiments were run on a TA 2920 calorimeter. Samples of approximately 4 mg were sealed in aluminum pans and heated at a rate of 5° min^{-1} . TGA experiments were performed on a TA 2050 analyzer under flow of a N_2 at 50 mL min^{-1} . Sample sizes were approximately 8 mg; heating rate 5° min^{-1} .
- [20] *Inclusion Compounds* (Eds.: J. L. Atwood, J. E. D. Davies, D. D. MacNicol), Academic, London, **1984**.
- [21] a) C. H. Görbitz, *Chem. Eur. J.* **2001**, *7*, 5153–5159; b) C. H. Görbitz, *New J. Chem.* **2003**, *27*, 1789–1793.
- [22] a) C. Landon, P. Berthault, F. Vovelle, H. Desvaux, *Protein Sci.* **2001**, *10*, 762–770; b) B. M. Goodson, *J. Magn. Reson.* **2002**, *155*, 157–216; c) S. M. Rubin, S. Y. Lee, E. J. Ruiz, A. Pines, D. E. Wemmer, *J. Mol. Biol.* **2002**, *322*, 425–440.

Are NMR-Derived Model Structures for β -Peptides Representative for the Ensemble of Structures Adopted in Solution?*

Alice Glättli and Wilfred F. van Gunsteren*

Connecting an NMR observable \vec{q}^{obs} , such as an interproton distance derived from nuclear Overhauser effect (NOE) intensity or a 3J -coupling constant, with the underlying conformational ensemble $\{\vec{r}\}$ is a long-standing problem for the structure determination of peptides, proteins, and other biomolecules in solution.^[1–9] In particular, for flexible molecules such as peptides the assumption that all NMR signals originate from the same predominant conformer may not hold.^[10–13] In that case conventional NMR structure refinement procedures are not sufficient for the correct interpretation of the experimental data.

Molecular dynamics (MD) simulation can often complement the experimental tools for biomolecular structure determination such as NMR and circular dichroism spectroscopy.^[8,9,11,14,15] A sufficiently accurate simulation for comparison with and interpretation of experimental data requires:

- 1) the choice of the essential degrees of freedom appropriate to model the system of interest and to calculate the desired experimental observable,
- 2) a physically calibrated force field to describe the interactions along and between the chosen degrees of freedom,
- 3) equations of motion or a sampling method that generates a Boltzmann-weighted ensemble of conformers, and
- 4) the knowledge of the relation $\vec{q}(\vec{r})$ between the experimental observable \vec{q} and the molecular structure \vec{r} of the system of interest.

If the molecular model and the atomic interaction function (i.e. the force field) were perfect, and if a simulation could be carried out for an infinitely long time, the generated ensemble would exactly represent the real molecular system and there would be no need to carry out an NMR experiment on the system of interest. Furthermore, the connection

between experimentally measured observables and the underlying conformational ensemble would be perfectly understood, provided that the relation $\vec{q}(\vec{r})$, which connects the experimentally measured observables \vec{q} to a conformation \vec{r} , is exactly known. In practice, however, none of these conditions are completely fulfilled. Despite the enormous increase in computation power in recent years, the time required to sample the complete populated conformational space of a biomolecule is still beyond affordable simulation (sampling) for all but the shorter peptides. Additionally, even though current force fields for biomolecules are steadily improving in correctly modeling the structure, dynamics, and energetics of biomolecular systems,^[16] they are based on various approximations concerning polarizability, many-body interactions, quantum effects, etc. On the other hand, conventional structure determination makes use of force fields because the number of experimental observables is generally too small to uniquely derive the underlying set of conformations. Here, we compare two methods for the conformational interpretation of the NMR data of a β -hexapeptide (Figure 1):

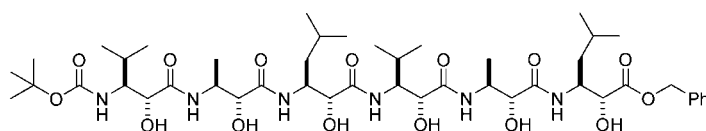


Figure 1. Chemical formula of the hydroxy β -hexapeptide studied. The peptide is protected by a *tert*-butoxycarbonyl group (N-Boc) at the N terminus and by a carbobenzoxy group (Z) at the C terminus. The hydroxy groups are attached to the C_α atoms and the side chains to the C_β atoms of the backbone.

firstly, conventional structure determination by simulated annealing in vacuo applying NOE distance and dihedral-angle restraints using a simple force field widely employed for structure determination of polypeptides, and secondly, free (unrestrained) MD simulation, which inherently generates Boltzmann-weighted ensembles, using a physically, thermodynamically calibrated force field and explicit treatment of solvent degrees of freedom. We show that the two methods yield rather different results and that the former one may lead to erroneous interpretation of NMR experiments.

The β -hexapeptide under investigation has been suggested by conventional NMR structure refinement to adopt a (*P*)- 2_8 -helical conformation in solution^[17] (Figure 2), representing the first example of the fourth helical secondary structure element adopted by β -peptides. By forming intramolecular hydrogen bonds, β -peptides adopt secondary structure elements that are very similar to those found in α -peptides and proteins,^[18,19] namely left- and right-handed helices (3_{14} ,^[20–22] 2.5_{12} ,^[23] $10/12$,^[24] and the previously mentioned 2_8 -helix^[17]), turns, and sheets.^[25] Starting from a fully extended conformation, the β -hexapeptide displayed in Figure 1 was simulated in explicit methanol solution at two different temperatures (298 K and 340 K) and at constant pressure (1 atm) using the GROMOS simulation package^[26,27] and the GROMOS biomolecular force field (version 45A3^[26,28]). For simulation details, see the Supporting Information. The ensembles of structures from the two 100-ns

[*] A. Glättli, Prof. W. F. van Gunsteren
Laboratorium für Physikalische Chemie, ETH
ETH Hönggerberg, HCI, 8093 Zürich (Switzerland)
Fax: (+41) 1-632-1039
E-mail: wfvgn@igc.phys.chem.ethz.ch

[**] We thank Prof. D. Seebach for challenging us to simulate the behavior of the peptide and Dr. K. Gademann for providing us with the 20 NMR model structures. Financial support from the Schweizer Nationalfonds (project number 2000-063590.00) and from the National Center of Competence in Research (NCCR) in Structural Biology of the Swiss National Science Foundation is gratefully acknowledged.

Supporting information for this article is available on the WWW under <http://www.angewandte.org> or from the author.



Figure 2. Superposition of the 20 NMR model structures with lowest energy from the ab initio simulated-annealing structure refinement runs^[17] with the 40 upper-bound distance restraints and 12 torsional-angle restraints derived from NMR data at 298 K in methanol.^[17] The simulated annealing runs were performed using the X-PLOR program and force field.^[29] The model structures suggest that the peptide adopts a (P)-2₈-helical conformation. The structures are superimposed using the backbone atoms of residues 2–5. The protection groups are omitted for clarity. Color scheme: C = yellow, H = white, N = blue, O = red.

0.03 nm. We also checked whether long proton–proton distances correspond to the absence of measured NOEs, although the latter may have other causes such as fast exchange, a particular overall tumbling time, and extensive spin–spin splitting. The 12 experimentally measured ³J-coupling constants are compared to the average ³J-coupling constants calculated for the trajectory structures from the simulations at 298 and 340 K and for the 20 X-PLOR structures using the Karplus relation^[30] as shown in Figure 3D–F. With an average absolute deviation of 0.4 Hz, the average ³J-coupling constants calculated from the ensemble of structures generated at room temperature agree very well with the experimentally measured values. Only one deviation exceeding 1 Hz, for HN–HC_β of residue 1, is observed. The 20 X-PLOR structures agree slightly worse with the experimental values than the simulation at room temperature with deviations of more than 1 Hz for the H–C_β–C_α–H torsions of residues 1 and 4, resulting in an average absolute deviation of 0.6 Hz.

trajectories were analyzed regarding the level of agreement with the NMR-derived data and regarding the conformational space sampled by the peptide in the simulation compared to the one covered by the 20 NMR model structures obtained by standard structure refinement using the program X-PLOR.^[29]

In Figure 3 the simulated and the NMR-derived data are compared in terms of 40 NOE distances and 12 ³J-coupling constants. The average effective violations of the upper-bound distances from all recorded structures in both simulations and from the 20 X-PLOR structures are displayed in Figure 3A–C. The upper-bound nature of NOE-derived distances implies that only violations with positive values are true violations. Essentially all experimentally observed NOEs are satisfied both in the X-PLOR structures and in the simulations at 298 and 340 K. The ensemble of structures at 298 K marginally violates two interresidue NOE distances: HC_γ(2)/HC_β(1) (NOE sequence number 3) and NH(2)/NH(3) (NOE sequence number 16) are both violated by 0.05 nm. The simulation at 340 K violates only one NOE distance (sequence number 3) by

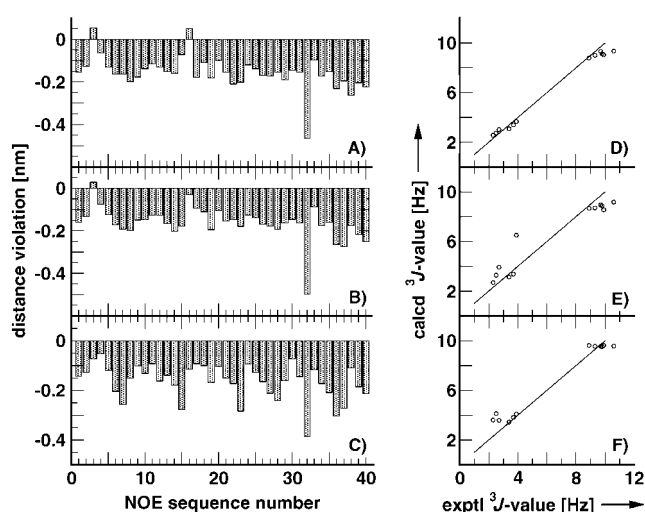


Figure 3. Panels A–C: Average (r^{-6} -averaging) distance violations of the upper-bound distances over all the recorded structures (2×10^5) in the MD simulations at 298 K (A) and 340 K (B) and the over the 20 X-PLOR structures^[17] (C). The upper-bound distances are inferred from 40 experimental NOE intensities observed in the ROESY NMR spectrum at 298 K.^[17] Panels D–F: Comparison of the 12 ³J-coupling constants (6 HN–HC_β, 6 HC_β–HC_α) extracted from the one-dimensional ¹H NMR spectrum measured at 298 K^[17] with the corresponding calculated ³J-coupling constants averaged over all structures from the MD simulations at 298 K (D) and at 340 K (E) and averaged over the 20 X-PLOR structures^[17] (F). The Karplus equation^[30] with $a = 6.4$ Hz, $b = -1.4$ Hz, and $c = 1.9$ Hz^[40] for ³J(HN,HC) and with $a = 9.5$ Hz, $b = -1.6$ Hz, and $c = 1.8$ Hz^[41] for ³J(HC,HC) was used. Tables of the experimental NOE upper-bound distances and ³J-coupling constants, of NOE distance bound violations of the r^{-6} -averaged distances and the calculated ³J-coupling constants averaged over the X-PLOR structures and the structures from the MD simulations are included in the Supporting Information.

Based on purely geometric criteria, the occurrence of hydrogen bonds in the 20 X-PLOR structures and in the ensemble of structures recorded in the simulations at 298 and 340 K has been determined (Table 1). Interestingly, eight-membered hydrogen-bonded rings (HB₈), characteristic for a (P)-2₈-helix, appear only at very low percentages in the two simulations ($\leq 4\%$), while they are to some extent present in the X-PLOR bundle of structures. This indicates that the suggested (P)-2₈-helix is only scarcely, if at all, populated in the simulations at 298 and 340 K. The hydrogen-bond analysis also shows that no regular secondary structure is sampled at room temperature, while at elevated temperature the occurrence of four 12-membered hydrogen-bonded rings hints at the formation of a (P)-2.5₁₂-helix. Additional simulations starting from either a (P)-2.5₁₂-helix or one of the 20 X-PLOR structure, which are suggested to represent a (P)-2₈-helix,^[17] show the (P)-2.5₁₂-helical conformation to be stable once the peptide has adopted it, while the X-PLOR structures are rather unstable (see the Supporting Information). In addition to the backbone–backbone hydrogen bonds, various hydrogen bonds between the α -hydroxy hydrogen and carbonyl oxygen atoms are present at the two temperatures. However, hydrogen bonds of the type OH(*i*)–O(*i*) (HB₅), proposed to

stabilize the (*P*)- 2_8 -helical conformation,^[17] are observed neither in the simulations nor in the 20 X-PLOR structures.

The results of the conformational clustering analysis over the combined ensembles (10 000 structures from each simulation (at 298 K and 340 K) and the 500 copies of each of the 20 X-PLOR structures) are displayed in Figure 4. The conformational clustering analysis groups the structures of the ensembles according to their positional root-mean-square deviation (rmsd) of the backbone (N, C $_{\beta}$, C $_{\alpha}$, C) atoms (excluding the first and last residue with the protecting groups) between each other structure favoring the most populated cluster.^[31] When a rather stringent rmsd similarity criterion of 0.04 nm is used (Figure 4A), the

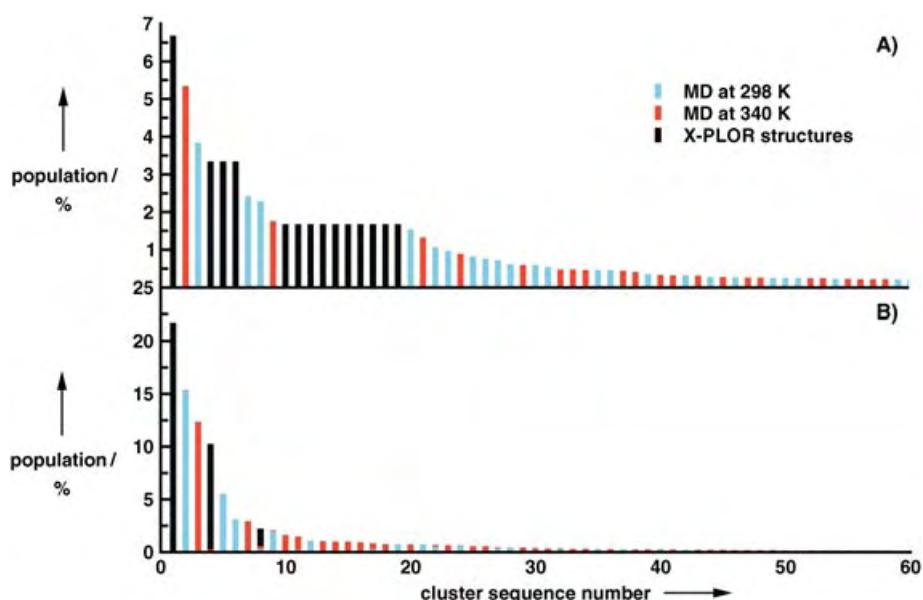


Figure 4. Conformational clustering analysis combining the “ensemble” of 500 copies of each of the 20 NMR model structures (i.e. equally weighing each NMR model structure) with the ensembles of 10 000 structures each (1 per 10 ps) sampled in the MD simulations at 298 and at 340 K. The plots show the population in percentage per cluster (conformers) and the portion of structures per cluster belonging to the “ensemble” of NMR model structures (black) and to the ensemble of structures generated at 298 K (blue) and at 340 K (red) by unrestrained MD simulation. In order to illustrate the conformational spread of the various ensembles, two different rmsd-similarity criteria are used: A more stringent one of 0.04 nm (A) and the standard criterion for a β -hexapeptide of 0.08 nm (B). With the first criterion a total of 2772 clusters are found, of which clusters 1–20 represent more than 50%, clusters 1–120 more than 75%, clusters 1–625 more than 90%, and clusters 1–1272 more than 95% of the total population. With the second criterion a total of 237 clusters are found, of which clusters 1–4 represent more than 50%, clusters 1–10 more than 75%, clusters 1–28 more than 90%, and clusters 1–51 more than 95% of the total population. For both rmsd criteria, only the populations of the first 60 most populated clusters are shown.

Table 1: Occurrence of intramolecular hydrogen bonds. A hydrogen bond is considered to exist when the donor-hydrogen-acceptor angle is larger than 135° and the hydrogen-acceptor distance is less than 0.25 nm. The hydrogen bonds are grouped according to the type of hydrogen-donor (NH or OH group) and the size (in terms of number of atoms) of the resulting hydrogen-bonded ring (e.g. a hydrogen bond between NH of residue *i* and C=O of residue (*i*–2) results in an eight-membered hydrogen-bonded ring, denoted as HB₈). O(0) corresponds to the carbonyl oxygen of the Boc protecting group. Only hydrogen bonds with a population larger than 10% in one of the sets of structures are shown.

Donor–Acceptor	Occurrence of hydrogen bonds [%]		
	MD simulation 298 K	MD simulation 340 K	Refinement X-PLOR
NH(<i>i</i>)–O(<i>i</i> –2) [HB ₈]			
NH(3)–O(1)	0	1	20
NH(4)–O(2)	0	1	25
NH(5)–O(3)	2	4	10
NH(<i>i</i>)–O(<i>i</i> –3) [HB ₁₂]			
NH(3)–O(0)	0	30	0
NH(4)–O(1)	0	26	0
NH(5)–O(2)	0	35	0
NH(6)–O(3)	1	18	0
NH(<i>i</i>)–O(<i>i</i> +1) [HB ₁₀]			
NH(2)–O(3)	11	0	0
NH(5)–O(6)	11	1	0
OH(<i>i</i>)–O(<i>i</i> –1) [HB ₇]			
OH(6)–O(5)	0	14	0
OH(<i>i</i>)–O(<i>i</i> –2) [HB ₁₁]			
OH(4)–O(2)	0	8	10
OH(5)–O(3)	1	22	0
OH(6)–O(4)	1	10	0
OH(<i>i</i>)–O(<i>i</i> –3) [HB ₁₅]			
OH(4)–O(1)	1	26	0
OH(5)–O(2)	0	10	0
OH(<i>i</i>)–O(<i>i</i> +2) [HB ₁₃]			
OH(3)–O(5)	38	0	0

three ensembles do not share any part of conformational space; each cluster is populated by members of only one of the three ensembles. With a larger rmsd criterion of 0.08 nm the ensembles slightly overlap at their peripheries (Figure 4B). Cluster 8 represents the only cluster containing structures from all three ensembles (MD at 298 K: 12%; MD at 340 K: 12%; X-PLOR: 76%). Figure 4 also illustrates that the Boltzmann-weighted ensembles generated by free (unrestrained) molecular dynamics simulations bear a much larger conformational variability than the bundle of structures obtained by restrained simulated annealing.

Summarizing, we find that even though the 20 model structures obtained from simulated annealing and the two ensembles generated by free MD simulations show different hydrogen-bond patterns and access different parts of the conformational space of the peptide, they all agree with the available NMR data. First, this indicates that for a given set of experimental observables, depending on the structural properties of a peptide, more than one solution structure is possible. Consequently, a single structure may not be representative for the ensemble of structures in solution.

Second, this study demonstrates that unbiased MD simulation using a thermodynamically calibrated force field reproduces experimental NMR data such as NOE upper-bound distances and 3J -coupling constants just as well or even better than a set of NMR model structures derived by classical single-structure simulated-annealing refinement techniques using a simple force field in vacuo and the NOE upper bounds and J -value derived torsional-angle values as restraints. The fact that the MD simulations using the GROMOS force field do not need 40+12 restraints to satisfy the NMR data on the peptide demonstrates the accuracy of this force field and of the inclusion of explicit solvent compared to results from the use of the X-PLOR force field in vacuo. Therefore, standard NMR refinement procedures for flexible molecules such as small peptides as well as for proteins should be revised by completing the refinement process with molecular dynamics simulation in explicit solvent with a thermodynamically calibrated force field in order to generate a proper Boltzmann-weighted ensemble of structures. This should lead to a more reliable structural interpretation of the experimentally measured NMR observables. In the present case of the β -hexapeptide the MD simulations show that a (P)- 2_8 -helical conformation is not stable and therefore probably not representative for the ensemble of solution structures. It cannot be excluded that the finding that the simulation using the GROMOS force field prefers the formation of a (P)- 2_{12} -helix over a (P)- 2_8 -helix might be an artifact of the force field. Yet, the simulations agree with the experimental data and the GROMOS force field has very well reproduced experimental findings in previous peptide folding investigations.^[11,14,15,31–39] Finally, we note once more that the comparison of modeling or simulation results with experiment should always be done with primary, measured data such as NOE intensities, and maybe distances, or 3J -values and not only with secondary, derived data such as molecular structures and torsional-angle values in order to avoid spurious conclusions regarding (dis)agreement with experimental data.

Received: April 20, 2004

Keywords: β -peptides · conformation analysis · molecular dynamics · NMR spectroscopy · structure elucidation

- [1] O. Jardetzky, *Biochim. Biophys. Acta* **1980**, 621, 227–232.
- [2] J. Tropp, *J. Chem. Phys.* **1980**, 76, 6035–6043.
- [3] W. F. van Gunsteren, R. M. Brunne, P. Gros, R. C. van Schaik, C. A. Schiffer, A. E. Torda in *Methods in Enzymology: Nuclear Magnetic Resonance*, Vol. 239 (Eds.: T. James, N. Oppenheimer), Academic Press, New York, **1994**, pp. 619–654.
- [4] R. Abseher, S. Lüdemann, H. Schreiber, O. Steinhauser, *J. Mol. Biol.* **1995**, 249, 604–624.
- [5] A. M. J. J. Bonvin, A. T. Brünger, *J. Biomol. NMR* **1996**, 7, 72–76.
- [6] T. R. Schneider, A. T. Brünger, M. Nilges, *J. Mol. Biol.* **1999**, 285, 727–740.
- [7] C. A. E. M. Spronk, B. Sander, A. M. J. J. Bonvin, E. Krieger, G. W. Vuister, G. Vriend, *J. Biomol. NMR* **2003**, 25, 225–234.
- [8] A. E. Torda, W. F. van Gunsteren in *Reviews in Computational Chemistry*, Vol. III (Eds.: K. Lipkowitz, D. Boyd), VCH, New York, **1992**, pp. 143–172.
- [9] W. R. P. Scott, A. E. Mark, W. F. van Gunsteren, *J. Biomol. NMR* **1998**, 12, 501–508.
- [10] R. Abseher, S. Lüdemann, H. Schreiber, O. Steinhauser, *J. Am. Chem. Soc.* **1994**, 116, 4006–4018.
- [11] X. Daura, K. Gademann, B. Jaun, D. Seebach, W. F. van Gunsteren, A. E. Mark, *Angew. Chem.* **1999**, 111, 249–253; *Angew. Chem. Int. Ed.* **1999**, 38, 236–240.
- [12] X. Daura, I. Antes, W. F. van Gunsteren, A. E. Mark, *Proteins Struct. Funct. Genet.* **1999**, 36, 542–555.
- [13] R. Bürgi, J. Pitera, W. F. van Gunsteren, *J. Biomol. NMR* **2001**, 19, 305–320.
- [14] C. Peter, X. Daura, W. F. van Gunsteren, *J. Biomol. NMR* **2001**, 20, 297–310.
- [15] A. Glättli, X. Daura, D. Seebach, W. F. van Gunsteren, *J. Am. Chem. Soc.* **2002**, 124, 12972–12978.
- [16] T. Hansson, C. Oostenbrink, W. F. van Gunsteren, *Curr. Opin. Struct. Biol.* **2002**, 12, 190–196.
- [17] K. Gademann, A. Häne, M. Rueping, B. Jaun, D. Seebach, *Angew. Chem.* **2003**, 115, 1573–1575; *Angew. Chem. Int. Ed.* **2003**, 42, 1534–1537.
- [18] D. Seebach, J. L. Matthews, *Chem. Commun.* **1997**, 79, 2015–2022.
- [19] R. P. Cheng, S. H. Gellman, W. F. DeGrado, *Chem. Rev.* **2001**, 101, 3219–3232.
- [20] D. Seebach, M. Overhand, F. N. M. Kühnle, B. Martinoni, L. Oberer, U. Hommel, H. Widmer, *Helv. Chim. Acta* **1996**, 79, 913–941.
- [21] D. Seebach, P. E. Ciceri, M. Overhand, B. Jaun, D. Rigo, L. Oberer, U. Hommel, H. Widmer, *Helv. Chim. Acta* **1996**, 79, 2043–2066.
- [22] D. H. Appella, L. A. Christianson, I. L. Karle, D. R. Powell, S. H. Gellman, *J. Am. Chem. Soc.* **1996**, 118, 13071–13072.
- [23] D. H. Appella, L. A. Christianson, D. A. Klein, D. R. Powell, X. Huang, J. J. Brachi, Jr., S. H. Gellman, *Nature* **1997**, 387, 381–384.
- [24] D. Seebach, S. Abele, K. Gademann, G. Guichard, T. Hintermann, B. Jaun, J. L. Matthews, J. V. Schreiber, L. Oberer, U. Hommel, H. Widmer, *Helv. Chim. Acta* **1998**, 81, 932–982.
- [25] D. Seebach, S. Abele, K. Gademann, B. Jaun, *Angew. Chem.* **1999**, 111, 1700–1703; *Angew. Chem. Int. Ed.* **1999**, 38, 1595–1597.
- [26] W. F. van Gunsteren, S. R. Billeter, A. A. Eising, P. H. Hünenberger, P. Krüger, A. E. Mark, W. R. P. Scott, I. G. Tironi, *Biomolecular Simulation: The GROMOS96 Manual and User Guide*, vdf Hochschulverlag, ETH Zürich, Switzerland, **1996**.
- [27] W. R. P. Scott, P. H. Hünenberger, I. G. Tironi, A. E. Mark, S. R. Billeter, J. Fennen, A. E. Torda, T. Huber, P. Krüger, W. F. van Gunsteren, *J. Phys. Chem.* **1999**, 103, 3596–3607.
- [28] L. D. Schuler, X. Daura, W. F. van Gunsteren, *J. Comput. Chem.* **2001**, 22, 1205–1218.
- [29] A. T. Brünger, *X-PLOR. A System for X-ray Crystallography and NMR*, Yale University Press, New Haven, CT, USA, **1992**.
- [30] M. Karplus, *J. Chem. Phys.* **1959**, 30, 11–15.
- [31] X. Daura, W. F. van Gunsteren, A. E. Mark, *Proteins Struct. Funct. Genet.* **1999**, 34, 269–280.
- [32] X. Daura, B. Jaun, D. Seebach, W. F. van Gunsteren, A. E. Mark, *J. Mol. Biol.* **1998**, 280, 925–932.
- [33] W. F. van Gunsteren, R. Bürgi, C. Peter, X. Daura, *Angew. Chem.* **2001**, 113, 363–367; *Angew. Chem. Int. Ed.* **2001**, 40, 351–355.
- [34] X. Daura, K. Gademann, H. Schäfer, B. Jaun, D. Seebach, W. F. van Gunsteren, *J. Am. Chem. Soc.* **2001**, 123, 2393–2404.
- [35] C. Peter, X. Daura, W. F. van Gunsteren, *J. Am. Chem. Soc.* **2000**, 122, 7461–7466.
- [36] R. Bürgi, X. Daura, A. E. Mark, M. Bellanda, B. Mammi, E. Peggion, W. F. van Gunsteren, *J. Pept. Res.* **2001**, 57, 107–118.

- [37] X. Daura, A. Glättli, P. Gee, C. Peter, W. F. van Gunsteren, *Adv. Protein Chem.* **2002**, 62, 341–360.
- [38] C. Peter, M. Rueping, H. J. Wörner, B. Jaun, D. Seebach, W. F. van Gunsteren, *Chem. Eur. J.* **2003**, 9, 5838–5849.
- [39] H. Yu, X. Daura, W. F. van Gunsteren, *Proteins Struct. Funct. Genet.* **2004**, 54, 116–127.
- [40] A. Pardi, M. Billeter, K. Wüthrich, *J. Mol. Biol.* **1984**, 180, 741–751.
- [41] A. de Marco, M. Llinás, K. Wüthrich, *Biopolymers* **1978**, 17, 617–636.

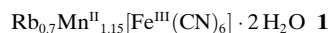
Mixed-Valence Compounds

Large Lattice Responses in a Mixed-Valence Prussian Blue Analogue Owing to Electronic and Spin Transitions Induced by X-ray Irradiation**

Serena Margadonna,* Kosmas Prassides, and Andrew N. Fitch

Mixed-valence metal cyanides with general formula $A_xM^{II}_y[M'^{III}(CN)_6]_n \cdot nH_2O$ (where A is an alkali-metal cation, and M and M' are divalent and trivalent transition-metal cations, respectively) have attracted considerable interest because of their unusual electronic and magnetic properties.^[1] In addition to molecular-based ferromagnetic properties with Curie temperatures higher than room temperature,^[2–4] the availability of degenerate or quasidegenerate electronic states has made them ideal systems with which to explore switching phenomena at the molecular level.^[5] For example, in some of these materials visible-light irradiation at low temperatures can drive optically controlled phase transitions to long-lived metastable states where the optical and/or magnetic properties change dramatically, thereby raising the potential of applications in memory devices and magneto-optical switching.^[6–10] Metal-to-metal electron transfer was also induced by X-ray irradiation at very low temperatures in the Prussian blue analogue, $Rb_{1.8}Co_4[Fe(CN)_6]_{3.3} \cdot 13H_2O$ with the resulting phase transformation monitored by energy-dispersive syn-

chrotron X-ray diffraction.^[11] Herein, we show that X-ray irradiation can also induce interconversion between the ground and excited states in another such compound **1**, over a broad temperature range (between room temperature and 10 K). Depending on the experimental conditions, a variety of internal charge-transfer processes and spin transitions are triggered resulting in either continuous or abrupt phase transformations that are accompanied by large lattice relaxations and can be accurately monitored by high-resolution angle-dispersive synchrotron X-ray diffraction.



Important information concerning the thermo- and photoinduced magnetization/demagnetization behavior of transition-metal cyanides has been recently obtained by studying the cubic $RbMn^{II}[Fe^{III}(CN)_6]$ system.^[12] At room temperature, the Mn^{II} ions are in their high-spin (HS, $t_{2g}^3e_g^2$, $S = 5/2$) state and the Fe^{III} ions in the low-spin (LS, $t_{2g}^5e_g^0$, $S = 1/2$) state, and these ions couple antiferromagnetically. Cooling induces a charge transfer from manganese to iron leading to Mn^{III} in the HS ($t_{2g}^3e_g^1$, $S = 2$) and Fe^{II} in the LS state ($t_{2g}^6e_g^0$, $S = 0$) and is accompanied by a cubic–tetragonal phase transition, driven by the Jahn–Teller distortion of the $Mn^{III}N_6$ octahedra^[13,14] and the appearance of ferromagnetism at approximately 10 K.^[15] Green light irradiation at low temperatures induces the reverse electron transfer and the low lying Mn^{II} – Fe^{III} excited state can then be populated.^[16] Herein, we report on the internal redox reactions triggered by synchrotron X-ray radiation as a function of temperature and time in the related mixed-valence metal cyanide, **1**. As excited metastable electronic and spin states are populated and evolve with illumination time at different temperatures, the angle-dispersive synchrotron X-ray diffraction technique allows simultaneous complete crystal structure refinements, which leads to the elucidation of the resulting rich phase diagram in unprecedented detail.

We examined the synchrotron X-ray diffraction profiles of **1** collected at 295 K and at 100 and 10 K after cooling in the absence of X-ray illumination. No reflections violating face-centered cubic (*fcc*) extinction rules are evident and the crystal structure remains strictly cubic down to 10 K. Rietveld analysis (Figure 1a, see Supporting Information) proceeded smoothly with the generic structural model of mixed-valence metal cyanides,^[17] comprising a three-dimensional network of $\{Mn(NC)_6\}$ and $\{Fe(CN)_6\}$ octahedra linked by the CN ligands (space group $Fm\bar{3}m$, $a = 10.54314(4)$ Å at 295 K). The $Fe(CN)_6$ vacancy positions (13%) are occupied by H_2O molecules completing the coordination sphere of neighboring Mn^{II} cations while the Rb^+ ions are disordered in the tetrahedral interstices of the framework structure (inset Figure 1a). The Mn–N and Fe–C bond lengths of the $\{Mn(NC)_6\}$ and $\{Fe(CN)_6\}$ octahedra refine to 2.249(4) and 1.900(5) Å, respectively, consistent with the Mn^{II} –NC– Fe^{III} ground state (GS) assignment of the metal valence states. This result is also in agreement with the magnetic susceptibility data (measured $\chi T = 5.17$ cm³ K mol^{−1} at 295 K; spin-only value calculated for $Mn^{II}(HS, S = 5/2)$ – $Fe^{III}(LS, S = 1/2)$, $\chi T = 5.41$ cm³ K mol^{−1}). In contrast to stoichiometric

[*] Dr. S. Margadonna
Department of Chemistry
University of Cambridge
Cambridge CB2 1EW (UK)
Fax: (+44) 1223-336-362
E-mail: sm413@cam.ac.uk

Prof. K. Prassides
Department of Chemistry
University of Sussex, Brighton BN1 9QJ (UK)
Dr. A. N. Fitch
European Synchrotron Radiation Facility
38042 Grenoble (France)

[**] We thank the ESRF for synchrotron X-ray beamtime, the Royal Society for a Dorothy Hodgkin Research Fellowship (S.M.), and Dr. M. Kurmoo (Strasbourg) for useful discussions.

Supporting information for this article is available on the WWW under <http://www.angewandte.org> or from the author.

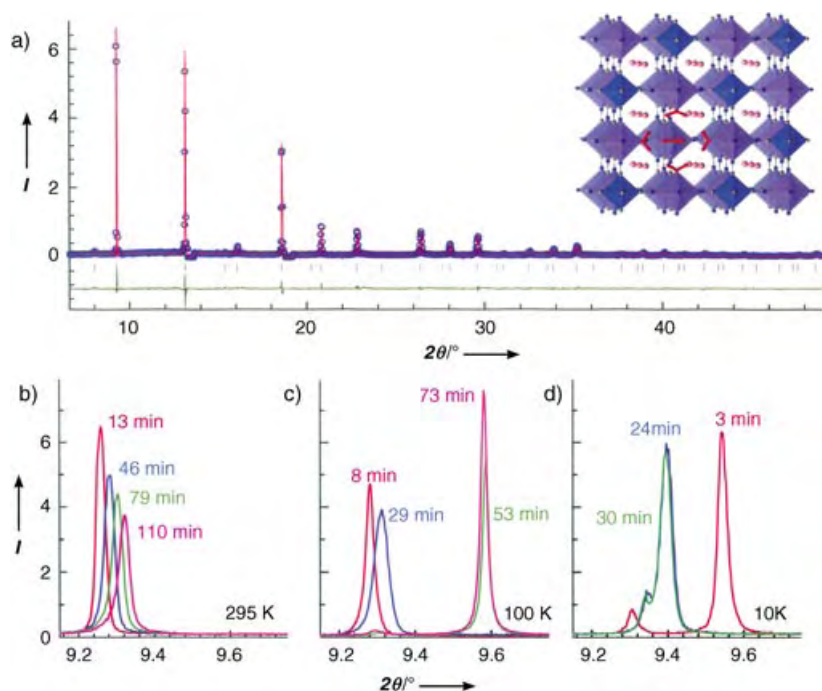


Figure 1. a) Final observed (blue circles) and calculated (red solid line) synchrotron X-ray powder diffraction profiles ($\lambda = 0.85066 \text{ \AA}$) for **1** at 295 K after 17 min of X-ray illumination. The lower green solid line shows the difference profile and the tick marks show the reflection positions. Two impurity peaks were excluded from the refinement. Inset: Building block of the cubic framework structure of **1**. Alternating $\{\text{Mn}(\text{NC})_6\}$ (light violet) and $\{\text{Fe}(\text{CN})_6\}$ (dark violet) octahedra are bridged by CN ligands. Pink spheres Rb^+ ions, red H_2O molecules residing in the $\text{Fe}(\text{CN})_6$ vacancies. b)–d) Selected region of representative diffraction profiles showing the evolution of the (200) Bragg reflection with increasing X-ray illumination time. b) 295 K, c) 100 K, d) 10 K. Each curve is labeled with the corresponding illumination time.

$\text{RbMn}[\text{Fe}(\text{CN})_6]$, which is tetragonal at low temperatures^[13,14] after an internal electron transfer to give ferromagnetically coupled $\text{Mn}^{\text{III}}(\text{HS}, S=2)\text{--Fe}^{\text{II}}(\text{LS}, S=0)\text{--Mn}^{\text{III}}(\text{HS}, S=2)$ units, no phase change is observed for **1** down to 10 K. This result can be understood in terms of the disorder associated with the water molecules which fill the $\text{Fe}(\text{CN})_6$ vacancies, thereby suppressing the cubic–tetragonal phase transition of stoichiometric $\text{RbMn}[\text{Fe}(\text{CN})_6]$ and is consistent with the temperature dependence of the magnetic data (see Supporting Information), which show 1) a change in χT below 180 K to $4.5 \text{ cm}^3 \text{ K mol}^{-1}$, implying that the thermally induced charge transfer to give $\text{Mn}^{\text{III}}(\text{HS}, S=2)\text{--Fe}^{\text{II}}(\text{LS}, S=0)$ occurs only partially ($<20\%$) on cooling, 2) a negative Weiss temperature of -5.4 K implying predominant $\text{Mn}^{\text{II}}\text{--Fe}^{\text{III}}$ antiferromagnetic interactions at low temperatures, and 3) the appearance of weak ferrimagnetism below approximately 10 K (coercive field = 235 Oe, remnant magnetization = $240 \text{ cm}^3 \text{ G mol}^{-1}$).

We monitored the evolution of the diffraction profiles at various temperatures with increasing exposure time to the X-ray radiation. A striking feature of the data at 295 K is that, although the structure remains cubic, the diffraction peaks continuously shift to higher angles (Figure 1 b), which implies that the material rapidly contracts at a rate of $0.238(3) \text{ \AA}^3 \text{ min}^{-1}$ (Figure 2 a) and shows an overall volume

decrease after 150 min of 2.9%. It is remarkable that the lattice contraction at 295 K for the illuminated sample is large enough to produce a cell volume considerably smaller than that of the non-illuminated sample at 10 K (overall volume decrease ca. 0.5%). Rietveld refinements with the same $Fm\bar{3}m$ structural model reveal a monotonic decrease of the Mn–N bond length to $2.203(4) \text{ \AA}$ after 150 min of exposure of the sample to the X-ray beam (Figure 2 b) at room temperature. This result is consistent with a progressive generation of $\text{Mn}^{\text{III}}\text{--NC--Fe}^{\text{II}}$ centers with increased X-ray illumination time and shrinking of the Mn–N bonds upon oxidation of the Mn^{II} centers. In contrast, the iron coordination sphere changes very little upon reduction as expected (in $\text{K}_3[\text{Fe}(\text{CN})_6]$ $\text{Fe}^{\text{III}}\text{--C}$ 1.93 \AA , and in $\text{K}_4[\text{Fe}(\text{CN})_6]$ $\text{Fe}^{\text{II}}\text{--C}$ 1.91 \AA ^[8]). Though there is no unique real-space description of this internal charge-transfer effect, the observation that the width of the diffraction peaks also progressively increases (see Figure 1 b) leads us to describe the observed X-ray induced transformation as the formation of $\text{Mn}^{\text{III}}\text{--NC--Fe}^{\text{II}}$ islands which progressively grow in size within a matrix of the original $\text{Mn}^{\text{II}}\text{--NC--Fe}^{\text{III}}$ units and with a local structure different from that of the average bulk structure.

The behavior of **1** is even more intriguing when the X-ray irradiation is switched on at 100 K after cooling without illumination (Figure 1 c). The diffraction peaks initially shift continuously to higher angles as at 295 K but, after an incubation period of approximately 20 min, all the diffraction peaks are accompanied by a partner at significantly higher angle, thereby providing the signature of a sudden transformation of the high-temperature structure to an isostructural one (PT-1) with drastically reduced lattice dimensions (Figure 2 a). The fraction of the contracted phase grows rapidly in a very short time and is accompanied by a notable sharpening of the diffraction peaks, which indicates the occurrence of a phase transition in the bulk. The abrupt collapse in the unit cell dimensions ($\Delta V/V \approx -10.3\%$) can be again understood in terms of the X-ray induced internal redox process $\text{Mn}^{\text{II}}(\text{HS})\text{--NC--Fe}^{\text{III}}(\text{LS}) \rightarrow \text{Mn}^{\text{III}}(\text{HS})\text{--NC--Fe}^{\text{II}}(\text{LS})$, which occurs even more efficiently at this temperature. This process leads to a large fraction of photoconverted units that exceeds the percolation threshold and thereby a cooperative first-order phase transformation is abruptly triggered. Rietveld refinements (see Supporting Information) indicate that in the contracted phase, the Mn–N bond length further shortens significantly to $2.056(5) \text{ \AA}$, while the Fe–C bond lengthens only slightly to $1.920(5) \text{ \AA}$ (Figure 2 b). We note that the abrupt phototransformation to the collapsed phase is accompanied by the appearance of a small fraction (ca. 5%) of a coexisting minority phase whose lattice

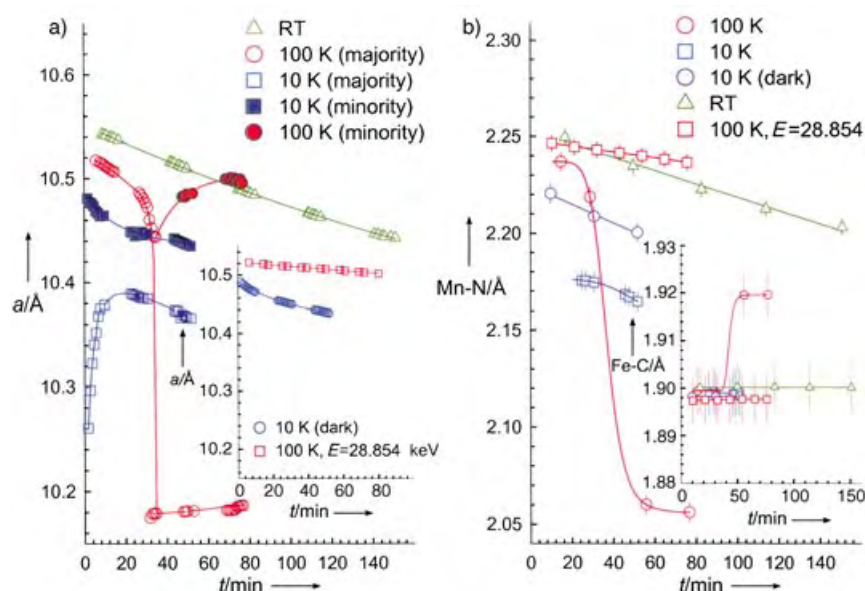


Figure 2. a) Evolution with increasing X-ray ($E = 14.575$ keV) illumination time of the cubic lattice constant in **1** at different temperatures: 295 K (green triangles), 100 K (red circles), 10 K (blue squares). Open symbols represent the lattice constants of the majority (full symbols the minority) phases at 100 and 10 K. Inset: the time dependence of the lattice constants at 10 K ($E = 14.575$ keV) after cooling in the dark (blue circles) and at 100 K for an incident photon energy of 28.854 keV (red squares). b) The corresponding time evolution of the Mn–N (inset: Fe–C) bond lengths as obtained from Rietveld refinements of the synchrotron X-ray powder diffraction profiles. Symbols are as described in (a).

size rapidly increases and approaches that expected for the untransformed material at this temperature (Figure 2a). Complementary experiments at 100 K with an X-ray beam of energy 28.854 keV were not able to induce the same first-order transition even after 80 min of irradiation and led only to a very slow decrease of the lattice dimensions at a rate of $0.083(2) \text{ Å}^3 \text{ min}^{-1}$ (inset Figure 2a). This can be understood by the now significantly reduced (by a factor between about 40–80) energy per unit volume per second deposited at the sample rendering the phototransformation extremely inefficient. This conclusion is also supported by the extracted lattice constant ($a = 10.49667(4) \text{ Å}$) being similar to that of the untransformed minority phase at 14.575 keV ($a = 10.4877(7) \text{ Å}$). In a complementary series of diffraction experiments at 100 K with a synchrotron X-ray beam of energy 28.850 keV, the first-order transformation to the collapsed phase was also successfully triggered by continuous wave (CW) green laser light illumination ($\lambda = 532 \text{ nm}$, power = 50 mW).^[18]

Substantial changes to the diffraction profile of the phototransformed PT-1 material are also observed on cooling to 10 K (Figure 1d). An extremely rapid phase change sets in as soon as the X-ray light is switched on and the lattice size inflates within the first 10 min by $\Delta V/V \approx +6.3\%$. Apparently the PT-1 phase, which was accessed at 100 K by X-ray irradiation now becomes highly unstable and transforms to a new bulk phase (PT-2) whose lattice constants straddle those of PT-1 and of the non-irradiated phase (GS; see Supporting Information). Undoubtedly, the formation of PT-2 is triggered by the reverse internal redox process, which led to the

formation of PT-1 from GS, namely $\text{Mn}^{\text{III}}\text{-NC-Fe}^{\text{II}} \rightarrow \text{Mn}^{\text{II}}\text{-NC-Fe}^{\text{III}}$. However, both the reduced lattice dimension ($a = 10.36940(6) \text{ Å}$) and refined Mn–N bond distance of $2.168(5) \text{ Å}$ (Figure 2) are inconsistent with a description of the electronic states of the bridging motifs as identical to those of GS, namely $\text{Mn}^{\text{II}}(\text{HS})\text{-NC-Fe}^{\text{III}}(\text{LS})$. Additional support for the conclusion that the phototransformed PT-2 phase should not be identified with GS comes from the presence of a co-existing minority phase (9.9(1)%) with a lattice size identical to that of the material when cooled to 10 K in the dark (Figure 2a) and therefore comprising $\text{Mn}^{\text{II}}(\text{HS})\text{-NC-Fe}^{\text{III}}(\text{LS})$ units.

To our knowledge, such a sensitivity to X-ray light with facile interconversion between a number of metastable states with differing charge (electronic) and spin (magnetic) states through both continuous (second order) and discontinuous (first order) phase transitions at temperatures ranging from 10 K to room temperature has not been reported for a single molecular system. It is reminiscent of the transitions from an insulating antiferromagnetic to a metallic ferromagnetic state in the $\text{Pr}_{0.7}\text{Ca}_{0.3}\text{MnO}_3$ manganite^[19,20] and from a charge-ordered spin-dimerized to a disordered dimer state in the CuIr_2S_4 spinel^[21] that were driven by X-ray illumination at low temperatures ($< 40 \text{ K}$ and $< 10 \text{ K}$, respectively). Stabilization of the photoinduced states in the manganites has been strongly linked to the structural changes, which accompany the absorption of X-ray photons and the relaxation of the lattice distortion associated with the $\{\text{Mn}^{\text{III}}\text{O}_6\}$ octahedra. This is a similar mechanism to that developed herein for the mixed-valence metal cyanides in which the photoinduced long-range-ordered states at 100 and 10 K are stabilized by the large lattice relaxations after electron removal from the $\{\text{Mn}^{\text{II}}(\text{NC})_6\}$ octahedra or electron addition to $\{\text{Mn}^{\text{III}}(\text{NC})_6\}$ octahedra. Moreover, our picture of the inhomogeneous character of the continuous phototransformation at room temperature is also analogous to that proposed for both the manganites and the spinels,^[19–21] in which the X-ray induced states are similarly characterized by structural inhomogeneities, as evidenced by the observed peak broadening and gradual evolution in the unit cell dimensions and metal–ligand bond lengths.

In conclusion, the initial results presented herein open the way for the study of the structural relaxations of otherwise inaccessible metastable electronic states of various multi-stable molecular materials following the absorption of photons. In addition, given the energy tunability of synchrotron X-ray light, the kinetics of the phototransformations can be controlled and moved between different time windows even at ambient temperature. We also note the considerably persistent character of the photoinduced transitions. To explain this, we can invoke the large lattice relaxations, which in these materials accompany the internal charge transfer and spin rearrangements (strong electron–phonon

coupling) and need large energies in order to be annealed. Figure 3 summarizes the postulated electronic and spin configurations of the transition-metal ions following the X-

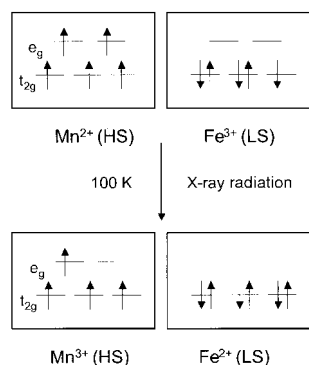


Figure 3. Schematic representation of the postulated electronic and spin configurations of the Mn and Fe ions following the X-ray-induced first-order phase transitions at 100 K in **1** at an incident photon energy of 14.575 keV.

ray-driven first-order phase transition at 100 K. Although the optical and magnetic properties of the two photoinduced bulk states, PT-1 and PT-2 are not probed in the present diffraction experiments directly, we anticipate that both their color and their magnetization should also significantly change. For instance, the color of the material exposed to X-ray light at room temperature changes from light to dark brown. Comparing the magnetic properties, we note that the untransformed material comprises antiferromagnetically coupled $\text{Mn}^{\text{II}}(\text{HS}, S=5/2)$ and $\text{Fe}^{\text{III}}(\text{LS}, S=1/2)$ ions and becomes ferrimagnetic at about 10 K. On the other hand, the exchange coupling between near-neighbor $\text{Mn}^{\text{III}}(\text{HS}, S=2)$ ions in PT-1 is mediated by the $\text{Fe}^{\text{III}}(\text{LS}, S=0)$ degenerate t_{2g} orbitals and is of ferromagnetic nature. As a result, conversion into the phototransformed excited states should be accompanied by drastic changes of the magnetization.

Experimental Section

1 was prepared as a light brown solid by reaction of aqueous solutions of MnCl_2 (0.1M), RbCl (1M), and $\text{K}_3\text{Fe}(\text{CN})_6$ (0.1M) and its stoichiometry established by elemental ($\text{Rb}:\text{Mn}:\text{Fe}=0.72:1.13:1$) and thermogravimetric analysis. Temperature- and field-dependent magnetization measurements were performed with a Quantum Design MPMS5 SQUID susceptometer. For the angle-dispersive synchrotron X-ray diffraction measurements, samples were sealed in thin-wall glass capillaries 0.5 mm in diameter. With the sample inside a continuous-flow cryostat, synchrotron X-ray powder diffraction data ($\lambda=0.85066 \text{ \AA}$, $E=14.575 \text{ keV}$, beamsize approximately $2.3 \times 1.4 \text{ mm}^2$) were collected on cooling at 295, 100, and 10 K as a function of illumination time using the high-resolution powder X-ray diffraction beamline ID31 at the European Synchrotron Radiation Facility (ESRF), Grenoble, France. Complementary diffraction data were also collected at 100 K using X-rays with $\lambda=0.42970 \text{ \AA}$ ($E=28.854 \text{ keV}$). Data analysis was performed with the GSAS suite of Rietveld analysis programs.

Received: May 9, 2004

Revised: August 2, 2004

Keywords: electron transfer · mixed-valence compounds · phase transitions · photochemistry · Prussian blue analogues · solid-state structures

- [1] P. Gülich, Y. Garcia, T. Woike, *Coord. Chem. Rev.* **2001**, 219, 839.
- [2] S. Ferlay, T. Mallah, R. Ouahes, P. Veillet, M. Verdaguer, *Nature* **1995**, 378, 701.
- [3] Ø. Hatlevik, W. E. Buschmann, J. Zhang, J. L. Manson, J. S. Miller, *Adv. Mater.* **1999**, 11, 914.
- [4] S. M. Holmes, G. S. Girolami, *J. Am. Chem. Soc.* **1999**, 121, 5593.
- [5] S. Ohkoshi, K. Hashimoto, *J. Photochem. Photobiol. C* **2001**, 2, 71.
- [6] O. Sato, T. Iyoda, A. Fujishima, K. Hashimoto, *Science* **1996**, 272, 704.
- [7] O. Sato, Y. Einaga, A. Fujishima, K. Hashimoto, *Inorg. Chem.* **1999**, 38, 4405.
- [8] A. Bleuzen, C. Lomenech, V. Escax, F. Villain, F. Varret, C. Cartier dit Moulin, M. Verdaguer, *J. Am. Chem. Soc.* **2000**, 122, 6648.
- [9] H. W. Liu, K. Matsuda, Z. Z. Gu, K. Takahashi, A. L. Cui, R. Nakajima, A. Fujishima, O. Sato, *Phys. Rev. Lett.* **2003**, 90, 167403.
- [10] M. Hanawa, Y. Moritomo, A. Kuriki, J. Tateishi, K. Kato, M. Takata, M. Sakata, *J. Phys. Soc. Jpn.* **2003**, 72, 987.
- [11] V. Escax, A. Bleuzen, J. P. Itie, P. Munsch, F. Varret, M. Verdaguer, *J. Phys. Chem. B* **2003**, 107, 4763.
- [12] S. Ohkoshi, H. Tokoro, M. Utsunomiya, M. Mizuno, M. Abe, K. Hashimoto, *J. Phys. Chem. B* **2002**, 106, 2423.
- [13] Y. Moritomo, K. Kato, A. Kuriki, M. Takata, M. Sakata, H. Tokoro, S. Ohkoshi, K. Hashimoto, *J. Phys. Soc. Jpn.* **2002**, 71, 2078.
- [14] K. Kato, Y. Moritomo, M. Takata, M. Sakata, M. Umekawa, N. Hamada, S. Ohkoshi, H. Tokoro, K. Hashimoto, *Phys. Rev. Lett.* **2003**, 91, 255502.
- [15] Y. Moritomo, A. Kuriki, K. Ohoyama, H. Tokoro, S. Ohkoshi, K. Hashimoto, N. Hamada, *J. Phys. Soc. Jpn.* **2003**, 72, 456.
- [16] Y. Moritomo, M. Hanawa, Y. Ohishi, K. Kato, M. Takata, A. Kuriki, E. Nishibori, M. Sakata, S. Ohkoshi, H. Tokoro, K. Hashimoto, *Phys. Rev. B* **2003**, 68, 144106.
- [17] H. J. Buser, D. Schwarzenbach, W. Petter, A. Lüdi, *Inorg. Chem.* **1977**, 16, 2704.
- [18] The observed photoinduced effects are of persistent nature. Upon switching off the X-ray beam and warming the sample in the dark to room temperature, the lattice contraction partially survives for many hours (after 10 h, the fraction of the collapsed phase is still about 20%), which implies that the lattice strains accompanying electron transfer are large enough that relaxation does not occur immediately even at room temperature. However, we note that if in the course of warming to room temperature the sample is continuously illuminated by green laser light, the pristine room temperature phase (GS) is completely recovered.
- [19] V. Kiryukhin, D. Casa, J. P. Hill, B. Keimer, A. Vigliante, Y. Tomioka, Y. Tokura, *Nature* **1997**, 386, 813.
- [20] D. E. Cox, P. G. Radaelli, M. Marezio, S.-W. Cheong, *Phys. Rev. B* **1998**, 57, 3305.
- [21] H. T. Ishibashi, Y. Koo, Y. S. Hor, A. Borissov, P. G. Radaelli, Y. Horibe, S.-W. Cheong, V. Kiryukhin, *Phys. Rev. B* **2002**, 66, 144424.

Protein Conformation

Design of a Conformation-Sensitive Xenon-Binding Cavity in the Ribose-Binding Protein**

Thomas J. Lowery, Seth M. Rubin, E. Janette Ruiz, Alexander Pines, and David E. Wemmer*

NMR spectroscopy with laser-polarized ^{129}Xe has been used to investigate biomolecular systems, for example, detecting protein cavities in myoglobin, lipoxxygenase, lysozyme, and a lipid-transfer protein, through interaction-induced chemical shift changes.^[1–4] With the maltose-binding protein (MBP) from *E. coli*^[2] and the chemotaxis protein Y^[3] the chemical shift of interacting ^{129}Xe was found to respond to the protein conformation because of cavities that change size or shape in different conformers,^[3,4] altering the shift of bound ^{129}Xe or the xenon binding affinity. Xenon probing requires no protein derivatization, and exploits simple spectra with no background signals and high sensitivity through optical polarization.^[2,3]

It has been estimated that about half of the natural proteins contain cavities of sufficient size to bind xenon,^[5] but only a few can be expected to bind xenon in a conformation-sensitive manner. Our studies of the conformation-sensitive xenon binding in MBP^[4] led us to attempt to engineer a cavity for conformation-sensitive xenon binding into the ribose-binding protein (RBP), which lacks an intrinsic site of this type.

[*] T. J. Lowery, Dr. S. M. Rubin, Prof. D. E. Wemmer
Department of Chemistry
University of California at Berkeley
Berkeley, CA 94720 (USA)
and

Physical Biosciences Division
Lawrence Berkeley National Laboratory
1 Cyclotron Road, Berkeley, CA 94720 (USA)
Fax: (+1) 510-486-6059
E-mail: dewemmer@lbl.gov

Dr. E. J. Ruiz, Prof. A. Pines
Department of Chemistry
University of California at Berkeley
Berkeley, CA 94720 (USA)
and

Material Sciences Division
Lawrence Berkeley National Laboratory
1 Cyclotron Road, Berkeley, CA 94720 (USA)

[**] This work was supported by the Director, U.S. Department of Energy, under Contract No. DE-AC03-76F00098, through the Office of Naval Research (MDI-II), and through the Laboratory Directorate Research and Development Program of Lawrence Berkeley National Laboratory. We thank Prof. S. Mowbray for the ribose-binding-protein gene, H. Yokota for helpful advice with cloning, Dr. S. Burley for the pSKB3 plasmid, Dr. D. King for mass spectrometry, Prof. S. Marqusee and Dr. C. Park for providing an isothermal titration calorimeter and guidance with urea melt experiments. S.M.R. acknowledges the National Science Foundation and E.J.R. Lucent Technologies/Bell Laboratories for predoctoral fellowships.

Supporting information for this article is available on the WWW under <http://www.angewandte.org> or from the author.

Periplasmic transport proteins, including MBP and RBP, close around their ligands in a “clam-shell”-like manner as they bind.^[6] The ^{129}Xe chemical shift in RBP solutions responds only slightly to this process (Figure 1). Xenon in

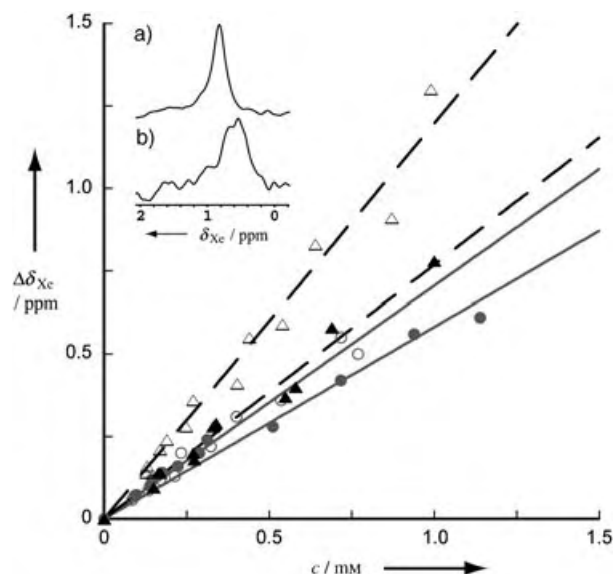


Figure 1. Change in ^{129}Xe chemical shift ($\Delta\delta_{\text{Xe}}$) with protein concentration (c) for the open (○, solid gray line) and closed (●, solid gray line) conformations of wild-type RBP and for the open (△, black dashed line) and closed (▲, black dashed line) conformations of L19A RBP. $\Delta\delta_{\text{Xe}}$ is the difference between the ^{129}Xe chemical shifts of each titration point and the buffer. Insets: a) ^{129}Xe NMR spectrum for 0.64 mM L19A RBP in the open conformation at a chemical shift of 0.83 ppm. b) ^{129}Xe NMR spectrum for 0.69 mM L19A RBP in the closed conformation at a chemical shift of 0.58 ppm. The ^{129}Xe chemical shift and line-width are sensitive to the conformation of L19A RBP but not to that of wild-type RBP. The source of linewidth sensitivity is under current investigation.

protein solutions exchanges rapidly among all available sites of interaction giving a single observed chemical shift (δ_{obs}), which is an average over all site-specific chemical shifts (δ_i) weighted by their respective binding constants (K_i) [Eq. (1)].^[3,7,8]

$$\delta_{\text{obs}} = \left(\sum \delta_i K_i \right) c(\text{protein}) \quad (1)$$

The concentration-normalized chemical shift ($\sum \delta_i K_i$) values (slopes of the lines) for the open and closed conformations of RBP are (0.7 ± 0.1) and $(0.6 \pm 0.1) \text{ ppm mm}^{-1}$, respectively, whereas for MBP these are (1.2 ± 0.1) and $(2.1 \pm 0.1) \text{ ppm mm}^{-1}$.^[2] The low sensitivity of the ^{129}Xe shift to the RBP conformation indicates that wild-type RBP does not contain a conformation-sensitive xenon-binding cavity.^[3,4] A search of the RBP structures with the program VOIDOO, which identifies internal voids, found a cavity located away from the ligand-binding cleft (Figure 2). Its size, about 50 \AA^3 , is the same in the open and closed conformations.

Mutating a buried, nonpolar side chain, such as Leu, Ile, or Phe, to a smaller nonpolar side chain, such as Ala, can create a cavity of sufficient size to bind xenon.^[4,5,9] Bulky

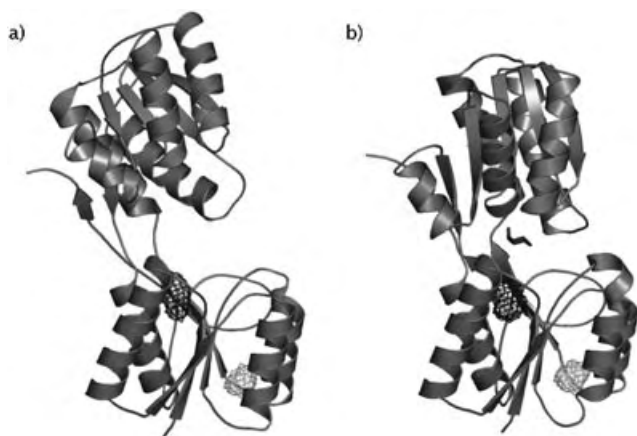


Figure 2. Cartoon backbone depictions of a) the open, or ligand-free, b) the closed, or ligand-bound, conformation of RBP.^[6,11] Shown in light gray mesh is the surface of the cavity present in wild-type RBP that does not bind xenon; it is located away from the binding site and is the same size in both conformations. The black mesh shows the cavity created by the L19A mutation. Its increased size in the closed conformation is apparent as well as its proximity to bound ribose (with the ring shown by black sticks) and the loops that connect the two domains.

nonpolar side chains in regions that change structure between the two conformers were inspected and six potential sites for mutation were selected for initial screening: L19, L88, F187, F214, I233, and I240. The effect of a change to alanine at each site was evaluated by deleting atoms in the PDB file and calculating the size of the resulting cavity. Two changes produced cavities that differed significantly in size ($\sim 30 \text{ \AA}^3$) between the two conformations, and L19A RBP was selected to test experimentally. The cavity sizes estimated by VOIDOO for the open and closed conformations of L19A RBP are 74 and 102 \AA^3 , respectively. Smaller cavities can result if residues surrounding a cavity created by mutation relax.^[9,10] This was not considered a significant problem in the design process because xenon has been shown to bind to small flexible cavities, increasing the cavity volume by restoring the lining residues to their original positions.^[9]

Figure 2 shows that the cavity of L19A RBP is directly below the ribose-binding cleft near loops that serve as a hinge during ligand binding. Of the residues that line the cavity, F15, F16, N64, and D89 make direct contact with ribose in the closed conformation.^[11] The proximity of the cavity to functionally critical residues could affect the conformation change and decrease affinity for ribose. The affinities of wild-type and L19A RBP for ribose were measured using isothermal titration calorimetry (ITC) which gave K_d values of $(0.11 \pm 0.01) \mu\text{M}$ for wild-type (in agreement with previous work^[12]) and $(0.30 \pm 0.05) \mu\text{M}$ for L19A RBP. The concentration-normalized ^{129}Xe shifts for open $((1.2 \pm 0.1) \text{ ppm mm}^{-1})$ and closed L19A RBP $((0.8 \pm 0.1) \text{ ppm mm}^{-1})$ were determined (Figure 1). The mutation increases the ^{129}Xe shift of the open conformation by 0.5 ppm mm^{-1} and of the closed conformation by 0.2 ppm mm^{-1} , enhancing the discrimination of open and closed conformations.

To verify that xenon binds in the designed cavity, ^1H - ^{15}N correlation spectra (HSQC) were obtained in the presence

and absence of xenon as done previously for MBP and other proteins.^[4,13] Resonance signals that shift upon xenon addition are primarily from amide protons that line the cavity.^[4,13] ^1H - ^{15}N HSQC spectra of open and closed wild-type RBP were collected in the presence and absence of 90 mM xenon. The overlaid spectra of wild-type RBP show that 90 mM xenon does not shift signals in either wild-type conformer, indicating that xenon does not bind to the wild-type cavity.^[14] In the L19A RBP spectra a subset of the signals shift relative to their wild-type counterparts, reflecting perturbations from introducing the L19A mutation (Figure 3). For both open and

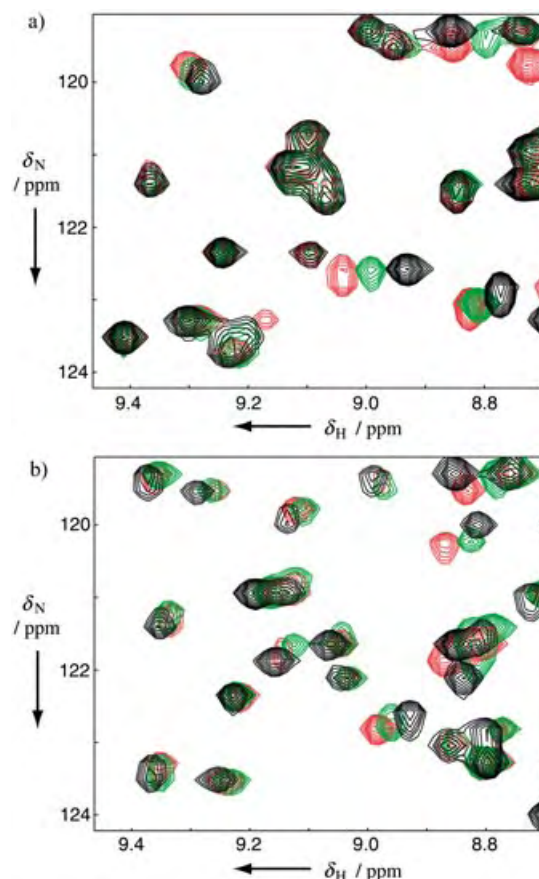


Figure 3. Representative portions of the ^1H - ^{15}N HSQC spectra for the open (a) and closed (b) conformations of wild-type RBP in the absence of xenon (black), L19A RBP in the absence of xenon (red), and L19A RBP in the presence of 93 (a) or 72 mM (b) xenon (green).

closed L19A RBP specific resonance signals shift with increasing xenon concentration, indicating specific binding.^[4] Every signal that shifts with increasing xenon concentration also shifts upon introduction of the L19A mutation, indicating that residues affected by xenon binding are associated with the introduced cavity, verifying creation of a specific xenon-binding site. Several signals affected by xenon binding shift toward the wild-type signals, suggesting that xenon restores these residues to their original environments, as in T4 lysozyme.^[9]

The xenon binding affinity was measured by following the change in amide shift with xenon concentration (Figure 4).^[4] Five resonance signals that shifted at least ten Hertz in each conformation were fitted as previously described^[4] and averaged to give values of (70 ± 30) and $(40 \pm 20) \text{ M}^{-1}$ for the open and closed conformations, respectively, yielding affinities similar to those for MBP.^[4]

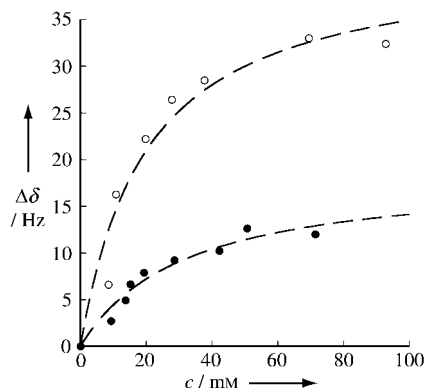


Figure 4. The total change in amide ^1H chemical shift ($\Delta\delta$) versus xenon concentration (c) for the same resonance signal in the open (○) and closed (●) conformations of L19A RBP. Similar binding curves and fits were obtained for four other resonance signals. The different xenon binding affinity of the open and closed conformations reflects the conformation-sensitive nature of the xenon-binding cavity created by the L19A mutation.

The limiting xenon chemical shifts relative to the shift in buffer, (δ_i) [Eq. (1)], in the xenon-binding cavity were determined by comparing titrations in which the cavity was available and blocked,^[4] giving $\delta_{\text{open}} = (7 \pm 3)$ and $\delta_{\text{closed}} = (5 \pm 3)$ ppm. Cavity-induced downfield shifts have been shown to be inversely proportional to cavity volume in proteins, zeolites, and clathrates.^[4,15,16] The shift values for the cavity of L19A RBP indicate that it is smaller in the open conformation, as predicted by the design process.

Cavity-creating mutations in T4 lysozyme were shown to decrease the Gibbs energy of unfolding in proportion to the size of the cavity.^[11] Urea-induced unfolding of open wild-type and L19A RBP was followed by circular dichroism, and analyzed to give ΔG_u values of (5.8 ± 0.1) and $(3.3 \pm 0.1) \text{ kcal mol}^{-1}$, respectively. Combining this with ribose affinity measurements from ITC and the calibration from T4 lysozyme^[11] gives estimates of 25 \AA^3 (open) and 54 \AA^3 (closed) for the cavities in RBP, a change of about 30 \AA^3 as modeled.^[14]

Analysis of the L19A- ^{129}Xe interaction shows that the conformational responsiveness arises from both a higher xenon affinity and a larger shift induced by the cavity in the open conformation contributing to the averaged limiting ^{129}Xe chemical shift (δ_{obs}) [Eq. (1)]. The higher xenon binding affinity of the smaller cavity likely arises from increased van der Waals contact in the smaller cavity.^[9]

We were able to introduce a conformation-sensitive xenon-binding cavity into the ribose-binding protein with a straightforward design process, demonstrating the feasibility

of engineering ^{129}Xe NMR reporter sites into proteins of interest for assaying ligand binding or conformation changes. The idea of designed sites for xenon can be further generalized^[17] and is being applied to biological problems.

Received: May 12, 2004

Keywords: hydrophobic cavities · NMR spectroscopy · protein engineering · protein structures · xenon

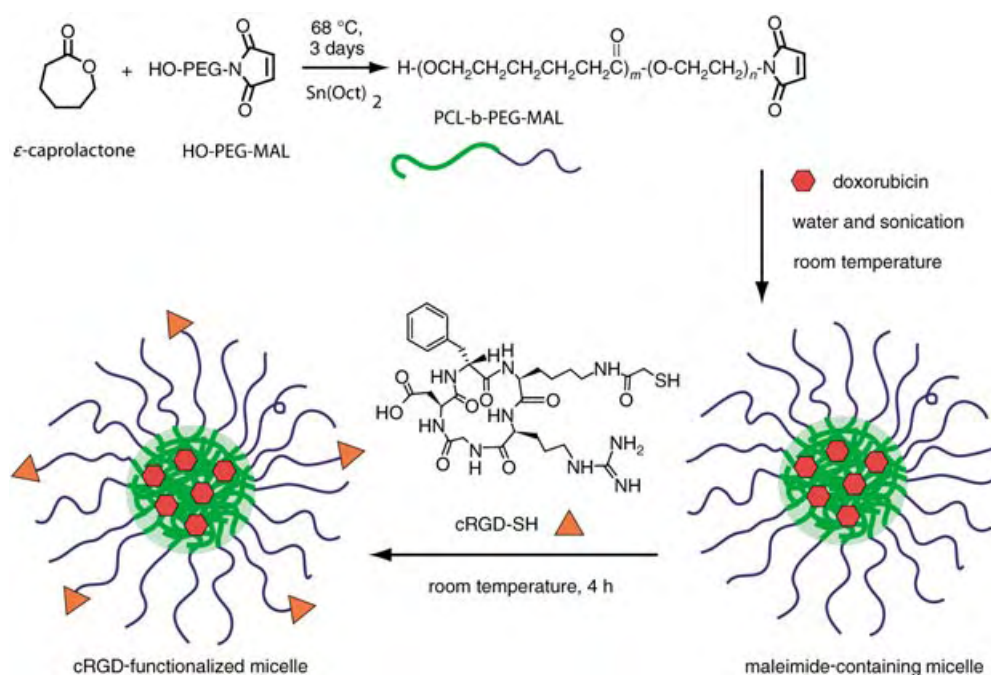
- [1] a) B. C. Schoenborn, H. C. Watson, J. C. Kendrew, *Nature* **1965**, 207, 28–30; b) R. F. Tilton, Jr., I. D. Kuntz, Jr., *Biochemistry* **1982**, 21, 6850–6857; c) C. R. Bowers, V. Storhaug, C. E. Webster, J. Bharatam, A. Cottone III, R. Gianna, K. Betsey, B. J. Gaffney, *J. Am. Chem. Soc.* **1999**, 121, 9370–9377; d) C. Landon, P. Berthault, F. Vovelle, H. Desvaux, *Protein Sci.* **2001**, 10, 762–770.
- [2] S. M. Rubin, M. M. Spence, I. E. Dimitrov, E. J. Ruiz, A. Pines, D. E. Wemmer, *J. Am. Chem. Soc.* **2000**, 122, 8616–8617.
- [3] T. J. Lowery, S. M. Rubin, E. J. Ruiz, M. M. Spence, N. Wisinger, P. G. Schultz, A. Pines, D. E. Wemmer, *Magn. Reson. Imaging* **2003**, 21, 1235–1239.
- [4] S. M. Rubin, S. Y. Lee, E. J. Ruiz, A. Pines, D. E. Wemmer, *J. Mol. Biol.* **2002**, 322, 425–440.
- [5] M. L. Quillin, B. W. Matthews, *Acta Crystallogr. Sect. D* **2002**, 58, 97–103.
- [6] A. J. Björkman, S. L. Mowbray, *J. Mol. Biol.* **1998**, 279, 651–664.
- [7] S. M. Rubin, M. M. Spence, A. Pines, D. E. Wemmer, *J. Magn. Reson.* **2001**, 152, 79–86.
- [8] a) S. M. Rubin, M. M. Spence, B. M. Goodson, D. E. Wemmer, A. Pines, *Proc. Natl. Acad. Sci. USA* **2000**, 97, 9472–9475; b) E. Locci, Y. Dehouck, M. Casu, G. Saba, A. Lai, M. Luhmer, J. Reisse, K. Bartik, *J. Magn. Reson.* **2001**, 150, 167–174.
- [9] M. L. Quillin, W. A. Breyer, I. J. Griswold, B. W. Matthews, *J. Mol. Biol.* **2000**, 302, 955–977.
- [10] A. E. Eriksson, W. A. Baase, X.-J. Zhang, D. W. Heinz, M. Blaber, E. P. Baldwin, B. W. Matthews, *Science* **1992**, 255, 178–183.
- [11] S. L. Mowbray, L. B. Cole, *J. Mol. Biol.* **1992**, 225, 155–175.
- [12] R. C. Willis, C. E. Furlong, *J. Biol. Chem.* **1974**, 249, 6926–6929.
- [13] C. Gröger, A. Möglich, M. Pons, B. Koch, W. Hengstenberg, H. R. Kalbitzer, E. Brunner, *J. Am. Chem. Soc.* **2003**, 125, 8726–8727.
- [14] See Supporting Information for details.
- [15] J. A. Ripmeester, C. I. Ratcliffe, J. S. Tse, *J. Chem. Soc. Faraday Trans.* **1988**, 84, 3731–3745.
- [16] J. Bonardet, J. Fraissard, A. Gédéon, M. Springuelhuet, *Catal. Rev. Sci. Eng.* **1999**, 41, 115–225.
- [17] M. M. Spence, S. M. Rubin, I. E. Dimitrov, E. J. Ruiz, D. E. Wemmer, A. Pines, S. Q. Yao, F. Tian, P. G. Schultz, *Proc. Natl. Acad. Sci. USA* **2001**, 98, 10654–10657.

cRGD-Functionalized Polymer Micelles for Targeted Doxorubicin Delivery**

Norased Nasongkla, Xintao Shuai, Hua Ai, Brent D. Weinberg, John Pink, David A. Boothman, and Jinming Gao*

Low water solubility, rapid phagocytic and renal clearance, and systemic toxicity represent three major barriers that limit the therapeutic use of many hydrophobic antitumor agents such as doxorubicin (DOXO) and paclitaxel.^[1] Various drug-

delivery systems, among which polymeric micelles have emerged as a very important system, have been developed to overcome these limitations and deliver various drugs with remarkable in vitro and in vivo success.^[2,3] Polymeric micelles are nanoscopic (10 to 100 nm) colloidal particles self-assembled from amphiphilic block or graft copolymers in aqueous media. The hydrophobic core of the micelles is a carrier compartment that accommodates antitumor drugs, and the shell consists of a brushlike protective corona that stabilizes the nanoparticles in aqueous solution.^[4] The basic requirements for polymeric micelles in drug-delivery applications include high drug-loading capacity, biodegradability, long blood circulation times, and controllable drug-release profiles. Research on micelles has been greatly advanced in the



Scheme 1. Synthesis of MAL-PEG-PCL copolymer and preparation of cRGD-functionalized, DOXO-loaded micelles.

[*] N. Nasongkla,^[1] Dr. X. Shuai,^[1] Dr. H. Ai, B. D. Weinberg, Prof. Dr. J. Gao

Department of Biomedical Engineering
Case Western Reserve University, 10900 Euclid Avenue
Cleveland, Ohio 44106 (USA)

Tel: (+1) 216-368-1083

Fax: (+1) 216-368-4969

E-mail: jinming.gao@case.edu

Dr. J. Pink, Prof. D. A. Boothman

Department of Radiation Oncology
Case Western Reserve University, 10900 Euclid Avenue
Cleveland, Ohio 44106 (USA)

[*] These authors contributed equally to this work

[**] This research is supported by the National Institutes of Health (R01-CA-90696). N.N. acknowledges the Royal Thai Government for a predoctoral fellowship support. X.T.S. acknowledges fellowship support from the Ohio Biomedical Research and Technology Trust fund. We thank Dr. Steven Eppell and Zhilei Liu for their help with atomic force microscopy.

Supporting information for this article is available on the WWW under <http://www.angewandte.org> or from the author.

past decade.^[5–8] However, the ability to achieve high targeting efficiency at the tumor site and associated cells remains a significant challenge for the development of micelle-mediated drug-delivery systems. Although nanosized micelles are known to spontaneously accumulate in tumors with leaky vasculature by an enhanced permeability and retention (EPR) effect,^[9] micelles are also observed to accumulate quite significantly in reticuloendothelial sites such as the liver, spleen, and kidney.^[10] Consequently, insufficient uptake in tumor sites will decrease the therapeutic effect of the administered drug dose, and nonspecific spreading to healthy tissues will lead to serious side effects and limit the dosage that can be applied. These limitations prevent these drugs from achieving the potential cures that they might otherwise attain.^[11]

One strategy to achieve cancer-targeted drug delivery is the utilization of unique molecular markers that are specifically overexpressed in the cancerous tissues. It is well known that tumor endothelial cells show increased expression of

several cell-surface molecules that potentiate cell invasion and proliferation during tumor vascular remodeling and angiogenesis.^[12,13] One such molecule is the $\alpha_v\beta_3$ integrin, which plays a key role in endothelial cell survival during angiogenesis.^[14] Enlightened by the early discovery that viruses, such as rotavirus and adenovirus, can utilize this receptor to facilitate gene transfer by selective recognition between $\alpha_v\beta_3$ on the targeted cell membrane and the viral surface, researchers have exploited ligands such as the Arg-Gly-Asp (RGD) peptide. In fact, $\alpha_v\beta_3$ was recently used as an endothelial cell target in several therapeutic approaches such as nonviral gene delivery.^[15,16]

Unfortunately, ligand-directed delivery of hydrophobic drugs with polymeric micelles has been reported only in a few cases.^[17,18] Herein, we develop polymeric micelles that can selectively deliver hydrophobic drugs, such as doxorubicin, to angiogenic tumor endothelial cells with over-expressed $\alpha_v\beta_3$ integrins. To this end, we attached a cyclic pentapeptide c(Arg-Gly-Asp-D-Phe-Lys) (cRGDfK, also referred to as cRGD herein) as an $\alpha_v\beta_3$ ligand to the surface of doxorubicin-loaded poly(ϵ -caprolactone)-poly(ethylene glycol) (PCL-PEG) micelles. cRGDfK was selected as the targeting ligand since it can selectively bind to the $\alpha_v\beta_3$ integrin with high affinity.^[19,20] Although the coupling of doxorubicin to RGD peptides (for example, RGD-4C) was found to be able to target tumor blood vessels,^[21] RGD-directed doxorubicin delivery using polymeric micelles has not been reported to date.

The synthesis of the maleimide-terminated block copolymer (MAL-PEG-PCL, $M_n = 5.5$ kD) and preparation of the cRGDfK-functionalized micelles with DOXO loading are outlined in Scheme 1. In contrast to the reported procedure for the polymerization of ϵ -caprolactone with stannous(II) octoate as a catalyst,^[22] the synthesis of MAL-PEG-PCL must be conducted at a lower temperature because of the thermal susceptibility of the maleimide end groups. We found that reaction at 68 °C led to PCL segments of the desired molecular weights (for example, 2.4 kD), while reducing the thermal decomposition of maleimide to a negligible level (see the Supporting Information). DOXO-loaded MAL-PEG-PCL micelles were prepared by a solvent-evaporation method.^[23] Different amounts of methoxy-terminated MPEG-PCL copolymer were also introduced to control the density of maleimide at the micelle surface, which subsequently controls the cRGD density (5, 16, and 76% of all PEG chains). The typical DOXO loading content (DLC) in the micelle preparations was 3.10 wt %.

Figure 1a shows the ^1H NMR spectrum of MAL-PEG-PCL copolymer in CDCl_3 . Resonances of the PEG methylene protons (mainly at $\delta = 3.64$ ppm) and PCL protons ($\delta = 1.38, 1.65, 2.31$, and 4.06 ppm) were observed. The small triplet at $\delta = 4.2$ ppm was attributed to the proton resonance of the methyleneoxyl group linking the PCL and PEG blocks. The intensity of the integrals for the maleimide vinylic protons at $\delta = 6.74$ ppm confirms that the maleimide group in MAL-PEG-PCL copolymers remained intact, as in the MAL-PEG-OH. These data strongly demonstrated that the desired block copolymers were successfully synthesized. The number-averaged molecular weight of PCL blocks was calculated to be

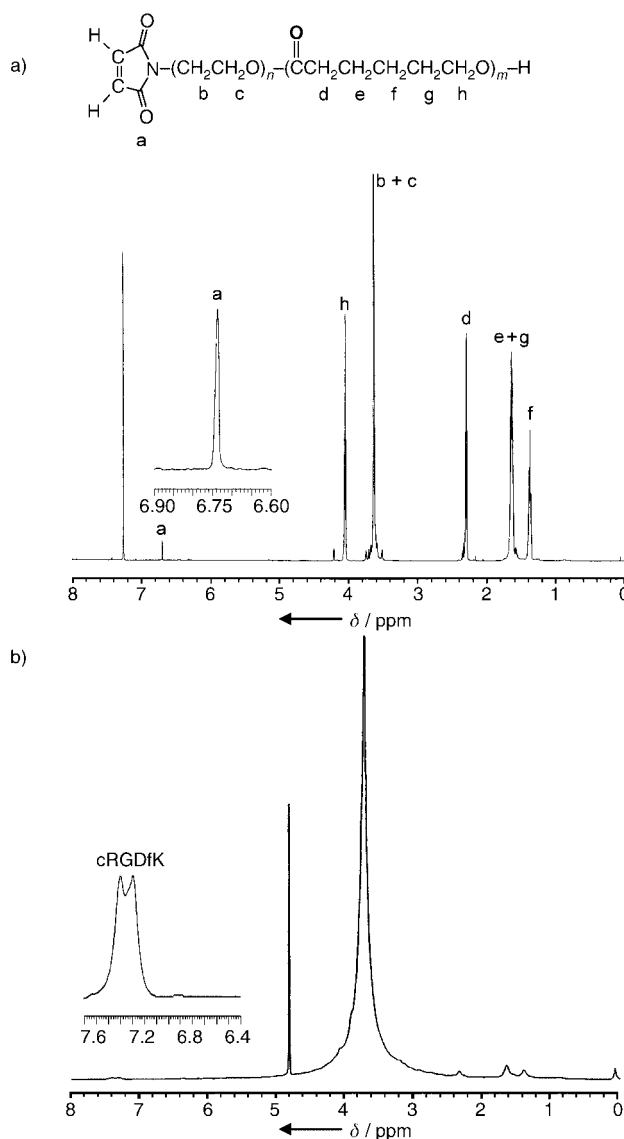


Figure 1. ^1H NMR spectra (600 MHz, 25 °C) of a) MAL-PEG-PCL copolymer in CDCl_3 and b) cRGD-functionalized, DOXO-loaded micelles in D_2O . The inset in (a) shows the proton signal from maleimide groups ($\delta = 6.74$ ppm), and the inset in (b) shows the absence of the maleimide signal and the presence of aromatic protons from the Phe residue in cRGDfK, thus indicating a complete conversion of the maleimide group after cRGD conjugation.

2.4 kD from the integral of the PCL protons at $\delta = 2.31$ ppm versus that of the PEG proton at $\delta = 3.64$ ppm. A postmicellar modification strategy was used to prepare cRGD-functionalized micelles (Scheme 1). The NMR spectrum of the freeze-dried micelles in D_2O strongly suggests the formation of the core-shell structure of DOXO-loaded micelles (Figure 1b). The micelle corona (shells) consisting of PEG blocks were solvated to a high degree in D_2O and showed clear ^1H NMR signals. In contrast, DOXO was loaded inside the solid PCL cores of micelles, and thus the resonances of both the PCL blocks and DOXO molecules were significantly reduced because of their insufficient mobility in D_2O . Moreover, successful conjugation of cRGDfK onto the solvated PEG

shells was verified by the resonances of the phenyl protons of cRGDfK at $\delta = 7.4$ ppm and complete disappearance of the maleimide signal at $\delta = 6.74$ ppm (Figure 1 b).

It is well known that the size of nanocarriers plays an important role in cellular internalization process. Before evaluating the cellular uptake of non- and cRGD-functionalized micelles, we studied the size and morphology of the micelles by atomic force microscopy (AFM) and dynamic light scattering (DLS). AFM studies showed that micelles with 76 % cRGD attachment had a mean size (43.2 ± 3.9 nm) similar to that of cRGD-free micelles (37.5 ± 2.6 nm). Both unfunctionalized and 76 % cRGD-containing micelles appeared to be discrete and round-shaped nanoparticles. Aggregation of micelle particles was not observed. The DLS measurements showed that the size of the cRGD-functionalized micelles was also close to that of the unfunctionalized micelles (20.9 ± 1.7 and 24.4 ± 2.7 nm for non- and cRGD-functionalized micelles, respectively; Figure 2). Two major factors may have contributed to the larger diameter of the micelle determined by AFM measurement. First, the height of the micelle particles was approximately 5 nm by AFM, which is significantly smaller than the diameter of the micelle determined by DLS (20–25 nm). The decreased height in the solid state indicates that particle-flattening events occur during the sample dewetting process on the mica surface, which can increase the apparent particle diameter in the *x,y* plane for AFM measurement. Second, it is well known

that AFM can give an overestimation of particle size as a result of the AFM tip-broadening effect.^[24] The magnitude of the tip dilation effect depends on the height of the object, the ambient humidity, and the size and shape of the AFM tip.^[25,26] The morphology reconstruction method can potentially be applied to correct the dilation effect and provide a more accurate determination of the particle sizes.^[26]

Finally, we used flow cytometry and confocal laser scanning microscopy to study the uptake of micelles into SLK tumor endothelial cells (derived from human Kaposi's sarcoma) that over-express the $\alpha_v\beta_3$ integrin.^[27] We quantified the cellular internalization efficiency of the cRGD-micelles by measuring the increase in fluorescence intensity after the DOXO-loaded micelles had been transported into the cells. Figure 3a shows the percentage of SLK cells with micelle uptake as a function of cRGD density on the polymer micelles after 2 h incubation. We observed a remarkable increase in the uptake of micelles in the cells upon attachment of cRGD molecules to the micelle surface. A higher density of cRGD molecules led to a higher level of cellular internalization of these micelles over the entire cRGD density range (0–76 %) examined. A maximum 30-fold enhancement was achieved with 76 % cRGD-functionalized DOXO-loaded micelles relative to unfunctionalized DOXO-loaded micelles. It is noteworthy that Kissel and co-workers recently reported that linear RGD molecules attached to DNA/PEI-PEG (PEI = polyethyleneimine) nanocomplexes through PEG spacers did

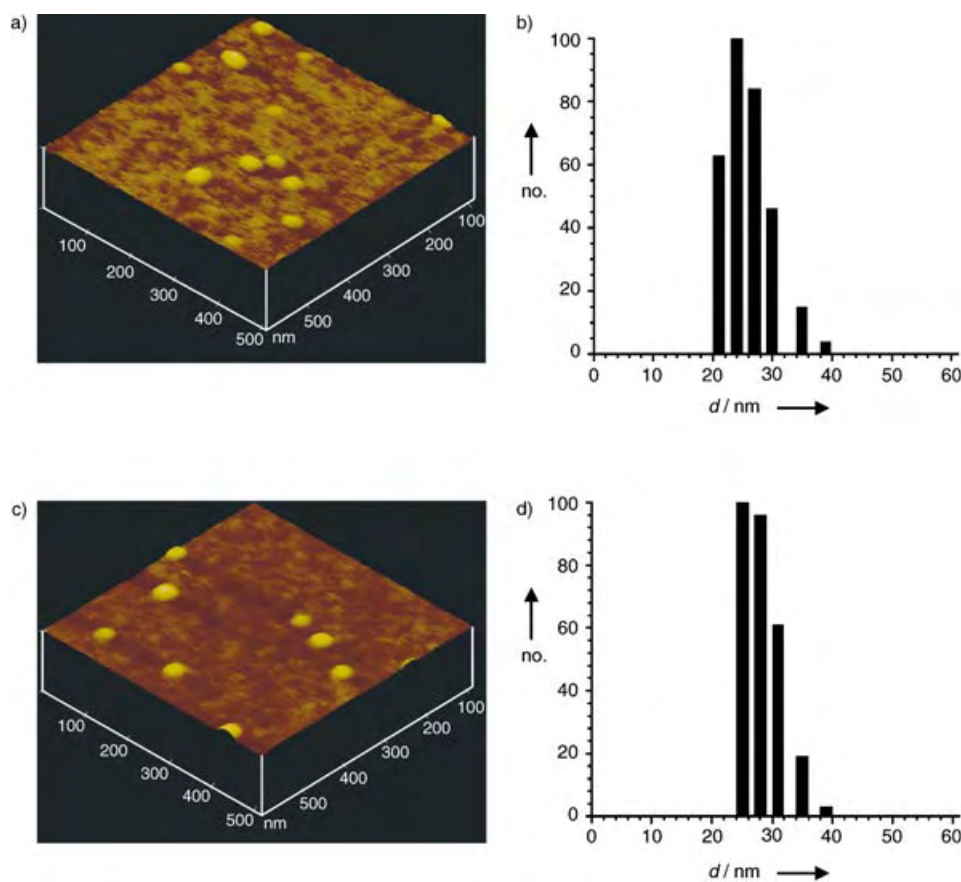


Figure 2. Size characterization of 0% (a, b) and 76% (c, d) cRGD-functionalized DOXO-loaded micelles by atomic force microscopy (a, c) and dynamic light scattering (b, d).

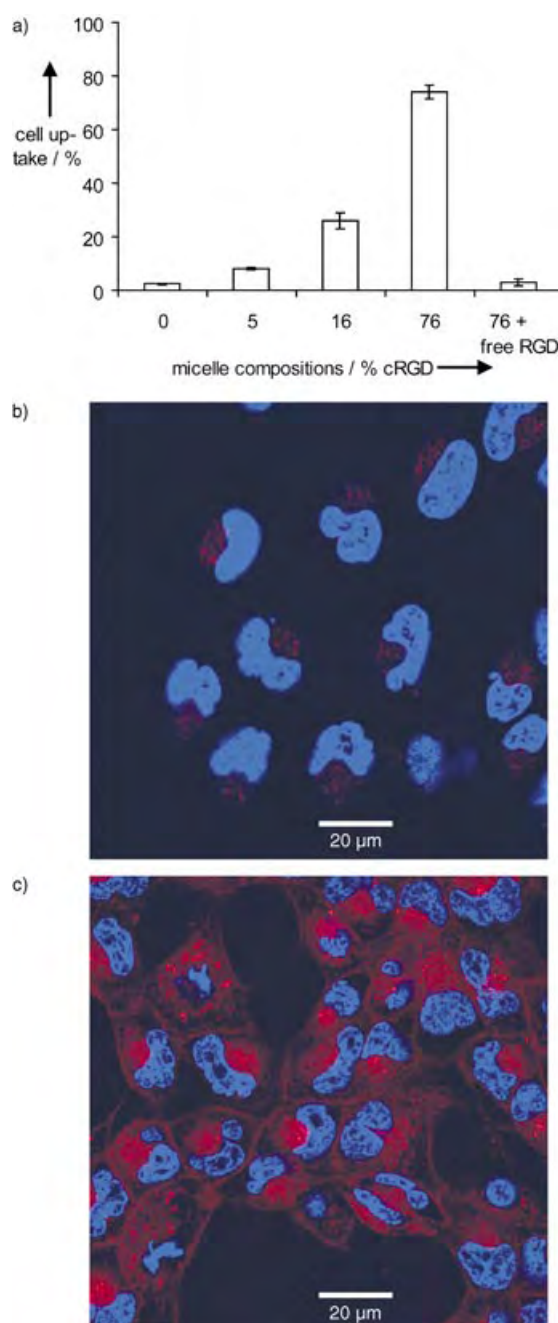


Figure 3. a) Percentage of micelle uptake in SLK tumor endothelial cells measured by flow cytometry as a function of cRGD density (0–76%) on the micelle surface. The last bar shows that the cell uptake of 76% cRGD-functionalized micelles is inhibited by the presence of free RGD ligands (9 mM) in solution. b, c) Confocal laser scanning microscopy images of SLK cells treated with 0% (b) and 16% (c) cRGD-functionalized micelles after incubation for 2 h. Cell nuclei were stained blue by Hoechst 33342 ($\lambda_{\text{ex}} = 352 \text{ nm}$, $\lambda_{\text{em}} = 455 \text{ nm}$) and overlaid with DOXO fluorescent images ($\lambda_{\text{ex}} = 485 \text{ nm}$, $\lambda_{\text{em}} = 595 \text{ nm}$).

not lead to effective targeting to $\alpha_v\beta_3$ -expressing cells.^[28] We believe the higher affinity of cyclic RGDfK to $\alpha_v\beta_3$ over the linear RGD peptides (> 200 times)^[19] in our current system has primarily contributed to the higher targeting efficiency by our cRGD micelles.

This cRGD-directed micelle targeting to $\alpha_v\beta_3$ -overexpressed tumor endothelial cells was further demonstrated in a control experiment, in which SLK cells were first incubated with a free AARGDY blocking ligand (9 mM), and then co-incubated with 76% cRGD-functionalized micelles (see the Supporting Information). The cellular uptake level of cRGD-functionalized micelles in the presence of blocking ligand was dramatically reduced and became essentially equivalent to that of unfunctionalized micelles (Figure 3a). These data demonstrate that the $\alpha_v\beta_3$ receptor is essential for the uptake of cRGD-functionalized micelles in SLK tumor endothelial cells.

Confocal laser scanning microscopy was then used to characterize and compare the cell uptake and intracellular distribution of cRGD-free and 16% cRGD-functionalized DOXO micelles after incubation for two hours (Figure 3b,c). Significantly increased intracellular DOXO fluorescence intensity was observed with cRGD-functionalized micelles, thus demonstrating again the enhanced cellular uptake by the cRGD- $\alpha_v\beta_3$ -mediated endocytosis as shown by flow cytometry. Similar to cRGD-free micelles, cRGD-functionalized micelles were localized in the cytoplasm rather than the nuclei where free DOXO accumulated quickly after membrane diffusion.^[8,23] Recently, Maysinger and co-workers detected intracellular localization of modified PCL-PEG micelles (20 to 45 nm) in several intracellular organelles including mitochondria, Golgi apparatus, and acidic organelles such as lysosomes in PC12 and NIH 3T3 cells. They suggested the multiple cytoplasmic-targeting of modified PCL-PEG micelles.^[4] On the basis of the $\alpha_v\beta_3$ receptor mediated endocytosis pathway of the cRGD-functionalized micelles, we suggest that in our system the cRGD-functionalized micelles were more likely entrapped in the endosomal compartments. Indeed, as shown in Figure 3b, a large amount of dot-shaped DOXO fluorescence was observed in the cytoplasm of treated cells, which suggests the presence of internalized micelles in the endosomes.^[8]

In summary, a very effective $\alpha_v\beta_3$ ligand (cRGDfK) was successfully conjugated to DOXO-loaded PEG-PCL micelles by using a postmicelle modification method. Attachment of the cyclic RGD ligand greatly enhanced internalization of the micelles in tumor endothelial cells that overexpress $\alpha_v\beta_3$ integrins, apparently through receptor-mediated endocytosis. Although preliminary, our results illustrate the tremendous potential of cRGD-functionalized micelles for targeting the tumor neovasculature. To verify this hypothesis, we are conducting in vitro cytotoxicity tests and animal studies with cRGD-functionalized, DOXO-loaded micelles.

Received: May 26, 2004

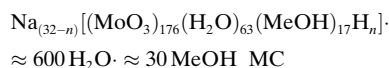
Keywords: antitumor agents · bioorganic chemistry · drug delivery · micelles · peptides

- [1] A. M. Fernandez, K. Van Derpoorten, L. Dasnois, K. Lebtahi, V. Dubois, T. J. Lobl, S. Gangwar, C. Oliyai, E. R. Lewis, D. Shochat, A. Trouet, *J. Med. Chem.* **2001**, *44*, 3750–3753.
- [2] M. Yokoyama, T. Okano, Y. Sakurai, H. Ekimoto, C. Shibazaki, K. Kataoka, *Cancer Res.* **1991**, *51*, 3229–3236.

- [3] K. Kataoka, T. Matsumoto, M. Yokoyama, T. Okano, Y. Sakurai, S. Fukushima, K. Okamoto, G. S. Kwon, *J. Controlled Release* **2000**, *64*, 143–153.
- [4] R. Savic, L. Luo, A. Eisenburg, D. Maysinger, *Science* **2003**, *300*, 615–618.
- [5] G. S. Kwon, K. Kataoka, *Adv. Drug Delivery Rev.* **1995**, *16*, 295–309.
- [6] K. Kataoka, A. Harada, Y. Nagasaki, *Adv. Drug Delivery Rev.* **2001**, *47*, 113–131.
- [7] R. Haag, *Angew. Chem.* **2004**, *116*, 280–284; *Angew. Chem. Int. Ed.* **2004**, *43*, 278–282; .
- [8] Y. Bae, S. Fukushima, A. Harada, K. Kataoka, *Angew. Chem.* **2003**, *115*, 4788–4791; *Angew. Chem. Int. Ed.* **2003**, *42*, 4640–4643; .
- [9] K. Greish, J. Fang, T. Inustuka, A. Nagamitsu, H. Maeda, *Clin. Eur. Clin. Pharmacokinet.* **2003**, *42*, 1089–1105.
- [10] Y. Yamamoto, Y. Nagasaki, Y. Kato, Y. Sugiyama, K. Kataoka, *J. Controlled Release* **2001**, *77*, 27–38.
- [11] D. Needham, M. W. Dewhirst, *Adv. Drug Delivery Rev.* **2001**, *53*, 285–305.
- [12] G. D. Yancopoulos, M. Klagsbrun, J. Folkman, *Cell* **1998**, *93*, 661–664.
- [13] B. P. Eliceiri, D. A. Cheresh, *Curr. Opin. Cell Biol.* **2001**, *13*, 563–568.
- [14] P. C. Brooks, A. M. Montgomery, M. Rosenfeld, R. A. Reisfeld, T. Hu, G. Klier, D. A. Cheresh, *Cell* **1994**, *79*, 1157–1164.
- [15] T. J. Wickham, *Nature Med.* **2003**, *9*, 135–139.
- [16] J. D. Hood, M. Bednarski, R. Frausto, S. Guccione, R. A. Reisfeld, R. Xiang, D. A. Cheresh, *Science* **2002**, *296*, 2404–2407.
- [17] V. P. Torchilin, A. N. Lukyanov, Z. Gao, B. Papahadjopoulos-Sternberg, *Proc. Natl. Acad. Sci. USA* **2003**, *100*, 6039–6044.
- [18] E. S. Lee, K. Na, Y. H. Bae, *J. Controlled Release* **2003**, *91*, 103–113.
- [19] R. Haubner, R. Gratias, B. Diefenbach, S. L. Goodman, A. Jonczyk, H. Kessler, *J. Am. Chem. Soc.* **1996**, *118*, 7461–7472.
- [20] M. Kantlehner, D. Finsinger, J. Meyer, P. Schaffner, A. Jonczyk, B. Diefenbach, B. Nies, H. Kessler, *Angew. Chem.* **1999**, *111*, 587–590; *Angew. Chem. Int. Ed.* **1999**, *38*, 560–562; .
- [21] W. Arap, R. Pasqualini, E. Ruoslahti, *Science* **1998**, *279*, 377–380.
- [22] X. Shuai, T. Merdan, A. K. Schaper, F. Xi, T. Kissel, *Bioconjugate Chem.* **2004**, *15*, 441–448.
- [23] X. Shuai, H. Ai, N. Nasongkla, S. Kim, J. Gao, *J. Controlled Release* **2004**, *98*, 415–426.
- [24] D. L. Wilson, K. S. Kump, S. J. Eppell, R. E. Marchant, *Langmuir* **1995**, *11*, 265–272.
- [25] W. A. Ducker, T. J. Senden, R. M. Pashley, *Nature* **1991**, *353*, 239–241.
- [26] B. A. Todd, S. J. Eppell, *Surf. Sci.* **2001**, *491*, 473–483.
- [27] F. Samaniego, D. Young, C. Grimes, V. Prospero, M. Christofidou-Solomidou, H. M. Delisser, O. Prakash, A. A. Sahin, S. Wang, *Cell Growth Differ.* **2002**, *13*, 387–395.
- [28] K. Kunath, T. Merdan, O. Hegener, H. Häberlein, T. Kissel, *J. Gene Med.* **2003**, *5*, 588–599.

A Molybdenum Crown Cluster Forms Discrete Inorganic–Organic Nanocomposites with Metalloporphyrins***Akihiko Tsuda,* Eri Hirahara, Yeong-Sang Kim, Hiroyuki Tanaka, Tomoji Kawai,* and Takuzo Aida**

Molybdenum blue (MB), formed by partial reduction of Mo^{VI} in an acidic aqueous solution, is a striking inorganic material due to its vivid blue color. It is a mixture of polyoxomolybdate (POM) clusters consisting of mixed-valent Mo^V and Mo^{VI} centers.^[1–3] Although the initial exploration was made more than 200 years ago,^[4] the first success in structural analysis of POM clusters was only reported in 1995, when Müller and co-workers isolated a crown-shaped POM cluster and obtained its crystal structure.^[5] To date, they have also succeeded in structural determination of large POM clusters with hollow and spherical shapes.^[6,7] Despite their interesting potentials in materials sciences, no examples have yet been reported of the utilization of such inorganic nano-objects for the fabrication of discrete inorganic/organic nanocomposite materials. Herein we report that the crown-shaped POM (molybdenum crown cluster; MC), upon mixing with metalloporphyrins having meso-aminophenyl substituents, forms discrete inclusion complexes, where the inorganic cavity of MC can accommodate up to three molecules of the guest compounds, to give spatially isolated metalloporphyrin molecules (Scheme 1).



MC has a large cavity with a diameter of approximately 2.3 nm.^[7] We expected that this cavity can incorporate proton acceptors through a hydrogen-bonding interaction, since a

[*] Dr. A. Tsuda, E. Hirahara, Dr. Y.-S. Kim, Prof. Dr. T. Aida
Department of Chemistry and Biotechnology
School of Engineering, The University of Tokyo
7-3-1 Hongo, Bunkyo-ku, Tokyo 113-8656 (Japan)
Fax: (+81) 3-5841-7310
E-mail: tsuda@macro.t.u-tokyo.ac.jp
aida@macro.t.u-tokyo.ac.jp

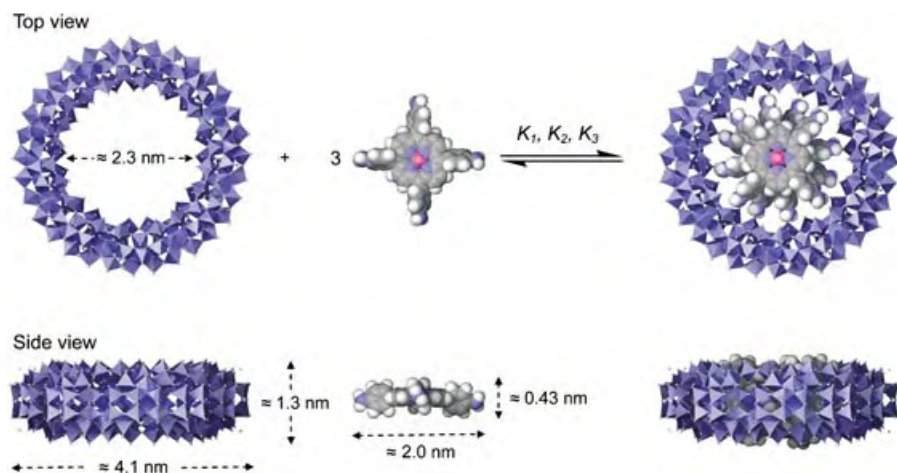
Dr. H. Tanaka,^[†] Prof. Dr. T. Kawai
The Institute of Scientific and Industrial Research
Osaka University
8-1 Mihogaoka, Ibaraki, Osaka 567-0047 (Japan)
E-mail: kawai@sanken.osaka-u.ac.jp

[†] Responsible for scanning tunneling microscopy.

[**] The present work was supported by a Grants-in-Aid for Scientific Research (No. 15350128) and Encouragement of Young Scientists (No. 15750028) from the Ministry of Education, Science, Sports, and Culture, Japan. A.T. thanks the Kurata Memorial Hitachi Science and Technology Foundation, and the Tokuyama Science Foundation.



Supporting information for this article is available on the WWW under <http://www.angewandte.org> or from the author.



Scheme 1. Schematic representations of the complexation of molybdenum crown cluster (MC; blue polyhedra) with zinc 5,10,15,20-*tetrakis*(4-aminophenyl)porphyrin (**1**(*p*-NH₂)_{Zn}; space-filling model: pink Zn, blue N, gray C, white H). Molecular models of MC and **1**(*p*-NH₂)_{Zn} are based on X-ray crystallography (see ref. [7]) and MM2 calculation, respectively.

great number of proton-donating $\mu_3\text{-O}\cdots\text{H}$ species are concentrated in its inner surface.

MC was prepared according to a literature method,^[7] and characterized by means of MALDI-TOF mass spectrometry and scanning tunneling microscopy (STM), along with UV/Vis and IR spectroscopy.^[8] The MC, thus obtained, was highly soluble in MeCN to give a clear blue solution, which showed characteristic broad absorption bands at 730 and 1058 nm (Figure 1 a). For the complexation studies with MC, we chose as potential guest molecules zinc complexes of 5,10,15,20-

tetrakis(aminophenyl)porphyrins, such as **1**(*p*-NH₂)_{Zn}, **1**(*m*-NH₂)_{Zn}, and **1**(*o*-NH₂)_{Zn}, and **1**(*p*-NH₂)_{Cu}, a copper analogue of **1**(*p*-NH₂)_{Zn}. Compounds **2**_{Zn} having 4-aminobiphenyl groups and **3**_{Zn} bearing 3,5-dihydroxyphenyl groups at the meso-positions were used as references. According to molecular models, **1**(*p*-NH₂)_{Zn}, **1**(*p*-NH₂)_{Cu}, **1**(*m*-NH₂)_{Zn}, **1**(*o*-NH₂)_{Zn}, and **3**_{Zn} are 2.0, 2.0, 1.8, 1.6, and 1.8 nm in diameter (longer molecular axis), respectively,^[9] and smaller than the cavity of MC, whereas compound **2**_{Zn} is much larger (2.8 nm). Compound **3**_{Zn} is different from these complexes, in that it has Brønsted acidic OH functionalities in place of the amino functionalities.

Electronic absorption spectroscopy in MeCN with the five zinc porphyrin complexes indicated that **1**(*p*-NH₂)_{Zn} and **1**(*m*-NH₂)_{Zn} interact with MC. For example, upon

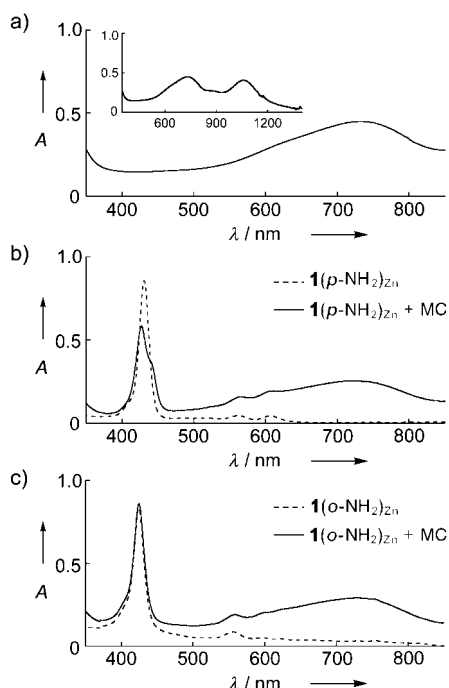
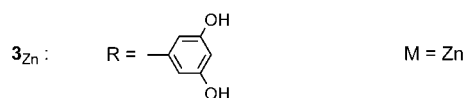
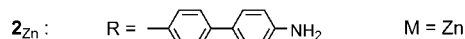
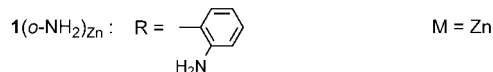
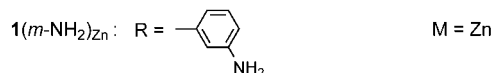
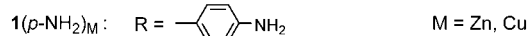
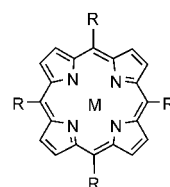


Figure 1. Absorption spectra (350–850 nm) of a) MC (2.2×10^{-6} M)^[10] (inset: 350–1400 nm), and zinc porphyrins, b) **1**(*p*-NH₂)_{Zn} (2.4×10^{-6} M), and c) **1**(*o*-NH₂)_{Zn} (2.5×10^{-6} M) in the absence and presence of MC (0.5 equiv) in MeCN at 20 °C.

titration of **1**(*p*-NH₂)_{Zn} which has 4-aminophenyl groups with MC, the Soret-band at 430 nm decreased in intensity with a small blue shift to 427 nm, while a red-shifted shoulder appeared at 440 nm (Figure 1 b). Compound **1**(*m*-NH₂)_{Zn} which has 3-aminophenyl groups also showed a spectral change upon titration with MC, a considerable broadening of the Soret band in the longer wavelength region took place.^[8] In contrast, **1**(*o*-NH₂)_{Zn} bearing amino groups directed towards the porphyrin unit (Figure 1 c) and the larger sized **2**_{Zn}^[8] hardly showed spectral changes under similar titration conditions. Likewise, the absorption spectrum of **3**_{Zn} having phenolic OH functionalities was virtually unchanged upon addition of MC. These contrasting observations indicate that the complexation of the zinc porphyrins with MC is chemo-

regio-, and size-selective. Namely, the peripheral amino groups are crucial for the complexation with MC, but they should be oriented away from the porphyrin ring, and such guest molecules should be smaller than the MC cavity. Therefore, MC accommodates $\mathbf{1}(p\text{-NH}_2)_{\text{Zn}}$ and $\mathbf{1}(m\text{-NH}_2)_{\text{Zn}}$ inside the cavity through the formation of multiple hydrogen bonds (e.g., $\mu_3\text{-O}\cdots\text{H}\cdots\text{N}$), to give inclusion complexes $[\text{MC}\supset\mathbf{1}(p\text{-NH}_2)_{\text{Zn}}]$, and $[\text{MC}\supset\mathbf{1}(m\text{-NH}_2)_{\text{Zn}}]$, respectively. Copper complex $\mathbf{1}(p\text{-NH}_2)_{\text{Cu}}$, upon titration with MC, also showed an essentially identical spectral change profile to that of $\mathbf{1}(p\text{-NH}_2)_{\text{Zn}}$.^[8]

To determine the stoichiometry of the complexation, spectroscopic titration of MC with $\mathbf{1}(p\text{-NH}_2)_{\text{Zn}}$ was conducted in MeCN (Figure 2a), where MC showed stepwise spectral

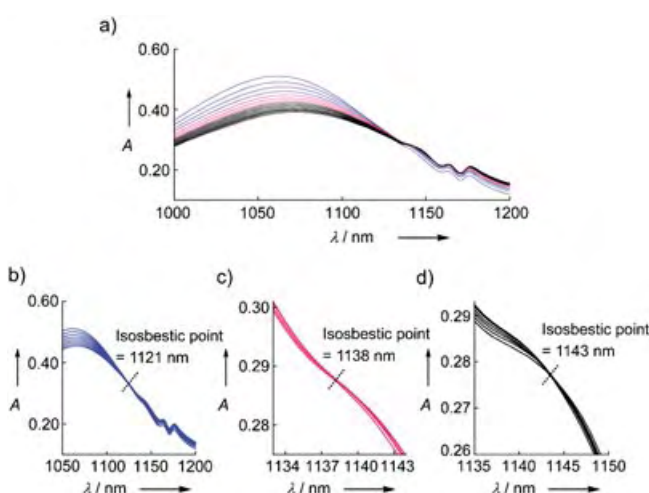


Figure 2. Spectroscopic titration of MC (2.5×10^{-6} M)^[10] with $\mathbf{1}(p\text{-NH}_2)_{\text{Zn}}$ in MeCN at 20°C. $[\mathbf{1}(p\text{-NH}_2)_{\text{Zn}}]$ = a) $0\text{--}2.1 \times 10^{-5}$ M (overall spectral change), b) $0\text{--}0.5 \times 10^{-5}$ M, c) $0.6 \times 10^{-5}\text{--}1.0 \times 10^{-5}$ M, and d) $1.2 \times 10^{-5}\text{--}2.1 \times 10^{-5}$ M.

changes in response to $[\mathbf{1}(p\text{-NH}_2)_{\text{Zn}}]/[\text{MC}]$ at 0–2, 2–4, and 4–10 (Figure 2b–d),^[10] with isosbestic points at 1121, 1138, and 1143 nm, respectively. This observation indicates the stepwise formation of 1:1, 1:2, and 1:3 complexes between MC and $\mathbf{1}(p\text{-NH}_2)_{\text{Zn}}$.^[11] Slow evaporation of a concentrated MeCN solution of a 1:3 mixture of MC and $\mathbf{1}(p\text{-NH}_2)_{\text{Zn}}$ allowed the isolation of $[\text{MC}\supset\mathbf{1}(p\text{-NH}_2)_{\text{Zn}}]$ as a green precipitate, which was subjected to inductively coupled plasma atomic emission spectroscopy (ICP-AES) to give a Mo/Zn ratio of 61.9. This value is in good agreement with that calculated for the 1:3 inclusion complex between MC and $\mathbf{1}(p\text{-NH}_2)_{\text{Zn}}$ (58.7). According to the crystal structure,^[7] the cavity of MC is 1.3 nm deep and large enough to accommodate up to three molecules of $\mathbf{1}(p\text{-NH}_2)_{\text{Zn}}$ when they are stacked face to face (Scheme 1). Thus, the spectral changes observed for the complexation of $\mathbf{1}(p\text{-NH}_2)_{\text{Zn}}$ (Figure 1b) and $\mathbf{1}(m\text{-NH}_2)_{\text{Zn}}$ ^[8] with MC are considered to reflect such a stacking association of these guest molecules in the MC cavity, as well as the proton-donation from their peripheral amino groups.

Ultrahigh-vacuum scanning tunneling microscopy (UHV-STM)^[12] (Figure 3) demonstrated that the product upon complexation of MC with $\mathbf{1}(p\text{-NH}_2)_{\text{Zn}}$ is indeed an inclusion complex $[\text{MC}\supset\mathbf{1}(p\text{-NH}_2)_{\text{Zn}}]$. Thus, a dilute aqueous solution

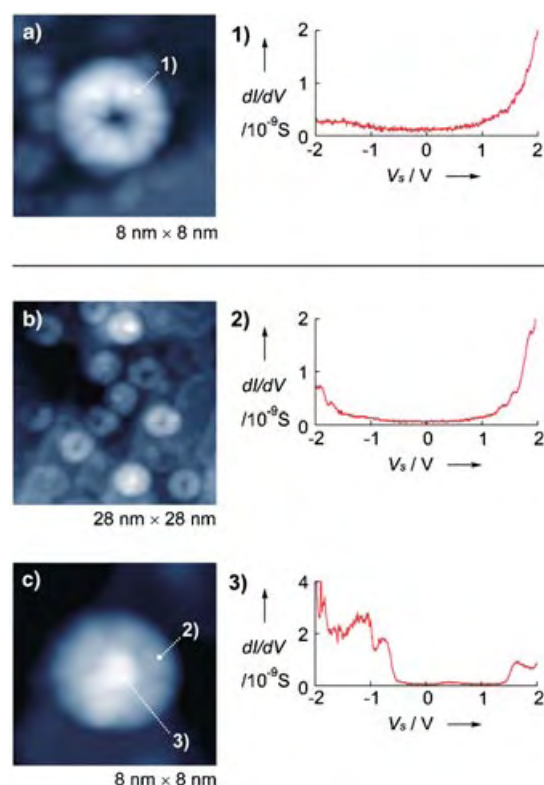


Figure 3. Left: ultrahigh-vacuum scanning tunneling microscopy (UHV-STM) images and right: scanning tunneling spectroscopy (STS) data on Cu(111) surfaces at 80 K. UHV-STM images of a) intact MC (imaging conditions: $I = 2.0$ pA, $V_s = 1.0$ V), b) a 1:3 mixture of MC and $\mathbf{1}(p\text{-NH}_2)_{\text{Zn}}$ ($I = 2.0$ pA, $V_s = 3.0$ V), and c) $[\text{MC}\supset\mathbf{1}(p\text{-NH}_2)_{\text{Zn}}]$ ($I = 2.0$ pA, $V_s = 1.0$ V). STS differential conductance (dI/dV)–sample bias voltage (V_s) correlations of area (1) an intact MC observed in (a), and areas (2) the shell and (3) the core of $[\text{MC}\supset\mathbf{1}(p\text{-NH}_2)_{\text{Zn}}]$ observed in (c).

of a mixture of MC and $\mathbf{1}(p\text{-NH}_2)_{\text{Zn}}$ (1:3)^[10] was sprayed by the pulse injection technique onto a clear flat Cu(111) surface. The UHV-STM image showed the presence of numerous doughnut-like discrete nano-objects with a diameter of 4–5 nm (Figure 3b), which is consistent with the reported dimension of crystallographically defined MC.^[7] Some of these nano-objects in the STM image (Figure 3c) appear to have a filled cavity.^[13] By means of scanning tunneling spectroscopy (STS)^[14] on one of these filled objects, correlations between differential conductance (dI/dV) and sample bias voltage (V_s) were measured separately for the shell and core parts.^[8] As shown in Figure 3, these two parts exhibit different dI/dV – V_s profiles. Although the shell part, as with intact MC, displays a gradual increase in dI/dV with either decreasing or increasing V_s , the core part, in contrast, shows two bands at -0.7 and $+1.6$ V, which are assignable to resonant tunneling currents through the HOMO and LUMO of the guest compound.^[15] Since the energy gap of 2.3 eV, thus observed, is consistent with the optical HOMO–LUMO energy gap of $\mathbf{1}(p\text{-NH}_2)_{\text{Zn}}$ (2.1 eV), it is clear that the object with a filled cavity (Figure 3c) is $[\text{MC}\supset\mathbf{1}(p\text{-NH}_2)_{\text{Zn}}]$.

We also conducted an electron paramagnetic resonance (EPR) study on the inclusion complex of MC with copper porphyrin $\mathbf{1}(p\text{-NH}_2)_{\text{Cu}}$ ($[\text{MC}\supset\mathbf{1}(p\text{-NH}_2)_{\text{Cu}}]$). MC is diamag-

netic at the ground state, while copper porphyrins are paramagnetic ($S = 1/2$) and generally show anisotropic EPR spectra with two distinct g_{\parallel} and g_{\perp} values and hyperfine splittings induced by copper ($I = 3/2$) and nitrogen ($I = 1$) nuclei.^[16] In contrast, **1**(*p*-NH₂)_{Cu} alone in MeCN at 103 K displayed an isotropic EPR pattern possibly arising from an irregular aggregation caused by hydrogen-bonding interactions at the peripheral amino groups (Figure 4). On the other

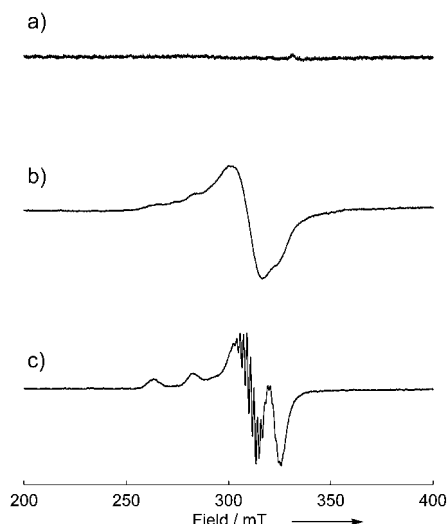


Figure 4. EPR spectra at 103 K in MeCN. a) MC (3.0×10^{-5} M), b) **1**(*p*-NH₂)_{Cu} (3.0×10^{-5} M), c) a mixture of **1**(*p*-NH₂)_{Cu} (3.0×10^{-5} M) and MC (1.0×10^{-5} M).^[10]

hand, when **1**(*p*-NH₂)_{Cu} was mixed with MC at a 1:3 molar ratio,^[10] the resulting inclusion complex [MC⊃**1**(*p*-NH₂)_{Cu}] showed in its EPR spectrum an anisotropic pattern with g_{\parallel} and g_{\perp} values of 2.187 and 2.085, respectively, along with sharp hyperfine arising from the copper ($a_{\parallel} = 19.3$ mT) and nitrogen nuclei. Thus, **1**(*p*-NH₂)_{Cu} is freed from its hydrogen-bonded irregular assembly and incorporated into the MC cavity to form a uniform assembly in the confined nanospace.

In conclusion, we have demonstrated the first example of organic functionalization of doughnut-like molybdenum crown cluster (MC). In its nanocavity MC can accommodate metal complexes of aminophenyl-substituted porphyrins, such as **1**(*p*-NH₂)_M (M = Zn, Cu) and **1**(*m*-NH₂)_{Zn} as a result of hydrogen-bonding interactions, to form discrete inorganic/organic nanocomposite materials. The results indicate a new potential for MC as an inorganic host in supramolecular chemistry and also as a building block for nanoscopic materials science.

Experimental Section

MC, **1**(*m*-NH₂)_{Zn}, and **1**(*o*-NH₂)_{Zn} were synthesized according to literature methods,^[7,17] while 5,10,15,20-tetrakis(4-aminophenyl)-21*H*,23*H*-porphine **1**(*p*-NH₂)_H and 5,10,15,20-tetrakis(3,5-dihydroxyphenyl)-21*H*,23*H*-porphine **3**_H were obtained from commercial sources. Column chromatography was carried out with Wakogel C-400 or alumina (Merck Ltd.). ¹H NMR spectra were recorded in CDCl₃ on a JEOL model α-500 spectrometer, where chemical shifts (δ in ppm) were determined with respect to tetramethylsilane (TMS) as internal standard. Electronic absorption spectra were recorded on a JASCO model V-570 spectrometer equipped with a temperature

controller. IR spectra were recorded on a JASCO model FT/IR-610 spectrometer. MALDI-TOF mass spectrometry was performed on a Perceptive Biosystems model Voyager-DE spectrometer with 9-nitroanthracene as matrix. ICP-AES was performed on a Seiko Instruments Inc. model SPS4000 inductively coupled plasma atomic emission analyzer. Ultrahigh-vacuum scanning tunneling microscopy (UHV-STM) was performed on a Unisoku Japan model USM-1200.

Metalation of porphyrins: Typically, a saturated MeOH solution of Zn(OAc)₂ or Cu(OAc)₂ was added to a CHCl₃ solution of a free-base porphyrin, and the resulting mixture was heated under reflux for 1–2 h. After the complete metalation was confirmed by thin layer chromatography (TLC) or MALDI-TOF MS, the mixture was poured into water and extracted with CHCl₃. The combined organic extract was washed with water and brine, dried over anhydrous Na₂SO₄, and then evaporated to dryness. Recrystallization of the residue from THF/hexane gave the corresponding metalloporphyrin in an analytically pure form.

2_{Zn}: (1,1'-Biphenyl)-4-nitro-4'-carboxaldehyde (786 mg, 3.5 mmol) and pyrrole (232 mg, 3.5 mmol) were heated in refluxing propionic acid (25 mL) for 3 h. A crystalline precipitate, obtained from the reaction mixture on cooling, was isolated by filtration and washed with water and MeOH. The precipitate (70 mg) and anhydrous SnCl₂ (250 mg, 1.1 mmol) were dissolved in concentrated aq. HCl/THF (2:1; 15 mL), and the resulting solution was stirred for 24 h at 50 °C. Aqueous KOH was added to the mixture until it turned basic, and the mixture was extracted with CH₂Cl₂ (4 × 50 mL). The combined organic extract was dried over anhydrous Na₂SO₄ and evaporated to dryness. The residue was purified by chromatography on silica gel with CHCl₃:MeOH (95:5) as eluent, and a reddish purple fraction isolated was stirred with excess Zn(OAc)₂ in CHCl₃ for 1 h. The reaction mixture was evaporated to dryness under reduced pressure, and the residue was extracted with CHCl₃/water. The combined organic extract was dried over anhydrous Na₂SO₄ and evaporated to dryness. Recrystallization of the residue from THF/hexane gave **2_{Zn}** (5 mg, 4.7 μmol) as purple powdery substance. MALDI-TOF MS *m/z* 1040, calcd for C₆₈H₄₈N₈Zn 1040; UV/Vis (CHCl₃): λ_{max} = 427, 522, 559, and 600 nm; ¹H NMR (500 MHz, [D₈]THF, 25 °C): δ = 4.61 (s, 8H, NH₂), 6.72 (d, *J* = 10.0 Hz, 8H, biphenyl), 7.62 (d, *J* = 10.0 Hz, 8H, biphenyl), 7.87 (d, *J* = 10.0 Hz, 8H, biphenyl), 8.14 (d, *J* = 10.0 Hz, 8H, biphenyl), and 8.88 ppm (s, 8H, pyrrole-β).

Received: June 16, 2004

Keywords: inorganic/organic nanocomposites · polyoxomolybdates · porphyrinoids · scanning probe microscopy · supramolecular chemistry

- [1] J. J. Berzelius, *Poggendorff's Ann. Phys.* **1826**, 6, 369–392.
- [2] F. B. Schirmer, Jr., L. F. Aurieth, S. T. Gross, D. S. McClellan, L. J. Seppi, *J. Am. Chem. Soc.* **1942**, 64, 2543–2545.
- [3] a) R. I. Buckley, R. J. H. Clark, *Coord. Chem. Rev.* **1985**, 65, 167–218; b) H. K. Chae, W. G. Marquardt, *Coord. Chem. Rev.* **1993**, 128, 209–224.
- [4] C. W. Scheele in *Sämtliche Physische und Chemische Werke, Vol. 1* (Ed.: D. S. F. Hermbstädt), Martin Sändig oHG: Niederwalluf/Wiesbaden, **1971**, pp. 185–200 (reprint: original 1793).
- [5] A. Müller, E. Krickemeyer, J. Meyer, H. Bögge, F. Peters, W. Plass, E. Diemann, S. Dillinger, F. Nonnenbruch, M. Randerath, C. Menke, *Angew. Chem.* **1995**, 107, 2293–2295; *Angew. Chem. Int. Ed. Engl.* **1995**, 34, 2122–2124.
- [6] Recent reviews: a) A. Müller, C. Serain, *Acc. Chem. Res.* **2000**, 33, 2–10; b) A. Müller, P. Kögerler, A. W. M. Dress, *Coord. Chem. Rev.* **2001**, 222, 193–218; c) A. Müller, S. Roy, *Coord. Chem. Rev.* **2003**, 245, 153–166.

- [7] A. Müller, M. Koop, H. Bögge, M. Schmidtman, C. Beugholt, *Chem. Commun.* **1998**, 1501–1502.
- [8] See Supporting Information.
- [9] Molecular models of metalloporphyrins were obtained using a MM2 force field.
- [10] Concentrations of MC are estimated to include, at most, 18 % deviations arising from its loosely bound crystal water.
- [11] K. Yamamoto, M. Higuchi, S. Shiki, M. Tsuruta, H. Chiba, *Nature* **2002**, 415, 509–511.
- [12] a) H. Tanaka, T. Kawai, *J. Vac. Sci. Technol. B* **1997**, 15, 602–604; b) H. Tanaka, T. Kawai, *Surf. Sci.* **2003**, 539, 531–536.
- [13] Some of the inclusion complexes presumably lost the guest molecule in the injection process.
- [14] a) M. Pomerantz, A. Aviram, R. A. McCorkle, L. Li, A. G. Schrott, *Science* **1992**, 255, 1115–1118; b) P. Guaino, A. A. Cafolla, O. McDonald, D. Carty, G. Sheerin, G. Hughes, *J. Phys. Condens. Matter* **2003**, 15, 2693–2698.
- [15] Similar spectral patterns have been reported for thin films of metalloporphyrins on an Au(111) surface, see: L. Scudiero, D. E. Barlow, K. W. Hipps, *J. Phys. Chem. B* **2002**, 106, 996–1003.
- [16] a) S. S. Eaton, G. R. Eaton, C. K. Chang, *J. Am. Chem. Soc.* **1985**, 107, 3177–3184; b) M. C. Feiters, M. C. T. Fyfe, M.-V. Martínez-Díaz, S. Menzer, R. J. M. Nolte, J. F. Stoddart, P. J. M. V. Kan, D. J. Williams, *J. Am. Chem. Soc.* **1997**, 119, 8119–8120.
- [17] a) M. Momenteau, J. Mispelter, B. Looock, J.-M. Lhoste, *J. Chem. Soc. Perkin Trans. 1* **1985**, 221–231; b) B. C. Bookser, T. C. Bruice, *J. Am. Chem. Soc.* **1991**, 113, 4208–4218.

handling relative to their radioactive counterparts.^[1–3] Combinatorial chemistry is now widely used in the medicinal/pharmaceutical field and in chemical biology for the discovery of novel biologically active molecules or drug candidates,^[4,5] yet the application of this method to fluorescence dyes is only in its infancy. A few early examples include oligopyridines,^[6] coumarins,^[7,8] oligonucleotides,^[9] and conjugated polymers.^[10] We previously reported the first combinatorial wide-color-range fluorescent styryl library by solution-phase chemistry and their potential application as organelle-specific probes.^[11] Here we report the first solid-phase synthesis of a styryl library and its application as amyloid sensors.

Amyloids result when protein misfolding leads to the formation of ordered secondary structures rich in cross- β -sheets, which are present as fibrillar deposits in tissues.^[12] The formation of amyloids has been associated with a large number of protein-misfolding diseases including type II diabetes, Alzheimer's, Parkinson's, Huntington's, mad-cow disease, and others.^[13,14] Of the many amyloidoses, Alzheimer's disease (AD) is the fourth leading cause of death in the United States and the most common cause of adult-onset dementia.^[15,16] The deposition of β -amyloid (A β) aggregates in brain tissue is one of the hallmark characteristics of AD, and the histological staining of the deposits is crucial for the diagnosis of AD.^[17] Whereas thioflavin T or S (ThT or ThS) and Congo red (CR) are widely used as detection agents for amyloids, neither of these are considered accurate enough for the quantitative estimation of fibril formation.^[18–21] Congo red is not fluorescent (thus the sensitivity is low), whereas ThT (or S) is a blue-emission dye, which often interferes with autofluorescence from tissue or other small-molecule components in the assay system. Therefore, sensor dyes that are more sensitive and assay-friendly which can stain biological tissue have been sought.

The styryl scaffold is formed by a condensation reaction of aldehydes and pyridinium salts, which are widely available commercially and easily prepared starting materials. A series of resins and reaction routes were tested, however, the best results, both in yield and purity, were obtained when 2-chlorotrityl resin **1** (BeadTech Inc., Korea) was used as the first linker-protecting group (Scheme 1). Two different aminoalcohols with 2- or 6-carbon-atom chains were loaded onto the 2-chlorotrityl resin, and the alcohol groups were mesylated for subsequent treatment with picoline moieties. Four picoline and three quinoline derivatives were chosen as R¹ building blocks to give solid-supported pyridinium salts **5**. 64 aldehyde R² building blocks that contain various functionalities and have various lengths and electron-donating or withdrawing properties are outlined in Scheme 2 (page 6333). Condensation of the solid-supported pyridinium salts **5** and the aldehydes was effectively performed under microwave irradiation. The addition of diluted TFA (1 %) then led to the facile release of the final styryl dye compounds **7** from the resin (10 min). All of the synthesized compounds were analyzed by LC/MS, and 320 components were selected based on their purity for further study (average purity: 82 %; purity data for individual compounds are available in the Supporting Information). Also, the λ_{max} values of the fluorescence excitation and emission bands of the library compounds

Fluorescent Probes

Solid-Phase Synthesis of Styryl Dyes and their Application as Amyloid Sensors**

Qian Li, Jun-Seok Lee, Chanki Ha, Chan Beum Park, Guang Yang, Wen Biao Gan, and Young-Tae Chang*

Fluorescent sensors and probes have attracted attention because of their high sensitivity and exceptional ease of

[*] Q. Li, J.-S. Lee, Prof. Dr. Y.-T. Chang

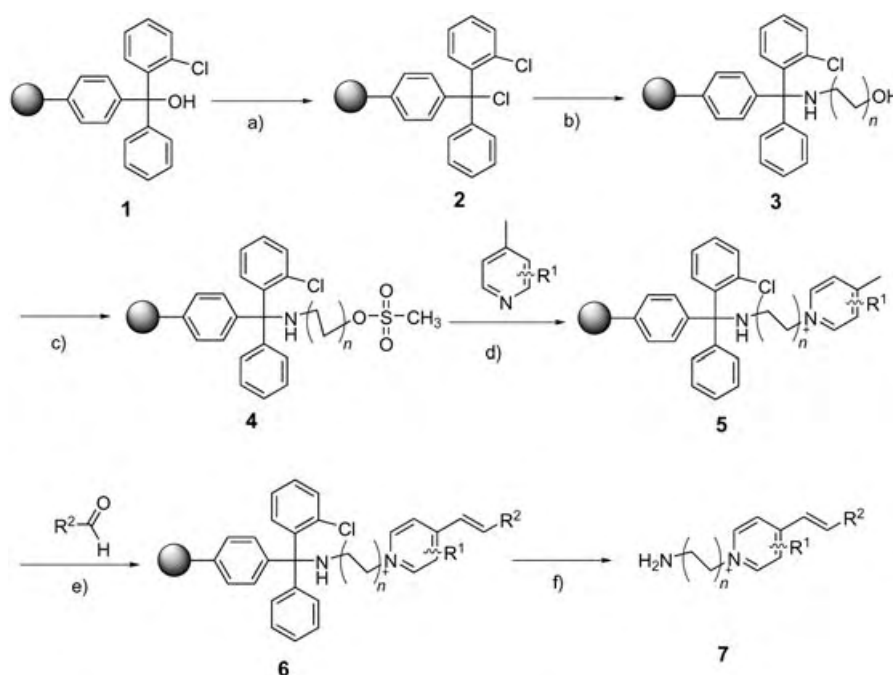
Department of Chemistry
New York University
New York, NY 10003 (USA)
Fax: (+1) 212-995-4203
E-mail: yt.chang@nyu.edu

C. Ha, Prof. Dr. C. B. Park
Department of Chemical & Materials Engineering
Arizona State University
Tempe, AZ 85287-6006 (USA)
Fax: (+1) 480-965-0037

G. Yang, Prof. Dr. W. B. Gan
Skirball Institute of Biomolecular Medicine
New York University School of Medicine
540 First Avenue
New York, NY 10016-6481 (USA)
Fax: (+1) 212-263-8214

[**] We thank BeadTech Inc., Korea, for technical support of this work.

Supporting information for this article is available on the WWW under <http://www.angewandte.org> or from the author.



Scheme 1. Solid-phase synthesis of the styryl dyes **7**: a) thionyl chloride, CH_2Cl_2 , room temperature, 2 h; b) ethanolamine ($n=1$) or 6-amino-1-hexanol ($n=3$), CH_2Cl_2 , room temperature, 3 h; c) methanesulfonyl chloride, NEt_3 , CH_2Cl_2 , room temperature, overnight; d) pyridine derivative (R^1), NMP, 80–90 °C, overnight; e) aldehyde (R^2), pyrrolidine, NMP, 80 W microwave, 6 min; f) TFA (1 %) in CH_2Cl_2 , 10 min. NMP = *N*-methylpyrrolidone.

were recorded with a Gemini XS fluorescent plate reader (data available in Supporting Information). The compounds in the library cover practically the whole color range from blue to red. These 320 compounds were tested for amyloid sensing without further purification.

Primary screening of amyloid sensing was carried out with insulin amyloid fibrils generated from fresh insulin which were induced to aggregate at low pH conditions to form a cross- β -sheet secondary structure.^[22] (A representative atomic force microscope (AFM) picture of the insulin amyloid fibrils used in this work is provided in the Supporting Information). The formation of insulin amyloids, a characteristic of injection-localized amyloidosis, occurs through kinetic mechanisms that are similar to those for other amyloidogenic

proteins such as A β peptides, α -synuclein, and transthyretin, and its rate is highly accelerated under stressful conditions such as elevated temperature or low pH.^[23,24] 13 compounds from the 320 compounds in the library were selected based on the observed increases in their fluorescence intensities upon addition of insulin amyloid fibril (relative to the dye or fresh insulin alone; see Figure 1), and their spectroscopic properties are summarized in Table 1. Promisingly, some of the compounds, such as 2C32 and 2C9, displayed dramatic increases in fluorescence intensity (663- and 736-fold) that were much better than the known standard dye ThS (42-fold). The fluorescence of many of the compounds demonstrated a red shift after binding with insulin amyloid fibril (Figure 1) which is a favorable property for the reduction of background signals and also for ratiometric measurements. The longer emission wavelengths of 2C32 and 2C9 may also allow for the screening of blue-green fluores-

cent inhibitors of amyloid formation, which was not possible with ThS or ThT.

We further tested the 13 selected compounds in synthetic A β 40 and A β 42 aggregates. The two A β variants, A β 40 and A β 42, which differ by truncation at the carboxyl terminus, are the predominant plaque proteins in AD.^[25] All of the dyes showed comparable increases in their fluorescence emissions. Interestingly, all of the styryl compounds showed higher sensitivities to fibril A β 40 than to fibril A β 42 (A β 40:A β 42 = 0.8–3.5), in contrast to ThS (A β 40:A β 42 = 0.4). Furthermore, the 13 candidates and ThS were tested for the *in vitro* staining of fixed AD mouse-brain sections. Images of the amyloid stained with the two most-effective compounds, 2C40 and 2E10, are shown in Figures 2 and 3. As 2C40 displays red

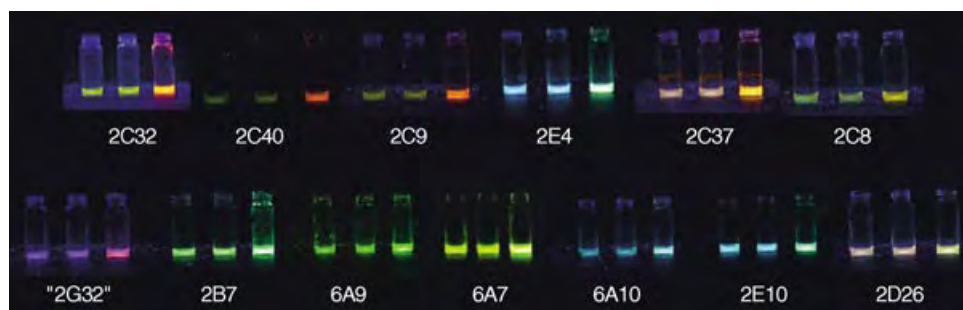
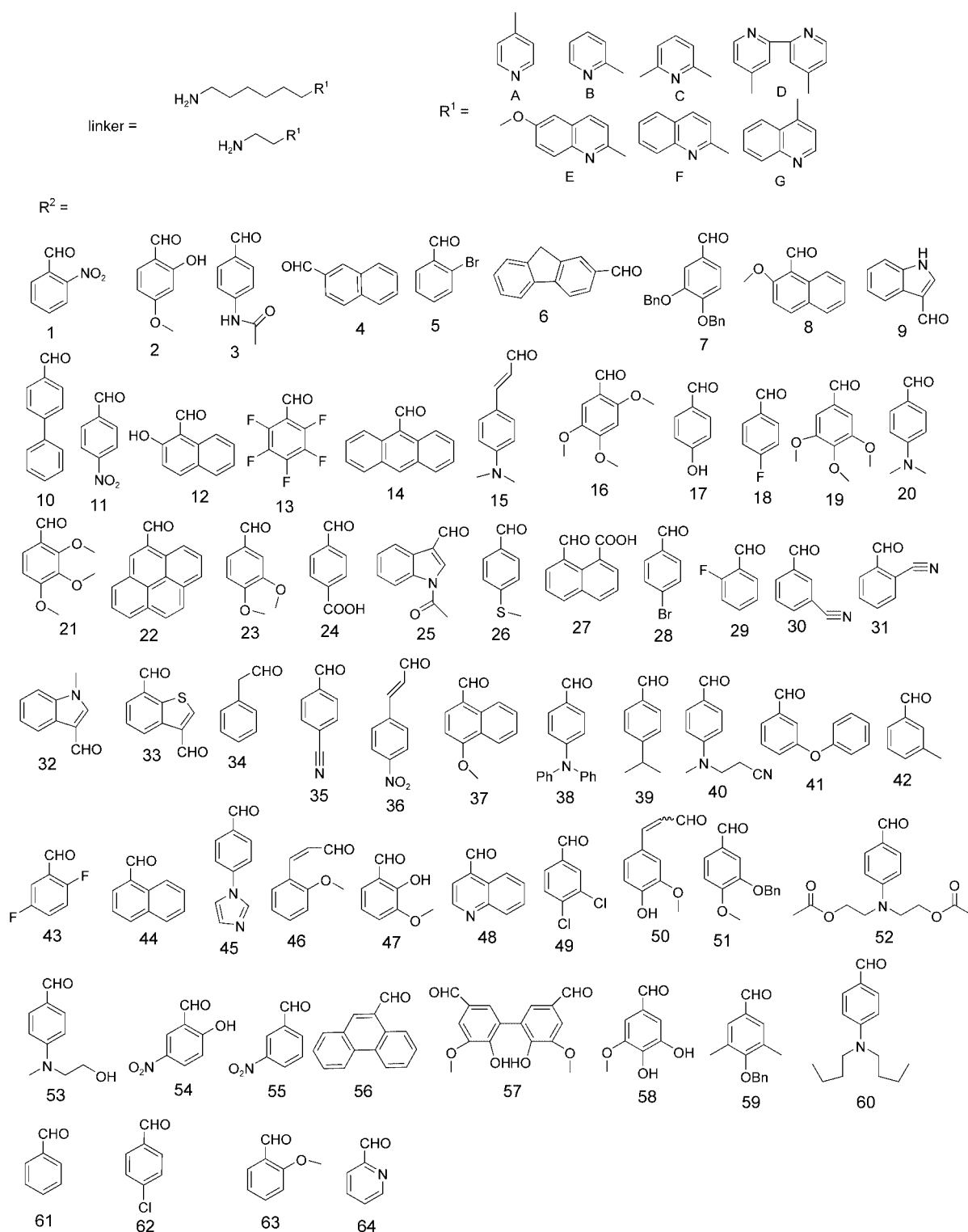


Figure 1. Color changes of the 13 “hit” compounds observed under irradiation with a Blak-Ray 365-nm UV lamp. Each set of 3 samples contains the dye (200 μM) alone in HCl (0.5 mL, pH 1.4; left), with fresh insulin (1 mg mL^{-1} , 0.5 mL, pH 1.4; center), and with insulin amyloid fibrils (1 mg mL^{-1} , 0.5 mL, pH 1.4; right). The dyes are numbered according to the length of the linker (2 or 6), the letter corresponding to R^1 (A–G), and the number corresponding to R^2 (1–64; see Scheme 2).



Scheme 2. Components (linkers, pyridine derivatives R^1 , and aldehydes R^2) for the parallel syntheses of the styryl dyes. Bn = benzyl.

fluorescence and 2E10 displays green fluorescence, these compounds may be good complementary-color dye substitutes for ThS (blue). We observed that our new dyes are at least as sensitive as ThS in terms of labeling aggregates and showed 100% colocalization with ThS-labeling in 50 plaques assayed (two brain-slices each). Interestingly, compared to

ThS, which stains the peripheral area of the plaque, our compounds mainly stained the core of the amyloid plaque.

In summary, we have reported the first solid-phase parallel synthesis of a styryl dye library that comprises 320 dye compounds. Through in vitro amyloid screening, 13 new amyloid sensors were identified of which two show outstand-

Table 1: Fluorescent properties of the 13 “hit” compounds from the styryl library.

Compound Code ^[a]	Buffer ^[b]		Fresh Insulin ^[b]		Insulin Amyloid Fibrils ^[b]		Insulin Amyloid Fibrils ^[c]	<i>n</i> -Fold Increase A β 40 Fibrils ^[d]	A β 42 Fibrils ^[d]
	λ_{ex} [nm]	λ_{em} [nm]	λ_{ex} [nm]	λ_{em} [nm]	λ_{ex} [nm]	λ_{em} [nm]			
ThS	385	445	385	445	450	482	42	10	23
2C32	425	537	426	539	548	593	663	276	85
2C40	433	565	432	568	505	590	20	27	20
2C9	392	536	390	537	538	585	736	173	62
2E4	366	443	367	445	447	522	29	23	9
2C37	406	545	405	545	453	572	8	7	5
2C8	423	529	421	536	450	547	7	11	14
2G32	473	590	473	594	453	585	7	7	2
2B7	375	515	371	513	417	509	18	9	6
6A9	417	526	424	527	447	515	6	9	7
6A7	371	521	372	525	392	520	6	6	5
6A10	361	495	361	494	379	494	6	5	6
2E10	441	491	441	492	464	503	185	30	16
2D26	394	550	395	550	434	527	4	4	3

[a] The styryl dyes are numbered according to the length of the linker (2 or 6), the letter corresponding to R¹ (A–G), and the number corresponding to R² (1–64): see Scheme 2. [b] λ_{max} values for the excitation and emission bands of ThS and the “hit” compounds as solutions in aqueous HCl (pH 1.4) recorded with a Hitachi F-2500 FL Spectrophotometer. [c] *n*-fold increase in fluorescence intensity of the dye in insulin amyloid fibrils relative to the control (EDTA (1 mM) in PBS) at pH 4.0. [d] *n*-fold increase in fluorescence intensity of the dye in A β 40 and A β 42 fibrils relative to the control (EDTA (1 mM) in PBS, pH 7.4) measured with a Gemini XS plate reader.

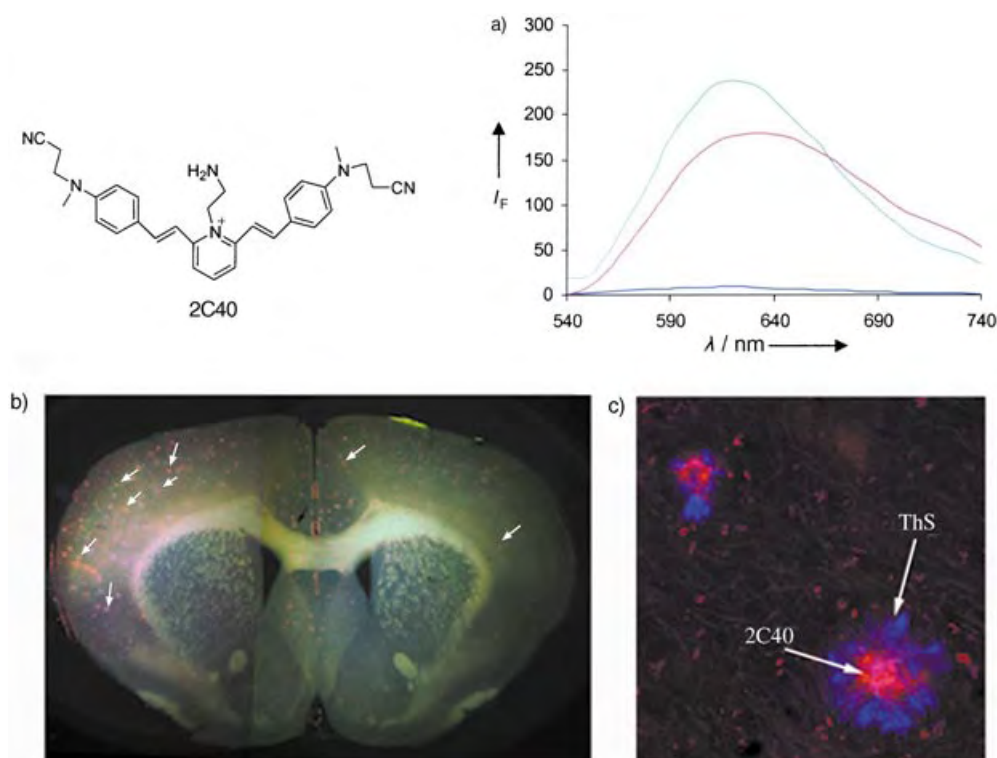


Figure 2. a) Fluorescence spectra of 2C40 (25 μM) with A β 40 fibril (green line; 30 μL of a 0.5-mg mL^{−1} solution in PBS (pH 7.4) containing EDTA (1 mM)), and A β 42 fibril (purple line; 30 μL of a 0.5-mg mL^{−1} solution in PBS solution (pH 7.4) containing EDTA (1 mM)) compared to a control buffer solution (dark blue line; 30 μL of a solution of PBS (pH 7.4) containing EDTA (1 mM)). b) Labeling of amyloid deposits with 2C40 in a slice of mouse brain (red, indicated by arrows). The image was taken with a charge-coupled device camera. c) Confocal microscopy image of amyloid deposits labeled with 2C40 (red) and ThS (blue); note that 2C40 preferentially labels the core of deposits.

ing promise as assay probes (2C32 and 2C9) and two others show promise as brain-imaging agents (2C40 and 2E10). This report demonstrates the high potential of the combinatorial approach in the development of novel sensors as well as in the established medicinal chemistry field. The study of systematic

structure–property relationships of the library compounds, and in vivo amyloid imaging studies are currently underway.^[26]

Received: August 10, 2004

Revised: August 30, 2004

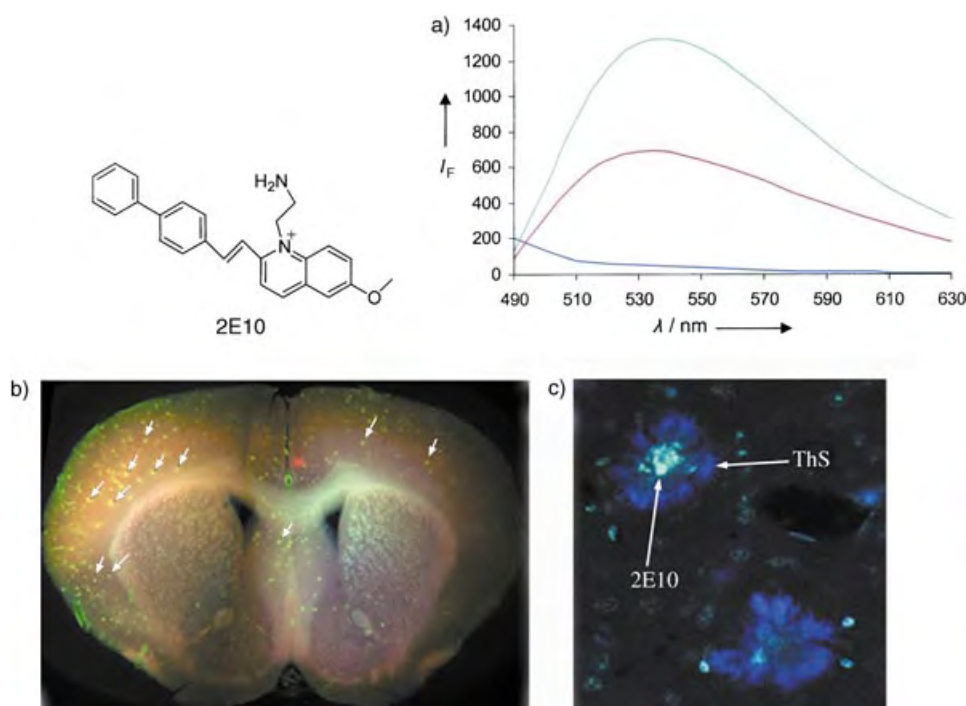


Figure 3. a) Fluorescence spectrum of 2E10 (25 μM) with A β 40 fibril (green line; 30 μL of a 0.5 mg mL^{-1} solution in PBS solution (pH 7.4) containing EDTA (1 mM)), and A β 42 fibril (purple line; 30 μL of a 0.5 mg mL^{-1} solution in PBS solution (pH 7.4) containing EDTA (1 mM)) compared to a control buffer solution (dark blue line; 30 μL of a solution in PBS (pH 7.4) containing EDTA (1 mM)). b) Labeling of amyloid deposits in a slice of mouse brain with 2E10 (green, indicated by arrows). c) Confocal microscopy image of amyloid deposits labeled with 2E10 (green) and ThS (blue); note that 2E10 preferentially labels the core of deposits.

Keywords: combinatorial chemistry · dyes/pigments · fluorescent probes · imaging agents · solid-phase synthesis

- [1] *Fluorescent Chemosensors for Ion and Molecule Recognition* (Ed.: A. W. Czarnik), American Chemical Society, Washington DC, **1992**.
- [2] W. Rettig, B. Strehmel, J. Schrader, H. Seifert, *Applied Fluorescence in Chemistry, Biology, and Medicine*, Springer, Berlin, **1999**.
- [3] J. R. Lakowicz, *Principles of Fluorescence Spectroscopy*, Kluwer Academic/Plenum Publishers, New York, **1999**.
- [4] K. C. Nicolaou, R. Hanko, W. Hartwig, *Handbook of Combinatorial Chemistry: Drugs, Catalysts, Materials*, Wiley-VCH, Weinheim, **2002**.
- [5] S. Miertus, G. Fassina, *Combinatorial Chemistry and Technology: Principles, Methods, and Applications*, Book News, New York, **1999**.
- [6] J. C. Loren, J. S. Siegel, *Angew. Chem.* **2001**, *113*, 776–779; *Angew. Chem. Int. Ed.* **2001**, *40*, 754–757.
- [7] M. S. Schiedel, C. A. Briehn, P. Bauerle, *Angew. Chem.* **2001**, *113*, 4813–4816; *Angew. Chem. Int. Ed.* **2001**, *40*, 4677–4680.
- [8] A. M. Song, J. H. Zhang, K. S. Lam, *J. Comb. Chem.* **2004**, *6*, 112–120.
- [9] J. M. Gao, C. Strassler, D. Tahmassebi, E. T. Kool, *J. Am. Chem. Soc.* **2002**, *124*, 11 590–11 591.
- [10] O. Lavastre, I. Illitchev, G. Jegou, P. H. Dixneuf, *J. Am. Chem. Soc.* **2002**, *124*, 5278–5279.
- [11] G. R. Rosania, J. W. Lee, L. Ding, H. S. Yoon, Y. T. Chang, *J. Am. Chem. Soc.* **2003**, *125*, 1130–1131.
- [12] J. D. Sipe, A. S. Cohen, *J. Struct. Biol.* **2000**, *130*, 88–98.
- [13] J. W. Kelly, *Curr. Opin. Struct. Biol.* **1996**, *6*, 11–17.
- [14] R. M. Murphy, *Annu. Rev. Biomed. Eng.* **2002**, *4*, 155–174.
- [15] C. M. Clark, *Neurodegenerative Dementias: Clinical Features and Pathological Mechanisms*, McGraw-Hill, New York, **2000**.
- [16] T. A. Bayer, O. Wirths, K. Majtenyi, T. Hartmann, G. Multhaup, K. Beyreuther, C. Czech, *Brain Pathol.* **2001**, *11*, 1–11.
- [17] J. Hardy, D. J. Selkoe, *Science* **2002**, *297*, 353–356.
- [18] J. D. Harper, S. S. Wong, C. M. Lieber, P. T. Lansbury, *Chem. Biol.* **1997**, *4*, 119–125.
- [19] J. D. Harper, P. T. Lansbury, *Annu. Rev. Biochem.* **1997**, *66*, 385–407.
- [20] G. T. Westermark, K. H. Johnson, P. Westermark, *Methods Enzymol.* **1999**, *309*, 3–25.
- [21] B. Urbanc, L. Cruz, R. Le, J. Sanders, K. H. Ashe, K. Duff, H. E. Stanley, M. C. Irizarry, B. T. Hyman, *Proc. Natl. Acad. Sci. USA* **2002**, *99*, 13 990–13 995.
- [22] A. Arora, C. Ha, C. B. Park, *FEBS Lett.* **2004**, *564*, 121–125.
- [23] L. Nielsen, R. Khurana, A. Coats, S. Frokjaer, J. Brange, S. Vyas, V. N. Uversky, A. L. Fink, *Biochemistry* **2001**, *40*, 6036–6046.
- [24] A. Ahmad, I. S. Millett, S. Doniach, V. N. Uversky, A. L. Fink, *Biochemistry* **2003**, *42*, 11 404–11 416.
- [25] G. Bitan, M. D. Kirkitadze, A. Lomakin, S. S. Vollers, G. B. Benedek, D. B. Teplow, *Proc. Natl. Acad. Sci. USA* **2003**, *100*, 330–335.
- [26] R. H. Christie, B. J. Bacskai, W. R. Zipfel, R. M. Williams, S. T. Kajdasz, W. W. Webb, B. T. Hyman, *J. Neurosci.* **2001**, *21*, 858–864.

Luminescent Materials

Improving Quantum Efficiencies of Siloles and Silole-Derived Butadiene Chromophores through Structural Tuning**

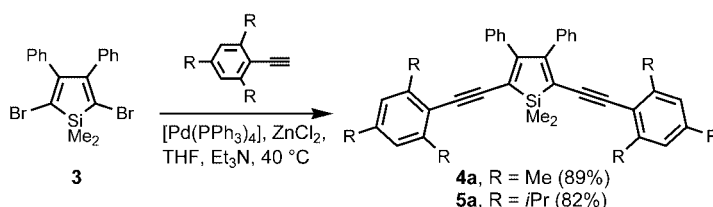
Andrew J. Boydston and Brian L. Pagenkopf*

Over the last decade, Tamao's *endo-endo* cycloreduction of bis(phenylethynyl)silanes has emerged as a powerful tool for generating 2,5-dilithiosiloles that can be trapped by various electrophiles *in situ*.^[1] The strategy has been used for the construction of various silole-containing monomeric, oligomeric, and polymeric systems,^[2] but a significant structural limitation for cycloreduction is the requirement for arene rings at the alkyne termini. Unfortunately, 3,4-diarylsiloles are virtually non-emissive in solution, exhibiting low quantum efficiencies from 0.1–11%.^[3,4] Their poor luminescence has been ascribed directly to effects arising from 3,4-substitution, given that the corresponding unsubstituted systems consistently show greater emission intensities.^[5] The lackluster luminescence of 3,4-diarylsilole chromophores condemns them to a dark future, which is unfortunate given the ease with which they can be prepared by cycloreduction methods.

We recently observed from silole **1a** a curiously high quantum efficiency of 9%,^[6] and in our studies of conjugated silole oligomers^[7] we observed a 20% quantum efficiency from the silole-capped extended chromophore **2**. The emission intensities of **1a** and **2** suggested that silole luminescence attenuation classically ascribed to the 3,4-diphenyl rings can be circumvented by

manipulation of the C2, C5, and Si substituents. Increased chromophore rigidity often leads to improved luminescence by dually facilitating electron delocalization and minimizing vibrational–rotational events in the excited state.^[8] With consideration of the silole nucleus, it seemed likely that increasing steric bulk about silicon and the 2,5-substituents would increase the energy barriers for non-emissive decay processes and ultimately result in increased photoluminescence. Thus, we explored synthetically practical silole modifications intended to impart “rigidity” to analogues of the parent chromophore **1a**. Herein, we report the structural optimization of a series of siloles ultimately resulting in the first highly luminescent 3,4-diphenylsilole chromophores.

The dimethylsilolene chromophores (**4a** and **5a**) were prepared by Negishi cross-coupling reactions with dibromide **3**^[6] (Scheme 1). These new siloles were crystalline solids that were purified by recrystallization from the crude reaction mixtures.



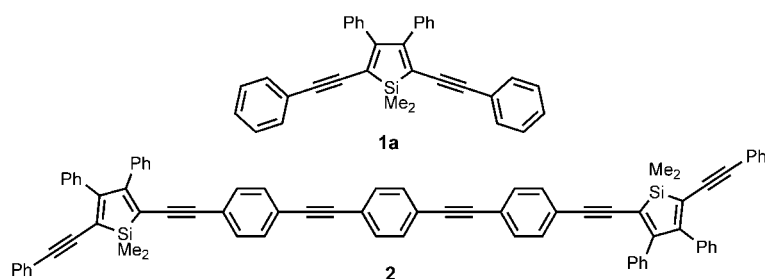
Scheme 1. Synthesis of 1,1-dimethylsilole fluorophores.

For the synthesis of di-*tert*-butylsilolene systems (Scheme 2) we found that isolation of dibromide intermediate **7** was not necessary and good yields were obtained by carrying out the entire reaction sequence from silane **6** through to siloles **1b**, **4b**, or **5b**. As with **4a** and **5a**, this simple process provided the desired siloles as crystalline solids that could be purified by recrystallization from the crude product mixtures.

Chlorosilole **10** was prepared via known intermediate **9**^[6] in 72% overall yield from silane **8** (Scheme 3). Cross-coupling with phenylacetylene provided asymmetric “mixed” silole **11a** in 86% isolated yield after recrystallization. Similarly, bromosilole **12** was used en route to “mixed” silole **11b**.

We found that treatment of the 1,1-dimethylsiloles with Bu₄NF in THF accomplished stereospecific^[9] desilylation in nearly quantitative yield after only a few minutes at room temperature (Scheme 4). As can be seen from X-ray crystal structures (Figure 1), the backbone of the chromophore achieves a nearly completely planar orientation upon removal of the silolene moiety and, as expected, the butadiene moiety adopts an *s-trans* conformation. The efficiency and simplicity of this desilylation method provided **1c**, **4c**, and **5c** essentially gratis.^[10]

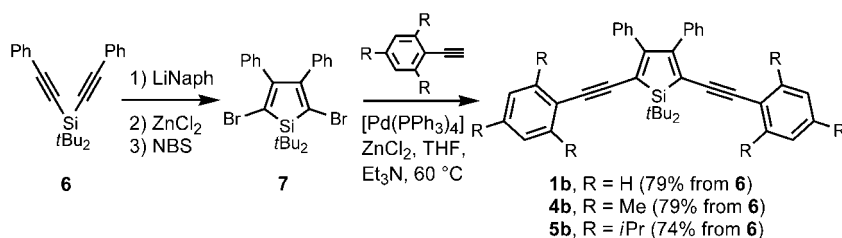
All of the new silole chromophores absorb in the visible region (Table 1) and have moderate molar absorptivities. In comparison with **1a**, siloles bearing larger arenes (**11a**, **4a**, and **5a**) display sequential bathochromic shifts in absorption maxima consistent with having greater electron density.



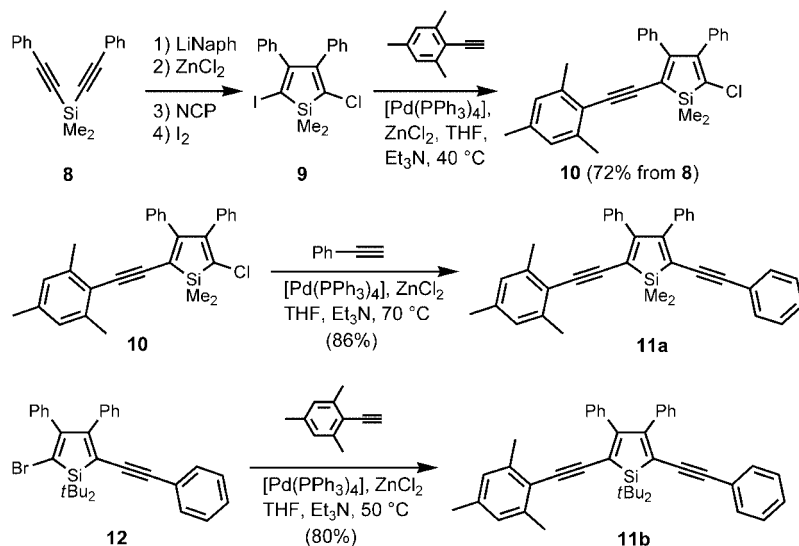
[*] A. J. Boydston, Prof. B. L. Pagenkopf
Department of Chemistry and Biochemistry
The University of Texas at Austin
1 University Station A5300, Austin, TX 78712-0165 (USA)
Fax: (+1) 512-471-8696
E-mail: pagenkopf@mail.utexas.edu

[**] We are grateful to the Robert A. Welch Foundation and donors of the American Chemical Society Petroleum Research fund for partial financial support of this research. A.J.B. thanks the Robert A. Welch Foundation for a Welch Summer Research Fellowship. We are indebted to Dr. Vincent Lynch for determination of crystal structures. We thank FMC Lithium, a division of FMC Corporation, for a generous donation of *t*Bu₂Si(OTf)₂.

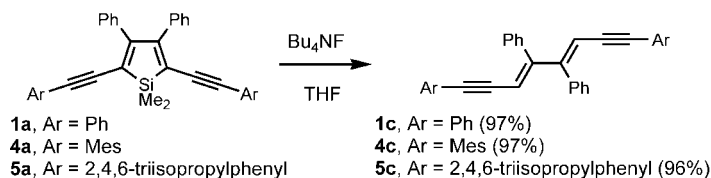
Supporting information for this article is available on the WWW under <http://www.angewandte.org> or from the author.



Scheme 2. Synthesis of 1,1-di-*tert*-butylsilole fluorophores; NBS = 1-bromo-2,5-pyrrolidine-dione.



Scheme 3. Synthesis of asymmetric silole fluorophores; NCP = *N*-chlorophthalimide.



Scheme 4. Protodesilylation for synthesis of butadiene chromophores.

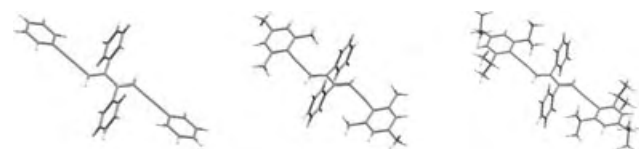


Figure 1. X-ray structures of siloles **1c** (left), **4c** (middle), and **5c** (right).

Increasing steric bulk about silicon alone causes a small hypsochromic shift in the absorption maxima (**1a** vs. **1b**, **4a** vs. **4b**, **5a** vs. **5b**, **11a** vs. **11b**). Relative to the least hindered silole **1a**, a hypsochromic shift (decrease in absorption intensity) is observed for each of the bulkier systems suggesting a decrease in planarity. In all cases, desilylation causes nearly equivalent hypsochromic shifts (that is, blue shifts) in absorption maxima (**1a**→**1c** $\Delta\lambda_{\text{max}} = -66$ nm; **4a**→

4c $\Delta\lambda_{\text{max}} = -64$ nm, **5a**→**5c** $\Delta\lambda_{\text{max}} = -66$ nm, Table 1) as a result of the loss of butadiene tethering and electronic interactions with the silicon atom. Increasing the size of the alkyl groups on the terminal arenes (i.e. **4c** and **5c** vs. **1c**) also causes longer wavelength absorption maxima and decreased molar absorptivity for the butadienes. Notably, blue emission was obtained from both **4c** and **5c**, which emit with 20% and 25% efficiency, respectively.

These structural modifications resulted in significant stepwise increases in quantum efficiencies (Φ_f) with minimal impact on emission wavelengths (Figure 2, Table 1). Compared with the parent silole **1a** ($\Phi_f = 9\%$), emission intensities improved when larger terminal arenes were employed. Replacing a single phenyl group on **1a** ($\Phi_f = 9\%$) with a mesityl (**11a**, $\Phi_f = 10\%$) had a marginal effect, but exchanging both phenyl groups for mesityl groups results in a marked increase in luminescence (**4a**, $\Phi_f = 30\%$). Replacing the mesityl groups with triisopropylphenyl groups gave only slight enhancement (**5a**, $\Phi_f = 41\%$). Substituting the dimethylsilolene for a di-*tert*-butylsilolene has a greater influence on Φ_f than changes to the terminal arene units. For the parent silole **1a** ($\Phi_f = 9\%$), the exchange brought Φ_f to 25% (**1b**). Incorporation of a single mesityl group again lead to only a modest improvement (**11b**, $\Phi_f = 32\%$), but when two mesityl groups were used in combination with the di-*tert*-butylsilolene (**4b**) a quantum efficiency of 63% was observed. No further increase was observed, however, with silole **5b** ($\Phi_f = 56\%$). To our knowledge, these quantum efficiencies are the highest ever reported for 3,4-diphenylsilole chromophores in solution.

Table 1: Electronic absorption and emission data in solution.

Silole	Butadiene	Absorption		Emission	
		λ_{max}	$\log(\epsilon)$	λ_{max}	$\Phi_f^{[b]}$
1a	–	429	4.74	520	0.09
1b	–	428	4.36	516	0.25
4a	–	443	4.49	532	0.30
4b	–	439	4.48	529 (536) ^[a]	0.63
5a	–	447	4.43	523	0.41
5b	–	439	4.51	507 (512) ^[a]	0.56
11a	–	436	4.42	532	0.10
11b	–	434	4.43	522	0.32
–	1c	363	5.03	428	0.02 ^[c]
–	4c	379	4.99	448	0.20 ^[c]
–	5c	381	4.85	426	0.25 ^[c]

[a] Emission maxima of thin films given in parentheses. [b] Determined with reference to fluorescein unless stated otherwise. [c] Determined with reference to 9,10-diphenylanthracene.

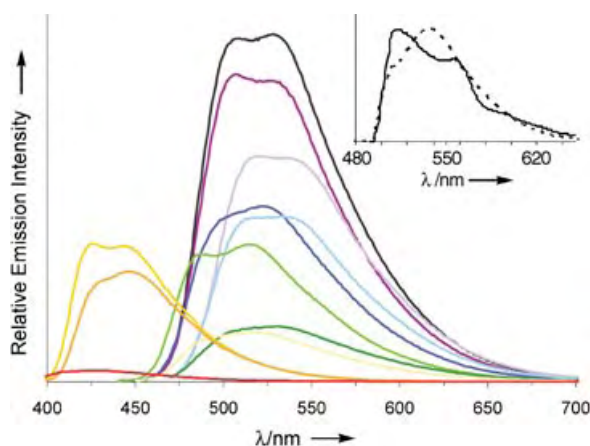


Figure 2. Photoluminescence spectra in CH_2Cl_2 at room temperature. **4b** (—), **5b** (—), **5a** (—), **11b** (—), **4a** (—), **1b** (—), **11a** (—), **1a** (—), **5c** (—), **4c** (—), **1c** (—). Inset: normalized emission spectra of thin films of **4b** (dashed line) and **5b** (solid line).

Although the solution photoluminescence (PL) efficiency is a good first measure of performance and is paramount in areas such as nitroaromatic detection,^[11] the solid-state behavior will more likely dictate the feasibility of deploying these compounds in electronic devices. In this regard, thin-films of **4b** and **5b** were prepared by spin-coating,^[12] and their PL spectra examined (Figure 2, inset). Intense green light emission was observed from the thin film of each fluorophore and the emission spectra revealed slight bathochromic shifts in the solid state relative to the solution PL spectra.

In conclusion, simple structural modifications have provided new luminescent silole chromophores with the highest quantum efficiencies for fully substituted monomeric siloles in solution. Importantly, these discoveries welcome siloles prepared by practical cycloreduction methods into the fold of useful fluorophores. The PL intensity was selectively modified without impact on the emission wavelength. This work establishes structure–property relationships that refute the notion that 3,4-disubstituted siloles possess intrinsically low quantum efficiencies, and illustrates enhanced performance through substituent tuning at C2, C5, and Si.

Received: August 31, 2004

Keywords: alkynes · fluorescence spectroscopy · luminescence · silicon · siloles

- [1] K. Tamao, S. Yamaguchi, M. Shiro, *J. Am. Chem. Soc.* **1994**, *116*, 11 715–11 722.
- [2] a) S. Yamaguchi, K. Tamao, *J. Organomet. Chem.* **2002**, *653*, 223–228; b) M. Hissler, P. W. Dyer, R. Réau, *Coord. Chem. Rev.* **2003**, *244*, 1–44.
- [3] a) S. Yamaguchi, T. Endo, M. Uchida, T. Izumizawa, K. Furukawa, K. Tamao, *Chem. Eur. J.* **2000**, *6*, 1683–1692; b) J. Lee, Q.-D. Liu, M. Motala, J. Dane, J. Gao, Y. Kang, S. Wang, *Chem. Mater.* **2004**, *16*, 1869–1877. Increased quantum yields (21 %) have been obtained from 3,4-diarylsiloles by aggregation-induced emission, see: c) J. Luo, Z. Xie, J. W. Y. Lam, L. Cheng,

H. Chen, Q. Chengfeng, H. S. Kwok, X. Zhan, Y. Lui, D. Zhu, B. Z. Tang, *Chem. Commun.* **2001**, 1740–1741; d) J. Chen, Z. Xie, J. W. Y. Lam, C. C. W. Law, B. Z. Tang, *Macromolecules* **2003**, *36*, 1108–1117; e) J. Chen, C. C. W. Law, J. W. Y. Lam, Y. Dong, S. M. F. Lo, I. D. Williams, D. Zhu, B. Z. Tang, *Chem. Mater.* **2003**, *15*, 1535–1546.

- [4] To our knowledge, at its current state of development the method is limited to phenyl groups.
- [5] a) S. Yamaguchi, K. Tamao, *J. Chem. Soc. Dalton Trans.* **1998**, 3693–3702; b) M. Katkevics, S. Yamaguchi, A. Toshimitsu, K. Tamao, *Organometallics* **1998**, *17*, 5796–5800.
- [6] A. J. Boydston, Y. Yin, B. L. Pagenkopf, *J. Am. Chem. Soc.* **2004**, *126*, 3724–3725.
- [7] A. J. Boydston, Y. Yin, B. L. Pagenkopf, *J. Am. Chem. Soc.* **2004**, *126*, 10350–10354.
- [8] X.-C. Li and S. C. Moratti in *Photonic Polymeric System: Fundamentals, Methods and Applications*, (Eds.: D. L. Wise, G. E. Wnek, D. J. Trantolo, T. M. Cooper, J. D. Gresser), Marcel Dekker, New York, **1998**, chap. 10, pp. 335–371.
- [9] Determined by ^1H NMR spectroscopy and X-ray analysis.
- [10] Similar silole desilylations have been reported using 50 equiv of KOH in refluxing $\text{PhCH}_3/\text{H}_2\text{O}$ for approximately 20 h, see ref. [3a].
- [11] a) H. Sohn, M. J. Sailor, D. Magde, W. C. Trogler, *J. Am. Chem. Soc.* **2003**, *125*, 3821–3830; b) H. Sohn, R. M. Calhoun, M. J. Sailor, W. C. Trogler, *Angew. Chem.* **2001**, *113*, 2162–2163; *Angew. Chem. Int. Ed.* **2001**, *40*, 2104–2105.
- [12] Thin films were prepared onto glass substrates by spin-coating solutions of the recrystallized siloles.

Magnetic Properties**A Reductive-Aggregation Route to $[\text{Mn}_{12}\text{O}_{12}(\text{OMe})_2(\text{O}_2\text{CPh})_{16}(\text{H}_2\text{O})_2]^{2-}$ Single-Molecule Magnets Related to the $[\text{Mn}_{12}]$ Family****

*Anastasios J. Tasiopoulos, Wolfgang Wernsdorfer, Khalil A. Abboud, and George Christou**

An exciting development in nanoscale magnetic materials occurred in 1993 when $[\text{Mn}_{12}\text{O}_{12}(\text{O}_2\text{CMe})_{16}(\text{H}_2\text{O})_4]$ (**1**) was identified as a nanoscale magnet,^[1] the first to comprise discrete, (magnetically) non-interacting molecular units rather than a 3D extended lattice (as in metals and metal oxides, for example). This discovery initiated the field of

[*] Dr. A. J. Tasiopoulos,^[†] Dr. K. A. Abboud, Prof. Dr. G. Christou
Department of Chemistry
University of Florida
Gainesville, FL 32611-7200 (USA)
Fax: (+1) 352-392-8757
E-mail: christou@chem.ufl.edu
Dr. W. Wernsdorfer
Laboratoire Louis Néel-CNRS
BP 166, 25 Avenue des Martyrs, 38042 Grenoble, Cedex 9 (France)

[†] present address:
Department of Chemistry
University of Cyprus, 1678 Nicosia (Cyprus)

[**] This work was supported by the National Science Foundation.

molecular nanomagnetism and such molecules have since been termed single-molecule magnets (SMMs).^[2] They derive their properties from the combination of a large spin (S) and an Ising (easy-axis) magnetoanisotropy (negative zero-field splitting parameter, D). Although several classes of SMMs are now known,^[1–10] there is still a need for new examples to improve our understanding of this phenomenon. Efforts along these lines have been concentrated in two directions: 1) development of synthetic routes to new high nuclearity metal complexes,^[4,5] and 2) modifications of known SMMs in a controlled fashion.^[6–10] The best and most thoroughly studied SMMs to date are members of the $[\text{Mn}_{12}\text{O}_{12}(\text{O}_2\text{CR})_{16}(\text{H}_2\text{O})_4]$ ($[\text{Mn}_{12}]$) family. A number of $[\text{Mn}_{12}]$ derivatives have been prepared in their neutral,^[1,6–8] one-electron^[6f,9] or two-electron^[10] reduced versions with a variety of carboxylate,^[6,9,10] mixed carboxylate,^[7] and mixed carboxylate/non-carboxylate^[8] ligands. In all such modifications, the $[\text{Mn}_{12}(\mu_3\text{-O})_{12}]$ core remains essentially the same.

Herein, we report three new developments: 1) a new synthetic procedure in manganese cluster chemistry involving reductive aggregation of permanganate ($[\text{MnO}_4]^-$) ions in MeOH/benzoic acid solution; 2) its employment to synthesize NnBu_4^+ salts of the new $[\text{Mn}_{12}\text{O}_{12}(\text{OMe})_2(\text{O}_2\text{CPh})_{16}(\text{H}_2\text{O})_2]^{2-}$ cluster ion, which is a structural derivative of the well studied $[\text{Mn}_{12}]$ complexes; and 3) the establishment that this anion is a new SMM.

The synthesis of normal $[\text{Mn}_{12}]$ compound **1** consists of the comproportionation reaction between $\text{Mn}(\text{O}_2\text{CMe})_2 \cdot 4\text{H}_2\text{O}$ and KMnO_4 in 60 % aqueous acetic acid.^[11] In contrast, the new synthetic procedure herein is part of a wider investigation of the reduction of $[\text{MnO}_4]^-$ in alcohol/carboxylic acid mixtures. The present results were obtained from a MeOH/ PhCO_2H medium. Thus, addition of $(\text{NnBu}_4)\text{MnO}_4$ to a methanolic solution of benzoic acid results in the formation of a dark brown solution from which subsequently were obtained essentially black crystals. Recrystallization from CH_2Cl_2 /hexanes results in the formation of two types of black crystals in a total, overall yield of 15 %.

Both types of crystals, diamond-like **2a** and needle-like **2b**, were crystallographically characterized. Both contain the same dianion, abbreviated $[\text{Mn}'_{12}]^{2-}$.



Complex **2a**^[12] crystallizes in the orthorhombic space group $Pbca$ with its asymmetric unit containing half the $[\text{Mn}'_{12}]^{2-}$ cluster and one $[\text{NnBu}_4]^+$ ion, as well as one H_2O and two disordered CH_2Cl_2 solvent molecules. The $[\text{Mn}'_{12}]^{2-}$ ion of **2a** (Figure 1) contains a central $[\text{Mn}^{\text{IV}}_4(\mu_3\text{-O})_2(\mu\text{-O})_2(\mu\text{-OMe})_2]^{6+}$ unit surrounded by a nonplanar ring of eight Mn^{III} atoms that are connected to the central Mn_4 unit by eight bridging $\mu_3\text{-O}^{2-}$ ions. The metal oxidation states and their trapped-valence nature were determined by inspection of the Mn–O bond lengths, manganese bond valence sum calculations,^[13] and the presence of Mn^{III} Jahn–Teller elongation axes for the manganese atoms in the outer ring. The outer Mn_8 ring is very similar to that in normal $[\text{Mn}_{12}]$ compound **1**, but **1** has

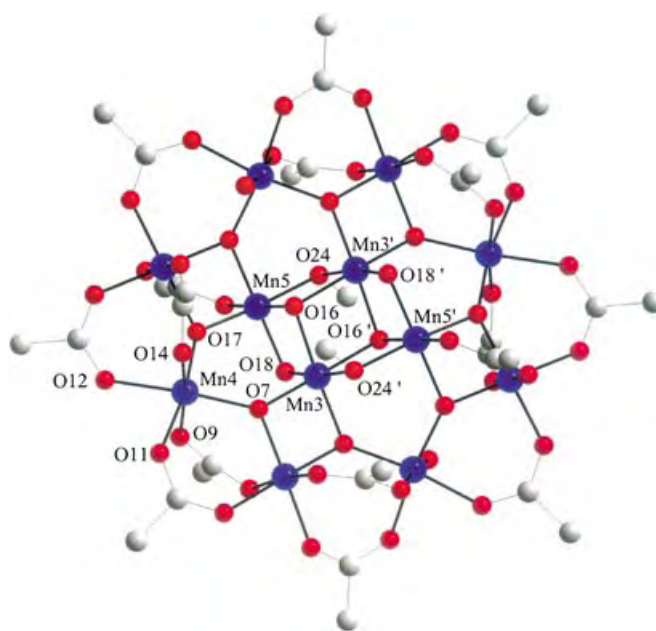


Figure 1. ORTEP plot (thermal ellipsoids set at 50% probability) of the anion of **2a**. For clarity, the benzoate rings have been omitted, except for the *ipso*-carbon atom of each ring; Mn blue, O red, C gray.

a central $[\text{Mn}_4(\mu_3\text{-O})_4]^{8+}$ cubane. The central $[\text{Mn}^{\text{IV}}_4\text{O}_4(\text{OMe})_2]^{6+}$ unit of **2a** comprises a planar Mn_4 rhombus with two $\mu_3\text{-O}^{2-}$ ions (O16, O16'), one above and one below the Mn_4 plane, and a $\mu\text{-O}^{2-}$ (O18, O18') or $\mu\text{-MeO}^-$ (O24, O24') ion bridging each edge of the rhombus. The central unit can thus be described either as a face-sharing dicubane unit with two missing vertices, or as two edge-sharing, oxide-capped Mn_3 triangular units; tetranuclear complexes possessing a core very similar to this central unit have been observed with manganese,^[5a,b] as well as with other transition metals.^[14] Peripheral ligation is completed by 16 bridging benzoate groups and two terminal water molecules. All the manganese atoms are six-coordinate with near octahedral coordination geometries.

Complex **2b** crystallizes in the triclinic space group $P\bar{1}$,^[12a] and its asymmetric unit consists of a half cluster and two halves of $[\text{NnBu}_4]^+$ ions disordered around inversion centers, as well as one disordered H_2O molecule and half a CH_2Cl_2 . The structure of the anion of **2b** is essentially identical to that of **2a**, except for some disorder in the peripheral benzoate rings.

For both **2a** and **2b**, there are Jahn–Teller (JT) distortions at the Mn^{III} ions in the outer ring, consistent with high-spin Mn^{III} centers with near-octahedral coordination geometry. The JT distortion takes the form of an axial elongation, with the elongation axes axial to the Mn_{12} disk-like core and thus roughly parallel to each other. Axially elongated Mn–O bonds are typically at least 0.1–0.2 Å longer than the others. However, there is one anomaly: for **2a** (Figure 1), the JT elongated bonds at Mn4 (Mn4–O9 2.074(4), Mn4–O14 2.080(5) Å) are not as long as those found at the other Mn^{III} ions (2.112(5)–2.250(5) Å), and the *trans* bonds Mn4–O7 (1.958(4) Å) and Mn4–O12 (2.060(5) Å) are longer than expected, especially Mn4–O7, which is unusually long for an

Mn–O^{2−} bond (compare Mn–O^{2−} bonds at the other Mn^{III} ions of 1.876(4)–1.905(4) Å). A similar anomalous situation is present at Mn1 of **2b**. This structural feature at manganese atoms Mn4 of **2a** and Mn1 of **2b** is crucial to understanding the magnetic data (see below).

The anions of complexes **2a** and **2b** are remarkably similar to normal [Mn₁₂] clusters, such as **1**, with the main difference being the structure of the central cores (Figure 2).

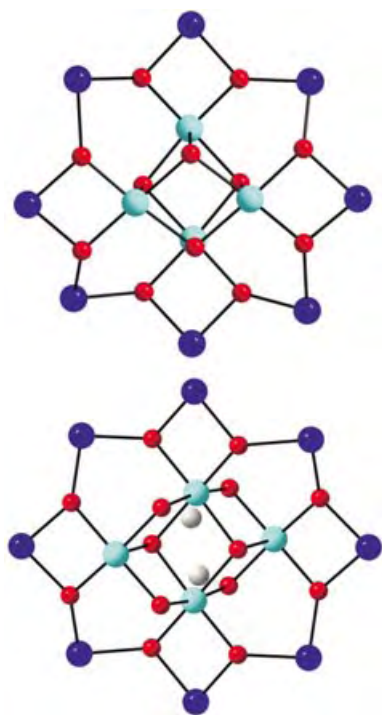


Figure 2. Comparison of the cores of normal [Mn₁₂] complex **1** (top) and the anion of **2a** (bottom); Mn⁴⁺ cyan, Mn³⁺ blue, O red, C gray.

The core of the anions of **2a** and **2b** could be considered the result of partial methanolysis of the central [Mn₄O₄]⁸⁺ cubane of **1**, leading to incorporation of two MeO[−] bridges and a change in the core structure (although we do not claim that this corresponds to its means of formation in the reaction mixture). Note that complexes **1** and **2** are the smallest nuclearity members of a larger family of [Mn^{III}_xMn^{IV}_y] clusters in which there is an outer Mn^{III}_x ring around a central Mn^{IV}_y core. This family currently comprises normal [Mn₁₂] complexes (such as **1**) and **2a/2b** ($x=8$, $y=4$), the Mn₁₆ cluster [Mn₁₆O₁₆(OMe)₆(O₂CMe)₁₆(MeOH)₃(H₂O)₃] ($x=10$, $y=6$),^[4c,15] and the Mn₂₁ cluster [Mn₂₁O₂₄(OMe)₈(O₂CCH₂-*i*Bu)₁₆(H₂O)₁₀] ($x=12$, $y=9$).^[16]

The structural similarity between complexes **1** and **2** suggested that **2** might also be an SMM. Thus AC magnetic susceptibility measurements were performed on a polycrystalline sample of **2** (containing both **2a** and **2b**) in the temperature range 1.8–10 K using a 3.5 G AC field oscillating at 5–500 Hz frequencies (ν). These studies revealed two frequency-dependent out-of-phase (χ_m'') AC signals (Figure 3), one in the higher temperature (HT) range of 3–5 K, and a second one at lower temperatures (LT) whose

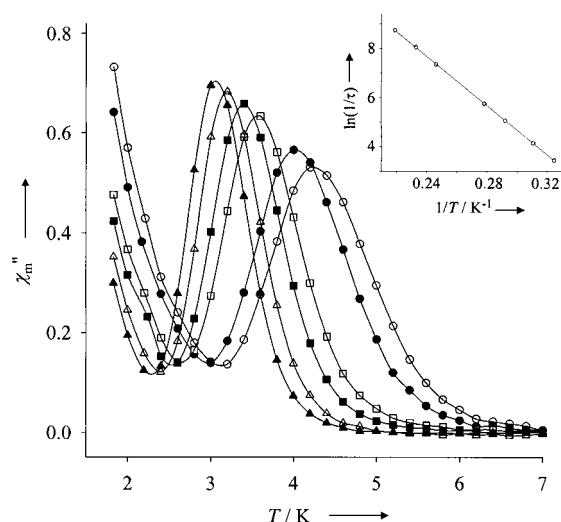


Figure 3. Plot of χ_m'' versus T for a microcrystalline sample of **2** suspended in solid eicosane at 500 (○), 250 (●), 50 (□), 25 (■), 10 (△), 5 Hz (▲). Inset: Plot of the natural logarithm of relaxation rate, $\ln(1/\tau)$ versus inverse temperature using the χ_m'' versus T data for the slower relaxing species (higher temperature data). The solid line is a fit to the Arrhenius equation; see the text for the fitting parameters.

peaks clearly occur at temperatures below the operating limit of our SQUID (superconducting quantum interference device) instrument (1.8 K). The LT and HT χ_m'' signals correspond to faster and slower relaxation rates, respectively. The peak of a χ_m'' versus T plot represents the temperature at which the magnetization relaxation rate equals the angular frequency $\omega (=2\pi\nu)$, and the χ_m'' versus T data at different frequencies (ν) were therefore used as a source of kinetic data to construct an Arrhenius plot (Figure 3, inset) based on the Arrhenius equation in Equation (1), where $1/\tau$ is the relax-

$$1/\tau = 1/\tau_0 \exp(-U_{\text{eff}}/kT) \quad (1)$$

ation rate (τ is the relaxation time), $1/\tau_0$ is the pre-exponential factor, U_{eff} is the effective relaxation barrier, and k is the Boltzmann constant. The fit of the data to Equation (1) gave $U_{\text{eff}} = 50.1$ K and $1/\tau_0 = 3.61 \times 10^8 \text{ s}^{-1}$. This U_{eff} value is smaller than that of normal [Mn₁₂] complexes; complex **1**, for example, has a U_{eff} of 60–65 K.

The observation of out-of-phase AC signals suggests that **2** might be an SMM, although such signals by themselves are not proof of an SMM. It is also tempting to assume that the two χ_m'' signals in Figure 3 are due to the two crystal forms, diamondlike **2a** and needlelike **2b**. To confirm whether **2a** and/or **2b** are indeed SMMs, and to assess any difference between the two forms, magnetization versus DC field sweep studies were performed on single crystals of **2a** and **2b** by using a micro-SQUID apparatus.^[17] The resulting hysteresis loops are shown in Figure 4, and their coercivities 1) increase with decreasing T at a constant field sweep rate, and 2) increase with increasing sweep rate at a constant T (not shown). This situation is as expected for the superparamagnet-like properties of an SMM.

However, it is clear that the observed properties (hysteresis loops) of **2a** and **2b** are very similar, and this is totally

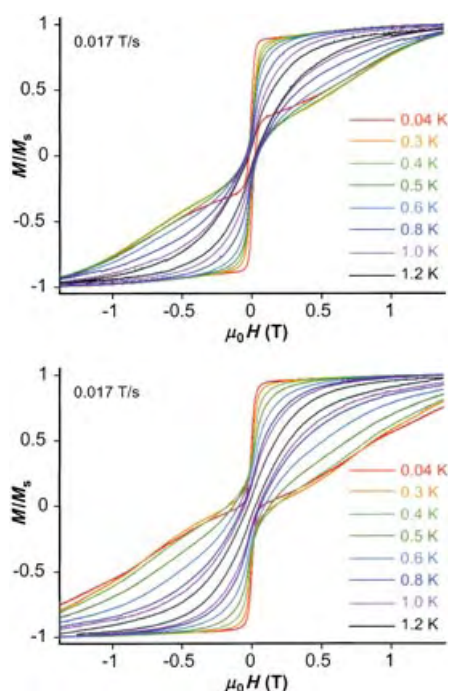


Figure 4. Magnetization (M) versus applied magnetic field ($\mu_0 H$) hysteresis loops for a single crystal (wet with mother liquor) of **2a** (top) and **2b** (bottom) at the indicated temperatures. M is normalized to its saturation value, M_s .

inconsistent with the two very different AC signals in Figure 3 and the at-first-glance “obvious” conclusion that the two signals are due to the two crystal forms. In fact, the hysteresis loops of both **2a** and **2b** suggest a mixture of faster relaxing (LT) and slower relaxing (HT) forms, the faster relaxing being responsible for the large decrease in magnetization at zero field, and the slower relaxing being responsible for the subsequent feature at higher fields. The relative proportions of these two features suggest comparable amounts of the LT and HT forms in each crystal, with perhaps a slightly greater amount of the LT, and this situation is again consistent with the relative proportion of LT and HT AC signals shown in Figure 3. Note that the hysteresis studies were performed on wet single-crystals and the AC studies on microcrystals suspended in solid eicosane, and thus not strictly speaking on the same material. Nevertheless, we conclude that 1) complex **2** is a new SMM, 2) the different space groups of diamond-like **2a** and needle-like **2b** lead to only small differences in the magnetic properties of the $[\text{Mn}_{12}\text{O}_{12}(\text{O}-\text{Me})_2(\text{O}_2\text{CPh})_{16}(\text{H}_2\text{O})_2]^{2-}$ ion, and 3) there are faster and slower relaxing forms of complex **2** that cocrystallize in the same crystal. In fact, the existence of cocrystallized faster and slower relaxing forms of **1** has long been known, with crystals of **1** containing about 5 % of the faster relaxing form;^[6f] in this respect complex **2** only differs from **1** in the relative amounts of the two forms.

For normal $[\text{Mn}_{12}]$ complexes, we have reported elsewhere that crystals of pure faster relaxing forms can be prepared with, for example, *tert*-butylacetate as the carboxylate group.^[6d,g] Crystallography on such crystals has allowed the origin of the faster relaxing form to be identified as the

abnormal orientation of one of the Mn^{III} JT elongation axes, being disposed equatorial rather than axial to the Mn_{12} disk-like plane, and thus this JT axis points towards a core O^{2-} ion. We have named this “Jahn–Teller isomerism”. The same effect is likely to be the origin of the two forms of **2**. Indeed, this phenomenon rationalizes the unusual Mn–O bond lengths at Mn4 for **2a** and Mn1 for **2b**. For **2a**, for example, an approximately equal mixture of a) slower relaxing species with the JT axis at Mn4 in the normal position along the O9–Mn4–O14 axis, and b) faster relaxing species with the JT axis at Mn4 abnormally aligned along the O7–Mn4–O12 axis, will lead to the crystallographic average result that the O9–Mn4–O14 bonds are shorter and the O7–Mn4–O12 bonds are longer than they should be, which is what is seen (similarly for **2b**). We thus feel that the crystallographic data support the conclusion from the magnetic studies that crystals of **2a** and **2b** comprise a mixture of slower and faster relaxing species which result from normal and abnormal orientations, respectively, of a Mn^{III} JT elongation axis. As with normal $[\text{Mn}_{12}]$ complexes, it will require crystallization of pure crystals of the different forms of **2** to allow more detailed study.

In summary, we have developed access to a variant of the $[\text{Mn}_{12}]$ family of SMMs by using a reductive-aggregation route. This structurally very similar variant is also an SMM and, like normal $[\text{Mn}_{12}]$ complexes, displays both faster and slower relaxing magnetization dynamics that we assign to the presence of Jahn–Teller isomerism. We have in the past obtained many derivatives of $[\text{Mn}_{12}]$ complexes, for example, by carboxylate substitution,^[6,7] one- and two-electron reduction,^[6f,9,10] introduction of non-carboxylate ligands,^[8] and similar derivatization of **2** may also prove possible, in which case it is merely the prototype of what could become a large new family of related SMMs.

Experimental Section

2: Freshly-prepared $(\text{NBu}_4)\text{MnO}_4$ (1.0 g, 2.8 mmol) was added in small portions to a solution of benzoic acid (5.0 g, 40.9 mmol) in MeOH (15 ml), and the mixture stirred for about 5 min. The resulting purple solution was left undisturbed at room temperature overnight. During this time, the color slowly turned dark brown, and black crystals slowly formed. These crystals, which were found to be poor diffractors of X-rays, were collected by filtration, washed with MeOH (2×10 mL) and dried in vacuo. The material was recrystallized from CH_2Cl_2 /hexanes to give a mixture of diamond-shaped crystals of **2a** and needle-shaped crystals of **2b** in an overall yield of 0.12 g (15 % based on Mn). These were collected by filtration, washed with hexanes, and dried in vacuo. Both **2a** and **2b** were good diffractors of X-rays, as long as they were kept in contact with the mother liquor to prevent solvent loss. Elemental analysis of dried solid: (%) calcd for $\text{C}_{146}\text{H}_{166}\text{N}_2\text{O}_{50}\text{Mn}_{12}$ (**2**·2 H_2O): C 51.45, H 4.91, N 0.82; found: C 51.26, H 4.72, N 0.70. Selected IR data (KBr pellet): $\tilde{\nu} = 3430$ (s, br), 3065 (w), 2965 (w), 2925 (w), 2875 (w), 1598 (s), 1560 (s), 1532 (s), 1492 (m), 1448 (m), 1417 (s), 1306 (w), 1177 (m), 1069 (w), 1026 (m), 838 (w), 718 (s), 675 (s), 625 (m, br), 499 (m) cm^{-1} .

Received: August 5, 2004

Keywords: cluster compounds · Jahn–Teller effect · manganese · O ligands · single-molecule magnets

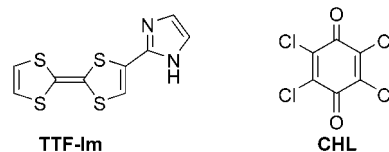
- [1] a) R. Sessoli, H.-L. Tsai, A. R. Schake, S. Wang, J. B. Vincent, K. Folting, D. Gatteschi, G. Christou, D. N. Hendrickson, *J. Am. Chem. Soc.* **1993**, *115*, 1804; b) R. Sessoli, D. Gatteschi, A. Caneschi, M. A. Novak, *Nature* **1993**, *365*, 141.
- [2] S. M. J. Aubin, M. W. Wemple, D. M. Adams, H.-L. Tsai, G. Christou, D. N. Hendrickson, *J. Am. Chem. Soc.* **1996**, *118*, 7746.
- [3] a) G. Christou, D. Gatteschi, D. N. Hendrickson, R. Sessoli, *MRS Bull.* **2000**, *25*, 66; b) D. Gatteschi, R. Sessoli, *Angew. Chem.* **2003**, *115*, 278; *Angew. Chem. Int. Ed.* **2003**, *42*, 268.
- [4] a) A. J. Tasiopoulos, W. Wernsdorfer, B. Moulton, M. J. Zaworotko, G. Christou, *J. Am. Chem. Soc.* **2003**, *125*, 15274; b) A. J. Tasiopoulos, A. Vinslava, W. Wernsdorfer, K. A. Abboud, G. Christou, *Angew. Chem.* **2004**, *116*, 2169; *Angew. Chem. Int. Ed.* **2004**, *43*, 2117; c) D. J. Price, S. R. Batten, B. Moubaraki, K. S. Murray, *Chem. Commun.* **2002**, 762; d) S. M. J. Aubin, N. R. Dilley, L. Pardi, J. Krzystek, M. W. Wemple, L.-C. Brunel, M. B. Maple, G. Christou, D. N. Hendrickson, *J. Am. Chem. Soc.* **1998**, *120*, 4991; e) M. Soler, W. Wernsdorfer, K. Folting, M. Pink, G. Christou, *J. Am. Chem. Soc.* **2004**, *126*, 2156; f) E. K. Brechin, M. Soler, G. Christou, M. Helliwell, S. J. Teat, W. Wernsdorfer, *Chem. Commun.* **2003**, 1276.
- [5] a) E. K. Brechin, J. Yoo, M. Nakano, J. C. Huffman, D. N. Hendrickson, G. Christou, *Chem. Commun.* **1999**, 783; b) J. Yoo, E. K. Brechin, A. Yamaguchi, M. Nakano, J. C. Huffman, A. L. Maniero, L.-C. Brunel, K. Awaga, H. Ishimoto, G. Christou, D. N. Hendrickson, *Inorg. Chem.* **2000**, *39*, 3615; c) E. K. Brechin, M. Soler, J. Davidson, D. N. Hendrickson, S. Parsons, G. Christou, *Chem. Commun.* **2002**, 2252; d) L. F. Jones, E. K. Brechin, D. Collison, A. Harrison, S. J. Teat, W. Wernsdorfer, *Chem. Commun.* **2002**, 2974; e) M. Moragues-Canovas, M. Helliwell, L. Ricard, E. Riviere, W. Wernsdorfer, E. Brechin, T. Mallah, *Eur. J. Inorg. Chem.* **2004**, 2219; f) C. J. Milios, C. P. Raptopoulou, A. Terzis, F. Lloret, R. Vicente, S. P. Perlepes, A. Escuer, *Angew. Chem.* **2004**, *116*, 212; *Angew. Chem. Int. Ed.* **2004**, *43*, 210; g) A. K. Boudalis, B. Donnadieu, V. Nastopoulos, J. M. Clemente-Juan, A. Mari, Y. Sanakis, J.-P. Tuchagues, S. P. Perlepes, *Angew. Chem.* **2004**, *116*, 2316; *Angew. Chem. Int. Ed.* **2004**, *43*, 2266; h) H. Andres, R. Basler, A. J. Blake, C. Cadiou, G. Chaboussant, C. M. Grant, H.-U. Güdel, M. Murrie, S. Parsons, C. Paulsen, F. Semadini, V. Villar, W. Wernsdorfer, R. E. P. Winpenny, *Chem. Eur. J.* **2002**, *8*, 4867.
- [6] a) S. M. J. Aubin, Z. Sun, I. A. Guzei, A. L. Rheingold, G. Christou, D. N. Hendrickson, *Chem. Commun.* **1997**, 2239; b) Z. Sun, D. Ruiz, E. Rumberger, C. D. Incarvito, K. Folting, A. L. Rheingold, G. Christou, D. N. Hendrickson, *Inorg. Chem.* **1998**, *37*, 4758; c) D. Ruiz, Z. Sun, B. Albela, K. Folting, J. Ribas, G. Christou, D. N. Hendrickson, *Angew. Chem.* **1998**, *110*, 315; *Angew. Chem. Int. Ed.* **1998**, *37*, 300; d) Z. Sun, D. Ruiz, N. R. Dilley, M. Soler, J. Ribas, K. Folting, M. B. Maple, G. Christou, D. N. Hendrickson, *Chem. Commun.* **1999**, 1973; e) S. M. J. Aubin, Z. Sun, H. J. Eppley, E. M. Rumberger, I. A. Guzei, K. Folting, P. K. Gantzel, A. L. Rheingold, G. Christou, D. N. Hendrickson, *Inorg. Chem.* **2001**, *40*, 2127; f) H. J. Eppley, H.-L. Tsai, N. de Vries, K. Folting, G. Christou, D. N. Hendrickson, *J. Am. Chem. Soc.* **1995**, *117*, 301; g) M. Soler, W. Wernsdorfer, Z. Sun, J. C. Huffman, D. N. Hendrickson, G. Christou, *Chem. Commun.* **2003**, 2672–2673.
- [7] M. Soler, P. Artus, K. Folting, J. C. Huffman, D. N. Hendrickson, G. Christou, *Inorg. Chem.* **2001**, *40*, 4902.
- [8] P. Artus, C. Boskovic, J. Yoo, W. E. Streib, L.-C. Brunel, D. N. Hendrickson, G. Christou, *Inorg. Chem.* **2001**, *40*, 4199; b) C. Boskovic, M. Pink, J. C. Huffman, D. N. Hendrickson, G. Christou, *J. Am. Chem. Soc.* **2001**, *123*, 9914; c) N. E. Chakov, W. Wernsdorfer, K. A. Abboud, D. N. Hendrickson, G. Christou, *Dalton Trans.* **2003**, 2243.
- [9] a) S. M. J. Aubin, Z. Sun, L. Pardi, J. Krzystek, K. Folting, L.-C. Brunel, A. L. Rheingold, G. Christou, D. N. Hendrickson, *Inorg. Chem.* **1999**, *38*, 5329; b) T. Kuroda-Sowa, M. Lam, A. L. Rheingold, C. Frommen, W. M. Reiff, M. Nakano, J. Yoo, A. L. Maniero, L.-C. Brunel, G. Christou, D. N. Hendrickson, *Inorg. Chem.* **2001**, *40*, 6469.
- [10] a) M. Soler, S. K. Chandra, D. Ruiz, E. R. Davidson, D. N. Hendrickson, G. Christou, *Chem. Commun.* **2000**, 2417; b) M. Soler, W. Wernsdorfer, K. A. Abboud, J. C. Huffman, E. R. Davidson, D. N. Hendrickson, G. Christou, *J. Am. Chem. Soc.* **2003**, *125*, 3576.
- [11] T. Lis, *Acta Crystallogr. Sect. B* **1980**, *36*, 2042.
- [12] a) Crystal structure data for $2\cdot 2\text{H}_2\text{O}\cdot 4\text{CH}_2\text{Cl}_2$ (**2a**): $\text{C}_{150}\text{H}_{174}\text{Cl}_8\text{Mn}_{12}\text{N}_2\text{O}_{50}$, $M_r=3747.90$, orthorhombic, *Pbca*, $a=25.476(2)$, $b=20.933(2)$, $c=31.206(2)$ Å, $V=16642(2)$ Å³, $T=173$ K, $Z=4$, $\rho_{\text{calcd}}=1.502$ g cm⁻³, 86166 reflections collected, 14638 unique ($R_{\text{int}}=0.1115$), $R1=0.0642$, $wR2=0.1585$, using 7705 reflections with $I>2\sigma(I)$. Crystal structure data for $2\cdot 2\text{H}_2\text{O}\cdot \text{CH}_2\text{Cl}_2$ (**2b**): $\text{C}_{147}\text{H}_{168}\text{Cl}_2\text{Mn}_{12}\text{N}_2\text{O}_{50}$, $M_r=3493.09$, triclinic, $P\bar{1}$, $a=16.357(1)$, $b=17.480(2)$, $c=17.617(2)$ Å, $\alpha=105.982(2)^\circ$, $\beta=111.329(2)^\circ$, $\gamma=108.680(2)^\circ$, $V=3982.5(4)$ Å³, $T=173$ K, $Z=1$, $\rho_{\text{calcd}}=1.348$ g cm⁻³, 26397 reflections collected, 17568 unique ($R_{\text{int}}=0.0489$), $R1=0.0696$, $wR2=0.1731$, using 8580 reflections with $I>2\sigma(I)$. The dichloromethane molecules of **2a** and the tetrabutylammonium cations of **2b** were disordered and could not be modeled properly, thus program SQUEEZE, a part of the PLATON package^[12b] of crystallographic software, was used to calculate the solvent disorder area and remove its contribution to the overall intensity data. CCDC-246482 (**2a**) and CCDC-246483 (**2b**) contain the supplementary crystallographic data for this paper. These data can be obtained free of charge via www.ccdc.cam.ac.uk/conts/retrieving.html (or from the Cambridge Crystallographic Data Centre, 12 Union Road, Cambridge CB21EZ, UK; fax: (+44) 1223-336-033; or deposit@ccdc.cam.ac.uk); b) PLATON: A. L. Spek, *Acta Crystallogr. Sect. A* **1990**, *46*, 1–34.
- [13] a) Bond valence sum calculations for Mn^{III} and Mn^{IV} ions of **2a** and **2b** gave oxidation state values of 2.89–3.02 (Mn^{III}) and 4.00–4.18 (Mn^{IV}); W. Liu, H. H. Thorp, *Inorg. Chem.* **1993**, *32*, 4102.
- [14] For example, see a) M. J. Manos, A. J. Tasiopoulos, E. J. Tolis, N. Laloti, J. D. Woolins, A. M. Z. Slawin, M. P. Sigalas, T. A. Kabanos, *Chem. Eur. J.* **2003**, *9*, 695; b) H. Kang, S. Liu, S. N. Shaikh, T. Nicholson, J. Zubietta, *Inorg. Chem.* **1989**, *28*, 920.
- [15] P. King, W. Wernsdorfer, K. A. Abboud, G. Christou, *Inorg. Chem.*, in press.
- [16] J. T. Brockman, J. C. Huffman, G. Christou, *Angew. Chem. Int. Ed.* **2002**, *41*, 2506.
- [17] W. Wernsdorfer, E. Bonet Orozco, K. Hasselbach, A. Benoit, D. Mailly, O. Kubo, H. Nakano, B. Barbara, *Phys. Rev. Lett.* **1997**, *79*, 4014.

A Purely Organic Molecular Metal Based on a Hydrogen-Bonded Charge-Transfer Complex: Crystal Structure and Electronic Properties of TTF-Imidazole-*p*-Chloranil**

Tsuyoshi Murata, Yasushi Morita,* Kozo Fukui, Kazunobu Sato, Daisuke Shiomi, Takeji Takui, Mitsuhiro Maesato, Hideki Yamochi, Gunzi Saito,* and Kazuhiro Nakasuji*

The control of the relative molecular orientation of redox-active molecules is of great importance for constructing organic conductors and superconductors.^[1] Ingenious manipulation of noncovalent interactions such as hydrogen bonding (H-bonding) is an efficient tool for creation of desired molecular arrangements.^[2] Thus, a variety of tetrathiafulvalene (TTF) derivatives with H-bonding functionality have been synthesized.^[3] However, most of these gave insulating or semiconducting charge-transfer (CT) complexes and salts,^[3] while CT salts of ethylenedithio-TTF-CONHMe with inorganic anions solely exhibited metallic behavior.^[3c,d] The imidazole ring system has been utilized as an interesting building block for H-bonded CT complexes^[4] and assembled metal complexes.^[5] Recently, we have designed TTF derivatives substituted with an imidazole moiety, TTF-Im, for exploring molecular conductors with highly ordered molecular aggregation by H-bonding.^[6] We report here the first purely organic molecular metal based on the H-bonded CT complex composed of TTF-Im and *p*-chloranil (CHL), in

which the component ratio and electron-accepting ability of CHL are controlled by H-bonding.^[7]



In CV measurements, TTF-Im shows the first oxidation potential at -0.06 V vs Fc/Fc^+ , which is close to that of TTF (-0.09 V).^[6] Single crystals of TTF-Im were obtained by the vapor diffusion method with hexane/THF.^[8] In the crystal structure of TTF-Im, the imidazole moiety is twisted by $15.5(1)^\circ$ from the TTF skeleton. The imidazole ring forms a one-dimensional chain by $\text{N}-\text{H}\cdots\text{N}$ H-bonding interaction (3.06 Å) along the *a* axis in a zigzag fashion similar to that of imidazole^[9] (Figure 1). The TTF-Im molecule uniformly

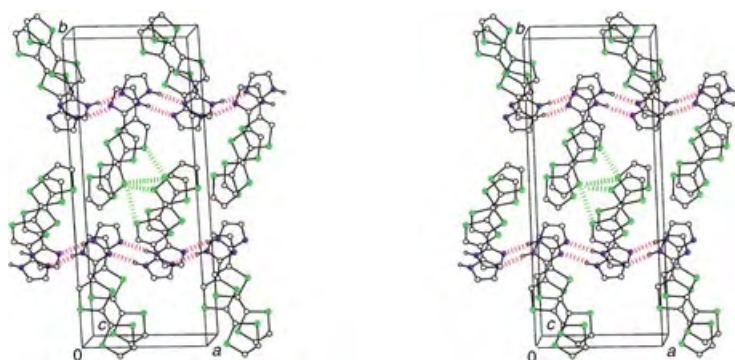


Figure 1. Stereoview of the crystal packing of TTF-Im, showing $\text{N}-\text{H}\cdots\text{N}$ H-bonding (red), π -stacking columns, and $\text{S}\cdots\text{S}$ contacts (green) between columns.

stacks and forms a columnar structure parallel to the *c* axis with a face-to-face distance of 3.66 Å. The column is connected by H-bonding and intercolumnar $\text{S}\cdots\text{S}$ contacts (3.48 and 3.57 Å) along the *a* axis (Figure 1) to give a three-dimensional network.

The CT complex $(\text{TTF-Im})_2(\text{CHL})$ was obtained as black needlelike crystals by diffusion of a solution of TTF-Im and CHL in acetonitrile containing 2 vol % ethanol in an H-shaped tube.^[7,10,11] The $\text{C}=\text{O}$ stretching frequency of 1532 cm^{-1} in the IR spectrum indicates that the CHL molecule exists as a radical anion.^[12] Thus, the ionicity of TTF-Im is estimated to be $+0.5$.^[13] Crystal structure analysis shows that the molecular structure of TTF-Im is nearly planar, with a small dihedral angle of $5.5(1)^\circ$ between the TTF and imidazole moieties, and the CHL molecule lies on the inversion center (Figure 2). The CHL forms a bifurcated triad with two TTF-Im molecules through double $\text{N}-\text{H}\cdots\text{O}$ H-bonding interactions. Because these H-bonds increase the electron-accepting ability of the CHL molecule, the CHL in the complex is a completely one-electron reduced.^[14] Each component molecule forms a uniform stacking column along the *a* axis with interplanar distances of 3.46 Å for TTF-Im and 3.19 Å for CHL. Furthermore, side-by-side $\text{S}\cdots\text{S}$ contacts

[*] T. Murata, Prof. Dr. Y. Morita, Prof. Dr. K. Nakasuji
Department of Chemistry, Graduate School of Science
Osaka University
Toyonaka, Osaka 560-0043 (Japan)
Fax: (+81) 6-6850-5395
E-mail: morita@chem.sci.osaka-u.ac.jp

Prof. Dr. M. Maesato, Prof. Dr. G. Saito
Division of Chemistry, Graduate School of Science
Kyoto University
Sakyo-ku, Kyoto 606-8502 (Japan)
Fax: (+81) 75-753-4035

Prof. Dr. K. Sato, Prof. Dr. D. Shiomi, Prof. Dr. T. Takui
Departments of Chemistry and Materials Science
Graduate School of Science
Osaka City University
Sumiyoshi-ku, Osaka 558-8585 (Japan)

Prof. Dr. H. Yamochi
Research Center for Low Temperature and Materials Science
Kyoto University
Sakyo-ku, Kyoto 606-8502 (Japan)

Prof. Dr. Y. Morita, Dr. K. Fukui
PRESTO, JST (Japan)

[**] This work was partially supported by PRESTO-JST, and by 21COE program "Creation of Integrated EcoChemistry of Osaka University".

Supporting information for this article is available on the WWW under <http://www.angewandte.org> or from the author.

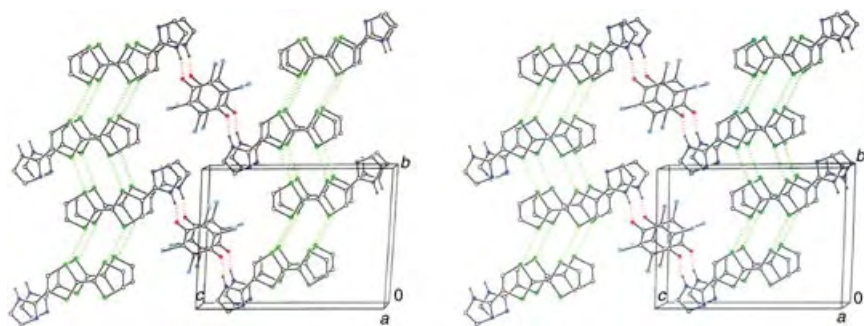


Figure 2. Stereoview of the crystal packing of $(\text{TTF-Im})_2(\text{CHL})$. The dashed lines show the intermolecular interactions: N–H...O H-bonding (red) and S...S contacts (green).

between TTF columns (3.51–3.57 Å) along the *b* axis form a two-dimensional donor layer parallel to the *ab* plane. Together with the double H-bonding of CHL, this results in a three-dimensional network of intermolecular interactions in the crystal.

Intermolecular overlap integrals of the HOMO of the donor molecules in the CT complex, calculated by the extended Hückel method, are summarized in Figure 3a.^[15]

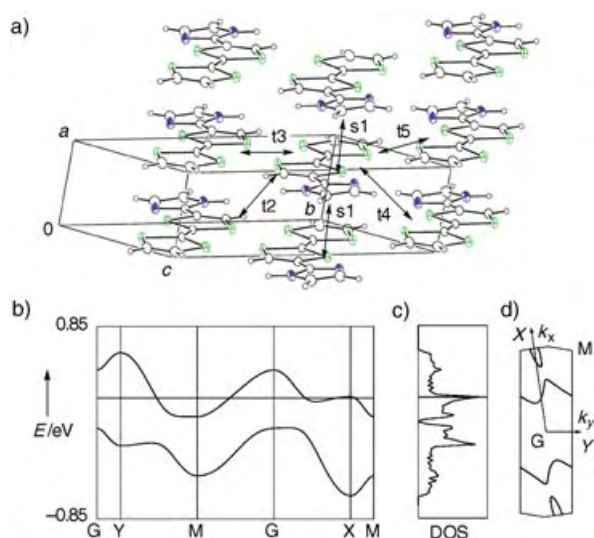


Figure 3. a) Packing pattern of the donor molecules; letters indicate intermolecular overlap integrals ($s_1 = -20.77$, $t_2 = 0.94$, $t_3 = -5.44$, $t_4 = 10.73$, $t_5 = -0.62$). b) Energy dispersion, c) density of states, and d) Fermi surface of $(\text{TTF-Im})_2(\text{CHL})$, calculated by the extended Hückel method with tight-binding approximation.

Although the strongest overlap integral (s_1) was observed along the stacking direction, interactions on the same order of magnitude (t_3 , t_4) were also calculated in the side-by-side directions. The tight-binding approximation gave the energy dispersion, density of states, and Fermi surfaces shown in Figure 3b–d. As shown in Figure 3b, the dispersion affords two bands having a gap of 0.05 eV, the upper one of which is half-filled. The main parts of the Fermi surfaces in Figure 3d exhibit a strongly warped one-dimensional feature. Along with these open surfaces, a hole pocket around point X was derived.

The static paramagnetic susceptibility χ_p of the polycrystalline sample showed nearly temperature-independent behavior in the range of 170–350 K, and its value of $+5.7 \times 10^{-4} \text{ emu mol}^{-1}$ per $(\text{TTF-Im})_2(\text{CHL})$ unit is consistent with Pauli paramagnetism (Figure 4). The χ_p value slightly decreased below 170 K, and after passing through a minimum at 90 K, a strongly temperature-dependent component appeared to increase the total χ_p in the lower temperature region (Figure 4). The magnetic field dependence of the magnetization at 1.9 K revealed that the temperature-dependent part of

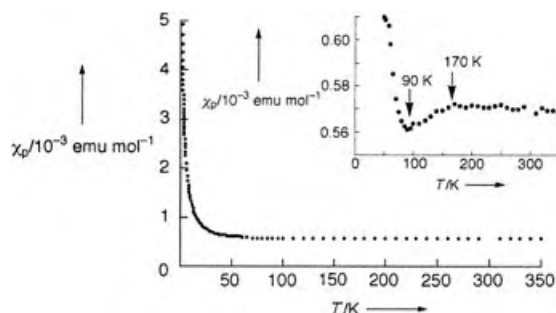


Figure 4. Temperature dependence of magnetic susceptibility after correction of Pascal diamagnetism for a polycrystalline sample of $(\text{TTF-Im})_2(\text{CHL})$. The inset shows a magnification of the plot.

χ_p is attributed to 1.1 % of nearly isolated $S = 1/2$ spins.^[16] No such temperature-dependent contribution was observed above 170 K, and this suggests that the generation of such a component may be associated with the subtle anomaly around 90–170 K.

The ESR spectra of the polycrystalline sample at 296 K showed a single Lorentzian absorption with $g = 2.0068$ (Figure 5). The ESR linewidth ΔB ^[17] steadily decreased on lowering the temperature (inset to Figure 5) and finally became sharp enough to resolve g anisotropy as (g_{xx} , g_{yy} , g_{zz}) =

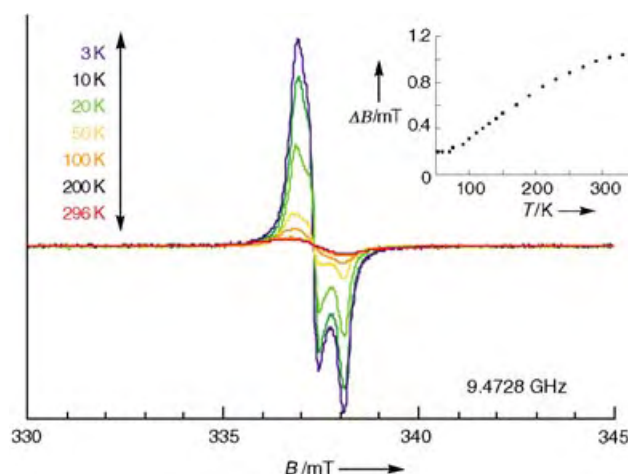


Figure 5. Temperature dependence of ESR spectra for a polycrystalline sample of $(\text{TTF-Im})_2(\text{CHL})$. The inset shows the temperature dependence of ESR linewidth ΔB .^[17]

(2.0101, 2.0075, 2.0028), which are characteristic values of TTF⁺ derivatives. The ESR signal intensity exhibits nearly identical behavior to χ_p at all temperatures. The above results show that the TTF-Im column acts a pathway for electrical conduction. In contrast, no ESR absorption originating from uniformly stacked CHL⁻ molecules was observed, probably because the short interplane distance of CHL⁻ (3.19 Å) and the large orbital overlaps induce a strong antiferromagnetic interaction that quenches paramagnetism. Density functional theory calculations gave support to this conjecture. For a pair of CHL⁻ molecules in the uniform column taken from the X-ray structure, the exchange coupling was calculated to be $2J/k_B = -2677$ K,^[18] which results in negligible paramagnetic contribution below 350 K as long as a one-dimensional magnetic chain is considered (Bonner–Fisher model^[19]).

The temperature dependence of electrical conductivity for the single crystal along the π -stacking direction confirms metallic behavior down to about 180 K, below which the resistivity increases gradually (activation energy 20 meV; Figure 6). The room-temperature electrical conductivity of

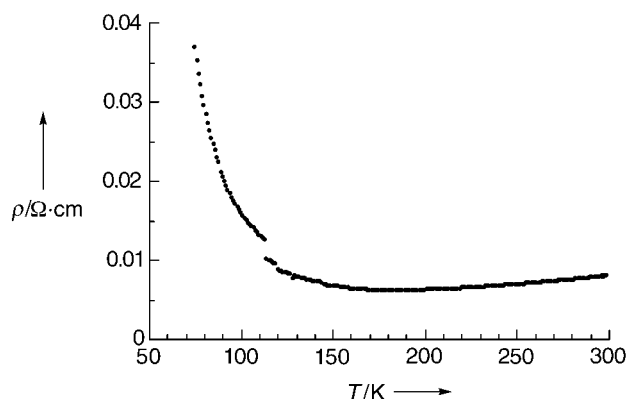


Figure 6. Temperature dependence of electrical resistivity of (TTF-Im)₂(CHL) measured by the four-probe method along the long axis (*a* axis) of a needlelike crystal.

this complex of $\sigma_{\text{rt}} = 124$ S cm⁻¹ is comparable to those of CT salts of ethylenedithio-TTF-CONHMe^[3c,d] and TTF-TCNQ complexes,^[20] and 10⁴–10⁷ orders of magnitude higher than those of CT complexes with organic electron acceptors based on H-bonded TTF derivatives.^[3] Clarification of the subtle anomaly in magnetic and electric properties at 90–180 K is the subject of further study.

In conclusion, we have prepared the first purely organic molecular metal based on an H-bonded CT complex. The absence of an abrupt change like the Peierls transition shows that the H-bonding interaction plays a vital role in transport properties by increasing dimensionality. Furthermore, we emphasize the ability of H-bonding interactions to control the electron-accepting ability of CHL and the donor/acceptor ratio by the formation of H-bonded triad of TTF-Im and CHL. We believe that these salient features of H-bonding interactions in purely organic CT complexes demonstrate a new concept for the molecular design of organic conductors.^[21]

Received: May 27, 2004

Keywords: conducting materials · crystal engineering · hydrogen bonds · magnetic properties

- a) M. R. Bryce, *J. Mater. Chem.* **1995**, 5, 1481; b) P. Batail, K. Boubekeur, M. Fourmigué, J.-C. P. Gabriel, *Chem. Mater.* **1998**, 10, 3005.
- For a recent overview of H-bonding, see *The Weak Hydrogen Bond* (Eds.: G. R. Desiraju, T. Steiner), Oxford University Press, New York, **1999**, chap. 1.
- Examples of H-bonded TTF derivatives: Hydroxymethyl: a) P. Blanchard, K. Boubekeur, M. Sallé, G. Duguay, M. Jubault, A. Gorgues, J. D. Martin, E. Canadell, P. Auban-Senzier, D. Jérôme, P. Batail, *Adv. Mater.* **1992**, 4, 579. Carboxy: b) A. Dolbecq, M. Fourmigué, P. Batail, *Bull. Soc. Chim. Fr.* **1996**, 133, 83; Amide: c) K. Heuzé, C. Mézière, M. Fourmigué, P. Batail, C. Coulon, E. Canadell, P. Auban-Senzier, D. Jérôme, *Chem. Mater.* **2000**, 12, 1898; d) K. Heuzé, M. Fourmigué, P. Batail, E. Canadell, P. Auban-Senzier, *Chem. Eur. J.* **1999**, 5, 2971; e) S. A. Baudron, N. Avarvari, P. Batail, C. Coulon, R. Clérac, E. Canadell, P. Auban-Senzier, *J. Am. Chem. Soc.* **2003**, 125, 11 583. Thioamide: f) A. J. Moore, M. R. Bryce, A. S. Batsanov, J. N. Heaton, C. W. Lehmann, J. A. K. Howard, N. Robertson, A. E. Underhill, I. F. Perepichka, *J. Mater. Chem.* **1998**, 8, 1541. Nucleic acid: g) Y. Morita, S. Maki, M. Ohmoto, H. Kitagawa, T. Okubo, T. Mitani, K. Nakasuji, *Org. Lett.* **2002**, 4, 2185. Pyrrole-fused: h) K. Zong, W. Chen, M. P. Cava, R. D. Rogers, *J. Org. Chem.* **1996**, 61, 8117; i) J. O. Jeppesen, K. Takimiya, F. Jensen, T. Brimert, K. Nielsen, N. Thorup, J. Becher, *J. Org. Chem.* **2000**, 65, 5794; j) K. A. Nielsen, J. O. Jeppesen, E. Levillain, J. Becher, *Angew. Chem.* **2003**, 115, 197; *Angew. Chem. Int. Ed.* **2003**, 42, 187; for a review, see: k) J. O. Jeppesen, J. Becher, *Eur. J. Org. Chem.* **2003**, 3245. Uracil-fused: l) O. Neilands, S. Belyakov, V. Tilika, A. Edzina, *J. Chem. Soc. Chem. Commun.* **1995**, 325; m) O. Neilands, V. Liepinsh, B. Turovska, *Org. Lett.* **1999**, 1, 2065; n) K. Balodis, S. Khasanov, C. Chong, M. Maesato, H. Yamochi, G. Saito, O. Neilands, *Synth. Met.* **2003**, 133–134, 353.
- a) T. Akutagawa, G. Saito, *Bull. Chem. Soc. Jpn.* **1995**, 68, 1753; b) T. Akutagawa, G. Saito, M. Kusunoki, K. Sakaguchi, *Bull. Chem. Soc. Jpn.* **1996**, 69, 2487.
- a) M. Tadokoro, H. Kanno, T. Kitajima, H. S. Umemoto, N. Nakanishi, K. Isobe, K. Nakasuji, *Proc. Natl. Acad. Sci. USA* **2002**, 99, 4950; b) Y. Morita, T. Murata, K. Fukui, M. Tadokoro, K. Sato, D. Shiomi, T. Takui, K. Nakasuji, *Chem. Lett.* **2004**, 33, 188.
- Y. Morita, T. Murata, H. Yamochi, G. Saito, K. Nakasuji, *Synth. Met.* **2003**, 135–136, 579. See also the Supporting Information.
- TTF-CHL is a neutral CT complex with 1:1 component ratio and is a semiconductor with low electrical conductivity ($\sigma_{\text{rt}} = \sim 10^{-4}$ S cm⁻¹): J. B. Torrance, J. J. Mayerle, V. Y. Lee, K. Bechgaard, *J. Am. Chem. Soc.* **1979**, 101, 4747.
- Crystal data for TTF-Im: C₉H₆N₂S₄, $M_r = 270.40$, crystal dimensions $0.25 \times 0.15 \times 0.05$ mm³, orthorhombic, space group *Pna*2₁ (no. 33), $a = 10.198(1)$, $b = 25.196(4)$, $c = 4.1681(5)$ Å, $V = 1071.0(2)$ Å³, $Z = 4$, $\rho_{\text{calcd}} = 1.677$ g cm⁻³, $\mu = 8.49$ cm⁻¹, $2\theta_{\text{max}} = 55.0^\circ$, $\lambda(\text{MoK}\alpha) = 0.71075$ Å, ω scan mode, $T = 200$ K, 9749 reflections, of which 2853 were unique and 2116 were included in the refinement [$I > 2.00\sigma(I)$], data corrected for Lorentzian and polarization effects; an empirical absorption correction resulted in transmission factors ranging from 0.8302 to 0.9582, solution by direct methods (MITHRIL 90) and refinement on $|F^2|$ by full-matrix least-squares procedures (SHELXL97), 136 parameters, the non-H atoms were refined anisotropically, H atoms were included but not refined, final values $R_1 = 0.032$, $wR_2 = 0.069$, GOF = 1.06, maximum positive and negative peaks in ΔF map were $\rho_{\text{max}} = 0.26$ e Å⁻³ and $\rho_{\text{min}} = -0.21$ e Å⁻³. CCDC-239640 contains the supplementary crystallographic data for this

paper. These data can be obtained free of charge via www.ccdc.cam.ac.uk/conts/retrieving.html (or from the Cambridge Crystallographic Data Centre, 12, Union Road, Cambridge CB21EZ, UK; fax: (+44)1223-336-033; or deposit@ccdc.cam.ac.uk).

- [9] a) S. Martinez-Carrera, *Acta Crystallogr.* **1966**, *20*, 783; b) B. M. Craven, R. K. McMullan, J. D. Bell, H. C. Freeman, *Acta Crystallogr. Sect. B* **1977**, *33*, 2585.
- [10] Crystal data for (TTF-Im)₂(CHL): C₁₂H₆N₂OS₄Cl₂, *M*_r = 393.34, crystal dimensions 0.30 × 0.05 × 0.02 mm³, triclinic, space group *P* $\bar{1}$ (no. 2), *a* = 3.7573(2), *b* = 12.2435(4), *c* = 15.8037(5) Å, α = 93.996(3), β = 85.915(3), γ = 82.138(3)°, *V* = 716.02(5) Å³, *Z* = 2, ρ_{calcd} = 1.824 g cm⁻³, μ = 95.20 cm⁻¹, $2\theta_{\text{max}}$ = 55.0°, $\lambda(\text{CuK}\alpha)$ = 1.54178 Å, ω scan mode, *T* = 293 K, 8786 reflections, of which 2521 were unique and 7895 were included in the refinement [*I* > 2.00σ(*I*)], data corrected for Lorentzian and polarization effects; an empirical absorption correction resulted in transmission factors ranging from 0.7196 to 1.0000, solutions by direct methods (SIR 97) and refinement on $|F^2|$ by full-matrix least-squares procedures, 192 parameters, the non-H atoms were refined anisotropically, H atoms were included but not refined, final values *R*₁ = 0.058, *wR*₂ = 0.171, GOF = 1.068, maximum positive and negative peaks in ΔF map were ρ_{max} = 0.42 e Å⁻³ and ρ_{min} = -0.42 e Å⁻³. CCDC 239641 contains the supplementary crystallographic data for this paper. These data can be obtained free of charge via www.ccdc.cam.ac.uk/conts/retrieving.html (or from the Cambridge Crystallographic Data Centre, 12, Union Road, Cambridge CB21EZ, UK; fax: (+44)1223-336-033; or deposit@ccdc.cam.ac.uk).
- [11] Selected physical data: (TTF-Im)₂(CHL), IR (KBr): $\tilde{\nu}$ = 3200–2700, 1532 cm⁻¹; UV/Vis (KBr): λ_{max} = 290, 386, 700, 834 nm; elemental analysis (%): calcd for (C₉H₆N₂S₄)₂(C₆O₂Cl₄): C 36.64, H 1.54, N 7.12; found: C 36.77, H 1.57, N 7.22.
- [12] A. Girlando, I. Zanon, R. Bozio, C. Pecile, *J. Chem. Phys.* **1978**, *68*, 22.
- [13] (TTF-Im)₂(CHL) shows the lower-energy absorption band at around 3000 cm⁻¹, which is characteristic of partial CT complexes with segregated stacking columns (see the Supporting Information).
- [14] The oxidation potential of TTF-based donor molecules with an amido moiety is strongly affected by formation of H-bonds to inorganic anions.^[3c]
- [15] Calculation method: T. Mori, A. Kobayashi, Y. Sasaki, H. Kobayashi, G. Saito, H. Inokuchi, *Bull. Chem. Soc. Jpn.* **1984**, *57*, 627.
- [16] The amount of the temperature-dependent contribution, 1.1 %, was determined by the saturation magnetization at 1.9 K (123.01 erg Oe⁻¹ mol⁻¹) under the assumption that a unit of (TTF-Im)₂(CHL) has nominally two *S* = 1/2 spins by complexation.
- [17] The ESR spectra observed at all temperatures were reproduced by spectral simulation for a randomly oriented system, which assumes temperature-independent *g* anisotropy (see text) and temperature-dependent peak-to-peak linewidths (inset of Figure 5).
- [18] The 2*J* value was calculated at the UB3LYP/6-31G(d) level according to the procedure developed by Yamaguchi et al.: Y. Takano, T. Taniguchi, H. Isobe, T. Kubo, Y. Morita, K. Yamamoto, K. Nakasuji, T. Takui, K. Yamaguchi, *J. Am. Chem. Soc.* **2002**, *124*, 11122, and references therein.
- [19] J. C. Bonner, M. E. Fisher, *Phys. Rev. A* **1964**, *135*, 640.
- [20] R. P. Groff, A. Suna, R. E. Merrifield, *Phys. Rev. Lett.* **1974**, *33*, 418.
- [21] A phase transition in H-bonded CT complex: K. Nakasuji, K. Sugiura, T. Kitagawa, J. Toyoda, H. Okamoto, K. Okaniwa, T. Mitani, H. Yamamoto, I. Murata, A. Kawamoto, J. Tanaka, *J. Am. Chem. Soc.* **1991**, *113*, 1862.

Photoswitchable Organic Nanoparticles and a Polymer Film Employing Multifunctional Molecules with Enhanced Fluorescence Emission and Bistable Photochromism**

Seon-Jeong Lim, Byeong-Kwan An, Sang Don Jung, Myung-Ae Chung, and Soo Young Park*

Among the various photon-mode molecular memory systems, bistable photoswitching of fluorescence emission is considered to be a promising signaling mode, not only because the fluorescence signals can be readily and sensitively recognized, but also because the small number of photons required for their excitation induce few side effects to spoil the digitalized signals.^[1–9] Multifunctional fluorescent (including phosphorescent) molecules combining bistable photochromism with built-in 1,2-bis(hien)ethylene (BTE) units have been successfully investigated with the aim of applications in ultrahigh-density optical memory media, and they show, in principle, reversible and bistable photoswitching.^[10–15] The important challenge still remaining unsolved, however, is the general problem of “concentration quenching” in the fluorescence signal, which certainly restricts the application of these multifunctional photochromic molecules to high-density optical memory systems.^[16] Herein, we demonstrate an innovative approach to this problem by employing a special class of multifunctional photochromic molecule which shows enhanced fluorescence emission with increasing concentration. It is readily expected that the high storage capability, high sensitivity, and high-contrast on/off signaling ratio are synergetically achieved with this molecule in neat nanoparticles or in a highly loaded polymer film.

Very recently, unconventional fluorescent molecules showing aggregation-induced enhanced emission (AIEE) have been reported by several groups including ours.^[17–19] Simple-structured 1-cyano-*trans*-1,2-bis-(4'-methylbiphenyl)-ethylene (CN-MBE) is a typical AIEE molecule that fluoresces strongly in the solid state even though it is virtually nonfluorescent in solution.^[19] The multifunctional fluorescent molecule for photoswitchable memory media **1a** was designed and synthesized by replacing one of the end tolyl groups of CN-MBE with the photochromic BTE moiety. Compound **2a**, the non-AIEE analogue of **1a** which lacks

[*] S.-J. Lim, B.-K. An, Prof. S. Y. Park
School of Materials Science and Engineering ENG445
Seoul National University
San 56-1, Shillim-dong, Kwanak-ku, Seoul 151-744 (Korea)
Fax: (+82) 2-886-8331
E-mail: parksy@plaza.snu.ac.kr
Dr. S. D. Jung, Dr. M.-A. Chung
Basic Research Laboratory
Electronics and Telecommunications Research Institute (ETRI)
161 Gajeong-dong, Yuseong-gu, Daejeon 305-350 (Korea)

[**] This work was supported in part by CRM-KOSEF and ETRI.



Supporting information for this article is available on the WWW under <http://www.angewandte.org> or from the author.

only the CN group, was also synthesized to properly compare the AIEE effect (see Figure 1 for the chemical structures and the Supporting Information for the synthetic details). Compounds **1a** and **2a** were fully identified by ^1H NMR spectroscopy, FTIR spectroscopy, MALDI-TOF mass spectrometry, and elemental analysis (analytical data are available in the Supporting Information).

Fluorescent photochromic organic nanoparticles (FPONs) of **1a** were prepared by a reprecipitation method to produce a highly concentrated photon-mode recording medium.^[20] Quite uniform and size-tuned nanoparticles of **1a** (see the scanning electron microscopy (SEM) photograph in Figure 1e) were obtained; the diameters of FPONs of **1a** were 40 ± 10 , 125 ± 25 , 200 ± 50 , and 275 ± 75 nm when prepared from THF/water concentrations of 2×10^{-5} , 4×10^{-5} , 1×10^{-4} , and 2×10^{-4} M, respectively (other images are available in the Supporting Information). According to the AIEE principle, FPONs of **1a** showed strongly enhanced fluorescence emission, although they were only weakly fluorescent in a THF solution of the same concentration (ca. 1700 times enhancement, compare (II) with (I) in Fig-

ure 1a). This observation contrasts strikingly with the behavior of conventional analogue **2a**, which shows significant concentration quenching in the nanoparticle (ca. 30 times reduction in fluorescence intensity, compare (VI) with (V) in Figure 1c). Such a totally different fluorescence behavior between **1a** and **2a** (AIEE versus quenching) is most probably related to the different aggregation states in their FPONs. In fact, the UV/Vis absorption spectra shown in Figure 2a,c suggest *J*-type and *H*-type aggregations for **1a** and **2a** FPONs, respectively. The absorption spectra of **1a** FPONs were characteristically red-shifted (Figure 2a) and exhibited Mie light scattering as a result of *J*-type aggregation and nanoparticle formation, respectively. Notably, the absorption maxima of FPONs of **1a** showed a gradual red-shift with increasing nanoparticle size; $\lambda_{\text{max}}^{\text{soln}} = 360$ nm, $\lambda_{\text{max}}^{\text{FPONs}} = 371$ – 382 nm with increasing FPON size of 40–275 nm. Concomitantly, FPONs of **1a** showed strongly enhanced fluorescence emission as shown in Figure 2b ($\Phi_{\text{F}}^{\text{FPONs}} = 3.2$ – 5.1 %, $\lambda_{\text{max}}^{\text{FPONs}} = 485$ – 493 nm) compared with the isolated **1a** dissolved in THF (2×10^{-4} M, $\Phi_{\text{F}}^{\text{soln}} = 0.002$ %, $\lambda_{\text{max}}^{\text{soln}} = 461$ nm).^[21,22] All of these spectral changes corroborate that the *J*-type aggregation and

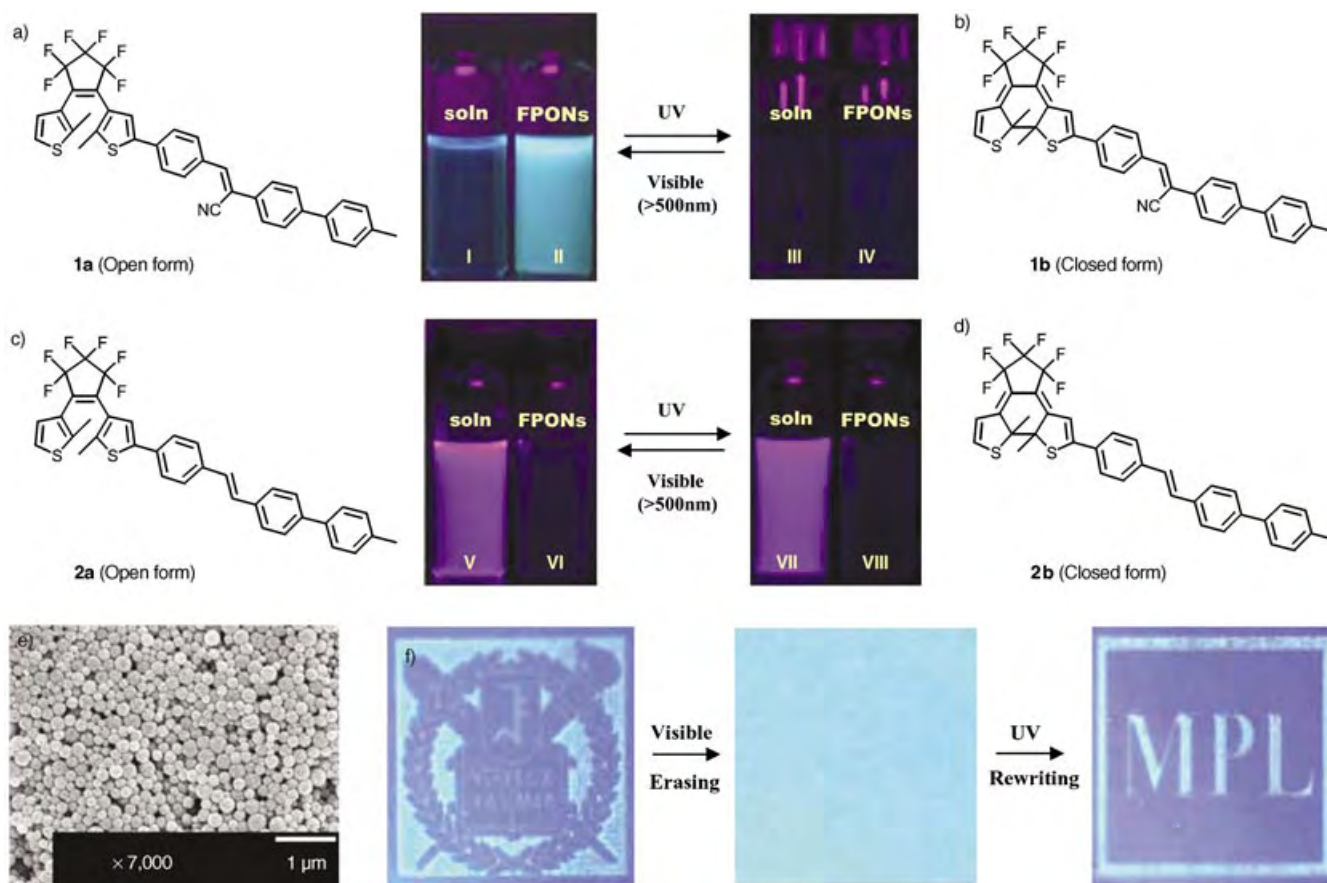


Figure 1. a) Chemical structure of **1a** and the fluorescence images of its THF solution (I, soln, 2×10^{-4} M) and the colloidal suspension (II) of fluorescent photochromic organic nanoparticles (FPONs; 2×10^{-4} M). b) Chemical structure of **1b** and the fluorescence images of its THF solution (III, 2×10^{-4} M) and the colloidal suspension of FPONs (IV, 2×10^{-4} M) in the photostationary state (PSS). c) Chemical structure of **2a** and the fluorescence images of its THF solution (V, 2×10^{-5} M) and the colloidal suspension of FPONs (VI, 2×10^{-5} M). d) Chemical structure of **2b** and the fluorescence images of its THF solution (VII, 2×10^{-5} M) and the colloidal suspension of FPONs (VIII, 2×10^{-5} M) in the PSS. e) FE-SEM image of FPONs of **1a** (275 ± 75 nm) prepared from a THF/water mixture (2×10^{-4} M). f) Photo-rewritable fluorescence imaging on the polymer film loaded with 20 wt% of **1a** by using UV (365 nm, hand-held lamp, 1.2 mW cm^{-2}) and visible light (> 500 nm). The dark regions represent the parts irradiated with UV light; the real size of the photomasks is about $1 \text{ cm} \times 1 \text{ cm}$.

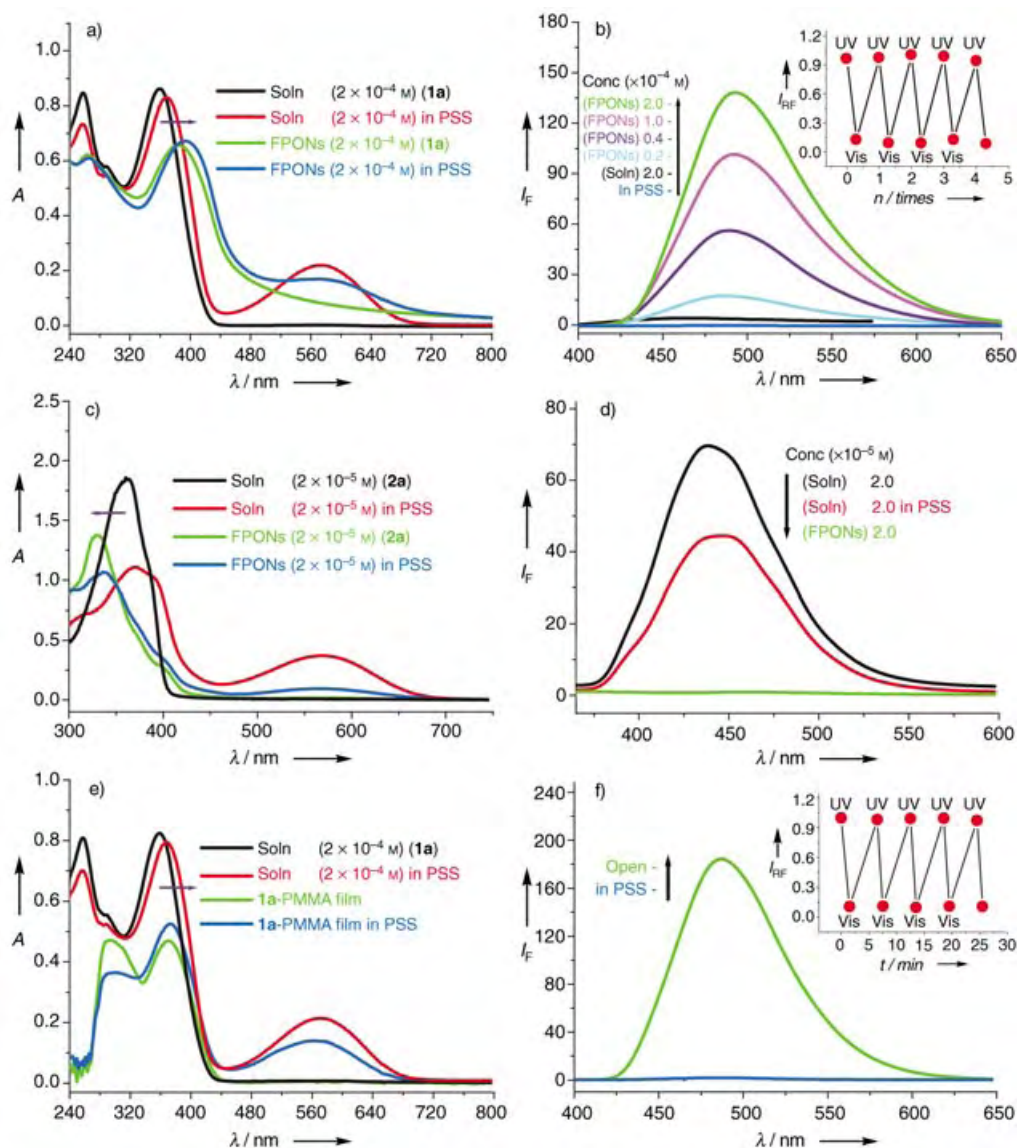


Figure 2. a) UV/Vis absorption spectra of **1a** in THF (2×10^{-4} M) and the colloidal suspension of FPONs of **1a** (2×10^{-4} M). b) PL spectra of FPONs of **1a** (275 ± 75 nm) in the PSS (bottom, blue line), **1a** in THF (2×10^{-4} M, black line), and size-tuned FPONs of **1a** of 40–275 nm (cyan–green line, respectively). The inset graph shows a relative PL intensity modulation of **1a** FPONs (275 ± 75 nm). c), d) UV/Vis absorption and PL spectra of **2a** in THF (2×10^{-5} M) and the colloidal suspension of **2a** FPONs (2×10^{-5} M). e) UV/Vis absorption spectra of **1a** in THF (2×10^{-4} M) and a 20 wt% **1a**-loaded PMMA film. f) PL spectra of the 20 wt% **1a**-loaded PMMA film. The inset graph shows the relative PL intensity modulation of the film.

molecular planarization of **1a** molecules were induced in their FPONs by specific intermolecular interactions.^[19,23] In contrast, the UV/Vis absorption spectra of **2a** FPONs were significantly blue-shifted ($\lambda_{\text{max}}^{\text{soln}} = 360$ nm, $\lambda_{\text{max}}^{\text{FPONs}} = 329$ nm) as shown in Figure 2c. Moreover, the fluorescence quantum yield of FPONs of **2a** was drastically reduced by 30 times from that of a solution of **2a** in THF (2×10^{-5} M, $\Phi_{\text{F}}^{\text{soln}} = 3.4\%$, $\lambda_{\text{max}}^{\text{soln}} = 439$ nm, $\Phi_{\text{F}}^{\text{FPONs}} = 0.1\%$) as indicated in Figure 2d. This blue-shifted UV absorption together with the salient concentration quenching in FPONs of **2a** is attributed to the formation of *H*-type aggregation through strong cofacial π -stacking interactions, which most likely provides a nonradiative decay route.^[24,25]

Compounds **1a** and **2a** with open-ring BTE units were converted into **1b** and **2b** with closed-ring BTE units when irradiated with UV light (365 nm, 1.2 mW cm⁻²). This process was easily monitored by the appearance of new absorption bands in the visible regions ($\lambda_{\text{max}}^{\text{1b}} = 574$ nm, $\lambda_{\text{max}}^{\text{2b}} = 570$ nm) as shown in Figure 2a,c (see the Supporting Information for details). Accompanied by this photochromic ring closure, the photoluminescence (PL) intensities of the **1a** FPONs were greatly reduced (compare (IV) with (II) in Figure 1a,b, and see the Supporting Information for details). The fluorescence quantum yields of the FPONs of **1a** in the photostationary state (PSS)^[15] were reduced by 16–170 times ($\Phi_{\text{F}}^{\text{FPONs}} = 0.20, 0.09, 0.04$, and 0.02% in the PSS, $\Phi_{\text{F}}^{\text{FPONs}} = 3.2, 5.1, 4.1$, and 3.4% in the **1a** form with increasing FPON size of 40–275 nm,

respectively).^[21,22] However, only a small amount of fluorescence modulation (29% reduction, see the Supporting Information for details) was achieved in a solution of **2a** (2×10^{-5} M, $\Phi_F^{\text{soln}} = 2.4\%$ in the PSS, $\Phi_F^{\text{soln}} = 3.4\%$ in the **2a** form).

It is known that there are two interconvertible conformations of BTE units: one is a parallel conformation and the other is an antiparallel conformation, of which only the latter allows an electrocyclic ring-closing reaction.^[15] Through the ¹H NMR spectroscopic study (2×10^{-4} M of CDCl₃ solution, 22 °C, 300 MHz) it was determined that the parallel and antiparallel conformations of **1a** were equally populated, and also that only about 35% of the **1a** forms were photoisomerized to the **1b** forms in the PSS under irradiation with 365 nm light.^[26,27] An even smaller extent of ring-closing reaction in the PSS is implied for FPONs of **1a**, because the net absorbance of the **1b** form at 574 nm is smaller in FPONs than in solution (see Figure 2a). It is reasonably supposed, therefore, that the photochromic interconversion between the two conformations was suppressed within a FPON (which is essentially a condensed solid state), or that the ring-closing reactions occurred only at the surfaces of the FPONs.^[28] Given that the extent of the ring-closing reaction is less than 35%, the experimentally observed extremely large reduction in the fluorescence quantum yield Φ_F (16–170-fold decrease) of FPONs of **1a** in the PSS must be achieved not only by intramolecular energy transfer between the fluorophore and the closed-ring form of BTE, although it is very likely that the 29% reduction of the Φ_F value of the **2a** solution occurs through this intramolecular energy transfer.^[2–5,7,8] It is presumed that the condensed-state FPONs also provide an additional quenching event, or intermolecular energy transfer between the unconverted **1a** forms and the neighboring **1b** forms, because of their proximity in FPONs. Consequently, extremely high contrast in the on/off signaling ratio is automatically implemented in the neat FPONs of **1a**, which is an additional advantage to the enhanced fluorescence and high storage capacity of the AIEE molecule.

Moreover, when the FPONs of **1a** in the “off” state were irradiated with visible light (> 500 nm), the PL intensities were perfectly recovered to those of the initial “on” state as a result of the reversible photochromic behavior of the BTE unit. The inset graph in Figure 2b shows a reversible photochromic modulation of relative fluorescence intensity in the suspension of FPONs of **1a** under alternating irradiation with UV and visible light (note the on/off fluorescence intensity ratio > 10).

To produce a more practical photo-rewritable imaging medium we prepared a strongly fluorescent poly(methyl methacrylate) (PMMA; $M_w = \text{ca. } 120\,000$) film containing a very high level (20 wt %, $\text{ca. } 3 \times 10^{-1}$ M) of **1a** molecules. This polymer film was optically clear and scatter-free, presumably because of the partial miscibility of PMMA and **1a**. The absence of light scattering and detectable aggregate features in the fluorescence-enhanced (FE) SEM image (down to $\text{ca. } 10$ nm scale, see Supporting Information), which are, however, accompanied by distinct *J*-type red-shifted absorption in the film ($\lambda_{\text{max}}^{\text{soln}} = 360$ nm, $\lambda_{\text{max}}^{\text{film}} = 372$ nm, see Figure 2e), suggests that the film comprises molecular-scale aggregates of

1a. The presence of molecular-scale aggregates is additionally evidenced by the strong effect of AIEE as the intense blue fluorescence ($\Phi_F^{\text{film}} = 5.8\%$, $\lambda_{\text{max}}^{\text{film}} = 487$ nm versus $\Phi_F^{\text{soln}} = 0.002\%$, $\lambda_{\text{max}}^{\text{soln}} = 461$ nm in 2×10^{-4} M solution) from this polymer film (see Figure 2f).^[21,29,30] The AIEE fluorescence from this PMMA/**1a** film was also photoswitched in a bistable manner by alternate UV and visible light irradiation with high contrast ($\Phi_F^{\text{film}} = 0.3\%$ in the PSS, $\Phi_F^{\text{film}} = 5.8\%$ in the **1a** form, or on/off fluorescence intensity ratio > 19), as shown in the inset graph in Figure 2f. In addition, the practical capability of rewritable fluorescence photoimaging on our AIEE polymer film was investigated by patterned illumination through photomasks. The emblem of Seoul National University was recorded as a first image (Figure 1f), which was subsequently erased and followed by the recording of a second image, the abbreviation of the Molecular Photonics Laboratory (MPL). This successful demonstration of rewritable photoimaging on the polymer film suggests immediate application of **1a** molecules to ultrahigh-density rewritable optical memory media or imaging processes.

In conclusion, we designed and synthesized a special class of multifunctional molecule **1a**, which shows a strongly enhanced fluorescence emission as well as bistable photochromism. High-contrast (> 10) on/off fluorescence switching was successfully implemented in the size-tuned neat nanoparticles of **1a** and also in a PMMA film highly loaded with **1a**.

Received: July 3, 2004

Keywords: aggregation · fluorescence · nanotechnology · photochromism · polymers

- [1] A. Fernandez, J.-M. Lehn, *Adv. Mater.* **1998**, *10*, 1519–1522.
- [2] T. Kawai, T. Sasaki, M. Irie, *Chem. Commun.* **2001**, 711–712.
- [3] K. Yagi, C. F. Soong, M. Irie, *J. Org. Chem.* **2001**, *66*, 5419–5423.
- [4] A. Osuka, D. Fujikane, H. Shinmori, S. Kobatake, M. Irie, *J. Org. Chem.* **2001**, *66*, 3913–3923.
- [5] T. B. Norsten, N. R. Branda, *J. Am. Chem. Soc.* **2001**, *123*, 1784–1785.
- [6] B. Chen, M. Wang, Y. Wu, H. Tian, *Chem. Commun.* **2002**, 1060–1061.
- [7] T. Kawai, M.-S. Kim, T. Sasaki, M. Irie, *Opt. Mater.* **2002**, *21*, 275–278.
- [8] M. Irie, T. Fukaminato, T. Sasaki, N. Tamai, T. Kawai, *Nature* **2002**, *420*, 759–760.
- [9] S. Murase, M. Teramoto, H. Furukawa, Y. Miyashita, K. Horie, *Macromolecules* **2003**, *36*, 964–966.
- [10] M. Irie, *Photoreactive Materials for Ultrahigh-Density Optical Memory*, Elsevier, Amsterdam, **1994**.
- [11] J. C. Crano, R. J. Guglielmetti, *Organic Photochromic and Thermochromic Compounds, Vol. 1*, Plenum, New York, **1999**.
- [12] S. Nakamura, M. Irie, *J. Org. Chem.* **1988**, *53*, 6136–6138.
- [13] Y. Nakayama, K. Hayashi, M. Irie, *J. Org. Chem.* **1990**, *55*, 2592–2596.
- [14] M. Hanazawa, R. Sumiya, Y. Horikawa, M. Irie, *J. Chem. Soc. Chem. Commun.* **1992**, 206–207.
- [15] M. Irie, *Chem. Rev.* **2000**, *100*, 1685–1716.
- [16] J. B. Birks in *Photophysics of Aromatic Molecules*, Wiley, London, **1970**.

- [17] J. Luo, Z. Xie, J. W. Y. Lam, L. Cheng, H. Chen, C. Qiu, H. S. Kwok, X. Zhan, Y. Liu, D. Zhu, B. Z. Tang, *Chem. Commun.* **2001**, 1740–1741.
- [18] H. Murata, Z. H. Kafafi, M. Uchida, *Appl. Phys. Lett.* **2002**, 80, 189–191.
- [19] B. K. An, S. K. Kwon, S. D. Jung, S. Y. Park, *J. Am. Chem. Soc.* **2002**, 124, 14410–14415.
- [20] Preparation of FPONs: All suspensions of FPONs were prepared by the reprecipitation method from THF solution with distilled water. Volume fractions of THF and water were adjusted to 20 and 80 %, respectively. See ref. [19] for details.
- [21] Fluorescence quantum yields: The fluorescence quantum yields (Φ_F) were relatively calculated using 9,10-diphenylanthracene (DPA) in benzene (see ref. [22]) and in PMMA (see refs. [29,30]) as a standard reference (1×10^{-3} M, $\Phi_F = 83$ %). Through this method, the Φ_F values of FPONs of **1a** were determined as 3.2, 5.1, 4.1, and 3.4 % ($\lambda_{\text{max em}}^{\text{FPONs}} = 485, 489, 491, \text{ and } 493 \text{ nm}$, $\lambda_{\text{max abs}}^{\text{FPONs}} = 371, 374, 378, \text{ and } 382 \text{ nm}$) in the **1a** form, and as 0.20, 0.09, 0.04, and 0.02 % in the PSS with increasing FPON size of 40 ± 10 , 125 ± 25 , 200 ± 50 , and $275 \pm 75 \text{ nm}$, respectively. It is reasonably considered that the slight reduction of the Φ_F values in 200 ± 50 and $275 \pm 75 \text{ nm}$ FPONs of **1a** results from the highly increased virtual absorbance values by increased light scattering. In fact, the extent of the apparent absorbance of the FPONs of **1a** at the excitation wavelength, that is at 360 nm, was almost linearly proportional to their suspension concentrations in spite of the inverse proportional relationship between the mean radius and the surface-to-volume ratio of the FPONs.
- [22] I. B. Berlman in *Handbook of Fluorescence Spectra of Aromatic Molecules*, Academic Press, New York, **1971**.
- [23] H. Auweter, H. Haberkorn, W. Heckmann, D. Horn, E. Lüddecke, J. Rieger, H. Weiss, *Angew. Chem.* **1999**, 111, 2325–2328; *Angew. Chem. Int. Ed.* **1999**, 38, 2188–2191.
- [24] A. V. Ruban, P. Horton, A. J. Young, *J. Photochem. Photobiol. B* **1993**, 21, 229–234.
- [25] L. Dahne, E. Biller, *Adv. Mater.* **1998**, 10, 241–245.
- [26] Determination of the conformational population and conversion rate: A ^1H NMR spectroscopic study (2×10^{-4} M of CDCl_3 solution, 22°C , 300 MHz) on the **1a** form showed that the parallel and antiparallel conformations were equally populated in solution, as evident by there only being two singlet resonances at $\delta = 1.98$ and 1.91 ppm without any splitting. These signals were assigned as the methyl protons at the 2-positions of the thiophene rings of the **1a** form (see ref. [27]). The conversion rate of about 35 % in the PSS was calculated by the integrated ratio between the singlet peaks of methyl protons in the **1a** form and those in the **1b** form, which newly appeared at $\delta = 2.15$ and 2.11 ppm .
- [27] M. Irie, K. Sakemura, M. Okinaka, K. Uchida, *J. Org. Chem.* **1995**, 60, 8305–8309.
- [28] F. Sun, F. Zhang, F. Zhao, X. Zhou, S. Pu, *Chem. Phys. Lett.* **2003**, 380, 206–212.
- [29] G. G. Guilbault, *Practical Fluorescence*, Marcel Dekker, New York, **1990**.
- [30] X. Zhang, A. S. Shetty, S. A. Jenekhe, *Macromolecules* **1999**, 32, 7422–7429.

Macroscopic Spinning Chirality Memorized in Spin-Coated Films of Spatially Designed Dendritic Zinc Porphyrin *J*-Aggregates**


Tatsuya Yamaguchi, Tatsumi Kimura, Hiro Matsuda, and Takuzo Aida*

The breaking of chiral symmetry can occur under nonequibrated conditions.^[1–4] Such a spontaneous induction of optical activity from achiral entities has attracted much attention in relation to the origin of chirality in nature. Representative examples can be seen in growth processes of large electrostatic assemblies of achiral chromophoric compounds such as cyanine dyes and porphyrin derivatives in aqueous media.^[5] In these cases, the assemblies are considered to adopt helical architectures, where either the *P* or *M* form is selected only accidentally at the initial stage of the self-organization event and develops predominantly in the subsequent stage. Hence, handedness of emerging chirality is unpredictable. Ribó et al.^[5c] have discovered, through studies on electrostatic *J*-aggregation of a 4-sulfonatophenylporphyrin in aqueous media, that the sense of such an optical activity can be selected by the spinning direction of vortex stirring initially applied to the solutions. Herein we report an interesting finding that spin-coated films of dendritic zinc porphyrin *J*-aggregates chiroptically memorize the spinning directions. The optical activities of the spin-coated films are thermally stable and preserved up to the melting temperatures of the *J*-aggregates. In contrast with the previous examples,^[5] the *J*-aggregates are optically inactive in solution.

Porphyrin *J*-aggregates have attracted attention because of their potential application as nonlinear optical materials.^[6] Although several examples of porphyrin *J*-aggregates have been reported, they are formed mostly in aqueous media;^[5b,c] however, there are few examples of *J*-aggregation in organic media^[7] which occur because of rather weak π -stacking interactions. We found that zinc porphyrins bearing carboxylic acid ($-\text{CO}_2\text{H}$) functionalities at the opposite meso positions undergo supramolecular polymerization by dimerization of the $-\text{CO}_2\text{H}$ groups to give *J*-aggregates in organic media. The *J*-aggregation takes great advantage of a multi-

[*] Dr. T. Yamaguchi, Prof. Dr. T. Aida
Aida Nanospace Project
Exploratory Research for Advanced Technology (ERATO)
Japan Science and Technology Agency (JST)
2-41 Aomi, Koto-ku, Tokyo 135-0064 (Japan)
Fax: (+81) 3-5841-7310
E-mail: aida@macro.t.u-tokyo.ac.jp
Dr. T. Kimura, Dr. H. Matsuda
Photonics Research Institute
National Institute of Advanced Industrial Science and Technology (AIST)
Tsukuba Central 5, 1-1-1 Higashi Tsukuba, Ibaraki 305-8565 (Japan)

[**] T.Y. thanks the JSPS Young Scientist Fellowship.

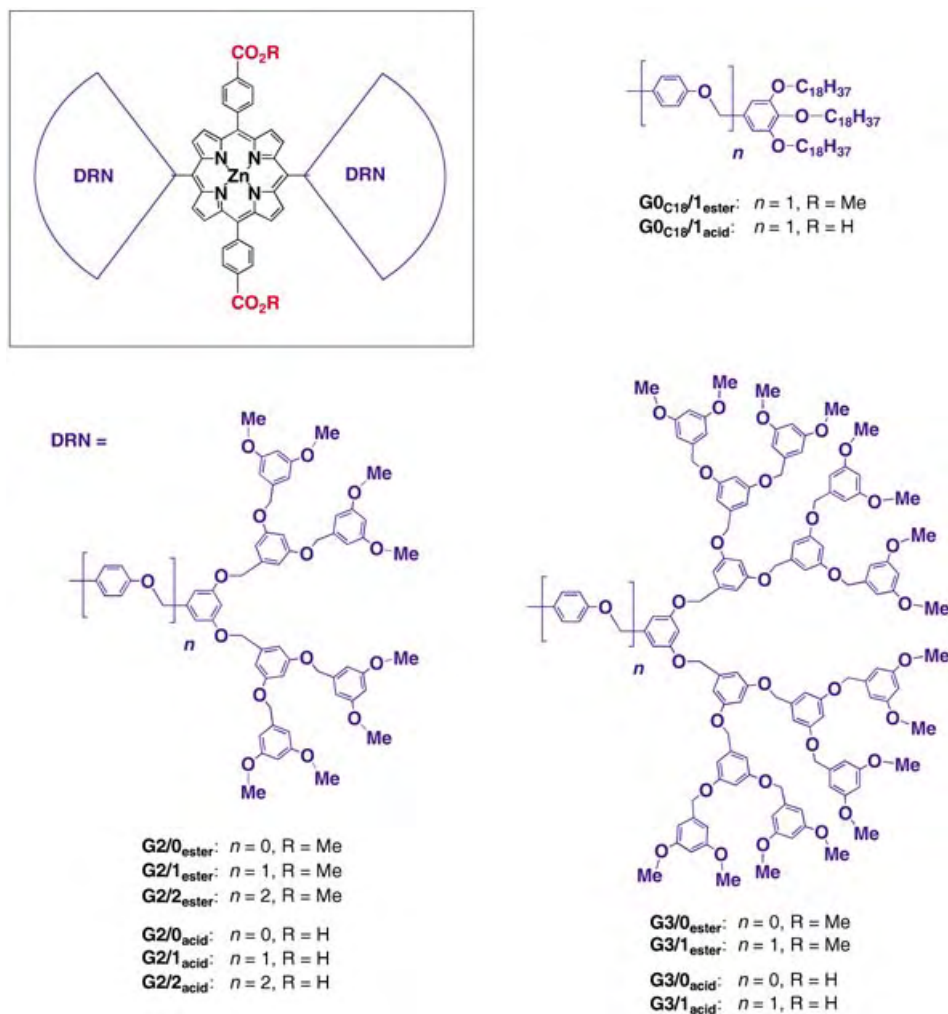
 Supporting information for this article is available on the WWW under <http://www.angewandte.org> or from the author.

point π -stacking interaction between the polymeric zinc porphyrin molecules. Our molecular design strategy also includes introduction of [G2] or [G3] dendritic wedges at the residual two meso positions (Gm/n_{acid} , where m is the generation number of the dendritic wedges (2 or 3) and n is the number of benzyl ether units (0–2) in the spacer parts of the dendritic wedges; Scheme 1). The dendritic wedges are essential not only for providing the resulting supramolecular polymers with sufficiently high solubilities but also for steric control over the π -stacking interaction among the polymeric focal cores. For comparison, we synthesized a zinc porphyrin dicarboxylic acid ($G0_{C18}/1_{acid}$) bearing long alkyl chains, and investigated the aggregation behavior of this nondendritic reference as well as those of ester versions Gm/n_{ester} , which were the synthetic precursors of Gm/n_{acid} .

For the synthesis of $G3/1_{acid}$ (Scheme 1), the zinc complex of 5,15-bis(4-methoxycarbonylphenyl)-10,20-bis(4-hydroxyphenyl)porphyrin was treated under alkaline conditions with [G3] poly(benzyl ether) dendron bromide, and the resulting ester ($G3/1_{ester}$) was hydrolyzed with KOH. After neutralization, the reaction mixture was subjected to preparative size-exclusion chromatography (SEC) to isolate $G3/$

1_{acid} . Other dendritic zinc porphyrins such as $G2/0_{acid}$ – $G2/2_{acid}$, $G3/0_{acid}$, and nondendritic $G0_{C18}/1_{acid}$ (Scheme 1) were synthesized in a similar manner to the above and unambiguously characterized.^[8] As the benzyl ether spacers between the zinc porphyrin unit and the dendritic wedges become longer, the zinc porphyrin core should possess a larger spatial freedom for the π -stacking interaction ($G2/0_{acid} < G2/1_{acid} < G2/2_{acid}$; $G3/0_{acid} < G3/1_{acid}$). On the other hand, the spatial freedom should become smaller as the dendritic wedges become larger ($G3/0_{acid} < G2/0_{acid}$; $G3/1_{acid} < G2/1_{acid}$). In contrast with the case of these dendritic versions Gm/n_{acid} , the zinc porphyrin unit in $G0_{C18}/1_{acid}$ is omitted because of the absence of dendritic wedges.

We found that [G2] dendritic zinc porphyrin dicarboxylic acids such as $G2/0_{acid}$ – $G2/2_{acid}$ all form stable *J*-aggregates in $CHCl_3$. For example, the electronic absorption spectrum of a $CHCl_3$ solution of $G2/2_{acid}$ (5 mM) at 25 °C displayed an intense red-shifted Soret band at 453 nm and a blue-shifted band at 413 nm (Figure 1c) which is characteristic of zinc porphyrin *J*-aggregates. $G2/1_{acid}$ with shorter benzyl ether spacers exhibited a virtually identical absorption spectral profile to $G2/2_{acid}$ (Figure 1b). Although $G2/0_{acid}$ without



Scheme 1. Structures of the dendritic and nondendritic zinc porphyrin dicarboxylic acids Gm/n_{acid} ($m = 0, 2, 3$, $n = 0–2$) and their esters Gm/n_{ester} ($m = 0, 2, 3$, $n = 0–2$).

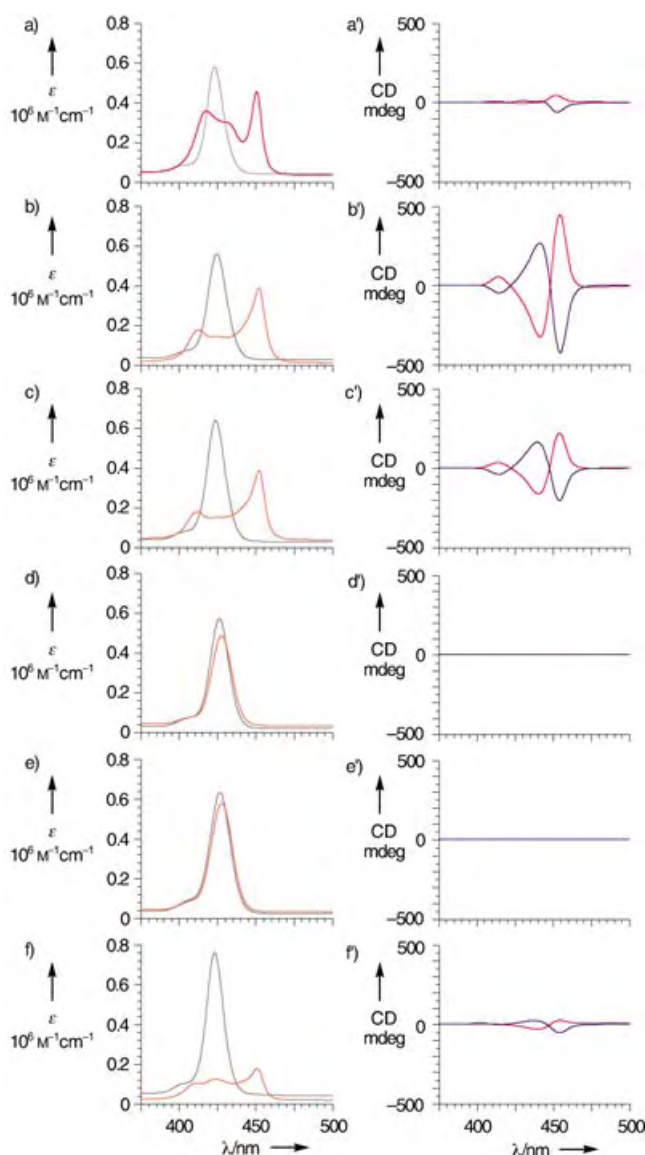
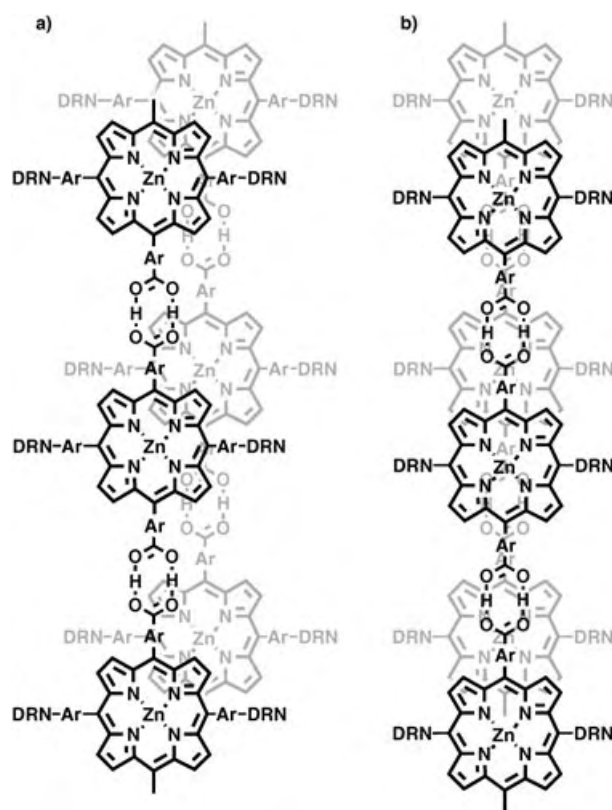


Figure 1. Electronic absorption spectra of solutions (5 mM) of **Gm/n_{acid}** ($m=0, 2, 3, n=0-2$; red curves) and **Gm/n_{ester}** ($m=0, 2, 3, n=0-2$; green curves) in CHCl_3 at 25 °C; a) **G2/0_{acid}** and **G2/0_{ester}** b) **G2/1_{acid}** and **G2/1_{ester}** c) **G2/2_{acid}** and **G2/2_{ester}** d) **G3/0_{acid}** and **G3/0_{ester}** e) **G3/1_{acid}** and **G3/1_{ester}** and f) **G0_{C18}/1_{acid}** and **G0_{C18}/1_{ester}**. CD spectra of thin films of **Gm/n_{acid}** ($m=2, 3, n=0-2$) prepared by spin-coating in clockwise (red curves) and counterclockwise (blue curves) spinning directions are also shown; a') **G2/0_{acid}**, b') **G2/1_{acid}**, c') **G2/2_{acid}**, d') **G3/0_{acid}**, e') **G3/1_{acid}**, f') **G0_{C18}/1_{acid}**.

benzyl ether spacers formed a *J*-aggregate, it displayed a slightly different absorption spectrum, with two red-shifted Soret bands at 451 and 432 nm (Figure 1a). The infrared spectra of solutions of **G2/n_{acid}** ($n=0-2$; 5 mM) in CHCl_3 all showed a carbonyl stretching vibration at 1688 cm^{-1} arising from a dimeric form of CO_2H , with only a negligibly small shoulder attributable to free CO_2H at 1725 cm^{-1} .^[8] Dynamic light scattering (DLS) studies on a dilute solution of *J*-aggregated **G2/1_{acid}** in CHCl_3 (0.05 mM), for example, showed the presence of large assemblies with an average radius of 200 nm.^[8] Thus, the zinc porphyrin cores of these dendritic

compounds are hydrogen bonded to one another to form supramolecular polymers. In contrast, their ester versions **G2/n_{ester}** ($n=0-2$) showed a single Soret band at 423 nm (Figure 1a-c; green curves), which is characteristic of non-aggregated zinc porphyrins. Therefore, it is concluded that the *J*-aggregation of zinc porphyrins can be induced in organic media by their hydrogen-bonding interactions. We assume that one-dimensional zinc porphyrin polymers formed by the dimerization of the CO_2H moieties stack up together, through a multipoint π -electronic interaction, to form a large, two-dimensional (2D) sheetlike assembly (Scheme 2). The differ-



Scheme 2. Structures of zinc porphyrin *J*-aggregates with a short, oblique slip (a) and a long, non-oblique slip (b).

ence in the absorption spectral profile between **G2/n_{acid}** ($n=1, 2$) and **G2/0_{acid}** (Figure 1a-c; red curves) is attributable to a difference in the π -stacking geometry of the zinc porphyrin units. Namely, the *J*-aggregates of **G2/1_{acid}** and **G2/2_{acid}** both involve a short, oblique slip of the π -stacked zinc porphyrin units (Scheme 2a), typical of *J*-aggregated tetraarylporphyrin derivatives, since such a geometry can reduce the steric interference from the meso-aryl groups on the zinc porphyrin units.^[9] On the other hand, the *J*-aggregate of **G2/0_{acid}**, which is devoid of any spacers between the dendritic wedges and the zinc porphyrin core, involves a long, non-oblique slip of the π -stacked zinc porphyrin units (Scheme 2b), possibly because of limited spatial freedom for the π -stacking interaction. The dendritic side chains, which are located presumably on both sides of the 2D sheet, are responsible for the high solubilities of the *J*-aggregates. For reference, the absorption spectral

profile of nondendritic **G0**_{C18}/**1**_{acid} in hot CHCl₃ (Figure 1 f) was analogous to those of *J*-aggregated **G2**/**1**_{acid} and **G2**/**2**_{acid}, but the compound gradually precipitated on standing at 25 °C.

In contrast with the [G2] dendritic zinc porphyrins **G2**/*n*_{acid} (*n* = 0–2), solutions of the one-generation higher systems **G3**/**0**_{acid} and **G3**/**1**_{acid} (5 mM) in CHCl₃ both displayed a single Soret band at 428 nm, similar to their ester versions, thus indicating that their zinc porphyrin cores are not assembled through π -stacking interactions (Figure 1 d,e). Infrared spectroscopic analysis of these compounds showed a considerable amount of free CO₂H groups at 1725 cm⁻¹, along with dimeric CO₂H groups at 1688 cm⁻¹.^[8] Therefore, it is likely that the large dendritic wedges attached to the zinc porphyrin core suppress both the hydrogen-bonding and π -stacking interactions. On the other hand, we also found that **G3**/**1**_{acid} gives a *J*-aggregate in an apolar solvent such as C₆H₆, where a dimeric form of CO₂H is stable. The electronic spectrum of a solution of **G3**/**1**_{acid} in C₆H₆ (5 mM) showed a red-shifted Soret band at 453 nm and a blue-shifted band at 414 nm (Figure 2 b; red

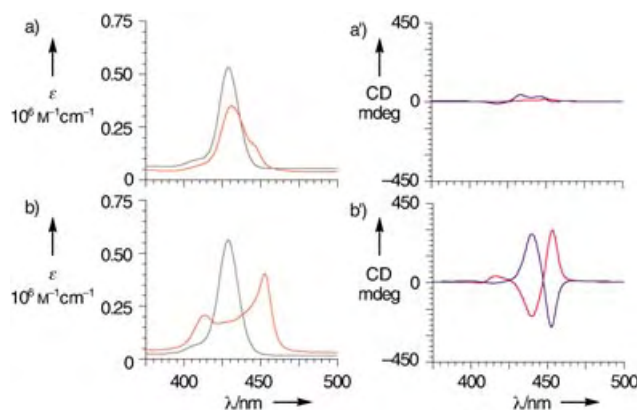


Figure 2. Electronic absorption spectra of solutions (5 mM) of **G3**/*n*_{acid} (*n* = 0, 1; red curves) and **G3**/*n*_{ester} (*n* = 0, 1; green curves) at 25 °C in C₆H₆; a) **G3**/**0**_{acid} and **G3**/**0**_{ester}, b) **G3**/**1**_{acid} and **G3**/**1**_{ester}. CD spectra of thin films of **G3**/*n*_{acid} (*n* = 0, 1) prepared by spin-coating in the clockwise (red curves) and counterclockwise (blue curves) directions are also shown; a') **G3**/**0**_{acid}, b') **G3**/**1**_{acid}.

curve), whereas ester **G3**/**1**_{ester}, under identical conditions, displayed an ordinary Soret band at 429 nm (Figure 2 b; green curve). Infrared spectroscopic analysis of **G3**/**1**_{acid} in C₆H₆ (5 mM), in contrast with the case in CHCl₃, showed a carbonyl stretching vibration predominantly at 1688 cm⁻¹ arising from the dimeric form of CO₂H. These observations again support our hypothesis that the zinc porphyrin units, when polymerized through hydrogen-bonding interactions, have an enhanced capability for π stacking. In contrast, **G3**/**0**_{acid}, with a sterically encumbered zinc porphyrin core, formed a weak gel in C₆H₆ whose absorption spectrum (Figure 2 a; red curve) was similar to that of non-aggregated **G3**/**0**_{ester} (Figure 2 a; green curve).

In the course of the above study we noticed that *J*-aggregated **G2**/*n*_{acid} (*n* = 0–2) gave birefringent films when cast from their CHCl₃ solutions on to glass plates. Spin-coating of these solutions also resulted in the formation of birefringent films, which showed the presence of rodlike

crystalline particles by polarized microscopy (Figure 3 a–c). The particles from **G2**/**0**_{acid} were smaller than those from the other two compounds. Quite interestingly, these films were optically active, although their solutions were silent in circular

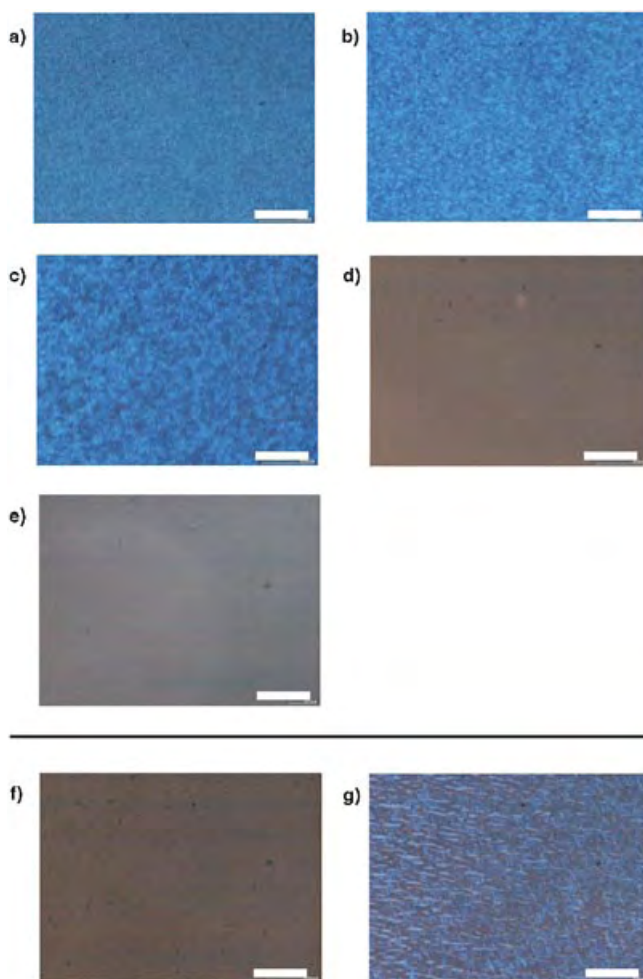


Figure 3. Polarized-light micrographs of spin-coated films from solutions of **Gm**/*n*_{acid} (*m* = 2, 3, *n* = 0–2) in CHCl₃ and solutions of **G3**/*n*_{acid} (*n* = 0, 1) in C₆H₆: a) **G2**/**0**_{acid}, b) **G2**/**1**_{acid}, c) **G2**/**2**_{acid}, d) **G3**/**0**_{acid}, e) **G3**/**1**_{acid}, f) **G3**/**0**_{acid}, g) **G3**/**1**_{acid}; scale bar, 50 μm.

dichroism (CD) spectroscopy. We also found that the spin-coated films displayed a chirality dominance in the statistical distributions that was dependent on the “spinning direction”, whereas the cast films did not show any dominance in chirality. For example, when a solution of **G2**/**2**_{acid} in CHCl₃ (5 mM) was spin-coated in a clockwise direction at 6000 rpm, the resulting film displayed intense CD bands at 413, 440, and 453 nm with positive, negative, and positive signs, respectively (Figure 1 c'; red curve). On the other hand, spin-coating of the same solution in a counterclockwise direction resulted in the appearance of a mirror-image CD spectrum (Figure 1 c'; blue curve). The intensities of the CD bands hardly changed when observed by rotating the samples along an axis perpendicular to the substrate surface,^[8] thus indicating a negligibly small contamination with linear dichroism. Furthermore, we prepared 10 samples for each spinning direction and confirmed a

complete dominance of the emerging chirality sense.^[8] Such a spinning direction dependent chirality dominance was also observed for spin-coated films of *J*-aggregated **G2/1_{acid}** (Figure 1b'). As already described, the *J*-aggregates of **G2/1_{acid}** and **G2/2_{acid}** both involve a short, oblique slip of the π -stacked zinc porphyrin units (red curves in Figure 1b and c, respectively). In sharp contrast, *J*-aggregated **G2/0_{acid}**, which is proposed to involve a long, non-oblique slip of the zinc porphyrin π stacks (Figure 1a; red curve), gave a spin-coated film that exhibited negligibly weak CD bands (Figure 1a') in the visible region. Similar weak CD bands resulted when nondendritic **G0_{C18}/1_{acid}**, which is *J*-aggregated in CHCl₃ (Figure 1f), was spin-coated (Figure 1f'). These observations indicate the importance of spatial design around the hydrogen-bonded zinc porphyrin chromophores for the emergence of chirality on spin-coating.

One-generation higher **G3/0_{acid}**, which is not associated through π interactions in CHCl₃ (Figure 1d) or even in C₆H₆ (Figure 2a), gave neither birefringent (Figure 3d, f) nor optically active films (Figure 1d', Figure 2a') on spin-coating. A nonbirefringent, optically inactive film (Figure 3e, Figure 1e') also resulted when non-assembled **G3/1_{acid}** in CHCl₃ (Figure 1e) was spin-coated. In contrast, spin-coating of a solution of *J*-aggregated **G3/1_{acid}** in C₆H₆ (Figure 2b) resulted in the formation of a birefringent, optically active film (Figure 3g, Figure 2b') that exhibited a spinning direction dependent CD response. On the other hand, non-assembled ester versions such as **Gm/n_{ester}** ($m = 2, 3, n = 0-2$) and **G0_{C18}/1_{ester}** (Figure 1a-f; green curves) gave CD-silent films on spin-coating, as expected.

Figure 4 shows a schematic representation of the suggested *J*-aggregated 2D sheet. This is composed of an offset stacking of hydrogen-bonded dendritic zinc porphyrin polymers (Scheme 2). A helical *J*-aggregate structure, proposed for the precedent examples,^[5b,c] seems unlikely in solutions,

because of a large steric repulsion between the dendritic wedges, along with the one-dimensionality of the backbone polymers. However, such 2D molecular sheets, when transferred to the solid state, are known to roll up to form coiled architectures.^[4,10] If this happens to the *J*-aggregated 2D sheet, the zinc porphyrin units are forced to adopt a twisted (chiral) geometry relative to one another, and the assembly can eventually be optically active when the parity of chirality is broken. On the other hand, when a large rotational shear force is applied to this roll-up event by spin-coating, either a right-handed or left-handed helical coil, depending on the spinning direction, may be selected. In other words, the spin-coated films can chiroptically memorize the macroscopic spinning direction. We found that the chiroptical memory thus fixed is thermally stable. For example, the spin-coated film of *J*-aggregated **G2/2_{acid}** still preserved its optically activity when heated at 200 °C for five minutes. Further heating the film up to 260 °C resulted in it losing its birefringence and becoming optically inactive.

In summary, we have demonstrated that spin-coating of hydrogen-bonded dendritic zinc porphyrin *J*-aggregates gives optically active films, where either of the two enantiomeric forms is selected by the spinning direction. This is the first successful example of the transformation of a macroscopic spinning chirality into a stable supramolecular chirality in the solid state. Extension of this finding to other self-assembling systems and application of the resulting optically active materials to absolute asymmetric synthesis and chiral separation are the challenging subjects worthy of further investigation.

Received: July 26, 2004

Keywords: chirality · dendrimers · *J*-aggregate · porphyrinoids · self-assembly

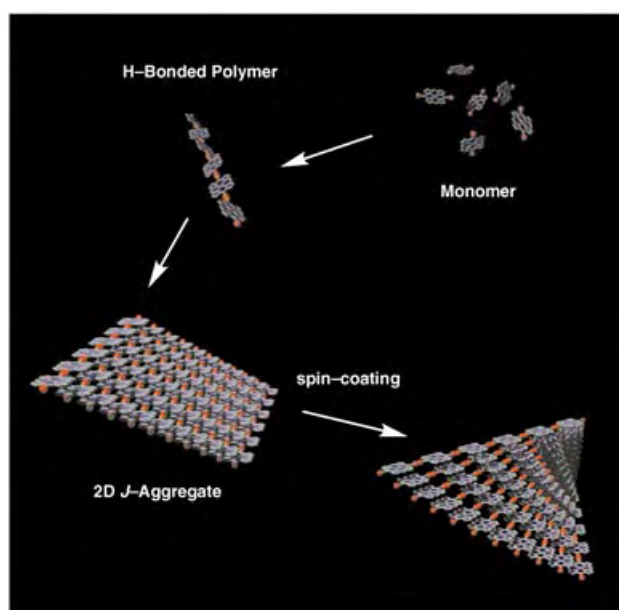


Figure 4. A proposed mechanism for the formation of a chiral zinc porphyrin *J*-aggregate.

- [1] J. Jacques, A. Collet, S. H. Wilen, *Enantiomers, Racemates, Resolutions*, Wiley, New York, 1998.
- [2] a) D. K. Kondepudi, R. J. Kaufman, N. Singh, *Science* **1990**, 250, 975–976; b) D. K. Kondepudi, K. L. Bullock, J. A. Digits, J. K. Hall, J. M. Miller, *J. Am. Chem. Soc.* **1993**, 115, 10211–10216; c) D. K. Kondepudi, J. Laudadio, K. Asakura, *J. Am. Chem. Soc.* **1999**, 121, 1448–1451.
- [3] D. R. Link, G. Natale, R. Shao, J. E. MacLennan, N. A. Clark, E. Körblava, D. M. Walba, *Science* **1997**, 278, 1924–1927.
- [4] X. Huang, C. Li, S. Jiang, X. Wang, B. Zhang, M. Liu, *J. Am. Chem. Soc.* **2004**, 126, 1322–1323.
- [5] a) U. De Rossi, S. Dähne, S. C. J. Meskers, H. P. J. M. Dekkers, *Angew. Chem.* **1996**, 108, 827–830; *Angew. Chem. Int. Ed. Engl.* **1996**, 35, 760–763; b) O. Ohno, Y. Kaizu, H. Kobayashi, *J. Chem. Phys.* **1993**, 99, 4128–4139; c) J. M. Ribó, J. Crusats, F. Sagues, J. M. Claret, R. Ruvires, *Science* **2001**, 292, 2063–2066.
- [6] a) C. Halvorson, A. Hays, B. Kraabel, R. Wu, F. Wudl, A. J. Heeger, *Science* **1994**, 265, 1215–1216; b) H. S. Nalwa, *Adv. Mater.* **1993**, 5, 341–358; c) K. Misawa, T. Kobayashi, *J. Chem. Phys.* **1999**, 110, 5844–5850.
- [7] a) S. Okada, H. Segawa, *J. Am. Chem. Soc.* **2003**, 125, 2792–2796; b) M. Shirakawa, S. Kawano, N. Fujita, K. Sada, S. Shinkai, *J. Org. Chem.* **2003**, 68, 5037–5044.
- [8] See Supporting Information.

- [9] J.-H. Furhop, C. Demoulin, C. Boettcher, J. König, U. Siggel, *J. Am. Chem. Soc.* **1992**, *114*, 4159–4165.
- [10] a) J. M. Schnur, *Science* **1993**, *262*, 1669–1676; b) R. Oda, I. Huc, M. Schmutz, S. J. Candau, F. C. MacKintosh, *Nature* **1999**, *399*, 566–569; c) E. D. Sone, E. R. Zubarev, S. I. Stupp, *Angew. Chem.* **2002**, *114*, 1781–1785; *Angew. Chem. Int. Ed.* **2002**, *41*, 1706–1709; d) J. P. Hill, W. Jin, A. Kosaka, T. Fukushima, H. Ichihara, T. Shimomura, K. Ito, T. Hashizume, N. Ishii, T. Aida, *Science* **2004**, *304*, 1481–1483.

Analytical Methods

Optimization Of “Wired” Enzyme O₂-Electroreduction Catalyst Compositions by Scanning Electrochemical Microscopy**

José L. Fernández, Nicolas Mano,* Adam Heller, and Allen J. Bard*

“Wired” enzyme electrodes, comprising enzymes connected electrically through redox polymers, which swell to give electron-conducting hydrogels,^[1] are already used in experimental subcutaneously implanted electrodes for the continuous monitoring of glucose in diabetics and may be used in future miniature, microwatt producing, membrane-less biofuel cells.^[2] The subcutaneously implanted electrodes comprise, in addition to the “wired” enzyme film that transduces the glucose flux to a current, a glucose flux-controlling membrane, which defines the measurable glucose concentration range, and optionally, a bioinert film.^[3] The membrane-less miniature biofuel cells comprise a “wired” glucose oxidase anode, and a “wired” bilirubin oxidase or laccase cathode. Optimizing the performance of these devices requires synthesis and characterization of new redox polymers,^[4,5] defining the optimal enzyme–cross-linker–redox-polymer compositions,^[6–9] and synthesis and optimization of flux controlling and bioinert membranes. A key parameter,

which is usually explored first, is the polymer/enzyme ratio. An excessive enzyme weight fraction can decrease the current density, because the enzyme, unlike the redox polymer, is an electronic insulator.^[10] Furthermore, if the enzyme weight fraction is high enough for the net negative charge of glucose oxidase to balance the positive charge of the redox polymer, an electrostatic adduct that shows poor electronic conductivity precipitates.^[6,7] Moreover, when the weight fraction of the redox polymer is excessive, the flux of electrons is reduced, because of the smaller number of enzyme molecules.^[11]

The effort and material expended in the optimization process^[6,7,11] can be reduced by combinatorial screening techniques^[12] exemplified by optimization through scanning electrochemical microscopy (SECM),^[13] a technique that has been extensively used for evaluating the activity of enzymatic systems^[14,15] and whose utility is demonstrated herein. Because only optimization of an exemplary parameter, the weight fraction of the multicopper oxidase bilirubin oxidase (BOD) or laccase, of a biofuel cell cathode was performed, the study does not provide as yet a fully optimized electrode, for which additional parameters, including the total loading and the weight % of the cross-linker, would have to be defined, along with the thickness of the electrode. The results obtained establish, nevertheless, that SECM screening of compositionally varying arrays of μm -size spot electrodes yields results identical with those obtained with discreet rotating disk electrodes, but much more efficiently in terms of speed and material required.

Ternary mixtures of enzyme, cross-linker, and redox polymer, with compositions ranging from pure enzyme to pure polymer, were prepared from aqueous solutions of BOD from *Trachyderma tsunodae* (8 mg mL^{-1} in pH 7.2 20-mM phosphate buffer) or laccase from *Coriolus hirsutus* (8.6 mg mL^{-1} in pH 5.0 20-mM citrate buffer), and PAA-PVI-[Os(4,4'-dichloro-2,2'-bipyridine)₂Cl]^{1+/2+} (8 mg mL^{-1}) or PAA-PVI-[Os(tpy)(dme-bpy)Cl]^{1+/2+} (8.6 mg mL^{-1}), respectively (PAA = poly(1-carboxy-1,2-ethanediyl), PVI = poly(1-imidazolyl-1,2-ethanediyl), tpy = 2,2':6',2''-terpyridine, dme-bpy = 4,4'-dimethyl-2',2-bipyridine). A solution of polyethylene glycol diglycidyl ether at 2 mg mL^{-1} (PEDGE, Polysciences Inc.) was used as the cross-linker. Arrays of spots containing these mixtures were deposited on glassy carbon (GC) plates $15 \times 15 \times 1\text{ mm}$ (Alfa) by using a piezo-based micro-arrayer, a device similar to that used by Schuhmann and co-workers for micro-patterning of enzymatic biosensors.^[15] A commercial piezo-dispenser MicroJet AB-01-60 (MicroFab) with an outlet aperture of $60\text{ }\mu\text{m}$, that dispenses on-demand picoliter-sized ($\approx 100\text{ pL}$) droplets by application of potential pulses (50 V , $25\text{ }\mu\text{s}$), was installed onto the head of a digital plotter (Houston Instruments DMP-5) to control its position with a resolution of $100\text{ }\mu\text{m/step}$. Figure 1 shows the preparation scheme. The dispenser was filled with polymer solution ($3\text{ }\mu\text{L}$), which was dispensed in a programmed number of drops at each site. To test for reproducibility, each composition was prepared in duplicate or triplicate. Thus, the arrays contained 11 rows and two columns of spots. Typically, the first two-spot row contained 10 drops per spot (pure polymer), the next row 9 drops per spot and so on down to and the tenth row with 1 drop per spot. The dispenser was

[*] Dr. J. L. Fernández, Prof. Dr. A. J. Bard
Chemistry and Biochemistry
University of Texas at Austin
Austin, TX 78712 (USA)
Fax: (+1) 512-471-0088
E-mail: ajbard@mail.utexas.edu

Dr. N. Mano, Prof. Dr. A. Heller
Department of Chemical Engineering and Texas Materials Institute
University of Texas at Austin
Austin, TX 78712 (USA)
Fax: (+1) 512-471-8799
E-mail: heller@che.utexas.edu

[**] Financial support for this work was provided by the Office of Naval Research (N00014-02-1-0144), the National Science Foundation (CHE 0109587), and the Robert A. Welch Foundation. J.L.F. thanks the Fundación Antorchas (Argentina) for a postdoctoral fellowship. N.M. thanks The Onozio de Nora Industrial Electrochemistry Fellowship of The Electrochemical Society.

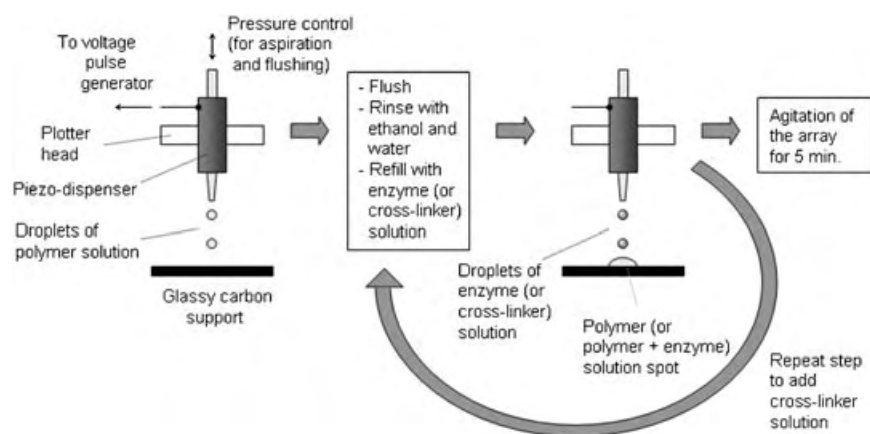


Figure 1. Schematic diagram of the preparation of the wired enzyme spot arrays.

emptied, thoroughly rinsed first with ethanol and then with water, and refilled with 3 μL of enzyme solution. Then the plotter positioned the dispenser exactly over the previously prepared polymer spots, and a number of drops of enzyme solution, sufficient for the sum of the enzyme drops and the polymer drops to always equal 10, were dispensed. About 80% of the polymer or enzyme solution used to fill the dispenser can be recovered. After polymer and enzyme were deposited, 3 drops of cross-linker solution were dispensed on each spot. The substrate was maintained under a water-saturated N_2 stream during the complete preparation procedure to avoid the premature evaporation of the spots. To mix the components, the array was then agitated under the water-saturated N_2 stream for 5 min in a Vortex Genie 2 agitator (Fisher), and the array was dried overnight in ambient air. Figure 2 shows an SEM picture of typical arrays and an optical micrograph of an individual spot. The center-to-center distance between the 150–200 μm diameter spots was about 400 μm . Before testing, the arrays were washed with Milli-Q water. The thickness of the spots, estimated by negative feedback mode SECM^[13] by using O_2 reduction on Au tips, over a spot and then over the neighboring GC, was 4–5 μm . The weight percent of enzyme (wt.%) at each spot was calculated from the number of drops (or volume fraction) and the concentrations of the polymer, enzyme, and cross-linker solutions used. The wt. % of the cross-linker was fixed at 6.9 for the BOD electrodes and at 6.5 for the laccase electrodes.

The SECM tip generation-substrate collection mode was used to image activity of the arrays.^[16] This mode of operation is well suited for imaging activity of surfaces with morphological features since it is relatively insensitive to changes of the tip-substrate distance.^[17] SECM images of O_2 reduction activity of the “wired” BOD arrays were obtained in 0.2 M pH 7.2 phosphate buffer, and of the “wired” laccase, in 0.2 M pH 5.0 citrate buffer, as previously described.^[16] Briefly, a 25 μm Pt tip situated at 40 μm from the GC surface was scanned in the xy plane (parallel to spot rows) at step intervals of 50 μm every 0.2 s while electrogenerating O_2 from H_2O at a constant current. Under these conditions, areas of 5×2 mm can be screened in about 1 h using the SECM (CH Instruments model 900B) with stepper-motor translators. The substrate array potential (E_s) was held at 0.3 and 0.4 V

versus Ag/AgCl (3 M KCl) for BOD and laccase, respectively, where the reduction of O_2 was diffusion controlled.^[6,7] The substrate current (i_s), measured as a function of tip position to produce the SECM image, was larger when the O_2 -generating tip passed over a more active spot. Thus, the measure of the electrocatalytic activity of any of the spot electrodes was the magnitude of i_s . Figure 3 presents SECM color-map images obtained for the BOD and the laccase arrays. To establish reproducibility, triplicate experiments were performed. Because of the time-dependent processes, such as diffusion of O_2 into the hydrogel and charge transport through the film, the response times were slower than for metallic electrodes, and individual spots were not well resolved in the direction of the

scan (x). As a result, the rows of the spots have a smeared, band-like appearance, particularly for the BOD films. Slower scanning can overcome the smearing, at the cost of increased imaging time.

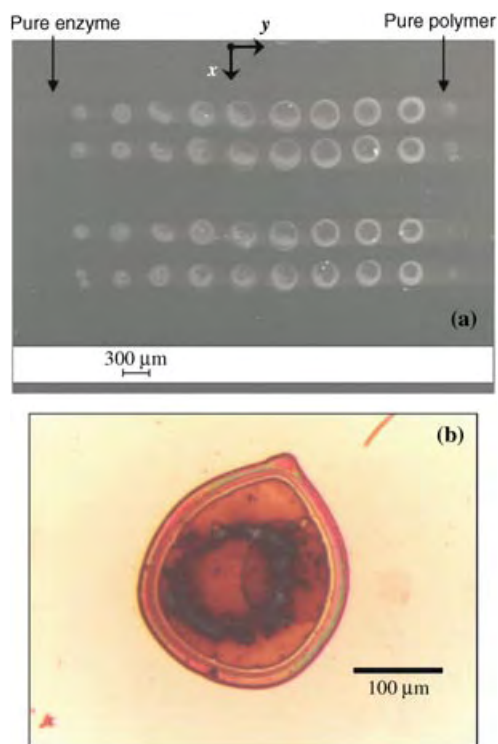


Figure 2. a) SEM photograph of two arrays of redox-polymer-laccase spots made with 6.5 wt. % cross-linker. Each two-dot row corresponds to a particular composition. b) Optical micrograph of the 46.5 wt. % enzyme, 46.6 wt. % polymer, 6.9 wt. % cross-linker “wired” BOD spot, prepared by mixing the component solutions in situ.

In the BOD arrays (Figure 3a), O_2 electroreduction was seen for a 20–80 wt. % BOD range. The largest oxygen reduction reaction (ORR) current (close to the highest expected) was for the 46.5 wt. % BOD spots. With the laccase arrays (Figure 3b), O_2 electroreduction was observed for a 15–70 laccase wt. % range, with a maximum at 46.7 wt. %

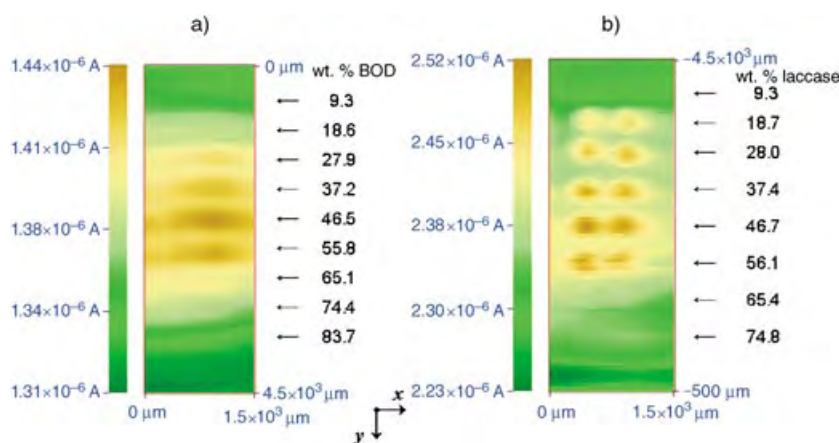


Figure 3. SECM images of "wired" enzyme arrays containing spots with different polymer/enzyme ratios. a) BOD (6.9 wt.% cross-linker) in pH 7.2 phosphate buffer, $i_T = -161$ nA (i_T = tip current), $E_s = 0.3$ V versus Ag/AgCl; b) laccase (6.5 wt.% cross-linker) in pH 5.0 citrate buffer, $i_T = -240$ nA, $E_s = 0.4$ V versus Ag/AgCl.

laccase. Figure 4 (solid symbols) summarizes the normalized ORR currents measured for each row as a function of enzyme wt.%. Each point is the average of three values measured from images obtained on three different arrays prepared under identical conditions.

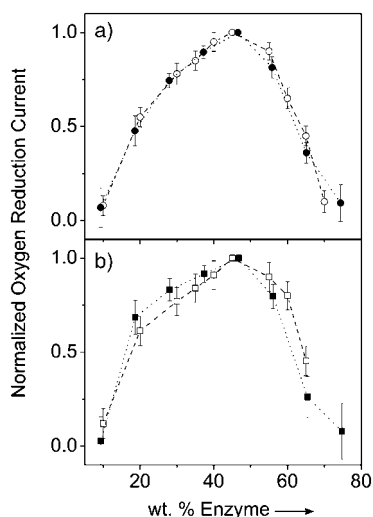


Figure 4. Dependence of the oxygen reduction current (normalized with respect to the highest current) on the enzyme wt.% for a) BOD in pH 7.2 phosphate buffer and for b) laccase in pH 5.0 citrate buffer. Solid symbols = results of the SECM screening, open symbols = results of the rotating disc experiments. 1 mVs^{-1} , 1000 rpm, 1 atm O_2 , total bioelectrocatalyst loading, 0.26 mg cm^{-2} .

To test the validity of the method, "wired" BOD and "wired" laccase GC rotating-disk electrodes were prepared, as described elsewhere, with different enzyme-polymer ratios.^[6,7] Polarization curves were measured by slow potentiodynamic scans (1 mVs^{-1}) in O_2 -saturated (1 atm) solutions at 1000 rpm in physiological buffer for BOD and in 0.2 M pH 5 citrate buffer for laccase. O_2 -electroreduction limiting currents were measured five times on each composition for BOD and seven times on laccase. The mean values are plotted in

Figure 4 (open symbols). The results obtained by the two methods were in good agreement. Sample preparation and testing by the SECM screening method required one day, while the preparation and testing of a rotating disk electrode required at least 10 days. The amounts of polymer and enzyme were reduced by a factor of 100 000 in the SECM test.

In conclusion, SECM screening of oxygen electroreduction activity on arrays of "wired" enzyme electrode spots, allows the optimization of a single-variable more rapidly and with less material than optimization utilizing discrete rotating disk electrodes. In the next phase, all parameters of the ORR films on carbon, including total loading, thickness, and weight % of the cross-linker will be optimized.

Received: August 3, 2004

Keywords: electrochemistry · enzyme electrodes · enzymes · polymers · scanning electrochemical microscopy

- [1] A. Heller, *Acc. Chem. Res.* **1990**, 23, 128.
- [2] A. Heller, *Phys. Chem. Chem. Phys.* **2004**, 6, 209.
- [3] A. Heller, *Annu. Rev. Biomed. Eng.* **1999**, 1, 153.
- [4] F. Mao, N. Mano, A. Heller, *J. Am. Chem. Soc.* **2003**, 125, 4951.
- [5] F. Barrière, Y. Ferry, D. Rochefort, Dónal Leech, *Electrochem. Commun.* **2004**, 6, 237.
- [6] N. Mano, H. Kim, Y. Zhang, A. Heller, *J. Am. Chem. Soc.* **2002**, 124, 6480.
- [7] S. Calabrese Barton, H. Kim, G. Binyamin, Y. Zhang, A. Heller, *J. Phys. Chem. B* **2001**, 105, 11917.
- [8] T. Chen, S. Calabrese Barton, G. Binyamin, Z. Gao, Y. Zhang, H. Kim, A. Heller, *J. Am. Chem. Soc.* **2001**, 123, 8630.
- [9] N. Mano, F. Mao, A. Heller, *J. Am. Chem. Soc.* **2003**, 125, 6588.
- [10] T. J. Ohara, R. Rajagopalan, A. Heller, *Anal. Chem.* **1994**, 66, 2451.
- [11] N. Mano, H. Kim, A. Heller, *J. Phys. Chem. B* **2002**, 106, 8842.
- [12] T. E. Mallouk, E. S. Smotkin in *Handbook of Fuel Cells—Fundamental and Applications*, Vol. 2, Part 3 (Eds.: W. Vielstich, A. Lamm, H. A. Gasteiger), Wiley, Chichester, **2003**, pp. 334–347.
- [13] *Scanning Electrochemical Microscopy* (Eds.: A. J. Bard, M. V. Mirkin), Marcel Dekker, New York, **2001**.
- [14] a) T. Wilhelm, G. Wittstock, *Angew. Chem.* **2003**, 115, 2350; *Angew. Chem. Int. Ed.* **2003**, 42, 2248; b) T. Wilhelm, G. Wittstock, *Langmuir* **2002**, 18, 9485; c) J. Zhou, C. Campbell, A. Heller, A. J. Bard, *Anal. Chem.* **2002**, 74, 4007; d) G. Wittstock, *Fresenius J. Anal. Chem.* **2001**, 370, 303.
- [15] a) M. Niculescu, S. Gáspár, A. Schulte, E. Csöregi, W. Schuhmann, *Biosens. Bioelectron.* **2004**, 19, 1175; b) S. Gáspár, M. Mosbach, L. Wallman, T. Laurell, E. Csöregi, W. Schuhmann, *Anal. Chem.* **2001**, 73, 4254; c) M. Mosbach, H. Zimmermann, T. Laurell, J. Nilsson, E. Gsöregi, W. Schuhmann, *Biosens. Bioelectron.* **2001**, 16, 827.
- [16] J. L. Fernández, A. J. Bard, *Anal. Chem.* **2003**, 75, 2967.
- [17] J. L. Fernández, A. J. Bard, *Anal. Chem.* **2004**, 76, 2281.

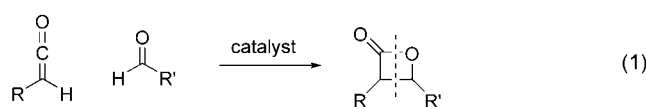
Lactone Synthesis

Asymmetric Synthesis of Highly Substituted β -Lactones by Nucleophile-Catalyzed [2+2] Cycloadditions of Disubstituted Ketenes with Aldehydes**

Jonathan E. Wilson and Gregory C. Fu*

The development of effective methods for the asymmetric synthesis of β -lactones is an important challenge for a variety of reasons.^[1] Numerous biologically active β -lactone-containing natural and unnatural products have been described, including Xenical (tetrahydrolipstatin), an anti-obesity drug developed by Roche.^[2,3] Furthermore, β -lactones serve as useful intermediates in an array of fields, including materials science and synthetic organic chemistry.^[1,4] The strain of the four-membered lactone provides an opportunity for a range of functionalizations; for example, nucleophiles can react either at the carbonyl group through an addition–elimination sequence or at a C–O single bond through an S_N2 process. Thus, a number of recent total syntheses, such as those of (–)-laulimalide,^[5] (–)-malyngolide,^[6] and trapoxin B,^[7] have exploited enantiopure β -lactones as intermediates.

One attractive route to β -lactones is the overall [2+2] cycloaddition of a ketene with an aldehyde [Eq. (1)]. Chiral

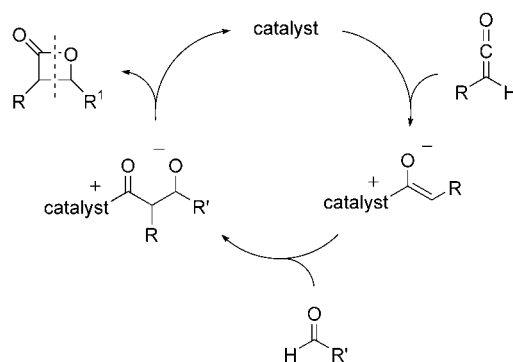


nucleophiles and chiral Lewis acids have both been shown to catalyze this process, sometimes with outstanding enantioselectivity (the postulated mechanism for the nucleophile-catalyzed cycloaddition is illustrated in Scheme 1).^[8–11] To date, all reports of asymmetric catalysis of this transformation have described reactions of ketene itself ($H_2C=C=O$) or of monosubstituted ketenes. Expanding the scope of such processes to include disubstituted ketenes would furnish access to α,α -disubstituted β -lactones, an important class of synthetic targets.^[12]

[*] J. E. Wilson, Prof. Dr. G. C. Fu
Department of Chemistry
Massachusetts Institute of Technology
Cambridge, MA 02139 (USA)
Fax: (+1) 617-324-3611
E-mail: gcf@mit.edu

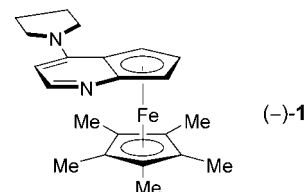
[**] We thank Ivory D. Hills for X-ray crystallographic studies. Support has been provided by the National Institutes of Health (National Institute of General Medical Sciences: R01-GM57034; National Cancer Institute: training grant CA009112), Merck, and Novartis. Funding for the MIT Department of Chemistry Instrumentation Facility has been furnished in part by NSF CHE-9808061 and NSF DBI-9729592.

Supporting information for this article is available on the WWW under <http://www.angewandte.org> or from the author.



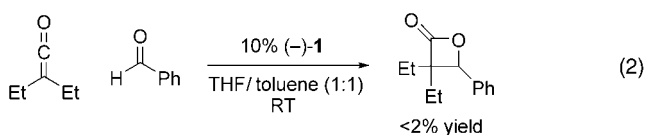
Scheme 1. Proposed pathway for the nucleophile-catalyzed enantioselective synthesis of β -lactones from ketenes and aldehydes.

We have been exploring the utility of planar-chiral DMAP and PPY derivatives (for example, **1**) as catalysts for a range of transformations,^[13] including an asymmetric Staudinger synthesis of β -lactams that likely proceeds by a pathway analogous to that depicted in Scheme 1 (DMAP = 4-(dimethylamino)pyridine, PPY = 4-pyrrolidin-1-ylpyridine).^[14]



We were intrigued by the possibility that these nucleophilic catalysts might also be useful for β -lactone synthesis. This sort of an “extension” from reactions of imines to reactions of aldehydes is not as straightforward as may appear; for example, in the case of cinchona alkaloid-based catalysts, an excellent method for enantioselective β -lactam synthesis from monosubstituted ketenes was reported several years ago,^[15] whereas general conditions for β -lactone synthesis from monosubstituted ketenes, which require a Lewis acid co-catalyst, have only been developed very recently.^[16] In this Communication, we demonstrate that PPY derivative **1** serves as an effective catalyst for [2+2] cycloadditions of disubstituted ketenes with aldehydes to furnish the first catalytic asymmetric route to α,α -disubstituted β -lactones.

In our earlier study, we established that **1** catalyzes a Staudinger-type cycloaddition of ketenes with imines to efficiently afford β -lactams with good enantioselectivity (76–98% yield; 81–98% *ee*).^[14] However, when we apply these conditions to the corresponding reaction of ketenes with aldehydes, we obtain essentially none of the desired β -lactone [Eq. (2)].



Interestingly, by lowering the reaction temperature, we can generate the targeted [2+2] cycloaddition product in high yield, and, equally significantly, in high enantiomeric excess (91% yield, 89% *ee*; Table 1, entry 1). Furthermore, the two-

Table 1: Catalytic asymmetric cycloaddition of diethylketene with benzaldehyde.

Entry	Catalyst	Conditions	Yield [%] ^[a]	<i>ee</i> [%] ^[a]
1	5% (–)- 1	THF/toluene (1:1), –78 °C	91	89
2	5% (–)- 1	THF, –78 °C	92	91
3	5% quinidine	THF/toluene (1:1), –78 °C → RT	< 5	–
4 ^[b]	10% O-TMS-quinidine, 2 equiv LiClO ₄	THF/CH ₂ Cl ₂ (1:1), –78 °C → RT	21	< 2

[a] Average of two runs. [b] Because the product β -lactone could not be separated from a side product, the β -lactone was reduced to a 1,3-diol with diisobutylaluminum hydride (DIBAL-H). TMS = trimethylsilyl.

solvent system that we employed for the synthesis of β -lactams is unnecessary—the formation of β -lactones proceeds in very good yield and *ee* in THF alone (entry 2). It is important to note that the alkaloid-based methods that have proved useful for catalytic asymmetric reactions of *mono*-substituted ketenes are not effective for the illustrated cycloaddition of a *disubstituted* ketene (entries 3^[10b] and 4^[10d]).

Our optimized conditions (Table 1, entry 2) are applicable to a range of [2+2] cycloadditions of disubstituted ketenes with aldehydes (Table 2). Thus, symmetrical ketenes, both acyclic and cyclic, couple with aldehydes with good enantioselectivity (entries 1–7). Cycloadditions of unsymmetrical disubstituted ketenes generate β -lactones that bear two contiguous stereocenters, one quaternary and one tertiary;^[17] we have determined that planar-chiral catalyst **1** preferen-

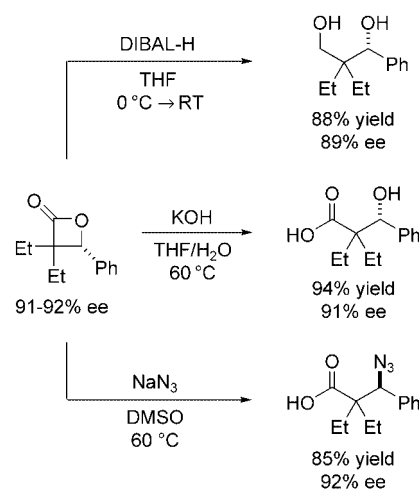
Table 2: Catalytic asymmetric synthesis of β -lactones by cycloadditions of disubstituted ketenes with aldehydes.

Entry	R ¹	R ²	R ³	<i>ee</i> [%] ^[a]	Yield [%] ^[a]
1	Et	Et	Ph	91	92
2	Et	Et	2-naphthyl	89	77
3	Et	Et	4-(CF ₃)C ₆ H ₄	80	74
4	Et	Et	4-(MeCO)C ₆ H ₄	81	76
5	Et	Et	4-MeC ₆ H ₄	89	67
6 ^[b]	Me	Me	Ph	76	68
7	–(CH ₂) ₆ –	–	Ph	82	71
8 ^[c]	<i>i</i> Pr	Me	Ph	91	48
9 ^[c]	cyclopentyl	Me	Ph	88	53

[a] Average of two runs. [b] 7% (–)-**1** was used. [c] *cis:trans* selectivity = 4.2–4.6:1. The *ee* value is for the *cis* diastereomer, and the yield is for both diastereomers.

tially furnishes the *cis* diastereomer (ca. 4.5:1 selectivity) with very good *ee* (ca. 90%; entries 8 and 9).^[18]

We have established that these sterically demanding α,α -disubstituted β -lactones can be derivatized through reactions with nucleophiles (Scheme 2). Reagents such as DIBAL-H



Scheme 2. Derivatization of α,α -disubstituted β -lactones.

and hydroxide add to the carbonyl group to furnish a 1,3-diol and a β -hydroxyacid, respectively. Sodium azide, on the other hand, reacts through an S_N2 process to generate a β -azidoacid.^[19,20] These functionalizations proceed in good to excellent yield with essentially no erosion in enantiomeric excess.^[21]

In conclusion, we have established for the first time that a chiral PPY derivative (**1**) can serve as an efficient catalyst for the asymmetric synthesis of β -lactones; this is the only catalyst reported to date that is effective for enantioselective cycloadditions of disubstituted ketenes, which generate α,α -disubstituted β -lactones. Furthermore, we have shown that these β -lactones, in addition to being useful structures in their own right, can be transformed into other important families of enantioenriched compounds. Additional studies of catalytic asymmetric reactions of ketenes are underway.

Received: May 18, 2004

Revised: September 10, 2004

Keywords: aldehydes · asymmetric catalysis · cycloaddition · ketenes · lactones

[1] For a review of the synthesis of optically active β -lactones, see: H. W. Yang, D. Romo, *Tetrahedron* **1999**, 55, 6403–6434.

[2] For reviews of naturally occurring β -lactones, see: a) C. Lowe, J. C. Vederas, *Org. Prep. Proced. Int.* **1995**, 27, 305–346; b) A. Pommier, J.-M. Pons, *Synthesis* **1995**, 729–744.

[3] For studies of analogues of lactacystin β -lactone (and leading references), see: a) E. J. Corey, W. Li, G. A. Reichard, *J. Am. Chem. Soc.* **1998**, 120, 2330–2336; b) F. Soucy, L. Grenier, M. L. Behnke, A. T. Destree, T. A. McCormack, J. Adams, L. Plamondon, *J. Am. Chem. Soc.* **1999**, 121, 9967–9976.

- [4] For an example of an application in material science, see: M. E. Gelbin, J. Kohn, *J. Am. Chem. Soc.* **1992**, *114*, 3962–3965.
- [5] S. G. Nelson, W. S. Cheung, A. J. Kassick, M. A. Hilfiker, *J. Am. Chem. Soc.* **2002**, *124*, 13654–13655.
- [6] Z. Wan, S. G. Nelson, *J. Am. Chem. Soc.* **2000**, *122*, 10470–10471.
- [7] J. Taunton, J. L. Collins, S. L. Schreiber, *J. Am. Chem. Soc.* **1996**, *118*, 10412–10422.
- [8] For leading references to methods for the catalytic asymmetric synthesis of β -lactones, see: C. Schneider, *Angew. Chem.* **2002**, *114*, 771–772; *Angew. Chem. Int. Ed.* **2002**, *41*, 744–746.
- [9] For industrial applications of catalytic asymmetric [2+2] cycloadditions of ketenes with aldehydes, see: P. Stutte in *Chirality in Industry* (Eds.: A. N. Collins, G. N. Sheldrake, J. Crosby), Wiley, New York, **1997**, chap. 18.
- [10] For chiral nucleophilic catalysts, see: a) D. Borrmann, R. Wegler, *Chem. Ber.* **1966**, *99*, 1245–1251; D. Borrmann, R. Wegler, *Chem. Ber.* **1966**, *99*, 1575–1579; b) H. Wynberg, E. G. J. Staring, *J. Am. Chem. Soc.* **1982**, *104*, 166–168; H. Wynberg, E. G. J. Staring, *J. Org. Chem.* **1985**, *50*, 1977–1979; P. E. F. Ketelaar, H. Wynberg, E. G. J. Staring, *Tetrahedron Lett.* **1985**, *26*, 4665–4668; c) R. Tennyson, D. Romo, *J. Org. Chem.* **2000**, *65*, 7248–7252; G. S. Cortez, R. L. Tennyson, D. Romo, *J. Am. Chem. Soc.* **2001**, *123*, 7945–7946; G. S. Cortez, S. H. Oh, D. Romo, *Synthesis* **2001**, 1731–1736; d) C. Zhu, X. Shen, S. G. Nelson, *J. Am. Chem. Soc.* **2004**, *126*, 5352–5353.
- [11] Chiral Lewis acid catalysts: a) for an overview, see: ref. [8]; b) for leading references, see: S. G. Nelson, C. Zhu, X. Shen, *J. Am. Chem. Soc.* **2004**, *126*, 14–15.
- [12] Salinosporamide A and omuralide are two examples of natural products that include an α,α -disubstituted β -lactone. For leading references, see: L. R. Reddy, P. Saravanan, E. J. Corey, *J. Am. Chem. Soc.* **2004**, *126*, 6230–6231.
- [13] a) For an early overview, see: G. C. Fu, *Acc. Chem. Res.* **2000**, *33*, 412–420; b) For more recent reports, see: A. H. Mermerian, G. C. Fu, *J. Am. Chem. Soc.* **2003**, *125*, 4050–4051; I. D. Hills, G. C. Fu, *Angew. Chem.* **2003**, *115*, 4051–4054; *Angew. Chem. Int. Ed.* **2003**, *42*, 3921–3924.
- [14] B. L. Hodous, G. C. Fu, *J. Am. Chem. Soc.* **2002**, *124*, 1578–1579.
- [15] A. E. Taggi, A. M. Hafez, H. Wack, B. Young, W. J. Drury III, T. Lectka, *J. Am. Chem. Soc.* **2000**, *122*, 7831–7832.
- [16] See ref. [11b]. Examples of cinchona alkaloid-based intramolecular reactions of monosubstituted ketenes had been described earlier (ref. [10c]).
- [17] For reviews of catalytic asymmetric methods that generate quaternary stereocenters, see: E. J. Corey, A. Guzman-Perez, *Angew. Chem.* **1998**, *110*, 403–415; *Angew. Chem. Int. Ed.* **1998**, *37*, 388–401; J. Christoffers, A. Mann, *Angew. Chem.* **2001**, *113*, 4725–4732; *Angew. Chem. Int. Ed.* **2001**, *40*, 4591–4597; see also: I. Denissova, L. Barriault, *Tetrahedron* **2003**, *59*, 10105–10146.
- [18] Notes: a) Under our standard conditions (Table 2), aryl alkyl ketenes, monosubstituted ketenes, very electron-rich aldehydes, and non-aromatic aldehydes are not suitable substrates. b) At the end of a reaction, we can typically recover about 80% of catalyst **1**.
- [19] A. Griesbeck, D. Seebach, *Helv. Chim. Acta* **1987**, *70*, 1326–1332. For a more recent study, see: S. G. Nelson, K. L. Spencer, *Angew. Chem.* **2000**, *112*, 1379–1381; *Angew. Chem. Int. Ed.* **2000**, *39*, 1323–1325.
- [20] For a review of the enantioselective synthesis of β -amino acids, see: a) E. Juaristi, *Enantioselective Synthesis of β -Amino Acids*, Wiley-VCH, New York, **1997**; b) M. Liu, M. P. Sibi, *Tetrahedron* **2002**, *58*, 7991–8035.
- [21] In preliminary experiments, we have not observed ring-opening upon reaction with RSH, R_2NH , or R_2NLi .

Large-Scale Synthesis of Micrometer-Scale Single-Crystalline Au Plates of Nanometer Thickness by a Wet-Chemical Route***Xuping Sun, Shaojun Dong,* and Erkang Wang**

In the past few years metal nanostructures have been the focus of intensive research as a result of their electronic, optical, magnetic, thermal, catalytic, and other properties being distinctly different from their bulk counterparts, and considerable attention, in terms of both fundamental and applied research, has been paid to synthesizing and characterizing metal nanostructures.^[1] It has also been demonstrated in nanometer-sized materials that the physical and chemical properties of the structures are closely related to their size and shape.^[2] For example, the surface plasmon resonance of metal particles is strongly shape-dependent: the transformation of spherical metal particles into nanometer-sized rods or triangular prisms results in a red-shift and even a split of the corresponding surface plasmon resonance into distinctive dipole and quadrupole modes.^[3] A variety of methods have so far been developed to prepare spherical metal nanoparticles,^[1d] however, the production of nanostructures by a shape-controlled procedure is still a challenge for materials scientists and there is great interest in developing new methods for fabricating shape-controlled nanoparticles. Many differently shaped nanostructures have been synthesized from metallic Ag by using various chemical approaches, with 1D Ag nanostructures having been fabricated by many research groups.^[4] Other Ag nanostructures, such as nanoprisms,^[3,5] nanocubes,^[6] nanoplates,^[7] nanodisks,^[8] and nanobelts,^[9] have also been fabricated. Much effort has also been made to fabricate Au nanostructures with specific shapes, and many methods have been developed to synthesis 1D Au nanostructures,^[10] however, there are very few reports on the synthesis of planar Au nanostructures such as nanodisks^[11] and nanoplates.^[12] We demonstrate herein a mild wet-chemical route to the large-scale synthesis of micrometer-scale Au nanoplates. In this process $\text{H}[\text{AuCl}_4]$ is reduced by *ortho*-phenylenediamine in an aqueous medium to form hexagonal single-crystalline Au nanoplates with a preferential growth direction along the Au(111) plane. This result suggests that the molar ratio of *ortho*-phenylenediamine to gold is key to producing Au nanoplates.

[*] Dr. X. Sun, Prof. S. Dong, Prof. E. Wang
State Key Laboratory of Electroanalytical Chemistry
Changchun Institute of Applied Chemistry
Chinese Academy of Sciences
Graduate School of the Chinese Academy of Sciences
Changchun 130022, Jilin (P.R. China)
Fax: (+86) 431-5689711
E-mail: dongsj@ns.ciac.jl.cn
ekwang@ciac.jl.cn

[**] We thank the National Natural Science Foundation of China for financial support of this research (Nos. 299750258 and 20075028).

The morphology of the precipitate was characterized by scanning electron microscopy (SEM, Figure 1). The lower magnification image (Figure 1a) indicates that the precipitate consists of a large amount of particles, while the higher

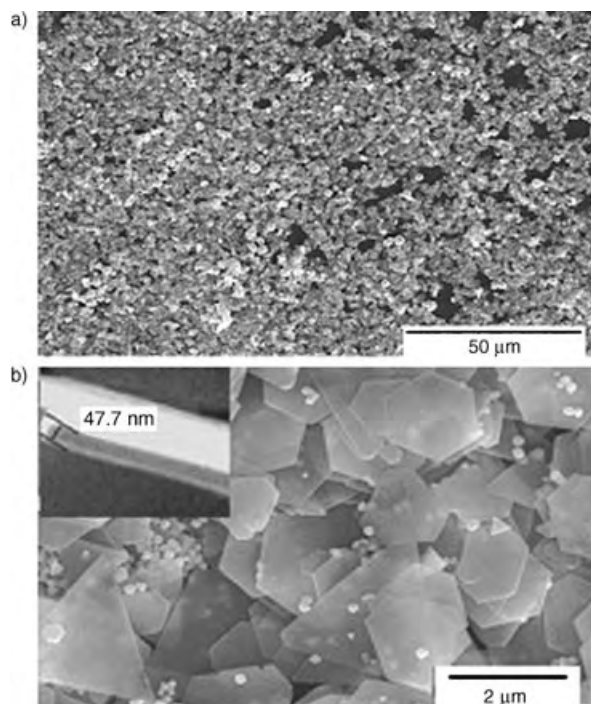


Figure 1. Low magnification (a) and high magnification (b) SEM images of the precipitate. The inset shows that the thickness of a single nanoplate is about 47.7 nm.

magnification image (Figure 1b) clearly reveals that the particles are micrometer-scale plates, mainly hexagonal in shape. We can conclude from measurements of the distance between two planes of one plate standing against the glass substrate that these plates are nanoplates, tens of nanometers thick (see Figure 1b, inset). Small quantities of spherical particles are also observed as by-products. The chemical composition of the particles was further determined by energy-dispersive X-ray spectroscopy (EDS). The EDS spectrum obtained from the precipitate only shows the peak corresponding to Au (data not shown), thus indicating that the particles are pure metallic Au.

Figure 2 shows the transmission electron microscopy (TEM) image (Figure 2a) of a single Au nanoplate as well

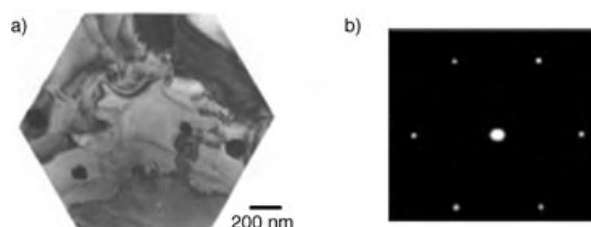


Figure 2. Typical TEM image (a) and corresponding electron diffraction pattern (b) of a single hexagonal Au nanoplate lying flat on a TEM grid.

as the related selected area electron diffraction (SAED) pattern (Figure 2b) obtained by focusing the electron beam on a nanoplate lying flat on the TEM grid. Interestingly, some patterns are observed on the nanoplate plane. The other four dark dots marked with arrows are spherical Au particles formed as by-products. The SAED pattern reveals that a hexagonal symmetry diffraction spot pattern is generated, thus demonstrating that the Au nanoplate is a single crystal with a preferential growth direction along the Au (111) plane.^[13]

The crystalline nature of the nanoplates was further confirmed by recording the X-ray diffraction (XRD) pattern. The XRD pattern (Figure 3) shows sharp peaks correspond-

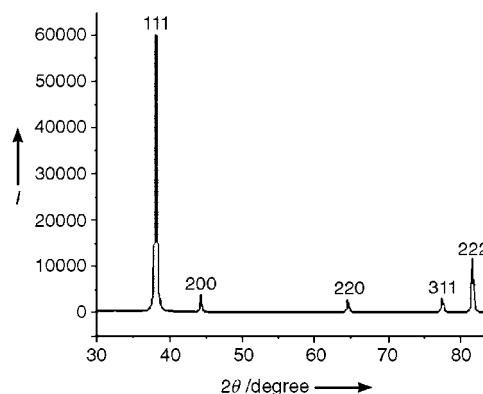


Figure 3. XRD pattern of the Au products.

ing to the (111), (200), (220), (311), and (222) diffraction peaks of metallic Au, and thus indicates that the precipitate is composed of pure crystalline Au.^[14] Note that the ratio of the intensity between the (200) and (111) diffraction peaks is much lower than the standard file (JCPDS; 0.061 versus 0.33). These observations confirm that our nanoplates are primarily dominated by (111) facets, and thus their (111) planes tend to be preferentially oriented parallel to the surface of the supporting substrate.

It is well-known that Au nanostructures dispersed in liquid media usually display a very intense color because of surface plasmon resonance (SPR). Figure 4 shows a photograph and an absorption spectrum of the resulting Au particles sus-

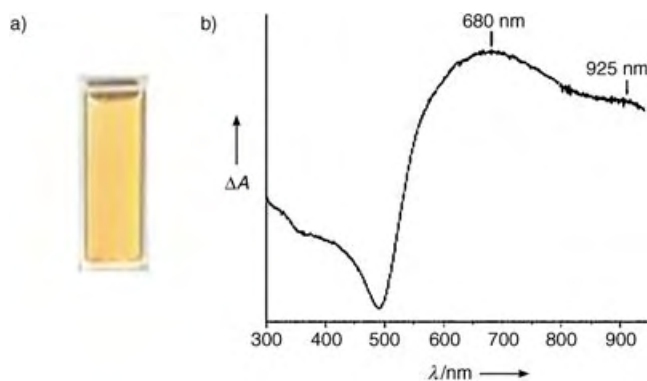


Figure 4. Photograph (a) and UV/Vis spectrum (b) of the Au particles suspended in water.

pended in water. It has been reported that a solution of spherical colloidal Au is red,^[15] but interestingly our suspension is gold-yellow in color (Figure 4a). It is also documented that the SPR band of Au nanostructures strongly depends on the size, shape, and aggregation of the nanostructures,^[16] and that spherical Au particles show an SPR band at approximately 520 nm that is usually red-shifted to longer wavelengths with increasing particle size.^[17] The resulting suspension shows two SPR bands located at about 680 and 925 nm which arise from the longitudinal plasmon resonance of Au particles,^[18] thus providing another piece of evidence for the formation of anisotropic Au particles.^[17]

We have found in our previous study that $\text{H}[\text{AuCl}_4]$ can be reduced by polyamine-containing polyelectrolytes and dendrimers to form Au nanoparticles.^[19] More recently, it has been shown that $\text{H}[\text{AuCl}_4]$ can also be reduced by *ortho*-phenylenediamine to form spherical Au particles with the concurrent formation of poly(*ortho*-phenylenediamine) nanobelts as a result of the oxidative polymerization of *ortho*-phenylenediamine monomers by $\text{H}[\text{AuCl}_4]$.^[20] In our present study we also obtained a precipitate of Au nanoplates and belts. Analysis of these belts by SEM shows that they contain C and N, thus indicating that they are oxidative products of *ortho*-phenylenediamine. These belts can be washed away with tetrahydrofuran (THF) to leave purified Au particles.

It is worthwhile mentioning that the quantity of *ortho*-phenylenediamine in the solution is an important factor in determining the morphology of the final Au particles. Control reactions in which excess *ortho*-phenylenediamine was added under otherwise identical conditions only gave isolated or aggregated spherical Au particles. Figure 5 shows typical SEM images of Au products obtained with initial *ortho*-phenylenediamine to gold ratios of 3:1 (Figure 5a) and 8:1

(Figure 5b), and clearly indicates the formation of aggregated and isolated spherical Au particles, respectively. Other control reactions also gave similar results. These results indicate that the quantity of *ortho*-phenylenediamine in the solution is key to yielding Au nanoplates. We suggest that *ortho*-phenylenediamine molecules serve as a soft template and kinetically control the growth rates of various faces of Au particles by selectively adsorbing on to the crystallographic planes, thus resulting in the formation of large single-crystalline Au nanoplates. However, it is not clear at present how the *ortho*-phenylenediamine molecules influence the growth of different crystal planes of the Au nanoplates, and the detailed mechanism needs further investigation.

In conclusion, we present our preliminary findings that micrometer-sized hexagonal single-crystalline Au nanoplates can be synthesized on a large scale by a mild wet-chemical route, carried out by the chemical reduction of $\text{H}[\text{AuCl}_4]$ with *ortho*-phenylenediamine in aqueous media at room temperature and ambient pressure. Two surface plasmon absorption bands at about 680 and 925 nm are found for these Au nanoplates. The study suggests that the quantity of *ortho*-phenylenediamine in the solution is key to producing Au nanoplates. The importance of the platelet-like gold particles is not restricted to optics; exceptionally interesting materials with unique mechanical properties can be obtained with such colloids.^[21]

Experimental Section

$\text{H}[\text{AuCl}_4]$ was purchased from Aldrich and *ortho*-phenylenediamine from Beijing Chem. Co. All reagents were used as received without further purification. The water used was purified through a Millipore system. In a typical experiment, an aqueous solution of 48 mM $\text{H}[\text{AuCl}_4]$ (3 mL) was added to water (5 mL). An appropriate volume of an aqueous solution of freshly prepared *ortho*-phenylenediamine (80 mM) was quickly added to the solution under vigorous stirring at room temperature to obtain a 1:1 molar ratio of *ortho*-phenylenediamine to gold. A large quantity of precipitate was observed several minutes later, which was collected by centrifugation, washed several times with THF and water, then suspended in water. The resulting suspension was used for further characterization.

The samples for SEM and XRD characterization were prepared by placing 100 μL of the suspension on a glass slide, and allowing the solvent to slowly evaporate at room temperature. The sample for the TEM study was similarly prepared by placing a drop of the suspension on a carbon-coated copper grid. The UV/Vis spectra were collected on a CARY 500 Scan UV/Vis/near IR spectrophotometer. The SEM images were obtained on a XL30 ESEM FEG scanning electron microscopy operating at 20 kV. The TEM images were recorded on a JEOL 2000 transmission electron microscopy operating at 200 kV. The XRD pattern was collected on a D/Max 2500 V/PC X-ray diffractometer using Cu (40 kV, 200 mA) radiation.

Received: June 19, 2004

Keywords: crystal growth · electron microscopy · gold · nanostructures · nanotechnology

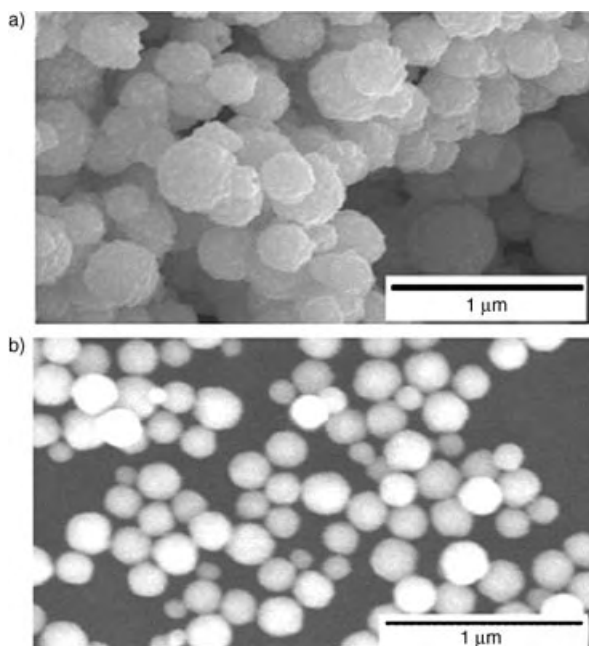


Figure 5. Typical SEM images of Au particles obtained with an initial *ortho*-phenylenediamine to gold ratio of 3:1 (a) and 8:1 (b).

- [1] a) *Nanoparticles and Nanostructured Films* (Ed.: J. H. Fendler), VCH, Weinheim, **1998**; b) *Nanoscale Materials in Chemistry* (Ed.: K. J. Klabunde), VCH, Weinheim, **2001**; c) G. Schmid,

- Chem. Rev.* **1992**, 92, 1709; d) A. Roucoux, J. Schulz, H. Patin, *Chem. Rev.* **2002**, 102, 3757.
- [2] M. A. El-Sayed, *Acc. Chem. Res.* **2001**, 34, 257.
- [3] R. Jin, Y. Cao, C. A. Mirkin, K. L. Kelly, G. C. Schatz, J. G. Zheng, *Science* **2001**, 294, 1901.
- [4] See, for example: a) M. Tian, J. Wang, J. Kurtz, T. E. Mallouk, M. H. W. Chan, *Nano Lett.* **2003**, 3, 919; b) E. Braun, Y. Eichen, U. Sivan, G. Ben-Yoseph, *Nature* **1998**, 391, 775.
- [5] R. Jin, Y. Cao, E. Hao, G. S. Métraux, G. C. Schatz, C. A. Mirkin, *Nature* **2003**, 425, 487.
- [6] Y. Sun, B. T. Mayers, Y. Xia, *Nano Lett.* **2002**, 2, 481.
- [7] a) D. O. Yener, J. Sindel, C. A. Randall, J. H. Adair, *Langmuir* **2002**, 18, 8692; b) S. Chen, D. L. Carroll, *Nano Lett.* **2002**, 2, 1003; c) F. Wang, Y. Ni, X. Ge, Z. Zhang, *Chem. Lett.* **2002**, 196.
- [8] See, for example: a) S. Chen, Z. Fan, D. L. Carroll, *J. Phys. Chem. B* **2002**, 106, 10777; b) M. Maillard, S. Giorgio, M.-P. Pileni, *Adv. Mater.* **2002**, 14, 1084; c) E. Hao, K. L. Kelly, J. T. Hupp, G. C. Schatz, *J. Am. Chem. Soc.* **2002**, 124, 15182.
- [9] Y. Sun, B. Mayers, Y. Xia, *Nano Lett.* **2003**, 3, 675.
- [10] See, for example, a) S. R. Nicewarner-Pena, G. P. Freeman, B. D. Reiss, L. He, D. J. Pena, I. D. Walton, R. Cromer, C. D. Keating, M. J. Natan, *Science* **2001**, 294, 137; b) E. Dujardin, L. B. Hsin, C. R. C. Wang, S. Mann, *Chem. Commun.* **2001**, 1264.
- [11] A. V. Simakin, V. V. Voronov, G. A. Shafeev, R. Brayner, F. Bozon-Verduraz, *Chem. Phys. Lett.* **2001**, 348, 182.
- [12] a) N. Malikova, I. Pastoriza-Santos, M. Schierhorn, N. A. Kotov, L. M. Liz-Marzan, *Langmuir* **2002**, 18, 3694; b) D. Ibane, Y. Yokota, T. Tominaga, *Chem. Lett.* **2003**, 32, 574; c) M. Tsuji, M. Hashimoto, Y. Nishizawa, T. Tsuji, *Chem. Lett.* **2003**, 32, 1114; d) Y. Shao, Y. Jin, S. Dong, *Chem. Commun.* **2004**, 1104; e) L. Wang, X. Chen, J. Zhan, Z. Sui, J. Zhao, Z. Sun, *Chem. Lett.* **2004**, 33, 720.
- [13] Y. Zhou, C. Y. Wang, Y. R. Zhu, Z. Y. Chen, *Chem. Mater.* **1999**, 11, 2310.
- [14] M. M. Maye, W. Zheng, F. L. Leibowitz, N. K. Ly, C.-J. Zhong, *Langmuir* **2000**, 16, 490.
- [15] I. Hussain, M. Brust, A. J. Papworth, A. I. Cooper, *Langmuir* **2003**, 19, 4831.
- [16] a) U. Kreibitz, L. Genzel, *Surf. Sci.* **1985**, 156, 678; b) Y. Yu, S. Chang, C. L. Lee, C. R. C. Wang, *J. Phys. Chem. B*, **1997**, 101, 6661; c) P. Novak, D. L. Feldheim, *J. Am. Chem. Soc.* **2000**, 122, 3979.
- [17] S. Link, M. A. El-Sayed, *J. Phys. Chem. B* **1999**, 103, 8410.
- [18] A. N. Shipway, M. Lahav, R. Gabai, I. Willner, *Langmuir* **2000**, 16, 8789.
- [19] a) X. Sun, X. Jiang, S. Dong, E. Wang, *Macromol. Rapid Commun.* **2003**, 24, 1024; b) B. Tang, *Heart Cut Dec* 22, **2003**, <http://www.chemistry.org>; c) X. Sun, S. Dong, E. Wang, *Polymer* **2004**, 45, 2181.
- [20] a) X. Sun, S. Dong, E. Wang, *Chem. Commun.* **2004**, 1182; b) *Chem. Sci.* **2004**, 1, C43; c) *Materials Today* **2004**, 7(10).
- [21] Z. Tang, N. A. Kotov, S. Magonov, B. Ozturk, *Nat. Mater.* **2003**, 2, 413.

High-Mobility Air-Stable n-Type Semiconductors with Processing Versatility: Dicyanoperylene-3,4:9,10-bis(dicarboximides)**

Brooks A. Jones, Michael J. Ahrens, Myung-Han Yoon, Antonio Facchetti, Tobin J. Marks,* and Michael R. Wasielewski*

Traditionally, inorganic materials have been the active charge-transporting components in numerous electronic devices. While inorganic materials are ideal for many applications, the rapid development of molecular/polymeric semiconductors for organic field-effect transistors (OFETs) promises materials better suited to inexpensive, flexible, large-area applications, such as displays, RF-ID tags, smart cards, and sensors.^[1] To this end, recent advances in p-type organic semiconductors have fulfilled many of the requirements for use in diverse applications,^[1c-e,2] however, n-type materials, needed for complementary circuits, continue to present challenges, such as low mobilities, instability in air, poor solubility for efficient film-casting, and large barriers to electron injection.^[1b,2]

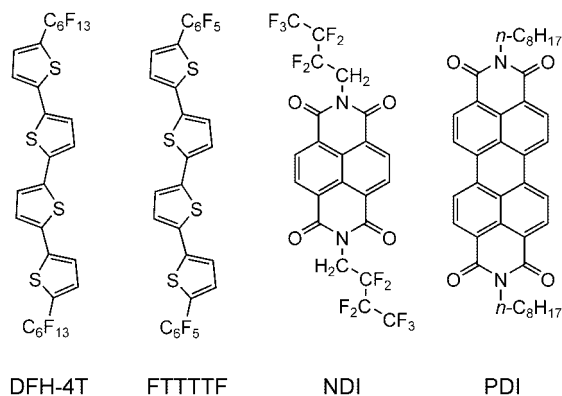
We have already demonstrated that high-mobility n-type organic semiconductors can be realized by functionalizing oligothiophene cores with electron-withdrawing perfluorinated groups (e.g. DFT-4T and FTTTTF).^[3] Furthermore, other research has demonstrated that electron-withdrawing imide substituents afford promising architectures for n-type naphthalene and perylene-based OFET materials (e.g., NDI and PDI).^[4] Thus, vapor-deposited and solution-cast films of *N*-fluorocarbon NDI derivatives exhibit air-stable n-type mobilities as high as $0.1 \text{ cm}^2 \text{ V}^{-1} \text{ s}^{-1}$, $I_{\text{on}}/I_{\text{off}} \approx 10^5$, and threshold voltages of approximately 20 V.^[4f-h] However, while *N*-alkyl NDI derivatives exhibit comparable or superior electrical performance, they fail to operate in air, possibly because of the less densely packed hydrocarbon tails.^[4f] While *N*-alkyl PDI films exhibit outstanding mobilities of approximately $0.6 \text{ cm}^2 \text{ V}^{-1} \text{ s}^{-1}$, OFET performance again degrades in air,

[*] B. A. Jones, M. J. Ahrens, M.-H. Yoon, Dr. A. Facchetti, Prof. T. J. Marks, Prof. M. R. Wasielewski
Department of Chemistry
Center for Nanofabrication and Molecular Self-Assembly
and the Materials Research Center
Northwestern University
2145 Sheridan Road, Evanston IL, 60208-3113 (USA)
Fax: (+1) 847-491-2290
E-mail: t-marks@northwestern.edu
wasielew@chem.northwestern.edu

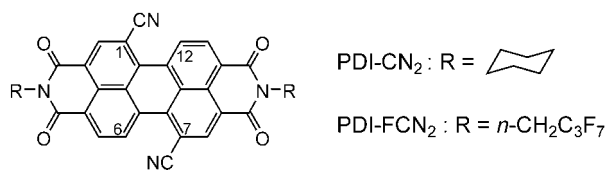
[**] We thank DARPA (MDA972-03-1-0023) and ONR (N00014-02-1-0909, N00014-02-1-0381) for support of this research, and the Northwestern Materials Research Center (NSF-MRSEC DMR-0076097) for characterization facilities. We also thank Charlotte Stern for single-crystal X-ray diffraction data collection and Matthew Russell for aid with SEM measurements.



Supporting information for this article is available on the WWW under <http://www.angewandte.org> or from the author.



devices exhibit very large threshold voltages of around 75 V, and these materials are not known to be solution processable.^[4d,i,k] In all instances, the focus of this prior work has been synthetic modification solely of the *N*-substituents. In other studies, microwave conductivity measurements of 1,6,7,12-substituted PDI derivatives demonstrated that modulation of π - π overlap by twisting of the normally flat core can drastically affect carrier mobility,^[4c] however, to date functionalization of the PDI core for OFET applications has gone unexplored. Herein we report two core-cyanated PDI derivatives, PDI-CN₂ and PDI-FCN₂, which exhibit the highest air-



stable n-type OFET carrier mobilities reported to date, in combination with low threshold voltages and substantial processing versatility.

The synthesis of PDI-CN₂ was reported elsewhere.^[5] This compound exhibits excellent air-stability and solubility in organic solvents, while reduced pressure thermogravimetric analysis (TGA) scans indicate slight (about 2%) decomposition during sublimation. The low-energy LUMO indicated by the first reduction potential, -0.07 V versus the saturated calomel electrode (SCE),^[5] suggests improved n-type charge-carrier stability over PDI (-0.43 V vs. SCE).^[6,7] Moreover, the results with PDI-CN₂-derived OFETs (see below) motivated the synthesis of a new PDI derivative, PDI-FCN₂, with additional electron-withdrawing substituents and greater volatility. The new compound was synthesized using modifications of published core cyanation^[5] and *N*-fluoroalkylation^[4f,j] procedures, and was characterized by NMR spectroscopy, mass spectrometry, optical absorption spectroscopy, photoluminescence, cyclic voltammetry, thermogravimetric analysis, and single-crystal X-ray diffraction. The electro-

chemical and optical data (Table 1) reveal further depression of the LUMO level of PDI-FCN₂ compared to PDI and PDI-CN₂, while TGA indicates quantitative sublimation.

For both cyanated PDI materials, a 1:1 mixture of isomers (cyanated at the 1,7 or 1,6 positions) is indicated by NMR spectroscopy, however this characteristic is found to be inconsequential for spectroscopic, electronic structural, and solid-state charge-transport properties (verified by measurements on the pure 1,7 isomer). Single crystals of PDI-FCN₂ were grown by sublimation, and the crystal structure (Figure 1) reveals a slightly twisted polycyclic core (torsion angle of about 5°) with slip-stacked face-to-face molecular packing and a minimum interplanar spacing of 3.40 Å.^[8] This

Table 1: Electronic and OFET characteristics of perylene diimide derivatives.

Compound	λ_{abs} [nm] ^[a]	λ_{em} [nm] ^[a]	$E_{(1)}$ [V] ^[b]	$E_{(2)}$ [V] ^[b]	μ [cm ² V ⁻¹ s ⁻¹]	$I_{\text{on}}/I_{\text{off}}$
PDI-CN ₂	530	547	-0.07	-0.40	0.10	10 ⁵
PDI-FCN ₂	530	545	+0.04	-0.31	0.64	10 ⁴

[a] measured in THF (10⁻⁵/10⁻⁶ M). [b] Measured in a solution of 0.1 M tetrabutylammonium hexafluorophosphate (TBA PF₆) in THF versus SCE.

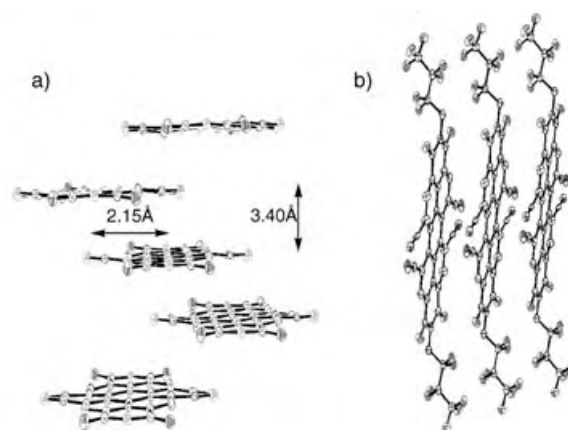


Figure 1. Crystal Structure of PDI-FCN₂. a) viewed along the unit cell diagonal, showing stacking relationships; fluoropropyl groups deleted for clarity. b) Viewed along the *ab* face diagonal, showing the segregation of arene and fluoroalkyl groups. Note the statistical disorder of the cyano substituents.^[10]

motif allows considerable intermolecular π - π overlap, which results in good charge-transport properties (see below). The positions of the disordered cyano substituents suggests that this structural feature does not greatly affect packing.

Top-contact configuration OFETs were fabricated with vapor-deposited PDI films (10⁻⁶ Torr, 0.2 Å s⁻¹ growth), and mobilities determined in the saturation regime by standard procedures.^[3] The microstructures and mobilities of the vapor-deposited films are found to be sensitive to substrate temperature during growth (see Supporting Information^[9]). Owing to the remarkable air-stability of these materials, all data presented herein were acquired under ambient atmosphere. PDI-CN₂-based OFETs display mobilities as high as 0.10 cm²V⁻¹s⁻¹, threshold voltages of approximately 15 V,

and $I_{\text{on}}/I_{\text{off}}(+100\text{ V}/0\text{ V}) \approx 10^5$, while PDI-FCN₂ devices exhibit mobilities as high as $0.64\text{ cm}^2\text{ V}^{-1}\text{ s}^{-1}$, threshold voltages between -20 V and -30 V , and $I_{\text{on}}/I_{\text{off}}(+100\text{ V}/-60\text{ V})$ as high as 10^4 . Figure 2 shows current–voltage (I – V) characteristics between source and drain electrodes recorded at different gate biases (V_G) for OFETs of PDI-CN₂ and PDI-FCN₂ operating in ambient atmosphere. Given the similarities in first reduction potentials for PDI-CN₂ and PDI-FCN₂, the striking difference in threshold voltages is presumably due to variations in trap densities in the two materials. Devices stored and tested under ambient conditions exhibit negligible degradation in mobility, threshold voltage, or $I_{\text{on}}/I_{\text{off}}$ over six months.

The microstructure of the vapor-deposited thin films was analyzed by X-ray diffraction (XRD), atomic force microscopy (AFM), and scanning electron microscopy (SEM), with XRD revealing d -spacings in highest-mobility devices of 17.9 Å for PDI-CN₂ and 20.3 Å for PDI-FCN₂. From a geometry-optimized, computed molecular length of 22.0 Å for PDI-CN₂^[11] and a crystallographically determined length of 22.8 Å for PDI-FCN₂, tilt angles relative to the substrate normal of 55° for PDI-CN₂ and 62° for PDI-FCN₂ are estimated. These results suggest favorable molecular orientations for source-to-drain electrode charge transport.

AFM and SEM analysis of film morphology confirms polycrystalline topologies with ribbon-like grains (ca. 400 – 800 nm long, and ca. 100 nm wide).^[9] Such large-grained polycrystalline features should promote charge-carrier mobility through efficient π – π intermolecular overlap and minimization of trap sites.^[1c,12]

To investigate material versatility for various applications, preliminary studies on bottom-contact OFETs and solution-cast films were performed. Bottom-contact devices are found to display air-stable mobilities from 10^{-3} – $10^{-4}\text{ cm}^2\text{ V}^{-1}\text{ s}^{-1}$. PDI-FCN₂ transistors, like many fluorinated organic semiconductors, require alkane thiol treatment of gold electrodes to better match surface energies at the metal/organic interface.^[4g] PDI-CN₂ devices function without the aid of thiolated electrodes, retaining the ability of PDI to function on unmodified substrates.^[4i] Top-contact devices fabricated from drip-cast films are also air-stable and exhibit mobilities of 10^{-3} – $10^{-5}\text{ cm}^2\text{ V}^{-1}\text{ s}^{-1}$. In contrast, solution casting of high-

quality films of PDI derivatives not having core functionalization is difficult owing to low solubility in common solvents. While the performance of the vapor-deposited top-contact devices is currently superior to the bottom-contact and solution-cast devices, efforts are being made to optimize device performance in these latter configurations.

One of the unique characteristics of the new PDI systems is the presence of significant charge-carrier densities at $V_G = 0\text{ V}$. Thus, the OFET threshold voltages for these materials are at $V_G = -20\text{ V}$ to -30 V , with the absence of charge carriers then defining the “off” state at -60 V , and classifying these devices as “always on” transistors.^[13] This characteristic is documented for very electron-deficient materials, and often attributed to unintentional doping.^[14] In some cases, the presence of charge carriers below $V_G = 0\text{ V}$ can be reversed by exposure to an oxidant, and for our devices, I₂ vapor increases the threshold voltage to $> -5\text{ V}$ and decreases the I_{SD} at $V_G = 0\text{ V}$ by up to an order of magnitude. Further studies of the nature and origin of the charge carriers are currently underway.

It is thought that ambient stability in n-type organic semiconductors benefits from electron-withdrawing fluorinated substituents, which electronically stabilize the charge carriers as well as promote close packing through fluorocarbon self-segregation. Judging from the present redox potentials, the charge carriers are not expected to be stable with respect to gaseous O₂;^[15] however, the close-packed fluorine functionalities may help provide a kinetic barrier to oxidation.^[1c] The strategic cyanation of PDI produces air-stable *N*-fluoroalkyl and *N*-alkyl materials, the air stability presumably reflecting carrier stabilization in the very low-lying LUMOs.

In summary, we report a promising new class of solution processable, cyano-polycyclic n-type organic semiconductors with high carrier mobility and air-stable OFET operation. Notable properties of this family reflect a combination of functionality at the core and imide positions. The cyano functionalities provide solubility for solution processing and stability of n-type charge carriers by lowering the LUMO to resist ambient oxidation. The electron-withdrawing *N*-functionalities further aid charge carrier stability by further lowering the LUMO energies, but may also induce close molecular packing for increased intermolecular π overlap and

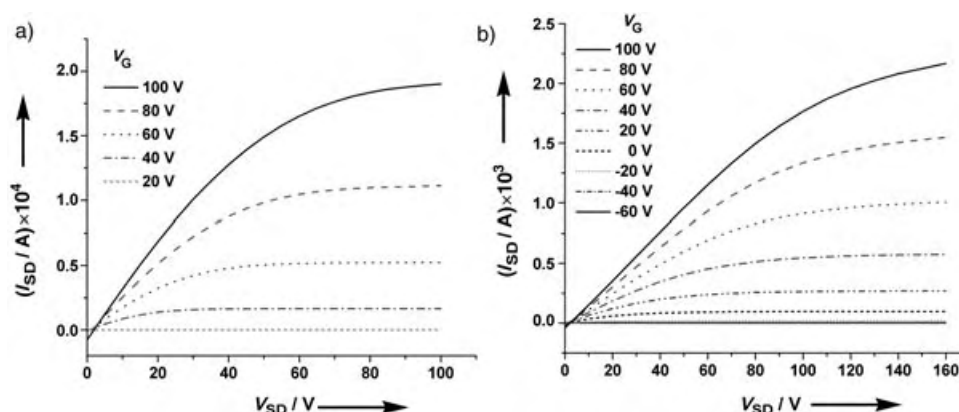


Figure 2. a) I – V characteristics of PDI-CN₂ exhibiting a mobility of $0.10\text{ cm}^2\text{ V}^{-1}\text{ s}^{-1}$ in ambient atmosphere b) I – V characteristics of a PDI-FCN₂ FET exhibiting a mobility of $0.64\text{ cm}^2\text{ V}^{-1}\text{ s}^{-1}$ in ambient atmosphere. V_{SD} = Voltage between source and drain, I_{SD} = current between source and drain, V_G = gate voltage.

more efficient charge transport. With the rich chemistry for PDI functionalization available, these derivatives should prove informative for elucidating structure–function relationships in organic n-type electronics.

Received: July 15, 2004

Keywords: conducting materials · electron transport · perylenes · semiconductors

- [1] a) B. Crone, A. Dodabalapur, A. Gelperin, L. Torsi, H. E. Katz, A. J. Lovinger, Z. Bao, *Appl. Phys. Lett.* **2001**, *78*, 2229; b) C. D. Dimitrakopoulos, D. J. Mascaró, *IBM J. Res. Dev.* **2001**, *45*; c) C. D. Dimitrakopoulos, P. R. L. Malenfant, *Adv. Mater.* **2002**, *14*, 99; d) A. Kraft, *ChemPhysChem* **2001**, *2*, 163; e) F. Würthner, *Angew. Chem.* **2001**, *113*, 1069; *Angew. Chem. Int. Ed.* **2001**, *40*, 1037.
- [2] Z. Bao, *Adv. Mater.* **2000**, *12*, 227.
- [3] a) A. Facchetti, Y. Deng, A. Wang, Y. Koide, H. Sirringhaus, T. J. Marks, R. H. Friend, *Angew. Chem.* **2000**, *112*, 4721; *Angew. Chem. Int. Ed.* **2000**, *39*, 4547; b) A. Facchetti, M. Mushrush, H. E. Katz, T. J. Marks, *Adv. Mater.* **2003**, *15*, 33; c) A. Facchetti, M.-H. Yoon, C. L. Stern, H. E. Katz, T. J. Marks, *Angew. Chem.* **2003**, *115*, 4030; *Angew. Chem. Int. Ed.* **2003**, *42*, 3900.
- [4] a) M. A. Angadi, D. Gosztola, M. R. Wasielewski, *J. Appl. Phys.* **1998**, *83*, 6187; b) M. A. Angadi, D. Gosztola, M. R. Wasielewski, *Mater. Sci. Eng. B* **1999**, *191*; c) Z. Chen, M. G. Debijs, T. Debaerdemaeker, P. Osswald, F. Würthner, *ChemPhysChem* **2004**, *5*, 137; d) R. J. Chesterfield, J. C. McKeen, C. R. Newman, C. D. Frisbie, P. C. Ewbank, K. R. Mann, L. R. Miller, *J. Appl. Phys.* **2004**, *95*, 6396; e) G. Horowitz, F. Kouki, P. Spearman, D. Fichou, C. Nogués, X. Pan, F. Garnier, *Adv. Mater.* **1996**, *8*, 242; f) H. E. Katz, A. J. Lovinger, J. Johnson, C. Kloc, T. Siegrist, W. Li, Y.-Y. Lin, A. Dodabalapur, *Nature* **2000**, *404*, 478; g) H. E. Katz, J. Johnson, A. J. Lovinger, W. Li, *J. Am. Chem. Soc.* **2000**, *122*, 7787; h) H. E. Katz, T. Siegrist, J. H. Schön, C. Kloc, B. Batlogg, A. J. Lovinger, J. Johnson, *ChemPhysChem* **2001**, *2*, 167; i) P. R. L. Malenfant, C. D. Dimitrakopoulos, J. D. Gelorme, L. L. Kosbar, T. O. Graham, A. Curioni, W. Andreoni, *Appl. Phys. Lett.* **2002**, *80*, 2517; j) M.-M. Shi, H.-Z. Chen, J.-Z. Sun, J. Ye, M. Wang, *Chem. Commun.* **2003**, *14*, 1710; k) C. W. Struijk, A. B. Sieval, J. E. J. Dakhorst, M. Van Dijk, P. Kimkes, R. B. M. Koehorst, H. Donker, T. J. Schaafsma, S. J. Picken, A. M. van de Craats, J. M. Warman, H. Zuilhof, E. J. R. Sudholter, *J. Am. Chem. Soc.* **2000**, *122*, 11057.
- [5] M. J. Ahrens, M. J. Fuller, M. R. Wasielewski, *Chem. Mater.* **2003**, *15*, 2684.
- [6] a) D. Gosztola, M. P. Niemczyk, W. Svec, A. S. Lukas, M. R. Wasielewski, *J. Phys. Chem. A* **2000**, *104*, 6545; b) For a compilation of redox potentials, see: F. Würthner, *Chem. Commun.* **2004**, 1564.
- [7] a) A. Facchetti, M.-H. Yoon, C. L. Stern, G. Hutchison, M. A. Ratner, T. J. Marks, *J. Am. Chem. Soc.* **2004**, *126*, 13480; b) A. Facchetti, M. Mushrush, M.-H. Yoon, G. R. Hutchison, M. A. Ratner, T. J. Marks, *J. Am. Chem. Soc.* **2004**, *126*, ASAP.
- [8] Single crystals were grown by slow vacuum sublimation. Crystal size: 0.345 mm × 0.106 mm × 0.022 mm. Triclinic, $P\bar{1}$, $Z = 1$. Cell dimensions: $a = 5.2320(14)$, $b = 7.638(2)$, $c = 18.819(5)$ Å; $\alpha = 92.512(5)^\circ$, $\beta = 95.247(5)^\circ$, $\gamma = 104.730(4)^\circ$, $V = 722.5(3)$ Å³, $2\theta_{\max} = 57.54^\circ$, $\rho_{\text{calcd}} = 1.849$ g cm⁻³. Of 6655 reflections, 3370 were independent ($R_{\text{int}} = 0.0967$), 272 parameters, $R1 = 0.0540$ (for reflections with $I > 2\sigma(I)$), $wR2 = 0.1258$ (for all reflections). All diffraction measurements were made on a Bruker SMART CCD diffractometer with graphite monochromated MoK α radiation. Data were collected at 153(2) K and the structure

solved by direct methods using SHELXTL. All non-hydrogen atoms were refined anisotropically. Hydrogen atoms were included in idealized positions and not refined. Intensities were corrected for absorption. CCDC-247498 contains the supplementary crystallographic data for this paper. These data can be obtained free of charge via www.ccdc.cam.ac.uk/conts/retrieving.html (or from the Cambridge Crystallographic Data Centre, 12 Union Road, Cambridge CB21EZ, UK; fax: (+44) 1223-336-033; or deposit@ccdc.cam.ac.uk).

- [9] See Supporting Information which includes: Experimental details, TGA plots, thin film XRD data, SEM, and AFM micrographs, redox properties of PDI derivatives, and details of device fabrication/measurement.
- [10] M. N. Burnett and C. K. Johnson, ORTEP-III: Oak Ridge Thermal Ellipsoid Plot Program for Crystal Structure Illustrations, Oak Ridge National Laboratory Report ORNL-6895, 1996.
- [11] Hyperchem (TM) 5.02, Hypercube, Inc., 1115 NW 4th Street, Gainesville, FL 32601, USA.
- [12] a) G. Horowitz, *Adv. Mater.* **1998**, *10*, 365; b) H. E. Katz, Z. Bao, *J. Phys. Chem. B* **2000**, *104*, 671.
- [13] S. M. Sze, *Semiconductor Devices*, Wiley, New York, **1985**.
- [14] a) R. C. Haddon, A. S. Perel, R. C. Morris, T. T. M. Palstra, A. F. Hebard, R. M. Fleming, *Appl. Phys. Lett.* **1995**, *67*, 121; b) T. M. Pappenfus, R. J. Chesterfield, C. D. Frisbie, K. R. Mann, J. Casado, J. D. Raff, L. L. Miller, *J. Am. Chem. Soc.* **2002**, *124*, 4184; c) J. G. Laquindanum, H. E. Katz, A. Dodabalapur, A. J. Lovinger, *J. Am. Chem. Soc.* **1996**, *118*, 11331.
- [15] D. M. de Leeuw, M. M. J. Simenon, A. R. Brown, R. E. F. Einerhand, *Synth. Met.* **1997**, *87*, 53.

Iridium Complexes

**An Iridium Difluoroketene Complex:
Synthesis and Isolation****

*Joseph G. Cordaro, Herman van Halbeek, and
Robert G. Bergman**

*Dedicated to Professor John E. Bercaw
on the occasion of his 60th birthday*

Despite substantial research on the chemistry of ketenes, efforts to isolate or characterize the electron-deficient difluoroketene ($\text{F}_2\text{C}=\text{C}=\text{O}$) have met with little success.^[1] While an early claim of the preparation of $\text{F}_2\text{C}=\text{C}=\text{O}$ exists,^[2] attempts to repeat this synthesis were not success-

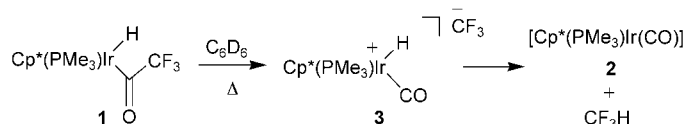
[*] J. G. Cordaro, H. van Halbeek, Prof. R. G. Bergman
Department of Chemistry
University of California Berkeley
CA 94720-1460 (USA)
Fax: (+1) 510-642-7714
E-mail: bergman@cchem.berkeley.edu

[**] Supported by the U.S. National Science Foundation through grant no. CHE-0094349. Funding for the AV-500 spectrometer was made available through grants from the NSF (CHE 0130862) and NIH (S10RR016634). We gratefully thank Ms. Cathleen M. Yung for assistance with low-temperature NMR experiments and Drs. Fred Hollander and Alan Oliver for X-ray analysis of compound 5.

ful.^[3] Difluoroketene has been generated transiently by zinc-induced dehalogenation of bromodifluoroacetyl halides, but its formation was only inferred from the isolation of a cycloaddition product with acetone and from the detection of CO and F₂C=CF₂, the presumed products of difluoroketene dissociation.^[3] Experiments designed to trap [2+2] adducts of cyclopentadiene and fluorinated ketenes generated in situ were successful with methylfluoroketene, phenylfluoroketene, and trifluoromethylfluoroketene, but failed when attempted with difluoroketene.^[4] Difluoroketene ethyl trimethylsilyl ketal, a masked variant of difluoroketene, has been employed in organic synthesis as a reagent for making fluoroorganic compounds.^[5–7]

In 1998, the generation and IR characterization of difluoroketene in a CO₂-doped argon matrix at 30 K was reported.^[8] This highly reactive ketene was also detected in the gas phase by mass spectrometry after ionization of perfluoromethylvinyl ether.^[9] However, until now neither the free ketene nor its metal complexes have been obtained on a preparative scale. Herein we report that research on the electron-rich organometallic fragment [Cp*(PMe₃)Ir] (Cp* = η⁵-C₅Me₅), has led to the discovery of an isolable difluoroketene complex.

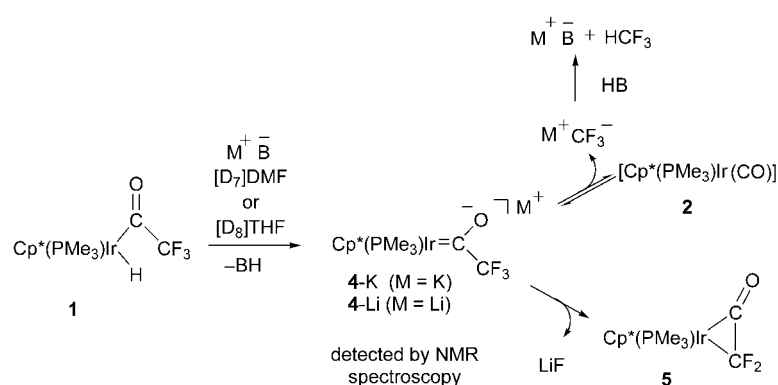
Recently, we reported that upon heating a solution of [Cp*(PMe₃)Ir(H){C(O)CF₃}] (**1**) in C₆D₆ at 105 °C, [Cp*(PMe₃)Ir(CO)] (**2**) and CF₃H were generated in quantitative yield.^[10] The proposed mechanism for this elimination involves CF₃[–] dissociation from **1** to give the intermediate ion pair **3** (scheme 1). Rapid proton transfer from the iridium carbonyl cation to the CF₃[–] ion yields the observed products (Scheme 1).^[10] While investigating the mechanism of this transformation, we discovered two different base-induced elimination reactions from **1**.



Scheme 1. Proposed mechanism for CF₃H loss from **1**.

Upon vacuum transferring [D₇]DMF to an NMR tube containing **1** and a catalytic amount of potassium *tert*-butoxide (0.2 equiv) at –196 °C, only **2**, CF₃H, and potassium *tert*-butoxide were detected in quantitative yield, by NMR spectroscopy upon warming to 22 °C. Using [D₈]THF as solvent gave similar results. The proposed mechanism for this transformation involves rapid deprotonation of **1** to generate the potassium iridate **4-K**. Elimination of CF₃[–] from **4-K** followed by deprotonation of *tert*-butanol, produces **2** and CF₃H, which regenerates the base (Scheme 2). Treatment of **1** with a base which would irreversibly deprotonate it, gave an unexpected result.

Compound **1** and 1.4 equivalents of *tert*-butyllithium were dissolved in [D₈]THF at low temperature and the subsequent reaction was monitored by NMR spectroscopy as the solution was warmed from –80 to 22 °C. At –80 °C one major species,



Scheme 2. Deprotonation of **1** leading to **2** and difluoroketene adduct **5**.

assigned as the lithium iridate **4-Li** was detected in the ¹⁹F NMR spectrum at δ = –69.2 ppm and in the ³¹P{¹H} NMR spectrum at δ = –39.9 ppm. Upon warming, the chemical shifts of all intermediates shifted slightly upfield. At –13 °C only the acyl iridate **4-Li** was detected;^[11] at –6 °C new products began to form. As the reaction mixture was warmed above 0 °C, elimination of CF₃Li gave iridium carbonyl **2**, and surprisingly, LiF elimination from **4-Li** furnished difluoroketene iridium adduct **5** in a 1:1 ratio (Scheme 2).

Isolation of the difluoroketene adduct **5** was by multiple precipitations and crystallizations from a mixture containing **2** and **5** in a solution of diethyl ether and pentane at –38 °C (ca. 30 % yield).^[12] As a solid at 22 °C under a N₂ atmosphere, the difluoroketene adduct **5** showed no signs of decomposition after two weeks. Heating a C₆D₆ solution of **5** at 75 °C resulted in slow decomposition to **2** and unidentifiable products which contained the {Cp*(PMe₃)Ir} fragment.

The characterization of **5** began with heteronuclear NMR spectroscopy experiments on the four NMR active nuclei. The ¹H NMR spectrum showed a singlet at δ = 1.75 ppm for the Cp* ligand, and a doublet at δ = 1.01 ppm with ²J_{H,P} = 10.4 Hz for the PMe₃ ligand. In the ¹⁹F NMR spectrum, two inequivalent signals were observed in the region typical of fluorine atoms bound to a sp²-hybridized carbon atoms. The signal at δ = –123.4 ppm was coupled to both phosphorus and fluorine atoms to give a doublet of doublets with ²J_{F,P} = 187 Hz and ³J_{F,P} = 33 Hz. The more upfield signal at δ = –132.1 ppm was coupled only to the other fluorine atom with ²J_{F,F} = 188 Hz. The ³¹P{¹H} NMR spectrum showed the signals for the PMe₃ ligand as a doublet coupled to one fluorine atom at δ = –41.6 ppm with ³J_{P,F} = 33 Hz. In the ¹³C{¹H} NMR spectrum, only singlets for the methyl and quaternary carbon atoms of the Cp* ligand at δ = 10.0 ppm and 96.1 ppm, respectively, and a doublet for the PMe₃ ligand at δ = 18.3 ppm with ²J_{C,P} = 42.3 Hz were found.

The difluoroketene carbon atom signals of **5** were observed in a ¹⁹F-detected 2D ¹⁹F/¹³C heteronuclear single- and multiple-bond correlation (HSMBC) experiment.^[13,14] This NMR experiment revealed ¹³C signals at δ = 178.0 and 207.2 ppm, through correlation peaks with each of the ¹⁹F signals (see Figure 1), mediated by ¹J_{C,F} (320–340 Hz) and ²J_{C,F} (5–10 Hz), respectively. Specifically, the ¹⁹F_a signal at –123.4 ppm appeared as a ddd (¹J_{F_a,C} = 344, ²J_{F_a,F_b} = 187,

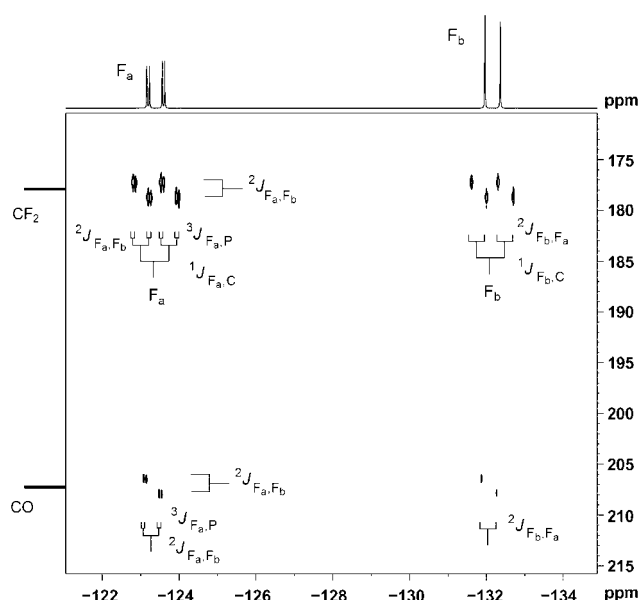


Figure 1. The 2D ^{19}F , ^{13}C HSMBC spectrum of **5** in C_6D_6 , recorded at 11.7 T and 19 °C. (The 1D ^{19}F NMR spectrum of **5** is displayed at the top.) The HSMBC experiment was carried out using a Bruker Avance 500 spectrometer equipped with a 5 mm (^1H , ^1X , ^{31}P) triple-resonance probehead with an actively shielded z-gradient coil. The inner (^1H) coil was tuned to the ^{19}F frequency (470.6 MHz), and the outer (X) coil to the ^{13}C frequency (125.8 MHz). The experiment used a gradient-enhanced 2D HMBC pulse sequence without a low-pass filter, allowing for observation of both $^1J_{\text{F,C}}$ and $^2J_{\text{F,C}}$ mediated correlations in one experiment. No ^{13}C -decoupling was applied during the detection period. For further experimental conditions see ref. [19].

$^3J_{\text{Fa,P}} = 34$ Hz) in its correlation peak with the signal at 178.0 ppm, which therefore arises from the CF_2 carbon atom; and as a dd ($^2J_{\text{Fa,Fb}} = 187$, $^3J_{\text{Fa,P}} = 34$ Hz, $^2J_{\text{Fa,C}}$ unresolved, that is, < 10 Hz) in the cross peaks with the CO signal at $\delta = 207.2$ ppm. Analogously, the $^{19}\text{F}_\text{b}$ fluorine signal at $\delta = -132.1$ ppm appeared as a dd ($^1J_{\text{Fb,C}} = 327$, $^2J_{\text{Fb,Fa}} = 187$ Hz) in its cross peaks with the CF_2 signal, and as a doublet ($^2J_{\text{Fb,Fa}} = 187$ Hz; $^2J_{\text{Fb,C}}$ unresolved, that is, < 8 Hz) in its correlation peaks with the CO signal. All four cross-peak patterns in the 2D spectrum are displaced by the $^2J_{\text{Fa,Fb}}$ coupling in both the ^{13}C and ^{19}F dimension. Reported ^{13}C NMR spectroscopic data for the $\eta^2\text{-(C,C)}$ carbon atoms of related phenyl- and diphenylketene iridium complexes were significantly upfield from these values.^[15] The downfield resonances for the $\eta^2\text{-(C,C)}$ carbon atoms are likely a result of the deshielding effects of the fluorine atoms.

Solid-state ZnSe attenuated total reflectance (ATR) FTIR spectroscopy of difluoroketene **5** showed strong bands at 1725, 1172, 954, 938, and 837 cm^{-1} . Medium to weak bands were recorded at 1424, 1384, and 1287 cm^{-1} . Using X-ray analysis and isotopic ^{18}O and ^{13}C labeling, Grotjahn and co-workers showed that the IR absorptions for a series of six bisphosphine chloro-iridium and rhodium ketene complexes were dependent on the coordination mode.^[15] When the ketene was coordinated through the carbonyl C=O bond an intense IR band, assigned to the C=O stretch, was found between 1632 and 1651 cm^{-1} . Alternatively, when the ketene

was coordinated through the C–C bond, a strong absorption was located between 1728 and 1802 cm^{-1} . Based on these data and the absorption at 1725 cm^{-1} for **5**, the coordination mode of our difluoroketene **5** was inferred to be $\eta^2\text{-(C,C)}$.

Pale yellow pyramidal crystals suitable for X-ray analysis were grown from a concentrated solution of difluoroketene **5** in diethyl ether at -38°C . The ketene adduct crystallized in the $\text{C}2/c$ space group with one molecule in the asymmetric unit.^[16] Coordination of the difluoroketene to iridium was confirmed to be $\eta^2\text{-(C,C)}$ (Figure 2). An unusually short C–O

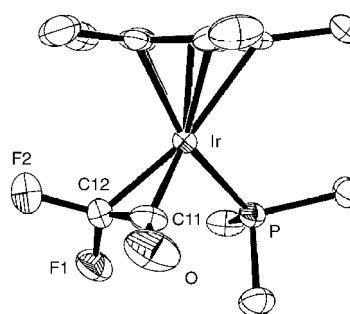


Figure 2. ORTEP diagram of **5** (thermal ellipsoids set at 50% probability). Hydrogen atoms have been omitted for clarity. Selected bond lengths [\AA] and angles [$^\circ$]: Ir–C11 1.799(9), Ir–C12 1.994(10), Ir–P 2.256(2), C12–F2 1.37(1), C12–F1 1.39(1), C12–C11 1.38(1), C11–O 1.11(1); P–Ir–C11 92.9(3), P–Ir–C12 91.1(3), Ir–C12–C11 61.3(5), Ir–C11–C12 76.6(6), C12–Ir–C11 42.1(4), F2–C12–C11 117.2(9), F1–C12–C11 124.1(8), F1–C12–F2 103.3(8), O–C11–C12 138(1), Ir–C11–O 143.9(9).

bond of 1.11(1) \AA for **5** compared to other iridium and rhodium $\eta^2\text{-(C,C)}$ -bound ketene complexes suggests that back-donation from the metal center to the ketene does not elongate the C–O bond.^[15,17] However, shorter Ir–C and C–C bonds were also measured, which indicate that the difluoroketene binds more closely than diphenyl- or phenylketene to iridium.^[18]

Overall loss of fluoride rather than the CF_3^- ion, when *tert*-butyllithium is used as the base to deprotonate **1**, may be attributed to reversible CF_3^- loss from iridate **4**. When **1** is deprotonated with $\text{KO}t\text{Bu}$ to give iridate **4-K** and $\text{HO}t\text{Bu}$, CF_3^- loss followed by protonation to yield CF_3H and **2** is irreversible. However, in the absence of a proton source, F^- loss becomes competitive with CF_3^- loss to give **5** (Scheme 2). Unfortunately, attempts to increase the yield of **5** by adding reagents which might assist in fluoride elimination were unsuccessful.

Difluoroketene iridium complex **5** joins an important group of complexes containing reactive organic fragments that are stabilized by coordination to transition-metal centers. The robust character of adduct **5** is attributed to the donating ability of the electron-rich organometallic fragment that coordinates to the electron-deficient difluoroketene. To our knowledge, this is the first example of a dihaloketene complex and the only structural data available for the difluoroketene fragment in any form.

Received: July 22, 2004

Keywords: fluorine · iridium · ketenes · NMR spectroscopy · structure elucidation

- [1] T. T. Tidwell, *Ketenes*, Wiley, New York, **1995**.
- [2] N. N. Yarovenko, S. P. Motornyi, L. I. Kirenskaya, *Zh. Obshch. Khim.* **1957**, 27, 2796.
- [3] D. C. England, C. G. Krespan, *J. Org. Chem.* **1968**, 33, 816.
- [4] W. R. Dolbier, S. K. Lee, O. Phanstiel, *Tetrahedron* **1991**, 47, 2065.
- [5] O. Kitagawa, A. Hashimoto, Y. Kobayashi, T. Taguchi, *Chem. Lett.* **1990**, 1307.
- [6] K. Iseki, *Tetrahedron* **1998**, 54, 13887.
- [7] K. Iseki, Y. Kuroki, D. Asada, Y. Kobayashi, *Tetrahedron Lett.* **1997**, 38, 1447.
- [8] C. Kottling, W. Sander, M. Senzlobler, H. Burger, *Chem. Eur. J.* **1998**, 4, 1611.
- [9] D. F. Dawson, J. L. Holmes, *J. Phys. Chem. A* **1999**, 103, 5217.
- [10] J. G. Cordaro, R. G. Bergman, *J. Am. Chem. Soc.* **2004**, 126, 3432.
- [11] This intermediate could be trapped with the electrophile MeI, to generate the methyl acyl compound $[\text{Cp}^*(\text{PMe}_3)\text{Ir}(\text{Me})\text{-}\{\text{C}(\text{O})\text{CF}_3\}]$, see ref. [10].
- [12] The synthesis of **5** was achieved on a larger scale as follows: A 250-mL thick-walled, resealable flask equipped with a stir bar was charged with **1** (125 mg, 0.25 mmol) and *tert*-butyllithium (22 mg, 0.35 mmol, recrystallized from pentane at -38°C until white). The flask was attached to a vacuum manifold and cooled to -196°C . THF (10 mL) was vacuum transferred from Na/benzophenone into the flask. The frozen reaction mixture was warmed to -78°C and then allowed to warm to room temperature over 15 h. The volatile materials were removed in vacuo to give a reddish-brown residue. Analysis of the crude reaction mixture by NMR spectroscopy revealed a 1:1 mixture of difluoroketene adduct **5** and iridium carbonyl **2** with a small amount of **1**. In a N_2 filled glove box, the crude material was filtered through a pad of silica gel on a medium-pore fitted glass frit eluting with diethyl ether. The resulting orange solution was concentrated in vacuo to 1 mL, layered with pentane, and allowed to stand at -38°C for crystallization. Dark reddish-brown clusters of crystals grew after 1 week. The mother liquor was removed by pipette and the solid was washed with pentane. Excess solvent was removed under reduced pressure. Yield: 38 mg (32%) EI HRMS: m/z calcd for $\text{C}_{15}\text{H}_{24}\text{F}_2\text{OPIr}$ 482.1162 $[M]^+$; found 482.1152.
- [13] A. Bax, M. F. Summers, *J. Am. Chem. Soc.* **1986**, 108, 2093.
- [14] S. Q. Sheng, H. van Halbeek, *J. Magn. Reson.* **1998**, 130, 296.
- [15] D. B. Grotjahn, L. S. B. Collins, M. Wolpert, G. A. Bikzhanova, H. C. Lo, D. Combs, J. L. Hubbard, *J. Am. Chem. Soc.* **2001**, 123, 8260.
- [16] CCDC-244081 (**5**) contains supplementary crystallographic data for this paper. These data can be obtained free of charge via www.ccdc.cam.ac.uk/conts/retrieving.html (or from the Cambridge Crystallographic Data Centre, 12, Union Road, Cambridge CB21EZ, UK; fax: (+44)1223-336-033; or deposit@ccdc.cam.ac.uk).
- [17] E. Bleuel, M. Laubender, B. Weberndorfer, H. Werner, *Angew. Chem.* **1999**, 111, 222; *Angew. Chem. Int. Ed.* **1999**, 38, 156.
- [18] In a separate experiment, compound **5** was co-crystallized with **2**. X-ray analysis of this crystal revealed a 2:1 mixture of **5** to **2** with the iridium carbonyl lying along the mirror plane of the unit cell. CCDC-244082 (**5/2**) contains supplementary crystallographic data for this paper. These data can be obtained free of charge via www.ccdc.cam.ac.uk/conts/retrieving.html (or from the Cambridge Crystallographic Data Centre, 12, Union Road, Cambridge CB21EZ, UK; fax: (+44)1223-336-033; or deposit@ccdc.cam.ac.uk).
- [19] The delay Δ was set to 25 ms; acquisition times t_2 and t_1 were 218 ms (^{19}F spectral width 9400 Hz, 4 K complex data points) and 5 ms (^{13}C spectral width 12,575 Hz, 128 real data points), respectively. The relaxation delay was 1 s; 128 scans were accumulated per t_1 increment. Gradient ratios $G_1:G_2:G_3$ were 3:1:3. The total acquisition time of the $^{19}\text{F},^{13}\text{C}$ HSMBC experiment on the difluoroketene sample (≈ 20 mg of **5** in 0.6 mL C_6D_6) was 5 h 45 min. ^{19}F Chemical shifts are referenced to external CFCl_3 at 0 ppm, ^{13}C chemical shifts to internal TMS at 0 ppm.

Nanostructures

Polymer–Monomer Pairs as a Reaction System for the Synthesis of Magnetic Fe₃O₄–Polymer Hybrid Hollow Nanospheres***Yin Ding, Yong Hu, Xiqun Jiang,* Leyang Zhang, and Changzheng Yang*

Recently, hollow spheres have attracted increasing interest because of their application in drug delivery,^[1–3] cell and enzyme transplantation,^[4] gene therapy,^[5] separation in biomedicine, and as contrast agents in diagnostics.^[6,7] Despite significant advances in the preparation of hollow inorganic or polymeric spheres,^[8–11] the construction of nanosized hybrid hollow spheres with both inorganic component and organic polymers as the shells remains a major challenge. Currently, a widely used approach for the synthesis of hybrid micro or submicron hollow spheres is the core-template-based strategy in which the inorganic components are coated on the polymer particles by sol–gel chemistry^[12] or layer-by-layer deposition.^[13] One advantage of such an approach is that the thickness of the coating layers is controllable. Although successful in the preparation of hollow hybrid spheres, the core-template-based approach faces limitations involving the selection in core composition and nanosized core templates. Furthermore, the core must be removed to create the hollow center. Hence, a core-template-free strategy for the production of hollow hybrid spheres is of particular interest. Previous efforts towards the preparation of hollow hybrid spheres with micrometer dimensions and in the absence of a core template include the assembly of inorganic nanoparticles into hollow spheres by using block copolymers,^[14] the

[*] Y. Ding, Dr. Y. Hu, Prof. X. Jiang, L. Zhang, Prof. C. Yang
Laboratory of Mesoscopic Chemistry and
Department of Polymer Science and Engineering
College of Chemistry and Chemical Engineering
Nanjing University
Nanjing, 210093 (P. R. China)
Fax: (+86) 25-8331-7761
E-mail: jiangx@nju.edu.cn

[**] Supported by the Natural Science Foundation of China (No.20374026, No.10334020) and the 973 Program of MOST (No.2003 CB 615 600).

assembly of positively charged polyelectrolytes and negatively charged inorganic nanoparticles,^[15] and liquid-phase deposition of inorganic nanoparticles on polymeric capsules.^[16] In previous work,^[17] we introduced a core-template-free approach to construct nanosized hollow polymeric spheres. The basis of this approach is that the reaction system is composed of water-soluble polymer–monomer pairs containing a cationic polymer and an anionic monomer. Depending on their concentration in aqueous solution, such polymer–monomer pairs can self-assemble to form micelles through electrostatic interactions, and hollow polymeric nanospheres are obtained by the polymerization of the anionic monomers inside the micelles.

As a significant advance in attempts to produce inorganic–organic hybrid hollow nanospheres, we present herein a robust, core-template-free method to prepare magnetic hollow Fe_3O_4 –polymer hybrid nanospheres in completely aqueous solution. The preparation procedure is schematically illustrated in Scheme 1. We selected chitosan (CS), which bears amino groups, as the cationic polymer and acrylic acid (AA), which bears acid groups, as the anionic monomer. The CS and AA polymer–monomer pair and Fe_3O_4 nanoparticles stabilized by poly(vinyl alcohol) (PVA) were mixed and formed micelles loaded with Fe_3O_4 nanoparticles; the cores consist of the polyionic complexes of CS and AA (i.e. positively charged protonated CS chains and negatively charged dissociated AA) and the shells consist of protonated CS chains. The formation of CS–AA micelles was confirmed by fluorescent probe, dynamic light scattering (DLS), and transmission electron microscopy (TEM).^[17] Initiation of the polymerization of AA with potassium persulfate ($\text{K}_2\text{S}_2\text{O}_8$) followed by cross-linking of the shells with glutaraldehyde (GA) at the end of polymerization led to the formation of magnetic hollow Fe_3O_4 –polymer hybrid nanospheres.

The size and morphology of the hybrid spheres were investigated by DLS in aqueous solution, and by TEM and magnetic force microscopy (MFM) in the solid state. The mean-number-average hydrodynamic diameter (D_h) for the synthesized hybrid spheres in aqueous solution was measured to be 76 ± 6.1 nm by DLS and the zeta potential to be 35 ± 2.6 mV by electrophoretic light scattering, suggesting that chitosan molecules with ionized amino groups are at the outermost layer of the hybrid spheres. Figure 1 shows representative TEM images of the synthetic materials. After the addition of Fe_3O_4 nanoparticles (4–6 nm in size) into an aqueous solution of CS–AA followed by polymerization of AA and selective cross-linking of CS at the end of polymerization, spheres with incorporated Fe_3O_4 nanoparticles were formed (Figure 1a). The average diameter of such a structure is 58 ± 11 nm, smaller than that determined by DLS in

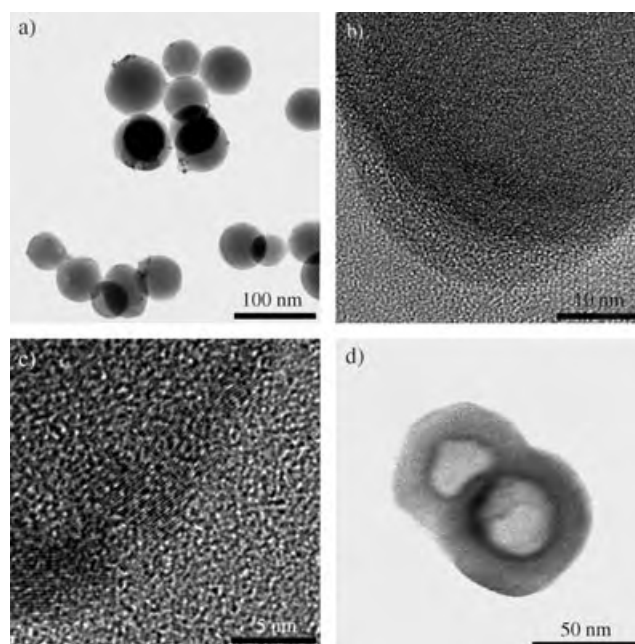
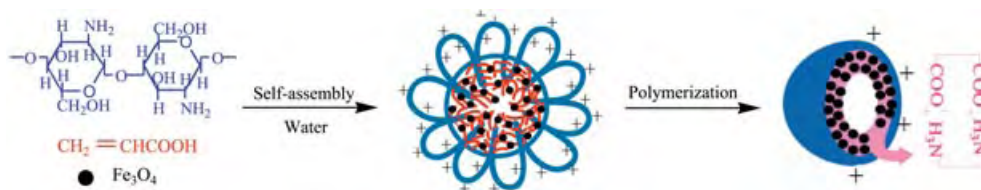


Figure 1. a) Direct-view TEM image of the synthesized Fe_3O_4 –polymer hybrid nanospheres; b) and c) Direct-view HRTEM images of the synthesized Fe_3O_4 –polymer hybrid nanospheres; d) Cut-section TEM image of the Fe_3O_4 –polymer hybrid nanospheres after microtomy at room temperature.

aqueous solution as a result of the sample being dry for TEM analysis. The electron-diffraction pattern recorded from these spheres confirms that magnetite nanoparticles with a minor amount of Fe_2O_3 were loaded into the nanospheres. A salient feature of Figure 1a is that these nanospheres have an intense dark circle within the shells of the spheres and dark spots at the surface of some spheres, which suggests that the distribution of the Fe_3O_4 nanoparticles is not concentrated in the core of the spheres. This is confirmed by high-resolution transmission electron microscopy (HRTEM) observation (Figure 1b,c). The lattice fringe planes of Fe_3O_4 nanoparticles arranged in the dark stripe region, indicative of the crystalline region of the Fe_3O_4 particles, are clearly observed inside the shell of the spheres or at the surface of the spheres. The size of the lattice fringe planes of individual Fe_3O_4 nanoparticles is estimated to be 4–6 nm, which corresponds well to the size of Fe_3O_4 nanoparticles used. The occurrence of Fe_3O_4 nanoparticles in the inner shell of the spheres indicates that the magnetic nanoparticles are trapped inside the micelles before polymerization by the interaction of AA and PVA attached to the Fe_3O_4 nanoparticles, as verified by FTIR. The presence of the magnetic nanoparticles the surface of the spheres suggests



Scheme 1. Illustration of the preparation process of hollow hybrid nanospheres.

that partial adsorption of Fe_3O_4 nanoparticles onto the spheres occurs during the reaction process. The most interesting feature of these nanospheres is their hollow interior, as revealed by the TEM image in Figure 1d obtained by microtomy of a hybrid nanosphere sample at room temperature which had been prepared by depositing hybrid nanospheres on a polyimide sheet followed by embedding in epoxy resin. The image shows the rings of sectioned spheres and the cavity in the interior, thus providing compelling evidence for a hollow sphere structure. Although the Fe_3O_4 nanoparticles are too small to be distinguished, elemental analysis (energy-dispersive spectrometer) provides evidence for the existence of Fe_3O_4 nanoparticles in the hollow spheres.

MFM imaging provides further evidence for the morphology of the hollow hybrid nanospheres and the distribution of magnetite nanoparticles in the nanospheres. As seen from the atomic force microscopy (AFM) image in Figure 2a, the hybrid nanospheres appear as intact spheres with an average height of 12 ± 2.5 nm and an average width of 47 ± 6.6 nm. In the MFM image (Figure 2b), a significant magnetic signal

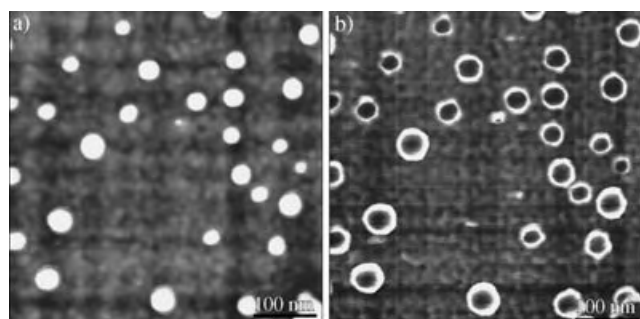


Figure 2. a) AFM and b) MFM images of hollow Fe_3O_4 -polymer hybrid nanospheres. Vertical scales (from dark to bright): 0 to 15 nm and -160° to -206° , respectively.

from the hollow hybrid nanospheres is detected. The rings, which correspond exactly to the positions of spheres in the AFM image, have diameters of 52 ± 4 nm; the thickness of the circular shells is 15 ± 2 nm. No magnetic signal in the center of the spheres is detected. Moreover, in an additional control experiment, no bright ring was detected in the MFM analysis of Fe_3O_4 -free hollow chitosan-poly(acrylic acid) nanospheres. This result indicates again that the magnetite nanoparticles are distributed in the shell wall of the hollow hybrid nanospheres.

We now turn to the formation of the hollow Fe_3O_4 -polymer nanospheres. Based on the $\text{p}K_a$ values of 4.26 for AA and 4.8 for poly(acrylic acid) (PAA),^[18] the conversion of AA monomers inside the micelles into PAA results in some dissociated carboxylic groups becoming protonated carboxylic groups. The original micellar core comprised of positively charged protonated CS and negatively charged dissociated AA gradually disintegrates owing to the polymerization of AA. On the other hand, the residual dissociated carboxylic groups in the produced PAA will interact with the protonated amino groups in CS to form water-insoluble polyelectrolyte complexes between CS and PAA, which causes a decrease in the size of the micelles, as determined by DLS.^[17] This process

experiences two kinds of force: The electrostatic attraction between CS and PAA shrinks the spheres, whereas the electrostatic repulsion from the shell tends to expand the spheres. The equilibrium between the two opposing forces results in the formation of the cavity in the center of the nanospheres, with CS-PAA polyelectrolyte complexes as the inner shell and protonated CS chains as the outer shell. As PVA attached to the Fe_3O_4 nanoparticles interacts with PAA by hydrogen bonding (as revealed by the shift of the carbonyl absorption band of PAA from 1753 to 1713 cm^{-1} in FTIR measurements), the Fe_3O_4 nanoparticles should occur in the inner shell where polyelectrolyte complexes between CS and PAA exist. This is confirmed by the TEM image shown in Figure 1b.

The hollow hybrid nanospheres were calcined as part of our efforts to use these materials. The polymers were removed at elevated temperatures (550°C) under argon for 1 h to afford the completely hollow inorganic nanospheres (Figure 3). The electron-diffraction pattern confirms that these hollow inorganic nanospheres are composed of Fe_3O_4 . The diameter and wall thickness of these hollow Fe_3O_4

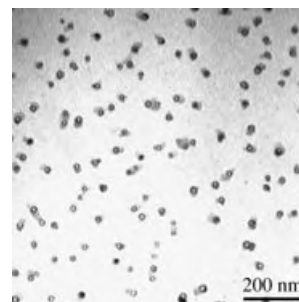


Figure 3. TEM image of hollow Fe_3O_4 nanospheres produced by calcination of hollow Fe_3O_4 -polymer hybrid nanospheres.

nanospheres are 20 ± 2 nm and 5 ± 1 nm, respectively, which are much smaller than those of uncalcined hollow hybrid spheres. Apparently, the hollow Fe_3O_4 nanospheres undergo significant shrinkage during the formation. In contrast to the shrinkage rate (below 30%)^[8] of hollow inorganic spheres prepared by colloidal templates, the shrinkage rate is more than 50% in our case. This may be due to the hollow interior of synthesized hybrid nanospheres and the distribution of Fe_3O_4 nanoparticles in the walls of hybrid nanospheres not being compact. Furthermore, the low polydispersity in the size of the hollow Fe_3O_4 nanospheres can be considered as indirect evidence that the synthesized hollow hybrid nanospheres have a relatively uniform size.

In summary, we have illustrated a successful synthesis of hollow Fe_3O_4 -polymer hybrid nanospheres by the addition of Fe_3O_4 nanoparticles to an aqueous solution of polymer-monomer pairs composed of the cationic polymer CS and the anionic monomer AA, followed by polymerization of AA and selective crosslinking of CS at the end of polymerization. The process is simple and allows the large-scale preparation of the nanospheres. There is also the possibility of extending this approach to other systems that involve different inorganic nanoparticles and different polymer-monomer pairs.

Experimental Section

Synthesis: The hollow Fe_3O_4 -polymer hybrid nanospheres were prepared by adding 10 mL of a PVA-stabilized magnetite nanoparticle suspension ($\approx 1 \times 10^{18}$ Fe_3O_4 particles mL^{-1}) to 50 mL of an aqueous solution of CS-AA, which consisted of 0.5 g of purified CS ($M_w = 200$ kDa, degree of deacetylation = 90%) and 0.22 g of AA, with a stoichiometric molar ratio of 1:1.1 (glucosamine unit/acid). Polymerization was then initiated by $\text{K}_2\text{S}_2\text{O}_8$ at 70 °C under a nitrogen stream. The concentration of $\text{K}_2\text{S}_2\text{O}_8$ in the reaction system is about 5 mM. As the reaction system appeared opalescent, the reaction was allowed to proceed for another 100 minutes at 50–60 °C. Afterwards, 0.5 mL of glutaraldehyde, a bifunctional crosslinker, was added to the reaction system at 40 °C to crosslink chitosan selectively. The resultant suspension was filtered to remove any possible aggregation and treated by repeated ultracentrifugation and washes. The nonloaded magnetite nanoparticles were separated in the ultracentrifugation process. The Fe_3O_4 loading content was determined to be 11% by thermogravimetric analysis.

Characterization: The mean particle size and zeta potential of the spheres were determined by DLS on a Brookhaven BI-9000AT instrument and a Zetaplus (Brookhaven Instruments Corporation, USA), respectively. All the measurements were repeated three times. TEM analysis was carried out on a JEOL JEM-2010 instrument at an acceleration voltage of 200 kV. For microtoming samples, an aqueous suspension of the crosslinked hollow Fe_3O_4 -polymer hybrid nanospheres was deposited on a polyimide sheet, and the sample was dried naturally. The polyimide sheet deposited with hollow Fe_3O_4 -polymer hybrid nanospheres was embedded in an epoxy resin, and sections approximately 70 nm thick were obtained by microtoming the resin sample at room temperature. MFM analysis was performed on a scanning-probe microscope (SPI3800, Seiko Instruments Inc, Japan) by using magnetic-moment MFM tips. Soft-tapping conditions were used. The lift mode (while tapping) was used to record the magnetic signal in the phase-detection mode. The samples for MFM analysis were coated with a 5-nm gold layer to avoid attachment of the nanospheres to the tip.

Calcination of hollow Fe_3O_4 -polymer hybrid nanospheres was carried out in a high-temperature oven under argon at 550 °C for 1 hour.

Received: April 22, 2004

Keywords: magnetic properties · micelles · nanostructures · polymerization · self-assembly

- [11] a) H. Dou, M. Jiang, H. Peng, D. Chen, Y. Hong, *Angew. Chem.* **2003**, *115*, 1554; *Angew. Chem. Int. Ed.* **2003**, *42*, 1516; b) X. Liu, M. Jiang, S. Yang, M. Chen, D. Chen, C. Yang, K. Wu, *Angew. Chem.* **2002**, *114*, 3074; *Angew. Chem. Int. Ed.* **2002**, *41*, 2950.
- [12] a) Z. Z. Zhong, Y. D. Yin, B. Gates, Y. Xia, *Adv. Mater.* **2000**, *12*, 206; b) I. Tissot, J. P. Reymond, F. Lefebvre, E. Bourgeat-Lami, *Chem. Mater.* **2002**, *14*, 1325; c) A. Imhof, *Langmuir* **2001**, *17*, 3579; d) H. Shiho, N. Kawahashi, *Colloid Polym. Sci.* **2000**, *278*, 270; e) H. Sertchook, D. Avnir, *Chem. Mater.* **2003**, *15*, 1690; f) Z. Yang, Z. Niu, Y. Lu, Z. Hu, C. C. Han, *Angew. Chem.* **2003**, *115*, 1987; *Angew. Chem. Int. Ed.* **2003**, *42*, 1943.
- [13] a) F. Caruso, R. A. Caruso, H. Mohwald, *Science* **1998**, *282*, 1111; b) N. Kawahashi, E. Matijevic, *J. Colloid Interface Sci.* **1990**, *138*, 534; c) F. Caruso, M. Spasova, A. Susa, M. Giersig, R. A. Caruso, *Chem. Mater.* **2001**, *13*, 109.
- [14] M. S. Wong, J. N. Cha, K. S. Choi, T. J. Deming, G. D. Stucky, *Nanolett.* **2002**, *2*, 583.
- [15] J. N. Cha, H. Birkedal, L. E. Euliss, M. H. Bartl, M. S. Wong, T. J. Deming, G. D. Stucky, *J. Am. Chem. Soc.* **2003**, *125*, 8285.
- [16] H. Stroh, M. Sgraja, J. Bertling, P. Lobmann, *J. Mater. Sci.* **2003**, *38*, 1605.
- [17] Y. Hu, X. Jiang, Y. Ding, Q. Chen, C. Z. Yang, *Adv. Mater.* **2004**, *16*, 933.
- [18] W. Arguelles-Monal, C. Peniche-Covas, *Makromol. Chem. Rapid Commun.* **1988**, *9*, 693.

- [1] *Hollow and Solid Spheres and Microspheres: Science and Technology Associated with Their Fabrication and Application*, Vol. 372 (Eds.: D. L. Wilcox, M. Berg, T. Bernat, D. Kellerman, J. K. Cochran), Materials Research Society Proceedings, Pittsburgh, **1995**.
- [2] J. Okada, S. Cohen, R. Langer, *Pharm. Res.* **1994**, *11*, 1568.
- [3] T. Ameller, W. Marsaud, P. Legrand, R. Gref, J. M. Renoir, *Int. J. Cancer* **2003**, *106*, 446.
- [4] I. Gill, A. Ballesteros, *J. Am. Chem. Soc.* **1998**, *120*, 8587.
- [5] T. Visted, T. Furmanek, P. Sakariassen, W. B. Foegler, K. Sim, H. Westphal, R. Bjerkvig, M. Lund-Johansen, *Hum. Gene Ther.* **2003**, *14*, 1429.
- [6] P. Tartaj, M. P. Morales, S. Veintemillas-Verdaguer, T. Gonzalez-Carreno, C. J. Serna, *J. Phys. D* **2003**, *36*, R182.
- [7] S. M. Marinakos, M. F. Anderson, J. A. Ryan, L. D. Martin, D. L. Feldheim, *J. Phys. Chem. B* **2001**, *105*, 8872.
- [8] F. Caruso, *Top. Curr. Chem.* **2003**, *227*, 145.
- [9] H. Huang, E. E. Remsen, T. Kowalewski, K. L. Wooley, *J. Am. Chem. Soc.* **1999**, *121*, 3805.
- [10] H. Shiho, N. Kawahashi, *J. Colloid Interface Sci.* **2000**, *226*, 91.

Organic Synthesis

Pd-Catalyzed Amination of Nucleoside Arylsulfonates to yield *N*⁶-Aryl-2,6-Diaminopurine Nucleosides**

*Padmaja Gunda, Larry M. Russon, and Mahesh K. Lakshman**

Palladium-catalyzed amination methods have become significantly important in organic synthesis over recent years, and major developments have been made in both the development of the catalysts as well as insight into mecha-

[*] P. Gunda, Prof. M. K. Lakshman
Department of Chemistry
The City College and The City University of New York
138th Street at Convent Avenue
New York, NY 10031 (USA)
Fax: (+1) 212-650-6107
E-mail: lakshman@sci.ccny.cuny.edu
Dr. L. M. Russon
Analytica of Branford Inc.
29 Business Park Drive
Branford, CT 06405 (USA)

[**] This work was supported by NSF grant CHE-0314326 and a PSC-CUNY 35 award. Acquisition of a 500 MHz NMR spectrometer was funded by NSF grant CHE-0210295. Professor S. L. Buchwald (MIT) is thanked for a sample of **L5**, and Dr. G. Li (CombiPhos Catalysts Inc.) is thanked for samples of **L6** and **L7**.



Supporting information for this article is available on the WWW under <http://www.angewandte.org> or from the author.

nisms.^[1] Application of such methods to the modification of biomolecules opens interesting new avenues for investigation, with a plethora of potential applications for the end products. In this context, we have focused our efforts on the understanding and development of Pd-catalyzed reactions of nucleosides because these compounds display some unusual reactivities that are often not comparable to simpler molecules. Our contributions to Pd-catalyzed C–N bond formation reactions, as well as the contributions of others, have led to the synthesis of unusual nucleosides that contain entities appended to the exocyclic amino groups of 2'-deoxyadenosine, 2'-deoxyguanosine, and C-8 aryl aminonucleosides.^[2–4] Unnatural nucleosides have long since held interest as novel pharmacophores and as probes of biofunction. These types of applications provide added importance to newer methods that lead to modification of nucleosides. For the synthesis of *N*⁶-aryl 2'-deoxyadenosine analogues, the readily available C-6 bromonucleoside **1** has been the substrate of choice, whereas the *O*⁶-benzyl-2-bromonucleoside **2** has been used for the synthesis of *N*²-modified 2'-deoxyguanosine derivatives.^[4] Although the *O*⁶-arylsulfonate derivatives of purine nucleosides, and particularly those of guanine, are readily available (**3a–c** in Figure 1),^[5] the utility of these compounds in Pd-catalyzed transformations has not been explored to date. Purine arylsulfonates, on the other hand, have been used for nucleophilic (S_NAr) displacement chemistry.^[5–7] By and large, direct displacement of leaving groups at the C-6 position of purines is possible with good nucleophiles, and amination reactions have been conducted with alkyl amines.^[7] There are not many examples of direct displacement reactions with aryl amines, and recently a few examples with bromonucleosides were reported.^[8] Among simpler aromatic systems, Pd-catalyzed amination reactions of arene arylsulfonates have been reported recently,^[9,10] and herein we report the first such studies that involve arylsulfonates of nucleosides.

From our recent studies on the Suzuki–Miyaura reactions of **3a**, it was clear that insertion of Pd into the C–sulfonate bond would occur quite readily.^[11] However, experience with amination reactions of **1** suggested that the product turnover could highly depend on the nature of the ligand.^[3] Therefore, two lines of investigation were initiated: One investigation

was directed towards the determination of conditions that lead to optimal coupling results, whereas the second involved an evaluation of the influence of the sulfonate group on these reactions. For this purpose, sulfonates **3a–c**, which differ in steric factors, were synthesized by known methods.

The supporting ligands chosen for this initial analysis are shown in Figure 2.^[12] The choice of these ligands originated from various results that we obtained in previous amination

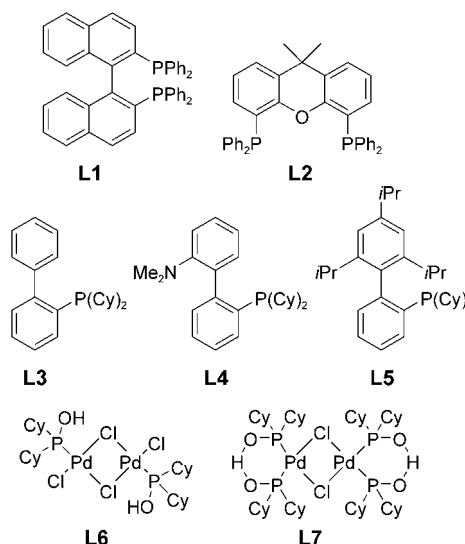


Figure 2. The ligands that were screened for the amination reactions. Cy = cyclohexyl.

reactions of nucleosides. So far, **L1** and **L4** had been successful for aminations, and **L2** was chosen based upon bite-angle considerations relative to **L1** (**L2** has a bite angle of 110° relative to 93° for **L1**).^[13] **L3** has been the preferred ligand for C–C bond-forming reactions of nucleosides and bears the core structure of **L4** and **L5**, a factor that may be useful in an analysis of the structural elements of ligands that can be used for these amination reactions. However, **L3** has so far not been very useful for amination reactions of nucleosides. **L6** and **L7** had not been tested for reactions of nucleosides and were chosen because they contain (Cy)₂P moieties bound to the metal, a factor that we have previously found to be important among the biphenyl-based phosphanes (*tert*-butyl groups in place of cyclohexyl (Cy) groups render the ligands ineffective for amination).^[2b]

The representative aryl amine chosen for the optimization experiments was 4-toluidine, and a Pd(OAc)₂/ligand ratio of 1:3 was employed. Based upon our experience with the C–C cross-coupling reaction, sulfonate **3a** was selected for the initial experiments.^[11] Parameters that were varied include the ligand, the solvent, and the base; the results of these experiments are summarized in entries 1–6 of Table 1. Certain interesting observations emerge from the data in Table 1. From entries 1 and 2, it becomes apparent that the

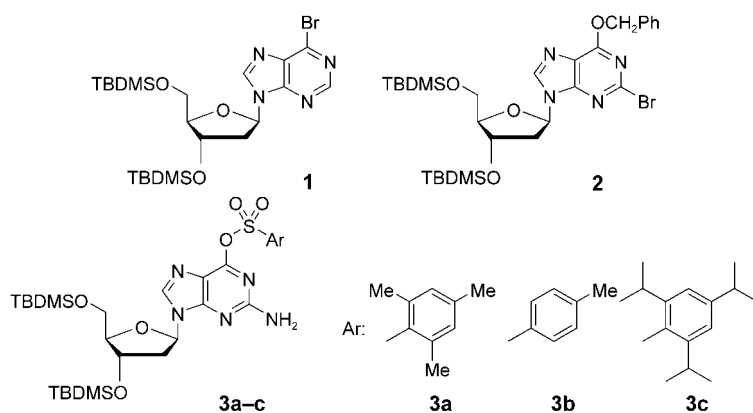
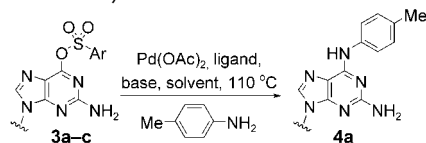


Figure 1. The substrates that were studied in Pd-catalyzed amination reactions. TBDMS = *tert*-butyldimethylsilyl.

Table 1: Coupling of the nucleoside arylsulfonates **3a–c** with 4-toluidine under various conditions.^[a]

Entry	Sulfonate	Ligand	Base	Solvent	Reaction time ^[b]	Yield [%] ^[c]
1	3a	L1	Cs ₂ CO ₃	PhMe	45 min	57
2	3a	L1	Cs ₂ CO ₃	1,4-Dioxane	30 min	[d]
3	3a	L2	Cs ₂ CO ₃	PhMe	1 h	55
4	3a	L3	Cs ₂ CO ₃	PhMe	11 h	[d]
5	3a	L4	Cs ₂ CO ₃	PhMe	1 h	63
6	3a	L4	K ₃ PO ₄	1,4-Dioxane	30 min	65
7	3b	L4	K ₃ PO ₄	1,4-Dioxane	30 min	75
8	3b	L4	K ₃ PO ₄	5:1 1,4-Dioxane/ <i>t</i> BuOH	30 min	77
9	3c	L4	K ₃ PO ₄	5:1 1,4-Dioxane/ <i>t</i> BuOH	30 min	[d]
10	3b	L5	K ₃ PO ₄	5:1 1,4-Dioxane/ <i>t</i> BuOH	30 min	71 ^[e]
11	3b	L6	K ₃ PO ₄	5:1 1,4-Dioxane/ <i>t</i> BuOH	5 h	0
12	3b	L7	K ₃ PO ₄	5:1 1,4-Dioxane/ <i>t</i> BuOH	24 h	[f]

[a] Reaction conditions: **3** (0.1 M in the respective solvent), aryl amine (2.0 equiv), Pd(OAc)₂ (10 mol %), **L** (30 mol %), base (1.5 equiv), 110 °C. [b] Disappearance of the sulfonate was monitored by tlc. [c] Yields reported are of isolated and purified **4a**. [d] The sulfonate was consumed, but an insignificant amount of product formed. [e] The product was impure after chromatography. [f] The sulfonate was still present in the reaction mixture, and an insignificant amount of product formed.

solvent has a significant influence on the reaction which involves **L1** as the ligand. However, this does not appear to be the case with **L4** as the difference in the yields in entries 5 and 6 is only marginal, with the combination of **L4**/K₃PO₄ in 1,4-dioxane producing a faster reaction. **L1** and **L2** produced comparable results which indicate that a change in the bite angle of the ligand does not seem to significantly alter the coupling. As expected, **L3** was ineffective which is consistent with previous aminations at the C-6 position of purine nucleosides.^[2b]

As a reasonable set of reaction parameters had been obtained, the coupling efficiency of the sulfonate **3b** was next studied. Interestingly, this less-hindered sulfonate substrate gave a 10 % increase in the yield of **4a** within 30 min (entry 7). Another factor was the importance of *t*BuOH for the aryl amination; this presented a critical deviation from the amination of simpler arene arylsulfonates. It has been reported that *t*BuOH is necessary for the amination reaction and reactions in 1,4-dioxane or toluene were very slow.^[9] This was not the case here, and although the addition of *t*BuOH appeared to provide a marginal improvement in yield and product quality, reactions in its presence or absence proceeded rapidly (entries 7 and 8).^[14] For this reason, all subsequent reactions were conducted in a mixture of 5:1 1,4-dioxane/*t*BuOH.

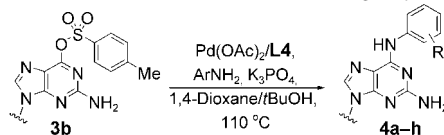
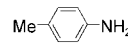
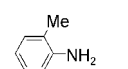
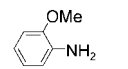
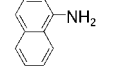
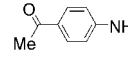
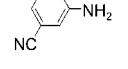
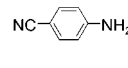
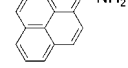
Reaction of the hindered tri(isopropyl)benzenesulfonate **3c** yielded another insight into a plausible steric effect. With this substrate, no product was recovered after 30 min although the sulfonate was consumed (entry 9): This apparently implies that product turnover diminishes with increased alkyl substitution proximal to the sessile C–O bond. With **L5** as the ligand, **4a** was furnished in a yield that was comparable to the yield obtained with **L4**, but the quality of the product was lowered (entry 10). Use of Pd₂(dba)₃

(5 mol %) and **L5** (30 mol %) led to a significant amount of unconverted **3b** even after 5 h. The use of ligands **L6** and **L7** did not provide any product from the amination step although **3b** was completely consumed in one case. In two cases (entries 2 and 9) in which consumption of the sulfonate occurred and very little product formation was observed, the ¹H NMR spectra of the reaction mixtures were analyzed. In both cases, formation of some product (also discernable by tlc) and nucleosidic resonances for another uncharacterized compound were observed. However, no starting material was present as resonances that correspond to the arylsulfonate unit had completely disappeared. No further attempt was made at determining what course these reactions had taken. Finally, to ascertain whether any product formation occurred

through a S_NAr displacement mechanism, **3b** was treated with 4-toluidine in the absence of Pd(OAc)₂ in the reaction mixture. After 24 h at 110 °C, a 12 % yield of highly impure **4a** was obtained which clearly indicates that under these conditions, the metal-catalyzed process is the significant contributor to the amination reaction.

These experiments provided a basis for a more detailed analysis of the scope of the amination reaction with respect to the steric and electronic nature of the aryl amine component as well as different catalyst and ligand concentrations. Thus, a series of experiments were conducted using several aryl amines in the presence of different ratios of ligand/Pd. Table 2 provides some interesting insight into these amination reactions. At a catalyst load of 10 mol % Pd(OAc)₂ and 30 mol % **L4**, all of the amines that were studied reacted smoothly within 30 min to afford the N⁶-aryl-2,6-diaminopurine nucleosides **4a–h**. The electron-deficient amines provided high yields, and the yields obtained with 4-toluidine, 1-naphthylamine, and 2-anisidine were also very good. A lower yield in the reaction of the sterically encumbered 2-toluidine (entry 2) was observed relative to that observed for 4-toluidine (entry 1): this is consistent with a steric influence and is reasonable when the yields obtained with 2-anisidine are also considered (entry 3). Upon lowering the catalyst loading to 5 mol % Pd(OAc)₂ and 15 mol % **L4**, the unhindered, electron-deficient amines and 4-toluidine again provided good (although slightly lower) yields. However, a dramatic effect was seen with the *ortho*-substituted amines and 1-naphthylamine (entries 2–4). In these cases, the reactions were incomplete which is consistent with a steric influence. The yield with 2-toluidine was significantly lower than that with the sterically less-hindered 2-anisidine. With 5 mol % Pd(OAc)₂ and 30 mol % **L4** (1:6 Pd/ligand), some other differences emerged. All of the reactions, with the

Table 2: Results of the amination reaction with various ratios of ligand/Pd.^[a]

					
Entry	ArNH ₂	Conditions ^[b]	Time ^[c]	Yield [%] ^[d]	Product
1		A	30 min	77	4a
		B	1 h	73	4a
		C	30 min	70	4a
2		A	30 min	58	4b
		B	5 h	22 ^[e]	4b
		C	30 min	27	4b
3		A	30 min	66	4c
		B	5 h	42 ^[e]	4c
		C	30 min	62	4c
4		A	30 min	79	4d
		B	8 h	56 ^[e]	4d
		C	30 min	75	4d
5		A	30 min	95	4e
		B	2.5 h	78	4e
		C	30 min	94	4e
6		A	30 min	97	4f
		B	30 min	87	4f
		C	30 min	96	4f
7		A	30 min	91	4g
		B	45 min	80	4g
		C	30 min	81	4g
8		A	30 min	87	4h
		B	2.5 h	63	4h

[a] General reaction conditions: **3b** (0.1 M in 5:1 1,4-dioxane/*t*BuOH), aryl amine (2.0 equiv), K₃PO₄ (1.5 equiv), 110 °C. [b] Conditions: A: Pd(OAc)₂ (10 mol %), **L4** (30 mol %); B: Pd(OAc)₂ (5 mol %), **L4** (15 mol %); C: Pd(OAc)₂ (5 mol %), **L4** (30 mol %). [c] Disappearance of **3b** was monitored by tlc. [d] Yields reported are of isolated and purified **4a–h**. [e] Incomplete reaction.

exception of 2-toluidine, proceeded to completion with yields that were comparable to those obtained when a higher loading of Pd was used. Therefore, these results suggest that with the exception of highly sterically congested *ortho*-substituted aryl amines, which require 10-mol % Pd(OAc)₂, most reactions run successfully at 5-mol % Pd(OAc)₂ as long as the ratio of Pd/**L4** ratio is ≈ 1:6. Finally, two reactions of **3b** and 4-toluidine were conducted at 10 and 5 mol % Pd(PPh₃)₄ in 1,4-dioxane and 1,4-dioxane/*tert*-BuOH, respectively. Both reactions were complete within 30 min to provide a yield of 78–84 % of **4a**. In contrast, even with 10 mol % Pd(PPh₃)₄, the amination of bromonucleoside **1** with 4-toluidine was incomplete after 5 h under the reaction conditions described here and those described previously.^[2a] Currently, complexes of **L4**/Pd appear to be generally good for amination reactions of nucleosides.

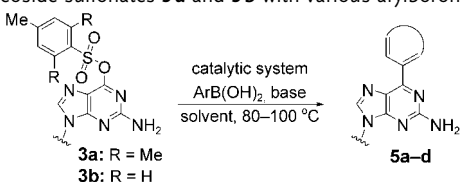
In light of the results of the amination studies, we reanalyzed the C–C cross-coupling reaction of **3a** and **3b**. In our earlier report on the Suzuki–Miyaura cross-coupling

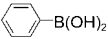
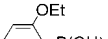
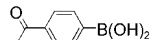
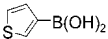
reaction using **L3**/Pd, **3a** was extensively studied and proved to be a generally good substrate, but one reaction with **3b** indicated that it might be comparable or superior to **3a**, whereas **3c** had again proven less useful.^[11] Therefore, the reactions of **3a** and **3b** with selected arylboronic acids were tested in the presence of Pd(OAc)₂/**L3** as well as Pd(PPh₃)₄, which has also found utility for such reactions, under conditions that were previously reported.^[11,15] The results of these experiments are summarized in Table 3.

In the presence of 5 mol % Pd(PPh₃)₄ and K₂CO₃ in toluene,^[15] the reaction of phenylboronic acid with **3b** was incomplete after 5 h; upon prolonged treatment (overnight), **5a** was obtained in 48 % yield (entry 1). The replacement of K₂CO₃ with K₃PO₄ gave significantly superior yields with a decreased reaction time (entry 2). Little improvement was observed upon increasing the Pd(PPh₃)₄ load to 10 mol % in 1,4-dioxane (entry 3). However, all of the subsequent reactions were performed at the higher load for comparison with our previous reaction conditions.^[11] All of the reactions of **3a** and **3b** gave good yields of the product (Table 3, entries 2–6), but **3a** appeared to be a better substrate. A similar trend was seen for reactions with 2-ethoxyphenylboronic acid (entries 7–10). Reaction

of the electron-deficient 4-acetylphenylboronic acid with **3b** produced **5c** in 45 % yield (entry 11) with a prolonged reaction time. On the other hand, with sulfonate **3a** the reaction was incomplete (entry 13). This is consistent with previous reports in which electron-deficient arylboronic acids gave low yields of the cross-coupled product with the Pd(PPh₃)₄ catalytic system.^[16] Both **3a** and **3b** gave a comparable yield of the product in the presence of Pd(OAc)₂, **L3**, and K₃PO₄ (entries 12 and 14).^[11] With 3-thienylboronic acid, good recoveries of the product were generally observed (entries 15–18), and Pd(PPh₃)₄ was somewhat superior to Pd(OAc)₂/**L3** despite the longer reaction times required and incomplete reaction observed with **3a** (entry 17). The results summarized in Table 3 also show that both **3a** and **3b** can be used for C–C bond-formation reactions, and that the Pd(OAc)₂/**L3** system is applicable with a variety of arylboronic acids.

Certain details on the nature of the catalytic systems warrant comment. The Pd(PPh₃)₄ catalyst shows applicability

Table 3: Reaction of nucleoside sulfonates **3a** and **3b** with various arylboronic acids.


Entry	ArB(OH) ₂	Sulfonate	Conditions ^[a]	Time ^[b]	Yield [%] ^[c]	Product
1		3b	A	17 h	48 ^[d]	5a
2		3b	B	45 min	78	5a
3		3b	C	30 min	81	5a
4		3b	D	30 min	66	5a
5		3a	C	30 min	89	5a
6		3a	D	30 min	76 ^[e]	5a
7		3b	C	5 h	72	5b
8		3b	D	5 h	27 ^[f]	5b
9		3a	C	5 h	76	5b
10		3a	D	5 h	65 ^[e]	5b
11		3b	C	4.5 h	45	5c
12		3b	D	2 h	64 ^[g]	5c
13		3a	C	4.5 h	27 ^[f]	5c
14		3a	D	30 min	64 ^[e]	5c
15		3b	C	1.5 h	95	5d
16		3b	D	30 min	83 ^[g]	5d
17		3a	C	4 h	87 ^[f]	5d
18		3a	D	30 min	78 ^[e]	5d

[a] Conditions: A: **3** (0.1 M), Pd(PPh₃)₄ (5 mol %), K₂CO₃ (1.5 equiv), PhMe, 100 °C; B: **3** (0.1 M), Pd(PPh₃)₄ (5 mol %), K₃PO₄ (1.5 equiv), PhMe, 100 °C; C: **3** (0.085–0.089 M), Pd(PPh₃)₄ (10 mol %), K₃PO₄ (2.0 equiv), 1,4-dioxane, 80 °C; D: **3** (0.085–0.089 M), Pd(OAc)₂ (10 mol %), **L3** (20 mol %), K₃PO₄ (2.0 equiv), 1,4-dioxane, 80 °C. [b] Disappearance of the sulfonate was monitored by tlc. [c] Yields reported are of isolated and purified **5a–d**. [d] Reaction incomplete after 5 h and was allowed to proceed overnight. [e] Yield reported in ref. [11]. [f] Reaction was incomplete at the time of workup. [g] Reactions were conducted as in ref. [11], but with K₃PO₄ (1.5 equiv).

for C–C bond-formation reactions and despite low yields with electron-deficient arylboronic acids, it can provide good to high yields when, in combination with K₃PO₄, other boronic acids are used. On the other hand, the biphenylphosphane-based catalysts appear to be more-broadly applicable, but they show some interesting differences. From the results presented in Table 1 and in our previous studies,^[2] **L3** appears to be ineffective for the formation of C–N bonds at the C-6 position of purine nucleosides, whereas both **L4** and **L5** produce effective catalysts. However, **L3** is an effective ligand for C–C cross-coupling reactions.^[2b,11] This leads us to speculate about the nature of the ligand–Pd interactions that may contribute to these two different reactions with the same substrate. With **L3**, an intramolecular η¹-arene coordination of the metal has been observed at room temperature.^[17] Such interactions or plausible cyclopalladation of the biphenyl entity, as has been reported with the di(*tert*-butyl) analogue,^[18] could perhaps provide an active catalyst for the formation of C–C bonds but not for C–N bonds. The prevention of cyclopalladation either through hemilabile heteroatom coordination to the metal in **L4** or the simple blockage of cyclopalladation centers in **L5** could lead to different types of non-cyclopalladated ligand–Pd complexes that display activity for C–N bond-formation reactions.

In summary, we have shown for the first time that an easily prepared arylsulfonate derivative of 2'-deoxyguanosine can be effectively utilized for Pd-catalyzed amination reactions with aryl amines to lead to *N*⁶-aryl-2,6-diaminopurine nucleoside analogues. Furthermore, the results from our studies on amination and C–C cross-coupling reactions seem to indicate a delicate interplay between the nature of the ligand, the substituents on the arylsulfonate, as well as the type of reaction that is conducted, all of which contribute to the success of these reactions.

Received: May 25, 2004

Revised: August 13, 2004

Keywords: amination · C–C coupling · nucleosides · palladium · phosphane ligands

- [1] For recent reviews on this topic, see: a) J. P. Wolfe, S. Wagaw, J.-F. Marcoux, S. L. Buchwald, *Acc. Chem. Res.* **1999**, *31*, 805–818; b) J. F. Hartwig, *Acc. Chem. Res.* **1999**, *31*, 852–860; c) C. G. Frost, P. Mendonca, *J. Chem. Soc. Perkin Trans. 1* **1998**, 2615–2623; d) B. H. Yang, S. L. Buchwald, *J. Organomet. Chem.* **1999**, *576*, 125–146; e) J. F. Hartwig, in *Modern Amination Methods*, (Ed.: A. Ricci), Wiley-VCH, Weinheim, **2000**, pp. 195–262; f) A. R. Muci, S. L. Buchwald, *Top. Curr. Chem.* **2002**, *219*, 131–209; g) D. Prim, J.-M. Campagne, D. Joseph, B. Andrioletti, *Tetrahedron* **2002**, *58*, 2041–2075.
- [2] a) M. K. Lakshman, J. C. Keeler, J. H. Hilmer, J. Q. Martin, *J. Am. Chem. Soc.* **1999**, *121*, 6090–6091; b) M. K. Lakshman, J. H. Hilmer, J. Q. Martin, J. C. Keeler, Y. Q. V. Dinh, F. N. Ngassa, L. M. Russon, *J. Am. Chem. Soc.* **2001**, *123*, 7779–7787; c) M. K. Lakshman, P. Gunda, *Org. Lett.* **2003**, *5*, 39–42; d) M. K. Lakshman, F. N. Ngassa, S. Bae, D. G. Buchanan, H.-G. Hahn, H. Mah, *J. Org. Chem.* **2003**, *68*, 6020–6030.
- [3] a) E. A. Harwood, S. T. Sigurdsson, N. B. F. Edfeldt, B. R. Reid, P. B. Hopkins, *J. Am. Chem. Soc.* **1999**, *121*, 5081–5082; b) F. De Riccardis, R. R. Bonala, F. Johnson, *J. Am. Chem. Soc.* **1999**, *121*, 10453–10460; c) E. A. Harwood, P. B. Hopkins, S. T. Sigurdsson, *J. Org. Chem.* **2000**, *65*, 2959–2964; d) R. Bonala, I. Shishkina, F. Johnson, *Tetrahedron Lett.* **2000**, *41*, 7281–7284; e) F. De Riccardis, F. Johnson, *Org. Lett.* **2000**, *3*, 293–295; f) Z. Wang, C. J. Rizzo, *Org. Lett.* **2001**, *3*, 565–568; g) E. Schoffers, P. D. Olsen, J. C. Means, *Org. Lett.* **2001**, *3*, 4221–4223; h) C. Meier, S. Gräsl, *Synlett* **2002**, 802–804; i) F. Johnson, R. Bonala, D. Tawde, M. C. Torres, C. R. Iden, *Chem. Res. Toxicol.* **2002**, *15*, 1489–1494; j) L. C. Gillet, O. D. Schärer, *Org. Lett.* **2002**, *4*, 4205–4208; k) D. Chakraborti, L. Colis, R. Schneider, A. K. Basu, *Org. Lett.* **2003**, *5*, 2861–2864; l) T. Takamura-Enya, S. Ishikawa, M. Mochizuki, K. Wakabayashi, *Tetrahedron Lett.* **2003**, *44*, 5969–5973.

- [4] For reviews on Pd-catalyzed C–N bond-forming reactions of nucleosides, see: a) M. K. Lakshman, *J. Organomet. Chem.* **2002**, 653, 234–251; b) M. K. Lakshman, *Curr. Org. Synth.* **2005**, in press.
- [5] a) H. P. Daskalov, M. Sekine, T. Hata, *Tetrahedron Lett.* **1980**, 21, 3899–3902; b) B. L. Gaffney, R. A. Jones, *Tetrahedron Lett.* **1982**, 23, 2253–2256; c) Y. Hayakawa, M. Hirose, R. Noyori, *J. Org. Chem.* **1993**, 58, 5551–5555; d) C. B. Reese, P. A. Skone, *J. Chem. Soc. Perkin Trans. I* **1984**, 1263–1271.
- [6] a) P. K. Bridson, W. T. Markiewicz, C. B. Reese, *J. Chem. Soc. Chem. Commun.* **1977**, 791–792; b) Y.-Z. Xu, Q. Zheng, P. F. Swann, *Tetrahedron* **1991**, 32, 2817–2820; c) C. R. Allerson, S. L. Chen, G. L. Verdine, *J. Am. Chem. Soc.* **1997**, 119, 7423–7433.
- [7] M. K. Lakshman, F. N. Ngassa, J. C. Keeler, Y. Q. V. Dinh, J. H. Hilmer, L. M. Russon, *Org. Lett.* **2000**, 2, 927–930.
- [8] E. A. Véliz, P. A. Beal, *J. Org. Chem.* **2001**, 66, 8592–8598.
- [9] X. Huang, K. W. Anderson, D. Zim, L. Jiang, A. Klapars, S. L. Buchwald, *J. Am. Chem. Soc.* **2003**, 125, 6653–6655.
- [10] A. H. Roy, J. F. Hartwig, *J. Am. Chem. Soc.* **2003**, 125, 8704–8705.
- [11] M. K. Lakshman, P. F. Thomson, M. A. Nuqui, J. H. Hilmer, N. Sevova, B. Boggess, *Org. Lett.* **2002**, 4, 1479–1482.
- [12] Ligands **L1** to **L5** are commercially available from Strem Chemicals, whereas **L6** and **L7** are available from CombiPhos Catalysts Inc.
- [13] a) P. C. J. Kamer, P. W. N. M. van Leeuwen, J. N. H. Reek, *Acc. Chem. Res.* **2001**, 34, 895–904; b) J. Yin, S. L. Buchwald, *J. Am. Chem. Soc.* **2002**, 124, 6043–6048; c) I. del Rio, N. Ruiz, C. Claver, L. van der Veen, P. W. N. M. van Leeuwen, *J. Mol. Catal.* **2000**, 161, 39–48.
- [14] Amination reactions of **3a** were also conducted with 2-anisidine and 4-aminoacetophenone in the presence of Pd(OAc)₂ (10 mol %) and **L4** (30 mol %) in toluene at 110 °C. The progress of these reactions was observed with product recoveries of 50 % (reaction time: 1.75 h) and 25 % (reaction time: 3 h), respectively.
- [15] a) M. Hocek, A. Holý, I. Votruba, H. Dvořáková, *J. Med. Chem.* **2000**, 43, 1817–1825; b) M. Hocek, A. Holý, I. Votruba, H. Dvořáková, *Collect. Czech. Chem. Commun.* **2000**, 65, 1683–1697; c) M. Hocek, A. Holý, I. Votruba, H. Dvořáková, *Collect. Czech. Chem. Commun.* **2001**, 66, 483–499.
- [16] a) M. Havelkova, M. Hocek, M. Česnek, D. Dvořák, *Synlett* **1999**, 1145–1147; b) M. Havelkova, D. Dvořák, M. Hocek, *Synlett* **2001**, 1704–1710.
- [17] S. M. Reid, R. C. Boyle, J. T. Mague, M. J. Fink, *J. Am. Chem. Soc.* **2003**, 125, 7816–7817.
- [18] D. Zim, S. L. Buchwald, *Org. Lett.* **2003**, 14, 2413–2415.

In Situ Magnetic Resonance Investigation of Styrene Oxidation over TS-1 Zeolites**

Jianqin Zhuang, Gang Yang, Ding Ma,* Xijie Lan, Xiumei Liu, Xiuwen Han, Xinhe Bao,* and Ulrich Mueller

As an efficient catalyst for the selective oxidation of various organic substrates,^[1] the titanium molecular sieve TS-1 has shown great potential in industry, as it is also environmentally benign. Over the past few decades, the synthesis of TS-1 as well as novel reactions based on it, including the mechanisms of these reactions, have attracted the attention of many researchers from experimental and computational fields.^[1–6]

For example, with aqueous H₂O₂ as the oxidant, alkenes are converted into epoxides with high efficiency under mild conditions. With FTIR spectroscopy, Frei and Lin observed the TiOOH species that was determined to be the active site in the oxidation of small olefins.^[6] When the reaction was extended to styrene, however, the main product was phenylacetaldehyde (PADH), and only a small amount of epoxide was obtained.^[1c,3] Accompanying by-products included benzaldehyde (BADH) from cleavage of the C–C bond and 1-phenyl-1,2-ethanediol (DIOL) from hydrolysis in the presence of water.^[3b] Some reports claimed that a synergic effect of TiOOH and a polar solvent (such as water) provided an acidic environment and thus promoted the isomerization or hydrolysis of styrene epoxide.^[3,4] However, contrary opinions have been voiced based on the fact that the rearrangement of styrene epoxide is difficult owing to its high stability under the reaction conditions.^[5] The oxidation of styrene may instead proceed by a radical mechanism with help from the aromatic π ring. Therefore, PADH might be obtained directly from

[*] Dr. J. Zhuang, G. Yang, Dr. D. Ma, X. Lan, X. Liu, Prof. X. Han, Prof. Dr. X. Bao
State Key Laboratory of Catalysis
Dalian Institute of Chemical Physics
Chinese Academy of Sciences
Dalian 116023 (P.R. China)
E-mail: dma@dicp.ac.cn
xhbao@dicp.ac.cn

Dr. D. Ma
School of Chemistry
University of Bristol
Bristol, BS8 1TS (UK)
Fax: (+44) 117-925-1295
Dr. J. Zhuang, Dr. U. Mueller
BASF Aktiengesellschaft
GCC/Z-M301
67056 Ludwigshafen (Germany)

[**] Financial support from the National Natural Science Foundation and the Ministry of Science and Technology of the People's Republic of China is gratefully acknowledged. The authors thank Dr. R. Hong and X. Ruan for helpful discussions and K. Perkin for his kind help in composing this paper.



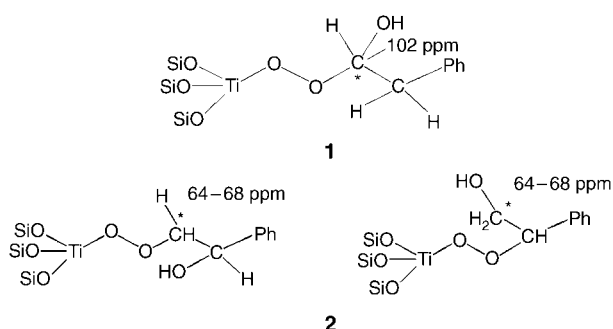
Supporting information for this article is available on the WWW under <http://www.angewandte.org> or from the author.

styrene, with the formation of styrene epoxide being a competitive process. Kumar et al. used EPR spectroscopy to observe the formation of Ti-superoxo radicals in TS-1 catalysts upon contact with H_2O_2 or urea-hydroperoxide (UHP). The key site was determined to be a Ti-superoxo species such as TiOOH or TiOO^\bullet .^[4a,6] However, there was no direct evidence for how PADH and styrene epoxide were formed, and the overall reaction is still far from being understood.

In the present work, in situ NMR spectroscopy, one of the most powerful tools for the study of catalytic mechanisms,^[7–9] was applied to study the oxidation of styrene over TS-1 zeolites with UHP. The role of the Brønsted acidic sites, the catalytically active sites, and the intermediates of PADH formation were investigated. To supplement the NMR data, EPR spectroscopy was also used. This technique is very sensitive to paramagnetic species with one or more unpaired electrons, and enables the detection of even small amounts of the active sites or reaction intermediates. Through the combination of density functional theory with the gauge-invariant atomic orbital (GIAO) method, the ^{13}C chemical shifts of some key products were calculated. Then, a mechanism for the overall reaction was proposed and verified by subsequent density functional calculations.

Two kinds of TS-1 zeolite samples were used in the study: one without Brønsted acidity (sample **A**) and one with Brønsted acidity (sample **B**). The acidity was confirmed by ^{31}P MAS NMR spectroscopy with trimethylphosphane (TMP) as the probe (see the Supporting Information). When β - ^{13}C -enriched styrene was adsorbed on sample **A**, two peaks centered at $\delta = 113.2$ and 128.0 – 140.0 ppm were observed (Figure 1A). These peaks correspond to the β carbon atom and the other carbon atoms in styrene, respectively. When styrene was adsorbed on premixed UHP and sample **A**, the conversion of styrene can be observed (Figure 1B). In

addition to the signals of the reactant, two narrow peaks centered at $\delta = 50.2$ and 102.2 ppm appeared. The former is a typical signal for the β carbon atom of styrene epoxide, which is formed by the epoxidation of styrene with UHP.^[4a,10] The latter signal is in the range for O-C-O species and assigned to a hemiacetal species **1** bound to framework Ti species of the zeolite. The local structure of the hemiacetal species was optimized by density functional calculations, and then the ^{13}C chemical shift was computed by the GIAO method (see the Supporting Information). The calculated chemical shift of this species is $\delta = 102.7$ ppm, in agreement with the experimental value of $\delta = 102.2$ ppm. In addition, a broad peak at $\delta = 64.0$ – 68.0 ppm appeared, which can be assigned to a glycol species bound to the framework Ti species. This assumption was confirmed by calculation of the chemical shift at $\delta = 64.7$ ppm for the corresponding structure **2** (see the Supporting Information).



When the sample was heated at 313 K after adsorption, the intensity of the signal for the hemiacetal species increased at the expense of that of styrene (Figure 1C, D). Meanwhile, the intensity of the signal for the styrene epoxide decreased slightly and, at the same time, a broad peak at $\delta = 64.0$ – 68.0 ppm appeared. In addition there were two other new peaks: one centered at $\delta = 163.2$ ppm is ascribed to formic acid, arising from further oxidation of styrene, and one at $\delta = 87.0$ ppm is due to an alkoxy group, whose nature needs further investigation. It is important that no signal at $\delta = 200$ ppm corresponding to PADH, the dominant product for styrene oxidation with aqueous H_2O_2 , was detected.

Based on these results, it is clear that, with UHP as the oxidant, styrene was mainly converted into the hemiacetal species when catalyzed by TS-1 zeolite without Brønsted acid sites. On the other hand, the concentration of the side product, styrene epoxide, decreases slightly with increasing reaction time (Figure 1B–D), suggesting that it may be in equilibrium with other minor products. The hemiacetal species are stabilized by the framework of the TS-1 zeolite and thus cannot be released. Therefore, without Brønsted acid sites, styrene could not be converted into PADH.

However, when TS-1 zeolite containing Brønsted acid sites (sample **B**) is used, a different picture is presented. Most importantly, after styrene reacted with a premixture of UHP and sample **B** (Figure 2C) for 15 min at 313 K, a new peak at around $\delta = 202.0$ ppm appeared. The intensity of the signals for the corresponding species increased as the reaction

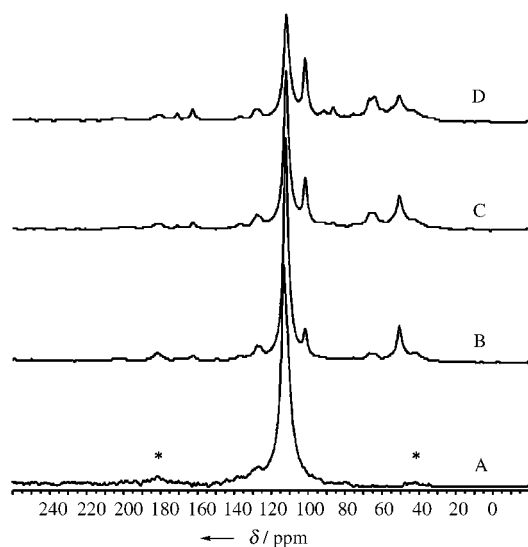


Figure 1. The in situ ^{13}C MAS NMR spectra of styrene adsorbed on sample **A** (A), and for the reaction of styrene with a mixture of sample **A** and UHP at 313 K after 0 min (B), 15 min (C), and 45 min (D). The asterisks represent side bands.

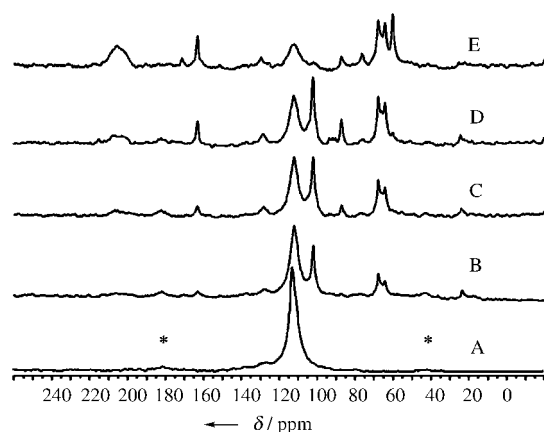


Figure 2. The in situ ^{13}C MAS NMR spectra of styrene adsorbed on sample **B** (A), and for the reaction of styrene with a mixture of sample **B** and UHP at 313 K after 0 min (B), 15 min (C), and 45 min (D). The asterisks represent side bands.

proceeded (Figure 2D, E). On the other hand, the intensity of the signal for the hemiacetal species ($\delta = 102.2$ ppm) increased at first and passed through a maximum at the same time as the depletion of styrene and the formation of PADH, strongly suggesting that the hemiacetal species are intermediates for PADH production. This rules out the previous assumption that PADH results from the rearrangement of styrene epoxide.^[4] The intermediate role of the hemiacetal species in the production of PADH is in agreement with the well-documented equilibrium between hemiacetal and acetal, that is, the hemiacetal can be converted into the acetal under acidic conditions.^[11] Significantly, the only difference between the two samples is that sample **B** contains Brønsted acid sites; that is, Brønsted acid sites catalyzed the conversion of hemiacetal into PADH. Without Brønsted acid sites, PADH is not formed, and the hemiacetal species remains bound to the zeolite framework (Figure 1).

Much to our surprise, if a mixture of sample **A** and UHP is put aside overnight at room temperature and then allowed to react with styrene, no hemiacetal species is formed (Figure 3).

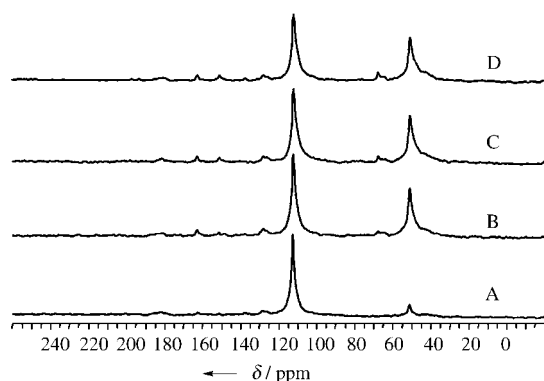


Figure 3. The ^{13}C MAS NMR spectra of styrene upon reaction with a mixture of UHP and sample **A** at 313 K after 0 min (A), 10 min (B), 20 min (C), and 40 min (D). Before the adsorption of styrene, the mixture of UHP and sample **A** was stored at room temperature overnight.

The sole product was a small amount of styrene epoxide ($\delta = 50.2$ ppm). As the reaction proceeded, trace amounts of two other minor products were observed, such as a glycol species at about $\delta = 68.0$ ppm; no aldehyde was detected. This result was completely different from that obtained upon the immediate adsorption of styrene onto the mixture of sample **A** and UHP (Figure 1), implying that the catalytic species responsible for the formation of the hemiacetal had decomposed during the long delay. This interesting phenomenon prompted us to investigate in detail the effect of delay time on the product distribution. Figure 4 depicts the ratio of the

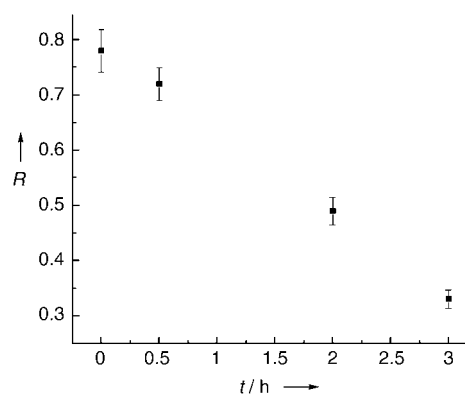


Figure 4. Plot showing the ratio R of hemiacetals to epoxide as a function of delay time before styrene adsorption/reaction. This ratio decreased with an increase in delay time. The intensities of the different species were obtained by integrating the area under corresponding peaks in the ^{13}C MAS NMR spectra.

hemiacetal species to epoxide as a function of delay time. The ratio decreased as the delay time increased, and after a 12-h delay, the hemiacetal species was no longer present (Figure 3).

We also followed the styrene oxidation by in situ EPR spectroscopy. Figure 5a shows the EPR spectra of sample **A** and UHP at room temperature with different delay times. Two distinct signals were observed, which indicated the existence of different Ti^{4+} sites in the mixture. The stronger signal ($g_x = 2.0023$, $g_y = 2.0090$, $g_z = 2.0280$) was assigned to the Ti-superoxo species from the interaction between the framework Ti and UHP. The other weak resonance at $g_z = 2.0200$ was caused by the $(\text{SiO})_2(\text{OH})\text{TiOO}^\cdot$ species, that is, the defects in the TS-1 zeolite^[12] or the superoxo anion dispersed on extra framework Ti sites.^[13] As time went on, the signal at $g_z = 2.0280$ gradually wore off, whereas the signal at $g_z = 2.0200$ remained almost unchanged, indicating that the Ti-superoxo species in the framework Ti sites was not stable and easily quenched. When this result is coupled with that from the NMR experiment, in which the ratio of hemiacetal to epoxide decreased with the delay time, it is clear that production of the hemiacetal species decreased with quenching of the Ti-superoxo species. Thus it is natural to conclude that the Ti-superoxo species was critical in the formation of the hemiacetal species, that is, it represents the active center for the formation of the hemiacetal species. To further support this conclusion, different amounts of styrene were

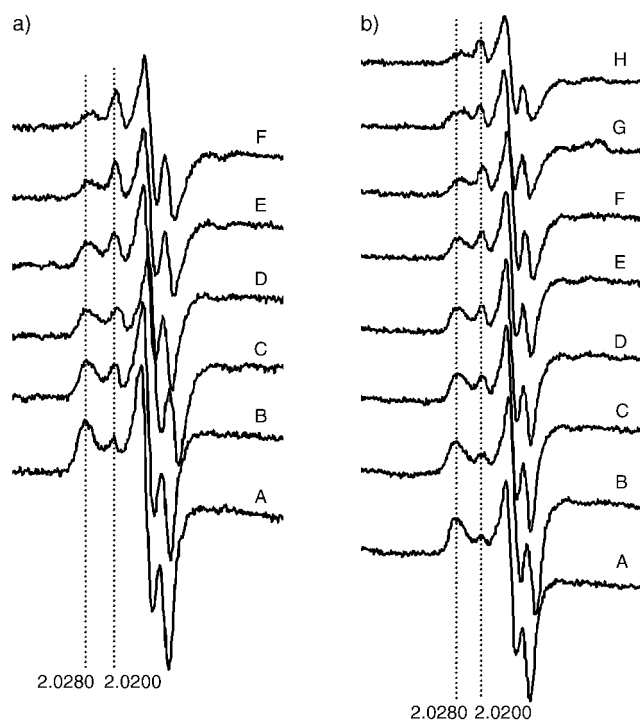
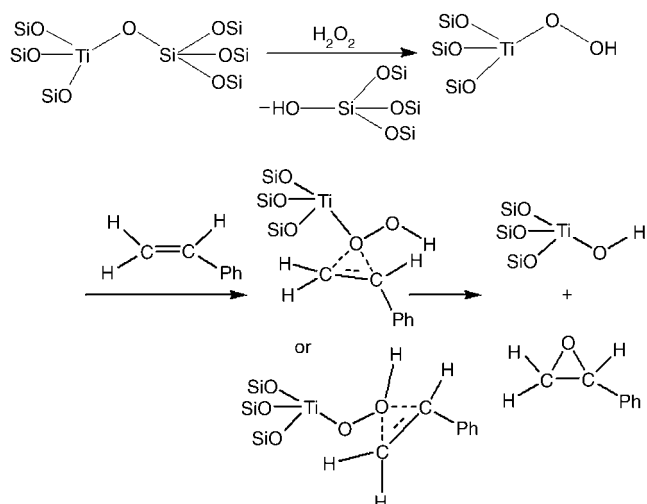


Figure 5. a) The EPR spectra of sample **A** after interaction with UHP at RT for different lengths of time: A) 0 min, B) 20 min, C) 30 min, D) 45 min, E) 55 min, F) 90 min. b) The EPR spectra of the reaction of sample **A** and UHP with different amounts of styrene: A) 0 mL, B) 0.05 mL, C) 0.10 mL, D) 0.15 mL, E) 0.20 mL, F) 0.25 mL, G) 0.50 mL, H) 0.75 mL.

added to the mixture of TS-1 and UHP at 293 K (without delay time). Indeed, the signal at $g_z = 2.0280$ decreased in intensity as the Ti-superoxo species was consumed by the additional styrene, whereas the signal at $g_z = 2.0200$ remained almost intact (Figure 5b). This again proved that the Ti superoxo radical species formed on tetrapodal Ti ions was involved in the oxidation of styrene and is responsible for the formation of the hemiacetal species.

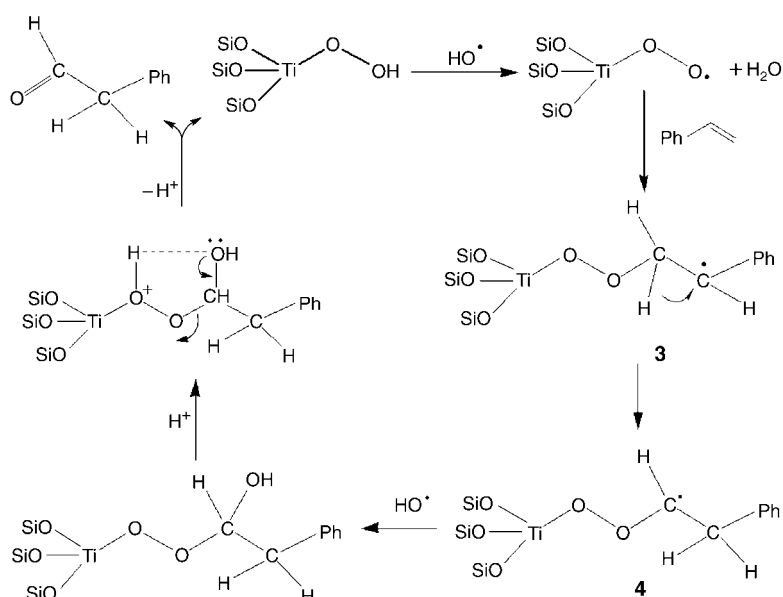
It is generally accepted that the first step in the oxidation by the TS-1/ H_2O_2 system is the formation of the TiOOH species, the species responsible for the epoxidation.^[1b,2d,14] While the production of the epoxide species was not disturbed by a delay in reaction, it is clear that it is formed at a different active center than the hemiacetal species, the precursor of PADH. This is different from previous studies that suggested that PADH is just the rearrangement product of epoxide.^[4] As TiOOH is the precursor for the generation of the Ti-superoxo species (by the reaction $\text{TiOOH} + \text{HO}^\bullet \rightarrow \text{TiOO}^\bullet + \text{H}_2\text{O}$),^[15] the epoxidation and the radical reaction to form the hemiacetal/PADH are competitive processes.

Based on these results and the theoretical calculations (see the Supporting Information), a mechanism for the oxidation of styrene is



Scheme 1. The proposed mechanism for the formation of TiOOH and styrene epoxide.

proposed (Schemes 1 and 2). First, the framework Ti species (which may be distorted^[16]) reacts with H_2O_2 to form TiOOH . Second, TiOOH either oxidizes styrene to styrene epoxide or reacts with the OH^\bullet radical (generated from the decomposition of H_2O_2) to form the Ti-superoxo radical species. Third, the superoxo species interacts with the C–C double bond of styrene to form a new organic radical **3**, which is immediately converted into another radical **4** through hydrogen transfer from the β -C atom to the α -C atom of the styrene side chain. According to the theoretical calculations this process is thermodynamically favorable (see the Supporting Information). Finally, the OH^\bullet radical terminates the chain reactions and form the hemiacetal species (^{13}C MAS NMR signal at $\delta = 102.2$ ppm). Without Brønsted acid sites (as with sample **A**,



Scheme 2. The proposed mechanism for the radical reaction leading to the hemiacetal species and PADH.

Figure 1) the hemiacetal species is stable on the catalyst surface and with Brønsted acid sites (sample **B**) it is converted into aldehyde and then released from the zeolite framework (Figure 2). At the same time, TiOOH is recovered and thus the catalytic cycle is accomplished.

In summary, the mechanism of styrene oxidation by TS-1/UHP is discussed in detail. It was verified that the Ti-superoxo radical is responsible for the formation of the hemiacetal species, while Brønsted acid sites offer the active centers for the transformation of the hemiacetal species to PADH. Without these Brønsted sites, the hemiacetal species remain stable on the framework of TS-1, and accordingly no PADH is formed. Therefore, styrene epoxide and PADH are formed by two competing processes: PADH does not result from further reaction of styrene epoxide, as previously suggested. Through the combination of experimental results and theoretical calculations, a more reasonable mechanism for styrene oxidation has been proposed.

Experimental Section

The two different TS-1 zeolites with (sample **B**) or without (sample **A**) Brønsted sites were synthesized according to a BASF Aktiengesellschaft patent (WO 01/14251). X-ray diffraction confirmed the MFI structure of both samples. Chemical analysis was performed with a SRS 3400 X-ray fluorescence spectrometer. The overall SiO₂/TiO₂ ratios of these samples are 50 (sample **A**) and 52 (sample **B**).

The acidity in the samples was characterized by ³¹P MAS NMR spectroscopy of trimethylphosphane (TMP) adsorbed on TS-1 zeolites. The samples were dehydrated by heating at 673 K under vacuum (below 10⁻² Pa) for 20 h. The adsorption of TMP (Acros Organics) was performed by exposing the dehydrated sample to a saturated vapor pressure at room temperature for 30 min. Each sample was then evacuated for 20 min to remove the TMP physisorbed on the surface. The sample was then filled into an NMR rotor and sealed without exposure to air.

In situ ¹³C MAS NMR spectra were measured by adsorbing β-¹³C-rich styrene (Cambridge Co.) on samples **A** and **B** with a homemade device. Before adsorption the samples were dehydrated by heating at 673 K under vacuum (below 10⁻² Pa) for 20 h and then used directly or mixed with urea-hydroperoxide (Acros Organics) uniformly under N₂. The mixture was evacuated at room temperature for 5 min and styrene was then loaded at -196 °C (liquid nitrogen). The sample was evacuated for 20 min to remove physisorbed styrene. Subsequently, it was treated at 313 K for a precisely controlled period of time, and then packed into the rotor.

All NMR spectra were obtained at room temperature on a Bruker DRX-400 spectrometer with a BBO MAS probe using 4-mm ZrO₂ rotors. The ³¹P MAS NMR spectra with high-power proton decoupling were obtained at 161.9 MHz by using a 2.0-μs pulse, 2-s repetition time, and 1024–2048 scans; the samples were spun at 6 kHz and referenced to 85% H₃PO₄. The ¹³C MAS NMR measurements were made at 100.6 MHz with high-power proton decoupling by using a 2-μs pulse and 2-s repetition time. For each ¹³C spectrum, 1600 free induction decays were accumulated with a sample spinning rate of 7 kHz. Adamantane was used as the reference of the chemical shift. The WINNMR program supplied by the instrument manufacturer was employed for spectral deconvolution by using Gaussian–Lorentzian lineshapes.

EPR spectra were recorded on a JEOL ES-EDX3 spectrometer. Prior to the measurements, the samples (100 mg) were dehydrated at 673 K for 2 h under He and then mixed with 30 mg of UHP. The EPR spectra were recorded at room temperature, operating at an X-band

frequency of 9.42 GHz and 100 kHz field modulation with a microwave power of 1 mW. The g factors were calculated by taking the signal of manganese as standard.

Received: June 29, 2004

Keywords: EPR spectroscopy · heterogeneous catalysis · NMR spectroscopy · styrene oxidation · zeolites

- [1] a) D. R. C. Huybrechts, L. De Braycker, P. A. Jacobs, *Nature* **1990**, 345, 240; b) M. G. Clerici, P. Ingallina, *J. Catal.* **1993**, 140, 71; c) J. Q. Zhuang, D. Ma, Z. M. Yan, X. M. Liu, X. Han, X. Bao, Y. Zhang, X. Guo, X. Wang, *Appl. Catal. A* **2004**, 258, 1; d) A. Thangaraj, R. Kumar, P. Ratnasamy, *J. Catal.* **1991**, 131, 294; e) A. Thangaraj, S. Sivasanker, P. Ratnasamy, *J. Catal.* **1991**, 131, 394.
- [2] a) M. Taramasso, G. Perego, B. Notari, US Patent 4410501, **1983**; b) G. Tozzola, M. A. Mantegazza, G. Ranghino, G. Petrini, S. Bordiga, G. Ricchiardi, C. Lamberti, R. Zulian, A. Zecchina, *J. Catal.* **1998**, 179, 64; c) G. N. Vayssilov, *Catal. Rev.* **1997**, 39, 209; d) S. Bordiga, A. Damin, F. Bonino, G. Ricchiardi, C. Lamberti, A. Zecchina, *Angew. Chem.* **2002**, 114, 4928; *Angew. Chem. Int. Ed.* **2002**, 41, 4734; e) P. E. Sinclair, C. R. A. Catlow, *J. Phys. Chem. B* **1999**, 103, 1084; f) P. F. Henry, M. T. Weller, C. C. Wilson, *J. Phys. Chem. B* **2001**, 105, 7452.
- [3] a) S. B. Kumar, S. P. Mirajkar, G. C. G. Pais, P. Kumar, *J. Catal.* **1995**, 156, 163; b) M. A. Uguina, D. P. Serrano, R. Sanz, J. L. G. Fierro, M. Lopez Granados, R. Mariscal, *Catal. Today* **2000**, 61, 263.
- [4] a) S. L. Laha, R. Kumar, *J. Catal.* **2001**, 204, 64; b) G. Bellussi, A. Carati, M. G. Clerici, G. Maddinelli, R. Millini, *J. Catal.* **1992**, 133, 220.
- [5] G. R. Wang, B. Wang, X. F. Zhang, Y. Z. Wang, H. O. Liu, X. W. Guo, X. S. Wang, *J. Dalian Univ. Technol.* **2000**, 40, 160.
- [6] W. Y. Lin, H. Frei, *J. Am. Chem. Soc.* **2002**, 124, 9292.
- [7] M. Hunger, J. Weitkamp, *Angew. Chem.* **2001**, 113, 3040; *Angew. Chem. Int. Ed.* **2001**, 40, 2954.
- [8] a) C. A. Fyfe, Y. Feng, H. Grondey, G. T. Kokotailo, H. Gies, *Chem. Rev.* **1991**, 91, 1525; b) I. I. Ivanova, E. G. Derouane, *Stud. Surf. Sci. Catal.* **1994**, 85, 357.
- [9] a) E. Karlsen, K. Schoffel, *Catal. Today* **1996**, 32, 107; b) M. Neurock, L. E. Manzer, *Chem. Commun.* **1996**, 1133.
- [10] a) D. Srinivas, P. Manikandan, S. C. Laha, R. Kumar, P. Ratnasamy, *J. Catal.* **2003**, 217, 160; b) S. C. Laha, R. Kumar, *J. Catal.* **2002**, 208, 339.
- [11] J. March, *Advanced Organic Chemistry: Reactions, Mechanisms and Structure*, McGraw-Hill, New York, **1977**, p. 804.
- [12] G. Sanker, J. M. Thomas, C. R. A. Catlow, C. M. Barker, D. Gleeson, N. Kaltsoyannis, *J. Phys. Chem. B* **2001**, 105, 9028.
- [13] Q. Zhao, X. H. Bao, Y. Wang, L. W. Lin, G. Li, X. W. Guo, X. S. Wang, *J. Mol. Catal. A* **2000**, 157, 265.
- [14] B. Notari, *Adv. Catal.* **1996**, 41, 253.
- [15] F. Geobaldo, S. Bordiga, A. Zecchina, E. Giamello, G. Leofanti, G. Petrini, *Catal. Lett.* **1992**, 16, 109.
- [16] J. Q. Zhuang, D. Ma, Z. M. Yan, F. Deng, X. M. Liu, X. W. Han, X. H. Bao, X. Wu Liu, X. Guo, X. Wang, *J. Catal.* **2004**, 221, 670.

Carbene Complexes

A Bis(thiophosphinoyl)methanediide Palladium Complex: Coordinated Dianion or Nucleophilic Carbene Complex?*

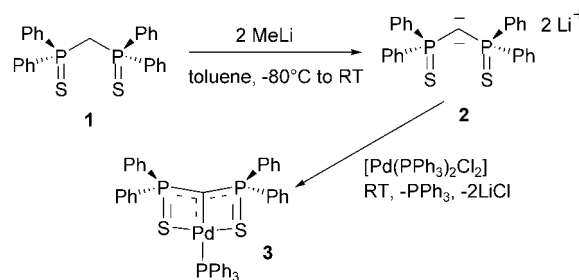
Thibault Cantat, Nicolas Mézailles, Louis Ricard, Yves Jean,* and Pascal Le Floch*

Transition-metal carbene complexes are one of the most widely studied organometallic species because of their high activity in numerous catalytic processes.^[1] Most efforts were recently focused on the synthesis of isolable free carbene ligands.^[2] However, new and rapid synthetic strategies allowing the generation of new carbenes in the coordination sphere of metals from easily available and cheap precursors have yet to be developed. In this perspective, phosphorus-substituted methane derivatives have attracted the attention of many groups as potential precursors.^[3,4] Besides the particular electronic properties of phosphorus, which markedly differ from that of their nitrogen counterparts, the interest of such derivatives also resides in the possibility of using phosphorus as an anchor for other heteroatoms through oxidation of its lone pair. This approach was elegantly demonstrated by Cavell and co-workers who successfully developed the chemistry of bis(iminophosphorano)methanediide complexes.^[5]

As part of a program aimed at exploring the use of thiophosphinoyl ligands in coordination chemistry and catalysis^[6] we recently explored the possibility of generating analogous carbene complexes from the bis(diphenylthiophosphinoyl)methane ligand. This work was also motivated by the tendency of thiophosphinoyl ligands to favor coordination of electron-rich metal centers. Furthermore, sulfur ligands were rarely employed as ancillary ligands in carbene chemistry.^[7] Herein, we report a new type of pincer ligand featuring a formal “carbenic” atom and two ancillary sulfide ligands.

The new dianion **2** was readily synthesized in quantitative yield through a double deprotonation of the methylene group in **1** using MeLi in toluene at low temperature (Scheme 1) following a similar procedure to that used for the deprotonation of bis(diphenyl-*N*-trimethylsilylphosphinimino)-methane.^[8] Formation of **2** was evidenced by vigorous evolution of methane at room temperature and the formation, over two hours, of a yellow turbid mixture. Dianion **2** which is highly

sensitive towards moisture gives rise to a singlet in the ³¹P NMR spectrum at $\delta = 20.6$ ppm (121.5 MHz, toluene, 25 °C, 85 % H₃PO₄ as external standard) and was used without purification for further reactions. The reaction of **2** with [(PPh₃)₂PdCl₂] yielded a burgundy red solution and a red precipitate. The ³¹P NMR spectrum of the new species is highly diagnostic. Indeed the new complex **3** gives rise to an AX₂ spin system ($\delta(A) = 21.5$ ppm; $\delta(X_2) = +39.8$ ppm, CD₂Cl₂, 298 K) revealing a symmetrical structure featuring three phosphorus atoms (Scheme 1).



Scheme 1.

After work-up aimed at eliminating the LiCl salt formed and the free PPh₃ ligand, complex **3** was fully characterized by NMR spectroscopic techniques (¹H and ¹³C) and elemental analyses. Though no ¹³C NMR signal could be recorded for the carbenic carbon atom (as was reported by Cavell and co-workers for some carbene complexes^[5g,h]), the absence of methylenic protons was confirmed by both ¹H and ¹³C NMR spectroscopy. Fortunately, X-ray-quality red crystals of **3** were obtained either from a concentrated CH₂Cl₂ solution or by diffusion of hexanes into a CH₂Cl₂ solution of the complex (Figure 1).^[9] Complex **3** was found to be remarkably resistant to moisture and it crystallizes with a molecule of CH₂Cl₂ a situation which already points towards a weak nucleophilic character. The shortest distances between the solvent and the C1 and Pd atoms are 5.0 and 5.9 Å, respectively.

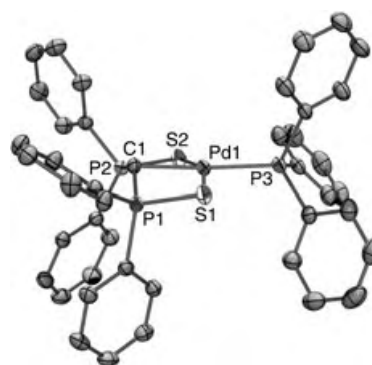


Figure 1. View of one molecule of **3** (thermal ellipsoids set at 50% probability). The hydrogen atoms and cocrystallized CH₂Cl₂ are omitted for clarity. Selected bond lengths [Å] and angles [°]: Pd1–C1 2.113(2), C1–P1 1.689(2), C1–P2 1.690(2), Pd1–S1 2.3741(6), Pd1–S2 2.3677(6), Pd1–P3 2.3030(6), P1–S1 2.0451(7), P2–S2 2.0424(8); P1–C1–P2 139.2(1), C1–Pd1–S1 80.63(6), S1–Pd1–P3 96.45(2), P3–Pd1–S2 103.78(2), S2–Pd1–C1 80.91(6), C1–Pd1–P3 174.61(6), S1–Pd1–S2 158.42(2).

[*] T. Cantat, Dr. N. Mézailles, Dr. L. Ricard, Prof. Y. Jean, Prof. P. Le Floch

Laboratoire Hétéroéléments et Coordination
UMR CNRS 7653 (DCPH)
Département de Chimie
Ecole Polytechnique
91128 Palaiseau cedex (France)
Fax: (+33) 1-6933-3990
E-mail: yves.jean@poly.polytechnique.fr
lefloch@poly.polytechnique.fr

[**] This work was supported by the CNRS and the Ecole Polytechnique.

Supporting information for this article is available on the WWW under <http://www.angewandte.org> or from the author.

The structure of **3** definitely establishes the presence of a central tricoordinate carbon atom that is bound to the Pd center and the two PPh₂S groups. However, the relatively long C1–Pd separation (2.113(2) Å) rules out the formation of a true double bond (2.005 Å).^[7] This bond is shorter than a classical single Pd–C bond (about 2.15 Å). Moreover, even though the overall geometry around the palladium center is square planar, the angle between the Pd–C1 bond and the plane defined by the “carbene moiety” measures 102.0°. Thus in **3**, the metal center seems to be located in a quasiperpendicular plane to the carbene fragment. Similar distortions, but to a lesser extent (angles varying between 0 and 37.7°), were also observed in some of Cavell’s complexes.^[5e] A striking feature is the very short P–C1 bonds of 1.689(2) and 1.690(2), which are similar to bond lengths found in carbodiphosphoranes and their complexes.^[10] These short bonds very likely result from negative hyperconjugation from carbon to phosphorus σ* orbitals. How can this geometry be rationalized? ONIOM calculations were carried out on the real system using the Gaussian03 set of programs^[11] (all phenyl groups were calculated at the MM level and the other atoms at the MQ level of theory).^[12] Theoretical data are very similar to those given by X-ray crystallography with the exception of the P–S bond lengths which were found to be slightly longer.

The electronic structure of **3** can be rationalized by looking at the molecular orbital (MOs) which involve the n_p and n_o nonbonding orbitals on the carbenic center.^[13] Owing to the almost perpendicular orientation of the carbene ligand, the sigma bonding MO results from the interaction between the n_p orbital and a metal-centered orbital directed along the Pd–C axis. This doubly occupied MO characterizes a σ Pd–C bond since its antibonding counterpart (the LUMO of the complex) is vacant (Figure 2, right). The n_o orbital interacts

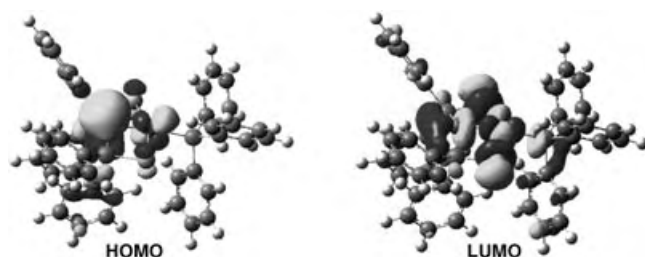


Figure 2. HOMO and LUMO of the theoretical structure of **3** as given by DFT calculations.

with the d_{xz} orbital through a π-type overlap. Note that both the bonding and the antibonding combinations are occupied, the latter being the HOMO of the complex (Figure 2, left). Therefore the π interaction does not lead to any π bonding character between the Pd and C1 centers. The bonding picture which emerges from this six-electron four-orbital analysis is that there is: 1) a single (σ) metal–carbon bond involving the n_p orbital on the carbenic center and 2) two nonbonding electron pairs on Pd and C1, the electron pair on the carbenic center is located approximately in the plane of the carbene (n_o orbital). A way to understand this particular electronic

structure is to consider that the complex results from the interaction between a d¹⁰PdL₃ fragment and a neutral carbene (Figure 3): an occupied MO of the metal fragment interacts with the vacant n_p orbital, leading to a nearly perpendicular orientation of the carbene ligand (distorted “open book” conformation).^[5e] A four-electron interaction develops between the n_o and d_{xz} orbitals.

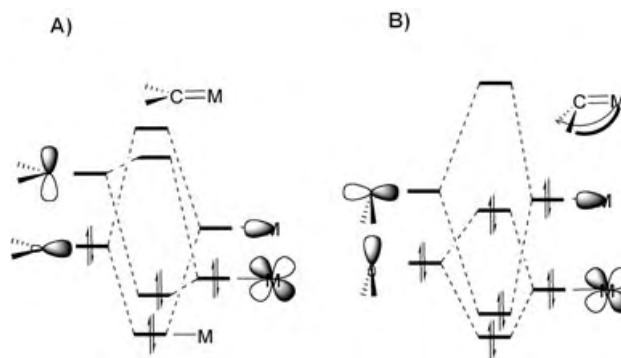


Figure 3. A) Usual bonding mode in carbene complexes, B) electronic situation in **3** assuming a d¹⁰PdL₃ fragment.

Or, one can assume the two electrons of the σ bond to be associated to the carbenic ligand as is usual for electron counting in transition-metal complexes. Then, the whole complex can be described as a d⁸ [PdL₃]²⁺ metal fragment interacting with a dianionic carbenic center. A further interpretation is found by using the isolobal analogy. The T-shape d¹⁰PdL₃ fragment is isolobal to CH₃[−], so that complex **3** is analogous to the CH₃–CH₂[−] ion (Figure 4) with a single C–C bond and a lone pair on the pyramidalized methylene moiety.^[14]

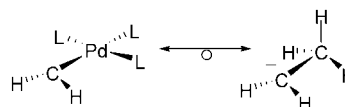
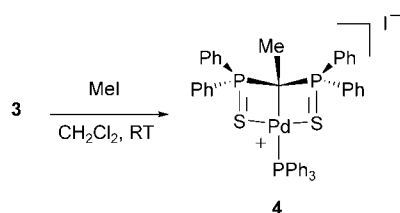


Figure 4. By the isolobal analogy complex **3** is analogous to the CH₃–CH₂[−] ion.

The nucleophilic character of the carbenic atom was confirmed by NBO calculations ($q_C = -1.39$ and $q_{Pd} = +0.37$). To demonstrate the presence of a reactive lone pair on this “carbenic” carbon atom, complex **3** was treated with various electrophiles. For example, the reaction with MeI, which was carried out in CH₂Cl₂ at room temperature, exclusively takes place on the carbon atom. The cationic complex **4** formed was isolated in a quantitative yield (Scheme 2).^[15]

This new complex was fully characterized by NMR spectroscopy, elemental analysis, and X-ray crystallography. Orange crystals of **4** were grown by a slow diffusion of hexanes into a dichloromethane solution of the complex (see Supporting Information).^[9] Interestingly, we note that the C–Pd bond in **4** (2.146(2) Å) is only slightly elongated with regard to **3** thus confirming the pronounced single-bond character of the C–Pd bond in **3** (2.113(2) Å). Theoretical



Scheme 2.

calculations using the ONIOM method (same level of theory than in **3**) yielded a structure which is very close to that experimentally observed. NBO calculations indicate that the palladium-bound carbon atom still bears a substantial negative charge ($q_C = -1.02$ and $q_{Pd} = +0.36$).

In conclusion, we have developed an easy synthetic access to a new type of nucleophilic “carbene” complex featuring two pendant thiophosphinoyl ancillary ligands. Theoretical calculations indicate that these new species can be either regarded as a coordinated dianion with a strong delocalization of the charge onto the two P–C bonds, or as a nucleophilic carbene complex.

Experimental Section

All experiments were carried out under dry argon or nitrogen atmosphere using distilled and degassed solvents.

3: Two equivalents of MeLi (0.84 mL, 1.6 M in diethyl ether, 1.34 mmol) were added to a solution of **1** (300 mg, 0.67 mmol) in toluene (5 mL) at -78°C . The mixture was warmed to room temperature and stirred for 2 h leading to the formation of a yellow suspension of **2**. Then $[\text{PdCl}_2(\text{PPh}_3)_2]$ (470 mg, 0.67 mmol) was added in one portion at room temperature. The resulting mixture immediately turned red and ^{31}P NMR spectroscopy showed the reaction to be complete by indicating the presence of complex **3** and PPh_3 . Complex **3** and LiCl are poorly soluble in toluene and were isolated by centrifugation. Pure complex **3** was finally obtained in 88% yield (480 mg, 0.59 mmol) after dissolution in CH_2Cl_2 (6 mL) followed by filtration to remove LiCl and evaporation of the solvent. Selected data: ^1H NMR (300 MHz, CD_2Cl_2 , 25°C): $\delta = 7.13\text{--}7.66$ ppm (m, 35 H; H of phenyl); $^{31}\text{P}\{^1\text{H}\}$ NMR (121.5 MHz, CD_2Cl_2 , 25°C , 85% H_3PO_4 as external standard): $\delta = 21.5$ (t, $^3J(\text{P,P}) = 14.6$ Hz; PPh_3), 39.8 ppm (d, $^3J(\text{P,P}) = 14.6$ Hz; PPh_2S); $^{13}\text{C}\{^1\text{H}\}$ NMR (75.465 MHz, CD_2Cl_2 , 25°C , CD_2Cl_2 $\delta = 53.73$ ppm as internal reference): $\delta = 125.4\text{--}139.1$ ppm (m; C of phenyl), C–Pd not observed; elemental analysis (%) calcd for $\text{C}_{43}\text{H}_{35}\text{P}_3\text{PdS}_2$: C 63.35, H 4.33, found: C 62.97, H 4.05.

4: Complex **4** was obtained by adding MeI (27 μL , 0.43 mmol) to a solution of **3** (350 mg, 0.43 mmol) in CH_2Cl_2 (10 mL) at room temperature. The mixture was stirred for five minutes and then taken to dryness. Complex **4** was thus isolated in a quantitative yield (100%, 410 mg, 0.43 mmol). Selected data: ^1H NMR (300 MHz, CD_2Cl_2 , 25°C): $\delta = 1.86$ (dt, $^3J(\text{H,P}) = 16.2$ Hz, $^4J(\text{H,P}) = 8.6$ Hz, 3 H; CH_3), 7.00–8.04 ppm (m, 35 H; H of phenyl); $^{31}\text{P}\{^1\text{H}\}$ NMR (121.5 MHz, CD_2Cl_2 , 25°C , 85% H_3PO_4 as external standard): $\delta = 22.8$ (t, $^3J(\text{P,P}) = 15.8$ Hz; PPh_3), 62.3 ppm (d, $^3J(\text{P,P}) = 15.8$ Hz; PPh_2S); $^{13}\text{C}\{^1\text{H}\}$ NMR (75.465 MHz, CD_2Cl_2 , 25°C , CD_2Cl_2 $\delta = 53.73$ ppm as internal reference): $\delta = 20.7$ (pq, $J(\text{C,P}) = 5.0$ Hz; CH_3), 125.6 (dt, $^1J(\text{C,P}) = 48.0$ Hz, $^2J(\text{C,P}) = 8.7$ Hz; C–Pd), 127.7–135.4 ppm (m; C of phenyl); elemental analysis (%) calcd for $\text{C}_{44}\text{H}_{38}\text{IP}_3\text{PdS}_2$: C 55.21, H 4.00; found: C 55.10, H 3.87.

Received: July 22, 2004

Revised: August 27, 2004

Keywords: carbenes · density functional calculations · palladium · phosphorus · sulfides

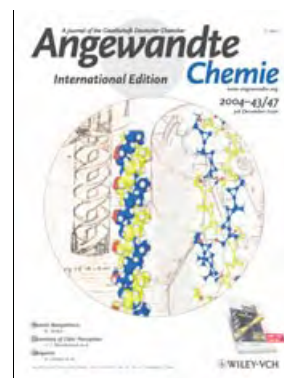
- [1] See for example: a) A. J. Arduengo III, *Acc. Chem. Res.* **1999**, 32, 913–921; b) W. A. Herrmann, T. Weskamp, V. P. W. Bohm, *Adv. Organomet. Chem.* **2001**, 48, 1–69; c) W. A. Herrmann, *Angew. Chem.* **2002**, 114, 1342–1363; *Angew. Chem. Int. Ed.* **2002**, 41, 1290–1309.
- [2] D. Bourissou, O. Guerret, F. P. Gabbaï, G. Bertrand, *Chem. Rev.* **2000**, 100, 39–91.
- [3] See for example: a) J. Ruiz, M. E. G. Mosquera, G. Garcia, E. Patron, V. Riera, S. Garcia-Granda, F. Van der Maelen, *Angew. Chem.* **2003**, 115, 4915–4919; *Angew. Chem. Int. Ed.* **2003**, 42, 4767–4771; b) T. Cantat, N. Mézailles, N. Maigrot, L. Ricard, P. Le Floch, *Chem. Commun.* **2004**, 1274–1275.
- [4] Phosphoniumphosphanylcarbene ions $[(\text{R}_2\text{P})(\text{R}_2\text{PH})\text{C}]^+$ exist as free species, see: M. Soleilhavoup, A. Baceiredo, O. Treutler, R. Ahlrichs, M. Nieger, G. Bertrand, *J. Am. Chem. Soc.* **1992**, 114, 10959–10961.
- [5] a) R. G. Cavell, R. P. Kamalesh Babu, A. Kasani, R. McDonald, *J. Am. Chem. Soc.* **1999**, 121, 5805–5806; b) R. P. Kamalesh Babu, R. McDonald, S. A. Drecker, M. Klobukowski, R. G. Cavell, *Organometallics* **1999**, 18, 4226–4229; c) R. P. Kamalesh Babu, R. McDonald, R. G. Cavell, *Organometallics* **2000**, 19, 3462–3465; d) K. Aparana, M. Ferguson, R. G. Cavell, *J. Am. Chem. Soc.* **2000**, 122, 726–727; e) R. G. Cavell, R. Kamalesh Babu, K. Aparana, *J. Organomet. Chem.* **2001**, 617–618, 158–169; f) K. Aparana, R. P. Kamalesh Babu, R. McDonald, R. G. Cavell, *Angew. Chem.* **2001**, 113, 4535–4537; *Angew. Chem. Int. Ed.* **2001**, 40, 4400–4402; g) N. D. Jones, G. Lin, R. A. Gossage, R. McDonald, R. C. Cavell, *Organometallics*, **2003**, 22, 2832–2841; h) G. Lin, N. D. Jones, A. Gossage, R. McDonald, R. G. Cavell, *Angew. Chem.* **2003**, 115, 4188–4191; *Angew. Chem. Int. Ed.* **2003**, 42, 4054–4057.
- [6] a) M. Doux, C. Bouet, N. Mézailles, L. Ricard, P. Le Floch, *Organometallics* **2002**, 21, 2785–2788; b) M. Doux, N. Mézailles, M. Melaimi, L. Ricard, P. Le Floch, *Chem. Commun.* **2002**, 1566–1567; c) M. Doux, N. Mézailles, L. Ricard, P. Le Floch, *Eur. J. Inorg. Chem.* **2003**, 3878–3894; d) M. Doux, N. Mézailles, L. Ricard, P. Le Floch, *Organometallics* **2003**, 22, 4624–4626; e) M. Doux, L. Ricard, F. Mathéy, P. Le Floch, N. Mézailles, *Eur. J. Inorg. Chem.* **2003**, 687–698.
- [7] N. Matsumura, J.-I. Kawano, N. Fukunishi, H. Inoue, *J. Am. Chem. Soc.* **1995**, 117, 3623.
- [8] a) A. Kasani, R. P. Kamalesh Babu, R. McDonald, R. G. Cavell, *Angew. Chem.* **1999**, 111, 1580–1582; *Angew. Chem. Int. Ed.* **1999**, 38, 1483–1484; b) C. M. Ong, D. W. Stephan, *J. Am. Chem. Soc.* **1999**, 121, 2939–2940.
- [9] Crystal data for **3** ($\text{C}_{43}\text{H}_{35}\text{P}_3\text{PdS}_2 \cdot \frac{1}{2}(\text{CH}_2\text{Cl}_2)$): space group $P2_1/c$, $a = 9.0270(10)$, $b = 36.1930(10)$, $c = 12.7440(10)$ Å, $\beta = 109.3620(10)^\circ$, $V = 3928.2(5)$ Å³, $Z = 4$, $\rho_{\text{calcd}} = 1.450$ g cm^{−3}, $F(000) = 1748$, $\text{MoK}\alpha$ radiation ($\lambda = 0.71073$ Å), $\mu = 0.800$ cm^{−1}; crystal dimensions $0.20 \times 0.10 \times 0.08$ mm. Data collection was performed on a Nonius KappaCCD single crystal diffractometer at $T = 150$ K. Crystal structure was solved with SIR97,^[16] refinement against F^2 (SHELXL97^[17]) with anisotropic thermal parameters for all non-hydrogen atoms, calculated hydrogen positions with riding isotropic thermal parameters. hkl ranges: $-6\ 12$; $-46\ 50$; $-17\ 17$, 22 119 reflections collected, 11 087 unique ($R_{\text{int}} = 0.0445$), 8922 data with $I > 2\sigma(I)$, 444 parameters refined, $\text{GOF}(F^2) = 1.013$, final R indices ($R1 = \Sigma |F_o| - |F_c| / \Sigma |F_o|$, $wR2 = [\Sigma w(F_o^2 - F_c^2)^2 / \Sigma w(F_c^2)^2]^{1/2}$, $R1 = 0.0403$, $wR2 = 0.1161$, max/min residual electron density $0.973(0.097)/-1.215(0.097)$ e Å^{−3}. Crystal data for **4** are given in the Supporting Information. CCDC-245083 (**3**) and CCDC-245084 (**4**) contains the supplementary crystallographic data for this paper. These data can be

- obtained free of charge via www.ccdc.cam.ac.uk/conts/retrieving.html (or from the Cambridge Crystallographic Data Centre, 12 Union Road, Cambridge CB2 1EZ, UK; fax: (+44) 1223-336-033; or deposit@ccdc.cam.ac.uk).
- [10] See for example: a) A. T. Vincent, P. J. Wheatley, *J. Chem. Soc. Dalton Trans.* **1972**, 617–622; b) G. E. Hardy, J. I. Zink, W. C. Kaska, J. C. Baldwin, *J. Am. Chem. Soc.* **1978**, *100*, 8001–8002; c) W. Petz, F. Weller, J. Uddin, G. Frenking, *Organometallics* **1999**, *18*, 619–626.
- [11] a) Gaussian03 (Revision A.1), M. J. Frisch, G. W. Trucks, H. B. Schlegel, G. E. Scuseria, M. A. Robb, J. R. Cheeseman, J. A. Montgomery, Jr., T. Vreven, K. N. Kudin, J. C. Burant, J. M. Millam, S. S. Iyengar, J. Tomasi, V. Barone, B. Mennucci, M. Cossi, G. Scalmani, N. Rega, G. A. Petersson, H. Nakatsuji, M. Hada, M. Ehara, K. Toyota, R. Fukuda, J. Hasegawa, M. Ishida, T. Nakajima, Y. Honda, O. Kitao, H. Nakai, M. Klene, X. Li, J. E. Knox, H. P. Hratchian, J. B. Cross, C. Adamo, J. Jaramillo, R. Gomperts, R. E. Stratmann, O. Yazyev, A. J. Austin, R. Cammi, C. Pomelli, J. W. Ochterski, P. Y. Ayala, K. Morokuma, G. A. Voth, P. Salvador, J. J. Dannenberg, V. G. Zakrzewski, S. Dapprich, A. D. Daniels, M. C. Strain, O. Farkas, D. K. Malick, A. D. Rabuck, K. Raghavachari, J. B. Foresman, J. V. Ortiz, Q. Cui, A. G. Baboul, S. Clifford, J. Cioslowski, B. B. Stefanov, G. Liu, A. Liashenko, P. Piskorz, I. Komaromi, R. L. Martin, D. J. Fox, T. Keith, M. A. Al-Laham, C. Y. Peng, A. Nanayakkara, M. Challacombe, P. M. W. Gill, B. Johnson, W. Chen, M. W. Wong, C. Gonzalez, J. A. Pople, Gaussian, Inc., Pittsburgh, PA, **2003**; b) The authors wish to thank the IDRIS center (University Paris-Sud XI Orsay, Institut du développement et des ressources en Informatiques Scientifique) for computational facilities.
- [12] Theoretical calculations were carried out using the ONIOM (B3PW91^[18]/UFF^[19]) method implemented in the Gaussian03 package. All the phenyl groups were considered as the second shell and were calculated using the UFF force field.^[18] The carbenic carbon atom, P, S, and Pd atoms were calculated using the B3PW91 functional. A 6-31+G* basis set was used for H and the 6-311+G** was used for the carbenic atom, S and P atoms. The quasirelativistic small-core ECP basis set (441/2111/31) developed by Hay–Wadt^[20] augmented with a f polarization function of exponent 1.472^[21] was used for the Pd atom. The same combination of basis set was chosen for calculation of the theoretical structure of **4** but the 6-31+G* basis set was used the H atoms of the methyl group.
- [13] Molecular orbitals of **3** were calculated at the MQ (B3PW91) level on the ONIOM structure using the 6-311+G** basis set for the carbenic atom, S, and P atoms and the 6-31G* for all phenyl groups (C and H atoms). Natural bond order (NBO) calculations were performed at the same level of theory for **3**.^[22] For the theoretical structure of **4**, the 6-31+G* basis set was used for calculating the H atoms of the methyl group.
- [14] An X-ray crystal analysis of a pyramidalized carbanion has been recently reported: F. Breher, J. Grunenberg, S. C. Lawrence, P. Mountford, H. Rügger, *Angew. Chem.* **2004**, *116*, 2575–2578; *Angew. Chem. Int. Ed.* **2004**, *43*, 2521–2524.
- [15] Complexes with an H atom replacing the methyl group have already been synthesized by trapping reactions of bis(imino-phosphorano)methanide anions with transition-metals fragments. a) S. Al-Benna, M. J. Sarsfield, M. Thornton-Pett, D. L. Ormsby, P. J. Maddox, P. Brès, M. Bochmann, *J. Chem. Soc. Dalton Trans.* **2000**, 4247–4257; b) D. A. Evans, M. S. Hill, P. B. Hitchcock, *Dalton Trans.* **2003**, 570–574.
- [16] A. Altomare, M. C. Burla, M. Camalli, G. Cascarano, C. Giacovazzo, A. Guagliardi, A. G. G. Moliterni, G. Polidori, R. Spagna, SIR97, an integrated package of computer programs for the solution and refinement of crystal structures using single crystal data, **1999**.
- [17] M. Sheldrick, SHELXL-97, Universität Göttingen, Göttingen, Germany, **1998**.
- [18] a) A. D. J. Becke, *J. Chem. Phys.* **1993**, *98*, 5648–5662; b) J. P. Perdew, Y. Wang, *Phys. Rev. B* **1992**, *45*, 13244–13249.
- [19] A. K. Rappé, C. J. Casewitt, K. S. Colwell, W. A. Goddard, W. M. Skiff, *J. Am. Chem. Soc.* **1992**, *114*, 10024–10035.
- [20] P. J. Hay, W. R. Wadt, *J. Chem. Phys.* **1985**, *82*, 299–310.
- [21] A. W. Ehlers, M. Böhme, S. Dapprich, A. Gobbi, A. Höllwarth, V. Jonas, K. F. Köhler, R. Stegman, A. Veldkamp, G. Frenking, *Chem. Phys. Lett.* **1993**, *208*, 111–113.
- [22] A. E. Reed, L. A. Curtiss, F. Weinhold, *Chem. Rev.* **1988**, *88*, 899–926.

Cover Picture

Armin de Meijere,* Alexander F. Khlebnikov, Sergei I. Kozhushkov, Kazutoshi Miyazawa, Daniel Frank, Peter R. Schreiner, B. Christopher Rinderspacher, Dmitrii S. Yufit, and Judith A. K. Howard

The rigid helical frameworks of the molecules of (*M*)-(-)-[7]triangulane-1,9-dimethanol associate through hydrogen bonds between their terminal hydroxy groups in supramolecular helices, two of which form a supramolecular double helix. In the cover picture, this is compared with the design by Leonardo da Vinci of a double-spiral staircase. The hydrocarbon (*M*)-(-)-[9]triangulane does not organize itself as a supramolecular double helix. For more information see the Communication by de Meijere et al. on page 6553 ff. The cover picture was created by Dipl.-Chem. Heiko Schill.



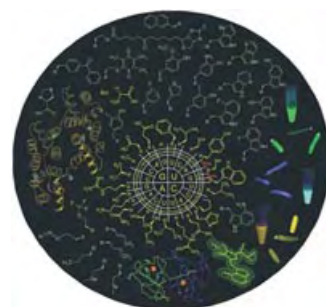
History of Science

The 100th anniversary is commemorated of the awarding of the Nobel Prize to Lord Rayleigh and Sir Ramsay for their discovery and characterization of the noble gases. J. M. Thomas describes in his Essay on page 6418 the important stages in the lives of these two great scientists.



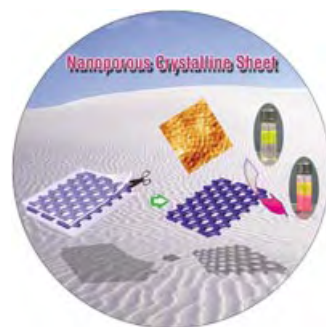
Protein Biosynthesis

In vitro and in vivo incorporation of noncanonical amino acids using an expanded genetic code and the perspectives of this method for the synthesis of tailor-made proteins are discussed in the Review by N. Budisa on p. 6426 ff.



Nanoporous Materials

Removal of the coil segments from an ordered rod-coil compound with a honeycomb-like structure to give a perforated crystalline sheet of hexagonally ordered nanopores is described by M. Lee and co-workers in their Communication on page 6466 ff.



Angewandte EarlyView®

The following Communications are available online (in Wiley InterScience). You can find them, as well as forthcoming Reviews, Highlights, and Essays, at www.angewandte.org, under Early View.

J. W. Yang, M. T. Hechavarria Fonseca, B. List*:

A Metal-Free Transfer Hydrogenation: Organocatalytic Conjugate Reduction of α,β -Unsaturated Aldehydes

DOI: 10.1002/anie.200461816

Published online: November 12, 2004

L. Kastrup, S. W. Hell*:

Absolute Optical Cross Section of Individual Fluorescent Molecules

DOI: 10.1002/anie.200461337

Published online: November 19, 2004

M. T. Kieber-Emmons, R. Schenker, G. P. A. Yap, T. C. Brunold, C. G. Riordan*:

Spectroscopic Elucidation of a Peroxo $\text{Ni}_2(\mu\text{-O}_2)$ Intermediate Derived from a Nickel(I) Complex and Dioxygen

DOI: 10.1002/anie.200460747

Published online: November 19, 2004

D. Fiedler, R. G. Bergman,* K. N. Raymond*:

Supramolecular Catalysis of a Unimolecular Transformation: Aza-Cope Rearrangement within a Self-Assembled Host

DOI: 10.1002/anie.200461776

Published online: November 19, 2004

Articles judged by the referees or the editor as being either very important or very urgent are immediately edited, proof-read, and electronically published once the manuscript has arrived in the editorial office in its final form. As long as there is no page number available these articles should be cited in the following manner:

Author(s), *Angew. Chem. Int. Ed.*, online publication date, DOI.

News

P. Yang Receives Pure Chemistry Award _____ **6406**

Inorganic Chemistry Award to W. J. Evans _____ **6406**

E. Iglesia Receives George A. Olah Award _____ **6406**

Books

Organic Chemistry Principles and Industrial Practice

Mark M. Green, Harold A. Wittcoff

reviewed by J. S. Siegel _____ **6407**

Protein Crystallography in Drug Discovery

Robert E. Babine, Sherin S. Abdel-Meguid

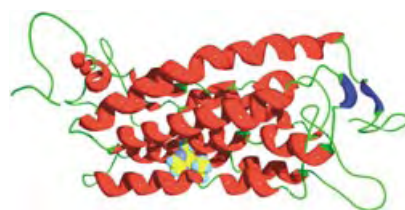
reviewed by L.-O. Essen _____ **6408**

Highlights

Chemistry of Odor Perception

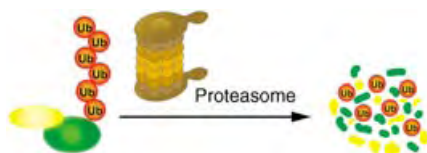
U. J. Meierhenrich,* J. Golebiowski, X. Fernandez, D. Cabrol-Bass _____ **6410–6412**

The Molecular Basis of Olfactory Chemoreception



The Nobel Prize in Medicine this year went to Richard Axel and Linda Buck, who

elucidated the molecular basis of the olfactory reception of fragrances and the neuronal preprocessing of information in the olfactory system. From the viewpoint of a chemist, these studies offer fascinating perspectives. For example, they enable an understanding of the perception of odors by transmembrane proteins (see picture).



The kiss of death for a protein is to be labeled with ubiquitin (Ub, see picture). The protein can then be recognized and

degraded by the 26S proteasome, an important target in drug research, as it regulates the concentration of certain proteins. Recognition by the proteasome is hindered by two novel proteasome inhibitors, ubistatins A und B, which were identified through a chemical genetic approach.

Proteasome Inhibitors

M. Biel, V. Wascholowski,
A. Giannis* _____ 6414–6416

A Fatal Affair: The Ubiquitinylation of Proteins



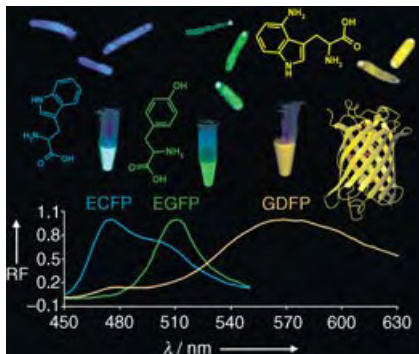
Noble gases and Nobel prizes: To mark the 100th anniversary of the awarding of the Nobel Prize to Lord Rayleigh (see picture; right) and Sir William Ramsay (left) for their discovery and characterization of the noble gases, tribute is paid to two scientific greats whose work goes far beyond their prize-winning discovery.

Essays

History of Science

J. M. Thomas* _____ 6418–6424

Argon and the Non-Inert Pair: Rayleigh and Ramsay



Room for one more: The genetic code of life consists of 64 coding units that control the incorporation of no more than 20 canonical amino acids in proteins—enough space remains for codon re-assignments, which render additional, noncanonical amino acids (see picture) translationally active substrates for the protein biosynthesis machinery. This review surveys methods, problems, and perspectives of this genetic code engineering.

Reviews

Protein Biosynthesis

N. Budisa* _____ 6426–6463

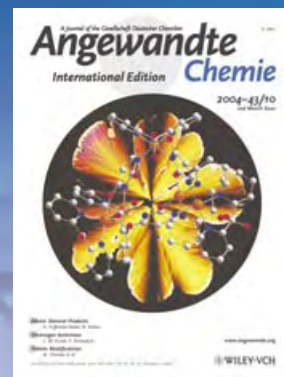
Prolegomena to Future Experimental Efforts on Genetic Code Engineering by Expanding Its Amino Acid Repertoire

For the USA and Canada:
ANGEWANDTE CHEMIE International Edition (ISSN 1433-7851) is published weekly by Wiley-VCH PO Box 191161, D 69451 Weinheim, Germany. Air freight and mailing in the USA by Publications Expediting Inc. 200 Meacham Ave., Elmont, NY 11003. Periodicals

postage paid at Jamaica NY 11431. US POSTMASTER: send address changes to *Angewandte Chemie*, Wiley-VCH, 111 River Street, Hoboken, NJ 07030. Annual subscription price for institutions: US\$ 4948.00/4498.00 (valid for print and electronic / print or electronic delivery); for individuals who are personal members of a

national chemical society, or whose institution already subscribes, or who are retired or self-employed consultants, print only: US\$ 394.00. Postage and handling charges included. All Wiley-VCH prices are exclusive VAT.

The best in chemistry – for more than hundred years



A Journal of the Gesellschaft Deutscher Chemiker
Angewandte
International Edition **Chemie**

www.angewandte.org

1888: The beginning
of a success story

Constant Innovations

- 1962:** First issue of the International Edition
- 1976:** Graphical abstracts
- 1979:** Cover pictures
- 1988:** Centenary of Angewandte
- 1989:** Routine use of color
- 1991:** New section: Highlights
- 1992:** Computerized editorial tracking system
- 1995:** Internet service for readers
- 1998:** Regular press service; full-text online
- 2000:** New section: Essays; EarlyView: Communications available online ahead of the printed version
- 2001:** New section: Microreviews
- 2002:** Online submission of manuscripts
- 2003:** Weekly publication; new section: News; new layout
- 2004:** Backfiles (1962-1997); ManuscriptXpress: Online system for authors and referees



Angewandte's advisors...

K.C. Nicolaou

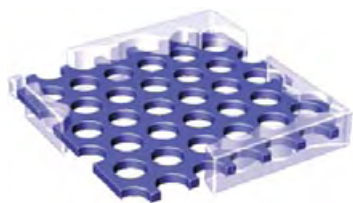
The Scripps Research Institute
and University of California
San Diego (La Jolla, USA)

» Angewandte Chemie has been highly influential in shaping the art of publishing chemical innovations and I feel privileged to be part of its Advisory Board. Eliciting admiration and respect from both readers and authors alike, its editorial staff should be commended for creating a new and exciting image of this most admired journal. «

Angewandte Chemie International Edition is
a journal of the German Chemical Society (GDCh)



Communications



Self-assembly of rod-coil molecules with an ester linkage gave a honeycomblike supramolecular structure with 3D hexagonal symmetry. Hydrolysis of the ester linkages and removal of the coil segments (light blue) from the perforated lamellar structure afforded crystalline sheets (dark blue) with in-plane arrays of nanopores whose hydrophobic interiors entrap nonpolar molecules.

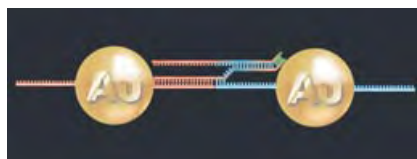
Nanoporous Sheets

M. Lee,* M.-H. Park, N.-K. Oh, W.-C. Zin, H.-T. Jung, D. K. Yoon — 6465 – 6468

Supramolecular Crystalline Sheets with Ordered Nanopore Arrays from Self-Assembly of Rigid-Rod Building Blocks

Switchable formation of materials:

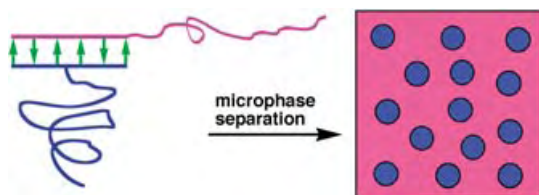
DNA-modified gold nanoparticles can aggregate reversibly by the employment of “fueling” oligomers that hybridize with the linker oligomers within the aggregated nanoparticles (see scheme). This approach paves the way to the generation of programmable functional materials.



Nanobiotechnology

P. Hazarika, B. Ceyhan, C. M. Niemeyer* — 6469 – 6471

Reversible Switching of DNA–Gold Nanoparticle Aggregation



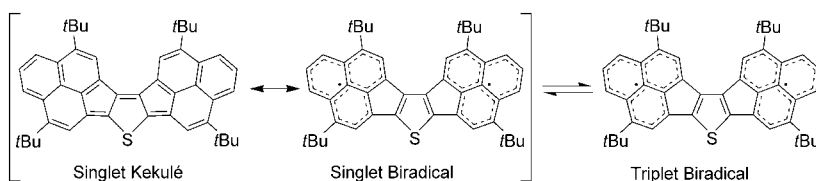
Hydrogen-bonded duplexes of incompatible polystyrene and poly(ethylene glycol) chains have been prepared that show microphase separation (see picture). Differential scanning calorimetric studies of

the phase transitions for these copolymers show that they behave like typical covalently bonded diblock copolymers at temperatures below 170 °C.

Polymer Chemistry

X. Yang, F. Hua, K. Yamato, E. Ruckenstein, B. Gong,* W. Kim, C. Y. Ryu* — 6471 – 6474

Supramolecular AB Diblock Copolymers



A phenalenyl-based singlet biradical that shows highly amphoteric redox properties (see scheme) has been prepared by a stepwise synthesis. Its singlet biradical

character originates from a small HOMO–LUMO gap, as suggested by quantum chemical calculations and experimental data.

Radical Reactions

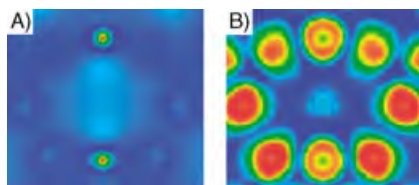
T. Kubo,* M. Sakamoto, M. Akabane, Y. Fujiwara, K. Yamamoto, M. Akita, K. Inoue, T. Takui, K. Nakasuji* — 6474 – 6479

Four-Stage Amphoteric Redox Properties and Biradicaloid Character of Tetra-*tert*-butyldicyclopenta[*b*; *d*]thieno[1,2,3-*cd*; 5,6,7-*c'**d'*]diphenalene

Inorganic Electrides

Z. Li, J. Yang,* J. G. Hou,
Q. Zhu ————— 6479–6482

Is Mayenite without Clathrated Oxygen an Inorganic Electride?

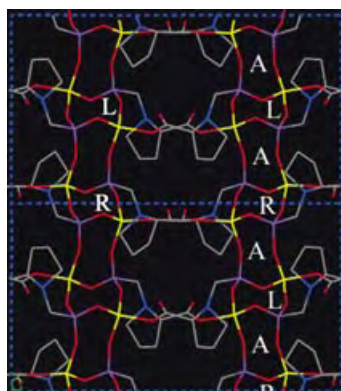


Yes or no? Mayenite without the clathrated oxygen *can* be classified as an inorganic electride based on combined charge-density (see picture, A) and electron-localization-function (ELF) analysis (B). Ionic chemical bonds are found to form between extra electrons and the positively charged crystal framework in this material.

Chiral Coordination Polymer

X. Shi, G. Zhu, S. Qiu,* K. Huang, J. Yu,
R. Xu ————— 6482–6485

$\text{Zn}_2[(S)\text{-O}_3\text{PCH}_2\text{NHC}_4\text{H}_7\text{CO}_2]_2$:
A Homochiral 3D Zinc Phosphonate with Helical Channels



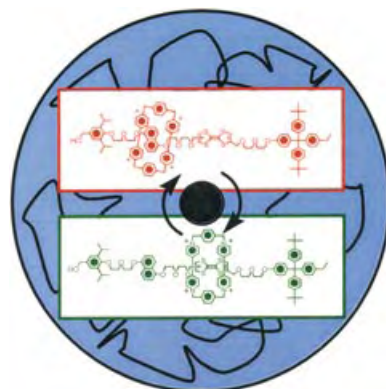
Three types of channel—right- (R) and left-handed (L) helical, and achiral (A)—alternate along the *c* axis in the structure of the title compound (see picture). The catalytically active groups of the 1-phosphonomethylproline ligands are directed into the channels, thus suggesting applications of this material in asymmetric catalysis.

Molecular Switches

D. W. Steuerman, H.-R. Tseng, A. J. Peters,
A. H. Flood, J. O. Jeppesen, K. A. Nielsen,
J. F. Stoddart,* J. R. Heath* 6486–6491

Molecular-Mechanical Switch-Based
Solid-State Electrochromic Devices

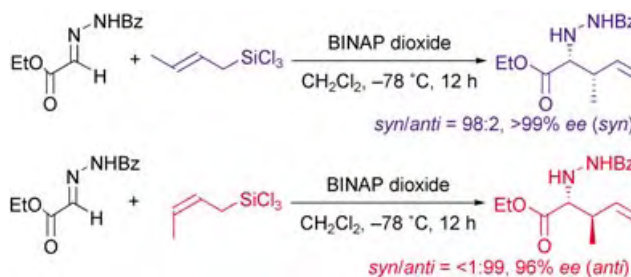
You only need eyes to appreciate the color change that occurs in a polymer matrix when the bistable rotaxane shown is switched between its ground-state (green) and metastable-state (red) co-conformers. Not only is an electrochromic device within reach, but a universal switching mechanism seems to be on the cards.



Asymmetric Synthesis

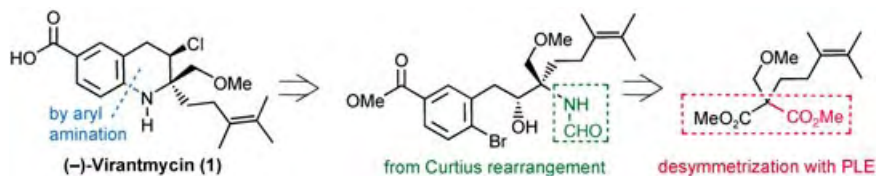
C. Ogawa, M. Sugiura,
S. Kobayashi* ————— 6491–6493

Stereospecific, Enantioselective Allylation of α -Hydrazono Esters by Using Allyltrichlorosilanes with BINAP Dioxides as Neutral-Coordinate Organocatalysts



Excellent diastereo- and enantioselectivities were obtained in the title reaction. (*E*)-Crotylsilanes gave *syn* adducts,

whereas *anti* adducts were obtained from (*Z*)-crotylsilanes (see scheme).



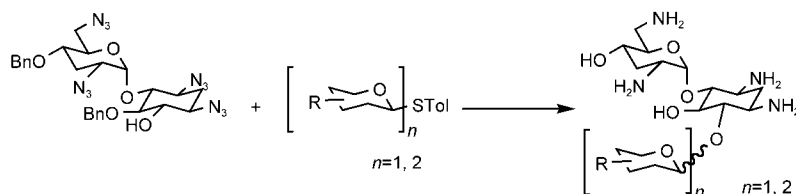
Both enantiomers of the antiviral agent virantmycin were synthesized in a sequence of reactions in which the key steps were a highly stereoselective porcine liver esterase (PLE) mediated desymmetrization of a prochiral diester and a

remarkably effective intramolecular aryl amination of an *ortho*-substituted aryl bromide with a highly hindered α -quaternary formamide (see retrosynthetic scheme).

Stereoselective Synthesis

T. G. Back,* J. E. Wulff — 6493 – 6496

A Stereodivergent Synthesis of Virantmycin by an Enzyme-Mediated Diester Desymmetrization and a Highly Hindered Aryl Amination



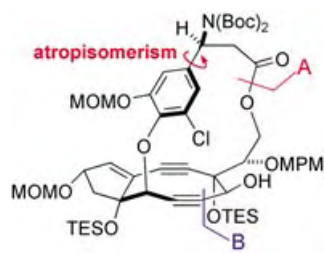
A library of 4,6-linked analogues of the drug tobramycin with various mono- or diaminosugars attached to the 6-position of the two-ring core has been prepared (see scheme; Bn = benzyl, Tol = *p*-tolyl).

The compounds were screened against different disease-related RNAs, and several of the synthetic analogues showed a high affinity and selectivity toward certain RNA sequences.

RNA Binding

F.-S. Liang, S.-K. Wang, T. Nakatani, C.-H. Wong* — 6496 – 6500

Targeting RNAs with Tobramycin Analogues

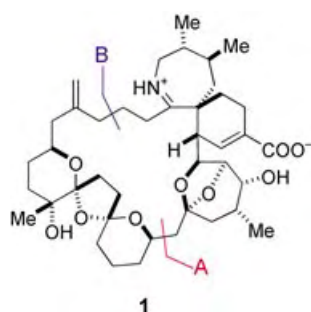


Long-range steric interactions of the protecting groups of the 1,5-diol were harnessed for the successful atropselective macrolactonization (A) in the synthesis of the C-1027 chromophore framework (see scheme). Subsequent $\text{LiN}(\text{SiMe}_3)_2/\text{CeCl}_3$ -promoted acetylide addition to an aldehyde (B) in the setting of a rigid macrocycle formed the target nine-membered ring system with a highly strained diyne.

Natural Products Synthesis

M. Inoue,* T. Sasaki, S. Hatano, M. Hirama* — 6500 – 6505

Synthesis of the C-1027 Chromophore Framework through Atropselective Macrolactonization



Powerful dithiane coupling (A) of two fragments and subsequent macrocyclization by ring-closing metathesis (B) produced the entire 27-membered carbocycle of (+)-pinnatoxin A (1), a major toxic principle responsible for outbreaks of shellfish poisonings in China and Japan.

Natural Products Synthesis

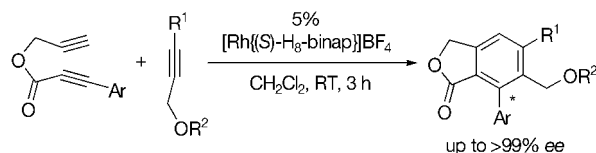
S. Sakamoto, H. Sakazaki, K. Hagiwara, K. Kamada, K. Ishii, T. Noda, M. Inoue,* M. Hirama* — 6505 – 6510

A Formal Total Synthesis of (+)-Pinnatoxin A

Biaryl Compounds

K. Tanaka,* G. Nishida, A. Wada,
K. Noguchi ————— 6510–6512

Enantioselective Synthesis of Axially Chiral Phthalides through Cationic $[\text{Rh}^I(\text{H}_8\text{-binap})]$ -Catalyzed Cross Alkyne Cyclotrimerization



Easy access to axially chiral phthalides that bear one or two oxymethylene functionalities is provided by an enantioselective cross alkyne cyclotrimerization in the

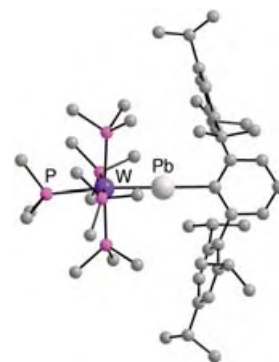
presence of the cationic complex $[\text{Rh}^I\{(\text{S})\text{-H}_8\text{-binap}\}]^+$. The axial chirality is introduced during the formation of the benzene ring with high enantioselectivity.

Lead Complexes

A. C. Filippou,* N. Weidemann,
G. Schnakenburg, H. Rohde,
A. I. Philippopoulos ————— 6512–6516

Tungsten–Lead Triple Bonds: Syntheses, Structures, and Coordination Chemistry of the Plumbidyne Complexes $\text{trans-[X(PMe}_3)_4\text{W=Pb(2,6-Trip}_2\text{C}_6\text{H}_3)]}$

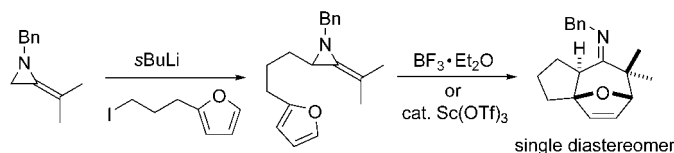
Plumb line: A series of compounds $\text{trans-[L(PMe}_3)_4\text{W=Pb(2,6-Trip}_2\text{C}_6\text{H}_3)]^{n+}$ ($n = 0$: $\text{L} = \text{Br, I}$; $n = 1$: $\text{L} = \text{PhCN, PMe}_3$; $\text{Trip} = 2,4,6\text{-}i\text{Pr}_3\text{C}_6\text{H}_2$; see structure of $\text{L} = \text{PMe}_3$ derivative) containing W–Pb triple bonds is reported. Quantum-chemical analyses of the W=Pb bond in the plumbidyne complex $[(\text{PMe}_3)_5\text{W=Pb(2,6-Trip}_2\text{C}_6\text{H}_3)]^+$ confirm the electronic analogy with Fischer-type carbyne complexes.



Cycloadditions

G. Prié, N. Prévost, H. Twin,
S. A. Fernandes, J. F. Hayes,
M. Shipman* ————— 6517–6519

A Lewis Acid Catalyzed Intramolecular $[4+3]$ Cycloaddition Route to Polycyclic Systems That Contain a Seven-Membered Ring



Two simple steps, including a new intramolecular $[4+3]$ cycloaddition, are required for the preparation of polycycles that contain a seven-membered ring from 2-methyleneaziridines (see scheme). The

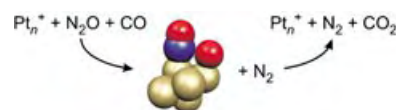
diene component is introduced by selective lithiation/alkylation at C3 of the aziridine ring. Lewis acid catalyzed cyclization leads to the products in good yields with stereocontrol.

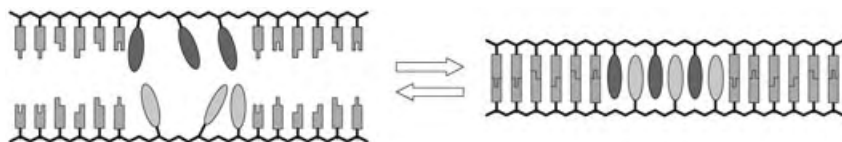
Oxidation

O. P. Balaj, I. Balteanu,
T. T. J. Roßteuscher, M. K. Beyer,*
V. E. Bondybey* ————— 6519–6522

Catalytic Oxidation of CO with N_2O on Gas-Phase Platinum Clusters

The complete catalytic cycle of CO oxidation with N_2O is shown to occur on Pt_n^+ (see scheme); for Pt_7^+ it involves six different elementary reactions. Poisoning of the catalyst by sequential addition of CO is observed. The extent of poisoning can be adjusted with the ratio of N_2O and CO partial pressures.





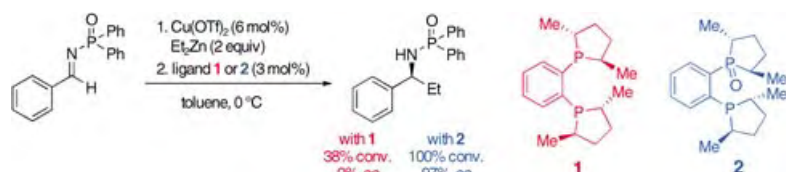
Seeing red: Aggregates in which methyl red and naphthyl red moieties are stacked alternately in a DNA duplex have been prepared by hybridization of two DNA-dye conjugates (see picture). A sharp

absorption band appears at 478 nm, which is different from that of the individual dyes. A strong CD effect is also induced by the interstrand heterostacking of the dyes.

Dye Aggregates

H. Kashida, H. Asanuma,*
M. Komiyama _____ 6522–6525

Alternating Hetero H Aggregation of Different Dyes by Interstrand Stacking from Two DNA-Dye Conjugates



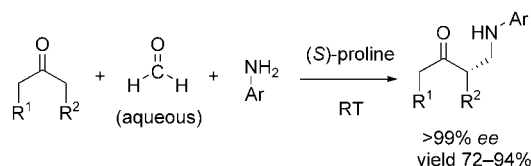
Mistaken identity: The active catalyst in the highly selective Cu-catalyzed nucleophilic addition of diorganozinc reagents to *N*-diphenylphosphinoylimines (see scheme) does not contain the bis(phosphine) ligand **1** but rather the hemilabile

monophosphine oxide **2**. Ligand **1** is oxidized when it is mixed with either copper(II) or copper(I) triflate. The analogous reaction under nonoxidizing conditions is slower and not enantioselective.

Reaction Mechanisms

A. Côté, A. A. Boezio,
A. B. Charette* _____ 6525–6528

Evidence for the Structure of the Enantioactive Ligand in the Phosphine-Copper-Catalyzed Addition of Diorganozinc Reagents to Imines



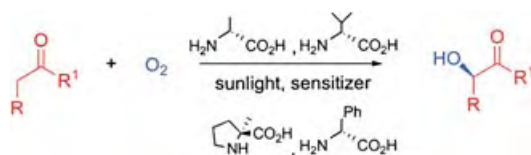
A proline-catalyzed Mannich reaction produces α -aminomethylated ketones in high yield and with excellent *ee* values (see scheme). The Mannich bases resulting from this highly practical one-pot three-

component asymmetric reaction are of particular interest, for example, as synthetic building blocks and precursors of pharmaceutically valuable 1,3-amino alcohols.

Asymmetric Synthesis

I. Ibrahim, J. Casas,
A. Córdova* _____ 6528–6531

Direct Catalytic Enantioselective α -Aminomethylation of Ketones



A possible prebiotic pathway for the asymmetric incorporation of molecular oxygen into organic compounds involves the amino acid catalyzed reaction of molecular singlet oxygen with ketones.

Amino acids and their derivatives mediate the reaction between oxygen and ketones with high efficiency to produce α -hydroxyketones (see scheme).

Oxidations

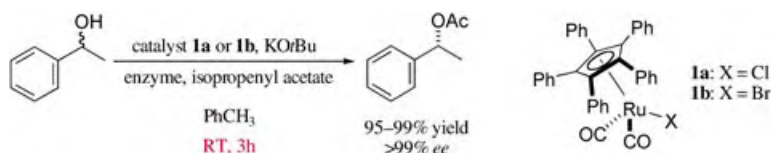
H. Sundén, M. Engqvist, J. Casas,
I. Ibrahim, A. Córdova* _____ 6532–6535

Direct Amino Acid Catalyzed Asymmetric α Oxidation of Ketones with Molecular Oxygen

Dynamic Kinetic Resolution

B. Martín-Matute, M. Edin, K. Bogár,
J.-E. Bäckvall* — 6535 – 6539

Highly Compatible Metal and Enzyme Catalysts for Efficient Dynamic Kinetic Resolution of Alcohols at Ambient Temperature



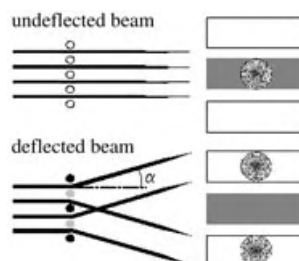
The combination of highly compatible metal and enzyme catalysts allows the fastest dynamic kinetic resolution of alcohols ever reported. The use of ruthenium catalyst **1a** (or **1b**) and an immobi-

lized lipase results in a highly efficient enantioselective synthesis of acetates in excellent yields at room temperature (see scheme).

Mass Spectrometry

O. Trapp, J. R. Kimmel, O. K. Yoon,
I. A. Zuleta, F. M. Fernandez,
R. N. Zare* — 6541 – 6544

Continuous Two-Channel Time-of-Flight Mass Spectrometric Detection of Electrosprayed Ions

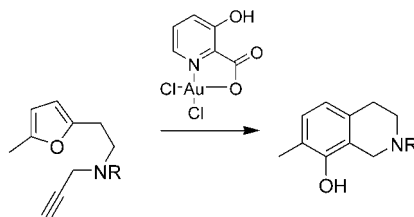


Flying to new destinations: Instrument modifications, which give three detection areas (see scheme) in a two-channel detection scheme, extend the achievable duty cycle of a Hadamard transform time-of-flight mass spectrometer (HT-TOFMS) to 100% and effectively converts TOFMS into a continuous detection technique. Beyond the improved signal-to-noise ratio, this advance gives an increase in the data-acquisition rate leading to a higher detection speed.

Homogeneous Catalysis

A. S. K. Hashmi,* J. P. Weyrauch,
M. Rudolph, E. Kurpejović — 6545 – 6547

Gold Catalysis: The Benefits of N and N,O Ligands

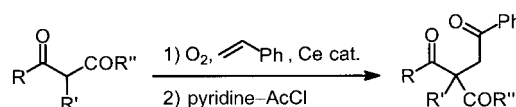


The golden key: The use of N and N,O ligands for gold(III) complexes leads to stable catalysts that facilitate an efficient synthesis of tetrahydroisoquinolines with substitution patterns difficult to access by classic methods (see picture).

C–C Coupling

M. Rössle, T. Werner, A. Baro, W. Frey,
J. Christoffers* — 6547 – 6549

Formation of 1,4-Diketones by Aerobic Oxidative C–C Coupling of Styrene with 1,3-Dicarbonyl Compounds



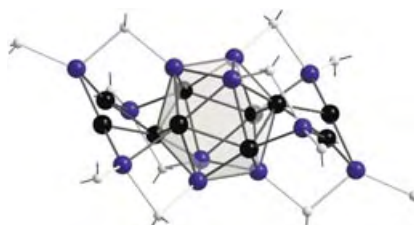
Convenient and direct: 1,4-Dicarbonyl compounds are readily obtained through a one-pot cerium-catalyzed oxidative C–C

coupling in the presence of oxygen and subsequent fragmentation. The products are suitable precursors for heterocycles.

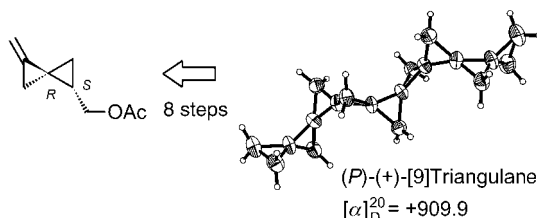
Element Modifications

J. Steiner, G. Stößer,
H. Schnöckel* — 6549 – 6552

[Ga₂₂(PtBu₂)₁₂]: Diversity in the Arrangement of 22 Gallium Atoms—A Unique Case in the Field of Metalloid Clusters?



Disproportionation of a metastable Ga^I chloride solution and substitution with phosphanides leads to a novel type of metalloid Ga₂₂ clusters ([Ga₂₂(PtBu₂)₁₂], see molecular structure, Ga: blue and black, P: gray). The four previously discovered Ga₂₂ structural isomers—which in solid-state chemistry would be referred to as different phases—reflect the diverse bonding possibilities in gallium modifications.



Remarkably high specific rotations, even at 589 nm, are exhibited by the enantiomerically pure σ -[9]helicenes (*M*)-(-)- and (*P*)-(+)-[9]triangulanes (see scheme). This significant power of rotation, which is

in very good agreement with calculated values, must be attributed to the rigid helical framework of σ bonds in these formally saturated hydrocarbons.

Spirocycles

A. de Meijere,* A. F. Khlebnikov, S. I. Kozhushkov, K. Miyazawa, D. Frank, P. R. Schreiner, B. C. Rinderspacher, D. S. Yufit, J. A. K. Howard – **6553 – 6557**

A Convergent Route to Enantiomerically Pure Higher [*n*–2]Triangulanedimethanol Derivatives and [*n*]Triangulanes (*n* ≥ 7)



Communications labeled with this symbol have been judged by two referees as being “very important papers”.

Looking for outstanding employees?

Do you need another expert for your excellent team?

... Chemists, PhD Students, Managers, Professors, Sales Representatives...

Place an advert in the printed version and have it made available online for 1 month, free of charge!

Angewandte Chemie International Edition

Advertising Sales Department: Marion Schulz

Phone: 0 62 01 - 60 65 65

Fax: 0 62 01 - 60 65 50

E-Mail: MSchulz@wiley-vch.de

Service

Keywords **6558**

Authors **6559**

Angewandte's
Sister Journals **6560 – 6561**

Preview **6563**



P. Yang Receives Pure Chemistry Award

The ACS (American Chemical Society) Award in Pure Chemistry is awarded to a young scientist based in North America for fundamental research of exceptional merit and originality in pure chemistry. The recipient for 2005 is Peidong Yang, Associate Professor of Chemistry at the University of California, Berkeley. Born in



P. Yang

1971, Yang completed his BS in Applied Chemistry at the University of Science and Technology of China in 1993. He continued his education in the USA, where he completed his MS and PhD (1997) at Harvard University under the guidance of Charles M. Lieber. Following a period as a postdoctoral fellow in the research group of Galen D.

Stucky at the University of California, Santa Barbara, Yang became Assistant Professor at Berkeley in 1999.

Yang's research is centered on the development of strategies for the rational synthesis and organization of low-dimensional nanoscale building blocks, which can be used to assemble complex architectures with novel electronic and photonic properties. He is particularly interested in the thermal stability, chemical stability, and optoelectronic properties of nanowires. His recent publication on the controlled synthesis of platonic gold nanocrystals in the form of tetrahedra, cubes, octahedra, and icosahedra was highlighted on the cover of *Angewandte Chemie*.^[1]

Inorganic Chemistry Award to W. J. Evans

William J. Evans is to receive the ACS Award in Inorganic Chemistry for 2005. Evans completed his BS in 1969 at the University of Wisconsin (USA), with research directed by Donald F. Gaines on penta-borane. After completion of his PhD in 1973 at the University of California, Los Angeles, where he studied metallocarboranes under the supervision of M. Frederick Hawthorne, he undertook postdoctoral research on molybdenum phosphite chemistry with Earl L. Muetterties at Cornell University. Evans then joined the faculty at the University of Chicago in 1975. He was promoted to associate professor there before moving in 1982 to the University of California, Irvine, where he has been ever since as a full professor.



W. J. Evans

Evans embarked on pioneering research into the chemistry of the lanthanide elements at the very beginning of his independent research career. His research program covers many aspects of the chemistry of the lanthanides, actinides, and early transition metals, including synthesis, mechanistic studies, and structural analysis. He is also interested in applications of these metals in organic synthesis, polymers, the development of high-technology materials, and dinitrogen fixation. In his most recent Communication in *Angewandte Chemie* he described the formation of dinitrogen derivatives of lanthanum from organometallic and heteroleptic precursors.^[2]

E. Iglesia Receives George A. Olah Award

Enrique Iglesia is the recipient for 2005 of the George A. Olah Award in Hydrocarbon or Petroleum Chemistry, admin-

istered by the ACS and awarded to a resident of the USA or Canada who has accomplished outstanding research in the chemistry of hydrocarbons or of petroleum and its products. Iglesia's research focuses on the design, synthesis, and structural and mechanistic characterization of catalysts for chemical reactions important in energy use, petrochemical synthesis, and environmental protection.

Iglesia completed his PhD in chemical engineering at Stanford University (USA) in 1982 under the guidance of Michel Boudart. After



E. Iglesia

gaining eleven years of experience in heterogeneous catalysis and reaction engineering at the Corporate Research Laboratories of Exxon Research and Engineering, he accepted a position as Professor of Chemical Engineering at the University of California, Berkeley in 1993. He is also a Faculty Scientist in the E. O. Lawrence Berkeley National Laboratory of the US Department of Energy, as well as the founding and current director of the Berkeley Catalysis Center. Iglesia has received a number of awards, including two for excellence in teaching from the American Institute of Chemical Engineers. He recently reported in *Angewandte Chemie* on the structural and mechanistic requirements for the activation of methane and its chemical conversion on supported iridium clusters.^[3]

- [1] F. Kim, S. Connor, H. Song, T. Kuykendall, P. Yang, *Angew. Chem.* **2004**, *116*, 3759; *Angew. Chem. Int. Ed.* **2004**, *43*, 3673.
- [2] W. J. Evans, D. S. Lee, C. Lie, J. W. Ziller, *Angew. Chem.* **2004**, *116*, 5633; *Angew. Chem. Int. Ed.* **2004**, *43*, 5517.
- [3] J. Wei, E. Iglesia, *Angew. Chem.* **2004**, *116*, 3771; *Angew. Chem. Int. Ed.* **2004**, *43*, 3685.

The Molecular Basis of Olfactory Chemoreception**

Uwe J. Meierhenrich,* Jérôme Golebiowski, Xavier Fernandez,
and Daniel Cabrol-Bass

Keywords:

bioorganic chemistry · fragrances · gene expression ·
protein models · protein structures

Dedicated to Professor R. Luft

Chemoreception is the aptitude of living organisms to identify natural or synthetic chemical compounds in their environment and to evaluate their concentration.^[1,2] In April 1970, the organic chemist Robert Luft was asked how volatile odorant molecules are perceived by the olfactory system. “*Si vous répondez à cette question,*” he replied, “*le Prix Nobel est à vous*”.^[3] The 2004 Nobel Prize in Medicine was awarded 34 years later to Richard Axel and Linda B. Buck of the Howard Hughes Medical Institute, who deciphered the molecular basis for the perception of odors and the corresponding information preprocessing in the olfactory system. From the viewpoint of a chemist, these studies offer fascinating perspectives.

Olfaction is initiated by a molecular interaction of chemical compounds called odorants with the olfactory neurons located in the epithelium of the nasal cavity. The required molecular properties of odorants were determined

to be a moderate molecular weight, low polarity, a certain water solubility, high vapor pressure, and lipophilicity.^[1] The existence of peripheral olfactory receptor (OR) proteins located in the cilia of sensory neurons in the epithelium had been postulated but remained unproven prior to the work of Axel and Buck.^[4] Numerous theories had been formulated concerning the mode of interaction between odorant molecules and the olfactory neurons, including the vibrational theory,^[5,6] the membrane-diffusion theory,^[7] the Piezzo effect,^[8] complexation,^[9] the polarization theory,^[10] the chromatography analogy,^[11] the hydrogen-bond-dispersion model,^[12] and the tunneling vibrational theory.^[13,14]

Since 1949, it had been thought that only the characteristic molecular shape of an odorant determined its odor.^[15,16] Based on the identification of a number of different types of anosmia (the lack of a sense of smell), it was concluded that as many (between 7 and 30) specific receptors with the capacity to recognize different molecular shapes must exist. Thus, the existence of an “alphabet” of odor types with corresponding molecular shapes was postulated. The combination of the letters of this alphabet should lead to the perception of a multitude of different odors.^[17] Since then, numerous chemical studies have been devoted to the elucidation of structure–odor relationships.^[18,19] Despite some success with specific series of molecules and their odors (e.g. musks, ambergris, sandalwood), numerous discrepancies and exceptions remained.^[1] Furthermore, it remained impossible to predict the odor of a molecule from its molecular structure. These difficulties are not surprising, as structure–odor relation-

ships are several orders of magnitude more complex than their pharmacological counterparts, structure–activity relationships.^[13] More recently, the simplifying “steric theory” of Amoore has evolved into the olfactophore concept. Olfactophores, like pharmacophores, describe the spatial molecular arrangement of interacting groups and were found to be helpful for the computer-aided design of new odorants.^[20] Such models were constructed without prior knowledge about the receptor site.

In 1991, Axel and Buck published a study that contributed considerably to our understanding of the molecular basis for the olfactory perception process.^[4] To assess the presence of potential receptors in the olfactory epithelium they postulated that OR proteins belong to the family of G-protein-coupled receptors (GPCR). GPCR proteins are embedded in the surface membrane of cells and cross this membrane seven times. They are made up of seven helices, which are joined together by three extracellular and three intracellular loops. These transduction proteins can receive chemical signals outside the cell and transmit them into the interior of the cell. The receptor activates the intracellular G protein, which causes effectors to produce a second signal inside the cell. This second signal causes the cell to react to the original external chemical signal. A simplified schematic representation of the transmembrane protagonists is presented in Figure 1.

Prior to their interaction with transmembrane OR proteins, odorants are thought to be associated with odorant-transport (OT) proteins present in mucus.^[21,22] OT proteins belong to a class of carrier proteins present in physiological

[*] Priv.-Doz. Dr. U. J. Meierhenrich,
Dr. J. Golebiowski, Dr. X. Fernandez,
Prof. Dr. D. Cabrol-Bass
Université de Nice-Sophia Antipolis
Faculté des Sciences
Laboratoire “Arômes, Synthèses et
Interactions”
Parc Valrose, 06108 Nice (France)
Fax: (+33) 4-9207-6125
E-mail: uwe.meierhenrich@unice.fr

Priv.-Doz. Dr. U. J. Meierhenrich
Laboratoire de Chimie Bioorganique
Unité Mixte de Recherche 6001 CNRS-
UNSA

[**] This Highlight was written to coincide with the awarding of the 2004 Nobel Prize in Medicine and is dedicated to Prof. Dr. R. Luft, initiator of research on odorants in the late 1960s at the Université de Nice-Sophia Antipolis.

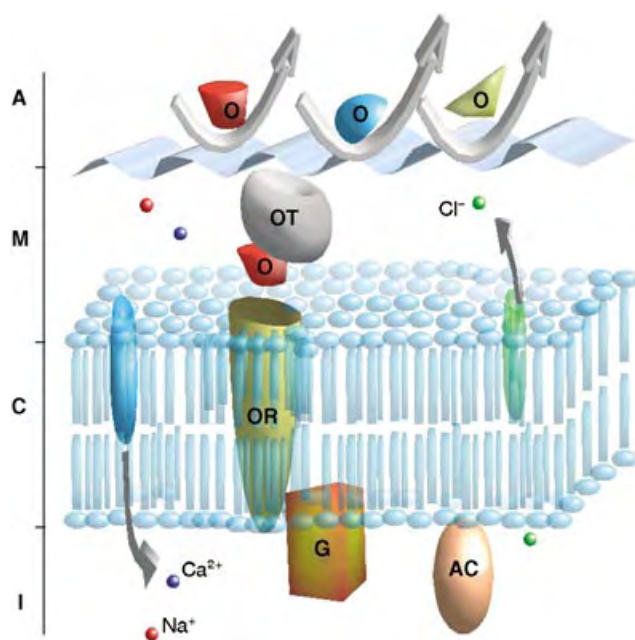


Figure 1. Schematic illustration of odorant binding and signal activation. The transduction mechanism of chemical reception through the cilia is initiated by the binding of an odorant molecule **O** from the gaseous phase **A** to a water-soluble **OT** protein,^[21] which transports the odorant to the **OR** protein through the olfactory mucus **M**. Subsequently, the intracellular (**I**) G protein **G** is activated, and this protein in turn activates adenylate cyclase **AC**, resulting in an opening of the ion channels located in the cell membrane **C**. The cell is depolarized through the entry of Ca^{2+} ions and leaving of Cl^- ions.

fluids. They contribute actively to the transportation of the odorant from the inhaled air stream through the mucus to the cilia of the olfactory neurons.

The basic approach of Axel and Buck was to design probes that could recognize DNA sequences that encode proteins located in the olfactory epithelium. A new class of genes were found that express a previously unknown family of GPCR-type proteins, the so-called OR proteins. The derived molecular structure of an OR protein is depicted in Figure 2 together with a complex of the odorant 2-isobutyl-3-methoxypyrazine with an OT protein.

Gene analysis revealed that the OR proteins had highly variable sequences and that they were only encoded in the olfactory epithelium. From then on, a tremendous number of studies were performed to determine the number and functions of OR proteins.^[24,25] By searching the human genome database, Buck and co-workers identified 339 intact OR genes and 297 OR pseudogenes. Sequence comparison led to the classification of the human OR proteins into 172 families.^[26] It was shown that a single OR protein can be activated by

multiple odorants,^[27–31] and that a single odorant can activate several OR proteins.^[29] As a consequence, different odorants are recognized by different combinations of receptors, some of which are closely related to one another. Numerous odorants activate distinct sets of OR proteins, even if overlaps between these sets can exist.^[29] From these results, the molecular basis for the first steps of olfaction was identified, namely, that olfactory perception proceeds through a *combinatorial* process. Indeed, given the large number of OR proteins, this combinatorial process could permit discrimination between a vast range of chemicals. Buck and co-workers estimated that even if an odorant activated only three receptors (in fact many more are activated), the number of theoretically discriminable odorants should be close to a billion.^[29] The biological method of chemical recognition is therefore far removed from the simple “lock and key” analogy. These findings are fully consistent with the potential discrimination of a very large number of chemical compounds with different structures and shapes, as well as distinct odors.



Figure 2. Three-dimensional structure of a complex between the odorant 2-isobutyl-3-methoxypyrazine and a water-soluble OT protein located in the mucus (top).^[23] It is assumed that the odorant molecule is transferred to the transmembrane GPCR olfactory receptor (bottom).^[22]

The sequence of the OR proteins was determined indirectly through examination of the DNA sequence. Generally, three-dimensional protein structures can be determined through direct measurements by X-ray crystallography, electron microscopy, and NMR spectroscopy. These techniques are, however, suitable only for water-soluble proteins, and not for GPCR proteins, which require precisely balanced physicochemical conditions for structural and functional integrity. As such conditions are difficult to achieve, new techniques, such as two-dimensional cryomicroscopy, have to be employed to attempt the elucidation of these structures.^[32] Therefore, the amount of

experimental information available on the three-dimensional structure of GPCR proteins is limited. So far, only the rhodopsin GPCR structure has been determined by direct measurements,^[33] and the structures of OR proteins have been derived from rhodopsin-based models.^[34] Recent studies started to evaluate the differential responses of a receptor to a broad variety of agonists.^[35] Much progress has been made towards understanding the molecular basis of olfactory perception, but many questions remain unanswered because of its combinatorial nature.

The pioneering transdisciplinary studies of Axel and Buck have tremendous implications for flavor and fragrance research. Knowledge about the molecular interactions between OR proteins and odorants can contribute to the evaluation of the interaction of a specific odorant with a given set of OR proteins, a strategy that has already been patented.^[36] The combinatorial aspect of information processing in the olfactory bulb and the perception of odor by pattern recognition throw light on the success and failure of previous approaches based on studies of structure–odor relationships and olfactory-phore modeling. After the confirmation of the three-dimensional OR protein structure, chemists will be in a better position to undertake the rational design of odorants for the activation of specific OR proteins. However, for practical applications, odorants are seldom used as pure compounds, but rather as mixtures, which may be very complex. Thus, the successful application of odorants will always depend on their formulation. The field for the search for new odorants, deodorants, and odor modifiers is wide open.

- [1] G. Ohloff, *Scent and Fragrances*, Springer, Heidelberg, **1994**, p. 9, and references therein.
- [2] S. Firestein, *Nature* **2001**, *413*, 211–218.

- [3] “If you can answer that question, the Nobel Prize is yours.” Nice-Matin, 2 April **1970**.
- [4] L. Buck, R. Axel, *Cell* **1991**, *65*, 175–181.
- [5] G. M. Dyson, *Chem. Ind.* **1938**, *57*, 647–651.
- [6] a) R. H. Wright, *Nature* **1972**, *239*, 226; b) R. H. Wright, *J. Theor. Biol.* **1977**, *64*, 473–502; c) R. H. Wright, *The sense of Smell*, CRC, Boca Raton, **1982**.
- [7] a) J. T. Davies, F. H. Taylor, *Nature* **1954**, *174*, 693–694; b) J. T. Davies, F. H. Taylor, *Proc. Int. Congr. Surf. Act.* **1957**, *4*, 329–340; c) J. T. Davies, F. H. Taylor, *Biol. Bull. (Woods Hole, MA, U.S.)* **1959**, *117*, 222–238.
- [8] M. H. Briggs, R. B. Duncan, *Nature* **1961**, *191*, 1310–1311.
- [9] B. Rosenberg, T. N. Misra, R. Switzer, *Nature* **1968**, *217*, 423–427.
- [10] a) H. G. B. De Jong, G. G. P. Saubert, *Proc. Acad. Sci. (Amsterdam)* **1937**, *40*, 302; b) H. G. B. De Jong, G. G. P. Saubert, *Protoplasma* **1937**, *28*, 329.
- [11] M. M. Mozell, *J. Gen. Physiol.* **1970**, *56*, 46–63.
- [12] M. Chastrette, D. Zakarya in *The Human Sense of Smell* (Eds.: D. G. Laing, R. L. Doty, W. Breipohl), Springer, Berlin, **1991**, pp. 77–92.
- [13] L. Turin, F. Yoshii in *Handbook of Olfaction and Gustation*, 2nd ed. (Ed.: R. L. Doty), Marcel Dekker, New York, **2002**, 275–294.
- [14] L. Turin, *J. Theor. Biol.* **2002**, *216*, 367–385.
- [15] a) R. W. Moncrieff, *Am. Perfum. Essent. Oil Rev.* **1949**, *54*, 453–454; b) R. W. Moncrieff in *The Chemical Senses*, 2nd ed., CRC, Cleveland, **1951**.
- [16] a) J. E. Amoore, *Molecular Basis of Odor*, Thomas CC, Springfield, **1970**; b) J. E. Amoore, *Perfum. Essent. Oil Rec.* **1952**, *43*, 321–330; c) J. E. Amoore, *Nature* **1963**, *198*, 271–272; d) J. E. Amoore, *Chemical Senses*, Springer, Berlin, **1971**.
- [17] J. E. Amoore, *Chem. Senses Flavour* **1977**, *2*, 267.
- [18] K. J. Rossiter, *Chem. Rev.* **1996**, *96*, 3201–3240, and references therein.
- [19] M. Chastrette, *SAR QSAR Environ. Res.* **1997**, *6*, 215–254, and references therein.
- [20] P. Kraft, J. A. Bajgrowicz, C. Denis, G. Fráter, *Angew. Chem.* **2000**, *112*, 3106–3138; *Angew. Chem. Int. Ed.* **2000**, *39*, 2980–3010.
- [21] Until now, the odorant-transport protein was denoted odorant-binding (OB) protein. Herewith, we suggest the label OT protein, because 1. the term “binding” is not specific enough to describe the hydrophobic chemical interaction between odorant and protein, and 2. the term “transport” can describe the processes of inclusion, delivery, and release of the odorant molecule to the OR protein.
- [22] P. Pelosi, *Crit. Rev. Biochem. Mol. Biol.* **1994**, *29*, 199–228.
- [23] The structure of the OT protein was taken directly from X-ray crystallographic data (PDB id. 1DZK). The three-dimensional structure of the OR protein was derived by analogy with the experimentally determined structure of rhodopsin; see reference [33].
- [24] J. M. Young, C. Friedman, E. M. Williams, J. A. Ross, L. Tonnes-Priddy, B. J. Trask, *Hum. Mol. Genet.* **2002**, *11*, 535–546.
- [25] X. Zhang, S. Firestein, *Nat. Neurosci.* **2002**, *5*, 124–133.
- [26] B. Malnic, P. A. Godfrey, L. B. Buck, *Proc. Natl. Acad. Sci. USA* **2004**, *101*, 2584–2589.
- [27] H. Zhao, L. Ivic, J. Otaki, M. Hasimoto, K. Mikoshiba, S. Firestein, *Science* **1998**, *279*, 237–242.
- [28] D. Krautwurst, K. W. Yau, R. R. Reed, *Cell* **1998**, *95*, 917–926.
- [29] A. B. Malnic, J. Hirono, T. Sato, L. B. Buck, *Cell* **1999**, *96*, 713–723.
- [30] K. Touhara, S. Sengoku, K. Inaki, A. Tsuboi, J. Hirono, T. Sato, H. Sakano, T. Haga, *Proc. Natl. Acad. Sci. USA* **1999**, *96*, 4040–4045.
- [31] C. H. Wetzel, M. Oles, C. Wellerdieck, M. Kuczkowiak, G. Gisselmann, H. Hatt, *J. Neurosci.* **1999**, *19*, 7426–7433.
- [32] G. Müller, *Curr. Med. Chem.* **2000**, *7*, 861–888.
- [33] K. Palczewski, T. Kumasaka, T. Hori, C. A. Behnke, H. Motoshima, B. A. Fox, I. Le Trong, D. C. Teller, T. Okada, R. E. Stenkamp, M. Yamamoto, M. Miyano, *Science* **2000**, *289*, 739–745.
- [34] W. B. Floriano, N. Vaidehi, W. A. Goddard III, M. S. Singer, G. M. Shepherd, *Proc. Natl. Acad. Sci. USA* **2000**, *97*, 10712–10716.
- [35] W. B. Floriano, N. Vaidehi, W. A. Goddard III, *Chem. Senses* **2004**, *29*, 269–290.
- [36] L. Buck, R. Axel, US 9217585; US 2002-064817.

A Fatal Affair: The Ubiquitylation of Proteins

Markus Biel, Veit Wascholowski, and Athanassios Giannis*

Keywords:

drug design · inhibitors · proteasome · ubiquitin

The activity, stability, and subcellular distribution of proteins can be modulated by different post-translational modifications. The awarding of the Nobel Prize in Chemistry for 2004 to Ciechanover, Hershko, and Rose pushed ubiquitylation into the center of scientific attention. Ubiquitylation is not only a signal for the degradation of unnecessary or defective proteins, but it also plays an important role in complex biological processes, such as cell-cycle control, DNA repair, apoptosis, and immune response.^[1]

Ubiquitin (Ub) is a 8-kDa protein made up of 76 amino acids. Usually it is bound to other proteins by an isopeptide bond between its C terminus and a lysine side chain of the protein (Figure 1).^[2] The ubiquitin-activating enzyme E1 adenylates the carboxy function of the C-terminal glycine residue of ubiquitin and transfers the activated species to an internal cysteine residue of the enzyme with the formation of a thioester bond. In a second step, Ub is transesterified from E1 to the ubiquitin-conjugating enzyme E2. A ubiquitin ligase E3 then selectively catalyzes its transfer from E2 to the target protein. As ubiquitin itself possesses internal lysine residues (e.g. lysine 48, lysine 63), the enzymatic cascade can be repeated several times to form a chain of Ub units.

Substrate molecules with a single Ub unit may be recognized by proteins that possess special ubiquitin-binding domains. The monoubiquitylation of his-

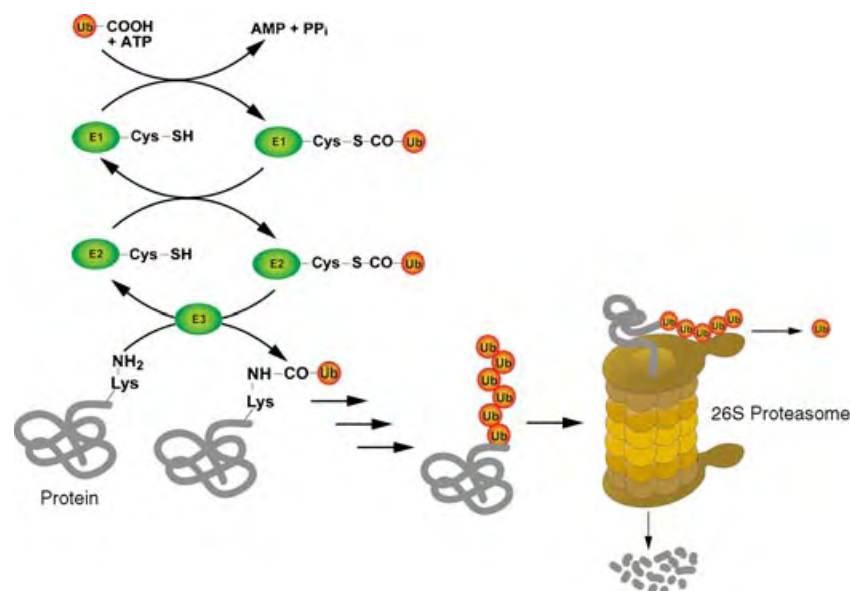


Figure 1. Mechanism of the E1/E2/E3-catalyzed attachment of ubiquitin to proteins; ubiquitylation marks a protein for degradation by the 26S proteasome.

tone H2B, which is part of the postulated histone code, serves as a signal for the activation of transcription,^[3] whereas the same modification at receptor tyrosine kinases (RTKs) leads to their endocytosis and subsequent transport to the lysosome. Polyubiquitylated species with Ub chains linked through lysine 63 are responsible for the mediation of nonproteolytic, reversible events,^[4] including the modulation of protein properties, such as activity, subcellular distribution, and protein–protein interactions. On the other hand, if polyubiquitin chains are linked through lysine 48, the labeled proteins are recognized by the 26S proteasome and degraded by this 2.4-MDa multisubunit enzyme.^[5]

The proteasome is present in both the nucleus and the cytoplasm of a cell and has a cylindrical shape. It consists of a catalytic 20S component, which is closed on both sides by a regulatory

19S component. This 19S unit recognizes and binds proteins with Ub chains that are linked through lysine 48 and forwards them, after cleavage of the ubiquitin chain and unfolding of the structure under ATP hydrolysis, to the catalytic 20S unit. The enzymatic mechanism^[6] is not based on the catalytic triad common to most proteases, but on a single, highly conserved N-terminal threonine as the active-site nucleophile. The products of degradation by the proteasome are peptides with a length of 3 to 25 amino acids.

The proteasome has become an interesting target for the development of drugs. Not only does it control gene expression, but it represents a further mechanism for regulating the concentration of certain proteins inside the cell.^[7] For example, cyclin-dependent kinases (CDKs) are regulators of cell-cycle progression,^[8] and their activity depends on cyclins, phosphatases such

[*] M. Biel, V. Wascholowski,
Prof. Dr. A. Giannis
Institute of Organic Chemistry
Universität Leipzig
Johannisallee 29, 04103 Leipzig (Germany)
Fax: (+49) 341-973-6599
E-mail: giannis@chemie.uni-leipzig.de

as CDC25, and different cellular inhibitors (WAF1, KIP1). The proteasome is responsible for the well-ordered degradation of cyclins and CDK inhibitors. Furthermore, it is linked to the stabilization of CDC25 during cell-cycle progression.^[9] The inhibition of proteasome-mediated degradation is an important possibility for the induction of a cell-cycle arrest and is therefore of clinical relevance, for example, in the treatment of malignant tumors. Moreover, ubiquitin–proteasome-mediated degradation is linked to the signaling pathways of p53,^[10,11] which serves as a signal for numerous cellular responses, such as DNA repair, cell-cycle arrest, differentiation, and apoptosis, and to the NF- κ B family^[12,13] of transcription factors (Figure 2).

Until now, proteasome inhibitors have been subdivided into five classes: peptide aldehydes (MG132), peptide vinyl sulfones (NLVS), peptide boronates (bortezomib), peptide epoxyketones (epoxymycin), and β -lactones (PS-519; Scheme 1).^[5a,6] They all contain an electrophilic group, which interacts with the threonine residue in the active site of the proteasome. As a result of metabolic instability and lack of enzyme specificity, only two proteasome inhibitors have reached the stage of clinical development: PS-519 (also known as MLN519) influences anti-inflammatory processes,

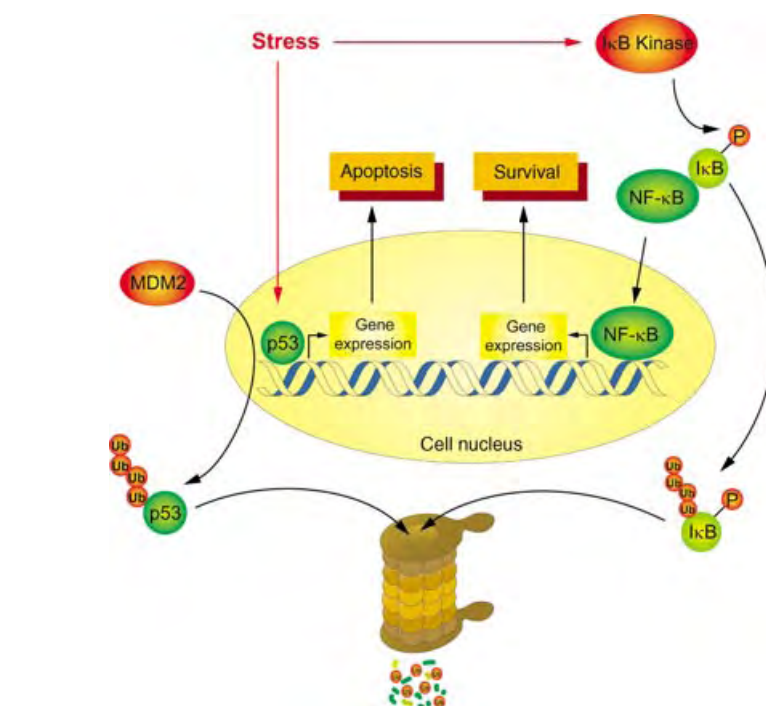
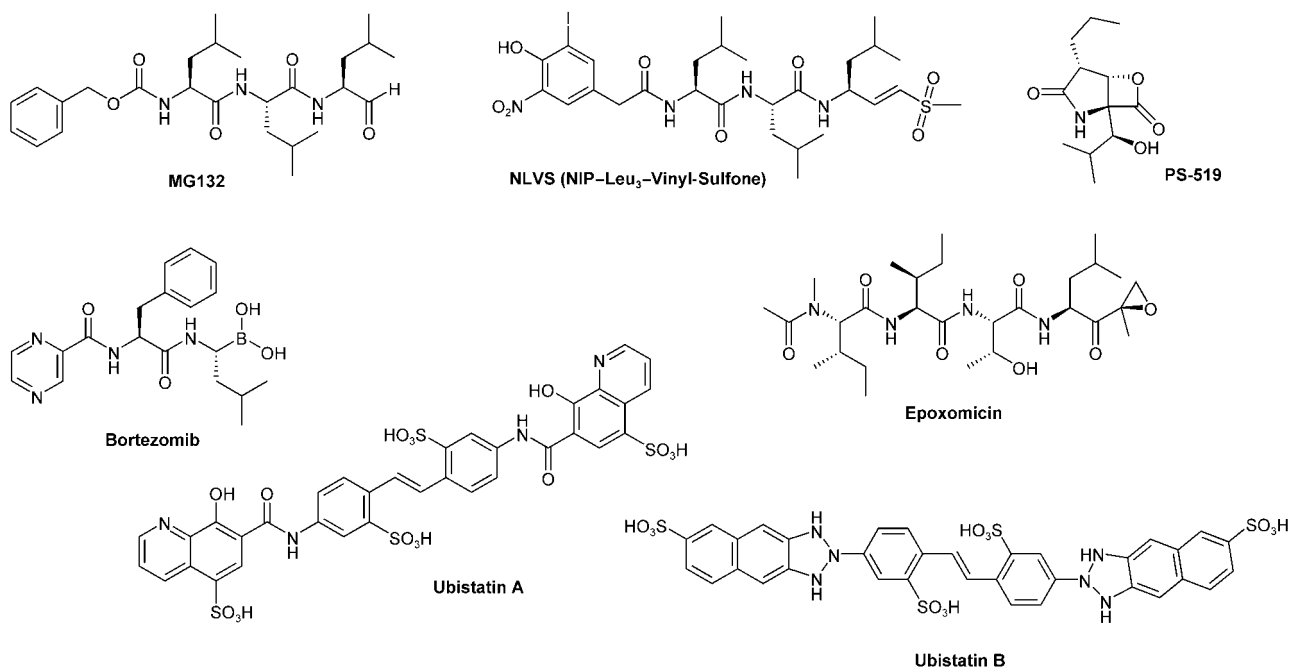


Figure 2. Cellular signaling pathways linked to the proteasome. Stress (e.g. radiation or chemicals) induces DNA damage and leads to the accumulation of the tumor suppressor p53, which activates gene expression. This process results in the induction of apoptosis. The ubiquitin ligase MDM2 blocks this pathway by ubiquitinylation and subsequent degradation of p53 in the proteasome. Proteasome inhibitors may prevent the destructive degradation of p53 in tumor cells which overexpress MDM2. Moreover, chemotherapy, radiation, viruses, and cytokines lead to the phosphorylation of the inhibitor of NF- κ B (I κ B) and thus to its degradation. Subsequently, the active NF- κ B enhances several signaling pathways, thus ensuring the survival of the cell. Therefore, NF- κ B is an important target for antineoplastic drugs.

whereas bortezomib (PS-341, velcade)—now a commercially available drug—shows significant antineoplastic effects in various tumor-cell lines. The



Scheme 1. Selected structures of inhibitors of proteasome degradation.

exact mechanism of action and the specificity of each proteasome inhibitor are still under investigation, but much is known about the role of the inhibitors in carcinogenesis, angiogenesis, and metastasis. The biological effects of inhibiting proteasome activity are apoptosis, increased sensitivity to chemotherapy and radiation therapy, and decreased resistance to these therapies.^[5a,6,7]

Recently, two new inhibitors of proteasome-dependent protein degradation, ubistatins A and B, were identified by a chemical genetic screen in *Xenopus* extracts.^[14] The ubistatins do not bind to the active site of the proteasome, but interact with the ubiquitin–ubiquitin interface of lysine 48 linked ubiquitin chains, thus preventing the recognition of these proteins, which are marked for degradation, by the regulatory 19S unit of the proteasome. The ubistatins therefore form a new class of proteasome inhibitors and belong to the small group of modulators that function by disrupting critical protein–protein interactions.^[15]

The experimental basis for this screening system is illustrated in Figure 3. The ubiquitinylation of cyclin B by the E3 ligase APC/C (anaphase-promoting complex/cyclosome) and its subsequent degradation is a prerequisite for exiting mitosis and progression into the next phase of the cell cycle. The use of a cyclin B–luciferase fusion protein allows the identification of compounds that block the degradation of cyclin B and therefore influence cell-cycle progression. Several control experiments were necessary to explore the exact mechanism of action of the most potent compounds. It was found that the ubistatins form specific protein–protein interactions with lysine 48 linked Ub chains and prevent their recognition by the proteasome. Titration experiments monitored by NMR spectroscopy with lysine 48 linked ubiquitin dimers showed that the inhibitors alter the molecular environment of specific hydrophobic sites of the ubiquitin units. Further investigation of these inhibitors in cellular assays may be hindered through their high polarity and low membrane permeability. Nevertheless, these results underline the importance of chemical genetic approaches for the discovery of new lead structures that wouldn't be found by using methods such as structure-based drug design or computer modeling.

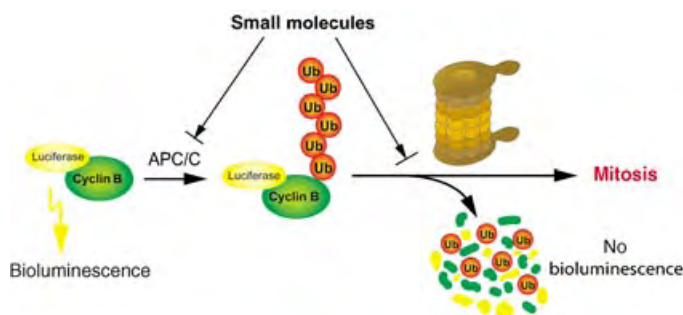


Figure 3. Schematic representation of the chemical genetic screen for the identification of ubistatins A and B. The luminescence of luciferase indicates the presence of cyclin B: Compounds that inhibit the degradation of cyclin B lead to continuous luminescence in this test system.

- [1] A. Hershko, A. Ciechanover, *Annu. Rev. Biochem.* **1998**, *67*, 425–479.
- [2] L. A. Passmore, D. Barford, *Biochem. J.* **2004**, *379*, 513–525.
- [3] M. Biel, V. Wascholzowski, A. Giannis, *Angew. Chem./Angew. Chem. Int. Ed.*, in press.
- [4] J. D. Schnell, L. Hicke, *J. Biol. Chem.* **2003**, *278*, 35857–35860.
- [5] a) J. Adams, *Nat. Rev. Cancer* **2004**, *4*, 349–360; b) D. Voges, P. Zwickel, W. Baumeister, *Annu. Rev. Biochem.* **1999**, *68*, 1015–1068.
- [6] A. F. Kisselev, A. L. Goldberg, *Chem. Biol.* **2001**, *8*, 739–758.
- [7] J. Adams, *Cancer Cell* **2004**, *5*, 417–421.
- [8] A. Huwe, R. Mazitschek, A. Giannis, *Angew. Chem.* **2003**, *115*, 2170–2187; *Angew. Chem. Int. Ed.* **2003**, *42*, 2122–2138.
- [9] M. Shirane, Y. Harumiya, N. Ishida, A. Hirai, C. Miyamoto, S. Hatakeyama, K. Nakayama, M. Kitagawa, *J. Biol. Chem.* **1999**, *274*, 13886–13893.
- [10] N. Sunder-Plassman, A. Giannis, *ChemBioChem* **2004**, *5*, in press.
- [11] Y. Haupt, R. Maya, A. Kazaz, M. Oren, *Nature* **1997**, *387*, 296–299.
- [12] a) M. L. Schmitz, I. Mattiolo, H. Buss, M. Kracht, *ChemBioChem* **2004**, *5*, 1348–1358; b) M. Karin, Y. Cao, F. R. Greten, Z. W. Li, *Nat. Rev. Cancer* **2002**, *2*, 301–310.
- [13] E. E. Varfolomeev, M. Schuchmann, V. Luria, N. Chiannikulchai, J. S. Beckmann, I. L. Mett, D. Rebrikov, V. M. Brodianski, O. C. Kemper, O. Kollet, T. Lapidot, D. Soffer, T. Sobe, K. B. Avraham, T. Goncharov, H. Holtmann, P. Lonai, D. Wallach, *Immunity* **1998**, *9*, 267–276.
- [14] R. Verma, N. R. Peters, M. D'Onofrio, G. P. Tochtrop, K. M. Sakamoto, R. Varadan, M. Zhang, P. Coffino, D. Fushman, R. J. Deshaies, R. W. King, *Science* **2004**, *306*, 117–120.
- [15] L. Pagliaro, J. Felding, K. Audouze, S. J. Nielsen, R. B. Terry, C. Krog-Jensen, S. Butcher, *Curr. Opin. Chem. Biol.* **2004**, *8*, 442–449.

Argon and the Non-Inert Pair: Rayleigh and Ramsay

John Meurig Thomas*

Keywords:

history of science · noble gases · Ramsay, William · Rayleigh, John William, Lord

In 1904 two London-based scientists became the first British citizens to be awarded the Nobel prize. Lord Rayleigh, at the Davy–Faraday Research Laboratories of the Royal Institution, won the Physics prize “for his investigation of the densities of the most important gases and for the discovery of argon in connection with these studies”; and Sir William Ramsay of University College, London, won the Chemistry prize “for his discovery of the inert gaseous elements in air, and his determination of their place in the periodic system.” The significance of their discoveries, in particular their remarkable joint paper (“Argon, a New Constituent of the Atmosphere”, *Philos. Trans. R. Soc. London Ser. A* **1895**, 186, 187–241) is seen to be even more profound now than it was a century ago. But it must not be thought that these two individuals, like some other scientists who have won the Nobel prize subsequently, were focused upon and conquered just one large problem. On the contrary, these two, in diverse ways, were scientific giants, in ways not revealed by the Nobel citation, and the lessons that present-day practitioners in chemical science may draw from the talents, insights, generosity of spirit, humanity, activity, and achievements of Rayleigh and Ramsay are not only instructive to ponder but inspirational to aspiring young scientists (Figure 1).

[*] Prof. Sir J. M. Thomas
Davy–Faraday Research Laboratory
Royal Institution of Great Britain
21 Albemarle Street, London W1S 4BS (UK)
and
Department of Materials Science
University of Cambridge
Pembroke Street, Cambridge CB2 3QZ (UK)
Fax: (+44) 1223-334-567
E-mail: robert@ri.ac.uk



Figure 1. Sir William Ramsay and Lord Rayleigh. The picture was taken shortly after the isolation of the first noble gas.

An Outline of Rayleigh's Career

Lord Rayleigh (1842–1919), last of the great British classical physicists, made contributions to every single branch of the physical sciences known in his day. His penetrating insight and prodigious capacity for detailed work enabled him to solve problems previously perceived by his progenitors and contemporaries as intractable as well as to suggest new lines of research that engendered the blossoming of much of 20th (and 21st) century science and technology. No name stands higher in the general esteem of physical scientists, engineers, and applied mathematicians

the world over than that of John William Strutt (Third Baron Rayleigh) who was “to the manor born” in rural Essex, some sixty miles from London. No name occurs more frequently in relation to phenomena, principles, and effects with which any student of classical physics must become acquainted than that of Rayleigh. “Rayleigh Scattering” (of electromagnetic waves and the explanation of the blue sky and red sunset), “Rayleigh Waves”, “Rayleigh Criterion” (governing resolving power in microscopes and telescopes), “Rayleigh Number” (in convection), “Rayleigh disc” (for measuring the absolute intensity of sound), “Rayleigh Fading and

Rayleigh Distance (terms used in the propagation of electromagnetic waves), "Rayleigh Damping", the "Rayleigh–Jeans Law" (for black body radiation)—these are by no means an exhaustive list of the impact of his work. They reflect but a fraction of the fields and phenomena in which his interests ranged with the most fruitful of results. For example, in 1885 Rayleigh published an article on the propagation of surface acoustic waves. This was a seminal paper that, for modern-day seismologists and earth scientists, is the basis for detecting and pin-pointing the location of distant earthquakes, and for electronic engineers forms that basis for practical delay lines in circuits used in radar and television.

Rayleigh was born John William Strutt at Terling Place in the county of Essex on November 12, 1842. As an infant he exhibited no sign of precocity, and he was almost three years old before he could talk. His schooling was rather fragmentary, short spells first at Eton then at Harrow (two of the premier private schools in the UK) being terminated by ill health. In the autumn of 1857 he was put under the care of Rev. George T. Warner, who took pupils at Torquay where he remained for four years. He entered Trinity College, Cambridge in October 1861 and was soon following the rigorous courses in mathematics given by or Edward J. Routh (of Peterhouse) a phenomenally successful tutor who, in 33 years of teaching produced 27 senior wranglers (the name given to the person who came top in the mathematical tripos examinations). J. W. Strutt was senior wrangler in January 1865. Sir James Jeans, the eminent astronomer and cosmologist, writing some 60 years later, said that "*there still lingers in Cambridge a tradition as to the lucidity and literary finish of his answers in the examination*". The fine sense of literary style which Strutt displayed even under pressure in the examinations never deserted him. Every paper he wrote—and there were some 450 over a fifty year period—even those dealing with the most abstruse subjects—is a model of clarity and simplicity, and conveys the impression of having been written with effortless ease.

After his triumph in the mathematics examination he took a course on

chemical analysis (from George D. Living, the newly appointed Professor of Chemistry at Cambridge). This choice of course was partly because young Strutt had a passion for experiment, but chiefly because no course was available in Cambridge dealing with experimental physics—an incredible state of affairs for the University where Newton had studied and taught.^[1] In 1866 he was elected a fellow of Trinity College but it was not until 1869 that his first scientific paper appeared bearing the title "On Some Electro-Magnetic Phenomena Considered in Connection with the Dynamical Theory"^[2] This paper was a brilliant example of the method and style that its author was to pursue throughout his career. The "dynamical theory" in question was James Clerk Maxwell's monumental work on the electromagnetic field, which Maxwell had cast in terms of complicated mathematical equations that were not readily transparent and fully appreciated by his contemporaries. Strutt elucidated and simplified this recondite theory—almost, as Jeans said later, made it intelligible to the average person. This simplification was done by showing that the intricate processes of the electromagnetic field found practically perfect analogies in such well-understood phenomena as the bursting of a water pipe under sudden pressure. And so, by adding to his towering mathematical skills the capacity for^[3] "*understanding everything just a little more deeply than anyone else, and the consequent capacity for exhibiting it in its simplest aspect*", Strutt began on his extraordinary scientific career, one marked by a catholicity of tastes and an exceptional combination of mathematical power and (later) experimental virtuosity.

Soon after his lucid interpretation of Maxwell's electromagnetic work, there came another major contribution which emerged from his reading the articles of Hermann von Helmholtz on sound. In 1860, Helmholtz had studied the acoustic resonator, now associated with his name. The 28 year old Strutt felt he could improve the mathematical treatment considerably, and this formed his first excursion into acoustics, which led to his classic paper entitled "On the Theory of Resonance"^[4] In this major paper he attacked the problem of the

oscillations of the air in the mouth of a resonator from the standpoint of energy; and he also introduced the invaluable concept of the acoustic conductivity of an orifice. He significantly extended Helmholtz's results, including (among other novelties) a discussion of coupled resonators. Ruminating over Helmholtz's famous treatise on tone,^[5] he realized that there existed no up-to-date book on acoustical problems that provided an adequate mathematical treatment of well-established experimental phenomena.^[6] No one had taken the trouble to summarize in a single text the classical memoirs of Euler, Lagrange, D'Alembert, Bernoulli, and other theorists of the eighteenth century.

By that time, 1871 to be precise, he had married Evelyn Balfour, sister of Arthur J. Balfour, the future Prime Minister, and later the author of the Balfour declaration that established a national home for the Jews.^[8] Shortly thereafter he was struck by a severe attack of rheumatic fever, which led to his devoting a winter to travel in Egypt and Greece. It was while he was holidaying on a houseboat on the Nile that he drafted—without access to a library—Volume One of his monumental two volume *The Theory of Sound*, in which he examined questions of vibrations and the resonance of elastic solids and gases.^[9] But before he left for the Middle East he had, in a two year period, published a dozen other outstanding papers. Arguably one of his most celebrated is entitled: "On the Light from the Sky: its polarization and colour"^[10] and it marked the beginning of his concern for the scattering of radiation in general. He arrived, in this paper, at both the intensity and polarization of the scattered light by use of dimensional analysis and properly explained why the sky is blue and the sunset is red.^[11] The amplitude of the Rayleigh scattered light is inversely proportional to the square of the wavelength.

In 1873, the year that his father died and when, therefore, he inherited the title of Lord (the Third Baron Rayleigh), he was elected Fellow of the Royal Society (FRS). Taking up residence in the family seat, Terling Place, he built a laboratory adjacent to the manor house. Although his primary interest was (and remained throughout

his life) scientific research, he now found himself compelled to devote a part of his time to the management of his estates. He acquired considerable knowledge of agriculture, which, combined with his general scientific knowledge and acumen led to his practice in estate management being in many regards in advance of its time.

This period saw the commencement of Rayleigh's lifelong interest in psychological research.^[13] According to Sir James Jeans,^[3] at first Rayleigh expected that investigation would rapidly lead to a definite conclusion, either positive or negative. Apparently he expected the former, in which case he was prepared to throw the greater part of his energies into a study of psychic phenomena. Rayleigh returned to orthodox scientific work when it became clear that no such definite conclusion was being attained.

Professor at Cambridge and at the Royal Institution of Great Britain

In 1879 James Clerk Maxwell, the first occupant of the Cavendish chair of experimental physics at Cambridge, died of intestinal cancer. Rayleigh agreed to serve as the second Cavendish professor for the period 1879–1884. He took his university duties very seriously both with respect to the instruction of students and to the carrying out of a vigorous research program that set about redetermining the values of electrical standards (the ohm, volt, and amp). A classical series of papers resulted from this ambitious project. But after a five-year tenure, he returned to his laboratory at Terling Place. Later he became (from 1887 to 1905) professor of Natural Philosophy at the Royal Institution.^[14] In the intervening time, he accepted the secretaryship of the Royal Society, vacated by the resignation of one of his former teachers, Sir George Gabriel Stokes. The duties of such a post were not onerous, and there was no falling off of Rayleigh's output throughout his eleven years of secretaryship.

The tenure of this office gave him the opportunity to discover (in 1891) and rescue from oblivion the valuable memoir in which John J. Waterston^[15] in

1846 had anticipated some of the important features of the kinetic theory of gases.

Helping Miss Pockels

An example of Rayleigh's scientific generosity was the support that he gave to some research by Miss Agnes Pockels. In January 1891, after he had published several papers relating to liquid surfaces and surface tension, Rayleigh received a long letter (in German) from Agnes Pockels (1862–1935) of Braunschweig



Figure 2. Agnes Pockels.

(Figure 2). She had read Rayleigh's paper in her brother Friedrich's^[16] journals and wanted to tell him of some experiments on surface forces that she had carried out in her kitchen sink. At that time no mechanism for the formal university training of women existed in Germany. So after she completed her education at the Municipal High School for Girls, she came under the tutelage of her scientifically adroit brother. In 1880, while still a teenager, she had begun a series of researches on the effect of oil films on the surface tension of water. To measure surface forces quantitatively, she had suspended a horizontal disk from one arm of a balance scale until the disk just touched the surface of the pure (or contaminated) water. Based on her "surface-balance" work, she sent letters outlining her results to various German scientists, but they displayed little interest in her work. It was her brother who urged her to write to Rayleigh, who

immediately saw that she had achieved several fundamental advances in the surface physics of liquids. Rayleigh then published her paper in *Nature* in 1891, with an introduction by himself commenting on the importance of her work.

This public recognition by a distinguished British scientist brought her instant fame: her later papers, it was alleged,^[12] were treated by journals with deferential respect. Professor Voigt of the Physical Institute, Braunschweig, offered her laboratory facilities. She later visited illuminati such as Quincke, Ostwald, and Weber, all eminent surface scientists. Irving Langmuir, a later Nobel laureate (1932), adopted essentially her method for measuring surface forces.

The Discovery of Argon^[7]

It was at the Royal Institution that Rayleigh largely conducted the work that earned him the Nobel Prize in Physics and brought him his greatest fame. Rayleigh had long been intrigued by Prout's hypothesis that the atomic weights should be integral numbers. If we assign hydrogen to be 1, oxygen should be 16, but it was not quite so. Was the discrepancy real? Rayleigh therefore determined the densities of hydrogen and oxygen; and then he moved on to nitrogen (in 1892). In a letter to *Nature* (submitted September 24 of that year, published September 29) he wrote:^[18]

I am much puzzled by some results on the density of nitrogen, and I shall be obliged if any of your chemical readers can offer suggestions as to the cause. According to the methods of preparation, I obtain two quite distinct values. The relative difference, amounting to about one part in 1000, is small in itself, but it lies entirely outside the errors of experiment, and can only be attributed to a variation of the character of the gas.

His two sources of nitrogen had been ordinary air with the oxygen removed by heated metallic copper, and a "lighter" nitrogen obtained by decomposition of ammonia. No illuminating response came at that time from the chemical public, but his colleague at the Royal Institution, Sir James Dewar, said that some of the atmospheric N₂ was in

an allotropic state, such as N_3 , just as some oxygen exists as ozone O_3 . Rayleigh was skeptical about this; and he continued (for two years) to prepare nitrogen by several methods. Such chemically produced nitrogen was always lighter in density than atmospheric nitrogen. One of Rayleigh's lecture-demonstrations at the Royal Institution was a repeat of some of Henry Cavendish's studies, carried out a century earlier, in which a globe of ordinary air was subjected to electrical sparking so as to consume the oxygen as an oxide of nitrogen (that could be absorbed by potash). In this manner, all of the nitrogen was removed, except, as Cavendish had noted, a very small residue. In other words, Rayleigh verified the reclusive Cavendish's results that had lain unnoticed in the literature for over 100 years.

Rayleigh expatiated on these puzzling facts in a lecture given to the Royal Society on April 19, 1894. This prompted a member of the audience, William Ramsay, to converse with Rayleigh. By the end of May of that year, Ramsay had shown that nitrogen gas, when repeatedly exposed to heated magnesium (to form the solid nitride) could be made progressively denser. Continuing his experiments through the summer, Ramsay produced in early August a gas, apparently unaffected by further treatment with magnesium (Figure 3). This result led to an exchange of letters. Sir William Crookes examined the gas and reported that it was new and quite distinct from nitrogen. Rayleigh told Ramsay that the residue was neither oxygen nor nitrogen. The two immediately joined forces, and on January 31, 1895 announced to

the Royal Society the discovery of a new gaseous element, apparently inert chemically, which they called argon (for inert, without work).

Rayleigh and Ramsay's 54-page joint paper gave the density, refractive index, solubility in water, ratio of specific heats (C_p/C_v), and atomic spectrum of the new gas, and they postulated a new zeroth column, for noble gases, in Mendeleeff's Periodic Table. Some scientists argued that so heavy an element could not possibly be a gas. Rayleigh, with aristocratic humor, replied:

...the result is, no doubt, very awkward. Indeed, I have seen some indications that the anomalous properties of argon are brought as a kind of accusation against us. But we had the very best intentions in the matter. The facts were too much for us, and all that we can do now is apologize for ourselves and for the gas.

In the process of isolating argon, Rayleigh designed the refractometer that bears his name, and the Rayleigh modification of the Huygens manometer. Lord Kelvin hailed argon as undoubtedly the greatest scientific event of the year. Specifically, he said:

If anything could add to the interest which we must all feel in this startling discovery, it is the consideration of the way by which it was found—arduous work—commenced in 1882, has been continued for 12 years by Rayleigh, with unremitting perseverance.

When Rayleigh received his Nobel Prize in 1904 the monetary value amounted to some £7700, a huge sum in those days. He donated his money to the University of Cambridge, and it was used to construct a new extension to the Cavendish Laboratory, the so-called Rayleigh Wing. This institution was built using wooden pegs and stone and cement instead of metal nails, to provide a facility better suited for sensitive electrical measurements. (Wilson's cloud-chamber measurements were carried out in this extension. All my present efforts in electron microscopy are also done in the Rayleigh wing). In his later years, honors and responsibilities fell much upon Rayleigh. He was one of the original recipients (1902) of the Order of Merit, and he accepted that Presidency of the Royal Society in 1905 (having earlier declined it).

According to Sir James Jeans:

...his massive, precise and perfectly balanced mind was utterly removed from that of the erratic genius who typifies the great scientist in the popular imagination...The outstanding qualities of his writings were thoroughness and clearness; he made everything seem obvious. Rayleigh died in Essex on 30 June 1919, having been at work on a scientific paper only five days previously...The inscription on his memorial in Westminster Abbey, 'An unerring leader in the advancement of natural knowledge', does not overstate the case.

Sir William Ramsay (1852–1916)

Rayleigh's co-discoverer of argon was born in Glasgow on October 2, 1852. He inherited scientific ability from both his parents; for, whilst his father was a civil engineer of no mean achievement and his paternal grandfather a well-known manufacturer of chemicals used by dyers, his mother was descended from a Scottish family which had produced many medical doctors of note.

As a child he showed remarkable skills with language and, like the polymath, Thomas Young (1773–1829), is said to have read the Bible when he was about four years of age. Brought up in a Calvinistic (Methodist) background he was exposed as a young child to long (and for him rather boring) sermons, during the course of which he acquired aptitude for German and French by reading the Bible in those languages. In his early teens while pursuing a conventional classical education (he was intended for the church) he broke his leg and spent a long convalescent period in bed. To while away the time, his father gave him chemicals with which he experimented. Ramsay later wrote:^[19,20]

I had the misfortune to break my leg at football. During my convalescence I read Graham's chemistry, chiefly, I must admit because I wanted to know how to make fireworks. I remember that my father gave me small quantities of potassium chlorate, phosphorus, sulphuric acid, and some small flasks and beakers and a spirit lamp, and with these I amused myself during several weary months.

4th August, 1894

Dear Lord Rayleigh,

I have isolated the gas. Its density is 19.075, and it is not absorbed by magnesium....

6th August, 1894

Dear Prof Ramsay,—

I believe that I too have isolated the gas, though in miserably small quantities...

Figure 3. The opening sentence of the letters in which Rayleigh and Ramsay report their simultaneous isolation of argon.

The thought that a young child had access to the potentially explosive mixtures of potassium chlorate and phosphorus in his bedroom fills one with alarm even now!

Young Ramsay attended an elementary (state) school and then proceeded to Glasgow Academy where he quickly revealed his flair for languages. Apart from knowing much of the Bible by heart, he acquired fluency in German and French (later he learned to speak Italian, Norwegian, Swedish, and Dutch and could read several other ancient and modern languages).

At Glasgow University, which he entered in 1866, Ramsay studied classics general literature, logic and mathematics; but after a year he decided to become a chemist. In 1869 he worked for a short while in the laboratory of the chemical supplier Robert Tatlock. At the close of the Franco-Prussian War he went to Heidelberg with the intention of studying under Robert W. Bunsen, but early in 1871 he changed to Rudolf Fittig's laboratory at Tübingen where he obtained the degree of Ph.D. for research on toluic acid (methylbenzoic acid) and nitro-toluic acids. In 1874 he became the assistant to the Professor of chemistry at the University of Glasgow, but in barely six years he became (1880) first, Professor of Chemistry at University College, Bristol, and then, a year later (shortly after his marriage to Margaret Buchanan) its principal. In 1887 he succeeded the renowned organic chemist A. William Williamson as head of general chemistry at University College, London. By the time he left Bristol, Ramsay had established himself as a formidable physical chemist, knowledgeable about critical phenomena, under which liquids and gases are in equilibrium, and dexterous in the design and imaginative use of his own apparatus for handling minute volumes of gases.

The meeting between him and Lord Rayleigh in 1894 after the latter's lecture (on the anomalous density of nitrogen) at the Royal Society marked a major turning point in Ramsay's career. Their joint discovery of argon was soon followed by another of equal importance. It came about after Sir Henry Miers (1858–1947) of the British Museum had suggested that argon might be

identical with an inert gas, supposedly nitrogen, that William Hillebrand (1853–1925), of the United States Geological Survey, had obtained by heating certain uranium containing minerals, such as cleveite (impure UO_3). Ramsay prepared this gas and found that it was not argon, but yet another, new inert gas, identical in its spectrum with the element helium, the presence of which in the sun had been spectroscopically detected during the eclipse of 1868 by Sir Norman Lockyer and Sir Edward Frankland.

Recognizing the remarkable inertness of both argon and helium, Ramsay divined that there must exist a whole related family of such inert elements. He set about, with almost frenetic speed (along with his galvanized collaborators, especially his pupil Morris W. Travers) to search for others (Figure 4); and after many months of hard work using the process of fractional distillation three new inert elementary gases, neon (the new one), krypton (the hidden one), and xenon (the strange one) were all isolated and identified in mid-summer, 1898. These gases were isolated by Ramsay and Travers from one hundred and

twenty tons of air which had been liquefied!

At the turn of the nineteenth and twentieth centuries, Ernest Rutherford and Fredrick Soddy^[21] discovered, at McGill University, Montreal, that thorium had associated with it, in minute quantities, a radioactive gas, which they designated thorium emanation. It, too, was chemically inert. In 1903 Soddy joined Ramsay's department at London and began to apply the refined techniques of analysis perfected earlier. The "emanation" gas showed no discharge spectrum, but after a time, the spectrum of helium developed. This was incontrovertible proof of the transmutation of elements, an idea that, in 1903, had been proposed by Rutherford and Soddy. In late 1910, the "emanation", later called radon, was weighed by one of Ramsay's colleagues (Whytlaw-Gray) with a balance of (then) unsurpassed sensitivity. They found that $6.58 \times 10^{-5} \text{ cm}^3$ of radon weighed $6.55 \times 10^{-7} \text{ g}$, and thus they arrived at the atomic weight (222), thereby completing the entire Nobel gas group of the Periodic Table.

Ramsay's Character, Style, and Humanity

Apart from being one of the greatest chemical discoverers—he and Humphry Davy between them discovered 14 of the elements of the Periodic Table—he was gifted with rare scientific insight and imagination, and was the possessor of a most wonderful skill and dexterity in the devising, constructing, and use of apparatus for the delicate and exact investigation of gases. According to one of his greatest protégés, Frederick George Donnan (1870–1956)—of membrane equilibria fame—who succeeded Ramsay as Professor in 1913, he was:

...a man of sanguine and courageous temperament, of tireless energy, and power of instant action, he fearlessly attacked problems the experimental difficulties of which would have dismayed and deterred most men.... Nothing was ever postponed. What an ordinary very active man would do on Monday morning, Ramsay did on Saturday afternoon. He was endowed with extraordinary personal charm, and a most kindly, generous and gentle disposition... An



Figure 4. Picture by the London cartoonist-Leslie Ward ("Spy" 1851–1922); Ramsey points to the eighth group of the Periodic Table which only contains elements that he discovered and isolated.

excellent linguist and musician, a witty and humorous speaker both in public and in private. The quickness and receptivity of his mind were remarkable, so that he was ever the enthusiastic friend and exponent of new advances in science. Thus he was one of the first chemists in England to teach and expound the work of Ostwald, Van't Hoff and Arrhenius with each of whom he could converse in their mother tongue.

Ramsay, like Rayleigh extended his activities in many directions: he found time to write a number of excellent texts on chemistry, was an ardent apostle of reform in converting the University of London into a great teaching University, and served as a member of the Royal Commission on sewage disposal and several other public bodies. Like many other truly great scientists, he could spot winners, two outstanding examples being Fredrick Soddy, Nobel Laureate 1921, and Sir Stafford Cripps, FRS (1889–1952) Statesman, Lawyer, Leader of the House of Commons in Winston Churchill's war-time cabinet, and chancellor of the exchequer in Clement R. Atlee's post-war government.^[22] The papers which won Cripps from Winchester a Natural Science Scholarship to New College, Oxford in 1907 were so remarkable that Ramsay, who had been asked to scrutinize, persuaded Cripps to prefer the better equipped laboratories of University College London. This change meant that Cripps was doing advanced research even as an undergraduate. It resulted in Cripps being a part author of a paper on the properties of xenon read before the Royal Society when he was twenty-two.^[23]

A Harmonious Partnership

It is fitting that this essay should end with reference to Helmholtz a natural philosopher greatly admired by both Rayleigh and Ramsay. Rayleigh heard Helmholtz give the Faraday Lecture at the Royal Institution in 1881, and it was Helmholtz's pioneering work that stimulated Rayleigh to write his *The Theory of Sound*. During the course of a memorable Friday evening Discourse at the Royal Institution on "Argon" in 1895, Rayleigh said:

In what I have to say from this point onwards, I must be understood as speaking on behalf of Professor Ramsay as for myself. At the first, the work which we did was to a certain extent independent. Afterwards we worked in concert, and all that we have published in our joint name, must be regarded as being equally the work of both of us. But, of course, Professor Ramsay must not be held responsible for any chemical blunder into which I may stumble tonight.

These are the very words uttered and written by Rayleigh in the enthralled account that he gave at the Royal Institution.^[24] Rayleigh ended his lecture with the following words:

It will be known to many that during the last few months of his life Helmholtz lay prostrate in a semi paralyzed condition, forgetful of many things, but still retaining a keen interest in science. Some little while after his death we had a letter from his widow, in which she described how interested he had been in our preliminary announcement (upon the subject of Argon), and how he desired the account to be read to him again. He added the remark, 'I always thought that there must be something more in the atmosphere'.

I acknowledge with gratitude the advice and guidance given to me by many: Professors Alwyn Davies, E. A. Davis, Arthur Humphrey, R. J. H. Clark, and C. R. Calladine and Dr. Andrea Sella and Dr. Aimee Morgan. I am also grateful for the kind assistance provided by Ms Joanna Corden (Royal Society), Ms Erica McDonald (Peterhouse), Ms Shazia Riaz (Davy Faraday Research Laboratory), and Dr. Robert Raja.

- [1] Sir George Gabriel Stokes (another senior wrangler), the Lucasian Professor of Mathematics, whom Strutt greatly admired, did carry out some lecture-demonstrations, and he also ran his own laboratory, where, he discovered the phenomenon of fluorescence. The only experimental courses available in Cambridge in the mid-1860s were those in chemistry, mineralogy, and certain biological sciences, a narrowness of choice which Strutt greatly resented.
- [2] J. W. Strutt, *Philos. Mag.* **1869**, 38, 1–15.
- [3] Sir James H. Jeans, *Dictionary of National Biography*, **1912–1921**, p. 515.

- [4] J. W. Strutt, *Philos. Trans. R. Soc. London* **1870**, 161, 77–118.
- [5] H. von Helmholtz, *Lehre von den Töneempfindungen*, Berlin, **1863** (translated by A. J. Ellis under the title *Sensations of Tone* (**1875**)).
- [6] Helmholtz's monograph specialized primarily^[7] in physiological and psychological acoustics and music.
- [7] R. B. Lindsay, *Lord Rayleigh: The Man and His Worth*, Pergamon, **1970**.
- [8] Evelyn Balfour was also the niece of another British Prime Minister, Lord Salisbury.
- [9] The first volume appeared in 1877, the second in 1878. This treatise soon became, and remains, the standard and authoritative text dealing with all aspects of the production and propagation of sound and acoustic attenuation in all kinds of elastic media.
- [10] J. W. Strutt, *Philos. Mag.* **1872**, 41, 107–120; J. W. Strutt, *Philos. Mag.* **1872**, 41, 274–279.
- [11] Dimensional analysis, pioneered as a mathematico-physical tool by Strutt, was later extended by others, notably the Nobel Laureate Percy W. Bridgman^[12].
- [12] "The Scientific Research of John William Strutt, Third Baron Rayleigh": J. N. Howard, *Proc. R. Inst. GB* **1988**, 60, 73–86.
- [13] One should not be surprised by the fact, for there were other contemporary, great scientists (like William Crookes, inventor of the radiometer and discoverer of the element thallium, and later, like Rayleigh, President of the Royal Society) who were deeply interested in psychical phenomena. That was a widely held view. In fact when the journal *Scientific American* published an editorial in 1920, under the heading "The Future Based on an Analysis of the last 70 Years", it was predicted that whereas the eighteenth century was characterized scientifically by advances in electricity the twentieth century would be equally remembered for advances in psychic research.
- [14] The basic duties at the Royal Institution were light: the incumbent was to give each year a course of six Saturday afternoon lectures before Easter, as well as one Friday evening Discourse per annum, the lectures to be illustrated by experiments. In return he would have the year-round use of a laboratory of three rooms in the Royal Institution. The real attraction, it seemed, was that the Royal Institution was wired for electricity (thanks to the effort of the then Director, Sir James Dewar), which his laboratory at Terling was not.
- [15] J. J. Waterston (1811–1883) developed the early Kinetic Theory of Gasses and

largely anticipated the theory put forward by R. J. E. Clausius in (1857).

- [16] Who is now remembered for his studies of the Pockels effect, used in electro-optical modulators.
- [17] Part of this account is based on the excellent Friday Evening Discourse given, at my invitation at the Royal Institution by J. N. Howard during my tenure of the Directorship. See ref. [12] for fuller details.
- [18] "Density of Nitrogen": Lord Rayleigh, *Nature* **1892**, 46, 512–513.
- [19] W. M. Travers, *A Life of Sir William Ramsay*, Arnold, London, 1956; see also obituary notice in *Proc. R. Soc. London Ser. A* **1956**, 93, 1916–1917.
- [20] I am greatly indebted to Professor Alwyn G. Davies FRS for making available to me his notes for a lunchtime lecture (on Ramsay) given at University College London, March 19, **2004**.
- [21] Ramsay had spotted Soddy in 1898 as a bright young student at the University of Oxford where he was external examiner and Soddy had headed the honours list in chemistry.
- [22] Other members of Ramsay's team in London, included M. W. Travers, E. C. C. Baly, N. Collie, F. Soddy, R. Whytlaw-Gray, and E. Egerton, all of whom, like Donnan, became Fellow of the Royal Society.
- [23] H. S. Patterson, R. S. Cripps, R. Whytlaw-Gray, *Proc. R. Soc. London Ser. A* **1912**, 86, 579–590.
- [24] Lord Rayleigh, *Proc. R. Inst. GB* **1895**, 14, 524–538.

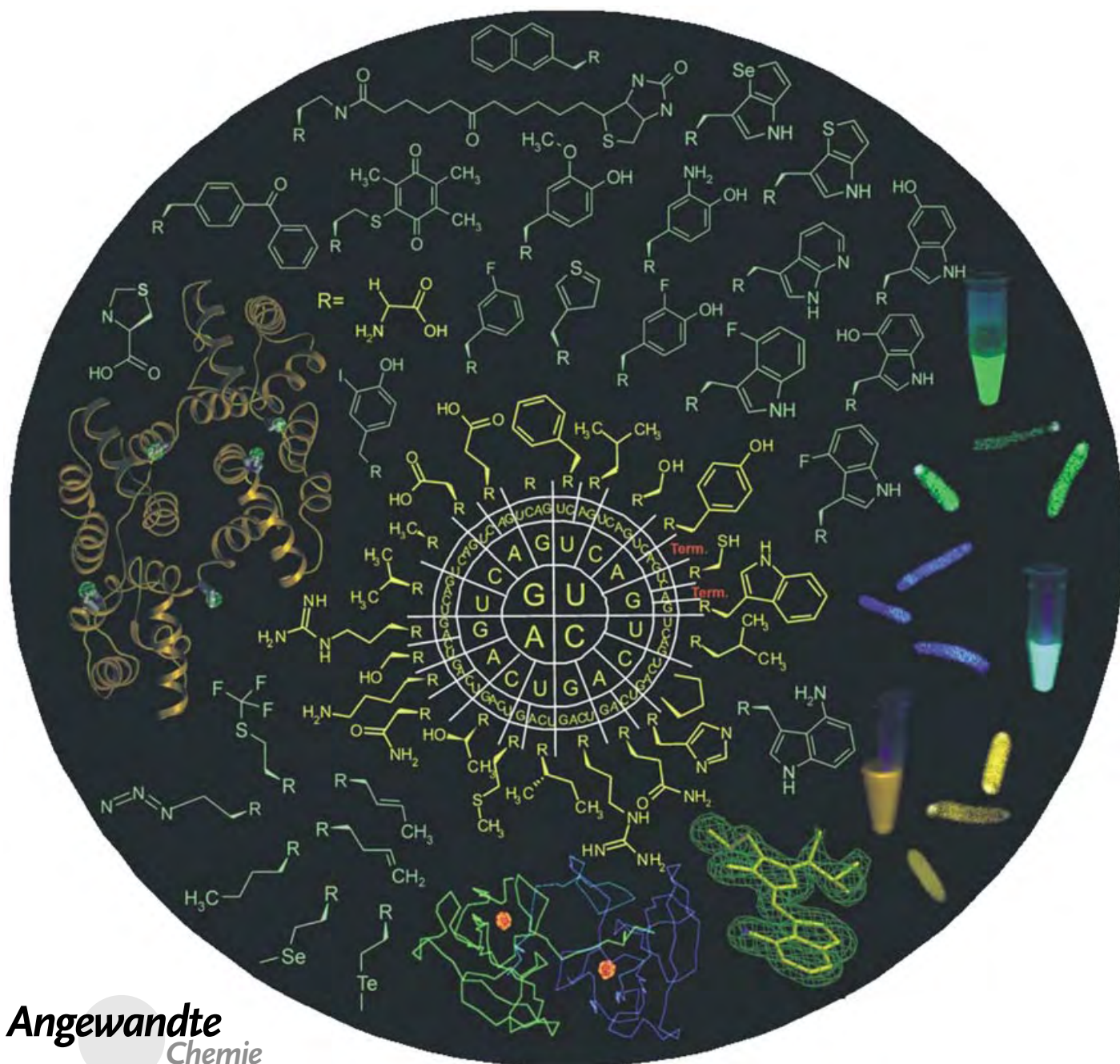
Protein Biosynthesis

Prolegomena to Future Experimental Efforts on Genetic Code Engineering by Expanding Its Amino Acid Repertoire

Nediljko Budisa*

Keywords:

amino acids · biosynthesis · evolution · genetic code · proteins



Angewandte
Chemie

Protein synthesis and its relation to the genetic code was for a long time a central issue in biology. Rapid experimental progress throughout the past decade, crowned with the recently elucidated ribosomal structures, provided an almost complete description of this process. In addition important experiments provided solid evidence that the natural protein translation machinery can be reprogrammed to encode genetically a vast number of non-coded (i.e. noncanonical) amino acids. Indeed, in the set of 20 canonical amino acids as prescribed by the universal genetic code, many desirable functionalities, such as halogeno, keto, cyano, azido, nitroso, nitro, and silyl groups, as well as $C=C$ or $C\equiv C$ bonds, are absent. The ability to encode genetically such chemical diversity will enable us to reprogram living cells, such as bacteria, to express tailor-made proteins exhibiting functional diversity. Accordingly, genetic code engineering has developed into an exciting emerging research field at the interface of biology, chemistry, and physics.

From the Contents

1. Introduction	6427
2. Basic Features and Requirements for Cellular Protein Synthesis	6429
3. Traditional Auxotroph-Based Methods	6432
4. Power and Limits of Selective Pressure: Engineering a Second Code	6438
6. Other Aspects Related to an Expanded Amino Acid Repertoire	6444
7. Some Practical Applications of Noncanonical Monomers	6449
8. The Future of Genetic Code Engineering	6452

“Wenn es uns gelingt, in dem dunklen Gebiet der organischen Natur auf einen lichten Punkt zu treffen, der uns wie einer der Eingänge erscheint, durch die wir vielleicht auf die wahren Wege zur Erforschung und Erkennung dieses Gebietes gelangen können, so hat man immer Ursache sich Glück zu wünschen, selbst wenn man sich der Unerschöpftheit des vorgesetzten Gegenstandes bewusst ist.”^[*]

F. Wöhler and J. Liebig, *Ann. Pharm.* **1833**, 3, 249

1. Introduction

1.1. Genetic Program and Natural Laws

Life is a continuous interaction of an autonomous self-perpetuating system, composed of organic matter, with its physicochemical environment. Two factors shape this process: first, the deterministic laws of chemistry and physics (Natural laws) and second, the genetic program which determines all biological activities and phenomena. The existence of such a genetic program distinguishes living and non-living matter.^[1] In the frame of such a program nucleic acids encode information and proteins replicate it.

The genetic information is defined by a precise sequence, either of bases in nucleic acids, or of amino acids in proteins. The information stored in deoxyribonucleic acid (DNA) may

be retained as regulatory DNA, transferred to ribonucleic acid (RNA) and retained as tRNA, rRNA, snRNA, tmRNA etc., “reversed” from messenger RNA (mRNA) back to DNA (by a reverse transcriptase), or further transferred from RNA (through mRNA) to a protein. The “central dogma” of molecular biology, proposed originally by Crick,^[2] was the first hypothesis capable of predicting a direction of transfer of genetic information in living beings. It states that “the transfer of information from nucleic acid to nucleic acid or from nucleic acid to protein may be possible, but transfer from protein to protein, or from protein to nucleic acid is impossible.” This transfer is governed by the genetic code as a set of rules that precisely relates the sequence of base triplets in nucleic acids (polynucleotides) with a sequence of amino acid residues in proteins (polypeptides). After the elucidation of the triplet genetic code,^[3,4] it became clear how information for linear amino acid sequences was contained in the collinear nucleic acid sequences. That the 20 standard or canonical amino acids are assigned by 61 coding triplet combinations and three termination signals (Figure 1) is now considered as basic biochemical knowledge.

[*] When we are successful in finding a glimmer of light in the dark field of organic nature, which seems to provide us with a comprehensible entry to research in this field, one has always enough reasons to consider himself as lucky, even when one is fully aware of how inexhaustible this matter is.

[*] Dr. N. Budisa
Max-Planck-Institut für Biochemie
Junior Research Group “Molekulare Biotechnologie”
Am Klopferspitz 18a
82152 Martinsried bei München (Germany)
Fax: (+49) 89-8578-3516
E-mail: budisa@biochem.mpg.de



Supporting information for this article is available on the WWW under <http://www.angewandte.org> or from the author.

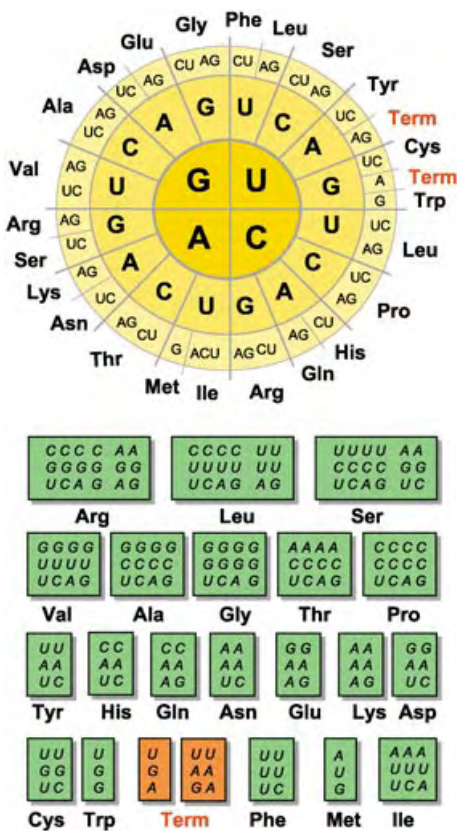


Figure 1. The structure of the genetic code. Twenty amino acids are encoded by 61 triplet coding units or codons (“sense” codons), while the remaining three codons (UAA, UGA, UAG) serve as termination signals in protein translation (“nonsense” codons). The set of 20 canonical amino acids is the result of the evolutionary assignment of coding triplets (codons) or codon families to particular amino acids (below). Note the increased redundancy in coding of strictly polar and apolar amino acids with the highly synonymous quotas for Arg, Ser (XGX codons), Leu and other hydrophobic amino acids (XUX codons). On the other hand, amino acids such as Met (AUG) or Trp (UGG) are assigned with only a single coding triplet.

1.2. What Is Genetic Code Engineering?

Experimental approaches for the expansion of the number of amino acids that can serve as basic building blocks in ribosome-mediated protein synthesis are described



Nediljko Budisa, born 1966 in Sibenik (Croatia), studied chemistry, biology, molecular biology, and biophysics at the University of Zagreb (Croatia). He carried out his Ph.D. work in the laboratory of Robert Huber at the Max-Planck-Institute für Biochemie in Martinsried and defended his Ph.D. thesis in 1997 at the Technical University, Munich. He continued his Postdoctoral work in Martinsried in the laboratories of Robert Huber and Luis Moroder where was been leading a "protein engineering" research team since 2000. He is currently finishing his Habilitation work (started 2001) at the Technical University in Munich.

in the literature under different names. Examples include “expanded scope of protein synthesis”,^[5] “expanded amino acid repertoire”,^[6] “expanded genetic code”,^[7] “tRNA-mediated protein engineering” (TRAMPE),^[8] “site-directed non-native amino acid replacement” (SNAAR).^[9] All these approaches have in common experimental re-coding, read-through, or changes in meaning of coding triplets in the frame of the existing universal genetic code. In principle, experimental readthrough can be achieved either by the reassignment of evolutionary assigned coding triplets (i.e. sense codons), or by suppression of termination triplets (UGA, UGG, UGU) or non-triplet coding units. In the context of protein expression, this can be achieved by controlling environmental factors (i.e. selective pressure) and/or by supplementation with redesigned translation components. The result of these experimental interventions at the level of the universal genetic code is an increase in its coding capacity by expanding the amino acid repertoire. In other words, the changes in the interpretation of the genetic code lead to the expanded scope of ribosome-mediated protein synthesis. The term “engineering of the genetic code” unifies all these aspects as it strictly refers to experiments aimed at changing the interpretation of the universal genetic code and thus at changing the structure of the code by introduction of novel coding units.

1.3. Terminology of Code Engineering

Engineering of the genetic code can be regarded as a novel interdisciplinary research field. This causes some difficulties in gaining a comprehensive overview of the field. For example, the subdiscipline of genetics brings with it a rather complex terminology. Widely used terms such as “functional genomics” or “proteomics” cover gene actions and interactions for the genome and proteome, respectively, and include at least four levels of complexity: genes (the genome), messenger RNA (the transcriptome), proteins (the proteome), and metabolism (the metabolome).^[10] It becomes even more complicated when other aspects such as post-translational modifications or pharmacological properties are included since each of these research areas uses its own terminology.

There is currently no generally accepted nomenclature for the field of code engineering. A simplified terminology^[6] classifies amino acids in two general groups: canonical and noncanonical. Other distinctions include cognate/non-cognate, coded/non-coded, proteinogenic/non-proteinogenic, standard/nonstandard, natural/unnatural/non-natural, special canonical amino acids and biogenic amino acids. Amino acids isosteric or similar to the canonical ones are regarded as analogues or surrogates, and their mode of translation in proteins can be position-specific (directed by reassignments of rare codons and by suppression of termination or frameshifted coding units) or multiple-site (usually directed by reassignments of common coding triplets or codon families in the target sequence).

1.4. Routes towards an Expanded Amino Acid Repertoire

The current methodological developments in the field of genetic code engineering can be divided into two methodologically different, but equally valuable and promising approaches based on different traditions. The first approach, which is based on the use of auxotrophic strains, can be traced back to the classical experiment performed by Cowie and Cohen in 1957.^[11] It relies on classical genetics based on breeding, strain construction, and selection of intentionally induced genetic variations in intact host expression cells that are forced to make “mis-incorporations” by environment control and manipulation, that is, by an externally imposed selective pressure. Usual terms used for this experimental approach are codon reassignments and multiple-site mode of incorporation.

The second approach can also be dated back to early experiments performed in an attempt to elucidate the genetic code and to get insights into the process of protein synthesis. The most prominent example is the classical discovery by Chapeville et al.^[12] in 1962 which demonstrated that misacylated tRNAs (i.e. tRNAs charged with non-cognate amino acids) are able to participate in peptide bond formation at the ribosome in a fashion consistent with the adapter hypothesis. This discovery can be regarded as the birth of the experimental approaches that use mostly tRNAs with changed identity, usually suppressor tRNAs. By the use of chemically or enzymatically aminoacylated tRNAs the original meaning of coding units is “suppressed” leading to suppression-based methodologies, usually associated with the position-specific mode of incorporation.

1.5. Scope of This Review

The intention of this article is to provide a broader context for discussing the importance of selective-pressure-based methods in the field of genetic code engineering.^[6,13–17] This is indeed necessary due to the lack of recent comprehensive and critical reviews covering this topic. In addition, for a complete overview of this field a critical and systematic review of suppression-based methodologies is also provided. The diversity of topics and themes in chemistry and biology touched by this novel research field will be illustrated through discussions of challenging problems in contemporary biological chemistry. Apart from the attempt to contribute to a clarification of the taxonomic issues, this study will also address possible future research ventures. In this context, it is also important to consider potential global impacts of code engineering on the society.

A great deal of the discussions in this review of code engineering is actually related to the chemistry of *Escherichia coli* which till date, remains the main model microorganism for protein expression in biochemistry. A major task for future experiments is to realize engineering of the genetic code in eukaryotic cells to larger extents, which will certainly provide additional, novel, and exciting insights and concepts. Related fields such as protein modifications, peptide synthesis, recombinantly expressed protein and native ligation,

and in vitro use of chemically misacylated tRNAs will not be addressed since numerous reviews and textbooks are available on these topics.

2. Basic Features and Requirements for Cellular Protein Synthesis

2.1. Chemistry and Metabolism of Canonical and Noncanonical Amino Acids

One of the greatest successes of 19th century biochemistry was the establishment of the nitrogen-balance concept, which is closely related to amino acid metabolism.^[18] Only after the advent of radioactive labeling in metabolic studies it became clear that this concept can be understood in terms of a balance between protein synthesis and catabolism. Because of this balance, amino acids are found in living organisms in both their free (modified or unmodified) forms, covalently integrated into peptides and proteins, or conjugated into other structures. Since life is based on protein chemistry, through its evolution on earth, a large variety of organisms has developed idiosyncratic ways of handling amino acids. Therefore, many findings regarding 1) mechanisms of amino acids formation, 2) their chemical nature, and 3) their intracellular transport turnover and discharge properties in *Escherichia coli* apply equally well to mammalian and other cell types.^[19] In general, amino acids are either metabolically generated or are imported into tissues by means of active transport.

They may undergo different metabolic pathways serving as substrates for deamination that result in keto acid residues capable of entering the glycolytic pathway at the level of pyruvate or acetyl CoA or alternatively enter the Krebs cycle. In addition, they are both fundamental building blocks for protein synthesis as well as important components in the biosynthesis of numerous bioactive molecules such as nucleic acids, glutathione, nicotinamide sphingosins, porphyrin derivatives, various metabolic cofactors, neurotransmitters, and pigments.^[10]

Under the normal physiological conditions and along with the steady state conditions of the growth medium, the amino acid levels in intracellular pools remain constant—oscillations and changes are associated with the cell cycle phase.^[20] The transport of amino acids across the plasma membrane is an active process mediated by membrane permeases grouped according to their preference for certain types of amino acids. Living cells inspect many substances that can and do interfere with their metabolism. However transport systems are quite promiscuous and are also not capable of distinguishing between chemically and sterically similar amino acids (and other small molecules) and thus, cells pay the penalty of being penetrated by harmful substances.^[19] Therefore, the formation of a pool of noncanonical amino acids is expected to take place just as much as of those of canonical ones.

Because of such a lack of specificity in the cellular uptake mechanisms, a particular cell would treat D- and L-forms in a similar, if not, identical manner and allow the incursion of all kinds of small molecules, which leads to the formation of intracellular pools of β -imino, β -, and γ -amino acids, cyclized

forms etc. Once such substances are present in the cytosol, they may affect a variety of metabolic, synthetic, and other physiological functions. In general, these amino acids have several effects: 1) They influence the amino acid biosynthesis, 2) they interact with catabolic enzymes, 3) they act as mechanism-based irreversible enzyme inhibitors, 4) they interfere with the amino acid transport and storage, and finally 5) they act in the translation process by serving as substrates for protein synthesis (i.e. they enter the genetic code).^[19,21]

2.2. Why Are There Only 20 Canonical Amino Acids?

Numerum combinationum in terminis etiam numero finitis esse infinitum; si rite omnia expendantur. In ipso immenso combinatorium numero in immensum plures esse combinationes inordinatas, quam ordinatas.

(Careful examination reveals the infinite number of combinations between the finite numbers of terms. In this large number of combinations there are far more without order than with it.)

R. J. Boscovich, *Theoria philosophiae naturalis redacta ad unicam legem virium in natura existentium*, Venetiis, Ex Typographia Remondiana, **1763**, p. 254–256.

Assembling polymeric molecules from building blocks by means of predefined combination rules would certainly lead to combinatorial explosions.^[22] The number of the monomeric building blocks is defined, whereas their transient assemblies (i.e. polymers) become entities of great variety, some of which are capable of function. The organized polymeric structures in living beings originate by a self-organization process under nonequilibrium conditions that is facilitated by self-enhancement or cooperativity.^[23] These structures are constructed around a template and the choice of their fundamental building blocks is dictated by the need to implement the biological functions carried out by them. In this process of assembly, evolution led to the accumulation of structures/functions on account of their selective advantages. The main questions in this respect are as follows. What basic features should such polymers have? What limits their size, diversity, and complexity?

A few decades ago, Miller and Weber^[24] were considering the hypothetical scenario for the independent origin of life on another planet in which proteins would function as catalysts. Which basic building blocks would then be used for the synthesis of the proteins? Applying physicochemical, genetic, and historical argumentation^[25] for such a scenario, Miller and Weber concluded that about two-thirds of the basic building blocks would be of the same physicochemical nature as those on earth. According to this concept, amino acids that have adverse effects on protein structure, stability, and function, were excluded from the code. The explanation for the exclusion of other amino acid types that do not violate these rules is most probably historical, such as their unavailability or insufficient evolutionary time to produce them metabolically.^[26]

Therefore, the answer to the question as to why only 20 amino acids represent the standard repertoire of the universal genetic code is an evolutionary one. The establishment of this set was certainly a historical process, a sort of “bottleneck” event to which all coding properties could be traced.^[27] The establishment of the standard repertoire of 20 amino acids might be depicted either as the “last universal common ancestor”,^[28] as “progenote” local populations.^[29] In other words, in their evolutionary development living beings must have reached a stage when any further amino acid repertoire expansion (i.e. further invasion or reassignments of coding triplets) were not possible without lethal effects. Indeed, genome and proteome complexity of evolutionary advanced eukaryotic cells allows further functional diversification by other means as has been extensively discussed elsewhere.^[27]

In this way, the amino acid repertoire of the genetic code can be regarded as conserved. Canonical amino acids as basic monomers of protein structure have a capacity to allow foldable, properly stable, and functionally active structures with well-balanced and optimized sequence compositions, fully integrated into the cell metabolism and bioenergetics. As a result of these evolutionary optimizations, characteristic folds and stable conformations in proteins are largely preserved despite their great variations in their sequences.

In spite of such strict conservation in the code repertoire, it has been possible for decades to substitute, to a certain extent, in the whole proteome one canonical amino acid with a similar noncanonical one by simple experimental design. This procedure foresees simple selective pressure experiments based on the phenotype selection (metabolically engineered cells, e.g., auxotrophs), together with the fermentation conditions and amino acid supply control. Recombinant DNA technology brings these possibilities down to the level of single proteins (see Section 3.4).

Novel “intrinsic” codon reassignments designed experimentally should be chemically plausible. Every amino acid “privileged” for entry in such a “tailored” genetic code must be optimally designed to fulfil the selective requirement, for example, for polarity, hydrophathy, molecular volume, isoelectric point, position in the protein structure with optimized codon template. Correspondingly, it was expected that a carefully designed selective pressure experiment should exploit the fact that there is sufficient room for increasing the diversity of the genetic code vocabulary.

2.3. Basic Features of Ribosome-Mediated Protein Synthesis

The genes involved in replication, transcription, aminoacylation and translation are almost universally conserved among the living kingdoms. Protein synthesis, a key step in realizing templated genetic information is performed by ribosomes in all living organisms. These translate the genetic information, previously transcribed from the DNA template to an mRNA (template replica), into the amino acid sequence of a protein. The DNA-replication, RNA-transcription, and protein translation are mutually interdependent processes that are intrinsically coupled with the proper folding of a target protein^[6] (see Figure 2).

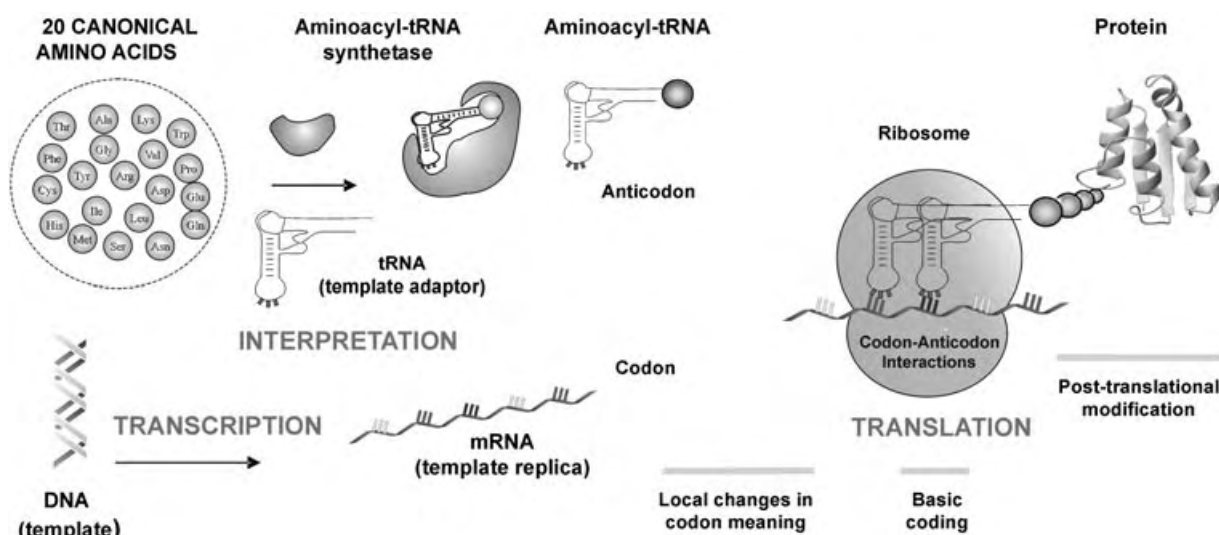


Figure 2. Flow chart depicting the transmission of genetic information. The accuracy of the translational process depends largely on two successive independent recognition events: 1) selection, activation, and covalent linkage of cognate amino acids with cognate tRNAs (aminoacylation) and 2) noncovalent interactions between charged tRNA with ribosome-bound mRNA (translation in *sensu strictu*). The basic coding is achieved through the conservative mRNA–tRNA codon–anticodon specific base pairing; the meaning of each codon is interpreted through the stringent substrate specificity of aminoacyl-tRNA synthetases (aaRS) in the aminoacylation reaction. Local changes in codon meaning and post-translation modifications provide a means to diversify protein functionality beyond its basic coding.

The protein translation process is shaped by two crucial molecular recognition events: codon–anticodon interaction between tRNAs and mRNAs on the ribosome (translation of the genetic information in *sensu strictu*) and a specific selection of the amino acid substrates by the enzyme actions of the aminoacyl-tRNA synthetases^[30] (interpretation of the genetic code). It means that translation of the genetic message relies on interactions between nucleic acids (i.e. base pairing), whereas interpretation of the genetic message relies on the enzyme catalytic actions (i.e. enzyme–substrate interactions)^[31] of the aminoacyl-tRNA synthetase (aaRS), and in exceptions on other enzymes as well. In fact, this second recognition event is the tRNA-aminoacylation catalyzed by corresponding enzymes, the aminoacyl-tRNA synthetases, which are highly specific for particular amino acids and their cognate tRNA isoacceptors. Therefore, aaRSs and tRNAs are central players in translation,^[32] catalyzing the amino acid activation and accurate biosynthesis of aminoacyl-tRNAs, the immediate precursors for encoded proteins.

Transfer RNA plays a role of an adapter between amino acids and mRNA molecules^[2] since it links in a collinear manner the information coded in the nucleotide sequence of mRNA with the amino acid sequence of the corresponding protein. Because of the degeneracy of the genetic code, there are more than forty adapters in *E. coli* alone. The basic architecture of tRNA molecules^[33,34] consists of an acceptor stem capable of being loaded with one amino acid and an anticodon loop which provides complementarity for coding triplets at the mRNA. Such a design predisposes the tRNA molecule to participate in both recognition events crucial for correct translation of a particular mRNA into the target protein sequence.

The original proposal of the adaptor hypothesis postulates that the synthesis of proteins from messenger RNA is possible

since each cognate tRNA would be aminoacylated by a unique enzyme.^[2] However, it is now well documented that many *Archaea* bacteria possess only 16 of the 20 canonical aaRSs. The absence of particular aaRSs (such as AsnRS and GlnRS) is often compensated in indirect ways, that is, by the recruitment of enzymes of intermediary metabolism.^[32] Interestingly, the absence of CysRS is compensated by the dual function of the ProRS (which obviously recognizes both substrates).^[35] These surprising findings will most probably be further extended in future genome and proteome mapping among different life kingdoms.

Other features of the translational apparatus include the existence of quality control mechanisms responsible for discrimination between the cognate/noncognate/biogenic amino acid.^[36–38] Each tRNA from the cellular pool has its own “identity”, which is defined as a sum of properties that enable its recognition through cognate aminoacyl-tRNA synthetase and prevent binding of other enzymes.^[39,40] Similarly, the “identity problem” of amino acids can be faced in the frame of the expanded amino acid repertoire as well. It is conceivable that one amino acid serves as a substrate for two synthetases. The two different tRNA species are then loaded as isoacceptors with the same amino acid and have the same “identity”. For example, Tirrell and co-workers^[41] clearly demonstrated that norleucine and norvaline are not only substrates for MetRS but also for LeuRS with attenuated editing activity. Similarly, chlorinated and brominated Phe analogues were equally good substrates for engineered PheRS from *E. coli*^[42] as well as TyrRS from *M. jannaschii*.^[43] Thus, it is reasonable to expect that future experimental manipulations with the intracellular concentrations as well as substrate specificities of aaRS will certainly yield “identity switches” of particular noncanonical amino acids between different coding triplets in the protein translation.

3. Traditional Auxotroph-Based Methods

It is well known from the evolution theory that mutations in living organisms occur spontaneously regardless of their fitness,^[1,44] that is, they are random and the environment (selection) acts as a filter to those that are beneficial.^[45] The transmission of this strategy from nature into the laboratory facilitates an anthropogenic selection of the phenotype of interest. Rapidly evolving organisms such as viruses, bacteria, protozoa or some organelles or fast growing mammalian cells in culture are usually selected for work in laboratory conditions on very short human time scales. A special class of mutants of bacterial or eukaryotic cells deprived of its own amino acid supply (auxotrophs) can be bred and selected by using methods of classical genetics.^[46] The engineering of the genetic code benefits from such cells which are, in fact, either metabolically engineered microorganisms or eukaryotic cells. Cells selected in this way offer an almost ideal platform to affect the selection of the amino acids for protein biosynthesis, that is, to expand its amino acid repertoire. In general, to obtain new amino acids as building blocks for proteins, the selective pressure should be specifically designed for such a compound of interest. Successful experiments include 1) uptake of the noncanonical amino acid, 2) its attachment onto tRNA, and 3) its incorporation into the nascent polypeptide chain.

At the level of the genetic code and genetic message translation, this traditional auxotrophic approach results in sense-codon reassignments, which result in a canonical → noncanonical amino acid substitution in the protein sequence. Substitution experiments were done at the level of the whole proteome.^[11] Later, when extra-chromosomal plasmid-directed protein expression systems became available, it was possible to replace amino acids in single target proteins (for example, see refs. [13,17,47–49]).

3.1. Early Experiments

The substitution of canonical amino acids with non-canonical ones is a relatively old approach in protein chemistry.^[50,51] The recent revival of these methods can be seen as a renaissance of the pioneering work and ideas from the 1950s and 1960s.^[52] Numerous observations and findings from these early studies are still relevant for the development of current methods. In the pioneering work, *Escherichia coli* had still not become a “model” organism for protein expression. Indeed, other microorganisms (*Staphylococcus*, *Bacillus*, *Lactobacillus*, *Salmonella*, *Leuconostoc*) and a variety of eukaryotic cells types (*Saccharomyces*, *Neurospora*, *Tetrahymena*, different carcinoma cell lines such as *HeLa*, hepatocytes, and lymphocytes) were used for incorporation experiments as well.^[52]

The initial attempts to introduce variations into the amino acid composition in proteins were made by the fermentation of microorganisms in the presence of structural analogues of amino acids.^[53] The basic criterion for one substance to be regarded as an “analogue” was the requirement of having a shape and size similar to those of the naturally occurring

molecule without dramatic differences in biophysical properties. Such amino acid analogues that are sterically almost identical to the canonical ones are named isosteres (e.g., Met/SeMet^[11] or Arg/canavanine^[54]). Modifications that include addition/deletion of one or more methylene group in the side chain (e.g., Met/ethionine^[53]) or other groups resulted in homologues of the amino acids. In recent research such amino acids are usually termed as “surrogates” (for examples see Chapter 4).

The first property of such analogues/surrogates observed was their potential to serve as antimetabolites and to penetrate into the amino acid pool of bacteria by the same route as their canonical counterparts. These pools are in dynamic equilibrium with the protein-synthesizing machinery. It was also shown that certain analogues, such as 3- α -indoleacrylic acid, indeed inhibits the endogenous supply (i.e. biosynthesis) of tryptophan.^[55] In the context of the fermentation experiments such antimetabolic actions were observed as an emergence of “linear” instead of exponential growth in the cultures supplemented with these analogues.^[56] This linear growth was correctly attributed to the incorporation of amino acid analogues into the vital cellular enzymes, which reduces or even abolishes the enzyme function. Almost all documented fermentation experiments with a variety of analogues (except SeMet) reported a linear growth of the culture upon addition of an analogue into the synthetic growth media.^[57] These pioneering experiments confirm that the composition of proteins can be influenced by environmental changes, that is, by experimentally imposed selective pressure. Since then, experimental effort has focused towards more specifically defined goals to shed more light on the factors that determine amino acid incorporation into proteins. However, neither these earlier studies nor recent developments in this field, yielded general rules that are capable of predicting which changes will produce translationally active amino acid analogues. To date there are only empirical observations that are concerned with the chemical reactivity, molecular structure, volume, and other properties of the analogues/surrogates.

Nonetheless, these early studies paved the way for more extensive studies of the effects of the exchange of canonical for noncanonical amino acids on the enzymatic and immunological properties of selected proteins. Numerous historical examples of amino acid analogue applications in various fields ranging from microbiology to biomedicine are extensively reviewed elsewhere.^[50,51,58]

3.2. The Importance of Cellular Extracts for Early Incorporation Experiments

As early as the beginning of 1950s it had been shown by several investigators that ribosome-mediated protein synthesis does not require the integrity of the cell and can continue after cell disruption.^[59] Ribosomes in these cell extracts were programmed with endogenous DNA templates. These systems were invaluable in studies of molecular mechanisms of protein biosynthesis, requirements for protein synthesis, and elucidation of the genetic code. The introduc-

tion of the exogenous messengers as demonstrated by Nirenberg and Matthaei^[3,4,60] paved the way not only to unambiguous deciphering of the genetic code, but also to the development of modern cell-free systems with dramatically improved performance. The availability of these cell-free extracts was also important for studying the requirements for protein translation with amino acid analogues/surrogates.

That a large number of amino acid analogues could be activated was well documented, even before a clear picture of the aminoacylation reaction emerged. In these initial experiments, extracts of *E. coli* were used to study the activation of noncanonical amino acids. Norvaline, α -amino- β -chloro-butyric acid, *p*-fluorophenylalanine, Nle, SeMet, and ethionine were activated by *E. coli* extracts.^[52] The most important observation in these studies was that the rate of activation does not directly correlate with the translation of amino acid analogues into protein sequences. For example, extracts of a Phe-requiring *E. coli* strain were capable of activating β -2-thienylalanine at the same rate as Phe. On the other hand it is a poor substrate for protein synthesis in intact *E. coli* cells. The lesson from these experiments was obvious: activation of a particular amino acid does not automatically mean that it leads to translational activity. Later, extracts of the microbial auxotrophic strains as working material were replaced with purified aminoacyl-tRNA synthetases (aaRS) and activation was directly tested in ATP-pyrophosphate exchange reactions. By the end of 1970s an impressive number of non-canonical analogues capable of participating in activation reactions were known.^[61]

3.3. Proteome-Wide Replacements: An “Unnatural Microorganism”

By the 1950s it was well known that amino acid analogues could be incorporated into the proteins of *E. coli* as well as that those substitutions might result in various biological effects.^[52] However, the most important and far-reaching finding was the SeMet-incorporation into proteins made by Cowie and Cohen by use of the Met-auxotrophic *E. coli* ML304d strain.^[11] Since the growth rate of the culture was dependent on the external Met supply, it was possible to design a defined synthetic medium in which Met was replaced by SeMet. In such cultures, ML304d cells grow more slowly than in cultures supplied with Met, but the shape of the growth curve was nevertheless exponential. SeMet, when offered as a sole source of replacement for Met, was found to completely and uniformly substitute Met in all cellular proteins retaining exponential growth. In other words, the cellular viability was not dramatically harmed by SeMet replacements and this first “unnatural” organism had similar properties to its Met-containing parental cells.

This landmark experiment by Cowie and Cohen^[11] was certainly the first demonstration of proteome-wide substitution of Met residues through selenomethionine. SeMet is one of the few analogues for which a great substitution capacity has been demonstrated. Moreover, the work of Cowie and Cohen^[11] is an excellent example of experimentally imposed changes in the interpretation of the genetic code (that is, the

Met→SeMet reassignment for the AUG coding triplet) by use of metabolically engineered cells (Met-auxotrophs). In the following decades, the focus was on the mechanism of the incorporation of SeMet in different cells as well as its role in aminoacylation reactions and protein synthesis. The recent renaissance of SeMet incorporation into proteins was possible only after Hendrickson^[62] rediscovered the approach adopted by Cowie and Cohen as an important tool for structural biology. Namely, the replacement of sulfur for selenium in Met residues of proteins was recognized as a very effective anomalous scatterer of X-rays, a main prerequisite for multiwavelength anomalous diffraction (MAD) for solving the phase problem in X-ray crystallography of proteins.^[63] The ever increasing number of protein structures resolved by MAD is a clear sign that SeMet proteins are not just another ephemeral trend in biochemical sciences.^[64]

A second example of an “unnatural” microorganism was provided by Wong who reported a series^[65] of microorganisms capable of intrinsically changing their preference for amino acids. In this experiment, *Bacillus subtilis* QB928 Trp-auxotroph was serially mutated and cultured for many generations in a defined minimal medium containing 4-fluorotryptophan. The resulting *Bacillus subtilis* mutant HR15, which shows a higher preference for 4-fluorotryptophan than for canonical Trp, has been described as the “first free-living organism in the past couple of billion years to have learnt to thrive on a genetic code that departs from the universal code”. Unfortunately, an accompanying genotype analysis was not presented and experiments that would reproduce these exciting findings have not been done yet, to the best of our knowledge. Since 4-fluorotryptophan exhibits no characteristic fluorescence at room temperature, related labeled proteins should exhibit “silent” (i.e. suppressed) fluorescence. This was demonstrated in a study of ribosomal proteins isolated from *B. subtilis* HR15, which upon Trp/4-fluorotryptophan replacement lost their fluorescence.^[66] The importance of Wong’s experiments, however, lies in the fact that he demonstrated the power of genetic selection and the possibility of imposing experimental pressure on the membership mutation of the genetic code, that is, of making a microorganism with a changed genetic code vocabulary.

The approach adopted by Wong to design an “unnatural organism” has recently been revived by Ellington and Bacher. In 2001 they attempted to evolve *E. coli* variants that could survive on 4-fluorotryptophan ((4-F)Trp),^[253] the growth-inhibitory properties of which are well known. They hypothesized that a relatively small number of proteins might be adversely affected, and some cells might mutate and emerge through many generations created in a simple serial transfer experiment in a way that (4-F)Trp could be accommodated in the proteome. After continuous evolution for 250 h and 14 serial transfers, the parent strain was adapted to 99% of (4-F)Trp in the medium. Although mutant strains capable of growing on 99.97% of (4-F)Trp in the synthetic medium have been isolated, the evolved strains maintained an absolute requirement for Trp. The authors concluded “that the incorporation of unnatural amino acids into organismal proteomes may be possible but that extensive evolution might be required to reoptimize proteins and metabolism to

accommodate such analogues". In their most recent contribution, Bacher, Bull, and Ellington switched to bacteriophage Q β as a model system for the generation of chemically ambiguous proteomes.^[254] The Q β phage is a relatively simple model system, defined as a quasi-species since its genome is a weighted average of a large number of different individual sequences. The replication of this phage was examined in *E. coli* Trp-auxotroph in the presence of a series of monofluorinated Trp analogues. Even though the fitness of the phage after 25 serial passages increased substantially, an absolute requirement for traces of L-Trp remained.

Genetic selection was also the tool of choice for ambitious experiments performed by Marliere and co-workers^[67] in which the goal was to design "microbial strains with a clear-cut requirement for an additional amino acid that should be instrumental for widening the genetic code experimentally".^[68] Mutagenesis/selection cycles that resulted in *E. coli* mutant strains capable of installing translational pathways specific for additional amino acids *in vivo*, were selected. In this particular experiment, an *E. coli* mutant was grown with a defective thymidylate synthase; thus it lacked an essential enzyme for growth and viability. After the essential arginine codon (for Arg126) in the gene of the thymidylate synthase had been mutated to a leucine-codon, cells were able to grow only in the presence of azaleucine, that is, the activity of this enzyme could be restored only when azaleucine (whose structure mimics leucine, but serves as a functional substitute for arginine) was incorporated at position 126 of the enzyme. In other words, carefully designed selective pressure led to phenotypic suppression that causes Arg compensation with the antibiotic amino acid azaleucine. In the subsequent experiments, Döring and Maliere^[69] selected stable bacterial strains with coding triplets that can be read ambiguously. The captured coding signal was the rare isoleucine codon AUA, and cysteine was used as "codon captor" due to the rarity of its codons in genomes. The possibility for total reassignment in *E. coli* by proper selection under experimentally defined pressure was proposed for the rare codon AUA. Most recently Marliere and co-workers^[67] constructed an *E. coli* strain with a defective editing function of ValRS (Thr222Pro) capable of overall amino acid replacements by almost 24% valine with α -amino butyric acid in the cellular proteome.

3.4. Substitutions in Single Target Proteins under Selective Pressure

It is a general rule that nearly all amino acids outside the 20 canonical and metabolic intermediates are toxic (i.e. they do not support cellular growth at all). An exception to this rule is SeMet,^[70] and it was shown very early that *E. coli* Met-auxotroph ML304d substitutes completely Met with SeMet in cellular proteins.^[11] On the other hand, it was also observed that toxic analogues (fluorinated phenylalanines, norleucine, and canavanine) might serve as substrates in protein synthesis. However, when such toxic analogues are supplied together with their canonical counterparts in the synthetic growth media, usually lower incorporation levels in all cellular proteins can be achieved. For example, the Met

analogue norleucine leads to replacement of only 38% of the total cellular Met in proteins accompanied by greatly impaired viability of *E. coli* ML304d.^[57] More recent experiments have shown that it is possible to replace about 50% of the total cellular proteins in this way, since one further division of bacterial cells takes place after Met was exhausted in the intracellular pool and extra-cellular medium.^[71,72]

The basic problem to overcome to achieve full substitution in target proteins was how to retain the translation capacity and at the same time exclude the metabolic toxicity. The use of auxotrophic mutants of bacteria provided a solution to circumvent toxic metabolic effects. Namely, such cells are suitable for design of successful replacement experiments because preferential incorporation of a noncanonical amino acid over a canonical one can be achieved. A particularly effective approach was to starve host cells of a specific canonical amino acid and to induce the synthesis of a specific protein, with concomitant addition of the analogue to the culture medium. Sykes et al.^[73] succeeded in this way in replacing 10% of all Tyr residues in alkaline phosphatase. Bacteriophage-coded proteins labeled with fluorinated amino acids have been prepared in a similar manner by simultaneous initiation of bacteriophage infection and amino acid analogue addition.^[50]

However, the auxotrophic approach for complete labeling of target proteins could be fully generalized to a single target protein only after the introduction of recombinant DNA techniques. Cohen, Boyer, and co-workers^[74] found a means to reassemble isolated DNA fragments and genes in new arrangements and to propagate these fragments in living cells. With this method at hand, highly efficient expression systems capable of generating heterologous proteins in large amounts become available. On the other hand, such controlled extrachromosomally encoded protein expression systems provide an excellent platform for the expansion of the amino acid repertoire. In particular, the stringent control of a heterologous gene expression allows the full exercise of selective pressure on the translation apparatus to produce a single substituted target protein in the context of the host cell with an unchanged proteome.

Most importantly, the desired noncanonical amino acids can be incorporated in single target proteins without harmful global effects on the expression host. The basic requirements include: 1) selection of proper cell and expression system, 2) control of fermentation conditions (i.e. environment), 3) selective pressure for the replacement of the amino acid (i.e. the reassignment of the sense-codon(s)) in a single protein.^[13] This approach is termed as the selective pressure incorporation (SPI) method since it is based on the principle that the choice of the amino acids for protein synthesis could be conditioned by the control of environmental factors such as amino acid supply and fermentation parameters, that is by an experimentally imposed selective pressure.^[6]

The SPI method has been practised under various names by different research groups (e.g. the auxotroph method, media-shift) in the past decade. In the course of this research, a large number of noncanonical amino acids have been incorporated into proteins. The experimental pressure on a selected expression host has been exercised as follows. The

target gene activity is kept silent while the host cells are grown to an appropriate density. After sufficient “healthy” cells are produced, the synthesis of the target protein is induced. From this point on, the host cells serve only as a “factory” to produce the desired recombinant protein. The fermentation in minimal media with growth-limiting concentrations of the native amino acid as natural substrate leads to its depletion in the medium. At this point, the noncanonical amino acid is added and the protein synthesis is induced. As a result of such a pressure on the translation apparatus, the target protein containing exclusively noncanonical amino acid(s) is accumulated. This procedure leads to the arrest of cellular growth, but in the light of a successful expression of target protein variants, this fact is of less importance.^[15] Thus, the toxicity can be circumvented in quite a simple and straightforward way. Alternatively, biosynthetic pathways of host cells, as the endogenous supply, can be blocked by intracellular supplementation with proper inhibitors during incorporation experiments.

In fact, the SPI approach as an extension of the heterologous expression is based on the incapability of aaRS, as crucial enzymes in the interpretation of the genetic code, to distinguish between a variety of structurally and chemically similar substrate analogues in the aminoacylation reaction (Figure 3).^[6] It enables generally a reassignment of the coding triplets, that is, changes in the interpretation of the genetic code under the experimentally imposed selective pressure in the context of an intact proteome of the host cell. The basic advantages of the SPI method lie in the possibilities

for sense-codon-directed (residue-specific) substitutions, expression and purification of variant proteins at wild-type levels, as well as in the simple, reproducible methodology. For these reasons, SPI is still the method of choice for the production of labeled proteins on a larger scale, for example, for sample-intensive methods of structural biology (such as NMR spectroscopy^[73,75] or X-ray crystallography of proteins^[63,70,76]) or the production of therapeutic proteins on an industrial scale (Section 7).^[14,15,77]

3.5. Enhanced Translation System for the Biosynthesis of Proteins

Selective pressure based methods can be further improved by a manipulation of the activity of particular translation components. For example, Tirrell and co-workers tested a library of nine unsaturated Met analogues for translation activity (Figure 4)^[5] in order to introduce the various terminally saturated Met analogues. However, only *trans*-crotylglycine acid (**12**) was incorporated into a model protein. The other Met-surrogate, *cis*-crotylglycine (**17**), was not translationally active in spite of its modest activation capacity. An efficient incorporation (over 90%) of the latter into model proteins has been achieved only after endogenous co-expression of recombinant MetRS.^[78] This clearly demonstrates an obvious correlation between activation and translation capacity at least in aaRS (Tyr, Met) without any additional editing function. In this way, a whole repertoire of the Met analogues was incorporated into proteins after

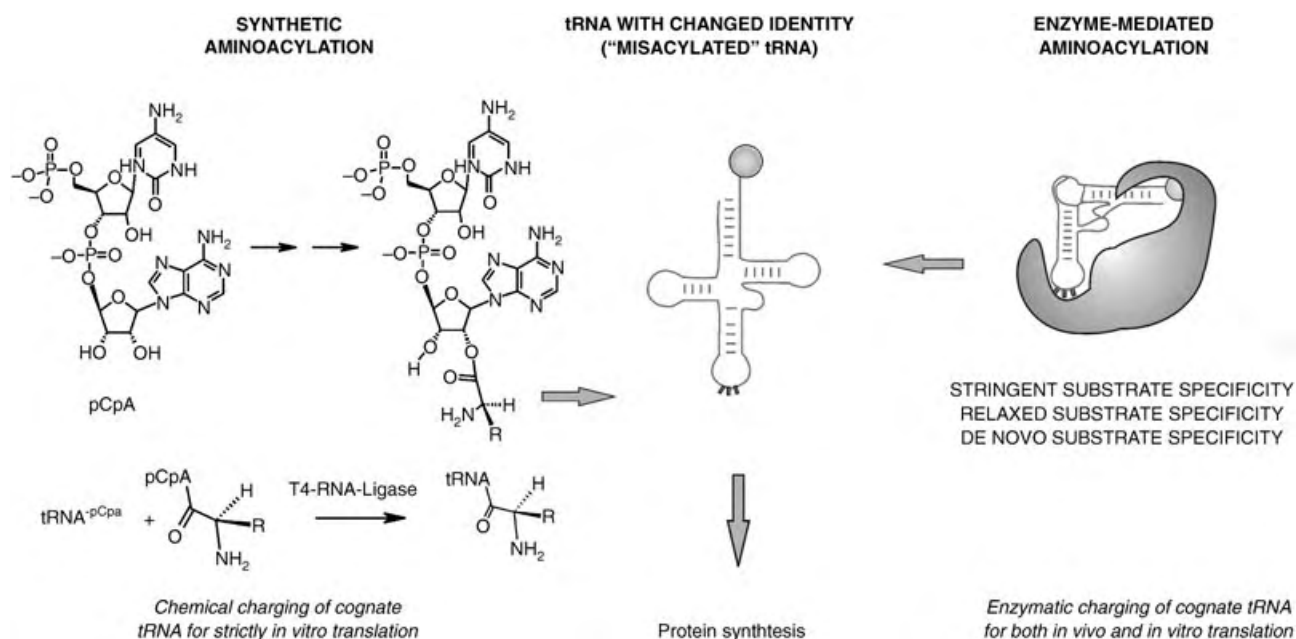


Figure 3. The main routes towards the expanded amino acid repertoire for ribosome-mediated protein synthesis. In the center of these experimental efforts is the tRNA with a changed identity or tRNA aminoacylated with the desired noncanonical amino acid. Such a aminoacylated tRNA can be created either by chemical synthesis (left), or by the use of cognate aminoacyl-tRNA synthetases (aaRS, right). The construction of chemically aminoacylated tRNAs takes advantage of the fact that all tRNAs have a common acceptor sequence (-CCA). Controlled digestion allows the removal of two terminal nucleotides (-CA) in every type of tRNA.^[158] The amino acid of interest can be chemically acylated to the dinucleotide p(d)CpA and then attached to the suitably prepared suppressor tRNA by T4 RNA ligase.^[166] Such tRNAs can be mainly used for in vitro protein synthesis and only in special cases in vivo. On the other hand, enzyme-mediated aminoacylation can be performed either in vivo or in vitro. Since native aaRS are often promiscuous in their substrate specificity, a rather large number of noncanonical amino acids can be loaded onto cognate tRNAs and translated into the target protein sequences.^[6]

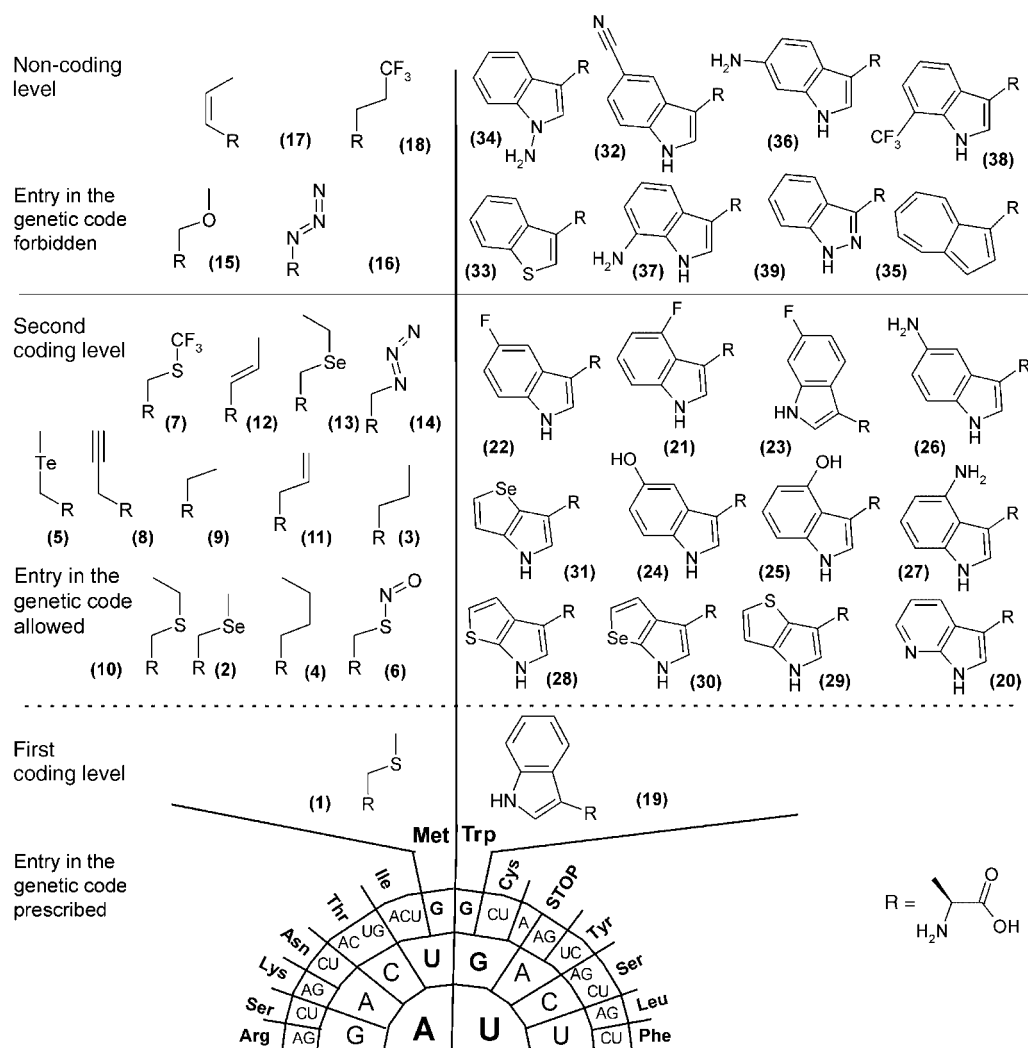


Figure 4. Expansion of the coding capacities of AUG and UGG triplets, which are in the genetic code assigned to the canonical amino acids methionine (**1**)^[13,76] and tryptophan (**19**),^[17,74,75,102–106] respectively. These evolutionary codon assignments make Met and Trp obligatory building blocks in protein synthesis, as they both belong to the first coding level. Experimental reassignments of AUG and UGG coding triplets enable entire libraries of mostly isosteric, noncanonical amino acid analogues and surrogates to serve as substrates for ribosome-mediated protein synthesis, building in this way a second or facultative coding level in the genetic code. Noncoding levels consist of amino acid substrates for which experimental attempts at incorporation were unsuccessful to date. One of the main tasks of code engineering is to “move” translationally inactive amino acids from the noncoding level to coding levels. Most of the translationally active amino acids presented here were incorporated into proteins by the groups of Budisa and Tirrell. Note that translationally active allylglycine, 2-butyrylglycine (not shown) as well as norvaline (**9**), norleucine (**3**), homoallylglycine (**11**), and homopropargylglycine (**8**) might serve as substrates for engineered LeuRS as well.^[102–106] This novel feature in the translational process (“identity problem”) is discussed in detail in the text. Methionine analogues and surrogates: selenomethionine (SeMet, **2**), 2-aminoheptanoic acid (**4**), telluromethionine (TeMet, **5**), S-nitrosomethionine (**6**), trifluoromethionine (**7**), ethionine (**10**), *trans*-crotlylglycine (**12**), selenoethionine (**13**), azidohomoalanine (**14**), metoxinine (**15**), azidoalanine (**16**), *cis*-crotlylglycine (**17**), and trifluoronorleucine (**18**). Translationally active tryptophan analogues and surrogates: 7-azatryptophan (**20**), 4-, 5-, and 6-fluorotryptophan (**21–23**), 5- and 4-hydroxytryptophan (**24** and **25**), 5- and 4-aminotryptophan (**26** and **27**), L-β-(thieno[2,3-*b*]pyrrolyl)alanine (**28**), L-β-(thieno[3,2-*b*]pyrrolyl)alanine (**29**), β-selenolo[2,3-*b*]pyrrolyl-L-alanine (**30**), and β-selenolo[3,2-*b*]pyrrolyl-L-alanine (**31**). The 7-fluorotryptophan, and 4-methyltryptophan are not shown. Translationally inactive Trp analogues and surrogates: 5-cyanotryptophan (**32**), benzothienopenalanine (**33**), azulene (**35**), 1-, 6-, and 7-aminotryptophan (**34**, **36**, **37**), 7-trifluoromethyltryptophan (**38**), and azatryptophan (**39**). The IUPAC names of the compounds are available in the Supporting Information.

fermentation and expression of target proteins in Met-depleted cultures of *E. coli* in which MetRS was overexpressed and the medium supplemented with the analogue at millimolar concentrations.

In addition, this approach can be employed even with synthetases with well documented editing activity, but only if

the desired noncanonical amino acid is not a substrate for editing reactions. For example, the leucine analogue trifluoroleucine is about 200-fold less active than leucine in the ATP-pyrophosphate exchange activation assay.^[79] Nevertheless, it can easily be incorporated into relatively small coiled-coil proteins under normal expression conditions.^[80] On the other

hand, the leucine analogue hexafluoroleucine does not support protein synthesis because it is activated approximately 4000-fold more slowly than leucine. The elevated intracellular concentrations of leucyl-tRNA synthetase proved to be a crucial factor for the incorporation of hexafluoroleucine as a response to the leucine-coding triplets in the mRNA sequence of coiled-coil protein HA1.^[81]

It now becomes clear that at least some of the non-canonical amino acids that do not support protein synthesis under conventional expression conditions, can indeed be efficiently incorporated into proteins after the amount of intracellular aaRS is increased in the microbial host.

3.6. Engineering the Catalytic and Editing Function of aaRS

The aminoacylation reaction is one of the main “filters” for the entry of noncanonical/non-cognate amino acids into the genetic code.^[38] The “classical” SPI approach simply exploits a “promiscuity” of the wild-type aaRSs to expand the amino acid repertoire.^[6] Nevertheless, the number of non-canonical amino acids capable of entering the genetic code by this route is regarded to be relatively small and the range of desired chemical diversity is rather modest when compared to that obtained with the suppression-based methodologies that exploit chemical tRNA aminoacylation. Therefore, the *in vivo* expansion of the amino acid repertoire by using the SPI approach must profit to a greater extent, if aaRSs of the microbial host would be supplemented or replaced with designed enzymes with changed or relaxed substrate specificity.

Kast and Hennecke^[82] reported an engineered mutant of phenylalanyl-tRNA synthetase (PheRS) with a mutation in the binding pocket (Ala294Gly) which charges tRNA^{Phe} with *p*-chlorophenylalanine. Later, Ibba, Tirrell, and co-workers^[42, 83] demonstrated that it was possible to introduce amino acids such as *p*-chlorophenylalanine (**45**) and *p*-bromophenylalanine (**52**) into recombinant luciferase and dihydrofolate reductase by using bacterial hosts extra-chromosomally supplemented with this PheRS variant, which exhibits relaxed substrate specificity. A novel mutant of *E. coli* PheRS computationally designed with the additional mutation Thr251Gly further relaxed the substrate specificity. The *E. coli* expression host supplemented with this enzyme was capable of incorporating a whole set of Phe analogues and surrogates such as *O*-acetyltyrosine (**65**), *p*-bromophenylalanine (**52**), *p*-iodophenylalanine (**46**), *p*-cyanophenylalanine, *p*-ethynylphenylalanine (**66**), *p*-azidophenylalanine (**59**), and 2-, 3-, and 4-azaphenylalanine (**53**, **55**, **56**)^[83, 84] into the model protein dihydrofolate reductase (Figure 5).

Aminoacyl-tRNA synthetases without editing activity such as TyrRS are especially attractive targets for substrate-specificity engineering. For example, the mutant Phe130Ser of TyrRS from *E. coli*, whose affinity for 2-azatyrosine (**61**) is elevated, was selected by screening of *E. coli* cells transformed with the mutant TyrRS gene (*tyrS*) harboring plasmids.^[85] Similarly, yeast TyrRS-engineering based on the available three-dimensional structure of the enzyme from *Bacillus stearothermophilus*, yielded the mutant Tyr43Gly-

TyrRS which was able to utilize several 3-substituted Tyr analogues as substrates for aminoacylation.^[86] Moreover, this yeast Tyr43Gly-TyrRS imported into *E. coli* preferentially recognizes 3-iodotyrosine (**49**) rather than Tyr itself. Schultz and co-workers^[87] chose the TyrRS from *Methanococcus jannaschii* to produce a library of its mutants with novel substrate specificity. In this way they selected a mutant with higher specificity for *O*-methyltyrosine (**60**) than for Tyr itself.^[88]

A more sophisticated system was reported recently based on combined genetic selection and screening. This system allowed rapid evolution of the substrate specificity of TyrRS from *M. jannaschii*. An antibiotic marker was used in combination with the amplifiable fluorescence reporter to screen for variants with the desired change in amino acid specificity.^[43] An advantage of this approach is that the amplifiable fluorescence reporter allows evaluation of aaRS activity and selectivity. In this way, the amino acid binding pocket of a TyrRS from *M. jannaschii* was systematically mutated, which allowed one to select a series of novel TyrRS variants that leads to specific aminoacylation of various Tyr analogues, that is, Tyr-like (or Phe-like) amino acids substituted with different functional moieties such as methoxy,^[88] amino,^[89] alkenyl,^[90] keto,^[91] azido,^[92] and naphthyl groups^[93] as well as substrates with photocrosslinking groups^[94] (Figure 5).

Another way to achieve a greatly expanded amino acid repertoire for one particular system is the use of synthetases with deleted or attenuated editing activity. Recently, Murzin and Martinis^[95] reported a rational design that led to a blocking of amino acid editing in LeuRS from *E. coli*. In this enzyme a single Thr at position 252 (in the amino acid binding pocket of the editing active site) plays a critical role in the editing reaction; its mutation with bulky amino acids such as Phe or Tyr results in the loss of the editing reaction. Such inactivated LeuRS has the potential to provide an efficient and facile enzymatic synthetic route to generate tRNAs loaded with noncanonical amino acids. Tirrell and co-workers isolated and characterized three LeuRS mutants (Thr252Tyr; Thr252Leu; Thr252Phe) with attenuated editing activity.^[41] The LeuRS Thr252Tyr mutant was endogenously overexpressed together with target proteins, which allows the incorporation of the noncanonical amino acids norvaline (**9**) and allylglycine. In addition, noncanonical amino acids described as Met-surrogates were incorporated at the Leu positions of the model protein, for example, homoallylglycine (**11**), homopropargylglycine (**8**, Figure 4), and 2-butyryllylglycine.^[41]

Finally, a computational approach for predicting the relative energies of the binding of different noncanonical amino acids into the binding site of aaRS on the basis of crystal structures or homology-derived models represents a useful approach for virtual screening of amino acid analogues. In this context, Goddard et al. reported that the calculated binding energies of some Phe analogues to PheRS correlate well with their translation activities in *E. coli*.^[96] Another recently reported example includes a computing procedure termed as the “clash opportunity progressive computational method” for designing mutants of aaRS with higher preference for noncanonical amino acids.^[97]

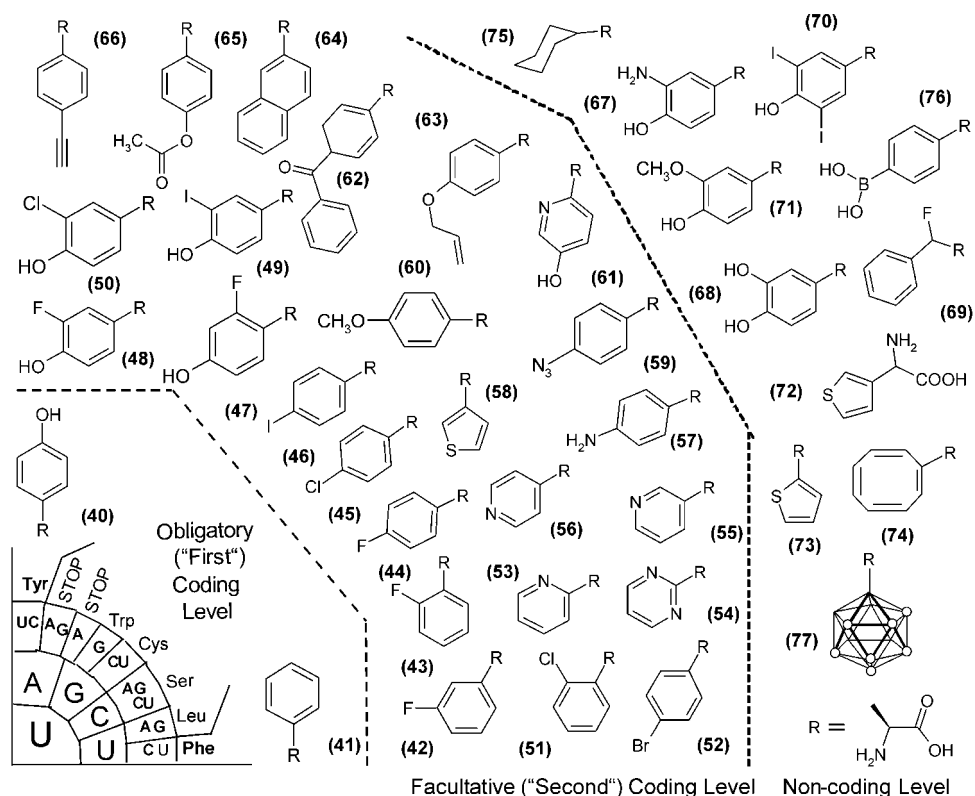


Figure 5. Canonical amino acids Phe and Tyr, encoded with two coding triplets are especially attractive substitution targets for amino acid repertoire expansion. Their “second” coding levels include at least 25 analogues and surrogates. Note that in terms of “identity”, many of them can be assigned either as Tyr or Phe analogues, or surrogates, depending on the system in which they were used. For example, *p*-iodophenylalanine (46) and *p*-bromophenylalanine (52) can be incorporated into proteins either by using *E. coli* cells whose PheRS exhibit relaxed substrate specificity or by using plasmids harboring TyrRS from *M. jannaschii* with novel substrate specificity. Although analogues such as *p*-aminophenylalanine (57), *p*-azidophenylalanine (59), *p*-benzoylphenylalanine (62), and 2-naphthylalanine (64) are introduced into model proteins in a response to the termination UGA coding unit by using suppressor tRNA, there is no doubt that they can be translated into proteins in a response to UAU or UAC sense coding triplets by using designed TyrRS and cognate tRNAs (see text for more details). Presented amino acids: tyrosine (40), phenylalanine (41), *o*-, *m*-, and *p*-fluorophenylalanine (42–44), *o*- and *p*-chlorophenylalanine (51, 45), *o*- and *m*-fluorotyrosine (47, 48), *m*-iodo- and *m*-chlorotyrosine (49, 50), 2-, 3-, and 4-azaphenylalanine (53, 55, 56), 2,6-diazaphenylalanine (54), 2- and 3-thienylalanine (73, 58), *O*-methyltyrosine (60), 2-azatyrone (61), *O*-allyltyrosine (63), *O*-acetyltyrosine (65), *p*-ethynylphenylalanine (66), *m*-amino- and *m*-methoxytyrosine (67, 71), *m*-hydroxytyrosine (DOPA, 68), β -fluorophenylalanine (69), 3,5-diiodotyrosine (70), 3-thienylglycine (72), cyclooctatetraenylalanine (74), cyclohexylalanine (75) (4-boronic acid)phenylalanine (76), carbonylalanine (77). The IUPAC names of the compounds are available in the Supporting Information.

4. Power and Limits of Selective Pressure: Engineering a “Second” Code

Expansion of the amino acid repertoire, especially in vivo is constrained by general limits imposed by this specific experimental milieu. These limits are metabolic constraints (related to the metabolic toxicity of most of the amino acids outside the canonical 20 as prescribed by the genetic code), proofreading mechanisms in the transmission of genetic information that are providing the fidelity of protein translation, and finally protein folding rules that are closely related to the structure of the genetic code and physicochemical properties of the amino acids. To challenge these constraints and to find means to bypass, change, or modulate aaRSs activities is one of the most fundamental problems of the engineering of the genetic code.

The expansion of the amino acid repertoire as presented in Figure 6 reveals that the postulated universality of the genetic code should not be limited to its first (restricted) part,

but also to its second part (relaxed or second code) which can be experimentally assessed.^[6] Three levels in the structure of the genetic code can be postulated (Figure 4 and 5): the first coding level includes canonical amino acids whose entry in the genetic code is obligatory; the second coding level includes noncanonical amino acids whose entry is allowed in the code (i.e. entry is facultative); the third or non-coding level includes all amino acid analogues whose entry in the genetic code by sense-codon reassignments is not allowed (i.e. entry is forbidden) at this level of the method development. In other words, for each amino acid in the standard genetic code table it should be possible to establish or define a whole library of translationally active substances, capable of being incorporated in proteins. The final goal would be to build up an extended structure of the genetic code that would have an additional (i.e. second) coding level with a defined library of translationally active analogues and surrogates for each canonical amino acid. Alternatively, the goal can be defined as an attempt to move amino acids from the non-coding to

possibility of using L-DOPA (**68**) for incorporation into proteins was not supported by recent experiments^[116] (Figure 5).

The investigations into the modification of tyrosyl-tRNA synthetase (TyrRS) from *E. coli* yielded a mutant Phe130Ser-TyrRS capable of introducing the Tyr analogue azatyrosine (**61**) into cellular proteins. Yokoyama and co-workers^[86] developed a suppressor tRNA^{Tyr} and a mutant TyrRS that incorporate *m*-iodotyrosine (**49**) into proteins in mammalian cells. The research group of Schultz have evolved a couple of orthogonal *M. jannaschii* TyrRS/tRNA^{Tyr}_{CUA} pairs with an impressive wide range of substrate specificity.^[43] Amino acids such as *O*-methyltyrosine (**60**), *O*-acetyltyrosine (**65**), *O*-allyltyrosine (**63**), 2-naphthylalanine (**64**), *p*-aminophenylalanine (**57**), *p*-iodophenylalanine (**46**), *p*-bromophenylalanine (**52**), *p*-azidophenylalanine (**59**), *p*-benzoylphenylalanine (**62**) were incorporated into the green fluorescent proteins,^[89] glutathione-S-transferase^[117] and dehydrofolate reductase^[88] as a result of efficient suppression of the UGA termination codon (Figure 5).

Interestingly, a structural homology of TyrRS and TrpRS indicates that the two enzymes can be described as conformational isomers. It remains to be seen whether this feature can be used for a switch or relaxation in their substrate specificity and thus allow an additional expansion of the amino acid repertoire.

4.3. Phenylalanine

Fluorinated phenylalanine analogues were used in the initial incorporation experiments as well as in the last few years mainly for protein NMR spectroscopy. Yoshida^[118] found the stability of *Bacillus subtilis* α -amylase remains unchanged upon partial replacement of Phe with *p*-fluorophenylalanine (**44**) but its activity was altered. Conversely, Richmond^[52] found that *Bacillus cereus* exopencillinase changed its immunological properties upon substitution with *p*-fluorophenylalanine. On the other hand, for alkaline phosphatase from *E. coli*, replacement of 56% of the Phe groups with *p*-fluorophenylalanine had no detectable effects on stability and activity. More recently, *o*-, *m*-, and *p*-fluorophenylalanine (**42**, **43**, **44**) were systematically incorporated into recombinant proteins or recombinantly produced materials^[119] providing them with interesting optical^[120] and thermal properties as well as with altered kinetics. Janacek and Rickenberg^[121] have shown that β -galactosidase expressed in the presence of the Phe surrogate 2-thienylalanine (**73**) is more labile than the normal enzyme. They also found that this 2-thienylalanine although a substrate for protein synthesis, inhibits permease action, that is, its active transport in the cytosol. This is the reason why incorporation of this analogue is quite poor in auxotrophic strains with intact permease function. More recently, the Phe analogue 3-thienylalanine (**58**) was incorporated into a recombinant periodic protein that forms lamellar crystals comprising regularly folded β -sheets.^[122] Koide et al.^[123] reported the incorporation of Phe analogues with pyridyl groups in recombinant human epidermal growth factor. These ana-

logues, for example 2-azaphenylalanine (**53**), 3-azaphenylalanine (**55**), and 4-azaphenylalanine (**56**), are protonated in acidic solutions (Figure 5).

The discovery of a bacterial PheRS variant with relaxed substrate specificity by Kast and Hennecke^[82] paved the way for further expansion of the translationally active Phe surrogates and analogues. The halogenated analogues *p*-chloro- (**45**), or *p*-bromophenylalanine (**52**) were incorporated into full-length luciferase in vitro.^[42] Further redesign of the active site of PheRS and its use for a coexpression in *E. coli* resulted in replacement of Phe residues by *O*-acetyltyrosine (**65**), *p*-aminophenylalanine (**57**), *p*-iodophenylalanine (**46**), *p*-bromophenylalanine (**52**), *p*-azidophenylalanine (**59**), *p*-chlorophenylalanine (**45**), *p*-cyanophenylalanine, *p*-ethynylphenylalanine, (**66**) *p*-azidophenylalanine (**59**), and 2,6-diazaphenylalanine (**54**) in dihydrofolate reductase.^[83,124] These designed PheRS variants allow efficient in vivo incorporation of aryl ketone functionality into proteins, which is normally rejected by the cellular translational machinery.^[84] Several Phe-based amino acid substrates such as *p*-bromophenylalanine and *p*-iodophenylalanine were incorporated into proteins as a response to the amber stop codon using engineered TyrRS from *M. jannaschii*.^[43] In this way, all these amino acids can have a “dual identity” serving as substrates for both systems (Figure 5).

4.4. Histidine

Histidine analogues 1,2,4-triazolyl-3-alanine and 2-methylhistidine have been successfully incorporated into *E. coli* alkaline phosphatase. The resulting enzyme was inactive since it could not dimerize.^[58] The same analogues were incorporated into aspartate transcarbamylase and a mutant phospholipase A2. The products of these modifications differ dramatically from the native enzyme with regard to the activity–pH profiles.^[125] In fact, the replacement of His by its noncanonical counterpart 1,2,4-triazolyl-3-alanine yields an enzyme with high activity at acidic pH.^[126] A similar effect was achieved by the incorporation of 2-fluorohistidine^[127] and 4-fluorohistidine; the p*K*_a value reduced by approximately 5 pH units.^[58] Such a dramatic increase in the acidity of the imidazole ring dramatically alters the activity and properties of the fluorohistidine-containing proteins. This strong effect on p*K*_a possibly induces a loss in enzymatic activity in many proteins in the physiological milieu making such His replacements with 2-fluorohistidine and 4-fluorohistidine responsible for the toxicity of these substances.^[58] These considerations were fully confirmed in the studies of ribonuclease S with semi-synthetically incorporated 4-fluorohistidine.^[128] Recently, Ikeda et al. demonstrated the possibility of preparing a versatile set of histidine analogues as efficient substrates for protein synthesis.^[129]

His residues are specially attractive for engineering enzyme activity and catalysis since they are often found in the active sites of different enzymes, functioning as catalysts in acid–base and nucleophilic processes. Isosteric replacements in the frame of some canonical amino acids such as Ser/Cys, Thr/Val represent an excellent tool to study the nature of

the catalytic mechanism of residues directly involved in enzyme catalysis. However such replacements are not possible for His side chains. Therefore, engineering of histidyl-tRNA synthetase (HisRS) to extend its substrate specificity will greatly expand the scope and versatility of the enzyme catalysis.

4.5. Leucine, Valine, Isoleucine

Pioneering work by Anker and co-workers demonstrated that 5',5',5'-trifluoroleucine was incorporated by bacteria but not by eukaryotic systems. These early results were recently confirmed by Tirrell and Tang^[80] who in addition succeeded in incorporating hexafluoroleucine into peptides expressed *in vivo*.^[81] *Lactobacillus casei* dihydrofolate reductase expressed in *E. coli* was substituted with (2*S*,4*S*)-5-fluoroleucine to study conformational changes of the protein upon ligand binding with ¹⁹F NMR spectroscopy.^[130] The translational activity of *threo*-3-hydroxyleucine was reported by Hortin and Boime.^[50] More recently, Apostol et al.^[131] found that norvaline (**9**) can be incorporated in place of leucine in recombinant proteins. By using the T252Y mutant of leucyl-tRNA synthetase with attenuated editing activity in *E. coli* under conditions of its constitutive overexpression, the noncanonical amino acids norvaline (**9**), norleucine (**3**), allylglycine, homoallylglycine (**11**), homopropargylglycine (**8**), and 2-butynylalanine were inserted efficiently at the leucine sites of recombinant proteins.^[41]

The valine analogues 2-amino-3-chlorobutyronoic acid, cyclobutaneglycine, penicillamine, and *allo*-isoleucine have been used to probe the process of membrane transversion of secretory proteins through the endoplasmic reticulum.^[51] However, the extent of their incorporation to date is still unclear. For example, Porter et al.^[132] reported that "cyclobutaneglycine is activated by ValRS and forms cyclobutylglycyl-tRNA^{Val}, and presumably is incorporated into proteins in lieu of valine". Therefore, additional experiments are necessary to resolve these ambiguities. On the other hand, a recent experiment by Marliere and co-workers unambiguously demonstrated proteome-wide substitution of valine up to 24% by α -aminobutyrate in an engineered *E. coli* strain with attenuated ValRS editing function.^[67]

Isoleucine analogues, such as 4-thiaisoleucine, *O*-ethylthreonine, *O*-methylthreonine, 4-fluoroisoleucine, and *allo*-isoleucine were used in pioneering experiments.^[50–52] Novel isoleucine analogues incorporated more recently into a few model target proteins include furanomycin and trifluoroisoleucine.^[133]

The systems for the selection and tRNAs aminoacylation of leucine, valine, and isoleucine evolved in their synthetases additional domains for a "double sieve" discrimination^[36] of cognate from non-cognate, noncanonical and biogenic amino acids. Engineered valyl-tRNA synthetase or leucyl-tRNA synthetase with inactivated or attenuated editing function should have a great potential to fill up the second coding levels of leucine, valine, and isoleucine with a large number of analogues, surrogates, or similar amino acids.

4.6. Methionine

Methionine residues in proteins contribute to their structures with both hydrophobic interactions and hydrogen bonding; they are relatively rare (1.5% of all side chains in proteins of known structures), and usually located in positions inaccessible to the bulk solvent with only 15% of all Met residues exposed to the surface.^[134] Met (**1**) has always been an attractive replacement target in proteins and peptides because of its facile reversible conversion into a hydrophilic sulfoxide form upon oxidation. Using natural translation machinery in *E. coli* or even yeast and mammalian cells, it was possible to substitute Met residues with SeMet (**2**),^[11] Nle (**3**),^[49,71,72] ethionine (**10**),^[13,52] and even telluromethionine (**5**).^[13,135] Honek and co-workers demonstrated the possibility of incorporation of trifluoromethionine (**7**) into phage lysozyme.^[136]

A target of the editing activity of the MetRS is the Met metabolic precursor homocysteine.^[137] In general, all Met-like amino acids smaller in size than Met itself are edited (with Nle on the border of this size-based exclusion).^[138] More recently, Jakobowski showed that *S*-nitrosomethionine (**6**) can be transferred to tRNA^{Met} by MetRS and incorporated into proteins in *E. coli* and in the rabbit reticulocyte system.^[139] Removal of the nitroso group from *S*-nitrosomethionine-tRNA^{Met} results in homocysteinyl-tRNA^{Met}, and subsequently, its *in vitro* incorporation into proteins in place of Met side chains.

The increase in the intracellular MetRS concentration by coexpression experiments in the *E. coli* Met auxotroph CAG18491 and the model protein dihydrofolate reductase^[140] allowed further extension of the number of Met-based amino acid analogues and surrogates: homoallylglycine (**11**), homopropargylglycine (**8**), *cis*-crotylglycine (**17**), *trans*-crotylglycine (**12**), allylglycine, 2-butynylglycine, 2-aminoheptanoic acid (**4**), norvaline (**9**), and azidohomoalanine (**14**)^[141] (Figure 4). Some of these amino acids have a "dual identity", such as norvaline (**9**), 2-butynylglycine, homoallylglycine (**11**), and allylglycine, since they can serve as substrates for both MetRS and LeuRS with attenuated editing activity.^[41]

4.7. Proline

Proline is a unique imino acid that has a cyclic side chain with a fixed ϕ angle, which acts as a classical breaker of both the α -helical and β -sheet structures in water-soluble proteins and peptides. In addition, the rate-limiting step in the slow folding reactions of many proteins involves *cis/trans* isomerization about peptidyl-prolyl-amide bonds.^[142] Thus, proline is able to play these important roles due to its unique ring size and geometry. In protein and peptide sequences it is often post-translationally hydroxylated, but has no similar counterparts among the remaining 19 canonical amino acids. Therefore, proline can be co-translationally substituted only with an expanded amino acid repertoire.

Early reports assigned 3,4,-dehydroproline, 4-thiaproline, 4-selenoproline, *cis*-4-hydroxyproline, *cis*-4-fluoroproline, *trans*-4-fluoroproline, and azetidine-2-carboxylic acid as

potential proline analogues in protein synthesis.^[50–52] Recent research confirmed that *cis*-4-fluoroproline, *trans*-4-fluoroproline, difluoroproline, and thiaproline can indeed be incorporated into recombinant proteins.^[143] In addition, the proline analogue 3,4-dehydropyrolidine was incorporated in a repetitive periodic protein with lamellar morphology.^[144]

In peptide synthesis, pseudoprolines are well known from peptidomimetic studies as serine-, or threonine-derivatized oxazolidines, and cysteine-derived thiazolidines.^[145] Chemical aminoacylation of suppressor tRNAs revealed that various proline-based analogues and surrogates that influence the backbone structures of proteins can indeed be incorporated into proteins. They include pipecolic acid, homopipecolic acid, cyclopropylglycine, azetidine-2-carboxylic acid, and hydroxyproline.^[146] Although *in vivo* incorporation of these analogues and surrogates and their derivatives has still not been achieved, there is no doubt that engineering or simple elevation of intracellular levels of prolyl-tRNA synthetase (ProRS) in the context of carefully designed experimental selective pressure, will result in their translational activity.

4.8. Arginine

Canavanine, a very potent toxin from the raw seeds of *Canavalia ensiformis*, is, so far, the only studied analogue of arginine as the substrate for protein synthesis. Pioneering studies from the 1950s and 1960s established that incorporation of canavanine into proteins resulted in altered conformation and disruption of its function.^[54] The production of functionally impaired, canavanyl-containing proteins affects cell development and has growth-inhibiting properties. Thus, anticancer and antiviral properties of this substance have been intensively studied.^[51]

4.9. Lysine

Lysine residues in proteins play an important role either as targets for chemical derivatization or post-translation modifications. Early studies reported a few analogues of lysine with the potential to be translated into proteins: *S*-2-aminoethylcysteine, 6-*C*-methyllysine, 5-hydroxylysine, *trans*-4,5-dehydrolysine, 2,6-diamino-4-hexanoic acid, 4-oxalysine, 4-selenalysine.^[145] However, there are no reports about any recent research in this field. On the other hand, lysyl-tRNA synthetase (LysRS) could be an attractive target for engineering to relax or even exchange its substrate specificity in the desired direction.

The specificity of the aminoacylation reaction (termed as discrimination or *D*-factor) with regards to the 20 canonical amino acids varies considerably among different aaRS *in vitro*.^[137] The highest *D*-factor (between 28 000 and > 500 000) is found for TyrRS, whereas the lowest values (between 130 and 1700) were observed for LysRS. Therefore one of the most important tasks for future experiments is to find out whether this observation of “intrinsically relaxed” LysRS substrate specificity can be generalized for further chemical diversification of the proteins based on lysine-derived ana-

logues and surrogates. In addition, the existence of two unrelated forms of LysRS with the same affinity for lysine but different preferences toward noncanonical amino acids such as thialysine^[147] can be also exploited for expanding the lysine-like amino acid repertoire. Since Lys residues in proteins are mainly distributed at surfaces, it is reasonable to expect that LysRS-based orthogonal systems that utilize templates with optimized Lys-codons distributions, would most probably replace complicated suppressor-based approaches for chemical diversification of protein surfaces.^[117]

4.10. Metabolic Toxicity and Recruitment of Secondary Metabolism Intermediates for Protein Biosynthesis

Canonical amino acids are like “multi-tasking” substrates perfectly integrated into the fine network of cellular biosynthetic, metabolic, and energetic functions. Their synthesis or uptake has to be regulated, not only to enable protein translation, but also to provide a proper balance of metabolites in the cell. Under normal physiological conditions a small amount of toxic amino acid can be tolerated without gross effects on cellular viability, whereas larger amounts might cause cell death.

The message from these and other similar observations is clear: isosteric amino acids are also physiologically “orthogonal” to canonical amino acids in the sense that they act as antagonists in the given cellular milieu. Such metabolic choices have to be taken into consideration in any attempt to engineer cellular expression hosts for an expanded amino acid repertoire. For these reasons, the simplest approach to proteome-wide substitutions would be to metabolically engineer microbial strains whose simple “nonfunctional” aliphatic amino acids such as alanine, leucine, and valine (which have relatively limited metabolic choices) could be suitable targets for global substitutions, since their replacement would be less harmful. Thus, they are candidates that are most probably the best suited for future noncanonical amino acid translations into the total cellular protein output.

Alternatively, more than 700 biogenic amino acids (among them at least 300 from plants)^[148] represent a larger natural reservoir of potential substrates for protein biosynthesis, that is, entry into the genetic code. In organisms of all life kingdoms α -amino acids are the end products of secondary metabolism, intermediates of metabolic pathways, or originate from the metabolism and detoxification of foreign substances.

For years, metabolic engineering has allowed us to generate or design a novel endogenous supply route of substances of interest (vitamins, hormones, metabolic intermediates). In the case of *E. coli* bacterial hosts, it should be possible to generate the desired amino acid from carbon sources. The combination of metabolic engineering and *in vivo* incorporation of noncanonical amino acids has been demonstrated by Mehl et al.^[149] Gene-loci encoding production of *p*-aminophenylalanine (**57**) (*papA*, *papB*, and *papC*) as a metabolic intermediate identified in *Streptomyces venezuelae* were “borrowed” and put into *E. coli*. Genes for these enzymes were imported by a low-copy plasmid into *E. coli*,

making this microbe capable of intracellular production of *p*-aminophenylalanine from chorismate. *p*-Aminophenylalanine was incorporated with fidelity and efficiency similar to those of the canonical amino acids by use of a corresponding orthogonal pair. The intracellularly generated *p*-aminophenylalanine pool does not dramatically interfere or compete with the intracellular pools of the canonical amino acids. This expression host supplied with orthogonal components, heterologous target gene, and metabolic pathway is an instructive example of the combination and engineering of components that originate from different species in one unique system.

It is now clear that metabolic engineering of bacterial or any other expression host can be done by two opposite approaches. The first relies on full or partial addition of novel biosynthetic pathways, whereas the second includes knock-out, modulation, or attenuation of the existing biosynthetic supply pathways. For practical purposes, the *in vivo* expression system in which cells use the desired noncanonical amino acids directly from the growth media is much more advantageous in many cases. On the other hand, the expression of recombinant proteins with *p*-aminophenylalanine in *E. coli* might represent an interesting system for studying the effects of selective pressures on shaping the amino acid repertoire of living cells. Future tighter bridging of natural products chemistry and engineering of the genetic code could lead to a larger scale screening for suitable amino acids as “candidates” for entry into the genetic code from the intermediary metabolism of various species.

4.11. Cellular Proofreading

Under the influence of various selective pressures, living cells evolved molecules of the most efficient size and shape for their function. Basic monomeric protein building blocks having an average size of an amino acid can be divided into 20 unambiguous types apparently fulfilling these criteria. One can speculate that with more building blocks used in protein synthesis, mistakes could be so frequent that they would seriously outweigh the advantage of having more types. There are however, remarkable similarities between the members of the encoded amino acids. Several are isosters (Val/Thr, Cys/Ser), have the same molecular volume (Ile/Val, Pro/Cys), or very similar chemistry (Ser/Thr). Thus, the foremost practical criterion for the distinguishability between them must be their facile differentiation in the recognition process. Indeed, almost perfect discrimination between closely related structures is the hallmark of biochemical systems.^[150]

It should always be kept in mind that amino acid activation and tRNA charging are not the only “checked” steps in translation. For example, in the experimental attempts to expand the amino acid repertoire in proteins by using the SPI approach, it was demonstrated that it is possible to incorporate 4-aminotryptophan into the green fluorescent protein (GFP) from *Aequorea*, but not 5-aminotryptophan and 4- or 5-hydroxytryptophan.^[104] On the other hand, all these substrates are translationally active, since they could be incorporated into another protein barstar.^[105] Other examples are thiaproline, and selenoproline, both of which have been

recognized, selected, and loaded onto cognate tRNAs in the aminoacylation reaction, but only thiaproline can be fully translated into target proteins.^[14] The reasons for such behavior are still unclear, but certain still unknown editing mechanisms during the ribosomal synthetic cycles or co-translational folding must be at work. To date, studies of co-translational or assisted (i.e. chaperone-mediated) protein folding, as well as ribosome fidelity with various noncanonical amino acids are rare.

The need for a strong discrimination goes beyond the canonical 20 amino acids, since the cellular milieu is full of metabolic intermediates and other biogenic amino acids as well. On the other hand, editing was not evolved against specific features of chemically or sterically similar synthetic amino acids, since living cells never encountered them in their evolution. Such a lack of the absolute substrate specificity of aaRS has been well documented in many systems for decades, and was recognized very early as a route for the expansion of the amino acid repertoire *in vivo*.

4.12. Protein Folding and the Genetic Code: Are There General Rules for Codon Reassignments?

Amino acid analogues incorporated into proteins using the traditional auxotrophic approach, at the level of the genetic code, represent codon reassignments that occur by obeying a simple “similar replaces similar” rule.^[6] In fact, it is well known that experimental or natural codon redefinition occur always among similar amino acids. For example, the Met codon AUG could be reassigned to Ile (noncognate) or Nle (noncanonical) but never to arginine (nocognate) or methoxinine (Figure 7), because this reassignment would be fatal for efficient folding and consequently for the biological activity of the encoded protein structure.^[27] In other words, the codon reassignment usually takes place by obeying a simple “similar replaces similar” rule, because disruption of the resulting protein structure is minimized by such modest alterations in the amino acid side chain. In the evolution of proteins, amino acid substitutions are found to occur more frequently between similar amino acids than between dissimilar ones. Sonneborn^[151] conceptualized these observations about coding similarities between amino acids with similar physical properties in the form of a “translation-error minimization” theory about the nature of the genetic code. It postulates that the main function of the structure of the genetic code is to maintain the structural stability of globular proteins. From this point of view, the structure of the genetic code is the direct product of natural selection for a system that minimizes phenotypic impact of the genetic error.^[152,153]

Therefore, the simplest rule to be obeyed is the general “apolar in—polar out” principle. Namely, the basic architectural pattern for proteins is to fold into tight particles, which have an internal hydrophobic core that is shielded from the surrounding solvent. This binary partitioning of polar and nonpolar amino acids is an intrinsic part of the genetic code. In its structure, these relations are visibly regular: all codons with a central “U” are cognate to amino acids with chemically relatively uniform, hydrophobic side chains (“convergent

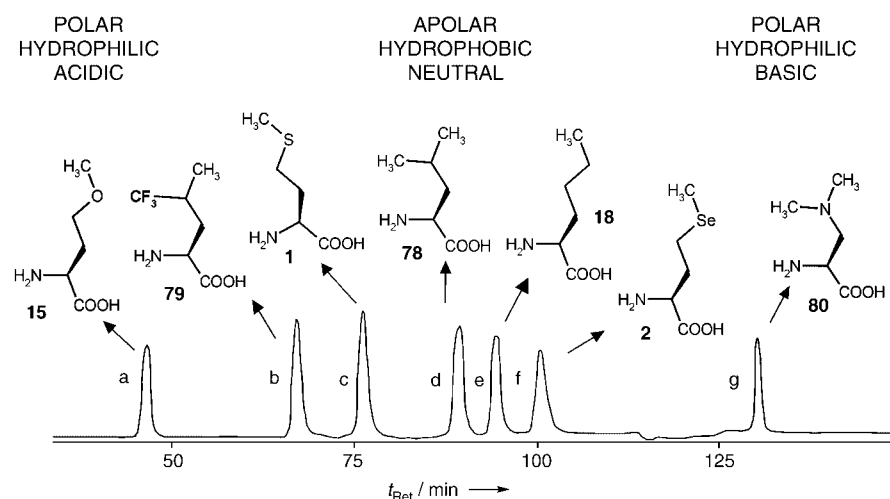


Figure 7. Chromatographic mobility of various ninhydrine derivatives of canonical and noncanonical amino acids as a function of their molecular size, polarity, hydrophobicity, and pI values.^[220] The elution profiles of Met (**1**, signal c) and its isosteric analogues Nle (**18**, e), SeMet (**2**, f), and metoxinine (**15**, a) as well as of leucine (**78**, d) and its isosteric analogues 5'5'5'-trifluoroisoleucine (**79**, a) and Aza-leucine (**80**, g) were superimposed on the same retention time (t_{Ret}) scale. Since canonical amino acids and their counterparts are almost identical in terms of molecular shape, their separation is based mainly on differences in polarity and pI values. Translational cellular machinery recognizes hydrophobic amino acids Leu and Met as native substrates, whose signals are chromatographically positioned in the “neutral apolar area”. Conversely, in the acidic and basic “polar areas” are their isosteric analogues metoxinine (**15**) and azaleucine (**80**), which are not substrates for protein biosynthesis. Namely, hydrophobic and neutral amino acids from the XUX codon family (Val, Ile, and Phe) cannot be globally substituted with these polar amino acids, since it would have an adverse effect on protein folding. Therefore, the positions of the chromatographic peaks revealed which of these noncanonical analogues are allowed to enter into the genetic code.

types”). On the other hand, coding triplets with a central “A” are cognate to amino acids with chemically variable, polar side chains (“divergent types”).

Not only is such a chemical order apparent by careful inspection, it can be also quantitatively measured in a simple chromatographic experiment. Woese et al.^[154] measured the chromatographic mobility of amino acids on paper in various solvents. The observed mobility correlated with the number of water molecules required for solvation. On this basis, the “polar requirement” index was developed.^[155] This index reflects remarkably well the order in the coding table, clearly indicating that the genetic code assigns amino acids to related triplets on the basis of polarity/hydrophobicity. Later studies by Wolfenden and co-workers^[156,157] confirmed that the relative distributions of amino acids between surfaces and the interiors of native globular proteins are indeed shaped with a sharp bias imposed by the genetic code.

This is also true for reassignment or substitution of canonical amino acids with noncanonical ones. The chromatographic mobility test for the series of isosteric canonical and noncanonical amino acids starting with Met and its isosteric analogues Nle, SeMet, and metoxinine (**15**) as well as Leu and its isosteric analogues 5'5'5'-trifluoroisoleucine and azaleucine, is presented in Figure 7. The observed mobility revealed a full agreement between amino acid polarities and their capacities for incorporation into proteins: neutral and hydrophobic (apolar) noncanonical amino acids such as Nle, SeMet, and trifluoroisoleucine indeed serve as substitution substrates for the

canonical amino acids Met and Leu. On the other hand, their isosteric but hydrophilic (polar) counterparts azaleucine and metoxinine were never successfully incorporated into target proteins. Not surprisingly, Marliere and co-workers^[68] used azaleucine as a functional analogue for arginine.

The main lesson from this observation is that novel reassignments of coding triplets are strongly correlated with the biophysical relationships among the sterically similar amino acids. The simple experiments described above teach us also about the existence of a firm boundary between “allowable” and non-permissive amino acids in the genetic code, which can be delineated by simply measuring the differences in their physico-chemical properties. In this context, it would be interesting to see if there is a quantitative value (i.e. index) for the possibility of a desired synthetic amino acid to enter the genetic code. Future work in the code engineering field should decide which criteria (e.g., polarity, hydrophobicity, molecular volume, isoelectric point, position in the genetic code table, and putative protein structure) could be more (or less) important in developing such indices.

5. Suppression-Based Methods

The most common codon reassignment in nature among different organisms occurs from one canonical amino acid to another. For example, vertebrate mitochondria read AUA as Met, whereas in the vertebrate cytosol this codon is assigned to code for isoleucine.^[158] On the other hand, according to Osawa and co-workers “central to codon reassignment is the principle that a codon cannot have two assignments simultaneously, because this would be lethal to an organism”.^[159] However, an exceptional and unique example is the UGA codon that reads for stop, selenocysteine (SeCys), pyrrolysine, Trp, and cysteine.^[160] In addition, other examples were identified as well, such as the universal CUG leucine codon, which is translated as serine in some *Candida* species.^[161] This coding unit which is capable of assigning a few distinct amino acids was termed a “polysemous codon”.^[162] Such diversity in the assignment of certain codons in the universal code suggests that it should be possible to experimentally accommodate additional amino acids into proteins.^[9]

Traditional approaches based on auxotrophism have only in exceptional cases the capacity to replace amino acids at any chosen position in a protein, as is possible by the use of site-directed mutagenesis. In the case of SeCys insertions, selective pressure during evolution yielded tolerable levels of nonsense suppression. Three-dimensional structural elements of mRNA and a special elongation factor are the crucial elements for local change in the codon meaning. The experimental extension of local changes leads to “an

expanded" genetic code^[7] and refers to numerous amino acids experimentally translated into protein sequences by suppression of termination or frameshifted codons.^[163] The large variety of chemically or enzymatically aminoacylated suppressor tRNAs able to participate in ribosome-mediated protein synthesis, are the basis for suppression-based methodologies capable of position-specific and multiple-site incorporations of amino acids.

5.1. The Concept of Suppression in Protein Translation

When a nonsense (stop) mutation occurs in the middle of a genetic message, an incomplete polypeptide is released from the ribosome owing to premature chain termination. In many cases incomplete chains have no biological activity, which makes most nonsense mutations harmful for cells. Such harmful effects can be reversed by further changes (suppressor mutations) at different genes of mutant tRNAs. These genetic changes might take place in tRNA anticodons, or more rarely in some other tRNA identity elements. Suppressor tRNAs can insert different canonical amino acids in response to the *nonsense* (when one of the three terminator codons appears in mRNA) or *missense* codons (i.e. alteration of one sense codon to another so that different amino acids are determined) or *frameshift* mutation in the parent gene. In this way, the normal functions of these termination or sense codons are suppressed by tRNAs with changed identity.^[158]

The existence of suppressor tRNAs raised the question of how they compete with release factors for termination codons especially those for UAG and UGA, which appear quite frequently at the end of genes. In addition, it is still not clear why the UGA and UAG suppressor tRNAs do not generate an unacceptable number of abnormally long proteins.^[164] Evidently, there is no advantage for a normal cell to harbor suppressor mutations, even if only a small fraction of proteins would be non-functional. Therefore, suppressions either *nonsense* or *missense* should be regarded as exceptional natural phenomena. The response of a particular suppressor tRNA to a particular nonsense codon (read-through) can vary by as much as tenfold, depending on its location in the mRNA, a phenomenon known as the "context effect". There are also suppressor tRNAs capable of masking the effects of certain frameshift mutations created by the insertion of nucleotides and subsequently to restore a reading frame.^[165]

5.2. Chemical tRNA Misacylations and In Vitro Amber (UAG) Suppression Methodology

Lipmann and co-workers demonstrated that misacylated tRNA could be chemically synthesized; they prepared Ala-tRNA^{Cys} by chemical desulfurization (Raney nickel) of Cys-tRNA^{Cys}.^[12] Indeed, misacylated tRNA could substitute Cys with Ala at all positions in haemoglobin, which was taken as a model protein. This finding supported the view that fidelity of protein synthesis was controlled largely at the level of amino acid activation and correct tRNA charging by the aaRS. Later, Hecht and co-workers^[166] demonstrated the utility of

the misacylated tRNAs for effecting amino acid substitutions at predetermined sites in polypeptides. In this way, it was shown that lysyl-tRNA acetylated at the N^ε-amino group can be incorporated into the rabbit haemoglobin with nearly the same efficiency as the unmodified one.^[166] The general method for the preparation of misacylated (either suppressor or normal) tRNAs developed by Hecht and his group has been the subject of numerous reviews.^[163,167]

The wide variety of chemically acylated suppressor tRNAs for the terminator codon UAG (Amber codon) are able to participate in the peptide bond formation at the ribosome. Suppressor tRNA species containing the anticodon CUA can be prepared either by chemical modification of some commercially available tRNAs (e.g. yeast tRNA^{Phe}) or by runoff transcription of a suppressor tRNA gene. The basic scheme for the chemical aminoacylation of these tRNAs is described in Figure 3. Such tRNAs added in a suitably programmed in vitro translation system contribute directly in ribosome-mediated protein synthesis. In this way, an interpretation step in the flow of the genetic information is efficiently avoided (i.e. in vivo selection, activation, and aminoacylation of desired amino acid). It is therefore not surprising that a wide variety of modified amino acids can indeed participate in protein synthesis.^[168] More recently, Schultz,^[169] Chamberlin,^[170] Sisido^[163] and their co-workers, in a series of in vitro experiments using termination or frameshift suppressor tRNAs, extended the early Hecht approach and demonstrated an extraordinary capacity of the ribosome to allow translation of more than a hundred special non-canonical amino acids (Figure 8).

The in vitro experimental extension of missense or nonsense suppression phenomena for the expansion of the amino acid repertoire was accomplished by chemical misacylation of suppressor or cognate tRNAs. Their addition to a translation system programmed with a gene containing nonsense suppression sites results in the incorporation of the special noncanonical amino acid at the corresponding position in the protein. Site-directed incorporation of 3-iodotyrosine into the 16-residue peptide product translated in vitro with a rabbit reticulocyte system was reported by Chamberlin and co-workers.^[171] Similarly, by using a nonsense suppressor tRNA from yeast, Noren et al.^[7] incorporated several Phe analogues. This position-specific replacement strategy was first postulated by Kwok and Wong,^[172] who have shown that *E. coli* PheRS can aminoacylate yeast tRNA^{Phe} with an efficiency of less than 1 % of that of *E. coli* tRNA^{Phe}. Thus, the amber suppressor tRNA derived from yeast tRNA^{Phe} was especially suitable for in vitro incorporation experiments with a coupled transcription/translation system based on *E. coli*. These tRNAs insert the desired amino acid efficiently into the β -lactamase; positions were taken that correspond to those of the UAG codon on its mRNA. On the other hand, they were not acylated or deacylated by any of the *E. coli* aaRS present in the cell-free lysate. After the suppression reaction in the Zubay transcription/translation system, 2.8–7.5 $\mu\text{g mL}^{-1}$ of the replaced β -lactamase was produced, which is about 15–20 % of the native protein yield (30–45 μg).^[7] These successes were possible because four essential requirements for the application of suppression

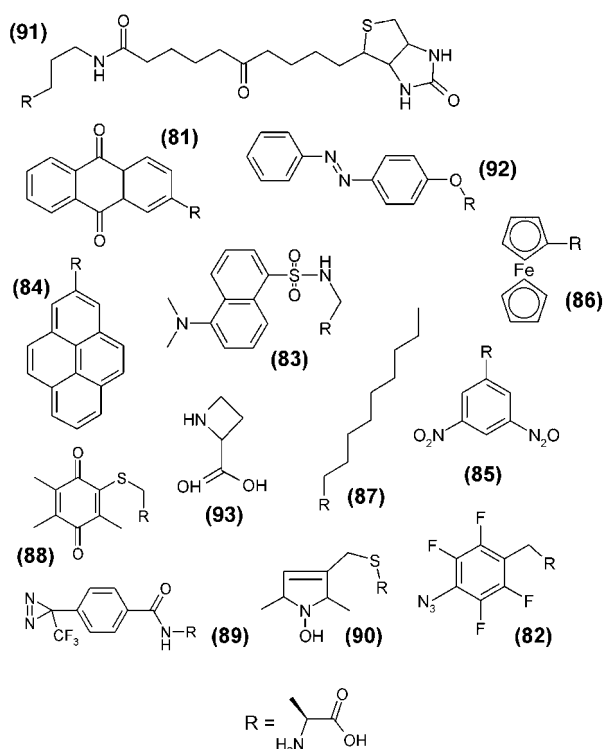


Figure 8. Some of the translationally active amino acids delivered to the ribosome by chemical aminoacylation of suppressor tRNAs. The large number of synthetic amino acids incorporated into proteins by these approaches demonstrates almost unlimited possibilities for chemical diversifications on protein surfaces. For example, such compounds might be used as markers for hydrophobic/polar interactions, to restrain the protein backbone, to serve as spin labels, or as photo-reactive side chains. On the other hand, these amino acids can be packed into the protein core only in exceptional cases. See the reviews by Schultz et al.,^[87,167,169,174] Dougherty et al.,^[179,180] and Hoshida and Sisido.^[163] The IUPAC names of the compounds are available in the Supporting Information.

methodology were fulfilled: 1) the suppressible amber (UAG) mutation was generated in the gene of interest by conventional site-directed mutagenesis; 2) the design of an efficient suppressor tRNA was achieved; 3) the suppressor tRNA was chemically acylated, and 4) a suitable in vitro protein synthesis system was available.

5.3. Limits of Suppression-Based Methodologies

The use of misacylated suppressor tRNAs has provided proteins containing various noncanonical amino acids at single predetermined positions. Most of these studies involved a read-through of the UAG codon. The main drawback of all suppressor-based approaches is the limited capacity of chemically misacylated synthetic suppressor tRNA charged with noncanonical amino acids to fully decode (suppress, read-through) nonsense (triplet or quadruplet) codons. This is not surprising since the suppressions are exceptional phenomena that are *context-dependent*, that is, each desired position in a protein sequence cannot be

always suppressed. It has been observed and documented that *release*, that is, intervention of so-called *release factors*, is so effective at some sites that the natural function of the amber stop codon is not suppressed even when the suppressor tRNA is charged with the amino acid that normally appears at that point in the wild-type protein.^[173] Other unresolved issues include the stability of mRNA containing terminating codons as well as the stability of protein with noncanonical amino acids.

Therefore, the main bottleneck of this system is not the relatively low yield of the expressed proteins due to the inefficiency of the in vitro system,^[169] but the rather low efficiency of the suppression. This parameter depends mainly on the nature of the amino acid to be incorporated into target proteins. For example, Nle can be incorporated into T4 lysozyme with a 100% suppression efficiency, whereas α -methylleucine can be incorporated with only 14%.^[174] Unfortunately, suppression efficiencies cannot be reliably predicted, and there are only empirical observations such as read-through being very poor for polar amino acids. Bypassing the suppression's "side effects" can at least be in part achieved by the generation of a completely unique quadruplet composed of canonical bases for particular aaRS/tRNA pairs with orthogonal function^[175] or by choosing non-toxic amino acids such as substituted analogues of aromatic amino acids. More recently, Frankel and Roberts^[176] have described a selection approach for identifying coding triplets especially susceptible to suppression. However, the most efficient way to circumvent completely these limits is to switch to the use of sense codons^[177,178] in the context of codon-optimized target gene sequences (Section 5.7).

The generally impaired cellular viability upon in vivo introduction of orthogonal translation components is not the only "side effect" of these experimental interventions. The efficiency of translation can also be substantially reduced, resulting in decreased yields of the desired protein mutants. For example, in rich media, *E. coli* with heterologous wtTyrRS/tRNA_{CUA}^{Tyr} expresses dihydrofolate reductase in yields of 67 mg L⁻¹, whereas by transfer in designed minimal medium, the yield drops by more than 95% to 2.6 mg L⁻¹.^[188] Nevertheless, this approach might be useful in those studies where minute amounts of labeled proteins are necessary in the context of the living cells.^[179,180]

It should be always kept in mind that such experiments have been performed with model proteins such as dehydrofolate reductase, streptavidin, luciferase, smaller coiled peptides, lactamase, lysozyme, or GFP, whereas "difficult" proteins such as single-chain antibodies are most probably not permissive of such incorporations at all. In addition, suppression-based approaches that incorporate amino acids, such as ϵ -(7-nitrobenz-2-oxa-1,3-diazol-4-yl)-L-lysine or dansyllysine, might be useful only for the chemical diversification of the protein surfaces.^[181] On the other hand, there are a large number of the widely used efficient and much simpler protocols for chemical modifications of the protein surfaces.^[117] Therefore, in vitro suppression-based approaches will not be of much use in biological sciences, until currently available protocols for incorporations are considerably simplified.

The identities of amino acids and their nature show a certain correlation with its suppression efficiencies. For example, larger hydrophobic amino acids were incorporated with higher efficiency than smaller or charged ones. Not surprisingly, numerous large polyaromatic amino acids were incorporated in vitro (Figure 8), whereas most of noncanonical amino acids recently incorporated by in vivo suppression are in fact substituted aromatic derivatives of Phe and Tyr (Figure 5). Other factors that might dramatically influence suppression efficiency are polarity, stereochemistry, and amino acid geometry. For example, D-amino acids and β -amino acids are not substrates for translation by nonsense suppression methodologies.^[169,174] An interesting question that remains to be tackled is to investigate whether there are correlations between suppression efficiencies, amino acid nature, and the already discussed general rules for codon reassignments.

5.4. In Vitro Frameshift Suppression Methodology

The maintenance of the frame during translation is not absolute and the frameshift mutations can be externally suppressed. Early experiments in the 1960s and 1970s demonstrated that the mutant tRNA in *Salmonella* and yeast with extended anticodons can read non-triplet codons but their read-through efficiency was comparatively low.^[158] Recently, it was shown that the efficiency of UAGA quadruplet decoding for a tRNA^{Leu} with engineered 3'AUCU^{5'} anticodon could be elevated to the range of 20–40%.^[182]

An in vitro approach based on frameshift suppressions has been developed by Sisido and co-workers over the last decade.^[183] A combination of four base codons AGGN and the corresponding anticodons NCCU was used to examine the scope and possibilities for in vitro frameshift suppression for the incorporation of particular canonical amino acids. Indeed streptavidin was substituted with 2-anthranylanine by using all combinations of quadruplets: AGGG, AGGA, AGGC, AGGU.^[184] The target gene sequence was optimized in a way that its mRNA contains extra downstream stop codons to terminate non-frameshifted products, that is, to abort protein synthesis in the absence of frameshift suppression.^[175]

Sisido and co-workers^[185] observed that incorporation of certain noncanonical aromatic amino acids is dependent on their adaptability at the active center of the ribosomal A-site. The regularity that emerged from these experiments was that noncanonical amino acids with linearly expanded aromatic groups (e.g. 2-naphtylalanine, *p*-biphenylalanine, (*p*-phenylazo)phenylalanine) are more favorable than those with widely expanded or bent aromatic groups (e.g. 9-phenylanthrylalanine). The transfer of these components into a cell-free rabbit reticulocyte-based system resulted in essentially the same observations.^[184]

The use of quadruplets has aroused great interest because of the possibility of incorporating two or more different amino acids into a single protein. For example, streptavidin mRNA containing CGGG and AGGU quadruplets was translated in the presence of aminoacyl-tRNA_{CCCG} and aminoacyl-tRNA_{ACCU} charged with ϵ -(7-nitrobenz-2-oxa-1,3-

diazol-4-yl)lysine (CGGG signal in mRNA) and 2-naphthylalanine (AGGU signal in mRNA). Sisido and co-workers convincingly showed that the use of quadruplets in vitro protein biosynthesis provides a strategy for the introduction of noncanonical amino acids at several sites in a single protein.^[186] Although it was expected that the basic advantage of this strategy should be the circumvention of the competition with the release factors, the rules that govern the different suppression efficiencies for different quadruplets are unclear as well. For example, it was argued that some sites in mRNA cause more frameshifts than others.^[187] Therefore, this strategy has been limited both by the overall read-through efficiency of the suppressor tRNAs as well as by the occasional apparent misfolding of nascent proteins containing modified amino acids.

The general aspects related to the limits of anticodon size that would help to identify efficient tRNA suppressors of two-, three-, four-, five-, or even six-base codons have recently been the subject of detailed studies.^[188,189] For example it was demonstrated that pentaplets (i.e. five-base codons) are indeed suitable for incorporation of special canonical amino acids into proteins.^[189] Extensive examinations performed by Schultz et al. have shown that the translation apparatus indeed permits decoding of codons consisting of three to five bases and that each codon type requires different tRNAs. However, six-base codons are incompatible with the translation machinery and pentaplets cannot be suppressed with the same efficiency as quadruplets. Such limits in codon size are most probably governed by the ribosome itself where the tRNA is a sort of "molecular ruler" that measures codon size during translation.^[188]

5.5. Species-Specific Features of Aminoacylation and Orthogonal aaRS/tRNA Pairs

At the level of the interpretation of the genetic code, that is, aminoacylation, orthogonality is defined as a lack of cross-reactivity between heterologous aaRSs and tRNAs with the endogenous synthetases, amino acids, and tRNAs of the natural host. Indeed, the most important requirement for the generation of orthogonal translation components is the strict absence of cross-reactivity with the protein-synthesis apparatus of the host. The tRNA as the carrier of adapter function in translation is the most attractive target for orthogonality engineering. This, however, requires a detailed knowledge of the tRNA identity rules. The rational design of both positive and negative recognition elements of tRNAs is difficult and the experimental results often rely on serendipitous findings. Sometimes it is necessary to search for identity elements outside the anticodon as suitable markers for the design of efficient suppressor tRNA. Nevertheless, the search for orthogonal pairs with in vivo and in vitro suppression methods can be summarized as follows: first, an orthogonal amber suppressor tRNA_{CUA} has to be generated that is capable of incorporating the noncanonical amino acid in response to a UAG codon in the mRNA encoding the protein of interest. Second, an orthogonal aminoacyl-tRNA synthetase has to be designed by using mutagenesis and screening

approaches. Such an orthogonal aaRS should recognize exclusively related orthogonal-tRNA, but not any of the endogenous tRNAs. Finally, a library of mutants of the orthogonal tRNAs and aaRS has to be screened to find orthogonal aaRS/tRNA pairs capable of activating and transferring the desired noncanonical amino acid preferentially over canonical ones.^[190]

The first systematic efforts in this direction were made by using the three-dimensional structures of the GlnRS/tRNA₂^{Gln} pair from *E. coli* as a starting point to generate several mutant suppressor tRNAs capable of serving as adapters for in vivo protein synthesis.^[191] These tRNAs were indeed not substrates for any endogenous aaRSs including GlnRS, which is an important orthogonal component in a nontoxic in vivo aminoacylation system.^[192] Parallel attempts to design an orthogonal GlnRS did not yield a mutant enzyme capable of charging orthogonal tRNA better than the native enzyme.^[190] Thus, efforts to create an *E. coli* GlnRS/tRNA₂^{Gln} orthogonal pair even when heterologues tRNA₂^{Gln} from yeast was included, had only limited success.

There are two general difficulties in any attempt to create 21 aaRS/tRNA pairs in the context of a living cell. First, such designed enzymes will selectively be eliminated the living cells due to their redundancy; they can be kept only under experimentally imposed selective pressure. Second, there is the problem to specify which component from the remaining tRNAs and enzymes from the cellular pool directly interferes with the engineered enzyme.^[193] For example, RajBhandary and co-workers initially found that the introduction of yeast TyrRS into *E. coli* is lethal, since this enzyme misacylates *E. coli* tRNA^{Pro} with Tyr.^[194] Therefore, yeast TyrRS was modified so that it would no longer mischarge the *E. coli* tRNA^{Pro}. Only a mutant (generated by error-prone PCR) with very low rates of misacylation of *E. coli* tRNA^{Pro} could serve as orthogonal aaRS.

The development of orthogonal aaRS/tRNA pairs proved to be very successful when both the components, namely suppressor tRNA and aaRS, were imported from another organism.^[195] It is now clear that exploitation of the species-specificity of aminoacylation is the most promising route to design orthogonal pairs. For example, after analysis of biochemical data for the TyrRS/tRNA^{Tyr} pair from a variety of organisms, Wang et al. found that TyrRS/tRNA_{CUA}^{Tyr} from *Methanococcus jannaschii* might serve as a valuable orthogonal pair for recombinantly expressed target proteins in *E. coli*.^[196] The basis for the orthogonality in the Tyr systems can be derived from fundamentally different modes of recognition of tRNA^{Tyr} by TyrRS in archaea/eukarya and eubacteria.^[197] In this way, a cross-aminoacylation in such a hybrid translation system is not possible. In addition, TyrRS from *M. jannaschii* does not have documented editing mechanisms and its cognate tRNA^{Tyr} can be efficiently transformed into suppressor tRNA without much decline in aminoacylation efficiency.^[196] The transfer of amber and ochre suppressor tRNAs derived from *E. coli* initiator tRNAs into mammalian COS1 cells was also demonstrated. These tRNAs were not substrates for any mammalian aaRS and their aminoacylation with amino acid analogues opens a perspective for their position-specific insertion in mammalian cells.^[198]

5.6. In Vivo Orthogonal aaRS/tRNA Pairs

Chemical aminoacylations are complex experiments, and in vitro expression systems still suffer from low protein yields. This certainly sped up efforts to transfer suppression-based methods to in vivo systems. Although the efforts to create an *E. coli*-based efficient GlnRS/tRNA₂^{Gln} orthogonal pair^[190] failed, these experiments yielded a methodological breakthrough in the development of an efficient system for positive/negative selection of mutant aaRS enzymes and tRNAs.^[43,88] They also brought into focus other important aspects and issues that should be taken into consideration in host strain engineering. For example, amino acid uptake proved to be a critical issue since it is well known that transport of amino acids into cells is not purely passive. Indeed, most of the translationally active noncanonical amino acids are about the same size as canonical amino acids. Thus, it is not surprising that “exotic” amino acids such as (*p*-phenylazo)phenylalanine are hardly acceptable as substrates for cellular amino acid permease systems. Therefore, the systematic generation of the libraries of cell-permeable amino acids represents an important future research avenue.^[199]

Extra-chromosomally controlled heterologous expression systems in microorganisms are especially practical as platforms for expanding the amino acid repertoire because of their easy maintenance, propagation, and handling. These expression systems can be programmed either for position-specific or multiple-site incorporation of noncanonical amino acids by supplementation with additional translation components. These goals can be achieved in the context of living cells only if four basic requirements are fulfilled: 1) the availability of coding units programming the translation of noncanonical amino acids; 2) tRNAs capable of decoding these units, and 3) an enzyme capable of charging the tRNA. 4) Both aaRS and its corresponding tRNA should be free from cross-aminoacylation and compatible with host translation machinery and physiology.^[87]

Forster^[200] developed for the first time a general approach for the implementation of these criteria for position-specific in vivo incorporation of noncanonical amino acids. The Phe analogue *p*-fluorophenylalanine was incorporated at position 5 as a response to a UGA coding triplet in the mRNA sequence of recombinantly expressed dehydrofolate reductase. This was achieved by introducing yeast PheRS/amber suppressor tRNA^{Phe} into the expression host *E. coli*. There is almost no cross-reactivity between the PheRS from yeast and *E. coli* since identity elements in their tRNAs evolved in a completely different manner. The *E. coli* strain used was a Phe-auxotrophic one and was resistant to *p*-fluorophenylalanine, that is, its PheRS prevents tRNA^{Phe} from being charged with *p*-fluorophenylalanine. In contrast, for yeast PheRS, *p*-fluorophenylalanine is almost as good a substrate as Phe. Thus the system would not be sufficiently defined, since the UGA coding triplet at position 5 of dehydrofolate reductase would be read as both Phe and *p*-fluorophenylalanine. This problem was circumvented by a careful experimental design of the fermentation, resulting in replacement of 64–75% at the amber position 5 in dehydrofolate reductase. This is indeed the first demonstration of the introduction of a new redun-

dant aminoacylation pathway and a new design of the hybrid translation system. When such an expression host is exposed to the efficiently imposed experimental pressure, the non-canonical amino acid is preferentially incorporated over the canonical one.

A further advance was made by the use of the TyrRS/tRNA_{CUA}^{Tyr} orthogonal pair from *M. jannaschii*^[196] in the expression host *E. coli* for the position-specific incorporation of *O*-methyltyrosine into dihydrofolate reductase in yields of about 2 mg L⁻¹.^[88] This was demonstrated in the case of green fluorescent protein (GFP)^[89] as well, where a variety of Tyr analogues were incorporated into the chromophore of this protein. The hybrid translation system with the TyrRS/tRNA_{CUA}^{Tyr} pair from *M. jannaschii* imported into *E. coli* is technically a much more advanced system than the one used by Furter^[200] as it is much more stringent. In other words, the orthogonality is almost fully achieved, since amber positions on the mRNA are translated with great fidelity into target proteins with minimal suppression-associated toxic effects. Finally, the use of substituted analogues of aromatic amino acids proved to be advantageous for this system.

It remains to be seen whether these *in vivo* expression systems can be developed further for use in molecular biology and biochemistry. Limited success in experiments with GlnRS/tRNA_{Gln}^[190] poses a dilemma as to whether all synthetase/tRNA systems are generally suited for such design. In addition, the orthogonal synthetase/suppressor tRNA pair for each specific noncanonical amino acid has to be generated through a series of complicated mutagenesis and selection cycles. It also remains to be clarified whether the *in vivo* transfer resolves the problems associated with context-dependent suppression phenomena (i.e. the problem of equal suppressability of all positions in a desired protein sequence). The *in vivo* approach also brings additional difficulties associated with the metabolic toxicity and bioavailability of the desired amino acids, that is, their transfer into the cytoplasm.

5.7. Sense Codon-Dependent Method with Chemoenzymatically Charged tRNAs

The reassignment of sense coding triplets by chemically or enzymatically charged tRNAs might be an attractive alternative to bypass the complications arising from context effects encountered in suppression-based approaches. Takai et al.^[177] inactivated tRNA^{Asp} and tRNA^{Phe} within crude S30 extracts from *E. coli* by antisense treatment or by digesting most of the tRNA without essential damage to the ribosomal activity. Using HIV-1 protease as a model protein in RNase-treated cell-free S30 extracts with pre-charged tRNAs, they succeeded in substituting aspartic acid and Phe residues with 2-naphthylalanine and (*p*-phenylazo)phenylalanine, respectively. However they were not able to estimate the specific yield of fully substituted protein, probably because folding of the resulting protein was seriously impaired.

A similar approach by Sisido and co-workers^[175,184] was based on the use of rare codons that can be placed at any position in the target mRNA sequence. Such codon-optimi-

zation of the target gene sequence allows position-specific or multiple-site incorporation of one or more different amino acids. For example, the rarest arginine-codon AGG (which contributes on average to less than 3 % of the total tRNA^{Arg} pool) is a suitable binding partner for chemically acylated tRNA_{CCU}, which can be used for the incorporation of various photoactive amino acids (*p*-aminophenylalanine, 2-anthrylalanine, 1-naphthylalanine, 2-naphthylalanine, *p*-biphenylalanine).^[201]

Sense codon reassignments using externally charged tRNAs should be an interesting approach, since it is based on the use of codon-optimized DNA in the context of *in vitro* protein synthesis. For example, the canonical amino acid Thr is coded with four coding triplets (Figure 1), with ACA being the rarest codon in *E. coli*. Using sophisticated *in vitro* systems such as PURE,^[202] where addition of all components can be precisely controlled, it should be possible to introduce the desired amino acid either in the position-specific or multiple-site mode. With the help of site-directed mutagenesis, the target DNA sequence can be optimized so that ACA is present only once, twice, etc. in the sequence. The corresponding tRNA (tRNA^{Thr} (3'UGU⁵)) can be enzymatically charged with the desired noncanonical amino acids, while the rest of the tRNA^{Thr} isoacceptors are charged with Thr. Addition of these preacylated tRNAs into the cell-free system devoid of deacylation problems should lead to the desired mode (position-specific, multiple-site) of incorporation.^[255] Similarly, Forster et al.^[203] combined a purified translation system free of aaRS with chemoenzymatically synthesized cognate tRNAs, which enabled arbitrarily chosen coding triplets to be completely reassigned to noncanonical amino acids *in vitro*.

Finally, there is a recent report of a successful experiment on the reassignment of coding triplets in the frame of codon families. Tirrell and co-workers^[178] used mutant yeast tRNA^{Phe} to reassign one of two degenerate Phe codons to the non-canonical amino acid 2-naphthylalanine. However, this is essentially a missense suppression-based approach and therefore suffers from the "child disease" of all these methodologies: reassignment is incomplete, canonical amino acids are often preferentially incorporated as a response to "reassigned" coding units during translation. For all these reasons, the best approach to achieve full noncanonical amino acid translations might be the use of the codon-optimized DNA/mRNA templates. Such templates would contain rare sense coding units placed in position-specific or multiple-mode sites in a target gene sequences. Therefore, the *in vivo* or *in vitro* translation of such codon-optimized DNA/mRNA templates with noncanonical amino acids is most probably the approach that will replace the suppression-based methods to a great extent.

6. Other Aspects Related to an Expanded Amino Acid Repertoire

6.1. *In Vitro* versus *In Vivo* Translation for the Extension of the Amino Acid Repertoire

The classical experiments by Chapeville et al.,^[12] which clearly demonstrated that misacylated tRNA is capable of

participating in protein synthesis, applied in vitro translation. In fact, cell-free systems with chemically aminoacylated tRNAs demonstrated remarkable ribosome plasticity in terms of the number, as well as the structural, steric, and chemical properties of the amino acids that can be translated into proteins. This chemical diversity can be lost to a great extent on transfer to an in vivo method. A recent example shows that an “orthogonal pair” in an in vivo system derived from the orthogonal system TyrRS/tRNA_{CUA}^{Tyr} from *M. jannaschii* allows mainly the translation of Tyr or Phe analogues (Figure 5). Evidently, to make fairly exotic amino acids such as ϵ -(7-nitrobenz-2-oxa-1,3-diazol-4-yl)-L-lysine, or the biotin derivative **91** (Figure 8), intracellularly bioavailable, experimental intervention for “rational re-design” of many components in the living cell is necessary. The range of the intervention is such that it would require simultaneous remodeling and non-invasive changes for the amino acid transport into cells. Furthermore, ways need to be found to avoid metabolic activation or modifications, as well as to pass translation editing check points of intact cellular physiology.

It should always be kept in mind that protein synthesis by the in vivo gene expression is carried out in cells, which because of their cell walls and membranes form a closed system. The alternative, open system, is represented by in vitro protein synthesis. Thus, the in vitro coupled transcription/translation, which is devoid of the problems associated with the mechanisms of cellular physiological functions, could be optimized as a platform for engineering the genetic code with a significantly wider spectrum than in living organisms.^[204] This explains the significant interest in the development of high-yield cell-free translation systems. Various improvements, including optimized batch reactions, addition of chaperones, replenishment of consumable factors, continuous flow or optimization of the relative concentrations of various lysate components, etc. are extensively described in current literature. Therefore, novel generations of even more sophisticated in vitro systems with improved performance in terms of protein yield and control of translation conditions would certainly serve as attractive platforms for the expansion of the amino acid repertoire.

6.2. Site-Directed versus “Statistical” Incorporation

In the early stages of the development of any novel research field, precise terminology cannot usually be formulated because not enough is known to permit such accurate definitions. A pragmatic strategy is to accept provisional, rough terminological characterizations that can provide leverage to the field’s first developmental stages with taxonomic refinements emerging as the related facts become clear. In the field of code engineering, the “site-directedness” as a highly desirable feature for the hybrid translation system is a term that demonstrates the confusion that might appear as a consequence of an immature terminology. For example, it was often claimed that the suppression-based read-through methods for noncanonical amino acid incorporation are “site-specific”, because it is theoret-

ically possible to insert a suppressible stop-codon at any desired position in the protein sequence. It is most probably not fully correct due to the well known fact that misacylated tRNA must compete with release factors that often result not only in low-suppression efficiency but complete absence of the suppression. In this case it would certainly be necessary to screen for permissible positions that allow a high-level suppression (lowest possible “leakage” of the system). However, it is hard to imagine this approach as “site-directed” in the terms used in routine oligonucleotide-directed DNA mutagenesis experiments.

The term “statistical” incorporation mode (labeling) is likewise not suitable for the following reasons. It is open to discussion whether the reported incorporation for particular amino acids by the use of read-through methods where suppression efficiency is 10%, is “statistical” or “site-directed”; whether the 99% reassignment of a single UGG codon (i.e. Trp substitution) in one particular gene sequence is “statistical” or “multisite” or “site-directed”. Such unclear taxonomic considerations might lead to statements like those that selective-pressure incorporation methods has “comparatively little impact on the field of protein engineering”.^[104] This is indeed misleading when for example the importance of SeMet incorporation into proteins based on the traditional use of auxotrophic strains for structural biology is considered. Also for the design of therapeutic proteins for drug delivery such “multisiteness” might even be a desirable feature of the system (see Section 7). Last but not least, whether SeMet incorporation is “multisite”, “statistical”, or “site-directed” depends upon the number of AUG codons that can be easily experimentally manipulated by recombinant DNA technology.

To avoid such terminological ambiguities one might simply accept that in naturally occurring proteins the problem of “site-specificity” is solved with the evolutionary optimized appearance of the codon (frequency) in particular sequences. This is especially true for relatively rare amino acids such as Trp, Cys, and Met. In this context, the question of whether one amino acid is “site-directed” or “multisite” incorporated is, in the first place, a matter of codon composition of its coding template. In practice, codon-optimized gene sequences, that is, target gene sequences with controlled codon composition, can be used in incorporation experiments with noncanonical amino acids. Furthermore, one can choose as replacement targets those amino acids that are naturally less abundant such as Trp (1.1%) or Met (1.5%), but which often play crucial roles in protein functionality. Finally there should be numerous protein sequences for which the problem of “multisite” replacements can be circumvented by a simple combination of site-directed mutagenesis and an expanded amino acid repertoire.

6.3. Other Approaches

Experimental intervention at all important levels of transmission of the genetic information might result in the engineering of the genetic code in terms of an expanded

number of amino acids as protein basic building blocks. At the level of the DNA/RNA sequence it is possible to manipulate the nature and lengths of the basic coding/decoding units (i.e. codons/anticodons). The aminoacylation reaction is the interpretation level of the genetic code and therefore the most attractive point for experimental interventions. Since codon–anticodon interactions are insensitive to the nature of the amino acid attached to the acceptor stem of tRNA, the influence of an amino acid charging process is the most obvious way to get novel amino acids into the genetic code. Finally, the ribosome itself can be altered to affect the interpretation of the genetic code. The use of noncanonical nucleotides to form a novel Watson–Crick base pair has already been extensively discussed.^[205–207]

Kowal and Oliver^[173] explored the use of nonassigned codons in *Micrococcus luteus* to circumvent problems associated with competitions by release factors in suppression-based methods. In this microorganism, six codons are unassigned (or very rarely assigned) allowing one to evaluate the possibility of inserting such codons into the DNA template for either position-specific or multiple-site incorporation of noncanonical amino acids. In vitro reaction in a lysate from *M. luteus* supplied with a plasmid-encoded target gene and *E. coli* tRNAs for unassigned or rare codons led to complete translation.

Besides the engineering of aaRS, specially selected ribozymes capable of transferring amino acids to the 3'-end of specific tRNAs might also provide an additional means of generating aminoacylated tRNAs with noncanonical amino acids.^[208,209] However, this methodology at the current level of development suffers from serious shortcomings such as inefficient amino acid transfer, complicated ribozyme construction (which requires chemical methods at least in part), and high concentrations of aminoacylated ribozyme.

Manipulation of the ribosome structure might be another way to expand the genetic code. Little is known about the recognition elements that have to be altered to allow the introduction of versatile chemical functionalities into proteins. For example, Dedkova et al.^[210] have shown that the mutations in 23S rRNA in the region of the peptidyltransferase center and the helix 89 led to a conformational change, which diminished the normal mechanisms for discrimination between D- and L-amino acids in the ribosomal A site. Such modified ribosomes might exhibit altered translation properties, a feature that can be exploited for the expansion of the amino acid repertoire. The addition of suppressor tRNA_{CUA} in a cell-free system containing such ribosomes allowed the synthesis of luciferase with D-Met and D-Phe.

Future research should demonstrate whether all these approaches will reach the efficiency of the currently available methodologies for genetic code expansion.

6.4. Future Avenues: Shuttle Orthogonal Pair and Hybrid Translation Systems with Codon Capture

Practical applications either in research or industry will dictate to a great extent current and future development and

trends in genetic code engineering. The main focus will be the development of efficient in vitro or in vivo hybrid translation systems, capable of producing elevated levels of tailor-made proteins. The most conceivable way to reach high levels of production of tailor-made therapeutic proteins would be the experimental design of specialized prokaryotic or eukaryotic cells capable of synthesizing protein variants with a high fidelity. Metabolism, bioenergetics, synthetic and supply routes as well as amino acid pools of such cells should be controllable, tightly regulated, and properly balanced. Coupling metabolic engineering with code engineering therefore clearly has a great future.

On the other hand, in vivo expression of tailor-made proteins as tags in mammalian cells is also highly desirable. In this case, the amount of the labeled proteins does not necessarily need to be elevated, since minimal amounts of the tailored protein can easily be detected by fluorescence, for example.^[180,211] Finally, the capability to shuttle such systems between cells of different life kingdoms (archaea, eubacteria, eukarya) would be of a great advantage. Indeed, a recent report about the use of the orthogonal system TyrRS/tRNA_{CUA}^{Tyr} from *M. jannaschii* in yeast is the first step in this direction.^[212]

The initial results on the engineering of the genetic code reveal that new amino acids can be incorporated into the existing repertoire. In most cases, this was readily possible since the goal was not to produce “unnatural organisms”, but rather to generate a system that works with an expanded amino acid repertoire. This system is compatible with the translation machinery of the host which serves only as a platform for codon-reassignment experiments. However, currently available methods for the expansion of the amino acid repertoire are characterized by temporal changes termed as read-throughs, suppressions, codon reassignments, etc., which are achieved by changes in the genotype and physiology of the living cells, and by controlled experimental conditions. The goal is, however, permanent reassignments or novel assignments of the coding units that is, codon capture either at the level of the expression system or at the level of the living cell (Figure 9).

This codon capture should be 1) nonlethal and 2) an intrinsic property of the system. Expression host cells with such a nonlethal codon capture (e.g. an organism without a seriously impaired viability upon an insertion of a novel amino acid in its repertoire) would be the most advanced system to expand the coding capacities of the universal genetic code in vivo. Codon capture can be achieved by a permanent reassignment of coding units in the frame of the existing structure of the universal genetic code. Another and a much more challenging venture is to introduce novel coding units by the generation of novel nucleic acid base pairs. In both cases, the protein translation would be enriched with truly novel canonical amino acids. Such codon capture in an organism with a tailor-made (or target-engineered) genetic code and with an intrinsically expanded amino acid repertoire is the most challenging aspect of future experimental approaches in code engineering.

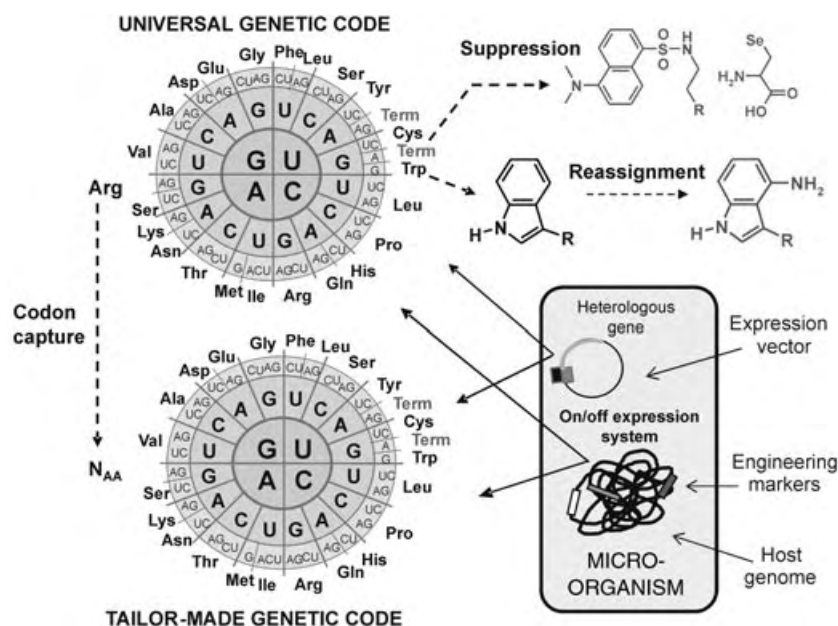


Figure 9. Codon capture as a vehicle to expand the coding capacities of the universal genetic code. Microorganisms used for genetic code engineering to date, are required to be able to read-through sense, nonsense, and non-triplet coding units, which were reassigned or suppressed, mainly at the level of a single protein and rarely at the proteome-wide level. Alternatively to this temporal re-coding, the existing genetic code can be tailored (or target engineered) with a codon capture. Hereby particular coding units are permanently reassigned, either at the level of the expression system or proteome-wide at the level of a whole living cell. The Arg coding triplets AGA and AGG were chosen as an example for permanent reassignment (codon capture) to a hypothetical novel amino acid (N_{AA}). However, any other combination is conceivable as well.

6.5. Is It Possible To Create the “First Autonomous Synthetic Life Form”?

As discussed before, the codon capture should be a nonlethal intrinsic property of an “unnatural” microorganism with a tailor-made genetic code that has an expanded coding capacity. Recent reports about the “first synthetic form of life”^[213] with a recombinantly expressed protein, which contains *p*-aminophenylalanine through suppression of the amber termination codon,^[149] meets this criteria only partially. Even if *p*-aminophenylalanine is accepted in the proteome of an *E. coli* expression host, which is supplied with a hybrid translation system (i.e. orthogonal components), partially imported metabolic pathways, and the termination stop-codon capture, this only occurs with the aid of an extra-chromosomally placed expression system (Figure 9). Therefore, this “truly unnatural organism”^[213] remains what it taxonomically always was, namely *Escherichia coli*. It remains to be seen whether *p*-aminophenylalanine as a “codon captor” of UGA termination signals could invade the genome and the proteome without imperilling the viability of this microorganism.

The first step in this direction would be the invasion of a novel amino acid in the existing repertoire by codon capture. Such cells would be supplied extra-chromosomally or in a compartmental manner with tailored genetic codes. However, one has always to keep in mind the immense complications in these trials. The more we understand the full complexity of

the biological machinery, the clearer it becomes that the components of a living cell interact in so many ways that a change in any key component requires compensatory changes in many others. For example, noncanonical base pairs for an in vivo expansion of the code requires experimental redesign of DNA replication, transcription, editing mechanisms, design of novel tRNA genes, and the necessity for recognition of novel bases and coding units that contain these bases. Similarly, one “rationally” designed orthogonal aaRS/tRNA pair might introduce a massive mutagenesis and finally cell death. Thus, an old principle of continuity expressed by Lucretius as “*Natura non saltus fecit*” (“Nature never makes a leap”), holds true for living organisms as well.

The alterations in the genetic code structure are now a well documented fact in nearly all living beings. For example, each eukaryotic cell is provided with two slightly different code assignment arrangements, but with the same standard amino acid repertoire. This means that one cell can shift one of the 20 canonical amino acids between different codons despite a complex genome encoding a highly complex proteome. The possibility to introduce alternative repertoires into the existing code structure has been described as a “Copernican turn”.^[27] It postulates that the amino acid repertoire of the genetic code of all living beings is universal and is therefore of prime importance, whereas smaller deviations in codon reassignments

are tolerated. Whereas living beings could survive codon reassignments (in the frame of the standard amino acid repertoire), the insertion of a novel amino acid into the existing repertoire is supposed to be harmful or even lethal. In this context, the prime goal of the research field described in this study is to derive new cells with nonlethal codon captures, that is, cells that survive an insertion of a novel amino acid in its repertoire. In this way, an experimental evolution of a “standard” to an “alternative” amino acid repertoire in the genetic code would be fully achievable. Whether and to which extent these cells with nonlethal codon captures and tailored genetic codes derived from natural parent cells can be regarded as a new taxonomic species or subspecies remains to be established.

7. Some Practical Applications of Noncanonical Monomers

7.1. Protein Chemistry in the Era of Genetic Code Engineering

Many interesting noncanonical amino acids contain desirable functional groups such as halogens, keto, and silyl groups, alkenes, or alkynes, could promote considerable functional advantages once incorporated into proteins. The possibility to encode genetically such chemical diversity should enable us to program living cells such as bacteria to do quite sophisticated syntheses with water, salts, and simple

carbon-sources being the only essential external requirements. Therefore, protein chemists will inevitably encounter the challenge of engineering the genetic code in the coming decades. Advances in polymer and peptide chemistry as well as in peptidomimetic chemistry teach us about the potentially vast chemical diversity that can be achieved if these are transferred onto proteins.^[214] Indeed, in the foreseeable future the increased demands for proteins with novel properties and functions, or as therapeutic agents, is easy to predict. Thus, the production of such tailor-made, custom-tailored proteins or alloproteins, (Figure 6) by use of programmed templates in metabolically engineered host cells will certainly be one of the main driving forces for the engineering of the genetic code by expanding its amino acid repertoire.

7.2. The Concept of Isomorphous Replacement in Biochemistry

More than two decades ago Wilson and Hatfield^[51] described that analogues of canonical amino acids were able to “induce predictable perturbation in protein structure”. This is equivalent to the concept of isomorphous replacement in protein X-ray crystallography: a heavy-metal containing

analogue can be incorporated in a protein without the occurrence gross changes with regard to the conformation of the molecules in the crystal. This incorporation influences in a predictable way, diffraction patterns of protein crystals, thus enabling their structure elucidation. The most prominent example is the presently routine SeMet incorporation into proteins, which provides selenium as a diffraction label for structure elucidation.^[13,63,215] In the meantime, the number of selenium-containing amino acid analogues or surrogates available for this purpose was further increased (Figure 10).^[70,76,103,216,217]

Similarly ¹⁹F NMR studies have taken advantage of the extreme sensitivity of ¹⁹F chemical shifts to the changes in local environments. This makes ¹⁹F NMR spectroscopy a powerful technique as it allows subtle conformational changes and intrinsic dynamic features of proteins to be probed.^[75] Furthermore, fluorinated proteins certainly represent potent tools for in vivo ¹⁹F magnetic resonance imaging and spectroscopy for diagnostic purposes in medicine due to their biocompatibility. The potentials of amino acid analogues in spectroscopy, protein folding and stability studies, material sciences, and enzymology have been extensively discussed elsewhere.^[6,15]

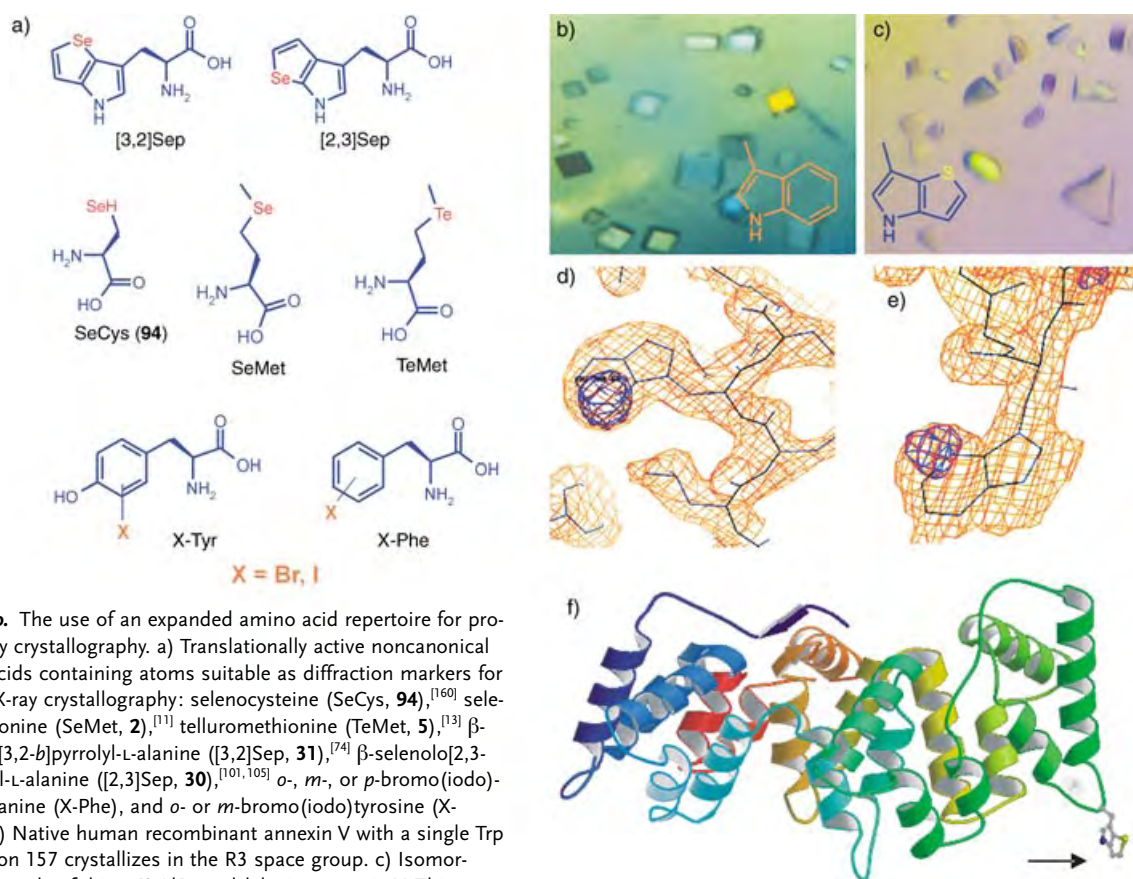


Figure 10. The use of an expanded amino acid repertoire for protein X-ray crystallography. a) Translationally active noncanonical amino acids containing atoms suitable as diffraction markers for protein X-ray crystallography: selenocysteine (SeCys, **94**),^[160] selenomethionine (SeMet, **2**),^[11] telluromethionine (TeMet, **5**),^[13] β -selenolo[3,2-*b*]pyrrolyl-L-alanine ([3,2]Sep, **31**),^[74] β -selenolo[2,3-*b*]pyrrolyl-L-alanine ([2,3]Sep, **30**),^[101,105] *o*-, *m*-, or *p*-bromo(iodo)-phenylalanine (X-Phe), and *o*- or *m*-bromo(iodo)tyrosine (X-Tyr).^[81] b) Native human recombinant annexin V with a single Trp at position 157 crystallizes in the R3 space group. c) Isomorphous crystals of thieno[3,2-*b*]pyrrolylalanine-annexin V. This amino acid is a pharmacologically active substance. d) Experimentally determined electron density maps confirmed the complete replacement of the benzyl group of Trp by selenophene units of [3,2]Sep at position 53 in the protein barstar (Figure 11). For this residue the difference Fourier maps ($F_o - F_c$) are superimposed with 3.5 σ (blue) of the 2 $F_o - F_c$ continuous electron density map at 1 σ (orange). e) Representation as for (d) for the replacement of Trp for [3,2]Sep at position 157 in recombinant human annexin V ($F_o - F_c$ at 3.0 σ and 2 $F_o - F_c$ at 1 σ). f) Structure of human recombinant annexin V with [3,2]Sep at position 157. For both proteins (annexin V and barstar), incorporation of the analogue was fully isomorphous, since their overall fold and structures are practically identical with that of the parent protein.

For a biophysicist, replacements at the level of single atoms or small groups such as H/F, CH₂/S/Se/Te represent a type of “atomic mutations”.^[134,218–220] They cause minimal changes in the local geometry often far beyond the resolution of X-ray and NMR protein analyses, but can often induce significant changes in marginally stable protein structures. In fact, they introduce novel interactions in proteins such as enhanced or decreased polarity and offer the unique possibility to study and understand how these properties are integrated, propagated, and modulated into the cooperatively folded protein structure.

The concept of predictable perturbation or isomorphous replacement can be generally extended from structural biology and biophysics to biomedicine. Some potential applications of the concept will be dealt with in more detail in the following sections.

7.3. DNA Nucleotide Analogues

In addition to protein chemistry, the concept of analogues is widely practiced in other research fields as well. The most prominent example is the observation of the possibility for enzymatic incorporation of dideoxynucleotide analogues (dNTPs) into a growing DNA strand. Sanger and co-workers developed a method based on these experiments that is currently central to almost all current DNA sequencing technologies. The modified dNTPs with detectable reporter groups such as digoxigenin or biotin, fluorochromes or aliphatic side chains covalently attached to the base are able to terminate DNA synthesis mediated by a number of DNA-polymerases.^[158]

On the other hand, the same approach could be applied to biomedicine. For example, the human immunodeficiency virus and other retroviruses do not encode specific enzymes required for the metabolism of the purine or pyrimidine nucleosides. Therefore, many of such compounds that exhibit antimetabolic effects or antiviral action that are currently in use, or under advanced clinical trial, for the treatment of HIV infection, belong to different classes of nucleoside/nucleotide analogues that act as reverse transcriptase inhibitors, for example zidovudine (AZT), didanosine (ddI), zalcitabine (ddC), and stavudine (d4T).^[221]

Finally, there are attempts to use similar approaches to expand the genetic code through the creation of a 65th codon–anticodon pair from noncanonical nucleoside bases having non-standard hydrogen-bonding or even inter-base hydrophobic interaction patterns. This new DNA base pair would allow an expansion of the information content of DNA by extension of the genetic alphabet with a third base pair.^[205,206,222]

7.4. Protein-Based Sensors and “Golden” Fluorescence

Absorbance in the near UV region and fluorescence are intrinsic properties of proteins, which are attributed to the presence of aromatic amino acid residues in the structure; the contributions of these residues to the spectral properties are

additive. The amino acid Trp has been the target for substitution studies for a long time since the mean UV absorbance of proteins is mainly dominated by the its spectral contribution.^[120] A recent review by Szabo, Ross, and Hogue^[17] details the potential applications of 5-hydroxytryptophan, 7-azatryptophan, and fluorinated Trp analogues for fluorescence spectroscopy. The most recent advances included incorporation of selenium-containing Trp surrogates (for structural biology), and pharmacologically active sulfur surrogates (Figure 10) as well as pH-sensitive aminotryptophan analogues, which open up perspectives for a relatively simple approach for the general design of protein-based sensors (Figure 11).^[105]

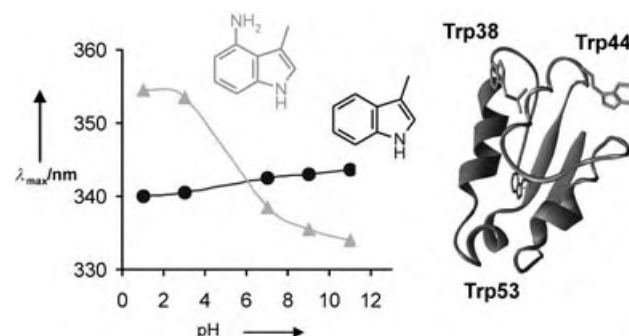


Figure 11. Replacement of Trp residues in barstar with 4-aminotryptophan converts the pH-insensitive parent protein into a pH-sensitive fluorescent protein. Note that the positions of the fluorescence emission maxima (λ_{max}) are pH-dependent only in (4-NH₂)Trp-barstar.

A step further towards the use of aminoindoles was their integration into the chromophore of the green fluorescent protein (GFP) from the jellyfish *Aequoria victoria* (av), which has recently become a standard reporter in cellular and molecular biology as well as a model for studies of chromophore photophysics.^[223] The avGFP chromophore, completely encoded in the amino acid sequence (4-(*p*-hydroxybenzylidene)imidazolid-5-one) is autocatalytically formed in the post-translational reaction of residues Ser65, Tyr66, and Gly67.^[224] Chromophore-building residues of avGFP are almost ideal models for such substitutions, since the produced effects are immediately observable in the optical properties. Importantly, the placement of any aromatic amino acid in position 66 is crucial for the emergence of a fluorescently active avGFP chromophore.^[225] The standard amino acid repertoire limits the possibilities to gain altered spectral windows by direct re-design of avGFP-chromophore, since only four aromatic rings are available (Phe, His, Tyr, and Trp). It is, therefore, not surprising that despite years of effort on its variations by classical protein engineering approaches, no significantly red-shifted variants of *A. victoria* GFP were found ($\lambda_{\text{max}} < 530$ nm). Clearly, a further re-design of avGFP-chromophores requires an expanded amino acid repertoire.

The mutation Tyr66Trp (e.g. Ser65Thr/Tyr66Trp) leads to enhanced cyan fluorescent proteins (ECFPs) with a characteristic blue-green emission and an indole ring as an integral part of the chromophore. The replacement of the indole ring by an electron-donating 4-aminoindole in ECFP results in a

“gold” fluorescent protein (GdFP) which is, with its Stokes shift of about 100 nm, the most red-shifted *Aequoria* GFP-variant known to date (Figure 12).^[104] The GdFP is further characterized by a dramatically increased thermostability and stability of the monomeric state. It was expressed and purified by using a Trp-auxotrophic *E. coli* strain in the yields similar to that of the parent ECFP ($\approx 30 \text{ mg L}^{-1}$ of the culture). This allowed the crystallization of the protein, the elucidation of its structure, as well as the determination of various biochemical and biophysical parameters for the dynamics of the chromophore.

With the *av*GFP variants available to date, however, there is only one pair of proteins, which are excited at the same wavelength, but which can be detected at two different wavelengths. The design of the GdFP expands these possibilities, since three populations of Trp-auxotrophic *E. coli* cells expressing “cyan”, “green”, and “gold” fluorescent proteins can be unambiguously detected upon excitation at a single wavelength, clearly opening new ways for multiple labeling applications (Figure 12). It also represents an excellent example of custom-tailored or tailor-made protein.

However, the use of these tailor-made *av*GFPs as fusion tags in mammalian cells is limited, since they need either auxotrophic bacterial strains or bacterial strains that host suitable orthogonal pairs. Therefore, the ideal goal in this particular case would be to provide mammalian cells under investigation with suitable orthogonal pairs or orthogonal translation components to study expression of a larger number of *av*GFP-fusion proteins simultaneously. That requires the development of expressible reporter systems for use in mammalian cells as was recently reported.^[198,211,180]

7.5. Analogues, Isosteres and Surrogates for Biomedicine

Bioisosteric compounds with nearly identical structures, shapes, and volumes, as well as similar distributions of electrons might affect biochemically associated systems as agonist or antagonists and thereby produce biological properties that are related to each other. Early studies on non-canonical amino acids as antimetabolites which were extensively reviewed by Richmond,^[52] Hortin and Boime,^[50] Wilson and Hartfield,^[51] and Kirk,^[58] clearly demonstrated the strong

antimicrobial, antimycotic, and antitumor activities of such compounds. However, little attention was paid to these interesting pharmacological properties that might possibly have a great potential in biomedicine.^[15] The roles of non-canonical amino acids other than participation in protein synthesis are specific interactions with metabolic and catabolic enzymes (inhibition, activation, modulation) and interference in the process of amino acid biosynthesis, turnover, transport, and storage.

Most of the noncanonical amino acids are toxic; often this toxicity is the result of their conversion into toxic substances by a relatively complex metabolic route. Microorganisms and fungi produce many unusual amino acid containing toxic substances that are physiologically highly active in mammals or other microorganisms, usually in a highly deleterious manner such as cephalosporines or penicillins. Plants are the best chemists among living organisms because of their remarkable capacity to produce a wide variety of secondary metabolites such as alkaloids, terpenes, and tannins to protect themselves from predators, parasites, and infection by viruses. Many novel plant amino acids are structurally very similar to the canonical ones and have the poten-

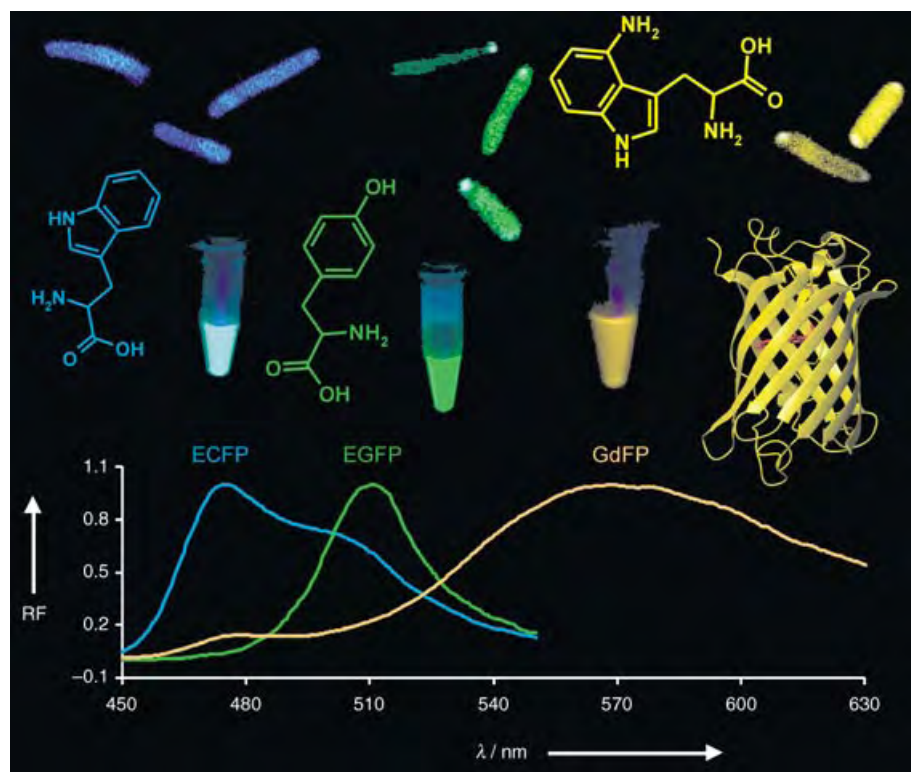


Figure 12. Top: Single color excitation of differently emitting *av*GFP mutants and variants expressed in bacterial cells and imaged on a standard confocal microscope by using different emission filters. The fluorophores are excited at one wavelength and differ with respect to their emission wavelengths. The experiment shown is an example for in vivo non-invasive multiple labelling: Trp-auxotrophic *E. coli* ATCC49980 cells^[102] expressing “enhanced cyan” *av*GFP (ECFP, Ser65Thr/Tyr66Trp), “enhanced green” *av*GFP (EGFP, Phe64Leu/Ser65Thr), and “gold” fluorescent protein (GdFP) are clearly distinguishable upon simultaneous excitation at a single wavelength (457 nm). Bottom: Comparison of normalized fluorescence emission spectra of these *av*GFP classes. The fluorescence of ECFP is characterized by two emission maxima ($\lambda_{\text{max}1}=475 \text{ nm}$; $\lambda_{\text{max}2}=506 \text{ nm}$). The emission maximum of the likewise “classical” mutant EGFP (with Tyr66 as an integral part of the chromophore) is further red-shifted ($\lambda_{\text{max}}=508 \text{ nm}$).^[223] The tailor-made GdFP (with (4-NH₂)Trp66 as an integral part of the chromophore) shows the largest red shift ($\lambda_{\text{max}2}=576 \text{ nm}$). RF = normalized fluorescence intensity.

tial to affect deleteriously the metabolism in other organisms. For example, the noncanonical amino acid mimosine causes loss of hair and wool in cattle and sheep grazing on *Leucaena leucocephala* or *Mimosa pudica*, while the numerous selenium- or sulfur-containing amino acids are found in a variety of plants that have wide-ranging toxic effects on grazing animals.^[148]

The particularly well-documented toxicity of 3-fluorotyrosine, 3-fluorophenylalanine, and 5-fluorotryptophan is due to the formation of fluoroacetate formed by the dominant Tyr metabolic pathway, which was discovered over 30 years ago.^[226–228] The toxic fluoroacetate is the most ubiquitous among the organofluorine compounds and has been identified in more than 40 tropical and subtropical plant species. It is also produced by some microorganisms when grown on media containing fluoride. Whether such a principle can be “borrowed” from nature to kill tumor cells and spare normal ones, is still unknown. Indeed, in drug design for chemotherapy the best way to achieve the specificity of action and selectivity of delivery is to use proteins as delivery vehicles (protein shuttles; Figure 13). For example, it is known that lethal metabolic intermediates such as fluorocitrate and fluoroacetate are formed from 3-fluorotyrosine in mammalian tissues.^[58] The same must hold true for tumor cells, if this cytotoxic amino acid would be specifically delivered to them (Figure 14). Free cytotoxic amino acids generally have two choices: 1) the re-incorporation into other proteins (i.e. re-entering protein translation), and 2) the entry into the intracellular metabolism. The cytotoxic action most probably follows the general principle postulated by Pattison that “any compound which can form fluoroacetic acid by some simple biochemical process is toxic”.^[229]

7.6. Noncanonical Amino Acid Surrogates in the Brain?

Many surrogates are more active than their parent molecules. A widely known example is the lactose surrogate isopropyl- β -thiogalactoside (IPTG), which is a much stronger inducer of the *lac*-operon than lactose itself. Neuroregulatory amino acids and their derivatives play critical biochemical roles not only in the brain, but also in the whole nervous system. Indeed, numerous neurologically active substances have amino acids as precursors. The uptake of amino acids into the brain is particularly important for the control of brain functions. The composition of free amino acid pools in the

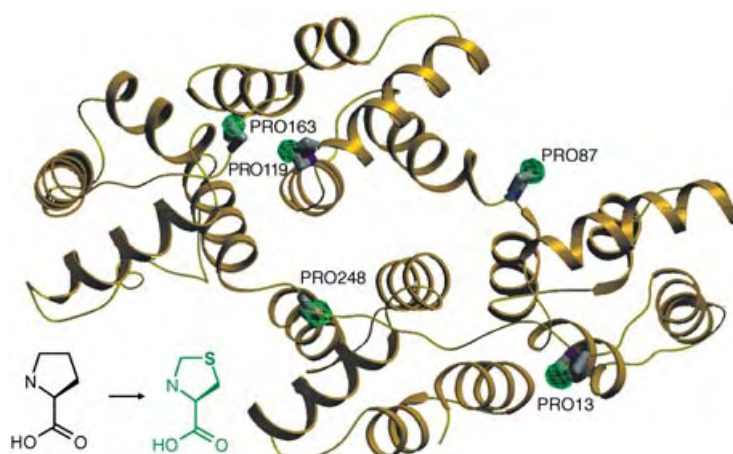


Figure 14. Human recombinant annexin V isomorphously substituted with the pharmacologically active noncanonical amino acid thiaproline.^[14] The overall protein structure is not changed by the replacement. Cytotoxic amino acids, such as thiaproline, that might serve as diagnostic markers, are covalently integrated into the polypeptide as an inactive prodrug and should exert no toxicity during delivery. This approach is expected to introduce as few perturbations as possible in the structural, functional, and immunogenic properties of the protein carrier (e.g. antibodies, cytokines, growth factors, tissue-specific proteins).

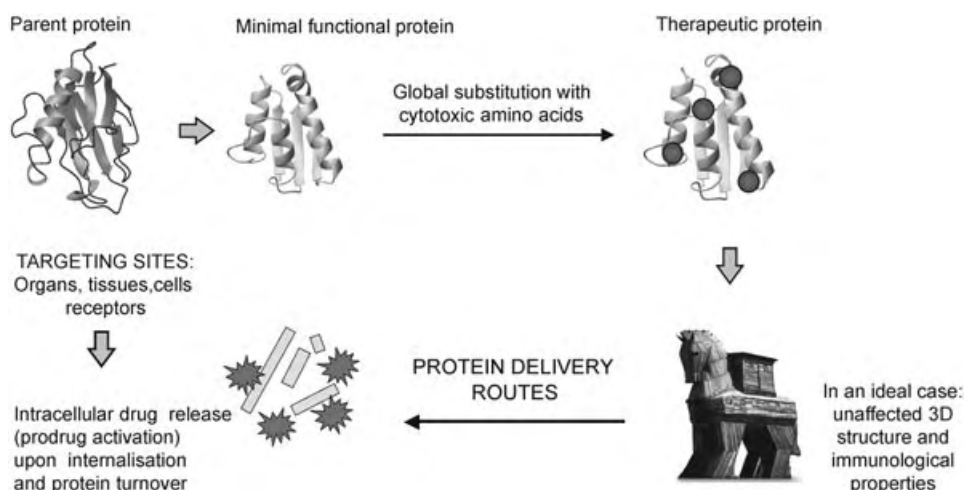


Figure 13. Schematic representation of the concept of use of proteins “armed” with cytotoxic amino acids as possible non-invasive carriers for drug delivery.^[15] Antibiotic amino acids such as penicillamine, azaleucine, azatyrosine, thiaproline, furanomycin, or strong antimetabolites such as fluorinated amino acids, or canavanine can be incorporated into proteins. Recombinant proteins that contain such pharmaceutically active amino acids are expected to act as specific delivery vehicles “shuttles”, “Trojan horses” or even “magic bullets” due to their potential ability for selective delivery and targeting in the human body.

brain differs largely from those of other tissues. The availability (i.e. uptake) and utilization of such amino acids are often the rate-limiting step in the neurological actions of their derivatives. For instance, the administration of large amounts of Trp in rats leads to an increase in the synthesis of the neurohormone 5-hydroxytryptamine (serotonin).^[230]

The neurological activity of some noncanonical amino acid analogues, surrogates, and their derivatives has been known for a long time.^[231,232] The delivery of such substrates alone or as a part of peptide or protein carriers that pass the blood–brain barrier might provide the brain with novel substances of anthropogenic origin that can exhibit interesting and useful properties.

Relatively well documented “relaxed” substrate specificity of brain enzymes can be exemplified by the nonspecificity of the aromatic amino acid decarboxylase and dopamine- β -hydroxylase, which are responsible for the conversion of a number of Tyr derivatives into analogues of norepinephrine, or the 5-hydroxytryptophan-based serotonin enzymatic system. Furthermore, the storage mechanism between processed (e.g. decarboxylated) canonical amino acids and their amino acid surrogates is nonselective as well.^[233] These features might help to modulate synaptic activity by the use of noncanonical amino acid analogues or surrogates because they might enter some of the metabolic pathways of their canonical counterparts and form metabolic derivatives that might displace natural neurotransmitters.

Since neurohormones based on amino acids are responsible for many aspects of neural and brain functions, it is conceivable that the changes in their balance caused by surrogates and analogues released in the bloodstream might be responsible even for different consciousness states. In other words, approaching the chemistry of the brain by way of amino acid surrogates should provide an efficient and valuable tool for studying not only the molecular principles of thought, memory, and sensory perception but also might be able to act as effective medicines.^[234]

8. The Future of Genetic Code Engineering

8.1. Protein Chemistry and Genetics: History and Current Status

By the end of the 19th century, protein chemists had identified most of the amino acids, which were known to be the main building blocks of all proteins. At the same time, Fischer and Hofmeister^[235,236] conceptually solved the problem of amino acid linkages in proteins with the “peptide hypothesis” (i.e. peptide bond concept). The development of a variety of analytical techniques took almost half a century before this hypothesis was fully confirmed with the successful insulin sequencing by Sanger.^[237] How amino acids are linked to polypeptide chains was first fully understood only when it had been demonstrated experimentally that RNA templates direct the synthesis of each protein. At this point, the direct connection between intracellular protein synthesis of living matter and its genetic program was clear.

After the unambiguous experimental identification of DNA as the hereditary molecule made by Avery, Hershey,

and Chase,^[238,239] biologists, chemists, and physicists directed their interest to DNA. Beadle’s “one gene \rightarrow one protein” concept^[240,241] certainly paved the way for the discovery of the regulation of the gene expression by Jacob and Monod.^[242] After the genetic code had been deciphered^[3,4] further rapid development continued unabated. In the early 1970s almost all crucial concepts of genetics were established and are now an integral part of common biochemical knowledge. The concept “one gene \rightarrow one protein” certainly does not fit into the current picture of the multidimensionality of a proteome; however, its historical impact is based on the fact that it was used (and still is a common practical guide in laboratory routine) as a working hypothesis leading to important discoveries and developments.

The incorporation of noncanonical amino acids into proteins emerged as a research field as early as the 1950s.^[52] However, only after the advent of recombinant DNA technology did it become possible to advance in the direction of an expanded amino acid repertoire. As with the deciphering of the triplet genetic code, organic chemistry and genetics had to work closely together. The new venture is not just a renaissance of old dreams about generating proteins with synthetic amino acids, but is centered on about how to change the universal genetic code experimentally and how affect its evolution.

8.2. Theories on the Genetic Code and Its Engineering

While investigations into the emerging questions about the nature and history of the genetic code evolution were taking place mainly in theoretical biology, research into the possibilities of an expansion of the amino acid repertoire in the genetic code was developed in the field of protein chemistry. The field of molecular evolution in the last few decades was marked by the emergence of a rather large number of studies on the different models for evolution of the genetic code, whose influence on the experimental engineering of the genetic code was rather minimal.

Classical experiments by Miller^[25] about the spontaneous prebiotic synthesis of amino acids mark the historical start of the era of the experimental approach to the problem of the origin of life. Regarding the genetic code itself, the vast majority of the contributions deal with theoretical aspects; only a few authors have contributed in both theoretical as well as practical research directions. Recently, Yarus wrote “the immediate future of the code origin appears to be in hands of experimentalists”.^[243] Wong et al. made historically important contributions to the attempts to expand the amino acid repertoire.^[66,172] In addition, Wong postulated the co-evolution theory of the origin of the genetic code, which states that the genetic code expansion took place by the recruitment of precursor amino acids from developing biosynthetic pathways.^[244] This means that an expansion of the coding capacities of the existing genetic code can be achieved if host microorganism cells are additionally provided with novel biosynthetic pathways that produce amino acids compatible with their physiology and metabolism. In other words, the amino acid repertoire cannot be freely expanded to maximize

the efficiency of a single function, but must instead co-evolve with the expansion of other cellular metabolic and biosynthetic capacities. Indeed, recent experiments by Mehl et al.^[149] seem to confirm such possibilities.

The other hypotheses of the code evolution such as how it was shaped by various selective pressures, its capacity for translation-error minimization and flexibility might indeed serve to certain extents as a good guide or conceptual framework in experimental attempts for code engineering. Taking into account the immense complexity of the biological systems we are dealing with, it should not be a surprise that in spite of the large volume of recent and older literature on the genetic code evolution, there are no generally accepted concepts.

Most probably, we might forever remain agnostic about the exact historical sequence of events in code origin and establishment. The genetic code itself is a product of Darwinian evolution,^[44,245] and Darwinism per se is a historical concept. Therefore, for genetic code engineering, the experiment always remains the ultima ratio to analyze any prediction, hypothesis, or expectation. Even then, the non-resolvable complexities and controversies are often difficult to avoid. For example, the second position of U in the coding triplets, encodes hydrophobic amino acids, that is, the genetic code conserves hydrophobicity against random nucleotide mutations. Not surprisingly, this residue property is also an essential driving force in protein folding. On the other hand, in the context of the standard repertoire, it is often notoriously difficult to characterize a single property such as the hydrophobic nature of Trp.^[246,247] Namely, there are more than forty published hydrophobicity scales in the literature with many cases of contradictions about the hydrophobic/hydrophilic nature of Trp.^[248]

8.3. Code Engineering and De Novo Protein Design

The terms “protein engineering” and “protein design” used in numerous contemporary research reports, usually refer to the modification or redesign of pre-programmed protein modules. These are normally identified by pattern recognition or exchange (permutation) among the canonical 20 amino acids. Both these pathways have been selected, shaped, and optimized for billions of years by various selective pressures during evolution. Two fundamentally different approaches have emerged over the last twenty years: 1) A “rational” redesign by site-directed mutagenesis. This method requires knowledge of the three-dimensional structure of the protein or the capacity to predict the effect of exchanges among the canonical 20 amino acids. 2) Random mutational techniques such as DNA shuffling, based on a mutation/selection approach, which imitates the natural selection process.

Unfortunately, despite numerous published studies and experimental observations concerning folding properties of proteins, there are still no general rules for a successful de novo protein design.^[249] The rapid progress in structural biology, as reflected by the dramatic increase in the number of resolved three-dimensional structures, was surprisingly of

little help in coping with the problems of rational design. Even for genetic code engineering, the availability of three-dimensional structures of all translational components, including that of the ribosome,^[250] although spectacular, has until now, contributed only marginally, to enable and teach us how to expand the genetic code experimentally. For example, the recently determined structure of the TyrRS/tRNA_{CUA}^{Tyr} pair from *Methanococcus jannaschii*^[251] explained the structural basis for orthogonality—but it was a posteriori, that is, after the novel aaRS substrate specificity had already been established. Although three-dimensional structures are invaluable starting points for design attempts, it is clear that difficult and challenging problems associated with protein rational design as well as code engineering cannot be based solely on such predominantly mechanistic, descriptive, and reductive approaches. One might hope that protein chemistry through code engineering will turn future research trends in biochemical sciences from the currently prevailing dry descriptiveness to a research dominated by conceptual intuition and inventive spirit.

The problem of the de novo design of proteins will not be solved by an expansion of the amino acid repertoire itself. At this stage of the development in the field, many cases are well-documented for which translationally active amino acids exhibit adverse effects on the folding and structural integrity of target proteins. In other words, many interesting non-canonical amino acids simply cannot be accommodated in the existing natural protein scaffolds without their redesign or de novo design. Literally speaking, we are in the same position as those builders from the beginning of dark Middle Ages of Western culture who were borrowing building materials from sophisticated Greek and Roman structures.

8.4. Future Progress and the Global Impact of Code Engineering

Progress in natural science in general, as well as in genetic code engineering in particular, would usually have an impact on society in terms of the novel technical advances and perspectives that it brings. On the other hand, such progress often cannot occur without having an impact on numerous traditional philosophical, religious, and ethical issues. It might cause or catalyze critical re-evaluation, disappearance of the obsolete, and even the emergence of novel ideological, religious, or ethical systems in certain societies. For example, Darwinism offers a frame in which one would see the genetic code as an integral part of cellular chemistry whose function is to increase the survival fitness in a given environment.^[45] It also postulates that in the process of the emergence of biologically active natural proteins as well as living organisms, no conscious effort is involved.^[252] On the other hand, the engineering of novel functions of artificial proteins or even cells with an expanded amino acid repertoire would be an example of human-made conscious design.

At the more practical level, sound experimental research in coming decades will mainly concentrate on using current knowledge of the basic determinants behind the organization of the present-day genetic code to make it more accessible for further experimental manipulations. The strategy of evolution

will be borrowed from nature to much larger extents than now. Namely, natural selection is a nonrandom process determined by the environment; a sort of statistical bias that increases the probability of otherwise extremely improbable but successful adaptive genetic and phenotypic combinations. This process is highly innovative and teleonomic in its very nature, since the end result of it is improved functional performance in a given environment.

The emergence of such tailor-made (or custom-made) proteins, produced in specialized cells (with target-engineered genetic codes) and intentionally designed for performance in user-defined environments probably mark the start of the “post-proteome” era. Nonetheless, it would always be desirable to refrain from the claim to describe current as well as future progress in the field as “revolutionary”—serendipity and intuition cannot be excluded as important factors for breakthrough discoveries. One more reason always to be sceptical of revolutionary talk is the fact that the only context in which such developments could take place is continuous skilled and dedicated experimental labor. Furthermore, it is hard to imagine that progress anticipated in this way represents a sort of a “paradigm shift”. It should be rather taught in terms of a gradual change of concepts and experimental possibilities that are deeply rooted in Mendelian and Darwinian tradition with the necessary requirement for its constant and critical re-evaluation and improvement.

Addendum

Since the submission of this review a series of novel, important, and relevant contributions in this rapidly developing field have appeared.

Proline and phenylalanine analogues and surrogates: The expectation of this study that engineering or a simple elevation of intracellular levels of prolyl-tRNA synthetase (ProRS) will result in a full translational activity of the proline analogues and surrogates such as *trans*- and *cis*-4-hydroxyproline, piperidine-2-carboxylic acid, and azetidine-2-carboxylic acid (Section 4.7) has been fulfilled by Conticello and co-workers.^[256] They succeeded in incorporating these amino acids efficiently into recombinant elastin by using Pro-auxotrophic strains with native genomic background activity of ProRS, or Pro-deficient strains supplemented with elevated amounts of native or mutated ProRS expressed under the control of an orthogonal promoter system. Similarly, by using the PheRS mutant with broadened substrate specificity (PheRS- α Ala294Gly), Bentin et al. reported the incorporation of large amounts of the photoreactive bicyclic amino acid benzofuranylaniline into a model protein.^[257]

Identity problem: An important contribution that fully highlighted the problem of amino acid “identity” (Section 2.3), as a novel feature of the protein translation apparatus was made by Tirrell and Kumar.^[258] Therein they fully confirm the hypothesis that there must “be a case when one amino acid is a substrate for two synthetases and subsequently, the isoacceptor from two different tRNA species which are loaded with the same amino acid, that is having the same ‘identity’”. It is well known (see for example

refs. [259] and [260]) that the fidelity of the aminoacylation reaction is determined not only by the catalytic specificity of aaRS but also by its specific intracellular concentrations in cytosol. In this work, it is explicitly demonstrated how variations of cytosol concentrations of aaRS in bacterial expression hosts can allow a single RNA message to be read in different ways. More specifically, Tirrell, Kumar, and co-workers have shown that the identity of the noncanonical amino acid (2*S*,3*R*)-4,4,4-trifluorovaline can be changed in the protein translation by its assignment either to isoleucine or to valine codons, depending on intracellular levels of the isoleucyl- or the valyl-tRNA synthetase in the bacterial expression host. This is an excellent example of how kinetic knowledge about relative rates of competing aminoacylation reactions could be used to expand the amino acid repertoire.

Bridging the gap between theory and experiment: The results described in reference [254] proved to have implications for the understanding of the origins of alternate genetic codes, favoring the “ambiguous intermediate” hypothesis of Schultz and Yarus.^[261,262] Two papers have appeared recently that demonstrate that the community of theoretical biologists concerned with the evolutionary establishment of the genetic code are slowly becoming keen on the experiments of code engineering, continuing in this way a tradition established earlier (see Section 2.2, ref. [27]). Namely, a review by Bacher, Hughes, Wong, and Ellington^[263] and a short commentary by Cavalcanti and Landweber^[264] elaborated different hypotheses regarding genetic code evolvability in light of the results of novel code engineering experiments.

Other contributions and reviews in the field: In the meantime, Schultz and co-workers have reported the use of orthogonal TrpRS/tRNA^{Trp}, which is capable of efficient opal suppression for selective incorporation of (5-OH)Trp into proteins in mammalian cells.^[265] Another breakthrough from this group is the report of the design and generation of an orthogonal synthetase/tRNA pair derived from archeal tRNA^{Lys} sequences that are capable of frameshift suppression of the quadruplet codon AGGA.^[266] This pair proved to be compatible with the amber-orthogonal system; thus, enabling the simultaneous incorporation of homoglutamine and *O*-methyltyrosine at distinct positions within myoglobin. The most recent reviews by Link et al.,^[267] Hahn et al.,^[268] as well as by Anthony-Cahill and Maglieri,^[269] provide a balanced view on the whole field, whereas specialized reviews have focused on site-specific labeling using chemoenzymatically acylated tRNAs^[270,271] and subsequent post-translation chemistry of the resulting proteins.^[272]

Noncanonical DNA base pairs: The approach pioneered by Benner and co-workers (1989) on the use of complementary nucleotides to generate novel Watson–Crick base pairs culminated recently in the finding by Yokoyama and co-workers^[273] that DNA with unusual base pairs can be transcribed into RNA molecules. The rapid progress in the design and construction of noncanonical base pairs based on research by Benner, Eaton, Kool, Hirao, Rombesberg, Yokoyama, Schultz and their respective groups was recently comprehensively reviewed by Bergstrom.^[274]

Beside experimental results and critical observations, this study presents certain themes and insights, which have interested me for a long time. The development of novel ideas, concepts, and innovative work in general is much more probable in those places where the precious institution of freedom is cultivated, that is, where heads and leaders allow sometimes members of their groups to step beyond the strict boundaries of their charge. I was lucky to be in such a place during the last eleven years of my research work. Therefore I wish to express my thanks and deep gratitude to my mentors Robert Huber and Luis Moroder who provided me with the infrastructure in their laboratories, the staff support, and encouragement for work, but above all for freedom. I am also grateful to Waltraud Wenger, Tatjana Krywcun, and Petra Birle for their excellent technical assistance, and for providing a friendly, congenial, and creative working atmosphere. Finally I am also in debt to my family especially my dear wife Monika for her love, understanding, and support for my "scientific" way of life.

Received: December 29, 2003

Revised: April 5, 2004

- [1] E. Mayr, *What Evolution Is*, Perseus Books, New York, **2001**.
- [2] F. H. C. Crick, *Symp. Soc. Exp. Biol.* **1957**, 12, 138.
- [3] M. W. Nirenberg, *Trends Biochem. Sci.* **2004**, 29, 46.
- [4] M. W. Nirenberg, *Methods Enzymol.* **1963**, 6, 17.
- [5] K. L. Kiick, J. C. M. van Hest, D. A. Tirrell, *Angew. Chem.* **2000**, 112, 2232; *Angew. Chem. Int. Ed.* **2000**, 39, 2148.
- [6] N. Budisa, C. Minks, S. Alefelder, W. Wenger, F. M. Dong, L. Moroder, R. Huber, *FASEB J.* **1999**, 13, 41.
- [7] C. J. Noren, S. J. Anthony-Cahill, M. C. Griffith, P. G. Schultz, *Science* **1989**, 244, 182.
- [8] K. J. Rothschild, S. Gite, *Curr. Opin. Biotechnol.* **1999**, 10, 64.
- [9] M. Ibba, H. Hennecke, *Bio/Technology* **1994**, 12, 678.
- [10] G. Michal, *Biochemical pathways: An Atlas of Biochemistry and Molecular Biology*, Wiley, New York, **1999**.
- [11] D. B. Cowie, G. N. Cohen, *Biochim. Biophys. Acta* **1957**, 26, 252.
- [12] F. Chapeville, G. V. Ehrenstein, S. Benzer, B. Weisblum, W. J. Ray, F. Lipmann, *Proc. Natl. Acad. Sci. U.S.A.* **1962**, 48, 1086.
- [13] N. Budisa, B. Steipe, P. Demange, C. Eckerskorn, J. Kellermann, R. Huber, *Eur. J. Biochem.* **1995**, 230, 788.
- [14] N. Budisa, C. Minks, F. J. Medrano, J. Lutz, R. Huber, L. Moroder, *Proc. Natl. Acad. Sci. U.S.A.* **1998**, 95, 455.
- [15] C. Minks, S. Alefelder, L. Moroder, R. Huber, N. Budisa, *Tetrahedron* **2000**, 56, 9431.
- [16] K. L. Kiick, D. A. Tirrell, *Tetrahedron* **2000**, 56, 9487.
- [17] J. B. A. Ross, A. G. Szabo, C. W. V. Hogue, *Fluoresc. Spectrosc.* **1997**, 278, 151.
- [18] C. Tanford, J. Reynolds, *Nature's robots: A history of proteins*, Oxford University Press, New York, **2001**.
- [19] D. N. Wheatley, M. S. Inglis, P. C. Malone, *Curr. Top. Cell. Regul.* **1986**, 28, 107.
- [20] D. M. Kipnis, E. Helmreich, E. Reiss, *Biochim. Biophys. Acta* **1961**, 51, 519.
- [21] K. L. Kirk, J. Y. Nie, *Biomed. Front. Fluorine Chem.* **1996**, 639, 312.
- [22] P. Schuster, *Proc. Natl. Acad. Sci. U.S.A.* **2000**, 97, 7678.
- [23] I. Prigogine, *Cell Biophys.* **1986**, 9, 217.
- [24] A. L. Weber, S. L. Miller, *J. Mol. Evol.* **1981**, 17, 273.
- [25] S. L. Miller, *Science* **1953**, 117, 528.
- [26] D. H. Ardell, G. Sella, *J. Mol. Evol.* **2001**, 53, 269.
- [27] N. Budisa, L. Moroder, R. Huber, *Cell. Mol. Life Sci.* **1999**, 55, 1626.
- [28] P. Forterre, *Curr. Opin. Genet. Dev.* **1997**, 7, 764.
- [29] C. Woese, *Proc. Natl. Acad. Sci. U.S.A.* **1998**, 95, 6854.
- [30] M. B. Hoagland, P. C. Zamecnik, *Fed. Proc.* **1957**, 16, 197.
- [31] F. H. C. Crick, *Science* **1963**, 139, 461.
- [32] M. Ibba, H. D. Becker, C. Stathopoulos, D. L. Tumbula, D. Soll, *Trends Biochem. Sci.* **2000**, 25, 311.
- [33] R. W. Holley, J. Apgar, G. A. Everett, J. T. Madison, S. H. Merrill, J. R. Penswick, A. Zamir, *Fed. Proc.* **1965**, 24, 216.
- [34] S. H. Kim, F. L. Suddath, G. J. Quigley, A. McPherson, J. L. Sussman, A. H. J. Wang, N. C. Seeman, A. Rich, *Science* **1974**, 185, 435.
- [35] C. Stathopoulos, T. Li, R. Longman, U. C. Vothknecht, H. D. Becker, M. Ibba, D. Soll, *Science* **2000**, 287, 479.
- [36] A. R. Fersht, *Proc. R. Soc. London Ser. B* **1981**, 212, 351.
- [37] G. D. Gay, H. W. Duckworth, A. R. Fersht, *FEBS Lett.* **1993**, 318, 167.
- [38] M. Ibba, D. Soll, *Annu. Rev. Biochem.* **2000**, 69, 617.
- [39] L. H. Schulman, J. Abelson, *Science* **1988**, 240, 1591.
- [40] W. H. McClain, *FASEB J.* **1993**, 7, 72.
- [41] Y. Tang, D. A. Tirrell, *Biochemistry* **2002**, 41, 10635.
- [42] M. Ibba, P. Kast, H. Hennecke, *Biochemistry* **1994**, 33, 7107.
- [43] S. W. Santoro, L. Wang, B. Herberich, D. S. King, P. G. Schultz, *Nat. Biotechnol.* **2002**, 20, 1044.
- [44] C. Darwin, *On the Origin of Species*, John Murray, London, **1859**.
- [45] F. J. Ayala, *Sci. Am.* **1978**, 239, 56.
- [46] F. C. Neidhardt, *Escherichia coli & Salmonella typhimurium: Cellular & Molecular Biology*, American Society for Microbiology, Washington, DC, **1987**.
- [47] S. Schlesinger, *J. Biol. Chem.* **1968**, 243, 3877.
- [48] S. Schlesinger, M. J. Schlesinger, *J. Biol. Chem.* **1967**, 242, 3369.
- [49] C. B. Anfinsen, L. G. Corley, *J. Biol. Chem.* **1969**, 244, 5149.
- [50] G. Hortin, I. Boime, *Methods Enzymol.* **1983**, 96, 777.
- [51] M. J. Wilson, D. L. Hatfield, *Biochim. Biophys. Acta* **1984**, 781, 205.
- [52] M. H. Richmond, *Bacteriol. Rev.* **1962**, 26, 398.
- [53] M. Levine, H. Tarver, *J. Biol. Chem.* **1951**, 192, 835.
- [54] M. H. Richmond, *Biochem. J.* **1959**, 73, 261.
- [55] P. Fildes, *Br. J. Exp. Pathol.* **1945**, 26, 416.
- [56] G. N. Cohen, R. Munier, *Biochim. Biophys. Acta* **1959**, 31, 347.
- [57] R. Munier, G. N. Cohen, *Biochim. Biophys. Acta* **1959**, 31, 378.
- [58] K. L. Kirk, *Biochemistry of Halogenated Organic Compounds*, Plenum, New York, **1991**.
- [59] M. B. Hoagland, *The Relationship of Nucleic Acid and Protein Synthesis as Revealed by Cell-free Systems*, Academic Press, New York, **1960**.
- [60] J. H. Matthaei, M. W. Nirenberg, *Proc. Natl. Acad. Sci. U.S.A.* **1961**, 47, 1580.
- [61] G. L. Igloi, F. Von der Haar, F. Cramer, *Biochemistry* **1977**, 16, 1696.
- [62] W. A. Hendrickson, *Science* **1991**, 254, 51.
- [63] W. A. Hendrickson, C. M. Ogata, *Macromol. Crystallogr. Part B* **1997**, 276, 494.
- [64] W. A. Hendrickson, *Trends Biochem. Sci.* **2000**, 25, 637.
- [65] J. T. F. Wong, *Proc. Natl. Acad. Sci. U.S.A.* **1983**, 80, 6303.
- [66] P. M. Bronskill, J. T. F. Wong, *Biochem. J.* **1988**, 249, 305.
- [67] V. Doring, H. D. Mootz, L. A. Nangle, T. L. Hendrickson, V. de Crecy-Lagard, P. Schimmel, P. Marliere, *Science* **2001**, 292, 501.
- [68] B. Lemeignan, P. Sonigo, P. Marliere, *J. Mol. Biol.* **1993**, 231, 161.
- [69] V. Doring, P. Marliere, *Genetics* **1998**, 150, 543.
- [70] N. Budisa, W. Karnbrock, S. Steinbacher, A. Humm, L. Prade, T. Neuefeind, L. Moroder, R. Huber, *J. Mol. Biol.* **1997**, 270, 616.

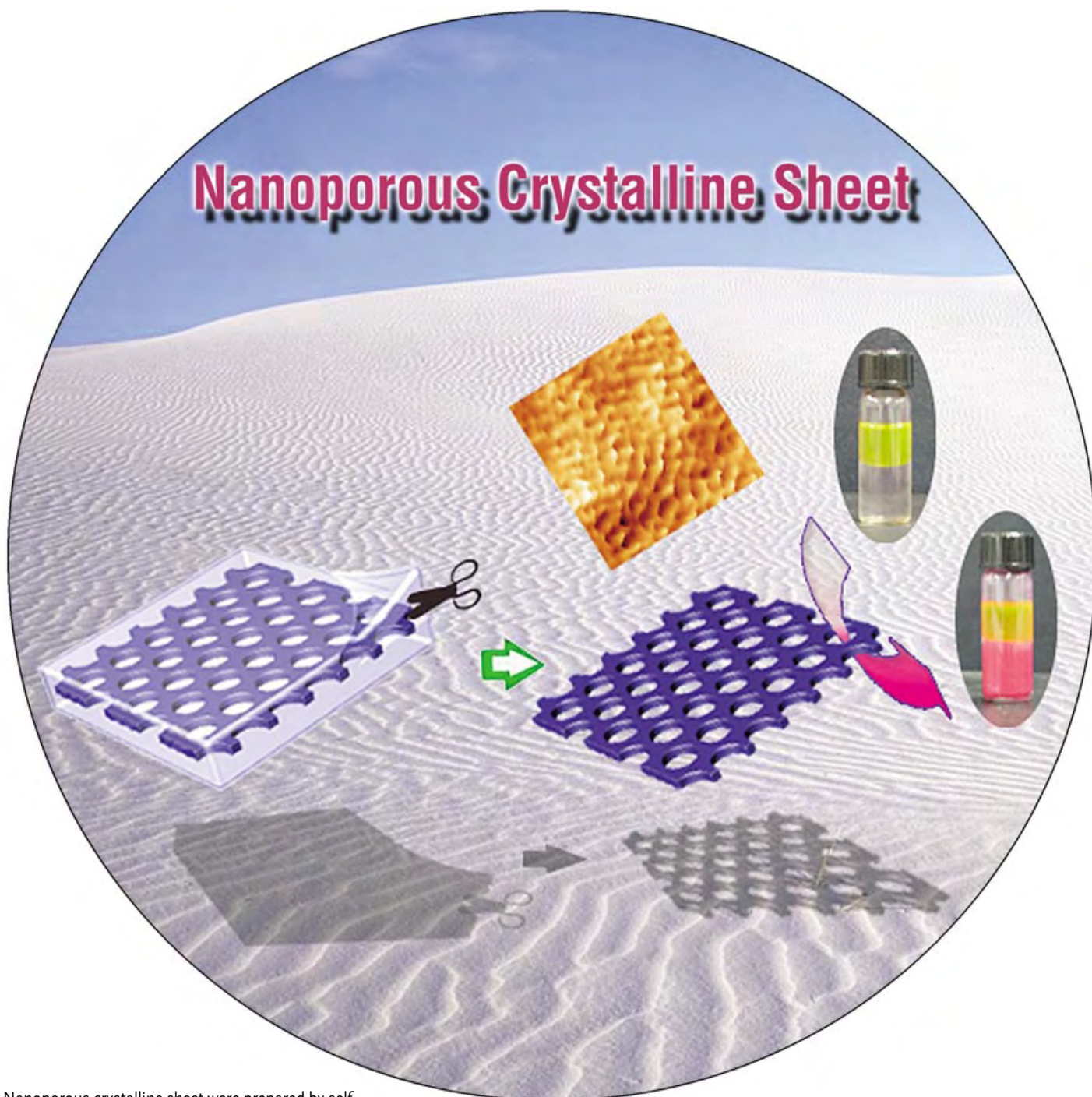
- [71] A. M. Gilles, P. Marliere, T. Rose, R. Sarfati, R. Longin, A. Meier, S. Femandjian, M. Monnot, G. N. Cohen, O. Barzu, *J. Biol. Chem.* **1988**, 263, 8204.
- [72] G. Bogosian, B. N. Violand, E. J. Dorwardking, W. E. Workman, P. E. Jung, J. F. Kane, *J. Biol. Chem.* **1989**, 264, 531.
- [73] B. D. Sykes, H. Weingart, M. J. Schlesinger, *Proc. Natl. Acad. Sci. U.S.A.* **1974**, 71, 469.
- [74] S. N. Cohen, A. C. Y. Chang, H. W. Boyer, R. B. Helling, *Proc. Natl. Acad. Sci. U.S.A.* **1973**, 70, 3240.
- [75] M. H. Seifert, D. Ksiazek, M. K. Azim, P. Smialowski, N. Budisa, T. A. Holak, *J. Am. Chem. Soc.* **2002**, 124, 7932.
- [76] J. H. Bae, S. Alefelder, J. T. Kaiser, R. Friedrich, L. Moroder, R. Huber, N. Budisa, *J. Mol. Biol.* **2001**, 309, 925.
- [77] N. Budisa, S. Alefelder, J. H. Bae, R. Golbik, C. Minks, R. Huber, L. Moroder, *Protein Sci.* **2001**, 10, 1281.
- [78] K. L. Kiick, R. Weberskirch, D. A. Tirrell, *FEBS Lett.* **2001**, 505, 465.
- [79] Y. Tang, G. Ghirlanda, W. A. Petka, T. Nakajima, W. F. DeGrado, D. A. Tirrell, *Angew. Chem.* **2001**, 113, 1494; *Angew. Chem. Int. Ed.* **2001**, 40, 1494.
- [80] Y. Tang, D. A. Tirrell, *Abstr. Pap. Am. Chem. Soc.* **1999**, 218, 416.
- [81] Y. Tang, D. A. Tirrell, *J. Am. Chem. Soc.* **2001**, 123, 11089.
- [82] P. Kast, H. Hennecke, *J. Mol. Biol.* **1991**, 222, 99.
- [83] K. Kirshenbaum, I. S. Carrico, D. A. Tirrell, *ChemBioChem* **2002**, 3, 235.
- [84] D. Datta, P. Wang, I. S. Carrico, S. L. Mayo, D. A. Tirrell, *J. Am. Chem. Soc.* **2002**, 124, 5652.
- [85] F. Hamano-Takaku, T. Iwama, S. Saito-Yano, K. Takaku, Y. Monden, M. Kitabatake, D. Soll, S. Nishimura, *J. Biol. Chem.* **2000**, 275, 40324.
- [86] D. Kiga, K. Sakamoto, K. Kodama, T. Kigawa, T. Matsuda, T. Yabuki, M. Shirouzu, Y. Harada, H. Nakayama, K. Takio, Y. Hasegawa, Y. Endo, I. Hirao, S. Yokoyama, *Proc. Natl. Acad. Sci. U.S.A.* **2002**, 99, 9715.
- [87] L. Wang, P. G. Schultz, *Chem. Commun.* **2002**, 1.
- [88] L. Wang, A. Brock, B. Herberich, P. G. Schultz, *Science* **2001**, 292, 498.
- [89] L. Wang, J. M. Xie, A. A. Deniz, P. G. Schultz, *J. Org. Chem.* **2003**, 68, 174.
- [90] Z. W. Zhang, L. Wang, A. Brock, P. G. Schultz, *Angew. Chem.* **2002**, 114, 2840; *Angew. Chem. Int. Ed.* **2002**, 41, 2840.
- [91] L. Wang, Z. W. Zhang, A. Brock, P. G. Schultz, *Proc. Natl. Acad. Sci. U.S.A.* **2003**, 100, 56.
- [92] J. W. Chin, S. W. Santoro, A. B. Martin, D. S. King, L. Wang, P. G. Schultz, *J. Am. Chem. Soc.* **2002**, 124, 9026.
- [93] L. Wang, A. Brock, P. G. Schultz, *J. Am. Chem. Soc.* **2002**, 124, 1836.
- [94] J. W. Chin, A. B. Martin, D. S. King, L. Wang, P. G. Schultz, *Proc. Natl. Acad. Sci. U.S.A.* **2002**, 99, 11020.
- [95] R. S. Mursinna, S. A. Martinis, *J. Am. Chem. Soc.* **2002**, 124, 7286.
- [96] P. Wang, N. Vaidehi, D. A. Tirrell, W. A. Goddard III, *J. Am. Chem. Soc.* **2002**, 124, 14442.
- [97] D. Q. Zhang, N. Vaidehi, W. A. Goddard III, J. F. Danzer, D. Debe, *Proc. Natl. Acad. Sci. U.S.A.* **2002**, 99, 6579.
- [98] A. B. Pardee, V. G. Shore, L. S. Prestidge, *Biochim. Biophys. Acta* **1956**, 21, 406.
- [99] G. Brawerman, M. Ycas, *Arch. Biochem. Biophys.* **1957**, 68, 112.
- [100] E. A. Pratt, C. Ho, *Fed. Proc.* **1974**, 33, 1463.
- [101] D. F. Senear, R. A. Mendelson, D. B. Stone, L. A. Luck, E. Rusinova, J. B. A. Ross, *Anal. Biochem.* **2002**, 300, 77.
- [102] S. M. Twine, A. G. Szabo, *Biophotonics Part A* **2003**, 360, 104.
- [103] J. O. Boles, J. Henderson, D. Hatch, L. A. Silks, *Biochem. Biophys. Res. Commun.* **2002**, 298, 257.
- [104] J. H. Bae, M. Rubini, G. Jung, G. Wiegand, M. H. J. Seifert, M. K. Azim, J. S. Kim, A. Zumbusch, T. A. Holak, L. Moroder, R. Huber, N. Budisa, *J. Mol. Biol.* **2003**, 328, 1071.
- [105] N. Budisa, M. Rubini, J. H. Bae, E. Weyher, W. Wenger, R. Golbik, R. Huber, L. Moroder, *Angew. Chem.* **2002**, 114, 4238; *Angew. Chem. Int. Ed.* **2002**, 41, 4066.
- [106] S. Barlati, O. Ciferri, *J. Bacteriol.* **1970**, 101, 166.
- [107] N. Budisa, P. P. Pal, S. Alefelder, P. Birle, T. Krywcun, M. Rubini, W. Wenger, J. H. Bae, T. Steiner, *Biol. Chem.* **2004**, 385, 191.
- [108] G. Loidl, H. J. Musiol, N. Budisa, R. Huber, S. Poirrot, D. Fourmy, L. Moroder, *J. Pept. Sci.* **2000**, 6, 139.
- [109] Z. J. Xu, M. L. Love, L. Y. Y. Ma, M. Blum, P. M. Bronskill, J. Bernstein, A. A. Grey, T. Hofmann, N. Camerman, J. T. F. Wong, *J. Biol. Chem.* **1989**, 264, 4304.
- [110] R. L. Munier, G. Sarrazin, *C. R. Hebd. Seances Acad. Sci.* **1963**, 256, 3376.
- [111] P. Lu, M. Jarema, K. Mosser, *Fed. Proc.* **1976**, 35, 1456.
- [112] M. Ring, I. M. Armitage, R. E. Huber, *Biochem. Biophys. Res. Commun.* **1985**, 131, 675.
- [113] M. Ring, R. E. Huber, *Biochem. Cell Biol.* **1993**, 71, 127.
- [114] B. Brooks, R. S. Phillips, W. F. Benisek, *Biochemistry* **1998**, 37, 9738.
- [115] R. Calendar, P. Berg, *Biochemistry* **1966**, 5, 1690.
- [116] C. Minks, PhD thesis, Technische Universität München, **1999**.
- [117] Z. W. Zhang, B. A. C. Smith, L. Wang, A. Brock, C. Cho, P. G. Schultz, *Biochemistry* **2003**, 42, 6735.
- [118] A. Yoshida, *Biochim. Biophys. Acta* **1960**, 41, 98.
- [119] E. Yoshikawa, M. J. Fournier, T. L. Mason, D. A. Tirrell, *Macromolecules* **1994**, 27, 5471.
- [120] C. Minks, R. Huber, L. Moroder, N. Budisa, *Anal. Biochem.* **2000**, 284, 29.
- [121] J. Janacek, H. V. Rickenberg, *Biochim. Biophys. Acta* **1964**, 81, 108.
- [122] S. Kothakota, T. L. Mason, D. A. Tirrell, M. J. Fournier, *J. Am. Chem. Soc.* **1995**, 117, 536.
- [123] H. Koide, S. Yokoyama, Y. Katayama, Y. Muto, T. Kigawa, T. Kohno, H. Takusari, M. Oishi, S. Takahashi, K. Tsukumo, T. Sasaki, T. Miyake, T. Fuwa, G. Kawai, T. Miyazawa, *Biochemistry* **1994**, 33, 7470.
- [124] N. Sharma, R. Furter, P. Kast, D. A. Tirrell, *FEBS Lett.* **2000**, 467, 37.
- [125] S. H. W. Beiboer, B. van den Berg, N. Dekker, R. C. Cox, H. M. Verheij, *Protein Eng.* **1996**, 9, 345.
- [126] P. Soumillion, J. Fastrez, *Protein Eng.* **1998**, 11, 213.
- [127] D. C. Klein, J. L. Weller, K. L. Kirk, R. W. Hartley, *Mol. Pharmacol.* **1977**, 13, 1105.
- [128] B. M. Dunn, C. Dibello, K. L. Kirk, L. A. Cohen, I. M. Chaiken, *J. Biol. Chem.* **1974**, 249, 6295.
- [129] Y. Ikeda, S. Kawahara, M. Taki, A. Kuno, T. Hasegawa, K. Taira, *Protein Eng.* **2003**, 16, 699.
- [130] J. Feeney, J. E. McCormick, C. J. Bauer, B. Birdsall, C. M. Moody, B. A. Starkmann, D. W. Young, P. Francis, R. H. Havlin, W. D. Arnold, E. Oldfield, *J. Am. Chem. Soc.* **1996**, 118, 8700.
- [131] I. Apostol, J. Levine, J. Lippincott, J. Leach, E. Hess, C. B. Glascock, M. J. Weickert, R. Blackmore, *J. Biol. Chem.* **1997**, 272, 28980.
- [132] T. H. Porter, S. C. Smith, W. Shive, *Arch. Biochem. Biophys.* **1977**, 179, 266.
- [133] P. Wang, Y. Tang, D. A. Tirrell, *J. Am. Chem. Soc.* **2003**, 125, 6900.
- [134] N. Budisa, R. Huber, R. Golbik, C. Minks, E. Weyher, L. Moroder, *Eur. J. Biochem.* **1998**, 253, 1.
- [135] J. O. Boles, K. Lewinski, M. Kunkle, J. D. Odom, R. B. Dunlap, L. Lebioda, M. Hatada, *Nat. Struct. Biol.* **1994**, 1, 283.

- [136] H. Duewel, E. Daub, V. Robinson, J. F. Honek, *Biochemistry* **1997**, 36, 3404.
- [137] H. Jakubowski, E. Goldman, *Microbiol. Rev.* **1992**, 56, 412.
- [138] A. R. Fersht, C. Dingwall, *Biochemistry* **1979**, 18, 1250.
- [139] H. Jakubowski, *J. Biol. Chem.* **2000**, 275, 21813.
- [140] J. C. M. van Hest, K. L. Kiick, D. A. Tirrell, *J. Am. Chem. Soc.* **2000**, 122, 1282.
- [141] K. L. Kiick, E. Saxon, D. A. Tirrell, C. R. Bertozzi, *Proc. Natl. Acad. Sci. U.S.A.* **2002**, 99, 19.
- [142] U. Reimer, G. Scherer, M. Drewello, S. Kruber, M. Schutkowski, G. Fischer, *J. Mol. Biol.* **1998**, 279, 449.
- [143] C. Renner, S. Alefelder, J. H. Bae, N. Budisa, R. Huber, L. Moroder, *Angew. Chem.* **2001**, 113, 923; *Angew. Chem. Int. Ed.* **2001**, 40, 923.
- [144] T. J. Deming, M. J. Fournier, T. L. Mason, D. A. Tirrell, *J. Macromol. Sci. Pure Appl. Chem.* **1997**, 34, 2143.
- [145] J. F. Guichou, L. Patiny, M. Mutter, *Tetrahedron Lett.* **2002**, 43, 4389.
- [146] T. J. Deming, M. J. Fournier, T. L. Mason, D. A. Tirrell, *Macromolecules* **1996**, 29, 1442.
- [147] B. C. Jester, J. D. Levengood, H. Roy, M. Ibba, K. M. Devine, *Proc. Natl. Acad. Sci. U.S.A.* **2003**, 100, 14351.
- [148] G. Rosenthal, *Plant nonprotein amino and imino acids. Biological, Biochemical and Toxicological Properties*, Academic Press, New York, **1982**.
- [149] R. A. Mehl, J. C. Anderson, S. W. Santoro, L. Wang, A. B. Martin, D. S. King, D. M. Horn, P. G. Schultz, *J. Am. Chem. Soc.* **2003**, 125, 935.
- [150] M. Ibba, D. Soll, *Science* **1999**, 286, 1893.
- [151] T. M. Sonneborn, *Degeneracy of the Genetic Code: Extent, Nature and Genetic Implications*, Academic Press, New York, **1965**.
- [152] S. J. Freeland, R. D. Knight, L. F. Landweber, L. D. Hurst, *Mol. Biol. Evol.* **2000**, 17, 511.
- [153] S. J. Freeland, T. Wu, N. Keulmann, *Origins Life Evol. Biosphere* **2003**, 33, 457.
- [154] C. R. Woese, D. H. Dugre, S. A. Dugre, M. Kondo, W. C. Saxinger, *Cold Spring Harbor Symp. Quant. Biol.* **1966**, 31, 723.
- [155] D. Haig, L. D. Hurst, *J. Mol. Evol.* **1991**, 33, 412.
- [156] A. Radzicka, R. Wolfenden, *Biochemistry* **1988**, 27, 1664.
- [157] G. D. Rose, R. Wolfenden, *Annu. Rev. Biophys. Biomol. Struct.* **1993**, 22, 381.
- [158] J. D. Watson, N. H. Hopkins, J. W. Roberts, J. A. Steitz, A. M. Weiner, *Molecular Biology of the Gene*, Benjamin/Cummings Publishing, Amsterdam, **1988**.
- [159] S. Osawa, T. H. Jukes, K. Watanabe, A. Muto, *Microbiol. Rev.* **1992**, 56, 229.
- [160] A. Bock, K. Forchhammer, J. Heider, W. Leinfelder, G. Sawers, B. Veprek, F. Zinoni, *Mol. Microbiol.* **1991**, 5, 515.
- [161] M. F. Tuite, M. A. S. Santos, *Biochimie* **1996**, 78, 993.
- [162] T. Suzuki, T. Ueda, K. Watanabe, *EMBO J.* **1997**, 16, 1122.
- [163] T. Hohsaka, M. Sisido, *Curr. Opin. Chem. Biol.* **2002**, 6, 809.
- [164] G. Eggertsson, D. Soll, *Microbiol. Rev.* **1988**, 52, 354.
- [165] J. R. Roth, *Cell* **1981**, 24, 601.
- [166] T. G. Heckler, L. H. Chang, Y. Zama, T. Naka, M. S. Chorghade, S. M. Hecht, *Biochemistry* **1984**, 23, 1468.
- [167] V. W. Cornish, D. Mendel, P. G. Schultz, *Angew. Chem.* **1995**, 107, 677; *Angew. Chem. Int. Ed. Engl.* **1995**, 34, 621.
- [168] T. Arslan, S. V. Mamaev, N. V. Mamaeva, S. M. Hecht, *J. Am. Chem. Soc.* **1997**, 119, 10877.
- [169] D. Mendel, V. W. Cornish, P. G. Schultz, *Annu. Rev. Biophys. Biomol. Struct.* **1995**, 24, 435.
- [170] L. E. Steward, A. R. Chamberlin in *Protein Synthesis—Methods and Protocols*, Vol. 77 (Ed.: R. Martin), Humana Press, Totowa, New Jersey, **1998**, p. 325.
- [171] J. D. Bain, C. G. Glabe, T. A. Dix, A. R. Chamberlin, E. S. Diala, *J. Am. Chem. Soc.* **1989**, 111, 8013.
- [172] Y. Kwok, J. T. F. Wong, *Can. J. Biochem.* **1980**, 58, 213.
- [173] A. K. Kowal, J. S. Oliver, *Nucleic Acids Res.* **1997**, 25, 4685.
- [174] J. Ellman, D. Mendel, S. Anthony-Cahill, C. J. Noren, P. G. Schultz, *Methods Enzymol.* **1991**, 202, 301.
- [175] T. Hohsaka, Y. Ashizuka, H. Murakami, M. Sisido, *J. Am. Chem. Soc.* **1996**, 118, 9778.
- [176] A. Frankel, R. W. Roberts, *RNA* **2003**, 9, 780.
- [177] T. Kanda, K. Takai, T. Hohsaka, M. Sisido, H. Takaku, *Biochem. Biophys. Res. Commun.* **2000**, 270, 1136.
- [178] I. Kwon, K. Kirshenbaum, D. A. Tirrell, *J. Am. Chem. Soc.* **2003**, 125, 7512.
- [179] M. W. Nowak, J. P. Gallivan, S. K. Silverman, C. G. Labarca, D. A. Dougherty, H. A. Lester, *Methods Enzymol.* **1998**, 293, 504.
- [180] S. L. Monahan, H. A. Lester, D. A. Dougherty, *Chem. Biol.* **2003**, 10, 573.
- [181] L. E. Steward, C. S. Collins, M. A. Gilmore, J. E. Carlson, J. B. A. Ross, A. R. Chamberlin, *J. Am. Chem. Soc.* **1997**, 119, 6.
- [182] B. Moore, B. C. Persson, C. C. Nelson, R. F. Gesteland, J. F. Atkins, *J. Mol. Biol.* **2000**, 298, 195.
- [183] T. Hohsaka, Y. Ashizuka, H. Taira, H. Murakami, M. Sisido, *Biochemistry* **2001**, 40, 11060.
- [184] T. Hohsaka, D. Kajihara, Y. Ashizuka, H. Murakami, M. Sisido, *J. Am. Chem. Soc.* **1999**, 121, 34.
- [185] T. Hohsaka, K. Sato, M. Sisido, K. Takai, S. Yokoyama, *FEBS Lett.* **1993**, 335, 47.
- [186] T. Hohsaka, Y. Ashizuka, H. Sasaki, H. Murakami, M. Sisido, *J. Am. Chem. Soc.* **1999**, 121, 12194.
- [187] T. J. Magliery, J. C. Anderson, P. G. Schultz, *J. Mol. Biol.* **2001**, 307, 755.
- [188] J. C. Anderson, T. J. Magliery, P. G. Schultz, *Chem. Biol.* **2002**, 9, 237.
- [189] T. Hohsaka, Y. Ashizuka, H. Murakami, M. Sisido, *Nucleic Acids Res.* **2001**, 29, 3646.
- [190] D. R. Liu, P. G. Schultz, *Proc. Natl. Acad. Sci. U.S.A.* **1999**, 96, 4780.
- [191] D. R. Liu, T. J. Magliery, P. G. Schultz, *Chem. Biol.* **1997**, 4, 685.
- [192] D. R. Liu, T. J. Magliery, M. Pasternak, P. G. Schultz, *Proc. Natl. Acad. Sci. U.S.A.* **1997**, 94, 10092.
- [193] P. Schimmel, D. Soll, *Proc. Natl. Acad. Sci. U.S.A.* **1997**, 94, 10007.
- [194] A. K. Kowal, C. Kohrer, U. L. RajBhandary, *Proc. Natl. Acad. Sci. U.S.A.* **2001**, 98, 2268.
- [195] L. Wang, P. G. Schultz, *Chem. Biol.* **2001**, 8, 883.
- [196] L. Wang, T. J. Magliery, D. R. Liu, P. G. Schultz, *J. Am. Chem. Soc.* **2000**, 122, 5010.
- [197] M. Pasternak, T. J. Magliery, P. G. Schultz, *Helv. Chim. Acta* **2000**, 83, 2277.
- [198] C. Kohrer, L. Xie, S. Kellerer, U. Varshney, U. L. RajBhandary, *Proc. Natl. Acad. Sci. U.S.A.* **2001**, 98, 14310.
- [199] K. Koide, J. M. Finkelstein, Z. Ball, G. L. Verdine, *J. Am. Chem. Soc.* **2001**, 123, 398.
- [200] R. Furter, *Protein Sci.* **1998**, 7, 419.
- [201] T. Hohsaka, K. Sato, M. Sisido, K. Takai, S. Yokoyama, *FEBS Lett.* **1994**, 344, 171.
- [202] Y. Shimizu, A. Inoue, Y. Tomari, T. Suzuki, T. Yokogawa, K. Nishikawa, T. Ueda, *Nat. Biotechnol.* **2001**, 19, 751.
- [203] A. C. Forster, Z. P. Tan, M. N. L. Nalam, H. N. Lin, H. Qu, V. W. Cornish, S. C. Blacklow, *Proc. Natl. Acad. Sci. U.S.A.* **2003**, 100, 6353.
- [204] N. Budisa in *Cell Free Protein Expression* (Ed.: J. R. Swartz), Springer, Berlin, **2003**, p. 89.
- [205] Y. Q. Wu, A. K. Ogawa, M. Berger, D. L. McMinn, P. G. Schultz, F. E. Romesberg, *J. Am. Chem. Soc.* **2000**, 122, 7621.
- [206] T. Mitsui, A. Kitamura, M. Kimoto, T. To, A. Sato, I. Hirao, S. Yokoyama, *J. Am. Chem. Soc.* **2003**, 125, 5298.

- [207] I. Hirao, T. Ohtsuki, T. Fujiwara, T. Mitsui, T. Yokogawa, T. Okuni, H. Nakayama, K. Takio, T. Yabuki, T. Kigawa, K. Kodama, K. Nishikawa, S. Yokoyama, *Nat. Biotechnol.* **2002**, 20, 177.
- [208] K. Tamura, P. Schimmel, *Nat. Biotechnol.* **2002**, 20, 669.
- [209] Y. Bessho, D. R. W. Hodgson, H. Suga, *Nat. Biotechnol.* **2002**, 20, 723.
- [210] L. M. Dedkova, N. E. Fahmi, S. Y. Golovine, S. M. Hecht, *J. Am. Chem. Soc.* **2003**, 125, 6616.
- [211] K. Sakamoto, A. Hayashi, A. Sakamoto, D. Kiga, H. Nakayama, A. Soma, T. Kobayashi, M. Kitabatake, K. Takio, K. Saito, M. Shirouzu, I. Hirao, S. Yokoyama, *Nucleic Acids Res.* **2002**, 30, 4692.
- [212] J. W. Chin, T. A. Cropp, J. C. Anderson, M. Mukherji, Z. W. Zhang, P. G. Schultz, *Science* **2003**, 301, 964.
- [213] R. F. Service, *Science* **2003**, 299, 640.
- [214] M. J. Dougherty, S. Kothakota, M. T. Krejci, G. H. Zhang, T. L. Mason, D. A. Tirrell, M. J. Fournier, *Makromol. Chem. Macromol. Symp.* **1992**, 62, 225.
- [215] J. O. Boles, R. J. Cisneros, M. S. Weir, J. D. Odom, J. E. Villafranca, R. B. Dunlap, *Biochemistry* **1991**, 30, 11073.
- [216] W. Karnbrock, E. Weyher, N. Budisa, R. Huber, L. Moroder, *J. Am. Chem. Soc.* **1996**, 118, 913.
- [217] D. Besse, N. Budisa, W. Karnbrock, C. Minks, H. J. Musiol, S. Pegoraro, F. Siedler, E. Weyher, L. Moroder, *Biol. Chem.* **1997**, 378, 211.
- [218] N. Budisa, G. Pifat, *Croat. Chem. Acta* **1998**, 71, 179.
- [219] M. Pieper, M. Betz, N. Budisa, F.-X. Gomis-Rüth, W. Bode, H. Tschesche, *J. Protein Chem.* **1997**, 16, 637.
- [220] C. Minks, R. Huber, L. Moroder, N. Budisa, *Biochemistry* **1999**, 38, 10649.
- [221] R. M. W. Hoetelmans, *Antiviral Ther.* **1999**, 4, 29.
- [222] J. D. Bain, C. Switzer, A. R. Chamberlin, S. A. Benner, *Nature* **1992**, 356, 537.
- [223] M. Zimmer, *Chem. Rev.* **2002**, 102, 759.
- [224] O. Shimomura, *FEBS Lett.* **1979**, 104, 220.
- [225] G. J. Palm, A. Wlodawer, *Green Fluoresc. Protein* **1999**, 302, 378.
- [226] B. K. Koe, A. Weissman, *Biochem. Pharmacol.* **1966**, 15, 2134.
- [227] B. K. Koe, A. Weissman, *J. Pharmacol. Exp. Ther.* **1967**, 157, 565.
- [228] A. Weissman, B. K. Koe, *J. Pharmacol. Exp. Ther.* **1967**, 155, 135.
- [229] F. L. M. Pattison, *Nature* **1953**, 172, 1139.
- [230] C. S. Evans, E. A. Bell, *Trends Neurosci.* **1980**, 3, 70.
- [231] B. K. Koe, A. Weissman, *Fed. Proc.* **1966**, 25, 452.
- [232] P. Stark, R. W. Fuller, *Fed. Proc.* **1971**, 30, A504.
- [233] L. Stryer, *Biochemistry*, New York, **2001**.
- [234] D. A. Dougherty, *J. Phys. Org. Chem.* **1998**, 11, 334.
- [235] E. Fischer, *Ber. Dtsch. Chem. Ges.* **1906**, 39, 530.
- [236] F. Hofmeister, *Ergeb. Physiol. Biol. Chem. Exp. Pharmacol.* **1902**, 1, 759.
- [237] F. Sanger, E. O. P. Thompson, *Biochem. J.* **1952**, 52, R3.
- [238] A. D. Hershey, M. Chase, *J. Gen. Physiol.* **1952**, 36, 39.
- [239] O. T. Avery, C. M. MacLeod, M. McCarty, *J. Exp. Med.* **1944**, 79, 137.
- [240] G. W. Beadle, *J. Allergy* **1957**, 28, 392.
- [241] G. W. Beadle, *Harvey Lect.* **1945**, 40, 179.
- [242] F. Jacob, J. Monod, *J. Mol. Biol.* **1961**, 3, 318.
- [243] M. Yarus, *RNA* **2000**, 6, 475.
- [244] J. T. F. Wong, *Proc. Natl. Acad. Sci. U.S.A.* **1975**, 72, 1909.
- [245] R. Dawkins, *The Selfish Gene*, Oxford University Press, **1976**.
- [246] R. Wolfenden, A. Radzicka, *Trends Biochem. Sci.* **1986**, 11, 69.
- [247] J. L. Fauchere, V. Pliska, *Eur. J. Med. Chem.* **1983**, 18, 369.
- [248] G. Trinquier, Y. H. Sanejouand, *Prot. Eng.* **1998**, 24, 153.
- [249] W. F. DeGrado, C. M. Summa, V. Pavone, F. Nastri, A. Lombardi, *Annu. Rev. Biochem.* **1999**, 68, 779.
- [250] D. N. Wilson, K. H. Nierhaus, *Angew. Chem.* **2003**, 115, 3464; *Angew. Chem. Int. Ed.* **2003**, 42, 3464.
- [251] T. Kobayashi, O. Nureki, R. Ishitani, A. Yaremchuk, M. Tukalo, S. Cusack, K. Sakamoto, S. Yokoyama, *Nat. Struct. Biol.* **2003**, 10, 425.
- [252] E. O. Wilson, *On Human Nature*, Harvard University Press, Cambridge, MA, **1978**.
- [253] J. M. Bacher, A. D. Ellington, *J. Bacteriol.* **2001**, 183, 5414.
- [254] J. M. Bacher, J. J. Bull, A. D. Ellington, *BMC Evol. Biol.* **2003**, 3.
- [255] P. Hess, N. Budisa, unpublished results.
- [256] W. Y. Kim, A. George, M. Evans, V. P. Conticello, *ChemBioChem* **2004**, 5, 928.
- [257] T. Bentin, R. Hamzavi, J. Salomonsson, H. Roy, M. Ibba, P. E. Nielsen, *J. Biol. Chem.* **2004**, 279, 19839.
- [258] P. Wang, A. Fichera, K. Kumar, D. A. Tirrell, *Angew. Chem.* **2004**, 116, 3750; *Angew. Chem. Int. Ed.* **2004**, 43, 3664.
- [259] H. Putzer, M. Grunberg-Manago, M. Springer in *tRNA: Structure, Biosynthesis and Function* (Ed.: D. Söll, U. RajBhandary), American Society for Microbiology, Washington, DC, **1995**, p 293.
- [260] T. Meinel, Y. Mechulam, S. Blanquet in *tRNA: Structure, Biosynthesis and Function* (Hrsg.: D. Söll, U. RajBhandary), American Society for Microbiology, Washington DC, **1995**, S. 251.
- [261] D. W. Schultz, M. Yarus, *J. Mol. Evol.* **1996**, 42, 597.
- [262] M. Yarus, D. W. Schultz, *J. Mol. Evol.* **1997**, 45, 3.
- [263] J. M. Bacher, R. A. Hughes, J. T. F. Wong, A. D. Ellington, *Trends Ecol. Evol.* **2004**, 19, 69.
- [264] A. R. O. Cavalcanti, L. F. Landweber, *Curr. Biol.* **2003**, 13, R884.
- [265] Z. W. Zhang, L. Alfonta, F. Tian, B. Bursulaya, S. Uryu, D. S. King, P. G. Schultz, *Proc. Natl. Acad. Sci. U.S.A.* **2004**, 101, 8882.
- [266] J. C. Anderson, N. Wu, S. W. Santoro, V. Lakshman, D. S. King, P. G. Schultz, *Proc. Nat. Acad. Sci. U.S.A.* **2004**, 101, 7566.
- [267] A. J. Link, M. L. Mock, D. A. Tirrell, *Curr. Opin. Biotechnol.* **2003**, 14, 603.
- [268] U. Hahn, G. J. Palm, W. Hinrichs, *Angew. Chem.* **2004**, 116, 1210; *Angew. Chem. Int. Ed.* **2004**, 43, 1190.
- [269] J. S. Anthony-Cahill, T. J. Magliery, *Curr. Pharm. Res.* **2002**, 3, 299.
- [270] J. H. van Maarseveen, J. W. Back, *Angew. Chem.* **2003**, 115, 6106; *Angew. Chem. Int. Ed.* **2003**, 42, 5926.
- [271] T. Hohsaka, *Bull. Chem. Soc. Jpn.* **2004**, 77, 1041.
- [272] A. Stromgaard, A. A. Jensen, K. Stromgaard, *ChemBioChem* **2004**, 5, 909.
- [273] M. Kimoto, M. Endo, T. Mitsui, T. Okuni, I. Hirao, S. Yokoyama, *Chem. Biol.* **2004**, 11, 47.
- [274] D. E. Bergstrom, *Chem. Biol.* **2004**, 11, 18.

Communications

Nanoporous Crystalline Sheet



Nanoporous crystalline sheet were prepared by self-assembly of roil-coil molecules. Removal of coil segments from the organized structure produced a crystalline layer with a planar nanopore array. The nanoporous solid is capable of entrapping highly nonpolar hexane soluble dyes, such es Nile red, in aqueous solution. For more details see the Communication by M. Lee and co-workers on the following pages..

Nanoporous Sheets

Supramolecular Crystalline Sheets with Ordered Nanopore Arrays from Self-Assembly of Rigid-Rod Building Blocks**

Myongsoo Lee,* Myoung-Hwan Park, Nam-Keun Oh, Wang-Cheol Zin, Hee-Tae Jung, and Dong Ki Yoon

The design and construction of well-defined nanoporous materials is an area of great interest, because they have broad applications in catalysis, lithography, membrane filtration, and ion-selective membranes.^[1–6] Development of such well-defined porous materials requires the rational design of molecular components that are programmed to assemble through noncovalent intermolecular forces. We previously demonstrated that self-assembled structures based on rod building blocks could be manipulated through attachment of flexible parts with different lengths to their ends.^[7] Depending on the relative length of the rigid segments, these blocks self-assemble into perforated supramolecular layers with in-plane, ordered coil perforations that are able to self-organize into a three-dimensional (3D) hexagonal superlattice.^[8] One can envision that selective removal of coil segments from this ordered structure would provide a novel strategy to generate nanoporous layered materials with in-plane nanopore arrays.

Here we report the preparation of supramolecular crystalline sheets with in-plane nanopore arrays by hydrolysis with aqueous KOH and subsequent removal of coil segments from the perforated layered structure (Figure 1). The synthesis of a self-assembling rod-coil molecule consisting of penta-*p*-phenylene and poly(propylene oxide) was performed in a stepwise fashion starting with esterification of poly(propylene oxide) and 4-bromobenzoic acid, and continuing with Suzuki cross-coupling to generate the rod building block. The rod-coil molecule was characterized by ¹H and ¹³C NMR spectroscopy, elemental analysis, and gel-permeation chromatography (GPC) and shown to be in full agreement with

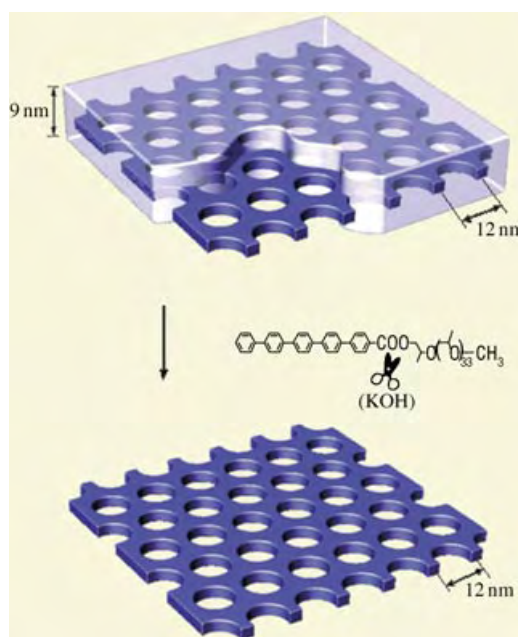


Figure 1. Preparation of supramolecular porous crystalline sheets by selective removal of coil segments from a perforated layer structure.

the structure presented. The ester linkage grafting the rod and coil segments can be easily cleaved by hydrolysis with alkali metal hydroxide solution.

The rod-coil compound melts into an isotropic liquid at 203°C, as evidenced by differential scanning calorimetry (DSC) and thermal optical polarized microscopy. The TEM image of a microtomed film of the material (stained with RuO₄) showed a honeycomblike supramolecular structure with a hexagonal array of light coil perforations in a dark rod matrix (Figure 2a). Small-angle X-ray scattering (SAXS) measurements showed a number of well-resolved reflections, which can be indexed as a 3D hexagonal order (*P*6₃/*mmc* space-group symmetry) with lattice constants *a* = 12.7 and *c* = 18.0 nm (Figure 2b).^[8] The diameter of a perforation, determined from the lattice constants and density measurements, appeared to be 9 nm, consistent with the TEM analysis.

Wide-angle X-ray diffraction patterns showed three sharp reflections (Figure 3a), that is, the rod segments are packed

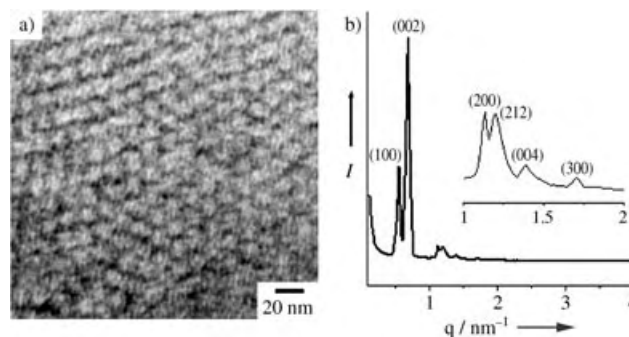


Figure 2. a) TEM image of a microtomed film of the rod-coil compound stained with RuO₄. b) Small-angle XRD pattern of the rod-coil compound. Inset: SAXS reflections for *q* = 1.0–2.0 nm^{−1} with an intensity scale expansion of ×10.

[*] Prof. M. Lee, M.-H. Park
Center for Supramolecular Nanoassembly and
Department of Chemistry
Yonsei University, Shinchon 134, Seoul 120-749 (Korea)
Fax: (82) 2-393-6096
E-mail: mslee@yonsei.ac.kr

N.-K. Oh, Prof. W.-C. Zin
Department of Materials Science and Engineering
Pohang University of Science and Technology
Pohang 790-784 (Korea)
Prof. H.-T. Jung, D. K. Yoon
Department of Chemical and Biomolecular Engineering
Korea Advanced Institute of Science and Technology
Daejeon 305-701 (Korea)

[**] This work was supported by the Creative Research Initiative Program of the Ministry of Science and Technology, Korea. We thank the Pohang Accelerator Laboratory, Korea (for synchrotron radiation experiments).

Supporting information for this article is available on the WWW under <http://www.angewandte.org> or from the author.

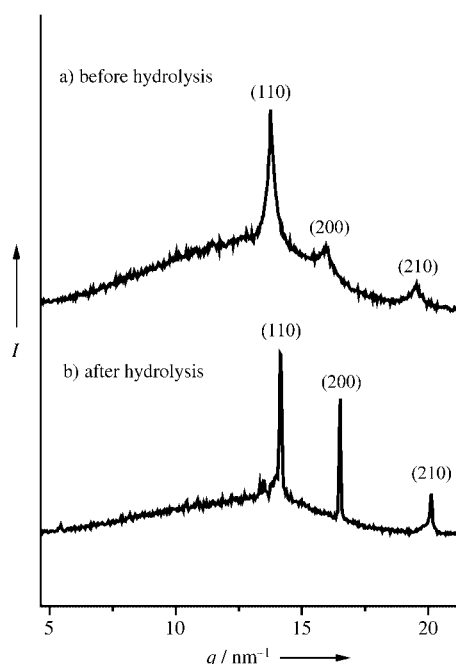


Figure 3. Wide-angle XRD patterns measured a) before and b) after hydrolysis of the rod-coil compound at 25 °C.

into a rectangular lattice ($P2gg$ space group) with unit cell dimensions $a = 0.79$ and $b = 0.56$ nm. These results demonstrate that the rod segments crystallize into a perforated layered structure, in which perforations are filled by coil segments, and subsequently the perforations organize into a 3D hexagonal superlattice.

Cleavage of the ester groups followed by selective removal of coil segments in the ordered state is a possible strategy for constructing nanoporous supramolecular crystalline sheets with well-defined pore size. To obtain initial proof of this concept, the thin film with coil perforations was placed in water/methanol containing potassium hydroxide at room temperature to cleave the ester groups grafting the rod and coil segments. Under these conditions, the crystalline layers consisting of rod segments are insoluble and inert. After one week, the rigid and insoluble film was removed from the hydrolysis solution, thoroughly washed with aqueous HCl and methanol, and dried at room temperature under vacuum.

Solid-state ^{13}C NMR spectra of the films showed that the signals associated with the poly(propylene oxide) chain had completely disappeared after hydrolysis (Figure 4). The FT-IR spectrum showed a broad O–H absorption in the region from 3400 to 2400 cm^{-1} and a C=O stretching band centered at 1720 cm^{-1} , which shifts to 1690 cm^{-1} after hydrolysis, indicative of conversion of an ester to a carboxylic acid. These data are consistent with the formation of rigid organic frameworks consisting only of aromatic rod segments by selective removal of the poly(propylene oxide) coils. The resulting film is completely insoluble in water and common organic solvents such as CHCl_3 , methanol, CH_2Cl_2 , toluene, hexane, and ethyl acetate and does not exhibit any noticeable swelling.

The TEM image of a microtomed film of the hydrolyzed sample stained with RuO_4 showed nanopore arrays (Figure 5a), indicative of the formation of nanoholes on hydroly-

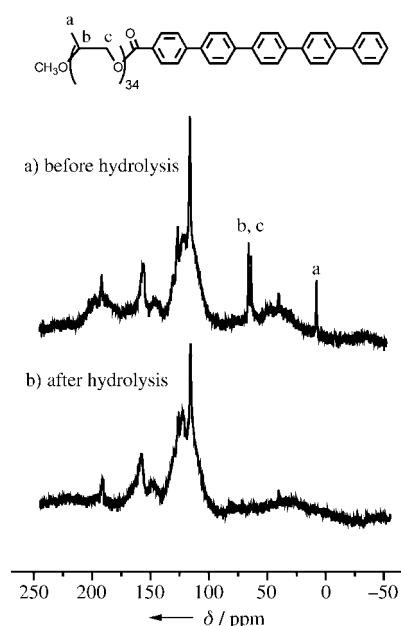


Figure 4. Solid-state ^{13}C NMR spectra of the rod-coil compound a) before and b) after hydrolysis.

ysis. This was also confirmed by atomic force microscopy (AFM) images. The amplitude images of a hydrolyzed film showed an ordered array of circular pores at the positions of the coil perforations (Figure 5b and 5c). The line scan in Figure 5b (inset) shows a pore to pore distance of approximately 12 nm, that is, the fundamental spacing is not changed on hydrolysis. The SAXS pattern exhibited four sharp scattering peaks corresponding to a lamellar structure with

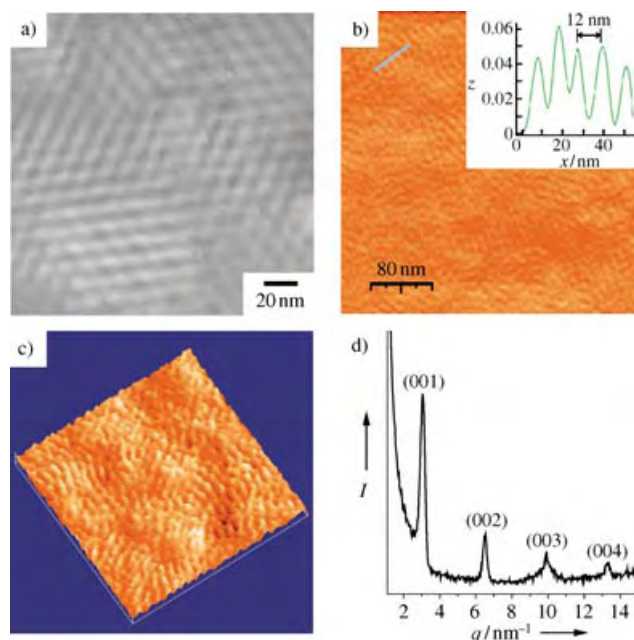


Figure 5. a) TEM image of a hydrolyzed film stained with RuO_4 . Tapping-mode AFM amplitude images presented as b) two- and c) three-dimensional graphics ($250\text{ nm} \times 250\text{ nm}$ area). d) Small-angle XRD pattern of the hydrolyzed sample.

a layer thickness of 2.1 nm (Figure 5d), which implies that perforation order is not maintained on removal of the coil segments. Since the length of carboxylic-acid-terminated penta-*p*-phenylene is 2.1 nm, the measured lattice constant indicates that the coil segments are extracted from the perforated layered structure after hydrolysis. These results demonstrate that the crystalline rod layers with in-plane nanopore arrays are stacked into a lamellar structure with a thickness corresponding to the length of a rod, while pore order along the *c* direction is lost on extraction of PPO coil segments. The wide-angle XRD pattern of the hydrolyzed sample revealed the same diffraction pattern but with peak narrowing compared to that of the rod-coil molecule (Figure 3b).^[9] These data are consistent with the preservation of the crystal structure within the rod layers, with enhanced crystallinity due to selective etching of the amorphous coil segments from the perforated layers. These results demonstrate that hydrolysis and subsequent removal of the flexible-coil segments in ordered nanostructures formed by rod-coil systems can provide a strategy for constructing nanoporous crystalline materials with uniform pore size.

Remarkably, the nanoporous solid proved capable of entrapping highly nonpolar dyes such as Nile Red in aqueous solution; this is indicative of the presence of nanoholes with hydrophobic interiors. In one experiment, Nile Red was dissolved in hexane and added to an aqueous dispersion of the nanoporous solid. The mixture was treated by ultrasonication

for 12 h. After this time, the water subphase turned violet, and the significant decrease in the intensity of the absorption peak corresponding to Nile Red in the hexane phase indicated that dye molecules had been transferred to the aqueous phase (Figure 6). This unique amphiphilic behavior is most probably attributable to hydrophobic and π - π interactions between the hydrophobic interiors of the nanopores and aromatic dye molecules.

In summary, a rod-coil compound in which an ester linkage grafts rod and coil segments exhibited a honeycomb-like supramolecular structure with 3D hexagonal symmetry. Hydrolysis with aqueous KOH and subsequent removal of the coil segments from the ordered structure with in-plane, hexagonally ordered perforations produced a crystalline layer with in-plane nanohole arrays. These results indicate that this approach allows novel, highly ordered nanoporous crystalline sheets to be produced, which potentially have applications as diverse as biomimetic transport membranes,^[1d] periodic porous materials,^[10] and nanopatterning.^[11]

Received: April 20, 2004

Revised: June 6, 2004

Keywords: nanostructures · rod-coil molecules · self-assembly · supramolecular chemistry

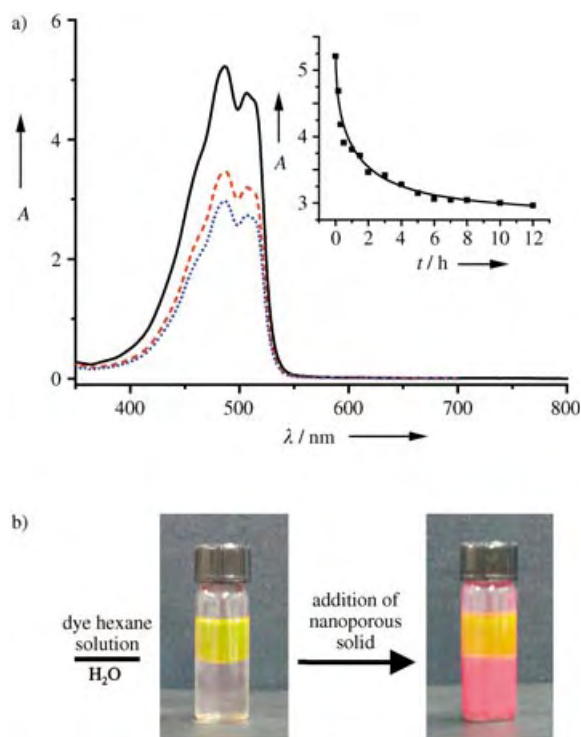


Figure 6. a) UV/Vis spectra of Nile Red in the hexane phase with a pure water phase before sonication (solid line) and with the water phase containing 7 wt% of the nanoporous crystals after 2 h (dashed red line) and 12 h sonication (dotted blue line). Inset: UV/Vis absorbance at $\lambda_{\text{max}} = 486$ nm as a function of time. b) Encapsulation of non-polar guest molecules in the nanoporous solid in an aqueous environment.

- [1] a) G. J. de A. A. Soler-Illia, C. Sanchez, B. Lebeau, J. Patarin, *Chem. Rev.* **2002**, *102*, 4093; b) S. A. Jenekhe, X. L. Chen, *Science* **1999**, *283*, 372; c) T. Thurn-Albrecht, J. Schotter, G. A. Kaestle, N. Emley, T. Shibauchi, L. Krusin-Elbaum, K. Gaurini, C. T. Black, M. T. Touminen, T. P. Russell, *Science* **2000**, *290*, 2126; d) L.-Q. Gu, O. Braha, S. Conlan, S. Cheley, H. Bayley, *Nature* **1999**, *398*, 686; e) R. G. H. Lammertink, M. A. Hempenius, J. E. van den Enk, V.-H. Chan, E. L. Thomas, G. J. Vancso, *Adv. Mater.* **2000**, *12*, 98; f) D. L. Gin, W. Gu, B. A. Pindzola, W. -J. Zhou, *Acc. Chem. Res.* **2001**, *34*, 973; g) G. Liu, J. Ding, T. Hashimoto, K. Kimishima, F. M. Winnik, S. Nigam, *Chem. Mater.* **1999**, *11*, 2233.
- [2] T. Thurn-Albrecht, R. Steiner, J. DeRouchey, C. M. Stafford, E. Huang, M. Bal, M. Touminen, C. J. Hawker, T. P. Russell, *Adv. Mater.* **2000**, *12*, 787.
- [3] R. Maeki-Ontto, K. de Moel, W. de Ondorico, J. Ruokolainen, M. Stamm, G. ten Brinke, O. Ikkala, *Adv. Mater.* **2001**, *13*, 117.
- [4] a) A.-S. Zalusky, R. Olayo-Valles, C.-J. Taylor, M. A. Hillmyer, *J. Am. Chem. Soc.* **2001**, *123*, 1519; b) A.-S. Zalusky, R. Olayo-Valles, J. H. Wolf, M. A. Hillmyer, *J. Am. Chem. Soc.* **2002**, *124*, 12761.
- [5] R.-M. Ho, Y.-W. Chiang, C.-C. Tsai, C.-C. Lin, B.-T. Ko, B.-H. Huang, *J. Am. Chem. Soc.* **2004**, *126*, 2704.
- [6] Q. Zhang, K. Ariga, A. Okabe, T. Aida, *J. Am. Chem. Soc.* **2004**, *126*, 988.
- [7] a) M. Lee, B.-K. Cho, W.-C. Zin, *Chem. Rev.* **2001**, *101*, 3869; b) M. Lee, Y.-S. Yoo, *J. Mater. Chem.* **2002**, *12*, 2161.
- [8] a) M. Lee, B.-K. Cho, K. J. Ihn, W.-K. Lee, N.-K. Oh, W.-C. Zin, *J. Am. Chem. Soc.* **2001**, *123*, 4647; b) J.-H. Ryu, N.-K. Oh, W. C. Zin, M. Lee, *J. Am. Chem. Soc.* **2004**, *126*, 3551.
- [9] The unit cell dimensions of the rectangular lattice decrease slightly after hydrolysis ($a = 0.76$, $b = 0.55$ nm).
- [10] Y. Sakamoto, M. Kaneda, O. Terasaki, D. Y. Zhao, J. M. Kim, G. Stucky, H. J. Shin, R. Ryoo, *Nature* **2000**, *408*, 449.
- [11] M. Park, C. Harrison, P. M. Chaikin, R. A. Register, D. H. Adamson, *Science* **1997**, *276*, 1401.

Reversible Switching of DNA–Gold Nanoparticle Aggregation**

Pompi Hazarika, Bülent Ceyhan, and
Christof M. Niemeyer*

The utilization of the tremendous recognition properties and functionality of proteins and nucleic acids as building blocks in the “bottom-up” self-assembly of nanometer-scaled functional devices has led, in the past few years, to a new research discipline, descriptively termed as nanobiotechnology.^[1] Applications include, for instance, the organization of metal and semiconductor nanoclusters,^[2] numerous bioanalytical techniques,^[3] as well as biomolecular electronics^[4] and nanomechanical devices. In the development of the latter, an increasing number of reports is currently being devoted to the construction of nanomechanical devices from DNA.^[5] Examples include the construction of devices from DNA molecules whose functionality is based on conformational changes induced by the binding of intercalators,^[6] Co³⁺-ion-dependent B- to Z-DNA transformation,^[7] Mg²⁺-ion-dependent DNA supercoiling,^[8] pH-dependent formation of intramolecular cytosin quartet structures,^[9] or by intermolecular hybridization with so-called fueling oligonucleotides.^[10–14] In this concept, a given DNA conformation is changed upon hybridization with an effector oligomer, which, in turn, can be removed from the complex by hybridization with a second oligomer. Although various examples have proven the suitability of this approach for switching dye-tagged DNA molecules, to the best of our knowledge, its application to the reversible formation of materials has not been realized yet.

Herein we report the reversible aggregation of DNA-modified gold nanoparticles by taking advantage of two complementary fueling oligonucleotides, F_a and F_d (Figure 1). The base sequence of F_a is comprised of three stretches, a' , b' (which are complementary to ≈ 23 -nm Au nanoparticle-bound 12-mer oligomers a and b , respectively) as well as stretch c' (which promotes hybridization of F_a and F_d). The transformation cycle starts with state I (Figure 1) in which the DNA nanoparticles are dispersed and reveal a characteristic plasmon absorption maximum at 526 nm (Figure 2). Upon addition of 32 equivalents of oligomer F_a , the particles

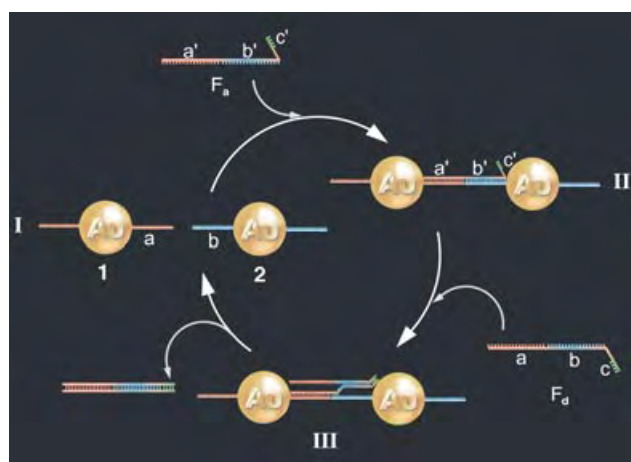


Figure 1. Schematic drawing of the reversible aggregation of DNA-modified gold nanoparticles utilizing fueling oligonucleotides F_a and F_d . F_a contains three stretches (a' , b' , and c'), which are complementary to the gold-nanoparticle-bound 12-mer oligomers, a and b . Stretch c' forms a dangling end in the aggregated particles (state II), which promotes the hybridization of F_a and F_d (intermediate state III).

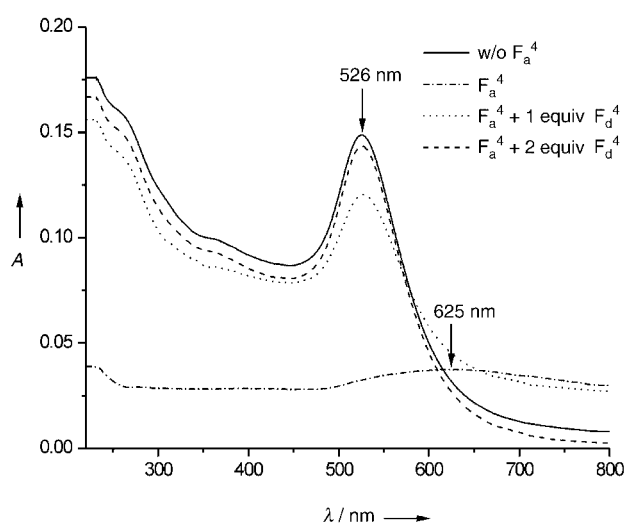


Figure 2. UV/Vis spectra of nanoparticle aggregation and redispersion. The absorbance maxima at 526 nm and 625 nm indicate the formation of dispersed and aggregated particles, respectively. The fueling oligomers F_a^4 and F_d^4 employed contain a stretch c' and c that are 4 bases in length. Notably, 2 equivalents of oligomer F_d^4 (with respect to F_a^4) are required to restore the original extinction of the dispersed particles.

aggregate (state II, Figure 1), and, consequently, the plasmon absorption band is damped and shifted towards longer wavelengths (≈ 625 nm; Figure 2). In the next step, oligomer F_d is added; F_d is fully complementary to and hybridizes with F_a , starting at the dangling-end stretch c' of the duplex DNA that interconnects the nanoparticles. This process, schematically shown as the intermediate state III in Figure 1, leads to the formation of a waste duplex and the redispersion of the nanoparticles. Hence, an increase in absorbance at 526 nm is observed (Figure 2).

Experimental variations revealed that 2 equivalents of oligomer F_d (with respect to F_a) were needed to retain the

[*] P. Hazarika, Dr. B. Ceyhan, Prof. Dr. C. M. Niemeyer
Fachbereich Chemie, Biologisch-Chemische Mikrostrukturtechnik
Universität Dortmund
Otto-Hahn Strasse 6, 44 227 Dortmund (Germany)
Fax: (+49) 231-755-7082
E-mail: cmn@chemie.uni-dortmund.de

[**] This work was supported by Deutsche Forschungsgemeinschaft (DFG) in Schwerpunktprogramm 1072. We acknowledge financial support by the research program “Molecular Basics of Biosciences” of the University of Dortmund. We thank Michael Adler for help with the figures.

Supporting information for this article is available on the WWW under <http://www.angewandte.org> or from the author.

extinction of the original nanoparticle solution (Figure 2). It is likely that the excess F_d is necessary owing to a limited accessibility of linking strands F_a within the aggregates and, hence, decreased hybridization kinetics. Additional studies on the influence of the length and base composition of sequence stretch c within the fueling oligomer F_a and F_d showed that four base pairs are sufficient to promote complete removal of the DNA strands that interconnect the particles (see Supporting Information).

To demonstrate the reversible switching of the nanoparticle aggregation, we carried out seven consecutive cycles of aggregation and redispersion by adding fuelling oligomers F_a and F_d , respectively. After each addition, UV/Vis spectra of the samples were recorded (see Supporting Information) and the extinction at 526 nm and 700 nm, which are indicative for dispersed and aggregated particles, respectively, was plotted against the number of steps (Figure 3). The results clearly

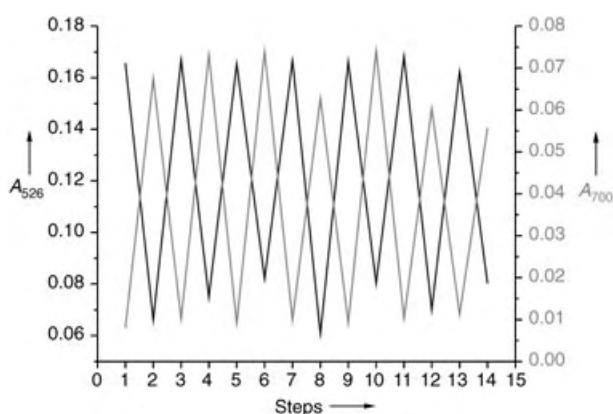


Figure 3. Reversible switching of the nanoparticle aggregation. Plot of the extinction measured at 526 nm (black) and 700 nm (gray) versus the number of steps of the addition of either oligomer F_a (even numbers) or F_d (odd numbers). Notably, a high extinction at 526 nm and 700 nm indicates the presence of dispersed and aggregated particles, respectively.

demonstrate the feasibility of using fueling oligomers for the reversible switching of nanoparticle aggregation. Nonetheless, careful analysis of the absorbance maxima observed for the aggregated particles indicated a decrease in the red shift of the plasmon absorption band from 619 nm in cycle 1 to 556 nm in cycle 7 (Supporting Information). As the magnitude of the shift is indicative of the size of the particle aggregates formed,^[15,16] this observation suggests that the aggregation efficiency is diminished owing to increasing concentrations of free F_a oligomers.

In conclusion, we have shown that the reversible switching of DNA–gold nanoparticle aggregation can be carried out by the employment of complementary fueling oligonucleotides that contain a short dangling-end sequence for the initiation of strand removal from the aggregates. Further optimization of this concept by variation of temperature, salt concentration, and pH value, by using oligofunctional DNA nanoparticles^[17] and, in particular, by careful design of the oligomer sequences^[18,19] should pave the way towards nanostructured materials with programmable functionalities for a broad range of applications in nanobiotechnology.

Experimental Section

The preparation of DNA–gold nanoparticle conjugates was carried out as described earlier.^[17] The size of the citrate-stabilized gold nanoparticles used was 22.9 ± 5.7 nm. Thiol-modified DNA oligomers (sequence a: 5'-SH-GGT GAA GAG ATC-3'; sequence b: 5'-AAG ACC ATC CTG-SH-3') were purchased from Thermo Electron, Germany.

To aggregate the DNA-modified particles, generally 32.5 equivalents^[20] of oligonucleotide F_a (5'-TAC GCA GGA TGG TCT TGA TCT CTT CAC C-3') was added to a mixture of DNA–gold nanoparticle conjugates **1** and **2** (each 1.54 nm) in TETBS buffer (0.3 M NaCl, 20 mM Tris-HCl, pH 7.35 containing 5 mM EDTA and 0.05% Tween 20). The solution was incubated for 24 h at room temperature. Subsequently, the aggregates were redispersed by adding oligonucleotide F_d (5'-GGT GAA GAG ATC AAG ACC ATC CTG CGT A-3'; 2.2 equiv with respect to F_a), and the solution was incubated for 24 h at 37 °C.

For the repeated switching of particle aggregation, seven cycles of aggregation/redispersion were performed as described above with the following amounts of fuelling oligomers: Cycle 1: 32.5 equiv (1.5 pmol) F_a and 73.7 equiv (3.4 pmol) F_d ; cycle 2: 84.5 equiv (3.9 pmol) F_a and 192.8 equiv (8.9 pmol) F_d ; cycle 3: 212.3 equiv (9.8 pmol) F_a and 467.9 equiv (21.6 pmol) F_d ; cycle 4: 511.2 equiv (23.6 pmol) F_a and 1109.0 equiv (51.2 pmol) F_d ; cycle 5: 1193.5 equiv (55.1 pmol) F_a and 2558.1 equiv (118.1 pmol) F_d ; cycle 6: 2729.2 equiv (126.0 pmol) F_a and 5796.3 equiv (267.6 pmol) F_d ; cycle 7: 6138.5 equiv (283.4 pmol) F_a . To prevent changes in absorbance due to dilution of the samples, 14 different aliquots of gold nanoparticles were prepared and F_a , F_d oligonucleotide solutions were added until a distinct step was reached. In the remaining steps, only buffer was added to these particular samples. After the final addition of either oligomer or buffer solution to all 14 aliquots of the nanoparticle samples, the UV/vis spectra were recorded on a Varian-Cary 100 UV/Vis spectrophotometer.

Received: September 3, 2004

Keywords: DNA · gold · nanostructures · supramolecular chemistry

- [1] C. M. Niemeyer, C. A. Mirkin, *NanoBiotechnology: Concepts, Methods and Applications*, Wiley-VCH, Weinheim, 2004.
- [2] J. J. Storhoff, C. A. Mirkin, *Chem. Rev.* **1999**, 99, 1849–1862.
- [3] C. M. Niemeyer, *Angew. Chem.* **2001**, 113, 4254–4287; *Angew. Chem. Int. Ed.* **2001**, 40, 4128–4158.
- [4] E. Braun, Y. Eichen, U. Sivan, G. Ben-Yoseph, *Nature* **1998**, 391, 775–778.
- [5] C. M. Niemeyer, M. Adler, *Angew. Chem.* **2002**, 114, 3933–3937; *Angew. Chem. Int. Ed.* **2002**, 41, 3779–3783.
- [6] X. Yang, A. V. Vologodskii, B. Liu, B. Kemper, N. C. Seeman, *Biopolymers* **1998**, 45, 69–83.
- [7] C. Mao, W. Sun, Z. Shen, N. C. Seeman, *Nature* **1999**, 397, 144–146.
- [8] C. M. Niemeyer, M. Adler, S. Lenhert, S. Gao, H. Fuchs, L. F. Chi, *ChemBioChem* **2001**, 2, 260–265.
- [9] D. Liu, S. Balasubramanian, *Angew. Chem.* **2003**, 115, 5912–5914; *Angew. Chem. Int. Ed.* **2003**, 42, 5734–5736.
- [10] B. Yurke, A. J. Turberfield, A. P. Mills, Jr., F. C. Simmel, J. L. Neumann, *Nature* **2000**, 406, 605–608.
- [11] J. J. Li, W. Tan, *Nano Lett.* **2002**, 2, 315–318.
- [12] H. Yan, X. Zhang, Z. Shen, N. C. Seeman, *Nature* **2002**, 415, 62–65.
- [13] W. U. Dittmer, E. Reuter, F. C. Simmel, *Angew. Chem.* **2004**, 116, 3634–3637; *Angew. Chem. Int. Ed.* **2004**, 43, 3554–3557.
- [14] Y. Chen, M. Wang, C. Mao, *Angew. Chem.* **2004**, 116, 3638–3641; *Angew. Chem. Int. Ed.* **2004**, 43, 3550–3553.

- [15] J. J. Storhoff, A. A. Lazarides, R. C. Mucic, C. A. Mirkin, R. L. Letsinger, G. C. Schatz, *J. Am. Chem. Soc.* **2000**, *122*, 4640–4650.
- [16] The quantitative determination of the size of the nanoparticle aggregates formed has not been carried out. Comparison of the spectroscopic data with values known from the literature,^[15] however, suggests that dimensions of up to 3 μm in diameter are reached.
- [17] C. M. Niemeyer, B. Ceyhan, P. Hazarika, *Angew. Chem.* **2003**, *115*, 5944–5948; *Angew. Chem. Int. Ed.* **2003**, *42*, 5766–5770.
- [18] A. J. Turberfield, J. C. Mitchell, B. Yurke, A. P. Mills, Jr., M. I. Blakey, F. C. Simmel, *Phys. Rev. Lett.* **2003**, *90*, 118102.
- [19] U. Feldkamp, R. Wacker, W. Banzhaf, C. M. Niemeyer, *Chem-PhysChem* **2004**, *5*, 367–372.
- [20] We previously showed that nanoparticles of similar size contain about 260 oligomers bound to their surface^[17] and we observed that a maximum aggregation is obtained when 32 equivalents of linker oligomers are added per mole of particles: B. Ceyhan, Ph.D. thesis, University of Dortmund, **2004**; this value corresponds to a hybridization efficiency of the particle-bound oligomers of $\approx 12\%$, which is in good agreement with hybridization efficiency data reported earlier: L. M. Demers, C. A. Mirkin, R. C. Mucic, R. A. Reynolds, R. L. Letsinger, R. Elghanian, G. Viswanadham, *Anal. Chem.* **2000**, *72*, 5535–5541.

Polymer Chemistry

Supramolecular AB Diblock Copolymers**

Xiaowu Yang, Fengjun Hua, Kazuhiro Yamato,
Eli Ruckenstein, Bing Gong,* Won Kim, and
Chang Y. Ryu*

Coupling incompatible oligomeric or polymeric chains at their ends leads to the formation of block copolymers. Block copolymers have a fascinating tendency to attain, through self-assembly and microphase separation, various ordered

morphologies that have characteristic dimensions on the nanometer scale.^[1] In recent years, efforts to develop supramolecular polymers, that is, macromolecules which consist of monomeric building blocks that are linked together by noncovalent forces, have generated great enthusiasm.^[2] A successful design of supramolecular polymers relies on the availability of noncovalent association units that can link various structural modules together. Although strategies that lead to a variety of chains or networks have been reported, association units with reasonable affinity and specificity have only recently become available. The groups of Zimmerman^[3] and Meijer^[4] have developed self-complementary, quadruply hydrogen-bonded complexes that serve as associating end groups for the construction of supramolecular polymers of high molecular weights. Other polymeric systems that involve supramolecular interactions are also known.^[5] Despite the progress made, few hydrogen-bonded supramolecular block copolymers have been reported so far.^[5] Owing to the unavailability of heterodimeric hydrogen-bonded units of sufficient strength and specificity, supramolecular block copolymers that display microphase separation have not been reported. Lohmeijer and Schubert recently reported an exciting example of supramolecular block copolymers by using unsymmetrical metal complexes which were obtained with 30–50% yield after purification (column chromatography).^[6]

To ensure microphase separation of designed supramolecular block copolymers and to couple different blocks, ideally, association units that link the different blocks together should exhibit both high stability and high non-self-complementary specificity, and at the same time the linkages should be kinetically reversible. Indeed, this is an unsolved problem. Many metal complexes are highly stable but are kinetically inert, whereas most hydrogen-bonded complexes lack high binding affinities and specificities.

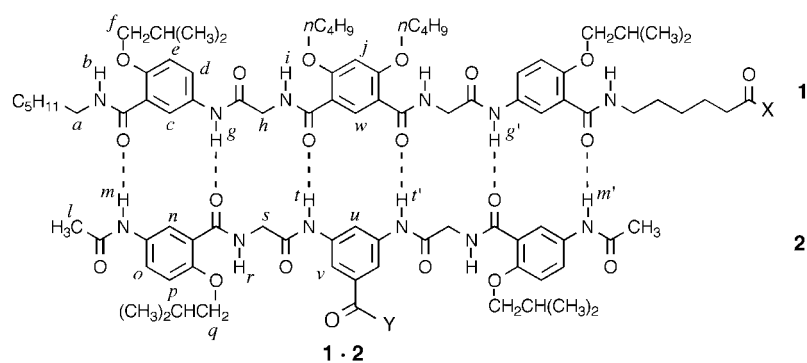
We report herein a new class of supramolecular, AB-type diblock copolymers that rely on hydrogen-bond-enforced association of incompatible polymer chains. In the general structures **1** and **2**, hydroxyl-terminated polystyrene (PS) and poly(ethylene glycol) monomethyl ether (PEG) chains were coupled to two different oligoamide strands. We previously showed that oligoamide strands such as **1'** and **2'** paired into a hexa-hydrogen-bonded heteroduplex with an association constant $K_a > 10^9 \text{ M}^{-1}$ in chloroform.^[7] Thus, mixing the modified PS with the PEG chains in a ratio of 1:1 in a common solvent (chloroform) should also lead to hydrogen-bonded supramolecular diblock copolymers. We also reported that the pairing of oligoamides similar to **1'** and **2'** was accompanied by significant downfield shifts of the signals for the protons of the amide groups: *g* (*g'*), *m* (*m'*), and *t* (*t'*; see structures **1** and **2** for atom labels).^[7b] Here, the 1D ¹H NMR spectra of **1'·2a**, **1a·2a**, and **1c·2c** exhibited similar downfield shifts of N–H protons to those of the duplex **1'·2'**^[8] which indicates that the PEG and PS strands are linked by intermolecular hydrogen bonds. Results from 2D ¹H NMR (NOESY) studies on **1a·2a** and **1c·2c** revealed interstrand NOEs that are also consistent with the formation of hydrogen-bonded duplexes, that is, the noncovalent coupling of PEG and PS strands.^[8]

[*] Dr. X. Yang, Dr. F. Hua, Dr. K. Yamato, Prof. E. Ruckenstein, Prof. B. Gong
Department of Chemistry and
Department of Chemical and Biological Engineering
University at Buffalo
The State University of New York
Buffalo, NY 14260 (USA)
Fax: (+1) 716-645-6963
E-mail: bgong@chem.buffalo.edu

W. Kim, Prof. C. Y. Ryu
Department of Chemistry and Chemical Biology
Rensselaer Polytechnic Institute
Troy, NY 12180 (USA)
Fax: (+1) 518-276-4887
E-mail: ryuc@rpi.edu

[**] We thank the donors of the Petroleum Research Fund, administered by the ACS, for support of this research (37200-AC4). The NIH, NSF, and ONR are acknowledged for partial funding. We are also grateful for a Mettler–Toledo Thermal Analysis Education Grant in honor of Professor Edith Turi (2001).

Supporting information for this article is available on the WWW under <http://www.angewandte.org> or from the author.



- 1': X = -OCH₃
 1a: X = -O-PS ($M_w = 1.7 \times 10^3$)
 1b: X = -O-PS ($M_w = 3.2 \times 10^3$)
 1c: X = -O-PS ($M_w = 20 \times 10^3$)
 2': Y = -OC(CH₃)₃
 2a: Y = -O-PEG ($M_w = 350 \times 10^3$)
 2b: Y = -O-PEG ($M_w = 2.0 \times 10^3$)
 2c: Y = -O-PEG ($M_w = 5.0 \times 10^3$)



Hydrogen-bond-mediated association of the modified PS and PEG chains was further confirmed by gel permeation chromatography (GPC). The **1c·2c** pair, relative to **1c** or **2c** alone, had the fastest elution time (23.00 min), followed by **1c** (23.45 min), and then **2c** (24.99 min; Figure 1 a). Upon elution

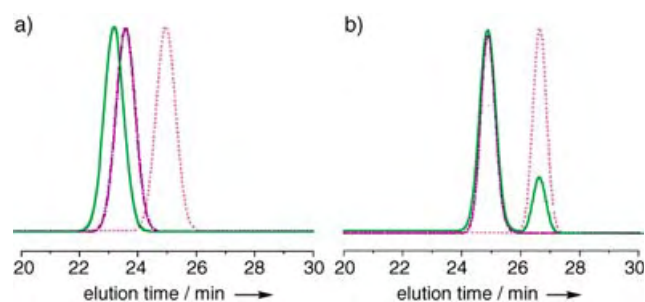


Figure 1. GPC traces of **1c·2c** (green), **1c** (---, purple), and **2c** (—, pink) eluted with a) DMF/toluene (10:90, v/v) and b) DMF, both at 60 °C. DMF = *N,N*-Dimethylformamide.

with the polar solvent DMF (Figure 1 b), **1c·2c** appeared as two peaks that coincided with the positions of **1c** and **2c** which again confirmed the hydrogen-bonded nature of **1c·2c**. Similar results were obtained from GPC analyses of another duplex, **1b·2b**, and its corresponding constituent blocks **1b** and **2b**.^[8]

The above NMR and GPC results clearly establish that PS and PEG strands can indeed be linked through hydrogen bonding. In the bulk phase, under conditions that favor the formation of intermolecular hydrogen bonds, these supramolecular block copolymers may demonstrate properties that are characteristic of typical covalent block copolymers. On the other hand, under conditions that disrupt intermolecular hydrogen bonds, these supramolecular diblock copolymers may dissociate and behave like A/B polymer blends. One of the most important properties of block copolymers involves

microphase separation, which depends on the incompatibility or immiscibility of the two constituent polymer blocks and the volume fraction of the blocks.^[1] If the molecular weights of the blocks are low, the constituent blocks are miscible and the corresponding block copolymers will be disordered and therefore not show microphase separation. As their molecular weights increase, the constituent blocks will eventually become immiscible and the corresponding block copolymers will show microphase separation.

According to the method described by Cheng and co-workers,^[9] the interaction parameters (χ_N ; 60 °C) of the PS and PEG chains in the diblock copolymer architecture were estimated to have values of 2.8, 4.5, 17.3, and 19.8 for **1b·2a**, **1b·2b**, **1c·2b**, and **1c·2c**, respectively. In terms of polymer–polymer interactions in the phase diagram of diblock copolymers,^[10] these χ_N values mean that 1) **1b·2a** and **1b·2b** should exist as disordered hydrogen-bonded block copolymers, which

do not exhibit PS/PEG microphase separation owing to their low χ_N values, 2) **1c·2b** may still be disordered owing to its low PEG volume fraction (9.5%), although it has a reasonably large χ_N value, and 3) **1c·2c** with its χ_N value of 19.8 and PEG volume fraction of 20.9% should show microphase separation, which would lead to discontinuous nanoscale PEG domains embedded in the PS matrix. These predictions based on the χ_N values are fully consistent with results from differential scanning calorimetry (DSC) studies.

Figure 2 shows the DSC heating diagrams of four PS–PEG pairs, **1b·2a**, **1b·2b**, **1c·2b**, and **1c·2c**. The similar results obtained during the first heating scans for **1b·2a**, **1b·2b**, and **1c·2b** indicate the absence of ordered PEG domains, which suggests that these three duplexes are disordered block copolymers. This is consistent with the above theoretical predictions on **1b·2a**, **1b·2b**, and **1c·2b**. In contrast, the first DSC heating diagram of **1c·2c** revealed a sharp melting peak for PEG near 60 °C and a glass transition of PS near 100 °C. This heating diagram is very similar to those of ordered, covalent PS–PEG diblock copolymers^[9] and suggests that **1c·2c** self-assembles into an ordered morphology. The endothermic peaks observed for **1b·2a** (175 °C), **1b·2b** (174 °C), and **1c·2b** (190 °C) during the first heating scans are likely brought about by the dissociation of the hydrogen-bonded duplex units because a similar peak (192 °C) was also observed in the heating diagram of duplex **1'·2'**, which does not carry a polymer chain. The first heating scans of **1c·2c** revealed a broad exothermic peak centered around 179 °C, which indicates that the hydrogen-bonded duplex unit of **1c·2c** is in an environment that is very different from those in the three supramolecular pairs that exist in the disordered state. The endothermic peaks were reproduced in the second heating of **1b·2a** (172 °C) and **1b·2b** (174 °C). The corresponding endo- or exothermic peak was absent in the diagram of **1c·2b** or **1c·2c** during the second heating cycle. Instead, melting peaks of PEG were observed for both **1c·2b** and **1c·2c**, which suggests that the blocks of **1b·2a** and **1b·2b** remain as miscible blends after the hydrogen-bonded duplex unit dissociates at high temperatures. Upon cooling, the two

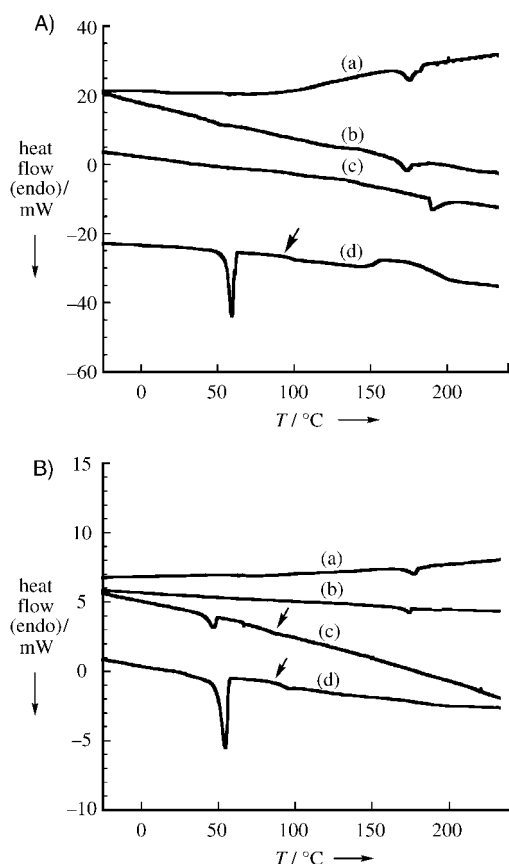


Figure 2. DSC profiles from the A) first and B) second heating at $5^{\circ}\text{C min}^{-1}$ of a) **1b-2a**, b) **1b-2b**, c) **1c-2b**, and d) **1c-2c**. Prior to the second heating, the samples were cooled from 250°C to -50°C at $5^{\circ}\text{C min}^{-1}$. Arrows are used to indicate the glass transition from the PS domains of either ordered or macrophase-separated PS/PEG.

blocks were linked through hydrogen bonds to form the diblock copolymers from the homogeneous mixtures of the melts. As for **1c-2b** and **1c-2c**, the separated PS and PEG macrophases did not allow the pairing of their hydrogen-bonded duplex units and thus the block copolymers within the timeframe of the cooling cycle. This conclusion is further supported by comparison of the behavior of **1c-2c** with that of a PS/PEG (M_M : 20000:5000) blend by DSC studies, which revealed significant differences between the two.^[8] The first heating scan gave results that were consistent with microphase separation for **1c-2c** and macrophase separation for the PS/PEG blend. After cooling down from the first heating scan, the second heating scan on the same samples led to DSC results that indicated macrophase separation of both samples relative to the original **1c-2c** duplex and the PS/PEG blend.

The microphase separation of **1c-2c** was also confirmed by the AFM image of its spin-coated film from benzene (Figure 3). It was reported that PEG cylinders could be aligned normal to the substrate by spin-coating PS-PEG diblock copolymers from benzene.^[11] From the AFM image (Figure 3), the well-dispersed discontinuous PEG domains (dark regions) with an average diameter of 24 nm indicate that the **1c-2c** sample has a typical PS-PEG diblock copoly-

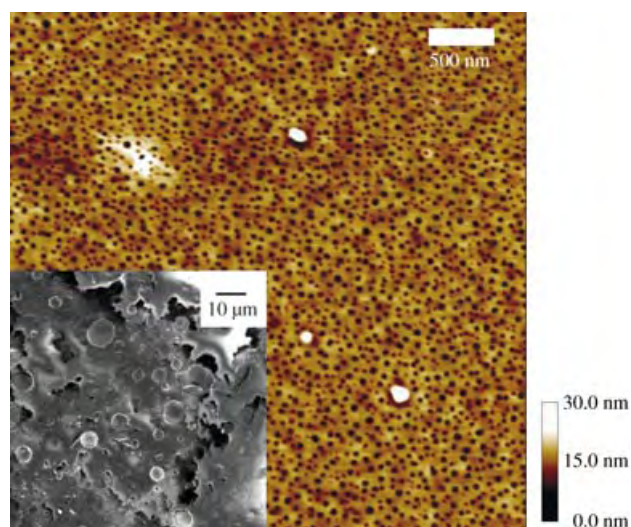


Figure 3. Tapping mode AFM image (height) of a film of **1c-2c** by spin-coating from benzene solution. Inset: SEM image of freeze-fractured surface of a sample of **1c-2c**, which had been heated to 250°C and cooled to -50°C at $5^{\circ}\text{C min}^{-1}$ (that is, after the DSC experiments).

mer-like microphase separation,^[11] although it is not clear at this moment whether the PEG domains are vertically oriented cylinders or dispersed spheres. The morphology of a cryogenically fractured surface of the **1c-2c** sample was examined by scanning electron microscopy (SEM) after the DSC experiments, which revealed that the sample had indeed undergone a macroscopic phase separation after the heating and cooling cycles in the DSC analyses. The AFM images of **1c-2c** before and after dipping into a mixture of methanol/water (1:1 v/v) at room temperature for one hour show that the methanol/water-treated sample contains nanoscale local swellings in the PEG domains, which is presumably due to the disruption of the six hydrogen-bonded association units and the swelling of PEG.^[8] Furthermore, the AFM image of **1d-2d**, with its higher ratio of PEG relative to that for **1c-2c**, contains enlarged dark regions,^[8] which supports our contention that the dark regions in the AFM image of **1c-2c** correspond to microphase-separated PEG domains.

In summary, the supramolecular diblock copolymers described here demonstrate the phase behavior that is typical of diblock copolymers. The perturbation of the hydrogen-bonded duplex units on the phase behavior of the diblock assemblies, such as **1c-2c** and **1d-2d**, with long PS and PEG blocks is surprisingly small. Relative to covalent block copolymers, these supramolecular block copolymers offer unique advantages such as 1) the rapid generation of numerous block combinations, 2) the preparation of block copolymers consisting of blocks that can only be prepared separately by using drastically different methods, 3) the hydrogen-bonded bridging units can be formed or cleaved under mild conditions, and 4) the ability of the designed system to undergo self-repair (or error-correcting). Coupled with the programmable sequence-specificity and high stability of our hydrogen-bonded duplexes, the described strategy can be easily extended to the creation of tri- and multiblock

copolymers, which will greatly enhance the diversity of the corresponding self-assembled nanoarchitectures.

Received: April 28, 2004

Revised: August 17, 2004

Keywords: block copolymers · hydrogen bonds · nanostructures · phase transitions · supramolecular chemistry

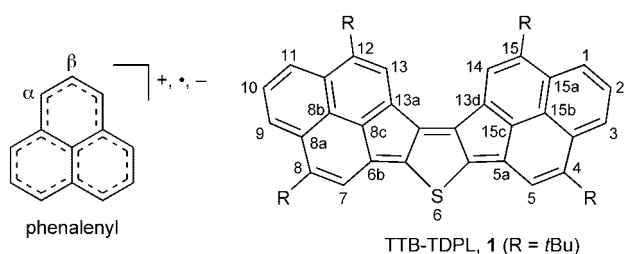
- [1] a) F. S. Bates, G. H. Fredrickson, *Phys. Today* **1999**, 52, 32; b) G. H. Fredrickson, F. S. Bates, *Annu. Rev. Mater. Sci.* **1996**, 26, 501; c) W. Meier, *Chem. Soc. Rev.* **2000**, 29, 295; d) I. W. Hamley, *The Physics of Block Copolymers*, Oxford University Press, **1998**.
- [2] a) J. S. Moore, *Curr. Opin. Colloid Interface Sci.* **1999**, 4, 108; b) L. Brunsveld, B. J. B. Folmer, E. W. Meijer, R. P. Sijbesma, *Chem. Rev.* **2001**, 101, 4071; c) S. C. Zimmerman, L. J. Lawless, *Top. Curr. Chem.* **2001**, 217, 95.
- [3] S. C. Zimmerman, P. S. Corbin, *Struct. Bonding (Berlin)* **2000**, 96, 63.
- [4] R. P. Sijbesma, F. H. Beijer, L. Brunsveld, B. J. B. Folmer, J. H. K. K. Hirschberg, R. F. M. Lange, J. K. L. Lowe, E. W. Meijer, *Science* **1997**, 278, 1601.
- [5] a) V. M. Artzner, L. Jullien, T. Gulik-Krzywicki, J.-M. Lehn, *Chem. Commun.* **1997**, 117; b) L. L. Freitas, M. M. Jacobi, G. Gonçalves, R. Stadler, *Macromolecules* **1998**, 31, 3379; c) J. F. Gohy, R. Jerome, *Prog. Polym. Sci.* **2001**, 26, 1061; d) R. J. Thibault, P. J. Hotchkiss, M. Gray, V. M. Rotello, *J. Am. Chem. Soc.* **2003**, 125, 11249; e) R. K. Castellano, J. Rebek, *J. Am. Chem. Soc.* **1998**, 120, 3657; f) E. A. Fogleman, W. C. Yount, J. Xu, S. L. Craig, *Angew. Chem.* **2002**, 114, 4198; *Angew. Chem. Int. Ed.* **2002**, 41, 4026; g) K. Yamauchi, J. R. Lizotte, D. M. Hercules, M. J. Vergne, T. E. Long, *J. Am. Chem. Soc.* **2002**, 124, 8599; h) H. W. Gibson, N. Yamaguchi, J. W. Jones, *J. Am. Chem. Soc.* **2003**, 125, 3522; i) W. H. Binder, M. J. Kunz, C. Kluger, G. Hayn, R. Saf, *Macromolecules* **2004**, 37, 1749.
- [6] B. G. G. Lohmeijer, U. S. Schubert, *Angew. Chem.* **2002**, 114, 3980; *Angew. Chem. Int. Ed.* **2002**, 41, 3825.
- [7] a) B. Gong, Y. Yan, H. Q. Zeng, E. Skrzypczak-Jankunn, Y. W. Kim, J. Zhu, H. Ickes, *J. Am. Chem. Soc.* **1999**, 121, 5607; b) H. Q. Zeng, R. S. Miller, R. A. Flowers, B. Gong, *J. Am. Chem. Soc.* **2000**, 122, 2635; c) H. Q. Zeng, X. W. Yang, A. L. Brown, S. Martinovic, R. D. Smith, B. Gong, *Chem. Commun.* **2003**, 1556; d) H. Q. Zeng, H. Ickes, R. A. Flowers, B. Gong, *J. Org. Chem.* **2001**, 66, 3574; e) B. Gong, *Synlett* **2001**, 582; f) X. W. Yang, S. Martinovic, R. D. Smith, B. Gong, *J. Am. Chem. Soc.* **2003**, 125, 9932; g) H. Q. Zeng, X. W. Yang, R. A. Flowers, B. Gong, *J. Am. Chem. Soc.* **2002**, 124, 2903.
- [8] See Supporting Information.
- [9] L. Zhu, S. Z. D. Cheng, B. H. Calhoun, Q. Ge, R. P. Quirk, E. L. Thomas, B. S. Hsiao, F. Yeh, B. Lotz, *Polymer* **2001**, 42, 5829.
- [10] M. W. Matsen, F. S. Bates, *J. Polym. Sci. Part B* **1997**, 35, 945.
- [11] Z. Q. Lin, D. H. Kim, X. D. Wu, L. Boosahda, D. Stone, L. LaRose, T. P. Russell, *Adv. Mater.* **2002**, 14, 1373–1376.

Four-Stage Amphoteric Redox Properties and Biradicaloid Character of Tetra-*tert*-butyldicyclopenta[*b*; *d*]thieno[1,2,3-*cd*;5,6,7-*c'**d'*]diphenylene**

Takashi Kubo,* Maki Sakamoto, Minako Akabane, Yoshinori Fujiwara, Kageyoshi Yamamoto, Motoko Akita, Katsuya Inoue, Takeji Takui, and Kazuhiro Nakasuji*

Dedicated to Emeritus Professor Ichiro Murata on the occasion of his 75th birthday

Phenalenyl-based hydrocarbons possess highly amphoteric redox properties that give low oxidation and high reduction potentials and afford stable multivalent redox species.^[1] These



α -position: 1,3,4,5a,6b,8,9,11,12,13a,13d,15
 β -position: 2,5,7,10,13,14

compounds have frontier orbitals with a nonbonding molecular orbital (NBMO) character that results from a weak perturbation between singly occupied molecular orbitals (SOMOs) of the phenalenyl radical and the frontier orbitals of a central conjugated system. This perturbation leads to a

[*] Dr. T. Kubo, M. Sakamoto, M. Akabane, Y. Fujiwara, Prof. Dr. K. Yamamoto, Prof. Dr. K. Nakasuji
 Department of Chemistry
 Graduate School of Science, Osaka University
 Machikaneyama 1-1, Toyonaka, Osaka 560-0043 (Japan)
 Fax: (+81) 6-6850-5395
 E-mail: kubo@chem.sci.osaka-u.ac.jp
 nakasuji@chem.sci.osaka-u.ac.jp

Dr. M. Akita, Prof. Dr. K. Inoue
 Department of Applied Molecular Science
 Institute for Molecular Science
 Okazaki 444-8585 (Japan)

Prof. Dr. T. Takui
 Departments of Chemistry and Materials Science
 Graduate School of Science, Osaka City University
 Sumiyoshi-ku, Osaka 558-8585 (Japan)

[**] This work was supported by a Grant-in-Aid for Scientific Research on Priority Areas (No. 15750034, Area No. 769, Proposal No. 15087202) from the Ministry of Education, Culture, Sports, Science, and Technology (MEXT), Japan.



Supporting information for this article is available on the WWW under <http://www.angewandte.org> or from the author.

small gap between the highest occupied molecular orbital (HOMO) and the lowest unoccupied molecular orbital (LUMO). This amphoteric redox property makes the phenalenyl moiety an important species in redox chemistry. Herein, the synthesis and properties of a new phenalenyl-based conjugated system that has amphoteric redox properties (Scheme 1) and a biradicaloid character originating from a small HOMO–LUMO gap is reported.

The synthetic procedure for **1** is shown in Scheme 2. The key intermediates **3** were obtained as an isomeric mixture of 3,10-, 3,11-, and 4,10-dimethyl compounds by treatment of acenaphthene derivative **2** with sulfur.^[2] Isolation of the individual isomers was not carried out as **1** could be prepared from each of them. Bis(propionic acid) derivatives **6** were obtained in three steps. Intramolecular Friedel–Crafts cyclization of the acyl chloride of **6** with AlCl_3 gave diketones **7**, which were reduced and subsequently dehydrated to afford dihydro compounds **9**. Dehydrogenation of **9** with *p*-benzoquinone provided the target compound **1** as black prisms. Compound **1** was found to be stable in the solid state at room temperature even in air. The structure of **1** was confirmed by X-ray crystographic analysis (see below).

The cyclic voltammogram of **1** gave four reversible redox waves, with two oxidation potentials ($E_2^{\text{ox}} = +0.94$ V and $E_1^{\text{ox}} = +0.47$ V) and two reduction potentials ($E_1^{\text{red}} = -0.53$ V and $E_2^{\text{red}} = -0.90$ V; Figure 1). The reversibility of the redox waves indicates the persistency of the mono- and divalent ionic species. Furthermore, the low E_1^{ox} and high E_1^{red} values suggest that the oxidized and reduced species that are generated have high thermodynamic stabilities. The E_1^{sum} value^[3a] of 1.00 V is

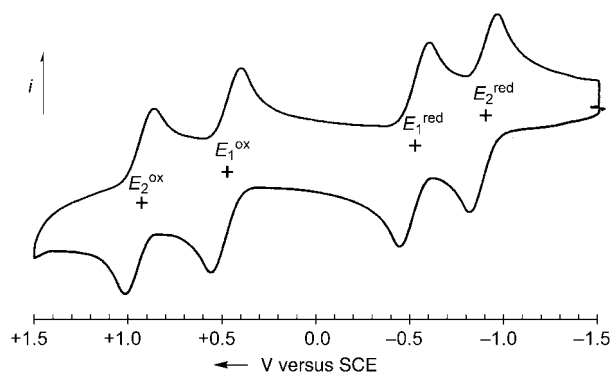
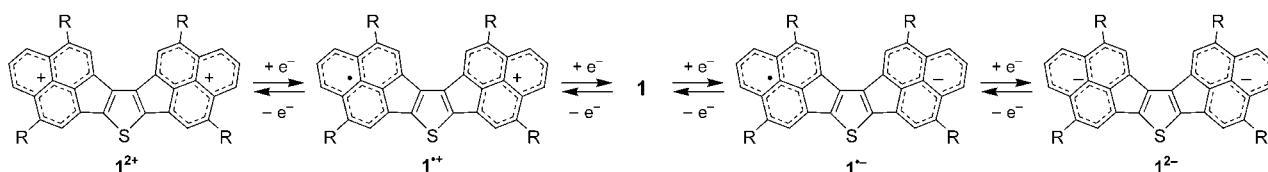
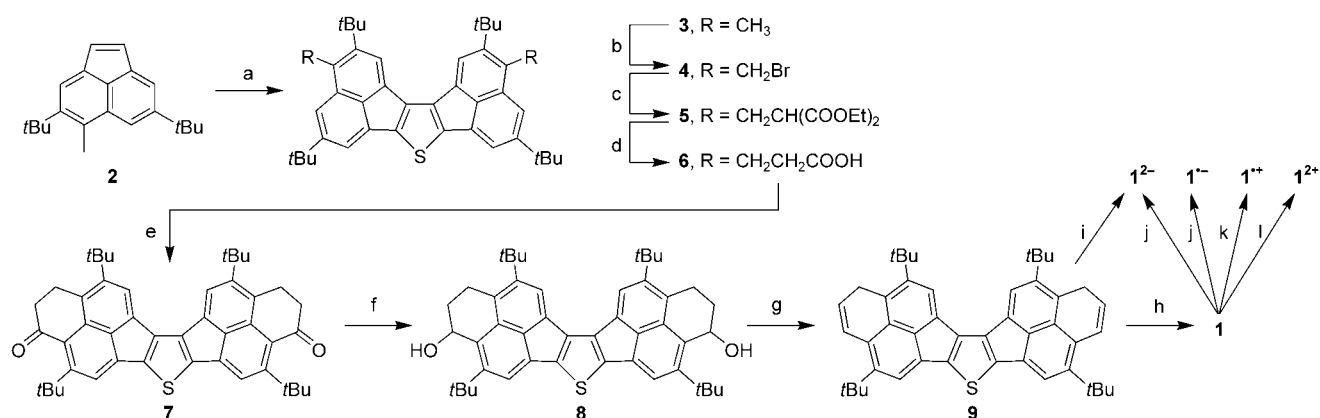


Figure 1. Cyclic voltammogram (versus saturated calomel electrode) of **1** in CH_2Cl_2 with 0.1 M Bu_4NClO_4 as the supporting electrolyte at room temperature; sweep rate = 100 mV s^{-1} .

comparable to that of pentaleno[1,2,3-*cd*;4,5,6-*c'd'*]diphenylene (PDPL, $0.99 \text{ V}^{[3b]}$), which is the smallest value reported for closed-shell hydrocarbons.^[1c] Thus, **1** possesses a high amphoteric redox ability, which indicates that it has a small HOMO–LUMO gap. Such a small gap is also confirmed by the electronic absorption spectrum of **1**, where an extraordinarily low energy band at 800–2000 nm is seen (Figure 2). The band is assignable to a HOMO–LUMO transition, which is consistent with the value of 1520 nm ($f = 0.08$) calculated by time-dependent density functional theory (TD-DFT; RB3LYP/6-31G**) calculations.^[4] The low energy band is independent of the sample concentration (5×10^{-4} and $5 \times 10^{-5} \text{ mol L}^{-1}$) and the solvent polarity (cyclohexane, tetrahy-



Scheme 1. Four-stage amphoteric redox behavior of **1**.



Scheme 2. Synthesis of neutral **1** and ionic redox species 1^{2+} , $1^{+•}$, $1^{•-}$, and 1^{2-} . Reaction conditions: a) Sulfur, DMF, reflux, 2 h, 90%; b) *N*-bromosuccinimide (NBS), benzoyl peroxide, benzene, reflux, 10 min; c) NaOEt, $\text{CH}_2(\text{CO}_2\text{Et})_2$, benzene+ethanol, RT, 21 h, 67% (2 steps); d) 1. 10% aq KOH, ethanol, reflux, 3 h, 2. 3 N HCl, reflux, 12 h, 89%; e) 1. $(\text{COCl})_2$, reflux, 2 h, 2. AlCl_3 , CH_2Cl_2 , -30°C , 2 h, 75%; f) LiAlH_4 , THF, RT, 4 h, 86%; g) cat. *p*-toluenesulfonic acid, benzene, reflux, 5 min, 99%; h) *p*-chloranil, benzene, reflux, 5 min, 87%; i) KH, under vacuum, THF, RT, 1 week; j) K mirror, THF, RT; k) 1 equiv. of SbCl_5 , CH_2Cl_2 ; l) D_2SO_4 , RT, 10 days.

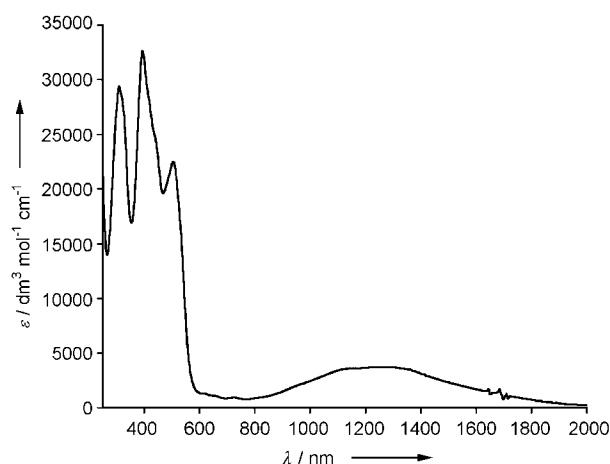


Figure 2. Electronic absorption spectrum of **1** in CH₂Cl₂ at room temperature.

drofuran, dichloromethane, and acetonitrile). Such observations exclude the possibility that the band is an intermolecular charge-transfer (CT) absorption band.

The high amphotericity indicates that **1** should yield cationic and anionic species readily. The ionic redox species of **1** were generated with no difficulties and showed no appreciable decomposition over several weeks at room temperature. The reaction conditions are summarized in Scheme 1. The monovalent radical species **1**^{•+} and **1**^{•−} gave rise to well-resolved ESR signals without detectable changes in the spectra at 183–293 K. The coupling constants of the ring protons are given in Table 1 along with the theoretical

Table 1: Experimental and theoretical hyperfine coupling constants (in mT) of **1**^{•+} and **1**^{•−}.

position	1 ^{•+} [a]		1 ^{•−} [b]	
	exptl.	theor.[c]	exptl.	theor.[c]
1,11	0.218	−0.225	0.150	−0.163
2,10	0.060	+0.045	0.004	+0.004
3,9	0.218	−0.204	0.154	−0.164
5,7	0.029	+0.003	0.068	+0.045
13,14	0.060	+0.054	0.008	−0.004

[a] Recorded in CH₂Cl₂ at −70 °C. The *g* value was 2.0045. [b] Recorded in THF at −70 °C. The *g* value was 2.0034. [c] Calculated at the SVWN/6-31G** level and with the McConnell equation (*Q* = −2.5 mT for **1**^{•+} and −2.4 mT for **1**^{•−}).

coupling constants calculated by the DFT (SVWN/6-31G**) method and the McConnell equation.^[5] The agreement between the experimental and the theoretical hyperfine coupling constants indicates that the unpaired electron is not confined to one phenalenyl moiety (A) but is delocalized over the entire molecule (B).^[6] The spin-density calculation indicates that the π spin of **1**^{•+} and **1**^{•−} resides on the two phenalenyl moieties with a similar spin distribution pattern to that of the phenalenyl radical (Figure 3). The similarity of the distribution pattern on two phenalenyl moieties supports the idea that both the HOMO and LUMO of **1** should have a

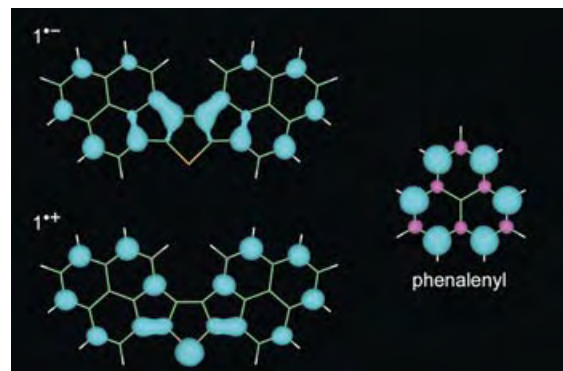
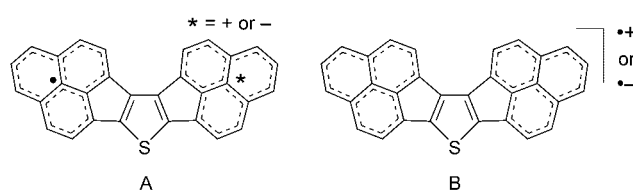


Figure 3. Spin density of **1**^{•+}, **1**^{•−}, and the phenalenyl radical calculated at the SVWN/6-31G** level.

large contribution from the nonbonding molecular orbital (NBMO) in the phenalenyl radical.

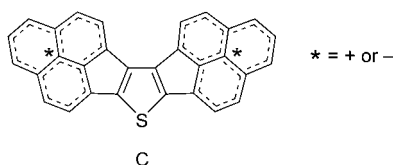
The π -charge distribution of the divalent species **1**²⁺ and **1**^{2−} should closely relate to the π -spin distribution of the monovalent species **1**^{•+} and **1**^{•−}. The removal and addition of two electrons in the divalent species occurs in the same molecular orbitals as those of a single electron in the monovalent species, that is the HOMO and LUMO, respectively. The divalent species **1**²⁺ and **1**^{2−} gave rise to only seven signals in the ¹H NMR spectra (two from the *tert*-butyl groups and five from the ring protons; Table 2). This simple ¹H NMR

Table 2: ¹H and ¹³C NMR spectroscopic data (δ) of **1**²⁺ and **1**^{2−}, and ¹³C NMR chemical shift changes on going from **1**²⁺ to **1**^{2−}.^[a]

position	1 ²⁺		1 ^{2−}		position ^[b]	$\Delta\delta_c$ ^[c]
	¹ H	¹³ C	¹ H	¹³ C		
1,11	8.75	148.8	8.08	115.4	α	33.4
2,10	7.39	131.0	7.50	118.2	β	12.8
3,9	8.75	150.0	8.06	115.7	α	34.3
3a,8a		134.0		129.6		4.4
4,8		185.0		128.8	α	56.2
5,7	7.14	123.6	8.07	116.0	β	8.6
5a,6b		155.2		111.1	α	44.1
8c,15c		139.0		127.8		11.2
13a,13d		147.6		108.7	α	38.9
13,14	7.27	125.0	8.93	119.2	β	5.8
12,15		180.0		128.1	α	51.9
11a,15a		133.9		129.9		4.0
8b,15b		129.1		129.5		−0.4
5b,6a		159.5		119.7		39.8
13b,13c		150.4		123.4		27.0

[a] Compound **1**²⁺ was recorded in D₂SO₄ at room temperature. Compound **1**^{2−} was recorded in [D₈]THF at room temperature. [b] α and β denote the positions shown in the first formula. [c] $\Delta\delta_c = {}^{13}\text{C}(\text{1}^{2+}) - {}^{13}\text{C}(\text{1}^{2-})$.

spectroscopic pattern reflects the C_2 -symmetry of the divalent species. The changes in the ^{13}C NMR chemical shifts of the sp^2 carbon atoms on going from $\mathbf{1}^{2+}$ to $\mathbf{1}^{2-}$ are 744.0 ppm (or 186.0 ppm per electron), which supports the complete generation of the dication and the dianion.^[7] The changes observed in chemical shifts for the individual carbon atoms are large at the α position and small at the β position. A similar trend is found with the changes found for the chemical shifts for the phenalenyl species: large (51.8 ppm) at the α position and small (4.9 ppm) at the β position.^[8] These NMR spectroscopic studies show that the electronic structures of the phenalenyl cation and anion contribute largely to the divalent species $\mathbf{1}^{2+}$ and $\mathbf{1}^{2-}$, as shown in formula C. Thus, it can be concluded that the high amphotericity of $\mathbf{1}$ results from the NBMO character of its frontier orbitals.



A large exchange interaction ($K_{\text{H,L}}$) in the frontier orbitals is expected for a compound with a small HOMO–LUMO gap and a large spatial overlap between these orbitals which would lead to a pronounced biradical character.^[9] The frontier orbitals in the two phenalenyl moieties in $\mathbf{1}$ have a very similar pattern to the NBMO of the phenalenyl radical, and therefore substantial spatial overlap between the HOMO and LUMO is expected (Figure 4). ESR measurements of solid $\mathbf{1}$ afforded a

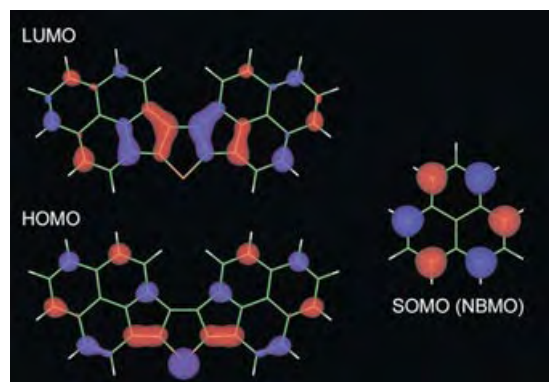


Figure 4. HOMO and LUMO of $\mathbf{1}$ as well as the singly occupied molecular orbital (SOMO) of the phenalenyl radical calculated at the B3LYP/6-31G** level.

typical spectra for triplet species ($|D| = 17.2$ mT, $|E| = 3.9$ mT). Furthermore, the temperature dependence of the half-field signal indicated a thermal excitation to the triplet state with an energy gap ($\Delta E_{\text{S-T}}$) of ~ 5 kJ mol $^{-1}$. The average distance between the two interacting spins is estimated from the D value to be 5.5 Å, which is smaller than the intramolecular distance between the centers of the two phenalenyl moieties of $\mathbf{1}$ (8.4 Å). This finding suggests that an unpaired

electron is not confined to one phenalenyl moiety but can delocalize on the central thiophene ring. The unpaired electron spin of a triplet state generally broadens NMR resonance signals by thousands of hertz. No signals arising from the ring protons were observed in the ^1H NMR spectrum of $\mathbf{1}$ recorded in CD_2Cl_2 . Although a weak and broad signal was recognized between 4 and 9 ppm below -70°C , sharp signals could not be obtained even at -90°C (see the Supporting Information). An equilibrium with the thermally accessible triplet state would cause line broadening of the NMR resonance signals. Such a thermal accessibility to the triplet state supports the existence of a small HOMO–LUMO gap and the large exchange interaction ($K_{\text{H,L}}$) in $\mathbf{1}$.

The large exchange interaction ($K_{\text{H,L}}$) is another fascinating property that describes the ground-state configuration.^[10] A configuration interaction (CI) calculation at the CASSCF(2,2)/6-31G(d,p) level afforded an admixture (4%) of the double excitation $^1\Phi_{\text{H,H} \rightarrow \text{L,L}}$ into the ground configuration $^1\Phi_0$. The singlet diradical index, proposed by Neese and co-workers recently,^[11] was estimated to be approximately 35% based on the CI calculation for $\mathbf{1}$. The singlet diradical picture was supported by the DFT calculation at the UB3LYP/6-31G(d,p) level, which afforded an energy lowering of 7 kJ mol $^{-1}$ induced by symmetry breaking of the DFT solution. Fortunately, we obtained two indicative results for the singlet biradicaloid character.

The first indicative result is the X-ray crystal structure showing that $\mathbf{1}$ formed two kinds of dimeric pairs with substantially short nonbonding contacts of about 3.1 Å between each thiophene ring, as shown in Figure 5. The terminal rings were separated by over 4.2 Å because of the steric repulsion between the *tert*-butyl groups and the six-membered rings. The van der Waals contact between carbon atoms only exist within the central dicyclopenta[*b,d*]thiophene moieties. The attractive forces leading to dimerization would probably be an intermolecular CT interaction. Therefore, there will be intermolecular delocalization of electrons in the dimer of $\mathbf{1}$.^[12] There are two possible explanations for

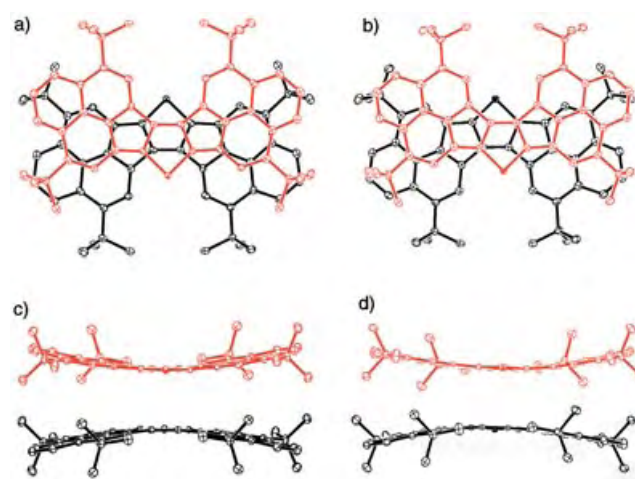


Figure 5. Crystal structures of $\mathbf{1}$. Top view of the dimeric pair A (a) and B (b), and side view of the dimeric pair A (c) and B (d). Hydrogen atoms are omitted for clarity.

the dimerization of **1** through CT interactions: The first is the attractive forces resulting from electron transfer between occupied and unoccupied molecular orbitals (MOs) in each of the monomers in the dimers. In general, the most important terms are related to an intermolecular HOMO–LUMO interaction; however, with **1** the HOMO–LUMO interaction should lead to no or only slight stabilization of the system because of the orbital symmetry mismatching in the dimeric arrangement described above. In contrast, the next highest occupied molecular orbital (NHOMO)–LUMO interaction should result in the formation of a bonding intermolecular orbital (Figure 6a). The second explanation is an attractive

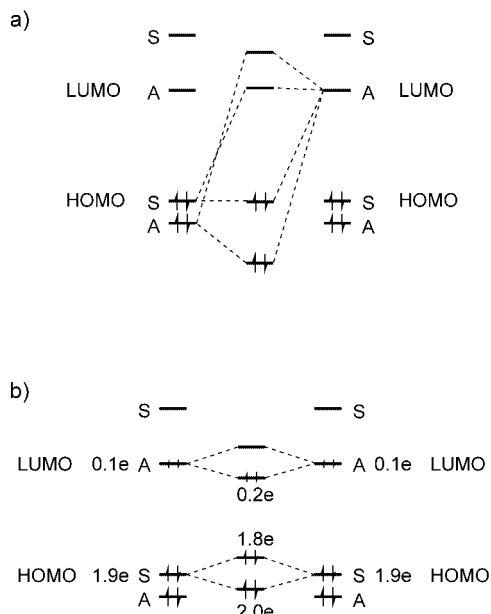
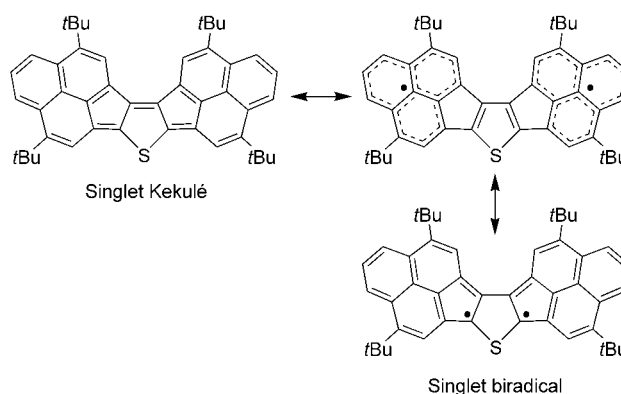


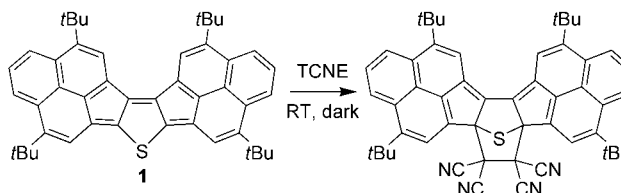
Figure 6. Schematic drawing of the molecular orbital interaction of dimeric **1** through electron transfer between occupied and unoccupied molecular orbitals (a), and through the double excitation configuration $^1\Phi_{H,H\rightarrow L,L}$ (b). S and A denote the symmetry of the molecular orbitals.

interaction through the double excitation configuration $^1\Phi_{H,H\rightarrow L,L}$, that is, a singlet biradical contribution. Based on the CASSCF(2,2) calculation of **1**, the occupation numbers of HOMO and LUMO are 1.9 and 0.1, respectively. In this case, a LUMO–LUMO interaction will lead to stabilization of the system because a newly formed “LUMO” of the dimer, which is more stable than the original LUMO, can accommodate at least 0.2 electrons (Figure 6b). In addition, a HOMO–HOMO interaction seems likely to stabilize the system because a newly formed “HOMO” of the dimer would contain only 1.8 electrons. This would suppress a four-electron repulsion that would result from the interaction between fully occupied orbitals. A valence-bond picture is helpful for understanding the singlet biradical structure. The Kekulé form of **1** loses aromatic stabilization in the central thiophene ring, whereas thiophene and phenalenyl radical structures appear in a singlet biradical form of **1**. Therefore, mixing of the singlet biradical configuration with the ground state is promoted. The broken symmetry DFT solution affords a large π -spin population on the phenalenyl moieties



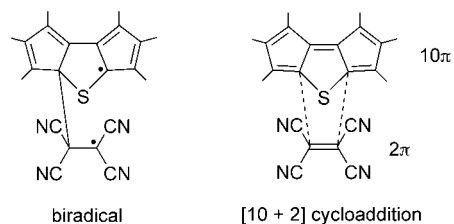
with a little delocalization to the thiophene ring (see the Supporting Information).

The second indicative result is a cycloaddition reaction of **1** with tetracyanoethylene (TCNE). Mixing a solution of **1** and TCNE in C_6D_6 exclusively afforded a TCNE adduct within 10 seconds in the dark at room temperature (Scheme 3). The



Scheme 3. Reaction of **1** with tetracyanoethylene (TCNE).

structure of the adduct was confirmed by NMR spectroscopy (1H , ^{13}C , NOESY, HMBC, and HMQC experiments). The reaction may proceed by a stepwise process involving a biradical or a symmetry-forbidden thermal concerted [10+2] process. At this stage the reaction mechanism is still



undetermined. However, discussion of symmetry being “forbidden” or “allowed” becomes meaningless for the concerted reaction of biradicaloid compounds because the double excitation configuration should lower the symmetry-imposed activation energy.^[9]

In conclusion, the amphoteric redox compound **1** was prepared by a stepwise synthesis and showed highly amphoteric redox properties. Notably, a singlet biradical character of **1** is suggested by quantum chemical calculations and supported by experimental results. The chemistry of amphoteric redox systems are expected to contribute to investigations

into the solid-state properties of conjugated singlet biradicals, such as crystal packing, magnetism, and electroconductive behavior. Closed-shell conjugated systems based on the phenalenyl radical could lead to conjugated biradicaloid compounds that could be isolated in the air.

Experimental Section

The detailed synthetic procedure for **1** is described in the Supporting Information.

Crystal data for **1**: $C_{52}H_{60}S$, $M = 717.11$, triclinic, space group $P\bar{1}$ (no. 2), $a = 12.901(2)$, $b = 17.000(3)$, $c = 20.674(4)$ Å, $\alpha = 82.243(3)$, $\beta = 89.589(3)$, $\gamma = 69.229(3)^\circ$, $V = 4196(1)$ Å³, $Z = 4$, $\mu(Mo_{K\alpha}) = 0.111$ cm⁻¹, $\rho_{\text{calcd.}} = 1.135$ g cm⁻³, $R1(wR2) = 0.071$ (0.187) for 982 parameters and 15174 unique reflections with $I > 2\sigma(I)$, GOF = 1.004. Data collection were performed on Enraf-Nonius CAD-4 diffractometer ($Mo_{K\alpha}$, $\lambda = 0.71069$ Å) at 9 K. The structure was solved with direct methods and refined with full-matrix least squares (teXsan). CCDC-237621 contains the supplementary crystallographic data for this paper. These data can be obtained free of charge from www.ccdc.cam.ac.uk/conts/retrieving.html (or from the Cambridge Crystallographic Data Centre, 12 Union Road, Cambridge CB21EZ, UK; fax: (+44) 1223-336-033; or deposit@ccdc.cam.ac.uk).

Received: May 6, 2004

Keywords: charge transfer · conjugation · density functional calculations · radicals · redox chemistry

P. M. W. Gill, B. G. Johnson, W. Chen, M. W. Wong, J. L. Andres, M. Head-Gordon, E. S. Replogle, J. A. Pople, Gaussian, Inc., Pittsburgh, PA, 1998.

- [5] H. M. McConnell, *J. Chem. Phys.* **1956**, *24*, 764.
- [6] The highly delocalized structure of the charge and the spin suggests that the monovalent radicals $1^{\cdot+}$ and $1^{\cdot-}$ can be placed in the class III category in the classification of mixed-valence species, which is consistent with the quite large values between the first and the second redox potentials ($E_2^{\text{ox}} - E_1^{\text{ox}} = 0.47$ V, $E_1^{\text{red}} - E_2^{\text{red}} = 0.37$ V). The properties of mixed valence compounds depend on the extent of the electronic interaction between the redox centers and its range. The common classification is: small or nonexistent (class I), slight (class II), and strong interaction (class III, including the completely delocalized molecules). See M. B. Robin, P. Day, *Adv. Inorg. Chem. Radiochem.* **1967**, *10*, 247.
- [7] H. Spiesecke, W. G. Schneider, *Tetrahedron Lett.* **1961**, *2*, 468.
- [8] I. Sethso, D. Johnels, U. Edlund, A. Sygula, *J. Chem. Soc. Perkin Trans. 2* **1990**, 1339.
- [9] The term “ π , π -biradicaloid” was used previously for a compound possessing two approximately nonbonding π -orbitals. See, J. Kolc, J. Michl, *J. Am. Chem. Soc.* **1973**, *95*, 7391.
- [10] D. R. McMasters, J. Wirz, *J. Am. Chem. Soc.* **2001**, *123*, 238.
- [11] D. Herebian, K. E. Wieghardt, F. Neese, *J. Am. Chem. Soc.* **2003**, *125*, 10997.
- [12] In general, the π - π interactions of aromatic systems is affected by various electronic factors. The well-known attractive forces are derived from electrostatic interactions between electron-deficient and electron-rich sites. However, this interaction is not likely to be effective in the dimeration of **1** because there is only a small overlap of positive and negative charges as found from the Mulliken charge analysis (see the Supporting Information).

- [1] a) K. Nakasuji, K. Yoshida, I. Murata, *J. Am. Chem. Soc.* **1982**, *104*, 1432; b) K. Nakasuji, K. Yoshida, I. Murata, *Chem. Lett.* **1982**, 969; c) K. Nakasuji, K. Yoshida, I. Murata, *J. Am. Chem. Soc.* **1983**, *105*, 5136; d) I. Murata, S. Sasaki, K.-U. Klabunde, J. Toyoda, K. Nakasuji, *Angew. Chem.* **1991**, *103*, 198; *Angew. Chem. Int. Ed. Engl.* **1991**, *30*, 172; e) K. Ohashi, T. Kubo, T. Masui, K. Yamamoto, K. Nakasuji, T. Takui, Y. Kai, I. Murata, *J. Am. Chem. Soc.* **1998**, *120*, 2018; f) T. Kubo, K. Yamamoto, K. Nakasuji, T. Takui, *Tetrahedron Lett.* **2001**, *42*, 7997; g) T. Kubo, K. Yamamoto, K. Nakasuji, T. Takui, I. Murata, *Angew. Chem.* **1996**, *108*, 456; *Angew. Chem. Int. Ed. Engl.* **1996**, *35*, 439; h) T. Kubo, K. Yamamoto, K. Nakasuji, T. Takui, I. Murata, *Bull. Chem. Soc. Jpn.* **2001**, *74*, 1999.
- [2] J. Nakayama, Y. Ito, *Sulfur Lett.* **1989**, *9*, 135.
- [3] a) To evaluate the amphoteric redox abilities of a molecule, the numerical sum (E^{sum}) of the oxidation potential (E^{ox}) and the reduction potential (E^{red}), $E^{\text{sum}} = E^{\text{ox}} + (-E^{\text{red}})$, is used; see V. D. Parker, *J. Am. Chem. Soc.* **1976**, *98*, 98, and ref [1a]. b) The measurement condition for PDPL is different from that for **1**. The condition for PDPL is as follows; temperature, -50°C ; solvent, DMF; supporting electrolyte, 0.1M Et_4NClO_4 , sweep rate, 30 mVs⁻¹; working electrode, Pt; reference electrode, saturated calomel electrode (SCE).
- [4] All DFT and CASSCF calculations were done using Gaussian 98 (Revision A.7), M. J. Frisch, G. W. Trucks, H. B. Schlegel, G. E. Scuseria, M. A. Robb, J. R. Cheeseman, V. G. Zakrzewski, J. A. Montgomery, R. E. Stratmann, J. C. Burant, S. Dapprich, J. M. Millam, A. D. Daniels, K. N. Kudin, M. C. Strain, O. Farkas, J. Tomasi, V. Barone, M. Cossi, R. Cammi, B. Mennucci, C. Pomelli, C. Adamo, S. Clifford, J. Ochterski, G. A. Petersson, P. Y. Ayala, Q. Cui, K. Morokuma, D. K. Malick, A. D. Rabuck, K. Raghavachari, J. B. Foresman, J. Cioslowski, J. V. Ortiz, B. B. Stefanov, G. Liu, A. Liashenko, P. Piskorz, I. Komaromi, R. Gomperts, R. L. Martin, D. J. Fox, T. Keith, M. A. Al-Laham, C. Y. Peng, A. Nanayakkara, C. Gonzalez, M. Challacombe,

Inorganic Electrides

Is Mayenite without Clathrated Oxygen an Inorganic Electride?*

Zhenyu Li, Jinlong Yang, J. G. Hou, and Qingshi Zhu*

With electrons as their anions, electrides have attracted a much interest recently in broad fields of research.^[1] Despite their importance both in fundamental science and industrial

[*] Dr. Z. Li, Prof. Dr. J. Yang, Prof. Dr. J. G. Hou, Prof. Dr. Q. Zhu
Hefei National Laboratory for Physical Science at Microscale
Laboratory of Bond-Selective Chemistry and
Structure Research Laboratory
University of Science and Technology of China
Hefei, 230026 Anhui (China)
Fax: (+86) 551-360-2969
E-mail: jlyang@ustc.edu.cn

[**] This work is partially supported by the National Project for the Development of Key Fundamental Sciences in China (G1999075305, G2001CB3095), by the National Natural Science Foundation of China (50121202, 20025309, 10074058), by the Foundation of Ministry of Education of China, and by the Foundation of the Chinese Academy of Science. We thank Prof. James L. Dye for helpful discussions.

applications, traditional organic electrides are stable only at cryogenic temperatures and are air- and water-sensitive. It is therefore interesting and important to explore room-temperature stable inorganic electrides.^[2] Existing model systems towards this direction include Na_4^{3+} clusters in the sodalite cage of Na^+Y^{3-} and alkali metals in the channels of zeolite ITQ-4.^[4] Recently, Matsuishi et al.^[5] removed the clathrated oxygen ions from the crystallographic cages of mayenite $12\text{CaO} \cdot 7\text{Al}_2\text{O}_3$ (C12A7) through a base-metal oxidation process. They suggested that their treatment inject extra electrons in place of the free O^{2-} with a spherical $1s$ wave function of an F^+ -like center, and thus produce an inorganic electride.

To gain insight into the electronic properties of this kind of mayenite with removed clathrated oxygen (C12A7: $2e^-$) and to verify the electride model, it is important to investigate this material theoretically. Unfortunately, the existing theoretical studies give contradictory conclusions. The first theoretical work by Sushko et al.^[6] supports the electride model with localized extra electrons, whereas a recent study by Medvedeva and Freeman^[7] reveals that the extra electrons are highly delocalized both in the cavities and in the regions occupied by cations, and thus opposes the electride model. We noticed that both studies do not provide a satisfactory conclusion with respect to the real physical picture of the extra electrons in this novel material. Sushko et al.^[6] used an embedded cluster model, which is only suitable for the dilute extra electron limit, and Medvedeva and Freeman^[7] used the linear muffin-tin orbital (LMTO) method with a simple atomic sphere approximation, which may not be accurate enough to describe the charge-density distribution in this complex system. Moreover, the geometry was not fully optimized in either of the studies. To clarify this issue, we report herein a careful plane-wave pseudopotential study on the geometrical and electronic structure of this material.

The crystal structure of C12A7, with two formula units per unit cell, is characterized by a positively charged lattice framework $[\text{Ca}_{24}\text{Al}_{28}\text{O}_{64}]^{4+}$ that forms twelve crystallographic cages per unit cell ($I\bar{4}3d$ space group). The remaining two oxygen ions are clathrated in the cages to maintain charge neutrality. We optimized the geometry of C12A7 with its lattice parameter fixed to the experimental value (11.989 Å).^[8] As shown in Figure 1, cages with free oxygen inside have a relatively large distortion after optimization, where it can be clearly seen that two opposite Ca atoms at the cage wall are strongly pulled towards the center of the cage. Therefore, after optimization, the cages in C12A7 are no longer identical.

When considering the geometry of the system without clathrated oxygen, one must take special care. In the work of Medvedeva and Freeman,^[7] they simply assumed that all cages in C12A7: $2e^-$ are identical. But considering the possibility that the extra electrons may be captured in some cages with other cages being kept empty,^[5,6] this assumption is far from obvious. In this work, we optimized the geometry of C12A7: $2e^-$ from two initial configurations. The first optimization starts from a framework of undistorted cages, and the second starts from the previously relaxed distorted framework, but without clathrated oxygen. Within numerical

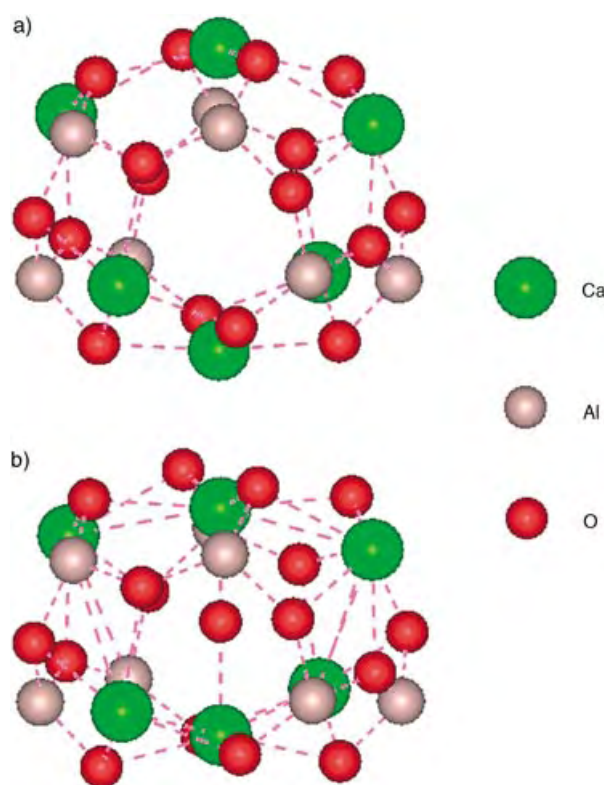


Figure 1. Perspective view of a) an undistorted cage and b) a distorted cage in mayenite. There is a clathrated oxygen inside the distorted cage, and the upper and lower Ca (green) at the cage wall are strongly pulled towards the center O (red).

precision, both optimizations led to the same final structure, and the distortion of the second initial geometry finally disappeared. Therefore, the simple assumption of Medvedeva and Freeman^[7] turns out to be correct, but it must be emphasized that we can only be confident with the following calculations on electronic structure after such a careful examination of the geometry.

The identical-cage geometry strongly suggests that the picture^[5,6] of two types of cages (electron trapping and empty) in C12A7: $2e^-$ may be incorrect. We noticed that in the embedded cluster calculation^[6] the two quantum-mechanical (QM) cages are geometrically different on account of different classical neighboring cages. This artificial difference between the two QM cages may be the reason that leads to the extra electron being localized in only one of the two cages.

Based on the optimized geometries, we calculated the band structures of C12A7 and C12A7: $2e^-$, and the result is shown in Figure 2. For C12A7, there are two very narrow bands below the Fermi level, which mainly come from the p orbitals of the clathrated oxygen, as suggested by Medvedeva and Freeman.^[7] Above these two interstitial bands, there is a band manifest (from about 2.0 to 3.8 eV) that corresponds to the cavities. After the clathrated oxygen is removed, the interstitial bands disappear, and the cavity bands become partially occupied by the extra electrons. Because of the disappearance of the distortion, the cavity bands become more degenerate for C12A7: $2e^-$.

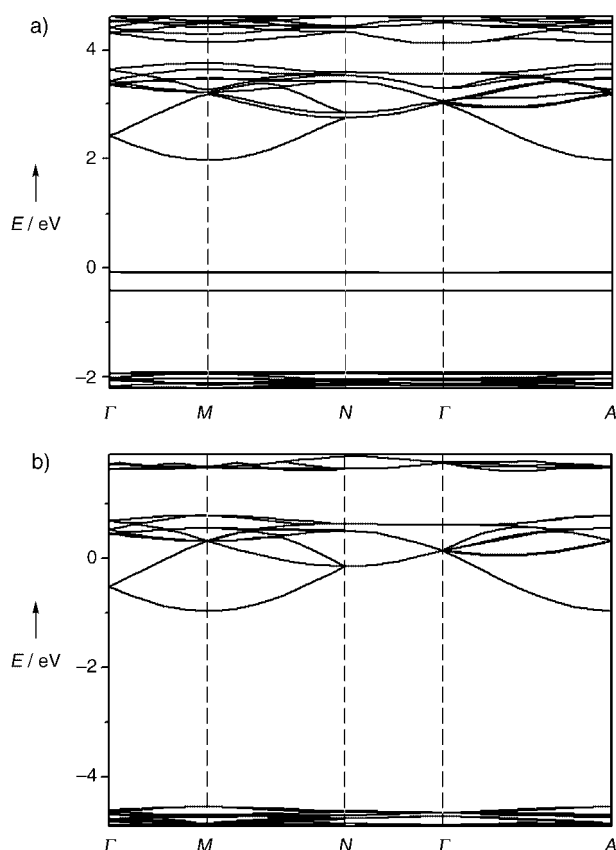


Figure 2. Band structures of a) C12A7 and b) C12A7:2e⁻. The Fermi energy is at 0. $\Gamma = (0,0,0)$, $M = (1/2,0,0)$, $N = (1/2,1/2,0)$, and $A = (0,0,1/2)$.

To address the validity of the electrider model, we calculated the charge density in a 1.5 eV window below E_F which gives the spatial distribution of the extra electrons. We found that the density is equally distributed in the twelve cages and that most of the charge density is inside the cages (Figure 3 a, b). Although it is still not perfectly localized, our charge density is already different from that of Medvedeva and Freeman.^[7] To evaluate the degree of localization quantitatively, we integrated the charge density inside the cage with the ionic radii of Ca, Al, and O set to 0.99, 0.51, and 1.32 Å, respectively. We found that 75 % of the extra electron density is distributed in the twelve cages. Although this value is not very high, it is comparable to those of organic electrideres. For example, in Cs⁺[(15]crown-5)₂e⁻,^[9] a well-studied electrider, we determined the ratio of the in-cavity extra electron as 83 % by performing a similar analysis. Therefore, our pseudopotential plane-wave calculations show that the extra electrons are generally localized in the cages, and thus support an electrider model for C12A7:2e⁻.

Further important theoretical evidence for the electrider model comes from the types of chemical bond between the extra electrons and the positively charged lattice framework. Ionic bonding would support the electrider model, whereas metallic bonding would lead to the opposite conclusion. Following the seminal work of Silvi and Savin,^[10] we used the topological analysis of electron-localization functions

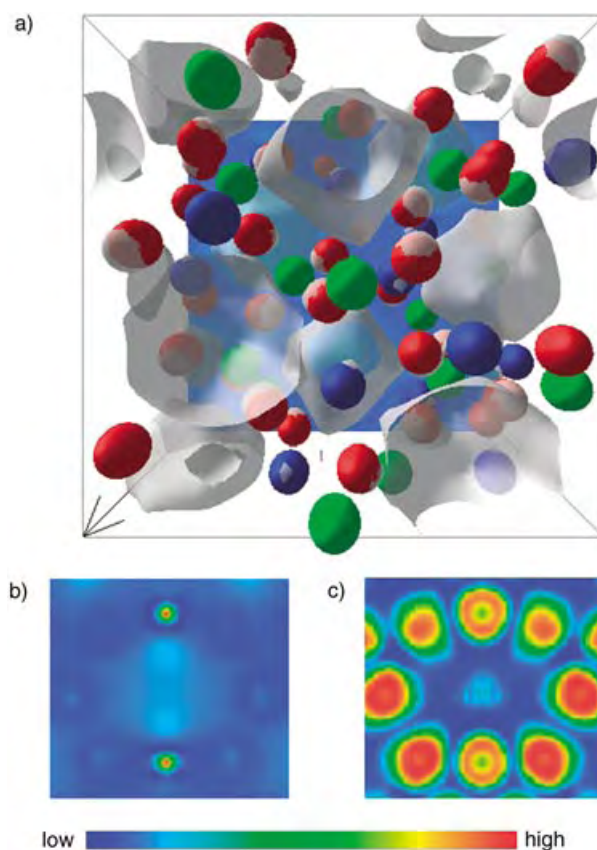


Figure 3. a) Isosurface and b) contour map of the charge density of extra electrons in C12A7:2e⁻, and c) contour map of the C12A7:2e⁻ electron-localization function. The isosurface is plotted within a unit cell, and the contour maps are plotted on a profile crossing one cage. The value of the isosurface is 7.0 electrons per unit cell.

(ELF)^[11] to classify chemical bonds rigorously. The key topological character of ELF is its local maxima, namely the localization attractors. There are three types of attractors: bonding, nonbonding, and core. For systems with shared-electron interactions (covalent, dative, and metallic bonds), there is always a point or ring bonding attractor on the bond path, whereas for the unshared-electron interactions (ionic, hydrogen, electrostatic, and van der Waals bonds) there is nothing between the core attractors. A previous study also showed that ELF topological analysis of metallic bonds is characterized by di- or polysynaptic bonding attractors and a tridimensional network of channels.^[12] For F or F⁺ centers, which are chemically bonded (ionic type) to the host lattice as a quantum-mechanical subsystem, the ELF topology is characterized by a localization attractor at the vacancy site.^[13]

As shown in Figure 3 c, the calculated ELF for C12A7:2e⁻ gives only one localization attractor at the center of the cavity, which is very different from the case of the typical metallic bond,^[12] but similar to the ELF topology for F or F⁺ centers.^[13] Therefore our ELF topological analysis supports the fact that the extra electrons act as coreless anions, and there is ionic bonding between these anionic electrons and the positively charged host lattice. The electrider model of C12A7:2e⁻ is thus also supported by the criterion of the bond type. This new criterion based on powerful ELF topological analysis is much

more conclusive and easy to use than the previous charge-density criterion, which is more frequently used in the literature. In fact, the charge-density criterion may be difficult to apply even for some classical organic electrides that contain delocalized electrons.^[1]

Although C12A7:2e⁻ should be considered as an inorganic electride based on the above discussions, it is very different from the originally suggested electride model.^[5,6] The integrated extra electron density within the cavity only approaches 1/3 instead of one electron, and the ELF value of the corresponding localization attractor is also relatively small (about 0.45). Therefore, C12A7:2e⁻ can be considered as a nonstoichiometric (between extra electrons and cages) electride with only 1/3 of the electron localized in a cage. Accordingly, the chemical formula can be written as [Ca₂₄Al₂₈O₆₄]⁴⁺·(1/3e⁻)₁₂. We point out that before a stoichiometric inorganic electride can be found, it is essential to obtain a stoichiometric ratio between cavities and extra electrons.

In conclusion, by carefully checking the distribution of the extra electron density and the type of bonding between these extra electrons and the host lattice, we obtained a conclusive result on whether mayenite without clathrated oxygen is an electride. This study is useful for pursuing a rigorous definition of electrides in future, and demonstrates that ELF topological analysis may play an important role in this topic. The results presented herein may also shed light on the behavior of a confined electron gas of different topology and suggest new designs for stoichiometric inorganic electrides and related functional materials.

Experimental Section

Computational methodology: Electronic-structure calculations were performed with a pseudopotential plane-wave method within the generalized gradient approximation (GGA) for exchange and correlation. A projector-augmented wave (PAW) pseudopotential^[14] for electron-ion interactions and the Perdew-Wang form^[15] of the GGA functional were used. A plane-wave kinetic-energy cutoff of 500 eV and a 6 × 6 × 6 Monkhorst-Pack *k*-mesh were used to calculate the total energy and charge density. The calculations were performed with the Vienna Ab initio Simulation Package (VASP)^[16] on an HP RX2600 cluster and an HP superdome server of the USTC-HP Laboratory for High-Performance Computing.

Received: May 25, 2004

Revised: September 26, 2004

Keywords: cage compounds · clathrates · computer chemistry · electrides · electronic structure

- [1] a) R. H. Huang, M. K. Faber, K. J. Moeggenborg, D. L. Ward, J. L. Dye, *Nature*, **1988**, 331, 599; b) J. L. Dye, *Nature* **1993**, 365, 10; c) J. L. Dye, *Inorg. Chem.* **1997**, 36, 3816.
- [2] a) J. L. Dye, *Science* **2003**, 301, 607; b) Z. Li, J. Yang, J. G. Hou, Q. Zhu, *Chem. Eur. J.* **2004**, 10, 1592.
- [3] a) P. P. Edwards, P. A. Anderson, J. M. Thomas, *Acc. Chem. Res.* **1996**, 29, 23; b) V. I. Srdanov, G. D. Stucky, E. Lippmaa, G. Engelhardt, *Phys. Rev. Lett.* **1998**, 80, 2449.
- [4] a) A. S. Ichimura, J. L. Dye, M. A. Camblor, L. A. Villaescusa, *J. Am. Chem. Soc.* **2002**, 124, 1170; b) V. Petkov, S. J. L. Billinge, T.

- Vogt, A. S. Ichimura, J. L. Dye, *Phys. Rev. Lett.* **2002**, 89, 75502; c) Z. Li, J. Yang, J. G. Hou, Q. Zhu, *J. Am. Chem. Soc.* **2003**, 125, 6050; d) Z. Li, J. Yang, J. G. Hou, Q. Zhu, *J. Chem. Phys.* **2004**, 120, 9725.
- [5] S. Matsuishi, Y. Toda, M. Miyakawa, K. Hayashi, T. Kamiya, M. Hirano, I. Tanaka, H. Hosono, *Science* **2003**, 301, 626.
- [6] P. V. Sushko, A. L. Shluger, K. Hayashi, M. Hirano, H. Hosono, *Phys. Rev. Lett.* **2003**, 91, 126401.
- [7] J. E. Medvedeva, A. J. Freeman, *Appl. Phys. Lett.* **2004**, 85, 955.
- [8] H. Bartl, T. Scheller, *Neues Jahrb. Mineral. Monatsh.* **1970**, 35, 547.
- [9] a) D. L. Ward, R. H. Huang, M. E. Kuchenmeister, J. L. Dye, *Acta Crystallogr. Sect. C* **1990**, 46, 1831; b) D. J. Singh, H. Krakauer, C. Haas, W. E. Pickett, *Nature* **1993**, 365, 39.
- [10] B. Silvi, A. Savin, *Nature* **1994**, 371, 683.
- [11] A. D. Becke, K. E. Edgecombe, *J. Chem. Phys.* **1990**, 92, 5397.
- [12] B. Silvi, C. Gatti, *J. Phys. Chem. A* **2000**, 104, 947.
- [13] P. Mori-Sanchez, J. M. Recio, B. Silvi, C. Sousa, A. M. Pendas, V. Luana, F. Illas, *Phys. Rev. B* **2002**, 66, 75103.
- [14] G. Kresse, D. Joubert, *Phys. Rev. B* **1996**, 59, 1758.
- [15] J. P. Perdew, J. A. Chevary, S. H. Vosko, K. A. Jackson, M. R. Pederson, D. J. Singh, C. Fiolhais, *Phys. Rev. B* **1992**, 46, 6671.
- [16] G. Kresse, J. Furthmüller, *Comput. Mater. Sci.* **1996**, 6, 15.

Chiral Coordination Polymer

Zn₂[(S)-O₃PCH₂NHC₄H₇CO₂]₂: A Homochiral 3D Zinc Phosphonate with Helical Channels**

Xin Shi, Guangshan Zhu, Shilun Qiu, Kunlin Huang, Jihong Yu, and Ruren Xu*

Chiral metal–organic coordination polymers with open frameworks have attracted much attention because of their potential applications in enantioselective separation and catalysis.^[1–4] Such materials are generally prepared by enantioselective synthesis or spontaneous resolution. Spontaneous resolution on crystallization without any chiral auxiliary will result in a racemic mixture of enantiomeric crystals. Moreover, spontaneous resolution is relatively rare and cannot be predicted because its mechanism is not yet fully under-

[*] Dr. X. Shi, Dr. G. Zhu, Prof. S. Qiu, Dr. K. Huang, Prof. J. Yu, Prof. R. Xu
State Key Laboratory of Inorganic Synthesis & Preparative Chemistry
Department of Chemistry, Jilin University
Changchun 130012 (China)
Fax: (+86) 431-5168589
E-mail: sqiu@mail.jlu.edu.cn

[**] We are grateful for financial support from the State Basic Research Project (G2000077507) and the National Nature Science Foundation of China (Grant no. 29873017, 20101004 and 20371020). We thank Professor Guangdi Yang and Dr. Guanghua Li (Department of Chemistry, Jilin University) for their help in the analysis of the single-crystal structure.



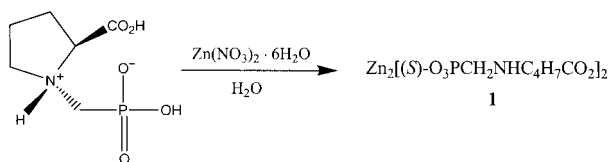
Supporting information for this article is available on the WWW under <http://www.angewandte.org> or from the author.

stood.^[4–6] Enantioselective synthesis, however, is a direct and effective method for the synthesis of enantiopure chiral open frameworks by using enantiopure organic building units as reactant precursors.^[3,7,8] By enantioselective synthesis, many chiral open frameworks with high thermal stability have been obtained in recent years, and they showed encouraging results in enantioselective separation and catalysis.^[9–11]

Some enantiopure organic compounds are good homogeneous catalysts in asymmetric synthesis, for example, (*S*)-proline and its derivatives show highly enantioselective catalysis and afford good yields in many reactions such as α -amination of aldehydes or ketones and aldol, Mannich, and Michael reactions.^[12–14] An intriguing idea is to synthesize a porous material with such enantiopure catalysts as building units. The resulting open-framework material might be used as a heterogeneous asymmetric catalyst.

We chose an enantiomerically pure derivative of (*S*)-proline, namely, 1-phosphonomethylproline, as a chiral building unit and successfully prepared a homochiral 3D zinc phosphonate $\text{Zn}_2[(S)\text{-O}_3\text{PCH}_2\text{NHC}_4\text{H}_7\text{CO}_2]_2$ (**1**) with alternately arranged left- and right-handed helical channels. Of particular interest is that the active sites of 1-phosphonomethylproline for asymmetric catalysis—the amino group and the partially uncoordinated carboxylate group—are retained and directed into the channels, in contrast to a recently reported similar metal phosphonate.^[16c,d] Many open frameworks constructed from enantiopure phosphonic acids have been reported previously,^[11,15,16] but a chiral metal phosphonate containing not only helical channels but also active sites for asymmetric catalysis in achiral channels has not been found so far.

The chiral building unit 1-phosphonomethylproline was prepared by using a modified literature method.^[16c] Enantiopure 1-phosphonomethylproline reacts with $\text{Zn}(\text{NO}_3)_2 \cdot 6\text{H}_2\text{O}$ in the presence of triethylamine as base under hydrothermal conditions to give the homochiral 3D open framework $\text{Zn}_2[(S)\text{-O}_3\text{PCH}_2\text{NHC}_4\text{H}_7\text{CO}_2]_2$ (**1**; Scheme 1). Compound **1**



Scheme 1. Synthesis of **1**.

crystallizes in the orthorhombic space group $P2_12_12$ (No. 18). It consists of 4,8-nets formed by alternately arranged left- and right-handed helices that are connected through 1-phosphonomethylproline ligands to generate a 3D open framework. Each asymmetric unit contains two unique Zn atoms and two unique P atoms. The Zn atoms adopt tetrahedral geometry by coordination of three phosphonate oxygen atoms and one carboxylate oxygen atom of the ligand, while the other carboxylate oxygen atom is uncoordinated. The 3D framework is based on two crystallographically distinct ZnO_4 tetrahedra and two distinct O_3PC tetrahedra. Each Zn atom shares three vertex oxygen atoms with adjacent P atoms (Zn–

O 1.922(4)–1.978(4) Å), and each O_3PC tetrahedron also shares three oxygen atoms with adjacent Zn atoms. The P–O_{bridging} bond lengths are in the range between 1.501(4) and 1.523(4) Å. The Zn- and P-centered tetrahedra alternate to form 4,8-net sheets by sharing oxygen atoms on the *bc* plane, which are linked by the ligands along the *a* axis to generate a 3D open framework.

Figure 1 shows the framework of **1** viewed along the [100] direction. The structure contains four- and eight-membered

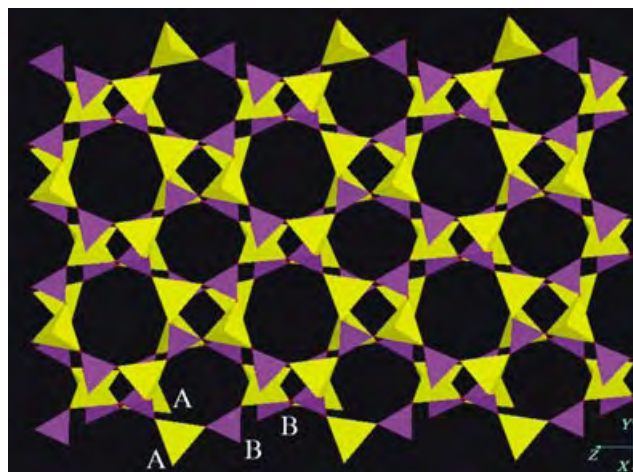


Figure 1. A polyhedral view of the framework along the [100] direction. 4,8-Nets consist of left-handed (A) and right-handed helices (B), which are arranged AA and BB along the *a* axis. 1-phosphonomethylproline ligands are omitted for clarity; Zn yellow, P purple.

rings (7×8 Å, estimated by measuring the distances between the centers of opposite atoms; hereafter, all dimensions are reported in this way), similar to the reported example,^[17] which are made of two different helical chains A and B. These chains run along the *b* axis and are arranged AA and BB along the *a* axis, respectively.

The framework of **1** contains two types of microchannels with dimensions of 4×6 and 5×12 Å, seen in a view along the [001] direction in Figure 2. These channels are made of helical chains of the same handedness (either chain A or chain B) and 1-phosphonomethylproline ligands. These helical chains run along the *b* axis and are arranged ABAB along the *c* axis.

Figure 3a shows a view of the framework of **1** along the [010] direction. Three different four-membered-ring channels (left-handed helical, right-handed helical, and achiral channels) and eight-membered-ring channels (7×7 Å) can be seen. Along the *c* axis, left-handed helical channels, achiral channels, and right-handed helical channels alternate. These chiral channels are enclosed by two types of helical chains, as shown in Figure 3b and c. Interestingly, *L*-handed helices consist of Zn1 and P2 atoms, while *R*-handed helices consist of Zn2 and P1 atoms.

Notably, in the structure of **1**, coordination of the 1-phosphonomethylproline ligand to the zinc atom through the phosphonate group and the monodentate carboxylate group leaves a carboxylate oxygen atom uncoordinated and the amino group free, and the functionality of the material is thus

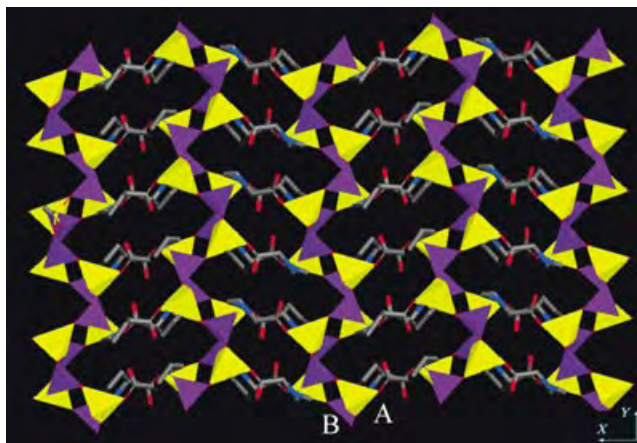


Figure 2. View along the [001] direction. Two types of microchannels with dimensions of 4×6 and 5×12 Å are made of 1-phosphonomethylproline ligands and left-handed helical chains (A) and right-handed helical chains (B). The two kinds of chiral chains are arranged ABAB along the c axis (Zn yellow, P purple, O red, N blue, C gray).

retained. The uncoordinated carboxylate oxygen atoms and the amino groups with N–H bonds, which are the active sites for asymmetric catalysis, are directed into the achiral six- and ten-membered-ring channels along the [001] direction (Figure 2) and eight-membered-ring channels along the [010] direction (Figure 3a).

Thermogravimetric analysis (TGA) was performed to gauge the thermal stability. No weight loss occurred below 400°C , which shows that the open framework is stable below

that temperature. The presence of active sites for asymmetric catalysis in channels along with the high thermal stability of the homochiral zinc phosphonate open framework promises applications in heterogeneous asymmetric catalysis. Research on asymmetric catalysis is currently underway.

Experimental Section

(*S*)- $\text{HO}_3\text{PCH}_2\text{NHC}_4\text{H}_7\text{CO}_2\text{H}$: HCHO (40 mmol, 36% in water) was added dropwise to a mixture of (*S*)-proline (10 mmol), H_3PO_3 (11 mmol), and HCl (30 mL of a 6.0 M aqueous solution) under reflux. The resultant solution was then heated at reflux for a further 12 h. A white solid was recovered in a yield of 90% after removal of water, and recrystallized from EtOH/propylene oxide. M.p. $257\text{--}259^\circ\text{C}$. $[\alpha]_{\text{D}}^{25} = -63^\circ$ ($c = 1.6$ in water). Elemental analysis (%): calcd for $\text{C}_6\text{H}_{12}\text{NO}_3\text{P}$ (209.14): C 34.44, N 6.69, H 5.74; found: C 34.25, N 6.80, H 5.67. ^{31}P MAS NMR (161.9 MHz, 298 K): $\delta = 8.7$ ppm.

$\text{Zn}_2[(\text{S})\text{-O}_3\text{PCH}_2\text{NHC}_4\text{H}_7\text{CO}_2]_2 \cdot \text{Zn}(\text{NO}_3)_2 \cdot 6\text{H}_2\text{O}$ (0.074 g) and (*S*)- $\text{HO}_3\text{PCH}_2\text{NHC}_4\text{H}_7\text{CO}_2\text{H}$ (0.053 g) were dissolved in H_2O (10 mL), and then triethylamine (0.5 mL) was added while stirring to adjust the pH of the mixture. The mixture ($\text{pH} \approx 6$) was sealed in a Teflon-lined stainless steel autoclave after stirring for 10 min and heated at 160°C for 2 d. Colorless block single crystals were filtered off, washed with distilled water, and dried at room temperature to yield **1** (0.079 g, 58%). ^{31}P MAS NMR (161.9 MHz, 298 K): $\delta = -24.5$ ppm. The CD spectrum (Figure 3 of Supporting Information) clearly shows a positive Cotton effect, in agreement with that of the original chiral ligand, which indicates that the chiral ligand retained its original chirality even after the hydrothermal reaction.

Inductively coupled plasma (ICP) analysis (Perkin-Elmer Optima 3300 DV ICP instrument): Zn 24.08, P 11.45% (calcd: Zn 23.96, P 11.37%). Elemental analysis (Perkin-Elmer 2400 elemental analyzer): C 26.51, H 3.54, N 5.22% (calcd: C 26.45, H 3.70, N 5.14%).

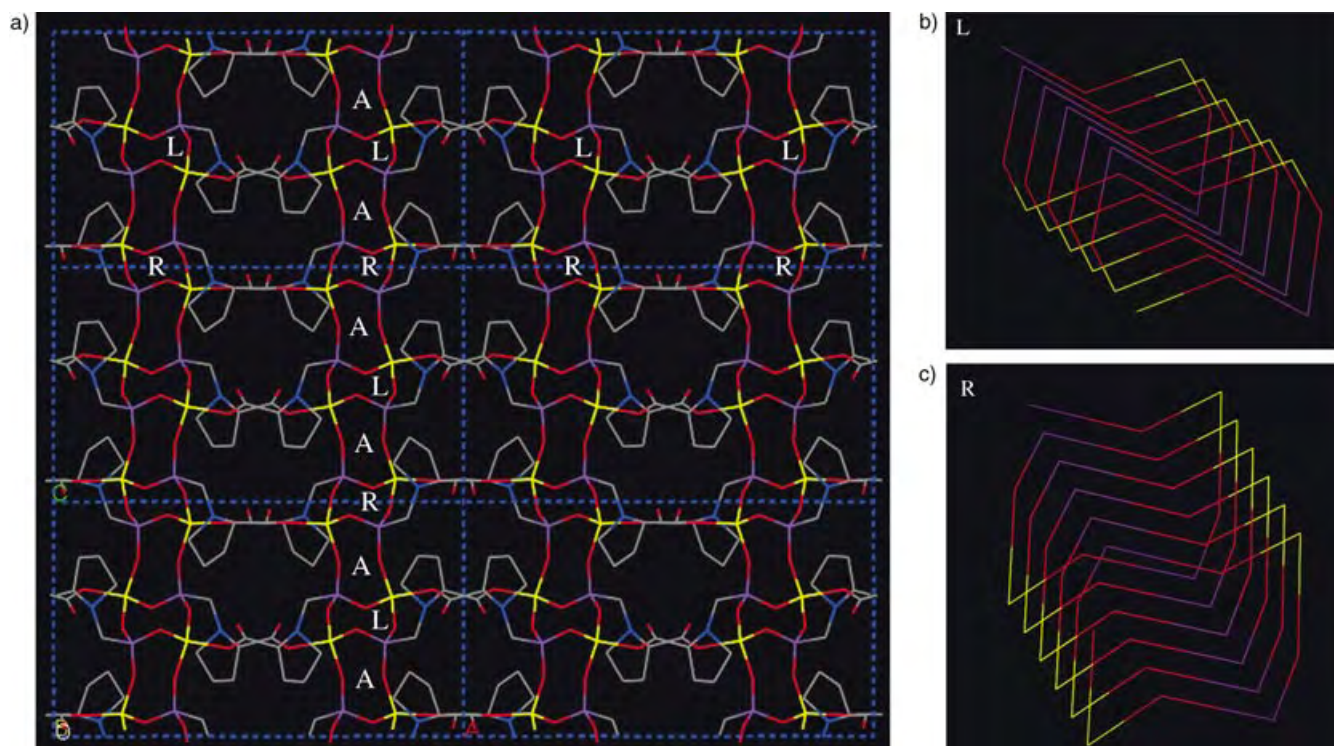


Figure 3. a) The framework viewed along the [010] direction, showing two types of helical channels and achiral channels which are alternately arranged along the c axis (A: achiral channel, L: left-handed helical channel, R: right-handed helical channel). b, c) The left-handed (L) and right-handed (R) helical channels (Zn yellow, P purple, O red, N blue, C gray).

Thermogravimetric analysis was performed on a Perkin-Elmer TGA7 unit in air. A weight loss was observed in the 400–450 °C temperature range, which indicated decomposition of the metal phosphonate.

Structure determination: A suitable single crystal with dimensions of 0.58 × 0.47 × 0.14 mm was selected for single-crystal X-ray diffraction analysis. Crystallographic data were collected at 293(2) K on a Bruker-AXS Smart CCD diffractometer using Mo_Kα radiation (λ = 0.71073 Å). The structure was solved by direct methods^[18] and refined by the full-matrix least-squares method against *F*² (SHELXL-97).^[19] All non-hydrogen atoms were refined anisotropically. Hydrogen atoms of organic ligands (except H1 and H2) were located geometrically.

Crystal data: Zn₂[(S)-O₃PCH₂NHC₄H₇CO₂]₂ (**1**), *M*_r = 544.98, orthorhombic, space group *P*₂₁₂₁₂ (No. 18), *a* = 18.425(8), *b* = 9.168(2), *c* = 10.554(3) Å, *V* = 1782.7(9) Å³, *Z* = 4, *μ* = 2.929 mm⁻¹, *ρ*_{calc} = 2.031 g cm⁻³, 2781 reflections measured, of which 2207 were unique (*R*_{int} = 0.0424). The final *wR*(*F*²) was 0.0788 (all data), and *R*(*F*) was 0.0523 (all data). CCDC-239389 contains the supplementary crystallographic data for this paper. These data can be obtained free of charge via www.ccdc.cam.ac.uk/conts/retrieving.html (or from the Cambridge Crystallographic Data Centre, 12, Union Road, Cambridge CB2 1EZ, UK; fax: (+44) 1223-336-033; or deposit@ccdc.cam.ac.uk).

Received: May 20, 2004

Keywords: amino acids · helical structures · hydrothermal synthesis · zinc

- [1] a) C. J. Kepert, T. J. Prior, M. J. Rosseinsky, *J. Am. Chem. Soc.* **2000**, *122*, 5158–5168; b) H. Kumagai, K. Inoue, *Angew. Chem.* **1999**, *111*, 1694–1696; *Angew. Chem. Int. Ed.* **1999**, *38*, 1601–1603; c) R. Andrés, M. Brissard, M. Gruselle, C. Train, J. Vaissermann, B. Malézieux, J.-P. Jamet, M. Verdager, *Inorg. Chem.* **2001**, *40*, 4633–4640; d) T. J. Prior, M. J. Rosseinsky, *Inorg. Chem.* **2003**, *42*, 1564–1575; e) G. Seeber, A. L. Pickering, D.-L. Long, L. Cronin, *Chem. Commun.* **2003**, 2002–2003; f) K. Inoue, H. Imai, P. S. Ghalsasi, K. Kikuchi, M. Ohba, H. Ōkawa, J. V. Yakhmi, *Angew. Chem.* **2001**, *113*, 4372–4375; *Angew. Chem. Int. Ed.* **2001**, *40*, 4242–4245.
- [2] a) M. Minguet, D. Luneau, E. Lhotel, V. Villar, C. Paulsen, D. B. Amabilino, J. Veciana, *Angew. Chem.* **2002**, *114*, 606–609; *Angew. Chem. Int. Ed.* **2002**, *41*, 586–589; b) C. Qin, L. Xu, Y. Wei, X. Wang, F. Li, *Inorg. Chem.* **2003**, *42*, 3107–3110; c) U. Siemeling, I. Schepplmann, B. Neumann, A. Stammer, H.-G. Stammer, J. Frelek, *Chem. Commun.* **2003**, 2236–2237; d) M. Vázquez, A. Taglietti, D. Gatteschi, L. Sorace, C. Sangregorio, A. M. González, M. Maneiro, R. M. Pedrido, M. R. Bermejo, *Chem. Commun.* **2003**, 1840–1841; e) A. Jouaiti, M. W. Hosseini, N. Kyritsakas, *Chem. Commun.* **2003**, 472–473; f) E. Coronado, C. J. Gómez-García, A. Nuez, F. M. Romero, E. Rusanov, H. Stoeckli-Evans, *Inorg. Chem.* **2002**, *41*, 4615–4617.
- [3] U. Knof, A. von Zelewsky, *Angew. Chem.* **1999**, *111*, 312–333; *Angew. Chem. Int. Ed.* **1999**, *38*, 302–322.
- [4] L. Pérez-García, D. B. Amabilino, *Chem. Soc. Rev.* **2002**, *31*, 342–356.
- [5] a) E. Coronado, J. R. Galán-Mascarós, C. J. Gómez-García, J. M. Martínez-Agudo, *Inorg. Chem.* **2001**, *40*, 113–120; b) E. Gao, S. Bai, Z. Wang, C. Yan, *J. Am. Chem. Soc.* **2003**, *125*, 4984–4985; c) J. Sun, L. Weng, Y. Zhou, J. Chen, Z. Chen, Z. Liu, D. Zhao, *Angew. Chem.* **2002**, *114*, 4651–4653; *Angew. Chem. Int. Ed.* **2002**, *41*, 4471–4473.
- [6] a) M. Hernández-Molina, F. Lloret, C. Ruiz-Pérez, M. Julve, *Inorg. Chem.* **1998**, *37*, 4131–4135; b) S. Han, J. L. Manson, J. Kim, J. S. Miller, *Inorg. Chem.* **2000**, *39*, 4182–4185; c) E. Gao, Y. Yue, S. Bai, Z. He, C. Yan, *J. Am. Chem. Soc.* **2004**, *126*, 1419–1429.
- [7] a) K. Inoue, K. Kikuchi, M. Ohba, H. Ōkawa, *Angew. Chem.* **2003**, *115*, 4958–4961; *Angew. Chem. Int. Ed.* **2003**, *42*, 4810–4813; b) P. Grosshans, A. Jouaiti, V. Bulach, J.-M. Planeix, M. W. Hosseini, J.-F. Nicoud, *Chem. Commun.* **2003**, 1336–1337; c) Y. Cui, S. J. Lee, W. Lin, *J. Am. Chem. Soc.* **2003**, *125*, 6014–6015.
- [8] a) J. D. Ranford, J. J. Vittal, D. Wu, *Angew. Chem.* **1998**, *110*, 1159–1162; *Angew. Chem. Int. Ed.* **1998**, *35*, 1114–1116; b) C. Wu, C. Lu, S. Lu, H. Zhuang, J. Huang, *J. Chem. Soc. Dalton Trans.* **2003**, 3192–3198; c) Y. Cui, O. R. Evans, H. L. Ngo, P. S. White, W. Lin, *Angew. Chem.* **2002**, *114*, 1207–1210; *Angew. Chem. Int. Ed.* **2002**, *41*, 1159–1160.
- [9] J. S. Seo, D. Whang, H. Lee, S. I. Jun, J. Oh, Y. J. Jeon, K. Kim, *Nature* **2000**, *404*, 982–986.
- [10] R. Xiong, X. You, B. F. Abrahams, Z. Xue, C. Che, *Angew. Chem.* **2001**, *113*, 4554–4557; *Angew. Chem. Int. Ed.* **2001**, *40*, 4422–4425.
- [11] O. R. Evans, H. L. Ngo, W. Lin, *J. Am. Chem. Soc.* **2001**, *123*, 10395–10396.
- [12] A. Bøgevig, K. Juhl, N. Kumaragurubaran, W. Zhuang, K. A. Jørgensen, *Angew. Chem.* **2002**, *114*, 1868–1871; *Angew. Chem. Int. Ed.* **2002**, *41*, 1790–1793.
- [13] A. G. M. Barrett, A. S. Cook, A. Kamimura, *Chem. Commun.* **1998**, 2533–2534.
- [14] Reviews: R. O. Duthaler, *Angew. Chem.* **2003**, *115*, 1005–1008; *Angew. Chem. Int. Ed.* **2003**, *42*, 975–978; P. Dalko, L. Moisan, *Angew. Chem.* **2004**, *116*, 5248–5286; *Angew. Chem. Int. Ed.* **2004**, *43*, 5138–5175.
- [15] a) O. R. Evans, D. R. Manke, W. Lin, *Chem. Mater.* **2002**, *14*, 3866–3874; b) H. L. Ngo, W. Lin, *J. Am. Chem. Soc.* **2002**, *124*, 14298–14299.
- [16] a) F. Fredoueil, M. Evain, M. Bujoli-Doeuff, B. Bujoli, *Eur. J. Inorg. Chem.* **1999**, 1077–1079; b) F. Fredoueil, M. Evain, D. Massiot, M. Bujoli-Doeuff, B. Bujoli, *J. Mater. Chem.* **2001**, *11*, 1106–1110; c) A. Turner, P.-A. Jaffrès, E. J. MacLean, D. Villemin, V. McKee, G. B. Hix, *J. Chem. Soc. Dalton Trans.* **2003**, 1314–1319; d) B. Yang, J. Mao, Y. Sun, H. Zhao, A. Clearfield, *Eur. J. Inorg. Chem.* **2003**, 4211–4217.
- [17] J. Liang, Y. Wang, J. Yu, Y. Li, R. Xu, *Chem. Commun.* **2003**, 882–883.
- [18] G. M. Sheldrick, SHELXS-97, Program for Crystal Structure Solution, Göttingen University, Germany, **1997**.
- [19] G. M. Sheldrick, SHELXL-97, Program for Crystal Structure Refinement, Göttingen University, Germany, **1997**.

Molecular Switches

Molecular-Mechanical Switch-Based Solid-State Electrochromic Devices**

David W. Steuerman, Hsian-Rong Tseng, Andrea J. Peters, Amar H. Flood, Jan O. Jeppesen, Kent A. Nielsen, J. Fraser Stoddart,* and James R. Heath*

The dynamics of electrochemically driven, bistable molecular mechanical switches—such as certain nondegenerate, two-station, donor–acceptor [2]catenanes and [2]rotaxanes—have been the subject of numerous experimental investigations^[1–3] in the solution phase, in which the general mechanistic details of the redox-activated switching processes are becoming increasingly well understood.^[4] These molecular machines may have many technological applications,^[5] although few are likely to be liquid-solution-phase based.^[6–9] Thus, significant effort has been directed towards understanding and exploiting the bistability of [2]catenanes and [2]rotaxanes in other environments, including both Langmuir–Blodgett (LB)^[10,11] and self-assembled monolayers (SAMs),^[12] and in solid-state molecular-switch tunnel junctions (MSTJs).^[13–16]

Herein we explore, at a fundamental level, the solid-state application of electrochromic devices by taking advantage of the colorimetric changes that accompany the electrochemically driven switching of certain bistable [2]catenanes and [2]rotaxanes. The molecular switches were immobilized within a solid-state polymer electrolyte, and a microfabricated, planar, three-terminal equivalent of a standard electrochemical cell was used for electrical addressing. The polymer environment significantly slows down certain steps within the molecular-mechanical switching cycle, but the overall mechanism remains unchanged from that observed in other environments. We also find that by varying the molecular structure of the switch, the colorimetric retentions times of

these devices could be controlled over a dynamic range of 10^3 to 10^4 s. The fundamental properties of these devices were quantified through time- and temperature-dependent cyclic voltammetry (CV) measurements. In this way, the kinetic parameters (ΔG^\ddagger , ΔH^\ddagger , ΔS^\ddagger , and E_a) of the rate-limiting step in the switching cycle of the device could be evaluated for several different molecular switches.

Four bistable molecular-mechanical systems^[2,3a,17,18]—two [2]catenanes **C1**⁴⁺ and **C2**⁴⁺ and two [2]rotaxanes **R1**⁴⁺ and **R2**⁴⁺—along with appropriate control compounds, were investigated (Figure 1) for electrochromic device applica-

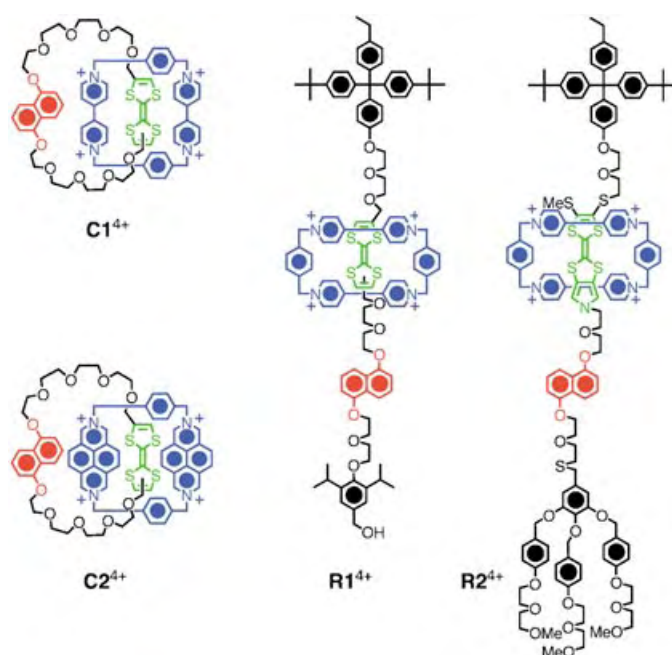


Figure 1. The structural formulas of the two bistable [2]catenanes **C1**⁴⁺ and **C2**⁴⁺ and the two bistable [2]rotaxanes **R1**⁴⁺ and **R2**⁴⁺ investigated within solid-state polymer electrolyte environments. The use of color—namely, red, blue, and green—for certain units and components relates to the graphical representations shown in Figure 2.

[*] Dr. D. W. Steuerman, Dr. H.-R. Tseng, Dr. A. J. Peters, Dr. A. H. Flood, Dr. J. O. Jeppesen, K. A. Nielsen, Prof. J. F. Stoddart
The California NanoSystems Institute, and
Department of Chemistry and Biochemistry
University of California, Los Angeles
405 Hilgard Avenue, Los Angeles, CA 90095-1569 (USA)
Fax: (+1) 310-206-1843
E-mail: stoddart@chem.ucla.edu

Prof. J. R. Heath
Division of Chemistry and Chemical Engineering, MC 127-72
California Institute of Technology
1200 East California Boulevard, Pasadena, CA 91125 (USA)
Fax: (+1) 626-395-2355
E-mail: heath@caltech.edu

[**] This research was funded by the Office of Naval Research, the National Science Foundation, and the Moletronics Program of the Defense Advanced Research Projects Agency, the Microelectronics Advanced Research Corporation, its Focus Centers on Functional Engineered NanoArchitectonics and Advanced Materials and Devices, and the Center for Nanoscale Innovation for Defense.

Supporting information for this article is available on the WWW under <http://www.angewandte.org> or from the author.

tions. Most of these compounds have been studied^[2,3,19] in the liquid-solution phase by using ¹H NMR spectroscopy and temperature-dependent electrochemistry. In addition, the switching cycle of a SAM^[12] formed from a [2]rotaxane that is closely related to **R1**⁴⁺ was previously reported. Herein, we present a description of the general switching cycle mechanism that is applicable to all four molecules, followed by a brief description of how certain details of this cycle vary between the four molecules.

The switching cycle mechanism for the bistable [2]catenanes and [2]rotaxanes is illustrated in Figure 2. There is always an equilibrium ($K_{(D,T)^+}$) established between the cyclobis(paraquat-*p*-phenylene) (CBPQT⁴⁺) ring encircling the tetrathiafulvalene (TTF) site (labeled as the ground-state co-conformer or GSCC) and the dioxynaphthalene (DNP) site (labeled as the metastable-state co-conformer or MSCC).^[20] These labels reflect the fact that the equilibrium is most commonly shifted toward the CBPQT⁴⁺ ring encircling the TTF site. The first oxidation state of the GSCC

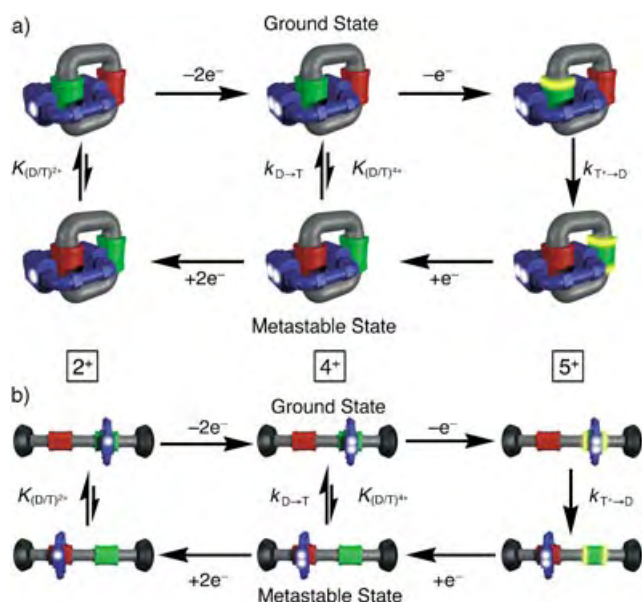


Figure 2. The analogous switching cycles for a) the bistable catenanes and b) the bistable rotaxanes, starting from the centrally located ground-state co-conformers. The green and red sites on the ring and dumbbell components refer to the TTF- and DNP-recognition units, respectively. When the TTF unit is oxidized, it is drawn as a highlighted green unit carrying yellow ends. The CBPQT⁴⁺ ring is modeled as the blue ring encircling the green site with positive charges indicated as white spots. The metastable co-conformers are isomeric (and isoelectronic) with the appropriate ground-state co-conformers.

corresponds to removal of an electron from the TTF site, and is accompanied by a rapidly driven shuttling (Coulombic repulsion) of the CBPQT⁴⁺ ring to the DNP site with a rate described by the constant, $k_{T^+ \rightarrow D}$. Upon reduction of the TTF site back to its charge-neutral state, the MSCC is formed. The MSCC and GSCC are readily distinguished from each other by using CV because the oxidation potential of the (bare) TTF unit on the MSCC is approximately 200 mV less^[12] positive than that for the GSCC (vs. a Pt reference electrode)—a result that is valid for both the bistable [2]catenanes and the bistable [2]rotaxanes. The return of the MSCC to the GSCC, which is really a recovery of the equilibrium distribution described by $K_{(D/T)^{4+}}$, is thermally activated. This recovery is typically too fast to observe at room temperature in the solution phase.

CV measurements on the bistable [2]rotaxane SAMs^[12] revealed that the rate of recovery of the equilibrium distribution was strongly dependent^[21] on the physical environment—the rate was much slower for the SAM environment than for the solution phase. For the SAM, it was also demonstrated that the GSCC/MSCC equilibrium distribution may be recovered at least 1000 times faster through the pathway that accesses the two-electron reduction of the CBPQT⁴⁺ ring to its bis-radical cation, CBPQT^{2,2+} (Figure 2).^[12] This pathway is precisely that proposed originally as the mechanism for “opening” a MSTJ device.^[13]

The solid-state polymer environment, which can be considered as a highly viscous solvent, should also affect the rate of recovery of the equilibrium distribution from the

MSCC to the GSCC. There is a long history, dating back to the early work of Kramers,^[22] of investigations into molecular-mechanical processes within high-viscosity solvents,^[23,24] although those studies have typically focused on low-amplitude molecular motions with energy barriers of only a few kcal mol⁻¹. Based on the assumption that the large-amplitude, high-energy-barrier motions in our systems follow similar trends, the expectation is that the rate constant for the recovery of the equilibrium distribution will scale as $k = \eta^{-\gamma}$ (η is the solvent viscosity and γ has a value between 0.5 and 0.75).^[25]

The molecular switches investigated herein exhibit significant differences from one another that should be reflected in the switching characteristics of the electrochromic devices. **R1**⁴⁺ and **R2**⁴⁺ are characterized^[3] by very different equilibrium dynamics in solution. **R1**⁴⁺ contains a simple TTF unit, and the room-temperature affinity of the CBPQT⁴⁺ ring for this TTF unit over the DNP ring system is 10:1. **R2**⁴⁺ does not have a simple TTF unit and the CBPQT⁴⁺ ring has an equal probability for being located on the “quasi-TTF” or the DNP at 298 K, although this equilibrium is temperature-dependent. As chemical constitution impacts the dynamic equilibrium between translational isomers^[26] in solution for **R1**⁴⁺ and **R2**⁴⁺, we expect a similar situation to pertain within the solid-state polymer environment.

C1⁴⁺ and **C2**⁴⁺, on the other hand, are characterized^[2,16] by similar equilibrium dynamics. For both structures, the ground-state equilibrium strongly favors the CBPQT⁴⁺ ring encircling the TTF unit. However, the molecular-mechanical motion in **C2**⁴⁺, with its two bulky diazapyrenium units, is significantly more sterically hindered than that in **C1**⁴⁺, and this constitutional feature is expected, in any environment, to slow the recovery of **C2**⁴⁺ from the MSCC to the GSCC substantially relative to that of **C1**⁴⁺.

Figure 3 shows two successive CVs collected from a solid-state polymer device containing **R1**⁴⁺ as well as measurements

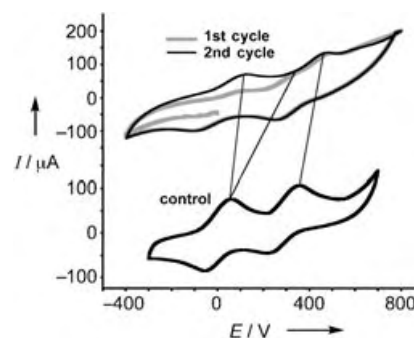


Figure 3. The first and second CVs (298 K, scan rate = 150 mV s⁻¹) of the **R1**⁴⁺-containing solid-state polymer electrolyte device. The initial scan (gray trace) reveals a weak feature at 115 mV and two oxidation peaks (partially resolved) at 315 and 465 mV. For the second scan (black trace) virtually all the signal corresponding to the feature at 315 mV has shifted to 115 mV. The features at 115 and 315 mV were assigned as the first oxidation state of the metastable and ground-state co-conformers, respectively. A control device that contains only the dumbbell component of **R1**⁴⁺ reveals two well-separated oxidation peaks at 55 and 355 mV that do not change between the first and second scans.

from a control device containing the dumbbell component of **R1**⁴⁺. This bistable [2]rotaxane exhibits an equilibrium GSCC/MSCC population of about 10:1 under ambient conditions, similar to that observed in solution at 298 K. The first CV trace reflects this distribution—three oxidation features are recorded at 115, 315, and 465 mV. The relatively weak feature at 115 mV corresponds to the TTF→TTF^{•+} oxidation of the low-abundance MSCC. The feature at 315 mV arises from the TTF→TTF^{•+} oxidation of the GSCC, and the feature at 465 mV is the second oxidation (TTF^{•+}→TTF²⁺) of **R1**⁴⁺. This second oxidation step is independent of the co-conformer as the CBPQT⁴⁺ ring encircles the DNP site once the TTF site is singly oxidized. For the second scan, nearly all the integrated current under the 315 mV feature has moved to 115 mV. This assignment is consistent with the control device measurements, which reveal two well-separated oxidation peaks at 55 and 355 mV.

The hysteretic response in the successive CV curves of **R1**⁴⁺ reflects the slow recovery of the ground-state equilibrium distribution (described by $K_{(D/T)^{++}}$), and is similar to that observed for the bistable [2]rotaxane SAMs.^[12] By varying the time between the first and second CV scans as well as the temperature of the experiment, the various kinetic parameters for relaxation from the MSCC to the GSCC were determined. Figure 4a shows a scan-rate series of (second) CVs. Figure 4b displays a graph of the scan-rate series condensed into a single plot that exhibits an exponential decay. In this case, we have taken into account the rates based on the integrated current of the MSCC oxidation peak at 115 mV relative to the total current of the first-oxidation peaks of the MSCC and GSCC. For all data sets, at least one point was taken at scan rates that were much slower than the measured relaxation times—the $\Delta t = 100$ s in Figure 4b, for example—and that point was fixed in the exponential decay fit. Figure 4c is an Eyring plot of several such series, each collected at a different temperature. From this plot, we can extract the various kinetic parameters that describe the recovery of the ground-state equilibrium distribution. Those parameters, along with the analogous measurements for **C1**⁴⁺, **C2**⁴⁺, and **R2**⁴⁺, are summarized in Table 1. The data for **C2**⁴⁺ were only collected under ambient conditions, and so only τ_{298} and ΔG_{298}^\ddagger are reported.

The polymer utilized in this case has a viscosity approximately 10⁴ times greater than that of MeCN, which is the commonly used solvent in the investigation of the electrochemical properties of these molecules in solution. Thus, the implication is that the relaxation rates in solution should be between 10² and 10³ times faster than those observed. Thus, under cryogenic conditions, it should be possible to observe the MSCC→GSCC relaxation in the liquid-solution phase, and we have now confirmed that this prediction does, indeed, hold true.^[19]

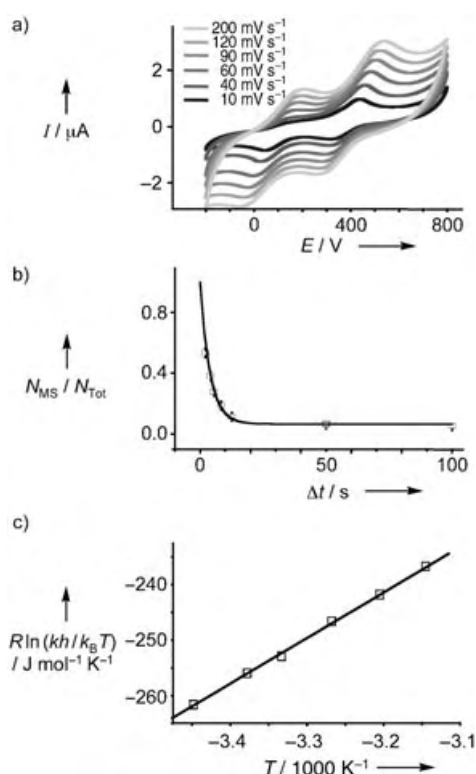


Figure 4. Experimental data utilized to extract the kinetic parameters of the metastable→ground-state relaxation process of **R1**⁴⁺ within the solid-state polymer electrolyte environment. a) Representative (second scan) CVs recorded at 296 K at various scan rates. b) The population ratios of the metastable state and the relaxation times fitted to a first-order decay model. c) The temperature dependence of the relaxation kinetics expressed as an Eyring plot.

Table 1: The 1/e decay times (τ_{298}) and free energies of activation (ΔG_{298}^\ddagger) obtained by using cyclic voltammetry together with the thermodynamic data, obtained after an analysis of variable-temperature cyclic voltammetry studies using the Eyring (ΔH^\ddagger , ΔS^\ddagger) and the Arrhenius (E_a) relationships for a series of bistable rotaxanes and catenanes in solution and in a solid-state polymer electrolyte.^[a]

Compound	τ_{298} [s]	k_{298} [s ⁻¹]	ΔG_{298}^\ddagger [kcal mol ⁻¹]	ΔH^\ddagger [kcal mol ⁻¹]	ΔS^\ddagger [cal mol ⁻¹ K ⁻¹]	E_a^\ddagger [kcal mol ⁻¹]
[2] R1 ⁴⁺ [b]	3.50(±0.02)	0.286(±0.002)	18.1(±0.2)	19.5(±0.2)	4.7(±1.4)	19.6(±0.2)
[2] R2 ⁴⁺	≤1	≥1	15.8(±0.4)	9.1(±0.4)	-22(±3)	9.7(±0.5)
[2] C1 ⁴⁺	0.6	1.7	17.0(±0.4)	14.8(±0.4)	-7.5(±2.5)	15.4(±0.4)
[2] C2 ⁴⁺	800	0.00125	21.0	—	—	—

[a] Solid-state polymer data obtained from samples mixed within a polymer matrix (MeCN/PPMA/PC/LiClO₄ (w/w/w) = 70:7:20:3) at a Pt electrode over a range of temperatures **R1**⁴⁺ (290–320 K). [b] Self-assembled monolayers of the analogue to **R1**⁴⁺, bearing a disulfide tether, was characterized by variable-temperature CV to obtain thermodynamic data: $k_{293} = 0.39$ s⁻¹, $\Delta G_{298}^\ddagger = 18.0$ kcal mol⁻¹, $\Delta H^\ddagger = 17.6 \pm 3.0$ kcal mol⁻¹, $\Delta S^\ddagger = -1.4 \pm 10$ cal mol⁻¹ K⁻¹, $E_a = 17.7 \pm 2.8$ kcal mol⁻¹.

The viscosity of the polymer matrix changes by approximately a factor of two over the temperature range of these investigations (280–320 K). This trend can certainly impact the measured thermodynamic parameters—most notably ΔS^\ddagger . However, τ_{298} , k_{298} , ΔG_{298}^\ddagger and E_a are less sensitive and so it is in the case of these parameters that we have the most confidence. In reference to these values, we find that the MSCC→GSCC relaxation rates, within the polymer environment, are under significant chemical control. In fact, they

varied by more than 1000 times in moving from $R2^{4+}$ to $C2^{4+}$. This result directly translates into chemical control over colorimetric retention times in these electrochromic devices. In Figure 5, we present a demonstration of such a device

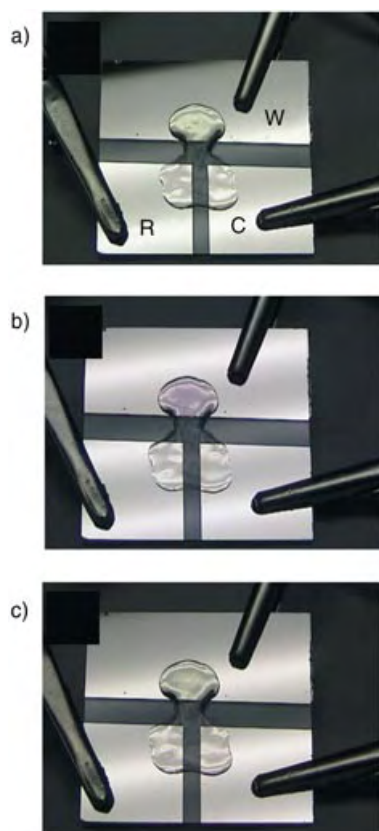


Figure 5. The electrochromic response of the solid-state polymer devices. The working (W), counter (C), and reference (R) electrodes are indicated. a) The device with the working electrode grounded. The green color correlates with the color of the ground-state co-conformer of $R1^{4+}$, with the CBPQT $^{4+}$ ring encircling the TTF site. b) After a +1 V oxidizing potential has been applied to the working electrode, the color change to red/purple correlates with the translational isomerization having occurred to the metastable state. c) Several seconds after the working electrode has been returned to 0 bias and $R1^{4+}$ has relaxed back to the ground-state co-conformer.

containing $R1^{4+}$ that was cycled from the green to the red state, and then back to the green state again. This electrochromic device^[27] contained substantially higher concentrations of $R1^{4+}$ than did other devices discussed herein, but was, in all other ways, identical to them.

In summary, we find that a single mechanistic picture can be applied to describe the electrochemically driven switching cycle of bistable [2]catenanes and [2]rotaxanes in solid-state polymer electrolytes. This mechanistic picture is qualitatively identical to that initially proposed to describe the behavior of a MSTJ device,^[13] and is also analogous to that observed for the switching cycle of a [2]rotaxane SAM.^[12] We find that the MSCC→GSCC relaxation rate is strongly dependent upon both physical environment and molecular structure. In particular, by varying the molecular structure we could vary

this relaxation rate by more than 1000 times. This variation has interesting implications for controlling the colorimetric retention times (and hence power efficiencies) in solid-state electrochromic devices,^[27] and we have demonstrated such a device. Finally, these results suggest that electrochemical measurements^[19] on these same molecules in cryogenic solutions should go far toward quantifying how the kinetic parameters that describe the switching cycle are impacted by the physical environment of the molecular switches.

Experimental Section

A three-terminal, microfabricated device, operated as a function of voltage scan rate and temperature, was employed to interrogate the kinetics of electrochemically-induced molecular mechanical switching within a solid-state polymer. The polymer electrolyte matrix was a standard solid-state electrolyte prepared from a solution in MeCN that contained polymethylmethacrylate (PMMA, $M_w = 300\,000$), propylene carbonate, (PC)—as a plasticizer—and $LiClO_4$ (MeCN/PMMA/PC/ $LiClO_4$ (w/w/w/w) = 70:7:20:3). These materials were handled only in flame-dried glassware under an inert atmosphere of Ar. The $LiClO_4$ was purified by fusion under vacuum. The MeCN was dried either by passage through steel columns containing activated alumina under Ar using a solvent purification system (Anhydrous Engineering) or by distillation over CaH_2 . Finally, the MeCN was deoxygenated prior to use through three freeze/pump/thaw cycles.

The solid-state electrolyte devices were fabricated with traditional CV experiments in mind. A planar three-electrode—working, counter, reference—configuration was implemented, and each electrode consisted of 10 nm of Ti covered with 50 nm of Pt. The electrodes were patterned by using standard lithographic and metal evaporation procedures onto a glass substrate. The fabricated substrates were placed in a glove box under a N_2 environment. The electrochemically active species were then combined with the electrolyte and drop cast onto the three electrodes. These devices were allowed to stand for 20 min to facilitate drying, and then were pumped for a further 20 min to a final pressure of 100 mTorr. The working devices were firm to the touch, with a consistency similar to that of a stiff rubber band. The viscosity of similarly prepared polymer electrolytes has been reported,^[28] and, at 298 K, it is more than 10^4 times larger than that for the solvent MeCN.

CV measurements were performed in a sealed container on an EG&G VersaStat II Potentiostat with the aid of three electrical feedthroughs and a thermocouple fed back to a hot-plate for thermal control. The key experimental variables were scan rate and temperature and—for a given device—these parameters were varied randomly to avoid the influence of systematic errors.

Received: August 19, 2004

Keywords: catenanes · electrochromic devices · metastable compounds · polymers · rotaxanes

- [1] R. A. Bissell, E. Córdova, A. E. Kaifer, J. F. Stoddart, *Nature* **1994**, 369, 133–137.
- [2] a) M. Asakawa, P. R. Ashton, V. Balzani, A. Credi, C. Hamers, G. Matternsteig, M. Montalti, A. N. Shipway, N. Spencer, J. F. Stoddart, M. S. Tolley, M. Venturi, A. J. P. White, D. J. Williams, *Angew. Chem.* **1998**, 110, 357–361; *Angew. Chem. Int. Ed.* **1998**, 37, 333–337; b) V. Balzani, A. Credi, G. Matternsteig, O. A. Matthews, F. M. Raymo, J. F. Stoddart, M. Venturi, A. J. P. White, D. J. Williams, *J. Org. Chem.* **2000**, 65, 1924–1936.
- [3] a) J. O. Jeppesen, K. A. Nielsen, J. Perkins, S. A. Vignon, A. Di Fabio, R. Ballardini, M. T. Gandolfi, M. Venturi, V. Balzani, J.

- Becher, J. F. Stoddart, *Chem. Eur. J.* **2003**, *9*, 2982–3007; b) T. Yamamoto, H.-R. Tseng, J. F. Stoddart, V. Balzani, A. Credi, F. Marchioni, M. Venturi, *Collect. Czech. Chem. Commun.* **2003**, *68*, 1488–1514; c) H.-R. Tseng, S. A. Vignoni, P. C. Celestre, J. Perkins, J. O. Jeppesen, A. Di Fabio, R. Ballardini, M. T. Gandolfi, M. Venturi, V. Balzani, J. F. Stoddart, *Chem. Eur. J.* **2004**, *10*, 155–172.
- [4] V. Balzani, A. Credi, M. Venturi, *Molecular Devices and Machines—A Journey into the Nano World*, Wiley-VCH, Weinheim, **2003**.
- [5] a) J. F. Stoddart, *Chem. Aust.* **1992**, *59*, 576–577, 581; b) A. N. Shipway, I. Willner, *Acc. Chem. Res.* **2001**, *34*, 421–432; c) B. X. Colasson, C. Dietrich-Buchecker, M. C. Jimenez-Molero, J.-P. Sauvage, *J. Phys. Org. Chem.* **2002**, *15*, 476–483; d) M. Cavallini, F. Biscarini, S. Leon, F. Zerbetto, G. Bottari, D. A. Leigh, *Science* **2003**, *299*, 531–531; e) A. H. Flood, R. J. A. Ramirez, W.-Q. Deng, R. P. Muller, W. A. Goddard III, J. F. Stoddart, *Aust. J. Chem.* **2004**, *57*, 301–322; f) P. H. Kwan, M. J. MacLachlan, T. M. Swager, *J. Am. Chem. Soc.* **2004**, *126*, 8638–8639.
- [6] a) For an example of working supramolecular machines in the form of [2]pseudorotaxanes trapped in glass and mounted on the surface of a silica film, see: S. Chia, J. Cao, J. F. Stoddart, J. I. Zink, *Angew. Chem.* **2001**, *113*, 2513–2517; *Angew. Chem. Int. Ed.* **2001**, *40*, 2447–2451; b) for a recent example in which a [2]pseudorotaxane, as a self-assembled monolayer on gold, was shown to undergo reversible dethreading and rethreading of its ring, and so exhibit ion-gating behavior; see: K. Kim, W. S. Jeon, J.-K. Kang, J. W. Lee, S. Y. Jon, T. Kim, K. Kim, *Angew. Chem.* **2003**, *115*, 2395–2398; *Angew. Chem. Int. Ed.* **2003**, *42*, 2293–2296; c) for a detailed discussion on the assembly of an electronically switchable rotaxane on the surface of a titanium dioxide nanoparticle, see: B. Long, K. Nikitin, D. Fitzmaurice, *J. Am. Chem. Soc.* **2003**, *125*, 15490–15498; d) for a very recent example of a functioning nanomachine in the form of a supramolecular nanovalve that opens and closes the orifices to molecular-sized pores and releases a small number of molecules on demand, see: R. Hernandez, H.-R. Tseng, J. W. Wong, J. F. Stoddart, J. I. Zink, *J. Am. Chem. Soc.* **2004**, *126*, 3370–3371; e) in a very recent study, a novel method was demonstrated for the electrical contacting of a redox enzyme by using the CBPQT⁴⁺ ring as a rotaxane-derived electronic relay on a molecular wire connecting the enzyme to the electrode; see: E. Katz, L. Sheeney-Haj-Idia, I. Willner, *Angew. Chem.* **2004**, *116*, 3354–3362; *Angew. Chem. Int. Ed.* **2004**, *43*, 3292–3300.
- [7] For a very early example of self-assembling a donor–acceptor [2]catenane-like structure on a gold surface, see: T. Lu, L. Zhang, G. W. Gokel, A. E. Kaifer, *J. Am. Chem. Soc.* **1993**, *115*, 2542–2543.
- [8] For a discussion of the current/voltage characteristics of Langmuir–Blodgett monolayers of redox-switchable [2]catenanes on gold, see: M. Asakawa, M. Higuchi, G. Mattersteig, T. Nakamura, A. R. Pease, F. M. Raymo, T. Shimizu, J. F. Stoddart, *Adv. Mater.* **2000**, *12*, 1099–1107.
- [9] Recently, it was demonstrated that an array of microcantilever beams, when coated with a SAM of palindromic, bistable [3]rotaxane molecules, undergoes controllable and reversible bending when it is exposed to chemical oxidants and reductants; see: T. J. Huang, B. Brough, C.-M. Ho, Y. Liu, A. H. Flood, P. A. Bonvallet, H.-R. Tseng, J. F. Stoddart, M. Baller, S. Magonov, *Appl. Phys. Lett.* **2004**, *85*, in press.
- [10] I. C. Lee, C. W. Frank, T. Yamamoto, H.-R. Tseng, A. H. Flood, J. F. Stoddart, J. O. Jeppesen, *Langmuir* **2004**, *20*, 5809–5828.
- [11] For evidence that redox-controllable molecular shuttles, in the form of amphiphilic, bistable [2]rotaxanes, are mechanically switchable with chemical reagents in closely packed Langmuir films, and in Langmuir–Blodgett bilayers mounted on solid substrates, see: T. J. Huang, H.-R. Tseng, J. Sha, W. Lu, B. Brough, A. H. Flood, B.-D. Yu, P. C. Celestre, J. P. Chang, J. F. Stoddart, C.-M. Ho, *Nano Lett.* **2004**, *4*, ASAP.
- [12] H.-R. Tseng, D. Wu, N. X. Fang, X. Zhang, J. F. Stoddart, *ChemPhysChem* **2004**, *5*, 111–116.
- [13] C. P. Collier, G. Mattersteig, E. W. Wong, Y. Luo, K. Beverly, J. Sampaio, F. M. Raymo, J. F. Stoddart, J. R. Heath, *Science* **2000**, *289*, 1172–1175.
- [14] C. P. Collier, J. O. Jeppesen, Y. Luo, J. Perkins, E. W. Wong, J. R. Heath, J. F. Stoddart, *J. Am. Chem. Soc.* **2001**, *123*, 12632–12641.
- [15] Y. Luo, C. P. Collier, J. O. Jeppesen, K. A. Nielsen, E. De Iono, G. Ho, J. Perkins, H.-R. Tseng, T. Yamamoto, J. F. Stoddart, J. R. Heath, *ChemPhysChem* **2002**, *3*, 519–525.
- [16] M. R. Diehl, D. W. Steuerman, H.-R. Tseng, S. A. Vignoni, A. Star, P. C. Celestre, J. F. Stoddart, J. R. Heath, *ChemPhysChem* **2003**, *4*, 1335–1339.
- [17] P. R. Ashton, S. E. Boyd, A. Brindle, S. J. Langford, S. Menzer, L. Pérez-García, J. A. Preece, F. M. Raymo, N. Spencer, J. F. Stoddart, A. J. P. White, D. J. Williams, *New J. Chem.* **1999**, *23*, 587–602.
- [18] The synthesis of rotaxane **R1**⁴⁺ and its corresponding dumbbell are reported in the Supporting Information.
- [19] A. H. Flood, A. J. Peters, S. A. Vignoni, D. W. Steuerman, H.-R. Tseng, J. R. Heath, J. F. Stoddart, *Chem. Eur. J.* **2004**, *10*, 6558–6561.
- [20] Previously, we had advocated (M. C. T. Fyfe, P. T. Glink, S. Menzer, J. F. Stoddart, A. J. P. White, D. J. Williams, *Angew. Chem.* **1997**, *109*, 2158–2160; *Angew. Chem. Int. Ed. Engl.* **1997**, *36*, 2068–2070) the use of the term “co-conformation” to designate the different three-dimensional spatial arrangements of the components of mechanically interlocked molecular systems. Also, in identifying the ON and OFF states of the bistable [2]catenane employed in the first MSTJ crossbar device,^[16] we employed the term “co-conformer” to the two states. See, especially Figure 1 in reference [16]. In other words, in proposing our original mechanism, we appreciated correctly that the ON and OFF states are both isomeric and, of course, isoelectronic.
- [21] SAMs of copper catenates have been prepared; however, the electrochemically-triggered circumrotations are either significantly slower than the corresponding motions in solution or completely frozen out; see: L. Raehm, J.-M. Kern, J.-P. Sauvage, C. Hamann, S. Palacin, J.-P. Bourgoign, *Chem. Eur. J.* **2002**, *8*, 2153–2162.
- [22] H. A. Kramers, *Physica* **1940**, *7*, 284–304.
- [23] D. Raftery, R. J. Sensen, R. M. Hochstrasser in *Activated Barrier Crossings* (Eds: G. Fleming, R. Hanggi), World Scientific, Hackensack, NJ, **1993**, p. 163.
- [24] a) R. F. Grote, J. T. Hynes, *J. Chem. Phys.* **1980**, *73*, 2715–2732; b) R. F. Grote, J. T. Hynes, *J. Chem. Phys.* **1981**, *74*, 4465–4475.
- [25] a) H. Sumi, R. A. Marcus, *J. Chem. Phys.* **1986**, *84*, 4894–4914; b) H. Sumi, *J. Mol. Liq.* **1993**, *65*, 65–73.
- [26] G. Schill, K. Rissler, W. Vetter, *Angew. Chem.* **1981**, *93*, 197–201; *Angew. Chem. Int. Ed. Engl.* **1981**, *20*, 187–189.
- [27] a) For a general discussion of electrochromic devices, see: D. R. Rossinsky, R. J. Mortimer, *Adv. Mater.* **2001**, *13*, 783–793; b) see also the Special Issue covering the Third International Meeting on Electrochromics (IME-3) in *Electrochimica Acta* **1999**, *44*(18), 2969–3258; c) Electrochromic devices have been developed out of a variety of different materials; for examples of molecular systems, see: R. J. Mortimer, *Electrochim. Acta* **1999**, *44*, 2971–2981, and, for an example in which an electrochromic molecule that has been attached to a solid support, see: R. Cinnsealach, G. Boschloo, S. Nagaraja Rao, D. Fitzmaurice, *Sol. Energy Mater. Sol. Cells* **1999**, *57*, 107–125; for examples of polymers, see: F. Fungo, S. A. Jenekhe, A. J. Bard, *Chem. Mater.* **2003**, *15*, 1264–1272, and, for a very recent report on polymeric

- systems, see: G. Sonmez, C. K. F. Shen, Y. Rubin, F. Wudl, *Angew. Chem.* **2004**, *116*, 1524–1528; *Angew. Chem. Int. Ed.* **2004**, *43*, 1498–1502; for examples of metal-oxide thin films, see: S. Papaefthimiou, G. Leftheriotis, P. Yianoulis, *Electrochim. Acta* **2001**, *46*, 2145–2150; d) for the use of polymer-gel electrolytes in electrochromic devices, see: J. Vondrák, M. Sedlarikova, J. Reiter, T. Hodal, *Electrochim. Acta* **1999**, *44*, 3067–3073.
- [28] M. Deepa, N. Sharma, S. A. Agnihory, S. Singh, T. Lal, R. Chandra, *Solid State Ionics* **2002**, *152–153*, 253–258.

Asymmetric Synthesis

Stereospecific, Enantioselective Allylation of α -Hydrazono Esters by Using Allyltrichlorosilanes with BINAP Dioxides as Neutral-Coordinate Organocatalysts**

Chikako Ogawa, Masaharu Sugiura, and
Shū Kobayashi*

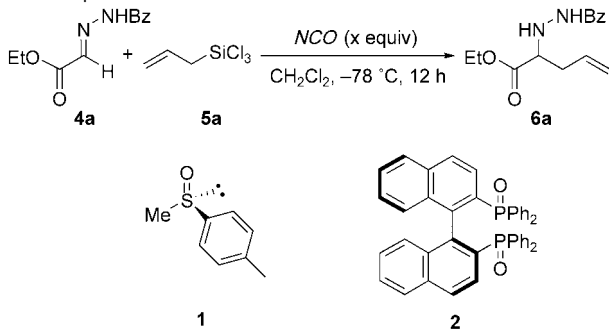
Enantioselective allylation of α -imino esters or their equivalents provides one of the most efficient routes to optically active natural and unnatural α -amino acids. Lectka et al. reported enantioselective allylation of a hemiacetal of a *N*-sulfonyl α -imino ester with trimethyl(2-phenylallyl)silane and related silanes using a chiral Cu^I catalyst.^[1] Jørgensen et al. also reported at almost the same time that the chiral Cu^I catalyst had lower activity for the reaction with allylsilanes. His group used allylstannanes instead of allylsilanes.^[2] However, in both cases, the enantioselectivities obtained were still unsatisfactory, and were dependent on the structure of allylsilanes. Recently, our group also reported that enantioselective allylation of α -hydrazono esters with allyltrimethoxysilanes proceeded smoothly in aqueous media in the presence of a ZnF₂-chiral diamine complex.^[3] However, also in this case the enantioselectivities obtained were less than 90% *ee*. Furthermore, only a few examples of diastereo- and enantioselective addition of γ -substituted allyl metals to α -imino esters have been reported,^[1b,2,4] no *stereospecific*, enantioselective allylation has been attained to date.

Recently, we have found that neutral (uncharged) organic molecules such as *N,N*-dimethylformamide (DMF) and

hexamethylphosphoramide (HMPA) mediate allylation of aldehydes^[5] and *N*-acylhydrazones^[6] with allyltrichlorosilanes. Remarkably, the reactions proceeded without the use of any metal catalyst. These organic molecules coordinate to allyltrichlorosilanes to form hypervalent silicon compounds^[7] that react with electrophiles efficiently; thus, we defined these molecules as neutral coordinate-organocatalysts (NCOs).^[8] Quite recently, we have achieved stereospecific, enantioselective allylation of *N*-acylhydrazones by using chiral sulfonides as chiral NCOs.^[9] We have also found that phosphine oxides are effective for the allylation of *N*-acylhydrazones.^[10] On the basis of this background, we decided to develop the stereospecific, enantioselective allylation of α -imino ester derivatives.

We selected α -hydrazono esters as α -imino ester surrogates because of their stability compared to the corresponding α -imino esters. Indeed, most α -hydrazono esters are crystalline, easily purified by simple recrystallization, and can be stored for several months at room temperature.^[3,11] First, the reaction of α -hydrazono ester **4a** (prepared from ethyl glyoxylate and benzhydrazide) with allyltrichlorosilane (**5a**) was chosen as a model, and several enantiopure catalysts were tested (Table 1). When sulfoxide **1** was used as a chiral

Table 1: Optimization of reaction conditions.



Entry	NCO	x	Conc. [M]	Yield [%]	<i>ee</i> [%]
1	1	3.0	0.15	60	23 (<i>S</i>)
2	2	0.2	0.30	11	56 (<i>R</i>)
3	2	0.4	0.30	38	69 (<i>R</i>)
4	2	1.0	0.30	62	96 (<i>R</i>)
5	2	1.0	0.05	72	95 (<i>R</i>)
6	2	2.0	0.05	91	98 (<i>R</i>)

catalyst, the reaction proceeded to afford the desired allylated adduct **6a** in 60% yield but with disappointingly low enantioselectivity (23% *ee*; Table 1, entry 1). Although several reaction conditions were examined using **1**, little improvement of the yield and the selectivity was observed. We then decided to search for other chiral catalysts for this reaction. After screening several catalysts, we found that 2,2'-bis(diphenylphosphanyl)-1,1'-binaphthyl dioxides (**2**, BINAP dioxides) were promising. When 1.0 equivalent of (*S*)-BINAP dioxide (**2**) was used in the reaction between **4a** and **5a**, the reaction proceeded in dichloromethane at -78°C to give the desired adduct **6a** in 62% yield with 96% *ee* (Table 1, entry 4). Unfortunately, use of smaller amounts of (*S*)-BINAP dioxide gave lower yields and enantioselectivities (Table 1,

[*] Dr. C. Ogawa, Dr. M. Sugiura, Prof. Dr. S. Kobayashi
Graduate School of Pharmaceutical Sciences
The University of Tokyo
Hongo, Bunkyo-ku, Tokyo 113-0033 (Japan)
Fax: (+81) 3-5684-0634
E-mail: skobayas@mol.f.u-tokyo.ac.jp

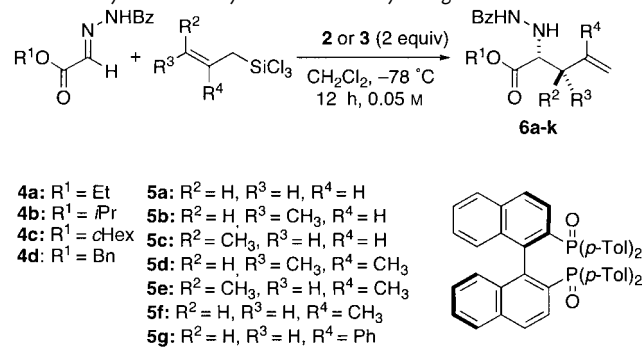
[**] This work was partially supported by CREST, SORT, ERATO, the Japan Science Technology Corporation (JST), and a Grant-in-Aid for Scientific Research from the Japan Society of the Promotion of Sciences (JSPS). BINAP = 2,2'-Bis(diphenylphosphanyl)-1,1'-binaphthyl.

Supporting information for this article is available on the WWW under <http://www.angewandte.org> or from the author.

entries 2 and 3). The yield and the selectivity were further improved when two equivalents of **2** were used under lower concentration conditions; thus, the desired adduct **6a** was obtained in 91 % yield with 98 % *ee* (Table 1, entry 6). After the reaction, **2** was recovered almost quantitatively without loss of optical purity. It is noted that the use of chiral phosphine oxides in asymmetric catalysis has been limited,^[12] whereas innumerable usage of BINAP has been reported.^[13]

We then examined other α -hydrazono esters and allyltrichlorosilanes, and the results are summarized in Table 2. For

Table 2: Allylation of α -hydrazono esters by using BINAP dioxides.



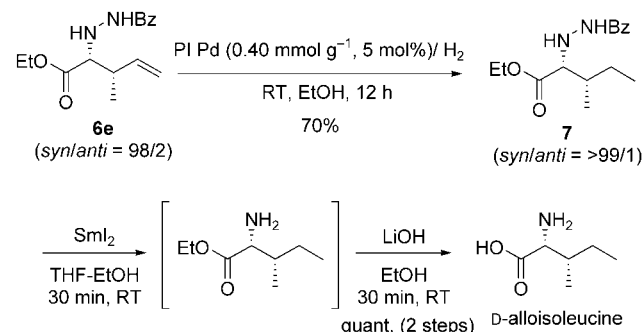
Entry	Electrophile	Silane	Yield [%]	<i>syn/anti</i>	<i>ee</i> [%]
1	4a	5a	91 (6a)	–	98 (<i>R</i>)
2	4b	5a	70 (6b)	–	97
3	4c	5a	28 (6c)	–	98
4	4d	5a	12 (6d)	–	91
5	4a	5b	92 (6e)	98/2	> 99 (2 <i>R</i> , 3 <i>S</i>)
6	4a	5c	96 (6f)	< 1/ > 99	96 (2 <i>R</i> , 3 <i>R</i>)
7 ^[a]	4a	5d	80 (6g)	98/2	96 (2 <i>S</i> , 3 <i>R</i>)
8 ^[a]	4a	5e	80 (6h)	< 1/ > 99	81 (2 <i>S</i> , 3 <i>S</i>)
9 ^[b]	4a	5f	83 (6i)	–	94 (<i>R</i>)
10 ^[a]	4a	5g	50 (6j)	–	95

[a] Compound **3** was used instead of **2**. Reaction time was 15 h.

[b] Reaction time was 6 h.

α -hydrazono esters, larger ester groups gave lower yields, whereas high enantioselectivities were maintained in some cases. For allyltrichlorosilanes, we carefully examined crotylation using (*E*)- and (*Z*)-crotyltrichlorosilanes. It was exciting to find that the reactions proceeded stereospecifically; (*E*)-crotyltrichlorosilane **5b** gave the *syn* adduct **6e** (Table 2, entry 5), whereas the *anti* adduct **6f** was produced from (*Z*)-crotyltrichlorosilane **5c** (Table 2, entry 6).^[14] In both cases, yields were high, and excellent diastereo- and enantioselectivities were obtained. When (*E*)- and (*Z*)-allylic trichlorosilanes, **5d** and **5e**, were employed, both *syn* and *anti* adducts were also obtained stereospecifically, although (*R*)-2,2'-bis(di-*p*-tolylphosphanyl)-1,1'-binaphthyl dioxides (**3**, (*R*)-*p*-tol-BINAP dioxides) as an *NCO* gave better results than **2** (Table 2, entries 7 and 8). It is noteworthy that this is the first example of stereospecific, enantioselective allylation of α -imino ester equivalents. Other allylic silanes **5f** and **5g** also worked well to afford the desired adducts with high enantioselectivities (Table 2, entries 9 and 10).

The present allylation was successfully applied to the enantioselective synthesis of D-alloisoleucine, an uncommon α -amino acid observed in biologically important peptides;^[15] however, there are several reports on enantioselective synthesis of this molecule.^[16] Our synthesis is outlined in Scheme 1. The starting material **6e** is an allylated adduct



Scheme 1. Facile synthesis of D-alloisoleucine.

prepared from **4a** and **5b** (Table 2, entry 5). The olefin moiety of **6e** was reduced by using polymer incarcerated Pd (PI Pd)^[17] to give **7** in 70 % yield. Successive reductive cleavage of the N–N bond of **7** using SmI₂,^[18] followed by ester hydrolysis gave D-alloisoleucine (quantitative yield for two steps). Thus, D-alloisoleucine has been synthesized from α -hydrazono ester **4a** in four steps in an overall yield of 64 %. This efficient synthesis demonstrates the utility of the BINAP dioxides-catalyzed enantioselective allylation reaction for amino acid synthesis.

In conclusion, we have found that BINAP dioxides are excellent chiral neutral-coordinate organocatalysts for the enantioselective allylation of α -hydrazono esters using allyltrichlorosilanes. The reactions proceeded stereospecifically; (*E*)-allylic silanes gave *syn* adducts, whereas *anti* adducts were obtained from (*Z*)-allylic silanes. This is the first example of the stereospecific, enantioselective allylation of α -imino ester equivalents. Diastereo- and enantioselectivities obtained in this allylation are very high compared to those reported by previous methods. In addition, the present reaction was successfully applied to the efficient synthesis of D-alloisoleucine. A drawback of this reaction is the use of two equivalents of BINAP dioxides, but the chiral source could be recovered almost quantitatively without loss of optical purity. Further investigations to reduce the amounts of BINAP dioxides are now in progress.

Received: July 15, 2004

Keywords: allylation · amino acids · asymmetric catalysis · asymmetric synthesis · hydrazones

- [1] a) D. Ferraris, T. Dudding, B. Young, W. J. Drury III, T. Lectka, *J. Org. Chem.* **1999**, *64*, 2168; b) D. Ferraris, B. Young, C. Cox, T. Dudding, W. J. Drury III, L. Ryzhkov, A. E. Taggi, T. Lectka, *J. Am. Chem. Soc.* **2002**, *124*, 67.
- [2] X. Fang, M. Johannsen, S. Yao, N. Gathergood, R. G. Hazel, K. A. Jørgensen, *J. Org. Chem.* **1999**, *64*, 4844.

- [3] T. Hamada, K. Manabe, S. Kobayashi, *Angew. Chem.* **2003**, *115*, 4057; *Angew. Chem. Int. Ed.* **2003**, *42*, 3927.
- [4] For a diastereo- and enantioselective allylation of imines, see: T. Gastner, H. Ishitani, R. Akiyama, S. Kobayashi, *Angew. Chem.* **2001**, *113*, 1949; *Angew. Chem. Int. Ed.* **2001**, *40*, 1896.
- [5] a) S. Kobayashi, K. Nishio, *Tetrahedron Lett.* **1993**, *34*, 3453; b) S. Kobayashi, K. Nishio, *J. Org. Chem.* **1994**, *59*, 6620.
- [6] a) S. Kobayashi, R. Hirabayashi, *J. Am. Chem. Soc.* **1999**, *121*, 6942; b) R. Hirabayashi, C. Ogawa, M. Sugiura, S. Kobayashi, *J. Am. Chem. Soc.* **2001**, *123*, 9493; c) C. Ogawa, M. Sugiura, S. Kobayashi, *J. Org. Chem.* **2002**, *67*, 5359.
- [7] a) C. C. Chuit, R. J. Corriu, C. Reye, J. C. Young, *Chem. Rev.* **1993**, *93*, 1371; b) H. Sakurai, *Synlett* **1989**, 1.
- [8] S. Kobayashi, M. Sugiura, C. Ogawa, *Adv. Synth. Catal.* **2004**, *346*, 1023.
- [9] S. Kobayashi, C. Ogawa, H. Konishi, M. Sugiura, *J. Am. Chem. Soc.* **2003**, *125*, 6610.
- [10] C. Ogawa, H. Konishi, M. Sugiura, S. Kobayashi, *Org. Biomol. Chem.* **2004**, *2*, 446.
- [11] a) K. Manabe, H. Oyamada, K. Sugita, S. Kobayashi, *J. Org. Chem.* **1999**, *64*, 8054; b) S. Kobayashi, T. Hamada, K. Manabe, *J. Am. Chem. Soc.* **2002**, *124*, 5640.
- [12] a) K. Mikami, M. Yamaoka, *Tetrahedron Lett.* **1998**, *39*, 4501; b) Q.-H. Fan, G.-H. Liu, G.-J. Deng, X.-M. Chen, A. S. C. Chan, *Tetrahedron Lett.* **2001**, *42*, 9047; c) J. Bayaeldon, M. Cavazzini, D. Maikkard, G. Pozzi, S. Quici, D. Sinou, *Tetrahedron: Asymmetry* **2003**, *14*, 2215; d) A. M. Maj, K. M. Pietrusiewicz, I. Suisse, F. Agbossou, A. Mortreux, *Tetrahedron: Asymmetry* **1999**, *10*, 831; e) S. Matsukawa, H. Sugama, T. Imamoto, *Tetrahedron Lett.* **2000**, *41*, 6461.
- [13] *Catalytic Asymmetric Synthesis* (Ed.: I. Ojima), 2nd ed., Wiley-VCH, New York, **2000**.
- [14] The stereochemistry of the adducts was tentatively assigned at this stage based on previous data (see ref [3]). It was finally confirmed after converting to D-alloisoleucine (Scheme 1).
- [15] See, for example: K. Takesato, K. Ikai, F. Haruna, M. Endo, K. Shimanaka, E. Sono, T. Nakamura, I. Kato, *J. Antibiot.* **1991**, *44*, 919.
- [16] a) W. Oppolzer, O. Tamura, *Tetrahedron Lett.* **1990**, *31*, 991; b) M. Bakke, H. Ohta, U. Kazmaier, T. Sugai, *Synthesis* **1999**, 9, 1671; c) P. Portonovo, B. Liang, M. Joullie, *Tetrahedron: Asymmetry* **1999**, *10*, 1451; d) X. Wang, M. Xu, J. Chen, Y. Pan, Y. Shi, *Synth. Commun.* **2000**, *30*, 2253; e) W. Oppolzer, R. Pedrosa, R. Moretti, *Tetrahedron Lett.* **1986**, *27*, 831; f) W. Oppolzer, O. Tamura, J. Deeberg, *Helv. Chim. Acta* **1992**, *75*, 1965; g) P. Lloyd-William, P. Moneris, I. Gonzalez, G. Jou, E. Giralt, *J. Chem. Soc. Perkin Trans. 1* **1994**, 1969; h) H. Noda, K. Sakai, H. Murakami, *Tetrahedron: Asymmetry* **2002**, *13*, 2649.
- [17] R. Akiyama, S. Kobayashi, *J. Am. Chem. Soc.* **2003**, *125*, 3412.
- [18] M. J. Burk, J. E. Feaster, *J. Am. Chem. Soc.* **1992**, *114*, 6266.

A Stereodivergent Synthesis of Virantmycin by an Enzyme-Mediated Diester Desymmetrization and a Highly Hindered Aryl Amination**

Thomas G. Back* and Jeremy E. Wulff

(–)-Virantmycin (**1**) is an unusual chlorinated tetrahydroquinoline that was isolated from a strain of *Streptomyces nitrosporeus* in 1980.^[1] It was found to possess both strong inhibitory activity against RNA and DNA viruses, and antifungal activity.^[2] The initial structure elucidation of virantmycin was reported in the 1980s,^[2,3] but not until 1990 was the correct stereochemistry established by NMR methods,^[4] and later confirmed by synthesis.^[5] To date, racemic syntheses of **1** have been completed by Hill and Raphael,^[6] Morimoto, Shirahama et al.,^[5,7] and by Steinhagen and Corey.^[8] The preparation of the (+)-antipode of the naturally occurring antibiotic has also been reported.^[9] Very recently, Kogen et al. achieved the first enantioselective synthesis of (–)-**1** from (*S*)-indoline-2-carboxylic acid.^[10] The latter report prompted us to disclose our own efforts in this area, which have resulted in a stereodivergent route to both (+)-**1** and (–)-**1**.

The principal challenge in the synthesis of virantmycin involves the stereoselective construction of the two contiguous stereocenters, which include the quaternary carbon atom at C2. Our plan was to construct the latter center by the desymmetrization of a key intermediate diester **2** by an enzyme-mediated partial hydrolysis. After appending the aryl moiety by a Claisen-like condensation, we envisaged the stereoselective introduction of the amino group to the highly hindered stereocenter by a Curtius rearrangement and ring-closure to complete the tetrahydroquinoline skeleton by an intramolecular aryl amination reaction (Scheme 1).

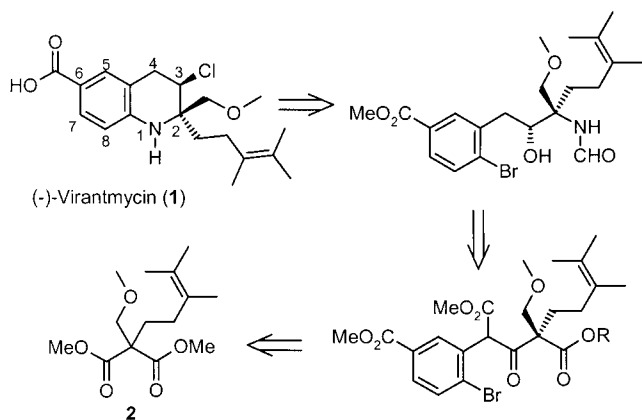
Diester **2** was readily obtained by sequential alkylation of the enolate derived from dimethyl malonate by using NaH with 5-iodo-2,3-dimethyl-2-pentene^[11] and methoxymethyl chloride. Scheme 2 illustrates the desymmetrization of **2**, which was achieved by partial hydrolysis with porcine liver esterase (PLE)^[12] to afford the half-ester **3** in 89 % yield and 95 % *ee*, as determined by integration of the NMR spectrum of the salt formed from **3** and (*S*)-(–)- α -methylbenzylamine.

[*] Prof. Dr. T. G. Back, J. E. Wulff
Department of Chemistry
University of Calgary
Calgary, AB, T2N 1N4 (Canada)
Fax: (+1) 403-289-9488
E-mail: tgback@ucalgary.ca

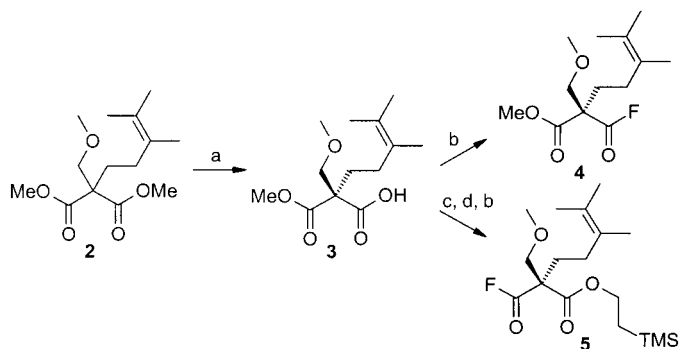
[**] We thank the Natural Sciences and Engineering Research Council of Canada (NSERC) for financial support. J.E.W. thanks, the NSERC, the Alberta Heritage Foundation for Medical Research, and the Izaak Walton Killam Foundation for Postgraduate Scholarships. We thank Dr. B. A. Keay for helpful discussions and a generous gift of BINAPFu.



Supporting information for this article is available on the WWW under <http://www.angewandte.org> or from the author.



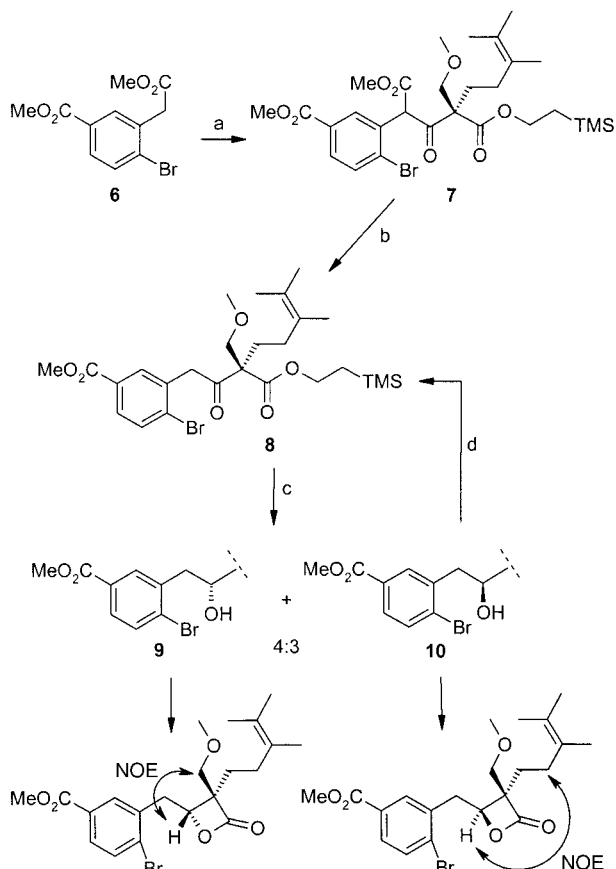
Scheme 1. Retrosynthesis of (–)-virantmycin (**1**).



Scheme 2. Desymmetrization of diester **2** to generate chiral intermediates **4** and **5**: a) porcine liver esterase (PLE), DMSO-pH 8.0 phosphate buffer (1:4), 7 days, RT, 89%, 95% *ee*; b) cyanuric fluoride, pyridine, dichloromethane, 1 h, 0°C, 71% for **4** and 75% for **5**; c) 2-(trimethylsilyl)ethanol, 1,3-dicyclohexylcarbodiimide (DCC), *N,N*-dimethylamino-pyridine (DMAP), dichloromethane, 3 days, RT, 77%; d) 10% aqueous KOH, methanol, 15 h, 45°C, 88% (based on 20% of recovered **3**).

The absolute configuration of **3** was assumed to be (S) on the basis of earlier studies^[12b,c] of PLE-mediated hydrolyses of other β -diesters, and this assignment was confirmed unequivocally by the ultimate conversion of **3** to essentially pure enantiomers of the final products. Thus, half-ester **3** was converted separately into each of the pseudo-enantiomeric acyl fluorides **4** and **5** (Scheme 2),^[13] which in turn served as respective precursors of (+)-**1** and (–)-**1**. Acylation of the enolate of diester **6**^[14] with **5** afforded triester **7** (Scheme 3), which was subjected to selective Krapcho decarboxylation^[15] of the less hindered β -keto ester moiety to furnish **8**. The reduction of the ketone group of **8**, which was required to introduce a hydroxy group to serve as the chlorination site for the final product, resulted in poor stereoselectivity under a variety of conditions. However, the undesired epimer **10** was easily separated from **9** and recycled back to ketone **8** with PCC. The configurations of epimers **9** and **10** were assigned on the basis of NOE experiments conducted on the corresponding β -lactones (Scheme 3).

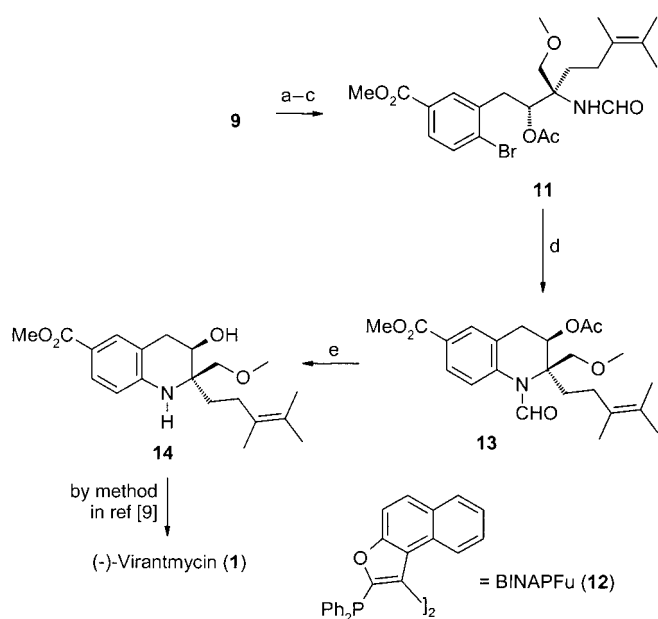
Alcohol **9** was acetylated and the trimethylsilylethyl ester was selectively removed with fluoride ion. The resulting carboxylic acid was subjected to a Curtius rearrangement



Scheme 3. Coupling of diester **6** with chiral intermediate **5**: a) lithium hexamethyldisilazide (LiHMDS), Et₂O, 0 °C, 10 min; then **5**, Et₂O, 1 h at 0 °C—20 h at RT, 63%; b) 10% aqueous NaCl, DMSO, 20 h, 125 °C, 78%; c) NaBH₄, methanol, 2.5 h, 0 °C, 83%; d) pyridinium chlorochromate (PCC), dichloromethane, 3 days, RT, 77%.

mediated by diphenylphosphoryl azide (DPPA),^[16] followed by workup with sodium borohydride, to afford formamide **11** (Scheme 4). The crucial intramolecular Buchwald–Hartwig aryl amination^[17] step was then attempted under a variety of conditions, with generally unsatisfactory results. However, we were pleased to discover that the treatment of formamide **11** with [Pd₂(dba)₃] in the presence of the Keay ligand BINAPFu (**12**)^[18] under the conditions shown in Scheme 4 resulted in quantitative cyclization to **13**.

The selection of BINAPFu as the Pd ligand of choice was based on model studies of the aryl aminations of other α -quaternary amines (1-adamantylamine and methyl α,α -dimethylglycinate) with methyl 4-bromo-3-methylbenzoate. Other ligands, such as BINAP,^[19a] DPPF,^[19b] PCy₃,^[19c] *o*-biphenyl-PCy₂,^[19d] *o*-biphenylPrBu₂,^[19d] DPEphos,^[19e] MAP,^[19f] and IMES hydrochloride^[19g] failed to effect coupling or produced very low yields of the corresponding aryl amines under a wide variety of conditions. The successful intramolecular aryl amination of formamide **11** using the BINAPFu ligand is particularly noteworthy because very few examples of aryl aminations of aliphatic amines containing α -quaternary centers are known.^[20] BINAPFu is a less strongly donating ligand than other commonly employed bidentate phosphines such as BINAP.^[18] Moreover, the reductive elimination steps

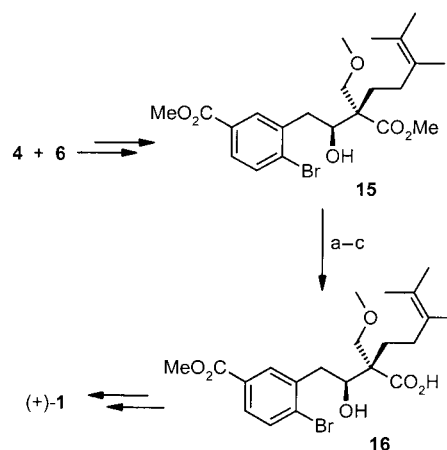


Scheme 4. Synthesis of (–)-virantmycin (**1**) from intermediate **9**: a) *N,N*-dimethylaminopyridine (DMAP), pyridine, acetic anhydride, 3 days, RT; b) 1.0 M tetrabutylammonium fluoride in tetrahydrofuran, 1 h, RT; c) diphenylphosphoryl azide (DPPA), *N,N*-dimethylaminopyridine (DMAP), triethylamine, toluene, 2.25 h, reflux; then NaBH₄, tetrahydrofuran, 12.5 h, RT, 84% overall yield for steps a–c; d) [Pd₂(dba)₃], **12**, Cs₂CO₃, toluene, 6.5 h, 90°C, 100%; e) 0.13 M NaOH in methanol, 24 h, RT, 84%.

of aryl aminations and related Pd-catalyzed coupling reactions are enhanced by weakly coordinating phosphine ligands.^[21] It is therefore possible that reductive elimination is the rate-determining step in the present case because of the high degree of steric hindrance associated with coupling an *ortho*-substituted aryl bromide with an α -quaternary amine derivative. The particular efficacy of BINAPFu may be attributed to its ability to facilitate this step.

Deacetylation and concomitant deformylation of tetrahydroquinoline **13** provided the free alcohol **14**, which was converted into (–)-**1** by the same method used previously by Morimoto and Shirahama^[9] in their synthesis of (+)-**1** (Scheme 4). The product displayed NMR spectra consistent with the literature^[4,6,9] and gave a specific rotation $[\alpha]_D^{20} = -11^\circ$ ($c = 0.13$, chloroform) that compared favorably with that reported for the natural product: $[\alpha]_D^{24} = -11.1^\circ$ ($c = 0.175$, chloroform).^[9]

Finally, acyl fluoride **4** was converted into the unnatural antipode (+)-**1** by a similar process (Scheme 5), except that the aromatic and aliphatic ester moieties of **15** were converted to the free carboxylic acids in **16** by saponification of the former and dealkylation with sodium propanethiolate of the latter, followed by selective reesterification of the remaining carboxylic acid and Curtius rearrangement of the remaining aliphatic acid (Scheme 5). Completion of the synthesis was achieved as in the case of (–)-**1**. The NMR spectra of the product were identical to those of (–)-**1** and the optical rotation data $[\alpha]_D^{20} = +13^\circ$ ($c = 0.14$, chloroform), compared



Scheme 5. Synthesis of (+)-virantmycin from acyl fluoride **4**: a) 10% aqueous KOH, methanol, 20 h, RT; b) NaH, *n*PrSH, HMPA, 4.75 h, RT; c) SOCl₂, methanol, 1 h at –10°C → 3 h at reflux, 46% overall yield for steps a–c.

favourably with the literature value $[\alpha]_D^{24} = +11.2^\circ$ ($c = 0.125$, chloroform).^[9]

In conclusion, the present method provides a new route to both enantiomers of the antiviral agent virantmycin (**1**). It employs as key steps a highly enantioselective enzyme-mediated desymmetrization and a remarkably effective intramolecular aryl amination of a hindered α -quaternary aliphatic amine. The procedure is also potentially amenable to the preparation of analogues for the purpose of structure–activity studies.

Received: July 16, 2004

Keywords: aryl amination · enzyme catalysis · esterases · natural products · total synthesis

- [1] S. Ōmura, A. Nakagawa, H. Hashimoto, R. Oiwa, Y. Iwai, A. Hirano, N. Shibukawa, Y. Kojima, *J. Antibiot.* **1980**, *33*, 1395.
- [2] A. Nakagawa, Y. Iwai, H. Hashimoto, N. Miyazaki, R. Oiwa, Y. Takahashi, A. Hirano, N. Shibukawa, Y. Kojima, S. Ōmura, *J. Antibiot.* **1981**, *34*, 1408.
- [3] Y. Morimoto, K. Oda, H. Shirahama, T. Matsumoto, S. Ōmura, *Chem. Lett.* **1988**, 909.
- [4] C. M. Pearce, J. K. M. Sanders, *J. Chem. Soc. Perkin Trans. 1* **1990**, 409.
- [5] Y. Morimoto, F. Matsuda, H. Shirahama, *Synlett* **1991**, 202.
- [6] a) M. L. Hill, R. A. Raphael, *Tetrahedron Lett.* **1986**, *27*, 1293; b) M. L. Hill, R. A. Raphael, *Tetrahedron* **1990**, *46*, 4587.
- [7] Y. Morimoto, F. Matsuda, H. Shirahama, *Tetrahedron* **1996**, *52*, 10609.
- [8] H. Steinhagen, E. J. Corey, *Org. Lett.* **1999**, *1*, 823.
- [9] Y. Morimoto, H. Shirahama, *Tetrahedron* **1996**, *52*, 10631.
- [10] M. Ori, N. Toda, K. Takami, K. Tago, H. Kogen, *Angew. Chem.* **2003**, *115*, 2644; *Angew. Chem. Int. Ed.* **2003**, *42*, 2540.
- [11] a) T. G. Back, R. J. Bethell, M. Parvez, D. Wehrli, *J. Org. Chem.* **1998**, *63*, 7908; b) A. N. De Silva, C. L. Francis, A. D. Ward, *Aust. J. Chem.* **1993**, *46*, 1657.
- [12] a) For a general review, see: H. G. Davies, R. H. Green, D. R. Kelly, S. M. Roberts, *Biotransformations in Preparative Organic Chemistry*, Academic Press, London, **1989**, chap. 2; b) F. Björk-

- ling, J. Boutelje, S. Gatenbeck, K. Hult, T. Norin, P. Szmulik, *Tetrahedron* **1985**, 41, 1347; c) E. J. Toone, M. J. Werth, J. B. Jones, *J. Am. Chem. Soc.* **1990**, 112, 4946.
- [13] The acyl fluorides were prepared by the general method of: S. Groß, S. Laabs, A. Scherrmann, A. Sudau, N. Zhang, U. Nubbemeyer, *J. Prakt. Chem.* **2000**, 342, 711.
- [14] Diester **6** was prepared by treatment of methyl 4-bromo-3-bromomethylbenzoate with NaCN, followed by alkaline hydrolysis of the corresponding benzyl nitrile and Fischer esterification with methanol.
- [15] A. P. Krapcho, A. J. Lovey, *Tetrahedron Lett.* **1973**, 957.
- [16] T. Shioiri, K. Ninomiya, S. Yamada, *J. Am. Chem. Soc.* **1972**, 94, 6203.
- [17] For selected reviews, see: a) J. P. Wolfe, S. Wagaw, J.-F. Marcoux, S. L. Buchwald, *Acc. Chem. Res.* **1998**, 31, 805; b) J. F. Hartwig, *Acc. Chem. Res.* **1998**, 31, 852; c) J. F. Hartwig in *Handbook of Organopalladium Chemistry for Organic Synthesis*, Vol. 1 (Ed.: E. Negishi), Wiley, Hoboken, NJ, **2002**, pp. 1051–1096.
- [18] a) N. G. Andersen, M. Parvez, R. McDonald, B. A. Keay, *Can. J. Chem.* **2004**, 82, 145; b) for a review of 2-furylphosphine ligands in transition-metal-mediated reactions, see: N. G. Andersen, B. A. Keay, *Chem. Rev.* **2001**, 101, 997.
- [19] a) BINAP = 2,2'-bis(diphenylphosphanyl)-1,1'-binaphthyl: J. P. Wolfe, S. Wagaw, S. L. Buchwald, *J. Am. Chem. Soc.* **1996**, 118, 7215; b) DPPF = 1,1'-bis(diphenylphosphanyl)ferrocene: M. S. Driver, J. F. Hartwig, *J. Am. Chem. Soc.* **1996**, 118, 7217; c) PCy₃: N. P. Reddy, M. Tanaka, *Tetrahedron Lett.* **1997**, 38, 4807; d) *o*-biphenylPCy₂ and *o*-biphenylPtBu₂: J. P. Wolfe, H. Tomori, J. P. Sadighi, J. Yin, S. L. Buchwald, *J. Org. Chem.* **2000**, 65, 1158; e) DPEphos = 2,2'-bis(diphenylphosphanyl)-1,1'-diphenyl ether: J. P. Sadighi, M. C. Harris, S. L. Buchwald, *Tetrahedron Lett.* **1998**, 39, 5327; f) MAP = 2'-dimethylamino-2-(diphenylphosphanyl)-1,1'-binaphthalene: S. Vyskočil, M. Smrčina, P. Kočovský, *Tetrahedron Lett.* **1998**, 39, 9289; g) IMES hydrochloride = 1,3-bis(2,4,6-trimethylphenyl)imidazol-2-ylidene hydrochloride: G. A. Grasa, M. S. Viciu, J. Huang, S. P. Nolan, *J. Org. Chem.* **2001**, 66, 7729.
- [20] For an aryl amination with *tert*-butylamine, see: a) H. Siebeneicher, I. Bytschkov, S. Doye, *Angew. Chem.* **2003**, 115, 3151; *Angew. Chem. Int. Ed.* **2003**, 42, 3042; b) I. Bytschkov, H. Siebeneicher, S. Doye, *Eur. J. Org. Chem.* **2003**, 2888; for an aryl amination with *N*-*tert*-butylaniline, see: c) M. Prashad, X. Y. Mak, Y. Liu, O. Repič, *J. Org. Chem.* **2003**, 68, 1163.
- [21] G. Mann, Q. Shelby, A. H. Roy, J. F. Hartwig, *Organometallics* **2003**, 22, 2775.

Targeting RNAs with Tobramycin Analogues**

*Fu-Sen Liang, Sheng-Kai Wang, Takuji Nakatani, and
Chi-Huey Wong**

There are growing interests in developing small molecules to specifically target RNA because of the potential therapeutic applications.^[1] Aminoglycosides and macrolides, for example, have been known to exhibit antibiotic activities by interacting with the bacterial ribosomal RNA.^[2] Recent discoveries of other small molecules that control gene expression in living cells by attenuating RNA activities have shed more light on the promising potential of developing RNA-binding molecules as drugs.^[3] Many aminoglycosides have been developed to target not only the bacterial ribosomal RNA 16S A-site, but also other RNA sequences, including the regulatory domains of HIV-1 mRNA, the oncogenic Bcr-Abl mRNA sequence, and the group I intron.^[4]

From NMR and X-ray crystallographic studies,^[2,5] it is clear that the two-ring cores (rings I and II) of both tobramycin (**1**) and paromomycin (**2**), which are 4,5- and 4,6-linked aminoglycosides, respectively (see Figure 1), sit in the bulges of A¹⁴⁰⁸, A¹⁴⁹², and A¹⁴⁹³ of the A-site and make very similar contacts with the RNA bases and the phosphate backbones. The surface plasmon resonance (SPR) binding studies of the naturally occurring aminoglycosides with the wild-type or mutant 16S A-site RNAs show that the binding affinity and specificity vary when the compositions or the linking positions of the additional sugar moieties change.^[6] Previous studies also suggest that both neamine and nebramine are basic cores for binding to various RNA sequences and for cell permeability.^[7] It is possible that by keeping the

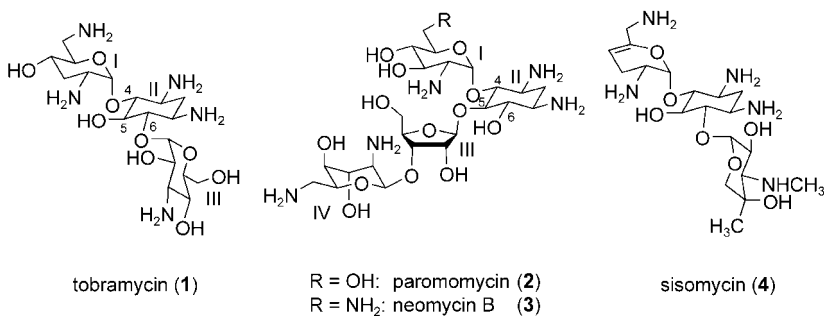



Figure 1. The structures of 4,6- and 4,5-linked aminoglycosides.

[*] F.-S. Liang, S.-K. Wang, Dr. T. Nakatani, Prof. C.-H. Wong
Department of Chemistry and
The Skaggs Institute of Chemical Biology
The Scripps Research Institute
10550 N. Torrey Pines Road, La Jolla, CA 92037 (USA)
Fax: (+1) 858-784-2409
E-mail: wong@scripps.edu

[**] Supported by the NIH.

 Supporting information for this article is available on the WWW under <http://www.angewandte.org> or from the author.

two-ring core and changing the carbohydrate unit attached to position 5 or 6 of the core may affect both affinity and specificity.

Most of the aminoglycoside analogues developed to date have been modified by the attachment of various nonsugar moieties to the original aminoglycosides or to the two-ring core through different linkers. Here, we designed and synthesized a new library of 4,6-linked tobramycin analogues with various mono- or diaminosugars attached to the 6-position of the deoxystreptamine ring (Figure 2). With the relatively rigid conformation of the carbohydrate framework, it was hoped that new aminoglycosides with higher binding affinities and selectivities would be found.

The protected nebramine core **5** was derived from tobramycin (**1**; Scheme 1). The amine groups of tobramycin (**1**) were first converted into azides as protecting groups by the diazo transfer reaction.^[8] This was followed by benzylation of the alcohol groups to give the fully protected tobramycin derivative **6**. Cleavage of the glycosidic bond between the nebramine core and the third ring was catalyzed by a Lewis acid in the presence of *p*-thiocresol as nucleophile.^[9] The advantage of this method, instead of HCl or copper chloride catalyzed cleavage, is that the resulting cleaved third ring can

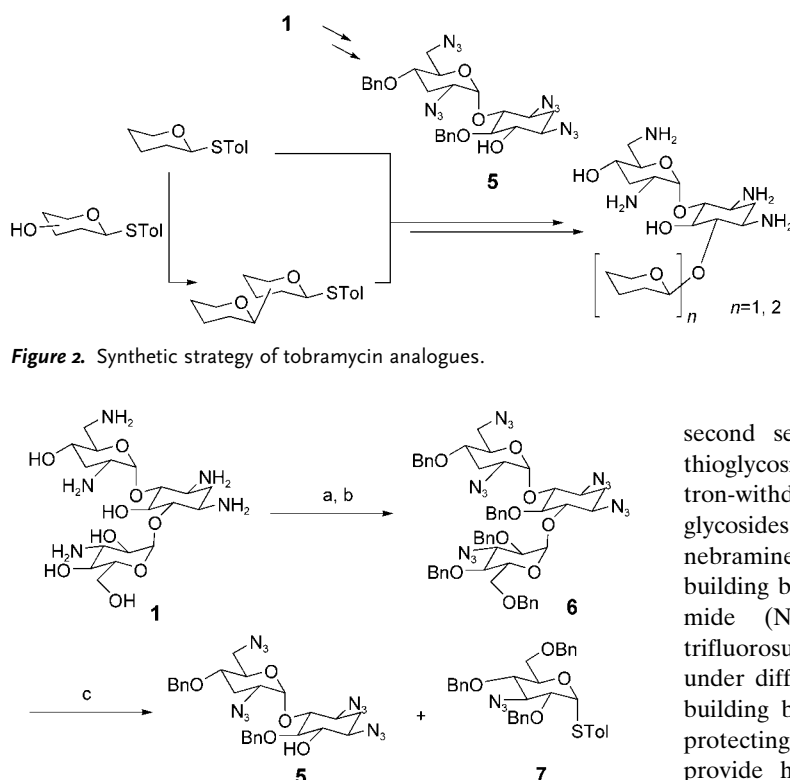


Figure 2. Synthetic strategy of tobramycin analogues.

Scheme 1. Synthesis of the protected nebramine core: a) TFN_3 , ZnCl_2 (cat.), NEt_3 , CH_2Cl_2 , H_2O , MeOH ; b) NaH , BnBr , TBAI , DMF , 82% (two steps); c) $p\text{-TolSH}$, $\text{BF}_3 \cdot \text{Et}_2\text{O}$, CH_2Cl_2 , **5** 43%, **7** 47%. Tf = triflate (CF_3SO_2), Bn = benzyl, TBAI = tetra-*n*-butylammonium iodide, DMF = *N,N*-dimethylformamide.

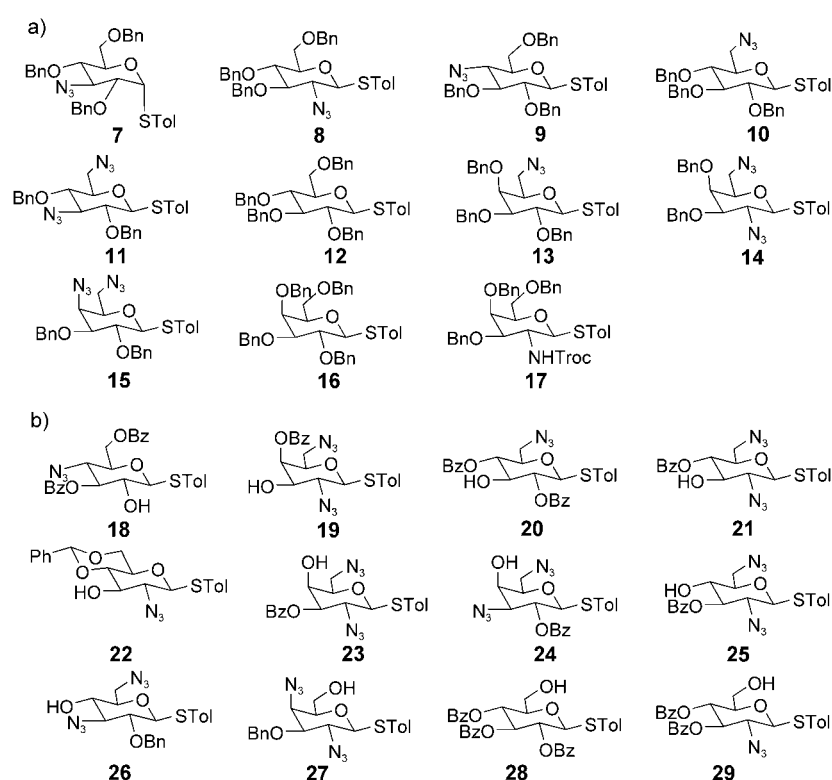
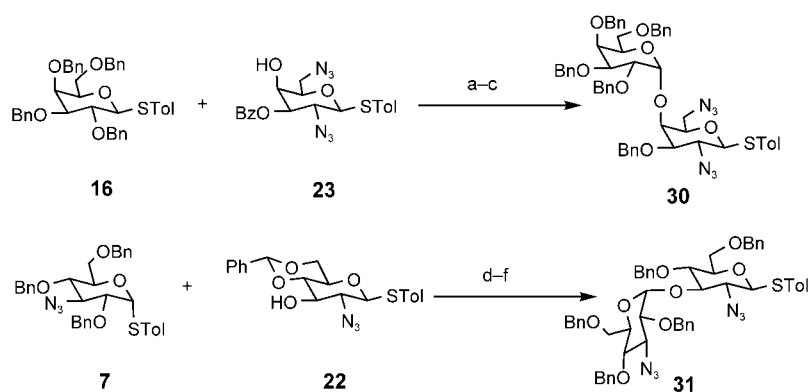


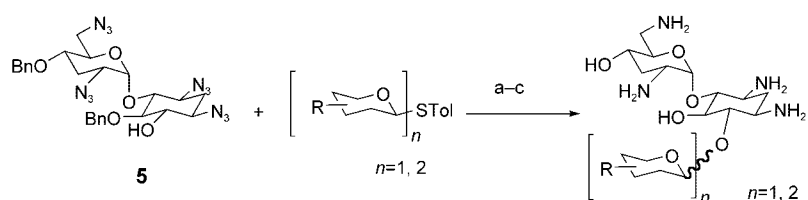
Figure 3. Thioglycoside building blocks as a) the first donors and b) the second donors. Tol = *p*-tolyl, Troc = trichloroethoxycarbonyl ($\text{CCl}_3\text{CH}_2\text{OC}(\text{O})-$), Bz = benzoyl.

be recovered as a thioglycoside building block and used in library synthesis.

A group of protected monosaccharide building blocks, which contained one or more amine groups, was then selected and synthesized from our thioglycoside building block database (Figure 3). Two sets of building blocks were chosen with significant differences in reactivity as glycosylation donors.^[10] The first set, which includes compounds **7–17**, contains thioglycoside donors with high reactivity which were designed by the introduction of electron-donating protecting groups (Figure 3a). The second set, which includes compounds **18–29**, contains thioglycoside donors with lower reactivity, tuned by electron-withdrawing protecting groups (Figure 3b). Thioglycosides **7–17** were either directly coupled to the protected nebramine core **5** or were used to assemble disaccharide building blocks with thioglycosides **18–29** by *N*-iodosuccinimide (NIS)- TfOH promoted glycosylation (TfOH = trifluoromethanesulfonic acid).^[11] After several unsuccessful attempts under different glycosylation conditions, these disaccharide building blocks were found to be relatively inactive. The protecting groups were then changed to benzyl groups to provide higher reactivity toward the nebramine core **5** (Scheme 2). Benzenesulfonylpiperidine (BSP) and Tf_2O were used as promoters for these glycosylation reactions (Scheme 3).^[12] Stereoisomers at the anomeric positions (α or β linkage) were usually formed in these glycosylation reactions and these were separated by column chromatog-



Scheme 2. Representative synthesis of disaccharide building blocks. a) NIS, TfOH, CH₂Cl₂, mol. sieves (4 Å), –45 °C; b) NaOMe/MeOH; c) NaH, BnBr, TBAI, DMF, 54 % (three steps); d) NIS, TfOH, CH₂Cl₂, mol. sieves (4 Å), –45 °C; e) AcOH, H₂O, 80 °C; f) NaH, BnBr, TBAI, DMF, 41 % (three steps). NIS = N-iodosuccinimide.



Scheme 3. Synthesis of tobramycin analogues. a) BSP, Tf₂O, CH₂Cl₂, mol. sieves (4 Å), –45 °C, 32–78 %; b) Raney Ni, N₂H₄, EtOH, dioxane; c) HCl (0.1 N), H₂, Pd(OH)₂ (20 %), MeOH/H₂O, 19–65 % (two steps). BSP = benzenesulfinylpiperidine.

raphy (silica gel). The number of different protecting groups used was kept to a minimum, with the use of only azido and benzyl groups to simplify the deprotection steps afterward.

Deprotection was completed by first, the reduction of the azido groups with Raney Nickel and anhydrous hydrazine and second, palladium hydroxide catalyzed hydrogenation under acidic conditions to remove the benzyl groups (Scheme 3), to give the tobramycin analogues **32–92** (Figure 4 and Supporting Information). An attempt to remove both groups in one step by hydrogenation in the presence of different palladium catalysts only gave mixtures of incompletely deprotected products probably owing to the poisoning of the catalysts by amines.^[13]

The SPR assay was then used to study the binding affinity and specificity of these tobramycin analogues with a number of short RNA sequences (24 to 48 bps), which were identified from sequence-conserved and functionally important regions of several disease-related bacterial, viral, or human RNAs, such as the bacterial ribosomal 16S A-site, *E. coli* transglycosidase mRNA, Hepatitis C virus (HCV) internal ribosome entry site (IRES) RNAs,^[14] HIV frameshift signal,^[15] HIV protease mRNA, human oncogenic Bcr-Abl mRNA,^[16] and human tyrosine sulfotransferase mRNA (Figure 5). The synthetic compound library as well as commercially available aminoglycosides and

macrolides were first screened at 1 μM against the above RNA molecules. By using tobramycin (**1**) and neomycin B (**3**) as standards, compounds with high binding signals were selected for the determination of dissociation constants (*K_d*).^[17] The *K_d* values of selected compounds from each RNA screening were determined for all RNA sequences in this study to examine the binding specificity (Table 1).

From the results of the binding assay, several molecules displayed an affinity in the nanomolar range to specific RNA sequences. Whereas all of the selected compounds showed some limited affinity toward the RNAs tested, several compounds exhibited higher affinity to specific RNAs. Tobramycin (**1**) showed a higher affinity to the HIV frameshift signal (0.64 μM, 2–100-fold selectivity); neomycin B (**3**) was more specific to the bacterial 16S A-site and the human tyrosine sulfotransferase mRNA (0.2 μM and 0.3 μM, 8–14-fold); sisomycin (**4**) was selective for the HCV IRES IIIId domain (0.26 μM, 5 to >100-fold); **33** displayed a relatively high affinity to the HCV IRES IIIId (0.7 μM, 1.6–5-fold); **34** also showed a high affinity to the HCV IRES IIIId (0.25 μM, 1.7–38-fold); **35** was selective for the HIV frameshift signal (0.32 μM, 5.6–

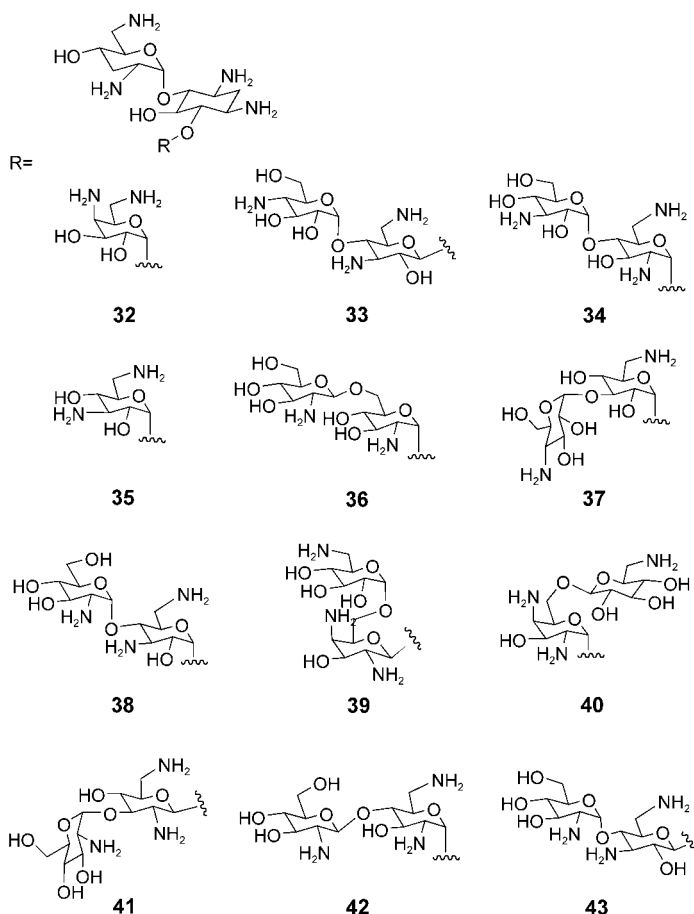


Figure 4. Selected tobramycin analogues (with R groups as shown) which were active in the SPR studies (structures of other synthesized analogues can be found in the Supporting Information).

bacterial ribosomal RNA 16S A-site (16S-AS)

5'-GGCGUCACACCUUCGGGUGAAGUCGCC-3'

E. coli transglycosidase mRNA (EcTG)

5'-GAAGACAGCCGCUUCUACGAGCAU-3'

HCV IRES domain IIb (HCV2b)

5'-CUGUCUUCACGCAGAAAGCGUCUAGCCAUGGCGUUAGUAUGAGUGUCG-3'

HCV IRES domain IIIId (HCV3d)

5'-GGCCGAGUAGUGUUGGGUCGCGAAAGGCC-3'

HIV frameshift signal (HIV-FSS)

5'-UUUUUUAGGGAAGAUUCGGCCUCCUACAAGGGAAGGCCAGGAAU-3'

HIV protease active site mRNA (HIV-PAS)

5'-GAAGCUUUUAGUAUACAGGAGCAGAUACAGUAUUA-3'

human oncogenic Bcr-Abl mRNA (hBcr-Abl)

5'-GGCUGACCAUCAAUAGGAAGAAGCCUUCACGGGCCAGUA-3'

human tyrosine sulfotransferase mRNA (hTSuT)

5'-GCCAACCCACCUAACUACGGAAACCUGAUCC-3'

Figure 5. RNA sequences used for the SPR binding assay. All RNA sequences were 5'-biotin-labeled and were heated to 80°C for 2 min and allowed to cool down slowly to refold into the most stable conformations before immobilization onto a streptavidin-coated sensor chip. SPR experiments were performed according to the procedure reported previously.^[17]

Table 1: K_d values [μ M] for selected compounds screened against different RNAs.^[a, b]

Compound	16S-AS	EcTG	HCV2b	HCV3d	HIV-FSS	HIV-PAS	hBcr-Abl	hTSuT
1	2.1	19	2.7	2.2	0.64	14	1.3	65
3	0.2	2.8	2.9	2.9	1.6	2	2	0.3
4	1.3	12	4.3	0.26	2.7	15	10	37
32	5.9	11	12	6.8	4.7	19	3.2	25
33	1.7	1.8	3	0.7	1.2	1.1	3.5	1.6
34	4.3	0.62	0.42	0.25	3.4	0.83	0.75	9.4
35	3	4.9	1.8	2.7	0.32	6.8	3.8	8.1
36	1.8	5.3	9.4	—	1	5.1	3.2	—
37	3.8	14	0.28	2.3	0.71	3	0.7	52
38	6.6	1	12	2.3	4.6	5	5	14
39	2.6	0.42	2.6	4	1.7	4	4	9.6
40	4.6	8	3.8	3.3	2	14	8.5	13
41	3.6	0.67	3.5	0.53	7.6	1.2	6.4	9.4
42	2.3	2.5	3.1	2	1.6	7	3.5	3.9
43	3.7	1.7	9.5	1	4.5	6	14	5.1

[a] RNA abbreviations used: 16S-AS: Bacterial 16S A-site; EcTG: *E. coli* transglycosidase mRNA; HCV2b: HCV IRES domain IIb; HCV3d: HCV IRES domain IIIId; HIV-FSS: HIV frameshift signal; HIV-PAS: HIV protease active site mRNA; Bcr-Abl: human oncogenic Bcr-Abl mRNA; hTSuT: human tyrosine sulfotransferase mRNA; [b] Errors of K_d values range from $\pm 5\%$ to $\pm 29\%$.

25-fold); **37** bound better to the HCV IRES IIb domain (0.28 μ M, 2.5 to >100-fold); **39** selectively bound the *E. coli* transglycosidase mRNA (0.42 μ M, 4–23-fold); **41** exhibited a high affinity to the HCV IRES IIIId domain and the *E. coli* transglycosidase mRNA (0.53 μ M and 0.67 μ M, 2–16-fold). The charges of the aminoglycosides tested range from +5 to +7. However, upon comparing the K_d values and the number of charges, no direct correlations were found.

In conclusion, we have developed an efficient method to replace a monosaccharide unit of tobramycin with another

monosaccharide or disaccharide moiety to form analogues of tobramycin. The SPR studies of the interactions of these analogues with certain RNA sequences show that new aminoglycosides can be created to target RNA in a sequence-selective manner. Work is in progress to further study the interactions of selected compounds and RNAs to understand the origin of selectivity and to design better RNA-binding molecules as inhibitors of translational processes in cell-based systems.

Received: May 5, 2004

Revised: June 15, 2004

Keywords: carbohydrates · drug design · glycosylation · RNA recognition · surface plasmon resonance

- [1] a) D. Ecker, R. H. Griffey, *Drug Discovery Today* **1999**, 4, 420; b) S. J. Sucheck, C.-H. Wong, *Curr. Opin. Chem. Biol.* **2000**, 4, 678; c) T. Hermann, *Angew. Chem.* **2000**, 112, 1962; *Angew. Chem. Int. Ed.* **2000**, 39, 1890; d) J. Gallego, G. Varani, *Acc. Chem. Res.* **2001**, 34, 836.

- [2] a) N. Ban, P. Nissen, J. Hansen, P. B. Moore, T. A. Steitz, *Science* **2000**, 289, 905; b) D. Moazed, H. F. Noller, *Nature* **1987**, 327, 389; c) F. Schlünzen, R. Zarivach, J. Harms, A. Bashan, A. Tocilj, R. Albrecht, A. Yonath, F. Franceschi, *Nature* **2001**, 413, 814; d) D.

Fourmy, M. I. Recht, S. C. Blanchard, J. D. Puglisi, *Science* **1996**, 274, 1367; e) Q. Vicens, E. Westhof, *ChemBioChem* **2003**, 4, 1018; f) Y. Tor, *ChemBioChem* **2003**, 4, 998.

- [3] a) M. Howard, R. A. Frizzell, D. M. Bedwell, *Nat. Med.* **1996**, 2, 467; b) G. Werstuck, M. R. Green, *Science* **1998**, 282, 296; c) W. Winkler, A. Nahvi, R. R. Breaker, *Nature* **2002**, 419, 952.

- [4] a) M. L. Zapp, S. Stern, M. R. Green, *Cell* **1993**, 74, 969; b) S. Wang, P. W. Huber, M. Cui, A. W. Czarnik, H.-Y. Mei, *Biochemistry* **1998**, 37, 5549; c) S. J. Sucheck, W. A. Greenberg, T. J. Tolbert, C.-H. Wong, *Angew. Chem.* **2000**, 112, 1122; *Angew. Chem. Int. Ed.* **2000**, 39, 1080; d) U. von Ahsen, J. Davies, R. Schroeder, *Nature* **1991**, 353, 368.

- [5] a) D. Fourmy, S. M. I. Recht, J. D. Puglisi, *J. Mol. Biol.* **1998**, 277, 347; b) S. Yoshizawa, D. Fourmy, J. D. Puglisi, *EMBO J.* **1998**, 17, 6437; c) A. P. Carter, W. M. J. Clemons,

D. E. Brodersen, R. J. Morgan-Warren, B. T. Wimberly, V. Ramakrishnan, *Nature* **2000**, 407, 340; d) Q. Vicens, E. Westhof, *Structure* **2001**, 9, 647; e) Q. Vicens, E. Westhof, *Chem. Biol.* **2002**, 9, 747.

- [6] C.-H. Wong, M. Hendrix, E. S. Priestley, W. A. Greenberg, *Chem. Biol.* **1998**, 5, 397.

- [7] a) S. R. Kirk, N. W. Luedtke, Y. Tor, *J. Am. Chem. Soc.* **2000**, 122, 980; b) S. J. Sucheck, A. L. Wong, K. M. Koeller, D. D. Boehr, K.-a. Draker, P. S. Sears, G. D. Wright, C.-H. Wong, *J. Am. Chem. Soc.* **2000**, 122, 5230; c) J. Haddad, L. P. Kotra, B. Llano-Sotelo, C. Kim, E. F. Azucena, Jr., M. Liu, S. B. Vakulenko, C. S. Chow, S. Mobashery, *J. Am. Chem. Soc.* **2002**, 124, 3229; d) S.

- Hanessian, M. Tremblay, E. E. Swayze, *Tetrahedron* **2003**, *59*, 983.
- [8] P. T. Nyffeler, C.-H. Liang, K. M. Koeller, C.-H. Wong, *J. Am. Chem. Soc.* **2002**, *124*, 10773.
- [9] B. Wu, J. Yang, Y. He, E. E. Swayze, *Org. Lett.* **2002**, *4*, 3455.
- [10] T. K. Ritter, K.-K. T. Mong, H. Liu, T. Nakatani, C.-H. Wong, *Angew. Chem.* **2003**, *115*, 4805; *Angew. Chem. Int. Ed.* **2003**, *42*, 4657.
- [11] a) P. Konradsson, U. E. Udodong, B. Fraser-Reid, *Tetrahedron Lett.* **1990**, *31*, 4313; b) Z. Zhang, I. R. Ollmann, X.-S. Ye, R. Wischnat, T. Baasov, C.-H. Wong, *J. Am. Chem. Soc.* **1999**, *121*, 734.
- [12] a) D. Crich, M. Smith, *J. Am. Chem. Soc.* **2001**, *123*, 9015; b) K.-K. T. Mong, H.-K. Lee, S. G. Durón, C.-H. Wong, *Proc. Natl. Acad. Sci. USA* **2003**, *100*, 797.
- [13] B. P. Czech, R. A. Bartsch, *J. Org. Chem.* **1984**, *49*, 4076.
- [14] a) P. J. Lukavsky, G. A. Otto, A. M. Lancaster, P. Sarnow, J. D. Puglisi, *Nat. Struct. Biol.* **2000**, *7*, 1105; b) C. M. T. Spahn, J. S. Kieft, R. A. Grassucci, P. A. Penczek, K. Zhou, J. A. Doudna, J. Frank, *Science* **2001**, *291*, 1959.
- [15] T. Jacks, M. D. Power, F. R. Masiarz, P. A. Luciw, P. J. Barr, H. E. Varmus, *Nature* **1988**, *331*, 280.
- [16] E. Shtivelman, B. Lifshitz, R. P. Gale, E. Canaani, *Nature* **1985**, *315*, 550.
- [17] C.-H. Wong, F.-S. Liang, *Methods Enzymol.* **2003**, *362*, 340.

(Figure 1) has extremely limited stability in solution and has been shown to undergo spontaneous Masamune–Bergman rearrangement without any external activator.^[6] Through this rearrangement, **1** generates *p*-benzyne biradical **2**, which

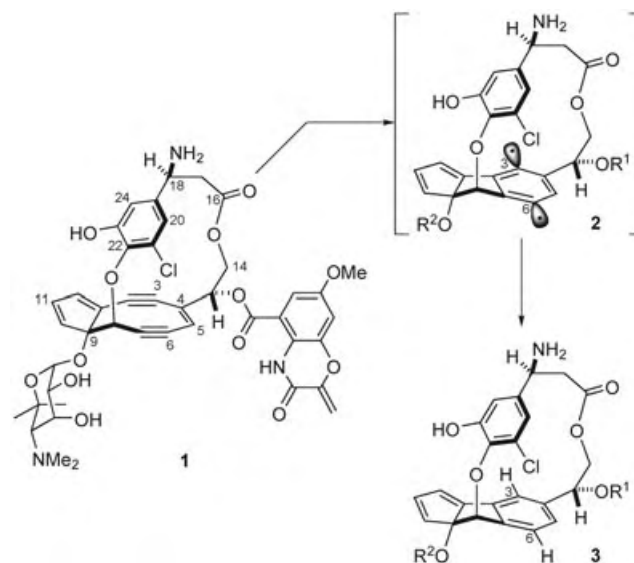


Figure 1. Structure of the C-1027 chromophore **1** and its Masamune–Bergman rearrangement to **3**.

Natural Products Synthesis

Synthesis of the C-1027 Chromophore Framework through Atropselective Macrolactonization^{**,*}

Masayuki Inoue,^{*} Takeo Sasaki, Suguru Hatano, and Masahiro Hirama^{*}

C-1027 is a chromoprotein enediyne natural product with potent in vitro and in vivo cytotoxicity against a variety of cancer cell lines.^[1] It is a member of the subset of enediyne antibiotics that includes neocarzinostatin,^[2] kedarcidin,^[3] and maduropeptin.^[4,5] Each of these agents is composed of protein and small-molecule (chromophore) components, which form a 1:1 complex. The C-1027 chromophore **1**

exerts its potent toxicity by abstracting hydrogen atoms (**2** → **3**) from the backbone of DNA to cleave the double strand.^[7] This chemical instability and its complex structure distinguish **1** as a challenging target for total synthesis.^[8–11]

The structure of **1** is highly unusual, characterized by a chlorocatechol-containing ansa-bridge, a strained bicyclo[7.3.0]dodecatrienediynyl, an appended benzoxazine,^[12] and an aminosugar.^[13] The synthetic challenge presented by **1** is heightened by the presence of nonbiaryl atropisomerism arising from hindered rotation of the chlorocatechol ring in the ansa-bridge.^[14,15] Herein we present the synthesis of the C-1027 chromophore framework through a newly designed atropselective macrocyclization.

Our synthetic strategy is outlined in Scheme 1. The total synthesis of **1** would be attained from its framework **4** by attaching the amino sugar^[16] and the benzoxazine, followed by introducing two olefins (C4–C5 and C11–C12).^[17] As the nine-membered diyne of **4** could be chemically unstable, as suggested by experiments on a model compound,^[18] the macrolactone system would have to be constructed prior to the nine-membered ring.^[19] We planned to form this strained nine-membered diyne **4** by LiN(TMS)₂/CeCl₃-promoted cyclization of **5**.^[16,17,19b,20] The highly unsaturated macrocycle **5** was to be synthesized through the coupling of the three fragments **6**, **7**, and **8** in a convergent manner.

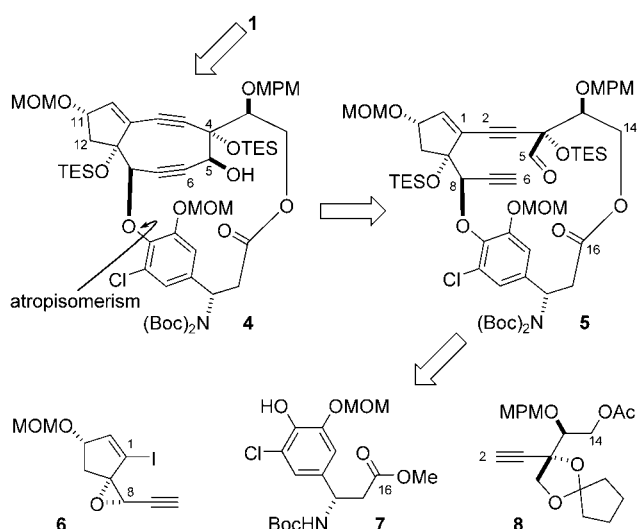
The synthesis of the five-membered ring **14** bearing the β-tyrosine moiety was improved from a previously published procedure,^[21] and started with the known intermediate **9** (Scheme 2).^[22] Nucleophilic addition of vinylmagnesium bromide to enone **9** occurred from the opposite side of the bulky TBS ether to afford tertiary alcohol **10** as the sole isomer.

[*] Prof. Dr. M. Inoue, Dr. T. Sasaki, S. Hatano, Prof. Dr. M. Hirama
Department of Chemistry
Graduate School of Science, Tohoku University
Sendai 980-8578 (Japan)
Fax: (+81) 22-217-6566
E-mail: inoue@ykbsc.chem.tohoku.ac.jp
hirama@ykbsc.chem.tohoku.ac.jp

Prof. Dr. M. Inoue
Research and Analytical Center for Giant Molecules
Graduate School of Science, Tohoku University
Sendai 980-8578 (Japan)

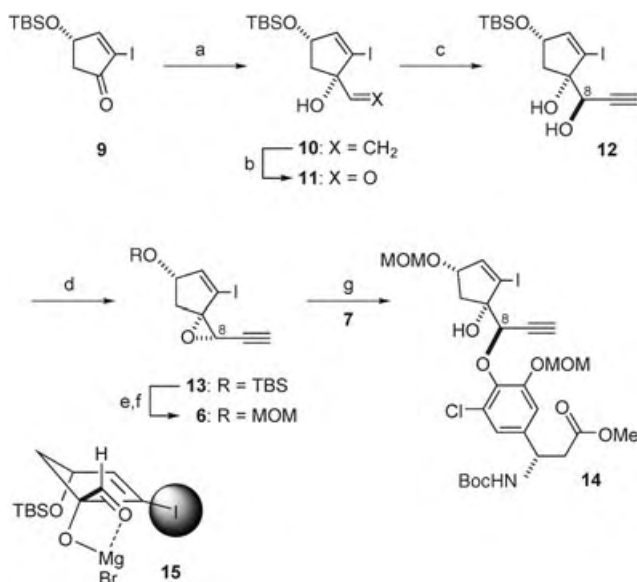
[**] This work was supported by CREST, Japan Science and Technology Agency (JST). A fellowship to T.S. from the Japanese Society for the Promotion of Science (JSPS) is gratefully acknowledged.

Supporting information for this article is available on the WWW under <http://www.angewandte.org> or from the author.



Scheme 1. Retrosynthesis of the C-1027 chromophore.

MOM = methoxymethyl, MPM = *p*-methoxyphenylmethyl, TES = triethylsilyl, Boc = *tert*-butoxycarbonyl.



Scheme 2. Reagents and conditions: a) $\text{CH}_2=\text{CHMgBr}$, Et_2O , $-70 \rightarrow 0^\circ\text{C}$, 83%; b) O_3 , $\text{CH}_2\text{Cl}_2/\text{MeOH}/\text{pyridine}$ (4:4:1), -80°C ; then Me_2S , $-60^\circ\text{C} \rightarrow \text{RT}$; c) $\text{HC}\equiv\text{CMgBr}$, toluene, $-85^\circ\text{C} \rightarrow \text{RT}$, 62% (over two steps); d) MsCl , CH_2Cl_2 , -70°C ; then DBU, $-70^\circ\text{C} \rightarrow \text{RT}$, 69%; e) TBAF, THF, 0°C , 95%; f) MOMCl, $i\text{Pr}_2\text{NEt}$, $(\text{CH}_2\text{Cl})_2$, 40°C , 86%; g) **7** (1.1 equiv), CsF, DMF, 75°C , 77%. TBS = *tert*-butyldimethylsilyl; Ms = methanesulfonyl; DBU = 1,8-diazabicyclo[5.4.0]undec-7-ene; TBAF = tetrabutylammonium fluoride; MOM = methoxymethyl; DMF = *N,N*-dimethylformamide.

Selective ozonolysis of the terminal olefin of **10** and subsequent reductive workup generated aldehyde **11**. Treatment of **11** with ethynylmagnesium bromide in toluene exclusively produced diol **12** bearing the β -hydroxy group at C8. The stereochemical outcome of the reaction was presumably governed by magnesium chelation and the presence of the bulky iodine, forcing the nucleophile to attack from the

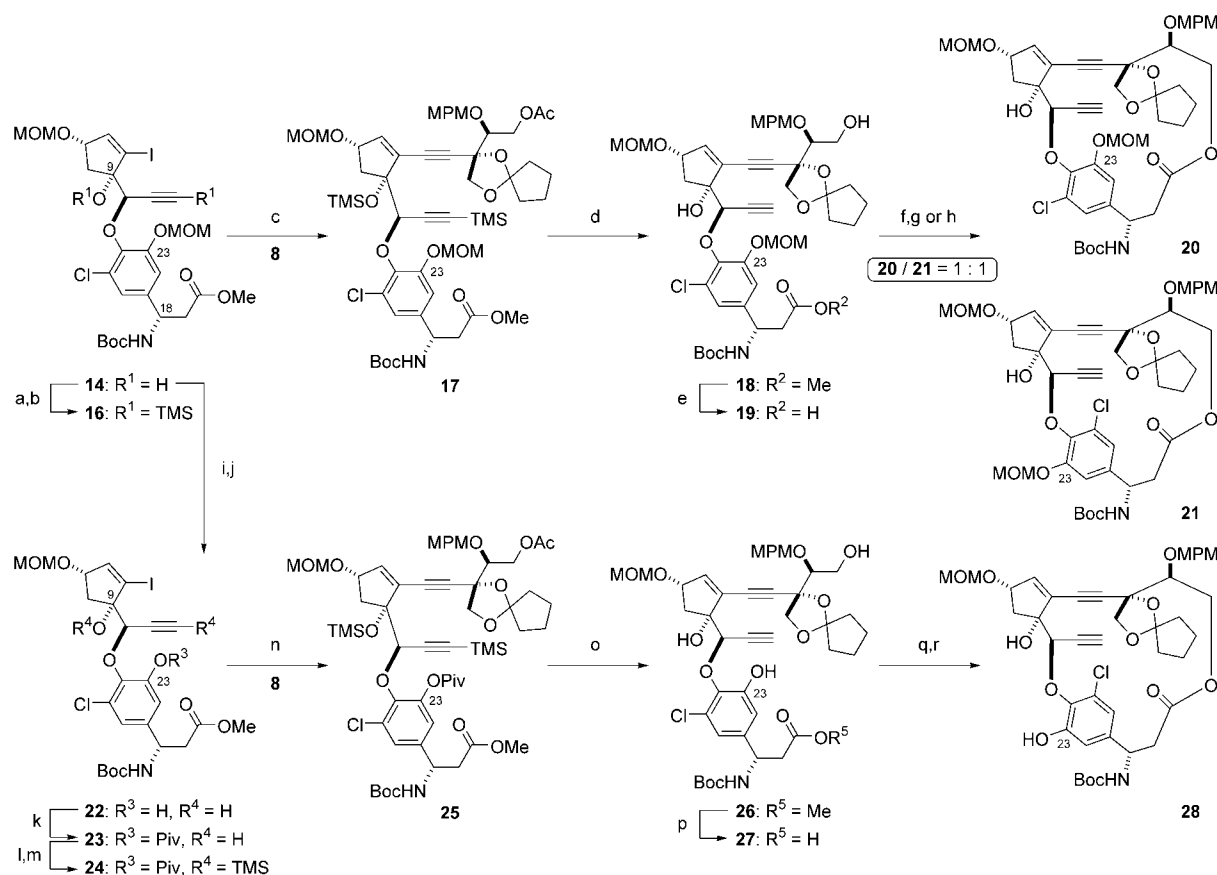
less hindered side of the five-membered chelate **15**. The secondary alcohol of **12** was selectively mesylated with MsCl and Et_3N , and the monomesylate was converted into epoxide **13** by the addition of DBU (one-pot reaction). Next, the TBS group of **13** was replaced by a MOM group to give **6** in a two-step sequence. Finally, the β -tyrosine moiety **7**^[21] was coupled to **6** by the action of CsF in DMF,^[23] leading to adduct **14**.

To evaluate potential strategies for the desired atropselective macrolactonization, substrate **19** was first synthesized (Scheme 3). The tertiary alcohol of **14** was converted into the TMS ether, and the TMS group was also introduced to the terminal acetylene to afford **16**. Sonogashira coupling^[24] of **16** with acetylene moiety **8**^[19a] in the presence of catalytic $[\text{Pd}(\text{PPh})_4]$ and CuI led to **17**. Treatment of **17** with K_2CO_3 in methanol resulted in simultaneous removal of the acetyl and two TMS groups to produce **18**, and subsequent saponification of the methyl ester of **18** with KOH gave rise to seco-acid **19**.

Macrolactonization of **19** was successfully realized by two methods, but with a non-atropselective outcome. Carboxylic acid **19** was treated with 2,2'-dipyridyl disulfide and PPh_3 to give the corresponding thioester, which was heated at reflux in toluene,^[25] resulting in the formation of macrolactone **20** and **21** in 50% yield (1:1).^[19a] A higher yield of **20** was achieved by the powerful method recently developed by Shiina and co-workers.^[26] Treatment of **19** with MNBA and DMAP at 40°C produced macrolactones **20** and **21** (1:1.1 ratio in 65% combined yield). Importantly, the ratio of the atropisomers was unaffected under the two different conditions, and thus the structure of the substrate was likely to be the decisive factor in the selectivity of the reaction. Furthermore, isomerization to enrich the desired atropisomer **20** was unsuccessful. Separate heating of atropisomers **20** and **21** at 160°C in deuterated 1,2-dichlorobenzene for 12 h did not result in isomerization, which suggests that these macrocycles are highly rigid.^[27,28] Consequently, selective formation of the desired atropisomer would be possible only by controlling the transition state of the macrolactonization by using an appropriately functionalized substrate.

To examine the effect of substituents of the aromatic ring on selectivity, the OMOM group at C23 of **19** was replaced with OH in the alternative substrate **27** (Scheme 3). First, bis-MOM ether **14** was successfully transformed into mono-MOM ether **22** by treatment with TFA and subsequent reattachment of Boc to the C18 amine. After conversion of phenol **22** into pivalate ester **23**, TMS groups were introduced at 9-OH and at the C6-methyne to produce Sonogashira coupling substrate **24**. Adduct **25** was then obtained by coupling **24** with **8** in the presence of catalytic Pd^0 and CuI. Deprotection of four protecting groups (two TMS, Ac, and Piv) from **25** with K_2CO_3 in methanol and subsequent treatment with KOH resulted in seco-acid **27** with the free 23-OH group. Surprisingly, macrolactonization of **27** by using the Corey–Nicolaou thioester method generated solely the undesired atropisomer **28** in modest yield.

From NOESY data and molecular modeling (Macro-Model Ver 8.0),^[29] all the macrolactones (**20**, **21**, and **28**) were found to have similar conformations. The structure of **28** is shown as a representative example (Figure 2), in which it can



be seen that the terminal acetylene and the chlorocatechol are perpendicular to the macrocycle plane. It is evident that the

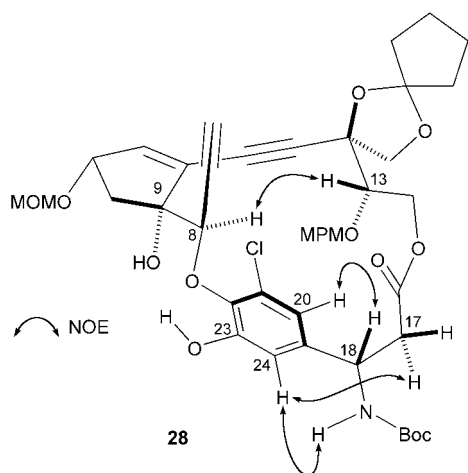


Figure 2. Three-dimensional structure of **28** based on NOESY data (C₆D₆) and molecular modeling.

1,5 hydroxy groups (9-OH and 23-OH) are in spatial proximity, suggesting hydrogen bonding. This hydrogen bonding could also fix the conformation of the transition state (Figure 3), which explains the sole formation of **28** from **27**. In the cyclization of **19**, the larger unfavorable steric

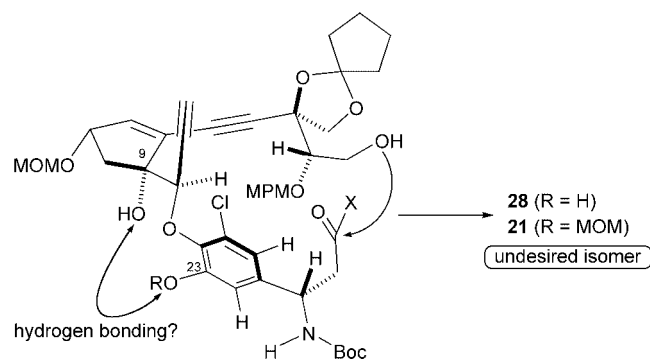


Figure 3. Potential hydrogen bonding in the transition state of the macrolactonization reaction.

interaction between the 23-OMOM group and the tertiary 9-OH group could counteract the attractive hydrogen bond, which could be the reason for the nonstereoselective outcome observed. Hence, the atropselectivity of the macrolactonization appears to be controlled by the balance between steric interaction and hydrogen bonding of the substituents at C9 and C23.

From these considerations, placement of a bulky protecting group on the tertiary 9-OH group could force an atropselective macrolactonization to the desired isomer, because both increased steric interaction with the 23-OMOM group and elimination of the hydrogen bond would impose an energetic penalty on the transition state of the unwanted atropisomer. For undertaking an experimental verification of this hypothesis, we designed a new macrolactonization substrate **31**, which bears 23-OMOM and 9-OTES groups (Scheme 4).

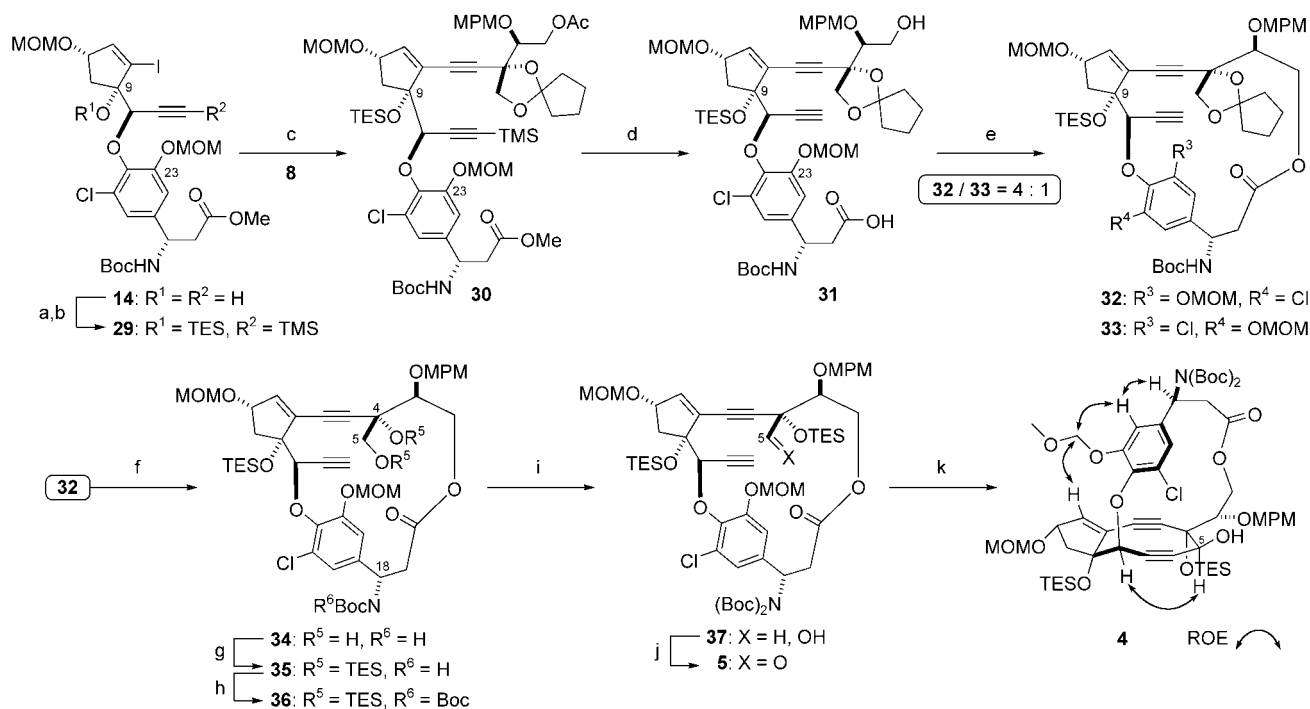
As shown in Scheme 4, seco-acid **31** was synthesized from **14** in a route similar to that used for **19**. The TES group was introduced at the tertiary alcohol function of **14**, and the acetylene moiety was transformed to its TMS-protected form **29**. Condensation of **8** and **29** under Sonogashira conditions led to diyne **30**, whose acetate, methyl esters, and TMS group were hydrolyzed with KOH in THF/MeOH/H₂O, without affecting the TES ether, giving **31**.

Atropselective macrolactonization of seco-acid **31** was effected by using the MNBA method. Upon treatment of **31** with MNBA and DMAP in refluxing CH₂Cl₂, the desired isomer **32** was formed with 4:1 atropselectivity and isolated in

61% yield.^[31] Remarkably, the yield of the desired atropisomer (**32** versus **20**) was doubled by strategic protection of the 9-OH group.

With the desired ansa macrolide **32** in hand, our next focus was to construct the nine-membered diyne ring. Before doing so, the reaction conditions of protecting- and functional-group manipulations were carefully tuned. First, the cyclopentylidene ketal of **32** was selectively removed with TFOH in CF₃CH₂OH/THF^[30] without affecting other acid-labile protecting groups (MOM, TES, MPM, and Boc) to afford 1,2-diol **34**. After conversion of **34** into tris-TES ether **35**, another Boc group was introduced by using (Boc)₂O and DMAP to mask the acidic 18-NH proton of **35**, leading to biscarbamate **36**.^[32] The primary alcohol at C5 was selectively deprotected by using HF·py to produce **37**, which was oxidized to aldehyde **5** with (COCl)₂ and DMSO.

Cyclization of **5** was promoted by a 1:1 mixture of LiN(TMS)₂ and CeCl₃ in THF from –50°C to room temperature, giving rise to the strained nine-membered diyne **4** as the sole isomer in 30% yield. Thus, this LiN(TMS)₂/CeCl₃ reagent combination proved to be applicable to the highly complex and conformationally rigid system **5**. The stereochemical structure of **4**, including the newly formed β secondary alcohol, was unambiguously determined by ROESY experiments in [D₆]DMSO. The correct atropisomerism of **4** was again confirmed at this stage, indicating the high energy barrier to rotation of the chlorocatechol in all the synthetic intermediates. Diyne **4** slowly decomposed at room temperature, presumably through Cope rearrangement, as



Scheme 4. Reagents and conditions: a) TESCl, imidazole, DMF, room temperature, 98%; b) TMSCl, LiN(TMS)₂, THF, –78°C, 87%; c) **8** (1.2 equiv), [Pd(PPh₃)₄] (20 mol%), CuI (40 mol%), iPr₂NEt, DMF, room temperature, 80%; d) KOH, THF/H₂O/MeOH (5:1:1), 90%; e) MNBA (2.4 equiv), DMAP (4.8 equiv), CH₂Cl₂ (1 mm), 40°C, slow addition of **31** over 12 h, 61% (**32**), 15% (**33**), 5% (dimer); f) TFOH, CF₃CH₂OH/THF (5:1), 65%; g) TESCl, imidazole, DMF, 40°C, 93%; h) (Boc)₂O, DMAP, MeCN, 40°C, 100%; i) HF·py, THF, 0°C, 78%; j) (COCl)₂, DMSO, Et₃N, CH₂Cl₂, –78°C, 100%; k) LiN(TMS)₂ (58 equiv), CeCl₃ (61 equiv), THF (1 mm), –50→0°C, 30%. Tf = trifluoromethanesulfonyl, DMSO = dimethyl sulfoxide.

demonstrated with previously synthesized model compounds.^[33]

In conclusion, we achieved the stereoselective synthesis of the C-1027 chromophore framework through atropselective macrolactonization. The key features in this synthesis were 1) strategic protection of a 1,5-diol to attain atropselective macrocyclization, and 2) LiN(TMS)₂/CeCl₃-promoted acetylide-aldehyde condensation to build the nine-membered diyne ring in a highly unsaturated and heavily substituted macrocycle. Further studies on the total synthesis of the C-1027 chromophore from **4** are currently underway in this laboratory.

Received: July 26, 2004

Keywords: alkynes · antitumor agents · atropisomerism · lactones · macrocycles

- [1] a) T. Otani, Y. Minami, T. Marunaka, R. Zhang, M.-Y. Xie, *J. Antibiot.* **1988**, *41*, 1580–1585; b) Y. Zhen, S. Ming, Y. Bin, T. Otani, H. Saito, Y. Yamada, *J. Antibiot.* **1989**, *42*, 1294–1298.
- [2] *Neocarzinostatin* (Eds.: H. Maeda, K. Edo, N. Ishida), Springer, Tokyo, **1997**.
- [3] a) J. E. Leet, D. R. Schroeder, S. J. Hofstead, J. Golik, K. L. Colson, S. Huang, S. E. Kloor, T. W. Doyle, J. A. Matson, *J. Am. Chem. Soc.* **1992**, *114*, 7946–7948; b) S. Kawata, S. Ashizawa, M. Hiram, *J. Am. Chem. Soc.* **1997**, *119*, 12012–12013.
- [4] D. R. Schroeder, K. L. Colson, S. E. Kloor, N. Zein, D. R. Langley, M. S. Lee, J. A. Matson, T. W. Doyle, *J. Am. Chem. Soc.* **1994**, *116*, 9351–9352.
- [5] For a review on chromoprotein antibiotics and other enediyne natural products, see: Z. Xi, I. H. Goldberg in *Comprehensive Natural Products Chemistry*, Vol. 7 (Eds.: D. H. R. Barton, K. Nakanishi), Elsevier, Dordrecht, **1999**, pp. 553–592.
- [6] a) Y. Minami, K. Yoshida, R. Azuma, M. Saeki, T. Otani, *Tetrahedron Lett.* **1993**, *34*, 2633–2636; b) K. Yoshida, Y. Minami, R. Azuma, M. Saeki, T. Otani, *Tetrahedron Lett.* **1993**, *34*, 2637–2640; c) K. Yoshida, Y. Minami, T. Otani, Y. Tada, M. Hiram, *Tetrahedron Lett.* **1994**, *35*, 5253–5256; d) K. Iida, S. Fukuda, T. Tanaka, M. Hiram, S. Imajo, M. Ishiguro, K. Yoshida, T. Otani, *Tetrahedron Lett.* **1996**, *37*, 4997–5000.
- [7] a) Y. Sugiura, T. Matsumoto, *Biochemistry* **1993**, *32*, 5548–5553; b) Y. Xu, X. Zhen, Y. Zhen, I. H. Goldberg, *Biochemistry* **1995**, *34*, 12451–12460.
- [8] Total syntheses of the nine-membered ring enediynes were reported: N-1999A2: a) S. Kobayashi, S. Ashizawa, Y. Takahashi, Y. Sugiura, M. Nagaoka, M. J. Lear, M. Hiram, *J. Am. Chem. Soc.* **2001**, *123*, 11294–11295; neocarzinostatin chromophore: b) A. G. Myers, J. Liang, M. Hammond, P. M. Harrington, Y. Wu, E. Y. Kuo, *J. Am. Chem. Soc.* **1998**, *120*, 5319–5320; c) A. G. Myers, R. Glatthar, M. Hammond, P. M. Harrington, E. Y. Kuo, J. Liang, S. E. Schaus, Y. Wu, J.-N. Xiang, *J. Am. Chem. Soc.* **2002**, *124*, 5380–5401.
- [9] For recent synthetic studies of the enediyne natural products from this laboratory, see: neocarzinostatin chromophore: a) K. Toyama, S. Iguchi, H. Sakazaki, T. Oishi, M. Hiram, *Bull. Chem. Soc. Jpn.* **2001**, *74*, 997–1008; kedarcidin: b) F. Yoshimura, S. Kawata, M. Hiram, *Tetrahedron Lett.* **1999**, *40*, 8281–8285; c) I. Ohashi, M. J. Lear, F. Yoshimura, M. Hiram, *Org. Lett.* **2004**, *6*, 719–722; maduropeptin: d) N. Kato, S. Shimamura, Y. Kikai, M. Hiram, *Synlett* **2004**, 2107–2110, and references therein.
- [10] For the synthesis of the protected kedarcidin chromophore aglycon, see: A. G. Myers, P. C. Hogan, A. R. Hurd, S. D. Goldberg, *Angew. Chem.* **2002**, *114*, 1104–1109; *Angew. Chem. Int. Ed.* **2002**, *41*, 1062–1066.
- [11] For reviews on the syntheses of enediyne compounds, see: a) K. C. Nicolaou, W.-M. Dai, *Angew. Chem.* **1991**, *103*, 1453–1481; *Angew. Chem. Int. Ed. Engl.* **1991**, *30*, 1387–1416; b) S. J. Danishefsky, M. D. Shair, *J. Org. Chem.* **1996**, *61*, 16–44.
- [12] M. Shibuya, H. Sakurai, T. Maeda, E. Nishiwaki, M. Saito, *Tetrahedron Lett.* **1986**, *27*, 1351–1354.
- [13] a) K. Iida, T. Ishii, M. Hiram, T. Otani, Y. Minami, K. Yoshida, *Tetrahedron Lett.* **1993**, *34*, 4079–4082; b) M. F. Semmelhack, Y. Jiang, D. Ho, *Org. Lett.* **2001**, *3*, 2403–2406.
- [14] For a review, see: P. Lloyd-Williams, E. Giralt, *Chem. Soc. Rev.* **2001**, *30*, 145–157.
- [15] Only a few examples have been reported on the stereoselective synthesis of nonbiaryl stereogenic axes in natural product syntheses; see: a) D. A. Evans, M. R. Wood, B. W. Trotter, T. I. Richardson, J. C. Barrow, J. L. Katz, *Angew. Chem.* **1998**, *110*, 2864–2868; *Angew. Chem. Int. Ed.* **1998**, *37*, 2700–2703; b) D. A. Evans, C. J. Dinsmore, P. S. Watson, M. R. Wood, T. I. Richardson, B. W. Trotter, J. L. Katz, *Angew. Chem.* **1998**, *110*, 2868–2872; *Angew. Chem. Int. Ed.* **1998**, *37*, 2704–2708; c) M. E. Layton, C. A. Morales, M. D. Shair, *J. Am. Chem. Soc.* **2002**, *124*, 773–775; d) K. C. Nicolaou, C. N. C. Boddy, *J. Am. Chem. Soc.* **2002**, *124*, 10451–10455; see also references [9b] and [10].
- [16] I. Sato, Y. Akahori, T. Sasaki, T. Kikuchi, M. Hiram, *Chem. Lett.* **1999**, 867–868.
- [17] M. Inoue, S. Hatano, M. Kodama, T. Sasaki, T. Kikuchi, M. Hiram, *Org. Lett.* **2004**, *6*, 3833–3836.
- [18] K. Iida, M. Hiram, *J. Am. Chem. Soc.* **1994**, *116*, 10310–10311.
- [19] a) T. Sasaki, M. Inoue, M. Hiram, *Tetrahedron Lett.* **2001**, *42*, 5299–5303; b) M. Inoue, T. Kikuchi, M. Hiram, *Tetrahedron Lett.* **2004**, *45*, 6439–6442.
- [20] For other studies on bicyclo[7.3.0]dodecadiyne formation, see: a) P. A. Wender, M. Harmata, D. Jeffery, C. Mukai, J. Suffert, *Tetrahedron Lett.* **1988**, *29*, 909–912; b) P. A. Wender, J. A. McKinney, C. Mukai, *J. Am. Chem. Soc.* **1990**, *112*, 5369–5370; c) T. Doi, T. Takahashi, *J. Org. Chem.* **1991**, *56*, 3465–3467; d) P. Magnus, R. Carter, M. Davies, J. Elliott, T. Pittner, *Tetrahedron* **1996**, *52*, 6283–6306; e) H. Tanaka, H. Yamada, A. Matsuda, T. Takahashi, *Synlett* **1997**, 381–383; f) S. Caddick, V. M. Delisser, V. E. Doyle, S. Khan, A. G. Avent, S. Vile, *Tetrahedron* **1999**, *55*, 2737–2754, and references therein.
- [21] I. Sato, T. Kikuchi, M. Hiram, *Chem. Lett.* **1999**, 511–512.
- [22] a) M. Hiram, T. Gomibuchi, K. Fujiwara, Y. Sugiura, M. Uesugi, *J. Am. Chem. Soc.* **1991**, *113*, 9851–9853; b) C. R. Johnson, M. P. Braun, *J. Am. Chem. Soc.* **1993**, *115*, 11014–11015.
- [23] S. Kawata, M. Hiram, *Tetrahedron Lett.* **1998**, *39*, 8707–8710.
- [24] K. Sonogashira in *Comprehensive Organic Synthesis*, Vol. 3 (Eds.: B. M. Trost, I. Fleming), Pergamon, London, **1990**, pp. 521–549.
- [25] E. J. Corey, K. C. Nicolaou, *J. Am. Chem. Soc.* **1974**, *96*, 5614–5616.
- [26] a) I. Shiina, M. Kubota, R. Ibuka, *Tetrahedron Lett.* **2002**, *43*, 7535–7539; b) I. Shiina, M. Kubota, H. Oshiumi, M. Hashizume, *J. Org. Chem.* **2004**, *69*, 1822–1830.
- [27] For an excellent example of the selective isomerization of atropisomers in the context of a total synthesis of vancomycin, see: D. L. Boger, S. Miyazaki, S. H. Kim, J. H. Wu, S. L. Castle, O. Loiseleur, Q. Jin, *J. Am. Chem. Soc.* **1999**, *121*, 10004–10011.
- [28] Interestingly, the facile atropisomerism of kedarcidin synthetic intermediates has been observed: A. G. Myers, A. R. Hurd, P. C. Hogan, *J. Am. Chem. Soc.* **2002**, *124*, 4583–4585. see also reference [10].

- [29] F. Mohamadi, N. G. J. Richards, W. C. Guida, R. Liskamp, M. Lipton, C. Caufield, G. Chang, T. Hendrickson, W. C. Still, *J. Comput. Chem.* **1990**, *11*, 440–467.
- [30] J. L. Halcombe, T. Livinghouse, *J. Org. Chem.* **1986**, *51*, 111–114.
- [31] Yamaguchi lactonization of **31** gave **32** in lower yield (**32**: 33 %, **33**: 6 %, dimer: 30 %): J. Inanaga, K. Hirata, H. Saeki, T. Katsuki, M. Yamaguchi, *Bull. Chem. Soc. Jpn.* **1979**, *52*, 1989–1993.
- [32] Bis-Boc protection of the amine was found to have a dramatic effect on the yield of the nine-membered ring cyclization.^[19b]
- [33] Cope rearrangement of the nine-membered cyclic 1,5-diyne to the bisallene is considered to be the major decomposition pathway.^[18]

Natural Products Synthesis

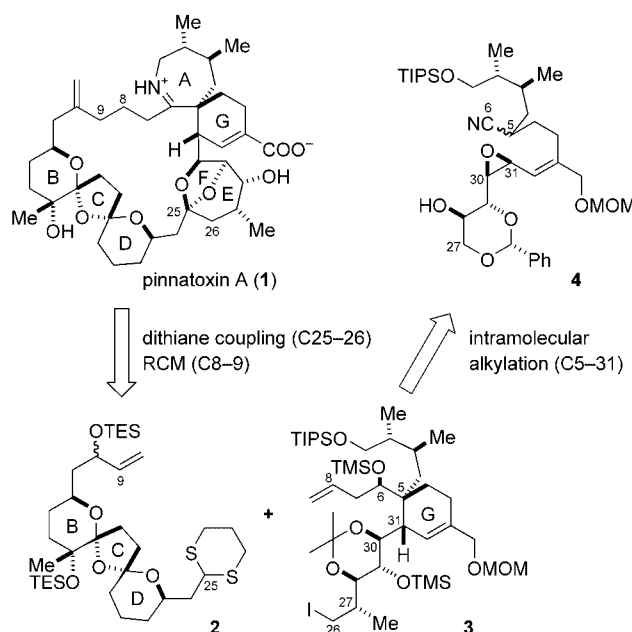
A Formal Total Synthesis of (+)-Pinnatoxin A**

Satoshi Sakamoto, Hayato Sakazaki, Koji Hagiwara,
Kei Kamada, Kento Ishii, Takeshi Noda,
Masayuki Inoue,* and Masahiro Hirama*

In 1995, Uemura and co-workers reported the isolation and characterization of pinnatoxin A (**1**, Scheme 1),^[1,2] one of the major toxic principles responsible for outbreaks of *Pinna* shellfish poisonings in China and Japan. The precise biological activity has not been clarified, but **1** has been suggested to be a Ca²⁺-channel activator.^[3] Structurally, **1** features a spiro-linked cyclic imine along with trioxadispiro- and bicycloacetal substructures within a 27-membered macrocycle. The novel

chemical and biological aspects of **1** render it an intriguing and challenging target. Indeed, a number of synthetic approaches have been described to date.^[4–6] The only total synthesis of **1** was reported by Kishi in 1998,^[7] an achievement further highlighted by the determination of the absolute configuration of **1** and the development of a biomimetic intramolecular Diels–Alder reaction to construct the G ring along with the macrocycle. Herein, we describe our own efforts in this area which have culminated in a formal total synthesis of natural (+)-pinnatoxin A.

Our synthetic strategy toward (+)-**1** targeted an optimally convergent route in which two complex fragments (**2** and **3**) were to be constructed, coupled, and elaborated to form the macrocyclic system (Scheme 1). We envisaged assembling **2**



Scheme 1. Retrosynthesis of pinnatoxin A. MOM = methoxymethyl; TES = triethylsilyl; TIPS = triisopropylsilyl; TMS = trimethylsilyl.

and **3** through a dithiane coupling reaction at C25; the polyether macrocycle would then emerge from ring-closing olefin metathesis reaction (RCM)^[8] to link C8 and C9, and subsequent EF-ring formation. Ring G was to be constructed by using intramolecular cyclization of epoxy nitrile **4**,^[9] which would set the stereochemistry of the C5 quaternary center, as demonstrated in our model studies on simple substrates.^[4c,d]

The synthesis of the BCD bispiroacetal **2** began with previously reported compound **5**^[4a] (Scheme 2). Sharpless asymmetric epoxidation^[10] of allylic alcohol **5** with (+)-diethyl tartrate provided **6**. Oxidation of alcohol **6** to aldehyde **7** with SO₃·py/DMSO followed by treatment with vinylmagnesium bromide produced epoxy alcohol **8** as a 1:1 diastereomeric mixture. Subsequent reductive opening of epoxide **8** with Red-Al in Et₂O resulted in the formation of 1,3-diol **9** as the major isomer.^[11] After protection of **9** as its acetone, chemo- and enantioselective dihydroxylation of the C15–C16 olefin was realized under Sharpless conditions in the presence of (DHQD)₂PHAL,^[12] which exclusively produced the desired

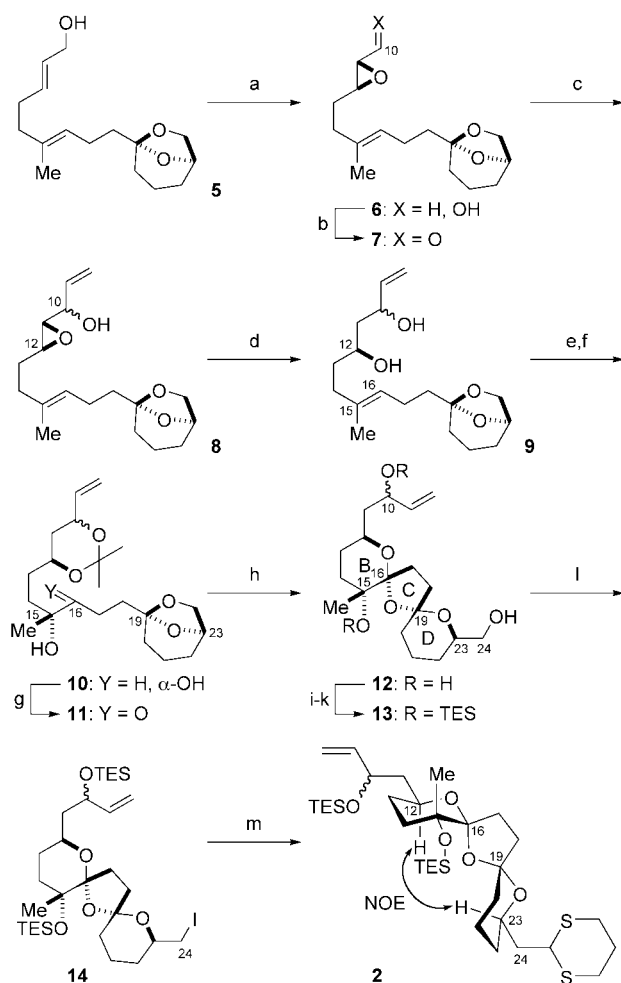
[*] Dr. S. Sakamoto, H. Sakazaki, K. Hagiwara, K. Kamada, K. Ishii, Prof. Dr. M. Inoue, Prof. Dr. M. Hirama
Department of Chemistry
Graduate School of Science, Tohoku University
Sendai 980-8578 (Japan)
Fax: (+81) 22-217-6566
E-mail: inoue@ykbsc.chem.tohoku.ac.jp
hirama@ykbsc.chem.tohoku.ac.jp

Prof. Dr. T. Noda
Department of Applied Chemistry
Faculty of Engineering, Kanagawa Institute of Technology
Atsugi 243-0292, (Japan)

Prof. Dr. M. Inoue
Research and Analytical Center for Giant Molecules
Graduate School of Science, Tohoku University
Sendai 980-8578 (Japan)

[**] This work was supported by CREST, Japan Science and Technology Agency (JST). A fellowship to H.S. from the Japan Society for the Promotion of Science (JSPS) is gratefully acknowledged. We thank Professor Y. Kishi (Harvard University) for providing NMR spectra of synthetic intermediates, Professor D. Uemura (Nagoya University) for providing natural pinnatoxin A, and Professor K. Nagasawa (Tokyo University of Agriculture and Technology) for helpful discussions.

Supporting information for this article is available on the WWW under <http://www.angewandte.org> or from the author.



Scheme 2. Reagents and conditions: a) *t*BuOOH, Ti(O*i*Pr)₄ (0.2 equiv), (+)-DET (0.2 equiv), molecular sieves (4 Å), CH₂Cl₂, –20 °C, 83%; b) SO₃·py, Et₃N, DMSO, CH₂Cl₂, room temperature; c) CH₂=CHMgBr, THF, –40 °C, 74% (over two steps); d) NaAlH₂(OCH₂CH₂OCH₃)₂, Et₂O, –20→0 °C; then NaIO₄, THF/H₂O (1:1), room temperature, 90%; e) 2-methoxypropene, *p*-TsOH, DMF, room temperature, 91%; f) OsO₄ (1 mol%), (DHQD)₂PHAL (1.5 mol%), K₂[Fe(CN)₆] (3 equiv), K₂CO₃ (3.5 equiv), MeSO₂NH₂ (1 equiv), *t*BuOH/H₂O (1:1), 0 °C; g) SO₃·py, Et₃N, DMSO, room temperature, 82% (over two steps); h) CSA (0.1 equiv), MeOH, room temperature, 3 h; then CSA, toluene, room temperature, 2 days, 84% (**12**), 11% (C19-epimer); i) PivCl, CH₂Cl₂/pyridine (2:1), 0 °C→RT; j) TESOTf, 2,6-lutidine, CH₂Cl₂, 0 °C; k) DIBAL-H, THF, –78 °C, 75% (over three steps); l) I₂, Ph₃P, imidazole, THF, room temperature, 91%; m) 1,3-dithiane, *n*BuLi, THF/HMPA (4:1), –78 °C, 83%. DET = diethyl tartrate; DMSO = dimethyl sulfoxide; Ts = *p*-toluenesulfonyl; DMF = *N,N*-dimethylformamide; (DHQD)₂PHAL = hydroquinidine 1,4-phthalazinediyl diether; CSA = (+)-camphorsulfonic acid; Piv = pivaloyl; Tf = trifluoromethanesulfonyl; DIBAL-H = diisobutylaluminum hydride; HMPA = hexamethylphosphoramide.

1,2-diol **10** without oxidizing the terminal olefin. Then, oxidation with SO₃·py converted secondary alcohol **10** into ketone **11**.

The crucial bispiroacetalization of **11** necessitated fine-tuning of the reaction conditions.^[13] First, **11** was exposed to camphorsulfonic acid in methanol at room temperature to remove the acetonide, and then methanol was replaced with

toluene to increase the ratio of the desired isomer **12**. In this way, **12** was selectively generated out of four possible isomers in 84% yield. As depicted in Figure 1, favorable intramolecular hydrogen bonding between free hydroxy groups at C10

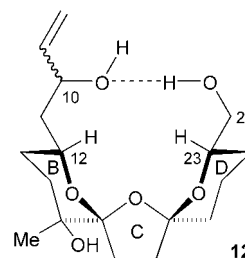


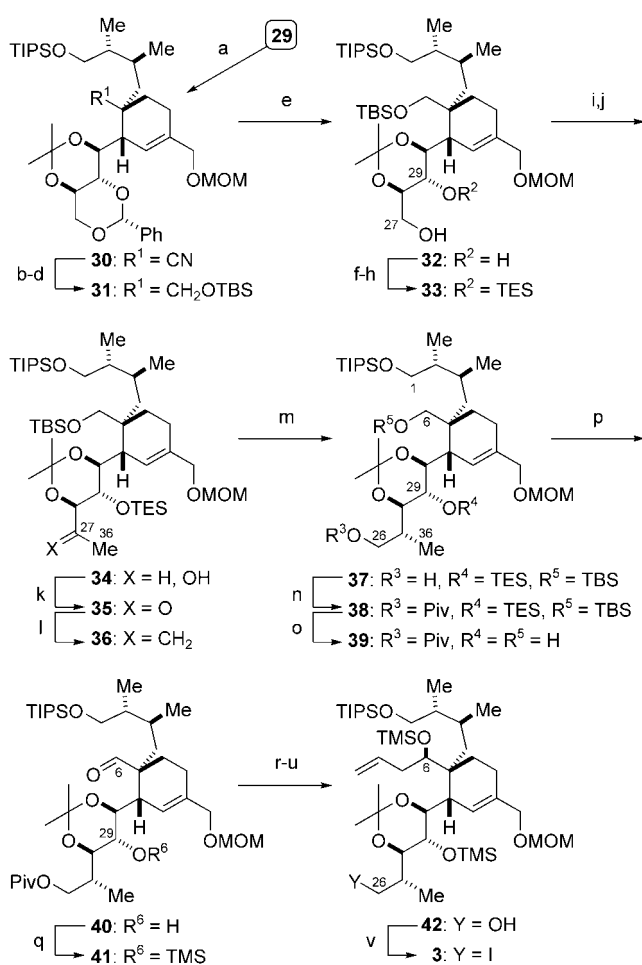
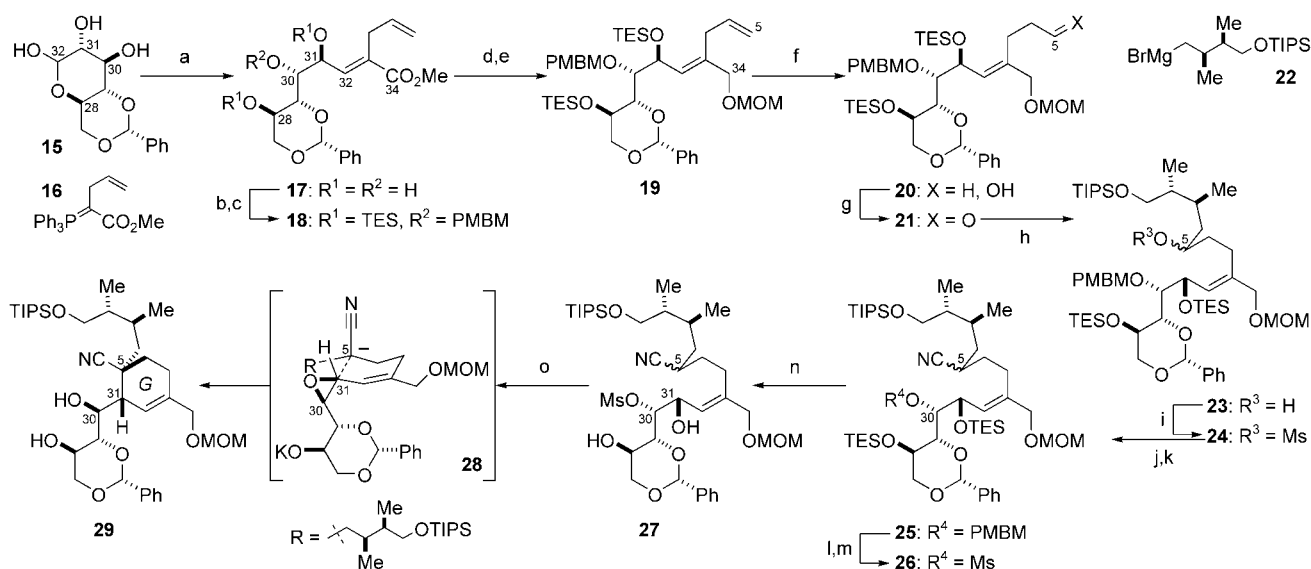
Figure 1. Potential intramolecular hydrogen bond in **12**.

and C24 is considered to influence the high selectivity for **12**.^[14] Next, the 10-OH and 15-OH groups of **12** were protected as their TES ethers through a three-step sequence to afford **13**, whose 24-OH function was converted into iodide to give **14**. Finally, nucleophilic attack of lithiodithiane at **14** delivered the BCD-ring fragment **2**, suitably functionalized for assembly of the fragments. The configurations of the C16 and C19 stereocenters established during the spiroacetalization were unambiguously determined by NOE experiments at this stage.

Synthesis of the other half of the molecule began with 4,6-*O*-benzylidene-D-glucose (**15**)^[15] (Scheme 3). Wittig reaction of **15** with ylide **16**^[16] in refluxing THF afforded olefin (*E*)-**17**. The hydroxy groups at C28 and C31 of **17** were selectively protected as TES ethers, and PMBM^[17] was introduced to protect the remaining 30-OH to produce **18**. Reduction with DIBAL-H and subsequent protection with MOMCl converted ester **18** into MOM ether **19**. Then, chemoselective hydroboration^[18] of the terminal olefin of diene **19** generated alcohol **20**, which was oxidized to aldehyde **21** with SO₃·py. Addition of Grignard reagent **22**^[4d] to **21** extended the carbon chain corresponding to the A-ring to furnish **23**. The secondary alcohol of **23** was derivatized to mesylate **24**, after which the mesylate was replaced by a nitrile group through the action of Et₄NCN to provide **25** after reattachment of the partially cleaved TES groups (1:1 diastereomeric mixture at C5). Replacement of the PMBM group of **25** with the Ms group in two steps and subsequent selective removal of TES from **26** with HF·py resulted in diol **27**.

Stereoselective G-ring formation from **27** was induced by an excess of KN(TMS)₂.^[4c,d] After treating mesylate **27** with KN(TMS)₂ (2.5 equiv) in THF to promote the C30–C31 epoxide formation,^[19] additional KN(TMS)₂ (1.5 equiv) was introduced to the reaction mixture, giving rise to the desired product **29** as the sole isomer in 72% yield.^[20] Not only is the stereoselectivity quite remarkable, but the reactions efficiently install consecutive C5 quaternary and C31 tertiary centers. The selectivity is consistent with cyclization through transition state **28** in which the large branched carbon chain preferentially adopts the equatorial orientation.

Having constructed the G-ring, we turned our attention to stereoselective introduction of the C36-methyl group and



elongation of the carbon chain at C6 (Scheme 4). First, 1,3-diol **29** was converted into acetone **30**, of which stepwise reduction to the alcohol and subsequent protection with TBS afforded **31**. Then, deprotection of the benzylidene acetal of **31** under Birch conditions produced diol **32**, and the secondary alcohol at C29 was quantitatively protected as its TES ether to give **33** in a three-step sequence. Oxidation of the remained primary alcohol of **33** with SO₃·py followed by addition of MeMgBr led to secondary alcohol **34**, which was further oxidized to ketone **35**. Treatment of **35** with the Tebbe reagent^[21] resulted in exo olefin **36**. Regio- and stereo-selective hydroboration of diene **36** was realized with 9-BBN to generate **37** with the desired C36-methyl stereochemis-

try.^[22] Primary alcohol **37** was in turn transformed into pivaloyl ester **38**, from which the silyl protecting groups (except TIPS) were removed with TBAF to afford **39**. After selective oxidation of diol **39** with PDC to form aldehyde **40**, the 29-OH group was converted into the TMS ether to afford **41**. Addition of allylmagnesium bromide to the C6 aldehyde of **41** and a subsequent reprotection-deprotection sequence gave **42**. Lastly, introduction of iodine at C26 of alcohol **42** furnished **3**, appropriately functionalized for the next coupling reaction.

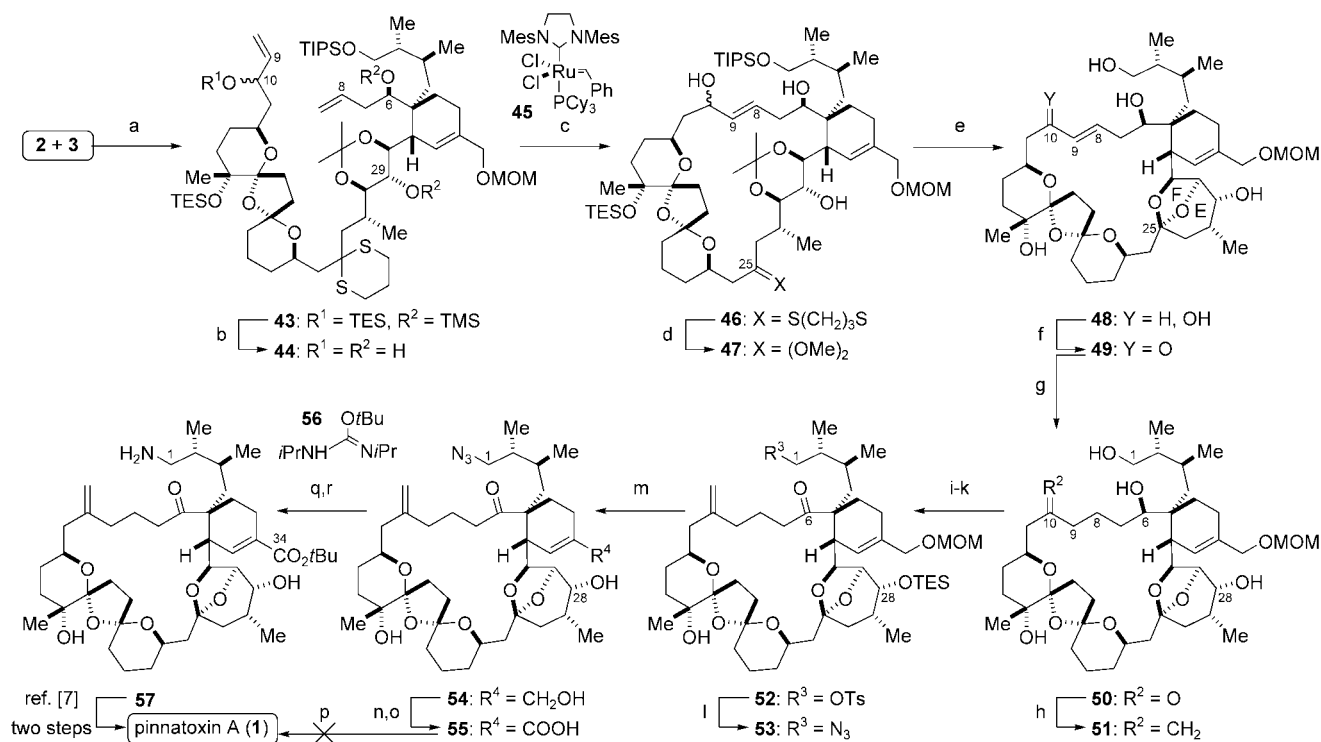
The stage was now set for union of the two highly complex structural fragments **2** and **3** and subsequent macrocyclization by RCM (Scheme 5). Lithiation of dithiane **2** with *t*BuLi in THF/HMPA at -78°C was immediately followed by addition of a precooled solution of iodide **3**,^[23] delivering the coupling adduct **43** in 95% yield based on recovered **3**. After many unsuccessful attempts to effect the macrocyclization of **44**, it was found that the silyl protecting groups proximal to the terminal olefins impeded the RCM reaction, presumably owing to steric shielding of the reaction sites. Therefore, the TES (10-OH) and two TMS groups (6-, 29-OH) were selectively removed with TBAF at 0°C to produce triol **44**. Gratifyingly, macro-RCM reaction of **44** was enabled by the action of Grubbs catalyst **45**,^[24] resulting in the formation of 27-membered carbocycle **46** with the *E* olefin (75% yield).

Prior to construction of the EF-ring system within the obtained macrocycle, dithiane **46** was transformed into

dimethyl acetal **47** with the Stork reagent $((\text{CF}_3\text{CO}_2)_2\text{I}^+\text{Ph}, \text{MeOH})$.^[25] Then, **47** was sequentially subjected to TFA/MeOH and CSA/MeOH,^[26] which led to deprotection of the acetonide and silyl protecting groups, and concomitant cyclization of the desired EF-ring of **48** in 71% yield over the sequence. Notably, the preexisting trioxadispiroacetal moiety was left intact under these acidic conditions.

With the synthesis of the entire macrocyclic structure of **1** completed, the end game for the total synthesis entailed specific functional-group manipulations of the highly complicated molecule. The C10 allylic alcohol of pentaol **48** was oxidized with DDQ to afford α,β -unsaturated ketone **49**,^[27] which was converted into ketone **50** by 1,4-reduction of the C8–C9 double bond with the Stryker reagent.^[28] The exo methylene group was then introduced at C10 of **50** by Wittig reaction to provide **51**. The Ts and TES groups were sequentially introduced to 1-OH and 28-OH of **51**, respectively, and the 6-OH group was oxidized with Dess–Martin periodinane^[29] to give ketone **52**. Displacement of tosylate by azide generated **53**, which was treated with acid to remove the MOM and TES groups, affording triol **54**. Allylic alcohol **54** was then oxidized to carboxylic acid **55** in a two-step sequence (MnO_2 ^[30] then NaClO_2).

To obtain pinnatoxin A (**1**) directly from **55**, intramolecular aza-Wittig reaction of azide **55** was attempted in the presence of PMe_3 .^[4d] However, **1** was not detected in the reaction products, and the amine was only obtained through



Scheme 5. Reagents and conditions: a) *t*BuLi (1.9 equiv), **2** (1.7 equiv), THF/HMPA (9:1), -78°C , 95% based on recovered **3** (41%); b) TBAF, THF, 0°C , 89%; c) **45** (0.1 equiv), CH_2Cl_2 , reflux, 75%; d) $(\text{CF}_3\text{CO}_2)_2\text{I}^+\text{Ph}$, molecular sieves (3 Å), MeOH/ CH_2Cl_2 (20:9), room temperature; e) TFA/MeOH (1:20), room temperature; then CSA, MeOH, room temperature, 71% (over two steps); f) DDQ, 1,4-dioxane/ CH_2Cl_2 (1:1), 40°C , 67%; g) $[(\text{Ph}_3\text{P})\text{CuH}]_3$ (0.1 equiv), toluene/ H_2O (100:1), room temperature, 64%; h) $\text{Ph}_3\text{PCH}_3\text{Br}$, *t*BuOK, THF, 0°C , 64%; i) *p*-TsCl, Et_3N , DMAP, molecular sieves (4 Å), CH_2Cl_2 , room temperature; j) TESCl, imidazole, CH_2Cl_2 , room temperature, 51% (over two steps); k) Dess–Martin periodinane, CH_2Cl_2 ; l) NaN_3 , DMF, 80°C , 68% (over two steps); m) aqueous HCl (2 N)/THF (1:10), 40°C , 96%; n) MnO_2 , CH_2Cl_2 , room temperature; o) NaClO_2 , NaH_2PO_4 , 2-methyl-2-butene, *t*BuOH/ H_2O (4:1), 0°C ; p) PMe_3 , THF, 60°C , 0% (**1**); q) **56**, toluene, 70°C , 34% (over three steps); r) PMe_3 , THF/ H_2O (10:1), room temperature, 60%.

hydrolysis of the resultant N=P bond. Therefore, we elected to complete the formal total synthesis of **1** simply by reduction of the C1 azide and esterification of the C34 carboxylic acid. Introduction of *t*Bu to **55** with **56**^[31] and subsequent treatment with PMe₃ in THF/H₂O^[32] gave rise to amine **57**, which had been transformed into **1** by Kishi in two steps.^[33] Our synthetic **57** showed ¹H NMR data that was identical to that provided by Professor Kishi.

In summary, we have reported the formal total synthesis of (+)-pinnatoxin A in a highly convergent fashion. The salient methodologies employed in our successful campaign include 1) stereoselective bis-acetalization to yield the BCD-ring fragment **2** effected by exploiting intramolecular hydrogen bonding; 2) intramolecular alkylation of epoxynitrile **4** to construct the G-ring; 3) powerful dithiane coupling to unify the two halves of the molecule (**2** and **3**); 4) macrocyclization of 27-membered carbocycle **46** by utilizing olefin metathesis reaction; and 5) intramolecular acetalization of the complex macrocycle to construct EF-ring **49**.

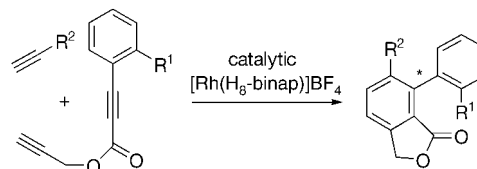
Received: August 27, 2004

Keywords: heterocycles · macrocycles · natural products · spiro compounds · total synthesis

- [1] a) D. Uemura, T. Chou, T. Haino, A. Nagatsu, S. Fukuzawa, S. Zheng, H. Chen, *J. Am. Chem. Soc.* **1995**, *117*, 1155–1156; b) T. Chou, O. Kamo, D. Uemura, *Tetrahedron Lett.* **1996**, *37*, 4023–4026.
- [2] For the structural determination of related molecules, see: pinnatoxin B,C: a) N. Takada, N. Umemura, K. Suenaga, T. Chou, A. Nagatsu, T. Haino, K. Yamada, D. Uemura, *Tetrahedron Lett.* **2001**, *42*, 3491–3494; pinnatoxin D: b) T. Chou, T. Haino, M. Kuramoto, D. Uemura, *Tetrahedron Lett.* **1996**, *37*, 4027–4030; spiroolides: c) T. Hu, J. M. Curtis, Y. Oshima, M. A. Quilliam, J. A. Walter, W. M. Watson-Wright, J. L. C. Wright, *J. Chem. Soc. Chem. Commun.* **1995**, 2159–2161; d) M. Falk, I. W. Burton, T. Hu, J. A. Walter, J. L. C. Wright, *Tetrahedron* **2001**, *57*, 8659–8665; pteriattoxins: e) N. Takada, N. Umemura, K. Suenaga, D. Uemura, *Tetrahedron Lett.* **2001**, *42*, 3495–3497.
- [3] S. Z. Zheng, F. L. Huang, S. C. Chen, X. F. Tan, J. B. Zuo, J. Peng, R. W. Xie, *Chin. J. Mar. Drugs* **1990**, *33*, 33–35.
- [4] For synthetic studies of **1** from this laboratory, see: a) T. Noda, A. Ishiwata, S. Uemura, S. Sakamoto, M. Hiram, *Synlett* **1998**, 298–300; b) A. Ishiwata, S. Sakamoto, T. Noda, M. Hiram, *Synlett* **1999**, 692–694; c) A. Nitta, A. Ishiwata, T. Noda, M. Hiram, *Synlett* **1999**, 695–696; d) J. Wang, S. Sakamoto, K. Kamada, A. Nitta, T. Noda, H. Oguri, M. Hiram, *Synlett* **2003**, 891–893.
- [5] For synthetic studies of **1** from other laboratories, see: a) T. Sugimoto, J. Ishihara, A. Murai, *Tetrahedron Lett.* **1997**, *38*, 7379–7382; b) J. Ishihara, T. Sugimoto, A. Murai, *Synlett* **1998**, 603–606; c) B. D. Suthers, M. F. Jacobs, W. Kitching, *Tetrahedron Lett.* **1998**, *39*, 2621–2624; d) T. Sugimoto, J. Ishihara, A. Murai, *Synlett* **1999**, 541–544; e) J. Ishihara, S. Tojo, A. Kamikawa, A. Murai, *Chem. Commun.* **2001**, 1392–1393; f) S. Nakamura, J. Inagaki, T. Sugimoto, M. Kudo, M. Nakajima, S. Hashimoto, *Org. Lett.* **2001**, *3*, 4075–4078; g) S. Nakamura, J. Inagaki, M. Kudo, T. Sugimoto, K. Obara, M. Nakajima, S. Hashimoto, *Tetrahedron* **2002**, *58*, 10353–10374; h) S. Nakamura, J. Inagaki, T. Sugimoto, Y. Ura, S. Hashimoto, *Tetrahedron* **2002**, *58*, 10375–10386.
- [6] For synthetic studies of spiroolides, see: a) D. P. Furkert, M. A. Brimble, *Org. Lett.* **2002**, *4*, 3655–3658; b) M. Trzoss, M. A. Brimble, *Synlett* **2003**, 2042–2046, and references therein.
- [7] a) J. A. McCauley, K. Nagasawa, P. A. Lander, S. G. Mischke, M. A. Semones, Y. Kishi, *J. Am. Chem. Soc.* **1998**, *120*, 7647–7648; b) K. Nagasawa, *J. Synth. Org. Chem. Jpn.* **2000**, *58*, 877–886.
- [8] For reviews, see: a) A. Fürstner, *Angew. Chem.* **2000**, *112*, 3140–3172; *Angew. Chem. Int. Ed.* **2000**, *39*, 3013–3043; b) T. M. Trnka, R. H. Grubbs, *Acc. Chem. Res.* **2001**, *34*, 18–29; c) *Handbook of Metathesis*, Vol. 2 (Ed.: R. H. Grubbs), Wiley-VCH, Weinheim, **2003**.
- [9] a) G. Stork, L. D. Cama, D. R. Coulson, *J. Am. Chem. Soc.* **1974**, *96*, 5268–5270; b) G. Stork, J. F. Cohen, *J. Am. Chem. Soc.* **1974**, *96*, 5270–5272; for a review, see: c) F. F. Fleming, B. C. Shook, *Tetrahedron* **2002**, *58*, 1–23.
- [10] a) Y. Gao, R. M. Hanson, J. M. Klunder, S. Y. Ko, H. Masamune, K. B. Sharpless, *J. Am. Chem. Soc.* **1987**, *109*, 5765–5780; b) T. Katsuki, V. S. Martin, *Org. React.* **1996**, *48*, 1–299.
- [11] J. M. Finan, Y. Kishi, *Tetrahedron Lett.* **1982**, *23*, 2719–2722.
- [12] a) G. A. Crispino, K. S. Jeong, H. C. Kolb, Z. M. Wang, D. Xu, K. B. Sharpless, *J. Org. Chem.* **1993**, *58*, 3785–3786; b) P. G. Andersson, K. B. Sharpless, *J. Am. Chem. Soc.* **1993**, *115*, 7047–7048; for a review, see: b) H. C. Kolb, M. S. VanNieuwenhze, K. B. Sharpless, *Chem. Rev.* **1994**, *94*, 2483–2547.
- [13] For a recent review on synthesis of bis-spiroacetals, see: M. A. Brimble, F. F. Farès, *Tetrahedron* **1999**, *55*, 7661–7706.
- [14] Existence of this intramolecular hydrogen bond was suggested from the X-ray analysis of a closely related substrate with free hydroxy groups at C10 and C24.^[4a] Furthermore, acidic treatment of a 10-OH-protected substrate resulted in nonselective formation of the desired spiroacetal and its C19-epimer despite the seemingly favorable anomeric effect at C19 of the desired compound.
- [15] P. L. Barili, G. Berti, G. Catelani, C. Cini, F. D'Andrea, E. Mastrorilli, *Carbohydr. Res.* **1995**, *278*, 43–57.
- [16] a) H. J. Bestmann, *Angew. Chem.* **1965**, *77*, 651–666; *Angew. Chem. Int. Ed. Engl.* **1965**, *4*, 645–660; b) R. S. Mali, S. G. Tilve, S. N. Yeola, A. R. Manekar, *Heterocycles* **1987**, *26*, 121–127.
- [17] A. P. Kozikowski, J.-P. Wu, *Tetrahedron Lett.* **1987**, *28*, 5125–5128.
- [18] H. C. Brown, R. Liotta, C. G. Scouten, *J. Am. Chem. Soc.* **1976**, *98*, 5297–5301.
- [19] The intermediacy of epoxide **4** was supported by its isolation without the subsequent addition of KN(TMS)₂.
- [20] The stereochemistry of C5 and C31 were determined by X-ray crystallographic analysis of an analogue derivatized from **29**; see Supporting Information for detail.
- [21] F. N. Tebbe, G. W. Parshall, G. S. Reddy, *J. Am. Chem. Soc.* **1978**, *100*, 3611–3613.
- [22] W. C. Still, J. C. Barrish, *J. Am. Chem. Soc.* **1983**, *105*, 2487–2489.
- [23] a) D. R. Williams, S.-Y. Sit, *J. Am. Chem. Soc.* **1984**, *106*, 2949–2954; b) A. B. Smith III, S. M. Condon, J. A. McCauley, J. L. Leazer, Jr., J. W. Leahy, R. E. Maleczka, Jr., *J. Am. Chem. Soc.* **1997**, *119*, 947–961; c) A. B. Smith III, S. M. Condon, J. A. McCauley, *Acc. Chem. Res.* **1998**, *31*, 35–46.
- [24] M. Scholl, S. Ding, C. W. Lee, R. H. Grubbs, *Org. Lett.* **1999**, *1*, 953–956.
- [25] G. Stork, K. Zhao, *Tetrahedron Lett.* **1989**, *30*, 287–290.
- [26] While initial treatment with TFA mainly removed the TMS and TES groups, the TIPS and acetonide groups were deprotected by subjection to CSA/MeOH. This stepwise deprotection scheme appears to be superior to a single-step approach in terms of yield.
- [27] a) H.-D. Becker, A. Björk, E. Adler, *J. Org. Chem.* **1980**, *45*, 1596–1600; b) E. J. Corey, C. Shih, N.-Y. Shih, K. Shimoji, *Tetrahedron Lett.* **1984**, *25*, 5013–5016.

- [28] W. S. Mahoney, D. M. Brestensky, J. M. Stryker, *J. Am. Chem. Soc.* **1988**, *110*, 291–293.
- [29] D. B. Dess, J. C. Martin, *J. Am. Chem. Soc.* **1991**, *113*, 7277–7287.
- [30] T. Aoyama, N. Sonoda, M. Yamauchi, K. Toriyama, M. Anzai, A. Ando, T. Shioiri, *Synlett* **1998**, 35–36.
- [31] L. J. Mathias, *Synthesis* **1979**, 561–576.
- [32] For related examples, see: a) B. M. Trost, S. R. Pulley, *Tetrahedron Lett.* **1995**, *36*, 8737–8740; b) J. Zhu, D. Ma, *Angew. Chem.* **2003**, *115*, 5506–5509; *Angew. Chem. Int. Ed.* **2003**, *42*, 5348–5351.
- [33] Kishi reported that heating **57** at 200 °C under vacuum and treating the resultant imine with TFA afforded pinnatoxin A (**1**).^[7]

cyclotrimerization of terminal alkynes and an electron-deficient alkyne (diethyl acetylene dicarboxylate) catalyzed by the cationic $[\text{Rh}^{\text{I}}(\text{H}_8\text{-binap})]$ complex.^[10] We anticipated that cross cyclotrimerization of terminal alkynes and electron-deficient 1,6-diynes (bearing a *ortho*-substituted phenyl group and a hydrogen atom at each terminal position) would install the axial chirality during the formation of the benzene rings (Scheme 1).^[11–14] Very recently, Gutnov, Heller, and co-work-



Scheme 1. Cationic $[\text{Rh}^{\text{I}}(\text{H}_8\text{-binap})]$ -catalyzed cross alkyne cyclotrimerization to give axially chiral phthalides.

Biaryl Compounds

Enantioselective Synthesis of Axially Chiral Phthalides through Cationic $[\text{Rh}^{\text{I}}(\text{H}_8\text{-binap})]$ -Catalyzed Cross Alkyne Cyclotrimerization**

Ken Tanaka,* Goushi Nishida, Azusa Wada, and Keiichi Noguchi

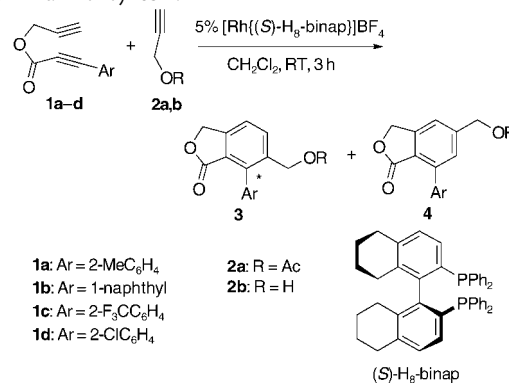
Axially chiral biaryl compounds are widely found as key structures of effective chiral ligands and biologically active compounds. Therefore, several catalytic enantioselective syntheses of these compounds have been developed to date. These methods are based on three types of asymmetric cross-coupling approaches: 1) cross-coupling of aryl compounds (such as the Kumada coupling,^[1] Suzuki coupling,^[2] and oxidative coupling^[3]), 2) cross-coupling of biaryl ditriflates,^[4] and 3) cross-coupling of dinaphthothiophene.^[5] In these reactions, the axial chirality is constructed during the formation of the biaryl link, the selective substitution of one of two triflates, and the selective cleavage of one of two carbon–sulfur bonds, respectively.^[6,7]

Cyclotrimerization of alkynes is an attractive method for the synthesis of substituted benzenes, and various transition-metal complexes catalyze this reaction.^[8] We recently reported the chemo- and regioselective intermolecular cross

ers reported the synthesis of axially chiral 2-aryl pyridines through the Co^{I} -catalyzed asymmetric $[2 + 2 + 2]$ cycloaddition of alkynes and nitriles,^[15] and Shibata et al. reported the synthesis of axially chiral teraryl compounds through a neutral $[\text{Ir}^{\text{I}}(\text{Me-duphos})]$ complex catalyzed asymmetric $[2 + 2 + 2]$ cycloaddition of symmetrical α,ω -diynes and symmetrical monoynes.^[16] Herein we describe a highly enantioselective synthesis of axially chiral phthalides by the cationic $[\text{Rh}^{\text{I}}(\text{H}_8\text{-binap})]$ complex catalyzed cross alkyne cyclotrimerization of unsymmetrical α,ω -diynes and unsymmetrical or symmetrical monoynes.^[17]

The reaction of 2-methylphenyl-substituted 1,6-diyne **1a** with various terminal monoynes was investigated in the presence of the cationic complex $[\text{Rh}^{\text{I}}((S)\text{-H}_8\text{-binap})]$. We were pleased to find that the use of propargyl acetate (**2a**; 5 equiv) furnished axially chiral phthalide (+)-**3aa** in high yield with high enantioselectivity (Table 1, entry 1). Not only

Table 1: Enantioselective cross alkyne cyclotrimerization of 1,6-diynes **1** and terminal monoynes **2**.



Entry	1	2	Phthalide	Yield [%] ^[a]	3/4	ee (3) [%]
1	1a	2a	(+)- 3aa / 4aa	79	90:10	87
2	1b	2a	(-)- 3ba / 4ba	91	88:12	82
3	1c	2a	(-)- 3ca / 4ca	86	66:34	81
4	1d	2a	(-)- 3da / 4da	91	87:13	73
5	1a	2b	(+)- 3db / 4db	90	70:30	78

[a] Yields of isolated products.

[*] Prof. Dr. K. Tanaka, G. Nishida, A. Wada
Department of Applied Chemistry, Graduate School of Engineering
Tokyo University of Agriculture and Technology
Koganei, Tokyo, 184-8588 (Japan)
Fax: (+81) 42-388-7037
E-mail: tanaka-k@cc.tuat.ac.jp

Prof. Dr. K. Noguchi
Instrumentation Analysis Center
Tokyo University of Agriculture and Technology
Koganei, Tokyo 184-8588 (Japan)

[**] This work was supported by Mitsubishi Chemical Corporation Fund and Asahi Glass Fund. We thank Takasago International Corporation for the gift of $\text{H}_8\text{-binap}$.

Supporting information for this article is available on the WWW under <http://www.angewandte.org> or from the author.

2-methylphenyl-, but also 1-naphthyl- (**1b**, Table 1, entry 2), 2-trifluoromethylphenyl- (**1c**, Table 1, entry 3), and 2-chlorophenyl-substituted 1,6-diynes (**1d**, Table 1, entry 4) were suitable substrates in this process. Importantly, the generation of sterically demanding regioisomers **3** was predominant. In the case of **1d**, the use of propargyl alcohol (**2b**) improved the enantioselectivity (Table 1, entry 5).

Interestingly, the use of symmetrical internal monoyne, 1,4-diacetoxy-2-butyne (**2c**; 5 equiv), enhanced the enantioselectivity to yield axially chiral phthalides **3ac–dc** in good yield with excellent enantioselectivity (Table 2, entries 1–4).

Table 2: Enantioselective cross alkyne cyclotrimerization of 1,6-diynes **1** and internal monoynes **2**.

Entry	1	2	Phthalide	Yield [%] ^[a]	ee [%]
1	1a	2c	(+)- 3ac	67	> 99
2	1b	2c	(+)- 3bc	57	94
3	1c	2c	(+)- 3cc	73	> 99
4	1d	2c	(+)- 3dc	45	86
5 ^[b]	1a	2d	(+)- 3dd	63	> 99

[a] Yields of isolated products. [b] Solvent: THF.

In the case of **1d**, the use of 2-butyne-1,4-diol (**2d**) improved the yield and enantioselectivity (Table 2, entry 5). The absolute configuration of the diol (+)-**3dd** was determined to be *R* by an anomalous dispersion method, and that of the diacetate (+)-**3dc** was also determined to be *R* (Figure 1).^[18]

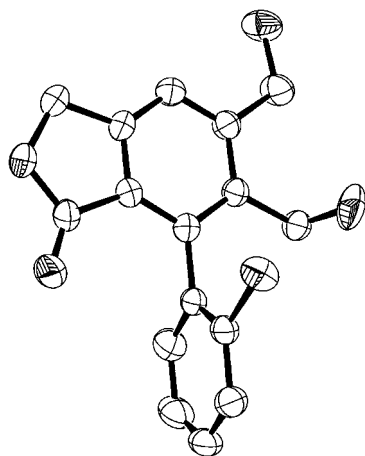
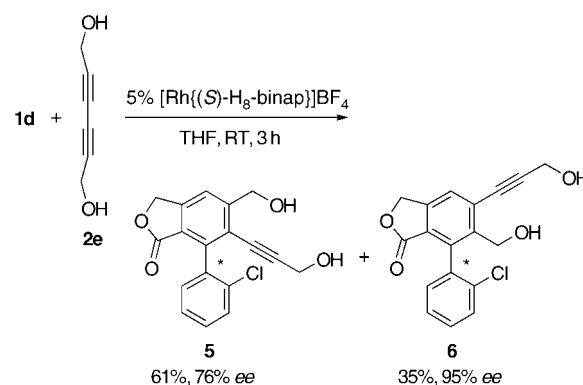


Figure 1. ORTEP Diagram of (R)-(+)-**3dd** drawn at the 50% probability level. Hydrogen atoms have been omitted for clarity.

The present enantioselective cross alkyne cyclotrimerization was applied to the symmetrical internal diyne **2e**, and the chiral phthalides **5** and **6** were obtained in excellent yield with high enantioselectivity (Scheme 2).



Scheme 2. Cross alkyne cyclotrimerization of **1d** and symmetrical internal diyne **2e**.

In conclusion, we have discovered an enantioselective cross alkyne cyclotrimerization of unsymmetrical 1,6-diynes and both terminal and internal alkynes. This method provides easy access to axially chiral phthalides that bear one or two oxymethylene functionalities. Work toward developing a wide variety of asymmetric reactions in the presence of cationic complexes of Rh^I and modified binap is underway in our laboratory.

Experimental Section

Full procedures and characterization data are given in the Supporting Information. **3ac**: Under an Ar atmosphere, (S)-H₈-binap (7.9 mg, 0.0125 mmol) and [Rh(cod)₂]₂BF₄ (5.1 mg, 0.0125 mmol) were dissolved in CH₂Cl₂ (1.0 mL), and the mixture was stirred for 5 min. H₂ was introduced to the resulting solution in a Schlenk tube. The resulting mixture was stirred for 30 min at room temperature and then concentrated to dryness. The residue was taken up in CH₂Cl₂ (1.0 mL), and to this solution was added a solution of **1a** (49.8 mg, 0.250 mmol) and **2c** (212.7 mg, 1.25 mmol) in CH₂Cl₂ (1.0 mL) at room temperature; the vial was rinsed with CH₂Cl₂ (0.5 mL). The mixture was stirred at room temperature for 3 h. The resulting mixture was concentrated and purified by preparative TLC to furnish (+)-**3ac** (61.7 mg, 0.167 mmol, 67%, > 99% ee) as a yellow solid. M.p. 95.0–97.5°C; [α]_D²⁵ = +17.3° (c = 0.274, CHCl₃); IR (neat): $\tilde{\nu}$ = 1740, 1220, 1020 cm^{−1}; ¹H NMR (CDCl₃, 400 MHz): δ = 7.60 (s, 1H), 7.22–7.36 (m, 3H), 7.01 (dd, *J* = 7.6 and 1.2 Hz, 1H), 5.33 (s, 2H), 5.29 (d, *J* = 3.2 Hz, 2H), 4.99 (d, *J* = 12.8 Hz, 1H), 4.88 (d, *J* = 12.8 Hz, 1H), 2.17 (s, 3H), 1.98 (s, 3H), 1.97 ppm (s, 3H); ¹³C NMR (CDCl₃, 100 MHz): δ = 170.3, 170.0, 168.6, 147.5, 143.2, 142.6, 135.8, 133.7, 133.2, 129.7, 128.6, 128.5, 125.5, 123.4, 121.5, 68.2, 63.4, 59.8, 20.9, 20.6, 20.0 ppm; HRMS (EI): calcd for C₂₁H₂₀O₆ [M]⁺: 368.1260; found: 368.1226; CHIRALPAK AS, hexane/iPrOH 80:20, 0.8 mL min^{−1}, retention times: 28.6 min (minor isomer) and 30.3 min (major isomer).

Received: August 4, 2004

Keywords: asymmetric catalysis · atropisomerism · biaryls · cyclotrimerization · rhodium

- [1] a) T. Hayashi, K. Hayashizaki, Y. Ito, *Tetrahedron Lett.* **1989**, 30, 215; b) T. Hayashi, K. Hayashizaki, T. Kiyoi, Y. Ito, *J. Am. Chem. Soc.* **1988**, 110, 8153.
- [2] a) J. Yin, S. L. Buchwald, *J. Am. Chem. Soc.* **2000**, 122, 12051; b) A. N. Cammidge, K. V. L. Crépy, *Chem. Commun.* **2000**, 1723.

- [3] a) X. Li, J. B. Hewgley, C. A. Mulrooney, J. Yang, M. C. Kozlowski, *J. Org. Chem.* **2003**, 68, 5500; b) Z. Luo, Q. Liu, L. Gong, X. Cui, A. Mi, Y. Jiang, *Chem. Commun.* **2002**, 914; c) C. -Y. Chu, D.-R. Hwang, S.-K. Wang, B.-J. Uang, *Chem. Commun.* **2001**, 980; d) S. Saito, T. Kano, H. Muto, H. Nakadai, H. Yamamoto, *J. Am. Chem. Soc.* **1999**, 121, 8943; e) M. Nakajima, K. Kanayama, I. Miyoshi, S.-I. Hashimoto, *Tetrahedron Lett.* **1995**, 36, 9519.
- [4] a) T. Kamikawa, T. Hayashi, *Tetrahedron* **1999**, 55, 3455; b) T. Hayashi, S. Niizuma, T. Kamikawa, N. Suzuki, Y. Uozumi, *J. Am. Chem. Soc.* **1995**, 117, 9101.
- [5] a) Y.-H. Cho, A. Kina, T. Shimada, T. Hayashi, *J. Org. Chem.* **2004**, 69, 3811; b) T. Shimada, Y.-H. Cho, T. Hayashi, *J. Am. Chem. Soc.* **2002**, 124, 13396.
- [6] For the synthesis of axially chiral biaryl compounds through chirality exchange from sp^3 central chirality to axial chirality, see: Y. Nishi, K. Wakasugi, K. Koga, Y. Tanabe, *J. Am. Chem. Soc.* **2004**, 126, 5358.
- [7] For the synthesis of axially chiral biaryl compounds by utilizing a planar chiral arene–chromium complex, see: a) T. Watanabe, Y. Tanaka, R. Shoda, R. Sakamoto, K. Kamikawa, M. Uemura, *J. Org. Chem.* **2004**, 69, 4152; b) K. Kamikawa, T. Sakamoto, Y. Tanaka, M. Uemura, *J. Org. Chem.* **2003**, 68, 9356, and references therein.
- [8] For reviews, see: a) S. Saito, Y. Yamamoto, *Chem. Rev.* **2000**, 100, 2901; b) M. Lautens, W. Klute, W. Tam, *Chem. Rev.* **1996**, 96, 49.
- [9] X. Zhang, K. Mashimo, K. Koyano, N. Sayo, H. Kumobayashi, S. Akutagawa, H. Takaya, *Tetrahedron Lett.* **1991**, 32, 7283.
- [10] K. Tanaka, K. Shirasaka, *Org. Lett.* **2003**, 5, 4697.
- [11] For the $[RhCl(PPh_3)_3]$ -catalyzed non-asymmetric synthesis of phthalides with acetylene gas, see: B. Witulski, A. Zimmermann, *Synlett* **2002**, 1855.
- [12] For the nickel-catalyzed non-asymmetric synthesis of phthalides, see: Y. Sato, K. Ohashi, M. Mori, *Tetrahedron Lett.* **1999**, 40, 5231.
- [13] For the nickel-catalyzed asymmetric construction of sp^3 central chirality, see: Y. Sato, T. Nishimata, M. Mori, *Heterocycles* **1997**, 44, 443.
- [14] For the nickel-catalyzed asymmetric synthesis of a chiral helicene, see: I. G. Stara, I. Stary, A. Kollarovic, F. Teplý, S. Vyskocil, D. Saman, *Tetrahedron Lett.* **1999**, 40, 1993.
- [15] A. Gutnov, B. Heller, C. Fischer, H.-J. Drexler, A. Spannenberg, B. Sundermann, C. Sundermann, *Angew. Chem.* **2004**, 116, 3883; *Angew. Chem. Int. Ed.* **2004**, 43, 3795.
- [16] T. Shibata, T. Fujimoto, K. Yokota, K. Takagi, *J. Am. Chem. Soc.* **2004**, 126, 8382.
- [17] Shibata et al. reported one example of an asymmetric $[2+2+2]$ cycloaddition of an unsymmetrical α,ω -diyne and a symmetrical monoyne (neutral $[Ir^I(Et\text{-}diphos)]$ catalyst, 81 % ee).^[16]
- [18] CCDC-246690 (**3dd**) contains the supplementary crystallographic data for this paper. These data can be obtained free of charge via www.ccdc.cam.ac.uk/conts/retrieving.html (or from the Cambridge Crystallographic Data Centre, 12, Union Road, Cambridge CB21EZ, UK; fax: (+44) 1223-336-033; or deposit@ccdc.cam.ac.uk).

Tungsten–Lead Triple Bonds: Syntheses, Structures, and Coordination Chemistry of the Plumbidyne Complexes *trans*-[X(PMe₃)₄W≡Pb(2,6-Trip₂C₆H₃)]**

Alexander C. Filippou,* Nils Weidemann,
Gregor Schnakenburg, Holger Rohde, and
Athanasios I. Philippopoulos

Compounds containing a multiple bond between lead and another main-group element are very rare.^[1] In fact, only a few diplumbenes, [Pb₂R₄] (R = aryl, silyl),^[2] have been isolated to date,^[3,4] whereas alkenes are ubiquitous in organic chemistry. Similarly, very few transition-metal plumbanediyl (plumbylene) complexes have been reported,^[5] whereas carbene complexes are a common class of organometallic compounds.^[6] Other prominent examples of compounds containing transition-metal–lead multiple bonds are the heterocumulenes [(η⁵-C₅H₄R)(CO)₂Mn=Pb=Mn(CO)₂(η⁵-C₅H₄R)] (R = H, Me).^[7] Two major reasons have emerged from quantum chemical studies for the distinct reluctance of lead to participate in multiple bonding. These are the comparatively low bond energies^[8] and the reduced hybridization of its 6s and 6p valence orbitals.^[9,10] However, these are not inherent properties of lead, as recently demonstrated by our synthesis of the plumbidyne complex *trans*-[Br(PMe₃)₄Mo≡Pb(2,6-Trip₂C₆H₃)], which features a triply bonded, linear-coordinated lead atom.^[11] We have now characterized compounds with tungsten–lead triple bonds. First results of the coordination chemistry of these compounds are also presented, providing experimental evidence for their electronic analogy with Fischer-type carbyne complexes.^[12]

Starting materials were the dinitrogen complexes *cis*-[W(N₂)₂(PMe₃)₄] and [W(N₂)(PMe₃)₅]^[13] and the aryllead(II) halides [[Pb(2,6-Trip₂C₆H₃)X]₂] (X = Br (**1-Br**), I (**1-I**)). Compound **1-I** was prepared by metathetical exchange of **1-**

[*] Prof. Dr. A. C. Filippou, Dipl.-Chem. N. Weidemann, Dipl.-Chem. G. Schnakenburg, Dipl.-Chem. H. Rohde
Institut für Chemie
Humboldt-Universität zu Berlin
Brook-Taylor Strasse 2, 12489 Berlin (Germany)
Fax: (+49) 30-2093-6939
E-mail: filippou@chemie.hu-berlin.de
Dr. A. I. Philippopoulos
Institute of Physical Chemistry, NCSR Demokritos
Ag. Paraskevi Attikis, 15310 Athens (Greece)

[**] We are grateful to the Humboldt-Universität zu Berlin and the Deutsche Forschungsgemeinschaft (project FI 445/6-1) for the generous financial support of this work, Dr. B. Ziemer and P. Neubauer for the X-ray diffraction studies, Dr. U. Hartmann and U. Kästel for the elemental analyses, and W.-D. Bloedorn and A. Thiesies for the 2D NMR spectra. N. Weidemann thanks the Fonds der Chemischen Industrie for a fellowship. X = Br, I; Trip = 2,4,6-iPr₃C₆H₂.



Supporting information for this article is available on the WWW under <http://www.angewandte.org> or from the author.

Br^[14] with NaI in diethyl ether. It was isolated in 82 % yield as an air-sensitive, bright orange solid, which melts at 222 °C and decomposes at 235 °C to give an oily, red mass.^[15] Compound **1-I** is the first organolead(II) iodide to be structurally characterized.^[16] It crystallizes as a centrosymmetric iodide-bridged dimer, which features a Pb₂I₂ parallelogram with a Pb...Pb separation of 4.603(1) Å^[17] and two quite different Pb–I bond lengths (2.9499(7) and 3.2764(8) Å) and internal bond angles (84.81(2) and 95.19(2)°; Figure 1). The Pb–C_{aryl} bond length of **1-I** at 2.326(6) Å compares well with those of

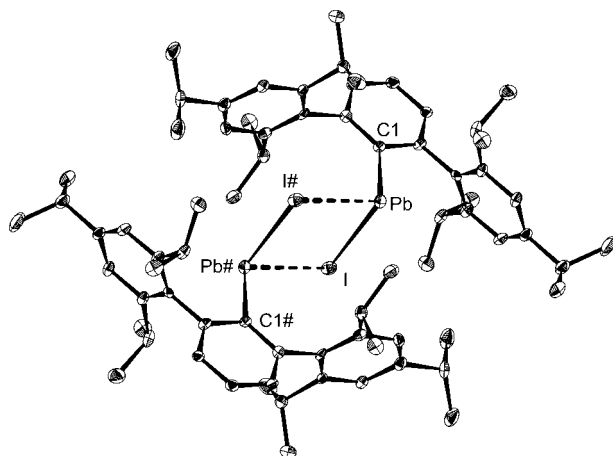
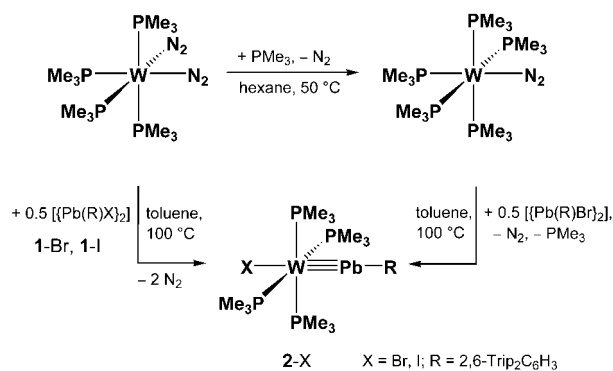


Figure 1. DIAMOND plot of the molecular structure of **1-I** in the solid state. Thermal ellipsoids are set at 30 % probability. Hydrogen atoms are omitted for clarity. Selected bond lengths [Å] and angles [°]: Pb–I 2.9499(7), Pb–I# 3.2764(8), Pb–C1 2.326(6); C1–Pb–I 97.3(2), C1–Pb–I# 115.1(2), I–Pb–I# 84.81(2), Pb–I–Pb# 95.19(2).

1-Br (2.306(13) and 2.329(11) Å).^[14] Heating a solution of *cis*-[W(N₂)₂(PMe₃)₄] with a stoichiometric amount of **1-Br** or **1-I** in toluene at 100 °C was accompanied by a rapid color change from orange to red-brown to afford the plumbidyne complex **2-Br** and **2-I**, respectively (Scheme 1).^[15,18] Compounds **2-Br** and **2-I** were purified by crystallization from pentane and isolated as red-brown, air-sensitive, microcrystalline solids in 66 (**2-Br**) and 58 % (**2-I**) yields. Both complexes are very soluble in pentane and decompose upon melting at 195 and 192 °C, respectively. The plumbidyne complex **2-Br** was also obtained in a straightforward manner by the reaction



Scheme 1. Syntheses of the plumbidyne complexes **2-X** (X = Br, I).

of [W(N₂)(PMe₃)₅] with 0.5 equivalents of **1-Br** in toluene at 100 °C (Scheme 1).^[15] This reaction provides another example for the aptitude of electron-rich^[19] Group 6 metal dinitrogen complexes with a d⁶ electron configuration to form triple bonds to lead. Compounds **2-Br** and **2-I** are essentially isotopic (Figure 2).^[15] The isostructural, *trans*-configured

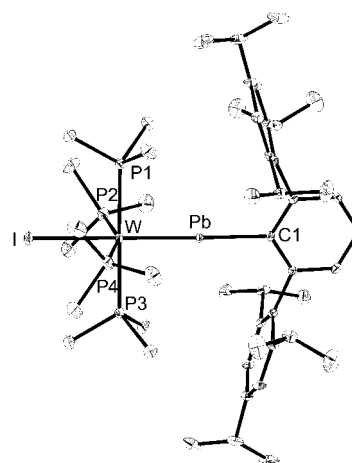
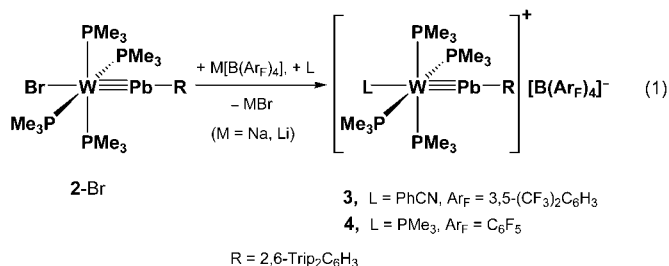


Figure 2. DIAMOND plot of the molecular structure of **2-I** in the solid state. Thermal ellipsoids are set at 30 % probability. Hydrogen atoms are omitted for clarity. Selected bond lengths [Å] and angles [°] of **2-I** and **2-Br**: W–Pb 2.5477(3) [2.5464(5)], W–I 2.8656(4) [W–Br 2.6798(9)], W–P1 2.4776(9) [2.474(2)], W–P2 2.481(1) [2.484(2)], W–P3 2.4663(9) [2.461(2)], W–P4 2.486(1) [2.485(2)], Pb–C1 2.258(3) [2.254(6)]; W–Pb–C1 175.79(8) [177.5(2)], I–W–Pb 177.857(8) [Br–W–Pb 179.05(3)], Pb–W–P1 90.00(2) [90.17(5)], Pb–W–P2 98.17(2) [100.88(5)], Pb–W–P3 89.01(2) [89.17(4)], Pb–W–P4 102.45(3) [102.84(6)].

octahedral complexes have approximate C₂ point group symmetry,^[20] and display almost linear W–Pb–C_{aryl} linkages (**2-Br**, 177.5(2)°; **2-I**, 175.79(8)°) and the shortest W–Pb bonds (**2-Br**, 2.5464(5) Å; **2-I**, 2.5477(3) Å) reported to date.^[21] In fact, the W–Pb bond lengths of **2-Br** and **2-I** are 0.20 Å shorter than those of the bridged plumbidyne complex [(W(CO)₄)₂(μ-Br){μ-Pb(2,6-Trip₂C₆H₃)}] (2.7423(3) and 2.7517(3) Å), which contains a three-coordinate lead center with trigonal-planar geometry,^[14] and approximately 0.45 Å shorter than the W–Pb single bonds of the V-shaped tungstenplumbylene [Pb(2,6-Trip₂C₆H₃){W(η⁵-C₅H₅)(CO)₃}] (2.9809(10) and 3.0055(6) Å).^[21d] The Pb–C_{aryl} bonds of **2-Br** (2.254(6) Å) and **2-I** (2.258(3) Å) are shorter than those of **1-Br** and **1-I** (Figure 1), or those reported for the plumbylenes [Pb(2,6-Trip₂C₆H₃)R] (R = Me, *t*Bu, Ph: Pb–C_{aryl} 2.272(9)–2.321(3) Å)^[14] and metalloplumbylens [Pb(2,6-Trip₂C₆H₃){M(η⁵-C₅H₅)(CO)₃}] (M = Cr, Mo, W: Pb–C_{aryl} 2.278(9)–2.294(4) Å),^[21d] and indicate that the triply bonded lead atom uses sp-hybrid orbitals for σ bonding. The composition of **2-Br** and **2-I** was confirmed by elemental analyses and IR, ¹H, ³¹P{¹H} and ¹³C{¹H} NMR spectroscopy.^[15] The number and relative intensity of the ¹H NMR spectroscopy signals of the *m*-terphenyl substituent and the PMe₃ ligands suggest an averaged C_{2v} symmetry of the plumbidyne complexes **2-Br** and **2-I** in solution, and their ³¹P{¹H} NMR spectra in C₆D₆ showed a singlet for the four chemically equivalent PMe₃ ligands, which appears up field (**2-Br**, δ =

–43.6 ppm; **2-I**, $\delta = -53.9$ ppm) of those of the lighter Group 14 element analogues *trans*-[Cl(PMe₃)₄W≡E-R] (E = C, R = Me: $\delta_P = -20.8$ ppm, $^1J(W,P) = 285$ Hz;^[22] E = Ge, R = C₆H₃-2,6-Dipp₂ (Dipp = 2,6-*i*Pr₂C₆H₃): $\delta_P = -31.1$ ppm, $^1J(W,P) = 258$ Hz; E = Sn, R = 2,6-Dipp₂C₆H₃: $\delta_P = -30.8$ ppm, $^1J(W,P) = 256$ Hz).^[23] The ³¹P NMR signals are flanked by one pair of satellites arising from coupling with the ¹⁸³W nucleus,^[24] the $^1J(W,P)$ coupling constants (**2-Br**, 257 Hz; **2-I**, 258 Hz) comparing well with those of the ylidene complexes *trans*-[Cl(PMe₃)₄W=E-R] (E = Ge, Sn; R = aryl, see above). The ¹³C{¹H} NMR spectra of the plumbidyne complexes **2-Br** and **2-I** display a characteristic downfield-shifted signal for the lead-bonded C_{ipso} atom at $\delta = 270.2$ (**2-Br**) and 267.9 ppm (**2-I**), as do those of the aryllead(II) halides **1-Br** ($\delta_C = 287.9$ ppm)^[14] and **1-I** ($\delta_C = 276.7$ ppm).^[15]

Electrophile-induced halide abstraction was shown to be a very efficient method for the preparation of cationic Fischer-type carbyne complexes from neutral precursors.^[25] Application of this method to **2-Br** and **2-I** was envisaged as an approach to cationic plumbilydine complexes, given the electronic analogy of **2-Br** and **2-I** with Fischer-type carbyne complexes.^[12] In fact, treatment of **2-Br** with Na[B(3,5-(CF₃)₂C₆H₃)₄]^[26] and PhCN in toluene afforded the brown benzonitrile complex salt **3**, and bromide abstraction from **2-Br** by Li[B(C₆F₅)₄] \cdot 2.5 Et₂O^[27] in fluorobenzene gave in the presence of PMe₃ the olive-green to brown plumbilydine complex salt **4** [Eq. (1)].^[15] Both salts are soluble in THF, and decompose upon melting at 181–182 (**3**) and 149–150 °C (**4**).



The structures of the complex cations in **3** and **4** (Figures 3 and 4) reveal the same bonding features of the plumbilydyne ligand as observed in **2-Br** and **2-I**. These are the almost linear coordination geometry at lead (W-Pb-C_{aryl} = 171.7(1) (**3**), 177.5(1)° (**4**)), the short W-Pb triple bonds (2.5520(6) (**3**), 2.5744(2) Å (**4**)), and the comparatively short Pb-C_{aryl} bonds of 2.228(5) Å (**3**) and 2.289(4) Å (**4**). The W-P bond of the *trans*-disposed PMe₃ ligand in **4** is longer (2.565(1) Å) than those of the *cis*-coordinated PMe₃ ligands (2.490(1)–2.513(1) Å), reflecting the *trans*-influence of the plumbilydyne ligand.^[28] ¹H, ³¹P{¹H}, ¹⁹F{¹H}, and ¹³C{¹H} NMR spectroscopic studies corroborated the X-ray structures of **3** and **4**.^[15] Thus, the IR spectrum of **3** in nujol displays a characteristic $\nu(\text{C}\equiv\text{N})$ band of the benzonitrile ligand at 2171 cm^{−1}, which is at lower wavenumbers than that of free PhCN ($\nu(\text{C}\equiv\text{N})$ in nujol = 2230 cm^{−1}) and indicates some tungsten–nitrile back-bonding.^[29] In addition, the ³¹P{¹H} NMR spectrum of **3** shows a singlet resonance at $\delta = -36.8$ ppm ($^1J(\text{W,P}) = 262$ Hz) for the PMe₃ ligands, which confirms the *trans*-configuration of the complex cation in **3**. In

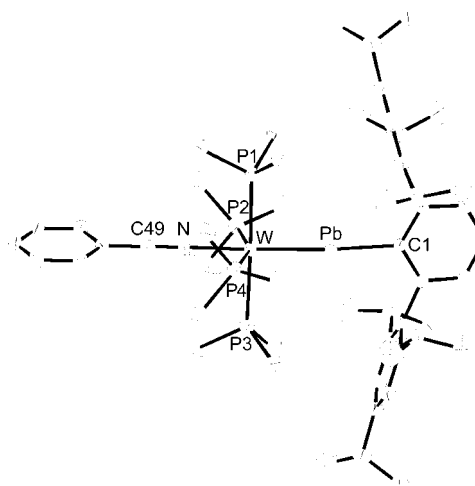


Figure 3. DIAMOND plot of the structure of the complex cation in **3**. Thermal ellipsoids are set at 30% probability. Hydrogen atoms are omitted for clarity. Selected bond lengths [Å] and angles [°]: W-Pb 2.5520(6), W-N 2.099(4), W-P1 2.469(1), W-P2 2.472(2), W-P3 2.493(2), W-P4 2.496(2), Pb-C1 2.228(5), C49-N 1.137(7); W-Pb-C1 171.7(1), N-W-Pb 174.9(1), Pb-W-P1 90.28(4), Pb-W-P2 95.69(4), Pb-W-P3 91.56(4), Pb-W-P4 104.96(4), W-N-C49 179.1(5).

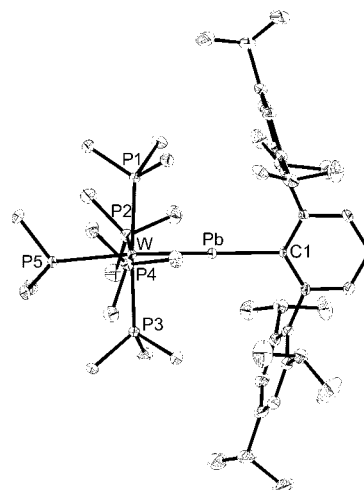


Figure 4. DIAMOND plot of the structure of the complex cation in **4**. Thermal ellipsoids are set at 30% probability. Hydrogen atoms are omitted for clarity. Selected bond lengths [Å] and angles [°]: W-Pb 2.5744(2), W-P1 2.500(1), W-P2 2.490(1), W-P3 2.513(1), W-P4 2.495(1), W-P5 2.565(1), Pb-C1 2.289(4); W-Pb-C1 177.5(1), Pb-W-P1 87.10(3), Pb-W-P2 93.90(3), Pb-W-P3 88.93 (3), Pb-W-P4 92.93(3), Pb-W-P5 174.87(3).

comparison, the $^{31}\text{P}\{^1\text{H}\}$ NMR spectrum of **4** reveals the signal pattern expected for a nonfluxional, square-pyramidal $\text{W}(\text{PMe}_3)_5$ fragment, that is, one doublet at $\delta = -52.1$ ppm ($^2J(\text{P,P}) = 31$ Hz, $^1J(\text{W,P}) = 249$ Hz) and one quintet at $\delta = -65.6$ ppm ($^2J(\text{P,P}) = 31$ Hz) in the intensity ratio of 4:1.^[15] The structures of **3** and **4** are also confirmed by the Pb- C_{ipso} resonance signal in the $^{13}\text{C}\{^1\text{H}\}$ NMR spectra at $\delta = 278.7$ (**3**) and 279.1 ppm (**4**). The C_{ipso} signal of **4** is split into a doublet as a result of coupling with the *trans*-disposed PMe_3 ligand ($^3J(\text{P,C}) = 22$ Hz).

The similarity of the plumbidyne complex $[(\text{PMe}_3)_5\text{W}\equiv\text{Pb}(\text{2,6-Trip}_2\text{C}_6\text{H}_3)]^+$ with the Fischer-type carbyne complexes

Table 1: Results of the bonding analyses of the cation of **4**.

center	NPA ^[b] charges	NBO analysis ^[a]				hybrid.	WBI	BDE ^[c] [kJ mol ⁻¹]	ΔE_{Pauli}	EDA ^[d] [kJ mol ⁻¹]		
		occupancy	%(W)	hybrid.	%(Pb)					ΔE_{elstat}	ΔE_{orb}	ΔE_{int}
W	−1.58	σ : 1.71	41.1	sd ^{1.54}	58.9	sp ^{0.77}	1.42	149.7	+472.0	−352.0	−530.9	−410.9
Pb	+1.21	π_1 : 1.85	81.0	d	19.0	p						
		π_2 : 1.83	81.0	d	19.0	p						

[a] BP86/LANL2DZ; Natural bond orbital analysis of the W–Pb bond: NBO occupancies, bond polarization in %W and %Pb, orbital hybridization, and Wiberg bond index. [b] Natural population analysis. [c] Gibbs free dissociation energy (298.15 K, 1 atm) of the W–Pb bond to the fragments in their relaxed geometries and electronic ground states (zero point energy (ZPE) corrected). [d] Energy decomposition analysis (BP86/TZ2P for Pb, W, and P, and DZP for C and H): Pauli repulsion (ΔE_{Pauli}), electrostatic interaction (ΔE_{elstat}), orbital interaction (ΔE_{orb}), and total interaction energy ΔE_{int} between the fragments $[\text{W}(\text{PMe}_3)_5]$ and $[\text{Pb}(2,6\text{-Trip}_2\text{C}_6\text{H}_3)]^+$ at their frozen geometries in the complex cation.

$[(\text{CO})_5\text{M}\equiv\text{C}-\text{NEt}_2]^+$ (M = Cr, Mo, W) is noticeable.^[30] This fact prompted us to study the nature of the W–Pb bond in **4** by various quantum chemical methods. Optimization of the structure of the complex cation at the BP86/LANL2DZ level of theory led to a minimum structure with a W–Pb separation of 2.609 Å and a bond angle at the lead atom of 174.9° in good agreement with the experimental values (Figure 4). Analysis of the electronic charge distribution by the natural bond orbital (NBO) method^[31] gives an optimal Lewis structure with a W–Pb triple bond. The W–Pb bond is composed of a σ component that is polarized towards the lead atom, and two nearly degenerate π bonds, which are strongly polarized towards the tungsten center (Table 1). The high polarity of the W–Pb bond is further reflected in the natural population analysis (NPA) partial charges of the Pb (+1.21) and W atom (−1.58) and the Wiberg bond index (WBI) of 1.42 (Table 1), which is slightly lower than that of the model compound *trans*- $[\text{Br}(\text{PH}_3)_4\text{Mo}\equiv\text{Pb}-\text{Ph}]$ (WBI = 1.51).^[11] Partitioning of the total interaction energy ΔE_{int} (−410.9 kJ mol⁻¹) between the frozen fragments $[\text{W}(\text{PMe}_3)_5]$ and $[\text{Pb}(2,6\text{-Trip}_2\text{C}_6\text{H}_3)]^+$ into the attractive Coulomb term ΔE_{elstat} of −352.0 kJ mol⁻¹, the repulsive Pauli term ΔE_{Pauli} of +472.0 kJ mol⁻¹, and the orbital interaction term ΔE_{orb} of −530.9 kJ mol⁻¹ affords a covalent character of 60 % for the W≡Pb bond.^[32] All these results suggest that the W–Pb triple bond of **4** can be reasonably described with the Dewar–Chatt–Duncanson model as a donor–acceptor interaction involving a $[\text{PbR}]^+ \rightarrow [\text{W}(\text{PMe}_3)_5] \sigma$ donation and two $[\text{W}(\text{PMe}_3)_5] \rightarrow [\text{PbR}]^+ \pi$ back-donations.^[33]

Finally, the Gibbs free dissociation energy of **4** to give the fragments $[\text{W}(\text{PMe}_3)_5]$ and $[\text{Pb}(2,6\text{-Trip}_2\text{C}_6\text{H}_3)]^+$ in their electronic ground states and minimum geometries^[34,35] was calculated to be only 149.7 kJ mol⁻¹, which suggests that the complex cation might be useful as a $[\text{Pb}-\text{R}]^+$ transfer reagent.

Several applications of these compounds in stoichiometric reactions might be envisaged given their structural and electronic analogy with Fischer-type carbyne complexes.

Received: August 19, 2004

Keywords: density functional calculations · lead · plumbilydine ligands · triple bonds · tungsten

[1] Review articles on multiple bonds of the heavier group homologues of carbon: a) G. Raabe, J. Michl, *Chem. Rev.* **1985**, 85, 419; b) A. G. Brook, K. M. Baines, *Adv. Organomet. Chem.*

1986, 25, 1; c) R. West, *Angew. Chem.* **1987**, 99, 1231; *Angew. Chem. Int. Ed. Engl.* **1987**, 26, 1201; d) J. Barrau, J. Escudié, J. Satgé, *Chem. Rev.* **1990**, 90, 283; e) T. Tsumuraya, S. A. Batcheller, S. Masamune, *Angew. Chem.* **1991**, 103, 916; *Angew. Chem. Int. Ed. Engl.* **1991**, 30, 902; f) R. S. Grev, *Adv. Organomet. Chem.* **1991**, 33, 125; g) M. Weidenbruch, *Coord. Chem. Rev.* **1994**, 130, 275; h) J. Escudié, C. Couret, H. Ranaivonjatovo, J. Satgé, *Coord. Chem. Rev.* **1994**, 130, 427; i) R. Okazaki, R. West, *Adv. Organomet. Chem.* **1996**, 39, 231; j) M. Driess, H. Grützmacher, *Angew. Chem.* **1996**, 108, 900; *Angew. Chem. Int. Ed. Engl.* **1996**, 35, 828; k) K. M. Baines, W. G. Stibbs, *Adv. Organomet. Chem.* **1996**, 39, 275; l) J. Escudié, C. Couret, H. Ranaivonjatovo, *Coord. Chem. Rev.* **1998**, 178, 565; m) J. Escudié, H. Ranaivonjatovo, *Adv. Organomet. Chem.* **1999**, 44, 113; n) M. Weidenbruch, *Eur. J. Inorg. Chem.* **1999**, 373; o) P. P. Power, *Chem. Rev.* **1999**, 99, 3463; p) M. Weidenbruch, *J. Organomet. Chem.* **2002**, 646, 39.

[2] The name diplumbene underlines the similar composition of $[\text{Pb}_2\text{R}_4]$ and alkenes, and is used herein instead of the term bis(plumbanediyl) which is more appropriate to describe the physical properties, structures, and chemical behavior of these compounds, which bear little resemblance to those of alkenes.

[3] a) K. W. Klinkhammer, T. F. Fässler, H. Grützmacher, *Angew. Chem.* **1998**, 110, 114; *Angew. Chem. Int. Ed.* **1998**, 37, 124; b) M. Stürmann, M. Weidenbruch, K. W. Klinkhammer, F. Lissner, H. Marsmann, *Organometallics* **1998**, 17, 4425; c) M. Stürmann, W. Saak, H. Marsmann, M. Weidenbruch, *Angew. Chem.* **1999**, 111, 145; *Angew. Chem. Int. Ed.* **1999**, 38, 187; d) M. Stürmann, W. Saak, M. Weidenbruch, K. W. Klinkhammer, *Eur. J. Inorg. Chem.* **1999**, 579.

[4] A Pb–Pb multiple bond has been also formulated in the complex anion $[(\text{W}(\text{CO})_5)_4\text{Pb}_2]^{2-}$: P. Rutsch, G. Huttner, *Angew. Chem.* **2000**, 112, 3852; *Angew. Chem. Int. Ed.* **2000**, 39, 3697.

[5] a) J. D. Cotton, P. J. Davidson, M. F. Lappert, *J. Chem. Soc. Dalton Trans.* **1976**, 2275; b) M. F. Lappert, P. P. Power, *J. Chem. Soc. Dalton Trans.* **1985**, 51; c) H.-J. Kneuper, E. Herdtweck, W. A. Herrmann, *J. Am. Chem. Soc.* **1987**, 109, 2508; d) M. F. Lappert, R. S. Rowe, *Coord. Chem. Rev.* **1990**, 100, 267.

[6] Selected recent review articles on carbene complexes: a) M. A. Sierra, *Chem. Rev.* **2000**, 100, 3591; b) A. de Meijere, H. Schirmer, M. Duetsch, *Angew. Chem.* **2000**, 112, 4124; *Angew. Chem. Int. Ed.* **2000**, 39, 3964; c) T. M. Trnka, R. H. Grubbs, *Acc. Chem. Res.* **2001**, 34, 18; d) A. H. Hoveyda, R. R. Schrock, *Chem. Eur. J.* **2001**, 7, 945; e) W. A. Herrmann, *Angew. Chem.* **2002**, 114, 1342; *Angew. Chem. Int. Ed.* **2002**, 41, 1290; f) J. W. Herndon, *Coord. Chem. Rev.* **2003**, 243, 3; g) W. Kirmse, *Angew. Chem.* **2003**, 115, 1120; *Angew. Chem. Int. Ed.* **2003**, 42, 1088.

[7] a) W. A. Herrmann, H.-J. Kneuper, E. Herdtweck, *Angew. Chem.* **1985**, 97, 1060; *Angew. Chem. Int. Ed. Engl.* **1985**, 24, 1062; b) F. Ettel, G. Huttner, L. Zsolnai, *Angew. Chem.* **1989**, 101, 1525; *Angew. Chem. Int. Ed. Engl.* **1989**, 28, 1496; c) F. Ettel, M. Schollenberger, B. Schiemenz, G. Huttner, L. Zsolnai, *J. Organomet. Chem.* **1994**, 476, 153.

- [8] a) M. J. S. Dewar, M. K. Holloway, G. L. Grady, J. J. P. Stewart, *Organometallics* **1985**, *4*, 1973; b) G. Trinquier, *J. Am. Chem. Soc.* **1990**, *112*, 2130; c) H. Jacobsen, T. Ziegler, *J. Am. Chem. Soc.* **1994**, *116*, 3667.
- [9] W. Kutzelnigg, *Angew. Chem.* **1984**, *96*, 262; *Angew. Chem. Int. Ed. Engl.* **1984**, *23*, 272.
- [10] For the relativistic contraction of the 6s orbital of lead and the increase of the 6s–6p orbital energy gap causing the inert-pair effect see: a) P. Pyykkö, *Chem. Rev.* **1988**, *88*, 563; b) N. Kaltsoyannis, *J. Chem. Soc. Dalton Trans.* **1997**, 1.
- [11] A. C. Filippou, H. Rohde, G. Schnakenburg, *Angew. Chem.* **2004**, *116*, 2293; *Angew. Chem. Int. Ed.* **2004**, *43*, 2243.
- [12] a) E. O. Fischer, *Adv. Organomet. Chem.* **1976**, *14*, 1; b) H. Fischer, P. Hofmann, F. R. Kreißl, R. R. Schrock, K. Weiss, *Carbyne Complexes*, VCH, Weinheim, **1988**; c) A. Mayr, H. Hoffmeister, *Adv. Organomet. Chem.* **1991**, *32*, 227.
- [13] E. Carmona, A. Galindo, M. L. Poveda, R. D. Rogers, *Inorg. Chem.* **1985**, *24*, 4033.
- [14] L. Pu, B. Twamley, P. P. Power, *Organometallics* **2000**, *19*, 2874.
- [15] The Supporting Information contains the experimental section including the syntheses, spectroscopic, and crystallographic data of **1-I** and of the plumbidyne complexes **2-Br**, **2-I**, **3**, and **4**. It also contains IR and NMR spectroscopic data of the dinitrogen complexes *cis*-[W(N₂)₂(PMe₃)₄] and [W(N₂)(PMe₃)₅] and details of the electronic structure calculations of the complex cation [(PMe₃)₅W≡Pb(2,6-Trip₂C₆H₃)]⁺. CCDC-247928 (**1-I**-(*n*-C₅H₁₂)), CCDC-247927 (**2-Br**), CCDC-247929 (**2-I**-0.5(*n*-C₅H₁₂)), CCDC-247931 (**3**) and CCDC-247930 (**4**-0.705(C₆H₅F)) contains the supplementary crystallographic data for this paper. These data can be obtained free of charge via www.ccdc.cam.ac.uk/conts/retrieving.html (or from the Cambridge Crystallographic Data Centre, 12 Union Road, Cambridge CB21EZ, UK; fax: (+44) 1223-336-033; or deposit@ccdc.cam.ac.uk).
- [16] The only other known organolead(II) iodide is [Pb(η-C₅H₅)I]: A. K. Holliday, P. H. Makin, R. J. Puddephatt, *J. Chem. Soc. Dalton Trans.* **1976**, 435.
- [17] The Pb···Pb separation of **1-I** is much longer than the interatomic distance in elementary lead (3.494 Å): a) H. P. Klug, *J. Am. Chem. Soc.* **1946**, *68*, 1493; b) A. F. Wells, *Structural Inorganic Chemistry*, 5th ed., Clarendon, Oxford, **1984**, p. 1288.
- [18] IR spectra of the reaction solutions and the ¹H and ³¹P{¹H} NMR spectra of the crude products, that were isolated after completion of the reaction, revealed the concomitant formation of two by-products. These were identified to be [W(N₂)(PMe₃)₅] and 1,3-Trip₂C₆H₄ by comparison with authentic samples (Supporting Information). A gray-green solid, which is soluble in THF, but insoluble in pentane was also formed in these reactions. This solid burned upon exposure to air in dried form and was not further characterized.
- [19] The term “electron-rich” is used herein to emphasize the strong π-electron donating ability of the metal centers in these complexes: a) A. J. L. Pombeiro, R. L. Richards, *Coord. Chem. Rev.* **1990**, *104*, 13; b) A. J. L. Pombeiro, M. F. C. Guedes da Silva, R. A. Michelin, *Coord. Chem. Rev.* **2001**, *218*, 43.
- [20] The orientation of the *para*-positioned isopropyl substituents lowers the molecular symmetry of **2-Br** and **2-I** from roughly C_{2v} to C₂. The terphenyl substituent adopts in both plumbidyne complexes an eclipsed conformation, as shown by the interplane angle of 5.9(2) (**2-Br**) and 9.0(1)° (**2-I**) between the central aryl ring and the least-square plane through the atoms Br (I), W, P1, and P3.
- [21] Only a few compounds with W–Pb bonds have been structurally characterized. The W–Pb bond lengths range in these compounds from 2.7423(3) to 3.339(1) Å depending on the bond order, the oxidation states, and the coordination numbers of lead and tungsten: a) ref. [4]; b) ref. [14]; c) S. Seebald, G. Kickelbick, F. Möller, U. Schubert, *Chem. Ber.* **1996**, *129*, 1131; d) L. Pu, P. P. Power, I. Boltes, R. Herbst-Irmer, *Organometallics* **2000**, *19*, 352; e) N. Seidel, K. Jacob, A. K. Fischer, *Organometallics* **2001**, *20*, 578; f) J. Campbell, H. P. A. Mercier, H. Franke, D. P. Santry, D. A. Dixon, G. J. Schrobilgen, *Inorg. Chem.* **2002**, *41*, 86.
- [22] L. M. Atagi, J. M. Mayer, *Polyhedron* **1995**, *14*, 113.
- [23] A. C. Filippou, N. Weidemann, H. Rohde, unpublished results.
- [24] No ²⁰⁷Pb satellites were observed in the ³¹P{¹H} NMR spectra of **2-Br**, **2-I**, **3**, and **4** at room temperature, and attempts to detect the ²⁰⁷Pb NMR signal of **2-Br** in C₆D₆ at ambient temperature were not successful to date.
- [25] a) A. C. Filippou, E. O. Fischer, *J. Organomet. Chem.* **1990**, 383, 179; b) A. C. Filippou, C. Mehnert, K. M. A. Wanninger, M. Kleine, *J. Organomet. Chem.* **1995**, 491, 47; c) A. C. Filippou, D. Wössner, G. Kociok-Köhn, I. Hinz, L. Grubert, *J. Organomet. Chem.* **1997**, 532, 207; d) F. W. Lee, M. C. W. Chan, K. K. Cheung, C. M. Che, *J. Organomet. Chem.* **1998**, 563, 191; e) E. Bannwart, H. Jacobsen, R. Hübener, H. W. Schmalle, H. Berke, *J. Organomet. Chem.* **2001**, 622, 97.
- [26] a) S. R. Bahr, P. Boudjouk, *J. Org. Chem.* **1992**, *57*, 5545; b) R. Taube, S. Wache, *J. Organomet. Chem.* **1992**, 428, 431.
- [27] a) A. G. Massey, A. J. Park, *J. Organomet. Chem.* **1964**, *2*, 245; b) J. B. Lambert, S. Zhang, S. M. Ciro, *Organometallics* **1994**, *13*, 2430.
- [28] For the *trans*-influence of carbyne and germylidyne ligands see: a) ref. [12b]; b) E. Bannwart, H. Jacobsen, F. Furno, H. Berke, *Organometallics* **2000**, *19*, 3605; c) F. Furno, T. Fox, H. W. Schmalle, H. Berke, *J. Organometallics* **2000**, *19*, 3620; d) A. C. Filippou, P. Portius, A. I. Philippopoulos, *Organometallics* **2002**, *21*, 653.
- [29] For d⁶ tungsten nitrile complexes revealing dπ(tungsten)→π*(nitrile) back-bonding see: a) J. Chatt, G. J. Leigh, H. Neukomm, C. J. Pickett, D. R. Stanley, *J. Chem. Soc. Dalton Trans.* **1980**, 121; b) B. J. Carter, J. E. Bercau, H. B. Gray, *J. Organomet. Chem.* **1979**, 181, 105; c) H. Seino, Y. Tanabe, Y. Ishii, M. Hidai, *Inorg. Chim. Acta* **1998**, *280*, 163; d) C. M. Habeck, N. Lehnert, C. Näther, F. Tuzcek, *Inorg. Chim. Acta* **2002**, 337, 11.
- [30] a) U. Schubert, E. O. Fischer, D. Wittmann, *Angew. Chem.* **1980**, *92*, 662; *Angew. Chem. Int. Ed. Engl.* **1980**, *19*, 643; b) U. Schubert, D. Neugebauer, P. Hofmann, B. E. R. Schilling, H. Fischer, A. Motsch, *Chem. Ber.* **1981**, *114*, 3349; c) E. O. Fischer, D. Wittmann, D. Himmelreich, U. Schubert, K. Ackermann, *Chem. Ber.* **1982**, *115*, 3141; d) E. O. Fischer, D. Wittmann, D. Himmelreich, R. Cai, K. Ackermann, D. Neugebauer, *Chem. Ber.* **1982**, *115*, 3152.
- [31] A. E. Reed, L. A. Curtiss, F. Weinhold, *Chem. Rev.* **1988**, *88*, 899.
- [32] The Δ*E*_{orb} term could not be broken down into the σ and π bond energy contributions owing to the lack of symmetry. The percentage contribution of Δ*E*_{orb} to the total attractive interactions (Δ*E*_{orb} and Δ*E*_{elstat}) reflects the covalent character of the bond.
- [33] G. Frenking, N. Fröhlich, *Chem. Rev.* **2000**, *100*, 717 and references therein.
- [34] [W(PMe₃)₅] has a singlet ground-state configuration and adopts a distorted trigonal-bipyramidal minimum geometry, in which one of the equatorial PMe₃ ligands displays a C–H agostic interaction with the metal center (see Supporting Information). [W(PMe₃)₅] has been suggested as an intermediate in the cyclometallation reaction of [W(PMe₃)₆] to afford [W(PMe₃)₄(η²-CH₂PMe₂)H] and PMe₃: D. Rabinovich, G. Parkin, *J. Am. Chem. Soc.* **1990**, *112*, 5381.
- [35] The ion [Pb(2,6-Trip₂C₆H₃)]⁺ has a singlet ground state (see Supporting Information). The toluene adduct of [Pb(2,6-Trip₂C₆H₃)]⁺ was isolated recently with the counterion [B(Me)(C₆F₅)₃][−]: S. Hino, M. Brynda, A. D. Phillips, P. P. Power, *Angew. Chem.* **2004**, *116*, 2709; *Angew. Chem. Int. Ed.* **2004**, *43*, 2655.

Cycloadditions

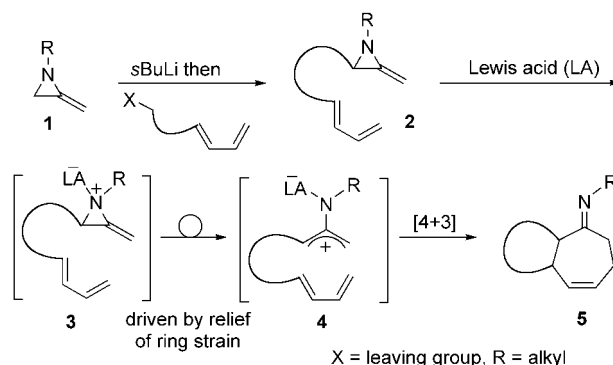
A Lewis Acid Catalyzed Intramolecular [4+3] Cycloaddition Route to Polycyclic Systems That Contain a Seven-Membered Ring**

Gildas Prié, Natacha Prévost, Heather Twin,
Stephanie A. Fernandes, Jerome F. Hayes, and
Michael Shipman*

Oxyallyl cations are important intermediates in the synthesis of seven-membered rings by way of [4+3] cycloadditions with 1,3-dienes.^[1] The products commonly serve as useful templates in organic synthesis.^[2] Intramolecular cycloadditions of oxyallyl cations are especially useful for the construction of complex polycyclic systems.^[1c,f,3] For example, Harmata and co-workers have used this approach to make aphanamol I, widdrol, and (+)-dactylol.^[1e] Less well-studied are 2-aminoallyl cations, which also participate in [4+3] cycloadditions.^[4] Interestingly, these *N*-substituted cations appear to have some advantages over the more extensively studied oxyallyl cations. For example, Cha and co-workers have shown that in some situations cycloadditions that involve 2-aminoallyl cations proceed in higher yields and/or with enhanced stereocontrol.^[4g] Furthermore, Kende and Huang have shown that asymmetric induction (up to 60% *ee*) is possible in [4+3] cycloadditions that involve 2-aminoallyl cations by incorporating a chiral, nonracemic element into the cation.^[4h] Despite these potential benefits, 2-aminoallyl cations are not widely used because methods for their generation are rather limited. Typically, they involve the solvolysis of unstable α -chloroamines^[4a,d-g] or 2-chloroimines^[4c,h] with stoichiometric amounts of silver(I) salts.

As part of a program aimed at exploring the scope and utility of 2-methyleneaziridines **1** in organic synthesis,^[5] we realised that these heterocycles might serve as alternative precursors to 2-aminoallyl cations. As methyleneaziridines can be functionalised readily at C3,^[5c] we felt that this methodology might be especially useful for the development of intramolecular [4+3] cycloadditions. The general strategy

is depicted in Scheme 1. Lithiation and alkylation of **1** with an appropriately functionalized 1,3-diene is expected to provide direct entry to cycloaddition precursor **2**. Complexation of the nitrogen atom of **2** to a suitable Lewis acid might then



Scheme 1. Proposed Lewis acid catalyzed intramolecular [4+3] cycloaddition of 2-methyleneaziridines.

generate the highly strained and reactive aziridinium ion **3**,^[6] which could be expected to undergo fragmentation to Lewis acid complexed 2-aminoallyl cation **4**. Further intramolecular reaction with the appended 1,3-diene would lead to cycloheptenone imine **5**. Thus, in just two synthetic operations, polycyclic systems might be produced from the readily accessible methyleneaziridine **1**. Herein we report our initial studies, which demonstrate the validity of this new approach to seven-membered rings.

A variety of cycloaddition precursors **6–12** were made to probe this chemistry in detail with respect to changes in the 1,3-diene and aziridine components as well as in the nature of the linking tether (Table 1). Lithiation of *N*-benzyl-2-isopropylideneaziridine (*s*BuLi, TMEDA, -78°C , THF, 5 h) and further reaction with 2-(3-iodopropyl)furan (**13**), 2-(4-iodobutyl)furan (**14**), and 7-iodo-hepta-1,3-diene provided **6** (67%), **7** (71%) and **8** (83%), respectively, after column chromatography. Similarly, reaction of *N*-benzyl-2-cyclohexylideneaziridine with **13**, and separately **14**, gave **9** (61%) and **10** (62%), respectively. We used geometrically pure (*Z*)- and (*E*)-*N*-benzyl-2-ethyleneaziridine,^[5d] to produce (*Z*)-**11** (59%) and (*E*)-**11** (71%), respectively, by lithiation and reaction with **13**. Finally, deprotonation and diastereocontrolled alkylation of (*S*)-*N*-(1-phenylethyl)-2-isopropylideneaziridine gave **12** (63%) as a single diastereomer whose relative configuration was assigned by correlation with literature data.^[5c]

Initial cycloaddition studies were conducted on furan-tethered aziridine **6**, which bears a three-carbon linking chain between the reaction partners. After some experimentation, it was determined that treatment of **6** with excess $\text{BF}_3\cdot\text{OEt}_2$ (150 mol%) in dichloromethane at room temperature for 16 h yielded tricyclic imine **15** in 67% yield as a single stereoisomer after silica-gel chromatography (Table 1, entry 1). The structure and stereochemistry of **15** were unambiguously confirmed by X-ray crystallography after reduction of the imine from the *Si* face with sodium cyanoborohydride and conversion of the resulting amine

[*] G. Prié, S. A. Fernandes, M. Shipman
Department of Chemistry
University of Warwick
Coventry, CV4 7AL (UK)
Fax: (+44) 24-7652-4429
E-mail: m.shipman@warwick.ac.uk

N. Prévost, H. Twin
Department of Chemistry
University of Exeter
Stocker Road, Exeter, EX4 4QD (UK)

J. F. Hayes
GlaxoSmithKline
Old Powder Mills
Tonbridge, Kent, TN11 9AN (UK)

[**] This work was supported by the Engineering and Physical Sciences Research Council (Grant no. GR/R82586/02) and GlaxoSmithKline.

Supporting information for this article is available on the WWW under <http://www.angewandte.org> or from the author.

Table 1: Lewis acid catalyzed intramolecular [4+3] cycloaddition of 2-methyleneaziridines **6–12**.

Entry	Aziridine	Lewis acid (method) ^[a]	Cycloadducts	Yield [%] ^[b]	Ratio
1 2		BF ₃ ·OEt ₂ (A) Sc(OTf) ₃ (B)		67 ^[d] 57	–
3 4		BF ₃ ·OEt ₂ (C) Sc(OTf) ₃ (D)		70 ^[e] 60	–
5		BF ₃ ·OEt ₂ (E)		53	56:44
6		BF ₃ ·OEt ₂ (A)		67 ^[f]	–
7		BF ₃ ·OEt ₂ (C)		65 ^[e]	–
8		BF ₃ ·OEt ₂ (C) ^[c]		56 ^[f]	20/21 80:20
9		BF ₃ ·OEt ₂ (C) ^[c]		45 ^[f]	20/21 32:68
10		BF ₃ ·OEt ₂ (A)		72	45:55

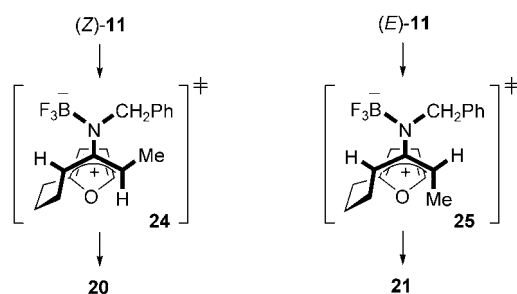
[a] Method A: BF₃·OEt₂ (150 mol%), CH₂Cl₂, –30°C, 1 h; then room temperature, 16 h; method B: Sc(OTf)₃ (10 mol%), CH₂Cl₂, –30°C, 1 h; then room temperature, 16 h; method C: same as method A; then aqueous H₂SO₄ (10%), MeOH, 16 h, room temperature; method D: same as method B; then aqueous H₂SO₄ (10%), MeOH, 16 h, room temperature; method E: BF₃·OEt₂ (150 mol%), ClCH₂CH₂Cl, –60°C to reflux, 48 h; then aqueous H₂SO₄ (10%), MeOH, 16 h. [b] Yield of isolated product. [c] Cycloaddition and hydrolysis conducted at 50°C. [d] Structure determined by X-ray crystallography after reduction of the imine and formation of the HCl salt (see text). [e] Structure determined by X-ray crystallography. [f] Ring junction stereochemistry confirmed by NOE difference experiments.

into its crystalline hydrochloride salt (data not shown). Significantly, **6** could also be converted into **15** by using just a catalytic amount (10 mol%) of scandium(III) triflate (Table 1, entry 2).^[7] Representative procedures are provided in the Supporting Information. Ketone products can be isolated from these reactions by inclusion of an acidic workup step. For example, reaction of aziridine **7** with either BF₃·OEt₂ or Sc(OTf)₃ provided tricyclic ketone **16**, again as a single

diastereomer, after workup with aqueous H₂SO₄ in methanol (Table 1, entries 3 and 4). The reaction is not limited to electron-rich dienes such as furan. For example, aziridine **8**, which incorporates a simple monosubstituted 1,3-diene, reacts to give **17** as a mixture of diastereomers. In this case, better yields were obtained by heating **8** and BF₃·Et₂O in 1,2-dichloroethane at reflux for 48 h prior to acidic hydrolysis (Table 1, entry 5). The reaction also accommodates changes in the nature of the structure of the methyleneaziridine component (Table 1, entries 6–10). However, we have been unable to determine if intramolecular cycloadditions proceed with methyleneaziridines that do not bear carbon substituents on the alkene terminus.^[8] Interestingly some stereochemical “memory” is apparent in the cycloaddition of (*Z*)- and (*E*)-**11**. Both produce **20** and **21**, but the relative amounts of these two diastereomers is dependent on the alkene geometry in the starting material (Table 1, entries 8 and 9). The assignment of the relative stereochemistry within **20** and **21** was made on the basis of the vicinal coupling constant between 7-H and 8-H (**20**: *J*_{7,8} = 5.3 Hz; **21**: *J*_{7,8} = 0.0 Hz).^[9] The conversion of diastereomerically pure **12** into near equal quantities of tricycles **22** and **23** is mechanistically significant as it reveals that the stereochemical homogeneity at C3 of **12** is almost completely lost during the cycloaddition (Table 1, entry 10).

We propose that the cycloadditions of **6**, **8**, **9**, **11**, and **12** proceed via a compact transition state, with the tethering arm orientating itself *anti* to the bulky Lewis acid complexed amino substituent. This is illustrated for the conversion of (*Z*)- and (*E*)-**11** into the major products **20** and **21** via **24** and **25**, respectively (Scheme 2). In support of this hypothesis, it is known that cyclic 2-aminoallyl cations favor compact transition states.^[4a] Furthermore, the loss of stereochemical integrity in the conversion of **12** into **22** and **23** is consistent with the formation of a planar 2-aminoallyl cation. To account for the switch in stereochemical outcome in the preparation of **16** (and **19**), an extended transition state may prevail

with a longer linking tether.^[10] However, in considering the analysis of these reactions, it is important to bear in mind that other mechanistic alternatives cannot be ruled out. For example, the formation of **15–23** might proceed in a stepwise manner by direct nucleophilic attack of the 1,3-diene unit onto the aziridinium cation **3**, followed by subsequent ring closure of the resulting enamine onto the allylic cation derived from the diene.^[11] Efforts to obtain direct evidence



Scheme 2. Postulated transition states for the formation of **20** and **21**.

for the involvement of allylic cation **4** have thus far proved unsuccessful.^[12]

To conclude, a very concise new entry into a range of polycyclic systems that contain seven membered rings has been devised based on an intramolecular Lewis acid catalyzed [4+3] cycloaddition of methyleneaziridines. Efforts to develop asymmetric variants of this chemistry by using chiral Lewis acid catalysts or chiral, nonracemic methyleneaziridines are currently ongoing in our laboratory.

Received: June 25, 2004

Keywords: aziridines · cycloaddition · Lewis acids · nitrogen heterocycles · strained molecules

- [7] Examples of catalytic [4+3] cycloadditions of allyl cations are uncommon; for a recent example with scandium(III) triflate, see: M. Harmata, U. Sharma, *Org. Lett.* **2000**, 2, 2703.
- [8] Attempts to make substrates that bear two hydrogen atoms on the exocyclic double bond of the methyleneaziridine have been hampered by their lack of stability during silica-gel chromatography. However, preliminary experiments establish that 2-methyleneaziridines do participate in *intermolecular* [4+3] cycloadditions. For example, the reaction of 1-(1-phenylethyl)-2-methyleneaziridine with excess furan ($\text{BF}_3 \cdot \text{Et}_2\text{O}$ (1.5 equiv), CH_2Cl_2 , room temperature, 16 h; then aqueous AcOH (1M), 2 h) yields 8-oxabicyclo[3.2.1]octan-3-one in 24% yield (unoptimized).
- [9] A. M. Montaña, S. Ribes, P. M. Grima, F. Garcia, *Magn. Reson. Chem.* **1998**, 36, 174.
- [10] In the case of **16** (and **19**), it is conceivable that the switch in the preferred diastereomer is not due to a change in the cycloaddition transition state but results from thermodynamic equilibration of the α stereocenter of the ketone during hydrolysis. From labeling experiments, we know that hydrolysis ($\text{D}_2\text{SO}_4/\text{D}_2\text{O}$ in CD_3OD) leads to some deuterium incorporation ($\approx 36\%$ D) into **16** at the center α to the ketone.
- [11] For recent theoretical studies on [4+3] cycloadditions that support stepwise mechanisms, see: M. Harmata, P. R. Schreiner, *Org. Lett.* **2001**, 3, 3663; J. A. Sáez, M. Arnó, L. R. Domingo, *Org. Lett.* **2003**, 5, 4117.
- [12] A large downfield shift of the signal for the aziridine methylene group is observed in the ^1H NMR spectrum (400 MHz, CD_2Cl_2) of *N*-benzyl-2-isopropylideneaziridine upon addition of $\text{BF}_3 \cdot \text{Et}_2\text{O}$ (150 mol %) which suggests coordination of the nitrogen atom of the aziridine to the Lewis acid. Selected data: uncomplexed: $\delta = 2.37$ ppm (2H, s); complexed: $\delta = 3.09$ (1H, s), 2.52 ppm (1H, s). However, signals for the allylic cation were not observed.

- [1] For reviews, see: a) R. Noyori, Y. Hayakawa, *Org. React.* **1983**, 29, 163; b) H. M. R. Hoffmann, *Angew. Chem.* **1984**, 96, 29; *Angew. Chem. Int. Ed. Engl.* **1984**, 23, 1; c) J. Mann, *Tetrahedron* **1986**, 42, 4611; d) J. H. Rigby, F. C. Pigge, *Org. React.* **1997**, 51, 351; e) M. Harmata, *Acc. Chem. Res.* **2001**, 34, 595; f) M. Harmata, P. Rashatasakhon, *Tetrahedron* **2003**, 59, 2371.
- [2] M. Lautens, *Synlett* **1993**, 177; I. V. Hartung, H. M. R. Hoffmann, *Angew. Chem.* **2004**, 116, 1968; *Angew. Chem. Int. Ed.* **2004**, 43, 1934.
- [3] For a recent example, see: C. Rameshkumar, R. P. Hsung, *Angew. Chem.* **2004**, 116, 625; *Angew. Chem. Int. Ed.* **2004**, 43, 615.
- [4] a) R. Schmid, H. Schmid, *Helv. Chim. Acta* **1974**, 57, 1883; b) B. Ernst, C. Ganter, *Helv. Chim. Acta* **1978**, 61, 1775; c) N. De Kimpe, M. Palamareva, R. Verhe, L. De Buyck, N. Schamp, *J. Chem. Res. Synop.* **1986**, 190; d) J. Oh, J. Lee, S.-J. Jin, J. K. Cha, *Tetrahedron Lett.* **1994**, 35, 3449; e) J. Lee, J. Oh, S.-J. Jin, J.-R. Choi, J. L. Atwood, J. K. Cha, *J. Org. Chem.* **1994**, 59, 6955; f) H. Kim, C. Ziani-Cherif, J. Oh, J. K. Cha, *J. Org. Chem.* **1995**, 60, 792; g) S.-J. Jin, J.-R. Choi, J. Oh, D. Lee, J. K. Cha, *J. Am. Chem. Soc.* **1995**, 117, 10914; h) A. S. Kende, H. Huang, *Tetrahedron Lett.* **1997**, 38, 3353.
- [5] a) N. Prévost, M. Shipman, *Org. Lett.* **2001**, 3, 2383; b) J. F. Hayes, M. Shipman, H. Twin, *J. Org. Chem.* **2002**, 67, 935; c) J. F. Hayes, N. Prévost, I. Prokes, M. Shipman, A. M. Z. Slawin, H. Twin, *Chem. Commun.* **2003**, 1344; d) J. J. Shiers, M. Shipman, J. F. Hayes, A. M. Z. Slawin, *J. Am. Chem. Soc.* **2004**, 126, 6868, and references therein.
- [6] Protonation and methylation of *N*-substituted methyleneaziridines with $\text{HFSO}_3/\text{SbF}_5$ and $[\text{Me}_2\text{Cl}]^+[\text{SbF}_6]^-$, respectively, are known to produce the corresponding methyleneaziridinium cations; see: E. Jongejan, H. Steinberg, T. J. de Boer, *Recl. Trav. Chim. Pays-Bas* **1978**, 97, 145.

Oxidation

Catalytic Oxidation of CO with N₂O on Gas-Phase Platinum Clusters**

O. Petru Balaj, Iulia Balteanu, Tobias T. J. Roßteuscher, Martin K. Beyer, and Vladimir E. Bondybey**

Herein we report the observation of the full catalytic cycle of CO oxidation with N₂O on cationic platinum clusters for Pt_n⁺, *n* = 6–8, in the gas phase studied by Fourier-transform ion cyclotron resonance (FT-ICR) mass spectrometry. Platinum is

[*] O. P. Balaj, I. Balteanu, T. T. J. Roßteuscher,
Priv.-Doz. Dr. M. K. Beyer, Prof. Dr. V. E. Bondybey
Department Chemie, Lehrstuhl 2 für Physikalische Chemie
Technische Universität München
Lichtenbergstrasse 4, 85 747 Garching (Germany)
Fax: (+49) 89-289-13416
E-mail: beyer@ch.tum.de
ve.bondybey@ch.tum.de

[**] Financial support by the Deutsche Forschungsgemeinschaft and the Fonds der Chemischen Industrie is gratefully acknowledged.

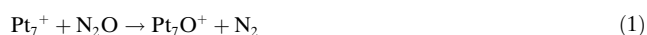


Supporting information for this article is available on the WWW under <http://www.angewandte.org> or from the author.

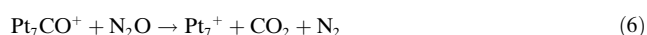
the key catalytic metal for a variety of industrial and environmental applications, for example, it catalyzes the oxidation of CO with O₂ in catalytic converters. This reaction has been studied in detail on surfaces.^[1] In the present study, N₂O was chosen as oxidant because small platinum clusters can undergo loss of platinum atoms by formation of PtO₂ by reaction with O₂.^[2] Gas-phase reactivity studies with bare transition-metal ions and clusters have been a useful tool to elucidate elementary steps in catalysis.^[3–6] Irion and co-workers demonstrated the catalytic formation of benzene from ethylene catalyzed by Fe₄⁺ in the gas phase,^[7] during which collision-induced desorption of C₆H₆ from the cluster was necessary to close the catalytic cycle. Ervin and co-workers demonstrated that the elementary steps of the catalytic cycle of the oxidation of CO with N₂O are possible on anionic platinum clusters.^[8–11] Schwarz and co-workers showed that the platinum cation Pt⁺ already exhibits catalytic activity, including full cycles of CO and methane oxidation.^[12–18] Andersson and Rosén provided strong evidence for catalytic oxidation of H₂ with O₂, forming H₂O on neutral platinum clusters in a flow reactor, albeit without resolving the detailed kinetics of the reaction.^[19] Previous studies of gas-phase platinum clusters^[1,8–11,19–28] were limited in size range and mass resolution by the use of platinum targets with natural isotope distribution. A laser vaporization source requires only minor amounts of materials, permitting work with isotopically enriched samples.^[29] We recently showed that full kinetic information of gas-phase reactions of cationic and anionic platinum clusters with up to 24 atoms can be obtained by using nearly pure ¹⁹⁵Pt.^[30] This size range is vital for comparison with the reactivities of size-selectively deposited clusters on surfaces, as studied for example, by Heiz et al.^[31,32]

When platinum cluster cations in a size range from 5 to 10 are stored in the ICR cell together with a 1:6 mixture of CO and N₂O, for some cluster sizes sequential addition of CO is observed, while for others, a steady state between the bare platinum cluster and its oxides is established. Although Pt₅⁺ forms Pt₅O⁺ and Pt₅O₂⁺, it efficiently reacts by attaching CO molecules. Pt₆⁺ reaches a steady state with Pt₆O⁺, and, to a small extent, Pt₆O₂⁺ and Pt₆O₃⁺ are also visible. Pt₇⁺ establishes a steady state with Pt₇O⁺ and Pt₇O₂⁺ in a ratio of about 1:2:4. Pt₈⁺ behaves somewhat similarly to Pt₇⁺, with Pt₈⁺ and Pt₈O⁺ as dominant species. Pt₉⁺ and Pt₉O⁺ keep a constant branching ratio, but their intensities decrease, because Pt₉⁺ sequentially attaches CO ligands. Pt₁₀⁺ efficiently attaches CO without any indication of catalytic activity.

Mass-selection experiments confirm that a steady state is indeed established for the Pt₇⁺ group. When Pt₇O⁺ was mass selected after 2 s, the constant intensity ratio between Pt₇⁺, Pt₇O⁺, and Pt₇O₂⁺ is again established within 3 s after mass selection, which proves that catalytic oxidation of CO takes place, involving the four reactions [Eqs. (1)–(4)]:



After very long reaction delays of 150 s, Pt₇CO_{8–10}⁺ species are observed to a very small extent. Evidently, by addition of multiple CO molecules, some bare Pt₇⁺ ions are removed from the catalytic cycle. To learn more about this process of catalyst poisoning, and to establish the number of CO molecules necessary to quench the oxidation reaction, we changed the experimental conditions in favor of poisoning. A 5:3 mixture of CO and N₂O was used in the ICR cell, and Pt₇CO⁺ was mass selected after 1 s. Subsequently, Pt₇CO⁺ is (with almost equal probability) either converted back into Pt₇⁺, which becomes available for the catalytic cycle described above, or it attaches a second CO molecule to form Pt₇(CO)₂⁺ [Eqs. (5)–(7)]:



Mass selection of Pt₇(CO)₂⁺ under otherwise similar conditions shows efficient addition of further CO molecules, whereas Pt₇CO⁺ is barely visible over the full course of the reaction. This observation unambiguously shows that a second CO ligand effectively poisons the cluster, although a minor contribution of CO₂ formation, at most 10 % of the efficiency for Pt₇CO⁺, cannot be fully excluded. The cluster then presumably adds CO molecules until the surface is fully saturated [Eq. (8)]:

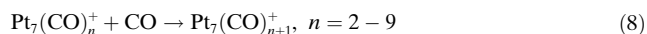


Figure 1 shows the kinetics of the Pt₇⁺ catalytic cycle when using a 1:6 mixture of CO and N₂O without mass selection, as this yields the best signal to noise ratio. To decrease the number of fit parameters, we have used the previously published absolute rate constants of Equations (1) and (2).^[30] In addition, the rate constant of Equation (6) was taken from the mass selection of Pt₇CO⁺. Absolute rate constants and reaction efficiencies of Equations (1)–(7) are summarized in Table 1. As seen in Figure 1, the steady state between Pt₇⁺, Pt₇O⁺, Pt₇O₂⁺, and Pt₇CO⁺ is established within 5 s. Towards longer reaction times, the intensities slowly decrease, and the poisoned clusters become more and more intense. By extrapolating the exponential decrease of the ions involved in the catalytic cycle, the active lifetime of a cluster in the cycle is estimated to be 750 s. From the reaction rate constants and the intensities of the reactant ions in Equations (3), (4), and (6), one can estimate that each Pt₇⁺ cluster converts 0.687 CO molecules into CO₂ per second. Over the lifetime of the cluster in the cycle, this amounts to a total of 515 CO₂ molecules formed.

The full catalytic cycle together with the poisoning mechanism is summarized in Scheme 1. Efficient catalytic conversion of CO into CO₂ is achieved in three different ways, either by CO colliding with the oxide species Pt₇O⁺ or Pt₇O₂⁺ (Equations (3) and (4)), or by N₂O oxidizing preadsorbed CO

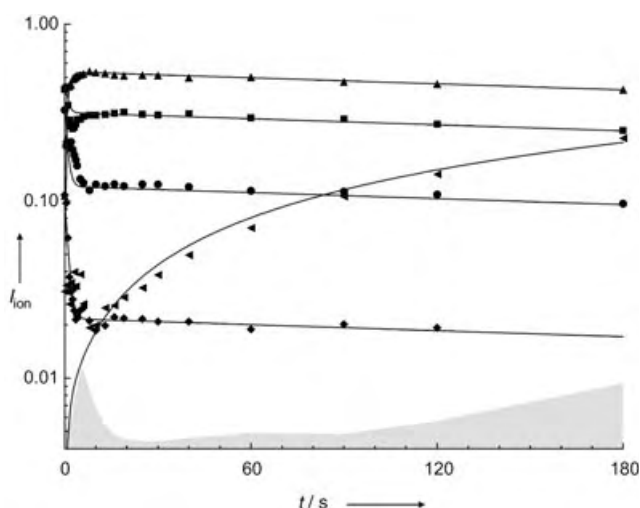
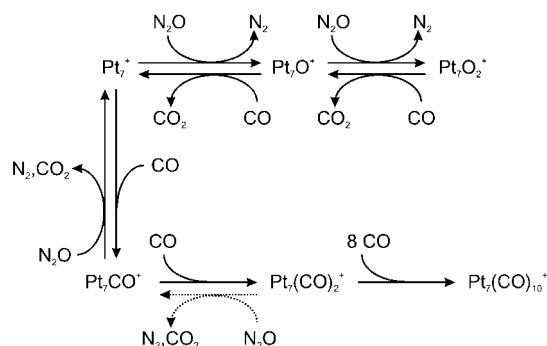


Figure 1. Kinetic fit of the Pt_7^+ reactions with a 1:6 mixture of CO and N_2O . Pt_7^+ (●) reacts very fast to form Pt_7O^+ (■) and Pt_7O_2^+ (▲). The described steady state is established between the three species within 5 s. Pt_7^+ also reacts efficiently with CO to form Pt_7CO^+ (◆), which, in turn, can either revert back to Pt_7^+ (●) or can very slowly attach a second CO molecule to form $\text{Pt}_7(\text{CO})_2^+$. Additional CO molecules are then attached until the cluster is fully saturated. The final product of CO attachment is $\text{Pt}_7(\text{CO})_{10}^+$. The visible $\text{Pt}_7(\text{CO})_n^+$, $n = 2, 8, 9, 10$, are summed together for clarity. Owing to the low intensity of $\text{Pt}_7(\text{CO})_2^+$, it was not possible to include it separately in the fit. The gray area denotes the noise level.

Table 1: Absolute rate constants k_{abs} and efficiencies calculated from ADO theory^[37,38] for the reactions of Pt_7^+ .

Reaction	$k_{\text{abs}} [10^{-11} \text{ cm}^3 \text{ s}^{-1}]$	Efficiency [%]
[Eq. (1)]	96.2	154.1 ^[a]
[Eq. (2)]	48.9	78.4
[Eq. (3)]	179.8	287.9 ^[a]
[Eq. (4)]	231.1	370.1 ^[a]
[Eq. (5)]	71.9	115.1 ^[a]
[Eq. (6)]	61.7	98.8
[Eq. (7)]	15.4	24.7

[a] Efficiencies above 100% are obtained because the collision rate is calculated by using a point-charge model, whereas the cluster has a finite size.



Scheme 1. Catalytic cycle of the Pt_7^+ ion in a 1:6 mixture of CO and N_2O . The catalytic cycle is running efficiently between Pt_7^+ , Pt_7O^+ , Pt_7O_2^+ , and Pt_7CO^+ . Additional CO molecules increasingly poison the cluster. Conversion of $\text{Pt}_7(\text{CO})_2^+$ back into Pt_7CO^+ might contribute to a minor extent to the catalytic cycle.

on Pt_7CO^+ (Equation (6)). A minor contribution from $\text{Pt}_7(\text{CO})_2^+$ to CO_2 formation is possible, but the absence of $\text{Pt}_7(\text{CO})_n^+$ with $n = 3-7$ and the appearance of the $n = 8-10$ species in the mass spectra clearly indicate that CO addition is the only significant process for $n = 3-9$.

If N_2O is present in sufficient excess, the concentration of Pt_7^+ in the steady state is small, and the catalytic cycle runs mostly through Equations (2) and (3) between Pt_7O^+ and Pt_7O_2^+ . Very few Pt_7CO^+ ions are formed and these are, in turn, almost entirely converted back into Pt_7^+ , before attachment of a second or third CO molecule can occur. This gas-phase catalytic cycle thus exhibits a typical characteristic of large-scale catalytic processes: The partial pressures of the reactants can be adjusted to suppress catalyst poisoning.

Our preliminary data for other cluster sizes indicate that the catalytic activity with respect to CO oxidation by N_2O is determined by the reactivity of the bare cluster with N_2O .^[30] This seems eminently reasonable: A high reactivity with N_2O shifts the cluster intensities in the steady state in favor of the oxide species and thus hinders the poisoning reaction by sequential CO addition to the bare cluster. For larger clusters, however, the picture becomes more complicated. Owing to their larger surface, adsorption of CO on Pt_nO^+ becomes feasible, presumably at a site that is remote from the oxygen atom. For example, for Pt_{20}^+ , it seems that $\text{Pt}_{20}\text{OCO}^+$ becomes an observable intermediate in the catalytic cycle. Such larger clusters, as well as anionic species, are currently under investigation.

Experimental Section

The experiments were performed on a modified Bruker/Spectrospin CMS47X mass spectrometer, equipped with an Apex III data station and an external homebuilt laser vaporization source described previously.^[33-36] Platinum clusters Pt_n^+ were produced by laser vaporization of a solid platinum target with the 5-ns pulse of a frequency-doubled Nd:YAG laser (Continuum Surelite II, 10 Hz, 5-mJ pulse energy), followed by supersonic expansion of the hot plasma entrained in a 50- μs helium pulse. The Pt_n^+ ions formed were transferred by a series of electrostatic lenses through four stages of differential pumping, decelerated, and stored in the ICR cell. To minimize problems associated with the isotope pattern of larger clusters, isotopically enriched platinum (97.3% ^{195}Pt , Oak Ridge National Laboratories) was used as described previously.^[30] The reactant gases CO (99.98%) and N_2O (99.8%) were admitted through two needle valves into the UHV region of the FT-ICR instruments at constant partial pressures. In the 1:6 mixture, $p(\text{CO}) = 1.6 \times 10^{-8}$ mbar and $p(\text{N}_2\text{O}) = 9.9 \times 10^{-8}$ mbar. In the 5:3 mixture, $p(\text{CO}) = 1.6 \times 10^{-8}$ mbar and $p(\text{N}_2\text{O}) = 9.8 \times 10^{-9}$ mbar. Relative rate constants were obtained by fitting the experimental data to pseudo-first-order reaction kinetics and converted into absolute rate constants and reaction efficiencies by using average dipole orientation (ADO) theory.^[37,38]

Received: July 6, 2004

Keywords: catalyst poisoning · cluster compounds · gas-phase reactions · heterogeneous catalysis · platinum

- [1] R. Imbühl, M. P. Cox, G. Ertl, *J. Chem. Phys.* **1986**, *86*, 3519–3534.
- [2] K. Koszinowski, D. Schröder, H. Schwarz, *J. Phys. Chem. A* **2003**, *107*, 4999–5006.
- [3] a) P. B. Armentrout, *Annu. Rev. Phys. Chem.* **2001**, *52*, 423–461; b) V. E. Bondybey, M. K. Beyer, *J. Phys. Chem. A* **2001**, *105*, 951–960; c) M. P. Irion, *Int. J. Mass Spectrom. Ion Processes* **1992**, *121*, 1–47; d) M. B. Knickelbein, *Annu. Rev. Phys. Chem.* **1999**, *50*, 79–115; e) K. M. Ervin, *Int. Rev. Phys. Chem.* **2001**, *20*, 127–164.
- [4] L. D. Socaciu, J. Hagen, T. M. Bernhardt, L. Wöste, U. Heiz, H. Hakkinen, U. Landman, *J. Am. Chem. Soc.* **2003**, *125*, 10437–10445.
- [5] M. M. Kappes, R. H. Staley, *J. Am. Chem. Soc.* **1981**, *103*, 1286–1287.
- [6] B. Blagojevic, M. J. Y. Jarvis, E. Flaim, G. K. Koyanagi, V. V. Lavrov, D. K. Bohn, *Angew. Chem.* **2003**, *115*, 5073–5077; *Angew. Chem. Int. Ed.* **2003**, *42*, 4923–4927.
- [7] P. Schnabel, K. G. Weil, M. P. Irion, *Angew. Chem.* **1992**, *104*, 633–635; *Angew. Chem. Int. Ed. Engl.* **1992**, *31*, 636–638.
- [8] P. A. Hintz, K. M. Ervin, *J. Chem. Phys.* **1995**, *103*, 7897–7906.
- [9] P. A. Hintz, K. M. Ervin, *J. Chem. Phys.* **1994**, *100*, 5715–5725.
- [10] X. L. Ren, P. A. Hintz, K. M. Ervin, *J. Chem. Phys.* **1993**, *99*, 3575–3587.
- [11] Y. Shi, K. M. Ervin, *J. Chem. Phys.* **1998**, *108*, 1757–1760.
- [12] M. Brönstrup, D. Schröder, I. Kretschmar, H. Schwarz, J. N. Harvey, *J. Am. Chem. Soc.* **2001**, *123*, 142–147.
- [13] R. Wesendrup, D. Schröder, H. Schwarz, *Angew. Chem.* **1994**, *106*, 1232–1234; *Angew. Chem. Int. Ed. Engl.* **1994**, *33*, 1174–1176.
- [14] M. Pavlov, M. R. A. Blomberg, P. E. M. Siegbahn, R. Wesendrup, C. Heinemann, H. Schwarz, *J. Phys. Chem. A* **1997**, *101*, 1567–1579.
- [15] M. Aschi, M. Brönstrup, M. Diefenbach, J. N. Harvey, D. Schröder, H. Schwarz, *Angew. Chem.* **1998**, *110*, 858–861; *Angew. Chem. Int. Ed.* **1998**, *37*, 829–832.
- [16] M. Brönstrup, D. Schröder, H. Schwarz, *Organometallics* **1999**, *18*, 1939–1948.
- [17] H. Schwarz, *Angew. Chem.* **2003**, *115*, 4580–4593; *Angew. Chem. Int. Ed.* **2003**, *42*, 4442–4454.
- [18] M. Diefenbach, M. Brönstrup, M. Aschi, D. Schröder, H. Schwarz, *J. Am. Chem. Soc.* **1999**, *121*, 10614–10625.
- [19] M. Andersson, A. Rosén, *J. Chem. Phys.* **2002**, *117*, 7051–7054.
- [20] U. Achatz, C. Berg, S. Joos, B. S. Fox, M. K. Beyer, G. Niedner-Schatteburg, V. E. Bondybey, *Chem. Phys. Lett.* **2000**, *320*, 53–58.
- [21] D. J. Trevor, D. M. Cox, A. Kaldor, *J. Am. Chem. Soc.* **1990**, *112*, 3742–3749.
- [22] D. J. Trevor, R. L. Whetten, D. M. Cox, A. Kaldor, *J. Am. Chem. Soc.* **1985**, *107*, 518–519.
- [23] A. Grushow, K. M. Ervin, *J. Am. Chem. Soc.* **1995**, *117*, 11612–11613.
- [24] A. Grushow, K. M. Ervin, *J. Chem. Phys.* **1997**, *107*, 8210–8210.
- [25] Y. Shi, V. A. Spasov, K. M. Ervin, *Int. J. Mass Spectrom.* **2001**, *204*, 197–208.
- [26] G. S. Jackson, F. M. White, C. L. Hammill, R. J. Clark, A. G. Marshall, *J. Am. Chem. Soc.* **1997**, *119*, 7567–7572.
- [27] T. Hanmura, M. Ichihashi, T. Kondow, *J. Phys. Chem. A* **2002**, *106*, 11465–11469.
- [28] K. Koszinowski, D. Schröder, H. Schwarz, *Organometallics* **2003**, *22*, 3809–3819.
- [29] V. E. Bondybey, *Science* **1985**, *227*, 125–131.
- [30] I. Balteanu, O. P. Balaj, M. K. Beyer, V. E. Bondybey, *Phys. Chem. Chem. Phys.* **2004**, *6*, 2910–2913.
- [31] U. Heiz, A. Sanchez, S. Abbet, W. D. Schneider, *Eur. Phys. J. D* **1999**, *9*, 35–39.
- [32] U. Heiz, A. Sanchez, S. Abbet, W. D. Schneider, *J. Am. Chem. Soc.* **1999**, *121*, 3214–3217.
- [33] V. E. Bondybey, J. H. English, *J. Chem. Phys.* **1981**, *74*, 6978–6979.
- [34] T. G. Dietz, M. A. Duncan, D. E. Powers, R. E. Smalley, *J. Chem. Phys.* **1981**, *74*, 6511–6512.
- [35] S. Maruyama, L. R. Anderson, R. E. Smalley, *Rev. Sci. Instrum.* **1990**, *61*, 3686–3693.
- [36] C. Berg, T. Schindler, G. Niedner-Schatteburg, V. E. Bondybey, *J. Chem. Phys.* **1995**, *102*, 4870–4884.
- [37] T. Su, M. T. Bowers, *J. Chem. Phys.* **1973**, *58*, 3027–3037.
- [38] L. Bass, T. Su, M. T. Bowers, *Int. J. Mass Spectrom. Ion Phys.* **1978**, *28*, 389–399.

Dye Aggregates

Alternating Hetero H Aggregation of Different Dyes by Interstrand Stacking from Two DNA–Dye Conjugates**

Hiromu Kashida, Hiroyuki Asanuma, and Makoto Komiyama*

DNA is a naturally occurring supramolecule that spontaneously forms a stable duplex with its complementary strand. Recent developments in phosphoramidite chemistry have made it possible to introduce various functional molecules or metal complexes into DNA.^[1] In these modified DNA structures, non-natural molecules or metal ions are aligned in an ordered manner and exhibit interesting properties that are rarely found in the monomeric state, such as the “fluorosides” demonstrated by Kool and co-workers.^[2]

Dye aggregates are known to exhibit properties that the corresponding monomers do not show. Control of the aggregation is important,^[3] especially in the fields of photo-induced electron transfer^[4] and enhancement of nonlinear optical properties.^[5] Previously, we introduced multiple methyl red moieties into DNA and successfully prepared stable H* and H aggregates that are characterized by a

[*] H. Kashida, Prof. Dr. H. Asanuma,^[†] Prof. Dr. M. Komiyama
Research Center for Advanced Science and Technology
The University of Tokyo
Komaba, Meguro-ku, Tokyo 153-8904 (Japan)
Fax: (+81) 3-5452—5202
E-mail: asanuma@mkomi.rcast.u-tokyo.ac.jp

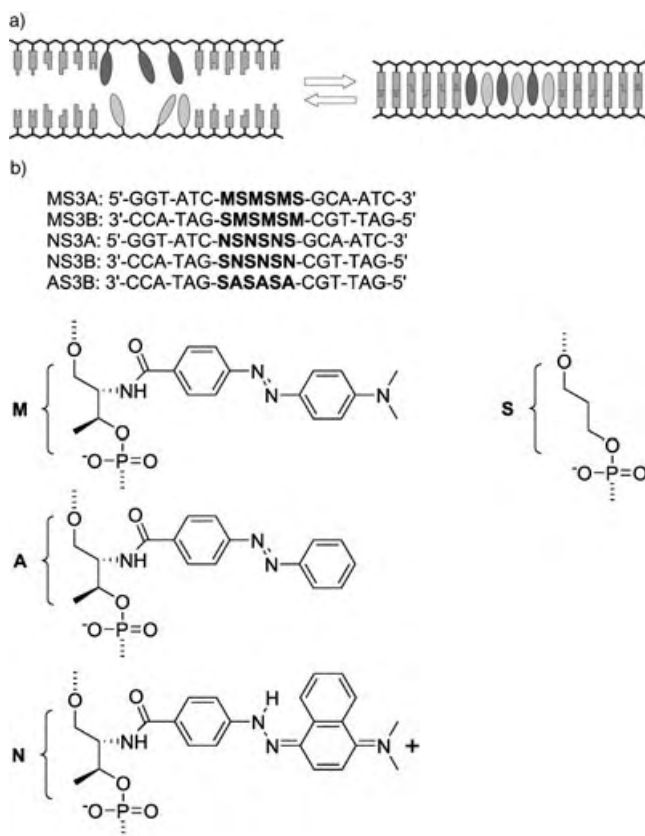
[†] PRESTO, Japan Science and Technology Corporation (JST)
Kawaguchi 332-0012 (Japan)

[**] This work was supported by Precursory Research for Embryonic Science and Technology (PRESTO), Japan Science and Technology Corporation (JST). Partial supports by a Grant-in-Aid for Scientific Research from the Ministry of Education, Culture, Sports, Science, and Technology, Japan, and by the Bio-oriented Technology Research Advancement Institution are also acknowledged.



Supporting information for this article is available on the WWW under <http://www.angewandte.org> or from the author.

narrowing of the absorption band as well as hypsochromic shift.^[6,7] The number of dye molecules and their orientation are easily controlled by programming the automated DNA synthesizer with the correct sequence. Various aggregates that are impossible to prepare by self-association of dyes are easily programmable through the covalent attachment of dye to DNA (conjugation of dye and DNA). One example of this is a heteroaggregate in which two different dyes are stacked alternately (Scheme 1a). Dye aggregates are conventionally



Scheme 1. Schematic illustration of a) preparation of heteroaggregates and b) modified DNA synthesized in this study.

prepared by the spontaneous self-association of dye monomers,^[3] so alternating alignment of two different dyes is very difficult in solution. In our study, dye molecules are introduced into each strand and dye aggregates are prepared by hybridization of these strands. As far as we know, preparation of this type of heteroaggregate has not yet been reported. It is widely known that H aggregation of identical dyes (homo H aggregate) shows both a narrowing and hypsochromic shift of the band because of the strong exciton coupling, as predicted by McRae and Kasha.^[8] However, there has been little investigation of whether similar narrowing of the band occurs in heteroaggregation, both from experimental and theoretical viewpoints.

Here, we report for the first time hetero H aggregates, which are difficult to prepare with a conventional method,^[3] by the use of two DNA–dye conjugates (Scheme 1a). This heteroaggregate showed a new sharp absorption band that

was different from those of the individual dyes, which indicates that exciton coupling occurs even between the different dyes.

Methyl red and naphthyl red (designated as **M** and **N**, respectively, in Scheme 1b) were introduced into the DNA on D-threoninol linkers from the corresponding phosphoramidite monomers, as reported previously.^[6,9] The pK_a values of methyl red and naphthyl red in the single-stranded DNA were 4.1 and 5.8,^[9] respectively, as determined from the change of their absorption maxima. At pH 5.0, where all the spectroscopic experiments were conducted, methyl red was neutral whereas naphthyl red was protonated (Scheme 1b). 1,3-Propanediol (**S** residue in Scheme 1b) and dye residues were alternated in the middle of the sequence.^[10,11] Aqueous solutions of **MS3A** and **NS3B** exhibited absorption maxima at 462 and 520 nm, respectively (Figure 1).^[12] Interestingly, a

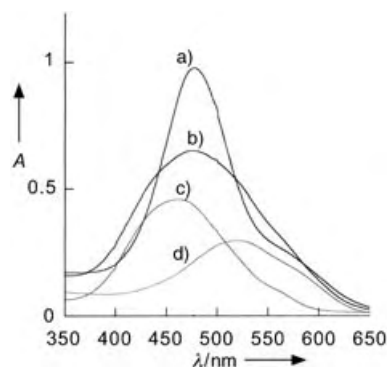


Figure 1. UV/Vis spectra of **MS3A/NS3B** duplex (a), single-stranded **MS3A** (c), **NS3B** (d), and simple sum of the spectra of **MS3A** and **NS3B** (b) at 0°C, pH 5.0 (10 mM MES buffer) in the presence of 100 mM NaCl.

new single sharp band appeared at 478 nm when these two strands **MS3A** and **NS3B** were hybridized (Figure 1). A simple sum of the spectra of the single-stranded **MS3A** and **NS3B** solution was very broad and different from the spectrum of the **MS3A/NS3B** duplex (compare the lines in Figure 1). In addition to the new absorption band, a single strong circular dichroism (CD) band with a sharp and symmetrical positive Cotton effect was induced at around 480 nm (Figure 2b). These spectroscopic behaviors demonstrate that methyl red and naphthyl red in the heteroaggregates optically interacted with each other (H band) and had different spectroscopic properties from those in the monomeric states.

This sharp new band became broad on elevating the temperature, and at 60°C, which is higher than the melting temperature T_m of the **MS3A/NS3B** duplex,^[13] the spectrum almost coincided with the simple sum of the two individual spectra of **MS3A** and **NS3B** (Figure 2a). This result also supports the hypothesis that the new band is attributed to heteroaggregation. Concurrently, the strong induced CD signal disappeared at 60°C (Figure 2b).

The peak maximum of the heteroaggregates appeared in the middle of those for homoaggregates (H aggregates) of methyl red (**MS3A/MS3B**) and naphthyl red (**NS3A/NS3B**) in

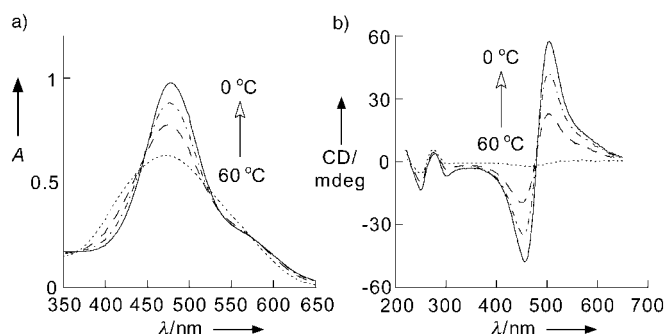


Figure 2. Effect of the temperature on a) UV/Vis and b) CD spectra of **MS3A/NS3B** duplex (20 °C interval) at pH 5.0 (10 mM MES buffer) in the presence of 100 mM NaCl.

both UV/Vis and CD spectra (Figure 3). This fact indicates that the new narrow band for the heteroaggregates is an H band derived from exciton coupling among the chromo-

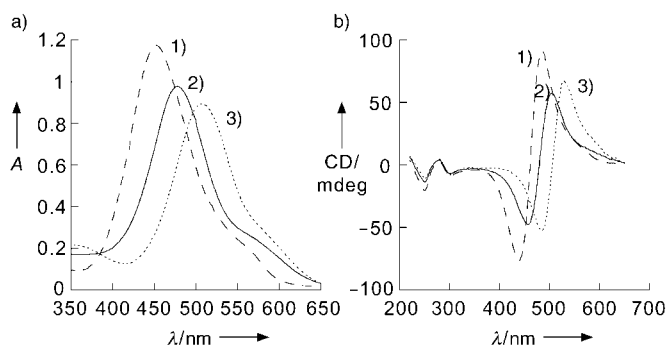


Figure 3. a) UV/Vis and b) CD spectra of heteroaggregates (**MS3A/NS3B**; 2), naphthyl red homoaggregates (**NS3A/NS3B**; 3), and methyl red homoaggregates (**MS3A/MS3B**; 1) at 0 °C, pH 5.0 (10 mM MES buffer) in the presence of 100 mM NaCl.

phores.^[14–16] This assignment is further supported by the fact that an increase in the aggregation number resulted in a larger hypsochromic shift (see the Supporting Information).^[8] To our knowledge, the appearance of an H band from two different kinds of dyes has rarely been reported and is not even predicted in the exciton theory.^[17]

Notably, not all combinations of chromophores exhibit a hetero H band. In the case of the methyl red/naphthyl red combination, a new sharp H band appeared. But when **MS3A** or **NS3A** was hybridized with **AS3B** involving azobenzenes in which the absorption maximum was located at 330 nm, no significant optical interaction was observed (Figure 4): the UV/Vis spectrum of either **MS3A/AS3B** or **NS3A/AS3B** almost coincided with the simple sum of that of each strand (see the Supporting Information).^[18] A certain degree of spectral overlap between the two chromophores is required to produce a hetero H band.^[19]

In conclusion, heteroaggregates in which two dyes are stacked alternately can be prepared by interstrand stacking from two DNA–dye conjugates. Even different dyes can exhibit an H band as a result of aggregation. The present method is applicable to other functional molecules, and

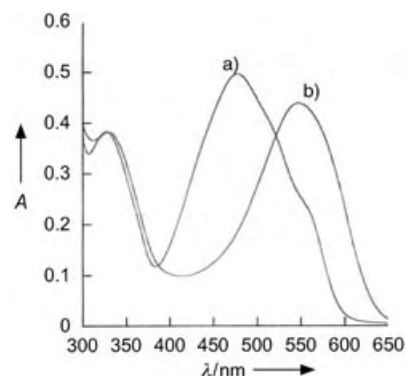


Figure 4. UV/Vis spectra of **MS3A/AS3B** (a) and **NS3A/AS3B** (b) at 0 °C, pH 5.0 (10 mM MES buffer) in the presence of 100 mM NaCl.

various novel materials can be produced by the attachment of dyes to DNA.^[17]

Experimental Section

Synthesis of the modified DNA involving dyes: The modified DNA molecules carrying **A**, **M**, **N**, and **S** residues were synthesized with an automated DNA synthesizer by using the corresponding phosphoramidite monomer prepared according to previous papers,^[6,9,20] and conventional ones. All the modified DNA molecules listed in Scheme 1b were purified by reversed-phase HPLC and characterized by MALDI-TOF mass spectrometry.

MALDI-TOF mass spectrometry: **NS3A**: found m/z 5463 (calcd for $[\text{NS3A-H}]^+$: m/z 5462); **NS3B**: found m/z 5464 (calcd for $[\text{NS3B-H}]^+$: m/z 5462); **MS3A**: found m/z 5311 (calcd for $[\text{MS3A-H}]^+$: m/z 5311); **MS3B**: found m/z 5311 (calcd for $[\text{MS3B-H}]^+$: m/z 5311); **AS3B**: found m/z 5183 (calcd for $[\text{AS3B-H}]^+$: m/z 5182).

Spectroscopic measurements: The UV/Vis spectra and CD spectra were measured on JASCO model V-530 and JASCO model J-725 instruments with 10-mm quartz cells, respectively. Both of them were equipped with programmed temperature controllers. The conditions for the sample solutions were: $[\text{NaCl}] = 100 \text{ mM}$, pH 5.0 (10 mM β -morpholinoethanesulfonic acid (MES) buffer), $[\text{DNA}] = 5 \mu\text{M}$. The T_m value was determined from the maximum in the first derivative of the melting curve, which was obtained by measuring the absorbance at 260 nm as a function of temperature. The temperature ramp was $1.0^\circ\text{C min}^{-1}$.

Received: June 4, 2004

Keywords: aggregation · conjugation · DNA · dyes/pigments

- [1] a) E. T. Kool, *Chem. Rev.* **1997**, 97, 1473–1488; b) K. Tanaka, M. Shionoya, *J. Org. Chem.* **1999**, 64, 5002–5003; c) A. K. Ogawa, Y. Wu, D. L. McMinn, J. Liu, P. G. Schultz, F. E. Romesberg, *J. Am. Chem. Soc.* **2000**, 122, 3274–3287; d) M. Smietana, R. B. Johnson, Q. M. Wang, E. T. Kool, *Chem. Eur. J.* **2004**, 10, 173–181, and references therein.
- [2] a) J. Gao, C. Strässler, D. Tahmassebi, E. T. Kool, *J. Am. Chem. Soc.* **2002**, 124, 11590–11591; b) E. T. Kool, *Acc. Chem. Res.* **2002**, 35, 936–943.
- [3] Dye aggregates are conventionally prepared by the self-association of individual dye monomers in solution (e.g., by addition of a salt to the aqueous dye solution), so the size of aggregates is difficult to control. Moreover, higher aggregates always precip-

- itate from the solution: S. Makio, N. Kanamaru, J. Tanaka, *Bull. Chem. Soc. Jpn.* **1980**, 53, 3120–3124.
- [4] a) H. Asanuma, T. Tani, *J. Phys. Chem. B* **1997**, 101, 2149–2153; b) T. Tani in *Photographic Sensitivity*, Oxford University Press, Oxford, **1995**, p. 111.
- [5] a) V. V. Shelkovnikov, R. V. Markov, A. I. Plekhanov, A. E. Simanchuk, Z. M. Ivanova, *High Energy Chem.* **2002**, 36, 260–264; b) F. Wurthner, S. Yao, T. Debaerdemaeker, R. Wortmann, *J. Am. Chem. Soc.* **2002**, 124, 9431–9447.
- [6] a) H. Asanuma, K. Shirasuka, M. Komiyama, *Chem. Lett.* **2002**, 490–491; b) H. Asanuma, K. Shirasuka, T. Takarada, H. Kashida, M. Komiyama, *J. Am. Chem. Soc.* **2003**, 125, 2217–2223.
- [7] An H aggregate is a dye cluster that causes a hypsochromic shift in the absorption spectrum with respect to the monomer spectrum. Dye molecules in H aggregates are known to be stacked in a face-to-face manner. See the Supporting Information.
- [8] a) E. G. McRae, M. Kasha, *J. Chem. Phys.* **1958**, 28, 721–722; b) M. Kasha, *Radiat. Res.* **1963**, 20, 55–71.
- [9] H. Asanuma, H. Kashida, X. G. Liang, M. Komiyama, *Chem. Commun.* **2003**, 1536–1537.
- [10] Recently, Brotschi and Leumann reported interstrand stacking of bipyridyl C-nucleotides that were consecutively introduced into the DNA. In our design, dye moieties are separated by **S** residues to avoid firm H* aggregation of methyl red moieties in the single-stranded state. See Refs. [6] and [11].
- [11] C. Brotschi, C. J. Leumann, *Angew. Chem.* **2003**, 115, 1694–1697; *Angew. Chem. Int. Ed.* **2003**, 42, 1655–1658.
- [12] Absorption maxima of monomers of methyl red and naphthyl red in the DNA appeared at around 484 and 546 nm, respectively. See the Supporting Information.
- [13] The melting temperature of **MS3A/NS3B** was 50.7°C, as estimated from the change in absorbance at 260 nm as a function of temperature. See the Supporting Information for the actual melting curve.
- [14] The possibility of a charge-transfer band is ruled out because the absorption band of the charge-transfer complex usually appears at a longer wavelength than those of individual dyes. See Ref. [15].
- [15] S. A. Lee, S. Hotta, F. Nakanishi, *J. Phys. Chem. A* **2000**, 104, 1827–1833.
- [16] The relative alignment of the chromophores will be discussed in detail elsewhere.
- [17] Since exciton coupling occurs over very short ranges (within 1.0 nm), our present finding would be applicable to the detection of short-distance interaction.
- [18] A contribution of the reduction of the conformers or local polarity change to the band narrowing of **MS3A/NS3B** is unlikely, because significant narrowing was not observed for the combination with **AS3B** involving **A** residues that are structurally similar to **M**.
- [19] We attributed the optical inactivity of the azobenzene/naphthyl red or azobenzene/methyl red combinations to the large difference in the absorption maximum, but more detailed analyses are needed.
- [20] H. Asanuma, T. Takarada, T. Yoshida, D. Tamaru, X. G. Liang, M. Komiyama, *Angew. Chem.* **2001**, 113, 2743–2745; *Angew. Chem. Int. Ed.* **2001**, 40, 2671–2673.

Evidence for the Structure of the Enantioactive Ligand in the Phosphine–Copper-Catalyzed Addition of Diorganozinc Reagents to Imines**

Alexandre Côté, Alessandro A. Boezio, and
André B. Charette*

Substantial efforts have been invested recently in the design and development of new chiral ligands for the asymmetric catalytic synthesis of simple chiral building blocks. Among the most effective and popular coordinating groups for chiral ligands are phosphorus-based groups due to their inherent ability to bind strongly but reversibly to several transition metals. However, even though redox processes have been reported between the phosphorus ligand and some transition metals,^[1] this potentially harmful process that could lead to important ligand modification has never been highlighted in asymmetric copper-catalyzed reactions. One well-known example is the reduction of Pd^{II} salts into Pd⁰ with Ph₃P to produce Ph₃P=O as the by-product.^[2] It has also been reported that Cu^{II} salts are reduced by 1,2-bis(diphenylphosphino)ethane to produce several phosphine/phosphine oxide ligands.^[3] It is surprising to see that even though Cu–phosphine complexes have been used extensively in asymmetric catalysis (conjugate additions and reduction,^[4] nucleophilic addition to ketones,^[5] enamines^[6] and imines^[7]) the in situ oxidation of the ligand has never been observed nor highlighted as the key step for high asymmetric induction. In this communication, we demonstrate that the oxidation of Me-duphos (**1**) by Cu^{II} salts to produce the highly effective monoxide ligand **2** (see Figure 1) is a key event for the high asymmetric induction of the Cu-catalyzed addition of di-

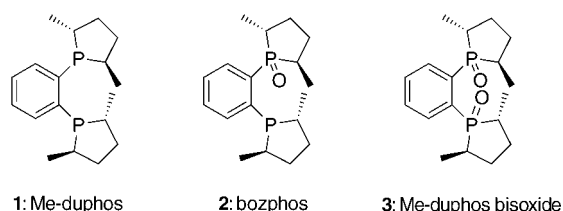


Figure 1. Phosphine and phosphine oxide ligands derived from Me-duphos.

[*] A. Côté, A. A. Boezio, Prof. A. B. Charette
Département de Chimie
Université de Montréal
P.O. Box 6128, Station Downtown
Montréal, Québec H3C 3J7 (Canada)
Fax: (+1) 514-343-5900
E-mail: andre.charette@umontreal.ca

[**] This work was supported by the NSERC, Merck Frosst Canada, Boehringer Ingelheim (Canada), and the Université de Montréal. A.C. is grateful to NSERC (ES). A.A.B. is grateful to the NSERC (PGF B) and F.C.A.R. (B2) for postgraduate fellowships.

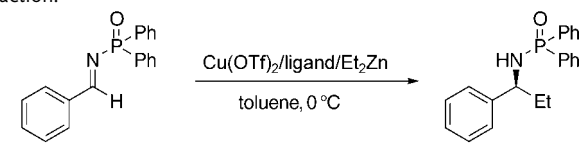


Supporting information for this article is available on the WWW under <http://www.angewandte.org> or from the author.

organozinc to *N*-phosphinoylimines. We also report that the efficiency of the oxidation is highly dependent upon the nature of the copper salt and the counterion used in the process.

We recently reported that Cu-**1** is an efficient catalyst for the addition of diorganozinc compounds to imines^[8] (Table 1, entry 1). We later disclosed that the replacement of one phospholane group by the hemilabile phosphine oxide (ligand **2**) led to a significant increase of the reaction rate and enantiomeric excesses (Table 1, entry 2).^[9]

Table 1: Effect of the order of addition in the Me-duphos-catalyzed reaction.



Entry	Method ^[a]	Ligand	Conv. [%]	ee [%]
1	A	1	92	89
2	A	2	100	97
3	B	1	38	0
4	B	2	100	97

[a] Method A: 1) Cu(OTf)₂ (6 mol%) and ligand **1** or **2** (3 mol%), 2) addition of Et₂Zn (2 equiv); method B: 1) Cu(OTf)₂ (6 mol%) and Et₂Zn (2 equiv), 2) addition of ligand **1** or **2** (3 mol%).

Although these two reactions appear to differ simply by the selection of the ligand, we were puzzled by the observation that the level of enantiocontrol was greatly dependant upon the order of addition to the reagents. For example, a high level of stereocontrol was observed with both ligands if Cu(OTf)₂ was mixed with Me-duphos or bozphos prior to the addition of Et₂Zn. In sharp contrast, no enantioselection was observed with Me-duphos if the Cu^{II} salt was initially reduced with Et₂Zn (to generate EtCu) followed by the addition of the chiral ligand (Table 1, entry 3). Conversely, the order of addition did not affect the *ee* value of the product if bozphos was used (Table 1, entry 4). One explanation for this behavior is that the Cu-**1** complex is only a precatalyst for the reaction, and it needs to undergo phosphine oxidation to generate the more reactive and selective Cu-**2** complex. To demonstrate whether Me-duphos oxidation is a viable pathway under the reaction conditions, we undertook a systematic spectroscopic investigation of the reaction to identify whether **2** or **3** is formed upon treatment with Cu salts. Unfortunately, the reaction could not be followed by in situ NMR methods due to the presence of paramagnetic Cu^{II}/Cu⁰ species and the rapid equilibration and disproportionation between various complexes.

To overcome this problem, we removed the residual Cu salts from the crude reaction mixture by treatment with aqueous KCN under deoxygenated conditions. This is a nice alternative to the use of dithiocatechol dilithium salts, which have been used to scavenge and recover phosphine ligands.^[10] Each ligand (**1–3**) was submitted to Cu(OTf)₂/Et₂Zn by the normal or reverse-addition protocol. After a standard KCN workup, the crude mixture was analyzed by ³¹P NMR

spectroscopy (Table 2). The first striking observation is that significant oxidation (up to 20 %) of one of the free phosphine of Me-duphos was observed when the ligand was initially premixed with Cu(OTf)₂ (Table 2, entry 2). Conversely,

Table 2: Oxidation of ligands **1–3** by Cu(OTf)₂.

1, 2, or 3 $\xrightarrow[\text{(2 equiv)}]{\text{Cu(OTf)}_2^{[a]}}$ mixture of **1, 2, and 3**

Entry	Starting ligand	Method ^[b]	Prod. ratio ^[c] 1:2:3
1	1	A	96:3:1
2	1	B	76:20:4
3	2	A	0:98:2
4	2	B	0:94:6
5	3	A	0:0:100
6	3	B	0:0:100

[a] Cu(OTf)₂ was purchased from Strem Chemical Inc. [b] Method A: 1) Cu(OTf)₂ (2 equiv) and Et₂Zn (10 equiv), 2) addition of ligand **1, 2, or 3** (1 equiv); method B: 1) Cu(OTf)₂ (2 equiv) and ligand **1, 2, or 3** (1 equiv), 2) addition of Et₂Zn (10 equiv). [c] The ratios were determined by quantitative ³¹P NMR spectroscopy, and the mass recovery was > 70%. See the Supporting Information for details.

inverting the order of addition almost completely suppressed the oxidation of the phosphine (only 3 % of bozphos was formed; Table 2, entry 1). The same series of experiments carried with bozphos (**2**) indicated that very little oxidation to give **3** (2–6 %) was observed regardless of the order of addition. This is not too surprising since the monoxide should be less prone to oxidation than Me-duphos. The relatively low level of oxidation with procedure A could be attributed to the background oxidation during the workup under a noninert atmosphere and not to a formal oxidation of phosphorus by the in situ formed EtCu.

The next step was to establish whether other species present in the reaction mixture could potentially oxidize Me-duphos to give bozphos (Table 3). CuOTf also led to significant oxidation of Me-duphos (up to 39 %; Table 3, entry 2). Conversely, both CuCl and CuOAc led to lower levels of phosphine oxidation, indicating that the nature of the counterion is also important. Since the level of oxidation appeared to be somewhat dependant upon the source of the copper salt used, we began to suspect that the presence of water could accelerate the oxidation process. Indeed, a much higher amount of oxidized product **2** was observed if a

Table 3: Oxidation of **1** with various copper salts.

1 $\xrightarrow[\text{(2 equiv)}]{\text{CuX}}$ **1+2+3**

Entry	CuX	Source	Prod. ratio ^[a] 1:2:3
1	(CuOTf) ₂ ·benzene	freshly prepared	75:20:5
2	(CuOTf) ₂ ·toluene	commercial	55:39:6
3	CuOAc	commercial	90:8:2
4	CuCl	commercial	96:3:1
5	Cu(OTf) ₂ ·2.3 H ₂ O	freshly prepared ^[b]	52:42:6

[a] The ratios were determined by quantitative ³¹P NMR spectroscopy. [b] Hydration of commercial Cu(OTf)₂ and analyzed by elemental analysis.

partially hydrated form of $\text{Cu}(\text{OTf})_2$ was used (Table 3, entry 5). We also noticed that the nature of the phosphine is also very important since the replacement of Me-duphos by PPh_3 under the conditions given in Table 3, entry 2 led to about 5 % of $\text{Ph}_3\text{P}=\text{O}$.

Plots of the course of the reaction with (Table 1, entries 3 and 4) with different ligands using the reverse-addition procedure are shown in Figure 2. The data strongly suggest

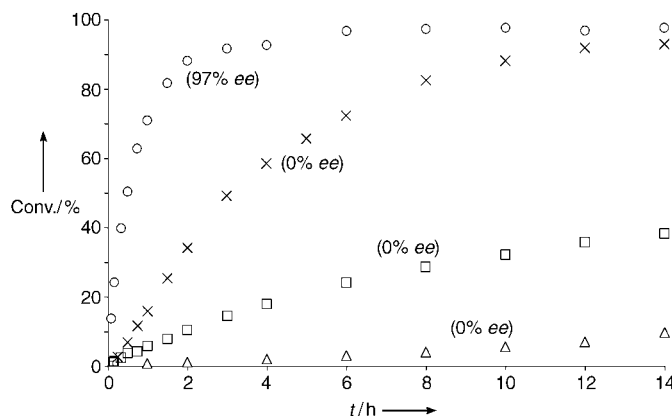


Figure 2. Plot of the course of the reaction with ligands 1–3 (3 mol% ligand/6 mol% $\text{Cu}(\text{OTf})_2$). \square = Me-duphos (1), \circ = bozphos (2), \triangle = bozphos (2) without Cu, \times = Me-duphos bisoxide (3).

that the ligand **2** is responsible for the highly enantioselective pathway. One striking feature is the difference in the reactivity between complex Cu^{I} -**1** and Cu^{I} -**2** in the reaction. This accounts for the observation that high enantioselectivities are obtained even when both complexes are present (Table 1, entry 1). The excellent catalytic activity of bis(phosphine) monoxide complexes has been observed in several reactions.^[11–13] Further evidence for the structure of the active catalyst resides in the demonstration that the reaction displays first-order kinetics in catalyst (1:1 stoichiometry ligand:Cu; Figure 3).

In conclusion, this paper highlights the very important observation that this copper–phosphine-catalyzed process

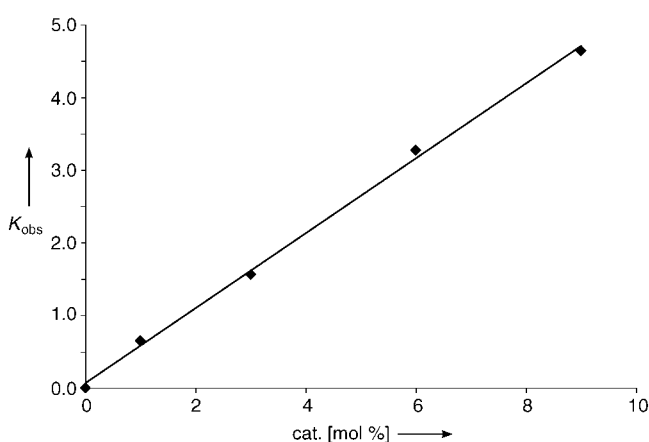


Figure 3. Plot showing that the reaction is first order in catalyst. Ratio bozphos/ $\text{Cu}(\text{OTf})_2$ = 1:1.

involve an initial phosphine oxidation, leading to a more reactive and selective metal complex.

Received: September 8, 2004

Published Online: November 11, 2004

Keywords: copper · imino compounds · nucleophilic addition · oxidation · phosphine ligands

- [1] I. Shimizu, Y. Matsumoto, K. Shoji, T. Ono, A. Satake, A. Yamamoto, *Tetrahedron Lett.* **1996**, 37, 7115–7118.
- [2] a) V. V. Grushin, *J. Am. Chem. Soc.* **1999**, 121, 5831–5831; b) F. Ozawa, A. Kubo, Y. Matsumoto, T. Hayashi, E. Nishioka, K. Yanagi, K. Moriguchi, *Organometallics* **1993**, 12, 4188–4196; c) C. Amatore, E. Carré, A. Jutand, M. A. M'Barki, *Organometallics* **1995**, 14, 1818–1826; d) C. Bianchini, A. Meli, W. Oberhauser, *Organometallics* **2003**, 22, 4281–4285; e) C. Amatore, M. A. M'Barki, *Organometallics* **1992**, 11, 3009–3013; f) M. R. Mason, J. G. Verkade, *Organometallics* **1992**, 11, 2212–2220; g) V. V. Grushin, C. Bensimon, H. Alper, *Inorg. Chem.* **1994**, 33, 4804–4806; h) W. J. Marshall, V. V. Grushin, *Organometallics* **2003**, 22, 555–562; i) F. Ozawa, A. Kubo, T. Hayashi, *Chem. Lett.* **1992**, 2177–2188; j) C. Amatore, A. Jutand, A. Thuilliez, *Organometallics* **2001**, 20, 3241–3249.
- [3] S. J. Berners-Price, R. K. Johnson, C. K. Mirabelli, L. F. Faucette, F. L. McCabe, P. Sadler, *Inorg. Chem.* **1987**, 26, 3383–3387.
- [4] a) V. Jurkauskas, S. L. Buchwald, *J. Am. Chem. Soc.* **2002**, 124, 2892–2893; b) A. H. M. de Vries, A. Meetsma, B. L. Feringa, *Angew. Chem.* **1996**, 108, 2526–2528; *Angew. Chem. Int. Ed. Engl.* **1996**, 35, 2374–2376; c) X. Hu, H. Chen, X. Zhang, *Angew. Chem.* **1999**, 111, 3720–3723; *Angew. Chem. Int. Ed.* **1999**, 38, 3518–3521; d) A. Alexakis, C. Benhaim, S. Rosset, M. Humam, *J. Am. Chem. Soc.* **2002**, 124, 5262–5263.
- [5] R. Wada, K. Oisaki, M. Kanai, M. Shibasaki, *J. Am. Chem. Soc.* **2004**, 126, 8910–8911.
- [6] a) C. Koradi, N. Gommermann, K. Polborn, P. Knochel, *Chem. Eur. J.* **2003**, 9, 2797–2811; b) C. Koradin, K. Polborn, P. Knochel, *Angew. Chem.* **2002**, 114, 2651–2654; *Angew. Chem. Int. Ed.* **2002**, 41, 2535–2538; c) N. Gommermann, K. Polborn, P. Knochel, *Angew. Chem.* **2003**, 115, 5941–5944; *Angew. Chem. Int. Ed.* **2003**, 42, 5763–5766.
- [7] a) B. H. Lipshutz, H. Shimizu, *Angew. Chem.* **2004**, 116, 2278–2280; *Angew. Chem. Int. Ed.* **2004**, 43, 2228–2230; b) T. Soeta, K. Nagai, H. Fujihara, M. Kuriyama, K. Tomioka, *J. Org. Chem.* **2003**, 68, 9723–9727; c) H. Fujihara, K. Nagai, K. Tomioka, *J. Am. Chem. Soc.* **2000**, 122, 12055–12056.
- [8] A. A. Boezio, A. B. Charette, *J. Am. Chem. Soc.* **2003**, 125, 1692–1693.
- [9] a) A. A. Boezio, J. Pytkowicz, A. Côté, A. B. Charette, *J. Am. Chem. Soc.* **2003**, 125, 14260–14261; b) A. Côté, A. A. Boezio, A. B. Charette, *Proc. Natl. Acad. Sci. USA* **2004**, 101, 5405–5410.
- [10] B. H. Lipshutz, B. Frieman, H. Birkedal, *Org. Lett.* **2004**, 6, 2305–2308.
- [11] Review on bis(phosphine) monoxides: V. V. Grushin, *Chem. Rev.* **2004**, 104, 1629–1662.
- [12] Asymmetric applications of bis(phosphine) monoxides: a) J. W. Fallar, B. J. Grimmond, D. G. D'Allesio, *J. Am. Chem. Soc.* **2001**, 123, 2525–2529; b) S. Gladiali, R. Taros, R. M. Ceder, M. Rocamora, G. Muller, X. Solan, M. Font-Bardia, *Tetrahedron: Asymmetry* **2004**, 15, 1477–1485; c) S. Gladiali, S. Pulacchini, D. Fabbri, M. Sansoni, *Tetrahedron: Asymmetry* **1998**, 9, 391–395.
- [13] For some examples of monophosphane ligands bearing an additional coordinating heteroatom used in asymmetric catalysis: a) P. von Matt, A. Pfaltz, *Angew. Chem.* **1993**, 105, 614–

615; *Angew. Chem. Int. Ed. Engl.* **1993**, 32, 566–568; b) J. M. Brown, D. I. Hulmes, P. I. Guiry, *Tetrahedron* **1994**, 50, 4493–5006; c) H. Kodama, T. Taiji, T. Ohta, I. Furukawa, *Tetrahedron: Asymmetry* **2000**, 11, 4009–4015; d) Y. Uozumi, T. Hayashi, *J. Am. Chem. Soc.* **1991**, 113, 9887–9888; e) S. Vyskocil, M. Smrcina, V. Hanus, M. Polasek, P. Kocovsky, *J. Org. Chem.* **1998**, 63, 7738–7748; f) T. Hamada, A. Chieffi, J. Åhman, S. L. Buchwald, *J. Am. Chem. Soc.* **2002**, 124, 1261–1268; g) T. Hayashi, H. Iwamura, M. Naito, Y. Matsumoto, Y. Uozumi, *J. Am. Chem. Soc.* **1994**, 116, 775–776; h) A. Chieffi, K. Kamikawa, J. Åhman, J. M. Fox, S. L. Buchwald, *Org. Lett.* **2001**, 3, 1897–1903; i) J. Sprinz, G. Helmchen, *Tetrahedron Lett.* **1993**, 34, 1769–1772; Ref. [6], [7b,c].

Asymmetric Synthesis

Direct Catalytic Enantioselective α -Aminomethylation of Ketones**

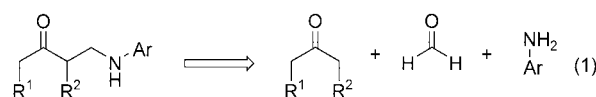
Ismail Ibrahim, Jesús Casas, and Armando Córdova*

The classical Mannich reaction,^[1] in which an aminomethyl group is introduced in the position α to a carbonyl function, has found a multitude of applications in organic chemistry.^[2] The resulting Mannich bases are of particular interest due to their biological activity as analgesics, antioplastics, and antibiotics, and as synthetic building blocks and precursors of pharmaceutically valuable γ -amino alcohols.^[2] However, regardless of the immense importance of this reaction only a few stereoselective α -aminomethylation reactions have been developed.^[3] For example, Enders et al. employed enantiomerically pure α -silyl ketones in diastereoselective α -aminomethylation reactions.^[4]

Chemists have developed several stoichiometric, indirect, stereoselective Mannich transformations that utilize preformed enol equivalents or imines.^[5] More recently, the first successful examples of catalytic asymmetric additions of enolates to imines were reported by Kobayashi and co-workers,^[6] which has led to intense research into catalytic indirect Mannich reactions.^[7] For example, Hoveyda and co-workers developed an elegant one-pot three-component silver-mediated Mannich-type reaction.^[8] Recently, Shibasaki and co-workers reported that heterodimetallic complexes are catalysts for the direct asymmetric Mannich reaction.^[9] Shibasaki and co-workers^[10] and Trost and Terrell^[11] also developed binuclear organozinc complexes that catalyze

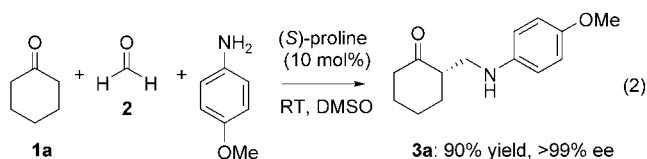
highly enantioselective Mannich-type reactions between hydroxyaryl ketones and preformed imines. Jørgensen and co-workers developed direct asymmetric Mannich reactions involving activated ketones as donors which are catalyzed by chiral copper(II) bisoxazoline (BOX) complexes.^[12] It was not until recently that researchers demonstrated that amino acid derivatives function as metal-free catalysts for direct asymmetric intermolecular reactions.^[13,14] List et al.,^[15] Barbas and co-workers,^[16] and we have developed direct organocatalytic asymmetric Mannich reactions of this type that involve ketones as donors.^[17] Asymmetric Mannich-type reactions with aldehydes as nucleophiles and preformed α -imino glyoxylate esters as the electrophiles have also been developed.^[18] More recently, we developed direct organocatalytic one-pot three-component cross-Mannich reactions.^[19] In addition, Jacobsen and Wenzel,^[20a] Terada and Uruguchi,^[20b] and others have reported excellent organocatalytic asymmetric Mannich-type reactions.^[20]

Despite the intense research on the catalytic enantioselective Mannich reaction, there is to our knowledge only one example of a catalytic one-pot three-component α -aminomethylation reaction. In this example, Shibasaki and co-workers demonstrated a catalytic enantioselective reaction between a ketone, amine, and formaldehyde, which furnished the corresponding Mannich base in 16 % yield with 64 % *ee*.^[9] Based on this initial investigation and our recently developed organocatalytic asymmetric α -hydroxymethylation reaction,^[21] we became interested in whether organocatalysis could be applied to this transformation. An amino acid catalyzed one-pot three-component reaction would be a more effective and economical process, which would provide a new tool for the α -aminomethylation of ketones [Eq. (1)].



Herein, we disclose one-pot three-component direct organocatalytic Mannich reactions between aqueous formaldehyde and ketones that furnished α -aminomethylated ketones with yields of up to 94 % and >99 % *ee*. The reactions were catalyzed by proline and its derivatives with excellent chemo- and enantioselectivity.

In an initial experiment we treated cyclohexanone **1a** (2 mmol) with formaldehyde **2** (1 mmol, 36 % aqueous solution) and *para*-anisidine (1.1 mmol) in the presence of a catalytic amount of (*S*)-proline (10 mol %) in dimethylsulfoxide (DMSO, 4 mL) at room temperature [Eq. (2)]. The reaction was quenched after 20 h, and α -aminomethylated ketone **3a** was isolated in 90 % yield with >99 % *ee* by column chromatography using neutral aluminium oxide as the



[*] I. Ibrahim, Dr. J. Casas, Prof. Dr. A. Córdova
Department of Organic Chemistry
The Arrhenius Laboratory, Stockholm University
10691 Stockholm (Sweden)
Fax: (+46) 8-154-908
E-mail: acordova@organ.su.se

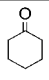
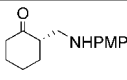
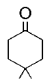
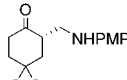
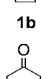
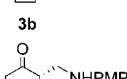
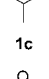
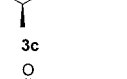
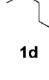
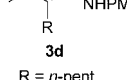
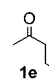
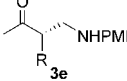
[**] We gratefully acknowledge the Swedish National Research council and Wenner-Gren-Foundation for financial support.

stationary phase.^[22] The reactions were also readily performed in *N,N*-dimethylformamide (DMF) and *N*-methylpyrrolidinone (NMP) without decreasing the enantioselectivity.

We also performed a catalyst screen using high-throughput chiral-phase high-performance liquid chromatography (HPLC) analyses and found that hydroxyproline derivatives, 5-pyrrolidine-2-yltetrazole, and proline-derived dipeptides catalyzed the α -aminomethylation reactions. For example, *trans*-4-hydroxyproline catalyzed the reaction between ketone **1a**, formaldehyde **2**, and anisidine furnishing **3a** with 90% *ee*.

Next, we performed the corresponding reaction with a set of different aliphatic ketones (Table 1). The reactions were effective, and the corresponding α -aminomethylated ketones **3a–3f** were isolated in high yield with predominantly > 99% *ee*. The reactions proceeded with excellent chemoselectivity, and no aldol adducts could be detected. For acyclic ketones, the reactions were regioselective and the α -aminomethylation occurred predominantly at the methylene carbon atoms of the ketones. For example, α -aminomethylated

Table 1: Proline-catalyzed one-pot three-component direct α -aminomethylation of different ketones.^[a]

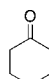
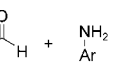
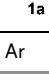
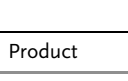
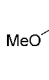
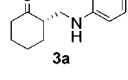
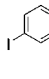
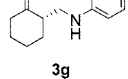
Entry	Ketone	Product	Yield [%] ^[b]	3:3' [%]	Sel. 3 [% <i>ee</i>] ^[c]
1			90	–	> 99
2			85	–	> 99
3			85 ^[d]	–	> 99 ^[e]
4			80	2:1	> 99
5			94	4:1	84
6			72	6:1	> 99

[a] Experimental conditions: a mixture of **1** (2 mmol, 2 equiv), **2** (1 mmol), and (*S*)-proline was stirred at room temperature for 16–17 h. The crude product obtained after aqueous workup was purified by column chromatography. PMP = *para*-methoxyphenyl. [b] Yield of the pure products isolated after column chromatography using neutral alumina as the stationary phase. [c] Determined by chiral-phase HPLC analyses. [d] *trans/cis* = 3:1. [e] *ee* of the *trans* isomer.

ketones **3f** and **3f'** were isolated (**3f/3f'** 6:1) in 72% yield for the combined products and with > 99% *ee* for **3f**. The reactions were readily performed on a 10-gram scale in aqueous solvents and in the presence of air without decreasing the yield and the *ee* of the product.

We also examined the variation of the amine component for the catalytic α -aminomethylation reaction. Hence, substituted aniline derivatives were treated with cyclohexanone and formaldehyde in the presence of a catalytic amount of (*S*)-proline (10 mol%; Table 2). In all cases, the reaction furnished the α -arylamino-methylated ketones with > 99% *ee*.

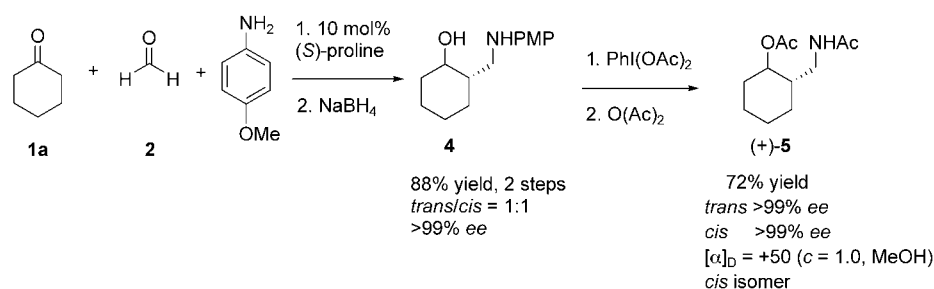
Table 2: Direct catalytic one-pot three-component α -aminomethylation reactions with different aromatic amines.^[a]

Entry	Ar	Product	Yield [%] ^[b]	Sel. [% <i>ee</i>] ^[c]
1			90	> 99
2			45	> 99
3			71	> 99
4			92	> 99

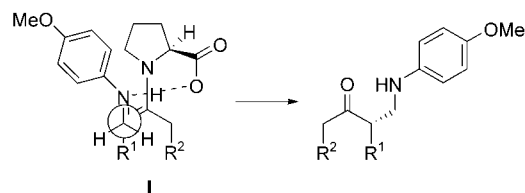
[a] Experimental conditions: a mixture of **1** (2 mmol, 2 equiv), **2** (1 mmol), and (*S*)-proline was stirred at room temperature for 16–24 h. The crude product obtained after aqueous workup was purified by column chromatography. [b] Combined yield of products isolated after column chromatography using neutral alumina as the stationary phase. [c] Determined by chiral-phase HPLC analyses.

The α -aminomethylated ketone **3a** was readily reduced with NaBH₄ in situ to give the corresponding monoprotected amino alcohol **4**, which was isolated in 88% yield over the two steps with d.r. (*trans/cis*) 1:1 and > 99% *ee* (Scheme 1). Removal of the *para*-methoxyphenyl (PMP) group under oxidative conditions followed by acetylation afforded the *cis*- and *trans*-diacetylated amino alcohols **5** in 72% yield for the combined products. Optical rotation studies of the *cis* isomer and comparison with published reports revealed that the absolute configuration of the product was *cis*-(1*S*,2*S*)-**5**.^[23] As selective reduction of β -amino ketones to both *syn*- and *anti*-1,3-amino alcohols is known, the present procedure is one practical route for the preparation of all of the possible stereoisomers of chiral 1,3-amino alcohols.^[24]

Based on the absolute configuration of the product, we propose transition-state model **I** to account for the regio- and enantioselectivity of the α -aminomethylation reaction of unmodified substituted ketones (Scheme 2). Hence, the (*S*)-



Scheme 1. Asymmetric synthesis of diacetylated *cis*- and *trans*-5.



Scheme 2. Transition-state model I is evoked to account for the enantioselectivity of the (S)-proline-catalyzed reaction.

proline derivative forms an enamine with the ketone that is attacked by the imine from its *si* face, providing (2*S*)- α -aminomethylated ketones. This is in accordance with the transition states of previously reported proline-catalyzed Mannich reactions, in which a *si*-facial attack occurs.^[15–19,25]

In conclusion, we have developed a direct catalytic enantioselective method that provides α -aminomethylated ketones in high yield with up to > 99% *ee*. The reactions were performed without tedious elaboration in wet solvents, were carried out in the presence of air, and could be readily scaled-up. In addition, a high-throughput screen revealed that other proline-derivatives including dipeptides catalyze the reaction with excellent enantioselectivity. To the best of our knowledge, this procedure is the first practical applicable a one-pot three-component catalytic asymmetric α -aminomethylation reaction. Further elaboration of this transformation and its synthetic applications is ongoing in our laboratory.

Experimental Section

Typical experimental procedure (Table 1, entry 1): Ketone **1a** (2 mmol) was added to a vial containing **2** (1 mmol, 36% aqueous solution) and a catalytic amount of (S)-proline (10 mol%) in DMSO (4 mL). After 20 h of vigorous stirring, the reaction was quenched by addition of aqueous NH₄Cl, and the aqueous phase was extracted three times with EtOAc. The combined organic layers were dried with MgSO₄, which was subsequently removed by filtration. Next, the solvent was removed under reduced pressure, and the crude product mixture was purified by column chromatography using neutral aluminum oxide as the stationary phase (EtOAc/pentane 1:10) to afford α -aminomethylated ketone **3a** in 90% yield as pale yellow solid. The *ee* value of **3a** was > 99% as determined by chiral-phase HPLC analysis. **3a**: ¹H NMR (CDCl₃): δ = 1.49 (m, 2H), 1.67 (m, 2H), 2.10 (m, 2H), 2.35 (m, 2H), 3.05 (dd, *J* = 13.3, 9.3 Hz, 1H), 3.37 (dd, *J* = 12.8, 7.8 Hz, 1H), 3.74 (s, 3H), 6.63 (d, *J* = 8.4 Hz, 2H), 6.77 ppm (d, *J* = 8.4 Hz, 2H); ¹³C NMR: δ = 25.1, 28.0, 32.3, 42.5, 45.6,

50.0, 56.1, 114.9, 115.18, 142.2, 152.6, 213.56 ppm; HPLC (Daicel Chiralpak AD, hexanes/*i*PrOH (96:4), flow rate = 0.5 mL min⁻¹, λ = 254 nm): major isomer: *t*_R = 44.31 min; minor isomer: *t*_R = 58.79 min; [α]_D = +4.1 (c = 2.0, CHCl₃); MALDI-TOF-MS: *m/z* = 256.1008; C₁₄H₁₉NO₂ (M + Na⁺: calcd 256.1313).

Received: May 15, 2004

Keywords: amino alcohols · asymmetric catalysis · ketones · Mannich reaction

- [1] C. Mannich, W. Krösche, *Arch. Pharm.* **1912**, 250, 647.
- [2] For excellent reviews see: a) E. F. Kleinmann in *Comprehensive Organic Synthesis*, Vol. 2 (Eds.: B. M. Trost, I. Fleming), Pergamon Press, New York, **1991**, Chapter 4.1; b) M. Arend, B. Westerman, N. Risch, *Angew. Chem.* **1998**, 110, 1096; *Angew. Chem. Int. Ed.* **1998**, 37, 1044; c) S. Denmark, O. J.-C. Nicaise in *Comprehensive Asymmetric Catalysis*, Vol. 2 (Eds.: E. N. Jacobsen, A. Pfaltz, H. Yamamoto), Springer, Berlin, **1999**, p. 93; d) M. Tramontini, L. Angiolini, *Tetrahedron* **1990**, 46, 1791; e) H. Hellmann, G. Opitz, α -Aminoalkylierung, Verlag Chemie, Weinheim, **1960**, p. 1; f) For examples, see: *Enantioselective Synthesis of β -Amino Acids* (Ed.: E. Juaristi), Wiley-VCH, Weinheim, **1997**.
- [3] a) N. Risch, A. Esser, *Liebigs Ann.* **1992**, 233; b) N. Risch, M. Arend in *Houben-Weyl: Methoden der Organischen Chemie*, Vol. E21b (Ed.: E. Müller), Thieme, Stuttgart, **1995**, p. 1908; c) V. Vinkovic, V. Sunjic, *Tetrahedron* **1997**, 53, 689.
- [4] a) D. Enders, D. Ward, J. Adam, G. Raabe, *Angew. Chem.* **1996**, 108, 1059; *Angew. Chem. Int. Ed. Engl.* **1996**, 35, 981; b) D. Enders, S. Oberbörsh, J. Adam, D. Ward, *Synthesis* **2002**, 18, 1737.
- [5] a) R. Kober, K. Papadopoulos, W. Miltz, D. Enders, W. Steglich, H. Reuter, H. Puff, *Tetrahedron* **1985**, 42, 1963; b) D. Enders, S. Oberbörsh, J. Adam, *Synlett* **2000**, 644; c) D. Seebach, M. Hoffmann, *Eur. J. Org. Chem.* **1998**, 1337; d) Y. Aoyagi, R. P. Jain, R. M. Williams, *J. Am. Chem. Soc.* **2001**, 123, 3472, and references therein; e) U. Schöllkopf in *Topics in Current Chemistry*, Vol. 109 (Ed.: F. L. Boschke), Springer, Berlin, **1983**, pp. 45–85; f) D. A. Evans, F. Urpi, T. C. Somers, J. S. Clark, M. T. Bilodeau, *J. Am. Chem. Soc.* **1990**, 112, 8215; g) C. Palomo, M. Oiarbide, A. Landa, M. C. Gonzales-Rego, J. M. Garcia, A. Gonzalez, J. M. Odriozola, M. Martin-Pastor, A. Linden, *J. Am. Chem. Soc.* **2002**, 124, 8637, and references therein.
- [6] a) S. Kobayashi, H. Ishitani, *Chem. Rev.* **1999**, 99, 1069; b) H. Ishitani, M. Ueno, S. Kobayashi, *J. Am. Chem. Soc.* **1997**, 119, 7153; c) S. Kobayashi, T. Hamada, K. Manabe, *J. Am. Chem. Soc.* **2002**, 124, 5640; d) H. Ishitani, M. Ueno, S. Kobayashi, *Org. Lett.* **2002**, 4, 143; e) H. Ishitani, S. Ueno, S. Kobayashi, *J. Am. Chem. Soc.* **2000**, 122, 8180.
- [7] a) E. Hagiwara, A. Fujii, M. Sodeoka, *J. Am. Chem. Soc.* **1998**, 120, 2474; b) A. Fujii, E. Hagiwara, M. Sodeoka, *J. Am. Chem. Soc.* **1999**, 121, 545; c) Y. Hamashima, K. Yagi, H. Tamas, M. Sodeoka, *J. Am. Chem. Soc.* **2002**, 124, 14530; d) Y. Hamashima, M. Hotta, M. Sodeoka, *J. Am. Chem. Soc.* **2002**, 124, 11240; e) D. Ferraris, B. Young, T. Dudding, T. Lectka, *J. Am. Chem. Soc.* **1998**, 120, 4548; f) D. Ferraris, B. Young, C. Cox, W. J. Drury III, T. Dudding, T. Lectka, *J. Org. Chem.* **1998**, 63, 6090; g) D. Ferraris, B. Young, C. Cox, T. Dudding, W. J. Drury III, L. Ryzhkov, T. Taggi, T. Lectka, *J. Am. Chem. Soc.* **2002**, 124, 67.
- [8] W. S. Josephsohn, M. L. Snapper, A. H. Hoveyda, *J. Am. Chem. Soc.* **2004**, 126, 3734.

- [9] S. Yamasaki, T. Iida, M. Shibasaki, *Tetrahedron Lett.* **1999**, *40*, 307.
- [10] S. Matsunaga, N. Kumagai, N. Harada, S. Harada, M. Shibasaki, *J. Am. Chem. Soc.* **2003**, *125*, 4712.
- [11] B. M. Trost, L. M. Terrell, *J. Am. Chem. Soc.* **2003**, *125*, 338.
- [12] a) K. Juhl, N. Gathergood, K. A. Jørgensen, *Angew. Chem.* **2001**, *113*, 3083; *Angew. Chem. Int. Ed.* **2001**, *40*, 2995; b) M. Marigo, A. Kjaersgaard, K. Juhl, N. Gathergood, K. A. Jørgensen, *Chem. Eur. J.* **2003**, *9*, 2395; c) L. Bernardi, A. S. Gothelf, R. G. Hazell, K. A. Jørgensen, *J. Org. Chem.* **2003**, *68*, 2583.
- [13] a) P. I. Dalko, L. Moisan, *Angew. Chem.* **2001**, *113*, 3840; *Angew. Chem. Int. Ed.* **2001**, *40*, 3726; b) B. List, *Tetrahedron* **2002**, *58*, 5573; c) E. R. Jarvo, S. J. Miller, *Tetrahedron* **2002**, *58*, 2481; d) R. O. Duthaler, *Angew. Chem.* **2003**, *115*, 1005; *Angew. Chem. Int. Ed.* **2003**, *42*, 975.
- [14] Aldol reactions see: a) B. List, R. A. Lerner, C. F. Barbas III, *J. Am. Chem. Soc.* **2000**, *122*, 2395; b) W. Notz, B. List, *J. Am. Chem. Soc.* **2000**, *122*, 7386; c) K. Saktihvel, W. Notz, T. Bui, C. F. Barbas III, *J. Am. Chem. Soc.* **2001**, *123*, 5260; d) A. Córdova, W. Notz, C. F. Barbas III, *J. Org. Chem.* **2002**, *67*, 301; e) B. List, P. Pojarliev, C. Castello, *Org. Lett.* **2001**, *3*, 573; f) A. Córdova, W. Notz, C. F. Barbas III, *Chem. Commun.* **2002**, *67*, 3034; g) A. Bøgevig, K. Juhl, N. Kumaragurubaran, K. A. Jørgensen, *Chem. Commun.* **2002**, 620; h) A. B. Northrup, D. W. C. MacMillan, *J. Am. Chem. Soc.* **2002**, *124*, 6798; i) N. S. Chowdari, D. B. Ramachary, A. Córdova, C. F. Barbas III, *Tetrahedron Lett.* **2002**, *43*, 9591; j) C. Pidathala, L. Hoang, N. Vignola, B. List, *Angew. Chem.* **2003**, *115*, 2797; *Angew. Chem. Int. Ed.* **2003**, *42*, 2785; k) Z. Tang, F. Jiang, L.-T. Yu, X. Cui, L.-Z. Gong, A.-Q. Mi, Y.-Z. Jiang, Y.-D. Wu, *J. Am. Chem. Soc.* **2003**, *125*, 5262; α -Aminations see: a) A. Bøgevig, K. Juhl, N. Kumaragurubaran, W. Zhuang, K. A. Jørgensen, *Angew. Chem.* **2002**, *114*, 1868; *Angew. Chem. Int. Ed.* **2002**, *41*, 1790; b) B. List, *J. Am. Chem. Soc.* **2002**, *124*, 5656; c) N. Kumaragurubaran, K. Juhl, W. Zhuang, A. Bøgevig, K. A. Jørgensen, *J. Am. Chem. Soc.* **2002**, *124*, 6254; α -Oxidations see: a) A. Bøgevig, H. Sundén, A. Córdova, *Angew. Chem.* **2004**, *116*, 1129; *Angew. Chem. Int. Ed.* **2004**, *43*, 1109; b) M. Hayashi, J. Yamaguchi, T. Sumaiya, M. Shoji, *Angew. Chem.* **2004**, *116*, 1132; *Angew. Chem. Int. Ed.* **2004**, *43*, 1112; c) G. Zhong, *Angew. Chem.* **2003**, *115*, 4379; *Angew. Chem. Int. Ed.* **2003**, *42*, 4247; d) S. P. Brown, M. P. Brochu, C. J. Sinz, D. W. C. MacMillan, *J. Am. Chem. Soc.* **2003**, *125*, 10808; Michael reactions see: a) B. List, P. Pojarliev, H. J. Martin, *Org. Lett.* **2001**, *3*, 2423; b) S. Hanessian, V. Pham, *Org. Lett.* **2000**, *2*, 2975; c) J. M. Betancort, K. Saktihvel, R. Thayumanavan, C. F. Barbas III, *Tetrahedron Lett.* **2001**, *42*, 4441; d) J. M. Betancort, C. F. Barbas III, *Org. Lett.* **2001**, *3*, 3737; e) D. J. Hortsmann, D. J. Guerin, S. J. Miller, *Angew. Chem.* **2000**, *112*, 3781; *Angew. Chem. Int. Ed.* **2000**, *39*, 3635; f) A. Alexakis, O. Andrey, *Org. Lett.* **2002**, *4*, 3611; g) D. J. Guerin, S. J. Miller, *J. Am. Chem. Soc.* **2002**, *124*, 2134; h) N. Halland, P. S. Aburel, K. A. Jørgensen, *Angew. Chem.* **2003**, *115*, 685; *Angew. Chem. Int. Ed.* **2003**, *42*, 661; i) N. Halland, R. G. Hazell, K. A. Jørgensen, *J. Org. Chem.* **2002**, *67*, 8331; j) O. Andrey, A. Alexakis, G. Bernardinelli, *Org. Lett.* **2003**, *5*, 2559; k) D. Enders, A. Seki, *Synlett* **2002**, 26; Diels–Alder reactions see: a) A. B. Northrup, D. W. C. MacMillan, *J. Am. Chem. Soc.* **2002**, *124*, 2458; b) K. A. Ahrendt, C. J. Borths, D. W. C. MacMillan, *J. Am. Chem. Soc.* **2000**, *122*, 4243; hetero-Diels–Alder reactions see: a) K. Juhl, K. A. Jørgensen, *Angew. Chem.* **2003**, *115*, 1536; *Angew. Chem. Int. Ed.* **2003**, *42*, 1498; b) Y. Huang, K. Unni, A. N. Thadani, V. H. Rawal, *Nature* **2003**, *424*, 146; alkylation of electron-rich benzene systems see: a) N. A. Paras, D. W. C. MacMillan, *J. Am. Chem. Soc.* **2001**, *123*, 4370; b) J. F. Austin, D. W. C. MacMillan, *J. Am. Chem. Soc.* **2002**, *124*, 1172; c) N. A. Paras, D. W. C. MacMillan, *J. Am. Chem. Soc.* **2002**, *124*, 7894; 1,3-dipolar cycloadditions see: a) W. S. Jen, J. J. M. Wiener, D. W. C. MacMillan, *J. Am. Chem. Soc.* **2000**, *122*, 9874; b) S. Karlsson, H. Högberg, *Tetrahedron: Asymmetry* **2002**, *13*, 923; other reactions see: a) A. E. Taggi, A. M. Hafez, H. Wack, B. Young, W. J. Drury III, T. Lectka, *J. Am. Chem. Soc.* **2000**, *121*, 7831; b) B. R. Sculimbrene, A. J. Morgan, S. J. Miller, *J. Am. Chem. Soc.* **2002**, *124*, 11653; c) M. Harmata, S. K. Ghosh, X. Hong, S. Wacharasindhu, P. Kirchhoefer, *J. Am. Chem. Soc.* **2003**, *125*, 2058; d) N. Bremeyer, S. C. Smith, S. V. Ley, M. J. Gaunt, *Angew. Chem.* **2004**, *116*, 2735; *Angew. Chem. Int. Ed.* **2004**, *43*, 2681.
- [15] a) B. List, *J. Am. Chem. Soc.* **2000**, *122*, 9336; b) B. List, P. Porjaliev, W. T. Biller, H. J. Martin, *J. Am. Chem. Soc.* **2002**, *124*, 827.
- [16] W. Notz, K. Saktihvel, T. Bui, G. Zhong, C. F. Barbas III, *Tetrahedron Lett.* **2001**, *42*, 199.
- [17] A. Córdova, W. Notz, G. Zhong, J. M. Betancort, C. F. Barbas III, *J. Am. Chem. Soc.* **2002**, *124*, 1842.
- [18] a) A. Córdova, S. Watanabe, F. Tanaka, W. Notz, C. F. Barbas III, *J. Am. Chem. Soc.* **2002**, *124*, 1866; b) A. Córdova, C. F. Barbas III, *Tetrahedron Lett.* **2002**, *43*, 7749; c) A. Córdova, C. F. Barbas III, *Tetrahedron Lett.* **2003**, *44*, 1923; d) S.-i. Watanabe, A. Córdova, F. Tanaka, C. F. Barbas III, *Org. Lett.* **2002**, *4*, 4519.
- [19] a) A. Córdova, *Chem. Eur. J.* **2004**, *10*, 1987; b) A. Córdova, *Synlett* **2003**, 1651; c) Y. Hayashi, W. Tsuboi, I. Ashimine, T. Urushima, M. Shoji, K. Sakai, *Angew. Chem.* **2003**, *115*, 3805; *Angew. Chem. Int. Ed.* **2003**, *42*, 3677; d) A. Córdova, *Acc. Chem. Res.* **2004**, *37*, 102.
- [20] a) E. N. Wenzel, E. N. Jacobsen, *J. Am. Chem. Soc.* **2002**, *124*, 12964; b) D. Uraguchi, M. Terada, *J. Am. Chem. Soc.* **2004**, *126*, 5356; c) T. Akiyama, J. Itoh, K. Yokota, K. Fuchibe, *Angew. Chem.* **2004**, *116*, 1592; *Angew. Chem. Int. Ed.* **2004**, *43*, 1566; d) A. J. A. Cobb, D. M. Shaw, S. V. Ley, *Synlett* **2004**, 558; e) T. Itoh, M. Yokoya, K. Miyauchi, K. Nagata, A. Ohsawa, *Org. Lett.* **2003**, *5*, 4301.
- [21] a) J. Casas, H. Sünden, A. Córdova, *Tetrahedron Lett.* **2004**, *45*, 6117; b) Yamamoto, Saito and co-workers have also reported two excellent examples of organocatalytic asymmetric α -hydroxymethylation of ketones see: H. Torii, M. Nakadai, K. Ishihara, S. Saito, H. Yamamoto, *Angew. Chem.* **2004**, *116*, 2017; *Angew. Chem. Int. Ed.* **2004**, *43*, 1983.
- [22] The compounds are sensitive and racemize upon column chromatography with silica gel as the stationary phase. The Mannich base products should be stored at -35°C .
- [23] $[\alpha]_{\text{D}} = +50$ ($c = 1.0$, MeOH), (literature: $[\alpha]_{\text{D}} = +49.5$ ($c = 0.8$, MeOH), J. Kaman, E. Forro, F. Fülöp, *Tetrahedron: Asymmetry* **2001**, *12*, 1881).
- [24] R. A. Pili, D. Russowsky, L. C. Dias, *J. Chem. Soc. Perkin Trans. I* **1990**, 213.
- [25] S. Bahmanyar, K. N. Houk, *Org. Lett.* **2003**, *5*, 1249 and references therein.

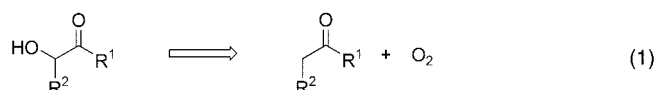
Oxidations

Direct Amino Acid Catalyzed Asymmetric α Oxidation of Ketones with Molecular Oxygen**

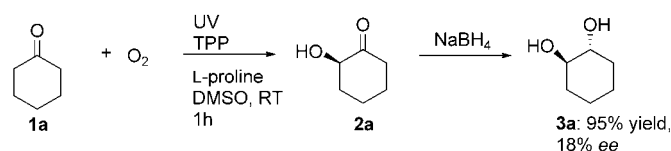
Henrik Sundén, Magnus Engqvist, Jesús Casas, Ismail Ibrahim, and Armando Córdoba*

Molecular oxygen is fundamental for the existence of complex multicellular life on earth. The initially very small amounts of molecular oxygen is believed to have been formed around 4 billion years ago by the decomposition of CO_2 and water promoted by UV irradiation from the sun.^[1] Molecular oxygen can be transferred between its more reactive singlet state ($^1\text{O}_2$) and its non-excited triplet state ($^3\text{O}_2$).^[2] Singlet molecular oxygen ($^1\text{O}_2$) plays a significant role in several biochemical processes. For example, it is involved in the development of different diseases and biochemical oxidations.^[3,4] Furthermore, chemists have utilized photo- or chemically generated molecular $^1\text{O}_2$ as an oxygen source for several synthetic transformations.^[1,5] For example, it is used in the formation of allylic hydroperoxides (analogous to the “ene” reaction) and to generate cyclic peroxides (analogous to a Diels–Alder-type reaction). There is a demand in today’s society for the development of sustainable chemistry from renewable resources.^[6] The content of molecular oxygen in air is 21 %, which allows its use in oxidation reactions. Thus, molecular oxygen is one of the ultimate oxidants for oxidation of organic molecules and the development of sustainable chemistry.

Asymmetric reactions that are catalyzed by small organic molecules have received increased attention in recent years.^[7] Among several transformations, amine-catalyzed asymmetric epoxidations with dioxirane have been reported.^[8] The employment of non-toxic, small organic molecules has the potential for allowing environmentally benign reaction conditions. Based on our previous investigations of organic reactions that are mediated by metal-free organic molecules,^[9] we became interested in whether an amino acid would allow the catalytic incorporation of molecular oxygen into ketones [Eq. (1)].^[10–11] Moreover, this potential amino acid catalyzed transformation may warrant investigation as a prebiotic pathway for the synthesis of α -hydroxyketones, which are the building blocks of sugars.^[12] Herein, we report the unprecedented direct amino acid catalyzed asymmetric incorporation of singlet molecular oxygen into ketones. This α oxidation of ketones with molecular oxygen or air furnished α -hydroxyketones and diols.



In an initial experiment, cyclohexanone **1a** (1 mmol) was added to a vial containing dimethyl sulfoxide (DMSO) (1 mL), L-proline (20 mol %) and tetraphenylporphine (TPP) (1 mol %). A continuous flow of O_2 or air was bubbled through the vial and the reaction was exposed to visible light from a 250-W high-pressure sodium lamp (Scheme 1). To our



Scheme 1. Amino acid catalyzed asymmetric α oxidation of cyclohexanone to give **2a** and in situ reduction to diol **3a**.

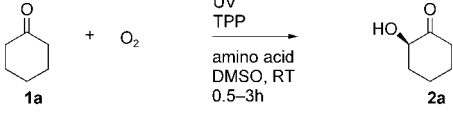
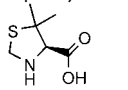
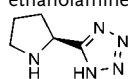
delight, complete conversion had occurred after one hour, and the reaction was quenched by aqueous workup. The crude ketone **2a** existed as a mixture of dimeric and oligomeric products. The crude product mixture was purified by silica-gel column chromatography to yield α -hydroxyketone **2a** with 18 % *ee*.^[13,14] We also performed the reaction with in situ reduction of α -hydroxyketone **2a** with NaBH_4 to afford the corresponding optically active *trans*- and *cis*-diols **3a** (*trans/cis* = 3:1) in 95 % combined yield after silica-gel column chromatography. The enantiomeric excess of the pure *trans*-**3a** diol was determined by chiral-phase GC analyses to be 18 % *ee*.

Next, we screened several natural amino acids and their derivatives for their potential in catalyzing the introduction of $^1\text{O}_2$ at the α position of **1a** and to improve the stereoselectivity of the reaction (Table 1). We found that several of the amino acids investigated catalyzed the α oxidations with molecular $^1\text{O}_2$ with high efficiency and chemoselectivity. The simple amino acids alanine and valine mediated the reaction with the highest stereoselectivity. In fact, this is the first case in which an acyclic amino acid provides higher asymmetric induction than proline and its derivatives in organic solvents. In previously reported direct organocatalytic intermolecular transformations, the catalyst required a cyclic five-membered ring to allow high efficiency and enantioselectivity.^[7] However, a higher enantioselectivity was obtained with L- α -methylproline than with L-proline (increase from 18 to 48 % *ee* for **2a**). Thus, the presence of a methyl group at the α position of proline significantly increased the stereoselectivity. In contrast, this effect was not observed when comparing valine with α -methylvaline. The asymmetric α oxygenation reactions that were catalyzed by a D-amino acid afforded the opposite enantiomer of **2a** to that obtained in the reactions catalyzed by the corresponding L-amino acid, without affecting the asymmetric induction. Furthermore, amino alcohols, dipeptides, amino acids with amide and amine functionalities, and synthetic amino acid derivatives catalyzed the direct asymmetric introduction of molecular oxygen into

[*] H. Sundén, M. Engqvist, Dr. J. Casas, I. Ibrahim, Prof. Dr. A. Córdoba
Department of Organic Chemistry, The Arrhenius Laboratory
Stockholm University, 10691 Stockholm (Sweden)
Fax: + (46) 8-154-908
E-mail: acordova1a@netscape.net
E-mail: acordova@organ.su.se

[**] We thank the Swedish National Research council, the Wenner-Gren Foundation and the Lars-Hierta Foundation for financial support. We thank Prof. J.-E. Bäckvall for sharing chemicals and one of the reviewers for suggesting the direct isolation of the α -hydroxyketone.

Table 1: Direct amino acid-catalyzed introduction of $^1\text{O}_2$ to **1a**.^[a]

				
Entry	Amino acid	Product	Yield [%] ^[b]	ee [%] ^[c]
1	L-alanine	ent- 2a	93	56
2	D-alanine	2a	88	57
3	L-valine	ent- 2a	78	49
4	D-valine	2a	77	48
5	L-proline	2a	95	18
6	D-proline	ent- 2a	93	16
7	L-hydroxyproline	2a	88	11
8	L- α -methylproline	2a	20	48
9	L- α -methylvaline	ent- 2a	15	6
10	L- α -phenylglycine	ent- 2a	70	20
11	L-phenylalanine	ent- 2a	89	38
12	D- α -phenylglycine	2a	71	21
13	L-threonine	ent- 2a	20	10
14	L-phenylalinal	ent- 2a	67	< 2
15		2a	62	11
16	glycine	2a	85	—
17	ethanolamine	2a	81	—
18		2a	97	< 5

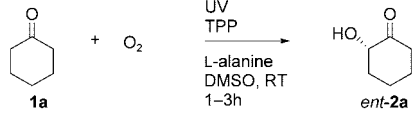
[a] See experimental section. [b] Yields of isolated product after column chromatography on silica gel of the pure **3a** furnished after reduction of **2a**. [c] Determined by chiral-phase GC analyses. The racemic product derived by glycine catalysis was used as reference material. The absolute configuration was determined by comparison with commercially available diols and literature data.

ketones with a similar efficiency to that of the amino acids. However, the amino acid catalysts were superior to the amino alcohols with regards to stereoselectivity. It should be noted that the direct introduction of $^1\text{O}_2$ into ketones was also readily catalyzed by glycine and ethanolamine, providing a novel inexpensive entry to α -oxygenated compounds.

We also performed a solvent screen of the L-alanine-catalyzed asymmetric incorporation of molecular oxygen into **1a** in different solvents (Table 2). Direct L-alanine-catalyzed asymmetric α oxidations with $^1\text{O}_2$ proceeded smoothly in DMSO, *N*-methylpyrrolidinone (NMP), and *N,N*-dimethylformamide (DMF). In contrast, L-alanine only furnished trace amount of product in MeOH, trifluoroethanol (TFE), and CHCl_3 . Hence, the best selectivity and efficiency is obtained in the more polar aprotic solvents. We did not observe any significant temperature dependence of the stereoselectivity in DMSO. Furthermore, the reactions were also efficient in aqueous media with air as the molecular oxygen source, which could allow the development of environmentally benign reaction conditions.

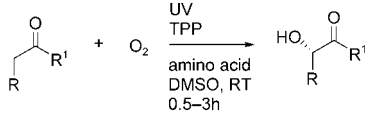
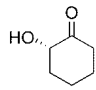
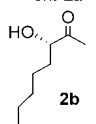
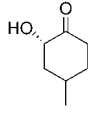
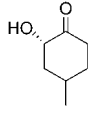
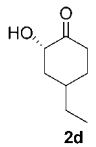
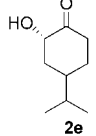
Next, we investigated the amino acid catalyzed asymmetric α oxidations with molecular oxygen of various ketones (Table 3). The direct amino acid catalyzed asymmetric α -oxygenation reactions progressed with excellent chemoselectivity and furnished the corresponding α -oxygenated adducts **ent-2a** and **2b–e** with good enantioselectivity. For example,

Table 2: Solvent screen of the L-alanine-catalyzed incorporation of $^1\text{O}_2$ to ketones.^[a]

				
Entry	Solvent	T [°C]	Yield [%] ^[b]	ee [%] ^[c]
1	MeOH	RT	traces	n.d.
2	DMSO	40	79	55
3	DMSO	RT	93	56
4	DMSO	0 \rightarrow RT	80	48
5	DMSO ^[d]	RT	82 ^[d]	56 ^[d]
6	NMP	RT	86	48
7	DMF	RT	82	49
8	TFE	RT	traces	n.d.
9	phosphate buffer ^[e]	RT	80 ^[e]	18 ^[e]
10	H_2O ^[e]	RT	77 ^[e]	19 ^[e]
11	CHCl_3	RT	traces	n.d.

[a] See experimental section. [b] Yields of isolated product after column chromatography on silica gel of the pure **ent-3a** furnished after reduction of **ent-2a**. [c] Determined by chiral-phase GC analyses. [d] Reaction performed with air as the O_2 source. [e] Protoporphine (1 mol%) was used as the sensitizer and DMSO (40% v/v).

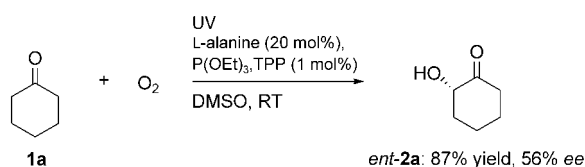
Table 3: Direct catalytic asymmetric incorporation of molecular oxygen to ketones.^[a]

				
Entry	Product	Amino acid	Yield [%] ^[b]	ee [%] ^[c]
1		L-alanine	93	56
2		L-valine	50	28
3		L-valine	75	69
4		L-alanine	67	72
5		L-alanine	61 ^[d]	60
6		L-alanine	58 ^[d]	52

[a] See experimental section. [b] Yields of isolated products after column chromatography on silica gel of the diol **3**. [c] Determined by chiral-phase GC analyses. The racemic products were derived by glycine or D-, L-proline catalysis and were used as reference materials. [d] Reaction performed in NMP.

L-alanine catalyzed the formation of **2c** in 67% yield with 72% *ee*. Furthermore, the amino acid catalyzed reactions with linear acyclic ketones progressed with excellent regioselectivity, and molecular oxygen was asymmetrically incorporated at the most substituted side of the ketone. Moreover, the reactions were readily scaled up and performed on the gram scale. The amino acids were also able to catalyze the asymmetric incorporation of molecular oxygen into unmodified aldehydes.^[15] For example, L-methylproline furnished (*R*)-2-hydroxy-3-phenylpropanal with 65% *ee*. The direct amino acid catalyzed α oxygenation with molecular $^1\text{O}_2$ may be considered as a new, simple, metal-free entry into the synthesis of α -hydroxyketones and diols.

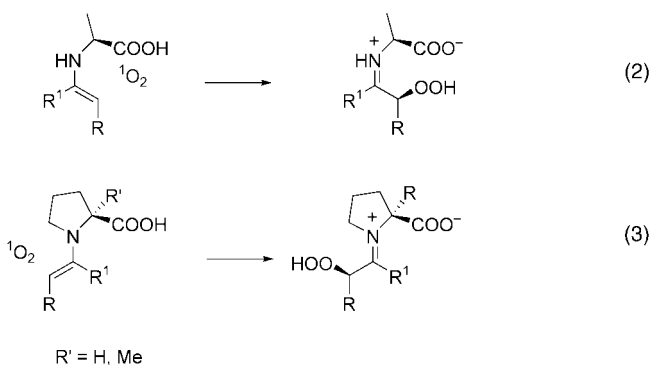
We also tested the amino acid-catalyzed α -oxidations of unmodified ketones with molecular $^3\text{O}_2$ as the electrophile in the presence of triethylphosphite.^[16] The reactions with molecular $^3\text{O}_2$ did not provide the α -hydroxyketone adducts **2** or the diol **3**. Thus, molecular $^1\text{O}_2$ is the more reactive electrophile and not $^3\text{O}_2$. Moreover, no products were formed in the absence of the amino acid catalysts. We also investigated the possibility of background oxidation by α -hydroperoxide ketone intermediates or another peroxide intermediate that potentially could influence the enantioselectivity of the reaction.^[13–14] However, the use of excess (5 equiv) H_2O_2 , NaClO, *m*-chloroperbenzoic acid (MCPBA), or oxone as the oxidants for cyclohexanone (1 mmol) in the presence of a catalytic amount of L-proline or L-alanine (20 mol%) in DMSO only provided trace amounts of the diol **3a** after in situ reduction with NaBH_4 . Furthermore, the L-alanine-catalyzed α oxygenation with $^1\text{O}_2$ in the presence of triethylphosphite furnished *ent*-**2a** in 87% yield with 56% *ee*, which is the same *ee* value of *ent*-**2a** obtained without the addition of phosphite (Scheme 2).



Scheme 2. Direct L-alanine-catalyzed introduction of molecular $^1\text{O}_2$ to **1a** in the presence of triethylphosphite.

These results indicated that the potential background oxidation by peroxide intermediates was not significant under the set reaction conditions. We were also able to rule out a 1,2-cycloaddition between $^1\text{O}_2$ and the catalytic chiral enamine to form a dioxetane intermediate, as no cleavage products from such an intermediate was detected. The stereochemical outcome of the reaction was determined by optical rotation and chiral-phase GC analyses of **2a** and *trans*-**3a**, which revealed that acyclic L-amino acids provided (*2S*)- α -hydroxycyclohexanone *ent*-**2a** and (1*S*, *2S*)-*trans*-cyclohexane-1,2-diol (*ent*-**3a**). In contrast, L-proline and its derivatives furnished (*2R*)- α -hydroxycyclohexanone (**2a**). The reaction plausibly proceeds through a catalytic enamine mechanism [Eq. (2) and (3)]. Hence, the tentative (*2S*)- α -hydroperoxide intermediate

is formed through proton abstraction by molecular $^1\text{O}_2$ from the carboxy group of the acyclic L-amino acids,^[14] which provides the stereochemical information, together with addition to the *Re* face of the amino acid derived enamine to furnish (*2S*)- α -hydroxyketone [Eq. (2)]. In the case of α oxygenation mediated by a cyclic L-amino acid, the addition of $^1\text{O}_2$ occurs at the *Si* face of the enamine to provide the (*2R*)- α -hydroxyketone [Eq. (3)].



We also established that natural amino acids catalyze the asymmetric incorporation of molecular oxygen into ketones in aqueous buffer. For example, L-alanine catalyzed the direct asymmetric synthesis of *ent*-**2a** in phosphate buffer at 37°C. Moreover, the amino acids mediated the direct catalytic asymmetric α oxidations in air with the sun as the light source. Hence, terrestrial and extraterrestrial amino acids were able to catalyze the introduction of molecular oxygen under prebiotic conditions to form α -hydroxyketones. In fact, the amino acids were able to catalyze the α oxidation of acetone with $^1\text{O}_2$ to furnish hydroxyacetone and dihydroxyacetone, which are the building blocks and donors in amino acid catalyzed asymmetric synthesis of sugars under prebiotic conditions.^[12a,17] Thus, the amino acid catalyzed introduction of molecular oxygen may plausibly have served as the first step in their homochirality transfer of their asymmetry to polyhydroxylated compounds, even in the presence of small amounts of oxygen.^[12]

In conclusion, we have disclosed the unprecedented ability of amino acids to catalyze the direct asymmetric incorporation of singlet molecular oxygen into ketones. The smallest amino acids alanine and valine catalyzed the transformation with the highest stereoselectivity. The direct catalytic α oxygenations are a novel, inexpensive, operationally simple, and environmentally benign entry to the preparation of α -hydroxyketones and diols. All materials in this process stem from renewable sources, thus allowing a highly sustainable catalytic process. Readily available amino acids allow catalytic asymmetric oxidations with molecular oxygen or air, which has previously been considered to be in the domains of enzymes and chiral transition-metal complexes.

Experimental Section

Typical experimental procedure (Table 1, entry 1): Cyclohexanone (1 mmol) was added to a vial containing TPP (1 mol%) and a catalytic amount of L-alanine (20 mol%) in DMSO (1 mL). A

continuous flow of O₂ or air was bubbled through the vial, and the reaction was exposed to visible light by a 250-W high-pressure sodium lamp. After 1 hour, complete conversion had occurred, and the reaction was quenched either by the addition of brine followed by extraction with EtOAc to furnish α -hydroxyketone **ent-2a** or by in situ reduction with NaBH₄ to afford the corresponding optically active crude diol **ent-3a** (*trans/cis* 3:1). The crude **ent-2a** existed as an oligomeric mixture that, upon standing, formed the dimer, which was isolated by silica-gel column chromatography (EtOAc/pentane 1:20) with 56% *ee* (determined by chiral-phase GC-analysis). GC: (CP-Chirasil-Dex CB); *T*_{inj} = 250 °C, *T*_{det} = 275 °C, flow = 1.8 mL min⁻¹, *t*_i = 60 °C (9 min), rate = 85 °C min⁻¹, *t*_f = 200 °C (5 min); retention times of **2a**: *t*_{maj} = 10.64 min, *t*_{min} = 10.66 min. The *trans-3a* and *cis-3a* diols were isolated by silica-gel column chromatography (EtOAc/pentane 1:1) in a combined yield of 92% with 56% *ee* of the pure *trans-3a* diol (determined by GC analyses). (1*S*, 2*S*)-*trans*-cyclohexane-1,2-diol: [α]_D = +21 (*c* = 0.2, CHCl₃); GC: (CP-Chirasil-Dex CB); *T*_{inj} = 250 °C, *T*_{det} = 275 °C, flow = 1.8 mL min⁻¹, *t*_i = 90 °C (2 min), *t*_f = 110 °C, rate = 0.3 °C min⁻¹; retention times of acetylated compound: *t*_{maj} = 9.75 min, *t*_{min} = 9.61 min.

Received: April 12, 2004

Revised: August 12, 2004

Keywords: amino acids · asymmetric catalysis · ketones · molecular oxygen · oxidation

- [1] a) H. D. Holland, *The Chemistry of the Atmosphere and Oceans*, Wiley, New York, **1978**; b) J. F. Kasting, T. P. Ackerman, *Science* **1986**, 234, 1383; c) J. H. Carver, *Nature* **1981**, 292, 136; d) K. Plankensteiner, H. Reiner, B. Schranz, B. M. Rode, *Angew. Chem.* **2004**, 116, 1922; *Angew. Chem. Int. Ed.* **2004**, 43, 1886.
- [2] a) C. S. Foote, *Acc. Chem. Res.* **1968**, 1, 104; b) C. Schweitzer, R. Schmidt, *Chem. Rev.* **2003**, 103, 1685.
- [3] a) B. Halliwell, M. C. John, *Free Radical in Biology and Medicine*, 2nd ed., Clarendon, Oxford, **1982**; b) N. I. Krinsky in *Biological roles of singlet oxygen*, Vol. 40 (Ed.: H. H. Wasserman), Academic Press, New York, **1979**, pp. 597–641.
- [4] a) B. Samuelsson, *J. Am. Chem. Soc.* **1965**, 87, 3011; b) P. Wentworth, Jr., L. H. Jones, A. D. Wentworth, X. Zhu, N. A. Larsen, I. A. Wilson, X. Xu, W. A. Goddard III, K. D. Janda, A. Eschenmoser, R. A. Lerner, *Science* **2001**, 293, 1806.
- [5] a) For an example in total synthesis see: K. C. Nicolaou, Z. Yang, G.-q. Shi, J. L. Gunzner, K. A. Agrios, P. Gärtner, *Nature* **1998**, 392, 264; b) For diastereoselective photooxygenations, see: M. Prein, W. Adam, *Angew. Chem.* **1996**, 108, 519; *Angew. Chem. Int. Ed. Engl.* **1996**, 35, 477.
- [6] M. Eissen, J. O. Metzger, E. Schmidt, U. Schneidewind, *Angew. Chem.* **2002**, 114, 402; *Angew. Chem. Int. Ed.* **2002**, 41, 414.
- [7] a) P. I. Dalko, L. Moisan, *Angew. Chem.* **2001**, 113, 3840; *Angew. Chem. Int. Ed.* **2001**, 40, 3726; b) B. List, *Tetrahedron* **2002**, 58, 5573; c) E. R. Jarvo, S. J. Miller, *Tetrahedron* **2002**, 58, 2481; d) R. O. Duthaler, *Angew. Chem.* **2003**, 115, 1005; *Angew. Chem. Int. Ed.* **2003**, 42, 975.
- [8] a) L. Bohe, G. Hanquet, M. Lusinch, X. Lusinch, *Tetrahedron Lett.* **1993**, 34, 7271; b) M. F. A. Adamo, V. K. Aggarwal, M. A. Sage, *J. Am. Chem. Soc.* **2000**, 122, 8317; c) A. Armstrong, *Angew. Chem.* **2004**, 116, 1484; *Angew. Chem. Int. Ed.* **2004**, 43, 1460, and references therein.
- [9] a) A. Bøgevig, H. Sundén, A. Córdova, *Angew. Chem.* **2004**, 116, 1129; *Angew. Chem. Int. Ed.* **2004**, 43, 1109; b) A. Córdova, H. Sundén, A. Bøgevig, M. Johansson, F. Himo, *Chem. Eur. J.* **2004**, 10, 3673; c) A. Córdova, *Chem. Eur. J.* **2004**, 10, 1937; d) A. Córdova, *Tetrahedron Lett.* **2004**, 45, 3949; e) A. Córdova, *Acc. Chem. Res.* **2004**, 37, 102; f) A. Córdova, *Synlett* **2003**, 1651, and references therein.
- [10] For proline-catalyzed α -aminooxylation reactions reported by other groups, see: a) G. Zhong, *Angew. Chem.* **2003**, 115, 4379; *Angew. Chem. Int. Ed.* **2003**, 42, 4247; b) S. P. Brown, M. P. Brochu, C. J. Sinz, D. W. C. MacMillan, *J. Am. Chem. Soc.* **2003**, 125, 10808; c) M. Y. Hayashi, J. Yamaguchi, T. Sumaiya, M. Shoji, *Angew. Chem.* **2004**, 116, 1132; *Angew. Chem. Int. Ed.* **2004**, 43, 1112; d) M. Y. Hayashi, J. Yamaguchi, K. Hibino, M. Shoji, *Tetrahedron Lett.* **2003**, 44, 8293; for the use of proline derivatives as catalysts, see: N. Momiyama, H. Torii, S. Saito, H. Yamamoto, *Proc. Natl. Acad. Sci. USA* **2004**, 101, 5374, and reference [9b].
- [11] For examples of proline-catalyzed α aminations, see: a) A. Bøgevig, K. Juhl, N. Kumaragurubaran, W. Zhuang, K. A. Jørgensen, *Angew. Chem.* **2002**, 114, 1868; *Angew. Chem. Int. Ed.* **2002**, 41, 1790; b) B. List, *J. Am. Chem. Soc.* **2002**, 124, 5656.
- [12] a) S. Pizzarello, A. L. Weber, *Science* **2004**, 303, 1151; b) L. E. Orgel, *Science* **2000**, 290, 1306.
- [13] In addition to the α oxidation of **1a**, the DMSO was also oxidized to the corresponding dimethyl sulfone at prolonged reaction times.
- [14] We were only able to isolate the α -hydroxyketone adducts and not a potential α -hydroperoxide intermediate. Hence, we believe that the α -hydroperoxide intermediate is rapidly converted into the α -hydroxyketone product.
- [15] A. Córdova, H. Sundén, M. Engqvist, I. Ibrahim, J. Casas, *J. Am. Chem. Soc.* **2004**, 126, 8914.
- [16] a) E. J. Corey, H. E. Ensley, *J. Am. Chem. Soc.* **1975**, 97, 6908; b) E. F. J. de Vries, L. Ploeg, M. Colao, J. Brussee, A. van der Gen, *Tetrahedron: Asymmetry* **1995**, 6, 1123.
- [17] A. Córdova, W. Notz, C. F. Barbas III, *Chem. Commun.* **2002**, 24, 3024. For a Zn–amino acid mediated sugar synthesis under prebiotic conditions, see: J. Kofoed, M. Machuqueiro, J.-L. Reymond, T. Darbre, *Chem. Commun.* **2004**, 26, 1540.

Dynamic Kinetic Resolution

**Highly Compatible Metal and Enzyme Catalysts
for Efficient Dynamic Kinetic Resolution of
Alcohols at Ambient Temperature****

*Belén Martín-Matute, Michaela Edin, Krisztián Bogár,
and Jan-E. Bäckvall**

The demand for chiral compounds as single enantiomers has increased dramatically in recent years, driven by the pharmaceutical industry and also by other applications, such as

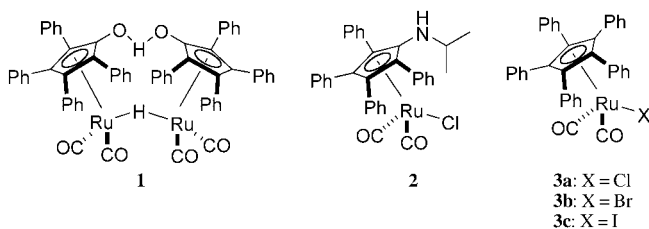
[*] Dr. B. Martín-Matute, M. Edin, K. Bogár, Prof. Dr. J.-E. Bäckvall
Department of Organic Chemistry, Arrhenius Laboratory
Stockholm University
10691 Stockholm (Sweden)
Fax: (+46) 8-154-908
E-mail: jeb@organ.su.se

[**] We are grateful for financial support from the Swedish Research Council, the Swedish Foundation for Strategic Research, and the Ministerio de Educación y Ciencia of Spain.



Supporting information for this article (NMR data for **3a** and **5g**) is available on the WWW under <http://www.angewandte.org> or from the author.

agrochemicals, flavors, fragrances, and materials. Dynamic kinetic resolution (DKR) is a powerful tool to transform a racemic mixture into one enantiomer.^[1] This strategy overcomes the limitation of the maximum 50 % yield in a kinetic resolution (KR) by combining it with an in situ racemization of the substrate. Recently the coupling of enzymes and transition metals for the DKR of alcohols has attracted considerable attention.^[2,3] In these reactions, in situ racemization by a metal occurs during the enzymatic resolution. The first example was reported by Williams and co-workers who used a rhodium catalyst and a lipase to obtain a DKR of secondary alcohols with moderate efficiency.^[4] In 1997 our group reported^[5] an efficient DKR process for the synthesis of enantiopure secondary alcohols by the use of ruthenium catalyst **1**^[6] in combination with an immobilized lipase. This



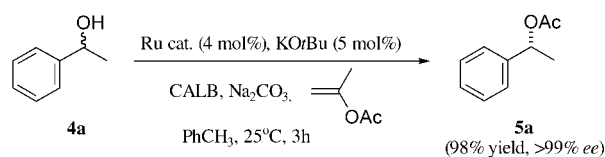
method has also been applied to the DKR of different functionalized alcohols, such as hydroxyacid derivatives,^[7] hydroxynitriles,^[8] azidoalcohols,^[9] haloalcohols,^[10] hydroxyphosphonates,^[11] and diols.^[12] Kim, Park, and co-workers have also employed catalyst **1** in the DKR of protected hydroxyacids, diols, and hydroxyaldehydes,^[13] and in the asymmetric transformation of ketones and enol acetates to chiral acetates.^[14] In general, good yields and enantioselectivities were attained. However, complex **1** suffers from some drawbacks: it is activated at high temperature and therefore a thermally stable enzyme is required. Also, the addition of an appropriate hydrogen source is needed in some cases to prevent ketone formation.

Various ruthenium, rhodium, and iridium complexes are known to catalyze fast racemization of alcohols.^[2c,4,5,15,16] Unfortunately, almost all of these catalysts do not work in the DKR of alcohols when combined with the enzyme. Recently, Kim, Park, and co-workers reported that ruthenium catalyst **2** racemizes alcohols within 30 min at room temperature.^[17] However, when combined with an enzyme (lipase) in DKR at room temperature, very long reaction times (1.3–7 days) were required, in spite of the fact that the enzymatic reaction (in KR) takes only a few hours.

Very recently we found that complexes **3a–c** catalyze the racemization of chiral alcohols highly efficiently at room temperature after being activated by KOtBu.^[18] For example, **3a** (0.5 mol %) racemized (*S*)-1-phenylethanol within 10 min and resulted in 50 % racemization after less than 2 min.

Initial attempts to combine catalyst **3a** (or **3b**) with an enzymatic resolution were unsuccessful and gave either no DKR or led to very long reaction times for the DKR (several days). This was frustrating, as the isolated reactions (racemization and enzymatic resolution) are very fast. Finally, after

some fine-tuning and optimization, we were able to find reaction conditions under which the DKR process has almost the same rate as the kinetic resolution. Herein we report a DKR process (Scheme 1) that is more than two orders of



Scheme 1. DKR of 1-phenylethanol.

magnitude faster than our previous procedures^[2,5] and one order of magnitude faster than the hitherto fastest procedure reported.^[17] We also provide evidence for the intermediacy of a ruthenium alkoxide complex.

In one experiment a solution of 1-phenylethanol (**4a**) in toluene (0.3 M) was added to a mixture of KOtBu and ruthenium complex **3b**, under an argon atmosphere. After stirring for 5 min, Na₂CO₃, *Candida antarctica* lipase B (CALB^[19]), and isopropenyl acetate were added. After 4 h, only 55 % yield of enantiopure (*R*)-1-phenylethanol acetate (**5a**) was obtained (Table 1, entry 1).^[20] Surprisingly, when the

Table 1: Dynamic kinetic resolution of 1-phenylethanol.^[a]

Entry	Ru catalyst	<i>t</i> [h]	Yield [%] ^[b]	ee [%] ^[b]
1 ^[c]	3b	4	55	> 99
2 ^[d]	3b	4	99 (97) ^[e]	> 99
3	3b	3	98	> 99
4	3a	3	95 (92) ^[e]	> 99
5 ^[f]	3b	15	60	> 99

[a] Unless otherwise noted, Ru catalyst (4 mol %) and KOtBu (5 mol %) were stirred in toluene (2 mL) for 6 min before adding **4a** (1 mmol). After 4 min CALB (6 mg), Na₂CO₃ (1 mmol), and isopropenyl acetate (1.5 mmol) were added and the mixture was stirred under an argon atmosphere. [b] Determined by chiral GC. [c] A solution of **4a** in toluene (3.3 mL) was added to a mixture of Ru catalyst and KOtBu. [d] Toluene: 3.3 mL. [e] Yield of isolated product. [f] Under an air atmosphere.

mixture of KOtBu and complex **3b** was stirred for 6 min in toluene before adding the alcohol **4a**, acetate **5a** was obtained in 99 % yield with > 99 % ee in 4 h (Table 1, entry 2). When the concentration of **4a** was increased to 0.5 M, **5a** was obtained after only 3 h in 98 % yield (> 99 % ee) (Table 1, entry 3). Similar results were obtained with catalyst **3a** under the same reaction conditions (Table 1, entry 4). It was observed that the system is very sensitive to molecular oxygen; thus when the reaction was run under an air atmosphere, only 60 % yield was attained after 15 h (Table 1, entry 5).

To study the scope of the reaction, a variety of substrates were tested with the reaction conditions used in Table 1, entry 4.^[21] For most substrates we obtained the best results when employing 5 mol % of **3a**. The amount of KOtBu needed depends on the substrate and on the amount of CALB employed;^[22] therefore it was optimized for each entry. The

results are summarized in Table 2. Similarly to **5a** (Table 2, entries 1 and 2), the naphthyl derivative **5b** was obtained in 93% yield after 3 h (Table 2, entry 3). The ethyl carbinol **4c** reacts slower with the enzyme and required the use of 40 mg

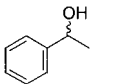
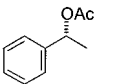
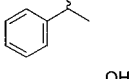
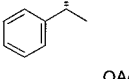
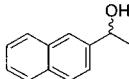
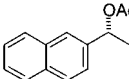
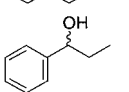
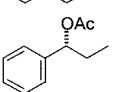
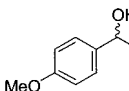
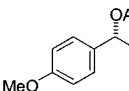
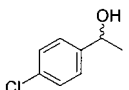
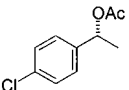
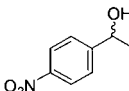
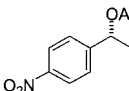
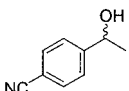
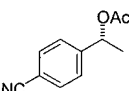
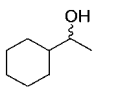
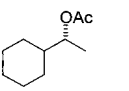
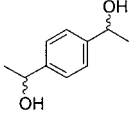
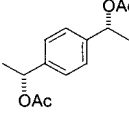
coordination to the ruthenium center. Excellent selectivity and yield were also obtained with the aliphatic substrate **4h** (Table 2, entry 9). DKR of diol **6** is also possible when using 5 mol % of catalyst **3a** at room temperature, although 72 h

were needed to attain 93% yield. However, at 50°C enantiopure diacetate **7** was obtained after 10 h in 94% yield (Table 2, entry 10).

The necessity for premixing complex **3a** (or **3b**) with KOtBu in toluene suggests that a new ruthenium complex is formed and this is supported by a color change from yellow to dark red within a few minutes. This intermediate is most likely ruthenium alkoxide **8**, which is crucial for initiating the racemization under DKR conditions. The formation of intermediate **8** is inhibited or slowed down when the substrate alcohol is present in the reaction mixture. A ligand-exchange reaction of **8** with the substrate gives alkoxide **9**, which undergoes β -hydride elimination and forms ruthenium hydride **10** and the oxidized product **11**. Insertion of the ketone into the Ru–H bond produces the racemic alkoxide complex **12**. Alkoxide exchange with *S* alcohol releases *rac* alcohol and regenerates intermediate **9** (Scheme 2).

Alcohol complexes of tungsten, rhenium, and molybdenum have previously been prepared.^[23] Recently, Casey et al. observed a Ru–alcohol complex by NMR spectroscopy.^[24] Unfortunately, attempts to prepare the alkoxide complex by deprotonation with a base were unsuccessful.^[24] The postulated ruthenium alkoxide complex **8** in Scheme 2, would be

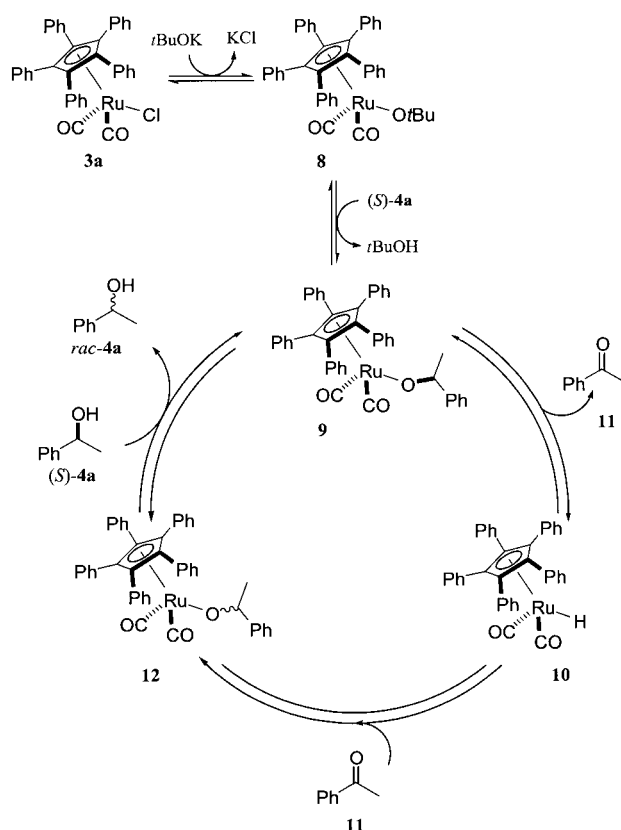
Table 2: DKR of various alcohols.^[a]

Entry	Alcohol	KOtBu (mol %)	t [h]	Product	Yield [%] ^[b,c]	ee [%] ^[b]
1 ^[d]		4a 5	3		5a 98	> 99
2		4a 5	3		5a 95 (92)	> 99
3		4b 6.25	3		5b 93	> 99
4 ^[e]		4c 8	17		5c 92 (90)	> 99
5		4d 7.5	6		5d 96 (94)	> 99
6		4e 5	6		5e 93 (91)	> 99
7		4f 5	20		5f 99 (97)	> 99
8		4g 5	20		5g 98 (95)	> 99
9		4h 7	17		5h 98 ^[f]	> 99
10 ^[g]		6 6	10		7 94 (90)	> 99 (99:1 d.r.)

[a] Unless otherwise noted, Ru catalyst **3a** (5 mol %), CALB (6 mg), Na₂CO₃ (1 mmol), and KOtBu were stirred in toluene (2 mL) at room temperature for 6 min before adding the alcohol (1 mmol). After 4 min, isopropenyl acetate (1.5 mmol) was added and the mixture was stirred at room temperature under an argon atmosphere. [b] Determined by chiral GC. [c] Yield of isolated product in parenthesis. [d] **3b**: 4 mol %. [e] CALB: 40 mg. [f] Yield determined by ¹H NMR spectroscopy. [g] 50°C.

of CALB and 8 mol % of KOtBu. Although a longer reaction time is needed (17 h), **5c** was obtained in high yield and enantioselectivity (92%, > 99% ee) (Table 2, entry 4). Electron-rich alcohol **4d** did not significantly change the rate or selectivity of the reaction and gave enantiomerically pure **5d** in 96% yield after 6 h (Table 2, entry 5). Similarly, electron-withdrawing groups on the phenyl ring gave enantiopure acetates in excellent yields. Thus, **5e** was obtained in 93% yield in 6 h (Table 2, entry 6). Despite the prolonged reaction times needed for alcohols **4f** and **4g**, this is the first time that acetates **5f** and **5g** are obtained through DKR (Table 2, entries 7 and 8). A plausible explanation that accounts for the need for longer reaction times is that the nitrogen-containing substituents on the substrates slow down the reaction rate by

easy to observe as it cannot undergo β -hydride elimination. When complex **3a** and KOtBu were mixed in [D₈]toluene in an NMR tube and shaken vigorously, a fine new precipitate of KCl was formed that was allowed to settle. The quantitative formation of a new ruthenium complex was observed by ¹³C NMR spectroscopy. The resonance of the five equivalent quaternary carbons of the cyclopentadienyl ring of **8** is shifted to higher frequency (δ = 108.8 ppm) than that of **3a** (δ = 107.1 ppm) in [D₈]toluene. Similar changes are observed for the resonance of the CO ligands (δ = 202.8 ppm in **8** and 198.0 ppm in **3a**). The resonances of the *tert*-butoxide ligand are also observed (δ = 34.3 and 73.1 ppm), and differ from those of *t*BuOH (δ = 31.3 and 68.2 ppm) and of KOtBu (δ = 37.6 and 66.5 ppm) in [D₈]toluene. Furthermore, when an



Scheme 2. Proposed mechanism for the racemization.

excess of 1-phenylethanol (**4a**) was added to the NMR tube, the formation of acetophenone (**11**) was immediately observed.

In summary, we have developed a highly efficient DKR of secondary alcohols at room temperature that for the first time provides enantiopure products in high yields in very short reaction times. Furthermore, isopropenyl acetate can be employed as the acyl donor, which makes the purification of the products very easy. We have also proven the intermediacy of Ru alkoxides in this process. This mild procedure makes it possible to use sensitive and/or less-thermostable enzymes in future applications.

Experimental Section

Complexes **3a** and **3b** were prepared as described in the literature.^[18,25] Toluene was dried over CaH₂ overnight, distilled under argon, and stored over 4-Å molecular sieves. Isopropenyl acetate was washed with saturated K₂CO₃, dried with CaCl₂, and distilled under argon. ¹H NMR and ¹³C NMR spectra of acetates were in good agreement with the data previously reported in the literature.^[26]

Dynamic kinetic resolution of 1-phenylethanol (4a): A solution of KOtBu (0.5 M in THF; 100 µL, 0.05 mmol) was added to a 10-mL Schlenk flask. The THF was carefully removed under vacuum, and the flask was filled with argon. CALB^[19] (6 mg), Na₂CO₃ (106 mg, 1 mmol) and Ru catalyst **3a** (25 mg, 0.04 mmol) were quickly added. The Schlenk flask was evacuated and filled with argon. Toluene (2 mL) was added, and the mixture was stirred for 6 min.^[27] 1-Phenylethanol (**4a**) (120 µL, 1 mmol) was then added, and after 4 min isopropenyl acetate (165 µL, 1.5 mmol) was added. After being stirred for 3 h at ambient temperature, the reaction mixture was

filtered and concentrated. Purification by column chromatography (SiO₂; pentane/Et₂O 98:2) afforded (*R*)-1-phenylethanol acetate (**5a**) as a colorless oil (151 mg, 92 % yield, > 99 % *ee*).

Received: July 23, 2004

Keywords: enantioselectivity · enzyme catalysis · kinetic resolution · reaction mechanisms · ruthenium

- [1] For examples, see: a) K. Faber, *Chem. Eur. J.* **2001**, *7*, 5005–5010; b) R. Noyori, M. Tokunaga, M. Kitamura, *Bull. Chem. Soc. Jpn.* **1995**, *68*, 36–56; c) R. S. Ward, *Tetrahedron: Asymmetry* **1995**, *6*, 1475–1490.
- [2] For chemoenzymatic DKR, see: a) O. Pàmies, J.-E. Bäckvall, *Trends Biotechnol.* **2004**, *22*, 130–135; b) O. Pàmies, J.-E. Bäckvall, *Chem. Rev.* **2003**, *103*, 3247–3262; c) F. F. Huerta, A. B. E. Minidis, J.-E. Bäckvall, *Chem. Soc. Rev.* **2001**, *30*, 321–331; d) M.-J. Kim, Y. Ahn, J. Park, *Curr. Opin. Chem. Biol.* **2002**, *13*, 578–587; e) M. T. El Gihani, J. M. J. Williams, *Curr. Opin. Chem. Biol.* **1999**, *3*, 11–15; f) R. Stürmer, *Angew. Chem.* **1997**, *109*, 1221–1222; *Angew. Chem. Int. Ed. Engl.* **1997**, *36*, 1173–1174.
- [3] For a related DKR of amines, see: M. T. Reetz, K. Schimossek, *Chimia* **1996**, *50*, 668–669.
- [4] P. M. Dinh, J. A. Howarth, A. R. Hudnott, J. M. J. Williams, *Tetrahedron Lett.* **1996**, *37*, 7623–7626.
- [5] a) A. L. E. Larsson, B. A. Persson, J.-E. Bäckvall, *Angew. Chem.* **1997**, *109*, 1256–1258; *Angew. Chem. Int. Ed. Engl.* **1997**, *36*, 1211–1212; b) B. A. Persson, A. L. E. Larsson, M. Le Ray, J.-E. Bäckvall, *J. Am. Chem. Soc.* **1999**, *121*, 1645–1650.
- [6] N. Menasche, Y. Shvo, *Organometallics* **1991**, *10*, 3885–3891.
- [7] a) F. F. Huerta, J.-E. Bäckvall, *Org. Lett.* **2001**, *3*, 1209–1212; b) A.-B. Runmo, O. Pàmies, K. Faber, J.-E. Bäckvall, *Tetrahedron Lett.* **2002**, *43*, 2983–2986; c) F. F. Huerta, Y. R. S. Laxmi, J.-E. Bäckvall, *Org. Lett.* **2000**, *2*, 1037–1040; d) O. Pàmies, J.-E. Bäckvall, *J. Org. Chem.* **2002**, *67*, 1261–1265.
- [8] a) O. Pàmies, J.-E. Bäckvall, *Adv. Synth. Catal.* **2001**, *343*, 726–731; b) O. Pàmies, J.-E. Bäckvall, *Adv. Synth. Catal.* **2002**, *344*, 947–952.
- [9] O. Pàmies, J.-E. Bäckvall, *J. Org. Chem.* **2001**, *66*, 4022–4025.
- [10] O. Pàmies, J.-E. Bäckvall, *J. Org. Chem.* **2002**, *67*, 9006–9010.
- [11] O. Pàmies, J.-E. Bäckvall, *J. Org. Chem.* **2003**, *68*, 4815–4818.
- [12] a) B. A. Persson, F. F. Huerta, J.-E. Bäckvall, *J. Org. Chem.* **1999**, *64*, 5237–5240; b) M. Edin, J. Steinreiber, J.-E. Bäckvall, *Proc. Natl. Acad. Sci. USA* **2004**, *101*, 5761–5766; c) B. Martín-Matute, J.-E. Bäckvall, *J. Org. Chem.*, in press.
- [13] M.-J. Kim, Y. K. Choi, M. Y. Choi, M. J. Kim, J. Park, *J. Org. Chem.* **2001**, *66*, 4736–4738.
- [14] a) H. M. Jung, J. H. Koh, M.-J. Kim, J. Park, *Org. Lett.* **2000**, *2*, 409–411; b) H. M. Jung, J. H. Koh, M.-J. Kim, J. Park, *Org. Lett.* **2000**, *2*, 2487–2490.
- [15] O. Pàmies, J.-E. Bäckvall, *Chem. Eur. J.* **2001**, *7*, 5052–5058.
- [16] J. H. Koh, H. M. Jung, J. Park, *Tetrahedron Lett.* **1998**, *39*, 5545–5548.
- [17] a) J. H. Choi, Y.-H. Kim, S. H. Nam, S. T. Shin, M.-J. Kim, J. Park, *Angew. Chem.* **2002**, *114*, 2479–2482; *Angew. Chem. Int. Ed.* **2002**, *41*, 2373–2376; b) J. H. Choi, Y. K. Choi, Y. H. Kim, E. S. Park, E. J. Kim, M. J. Kim, J. Park, *J. Org. Chem.* **2004**, *69*, 1972–1977.
- [18] G. Csajnyik, K. Bogár, J.-E. Bäckvall, *Tetrahedron Lett.* **2004**, *45*, 6799–6802.
- [19] Immobilized and commercially available as Novozym-435.
- [20] Under the same reaction conditions, (2-naphthyl)-1-ethanol gave (2-naphthyl)-1-ethanol acetate in 100 % yield but 0 % *ee*.
- [21] To avoid opening of the reaction vessel, the order of addition of reagents was changed slightly: Toluene was added to a mixture

- of KO^tBu, Ru complex, CALB, and Na₂CO₃. After 6 min the alcohol was added and the mixture was stirred for 4 min. Finally, isopropenyl acetate was added.
- [22] To control the water activity, the enzyme was stored in a sealed container with a saturated solution of LiCl for a minimum of 24 h. An excess of KO^tBu is needed to consume the water in the reaction mixture. To test this hypothesis, DKR of **4a** was carried out under the same reaction conditions as in Table 1, entry 4, but employing 40 mg of CALB instead of 6 mg. Acetate **5a** was obtained in only 57% yield after 3 h.
- [23] a) R. M. Bulloc, *Chem. Eur. J.* **2004**, *10*, 2366–2374, and references therein; b) V.-I. Bakhmutov, E. V. Vorontsov, D. Y. Antonov, *Inorg. Chim. Acta* **1998**, *278*, 122–126.
- [24] C. P. Casey, T. E. Vos, G. A. Bikzhanova, *Organometallics* **2003**, *22*, 901–903.
- [25] N. G. Connelly, I. Manners, *J. Chem. Soc. Dalton Trans.* **1989**, 283–288.
- [26] NMR data can be found in the following references: **5a**: D. Bianchi, P. Cesti, E. Battistel, *J. Org. Chem.* **1988**, *53*, 5531–5535; **5b**: J. Y. Legros, M. Toffano, J.-C. Fiaud, *Tetrahedron* **1995**, *51*, 3235–3246; **5c**: B. R. Rao, M. E. N. Nambudiry, *Synth. Commun.* **1991**, *21*, 1721–1727; **5d**: S. M. Brown, S. G. Davies, J. A. A. de Sousa, *Tetrahedron: Asymmetry* **1993**, *4*, 813–822; **5e**: Y. Kita, Y. Takebe, K. Murata, T. Naka, S. Akai, *J. Org. Chem.* **2000**, *65*, 83–88; **5f**: A. Kamal, M. Sandbhor, K. V. Ramana, *Tetrahedron: Asymmetry* **2002**, *13*, 815–820; **5h**: reference [5b]; **7**: J. S. Wallace, B. W. Baldwin, C. J. Morrow, *J. Org. Chem.* **1992**, *57*, 5231–5239.
- [27] Stirring for 10 min gave essentially the same result but stirring for 1.5 h gave less-reproducible results.

Continuous Two-Channel Time-of-Flight Mass Spectrometric Detection of Electrosprayed Ions**

Oliver Trapp, Joel R. Kimmel, Oh Kyu Yoon,
Ignacio A. Zuleta, Facundo M. Fernandez, and
Richard N. Zare*

Time-of-flight mass spectrometry (TOFMS) is a widely used technique that is recognized for offering high analytical performance at a reasonable cost. Development of this technique is ongoing, and advances in areas such as ion optics and ion-detection hardware have pushed the mass resolution and mass accuracy of TOFMS to regimes that are appropriate for the identification of components of complex mixtures.^[1] The technique's intrinsic high ion transmission and capability to measure wide mass ranges without scanning, yields high sensitivity and fast spectral acquisition rates. Based on these characteristics, TOFMS seems to be an ideal detector for fast separations of analytes with a broad range of molecular weights.^[2] Such applications, which include the in-line separation of pharmaceuticals, peptides, or proteins followed by electrospray ionization, are becoming increasingly important.^[3] Unfortunately, the pulsed nature of TOFMS yields inherent losses when analyzing ions emerging from continuous ion sources. Minimization of these losses can be achieved only at the expense of a reduction in the sampled mass range and potentially the mass resolution if the flight path is shortened. In conventional TOFMS, packets of ions are periodically pulsed into the entrance of a field-free drift chamber. To avoid overlap of the recorded flight times, the duration between start pulses is set to be longer than the flight time of the heaviest analyte ion. Ions reaching the entrance of the flight chamber between start pulses are lost. Thus, the ion sampling efficiency (duty cycle) and spectral acquisition speed are directly related to the ratio of the duration of the start pulse to the time between pulses, and these figures of merit decrease as the sampled mass range or flight path are increased.

An ideal detector for capillary and chip-format separations should provide universal detection, sufficient spectral selectivity, and high sensitivity without degrading separation efficiency.^[4] If TOFMS is to become the detector of choice for these applications, optimization of its transmission, speed, and efficiency is essential. One approach to improve the duty cycle is to modulate the continuous ion beam of a conventional TOF instrument to receive encoded single-ion packets, for example, by Fourier transform techniques.^[5] The mass spectrum is then obtained by mathematical deconvolution and the analyzer duty cycle can be increased to about 25 %.

The most widely used strategy for improving the duty cycle of TOFMS is orthogonal extraction (OE).^[6] In this TOFMS configuration the fraction of the ion beam that is sampled is proportional to the length of the extraction region in the dimension orthogonal to the field-free flight trajectory. This region tends to be much larger than the sampling volume defined by ion gates used in an on-axis configuration. Thus, OE-TOFMS has a higher duty cycle than conventional on-axis TOFMS. But, because the flight times of ions traversing the extraction region depend on m/z , the duty cycle of OE-TOFMS decreases with m/z . More importantly, the overall performance of OE-TOFMS is still limited by trade-offs between efficiency, mass resolution, and mass range.

In an effort to decouple these figures of merit, we continue to explore a TOFMS strategy based on Hadamard-type, pseudorandom modulation.^[7] In this case a finely spaced Bradbury–Nielson gate (BNG)^[8] is used to rapidly modulate (MHz frequency range) a continuous ion beam on and off the axis of detection following a known pseudorandom binary sequence. Encoding sequences are applied to the ion beam by alternating the voltage of this gate between two set limits; a sequence element “1” fixes the gate electrodes at relative ground and allows ions to pass undeflected, while a sequence element “0” shifts the gate electrodes to a deflecting state. The acquired spectrum corresponds to the sum of time-shifted spectra of multiple packets. Knowledge of the encoding sequence allows mathematical deconvolution and recovery of the TOF mass spectrum. The length of the applied encoding sequence is chosen based on the range of flight times (i.e. mass range) being monitored. All encoding sequences contain approximately equal numbers of 1s and 0s (on and off signals), so by detecting all ions of state “1”, a one-channel Hadamard transform (HT) TOF mass spectrometer offers a 50 % duty cycle, independent of other instrument parameters.

In an attempt to extend the duty cycle of HT-TOFMS to 100 % and to increase the overall performance of the technique, for example, the signal-to-noise ratio (SNR), a next generation instrument has been developed as shown in Figure 1a. Improvements include new modulation electronics^[9] which integrate the Bradbury–Nielson gate on the driver board to minimize the length of the transmission lines for the amplified modulation sequence for more precise and also faster modulation, and software for simultaneous data acquisition and real-time Hadamard transformation. New focusing optics allow us to obtain a highly focused ion beam with a narrow energy distribution that can be precisely deflected at the BNG with a switching frequency between 5 and 50 MHz corresponding to an encoding element width of

[*] Dr. O. Trapp, J. R. Kimmel, O. K. Yoon, I. A. Zuleta,
Prof. Dr. F. M. Fernandez,† Prof. Dr. R. N. Zare
Department of Chemistry
Stanford University
Stanford CA 94305-5080 (USA)
Fax: (+1) 650-723-9262
E-mail: zare@stanford.edu

[†] Present address:
School of Chemistry and Biochemistry
Georgia Institute of Technology
Atlanta, GA 30332-0400 (USA)

[**] This work was supported by the US Air Force Office of Scientific Research (AFOSR Grant FA9550-04-1-0076) and Predicant Biosciences, South San Francisco. O.T. thanks the Deutsche Forschungsgemeinschaft (DFG) for an Emmy Noether-Fellowship (TR542/1-1/2) and F.M.F. thanks the Fundacion Antorchas for a postdoctoral fellowship. J.R.K. was supported by an American Chemical Society Division of Analytical Chemistry Fellowship, sponsored by Merck & Co.

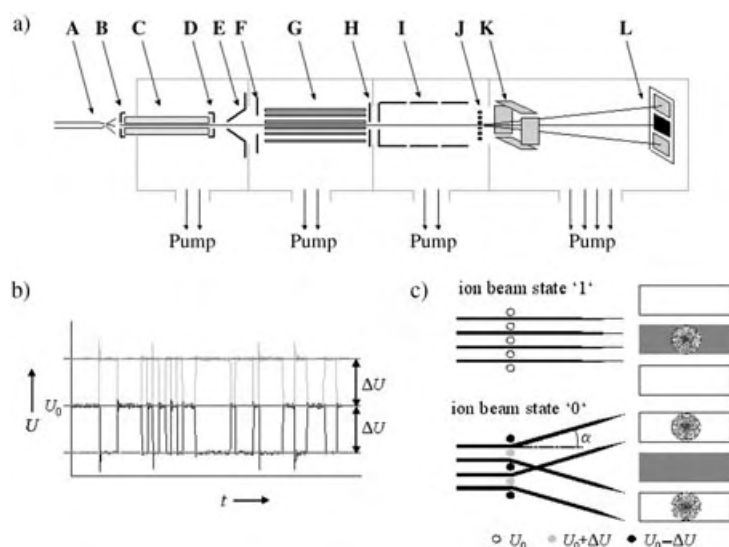


Figure 1. a) Schematic experimental setup of the new HT-TOF mass spectrometer. A) Electrospray needle, B) counter electrode, C) heated glass capillary, D) capillary exit electrode, E) skimmer, F) focusing lens, G) hexapole, H) conductance limiting exit lens, I) Einzel lens, J) Bradbury-Nielson gate, K) x,y steering plates, and L) masked dual-anode detector. b) Oscilloscope traces of the positive and negative phases of a Hadamard modulation sequence segment (11111100001111101010110000010000100000110011100) applied to the Bradbury-Nielson gate. c) Dual-detection scheme demonstrating the ion-beam states "0" and "1".

200 and 20 ns, respectively. The deflection angle α of the modulated ion beam (see Figure 1c) can be controlled by varying the voltage (ΔU) applied to the BNG. With sufficient modulation voltage applied to the BNG two spatially resolved modes of the ion beam can be experimentally observed at the detector plane: a centered, focused beam, and the two deflected ion beam branches that arrive above and below the detector center. To monitor both spatial modes, we have designed and installed a dual-anode multichannel plate (MCP) detector with isolated active charge-collection areas and a mask that is dimensioned to reflect the spatial profile of the modulated ion beam (Figure 1c).

The maximum duty cycle of a one-channel HT-TOF mass spectrometer is 50%. The experimentally achieved value depends on the percentage of ions entering the mass analyzer that strike the detector and, further, on the fraction of these ions that are modulated on and off of the detector [Eq. (1)] where n_{tot} is the total number of ions entering the mass analyzer, n_t is the number of ions striking the detector in the transmitted mode, and n_{nt} is the number of ions striking the detector (ideally zero) in the non-transmitted mode.

$$\text{duty cycle} = 50\% \left(\frac{n_t}{n_{\text{tot}}} \right) \left(\frac{n_t - n_{\text{nt}}}{n_t} \right) \quad (1)$$

The first ratio in Equation (1) represents ion-beam clipping, which can result if the ion beam and the detector are not properly aligned. The second ratio describes the deflection efficiency during modulation of the ion beam. The "0"-state ions that are insufficiently deflected and strike the

detector yield no TOF information and contribute to background noise.

Two-channel HT-TOF mass spectrometry involves the simultaneous optimization of paired one-channel HT-TOFMS experiments. Detecting high-quality spectra on the outer channel requires that deflection not only moves ions off the central axis of detection, but also that the deflection is repeatable and well-defined. While the inner channel records the static, focused component of the modulated ion beam, the outer channel detects ions that have undergone a time- and energy-dependent deflection (impulse sweep mode).^[10] Optimized conditions for both channels require reducing the kinetic-energy spread of the ions and matching the images of the deflected and undeflected ion-beam modes at the plane of the detector with the detector dimensions.

Images of the deflected and undeflected ion-beam modes were collected for the "0" and "1" modulation states using various optical configurations. The voltages applied to the set of four steering plates (see Figure 1a) at the entrance of the TOF chamber were scanned to move the ion beam about the three active areas of the detector. Synchronized measurements of total ion current (TIC) were used to generate two-dimensional ion-current plots. These plots represent the convolution of the detector shape and the beam shape. In the situation where the beam cross section is small compared to the detector area, the ion-current plot will have the shape of the beam, and knowledge of the detector dimensions can be used to estimate beam size. These data were used to optimize beam focus and position and to choose appropriate modulation conditions. Figure 2 displays the beam images at optimized conditions. The focused ion beam has dimensions comparable to the inner anode and can be moved vertically between the three active areas. The deflected ion beam has two well-defined centers that exist above and below the focused mode (Figure 2c and d).

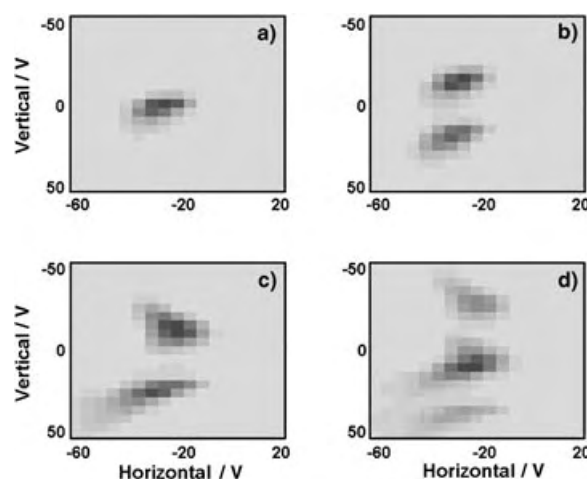


Figure 2. Two-dimensional images of the position, shape, and size of the temporally and spatially modulated ion beam obtained by x,y-steering of the undeflected or deflected ion beam across the two detection anodes. a) Undeflected ion beam detected at the inner anode, b) undeflected ion beam detected at the outer anode, c) deflected ion beam ($\Delta U = 13$ V) detected at the inner anode, d) deflected ion beam at the outer anode.

Subtracting deflected data from the undeflected data collected under identical scanning conditions provides a measure of how many ions are modulated about each detector at a specific beam position and focus. High duty cycle requires that ion current moves between the two channels of detection. Poor alignment or non-ideal deflection yield asymmetry in the data obtained for the two channels. Figure 3 shows an

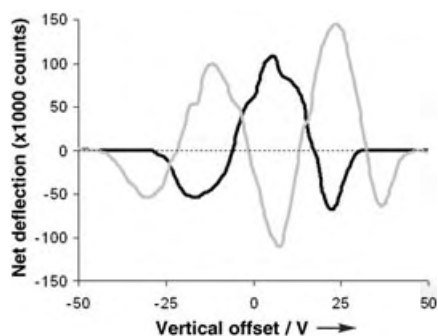


Figure 3. Net deflection plots of reserpine ($C_{33}H_{40}N_2O_9$) extracted by subtracting the vertical cross-sections of the deflected mode from the vertical cross sections of the undeflected mode of the ion beam. The black and gray curves represent the inner and outer detection anodes, respectively.

example of such data extracted from vertical cross sections with a modulation voltage $\Delta U = 13$ V applied to the BNG. The changes in the sign and magnitude of the deflection verify that the deflection process is vertical and that the deflected mode of the ion beam has two branches. At the ideal position, the BNG moves the entire ion beam from the inner to the outer anode.

Figure 4 shows deconvoluted spectra of polypropylene glycol (PPG 450) acquired at the inner and outer anodes. The spectrum of the outer anode is inverted owing to the mathematical formalism of the multiplication of the inverse Hadamard matrix (in our experiment a simplex matrix)^[11] with the raw spectrum of the outer anode, where each on state of the beam at the inner channel corresponds to the off state of the beam at the outer and vice versa. Similar data were collected for analytes across an m/z range of 200 to 2000 amu, including: caffeine, tetrabutylammonium acetate, *N*-hydroxyethyl-*N,N*-dimethylbenzylammonium chloride, bradykinin, reserpine, PPG 1000, and gramicidin. In each case, the flight times measured on the two channels were identical, and data subtraction did not require peak matching of the two spectra. At faster modulation and acquisition rates the slight difference in the flight paths to the two channels could require a different procedure to match and calibrate data.

Under ideal conditions the combination of the two channels of data yields an improvement of 41% ($\sqrt{2}$) in SNR over the one-channel experiment (only the inner detector). Experimentally we observe an average SNR improvement of 29%. Small deviations in the beam-detector proportions primarily cause this difference. Two-channel experiments were also carried out with a two-stage reflectron installed. Resolvable ion beamlets were observed in beam-

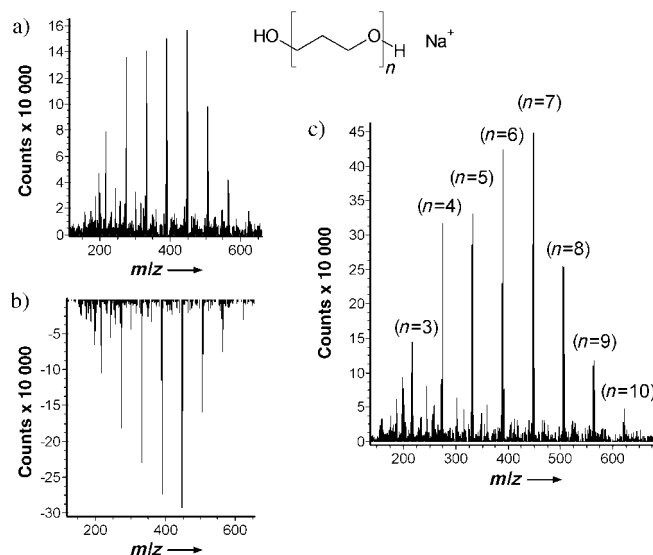


Figure 4. Spectra of PPG 450 simultaneously collected at the inner (a) and outer (b) anodes of the detector. Spectrum (c) represents the difference of spectrum (a) and spectrum (b) with an experimental improvement of the SNR of 29%. Conditions are 11-bit modulation sequence (2047 elements), 20 MHz modulation frequency, and 30 s acquisition time.

imaging experiments, but the extension of the flight path (2.2 m) caused a majority of the deflected ions to miss the outer detector at even our lowest deflection voltage ($\Delta U = 13$ V). Thus, the duty cycle on this detector was limited by the beam clipping term in Equation 1. Using current knowledge of the ion-beam dimensions and deflection profiles, appropriately sized detection areas will be designed to detect all ions.

With the implemented instrumental modifications, this two-channel detection scheme extends the achievable duty cycle of HT-TOFMS to 100% and effectively converts TOFMS into a continuous detection technique. Beyond the improved SNR, this advance gives an increase in the data acquisition rate (several thousand full spectra per second). More generally, this work suggests that temporal and spatial encoding of ion beams combined with multichannel detection schemes is a promising strategy for increasing the information density of TOFMS experiments.

Efficient multiplexing enables novel approaches to tandem MS detection. For example, the three spatially defined regions in this experiment (Figure 2) could be used for different MS experiments. It can be envisioned that one of the beams might be used for high-speed HT-TOFMS while the other two ion beams could be transferred into a high-mass resolution ion-trapping instrument, such as a Fourier transform ion cyclotron resonance mass spectrometer (FT-ICR-MS)^[12] for MSⁿ experiments.

Experimental Section

Figure 1 illustrates the experimental setup of the ESI-HT-TOF mass spectrometer at Stanford University. Ions are produced by an ESI source consisting of three differentially pumped stages. A borosilicate

glass capillary (0.4 mm i.d., length 124 mm), treated with chlorotrimethylsilane (Fluka) to minimize analyte surface interactions, was used as the transfer line between atmospheric pressure and the first pumping stage. A fused silica capillary, mechanically sharpened and coated with gold was used as spray needle. Analyte solutions were infused into this fused silica capillary at flow rates between 0.1 and 10 $\mu\text{L min}^{-1}$ by application of back pressure. The typical electrospray conditions were: spray-needle voltage of +2.4 to +3.6 kV, needle-capillary separation of 5–8 mm, and a spray source temperature of 220°C. The metal front and end cap of the heated transfer capillary were set between +30 and +80 V. Ions were extracted from the silent zone of the mach disk emerging from the metal spray nozzle with a skimmer (1 mm orifice i.d., +20 to +50 V). The second pumping stage of the ion source consists of a focusing lens (+14 to +24 V), a hexapole ion guide (length 21.9 cm, frequency 2.9 MHz, amplitude between 200 and 2500 V; ABB Inc, Pittsburgh), and a focusing exit lens (–2 to –25 V). The ions were accelerated to kinetic energies of 1500 eV by the first segment of a modified Einzel-type lens. Angular spread caused by the acceleration is focused by varying the voltage of the middle lens of the Einzel lens (–420 to –500 V). After the Einzel lens, a Bradbury–Nielson gate modulates the ion beam. The modulator grid consists of interspersed wire sets positioned normal to the ion beam. The wire sets were made from 20- μm diameter gold-plated tungsten wire and spaced 100 μm apart.^[8b] The pseudorandom sequence generator (Predicant Biosciences) is based on a feedback shift register circuit producing variable length sequences between 255 (8-bit) and 16383 (14-bit) elements. The modulation frequency can be set between 2 and 50 MHz and was kept at 20 MHz for all the experiments reported herein. The low-voltage signals of the binary sequence are transmitted to a driver board which is mounted on a heat sink cooled by a water/Peltier element. The cooling system is rated to dissipate up to 80 W of heat generated during operation. At the driver board the low voltage modulation signal is split into two phases that are 180° out of phase, amplified to voltages between $\Delta U = 13$ and 24 V, and applied to the wire sets of the Bradbury–Nielson gate, which floats at the flight tube potential (–1500 V). The ion beam passes undeflected when both wire sets are at the same potential, corresponding to the beam “on” state (1). When opposing potentials (between $\Delta U = 13$ and 24 V) are applied to the wire sets, the beam is split into two deflected beams, corresponding to the beam “off” state (0). The effective flight path in the non-reflectron configuration corresponds to approximately 1.1 m. The ions, passing through the slits of mask in front of the detector, are post-accelerated to an energy of 2300 eV before they are detected by a set of multichannel plates (MCPs; Quantar Technology). The MCP signals from the two anodes are amplified and fed into two multichannel scalers (Turbo MCS, EG&G Ortec, Oak Ridge, TN) for counting purposes. Synchronization of the data acquisition with the modulation electronics is achieved by triggering the start pulse of the data acquisition from the sequence generator at the beginning of the first sequence element. The digitized waveform acquired by the multichannel scaler is transferred to a computer (700 MHz Pentium III-based PC, with 384 MB RAM). Real-time deconvolution and data processing is performed with a program written in Delphi.

Mass calibration was achieved by quadratic regression analysis between the flight times and the known molecular weights of caffeine, polypropylene glycol (PPG450), bradykinin, and reserpine.

Solvents used for preparing the solutions were reagent grade. Bradykinin, caffeine, reserpine (Sigma), and polypropylene glycol standard (PPG450, narrow molecular-weight distribution; Scientific Polymer Products) were used as received without further purification. The analytes were dissolved in a water:methanol mixture (70:30 v/v). To improve the electrospray ionization efficiency 10 μL of 50 mM sodium acetate solution were added per mL of sample solutions of bradykinin, reserpine, and polypropylene glycol.

Received: July 8, 2004

Keywords: analytical methods · mass spectrometry · time of flight

- [1] M. Guilhaus, *J. Mass Spectrom.* **1995**, *30*, 1519–1532; b) M. Guilhaus, V. Mlynski, D. Selby, *Rapid Commun. Mass Spectrom.* **1997**, *11*, 951–962; c) R. J. Cotter, *Anal. Chem.* **1999**, *71*, 445A–451A; d) B. A. Mamyrin, *Int. J. Mass Spectrom.* **2001**, *206*, 251–266.
- [2] S. D. Koning, H.-G. Janssen, M. V. Deursen, U. A. T. Brinkman, *J. Sep. Sci.* **2004**, *27*, 397–409; b) M. T. Roberts, J.-P. Dufour, A. C. Lewis, *J. Sep. Sci.* **2004**, *27*, 473–478.
- [3] J. B. Fenn, *Angew. Chem.* **2003**, *115*, 3999–4024; *Angew. Chem. Int. Ed.* **2003**, *42*, 3871–3894; b) J. S. Rossier, N. Youhnovski, N. Lion, E. Damoc, S. Becker, F. Reymond, H. H. Girault, M. Przybylski, *Angew. Chem.* **2003**, *115*, 55–60; *Angew. Chem. Int. Ed.* **2003**, *42*, 53–58.
- [4] J. A. Olivares, N. T. Nguyen, C. R. Yonker, R. D. Smith, *Anal. Chem.* **1987**, *59*, 1230–1232.
- [5] a) F. J. Knorr, M. Ajami, D. A. Chatfield, *Anal. Chem.* **1986**, *58*, 690–694; b) G. Hars, I. Maros, *Int. J. Mass Spectrom.* **1999**, *225*, 101–114.
- [6] I. V. Chernushevich, W. Ens, K. G. Standing, *Anal. Chem.* **1999**, *71*, 452A–461A; b) M. Guilhaus, D. Selby, V. Mlynski, *Mass Spectrom. Rev.* **2000**, *19*, 65–107.
- [7] a) A. Brock, N. Rodriguez, R. N. Zare, *Anal. Chem.* **1998**, *70*, 3735–3741; b) A. Brock, N. Rodriguez, R. N. Zare, *Rev. Sci. Instrum.* **2000**, *71*, 1306–1318; c) F. M. Fernandez, J. M. Vadillo, F. Engelke, J. R. Kimmel, R. N. Zare, N. Rodriguez, M. Wetterhall, K. Markides, *J. Am. Soc. Mass Spectrom.* **2001**, *12*, 1302–1311; d) F. M. Fernandez, J. M. Vadillo, J. R. Kimmel, M. Wetterhall, K. Markides, N. Rodriguez, R. N. Zare, *Anal. Chem.* **2002**, *74*, 1611–1617; e) J. R. Kimmel, F. M. Fernandez, R. N. Zare, *J. Am. Soc. Mass Spectrom.* **2003**, *14*, 278–286; f) R. N. Zare, F. M. Fernandez, J. R. Kimmel, *Angew. Chem.* **2003**, *115*, 30–36; *Angew. Chem. Int. Ed.* **2003**, *42*, 30–35.
- [8] a) N. E. Bradbury, R. A. Nielsen, *Phys. Rev.* **1936**, *49*, 388; b) J. R. Kimmel, F. Engelke, R. N. Zare, *Rev. Sci. Instrum.* **2001**, *72*, 4354–4357.
- [9] C. Bolton, *Electronic Design News (EDN)*, October 3, **2002**, 88.
- [10] G. E. Yefchak, G. A. Schutz, J. Allison, C. G. Enke, J. F. Holland, *J. Am. Soc. Mass Spectrom.* **1990**, *1*, 440–447.
- [11] a) M. Harwit, N. J. A. Sloane, *Hadamard Transform Optics*, Academic Press, New York, **1979**; b) A. G. Marshall, *Fourier, Hadamard, and Hilbert Transforms in Chemistry*, Plenum, New York, **1982**.
- [12] M. B. Comisarow, A. G. Marshall, *Chem. Phys. Lett.* **1974**, *25*, 282–283; b) M. B. Comisarow, A. G. Marshall, *Chem. Phys. Lett.* **1974**, *26*, 489–490.

Homogeneous Catalysis

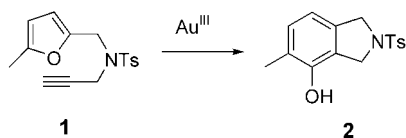
Gold Catalysis: The Benefits of N and N,O Ligands**

A. Stephen K. Hashmi,* Jan P. Weyrauch,
Matthias Rudolph, and Elzen Kurpejović

Dedicated to Professor Johann Mulzer
on the occasion of his 60th birthday

The catalysis of organic reactions by gold compounds has been recently shown to be a powerful tool in synthesis.^[1,2] When gold(I) compounds are used as precatalysts, ligands such as phosphanes^[3–8] or phosphites^[9] can be applied. The gold(III) precatalysts are mainly simple halides;^[2] other examples include one thioether-containing,^[10] one phosphite-containing,^[9] and organogold(III)^[11] compounds.

For the gold-catalyzed phenol synthesis,^[12] AuCl₃ usually delivers good results with simple substrates, but with more complicated ones a significant loss of activity is observed. At lower temperature, kinetic studies with our most simple test-substrate **1** (see Scheme 1) showed that the problem with



Scheme 1. Conversion of the test-substrate **1** with AuCl₃ as the precatalyst; Ts = tosyl (reaction conditions see Figure 1).

regard to the loss of activity occurs even with as much as 5 mol % of catalyst (Figure 1). With small amounts of catalyst, the conversion remains incomplete.

We have now tested several gold(I) and gold(III) complexes with different ligands as catalysts for this reaction. Gold(I) complexes showed low selectivity and led to several side products. Satisfactory results in terms of activity, long-term stability and product-selectivity were obtained only with gold(III) complexes with pyridine derivatives, some of which contained chelating oxygen functionalities. The most interesting complexes were precatalysts **3–6**.^[13] The complexes did not suffer deactivation, as shown in Figure 2 for **3**—the activity even holds in a second catalytic run. Unlike with AuCl₃, a mechanistically interesting induction period was

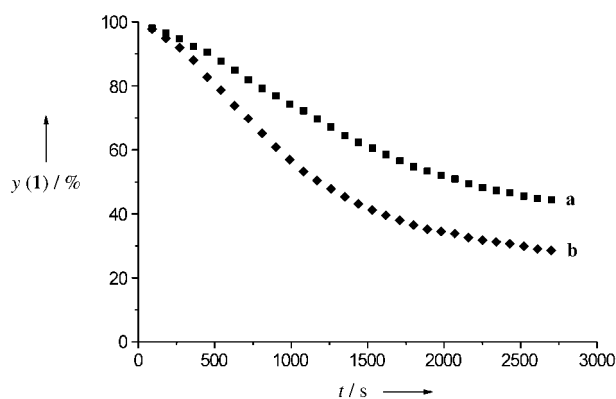


Figure 1. Reaction of **1** with AuCl₃. Reaction conditions: CD₃CN, 10 °C, a) 3.3 mol % AuCl₃; b) 5.0 mol % AuCl₃.

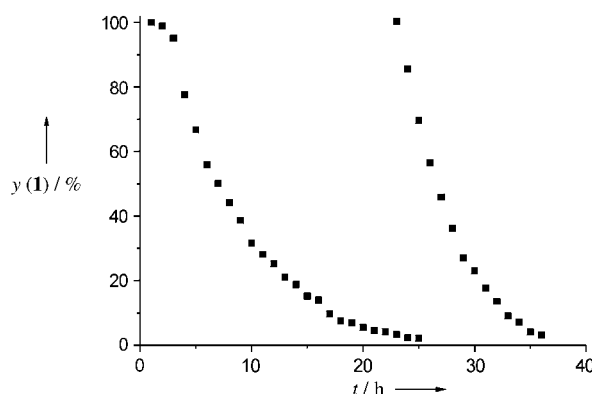
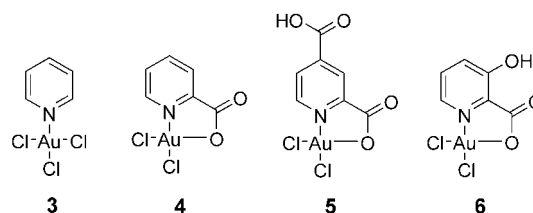


Figure 2. Reaction of **1** with the precatalyst **3**. Reaction conditions: CD₃CN, 45 °C, 5 mol % **3**. After 25 h the same amount of **1** was added.

observed for **3–6**, clearly proving that here the complexes are precatalysts. This is also the reason for the higher activity in the second run, since the catalytically active species is already present and does not have to be formed in a slow reaction.

With as little as 0.07 mol % of **3** a complete conversion could be achieved; this corresponds to 1180 instead of the usual 20–50 turnovers. The complexes **4–6** are also highly stable catalysts; a comparison of their activity is depicted in Figure 3: the acceptor-substituted pyridine carboxylate **5** is the most reactive one, followed by the unsubstituted **4** and the donor-substituted **6**. Nevertheless, the initial activity of **3**, **4**, and **6** is lower than that of AuCl₃. In part, this problem can be solved by switching to dichloromethane/acetonitrile mixtures or even pure dichloromethane (as shown for **3** in Figure 4). In

[*] Prof. Dr. A. S. K. Hashmi, Dipl.-Chem. J. P. Weyrauch, Dipl.-Chem. M. Rudolph, Dipl.-Chem. E. Kurpejović
Institut für Organische Chemie
Universität Stuttgart
Pfaffenwaldring 55, 70569 Stuttgart (Germany)
Fax: (+49) 711-685-4321
E-mail: hashmi@hashmi.de

[**] This work was supported by the Fonds der Chemischen Industrie, J.P.W. is grateful for a Doktoranden-Stipendium. A number of gold complexes were generously provided by Johnson Matthey.

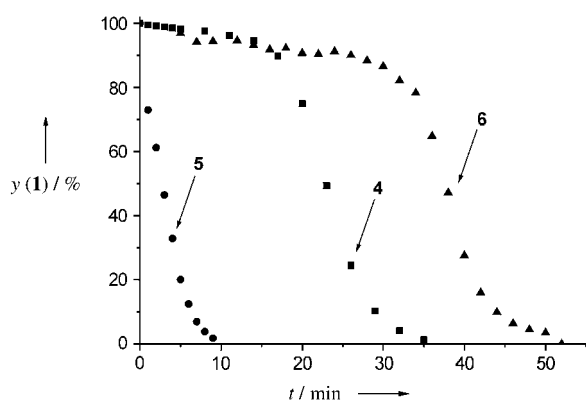


Figure 3. Comparison of the activities of 4–6 (with test-substrate 1). Reaction conditions: room temperature, 5 mol % of catalyst, MeCN.

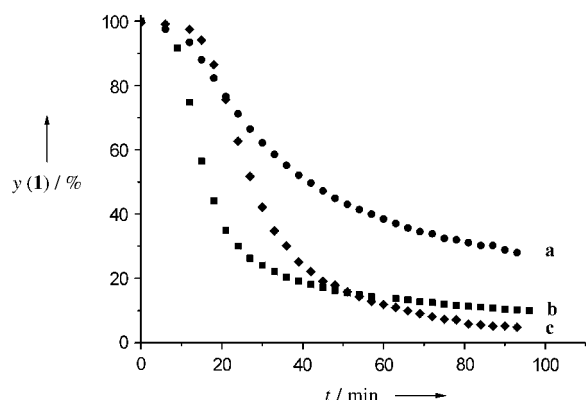


Figure 4. Activity of 3 in the conversion of 1 in different solvents. Reaction conditions: room temperature, 5 mol % 3, a) $\text{CH}_2\text{Cl}_2/\text{MeCN} = 80:20$; b) $\text{CH}_2\text{Cl}_2/\text{MeCN} = 100:0$; c) $\text{CH}_2\text{Cl}_2/\text{MeCN} = 90:10$.

spite of the slower conversion, these complexes are superior to other transition-metal complexes known to catalyze this reaction (Figure 5).^[12c,14]

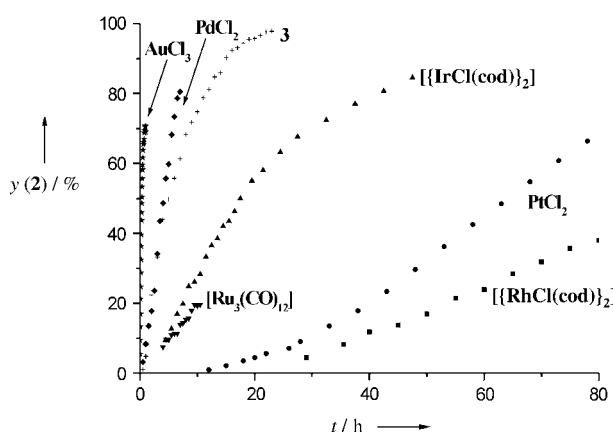
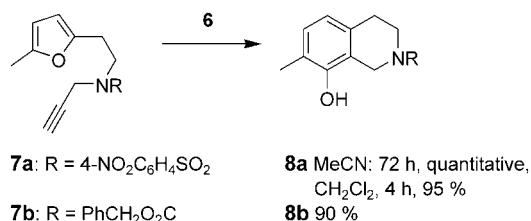


Figure 5. Comparison of the activity of 3 with the activities of different transition-metal catalysts (product 2). Reaction conditions: 5 mol % catalyst, AuCl_3 : 10 °C, MeCN; 3: 45 °C, MeCN; PdCl_2 : 45 °C, MeCN; $[\text{IrCl}(\text{cod})]_2$: 45 °C, MeCN; $[\text{Ru}_3(\text{CO})_{12}]$: 45 °C, benzene; PtCl_2 : 45 °C, MeCN; $[\text{RhCl}(\text{cod})]_2$: 45 °C, MeCN.

The major benefit in preparative terms of using these precatalysts in this reaction is that they enable the preparation of benzoannulated heterocycles with a phenolic hydroxy group in a position which is difficult to achieve by employing classic synthetic methodology.^[12d] The most significant targets are antitumor antibiotics from the tetrahydroisoquinoline family,^[15] which—with this substitution pattern—are not readily accessible by the Pictet–Spengler or related reactions.^[16] As reported previously, with 5 mol % or less AuCl_3 no complete conversion could be achieved,^[12a] but 6 gave a quantitative conversion of 7a at room temperature (Scheme 2). And even the Z-protected substrate 7b (Z = $\text{CO}_2\text{CH}_2\text{Ph}$) gave a clean reaction with 6. With cationic gold(i) complexes we could not achieve the product selectivity reported here.



Scheme 2. Conversion of the substrates 7a and 7b with the precatalyst 6.

In conclusion, the development of the gold(III) precatalysts 3–6 represents a first step in catalyst-tuning by ligand design, a major focus of research for most other transition metals. These results provide good evidence for the establishment of significantly more effective gold catalysts.

Experimental Section

Complex 7a (300 mg, 861 μmol) and complex 6 (15.7 mg, 38.7 μmol ; 4.5 mol %) in CH_2Cl_2 (1.50 mL) were stirred at room temperature for 4 h. The solvent was removed in vacuo, and column chromatography yielded 8a (284 mg; 95 %).

8a: M.p. 166–167 °C. R_f (petroleum ether/dichloromethane/ethyl acetate, 10:3:1) = 0.10; IR (neat): $\tilde{\nu} = 3514, 1587, 1530, 1467, 1346, 1311, 1260, 1235, 1216, 1161, 992, 958, 873, 854, 805, 763, 737, 691, 619, 600, 580 \text{ cm}^{-1}$; ^1H NMR (CDCl_3 , 250 MHz): $\delta = 2.20$ (s, 3H), 2.88 (t, $J = 5.9 \text{ Hz}$, 2H), 3.43 (t, $J = 5.9 \text{ Hz}$, 2H), 4.31 (s, 2H), 4.82 (s, 1H), 6.60 (d, $J = 7.7 \text{ Hz}$, 1H), 6.93 (d, $J = 7.7 \text{ Hz}$, 1H), 8.04 (d, $J = 9.0 \text{ Hz}$, 2H), 8.36 ppm (d, $J = 9.0 \text{ Hz}$, 2H); ^{13}C NMR (CDCl_3 , 126 MHz): $\delta = 15.57$ (q), 28.93 (t), 43.82 (t), 43.85 (t), 118.63 (s), 120.12 (s), 121.06 (d), 124.74 (d, 2C), 129.12 (d, 2C), 129.29 (d), 132.53 (s), 143.38 (s), 150.51 (s), 150.53 ppm (s); MS (70 eV): m/z (%): 348 (31) [M^+], 161 (100), 134 (41), 91 (10). C, H, N analysis calcd (%) for $\text{C}_{16}\text{H}_{16}\text{N}_2\text{O}_5\text{S}$ (348.38): C 55.16, H 4.63, N 8.04; found: C 55.16, H 4.66, N 8.07.

Received: April 6, 2004

Keywords: alkynes · gold · heterocycles · homogeneous catalysis · N,O ligands

[1] G. Dyker, *Angew. Chem.* **2000**, *112*, 4407–4409; *Angew. Chem. Int. Ed.* **2000**, *39*, 4237–4239.

- [2] a) A. S. K. Hashmi, *Gold Bull.* **2003**, 36, 3–9; b) A. S. K. Hashmi, *Gold Bull.* **2004**, 37, 51–65.
- [3] Y. Ito, M. Sawamura, T. Hayashi, *J. Am. Chem. Soc.* **1986**, 108, 6405–6406.
- [4] a) J. H. Teles, M. Schulz (BASF AG), WO-A1 9721648, **1997** [*Chem. Abstr.* **1997**, 127, 121499]; b) J. H. Teles, S. Brode, M. Chabanas, *Angew. Chem.* **1998**, 110, 1475–1478; *Angew. Chem. Int. Ed.* **1998**, 37, 1415–1418.
- [5] a) E. Mizushima, K. Sato, T. Hayashi, M. Tanaka, *Angew. Chem.* **2002**, 114, 4745–4747; *Angew. Chem. Int. Ed.* **2002**, 41, 4563–4565; b) E. Mizushima, T. Hayashi, M. Tanaka, *Org. Lett.* **2003**, 5, 3349–3352.
- [6] a) F. Shi, Y. Deng, H. Yang and T. SiMa, *J. Chem. Soc. Chem. Commun.* **2001**, 345–346; b) F. Shi, Y. Deng, *J. Chem. Soc. Chem. Commun.* **2001**, 443–444.
- [7] S. Komiya, T. Sone, Y. Usui, M. Hirano, A. Fukuoka, *Gold Bull.* **1996**, 29, 131–136.
- [8] a) R. T. Baker, P. Nguyen, T. B. Marder, S. A. Westcott, *Angew. Chem.* **1995**, 107, 1451–1452; *Angew. Chem. Int. Ed. Engl.* **1995**, 34, 1336–1338; b) R. T. Baker, J. C. Calabrese, S. A. Westcott, *J. Organomet. Chem.* **1995**, 498, 109–117.
- [9] J. Sundermeyer, C. Jost, DE 10041510, **1999** [*Chem. Abs.* **2001**, 134, 280723].
- [10] E. Boring, Y. V. Geletii, C. L. Hill, *J. Am. Chem. Soc.* **2001**, 123, 1625–1635.
- [11] R. Casado, M. Contel, M. Laguna, P. Romero, S. Sanz, *J. Am. Chem. Soc.* **2003**, 125, 11925–11935.
- [12] a) A. S. K. Hashmi, T. M. Frost, J. W. Bats, *J. Am. Chem. Soc.* **2000**, 122, 11553–11554; b) A. S. K. Hashmi, T. M. Frost, J. W. Bats, *Org. Lett.* **2001**, 3, 3769–3771; c) A. S. K. Hashmi, T. M. Frost, J. W. Bats, *Catal. Today* **2002**, 72, 19–72; d) A. S. K. Hashmi, L. Ding, J. W. Bats, P. Fischer, W. Frey, *Chem. Eur. J.* **2003**, 9, 4339–4345.
- [13] Complexes **4** and **5** were kindly provided by Johnson Matthey from their polyarthritis research. Complex **3** was prepared according to H.-N. Adams, J. Strähle, *Z. Anorg. Allg. Chem.* **1982**, 485, 65–80; H.-N. Adams, W. Hiller, J. Strähle, *Z. Anorg. Allg. Chem.* **1982**, 485, 81–91. Complex **6** was prepared according to A. Dar, K. Moss, S. M. Cottrill, R. V. Parish, C. A. McAuliffe, R. G. Pritchard, B. Beagley, J. Sandbank, *J. Chem. Soc. Dalton Trans.* **1992**, 1, 1907–1913.
- [14] a) B. Martín-Matute, D. J. Cardenas, A. M. Echavarren, *Angew. Chem.* **2001**, 113, 4890–4893; *Angew. Chem. Int. Ed.* **2001**, 40, 4754–4757; b) B. Martín-Matute, C. Nevado, D. J. Cárdenas, A. M. Echavarren, *J. Am. Chem. Soc.* **2003**, 125, 5757–5766.
- [15] J. D. Scott, R. M. Williams, *Chem. Rev.* **2002**, 102, 1669–1730.
- [16] A. Pictet, T. Spengler, *Chem. Ber.* **1911**, 44, 2030–2036; W. M. Whaley, T. R. Govindachari, *Org. React.* **1951**, 6, 151–206. Usually the annelation is directed to the *para* position of an oxygen substituent on the arene and not to the *ortho* position.

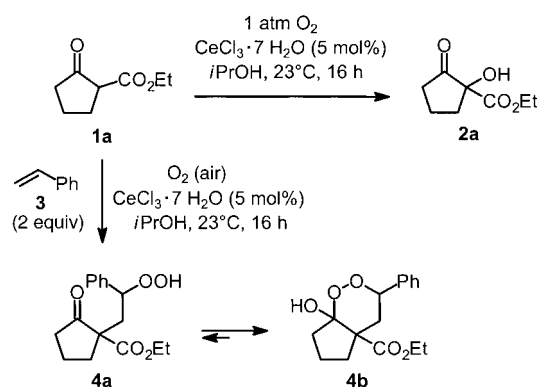
C–C Coupling

Formation of 1,4-Diketones by Aerobic Oxidative C–C Coupling of Styrene with 1,3-Dicarbonyl Compounds**

Michael Rössle, Thomas Werner, Angelika Baro, Wolfgang Frey, and Jens Christoffers*

1,4-Dicarbonyl compounds^[1] are versatile precursors for the synthesis of various heterocyclic structural motifs, for example, furan,^[2] thiophene, and pyrrole derivatives.^[3] The conversion of α -halo ketones with enolates represents a classic route to 1,4-dicarbonyl compounds (Feist–Bénary synthesis of furan derivatives).^[4] A modern concept utilizes the umpolung of aldehydes, for example, by application of the Stetter reagent^[5] or 1,3-dithiane derivatives.^[6]

Recently, we reported the cerium-catalyzed α hydroxylation of 1,3-dicarbonyl compounds **1** (Scheme 1).^[7] With



Scheme 1. Cerium-catalyzed α hydroxylation of β -oxoester **1a** with O_2 and oxidative C–C coupling with styrene **3**.

respect to economical and ecological considerations, the use of molecular oxygen is superior to other reagents applied in this type of conversion. Based on the assumption of radical intermediates along the hydroxylation pathway, the conversion has been performed in the presence of olefins such as styrene (**3**), and indeed, hydroperoxides **4** were obtained as the major products. Compounds **4** were isolated as hemiacetals such as **4b** with an endoperoxide 1,2-dioxane ring.^[8]

Surprisingly, these crystalline endoperoxides have a remarkable stability indicated by defined melting points between 50 and 150 °C, but, unfortunately, they were obtained as hardly separable mixtures of diastereoisomers. Thus, purification and characterization are difficult, resulting in a

[*] M. Rössle, Dr. T. Werner, Dr. A. Baro, Dr. W. Frey, Prof. J. Christoffers
Institut für Organische Chemie, Universität Stuttgart
Pfaffenwaldring 55, 70569 Stuttgart (Germany)
Fax: (+49) 711-685-4269
E-mail: jchr@oc.uni-stuttgart.de

[**] This work was generously supported by the Deutsche Forschungsgemeinschaft and the Fonds der Chemischen Industrie.

restricted application for further synthetic purposes. We were therefore interested in the conversion of 1,2-dioxanes into diastereomerically unique products, either by oxidation, reduction or by disproportionation of the peroxide unit.^[9] After considerable experimentation with a number of transition-metal-assisted transformations,^[10] we focused our interest on the Kornblum–DeLaMare fragmentation mediated by a pyridine/acetyl chloride system.^[11] Owing to the difficult purification of the diastereomeric endoperoxide mixtures, we investigated a sequential one-pot procedure for oxidative C–C bond formation and Kornblum–DeLaMare fragmentation. Herein we report an optimized protocol as the result of these studies.

1,3-Dicarbonyl compounds **1a–h** were converted with styrene (**3**) under $\text{CeCl}_3 \cdot 7\text{H}_2\text{O}$ catalysis (10 mol %) in 2-propanol at ambient temperature under an atmosphere of air as the oxidant (Table 1). Under higher partial pressures of O_2 the formation of undesired α -hydroxylated products **2** is favored.

Table 1: Formation of 1,4-dicarbonyl compounds **5** by a two-step one-pot reaction consisting of cerium-catalyzed C–C coupling with **3** and subsequent Kornblum–DeLaMare fragmentation.^[a]

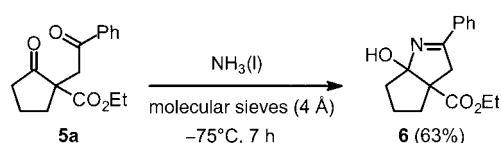
$\text{R}^1\text{C(=O)CH(R}^2\text{)COR}^3 + \text{CH}_2=\text{CHPh} \xrightarrow[\text{2) pyridine–AcCl, 16 h}]{\text{1) CeCl}_3 \cdot 7\text{H}_2\text{O (10 mol \%), iPrOH, 23}^\circ\text{C, 24 h, O}_2 \text{ (air)}} \text{R}^1\text{C(=O)CH(R}^2\text{)CH(R}^3\text{)COPh}$			
1a–h	3	5a–h	
Product	Yield [%] ^[b]	Product	Yield [%] ^[b]
5a	71	5e	50 ^[c]
5b	62	5f	71
5c	87 ^[c]	5g	68
5d	72	5h	72

[a] See Experimental Section for reaction conditions. [b] Overall yield over two steps. [c] 5 mol % of $\text{CeCl}_3 \cdot 7\text{H}_2\text{O}$.

As **3** is partly consumed by polymerization, the reaction was started with the addition of 2 equivalents followed by a further 1 equivalent of **3** after 4 h. The reaction mixture was stirred for a further 20 h, and then all volatile materials were removed under vacuum, leaving a mixture of crude endoperoxides **4**, polystyrene, and cerium-containing materials. This residue was directly treated with a mixture of pyridine (5 equiv) and AcCl (6 equiv) in CH_2Cl_2 and stirred for 16 h at ambient temperature. Filtration through SiO_2 and chromatography gave unique 1,4-diketones **5** in the range of 50–90% overall yield over two steps (Table 1).

Apart from carbocyclic and open-chain β -oxoesters and 1,3-diketones, heterocyclic compounds were also investigated. As can be seen from Table 1, the best result was realized for lactone **5c** (87% overall yield), whereas of cyclohexanone derivative **5e** was obtained in 50% yield. All other substrates, which include lactam **5d** and carbocyclic and open-chain derivatives, were isolated in 62–72% yield. The reaction sequence could also be extended to the seven-membered ring product **5f** (71%). In contrast to α -hydroxylations, even the α -unsubstituted substrate **1h** ($\text{R}' = \text{H}$) cleanly reacted in this manner with **3** to give **5h** in 72% yield (Table 1).

To prove the utility of the 1,4-diketones **5** (which bear a quaternary C atom) as building blocks in the synthesis of heterocycles, compound **5a** was treated with liquid NH_3 . After chromatographic workup, the novel bicyclic 3,4-dihydro-2H-pyrrole derivative **6** was isolated as a single diastereomer in 63% yield (Scheme 2). The molecular structure of **6**



Scheme 2. Interrupted Paal-Knorr reaction of the 1,4-dicarbonyl compound **5a** to pyrrole derivative **6**.

was confirmed by X-ray single-crystal analysis (Figure 1)^[12] and can be seen as a product of an interrupted Paal–Knorr pyrrole synthesis. The final elimination of water is inhibited by the quaternary center, and the position of the formed double bond is unexpected for this type of reaction.^[4a,b]

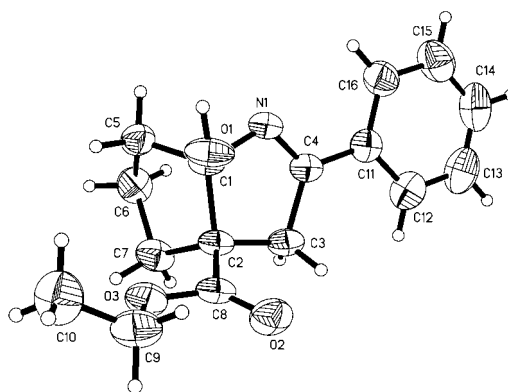


Figure 1. ORTEP view of 3,4-dihydro-2H-pyrrole derivative **6** drawn at the 50% probability level.

In summary, 1,4-diketones **5** are readily accessible in a two-step one-pot reaction in 50–87% overall yields. Our synthetic concept, which may be a valuable alternative to other umpolung strategies, combines an oxidative cerium-catalyzed C–C coupling of 1,3-dicarbonyl compounds **1** with styrene (**3**) and a pyridine/ AcCl -mediated Kornblum–DeLaMare fragmentation. A follow-up reaction of **5a** with

NH₃ to afford the new dihydro-2H-pyrrole derivative **6** demonstrates that 1,4-diketones **5** are suitable precursors for heterocyclic compounds.

Experimental Section

Typical procedure: Styrene (**3**; 2.0 equiv) and the respective 1,3-dicarbonyl compound **1** (1 mmol, 1.0 equiv) were added to a stirred suspension of CeCl₃·7H₂O (0.1 equiv) in *i*PrOH (0.65 mL/mmol **1**). After 4 h, more **3** (1.0 equiv) was added, and the reaction mixture was stirred for a further 20 h at room temperature. All volatile materials were removed under vacuum, and the residue was suspended in CH₂Cl₂ (2 mL/mmol **1**). Pyridine (5.0 equiv) and acetyl chloride (6.0 equiv) were added at 0°C, and the resulting mixture was stirred for 16 h at room temperature. The reaction mixture was filtered through SiO₂ (petroleum ether/EtOAc 2:1) and subsequently purified by silica-gel column chromatography (petroleum ether/EtOAc 5:1) to give 1,4-diketones **5** as the major products.

Received: July 23, 2004

Keywords: dicarbonyl compounds · C–C coupling · cerium · heterocycles · homogeneous catalysis

- [11] a) N. Kornblum, H. E. DeLaMare, *J. Am. Chem. Soc.* **1951**, *73*, 880–881; b) S. J. Blanksby, G. B. Ellison, V. M. Bierbaum, S. Kato, *J. Am. Chem. Soc.* **2002**, *124*, 3196–3197.
[12] CCDC-245445 contains the supplementary crystallographic data for this paper. These data can be obtained free of charge via www.ccdc.cam.ac.uk/conts/retrieving.html (or from the Cambridge Crystallographic Data Centre, 12, Union Road, Cambridge CB21EZ, UK; fax: (+44)1223-336-033; or deposit@ccdc.cam.ac.uk).

- [1] For a selection of other new syntheses of 1,4-diketones, see: a) M. Yuguchi, M. Tokuda, K. Orito, *J. Org. Chem.* **2004**, *69*, 908–914; b) R. Ballini, L. Barboni, G. Giarlo, *J. Org. Chem.* **2003**, *68*, 9173–9176; c) Y. Yamamoto, H. Maekawa, S. Goda, I. Nishiguchi, *Org. Lett.* **2003**, *5*, 2755–2758; d) M. Yasuda, S. Tsuji, Y. Shigeyoshi, A. Baba, *J. Am. Chem. Soc.* **2002**, *124*, 7440–7447.
[2] a) H. S. P. Rao, S. Jothilingam, *J. Org. Chem.* **2003**, *68*, 5392–5394; b) B. W. Greatrex, M. C. Kimber, D. K. Taylor, E. R. T. Tiekink, *J. Org. Chem.* **2003**, *68*, 4239–4246; c) D. S. Mortensen, A. L. Rodriguez, K. E. Carlson, J. Sun, B. S. Katzenellenbogen, J. A. Katzenellenbogen, *J. Med. Chem.* **2001**, *44*, 3838–3848.
[3] a) G. Minetto, L. F. Raveglia, M. Taddei, *Org. Lett.* **2004**, *6*, 389–392; b) R. Dhawan, B. A. Arndtsen, *J. Am. Chem. Soc.* **2004**, *126*, 468–469; c) B. K. Banik, S. Samajdar, I. Banik, *J. Org. Chem.* **2004**, *69*, 213–216; d) R. U. Braun, K. Zeitler, T. J. J. Müller, *Org. Lett.* **2001**, *3*, 3297–3300.
[4] Recent examples: a) M. A. Calter, C. Zhu, *Org. Lett.* **2002**, *4*, 205–208; b) M. A. Calter, C. Zhu, R. J. Lachicotte, *Org. Lett.* **2002**, *4*, 209–212; c) F. Stauffer, R. Neier, *Org. Lett.* **2000**, *2*, 3535–3537.
[5] D. Enders, T. Balensiefer, *Acc. Chem. Res.* **2004**, *37*, 534–541.
[6] A. B. Smith III, C. M. Adams, *Acc. Chem. Res.* **2004**, *37*, 365–377.
[7] a) J. Christoffers, T. Werner, *Synlett* **2002**, 119–121; b) J. Christoffers, T. Werner, S. Unger, W. Frey, *Eur. J. Org. Chem.* **2003**, 425–431; c) J. Christoffers, T. Werner, W. Frey, A. Baro, *Chem. Eur. J.* **2004**, *10*, 1042–1045.
[8] J. Christoffers, T. Werner, W. Frey, A. Baro, *Eur. J. Org. Chem.* **2003**, 4879–4886.
[9] a) B. W. Greatrex, D. K. Taylor, E. R. T. Tiekink, *J. Org. Chem.* **2004**, *69*, 2580–2583; b) B. Greatrex, M. Jevric, M. C. Kimber, S. J. Krivickas, D. K. Taylor, E. R. T. Tiekink, *Synthesis* **2003**, 668–672; c) B. W. Greatrex, M. C. Kimber, D. K. Taylor, G. Fallon, E. R. T. Tiekink, *J. Org. Chem.* **2002**, *67*, 5307–5314; d) M. C. Kimber, D. K. Taylor, *J. Org. Chem.* **2002**, *67*, 3142–3144; e) T. D. Avery, G. Fallon, B. W. Greatrex, S. M. Pyke, D. K. Taylor, E. R. T. Tiekink, *J. Org. Chem.* **2001**, *66*, 7955–7966.
[10] a) J. Yoshida, S. Nakatani, K. Sakaguchi, S. Isoe, *J. Org. Chem.* **1989**, *54*, 3383–3389; b) J.-Q. Yu, E. J. Corey, *J. Am. Chem. Soc.* **2003**, *125*, 3232–3233.

Element Modifications

[Ga₂₂(PtBu₂)₁₂]: Diversity in the Arrangement of 22 Gallium Atoms—A Unique Case in the Field of Metalloid Clusters?*

Jochen Steiner, Gregor Stößer, and
Hansgeorg Schnöckel*

*Dedicated to Professor Nils Wiberg
on the occasion of his 70th birthday*

With the formation of three different Ga₂₂ frameworks in metalloid clusters, the element gallium assumes a unique position in the field of metal clusters,^[1] since to our knowledge, structural isomers of large metalloid clusters are not known to date for any other metal. Here we report an additional structural variation in the arrangement of 22 gallium atoms, in which for the first time an icosahedral Ga₁₂ core is retained despite extensive reduction of the Ga₂₂ framework (average oxidation number 0.55). We have previously achieved low oxidation numbers for Ga₂₂ clusters only when gallium-centered arrangements were present in the cluster core (oxidation number 0.36, Figure 1): [Ga₂₂R₈] (**1**) with R = Si^tBu₃ (**1a**),^[2] Si(SiMe₃)₃ (**1b**),^[3] and Ge(SiMe₃)₃ (**1c**)^[4] as well as [Ga₂₂R₁₀]^{2−} (**2**) with R = N(SiMe₃)₂,^[5] the coordination numbers of the central Ga atoms are 13 for **1** and 11 for **2**. In contrast, in the case of the only previously obtained Ga₂₂ cluster with an icosahedral Ga₂₂ core (without a central Ga atom), [Ga₂₂[N(SiMe₃)₂]₁₀Br₁₀]^{2−} (**3**),^[6] the average oxidation number of 0.82 is not very different from that of the GaX starting material. This is also true for the first polyhedral gallium subhalide [Ga₂₄X₂₂] (**4**)^[7] (average oxidation number 0.92), which can be viewed as a common precursor (possibly in a slightly modified form, such as [Ga₂₂X₂₀], which is analogous to the well-known [Al₂₂X₂₀]^[8]) for the numerous

[*] Dr. J. Steiner, Dr. G. Stößer, Prof. Dr. H. Schnöckel
Institut für Anorganische Chemie
Universität Karlsruhe (TH)
Engesserstrasse 15, Gebäude 30.45, 76128 Karlsruhe (Germany)
Fax: (+49) 721-608-4854
E-mail: Hansgeorg.Schnoeckel@chemie.uni-karlsruhe.de

[**] This work was supported by the Deutsche Forschungsgemeinschaft and the Fonds der Chemischen Industrie.

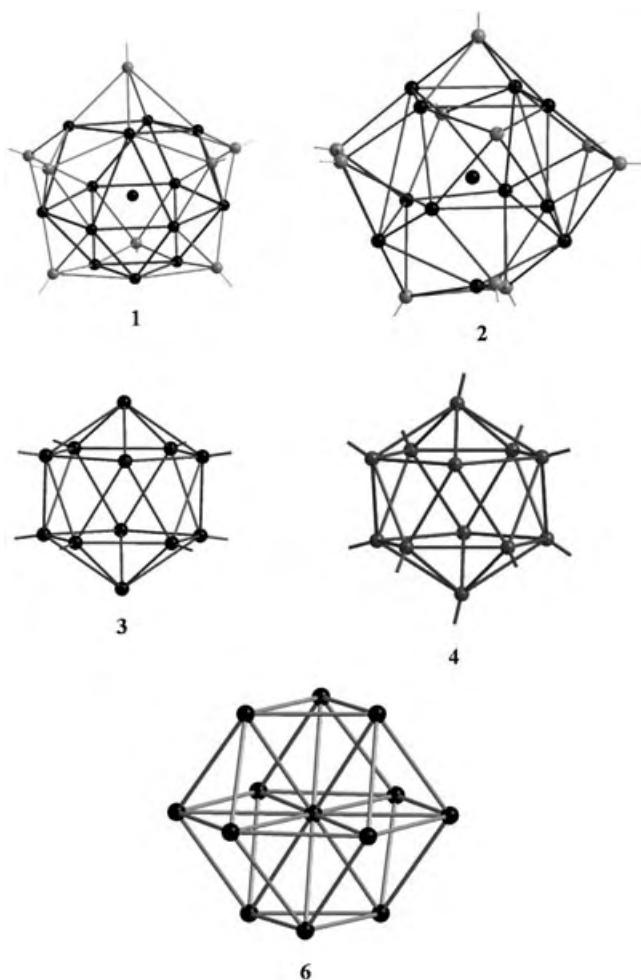


Figure 1. Ball-and-stick representations of the different arrangements of the inner (black) 12, 13, or 14 gallium atoms in the metalloid clusters **1** (1 + 13), **2** (1 + 11), **3** (12), **4** (12), and **6** (1 + 12). The information given in parentheses indicates that, for example, the central Ga atom in **6** is surrounded by 12 Ga atoms in the first coordination sphere.

Ga_{22} clusters (Figure 1). With the PtBu_2 ligand used here, as in previous cases such as the metalloid clusters $[\text{Ga}_{16}(\text{PtBu}_2)_{10}]$ (**5**)^[9] and $[\text{Ga}_{51}(\text{PtBu}_2)_{14}\text{Br}_6]^{3-}$ (**6**),^[10] we find that the cluster core is linked to the outer shell by additional bonds to bridging P atoms, which facilitates the isolation of unusual Ga_n frameworks. Such clusters have fewer ligands for a given number of metal atoms than clusters with purely terminally coordinated ligands. Therefore, it is possible to achieve a lower oxidation state for the gallium framework.

After slowly heating a metastable solution of GaCl , synthesized by the co-condensation of GaCl with a toluene/diethyl ether (4:1) mixture, from -78°C to -65°C and then to -50°C to induce disproportionation to Ga_n clusters, the metathesis reaction is spontaneous, if at these temperatures, initially only $1/3$ and then $2/3$ of the amount of LiPtBu_2 required for full substitution is added as a toluene suspension. Removal of the volatile components under vacuum and washing with pentane yields a dark extract from which large black crystals of $[\text{Ga}_{22}(\text{PtBu}_2)_{12}]$ (**7**) can be obtained reproducibly within a few days at $+60^\circ\text{C}$. The crystal structure

analysis^[11] of **7** reveals the neutral $[\text{Ga}_{22}(\text{PtBu}_2)_{12}]$ cluster depicted in Figure 2. The arrangement of the cluster molecules within the crystal corresponds to that of a distorted primitive hexagonal structure with the coordination numbers

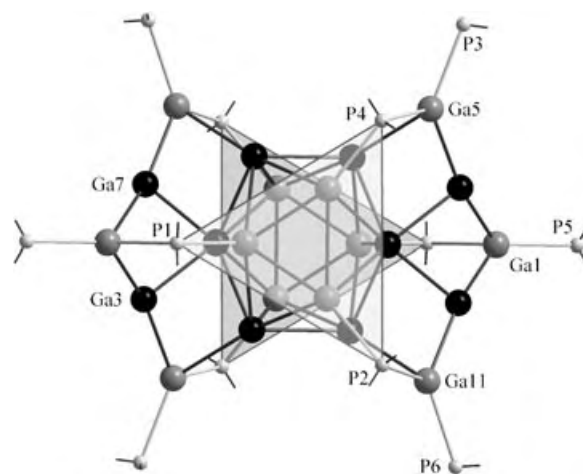


Figure 2. Ball-and-stick representation of the Ga_{22} cluster **7**; for clarity, only the bonds from the central phosphorus atom to the α -carbon atom of the $t\text{Bu}$ groups are shown, the bare Ga atoms are shown in black. The octahedrally arranged P atoms of the bridging phosphanides are drawn as polyhedra (with a view of the parallel triangular faces of the icosahedron and octahedron).

[4 + 4 + 8]. The distances between the centers of the clusters are 15.41, 17.62, and 23.62 \AA , respectively, for the above-mentioned coordination numbers. The central icosahedral Ga_{12} framework is bound through bridging P atoms to three Ga atoms in each of two neighboring Ga_5 units (see below). These six bridging P atoms enclose the Ga_{12} icosahedron in an octahedron (Figure 2). The six remaining Ga atoms of the icosahedron, which are arranged in a chair conformation, are bound directly to other Ga atoms, which surround the icosahedron in the form of two chainlike fragments. Each of the Ga_5 chains contains two naked Ga atoms and three Ga atoms that are each bound to two PtBu_2 groups—one bridging (to the light-colored Ga atoms of the central icosahedron in Figure 2) and one terminal. The ten naked Ga atoms are depicted in black in Figure 2.

The distinctive feature of the $[\text{Ga}_{22}(\text{PtBu}_2)_{12}]$ cluster (**7**) is that the GaR units surrounding the icosahedral core are bound very tightly to it by the additional bridges. Therefore, they cannot be removed as GaR units like other nonbridging ligands (such as $\text{C}(\text{SiMe}_3)_3$, $\text{Si}(\text{SiMe}_3)_3$, and $\text{N}(\text{SiMe}_3)_2$) under comparable reaction conditions;^[12] this prevents further cluster growth (in contrast to the formation of the Ga_{84} cluster, for example). The strong bonds between the PtBu_2 ligands and the cluster core on the one hand, and their high reactivity as phosphanide anions on the other, make it possible to take snapshots of the cluster's growth.^[13]

Through the stabilization provided by the bridging phosphanide ligands in **7**, an icosahedral Ga_{12} unit has been obtained for the first time whose average oxidation number is strongly shifted toward that of metallic gallium. Figure 3 (left) shows that the arrangement of the 22 Ga atoms of **7** is strongly

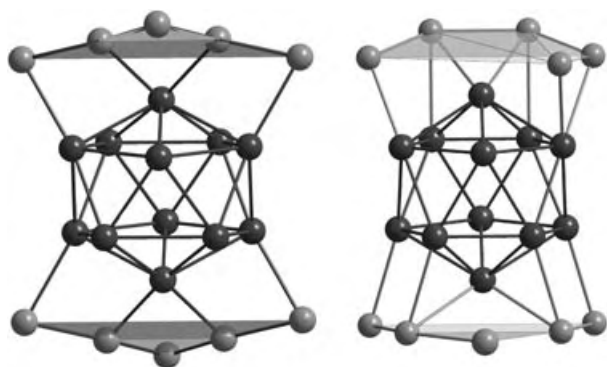


Figure 3. Comparison of the gallium substructure in the Ga_{22} cluster (**7**, left) with the corresponding section of the δ -modification of gallium (right).

reminiscent of that of the atoms in δ -gallium^[15] (Figure 3, right). The average Ga–Ga distances in the icosahedral substructure of **7** (2.68 Å) are shorter than those in δ -gallium (2.82 Å); this is not unexpected, in respect of the higher coordination number in δ -gallium. In addition, the increase in oxidation number from 0 in δ -gallium to 0.55 in **7** leads to a decrease in the Ga–Ga distances. This influence of the oxidation number on the volume of the icosahedral Ga_{12} cluster could also be confirmed by single-point calculations^[16] for **7** and **3**: **3** (oxidation number +0.82) 377 Å³ and **7** (oxidation number +0.59) 395 Å³. As expected, analogous calculations reveal the volume of the Ga_{12} icosahedron in δ -gallium to be considerably larger, 431 Å³.

Unfortunately, each of the Ga_{22} clusters obtained to date represents only one of many snapshots on the way from the Ga^{I} species to gallium metal. However, these snapshots demonstrate that this fundamental process of metal formation^[17] through disproportionation of metastable solutions is influenced in complex ways by many parameters (e.g. temperature, the type of ligand, the type of donor, and the donor concentration). Similar complexity is certainly expected for the formation of other metals as well. However, since elemental gallium has seven modifications, which are possibly only attained by different reaction paths, the clarification of the formation mechanisms may be exceptionally difficult in this case. Of particular interest here is the question under which conditions the formation of an icosahedral structure as in **3**, **4**, and **7** versus a centered cubic octahedral structure as in **1**, **6**, and $[\text{Ga}_{19}\text{R}_6]^-$ ($\text{R} = \text{C}(\text{SiMe}_3)_3$)^[19] (**8**) is favored. Many experimental and quantum-chemical investigations will be necessary to find an answer to this question. Here, we have initially investigated the volume requirements of the gallium atoms in several Ga_{12} and Ga_{13} units. As a result of such single-point calculations of volume requirements, we have found an approximately linear relationship between atom volume and the corresponding average oxidation state within both the icosahedral Ga_{12} units and the central Ga_{13} units (Table 1).

These calculations, based on the experimentally determined structures of the Ga_{12} and Ga_{13} units, demonstrate that the average atomic volumes of the core gallium atoms differ significantly, depending on the coordination polyhedron.

Table 1: Calculated atomic volumes in icosahedral and body-centered centers of metalloid gallium clusters and element modifications.

	Ox. ^[a]	Vol. [Å ³]/ Σ (Atoms)	Vol. [Å ³]/Atom
δ -gallium	0	431 (12)	35.92
7	0.55	395 (12)	32.92
3	0.82	377 (12)	31.41
4	0.92	379 (12)	31.58
fcc $\text{Ga}^{\text{IV}[b]}$	0	501 (13)	38.54
fcc $\text{Ga}^{\text{IV}[c]}$	0	397 (13)	30.54
8	0.26	462 (13)	35.54
6	0.33	455 (13)	35.00
1b	0.36	484 (13 + 1)	34.57

[a] Average oxidation state. [b] Volume of the Ga_{13} core extrapolated to standard pressure. [c] Volume of the Ga_{13} core calculated from the lattice constant at 68 GPa.

Whereas an icosahedral arrangement of the Ga_{12} core led to an atomic volume between 35.92 and 31.41 Å³, for cubic octahedral coordination patterns this rose to values ranging from 38.54 to 34.57 Å³. Within both groups, the atoms of the formally zero-valent element modification (fcc- or δ -gallium) assume the maximum volume; as expected, this decreases as the oxidation state of the molecule increases. It is thus the goal of continuing investigations to synthesize molecules whose average oxidation states lie in the range between 0.4 and 0.5. By using identical ligands, slight variations of the reaction conditions could make it possible to obtain both structures (icosahedron or cubic octahedron) with the same ligand shell. This would allow us to determine the influence of the average oxidation state on the arrangements of the cluster cores during formation of the element.

These investigations, which bring the number of different arrangements for 22 Ga atoms in metalloid clusters to four, illustrate the complexity involved in the formation of a bulk metallic phase from precursor salts. The isolation of individual metalloid clusters as intermediates of this process and the determination of their structures is currently the only direct approach to the solution of this fundamental problem. In principle, in situ NMR investigations should be ideal for answering these questions, but for a variety of reasons they often do not achieve this goal: low solubility of the cluster compounds, large half-widths of the gallium signals, and the large number of different gallium atoms in the clusters, which according to calculations result in different NMR chemical shifts (these are mixed-valent compounds, for example, the Ga_{84} cluster^[20] contains 42 different Ga atoms; quantum-chemical calculations indicate that these should also have different chemical shifts^[21]). Understanding the interactions of the metalloid clusters within the crystal is even more difficult to achieve than knowledge of their structures and mechanisms of formation—as in the case of the unsuccessful interpretation of the electrical conductivity and superconductivity of the Ga_{84} cluster compound.^[22,23]

Experimental Section

LiPrBu_2 (1.38 g, 9 mmol) was suspended in toluene (30 mL) at room temperature. In a flask cooled to -78°C , a 0.32 M $\text{Ga}^{\text{I}}\text{Cl}$ solution (20 mL; 6.4 mmol) in toluene/ Et_2O (4:1) was slowly warmed to

–65 °C and the LiPrBu₂/toluene suspension (10 mL) was added by pipette. The reaction solution was maintained at –50 °C for 2 h before the remaining ligand suspension (20 mL) was added. The mixture was then warmed to room temperature over 12 h. This resulted in a deep black solution with no residue. The solvent was removed under vacuum and the resulting residue was extracted with pentane.

The deep black pentane extract was filtered to remove the LiCl precipitate and then transferred to a Schlenk flask and heated to 60 °C for 2 h. The mixture was allowed to slowly cool to room temperature, and the Ga₂₂ cluster crystallized within a few days as black rhombuses, which could then not be redissolved (yield: 210 mg, 0.064 mmol). It was thus impossible to carry out any NMR spectroscopic or ESI mass spectrometric investigations. Mass spectrometric investigations with the MALDI technique led to unspecific fragmentations.

Received: May 25, 2004

Keywords: cluster compounds · gallium · main group elements · metalloids · structure determination

- [1] A. Schnepf, H. Schnöckel, *Angew. Chem.* **2002**, *114*, 3682; *Angew. Chem. Int. Ed.* **2002**, *41*, 3533.
- [2] A. Donchev, A. Schnepf, G. Stöber, E. Baum, H. Schnöckel, T. Blank, N. Wiberg, *Chem. Eur. J.* **2001**, *7*, 3348.
- [3] A. Schnepf, E. Weckert, G. Linti, H. Schnöckel, *Angew. Chem.* **1999**, *111*, 3578; *Angew. Chem. Int. Ed.* **1999**, *38*, 3381.
- [4] G. Linti, A. Rodig, *Chem. Commun.* **2000**, 127.
- [5] A. Schnepf, G. Stöber, H. Schnöckel, *Angew. Chem.* **2002**, *114*, 1959; *Angew. Chem. Int. Ed.* **2002**, *41*, 1882.
- [6] A. Schnepf, R. Köppe, E. Weckert, H. Schnöckel, *Chem. Eur. J.* **2004**, *10*, 1977.
- [7] T. Duan, E. Baum, R. Burgert, H. Schnöckel, *Angew. Chem.* **2004**, *116*, 3252; *Angew. Chem. Int. Ed.* **2004**, *43*, 3190.
- [8] C. Klemp, R. Köppe, E. Weckert, H. Schnöckel, *Angew. Chem.* **1999**, *111*, 1851; *Angew. Chem. Int. Ed.* **1999**, *38*, 1740.
- [9] J. Steiner, G. Stöber, H. Schnöckel, *Angew. Chem.* **2003**, *115*, 2016; *Angew. Chem. Int. Ed. Engl.* **2003**, *42*, 1971.
- [10] J. Steiner, G. Stoesser, H. Schnöckel, *Angew. Chem.* **2004**, *116*, 305; *Angew. Chem. Int. Ed.* **2004**, *43*, 2302.
- [11] Crystal structure data for **7**: *M_r* = 3564.75. Crystal dimensions: 0.2 × 0.3 × 0.2 mm, monoclinic, space group *P*2(1)/*c*, *a* = 17.620(4), *b* = 25.226(5), *c* = 17.619(4) Å, β = 96.89(3)°, *V* = 7775.0(3) Å³, *Z* = 2, ρ_{calcd} = 1.523 g cm^{–3}, μ = 3.90 mm^{–1}, θ_{max} = 19.78°, 24091 measured reflections, 7029 independent reflections (*R*_{int} = 0.0476), absorption correction numeric (min./max. transmission: 0.3758/0.6445), *R*₁ = 0.037, *wR*₂ = 0.0818, GOOF = 1.014, Stoe IPDS-diffractometer (MoK_α radiation, (λ = 0.71073 Å, 180 K). The structure was solved by direct methods and refined against *F*² for all observed reflections. Programs used: Shelxs and Shelxl (G. M. Sheldrick, Universität Göttingen). CCDC-238624 contains the supplementary crystallographic data for this paper. These data can be obtained free of charge at www.ccdc.cam.ac.uk/conts/retrieving.html (or from the Cambridge Crystallographic Data Centre, 12 Union Road, Cambridge CB21EZ; Fax: (+44)1223-336-033; or deposit@ccdc.cam.ac.uk).
- [12] K. Weiß, R. Köppe, H. Schnöckel, *Int. J. Mass Spectrom.* **2002**, *214*, 383.
- [13] In a virtual experiment, it is possible to imagine the formation of **7** by the following route: Separation of Ga₂X₄ units from a subhalide such as the recently described [Ga₂₄X₂₂] cluster (**4**)^[7] could lead to the formation of a hypothetical [Ga₂₂X₁₈]^[14] cluster, in which twelve halogen atoms are spontaneously replaced by PrBu₂ fragments. Through bridging, six halogen ligands could be removed from the [Ga₂₂X₆R₁₂] cluster formed in this manner and the [Ga₂₂R₁₂]⁶⁺ ion could be simultaneously reduced to the neutral [Ga₂₂R₁₂] cluster (**7**) in the strongly reducing environment.
- [14] The hypothetical [Ga₂₂X₁₈] cluster would have a structure analogous to that of the [Al₂₂X₂₀] cluster,^[8] in which two terminal GaX₂ groups would be replaced by GaX groups.
- [15] L. Bosio, H. Curien, M. Dupont, A. Rimsky, *Acta Crystallogr. Sect. B* **1973**, *29*, 367.
- [16] The molecular volumes were calculated with the Gaussian98 program package at the SCF level with a 3-21G* basis set. For this we carried out single-point calculations based on the experimentally determined geometries of the cluster compounds (**1b**, **3**, **4**, **6**, **7**, **8**), as well as δ-gallium and Ga^{IV}; in these calculations, the ICPM solvation model was used to place a shell of uniform electron density (4 × 10^{–3} e Å^{–3}) around the Ga_n unit. Clusters **5** and **6** have previously been discussed in an analogous fashion.^[9,10] a) IPCM: J. B. Foresman, T. A. Keith, K. B. Wiberg, J. Snoonian, M. J. Frisch, *J. Phys. Chem.* **1996**, *100*, 16098; b) Gaussian 98 (Revision A.7), M. J. Frisch, G. W. Trucks, H. B. Schlegel, G. E. Scuseria, M. A. Robb, J. R. Cheeseman, V. G. Zakrzewski, J. A. Montgomery, R. E. Stratmann, J. C. Burant, S. Dapprich, J. M. Millam, A. D. Daniels, K. N. Kudin, M. C. Strain, O. Farkas, J. Tomasi, V. Barone, M. Cossi, R. Cammi, B. Mennucci, C. Pomelli, C. Adamo, S. Clifford, J. Ochterski, G. A. Petersson, P. Y. Ayala, Q. Cui, K. Morokuma, D. K. Malick, A. D. Rabuck, K. Raghavachari, J. B. Foresman, J. Cioslowski, J. V. Ortiz, B. B. Stefanov, G. Liu, A. Liashenko, P. Piskorz, I. Komaromi, R. Gomperts, R. L. Martin, D. J. Fox, T. Keith, M. A. Al-Laham, C. Y. Peng, A. Nanayakkara, C. Gonzalez, M. Challacombe, P. M. W. Gill, B. G. Johnson, W. Chen, M. W. Wong, J. L. Andres, M. Head-Gordon, E. S. Replogle, J. A. Pople, Gaussian, Inc., Pittsburgh, PA, **2001**.
- [17] This process is also expected to be highly complex because different equilibrium conditions apply for nanoscale gallium particles (such as for β- and γ-gallium) than in the bulk solid phase.^[18]
- [18] S. Pochon, K. F. MacDonald, R. J. Knize, N. I. Zheludev, *Phys. Rev. Lett.* **2004**, *92*, 145702.
- [19] A. Schnepf, G. Stöber, H. Schnöckel, *J. Am. Chem. Soc.* **2000**, *122*, 9178.
- [20] A. Schnepf, H. Schnöckel, *Angew. Chem.* **2001**, *113*, 733; *Angew. Chem. Int. Ed.* **2001**, *40*, 712.
- [21] J. Hartig, H. Schnöckel, unpublished results.
- [22] O. N. Bakharev, N. Zelders, H. B. Brom, A. Schnepf, H. Schnöckel, L. J. de Jongh, *Eur. Phys. J. D* **2003**, *6*, 101.
- [23] J. Hagel, M. T. Kelemen, G. Fischer, B. Pilawa, J. Wosnitza, E. Dormann, H. v. Löhneysen, L. Jos de Jongh, A. Schnepf, H. Schnöckel, U. Neisel, J. Beck, *J. Low Temp. Phys.* **2002**, *129*, 133.

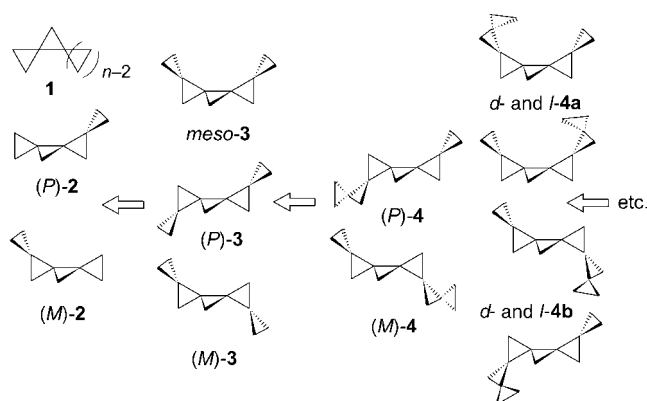
Spirocycles

A Convergent Route to Enantiomerically Pure Higher $[n-2]$ Triangulanedimethanol Derivatives and $[n]$ Triangulanes ($n \geq 7$)**

Armin de Meijere,* Alexander F. Khlebnikov, Sergei I. Kozhushkov, Kazutoshi Miyazawa, Daniel Frank, Peter R. Schreiner, B. Christopher Rinderspacher, Dmitrii S. Yufit, and Judith A. K. Howard

Dedicated to Professor Lawrence T. Scott on the occasion of his 60th birthday

$[n]$ Triangulanes **1**,^[1] that is, hydrocarbons that consist of spiroannulated (and thereby mutually orthogonal) cyclopropane rings only, with $n = 4$ (**2**) and $n = 5$ (**3**) were recently prepared in enantiomerically pure form.^[2,3] The extraordinarily high specific rotations of these hydrocarbons (P)-**2**, **3** and (M)-**2**, **3**, which do not bear any chromophore that absorbs above 200 nm, must be attributed to their unique helical σ -bond framework.^[4] In the same way as it was proved for the higher π - $[n]$ helicenes with $n \geq 8$,^[5] the higher ($n \geq 6$) σ - $[n]$ helicenes, as these $[n]$ triangulanes with $n \geq 4$ may be termed,^[6] must be expected to exhibit ever larger specific rotations, at least for a



significant series of derivatives with an increasing number of spiroannulated three-membered carbocycles.

To test this prediction, we set out to prepare higher analogues of **2** and **3** in enantiomerically pure form. In view of the rapidly growing number of possible stereoisomers of these $[n]$ triangulanes with increasing n (e.g., the family of $[9]$ triangulanes consists of four *meso* diastereomers and 16 pairs of enantiomers),^[7] a linear strategy to approach any enantiomerically pure continuously helical $[n]$ triangulane with $n \geq 4$ would not be feasible (there is only one enantiomeric pair of σ - $[6]$ helicenes and two additional pairs of enantiomeric $[6]$ triangulanes).^[7] We therefore conceived a reasonably general convergent strategy, and report herein our first results on its successful application in the synthesis of enantiomerically pure σ - $[9]$ helicenes.

Enantiomerically pure [(1*R*,3*S*)-4-methylenespiropentyl]-methanol [(1*R*,3*S*)-**5**] and the corresponding enantiomeric acetate (1*S*,3*R*)-**6**, which are easily accessible in more than 100-g quantities by enantioselective enzymatic acylation of the racemic alcohol *rac*-**5** with lipase PS,^[3,8] were chosen as appropriate starting materials. The addition of dibromocarbene to the double bond in the THP-protected alcohol (1*R*,3*S*)-**7** or the acetate (1*S*,3*R*)-**6**,^[8] adopting a well-established protocol,^[9] was followed by deprotection and chromatographic separation to furnish 5,5-dibromodispiro[2.0.2.1]-methanols (1*R*,3*S*,4*S*)-, (1*R*,3*S*,4*R*)-, (1*S*,3*R*,4*S*)-, and (1*S*,3*R*,4*R*)-**8** in 27, 25, 32 and 28% yield, respectively (Scheme 1).

The absolute configuration of all four diastereomers was assigned on the basis of the X-ray crystal-structure analysis^[10] of an arbitrarily selected dibromocyclopropane derivative of type **8**, prepared from (1*R*,3*S*)-**7**, the known absolute configuration of the starting materials,^[8] and comparison of the NMR spectra. THP ethers (1*R*,3*S*,4*S*)-**9** and (1*S*,3*R*,4*R*)-**9** were prepared from the corresponding alcohols with an *anti*-arrangement of their hydroxymethyl and dibromomethylene groups. An improved version of the protocol of Neuen-schwander et al.^[11] was used for the reductive dimerization of (1*R*,3*S*,4*S*)-**9** and (1*S*,3*R*,4*R*)-**9** to yield mixtures of the diastereomeric bicyclopropylidene derivatives^[12] (*E*)-**10** and (*Z*)-**10** after cleavage of the resulting THP ethers (Scheme 1). The dimerization probably proceeds via a copper carbenoid generated by treatment of the dibromocyclopropanes **9** with *n*-butyllithium in the presence of copper(II) chloride. After

[*] Prof. Dr. A. de Meijere, Dr. S. I. Kozhushkov, D. Frank
Institut für Organische und Biomolekulare Chemie
Georg-August-Universität Göttingen
Tammannstrasse 2, 37077 Göttingen (Germany)
Fax: (+49) 551-39-9475
E-mail: armin.demeijere@chemie.uni-goettingen.de

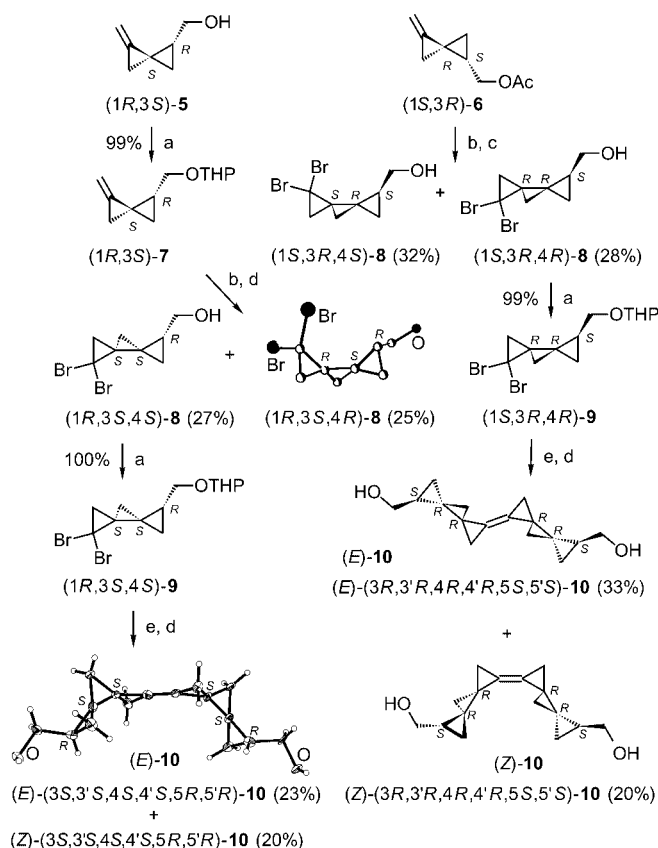
Prof. Dr. A. F. Khlebnikov
Department of Chemistry
St. Petersburg State University
Universitetskii Prospekt 26
Petrodvorets 198 504, St. Petersburg (Russia)

Dr. K. Miyazawa
Chisso Petrochemical Corporation
Specialty Chemicals Research Center
5-1 Goikaigan, Ichihara, Chiba 290-8551 (Japan)

Prof. Dr. P. R. Schreiner, Dipl. Chem. B. C. Rinderspacher
Institut für Organische Chemie
Justus-Liebig-Universität Giessen
Heinrich-Buff-Ring 58, 35392 Giessen (Germany)

Dr. D. S. Yufit, Prof. Dr. J. A. K. Howard
Department of Chemistry
University of Durham
Durham, South Rd., DH1 3LE (UK)

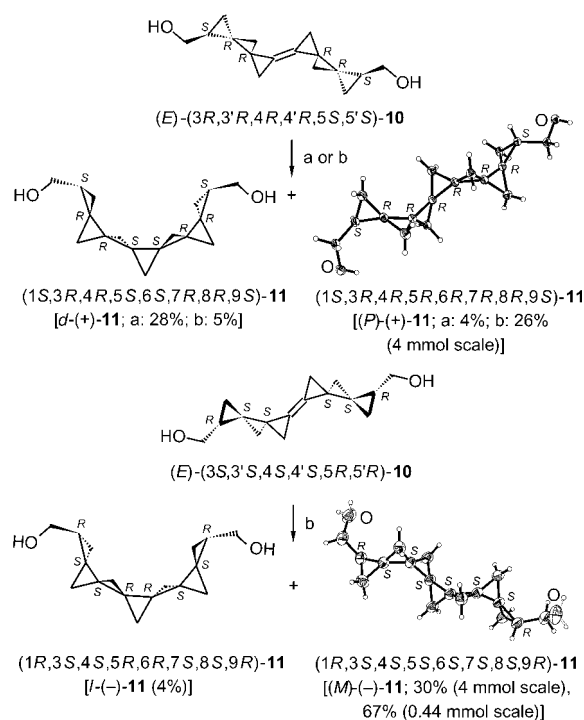
[**] This work was supported by the State of Niedersachsen, the Fonds der Chemischen Industrie, and the EPSRC (UK). The authors are grateful to the companies Chemetall GmbH and Chisso Petrochemical Corporation (K.M.) for generous gifts of chemicals. The authors are indebted to Dipl.-Chem. Heiko Schill, Universität Göttingen, for assembling the colored picture of the $[7]$ triangulanedimethanol, to Dipl.-Chem. Denis Vidović, Universität Göttingen, for the X-ray crystal-structure analysis of compound (1*R*,3*S*,4*R*)-**8**, to Evelin Pfeil, Universität Göttingen, for measuring optical rotations, and to Dr. Burkhard Knieriem, Universität Göttingen, for his careful reading of the final manuscript.



chromatographic separation from the corresponding *Z* isomers, diols (*E*)-(3*R*,3'*R*,4*R*,4'*R*,5*S*,5'*S*)-**10** and (*E*)-(3*S*,3'*S*,4*S*,4'*S*,5*R*,5'*R*)-**10** were obtained in 33 and 23 % yield, respectively. These products have the appropriate configurations required for the targeted, continuously helical [9]triangulanes. The assigned *E* configuration of (3*S*,3'*S*,4*S*,4'*S*,5*R*,5'*R*)-**10** was confirmed by X-ray crystal-structure analysis.^[10]

Among several attempted cyclopropanations of the diols (*E*)-(3*S*,3'*S*,4*S*,4'*S*,5*R*,5'*R*)-**10** and (*E*)-(3*R*,3'*R*,4*R*,4'*R*,5*S*,5'*S*)-**10** (e.g. with CH₂N₂/Pd(OAc)₂^[13] or with CH₂I₂/AlMe₃^[14]), only the modified Simmons–Smith-type cyclopropanation^[15] according to Shi et al. (with CH₂I₂/ZnEt₂/TFA)^[16] applied to (*E*)-(3*R*,3'*R*,4*R*,4'*R*,5*S*,5'*S*)-**10** gave a [7]triangulanedimethanol in moderate yield (28 %), which, disappointingly, turned out to have the incorrect configuration (1*S*,3*R*,4*R*,5*S*,6*S*,7*R*,8-*R*,9*S*)-**11** [*d*-(+)-**11**] with a horseshoe shape (Scheme 2). Apparently, the cyclopropanation of (*E*)-**10** under these conditions occurs on the sterically less-congested face of the bicyclopopylidene moiety.

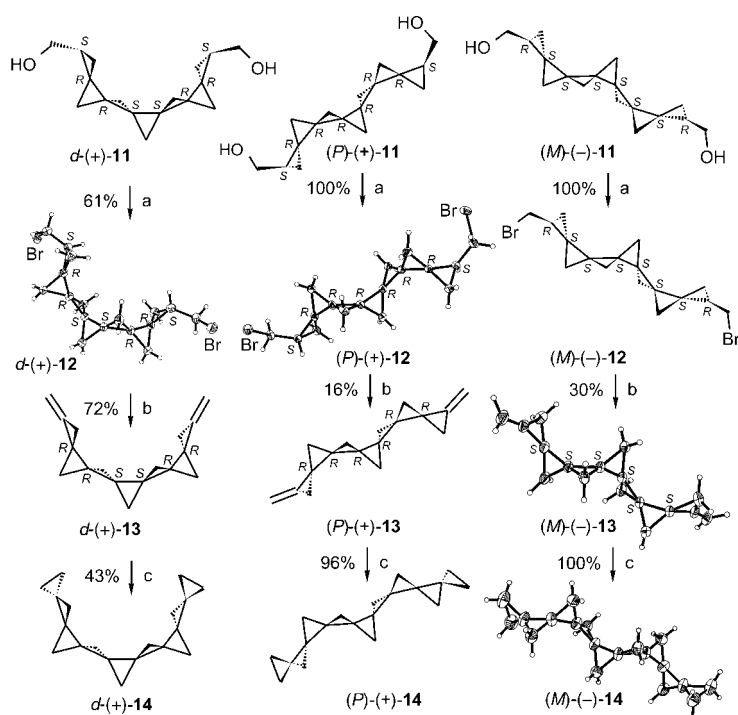
Fortunately, though, the old and nowadays rarely applied Gaspar–Roth cyclopropanation protocol (with CH₂N₂/



CuCl)^[17] gave the target (1*S*,3*R*,4*R*,5*R*,6*R*,7*R*,8*R*,9*S*)-**11** [(*P*)-(+)-**11**] and (1*R*,3*S*,4*S*,5*S*,6*S*,7*S*,8*S*,9*R*)-**11** [(*M*)-(-)-**11**] in 26 and 30 % yield, respectively, on a 4-mmol scale.^[18] However, a large excess of diazomethane and cuprous chloride was required. The absolute configurations of (*P*)-(+)-**11** and (*M*)-(-)-**11** were assigned on the basis of their relative configurations as disclosed by X-ray crystal-structure analyses.^[10]

The enantiomerically pure diols *d*-(+)-**11**, (*P*)-(+)-**11**, and (*M*)-(-)-**11** were transformed into the enantiomerically pure [9]triangulanes *d*-(+)-**14**, (*P*)-(+)-**14**, and (*M*)-(-)-**14**, respectively, in three routine steps for the preparation of triangulanes (Scheme 3).^[3] First, the diols were converted into the bis(bromomethyl)[7]triangulanes **12** by treatment with PPh₃·Br₂. Subsequent dehydrobromination of **12** with potassium *tert*-butoxide gave 1,9-dimethylene[7]triangulanes **13**, and cyclopropanation of the latter with diazomethane under Pd(OAc)₂ catalysis^[13] furnished the corresponding enantiomerically pure *d*-[*d*-(+)-**14**], (*M*)-[(*M*)-(-)-**14**], and (*P*)-[9]triangulanes [(*P*)-(+)-**14**] in 19, 15, and 30 % overall yield, respectively, (≥ 99 % *ee*) after chromatographic separation in the last step.^[19]

As expected, both (*P*)- and (*M*)-**14** exhibit remarkably high specific rotations even at 589 nm: [α]_D²⁰ = +909.9 (*c* = 0.96 in CHCl₃) and –890.5 (*c* = 1.01 in CHCl₃), respectively. The specific rotations increase drastically on going to shorter wavelengths: [α]₄₃₆²⁰ = +1907.0, [α]₃₆₅²⁰ = +3119.4 ((*P*)-(+)-**14**) and [α]₄₃₆²⁰ = –1866.2, [α]₃₆₅²⁰ = –3051.1 ((*M*)-(-)-**14**), indicating that these compounds must exhibit Cotton effects with large amplitudes in the optical rotatory dispersion (ORD)



Scheme 3. Preparation of enantiomerically pure [9]triangulanes *d*-(+)-**14**, (*M*)-(-)-**14**, and (*P*)-(+)-**14**. a) $\text{Ph}_3\text{P}\cdot\text{Br}_2$, py, CH_2Cl_2 , $-30\rightarrow 20^\circ\text{C}$, 5 h; b) *t*BuOK, DMSO, 55°C , 20 min; c) CH_2N_2 , $\text{Pd}(\text{OAc})_2$, Et_2O , -5°C . DMSO = dimethyl sulfoxide.

curve below 200 nm. DFT calculations at the B3LYP/6-31+G(d,p) level^[20–24] for the geometry optimization and time-dependent DFT calculations for determining optical rotations with a triple- ζ basis set (B3LYP/TZVP)^[25] for (*P*)-(+)-**14** in the gas phase gave specific rotations of $[\alpha]_{\text{D}}^{20} = 1006.5$, $[\alpha]_{436}^{20} = 2010.7$, and $[\alpha]_{365}^{20} = 3145.5$. These are in excellent agreement with the experimental values over the whole range of wavelengths and thus confirm the strong positive Cotton effect in the ORD curve, which is consistent with a large ellipticity in the CD below 200 nm. In contrast, the enantiomerically pure, but not continuously helical, horseshoe-shaped *d*-(+)-**14** has specific rotations of $[\alpha]_{\text{D}}^{20} = +244.9$ ($c = 1.13$ in CHCl_3), $[\alpha]_{436}^{20} = +511.2$, and $[\alpha]_{365}^{20} = +832.0$ only. A comparison of the values of $[\alpha]_{\text{D}}^{20}$ for the now known enantiomerically pure σ -[*n*]helicenes (*P*)-(+)-**14** (+909.9), (*P*)-(+)-**3** (+373.0), and (*M*)-(-)-**2** (–192.7)^[2,3] indicates a drastic increase in the specific rotation with an increasing number of three-membered rings (see reference [4]). This increase is neither proportional to the relative molecular masses nor to the number of cyclopropane rings.

Another extraordinary feature was observed for the crystal packing of (*M*)-(-)-**11**. In the crystals obtained from a solution in *n*-hexane containing some diethyl ether, the molecules are assembled as supramolecular helices through hydrogen bonds between the terminal hydroxy groups. Two such helices form a supramolecular double helix (Figure 1). A closer look disclosed that Et_2O molecules are incorporated in the grooves between two double helices. In spite of being severely disordered in the structure, these solvent molecules

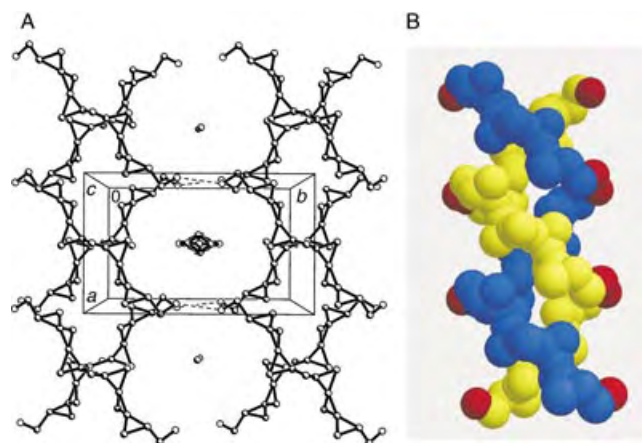


Figure 1. Section from the crystal packing of (*M*)-(-)-**11** (crystals from Et_2O /hexane) with supramolecular double-helical arrangement of hydrogen-bridged molecules as ball-and stick (A) and space-filling models (B). Yellow, blue: cyclopropane spirals; red: hydroxy groups.

apparently play an important role in gluing the double helices together; upon exposing the crystals to air, they rapidly disintegrate into powder, most probably because the Et_2O evaporates from the channels. The hydroxymethyl end groups in (*P*)- and (*M*)-**11** apparently are also essential for the supramolecular double-helix formation, as the hydrocarbons (*M*)-**13** and (*M*)-**14** do not form such a packing in their crystals.

Single, double, and even triple helical structures do play very important roles in biology and in polymer chemistry. However for relatively small nonbiological objects, this is not a common phenomenon^[26] in that they rarely form single helices,^[27] even less frequently double and triple helices.^[28]

Received: July 2, 2004

Keywords: ab initio calculations · chirality · helical structures · spirocycles · triangulanes

- [1] For reviews, see: a) A. de Meijere, S. I. Kozhushkov, *Chem. Rev.* **2000**, *100*, 93–142; b) A. de Meijere, S. I. Kozhushkov in *Advances in Strain in Organic Chemistry*, Vol. 4 (Ed.: B. Halton), JAI, London, **1995**, pp. 225–282; c) N. S. Zefirov, T. S. Kuznetsova, A. N. Zefirov, *Izv. Akad. Nauk* **1995**, 1613–1621; *Russ. Chem. Bull. (Engl. Transl.)* **1995**, 1613–1621.
- [2] A. de Meijere, A. F. Khlebnikov, R. R. Kostikov, S. I. Kozhushkov, P. R. Schreiner, A. Wittkopp, D. S. Yufit, *Angew. Chem.* **1999**, *111*, 3682–3685; *Angew. Chem. Int. Ed.* **1999**, *38*, 3474–3477.
- [3] A. de Meijere, A. F. Khlebnikov, S. I. Kozhushkov, R. R. Kostikov, P. R. Schreiner, A. Wittkopp, C. Rinderspacher, D. S. Yufit, J. A. K. Howard, *Chem. Eur. J.* **2002**, *8*, 828–842.
- [4] The recently reported helical hydrocarbons consisting of spiroannulated four-membered rings, which are conformationally flexible, not only disclosed significantly smaller specific rotations, but their specific rotations also decrease with an increasing number of spirocyclobutanes in the helix: a) L. Fitjer, R. Gerke, J. Weiser, G. Bunkoczi, J. E. Debreczeni, *Tetrahedron* **2003**, *59*,

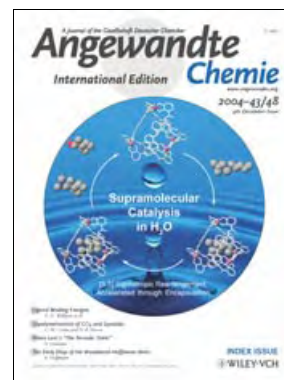
- 4443–4449; b) L. Fitjer, A. Kanschik, R. Gerke, *Tetrahedron* **2004**, *60*, 1205–1213.
- [5] a) R. H. Martin, V. Libert, *J. Chem. Res. Miniprint* **1980**, *4*, 1940–1950; b) R. H. Martin, M. J. Marchant, *Tetrahedron* **1974**, *30*, 343–345; c) R. H. Martin, M. J. Marchant, *Tetrahedron Lett.* **1972**, *13*, 3707.
- [6] See footnotes [4,5] in reference [3].
- [7] The stereochemical features of unbranched $[n]$ triangulanes **1** have been thoroughly analyzed: N. S. Zefirov, S. I. Kozhushkov, T. S. Kuznetsova, O. V. Kokoreva, K. A. Lukin, B. I. Ugrak, S. S. Tratch, *J. Am. Chem. Soc.* **1990**, *112*, 7702–7707.
- [8] a) K. Miyazawa, D. S. Yufit, J. A. K. Howard, A. de Meijere, *Eur. J. Org. Chem.* **2000**, 4109–4117; b) K. Miyazawa, Dissertation, Universität Göttingen, **1999**.
- [9] a) K. A. Lukin, N. S. Zefirov, *Zh. Org. Khim.* **1987**, *23*, 2548–2552; *J. Org. Chem. USSR (Engl. Transl.)* **1987**, *23*, 2249–2252; b) K. A. Lukin, A. A. Andrievskii, A. Yu. Masunova, N. S. Zefirov, *Dokl. Akad. Nauk SSSR Ser. Khim.* **1991**, *316*, 379–382; *Dokl. Chem. (Engl. Transl.)* **1991**, *316*, 19–21; for a review, see also: c) A. Jończyk, M. Fedoryński, *Methods of Organic Chemistry (Houben-Weyl)* (Ed.: A. de Meijere), Vol. E17a, Thieme, Stuttgart, **1997**, pp. 704–728.
- [10] CCDC-243441 ((1R,3S,4R)-**8**), 243444 ((E)-3S,3'S,4S,4'S,5R,5'R)-**10**), 243449 ((1S,3R,4R,5S,6S,7R,8R,9S)-**11**), 243442 ((1R,3S,4S,5S,6S,7S,8S,9R)-**11**), 243445 (*d*-(+)-**12**), 243448 ((*P*)-(+)-**12**), 243447 ((*M*)-(–)-**13**), and 243446 ((*M*)-(–)-**14**) contain the supplementary crystallographic data for this paper. These data can be obtained free of charge via www.ccdc.cam.ac.uk/conts/retrieving.html (or from the Cambridge Crystallographic Data Centre, 12, Union Road, Cambridge CB21EZ, UK; fax: (+44)1223-336-033; or deposit@ccdc.cam.ac.uk).
- [11] a) M. Borer, T. Loosli, M. Neuenschwander, *Chimia* **1991**, *45*, 382–386; b) T. Loosli, M. Borer, I. Kulakowska, A. Minder, M. Neuenschwander, P. Engel, *Helv. Chim. Acta* **1995**, *78*, 1144–1165; c) M. Borer, T. Loosli, A. Minder, M. Neuenschwander, P. Engel, *Helv. Chim. Acta* **1995**, *78*, 1311–1324; d) M. Borer, M. Neuenschwander, *Helv. Chim. Acta* **1997**, *80*, 2486–2501; e) R. Huwylar, X. Li, P. Bönzli, M. Neuenschwander, *Helv. Chim. Acta* **1999**, *82*, 1242–1249; f) A. de Meijere, M. von Seebach, S. Zöllner, S. I. Kozhushkov, V. N. Belov, R. Boese, T. Haumann, J. Benet-Buchholz, D. S. Yufit, J. A. K. Howard, *Chem. Eur. J.* **2001**, *7*, 4021–4034.
- [12] For reviews on bicyclopopylidenes, see: a) A. de Meijere, S. I. Kozhushkov, A. F. Khlebnikov, *Zh. Org. Khim.* **1996**, *32*, 1607–1626; *Russ. J. Org. Chem. (Engl. Transl.)* **1996**, *32*, 1555–1575; b) A. de Meijere, S. I. Kozhushkov, A. F. Khlebnikov, *Top. Curr. Chem.* **2000**, *207*, 89–147; c) A. de Meijere, S. I. Kozhushkov, *Eur. J. Org. Chem.* **2000**, 3809–3822; d) A. de Meijere, S. I. Kozhushkov, T. Späth, M. von Seebach, S. Löhr, H. Nüske, T. Pohlmann, M. Es-Sayed, S. Bräse, *Pure Appl. Chem.* **2000**, *72*, 1745–1756.
- [13] a) R. Paulissen, A. J. Hubert, P. Teyssie, *Tetrahedron Lett.* **1972**, *13*, 1465–1466; b) J. Kottwitz, H. Vorbrüggen, *Synthesis* **1975**, 636–637; c) A. J. Anciaux, A. J. Hubert, A. F. Noels, P. Teyssie, *J. Org. Chem.* **1980**, *45*, 695–702; for reviews, see also: d) Yu. V. Tomilov, V. A. Dokichev, U. M. Dzhemilev, O. M. Nefedov, *Usp. Khim.* **1993**, *62*, 847–886; *Russ. Chem. Rev.* **1993**, *62*, 799–838; e) L. R. Subramanian, K.-P. Zeller in *Methods of Organic Chemistry (Houben-Weyl)* (Ed.: A. de Meijere) Vol. E17a, Thieme, Stuttgart, **1997**, pp. 256–308.
- [14] J. M. Russo, W. A. Price, *J. Org. Chem.* **1993**, *58*, 3589–3590.
- [15] For reviews, see: reference [13e] and a) H. E. Simmons, T. L. Cairns, S. A. Vladuchik, C. M. Hoiness, in *Organic Reactions*, Vol. 20 (Ed.: W. G. Dauben), Wiley, New York, **1973**, pp. 1–132; b) P. Helquist in *Comprehensive Organic Synthesis*, Vol. 4 (Ed.: B. M. Trost), Pergamon, Oxford, **1991**, pp. 968–997.
- [16] Z. Yang, J. C. Lorentz, Y. Shi, *Tetrahedron Lett.* **1998**, *39*, 8621–8624.
- [17] W. von E. Doering, W. R. Roth, *Tetrahedron* **1963**, *19*, 715–737; for reviews, see also references [13d,e].
- [18] For unknown reasons, this cyclopropanation on a 4-mmol scale ceased after $\approx 50\%$ conversion, irrespective of the quantity of diazomethane and CuCl. The product and the starting material had to be isolated as a mixture by column chromatography and together subjected to repeated cyclopropanations until starting bicyclopopylidene had disappeared, as (*P*)-(+)-**11** is readily separable from *d*-(+)-**11**, but not from starting material. These necessary repeated chromatographic purification steps followed by recrystallization from hexane/Et₂O/CH₂Cl₂ decreased the yield significantly. However, on a 0.44-mmol scale the yield was 67%.
- [19] All new compounds were fully characterized by spectroscopic methods (¹H NMR, ¹³C NMR, MS), elemental analyses, and, whenever essential, X-ray crystal-structure analyses (see Schemes 1–3 and reference [10]). Physical data for some key compounds: (*M*)-(–)-**11**: Colorless crystals, m.p. 129–131°C (hexane/CH₂Cl₂/Et₂O); [α]_D²⁰ = –660.0 (*c* = 1.04 in CHCl₃); ¹H NMR (250 MHz, CDCl₃): δ = 3.71 (dd, *J* = 6.5, 11.0 Hz, 2H; CH₂O), 3.58 (dd, *J* = 7.1, 11.0 Hz, 2H; CH₂O), 1.70 (brs, 2H; 2 OH), 1.32–1.42 (m, 2H; Cpr-H), 1.21 (d, *J* = 3.9 Hz, 2H; Cpr-H), 1.16 (dd, *J* = 3.9, 11.0 Hz, 4H; Cpr-H), 1.04 (s, 2H; Cpr-H), 1.00 (d, *J* = 3.9 Hz, 2H; Cpr-H), 0.67 ppm (dd, *J* = 4.4 Hz, 2H; Cpr-H); ¹³C NMR (62.9 MHz, CDCl₃): δ = 66.3 (2CH₂), 18.5 (2CH), 18.2, 18.0, 17.4 (2C), 10.4, 9.0 (2CH₂), 8.8 (CH₂), 8.7 ppm (2CH₂). (*P*)-(+)-**11**: Colorless crystals, m.p. 130–131°C (hexane/CH₂Cl₂/Et₂O); [α]_D²⁰ = +673.9 (*c* = 1.92 in CHCl₃). (*P*)-(+)-**12**: Colorless crystals, m.p. 88–89°C (MeOH); [α]_D²⁰ = +527.7 (*c* = 1.25 in CHCl₃); ¹H NMR (250 MHz, CDCl₃): δ = 3.50 (s, 2H; CH₂Br), 3.47 (s, 2H; CH₂Br), 1.51–1.60 (m, 2H; Cpr-H), 1.31 (d, *J* = 3.9 Hz, 2H; Cpr-H), 1.25 (d, *J* = 4.0 Hz, 2H; Cpr-H), 1.18 (dd, *J* = 7.7, 4.7 Hz, 2H; Cpr-H), 1.12 (d, *J* = 3.8 Hz, 2H; Cpr-H), 1.03 (s, 2H; Cpr-H), 1.01 (d, *J* = 4.1 Hz, 2H; Cpr-H), 0.75 ppm (t, *J* = 4.5 Hz, 2H, Cpr-H); ¹³C NMR (62.9 MHz, CDCl₃): δ = 38.3 (2CH₂), 22.5 (2C), 19.1 (2CH), 18.2, 18.1 (2C), 13.3, 10.4 (2CH₂), 9.0 (CH₂), 8.1 ppm (2CH₂). (*P*)-(+)-**13**: Colorless crystals, m.p. 62°C (MeOH); [α]_D²⁰ = +1302.1 (*c* = 1.17 in CHCl₃); ¹H NMR (600 MHz, CDCl₃): δ = 5.31 (s, 2H; =CH₂), 5.23 (t, *J* = 1.9 Hz, 2H; =CH₂), 1.56 (d, *J* = 3.7 Hz, 2H), 1.43 (d, *J* = 3.7 Hz, 2H), 1.39 (d, *J* = 7.7 Hz, 2H), 1.37 (dt, *J* = 1.9, 7.7 Hz, 2H), 1.25 (d, *J* = 4.0 Hz, 2H), 1.15 (s, 2H), 1.08 ppm (d, *J* = 4.0 Hz, 2H); ¹³C NMR (150.8 MHz, CDCl₃): δ = 135.7 (2C), 99.3 (2CH₂), 21.9, 18.1, 15.9 (2C), 15.0, 10.7 (2CH₂), 8.6 ppm (3CH₂). (*M*)-(–)-**13**: Colorless crystals, m.p. 59–61°C (MeOH); [α]_D²⁰ = –1285.4 (*c* = 0.60 in CHCl₃); (*M*)-(–)-**14**: Colorless crystals, m.p. 85–87°C (EtOH); ¹H NMR (600 MHz, CDCl₃): δ = 1.20 (d, *J* = 3.8 Hz, 2H), 1.17 (d, *J* = 3.8 Hz, 2H), 1.13 (d, *J* = 3.8 Hz, 2H), 1.11 (s, 2H), 1.08 (d, *J* = 3.7 Hz, 2H), 1.06 (d, *J* = 3.7 Hz, 2H), 0.97 (d, *J* = 3.8, 2H), 0.86–0.83 (m, 2H), 0.79–0.74 (m, 4H), 0.70–0.67 ppm (m, 2H); ¹³C NMR (150.8 MHz, CDCl₃): δ = 18.1, 18.0, 17.4, 13.6 (2C), 11.2, 10.3 (2CH₂), 9.2 (CH₂), 9.1, 4.8, 4.6 ppm (2CH₂). (*P*)-(+)-**14**: Colorless crystals, m.p. 85–86°C (EtOH). NMR spectra of compounds (*P*)-(+)-**11**, (*M*)-(–)-**13**, and (*P*)-(+)-**14** were identical to those of their enantiomers.
- [20] Gaussian98 (Revision A.9), M. J. Frisch, G. W. Trucks, H. B. Schlegel, G. E. Scuseria, M. A. Robb, J. R. Cheeseman, V. G. Zakrzewski, J. A. Montgomery, R. E. Stratmann, J. C. Burant, S. Dapprich, J. M. Millam, A. D. Daniels, K. N. Kudin, M. C. Strain, O. Farkas, J. Tomasi, V. Barone, M. Cossi, R. Cammi, B. Mennucci, C. Pomelli, C. Adamo, S. Clifford, J. Ochterski, G. A. Petersson, P. Y. Ayala, Q. Cui, K. Morokuma, D. K. Malick, A. D. Rabuck, K. Raghavachari, J. B. Foresman, J. Cioslowski, J. V. Ortiz, B. B. Stefanov, G. Liu, A. Liashenko, P. Piskorz, I. Komaromi, R. Gomperts, R. L. Martin, D. J. Fox, T. Keith, M. A.

- Al-Laham, C. Y. Peng, A. Nanayakkara, C. Gonzalez, M. Challacombe, P. M. W. Gill, B. G. Johnson, W. Chen, M. W. Wong, J. L. Andres, M. Head-Gordon, E. S. Replogle, J. A. Pople, Gaussian, Inc., Pittsburgh, PA, **1998**.
- [21] A. D. Becke, *Phys. Rev. A* **1988**, 38, 3098–3100.
- [22] C. Lee, W. Yang, R. G. Parr, *Phys. Rev. B* **1988**, 37, 785–789.
- [23] R. G. Parr, W. Yang, *Density Functional Theory of Atoms and Molecules*, Oxford University Press, New York, **1989**.
- [24] W. J. Hehre, L. Radom, P. v. R. Schleyer, J. A. Pople, *Ab Initio Molecular Orbital Theory*, Wiley-Interscience, New York, **1986**.
- [25] a) R. Ahlrichs, Turbomole (Revision 5.3), Karlsruhe, **1998**; b) O. Treutler, R. Ahlrichs, *J. Chem. Phys.* **1995**, 102, 346–354; c) H. Weiss, R. Ahlrichs, M. Häser, *J. Chem. Phys.* **1993**, 99, 1262–1270; see also: d) S. Grimme, *Chem. Phys. Lett.* **1996**, 259, 128–137.
- [26] For a Highlight, see: C. Schmuck, *Angew. Chem.* **2003**, 115, 2552–2556; *Angew. Chem. Int. Ed.* **2003**, 42, 2248–2252.
- [27] a) T. B. Norsten, R. McDonald, N. R. Branda, *Chem. Commun.* **1999**, 719–720; b) L.-Y. Zhang, G.-F. Liu, S.-L. Zheng, B.-H. Ye, X.-M. Zhang, X.-M. Chen, *Eur. J. Inorg. Chem.* **2003**, 2965–2971; c) M. Ohkita, J.-M. Lehn, G. Baum, D. Fenske, *Chem. Eur. J.* **1999**, 5, 3471–3481; d) M. H. W. Lam, D. Y. K. Lee, S. S. M. Chiu, K. W. Man, W. T. Wong, *Eur. J. Inorg. Chem.* **2000**, 1483–1488; e) D. L. Reger, R. F. Semeniuc, M. D. Smith, *Eur. J. Inorg. Chem.* **2002**, 543–546; f) F. Bachechi, A. Buruni, R. Galassi, B. R. Pietroni, D. Tesei, *Eur. J. Inorg. Chem.* **2002**, 2086–2093; g) D. Sun, R. Cao, Y. Sun, W. Bi, X. Lo, M. Hong, Y. Zhao, *Eur. J. Inorg. Chem.* **2003**, 38–41; h) G. Blay, I. Fernández, J. R. Pedro, R. Ruiz-Garsia, M. C. Muñoz, J. Cano, R. Carrasco, *Eur. J. Org. Chem.* **2003**, 1627–1630; i) M. Gdaniec, W. Jankowski, M. J. Milewska, T. Połonski, *Angew. Chem.* **2003**, 115, 4033–4036; *Angew. Chem. Int. Ed.* **2003**, 42, 3903–3906; j) J. H. K. K. Hirschberg, R. A. Koevoets, R. P. Sijbesma, E. W. Meijer, *Chem. Eur. J.* **2003**, 9, 4222–4231.
- [28] a) G. Rapenne, B. T. Patterson, J.-P. Sauvage, F. R. Keene, *Chem. Commun.* **1999**, 1853–1854; c) S. Hanessian, R. Saladino, R. Margarita, M. Simard, *Chem. Eur. J.* **1999**, 5, 2169–2183; d) H. Borrmann, I. Persson, M. Sandström, C. M. Stålhandske, *J. Chem. Soc. Perkin Trans. 2* **2000**, 393–402; e) C. S. A. Fraser, D. J. Eisler, M. C. Jennings, R. J. Puddephatt, *Chem. Commun.* **2000**, 1224–1225; f) J. Stahl, J. C. Bohling, E. B. Bauer, T. B. Peters, W. Mohr, J. M. Martín-Avarez, F. Hampel, J. A. Gladysz, *Angew. Chem.* **2002**, 114, 1951–1957; *Angew. Chem. Int. Ed.* **2002**, 41, 1872–1876; g) Y. Cui, H. L. Ngo, W. Lin, *Chem. Commun.* **2003**, 1388–1389; h) M. Barboiu, G. Vaughan, N. Kuritsakas, J.-M. Lehn, *Chem. Eur. J.* **2003**, 9, 763–769.

Cover Picture

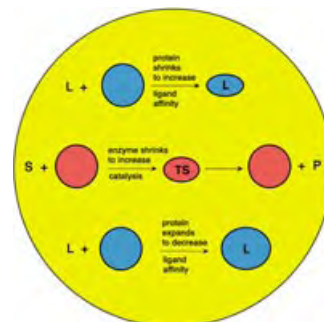
Dorothea Fiedler, Robert G. Bergman,* and Kenneth N. Raymond*

A supramolecular metal–ligand assembly catalyzes the [3,3]-sigmatropic rearrangement of enammonium guests in aqueous solution. The cover picture shows the proposed catalytic cycle. The space-restrictive host cavity forces the substrates to bind in a reactive chairlike conformation and thus accelerates the rate of rearrangement. Release and hydrolysis of the rearranged product enable catalytic turnover. For more information, see the Communication by R. G. Bergman, K. N. Raymond, and D. Fiedler on p. 6748 ff.



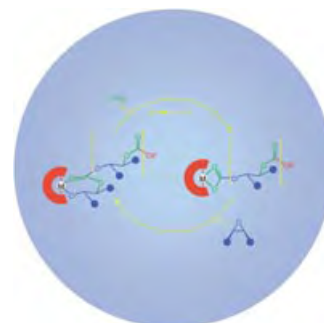
Noncovalent Interactions

The affinity of a ligand for its receptor depends both on the coordination itself and modification of the noncovalent interactions within the receptor. This phenomenon is described by D. H. Williams et al. in their Review on page 6596 ff.



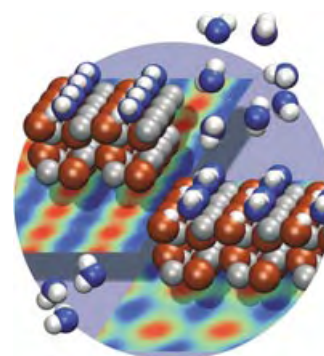
Polymerization Catalysts

Epoxides and CO₂ undergo copolymerization in the presence of well-defined homogeneous catalysts to produce polycarbonates. The latest developments in this field are summarized by G. W. Coates and D. R. Moore in their Review on page 6618 ff.



Water structure

The previous assumption that water adsorbs in a uniform monolayer on the surface of zinc oxide is disproved by B. Meyer, C. Wöll, and co-workers in their Communication on page 6641 ff. According to the findings a superstructure is formed that consists of partially dissociated water molecules.



The Woodward–Hoffmann Rules ...

... Were recognized as groundbreaking immediately upon their formulation, and “many chemists’ eyes were opened when they read the original publication by Woodward and Hoffmann in 1965 and the legendary Review in *Angewandte Chemie* in 1969”. These are the opinions of contemporary witnesses whom we asked for advice as to whether *Angewandte Chemie* should publish an article by Roald Hoffmann in which he responds to E. J. Corey’s claim to have given R. B. Woodward the incentive to develop what quickly became known as the Woodward–Hoffmann rules. In his acceptance speech during the award ceremony for the Priestley Medal, the highest accolade awarded by the American Chemical Society, in Spring 2004, E. J. Corey stated that:

“On May 4, 1964, I suggested to my colleague R. B. Woodward a simple explanation involving the symmetry of the perturbed (HOMO) molecular orbitals for the stereoselective cyclobutene / 1,3-butadiene and 1,3,5-hexatriene/cyclohexadiene conversions that provided the basis for the further development of these ideas into what became known as the Woodward–Hoffmann rules.” (published in *Chem. Eng. News* **2004**, 82(13), 42–44).

The audience/readership was astounded: Were the Woodward–Hoffmann rules not formulated by Woodward and Hoffmann after all? Should they rather be called the Corey–Woodward–Hoffmann rules? It was well known that Havinga, Schlatmann, and especially Oosterhoff had set some very important precedents (see: J. Berson, *Chemical Creativity*, Wiley-VCH, Weinheim, **1999**, pp. 26–31). However, Corey’s name had never before been mentioned in this

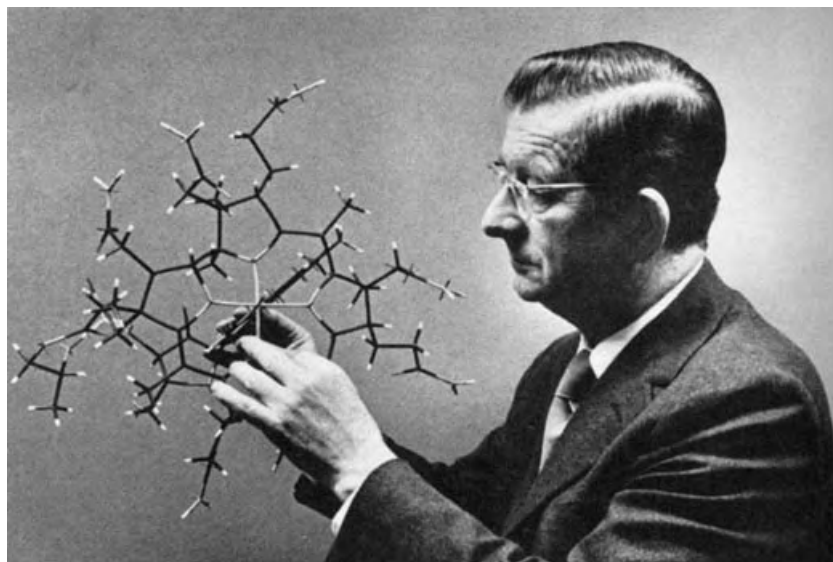


Figure 1. R. B. Woodward with a Dreiding model of cobyric acid. Copyright: Harvard University Archives.


context. As R. B. Woodward (Figure 1) died in 1979 at the age of 62, he can no longer say whether the conversation with Corey on May 4, 1964, enlightened him, gave him a decisive impetus, or merely confirmed his already well-thought-out ideas.

It is most fortunate for the history of science in general and for chemistry in particular that—triggered by E. J. Corey’s statement—Roald Hoffmann has penned his memories of that time. Entitled “A Claim on the Development of the Frontier Orbital Explanation of Electrocyclic Reactions”, his recollections of the early days of the development of the Woodward–Hoffmann rules and the time leading up to their publication can be read on page 6586 ff. It is unfortunate, but to be respected, that E. J. Corey, whom we of course asked to respond, chose not to say any more on

the subject other than reiterating: “I am sure that the statement I made in my Priestley presentation is absolutely true, and at a later time I will present the full story.”

For readers who practiced and shaped chemistry in the 1960s and 1970s, Roald Hoffmann’s contribution makes compelling reading. For all readers, the article is an opportunity to ponder how new theories develop and how important communication is: both personal, in the form of conversations and correspondence, and formal, from presentations to publications. And how easily the sender and receiver can interpret the same information in a completely different manner. *Angewandte Chemie* is a suitable forum for this contribution: The above-mentioned Review (*Angew. Chem.* **1969**, 81, 797–869; *Angew. Chem. Int. Ed. Engl.* **1969**, 8, 781–853), in which

the detailed Woodward–Hoffmann rules were lucidly presented, was published in this journal (see Figure 2). This Review is certainly one of the most-cited publications of *Angewandte Chemie* and, since the launch of the electronic Backfiles, has been one of the most-often downloaded files. Furthermore, the publication of a Correspondence article in a scientific journal has a more lasting character than in a magazine. May it now and in future find many readers and spur them on to reflect carefully on their own behavior.



Dr. Peter Göllitz
Editor

P.S. Another recommended read in this issue is the Essay by Amir Hoveyda, who delves into Primo Levi's literary masterpiece, *The Periodic Table* (page 6592 ff.).

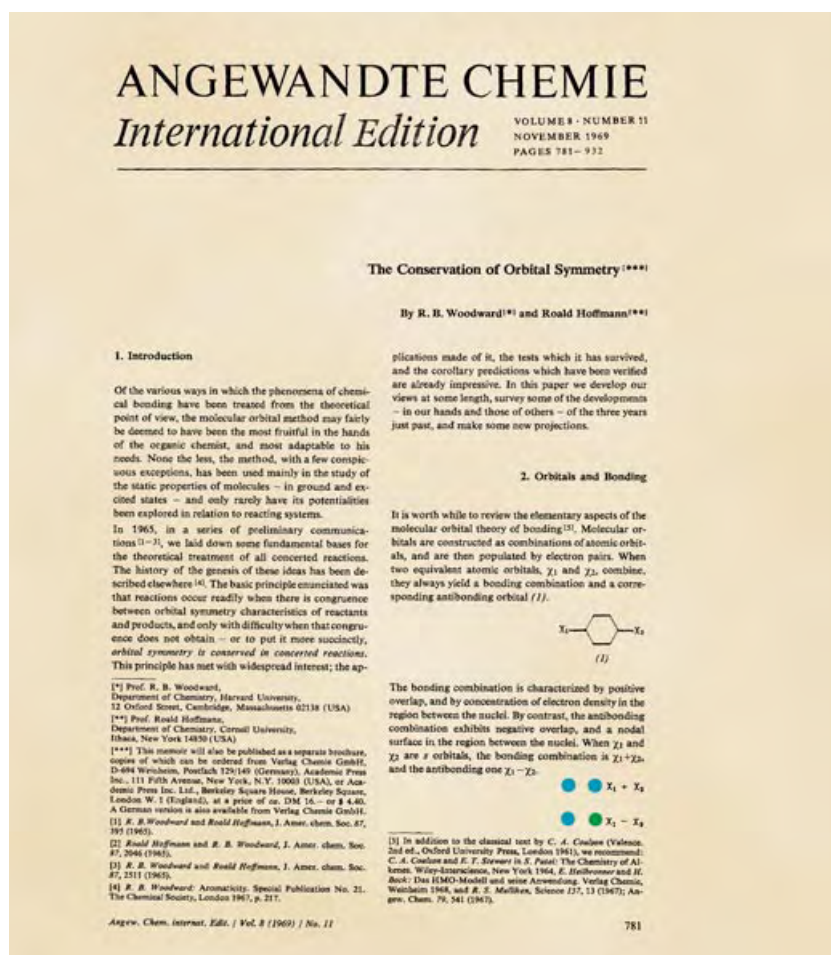


Figure 2. First page of the legendary Review by R. B. Woodward and R. Hoffmann in *Angewandte Chemie*.

Angewandte EarlyView®

The following Communications are available online (in Wiley InterScience). You can find them, as well as forthcoming Reviews, Highlights, and Essays, at www.angewandte.org, under Early View.

P. A. Troshin,* R. N. Lyubovskaya, I. N. Ioffe, N. B. Shustova,
E. Kemnitz, S. I. Troyanov*:
**Synthesis and Structure of the Highly Chlorinated [60]Fullerene
C₆₀Cl₃₀ with Drum-Shaped Carbon Cage**
DOI: 10.1002/anie.200461531
Published online: November 12, 2004

Y. Hu, G. Y. J. Chen, S. Q. Yao*:
**Activity-Based High-Throughput Screening of Enzymes by Using
a DNA Microarray**
DOI: 10.1002/anie.200461612
Published online: November 18, 2004

Articles judged by the referees or the editor as being either very important or very urgent are immediately edited, proof-read, and electronically published once the manuscript has arrived in the editorial office in its final form. As long as there is no page number available these articles should be cited in the following manner:

Author(s), *Angew. Chem. Int. Ed.*, online publication date, DOI.

Web Sites

http://www.cmbi.kun.nl/wetche/organic/	Mol4D—Molecules in the Fourth Dimension	E. Engel, M. Kruppa, B. König _____	6582
---	---	-------------------------------------	-------------

Books

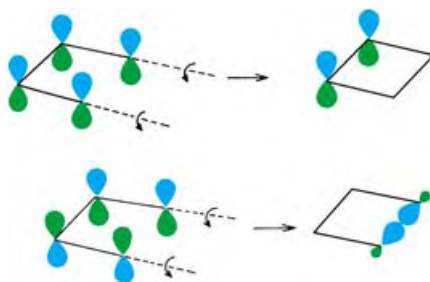
Chemical Micro-Process Engineering	Volker Hessel, Steffen Hardt, Holger Löwe	reviewed by C. de Bellefon _____	6583
Biocatalysis	Andreas S. Bommarius, Bettina R. Riebel	reviewed by U. Bornscheuer _____	6584
An Introduction to Chemical Kinetics	Margaret Robson Wright	reviewed by D. Peeters _____	6585

Correspondence

Woodward–Hoffmann Rules

R. Hoffmann* _____ **6586–6590**

A Claim on the Development of the
Frontier Orbital Explanation of
Electrocyclic Reactions



The well-known Woodward–Hoffmann rules explain how the feasibility and stereochemical outcome of pericyclic reactions are governed by the symmetry properties of the molecular orbitals of the reactants and products. Triggered by a recent claim by E. J. Corey, Roald Hoffmann recalls the first steps in the development of this theory.

Essays

Chemistry in Literature

A. H. Hoveyda* _____ **6592–6594**

Primo Levi's *The Periodic Table*. A Search
for Patterns in Times Past

In his book *The Periodic Table*, Primo Levi, with touching thoughtfulness, sketched the magic of the elements that make up this world. As with all enduring works of

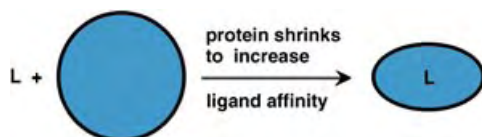
art, *The Periodic Table* is open to numerous interpretations. Another visit, a quarter of a century after its publication, proves to be most rewarding.

Reviews

Noncovalent Interactions

D. H. Williams,* E. Stephens,
D. P. O'Brien, M. Zhou — 6596–6616

Understanding Noncovalent Interactions: Ligand Binding Energy and Catalytic Efficiency from Ligand-Induced Reductions in Motion within Receptors and Enzymes



The strength lies within: This review proposes that receptors and enzymes (shown in blue in the scheme) derive an important contribution to binding their ligands and transition states (respec-

tively) by decreasing their dynamic behavior. Conversely, ligand binding energy is reduced where the binding process increases the dynamic behavior of the receptor protein.



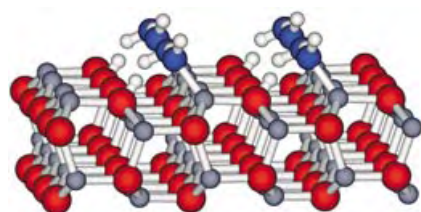
Given the non-renewable nature of synthetic polymers from petroleum feedstocks, there is increasing interest in developing routes to biodegradable polymeric materials from renewable resources. Polycarbonates made from CO₂ and

epoxides (see scheme) have the potential to meet these important goals. Reviewed here are well-defined catalysts for epoxide-CO₂ copolymerization and related reactions.

Polymerization Catalysts

G. W. Coates,* D. R. Moore — 6618–6639

Discrete Metal-Based Catalysts for the Copolymerization of CO₂ and Epoxides: Discovery, Reactivity, Optimization, and Mechanism



Half-dissociated: Experimental and computational findings conclude that water forms a highly ordered superstructure on defect-free surfaces of zinc oxide, in which every second water molecule is dissociated (see picture). The results are of general relevance for heterogeneous catalysis.

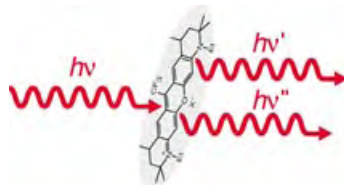
Communications

Water Structure

B. Meyer,* D. Marx, O. Dulub, U. Diebold,
M. Kunat, D. Langenberg,
C. Wöll* — 6641–6645

Partial Dissociation of Water Leads to Stable Superstructures on the Surface of Zinc Oxide

Light switches: The photon capture area of single fluorescent molecules has been directly measured by switching them “on and off” with light. Stimulated emission of single molecules (see picture) enables the precise control of the excited state population probability of an individual molecule at room temperature.



Single-Molecule Studies

L. Kastrup, S. W. Hell* — 6646–6649

Absolute Optical Cross Section of Individual Fluorescent Molecules

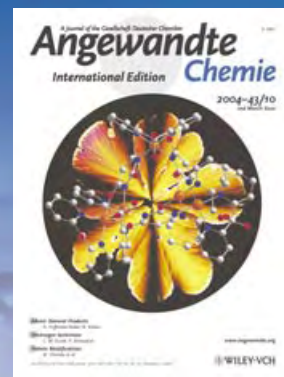
For the USA and Canada:

ANGEWANDTE CHEMIE International Edition (ISSN 1433-7851) is published weekly by Wiley-VCH PO Box 191161, D 69451 Weinheim, Germany. Air freight and mailing in the USA by Publications Expediting Inc. 200 Meacham Ave., Elmont, NY 11003. Periodicals

postage paid at Jamaica NY 11431. US POSTMASTER: send address changes to *Angewandte Chemie*, Wiley-VCH, 111 River Street, Hoboken, NJ 07030. Annual subscription price for institutions: US\$ 4948.00/4498.00 (valid for print and electronic / print or electronic delivery); for individuals who are personal members of a

national chemical society, or whose institution already subscribes, or who are retired or self-employed consultants, print only: US\$ 394.00. Postage and handling charges included. All Wiley-VCH prices are exclusive VAT.

The best in chemistry – for more than a hundred years



A Journal of the Gesellschaft Deutscher Chemiker
Angewandte Chemie
International Edition

www.angewandte.org

1888: The beginning
of a success story

Constant Innovations

- 1962:** First issue of the International Edition
- 1976:** Graphical abstracts
- 1979:** Cover pictures
- 1988:** Centenary of Angewandte
- 1989:** Routine use of color
- 1991:** New section: Highlights
- 1992:** Computerized editorial tracking system
- 1995:** Internet service for readers
- 1998:** Regular press service; full-text online
- 2000:** New section: Essays; EarlyView: Communications available online ahead of the printed version
- 2001:** New section: Minireviews
- 2002:** Online submission of manuscripts
- 2003:** Weekly publication; new section: News; new layout
- 2004:** Backfiles (1962-1997); ManuscriptXpress: Online system for authors and referees



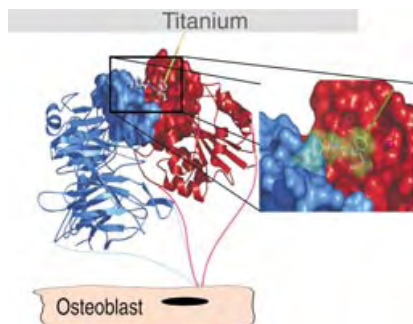
**Angewandte's
advisors...**

Manfred Reetz
Max-Planck-Institut für
Kohlenforschung, Mülheim

» *Angewandte Chemie* is extremely well-balanced in providing various types of information to the academic and industrial chemical community. If you inadvertently miss an issue, the mishap will catch up with you sooner or later. «

Angewandte Chemie International Edition is
a journal of the German Chemical Society (GDCh)





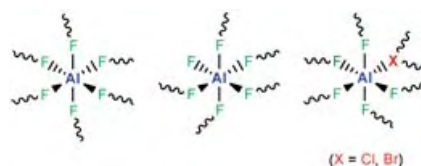
Giving cells some stick: Osteoblast adhesion to titanium, a common material for implants, is stimulated by coating with an optimized and highly specific nonpeptidic ligand for the $\alpha\beta3$ integrin (see picture). This new technology is advantageous to conventional coating by peptides or proteins in many practical aspects (selectivity and activity, stability against enzymatic degradation, sterilization, costs).

Biomaterials

C. Dahmen, J. Auernheimer, A. Meyer, A. Enderle, S. L. Goodman, H. Kessler* ————— **6649 – 6652**

Improving Implant Materials by Coating with Nonpeptidic, Highly Specific Integrin Ligands

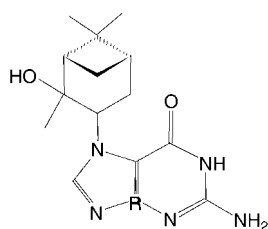
Different octahedral units form the basis of the structures of the very strong Lewis acids aluminum bromide fluoride (ABF) and aluminum chloride fluoride (ACF) (see picture). A structure model for these phases is established in which the octahedra are linked through μ -bridging fluorine atoms and μ_3 -bridging X atoms (X = Cl, Br). The bridging of three octahedra by a heavy halogen atom explains the results of NMR and EXAFS analysis.



Lewis Acids

T. Krah, E. Kemnitz* ————— **6653 – 6656**

Amorphous Aluminum Bromide Fluoride (ABF)

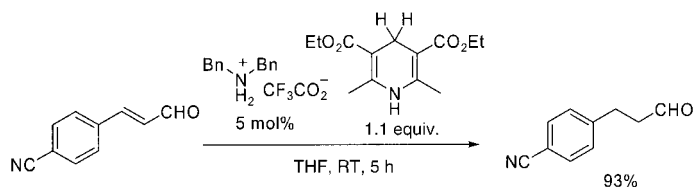


Markers by mass: The effect of terpenoids on organisms can be investigated by using DNA adducts as markers. High-resolution MS was used to characterize DNA/ α -pinene oxide adducts after enzymatic digestion. The reaction of α -pinene oxide with the N7 position of guanine leads to cleavage of the N-glycosidic bond and formation of the N7 guanine adducts (see picture).

DNA Adducts

W. Schrader,* S. Döring, W. Jopek ————— **6657 – 6660**

Mass Spectrometric Studies of DNA Adducts from a Reaction with Terpenoids



Impressive tolerance is displayed in the efficient and chemoselective organocatalytic transfer hydrogenation of α,β -unsaturated aldehydes in the presence of a Hantzsch dihydropyridine and a catalytic

amount of dibenzylammonium trifluoroacetate (see scheme). Various sensitive functional groups such as the nitro, cyano, alkenyl, and benzyloxy groups survive these reaction conditions.

Organocatalysis

J. W. Yang, M. T. Hechavarria Fonseca, B. List* ————— **6660 – 6662**

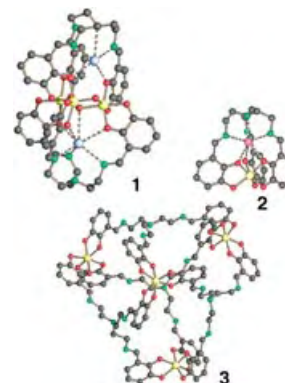
A Metal-Free Transfer Hydrogenation: Organocatalytic Conjugate Reduction of α,β -Unsaturated Aldehydes

Combinatorial Chemistry

M. Albrecht,* I. Janser, J. Runsink,
G. Raabe, P. Weis,
R. Fröhlich ————— **6662 – 6666**

Selecting Different Complexes from a
Dynamic Combinatorial Library of
Coordination Compounds

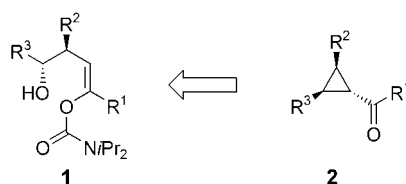
A choice selection: A dynamic combinatorial library of oligonuclear coordination compounds is formed from a flexible tris(catechol) ligand with titanium(IV) ions in the presence of lithium carbonate or potassium carbonate. A trinuclear complex (**1**) can be isolated by crystallization from DMF. In contrast, well-defined mononuclear (**2**) compounds are obtained by addition of Na⁺ as a template, and tetranuclear compounds (**3**) are isolated by changing the solvent to DMSO.



Cyclizations

R. Kalkofen, S. Brandau, B. Wibbeling,
D. Hoppe* ————— **6667 – 6669**

Synthesis of Stereohomogeneous Cyclopropanecarbaldehydes and Cyclopropyl Ketones by Cycloalkylation of 4-Hydroxy-1-alkenyl Carbamates

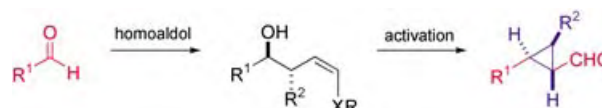


Small rings: Only a few methods are known for the synthesis of cyclopropane carbaldehydes and cyclopropyl ketones **2**. In a new, simple route to highly enantioenriched trisubstituted three-membered rings, 4-hydroxy-1-alkenyl *N,N*-diisopropyl carbamates **1** are treated with NaH, resulting in migration of the carbamoyl group and intramolecular enolate alkylation.

Cyclopropanes

C. A. Risatti, R. E. Taylor* — **6671 – 6672**

Enantioselective Synthesis of Cyclopropanes by Aldehyde Homologation



An efficient method for the enantioselective preparation of structurally diverse cyclopropanes has been developed. Sequential homoaldol coupling and activation steps result in a three-carbon

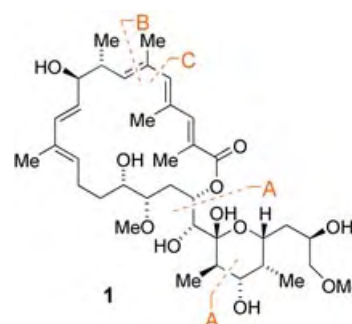
homologation of an aldehyde to give a nonracemic, stereochemically rich cyclopropylcarboxaldehyde (see scheme).

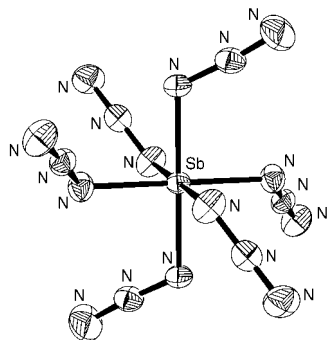
Natural Products

B. Wu, Q. Liu,
G. A. Sulikowski* ————— **6673 – 6675**

Total Synthesis of Apoptolidinone

The complex macrolide apoptolidinone (**1**) was synthesized in 19 steps (longest linear sequence) from (*S*)-malic acid. Key reactions include A) two stereoselective aldol reactions, B) a late-stage Grubbs cross-metathesis reaction to install a trisubstituted vinyl boronate, and C) an intramolecular Suzuki–Miyaura reaction.



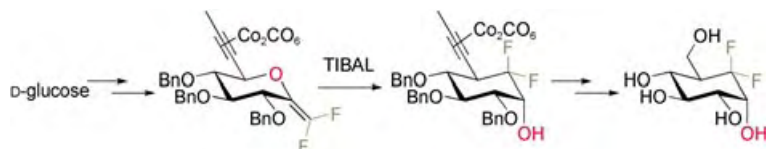


After all, neat $\text{As}(\text{N}_3)_5$ can be isolated: By analogy with AsCl_5 , neat $\text{As}(\text{N}_3)_5$ was predicted to be a highly unstable compound, and previous attempts at its synthesis had resulted in intense explosions. The successful syntheses and characterization of neat $\text{As}(\text{N}_3)_5$ and $\text{Sb}(\text{N}_3)_5$ and the crystal structure of the $[\text{Sb}(\text{N}_3)_6]^-$ ion (see picture) are now described.

Binary Group 15 Azides

R. Haiges,* J. A. Boatz, A. Vij, V. Vij, M. Gerken, S. Schneider, T. Schroer, M. Yousufuddin, K. O. Christe* _____ **6676–6680**

Polyazide Chemistry: Preparation and Characterization of $\text{As}(\text{N}_3)_5$, $\text{Sb}(\text{N}_3)_5$, and $[\text{P}(\text{C}_6\text{H}_5)_4][\text{Sb}(\text{N}_3)_6]$



A rearrangement strategy was used for the synthesis of α - and β -gem-difluorocarbap-D-glucose, which are close congeners of α - and β -D-glucose, in which the endocyclic oxygen atom has been replaced by a

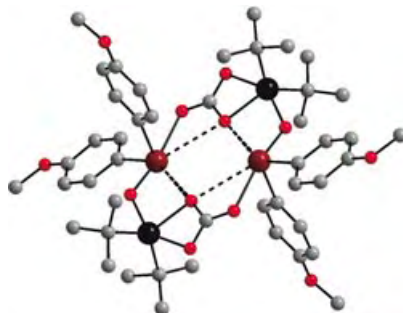
gem-difluoromethylene group (see scheme). The two anomers α or β were obtained stereoselectively by the use of steric or electronic control, respectively. TIBAL = triisobutylaluminum.

Carbohydrate Chemistry

A. Deleuze, C. Menozzi, M. Sollogoub,* P. Sinay* _____ **6680–6683**

Synthesis of gem-Difluorocarbap-D-glucose: A Step Further in Sugar Mimesis

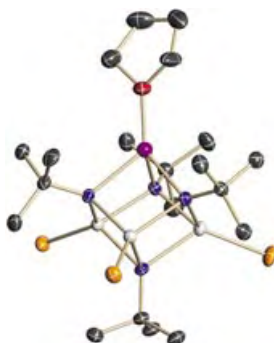
Hypervalency and secondary bonding are the driving forces behind the rapid absorption of gaseous carbon dioxide by two organotellurium and organotin oxides and the unexpected formation of a unique tellurastannoxane cluster (see structure; dark red Te, black Sn, gray C, light red O). The absorption is reversible with the liberation of carbon dioxide being observed at temperatures between 90 and 145 °C.



Cluster Compounds

J. Beckmann,* D. Dakternieks, A. Duthie, N. A. Lewcenko, C. Mitchell **6683–6685**

Carbon Dioxide Fixation by the Cooperative Effect of Organotin and Organotellurium Oxides



Three terminal $\text{Sn}=\text{E}$ bonds are present in the imidotin clusters $[(\text{thf})\text{LiSn}_3\text{E}_3(\mu_3\text{-NtBu})_4]^-$ ($\text{E} = \text{Se}, \text{Te}$; see picture: N blue; Sn gray; Te orange; Li purple; O red) that are readily obtained under mild conditions, as solvent-separated ion pairs with $[\text{Li}(\text{thf})_4]^+$ ($\text{E} = \text{Se}, \text{Te}$) or $[(\text{thf})\text{Li}([12]\text{-crown-4})]^+$ counterions ($\text{E} = \text{Se}$), by the reactions of the anionic cluster $[(\text{thf})\text{LiSn}_3(\mu_3\text{-NtBu})_4]^-$ with the appropriate chalcogen.

Cluster Compounds

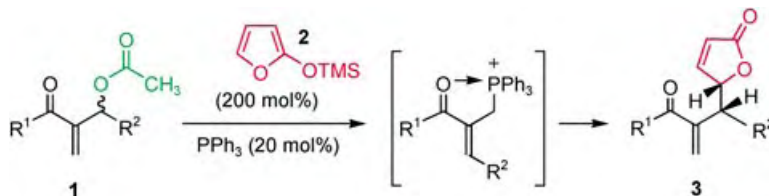
T. Chivers,* D. J. Eisler _____ **6686–6689**

Complete Chalcogenation of Tin(II) Centers in an Imidotin Cluster

Allylic Substitution

C.-W. Cho, M. J. Krische* — 6689–6691

Regio- and Stereoselective Construction of γ -Butenolides through Phosphine-Catalyzed Substitution of Morita–Baylis–Hillman Acetates: An Organocatalytic Allylic Alkylation



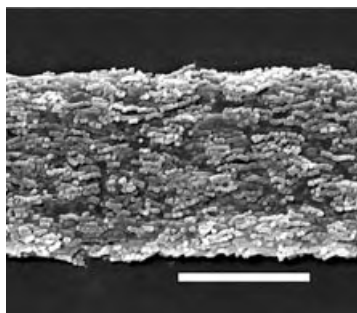
Hold the metal: Upon exposure of acetates **1** to substoichiometric quantities of triphenylphosphane in the presence of **2**, regioselective metal-free allylic substitution

occurs through a formal tandem $S_N2'-S_N2'$ substitution mechanism to provide γ -butenolides **3** with high levels of regio- and diastereocontrol (see scheme).

Nanotechnology

D. Walsh, A. Kulak, K. Aoki, T. Ikoma, J. Tanaka, S. Mann* — 6691–6695

Preparation of Higher-Order Zeolite Materials by Using Dextran Templating

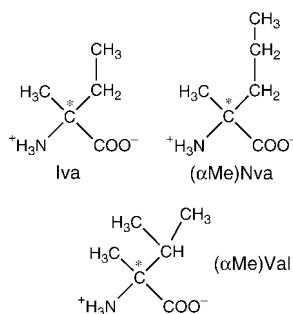


Template-directed processes involving polysaccharide, dextran, and preformed zeolite crystals/nanoparticles are used to prepare elaborate porous frameworks of interconnected filaments of NaY zeolite/silica nanoparticles, as well as macroscopic fibers of crystallographically aligned silicalite nanocrystals (see picture; bar is 5 μ m).

Chirality

M. Crisma, A. Moretto, F. Formaggio, B. Kaptein, Q. B. Broxterman, C. Toniolo* — 6695–6699

Meteoritic C^α -Methylated α -Amino Acids and the Homochirality of Life: Searching for a Link

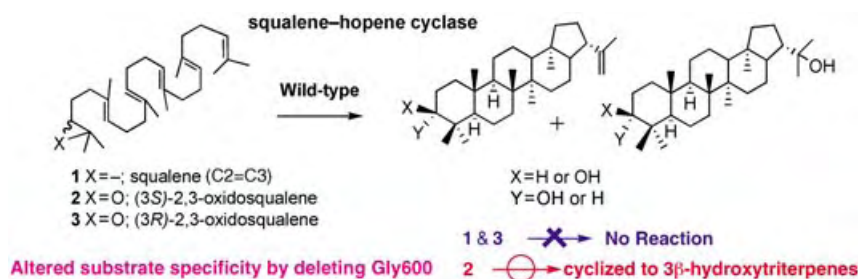


Catch a falling star: Peptides from chiral, C^α -methylated α -amino acids (see scheme) found in L enantiomeric excess in meteorites show diastereoselectivity when reacting with racemic proteinogenic amino acids. Accordingly, the prebiotic soup of proteinogenic amino acids may have evolved into a chirally unbalanced system, eventually seeding the homochirality of life.

Cyclization

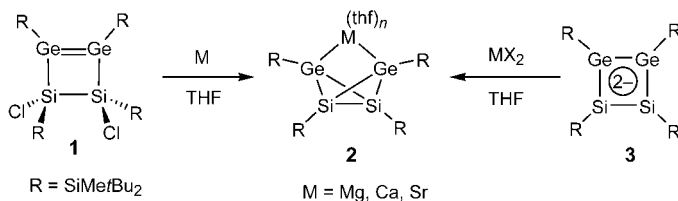
T. Hoshino,* K. Shimizu, T. Sato — 6700–6703

Deletion of the Gly600 Residue of *Alicyclobacillus acidocaldarius* Squalene Cyclase Alters the Substrate Specificity into that of the Eukaryotic-Type Cyclase Specific to (3S)-2,3-Oxidosqualene



Removal service: A deletion mutant lacking the Gly600 residue of a prokaryotic squalene-hopene cyclase was prepared. Surprisingly, the mutant cyclase has no enzyme activity for **1** and **3**, but shows a

high conversion ratio for **2** (see scheme). Deleting Gly600 alters the specificity from prokaryotic into that of eukaryotic-type cyclases.



Carbon copies: Alkaline-earth metal (Mg, Ca, and Sr) derivatives **2** of a silagerma-bicyclo[1.1.0]butane-2,4-diide are obtained by the treatment of **1** with magnesium or calcium in THF or by the reaction of the

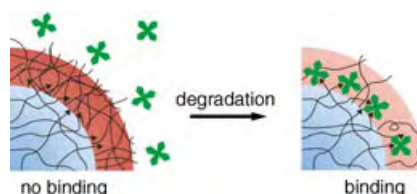
dianion **3** with MgBr_2 , CaI_2 , or SrI_2 in THF. Such stable derivatives of charged bicyclo[1.1.0]butanes have been elusive species until now.

Strained Molecules

V. Ya. Lee, K. Takanashi, M. Ichinohe, A. Sekiguchi* — 6703–6705

The First Bicyclo[1.1.0]butane Dianion of Heavier Group 14 Elements

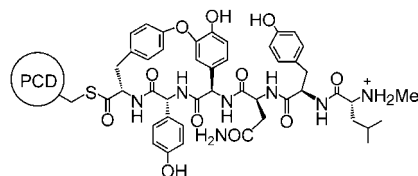
Sifting through the surface: Permselective core/shell microgels have been prepared by using a labile cross-linker, which can be cleaved stoichiometrically to control the porosity of the shell. Proteins that are smaller than the pore size are allowed to permeate through the shell to bind with the core-bound ligand (arrows; see picture).



Porous Structures

S. Nayak, L. A. Lyon* — 6706–6709

Ligand-Functionalized Core/Shell Microgels with Permselective Shells

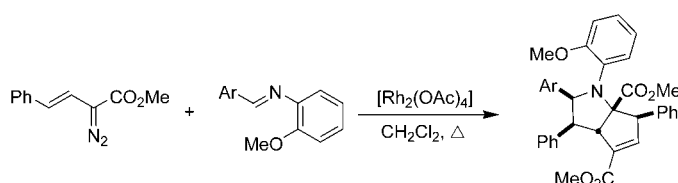


During the biosynthesis of glycopeptide antibiotics of the vancomycin family, several oxidative phenol coupling reactions take place. An oxygenase (OxyB) from the vancomycin producer catalyzes the first of these coupling reactions to a significant extent only when the putative hexapeptide substrate is linked as a thioester to a peptide carrier domain (PCD) derived from the non-ribosomal peptide synthetase (see picture).

Enzyme Catalysis

K. Zerbe, K. Wothke, D. B. Li, F. Vitali, L. Bigler, J. A. Robinson* — 6709–6713

An Oxidative Phenol Coupling Reaction Catalyzed by OxyB, a Cytochrome P450 from the Vancomycin-Producing Microorganism



Multiple C–C bonds are formed in an unprecedented reaction of an ylide with 2 equivalents of a rhodium-stabilized carbene. The cascade cyclization of the

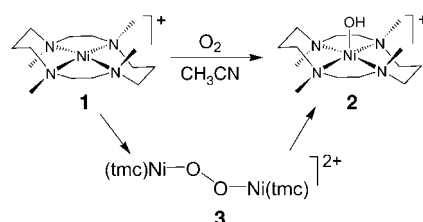
intermediate formed from the three components gives bicyclic pyrrolidine products with excellent diastereoselectivity (see scheme).

Carbenoid Reagents

M. Yan, N. Jacobsen, W. Hu, L. S. Gronenberg, M. P. Doyle,* J. T. Colyer, D. Bykowski — 6713–6716

Stereoselective Synthesis of Bicyclic Pyrrolidines by a Rhodium-Catalyzed Cascade Process

O₂ for you: The *trans*-μ₂-1,2-peroxo Ni₂ dimer **3**, a structural motif unknown previously in nickel coordination chemistry, was produced by reaction of the (tmc)nickel(I) precursor **1** with O₂. Thermal decomposition of **3** in CH₃CN leads to **2**, in which the atoms of the hydroxide ligand derive from O₂ and the hydrocarbon solvent.



Nickel Compounds

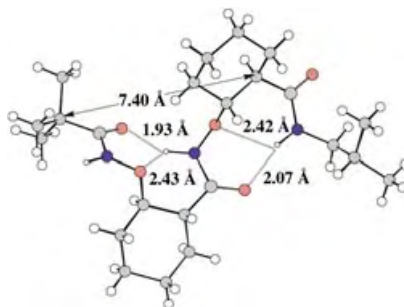
M. T. Kieber-Emmons, R. Schenker, G. P. A. Yap, T. C. Brunold, C. G. Riordan* — 6716–6718

Spectroscopic Elucidation of a Peroxo Ni₂(μ-O₂) Intermediate Derived from a Nickel(I) Complex and Dioxygen

Foldamer Structures

D. Yang,* D.-W. Zhang, Y. Hao, Y.-D. Wu, S.-W. Luo, N.-Y. Zhu — 6719–6722

$\beta^{2,3}$ -Cyclic Aminoxy Acids: Rigid and Ring-Size-Independent Building Blocks of Foldamers

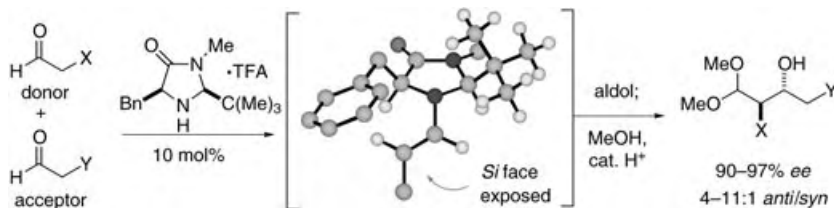


Independent of the ring size in the aliphatic side chains, peptides made up of $\beta^{2,3}$ -cyclic aminoxy acids, novel chiral building blocks of foldamers, adopt uniform secondary structures consisting of rigid β N–O turns and 1.8_9 -helix structures (see figure). This contrasts previous results from other groups with cyclic ring-constrained β -peptides.

Organocatalysis

I. K. Mangion, A. B. Northrup, D. W. C. MacMillan* — 6722–6724

The Importance of Iminium Geometry Control in Enamine Catalysis: Identification of a New Catalyst Architecture for Aldehyde–Aldehyde Couplings



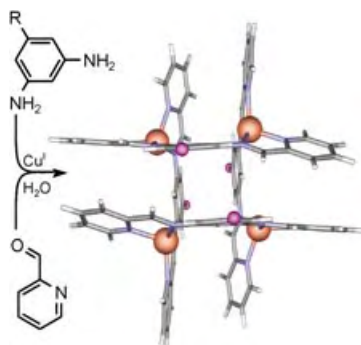
Central to the design of a new organocatalyst system for aldehyde–aldehyde aldol reactions is the necessity of iminium geometry control during the enamine addition step (see scheme). Significant

structural variation in both the aldol donor and aldol acceptor are possible while maintaining high reaction efficiency and enantioselectivity. TFA = trifluoroacetic acid.

Supramolecular Structures

J. R. Nitschke,* M. Hutin, G. Bernardinelli — 6724–6727

The Hydrophobic Effect as a Driving Force in the Self-Assembly of a [2 × 2] Copper(I) Grid



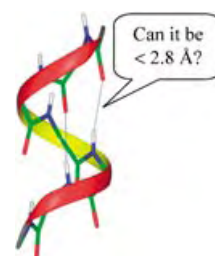
Spring-loaded supramolecular chemistry: Pyridine-2-carboxaldehyde reacts with the *m*-phenylenediamine shown in aqueous solution in the presence of Cu^{I} ions to give a tetracopper(I) grid complex (see structure). This structure is stable in water, but not in any of the organic solvents tried. The strain incorporated into the structure is compensated by a diffuse pressure applied by the hydrophobic effect. R = 2-hydroxyethylcarbamoyl.

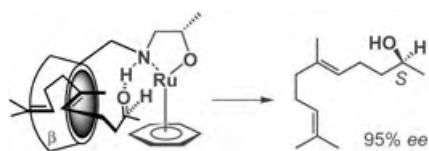
Peptide Structures

S. Aravinda, S. Datta, N. Shamala,* P. Balaram* — 6728–6731

Hydrogen-Bond Lengths in Polypeptide Helices: No Evidence for Short Hydrogen Bonds

The long and the short of it: N...O distances less than 2.8 Å (see picture) have been implicated in determining the 220 nm circular dichroism band intensity in helical peptides. An analysis of helical peptide crystal structures, however, reveals the average experimentally determined hydrogen-bond lengths are 2.978–3.113 Å (α helix) and 2.907–3.211 Å (3_{10} helix).



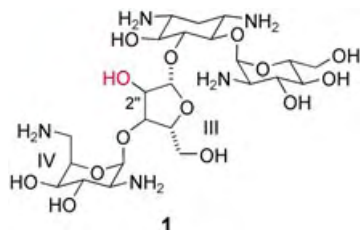


Water-soluble chiral Ru complexes with a β -cyclodextrin unit have been shown to catalyze the reduction of aliphatic ketones (see scheme) with up to 97% *ee* and in good to excellent yields in the presence of sodium formate. The β -cyclodextrin unit is an essential component of the catalyst. It contributes to the unprecedented levels of enantioselectivity observed through the preorganization of the substrates in the hydrophobic cavity.

Asymmetric Reduction

A. Schlatter, M. K. Kundu, W.-D. Woggon* — 6731 – 6734

Enantioselective Reduction of Aromatic and Aliphatic Ketones Catalyzed by Ruthenium Complexes Attached to β -Cyclodextrin

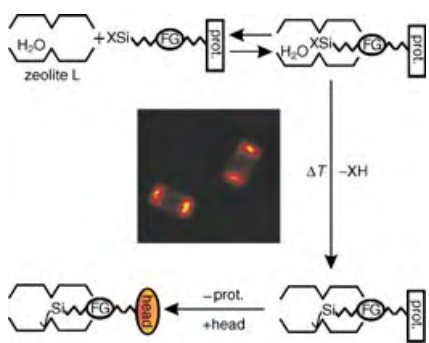


A new twist of RNA fate: Site-selective chemical functionalization at the C2''-OH group of paromomycin (**1**) afforded a novel analogue with potent inhibitory activity against several bacterial strains, including a multidrug-resistant *S. aureus* (MRSA) strain. X-ray cocrystal-structure determination of the complex with the A site of *E. coli* RNA revealed a new mode of binding in which significant conformational and positional changes had taken place in rings III and IV.

Drug Design

B. François, J. Szychowski, S. S. Adhikari, K. Pachamuthu, E. E. Swayze, R. H. Griffey, M. T. Migawa, E. Westhof,* S. Hanessian* — 6735 – 6738

Antibacterial Aminoglycosides with a Modified Mode of Binding to the Ribosomal-RNA Decoding Site

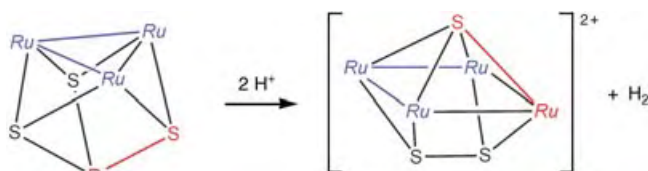


Protecting group chemistry was used to functionalize the channel entrances of zeolite L crystals. This approach is broadly applicable and can be used to obtain a wide range of new zeolite-based materials. The picture shows two microcrystals modified with amino groups at the channel entrances, which reacted further with a red-luminescent head molecule. FG = functionalizing group, prot. = protector.

Modified Zeolites

S. Huber, G. Calzaferri* — 6738 – 6742

Sequential Functionalization of the Channel Entrances of Zeolite L Crystals



Get into shape under redox: Rearrangement of $[\text{Ru}_4\text{S}_3(\text{arene})_4]$ accompanies redox processes and occurs in its reduction of H^+ to H_2 (see scheme;

$\text{Ru} = \text{Ru}(\text{cymene})$). The $[\text{Ru}_4\text{S}_3(\text{arene})_4]^{2+}$ ion is so crowded that arene rotation is hindered, which allows the detection of atropisomers.

Cluster Compounds

M. L. Kuhlman, T. B. Rauchfuss* — 6742 – 6745

Competing H–H, S–S, and M–M Bond Formation in the “Shape-Shifting” Cluster $[\text{Ru}_4\text{S}_3(\text{arene})_4]^{2+}$

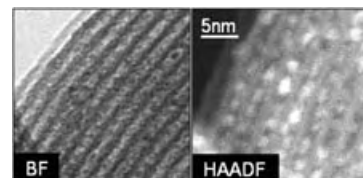


Electron Microscopy

J. M. Thomas,* P. A. Midgley,*
T. J. V. Yates, J. S. Barnard, R. Raja,
I. Arslan, M. Weyland — 6745–6747

The Chemical Application of High-Resolution Electron Tomography: Bright Field or Dark Field?

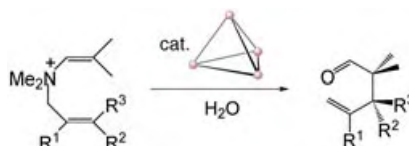
Visualizing 3D structures (especially of supported catalysts) by the nondestructive method of electron tomography is best accomplished by high-angle annular dark-field (HAADF) rather than by bright-field (BF) imaging; bimetallic clusters of $[\text{Ru}_{10}\text{Pt}_2]$ (diameter ca. 0.4 nm), supported on nanoporous silica, are invisible in BF but readily visible in HAADF images (see pictures).



Host–Guest Systems

D. Fiedler, R. G. Bergman,*
K. N. Raymond* — 6748–6751

Supramolecular Catalysis of a Unimolecular Transformation: Aza-Cope Rearrangement within a Self-Assembled Host



Catalytic containers: A supramolecular metal–ligand assembly $[\text{M}_4\text{L}_6]$ is utilized as a catalytic host for the unimolecular carbon–carbon bond-forming rearrangement of enammonium cations (see scheme). The restricted reaction space of the supramolecular structure forces the substrate to adopt a reactive conformation upon binding to the interior. The assembly achieves up to 850-fold rate acceleration of the rearrangement.



Communications labeled with this symbol have been judged by two referees as being “very important papers”.



The editorial staff and the publishers thank all readers, authors, referees, and advertisers for their interest and support over the past year and wish them all a Happy New Year.

Service

Keywords — 6752

Authors — 6753

Angewandte's Sister Journals — 6754–6755

Index — 6759

Preview — 6827



Open position at the Institute of Chemistry of the University of Osnabrück to be

W3-professorship: Organic Chemistry In the field of Organic Materials Sciences

Applications are to be sent by **15th of February, 2005**, to the **Dean of the Faculty of Biology and Chemistry, University of Osnabrück, Barbarastraße 7, D-49069 Osnabrück**.

Defaulted information is available on the web site: <http://www.chemie.uos.de/>.

YOUR HOTLINE FOR PLACING ADVERTS

MARION SCHULZ

MSCHULZ@WILEY-VCH.DE

+49(6201) 606-565 +49(6201) 606-550

Corrigendum

We have become aware of a report by Bergman and co-workers that the abstraction of a methyl group from $[\text{Cp}_2\text{ZrMe}_2]$ with $\text{B}(\text{C}_6\text{F}_5)_3$ leads to an acceleration of the intramolecular hydroamination reaction of an aminoallene substrate relative to the reaction in which only $[\text{Cp}_2\text{ZrMe}_2]$ is used (L. Ackermann, R. G. Bergman, R. N. Loy, *J. Am. Chem. Soc.* **2003**, 125, 11 956). We therefore correct our statement on p. 5543 that “alkyl metallocene cations have been used in organic synthesis, but to the best of our knowledge not in hydroamination reactions”, with reference to the above-mentioned publication.

In the legends to the Figures 3 and 4 the sweep rates and temperatures have been transposed. The correct values are as follows:

Figure 3: sweep rate 0.001 Ts^{-1} and $T = 0.04\text{--}0.5 \text{ K}$; Figure 4: sweep rate 0.007 Ts^{-1} and $T = 0.01\text{--}0.5 \text{ K}$.

The authors apologize for the error.

Hydroamination/Cyclization of Aminoalkenes Using Cationic Zirconocene and Titanocene Catalysts**

K. C. Hultzs, *

D. V. Gribkov — 5542—5546

Angew. Chem. Int. Ed. **2004**, 43

DOI 10.1002/anie.200460880

Building Molecular Minerals: All Ferric Pieces of Molecular Magnetite

G. W. Powell, H. N. Lancashire, E. K. Brechin, * D. Collison, * S. L. Heath, * T. Mallah, W. Wernsdorfer — 5772—5775

Angew. Chem. Int. Ed. **2004**, 43

DOI 10.1002/anie.200460636

Novartis is pleased to announce the 2004 recipients of the

Novartis European Young Investigator Award in Chemistry

Prof. J Stephen Clark
University of Nottingham
Nottingham, UK

for his outstanding contribution to the development of new carbenoid- and metathesis-based synthetic methodologies, and to the application to natural product synthesis

Prof. Jonathan P Clayden
University of Manchester
Manchester, UK

for his outstanding contribution to the development and application of new synthetic methodologies based on dearomatisation reactions, and on non-biaryl atropisomers

The Novartis European Young Investigator Award in Chemistry was created in 2002 to mark Novartis' commitment to science and innovation. The award, carrying an unrestricted research grant of CHF 100,000, is presented annually to an outstanding scientist under the age of 40 who is a European resident and is active in the areas of organic or bioorganic chemistry in the broadest sense.

Past winners:

Prof. Bernhard Breit, University of Freiburg (2002)

Prof. Thomas Carell, Philipps University, Marburg (2002)

Prof. Thorsten Bach, Technische Universität München (2003)

 NOVARTIS

A Claim on the Development of the Frontier Orbital Explanation of Electrocyclic Reactions

Roald Hoffmann*

Keywords:

history of science · molecular orbitals · pericyclic reactions · reaction mechanisms · theoretical chemistry

An important discovery took place in the period 1964–1969—it was the elaboration of the complex of ideas known variously as “the conservation of orbital symmetry” or “orbital symmetry control.” The stereochemistry and ease (or difficulty) of the elementary steps of many organic reactions found an explanation in the phase relationships of their molecular orbitals.

It was my fortune to collaborate with R. B. Woodward in this story. Our published work consisted of a series of five communications to the Editor of *J. Am. Chem. Soc.* in 1965,^[1] a paper in *Accounts of Chemical Research*,^[2] and, importantly, a final exposition of the ideas in an article of some length in *Angewandte Chemie*.^[3]

Woodward and I used a variety of theoretical approaches in our work—from simple frontier orbital (HOMO/LUMO) arguments, through orbital correlation diagrams, interaction diagrams, and perturbation theory arguments, to detailed molecular orbital calculations. There were good reasons not to use a single approach—symmetry was a way in to the solution, but its unthinking use would have imprisoned us. Still, there was a leitmotif in our work: orbitals and their symmetries mattered, and so did the number of electrons.

Woodward and I were lucky—we not only rationalized a large, piecewise

puzzling, body of chemistry, but also were able to make predictions that were verifiable by a community eminently capable and interested in probing experimentally the consequences of the theory. Orbital symmetry considerations were expeditiously tested; they were found to be portable and productive. The 1981 Nobel Prize in chemistry was awarded to Kenichi Fukui and me for this work; had R. B. Woodward lived, there isn't the least doubt that he would have shared in this recognition.

E. J. Corey's Public Claim

In his 2004 Priestley Medal address, published in *Chemical and Engineering News*,^[4] E. J. Corey writes,

“On May 4, 1964, I suggested to my colleague R.B. Woodward a simple explanation involving the symmetry of the perturbed (HOMO) molecular orbitals for the stereoselective cyclobutene/1,3-butadiene and 1,3,5-hexatriene/cyclohexadiene conversions that provided the basis for the further development of these ideas into what became known as the Woodward–Hoffmann rules.”

The same sentence appears in a 2004 *Journal of Organic Chemistry* perspective by E. J. Corey, “Impossible Dreams”.^[5] This terse reminiscence of a conversation, and a claim of its significance has given rise to considerable discussion and speculation in the community.

Let me recount what I know, remember (and don't remember), and what I infer about the events 40 years ago surrounding this claim. I cannot

speak about the contents of the conversation because I was unaware of it at the time; given that Woodward is no longer alive, we only have Corey's report on it. But in my opinion, the part of E. J. Corey's published statement that reads “...that provided the basis for the further development of these ideas” is not right in its characterization of an episode in an important discovery.

Corey's Claim, Made in Prior Conversations or Exchanges with Me on the Subject

In a visit to Cornell in the 1970s, Corey told me that he made my career by telling R. B. Woodward the HOMO explanation in 1964. To my knowledge, this was the first time he made this direct claim to me. I was puzzled, and I think I ignored the comment.

On November 2, 1981, after the Nobel Prize in Chemistry to Kenichi Fukui and me was announced, Corey wrote me a letter stating his claim in substantial detail. The original of this letter is deposited in my papers in the Cornell University Library (available to the public).^[6] In the letter Corey recounts a conversation he had with Woodward on the evening of May 4, 1964, in which he told Woodward, who posed the problem of the electrocyclic reactions to him (and who seemed, according to Corey, more interested in geometrical explanations), that the explanation might be found in the symmetry properties of the orbitals involved. Corey continues his account by relating how the next day Woodward appeared in Corey's office and told the same

[*] Prof. Dr. R. Hoffmann
Department of Chemistry and Chemical Biology
Cornell University, Baker Laboratory
Ithaca, NY 14853-1301 (USA)
Fax: (+1) 607-255-3419
E-mail: rh34@cornell.edu

explanation briefly to Douglas Applequist (a visitor to Harvard that semester) in Corey's presence, as his (Woodward's) "new idea." Corey goes on in his letter to say:

"...the fact is I conceived of the idea, not Bob. In a manner of which few would be capable he pirated the idea, evidently preferring that over my good will. Even more incredible than what Bob did was how he did it."

In his November 2, 1981 letter Corey expressed concern that I would tell the orbital symmetry story in my Nobel Lecture (I had already chosen to talk about something new, the isolobal analogy). And he wanted me to tell people of his, Corey's, contribution.

This letter, coming at the time that it did, and with such claims, disturbed me greatly. I answered it on November 8, 1981.^[6] I said that I would not tell people of Corey's claim—he chose not to do so himself in public (or to Woodward); it would be unfair to Woodward for me to do so then, in 1981, after his death in 1979.

Corey then wrote another letter to me (November 16, 1981)^[6] in which he reiterated and escalated his claims, in a manner that I felt as intimidating to threatening. Here are two excerpts from that letter, which convey its tone:

"You cannot deny that despite the possibility of appalling dishonesty at the roots of your collaboration with Bob, you elected to close your mind. The two of you in effect "stonewalled" my contribution so completely that you chose not even to make a perfunctory acknowledgement in your papers."

and

"Roald, please consider that history may not deal leniently in this matter, taking seriously the possibility not only of Bob's dishonesty, but of your own not unwitting participation in the extension of fraud."

In the spring of 1984, I visited Harvard for a semester. During that time Corey and I spoke for a couple of hours on the issue. He then sent me another letter on April 29, 1984^[6] in which he gives as the reason that he did not publish his claim in Woodward's lifetime as follows:

"I am amazed that you would think it possible that I would consider doing anything against Harvard, to which I was and am so devoted."

In his first letter to me on November 2, 1981, Corey gave another reason for not writing himself of the way he perceived things had happened:

"I had hoped that Bob himself would do it as he grew older, more considerate, and more sensitive to his own conscience."

To the best of my knowledge, Corey never made an attempt to set the record straight (according to his own perceptions) by speaking of it to Woodward in the 15 years between 1964 and 1979, when Woodward died. Or by publishing his claim. Corey made no public claims, as far as I know, until the statement in his Priestley Medal address in 2004.

Corey did talk to others at Harvard and elsewhere of the matter. In his November 2, 1981 letter to me, Corey writes that he told his story to E. B. Wilson in 1964. And I know he discussed the matter subsequently with Jeremy Knowles. Frank Westheimer and Elkan Blout knew about Corey's claim and agonized over the question for years while composing a memorial notice on Woodward. In the end, despite my objections, Elkan Blout included in his 2001 biographical memoir for Woodward the following sentence: *"In 1964, after a brief discussion with E. J. Corey and others of his thoughts and his chemical results, Woodward was able to formulate his important ideas in this area."*^[7]

Scientific and Personal Background to 1964 Events

To set the stage for my recollections of the period, let me recount the story of my relationship with E. J. Corey and R. B. Woodward.

I received my Ph.D. in 1962 with W. N. Lipscomb, Jr. and M. P. Gouterman, and began a Junior Fellowship in the summer of 1962. I was given an office in the basement of Conant Hall, a few doors down from Corey's office in Converse Hall. And I began to learn organic chemistry, applying the extend-

ed Hückel method that a group of us developed in the Lipscomb group to organic molecules. When I finished the first extended Hückel paper on hydrocarbons I sent a preprint (this was early 1963) to the organic chemists at Harvard—Woodward, Corey, Bartlett, and Westheimer—and then set up appointments to see all of them. This was the first time (after five years at Harvard) that I spoke to Woodward about science.

Of the people I saw, Corey responded most positively to my growing interest in organic chemistry. I was down the hall from him, and as busy as he was, he always welcomed me to talk. By telling me of hot subjects—nonclassical carbonium ions and organic photochemistry—he helped draw me into organic chemistry.

I began to go to organic seminars and went to one of the legendary evening Woodward meetings. In the spring of 1964, one of Corey's colleagues from Illinois, Douglas Applequist, visited Harvard for the semester. He gave a course on strained molecules which I listened to with great interest. Applequist and I talked to each other a lot. I was in the midst of discovering for myself the full beauty of organic chemistry.

My Recollections of the Specific Period in 1964

The simple frontier orbital explanation of the stereochemistry of electrocyclic reactions did not originate with me. It was brought to me by Woodward. Let me outline what I have a record of, what I remember, and what I don't recall, concerning my introduction to that frontier orbital explanation. And how my collaboration with Woodward began.

Woodward describes in two lectures the chemical and historical background of the advent of the orbital symmetry rules. In the first, his 1966 Sheffield lecture,^[8a] he uses the generic "we"; in his second account, the 1973 Cope Award Lecture (published long after, from a copy of a handwritten text by R. B. Woodward),^[8b] there is a direct first person account, as follows:

"I REMEMBER [capitals in the original] very clearly—and it still sur-

prises me somewhat—that the crucial flash of enlightenment came to me in algebraic, rather than in pictorial or geometric [all underlining is in original text] form. Out of the blue, it occurred to me that the coefficients of the terminal terms in the mathematical expression representing the highest occupied molecular orbital of butadiene were of opposite sign, while those of the corresponding expression for hexatriene possessed the same sign. From here it was but a short step to the geometric, and more obviously chemically relevant, view that in the internal cyclisation of a diene, the top face of one terminal atom should attack the bottom face of the other, while in the triene case, the formation of a new bond should involve the top (or *pari passu*, the bottom) faces of both terminal atoms.”

In this period I kept a hard-bound notebook. But I did not keep it carefully, with only occasional dates written in. There is in the notebook an April 17 date for a seminar by George Olah, and the next date in the notebook is May 5,

1964 (Figure 1) the day after the Corey and Woodward conversation (as reported by Corey).

The May 5 entry (p. 80; the entire notebook, covering roughly the period March to June 1964, is in the Cornell University Library, collection cited^[6]) says “Talk with Woodward and Applequist,” and below it contains the stereochemical essence of the four- and six-electron electrocyclic reaction, without orbitals. But clearly orbitals and their phases are in the discussion, because below these reactions I sketch the cyclopropyl to allyl opening and draw the lowest allyl orbital as presumably controlling the disrotatory motion in the cation.

This is the first mention of electrocyclic reactions in my notebook. But I believe I heard of the HOMO symmetry argument earlier (and prior to May 4, the date of the Corey–Woodward meeting) in—I think—a conversation I had with D. E. Applequist, who recounted it as an explanation that Woodward suggested and asked me for my reaction to

it. I have no written record of that early conversation. It must be said, however, that Applequist does not think he had such a conversation with me prior to May 5, 1964.^[9]

Returning to my notebook, after some thoughts on cyclopropyl cation, two pages later I sketch out a plan for studying what would later be called con- and disrotatory motion. These preoccupy me for quite a few pages/days (no further dates appear in the notebook until June 9, 1964); the discussion does not focus on orbitals but is “computational”. It is pretty well summarized in our first paper. At this point I was still a computational chemist, and even though I used orbitals and perturbation theory, explanations constructed in frontier orbital language were not yet a common part of my work and thought. They quickly became so. In fact, this—a recognition of the force of simple bonding arguments, and their utility in a theory–experiment dialogue—was on a personal level the main consequence for me of the orbital symmetry story.

Here’s how Woodward described the beginning of our interaction, in his Cope Award Lecture:

“AFTER a brief false start in extending these ideas, attributable clearly to my *gaucherie* in the details of quantum chemistry, I very soon realized that I needed more help than was available in my immediate circle, and I sought out Roald Hoffmann... I told him my story, and then, essentially, put to him the question ‘Can you make this respectable in more sophisticated theoretical terms?’”^[8b]

Woodward and I began to talk in that period. An important conversation I recall took place after a seminar by W. von E. Doering. By that time I had done the calculations and could confirm the ground- and excited-state stereochemical preferences. The electrocyclic reaction paper was submitted on November 30, 1964, and published in the January 20, 1965 issue of the *J. Am. Chem. Soc.*^[6a] Then R.B. Woodward and I went on to the rest of our orbital symmetry work. There was a lot to do...

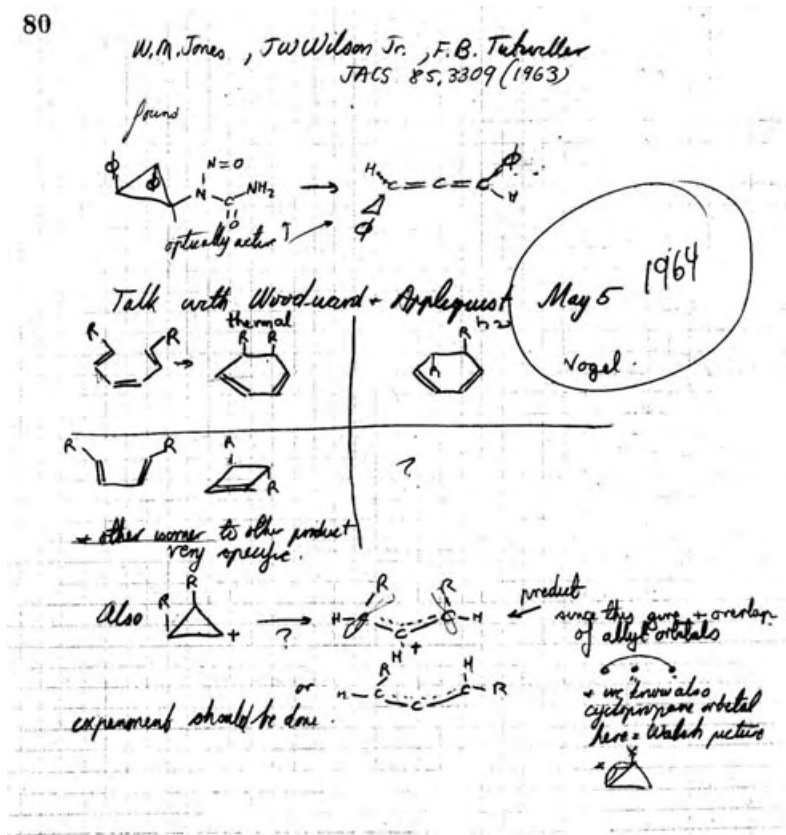


Figure 1. May 5, 1964, entry in Roald Hoffmann’s notebook. The year in the date was written in some time later.

Corey's Role in the Orbital Symmetry Story and Woodward's Denial of It

In the letter to me of November 16, 1981, E. J. Corey says that he told me in May 1964 that he had suggested to R. B. Woodward the HOMO explanation for the stereochemistry of electrocyclic reactions, and that Bob had taken over the idea from him. I spoke to Corey often in that period, but I have no recollection of such a conversation; I think Corey's statement would have been so striking (especially the part about Woodward taking the idea from Corey) that I would have remembered it.

Nevertheless, there *was* an idea in my mind then that Corey had a stake in the electrocyclic reaction story; my reconstruction today is that in the late spring and summer of 1964 Corey kept talking to me as if he did have such a role, as if the electrocyclic reaction research were joint work between Corey, Woodward, and me. Eventually, I was sufficiently puzzled by this that I did speak to Woodward. I do not remember when that was; I suspect it was later, in the fall of 1964, when we wrote our first paper.

When Woodward and I spoke of the matter—again, I cannot remember when it was—I asked him directly if Corey had a role in this work. He said “no”—this was our (R.B.W. and R.H.) work.

I did not question Woodward further. In retrospect, I regret not doing so, and I regret not asking Corey more directly to tell me his role in the work. R. B. Woodward was 47, the top synthetic organic chemist in the world. E. J. Corey was 36, a full Professor at Harvard. In May 1964 I was 26, a new Ph.D., a Junior Fellow to be sure, but just starting out in my career.

In the more than a year that I remained at Harvard (I left in June 1965), I kept on talking to Corey and learned a lot from him. I do not remember any cooling of our relationship, though I certainly spent more and more time with Woodward. Corey, in his correspondence with me, disagrees, saying that our previously frequent conversations stopped after I began working with Woodward.

My Perception of What Happened

I have no reason to doubt Corey's statement that there was a conversation between Corey and Woodward on May 4, 1964, even though we have only Corey's account of it.

But, I also do not think that the conversation “*provided the basis for the further development of these ideas into what became known as the Woodward–Hoffmann rules*,” as Corey writes. Here are some factors that go into my reasoning:

- Woodward had a habit of posing to people problems of great interest. And also of posing such problems as puzzles, even if he had the solution. Specifically, we know that he talked about the electrocyclic conundrum—to H.C. Longuet-Higgins, and Lionel Salem, for instance—as it was taking shape experimentally in the work of others and in the vitamin B₁₂ synthesis he was pursuing in collaboration with A. Eschenmoser's group.
- I think Woodward was perfectly capable of coming up with the frontier orbital explanation by himself. Though he began his career with VB arguments, I found Woodward in 1964 pretty well-versed in MO ideas. Woodward had learned a lot from William Moffitt, around the ferrocene and octant rule stories. Orbital ideas were in the air, the classic Streitwieser and Roberts books widely read, the success of the Hückel rule amply demonstrated. There was also the L. J. Oosterhoff “forerunner” (see below), which Woodward knew about.

One interesting piece of evidence for Woodward's knowledge of molecular orbitals is in a published comment he made after a lecture by Rolf Huisgen in a Welch Foundation Conference in 1961.^[10] Woodward draws quite explicitly the orbitals of a vinyl carbene (albeit without phases), and asks “*Do we have specific orbital geometric requirements [for Huisgen's reaction] and would they in this case preclude the operation of the mechanism which is so general in many of the cases?*”

My strong feeling is that Woodward had the frontier orbital idea before he spoke to Corey. I think that Corey's coming up with a similar way of thinking about the reaction in that May 4 conversation perhaps might have prompted Woodward to push on, and to ask for my assistance with calculations supporting the frontier orbital approach. For some reason, he was unsure of himself (not a characteristic one normally associated with Woodward...) and needed the support of a theoretical chemist.

Going back to the Corey–Woodward meeting of May 4, 1964, it would not be the first time that two people came away from a conversation with diametrically opposed ideas of what was said.

Crediting Suggestions: Then and Now

Assuming that the contents of the May 4, 1964 conversation were as E. J. Corey reports them, then I think that at best Corey has a claim to a rediscovery of the Oosterhoff orbital argument of 1961. In a paper by E. Havinga and J. L. M. A. Schlatmann, the authors write:

As Prof. Oosterhoff pointed out, another factor that possibly contributes to this stereochemical difference between the thermal and photoinduced ring closure may be found in the symmetry characteristics of the highest occupied π orbital of the conjugated hexatriene system.^[11]

The Oosterhoff “forerunner” to the orbital symmetry control ideas is mentioned in a footnote in our first 1965 paper; its role has been discussed by J. A. Berson in his book “Chemical Creativity.”^[12]

In 1963–1964, E. J. Corey and A. G. Hortmann accomplished the total synthesis of dihydrocostunolide. A crucial step involved a stereospecific electrocyclic reaction. The two papers on the work^[13] do not have any reference to an electronic factor in the stereoselectivity. Neither is the Havinga and Schlatmann paper mentioned. The full Corey and Hortmann paper was submitted on August 5, 1965, some months after publication of the first paper by Woodward and me.

The full paper on the dihydrocostunolide synthesis provided a place for Corey to state his electronic explanation. It was an opportunity not taken.

Should Corey's suggestion of the frontier orbital explanation for the stereochemistry of electrocyclic reactions have been credited in our first paper and subsequent ones? I can only speak for myself, and from today's perspective. We all make decisions, some easy, some hard, of what to reference/credit in our papers. If the substance of what E. J. Corey reports was said in that conversation with Woodward is true, then I believe it should have been credited. As Oosterhoff's suggestion was. I would be ready today to regret the omission and apologize to Corey for it. But, I am torn... between the conviction with which Corey tells his story in 1981 and today, torn between that and the impossibility of Woodward commenting on the decision today, as well as Woodward's 1964 denial to me of a role for Corey. With Woodward not alive, and no record except Corey's memory for the essence of that conversation, I just cannot say today that the conversation should have been credited.

A Claim Unfairly Made

The matter should have been argued out in 1964, by Corey persisting in telling Woodward of his (Corey's) perception of his contributions. Seventeen years later, Woodward gone, Corey,

without publishing his account, wanted me to tell others that *his* claim was valid.

People will form their own opinions of Corey's explanation of why he didn't press a public claim (that it would have hurt Harvard, that Woodward would eventually give him credit). Too bad he didn't speak out; had Corey done so in 1964, or in the period 1964–1979, we could have had Woodward's viewpoint.

I believe that E. J. Corey's perception of the consequences of what he told R. B. Woodward is just that—what he, Corey, believes. Based on the arguments I made above, and on what I remember, I don't think that the conversation in question influenced in any significant way the beginning of the orbital symmetry control story. And given that Corey's claim was (and is being) made after Woodward's death—when the claim could have been made for 15 years in Woodward's lifetime—that claim is also deeply and fundamentally unfair.

Published Online: November 19, 2004

- [1] a) R. B. Woodward, R. Hoffmann, *J. Am. Chem. Soc.* **1965**, *87*, 395–397; b) R. Hoffmann, R. B. Woodward, *J. Am. Chem. Soc.* **1965**, *87*, 2046–2048; c) R. B. Woodward, R. Hoffmann, *J. Am. Chem. Soc.* **1965**, *87*, 2511–2513; d) R. Hoffmann, R. B. Woodward, *J. Am. Chem. Soc.* **1965**, *87*, 4388–4389; e) R. Hoffmann, R. B. Woodward, *J. Am. Chem. Soc.* **1965**, *87*, 4389–4390.
- [2] R. Hoffmann, R. B. Woodward, *Acc. Chem. Res.* **1968**, *1*, 17–22.
- [3] R. B. Woodward, R. Hoffmann, *Angew. Chem.* **1969**, *81*, 797–870; *Angew. Chem. Int. Ed. Engl.* **1969**, *8*, 781–853 (reprinted in book form by Verlag Chemie and Academic Press).
- [4] E. J. Corey, *Chem. Eng. News* **2004**, *82*(13), 42–44.
- [5] E. J. Corey, *J. Org. Chem.* **2004**, *69*, 2917–2919.
- [6] R. Hoffmann, "Scientific Papers", [Collection No. 14/8/3360] Division of Rare and Manuscript Collections, Cornell University Library.
- [7] "Robert Burns Woodward": E. Blout, *Biographical Memoirs*, Vol. 80, The National Academy Press, Washington, D.C., **2001**, pp. 2–23.
- [8] a) R. B. Woodward, "The Conservation of Orbital Symmetry," in *Aromaticity*, special publication no. 21, London: The Chemical Society, London, **1967**, pp. 217–249; b) O. T. Benfey and P. J. T. Morris, *Robert Burns Woodward: Architect and Artist in the World of Molecules*, Chemical Heritage Foundation, Philadelphia, **2001**, pp. 415–452; this book also reprints reference [8a].
- [9] D. E. Applequist, personal communication to P. Göllitz, 2004.
- [10] R. Woodward in *Welch Foundation Conferences on Chemical Research IV. Molecular Structure and Organic Reactions*, (Ed.: W. O. Milligan), Welch Foundation, Houston, **1961**, p. 87.
- [11] E. Havinga, J. L. M. A. Schlatmann, *Tetrahedron* **1961**, 146–152.
- [12] J. A. Berson, *Chemical Creativity*, Wiley-VCH, Weinheim, **1999**, pp. 26–31.
- [13] E. J. Corey, A. J. Hortmann, *J. Am. Chem. Soc.* **1963**, *85*, 4033–4034; E. J. Corey, A. J. Hortmann, *J. Am. Chem. Soc.* **1965**, *87*, 5736–5742.

Primo Levi's *The Periodic Table*. A Search for Patterns in Times Past

Amir H. Hoveyda*

Keywords:

chemistry in literature · Levi, Primo

“But all at once it dawned on me that this was the real point, the contrapuntal theme; just this: not text, but texture; not the dream but topsy-turvical coincidence, Not flimsy nonsense, but a web of sense. Yes! It sufficed that I in life could find Some kind of link-and-bobolink, some kind Of correlated pattern in the game, Plexed artistry, and something of the same Pleasure in it as they who played it found.”

Vladimir Nabokov, *Pale Fire* (Canto Three)

He is not recognized for any contributions to science. He did not receive any scientific accolades, nor was he a university professor. Yet it is likely that Primo Levi will be remembered as a singularly influential chemist of the twentieth century.

A survivor of the world of concentration camps, Levi was trained as a chemist but is admired as a writer and an artist. Levi did not write because he felt that his life would be the stuff of drama that satisfies common curiosities. It was not a woolly relative, a wild whim, or a wily editor, tongue stained with tribal praise that urged him to author books. Writing for Levi was not a distraction from the everyday life—it was life itself.^[+]

“I had returned from captivity ... was living badly. The things I had seen and suffered were burning inside me; I felt closer to the dead than the living, and felt guilty at being a man, because men had built Auschwitz, and Auschwitz had gulped down millions of human beings, and many of my friends, and a woman who was dear to my heart. It seemed that I would be purified if I told its story. ... [By] writing I found peace for a while and felt myself become a man again, a person like everyone else, neither a martyr nor debased nor a saint ...”

In his creation *The Periodic Table*, Levi, with touching thoughtfulness, sketched the magic of the elements that make up this world. As with all enduring works of art, *The Periodic Table* is open to numerous interpretations—it rewards us with new vistas upon every re-reading. Levi portrayed the periodic table as a mirror for reflection, through which we might steal a glimpse at the meaning of our existence. Elements in *The Periodic Table* conjure memories, offering fresh notions meant to guide us, at a conscious as well as a subconscious level, in our search to understand Time and the scars that its tyranny leaves on our psyche. Through such meditative explorations we escape the prison of the hours and extend our consciousness beyond the oppressive cage of the immediate present.

The attributes of an element are used by Levi as a metaphor for his discussion in a particular essay; an element can be a nugget hiding a thought or an event that we are made privy to. For Levi, each element is the objects and sensations that cast their mysterious shadows in the writings of Proust: the celebrated Madeleine dipped in a tisane offered by Aunt Leonie

or the musty smell in uncle Adolphe's study. In *The Periodic Table* earthly elements hold ghosts of the past awaiting release initiated by an unexpected meeting, at an unforeseen date, at an unknown location. Reading *The Periodic Table* makes us wonder what do different elements mean to us. What mental reactions do they initiate in our subconscious? What fresh slices of the past have been faithfully sealed for us? We may have been taught as young students, and may now be convinced that Lithium, Europium, Vanadium and Iodine do not belong to the same family in the periodic table. *The Periodic Table* leads us to reconsider. We are encouraged to look again; Ar, Mo and Ir might well be connected in the land of dreams.

On the visible plane, the letter “K” represents potassium. But for Levi, this eleventh letter of our alphabet, unleashed anxieties, fears, sounds and smells of that frightful day when he nearly set his laboratory on fire. Unable to find pieces of sodium, as advised by the procedure that he was to follow for purification of benzene, Levi decided to substitute potassium. He was taught that potassium is

“sodium's twin, but it reacts with air and water even with greater energy. ... So I handled my ‘half-pea’ [of potassium] like a holy relic: I placed it on a piece of dry filter paper, wrapped it up in it, went down into the institute's courtyard, dug out a tiny grave, and buried the little bedeviled corpse ...”

I took now the empty flask, put it under a faucet, and turned on the water. I heard a rapid thump and from the neck of the flask came a flash of flame directed at the window that was next to the washbasin and the curtain around it caught fire. While I was stumbling

[*] Prof. Dr. A. H. Hoveyda
Department of Chemistry
Merkert Chemistry Center
Boston College
Chestnut Hill, MA 02467-3860 (USA)
Fax: (+1) 617-552-1442
E-mail: amir.hoveyda@bc.edu

[+] Quotations in this essay are from: Primo Levi, *The Periodic Table* (translation by R. Rosenthal), Everyman's Library, New York, 1995.

around looking for some even primitive means to extinguish it, the panels of the shutter began to blister and the room was now full of smoke. I managed to push over a chair and tear down the curtains; I threw them on the floor and stomped furiously on them, while the smoke half blinded me and my blood was throbbing violently in my temples.

... In a way it served me right: these are the things that happen to the profane, to those who dawdle and play before the portals of the temple instead of going inside. ... [The flask] must have contained, if nothing else the vapor of the benzene, beside of course the air that came in through its neck. But one has never seen the vapor of benzene, when cold, catch fire by itself: only the potassium could have set fire to the mixture, and I had taken out the potassium. All of it?

... I thought of another moral, ... and I believe that every militant chemist can confirm it: that one must mistrust almost-the-same (sodium is almost the same as potassium, but with sodium nothing would have happened), the practically identical, the approximate, the or-even, all surrogates, and all patchwork.

Potassium, the over-eager alkali metal represented to Levi the precariousness of life in a world of approximations. After all, one crucial thread that connects arts and sciences is the significance of subtleties. The importance of details is again brought forth in the chapter entitled *Vanadium*. Here, in a letter that Levi receives in response to his queries regarding the quality of a recent shipment of resin that his company had purchased from a German firm, he notices a misspelling. The correspondent, a Dr. L. Müller, writes "beta-naptylamin" in his letter instead of "beta-naphthylamine." Two h's missing; shaped like walking sticks, they lead Levi to a past that he did not necessarily wish to revisit.

"There was a Müller in my previous incarnation, but Müller is a very common name in Germany. ... Why continue to think about it? And yet, ... I could not quiet a doubt, a kind that refuses to be pushed aside and rasps slightly within you, like termites. Oh, come now, there must be two hundred thousand Müllers in Germany, forget it and think about the varnish ..."

Like all dedicated chemists, Levi followed his instinct. He was not about to trust his theory. "... [T]here is trouble in store for anyone who surrenders to the temptation of mistaking an elegant hypothesis for a certainty: the readers of detective stories know this quite well." After some deliberation, Levi managed to write to Müller, asking whether he was the man who was his "supervisor" at Auschwitz. Müller was the same man. His written response to Levi set free memories awaiting the right time, the right place to release and render lucid emotions that go far and deep in defining us as individuals. But it was not just memories that emerged from their shell.

"The Müller character was 'entpuppt', he had come out of his chrysalis, he was sharply defined, in perfect focus. Neither infamous nor a hero: after filtering off the rhetoric and the lies in good or bad faith there remained a typically gray human specimen, one of the not so few one-eyed men in the kingdom of the blind."

Much of what we label as the "real world" is the fruit of our imagination; reality frequently coincides with the imaginary world. Our senses become excited about the events that we can only imagine will take place in the future. When we recall the past, what we voluntarily remember, rarely remains unmodified by imagination. It is perhaps natural that once a set of events has occurred, imagination begins to alter memories, and gradually they grow to reflect who we are more than actually what happened. Memories, with time, are molded and remolded like pieces of clay in the hands of a sculptor. Unpleasant visits to relatives are remembered as touching experiences. We renew such visits, and by experiencing the original reality in its refreshed form, we realize the alteration that the persistent force of imagination has imposed on our past. It is for such reasons that an autobiography might be more the fruit of a writer's imagination than an impartial chronicle of events. In reading about Levi's past and his memories as he recalls and relates them, we gain insight about the unique contours of his imaginary world. The *Periodic Table* shows that remembering and searching for meaningful patterns in our past can prove to be a

promising gateway that can lead to a better understanding of who we are.

In a few segments such as *Lead* and *Mercury*, Levi speaks to us purely through the magic lantern of his imaginary world. In these stories Levi shows us that truth can be discovered anywhere, in any land, guided by imagination and invention. Through the story in *Lead* Levi deals with the symbiotic relationship between fiction and reality, observation and theory. While reading Levi's stories one wonders: What is the relationship between us the reader and Levi the storyteller? "*The crew chief came from Kriti and was a big liar: he told stories about a country where there lived men called Big Ears ...*" If one who tells tales is a liar, then who is the Levi who tells us the story of the crew chief? May we not also find some truth in Levi's other tales? If so, is only what we call "reality" the source of truth? Or can truth be found in our imagination and in our theories, in our stories? Is creativity how we see and interpret the world? Is there only one reality, one truth, one theory?

Levi, like many great artists, viewed everything through myriad dimensions. He cherished the unique power of imagination, but also recognized the freshness that rests within unspoiled facts. Facts were a source of inspiration to Levi. To be able to relate actual events in their original state, however, requires that we keep imagination at bay. Levi wanted his readers to see how "*the boredom of repetitious work was being transformed into nervous gaiety, as when as children you play hide and seek and discover your opponent clumsily squatting behind a bush.*" A frank account of struggles to decipher the mysteries of nature had its own unique poetry for Levi; it allowed him to see himself and nature in its own reality, clear from the fog and shifting images of an imaginary world. In the chapter *Silver* Levi confesses:

"... [T]he inadequacy of our preparation, and the need to make up for it with luck, intuition, stratagems and a river of patience. ... I wanted to put on display ... the strong and bitter flavor of our trade, which is only ... a more strenuous version of the business of living. ... [T]he stories of solitary chemistry, unarmed and on foot, at the measure

of man ... the chemistry of the founders, who did not work in teams but alone, surrounded by indifference of their time, generally without profit ..."

The *Periodic Table* may make one appreciate that to a large extent scientific papers represent the investigator's account of how a discovery is made. The manner in which we toil as scientists seldom coincides with our ideal world, a world where a total synthesis transpires exactly as we had originally planned it, or where we design that perfect catalyst on a first attempt. Renditions of reality reported by an investigator emanate from processed memory, which in turn is colored by the chronicler's ideals (his dream world). In scientific papers it is the data, it is only the uncompromising hard facts that bear no allegiance to, and remain unaltered by, a researcher's imagination.

One of the more prophetic chapters in *The Periodic Table* is *Zinc*; here, Levi reflected on a subject that is a perennial topic of interest to chemists: impurities. In thinking about this late transition metal, one that "... they make tubs out of ... for laundry, not a veteran covered with glory like copper ..." Levi recalls an early attempt, when as a student he attempted to purify zinc sulfate. The procedure called for sulfuric acid; the acid was first to be diluted. But, as always, certain details needed to be tended to first.

"[A] detail which at first reading had escaped me, namely, that the so tender and delicate zinc ... behaves ... in a different fashion when it is very pure; then it obstinately resists attack. One could draw from the two conflicting philosophical conclusions: the praise of purity, which protects from evil like a coat of mail; the praise of impurity, which gives rise to changes, in other words to life. I discarded the first, disgustingly moralistic, and I lingered to consider the second, which I found more congenial."

Levi's interpretation is poignant on two levels. It is ironic how as chemists we have become increasingly aware of the positive role that impurities can have on reluctant reactions. Curiously, once their (often unexpected) positive attributes are discovered, such impurities are referred to as additives. Combinatorial chemistry has turned our atten-

tion to the wonders of the chemistry of mixtures. Inorganic and organometallic chemists, in spite of an undying zeal for inert conditions, have provided us with reactive and colorfully impure alloys. Water and air, primordial necessities of life for all creatures on earth, and yet the angel of death to many of our fragile molecular creations, can prove at times to be the indispensable ingredients that push reluctant molecules forward over otherwise indomitable energy barriers.

On a more sublime but sobering level, Levi expanded his journey of self-discovery to include the role of impurities in the larger world, the one outside science:

"In order for the wheel to turn, for life to be lived, impurities are needed, and impurities of impurities in the soil, too, as is known, if it is to be fertile. Dissent, diversity, the grain of salt and mustard are needed: Fascism does not want them, forbids them, ... it wants everybody to be the same ..."

It was in the same laboratory that young Levi saw a "small zinc bridge" that he would negotiate to reach Rita while dispensing with his "masculine solitude." Rita was a quiet, thin, pale and sad but confident fellow student who happened to be "cooking [his] same dish." But Levi was to discover that all objects of desire, upon familiarity, lay bare their blemishes at which time the pleasures of imagination are reduced to their unimpressive, but still lovable, earthly dimensions.

Rita "got through exams with good marks, but without the genuine appetite that I felt," Levi explains. She read Mann's *Magic Mountain* only to discover "how far Hans would go with Madame Chauchat, and mercilessly skipped the fascinating (for me) ... metaphysical discussions between the humanist Settembrini and the Jewish Jesuit Naphtha." Levi was disappointed; "[I]t could even become an essential and fundamental discussion, because I too am Jewish, and she is not ..." Mundane zinc took Levi on a journey of self-discovery. "I am the impurity that makes zinc react, I am the grain of salt or mustard."

But impurities do not rejuvenate by being exclusionary. Impurities are not impurities if they only cling to other impurities.

"... I soon realized that Rita was different from me: she was not a grain of mustard. ... For her university was not at all the temple of knowledge: it was a thorny and difficult path which led to a degree, to a job. ... All this did not put a distance between us; on the contrary, I found it admirable ..."

[T]rembling with emotion, I slipped my arm under hers. ... I fell into step with her, and felt exhilarated and victorious. It seemed to me that I had won a small but decisive battle against the darkness, the emptiness, and the hostile years that lay ahead."

Through conceiving and writing *The Periodic Table*, Levi explored his personal reality. Levi aimed to unravel mysteries of human behavior and of nature, mysteries that test the limits of our reasoning and imagination. Levi's masterpiece bears tales of his struggles to understand the meaning of his existence and the world surrounding it. In a chapter entitled *Lead* Levi writes:

"This is a difficult thing to explain, but it has already happened more than once that someone, who knows when, coming from who knows where, at some remote time, perhaps before the Flood, finds a vein, does not say anything to anyone, tries by himself to dig out the rock, leaves his bones there, and the centuries pass. My father told me that in whatever tunnel or cave you may dig you find the bones of the dead."

Levi's writing encourages us to search the world in our own way and in our own time. It inspires us to see nature through our eyes, to try and take pleasure in solving her puzzles, anagrams and acrostics. Levi examined—voraciously—ideas, symbols, peoples, eras and kingdoms, songs, anecdotes, mirrored images, revelations, wonders, ruses, incredible tales, endless sufferings.

The Periodic Table invites us to travel the road that, however long and arduous, may be the only means through which we might catch a glimpse of the flicker of light that shines from the depth of a dark abyss. It is an infinite number of small steps, each taken by an instance of recognition that leads us towards the bottom of this unfathomable darkness. Perhaps, it is there that rests the answer to the meaning of it all.

Published Online: November 2, 2004

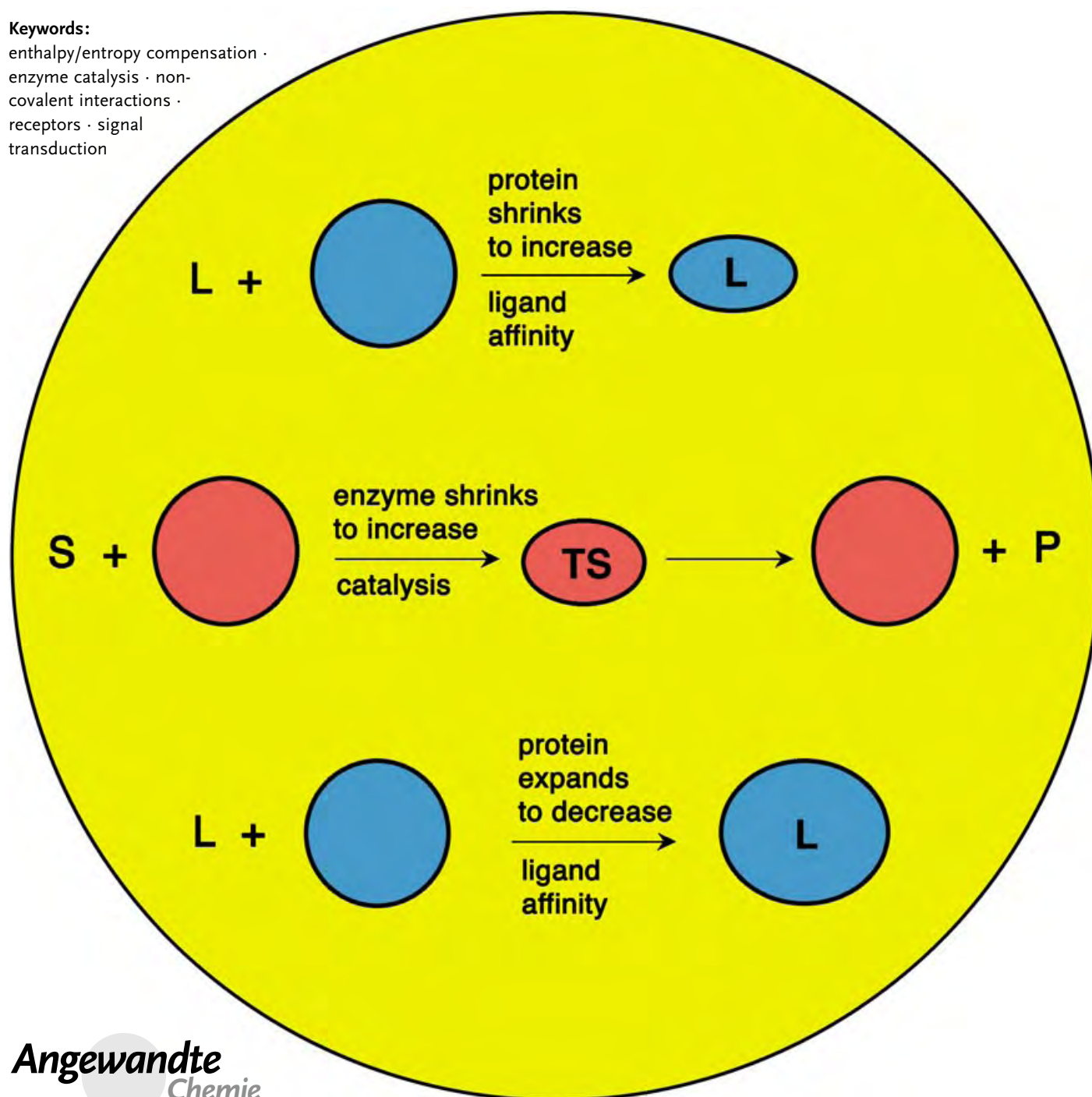
Ligand Binding Energies

Understanding Noncovalent Interactions: Ligand Binding Energy and Catalytic Efficiency from Ligand-Induced Reductions in Motion within Receptors and Enzymes

Dudley H. Williams,* Elaine Stephens, Dominic P. O'Brien, and Min Zhou

Keywords:

enthalpy/entropy compensation ·
enzyme catalysis · non-
covalent interactions ·
receptors · signal
transduction



Noncovalent interactions are sometimes treated as additive and this enables useful average binding energies for common interactions in aqueous solution to be derived. However, the additive approach is often not applicable, since noncovalent interactions are often either mutually reinforcing (positively cooperative) or mutually weakening (negatively cooperative). Ligand binding energy is derived (positively cooperative binding) when a ligand reduces motion within a receptor. Similarly, transition-state binding energy is derived in enzyme-catalyzed reactions when the substrate transition state reduces the motions within an enzyme. Ligands and substrates can in this way improve their affinities for these proteins. The further organization occurs with a benefit in bonding (enthalpy) and a limitation in dynamics (cost in entropy), but does not demand the making of new noncovalent interactions, simply the strengthening of existing ones. Negative cooperativity induces converse effects: less efficient packing, a cost in enthalpy, and a benefit in entropy.

1. Introduction

With the completion of a large part of the sequence of numerous genomes, a frontier research interest has now developed in the field of proteomics. This field is concerned with the more complete identification of proteins (for example, the identification of 1484 proteins from the yeast strain *S. cerevisiae*),^[1] with the interactions between these proteins, and with the way that they bind to ligands. The binding constants for these interactions depend on the differences in noncovalent bonding between free and bound states. Insofar as binding constants cannot be predicted, they are poorly understood, and in this sense the molecular basis of biological function is also poorly understood.

In this Review, an approach that treats systems of multiple interactions as the sum of their parts (the additive approach) is first described. It is a very useful approximation. However, in reality, the interactions are often (but not always) greater than the sum of their parts (positively cooperative) or less than the sum of their parts (negatively cooperative). Such cooperative interactions are covered in the second part of the Review. Some consequences for biology are described in Sections 9 and 11–14, with the implications for the understanding of ligand binding energy and enzyme catalysis being particularly important.

1.1. What Is It that Drives a Change?

The Second Law of Thermodynamics states that “in a spontaneous process, the entropy of the universe increases”. The simplest description of entropy S is that it is a measure of disorder; thus entropy increases with increasing disorder (more accessible arrangements). The Second Law therefore tells us that in a spontaneous process there will be an overall increase in disorder (increase in S). If the entropy of the

universe is S_0 before the change and S_1 after the change, then the overall entropy change is $\Delta S_{\text{overall}} = S_1 - S_0$. The more

From the Contents

1. Introduction	6597
2. The Additive Approach	6599
3. An Equation for the Estimation of Binding Constants	6600
4. Why is the Adverse ΔG_{int} Term Relatively Small?	6601
5. Cooperative Binding Processes: Definitions	6602
6. Cooperative Binding at a Single Interface	6603
7. Cooperative Binding over Multiple Interfaces	6604
8. Positive Cooperativity over Multiple Interfaces	6605
9. Negative Cooperativity over Multiple Interfaces—Hemoglobin	6606
10. Negative Cooperativity that Breaks Interfaces	6608
11. Reduced Dynamics within Protein Receptors as a Source of Ligand Binding Energy	6609
12. Ligand/Receptor Interactions that are Strongly Enthalpy or Entropy Driven	6610
13. Changes in the Aggregation of Receptors in Signal Transduction	6610
14. Volume Reductions within Enzymes can Promote Catalysis	6611
15. The General Structural Consequences of Positively Cooperative Binding	6613
16. Conclusion	6614

[*] Prof. Dr. D. H. Williams, Dr. E. Stephens, Dr. D. P. O'Brien, M. Zhou
Department of Chemistry
University of Cambridge
Lensfield Road, Cambridge, CB2 1EW (UK)
Fax: (+44) 1-223-336913
E-mail: dhw1@cam.ac.uk

positive is $\Delta S_{\text{overall}}$, the greater is the extent to which the process will occur. In considering the magnitude of $\Delta S_{\text{overall}}$ for any process, it is fruitful to divide the entropy change into two parts, namely, the entropy change in the system (what we are studying) and the change in order in the surroundings (the rest of the universe). Since the surroundings are in practice essentially infinite, the change within them is effectively diluted to zero in any finite element, but it is there.

The change in order in the surroundings of the system undergoing change is determined by the change in the enthalpy (exothermic: negative ΔH , endothermic: positive ΔH) of the process, and by the temperature T at which the change occurs. An exothermic process leads to more disorder in the surroundings (by increasing the motion in the surrounding universe). The extent of this increase in disorder is inversely proportional to the temperature. The reason for this latter relationship can be qualitatively understood: surroundings possessing little kinetic energy (low T) become proportionately more random by a given exothermicity than are those possessing more kinetic energy (higher T). Since an exothermic process (ΔH negative) gives a positive contribution to the total entropy change, the increase in entropy from this term is $-\Delta H/T$.

The second part of the entropy change (the change in order within the system undergoing change) is denoted as ΔS_{sys} , and positive values of ΔS_{sys} promote the change. Therefore, taking the two terms together, the propensity for spontaneous change can be quantitated [Eq. (1); for simplicity, the subscript "sys" is normally dropped].

$$\text{Increase in disorder that occurs in a process} = -\Delta H/T + \Delta S_{\text{sys}} \quad (1)$$

It is a consequence of the crucial insights of Boltzmann and Gibbs that we have this relationship. Perhaps confusingly

for generations of students, a new term ($-\Delta G/T$) was coined for this net increase in entropy in a spontaneous process. Thus, $-\Delta G/T = -\Delta H/T + \Delta S$, and leads to the famous Gibbs equation [Eq. (2)].

$$\Delta G = \Delta H - T\Delta S \quad (2)$$

The Gibbs equation states that ΔG (the free-energy change) is negative for a spontaneous change. Defining ΔG as the *negative* of the total entropy change for a process, multiplied by T , is not so strange as it may at first seem. Early in their careers, physical scientists tend to think in terms of spontaneous change being driven by a release of heat (exothermicity, which means that ΔH is negative). Although this is only one of the determining factors (see above), we therefore have early training to think of a driving force for a spontaneous change in terms of a parameter which has the units of energy and is negative in value. Continuity of thought is encouraged by taking the determinant of spontaneous change (a *positive* entropy change), changing its sign to make it negative, multiplying it by T to give it the units of energy, and calling it "free energy".

Not uncommonly, students are mystified by the spontaneous development of highly ordered organisms, which seems to them inconsistent with the Second Law. It is of course possible because, simultaneous with the development of the ordered organism, the surroundings of the organism are disordered to a greater degree.

Binding affinity can be expressed either in terms of the difference in free energy of free and bound states, or in terms of the equilibrium constant (K), where $\Delta G = -RT \ln K$ (where R is the gas constant and T is the temperature). The more negative ΔG is, the larger is the binding constant. For example, at 300 K, ΔG values of -5.7 and $-11.4 \text{ kJ mol}^{-1}$



Dudley Williams received his BSc and PhD degrees (in chemistry and organic chemistry, respectively) from the University of Leeds in 1958 and 1961. He subsequently carried out post-doctoral research at Stanford University (US) and in 1964 moved to the University of Cambridge (UK). He is a Fellow of Churchill College and Professor of Biological Chemistry. He was elected a Fellow of the Royal Society in 1983.



Dominic O'Brien received his BSc in Natural Sciences at the University of Cambridge (UK) in 1996. He gained his PhD degree under the supervision of Dudley Williams at the University of Cambridge in 1998 for studying the mode of action and biosynthesis of antibiotics of the vancomycin group. His most recent academic work has been concerned with studies of cooperativity in molecular recognition with Dudley Williams.



Elaine Stephens obtained her PhD under the supervision of Anne Dell at Imperial College, London, for studies of glycoproteins by mass spectrometry. She is currently working on biological applications of mass spectrometry in the Department of Chemistry at Cambridge University.



Min Zhou obtained her BSc and MSc degrees at Nanjing University, China. She is currently a doctoral student at Churchill College, and is studying for her PhD degree under the supervision of Dudley Williams at the University of Cambridge.

correspond to binding constants of 10 and 100 M^{-1} , respectively, etc. By using the Gibbs equation to understand binding we can monitor the effects of changes in bonding within the system (ΔH) and changes in the entropy of the system (in terms of $T\Delta S$). Although ΔS , rather than $T\Delta S$, is strictly the change in entropy, experiments carried out at one temperature show that the terms are proportional. $T\Delta S$ has the advantage that its effect upon ΔG can be directly compared with that of ΔH .

1.2. Enthalpy/Entropy Compensation

A key point in what follows is that a decrease in motion implies a decrease in entropy, since it results in fewer accessible arrangements. Consider the formation of a specific noncovalent bond (for example, $\text{A}\cdots\text{B}$ for the transformation $\text{A} + \text{B} \rightarrow \text{A}\cdots\text{B}$). An increase in its strength (which corresponds to an increasing negative contribution to ΔH , and a more favorable binding process) will be accompanied by an increasing restriction in the relative motion of **A** and **B** in $\text{A}\cdots\text{B}$ (which corresponds to a negative contribution to ΔS , and so unfavorable to binding). This opposing interplay between enthalpy and entropy is known as enthalpy/entropy compensation, and is a fundamental property of noncovalent interactions.^[2–4] Importantly, it is not confined to binding in aqueous solution,^[5] nor should it be ascribed to errors of measurement.^[6] It arises because bonding opposes motion and, also reciprocally, motion opposes bonding. The two effects can be traded off against each other because the strength of noncovalent bonds is, at room temperature, comparable to the thermal energies that oppose them. The idea of enthalpy/entropy compensation is therefore less important in the study of covalent bonds, which are typically too strong to be effectively opposed by thermal motions at room temperature.

2. The Additive Approach

When cooperativity is ignored, contributions of ΔG values to the total free energies of binding may be added together, and contributions of binding constants K are therefore multiplied.

2.1. Costs in the Formation of a Bimolecular Complex ($\text{L} + \text{R} \rightarrow \text{L}\cdots\text{R}$)

When a ligand **L** binds to a receptor **R** it loses some of its translational (t) and rotational (r) motion relative to the receptor. This cost of association is designated as $\Delta G_{\text{t+r}}$, and is an adverse entropy term ($\Delta G_{\text{t+r}} = -T\Delta S_{\text{t+r}}$).^[7–9] If the ligand lost *all* its motion relative to the receptor, then the cost of the association at room temperature for a ligand with a mass of a few hundred Daltons is approximately $+57\text{ kJ mol}^{-1}$ (opposing binding by a factor of 10^{-10}).^[7–9] However, in typical ligand/receptor complexes, the strengths of the noncovalent $\text{A}\cdots\text{X}$ and $\text{B}\cdots\text{Y}$ bonds (Figure 1) are comparable to thermal

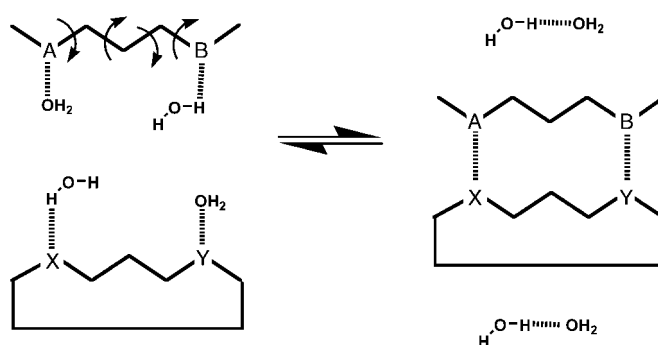


Figure 1. Complex formation between a ligand (containing polar functionalities **A** and **B**) and a receptor (containing polar functionalities **X** and **Y**) with exchange of four water molecules to the bulk solvent. (Broken lines indicate hydrogen bonds.)

energies and hence the bonds are highly elastic. Thus, the motional restriction occurring on ligand binding costs much less than $+57\text{ kJ mol}^{-1}$ (see Sections 3 and 4).

If a molecule has internal rotations that become more restricted on passing from the free to the bound state, then there is an entropic cost of $-T\Delta S_{\text{r}} = \Delta G_{\text{r}}$ to be paid for each restricted rotation. For example, the ligand shown in Figure 1 (top left) has four internal rotors (indicated by arrows) that allow much internal motion of the ligand prior to binding, but this motion is restricted upon formation of the complex. Binding is opposed by a contribution $4\Delta G_{\text{r}}$, and in the general case by $n\Delta G_{\text{r}}$, where n is the number of restricted rotors.

Complete restriction of an internal rotation has a free-energy cost (ΔG_{r}) of about 5 kJ mol^{-1} at room temperature.^[8,9] This value is also too large to be relevant to drug/receptor complexes, again because the energies of the interactions that are restraining the geometry of the complex are comparable to the thermal energies that tend to disrupt it. As a result, the internal rotors, although proscribed from undergoing full rotation, are able to undergo wagging motions in the bound state.

Molecules may bind to their receptors with the introduction of strain, or repulsive atom/atom interactions. Such effects are difficult to explore experimentally. For pragmatism, they are ignored in a simple approach to estimating binding affinities (Section 3), but are relevant in cases of negatively cooperative binding (Sections 6, 9, and 10).

2.2. Energy Benefits in the Formation of the Bimolecular Complex

The formation of a complex is favored when the ligand forms polar interactions to a receptor to give an overall negative change in free energy. The formation of two polar interactions ($\text{A}\cdots\text{X}$ and $\text{B}\cdots\text{Y}$) in water is illustrated in Figure 1. Water molecules which solvate the polar groups **A**, **B**, **X**, and **Y** prior to association become part of the bulk water after formation of the complex. These benefits can be semiquantified by including a benefit in the free energy (ΔG_{p}) for each interaction (which includes the changes in entropy associated with changes in solvent mobility).

The first attempt at a semiquantitation of drug–receptor interactions in terms of the costs and benefits outlined above was by Andrews, Craig, and Martin.^[10] We used a similar approach, but applied an additional term to account for the hydrophobic effect.^[11]

The hydrophobic effect is classically defined as a benefit to binding that is applicable when binding occurs in water.^[12,13] The benefit is a consequence of the removal of hydrocarbon surfaces from exposure to water upon formation of the complex. This effect can be measured by solvent-transfer experiments. For example, if **A** and **B** as well as **X** and **Y** are each separated by three methylene groups (Figure 1), the coming together of the hydrocarbon surfaces (with their concomitant removal from water exposure) will promote binding. The magnitude of the hydrophobic effect is proportional to the surface area of the hydrocarbon that is removed from exposure to water upon formation of the complex and can be estimated in terms of ΔG_h per unit of area A of hydrocarbon buried. The surface area of hydrocarbon that is removed from water exposure in the binding event is readily measured with the aid of computer graphics. Thus, the contribution to binding from the hydrophobic effect is $A\Delta G_h$.

The benefit of the removal of exposed hydrocarbon to water upon binding at room temperature derives from the fact that water molecules at hydrocarbon surfaces are more ordered than water molecules in bulk water.^[14] Therefore, the hydrophobic effect is normally largely entropy driven at room temperature, although it has a favorable enthalpy component in the special cases where water is expelled from an internalized cavity upon ligand binding.^[15]

3. An Equation for the Estimation of Binding Constants

Binding constants in aqueous solution can be estimated from Equation (3), which is derived from the above considerations.

$$\Delta G = \Delta G_{\text{tr}} + n\Delta G_r + A\Delta G_h + \sum \Delta G_p \quad (3)$$

ΔG is the observed free energy of binding, $\sum \Delta G_p$ is the sum of the free energies of binding for all the polar interactions made in the binding site,^[11] and the other terms are as defined in Section 2. Böhm^[16a] “trained” a variant of Equation (3) with a set of 45 interactions of experimentally known binding constants from the association of ligands of small molecular weight (66 to 1047 Daltons) with proteins through sets of known interactions (from X-ray structures). He divided the original ΔG_p values into two groups: those involving ionic interactions (ΔG_{ionic}) and those involving hydrogen bonds formed between neutral entities (the term ΔG_p was retained). Since the modified form of the equation has only five types of ΔG contributions and the 45 binding sites involve different combinations of these five types of ΔG contributions, average values for them can be obtained. The values obtained (Table 1) have proved very useful in the pharmaceutical industry.

Table 1: Average values for the parameters of Equation 3.

Parameter	Physical process	Value (kJ mol ^{−1})	Factor ^[a]
ΔG_{tr}	energy cost of bimolecular association	+5.4	(ca. 10)
ΔG_r	energy cost of restriction of an internal rotor	+1.4	(ca. 2 ^[b])
ΔG_h	benefit of the hydrophobic effect (per Å ² of buried hydrocarbon)	−0.17 (Å ^{−2})	(ca. 1 ^[c])
ΔG_p	benefit of making a neutral hydrogen bond of ideal geometry	−4.7	ca. 7
ΔG_{ionic}	benefit of making an ionic hydrogen bond of ideal geometry	−8.3	ca. 28

[a] Factor by which binding is promoted (opposed) at RT. [b] Per rotor. [c] Upon burial of 33 Å² of the hydrocarbon.

The use of the values given in Table 1 resulted in the equation reproducing the binding constants of the training set (which range experimentally from 40 M^{−1} to 2.5 × 10¹³ M^{−1}) with a standard deviation of 7.9 kJ mol^{−1}, which corresponds to a factor of 24 in binding affinity.^[16a] The standard deviation was a factor of 50 in binding affinity for a set of drugs outside the training set. This result represents an impressive outcome for a limited data set, although it should be noted that the inclusion of a larger variety of drug structures (for example, more heavily weighted with heterocyclic structures) somewhat decreased the success of the algorithm.^[16b] Several other relatively successful approaches for estimating binding constants have been published since this work, although the physical interpretation of the various terms (and coefficients) in these approaches is less simple.^[17,18]

The apparent binding energies obtained for the interactions (Table 1) are in good agreement with those obtained by other approaches, for example, from the mutation of proteins, which are also based on the partitioning of binding-energy contributions.^[19–21] Polar interactions (most commonly amide–amide hydrogen bonds and ionic interactions) are found to promote binding (negative values of ΔG) moderately in aqueous solution. The reason why the promotion of binding is relatively small is evident from Figure 1: the four hydrogen bonds of the dissociated state are replaced by four hydrogen bonds in the bound state.^[19]

The value for the hydrophobic effect is in reasonable accord with the values most commonly found in other studies. It is somewhat larger than those values estimated from the (low) solubility of hydrocarbons in water (0.10–0.14 kJ mol^{−1} per Å^{−2} of the hydrophobic surface buried from exposure to solvent).^[22–28] Yet it is smaller than those obtained by the deletion of methyl groups in binding sites, both within proteins or drug/receptor interactions (most frequently in the range 0.18–0.26 kJ mol^{−1} Å^{−2},^[20,29–32] although a range extending from 0.06 to 0.64 kJ mol^{−1} Å^{−2} has been reported.^[33–38] Presumably, the large range found in the literature reflects, at least in part, variations in positive and negative cooperative effects.

The localization of the drug at the binding site and restriction of internal rotations upon binding (see Section 2.1) spontaneously emerge from Equation (3) as factors which oppose binding (Table 1, positive values of ΔG_{tr} and ΔG_r , respectively). The average value $\Delta G_{\text{tr}} = +5.4 \text{ kJ mol}^{-1}$ is remarkably small, and represents only about one tenth of the maximum theoretical entropy loss corresponding to complete immobilization of the ligand (see Section 2). This small value presumably reflects, at least in part, the large residual motion that the drugs can exercise relative to the receptor to which they are bound. The average cost of restricting the rotation of an internal bond in the drugs ($+1.4 \text{ kJ mol}^{-1}$) is slightly less than that found for the formation of crystals from neat liquids that contain internal rotors ($2\text{--}3 \text{ kJ mol}^{-1}$).^[39] This finding probably reflects the fact that rotations are somewhat less restricted in these binding sites than they are in crystals. Most importantly, the application of the equation gives useful approximate binding constants in many cases.

4. Why is the Adverse ΔG_{tr} Term Relatively Small?

Given the assumption that the average value of ΔG_{tr} of $+5.4 \text{ kJ mol}^{-1}$ is representative of drugs as a whole, why is it so small? The stronger the noncovalent bonds that hold the complex together, the larger should be the restriction of overall motion (adverse entropy change, of which ΔG_{tr} is a measure). To test this hypothesis, it is necessary to examine associations where the entropy change can be put down solely, or largely, to ΔG_{tr} . Entropy changes arising from changes in solvation must be avoided, or minimized, which precludes the use of data for associations in water or other polar solvents. Additionally, the number of internal rotations that are restricted upon association must be zero, or limited, because interpretation of the entropy change must not be confused by the presence of a significant $n\Delta G_r$ term [Eq. (3)]. In the absence of these effects, the adverse entropy of association will be solely a consequence of, or dominated by, the ΔG_{tr} term.^[40]

The above considerations can be satisfied for simple bimolecular associations of relatively rigid entities occurring in the gas phase ($\text{A} + \text{B} \rightarrow \text{A} \cdots \text{B}$). Binding can only be promoted by a favorable enthalpy of interaction (ΔH), which measures the benefits of noncovalent bonding between the two portions of the complex. Binding can only be opposed by the unfavorable loss in translational and rotational entropy ($T\Delta S_{\text{tr}}$). The anticipated correlation between the heat given out (ΔH) and the order imposed ($T\Delta S_{\text{tr}}$, identical to $-\Delta G_{\text{tr}}$) is shown in Figure 2.^[2] There is a limit to the cost in entropy for bond formation in $\text{A} \cdots \text{B}$, which is reached when the bond strength is large compared to thermal energies, and at this point $\delta(\Delta H)/T\delta(\Delta S)$ is very large. However, when bond strengths are comparable to the thermal energy, the restraint is effectively opposed by the motion and $\delta(\Delta H)/T\delta(\Delta S)$ is smaller. Therefore, we can anticipate that the slope of the ΔH versus $T\Delta S$ graph (Figure 2) will increase as the bond strength increases through the “noncovalent region”.

Dunitz has indeed shown that a curve closely following the form of Figure 2 can be derived from a semiquantitative

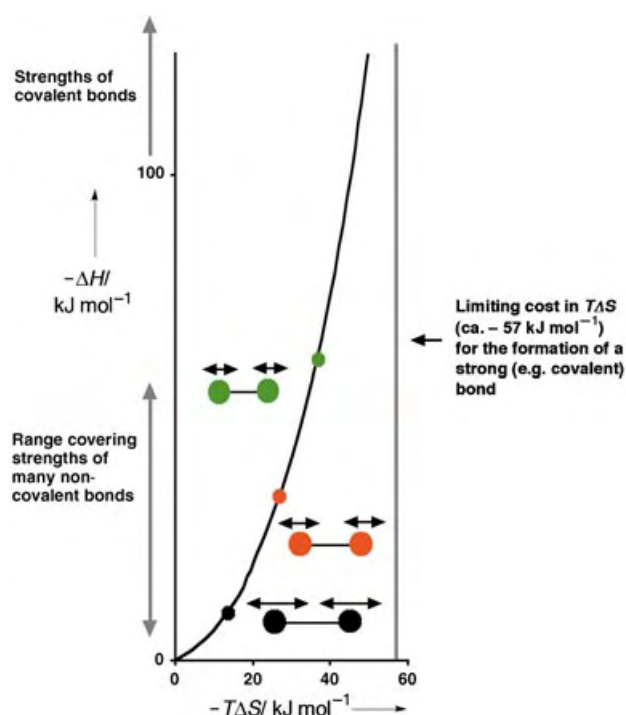


Figure 2. Anticipated relationship between the exothermicity (ΔH) and the cost in entropy ($T\Delta S$) for the complex formation $\text{A} + \text{B} \rightarrow \text{A} \cdots \text{B}$ in the gas phase or in a nonpolar solvent at 298 K (black curve). Under these conditions $-T\Delta S$ is a measure of ΔG_{tr} . When the relative motion of **A** and **B** in $\text{A} \cdots \text{B}$ is highly restricted, the entropy costs approach the limiting value of $T\Delta S \approx -57 \text{ kJ mol}^{-1}$. At room temperature the limit is reached at enthalpies corresponding to the formation of a covalent bond. As the $\text{A} \cdots \text{B}$ bond becomes weaker, there is increasing residual motion of **A** relative to **B**. The increasing motion, and the accompanying increase in bond length, is illustrated in the three sets of “dumbbells”, which correspond to the green, red, and black points on the curve. The adverse entropy of the association therefore becomes increasingly small.

approach based upon shallow energy wells.^[3] For such wells, bond extension and increased dynamics should become important as the depth of the well decreases. This point is illustrated schematically in Figure 2 for decreasingly exothermic associations (green, red, and black points on the curve). The decreasingly exothermic associations not only give rise to “looser” associations, but also to ones that give a less-favorable free energy of binding ($\Delta G = \Delta H - T\Delta S$) for population of the organized state. This last consequence follows because the weakest noncovalent interaction (black point) is, of the three, the one with the most efficient enthalpy/entropy compensation.^[3,4]

These conclusions are supported by experimental data. The adverse ΔG_{tr} term (expressed in terms of $T\Delta S_{\text{tr}}$) decreases as the favorable enthalpy of association is decreased (shallower well).^[2,40] The adverse ΔG_{tr} term is less than 13 kJ mol^{-1} in the cases of weakly exothermic associations (less than 20 kJ mol^{-1}). Put simply, “weak springs” give more residual motion at the binding interface.

A similar relationship should hold for corresponding noncovalent associations in nonpolar solvents because, to a useful approximation, these are like those in the gas phase.

This follows since the favorable entropy of desolvation of the polar groups that interact when the complex is formed should be relatively small. Experimental data for 233 such associations^[41] were examined to test this hypothesis.^[42] Although 215 of the data points produced a good correlation of the form predicted, 18 appeared anomalous (Figure 3). These 18 data points were subsequently shown to arise because of various kinds of errors.^[42]

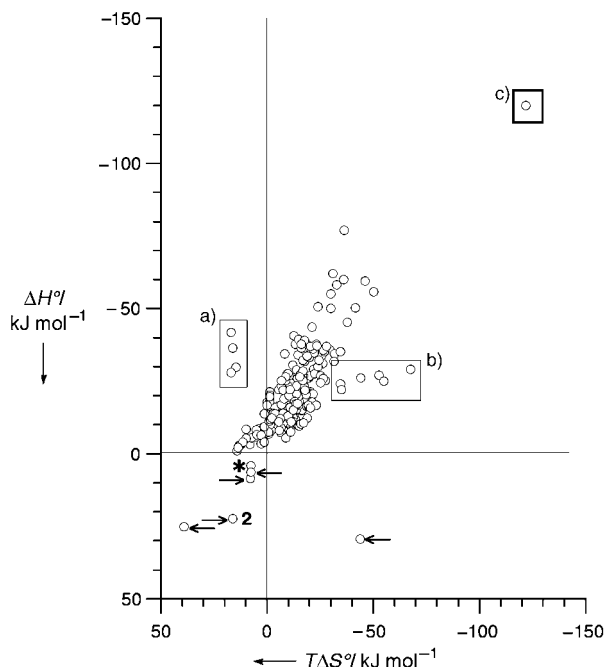


Figure 3. Enthalpy (ΔH) versus entropy ($T\Delta S$) diagram for the association of macrocycles with neutral molecules in a variety of nonpolar solvents.^[41] There are six groups of data points that appear to be inconsistent with the general form of the enthalpy/entropy compensation curve, but all of these are associated with errors^[42] (quite understandably arising in a valuable review^[41] of large breadth). Three examples of which follow: a) Four data points were transcribed with an incorrect sign for ΔS , thus requiring their transposition from the north-west quadrant to the north-east quadrant). b) Six data points were transcribed in the review with a conversion factor for ΔS that was too large (by a factor of 4.18 Joules/calories), thus requiring their transposition into the general region of the correlation). c) A point that is not an error in transcription was indicated by our experimental value to be erroneous. Given the correction of these errors, and others indicated by the arrows and asterisk,^[42] there is agreement between the general forms of Figures 2 and 3.

Many of the points lie in the north-west quadrant (Figure 3) for associations in nonpolar solvents that are less exothermic than 10 kJ mol^{-1} . This is because weakly exothermic associations lead to weakly ordered complexes $\mathbf{A} \cdots \mathbf{B}$ with only a very small cost in entropy. Hence, although the favorable entropy of desolvation will be small for associations in nonpolar solvents, it is large enough in the case of weakly exothermic associations to more than offset the small cost in entropy of the association.

There do not appear to be exceptions among the 233 data points to the general requirements of Figure 2, and the

generalization has been used to correct errors in the literature. This last point is important, because unifying concepts are unlikely to emerge when the literature accumulates errors. The idea that forming a more exothermic noncovalent interaction proceeds with a greater cost in entropy (greater restriction in motion) is confirmed.

Collectively, the data for the noncovalent associations occurring in the gas phase and in nonpolar solvents also confirm the conclusion from the training set of drug–receptor data used in conjunction with Equation (3)—noncovalent associations can have relatively small adverse ΔG_{itr} terms. On average, the drugs in the data set apparently have considerable motions relative to their receptors, that is, they are bound in a relatively dynamic manner.

5. Cooperative Binding Processes: Definitions

The aim in studying binding affinities is to understand the origins of the overall ΔG value in terms of structure. It is evident from the foregoing sections that the changes in the bonding (ΔH) and order ($T\Delta S$) terms for the binding of flexible molecules in aqueous solution are so numerous that the problem is a complex one. A useful approach is to separate the variables so that a deeper understanding can emerge. This has already been achieved at one level by separating the effects of noncovalent bonding in complex formation from those of desolvation (through the examination of complex formation in the gas phase and in nonpolar solvents, see Section 4). Cooperativity between noncovalent interactions has not so far been discussed. It will be seen that its effects upon the bonding (ΔH) and order ($T\Delta S$) terms can be predicted with some confidence, and so another layer of the complexity can be peeled away.

Noncovalent interactions are said to interact with each other in a positively cooperative manner when the binding energy that is derived from them acting together is greater than would be derived from the sum of their acting separately. Conversely, they are said to interact with each other in a negatively cooperative manner when the binding energy that is derived from them acting together is less than would be derived from the sum of their acting separately. Equation (3) was derived to remove part of the problem that arises from cooperativity. Equation (3) is based on the idea that the cost of an association (ΔG_{itr}) has to be paid only once. It was therefore reasoned that if this adverse term could be factored out from the other free-energy contributions then, to a useful approximation, all the free-energy terms could then be treated additively.

Figures 2 and 3 illustrate the inadequacy of this approach in the general case, since the adverse ΔG_{itr} term increases as association occurs with stronger bonding. The addition of an extra polar interaction at a binding interface can decrease the local dynamics and thereby increase the favorable free energy of adjacent interactions (see Section 6).^[40] It is this gradual switching on of positively cooperative effects, as a result of the interplay between motion and bonding, that precludes rigorous analysis of binding affinities in terms of sums of the parts.

Nevertheless, in many systems (particularly synthetic ones) there may be no significant cooperativity, and in these cases the binding energy will correspond to the sum of the parts. For example, the affinity of polyamines to DNA can be described simply as a function of the number of possible contributions of each ammonium center.^[43]

6. Cooperative Binding at a Single Interface

6.1. The Case of Positive Cooperativity

To illustrate how positive cooperativity can arise in a simple system of polar interactions, we consider a receptor that binds ligands **X**, **Y**, and **Z** with affinities ΔG_X , ΔG_Y , and ΔG_Z , respectively (Figure 4). Clearly, binding some combina-

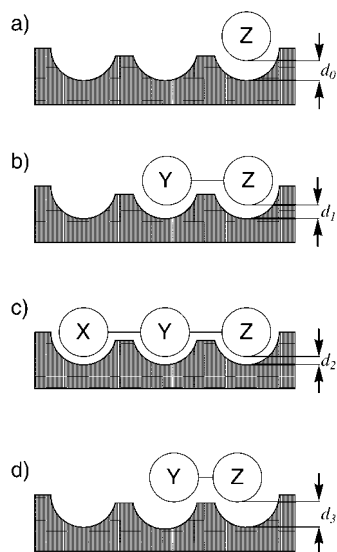


Figure 4. Schematic representation of a receptor that binds ligands **X**, **Y**, and **Z** with affinities ΔG_X , ΔG_Y , and ΔG_Z , respectively. a) Binding of **Z** results in a structure with an intermolecular distance d_0 . b) When **Y** and **Z** are connected by a rigid, strain-free linker (**Y–Z**) they bind to the receptor with positive cooperativity ($\Delta G_{Y,Z}$ more negative than $\Delta G_Y + \Delta G_Z$) and there is structural tightening ($d_1 < d_0$). c) If **X** is connected to **Y–Z** by a rigid, strain-free linker to form **X–Y–Z** then further structural tightening will occur ($d_2 < d_1$) leading to a further cooperative enhancement. d) The shorter linker between **Y** and **Z** does not allow both these binding interactions to occur with optimal geometry. **Y–Z** binds the receptor with negative cooperativity ($\Delta G_{Y,Z}$ more positive than $\Delta G_Y + \Delta G_Z$) and there is structural loosening ($d_3 > d_0$).

tion of these ligands, each as separate entities, will result in an overall free energy change that is represented by the sum of the contributions from each individual ligand. Let us now consider the case where **Y** and **Z** are connected by a linker (**Y–Z**) (Figure 4b). There is now the benefit of the classic entropic chelate effect to binding described by Jencks and Page.^[7–9] That is, if **Y** and **Z** each bound separately with an adverse $T\Delta S_{\text{tr}}$ term of N , then **Y–Z** will bind with a cost of less than $2N$. We now add the cooperative effects addressed in this review to this benefit to binding. First, the restrictions in motion that **Y** and **Z** impose on each other when binding as

Y–Z will increase the exothermicity of the noncovalent bonds that they make with the receptor; that is, there will be structural tightening of the receptor–ligand complex (Figure 4, $d_1 < d_0$). Second, the increased exothermicity associated with this first effect will in turn reduce the motions of **Y** and **Z** (in **Y–Z**) relative to the receptor. Therefore, these two effects will occur with a benefit in enthalpy and a cost in entropy relative to the situation occurring if there were no positive cooperativity of this nature. Analogous arguments allow us to conclude that if **X** is connected to **Y–Z** by a rigid strain-free linker to form **X–Y–Z** then further structural tightening will occur ($d_2 < d_1$) and lead to a further cooperative enhancement of binding (Figure 4c).

Studies with glycopeptide antibiotics established the reductions in distance modeled in Figure 4a–c.^[44] Several peptide ligands, all containing the carboxylate group depicted lower right in Figure 5, were separately bound to the anti-

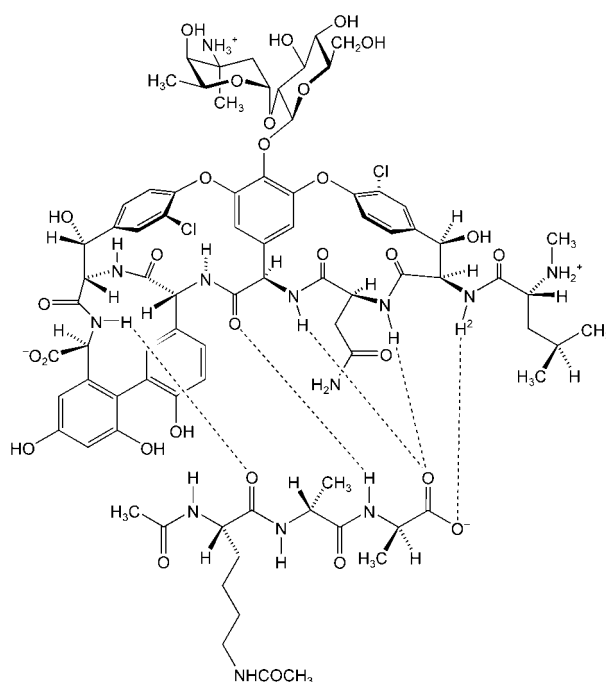


Figure 5. The binding interaction between the glycopeptide antibiotic vancomycin and the peptide ligand *N*- α -acetyl-Lys-(*N*- ϵ -acetyl)-D-Ala-D-Ala. Hydrogen bonds are indicated by dotted lines. The binding is also promoted by hydrophobic interactions, notably of the Ala methyl groups to the aromatic rings of the antibiotic. The amide NH proton H^2 discussed in the text is indicated.

biotics. In all cases, a large downfield chemical shift ($\Delta\delta = 1$ –3 ppm) of the antibiotic amide NH proton H^2 was observed upon binding of the ligand. A larger limiting downfield shift of this proton indicates a shorter and stronger carboxylate–NH hydrogen bond.^[44–46] This hydrogen bond was formed to a higher degree as the number of hydrogen bonds and other motional restrictions adjacent to the carboxylate–NH interaction was increased. The motional restriction of the carboxylate group, afforded by these adjacent motional restrictions, strengthens the hydrogen bonds directly made to the carboxylate group.

The dimers of the glycopeptide antibiotics (Figure 6) exhibit the same effect. The proton resonance H^4 at the dimer interface undergoes a downfield shift when the dimer is formed from the monomer. The extent of this downfield shift

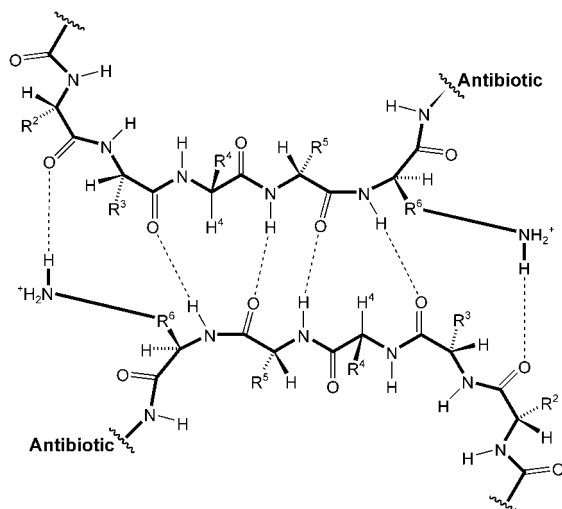


Figure 6. Backbone structure of the dimer of the glycopeptide shown in Figure 5. Hydrogen bonds are indicated by dashed lines. The α -proton H^4 mentioned in the text is indicated. The central four hydrogen bonds at the dimer interface are common to all glycopeptide dimers, whereas the two outer hydrogen bonds can only be made by antibiotics that possess an amino sugar attached to R^6 .

increases as additional bonding restraints, more distant from H^4 than the four central hydrogen bonds depicted in Figure 6, are added at the dimer interface. In analogy with the correlation observed between increased downfield changes in the chemical shifts of the α protons of β -strand structures as the interstrand distance decreases,^[47,48] these data indicate that remote bonding restraints reduce the interfacial distances in the dimer in the vicinity of H^4 .

Thus, structural tightening occurs in the bound state as a consequence of positive cooperativity.^[49] Furthermore, thermodynamic measurements indicate that the structural tightening occurs with a benefit in enthalpy (ΔH) and a smaller cost in entropy (in terms of $T\Delta S$).^[49]

6.2. The Case of Negative Cooperativity

The model of Figure 4 can also be used to illustrate how negative cooperativity may arise. Consider the case where **Y** and **Z** are rigidly held in a conformation that does not allow both binding interactions to occur with the preferred geometry shown in Figure 4b. This situation could be induced, for example, by introducing a linker between **Y** and **Z** that is too short (Figure 4d). The “pull” of **Y** towards its preferred binding geometry will adversely affect the binding of **Z** by forcing it away from its preferred binding geometry, and vice versa, with the consequence that ΔG_{Y-Z} will be less negative than the sum of $\Delta G_Y + \Delta G_Z$. **Y** binds with negative cooperativity with respect to **Z**, and vice versa. Based on the

arguments presented above, a consequence of this negative cooperativity should be loosening of the interaction of **Z** into its receptor cup (Figure 4d, $d_3 > d_0$), at a cost in enthalpy but with a benefit in entropy.

Studies on the melting of DNA duplexes support the models of negatively cooperative binding. For example, the self-complementary duplex **1** is formed in aqueous solution from its constituent single strands with an exothermicity of -430 kJ mol^{-1} .^[50] The magnitude of the exothermicity of duplex formation drops by 220 kJ mol^{-1} upon the introduction of only two mismatches into the sequence (formation of **2** with $X = {}^m\text{G}$, namely, methylation at the purine O6 site). This extremely large fall in the exothermicity of duplex formation is associated with a correspondingly dramatic fall in the adverse entropy for duplex formation ($-1164 \text{ J mol}^{-1} \text{ K}^{-1}$ for **1** versus $-577 \text{ J mol}^{-1} \text{ K}^{-1}$ for **2**).

CGCGAATTCGCG
GCGCTTAAGCGC
1

CGCXAATTTGCG
GCGTTTAAXCGC
2

Since the negative cooperativity associated with the introduction of the two mismatches reduces the melting temperature of the duplex, a correction must be made for the heat capacity change upon melting of the DNA.^[51–53] After allowing for heat capacity effects, it is found^[54] that the introduction of just two mismatches reduces the favorable enthalpy of duplex formation by $123 \pm 53 \text{ kJ mol}^{-1}$. Thus, there is a large reduction in the bonding in the duplex structure, even though formally it involves the removal of only two $\text{C=O} \cdots \text{HN}$ hydrogen bonds and the introduction of two repulsive $\text{C=O} \cdots \text{OR}_2$ interactions. Therefore, it appears likely that the introduction of the mismatched $\text{T} \cdots \text{X}$ interactions in **2** loosens adjacent interactions. A similar calculation for the entropy term indicates that the large reduction in bonding is accompanied by a large increase in the motional dynamics of **2** relative to **1**. There is enthalpy/entropy compensation, with the consequence that the introduction of the two mismatches has a much smaller effect on the relative stabilities ($\Delta\Delta G = 46 \text{ kJ mol}^{-1}$) of the two duplexes than would otherwise be the case.

7. Cooperative Binding over Multiple Interfaces

Although positively or negatively cooperative binding between interactions expressed at the same interface (Section 6) is important, such effects expressed over multiple interfaces are of supreme importance in biology. We first consider the free energy of positively and negatively cooperative binding when expressed over two interfaces.

Figure 7 shows a thermodynamic cycle for the formation of a dimer, which can occur either in the presence, or absence, of a ligand. The dimer can bind two molecules of ligand.^[55]

The transformation **A** \rightarrow **C** represents the free energy of dimerization and **A** \rightarrow **B** represents the free energy of binding two molecules of ligand to two of monomer. The transformation **C** \rightarrow **D** represents the free energy of binding two ligands to dimer in the absence of cooperativity, which by

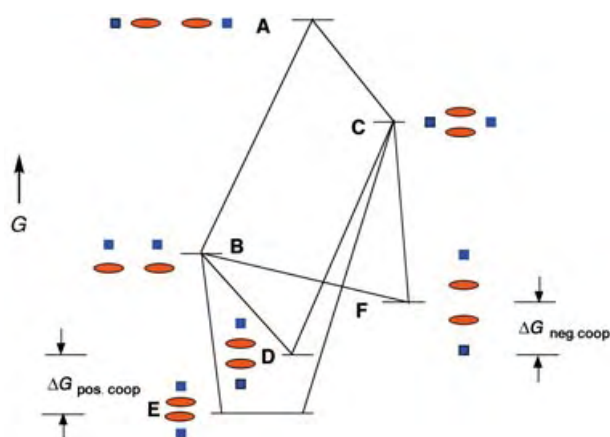


Figure 7. Formation of a fully coordinated dimer from the constituent elements of two ligand molecules (blue) and two antibiotic monomers (red). Vertically arranged species are bound, horizontally arranged species are not bound. Starting from the free components (**A**) the association can occur to give two ligand-bound monomers **B** or a ligand-free dimer **C**. The coordinated dimers may be formed without cooperativity (**D**), with positive cooperativity (**E**), or with negative cooperativity (**F**).

definition is therefore the same as the free-energy change for $A \rightarrow B$. The transformation $B \rightarrow D$ represents the free-energy change for dimerization of ligand-bound monomer in the absence of cooperativity, and is therefore by definition the same as the free-energy change for $A \rightarrow C$.

If the dimer and ligand interfaces are formed in a positively cooperative manner, then a more stable species **E** is formed instead of **D**. The difference between free energy levels **E** and **D** ($\Delta G_{\text{pos.coop}}$) represents the free energy benefit of the positive cooperativity. If the dimer and ligand interfaces are formed in a negatively cooperative manner, then a less-stable species **F** is formed instead of **D**. The

difference between free energy levels **F** and **D** ($\Delta G_{\text{neg.coop}}$) represents the free energy cost of the negative cooperativity.

Suppose the dimerization constant for the formation of a symmetrical dimer is increased by some factor x (for example, 100) by the occupation of both its ligand binding sites (positively cooperative binding, Figure 7). Then the binding constant for each ligand into the two identical binding sites of the dimer must be greater by \sqrt{x} (for example, 10) over binding to the monomer. More generally, if a receptor system is stabilized upon ligand binding, the ligand affinity for the receptor must thereby be increased. This important point is discussed in the general context in Section 11.

8. Positive Cooperativity over Multiple Interfaces

8.1. Monomeric Protein Receptors

A structural model^[56] to understand this phenomenon of positively cooperative binding is given in Figure 8a, and shows a portion of a protein receptor prior to (top) and after (bottom) binding to a ligand. First consider the free receptor (top): the formation of its two depicted hydrogen bonds is opposed by the relative motions of its two peptide backbones. The internal motions of the chain that is presented to the ligand can be reduced by the formation of hydrogen bonds from it to the ligand (Figure 8a, bottom). Since motion opposes bonding, the restriction of the internal motions of this chain upon ligand binding should result in the strengthening of the hydrogen bonds within the receptor.

The “damping down” of the motions of the depicted receptor residues upon ligand binding can, in turn, improve noncovalent bonding more deeply within the receptor. Such transmission will result in an improvement in noncovalent bonding at all sites within the receptor that are coupled with

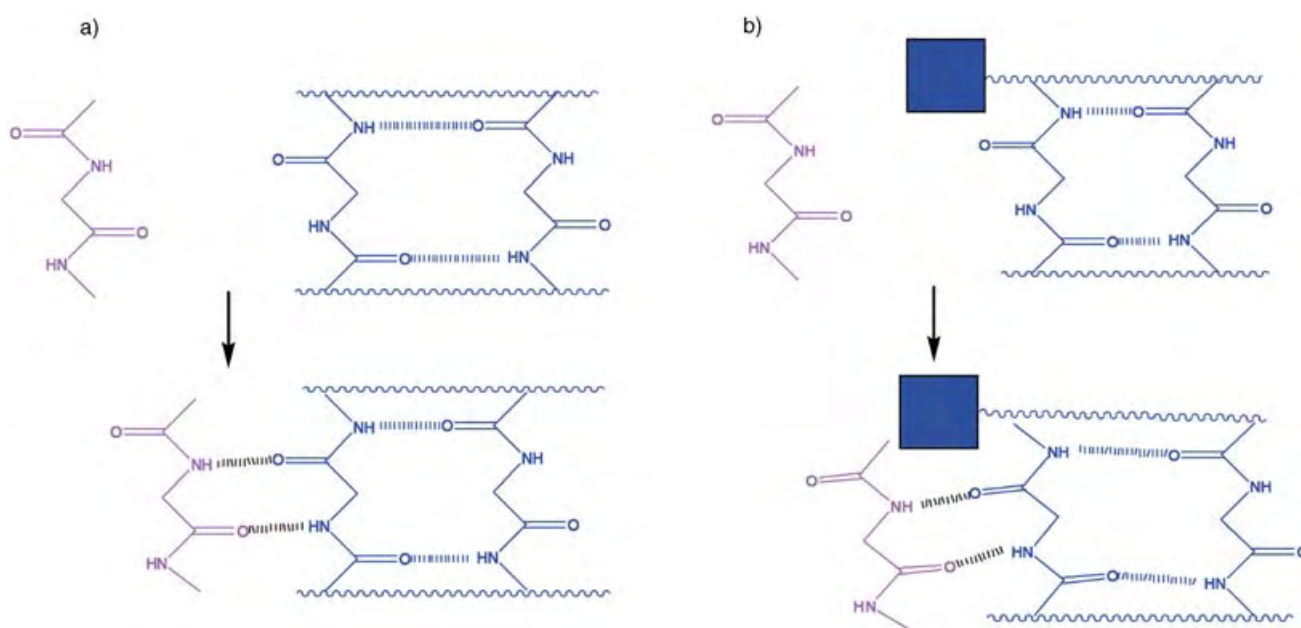


Figure 8. Structural models for positively cooperative binding (a) and for negatively cooperative binding (see text for details).

positive cooperativity to ligand binding. Ligand binding to the receptor is improved because the receptor is stabilized upon ligand binding.

A consequence of improved bonding within a receptor following positively cooperative ligand binding will be a reduced degree of H/D exchange of selected amide NH protons of the receptor (see Section 11).

8.2. Dimeric Receptors

The model of Figure 8a is equally useful in considering the case where the portion in blue represents not a single protein receptor, but rather two peptide chains that can come together through a bimolecular association (the wavy lines are ignored). Under these circumstances, the formation of the blue hydrogen bonds (for example, when a receptor dimer is formed) lead to the presentation of a more organized template to the ligand. For this reason, the cost in entropy in binding the ligand to the dimer will be less than in binding the ligand to the monomer. Molecular dynamics simulations illustrate that this contribution to positive cooperativity is a benefit to entropy.^[57]

It must now be considered how the above “templating” advantage of a dimeric over a monomeric receptor structure will cause “knock-on” effects on the structure. Since it is motion that opposes bonding, the presentation of a more-ordered surface (of a dimeric receptor) to a ligand will allow an improvement in interfacial ligand/receptor bonding (Figure 8a). In fact, there will tend to be mutual strengthening of all the hydrogen bonds between the chains in strain-free binding. A consequence of this strengthening of the hydrogen bonds must be to reduce the relative translational motions of the chains, and to further restrict their internal wagging motions, at a cost in entropy.

In summary, positively cooperative binding of a ligand to a dimeric receptor should be beneficial in enthalpy, that is, with a shortening of the noncovalent bonds involved. However, the overall entropy changes cannot be predicted from the model. Strain-free templating of binding gives an entropic benefit, whereas entropy/enthalpy compensation should give an entropic cost. Experiments are required to address this problem.

The structural and thermodynamic features of positive cooperativity expressed over multiple interfaces have been demonstrated experimentally. Dimers of glycopeptide antibiotics of the vancomycin group are typically further stabilized and, without reported exception, become less dynamic when they bind two molecules of the bacterial cell-wall analogues (Figure 9). This reduced dynamic behavior of the dimer receptor system occurs with distance reductions at the dimer interface, as indicated by NMR data.^[46] The reduction in the dynamic behavior of the dimeric receptor is greater for strongly binding ligands than for weakly binding ligands.^[58] The positive cooperativity is typically associated with a benefit in enthalpy and a cost in entropy.^[59] In such cases, the motional restriction that accompanies improved bonding outweighs the benefit in entropy of binding to a more-ordered template.

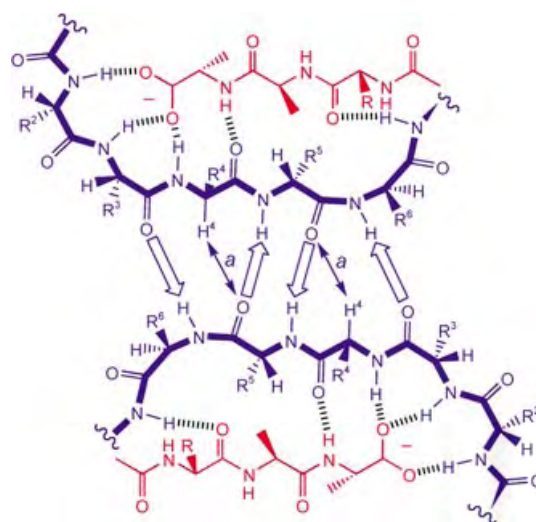


Figure 9. Peptide backbone of a glycopeptide antibiotic dimer (blue) that is simultaneously bound to two molecules of a bacterial cell peptide precursor analogue (red). The binding of the analogue occurs with positive cooperativity, such that the dimer system is stabilized and shortens the distances marked *a*. The effect affords a benefit in enthalpy and a cost in entropy.

The structural changes occurring upon positively cooperative binding bear analogy to the changes occurring upon cooling a substance. On reducing the temperature of a pure substance, whether liquid or solid, it is universally observed that the change is favorable in enthalpy and adverse in entropy.^[60] It is also almost universally observed that reducing the temperature leads to a volume reduction (the ice/water transition is an example of a relatively rare exception). The physical basis for this analogy is evident: both in the exercise of positive cooperativity and in cooling a substance, a reduction in dynamic behavior improves noncovalent bonding and shortens the average noncovalent bond lengths.

9. Negative Cooperativity over Multiple Interfaces—Hemoglobin

Since cooperative binding is a phenomenon of great importance in chemical biology, it might be assumed that a unified definition of the phenomenon would already be in use. This is not the case. For multiple ligand binding sites,^[61,62] positively cooperative binding is said to occur when binding ligands are successively bound with increasing affinities. Conversely, negatively cooperative binding is said to occur when binding ligands are successively bound with decreasing affinities.

Importantly, ligand binding can be positively cooperative if the above definition for multiple binding sites is used, while being negatively cooperative if the definition employed here is used (see Section 5). The advantage of the definition of positive cooperativity used in this Review is that it requires that the sets of noncovalent interactions are, when made together, mutually *reinforcing*. Such a condition would seem

to be a mandatory requirement for interactions that are “positively cooperative”. We now illustrate the nontrivial consequences of these considerations by reference to the binding of O_2 to hemoglobin.

A structural model to illustrate negatively cooperative binding over two interfaces is given in Figure 8b. Here, the surface chain of the protein receptor must incorporate a structural feature (for example, steric inhibition by the blue square) that inhibits ligand binding to the structure of the isolated receptor. As required for a structurally meaningful definition of “negatively cooperative”, the two sets of interactions (the preferred noncovalent interactions at the ligand/receptor interface and those preferred within the receptor) are mutually incompatible. Therefore, when ligand-binding occurs, the ground-state structure of the receptor must be distorted from its preferred geometry (Figure 8b, top) to a state (bottom) in which its internal noncovalent bonding is weakened. Thus, ligand binding that is negatively cooperative should cause receptors to loosen their structures and become more dynamic. Consequently, the extent of H/D exchange of the amide–NH protons of the peptide backbone of the receptor (upon exposure to D_2O) should increase upon ligand binding. In addition, the reduction in bonding efficiency within the receptor upon negatively cooperative ligand binding will make ligand binding less favorable in enthalpy, and more favorable in entropy than would otherwise be the case. Evidence to support these conclusions is presented below.

Hemoglobin, the protein that carries oxygen in the blood stream, exists as a tetramer. The classic work of Monod, Wyman, and Changeux (MWC)^[62] allows a deep insight into the changes that occur when O_2 binds to hemoglobin. The initially available form of the tetramer is described as a “tense” (T) form (Figure 10a). The geometry of this form

does not allow efficient binding of O_2 to it. The initially available T form is distorted to give a more “relaxed” structure (the R form, Figure 10a) to enable O_2 to bind more efficiently. The binding of just one O_2 molecule to the tetramer is envisioned as distorting all four subunits towards the R structure (Figure 10b), so that the subsequently binding O_2 molecules bind with higher affinity. The O_2 binding is therefore defined in the MWC model as positively cooperative. The energy required for the T→R conversion is largely carried out by the first O_2 molecule that binds. Therefore, subsequently binding O_2 molecules have the advantage of accessing a relatively high population of the R state, and bind with greater affinity.^[63]

However, in terms of the definition used here, the binding of O_2 to hemoglobin is negatively cooperative. The T state does not allow efficient binding of O_2 , and therefore the binding of O_2 distorts it to the R state (Figure 10a). This situation is analogous to the situation shown in Figure 8b.

The negatively cooperative binding does indeed force a loosening of the T state of the tetramer, through the breaking of ionic interactions between subunits.^[64] However, and importantly for the structural consequence of negatively cooperative binding developed here, widespread structural changes in the T to R transition seem possible: all non-covalent interactions within a receptor system that are coupled with negative cooperativity to ligand binding should loosen.

To test the above conclusion we determined^[65] the change in the dynamic behavior of the (horse) hemoglobin tetramer polypeptide backbone when it binds O_2 by ESI-mass spectrometry. Through the binding of oxygen, a further 7–8 exchangeable amide hydrogen atoms per α chain (5.2–6 % of the total number) and a further 16 per β chain (11.4 % of the total number) underwent solvent exchange. Thus, complete saturation of the hemoglobin tetramer by O_2 binding results in an increase of 46–48 backbone NH atoms undergoing exchange. The dramatic increase in amide NH exchange is in agreement with the predictions regarding the changes associated with negatively cooperative binding. This increase in dynamic behavior of the amide backbones of the hemoglobin subunits had not been uncovered by previous X-ray studies. Presumably, the changes in dynamic behavior, which are important for an understanding of binding interactions, are masked by crystal-packing forces.

The requirement that negative cooperativity, as exercised on the T state, will be accompanied by enthalpy/entropy compensation (in the sense of a benefit in entropy and a cost in enthalpy) is also satisfied. Thus, as O_2 binding promotes the T to R transition, there should be an uptake of heat by, and increase in disorder within, the hemoglobin tetramer. The following thermodynamic parameters (per subunit) were obtained for the case of O_2 binding to trout hemoglobin.^[66] The first O_2 molecule binds with $\Delta H = 0 \text{ kJ mol}^{-1}$ and a favorable $T\Delta S$ term of $+21 \text{ kJ mol}^{-1}$. In contrast, the fourth O_2 molecule binds exothermically ($\Delta H = -32 \text{ kJ mol}^{-1}$) and with a slightly unfavorable entropy term ($T\Delta S = -3 \text{ kJ mol}^{-1}$). The binding of O_2 to the iron atom of hemoglobin in isolation can confidently be assumed to be exothermic. However, since O_2 binding drives the T→R

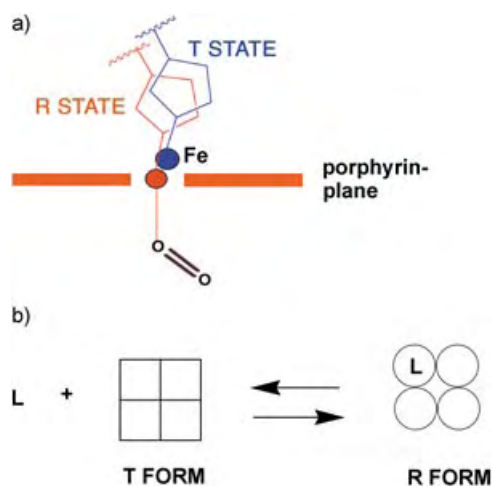


Figure 10. a) Negatively cooperative binding of O_2 to hemoglobin. In the T state (blue) the hemoglobin is unable to bind O_2 efficiently because the access of the O_2 to the T state is hindered by the plane of the porphyrin ring. The structure of the hemoglobin is therefore distorted (loosened, with a decrease in efficiency of its internal noncovalent bonding) to give the R state (red), which is better able to bind O_2 . b) MWC model for the binding of the first molecule of ligand (L) to a tetrameric protein existing in tense (T) and relaxed (R) forms.

conversion (Figure 10b), the associated loss in bonding within the hemoglobin structure offsets this exothermic gain. Hence, $\Delta H = 0 \text{ kJ mol}^{-1}$ for O_2 binding starting from the T form is understandable. The favorable $T\Delta S$ term of $+21 \text{ kJ mol}^{-1}$ reflects the loosening of the hemoglobin structure that accompanies its loss of internal bonding. Thus, it may be a useful approximation to isolate the binding event of O_2 to the R form of hemoglobin as being reflected by $\Delta H = -32 \text{ kJ mol}^{-1}$ and $T\Delta S = -3 \text{ kJ mol}^{-1}$. Indeed, O_2 binding *in isolation* should involve only a small adverse entropy change (reflecting the dynamic binding of a ligand of small mass to a receptor). This approximation isolates the thermodynamics of the T \rightarrow R transition in terms of $\Delta H = +32 \text{ kJ mol}^{-1}$ and $T\Delta S = +24 \text{ kJ mol}^{-1}$. These are plausible numbers for the generation of a structure that is less well bonded and exhibits more dynamic behavior (see the exchange data for horse hemoglobin above for comparison). Additionally, since $\Delta G = \Delta H - T\Delta S$, the T \rightarrow R transition is $\Delta G \approx +8 \text{ kJ mol}^{-1}$. Thus, at room temperature the free T state of trout hemoglobin should be more highly populated than the free R state by a factor of about 25. Seen in this light, the thermodynamic parameters make physical sense.

Analogous experiments on myoglobin are clearly of interest, since it exists as a monomeric species. In the original classic paper of Monod, Wyman, and Changeux it was assumed that “the subunits of the R form are closer to the conformation of the [hemoglobin] monomer” (cf. myoglobin) and that “myoglobin may be thought of as a relaxed subunit of hemoglobin”.^[62] According to this assumption, oxygen binds strongly to myoglobin, at least in part, because it does not have to pay the price of the T to R conversion (Figure 10).

However, it is important to recall that the internal structure of the R form has been shown above to be loosened relative to the T state, and this internal loosening must be driven by O_2 binding. Thus, the myoglobin structure might also be loosened internally by O_2 binding. The extent of H/D exchange of the amide protons on the peptide backbone of myoglobin in the absence, and presence, of bound oxygen was determined by ESI-MS. A further 13–15 exchangeable backbone amide hydrogen atoms were exposed to solvent exchange through the binding of oxygen.^[56] Myoglobin thus possesses a tight (or “tense”) internal structure, and not a relaxed one as originally seemed likely. This conclusion also makes physical sense because, as Perutz commented,^[67] it is the binding of O_2 that perturbs the protein structure. Both myoglobin and the T form of hemoglobin bind O_2 with negative cooperativity as defined by the model used here (see Figures 8b and 10a). Consistent with the model, the reduction in binding energy of the O_2 molecule to the T form of hemoglobin is widely spread, not only at the tetramer interfaces, but also among the internal network of non-covalent interactions of each monomeric unit.

The advantages of the negatively cooperative model for O_2 binding to hemoglobin are threefold: 1) it is part of a model for cooperativity (Figure 8) that is consistent with the sense in which the term “cooperativity” is most frequently used. Mutual *enhancement* of compatible sets of interactions is described as *positively* cooperative binding (Figure 8a, for example, as in protein folding^[68,69] and crystallization).

Mutual *weakening* of initially incompatible sets of interactions is described as *negatively* cooperative binding (Figure 8b, for example, as in the case of O_2 binding to hemoglobin (Figure 10a)). 2) The model postulates specific structural consequences. For example, since all noncovalent interactions within a receptor system that are coupled with negative cooperativity to ligand binding should loosen, it requires that the internal structure of each hemoglobin subunit be extensively loosened upon O_2 binding (this has been established by H/D exchange experiments^[65,70]). 3) The use of the terms T and R states^[62] is naturally accommodated, since negatively cooperative binding of O_2 forces a reduction in bonding in the T state (cost in enthalpy) to give the R state which is more dynamic (benefit in entropy).

If the binding of O_2 to hemoglobin were positively cooperative in a structural sense (in terms of noncovalent bonding), then the initial O_2 binding event would represent “normality”, and subsequent O_2 binding events would be accompanied by mutual enhancement of noncovalent interactions within the O_2 /hemoglobin system. This is not the case. Rather, nature has built the greatest adversity into the first O_2 -binding step, where the restriction of access of O_2 to the iron atom is the result of the steric hindrance of the porphyrin ring (Figure 10a). The successively stronger O_2 -binding steps that are described as positively cooperative in the Monod, Wyman, Changeux model are in fact successive steps of decreasing negative cooperativity.

Other literature data are consistent with the general properties proposed here for negatively cooperative binding. The binding of the cofactor (6R)-L-erythro-5,6,7,8-tetrahydrobiopterin to the tetrameric recombinant human tyrosine hydroxylase isoform 1 occurs with negative cooperativity.^[71] The cofactor-bound form of the enzyme shows, relative to the free form of the enzyme, a decreased resistance to limited tryptic proteolysis—as would be expected from a loosening of the enzyme structure. Additionally, a decreasing incremental affinity is observed for the binding of ligands with one, two, or three carbohydrate units to lectins.^[72,73] That is, the binding is negatively cooperative. The ligands with several carbohydrate units coordinate with more positive entropy of binding relative to the analogues with one unit,^[74] presumably reflecting the disorder produced in the lectins by the negatively cooperative binding of the second and third carbohydrate epitopes.

Lastly, a decrease in protein stability is induced by ligand binding which increases the flexibility of the protein.^[75]

10. Negative Cooperativity that Breaks Interfaces

If the free-energy change associated with negatively cooperative binding were sufficiently large, the free energy of **F** would lie above that of **B** (Figure 7). Under these circumstances, a ligand binds with negative cooperativity to a receptor that is in its dimeric state in the absence of ligand, and thereby induces dissociation of the dimer. Such cases are established,^[76] and, indeed, Monod, Wyman, and Changeux^[62] considered dissociation of an oligomeric species as the limit of structure loosening.

11. Reduced Dynamics within Protein Receptors as a Source of Ligand Binding Energy

In Sections 7 and 8 it was shown that in the positively cooperative binding of a ligand to a receptor (there a small dimer) the free-energy benefit of the positively cooperative binding is correlated with a tightening (that is, a local volume reduction) within the receptor system. A thermodynamic cycle shows that where a receptor system becomes more stable upon ligand binding it is axiomatic that ligand binding is thereby improved.^[55] This conclusion is represented schematically in Figure 11.

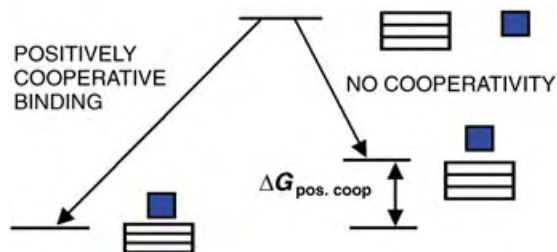


Figure 11. Schematic illustration showing that stabilization of a receptor system (oblong) upon ligand binding (blue square) increases ligand binding energy. In the absence of positively cooperative binding (right), the ligand binds without modification (tightening) of the receptor structure. In the presence of positively cooperative binding (left), the ligand binds with overall tightening of the receptor structure. The increase in ligand binding energy arising from positive cooperativity is because of increased stability of the ligand/receptor system. It may in principle be expressed at any of the noncovalent interfaces of the ligand/receptor system.

Has evolution exploited reduced dynamics within protein receptors as a source of ligand-binding energy? Clearly, the search for such effects should be through the examination of systems in which a localized view of noncovalent interactions would seem inadequate in understanding the observed affinities.

The binding of biotin to the streptavidin (STV) tetramer is so remarkably strong ($K = 10^{13.4} \text{ M}^{-1}$) that it finds widespread use in biology. It is poorly understood and typically found to be an “outlier” in comparison with other affinities.^[16,77] Specifically, it is about 1000 times stronger than expected on the basis that the binding should correspond to the sum of the parts.^[16,77] We used mass spectrometry to measure the extent of H/D exchange of the amide NH protons in STV both in the absence and presence of biotin. It was found that 22 backbone amide NH protons per STV monomer unit are protected from H/D exchange (RT, pH 8, 2 h) upon binding of biotin.^[65] The location of the backbone NH protons protected by biotin binding was obtained from a pepsin digest. The data show that the binding of biotin reduces the solvent accessibility of streptavidin backbone NH protons in much of the structure (Figure 12).

It is notable that the effects are much more marked in some parts of the structure than in others: thus, the improved packing induced within the receptor upon binding of biotin is not that which might be engendered upon simply carrying out

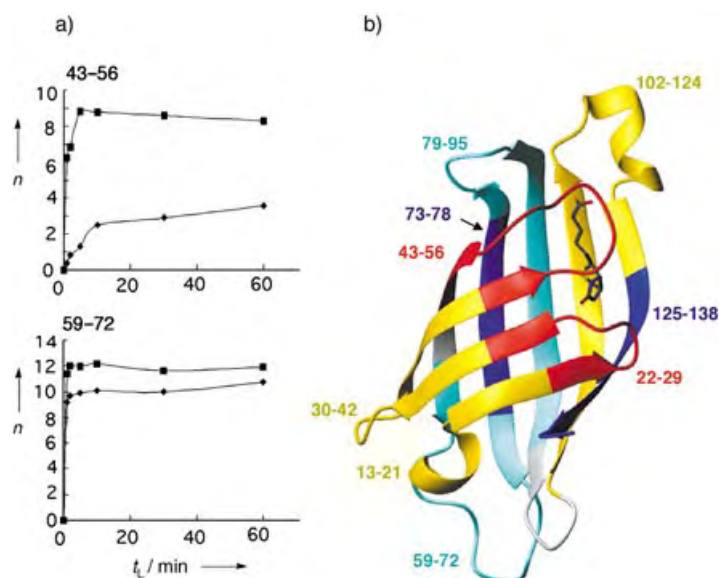


Figure 12. a) Deuterium incorporation into streptavidin in the absence (■) and presence (◆) of biotin as a function of time t_L . The level of deuterium incorporation in two peptides (43–56 and 59–72) obtained by pepsin digestion was investigated. b) Position of the peptides in a ribbon model of a STV subunit with bound biotin (the figure was prepared with the program MOLMOL^[108]). The degree of increased NH protection in the presence of biotin is indicated by color: red > 30%, yellow 20–30%, light blue 10–20%, and dark blue < 10%.

binding at a higher pressure. Rather, it is exercised only in the parts of the receptor where positively cooperative binding is expressed. It is clear that the binding energy of biotin to streptavidin is widely delocalized. X-ray crystallographic studies of the free and bound tetramer^[78–81] do not illustrate the widespread greater dynamic behavior of the free tetramer, presumably because this is damped down by crystal-packing forces. In this respect, we note that liquid to crystal transitions universally occur with improvements in noncovalent bonding that restrict dynamic behavior.

The streptavidin/biotin system provides a clear example where the binding affinity is the property of the whole system, rather than something that can be understood by examination of the ligand/receptor interface. This point is consistent with other, less structure specific, measurements. The effect of biotin binding on the thermal stability of STV has been evaluated by using differential scanning calorimetry (DSC).^[79,81] Biotin binding increases the thermally induced denaturation of STV in phosphate buffer from $T_m = 75$ to 112°C . Thus, the biotin/STV system is much more resistant to thermal unfolding than is STV in the absence of biotin, and clearly more stable than is the isolated STV. Additionally, the binding of biotin to STV is remarkably exothermic and adverse in entropy ($\Delta H = -134 \text{ kJ mol}^{-1}$ and $T\Delta S = -57 \text{ kJ mol}^{-1}$,^[81] also reported in another study as $\Delta H = -102 \text{ kJ mol}^{-1}$ and $T\Delta S = -26 \text{ kJ mol}^{-1}$).^[79] All the data satisfy the proposed effects of positively cooperative binding in which ligand binding energy is provided in part because the ligand reduces the dynamic behavior of the receptor. The formation of new noncovalent interactions within the receptor is not required, but simply the strengthening of existing

ones. In this sense, distinct conformational changes are not required.

The above conclusions also receive support from independent findings that an increase in protein stability is induced by ligand binding which reduces the flexibility of the protein.^[75] They are also in accord with the long-standing observation of Sturtevant that ligand binding to proteins commonly occurs with a reduction in heat capacity, which is consistent with the loss of many internal vibrational degrees of freedom.^[82] Notably, Cooper and Dryden have also concluded^[83] that positive cooperativity in ligand binding will induce a “stiffening” in the protein (corresponding to the “tightening” shown here). We note that although the H/D exchange experiments indicate the strengthening of hydrogen bonds, all the binding interactions that are positively coupled to the strength of these bonds will be enhanced.

An additional comment is necessary here. It is widely perceived that if there is a change in structure from the observed state of a free protein to a more packed state upon ligand binding, then there must be a cost in the free energy associated with the structural change of the protein. This idea is incorrect: once the ligand has bound to the protein, a new system (ligand-protein) has been generated. Since the ligand restricts the dynamic motion of the protein in positively cooperative binding (see above data), a more compact state is now the most favored in terms of free energy.

12. Ligand/Receptor Interactions that are Strongly Enthalpy or Entropy Driven

Since positive cooperativity promotes enthalpy-driven binding, and negative cooperativity promotes entropy-driven binding, these relationships can be used plausibly to infer the manner in which drugs are likely to order, or disorder, the receptors to which they bind. The thermodynamic parameters of the binding of 136 drugs to biological receptors has been plotted in a graph of ΔH° versus ΔS° (Figure 13).^[84] Some associations are endothermic by quantities in the region of 30 kcal mol^{-1} (125 kJ mol^{-1}), while at the other extreme, some

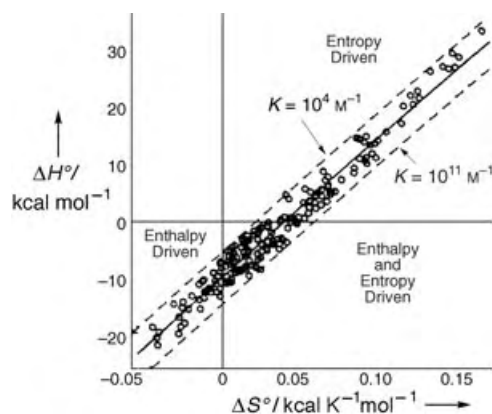


Figure 13. Plot of the standard enthalpies (ΔH°) versus standard entropies (ΔS°) for the binding equilibria of 136 different ligands to 10 biological receptors, one DNA, and two enzymes. The two dashed lines correspond to the ligand-macromolecule association constants K of 10^4 M^{-1} and 10^{11} M^{-1} . (Reproduced with permission from Ref. [84].)

are exothermic by about 20 kcal mol^{-1} (84 kJ mol^{-1}). The differences in these extremes are massive (ca. 200 kJ mol^{-1}) and can be ascribed to two scenarios:

- 1) The highly endothermic binding is associated with negative cooperativity and with associated decreased bonding within the receptor (in its drug-bound, relative to drug-free, state). The decreased bonding in the receptor upon binding the drug increases its internal motion, thus accounting for the very favorable positive entropy change ($T\Delta S$ is in the region of 160 kJ mol^{-1} at room temperature).
- 2) The highly exothermic binding is associated with positive cooperativity, and with associated improved bonding within the receptor (in its drug-bound, relative to drug-free, state). The increased bonding in the receptor upon binding the drug decreases its internal motion, thus accounting for the very unfavorable negative entropy change ($T\Delta S$ is in the region of -47 kJ mol^{-1} at room temperature).

It is of course possible that both positively and negatively cooperative interactions will occur within the same system, and the thermodynamic parameters will then reflect the net effect. Cases where enthalpy/entropy compensation occurs upon ligand binding to proteins have been highlighted, and examples where binding of ligand causes both increases and decreases in flexibility within the same protein are reported.^[85] Additionally, we note that we are only able to consider cases where cooperativity acts to loosen or tighten receptor structures. The situation becomes more complex than can be treated here when ligand binding induces the formation of receptor structures that contain new sets of noncovalent interactions within the receptor.

13. Changes in the Aggregation of Receptors in Signal Transduction

The extremes of enthalpy-driven versus entropy-driven binding were interpreted above as reflecting a tightening or loosening of the receptor system. A common feature of cell-signaling pathways is that membrane-bound receptors are induced to change the extent of their aggregation upon binding to the natural ligand (Figure 14).^[86] In some cases, agonists (which activate a receptor when they bind to it^[87]) induce aggregation of receptors.^[86] Such agonist binding should therefore be particularly beneficial in bonding (negative contribution to ΔH) and adverse in entropy (negative contribution to $T\Delta S$). These consequences (although not previously interpreted in this way) are seen in Figure 15 for the binding of agonists (●) to the β -adrenergic receptor.^[88]

In other cases agonists induce the dissociation of receptor multimers.^[86] Such agonist binding should therefore be relatively adverse in overall bonding and favorable in entropy. These consequences are seen in Figure 16 for the binding of agonists (●) to adenosine A_1 and A_2 receptors.^[89–91]

Antagonists are compounds that bind to such receptors but do not activate them.^[87] Therefore, antagonists must avoid induction of the same order of the receptor system that is

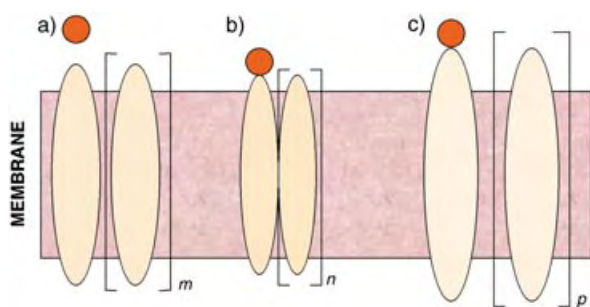


Figure 14. The binding of a ligand (red circle) to a receptor (ellipses) in a membrane: a) ligand-free receptor, b), c) receptors with ligands. b) The binding of a ligand induces greater oligomerization ($n > m$) and possibly also closer packing of the oligomers, c) the binding of the ligand induces dissociation of the receptor ($p < m$) and possibly also looser packing of the oligomers. The receptors may be partially bound (as shown in b and c) or fully saturated.

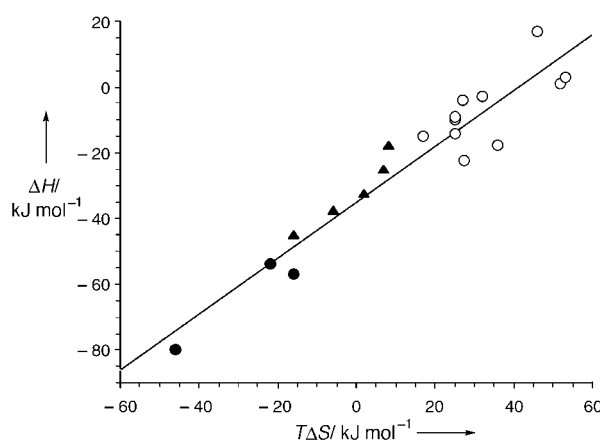


Figure 15. Plots of ΔH versus $T\Delta S$ for the binding of agonists (●), antagonists (○), and partial agonists (▲) to the β -adrenergic receptor.

induced by agonists. Thus, where the agonist induces receptor oligomerization (for example, the β -adrenergic receptor), the antagonist may avoid induction of oligomerization, or even induce the formation of monomeric receptor. Such antagonist binding should therefore be (in comparison to agonist binding) relatively adverse in overall bonding and favorable in entropy. This conclusion is consistent with the data points for antagonist binding to the β -adrenergic receptor (○ in Figure 15).

In contrast, if agonists induce the dissociation of receptor multimers (for example, the adenosine A_1 and A_2 receptors), antagonists may avoid the induction of this dissociation or even induce the formation of receptor oligomers. Such antagonist binding should therefore be (in comparison to agonist binding) relatively favorable in overall bonding and unfavorable in entropy. This conclusion is consistent with the data points for antagonist binding to the adenosine A_1 and A_2 receptors (○ in Figure 16).

Analogous effects are found in numerous systems.^[89–91] Thus, agonists and antagonists appear to frequently act differently in their effects on enthalpy/entropy compensation, and in such cases thermodynamic studies can be used to probe the changes in the oligomeric states of receptors upon ligand binding.

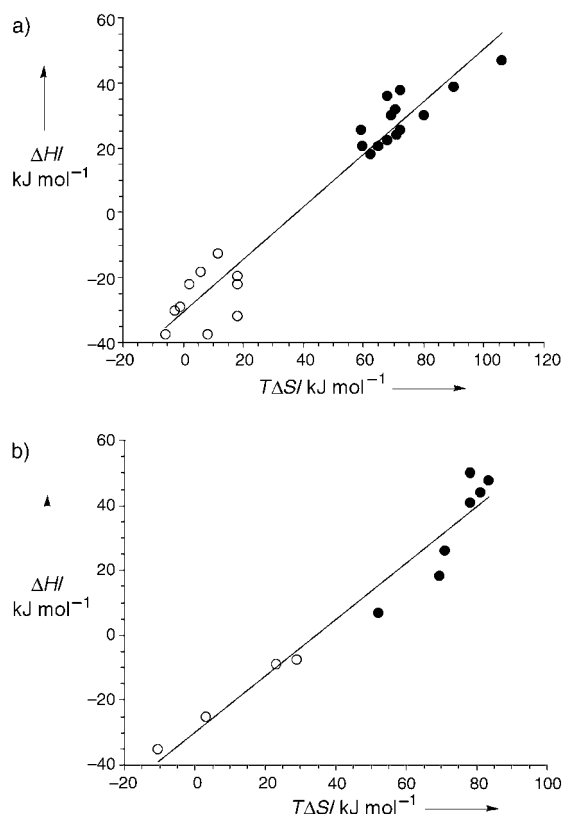
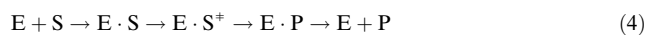


Figure 16. Plots of ΔH versus $T\Delta S$ for the binding of agonists (●) and antagonists (○) to the a) adenosine A_1 receptor and b) adenosine A_2 receptor.^[91]

14. Volume Reductions within Enzymes can Promote Catalysis

14.1. Benefits of Improved Bonding in Enzyme Catalysis

A reaction of substrate \rightarrow product ($S \rightarrow P$) catalyzed by an enzyme (E) benefits, relative to the reaction in free solution, because the adverse entropy of the reaction in free solution is reduced by the preorganization of the catalytic groups in relation to the substrate [Eq. (4)].^[63] Catalysis will also be promoted if the enzyme binds the substrate transition state (S^\ddagger) with positive cooperativity.



According to the model presented here, such positively cooperative binding will occur with a cost in entropy (because of reduced dynamics) and a benefit in enthalpy (because of noncovalent bond contractions) within parts of the enzyme structure in the transition state for reaction. The prediction is therefore that this latter cost in entropy will offset the advantage of the preorganization, but that a large benefit in enthalpy should be apparent in enzyme catalysis.

Relevant data are available for the reaction catalyzed by cytidine deaminase.^[92] The effect of enzyme catalysis is to increase the reaction rate by 10^{16} , as a result of a benefit in enthalpy ($\Delta\Delta H^\ddagger$) of -84 kJ mol^{-1} and a benefit in entropy

($T\Delta\Delta S^\ddagger$) of only 7 kJ mol^{-1} . From the Boltzmann equation, -5.7 kJ mol^{-1} corresponds to the rate of reaction at room temperature increasing by a factor of 10^1 . Thus, the benefit of improved bonding to the enzyme-catalyzed reaction is a factor of about 10^{15} , whereas the benefit from improved order is only a factor of about 10^1 (Figure 17). The data are consistent with catalysis being derived in part by improving the bonds *within the enzyme*, as a consequence of the transition-state structure of the substrate.

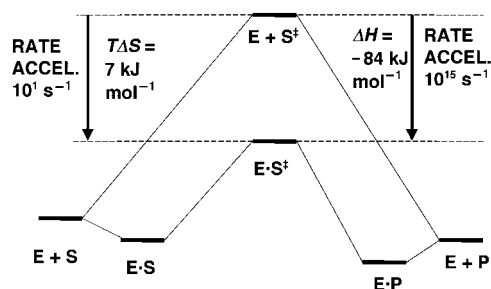


Figure 17. Free energy profiles for the uncatalyzed (upper profile, $E + S \rightarrow E + S^\ddagger \rightarrow E + P$) and catalyzed (lower profile, $E + S \rightarrow ES \rightarrow ES^\ddagger \rightarrow EP \rightarrow E + P$) deamination of cytidine (modified from [92]) The rate enhancement of the enzyme-catalyzed reaction (10^{16}) is obtained by deconvolution of the free energy benefit of catalysis and arises from overall improvements in bonding (10^{15}) and in order (10^1).

The relative reaction rates of six reactions (enzyme-catalyzed versus noncatalyzed, $k_{\text{cat.}}/k_{\text{uncat.}}$) have been measured by Wolfenden and co-workers.^[93,94] Strikingly, all the enzyme-catalyzed reactions are greatly accelerated as a result of the large improvement in bonding in the transition state (Table 2). One apparent source of this improved bonding is between the substrate transition state and the enzyme. The additional source proposed here is the strengthening of existing noncovalent bonds within the enzyme.

Table 2: Benefit in enthalpy ($\Delta\Delta H^\ddagger$) between some uncatalyzed and enzyme-catalyzed reactions.^[88,89]

Entry	Enzyme	$\Delta\Delta H^\ddagger$ [kJ mol ⁻¹]	$k_{\text{cat.}}/k_{\text{uncat.}}$ ^[a]
1	chorismate dismutase	-33	10^6
2	chymotrypsin	-66	10^{12}
3	staphylococcal nuclease	-63	10^{11}
4	bacterial α -glucosidase	-80	10^{14}
5	urease	-93	10^{16}
6	yeast OMP decarboxylase	-143	10^{25}

[a] Acceleration of the enzyme-catalyzed reaction relative to the uncatalyzed reaction as a consequence of $\Delta\Delta H^\ddagger$.

14.2. Reduced Dynamic Behavior of Enzyme Transition State Structures

If the above large benefits in bonding do indeed reflect changes within the enzyme to an important extent, rather than simply the formation of strong bonds between the enzyme and the substrate transition state, then enzymes should undergo markedly less H/D exchange when in the

form that binds this transition state. Two recent studies give convincing support to this idea.

Hydrogen/deuterium (H/D) exchange into backbone amide bonds in hypoxanthine-guanine phosphoribosyl transferase (HGPRT) was used to compare the dynamic properties of human HGPRT alone, in forms with bound reactant/product, and in a form with a bound transition-state analogue.^[95] It was found that out of a possible 207 amide H/D exchange sites in the enzyme, after 1 h at RT in D_2O , HGPRT alone exchanged 160, an equilibrium reactant/product complex exchanged 139, and the transition-state analogue complex exchanged 126 of these amide protons. Thus, the enzyme structure becomes better packed overall to provide binding energy for the reactant/product, and then the packing is improved further to provide even greater binding energy for the transition-state analogue.

Equally striking results are found for the binding of a transition-state analogue to a trimeric purine nucleoside phosphorylase (PNP).^[96] The transition-state analogue (immucillin-H) binds to the enzyme extremely strongly ($K_d = 23\text{ pM}$) when only one of the three catalytic sites is occupied. Deuterium exchange occurred at 167 slow-exchange sites in 2 h when no ligands were present at the catalytic site. A substrate analogue and product prevented H/D exchange at 10 of these sites. When only one of the three sites of the homotrimer was filled with the transition-state analogue immucillin-H, 27 of the slow-exchange protons were protected from exchange in all of the three subunits. The decisive function of the positively cooperative binding of the transition-state analogue is to reduce the dynamic behavior of the receptor (trimer) system to such a degree that a further 81 backbone NH protons are protected from exchange. The reduction in dynamic behavior occurs almost throughout the trimer,^[96] and the binding energy of the transition-state analogue can therefore be derived in a highly delocalized manner.

As in the case of positively cooperative binding of ligands to receptors (Section 11), the improved packing induced within enzyme/substrate transition states is different from that which can be induced by high pressures. Instead, it occurs selectively at those noncovalent interfaces where positively cooperative binding is induced by the substrate transition state (Figure 18).

14.3. Stabilization of the Enzyme in an Enzyme-Bound Intermediate

It can be expected that enzyme-bound intermediates (EBIs) will often bear structural similarities to the transition states for the reaction. Where this is the case, then catalysis should be aided if an EBI has 1) a higher melting temperature (T_m) and 2) a reduced susceptibility to trypsin digestion (relative to the enzyme from which it is formed). These properties have been demonstrated for a haloalkane dehalogenase (DhlA) that catalyzes the hydrolysis of haloalkanes via an alkyl-enzyme intermediate, which is then cleaved by a water molecule that is activated by His 289.^[97] When His 289 is replaced by Gln, the mutant enzyme (His289Gln-DhlA)

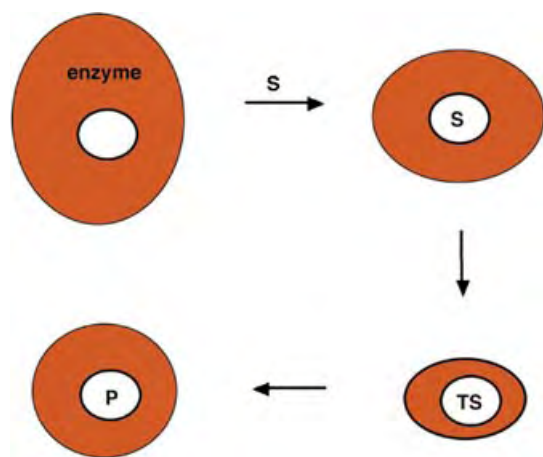


Figure 18. Improved packing of parts of an enzyme structure upon binding the substrate (S), the substrate transition state (TS), and the product (P). The magnitudes of the size and shape changes are grossly exaggerated to illustrate the principle.

accumulates the alkyl–enzyme intermediate. Both the mutant enzyme and the alkyl–enzyme intermediate generated from it through reaction with 1,2-dibromoethane retain the overall conformation of the wild-type protein. Unsurprisingly, the His289Gln-DhlA mutant is thermally less stable ($T_m = 41^\circ\text{C}$) than the native enzyme ($T_m = 48^\circ\text{C}$). However, the alkyl–enzyme intermediate is considerably more thermally stable ($T_m = 51^\circ\text{C}$) than the His289Gln-DhlA mutant from which it was derived. In accord with the conclusion that higher T_m values reflect less dynamic and more stable structures, a number of trypsin cleavage sites became far less susceptible in the enzyme intermediate than in the enzyme from which it was derived. The stabilization of the enzyme-intermediate structure is consistent with catalytic efficiency being derived in part through reduction in the dynamic behavior of the enzyme-intermediate structure.

15. The General Structural Consequences of Positively Cooperative Binding

We have argued here that when two sets of noncovalent bonds are made in a manner where each can restrict the motion associated with the other, there is a benefit in free energy to the ordered state. This conclusion is consistent with analogous (positively cooperative) changes that occur when the size of a homogeneous system is increased from n to $n + m$ molecules. The classical treatment of this effect was established by Hill.^[98] Consider a cluster of n molecules with a repeating geometry in the solid state. As the cluster increases in size, typically 1) the solid becomes thermodynamically more stable and 2) the transition to convert the solid into a liquid becomes sharper.^[99,100]

Table 3 shows the case of increasing numbers of layers of N_2 molecules adsorbed on a surface.^[99] The physical basis for this effect is that as the assemblies increase in size, any given molecule within the solid has other molecules extending out to greater distances that help to hold it in place. In larger

Table 3: Stabilities of N_2 layers as a function of the number of layers.

Number of layers	Melting temperature
2.2	ca. 52 K (very broad)
3.1	56 K (broad)
4.0	58 K (mod. broad)
4.8	61 K (mod. sharp)
infinite	63.14 K (very sharp)

assemblies, any given molecule has reduced dynamic behavior because the other $n-1$ molecules that hold it in place are increased in number. This reduced dynamic behavior means it is better bonded to its immediate neighbors.

The van't Hoff equation [Eq. (5)] requires that the greater the change in the equilibrium constant for a melting process in a given temperature range, the greater must be its enthalpy change.

$$\ln K = -\Delta H/RT + \Delta S/R \quad (5)$$

Thus, the sharper melting transitions undergone by systems as they increase in size (Table 3) reflect larger enthalpy changes. These larger enthalpy changes derive from two effects: 1) the increased size of the system (for example, 2.2 versus 4.8 layers) and 2) the more effective bonding of each molecule to its neighbors in the larger system. The addition of an extra layer of nitrogen molecules to the system is analogous to the binding of a ligand to a receptor in a strain-free manner. The contractions within such a system as it increases in size are illustrated schematically in Figure 19.

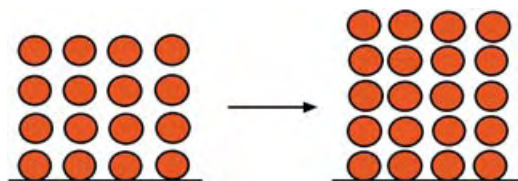


Figure 19. Improved packing and bonding within an ordered system of molecules upon addition of an extra layer.

A corollary of the above argument is that as systems of homogeneous solids become smaller the supramolecular assemblies that behave as an entity become smaller, and their van't Hoff enthalpies of fusion become smaller. It is for this reason that crystals usually exhibit lower (and broader) melting transitions as they are contaminated with increasing amounts of an impurity. In Table 3, the “impurities” are at the boundaries of the N_2 molecules below the surface and the gas above. In biological systems, the water at the surface of a receptor can behave as an “impurity” relative to more positively cooperative binding in the ligand–receptor system.

Consistent with the above generalizations, the incorporation of increasing quantities of cholesterol (as an impurity) progressively reduces the temperature, enthalpy, and cooperativity of the gel-to-liquid-crystalline phase transition of lipid bilayers constituted from phosphatidylserine.^[101]

16. Conclusion

An approach in which the simplification is made that noncovalent interactions have characteristic binding energies is useful in the estimation of binding energies. However, in reality each interaction is context-dependent. This context dependency is associated with enthalpy/entropy compensation.

Enthalpy/entropy compensation, sometimes proposed to be an artifact of experimental error, is a fundamental property of noncovalent interactions (Houk et al. have written a recent summary where either the physical validity or presumed lack of validity of enthalpy/entropy compensation is presented^[102]). It occurs in any solid/liquid transition, or when the temperature of any solid or liquid containing noncovalent bonds is changed. It is not only predicted from fundamental theoretical considerations,^[2–4] but is also in many experiments far too large to be an artifact arising from errors (see, for example, Figures 13 and 16). In this connection, it should be noted that the uncertainties in the determination of ΔG and ΔH values by calorimetry are not very different.^[59]

The correlations presented here between enthalpy/entropy compensation and the changes in dynamic behavior of proteins (as established by H/D exchange) establish the physical nature of a source of enthalpy/entropy compensation in biological systems. The enthalpy well for a local interaction

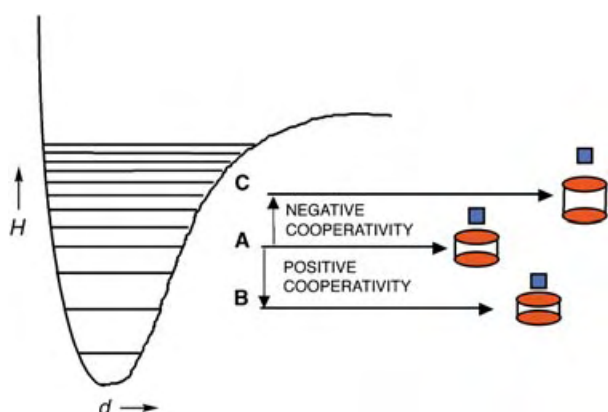


Figure 20. Relative vibrational levels occupied when the strength of a specified hydrogen bond of the receptor (red) and the coordination of the ligand (blue) are A) not cooperatively coupled, B) are coupled with positive cooperativity, and C) are coupled with negative cooperativity. The enthalpy of the interaction is more favorable (more negative) when it lies more deeply in the well. The asymmetry of the well means that when the interaction lies more deeply in the well its bond length is shorter.

influenced in this way is indicated in Figure 20. Promoting an interaction to lie more deeply in an enthalpy well provides a benefit in enthalpy at a cost in entropy; such a change is positively cooperative since ligands are able to bind better to organized templates. Conversely, inducing an interaction to lie more shallowly in the well gives a benefit in entropy at a cost in enthalpy; such a change is negatively cooperative in the general case since here ligands must distort their receptors, which thereby become more dynamic. When the

enthalpy barrier to breaking an interaction is very small, the available thermal energy will sometimes break the bond (that is, the interaction will be broken by “hopping” out of the well). Thus, when the bonding is extremely weak, the increases in bond length (that are associated with negative cooperativity or the removal of a positively cooperative effect) will also be associated with fraying.^[103]

Where ligand binding directly increases the electrostatic polarization of an interaction within the receptor (for example, of a receptor amide/amide hydrogen bond), the well shown in Figure 20 is additionally deepened, thus providing a further source of bond shortening. It is also clearly possible that distortion of a receptor upon ligand binding may occur in such a manner that the well of Figure 20 becomes less deep, and this effect further promotes the bond lengthening associated with negative cooperativity.

The total changes in the free energies in the organized systems (Figure 20) would be determined by summing over all the noncovalent interactions that are influenced in the manner indicated. Note that in a bound state, lying more deeply or shallowly inside a specified well (Figure 20) has the same consequences as lying in a deeper or shallower well (Figure 2).

Thus, evolution can lead to the use of better packing within parts of receptor structures, which occurs upon ligand binding, to aid ligand binding. It is perhaps useful to envision that the ligand causes a “pseudocrystallization” of parts of the receptor.^[56] In other cases, the loosening of parts of receptor structures occurs to weaken ligand binding. These changes are most simply represented as in Figures 18 and 21. The occurrence of the volume reductions indicated in Figure 18 and the upper panel of Figure 21 (grossly exaggerated) upon the positively cooperative binding of ligands to proteins is supported by the direct measurement of volume changes

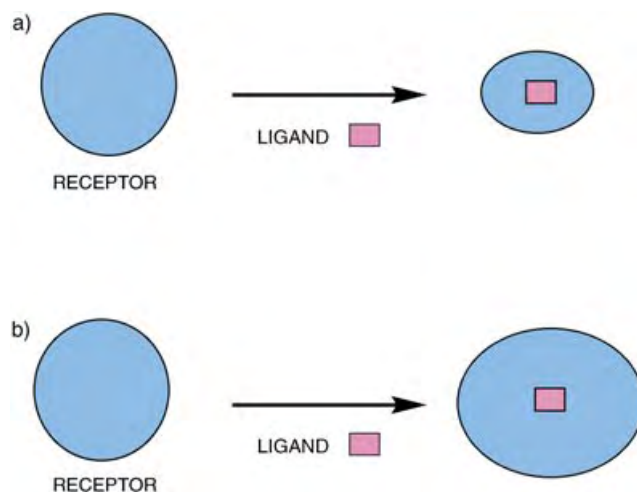


Figure 21. Changes in packing of parts of a receptor structure upon binding its ligand with a) positive cooperativity and b) negative cooperativity. The magnitudes of the size and shape changes are grossly exaggerated to illustrate the principle. The nonsymmetrical induced changes in the shape of the receptor illustrate that cooperativity will typically be exercised more in some parts of the structure than in others. The effects cannot therefore be equated with the ones that would simply be induced by changes in pressure.

occurring in such processes. Thus, it has been reported that decreases in volume (on the order of 1%) occur when *N*-acetyl-D-glucosamine oligomers bind to lysozyme.^[104] Importantly, the largest decreases in volume are observed for the ligand that exhibits the highest affinity.

Binding of a small molecule is promoted where the receptor protein shows some or all of the following properties:

- 1) reduced H/D exchange of the amide protons,^[59,87,88]
- 2) a raised T_m value,^[59,73]
- 3) improved internal bonding and reduced dynamic behavior (more negative values of ΔH and ΔS for ligand binding),^[65,81]
- 4) greater resistance to enzymic digestion and possibly also promotion of the stability of oligomeric forms of the protein.^[105]

In the examples cited here, negatively cooperative binding promotes converse effects.^[65,71]

Catalytic efficiency is promoted when substrate transition states extensively reduce the dynamic behavior of enzymes. Such a mechanism suggests a reason why enzymes are relatively large structures.

Addendum

It is clearly important to determine whether large binding energies can be provided in the delocalized manner envisioned in this Review. To establish this point, we have recently determined the reduction in the dynamic behavior of glyceraldehyde 3-phosphate dehydrogenase (GAPDH) upon successively binding four molecules of its cofactor (NAD⁺).^[107] We find that in the binding of the first NAD⁺ to the enzyme tetramer, 60 backbone amide NH protons are protected from H/D exchange, whereas in the binding of the fourth NAD⁺ molecule, there is no measurable protection of amide backbone NH protons from H/D exchange. The binding constant for the first NAD⁺ molecule is greater than that for the fourth NAD⁺ molecule by a factor of about 10^6 . Thus, it is clear that the binding constant can, in this case, be increased by a factor of a million because the dynamic behavior of the enzyme/cofactor system is reduced upon binding the first NAD⁺, but not upon binding the fourth NAD⁺ molecule.

We have also shown^[107] that under circumstances in which streptavidin is concluded to decrease its average amide hydrogen bond length by about 1%, (on decreasing its temperature from 55 to 5°C),^[108] its increased stability and reduced dynamic behavior decrease its extent of backbone amide H/D exchange from 99 to 61 (same conditions as reported in Section 11). This experiment, taken in conjunction with the data of Section 11 and the above GAPDH data, suggests that very large ligand binding energies, and increased catalytic efficiencies (of the order of a million-fold), can be derived by decreasing the lengths of the numerous hydrogen bonds of a protein (upon binding a small molecule) by as little as about 1%. It is therefore not surprising that X-ray studies

have not uncovered the structural basis of the effects proposed here.

Churchill College (M.Z.), the EPSRC (D.H.W. and D.O'B.) and the BBRSC (D.H.W. and E.S.) are thanked for financial support.

Received: December 4, 2003

Revised: March 5, 2004

- [1] M. P. Washburn, D. Wolters, J. R. Yates, *Nat. Biotechnol.* **2001**, 19, 242.
- [2] M. S. Searle, M. S. Westwell, D. H. Williams, *J. Chem. Soc. Perkin Trans. 2* **1995**, 141.
- [3] J. D. Dunitz, *Chem. Biol.* **1995**, 2, 709.
- [4] M. S. Searle, D. H. Williams, *Nucleic Acids Res.* **1993**, 21, 2051.
- [5] R. Lumry, S. Rajender, *Biopolymers* **1970**, 9, 1125.
- [6] O. Exner, *Prog. Phys. Org. Chem.* **1973**, 10, 411.
- [7] W. P. Jencks, *Proc. Natl. Acad. Sci. USA* **1981**, 78, 4046.
- [8] M. I. Page, W. P. Jencks, *Proc. Natl. Acad. Sci. USA* **1971**, 68, 1678.
- [9] M. I. Page, *Angew. Chem.* **1977**, 89, 456; *Angew. Chem. Int. Ed. Engl.* **1977**, 16, 449.
- [10] P. R. Andrews, D. J. Craik, J. L. Martin, *J. Med. Chem.* **1984**, 27, 1648.
- [11] D. H. Williams, J. P. L. Cox, A. J. Doig, M. Gardner, U. Gerhard, P. T. Kaye, A. L. Lal, I. A. Nichols, C. J. Salter, R. C. Mitchell, *J. Am. Chem. Soc.* **1991**, 113, 7020.
- [12] W. Kauzmann, *Adv. Protein Chem.* **1959**, 14, 1.
- [13] C. Tanford, *The Hydrophobic Effect: Formation of Micelles and Biological Membranes*, Wiley, New York, **1980**.
- [14] N. Muller, *Acc. Chem. Res.* **1990**, 23, 23.
- [15] D. B. Smithrud, T. B. Wyman, F. Diederich, *J. Am. Chem. Soc.* **1991**, 113, 5420.
- [16] a) H.-J. Böhm, *J. Comput.-Aided Mol. Des.* **1994**, 8, 243; b) H.-J. Böhm, personal communication.
- [17] M. D. Eldridge, C. W. Murray, T. R. Auton, G. V. Paolini, R. P. Mee, *J. Comput.-Aided Mol. Des.* **1997**, 11, 425.
- [18] R. D. Head, M. L. Smythe, T. I. Oprea, C. L. Waller, S. M. Green, G. R. Marshall, *J. Am. Chem. Soc.* **1996**, 118, 3959.
- [19] A. R. Fersht, *TIBS* **1987**, 12, 301.
- [20] M. S. Searle, D. H. Williams, U. Gerhard, *J. Am. Chem. Soc.* **1992**, 114, 10697.
- [21] B. A. Shirley, P. Stanssens, U. Hahn, C. N. Pace, *Biochemistry* **1992**, 31, 725.
- [22] C. Chothia, *Nature* **1974**, 248, 338.
- [23] C. Chothia, *Nature* **1975**, 254, 304.
- [24] R. B. Hermann, *J. Phys. Chem.* **1972**, 76, 2754.
- [25] G. I. Makhatadze, P. L. Privalov, *Adv. Protein Chem.* **1995**, 47, 307.
- [26] J. A. Reynolds, D. B. Gilbert, C. Tanford, *Proc. Natl. Acad. Sci. USA* **1974**, 71, 2925.
- [27] J. M. Sanchez-Ruiz, *J. Phys. Chem.* **1995**, 99, 12076.
- [28] J. M. Sanchez-Ruiz, *Eur. Biophys. J.* **1996**, 24, 261.
- [29] J. T. Kellis, K. Nyberg, A. R. Fersht, *Biochemistry* **1989**, 28, 4914.
- [30] A. Nicholls, K. A. Sharp, B. Honig, *Proteins Struct. Funct. Genet.* **1991**, 11, 281.
- [31] C. N. Pace, *J. Mol. Biol.* **1992**, 226, 29.
- [32] L. Serrano, J.-L. Neira, J. Sancho, A. R. Fersht, *Nature* **1992**, 356, 453.
- [33] K. Goto, *Biochem. Biophys. Res. Commun.* **1995**, 206, 497.
- [34] M. Matsumura, W. J. Becktel, B. W. Matthews, *Nature* **1988**, 334, 406.
- [35] P. D. Ross, M. V. Rekharsky, *Biophys. J.* **1996**, 71, 2144.

- [36] D. Shortle, W. E. Stites, A. K. Meeker, *Biochemistry* **1990**, 29, 8033.
- [37] K. Takano, Y. Yamagata, K. Yutani, *J. Mol. Biol.* **1998**, 280, 749.
- [38] B. Vallone, A. E. Miele, P. Vecchini, E. Chiancone, M. Brunori, *Proc. Natl. Acad. Sci. USA* **1998**, 95, 6103.
- [39] M. S. Searle, D. H. Williams, *J. Am. Chem. Soc.* **1992**, 114, 10690.
- [40] D. H. Williams, M. S. Westwell, *Chem. Soc. Rev.* **1998**, 27, 57.
- [41] R. M. Izatt, J. S. Bradshaw, K. Pawlak, R. L. Bruening, B. J. Tarbet, *Chem. Rev.* **1992**, 92, 1261.
- [42] M. S. Westwell, M. S. Searle, J. Klein, D. H. Williams, *J. Phys. Chem.* **1996**, 100, 16000.
- [43] H.-J. Schneider, A. Yatsimirsky, *Principles and Methods in Supramolecular Chemistry*, Wiley-VCH, Weinheim, **2000**.
- [44] M. S. Searle, G. J. Sharman, P. Groves, B. Benhamu, D. A. Beauregard, M. S. Westwell, R. J. Dancer, A. J. Maguire, A. C. Try, D. H. Williams, *J. Chem. Soc. Perkin Trans. 1* **1996**, 2781.
- [45] P. Groves, M. S. Searle, M. S. Westwell, D. H. Williams, *Chem. Commun.* **1994**, 1519.
- [46] D. H. Williams, A. J. Maguire, W. Tsuzuki, M. S. Westwell, *Science* **1998**, 280, 711.
- [47] G. Wagner, A. Pardi, K. Wüthrich, *J. Am. Chem. Soc.* **1983**, 105, 5948.
- [48] D. S. Wishart, B. D. Sykes, F. M. Richards, *J. Mol. Biol.* **1991**, 222, 311.
- [49] C. T. Calderone, D. H. Williams, *J. Am. Chem. Soc.* **2000**, 122, 6262.
- [50] G. A. Leonard, J. Thomson, W. P. Watson, T. Brown, *Proc. Natl. Acad. Sci. USA* **1990**, 87, 9573.
- [51] T. V. Chalikian, J. Voelker, J. G. E. Plum, K. J. Breslauer, *Proc. Natl. Acad. Sci. USA* **1999**, 96, 7853.
- [52] J. A. Holbrook, M. W. Capp, R. M. Saecker, M. T. Record, *Biochemistry* **1999**, 38, 8409.
- [53] I. Jelesarov, C. Crane-Robinson, P. L. Privalov, *J. Mol. Biol.* **1999**, 294, 981.
- [54] D. H. Williams, C. T. Calderone, D. P. O'Brien, R. J. Zerella, *Chem. Commun.* **2002**, 1266.
- [55] B. Bardsley, D. H. Williams, *Chem. Commun.* **1998**, 2305.
- [56] D. H. Williams, E. Stephens, M. Zhou, *Chem. Commun.* **2003**, 1973.
- [57] S. Jusuf, P. J. Loll, P. H. Axelsen, *J. Am. Chem. Soc.* **2002**, 124, 3490.
- [58] D. H. Williams, N. L. Davies, R. Zerella, B. Bardsley, *J. Am. Chem. Soc.* **2004**, 126, 2042.
- [59] D. McPhail, A. Cooper, *J. Chem. Soc. Faraday Trans.* **1997**, 93, 2283.
- [60] *CRC Handbook of Physics and Chemistry*, 73rd ed. (Ed.: D. R. Lide), New York, **1992–1993**.
- [61] D. E. Koshland, Jr., G. Nemethy, D. Filmer, *Biochemistry* **1996**, 35, 365.
- [62] J. Monod, J. Wyman, J.-P. Changeux, *J. Mol. Biol.* **1965**, 12, 88.
- [63] A. Fersht, *Structure and Mechanism in Protein Science*, Freeman, New York, **1999**.
- [64] M. F. Perutz, A. J. Wilkinson, M. Paoli, G. G. Dodson, *Annu. Rev. Biophys. Biomol. Struct.* **1998**, 27, 1.
- [65] D. H. Williams, E. Stephens, M. Zhou, *J. Mol. Biol.* **2003**, 329, 389.
- [66] A. Colosimo, M. Coletta, G. Falcioni, B. Giardina, S. J. Gill, M. Brunori, *J. Mol. Biol.* **1982**, 160, 531.
- [67] M. F. Perutz, *Annu. Rev. Biochem.* **1979**, 48, 327.
- [68] F. J. Blanco, G. Rivas, L. Serrano, *Nat. Struct. Biol.* **1994**, 1, 584.
- [69] P. E. Wright, H. J. Dyson, R. A. Lerner, *Biochemistry* **1988**, 27, 7167.
- [70] S. W. Englander, J. J. Englander, R. E. McKinnie, G. K. Ackers, G. J. Turner, J. A. Westrick, S. J. Gill, *Science* **1992**, 256, 1684.
- [71] T. Flatmark, B. Almas, P. M. Knappskog, S. V. Berge, R. M. Svebak, R. Chehin, A. Muga, A. Martinez, *Eur. J. Biochem.* **1999**, 262, 840.
- [72] T. K. Dam, R. Roy, S. K. Das, S. Oscarson, C. F. Brewer, *J. Biol. Chem.* **2000**, 275, 14223.
- [73] T. K. Dam, R. Roy, D. Page, C. F. Brewer, *Biochemistry* **2002**, 41, 1351.
- [74] T. K. Dam, R. Roy, D. Page, C. F. Brewer, *Biochemistry* **2002**, 41, 1359.
- [75] M. Celej, C. Montich, G. Fidelio, *Protein Sci.* **2003**, 12, 1496.
- [76] H.-P. Biemann, D. E. Koshland, Jr., *Biochemistry* **1994**, 33, 629.
- [77] I. D. Kuntz, K. Chen, K. A. Sharp, P. A. Kollman, *Proc. Natl. Acad. Sci. USA* **1999**, 96, 9997.
- [78] S. Freitag, I. Le Trong, L. Klumb, P. S. Stayton, R. E. Stenkamp, *Protein Sci.* **1997**, 6, 1157.
- [79] D. E. Hyre, I. Le Trong, S. Freitag, R. E. Stenkamp, *Protein Sci.* **2000**, 9, 878.
- [80] P. C. Weber, D. H. Ohlendorf, J. J. Wendoloski, F. R. Salemme, *Science* **1989**, 243, 85.
- [81] P. C. Weber, J. J. Wendoloski, M. W. Pantoliano, F. R. Salemme, *J. Am. Chem. Soc.* **1992**, 114, 3197.
- [82] J. Sturtevant, *Proc. Natl. Acad. Sci. USA*, **1977**, 74, 2236.
- [83] A. Cooper, D. T. F. Dryden, *Eur. Biophys. J.* **1984**, 11, 103.
- [84] P. Gilli, V. Ferretti, G. Gilli, P. A. Borea, *J. Phys. Chem.* **1994**, 98, 1515.
- [85] M. J. Stone, *Acc. Chem. Res.* **2001**, 34, 379.
- [86] A. Yesilaltay, D. D. Jenness, *Mol. Biol. Cell* **2000**, 11, 2873.
- [87] J. Kendrew, *The Encyclopedia of Molecular Biology*, Blackwell, Oxford, **1994**.
- [88] G. A. Weiland, K. P. Minneman, P. B. Molinoff, *Nature* **1979**, 281, 114.
- [89] P. A. Borea, K. Varani, L. Guerra, P. Gilli, G. Gilli, *Mol. Neuropharmacol.* **1992**, 2, 273.
- [90] P. A. Borea, A. Dalpiaz, K. Varani, L. Guerra, G. Gilli, *Biochem. Pharmacol.* **1995**, 49, 461.
- [91] P. A. Borea, K. Varani, S. Gessi, P. Gilli, A. Dalpiaz, *Farmaco* **1998**, 53, 249.
- [92] M. J. Snider, S. Gaunitz, C. Ridgeway, S. A. Short, R. Wolfenden, *Biochemistry* **2000**, 39, 9746.
- [93] A. Radzicka, R. Wolfenden, *Science* **1995**, 267, 90.
- [94] R. Wolfenden, M. Snider, C. Ridgway, B. Miller, *J. Am. Chem. Soc.* **1999**, 121, 7419.
- [95] F. Wang, W. Shi, E. Nieves, R. H. Angeletti, V. L. Schramm, C. Grubmeyer, *Biochemistry* **2001**, 40, 8043.
- [96] F. Wang, R. W. Miles, G. Kicsa, E. Nieves, V. L. Schramm, R. H. Angeletti, *Protein Sci.* **2000**, 9, 1660.
- [97] G. H. Krooshof, Ph.D. thesis, Groningen (Groningen), **2000**.
- [98] T. L. Hill, *Thermodynamics of Small Systems, Vol. 1*, Benjamin, New York, **1963**.
- [99] J. A. Morrison, L. E. Drain, J. S. Dugdale, *Can. J. Chem.* **1952**, 30, 890.
- [100] D. H. Williams, M. S. Westwell, *Chem. Biol.* **1996**, 3, 695.
- [101] T. P. W. McMullen, R. N. A. H. Lewis, R. N. McElhaney, *Biophys. J.* **2000**, 79, 2056.
- [102] K. N. Houk, A. G. Leach, S. P. Kim, X. Zhang, *Angew. Chem.* **2003**, 115, 5020; *Angew. Chem. Int. Ed.* **2003**, 42, 4872.
- [103] C. A. Hunter, *Chem. Biol.* **2003**, 10, 1023.
- [104] K. Gekko, K. Yamagami, *Chem. Lett.* **1998**, 839.
- [105] O. H. Laitinen, A. T. Marttila, J. Kari, K. J. Airene, T. Kulik, O. Livnah, E. A. Bayer, M. Wilchek, M. S. Kulomaa, *J. Biol. Chem.* **2001**, 276, 8219.
- [106] R. B. Koradi, M. Billeter, K. Wüthrich, *J. Mol. Graphics* **1996**, 14, 51.
- [107] D. H. Williams, M. Zhou, E. Stephens, unpublished results.
- [108] F. Cordier, S. Grzesiek, *J. Mol. Biol.* **2002**, 715, 739.

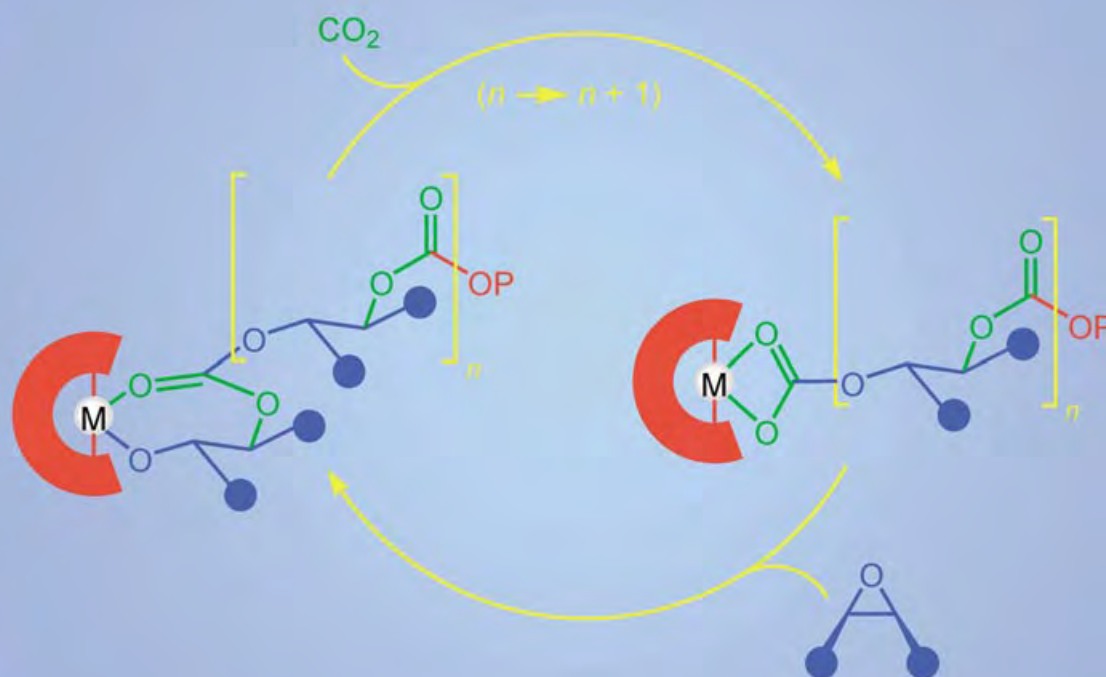
Polymerization Catalysts

Discrete Metal-Based Catalysts for the Copolymerization of CO₂ and Epoxides: Discovery, Reactivity, Optimization, and Mechanism

Geoffrey W. Coates* and David R. Moore

Keywords:

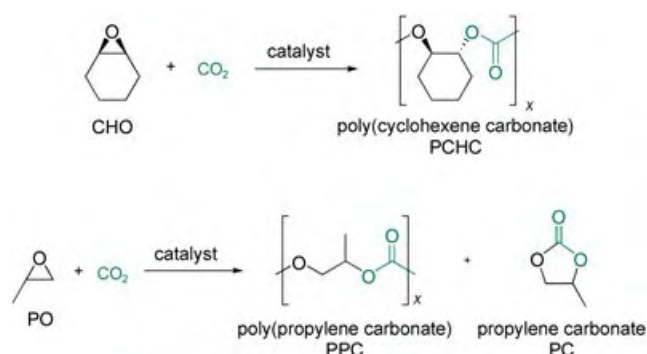
carbon dioxide · epoxides ·
homogeneous catalysis ·
polymers · renewable
resources



Most synthetic polymers are made from petroleum feedstocks. Given the non-renewable nature of these materials, there is increasing interest in developing routes to polymeric materials from renewable resources. In addition, there is a growing demand for biodegradable polymeric materials. Polycarbonates made from CO₂ and epoxides have the potential to meet these goals. Since the discovery of catalysts for the copolymerization of CO₂ and epoxides in the late 1960's by Inoue, a significant amount of research has been directed toward the development of catalysts of improved activity and selectivity. Reviewed here are well-defined catalysts for epoxide-CO₂ copolymerization and related reactions.

1. Introduction

Since petroleum resources are predicted to be exhausted within the next century at the current rate of consumption,^[1] there is a growing effort to develop new chemical processes using biorenewable resources.^[2–4] One such resource of particular interest is CO₂, a nontoxic, nonflammable, naturally abundant C₁ feedstock.^[5–8] The reaction of CO₂ with metal complexes has been extensively studied, revealing potential pathways for catalytic reactions.^[9–15] However the thermodynamic stability of CO₂ has hampered its utility as a reagent for chemical synthesis; in fact its high stability makes it an ideal medium for many chemical processes.^[7,16,17] To overcome this limitation, reactions employing CO₂ with highly reactive reagents have been explored. In particular, the catalytic coupling of CO₂ with heterocycles has received considerable attention over the past 35 years.^[18–23] A majority of these publications involve the reaction of CO₂ with epoxides to generate polycarbonates and/or cyclic carbonates (1,3-dioxolan-2-ones) (Scheme 1).



Scheme 1. Alternating copolymerization of cyclohexene oxide (CHO) and propylene oxide (PO) with CO₂.

Aliphatic polycarbonates have potential applications as packaging materials, as well as in the synthesis of engineering thermoplastics and resins, pyrotechnics, and interliners for

safety glass.^[24–26] Poly(propylene carbonate) (PPC)^[4] decomposes uniformly and controllably to cyclic propylene carbonate below 250 °C,^[27,28] making it particularly useful as a binder for ceramics, adhesives, and propellants.^[29] The glass transition temperature (*T_g*) of PPC is 35–40 °C, which hinders its broad utility as a bulk material.^[28] Therefore, efforts are being directed to employ aliphatic polycarbonates as additives and pore formers. Clearly one of the most promising applications of PPC is as a mid-segment of polyurethanes.^[25] PPCs with high ether linkage content (80 % ether) have been reported to exhibit excellent solubility in supercritical CO₂, a rare property for non-fluorinated polymers.^[30] Alicyclic polycarbonates, such as poly(cyclohexene carbonate) (PCHC), typically have much higher *T_g*'s (115 °C for PCHC) resulting in materials with properties very similar to poly(styrene).^[31] PCHC also has a higher decomposition temperature (≈ 300 °C), which allows melt-processing.^[26] Alicyclic polycarbonates are finding applications in lithographic processes for the construction of microfluidic devices.^[32–35] Cyclic carbonates are utilized industrially as polar aprotic solvents, substrates for small molecule synthesis, additives, antifoam agents for antifreeze, and plasticizers.^[36,37] The five-membered ring cyclic carbonates (1,3-dioxolan-2-ones) are generally incapable of ring-opening polymerization due to their thermodynamic stability, but do undergo polymerization with partial loss of CO₂ to yield macromolecules with both ether and carbonate linkages.^[38] Due to such uses, a number of syntheses of cyclic carbonates have been described over the

From the Contents

1. Introduction	6619
2. Early Discoveries and Background	6620
3. Aluminum and Manganese Catalysts	6622
4. Chromium Catalysts	6624
5. Cobalt Catalysts	6627
6. Lanthanide-Based Catalysts	6627
7. Zinc and Cadmium Catalysts	6628
8. Summary and Outlook	6636

[*] Prof. G. W. Coates, Dr. D. R. Moore
Department of Chemistry and Chemical Biology
Baker Laboratory
Cornell University
Ithaca, NY 14853-1301 (USA)
Fax: (+1) 607-255-4137
E-mail: gc39@cornell.edu

[†] A list of frequent abbreviations is given at the end of this Review.

last 30 years. For example, tetraalkylammonium salts, phosphanes, main-group and transition-metal complexes, and alkali metal salts convert epoxides and CO₂ to cyclic carbonates.^[20]

The moderate thermal stability and low temperature of thermal deformation of aliphatic polycarbonates, coupled with their high cost (ca. \$100 per lb) hamper their widespread use as bulk polymeric materials. More economically viable processes and the synthesis of new types of improved aliphatic polycarbonates would clearly increase the number of applications for these polymers, as well as lower their cost. A significant contributor to the cost of these materials is the low activity of the industrial zinc/dicarboxylic acid catalysts used to polymerize epoxides and CO₂. As a result, a significant amount of recent research has focused on the discovery and development of new catalysts for this process.

There are many parallels between the development of alkene polymerization catalysts and those for CO₂/epoxide polymerization. In each field, the catalysts initially discovered were heterogeneous; subsequent work focused on the empirical optimization to provide higher activity and selectivity for the polymerizations. Eventually, discrete, homogeneous metal complexes were explored in academic laboratories as a way to probe reaction mechanisms. It was envisaged that a detailed understanding of the polymerizations at the molecular level could be applied to the design of improved catalytic systems. In some cases, these new homogeneous catalysts have significant advantages over their heterogeneous counterparts.

Heterogeneous catalysts are the workhorse of many industrial processes. They have many processing advantages over their soluble counterparts, but often contain multiple active sites that result in polymers with broad polydispersity indices (PDIs) and composition distributions. In many cases, only a small percentage of the metal sites are active, and residual catalyst remains in the polymeric product. As a result of these drawbacks, a significant amount of research has been directed toward the development of well-defined, single-site homogeneous catalysts. Homogeneous catalysts are typically of the form L_nMR, where L_n is a set of permanently bound ligands, M is a metal center, and R is an efficient initiation group. These homogeneous catalysts are discrete species, rendering them amenable to precise modification as well as detailed mechanistic studies. Most of the major advances in metal-catalyzed polymerization, including stereoselective^[39]

and living^[40] alkene polymerization, lactide and lactone polymerization,^[41] olefin metathesis,^[42] and alkene/CO copolymerization,^[43] are the result of progress in homogeneous catalyst design. Homogeneous catalysts are being used to develop unique polymer architectures that lead to new, industrially relevant materials. However, it should be noted that the vast majority of industrial polymerization catalysts are still of the heterogeneous variety.

1.1. Scope of Review

The purpose of this review is to give a thorough account of the CO₂/epoxide polymerization literature,^[18–22] with a strong emphasis on single-site homogeneous catalysts and their mechanisms of operation. The review is organized according to the active metal center of the catalyst and although polymerization is the focus, the production of cyclic carbonates is discussed when appropriate. Activities in the form of turnover frequencies (TOFs) are given in mole epoxide converted to product per mole metal per hour (assuming all metal centers are active). The activity of a system is defined on the basis of TOFs as follows: low (< 5 TO h⁻¹), moderate (5–200 TO h⁻¹), and high (> 200 TO h⁻¹). For conformity, CO₂ pressures are reported in atm (1 atm = 14.7 psi = 1.013 bar = 1.013 × 10⁵ Pa).

2. Early Discoveries and Background

In 1969, Inoue and co-workers made the remarkable discovery that a mixture of ZnEt₂ and H₂O was active for catalyzing the alternating copolymerization of propylene oxide (PO) and CO₂ (Scheme 1), marking the advent of epoxide–CO₂ coupling chemistry.^[44,45] An optimum 1:1 ratio of ZnEt₂/H₂O gave the best yields of methanol-insoluble PPC with an activity of 0.12 h⁻¹ (mol of PO converted to polymer per mol Zn per h) at 80 °C and 20–50 atm CO₂ (Table 1). On the basis of elemental analysis, the copolymer contained 88 % carbonate linkages. Notably, a 1:1 mixture of ZnEt₂ and MeOH did not generate an active catalytic species for polycarbonate synthesis. Following this initial lead, Inoue investigated the use of dihydric sources, including resorcinol,^[46,47] dicarboxylic acids,^[48] and primary amines,^[49] in mixtures with ZnEt₂ for PO–CO₂ copolymerization. These



Geoffrey W. Coates, born in Evansville, Indiana in 1966, obtained a B.A. degree in chemistry from Wabash College in 1989 and a Ph.D. in organic chemistry from Stanford University in 1994. In his thesis work, under the direction of Robert M. Waymouth, he investigated the stereoselectivity of metallocene-based Ziegler–Natta catalysts. Following his doctoral studies, he was an NSF Postdoctoral Fellow with Robert H. Grubbs at the California Institute of Technology. In 1997, he joined the Department of Chemistry at Cornell University where he is currently Professor of Chemistry.



David R. Moore, born in Hamilton, New Jersey in 1976, graduated from Drew University in 1998 with a B.A. degree in chemistry and subsequently studied organic chemistry under the supervision of Geoffrey W. Coates at Cornell University. His doctoral research focused on the mechanism of alternating copolymerization of epoxides and carbon dioxide using β -diiminate–zinc catalysts. After graduating with a Ph.D. in 2003, he became a research scientist at the General Electric Global Research Center in Niskayuna, New York.

systems showed TOFs of 0.17, 0.43, and 0.06 h⁻¹, respectively (see Table 1).

Following Inoue's discoveries, Kuran and co-workers developed a copolymerization system using ZnEt₂ and trihydric phenols, including pyrogallol and 4-bromopyrogallol.

Table 1: Selected heterogeneous catalysts for PO-CO₂ copolymerization.^[a]

Complex	<i>p</i> (CO ₂) [atm]	<i>t</i> [h]	<i>T</i> [°C]	TON ^[b]	TOF [h ⁻¹] ^[c]	Ref.
ZnEt ₂ /H ₂ O ^[d]	20–50	48	80	5.9	0.12	[44]
ZnEt ₂ /resorcinol ^[d]	30	48	35	8.1	0.17	[46]
ZnEt ₂ /isophthalic acid ^[d]	40	44	35	19.1	0.43	[48]
ZnEt ₂ / <i>m</i> -hydroxybenzoic acid ^[d]	40	44	35	19.6	0.45	[48]
ZnEt ₂ /α-phenethylamine ^[d]	40	68	40	3.9	0.06	[49]
ZnEt ₂ /pyrogallol ^[e]	60	44	35	12.0	0.27	[50]
ZnEt ₂ /4-bromopyrogallol ^[e]	60	45	35	13.8	0.31	[51]
Zn(OH) ₂ /glutaric acid ^[f]	30	40	60	44.3	1.1	[53]
ZnO/glutaric acid ^[f]	25	40	60	134	3.4	[108]

[a] All polymerizations result in PPC, which is collected as the MeOH-insoluble fraction. [b] Moles of PO consumed per mole of zinc. [c] Moles of PO consumed per mole of zinc per hour. [d] 1:1 ratio of Zn to protic source, reaction in dioxane. [e] 2:1 ratio of ZnEt₂ to protic source, reaction in dioxane. [f] Reaction run in neat PO.

lol, that produced PPC with TOFs up to 0.3 h⁻¹ at 35 °C and 60 atm CO₂.^[50,51] In general, di- or tri-protic sources and ZnEt₂ produced PPC, while monoprotic sources, such as alcohols and secondary amines, only gave propylene carbonate (PC) (Schemes 1 and 2).^[52] In an effort to develop more active catalysts, Hattori and co-workers synthesized a heterogeneous catalyst from Zn(OH)₂ and glutaric acid. Under 30 atm CO₂ and 60 °C, the Zn(OH)₂/glutaric acid mixture yielded PPC with a TOF of 1.1 h⁻¹ (*M_n* = 12 000 g mol⁻¹).^[53]

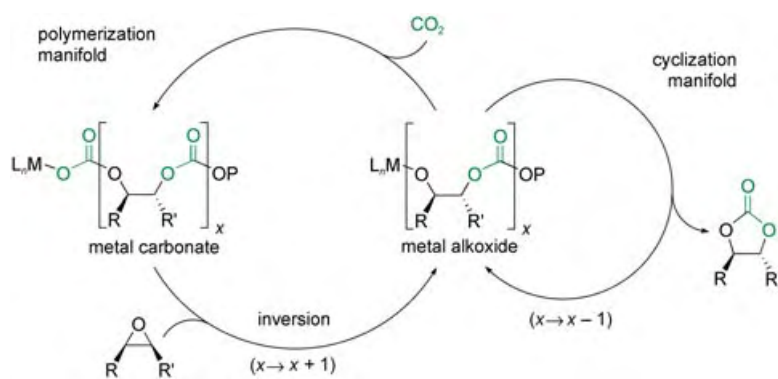
While the discoveries of ZnEt₂/R(OH)_x and Zn(OH)₂/glutaric acid catalysts for epoxide-CO₂ coupling marked salient scientific findings, the active species responsible for polymer and cyclic formation remain unknown. Nevertheless, several mechanistic studies indirectly support the theory that multi-site or polymeric catalysts are operative in the alternating copolymerization of CO₂ and epoxides.^[18,19,52,54–58] In the absence of multiple metal sites (i.e., 1 ZnEt₂ + 2 equivalents monohydric source), cyclic compounds are the predominant product of epoxide-CO₂ coupling. Epoxide-CO₂ copolymerization is generally accepted to proceed by a

coordination-insertion mechanism (Scheme 2). The mechanism includes several prevailing principles:

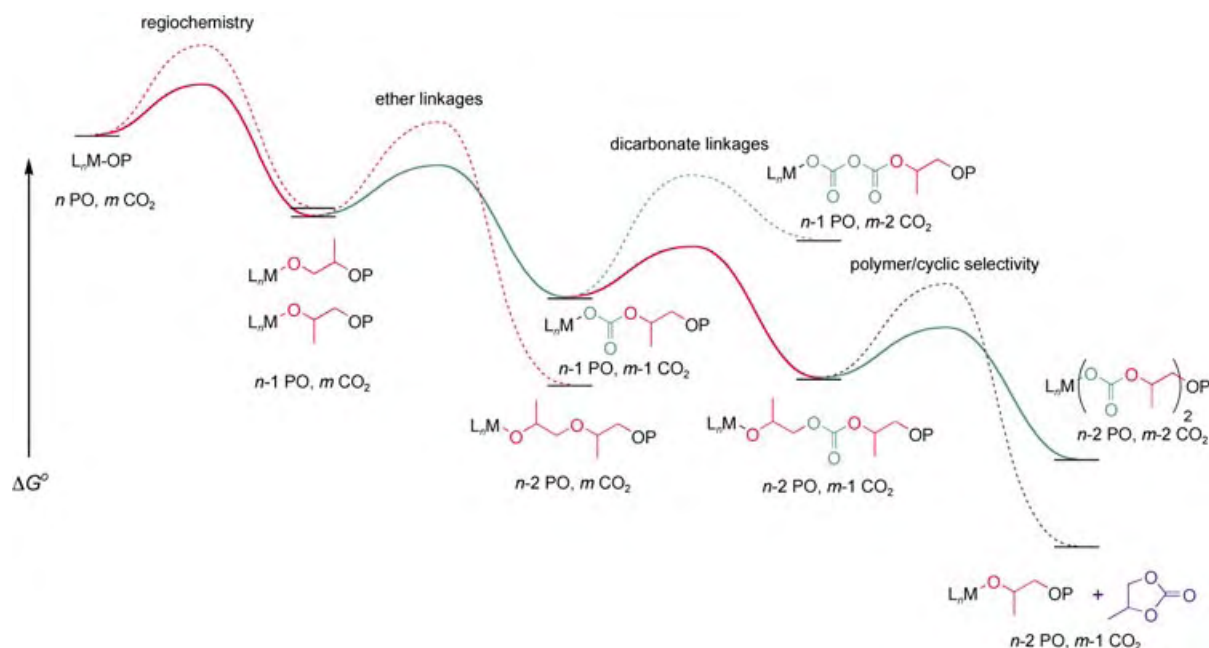
- 1) **Mechanism:** The alternating copolymerization of epoxides and CO₂ is a two-step process; the insertion of CO₂ into a metal alkoxide is followed by insertion of epoxide into a metal carbonate. Hence, most catalysts (polymerization initiators) are metal-alkoxide or metal-carboxylate species that are similar to the putative catalytic intermediates.
- 2) **Regiochemistry:** In the copolymerization of CO₂ and aliphatic epoxides (propylene oxide, etc.), epoxide ring-opening is typically favored at the least-hindered C–O bond, although cleavage is normally observed at both C–O bonds, giving regioirregular polymers.
- 3) **Stereochemistry:** In the copolymerization of CO₂ and alicyclic epoxides, such as cyclohexene

oxide (CHO), C–O bond cleavage typically occurs with inversion of configuration at the site of attack (S_N2-type mechanism) to give the *trans* ring-opened product.^[52,59] To date, there are no reports of catalysts that generate tactic polycarbonates by chain-end control mechanisms, presumably due to the distance between the stereogenic center of the chain end and the active metal center. There are examples of stereocontrol by site-control mechanisms using chiral metal catalysts (see Chapters 5, 7).

- 4) **Polymer/cyclic product selectivity:** Cyclic species are a common by-product of the copolymerization of CO₂ and aliphatic epoxides. Many systems produce predominantly cyclic species,^[20] which are thermodynamically more stable than polycarbonates. The percentage of polymer typically increases at lower reaction temperature. Systems can be tuned to favor cyclic-species or polymer formation depending on the catalyst, additives, CO₂ pressure, epoxide concentration, and temperature. Formation of cyclic species results from degradation of the growing polycarbonate chain by depolymerization or backbiting.^[51] In most cases, cyclic carbonates are thought to be generated by the backbiting of a metal-alkoxide into an adjacent carbonate linkage (Scheme 2).^[57]
- 5) **Ether and dicarbonate linkages:** The presence of ether linkages as a result of consecutive epoxide enchainment can be observed in some aliphatic polycarbonates. Most systems can be tuned to favor CO₂ incorporation by catalyst selection, CO₂ pressure, epoxide concentration, and polymerization temperature. The enthalpically disfavored consecutive insertion of two molecules of CO₂ to give dicarbonate linkages has not been reported.



Scheme 2. The basic mechanism of epoxide-CO₂ copolymerization and the formation of cyclic carbonates (*L_n* = ligand set, *M* = metal, *P* = polymer chain).



Scheme 3. Qualitative, ideal free-energy profile depicting alternating copolymerization of propylene oxide and CO₂, as well as potential side-reactions.

These prevailing principles are depicted in a qualitative free-energy profile for the copolymerization of epoxides and CO₂ (Scheme 3).

As observed in early studies, only a few metals are active for the coupling of epoxides and CO₂, including Al, Cr, Co, Mg, Li, Zn, Cu, and Cd.^[18,19] Studies have shown that large differences in catalytic efficacy result from the organic frameworks surrounding these metals, especially in the case of zinc. Accordingly, subsequent studies have largely focused on empirical modification of ligands to generate improved catalysts.

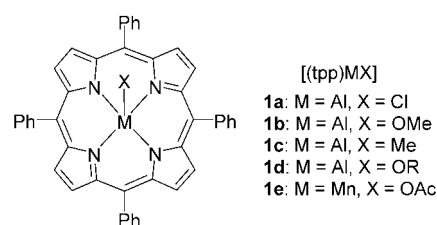
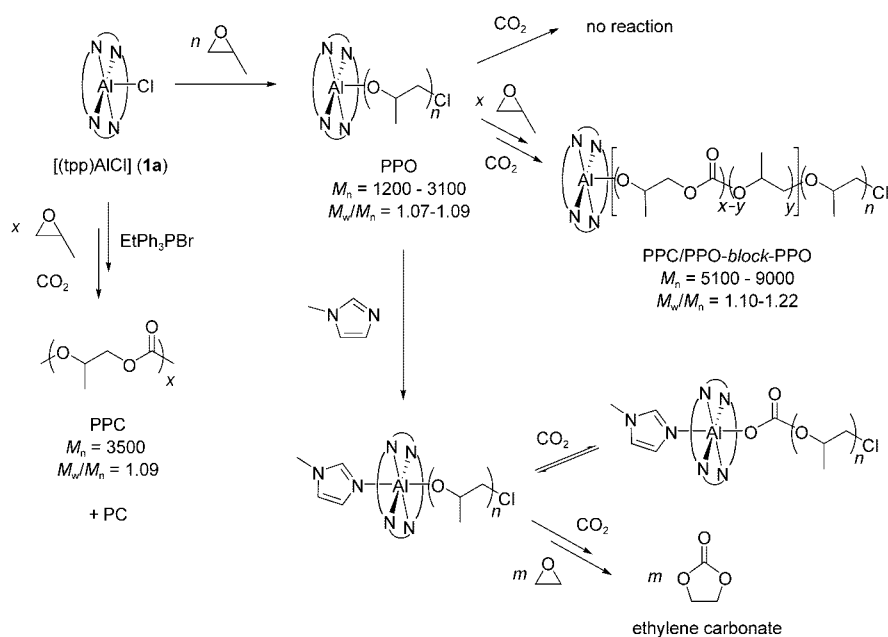


Figure 1. Aluminum and manganese porphyrins for the homopolymerization of epoxides and copolymerization of epoxides and CO₂ (R = alkyl, oligomer of PPO).

3. Aluminum and Manganese Catalysts

In 1978, Inoue developed the first single-site catalysts for epoxide–CO₂ copolymerization based on a tetraphenylporphyrin (tpp) ligand framework, **1a–d**.^[60] [(tpp)AlCl] (**1a**) and [(tpp)AlOMe] (**1b**) (Figure 1) were found to be living initiators for the homopolymerization of PO and of lactones, including lactide, β-butyrolactone, and ε-caprolactone, as well as for the copolymerization of CO₂ and epoxides and of PO and phthalic anhydrides.^[61–67] **1a** and **1b** reacted with PO to form poly(propylene oxide) (PPO) in a living polymerization with PDIs of 1.07–1.15 (Scheme 4). The chloride initiator ring-opened the least hindered C–O bond and generated a regioregular



Scheme 4. Reactivity of aluminum–porphyrin complexes.

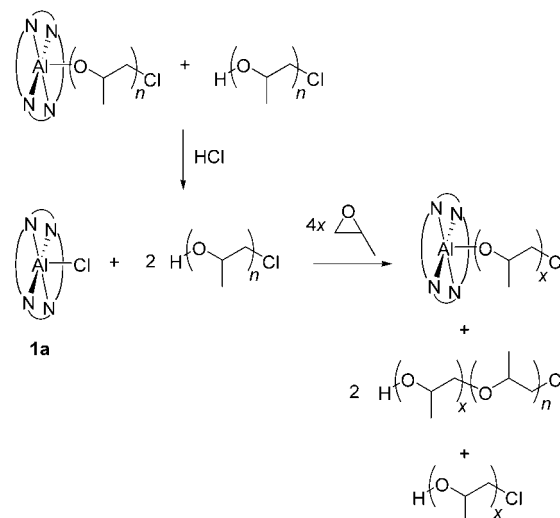
PPO. In addition, **1b** copolymerized PO and CO₂ at 20 °C and 8 atm CO₂, giving PPC ($M_n = 3900 \text{ g mol}^{-1}$; $M_w/M_n = 1.15$) with 40 % carbonate linkages over the course of 19 days.^[61,64] Although molecular weights were low and reaction times were long, this reaction marked the first example of mono-disperse polycarbonates having a narrow PDI.

Similarly to **1a**, [(tpp)AlOR] (**1d**), where R is an oligomer of PO, did not react with CO₂. However, upon addition of 1-methylimidazole (MeIm), reversible CO₂ insertion was observed. On the basis of ¹H NMR studies, MeIm was proposed to bind to aluminum in a *trans* fashion and activate the metal toward CO₂ insertion. The addition of ethylene oxide (EO) and CO₂ to **1d** catalytically produced cyclic ethylene carbonate (EC).^[65] The copolymer of PO and CO₂ was synthesized upon addition of ammonium or phosphonium salts. **1a** and 1 equivalent of EtPh₃PBr gave PPC ($M_n = 3500 \text{ g mol}^{-1}$, PDI = 1.09) with a TOF of 0.18 h⁻¹ at 20 °C and 48 atm CO₂. Both EtPh₃PBr and Et₄NBr were efficient cocatalysts, drastically increasing the percentage of carbonate linkages to > 99 %. Additionally, cyclic propylene carbonate was produced as a by-product in approximately 20 % yield relative to converted PO. **1a**/EtPh₃PBr was also active for EO-CO₂ and CHO-CO₂ alternating copolymerizations producing poly(ethylene carbonate) (PEC) with 70 % carbonate linkages, a M_n of 5500 g mol⁻¹, and a PDI of 1.14. Poly(cyclohexene carbonate) was produced with > 99 % carbonate linkages, a M_n of 6200 g mol⁻¹, and a PDI of 1.06 (TOF = 0.30 h⁻¹; Table 2). Even though this system yields PC, neither EC nor cyclohexene carbonate (CHC) was observed.

Finally, Inoue and co-workers synthesized several AB- and ABA-type block copolymers, incorporating PPO, PPC, and/or poly(PO-*alt*-phthalic anhydride), illustrating the “living” nature of the polymerizations.^[67] In 1999, Ree and co-workers also explored metalloporphyrins for PO-CO₂ copolymerization. In contrast to Inoue’s results, Ree found that **1a** and Et₄NBr cocatalyst gave PPC ($M_n = 1900 \text{ g mol}^{-1}$; $M_w/M_n = 1.10$) with only 75 % carbonate linkages at 20 °C and 52 atm CO₂.^[68] Aluminum porphyrins have also been utilized in the exclusive production of cyclic carbonates.^[69]

The low molecular weights of polymers produced by {(tpp)Al} catalysts suggest chain transfer, which supports

Inoue’s proposal of an “immortal” type polymerization.^[60] An immortal polymerization allows for multiple chains to propagate from one metal center, whereas a living polymerization grows only one chain per metal center. Protic sources facilitate chain swapping such that there are more polymer chains than active catalytic sites (Scheme 5). Free chains are



Scheme 5. “Immortal” polymerization of PO using aluminum-porphyrin complexes.

dormant, but continue to grow polymer when exchanged onto the active site. If the chain swapping is more rapid than propagation, polymer chains with narrow PDIs are produced. For example, addition of HCl does not quench the polymerization. Instead, it yields [(tpp)AlCl] which allows for new polymer chains to be initiated (see Scheme 5). [(tpp)AlCl] reinitiates polymerization and grows a new polymer chain in the same “immortal” manner, eventually giving a bimodal polymer distribution. Although no rate studies were reported for the alternating copolymerization of CO₂ and epoxides, Inoue showed a second-order dependence on the catalyst for the homopolymerization of δ -valerolactone^[70] and proposed a

Table 2: Selected homogeneous catalysts for epoxide-CO₂ copolymerization.^[a]

Complex	Epoxide	$p(\text{CO}_2)$ [atm]	t [h]	T [°C]	TON ^[b]	TOF [h ⁻¹] ^[c]	Carbonate linkages [%] ^[d]	M_n [kg mol ⁻¹] ^[e]	M_w/M_n	Ref.
1a + EtPh ₃ PBr (1:1)	CHO	48	336	20	100	0.30	> 99	6.2	1.06	[67]
8 + DMAP (1:1)	CHO	225	18	110	3120	173	97	3.9	1.16	[81]
10 + MeIm (1:5)	CHO	60	24	80	774	32.2	> 99	8.9 ^[f]	1.2 ^[f]	[87]
11 + DMAP (1:1)	PO	35	4	75	640	226 ^[g]	98	16.7	1.38	[90]
13a	PO	55	3	25	243	81 ^[h]	95	15.3	1.22	[93]
14a	CHO	135	24	100	210	8.8	93	17.0	6.4	[117]
17a	CHO	55	48	80	364	7.6	> 99	42.0	6.0	[125]
36a	CHO	7	0.5	50	180	360	95	15.8	1.11	[151]
39b	CHO	7	0.17	50	380	2290	90	22.9	1.09	[149]
46	PO	7	2	25	470	235 ^[i]	> 99	36.7	1.13	[150]

[a] Polymerizations using CHO and CO₂ result in PCHC, whereas those incorporating PO and CO₂ yield PPC. [b] Moles of epoxide consumed per mole of metal. [c] Moles of epoxide consumed per mole of metal per hour. [d] Calculated by integration of methine resonances in the ¹H NMR spectrum of the polymer. [e] Determined by gel-permeation chromatography, calibrated with polystyrene standards. [f] Molecular weight and molecular weight distribution were taken from a run without MeIm. [g] A 71:29 ratio of PPC/PC was observed by ¹H NMR spectroscopy. [h] > 99 % PPC/PC was observed by ¹H NMR spectroscopy. [i] A 75:25 ratio of PPC/PC was observed by ¹H NMR spectroscopy.

linear transition-state mechanism incorporating two aluminum–porphyrin complexes for the ring-opening of epoxides.^[71]

In 2003, Inoue and co-workers developed a related porphyrin system utilizing manganese as the active metal center.^[72] At 80 °C, [(tpp)MnOAc] (**1e**; Figure 1) reacted with CHO and 50 atm CO₂ to produce PCHC (99 % carbonate linkages; $M_n = 6700 \text{ g mol}^{-1}$; $M_w/M_n = 1.3$) with a moderate TOF of 16.3 h^{-1} . In this system, additives such as PPh₃, pyridine, or MeIm compromised polymerization rates and decreased the percentage of carbonate linkages. At 80 °C and only 1 atm of CO₂, **1e** catalyzed PCHC formation providing activities of up to 3.3 h^{-1} (95 % carbonate linkages; $M_n = 3000 \text{ g mol}^{-1}$; $M_w/M_n = 1.6$). Finally, the coupling of PO and CO₂ yielded PC, but gave no PPC.

Recently, a salicylaldimine(salen)–aluminum complex, **2a**, was found to be highly active for the cyclization of EO and CO₂ to ethylene carbonate (Figure 2).^[73,74] Lewis bases or

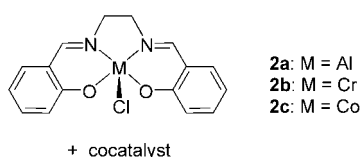


Figure 2. Salen catalyst systems (cocatalyst = tetrabutylammonium halide, pyridine, or MeIm) for the synthesis of ethylene carbonate.

quaternary ammonium salts, including pyridine, MeIm, and $n\text{Bu}_4\text{NX}$ ($X = \text{Cl}, \text{Br}, \text{I}$), were utilized as cocatalysts, enhancing rates by up to a factor of five. At 110 °C and in supercritical CO₂ (ca. 150 atm CO₂), a 1:1 mixture of **2a**/ $n\text{Bu}_4\text{NBr}$ catalyzed the conversion of EO to EC with a TOF of 2220 h^{-1} . Salen-chromium (**2b**) and -cobalt (**2c**) analogs also promoted cyclic-species formation showing rates of 2140 and 1320 h^{-1} , respectively (see Chapters 4, 5). Darensbourg and co-workers have reported AlCl_4^- -based complexes that exhibit TOFs up to 50 h^{-1} for the synthesis of propylene carbonate from PO and CO₂.^[75]

In 1998, Kuran and co-workers reported an aluminum calix[4]arene, **3**, derived from 25,27-dimethoxy-26,28-dihydroxy-*p*-tert-butylcalix[4]arene and diethylaluminum chloride (Figure 3).^[76] Complex **3** was found to be active for the alternating copolymerization of CO₂ with PO or CHO. At 60 atm CO₂ and 35 °C, PPC ($M_n = 5620 \text{ g mol}^{-1}$) was formed with a TOF of 0.11 h^{-1} . The polycarbonate contained low levels of carbonate linkages, comparable to the PPC made from [(tpp)AlCl] (**1a**) in the absence of quaternary salts. Under the same reaction conditions, **3** converted CHO and CO₂ to PCHC ($M_n = 1930 \text{ g mol}^{-1}$) with a TOF of only 0.05 h^{-1} . Additionally, cyclic PC and CHC were produced as by-products in 14 % and 4 % yield with respect to epoxide. Kuran et al. proposed a mechanism involving participation of two aluminum complexes in the alternating copolymerization, although no mechanistic studies were reported. Finally, **3** was active for the homopolymerization of PO and CHO, giving poly(alkene oxides) with fairly narrow PDIs ($M_w/M_n = 1.36\text{--}1.51$).

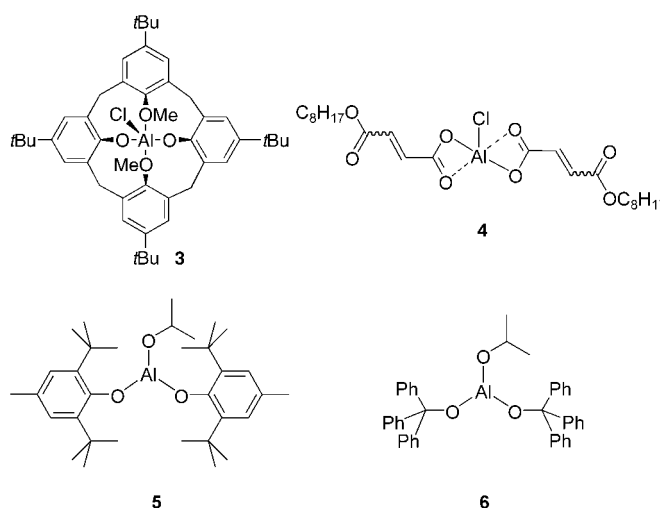


Figure 3. Aluminum complexes for the homopolymerization of epoxides and copolymerization of epoxides and CO₂.

Aluminum alkoxides have also been shown to convert epoxides and CO₂ to polycarbonates. Beckman and co-workers reported several aluminum complexes, including **4**, **5**, and **6** (Figure 3), that reacted with CHO and CO₂ to give PCHC with a maximum TOF of 2.7 h^{-1} .^[30,77,78] At 80 atm CO₂ and 60 °C, **4** produced PPC ($M_n = 5000 \text{ g mol}^{-1}$; $M_w/M_n = 2.89$) with only 22 % carbonate linkages and a TOF of 2.0 h^{-1} . These low-carbonate content polymers have shown promise as solubilizers in supercritical CO₂ (scCO₂).^[30] As expected, these complexes are also active for the homopolymerization of CHO.

Aluminum complexes are indeed active for the copolymerization of epoxides and CO₂; however, they are plagued by low activities and yield polycarbonates with high percentages of ether linkages. It appears that without additives, current aluminum catalysts do not cleanly generate alternating copolymer. Nevertheless, the “immortal” polymerization of [(tpp)AlX] compounds shows promise for the synthesis of a wealth of unique copolymers with varying levels of carbonate linkages provided the activities can be improved.

4. Chromium Catalysts

Kruper and Dellar discovered that [(tpp)CrX] (**7a,b**; Figure 4) in mixtures with 4–10 equivalents of a Lewis-basic amine cocatalyst (such as MeIm or (4-dimethylamino)pyridine (DMAP)) are moderately active for the cyclization of epoxides and CO₂.^[79,80] A wide range of epoxides, including PO, *trans*-2-butene oxide, epichlorohydrin, CHO, and cyclopentene oxide (CPO), were rapidly converted to the corresponding cyclic carbonates. For instance, under 50 atm CO₂ and at 80 °C, **7b** and MeIm converted PO to PC affording a TOF of 158 h^{-1} . **7a** and DMAP catalyzed CHC formation at 50 atm CO₂ and 95 °C, exhibiting activities of 103 h^{-1} . In this case, PCHC was isolated as the major product. Following thermolysis, a 95:5 ratio of *trans* and *cis* CHC was observed, suggesting the possibility of dual mechanisms. Unexpectedly,

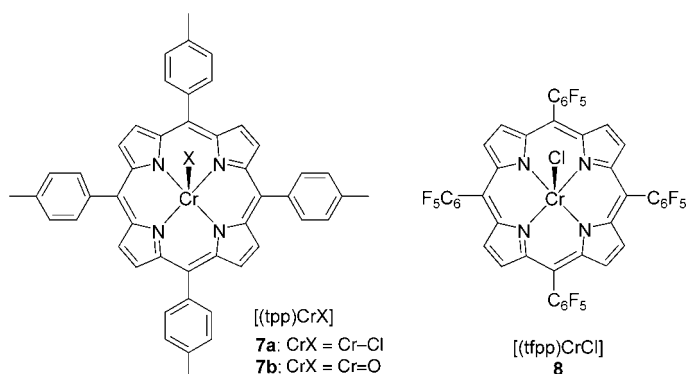
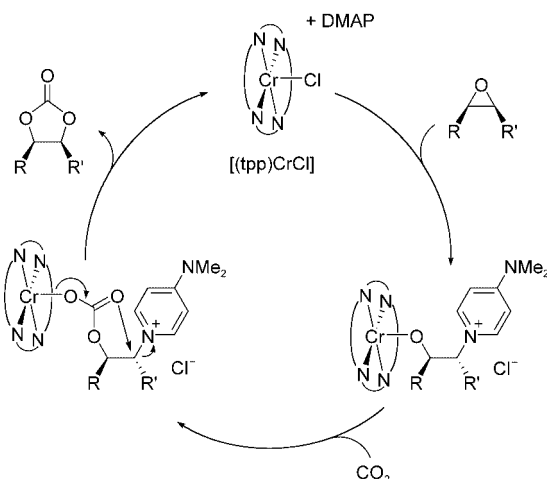


Figure 4. Chromium–porphyrin complexes for the coupling of epoxides and CO₂.

the conversion of CPO to cyclopentene carbonate gave the *cis* isomer as the exclusive product. To account for this, two mechanistic pathways were suggested: 1) double inversion leading to retention of configuration; and 2) inversion of configuration due to backbiting into a polymer chain. A possible mechanism to explain the double inversion is shown in Scheme 6.



Scheme 6. Proposed mechanism of dioxolanone synthesis using [(tpp)CrCl].

Following this lead, Holmes and co-workers developed [(tpp)CrCl] (**8**; Figure 4), which showed activities of up to 173 h^{−1} for the alternating copolymerization of CHO and CO₂ at 225 atm CO₂ (scCO₂) and 110 °C (Table 2).^[81,82] As with complexes **7a** and **7b**, the copolymerization only yielded polycarbonate when **8** was combined with a cocatalyst such as DMAP. The fluorinated aromatic moieties improved catalyst solubility in scCO₂, and consequently increased the yields of PCHC. Similar to aluminum–porphyrin catalysts for epoxide–CO₂ copolymerization, these chromium analogs yielded polycarbonates with narrow PDIs ($M_w/M_n = 1.08–1.50$) and low molecular weights ($M_n = 1500–9400$ g mol^{−1}). Furthermore, the resultant PCHC contained high percentages of carbonate linkages (97%). More recently, polymer supported chromium porphyrins have been found to be active for PCHC production.^[83]

Jacobsen and co-workers found [(salen)CrCl] complexes to be highly active in the asymmetric ring-opening of epoxides.^[84] This elegant work has since led to many crucial discoveries in the coupling of epoxides with CO₂; in fact the first report of (salen)chromium-mediated epoxide–CO₂ polymerization appeared in a 2000 patent by Jacobsen and co-workers.^[85] Nguyen and Paddock reported highly active [(salen)CrCl]/DMAP-based systems, **9a–c** and **10** (Figure 5), for the cycloaddition of CO₂ and a variety of terminal aliphatic epoxides, including PO, epichlorohydrin, butadiene monoepoxide, and styrene oxide (SO).^[86] *Cis*-[(salen)CrCl] (**9a**) was the most efficient catalyst and

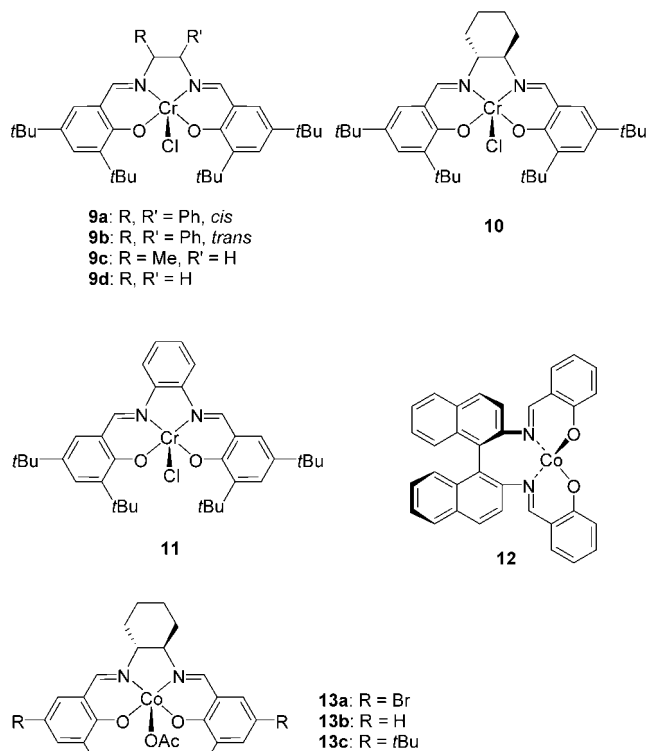


Figure 5. Salen–chromium and salen–cobalt complexes for the coupling of epoxides and CO₂.

was approximately twice as active as *trans*-[(salen)CrCl] (**9b**). At 100 °C and 7 atm CO₂, **9a** and 1 equivalent of DMAP rapidly converted PO to PC in 1 h, exhibiting a high TOF of 916 h^{−1}. Furthermore, activities were largely dependent on DMAP concentration. Cyclization activities increased when rising DMAP concentrations up to 2 equivalents, but trailed off significantly at higher cocatalyst loadings. Nguyen also reported that cycloaliphatic epoxides such as CHO are copolymerized with CO₂ in the presence of [(salen)CrCl] complexes. Holmes and Mang also reported the conversion of glycidol derivatives to cyclic carbonates using **10**/DMAP.^[82] More recently, He and co-workers reported the synthesis of ethylene carbonate using **2b**/cocatalyst mixtures.^[73,74]

Darensbourg and Yarbrough reported that the relatively air-stable complex **10** (Figure 5) is an effective catalyst for the alternating copolymerization of CHO and CO₂.^[87] At 80 °C

and 60 atm CO_2 , compound **10** converted CHO to PCHC with a moderate TOF of 10.4 h^{-1} . Analysis of the polycarbonate showed nearly 100 % carbonate linkages, a M_n of 8900 g mol^{-1} and a M_w/M_n of 1.2. Based on the TON and lack of cyclic by-product, the PCHC should exhibit a theoretical molecular weight of approximately 35000 g mol^{-1} . Like the aluminum^[60,67] and chromium^[79] porphyrin systems, activities increased upon addition of MeIm, such that 5 equivalents MeIm tripled the copolymerization rates to 32.2 h^{-1} (see Table 2). Although complex **10** is chiral, the resultant polymer was completely atactic, as determined by ^{13}C NMR. Additionally, complex **10** catalyzed the coupling of PO and CO_2 to PC and PPC; activities were not specified. At 80°C , cyclic PC is the predominant product, but as the temperature is reduced to 40°C , PPC production becomes a competitive pathway. Finally, silylated aliphatic epoxides, such as 2-(3,4-epoxycyclohexyl)ethyl-trimethoxysilane, and CO_2 can also be copolymerized by salen–chromium complexes and a MeIm cocatalyst.^[88] At 80°C and 55 atm CO_2 , **9d** (Figure 5) and 2.5 equivalents MeIm catalyzed the formation of the silylated polycarbonate with a TOF of 12.0 h^{-1} .

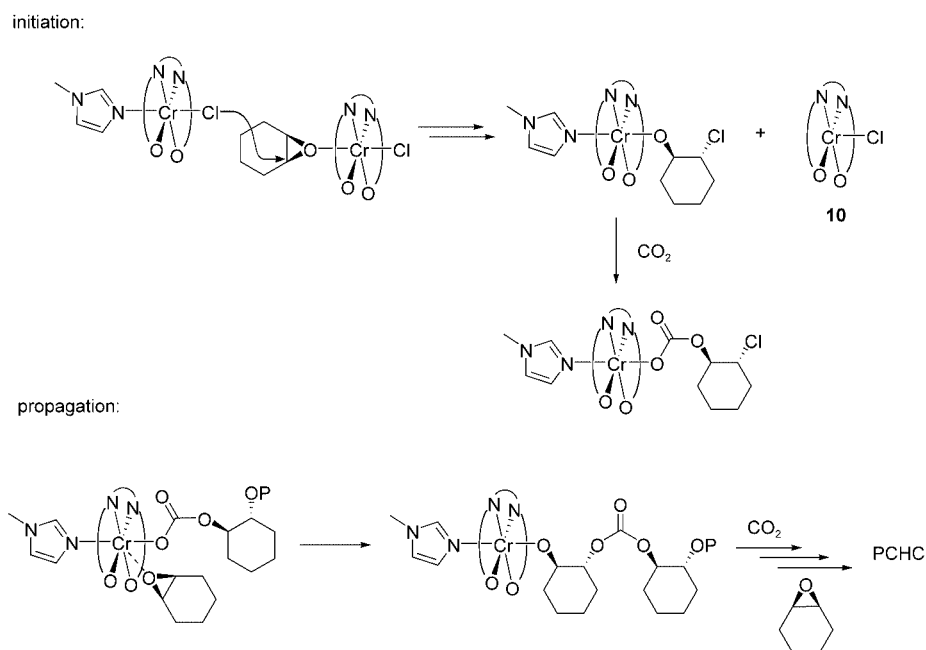
Subsequent work detailed the intricate energetics of polymer versus cyclic-species formation using compound **10**.^[89] In CHO– CO_2 coupling, the activation energies (E_a) for CHC and PCHC formation are 31.8 and $11.2 \text{ kcal mol}^{-1}$, illustrating markedly higher activation barriers for formation of the cyclic species. The activation barriers for PC and PPC in PO– CO_2 coupling were determined to be 24.0 and $16.2 \text{ kcal mol}^{-1}$, respectively. The significantly larger E_a for CHC versus PCHC is consistent with the exclusive formation of PCHC, while the slightly larger E_a for PC versus PPC is consistent with the formation of PC during PO– CO_2 copolymerization.

Recently, Rieger and co-workers found that a slightly modified complex, [(salen)CrCl] (**11**), and DMAP cocatalyst rapidly copolymerize PO and CO_2 (TOFs approaching 226 h^{-1} ; see Table 2) at 75°C and 35 atm CO_2 .^[90] Analysis of the PPC revealed molecular weights up to 16700 g mol^{-1} (lower than predicted assuming the lack of chain transfer reactions), PDIs as low as 1.38, and carbonate linkages as high as 98 %. The DMAP/**11** ratio drastically affected the product distribution in the coupling process. Without DMAP, no conversion to PC or PPC was observed. At 0.5 equivalents DMAP, the maximum ratio of PPC to PC formation (154:34) was observed. Higher DMAP/**11** ratios decreased the proportion of PPC to PC until only PC was observed. For example, when 2 equivalents of DMAP were added, only PC was observed

with a TOF of 602 h^{-1} . Interestingly, cocatalyst was not essential for copolymerization using **10**.^[87]

The proposed CO_2 –epoxide coupling mechanisms using seemingly similar catalysts **9a**/DMAP, **10**/MeIm, and **11**/DMAP differ considerably. At the current time, there is a lack of agreement regarding the mode of operation of these catalysts. Jacobsen proposed a bimetallic mechanism for the asymmetric ring-opening of epoxides based on the observation that bimetallic catalysts enhanced rates and enantiomeric excesses.^[84] Nguyen suggested a bimetallic mechanism for the formation of cyclic species.^[86] The *trans* coordination of DMAP to **9a** is proposed to activate CO_2 to give a [(salen)Cr{C(C=O)O[−]}] species. This intermediate is then proposed to attack PO bound to another salen–chromium complex in a cooperative bimetallic ring-opening process, followed by elimination of the cyclic product.

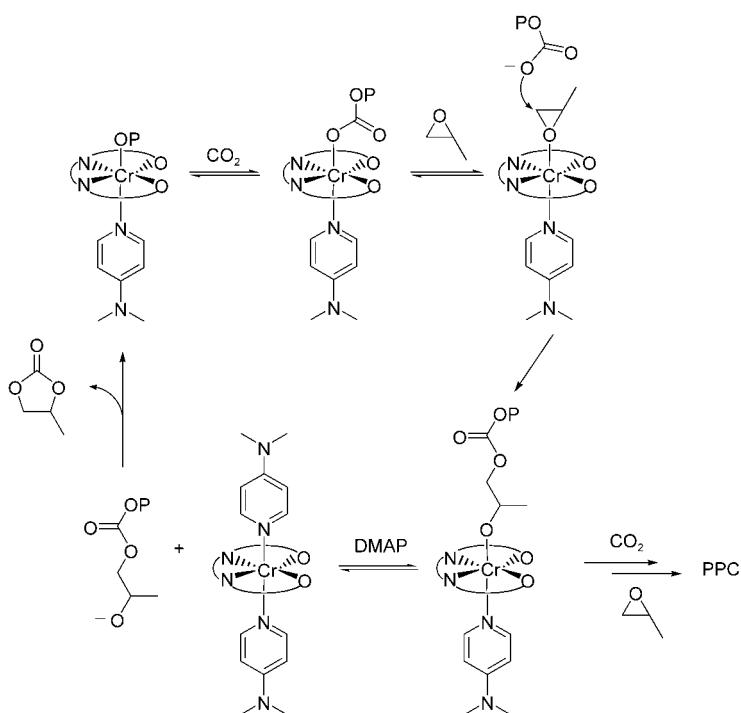
Darensbourg and co-workers offered a dual CHO– CO_2 copolymerization mechanism for the **10**/MeIm system. Here, initiation occurs by a bimetallic process and propagation operates by monometallic enchainment of epoxide.^[87,89] Initiation is accelerated by MeIm, which facilitates chloroligand attack on a CHO monomer bound to a second salen–chromium complex (Scheme 7). Subsequent CO_2 insertion



Scheme 7. Proposed CO_2 –CHO copolymerization mechanism using **10**/MeIm (P = polymer chain).

into the newly-generated chromium alkoxide generates a chromium carbonate. Because rate studies showed a first-order dependence on both CHO and catalyst, chain propagation was proposed to occur by a concerted epoxide ring-opening that proceeds through a four-membered transition state.

Alternatively, in PO– CO_2 copolymerization using **11**/DMAP, Rieger and co-workers proposed that DMAP coordinates strongly to Cr and facilitates dissociation of the polymer-chain alkoxide and carbonate (Scheme 8).^[90]



Scheme 8. Proposed PO–CO₂ copolymerization mechanism for **11**/DMAP catalyst system.

Under sufficient pressures of CO₂, the dissociated carbonate attacks PO-bound **11**/DMAP in a monometallic fashion. Subsequent CO₂ insertion into the newly-formed chromium alkoxide propagates the polycarbonate chain. The anionic nature of the chain-end promotes the degradative backbiting to cyclic propylene carbonate. Therefore, increased stoichiometric amounts of DMAP enhance formation of cyclic product and eventually exterminate copolymer formation.

Owing to similar catalysts and coupling processes, it is unlikely that all of the epoxide ring-opening steps discussed above are occurring simultaneously. Furthermore, no mechanism has accounted for the retention of configuration as reported by Kruper, or the low polymer molecular weights that are indicative of chain transfer or the formation of macrocycles. Studies generally agree that CO₂ reacts with a metal alkoxide and cyclic products are formed by backbiting of a metal alkoxide into an adjacent carbonate linkage. Indeed, detailed mechanistic studies must be performed to delineate the various intermediates and epoxide ring-opening steps involved in these highly active salen–chromium catalysts.

5. Cobalt Catalysts

In 1979, Co(OAc)₂ was reported to copolymerize PO and CO₂ with an extremely low TOF (0.06 h^{−1}).^[91] Since this report, few examples of cobalt-catalyzed coupling of epoxides and CO₂ have been found. He and co-workers reported the synthesis of ethylene carbonate using **2c**/cocatalyst mixtures.^[73,74] Shi et al. reported that related salen–cobalt com-

plexes such as **12** (Figure 5) can be activated with Lewis-basic amines for the synthesis of propylene carbonate (see Section 7.3).^[92] Recently, our group published that salen–cobalt complexes **13a–c** (Figure 5) exhibited moderate activities (up to 81 h^{−1} with **13a**) for the copolymerization of PO and CO₂.^[93] At 25 °C and 55 atm CO₂, **13a** catalyzed the copolymerization to yield PPC with no observable cyclic by-products, 95 % carbonate linkages, a *M_n* of 15 300 g mol^{−1}, and a *M_w*/*M_n* of 1.22. Pressures of 55 atm were essential for polymerization activity as lower pressures (40 atm) significantly hindered the copolymerization. In contrast to copolymerizations using the related salen–chromium catalysts, no heterocyclic additives were necessary. In addition, **13a–c** all showed unprecedented selectivities for PPC formation (> 99 % PPC versus PC). (*S*)-PO–CO₂ copolymerization using enantiomerically-pure **13c** yielded isotactic (*S*)-PPC (TOF = 71 h^{−1}, > 99 % PPC, 99 % carbonate linkages, *M_n* = 6900 g mol^{−1}, *M_w*/*M_n* = 1.58) with the highest reported level of head-to-tail linkages (93 %). Finally, **13c** exhibited a modest level of selectivity (*k_{rel}* = 2.8) in the kinetic resolution of PO. More recently, a catalyst system comprised of [(tpp)CoCl]/DMAP has been used for the synthesis of a range of dioxolanones from epoxides and CO₂,^[94] and **13c**/(*n*Bu)₄NX has been used to resolve racemic propylene oxide by forming PPC with *k_{rel}* values ranging from 1.1 to 9.0.^[95]

6. Lanthanide-Based Catalysts

Yttrium, aluminum, rare-earth metals, and combinations of multiple metal reagents have shown activity for the copolymerization of epoxides and CO₂. For example, PO–CO₂ copolymerization was effected by a rare-earth metal system comprised of yttrium tris[bis(2-ethylhexyl)phosphate], Al*i*Bu₃, and glycerol. The PPC produced contained only 10–30 % carbonate linkages, although molecular weights of up to 476 000 g mol^{−1} were achieved.^[96] This system also exhibited activity for the alternating copolymerization of CO₂ with epichlorohydrin^[97] and glycidyl ether monomers.^[98] Other rare-earth metal systems consisted of yttrium carboxylates [Y(CO₂CF₃)₃ or Y(CO₂RC₆H₄)₃ where R is H, OH, Me, or NO₂], ZnEt₂, and glycerine.^[99–101] The alternating copolymerization of CO₂ and PO yielded PPC with up to 98.5 % carbonate linkages, turnover frequencies up to 2.5 h^{−1}, and molecular weights reaching 100 000 g mol^{−1}. CHO–CO₂ copolymerization produced PCHC with 100 % carbonate linkages, molecular weights of 19 000–330 000 g mol^{−1}, and *M_w*/*M_n*'s of 3.5–12.5. It must be noted that control experiments indicated that ZnEt₂, but not Y(CO₂CF₃)₃, was essential for polymerization. Finally, ternary catalysts composed of Nd(CO₂CCl₃)₃, ZnEt₂, and glycerol were also reported to copolymerize PO and CO₂.^[102]

7. Zinc and Cadmium Catalysts

A variety of metal-based catalysts has shown activity for the coupling of epoxides and CO₂; however, few have exhibited the success associated with zinc-based complexes. Therefore, the majority of the work reported in this field has been performed using complexes with zinc as the active metal center. These catalysts have undergone a renaissance over the past ten years, shifting focus from heterogeneous mixtures to discrete and single-site catalysts which exhibit unprecedented reaction rates and selectivities.

7.1. Heterogeneous Zinc Catalysts

As described in Section 2, the first active species for the alternating copolymerization of epoxides and CO₂ were based on mixtures of: 1) ZnEt₂ with an assortment of di- and trihydric sources and 2) carboxylic acids and Zn(OH)₂. Subsequent to these groundbreaking discoveries, several companies pursued the commercialization of PPC using these and related catalysts.^[103–106] In 1999, Ree et al. reported a variant of the Zn(OH)₂/glutaric acid (zinc glutarate) system^[53] using ZnO as the zinc source. An optimal activity of 3.4 TO h⁻¹ was achieved for PO–CO₂ copolymerization at 60 °C and 25 atm CO₂, which at the time was the highest activity reported for zinc carboxylates (Table 1). Analysis of the PPC revealed a *M_n* of 210 000 g mol⁻¹, a PDI of 1.3, and a *T_g* of 38 °C.^[107–109] In addition, PO–CO₂ copolymerizations using zinc glutarate have been run in scCO₂, a suitable replacement for organic solvents.^[110] More recently, polycrystalline^[111] and single-crystal^[112] zinc glutarate have been studied using X-ray diffraction, which could play an important role in determining the mechanism of this catalyst. Ethylsulfinate capped zinc glutarates have also been reported.^[113] They have the potential to reduce the complexity inherent in these systems. Furthermore, terpolymerizations of CO₂, PO, and ε-caprolactone have been performed using zinc glutarate catalysts.^[114] PPC has also been synthesized using zinc glutarate produced by an ultrasonic method, giving TOFs up to 7.7 h⁻¹.^[29,111] Finally, carboxy-containing polymers, such as styrene and acrylic acid copolymers,^[115] and γ-alumina^[116] have been used as supports in zinc-catalyzed copolymerization of PO and CO₂.

A soluble counterpart to these systems was reported by Beckman et al., who observed that zinc oxide and a highly fluorinated carboxylic acid derived from a monoester of maleic acid^[105] (**14a**; Figure 6) is active for the alternating copolymerization of CHO with supercritical CO₂.^[117] The fluorination increased solubility of the catalyst mixture and

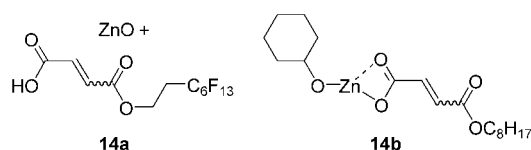


Figure 6. Zinc catalysts for the alternating copolymerization of CHO and CO₂.

facilitated PCHC formation with 8.8 TO h⁻¹ at 135 atm CO₂ and 100 °C (Table 2). Additionally, **14b** (Figure 6), a soluble Zn^{II}-based compound, produced PCHC (*M_n* = 2150, *M_w*/*M_n* = 4.4) with a TOF of only 1.2 h⁻¹ at 90 °C and 110 atm CO₂.^[77] In 1999, Darensbourg and Zimmer reported that zinc crotonate is a soluble catalyst precursor for this system.^[118] This catalyst afforded TOFs of approximately 16 h⁻¹ at 80 °C and 55 atm CO₂, yielding PCHC with 84 % carbonate linkages. A promising set of heterometallic catalysts are the double metal cyanide (DMC) catalysts originally reported by Kruper and Smart.^[119] Heterogeneous compounds of the form M_a^I(M^{II}(CN)_x)_b (*a* and *b*: 1, 2, 3; *x*: 4, 5, 6) were active for epoxide–CO₂ copolymerization. DMC catalysts such as zinc hexacyanoferrate(III) converted epoxides, including EO, PO, 1-butene oxide and CHO, to polycarbonates (50–95 % carbonate linkages and PDIs of 2–6) with TOFs of approximately 4 h⁻¹. Chen later reported similar DMC catalysts that exhibited better activities for PO–CO₂ copolymerization.^[120] (PEO)_aZn(Fe(CN)₆)_bCl_{2–3b}(H₂O)_c(KCl)_d (PEO = polyethylene oxide, *a* (mole ratio chelating atoms/Zn) = 2.2, *b* = 0.50, *c* = 0.76, *d* = 0.20) copolymerized PO and CO₂ at 60 °C and 50 atm CO₂ to give PPC (*M_n* = 20 000 g mol⁻¹) with 9.0 TO per mol zinc per h. To shed light on the origin of activity in DMC catalysts, Darensbourg et al. designed the related homogeneous complex **15**, which was prepared by the reaction of [KCpFe(CN)₂PPh₂(CH₂)_{1.5}]₂ (Cp = cyclopentadienyl) with ZnI₂ (Figure 7).^[121,122] Surprisingly, the coupling of CHO

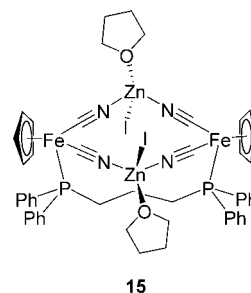


Figure 7. Soluble double metal cyanide complex.

and CO₂ gave predominantly cyclic *cis*-cyclohexene carbonate, a small percentage of low molecular weight polycarbonate was also isolated. Unfortunately, the intrinsic complexity of heterometallic catalysts hampers mechanistic studies, and currently the active species are unknown. Despite these difficulties, the ease of synthesis and inexpensive nature of these materials makes them highly attractive.

7.2. Zinc and Cadmium Phenoxides for Epoxide–CO₂ Coupling

Heterogeneous systems are often marred by poor reproducibility and the production of non-uniform polymers, caused by the presence of many different types of active sites that produce polymer with different activities and selectivities. To address these issues, Darensbourg and Holtcamp reported in 1995 the first discrete zinc complexes

for the alternating copolymerization of epoxides and CO₂ (Figure 8).^[123] This discovery marks an important step in the development of catalysts for the copolymerization of CO₂ and epoxides. Compound **16a**, which was synthesized from 2,6-diphenylphenol and Zn[N(SiMe₃)₂]₂, crystallized as a bis((2,6-

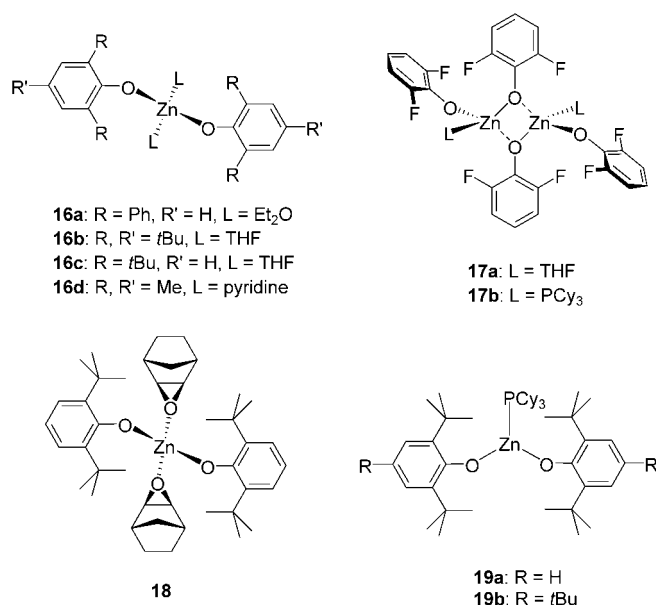


Figure 8. Zinc-bis(phenoxide) compounds for the alternating copolymerization of CHO and CO₂.

diphenyl)phenoxy)zinc complex containing two diethyl ether solvent molecules coordinated to a tetrahedral zinc center. Under 55 atm CO₂ and at 80°C, PCHC (91% carbonate linkages, $M_n = 38\,000\text{ g mol}^{-1}$, $M_w/M_n = 4.5$) was produced with a TOF of 2.4 h⁻¹. Additionally, **16a** catalyzed the random terpolymerization of CHO, PO, and CO₂, yielding polycarbonate with approximately 20% propylene carbonate linkages, 70% cyclohexene carbonate linkages, and 10% ether linkages. Approximately the same ratios of PO and CHO incorporation were observed regardless of feedstock composition.

Subsequent work investigated steric influences of N-aryl substituents, including 2,4,6-tri-*tert*-butyl (**16b**), 2,6-di-*tert*-butyl (**16c**), and 2,4,6-trimethyl (**16d**), on CHO-CO₂ copolymerization (see Figure 8).^[124] Complex **16d** displayed the highest activities (TOF = 9.6 h⁻¹), thus illustrating that bulky *ortho* substituents were not essential for high copolymerization rates. In the case of **16b**, only 50% carbonate linkages were observed in the resultant PCHC. In line with this result, the zinc phenoxides were also efficient catalysts for the homopolymerization of CHO. Electronic perturbations of the N-aryl *ortho* substituents revealed that electron-withdrawing groups resulted in higher activities for CHO-CO₂ copolymerization: F > Cl > Br.^[125] Addition of 2,6-dihalophenols to Zn[N(SiMe₃)₂]₂ gave four-coordinate, dimeric zinc phenoxides with coordinated THF solvent molecules. Compound **17a** showed a moderate TOF of 7.6 h⁻¹. Analysis of the PCHC revealed PDIs of 6.0, molecular weights of 42 000 g mol⁻¹, a T_g

of 115°C, and >99% carbonate linkages.^[31,125] In general, zinc-bis(phenoxide) compounds catalyzed PO-CO₂ copolymerization at 40°C and PO-CO₂ cyclization at 80°C in unspecified yields. Finally, zinc-bis(phenoxide) catalysts were active for CHO homopolymerization, CHO-CO₂ copolymerization, and CHO-PO-CO₂ terpolymerization, but did not readily react with bulky alicyclic epoxides such as α -pinene and *exo*-2,3-epoxynorbornane. Although no copolymerization activity was observed, X-ray analysis of **18** showed two molecules of *exo*-2,3-epoxynorbornane coordinated to zinc,^[126] providing a potential model compound for epoxide-bound intermediates in the polymerization.

Darensbourg et al. proposed that two coordination sites were required for polyether formation, while only one was necessary for copolymer formation.^[125,127] To probe this theory, phosphane (PCy₃, PMe₃, etc.) adducts of the zinc phenoxides were synthesized; these have only one open coordination site.^[127] Compounds **19a** and **b** (Figure 8) were found to be three-coordinate zinc compounds with a distorted trigonal planar geometry around zinc. While **16b** generated PCHC with only 50% carbonate linkages, **19b** facilitated the formation of PCHC with 100% carbonate linkages, without loss of catalytic activity. Furthermore, **17a**, which possesses only one open coordination site, produced PCHC with essentially 100% carbonate linkages whereas **17b** (the PCy₃ adduct of **17a**) was not active for the copolymerization of CHO and CO₂.

In a related study, Dinger and Scott reported that zinc-phenoxide cluster compounds showed activity for the alternating copolymerization of CHO and CO₂.^[128] A variety of solvent-dependent tri-, tetra-, penta-, and hexanuclear compounds were synthesized from tris(3,5-dialkyl-2-hydroxyphenyl)methane derivatives and ZnEt₂. For example, compound **20** (Figure 9) catalyzed the copolymerization of CHO and CO₂ to give PCHC with 81% carbonate linkages and a TOF of 1.3 h⁻¹.

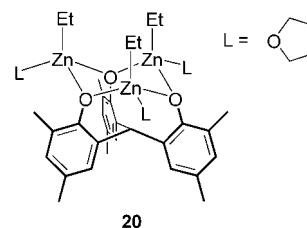


Figure 9. Trinuclear zinc-alkyl catalyst for CHO-CO₂ copolymerization.

Cadmium complexes have not shown significant activities for the coupling of epoxides and CO₂. Nevertheless, cadmium compounds can exhibit organometallic reactivity similar to their zinc analogs and therefore serve as good structural models (Figure 10). Perhaps the most intriguing insight derived from these models came from Darensbourg's discovery of tris(pyrazolylhydroborate)cadmium acetate complexes [(tp)CdOAc] (**21a-c**).^[129,130] Complexes **21a** and **b** contain bound PO and CHO and were proposed as possible models for initiation in epoxide-CO₂ polymerization. Darensbourg

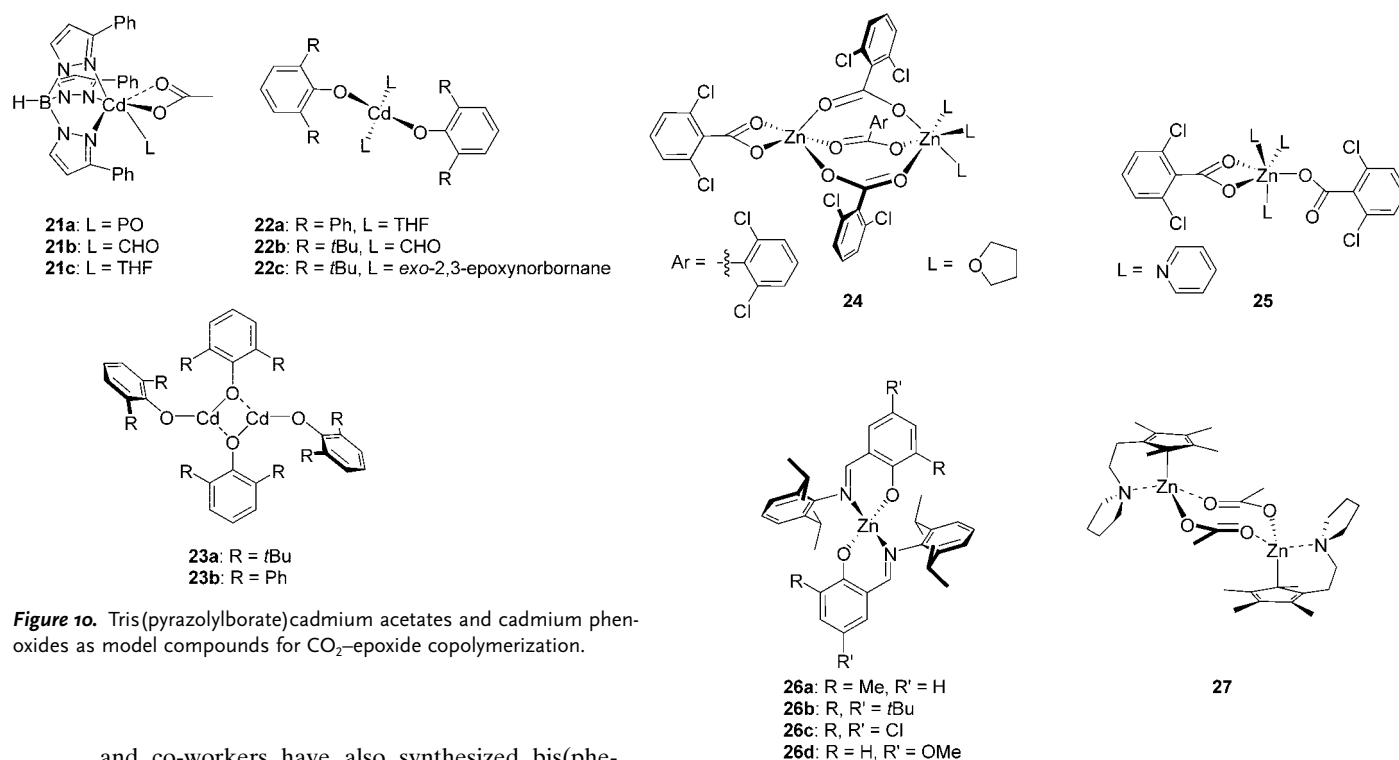


Figure 10. Tris(pyrazolylborate)cadmium acetates and cadmium phenoxides as model compounds for CO₂-epoxide copolymerization.

and co-workers have also synthesized bis(phenoxy) cadmium derivatives as model reagents.^[125,126,131–133] Compounds **22a–c** exhibited a distorted tetrahedral geometry around cadmium and illustrated the coordination of epoxides such as CHO and *exo*-2,3-epoxynorbornane. In the absence of coordinating solvents, dimeric three-coordinate cadmium phenoxides were synthesized (**23a,b**). Addition of coordinating solvents, such as THF, regenerated monomeric cadmium phenoxides. Finally, bis(phenoxy) cadmium and [(tp)CdOAc] complexes were not active for epoxide-CO₂ copolymerization; however, they did catalytically convert PO and CO₂ to PC at an unspecified rate.

Although the discrete catalysts above represent an important advance in catalyst design, the active species for the copolymerization remain unclear. Regarding these phenoxide-zinc complexes, one or more ligands are likely to act as polymerization initiators, and thus become the chain-end of the growing polymer chain.

7.3. Discrete Zinc Complexes for Epoxide-CO₂ Copolymerization

Given the success of zinc phenoxide compounds for copolymerization of CHO and CO₂, Darensbourg and co-workers investigated zinc benzoate (**24** and **25**),^[134] bis(salicylaldiminato)zinc (**26a–d**),^[135] and (dialkylamino)ethyltetramethylcyclopentadienyl (dec) zinc derivatives (**27**)^[136] (Figure 11). Zinc benzoate aggregates including compound **24** were synthesized by reaction of Zn[N(SiMe₃)₂]₂ with 2,6-disubstituted benzoic acids.^[134] Dimeric **24** was converted with pyridine to generate a monomeric complex with three coordinated pyridines (**25**). **24** displayed moderate CHO-CO₂ copolymerization activities (TOF = 7.7 h⁻¹) comparable to those observed with zinc phenoxide compounds. Addi-

Figure 11. Benzoate, bis(salicylaldiminato), and (dialkylamino)ethylcyclopentadienyl zinc catalysts for CHO-CO₂ copolymerization.

tionally, under 55 atm CO₂ at 80°C, PCHC was generated with essentially 100% carbonate linkages. A number of bis(salicylaldiminato)-zinc complexes (**26a–d**) were synthesized by reaction of Zn[N(SiMe₃)₂]₂ with 2 equivalents salicylaldimines.^[135] Complex **26a** was the most active catalyst copolymerizing CHO and CO₂ to give PCHC (>99% carbonate linkages, *M_n* = 41 000 g mol⁻¹, *M_w*/*M_n* = 10.3) with a TOF of 6.9 h⁻¹. Related zinc-bis(trimethylsilylamido) and zinc-phenoxide complexes have been reported by Chisholm et al.; however, no copolymerization activity was observed.^[137] The single-site catalyst [(dec)ZnOAc] (**27**) was synthesized by deprotonation of the dec ligands followed by reaction with Zn(OAc)₂.^[136] X-ray analysis of **27** revealed a dimeric compound featuring bridging acetates and η¹-coordination of the cyclopentadienyl moiety to zinc. At 30°C and 40 atm CO₂, **27** exhibited low activity (1.2 TOF⁻¹), and the resultant PCHC possessed 15–20% ether linkages.

Recently, Hampel et al. reported that quinoxaline-derived zinc alkoxide complexes, **28** and **29**, exhibited low activities for CHO-CO₂ copolymerization (Figure 12).^[138] At 80°C and 80 atm CO₂, compounds **28** and **29** showed TOFs of 4.9 and 3.6 h⁻¹, respectively. The PCHC yielded from **28** possessed 97% carbonate linkages, a *M_n* of 13 500 g mol⁻¹, and a PDI of 4.59.

Binaphthyldiamino (binap) salen-type metal complexes (**12**, **30a,b**) in combination with Lewis basic cocatalysts, including NEt₃, DMAP, and pyridine, were reported by Shi and co-workers for the cyclization of terminal epoxides and CO₂ (Scheme 9).^[92] At 35 atm CO₂ and 100°C, **30a**/NEt₃ (2 equiv) converts PO to PC with approximately 57 TOF⁻¹.

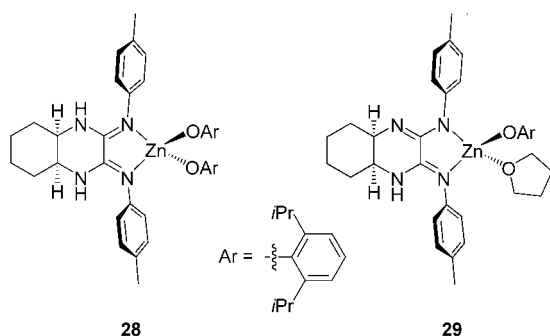
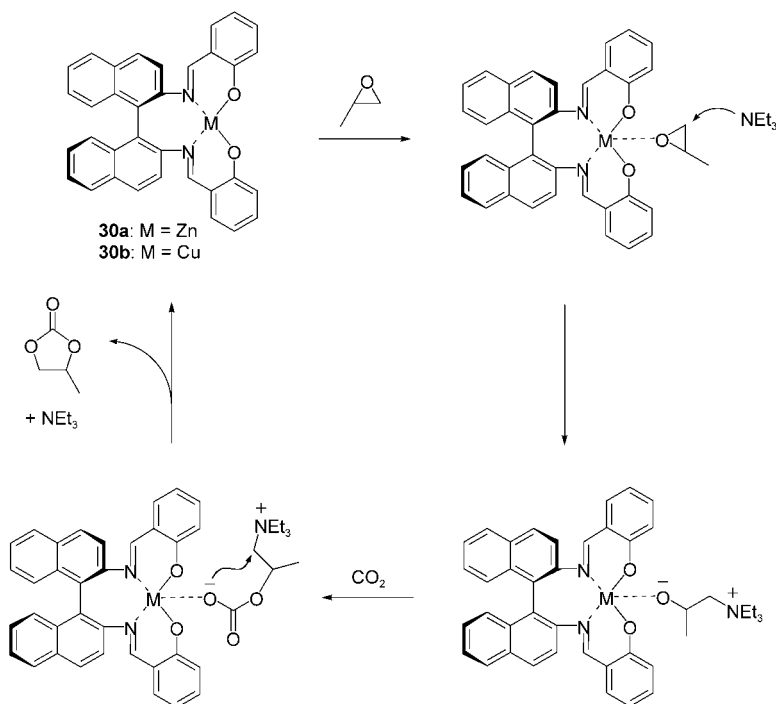


Figure 12. Quinoxaline-derived zinc phenoxides for CHO–CO₂ copolymerization.



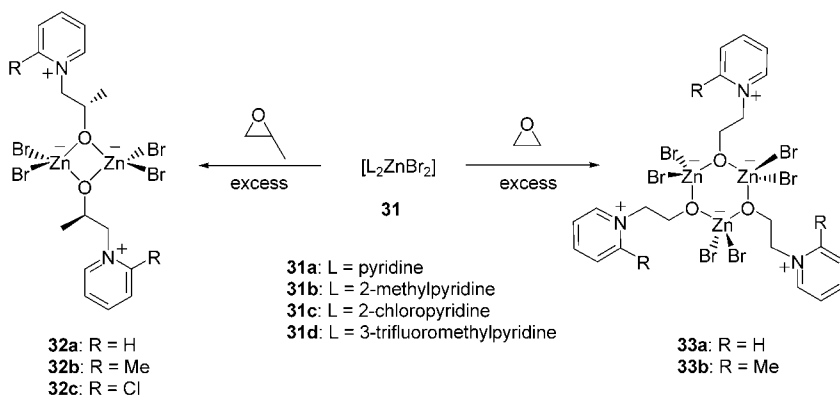
Scheme 9. Proposed catalytic cycle for the cyclization of terminal epoxides and CO₂ using chiral binap salen-type metal catalysts.

Copper complex **30b** and NEt₃ also catalyze the formation of **PC** with a TOF of 32 h^{−1}. Moreover, catalysts **30a,b** were discovered to transform a variety of terminal epoxides, such as butylene oxide, SO, and epichlorohydrin, to their corresponding cyclic carbonates. Isotope-labeling experiments using *trans*-deuterioethylene oxide derivatives indicated that epoxide ring-opening occurred by nucleophilic attack of a Lewis base (e.g., NEt₃) followed by CO₂ insertion (Scheme 9). Subsequent ring closure produced the *trans*-cyclic carbonate with overall retention of configuration. Although **30a,b** are chiral catalysts, virtually no asymmetric induction was observed.

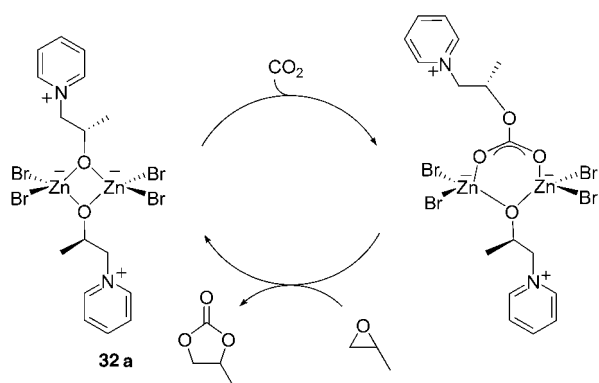
7.4. Pyridine–Zinc Halide Complexes for Epoxide–CO₂ Coupling

Despite extensive research on catalysts for cyclic carbonate synthesis, there are limited reports on catalyst intermediates or reaction mechanisms. Notably, Kim and co-workers addressed both of these issues using pyridinium alkoxy zinc dibromides.^[139,140] [(Pyridine)₂ZnBr₂] (**31a**) was found to couple PO and CO₂ to PC with a TOF of 308 h^{−1} at 100 °C and 35 atm CO₂. [(2-*R*-pyridine)₂ZnBr₂] (**31a** *R* = H, **31b** *R* = Me) reacted with excess PO to provide dimeric pyridinium alkoxy zinc dibromides (**32a** *R* = H, **32b** *R* = Me; Scheme 10). Complex **32a** crystallized as a dimeric compound containing a distorted tetrahedral geometry around both zinc centers. Interestingly, PO ring-opening occurred exclusively at the least hindered carbon and only the *meso* dimer crystallized. At 100 °C and 35 atm CO₂, **32a** converted PO and CO₂ to PC with a TOF of 340 h^{−1}, indicating the presence of a slight initiation time as **31a** reacts to form **32a**. A series of [(2-*R*-pyridine)₂ZnBr₂] (**31a–c**) with varying electronic properties were examined for activity. Electron-donating substituents promoted activity, while electron-withdrawing groups extinguished reactivity (Me > H > Cl), signifying the necessity for Lewis basic pyridine ligands. At 100 °C and 35 atm CO₂, **32b** exhibited an activity for PO–CO₂ cyclization of 530 TO h^{−1}.

In addition to PO–CO₂ cyclization, **32a** and **32b** were active for cyclic ethylene carbonate (EC) production with TOFs of 1200 h^{−1} and 1450 h^{−1}, respectively. Surprisingly, the reaction of EO with **31a** and **b** resulted in trimeric compounds (**33a** and **b**) containing an alternating zinc and oxygen six-membered ring at the core of the molecule (Scheme 10). Apparently, the sterics of the epoxide determine whether dimeric or trimeric intermediates are formed. Complex **33a** demonstrated activities almost identical to those of **32a** for both PC (327 TO h^{−1}) and EC (1180 h^{−1}), suggesting the same catalytic species. Kim proposed that the dimeric form was the active species for epoxide–CO₂ coupling (Scheme 11). Insertion of CO₂ in **32a** gave zinc



Scheme 10. Syntheses of dimeric and trimeric zinc pyridinium alkoxides.



Scheme 11. Proposed mechanism for the synthesis of propylene carbonate using dimeric zinc pyridinium alkoxides.

alkoxide carbonate dimer containing a six-membered ring, that subsequently eliminated PC. Species **32a** was regenerated upon reaction with PO.

Shortly thereafter, Darensbourg et al. illustrated that related pyridine–zinc halide adducts (Figure 13) were catalytically active for CHO–CO₂ copolymerization and cycliza-

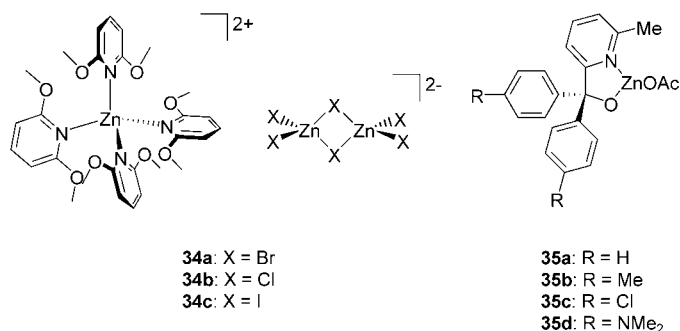


Figure 13. Zinc–pyridine complexes for CHO–CO₂ copolymerization.

tion with TOFs as high as 13.5 h^{−1}.^[141] 2,6-Dimethoxypyridine reacted with zinc halides to give [Zn(2,6-dimethoxypyridine)₄]²⁺[Zn₂X₆]^{2−} (**34a–c**) while 3-trifluoromethylpyridine reacted with ZnBr₂ to generate (3-CF₃-pyridine)₂ZnBr₂ (**31d**). The order of halide reactivity was Cl ≥ Br > I and the complex with 2,6-dimethoxypyridine was more active than that with 3-trifluoromethylpyridine. At 55 atm CO₂ and 80 °C, PCHC was produced with 80–91 % carbonate linkages, *M_n* up to 44 000 g mol^{−1}, and broad PDIs. In situ IR studies revealed a first-order dependence on catalyst concentration for polymerization, but an unusual fractional order of 1.5 for CHC formation. It was suggested that both dimeric and monomeric zinc active species accounted for the mixed order in zinc. Kim and co-workers recently reported that pyridine alkoxide ligated zinc acetates **35a–d** (Figure 13) catalyze the copolymerization of CHO and CO₂. Complex **35c** produces PCHC (*M_n* = 9500 g mol^{−1}, *M_w*/*M_n* = 2.5) with a TOF of 153 h^{−1}. The polycarbonate is unusual in that it has only 63 % carbonate linkages.^[142]

7.5. Single-Site β-Diiminate Zinc Catalysts for Epoxide–CO₂ Coupling

Our research group discovered a highly active, living epoxide–CO₂ copolymerization system using bulky β-diiminate (bdi) zinc catalysts, such as **36–39**, under low pressures (7 atm CO₂) and temperatures (50 °C) (Figure 14).^[143–153]

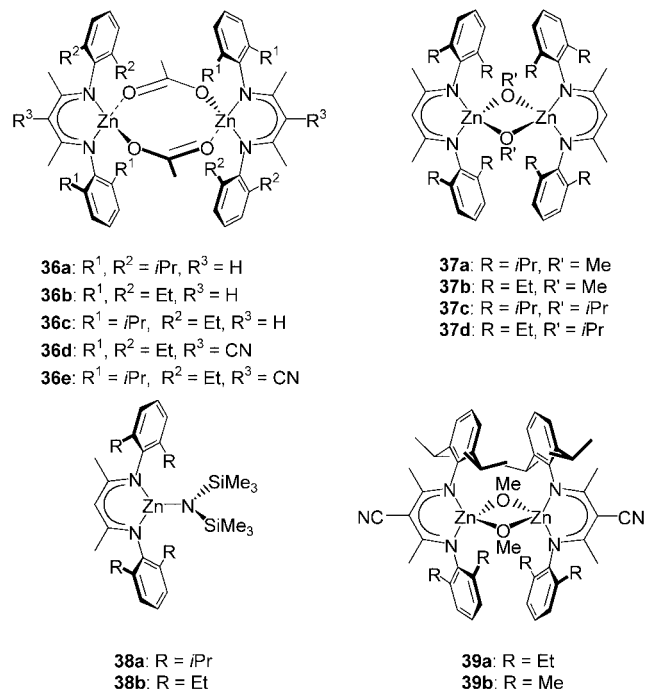
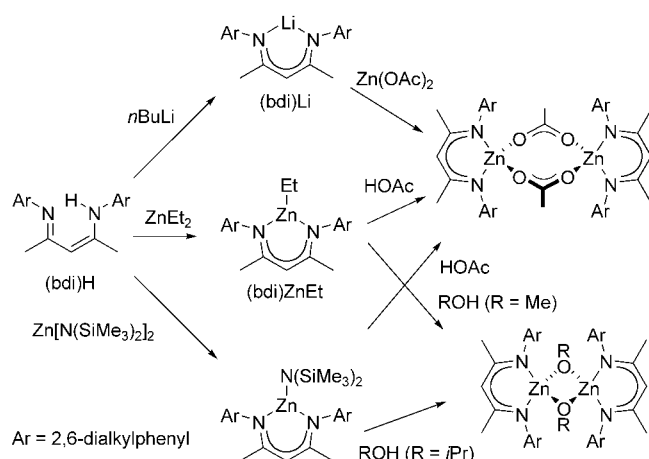


Figure 14. β-Diiminate–zinc catalysts for epoxide–CO₂ copolymerization.

Several key design features, including initiating groups, sterics, and electronics, drastically altered the efficacy of the catalysts. To model the growing polycarbonate chain, zinc–acetate (**36**), zinc–methoxide (**37a,b**), and zinc–isopropoxide (**37c,d**) complexes were synthesized as mimics for zinc carbonates and zinc alkoxides (Scheme 12). Zinc acetates were produced from the deprotonated (bdi)Li adducts and Zn(OAc)₂^[143,146] or by addition of acetic acid to [(bdi)ZnEt] compounds.^[150,151] (bdi)ZnEt was generated by addition of ZnEt₂ to (bdi)H ligands.^[143] [(bdi)ZnOAc] compounds crystallized as dimeric compounds with bridging μ,η²-acetates. The reaction of [(bdi)ZnEt] with MeOH provided dimeric [(bdi)ZnOMe] compounds (**37a,b**; **39a,b**).^[143,146] Deprotonation of (bdi)H using Zn[N(SiMe₃)₂]₂ gave monomeric, 3-coordinate [(bdi)ZnN(SiMe₃)₂] (**38a,b**).^[146,154] Subsequent alcoholysis with *i*PrOH yielded [(bdi)Zn(O*i*Pr)] complexes (**37c,d**) that are dimeric in the solid state. (bdi)Zn acetate, methoxide, isopropoxide, and bis(trimethylsilyl)amido complexes were all active for the alternating copolymerization of CHO and CO₂.^[143,145,146,149–151] In addition, [(bdi)Zn(O*i*Pr)] complexes were highly active for the living polymerization of lactide,^[154,155] ε-caprolactone, and β-butyrolactone.^[156] While X-ray crystallography revealed that [(bdi)ZnOAc], [(bdi)Zn(O*i*Pr)], and [(bdi)ZnOMe] compounds were dimeric,



Scheme 12. Synthesis of β -diimine-zinc complexes.

¹H NMR spectroscopy revealed that the solution states were highly dependent upon sterics.^[143,146,151,154] For instance, it was demonstrated that compounds **36a** and **37c** exhibited a monomer⇌dimer equilibrium under appropriate temperatures and concentrations.^[143,156] On the other hand, **36b**, **37b**, and **37d** were exclusively dimeric in solution, even at elevated temperatures.^[146,156] Concurrently, subtle modifications on the *N*-aryl *ortho* positions highly influenced polymerization activity. Sterically unencumbered methyl substituents exhibited no polymerization activity, whereas sterically congested ethyl and isopropyl substituents promoted the copolymerization giving TOFs of 431 h⁻¹ and 360 h⁻¹, respectively (Table 2).^[151] Furthermore, the unsymmetrical **36c** yielded PCHC (99% carbonate linkages, $M_n = 23\,300\text{ g mol}^{-1}$, $M_w/M_n = 1.15$) with a TOF of 729 h⁻¹. Electronics also played a dramatic role in activity, such that electron-withdrawing cyano substituents enhanced polymerization rates. Complex **36d** produced PCHC (90% carbonate linkages, $M_n = 17\,900\text{ g mol}^{-1}$, $M_w/M_n = 1.15$) with a TOF of 917 h⁻¹ in only 20 minutes. The combination of the unsymmetrical ligand geometries and the electron-withdrawing cyano substituent yielded the most active catalysts reported to date.^[149] At 50 °C and in only 10 minutes, **39a** and **39b** catalyzed the copolymerization of 1000 equivalents CHO and 7 atm CO₂ to give high molecular weight polymers ($M_n \approx 22\,000\text{ g mol}^{-1}$), narrow PDIs ($M_w/M_n = 1.09\text{--}1.11$), and extremely high TOFs of 2170 and 2290 h⁻¹, respectively (see Table 2).

In an attempt to isolate monomeric β -diimine complexes, Chisholm et al. investigated bulky initiators including *t*BuOH and Ph₃SiOH.^[157,158] As expected, monomeric compounds **40** and **41** (Figure 15) were active for CHO-CO₂ alternating copolymerization. Compound **41** also coupled PO and CO₂ to give propylene carbonate in unspecified yield. Unexpectedly, Chisholm's [(bdi)ZnNiPr₂], an analog of our compound **38a**, was not active for the copolymerization, although it readily reacted with CO₂ to generate **42**. Rieger et al. recently showed that an ethyl sulfinate is a viable initiator for the copolymerization.^[159] Compound **43** (Figure 15), synthesized by bubbling SO₂ through a [(bdi)ZnEt] solution, was also active for CHO-CO₂ copolymerization. Catalytic activities were comparable to **36a**, indicating

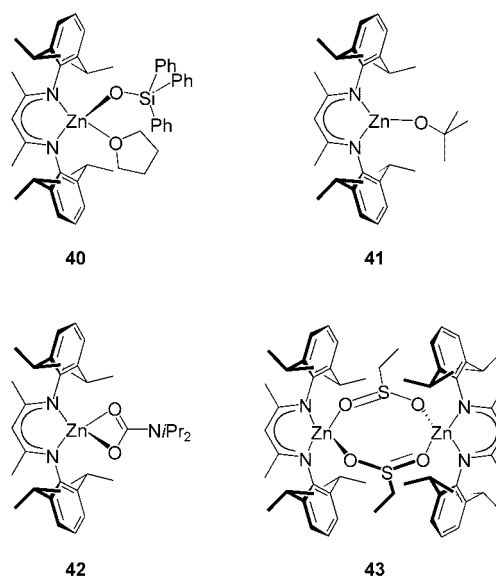


Figure 15. Monomeric and dimeric [(bdi)ZnOR] complexes.

similar active species. From bimodal gel permeation chromatography traces, monomeric and dimeric bdi-zinc species were believed to be active, although no mechanistic studies were conducted. Recently, oligomeric bdi ligands have been generated from 4,4'-methylenedianiline and 2,4-pentanedione. The zinc complexes have shown modest activity for CHO-CO₂ copolymerization (TOF = 11.3 h⁻¹).^[160–162]

Yu and Jones recently reported that β -diimine-zinc catalysts immobilized on silica exhibited moderate activities for CHO-CO₂ copolymerization.^[163] Compounds **44**, **45a**, and **45b** (Figure 16) are precursors to the silica-immobilized

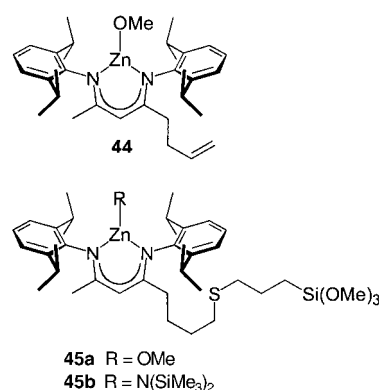


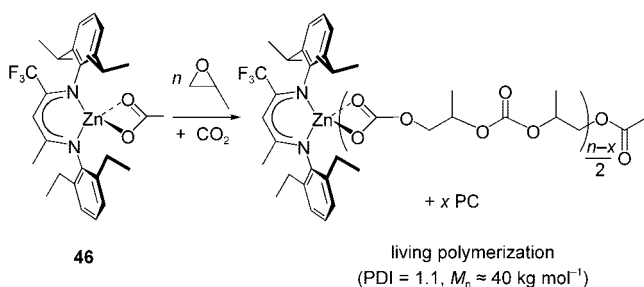
Figure 16. Precursors to silica-immobilized bdi-zinc catalysts.

complexes and show activities of 110, 60, and 65 h⁻¹, respectively, under 7 atm CO₂ at 50 °C. The resultant polycarbonates exhibited > 92% carbonate linkages, molecular weights of 8700–13 300 g mol⁻¹, and PDIs of 1.03–1.28. Complexes **45a** and **45b** were supported on mesoporous SBA-15 and controlled-pore glass, but the rates of PCHC formation (TOFs = 5–21 h⁻¹) and percent carbonate linkages (33–78%) decreased. A corresponding drop in molecular weights was

not observed indicating fewer active zinc centers. Finally, based on the activity observed with the silica-supported zinc catalysts, Yu and Jones suggested that the copolymerization proceeded via a monometallic mechanism.^[163] High-throughput equipment has been used to screen CHO–CO₂ copolymerization in the presence of β -diiminate–zinc catalysts, but so far this research has been limited to known compounds (**38a,b**).^[164]

Morokuma and co-workers performed theoretical studies using the hybrid molecular orbital method ONIOM on the alternating copolymerization of epoxides and CO₂ catalyzed by monomeric **37a**.^[165] The rate-determining step of the copolymerization was proposed to be epoxide insertion into a zinc–carbonate bond. Furthermore, in alicyclic epoxides such as CHO, the activation barrier for epoxide ring-opening by a zinc carbonate is drastically reduced due to ring, torsion, and angle strain. By contrast, the study predicted that aliphatic epoxides such as EO could not be copolymerized due to high activation barriers for epoxide ring-opening.

Subtle electronic and steric perturbations to [(bdi)ZnOR] (R = alkyl or acyl) complexes resulted in drastic enhancements in activity for CHO–CO₂ copolymerization.^[146,149,151] During the course of these studies, catalysts for PO–CO₂ coupling were also discovered by our research group.^[150] PO–CO₂ coupling proved to be highly sensitive on reaction conditions. Both temperature and pressure had a profound effect on product formation. At 50 °C and 20 atm CO₂, unsymmetrical **36e** yielded PC with a TOF of 50 h^{−1}. By simply reducing the temperature to 25 °C, PC formation was suppressed, and the selectivity for PPC/PC was 85:15 with a TOF of 47 h^{−1}. The polycarbonate exhibited > 99% carbonate linkages, a *T_g* of 38 °C, a *M_n* of 43 300 g mol^{−1}, and a PDI of 1.09. Furthermore, ¹³C NMR spectroscopy revealed a nearly regiorandom copolymer,^[166,167] indicating that ring-opening occurred at both C–O bonds. Further modifications of the ligand architecture generated complex **46** (Scheme 13), the

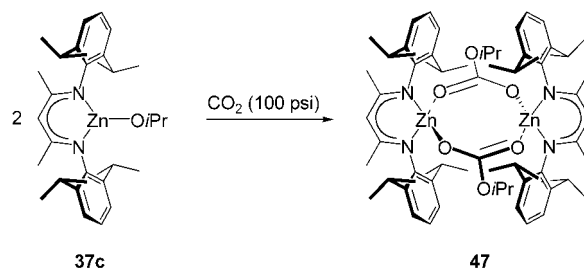


Scheme 13. Unsymmetrical, electron-deficient bdi–zinc complex for the copolymerization of PO and CO₂.

most potent catalyst reported to date for PO–CO₂ copolymerization. Complex **46** copolymerized PO and CO₂ at 25 °C and 7 atm CO₂ to give PPC (> 99% carbonate linkages, *M_n* = 36 700 g mol^{−1}, *M_w*/*M_n* = 1.13) with a TOF of 235 h^{−1} (Table 2). However, the selectivity for polymer was only 75%. Increasing the CO₂ pressure to 35 atm favored polymer formation with a selectivity of 93%, while only moderately attenuating catalytic activity (TOF = 138 h^{−1}). Finally, compound **46** is

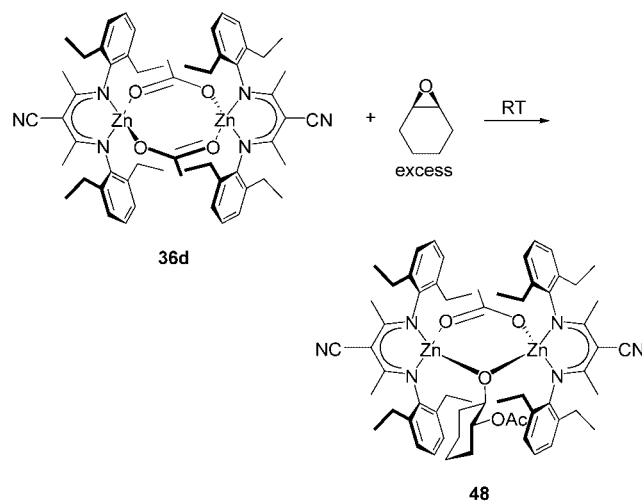
highly active for PC formation at high temperatures. At 75 °C, PC is produced with TOFs over 1000 h^{−1}.^[168]

Recently, our research group performed mechanistic studies on the [(bdi)ZnOR]-catalyzed copolymerization of CHO and CO₂.^[151] Stoichiometric reactions of the copolymerization initiation steps showed that zinc alkoxides insert CO₂, while zinc acetates react with CHO. For example, **37c**, which is a monomeric zinc alkoxide at room temperature ([Zn] = 0.01 M in [D₆]benzene) instantaneously reacted with CO₂ to give **47** (Scheme 14). X-ray analysis revealed that **47**



Scheme 14. Insertion reaction of CO₂ with [(bdi)Zn(OiPr)].

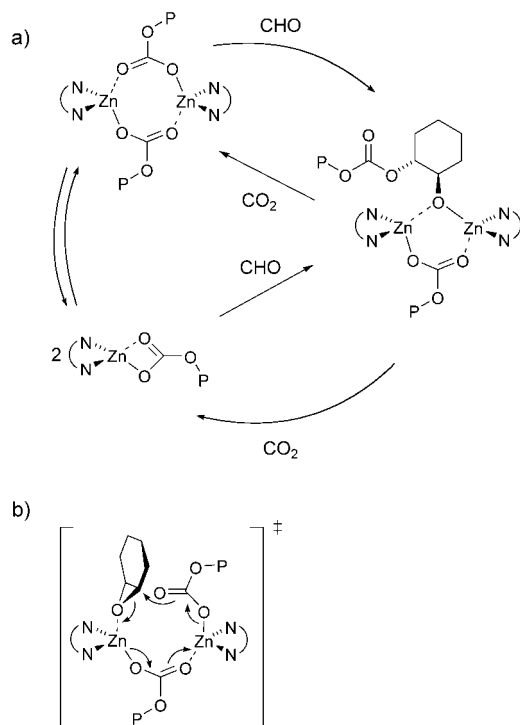
crystallized as a μ,η^2 -carbonate-bridged dimer. Complex **47** is virtually isostructural to **36a**, suggesting similar reactivity in the copolymerization. Complex **36d** inserted CHO to give **48** over the course of days (Scheme 15). X-ray analysis showed



Scheme 15. Insertion reaction of CHO with [(bdi)ZnOAc].

that **48** is a μ,η^2 -acetate- μ,η^1 -cyclohexyloxide acetate-bridged dimer in the solid state. Both **47** and **48** serve as model compounds for presumed intermediates in the copolymerization. Due to the expeditious reaction of CO₂ with **37c**, CHO insertion was predicted to be the rate-determining step. To monitor propagation, rate studies were performed on compounds **36a–c** using in situ FT-IR. The kinetic studies revealed a zeroth-order dependence in CO₂ and a first-order dependence in CHO. Hence, insertion of CHO into a zinc carbonate was indeed the rate-determining step. The copolymerization

of CHO (1.98 M in toluene) and 20 atm CO₂ at 50 °C using sterically-unhindered, dimeric **36b** resulted in an order of 1.02 ± 0.03 in [(bdi)ZnOR] concentration (R = alkyl, acyl, or polymer chain). However, under the same conditions, an order in [(bdi)ZnOR] concentration of 1.83 ± 0.04 was determined for **36c**. Therefore, the copolymerization of CHO and CO₂ using **36c** at 50 °C exhibited the following overall rate law: $d[P]/dt = k[\text{epoxide}]^{1.0}[\text{Zn}]^{1.83}$. At lower temperature (30 °C), a decrease in the order in [(bdi)ZnOR] concentration to 1.37 ± 0.02 was observed for **36c**. On the basis of [(bdi)ZnOR] solution studies (R = alkyl or acyl), stoichiometric insertion reactions, and rate studies, a bimetallic mechanism was proposed (Scheme 16a). Sterically



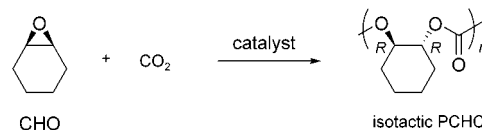
Scheme 16. a) Proposed copolymerization mechanism using bdi-zinc complexes; b) epoxide ring-opening transition state (P = polymer chain).

encumbered bdi-zinc complexes (**36a** and **36c**) ring-open CHO in a bimetallic transition state (Scheme 16b) with a predominantly monomeric ground state. Conversely, sterically unhindered bdi-zinc complexes (**36b**) insert CHO in a bimetallic transition state with a completely dimeric ground state.

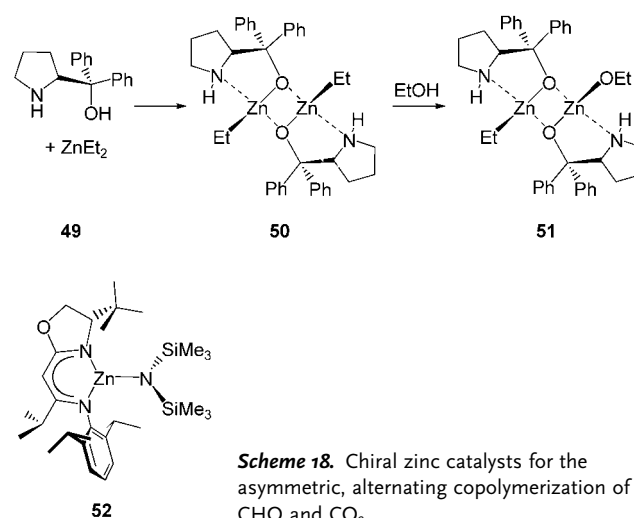
7.6. Zinc Catalysts for Asymmetric CHO–CO₂ Copolymerization

There is significant interest in controlling the absolute stereochemistry of ring-opening in epoxide–CO₂ copolymerization for several reasons. First, microstructure directly affects polymer properties.^[169] Second, the kinetic resolution of racemic epoxides or desymmetrization of *meso* epoxides by copolymerization is a potential route to valuable chiral

building blocks. CHO, a *meso* molecule, is an ideal substrate for desymmetrization using chiral catalysts.^[170] In 1999, Nozaki et al. reported that a 1:1 mixture of ZnEt₂ and (*S*)- α,α -diphenylpyrrolidine-2-yl-methanol (**49**) was active for stereoselective CHO–CO₂ copolymerization at 40 °C and 30 atm CO₂ (Schemes 17 and 18).^[171,172] The polycarbonate



Scheme 17. Asymmetric copolymerization of CHO and CO₂.



Scheme 18. Chiral zinc catalysts for the asymmetric, alternating copolymerization of CHO and CO₂.

exhibited 100 % carbonate linkages, a M_n of 8400 g mol⁻¹, and a PDI of 2.2. Hydrolysis of PCHC with base produced the corresponding *trans*-cyclohexane-1,2-diol with 73 % enantiomeric excess. ¹³C NMR spectroscopy studies of model polycarbonate oligomers afforded spectral assignments for isotactic dyads (153.7 ppm) and syndiotactic dyads (153.3–153.1 ppm).^[173] Finally, ring-opening proceeded by complete inversion of configuration (S_N2 mechanism), hence no *cis*-cyclohexane-1,2-diol was observed.

In a recent report, Nozaki and co-workers isolated presumed intermediates in the asymmetric alternating copolymerization.^[174] Reaction of ZnEt₂ and (*S*)- α,α -diphenylpyrrolidine-2-yl-methanol yielded dimeric **50**, which was structurally characterized by X-ray diffraction studies (Scheme 18). At 40 °C and 30 atm CO₂, **50** catalyzed the formation of isotactic PCHC ($M_n = 11800$ g mol⁻¹, $M_w/M_n = 15.7$, TOF = 0.6 h⁻¹) with a slightly lower enantiomeric excess of 49 %. When the copolymerization was attempted with **50** and 0.2 to 1.0 equivalents of EtOH, enantioselectivities increased up to 80 % *ee*, and better control of molecular weights and PDIs resulted. Compound **51** was proposed to be the active initiating species (see Scheme 18). End-group analysis by MALDI-TOF mass spectrometry revealed in the absence of EtOH signals assignable to the aminoalcohol-initiated polymerization. However, as EtOH addition was

increased from 0.2 to 1.0 equivalents, signals corresponding to the aminoalcohol-derived polycarbonate disappeared as peaks for the EtOH-initiated PCHC emerged. This was further confirmed by end-group analysis using ^1H NMR spectroscopy. Finally, mechanistic studies suggest that the dimeric form of the catalyst is in fact the active species.

In 2000, our research group developed C_1 -symmetric imine-oxazoline ligated zinc bis(trimethylsilyl)amido compounds for the stereoselective, alternating copolymerization of CHO and CO_2 (Scheme 18).^[145] Through multiple electronic and steric manipulations, compound **52** was found to exhibit the highest enantioselectivity (RR/SS ratio 86:14, 72% *ee*) in the copolymerization. The resultant PCHC exhibited 100% carbonate linkages, a M_n of $14\,700\text{ g mol}^{-1}$, a PDI of 1.35, and a T_g and T_m of 120 and 220°C , respectively. Furthermore, stereocontrol was also achieved in the alternating copolymerization of CPO and CO_2 , producing poly(cyclopentene carbonate) with a RR/SS ratio of 88:12 (76% *ee*). As revealed by ^{13}C NMR spectroscopy, the experimental carbonyl tetrad concentrations matched the predicted tetrad concentrations for an enantiomorphic-site control mechanism.^[145] The contributions described above represent an important step forward in the production of well-defined, tactic polycarbonates.

8. Summary and Outlook

Over the last decade, significant advances have been achieved in CO_2 -epoxide coupling chemistry. Homogeneous catalysts for CO_2 -epoxide copolymerization offer significant increases in rate as well as selectivity versus their heterogeneous counterparts. Well-defined, homogeneous catalysts have given new momentum to the field of CO_2 utilization, and have made possible a much deeper mechanistic understanding of these systems. Current catalysts provide reasonable routes to a variety of polycarbonates from inexpensive epoxides, including poly(cyclohexene carbonate), poly(propylene carbonate), and terpolymers of CHO, PO, and CO_2 . Moreover, living catalyst systems were found that provide block copolymers and polymers with molecular weights predetermined by monomer/initiator ratios. In addition, both polycarbonates and cyclic carbonates can be synthesized with high selectivities and rates, owing to subtle modification of the catalyst's architecture. Finally, precise control of cyclic carbonates and/or polycarbonate production is achieved by utilizing homogeneous catalysts with appropriate reaction conditions such as pressure, temperature, and cocatalyst additives.

Despite the recent breakthroughs, the future challenges are many. At the current time there are limited applications of epoxide- CO_2 copolymers due to their high cost and low thermal stability. Therefore it will be necessary to develop catalyst systems that are capable of producing these polymers economically. In addition, methods for producing polymers with increased thermal stability are needed. Surprisingly, only Cr, Co, and Zn compounds have shown significant activity for the copolymerization of CO_2 and epoxides. The unusual reactivity of these metals must be further exploited, and other metals such as Mg, Mn, Fe, and Ni should be explored.

Alternative comonomers, including lactones, isocyanates, aziridines, as well as new epoxides, such as limonene oxide and styrene oxide, could be promising reagents in the production of unique copolymers. By utilizing homogeneous living catalysts, there are infinite possibilities of new, exciting copolymer microstructures. Living systems allow for precise control of molecular weights, low PDIs, copolymer synthesis by sequential monomer addition, and the ability to functionalize chain ends. Because only one chain is produced by each metal center in homogeneous catalyst systems, the development of strategies related to Inoue's "immortal polymerization" may lead to more productive systems. Although the enantioselective copolymerization of CO_2 and epoxides has been accomplished, much higher levels of stereocontrol as well as regiocontrol are required for improved physical properties.

Undoubtedly, the future will witness continued research at this exciting interface of inorganic and polymer chemistry to the benefit of both fields. Homogeneous catalysts will lead to epoxide- CO_2 copolymers with unprecedented levels of architectural control, providing many new opportunities in polymer science.

Abbreviations

bdi	β -diiminate
CHC	cyclohexene carbonate
CHO	cyclohexene oxide
CPO	cyclopentene oxide
EC	ethylene carbonate
EO	ethylene oxide
PC	propylene carbonate
PCHC	poly(cyclohexene carbonate)
PEC	poly(ethylene carbonate)
PO	propylene oxide
PPC	poly(propylene carbonate)
PPO	poly(propylene oxide)
SO	styrene oxide
tpp	tetraphenylporphyrin

We gratefully acknowledge support from the NSF (CHE-9875261, CHE-0243605, DMR-0079992), the Cornell University Center for Biotechnology, Eastman Chemical and Sumitomo Chemicals, and the Packard, Sloan, and Beckman Foundations for support of our research involving CO_2 utilization. D.R.M. is grateful for a Corning Foundation Science Fellowship.

Received: April 26, 2004

Published Online: November 23, 2004

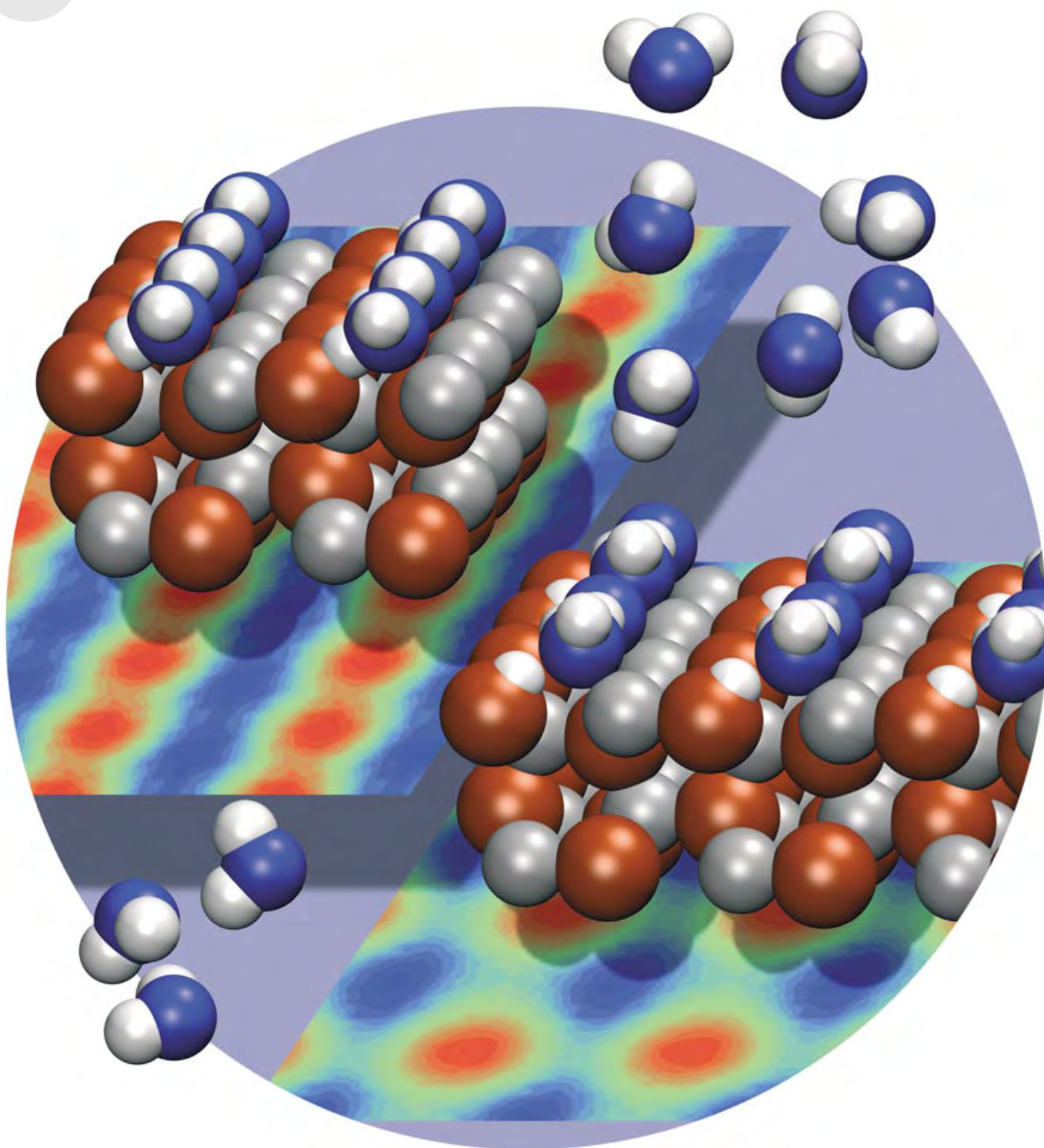
- [1] T. U. Gerngross, S. C. Slater, *Sci. Am.* **2000**, 283(2), 36–41.
- [2] R. A. Gross, B. Kalra, *Science* **2002**, 297, 803–807.
- [3] M. Okada, *Prog. Polym. Sci.* **2002**, 27, 87–133.
- [4] H. Danner, R. Braun, *Chem. Soc. Rev.* **1999**, 28, 395–405.
- [5] H. Arakawa, M. Aresta, J. N. Armor, M. A. Barteau, E. J. Beckman, A. T. Bell, J. E. Bercaw, C. Creutz, E. Dinjus, D. A. Dixon, K. Domen, D. L. DuBois, J. Eckert, E. Fujita, D. H.

- Gibson, W. A. Goddard, D. W. Goodman, J. Keller, G. J. Kubas, H. H. Kung, J. E. Lyons, L. E. Manzer, T. J. Marks, K. Morokuma, K. M. Nicholas, R. Periana, L. Que, J. Rostrup-Nielson, W. M. H. Sachtler, L. D. Schmidt, A. Sen, G. A. Somorjai, P. C. Stair, B. R. Stults, W. Tumas, *Chem. Rev.* **2001**, 101, 953–996.
- [6] W. Leitner, *C. R. Acad. Sci. Ser. IIc* **2000**, 3, 595–600.
- [7] A. I. Cooper, *J. Mater. Chem.* **2000**, 10, 207–234.
- [8] C. Bolm, O. Beckmann, O. A. G. Dabard, *Angew. Chem.* **1999**, 111, 957–959; *Angew. Chem. Int. Ed.* **1999**, 38, 907–909.
- [9] For leading references on CO₂ fixation and/or catalysis, see: a) G. Musie, M. Wei, B. Subramaniam, D. H. Busch, *Coord. Chem. Rev.* **2001**, 219, 789–820; b) W. Leitner, *Coord. Chem. Rev.* **1996**, 153, 257–284; c) W. Leitner, *Angew. Chem.* **1995**, 107, 2391–2405; *Angew. Chem. Int. Ed. Engl.* **1995**, 34, 2207–2221.
- [10] M. Shi, Y. M. Shen, *Curr. Org. Chem.* **2003**, 7, 737–745.
- [11] X. Yin, J. R. Moss, *Coord. Chem. Rev.* **1999**, 181, 27–59.
- [12] D. Walther, M. Ruben, S. Rau, *Coord. Chem. Rev.* **1999**, 182, 67–100.
- [13] A. Behr, *Carbon Dioxide Activation by Metal Complexes*, VCH, Weinheim, **1988**.
- [14] D. H. Gibson, *Chem. Rev.* **1996**, 96, 2063–2095.
- [15] D. Walther, *Coord. Chem. Rev.* **1987**, 79, 135–174.
- [16] P. G. Jessop, T. Ikariya, R. Noyori, *Chem. Rev.* **1999**, 99, 475–493.
- [17] J. L. Kendall, D. A. Canelas, J. L. Young, J. M. DeSimone, *Chem. Rev.* **1999**, 99, 543–563.
- [18] S. Inoue, *CHEMTECH* **1976**, 6, 588–594.
- [19] W. Kuran, *Prog. Polym. Sci.* **1981**, 23, 919–992.
- [20] D. J. Darensbourg, M. W. Holtcamp, *Coord. Chem. Rev.* **1996**, 153, 155–174.
- [21] M. S. Super, E. J. Beckman, *Trends Polym. Sci.* **1997**, 5, 236–240.
- [22] E. J. Beckman, *Science* **1999**, 283, 946–947.
- [23] D. X. Wang, M. Q. Kang, X. K. Wang, *Prog. Chem.* **2002**, 14, 462–468.
- [24] H. Pang, B. Liao, Y. H. Huang, G. M. Cong, *Chin. J. Appl. Chem.* **2001**, 18, 347–350.
- [25] <http://www.empowermaterials.com> (accessed April 25, 2004).
- [26] S. D. Thorat, P. J. Phillips, V. Semenov, A. Gakh, *J. Appl. Polym. Sci.* **2003**, 89, 1163–1176.
- [27] S. M. Peng, Y. An, C. Chen, B. Fei, Y. Zhuang, L. Dong, *Polym. Degrad. Stab.* **2003**, 80, 141–147.
- [28] B. Liu, L. Chen, M. Zhang, A. Yu, *Macromol. Rapid Commun.* **2002**, 23, 881–884.
- [29] S. J. Wang, L. C. Du, X. S. Zhao, Y. Z. Meng, S. C. Tjong, *J. Appl. Polym. Sci.* **2002**, 85, 2327–2334.
- [30] T. Sarbu, T. Styranec, E. J. Beckman, *Nature* **2000**, 405, 165–168.
- [31] C. Koning, J. Wildeson, R. Parton, B. Plum, P. Steeman, D. J. Darensbourg, *Polymer* **2001**, 42, 3995–4004.
- [32] C. K. Harnett, G. W. Coates, H. G. Craighead, *J. Vac. Sci. Technol. B* **2001**, 19, 2842–2845.
- [33] C. K. Harnett, K. M. Satyalakshmi, G. W. Coates, H. G. Craighead, *J. Photopolym. Sci. Technol.* **2002**, 15, 493–496.
- [34] D. A. Czaplewski, J. Kameoka, R. Mathers, G. W. Coates, H. G. Craighead, *Appl. Phys. Lett.* **2003**, 83, 4836–4838.
- [35] J. P. Jayachandran, H. A. Reed, H. Zhen, L. F. Rhodes, C. L. Henderson, S. A. B. Allen, P. A. Kohl, *J. Microelectromech. Syst.* **2003**, 12, 147–159.
- [36] A. G. Shaikh, *Chem. Rev.* **1996**, 96, 951–976.
- [37] J. H. Clements, *Ind. Eng. Chem. Res.* **2003**, 42, 663–674.
- [38] A. Rokicki, *Prog. Polym. Sci.* **2000**, 25, 259–342.
- [39] G. W. Coates, *Chem. Rev.* **2000**, 100, 1223–1252.
- [40] G. W. Coates, P. D. Hustad, S. Reinartz, *Angew. Chem.* **2002**, 114, 2340–2361; *Angew. Chem. Int. Ed.* **2002**, 41, 2236–2257.
- [41] B. J. O'Keefe, M. A. Hillmyer, W. B. Tolman, *J. Chem. Soc. Dalton Trans.* **2001**, 2215–2224.
- [42] R. H. Grubbs, *Handbook of Metathesis*, Wiley, New York, **2003**.
- [43] G. W. Coates, *J. Chem. Soc. Dalton Trans.* **2002**, 467–475.
- [44] S. Inoue, H. Koinuma, T. Tsuruta, *J. Polym. Sci. Part B* **1969**, 7, 287–292.
- [45] S. Inoue, H. Koinuma, T. Tsuruta, *Makromol. Chem.* **1969**, 130, 210–220.
- [46] M. Kobayashi, S. Inoue, T. Tsuruta, *Macromolecules* **1971**, 4, 658–659.
- [47] M. Kobayashi, Y. L. Tang, T. Tsuruta, S. Inoue, *Makromol. Chem.* **1973**, 169, 69–81.
- [48] M. Kobayashi, S. Inoue, T. Tsuruta, *J. Polym. Sci. Polym. Chem. Ed.* **1973**, 11, 2383–2385.
- [49] S. Inoue, M. Kobayashi, H. Koinuma, T. Tsuruta, *Makromol. Chem.* **1972**, 155, 61–73.
- [50] W. Kuran, S. Pasynkiewicz, J. Skupinska, A. Rokicki, *Makromol. Chem. Macromol. Chem. Phys.* **1976**, 177, 11–20.
- [51] P. Gorecki, W. Kuran, *J. Polym. Sci. Part C* **1985**, 23, 299–304.
- [52] W. Kuran, T. Listos, *Macromol. Chem. Phys.* **1994**, 195, 977–984.
- [53] K. Soga, E. Imai, I. Hattori, *Polym. J.* **1981**, 13, 407–410.
- [54] Y. Hino, *Polym. J.* **1984**, 16, 159–163.
- [55] T. Tsuruta, *Makromol. Chem.* **1986**, 6, 23–31.
- [56] W. Kuran, *Appl. Organomet. Chem.* **1991**, 5, 191–194.
- [57] W. Kuran, T. Listos, *Macromol. Chem. Phys.* **1994**, 195, 1011–1015.
- [58] W. Kuran, T. Listos, *Pol. J. Chem.* **1994**, 68, 1071–1083.
- [59] S. Inoue, H. Koinuma, Y. Yokoo, T. Tsuruta, *Makromol. Chem.* **1971**, 143.
- [60] S. Inoue, *J. Polym. Sci. Part A* **2000**, 38, 2861–2871.
- [61] N. Takeda, S. Inoue, *Makromol. Chem.* **1978**, 179, 1377–1381.
- [62] T. Aida, S. Inoue, *Macromolecules* **1981**, 14, 1162–1166.
- [63] T. Aida, S. Inoue, *Macromolecules* **1981**, 14, 1166–1169.
- [64] T. Aida, S. Inoue, *Macromolecules* **1982**, 15, 682–684.
- [65] T. Aida, S. Inoue, *J. Am. Chem. Soc.* **1983**, 105, 1304–1309.
- [66] T. Aida, S. Inoue, *J. Am. Chem. Soc.* **1985**, 107, 1358–1364.
- [67] T. Aida, M. Ishikawa, S. Inoue, *Macromolecules* **1986**, 19, 8–13.
- [68] J. H. Jung, M. Ree, T. Chang, *J. Polym. Sci. Part A* **1999**, 37, 3329–3336.
- [69] K. Kasuga, S. Nagao, T. Fukumoto, M. Handa, *Polyhedron* **1996**, 15, 69–72.
- [70] K. Shimasaki, T. Aida, S. Inoue, *Macromolecules* **1987**, 20, 3076–3080.
- [71] Y. Watanabe, T. Yasuda, T. Aida, S. Inoue, *Macromolecules* **1992**, 25, 1396–1400.
- [72] H. Sugimoto, H. Ohshima, S. Inoue, *J. Polym. Sci. Part A* **2003**, 41, 3549–3555.
- [73] X. B. Lu, X. J. Feng, R. He, *Appl. Catal. A* **2002**, 234, 25–33.
- [74] X. B. Lu, R. He, C. X. Bai, *J. Mol. Catal. A* **2002**, 186, 1–11.
- [75] D. J. Darensbourg, E. L. Maynard, M. W. Holtcamp, K. K. Klausmeyer, J. H. Reibenspies, *Inorg. Chem.* **1996**, 35, 2682–2684.
- [76] W. Kuran, T. Listos, M. Abramczyk, A. Dawidek, *J. Macromol. Sci. Pure Appl. Chem.* **1998**, 35, 427–437.
- [77] T. Sarbu, E. J. Beckman, *Macromolecules* **1999**, 32, 6904–6912.
- [78] T. Sarbu, T. J. Styranec, E. J. Beckman, *Ind. Eng. Chem. Res.* **2000**, 39, 4678–4683.
- [79] W. J. Kruper, D. V. Dellar, *J. Org. Chem.* **1995**, 60, 725–727.
- [80] W. J. Kruper, D. Dellar, US Patent 4,663,467, **1987** [*Chem. Abstr.* **1987**, 107, 98598b].
- [81] S. Mang, A. I. Cooper, M. E. Colclough, N. Chauhan, A. B. Holmes, *Macromolecules* **2000**, 33, 303–308.
- [82] A. B. Holmes, S. A. Mang (Secretary of State for Defence, UK; Qinetiq Ltd.), Brit. UK Pat. Appl. 2352449, **2001** [*Chem. Abstr.* **2001**, 134, 237964].

- [83] L. M. Stamp, S. A. Mang, A. B. Holmes, K. A. Knights, Y. R. de Miguel, I. F. McConvey, *Chem. Commun.* **2001**, 2502–2503.
- [84] For asymmetric ring-opening of epoxides using Cr or Co salen complexes, see the following and references therein: a) E. N. Jacobsen, *Acc. Chem. Res.* **2000**, *33*, 421–431; b) J. M. Ready, E. N. Jacobsen, *Angew. Chem.* **2002**, *114*, 1374–1377; *Angew. Chem. Int. Ed.* **2002**, *41*, 1374–1377; c) S. E. Schaus, B. D. Brandes, J. F. Larrow, M. Tokunaga, B. Hansen, A. E. Gould, M. E. Furrow, E. N. Jacobsen, *J. Am. Chem. Soc.* **2002**, *124*, 1307–1315; d) J. M. Ready, E. N. Jacobsen, *J. Am. Chem. Soc.* **2001**, *123*, 2687–2688; e) R. G. Konsler, J. Karl, E. N. Jacobsen, *J. Am. Chem. Soc.* **1998**, *120*, 10780–10781; f) K. B. Hansen, J. L. Leighton, E. N. Jacobsen, *J. Am. Chem. Soc.* **1996**, *118*, 10924–10925.
- [85] E. N. Jacobsen, M. Tokunaga, J. F. Larrow, PCT Int. Appl. WO 00/09463, **2000**.
- [86] R. L. Paddock, S. T. Nguyen, *J. Am. Chem. Soc.* **2001**, *123*, 11498–11499.
- [87] D. J. Darensbourg, J. C. Yarbrough, *J. Am. Chem. Soc.* **2002**, *124*, 6335–6342.
- [88] D. J. Darensbourg, J. L. Rodgers, C. C. Fang, *Inorg. Chem.* **2003**, *42*, 4498–4500.
- [89] D. J. Darensbourg, J. C. Yarbrough, C. Ortiz, C. C. Fang, *J. Am. Chem. Soc.* **2003**, *125*, 7586–7591.
- [90] R. Eberhardt, M. Allmendinger, B. Rieger, *Macromol. Rapid Commun.* **2003**, *24*, 194–196.
- [91] K. Soga, K. Uenishi, S. Ikeda, *J. Polym. Sci. Polym. Sci. Ed.* **1979**, *17*, 415–423.
- [92] Y. M. Shen, W. L. Duan, M. Shi, *J. Org. Chem.* **2003**, *68*, 1559–1562.
- [93] Z. Q. Qin, C. M. Thomas, S. Lee, G. W. Coates, *Angew. Chem.* **2003**, *115*, 5642–5645; *Angew. Chem. Int. Ed.* **2003**, *42*, 5484–5487.
- [94] R. Paddock, Y. Hiyama, J. McKay, S. Nguyen, *Tetrahedron Lett.* **2004**, *45*, 2023–2026.
- [95] X. B. Lu, B. Liang, Y. J. Zhang, Y. Z. Tian, Y. M. Wang, C. X. Bai, H. Wang, R. Zhang, *J. Am. Chem. Soc.* **2004**, *126*, 3732–3733.
- [96] X. H. Chen, Z. Q. Shen, Y. F. Zhang, *Macromolecules* **1991**, *24*, 5305–5308.
- [97] Z. Q. Shen, X. H. Chen, Y. F. Zhang, *Macromol. Chem. Phys.* **1994**, *195*, 2003–2011.
- [98] J. T. Guo, X. Y. Wang, Y. S. Xu, J. W. Sun, *J. Appl. Polym. Sci.* **2003**, *87*, 2356–2359.
- [99] C. S. Tan, T. J. Hsu, *Macromolecules* **1997**, *30*, 3147–3150.
- [100] T. J. Hsu, C. S. Tan, *Polymer* **2001**, *42*, 5143–5150.
- [101] Z. Quan, X. H. Wang, X. J. Zhao, F. S. Wang, *Polymer* **2003**, *44*, 5605–5610.
- [102] B. Y. Liu, X. J. Zhao, X. H. Wang, F. S. Wang, *J. Polym. Sci. Part A* **2001**, *39*, 2751–2754.
- [103] A. Rokicki (Air Products and Chemicals, Inc., and Arco Chemical Co.), US Pat. App., **1990**, US 4,943,677 [*Chem. Abstr.* **1990**, *113*, 192136].
- [104] S. A. Motika, T. L. Pickering, A. Rokicki, B. K. Stein (Air Products and Chemicals, Inc., Arco Chemical Co., and Mitsui Petrochemical Industries Ltd.), US Pat. App., **1991**, US Patent 5,026,676 [*Chem. Abstr.* **1991**, *115*, 93209].
- [105] H. N. Sun, (Arco Chemical Co.), US Pat. App., **1988**, US Patent 4,783,445 [*Chem. Abstr.* **1988**, *110*, 135920].
- [106] H. Kawachi, S. Minami, J. Armor, A. Rokicki, B. Stein, US Pat. App., **1991**, US Patent 4,981,948 [*Chem. Abstr.* **1990**, *113*, 24673].
- [107] M. Ree, J. Y. Bae, J. H. Jung, T. J. Shin, *Korea Polym. J.* **1999**, *7*, 333–349.
- [108] M. Ree, J. Y. Bae, J. H. Jung, T. J. Shin, *J. Polym. Sci. Part A* **1999**, *37*, 1863–1876.
- [109] M. Ree, J. Y. Bae, J. H. Jung, T. J. Shin, Y. T. Hwang, T. Chang, *Polym. Eng. Sci.* **2000**, *40*, 1542–1552.
- [110] D. J. Darensbourg, N. W. Stafford, T. Katsurao, *J. Mol. Catal. A* **1995**, *104*, L1–L4.
- [111] Y. Z. Meng, L. C. Du, S. C. Tiong, Q. Zhu, A. S. Hay, *J. Polym. Sci. Part A* **2002**, *40*, 3579–3591.
- [112] Y. Q. Zheng, J. L. Lin, H. L. Zhang, *Z. Kristallogr. New Cryst. Struct.* **2000**, *215*, 535–536.
- [113] R. Eberhardt, M. Allmendinger, M. Zintl, C. Troll, G. A. Luinstra, B. Rieger, *Macromol. Chem. Phys.* **2004**, *205*, 42–47.
- [114] Y. T. Hwang, J. H. Jung, M. Ree, H. S. Kim, *Macromolecules* **2003**, *36*, 8210–8212.
- [115] L. B. Chen, H. S. Chen, J. Lin, *J. Macromol. Sci. Chem.* **1987**, *24*, 253–260.
- [116] T. Listos, W. Kuran, R. Siwiec, *J. Macromol. Sci. Pure Appl. Chem.* **1995**, *32*, 393–403.
- [117] M. S. Super, E. Berluche, C. Costello, E. J. Beckman, *Macromolecules* **1997**, *30*, 368–372.
- [118] D. J. Darensbourg, M. S. Zimmer, *Macromolecules* **1999**, *32*, 2137–2140.
- [119] W. J. Kruper, D. J. Smart (The Dow Chemical Co.), US Patent 4,500,704, **1983**.
- [120] L. B. Chen, *Makromol. Chem. Macromol. Symp.* **1992**, *59*, 75–82.
- [121] D. J. Darensbourg, M. J. Adams, J. C. Yarbrough, *Inorg. Chem.* **2001**, *40*, 6543–6544.
- [122] D. J. Darensbourg, M. J. Adams, J. C. Yarbrough, A. L. Phelps, *Inorg. Chem.* **2003**, *42*, 7809–7818.
- [123] D. J. Darensbourg, M. W. Holtcamp, *Macromolecules* **1995**, *28*, 7577–7579.
- [124] D. J. Darensbourg, M. W. Holtcamp, G. E. Struck, M. S. Zimmer, S. A. Niezgoda, P. Rainey, J. B. Robertson, J. D. Draper, J. H. Reibenspies, *J. Am. Chem. Soc.* **1999**, *121*, 107–116.
- [125] D. J. Darensbourg, J. R. Wildeson, J. C. Yarbrough, J. H. Reibenspies, *J. Am. Chem. Soc.* **2000**, *122*, 12487–12496.
- [126] D. J. Darensbourg, J. R. Wildeson, S. J. Lewis, J. C. Yarbrough, *J. Am. Chem. Soc.* **2002**, *124*, 7075–7083.
- [127] D. J. Darensbourg, M. S. Zimmer, P. Rainey, D. L. Larkins, *Inorg. Chem.* **2000**, *39*, 1578–1585.
- [128] M. B. Dinger, M. J. Scott, *Inorg. Chem.* **2001**, *40*, 1029–1036.
- [129] D. J. Darensbourg, M. W. Holtcamp, B. Khandelwal, K. K. Klausmeyer, J. H. Reibenspies, *J. Am. Chem. Soc.* **1995**, *117*, 538–539.
- [130] D. J. Darensbourg, S. A. Niezgoda, M. W. Holtcamp, J. D. Draper, J. H. Reibenspies, *Inorg. Chem.* **1997**, *36*, 2426–2432.
- [131] S. C. Goel, M. Y. Chiang, W. E. Buhro, *J. Am. Chem. Soc.* **1990**, *112*, 6724–6725.
- [132] D. J. Darensbourg, S. A. Niezgoda, J. H. Reibenspies, J. D. Draper, *Inorg. Chem.* **1997**, *36*, 5686–5688.
- [133] D. J. Darensbourg, S. A. Niezgoda, J. D. Draper, J. H. Reibenspies, *J. Am. Chem. Soc.* **1998**, *120*, 4690–4698.
- [134] D. J. Darensbourg, J. R. Wildeson, J. C. Yarbrough, *Inorg. Chem.* **2002**, *41*, 973–980.
- [135] D. J. Darensbourg, P. Rainey, J. C. Yarbrough, *Inorg. Chem.* **2001**, *40*, 986–993.
- [136] D. J. Darensbourg, J. R. Wildeson, J. C. Yarbrough, *Organometallics* **2001**, *20*, 4413–4417.
- [137] M. H. Chisholm, J. C. Gallucci, H. H. Zhen, J. C. Huffman, *Inorg. Chem.* **2001**, *40*, 5051–5054.
- [138] O. Hampel, C. Rode, D. Walther, R. Beckert, H. Görls, *Z. Naturforsch. B* **2002**, *57*, 946–956.
- [139] H. S. Kim, J. J. Kim, B. G. Lee, O. S. Jung, H. G. Jang, S. O. Kang, *Angew. Chem.* **2000**, *112*, 4262–4264; *Angew. Chem. Int. Ed.* **2000**, *39*, 4096–4098.
- [140] H. S. Kim, J. J. Kim, S. D. Lee, M. S. Lah, D. Moon, H. G. Jang, *Chem. Eur. J.* **2003**, *9*, 678–686.

- [141] D. J. Darensbourg, S. J. Lewis, J. L. Rodgers, J. C. Yarbrough, *Inorg. Chem.* **2003**, 42, 581–589.
- [142] I. Kim, S. M. Kim, C. S. Ha, D. W. Park, *Macromol. Rapid Commun.* **2004**, 25, 888–893.
- [143] M. Cheng, E. B. Lobkovsky, G. W. Coates, *J. Am. Chem. Soc.* **1998**, 120, 11018–11019.
- [144] G. W. Coates, M. Cheng, E. B. Lobkovsky, *Abstr. Pap. Am. Chem. Soc.* **1999**, 217, 077-PMSE.
- [145] M. Cheng, N. A. Darling, E. B. Lobkovsky, G. W. Coates, *Chem. Commun.* **2000**, 2007–2008.
- [146] M. Cheng, D. R. Moore, J. J. Reczek, B. M. Chamberlain, E. B. Lobkovsky, G. W. Coates, *J. Am. Chem. Soc.* **2001**, 123, 8738–8749.
- [147] G. W. Coates, M. Cheng, US Pat. Appl., **2000**, US 6,133,402 [*Chem. Abstr.* **2000**, 132, 152332].
- [148] M. Cheng, Ph.D. Thesis, Cornell University, August **2000**.
- [149] D. R. Moore, M. Cheng, E. B. Lobkovsky, G. W. Coates, *Angew. Chem.* **2002**, 114, 2711–2714; *Angew. Chem. Int. Ed.* **2002**, 41, 2599–2602.
- [150] S. D. Allen, D. R. Moore, E. B. Lobkovsky, G. W. Coates, *J. Am. Chem. Soc.* **2002**, 124, 14284–14285.
- [151] D. R. Moore, M. Cheng, E. B. Lobkovsky, G. W. Coates, *J. Am. Chem. Soc.* **2003**, 125, 11911–11924.
- [152] D. R. Moore, Ph.D. Thesis, Cornell University, May **2003**.
- [153] S. D. Allen, D. R. Moore, E. B. Lobkovsky, G. W. Coates, *J. Organomet. Chem.* **2003**, 683, 137–148.
- [154] M. Cheng, A. B. Attygalle, E. B. Lobkovsky, G. W. Coates, *J. Am. Chem. Soc.* **1999**, 121, 11583–11584.
- [155] B. M. Chamberlain, M. Cheng, D. R. Moore, T. M. Ovitt, E. B. Lobkovsky, G. W. Coates, *J. Am. Chem. Soc.* **2001**, 123, 3229–3238.
- [156] L. R. Rieth, D. R. Moore, E. B. Lobkovsky, G. W. Coates, *J. Am. Chem. Soc.* **2002**, 124, 15239–15248.
- [157] M. H. Chisholm, J. C. Huffman, K. Phomphrai, *J. Chem. Soc. Dalton Trans.* **2001**, 222–224.
- [158] M. H. Chisholm, J. Gallucci, K. Phomphrai, *Inorg. Chem.* **2002**, 41, 2785–2794.
- [159] R. Eberhardt, M. Allmendinger, G. A. Luinstra, B. Rieger, *Organometallics* **2003**, 22, 211–214.
- [160] M. Zhang, L. B. Chen, B. Liu, Z. Yan, G. Qin, Z. Li, *Polym. Bull.* **2001**, 47, 255–260.
- [161] M. Zhang, L. B. Chen, G. Qin, Z. M. Li, *Acta Polym. Sin.* **2001**, 422–424.
- [162] M. Zhang, L. B. Chen, G. Qin, B. Liu, Z. Yan, Z. Li, *J. Appl. Polym. Sci.* **2003**, 87, 1123–1128.
- [163] K. Yu, C. W. Jones, *Organometallics* **2003**, 22, 2571–2580.
- [164] W. J. van Meerendonk, R. Duchateau, C. E. Koning, G. M. Gruter, *Macromol. Rapid Commun.* **2004**, 25, 382–386.
- [165] Z. W. Liu, M. Torrent, K. Morokuma, *Organometallics* **2002**, 21, 1056–1071.
- [166] M. H. Chisholm, D. Navarro-Llobet, *Macromolecules* **2002**, 35, 2389–2392.
- [167] M. H. Chisholm, D. Navarro-Llobet, Z. Zhou, *Macromolecules* **2002**, 35, 6494–6504.
- [168] S. D. Allen, G. W. Coates, unpublished results.
- [169] K. Nakano, N. Kosaka, T. Hiyama, K. Nozaki, *Dalton Trans.* **2003**, 4039–4050.
- [170] D. M. Hodgson, A. R. Gibbs, G. P. Lee, *Tetrahedron* **1996**, 52, 14361–14384.
- [171] K. Nozaki, K. Nakano, T. Hiyama, *J. Am. Chem. Soc.* **1999**, 121, 11008–11009.
- [172] K. Tamao, T. Hiyama, Y. Hori (Takasago Perfumery Co., Ltd.), Jpn. Kokai Tokkyo Koho 2000256454, **2000** [*Chem. Abstr.* **2000**, 133, 223229].
- [173] K. Nakano, K. Nozaki, T. Hiyama, *Macromolecules* **2001**, 34, 6325–6332.
- [174] K. Nakano, K. Nozaki, T. Hiyama, *J. Am. Chem. Soc.* **2003**, 125, 5501–5510.

Communications



Contrary to what was previously believed, water molecules do not adsorb intact on the surfaces of zinc oxide, but dissociate by an autocatalytic process and form a complex superstructure consisting of intact water molecules and hydroxy species. For more details, see the Communication by B. Meyer, C. Wöll et al. on the following pages.

Partial Dissociation of Water Leads to Stable Superstructures on the Surface of Zinc Oxide**

Bernd Meyer,* Dominik Marx, Olga Dulub, Ulrike Diebold, Martin Kunat, Deler Langenberg, and Christof Wöll*

Understanding wet surfaces and water/solid interfaces is of crucial importance in such diverse fields as corrosion, catalysis, mineralogy, and geology. For H_2O , the delicate interplay between chemical bonding, van der Waals forces, and hydrogen bonding gives rise to complex phenomena such as complete dissociation, partial dissociation at defects, multilayer formation, and wetting.^[1] Recently, an intriguing intermediate scenario was advanced, in which the interaction between the water molecules results in a partial dissociation of water on perfect surfaces, leading to superlattices with long-range order.^[2–5] In view of possible failures of common theoretical approaches and severe experimental difficulties^[5] this proposal has become the subject of a highly controversial debate.^[5–9] For a given surface a consistent picture can only be obtained by using a broad array of experimental and computational tools in concert. Applying such a strategy, we unambiguously demonstrate that water forms a simple, unusually stable two-dimensional superstructure on defect-free zinc oxide surfaces. Diffraction (He-atom scattering (HAS), low-energy electron diffraction (LEED)), real-space (scanning tunneling microscopy (STM)), and thermodynamic (He thermal desorption spectroscopy (He-TDS)) data show that water forms a (2×1) superstructure with long-range order that exists up to temperatures close to the boiling point of water. Car–Parrinello *ab initio* simulations^[10] reveal a superlattice in which every second water molecule is dissociated. The unusual thermal stability of this superstructure is a result of a favorable “key–lock” type structural arrangement in conjunction with hydrogen bonding. The computed struc-

ture and binding energy are in excellent agreement with those found in the experiment.

Zinc oxide is a material for which significant progress in understanding its surface properties was achieved recently,^[11–17] stimulated by its importance for a number of applications ranging from cosmetics and medicine to paints and heterogeneous catalysis. The nonpolar ZnO ($10\bar{1}0$) surface chosen for the present study is, in contrast to its polar counterparts,^[13,16] electrostatically stable and as such now well understood.^[12] Briefly, this Wurtzite-type surface consists of layers containing slightly tilted ZnO “dimers”, which are formed by three-fold coordinated Zn and O ions. These ZnO dimers, in turn, assemble to form characteristic rows separated by trenches (Figure 1). For the adsorption of

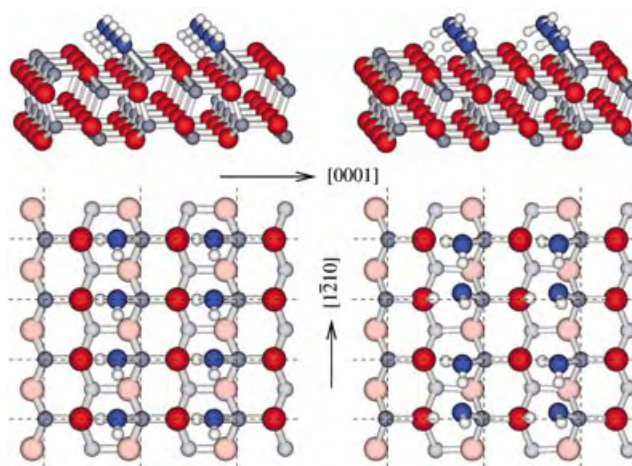


Figure 1. Side and top view of the atomic structure of the molecular adsorbed water monolayer with (1×1) symmetry (left) and the optimized half-dissociated $\text{H}_2\text{O}/\text{ZnO}(10\bar{1}0)$ adsorption geometry (right). The surface unit cells are shown by dashed lines. Zn, O, and H atoms are represented by grey, red, and white spheres, respectively, the O atoms of the water molecules are in blue. In the top views, the atoms in the second surface layer are indicated by lighter colors.

water on this surface one would expect that the oxygen atoms of the water molecules bind to the coordinatively unsaturated Zn ions on the surface. In a previous photoelectron spectroscopy study^[18] it was indeed concluded that H_2O chemisorbs at the Zn sites of the $\text{ZnO}(10\bar{1}0)$ surface. Since the distance between the Zn sites is fairly large (3.25 \AA versus 2.78 \AA between H_2O molecules in ice I_h), one would predict the formation of a simple water (1×1) monolayer.

In contrast to this prediction, we find that water on such a ZnO surface forms an ordered superstructure with a (2×1) periodicity. The He atom angular distributions (Figure 2) as well as LEED data clearly show sharp and well-defined half-order diffraction peaks. Also high-resolution STM measurements revealed a (2×1) periodicity of the adlayer. These findings effectively rule out that water is adsorbed on the $\text{ZnO}(10\bar{1}0)$ surface as a full monolayer of equivalent H_2O molecules as assumed previously. A (2×1) structure would come about if water would only occupy every other Zn site, with a total coverage of half a monolayer. If the water molecules were separated by two lattice constants, no hydro-

[*] Dr. B. Meyer, Prof. Dr. D. Marx
Lehrstuhl für Theoretische Chemie
Ruhr-Universität Bochum
44780 Bochum (Germany)
Fax: (+49) 234-32-14045
E-mail: bernd.meyer@theochem.ruhr-uni-bochum.de

Dr. M. Kunat, Dipl.-Chem. D. Langenberg, Prof. Dr. C. Wöll
Lehrstuhl für Physikalische Chemie I
Ruhr-Universität Bochum
44780 Bochum (Germany)
Fax: (+49) 234-32-14182
E-mail: woell@pc.ruhr-uni-bochum.de

Dr. O. Dulub, Prof. U. Diebold
Department of Physics
Tulane University
New Orleans, LA 70118 (USA)

[**] We thank Prof. Volker Staemmler for discussions and for carrying out the coupled-cluster reference calculations on the water dimers. This work was supported by the DFG (SFB 558), FCI, NSF (CHE-010908), and NASA.

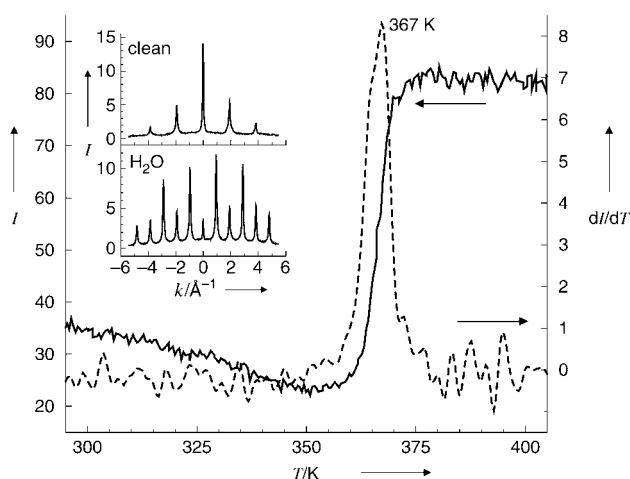


Figure 2. He-atom specular reflectivity of a ZnO(10 $\bar{1}$ 0) surface saturated with water at a temperature of 280 K (solid line) recorded for a heating rate of 1 K s $^{-1}$. The dashed line shows the corresponding derivative, revealing a desorption maximum at 367 K. Inset: He-atom diffraction patterns for the clean (top) and water-saturated (bottom) ZnO(10 $\bar{1}$ 0) surface recorded along the [01 $\bar{1}$ 0] azimuth. The (2 \times 1) periodicity of the water adlayer is clearly revealed by the prominent half-order diffraction peaks.

gen bonds between the water molecules would be present. However, the STM measurements show that for low water coverages the adsorbates form ordered two-dimensional islands (Figure 3), which implies a strong lateral attraction between adsorbed species. In addition, a quantitative determination of the H₂O coverage using X-ray photoelectron spectroscopy (XPS) shows that, at full coverage, the surface

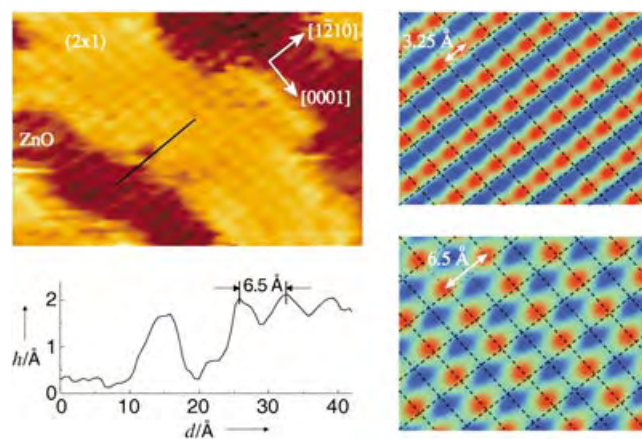


Figure 3. Left: STM image of a ZnO(10 $\bar{1}$ 0) surface after dosing 1 Langmuir of water at room temperature (tunneling conditions: +1.6 V sample bias and 4.7 nA tunneling current). The water molecules form well-ordered two-dimensional islands with a (2 \times 1) periodicity (bright spots) on the ZnO substrate (faint rows). The solid line shows the position where the line profile was taken. Right: Simulated STM images for the (hypothetical) molecular water monolayer with (1 \times 1) symmetry (top) and the half-dissociated H₂O/ZnO(10 $\bar{1}$ 0) structure (bottom). The height of the tip above the surface increases from blue through green to red. Bands in the energy range of 1 eV above the band gap are taken into account, mimicking positive sample bias and tunneling into the conduction band.

contains one H₂O molecule per surface Zn ion (see Experimental Section), so that a (2 \times 1) structure caused by only every second Zn site being occupied can be ruled out.

Important additional information about the adsorption of water can be gained from the binding energy of the molecules on the surface. The reliable determination of this quantity on metal oxide surfaces is, however, generally hampered by the presence of defects. In fact, most controversies on the question whether water adsorbs in a molecular form or dissociatively on a perfect surface stem from the problem that water may dissociate at defect sites, in particular at oxygen vacancies, which contributes to the overall signal.^[1] To rule out contributions of defects, a technique tailored to studying adsorbates on well-defined solid substrates was employed, namely the scattering of thermal energy He atoms. When monitoring the reflectivity of the ZnO(10 $\bar{1}$ 0) surface for thermal energy He atoms as a function of surface temperature (He-TDS) the desorption from perfect areas can be studied exclusively, allowing a precise determination of the adsorbate binding energies.^[13] He-TDS has been used previously to detect the desorption of water from oxide surfaces such as MgO^[19,20] or of CO and H₂ from ZnO surfaces.^[13,21] The He-TDS data (Figure 2) reveal a sharp, well-defined desorption maximum close to the boiling point of water at a temperature of 367 K. This corresponds to a binding energy of 1.02 eV, in excellent agreement with a value reported previously.^[18] This desorption temperature is astonishingly high. In general, such high desorption temperatures were only observed for a few other metal oxide surfaces for which it is known that water dissociates upon adsorption, for example, the Cr₂O₃ (0001)^[22] and the (2 \times 1) α -Fe₂O₃(01 $\bar{1}$ 2) surface.^[23] It therefore appears to be likely that also on this ZnO surface H₂O dissociates, hydroxylating a substrate O atom and adding an OH species on top of a Zn–substrate atom. Such a dissociation may in fact lead to a (2 \times 1) structure. Interestingly, we observed the formation of the (2 \times 1) phase already at temperatures as low as 200 K, a fact which would imply a very low activation energy for dissociation.

The precise value for the binding energy of H₂O adsorbed on defect-free regions of the ZnO(10 $\bar{1}$ 0) surface (the coherence length in the He-TDS measurement was of the order of 150 Å) opens the pathway for a *direct* comparison to and validation of theoretical calculations, which then in turn will provide the basis to rationalize the different experimental findings. To this end density functional theory (DFT) calculations were carried out within a periodic slab setup using six to eight ZnO layers. Special care was taken to electrostatically decouple the slabs to suppress artificial interactions.^[24] However, applying DFT to subtle molecule/surface interactions is often questionable in view of possible deficiencies for describing hydrogen bonding and van der Waals interactions. Thus, the gradient-corrected Perdew, Burke, and Ernzerhof (PBE) functional used here in conjunction with ultrasoft pseudopotentials and a 25 Rydberg plane wave cutoff (see ref. [12] for further details) was thoroughly tested for the system of interest. It is well known that the PBE functional describes very accurately the equilibrium structure and binding energy of water in isolated dimers and ice *I_h*.^[4,26] However, to probe the reliability of PBE

for water separations and orientations that are relevant here, we have calculated the binding energy of nearest and next-nearest water pairs as they appear in the undissociated (1×1) water monolayer on the $\text{ZnO}(10\bar{1}0)$ surface (see below). For these pairs with O–O separations of 3.25 and 5.21 Å, dimer binding energies of 0.085 and 0.011 eV, respectively, were found. This is in astonishing agreement with the results of 0.085 and 0.016 eV of very accurate coupled cluster-type (MC-CEPA^[25]) calculations. A similar accuracy was also previously demonstrated to hold for weakly bound molecules and adatoms on small ZnO clusters.^[13,14,27] Finally, the structure of bulk ZnO including its low-index surfaces has been calculated reliably within the described DFT/PBE setup.^[12] Based on all these gauges, it can be concluded that the PBE functional should capture the relevant interactions.

The adsorption properties of water on the $\text{ZnO}(10\bar{1}0)$ surface was studied for various coverages starting from a full monolayer and reducing to 1/2, 1/4, and 1/6 of a monolayer. In a first set of calculations, (1×1), (2×1), (2×2), and (3×2) surface unit cells containing one water molecule were used. This implies that the water molecules are kept equivalent by imposing translational symmetry. Under this constraint, only molecular adsorption of water is found for all coverages with a very similar orientation of the molecules (Figure 1). Dissociative adsorption, which may have been expected from the experimentally observed high desorption temperature, is not stable within this constraint. At a coverage of $1/4$ and $1/6$ monolayer the H_2O molecules basically do not interact, and the binding energy is 0.94 eV per molecule. It increases to 0.97 and 1.03 eV at half and full coverage, respectively. Despite the molecular adsorption, the binding energies are large and in good general agreement with the experimental value. This unexpectedly strong binding is due to a “key–lock” type interaction between the water molecules and the ZnO surface. The water molecules are stabilized by three different types of attractive interactions to both the substrate and neighboring adsorbate molecules. 1) The O atoms of the water molecules occupy the O sites of a hypothetical next ZnO layer on the $\text{ZnO}(10\bar{1}0)$ surface so that the surface Zn ions regain their four-fold tetrahedral coordination as in the underlying bulk, which leads to a strong Zn–O and thus ZnO/ H_2O bonding. 2) One of the H atoms forms a hydrogen bond across the ZnO trench of the surface to a neighboring substrate O atom. 3) In the case of a monolayer coverage, a water–water hydrogen bond to a neighboring adwater is formed by the second H atom. Thus, the full monolayer water film is significantly more stable than the half monolayer, in agreement with the XPS and STM data.

Although the key–lock configuration of a full monolayer of molecular water is a low-energy structure, it does not exhibit the (2×1) symmetry observed experimentally. Thus, in a second set of calculations, we explored the possibility that the (2×1) structure appears because of differently oriented water molecules. Two water molecules were randomly displaced in a (2×1) surface unit cell and a structural relaxation was performed. In all cases the adsorbed water molecules moved back toward the (1×1) monolayer structure and none of the modifications yielded an energy per water molecule lower than that obtained for the (1×1) coverage.

This picture changed when we explicitly considered the dynamics of the water molecules in full ab initio Car–Parrinello molecular dynamics (CPMD) simulations.^[10] In this approach, the system can evolve to a more stable structure, if there is any, without much bias. We set up slabs with (3×2) and (4×2) surface unit cells containing six and eight water molecules, respectively. Starting from the fully relaxed water monolayer structure with (1×1) symmetry, spontaneous dissociation of a *subset* of water molecules was observed at a simulation temperature of 300 K. After the initial dissociation the structures were stable and no further proton transfers occurred. Since the dissociation starts immediately after the beginning of the CPMD simulations, the activation energy has to be very low, which explains why the (2×1) phase already appears at temperatures below 200 K in the experiment.

Upon further structural optimization, the most stable structure turned out to be a configuration in which every second water molecule is dissociated, leading to a (2×1) superstructure (Figure 1). Interestingly, the undissociated water molecules remain in the stabilizing key–lock position akin to the molecular (1×1) structure described above. The molecules tilt a bit more toward the surface and thereby strengthen the hydrogen bond to their neighboring molecules. In every second water molecule one OH bond is cleaved and the H atom is transferred to a substrate O atom. Thus, two hydroxy groups are formed, one built from an adwater O atom and the second one originating from a substrate O atom. For this half-dissociated (2×1) structure, the overall binding energy per H_2O molecule is found to be slightly, but significantly, increased with regard to that of the molecular (1×1) structure (from 1.03 to 1.13 eV, respectively). This is one of the highest binding energies for water on structurally well-defined solid substrates.^[1] It is noteworthy that the interaction between the water molecules themselves “catalyzes” the dissociation reaction. As pointed out above, isolated water molecules do not dissociate on the $\text{ZnO}(10\bar{1}0)$ surface. However, calculations show that putting a second water molecule at a neighboring lattice site is already sufficient to trigger the dissociation. Between the two water molecules a hydrogen bond is formed that weakens the already activated OH bond across the ZnO trenches in the acceptor molecule. The molecule becomes unstable and the proton is transferred to a substrate O atom without noticeable activation energy.

To investigate if the half-dissociated monolayer structure is consistent with the observations in the STM experiments, STM images for both, the half-dissociated (2×1) and the molecular monolayer (1×1) were calculated by using the Tersoff–Hamann approximation.^[28] The experimental STM image in Figure 3 was recorded with a positive sample bias voltage, that is, under conditions where electrons tunnel into the conduction band (i.e. the LUMO). Under these conditions, the clean $\text{ZnO}(10\bar{1}0)$ surface is characterized by faint stripes that are attributed to the ZnO dimers (see Figure 1). The bright spots in the (2×1) superstructure of the H_2O islands are in registry with these stripes. The theoretical STM images reveal easily distinguishable differences between the two different adsorbate structures (Figure 3). The pattern

stemming from the half-dissociated superstructure matches the experimental STM image, which is clearly not the case for the molecular adlayer. The bright features in the image of the partially dissociated water layer are due to the OH groups of the dissociated water molecules, with a contrast that is predominantly geometric in nature.

Based on this consistent evidence, it can be concluded convincingly that half of the water molecules on the fully covered perfect ZnO(10 $\bar{1}$ 0) surface self-dissociate resulting in a well-defined (2 \times 1) superlattice. This superstructure is characterized by long-range order and structural simplicity but in particular by an unusually large stability range extending from 200 K up to the boiling point of liquid water. Transcending the specific case, these findings imply that when ionic materials such as minerals come in contact with water the possibility of water auto-dissociation has *always* to be considered both in experiment and theory—without necessarily invoking defects! This is of particular relevance to heterogeneous catalysis so that a number of reactions, such as methanol synthesis on ZnO or Cu/ZnO in which water is a side product, have to be reanalyzed.

Experimental Section

The measurements were carried out with an ultrahigh vacuum (UHV) molecular beam system that was described in detail in reference [21]. The mixed terminated ZnO(10 $\bar{1}$ 0) substrates were oriented to within 0.2° and polished mechanically. After installation in the UHV chamber the samples were first cleaned by cycles of Ar⁺ sputtering (800 V, \approx 1 μ A, 4–12 h, T = 650 K). After about 20 preparation cycles the XP spectra revealed contamination levels of less than 0.05 ML for carbon-containing species, and the surfaces exhibited (1 \times 1) diffraction peaks in HAS and LEED. The surface was exposed to water either by backfilling the UHV chamber using a leak valve or by dosing water through a capillary that ended about 5 cm in front of the ZnO substrate.

The STM experiments were carried out in a separate UHV chamber equipped with low-energy He⁺-ion scattering, LEED, and an STM operating at room temperature. The sample was prepared by sputtering (1 keV Ar⁺, 30 min) and annealing (1000 K, 15 min) cycles. Water was dosed by backfilling the UHV chamber.

Coverage calibration was carried out by ratioing the O1s signal seen for the H₂O monolayer at 533.5 eV to that measured for a (2 \times 1) CO₂ adlayer (with each (2 \times 1) unit cell containing one CO₂ molecule) at the same energy. The intensity ratio O1s_{OH}/O1s_{CO₂} was consistent with the presence of three OH species and one CO₂ molecule per (2 \times 1) unit cell. The activation energy for desorption was determined by using the Redhead formula with the experimental heating rate of 1 K s^{−1} and assuming first-order desorption with a preexponential factor of 10¹³ \times 1 s^{−1}.

Received: August 18, 2004

Keywords: ab initio calculations · surfaces · water structure · zinc oxide

- [5] D. Menzel, *Science* **2002**, 295, 58–59; Correction: D. Menzel, *Science* **2002**, 296, 264.
- [6] S. Meng, L. F. Xu, E. G. Wang, S. W. Gao, *Phys. Rev. Lett.* **2002**, 89, 176104; comment by P. J. Feibelman, *Phys. Rev. Lett.* **2003**, 91, 059601; reply: S. Meng, L. F. Xu, E. G. Wang, S. W. Gao, *Phys. Rev. Lett.* **2003**, 91, 059602.
- [7] H. Ogasawara, B. Brena, D. Nordlund, M. Nyberg, A. Pelmen-schikov, L. G. M. Pettersson, A. Nilsson, *Phys. Rev. Lett.* **2002**, 89, 276102.
- [8] R. Ludwig, *Angew. Chem.* **2003**, 115, 3580–3582; *Angew. Chem. Int. Ed.* **2003**, 42, 3458–3460.
- [9] C. Clay, S. Haq, A. Hodgson, *Phys. Rev. Lett.* **2004**, 92, 046102.
- [10] D. Marx, J. Hutter in *Modern Methods and Algorithms of Quantum Chemistry* (Ed.: J. Grotendorst), pp. 301–449 (NIC, FZ Jülich), **2000**, see: www.theochem.rub.de/go/cprev.html; CPMD code: J. Hutter et al., see: www.cpmd.org.
- [11] A. Wander, F. Schedin, P. Steadman, A. Norris, R. McGrath, T. S. Turner, G. Thornton, N. M. Harrison, *Phys. Rev. Lett.* **2001**, 86, 3811–3814.
- [12] B. Meyer, D. Marx, *Phys. Rev. B* **2003**, 67, 035403; B. Meyer, D. Marx, *Phys. Rev. B* **2003**, 67, 039902(E).
- [13] V. Staemmler, K. Fink, B. Meyer, D. Marx, M. Kunat, U. Burghaus, S. Gil Girol, C. Wöll, *Phys. Rev. Lett.* **2003**, 90, 106102.
- [14] B. Meyer, D. Marx, *J. Phys. Condens. Matter* **2003**, 15, L89–L94.
- [15] B. Meyer, *Phys. Rev. B* **2004**, 69, 045416.
- [16] O. Dulub, U. Diebold, G. Kresse, *Phys. Rev. Lett.* **2003**, 90, 016102.
- [17] G. Kresse, O. Dulub, U. Diebold, *Phys. Rev. B* **2003**, 68, 245409.
- [18] G. Zwicker, K. Jacobi, *Surf. Sci.* **1983**, 131, 179.
- [19] D. Ferry, A. Glebov, V. Senz, J. Suzanne, J. P. Toennies, H. Weiss, *J. Chem. Phys.* **1996**, 105, 1697–1701.
- [20] D. Ferry, A. Glebov, V. Senz, J. Suzanne, J. P. Toennies, H. Weiss, *Surf. Sci.* **1997**, 377–379, 634–638.
- [21] T. Becker, S. Hövel, M. Kunat, C. Boas, U. Burghaus, C. Wöll, *Surf. Sci.* **2001**, 486, L502–L506; Erratum: T. Becker, S. Hövel, M. Kunat, C. Boas, U. Burghaus, C. Wöll, *Surf. Sci.* **2001**, 511, 463.
- [22] M. A. Henderson, S. A. Chambers, *Surf. Sci.* **2000**, 449, 135–150.
- [23] M. A. Henderson, S. A. Joyce, J. R. Rustad, *Surf. Sci.* **1998**, 417, 66–81.
- [24] B. Meyer, D. Vanderbilt, *Phys. Rev. B* **2001**, 63, 205426.
- [25] R. Fink, V. Staemmler, *Theor. Chim. Acta* **1993**, 87, 129.
- [26] D. R. Hamann, *Phys. Rev. B* **1997**, 55, R10157–R10160.
- [27] B. Meyer, D. Marx, *Phys. Rev. B* **2004**, 69, 235420.
- [28] J. Tersoff, D. R. Hamann, *Phys. Rev. B* **1985**, 31, 805–813.

[1] M. A. Henderson, *Surf. Sci. Rep.* **2002**, 46, 1–308.

[2] P. J. D. Lindan, N. M. Harrison, M. J. Gillan, *Phys. Rev. Lett.* **1998**, 80, 762–765.

[3] L. Giordano, J. Goniakowski, J. Suzanne, *Phys. Rev. Lett.* **1998**, 81, 1271–1273.

[4] P. J. Feibelman, *Science* **2002**, 295, 99–102.

Absolute Optical Cross Section of Individual Fluorescent Molecules**

Lars Kastrup and Stefan W. Hell*

Besides having revealed transitions masked in the bulk,^[1,2] optical spectroscopy of single molecules has enabled the observation of elementary molecular quantum events, such as the absorption and emission of a photon.^[3–6] Single photon transitions are quantified by a cross section that can be regarded as the photon capture area of a molecule. Therefore, absolute optical cross sections can readily be measured in the bulk from the decrease (by absorption) or the gain (by stimulated emission) of the number of photons in a beam.^[7] Unfortunately, this method is not applicable to individual molecules, because the resulting change in intensity is negligible. If the fluorescence quantum efficiency Q_{em} is known, the molecular absorption cross section can be calculated from the fluorescence emission.^[8] However, this method re-introduces the hallmark of ensemble averaging, because Q_{em} is known only from the bulk. As a result, the absolute photon capture area of a specific molecule has remained elusive.

Here we report on the measurement of absolute cross sections of stimulated emission at room temperature. No a priori information about the individual molecule is needed. In addition, we demonstrate the instant control of a molecule's excited state by light and thus, as a matter of fact, also the viability of pump–probe experiments^[9] with individual molecules at room temperature.

Molecular optical absorption usually takes place from the vibrationally relaxed ground state S_0 to a hot Franck–Condon state S_1^* of the first excited singlet state (Figure 1a). After vibrational relaxation, which occurs on a (sub)picosecond time scale, organic fluorophores emit within a few nanoseconds with a probability given by the fluorescence quantum yield. Alternatively, the $S_1 \rightarrow S_0$ transition can be enforced by light, that is by stimulated emission.^[10] Stimulated emission has been employed to probe the temporal evolution of the excited state in a pump–probe fashion, as well as to alter the fluorescence lifetime and anisotropy^[11,12] of organic fluorophores in solution. Furthermore, stimulated emission depletion (STED) of the excited state has been introduced in fluorescence microscopy^[13,14] to break the diffraction reso-

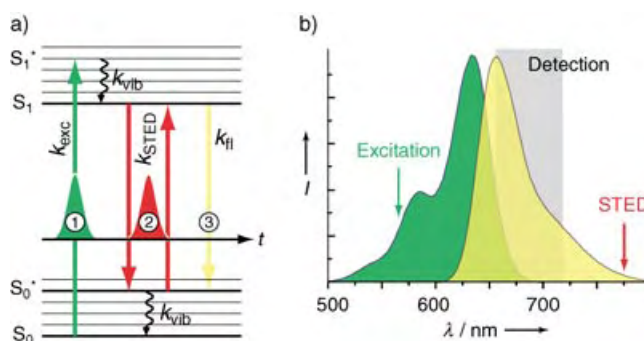
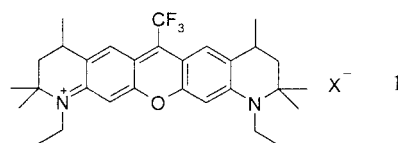


Figure 1. a) Jablonski diagram showing the transitions of the organic fluorophore involved: 1) excitation by the short-wavelength pulse, 2) stimulated emission and re-excitation by the STED pulse, and 3) fluorescence emission. The time axis indicates the succession of the pulses. b) Excitation and fluorescence spectrum of JA 26 showing the excitation and STED wavelengths, and detection regions.

lution barrier,^[15,16] but has recently also been used to measure cross sections in the bulk.^[17]

We attained single molecule sensitivity with a scanning confocal setup fed by two synchronized pulse trains: a first pulse at a wavelength of $\lambda = 565$ nm for excitation was followed by a red-shifted pulse at $\lambda = 778$ nm for STED, both adapted to the spectrum (Figure 1b) of the xanthene dye JA 26 (**1**). Efficient STED demands a STED pulse duration τ



of about 15 ps,^[13,15] because this is significantly shorter than the nanosecond lifetime of S_1 , but much longer than the sub-picosecond vibrational decay of S_0^* . Thus the $S_1 \leftrightarrow S_0^*$ system is effectively depleted.

Figure 2 illustrates the ability of the STED pulse to “switch off” single fluorescent molecules embedded in a poly(vinyl alcohol) film. The image was acquired with constant excitation intensity but with the STED beam intercepted at 250 Hz. The on- and off-periods of 4 ms were about three times shorter than the time span required for scanning the molecule through the focal spot along the x direction. As a result, the molecules appear as diffraction-limited fluorescence spots featuring dark, vertically (y) oriented stripes resulting from the on-times of the STED beam, during which the spontaneous emission is obviously suppressed. Importantly, fluorescence recovers with the interruption of the STED beam. Note that, besides STED, the image of individual molecules exhibits blinking and binary bleaching, as expected for individual molecules.^[18] Although depletion requires a much higher laser power than excitation (with pulse peak intensities of up to $1\text{--}2\text{ GW cm}^{-2}$), only a minor increase in photobleaching was observed during the action of the STED beam. In general, the dependence of the photobleaching rate on the STED intensity follows a higher

[*] L. Kastrup, Prof. S. W. Hell
Max Planck Institute for Biophysical Chemistry
Department of NanoBiophotonics
37077 Göttingen (Germany)
Fax: (+49) 551-201-1085
E-mail: shell@gwdg.de

[**] We thank Karl-Heinz Drexhage and Jutta Arden-Jacob (University of Siegen, Germany) for providing the dye JA 26. We gratefully acknowledge funding by the Volkswagen Foundation.

Supporting information for this article is available on the WWW under <http://www.angewandte.org> or from the author.

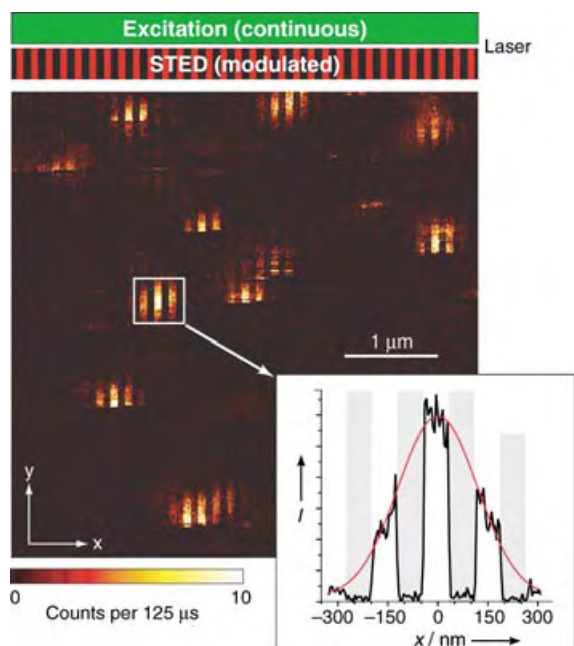


Figure 2. Stimulated emission of single JA 26 molecules. While scanning a $5 \times 5 \mu\text{m}^2$ area in the focal plane (xy) with continuous excitation, the STED beam was periodically interrupted as indicated by the red-black bar above the image. Synchronized with the x scan, stimulated emission is imprinted on the diffraction-limited fluorescence spot left by a molecule in the image: while the STED beam is effective, fluorescence is inhibited and, vice versa, fluorescence recovers within the time resolution of the measurement (i.e. the dwell time of a pixel of $125 \mu\text{s}$). This is highlighted in the inset, which displays the fluorescence intensity I of a selected molecule integrated in the y direction. The envelope of the fluorescence trace represents the spatial profile of the excitation spot along the x axis.

power law,^[19] that is the photobleaching increases strongly with the pulse peak intensity, but much less so if the power is elevated by extending the pulse duration.

If STED dominates over the other de-excitation channels, the normalized probability of a molecule to fluoresce after an excitation/STED pulse pair depends on the number of photons per unit area in the STED pulse and on the $S_1 \rightarrow S_0^*$ cross section σ_{xy} . Hence, measuring the fluorescence probability as a function of the STED laser power yields the $S_1 \rightarrow S_0^*$ cross section of a specific molecule in absolute terms. This evaluation relies on a three-level photokinetic model (Figure 1 a, levels drawn in bold) that applies once the molecule has arrived in the S_1 state. Starting at $t = 0$, the STED pulse acts with an intensity I_{STED} for the time span τ of about 15 ps. Besides the spontaneous and stimulated decay of S_1 , we also consider (re-)excitation by the STED pulse from S_0^* as well as the vibrational decay of the latter. Singlet-singlet absorption due to the STED pulse may, in principle, occur as well. However, since the subpicosecond decay of the higher singlet states is much shorter than τ (Kasha's rule), this mechanism is not expected to affect the efficiency of STED appreciably. Thus, our model is well described by two coupled differential equations. Under the assumption of a rectangular pulse shape, the solution to these equations is straightforward (see Supporting Information).

Further simplifications are obtained if one considers that the fluorescence rate $k_{\text{fl}} \approx (4 \text{ ns})^{-1}$ is much slower than the STED rate $k_{\text{STED}}(t) = \sigma_{\text{STED}} I_{\text{STED}}(t)$, which in turn is much slower than the vibrational relaxation $k_{\text{vib}} > (10^{12} \text{ s}^{-1})$, that is, $k_{\text{fl}} \ll k_{\text{STED}} \ll k_{\text{vib}}$. If these conditions are fulfilled, the level S_0^* remains virtually unpopulated. Moreover, the probability $P_1(I_{\text{STED}})$ of finding a molecule in S_1 after the STED pulse action is solely determined by the number of photons per pulse and unit area rather than by the intensity as a function of time. Hence, the pulse shape is insignificant. Under these conditions, the measured fluorescence follows a monoexponential decay [Eq. (1)]. Here, Δt denotes the integration time,

$$F(I_{\text{STED}}; \tau) = \Delta t Q_{\text{em}} Q_{\text{det}} P_1(0) \exp(-\sigma_{xy} I_{\text{STED}} \tau) \quad (1)$$

Q_{em} is the quantum efficiency of emission, and Q_{det} the detection sensitivity of the instrument. To determine *absolute* σ_{xy} values, Q_{em} and Q_{det} need not necessarily be known, since σ_{xy} is obtained from the simple ratio given in Equation (2).

$$\sigma_{xy} = \frac{1}{I_{\text{STED}} \tau} \ln \left[\frac{F(0; \tau)}{F(I_{\text{STED}}; \tau)} \right] \quad (2)$$

Higher precision is obtained by fitting the full decay with the exact analytical solution (see Supporting Information) that we actually pursued.

For each measurement, a single molecule was positioned in the overlapping foci of the two beams. Repetitive line scans across the molecule were performed while the STED beam was linearly ramped up from zero to a time-averaged focal power of $\bar{P}_{\text{STED}} = 3\text{--}10 \text{ mW}$ (Figure 3 a and b). After each power ramp, the STED beam was interrupted to verify the

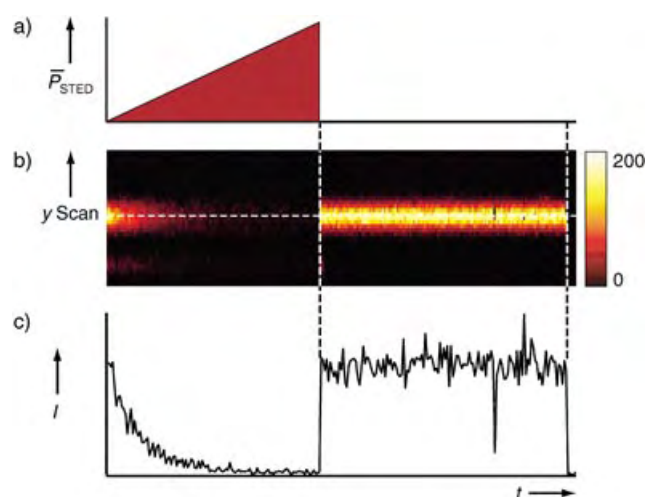


Figure 3. Measurement of saturated depletion of the excited state by stimulated emission of a single molecule. a) Sketch of the linear ramp of the average power \bar{P}_{STED} . b) Fluorescence of a single molecule that was repeatedly scanned through the focus in the y direction during the power ramp. Return to $\bar{P}_{\text{STED}} = 0$ leads to an instant recovery of the fluorescence intensity I , proving that the decrease in the signal was not due to irreversible photobleaching. c) Profile extracted from the center of gravity of the data shown in b), displaying the decrease and sudden onset of fluorescence intensity I as well as the final bleaching of the molecule.

recovery of the fluorescence. The fluorescence trace along the dotted line in Figure 3b is shown in Figure 3c, which exhibits a largely exponential decrease. A total of 65 traces on different molecules were acquired. Three representative traces are displayed in Figure 4a–c. Fitting with Equation (1)

Scaling with the ensemble emission spectrum (Figure 1b) or even better with the individual fluorescence spectrum of the molecule, yields the cross section for values other than at 778 nm. If the spectra are mirror symmetric, σ_{xy} allows one to extrapolate the cross section of absorption.^[20] This is interesting

because there is no purely analogous access to the absolute cross sections of absorption. If Q_{em} and Q_{det} are unknown, the absolute absorption cross sections must be extracted from the saturation of the excitation (see Supporting Information), which is heavily challenged by photobleaching.^[21]

In summary, we have demonstrated “instant fluorescence quenching and recovery” of a single molecule by light. The opportunity to repeatedly modify the probability of the same molecule to be in its excited state should disclose tangible new information. The values of the absolute optical cross sections of a molecular species have been given as a first example.

Recently, novel schemes were proposed to determine the full orientation of the molecular transition dipole moment in space. The synergistic combination with our method may finally also reveal the total radiative decay rate of each molecule in question. In conjunction with an excited state lifetime measurement by time-correlated single photon counting, this information could disclose the non-radiative rates as well, and could thus contribute to the full spectroscopic characterization of individual molecules at room temperature.

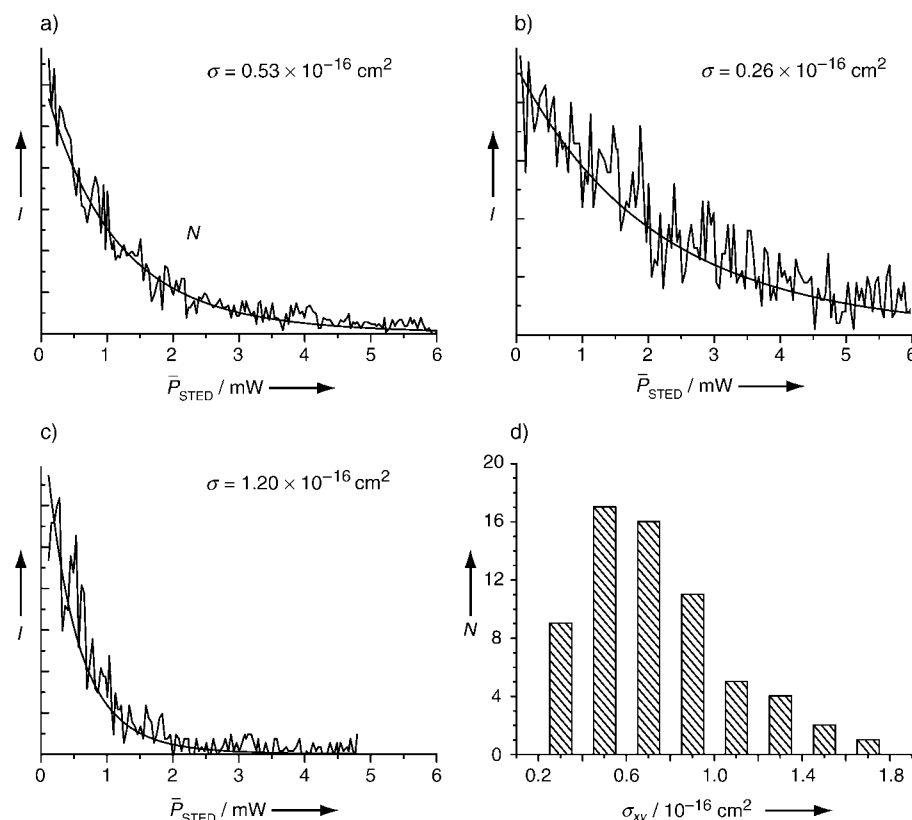


Figure 4. a–c) Typical fluorescence traces as a function of the average power \bar{P}_{STED} of the STED beam, which demonstrates saturated de-excitation. The curves fitted to the experiment yield the indicated cross sections. d) Histogram of 65 cross sections of individual JA 26 molecules in a PVA matrix. The largest values are attributed to molecules with transition dipole moments parallel to the focal plane. N = number of occurrences.

yields cross sections σ_{xy} of 0.44×10^{-16} , 0.23×10^{-16} , and $0.99 \times 10^{-16} \text{ cm}^2$, respectively, whereas application of the exact solution of the rate equations gives the values 0.53×10^{-16} , 0.26×10^{-16} , and $1.20 \times 10^{-16} \text{ cm}^2$. By varying the parameters entering our model, we estimated the total precision to be about 10%, which is at least comparable, if not superior, to that usually reached in the bulk.

For a molecule that includes an angle θ with the focal plane, only $\sigma_{xy} = \sigma \cos^2 \theta$ of the total cross section σ is effective in optical interactions. Figure 4d shows the σ_{xy} of all the molecules measured. The process of spin coating and arbitrary selection of the molecules is expected to introduce a certain bias in their orientational distribution. Nonetheless, the largest value $\sigma = 1.7 \times 10^{-16} \text{ cm}^2$ is an absolute lower limit for the total molecular cross section of JA 26. The molecular orientational distribution is equally required when absolute absorption cross sections are to be determined from ensemble measurements, but in most of these cases, a random distribution can safely be assumed.

Experimental Section

Excitation at $\lambda = 565 \text{ nm}$ of the dye JA 26 was accomplished by a frequency-doubled optical parametric oscillator (APE, Berlin, Germany) which was synchronously pumped by a femtosecond mode-locked titanium:sapphire laser (Coherent, Santa Clara, CA) operating at a pulse repetition rate of approximately 76 MHz. The fundamental mode of the latter was used for stimulated emission depletion at a wavelength of $\lambda = 778 \text{ nm}$. The laser power was adjusted with two liquid crystals (Cambridge Research & Instrumentation, Woburn, MA). The pulses of both lasers were stretched to 12 ps (excitation) and 15 ps (STED) with gratings and were temporally matched for maximal efficiency of STED. Quarterwave retardation plates ensured circular polarization of the beams which were coupled into a stage-scanning confocal microscope using dichroic beamsplitters (628dclpxr, 720drspxr, Chroma Technology, Rockingham, VT). The collected fluorescence was filtered by a bandpass filter (D680/60, Chroma Technology) and detected by a photon counting module (SPCM-AQR-13-FC, PerkinElmer, Canada). The samples were prepared by spin coating an aqueous solution of the dye JA 26 ($\sim 1 \text{ nM}$) containing 0.1% poly vinyl alcohol onto a cleaned glass coverslip and were purged with argon gas.

Received: July 16, 2004

Published online: November 19, 2004

Keywords: fluorescence spectroscopy · photophysics · single-molecule studies · stimulated emission

- [1] R. M. Dickson, A. B. Cubitt, R. Y. Tsien, W. E. Moerner, *Nature* **1997**, 388, 355.
- [2] M. Orrit, *J. Chem. Phys.* **2002**, 117, 10938.
- [3] W. E. Moerner, L. Kador, *Phys. Rev. Lett.* **1989**, 62, 2535.
- [4] M. Orrit, J. Bernard, *Phys. Rev. Lett.* **1990**, 65, 2716.
- [5] E. B. Shera, N. K. Seitzinger, L. M. Davis, R. A. Keller, S. A. Soper, *Chem. Phys. Lett.* **1990**, 174, 553.
- [6] T. Basché, W. E. Moerner, M. Orrit, U. P. Wild, *Single-Molecule Optical Detection, Imaging and Spectroscopy*, VCH, Weinheim, **1997**.
- [7] J. R. Lakowicz, *Principles of Fluorescence Spectroscopy*, Plenum, New York, **1983**.
- [8] M. F. Garcia-Parajo, G. M. J. Segers-Nolten, J.-A. Veerman, J. Greve, N. F. van Hulst, *Proc. Natl. Acad. Sci. USA* **2000**, 97, 7237.
- [9] P. Tamarat, F. Jelezko, C. Brunel, A. Maali, B. Lounis, M. Orrit, *Chem. Phys.* **1999**, 245, 121.
- [10] A. Einstein, *Phys. Z.* **1917**, 18, 121.
- [11] J. R. Lakowicz, I. Gryczynski, V. Bogdanov, J. Kusba, *J. Phys. Chem.* **1994**, 98, 334.
- [12] C. Y. Dong, P. T. C. So, T. French, E. Gratton, *Biophys. J.* **1995**, 69, 2234.
- [13] S. W. Hell, J. Wichmann, *Opt. Lett.* **1994**, 19, 780.
- [14] S. W. Hell, M. Schrader, K. Bahlmann, F. Meinecke, J. R. Lakowicz, I. Gryczynski, *J. Microsc.* **1995**, 180, RP1.
- [15] T. A. Klar, S. Jakobs, M. Dyba, A. Egner, S. W. Hell, *Proc. Natl. Acad. Sci. USA* **2000**, 97, 8206.
- [16] V. Westphal, L. Kastrup, S. W. Hell, *Appl. Phys. B* **2003**, 77, 377.
- [17] R. J. Marsh, D. A. Armoogum, A. J. Bain, *Chem. Phys. Lett.* **2002**, 366, 398.
- [18] E. Betzig, R. J. Chichester, *Science* **1993**, 262, 1422.
- [19] M. Dyba, S. W. Hell, *Appl. Opt.* **2003**, 42, 5123.
- [20] M. D. Rotter, B. Dane, *Opt. Commun.* **2001**, 198, 155.
- [21] C. Eggeling, J. Widengren, R. Rigler, C. A. M. Seidel, *Anal. Chem.* **1998**, 70, 2651.

Improving Implant Materials by Coating with Nonpeptidic, Highly Specific Integrin Ligands**

Claudia Dahmen, Jörg Auernheimer, Axel Meyer, Anja Enderle, Simon L. Goodman, and Horst Kessler*

Surface modification for enhanced cell adhesion to improve the properties of the critical interphase between an implant material and the biological tissue is an ongoing issue. Despite considerable improvements there is still a challenge to optimize the following criteria: the efficiency in stimulating cell adhesion, the selectivity for a specific cell type (e.g. osteoblast vs. platelet adhesion), the stability under physiological conditions, the stable covalent attachment to the material, the ease of handling under sterile conditions, and reasonable costs for the coating. Herein we present a new solution to these problems by using anchored nonpeptidic, highly α v-selective integrin ligands to coat titanium, a common implant material.

Osteoblast adhesion can be stimulated by extracellular matrix (ECM) proteins (e.g. fibronectin, collagen, laminine, and bone sialo protein),^[1] their fragments, or by RGD peptides^[2] which bind to α v β 3 integrin on osteoblast cells but bind to the platelet integrin α IIb β 3 as well.^[3] Selectivity for α v β 3 integrin could be achieved by using optimized cyclic pentapeptides.^[4–6] Coating poly(methyl methacrylate) (PMMA) with suitable modified cyclic pentapeptides stimulates osteoblast adhesion in vitro^[7] and bone formation in PMMA granulates in vivo (rabbit).^[8]

A number of nonpeptidic α v-selective RGD mimics have been developed by us and others^[9–12] as potential drugs to treat cancer, osteoporosis, acute renal failure, restenosis, arthritis, and retinopathy.^[13–18] Recently the X-ray structure of the α v β 3 head group containing the cyclic peptide cilengitide^[5] was reported.^[19] Modeling studies on the nonpeptidic α v β 3 ligands elucidated their binding mode.^[20] We used this data to identify suitable positions for anchor groups (linkers)

[*] Dr. C. Dahmen, Dipl.-Ing. J. Auernheimer, Dipl.-Chem. A. Meyer, Prof. Dr. H. Kessler
Department Chemie
Lehrstuhl Organische Chemie II
Technische Universität München
Lichtenbergstrasse 4, 85747 Garching (Germany)
Fax: (+49) 89-289-13210
E-mail: kessler@ch.tum.de

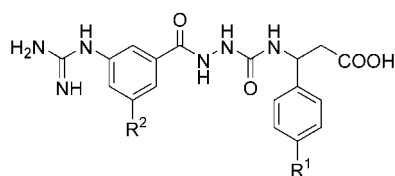
Dr. A. Enderle
Biomet Merck BioMaterials GmbH, Forschung
Frankfurter Strasse F129/250, 64271 Darmstadt (Germany)
Dr. S. L. Goodman
Merck KGaA, Oncology Research
Frankfurter Strasse 250, 64271 Darmstadt (Germany)

[**] This work was supported by the DFG, Sonderforschungsbereich 563, and by the German Federal Ministry of Education and Research under No. 03N4012.



Supporting information for this article is available on the WWW under <http://www.angewandte.org> or from the author.

that could be used to attach ligands to the surface without interfering with integrin binding. The guanidine and carboxy groups of the ligand are essential for binding to the integrin subunits α and β , respectively.^[21] Therefore we chose the two aromatic rings of our highly $\alpha\beta3$ -selective diacylhydrazine scaffold^[10] to position the anchor groups (Scheme 1). By using the AutoDock3 program^[22,23] two mimetics with different anchors at R^1 and R^2 were modeled into the X-ray structure of the $\alpha\beta3$ -cilengitide complex^[19] after removal of the peptide ligand. The binding modes were identical to those of the anchor-free mimetic ($R^1 = R^2 = H$; Figure 1),^[20] and the linkers showed no disturbing interaction with the integrin, hence we synthesized both variants with different linker groups.



Scheme 1. Substituted nonpeptidic diacylhydrazines with possible linker positions R^1 and R^2 for anchoring to surfaces.

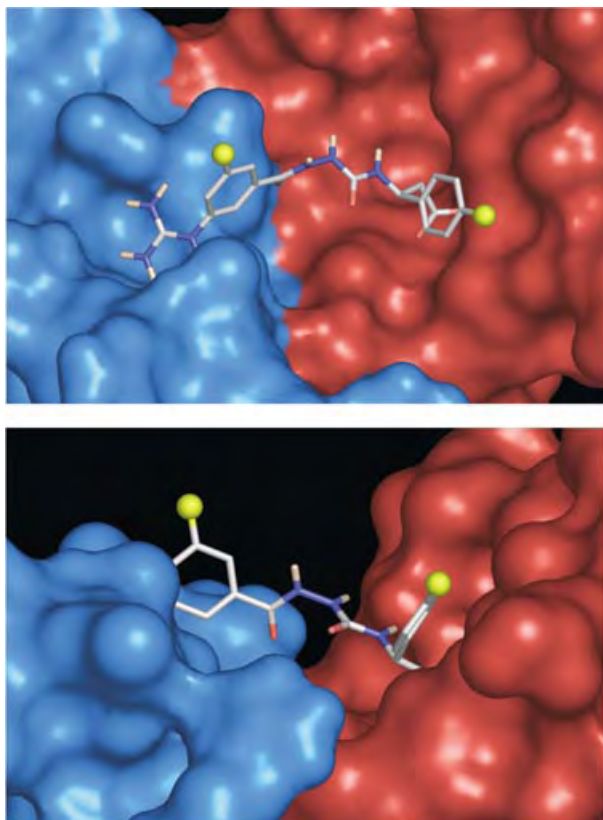
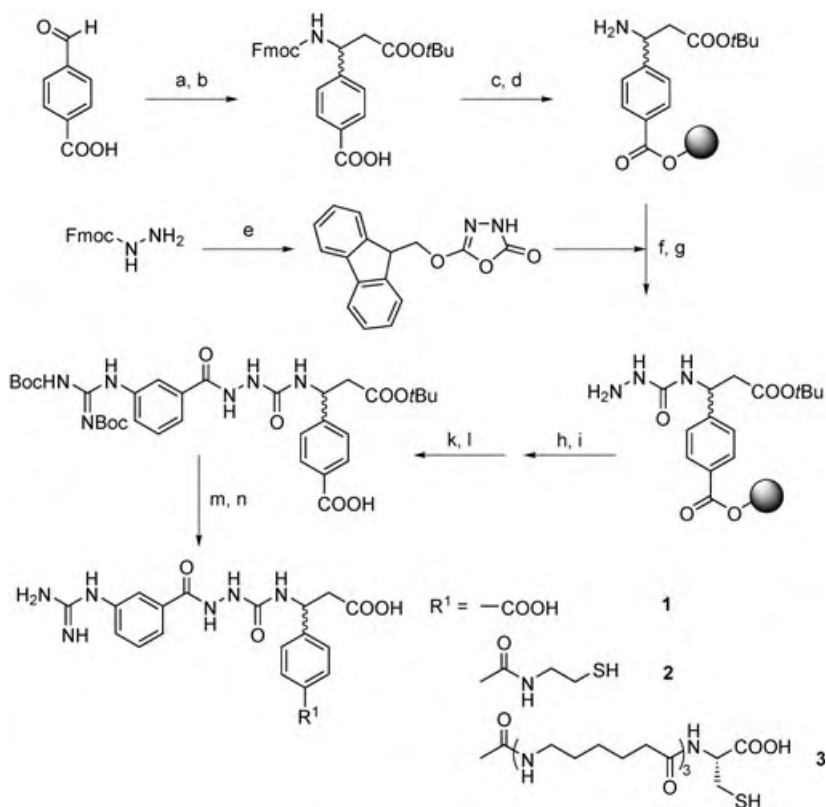


Figure 1. Results of the docking studies: Two diacylhydrazine molecules with anchors on the aromatic rings (stylized as yellow spheres) modeled into the crystal structure of the $\alpha\beta3$ integrin head group.^[19]



Scheme 2. Synthesis of R^1 substituted diacylhydrazines on a solid phase. a) NH_4OAc (2 equiv), malonic acid mono-*tert*-butyl ester (1 equiv), EtOH ; b) Fmoc-Cl (1.05 equiv), NaHCO_3 , dioxane; c) TCP-resin, CH_2Cl_2 , DIEA; d) 20% piperidine in NMP; e) COCl_2 (3 equiv; 1.9 M solution in toluene), sat. NaHCO_3 , CH_2Cl_2 ; f) 5-(9-*H*-fluoren-9-ylmethoxy)-1,3,4-oxadiazol-2-(3-*H*)-one (4 equiv), DMF; g) 20% piperidine in NMP; h) 3-(*N*-Fmoc)-aminobenzoic acid (2 equiv), HATU (1.94 equiv), collidine (22 equiv), NMP; i) 20% piperidine in NMP; j) *N,N'*-bis(Boc)guanylpurazole (10 equiv), CHCl_3 , 50°C; k) 20% HFIP in CH_2Cl_2 ; l) linker molecule (1 equiv), HATU (0.97 equiv), HOAt (1.1 equiv), collidine (11 equiv), DMF; m) 50% TFA, 2% triisopropyl silane; n) 2% water in CH_2Cl_2 . DIPEA = *N,N*-diisopropylethylamine.

Synthesis was performed on solid support (trityl chloride polystyrene resin = TCP-resin) by an Fmoc strategy (Fmoc = 9-fluorenylmethoxycarbonyl) similar to that described elsewhere.^[9,10,24] Starting from substituted β -amino acid immobilized on the resin, carbonylated Fmoc-protected hydrazine as the aza-glycine precursor^[24] and 3-(*N*-Fmoc)aminobenzoic acid were coupled. Guanidine was successfully incorporated using an excess of *N,N'*-bis(Boc)guanylpurazole (Boc = *tert*-butoxycarbonyl; Scheme 2). After cleavage (hexafluoroisopropanol (HFIP)/ CH_2Cl_2) the resulting Boc/OtBu-protected compound was coupled in solution on position R^1 with two thiol linkers of different length—cysteamine and 6-aminohexanoyl-6'-aminohexanoyl-6''-aminohexanoyl cysteine—and deprotected by trifluoroacetic acid (TFA). Purification was done by reverse-phase (RP) HPLC. The high $\alpha\beta3$ affinity of all the mimetics, with linkers (**2**, **3**) or not (**1**), was demonstrated in an established IC_{50} assay.^[10,25] Whereas the dicarboxy compound **1** is only active for the $\alpha\beta3$ integrin in the nanomolar range, the linked molecules are biselective

for $\alpha\beta3$ and $\alpha\beta6$ integrins (Table 1) as described for other nonpeptides of the diacylhydrazine type.^[9]

Steric effects cannot be the reason for the high $\alpha\beta3$ selectivity of compound **1** as compounds **1–3** are equally

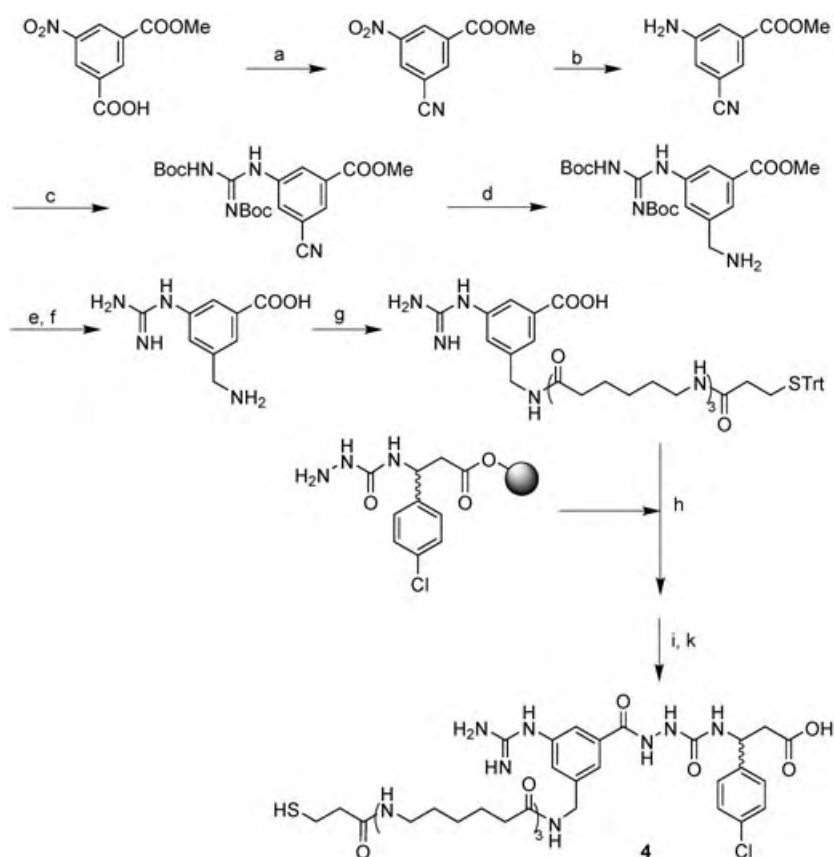
Substances **2–4** were tested for their cell adhesion properties on surfaces, the thiol linkers enable irreversible immobilization on titanium (an implant material). MC3T3E1 mouse osteoblasts, expressing the $\alpha\beta3$ integrin,^[8] were seeded onto

the modified titanium discs (Ti6Al4V, Ø1 cm), after 1 h the number of adherent cells was measured by detecting the hexamini-dase activity.^[27] Our study indicates that mouse osteoblasts bind to surfaces coated with compounds **2** or **3** (Figure 2). The plating efficiency was increased up to 42.9% (100 μM compound **3** in coating solution) compared to 9.4% on the unmodified titanium. Compound **3** stimulates cell adhesion as efficiently as the *cyclo*-(RGDfK[3-mercaptopropionyl]-) peptide.^[28] Compound **2** is slightly less potent, probably caused by the

significant shorter linker, which makes the integrin ligand less accessible to the integrin. Compound **4**, although having comparable activity in the binding assay of isolated $\alpha\beta3$

sterically demanding. Consistent with our theoretical studies on $\alpha\beta5$ homology models,^[26] the residues Lys180 and Asp252 of the SDL (selectivity determining loop) near the MIDAS region could effect an unfavored reorientation of ligand **1** in the binding pocket through electrostatic interactions with the carboxylate. There are uncharged residues at these positions in the $\beta3$ subunit and this could explain the strong impact of the carboxylic group in compound **1** for inhibiting the binding in $\alpha\beta5$.

R²-linked compound **4** was synthesized by a combined solution and solid-phase strategy (Scheme 3). *p*-Chlorophenyl-substituted β -alanine was chosen as the C-terminus of the molecule because it is found in very potent $\alpha\beta3$ integrin ligands.^[10] A complete solid-phase strategy could not realized, because after coupling of 3-amino-5-(*N*-Fmoc)aminomethylbenzoic acid stabilized with 4-methylbenzenesulfonic acid the coupling of ϵ -(*N*-Fmoc)-aminohexanoic acid after Fmoc deprotection (only possible with 2% 1,8-diazabicyclo[5.4.0]undec-7-ene (DBU)/2% piperidine in *N*-methylpyrrolidone (NMP)) did not work (probably caused by steric hindrance) even though different coupling reagents have been used. Therefore 3-aminomethyl-5-guanidinobenzoic acid was coupled with 3-(*S*-Trt)-mercaptopropionyl-Ahx-Ahx-Ahx-OH (Trt = trityl) in solution. The product was activated with *O*-(7-azabenzotriazol-1-yl)-1,1,3,3-tetramethyluroniumhexafluorophosphate (HATU) and coupled on resin-bound 3-(4-chlorophenyl)-3-[(hydrazinocarbonyl)-amino] propionic acid. Cleavage from the resin with HFIP/ CH_2Cl_2 , complete deprotection (TFA/ CH_2Cl_2), and subsequent purification by RP-HPLC gave in the integrin ligand **4** that is biselective for $\alpha\beta3/\alpha\beta6$ with an affinity in the subnanomolar range (Table 1).



Scheme 3. Synthesis of R² substituted diacylhydrazine **4**. a) $\text{SO}_2(\text{NH}_2)_2$ (1.2 equiv), SOCl_2 (3.6 equiv), sulfalane, 42 h reflux; b) Pd/C, H_2 , MeOH; c) $\text{SC}(\text{NH}(\text{Boc}))_2$ (1 equiv), NEt_3 (4 equiv), HgCl_2 (1.3 equiv), MeOH; d) Pd/C, H_2 , 20 bar, 2 M NH_3/EtOH , 50 °C; e) LiOH (3 equiv), MeOH/ H_2O ; f) 40% aqua.TFA (v/v); g) linker molecule (1 equiv), HATU (1 equiv), HOAt (1 equiv), collidine (10 equiv), DMF; h) HATU (1 equiv); i) 20% HFIP in CH_2Cl_2 ; k) 40% TFA, 2% triisopropyl silane,^[30] 2% water in CH_2Cl_2 .

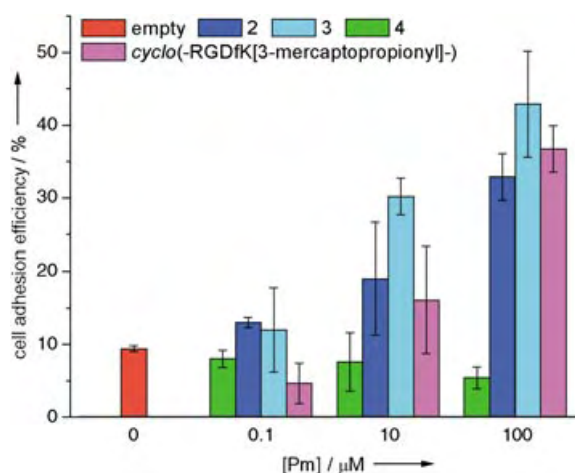


Figure 2. Adhesion of MC3T3E1 mouse osteoblasts on uncoated and coated titanium surfaces. The mean values of each point given is the result of triplicate determinations, the error bars represent standard deviations. [Pm] = mimic concentration in the coating solution.

integrin (Table 1), yielded no stimulation of osteoblast adhesion when bound to the titanium surface in repeated testing. An explanation could be that in spite of its huge linker the immobilized ligand has an unfavored orientation for integrin binding; the possibility that compound **4** does not immobilize on titanium is unlikely since we have investigated many peptidic derivatives of cyclo(-RGDfK[3-mercaptopropionyl]-) in the past (unpublished data) and all of them coated well on the titanium surfaces (checked by ELISA and cell adhesion assays, data not shown). In the case of the RGD mimic, immobilization could not be directly measured by ELISA because the antibody used recognizes only the cyclic RGD peptide and not the mimetics.

In conclusion, compounds **2** and **3** are the first nonpeptidic α_v -selective integrin ligands for surface coating which exhibit a potency for stimulated osteoblast adhesion similar to that of cyclo(-RGDfK[3-mercaptopropionyl]-) when immobilized on titanium. Compounds **2** and **3** are more stable to enzymatic degeneration, pH variations, and heat and their synthesis is much cheaper than that of the cyclic peptide.

Spectroscopic and analytical data for compounds **1–4** are included in the Supporting Information.

Received: May 25, 2004

Keywords: cell adhesion · cell recognition · materials science · peptide mimetics · titanium

- [1] J. M. Seeger, N. Klingman, *J. Surg. Res.* **1985**, 38, 641–647.
- [2] A. Wierzbka, U. Reichl, R. F. B. Turner, R. A. J. Warren, D. G. Kilburn, *Biotechnol. Bioeng.* **1995**, 46, 185–193.
- [3] E. Ruoslahti, *Annu. Rev. Cell Dev. Biol.* **1996**, 12, 697–715.
- [4] M. Aumailley, M. Gurrath, G. Müller, J. Calvete, R. Timpl, H. Kessler, *FEBS Lett.* **1991**, 291, 50–54.
- [5] M. A. Dechantsreiter, E. Planker, B. Mathä, E. Lohof, G. Hölzemann, A. Jonczyk, S. L. Goodman, H. Kessler, *J. Med. Chem.* **1999**, 42, 3033–3040.

- [6] R. Haubner, D. Finsinger, H. Kessler, *Angew. Chem.* **1997**, 109, 1440–1456; *Angew. Chem. Int. Ed. Engl.* **1997**, 36, 1374–1389.
- [7] M. Kantelehner, D. Finsinger, J. Meyer, P. Schaffner, A. Jonczyk, B. Diefenbach, B. Nies, H. Kessler, *Angew. Chem.* **1999**, 111, 587–590; *Angew. Chem. Int. Ed.* **1999**, 38, 560–562.
- [8] a) M. Kantelehner, P. Schaffner, D. Finsinger, J. Meyer, A. Jonczyk, B. Diefenbach, B. Nies, G. Hölzemann, S. L. Goodman, H. Kessler, *ChemBioChem* **2000**, 1, 107–114; b) U. Hersel, C. Dahmen, H. Kessler, *Biomaterials* **2003**, 24, 4385–4415.
- [9] C. Gibson, G. A. G. Sulyok, D. Hahn, S. L. Goodman, G. Hölzemann, H. Kessler, *Angew. Chem.* **2001**, 113, 169–173; *Angew. Chem. Int. Ed.* **2001**, 40, 165–169.
- [10] G. A. G. Sulyok, C. Gibson, S. L. Goodman, G. Hölzemann, M. Wiesner, H. Kessler, *J. Med. Chem.* **2001**, 44, 1938–1950.
- [11] G. Hölzemann, *IDrugs* **2001**, 4, 72–81.
- [12] J. S. Kerr, A. M. Slee, S. A. Mousa, *Expert Opin. Invest. Drugs* **2000**, 9, 1271–1279.
- [13] P. A. D'Amore, R. W. Thompson, *Annu. Rev. Physiol.* **1987**, 49, 453–464.
- [14] J. Folkman, Y. Shing, *J. Biol. Chem.* **1992**, 267, 10931–10934.
- [15] J. Folkman, *Nat. Med.* **1995**, 1, 27–31.
- [16] W. H. Miller, D. P. Alberts, P. K. Bhatnagar, W. E. Bondinell, P. K. Callahan, R. R. Calvo, R. D. Cousins, K. F. Erhard, D. A. Heerding, R. M. Keenan, C. Kwon, P. J. Manley, K. A. Newlander, S. T. Ross, J. M. Samanen, I. N. Uzinskas, J. W. Venslavsky, C. C.-K. Yuan, R. C. Haltiwanger, M. Gowen, S.-M. Hwang, I. E. James, M. W. Lark, D. J. Rieman, G. B. Stroup, L. M. Azzarano, K. L. Salyers, B. R. Smith, K. W. Ward, K. O. Johanson, W. F. Huffman, *J. Med. Chem.* **2000**, 43, 22–26.
- [17] M. W. Lark, G. B. Stroup, S. M. Hwang, I. E. James, D. J. Rieman, F. H. Drake, J. N. Bradbeer, A. Mathur, K. F. Erhard, K. A. Newlander, S. T. Ross, K. L. Salyers, B. R. Smith, W. H. Miller, W. F. Huffman, M. Gowen, *J. Pharmacol. Exp. Ther.* **1999**, 291, 612–617.
- [18] P. A. Burke, S. J. DeNardo, L. A. Miers, K. R. Lamborn, S. Matzku, G. L. DeNardo, *Cancer Res.* **2002**, 62, 4263–4272.
- [19] J.-P. Xiong, T. Stehle, R. Zhang, A. Joachimiak, M. Frech, S. L. Goodman, M. A. Arnaout, *Science* **2002**, 296, 151–155.
- [20] L. Marinelli, A. Lavecchia, K.-E. Gottschalk, E. Novellino, H. Kessler, *J. Med. Chem.* **2003**, 46, 4393–4404.
- [21] K.-E. Gottschalk, H. Kessler, *Angew. Chem.* **2002**, 114, 3919–3927; *Angew. Chem. Int. Ed.* **2002**, 41, 3767–3774.
- [22] G. M. Morris, D. S. Goodsell, A. J. Olson, AutoDock3 3.0 beta ed., **1993**.
- [23] G. M. Morris, D. S. Goodsell, R. S. Halliday, R. Huey, W. E. Hart, R. K. Belew, A. J. Olson, *J. Comput. Chem.* **1998**, 19, 1639–1662.
- [24] C. Gibson, S. L. Goodman, D. Hahn, G. Hölzemann, H. Kessler, *J. Org. Chem.* **1999**, 64, 7388–7394.
- [25] G. Thumshirn, U. Hersel, S. L. Goodman, H. Kessler, *Chem. Eur. J.* **2003**, 9, 2717–2725.
- [26] L. Marinelli, K.-E. Gottschalk, A. Meyer, E. Novellino, H. Kessler, *J. Med. Chem.* **2004**, 47, 4166–4177.
- [27] U. Landegren, *J. Immunol. Methods* **1984**, 67, 379–388.
- [28] B. Jeschke, J. Meyer, A. Jonczyk, H. Kessler, P. Adamietz, N. M. Meenen, M. Kantelehner, C. Goepfert, B. Nies, *Biomaterials* **2002**, 23, 3455–3463.
- [29] S. L. Goodman, G. Hölzemann, G. A. G. Sulyok, H. Kessler, *J. Med. Chem.* **2002**, 45, 1045–1051.
- [30] D. A. Pearson, M. Blanchette, M. L. Baker, C. A. Guindon, *Tetrahedron Lett.* **1989**, 30, 2739–2742.

Amorphous Aluminum Bromide Fluoride (ABF)**

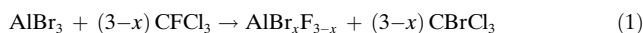
Thoralf Krahle and Erhard Kemnitz*

Dedicated to Professor Gerd-Volker Rösenthaller on the occasion of his 60th birthday

Amorphous aluminum chloride fluoride (ACF; $\text{AlCl}_x\text{F}_{3-x}$, $x = 0.05\text{--}0.3$), which is of high interest for catalytic reactions,^[1] was discovered at DuPont in 1992.^[2] It exhibits an extraordinarily high Lewis acidity similar to the acidity of SbF_5 , and in some cases, has even higher acidity. ACF is prepared by mild fluorination of AlCl_3 with chlorofluorocarbons such as CFCl_3 . However, the fluorination is never carried out to completion; the solid phase always contains some chlorine. The high Lewis acidity is surprising since pure aluminum chloride and phases of aluminum fluorides prepared in other ways are much weaker Lewis acids. We recently reported the investigation of ACF by several spectroscopic methods^[3] and presented our initial findings on the structure of this amorphous compound. However, the role of the residual chlorine in ACF is still unclear, but it has been shown that the structures of ACF and AlCl_3 differ with respect to the chlorine atoms.

Herein we report on the synthesis of amorphous aluminum bromide fluoride ABF ($\text{AlBr}_x\text{F}_{3-x}$, with $x = 0.13$), which is very similar to ACF. EXAFS measurements on the Br K edge of ABF enabled a more detailed study of the structure than for ACF. Partially fluorinated samples of AlBr_3 with the nominal composition AlBr_2F and AlBrF_2 were also investigated. From the analysis of the data measured by ^{19}F MAS NMR spectroscopy and Br K EXAFS, together with that gained during the investigation of ACF,^[3] a basic structural model of the compounds ABF and ACF is introduced for the first time.

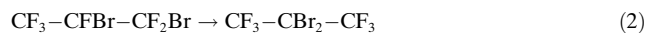
Solid AlBr_3 is built up of discrete Al_2Br_6 molecules,^[4a] whereas AlCl_3 has a layered structure.^[4b] The fluorination of AlBr_3 with CFCl_3 is highly exothermic and can be performed similar to that of ACF [Eq. (1)] to initially give CBrCl_3 and ABF.



The primary reaction product CBrCl_3 is not stable in the presence of a very strong Lewis acid such as ABF (see Experimental Section). Thus, it undergoes dismutation and slowly forms CCl_4 , CBr_2Cl_2 , CBr_3Cl , and CBr_4 . These products

have been observed by ^{13}C NMR spectroscopy. ABF is amorphous and shows no reflections in the XRD pattern. During heating, it crystallizes suddenly at 400°C , forms crystalline $\beta\text{-AlF}_3$ and AlBr_3 , and loses its very high Lewis acidity.

The Lewis acidity of ABF is very high. It catalyzes the isomerization reaction of 1,2-dibromohexafluoropropane to 2,2-dibromohexafluoropropane at room temperature [Eq. (2)], which requires an extremely strong Lewis acid.^[1d]



We chose this particular reaction because it can be carried out relatively easily. The acidity of certain Lewis acids has been recently expressed quantitatively by calculation of the fluoride ion affinity (FIA) at the MP2 level of theory. From this point of view, molecular SbF_5 is the strongest Lewis acid with the highest FIA.^[5] Molecular aluminum chloride and molecular aluminum fluoride have just slightly lower acidities. However, the acid strength of solid acids such as AlF_3 , ACF, and ABF cannot be expressed in such terms, but a ranking of the acid strengths can be done in terms of their reactivity. Reaction (2) requires a highly acidic catalyst; it runs easily at room temperature with the very strong Lewis acids SbF_5 , ACF, and ABF but not with the strong acids AlCl_3 and AlBr_3 .

The IR spectrum of ABF (Figure 1) is typical for a network of corner-sharing AlF_6 octahedra,^[3] which has the nominal composition of AlF_3 . Two intensive bands at around 665 and 350 cm^{-1} are attributed to the valence and deforma-

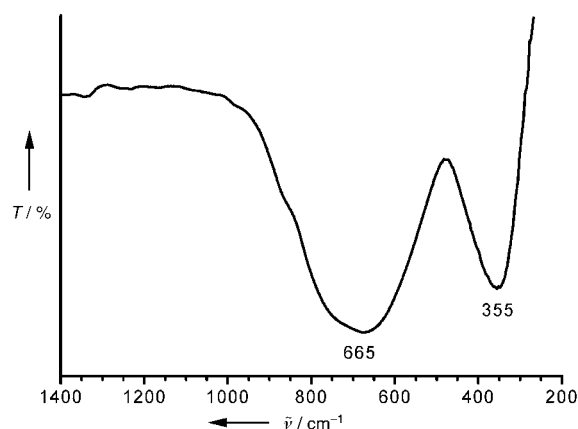


Figure 1. IR spectrum of ABF ($\text{AlBr}_{0.13}\text{F}_{2.87}$; CsI pellet).

tion vibrations of the AlF_6 octahedron, respectively. The large width of the band indicates the high degree of amorphicity of ABF. Interestingly, there is no significant difference between the IR spectra of ABF and ACF.^[3]

The ^{19}F MAS NMR spectra of ABF, partially fluorinated AlBr_3 , and ABF exposed to air are given in Figure 2. All spectra show the main signal between $\delta = -160$ and -170 ppm , which is typical for the $\mu\text{-F}$ atoms of corner-sharing AlF_6 octahedra and is also observed in amorphous and crystalline phases of AlF_3 .^[3,7] The spectrum of ABF shows an additional weak signal in the region from $\delta = -200$

[*] T. Krahle, Prof. Dr. E. Kemnitz
Institut für Chemie
Humboldt-Universität zu Berlin
Brook-Taylor-Strasse 2, 12489 Berlin (Germany)
Fax: (+49) 30-2093-7277
E-mail: erhard.kemnitz@chemie.hu-berlin.de

[**] This work was supported by the Deutsche Forschungsgemeinschaft (Ke 489/15-1). We thank Dr. J.-D. Grunwaldt and co-workers from the ETH Zurich for performing the EXAFS measurements.

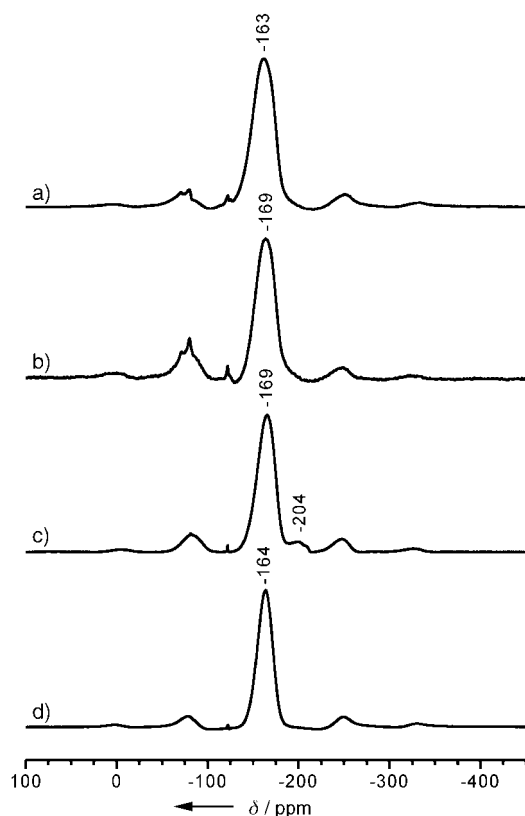


Figure 2. ^{19}F MAS NMR spectra of a) AlBr_2F , b) AlBrF_2 , c) ABF ($\text{AlBr}_{0.13}\text{F}_{2.87}$), and d) ABF exposed to air for 18 h.

to -210 ppm. According to the superposition model for the ^{19}F chemical shift, this signal is caused by terminal fluorine atoms bound to only one aluminum atom at a distance of around 1.7 \AA (t-F).^[6a] The appearance of such types of fluorine atoms has only been observed in ACF before and recently also in alumina fluorinated with CHClF_2 .^[7c] Deconvolution of the ^{19}F NMR spectrum of ABF with the program DMFIT^[6b] using Gaussian line shapes and two lines for each of the signals shows that the $\mu\text{-F}:\text{t-F}$ ratio of intensities of the fluorine signals is 92.3:7.7 (Figure 3 and Table 1). The small and narrow signals at chemical shifts of about $\delta = -80$ and -120 ppm can be assigned to the CF_3 and CF_2 groups of the organic residue. The signals of the terminal fluorine atoms disappear when the sample is exposed to atmospheric moisture (Figure 2d), and the structure of ABF changes irreversibly.

The fingerprint region of the X-ray absorption near edge spectra (XANES) of the Br K edge of AlBr_3 , AlBr_2F , AlBrF_2 , and ABF are shown in Figure 4. The spectra of ABF and AlBr_3 differ from each other, whereas the spectra of AlBr_2F and AlBr_3 are almost the same. The spectrum of AlBrF_2 is a superposition of the spectra of AlBr_3 and ABF—a linear combination of both data sets delivers the best fit result at 29% AlBr_3 and 71% ABF. From these results, it is evident that the bromine atoms in ABF and AlBr_3 differ from each other—the only partially fluorinated compound AlBrF_2 contains two different types of bromine atoms: one similar to the bromine in AlBr_3 and another similar to the bromine in

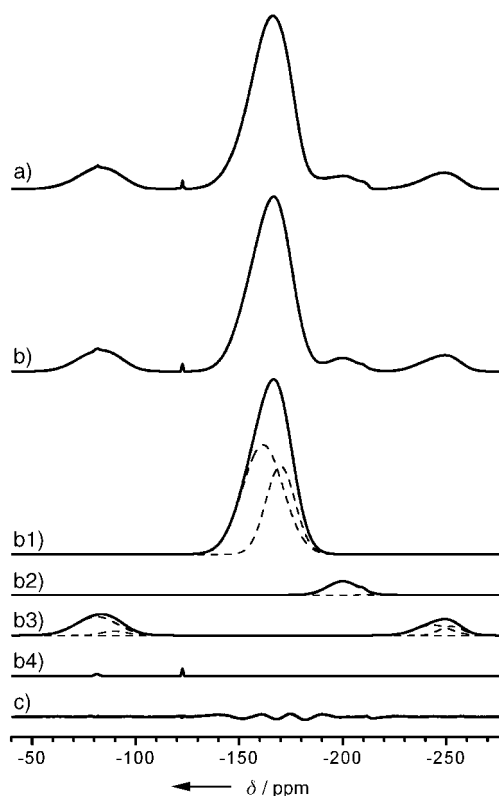


Figure 3. Measured (a) and simulated (b) ^{19}F MAS NMR spectrum of ABF. The fit (b) is the sum of the components (b1) to (b4). The parameters of the lines are shown in Table 1. b1) Main signal, lines 5 and 6; b2) shoulder, lines 7 and 8; b3) spinning side bands, lines 2, 3, 9, and 10; b4) organic residue, lines 1 and 4; c) difference between (a) and (b). The same scale was used for all components.

Table 1: Deconvolution of the ^{19}F MAS NMR spectrum of ABF.^[a]

No.	Amplitude [a.u.]	Position [ppm]	Width [kHz]	I_{rel} [%]	Comment
1	1.04	-81.31	1.06	—	organic
2	8.72	-80.18	8.60	—	s.s.b.
3	3.34	-89.80	6.18	—	s.s.b.
4	3.72	-122.64	0.35	—	organic
5	51.30	-161.41	8.89	48.8	bridging fluorine, 92.3 %
6	45.81	-169.84	6.56	43.5	
7	6.75	-200.00	6.02	6.4	terminal fluorine, 7.7 %
8	1.38	-210.00	1.19	1.3	
9	5.33	-243.32	7.34	—	s.s.b.
10	4.56	-252.38	5.15	—	s.s.b.

[a] The parameters of the Gaussian line fit are given. Only the lines 5 to 8 were considered for relative intensity. (I_{rel}) (s.s.b. = spinning side band).

ABF. Thus, the measurements confirm that AlBrF_2 is a mixture of the two phases, AlBr_3 and ABF, and that the remaining bromine in ABF does not derive from unreacted AlBr_3 .

The FT EXAFS spectra of the Br K edge of AlBr_3 and ABF (Figure 5) clearly show that the mean distance between bromine and the surrounding atoms in AlBr_3 is smaller than

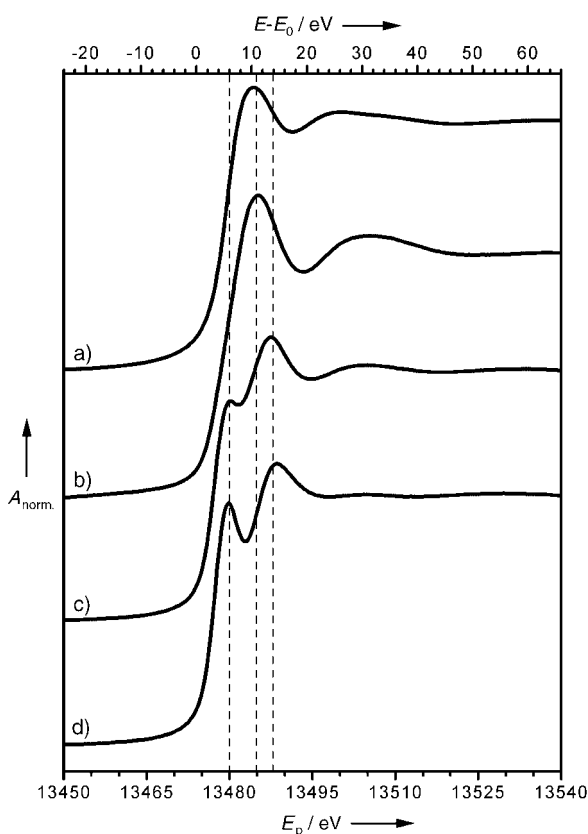


Figure 4. Br K-edge XANES spectra of a) AlBr_3 , b) AlBr_2F , c) AlBrF_2 , and d) ABF ($\text{AlBr}_{0.13}\text{F}_{2.87}$). The dashed lines indicate characteristic features. E_p = photon energy.

that found in ABF, that is the Al–Br bonds lengthen during the fluorination. The long Al–Br distances are surprising, but can be explained with the model established in the following.

The results gained from catalysis studies as well as IR and ^{19}F NMR measurements, and thermoanalysis show that the solid phases ABF and ACF are very similar to each other. Nevertheless, there are some spectroscopic methods, which could only be used with one of the phases (EXAFS for ABF, ESR for ACF^[3]). The combination of the results of work on ACF^[3] and the work on ABF presented here allows us to propose a simple geometric model for the structure of such compounds. It is assumed that ACF and ABF are built up of the same basic units; the structure is explained with a model based on linked polyhedra.

The following assumptions are made:

- 1) The aluminum atoms are octahedrally coordinated.
- 2) Three different types of octahedra are present (see Scheme 1):
 - 2a) $[\text{Al}(\mu\text{-F})_{\frac{5}{2}}]_0$ octahedra (**1**), in which all fluorine atoms link two octahedra,
 - 2b) $[\text{Al}(\mu\text{-F})_{\frac{5}{2}}(\text{t-F})]_{\frac{1}{2}}^-$ octahedra (**2**), in which five fluorine atoms link two octahedra and one fluorine atom is terminal,
 - 2c) $[\text{Al}(\mu_3\text{-X})_{\frac{1}{3}}(\mu\text{-F})_{\frac{5}{2}}]_{\frac{1}{6}}^+$ octahedral (**3**), in which one atom X (Cl or Br) links three octahedra and five fluorine atoms link two octahedra.

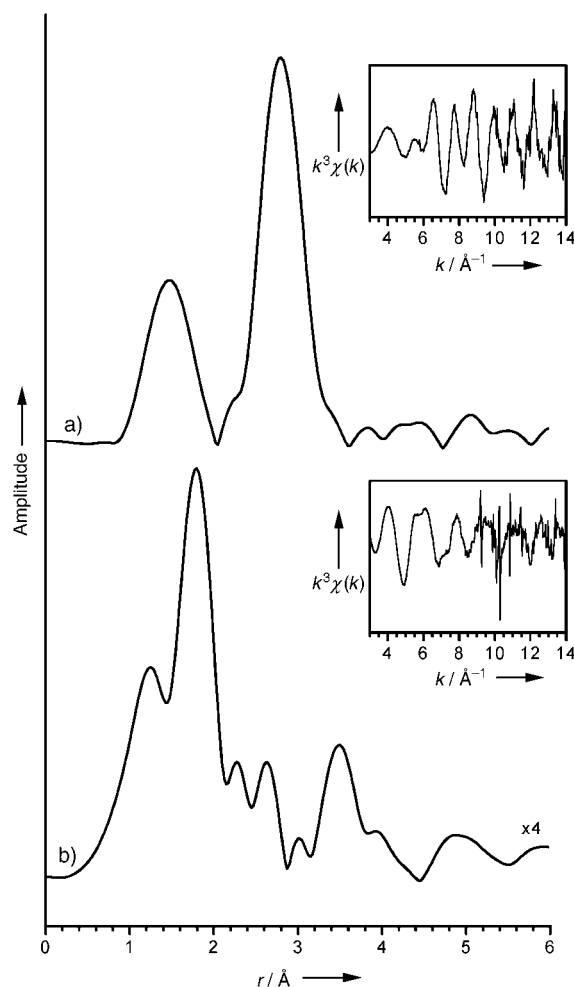
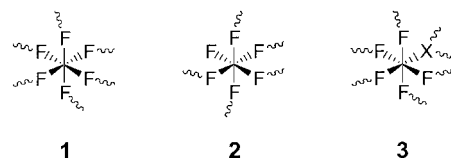


Figure 5. Fourier-transformed EXAFS spectra of the Br K-edge of a) $\text{AlBr}_{0.13}\text{F}_{2.87}$ (ABF) and b) AlBr_3 . The transformed spectra are not phase-corrected. The original EXAFS function is shown in the insets.



Scheme 1. Structural octahedral units proposed in ABF and ACF (X = Cl, Br). Al atoms in the middle of the octahedra are not shown. The sinuous lines indicate the bond to the next aluminum atom.

To ensure charge balance, the ratio between **2** and **3** must be 1:3. The overall sum formula can be formulated as $[\text{Al}(\mu\text{-F})_{\frac{5}{2}}(\text{t-F})] \cdot 3[\text{Al}(\mu_3\text{-X})_{\frac{1}{3}}(\mu\text{-F})_{\frac{5}{2}}] \cdot n[\text{Al}(\mu\text{-F})_{\frac{5}{2}}]$, where n is a variable parameter. This formula can be simplified to $\text{Al}_{4+n}\text{X}(\text{t-F})_x(\mu\text{-F})_{10+3n}$. Substitution of n as $\frac{1}{x}-4$ yields $\text{AlX}_x(\text{t-F})_x(\mu\text{-F})_{3-2x}$, or $\text{AlX}_x\text{F}_{3-x}$. For the ABF investigated in this publication n equals 3.69.

This model can explain the ^{19}F NMR and Br K EXAFS spectroscopic data. The following conclusions can be drawn:

- 1) The formal charge of the octahedra of type **3** is higher than that of the normal octahedra **1** found in AlF_3 . Thus, the

electron deficiency of the central Al atom of **3** is higher than that of the Al atoms in AlF_3 . Thus, ABF and ACF are more Lewis acidic than AlF_3 .

- 2) From $n \geq 0$ follows $x \leq 0.25$. $\text{AlX}_{0.25}\text{F}_{2.75}$ is the limiting composition for a compound called "ABF" or "ACF". This agrees quite well with the value 0.3 both given by duPont^[2] and determined by ^{19}F NMR spectroscopy for ACF.^[3]
- 3) The ABF structure investigated contains 7.7% terminal fluorine atoms with chemical shifts between $\delta = -200$ and -210 ppm in the ^{19}F NMR spectrum (Table 1). The amount of *t*-F and Br should be the same. Its formula can then be formulated as $\text{AlBr}_{0.13}(\text{t-F})_{0.22}(\mu\text{-F})_{2.65}$. The amount of *t*-F is a little higher than that of bromine.
- 4) The mean distance between a μ_3 -bridging halogen atom X and aluminum should be comparatively high. The EXAFS spectra (Figure 5) show clearly that the mean distance of bromine to its nearest neighboring atoms is higher in ABF than in crystalline AlBr_3 —the μ_2 -bridging Br atoms have an Al–Br distance of 2.38 Å and the terminal Br atoms have a Al–Br distance of 2.19 to 2.20 Å.^[4a]
- 5) Al–Br bonds are very sensitive to moisture. During exposure to air, not only are the acidic centers on the surface blocked, but the relevant structural elements explained above are destroyed. The resulting compound can be formulated approximately as $\text{Al}(\text{OH})_x\text{F}_{3-y}$. In the ^{19}F NMR spectrum no signals for terminal fluorine are seen, and the signals are shifted to slightly lower field (Figure 2D). The latter is also observed on comparing the spectra of AlF_3 and $\text{AlF}_3 \cdot 3\text{H}_2\text{O}$.^[3]

Experimental Section

Solid-state NMR spectra were measured with a Bruker AVANCE 400 MHz spectrometer equipped with a 2.5-mm Bruker MAS probe head at a rotation frequency of 30 kHz and a resonance frequency of 376 MHz for the ^{19}F nucleus.

Measurements of X-ray absorption spectra were carried out at HASYLAB on the beamline X1 (DESY, Hamburg, Germany) in transmission mode. The edge energy of the Br K-shell (13 474 eV) was calibrated with gold foil (Au L_2 -edge energy 13 733 eV). Samples were mixed with hexagonal boron nitride and pressed into pellets in a dry box.

All preparations were carried out under standard Schlenk conditions. Solvents were dried by condensing over molecular sieves (4 Å) before use. AlBr_3 (Reakhim, p.a.), CFCl_3 (Fluka, 99.5%), and perfluorooctane (ABCR, 95%) were used for the syntheses. The composition of the samples was checked by Br, C, and F analysis.

Synthesis of ABF: The reaction between AlBr_3 and CFCl_3 is strongly exothermic and should not be carried out at room temperature. AlBr_3 (11.0 g, 41.4 mmol) was placed with a magnetic stirrer in a 250-mL round-bottomed flask equipped with a dry ice condenser. The flask was evacuated and cooled with liquid nitrogen. Six equivalents of CFCl_3 (248 mmol) were condensed on the solid. The flask was warmed up to around 200 K (dry ice/2-propanol) and stirred at this temperature for 1 h. The start of the reaction was indicated by the yellow color of the solid. The flask was warmed to room temperature and refluxed for one more hour. The liquid was then evaporated in vacuum, and a fine orange-yellow powder was

obtained. The sample had a composition of $\text{AlBr}_{0.13}\text{F}_{2.87}$ and contained 0.8% carbon.

AlBr_2F and AlBrF_2 : The reaction was carried out similarly. Perfluorooctane was added until the solid AlBr_3 was totally immersed before the reaction. After mixture had been frozen, the desired amount of CFCl_3 (for AlBr_2F 1 equiv, for AlBrF_2 2 equiv) was condensed on the solid and then the workup proceeded as described for ABF.

Received: April 28, 2004

Keywords: aluminum · EXAFS spectroscopy · Lewis acids · NMR spectroscopy · structure elucidation

- [1] a) G. C. Krespan, V. A. Petrov, *Chem. Rev.* **1996**, *96*, 3269–3301; b) C. G. Krespan, D. A. Dixon, *J. Fluorine Chem.* **1996**, *77*, 117–126; c) V. A. Petrov, C. G. Krespan, B. E. Smart, *J. Fluorine Chem.* **1996**, *77*, 139–142; d) V. A. Petrov, C. G. Krespan, B. E. Smart, *J. Fluorine Chem.* **1998**, *89*, 125–130; e) V. A. Petrov, C. G. Krespan, *J. Fluorine Chem.* **2000**, *102*, 199–204.
- [2] A. C. Sievert, G. C. Krespan, F. J. Weigert (DuPont Co.), US-A 5.157.171, **1992**.
- [3] T. Krah, R. Stösser, E. Kemnitz, G. Scholz, M. Feist, G. Silly, J.-Y. Buzaré, *Inorg. Chem.* **2003**, *42*, 6474–6483.
- [4] a) S. I. Troyanov, *Zh. Neorg. Khim.* **1994**, *39*, 552–555; b) S. I. Troyanov, *Zh. Neorg. Khim.* **1992**, *37*, 266–272.
- [5] a) K. O. Christie, D. A. Dixon, D. McLemore, W. W. Wilson, J. A. Sheehy, J. A. Boatz, *J. Fluorine Chem.* **2000**, *101*, 151–153; b) H. D. B. Jenkins, H. K. Roobottom, J. Passmore, *Inorg. Chem.* **2003**, *42*, 2886–2893.
- [6] a) B. Bureau, G. Silly, J.-Y. Buzaré, J. Emery, *Chem. Phys.* **1999**, *249*, 89–104; b) D. Massiot, F. Fayon, M. Kapron, I. King, S. Le Calvé, B. Alonso, J.-O. Durand, B. Bujoli, Z. Gan, *Magn. Reson. Chem.* **2002**, *40*, 70–76.
- [7] a) P. J. Chupas, M. F. Circoalo, J. C. Hanson, C. P. Grey, *J. Am. Chem. Soc.* **2001**, *123*, 1694–1702; b) J. L. Delattre, P. J. Chupas, C. P. Grey, A. M. Stacy, *J. Am. Chem. Soc.* **2001**, *123*, 5364–5365; c) P. J. Chupas, C. P. Grey, *J. Catal.* **2004**, *224*, 69–79.

DNA Adducts

Mass Spectrometric Studies of DNA Adducts
from a Reaction with Terpenoids**

Wolfgang Schrader,* Sven Döring, and Werner Joppek

The phenomenon of blue haze above forests was described in the 1960s by Went,^[1] who correlated the formation of organic aerosols with biogenic plant emissions. Biogenic emissions, especially of mono- and sesquiterpenes, react with atmospheric oxidants to form a large number of products,^[2] which are thought to undergo a gas-to-particle conversion to form the organic aerosol. These particles in the atmosphere behave differently than the gaseous compounds, because they absorb or scatter the solar radiation, serve as cloud condensation nuclei, and are involved in multiphase atmospheric chemistry.^[3]

In addition to their atmospheric impact, terpenes and terpenoids are considered to be involved in plant-insect interactions.^[4] Indoor emissions of terpenes from furniture^[5] have been investigated as well as their impact on the nasal and respiratory system, and the risks of respiratory cancer for exposed woodworkers.^[6] The implication of terpenes and terpenoids in the generation of chronic pulmonary disease and acute bronchitis is well established.^[7] Their impact on the human organism is otherwise still unclear. Even pharmacokinetic data are not specific, and systematic studies on the metabolism have not been reported.^[7]

One marker used to observe the impact of xenobiotic compounds on organisms is the formation of DNA adducts, which in theory can lead to tumor development.^[8] Studies on DNA damage caused by oxidative stress or other natural compounds are of great interest to scientists.^[9] Randerath et al.^[10] were studying DNA modifications caused by polycyclic hydrocarbons using a ³²P-postlabeling assay when they found a significant number of DNA modifications in control samples from untreated animals. The authors suggested that these adducts arose from indigenous compounds and therefore called them "i-spots". The pattern of these i-spots is dependent on tissue, species, gender, and diet,^[11] and the number of i-spots increases with age.^[12] Recently, i-spots have been associated with cancer development.^[13] Unfortunately, the causes are still not fully understood. Some results indicate that compounds responsible for oxidative stress could cause some of the i-spots,^[9] although this does not sufficiently explain the complex pattern of the indigenous DNA modifications. Therefore other chemical compounds must be responsible for these lesions. One source that could have a substantial influence on base-level DNA damage is unsatu-

rated biogenic hydrocarbons, because they are ubiquitous. The only biogenic hydrocarbon that has been investigated in detail with regard to DNA-adduct formation is ethylene.^[14] Ethylene metabolizes to ethylene oxide, which is considered a strong carcinogen. Until now, there have been no studies on the impact of unsaturated hydrocarbons with regard to DNA adducts. Here, we report on a new class of xenobiotics and their effect in terms of base-level DNA damage.

Identification of xenobiotics contributing to base-level DNA damage is difficult, because the level is very low (about one adduct per 10⁸ nucleotides),^[15] which presents a challenge for analytical methods. The most sensitive technique is the ³²P-postlabeling assay, which allows detection of one adduct per about 10⁸–10¹⁰ bases.^[16] Since the adducts are detected by cochromatography, a synthetic standard is required and unknown adducts cannot be identified.

We have been studying the reactivity of terpenoids tentatively identified as products of the gas-phase ozonolysis of monoterpenes with regard to their reactivity with DNA and DNA constituents in vitro by applying enzymatic digestion followed by mass-spectrometric analysis to characterize the reaction products. Mass spectrometry is not as sensitive as ³²P-postlabeling, but the DNA adducts can be detected in small quantities and information about the structure of the adduct molecule can be extracted.^[17] For this purpose we use both an ion trap and a Fourier transform ion cyclotron resonance mass spectrometer (FTICR-MS) to study the reaction of α -pinene oxide with calf thymus DNA. While the ion trap MS can be used for fragmentation experiments induced through collision activation (CAD), FTICR-MS provides high-resolution mass data for the reaction products, which can be used to calculate the empirical formulas of the products in complex reaction mixtures.

Enzymatic DNA degradation is a standard tool for the study of these macromolecules. For a better understanding of the reaction, the DNA was digested using two different approaches: with the enzyme nuclease P1 and, alternatively, with a combination of the enzymes benzonuclease with an alkaline phosphatase. While nuclease P1 digests DNA to form mononucleotides, the benzonuclease produces a number of oligonucleotides of different chain lengths. The alkaline phosphatase removes the 5'-phosphates from the oligonucleotides, leading to oligonucleotides composed of *n* nucleosides and *n*–1 phosphate groups.^[17] Because MS provides only mass information about a nucleotide, the sequence specificity cannot be determined. Together, the two approaches provide an overview of possible DNA adducts resulting from the reaction with terpenoids.

Here, we report the first results obtained from the reaction of DNA with α -pinene oxide, an early product of α -pinene oxidation. Epoxides are reactive towards DNA,^[17] and their generation, by enzymatic oxidation through the cytochrome P 450, is often the first metabolic step in the removal of insoluble xenobiotics from the organism. A number of strong carcinogens are also activated in this way.^[18]

In addition to the DNA experiments we studied reactions of the four mononucleotides with α -pinene oxide in order to compare the results and facilitate the interpretation. The

[*] Dr. W. Schrader, S. Döring, W. Joppek
Max-Planck-Institut für Kohlenforschung
Kaiser-Wilhelm-Platz 1, 45470 Mülheim/Ruhr (Germany)
Fax: (+49) 208-306-2982
E-mail: wschrader@mpi-muelheim.mpg.de

[**] The authors thank Prof. Dr. A. Fürstner and Dr. J. Geiger for helpful discussions.

reaction of α -pinene oxide with DNA leads to a number of different adducts. Although their abundance is rather low, some specific DNA adducts could be detected and characterized. The DNA was detected as mononucleotides after nuclease P1 digestion; besides the not alkylated mononucleotides two adducts were detected. A signal at $m/z = 498$ was recorded for the deoxyguanylmorphosphate (dGMP) adduct and one at $m/z = 482$ for the deoxyadenylmorphosphate (dAMP) adduct. The other two bases did not form adducts under these conditions. MS/MS experiments with these adducts indicate that α -pinene oxide is coupled directly to the nucleobase. Corresponding results from FTICR-MS experiments confirm the findings and make it possible to obtain the empirical formulas of the respective adducts. When the reaction was conducted at 60 °C rather than at 37 °C, the dCMP and dTMP adducts with signals at $m/z = 473$ and 458, respectively, were observed. In comparison, pure mononucleotides showed adduct formation at 37 °C for all four nucleotides.

Spectra of the products of DNA degradation with benzonase and alkaline phosphatase show signals of oligonucleotides with different chain lengths. The most intensive signals were those of the dinucleotides, some of which also formed adducts. A total of seven different adducts with α -pinene oxide were characterized (Figure 1), and they are listed with the mononucleotide adducts in Table 1.

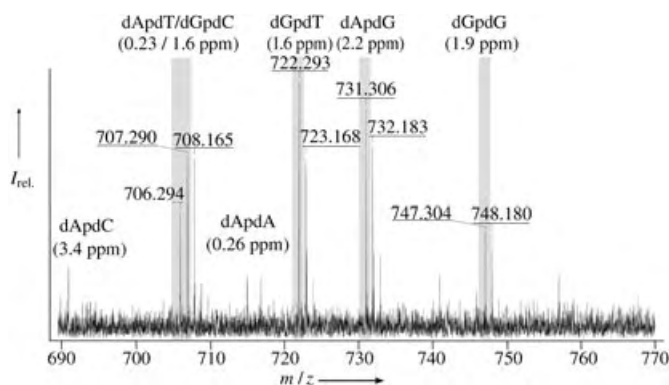


Figure 1. FTICR mass spectrum of enzymatically digested DNA. DNA adducts of α -pinene oxide shown as their dinucleotides are shown; seven of the possible ten dinucleotides are alkylated. The empirical formulas can be calculated from accurate mass determinations.

Table 1: DNA adducts resulting from the reaction with α -pinene oxide.

DNA adduct	m/z	Formula ^[a]	Accuracy [ppm]
dAMP	482.18072	C ₂₀ H ₂₉ N ₅ O ₇ P	0.6
dGMP	498.17611	C ₂₀ H ₂₉ N ₅ O ₈ P	0.38
dApdC	691.26342	C ₂₉ H ₄₀ N ₈ O ₁₀ P	3.4
dApdT	706.26088	C ₃₀ H ₄₁ N ₇ O ₁₁ P	0.23
dGpdC	707.25712	C ₂₉ H ₄₀ N ₈ O ₁₁ P	1.6
dApdA	715.27209	C ₃₀ H ₄₀ N ₁₀ O ₉ P	0.26
dGpdT	722.25681	C ₃₀ H ₄₁ N ₇ O ₁₂ P	1.6
dApdG	731.26880	C ₃₀ H ₄₀ N ₁₀ O ₁₀ P	2.2
dGpdG	747.26350	C ₃₀ H ₄₀ N ₁₀ O ₁₁ P	1.9

[a] Calculated formulas are based on the negatively charged ions [M-H]⁻.

MS/MS and MS³ spectra obtained from collision activation revealed that the adduct formation occurs primarily at the purine bases within the dinucleotides. No fragment ion could be detected that would indicate a reaction of α -pinene oxide with a pyrimidine base, while the fragments at $m/z = 286$ and $m/z = 302$ are characteristic for the adenine and guanine adducts, respectively. All the adducts were also characterized by FTICR-MS; the spectra confirmed the results from the ion trap measurements and the empirical formulas of the adducts were also determined (see Table 1). The results indicate that α -pinene oxide reacts with DNA at more or less random positions. The reaction seems to occur primarily with purine bases, while pyrimidine bases are less frequently involved.

In addition to the exocyclic sites in DNA, such as the N2 and O6 positions of guanine, the N7 position of guanine seems to be especially reactive. The FTICR spectrum in Figure 2

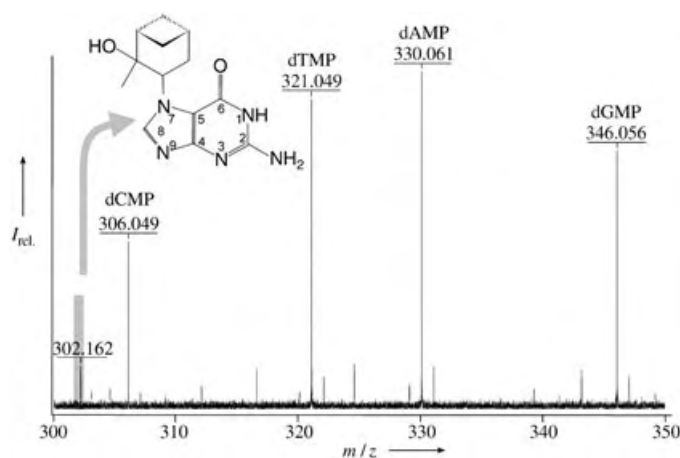
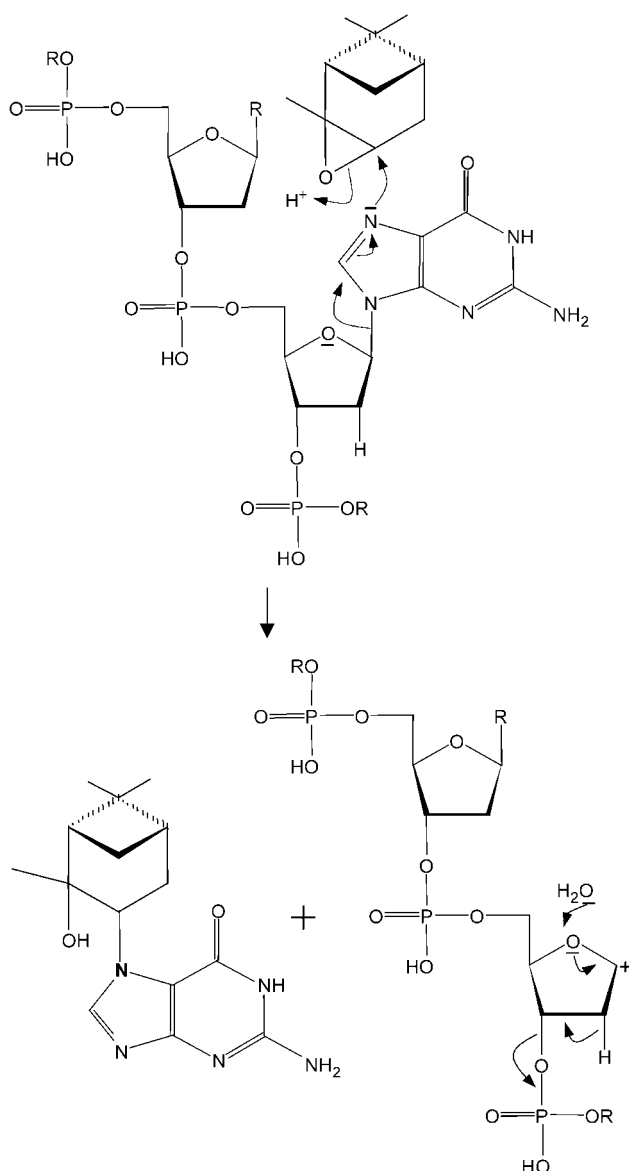


Figure 2. FTICR mass spectrum of enzymatically digested DNA showing the mononucleotides and the N7 guanine/pinene oxide adduct.

shows the four unreacted mononucleotides as well as the guanine adduct at $m/z = 302.16225$ (0.6 ppm). The accurate mass measurement led to a formula of C₁₅H₂₀N₅O₂, which corresponds to the α -pinene oxide/guanine adduct.

The enzymatic digestion used here should result in mononucleotides or oligonucleotides depending on the enzymes. The α -pinene oxide/guanine adduct in Figure 2 presumably results from reaction at the N7 position of guanosine, because alkylation at this site weakens the N-glycosidic bond, subsequently leading to bond cleavage and removal of the alkylated base from the DNA strand. This effect has been reported previously in studies of styrene oxide alkylation.^[19] Reaction at any other position of guanosine would not weaken the N-glycosidic bond and but would lead to either the corresponding mono- or oligonucleotide adduct depending on the enzyme. As a result of the hydrolytic cleavage of DNA, the very viscous reaction solution becomes fluid. A possible reaction mechanism is suggested in Scheme 1. No cleavage products could yet be identified for this hydrolysis of the remaining DNA. In addition to the guanine adduct, an adenine adduct could be found at $m/z = 286.16733$ (0.46 ppm), but the signal has lower intensity.



Scheme 1. The proposed reaction of α -pinene oxide at the N7 position of guanine, which leads to cleavage of the N-glycosidic bond and subsequent formation of the adduct.

The results reported here clearly indicate a reaction between α -pinene oxide and DNA. Although the concentrations used here are higher than in natural circumstances, the aim was to observe DNA adducts and provide sufficient structural information about a new class of xenobiotics that could have an effect on base-level DNA damage.

Experimental Section

Reaction: DNA (4–5 mg) was dissolved in 1 mL triply distilled water, combined with α -pinene oxide (25–100 μ L), and then incubated at 37°C for 24–72 h. The reaction mixture was enzymatically digested using a) a combination of benzonase (25 U mg⁻¹ DNA; Merck, Darmstadt, Germany) and alkaline phosphatase (1.75 U mg⁻¹ DNA; Roche Diagnostics, Mannheim, Germany) or b) nuclease P1 (6 U mg⁻¹ DNA; Roche Diagnostics, Mannheim, Germany) and incubated for 24 h at 37°C. The mononucleotides ($c = 1$ mg mL⁻¹)

were dissolved in triply distilled water, combined with α -pinene oxide (75 μ L), and also incubated at 37°C for 24 h. All reaction mixtures were analyzed without additional purification.

Mass spectrometric detection: A Bruker Esquire 3000 ion trap mass spectrometer was used. The mass range was scanned from $m/z = 50$ to 2000, and two scans were added for each spectrum. MS/MS and MS³ experiments were carried out inside the ion trap after the desired ion had been isolated; helium was used as the collision gas. Ions were isolated using a width of 0.5 Da. All samples were dissolved in acetonitrile in a ratio of 1:2 (v/v) and were introduced into the mass spectrometer using the direct-infusion mode with a flow rate of 2 μ L s⁻¹. In general, scans were recorded for 2 min and afterwards averaged for a better signal-to-noise ratio. High-resolution mass measurements were obtained from a Bruker APEX III FTICR-MS employing a 7 T magnet. The instrument was equipped with an Agilent electrospray ion source. After ionization ions were stored inside of a hexapole for sampling times between 0.3 and 0.8 s and afterwards transferred to the cyclotron cell. The mass range was scanned from $m/z = 80$ to 2000 with 512k data points. For detection of DNA adducts up to 100 scans were accumulated for a better signal-to-noise ratio.

Received: June 21, 2004

Revised: September 1, 2004

Keywords: DNA · i-spots · mass spectrometry · terpenoids

- [1] F. W. Went, *Nature* **1960**, 187, 641.
- [2] J. Yu, D. R. Crocker III, R. J. Griffin, R. C. Flagan, J. H. Seinfeld, *J. Atmos. Chem.* **1999**, 34, 207; b) H. Hakola, J. Arey, S. M. Aschmann, R. Atkinson, *J. Atmos. Chem.* **1994**, 18, 75; c) Y. Yokouchi, Y. Ambe, *Atmos. Environ.* **1985**, 19, 1271; d) U. Kückelmann, B. Warscheid, T. Hoffmann, *Anal. Chem.* **2000**, 72, 1905; e) W. Schrader, J. Geiger, T. Hoffmann, D. Klockow, E. H. Korte, *J. Chromatogr. A* **1999**, 864, 299; f) W. Schrader, J. Geiger, M. Godejohann, B. Warscheid, T. Hoffmann, *Angew. Chem.* **2001**, 113, 4129; *Angew. Chem. Int. Ed.* **2001**, 40, 3998.
- [3] M. O. Andreae, P. J. Crutzen, *Science* **1997**, 276, 1052; b) A. R. Ravishankara, *Science* **1997**, 276, 1058.
- [4] J. B. Harborne, *Ökologische Biochemie*, Spektrum Akademischer Verlag, **1995**, p. 62.
- [5] a) T. Salthammer, A. Schwarz, F. Fuhrmann, *Atmos. Environ.* **1995**, 33, 75; b) O. Jann, O. Wilke, D. Brödner, *Proc. of Healthy Buildings/IAQ, Vol. 3* (Eds.: J. E. Woods, D. T. Grimsrud, N. Bosch), **1997**, p. 593; c) T. Salthammer, F. Fuhrmann, *Proc. 7th Int. Conf. on Indoor Air and Climate, Vol. 3* (Eds.: K. Kimura, K. Ikeda, S. Tanabe, I. Iwata), **1996**, p. 607.
- [6] a) M. Ahman, M. Holmstrom, I. Cynkier, E. Soderman, *Occup. Environ. Med.* **1996**, 53, 112; b) T. P. Kauppinen, T. J. Partanen, S. G. Hernberg, J. I. Nickels, R. A. Luukkainen, T. R. Hakulinen, E. I. Pukkala, *Brit. J. Ind. Med.* **1993**, 50, 143.
- [7] C. Kohlert, I. van Rensen, R. März, G. Schindler, E. U. Graefe, M. Veit, *Planta Med.* **2000**, 66, 495.
- [8] A. C. Beach, R. C. Gupta, *Carcinogenesis* **1992**, 13, 1053.
- [9] L. J. Marnett, *Carcinogenesis* **2000**, 21, 361.
- [10] K. Randerath, M. Reddy, R. Disher, *Carcinogenesis* **1986**, 7, 1615.
- [11] a) D. H. Li, K. Randerath, *Cancer Res.* **1990**, 50, 3991; b) K. Randerath, K. L. Putman, E. Randerath, T. Zacharewsky, M. Harris, S. Safe, *Toxicol. Appl. Pharmacol.* **1990**, 103, 271.
- [12] D. H. Li, D. C. Xu, K. Randerath, *Carcinogenesis* **1990**, 11, 2227.
- [13] a) H. Bartsch, *Mutagenesis* **2002**, 17, 281; b) B. Bertram, H. Bartsch, *Forum DKG* **2003**, Spec. Iss. 1/03, 27.
- [14] a) H. Peter, H. J. Wiegand, H. M. Bolt, H. Greim, G. Walter, M. Berg, J. G. Filser, *Toxicol. Lett.* **1987**, 36, 9; b) H. M. Bolt, B.

- Jelitto, *Toxicology* **1996**, *113*, 328; c) R. Kreiling, R. J. Laib, H. M. Bolt, *Toxicol. Lett.* **1986**, *30*, 131.
- [15] D. H. Li, M. Y. Wang, J. G. Liehr, K. Randerath, *Mutat Res.-Gen. Toxicol.* **1995**, *344*, 117.
- [16] R. C. Gupta, M. V. Reddy, K. Randerath, *Carcinogenesis* **1982**, *3*, 1081.
- [17] W. Schrader, M. Linscheid, *J. Chromatogr. A* **1995**, *717*, 117; b) W. Schrader, M. Linscheid, *Arch. Toxicol.* **1997**, *71*, 588; c) P. Janning, W. Schrader, M. Linscheid, *Rapid Commun. Mass Spectrom.* **1994**, *8*, 1035.
- [18] F. P. Guengerich, *Arch. Biochem. Biophys.* **2003**, *409*, 59.
- [19] P. Vodicka, K. Heminki, *Carcinogenesis* **1988**, *9*, 1657.

Organocatalysis

A Metal-Free Transfer Hydrogenation: Organocatalytic Conjugate Reduction of α,β -Unsaturated Aldehydes**

Jung Woon Yang, Maria T. Hechavarria Fonseca, and Benjamin List*

Hydrogenations of double-bond-containing compounds such as carbonyls, imines, and olefins are crucial for living organisms as well as for the industrial production of chemicals. While chemical hydrogenations require metal catalysts or the use of stoichiometric amounts of metal hydrides, nature typically relies on organic cofactors such as nicotinamide adenine dinucleotide (NADH) in combination with metalloenzymes. Metal-free catalytic hydrogenations of olefins have been unknown both in nature and in chemical synthesis.^[1] Herein we disclose a highly efficient and remarkably chemoselective but completely metal-free catalytic transfer hydrogenation of α,β -unsaturated aldehydes.

The hydrogenation of α,β -unsaturated carbonyl compounds is a useful but challenging transformation. As both 1,2- and conjugate reductions readily occur, low selectivity for either of the two pathways is common. Catalytic hydrogenations of α,β -unsaturated aldehydes are possible, but the chemoselectivity is often low, and additional functional groups that are sensitive to hydrogenation conditions such as the benzyloxy, nitro, and nitrile groups are usually not tolerated.^[2] Alternative conjugate reductions have been realized with various substrate classes,^[3] but a mild, general, highly chemoselective, and catalytic variant that is applicable to α,β -unsaturated aldehydes has not been described.

Reported conjugate reductions of aldehydes are either non-catalytic and require stoichiometric amounts of an (organo)-metallic hydride source,^[4] require elevated temperatures,^[5] or show only modest selectivity.^[6] Clearly, a mild, catalytic, and highly chemoselective variant is highly desirable.

Recently iminium catalysis emerged as a powerful method for the asymmetric catalysis of cycloadditions and conjugate additions to enals and enones.^[7] We reasoned that this catalysis strategy might be applicable to the conjugate reduction of α,β -unsaturated carbonyl compounds if a suitable hydride donor could be identified.^[8] Such a process would constitute the first metal-free catalytic transfer hydrogenation.

We found that several ammonium salts (5 mol %) readily catalyze the conjugate reduction of *o*-nitrocinnamaldehyde (**3a**) to the corresponding saturated analogue **4a** when the Hantzsch ester **1** (1.1 equiv) is also added at room temperature [Eq. (1), Table 1]. No reduction was observed in the

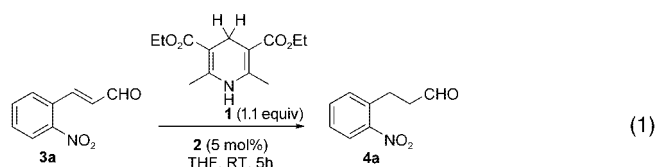


Table 1: Catalyst screening for the iminium catalytic conjugate reduction of α,β -unsaturated aldehydes.

Entry	Catalyst 2	Yield [%]
1	$\text{Bn-N}^+\text{H}_2\text{-Bn CF}_3\text{CO}_2^-$ 2a	2a 94
2	$\text{N}^+\text{H}_2\text{-O}^- \text{Cl}^-$ 2b	2b 65
3	$\text{C}_4\text{H}_8\text{NH}_2^+ \text{CF}_3\text{CO}_2^-$ 2c	2c 81
4	$\text{C}_4\text{H}_8\text{NH}_2^+ \text{CF}_3\text{CO}_2^-$ 2d	2d 92
5	$\text{C}_5\text{H}_{10}\text{NH}_2^+ \text{CF}_3\text{CO}_2^-$ 2e	2e 90
6	$\text{N}^+\text{H}_2 \text{Cl}^-$ 2f	2f 35

absence of catalyst after 48 h at room temperature. Cyclic as well as acyclic ammonium salts could be used, and the highest rate and yield was obtained with dibenzylammonium trifluoroacetate (**2a**). Interestingly, this catalyst was introduced in the 1970s by Corey et al. as an efficient catalyst for intramolecular aldol reactions of aldehydes.^[9] Under our reaction conditions aldolization did not occur to any measurable extent. In addition to catalyst **2a**, the corresponding pyrrolidinium, morpholinium, and piperidinium salts as well as the Weinreb salt **2b** can be used as catalysts.^[10] Ammonium salt **2b** has been used previously in the iminium catalysis of the Diels–Alder reaction.^[11]

After identifying an efficient and chemoselective iminium catalyst for the conjugate reduction of enal **3a**, we decided to explore the scope of this new process with a variety of

[*] Dr. J. W. Yang, Dr. M. T. Hechavarria Fonseca, Prof. Dr. B. List
Max-Planck-Institut für Kohlenforschung
Kaiser-Wilhelm-Platz 1, 45470 Mülheim an der Ruhr (Germany)
Fax: (+49) 208-306-2999
E-mail: list@mpi-muelheim.mpg.de

[**] We thank Degussa for donations of chemicals, Dr. Nicola Vignola for technical assistance, and the analytical departments of the Max-Planck-Institut für Kohlenforschung.

different aldehydes [Eq. (2), Table 2)]. The reduction works extremely well with a diverse set of unsaturated aldehydes, including substituted aromatic and aliphatic ones, and the

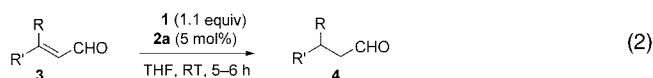


Table 2: Organocatalytic conjugate reduction of α,β -unsaturated aldehydes.

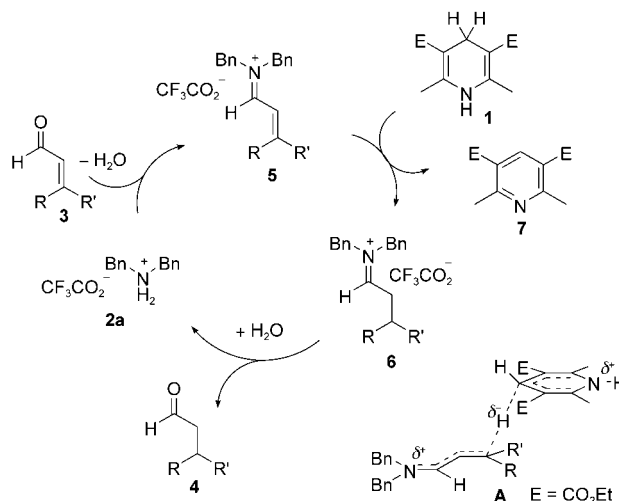
Entry	Substrate	Product	Yield [%] ^[a]
1			94
2			96
3			93
4			81 ^[b]
5			92
6			92
7			92 ^[c]
8			90
9			94
10			90 ^[b,c]
11			86 ^[b,c]
12			92

[a] Yield of isolated product. [b] Reaction time of 15 h. [c] Yield determined by GC.

yields exceed 90 % in almost all cases. Both β -mono- and β,β' -disubstituted enals can be reduced, although so far we have been unable to use enals with an additional substituent at the α -position. Besides the carbonyl group of aldehydes and ketones, a variety of functional groups that are sensitive to standard hydrogenation conditions are tolerated in the

process. These include the nitro, nitrile, benzyloxy, and alkenyl functional groups, which all survive the reaction conditions, illustrating the remarkable chemoselectivity of this novel organocatalytic reaction.

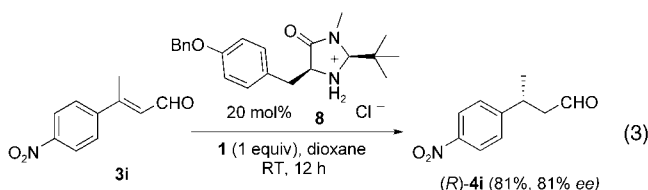
In terms of the mechanism we assume the reaction to proceed by the iminium catalysis cycle illustrated in Scheme 1. Accordingly, after an initial reversible formation



Scheme 1. Proposed mechanism of iminium catalysis.

of iminium ion **5** (which effectively lowers the LUMO energy of the substrate), conjugate hydride and proton transfer from dihydropyridine **1** follows. This step generates pyridine **7** along with iminium ion **6**. Hydrolysis then releases saturated aldehyde product **4** and regenerates catalyst **2a**. We suggest the hydride transfer to proceed via transition state **A**.

We are also developing an asymmetric variant of this reaction. For example, treating aldehyde **3i** with dihydropyridine **1** in the presence of catalyst **8** furnished (*R*)-**4i** in good yield and in 81 % *ee* [Eq. (3)].



In summary, we have developed the first metal-free catalytic transfer hydrogenation. This novel iminium catalytic conjugate reduction of α,β -unsaturated aldehydes is highly efficient and chemoselective. It requires low catalyst loadings and tolerates various functional groups that are sensitive to the conditions of standard hydrogenations and alternative conjugate reductions. Current work in our laboratory focuses on a) expanding the scope of the reaction even further to include other substrate classes such as ketones and α -substituted α,β -unsaturated aldehydes, b) improving the overall atom economy, potentially by regeneration of the cofactor in situ,^[12] c) including the reaction in tandem sequences

utilizing the presumed enamine intermediate,^[13] and d) developing an efficient catalytic asymmetric variant. First results will be reported shortly.

Experimental Section

General procedure for the transfer hydrogenation reaction: Synthesis of aldehyde **4a**: To a solution of *o*-nitrocinnamaldehyde (**3a**, 88.6 mg, 0.5 mmol) and catalyst **2a** (7.8 mg, 0.025 mmol, 5 mol %) in dry THF (2 mL) was added dihydropyridine **1** (140 mg, 0.55 mmol, 1.1 equiv). The reaction mixture was stirred at room temperature for 5 h under argon, after which the solvent was removed and the residue was chromatographed on silica gel (30 % diethyl ether/*n*-hexane) to give 84 mg (94 %) of **4a** as an oil. All aldehydes **3** and **4** are commercially available or have been described previously, and their analytical data match literature values.

Received: August 28, 2004

Published online: November 12, 2004

Keywords: chemoselectivity · Hantzsch dihydropyridine · iminium salts · organocatalysis · transfer hydrogenation

2003, 125, 1192–1194, and references therein; c) B. List, *Synlett* **2001**, 1675–1686.

- [8] For reported conjugate reductions of preformed α,β -unsaturated iminium ions with Hantzsch esters, see: a) T. Makino, N. Baba, J. Oda, Y. Inouye, *Chem. Ind.* **1977**, 277–278; b) N. Baba, T. Makino, J. Oda, Y. Inouye, *Can. J. Chem.* **1980**, 58, 387–392.
- [9] a) E. J. Corey, R. L. Danheiser, S. Chandrasekaran, P. Siret, G. E. Keck, J.-L. Gras, *J. Am. Chem. Soc.* **1978**, 100, 8031–8034; see also: b) A. Takahashi, M. Shibasaki, *Tetrahedron Lett.* **1987**, 28, 1893–1896; c) W. R. Roush, D. A. Barda, *Tetrahedron Lett.* **1997**, 38, 8785–8788.
- [10] S. Nahm, S. M. Weinreb, *Tetrahedron Lett.* **1981**, 22, 3815–3818.
- [11] J. L. Cavill, J. L. Peters, N. C. O. Tomkinson, *Chem. Commun.* **2003**, 728–729.
- [12] For an example of an enzymatic process in which the NADH cofactor can be regenerated in situ, see: M. R. Kula, C. Wandrey, *Methods Enzymol.* **1987**, 136, 9–21.
- [13] For elegant catalytic C–C coupling reactions that proceed by capture of hydrogenation intermediates, see: H.-Y. Jang, M. J. Krische, *Acc. Chem. Res.* **2004**, 37, 653–661.

- [1] For mechanistic studies on the base-catalyzed and transition-metal-free hydrogenation of ketones, see: a) A. Berkessel, T. J. S. Schubert, T. N. Müller, *J. Am. Chem. Soc.* **2002**, 124, 8693–8698; Also see: b) J. H. Teles, S. Brode, A. Berkessel, *J. Am. Chem. Soc.* **1998**, 120, 1345–1346; c) E. J. Lyon, S. Shima, G. Buurman, S. Chowdhuri, A. Batschauer, K. Steinbach, R. K. Thauer, *Eur. J. Biochem.* **2004**, 271, 195–204.
- [2] See for example: a) V. V. Grushin, H. Alper, *Organometallics* **1991**, 10, 831–833; b) J. M. Grosselin, C. Mercier, G. Allmang, F. Grass, *Organometallics* **1991**, 10, 2126–2133; c) M. Sommovigo, H. Alper, *Tetrahedron Lett.* **1993**, 34, 59–62, and references therein.
- [3] For selected examples: a) U. Leutenegger, A. Madin, A. Pfaltz, *Angew. Chem.* **1989**, 101, 61–62; *Angew. Chem. Int. Ed. Engl.* **1989**, 28, 60–61; b) M. Misun, A. Pfaltz, *Helv. Chim. Acta* **1996**, 79, 961–972; c) D. S. Hays, M. Scholl, G. C. Fu, *J. Org. Chem.* **1996**, 61, 6751–6752; d) D. H. Appella, Y. Moritani, R. Shintani, E. M. Ferreira, S. L. Buchwald, *J. Am. Chem. Soc.* **1999**, 121, 9473–9474; e) Y. Moritani, D. H. Appella, V. Jurkauskas, S. L. Buchwald, *J. Am. Chem. Soc.* **2000**, 122, 6797–6798; f) G. Hughes, M. Kimura, S. L. Buchwald, *J. Am. Chem. Soc.* **2003**, 125, 11253–11258; g) B. H. Lipshutz, J. M. Servesko, *Angew. Chem.* **2003**, 115, 4937–4940; *Angew. Chem. Int. Ed.* **2003**, 42, 4789–4792; h) C. Czekelius, E. M. Carreira, *Angew. Chem.* **2003**, 115, 4941–4943; *Angew. Chem. Int. Ed.* **2003**, 42, 4793–4795.
- [4] a) E. Keinan, N. Greenspon, *J. Am. Chem. Soc.* **1986**, 108, 7314–7325; b) D. M. Brestensky, J. M. Stryker, *Tetrahedron Lett.* **1989**, 30, 5677–5680; c) S. Saito, H. Yamamoto, *J. Org. Chem.* **1996**, 61, 2928–2929; d) H.-Y. Lee, M. An, *Tetrahedron Lett.* **2003**, 44, 2775–2778.
- [5] a) B. E. Norcross, P. E. Klinedinst, Jr., F. H. Westheimer, *J. Am. Chem. Soc.* **1962**, 84, 797–802; b) K. Nakamura, M. Fujii, A. Ohno, S. Oka, *Tetrahedron Lett.* **1984**, 25, 3983–3986; c) S. Torchy, G. Cordonnier, D. Barbry, J. J. Vanden Eynde, *Molecules* **2002**, 7, 528–533.
- [6] T. Suwa, I. Shibata, A. Baba, *Organometallics* **1999**, 18, 3965–3967.
- [7] See for example: a) K. A. Ahrendt, C. J. Borths, D. W. C. MacMillan, *J. Am. Chem. Soc.* **2000**, 122, 4243–4244; b) S. P. Brown, N. C. Goodwin, D. W. C. MacMillan, *J. Am. Chem. Soc.*

Combinatorial Chemistry

Selecting Different Complexes from a Dynamic Combinatorial Library of Coordination Compounds**

Markus Albrecht,* Ingo Janser, Jan Runsink,
Gerhard Raabe, Patrick Weis, and Roland Fröhlich

*Dedicated to Professor Heinz Balli
on the occasion of his 75th birthday*

Metallosupramolecular chemistry has developed over the last twenty years to an important and still growing field of research.^[1] Supramolecular aggregates of different shapes were obtained by the use of well-designed organic ligands in combination with appropriate metal ions or metal complex fragments. Although a series of different approaches have been discussed about how the formation of supramolecular

[*] Prof. Dr. M. Albrecht, I. Janser, Dr. J. Runsink, Prof. Dr. G. Raabe
Institut für Organische Chemie der RWTH-Aachen
Professor-Pirlet-Strasse 1, 52074 Aachen (Germany)
Fax: (+49) 241-80-92385
E-mail: markus.albrecht@oc.rwth-aachen.de

Dr. P. Weis
Institut für Physikalische Chemie der Universität Karlsruhe
Fritz-Haber-Weg, 76128 Karlsruhe (Germany)

Dr. R. Fröhlich
Organisch-Chemisches Institut der Universität Münster
Corrensstrasse 40, 48149 Münster (Germany)

[**] This work was supported by the Fonds der Chemischen Industrie and the Deutsche Forschungsgemeinschaft (SPP 1118). We thank Professor Dr. M. Kappes and the Nanotechnology Institute, Forschungszentrum Karlsruhe for facilitating the ESI-MS measurements.

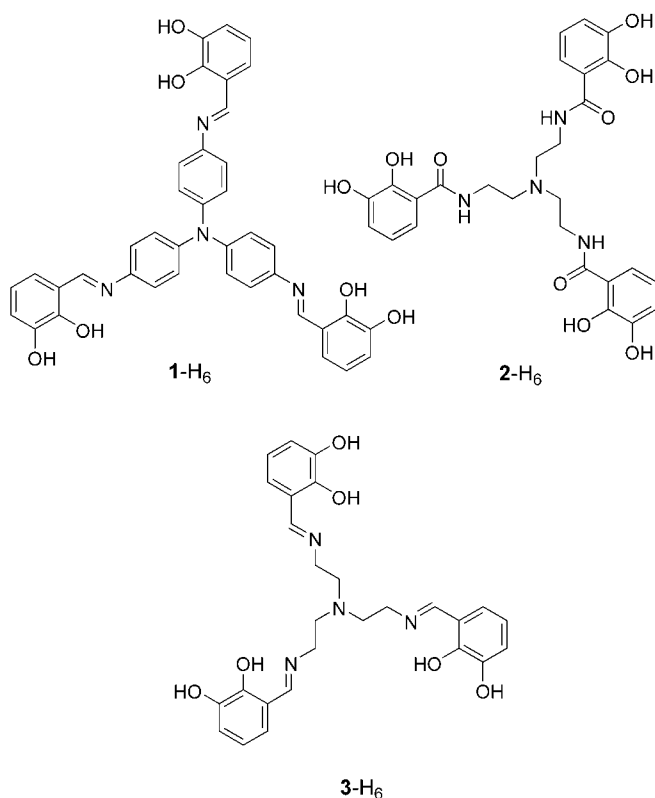


Supporting information for this article is available on the WWW under <http://www.angewandte.org> or from the author.

coordination compounds can be controlled,^[2] additional knowledge on the elementary processes of self-assembly is still required.

“Dynamic combinatorial chemistry” is a concept that uses the formation of dynamic combinatorial libraries (or virtual libraries) followed by a selection step which at the end ideally produces only one compound.^[3] A dynamic combinatorial library can be either formed by the introduction of labile covalent bonds or by noncovalent interactions between the molecular building blocks.^[4] In coordination chemistry it is relatively simple to obtain libraries (mixtures!) of compounds^[5] and some examples are known, for which it was possible to select and enhance one species from such a library.^[6] However, the selection of different species from the same library was described only in a few cases and still remains a challenge.^[7]

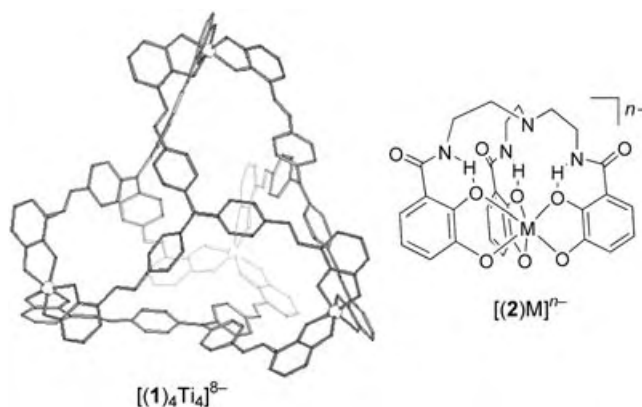
Recently we described the formation of the supramolecular tetrahedron $[(1)_4Ti_4]^{8-}$ from the rigid tris(catechol) ligand **1-H₆** (Scheme 1). The tetrahedron $[(1)_4Ti_4]^{8-}$ possesses



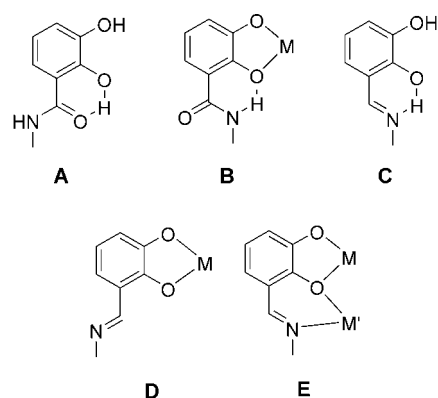
Scheme 1. C₃-symmetric ligands **1-H₆**–**3-H₆**, which form either tetranuclear $[(1)_4Ti_4]^{8-}$ or mononuclear $[(2)M]^{n-}$ coordination compounds.

a huge internal cavity for guest binding.^[8] A few similar molecular tetrahedra from rigid ligands were already known, which, however, did not possess internal cavities.^[9] We were interested to test if flexible ligands are also able to form M₄L₄ tetrahedra.

The well-known flexible tris(catechol) ligand **2-H₆** does not form a molecular tetrahedron, instead mononuclear complexes $[(2)M]^{n-}$ are obtained with metal ions.^[10–12] The conformation of flexible catechol amide ligands such as **2** is



dominated by intramolecular hydrogen bonding. In the free ligand, hydrogen bonds are formed between catechol-OH groups and the amide oxygen atom (**A**; Scheme 2) Deprotonation

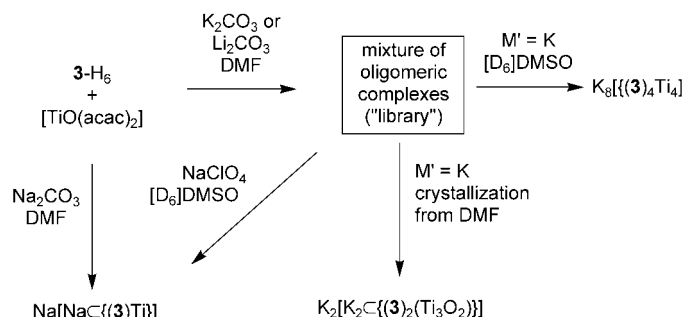


Scheme 2. Comparison of the preferred conformation at catechol amides with that of the corresponding catechol imines.

nation and metal complexation of the ligand leads to rotation of the C_{catechol}–C_{amide} bond, and hydrogen bonding occurs between the amide-NH and the catecholato-oxygen atom (**B**). This supports the formation of the mononuclear complex $[(2)M]^{n-}$.^[11,13] With catechol imines (e.g. **3**) the orientation of the catechol-C-N spacer moiety is opposite to that of the amides. In the free ligand, hydrogen bonding occurs between the catechol and the imine (**C**); in this case deprotonation and metal complexation lead to repulsion between the electron pairs at oxygen and nitrogen, and the conformation **D** is adopted.^[14] The difference in the conformation of coordinated catechol amides (**B**) and catechol imines (**D**) makes the imines superior ligands for the formation of molecular containers, if a huge cavity is desired.^[8] The cavity of the corresponding catechol amides will always be smaller. In addition, conformation **E** has to be discussed for the catechol imines. A templating metal ion M' binds to the internal catecholato oxygen atom as well as to the imine nitrogen atom, thus compensating the repulsion of the free O and N electron pairs.^[15]

The tris(catechol) derivative **3-H₆** with flexible connecting alkyl units was introduced by Vigato et al. to coordinate as an N₃O₃-Schiff base ligand to a series of metal ions.^[16] We were

interested in using **3**-H₆ as an O₆ ligand for transition metal ions (e.g. titanium(IV)).^[12] In our case, it should be possible to obtain different coordination compounds depending on the coordination mode (**D** or **E**) of the catechol imine unit. A conformation of type **D** should disfavor the formation of a mononuclear transition-metal complex and it is expected that the formation of a molecular tetrahedron is more likely. The conformation **E** with the bound cation M', which acts as a template and is encapsulated in the cavity of [(**3**)Ti]²⁻, should stabilize the mononuclear complex (Scheme 3)



Scheme 3. Formation of a mixture of titanium(IV) complexes ("library") of ligand **3** from which different coordination compounds can be obtained by selection or separation.

A coordination study of **3**-H₆ (1 equiv) with [TiO(acac)₂] (1 equiv; acac = acetylacetonate) was performed in the presence of lithium, sodium, and potassium carbonate (1 equiv) in DMF. Immediately after removal of the solvent and volatiles in vacuum, ¹H NMR spectra were measured in [D₆]DMSO (see the Supporting Information for the NMR spectra discussed). The spectra show that with lithium and potassium carbonate no defined coordination compounds could be obtained, but mixtures of different species are formed. Similar undefined spectra were obtained by recording the ¹H NMR spectrum of the mixture of complexes with potassium cations in [D₇]DMF. On the other hand, the use of sodium carbonate results in a nicely resolved NMR spectrum, in which the signal of the imine-hydrogen atom is shifted to $\delta = 8.14$ ppm—this is typical for conformation **E**. Orientation of the proton towards the catecholato oxygen atom (like in **D**) would result in an anisotropic shift and the resonance would be expected at $\delta = 8.5$ ppm or lower.^[14] This spectroscopic finding already supports the presence of a mononuclear complex of the type Na₂[(**3**)Ti]. The ²³Na NMR spectrum shows two signals at room temperature, indicating binding of one of the Na⁺ ions to the titanium complex [(**3**)Ti]²⁻. The signal of the solvated sodium ion is observed at $\delta = 0$ ppm, that of the other at $\delta = 10.4$ ppm, which is indicative for an O_xN_y coordination environment.^[17] At low temperature the signal at $\delta = 10.4$ ppm splits into two, a process which is not understood yet. As a hypothesis it is assumed that two diastereomers are formed with a homochiral or heterochiral relation between the sodium and titanium complex units. The epimerization barrier for the titanium(IV) complex can be estimated from ¹H NMR measurements in [D₇]DMF at variable temperature to be $\Delta G^\ddagger = 46.0$ kJ mol⁻¹.

The presence of a mononuclear titanium complex was shown by the X-ray structure analysis of Na[NaC{(3)Ti}].3DMF (Figure 1).^[18] Ligand **3** and titanium(IV) form a mononuclear complex in which the imine-nitrogen atoms

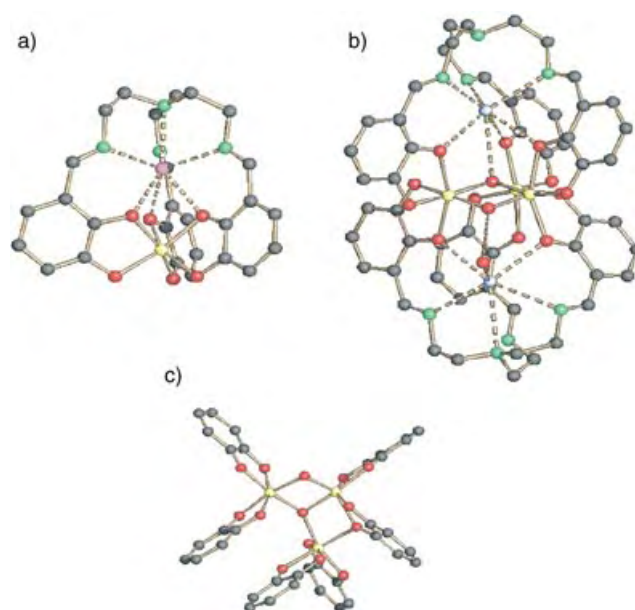


Figure 1. Representation of [NaC{(3)Ti}]⁻ (a) and [(H₂O)-K₂C{(3)₂(Ti₃O₂)}]²⁻ (b) as found in the solid state. c) The central tris(titaniumdioxo) cluster moiety of [(3)₂(Ti₃O₂)]⁴⁻. C: black; O: red; N: green; Ti: yellow; Na: pink; K: blue.

are orientated towards the interior. The cavity seems to be ideal for the uptake of a sodium ion which acts as a template. Lithium or potassium ions are not the correct size for this purpose. However, addition of sodium perchlorate to the mixture of oligomeric complexes, which is formed in the presence of Li⁺ or K⁺ ions, results in the quantitative formation of the metallacryptate [NaC{(3)Ti}]⁻.^[19]

The cavity of [(3)Ti]²⁻ is too small for the uptake of K⁺ ions. However, we were able to crystallize a titanium(IV) complex of ligand **3**, namely K₂[K₂C{(3)₂(Ti₃O₂)}], from DMF/diethyl ether in the presence of potassium ions.^[18] The complex was formed by K⁺ templating and possesses two cryptand-type units that are suitable for binding two of the potassium ions. Two ligands **3** coordinate to a tris(titaniumdioxo) cluster^[20] from its upper and lower side, respectively. One of the potassium ions coordinates to three imine-nitrogen and three catecholato-oxygen atoms of the first ligand **3** and additionally binds to the central oxygen atom of the Ti₃O₂ cluster. A second potassium ion binds to three catecholato oxygen atoms of the second ligand **3**, but to only two of the imine nitrogen atoms. In the solid state the coordination sphere at this potassium ion is completed by a water molecule, which functions as a bridge to a further potassium ion. Owing to the templating of the big potassium ions a trinuclear titaniumoxo cluster is stabilized by ligand **3**, providing an appropriate cavity for the template. The five catechol imines, which coordinate through their imine-nitrogen atoms to the potassium ions, possess conformation **E**,

while, as expected, the non-coordinating unit is orientated as shown in **D**.^[16]

A few crystals of $K_2[K_2C\{(3)_2(Ti_3O_2)\}]$ (ca. 0.1 mg) were dissolved in $[D_7]DMF$ and a 1H NMR spectrum was measured. The resonances of the ethylene units of **3** are not resolved. However, the signals of the aromatic moieties as well as of the imines are very informative. Five of the six imine protons are observed as singlets at $\delta = 8.49, 8.42, 7.98, 7.60$, and 7.56 ppm (1 H each). The sixth $-CH=N$ is probably hidden under the peak of the resonance of the DMF proton at $\delta = 8.06$ ppm. The protons of the aromatic groups in $K_2[K_2C\{(3)_2(Ti_3O_2)\}]$ appear at $\delta = 6.94$ (d, $J = 7.5$ Hz, 1 H), 6.81 (d, $J = 6.9$ Hz, 1 H), 6.63 (d, $J = 7.8$ Hz, 1 H), 6.56 (t, $J = 7.8$ Hz, 1 H), 6.49 (m, 2 H), 6.37 (m, 3 H), 6.26 (t, $J = 7.5$ Hz, 2 H), 6.18 (t, $J = 7.6$ Hz, 1 H), 5.98 (m, 5 H), and 5.67 ppm (t, $J = 8.3$ Hz, 1 H). The spectrum shows that $K_2[K_2C\{(3)_2(Ti_3O_2)\}]$ possesses the same low symmetry in solution as was observed in the solid state. Attempts to synthesize $K_2[K_2C\{(3)_2(Ti_3O_2)\}]$ in higher yield by choice of the correct ligand-to-metal stoichiometry did not result in the formation of a specific complex. Therefore $K_2[K_2C\{(3)_2(Ti_3O_2)\}]$ has to be considered as a side product of the reaction of **3** with titanium(IV) ions in the presence of potassium ions and can be separated by crystallization.

The NMR spectrum of a solution of the oligomeric complexes “ $[K_2\{(3)Ti\}]_n$ ” in $[D_7]DMF$ does not change over a period of several days. However, keeping a $[D_6]DMSO$ solution of the mixture for some hours at room temperature, leads to a simplification of the 1H NMR spectrum. Finally, besides the signals for trace amounts of side products, one dominating set of signals can be observed at $\delta = 8.58$ (s, imine-H), 6.86 (d, $J = 8.1$ Hz), 6.27 (t, $J = 8.1$ Hz), and 6.08 ppm (d, $J = 8.1$ Hz). Owing to the high symmetry associated with this spectrum, it can not be assigned to an unsymmetric species such as $K_2[K_2C\{(3)_2(Ti_3O_2)\}]$. In addition, the signals at $\delta = 8.6$ and 6.85 ppm indicate that an “outward” orientation of the imine-nitrogen atoms occurs (**D**). The imine proton hereby approaches the free electron pairs of the catecholato-oxygen atoms and experiences a low-field shift. A similar effect is observed for the aromatic proton of the catechol unit, which is located close to the imine-nitrogen atom. Owing to the electron pair at the N atom this aromatic proton is shifted to low field. From the orientation of the imine groups and the high symmetry of the compound, we deduce that the complex adopts the structure of a supramolecular tetrahedron $K_8[(3)_4Ti_4]$ (Figure 2). Negative-ion FT-ICR-MS (Fourier transform ion cyclotron resonance mass spectrometry) in DMSO shows peaks with the correct isotopic pattern at m/z 1213.5 $\{K_6[(3)_4Ti_4]\}^{2-}$, 795.6 $\{K_5[(3)_4Ti_4]\}^{3-}$, 783.3 $\{HK_4[(3)_4Ti_4]\}^{3-}$, 770.6 $\{H_2K_3[(3)_4Ti_4]\}^{3-}$, 587.7 $\{K_4[(3)_4Ti_4]\}^{4-}$, and 577.8 $\{HK_3[(3)_4Ti_4]\}^{4-}$, which confirm the presence of the molecular tetrahedron $K_8[(3)_4Ti_4]$.

Addition of $NaClO_4$ to a solution of $K_8[(3)_4Ti_4]$ in $[D_6]DMSO$ leads to a fast transformation of the tetrahedron into the mononuclear compound $[NaC\{(3)Ti\}]^-$, which can be nicely monitored by 1H NMR spectroscopy. This shows that this sodium ion stabilized mononuclear titanium(IV) complex is the thermodynamically most stable species in the presented system.

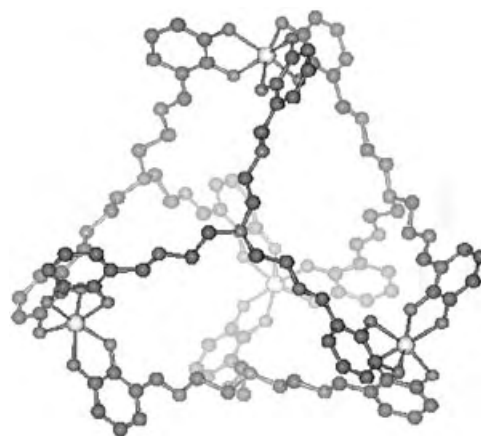


Figure 2. A model of the tetrahedral octaanion $[(3)_4Ti_4]^{8-}$, which was generated by using the Spartan O2 (MMFF) program^[21] and graphically represented by using the Schakal 99 program.

The described results represent a nice example for dynamic combinatorial chemistry, in which a dynamic library of complexes is formed in DMF solution in the presence of potassium ions. From this library three different coordination compounds $[NaC\{(3)Ti\}]^-$, $[(H_2O)K_2C\{(3)_2(Ti_3O_2)\}]^{2-}$, or $[(3)_4Ti_4]^{8-}$ can be obtained by addition of an appropriate template, by crystallization, or by equilibration of the mixture in DMSO. Competition experiments show that the mononuclear complex $[NaC\{(3)Ti\}]^-$ seems to be the thermodynamically most favored species. For the assembly of a M_4L_4 complex, sodium ions have to be excluded. We intend to extend this concept further, and to use it for the assembly of other large supramolecular aggregates.

Received: February 9, 2004

Revised: May 19, 2004 [Z53975]

Keywords: combinatorial chemistry · cryptands · self-assembly · template effect · titanium

- [1] J.-M. Lehn, *Supramolecular Chemistry—Concepts and Perspectives*, VCH, Weinheim, 1995.
- [2] a) R. W. Saalfrank, I. Bernt, *Curr. Opin. Solid State Mater. Sci.* **1998**, 3, 407; b) G. F. Swiegers, T. J. Malefetse, *Chem. Rev.* **2000**, 100, 3483; c) D. Caulder, K. N. Raymond, *J. Chem. Soc. Dalton Trans.* **1999**, 1185; d) S. Leininger, B. Olenyuk, P. J. Stang, *Chem. Rev.* **2000**, 100, 853; e) B. Olenyuk, A. Fechtenkötter, P. J. Stang, *J. Chem. Soc. Dalton Trans.* **1998**, 1707; f) M. Albrecht, *Angew. Chem.* **1999**, 111, 3671; *Angew. Chem. Int. Ed.* **1999**, 38, 3463.
- [3] a) A. Ganesan, *Angew. Chem.* **1998**, 110, 2989; *Angew. Chem. Int. Ed.* **1998**, 37, 2828; b) A. V. Eliseev, J. M. Lehn, *Curr. Top. Microbiol. Immunol.* **1999**, 243, 159; c) J.-M. Lehn, A. V. Eliseev, *Science* **2001**, 291, 2331.
- [4] a) P. A. Brady, J. K. M. Sanders, *Chem. Soc. Rev.* **1997**, 26, 327; b) J. K. M. Sanders, *Chem. Eur. J.* **1998**, 4, 1378; c) J.-M. Lehn, *Chem. Eur. J.* **1999**, 5, 2455; d) S. J. Rowan, S. J. Cantrill, G. R. L. Cousins, J. K. M. Sanders, J. F. Stoddart, *Angew. Chem.* **2002**, 114, 938; *Angew. Chem. Int. Ed.* **2002**, 41, 898; e) O. Storm, U. Lüning, *Chem. Eur. J.* **2002**, 8, 793.
- [5] a) Z. Grote, R. Scopelliti, K. Severin, *Angew. Chem.* **2003**, 115, 3951; *Angew. Chem. Int. Ed.* **2003**, 42, 3821; b) M. Ziegler, J. J. Miranda, U. N. Andersen, D. W. Johnson, J. A. Leary, K. N.

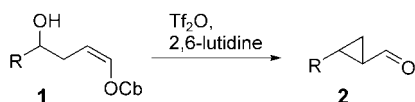
- Raymond, *Angew. Chem.* **2001**, *113*, 755; *Angew. Chem. Int. Ed.* **2001**, *40*, 733.
- [6] a) A. Bilyk, M. M. Harding, *J. Chem. Soc. Chem. Commun.* **1995**, 1697; b) M. Albrecht, O. Blau, *Chem. Commun.* **1997**, 345; c) M. A. Houghton, A. Bilyk, M. M. Harding, P. Turner, T. W. Hambley, *J. Chem. Soc. Dalton Trans.* **1997**, 2725; d) A. C. Try, M. M. Harding, D. G. Hamilton, J. K. M. Sanders, *Chem. Commun.* **1998**, 723; e) M. Albrecht, O. Blau, R. Fröhlich, *Chem. Eur. J.* **1999**, *5*, 48; f) M. Albrecht, O. Blau, R. Fröhlich, *Proc. Natl. Acad. Sci. USA* **2002**, *99*, 4876; g) M. Fujita, S. Nagao, K. Ogura, *J. Am. Chem. Soc.* **1995**, *117*, 1649; h) E. Stultz, S. M. Scott, A. D. Bond, S. J. Teat, J. K. M. Sanders, *Chem. Eur. J.* **2003**, *9*, 6039.
- [7] a) B. Hasenknopf, J.-M. Lehn, N. Boumediene, A. Dupont-Gervais, A. Van Dorsselaer, B. O. Kneisel, D. Fenske, *J. Am. Chem. Soc.* **1997**, *119*, 10956; b) B. Hasenknopf, J.-M. Lehn, N. Boumediene, E. Leize, A. Van Dorsselaer, *Angew. Chem.* **1998**, *110*, 3458; *Angew. Chem. Int. Ed. Engl.* **1998**, *37*, 3265; c) S. Hiraoka, M. Fujita, *J. Am. Chem. Soc.* **1999**, *121*, 10239; d) R. W. Saalfrank, I. Bernt, E. Uller, F. Hampel, *Angew. Chem.* **1997**, *109*, 2596; *Angew. Chem. Int. Ed. Engl.* **1997**, *36*, 2482; e) X. Wang, J. J. Vittal, *Inorg. Chem.* **2003**, *42*, 5135.
- [8] M. Albrecht, I. Janser, S. Meyer, P. Weis, R. Fröhlich, *Chem. Commun.* **2003**, 2854.
- [9] a) A. J. Amoroso, J. C. Jefferey, P. L. Jones, J. A. McCleverty, P. Thornton, M. D. Ward, *Angew. Chem.* **1995**, *107*, 1577; *Angew. Chem. Int. Ed. Engl.* **1995**, *34*, 1443; b) C. Brückner, R. E. Powers, K. N. Raymond, *Angew. Chem.* **1998**, *110*, 1937; *Angew. Chem. Int. Ed. Engl.* **1998**, *37*, 1837; c) D. Caulder, C. Brückner, R. E. Powers, S. König, T. N. Parac, J. A. Leary, K. N. Raymond, *J. Am. Chem. Soc.* **2001**, *123*, 8923; d) R. W. Saalfrank, H. Glaser, B. Demleitner, F. Hampel, M. M. Chowdhry, V. Schünemann, A. X. Trautwein, G. B. M. Vaughan, R. Yeh, A. V. Davis, K. N. Raymond, *Chem. Eur. J.* **2002**, *8*, 493.
- [10] S. J. Rodgers, C. W. Lee, C. Y. Ng, K. N. Raymond, *Inorg. Chem.* **1987**, *26*, 1622.
- [11] T. M. Garrett, P. W. Miller, K. N. Raymond, *Inorg. Chem.* **1989**, *28*, 128.
- [12] See also: F. E. Hahn, S. Rupprecht, K. H. Moock, *J. Chem. Soc. Chem. Commun.* **1991**, 224.
- [13] T. B. Karpishin, T. D. P. Stack, K. N. Raymond, *J. Am. Chem. Soc.* **1993**, *115*, 182.
- [14] M. Albrecht, I. Janser, S. Kamptmann, P. Weis, B. Wibbeling, R. Fröhlich, *Dalton Trans.* **2004**, 37.
- [15] M. Albrecht, S. Kamptmann, R. Fröhlich, *Polyhedron* **2003**, *22*, 643.
- [16] a) A. Aguiari, E. Bullita, U. Casellato, P. Guerriero, S. Tamburini, P. A. Vigato, U. Russo, *Inorg. Chim. Acta* **1994**, *219*, 135; b) A. Aguiari, E. Bullita, U. Casellato, P. Guerriero, S. Tamburini, P. A. Vigato, *Inorg. Chim. Acta* **1992**, *202*, 157.
- [17] J. P. Kintzinger, J.-M. Lehn, *J. Am. Chem. Soc.* **1974**, *96*, 3313.
- [18] X-ray crystal structure analysis of $\text{Na}[\text{NaC}\{(\text{3-Ti})\}]$: $\text{C}_{27}\text{H}_{24}\text{N}_4\text{O}_6$, $\text{Na}_2\text{Ti}_3\text{C}_3\text{H}_7\text{NO}$, $M_r = 813.66$, suitable crystals were obtained from dimethylformamide at room temperature. The compound crystallizes with three DMF molecules in the asymmetric unit. Crystal dimensions $0.54 \times 0.22 \times 0.12$ mm, monoclinic, $P2_1/n$ (no. 14), $a = 14.268(2)$, $b = 17.725(2)$, $c = 16.078(2)$ Å, $\beta = 105.84(1)^\circ$, $V = 3911.7(9)$ Å³, $Z = 4$, $\rho_{\text{calcd}} = 1.382$ g cm⁻³, a total of 16441 diffraction data were collected on an Enraf-Nonius CAD4 diffractometer at 268 K using graphite-monochromated MoK_α radiation ($\lambda = 0.71073$ Å, $\mu = 0.303$ mm⁻¹, no absorption correction) merged ($R_{\text{int}} = 0.1$) to give 3040 observed ($I > 2\sigma(I)$) reflections. The structure was solved by direct methods as implemented in the Xtal3.7 package of crystallographic routines (Xtal3.7 System, Eds.: S. R. Hall, D. J. du Boulay, R. Olthoff-Hazekamp. University of Western Australia, 2000) employing GENSIN to generate structure-invariant relationships and GENTAN for the general tangent phasing procedure. Full-matrix least-squares refinement on F including 496 parameters and 3027 reflections converged at $R = 0.098$, $R_w = 0.043$ ($w = \sigma(F)^{-2}$), $S = 1.513$, and a residual electron density of $-1.32/1.35$ e Å⁻³. The hydrogen atoms have been calculated in idealized positions and their isotropic displacement parameters have been fixed at 1.5 times the value of the corresponding heavy atom. The hydrogen parameters were not refined. $\text{K}_2[\text{K}_2\text{C}\{(\text{3-Ti})_2(\text{Ti}_3\text{O}_2)\}]$: formula $\text{C}_{54}\text{H}_{48}\text{N}_8\text{O}_{14}\text{Ti}_3\text{K}_4\text{H}_2\text{O} \cdot \text{C}_4\text{H}_{10}\text{O} \cdot 5\text{C}_3\text{H}_7\text{NO}$, $M_r = 1790.72$, orange crystal $0.20 \times 0.10 \times 0.03$ mm, $a = 15.075(1)$, $b = 21.742(1)$, $c = 25.522(1)$ Å, $\beta = 97.60(1)^\circ$, $V = 8291.6(7)$ Å³, $\rho_{\text{calcd}} = 1.434$ g cm⁻³, $\mu = 5.60$ cm⁻¹, empirical absorption correction ($0.896 \leq T \leq 0.983$), $Z = 4$, monoclinic, space group $P2_1/c$ (no. 14), $\lambda = 0.71073$ Å, $T = 198$ K, ω and ϕ scans, 66373 reflections collected ($\pm h$, $\pm k$, $\pm l$), $[(\sin\theta)/\lambda] = 0.59$ Å⁻¹, 14578 independent ($R_{\text{int}} = 0.130$) and 7696 observed reflections [$I \geq 2\sigma(I)$], 945 refined parameters, $R = 0.086$, $wR^2 = 0.195$, max. residual electron density 1.67 (-0.69) e Å⁻³, hydrogen atoms calculated and refined as riding atoms, three of the five dimethylformamide molecules and the diethyl ether molecule are refined with isotropic thermal parameters. Data set was collected with a Nonius KappaCCD diffractometer, equipped with a rotating anode generator Nonius FR591. Programs used: data collection COLLECT (Nonius B. V., 1998), data reduction Denzo-SMN (Z. Otwinowski, W. Minor, *Methods Enzymol.* **1997**, 276, 307), absorption correction SORTAV (R. H. Blessing, *Acta Crystallogr. Sect. A* **1995**, *51*, 33; R. H. Blessing, *J. Appl. Crystallogr.* **1997**, *30*, 421), structure solution SHELXS-97 (G. M. Sheldrick, *Acta Crystallogr. Sect. A* **1990**, *46*, 467), structure refinement SHELXL-97 (G. M. Sheldrick, Universität Göttingen, 1997), graphics SCHAKAL (E. Keller, Universität Freiburg, 1997). CCDC-230687 and CCDC-230007 contain the supplementary crystallographic data for this paper. These data can be obtained free of charge via www.ccdc.cam.ac.uk/conts/retrieving.html (or from the Cambridge Crystallographic Data Centre, 12, Union Road, Cambridge CB21EZ, UK; fax: (+44) 1223-336-033; or deposit@ccdc.cam.ac.uk).
- [19] a) R. W. Saalfrank, V. Seitz, D. Caulder, K. N. Raymond, M. Teichert, D. Stalke, *Eur. J. Inorg. Chem.* **1998**, 1313; b) M. S. Lah, B. R. Gibney, D. L. Tierney, J. E. Penner-Hahn, V. L. Pecoraro, *J. Am. Chem. Soc.* **1993**, *115*, 5857.
- [20] B. A. Borgias, S. R. Cooper, Y. B. Koh, K. N. Raymond, *Inorg. Chem.* **1984**, *23*, 1009.
- [21] *PC Spartan O2*, Wavefunction Inc., Irvine, 2002.

Cyclizations

Synthesis of Stereohomogeneous Cyclopropanecarbaldehydes and Cyclopropyl Ketones by Cycloalkylation of 4-Hydroxy-1-alkenyl Carbamates**

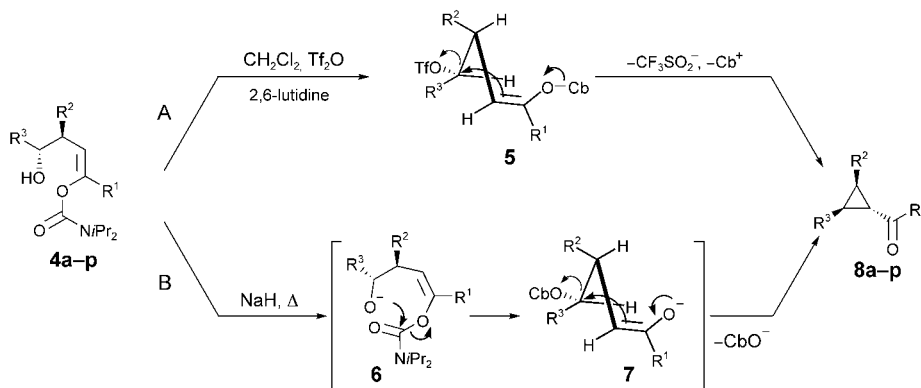
Rainer Kalkofen, Sven Brandau, Birgit Wibbeling, and Dieter Hoppe*

Only a few methods are known for the synthesis of optically active cyclopropanecarbaldehydes and cyclopropyl ketones by ring-forming reactions.^[1–3] Taylor et al.^[4] very recently described the synthesis of several racemic, disubstituted cyclopropanecarbaldehydes by intramolecular cycloalkylation of (*Z*)-4-hydroxy-2-alkenyl *N,N*-diisopropylcarbamates **1** by activation of the hydroxy group with trifluoromethanesulfonic anhydride (Tf₂O; Scheme 1).

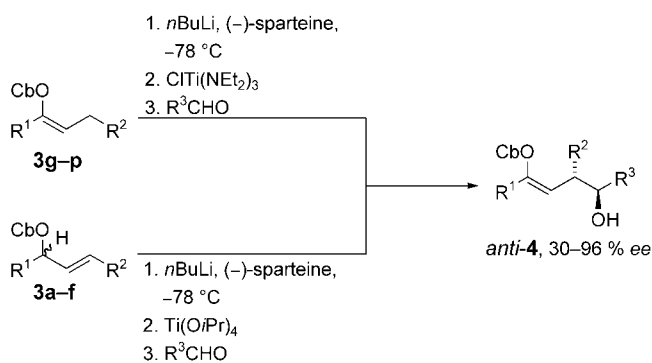


Scheme 1. Cyclopropane formation according to Taylor et al. Cb = CONiPr₂, Tf = triflate.^[4]

We found in our initial studies that this method can be extended to the synthesis of optically active, trisubstituted cyclopropanecarbaldehydes and cyclopropyl ketones **8** starting from compounds **4**, which in turn are readily obtained by enantioselective homoaldol reaction in the presence of (–)-sparteine^[5–7] (Scheme 2). According to Taylor et al., the (*Z*)-*anti* homoallylic alcohols **4** are converted into the corresponding triflates **5**, which undergo immediate intramolecular attack by the weakly nucleophilic enol carbamate moiety.^[8] The substitution step (Scheme 3, Method A) proceeds with complete stereoinversion, leading to a *cis* arrangement of R² and R³ and placing the acyl residue into the *trans* position to both of them via transition state **5**.



Scheme 3. Synthesis of highly enantioenriched disubstituted cyclopropanes.



Scheme 2. Enantioselective synthesis of 4-hydroxy-1-alkenyl carbamates **4**. **4 g–p**: R¹ = Ph, **4 a–f**: R¹ = H, R², and R³ in Table 1.

During the course of our work we made a surprising observation: simply treating the homoaldol adducts **4** with sodium hydride furnished the cyclopropanes **8** with excellent diastereoselectivity and complete chirality transfer (Method B, Scheme 3, Table 1). When alcohols **4** and sodium hydride were heated in THF or DMF for several hours, the cyclopropanes **8a–p** formed smoothly with the same efficiency as that observed for Method A. Apparently the *N,N*-diisopropylcarbamoyl group in alkoxide **6** migrates to the O4 atom,^[9] forming the (*Z*)-enolate **7**, which undergoes cycloalkylation by nucleophilic substitution of the carbamate group with strict stereoinversion. The enolate moiety occupies an *anti* position in transition state **7** in order to avoid steric repulsion with R² and R³. Method B also works well

even when a formyl group is generated (Table 1, entries 3 and 5).

The relative configuration of **8h** was confirmed by a single-crystal X-ray analysis.^[10] The absolute configuration of the precursor **4** is retained at C3, and the *ee* values of the products **8** correspond to those of the starting compounds **4** (Table 1). The combination of the cycloalkylation with the (–)-sparteine-mediated homoaldol reaction results in a two-step stereoselective route to cyclopropyl ketones.^[11] The *N,N*-diisopropylcarbamoyl group is required for the activation in the deprotonation step of the homoaldol reaction. Moreover,

[*] Dipl.-Chem. R. Kalkofen, Dipl.-Chem. S. Brandau, B. Wibbeling, Prof. Dr. D. Hoppe
Organisch-chemisches Institut
Westfälische Wilhelms-Universität Münster
Corrensstrasse 40, 48149 Münster (Germany)
Fax: (+49) 251-83-36531
E-mail: dhoppe@uni-muenster.de

[**] This work was supported by the Deutsche Forschungsgemeinschaft (SFB 424) and the Fonds der Chemischen Industrie. S. Brandau thanks V. Trepohl for her skillful experimental assistance.

Supporting information for this article is available on the WWW under <http://www.angewandte.org> or from the author.

Table 1:

Entry	Route	Solv.	Substr. (% ee)	Prod. (% ee)	R ¹	R ²	R ³	Yield [%]	d.r.	[α] _D ^{20[a]}
1	A	CH ₂ Cl ₂	4a (30) ^[b]	8a (30) ^[c]	H	(CH ₂) ₂ CH ₃	(CH ₂) ₂ Ph	70	98:2	+2
2	A	CH ₂ Cl ₂	4b (71) ^[b]	8b (71) ^[c]	H	CH ₃	Ph	> 99	95:5	+110
3	B	DMF	4b (71) ^[b]	8b (71) ^[b]	H	CH ₃	Ph	71	95:5	+110
4	A	CH ₂ Cl ₂	4c (87) ^[b]	8c (87) ^[c]	H	CH ₃	(CH ₂) ₂ Ph	48	95:5	+3
5	B	DMF	4c (87) ^[b]	8c (87) ^[b]	H	CH ₃	(CH ₂) ₂ Ph	58	98:2	+3
6	A	CH ₂ Cl ₂	4d (82) ^[c]	8d (82) ^[c]	H	CH ₃	CH(CH ₃) ₂	> 99	98:2	-4
7	A	CH ₂ Cl ₂	4e (83) ^[c]	8e (83) ^[c]	H	CH ₃	cyclopropyl	39	88:12	— ^[d]
8	A	CH ₂ Cl ₂	4f (86) ^[c]	8f (> 80) ^[c]	H	CH ₃	(CH ₂) ₄ CH ₃	61	98:2	+1
9	A	CH ₂ Cl ₂	4g (96) ^[b]	8g (96) ^[b]	Ph	CH ₃	Ph	80	98:2	+153
10	B	THF	4g (92) ^[b]	8g (91) ^[b]	Ph	CH ₃	Ph	98	98:2	+142
11	A	CH ₂ Cl ₂	4h (93) ^[b]	8h (93) ^[b]	Ph	CH ₃	C(CH ₃) ₃	83	98:2	-17
12	B	DMF	4h (95) ^[b]	8h (94) ^[b]	Ph	CH ₃	C(CH ₃) ₃	64	98:2	-17
13	A	CH ₂ Cl ₂	4i (91) ^[b]	8i (91) ^[b]	Ph	CH ₃	<i>p</i> -BrC ₆ H ₄	41	92:8	+148
14	B	THF	4i (93) ^[b]	8i (93) ^[b]	Ph	CH ₃	<i>p</i> -BrC ₆ H ₄	91	98:2	+151
15	B	DMF	4f (86) ^[b]	8f (> 80) ^[b]	H	CH ₃	(CH ₂) ₄ CH ₃	62	98:2	+1
16	B	THF	4j (94) ^[b]	8j (92) ^[b]	Ph	CH ₃	naphthyl	84	98:2	+206
17	B	THF	4k (92) ^[e]	8k (92) ^[e]	Ph	CH ₃	furyl	98	98:2	+177
18	B	THF	4l (91) ^[b]	8l ^[f]	Ph	CH ₃	CH ₃	84	98:2	—
19	B	THF	4m (95) ^[b]	8m ^[g]	Ph	CH ₃	CH ₂ CH ₃	96	98:2	-85
20	B	DMF	4n (96) ^[b]	8n (96) ^[b]	Ph	CH ₃	CH(CH ₃) ₂	62	98:2	-19
21	B	THF	4o (95) ^[b]	8o (95) ^[b]	Ph	CH ₃	cyclopropyl	74	98:2	-50
22	B	THF	4p (95) ^[b]	8p (95) ^[c]	Ph	CH ₃	cyclohexyl	78	98:2	-9

[a] $\epsilon = 0.15\text{--}0.92$, CHCl₃. [b] Determined by HPLC, column: Chira Grom-2. [c] Determined by chiral GC, column: β -Dex 120. [d] Due to the volatility of the compound it was not possible to determine the specific optical rotation. [e] Determined by HPLC, column: Chira Grom-1, solvent: *n*-hexane/isopropyl alcohol. [f] Achiral. [g] Not determined.

through the carbamoyl migration both the nucleophilic and the electrophilic properties of the stable precursors **4** are activated. These features fulfill in an exemplarily manner one demand of modern organic synthesis, namely minimizing the number of steps in a synthetic sequence.^[12]

Experimental Section

Synthesis of cyclopropanecarbaldehydes and cyclopropyl ketones:

Method A: A flame-dried flask was charged with **4b** (199 mg, 0.3 mmol, 1 equiv) in 10 mL CH₂Cl₂ under an argon atmosphere. 2,6-Lutidine (140 mg, 1.3 mmol, 4 equiv) was added by syringe, the solution was cooled to -78°C , and then freshly distilled triflic anhydride (314 mg, 1.1 mmol, 3 equiv) was injected. The reaction mixture was stirred for 1 h, quenched with 1 mL water, and allowed to warm to room temperature. The mixture was diluted with 25 mL CH₂Cl₂, the aqueous phase was separated, and the organic layer was washed with saturated NaHCO₃ solution (1 \times 10 mL). The organic phase was dried over MgSO₄ and the solvent evaporated in vacuum. The crude product was purified by flash chromatography on silica gel (diethyl ether/*n*-pentane 1:10).

Method B: To the *anti*-homoaldol adduct **4i** (169 mg, 0.37 mmol, 1 equiv) was added sodium hydride (60% in mineral oil; 20 mg, 0.5 mmol, 1.35 equiv). The flask was placed under argon, THF (2 mL) was injected, and the resulting solution was heated for 14 h at 60°C . When DMF was used as the solvent the solution was stirred 1 h at room temperature and then heated for 2–12 h at 60°C (tlc control). For workup 10 mL saturated sodium chloride solution was added. The aqueous phase was separated and extracted with diethyl ether (3 \times 25 mL). The combined organic extracts were dried over MgSO₄ and the solvents evaporated in vacuum. The crude product **8i** was purified by flash chromatography on silica gel (diethyl ether/*n*-pentane 1:5). For yields and enantiomeric excesses see Table 1.

Received: June 30, 2004

Keywords: asymmetric synthesis · cyclization · cyclopropanes · synthetic methods

- [1] Reviews: a) R. E. Taylor, F. Engelhardt, F. C. Schmitt, M. J. Schmitt, *Tetrahedron* **2003**, 59, 5623; b) H. Lebel, J.-F. Marcoux, C. Molinaro, A. B. Charette, *Chem. Rev.* **2003**, 103, 977; c) W. Kirmse, *Angew. Chem.* **2003**, 115, 1120; *Angew. Chem. Int. Ed.* **2003**, 42, 1088.
- [2] a) H. Abdallah, R. Greé, R. Carrié, *Tetrahedron Lett.* **1980**, 23, 503; b) H. M. Walborsky, L. E. Allen *Tetrahedron Lett.* **1969**, 11, 823; c) V. A. Aggarwal, E. Alonso, G. Fang, M. Ferra, G. Hynd, M. Porcelloni, *Angew. Chem.* **2001**, 113, 1482; *Angew. Chem. Int. Ed.* **2001**, 40, 1433; d) K. Yamaguchi, Y. Katzuta, H. Abe, A. Matsuda, S. Shuto, *J. Org. Chem.* **2003**, 68, 9255.
- [3] For other examples of asymmetric syntheses of cyclopropane derivatives mediated by (–)-sparteine see: a) M. Paetow, F. Hintze, D. Hoppe, *Angew. Chem.* **1993**, 105, 430; *Angew. Chem. Int. Ed. Engl.* **1993**, 32, 394; b) M. Paetow, M. Kotthaus, M. Grehl, R. Fröhlich, D. Hoppe, *Synlett* **1994**, 1034; c) S. Wiedemann, A. de Meijere, I. Marek, *Synlett* **2002**, 679.
- [4] a) R. E. Taylor, C. A. Risatti, F. Engelhardt, F. Conrad, M. J. Schmitt, *Org. Lett.* **2003**, 5, 1377; b) Prof. Taylor informed us after submission of our manuscript that he could successfully apply his cyclization conditions also to enantioenriched, higher substituted homoaldol products.
- [5] Reviews: a) D. Hoppe, T. Hense, *Angew. Chem.* **1997**, 109, 2376; *Angew. Chem. Int. Ed. Engl.* **1997**, 36, 2282; b) “Organolithiums in Enantioselective Synthesis”: D. Hoppe, F. Marr, M. Brüggenmann in *Topics in Organometallic Chemistry*, Vol. 5 (Ed.: D. M. Hodgson), Springer, Berlin, **2003**, p. 61; c) “Organolithiums in Enantioselective Synthesis”: P. Beak, T. A. Johnson, D. D. Kim, S. H. Lim in *Topics in Organometallic Chemistry*, Vol. 5 (Ed.: D. M. Hodgson), Springer, Berlin, **2003**, p. 134.
- [6] a) D. Hoppe, O. Zschage, *Angew. Chem.* **1989**, 101, 67; *Angew. Chem. Int. Ed. Engl.* **1989**, 28, 69; b) M. Özlügedik, J. Kristensen,

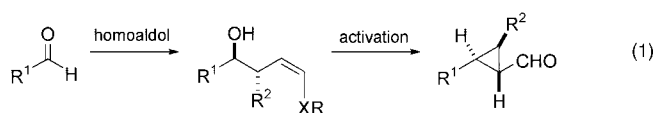
- B. Wibbeling, R. Fröhlich, D. Hoppe, *Eur. J. Org. Chem.* **2002**, 414.
- [7] a) M. Seppi, R. Kalkofen, J. Reupohl, R. Fröhlich, D. Hoppe, *Angew. Chem.* **2004**, *116*, 1447; *Angew. Chem. Int. Ed.* **2004**, *43*, 1423; b) J. Reuber, R. Fröhlich, D. Hoppe, *Org. Lett.* **2004**, *6*, 783.
- [8] For the direct reaction of vinyl carbamates as enolate equivalents: T. Krämer, C. F. Erdbrügger, E. Eggert, *Tetrahedron Lett.* **1989**, *30*, 1233.
- [9] For the generation of intermediate allenolates by carbamoyl migration: a) C. Schultz-Fademrecht, M. Tius, S. Grimme, B. Wibbeling, D. Hoppe, *Angew. Chem.* **2002**, *114*, 1610; *Angew. Chem. Int. Ed.* **2002**, *41*, 1532; b) M. Zimmermann, B. Wibbeling, D. Hoppe, *Synthesis* **2004**, 765.
- [10] X-ray crystal structure analysis of **8h**: $C_{15}H_{20}O$, $M_w = 216.31$, colorless crystal $0.50 \times 0.15 \times 0.10$ mm, $a = 5.975(1)$, $b = 10.359(1)$, $c = 11.161(1)$ Å, $\beta = 103.30(1)^\circ$, $V = 672.3(1)$ Å³, $\rho_{\text{calcd}} = 1.069$ g cm⁻³, $\mu = 4.96$ cm⁻¹, empirical absorption correction ($0.790 \leq T \leq 0.952$), $Z = 2$, monoclinic, space group $P2_1$ (No. 4), $\lambda = 1.54178$ Å, $T = 223$ K, ω and ϕ scans, 3002 reflections collected ($\pm h$, $\pm k$, $\pm l$), $[(\sin \theta)/\lambda] = 0.59$ Å⁻¹, 1640 independent ($R_{\text{int}} = 0.036$) and 1590 observed reflections [$I \geq 2\sigma(I)$], 149 refined parameters, $R = 0.039$, $wR^2 = 0.111$, Flack parameter 0.1(4), max. residual electron density 0.09 (−0.12) e Å⁻³, hydrogens calculated and refined as riding atoms. Data set was collected with a Nonius KappaCCD diffractometer. Programs used: data collection COLLECT (Nonius B. V., **1998**), data reduction Denzo-SMN (Z. Otwinowski, W. Minor, *Methods Enzymol.* **1997**, 276, 307–326), absorption correction SORTAV (R. H. Blessing, *Acta Crystallogr. Sect. A* **1995**, *51*, 33–37; R. H. Blessing, *J. Appl. Crystallogr.* **1997**, *30*, 421–426), structure solution SHELXS-97 (G. M. Sheldrick, *Acta Crystallogr. Sect. A* **1990**, *46*, 467–473), structure refinement SHELXL-97 (G. M. Sheldrick, Universität Göttingen, **1997**), graphics SCHAKAL (E. Keller, **1997**). CCDC-240544 contains the supplementary crystallographic data for this paper. These data can be obtained free of charge via www.ccdc.cam.ac.uk/conts/retrieving.html (or from the Cambridge Crystallographic Data Centre, 12, Union Road, Cambridge CB21EZ, UK; fax: (+44) 1223-336-033; or deposit@ccdc.cam.ac.uk).
- [11] For related work, see the following Communication in this issue: C. A. Risatti, R. E. Taylor, *Angew. Chem.* **2004**, *116*, 6839; *Angew. Chem. Int. Ed.* **2004**, *43*, 6671.
- [12] B. M. Trost, *Angew. Chem.* **1995**, *107*, 285; *Angew. Chem. Int. Ed. Engl.* **1995**, *34*, 259.

Cyclopropanes

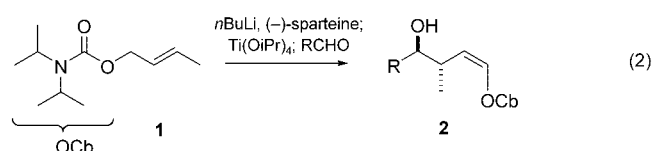
Enantioselective Synthesis of Cyclopropanes by Aldehyde Homologation**

Christina A. Risatti and Richard E. Taylor*

The prevalence of cyclopropane-containing compounds with biological activity, whether isolated from natural sources or rationally designed pharmaceutical agents, has inspired chemists to find novel and diverse approaches to their synthesis.^[1] We recently reported an efficient two-step homoaldol/activation sequence that resulted in the isolation of racemic 1,2-disubstituted cyclopropyl aldehydes.^[2] Herein we demonstrate the successful preparation of enantiomerically enriched and diastereomerically pure 1,2,3-trisubstituted cyclopropyl aldehydes by asymmetric metalation chemistry. In essence, this two-step procedure provides a three-carbon homologation of an aldehyde to give a nonracemic, stereochemically rich cyclopropyl aldehyde, [Eq. (1)].



Hoppe et al. have elegantly demonstrated that homoaldol adducts are readily available from (*E*)-butenyl *N,N*-diisopropylcarbamates **1** through deprotonation with *n*BuLi/(–)-sparteine complex and transmetalation with Ti(O*i*Pr)₄.^[3] Condensation with an aldehyde was shown to provide *O*-enecarbamates **2** with high diastereoselectivity and good enantioselectivity [Eq. (2)].



Carbamate **1** is readily prepared through condensation of *N,N*-diisopropyl carbamyl chloride with crotyl alcohol in refluxing pyridine. A series of aldehydes were applied to the described homoaldol conditions using the crotyl substrate as a

representative example. Aliphatic aldehydes, including sterically hindered substrates, resulted in high yields of (*Z*)-homoaldol adducts **3–5** with high *anti* selectivity as expected (Table 1). In addition aromatic aldehydes, including benzaldehyde and tolualdehyde, performed well in the coupling reaction to provide **6** and **7**, respectively (Table 1). In each case, the diastereoselectivity was >95:5 by crude ¹H NMR analysis.

Table 1: Trisubstituted cyclopropanes from *O*-enecarbamates.^[a]

Homoaldol adduct	Yield [%]	Cyclopropane	Yield [%], e.r.
	92		91, 93:7
	85		82, 92:8
	84		96, 93:7
	87		92, 83:17
	89		73, 90:10 ^[b]

[a] Reaction conditions: Tf₂O, 2,6-lutidine, toluene, –78 °C to –50 °C.
[b] Two minor diastereomers were also observed in this case (5:1:1 ratio).

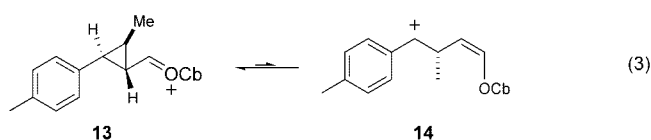
Exposure of homoaldol adducts **3–7** to triflic anhydride and 2,6-lutidine provided good to excellent yields of 1,2,3-trisubstituted cyclopropyl aldehydes **8a–12a** (Table 1). In contrast to our previous study,^[2] these cyclization substrates were more sensitive to the reaction conditions. When our standard activation conditions were employed, in CH₂Cl₂, multiple products were observed. However, when the reaction solvent was conducted in toluene, the inherent rate and alternative reaction pathways could be reduced such that the reaction was driven toward the formation of the desired cyclopropyl aldehyde products **8a–12a**. The enantiomeric purity of the cyclopropane derivatives was determined by reduction of the aldehyde with lithium aluminum hydride and analysis of the Mosher esters.^[4] The observed enantiomer ratios corresponded well with expected enantioselectivity of the starting homoaldol adducts,^[3] suggesting the cyclization step proceeds in a stereospecific manner.

The aliphatic systems provided high yields and diastereoselectivity for the cyclopropyl aldehyde products **8a–10a**. In each case, the ring closure takes place with inversion of configuration at the alcohol center.^[5] In contrast, reduced diastereoselectivity was observed upon activation of homoaldol adduct **7**. The inductively donating methyl group appears to promote equilibration of the oxonium ion intermediate **13** through the homoallylic cation **14** [Eq. (3)]. Under these conditions no products resulting from elimination were observed.

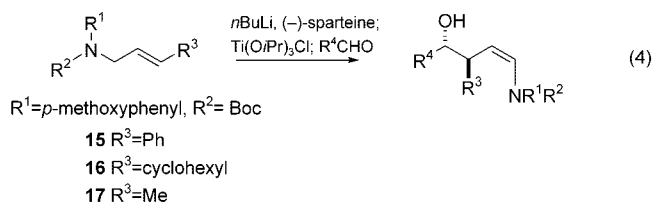
[*] C. A. Risatti, Prof. R. E. Taylor
Department of Chemistry and Biochemistry
University of Notre Dame
251 Nieuwland Science Hall, Notre Dame, IN 46556-5670 (USA)
Fax: (+1) 574-631-6652
E-mail: taylor.61@nd.edu

[**] Support of this work by the National Science Foundation (CHE-02-10918) is gratefully acknowledged. C.A.R. thanks Eli Lilly for support through an ACS Division of Organic Chemistry Graduate Fellowship.

Supporting information for this article is available on the WWW under <http://www.angewandte.org> or from the author.



Ideally one would like access to both enantiomers of the cyclopropyl aldehyde products. In fact, Beak et al. have demonstrated that *N*-(*tert*-butoxycarbonyl)-*N*-(*p*-methoxyphenyl)cinnamyl amine **15** and *N*-(*tert*-butoxycarbonyl)-*N*-(*p*-methoxyphenyl)-3-cyclohexylallylamine **16** undergo asymmetric deprotonation by an *n*BuLi/(–)-sparteine complex [Eq. (4)].^[6] However, in this case, transmetalation with Ti(O*i*Pr)₃Cl followed by quenching with an aldehyde furnished the enantiomeric, complementary homoaldol adducts.



The aldehydes used previously to generate the *O*-enecarbamates were subjected to the Beak homoaldol protocol. To complement the earlier work, the substrates were preformed with crotylamine **17**, and the yields and selectivities corresponded nicely with those observed by Beak for the cyclohexyl and cinnamyl systems. The (*Z*)-*N*-enecarbamates **18–22** were isolated with predominantly *anti* stereochemistry and the diastereoselectivity was >95:5 by crude ¹H NMR analysis (Table 2). Homoaldol adducts **18–22** were activated with triflic anhydride and 2,6-lutidine to provide aldehydes

Table 2: Trisubstituted cyclopropanes from *N*-enecarbamates.^[a]

Homoaldol adduct	Yield [%]	Cyclopropane	Yield [%], e.r.
	69		91, 90:10
	66		70, 94:6
	73		86, 91:9
	67		96, 94:6
	68		70, 92:8

[a] Reaction conditions: Tf₂O, 2,6-lutidine, toluene, –78 °C to –50 °C. R¹ = *para*-methoxyphenyl, R² = *tert*-butoxycarbonyl.

8b–12b in good to excellent yield. Again, the enantioselectivity of the cyclopropane products corresponded well with the expected enantiomer ratios from the homoaldol coupling, suggesting the cyclization step proceeds with complete stereospecificity.

In this system, cyclization of the aliphatic substrates **18–20** proceeded cleanly in CH₂Cl₂. However, care was taken with the activated aryl systems, and toluene was used as the reaction solvent. It is notable that, in contrast to *O*-enecarbamate substrate **7**, activation of *N*-enecarbamate **22** provided **12b** as a single diastereomer. The iminium ion intermediate, present in solution prior to quenching, is apparently more stable than the corresponding oxonium ion intermediate, and therefore, an equilibrium with its homoallylic cation is not relevant (Figure 1). Although the method

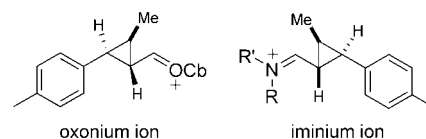


Figure 1.

has been applied to 1,2,3-trisubstituted cyclopropyl aldehydes containing a methyl substituent, alternative allylamine derivatives are expected to provide diversely substituted cyclopropanes and broaden the scope of this two-step three-carbon homologation procedure.

In conclusion we have demonstrated the stereospecific cyclization of enantiomerically enriched homoaldol adducts. This chemistry is a remarkably efficient method for the homologation of readily available aldehydes to give non-racemic, stereochemically rich 1,2,3-trisubstituted cyclopropyl aldehydes.^[7] Application of this method to the preparation of biologically relevant cyclopropanes is currently underway in our laboratories and will be reported in due course.

Received: June 28, 2004

Keywords: cations · cyclization · cyclopropanes · small ring systems · synthetic methods

- [1] H. Lebel, J.-F. Marcoux, C. Molinaro, A. B. Charette, *Chem. Rev.* **2003**, *103*, 977.
- [2] R. E. Taylor, C. A. Risatti, F. C. Engelhardt, M. J. Schmitt, *Org. Lett.* **2003**, *5*, 1377.
- [3] For a lead reference, see: K. R. K. Prasad, D. Hoppe, *Synlett* **2000**, 1067.
- [4] J. S. Dale, H. S. Mosher, *J. Am. Chem. Soc.* **1973**, *95*, 512.
- [5] R. E. Taylor, F. C. Engelhardt, M. J. Schmitt, H. Yuan, *J. Am. Chem. Soc.* **2001**, *123*, 2964.
- [6] a) M. C. Whisler, L. Vaillancourt, P. Beak, *Org. Lett.* **2000**, *2*, 2655; b) M. C. Whisler, P. Beak, *J. Org. Chem.* **2003**, *68*, 1207.
- [7] During review of this manuscript we learnt of a similar investigation. See the preceding Communication in this issue: R. Kalkofen, S. Brandau, B. Wibbeling, D. Hoppe, *Angew. Chem.* **2004**, *116*, 6836; *Angew. Chem. Int. Ed.* **2004**, *43*, 6667.

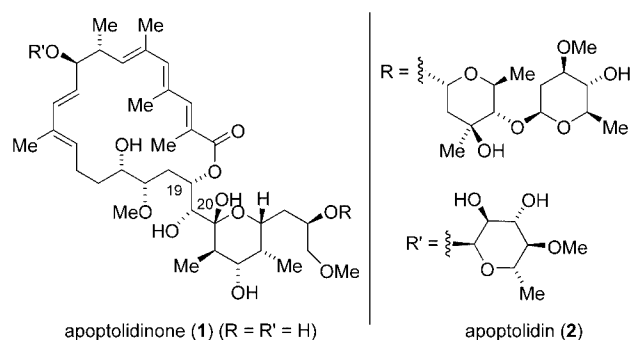
Natural Products

Total Synthesis of Apoptolidinone**

Bin Wu, Qingsong Liu, and Gary A. Sulikowski*

Dedicated to Professor Amos B. Smith, III
on the occasion of his 60th birthday.

Polyketide-derived secondary metabolites have long served as a source of structurally diverse and biologically active natural products.^[1] In the course of screening soil microorganisms for cell-specific apoptosis-inducing agents, Hayakawa and co-workers isolated the polyketide natural product apoptolidin (**2**) from *Nocardiopsis* sp.^[2] Apoptolidin induces

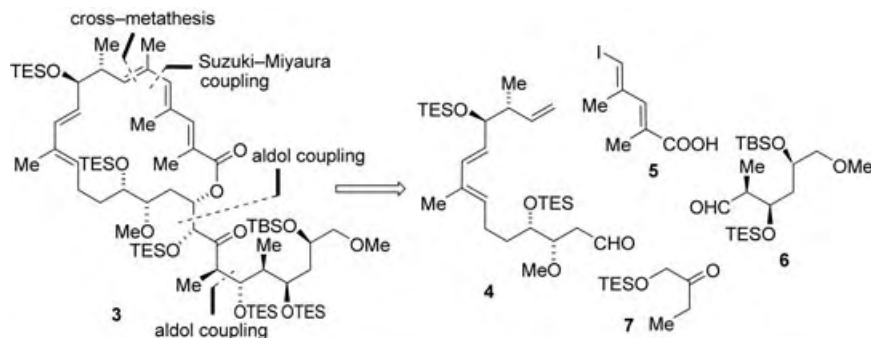


programmed cell death in E1A-transformed cells but not in normal cells.^[2a] Khosla, Salomon, and co-workers later correlated this cell-specific activity to the inhibition of mitochondrial F_0F_1 -ATPase by apoptolidin as well as other polyketide natural products.^[3] Structurally, apoptolidin features an unsaturated 20-membered macrocyclic hemiketal, a six-membered hemiketal, and three hexose sugars.^[2b] In 2001 Koert and co-workers reported the synthesis of apoptolidinone (**1**) and later the same year Nicolaou and co-workers described the total synthesis of apoptolidin.^[4–6] The latter total synthesis and other recent work has demonstrated that apoptolidin is a rather labile compound that undergoes a base-induced acyl migration from the C19 to C20 hydroxy group to produce isoapoptolidin,^[7] a compound that is less active against

mitochondrial F_0F_1 -ATPase.^[7a] Although evaluation of the cytotoxicity of select analogues has suggested the three hexose sugars of apoptolidin to contribute significantly to the overall cytotoxicity of **2**,^[3c,5e,8] biological evaluation of the aglycone, apoptolidinone (**1**), has not been reported. We describe herein the total synthesis of apoptolidinone.

Besides the synthetic approach to apoptolidin (**2**) described by Toshima and co-workers,^[6a] all previous synthetic strategies directed towards apoptolidin have relied on a linear approach in which the seco acid was assembled and subsequently subjected to a macrolactonization. To develop a more convergent assembly we retrosynthetically divided apoptolidinone into four fragments (**4–7**, Scheme 1). We planned to couple the four fragments through a combination of two diastereoselective aldol reactions, a Grubbs cross-metathesis reaction, and an intramolecular Suzuki–Miyaura cross-coupling reaction.

Construction of fragment **4** started from (*S*)-malic acid (**8**), which was converted into 3-methoxy- γ -butyrolactone (**9**) through a known four-step reaction sequence.^[9] Reduction of lactone **9** with DIBAL-H afforded lactol **10**, which on condensation with 1,3-propanedithiol afforded dithiane **11**. Swern oxidation of primary alcohol **11** provided aldehyde **12** in near quantitative yield. A five-carbon unit was introduced to aldehyde **12** by chelation-controlled addition of the Grignard reagent derived from bromide **13** to provide secondary alcohol **14** as a single isomer (Scheme 2). Bromide **13** was prepared from dihydrofuran according to the Kocien-



Scheme 1. Retrosynthetic analysis of apoptolidinone (**1**). TES = triethylsilyl, TBS = *tert*-butyldimethylsilyl.

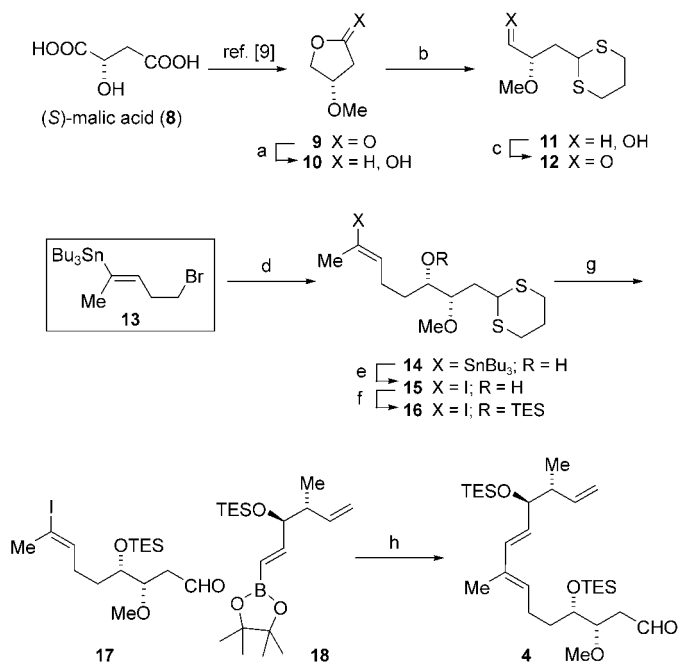
ski procedure described by Koert and co-workers in their reported synthesis of apoptolidinone.^[4a,10] A solution of **14** in dichloromethane was treated sequentially with iodine, triethylchlorosilane, and imidazole in one pot to provide vinyl iodide **16** in 90% overall yield from **14**. The dithiane group of **16** was hydrolyzed efficiently by using the Fetizon–Jurion procedure to provide aldehyde **17** in 68% yield (as well as recovered **16** (19%)).^[11]

Homoallylic silyl ether **18** was produced by the asymmetric addition of the diisopropyl tartrate ester derived (*Z*)-crotylboronate reagent developed by Roush et al.^[12] to the pinacol ester of 3-boronoacrolein,^[13] followed by silylation (TESOTf, 2,6-lutidine) of the crude crotylation product. The *syn* homoallylic ether **18** (single diastereomer, 80% *ee*) was

[*] B. Wu, Q. Liu, Prof. G. A. Sulikowski
Department of Chemistry, Vanderbilt University
7920 Stevenson Center, Nashville, TN 37235 (USA)
Fax: (+1) 615-343-1234
E-mail: gary.a.sulikowski@vanderbilt.edu

[**] We gratefully acknowledge support by the National Institutes of Health (CA 59515-09) and the Robert A. Welch Foundation (A-1230). The National Science Foundation (CHE-0077917) is acknowledged for providing funds for the purchase of NMR instrumentation.

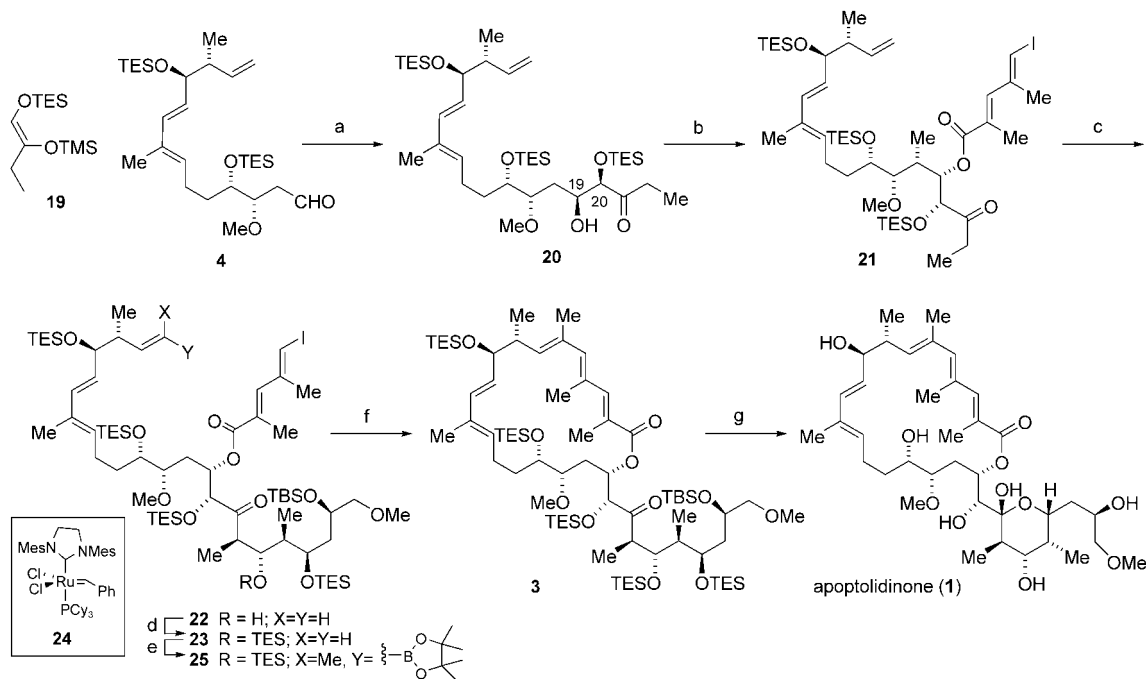
Supporting information for this article is available on the WWW under <http://www.angewandte.org> or from the author.



Scheme 2. Synthesis of fragment **4**. a) DIBAL-H, THF, -78°C ; b) 1,3-propanedithiol, $\text{BF}_3\cdot\text{OEt}_2$, CH_2Cl_2 , 28°C , 60% from **9**; c) $(\text{COCl})_2$, DMSO, $i\text{Pr}_2\text{NEt}$, $-78\rightarrow 0^{\circ}\text{C}$, 98%; d) **13**, Mg, 1,2-dibromoethane, Et_2O , -78°C , 68%; e) I_2 , CH_2Cl_2 , 0°C ; f) TESCl , 1mH, CH_2Cl_2 , 28°C , 90% from **14**; g) MeI (excess), K_2CO_3 , MeCN/pH 7 buffer (4:1), 28°C , 68% (plus 19% recovered **16**); h) **18**, $[\text{Pd}(\text{Ph}_3\text{P})_4]$, TIOH, THF/ H_2O (3:1), 28°C , 70%. DIBAL-H = diisobutylaluminum hydride, DMSO = dimethyl sulfoxide, 1mH = imidazole.

obtained in 43% yield over two steps. Suzuki–Miyaura cross-coupling between vinyl iodide **17** and vinyl boronate **18** provided diene **4** in 70% yield (Scheme 2).^[14]

The stereochemical relationship between C19 and C20 (see **20**) was established by a diastereoselective Mukaiyama aldol condensation between aldehyde **4** and enol silane (*Z*)-**19** (derived from 1,2-butanediol in three steps) to afford ketone **20** as the major product with a 4:1 ratio of isomers (Scheme 3). The assigned C19–C20 relative stereochemistry rested on the observed coupling constant of the aldol product ($J_{19,20} = 3.5$ Hz) and the 1,3-asymmetric induction model proposed by Evans and co-workers for β -methoxyaldehydes.^[15] Yamaguchi esterification of **20** with carboxylic acid **5** led to isolation of dienolate **21** in 83 % yield.^[16] Kinetic deprotonation (LHMDS, HMPA, THF, -78°C) of **21** followed by aldol condensation with aldehyde **6**^[17] afforded *syn* aldol product **22** as a single isomer in 41 % yield (plus 30 % recovered **21**).^[18] After silylation of **22** to give **23** we examined a series of cross-metathesis reactions with propenyl boronate to provide vinyl boronate **25**.^[19] The Grubbs second-generation catalyst **24** provided **25** in up to 30 % yield (plus 30 % recovered alkene **23**). Remarkably, this reaction provided **25** as a single isomer that was immediately subject to an intramolecular Suzuki–Miyaura cross-coupling to give macrolactone **3** in 47–60 % yield. Exhaustive desilylation of **3** provided apoptolidinone (**1**) in 61 % yield. Our synthetic apoptolidinone matched, in all respects, the spectral data reported by Koert and co-workers for their synthetic sample.^[4a]



Scheme 3. Synthesis of apoptolidinone (**1**). a) $\text{BF}_3 \cdot \text{OEt}_2$, CaH_2 , CH_2Cl_2 , -94°C , 50% (plus 34% recovered **4**); b) **5**, 2,4,6-trichlorobenzoyl chloride, Et_3N , DMAP, toluene, $-78 \rightarrow 28^\circ\text{C}$, 83%; c) LHMDS, THF, HMPA, -78°C , 2 h; then **6**, THF, 41% (plus 30% recovered **21**); d) TESOTf, 2,6-lutidine, CH_2Cl_2 , 0°C , 81%; e) **24**, isopropenyl pinacol boronic ester (18 equiv), CH_2Cl_2 , reflux, 6 h, 30% (plus 30% recovered **23**); f) $[\text{Pd}(\text{P}(\text{Ph})_3)_4]$, $\text{Ti}(\text{OEt})_4$, THF/ H_2O (3:1), 28°C , 30 min, 60%; g) HF-py, THF, -10°C , 12 h; then -5°C , 5 h, 61%. DMAP = 4-(dimethylamino)pyridine, LHMDS = lithium hexamethyldisilazide, HMPA = hexamethylphosphoramide, Tf = trifluoromethanesulfonyl.

In summary, apoptolidinone was synthesized from 3-methoxy- γ -butyrolactone (**9**) in 14 steps (longest linear sequence). Key steps of the synthesis include two diastereoselective aldol reactions, a cross-metathesis reaction, and two Suzuki–Miyaura cross-coupling reactions. We anticipate that this synthesis will provide access to modified derivatives of apoptolidin for utilization in studies on the cell-specific cytotoxicity of the parent natural product.^[20]

Received: July 28, 2004

Keywords: aldol reaction · diastereoselectivity · metathesis · natural products · total synthesis

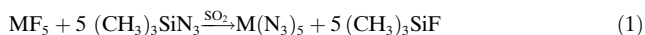
- [1] J. Stauton, K. J. Weisman, *Nat. Prod. Rep.* **2001**, *18*, 380–416.
- [2] a) J. W. Kim, H. Adachi, Y. K. Shin, Y. Hayakawa, H. Seto, *J. Antibiot.* **1997**, *50*, 628–630; b) Y. Hayakawa, J. W. Kim, H. Adachi, K. Shin-ya, K. Fujita, H. Seto, *J. Am. Chem. Soc.* **1998**, *120*, 3524–3525.
- [3] a) A. R. Salomon, D. W. Voehringer, L. A. Herzenberg, C. Khosla, *Chem. Biol.* **2001**, *8*, 71–80; b) A. R. Salomon, D. W. Voehringer, L. A. Herzenberg, C. Khosla, *Proc. Natl. Acad. Sci. USA* **2000**, *97*, 14766–14771; c) A. R. Salomon, Y. B. Zhang, H. Seto, C. Khosla, *Org. Lett.* **2001**, *3*, 57–59.
- [4] a) J. Schuppan, H. Wehlan, S. Keiper, U. Koert *Angew. Chem.* **2001**, *113*, 2125–2128; *Angew. Chem. Int. Ed.* **2001**, *40*, 2063–2066; b) J. Schuppan, B. Ziemer, U. Koert, *Tetrahedron Lett.* **2000**, *41*, 621–624; c) while this manuscript was in preparation, Koert and co-workers described the total synthesis of apoptolidin; see: H. Wehlan, M. Dauber, M.-T. M. Fernaud, J. Schuppan, R. Mahrwald, B. Ziemer, M.-E. J. Garcia, U. Koert, *Angew. Chem.* **2004**, *116*, 4698–4702; *Angew. Chem. Int. Ed.* **2004**, *43*, 4597–4601.
- [5] a) K. C. Nicolaou, Y. Li, K. C. Fylaktakidou, H. J. Mitchell, H. X. Wei, B. Weyershausen, *Angew. Chem.* **2001**, *113*, 3968–3972; *Angew. Chem. Int. Ed.* **2001**, *40*, 3849–3854; b) K. C. Nicolaou, Y. W. Li, K. C. Fylaktakidou, H. J. Mitchell, K. Sugita, *Angew. Chem.* **2001**, *113*, 3972–3976; *Angew. Chem. Int. Ed.* **2001**, *40*, 3854–3857; c) K. C. Nicolaou, Y. Li, B. Weyershausen, H.-x. Wei, *Chem. Commun.* **2000**, 307–308; d) K. C. Nicolaou, K. C. Fylaktakidou, H. Monenschein, Y. Li, B. Weyershausen, H. J. Mitchell, H. Wei, P. Guntupalli, D. Hepworth, K. Sugita, *J. Am. Chem. Soc.* **2003**, *125*, 15433–15442; e) K. C. Nicolaou, Y. Li, K. Sugita, H. Monenschein, P. Guntupalli, H. J. Mitchell, K. C. Fylaktakidou, D. Vourloumis, P. Giannakakou, A. O’Brate, *J. Am. Chem. Soc.* **2003**, *125*, 15443–15454.
- [6] For other synthetic studies toward apoptolidin, see: a) K. Toshima, T. Arita, K. Kato, D. Tanaka, S. Matsumura, *Tetrahedron Lett.* **2001**, *42*, 8873–8876; b) G. A. Sulikowski, W. M. Lee, B. Jin, B. Wu, *Org. Lett.* **2000**, *2*, 1439–1442; c) S. Chng, J. Xu, T. Loh, *Tetrahedron Lett.* **2003**, *44*, 4997–5000; d) Y. Chen, J. B. Evarts, Jr., E. Torres, P. L. Fuchs, *Org. Lett.* **2002**, *4*, 3571–3574; f) W. D. Paquette, R. E. Taylor, *Org. Lett.* **2004**, *6*, 103–106.
- [7] a) P. A. Wender, A. Gullledge, O. D. Jankowski, H. Seto, *Org. Lett.* **2002**, *4*, 3819–3822; b) J. D. Pennington, H. J. Williams, A. R. Salomon, G. A. Sulikowski, *Org. Lett.* **2002**, *4*, 3823–3825.
- [8] For the semisynthesis and biological evaluation of apoptolidin derivatives, see: a) P. A. Wender, O. D. Jankowski, E. A. Tabet, H. Seto, *Org. Lett.* **2003**, *5*, 587–590; b) P. A. Wender, O. D. Jankowski, E. A. Tabet, H. Seto, *Org. Lett.* **2003**, *5*, 2299–2302.
- [9] a) S. Saito, T. Hasegawa, M. Inaba, R. Nishida, *Chem. Lett.* **1984**, 1389–1392; b) C. E. Masse, M. Yang, J. Solomon, J. S. Panek, *J. Am. Chem. Soc.* **1998**, *120*, 4123–4134.
- [10] a) V. Fargeas, P. Le Menez, I. Berque, J. Ardisson, A. Pancrazi, *Tetrahedron* **1996**, *52*, 6613–6634; b) P. Kocienski, S. Wadman, K. Cooper, *J. Am. Chem. Soc.* **1989**, *111*, 2363–2364.
- [11] M. Fetizon, M. Jurion, *J. Chem. Soc. Chem. Commun.* **1972**, 382–383.
- [12] W. R. Roush, K. Ando, D. B. Powers, A. D. Palkowitz, R. L. Halterman, *J. Am. Chem. Soc.* **1990**, *112*, 6339–6348.
- [13] a) B. B. Touré, H. R. Hoveyda, J. Taylor, A. Ulaczyk-Lesanko, D. G. Hall, *Chem. Eur. J.* **2003**, *9*, 466–474; b) E. Jehanno, M. Vaultier, *Tetrahedron Lett.* **1995**, *36*, 4439–4442.
- [14] Owing to the modest enantioselectivity observed in the crotylation step used to prepare **18**, an initial 9:1 ratio of diastereomers was observed in the Suzuki–Miyaura coupled product **4**; the minor diastereomer was subsequently removed by flash chromatography following the sequence of two aldol reactions: a) N. Miyaura, K. Yamada, H. Suginome, A. Suzuki, *J. Am. Chem. Soc.* **1985**, *107*, 972–980; b) N. Miyaura, A. Suzuki, *Chem. Rev.* **1995**, *95*, 2457–2483; c) S. A. Frank, H. Chen, R. K. Kunz, M. J. Schnaderbeck, W. R. Roush, *Org. Lett.* **2000**, *2*, 2691–2694.
- [15] a) D. A. Evans, M. C. Yang, M. J. Dart, J. L. Duffy, A. S. Kim, *J. Am. Chem. Soc.* **1995**, *117*, 9598–9599; b) D. A. Evans, M. J. Dart, J. L. Duffy, M. C. Yang, *J. Am. Chem. Soc.* **1996**, *118*, 4322–4343.
- [16] J. Inanaga, K. Hirata, H. Saeki, T. Katsuki, M. Yamaguchi, *Bull. Chem. Soc. Jpn.* **1979**, *52*, 1989–1990.
- [17] The preparation of aldehyde **6** is described in the Supporting Information.
- [18] For related diastereoselective aldol reactions, see: a) S. F. Martin, T. Hida, P. R. Kym, M. Loft, A. Hodgson, *J. Am. Chem. Soc.* **1997**, *119*, 3193–3194; b) A. F. Sviridov, V. S. Borodkin, M. S. Ermolenko, D. V. Yashunsky, N. K. Kochetkov, *Tetrahedron* **1991**, *47*, 2317–2336.
- [19] a) A. K. Chatterjee, R. H. Grubbs, *Angew. Chem.* **2002**, *114*, 3303–3306; *Angew. Chem. Int. Ed.* **2002**, *41*, 3172–3174; b) J. T. Njardarson, K. Biswas, S. J. Danishefsky, *Chem. Commun.* **2002**, 759–761.
- [20] We employed the synthetic route described herein to produce 2–4 mg of apoptolidinone, which is currently undergoing biological evaluation in a side-by-side comparison with apoptolidin itself.

Polyazide Chemistry: Preparation and Characterization of As(N₃)₅, Sb(N₃)₅, and [P(C₆H₅)₄][Sb(N₃)₆][−]

Ralf Haiges,* Jerry A. Boatz, Ashwani Vij, Vandana Vij, Michael Gerken, Stefan Schneider, Thorsten Schroer, Muhammed Yousufuddin, and Karl O. Christe*

The binary arsenic and antimony azide species As(N₃)₃,^[1–3] [As(N₃)₄]⁺,^[4] [As(N₃)₄][−],^[4] [As(N₃)₆][−],^[4,5] Sb(N₃)₃,^[3,6] [Sb(N₃)₄]⁺,^[4] [Sb(N₃)₄][−],^[4] and [Sb(N₃)₆][−]^[4] have been reported, and the crystal structures of As(N₃)₃,^[3] Sb(N₃)₃,^[3] and [As(N₃)₆][−]^[4,5] determined.^[7] In addition, the Lewis base stabilized species M(N₃)₅·LB (M = As, Sb; LB = pyridine, quinoline, NH₃, N₂H₄, NH₂CN) are known.^[8] However, previous attempts^[4] to obtain the neat pentaazides of arsenic and antimony were not successful. Even at low temperatures, attempted syntheses resulted in explosions that were described as “so intense that only pulverized glass remained”.^[4] Furthermore, As(N₃)₅ was predicted^[4] to be a “highly unstable compound”, based on its analogy to AsCl₅.^[9] Herein, we communicate the synthesis and characterization of neat As(N₃)₅ and Sb(N₃)₅, and their conversion into the [As(N₃)₆][−] and [Sb(N₃)₆][−] ions, respectively. We also report the crystal structure of [P(C₆H₅)₄][Sb(N₃)₆].

The reactions of AsF₅ or SbF₅ in SO₂ with excess (CH₃)₃SiN₃ result in facile and complete fluoride–azide exchange and yield clear yellow solutions of As(N₃)₅ or Sb(N₃)₅, respectively, [Eq. (1); M = As, Sb].



Removal of the volatile compounds (SO₂, (CH₃)₃SiF, and excess (CH₃)₃SiN₃) results in the isolation of the neat pentaazides.

As expected for highly endothermic, covalent polyazides, As(N₃)₅ and Sb(N₃)₅ are highly shock sensitive and can

explode violently when touched with a metal spatula or by rapid change in temperature (e.g. freezing with liquid nitrogen). As(N₃)₅ was obtained as a yellow liquid. Its identity was established by the observed material balance, through ¹⁴N NMR and vibrational spectroscopy, and its conversion with [N₃][−] into the known^[4,5] [As(N₃)₆][−] ion. The observed low-temperature Raman spectrum of As(N₃)₅ is shown in Figure 1.

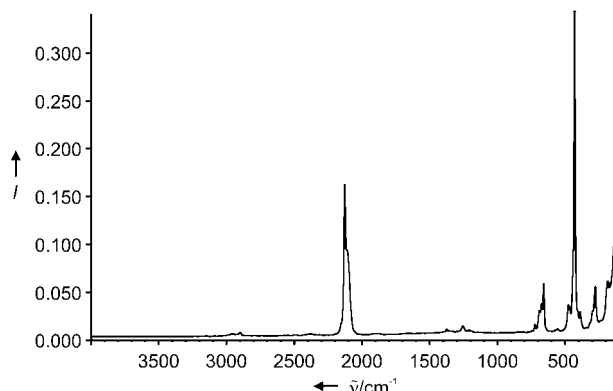


Figure 1. Low-temperature Raman spectrum of As(N₃)₅.

In contrast to a previous prediction,^[4] neat arsenic pentaazide was found to be kinetically stable at ambient temperature, but highly explosive. The presence of covalent azido ligands^[1–8,10–14] was confirmed by the observed ¹⁴N NMR shifts of δ = −149 ppm (N_β, Δν_{1/2} = 42 Hz), −160 ppm (N_γ, Δν_{1/2} = 96 Hz), and −282 ppm (N_α, extremely broad) in DMSO solution at 25 °C.

Sb(N₃)₅ was obtained as a pale yellow solid. It is even more sensitive than As(N₃)₅ and must be handled at reduced temperature. Warming the compound to ambient temperature results in violent decomposition and can cause serious damage. The identity of antimony pentaazide was established by the observed material balance, its Raman spectrum (Figure 2), and its reaction with [N₃][−] to give the [Sb(N₃)₆][−] ion. The calculated and observed vibrational frequencies and intensities for As(N₃)₅ and Sb(N₃)₅ are listed in Table 1. The agreement between the observed frequencies and those calculated for pentacoordinate trigonal-bipyramidal struc-

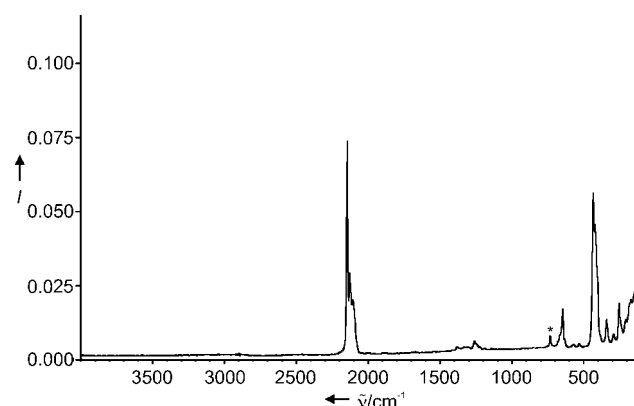


Figure 2. Low-temperature Raman spectrum of Sb(N₃)₅. The band marked by an asterisk is due to the Teflon-FEP sample tube.

[*] Dr. R. Haiges, Dr. M. Gerken, Dr. S. Schneider, Dr. T. Schroer, M. Yousufuddin, Prof. Dr. K. O. Christe
Loker Research Institute and Department of Chemistry
University of Southern California
Los Angeles, CA 90089-1661 (USA)
Fax: (+1) 213-740-6679
E-mail: haiges@usc.edu
kchriste@usc.edu

Dr. J. A. Boatz, Dr. A. Vij, V. Vij
Space and Missile Propulsion Division
Air Force Research Laboratory (AFRL/PRSP)
10 East Saturn Boulevard Bldg 8451, Edwards Air Force Base, CA 93524 (USA)

[**] This work was funded by the Defense Advanced Research Projects Agency, with additional support from the Air Force Office of Scientific Research and the National Science Foundation. R.H. thanks the Deutsche Forschungsgemeinschaft for a postdoctoral fellowship. We thank Prof. G. A. Olah, and Drs. A. Morrish, D. Woodbury, and M. Berman, for their steady support, and Prof. R. Bau and Dr. R. Wagner for their help and stimulating discussions.

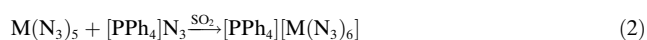
Table 1: Comparison of observed and calculated^[a] vibrational frequencies [cm⁻¹] and intensities^[b] for As(N₃)₅ and Sb(N₃)₅.

Band	Description	As(N ₃) ₅		Sb(N ₃) ₅	
		obsd Raman	calcd (IR) [Raman]	obsd Raman	calcd (IR) [Raman]
ν_1	$\nu_{as}N_3$	2162 [0.4]	2249 (366) [21]	2146 [10.0]	2198 (208) [35]
ν_2	$\nu_{as}N_3$	2135 [4.7]	2234 (775) [21]		2194 (936) [21]
ν_3	$\nu_{as}N_3$	2114 [2.6]	2210 (182) [35]	2127 [3.8]	2172 (282) [41]
ν_4	$\nu_{as}N_3$		2199 (417) [31]	2107 [2.6]	2166 (393) [25]
ν_5	$\nu_{as}N_3$		2191 (924) [24]	2097 [2.2]	2160 (941) [26]
ν_6	ν_sN_3	1262 [0.3]	1310 (48) [36]	1260 [0.7]	1262 (53) [32]
ν_7	ν_sN_3	1250 [0.3]	1305 (190) [8.8]	1249 [0.5]	1258 (151) [12]
ν_8	ν_sN_3		1284 (45) [21]	1239 [0.5]	1243 (17) [24]
ν_9	ν_sN_3		1283 (344) [3.1]	1221 [0.4]	1241 (290) [1.5]
ν_{10}	ν_sN_3		1276 (172) [9.3]		1238 (134) [7.9]
ν_{11}	δN_3	699 [0.8]	727 (91) [2.6]		661 (8) [1.5]
ν_{12}	δN_3	682 [1.0]	718 (16) [2.9]	667 [1.0]	658 (40) [3.9]
ν_{13}	δN_3		712 (29) [1.0]		653 (14) [1.9]
ν_{14}	δN_3		703 (59) [15]	646 [2.2]	647 (28) [15]
ν_{15}	δN_3	666 [1.7]	686 (9) [18]	630 [0.7]	634 (4) [28]
ν_{16}	δN_3		559 (9) [0.7]		540 (4) [1.3]
ν_{17}	δN_3		552 (3) [0.9]	532 [0.5]	529 (3) [0.9]
ν_{18}	δN_3		548 (5) [1.2]		525 (2) [1.2]
ν_{19}	δN_3		547 (4) [0.2]		524 (3) [1.3]
ν_{20}	δN_3		547 (12) [0.9]		522 (4) [1.1]
ν_{21}	$\nu_{as}MN$		514 (114) [3.1]	434 [7.5]	458 (74) [5.3]
ν_{22}	$\nu_{as}MN$		500 (100) [4.6]	421 [6.0]	452 (74) [5.8]
ν_{23}	$\nu_{as}MN$		488 (113) [4.6]		446 (69) [5.3]
ν_{24}	ν_sMN	437 [10.0]	463 (10) [49]	404 [3.8]	424 (4) [89]
ν_{25}	$\nu_{as}MN$	397 [0.8]	416 (6) [10]	382 [1.0]	400 (3) [14]
ν_{26}	δMN		333 (73) [0.7]		255 (62) [0.9]
ν_{27}	δMN		322 (47) [0.9]	291 [1.1]	250 (41) [1.6]
ν_{28}	δMN		314 (43) [2.6]	253 [2.5]	242 (11) [10]
ν_{29}	δMN	303 [0.8]	298 (6) [5.2]	239 [1.4]	234 (15) [5.2]
ν_{30}	δMN	284 [1.6]	291 (5) [9.4]	207 [1.6]	222 (29) [5.8]
ν_{31}	τ	194 [1.7]	183 (1) [4.2]	183 [2.3]	151 (2) [5.5]
ν_{32}	τ		173 (3) [1.5]	171 [2.6]	143 (4) [1.8]
ν_{33}	τ		167 (1) [4.4]		136 (1) [5.6]
ν_{34}	τ		148 (0.3) [0.7]		126 (1) [0.6]
ν_{35}	τ		112 (2) [3.2]		92 (2) [3.7]
ν_{36}	τ		95 (0) [8.5]		82 (1) [12]
ν_{37}	τ		92 (0.3) [9.5]		81 (0) [12]
ν_{38}	τ		83 (1) [4.4]		69 (1) [2.8]
ν_{39}	τ		53 (0) [4.6]		49 (0) [4.7]
ν_{40}	τ		45 (0) [6.3]		43 (0) [5.4]
ν_{41}	τ		43 (0) [7.7]		34 (0) [8.8]
ν_{42}	τ		31 (0) [4.5]		24 (0) [4.8]

[a] Our calculated MP2 minimum energy structures for As(N₃)₅ and Sb(N₃)₅ are derived from trigonal bipyramids and are very similar to those obtained at the B3LYP level.^[4] [b] Observed Raman intensities are relative intensities; calculated IR intensities [kmol⁻¹] and calculated Raman [Å⁴ amu⁻¹].

tures is good. However, it must be kept in mind that distinction between slightly different geometries based on the skeletal modes in these types of polyazido compounds is generally difficult, because the vibrational spectra are complex and not very sensitive to minor changes in the ligand arrangement.

The reactions of As(N₃)₅ and Sb(N₃)₅ with ionic azides, such as [PPh₄]⁺[N₃]⁻, produce the corresponding [As(N₃)₆]⁻^[4,5] and [Sb(N₃)₆]⁻ salts, respectively, [Eq. (2); M = As, Sb].



Both tetraphenylphosphonium salts were isolated as

colorless solids. The [PPh₄][Sb(N₃)₆] salt can also be prepared from the corresponding [SbCl₆]⁻ salt and (CH₃)₃SiN₃ in CH₃CN solution. However, the previously published^[4] reaction conditions, that is, one single treatment at 25 °C for 24 h, were found insufficient. Even after seven prolonged treatments with large amounts of fresh (CH₃)₃SiN₃ only four of the original six chlorine ligands were replaced by azido groups, as shown by Raman spectroscopy and single-crystal X-ray diffraction studies. Heating to 82 °C in refluxing CH₃CN was required to achieve further chloride substitution.

Single crystals of [PPh₄][Sb(N₃)₆] were obtained by recrystallization from CH₃CN solution. Because of the presence of a large counterion which serves as an inert spacer and suppresses detonation propagation, these salts are

much less shock sensitive than neat $\text{As}(\text{N}_3)_5$ and $\text{Sb}(\text{N}_3)_5$, and are thermally surprisingly stable. Thus, a crystalline sample of $[\text{PPh}_4][\text{Sb}(\text{N}_3)_6]$ could be heated to its melting point at 104–106 °C without decomposition.

$[\text{PPh}_4][\text{Sb}(\text{N}_3)_6]$ crystallizes in the monoclinic space group $C2/c$. Its X-ray structure (Figure 3)^[15] revealed the presence of

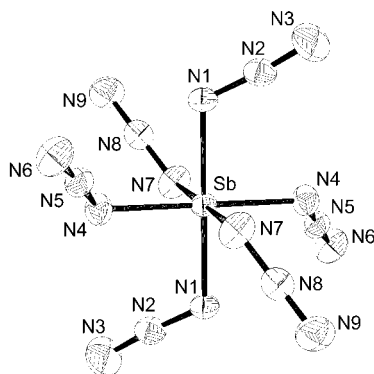


Figure 3. ORTEP drawing of the anionic part of the crystal structure of $[\text{PPh}_4][\text{Sb}(\text{N}_3)_6]$. Thermal ellipsoids are set at 50% probability. Selected bond lengths [Å] and angles [°]: Sb–N1 2.065(2), Sb–N4 2.079(2), Sb–N7 2.085(3), N1–N2 1.220(3), N2–N3 1.120(3), N4–N5 1.222(4), N5–N6 1.127(4), N7–N8 1.222(3), N8–N9 1.128(4); N1–N2–N3 175.1(3), N4–N5–N6 175.1(3), N7–N8–N9 174.7(4), N1–Sb–N4 92.00(9), N1–Sb–N7 88.33(11), N4–Sb–N7 88.45(11), Sb–N1–N2 116.7(2), Sb–N4–N5 116.4(2), Sb–N7–N8 116.6(2).

$[\text{PPh}_4]^+$ and $[\text{Sb}(\text{N}_3)_6]^-$ ions without significant cation–anion interaction. The closest Sb⋯N and N⋯N contacts between neighboring anions are 5.0 Å and 3.2 Å, respectively. The structure of the $[\text{Sb}(\text{N}_3)_6]^-$ ion is only slightly distorted from perfect S_6 symmetry and is analogous to those of $[\text{As}(\text{N}_3)_6]^-$,^[4,5] $[\text{Si}(\text{N}_3)_6]^{2-}$,^[16] $[\text{Ge}(\text{N}_3)_6]^{2-}$,^[17] and $[\text{Ti}(\text{N}_3)_6]^{2-}$,^[18] and contrary to that of $[\text{Te}(\text{N}_3)_6]^{2-}$.^[19] The structure of the $[\text{Sb}(\text{N}_3)_6]^-$ ion consists of an asymmetric SbN_9 unit with three azido groups covalently bonded in a trigonal pyramidal fashion to the antimony center. The remaining three coordination sites at the metal center are occupied by three symmetry related azido groups (symmetry operation $-x + 3/2, -y + 3/2, -z + 1$). All three Sb–N bond of 2.064(2), 2.079(2), and 2.084(2) Å are significantly shorter than the 2.119(4) Å found for $\text{Sb}(\text{N}_3)_3$.^[3]

Further support for the presence of the $[\text{Sb}(\text{N}_3)_6]^-$ ion is provided by the NMR spectrum. The ^{14}N NMR spectrum in DMSO shows resonances at $\delta = -141$ ppm (N_β , $\Delta\nu_{1/2} = 63$ Hz), -185 ppm (N_γ , $\Delta\nu_{1/2} = 103$ Hz), and -287 ppm (N_α , $\Delta\nu_{1/2} = 580$ Hz), that are characteristic for covalent azides.^[1–8,10–14] Our spectrum differs, particularly in the N_γ region, significantly from that previously reported^[4] (N_β : $\delta = -141$ ppm, $\Delta\nu_{1/2} = 45$ Hz; N_γ : $\delta = -154$ ppm, $\Delta\nu_{1/2} = 120$ Hz, $\delta = -163$ ppm, $\Delta\nu_{1/2} = 45$ Hz, $\delta = -173$ ppm, $\Delta\nu_{1/2} = 110$ Hz; N_α : $\delta = -244$ ppm, $\Delta\nu_{1/2} = 580$ Hz), for the $[\text{N}(\text{C}_2\text{H}_5)_4]^+$ salt in the same solvent and at the same temperature. We have observed similar shifts and multiple resonances for N_γ ($\text{N}_\alpha\delta = -245$ ppm; $\text{N}_\gamma\delta = -150, -160, -168$, and -169 ppm) in samples, prepared from $[\text{SbCl}_6]^-$, in which chlorine substitution was incomplete, as shown by Raman spectroscopy and

their crystal structures. This result is in accord with our finding that, under the previously reported conditions,^[4] the chloride/azide exchange is incomplete.

The observed Raman and IR spectra of $[\text{P}(\text{C}_6\text{H}_5)_4][\text{Sb}(\text{N}_3)_6]$ are shown in Figure 4, and the observed frequencies and intensities are listed in the Experimental Section.

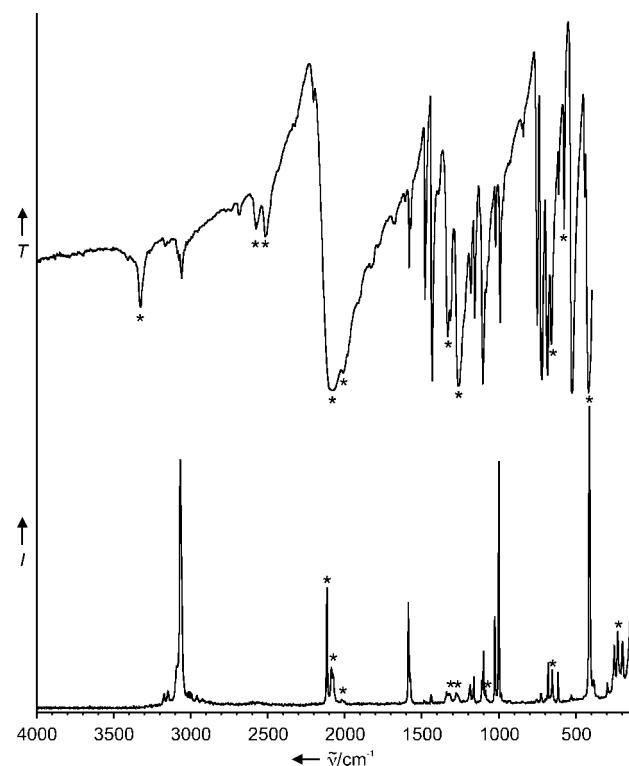


Figure 4. IR (top) and Raman (bottom) spectra of $[\text{P}(\text{C}_6\text{H}_5)_4][\text{Sb}(\text{N}_3)_6]$. The bands belonging to the $[\text{Sb}(\text{N}_3)_6]^-$ ion are marked with asterisks.

Assignments of the observed spectra were made by comparison with those calculated at the MP2/SBK + (d) level of theory and are given in the Experimental Section. The good agreement between the observed and calculated spectra confirms the results from the crystal-structure determination that, in its $[\text{PPh}_4]^+$ salt, the $[\text{Sb}(\text{N}_3)_6]^-$ ion closely approximates ideal S_6 symmetry.

Experimental Section

Caution! Arsenic and antimony azides are toxic, potentially hazardous, and can decompose explosively under various conditions! They should be handled only on a scale of less than 2 mmol with appropriate safety precautions (safety shields, safety glasses, face shields, leather gloves, protective clothing, such as leather suits, and ear plugs).^[3,18,19] Teflon containers should be used, whenever possible, to avoid hazardous shrapnel formation. Rapid changes in temperature of $\text{As}(\text{N}_3)_5$ and $\text{Sb}(\text{N}_3)_5$ (whether pure or in SO_2 solution) can result in violent explosions. The manipulation of these materials is facilitated by handling them, whenever possible, in solution to avoid detonation propagation, the use of large inert counterions as spacers, and anion formation which increases the partial negative charges on the terminal N_γ atoms and thereby reduces the N_β – N_γ triple-bond character and the

tendency for N_2 elimination. **Ignoring safety precautions can lead to serious injuries!**

All reactions were carried out in Teflon-FEP ampules (FEP = perfluoro ethylene propylene polymer) that were closed by stainless steel valves. Volatile materials were handled in a Pyrex glass vacuum line. All Teflon reaction vessels were passivated with ClF_3 prior to use. Nonvolatile materials were handled in the dry argon atmosphere of a glove box.

Raman spectra were recorded at -80°C in the range 4000–80 cm^{-1} on a Bruker Equinox 55 FT-RA spectrophotometer using a Nd-YAG laser at 1064 nm with power levels of 200 mW or less and a 180° geometry. Pyrex melting-point tubes that were baked out at 300°C for 48 h at 10 mTorr vacuum or Teflon-FEP tubes with stainless steel valves that were passivated with ClF_3 were used as sample containers. IR spectra were recorded in the range 4000–400 cm^{-1} on a Midac, M Series, FT-IR spectrometer using KBr or AgCl pellets. The pellets were prepared inside the glove-box using an Econo press (Barnes Engineering Co.).

^{14}N NMR spectra were recorded unlocked at 36.13 MHz on a Bruker AMX 500 spectrometer using solutions of the compounds in DMSO in sealed standard glass tubes. Neat CH_3NO_2 ($\delta = 0.00$ ppm) was used as the external reference.

The starting materials AsF_5 (Ozark Mahoning) and $[\text{P}(\text{C}_6\text{H}_5)_4]\text{I}$ (Aldrich) were used without further purification. $(\text{CH}_3)_3\text{SiN}_3$ (Aldrich) was purified by fractional condensation and SbF_5 (Ozark Mahoning) by distillation prior to use. Solvents were dried by standard methods and freshly distilled before being used. $[\text{P}(\text{C}_6\text{H}_5)_4]\text{N}_3$ was prepared from $[\text{P}(\text{C}_6\text{H}_5)_4]\text{I}$ and AgN_3 .

$\text{As}(\text{N}_3)_5$: $(\text{CH}_3)_3\text{SiN}_3$ (3.91 mmol) was condensed at -196°C onto a frozen solution of AsF_5 (0.570 mmol) in SO_2 (1 mL). The reaction mixture was kept at -25°C for 30 min and then slowly warmed to ambient temperature over a period of 4 h resulting in a yellow solution. Removal of all volatile material at ambient temperature in a dynamic vacuum resulted in the isolation of a colorless liquid (0.170 g, weight calculated for 0.570 mmol of $\text{As}(\text{N}_3)_5 = 0.162$ g). The obtained liquid was characterized by Raman and NMR spectroscopy.

$\text{Sb}(\text{N}_3)_5$: $(\text{CH}_3)_3\text{SiN}_3$ (4.84 mmol) was condensed at -196°C onto a frozen solution of SbF_5 (0.609 mmol) in SO_2 (14 mmol). The reaction mixture was warmed to -25°C and kept between -25°C and -15°C for 10 h resulting in a bright yellow solution. Removal of all volatile material at -15°C in a dynamic vacuum resulted in the isolation of an intense yellow solid (0.216 g, weight calculated for 0.609 mmol of $\text{Sb}(\text{N}_3)_5 = 0.202$ g).

$[\text{PPh}_4][\text{M}(\text{N}_3)_6]$ ($\text{M} = \text{As}, \text{Sb}$): Neat PPh_4N_3 (0.43 mmol) was added to a cooled solution of $\text{M}(\text{N}_3)_5$ (0.43 mmol) in SO_2 (15 mmol) at -64°C . The reaction mixture was kept at -25°C and occasionally agitated. After 2 h, all volatiles were removed at ambient temperature in a dynamic vacuum, leaving behind solid $[\text{PPh}_4][\text{M}(\text{N}_3)_6]$. $[\text{PPh}_4][\text{As}(\text{N}_3)_6]$: 0.285 g, weight calculated for 0.43 mmol = 0.288 g; $[\text{PPh}_4][\text{Sb}(\text{N}_3)_6]$: 0.313 g, weight calculated for 0.43 mmol = 0.307 g). Colorless single crystals of $[\text{PPh}_4][\text{Sb}(\text{N}_3)_6]$ were grown from a solution in CH_3CN by slow evaporation of the solvent in a dynamic vacuum. Raman spectrum of the $[\text{As}(\text{N}_3)_6]^-$ ion (50 mW, 20°C): $\tilde{\nu} = 2125(4.9)/2085(3.0)$ (ν_{asN_3}), 1331(0.6)/1269(1.0)/1251(0.6) (ν_{N_3}), 666(1.5)/631(0.5) (δN_3), 418(10.0) (ν_{asN}), 379(1.1) (ν_{asAsN}), 278(1.4) (δAsN), 165 (5.0) cm^{-1} . $[\text{Sb}(\text{N}_3)_6]^-$: IR (KBr): $\tilde{\nu} = 3329(\text{mw})/2583(\text{w})/2522(\text{w})$ (combination bands), 2086(vs)/2016(s) (ν_{asN_3}), 1337(m)/1318(m)/1264(s) (ν_{N_3}), 663(m)/580(w) (δN_3), 424(s) cm^{-1} (ν_{SbN}). Raman (50 mW, 20°C): $\tilde{\nu} = 2116(4.1)/2087(1.4)/2075(1.1)/2018(0.3)$ (ν_{asN_3}), 1319(0.5)/1275(0.5) (ν_{N_3}), 653(1.4) (δN_3), 412(10.0) (ν_{SbN}), 386(1.0) (ν_{asSbN}), 229(2.5) (δSbN), 147 (3.0) cm^{-1} .

Optimizations of all structures were performed using second-order perturbation theory.^[20,21] For the arsenic azides, the Binning and Curtis double-zeta valence basis set,^[22] augmented with a d polarization function^[23] was used for the arsenic and the 6-31G(d) basis set^[24,25] for the nitrogen atoms. For the antimony azides, the Stevens,

Basch, and Krauss (SBK) effective core potentials and the corresponding valence-only basis sets were used.^[26] The SBK valence basis set for nitrogen was augmented with a d polarization function^[25] and a diffuse s + p shell,^[27] whereas only a d polarization function^[28] was added to the antimony basis set. Hessians (energy second derivatives) were calculated for the final equilibrium structures to determine if they are minima (positive definite hessian) or transition states (one negative eigenvalue). All calculations were performed using the electronic structure code GAMESS.^[29]

Unscaled calculated frequencies (cm^{-1}) and (infrared, kmol^{-1}) and [Raman, $\text{\AA}^4\text{amu}^{-1}$] intensities for the $[\text{Sb}(\text{N}_3)_6]^-$ ion (C_{2h} symmetry): A_g : 2219 (0) [82], 2200 (0) [48], 1273 (0) [77], 1267 (0) [41], 659 (0) [6.0], 645 (0) [23], 596 (0) [18], 409 (0) [121], 385 (0) [8.8], 236 (0) [5.2], 215 (0) [12], 128 (0) [9.3], 68 (0) [20], 30 (0) [17]; B_g : 2202 (0) [33], 1267 (0) [42], 652 (0) [0.9], 590 (0) [0.1], 549 (0) [0.4], 372 (0) [5.4], 225 (0) [4.6], 128 (0) [8.4], 41 (0) [12], 24 (0) [9.9]; A_u : 2216 (1299) [0], 1268 (171) [0], 659 (5.8) [0], 590 (2.2) [0], 547 (5.8) [0], 424 (135) [0], 257 (122) [0], 195 (9.2) [0], 152 (1.0) [0], 68 (0.3) [0], 36 (1.1) [0], 19 (0.2) [0]; B_u : 2204 (1493) [0], 2193 (914) [0], 1271 (147) [0], 1268 (148) [0], 663 (25) [0], 650 (34) [0], 596 (7.0) [0], 429 (97) [0], 416 (112) [0], 247 (88) [0], 244 (52) [0], 166 (3.5) [0], 79 (4.1) [0], 71 (2.5) [0], 24 (0.5) [0].

Received: August 20, 2004

Keywords: antimony · arsenic · azides · theoretical chemistry

- [1] T. M. Klapötke, P. Geissler, *J. Chem. Soc. Dalton Trans.* **1995**, 3365.
- [2] P. Geissler, T. M. Klapötke, H.-J. Kroth, *Spectrochim. Acta Part A* **1995**, 51, 1075.
- [3] R. Haiges, A. Vij, J. A. Boatz, S. Schneider, T. Schroer, M. Gerken, K. O. Christe, *Chem. Eur. J.* **2004**, 10, 508.
- [4] K. Karaghiosoff, T. M. Klapötke, B. Krumm, H. Nöth, T. Schütt, M. Suter, *Inorg. Chem.* **2002**, 41, 170.
- [5] T. M. Klapötke, H. Nöth, T. Schütt, M. Warchhold, *Angew. Chem.* **2000**, 112, 2197; *Angew. Chem. Int. Ed.* **2000**, 39, 2108.
- [6] T. M. Klapötke, A. Schulz, J. McNamara, *J. Chem. Soc. Dalton Trans.* **1996**, 2985.
- [7] For recent reviews, see: a) W. Fraenk, T. M. Klapötke in *Inorganic Chemistry Highlights* (Eds.: G. Meyer, D. Naumann, L. Wesemann), Wiley-VCH, Weinheim, **2002**; b) A. Kornath, *Angew. Chem.* **2001**, 113, 3231; *Angew. Chem. Int. Ed.* **2001**, 40, 3135; c) T. M. Klapötke, *Chem. Ber.* **1997**, 130, 443.
- [8] T. M. Klapötke, T. Schütt, *J. Fluorine Chem.* **2001**, 109, 151.
- [9] a) K. Seppelt, *Z. Anorg. Allg. Chem.* **1977**, 434, 5; b) K. Seppelt, *Angew. Chem.* **1976**, 88, 410; *Angew. Chem. Int. Ed. Engl.* **1976**, 15, 377.
- [10] T. M. Klapötke, B. Krumm, P. Mayer, O. P. Ruscitti, *Inorg. Chem.* **2000**, 39, 5426.
- [11] T. M. Klapötke, B. Krumm, P. Mayer, H. Piotrowski, O. P. Ruscitti, A. Schiller, *Inorg. Chem.* **2002**, 41, 1184.
- [12] T. M. Klapötke, B. Krumm, P. Mayer, H. Piotrowski, I. Schwab, M. Vogt, *Eur. J. Inorg. Chem.* **2002**, 2701.
- [13] J. Mason in *Multinuclear NMR* (Ed.: J. Mason), Plenum, New York, **1987**.
- [14] S. Berger, S. Braun, H. O. Kalinowski, *NMR Spectroscopy of the Non-Metallic Elements*, Wiley, Chichester, **1997**.
- [15] Crystal data for $\text{C}_{24}\text{H}_{20}\text{N}_{18}\text{PSb}$: $M_r = 713.30$, monoclinic, space group $C2/c$, $a = 22.055(3)$, $b = 7.2656(7)$, $c = 18.994(2)$ Å, $\alpha = 90$, $\beta = 97.989(3)$, $\gamma = 90^\circ$, $V = 3014.1(5)$ Å³, $F(000) = 1424$, $\rho_{\text{calcd}} (Z = 4) = 1.572$ g cm⁻³, $\mu = 1.018$ mm⁻¹, approximate crystal dimensions $0.40 \times 0.18 \times 0.02$ mm³, θ range = 2.17 to 27.53° , $\text{MoK}\alpha$ ($\lambda = 0.71073$ Å), $T = 143(2)$ K, 7213 measured data (Bruker 3-circle, SMART APEX CCD with ξ -axis fixed at 54.74° , using the SMART V 5.625 program, Bruker AXS: Madison, WI, 2001), of

which 3130 ($R_{int}=0.0545$) unique. Lorentz and polarization correction (SAINT V 6.22 program, Bruker AXS: Madison, WI, 2001), absorption correction (SADABS program, Bruker AXS: Madison, WI, 2001). Structure solution by direct methods (SHELXTL 5.10, Bruker AXS: Madison, WI, 2000), full-matrix least-squares refinement on F^2 , data to parameters ratio: 15.6:1, final R indices [$I > 2\sigma(I)$]: $RI=0.0356$, $wR2=0.0669$, $RI=0.0455$, $wR2=0.0684$ (all data), GOF on $F^2=0.900$. CCDC-240155 contains the supplementary crystallographic data for this paper. These data can be obtained free of charge via www.ccdc.cam.ac.uk/conts/retrieving.html (or from the Cambridge Crystallographic Data Centre, 12, Union Road, Cambridge CB21EZ, UK; fax: (+44) 1223-336-033; or deposit@ccdc.cam.ac.uk).

- [16] A. C. Filippou, P. Portius, G. Schnakenburg, *J. Am. Chem. Soc.* **2002**, *124*, 12396.
- [17] A. C. Filippou, P. Portius, D. U. Neumann, K.-D. Wehrstedt, *Angew. Chem.* **2000**, *112*, 4524; *Angew. Chem. Int. Ed.* **2000**, *39*, 4333.
- [18] R. Haiges, J. A. Boatz, S. Schneider, T. Schroer, M. Yousufuddin, K. O. Christe, *Angew. Chem.* **2004**, *116*, 3210; *Angew. Chem. Int. Ed.* **2004**, *43*, 3148.
- [19] R. Haiges, J. A. Boatz, A. Vij, M. Gerken, S. Schneider, T. Schroer, K. O. Christe, *Angew. Chem.* **2003**, *115*, 5027; *Angew. Chem. Int. Ed.* **2003**, *42*, 5847.
- [20] a) C. Moeller, M. S. Plesset, *Phys. Rev.* **1934**, *46*, 618; b) J. A. Pople, J. S. Binkley, R. Seeger, *Int. J. Quantum Chem.* **1976**, *S10*, 1; c) M. J. Frisch, M. Head-Gordon, J. A. Pople, *Chem. Phys. Lett.* **1990**, *166*, 275.
- [21] R. J. Bartlett, D. M. Silver, *Int. J. Quantum Chem. Symp.* **1975**, *9*, 1927.
- [22] R. C. Binning, Jr., L. A. Curtiss, *J. Comput. Chem.* **1990**, *11*, 1206.
- [23] A d function polarization exponent of 0.293 was used.
- [24] W. J. Hehre, R. Ditchfield, J. A. Pople, *J. Chem. Phys.* **1972**, *56*, 2257.
- [25] The exponent of the d polarization function on N is 0.8; see P. C. Hariharan, J. A. Pople, *Theor. Chim. Acta* **1973**, *28*, 213.
- [26] W. J. Stevens, H. Basch, M. Krauss, *J. Chem. Phys.* **1984**, *81*, 6026.
- [27] The exponent of the diffuse s + p shell is 0.0639; see T. Clark, J. Chandrasekhar, G. W. Spitznagel, P. v. R. Schleyer, *J. Comput. Chem.* **1983**, *4*, 294.
- [28] The exponent of the d polarization function on Sb is 0.211; see S. Huzinaga, J. Andzelm, M. Klobukowski, E. Radzio-Andzelm, Y. Sakai, H. Tatewaki, *Gaussian Basis Sets for Molecular Calculations*, Elsevier, Amsterdam, **1984**.
- [29] M. W. Schmidt, K. K. Baldridge, J. A. Boatz, S. T. Elbert, M. S. Gordon, J. H. Jensen, S. Koseki, N. Matsunaga, K. A. Nguyen, S. Su, T. L. Windus, *J. Comput. Chem.* **1993**, *14*, 1347.

Synthesis of *gem*-Difluorocarba-D-glucose: A Step Further in Sugar Mimesis**

Aur lie Deleuze, Candice Menozzi,
Matthieu Sollogoub,* and Pierre Sina *

Chemical modifications of carbohydrates have been used extensively to understand the origin of the specificity in the recognition processes by sugar-binding proteins in aqueous solution. A classical example is the work by Lemieux, wherein chemoselective removal of hydroxyl groups from oligosaccharides led to the concept of key polar interactions.^[1] Along the same lines, the replacement of the endocyclic oxygen atom by a methylene group has provided hydrolytically stable glycoside mimetics called carbasugars, whose biochemical properties have been studied (Figure 1).^[2–8] Such a replace-

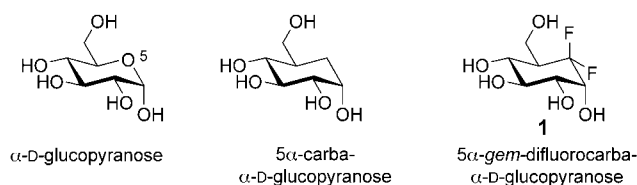


Figure 1. Glucopyranose and its carbocyclic congeners.

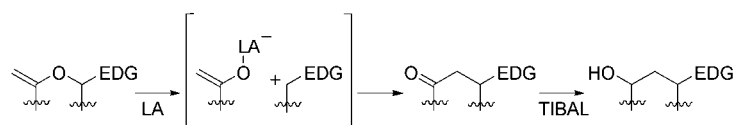
ment has the inherent disadvantage to suppress any possible hydrogen bond formation that involved this electronegative atom. This drawback clearly appeared in the case of carbalactoside, a close mimic of lactoside, which is no longer recognised by a β -galactosidase.^[9] A model has shown that the endocyclic oxygen atom (O-5) of the D-galactose moiety is involved in the interaction with hydrogen-donating groups of the active site of the enzyme.^[10] One way to circumvent this problem and to enlarge the probing spectrum of carbasugars is to replace the oxygen atom by other hydrogen-bond acceptors. Ideally, to fully understand the role of the endocyclic oxygen requires the two lone pairs to be discriminated so that they can be probed to see which of them, if any, is involved in hydrogen bonding in the active site of the enzyme. Fluorine atoms are not as strong hydrogen-bond acceptors as oxygen, but they still exhibit this property,^[11–13] and more interestingly they have been used as reporter groups of the active site of enzymes through ¹⁹F NMR spectroscopy.^[14] It is therefore foreseeable that

[*] A. Deleuze, C. Menozzi, Dr. M. Sollogoub, Prof. P. Sina 
D partement de Chimie
Ecole Normale Sup rieure
UMR 8642: CNRS-ENS-UPMC Paris 6
24 rue Lhomond
75231 Paris Cedex 05 (France)
Fax: (+33) 1-4432-3397
E-mail: matthieu.sollogoub@ens.fr
pierre.sina @ens.fr

[**] The authors would like to thank Dr. Corinne Aubert for useful discussions about cobalt.

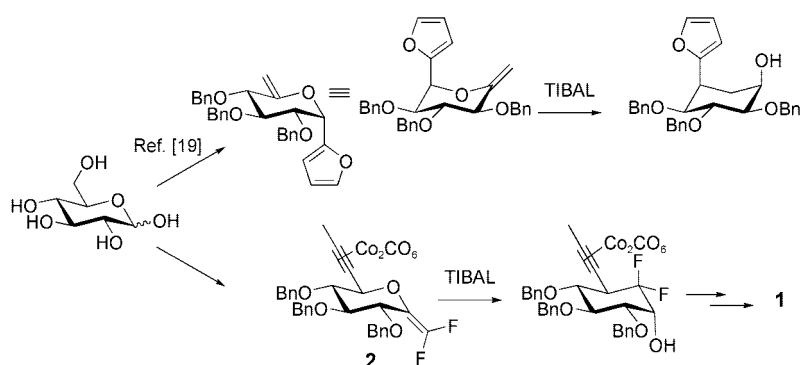
replacement of the endocyclic CH_2 group by a CF_2 moiety in a carbasugar would constitute a step further in the utilization of this family of sugar mimetics by enhancing their ability to be accepted by enzymes involving O-5 and allowing the study of their complexation by NMR spectroscopy.

We recently reported a novel sugar-to-carbocycle rearrangement promoted by triisobutylaluminum (TIBAL)^[15] or Cl_3TiOiPr .^[16] The proposed key step in this transformation is the opening of the ring to give a carbocationic intermediate. Indeed, this reaction is favored when this putative carbenium species can be stabilized by an electron-donating group (EDG).^[17] This is generally applicable to acyclic non-sugar-derived enol ethers (Scheme 1).^[18]



Scheme 1. General rearrangement of EDG-substituted vinyl ethers. EDG = electron-donating group, LA = Lewis acid, TIBAL = triisobutylaluminum.

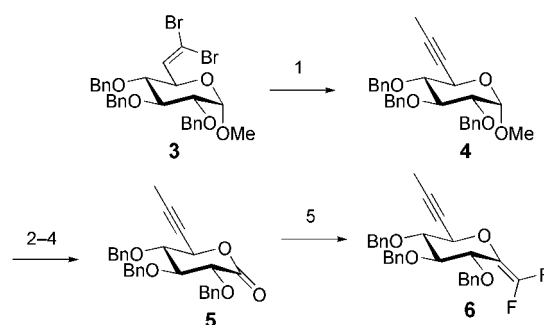
As an example, we recently synthesized a carbasugar with furanyl as the EDG which was easily introduced at the anomeric centre of D-glucose through a glycosylation process. In this synthesis, the anomeric center of the carba congener is derived from the C-5 carbon atom of D-glucose.^[19] Given the



Scheme 2. Synthetic strategies for carbasugars through TIBAL-promoted rearrangements. Bn = benzyl.

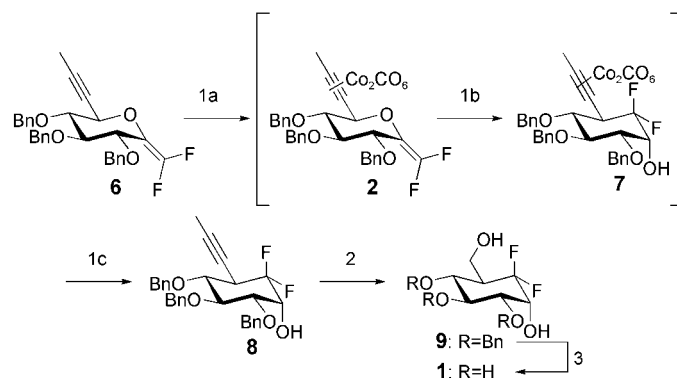
accessibility of ynopyranosides^[20] and the recent results of Harrity and co-workers^[21] who showed that dicobalt hexacarbonyl clusters^[22] could act as EDGs in a similar situation, we anticipated that our TIBAL-mediated reductive rearrangement applied to the difluoroalkene **2** might provide a convenient entry to our target molecule **1** (Scheme 2).

Synthesis of the ynopyranose **6**, the precursor of compound **2**, is depicted in Scheme 3. The known^[20] *gem*-dibromoalkene **3** was first converted into alkyne **4** through methylation of the acetylenic anion generated in situ. Acetolysis,^[23] followed by hydrolysis of the generated anomeric acetate, and oxidation of the hemiacetal afforded the corresponding lactone **5**. Difluoromethylation according to Motherwell et al.^[24] provided the desired *gem*-difluoroalkene precursor **6**.



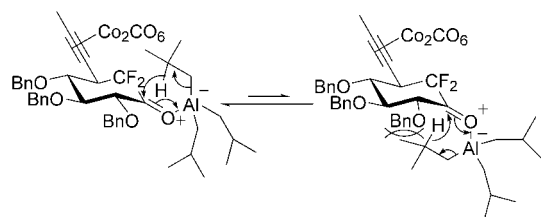
Scheme 3. Synthesis of the *gem*-difluoro-exo-glucal **6**. Reagents and conditions: 1) a) $n\text{BuLi}$ (2.1 equiv), THF, -78°C , 2 h; b) MeI (6 equiv), THF, -78°C , 30 min; c) HMPT (4 equiv), $-78^\circ\text{C} \rightarrow \text{RT}$, overnight, 75% over three steps; 2) H_2SO_4 (1 equiv), Ac_2O , 0°C , 3 min, 75%; 3) MeONa (4 equiv), MeOH, $0^\circ\text{C} \rightarrow \text{RT}$, 2 h, 90%; 4) PCC (3 equiv), 4-Å molecular sieves (3 equiv), CH_2Cl_2 , room temperature, 4 h, 74%; 5) a) HMPT (5 equiv), THF, $-40^\circ\text{C} \rightarrow \text{RT}$; b) CBr_2F_2 (5 equiv), HMPT (5 equiv), THF, RT \rightarrow reflux, 1 h, 95%. THF = tetrahydrofuran, HMPT = hexamethylphosphoric triamide, PCC = pyridinium chlorochromate.

As anticipated and much to our delight, the key rearrangement was performed through a two-step one-pot procedure that involved first, the complexation of the alkyne **6** by dicobalt octacarbonyl,^[25] followed by the reductive TIBAL-induced rearrangement of **2**.^[17] Decomplexation with CAN (ceric ammonium nitrate)^[26] of the crude compound **7** afforded alcohol **8** in 75% yield over three steps and only one purification step by chromatography. The 5a-*gem*-difluorocarba- α -D-glucopyranose **1**^[27] was then easily obtained by controlled reduction of the triple bond, reductive ozonolysis, and debenzoylation (Scheme 4). As previously observed,^[15] the rearrangement occurs with retention of configuration. The reduction of the putative transient



Scheme 4. Synthesis of the 5a-*gem*-difluorocarba- α -D-glucopyranose **1**. Reagents and conditions: 1) a) $[\text{Co}_2(\text{CO})_8]$ (1.5 equiv), CH_2Cl_2 , room temperature, 2 h; b) TIBAL (5 equiv), toluene, room temperature, 2.5 h; c) CAN (5 equiv), NEt_3 (1 equiv), acetone, 30 min, 65% over three steps; 2) a) Pd/CaCO_3 , H_2 , MeOH, room temperature, 4 h; b) O_3 , CH_2Cl_2 , -78°C , 5 min; c) NaBH_4 , CH_2Cl_2 , room temperature, 1 h, 76% over three steps; 3) Pd/C , H_2 , MeOH, room temperature, 1 h, 90%. CAN = ceric ammonium nitrate.

ketone is stereoselective and is classically explained by the attack of the hydride ion, which is attached to the isobutyl group, on the less-hindered face of the molecule to provide the axial hydroxyl group (Scheme 5).



Scheme 5. Stereoselectivity of the reduction of the transient ketone by TIBAL.

The reduction step described proceeds under steric control, whereas the electronic control admitted in such a case, the Ahn–Eisenstein effect,^[28] gives the opposite stereoselectivity. According to this model, the most stable transition-state structure has the axial C–F^[29,30] bond in the antiperiplanar position with respect to the forming H–C bond.

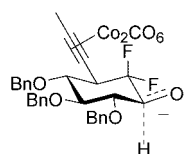
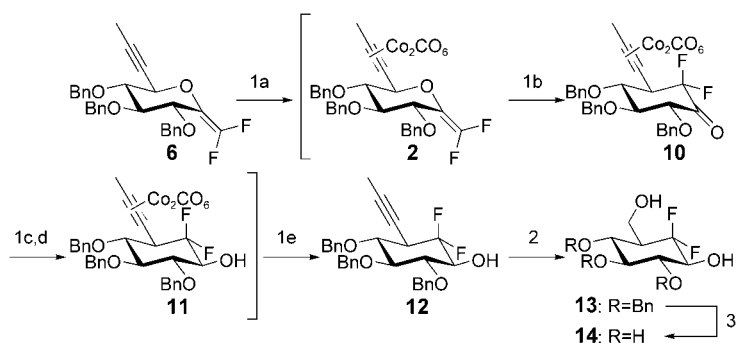


Figure 2. Ahn–Eisenstein effect to obtain the axial reduction.

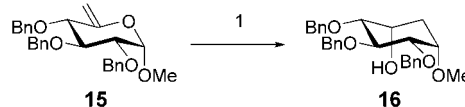
This model implies, as shown in Figure 2, which depicts the late transition state of the reduction step, a selective attack of the hydride ion to form the equatorial hydroxyl group.

Once again, a one-pot procedure was developed: After reaction of the alkyne **6** with dicobalt octacarbonyl to give cluster **2**, the rearrangement was, this time, induced by Cl₃TiOiPr^[16] to yield cyclohexanone **10**. The Lewis acid was then quenched with THF, and the ketone was reduced by means of the super hydride. The triple bond in the crude product **11** was decomplexed, and the expected equatorial alcohol **12** was obtained in 73% yield over five steps and only one purification step by column chromatography. The 5a-*gem*-difluorocarpa-β-D-glucopyranose **14**^[31] was then obtained as described above (Scheme 6).



Scheme 6. Synthesis of the 5a-*gem*-difluorocarpa-β-D-glucopyranose **14**. Reagents and conditions: 1) a) [Co₂(CO)₈] (1.5 equiv), CH₂Cl₂, room temperature, 2 h; b) TiCl₃OiPr (2 equiv), CH₂Cl₂, –78 °C, 1 h; c) THF (5 equiv), –78 °C, 15 min; d) Et₃BHLi (2 equiv), CH₂Cl₂, –78 °C, 30 min; e) CAN (5 equiv), NEt₃ (1 equiv), acetone, 1 h, 73% over five steps; 2) a) Pd/CaCO₃, H₂, MeOH, room temperature, 1.25 h; b) O₃, CH₂Cl₂, –78 °C, 5 min; c) NaBH₄, CH₂Cl₂, room temperature, 1 h, 78% over three steps; 3) Pd/C, H₂, MeOH, room temperature, 1 h, 90%.

The observed stereoselectivity of this reduction process is in sharp contrast to the case in which the fluorine atoms are absent from the molecule. Indeed, when the unsaturated sugar **15**^[32] was submitted to the same reaction conditions, only the axial alcohol **16**^[15] was obtained in 75% yield (Scheme 7). This result supports the directing role of fluorine in the reduction of the ketone.



Scheme 7. Rearrangement and reduction of **15**. Reagents and conditions: 1) a) TiCl₃OiPr (1 equiv), CH₂Cl₂, –78 °C; b) THF (5 equiv), –78 °C, 15 min; c) Et₃BHLi (2 equiv), CH₂Cl₂, –78 °C, 30 min, 73% over three steps.

In summary, we have synthesized, for the first time, two *gem*-difluorinated carba analogues of α- and β-D-glucopyranoses by using a rearrangement strategy and by taking advantage of the Ahn–Eisenstein effect to obtain the β analogue. They are attractive candidates for probing the role of endocyclic oxygen atoms in carbohydrates in sugar–protein interactions. This strategy is currently being extended to other carbohydrates.

Received: July 8, 2004

Keywords: carbohydrates · cyclization · fluorine · reduction · synthetic methods

- [1] a) R. U. Lemieux, *Chem. Soc. Rev.* **1989**, 18, 347–374; b) R. U. Lemieux, *Acc. Chem. Res.* **1996**, 29, 373–380.
- [2] T. Suami, S. Ogawa, *Adv. Carbohydr. Chem. Biochem.* **1990**, 48, 21–90.
- [3] S. Ogawa, N. Matsunaga, H. Li, M. M. Palcic, *Eur. J. Org. Chem.* **1999**, 3, 631–642.
- [4] M. Carpintero, A. Fernandez-Mayoralas, J. Jimenez-Barbero, *Eur. J. Org. Chem.* **2001**, 4, 681–689.
- [5] S. Ogawa, Y. Uematsu, S. Yoshida, N. Sasaki, T. Suami, *J. Carbohydr. Chem.* **1987**, 6, 471–478.
- [6] S. Ogawa, A. Maruyama, T. Odagiri, H. Yuasa, H. Hashimoto, *Eur. J. Org. Chem.* **2001**, 5, 967–974.
- [7] M. Carpintero, A. Bastida, E. Garcia-Junceda, J. Jimenez-Barbero, A. Fernandez-Mayoralas, *Eur. J. Org. Chem.* **2001**, 4, 4127–4135.
- [8] M. Kitaoka, S. Ogawa, H. Taniguchi, *Carbohydr. Res.* **1993**, 247, 355–359.
- [9] E. Montero, A. Garcia-Herrero, J. L. Asensio, K. Hirai, S. Ogawa, F. Santoyo-Gonzalez, F. J. Canada, J. Jimenez-Barbero, *Eur. J. Org. Chem.* **2000**, 1945–1952.
- [10] J. F. Espinosa, E. Montero, A. Vian, J. L. Garcia, H. Dietrich, M. Martin-Lomas, R. R. Schmidt, A. Imbert, F. J. Canada, J. Jimenez-Barbero, *J. Am. Chem. Soc.* **1998**, 120, 10862–10871.
- [11] L. A. Curtiss, D. J. Frurip, M. Blander, *J. Am. Chem. Soc.* **1978**, 100, 79–86.
- [12] D. A. Dixon, B. E. Smart, *J. Phys. Chem.* **1991**, 95, 1609–1612.
- [13] J. A. K. Howard, V. J. Hoy, D. O'Hagan, G. T. Smith, *Tetrahedron* **1996**, 52, 12613–12622.
- [14] J. Feeney, J. E. McCormick, C. J. Bauer, B. Birdsall, C. M. Moody, B. A. Starkmann, D. W. Young, P. Francis, R. H. Havlin,

- W. D. Arnold, E. Oldfield, *J. Am. Chem. Soc.* **1996**, *118*, 8700–8706.
- [15] S. K. Das, J.-M. Mallet, P. Sinaÿ, *Angew. Chem.* **1997**, *109*, 513–516; *Angew. Chem. Int. Ed. Engl.* **1997**, *36*, 493–496.
- [16] M. Sollogoub, J.-M. Mallet, P. Sinaÿ, *Tetrahedron Lett.* **1998**, *39*, 3471–3472.
- [17] M. Sollogoub, J.-M. Mallet, P. Sinaÿ, *Angew. Chem.* **2000**, *112*, 370–372; *Angew. Chem. Int. Ed.* **2000**, *39*, 362–364.
- [18] B. du Roizel, M. Sollogoub, A. J. Pearce, P. Sinaÿ, *Chem. Commun.* **2000**, 1507–1508.
- [19] M. Sollogoub, A. J. Pearce, A. Herault, P. Sinaÿ, *Tetrahedron: Asymmetry* **2000**, *11*, 283–294.
- [20] D. Rouzaud, P. Sinaÿ, *J. Chem. Soc. Chem. Commun.* **1983**, 1353–1354.
- [21] D. R. Carbury, S. Reigner, J. W. Myatt, N. D. Miller, J. P. A. Harrity, *Angew. Chem.* **2002**, *114*, 2699–2701; *Angew. Chem. Int. Ed.* **2002**, *41*, 2584–2587.
- [22] K. M. Nicholas, *Acc. Chem. Res.* **1987**, *20*, 207–214.
- [23] J. M. Aurrecoechea, B. Lopez, M. Arrate, *J. Org. Chem.* **2000**, *65*, 6493–6501.
- [24] W. B. Motherwell, M. J. Tozer, B. C. Ross, *J. Chem. Soc. Chem. Commun.* **1989**, 1437–1439.
- [25] K. M. Nicholas, M. Mulvaney, M. Bayer, *J. Am. Chem. Soc.* **1980**, *102*, 2508–2510.
- [26] D. Seyferth, A. T. Wehman, *J. Am. Chem. Soc.* **1970**, *92*, 5520–5522.
- [27] **1**: $[\alpha]_D^{20} = +2.4$ ($c = 0.9$, CH₃OH); ¹H NMR (400 MHz, CD₃OD, 25 °C, TMS): $\delta = 4.18$ (dd, ³*J*(5,6) = 4.8, ³*J*(6,6') = 11.6 Hz, 1H; H-6), 4.14 (dd, ³*J*(5,6') = 4.4, ³*J*(6,6') = 11.6 Hz, 1H; H-6'), 4.05 (ddd, ³*J*(1,2) = ³*J*(1,F_{eq}) = 3.9, ³*J*(1,F_{ax}) = 7.8 Hz, 1H; H-1), 3.83 (t, ³*J*(3,4) = ³*J*(3,2) = 9.4 Hz, 1H; H-3), 3.64–3.59 (m, 1H; H-2), 3.61 (t, ³*J*(3,4) = ³*J*(4,5) = 10.1 Hz, 1H; H-4), 2.50 ppm (ddq, ³*J*(5,6) = ³*J*(5,F_{eq}) = 4.2, ³*J*(5,F_{ax}) = 30.7, ³*J*(5,4) = 11.0 Hz, 1H; H-5); ¹³C NMR (100 MHz, CD₃OD, 25 °C): $\delta = 124.1$ (dd, ¹*J*(C,F) = 240.8, ¹*J*(C,F) = 251.8 Hz; CF₂), 75.6 (s; C-3), 73.5 (dd, ²*J*(C,F) = 22.1, ²*J*(C,F) = 32.3 Hz; C-1), 72.1 (d, ³*J*(C,F) = 11.0 Hz; C-2 or C-4), 72.0 (d, ³*J*(C,F) = 9.0 Hz; C-2 or C-4), 58.7 (t, ³*J*(C,F) = 2.9 Hz; C-6), 46.5 ppm (t, ²*J*(C,F) = 20.0 Hz; C-5). ¹⁹F NMR (235 MHz, CD₃OD, 25 °C): $\delta = -110.3$ (d, ²*J*(F,F) = 256.5 Hz; F_{eq}), -115.7 ppm (ddd, ²*J*(F,F) = 256.5, ³*J*(F,H-5) = 30.6, ³*J*(F,H-1) = 3.5 Hz; F_{ax}); DCI-MS (desorption chemical ionization; NH₃): *m/z*: 232 [*M*+NH₃+H]⁺, 215 [*M*+H]⁺; HRMS (DCI, NH₃): calcd for C₇H₁₃O₅F₂: 215.0731; found: 215.0726.
- [28] N. T. Anh, O. Eisenstein, *Nouv. J. Chim.* **1977**, *1*, 61–70.
- [29] S. S. Wong, M. N. Paddon-Row, *J. Chem. Soc. Chem. Commun.* **1990**, 456–458.
- [30] C. F. Bridge, D. O'Hagan, K. A. Reynolds, K. K. Wallace, *J. Chem. Soc. Chem. Commun.* **1995**, 2329–2330.
- [31] **14**: $[\alpha]_D^{20} = +1.0$ ($c = 1.2$, CH₃OH); ¹H NMR (400 MHz, CD₃OD, 25 °C, TMS): $\delta = 4.18$ (dd, ³*J*(5,6) = 4.6, ³*J*(6,6') = 12.0 Hz, 1H; H-6), 4.15 (dd, ³*J*(5,6') = 4.6, ³*J*(6,6') = 12.0 Hz, 1H; H-6'), 3.80–3.71 (m, 1H; H-2), 3.68–3.62 (m, 1H; H-4), 3.53–3.48 (m, 2H; H-1, H-3), 2.12 ppm (ddq, ³*J*(5,6) = ³*J*(5,F_{eq}) = 4.2, ³*J*(5,F_{ax}) = 28.6, ³*J*(5,4) = 11.6 Hz, 1H; H-5); ¹³C NMR (100 MHz, CD₃OD, 25 °C): $\delta = 122.8$ (dd, ¹*J*(C,F) = 245.4; ¹*J*(C,F) = 248.9 Hz; CF₂), 78.2 (d, ⁴*J*(C,F) = 1.2 Hz; C-3), 75.2 (t, ²*J*(C,F) = 20.3 Hz; C-1), 73.2 (d, ³*J*(C,F) = 9.5 Hz; C-2 or C-4), 71.7 (d, ³*J*(C,F) = 10.2 Hz; C-2 or C-4), 58.6 (t, ³*J*(C,F) = 3.1 Hz; C-6), 49.0 ppm (t, ²*J*(C,F) = 20.0 Hz; C-5). ¹⁹F NMR (235 MHz, CD₃OD, 25 °C): $\delta = -110.3$ (d, ²*J*(F,F) = 260.0 Hz; F_{eq}), -126.1 ppm (ddd, ²*J*(F,F) = 260.0, ³*J*(F,H-5) = 28.2, ³*J*(F,H-1) = 21.2 Hz; F_{ax}); DCI-MS (NH₃): *m/z*: 232 [*M*+NH₃+H]⁺; HRMS (DCI, NH₃): calcd for C₇H₁₆O₅NF₂: 232.0997; found 232.0999.
- [32] T. Iimori, H. Takahashi, S. Ikegami, *Tetrahedron Lett.* **1996**, *37*, 649–652.

Carbon Dioxide Fixation by the Cooperative Effect of Organotin and Organotellurium Oxides

Jens Beckmann,* Dainis Dakternieks, Andrew Duthie, Naomi A. Lewcenko, and Cassandra Mitchell

Dedicated to Professor Alwyn G. Davies

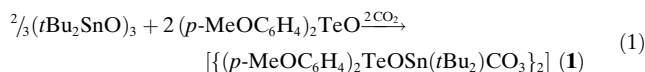
The recent interest in carbon dioxide fixation by organo-metallic species has occurred for two reasons:^[1] First, the increasing industrial emission of the “greenhouse gas” CO₂ into the atmosphere has been widely accepted as one of the main causes for global warming and climate changes, and therefore efficient solutions for the recovery of CO₂ are highly sought after. Second, being an inexpensive, nontoxic commodity, CO₂ holds considerable potential as a C₁ feed-stock for the preparation of key intermediates required by the chemical industry on a multitonne scale, such as urea and dimethyl carbonate (DMC). In this regard, organometallic complexes play a vital role for the activation of the comparatively inert C–O bonds in CO₂. Whilst a vast variety of transition-metal compounds are able to form complexes with CO₂, main-group organometallic species known to bind CO₂ are rare.^[1] Notable exceptions include triorganotin oxides, (R₃Sn)₂O, and triorganotin hydroxides, R₃SnOH, which react with gaseous CO₂ to give rise to the formation of polymeric triorganotin carbonates, (R₃Sn)₂CO₃ (R = alkyl).^[2] Industrially, triorganotin carbonates are used as catalysts for the preparation of organic carbonates from alkyl halides and potassium carbonate.^[1c] Di- and triorganotin alkoxides, R_nSn(OR')_{4–n} (R = alkyl, R' = alkyl, aryl; n = 2, 3) react with gaseous or supercritical CO₂ to give di- and triorganotin (alkoxy) carbonates, R₃Sn(O₂COR') and R₂Sn(OR')(O₂COR'), some of which produce DMC upon thermolysis.^[3]

We have now found that solutions containing of di-*tert*-butyltin oxide, (tBu₂SnO)₃,^[4] and di-*p*-anisyltellurium oxide, (p-MeOC₆H₄)₂TeO,^[5] (Sn/Te ratio = 1:1) readily absorb gaseous CO₂ to produce a unique molecular tellurastannoxane,^[6] [(p-MeOC₆H₄)₂TeOSn(tBu₂)CO₃]₂ (**1**) as an air-stable crystalline material [Eq. (1)]. The formation of this material is rapid (less than 15 min) at room temperature and almost quantitative when the solution is purged with an excess of CO₂. Smaller amounts of the same material were also formed

[*] Dr. J. Beckmann,^[a] Prof. Dr. D. Dakternieks, A. Duthie, N. A. Lewcenko, C. Mitchell
Centre for Chiral and Molecular Technologies
Deakin University
School of Biological and Chemical Sciences
Geelong 3217 (Australia)
E-mail: beckmann@chemie.fu-berlin.de

[†] Current address:
Institut für Anorganische und Analytische Chemie
Freie Universität Berlin
Fabeckstrasse 34–36, 14195 Berlin (Germany)
Fax: (+49) 30-838-53310

serendipitously, for the first time, when such a $(t\text{Bu}_2\text{SnO})_3/(p\text{-MeOC}_6\text{H}_4)_2\text{TeO}$ solution was exposed for several days to air.



The molecular structure of **1** (Figure 1),^[7] displays an almost planar inorganic $\text{Sn}_2\text{Te}_2\text{C}_2\text{O}_8$ core (largest deviation from the ideal plane: 0.393(2) Å), which lies across a crystallographic center of inversion. The geometry of the tin

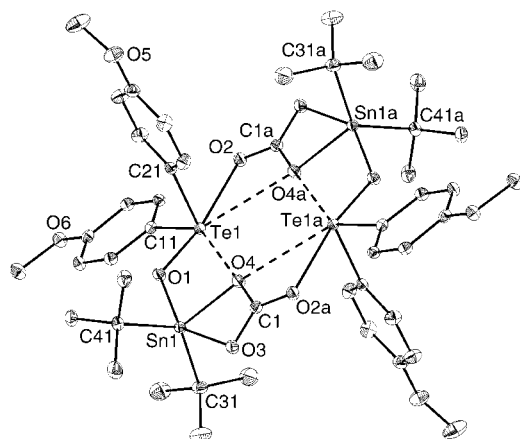


Figure 1. The X-ray crystal structure of **1**, thermal ellipsoids set at 30% probability. Selected interatomic separations [Å] and angles [°]: Te1–O1 1.921(2), Sn1–O3 2.307(2), Te1–O2 2.481(2), Sn1–O4 2.094(2), Te1...O4 3.279(2), Sn1–C31 2.166(3), Te1...O4a 3.059(2), Sn1–C41 2.166(3), Te1–C11 2.112(2), C1–O2a 1.259(3), Te1–C21 2.107(2), C1–O3 1.278(3), Sn1–O1 2.043(2), C1–O4 1.329(3); O1–Te1–O2 170.25(7), O1–Sn1–C31 102.18(9), O1–Te1–O4 59.32(7), O1–Sn1–C41 98.06(9), O1–Te1–O4a 138.14(7), O3–Sn1–O4 59.47(7), O1–Te1–C11 91.16(8), O3–Sn1–C31 97.27(9), O1–Te1–C21 93.11(9), O3–Sn1–C41 92.60(8), O2–Te1–O4 126.00(6), O4–Sn1–C31 113.94(9), O2–Te1–O4a 46.52(6), O4–Sn1–C41 115.82(8), O2–Te1–C11 84.55(8), C31–Sn1–C41 126.96(10), O2–Te1–C21 78.83(8), O2a–C1–O3 124.7(2), O4–Te1–O4a 79.51(5), O2a–C1–O4 120.9(2), O4–Te1–C11 149.18(7), O3–C1–O4 114.4(2), O4–Te1–C21 93.01(8), Te1–O1–Sn1 128.28(9), O4a–Te1–C11 130.67(7), C1–O2a–Te1a 110.26(15), O4a–Te1–C21 81.01(8), C1–O3–Sn1 88.94(14), C11–Te1–C21 97.62(9), C1–O4–Sn1 97.20(14), O1–Sn1–O3 145.36(7), C1–O4–Te1 172.53(16), O1–Sn1–O4 86.35(7), Sn1–O4–Te1a 171.65(9) (Symmetry operation used to generate equivalent atoms: a = –x, –y, –z).

atom is best described as a distorted trigonal bipyramid, in which two oxygen atoms are situated in the axial positions and two carbon atoms and one oxygen atom occupy the equatorial positions. The distortion seems to originate from the chelating coordination mode of the carbonate.

Taking into account the stereochemically active lone pair, the geometry of the tellurium atom may be described as a distorted octahedron with two carbon atoms mutually *cis* and two oxygen atoms mutually *trans*, and a deficiency in the primary coordination sphere along the vector defined by the two tellurium atoms (Te1...Te1a 4.875(1) Å). The O–Te–O linkage is rather asymmetric (Te1–O1 1.921(2), Te1–O2 2.481(2) Å) as opposed to the O–Te–O linkage in the polymeric parent compound, $(p\text{-MeOC}_6\text{H}_4)_2\text{TeO}$ (Te1–O1 2.100(2) Å, Te1–O1a 2.025(2) Å). Differences are also found

in the secondary bonding; while $(p\text{-MeOC}_6\text{H}_4)_2\text{TeO}$ lacks such interactions, two significant intramolecular secondary Te...O bonds are observed for the tellurium atoms of **1**, which involve O4 of the carbonate moiety.^[8]

Consistent with the molecular structure established by X-ray crystallography and the pentacoordinate geometry of the tin atoms, the ^{119}Sn magic angle spinning (MAS) NMR spectrum of **1** shows an isotropic chemical shift at $\delta_{\text{iso}} = -262.4$ ppm, which differs from that of $(t\text{Bu}_2\text{SnO})_3$ ($\delta_{\text{iso}} = -84.3$ ppm), which has tetracoordinate tin atoms.^[9] The ^{125}Te MAS NMR spectrum of **1** reveals an isotropic chemical shift at $\delta_{\text{iso}} = 1179$ ppm similar to that of the dimeric Ph_2TeO ($\delta_{\text{iso}} = 1103/1133$ ppm), but rather different to that of the polymeric $(p\text{-MeOC}_6\text{H}_4)_2\text{TeO}$ ($\delta_{\text{iso}} = 903$ ppm), which is apparently a reflection of the asymmetric O–Te–O linkage and the presence of secondary Te...O interactions in **1** and Ph_2TeO , as opposed to the rather symmetric O–Te–O linkage and the absence of secondary interactions in $(p\text{-MeOC}_6\text{H}_4)_2\text{TeO}$.^[5] At a MAS frequency of 9 kHz, both the ^{119}Sn and the ^{125}Te isotropic chemical shifts were accompanied by a set of spinning sidebands that were indicative for large shielding anisotropies (SA) and utilized for tensor analyses.^[10]

For solutions of **1** in CDCl_3 , the ^{119}Sn and ^{125}Te NMR spectra show signals at $\delta = -258.3$ and 1194.3 ppm, respectively, which suggest, by comparison with the respective solid-state NMR chemical shifts, that the molecular structure is retained in solution. Both signals show two identical pairs of satellites giving rise to two $^2J(^{119}\text{Sn}\text{--}^{125}\text{Te})$ couplings of 113 and 66 Hz, which unambiguously supports the idea that the secondary Te...O interactions also exist in solution.^[8] Independent evidence for the configurational stability of **1** in solution stems from osmometric molecular-weight determination in CHCl_3 at 40 °C (1282 Da found, 1301 Da calculated). The presence of the carbonate moiety is evident from the ^{13}C NMR spectra which show a signal at $\delta = 165.4$ ppm (in CDCl_3) and $\delta_{\text{iso}} = 165.6$ ppm (in the solid state), which increases significantly in intensity when using ^{13}C -labeled carbon dioxide for the preparation.

Solutions of $(t\text{Bu}_2\text{SnO})_3$ and $(p\text{-MeOC}_6\text{H}_4)_2\text{TeO}$ were treated separately with gaseous CO_2 . While the $(p\text{-MeOC}_6\text{H}_4)_2\text{TeO}$ was recovered unchanged, solutions of $(t\text{Bu}_2\text{SnO})_3$ also absorb CO_2 to produce $t\text{Bu}_2\text{SnCO}_3$ (**2**), albeit at a slower rate than in the formation of **1**. Owing to the virtual insolubility in all common organic solvents, we tentatively assign **2** a polymeric structure, thus acknowledging the fact that all known triorganotin carbonates, $(\text{R}_3\text{Sn})_2\text{CO}_3$ (R = alkyl) are also polymeric.^[2] This assignment is supported by ^{119}Sn MAS NMR spectroscopy of **2**, which shows an isotropic chemical shift at $\delta_{\text{iso}} = -285.5$.^[10]

Applications of organometallic species for the fixation and recovery of CO_2 require the reversibility of the absorption process, preferably at a low temperature to save energy costs.^[1] A thermographic analysis of **1** indicates mass loss between 90–145 °C (7.0% found, 6.8% calculated) associated with the liberation of CO_2 . It is well known that inorganic bases, such as aqueous KOH also absorb CO_2 from air, however these absorption processes are generally irreversible (e.g. K_2CO_3 is stable up to more than 900 °C).^[11] A bulk sample of **1** (300 mg) was heated at 145 °C for 60 min and the

released CO₂ was determined gravimetrically as BaCO₃ (recovery 80 %). The residual material was free of carbonate by indication of ¹³C NMR spectroscopy and the related ¹¹⁹Sn and ¹²⁵Te MAS NMR spectra exhibit signals at $\delta_{\text{iso}} = -228.3$ and 834 ppm, respectively, which are significantly different from those of **1** and the starting materials. The residual material was completely soluble in CDCl₃ and was used for the reabsorption of CO₂, after which the ¹¹⁹Sn and ¹²⁵Te NMR spectra of the crude product indicated the renewed quantitative formation of **1**.

In summary, we have demonstrated that solutions of (tBu₂SnO)₃ and (p-MeOC₆H₄)₂TeO (Sn/Te ratio = 1:1) rapidly absorb CO₂ to form an air-stable molecular tellurastannoxane [(p-MeOC₆H₄)₂TeOSn(tBu₂CO₃)₂] (**1**) showing significant intramolecular Te...O interactions in both solution and the solid state. In contrast, the absorption of CO₂ by (tBu₂SnO)₃ or triorganotin oxo species^[2] provides only polymeric organotin carbonates. The desorption of CO₂ occurs at rather low temperatures, which suggests applications of **1** for instance as phase-transfer catalyst^[12] or as precursor for the preparation of organic carbonates.^[3]

Experimental Section

1: A magnetically stirred solution of (tBu₂SnO)₃ (995 mg, 1.33 mmol)^[4] and (p-MeOC₆H₄)₂TeO (1.43 g, 4.00 mmol)^[5] in CHCl₃ (30 mL), was slowly purged with CO₂ for 15 min at room temperature. The solvent was removed in vacuo and the solid residue recrystallized from CH₂Cl₂/hexane to give colorless crystals. These crystals were dried in vacuum at 50 °C for 1 h to remove cocrystallized CH₂Cl₂. Single crystals suitable for X-ray diffraction were grown from a CHCl₃ solution, yield: 2.58 g, 1.98 mmol, 99%. M.p. 198 °C (decomp.) (crystals turn opaque at 120 °C). Elemental analysis (%) calcd for C₂₃H₃₂O₆SnTe (1301.74): C 42.44, H 4.96; found: C 42.39, H 5.03. ¹H NMR (300 MHz, CDCl₃): δ = 8.02 (d, ³J(¹H-¹H) = 9 Hz, 8H), 6.92 (d, ³J(¹H-¹H) = 9 Hz, 8H), 3.81 (s, 12H), 1.18 ppm (s, ³J(¹H-¹¹⁹Sn) = 109 Hz, 36H); ¹³C NMR (75 MHz, CDCl₃): δ = 165.4 (CO₃), 161.5 (p-C), 133.6 (o- or m-C), 129.5 (¹J(¹³C-¹²⁵Te) = 323 Hz; i-C), 114.7 (o- or m-C), 55.3 (OCH₃), 39.4 (¹J(¹³C-¹¹⁹Sn) = 562 Hz; CCH₃), 29.3 ppm (CCH₃).

2: A solution of (t-Bu₂SnO)₃ (249 mg, 0.33 mmol)^[4] in CHCl₃ (20 mL), was slowly purged with CO₂ for 30 min at room temperature. The colorless amorphous precipitate formed was collected by filtration and air dried. Yield: 228 mg, 0.78 mmol, 78%. M.p. 250 °C (decomp.) Elemental analysis (%) calcd for C₉H₁₈O₃Sn (292.97): C 36.90, H 6.19; found: C 36.91, H 6.20.

Received: March 30, 2004

Revised: June 6, 2004

Keywords: carbon dioxide fixation · hypervalent compounds · tellurium · tin

[1] For reviews, see: a) P. G. Jessop, T. Ikariya, R. Noyori, *Chem. Rev.* **1995**, 95, 259; b) D. H. Gibson, *Chem. Rev.* **1996**, 96, 2063; c) A.-A. G. Shaikh, S. Sivaram, *Chem. Rev.* **1996**, 96, 951; d) X. Yin, J. R. Moss, *Coord. Chem. Rev.* **1999**, 181, 27; e) M. Shi, Y.-M. Shen, *Curr. Org. Chem.* **2003**, 7, 737; f) A. Belli Dell'Amico, F. Calderazzo, L. Labella, F. Marchetti, G. Pampaloni, *Chem. Rev.* **2003**, 103, 3857.

[2] a) H. Sato, *Bull. Chem. Soc. Jpn.* **1967**, 40, 410; b) A. J. Bloodworth, A. G. Davies, S. C. Vasishtha, *J. Chem. Soc. C* **1967**, 1309;

c) S. J. Blunden, R. Hill, J. N. R. Ruddick, *J. Organomet. Chem.* **1984**, 267, C5; d) J. Kümmerlen, A. Sebald, H. Reuter, *J. Organomet. Chem.* **1992**, 427, 309.

[3] a) A. G. Davies, P. G. Harrison, *J. Chem. Soc. C* **1967**, 1313; b) T. Sakakura, Y. Saito, M. Okano, J.-C. Choi, T. Sako, *J. Org. Chem.* **1998**, 63, 7095; c) J.-C. Choi, T. Sakakura, T. Sako, *J. Am. Chem. Soc.* **1999**, 121, 3793; d) T. Sakakura, J.-C. Choi, Y. Saito, T. Masuda, T. Sako, T. Oriyama, *J. Org. Chem.* **1999**, 64, 4506; e) D. Ballivet-Tkatchenko, O. Douteau, S. Stutzmann, *Organometallics* **2000**, 19, 4563; f) H. Yasuda, J.-C. Choi, S.-C. Lee, T. Sakakura, *J. Organomet. Chem.* **2002**, 659, 133; g) D. Ballivet-Tkatchenko, T. Jerphagnon, R. Ligabue, L. Plasseraud, D. Poinot, *Appl. Catal. A* **2003**, 255, 93.

[4] H. Puff, W. Schuh, R. Sievers, W. Wald, R. Zimmer, *J. Organomet. Chem.* **1984**, 260, 271.

[5] J. Beckmann, D. Dakternieks, A. Duthie, F. Ribot, M. Schürmann, N. A. Lewcenko, *Organometallics* **2003**, 22, 3257.

[6] For the first work describing molecular tellurastannoxanes, see: J. Beckmann, D. Dakternieks, J. O'Connell, K. Jurkschat, M. Schürmann, *Eur. J. Inorg. Chem.* **2002**, 1484.

[7] a) Crystal data for 1·2CHCl₃ (C₄₆H₆₄O₁₂Sn₂Te₂·2CHCl₃): M_r = 1540.29, monoclinic, space group $P2(1)/c$, a = 14.4757(8), b = 12.2301(7), c = 18.3476(10) Å, β = 112.5350(10)°, V = 3000.2(3) Å³, Z = 2, ρ_{calcd} = 1.705 mg m⁻³, MoK α radiation (λ = 0.71073 Å), crystal dimensions 0.15 × 0.20 × 0.45 mm³. Of 18492 reflections collected on a Bruker SMART CCD area collector at 130(2) K, 6781 (6286) were observed and used for all calculations (SHELXL 97 implemented in WinGX 2000). After absorption correction the structure was solved by direct methods and refined anisotropically on F^2 . Final residuals R_1 = 0.0259, wR_2 = 0.0620 ($I > 2\sigma(I)$); R_1 = 0.0285, wR_2 = 0.0633 (all data). 316 parameters; b) CCDC-233184 contains the supplementary crystallographic data for this paper. These data can be obtained free of charge via www.ccdc.cam.ac.uk/conts/retrieving.html (or from the Cambridge Crystallographic Data Centre, 12 Union Road, Cambridge CB2 1EZ, UK; fax: (+44) 1223-336-033; or deposit@ccdc.cam.ac.uk).

[8] For another example of intramolecular secondary Te...O interaction, see: D. Dakternieks, R. Di Giacomo, R. W. Gable, B. F. Hoskins *J. Am. Chem. Soc.* **1988**, 110, 6541.

[9] J. Beckmann, K. Jurkschat, B. Mahieu, M. Schürmann, *Main Group Met. Chem.* **1998**, 21, 113.

[10] a) The tensor analyses were performed according to the method of Herzfeld and Berger: J. Herzfeld, X. Chen in *Encyclopedia of Nuclear Magnetic Resonance*, Vol. 7 (Eds.: D. M. Grant, R. K. Harris), Wiley, Chichester, **1996**, p. 4362; b) Computer program used: DmFit 2002: D. Massiot, F. Fayon, M. Capron, I. King, S. Le Calvé, B. Alonso, J.-O. Durand, B. Bujoli, Z. Gan, G. Hoatson, *Magn. Reson. Chem.* **2002**, 40, 70; c) Definitions δ_{iso} (ppm) = $-(\sigma_{11} + \sigma_{22} + \sigma_{33})/3$; ζ (ppm) = $\sigma_{33} - \sigma_{\text{iso}}$, and $\eta = (\sigma_{22} - \sigma_{11})/(\sigma_{33} - \sigma_{\text{iso}})$ where σ_{11} , σ_{22} , and σ_{33} (ppm) are the principal tensor components of the shielding anisotropy (SA), sorted as follows $|\sigma_{33} - \sigma_{\text{iso}}| > |\sigma_{11} - \sigma_{\text{iso}}| > |\sigma_{22} - \sigma_{\text{iso}}|$; d) Results obtained: ¹¹⁹Sn ζ 565, η 0.25; σ_{11} -1637, σ_{22} -1145, σ_{33} -755. ¹²⁵Te ζ -458, η 0.85; σ_{11} -91, σ_{22} 51, σ_{33} 827 for **1**. ¹¹⁹Sn ζ -538, η 0.50; σ_{11} -118, σ_{22} 151, σ_{33} 824 for **2**. e) For comparison: ¹¹⁹Sn ζ 215, η 0.00 reported for (tBu₂SnO)₃,^[9] ¹²⁵Te ζ 545, η 0.75 and ζ 570, η 0.60 reported for Ph₂TeO,^[5] ¹²⁵Te ζ 210, η 0.00 reported for (p-MeOC₆H₄)₂TeO.^[5]

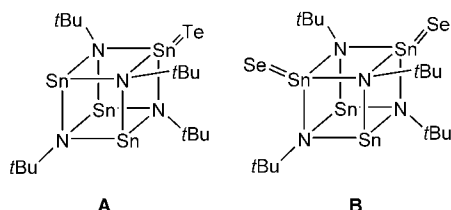
[11] R. L. Lehman, N. G. Glumac, J. S. Gentry, *Thermochim. Acta* **1998**, 316, 1.

[12] T. Fujinami, S. Sato, S. Sakai, *Chem. Lett.* **1981**, 749.

Complete Chalcogenation of Tin(II) Centers in an Imidotin Cluster**

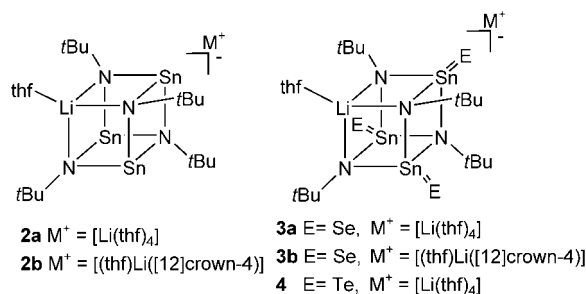
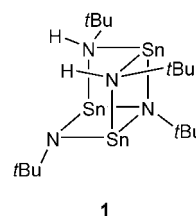
Tristram Chivers* and Dana J. Eisler

The use of inorganic rings or clusters as precursors to industrially important materials such as inorganic polymers,^[1] nanomaterials,^[2] or semiconductors^[3] represents an active area of contemporary inorganic chemistry. In the latter category the design of suitable precursors for the low band-gap semiconductors SnE (E = Se, Te), which have applications in thermoelectric devices and for optoelectronic materials, is of current interest.^[4,5] Suitably chosen complexes containing terminal Sn=E bonds would appear to be candidates for this purpose.^[6] In particular, imidotin chalcogenides of the type [(ESnμ₃-NR)₄] (E = Se, Te) may act as single-source precursors of these binary semiconductors by the energetically favorable elimination of the diazene RN=NR. However, investigations of the reactions of the neutral cluster [(Snμ₃-NtBu)₄] with chalcogens have revealed that oxidation is limited to one tin(II) center for E = Te (**A**) or two tin(II) centers in the case of E = Se (**B**).^[7] To address this synthetic



challenge, we have adopted a strategy that was successful for the generation of the previously inaccessible P–Te ligands [(TePPh₂)₂N][−] and [Te(NtBu)P(μ₂-NtBu)₂P(NtBu)Te]^{2−}.^[8] That approach involved the formation of anionic imidophosphorus(III) reagents by metalation with NaH or *n*BuLi, prior to reaction with tellurium.^[8]

Application of this methodology to imidotin cages involves the use of the amido/imido *seco*-cube [Sn₃(μ₃-NtBu)(μ₂-NtBu)(μ₂-NHtBu)₂] (**1**) reported by Veith et al.^[9] We disclose here that the anionic cluster in [Li(thf)₄][(thf)LiSn₃(μ₃-NtBu)₄] (**2a**), which is readily generated by dilithiation of **1** with *n*BuLi, exhibits a dramatic increase in the reactivity of the tin(II) centers towards chalcogens compared to that of the neutral cluster [(Snμ₃-NtBu)₄]. Complete chalcogenation to give the trichalcogenides



[Li(thf)₄][(thf)LiSn₃E₃(μ₃-NtBu)₄] (**3a**, E = Se; **4**, E = Te) occurs rapidly under mild conditions and in high yields. The characterization of these imidotin chalcogenides in the solid state by X-ray crystallography and in solution by multinuclear NMR spectroscopy (¹H, ⁷Li, ¹¹⁹Sn, ⁷⁷Se, and ¹²⁵Te) is reported.

The reaction of **1** with two equivalents of *n*-butyllithium in THF produces the anionic heterobimetallic cubane **2a** as a solvent-separated ion pair in 40% yield; complex **2b** was prepared from **2a** and [12]crown-4. Wright and co-workers have reported the formation of the related complex [Li(thf)₄][Sn₃Li(thf)(μ₃-NtBu)(μ₃-NC₁₀H₇)₃] by the reaction of [(Snμ₃-NtBu)₄] with three equivalents of C₁₀H₇NHLi.^[10] The ¹H NMR spectrum of complex **2a** exhibits two resonances in a 3:1 ratio for the *t*Bu protons, and a single resonance is observed in the ¹¹⁹Sn NMR spectrum; both of these observations are consistent with local C₃ symmetry for the anion in **2a**. The ⁷Li NMR spectrum of **2a** shows two well-separated resonances, indicating that the [Sn₃Li(μ₃-NtBu)₄] cluster remains intact, even in THF solution.

The reaction of **2a** with slightly more than three equivalents of selenium in THF readily produces the tristannaselenone **3a** in essentially quantitative yields within several minutes at room temperature. Complex **3b** was obtained in a similar manner from **2b** and selenium. The tristannatellone **4** can also be synthesized from **2a** and a slight excess of tellurium at room temperature in about 1 h. However, the reaction proceeds more rapidly with gentle heating (20 min, 40°C) to give **4** in 73% yield. The mild reaction conditions necessary to produce the fully chalcogenated complexes **3a**, **3b**, and **4** are in striking contrast to those used to prepare the partially chalcogenated complexes **A** and **B**, which require boiling toluene and long reaction times (24–48 h).^[7] Clearly, the negative charge in the anion of **2a** results in a dramatic enhancement of the susceptibility of the Sn^{II} centers towards oxidation. The complexes **3a**, **3b**, and **4** were characterized by multinuclear NMR spectroscopy, elemental analyses and, in the case of **3b** and **4**, by X-ray crystallography.

X-ray structural determinations of **3b**^[11] and **4**^[12] revealed the presence of three terminal Sn=E bonds in each complex (**3b**, E = Se; **4**, E = Te) (Figure 1 and 2, respectively). For **3b**

[*] Prof. T. Chivers, Dr. D. J. Eisler
Department of Chemistry
University of Calgary
Calgary, AB, T2N 1N4 (Canada)
Fax: (+1) 403-289-9488
E-mail: chivers@ucalgary.ca

[**] The authors gratefully acknowledge financial support from the Natural Sciences and Engineering Research Council (Canada).

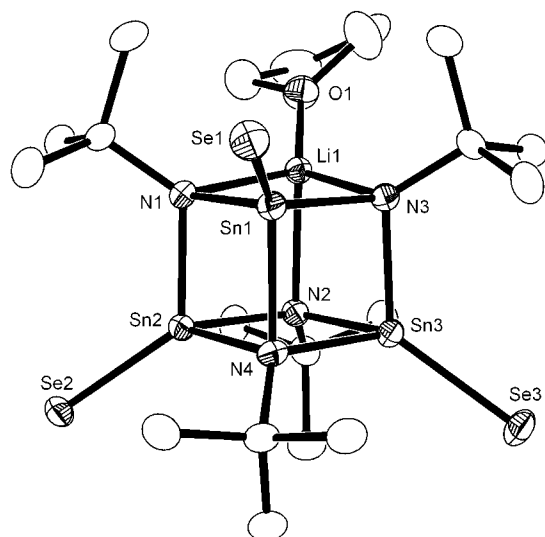


Figure 1. X-ray crystal structure of the anion in **3b**; selected bond lengths [Å]: Sn1–Se1 2.397(1), Sn2–Se2 2.391(1), Sn3–Se3 2.386(1). Thermal ellipsoids are shown at the 30% probability level.

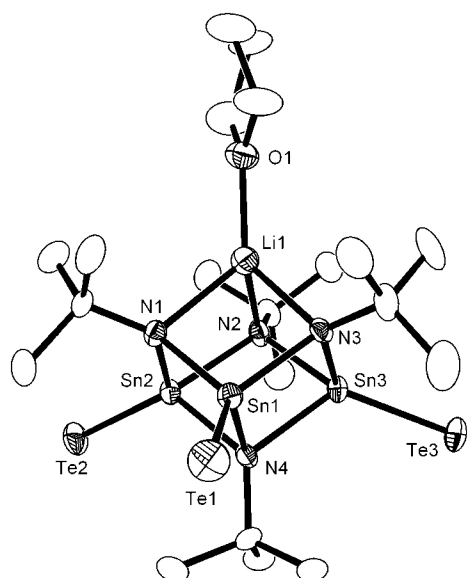


Figure 2. X-ray crystal structure of the anion in **4**; selected bond lengths [Å]: Sn1–Te1 2.613(1), Sn2–Te2 2.605(1), Sn3–Te3 2.610(1). Thermal ellipsoids are shown at the 30% probability level.

the Sn=Se bond lengths are nearly equal, with a mean value of 2.391(1) Å, slightly longer than the average Sn=Se bond length of 2.367(1) Å in the structurally related neutral complex **B**.^[7] The average Sn=Te bond length of 2.609(1) Å in **4** is significantly longer than the corresponding bond in **A** (2.589(1) Å),^[7] and slightly shorter than the distance of 2.618(1) Å observed in the five-coordinate complex $[\text{CH}(\text{SiMe}_3)\text{C}_9\text{H}_6\text{N-8}]_2\text{SnTe}$.^[13] The environments of the four-coordinate Sn^{IV} centers are highly distorted from tetrahedral in both structures, with bond angles in the range 83.6(2)–129.2(1)° in **3b** and 83.4(3)–129.0(2)° in **4**. The tin–nitrogen distances in **3b** and **4** show similar trends. The unique nitrogen center, which caps all three tin atoms, exhibits significantly

longer Sn–N distances (**3b**, 2.174(4)–2.184(4) Å; **4**, 2.15(1)–2.18(1) Å) in comparison to the nitrogen centers that bridge two tin atoms and the lithium atom (**3b**, 2.082(4)–2.105(4) Å; **4**, 2.07(1)–2.12(1) Å).

The solution NMR data for the complexes **3a**, **3b**, and **4** are consistent with the presence of a single species with local C_3 symmetry in each case. For example, the ^1H NMR spectra show two resonances in a 3:1 ratio for the *Nt*Bu protons, as expected. In the ^7Li NMR spectra of the complexes **3a**, **3b**, and **4**, the resonance in the region $\delta = 1.7$ –1.8 ppm is shifted significantly from that observed for the parent clusters **2a** or **2b** ($\delta = 2.6$ ppm), and is therefore attributed to the lithium cation that is part of the cubane cluster. For the complexes **3a** and **3b**, nearly identical NMR data were obtained, and so the data obtained for **3a** will serve as an example. The ^{119}Sn NMR spectrum of **3a** shows a single sharp resonance at $\delta = -133$ ppm, with well-resolved ^{77}Se satellites. The magnitude of $^1J_{\text{Sn,Se}}$ (3180 Hz) is comparable to the values in the range 2950–3450 Hz found for five-coordinate complexes.^[13,14] A single resonance is also observed in the ^{77}Se NMR spectrum, with well-resolved $^{117}\text{Sn}/^{119}\text{Sn}$ satellites. The room-temperature ^{119}Sn NMR spectrum of **4** exhibits a single resonance at $\delta = -450$ ppm, which is considerably broader than that observed for **3a** and no ^{125}Te satellites are observed, presumably as a result of chalcogen exchange. Consistently, at 213 K, this resonance becomes sharper, and ^{125}Te satellites can be detected. The value of the $^1J_{\text{Te,Sn}}$ coupling (8400 Hz) is consistent with an Sn=Te terminal bond.^[13] A single resonance at $\delta = -314$ ppm was observed in the ^{125}Te NMR spectrum of **4**, however poor solubility at low temperature prohibited the observation of well-resolved tin satellites.

The facile chalcogen exchange between clusters can be used advantageously for the synthesis of partially chalcogenated derivatives. Thus, stoichiometric addition of **2a** to solutions of **3a** or **4** results in the rapid and clean formation of the corresponding mono- and dichalcogenated clusters. This approach produces analytically pure products more readily than the direct reaction of **2a** with elemental chalcogens. Details of the synthesis and characterization of the partially chalcogenated complexes will be reported in a full account of this work.

In summary, we have developed a new, high-yield, synthetic route to completely chalcogenated imidotin clusters, which proceeds rapidly under mild conditions. The Sn^{II} centers of the anionic cubane in the solvent-separated ion pairs **2a** or **2b** show remarkable reactivity towards chalcogenation. Furthermore, the dilithio complexes **3** and **4** obtained by this route are potential synthons for the generation of a variety of heterobimetallic imidotin chalcogenides, which may serve as a source of ternary semiconductors by the thermal elimination of the diazene *t*BuN=N*t*Bu.^[15]

Experimental Section

All reactions and the manipulations of products were performed under an argon atmosphere by using standard Schlenk techniques or in an inert atmosphere glove box. NMR spectra were obtained on $[\text{D}_8]\text{THF}$ solutions at 298 K (unless otherwise noted) using a Bruker AMX 300 spectrometer. ^{77}Se , ^{119}Sn , and ^{125}Te NMR spectra were

referenced to the external standards (SePh)₂, SnMe₄, and (TePh)₂, respectively. The reagent **1** was prepared by modification of the literature procedure.^[9]

2a: A solution of **1** (9.00 g, 14.0 mmol) in THF (100 mL) was cooled to –78 °C to form a yellow slurry, and a cold (–78 °C) THF solution (60 mL) of *n*-butyllithium (1.6 M in hexane, 17.5 mL, 28.0 mmol) was added dropwise by using a cannula over 40 min. The resulting clear orange solution was stirred for 30 min at –78 °C, then allowed to warm slowly to room temperature, and stirred for an additional 45 min. The solvent was removed under vacuum and the yellow-orange residue was washed with hexanes (4 × 50 mL). The remaining solid was dissolved in diethyl ether (200 mL) and the solution was concentrated to about 100 mL, resulting in the precipitation of fine yellow crystals of **2a** (5.50 g, 39 %). Elemental analysis calcd (%) for **2a** (with loss of one THF) C₃₂H₆₈N₄Li₂O₅Sn₃: C 40.76, H 7.27, N 6.79; found: C 40.32, H 7.40, N 6.49; ¹H NMR: δ = 1.32 (s, 27H; NtBu), 1.35 (s, 9H; NtBu), 1.78 (m, 20H; THF), 3.63 ppm (m, 20H; THF); ⁷Li NMR: δ = –0.62 (s; [Li(thf)₄]⁺), 2.63 ppm (s; [(thf)LiSn₃(NtBu)₄][–]); ¹¹⁹Sn NMR: δ = 538 ppm (s).

2b: A solution of [12]crown-4 (0.40 mL, 2.42 mmol) in THF (25 mL) was added to a solution of **2a** (2.50 g, 2.46 mmol) in THF (50 mL) by using a cannula, and the mixture was stirred for 30 min at 25 °C. The solvent was removed under vacuum and the residue was washed with cold diethyl ether (50 mL) to give **2b** as a pale yellow solid (1.88 g, 78 %). Elemental analysis calcd (%) for **2b** (with loss of 0.5 THF) C₃₀H₆₄N₄Li₂O_{5.5}Sn₃: C 38.38, H 6.87, N 5.97; found: C 38.14, H 6.77, N 6.60; ¹H NMR: δ = 1.34 (s, 27H; NtBu), 1.37 (s, 9H; NtBu), 1.78 (m, 8H; THF), 3.63 (m, 8H; THF), 3.84 ppm (s, 16H; [12]crown-4); ⁷Li NMR: δ = –0.47 (s; [(thf)Li([12]crown-4)]⁺), 2.61 ppm (s; [(thf)LiSn₃(NtBu)₄][–]); ¹¹⁹Sn NMR: δ = 534 ppm (s).

3a: A mixture of **2a** (0.600 g, 0.59 mmol) and gray selenium powder (0.160 g, 2.03 mmol) in THF (20 mL) was stirred for 5 min at 25 °C. The resulting deep yellow solution was filtered through a 0.45 μm pore size filter disk, concentrated to about 5 mL, and **3a** was precipitated as a yellow solid (0.720 g, 97 %) by the addition of diethyl ether. Elemental analysis calcd (%) for C₃₆H₇₆N₄Li₂O₅Se₃Sn₃: C 34.54, H 6.12, N 4.48; found: C 33.74, H 5.86, N 4.58; ¹H NMR: δ = 1.47 (s, 27H; NtBu), 1.57 (s, 9H; NtBu), 1.77 (m, 20H; THF), 3.61 ppm (m, 20H; THF); ⁷Li NMR: δ = –0.60 (s; [Li(thf)₄]⁺), 1.75 ppm (s; [(thf)LiSn₃(NtBu)₄][–]); ⁷⁷Se NMR: δ = –174 ppm (s, ¹J_{119Sn,77Se} = 3185 Hz, ¹J_{117Sn,77Se} = 3065 Hz); ¹¹⁹Sn NMR: δ = –133 ppm (s, ²J_{119Sn,117Sn} = 305 Hz, ¹J_{119Sn,77Se} = 3180 Hz).

3b: This complex was prepared similarly from **2b** (0.200 g, 0.21 mmol) and gray selenium powder (0.053 g, 0.67 mmol) and obtained as a yellow solid (0.228 g, 91 %). Elemental analysis calcd (%) for C₃₂H₆₈N₄Li₂O₆Se₃Sn₃: C 31.72, H 5.66, N 4.62; found: C 31.84, H 5.87, N 4.47; ¹H NMR: δ = 1.50 (s, 27H; NtBu), 1.60 (s, 9H; NtBu), 1.78 (m, 8H; THF), 3.63 (m, 8H; THF), 3.85 ppm (s, 16H; [12]crown-4); ⁷Li NMR: δ = –0.44 (s; [(thf)Li([12]crown-4)]⁺), 1.72 ppm (s; [(thf)LiSn₃(NtBu)₄][–]); ⁷⁷Se NMR: δ = –172 ppm (s, ¹J_{119Sn,77Se} = 3174 Hz, ¹J_{117Sn,77Se} = 3030 Hz); ¹¹⁹Sn NMR: δ = –133 ppm (s, ²J_{119Sn,117Sn} = 312 Hz, ¹J_{119Sn,77Se} = 3200 Hz). X-ray quality crystals of **3b** were obtained by slow diffusion of *n*-hexane into a THF solution.

4: A mixture of **2a** (0.600 g, 0.59 mmol) and tellurium powder (0.260 g, 2.04 mmol) in THF (30 mL) was stirred for 20 min at 40 °C. The resulting deep orange solution was filtered through a 0.45 μm pore size filter disk, concentrated to about 5 mL, and diethyl ether (1 mL) was added to give **4** as red crystals (0.600 g, 73 %). Elemental analysis calcd (%) for C₃₆H₇₆N₄Li₂O₅Sn₃Te₃: C 30.93, H 5.48, N 4.01; found: C 30.79, H 5.61, N 4.07; ¹H NMR: δ = 1.52 (s, 27H; NtBu), 1.62 (s, 9H; NtBu), 1.78 (m, 20H; THF), 3.62 ppm (m, 20H; THF); ⁷Li NMR: δ = –0.70 (s; [Li(thf)₄]⁺), 1.82 ppm (s; [(thf)LiSn₃(NtBu)₄][–]); ¹¹⁹Sn NMR (213 K): δ = –439 ppm (s, ¹J_{125Te,119Sn} = 8400 Hz); ¹²⁵Te NMR: δ = –313 ppm. X-ray quality crystals of **4** were obtained by slow diffusion of *n*-hexane into a THF solution.

Received: June 14, 2004

Keywords: chalcogens · cluster compounds · cubanes · multiple bonds · tin

- [1] For recent reviews, see: a) C. A. Jaska, A. Bartole-Scott, I. Manners, *Dalton Trans.* **2003**, 4015–4021; b) A. R. McWilliams, H. Dorn, I. Manners, *Top. Curr. Chem.* **2002**, *220*, 141–167.
- [2] M. Afzaal, M. A. Malik, P. O'Brien, *Chem. Commun.* **2004**, 334–335.
- [3] a) M. Afzaal, D. Crouch, M. A. Malik, M. Motevalli, P. O'Brien, J. H. Park, J. D. Woollins, *Eur. J. Inorg. Chem.* **2004**, 171–177; b) M. Afzaal, K. Ellwood, N. L. Pickett, P. O'Brien, J. Raftery, J. Waters, *J. Mater. Chem.* **2004**, *14*, 1310–1315.
- [4] For examples, see: a) C. An, K. Tang, B. Hai, G. Shen, C. Wang, Y. Qian, *Inorg. Chem. Commun.* **2003**, *6*, 181–184; b) S. Schlecht, M. Budde, L. Kienle, *Inorg. Chem.* **2002**, *41*, 6001–6005; c) Y. Li, Z. Wang, Y. Ding, *Inorg. Chem.* **1999**, *38*, 4737–4740.
- [5] a) P. Boudjouk, M. P. Remington, Jr., D. G. Grier, W. Triebold, B. R. Jarabek, *Organometallics* **1999**, *18*, 4534–4537; b) A. L. Seligson, J. Arnold, *J. Am. Chem. Soc.* **1993**, *115*, 8214–8220.
- [6] For recent reviews, see: a) N. Tokitoh, R. Okazaki in *The Chemistry of Organic Germanium, Tin and Lead Compounds*, Vol. 2, Part 1 (Ed.: Z. Rapoport), Wiley, Chichester, UK, **2002**, pp. 843–901; b) N. Tokitoh, R. Okazaki, *Adv. Organomet. Chem.* **2001**, *47*, 121–166.
- [7] T. Chivers, T. J. Clark, M. Krahn, M. Parvez, G. Schatte, *Eur. J. Inorg. Chem.* **2003**, 1857–1860.
- [8] G. G. Briand, T. Chivers, M. Parvez, *Angew. Chem.* **2002**, *114*, 3618–3620; *Angew. Chem. Int. Ed.* **2002**, *41*, 3468–3470.
- [9] M. Veith, M.-L. Sommer, D. Jäger, *Chem. Ber.* **1979**, *112*, 2581–2587.
- [10] R. E. Allan, M. A. Beswick, N. L. Cromhout, M. A. Paver, P. R. Raithby, A. Steiner, M. Trevithick, D. S. Wright, *Chem. Commun.* **1996**, 1501–1502.
- [11] Crystal data for **3b**: 2 (C₃₂H₆₈N₄Li₂O₆Se₃Sn₃)·0.5(C₄H₈O), *M*_r = 2459.52, monoclinic, space group *P*2₁/*c*, *a* = 26.332(5), *b* = 10.920(2), *c* = 36.260(7) Å, β = 107.51(3)°, *V* = 9943(3) Å³, *Z* = 4, ρ_{calcd} = 1.643 g cm^{–3}, μ = 3.731 mm^{–1}, *T* = 173(2) K. A yellow platelike crystal (0.20 × 0.12 × 0.05 mm³) was coated with Paratone 8277 oil and mounted on a glass fiber. Data were collected on a Nonius Kappa CCD diffractometer by using MoK_α radiation (λ = 0.71073 Å). The structure was solved by Patterson techniques and refined by least-squares calculations (SHELXL-97). Of the 84930 reflections collected, 22 185 were unique (*R*_{int} = 0.071) and used to refine 891 parameters. Complex **3b** crystallizes with two independent but chemically equivalent molecules in the asymmetric unit. The disorder in the [12]crown-4 unit and the coordinated and lattice-bound THF molecules was treated by using appropriate models. Refinement was carried out on *F*² against all independent reflections and converged at *R*₁ = 0.050 (for 15995 reflections with *I* > 2σ(*I*)) and *wR*₂ = 0.133 (for all data).
- [12] Crystal data for **4**: 6 (C₃₆H₇₆N₄Li₂O₅Sn₃Te₃)·0.5(C₆H₁₄), *M*_r = 8429.63, triclinic, space group *P*1̄, *a* = 23.401(5), *b* = 26.126(5), *c* = 26.459(5) Å, α = 84.97(3), β = 84.26(3), γ = 83.01(3)°, *V* = 15929(6) Å³, *Z* = 2, ρ_{calcd} = 1.758 g cm^{–3}, μ = 3.053 mm^{–1}, *T* = 173(2) K. Crystal size : 0.16 × 0.06 × 0.06 mm³. Data collection, structure solution and refinement followed the procedures outlined above for **3b**. Of the 182994 reflections collected, 55941 were unique (*R*_{int} = 0.071) and used to refine 2556 parameters. Complex **4** crystallizes with six independent, but chemically equivalent molecules in the asymmetric unit. Disorder in the cubane and THF molecules was treated by using appropriate models. Refinement converged at *R*₁ = 0.071 (for 35294 reflections with *I* > 2σ(*I*)) and *wR*₂ = 0.177 (for all data). CCDC-241572 (**3b**) and CCDC-241573 (**4**) contain the supple-

mentary crystallographic data for this paper. These data can be obtained free of charge via www.ccdc.cam.ac.uk/conts/retrieving.html (or from the Cambridge Crystallographic Data Centre, 12, Union Road, Cambridge CB21EZ, UK; fax: (+44)1223-336-033; or deposit@ccdc.cam.ac.uk).

- [13] W.-P. Leung, W.-H. Kwok, Z.-Y. Zhou, T. C. W. Mak, *Organometallics* **2000**, *19*, 296–303.
- [14] M. C. Kuchta, G. Parkin, *J. Am. Chem. Soc.* **1994**, *116*, 8372–8373.
- [15] For examples, see a) A. E. Riley, S. H. Tolbert, *J. Am. Chem. Soc.* **2003**, *125*, 1551–1559; b) P. N. Trikalitis, K. K. Rangan, T. Bakas, M. G. Kanatzidis, *Nature* **2001**, *410*, 671–675.

Allylic Substitution

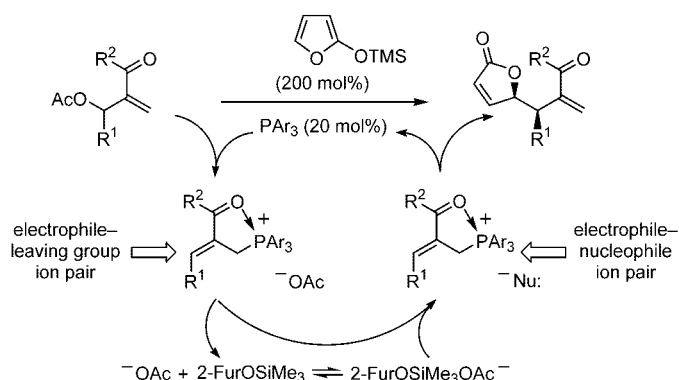
Regio- and Stereoselective Construction of γ -Butenolides through Phosphine-Catalyzed Substitution of Morita–Baylis–Hillman Acetates: An Organocatalytic Allylic Alkylation**

Chang-Woo Cho and Michael J. Krische*

The γ -butenolide ring system ranks among the most ubiquitous structural motifs found in naturally occurring organic molecules.^[1] Owing to the prevalence of γ -butenolides, their regio- and stereoselective synthesis has been the focus of intensive effort.^[2] In this regard, the use of 2-silyloxy furans as nucleophilic partners in Mukaiyama–aldol,^[3] Mukaiyama–Michael,^[4,5] and Mukaiyama–Mannich-type additions^[6] has emerged as an effective strategy. Even broader access to butenolide substructures would be possible through the development of new electrophilic partners amenable to 2-silyloxy furan addition. For example, the use of allylic carboxylates as electrophiles in silyloxy furan addition is unknown and would provide access to γ -butenolides with vicinal stereogenic centers. Herein we disclose that upon exposure of Morita–Baylis–Hillman (MBH) acetates **1a–12a** to substoichiometric amounts of triphenylphosphane (20 mol %) in the presence of 2-trimethylsilyloxy furan, regioselective allylic substitution occurs to provide the products of *C*-allylation, that is, γ -butenolides **1b–12b** (Table 1). Good to excellent yields, regioselectivities, and diastereose-

lectivities are attained and, in the case of the (–)-8-phenylmenthol ester **14a** (Scheme 3), the absolute stereochemical course of the substitution is controlled.

Recently, a two-step protocol for the amination of MBH acetates mediated by DABCO was reported.^[7a,b] A related two-step transformation employing quinidine subsequently appeared.^[7c] Following reports of these stoichiometric processes, the DABCO-catalyzed decarboxylative rearrangement of MBH carbamates was demonstrated.^[7d] Finally, (DHQD)₂PHAL was recently shown to catalyze regioselective allylic substitution of MBH acetates when using sodium bicarbonate as a nucleophile.^[7e] The corresponding MBH alcohols were produced in 25–42 % yield with 54–92 % *ee*. As part of a program in nucleophilic catalysis based on phosphine conjugate addition,^[8] the first *phosphine-catalyzed* allylic substitution of Morita–Baylis–Hillman (MBH) acetates was reported from our lab.^[8e] A key feature of this transformation appears to involve the generation of an electrophile–nucleophile ion pair, which suppresses direct addition of the nucleophile to the less substituted enone moiety of the starting MBH acetate. The enone immediately obtained upon addition of the phosphine may also benefit from activation through internal coordination to phosphorus (Scheme 1). In



Scheme 1. Postulated catalytic mechanism for γ -butenolide synthesis through tandem S_N2'–S_N2' substitution.

our initial study, an acid–base reaction between the leaving group (acetate) and the pronucleophile (4,5-dichlorophthalimide) served to generate the requisite electrophile–nucleophile ion pair. Given the propensity of organosilicon compounds to form hypervalent anions or “ate” complexes,^[9] the development of related catalytic C–C bond formations involving electrophile–nucleophile ion pair intermediates derived from enol silane based pronucleophiles was deemed feasible.

To explore this prospect, MBH acetate **1a** (100 mol %) derived from methyl vinyl ketone (MVK) was exposed to 2-trimethylsilyloxy furan (200 mol %) in the presence of triphenylphosphane (20 mol %) in THF solvent (0.3 M) at 0 °C. Gratifyingly, the desired product of allylic substitution, γ -butenolide **1b**, was isolated in 88 % yield as a single *syn* diastereomer. The regioisomeric substance **1c** was also formed in 9 % yield. Withstanding changes in reaction temperature, these conditions proved general across a range

[*] Dr. C.-W. Cho, Prof. M. J. Krische
University of Texas at Austin
Department of Chemistry and Biochemistry
1 University Station - A5300
Austin, TX 78712-1167 (USA)
Fax: (+1) 512-471-8696
E-mail: mkrische@mail.utexas.edu

[**] Acknowledgment is made to the Research Corporation Cottrell Scholar Award (CS0927), the Alfred P. Sloan Foundation, the Dreyfus Foundation, the NIH, and Eli Lilly for partial support of this research.

Supporting information for this article is available on the WWW under <http://www.angewandte.org> or from the author.

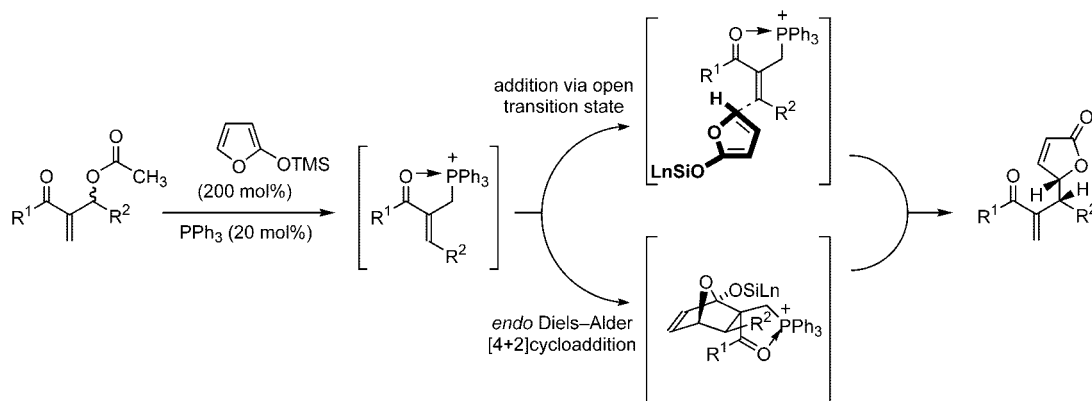
of related MVK-derived MBH acetates **2a–6a**, which bear aromatic, aliphatic, cyclopropyl, vinylic, and acetylenic substituents. All MVK-derived products **1b–6b** were obtained with diastereomeric ratios of $\geq 20:1$ (*syn/anti*). Similarly, the corresponding acrylate-derived MBH acetates **7a–12a** provide γ -butenolides **7b–12b** with excellent regioselectivity. Butenolides **7b, 8b, 11b**, and **12b**, which bear aromatic, vinylic, and acetylenic substituents, were obtained with excellent diastereoselectivity. However, acrylate-derived MBH acetates **9b** and **10b**, which bear *n*-alkyl and cyclopropyl substituents, respectively, were obtained with lower diastereoselectivities (Table 1).

The high levels of diastereoselectivity attained in these substitutions do not appear to be consistent with an open transition state. It is possible that the high diastereoselectivity arises as a consequence of a mechanism involving *endo*-selective Diels–Alder cycloaddition of the siloxy furan ate complex with the enone obtained upon the addition of the phosphine followed by subsequent Grob-type fragmentation. Structurally related silyloxy furan-enone [4+2] cycloadducts have been isolated. Notably, the high levels of diastereoselectivity observed in the formation of **1b–12b** require that the intermediate phosphine adducts appear as single enone geometrical isomers, irrespective of which mechanism is operative (Scheme 2).^[5b]

Table 1: Diastereoselective phosphine catalyzed allylic substitution of MBH acetates to form γ -butenolides.^[a,b]

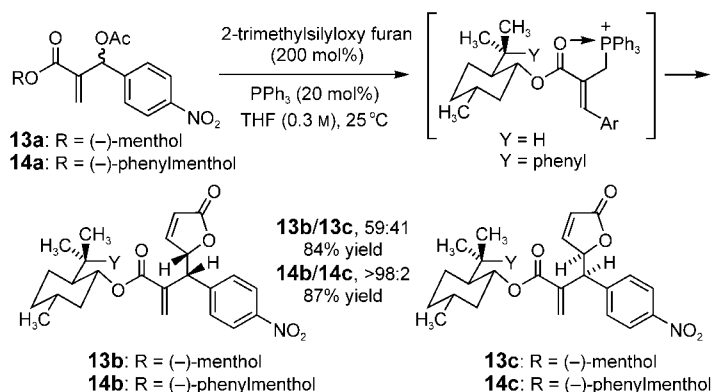
1a–12a	<i>syn</i> - 1b–12b	1c–12c
1b , 88%, > 95:5 d.r. 1c , 9%	2b , 80%, > 95:5 d.r. 2c , 5%	3b , 63%, > 95:5 d.r. 3c , 7%
4b , 80%, 20:1 d.r. 4c , 5%	5b , 45%, > 95:5 d.r. 5c , 10%	6b , 88%, 24:1 d.r. 6c , 5%
7b , 84%, > 95:5 d.r. 7c , 6%	8b , 86%, > 95:5 d.r. 8c , 1%	9b , 67%, 2.8:1 d.r. 9c , not observed
10b , 83%, 3.5:1 d.r. 10c , not observed	11b , 62%, > 95:5 d.r. 11c , not observed	12b , 94%, > 95:5 d.r. 12c , not observed

[a] Procedure: THF (1.6 mL, 0.3 M) was added to a reaction vessel charged with the MBH acetate (0.5 mmol, 100 mol%), 2-trimethylsilyloxy furan (1.0 mmol, 200 mol%), and PPh₃ (0.1 mmol, 20 mol%). The reaction mixture was allowed to stir at 0 °C (**1a, 6a, 7a**), 25 °C (**2a, 4a, 5a, 8a, 12a**), 50 °C (**3a**), or 80 °C (**9a–11a**) until complete consumption of starting material was observed, at which point the reaction mixture was adsorbed onto silica gel by evaporation of the solvent, and the product was isolated by silica-gel chromatography. [b] A diastereomeric ratio of >95:5 indicates that the minor isomer could not be detected by ¹H NMR spectroscopy.



Scheme 2. Alternate mechanisms postulated for the phosphine-catalyzed allylic substitution of MBH acetates to form γ -butenolides.

To control the absolute stereochemical course of this transformation, a chiral auxiliary approach was explored. Whereas (–)-menthol ester **13a** provides the γ -butenolides **13b** and **13c** in good yield, poor levels of asymmetric induction are observed. In contrast, the corresponding (–)-8-phenylmenthol ester **14a** provides the γ -butenolide **14b** in excellent yield and with complete levels of stereocontrol (Scheme 3). The diastereomeric butenolide **14c** was not observed. The stereochemical assignment of **14b**, which is supported by X-ray diffraction analysis, led to the indicated model for stereochemical induction.



Scheme 3. Controlling the absolute stereochemical course of allylic substitution through the use of (–)-8-phenylmenthol ester **14a**.

In summary, upon exposure of MBH acetates **1a–12a** to 2-trimethylsilyloxy furan in the presence of substoichiometric quantities of triphenylphosphine, highly regio- and stereo-selective substitution occurs to provide γ -butenolides **1b–12b**. Moreover, as demonstrated by the substitution of MBH acetate **14a**, the absolute stereochemical course of these transformations is controlled through the use of the (–)-8-phenylmenthol ester. Future studies will focus on the development of related transformations, including enantioselective variants of the transformation described herein.

Received: July 21, 2004

Keywords: allylic substitution · butenolides · C–C coupling · organocatalysis

- [1] For reviews encompassing major classes of butenolide-containing natural products, see: a) acetogenins: F. W. Alali, X.-X. Liu, J. L. McLaughlin, *J. Nat. Prod.* **1999**, 62, 504–540; b) cardiac steroids or cardenolides: J. R. Hanson, *Nat. Prod. Rep.* **2002**, 19, 381–389 and earlier reviews in this series; c) furanocembranoid diterpenes: A. D. Rodriguez, *Tetrahedron* **1995**, 51, 4571–4618; d) lignans: R. S. Ward in *Recent Advances in the Chemistry of Lignans*, Vol. 24, Part E (Ed.: Atta-ur-Rahman), Elsevier, Amsterdam, **2000**, p. 739–798.
- [2] For reviews encompassing synthetic approaches to butenolides, see: a) R. Brückner, *Curr. Org. Chem.* **2001**, 5, 679–718; b) D. W. Knight, *Contemp. Org. Synth.* **1994**, 1, 287–315; c) Y. S. Rao, *Chem. Rev.* **1976**, 76, 625–694.
- [3] For a review encompassing the use of the vinylogous aldol reaction in butenolide synthesis, see: G. Casiraghi, F. Zandari, G. Appendino, G. Rassu, *Chem. Rev.* **2000**, 100, 1929–1972.

- [4] For a review encompassing the use of the vinylogous Michael reaction in butenolide synthesis, see: J. Christoffers, *Synlett* **2001**, 723–732.
- [5] For recent examples of enantioselective vinylogous Michael reactions in butenolide synthesis, see: a) S. P. Brown, N. C. Goodwin, D. W. C. MacMillan, *J. Am. Chem. Soc.* **2003**, 125, 1192–1194; b) H. Kitajima, K. Ito, T. Katsuki, *Tetrahedron* **1997**, 53, 17015–17028.
- [6] For reviews encompassing the use of the vinylogous Mannich reaction in butenolide synthesis, see: a) S. K. Bur, S. F. Martin, *Tetrahedron* **2001**, 57, 3221–3242; b) S. F. Martin, *Acc. Chem. Res.* **2002**, 35, 895–904.
- [7] a) J. H. Gong, H. R. Kim, E. K. Ryu, J. N. Kim, *Bull. Korean Chem. Soc.* **2002**, 23, 789–790; b) J. N. Kim, H. J. Lee, K. Y. Lee, J. H. Gong, *Synlett* **2002**, 173–175; c) D. Basavaiah, N. Kumaragurubaran, D. S. Sharada, R. M. Reddy, *Tetrahedron* **2001**, 57, 8167–8172; d) M. Ciclosi, C. Fava, R. Galeazzi, M. Orena, J. Sepulveda-Arques, *Tetrahedron Lett.* **2002**, 43, 2199–2202; e) J. N. Kim, H. J. Lee, J. H. Gong, *Tetrahedron Lett.* **2002**, 43, 9141–9146.
- [8] a) L.-C. Wang, A.-L. Luiz, K. Agapiou, H.-Y. Jang, M. J. Krische, *J. Am. Chem. Soc.* **2002**, 124, 2402–2403; b) K. Agapiou, M. J. Krische, *Org. Lett.* **2003**, 5, 1737–1740; c) B. G. Jellerichs, J.-R. Kong, M. J. Krische, *J. Am. Chem. Soc.* **2003**, 125, 7758–7759; d) P. K. Koech, M. J. Krische, *J. Am. Chem. Soc.* **2004**, 126, 5350–5351; e) C.-W. Cho, J.-R. Kong, M. J. Krische, *Org. Lett.* **2004**, 6, 1337–1339.
- [9] For an authoritative review, see: C. Chuit, R. J. P. Corriu, C. Reye, J. C. Young, *Chem. Rev.* **1993**, 93, 1371–1448.

Nanotechnology

Preparation of Higher-Order Zeolite Materials by Using Dextran Templating**

*Dominic Walsh, Alexander Kulak, Kensuke Aoki, Toshiyuki Ikoma, Junzo Tanaka, and Stephen Mann**

The chemical construction of organized inorganic matter by using nanoparticle or microcrystal building blocks—nanotectonics^[1,2]—offers a novel approach to hierarchical, multi-

[*] Dr. D. Walsh, Dr. A. Kulak, K. Aoki, Prof. S. Mann
School of Chemistry
University of Bristol
Bristol BS8 1TS (UK)
Fax: (+44) 117 929 0509
E-mail: s.mann@bristol.ac.uk

Dr. D. Walsh, Dr. T. Ikoma, Dr. J. Tanaka
ICYS Centre/Advanced Material Group
National Institute for Material Science
1-1 Namiki, Tsukuba, Ibaraki 305-0051 (Japan)

K. Aoki
Central Technology Laboratory
Asahi Kasei Corporation
2-1 Samejima, Fuji, Shizuoka 416-8501 (Japan)

[**] We thank EPSRC (UK), JST(CREST) and Asahi Kasei Corp. for financial support.

functional materials with complex architectures. The multi-scale ordering, interlinking, and interfacing of preformed nanoparticles and small crystals can be directed internally by programmed assembly or externally by using a variety of structured organic templates. The former is achieved by self-coding of the inorganic building blocks with information-rich connectors, such as DNA duplexes,^[3] antibody–antigen complexes^[4] and streptavidin–biotin conjugates,^[5] complementary force fields based on electrostatic matching,^[6] or shape-directed hydrophobicity.^[7] In contrast, preformed nanoparticles can be organized within porous templates such as silica/polymer opals,^[8] polymer sponges^[9] or perfluorohexane foams^[10] to produce ordered macroporous inorganic replicas, or assembled onto polymer beads to form core–shell or hollow microspheres.^[11] Inorganic nanoparticles have also been assembled by using miniemulsion droplets,^[12] and recent studies involving sonicated water-in-oil emulsions have shown that highly complex spheroids can be assembled from silica/Au nanoparticles.^[13]

Exploitation of the above strategies in catalysis and separation science is timely as the chemical synthesis and fabrication of self-supported multifunctional materials with hierarchical porosity, complex formation, and multiscale ordering remains a significant challenge. Recently, nanoslabs of the aluminium-free zeolite, silicalite, were assembled into periodically ordered mesostructures by surfactant templating.^[14] Silicalite nanoparticles, about 50 nm in size, have also been organized on extended length scales to produce macroporous architectures by using multicellular bacterial threads,^[15] starch sponges,^[16] or polyurethane foams,^[17] or assembled around latex beads to produce hollow microspheres with hierarchical porosity.^[18] Other studies have demonstrated that zeolite crystals several micrometers in size can be organized into 2D arrays by using patterned solid substrates,^[19] or arranged into self-supporting complex hollow microspheres by sonication of aqueous dispersions in toluene.^[20]

Herein we demonstrate two new routes to the formation of higher-order zeolite materials based on template-directed processes that use the water-soluble polysaccharide, dextran and involve preformed zeolite crystals/nanoparticles as inorganic building blocks. In the first approach, which is based on a recent discovery in the preparation of metal and metal-oxide sponges,^[21] centimeter-sized macroporous framework monoliths of interconnected filaments composed of NaY crystals and amorphous silica nanoparticles are prepared by slow thermal processing of dextran/inorganic pastes. The zeolite crystals are embedded in the silica matrix to promote homogeneity in the distribution of active sites within the filamentous framework, and increase the strength of the macroporous monoliths. In the second approach, macroscopic threads of dextran are prepared and used to align linear chains of 100 nm-sized silicalite crystals to produce inorganic fibers with an ordered superstructure of crystallographically oriented prismatic crystals. The silicalite chains, which consist of up to 20 coaligned crystals, are prepared by a novel process involving hydrothermal synthesis in the presence of the cationic polymer, poly(diallyldimethylammonium hydroxide). Our results demonstrate that superstructural ordering of

zeolite crystals within complex macroscopic morphologies can be achieved, and suggest that further development of these proof-of-concept studies should provide a range of novel hierarchical multifunctional materials for potential use in catalysis and separation science.

Open-framework zeolite monoliths were prepared as follows. Dextran ($M_r = 70\,000$) was dissolved in an aqueous suspension, consisting of 20:1 wt ratio, respectively, of sub-micron-sized NaY zeolite crystallites (size range, 0.7–1 μm) and silica nanoparticles (diameter, 14 nm) to produce a viscous paste that was air dried for two days. Controlled heating of the paste resulted in thermal decomposition of the dextran matrix at around 270 °C with associated outgassing of steam and carbon dioxide to produce an expanded carbon-based foam that served as a template for patterning the thermally induced aggregation of the silica/zeolite particles. Increasing the temperature slowly to 470 °C at a heating rate of 2 °C min⁻¹ resulted in the gradual destruction and removal of the carbon foam, and the formation of an intact inorganic spongelike replica, 1–2 cm in size, that was further heated to 600 °C to remove residual organic constituents.

In general, the above procedure resulted in the preparation of self-supporting replicas that were fragile but sufficiently robust to be handled with care. SEM investigations indicated that the replicas consisted of a continuous open framework of interconnected filaments, about 15 μm in width and 100–150 μm in length (Figure 1). The filaments intersected at distinct three-point junctions to produce open cells that were usually five- or six-sided and 100–300 μm across. Interestingly, the inorganic frameworks exhibited a gradient in pore sizes, with cells produced close to the outer surface of the dextran paste generally larger than those formed deep

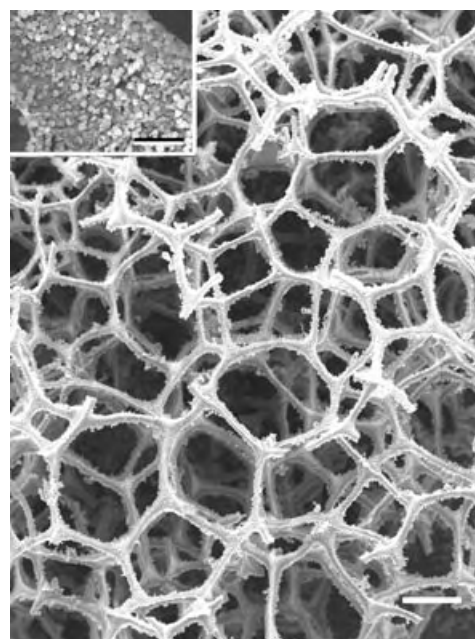


Figure 1. SEM micrograph showing open macroporous zeolite/silica framework prepared by dextran templating; scale bar = 100 μm . Inset; high magnification of a single-wall filament showing NaY crystals embedded in a continuous silica matrix; scale bar = 5 μm .

within the matrix. High-magnification images indicated that the filaments were composed of discrete micrometer-sized zeolite crystals embedded within a continuous matrix of condensed silica nanoparticles (Figure 1, inset). Significantly, X-ray diffraction studies showed almost identical reflections for the NaY crystals before and after heating the dextran composites to 600 °C, and BET analysis revealed no corresponding change in the type I isotherm, micropore size distribution, or surface area ($650 \text{ m}^2 \text{ g}^{-1}$), thus indicating that no degradation in the zeolite structure occurred during formation of the spongelike material.

Interestingly, closed-framework structures were obtained when NaY particles with size distribution of 0.3–0.4 μm were used in combination with colloidal silica solution at a respective weight ratio of 20:1. Under these conditions, the zeolite particles were small enough to stabilize the formation of thin self-supporting NaY/silica films across the 100–300 μm -sized apertures of the cellular framework (Figure 2). The supporting filamentous frame was typically 50 μm in width, whereas the membranes enclosing each cell were only

about 150 nm in thickness. Although the thin inorganic membranes were present throughout the framework monolith, they were very fragile and often split or destroyed when examined by SEM.

The above results indicate that spongelike silica/NaY composites with porosity at both the nano- and macroscale can be prepared by sacrificial dextran templating that involves the in situ formation of thermally induced dextran-derived foams. Other investigations showed that formation of the intact macroporous frameworks depended on the composition of the paste, as well as the heating rates used during thermal processing. For example, by using the above paste composition but with a higher heating rate of $10^\circ\text{C min}^{-1}$, samples that contained residual carbon even at 500 °C were produced. Consequently, it was necessary to heat the materials to 650 °C for several hours to prepare carbon-free replicas. However, these conditions resulted in the collapse of the NaY structure, as evidenced by the XRD data, to give frameworks with a low wall porosity of $20 \text{ m}^2 \text{ g}^{-1}$ (BET analysis). Whereas intact macroporous sponges could be prepared by using silica nanoparticles and dextran alone, significantly, samples synthesized by using NaY and dextran at a low heating rate 2°C min^{-1} in the absence of silica gave frameworks that were too fragile to be routinely handled. Similar results were also observed when mixtures of dextran and silicalite nanocrystals were used.

Dextran templating was also used to prepare intact macroscopic fibers of aligned silicalite crystals. Significantly, the crystals were preorganized in the form of discrete self-assembled chains (Figure 3a), which were prepared by hydrothermal synthesis in the presence of the water-soluble cationic polymer, poly(diallyldimethylammonium hydroxide). The chains were formed in situ within the reaction medium and consisted of prismatic particles that were coaligned with their crystallographic *b* axes parallel to the chain axis, as shown by TEM/electron diffraction analysis (data not shown) and XRD (Figure 4a,b). An aqueous suspension of the chains was mixed with dextran and long fibers up to 20 cm in length were pulled from the mixture, and air-dried. This process resulted in an intact composite fiber that consisted of a densely packed network of silicalite chains oriented preferentially along the morphological long axis, which was subsequently slowly heated to 550 °C to remove the dextran matrix. In general, this procedure resulted in intact inorganic replicas when the precursor threads were a few centimetres in length, whereas longer threads tended to disintegrate into smaller inorganic fibers. In each case, the calcined materials were highly textured and consisted of a superstructure of silicalite crystals. Significantly, materials prepared from dextran/silicalite threads, 20–30 μm in width, were highly ordered with chains of silicalite crystals preferentially aligned along the fiber axis (Figure 3b,c). Corresponding XRD measurements indicated that the silicalite micropore structure was retained after thermal treatment, and that the peak intensity of the (0100) reflection was reduced compared to a nonoriented control sample (Figure 4c). The data confirmed that under these conditions, the silicalite crystals within the oriented superstructure were preferentially aligned such that the crystallographic *b* axis was parallel to the fiber direction.

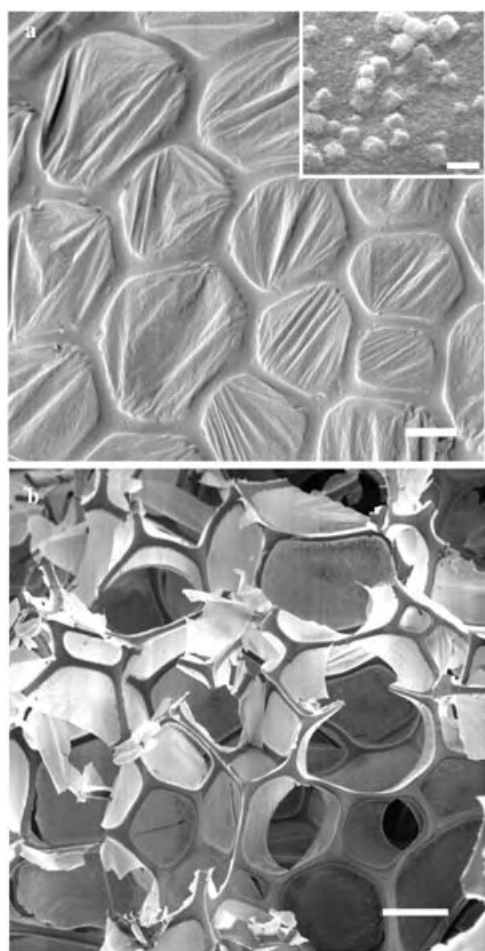


Figure 2. SEM images of closed cell NaY/silica frameworks. a) Top view showing underlying framework and intact aperture membrane; scale bar = 100 μm . Inset; high magnification image of the ultrathin membrane showing NaY crystals and silica matrix; scale bar = 0.5 μm . b) interior view showing details of closed cell architecture; scale bar = 100 μm .

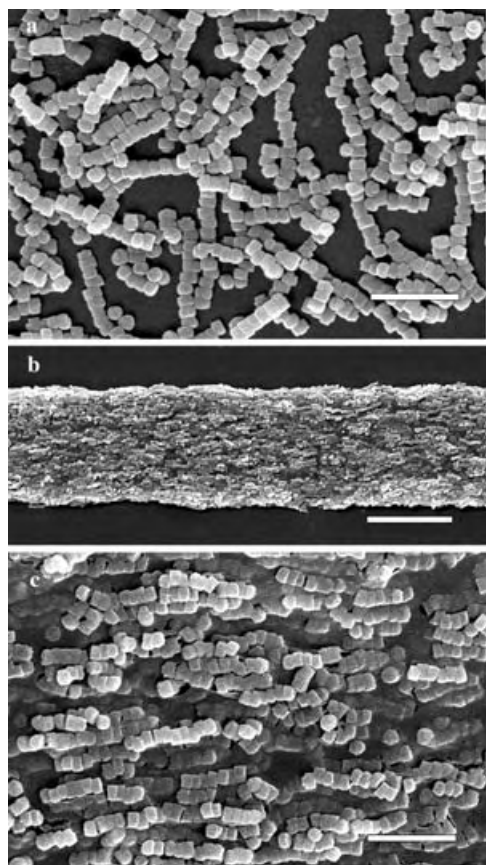


Figure 3. a) As-synthesized ordered chains of silicalite crystals viewed by SEM; scale bar = 1 μm . b) Inorganic fiber with ordered superstructure of silicalite crystals prepared from calcined dextran/silicalite thread; scale bar = 5 μm . c) High-magnification image showing iso-oriented texture of prismatic silicalite crystals aligned parallel to the fiber axis; scale bar = 1 μm .

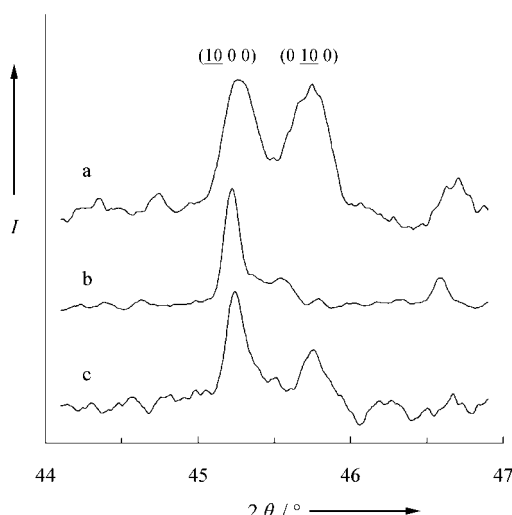


Figure 4. XRD data showing relative peak intensities for silicalite (1000) and (0100) reflections for a) control crystals (non-oriented), b) as-synthesized silicalite chains, and c) inorganic fiber with ordered silicalite superstructure. I is intensity, arbitrary units.

In contrast, the use of thicker dextran/silicalite precursor threads introduced increased levels of particle disorder and macroporous voids in the inorganic replicas, presumably due to enhanced entrapment of gas bubbles and associated disruption of the silicalite chains during thermal processing.

In conclusion, the above results indicate that dextran/inorganic composites can be used for the facile preparation of zeolite materials with higher-order structure, morphology, and porosity. The methods use the ability of dextran to be readily drawn into macrothreads from viscous solutions, or prepared as thick pastes as precursors to thermally induced foams. In both cases, the polysaccharide matrix is used as a sacrificial template to coalign or spatially pattern the zeolite crystals. Removal of dextran by heating the soft macrothreads results in minimal disruption to the constituent silicalite crystals, and the high level of crystal packing induced by the fiber-drawing process, as well as preorganization of the silicalite particles into chainlike assemblies, are sufficient to produce intact fibrous superstructures during sintering. In contrast, thermal decomposition of the pastes gives rise to an open framework of interconnected NaY-containing filaments due to temporary stabilization of CO_2 microbubbles in the lower-density matrix, which induces phase separation and spatial patterning of the zeolite crystals. However, in this case, the level of sintering between zeolite crystals is insufficient to form a self-supporting framework, and a silica “mortar” is required to stabilize the inorganic microfilaments. Interestingly, the presence of silica in association with NaY crystals of relatively small size (300–400 nm) produces intact frameworks in which the individual cell apertures are veiled in a thin micrometer-thick inorganic membrane. Although these structures are very fragile, the ability to prepare both open and closed frameworks of organized zeolite crystals could have interesting applications, for example in high-resolution separation processes. Further work is in progress to extend the above templating procedures to higher-order zeolite architectures with appropriate stability for applications testing and development.

Experimental Section

Preparation of NaY zeolite/silica framework monoliths: NaY zeolite crystals 0.7–1 μm in size were separated from a commercial sample (Aldrich Cat. No. 33, 444-8, $\text{SiO}_2/\text{Al}_2\text{O}_3$ mole ratio = 5.1; Na_2O wt % = 13) by fractional sedimentation in ethanol by using successive centrifugation at 3000 rpm for 3 min. The BET surface area was 450 m^2g^{-1} (as supplied) and 610 m^2g^{-1} (after heating at 2°Cmin^{-1} to 600°C). Alternatively, NaY particles with size a distribution of 0.3–0.4 μm were synthesized according to previous methods.^[22] An aqueous suspension consisting of NaY and silica particles at a respective weight ratio of 20:1 was prepared by the addition of 0.1 g of submicrometer-sized NaY crystals to 1 mL distilled water, followed by 0.025 g of a 20wt % colloidal silica suspension (Snowtex C, Nissan Chem. Co., particle size, 14 nm). Dextran (2 g, M_r 70000) was then dissolved in the suspension to form a viscous solution which was transferred to an open dish and left to air-dry for 2 days. The dried paste was heated to 600°C at a heating rate of 2°Cmin^{-1} , held at 600°C for 30 min, and then cooled to room temperature in the furnace. Samples were removed and investigated by SEM, XRD, TGA, FTIR spectroscopy and BET analysis (TGA is thermogravimetric analysis).

Preparation of silicalite chains and oriented multichain fibers: Linear chains of prismatic crystals of silicalite-1 were prepared as follows: Tetraethylorthosilicate (TEOS; 16 g, 76.8 mmol) was slowly added to a stirred aqueous solution that contained 1M tetrapropylammonium hydroxide (TPAOH; 27.32 g, 27.0 mmol) and 20wt% poly(diallyldimethylammonium hydroxide) (PDAC; 10 g, 0.015 mmol). After the reaction had been stirred for 24 h at room temperature, large agglomerates were removed and 10 ml of the resulting cloudy suspension poured into a 20 mL hydrothermal bomb, and placed in a preheated oven at 150°C and left at this temperature for 24 h. After cooling to room temperature, the white suspension was centrifuged and the supernatant fluid removed, and deionized water added and the precipitate resuspended by shaking. This washing procedure was repeated four times to give suspension 6–7wt% in solids that slowly sedimented over a period of a few days.

Inorganic macrofibers comprising coaligned chains of silicalite crystals were prepared as follows: 2.0 g of dextran (M_r 70000) was dissolved in 1 mL of an aqueous suspension containing about 3 wt% silicalite crystals in the form of linear chains to form a viscous solution. Dextran/silicalite threads, often 20–30 μm in width and up to 20 cm in length, were then drawn from the viscous solution by insertion and slow removal of a spatula tip. The composite threads were air-dried and then heated to 550°C at 2°C min⁻¹ for 12 h before cooling to room temperature in the furnace. The resulting intact inorganic fibers were removed and investigated by a range of physical methods.

Received: March 29, 2004

Revised: June 16, 2004

Keywords: higher-order assembly · inorganic building blocks · nanoparticles · template synthesis · zeolites

- [1] S. Mann, S. A. Davis, S. R. Hall, M. Li, K. H. Rhodes, W. Shenton, S. Vaucher, B. Zhang, *Dalton Trans.* **2000**, 3753.
- [2] S. A. Davis, M. Breulmann, K. H. Rhodes, B. Zhang, S. Mann, *Chem. Mater.* **2001**, *13*, 3218.
- [3] a) C. A. Mirkin, R. L. Lesinger, R. C. Mucic, J. J. Storhoff, *Nature* **1996**, *382*, 607; b) P. Alivasatos, K. P. Johnsson, X. Peng, T. E. Wilson, C. J. Loweth, M. Bruchez, P. G. Schultz, *Nature* **1996**, *382*, 609; c) A. N. Shipway, I. Willner, *Chem. Commun.* **2001** 2035; d) L. Josephson, J. M. Perex, R. Weissleder, *Angew. Chem.* **2001**, *40*, 3304; *Angew. Chem. Int. Ed.* **2001**, *40*, 3204; e) E. Dujardin, L. B. Hsin, C. R. C. Wang, S. Mann, *Chem. Commun.* **2001**, 1264.
- [4] W. Shenton, S. A. Davis, S. Mann, *Adv. Mater.* **1999**, *11*, 449.
- [5] a) S. Connolly, D. Fitzmaurice, *Adv. Mater.* **1999**, *11*, 1202; b) M. Li, K. K. W. Wong, S. Mann, *Chem. Mater.* **1999**, *11*, 23.
- [6] a) T. H. Galow, A. K. Boal, V. M. Rotello, *Adv. Mater.* **2000**, *12*, 576; b) A. K. Boal, T. H. Galow, F. Ilhan, V. M. Rotello, *Adv. Funct. Mater.* **2001**, *11*, 461.
- [7] M. Li, H. Schnablegger, S. Mann, *Nature* **1999**, *402*, 393.
- [8] a) B. T. Holland, C. F. Blanford, T. Do, A. Stein, *Chem. Mater.* **1999**, *11*, 795; b) Y. A. Vlasov, N. Yao, D. J. Norris, *Adv. Mater.* **1999**, *11*, 165; c) G. Subramania, V. N. Manoharan, J. D. Thorne, D. J. Pine, *Adv. Mater.* **1999**, *11*, 1261; d) O. D. Velev, P. M. Tessier, A. M. Lenhoff, E. W. Kaler, *Nature* **1999**, *401*, 548; f) O. D. Velev, E. W. Kaler, *Adv. Mater.* **2000**, *12*, 531.
- [9] M. Breulmann, S. A. Davis, S. Mann, H. P. Hentze, M. Antonietti, *Adv. Mater.* **2000**, *12*, 502.
- [10] F. Carn, F. A. Colin, M. F. Achard, H. Deleuze, Z. Saadi, R. Backov, *Adv. Mater.* **2004**, *16*, 140.
- [11] a) F. Caruso, R. A. Caruso, H. Möhwald, *Science* **1998**, *282*, 1111; b) A. Rogach, A. Susha, F. Caruso, G. Sukhorukov, A. Kornowski, S. Kershaw, H. Möhwald, A. Eychmüller, H. Weller, *Adv. Mater.* **2000**, *12*, 333; c) D. I. Gittens, A. S. Susha, B. Schoeler, F. Caruso, *Adv. Mater.* **2002**, *14*, 508.
- [12] B. zu Putlitz, K. Landfester, H. Fischer, M. Antonietti, *Adv. Mater.* **2001**, *13*, 500.
- [13] A. Kulak, S. A. Davis, E. Dujardin, S. Mann, *Chem. Mater.* **2003**, *15*, 528.
- [14] S. P. B. Kremer, C. E. A. Kirschhock, A. Aerts, K. Villani, J. A. Martens, O. I. Lebedev, G. V. Tendeloo, *Adv. Mater.* **2003**, *15*, 1705.
- [15] B. Zhang, S. A. Davis, N. H. Mendelson, S. Mann, *Chem. Commun.* **2000**, 781.
- [16] B. Zhang, S. A. Davis, S. Mann, *Chem. Mater.* **2002**, *14*, 1369.
- [17] L. Huerta, C. Guillem, J. Latorre, A. Beltran, D. Beltran, P. Amoros, *Chem. Commun.* **2003**, 1448.
- [18] a) K. H. Rhodes, S. A. Davis, F. Caruso, B. Zhang, S. Mann, *Chem. Mater.* **2000**, *12*, 2832; b) X. D. Wang, W. L. Yang, Y. Tang, Y. J. Wang, S. K. Fu, Z. Gao, *Chem. Commun.* **2000**, 2161; c) A. G. Dong, Y. J. Wang, Y. Tang, N. Ren, Y. H. Zhang, Z. Gao, *Chem. Mater.* **2002**, *14*, 3217; d) A. G. Dong, N. Ren, W. L. Yang, Y. J. Wang, Y. H. Zhang, D. J. Wang, H. H. Hu, Z. Gao, Y. Tang, *Adv. Funct. Mater.* **2003**, *13*, 943.
- [19] a) K. Ha, Y.-J. Lee, Y. S. Chun, Y. S. Park, G. S. Lee, K. B. Yoon, *Adv. Mater.* **2001**, *13*, 594; b) K. Ha, Y.-J. Lee, D.-Y. Jung, J. H. Lee, K. B. Yoon, *Adv. Mater.* **2000**, *12*, 1614.
- [20] A. Kulak, Y. J. Lee, Y. S. Park, H. S. Kim, G. S. Lee, K. B. Yoon, *Adv. Mater.* **2002**, *14*, 526.
- [21] D. Walsh, L. Arcelli, T. Ikoma, J. Tanaka, S. Mann, *Nat. Mater.* **2003**, *2*, 386.
- [22] G. S. Lee, Y.-J. Lee, K. Ha, K. B. Yoon, *Adv. Mater.* **2001**, *13*, 1491.

Chirality

Meteoritic C^α-Methylated α-Amino Acids and the Homochirality of Life: Searching for a Link

*Marco Crisma, Alessandro Moretto,
Fernando Formaggio, Bernard Kaptein,
Quirinus B. Broxterman, and Claudio Toniolo**

Growing evidence has recently accumulated on the occurrence of chiral, C^α-methylated α-amino acids with significant L (*S*) enantiomeric excess (*ee*; up to 15 %) in carbonaceous chondritic meteorites.^[1–3] The amino acids analyzed to date include isovaline (Iva), C^α-methyl norvaline [(αMe)Nva], C^α-

[*] Dr. M. Crisma, Dr. A. Moretto, Prof. F. Formaggio, Prof. C. Toniolo
Institute of Biomolecular Chemistry, CNR and
Department of Chemistry
University of Padova
via Marzolo 1, 35131 Padova (Italy)
Fax: (+39) 049-8275239
E-mail: claudio.toniolo@unipd.it
Dr. B. Kaptein, Dr. Q. B. Broxterman
DSM Research, Life Sciences
Advanced Synthesis and Catalysis
P.O. Box 18, 6160 MD Geleen (The Netherlands)



Supporting information for this article is available on the WWW under <http://www.angewandte.org> or from the author.

methyl valine [(α Me)Val], C $^{\alpha}$ -methyl isoleucine [(α Me)Ile], and C $^{\alpha}$ -methyl *allo*isoleucine [(α Me)*a*Ile] (Figure 1). In contrast, the α -amino acids lacking the C $^{\alpha}$ -methyl group (including the proteinogenic amino acids) have been found to be

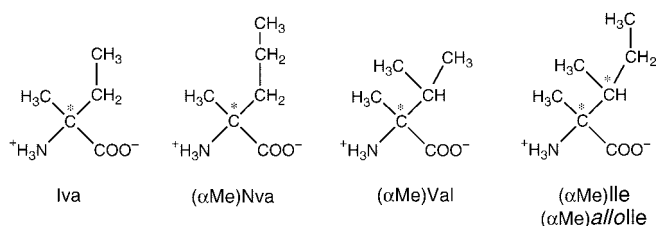


Figure 1. C $^{\alpha}$ -Methylated α -amino acids found in significant L enantiomeric excess in the Murchison and Murray meteorites. Chiral carbon atoms are starred.

racemic within experimental and terrestrial contamination errors.^[1–6] As opposed to C $^{\alpha}$ -methylated α -amino acids which are known to resist racemization, proteinogenic amino acids tend to racemize on an evolutionary time scale owing to their weakly acidic C $^{\alpha}$ -hydrogen.^[5,7–12] It has been calculated that during just one million years an amount of $\geq 10^{12}$ Kg of organic carbon was delivered by meteorites to the Earth.^[1–3] It has been also shown that C $^{\alpha}$ -methylated α -amino acids are generally abundant (10–100 ppm) in meteorites, although the ratios of C $^{\alpha}$ -methylated to C $^{\alpha}$ -nonmethylated α -amino acids (e.g., Iva/Ala) vary significantly (6.8/0.3) between samples. Other potentially chiral organic compounds largely found in meteorites are the α -hydroxy acids. For both classes of compounds (α -amino and α -hydroxy acids) a Strecker-like synthesis from aldehydes and ketones, HCN, water, and ammonia has been proposed.^[13] Taken together, these results have suggested that C $^{\alpha}$ -methylated α -amino acids of extraterrestrial origin, delivered by meteorites which heavily bombarded the early Earth, could have been homochirality seeds for life on our planet,^[14] which has developed upon proteinogenic amino acids of L-configuration. However, as C $^{\alpha}$ -methylated α -amino acids play a marginal role in contemporary biochemistry, this hypothesis implies that their *ee* values would have been somehow transferred to proteinogenic amino acids.^[14] The results reported herein represent an addition to the already postulated mechanisms of chiral transmission between biomolecules, the two most recently published mechanisms involve the stable homochiral Ser octameric cluster^[15] and Iva itself^[16] as key players. It was also proposed^[14] that initially life may have been based on the 3_{10} helix,^[17] the typical architecture of peptides rich in C $^{\alpha}$ -methylated α -amino acids,^[18,19] rather than on the α helix, the most stable regular secondary structure of proteinogenic amino acids.

Herein we describe the results of a study aimed at determining whether appropriately carboxy-activated, short peptides and long, 3_{10} helical peptides, based on chiral, C $^{\alpha}$ -methylated α -amino acids, can react with proteinogenic

amino acids and favor the incorporation in the sequence of one of their enantiomers over the other. Our investigation focused on L-Iva and L-(α Me)Nva, as they are some of the most abundant and frequently analyzed chiral C $^{\alpha}$ -methylated α -amino acids in terms of *ee* value in meteoritic samples,^[1–3] and on L-(α Me)Val, as a representative of the highly sterically hindered subclass of β -branched, C $^{\alpha}$ -methylated α -amino acids which also includes L-(α Me)Ile and L-(α Me)*a*Ile.^[1–3]

There is a general agreement on the view that some sort of chemical evolution occurred before the onset of life on Earth, this evolution led to the formation of polymers, or at least oligomers, of amino acids. Therefore, we developed a test system based on homochiral homooligomers of Iva, (α Me)Nva, and (α Me)Val (Figure 2). These peptides are acetylated (Ac) at the N-terminus and activated as 5(4*H*)-oxazolones (OXL) at the C-terminus. While *N*-acetylation favors peptide solubilization in organic solvents and prevents

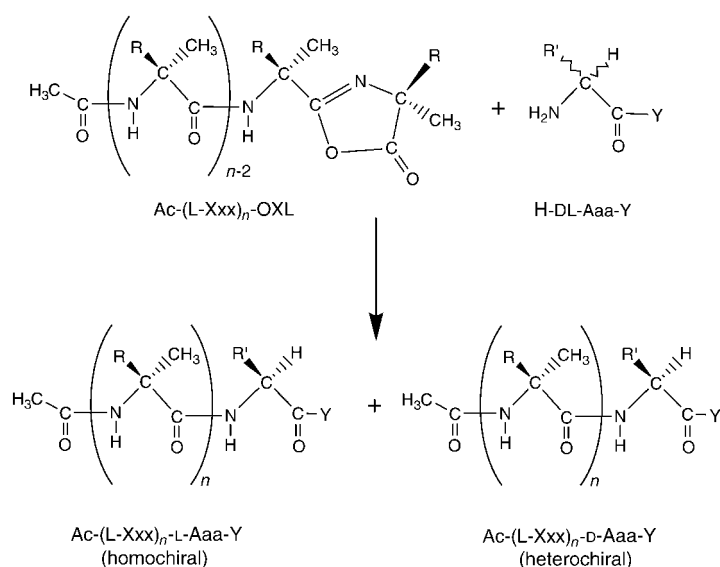


Figure 2. The test system developed for this study. Xxx represents a C $^{\alpha}$ -methylated α -amino acid (R = ethyl: Iva; *n*-propyl: (α Me)Nva; *iso*-propyl: (α Me)Val), while Aaa is a proteinogenic amino acid, either in its free form (Y = OH) or protected as the methyl ester (Y = OCH₃). The H-DL-Aaa-Y:Ac-(L-Xxx)_{*n*}-OXL molar ratio (in acetonitrile or acetonitrile–water mixtures) was 8:1, large enough to ensure thermodynamic rather than kinetic control of the stereochemical outcome of the reaction.

reactivity of the α -amino function, the use of OXL is because they are generated to a significant extent from C $^{\alpha}$ -methylated α -amino acid residues by nearly all activation methods used for peptide-bond formation.^[20] In particular, oxazolones are easily produced by intramolecular dehydration of C $^{\alpha}$ -methylated peptides with a free carboxy terminus. Thus, oxazolones represent an almost unavoidable entry to prebiotic peptide formation involving C $^{\alpha}$ -methylated α -amino acids. These peptide oxazolones were allowed to react with a large excess (8 equiv) of the racemate of a representative proteinogenic amino acid or its methyl ester (e.g. H-DL-Val-OH or H-DL-Val-OMe). Formation of the two resulting diastereomeric peptides (differing by the chirality of the incorporated,

C-terminal proteinogenic amino acid) was quantified chromatographically.

Initial experiments were performed in acetonitrile (a good solvent for reaction and HPLC analysis of terminally blocked peptides) with dipeptide oxazolones carrying one C^α-methylated L-residue at the C-terminus and the achiral α-amino-isobutyric acid (Aib, or C^α-methyl alanine), which is abundant in chondritic meteorites,^[21] at the penultimate position. Homochiral tripeptides are preferentially formed. Diastereoselection is temperature independent, and is comparable for L-Iva and L-(αMe)Nva while it is significantly higher for L-(αMe)Val (Table 1). By shifting the chiral residue to the penultimate position [for example, Ac-L-(αMe)Val-Aib-OXL] diastereoselection is completely suppressed (data not shown). These results would suggest that the chiral residue within the oxazolone ring is the only one involved in the stereoselection process. However, the related homodipeptide oxazolones behave differently (Table 1). The homochiral diastereoselectivities are temperature dependent and significantly lower than those obtained with the corresponding Ac-Aib-L-Xxx-OXLs, particularly at 30 °C and for the L-(αMe)Val oxazolone, thus pointing to a role of the penultimate residue as well in the diastereoselection process. These results can be explained on the basis of the reactant-like nature of the transition state of the step leading to peptide-bond formation through oxazolones,^[22] and of the likely occurrence of multiple conformers, differently populated at different temperatures, for the homodipeptide oxazolones. This occurrence of multiple conformers is particularly relevant for the relatively large temperature effect observed for the L-Iva homodipeptide oxazolone. Indeed, two independent molecules are present in the X-ray diffraction structure of Ac-(L-Iva)₂-OXL,^[23] differing by the signs of the φ, ψ backbone torsion angles at the penultimate residue.

Our investigation of the diastereoselection by the homochiral, homopeptide oxazolones was extended to the pentamer level for L-Iva and L-(αMe)Nva, and to the octamer for L-(αMe)Val (Table 1). For the L-Iva series preferential incorporation of the homochiral proteinogenic amino acid is observed. Diastereoselectivity tends to level off at the tetramer/pentamer level. In the L-(αMe)Nva series the L-selectivity decreases slightly but steadily with increasing peptide length, tending to a preference for the heterochiral

peptide at the pentamer level. For the L-(αMe)Val series reversal of diastereoselection from L to D is found at the trimer level, all longer oligomers giving large heterochiral diastereoselectivities. Along this series the largest variation is observed from trimer to tetramer.

These results led us to the hypothesis that the C^α-methylated residue within the oxazolone ring and the preceding one have opposite effects on diastereoselection. More specifically, the chiral, C^α-methylated residue within the oxazolone ring seems to favor the incorporation of the proteinogenic amino acid of the same chirality, whereas the preceding residue appears to preferentially induce formation of the heterochiral peptide. On this basis, a peptide oxazolone in which the penultimate and the C-terminal residues are of opposite chirality (e.g. L–D) should show an increased selectivity (compared to the L–L sequence) for the D-isomer of the proteinogenic amino acid. Indeed, the reaction of Ac-[L-(αMe)Val]₂-D-(αMe)Val-OXL with H-DL-Val-OMe in acetonitrile at 80 °C gave a D-selectivity of 42 % (not listed in Table 1), significantly higher than the value of 14 % obtained for the corresponding all-L trimer. The inversion of chirality at the C-terminal residue in the N-terminal acetylated (αMe)Val tetramer led to a variation of the D-selectivity in the same direction as in the above experiment with the trimer, but of much lower magnitude, from 47 % for Ac-[L-(αMe)Val]₄-OXL to 50 % for Ac-[L-(αMe)Val]₃-D-(αMe)Val-OXL (the latter is not listed in Table 1). However, we already noted for the all-L (αMe)Val series a sharp increase in heterochiral diastereoselectivity as the result of main-chain elongation from trimer to tetramer, which suggests the contribution of a conformational effect which may take place at the level of the tetramer.

N-terminal-acylated homotripeptides from Iva, (αMe)Nva, and (αMe)Val fold into β turns,^[24] stabilized by an intramolecular hydrogen bond between the NH group of the third residue and the carbonyl oxygen of the acyl group. Consecutive β turns are formed by the higher homologues, giving rise to ₃₁₀ helices.^[19,25,26] The L configurations of (αMe)Nva and (αMe)Val promote the onset of turns and helices with a largely predominant right-handed screw sense. For Iva, the amino acid of this family with the smallest difference in length between the two side chains, the relationship between residue chirality and helical screw

Table 1: Chirality of the incorporated proteinogenic amino acids in the reaction products Ac-Aib-Xxx-D,L-Val-OMe or Ac-(Xxx)_n-D,L-Val-OMe from the peptide oxazolones Ac-Aib-Xxx-OXL or Ac-(Xxx)_n-OXL and H-DL-Val-OMe in acetonitrile solution at 80 °C (or 30 °C, in parentheses).^[a]

Peptide oxazolone	X [%]	Peptide oxazolone	X [%]	Peptide oxazolone	X [%]
Ac-Aib-L-Iva-OXL	+25 (+25)	Ac-Aib-L-(αMe)Nva-OXL	+23 (+23)	Ac-Aib-L-(αMe)Val-OXL	+45 (+45)
Ac-(L-Iva) ₂ -OXL	+17 (–3)	Ac-[L-(αMe)Nva] ₂ -OXL	+16 (+13)	Ac-[L-(αMe)Val] ₂ -OXL	+12 (+7)
Ac-(L-Iva) ₃ -OXL	+12	Ac-[L-(αMe)Nva] ₃ -OXL	+10	Ac-[L-(αMe)Val] ₃ -OXL	–14
Ac-(L-Iva) ₄ -OXL	+20	Ac-[L-(αMe)Nva] ₄ -OXL	+8	Ac-[L-(αMe)Val] ₄ -OXL	–47
Ac-(L-Iva) ₅ -OXL	+22	Ac-[L-(αMe)Nva] ₅ -OXL	–3	Ac-[L-(αMe)Val] ₅ -OXL	–44
				Ac-[L-(αMe)Val] ₆ -OXL	–54
				Ac-[L-(αMe)Val] ₇ -OXL	–58
				Ac-[L-(αMe)Val] ₈ -OXL	–56

[a] Xxx = L-Iva, L-(αMe)Nva, L-(αMe)Val; the X values (defined as % L–% D, where L and D refer to the chirality of the incorporated proteinogenic amino acid) were determined by HPLC. For the assignment of the eluted peaks each diastereomer was prepared separately and used as a standard. The reported X values are the average of three independent experiments. Reproducibility is within 2 %.

sense is somewhat ambiguous.^[19,26,27] In an *N*-acylated peptide oxazolone, with the C-terminal residue lacking the hydrogen-bonding donor NH group, the minimal main-chain length required for the formation of a single β turn is four residues.^[28] Peptide oxazolones based on C $^{\alpha}$ -methylated residues and longer than tetramers are expected to fold into 3_{10} helices. Indeed, we show herein that in the crystal state the octameric oxazolone Z-[L-(α Me)Val]₈-OXL (Z, benzyloxycarbonyl) is folded into a right-handed 3_{10} helical conformation (Figure 3). The three-dimensional structural results reported herein, along with the conformational preferences of C $^{\alpha}$ -methylated peptides^[17–19,25–27] (discussed above), support Bada's hypothesis^[14] that if these peptides had some role during the origin of biological stereochemistry, then initially life may, at least in part, have been based on a different polypeptide architecture (the 3_{10} helix, instead of the classical α helix promoted by the proteinogenic C $^{\alpha}$ -hydrogen amino acids).

Overall, peptide oxazolones with a longer main-chain length and a bulky side chain (for example, as in L-(α Me)Val) preferentially incorporate a proteinogenic amino acid of the chirality opposite to that of the C $^{\alpha}$ -methylated residues, whereas a shorter main chain and a less bulky side chain in the peptide oxazolone (for example, as in L-Iva) direct the stereoselection towards the proteinogenic amino acid of the same chirality, but with lower efficiency. Such a bimodal distribution of diastereoselectivity is substantially retained in acetonitrile–water mixtures, as indicated by reactions of selected peptide oxazolones with either H-DL-Val-OMe or the racemates of the free amino acids Val, Phe, and Leu (Table 2), the free amino acids being prebiotically more relevant than their methyl esters. Thus, the stereochemical implications of our results are not hampered by addition of water (up to 70 %) to the reaction medium. Water, either in bulk or at the interface with organic layers, lipid vesicles, or mineral surfaces, is included in all current models of prebiotic chemical evolution on Earth.^[29–32] Acetonitrile itself may be not fully devoid of prebiotic relevance, as its occurrence in comets has been reported.^[33]

Prebiotic chemical evolution towards the emergence of peptides is thought to have occurred through a combination of cycles of peptide-bond formation and hydrolysis. A peptide bond between two C $^{\alpha}$ -methylated α -amino acid residues is sterically better protected from hydrolytic cleavage than a bond between a C $^{\alpha}$ -methylated and a proteinogenic amino acid residue. Thus, it is likely that the proteinogenic amino acids incorporated at the C-terminus of C $^{\alpha}$ -methylated peptide chains might have been subsequently released through hydrolysis to a greater extent than those released by the hydrolytic degradation of the fully C $^{\alpha}$ -methylated peptide chains. This process would seem to leave the racemic state of the prebiotic soup unaffected. However, significant epimerization can be expected to occur

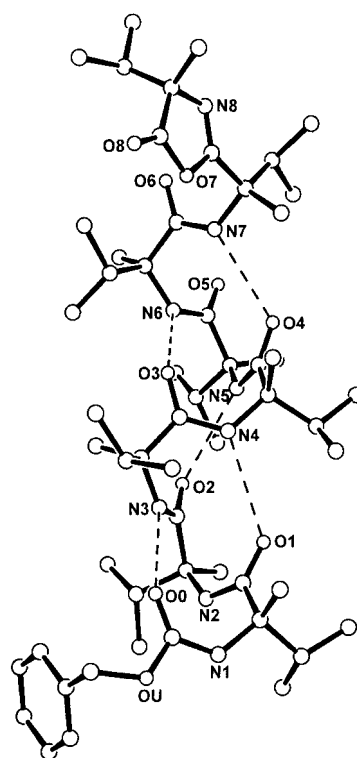


Figure 3. X-ray diffraction structure of Z-[L-(α Me)Val]₈-OXL. Only oxygen and nitrogen atoms are labeled. The five intramolecular C=O...H-N hydrogen bonds are indicated by dashed lines. The right-handed 3_{10} helix encompasses amino acid residues 1–6. The seventh residue, external to the helix, adopts a conformation with a screw sense opposite to that of the preceding residues. As a result, the oxazolone ring (N8, O7, O8) protrudes out of the helical envelope. Residue 8 is part of the oxazolone ring. The normal to the average plane of the oxazolone ring is nearly perpendicular to the helix axis.

Table 2: Chirality of the incorporated proteinogenic amino acids in the reaction products of selected *N*-acylated, C $^{\alpha}$ -methylated peptide 5(4*H*)-oxazolones with racemic proteinogenic amino acids or their methyl esters (H-DL-Aaa-Y) in H₂O/CH₃CN solution.^[a]

Peptide oxazolone	H-DL-Aaa-Y	X [%]	Solvent	<i>T</i> [°C]
Ac-Aib-L-(α Me)Val-OXL	H-DL-Val-OMe	+30	30% H ₂ O/CH ₃ CN	50
Ac-[L-(α Me)Val] ₅ -OXL	H-DL-Val-OMe	–40	30% H ₂ O/CH ₃ CN	50
Ac-[L-(α Me)Val] ₅ -OXL	H-DL-Val-OMe	–40	70% H ₂ O/CH ₃ CN	80
Ac-Aib-L-(α Me)Val-OXL	H-DL-Val-OH	+7	50% H ₂ O/CH ₃ CN	80
Ac-[L-(α Me)Val] ₅ -OXL	H-DL-Val-OH	–33	50% H ₂ O/CH ₃ CN	80
Ac-[L-(α Me)Val] ₅ -OXL	H-DL-Phe-OH	–16	50% H ₂ O/CH ₃ CN	80
Ac-[L-(α Me)Val] ₅ -OXL	H-DL-Leu-OH	–42	50% H ₂ O/CH ₃ CN	80

[a] Y=OH, OMe; the X values are defined as % L–% D, where L and D refer to the chirality of the incorporated proteinogenic amino acid.

in between incorporation and release of the proteinogenic amino acids, as a proteinogenic amino acid C-terminal to a peptide chain, upon activation, may undergo cyclization to oxazolone, thus becoming highly prone to racemization.^[34] Therefore, the chiral imbalance generated in the prebiotic soup of proteinogenic amino acids by their stereoselective incorporation into the C $^{\alpha}$ -methylated peptides can be retained to an extent which is directly proportional to the occurrence of oxazolone-mediated racemization of the pro-

teinogenic amino acids prior to their cleavage from the C $^{\alpha}$ -methylated peptide chain. Such a process could have been repeated in cycles, with C $^{\alpha}$ -methylated peptides providing a stable source of chiral bias. In the long run, the overall result would have been the enrichment of the primordial soup in proteinogenic amino acids of the chirality opposite to that preferentially incorporated by the C $^{\alpha}$ -methylated peptide chains. If the D-incorporation prevailed, then through amplification mechanisms^[35–40] the L-homochirality of life could have emerged.

In summary, our experimental results indicate the possibility that the proteinogenic amino acid homochirality on Earth may have originated from meteoritic C $^{\alpha}$ -methylated α -amino acids and that the 3_{10} helical structure may have played a significant role in this process, although concurrent or alternative pathways^[40–42] leading to the same final scenario are not excluded by the present results.

Received: June 8, 2004

Revised: July 16, 2004

Keywords: amino acids · chemical evolution · chirality · helical structures · peptides

- [1] J. R. Cronin, S. Pizzarello, *Science* **1997**, 275, 951–955.
- [2] S. Pizzarello, J. R. Cronin, *Geochim. Cosmochim. Acta* **2000**, 64, 329–338.
- [3] S. Pizzarello, M. Zolensky, K. A. Turk, *Geochim. Cosmochim. Acta* **2003**, 67, 1589–1595.
- [4] J. L. Bada, D. P. Glavin, G. D. McDonald, L. Becker, *Science* **1998**, 279, 362–365.
- [5] G. A. Goodfriend, M. J. Collins, M. L. Fogel, S. A. Macko, J. F. Wehmiller, *Perspective in Amino Acid and Protein Geochemistry*, Oxford University Press, Oxford, UK, **2000**.
- [6] U. J. Meierhenrich, G. M. Muñoz Caro, J. H. Bredehöft, E. K. Jessberger, W. H. P. Thiemann, *Proc. Natl. Acad. Sci. USA* **2004**, 101, 9182–9186.
- [7] J. L. Bada, S. L. Miller, *BioSystems* **1987**, 20, 21–26.
- [8] G. Nonadje, M. Nertz, F. Couderc, *J. Chromatogr. A* **1995**, 716, 331–334.
- [9] B. A. Cohen, C. F. Chyba, *Icarus* **2000**, 145, 272–281.
- [10] O. Trapp, V. Schurig, *Enantiomer* **2001**, 6, 193–194.
- [11] Y. Takano, J. Kudo, T. Kaneko, K. Kobayashi, Y. Ishikawa, K. Marumo, *Bull. Chem. Soc. Jpn.* **2004**, 77, 1029–1030.
- [12] V. A. Basiuk, *Adv. Space Res.* **2001**, 27, 335–340.
- [13] E. T. Peltzer, J. L. Bada, *Nature* **1978**, 272, 443–444.
- [14] J. L. Bada, *Science* **1997**, 275, 942–943.
- [15] Z. Takats, S. C. Nanita, R. G. Cooks, *Angew. Chem.* **2003**, 115, 3645–3647; *Angew. Chem. Int. Ed.* **2003**, 42, 3521–3523.
- [16] S. Pizzarello, A. L. Weber, *Science* **2004**, 303, 1151.
- [17] C. Toniolo, E. Benedetti, *Trends Biochem. Sci.* **1991**, 16, 350–353.
- [18] I. L. Karle, P. Balaran, *Biochemistry* **1990**, 29, 6747–6756.
- [19] C. Toniolo, M. Crisma, F. Formaggio, C. Peggion, *Biopolymers* **2001**, 60, 396–419.
- [20] F. Formaggio, Q. B. Broxterman, C. Toniolo in *Houben-Weyl Methods of Organic Chemistry, Vol. E22c* (Eds.: M. Goodman, A. Felix, L. Moroder, C. Toniolo), Thieme, Stuttgart, **2003**, pp. 292–310.
- [21] O. Botta, D. P. Glavin, G. Kminek, J. L. Bada, *Origins Life Evol. Biosphere* **2002**, 32, 143–163.
- [22] M. Crisma, G. Valle, F. Formaggio, C. Toniolo, A. Bagno, *J. Am. Chem. Soc.* **1997**, 119, 4136–4142.
- [23] M. Crisma, G. Valle, F. Formaggio, C. Toniolo, Q. B. Broxterman, J. Kamphuis, *Z. Kristallogr. New Cryst. Struct.* **1998**, 213, 315–316.
- [24] C. M. Venkatachalam, *Biopolymers* **1968**, 6, 1425–1426.
- [25] F. Formaggio, M. Crisma, C. Toniolo, Q. B. Broxterman, B. Kaptein, C. Corbier, M. Saviano, P. Palladino, E. Benedetti, *Macromolecules* **2003**, 36, 8164–8170.
- [26] M. Crisma, A. Moretto, M. Rainaldi, F. Formaggio, Q. B. Broxterman, B. Kaptein, C. Toniolo, *J. Pept. Sci.* **2003**, 9, 620–637.
- [27] B. Jaun, M. Tanaka, P. Seiler, F. N. M. Kühnle, C. Braun, D. Seebach, *Liebigs Ann.* **1997**, 1697–1710.
- [28] M. Crisma, F. Formaggio, C. Toniolo, *Acta Crystallogr. Sect. C* **2000**, 56, 695–696.
- [29] A. Brack, *Pure Appl. Chem.* **1993**, 65, 1143–1151.
- [30] D. Segre, D. Ben-Eli, D. W. Deamer, D. Lancet, *Origins Life Evol. Biosphere* **2001**, 31, 119–145.
- [31] J. P. Ferris, A. R. Hill, R. H. Liu, L. E. Orgel, *Nature* **1996**, 381, 59–61.
- [32] R. M. Hazen, T. R. Filley, G. A. Goodfriend, *Proc. Natl. Acad. Sci. USA* **2001**, 98, 5487–5490.
- [33] D. Bockelée-Morvan, D. C. Lis, J. E. Wink, D. Despois, J. Crovisier, R. Bachiller, D. J. Benford, N. Biver, P. Colom, J. K. Davies, E. Gérard, B. Germain, M. Houde, D. Mehringer, R. Moreno, G. Paubert, T. G. Phillips, H. Rauer, *Astron. Astrophys.* **2000**, 353, 1101–1114.
- [34] M. Goodman, W. H. J. McGahren, *Tetrahedron* **1967**, 23, 2031–2050.
- [35] G. Wald, *Ann. N. Y. Acad. Sci.* **1957**, 69, 353–368.
- [36] A. Brack, G. Spach, *Origins Life* **1981**, 11, 135–142.
- [37] H. R. Kricheldorf in *Models of Biopolymers by Ring-Opening Polymerization* (Ed.: S. Penczek), CRC, Boca Raton, FL, **1990**, pp. 46–62.
- [38] W. A. Bonner, *Origins Life Evol. Biosphere* **1991**, 21, 59–111.
- [39] T. H. Hitz, P. L. Luisi, *Origins Life Evol. Biosphere* **2004**, 34, 93–110.
- [40] I. Weissbuch, G. Bolbach, L. Leiserowitz, M. Lahav, *Origins Life Evol. Biosphere* **2004**, 34, 79–92.
- [41] S. F. Mason, *Chem. Soc. Rev.* **1988**, 17, 347–359.
- [42] W. J. Lough, I. W. Wainer, *Chirality in Natural and Applied Science*, CRC, Boca Raton, FL, **2002**.

Cyclization

Deletion of the Gly600 Residue of *Alicyclobacillus acidocaldarius* Squalene Cyclase Alters the Substrate Specificity into that of the Eukaryotic-Type Cyclase Specific to (3S)-2,3-Oxidosqualene**

Tsutomu Hoshino,* Kunio Shimizu, and Tsutomu Sato

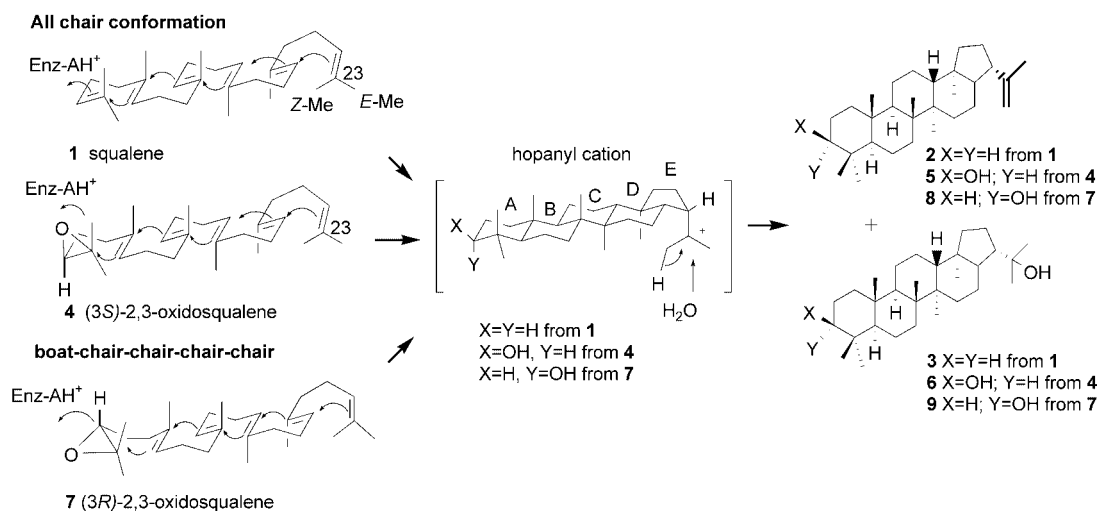
The acyclic molecule squalene (**1**) is cyclized into the pentacyclic triterpenes, hop-22(29)-ene (**2**) and hopan-22-ol (**3**; ca 5:1) by squalene-hopene cyclase (SHC) from prokaryotic species (Scheme 1).^[1] The polycyclization reaction proceeds with regio- and stereochemical specificity under precise enzyme control to form the 6/6/6/6/5-fused pentacyclic ring system and nine new stereocenters. The polycyclization mechanism is analogous to that of eukaryotic oxidosqualene cyclases (OSCs).^[1] SHC folds **1** into the all pre-chair conformation (a product-like conformation) inside the enzyme cavity, which leads to the final hopanyl cation through sequential ring-forming reactions. The proton elimination occurs exclusively from (23Z)-Me, but not from the *E*-Me, to form **2**.^[1a,2a] A nucleophilic attack by a water molecule on the cation affords **3**.

Recent three-dimensional X-ray crystallographic analyses^[3] and site-directed mutagenesis experiments^[1a,b] have

provided deeper insights into the polycyclization mechanism. Studies with the substrate analogues have also given important information on substrate recognition.^[1,2] The reaction cavity is lined with aromatic amino acid residues.^[3] Substrate specificity of bacterial SHCs is remarkably broad. Compounds (3S)-**4** and (3R)-oxidosqualenes **7** undergo the polycyclization reactions to form 3 β - and 3 α -hydroxyhopenes (**5** and **8**; ca. 1:1) and hopanediols (**6**; ca. 1:1), respectively, by a similar cyclization mechanism as **1**. Formation of the A-ring of **5** (scheme 1) proceeds by the chair conformation, while that of **8** by the boat structure.^[2a]

In contrast to bacterial SHCs, eukaryotic OSCs selectively recognize **4** as the substrate, and never accept **1** and **7**.^[1] Figure 1 shows a comparison of the amino acid alignment of some SHCs and OSCs. Gly600 is highly conserved among SHCs, but absent in OSCs.^[1a,b,4] To investigate the role of the G600 from *Alicyclobacillus acidocaldarius*, we constructed the Gly600-deletion mutant (Δ G600SHC) and then incubated with **1** or a racemic mixture of **4** and **7**. Interestingly, **1** and **7** were completely inert to the mutated cyclase (< 0.2% detection limit), while **4** underwent the cyclization to mono- and tricyclic skeletons which have a 3 β -hydroxy group. It is of note that the prokaryotic squalene cyclase could be altered into eukaryotic-type one, the substrate of which is limited to **4**.

The Δ G600SHC was constructed by using the polymerase chain reaction (PCR), in which oligonucleotide primers were designed in inverted tail-to-tail directions to amplify the



Scheme 1. Polycyclization pathway of squalene (**1**), (3S)-**4**, and (3R)-oxidosqualene (**7**) into the hopane skeleton.

[*] Prof. Dr. T. Hoshino, K. Shimizu, Dr. T. Sato
Department of Applied Biological Chemistry
Faculty of Agriculture and
Graduate School of Science and Technology
Niigata University, Ikarashi, Niigata 950-2181 (Japan)
Fax: (+81) 25-262-6854
E-mail: hoshitsu@agr.niigata-u.ac.jp

[**] This work was enabled by the financial support to T.H.
(No. 15380081), provided by the Ministry of Education, Science and
Culture of Japan.

Supporting information for this article is available on the WWW
under <http://www.angewandte.org> or from the author.

cloning vector together with the target sequence.^[5] One mg each of **1** or the racemic mixture of **4** and **7** was incubated at 40–70 °C for 16 h with 1 mL of the cell-free homogenates (ca. 200 μ g of the pure mutated SHC). The reaction was quenched by adding 15% KOH/MeOH and the lipophilic products were extracted with hexane. The GC analysis showed that no cyclization products were present in the incubation mixture from **1** (< 0.2% detection limit). On the other hand, six major products were detected in that of the racemate (**4** and **7**; total yield, 32%). The optimum catalytic

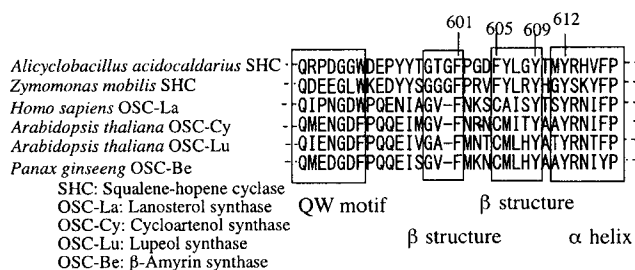


Figure 1. Amino acid alignment of some triterpene cyclases. The G598–Y605 alignment of *A. acidocaldarius* SHC corresponds to the G694–C700 sequence of human OSC, and these sequences constitute β -sheet domains.

temperature was 45 °C.^[6] The distribution ratios [%] of products **10–15** (Figure 2) was determined to be 11.3:2.9:2.9:3.4:8.6:2.9 and there was 68.0% recovered sub-

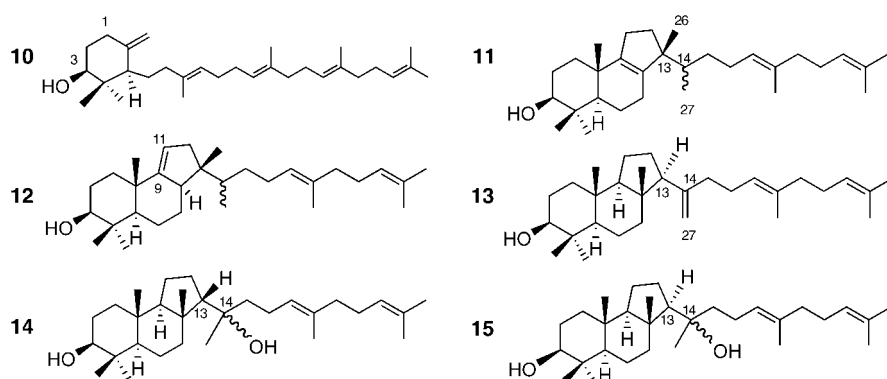


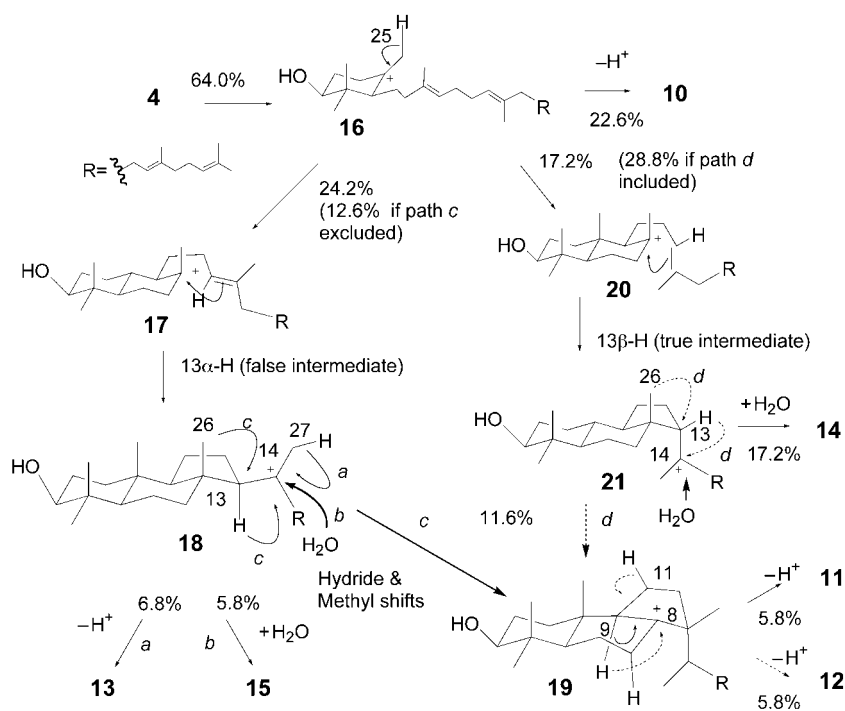
Figure 2. Cyclization products of **4** by the Δ G600 mutant.

strate, by the GC analysis. Products **10** and **13–15** were isolated in a pure state by the combination of normal and reverse-phase HPLCs, but separation of **11** and **12** was unsuccessful; column chromatography on SiO₂ impregnated with 5% AgNO₃ gave no separation. A mixture of acetates of **11** and **12**, prepared with Ac₂O/py, (Ac = acetyl, py = pyridine) was subjected to a careful column chromatography on SiO₂ (5% AgNO₃) which lead to the successful separation of **11** and **12** in part, but a large portion was still mixed.

Structures of all the isolated products as shown in Figure 2 were determined by NMR spectroscopy (¹H, ¹³C, DEPT, COSY 45, HOHAHA, NOESY, HMQC, HMBC).^[7] In particular, the H-3 signals of all the products were dd (*J* = 10–12 and 5–6 Hz), characteristic of axial–axial and axial–equatorial spin–spin couplings, thus all the products have a 3 β -hydroxy group. Product **10** was identified as achilleol.^[8a] Products **11–15** have three allyl methyl groups (δ_{H} = 1.69–1.88 ppm), which suggests the involvement of a tricyclic ring skeleton. Products **11** and **12** have a pododatriene skeleton^[8b] (podioda-8,17,21-trien-3 β -ol for **11** and

podioda-9(11)-17,21-trien-3 β -ol for **12**). Compound **11** was recently isolated as an *Arabidopsis* OSC product, and was named thalianol.^[8c] Compound **12** is a novel tricyclic triterpene. Product **13** is malabarica-14(27),17,21-trien-3 β -ol. Diols **14** and **15** have a similar skeleton to **13** bearing a second hydroxy group at C-14. The NOESY spectra of **13–15** clearly indicated that the stereochemistry at C-13 of **13** and **15** is opposite to that of **14** (13 α -H for **13** and **15**; 13 β -H for **14**). Production of 3 β -hydroxylated skeletons from the racemic mixture, but no formation of 3 α -hydroxylated one, indicated that only **4** underwent cyclization, while the enantiomer **7** was unaffected.^[2] The recovered epoxysqualene, further purified by normal-phase HPLC (hexane:2-PrOH = 100:2), showed an $[\alpha]_{\text{D}}^{25} = +1.17$ (*c* = 0.84, EtOH), further verifying that 3S-(–)-**4** was selectively converted.^[9] Thus, the conversion of **4** by the mutant cyclase was 64%.

Scheme 2 shows the mechanisms for the formation of products **10–15**. (3S)-Oxidosqualene **4** is cyclized into monocyclic cation **16**, then deprotonation from Me-25 yields **10**. Formation of bicyclic cations **17** and **20** guides further cyclization, leading to the 6/6/5-fused tricyclic Markovnikov cations **18** and **21**, respectively. The deprotonation from Me-27 of **18** affords **13** (path *a*). Attack by water on the C-14 cation gives diol **15** (path *b*). Sequential 1,2-shift reactions of hydride and Me-26 of **18** give cation **19** (path *c*). Deprotonation at C-9 of **19** gives **11** and hydride shift of H-9 to C-8 and the proton elimination of H-11 affords **12**. The



Scheme 2. Proposed polycyclization pathways of **4** into **10–15**; see text for details.

alternative route via **21** (path *d*) may be possible, but path *c* would be favorable owing to the antiparallel rearrangement reaction. A water attack on cation **21** gives **14**. Previously we have demonstrated that **21** (13 β -H) is a true intermediate, but **18** (13 α -H) is a false one.^[1a,10a]

The lack of reaction of **1** and **7** suggests that the terminal double bond of **1** and the epoxide ring of **7** may have failed to be in a close proximity to the D374XD376D377 motif,^[10b] which is responsible for the initiation of the polycyclization reaction. The specific activity of the mutant enzyme for **4** significantly decreased (ca. tenfold),^[6] compared to that of the native SHC, which suggests the looser binding of the epoxide ring of **4** to the mutant enzyme than to the wild-type. The secondary structures of the β -sheet and α -helix domains^[3,11] (Figure 1) may be disorganized by the loss of the G600, resulting in inappropriate positioning of F601,^[10a] F605,^[10c] Y609,^[10d,e] and Y612^[10d,e] in the reaction cavity, which are crucial for the sequential ring-forming reactions to give the fully cyclized **2**. Residues Y609 and Y612 are important in forming 6/6-fused bicyclic cations **17** and/or **20**,^[10d,e] thus monocycle **10** may have accumulated owing to the inappropriate positions of these residues. However, the Phe365, aligned prior to the G600, would still be correctly placed in the reaction cavity, which leads to the formation of **18** and **21** by the stabilization of cations **17** and **20**.^[12] The incorrect placement of the F601 and F605 residues, which are essential for the formation of tetra- and pentacycles,^[10,12] would interrupt the polycyclization reaction at the tricyclic ring stage, possibly because of the decreased cation/ π interaction. A high production (24.2%) of the false intermediate **18** (13 α -H)^[1a,10a] further indicated that the enzyme structure was disordered in part.

There are a few reports on the altered substrate specificity of the squalene cyclase. A triple mutant of D377C/V380E/V381A,^[13] a double mutant of D376C/C435S,^[14] and the single mutants^[10b,15] of D374N and D376N had no effect on **1**, but all the mutants had a cyclization activity for both enantiomers of **4** and **7**, albeit with significantly lower activity than the wild-type, which indicates that all the mutants had no stereospecificity for the racemic epoxides. The decreased acidity of the DXDD motif by the substitution with Cys or Asn would have led to no reaction for **1** and to a lowered activity for **4** and **7**. In contrast, the Δ G600 mutant selectively accepts **4**, but has no effect on **7**. Thus, the altered substrate specificity of the Δ G600 mutant is completely different from those of the previously reported mutants. The following differences are also noted: The Δ G600 mutant still had the original DXDD motif, and the location of the deleted G600 residue in the reaction cavity is distal from the initiation site of the DXDD motif.^[3] The X-ray structure of the wild-type SHC, which was cocrystallized with 2-azasqualene,^[3c] shows that the G600 is located in a close proximity to the D-ring formation site of **1**.

Why did the Δ G600 SHC accept only **4**? It is difficult to get a clear answer to this question at the present time, but one possible explanation is as follows. The recent study of the homology modeling of human OSC,^[16] based on the crystal structure information of the wild-type SHC,^[3] clearly indicates that the β -sheet domain of the OSC, consisting of the G694–C700 sequence (Figure 1), is more loosely packed

compared to that of the SHC, which is composed of the G598–Y605 sequence.^[16] Thus, the loss of the Gly600 makes the D-ring formation region less compact. The loosely packed domain structure of the mutant cyclase is more flexible, thus, a somewhat free motion of the substrate molecules can be allowed around the D-ring formation sites. The unconstrained motion of the substrates will influence the positions of the substrate heads; the epoxide ring of **4** could be located near to the DXDD motif, but the terminal double bond of **1** and the epoxide ring of **7** failed to have access to the motif. The proposed working hypothesis would agree with the previous reports^[10e,17] that the folding conformation and the polycyclization pathway of **1** are directed by the steric bulk size of active sites. However, other factors may be also involved in the alteration of substrate specificity. Further studies are necessary including the X-ray crystallographic analysis and the functional analyses of the related mutants, in order to gain the exact answer for the altered substrate specificity.

In conclusion, this is the first example in which the substrate specificity of prokaryotic cyclase could be successfully altered into that of the eukaryotic-type, which is quite interesting from the evolutionary aspect of squalene cyclases. This study also indicates how eukaryotic cyclases selectively accept **4**. The rationally engineered mutagenesis of bacterial SHC will lead to further creation of novel eukaryotic-type cyclases.

Experimental Section

A plasmid of pBH, which was a pUC119 derivative having the *Bam*HI–*Hind*III fragment of *shc* gene (1623–1896 nucleotide position),^[10b,d] was used as a template. A pair of primers, 5'-TTCCCAGGGGATTCTACCTCGGC-3' and 5'-GGTACCGGTG-TAGTACGGCTCATCCCAGC-3', was prepared for deleting a GGG codon of Gly600. The bold of **G** and **A** indicate the silent mutation for creating *Kpn*I site (*italics*).

The enzyme purification and incubation conditions were carried out according to the published methods.^[10b,d]

The hexane extract from the incubation mixture was subjected to column chromatography on SiO₂ with a step-wise gradient elution of hexane→hexane/EtOAc(100:10), to give residual oxidosqualene and **10** in a pure state, but the separation of **11**–**15** failed. Isolation of **14** and **15** was by normal-phase HPLC (hexane:2-PrOH = 100:2). A reverse-phase HPLC eluting with THF/H₂O (55:45) gave **13** in pure state. As a next step, the acetate mixture of **11** and **12**, prepared with Ac₂O/py, was subjected to a careful column chromatography on SiO₂ (5% AgNO₃) by eluting with hexane/EtOAc (100:0.05), leading to the separation of **11** and **12** in part.

NMR spectra were recorded in C₆D₆, the chemical shifts being relative to the solvent peak $\delta_{\text{H}} = 7.28$ and $\delta_{\text{C}} = 128.0$ ppm as the internal reference for ¹H and ¹³C NMR spectra, respectively. The product distribution pattern was monitored by GC. GC-MS and MS spectra were obtained with electronic impact at 70 eV using a DB-1 capillary column (0.32 mm \times 30 m), the oven temperature being elevated from 220 to 270 °C (3 °C min⁻¹). Specific rotation values were measured at 25 °C in EtOH. The CD spectra of the Δ G600 and the wild-type SHCs were measured in a solution of 10 mM sodium phosphate (pH 6.0) containing 0.6% Brij 35.

Received: August 3, 2004

Revised: August 30, 2004

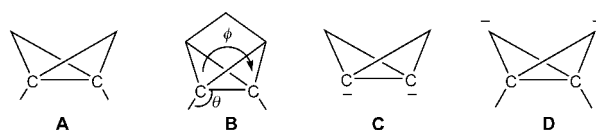
Keywords: cyclases · cyclization · enzymes · squalene · triterpenes

- [1] For reviews of triterpenes biosynthesis, see: a) T. Hoshino, T. Sato, *Chem. Commun.* **2002**, 291–301; b) K. U. Wendt, G. E. Schulz, E. J. Corey, D. R. Liu, *Angew. Chem.* **2000**, *112*, 2930–2952; *Angew. Chem. Int. Ed.* **2000**, *39*, 2812–2833; c) I. Abe, M. Rohmer, G. D. Prestwich, *Chem. Rev.* **1993**, *93*, 2189–2206.
- [2] a) T. Hoshino, S. Nakano, T. Kondo, T. Sato, A. Miyoshi, *Org. Biomol. Chem.* **2004**, *2*, 1456–1470; b) S. Nakano, S. Ohashi, T. Hoshino, *Org. Biomol. Chem.* **2004**, *2*, 2012–2022; c) T. Hoshino, Y. Kumai, I. Kudo, S. Nakano, S. Ohashi, *Org. Biomol. Chem.* **2004**, *2*, 2650–2657.
- [3] a) K. U. Wendt, K. Poralla, G. E. Schulz, *Science* **1997**, *277*, 1811–1815; b) K. U. Wendt, A. Lenhart, G. E. Schulz, *J. Mol. Biol.* **1999**, *286*, 175–187; c) D. J. Reinert, G. Balliano, G. E. Schulz, *Chem. Biol.* **2004**, *11*, 121–126.
- [4] a) A. Tippelt, L. Jahnke, K. Poralla, *Biochim. Biophys. Acta* **1998**, *1391*, 223–232; b) S. M. Godzina, M. A. Lovata, M. M. Meyer, K. A. Foster, W. K. Wilson, W. Gu, E. L. de Hostos, S. P. T. Matsuda, *Lipids* **2000**, *35*, 249–255.
- [5] Y. Imai, Y. Matsushima, T. Sugimura, M. Terada, *Nucleic Acids Res.* **1991**, *19*, 2785.
- [6] The optimum temperatures and specific activities (nmol min^{−1} mg^{−1}) for **4** were: 45 °C and 26.8 for the mutant; 62 °C and 234.0 for the wild-type.
- [7] Complete NMR assignments, EIMS data, and optical rotations for **10–15** are given in the Supporting Information.
- [8] a) A. F. Barrero, R. E. J. Alvarez-Manzanda, R. R. Alvarez-Manzanda, *Tetrahedron Lett.* **1989**, *30*, 3351–3352; b) Y. Arai, M. Hirohara, H. Ageta, *Tetrahedron Lett.* **1989**, *30*, 7209–7212; c) G. C. Fazio, R. Xur, S. P. T. Matsuda, *J. Am. Chem. Soc.* **2004**, *126*, 5678–5679.
- [9] T. Hoshino, E. Ishibashi, K. Kaneko, *Chem. Commun.* **1995**, 2401–2402. The literature value of optical rotation for **4**: $[\alpha]_D^{20} = -1.4$ ($c = 1.0$, EtOH), see Y. Yamada, C. W. Seo, H. Okada, *Agric. Biol. Chem.* **1981**, *45*, 1741–1742.
- [10] a) T. Hoshino, M. Kouda, T. Abe, S. Ohashi, *Biosci. Biotechnol. Biochem.* **1999**, *63*, 2038–2041; b) T. Sato, T. Hoshino, *Biosci. Biotechnol. Biochem.* **1999**, *63*, 2189–2198; c) T. Hoshino, M. Kouda, T. Abe, T. Sato, *Chem. Commun.* **2000**, 1485–1486; d) T. Sato, T. Hoshino, *Biosci. Biotechnol. Biochem.* **2001**, *65*, 2233–2242; e) C. Füll, K. Poralla, *FEMS Microbiol. Lett.* **2000**, *183*, 221–224.
- [11] With elevated temperatures, the circular dichroism (CD) spectrum of the mutant was more significantly altered than that of the wild-type, which indicates the disorganization of the ΔG600SHC. See the Supporting Information.
- [12] T. Hoshino, T. Sato, *Chem. Commun.* **1999**, 2005–2006.
- [13] T. Dang, G. D. Prestwich, *Chem. Biol.* **2000**, *7*, 643–649.
- [14] P. Milla, A. Lenhart, G. Grosa, F. Viola, W. A. Weinhofen, G. E. Schulz, G. Balliano, *Eur. J. Biochem.* **2002**, *269*, 2108–2116.
- [15] C. Feil, R. Sussmuth, G. Jung, K. Poralla, *Eur. J. Biochem.* **1996**, *242*, 51–55.
- [16] T. Schulz-Gasch, M. Stahl, *J. Comput. Chem.* **2003**, *24*, 741–753. The β-sheet domain of the G598–Y605 sequence of SHC and that of the corresponding G694–C700 sequence of the modeled human OSC are illustrated in the Figure 3 of this reference.
- [17] a) T. Hoshino, T. Abe, M. Kouda, *Chem. Commun.* **2000**, 441–442; b) T. Sato, S. Sasahara, T. Yamakami, T. Hoshino, *Biosci. Biotechnol. Biochem.* **2002**, *66*, 1660–1670; c) B. M. Joubert, L. Hua, S. P. T. Matsuda, *Org. Lett.* **2000**, *2*, 339–341; d) M. M. Meyer, R. Xu, S. P. T. Matsuda, *Org. Lett.* **2002**, *4*, 4459–4462.

The First Bicyclo[1.1.0]butane Dianion of Heavier Group 14 Elements**

Vladimir Ya. Lee, Kazunori Takanashi,
Masaaki Ichinohe, and Akira Sekiguchi*

The concept of the so-called “non-classical” compounds, which do not follow the generally accepted interpretation of the chemical bonds from the viewpoints of geometry, valency, and hybridization, is a fascinating topic in organic chemistry.^[1] Undoubtedly, among such non-classical molecules the highly strained bicyclo[1.1.0]butane and tricyclo[2.1.0.0^{2,5}]pentane, as well as their derivatives, are paramount examples of the most long-standing and attractive challenges for organic chemists (Scheme 1, **A** and **B**, respectively).^[2,3] Particularly



Scheme 1. Highly strained non-classical compounds bicyclo[1.1.0]butane (**A**) and tricyclo[2.1.0.0^{2,5}]pentane (**B**) and bridgehead 1,3- (**C**) and bridging 2,4-dianions (**D**) of **A**.

important is the question of the nature of the bridging bond in both compounds, which has been the subject of theoretical investigations and debates during the last two decades, especially for the derivatives of bicyclo[1.1.0]butane.^[2] Experimentally, the chemistry of bicyclo[1.1.0]butane, which has been known since 1959, has been developed, and many representatives of this unusual class of compounds, including their heavy analogues, have been synthesized.^[4] However, the stable, charged derivatives (both anionic and cationic) of bicyclo[1.1.0]butanes have remained elusive species until now: neither bridgehead 1,3- (Scheme 1, **C**) nor bridging 2,4-dianions (Scheme 1, **D**) of bicyclo[1.1.0]butane have ever been isolated and characterized.^[5] Very recently we have synthesized the ³Δ-1,2,3,4-disiladigermetene **1**,^[6] which appeared to be a most promising candidate for reduction to produce the corresponding dianion species. Indeed, by the reaction of **1** with alkali metals, the heavy analogues of the cyclobutadiene dianion were synthesized; their cyclic 6π-

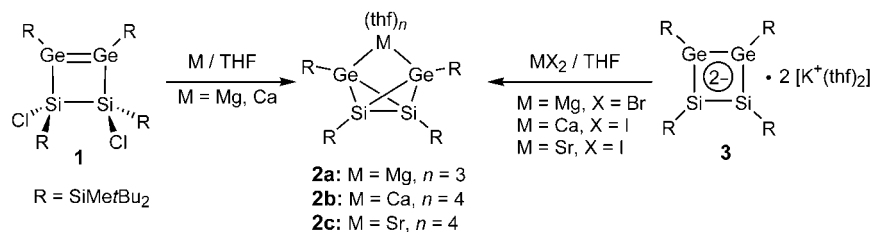
[*] Dr. V. Ya. Lee, Dipl.-Chem. K. Takanashi, Dr. M. Ichinohe, Prof. Dr. A. Sekiguchi
Department of Chemistry
Graduate School of Pure and Applied Sciences
University of Tsukuba
Tsukuba, Ibaraki 305-8571 (Japan)
Fax: (+81) 298-53-4314
E-mail: sekiguch@staff.chem.tsukuba.ac.jp

[**] This work was supported by a Grant-in-Aid for Scientific Research (Nos. 147078204, 16205008, 16550028) from the Ministry of Education, Science and Culture of Japan, and COE (Center of Excellence) Program.

electron system was demonstrated to be non-aromatic.^[7] To our surprise, the reduction of **1** with alkaline-earth metals gave a totally different structure with the bicyclo[1.1.0]butane 2,4-dianion skeleton, these compounds were isolated in the form of magnesium, calcium, and strontium salts, whose synthesis and structural characteristics we report herein.

The reduction of **1** with an excess of metallic magnesium or calcium in THF at room temperature resulted in the clean formation of the corresponding magnesium and calcium derivatives of tetrakis(di-*tert*-butylmethylsilyl)-1,3-disila-2,4-digermbicyclo[1.1.0]butane-2,4-diide **2a,b** isolated as highly air- and moisture-sensitive, bright orange crystals (Scheme 2). Of note is that both **2a** and **2b** can be prepared alternatively by the reaction of the dipotassium salt **3**^[7] with MX₂ (M = Mg, X = Br; M = Ca, X = I) in THF (Scheme 2). Employing this synthetic approach, we were able to synthesize dianion **2** with strontium as the coordinating counterion, compound **2c**.

Reflecting their symmetrical structure, ¹H and ¹³C NMR spectra of **2a–c** have only two sets of signals for the two kinds of *t*Bu₂MeSi substituents. The arrangement of the Si atoms at the bridgehead positions of **2** was clearly evident from the ²⁹Si NMR spectra, which show their very diagnostic greatly upfield-shifted signals: –231.9 ppm for **2a**, –220.2 ppm for **2b**, and –225.2 ppm for **2c**.



Scheme 2. Synthesis of 1,3-disila-2,4-digermbicyclo[1.1.0]butane-2,4-diide derivatives **2a–c**. R = SiMe*t*Bu₂.

The composition of all of the alkaline-earth-metal derivatives **2a–c** was unambiguously established by X-ray crystallography, as shown in Figure 1 for **2a**.^[8] With a capping alkaline-earth metal playing a bridge role, bicyclo[1.1.0]butane dianions **2** actually acquire the properties of tricyclo[2.1.0.0^{2,5}]pentane derivatives (Scheme 1, **B**). This relationship was clearly demonstrated by consideration of the structural characteristics of the Si₂Ge₂ skeleton of **2**: 1) the Si–Si bridging bonds are a little shortened in comparison with the normal Si–Si bond length, 2.3181(15) Å (**2a**), 2.323(2) Å (**2b**), and 2.3304(15) Å (**2c**); 2) the interplanar angles ϕ (see Scheme 1) are acute: 98.90 (**2a**), 102.30 (**2b**), and 104.90 for (**2c**); 3) bond angles θ are wide: 133.65(6) and 135.75(7) (**2a**), 132.76(9) and 132.89(9) (**2b**), and 128.60(8) and 136.42(8) (**2c**). All of these structural features match the properties of tricyclo[2.1.0.0^{2,5}]pentanes (Scheme 1, **B**),^[3] in which a small interplanar angle ϕ forces the hybrid orbitals of the bridged atoms towards each other to form short bent C–C bridging bonds. However, such a short Si–Si bridging bond in dianions

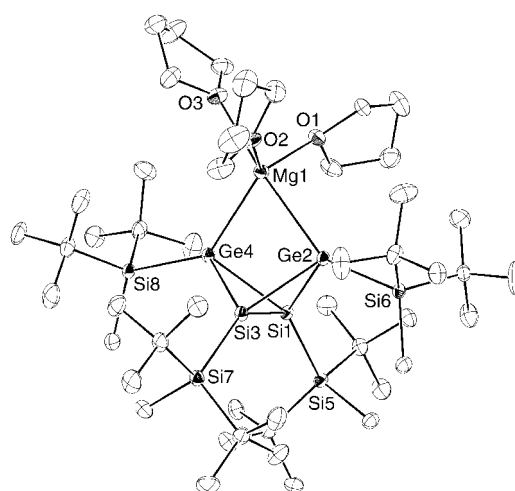
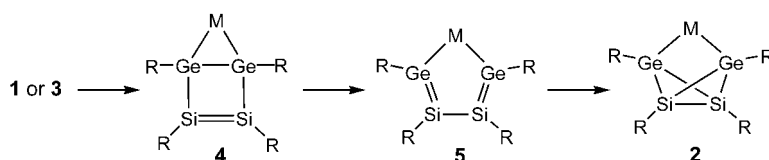


Figure 1. Structure of **2a** (ORTEP plot, thermal ellipsoids set at 30 % probability; hydrogen atoms omitted for clarity). Selected bond lengths [Å] and angles [°]: Si1–Si3 2.3181(15), Si1–Ge2 2.4911(11), Si1–Ge4 2.4480(11), Si3–Ge2 2.4691(12), Si3–Ge4 2.4523(12), Ge2–Mg1 2.7664(15), Ge4–Mg1 2.6259(14); Si3–Si1–Ge2 61.66(4), Si1–Si3–Ge2 62.62(4), Si1–Ge2–Si3 55.72(4), Si1–Si3–Ge4 61.67(4), Si3–Si1–Ge4 61.86(4), Si1–Ge4–Si3 56.46(4), Si3–Si1–Si5 133.65(6), Si1–Si3–Si7 135.75(7), Ge2–Mg1–Ge4 75.59(4).

2a–c is in complete contrast to our previously reported tricyclo[2.1.0.0^{2,5}]pentane analogue, which has an extremely long Ge–C bridging bond,^[9] owing to its significant biradical character.

The mechanism for the formation of compounds **2** may involve the initial reduction of the starting material **1** with alkaline-earth metals to form **4**, which has a bicyclo[2.1.0]pentene skeleton (Scheme 3). Valence isomerization to release the inherent strain of **4** might be imag-



Scheme 3. Proposed mechanism of formation of **2**.

ined as the next step, to produce the cyclopentadiene-like compound **5**, which finally undergoes intramolecular cross [2+2] cycloaddition to form tricyclo[2.1.0.0^{2,5}]pentane derivatives **2**.^[10] Starting from the cyclobutadiene dianion dipotassium salt **3**, the reaction with metal halides MX₂ resulted in the initial formation of **4**, following the isomerization steps described above. Such conclusions are supported by theoretical calculations, which showed that of all the cyclic R₄Si₂Ge₂Mg isomers **4**, **5**, and **2** (R = SiH₃), the tricyclo[2.1.0.0^{2,5}]pentane **2** is the most stable compound (0 kcal mol^{–1}), compared with the cyclopentadiene **5** (+12.12 kcal mol^{–1}) and the bicyclo[2.1.0]pentene **4** (+12.39 kcal mol^{–1}).^[11]

Experimental Section

2a: The mixture of **1** (96 mg, 0.106 mmol) and excess magnesium (35 mg, 1.44 mmol) in dry oxygen-free THF (2 mL) was stirred for two days at room temperature, during which time the color of the reaction mixture turned from yellow to dark brown. After filtration and evaporation of solvent from the filtrate, recrystallization from hexane–THF gave **2a** as bright-orange crystals (83 mg, 73%). M.p. 205 °C (dec.). ¹H NMR (400 MHz, [D₈]THF, TMS): δ = 0.16 (s, 6H, Me), 0.30 (s, 6H, Me), 1.16 (s, 36H, *t*Bu), 1.19 ppm (s, 36H, *t*Bu); ¹³C{¹H} NMR (100 MHz, [D₈]THF, TMS): δ = −2.6, −1.6, 22.4, 22.7, 31.4, 31.5 ppm; ²⁹Si{¹H} NMR (79 MHz, [D₈]THF, TMS): δ = −231.9 (bridgehead Si), 22.5 and 34.5 ppm (substituent Si).

2c: The mixture of **3** (127 mg, 0.106 mmol) and excess SrI₂ (60 mg, 0.176 mmol) in dry oxygen-free THF (2 mL) was stirred for 2 h at room temperature, during which time the color of the reaction mixture turned from dark green to orange. After filtration and evaporation of solvent from the filtrate, recrystallization from THF gave **2c** as bright-orange crystals (95 mg, 74%). M.p. 137 °C (dec.). ¹H NMR (400 MHz, [D₈]THF, TMS): δ = 0.14 (s, 6H, Me), 0.22 (s, 6H, Me), 1.16 (s, 36H, *t*Bu), 1.21 ppm (s, 36H, *t*Bu); ¹³C{¹H} NMR (100 MHz, [D₈]THF, TMS): δ = −1.9, −1.7, 22.6, 22.9, 32.1, 32.3 ppm; ²⁹Si{¹H} NMR (79 MHz, [D₈]THF, TMS): δ = −225.2 (bridgehead Si), 21.1 and 33.6 ppm (substituent Si).

Received: August 10, 2004

Keywords: alkaline-earth metals · germanium · heterobicyclobutanes · silicon · structure elucidation

- [1] F. A. Carey, R. J. Sundberg, *Advanced Organic Chemistry, Part A: Structure and Mechanisms*, 4th ed., Kluwer Academic/Plenum Publishers, New York, **2000**.
- [2] For bicyclo[1.1.0]butanes: a) P. H. M. Budzelaar, E. Kraka, D. Cremer, P. v. R. Schleyer, *J. Am. Chem. Soc.* **1986**, *108*, 561; b) P. v. R. Schleyer, A. F. Sax, J. Kalcher, R. Janoschek, *Angew. Chem.* **1987**, *99*, 374; *Angew. Chem. Int. Ed. Engl.* **1987**, *26*, 364; c) W. W. Schoeller, T. Dabisch, T. Busch, *Inorg. Chem.* **1987**, *26*, 4383; d) S. Nagase, T. Kudo, *J. Chem. Soc. Chem. Commun.* **1988**, *54*; e) J. A. Boatz, M. S. Gordon, *J. Phys. Chem.* **1988**, *92*, 3037; f) J. A. Boatz, M. S. Gordon, *J. Phys. Chem.* **1989**, *93*, 2888; g) D. B. Kitchen, J. E. Jackson, L. C. Allen, *J. Am. Chem. Soc.* **1990**, *112*, 3408; h) J. A. Boatz, M. S. Gordon, *Organometallics* **1996**, *15*, 2118.
- [3] For tricyclo[2.1.0.0^{2,5}]pentanes: a) P. Dowd, H. Irngartinger, *Chem. Rev.* **1989**, *89*, 985; b) M. D. Levin, P. Kaszynski, J. Michl, *Chem. Rev.* **2000**, *100*, 169.
- [4] For bicyclo[1.1.0]butane, see: a) K. B. Wiberg, R. P. Ciula, *J. Am. Chem. Soc.* **1959**, *81*, 5261; b) K. B. Wiberg, G. M. Lampman, *Tetrahedron Lett.* **1963**, *4*, 2173. For Si-containing bicyclo[1.1.0]butane derivatives, see: c) G. Fritz, S. Wartanessian, E. Matern, W. Hönle, H. G. v. Schnering, *Z. Anorg. Allg. Chem.* **1981**, *475*, 87; d) W. Ando, T. Shiba, T. Hidaka, K. Morihashi, O. Kikuchi, *J. Am. Chem. Soc.* **1997**, *119*, 3629; e) T. Iwamoto, D. Yin, C. Kabuto, M. Kira, *J. Am. Chem. Soc.* **2001**, *123*, 12730; f) S. Masamune, Y. Kabe, S. Collins, D. J. Williams, R. Jones, *J. Am. Chem. Soc.* **1985**, *107*, 5552; g) M. Driess, A. D. Fanta, D. R. Powell, R. West, *Angew. Chem.*, **1989**, *101*, 1087; *Angew. Chem. Int. Ed. Engl.* **1989**, *28*, 1038; h) R. P. Tan, N. M. Comerlato, D. R. Powell, R. West, *Angew. Chem.*, **1992**, *104*, 1251; *Angew. Chem. Int. Ed. Engl.* **1992**, *31*, 1217.
- [5] Attempts to generate derivatives of bicyclo[1.1.0]butane or tetrasilabicyclo[1.1.0]butane dianions caused the unavoidable breaking of the central bridging bond, which results in the formation of cyclobutane-1,3-diides, which were subsequently trapped with appropriate electrophiles: a) W. R. Moore, S. S. Hall, C. Largman, *Tetrahedron Lett.* **1969**, 4353; b) T. Kawase, S. A. Batcheller, S. Masamune, *Chem. Lett.* **1987**, 227.
- [6] V. Ya. Lee, K. Takanashi, M. Ichinohe, A. Sekiguchi, *J. Am. Chem. Soc.* **2003**, *125*, 6012.
- [7] V. Ya. Lee, K. Takanashi, T. Matsuno, M. Ichinohe, A. Sekiguchi, *J. Am. Chem. Soc.* **2004**, *126*, 4758.
- [8] Crystal structure analysis of **2a**, **2b**, and **2c**: The single crystals for X-ray analysis were grown from the THF/hexane solution for **2a** and THF solutions for **2b** and **2c**. Diffraction data were collected at 120 K on a MacScience DIP2030 K Image Plate Diffractometer employing graphite-monochromated MoK α radiation ($\lambda = 0.71070$ Å). Crystal data for **2a**: (tBu₂MeSi)₄Si₂Ge₂Mg(thf)₃, C₄₈H₁₀₈Ge₂MgO₃Si₆, *M_r* = 1071.37, orthorhombic, space group = *Pna*2₁, *a* = 13.1680(5), *b* = 21.5230(3), *c* = 21.5320(7) Å, *V* = 6102.5(3) Å³, *Z* = 4, ρ_{calcd} = 1.166 g cm^{−3}, GOF = 1.042. The final *R* factor was 0.0369 (*R_w* = 0.0990 for all data) for 6569 reflections with *I*₀ > 2σ(*I*₀). Crystal data for **2b**: (tBu₂MeSi)₄Si₂Ge₂Ca(thf)₄, C₅₂H₁₁₆CaGe₂O₄Si₆, *M_r* = 1159.25, triclinic, space group = *P*1̄, *a* = 13.7440(6), *b* = 13.7440(6), *c* = 21.4360(9) Å, α = 71.755(2), β = 71.749(2), γ = 60.250(2)°, *V* = 3277.1(2) Å³, *Z* = 2, ρ_{calcd} = 1.175 g cm^{−3}, GOF = 1.241. The final *R* factor was 0.0795 (*R_w* = 0.1888 for all data) for 12054 reflections with *I*₀ > 2σ(*I*₀). Crystal data for **2c**: (tBu₂MeSi)₄Si₂Ge₂Sr(thf)₄, C₅₂H₁₁₆Ge₂O₄Si₆Sr, *M_r* = 1206.79, monoclinic, space group = *Cc*, *a* = 23.7800(11), *b* = 13.9470(3), *c* = 21.4460(10) Å, β = 110.935(2)°, *V* = 6643.2(5) Å³, *Z* = 4, ρ_{calcd} = 1.207 g cm^{−3}, GOF = 0.953. The final *R* factor was 0.0383 (*R_w* = 0.0990 for all data) for 7000 reflections with *I*₀ > 2σ(*I*₀). All structures were solved by the direct method and refined by the full matrix Least-squares method using SHELXL-97 program. CCDC-246460 (**2a**), CCDC-246461 (**2b**), CCDC-246462 (**2c**) contain the supplementary crystallographic data for this paper. These data can be obtained free of charge via www.ccdc.cam.ac.uk/conts/retrieving.html (or from the Cambridge Crystallographic Data Centre, 12 Union Road, Cambridge CB21EZ, UK; fax: (+44) 1223-336-033; or deposit@ccdc.cam.ac.uk).
- [9] V. Ya. Lee, M. Ichinohe, A. Sekiguchi, *J. Am. Chem. Soc.* **2002**, *124*, 9962.
- [10] The possibility of such isomeric interconversion incorporating the heavier Group 14 elements has been experimentally observed and discussed; see: a) V. Ya. Lee, M. Ichinohe, A. Sekiguchi, *J. Am. Chem. Soc.* **2000**, *122*, 12604; b) see Ref. [9]; Recently this topic was also studied theoretically; see: c) I. Özkan, A. Kinal, M. Balci, *J. Phys. Chem. A* **2004**, *108*, 507.
- [11] All theoretical calculations were performed at the B3LYP/6-31(d) level with the GAUSSIAN-98 program package.

Ligand-Functionalized Core/Shell Microgels with Permselective Shells**

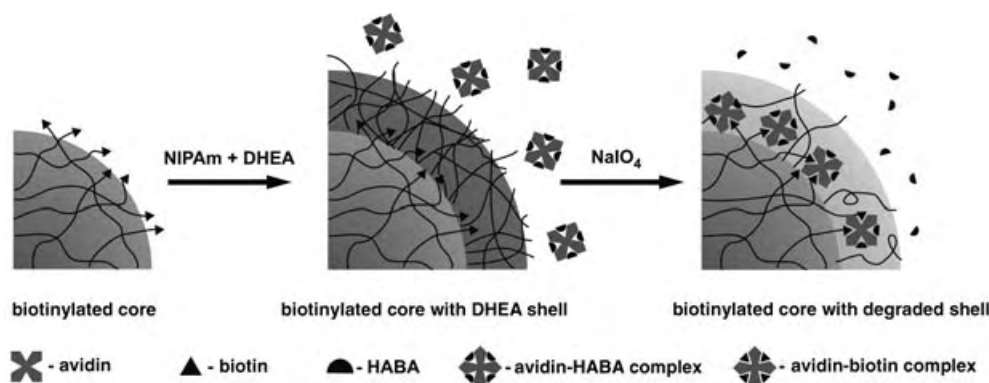
Satish Nayak and L. Andrew Lyon*

Recently the field of nanotechnology has received immense attention, which in part is owed to its potential impact on biotechnology. Nanometric materials find application in many fields such as chemical sensing^[1] and biosensing,^[2] catalysis,^[3] optics,^[4] separations,^[5] and drug delivery.^[6] Nanomaterials offer advantages in such arenas owing to the potential for new or enhanced optical, chemical, mechanical, or electrical properties. Of particular interest is the creation of multifunctional nanoparticles, which contain multiple chemistries such that they interact with their environment in a more-complex fashion. Here we report the synthesis of a well-defined, yet chemically and topologically complex colloidal particle. This structure comprises a porous, thermosensitive hydrogel “core” particle that is modified with a ligand (biotin). This particle is contained within a porous, thermoresponsive hydrogel “shell” that sterically excludes the transport and binding of the protein avidin, for which biotin is a tight-binding ligand. However, by using a cross-linker that can be chemically cleaved in the shell, the ability of avidin to

penetrate the particle and bind to the core can be chemically tuned with a high degree of fidelity.

The polymer used in the construction of these particles is mainly composed of poly(*N*-isopropylacrylamide) (pNIPAm), which is a classic stimuli-responsive polymer.^[7] Materials fabricated from pNIPAm are often deemed to be “smart” because they can be tuned to respond to temperature,^[8] pH,^[9] light,^[10] ionic strength,^[11] or biomolecules.^[12] pNIPAm can be cross-linked into nanoparticles by emulsion or precipitation polymerization processes with good size control over the range 10^{-8} – 10^{-5} m.^[13] We have developed precipitation polymerization methods to create a class of core/shell hydrogel particles derived from pNIPAm. The specific concept employed for the chemically and topologically complex particles presented herein is shown in Scheme 1. A biotinylated hydrogel core nanoparticle is coated with a hydrogel shell that contains the cleavable cross-linker *N,N'*-(1,2-dihydroxyethylene)bisacrylamide (DHEA). At the initial cross-link density, the pore size of the shell is too small to allow avidin molecules to pass through to the core where they bind biotin. Upon chemical cleavage of the cross-links, the pore size increases enough to allow avidin to pass through and bind biotin.

We have previously synthesized core/shell hydrogel nanoparticles by a multistage “seed and feed” method, whereby preformed thermoresponsive hydrogel nanoparticles are used as seeds for the addition of either chemically similar or



Scheme 1. A NIPAm/AAC core is biotinylated with biotin hydrazide and EDC, followed by addition of a NIPAm/DHEA shell. The cross-linker density of the shell is such that the pore size is smaller than the avidin–HABA complex which prevents the protein from passing through the shell. Upon treatment with periodate, the DHEA cross-linker degrades which subsequently increases the pore size to allow passage of avidin–HABA complex molecules. The K_d value for avidin–HABA (10^{-6}) is higher than the K_d value for avidin–biotin (10^{-15}). Therefore, HABA is released from avidin when biotin binds to avidin. The binding is detected by UV/Vis spectroscopy. NIPAm = *N*-isopropylacrylamide, AAC = acrylic acid, EDC = 1-ethyl-3-(3-dimethylaminopropyl)carbodiimide, DHEA = *N,N'*-(1,2-dihydroxyethylene)bisacrylamide, HABA = 2-(4'-hydroxyazobenzene)benzoic acid.

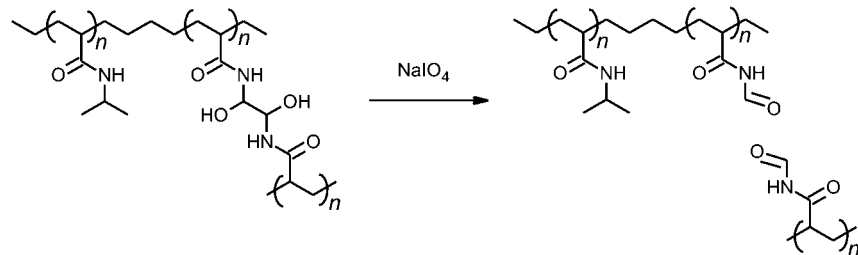
[*] S. Nayak, Prof. L. A. Lyon
School of Chemistry and Biochemistry
Georgia Institute of Technology
Atlanta, GA 30332-0400 (USA)
Fax: (+1) 404-894-7452
E-mail: lyon@chemistry.gatech.edu

[**] L.A.L. gratefully acknowledges financial support from the National Science Foundation, Division of Materials Research (DMR-0203707). Support through a Blanchard Foundation Fellowship is also acknowledged.

Supporting information for this article is available on the WWW under <http://www.angewandte.org> or from the author.

distinct hydrogel shells.^[14] In the present study, the core is predominantly composed of pNIPAm with acrylic acid (AAc) as a minor component (10 mol %). The acid groups are used for attaching biotin to the nanoparticles by carbodiimide coupling (see the Experimental Section in the Supporting Information). These biotinylated cores are then used as seed particles to which a shell is added. The shell also consists of pNIPAm, but it is cross-linked with the cleavable diol cross-linker DHEA. Traditionally, bulk gels that are cross-linked with DHEA have been used for electrophoretic protein

separation.^[15] As the vicinal diols in the cross-linker can be cleaved by stoichiometric amounts of sodium periodate, the pore size of the gel can be varied quantitatively by degradation of the cross-linker (Scheme 2). Figure 1 shows the



Scheme 2. Structure of the cleavable polymer. Sodium periodate cleaves the 1,2-glycol bond of DHEA through oxidation of the vicinal diols to aldehydes.

the absorption spectra of the avidin–HABA complex in the presence and absence of biotinylated core particles. The amount of biotin conjugated to the core particle was determined by titration of the acid groups before and after conjugation. Subtracting the number of moles of acid in the biotinylated sample from that in the non-biotinylated sample reveals that ≈ 160 mg of biotin is conjugated to one gram of core particles. From the avidin–HABA assay, only ≈ 25 mg of biotin was determined to be available for binding to avidin in one gram of core particles. This means that only $\approx 16\%$ of avidin is accessible from the total amount of biotin conjugated to the polymer.

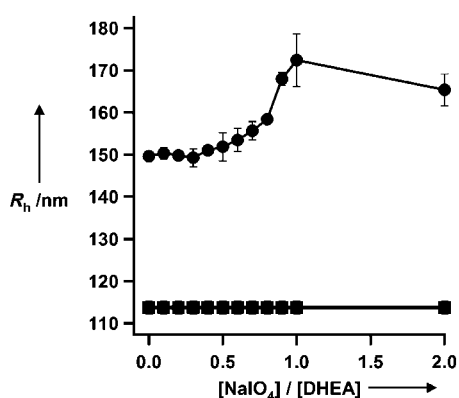


Figure 1. Hydrodynamic radius (R_h) of the core/shell particles (●) as a function of the ratio of periodate:DHEA. The R_h of the core is represented by ■. The error bars represent one standard deviation about the average of five separate measurements.

variation in the hydrodynamic radius (R_h) of the core/shell particle as a function of cleavage of the cross-links in the shell measured at 25 °C (filled circles). The filled squares represent the R_h values for the core. From this we see that the initial R_h value of the core is ≈ 115 nm, whereas that of the core/shell particle prior to the addition of periodate is ≈ 150 nm. Upon addition of periodate to the solution, the shell swells as suggested by the increase in the R_h values of the core/shell particle as a function of periodate concentration. This is expected, as a decrease in the concentration of cross-links in the network should result in a larger equilibrium swelling volume. Ultimately, the R_h value of the core/shell particle increases by ≈ 20 nm following complete cleavage of the periodate cross-links.

To detect the sieving of avidin through the shell we used the colorimetric 2-(4'-hydroxyazobenzene)benzoic acid (HABA) assay.^[16] Four equivalents of HABA bind weakly to avidin at the biotin binding site ($K_d = 10^{-6}$ M),^[17] and the resultant complex shows an absorption band at $\lambda = 500$ nm. In the presence of biotin, HABA is displaced from avidin ($K_d = 10^{-15}$ M for the avidin–biotin system),^[18] and the intensity of the absorbance band at $\lambda = 500$ nm decreases. Figure 2 shows

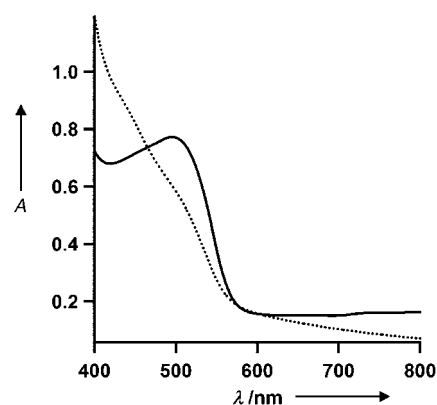


Figure 2. Absorption spectra of avidin–HABA complex in the presence (.....) and in the absence (—) of biotinylated core particles.

Figure 3 shows the variation in the absorbance of the avidin–HABA complex at $\lambda = 500$ nm as a function of the ratio of the concentrations of periodate/DHEA for particles with 20, 15, and 2% cross-linked shells. For the 20% cross-

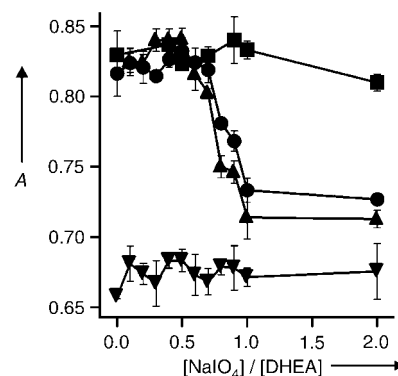


Figure 3. Absorbance of the avidin–HABA complex at $\lambda = 500$ nm as a function of the ratio of periodate:DHEA for 20% cross-linked shell particles (●), 15% cross-linked shell particles (▲), 2% cross-linked shell particles (▼) and biotin-free control particles (■). The error bars represent one standard deviation about the average of three different samples.

linked shell, the absorbance at $\lambda = 500$ nm remains essentially constant with increasing concentrations of periodate until approximately 70% of the diol groups are cleaved. The absorbance decreases precipitously beyond that concentration which is an indication of the displacement of HABA from avidin by the core-bound biotin. This clearly implies that until $\approx 70\%$ degradation, the pore size of the shell is not big enough to allow the passage of avidin–HABA. At $> 70\%$ degradation, the pore size becomes large enough to allow avidin–HABA to pass through the shell and bind biotin. Figure 3 also shows the variation in absorbance for control particles that do not have a biotinylated core. No substantial changes in the absorbance are observed for the control samples which further confirms that the changes in the absorbance observed for the biotinylated samples indeed arise from the binding of biotin to avidin. The 15% cross-linked shell shows the same trend as the 20% cross-linked sample, but the decrease in absorbance starts slightly earlier. This is presumably a result of the larger initial pore size in the 15% cross-linked shell relative to that in the 20% cross-linked shell. For 2% cross-linked shells, the absorbance for 0% degradation is already lower than that for the 20% and 15% cross-linked samples, which were treated with a twofold excess of periodate. This result indicates that the pore size for this cross-linking density is so large that it renders the shell permeable and thereby allows avidin to bind biotin in the core without any degradation of the shell. The increased degree of binding also suggests that more biotin molecules are accessible to avidin, as the more-open network structure of the 2% cross-linked shell imposes less steric hindrance to the transport of the protein. Also, further degradation does not lead to any substantial change in the absorbance which indicates that almost all of the biotin molecules are already accessible to avidin prior to any degradation.

To evaluate how a change in the radius of the protein impacts transport through the particle shell, we used an avidin–HRP (horseradish peroxidase) conjugate in which two moles of HRP were conjugated to one mole of avidin. The molecular weight of this conjugate is ≈ 154 kDa (compare to regular avidin: ≈ 66 kDa). Avidin–HRP binds both biotin and HABA with the same affinity as free avidin. Figure 4

shows the change in the absorbance at $\lambda = 500$ nm of the avidin–HRP–HABA complex as a function of the periodate/DHEA ratio for the 20% cross-linked shell particles. No significant decrease in absorbance is observed until an approximately twofold excess of periodate is added to the sample. Again, normal avidin begins to sieve through the shell at $\approx 70\%$ degradation. This indicates that the avidin–HRP complex is too big to sieve through the shell until all of the cross-links are cleaved. Presumably, the excess periodate is needed to drive the reaction in more highly cross-linked (less accessible) regions of the particle shell; the reaction proceeds under stoichiometrically equivalent conditions in free solution.

In conclusion, we have demonstrated the synthesis of complex hydrogel nanoparticles that bind to a protein through both native protein–ligand interactions as well as through steric sieving. These core/shell nanoparticles are formed by a simple “seed and feed” polymerization method, in which the shell has cleavable cross-links. The sieving of proteins through the shell to the core is simply controlled by the manipulation of the pore size of the shell through cleavage of those cross-links. At a particular cross-linker density, only avidin is allowed to sieve through the shell, whereas larger protein structures are excluded from binding. Such nanoparticles could find applications in protein separation processes—the shell could essentially behave as a molecular-weight cut-off membrane to eliminate the binding of macromolecules and assemblies that are larger than the protein of interest. Affinity-based sensors and assays that are required to work in complex biological fluids could also benefit from size-selecting structures. Finally, the specific biotin–avidin ligand/protein system used here has become important for a wide range of surface modification and bioconjugation methods. Thus, one could imagine applying this system to the preparation of a wide range of microgel bioconjugates in which access to the biomacromolecule can be reversibly tuned.

Received: June 25, 2004

Revised: August 27, 2004

Keywords: colloids · microporous materials · nanotechnology · polymerization · proteins

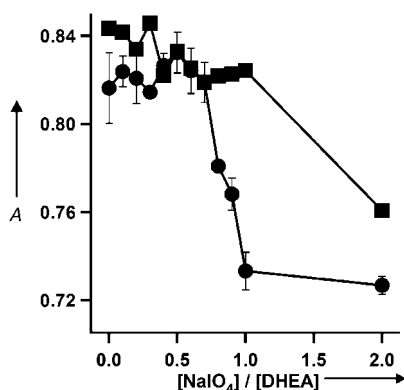


Figure 4. Absorbance of the avidin–HABA complex (●) and avidin–HRP–HABA complex (■) as a function of the percentage of degradation of 20% cross-linked shell particles. The error bars represent one standard deviation about the average of three different samples.

- [1] S.-Y. Lin, S.-W. Liu, C.-M. Lin, C.-H. Chen, *Anal. Chem.* **2002**, 74, 330.
- [2] R. C. Bailey, J.-M. Nam, C. A. Mirkin, J. T. Hupp, *J. Am. Chem. Soc.* **2003**, 125, 13541.
- [3] S. Shen, K. Hidajat, L. E. Yu, S. Kawi, *Adv. Mater.* **2004**, 16, 541.
- [4] C. D. Jones, L. A. Lyon, *J. Am. Chem. Soc.* **2003**, 125, 460.
- [5] E. Guihen, J. D. Glennon, *Anal. Lett.* **2003**, 36, 3309.
- [6] I. Brigger, C. Dubernet, P. Couvreur, *Adv. Drug Delivery Rev.* **2002**, 54, 631.
- [7] C. Wu, X. Wang, *Phys. Rev. Lett.* **1998**, 80, 4092.
- [8] T. Tanaka, D. J. Fillmore, *J. Chem. Phys.* **1979**, 70, 1214.
- [9] T. Tanaka, D. J. Fillmore, S.-T. Sun, I. Nishio, G. Swislow, A. Shah, *Phys. Rev. Lett.* **1980**, 45, 1636.
- [10] A. Suzuki, T. Tanaka, *Nature* **1990**, 346, 345.
- [11] D. Duracher, F. Sauzedde, A. Elaissari, C. Pichot, L. Nabzar, *Colloid Polym. Sci.* **1998**, 276, 920.

- [12] T. Miyata, N. Asami, T. Uragami, *Nature* **1999**, 399, 766.
- [13] R. Pelton, *Adv. Colloid Interface Sci.* **2000**, 85, 1.
- [14] C. D. Jones, L. A. Lyon, *Macromolecules* **2000**, 33, 8301.
- [15] P. B. H. O'Connell, C. J. Brady, *Anal. Biochem.* **1976**, 76, 63.
- [16] N. M. Green, *Biochem. J.* **1965**, 94, 23c.
- [17] H. Hofstetter, M. Morpurgo, O. Hofstetter, E. A. Bayer, M. Wilchek, *Anal. Biochem.* **2000**, 284, 354.
- [18] O. Livnah, E. A. Bayer, M. Wilchek, J. L. Sussman, *Proc. Natl. Acad. Sci. USA* **1993**, 90, 5076.
- [19] D. Gan, L. A. Lyon, *J. Am. Chem. Soc.* **2001**, 123, 7511.
- [20] C. D. Jones, L. A. Lyon, *Macromolecules* **2003**, 36, 1988.

Enzyme Catalysis

An Oxidative Phenol Coupling Reaction Catalyzed by OxyB, a Cytochrome P450 from the Vancomycin-Producing Microorganism**

Katja Zerbe, Katharina Woithe, Dong Bo Li, Francesca Vitali, Laurent Bigler, and John A. Robinson*

During the biosynthesis of vancomycin, three oxidative phenol coupling reactions take place which lead to cross-links between aromatic amino acid side chains in the heptapeptide glycopeptide aglycone (Figure 1).^[1] These cross-links constrain the peptide into a conformation that is optimal for binding to a *N*-acyl-D-Ala-D-Ala fragment, which arises during bacterial peptidoglycan biosynthesis.^[2] The binding of vancomycin to *N*-acyl-D-Ala-D-Ala inhibits peptidoglycan biosynthesis, an event that is lethal for Gram-positive bacteria.

Important information about the biosynthesis of glycopeptide antibiotics has been revealed through the analysis of biosynthetic gene clusters, in particular those of chloroeremomycin^[3] and balhimycin.^[4] Gene knockout experiments in the balhimycin producer (balhimycin shares the same aglycone with vancomycin) identified three oxygenase genes (*oxyA*, *oxyB*, and *oxyC*) in the cluster which encode cytochrome P450-like proteins and which are responsible for the three oxidative phenol coupling reactions (Figure 1).^[5] These knockout experiments indicated the order in which the

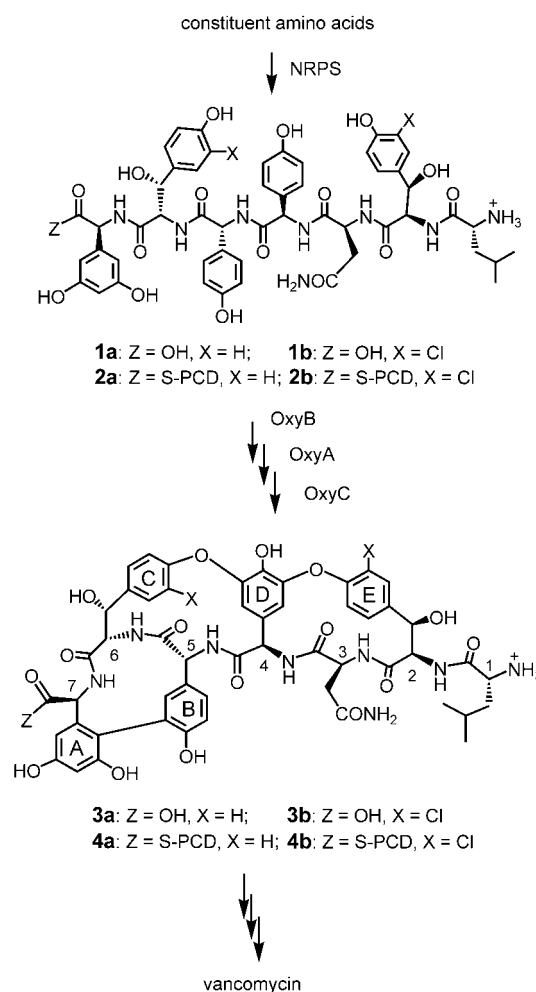


Figure 1. Outline of the biosynthesis of the glycopeptide antibiotic vancomycin. NRPS = non-ribosomal peptide synthetase, PCD = peptide carrier domain.

three coupling reactions occur. The first coupling occurs between rings C and D and is catalyzed by OxyB, the second reaction occurs between rings D and E and is catalyzed by OxyA, and the final coupling reaction takes place between rings A and B and is catalyzed by OxyC.^[6,7] So far, however, the preferred substrates of OxyA–C and hence at which step in the biosynthesis the coupling reactions occur remain unknown. Our earlier efforts to detect the turnover of the linear heptapeptides **1a** and **1b** by OxyB cloned from the vancomycin producer failed to reveal significant amounts of any product that arises from a phenol coupling reaction.^[8] One reason for this failure might be that the phenol coupling occurs *in vivo* whilst the peptide precursor is still attached as a thioester to a peptide carrier domain (PCD) of the glycopeptide non-ribosomal peptide synthetase (NRPS). The enzyme OxyB might, therefore, be unable to catalyze the coupling of phenols on the free heptapeptide, but rather would require the peptide to be present as a thioester derivative attached to its cognate PCD (as in **2a** and **2b**). Here we report results from experiments with OxyB from the vancomycin producer *Amycolatopsis orientalis* that support this conclusion.

[*] Dr. K. Zerbe, K. Woithe, Dr. D. B. Li, Dr. F. Vitali, Dr. L. Bigler, Prof. J. A. Robinson
Institute of Organic Chemistry
University of Zürich
Winterthurerstrasse 190
8057 Zürich (Switzerland)
Fax: (+41) 1-635-6833
E-mail: robinson@oci.unizh.ch

[**] The authors thank the EU (5th and 6th Framework Programs) and the Swiss National Science Foundation for supporting this work, Annelies Meier for technical assistance, Prof. Wolfgang Wohlleben and Prof. Roderich Süßmuth (University of Tübingen) for sharing unpublished results, and Dr. Matthias Witt (Bruker Daltonics, Bremen) for high resolution FT mass spectrometry measurements.

In our hands, it has so far proven difficult to produce **2a** or **2b** in sufficient quantities to perform assays with OxyB. Therefore, we sought to simplify the synthetic problem by synthesizing and testing the derivative **8** (Figure 2). This

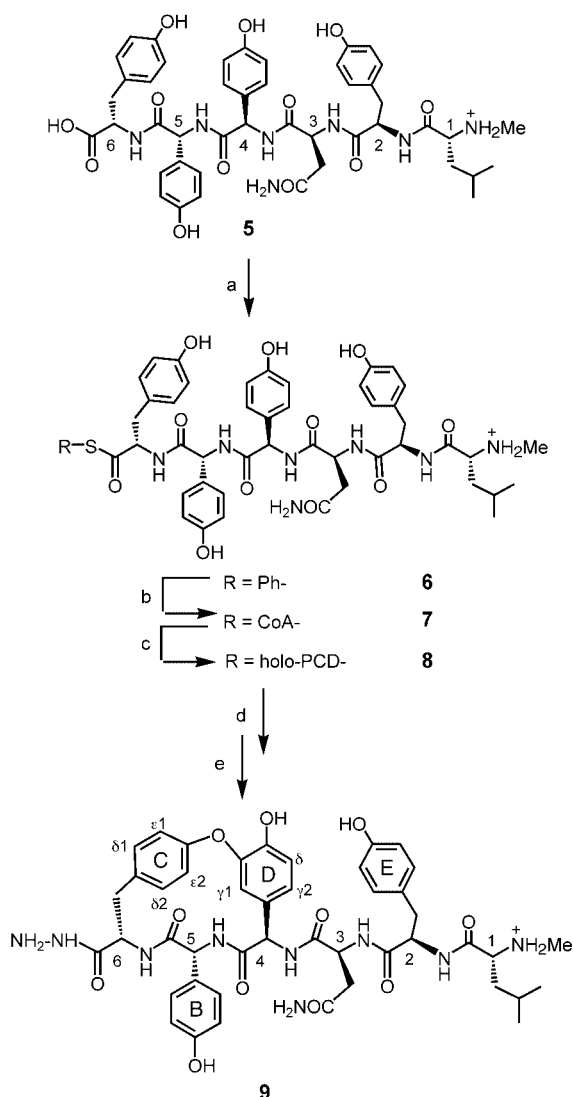
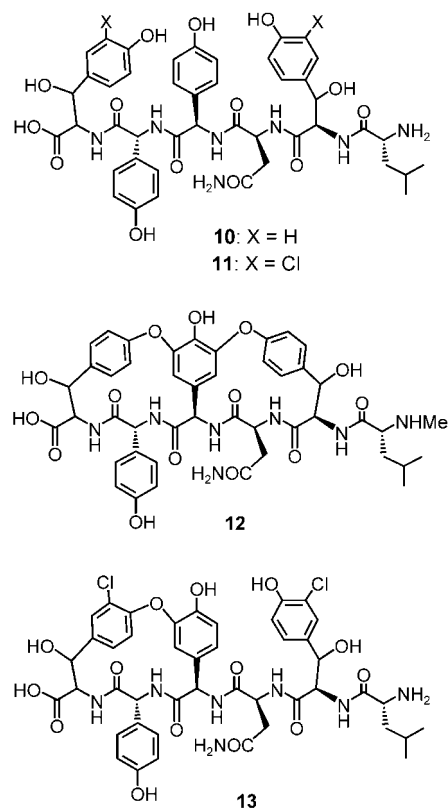


Figure 2. Synthetic route to the substrate **8**, and its assay with OxyB. a) PhSH, PyBOP; 95%; b) CoASH, pH 8.5; 50%; c) apo-PCD, phosphopantetheinyl transferase Sfp; 95%; d) OxyB, ferredoxin, ferredoxin-NADP⁺ reductase, NADPH, in air; e) NH₂NH₂. PyBOP = (benzotriazol-1-yloxy)tripyrrolidinophosphonium hexafluorophosphate.

molecule comprises a hexapeptide **5**, which contains tyrosine in place of *m*-chloro-3-hydroxytyrosine, linked to the sixth PCD from the vancomycin NRPS in *Amycolatopsis orientalis* DSM40040. Although the exact point at which the chlorination steps take place is not yet clear,^[9] the coupling reactions of the phenols can occur on non-chlorinated peptide chains.^[6] Also, both non-chlorinated linear hexapeptide **10** and bicyclic *N*-methylated hexapeptide **12** have been isolated from *oxyB* and *oxyC* knockout mutants, respectively, although these hexapeptides could conceivably arise by proteolytic degradation of a heptapeptide precursor in the fermentation broth.^[5,6]

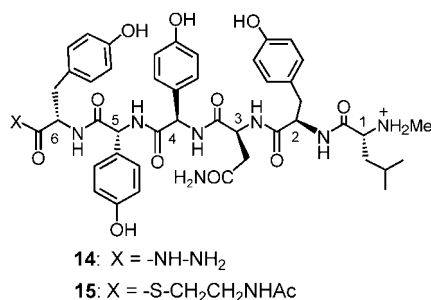


Of special interest, however, is the recent isolation of both the chlorinated linear and (in particular) monocyclic hexapeptides, **11** and **13**, respectively, from a mutant of the balhimycin producer in which a substantial portion of the *bpsC* gene has been deleted.^[10] The *bpsC* gene is responsible for the condensation of an NRPS-bound hexapeptide with the NRPS-bound seventh amino acid 3,5-dihydroxyphenylglycine. This last result clearly suggests that the corresponding linear hexapeptide linked to the NRPS can act as a substrate for OxyB.

The PCD we chose to produce here comprises 30 residues on the N-terminal side and 52 residues on the C-terminal side of the strictly conserved active site Ser residue.^[11,12] Furthermore, the Cys6 residue was modified to a Ser residue to avoid problems owing to disulfide-bridged dimer formation. This PCD, in its apo-form, was produced in *Escherichia coli* with a His₆ tag fused to the N terminus. The engineered apo-PCD was then purified to homogeneity by Ni-NTA (nickel-nitrilotriacetic acid) affinity chromatography followed by anion exchange chromatography. Electrospray ionization mass spectroscopy (ESI-MS) confirmed the expected mass of the protein (*m/z*: calcd: 11034; found: 11033 ± 1 ([*M*+H]⁺)).

The required hexapeptide **5** was synthesized by a concise solid-phase method using Alloc ((allyloxy)carbonyl) chemistry.^[13] This hexapeptide could then be converted at its C terminus into the corresponding activated phenylthioester **6** by following a previously reported method (see Figure 2).^[14] For this step to work efficiently, it is important that the N terminus is *N*-methylated (as in **6**) because no further protection is then necessary: the *N*-methylamino group does

not react with the thioester under these conditions. Next, the phenylthioester **6** was converted into a coenzyme A (CoA) thioester **7**. The hexapeptide–CoA thioester was then treated with the engineered apo-PCD and the phosphopantetheinyl transferase Sfp from *Bacillus subtilis*.^[15] The conversion into the hexapeptide–PCD **8** was followed by reverse-phase HPLC and found to proceed almost quantitatively. After purification by HPLC, the mass of the product **8** was confirmed by ESI-MS (m/z : calcd: 12239; found: 12239 ± 1 ($[M+H]^+$)). Upon treatment of the conjugate **8** with hydrazine, the thioester was cleaved, and the corresponding hydrazide derivative **14** was isolated and characterized by ESI-MS (m/z : calcd: 898.4; found: 898.4 ± 0.2 ($[M+H]^+$)).



An *N*-acetylcysteamine thioester derivative (S-NAC) **15** was also prepared by the direct coupling of *N*-acetylcysteamine to **5** because S-NAC thioesters are frequently used as simpler mimics of CoA and PCD thioesters.

To detect the turnover by OxyB, assays were performed with **8** (80 μ M) or other potential substrates in the presence of His₆-tagged OxyB^[8] (15 μ M), an engineered spinach ferredoxin, ferredoxin–NADP⁺ reductase (0.1 U, Sigma), an NADPH-regenerating system that comprises glucose-6-phosphate (2.5 mM) and glucose-6-phosphate dehydrogenase (1 U, Sigma), and NADPH (1 mM) in HEPES buffer (25 mM, pH 7.0) at 30 °C. When the free peptide **5** was tested in this way, no conversion into a monocyclic product could be detected by HPLC/MS which is consistent with earlier observations with putative free linear heptapeptide substrates (**1a** and **1b**).^[8] Following assays with the PCD derivative **8**, the assay mixture was treated directly with excess hydrazine, and the linear open chain and the monocyclic peptides, **14** and **9**, respectively, were analyzed by HPLC/MS. Assays were also performed with **6** and **7**, but these failed to reveal any conversion into a monocyclic product. An assay with **15** revealed a small degree of conversion ($\leq 5\%$) into a new product, whose molecular mass was lower by 2 Daltons (by HPLC/MS). The extent of conversion was too low, however, to allow a full characterization of this product. Assays with the PCD derivative **8**, however, typically showed up to 80% conversion into a new product (see Figure 3) to which we assign the structure **9** (high-resolution positive-ion ESI-MS (APEX Qe FT-ICR mass spectrometer (Bruker Daltonics) equipped

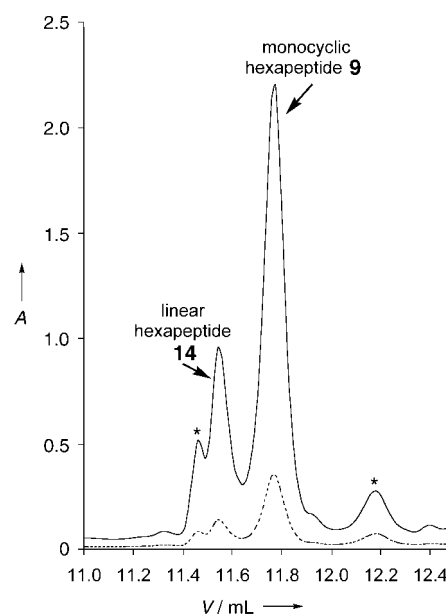


Figure 3. Analysis by HPLC (UV/Vis detection; — = 226 nm, ---- = 280 nm) of the products from the conversion of **8** with His₆-OxyB (see text for details). The peaks corresponding to linear (**14**) and monocyclic (**9**) products are shown; * = unknown. HPLC conditions: C18 Vydac column (218TP54), solvent A = water + 0.1% TFA, solvent B = MeCN + 0.1% TFA, gradient 5–40% B over 20 min, flow rate: 1 mL min⁻¹. TFA = trifluoroacetic acid, MeCN = acetonitrile.

with a 7 tesla magnet); exact mass calcd for C₄₅H₅₄N₉O₁₁: 896.3943 ($[M+H]^+$); found: 896.3938). No conversion of **8** into **9** took place under the assay conditions in the absence of OxyB nor in the absence of ferredoxin and ferredoxin–NADP⁺ reductase.

ESI-tandem mass spectra (ESI-MS/MS) of **9** and **14** are consistent with the location of a cross-link between rings C and D in the new product **9**. Thus, **14** showed the expected fragment ions b₂, b₃, b₄, and b₅, whereas **9** showed b₂ and b₃ fragments and additional z₃, y₄/z₄, and y₅/z₅ fragments with the expected (–2) masses (Figure 4).

The ¹H NMR and 2D COSY, TOCSY, NOESY, and ROESY spectra of **9** allowed a full assignment of the ¹H NMR spectrum (see Table 1) and strongly support the proposed connectivity. From 2D spectra, the connectivity of the peptide backbone was established by using standard methods.^[16] Also,

Table 1. ¹H NMR chemical shift assignments (ppm, 500 MHz) of monocyclic peptide **9** measured in [D₆]DMSO at 300 K.

Residue	NH	C(α)–H	C(β)–H	Others
Leu1	8.60(br)	3.58	1.49, 1.37	CH(γ) = 1.46, CH ₃ (δ) = 0.80, 0.73, NMe = 1.96
Tyr2	8.81	4.78	2.96, 2.57	C(δ)H = 7.04, C(ε)H = 6.62, OH = 9.17
Asn3	8.51	4.73	2.56, 2.38	N(δ)H(E) = 7.33, N(δ)H(Z) = 6.94
Hpg4	7.96	5.28	–	C(γ1)H = 5.95, C(γ2)H = 6.62, C(δ)H = 6.76, OH = 9.40
Hpg5	8.89	5.21	–	C(γ)H = 7.08, C(δ)H = 6.67, OH = 9.40
Tyr6	7.30	4.62	2.90	C(δ1)H = 7.21, C(δ2)H = 7.27, C(ε1)H = 6.90, C(ε2)H = 7.09
CONH.NH ₂	–	–	–	7.19, 7.08, 6.98

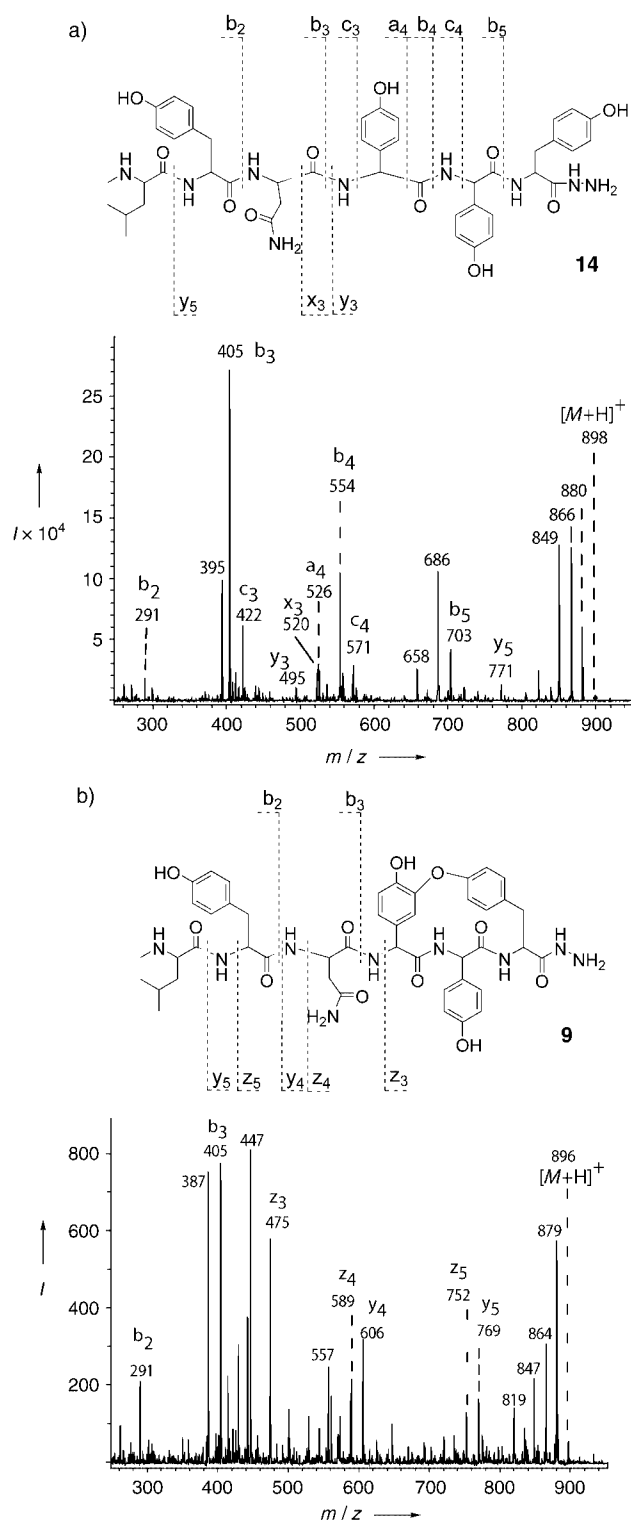


Figure 4. ESI-MS/MS of a) the linear peptide **14** and b) the monocyclic product **9**. The spectra were run on a Bruker ESQUIRE-LC quadrupole ion-trap mass spectrometer. Samples as solutions in MeOH/H₂O (1:2) with 0.05% TFA were introduced through the ES interface at 5 $\mu\text{L min}^{-1}$. The protonated quasi-molecular ions $[M+H]^+$ were selected and subjected to helium gas collision (fragmentation amplitude of 0.9 in the smart fragmentation mode).

the intact connectivity of the side chains of residues 1, 2, 3, and 5 was apparent in the 2D spectra. However, the side chains of residues 4 and 6 in this product had clearly been altered relative to the starting hexapeptide **5** (see Figure 2 for labeling of the rings, residues, and carbon atoms). The proton at C(α) of residue 4 showed NOE connectivities to a singlet peak at $\delta = 5.95$ ppm, which we assign to the hydrogen atom at C(γ 1) in the aromatic side chain. This aromatic proton is shifted upfield as expected from its close proximity to the face of the aromatic ring C in residue 6 in **9** (see Figure 2). The proton of the N-H group of residue 4 shows an NOE interaction with the hydrogen atom at C(γ 2) in ring D, with the latter hydrogen atom coupling to that at C(δ) to give rise to a doublet-of-doublets. In the case of residue 6, the protons of the aromatic ring C appear as two sets of doublet-of-doublets, which indicates hindered rotation of the aromatic ring and thus renders the two sides diastereotopic as would be expected for **9**. A weak NOE interaction is also observed between the hydrogen atoms at C(γ 1) in ring D and C(ϵ 2) in ring C, respectively. At a later stage, we hope to prepare **9** synthetically to prove the identity of this enzymic product by an alternative method, but at this point, the data from MS and NMR spectroscopy experiments strongly support the proposed structure of **9**.

These results provide the first direct evidence that OxyB can catalyze a phenol coupling reaction not on a free peptide but rather on a peptide attached as a thioester to a PCD. A simpler S-NAC thioester mimic, such as **15**, is not sufficient to render the peptide a viable substrate for OxyB. This further suggests that at least the OxyB-catalyzed coupling reaction, and perhaps all of the oxidative phenol couplings during glycopeptide antibiotic biosynthesis, occur whilst the peptide intermediates are attached to cognate PCDs within the NRPS as suggested indirectly by the results from other studies.^[10] However, many unanswered questions remain. A key uncertainty is whether the enzyme can also transform heptapeptides such as **2a** and **2b** (and whether this is more efficient), or whether the first phenol coupling reaction occurs preferentially on a hexapeptide (that is, before the last amino acid is added to the chain by the NRPS). Renewed efforts should now be made to prepare and perform assays with heptapeptide-PCD conjugates such as **2a** and **2b**. Evidence from gene knockout experiments suggest already that the biosynthetic enzymes may not have a strict substrate specificity.^[10] Clearly, a 3-hydroxy group in residue 6 is not necessary for the coupling reaction that is catalyzed by OxyB to occur. However, the influences of a β -hydroxy group and the chlorine atom in the *m*-chloro-3-hydroxytyrosine residue (compare **2a** and **2b** with **8**) on the rate of the reaction remain to be defined.

Received: July 12, 2004

Keywords: antibiotics · biosynthesis · enzymes · glycopeptides · natural products

[1] R. D. Süssmuth, W. Wohlleben, *Appl. Microbiol. Biotechnol.* **2004**, *63*, 344.

- [2] H. Shiozawa, B. C. S. Chia, N. L. Davies, R. Zerella, D. H. Williams, *J. Am. Chem. Soc.* **2002**, *124*, 3914.
- [3] A. M. A. van Wageningen, P. N. Kirkpatrick, D. H. Williams, B. R. Harris, J. K. Kershaw, N. J. Lennard, M. Jones, S. J. M. Jones, P. J. Solenberg, *Chem. Biol.* **1998**, *5*, 155.
- [4] S. Pelzer, R. D. Süssmuth, D. Heckmann, J. Recktenwald, P. Huber, G. Jung, W. Wohlleben, *Antimicrob. Agents Chemother.* **1999**, *43*, 1565.
- [5] R. D. Süssmuth, S. Pelzer, G. Nicholson, T. Walk, W. Wohlleben, G. Jung, *Angew. Chem.* **1999**, *111*, 2096; *Angew. Chem. Int. Ed.* **1999**, *38*, 1976.
- [6] D. Bischoff, S. Pelzer, B. Bister, G. J. Nicholson, S. Stockert, M. Schirle, W. Wohlleben, G. Jung, R. D. Süssmuth, *Angew. Chem.* **2001**, *113*, 4824; *Angew. Chem. Int. Ed.* **2001**, *40*, 4688.
- [7] D. Bischoff, S. Pelzer, A. Hölzel, G. J. Nicholson, S. Stockert, W. Wohlleben, G. Jung, R. D. Süssmuth, *Angew. Chem. Int. Ed.* **2001**, *113*, 1736; *Angew. Chem. Int. Ed.* **2001**, *40*, 1693.
- [8] K. Zerbe, O. Pylypenko, F. Vitali, W. W. Zhang, S. Rouse, M. Heck, J. W. Vrijbloed, D. Bischoff, B. Bister, R. D. Süssmuth, S. Pelzer, W. Wohlleben, J. A. Robinson, I. Schlichting, *J. Biol. Chem.* **2002**, *277*, 47476.
- [9] O. Puk, P. Huber, D. Bischoff, J. Recktenwald, G. Jung, R. D. Süssmuth, K. H. vanPee, W. Wohlleben, S. Pelzer, *Chem. Biol.* **2002**, *9*, 225.
- [10] D. Bischoff, B. Bister, M. Bertasso, V. Pfeifer, E. Stegmann, G. Nicholson, S. Keller, S. Pelzer, W. Wohlleben, R. D. Süssmuth, *ChemBioChem* **2004**, in press.
- [11] H. Mootz, M. Marahiel, *J. Bacteriol.* **1997**, *179*, 6843.
- [12] T. Weber, R. Baumgartner, C. Renner, M. A. Marahiel, T. A. Holak, *Structure* **2000**, *8*, 407.
- [13] E. Freund, F. Vitali, A. Linden, J. A. Robinson, *Helv. Chim. Acta* **2000**, *83*, 2572. Full details of the synthesis will be published elsewhere.
- [14] F. Vitali, K. Zerbe, J. A. Robinson, *Chem. Commun.* **2003**, 2718.
- [15] L. E. N. Quadri, P. H. Weinreb, M. Lei, M. M. Nakano, P. Zuber, C. T. Walsh, *Biochemistry* **1998**, *37*, 1585.
- [16] K. Wüthrich, *NMR of Proteins and Nucleic Acids*, Wiley, New York, **1986**.

Stereoselective Synthesis of Bicyclic Pyrrolidines by a Rhodium-Catalyzed Cascade Process**

Ming Yan, Neil Jacobsen, Wenhao Hu,
Luisa S. Gronenberg, Michael P. Doyle,* John T. Colyer,
and Darren Bykowski

The synthesis of complex products by a reaction between multiple components to form several carbon–carbon bonds in one operation is a strategy that has received considerable attention.^[1] Often referred to as tandem or cascade processes, these operations are useful for efficient molecular constructions. Ylide chemistry with metal-stabilized carbenes has provided numerous examples of these processes, often in the context of dipolar cycloaddition reactions.^[2] We recently reported versatile heterocycle syntheses by reactions of aryl and vinyl diazoacetates with aldehydes and imines catalyzed by dirhodium(II) acetate.^[3] These reactions proceed through the generation of an ylide intermediate to produce epoxides, aziridines, dihydropyrroles, and, in select cases, dihydroazepines with a high degree of stereoselectivity. More recently we reported alternative pathways for the highly selective synthesis of dihydropyrrole isomers that are catalyst dependent.^[4] During the course of this latter investigation, we obtained the isomeric compounds **2a,b** as minor products formed from two carbene units derived from methyl styryldiazoacetate and one imine (Scheme 1). However, the structure of **2a,b** was not determined. The constitution of these compounds was surprising, as the combination of two carbene units and an imine does not have precedence in diazo chemistry^[5] or ylide processes.^[1f,6] We now report the structure of this unusual product, the optimization of the reaction conditions to effect the synthesis of such compounds in good yield and selectivity, and the preliminary evaluation of the breadth of applicability of this reaction in synthesis.

The treatment of *N*-benzylidene-*p*-nitroaniline (1.0 equiv) with methyl styryldiazoacetate (1.1 equiv) in the presence of rhodium acetate (1 mol %) in refluxing dichloromethane gave a product mixture that contained two isomeric

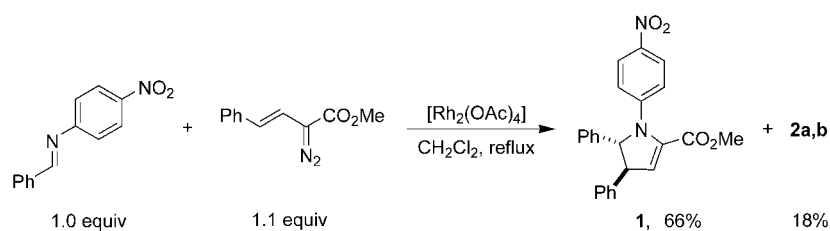
[*] Prof. M. P. Doyle, D. Bykowski
Department of Chemistry
University of Maryland
College Park, MD 20742 (USA)
Fax: (+1) 301-314-9121
E-mail: mdoyle3@umd.edu

M. Yan, Dr. N. Jacobsen, W. Hu, L. S. Gronenberg, J. T. Colyer
Department of Chemistry
University of Arizona
Tucson, AZ 85721-0041 (USA)

[**] We gratefully acknowledge the financial support provided by the NIH (grant GM46503) and NSF (grant CHE9816028). X-ray diffraction experiments were performed at the University of Arizona Molecular Structure Laboratory on a diffractometer provided by NSF grant CHE9610374.



Supporting information for this article is available on the WWW under <http://www.angewandte.org> or from the author.



Scheme 1. Synthesis of dihydropyrrole 1.

products whose structures were not fully revealed by their spectra (Scheme 1). The crystallization of one isomer produced a single crystal, which was identified by X-ray diffraction as **2a** (Figure 1).^[7] The relative stereochemistry

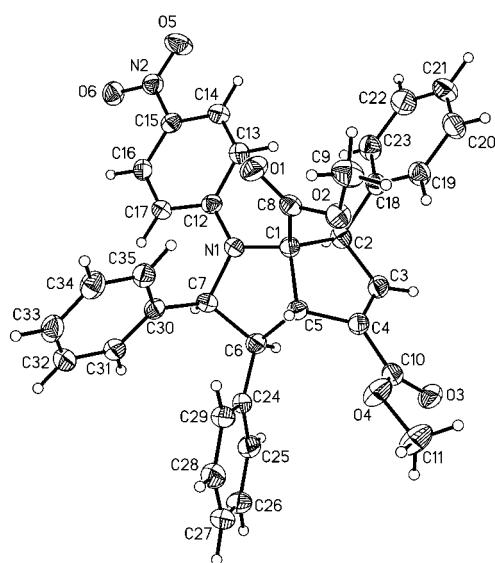
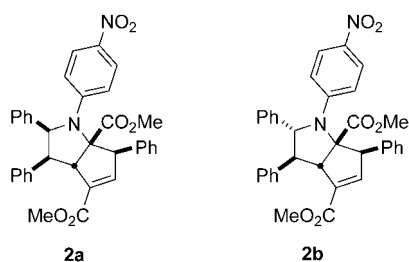


Figure 1. Crystal structure of **2a**. Selected bond lengths [Å] and angles [°]: N1-C1 1.469(2), N1-C12 1.377(2), C1-C5 1.557(2), N1-C1-C2 114.9(2), C7-N1-C12-C17 5.5(2), C30-C7-C6-C24 32.9(2).



of the second isomer was confirmed by NMR spectroscopy to be that of the *trans* diastereomer **2b**.^[8] No other isomers of **2** were observed.

Initial investigations focused on reaction stoichiometry and the influence of substituents on the *N*-benzylidene *p*-Z-aniline reagent on product formation in reactions with methyl styryldiazoacetate (2.0 equiv). In these reactions the yield of the bicyclic pyrrolidine was proportional to the number of equivalents of styryldiazoacetate used (up to 2.0 equiv). The

highest yields of the bicyclic pyrrolidine were obtained when Z was H (70% when the benzylidene group was unsubstituted); imines with *para* substituents on the benzylidene moiety were selected for further investigation of substitution effects on the reaction (Table 1).^[9]

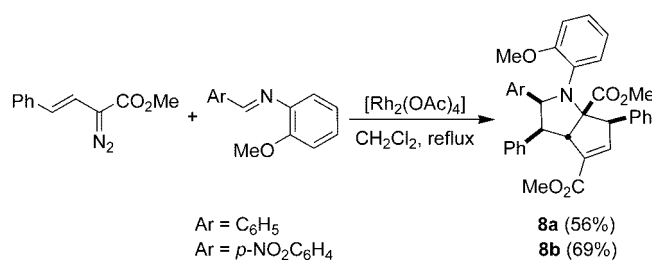
Variation of the substituents on the benzylidene group had no effect upon diastereoselectivity; however, the yield decreased with imines bearing elec-

Table 1: Preparation of bicyclic pyrrolidines from *N*-benzylidene *p*-Z-anilines.^[a]

Ar	Z	Product	a/b ^[b]	Yield [%] ^[c]
Ph	NO ₂	2	54:46	18 ^[d]
Ph	H	3	54:46	70
Ph	OMe	4	61:39	38
<i>p</i> -MeC ₆ H ₄	H	5	52:48	51
<i>p</i> -ClC ₆ H ₄	H	6	52:48	71
<i>p</i> -NO ₂ C ₆ H ₄	H	7	50:50	84

[a] A solution of methyl styryldiazoacetate (2.0 mmol) in CH₂Cl₂ (2 mL) was added by a syringe pump over 1 h to a solution of [Rh₂(OAc)₄] (0.01 mmol) and the imine (1.0 mmol) in CH₂Cl₂ (8 mL) at reflux. [b] Determined by the integration of characteristic ¹H NMR signals in the range δ = 5.47–4.22 ppm prior to chromatography. [c] Combined yield of product **a** and **b** after chromatography. [d] Compound **1** was isolated in 47% yield.

tron-donating substituents. Exclusive formation of the *cis* diastereomer of type **8** was observed when *ortho*-substituted imines were used (Scheme 2).

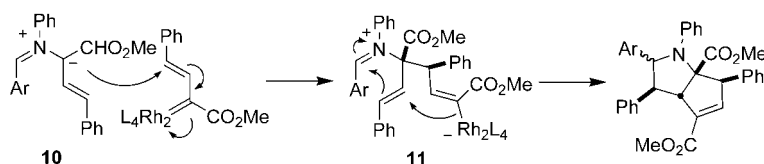


Scheme 2. Exclusive formation of the *cis* isomer in reactions with benzylidene *o*-anisidines.

Our previous investigations are consistent with the initial step being the generation of an azomethine ylide through reaction of the imine with a carbene unit formed by catalytic dinitrogen extrusion from the diazo compound. Initially, we considered the possibility that this ylide intermediate cyclized to form a dihydropyrrole, which then reacted with a second carbene unit to generate the bicyclic pyrrolidine. However,

the exposure of isolated **1** or **9** (formed from benzylideneaniline and methyl styryldiazoacetate) to methyl styryldiazoacetate (1.1 equiv) under the standard reaction conditions failed to produce any quantity of the corresponding bicyclic pyrrolidines, thus ruling out the intermediacy of the dihydropyrrole. Furthermore, *trans* dihydropyrroles are formed with a high degree of selectivity from styryldiazoacetate and *N*-benzylidene-*p*-Z-anilines (Scheme 1), whereas the bicyclic products **2–7** are mixtures of *cis* and *trans* isomers and could therefore not be derived from the *trans* dihydropyrrole isomer.

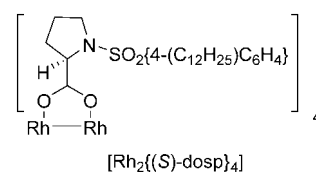
As dihydropyrroles are not intermediates in bicycle formation, an alternative explanation is that the azomethine ylide **10** reacts with a second metal–carbene unit prior to cyclization. Reports by Davies and co-workers have shown that rhodium(II)-stabilized vinyl carbenes are capable of undergoing nucleophilic attack at the vinylogous position.^[10] In a similar manner, this mode of nucleophilic addition of **10** to a rhodium(II)-stabilized vinyl carbene would, after the cascade ring closure of **11**, generate the observed products (Scheme 3).



Scheme 3. Mechanism of formation of bicyclic pyrrolidines.

To evaluate the propensity of the azomethine ylide to add to a second carbene unit rather than cyclize to the dihydropyrrole, we used an excess of the imine relative to methyl styryldiazoacetate. When methyl styryldiazoacetate was added to a tenfold excess of *N*-benzylideneaniline under dilute conditions, the ¹H NMR spectrum of the product mixture showed a 39:36:25 ratio of **3a**:**3b**:**9**.^[11] That the bicyclic pyrrolidine **3** remains the dominant product under conditions which are designed to force cyclization to the dihydropyrrole emphasizes the surprising efficiency of the vinylogous intermolecular reaction. The efficiency of this mode of reactivity was also illustrated upon attempts to trap ylide **10** with a series of dipolarophiles. Similar azomethine ylides have been trapped by electron-deficient olefins and acetylenes in [3+2] cycloadditions.^[2a] However, the addition of methyl styryldiazoacetate to imines in the presence of common dipolarophiles of this type, even in significant excess, failed to provide the [3+2] cycloadducts.^[12] The formation of bicyclic pyrrolidines was observed in all cases.

We have recently begun to develop an asymmetric variant of this reaction with chiral dirhodium catalysts; in initial investigations *N*-benzylideneaniline and the Davies catalyst [Rh₂[(*S*)-dosp]₄] were used.^[13] Although the yield of isolated **3a,b** decreased to 12% with no significant change in the ratio



of diastereomers, **3b** was formed with modest enantioselectivity (25% *ee*).^[14]

The potential for using simple, readily accessible starting materials to form stereochemically complex systems in good yields provides a new entry to nitrogen-based heterocycles. Of particular note are the high levels of diastereoselectivity and the promise of future progress in enantioselectivity. Attempts to exploit this reactivity mode in the synthesis of other heterocyclic systems are currently underway.

Received: August 19, 2004

Keywords: carbenoids · diastereoselectivity · diazo compounds · domino reactions · ylides

- [1] a) A. Ajamian, J. L. Gleason, *Angew. Chem.* **2004**, *116*, 3842; *Angew. Chem. Int. Ed.* **2004**, *43*, 3754; b) A. J. McCarroll, J. C. Walton, *Angew. Chem.* **2001**, *113*, 2282; *Angew. Chem. Int. Ed.* **2001**, *40*, 2224; c) S.-i. Ikeda, *Acc. Chem. Res.* **2000**, *33*, 511–519; d) L. F. Tietze, *Chem. Rev.* **1996**, *96*, 115; e) P. J. Parsons, C. S. Penkett, A. J. Shell, *Chem. Rev.* **1996**, *96*, 195; f) A. Padwa, M. D. Weingarten, *Chem. Rev.* **1996**, *96*, 223; g) D. F. Harvey, D. M. Sigano, *Chem. Rev.* **1996**, *96*, 271; h) R. A. Bunce, *Tetrahedron* **1995**, *51*, 13103; i) L. F. Tietze, U. Beifuss, *Angew. Chem.* **1993**, *105*, 137; *Angew. Chem. Int. Ed. Engl.* **1993**, *32*, 131; j) T. L. Ho, *Tandem Organic Reactions*, Wiley, New York, **1992**; k) G. H. Posner, *Chem. Rev.* **1986**, *86*, 831.

- [2] a) C. V. Galliford, M. A. Beenen, S. T. Nguyen, K. A. Scheidt, *Org. Lett.* **2003**, *5*, 3487; b) J. A. Veaneco, F. G. West, *Org. Lett.* **2002**, *4*, 2813; c) F. G. West, B. N. Naidu, *J. Am. Chem. Soc.* **1994**, *116*, 8420; d) A. Padwa, R. L. Chinn, S. F. Hornbuckle, Z. J. Zhang, *J. Org. Chem.* **1991**, *56*, 3271; e) A. Padwa, R. L. Chinn, S. F. Hornbuckle, L. Zhi, *Tetrahedron Lett.* **1989**, *30*, 301; g) T. Ibata, J. Toyoda, M. Sawada, T. Tanaka, *J. Chem. Soc. Chem. Commun.* **1986**, 1266.

- [3] a) M. P. Doyle, W. Hu, D. J. Timmons, *Org. Lett.* **2001**, *3*, 933; b) M. P. Doyle, W. Hu, D. J. Timmons, *Org. Lett.* **2001**, *3*, 3741.

- [4] M. P. Doyle, M. Yan, W. Hu, L. S. Gronenberg, *J. Am. Chem. Soc.* **2003**, *125*, 4692.

- [5] a) M. P. Doyle, M. A. McKerver, T. Ye, *Modern Catalytic Methods for Organic Synthesis with Diazo Compounds*, Wiley, New York, **1998**; b) M. Regitz, G. Maas, *Diazo Compounds: Properties and Syntheses*, Academic Press, Orlando, **1986**.

- [6] a) *Nitrogen, Oxygen, and Sulfur Ylide Chemistry*, (Ed.: J. S. Clark), Oxford University Press, Oxford, **2002**; b) A. Padwa, S. F. Hornbuckle, *Chem. Rev.* **1991**, *91*, 263.

- [7] X-ray diffraction experiments were performed with a Bruker SMART 1000 CCD detector X-ray diffractometer by using MoK_α radiation (λ = 0.71073 Å). The structures were solved by a full-matrix least-squares method (SHELXL-97, Bruker AXS Inc., Madison, WI, USA). Crystallographic data for **2a**: C₃₅H₃₁N₂O₆, triclinic, space group P1̄, a = 11.1175(8), b = 13.5357(9), c =

13.5623(9) Å, $\alpha = 112.090(2)$, $\beta = 94.205(2)$, $\gamma = 104.502(2)^\circ$, $V = 1798.6(2)$ Å³, $Z = 2$, $\rho_{\text{calcd}} = 1.061$ Mg m⁻³, $\mu = 0.09$ mm⁻¹, $T = 170$ K, $R(F, F^2) > 2\sigma = 0.0412$, $R_w(F^2, \text{all data}) = 0.0998$, $S = 0.0752$ for 7343 unique reflections ($\theta < 26.39^\circ$) and 469 refined parameters; final difference synthesis within ± 0.231 e Å⁻³. CCDC-240323 contains the supplementary crystallographic data for this paper. These data can be obtained free of charge via www.ccdc.cam.ac.uk/conts/retrieving.html (or from the Cambridge Crystallographic Data Centre, 12, Union Road, Cambridge CB21EZ, UK; fax: (+44)1223-336-033; or deposit@ccdc.cam.ac.uk).

- [8] Determination of the relative stereochemistry of **2a** allowed that of **2b** to be assigned by NMR, as detailed in the supporting information.
- [9] The reaction of the imine with $Z = \text{H}$, $\text{Ar} = p\text{-MeOC}_6\text{H}_4$ did not provide a significant quantity of the bicyclic pyrrolidine.
- [10] a) H. M. L. Davies, B. Xiang, N. Kong, D. G. Stafford, *J. Am. Chem. Soc.* **2001**, *123*, 7461; b) H. M. L. Davies, B. Hu, E. Saikali, P. R. Burzinski, *J. Org. Chem.* **1994**, *59*, 4535; c) H. M. L. Davies, B. Hu, *Tetrahedron Lett.* **1992**, *33*, 453.
- [11] A solution of methyl styryldiazoacetate (77 mg, 0.38 mmol) in CH_2Cl_2 (1 mL) was added by syringe pump over 1 h to a solution of $[\text{Rh}_2(\text{OAc})_4]$ (4.4 mg, 0.01 mmol) and benzylideneaniline (0.690 mg, 3.81 mmol) in CH_2Cl_2 (50 mL) at reflux. After the addition was complete, the solution was heated at reflux for a further 1 h. The reaction mixture was filtered through a plug of silica gel, which was then washed with CH_2Cl_2 . The product ratio was determined by ¹H NMR spectroscopy.
- [12] Reactions were carried out under the conditions described in Table 1. The dipolarophiles diethyl maleate, diethyl fumarate, dimethyl acetylenedicarboxylate, or *N*-phenylmaleimide (10–15 equiv) or methyl acrylate (100–200 equiv) were added prior to the addition of methyl styryldiazoacetate.
- [13] H. M. L. Davies, P. R. Burzinski, D. H. Lake, N. Kong, M. J. Fall, *J. Am. Chem. Soc.* **1996**, *118*, 6897.
- [14] Following the standard reaction protocol described in Table 1, methyl styryldiazoacetate was treated with benzylideneaniline in the presence of a catalytic amount of $[\text{Rh}_2((S)\text{-dosp})_4]$. Prior to purification, ¹H NMR spectroscopic analysis showed a 46:54 ratio of **3a/3b**. HPLC analysis of **3b** indicated 25% *ee*. (Chiralpak-OD, hexane/isopropyl alcohol 90:10, 1.0 mL min⁻¹, 220 nm; $R_t = 3.2$ min (major), 4.3 min (minor); $[\alpha]_D^{27} = +62.9$ ($c = 0.20$, CH_2Cl_2)).

Spectroscopic Elucidation of a Peroxo $\text{Ni}_2(\mu\text{-O}_2)$ Intermediate Derived from a Nickel(II) Complex and Dioxygen**

Matthew T. Kieber-Emmons, Ralph Schenker,
Glenn P. A. Yap, Thomas C. Brunold, and
Charles G. Riordan*

The preparative chemistry and reactivity of Ni-O_x intermediates has advanced significantly in the past few years with the identification of a number of new structure types. The most common synthetic approach, reaction of a nickel(II) precursor with H_2O_2 , has yielded bis- μ -oxo^[1-4] and bis- μ -superoxo complexes.^[4] An attractive alternate route utilizes the reaction of nickel(II) complexes with O_2 . This strategy relies on, and is limited by, the ability to prepare suitable nickel(II) species. We have utilized this latter approach to prepare $[(\text{PhTt}^{\text{tBu}}\text{Ni})_2(\mu\text{-O})_2]$ ^[5] (PhTt^{tBu} = phenyltris(*tert*-butylthio)methyl)borate) and the related side-on bound superoxo complex, $[(\text{PhTt}^{\text{Ad}}\text{Ni}(\text{O}_2))]$ (PhTt^{Ad} = phenyltris((1-adamantylthio)methyl)borate).^[6] During the course of these studies, we considered whether a μ -peroxo Ni_2 species was a possible intermediate along the reaction trajectory leading to the bis- μ -oxo dimer. Lacking experimental evidence, a μ - η^2, η^2 -peroxo bridged Ni_2 dimer supported by the tris(thioether) borato ligand was evaluated by density functional methods.^[7] This hypothetical species was deemed to be of high energy, significantly destabilized ($\Delta H^\circ = 32 \text{ kcal mol}^{-1}$) relative to the bis- μ -oxo dimer and, therefore, an unlikely intermediate. Consequently, we turned our attention to macrocyclic tetradentate ligands that coordinate in a planar array, reasoning that such an attribute would render access to the μ - η^2, η^2 -peroxo coordination more difficult. Herein, we report on the successful pursuit of this strategy, which led to the discovery of a $\text{Ni}_2(\mu\text{-O}_2)$ complex in which the peroxo moiety spans the metals in the μ -1,2 mode.

Addition of dry O_2 to $[\text{Ni}(\text{tmc})]\text{OTf}^{[8,9]}$ (**1**; tmc = 1,4,8,11-tetramethyl-1,4,8,11-tetraazadodecane, $\text{OTf} = [\text{CF}_3\text{SO}_3]^-$) in THF or acetonitrile at room temperature resulted in a color change from pale blue to clover green. The FT-IR spectrum of the paramagnetic product ($\mu_{\text{eff}} = 2.7(1) \mu_{\text{B}}$) included a prominent new feature at 3628 cm^{-1} assigned to the $\tilde{\nu}(\text{O-H})$ mode

[*] M. T. Kieber-Emmons, Dr. G. P. A. Yap, Prof. Dr. C. G. Riordan
Department of Chemistry and Biochemistry
University of Delaware
Newark, Delaware 19716 (USA)
Fax: (+1) 302-831-1073
E-mail: riordan@udel.edu

Dr. R. Schenker, Prof. Dr. T. C. Brunold
Department of Chemistry, University of Wisconsin-Madison
Madison, Wisconsin 53706 (USA)

[**] Acknowledgement is made to the NSF (CHE-0213260) to C.G.R., and to the University of Wisconsin-Madison to T.C.B. for financial support of this research.



Supporting information for this article is available on the WWW under <http://www.angewandte.org> or from the author.

of the $[\text{Ni}(\text{tmc})\text{OH}]^+$ ion. The assignment of a terminal hydroxy species was confirmed by the independent synthesis of $[\text{Ni}(\text{tmc})(\text{OH})\text{OTf}]$ (**2**) by metathesis of $[\text{Ni}(\text{tmc})](\text{OTf})_2$ and KOH. The $\tilde{\nu}(\text{O}-\text{H})$ band in the authentic sample of **2** was observed at identical frequency as in the product of the reaction between **1** and O_2 . Further, the corresponding ^1H NMR spectra are nearly indistinguishable (see Supporting Information). The monomeric nature of **2** was established through X-ray diffraction analysis, Figure 1.^[10] The geometry

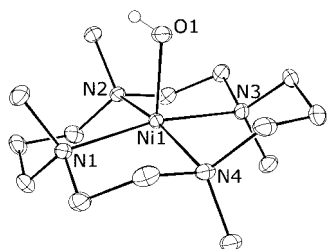


Figure 1. Molecular structure of the cation of **2** derived from an X-ray diffraction analysis. Thermal ellipsoids are set at 30% probability. The hydroxy proton was found in the Fourier difference map.

of the isolated cation is square pyramidal with the amine nitrogen atoms in the basal positions and the terminal hydroxy group in the apical position. The Ni–N bond lengths, which range from 2.116(2) to 2.138(2) Å, are similar to those found for other $[\text{Ni}(\text{tmc})\text{X}]^+$ species, all of which are high spin, $S=1$.^[9] Compound **2** is the first mononuclear, terminal hydroxy complex of nickel to be defined crystallographically; nonetheless, the Ni–O bond of 1.955(2) Å is consistent with a hydroxy ligand. Further, the hydrogen atom of the hydroxide was found in the difference Fourier map. Isotopic labeling experiments have identified the sources of the hydroxy oxygen and hydrogen atoms in **2**. Addition of $^{18}\text{O}_2$ to **1** generated the $[\text{Ni}(\text{tmc})(^{18}\text{OH})]\text{OTf}$ isotopomer as characterized by a new $\tilde{\nu}(^{18}\text{O}-\text{H})$ band at 3617 cm^{-1} ($\tilde{\nu}(^{16}\text{OH})/\tilde{\nu}(^{18}\text{OH})=1.003$; calcd 1.003 for an isolated harmonic oscillator). Oxygenation of **1** in CD_3CN resulted in isolation of $[\text{Ni}(\text{tmc})(\text{OD})]\text{OTf}$ (**2^D**) with $\tilde{\nu}(\text{O}-\text{D})$ at 2677 cm^{-1} , identical in magnitude to **2^D** prepared independently, implicating the solvent as the source of the hydrogen/deuterium. The magnitude of the isotopic shift is smaller than anticipated based on reduced-mass considerations for an isolated harmonic oscillator ($\tilde{\nu}(\text{OH})/\tilde{\nu}(\text{OD})=1.355$; calcd 1.414).

Low-temperature oxygenation of **1** results in formation of a red intermediate **3**, as indicated by the clean optical progression (isosbestic point at 388 nm, see Supporting Information). In the UV/Vis spectrum, compound **3** is characterized by $\lambda_{\text{max}}=465\text{ nm}$ (inset Figure 2; $\epsilon_{\text{M}}=2100\text{ M}^{-1}\text{ cm}^{-1}$ per nickel). The intermediate has a limited lifetime at -45°C in acetonitrile, decaying with $\tau_{1/2}=4\text{ min}$. This thermal instability precludes determination of the $\text{Ni}:\text{O}_2$ stoichiometry by spectrophotometric titration. The proton NMR spectrum of **3** in $[\text{D}_3]\text{acetonitrile}$ shows sharp, paramagnetically shifted resonance signals at 228 K (Supporting Information). Compound **3** is EPR silent between 4 and 77 K. These magnetic data suggest an integer-spin ground state, eliminating the possibility of a $1\text{ Ni}:1\text{ O}_2$ adduct, which would have an $S=1/2$ or $3/2$ ground state. To further elucidate the

molecular structure of **3**, resonance Raman (rR) studies were performed. Excitation of **3** in resonance with the visible absorption band ($\lambda_{\text{ex}}=502\text{ nm}$) at 77 K revealed two O_2 isotope sensitive features; namely, an intense band at 778 cm^{-1} and a weaker peak at 479 cm^{-1} . These features shift to 735 cm^{-1} and 456 cm^{-1} , respectively, in samples of **3** prepared with $^{18}\text{O}_2$ (Figure 2). The frequency and isotopic

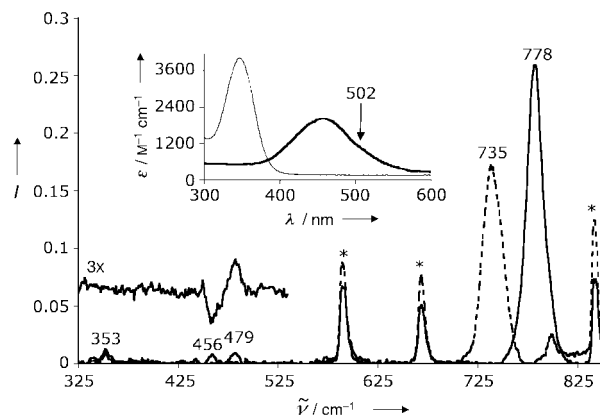
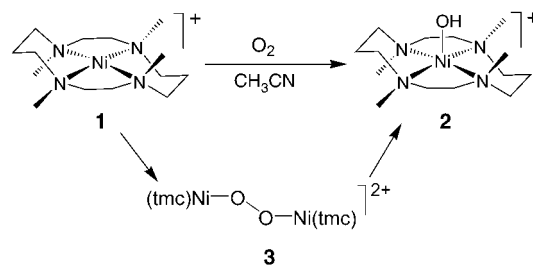


Figure 2. Resonance Raman spectra of **3** at 77 K obtained upon excitation at 502 nm in THF (*); (—) prepared with $^{16}\text{O}_2$, (----) prepared with $^{18}\text{O}_2$, offset: $\Delta(^{16}\text{O}_2$ and $^{18}\text{O}_2)$ traces. Inset: overlaid optical spectra of **1** (----) and **3** (—).

red-shift (-43 cm^{-1} ($\tilde{\nu}(^{16}\text{O}-^{16}\text{O})/\tilde{\nu}(^{18}\text{O}-^{18}\text{O})=1.058$; calcd 1.060 assuming an isolated O–O harmonic oscillator) of the dominant 778 cm^{-1} band are consistent with assignment of this band as an intraperoxo stretch.^[11–13] The lower frequency mode is ascribed to the $\tilde{\nu}(\text{Ni}-\text{O})$ mode associated with this peroxo intermediate, ($\tilde{\nu}(\text{Ni}-^{16}\text{O})/\tilde{\nu}(\text{Ni}-^{18}\text{O})=1.050$; calcd 1.048). The rR excitation profile of the 778 cm^{-1} mode closely parallels the dominant absorption band, which leads to the assignment of this absorption band as a peroxo $\rightarrow\text{Ni}^{2+}$ charge transfer (CT) transition. Together with the magnetic properties, the rR features are indicative of a dimeric μ -1,2-peroxo formulation for **3** (Scheme 1).^[14] We favor the *trans* conformation because this core structure is generally adopted by other unsupported peroxo-bridged species. Comparison with vibrational data of other *trans* end-on peroxo dimers lends credence to this assignment. In particular, in $[\text{Cu}(\text{tmpa})_2(\text{O}_2)]^{2+}$ (tmpa = tris(2-methylpyridyl)amine) the $\tilde{\nu}(\text{O}-\text{O})$ and $\tilde{\nu}(\text{Cu}-\text{O})$ stretching vibrations are at 832 cm^{-1} and 561 cm^{-1} , respectively.^[12] The frequency of $\tilde{\nu}(\text{M}-\text{O})$ vibration



Scheme 1.

is slightly lower than found in *trans* μ -1,2-peroxo dimers of copper(II) and cobalt(III)^[15] which is consistent with a weaker (that is, less covalent) metal–peroxo bonding interaction in the Ni₂ dimer owing primarily to the lower effective nuclear charge of nickel(II) relative to copper(II) and cobalt(III). Also, **3** differs from these other late-transition-metal examples in that the nickel center does not have a ligand *trans* to the peroxo group, as evidenced by the identical optical spectra of **3** in THF and CH₃CN, thus arguing against solvent ligation to the sixth coordination site. This lack of a *trans* axial ligand in **3** eliminates the possibility of mechanical coupling between the Ni–O and Ni–L_{trans} stretching motions, which otherwise could lead to a slight upshift of the $\tilde{\nu}(\text{Ni–O})$ vibration. The relative intensities of the Ni–O and O–O vibrational modes, specifically the extreme enhancement of $\tilde{\nu}(\text{O–O})$, strongly suggest that the kinematic coupling between the oxygen-derived modes is substantial. DFT computational studies and a normal coordinate analysis of **3** are underway to elucidate further the nature of the Ni₂(μ -O₂) unit and determine the factors that control the electronic and vibrational characteristics of this new chromophore.

In summary, we have identified a binuclear *trans*- μ -1,2-peroxo Ni₂ dimer, a structural motif unknown previously in nickel coordination chemistry, produced by reaction of a nickel(II) precursor with O₂. This structural assignment of **3** is supported by EPR, NMR, and rR spectral characteristics as well as DFT computations. Thermal decomposition of **3** in CH₃CN leads to **2**, in which the atoms constituting the hydroxide ligand derive from O₂ and the hydrocarbon solvent.

Experimental Section

2: Potassium hydroxide pellets (1.30 g, excess) were added to a slurry of [Ni(tmc)](OTf)₂^[16] (380 mg, 0.619 mmol) in THF (\approx 15 mL). The mixture was stirred for 1 h, resulting in a homogeneous green solution. The mixture was filtered to remove the remaining KOH, and the product was crystallized by diethyl ether vapor diffusion; 81% yield (0.240 g, 0.499 mmol). Green crystals suitable for diffraction analysis were obtained by vapor diffusion of pentanes into a saturated THF solution. Elemental analysis calcd (%) for N₄O_{4.6}SNiC₁₅F₃H_{34.3} (**2**·(2/3)H₂O): C 36.53, H 7.02, N 11.36; found: C 37.09, H 6.90, N 11.24. FT-IR (Nujol): $\tilde{\nu}(\text{OH})$ 3628 cm⁻¹ (w). Electronic absorption spectrum in MeCN, $\lambda_{\text{max}}(\epsilon_{\text{M}})$: 409 (41.4), 657 nm (30.1).

2^D: Potassium deuterioxide (KOD) was prepared from the reaction of potassium *tert*-butoxide (1.96 g, 17.5 mmol) with D₂O (5 mL, excess). Excess water and [D₁]*tert*-butanol were removed in vacuo overnight. **2^D** was prepared by a method analogous to that for **2**, using KOD in place of KOH and CD₃CN instead of THF. FT-IR (Nujol): $\tilde{\nu}(\text{OD})$ 2677 cm⁻¹ (w).

Received: May 23, 2004

Revised: August 4, 2004

Published online: November 19, 2004

Keywords: coordination modes · N ligands · nickel · oxygen · structure elucidation

[1] S. Hikichi, M. Yoshizawa, Y. Sasakura, M. Akita, Y. Moro-oka, *J. Am. Chem. Soc.* **1998**, *120*, 10567.

[2] S. Itoh, H. Bandoh, S. Nagatomo, T. Kitagawa, S. Fukuzumi, *J. Am. Chem. Soc.* **1999**, *121*, 8945–8946.

- [3] S. Itoh, H. Bandoh, M. Nakagawa, S. Nagatomo, T. Kitagawa, K. D. Karlin, S. Fukuzumi, *J. Am. Chem. Soc.* **2001**, *123*, 11168–11178.
- [4] K. Shiren, S. Ogo, S. Fujinami, H. Hayashi, M. Suzuki, A. Uehara, Y. Watanabe, Y. Moro-oka, *J. Am. Chem. Soc.* **2000**, *122*, 254–262.
- [5] B. S. Mandimutsira, J. L. Yamarik, T. C. Brunold, W. Gu, S. P. Cramer, C. G. Riordan, *J. Am. Chem. Soc.* **2001**, *123*, 9194–9195.
- [6] K. Fujita, R. Schenker, W. Gu, T. C. Brunold, S. P. Cramer, C. G. Riordan, *Inorg. Chem.* **2004**, *43*, 3324.
- [7] R. Schenker, B. S. Mandimutsira, C. G. Riordan, T. C. Brunold, *J. Am. Chem. Soc.* **2002**, *124*, 13842–13855.
- [8] N. Jubran, G. Ginzburg, H. Cohen, Y. Koresch, D. Meyerstein, *Inorg. Chem.* **1985**, *24*, 251.
- [9] M. S. Ram, C. G. Riordan, R. Ostrander, A. L. Rheingold, *Inorg. Chem.* **1995**, *34*, 5884–5892.
- [10] X-ray structural analysis for **2**: A single green crystal (0.40 × 0.20 × 0.15 mm) was mounted using Paratone oil onto a glass fiber and cooled to the data collection temperature of 150 K. Data were collected on a Bruker-AXS APEX CCD diffractometer with 0.7107 Å MoK α radiation. Unit cell parameters were obtained from 60 data frames, 0.3° Ω , from three different sections of the Ewald sphere yielding $a = 12.163(4)$, $b = 12.660(4)$, $c = 14.104(5)$ Å, $\alpha = 86.715(6)$, $\beta = 80.626(5)$, $\gamma = 89.312(5)^\circ$, $V = 2139.1(12)$ Å³. 14169 reflections ($R_{\text{int}} = 0.0117$) were collected (8939 unique) over $\theta = 2.05$ to 28.02° . No symmetry higher than triclinic was evident from the diffraction data. Solution in the centrosymmetric space group option *P1* yielded chemically reasonable and computationally stable results of refinement. The data-set was treated with SADABS absorption corrections based on redundant multiscan data (G. Sheldrick, Bruker-AXS, 2001) $T_{\text{max}}/T_{\text{min}} = 1.268$. A molecule was located in a general position while two-half molecules were also located at inversion centers yielding $Z = 2$, and $Z' = 2$. The molecule in general space has a coordinated hydroxide ligand on one metal face and a noncoordinated water molecule on the opposite face. The hydrogen atom on the hydroxy ligand was located from the electron-density-difference map and allowed to refine positionally with a riding isotropic model. The other symmetry unique molecules were assumed to be chemically identical and having water molecules disordered with hydroxy ligands. All non-hydrogen atoms were refined with anisotropic displacement parameters. All hydrogen atoms were treated as idealized contributions except those on the disordered hydroxy ligands and water molecules which were ignored. Structure factors are contained in the SHELXTL 6.12 program library (Sheldrick, G., Bruker-AXS, 2001). The goodness of fit on F^2 was 1.054 with $R1(wR2)$ 0.0348 (0.0905) for $[I > 2(I)]$ and with largest difference peak and hole of 0.776 and -0.466 e Å⁻³. CCDC-238390 (**2**) contains the supplementary crystallographic data for this paper. These data can be obtained free of charge via www.ccdc.cam.ac.uk/conts/retrieving.html (or from the Cambridge Crystallographic Data Centre, 12 Union Road, Cambridge CB21EZ, UK; fax: (+44) 1223-336-033; or deposit@ccdc.cam.ac.uk).
- [11] C. G. Barraclough, G. A. Lawrence, P. A. Lay, *Inorg. Chem.* **1978**, *17*, 3317.
- [12] M. J. Baldwin, P. K. Ross, J. E. Pate, Z. Tyeklar, K. D. Karlin, E. I. Solomon, *J. Am. Chem. Soc.* **1991**, *113*, 8671.
- [13] F. Tuczek, E. I. Solomon, *Inorg. Chem.* **1992**, *31*, 944.
- [14] Comparison of the relative energies of DFT geometry-optimized hypothetical μ -1,2-peroxo and μ - η^2 : η^2 -peroxo models of **3** reveals the former is more stable by approximately 85 kcal·mol⁻¹, thus supporting this structural assignment. See Supporting Information for details.
- [15] E. I. Solomon, F. Tuczek, D. E. Root, C. A. Brown, *Chem. Rev.* **1994**, *94*, 827.
- [16] F. Wagner, E. K. Barefield, *Inorg. Chem.* **1976**, *15*, 408–417.

Foldamer Structures

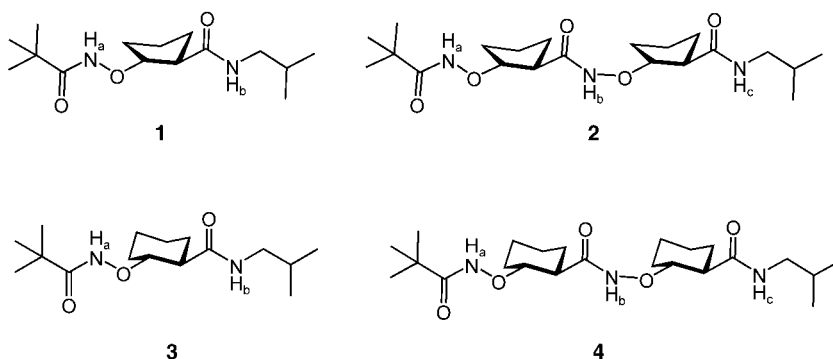
 $\beta^{2,3}$ -Cyclic Aminoxy Acids: Rigid and Ring-Size-Independent Building Blocks of Foldamers**

Dan Yang,* Dan-Wei Zhang, Yu Hao, Yun-Dong Wu, Shi-Wei Luo, and Nian-Yong Zhu

The exploration of foldamers having rigid conformations is an area of intensive research.^[1] Recently, the research groups led by Seebach and Gellman discovered independently that peptides of β -amino acids can fold into defined secondary structures.^[2] One special series of β -peptides, comprising cyclic ring-constrained β -amino acids, which were developed by Gellman and co-workers, form significantly stable helical structures in the solid state, in organic solvents,^[3] and even in aqueous solution.^[4] Increasing the number of cyclic ring-constrained residues can enhance the helical content of such β -peptides;^[5] this approach has become an important and powerful tool for structure–activity studies of the peptides.^[5b] Gellman et al. also found that the size of the side-chain rings in the β -peptides has significant impact on the secondary structures. The β -peptides of cyclohexane-containing amino acids prefer to form 14-helix structures, while those of cyclopentane-containing amino acids favor a very different helix, the 12-helix; these conformations result from the different torsional preferences of the C_α – C_β bonds in the cyclic rings of the individual residues.^[3b,6] To investigate whether this “ring-size effect” also plays an important role in determining the conformations of our aminoxy peptides, which represent another class of foldamers,^[7] we have explored, and report herein, the potential of $\beta^{2,3}$ -cyclic aminoxy acids, a subclass of β -aminoxy acids in which the α - and β -carbon atoms are part of an aliphatic ring (either a

cyclopentane and cyclohexane unit), to behave as new chiral building blocks for turns and helices.

Compounds **1** and **2**, which are derived from (*R,R*)-2-aminoxycyclopentanecarboxylic acid, and **3** and **4** derived



from (*R,R*)-2-aminoxycyclohexanecarboxylic acid, were synthesized by following the standard methods of peptide coupling. Table 1 summarizes the chemical shifts of all the amide protons in ¹H NMR spectra (5 mm in CDCl₃ at room

Table 1: ¹H NMR chemical shifts of the amide NH protons of **1–4** (5 mm in CDCl₃ at room temperature).^[a,b]

Cmpd.	$\delta(\text{NH}_a)$ [ppm]	$\delta(\text{NH}_b)$ [ppm]	$\delta(\text{NH}_c)$ [ppm]
1	8.45 (s)	7.33 (t)	
2	8.48 (s)	10.99 (s)	7.61 (t)
3	8.44 (s)	7.54 (t)	
4	8.58 (s)	11.78 (s)	8.58 (t)

[a] Abbreviations: s, singlet; t, triplet. [b] There is little change for chemical shifts of the amide NH protons of **1–4** below 5 mm (see the Supporting Information).

temperature). To confirm that intramolecular hydrogen bonds are formed, we also performed [D₆]DMSO titration studies and dilution studies with those four compounds; the chemical-shift changes of all the amide protons are presented in Table 2.

Notably, the signals of the NH_b protons of **1–4** and the NH_c protons of **2** and **4** are unusually downfield (Table 1), and they undergo little change when solutions of **1–4** are titrated gradually with [D₆]DMSO or diluted from 200 mm to 1.56 mm

Table 2: Changes in the ¹H NMR chemical shifts of the amide NH protons of **1–4**.^[a,b]

Cmpd.	$\Delta\delta(\text{NH}_a)$ [ppm]		$\Delta\delta(\text{NH}_b)$ [ppm]		$\Delta\delta(\text{NH}_c)$ [ppm]	
	[D ₆]DMSO	Dil.	[D ₆]DMSO	Dil.	[D ₆]DMSO	Dil.
1	1.82	0.74	0.48	0.31		
2	2.01	1.43	0.31	0.30	0.14	0.23
3	1.68	0.68	1.01	0.33		
4	2.04	1.60	0.47	0.52	0.15	0.31

[a] Titration study: [D₆]DMSO (50 μ L) was added gradually to a solution of the peptide (5 mm) in CDCl₃ (0.5 mL) at room temperature ($\Delta\delta_{\text{titration}} = \delta_{50 \mu\text{L DMSO}} - \delta_{0 \mu\text{L DMSO}}$). [b] Dilution study: solutions of the peptides in CDCl₃ were diluted from 200 mm to 1.56 mm at room temperature ($\Delta\delta_{\text{dilution}} = \delta_{200 \text{ mm}} - \delta_{1.56 \text{ mm}}$).

[*] Prof. Dr. D. Yang, Y. Hao, Dr. N.-Y. Zhu
Department of Chemistry, The University of Hong Kong
Pokfulam Road, Hong Kong (China)
Fax: (+852) 2859-2159
E-mail: yangdan@hku.hk

Prof. Dr. D. Yang, Dr. D.-W. Zhang
Department of Chemistry, Fudan University
Shanghai (China)

Prof. Dr. Y.-D. Wu, Dr. S.-W. Luo
Department of Chemistry
Hong Kong University of Science and Technology
Clear Water Bay, Kowloon, Hong Kong (China)

[**] This work was supported by The University of Hong Kong, Hong Kong University of Science and Technology, Hong Kong Research Grants Council (HKU7098/01P and HKUST6083/02M), HKU-Fudan Joint Laboratory on Molecular Design and Synthesis, and the National Natural Science Foundation of China (project no. 20202001). D.Y. acknowledges the Bristol-Myers Squibb Foundation for an Unrestricted Grant in Synthetic Organic Chemistry.

Supporting information for this article is available on the WWW under <http://www.angewandte.org> or from the author.

(Table 2). In contrast, the chemical shifts of N-oxy amide protons NH_a of **1–4** are rather upfield (Table 1) and change dramatically upon dilution or addition of $[\text{D}_6]\text{DMSO}$ (Table 2). These results suggest that the NH_b protons of **1–4** and the NH_c protons of **2** and **4** form intramolecular hydrogen bonds, but that the NH_a protons of **1–4** are not hydrogen-bonded and are solvent accessible. Similar conclusions were drawn from FT-IR spectroscopic studies (see the Supporting Information). This hydrogen-bonding pattern is very similar to that observed in $\beta^{2,2}$ -aminoxy peptides and, hence, suggests the presence of a β N–O turn in each peptide, in other words, an intramolecular hydrogen bond between $\text{C}=\text{O}_i$ and NH_{i+2} to form a nine-membered ring, which is stabilized by an extra hydrogen bond between NO_{i+1} and NH_{i+2} to form a six-membered ring.^[8]

Interestingly, the values of the chemical shifts of the NH_c protons of dimers **2** and **4** are much higher than those of the NH_b protons of monomers **1** and **3** (Table 1). In addition, the chemical-shift changes of the NH_c protons of dimers **2** and **4** that are caused by dilution or addition of $[\text{D}_6]\text{DMSO}$ are much smaller than those of the NH_b protons of monomers **1** and **3**. This observation suggests that hydrogen bonding is enhanced by increasing the number of N–O turns, that is, a cooperative effect exists.

Suitable crystals of **3** and **4** were obtained from CHCl_3/n -hexane solutions; their solid-state structures, obtained by X-ray crystallography, are presented in Figure 1.^[8] Similar to the $\beta^{2,2}$ -aminoxy peptides^[9] compound **3** adopts a β N–O turn that is characterized by a nine-membered-ring hydrogen bond between the $\text{C}=\text{O}_i$ and NH_{i+2} units ($\text{O}\cdots\text{H}$ distance = 2.20 Å) that is stabilized further by a six-membered-ring hydrogen

bond between the NO_{i+1} and NH_{i+2} units (Figure 1 a). The N–O bond is *anti* to the $\text{C}_\alpha\text{--C}_\beta$ bond with a dihedral angle $\angle\text{NOC}_\alpha\text{C}_\beta$ of 172°. Analogous to the 1.7₉-helix present in $\beta^{2,2}$ -aminoxy peptides,^[9] the solid-state structure of **4** (Figure 1 b) indicates the presence of a well-defined 1.8₉-helix composed of two consecutive β N–O turns with a basic hydrogen-bonding pattern similar to that existing in **3**. In the first N–O turn, the $\text{O}\cdots\text{H}$ distance in the hydrogen bond between the $\text{C}=\text{O}_i$ and NH_{i+2} units is 1.93 Å, which reflects the higher acidity of aminoxy amide protons relative to typical amide protons. In the second N–O turn, the $\text{O}\cdots\text{H}$ distance in the hydrogen bond between the $\text{C}=\text{O}_{i+1}$ and NH_{i+3} units (2.07 Å) is shorter than that in **3** (2.20 Å); this observation further corroborates the existence of the cooperative effects suggested by the ^1H NMR study.

Since suitable crystals of compounds **1** and **2** for X-ray analysis were not obtained, we utilized computational methods to calculate the most stable conformations of **5** and **6**,^[10] which are model compounds for **1** and **3**, respectively (Figure 2). The calculated structure of **6** and the crystal

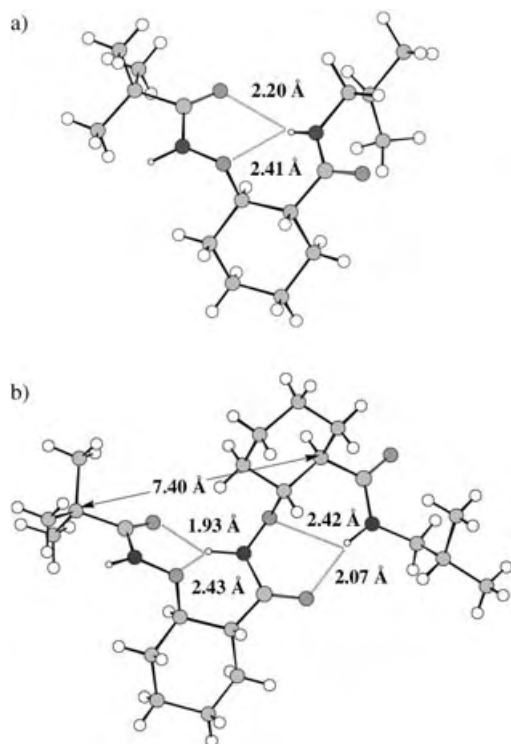


Figure 1. Pertinent hydrogen bonds present in the crystal structures of a) **3** and b) **4**.

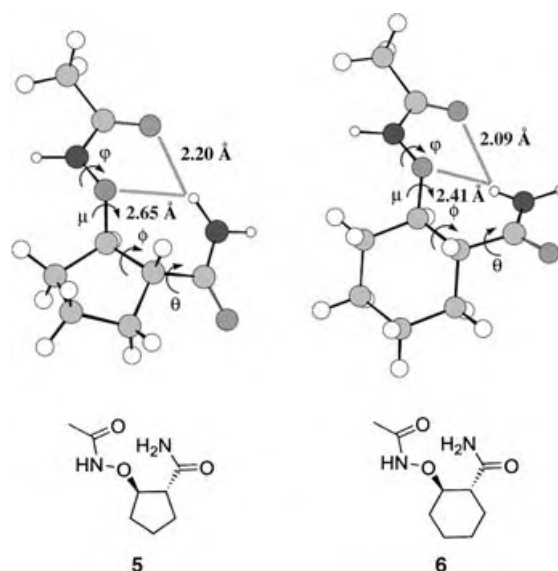


Figure 2. Pertinent hydrogen bonds present in the most stable conformations of **5** and **6**.

structure of **3** are almost superimposable, which strongly supports the correlation between the computational simulation and solid-state structure. The β N–O turn structures are found in the most stable conformations of both **5** and **6**, with little changes in the φ and μ angles but significant changes in the ϕ and θ angles (Table 3). In order to maintain the intramolecular hydrogen bonds of the N–O turns, the tor-

Table 3: Representative dihedral angles of the N–O turns of the most stable conformations of **5** and **6**.

Cmpd.	Dihedral angle [°]			
	φ	μ	ϕ	θ
5	−103.8	163.5	−101.0	51.8
6	−100.8	172.0	−59.6	−12.0

sional angle θ is adjusted accordingly to compensate for the changes in the torsional angle ϕ caused by the difference in ring size. As a result, the relative orientations of the two amide carbonyl groups ($\text{C}=\text{O}_i$ and $\text{C}=\text{O}_{i+1}$) are distinct in the most stable conformations of **5** and **6**. This difference is also reflected in the CD spectra of **1–4** (see the Supporting Information).

Figure 3 summarizes the observed nuclear Overhauser effects (NOEs) of compounds **1–4** obtained in 2D-NOESY experiments. All of the 2D NMR experiments were performed using 5 mM solutions in CDCl_3 at room temperature,

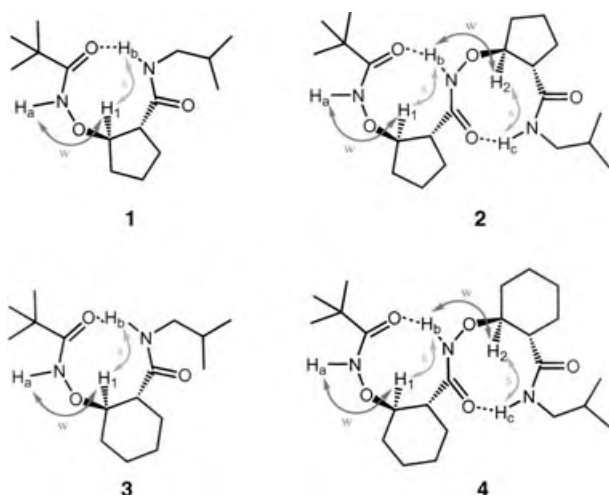


Figure 3. Summary of NOEs observed for compounds **1–3** (5 mM) and compound **4** (10 mM) in CDCl_3 at room temperature (s, strong NOE; w, weak NOE).

except for those for compound **4** (recorded at 10 mM to avoid overlap of the signals of the NH_a and NH_c protons). Compounds **1–4** exhibit very similar NOE patterns: weak NOEs exist between the NH_i and C_βH_i protons, but strong NOEs exist between the NH_{i+1} and C_βH_i protons. Moreover, these NOE patterns match well with the corresponding distances between protons of the N–O turns observed in the calculated structure of **5** and crystal structures of **3** and **4** (Table 4). This correlation suggests that, although the ring size of the side chain varies from five to six atoms, to a great extent compounds **1–4** adopt similar N–O turn structures in CDCl_3 , in contrast to Gellman's β -peptides.

Our β -aminoxy peptides can be considered as analogues of γ -peptides in which the γ -carbon is replaced by an oxygen atom. In fact, nine-membered-ring hydrogen-bonded structures have been observed for several γ -peptides. Dado and

Gellman studied a diamide of an unsubstituted γ -amino acid and found that a nine-membered-ring hydrogen-bonded conformation and a seven-membered-ring hydrogen-bonded conformation are in equilibrium in CH_2Cl_2 solution.^[11] Seebach et al. observed a nine-membered-ring hydrogen-bonded structure for a $\gamma^{2,3,4}$ -dipeptide in the solid state.^[12] However, a $\gamma^{2,3,4}$ -tetrapeptide was found to form a 2.6₁₄-helix (or 14-helix),^[12] which is also observed in several other types of γ -peptides.^[13] Theoretical calculations on α - and β -aminoxy acids have indicated that the N–O bond has a very strong conformational preference,^[7,9b] which contributes to the fact that peptides formed by α - and β -aminoxy acids have a tendency to form hydrogen bonds between adjacent residues.^[7,9] On the other hand, β - and γ -peptides have more flexible backbones and tend to form helical structures with hydrogen bonds involving more distant amino acid residues.^[2,12,13]

In summary, peptides of $\beta^{2,3}$ -cyclic aminoxy acids adopt rigid β N–O turns and 1.8₉-helix structures. These secondary structures exist independently of the ring size of the aliphatic side chains (either five or six atoms), unlike the case of the β -peptides having cyclically constrained backbones. The strong local conformational control exerted by the $\beta^{2,3}$ -cyclic aminoxy acids provides a powerful tool that allows the preparation of short peptides having rigid and predictable conformations.

Received: February 28, 2004

Revised: September 20, 2004 [Z54140]

Keywords: foldamers · helical structures · peptides · secondary structure · structure elucidation

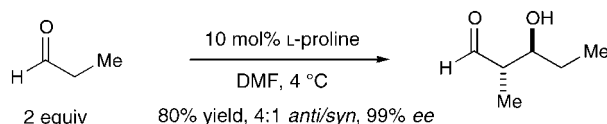
Table 4: Characteristic distances between the amide NH protons and β -protons of **5** in its most stable conformation as well as **3** and **4** in their crystal structures.

Cmpd.	$\text{H}_a\text{--H}_1$ [Å]	$\text{H}_1\text{--H}_b$ [Å]	$\text{H}_b\text{--H}_2$ [Å]	$\text{H}_2\text{--H}_c$ [Å]
5	3.27	2.50		
3	3.46	2.28		
4	3.15	2.35	3.02	2.14

- [1] a) S. H. Gellman, *Acc. Chem. Res.* **1998**, *31*, 173; b) D. J. Hill, M. J. Mio, R. B. Prince, T. S. Hughes, J. S. Moore, *Chem. Rev.* **2001**, *101*, 3893.
- [2] a) R. P. Cheng, S. H. Gellman, W. F. DeGrado, *Chem. Rev.* **2001**, *101*, 3219; b) P. I. Arvidsson, M. Rueping, D. Seebach, *Chem. Commun.* **2001**, 7, 649; c) D. Seebach, S. Abele, K. Gademann, B. Jaun, *Angew. Chem.* **1999**, *111*, 1700; *Angew. Chem. Int. Ed.* **1999**, *38*, 1595; d) K. Gademann, A. Häne, M. Rueping, B. Jaun, D. Seebach, *Angew. Chem.* **2003**, *115*, 1573; *Angew. Chem. Int. Ed.* **2003**, *42*, 1534; e) J. M. Langenhan, I. A. Guzei, S. H. Gellman, *Angew. Chem.* **2003**, *115*, 2504; *Angew. Chem. Int. Ed.* **2003**, *42*, 2402.
- [3] a) D. H. Appella, L. A. Christianson, I. L. Karle, D. R. Powell, S. H. Gellman, *J. Am. Chem. Soc.* **1996**, *118*, 13071; b) D. H. Appella, L. A. Christianson, D. A. Klein, D. R. Powell, X. Huang, J. J. Barchi, Jr., S. H. Gellman, *Nature* **1997**, *387*, 381; c) D. H. Appella, L. A. Christianson, D. A. Klein, M. R. Richards, D. R. Powell, S. H. Gellman, *J. Am. Chem. Soc.* **1999**, *121*, 7574; d) D. H. Appella, L. A. Christianson, I. L. Karle, D. R. Powell, S. H. Gellman, *J. Am. Chem. Soc.* **1999**, *121*, 6206; e) J. J. Barchi, Jr., X. Huang, D. H. Appella, L. A. Christianson, S. R. Durell, S. H. Gellman, *J. Am. Chem. Soc.* **2000**, *122*, 2711.
- [4] a) D. H. Appella, J. J. Barchi, Jr., S. R. Durell, S. H. Gellman, *J. Am. Chem. Soc.* **1999**, *121*, 2309; b) X. Wang, J. F. Espinosa, S. H. Gellman, *J. Am. Chem. Soc.* **2000**, *122*, 4821; c) T. L. Raguse, J. R. Lai, P. R. LePlae, S. H. Gellman, *Org. Lett.* **2001**, *3*, 3963; d) H.-S. Lee, F. A. Syud, X. Wang, S. H. Gellman, *J. Am. Chem. Soc.* **2001**, *123*, 7721; e) M. G. Woll, J. D. Fisk, P. R. LePlae, S. H. Gellman, *J. Am. Chem. Soc.* **2002**, *124*, 12447; f) E. A. Porter, X. Wang, M. A. Schmitt, S. H. Gellman, *Org. Lett.* **2002**, *4*, 3317.

- [5] a) P. R. LePlae, J. D. Fisk, E. A. Porter, B. Weisblum, S. H. Gellman, *J. Am. Chem. Soc.* **2002**, *124*, 6820; b) T. L. Raguse, E. A. Porter, B. Weisblum, S. H. Gellman, *J. Am. Chem. Soc.* **2002**, *124*, 12774; c) T. L. Raguse, J. R. Lai, S. H. Gellman, *J. Am. Chem. Soc.* **2003**, *125*, 5592; d) J.-S. Park, H.-S. Lee, J. R. Lai, B. M. Kim, S. H. Gellman, *J. Am. Chem. Soc.* **2003**, *125*, 8539.
- [6] Y. D. Wu, D. P. Wang, *J. Am. Chem. Soc.* **1998**, *120*, 13485.
- [7] a) D. Yang, F. F. Ng, Z. J. Li, *J. Am. Chem. Soc.* **1996**, *118*, 9794; b) D. Yang, J. Qu, B. Li, F. F. Ng, X. C. Wang, K. K. Cheung, D. P. Wang, Y. D. Wu, *J. Am. Chem. Soc.* **1999**, *121*, 589; c) Y. D. Wu, D. P. Wang, K. W. K. Chan, D. Yang, *J. Am. Chem. Soc.* **1999**, *121*, 11189; d) D. Yang, J. Qu, W. Li, Y. H. Zhang, Y. Ren, D. P. Wang, Y. D. Wu, *J. Am. Chem. Soc.* **2002**, *124*, 12410.
- [8] CCDC-250085 and CCDC-250086 (**3** and **4**) contains the supplementary crystallographic data for this paper. These data can be obtained free of charge via www.ccdc.cam.ac.uk/conts/retrieving.html (or from the Cambridge Crystallographic Data Centre, 12, Union Road, Cambridge CB21EZ, UK; fax: (+44)1223-336-033; or deposit@ccdc.cam.ac.uk).
- [9] a) D. Yang, Y. H. Zhang, N. Y. Zhu, *J. Am. Chem. Soc.* **2002**, *124*, 9966; b) D. Yang, Y.-H. Zhang, B. Li, D.-W. Zhang, J. C.-Y. Chan, S.-W. Luo, Y.-D. Wu, N.-Y. Zhu, *J. Am. Chem. Soc.* **2004**, *126*, 6956.
- [10] For details of the calculation method and results, see the Supporting Information.
- [11] D. P. Dado, S. H. Gellman, *J. Am. Chem. Soc.* **1994**, *116*, 1054.
- [12] D. Seebach, M. Brenner, M. Rueping, B. Jaun, *Chem. Eur. J.* **2002**, *8*, 573.
- [13] a) S. Hanessian, X. Luo, R. Schaum, S. Michnick, *J. Am. Chem. Soc.* **1998**, *120*, 8569; b) T. Hintermann, K. Gademann, B. Jaun, D. Seebach, *Helv. Chim. Acta* **1998**, *81*, 983.

molecular aldol reaction. Almost three decades later, studies by the groups of Barbas^[3a] and List^[3b] revealed that proline catalysis could be extended to a variety of transformations, including the direct enantioselective aldol reaction^[4] between ketones and aldehydes. Recently, our group advanced this proline-catalysis concept to the first example of a direct enantioselective cross-coupling of aldehyde substrates^[5] (Scheme 1), a powerful yet elusive aldol variant that had previously only been carried out within the realm of enzymatic catalysis.



Scheme 1. Proline-catalyzed aldehyde–aldehyde aldol reaction.

As part of an ongoing program to develop organocatalysts of broad utility to chemical synthesis, we recently initiated studies towards the identification of simple amines that mimic aldolase type I enzymes while providing complementary function or stereoselectivity to known enamine catalysts (e.g., proline). Herein we describe a mechanism-based investigation that has established imidazolidinones as efficient catalysts for direct and enantioselective aldehyde–aldehyde aldol reactions. More importantly, we demonstrate a new class of enamine catalyst with selectivity parameters that rival or complement benchmark amino acid catalysts (Scheme 2).

In 2001, Houk and Bahmanyar reported a computational study into the transition-state topographies involved in enamine aldol reactions.^[6] Besides providing further insight, this study described that secondary enamine additions typically proceed via a late transition state in which the

Organocatalysis

The Importance of Iminium Geometry Control in Enamine Catalysis: Identification of a New Catalyst Architecture for Aldehyde–Aldehyde Couplings**

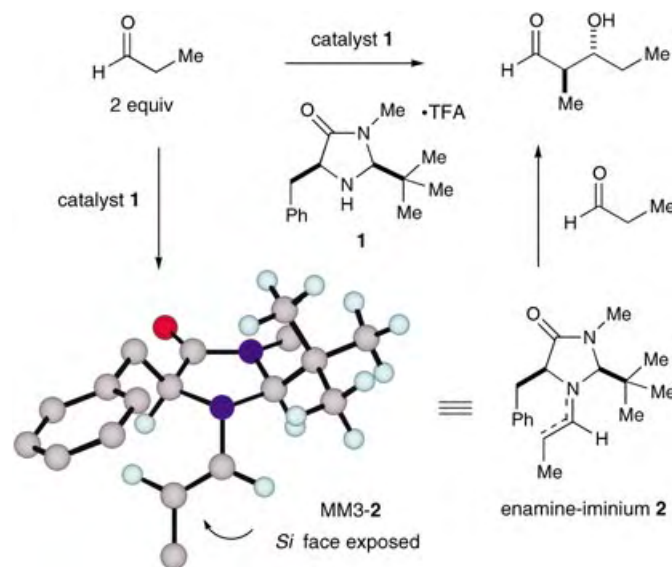
Ian K. Mangion, Alan B. Northrup, and David W. C. MacMillan*

In 1971, Hajos and Parrish^[1] and Eder, Sauer, and Wiechert^[2] independently described the first examples of enantioselective proline-catalyzed reactions in the form of an intra-

[*] I. K. Mangion, A. B. Northrup, Prof. D. W. C. MacMillan
Division of Chemistry and Chemical Engineering
California Institute of Technology
1200 E. California Blvd., MC 164-30, Pasadena, CA 91125 (USA)
Fax: (+1) 626-795-3658
E-mail: dmacmill@caltech.edu

[**] Financial support was provided by the NIHGMs (R01 GM66142-01) and kind gifts from Bristol-Myers Squibb, Eli Lilly, and Merck Research Laboratories. I.K.M. and A.B.N are grateful for NSF predoctoral fellowships.

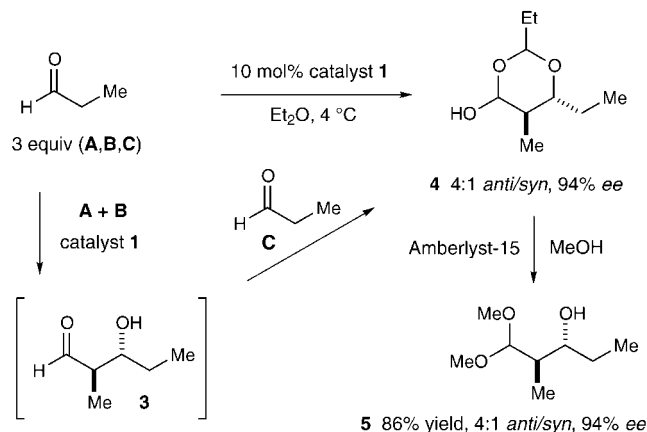
Supporting information for this article is available on the WWW under <http://www.angewandte.org> or from the author.



Scheme 2. Imidazolidinone-catalyzed aldehyde–aldehyde aldol reaction.

development of the iminium π bond precedes the formation of the carbon–carbon bond. On this basis, we hypothesized that enantiofacial discrimination in enamine additions might be governed, in part, by the ability of an amine catalyst to control iminium geometry during the transition state. Given the success of imidazolidinones as asymmetric catalysts that confer iminium activation and geometry control,^[7] we rationalized that amines of type **1** might readily function as enantioselective enamine-aldol catalysts. This hypothesis was further substantiated by the computational model MM3-2, which predicts π -facial differentiation of enamine-iminiums derived from **1** on the basis of 1) selective formation of the *E* iminium isomer during the transition state to avoid nonbonding interactions with the bulky *tert*-butyl group, and 2) the benzyl group on the catalyst framework which effectively prevents the *Re* face of the enamine from participating in carbonyl addition.

Initial investigations revealed that the (2*S*,5*S*)-5-benzyl-2-*tert*-butylimidazolidinone catalyst **1** (10 mol %) does, indeed, promote the aldol self-coupling of propionaldehyde to provide the putative aldol adduct **3** in $\geq 86\%$ yield with 94% *ee* (Scheme 3). Unexpectedly, the initial aldol dimeriza-



Scheme 3. Imidazolidinone-catalyzed aldol reaction: initial results.

tion adduct **3** undergoes rapid formation to the hemiacetal system **4**, a self-termination step that fortuitously protects the product from participation in further aldol processes. To our delight, methanolysis of this aldol hemiacetal product in situ allows direct access to the bench-stable β -hydroxy dimethoxyacetal **5** without loss in enantiopurity or diastereocontrol. Notably, the observed sense of asymmetric induction is in accord with the calculated enamine-iminium model MM3-2. In contrast to the proline variant, this enantioselective aldehyde coupling is readily accomplished in a wide variety of solvents,^[8] with low dielectric media (e.g., hexane: 90% *ee*; dioxane: 94% *ee*) being generally most efficient. The superior levels of asymmetric induction and efficiency exhibited by the amine salt **1** in Et₂O to afford the dimethoxy-protected aldol (2*R*)-**5** in 86% yield with 94% *ee* in one chemical process prompted us to select these catalytic conditions for further exploration.

The ability of imidazolidinone **1** to catalyze enantioselective cross-aldol reactions between non-equivalent aldehydes was examined next. As highlighted in Table 1, addition of α -methylenealdehyde donors by means of a syringe pump to a

Table 1: Imidazolidinone-catalyzed direct aldol condensation: reaction scope.

		donor	acceptor	10-20 mol% 1 , Et ₂ O, 4 °C; Amberlyst-15, MeOH			
Entry	R ¹	R ²	Product	Yield [%] ^[a]	<i>anti</i> / <i>syn</i> ^[b]	<i>ee</i> [%] ^[c,d]	
1	Me	Me		86	4:1	94	
2	Me	<i>i</i> Pr		90	5:1	95	
3	Me	<i>c</i> -C ₆ H ₁₁		81	5:1	97	
4	Me	Ph		61	4:1	93	
5	<i>n</i> Bu	<i>i</i> Pr		72	6:1	91	
6	Bn	<i>i</i> Pr		80	5:1	91	
7	Me	OPiv		58	4:1	90	
8	OBn	OBn		64	4:1	92	
9	SBn	SBn		84	11:1	97	
10 ^[e]	OTIPS	OTIPS		84	1:4	92	

[a] Absolute and relative stereochemistry assigned by chemical correlation. [b] Determined by chiral GLC or Mosher ester analysis. [c] Enantiomeric excess of major diastereomer. [d] Performed in dioxane. [e] Et₂NH/SiO₂ in place of MeOH/Amberlyst-15. TIPS = triisopropylsilyl, Piv = pivaloyl.

variety of formyl acceptors effectively prevents homodimerization while providing the desired cross-aldol products in excellent yields (Table 1, entries 1–10, 58–90% yield). Significant electronic and structural modification in the acceptor component can be realized to incorporate α -alkyl, α -aromatic, and α -oxy functionality (Table 1, entries 1–7, 90–97% *ee*).

Whereas it has been documented that α -acyloxy-substituted aldehydes are inert to proline catalysis,^[9] we have found that these substrates readily participate as electrophilic aldol partners in the presence of amine **1** (Table 1, entry 7, 58 % yield, 90 % ee).

We next examined the capacity of imidazolidinone **1** to catalyze the homodimerization of α -heterosubstituted aldehydes (Table 1). It has been established that proline catalysis in this venue provides erythrose architecture in one step,^[9] a transformation that enables the selective production of mannose, glucose, or allose in only two chemical reactions.^[10] As shown in Table 1, entries 8 and 9, exposure of catalyst **1** to α -benzyloxy or α -benzylsulfide aldehydes also provides the erythrose aldol adduct with high levels of enantiocontrol (92–97 % ee). In contrast, α -silyloxy aldehydes provide the corresponding threose aldehyde product upon hydrolysis of the corresponding hemiacetal over silica gel (Table 1, entry 10, 4:1 *syn/anti*, 92 % ee). As such, we anticipate that the imidazolidinone catalyst will be valuable in the production of hexose carbohydrates that are not available through proline catalysis (e.g. idose, gulose, galactose).^[11] More importantly, this result demonstrates the capacity for orthogonal enamine selectivities as a function of amine catalyst architecture.

In summary, we have documented the first asymmetric organocatalytic aldol reaction in the presence of imidazolidinone catalysts. This method allows enantioselective access to β -hydroxy dimethoxyacetals, bench-stable adducts that functionally complement the β -hydroxyaldehyde adducts derived from proline-catalyzed aldol reactions.

Received: September 1, 2004

Keywords: aldehydes · aldol reaction · nitrogen heterocycles · organocatalysis · synthetic methods

- [1] "Asymmetric Synthesis of Optically Active Polycyclic Organic Compounds": a) Z. G. Hajos, D. R. Parrish, German Patent DE2102623, July 29, **1971**; b) Z. G. Hajos, D. R. Parrish, *J. Org. Chem.* **1974**, 39, 1615.
- [2] a) "Optically active 1,5-Indanone and 1,6-Naphthalenedione": U. Eder, G. Sauer, R. Wiechert (Schering AG), German Patent DE2014757, Oct. 7, **1971**; b) U. Eder, G. Sauer, R. Wiechert, *Angew. Chem.* **1971**, 83, 492; *Angew. Chem. Int. Ed. Engl.* **1971**, 10, 496.
- [3] a) K. Sakthivel, W. Notz, T. Bui, C. F. Barbas III, *J. Am. Chem. Soc.* **2001**, 123, 5260; b) W. Notz, B. List, *J. Am. Chem. Soc.* **2000**, 122, 7386.
- [4] For examples of metal-mediated direct aldol reactions, see: a) Y. M. A. Yamada, N. Yoshikawa, H. Sasai, M. Shibasaki, *Angew. Chem.* **1997**, 109, 1290; *Angew. Chem. Int. Ed. Engl.* **1997**, 36, 1871; b) N. Yoshikawa, N. Kumagai, S. Matsunaga, G. Moll, T. Oshima, T. Suzuki, M. Shibasaki, *J. Am. Chem. Soc.* **2001**, 123, 2466; d) N. Kumagai, S. Matsunaga, N. Yoshikawa, T. Oshima, M. Shibasaki, *Org. Lett.* **2001**, 3, 1539; e) B. M. Trost, H. Ito, *J. Am. Chem. Soc.* **2000**, 122, 12003; f) B. M. Trost, E. R. Silcoff, H. Ito, *Org. Lett.* **2001**, 3, 2497; g) D. A. Evans, J. S. Tedrow, J. T. Shaw, C. W. Downey, *J. Am. Chem. Soc.* **2002**, 124, 392.
- [5] A. B. Northrup, D. W. C. MacMillan, *J. Am. Chem. Soc.* **2002**, 124, 6798.

- [6] S. Bahmanyar, K. N. Houk, *J. Am. Chem. Soc.* **2001**, 123, 11273.
- [7] a) K. A. Ahrendt, C. J. Borths, D. W. C. MacMillan, *J. Am. Chem. Soc.* **2000**, 122, 4243; b) J. F. Austin, D. W. C. MacMillan, *J. Am. Chem. Soc.* **2002**, 124, 1172.
- [8] Solvent study for propionaldehyde dimerization with amine **1**: hexane: 89 % yield, 3:1 *anti/syn*, 90 % ee; CH₂Cl₂: 66 % yield, 4:1 *anti/syn*, 93 % ee; CHCl₃: 42 % yield, 4:1 *anti/syn*, 91 % ee; toluene: 80 % yield, 3:1 *anti/syn*, 87 % ee; THF: 22 % yield, 2:1 *anti/syn*, 90 % ee; Et₂O: 86 % yield, 4:1 *anti/syn*, 94 % ee; dioxane: 92 % yield, 4:1 *anti/syn*, 94 % ee.
- [9] A. B. Northrup, I. K. Mangion, F. Hettche, D. W. C. MacMillan, *Angew. Chem.* **2004**, 116, 2204; *Angew. Chem. Int. Ed.* **2004**, 43, 2152.
- [10] A. B. Northrup, D. W. C. MacMillan, *Science* **2004**, 305, 1752.
- [11] We recently determined that this imidazolidinone-catalyzed aldol reaction allows enantioselective access to gulose in two steps.

Supramolecular Structures

The Hydrophobic Effect as a Driving Force in the Self-Assembly of a $[2 \times 2]$ Copper(I) Grid**

Jonathan R. Nitschke,* Marie Hutin, and
Gérald Bernardinelli

*Dedicated to Professor Jean-Marie Lehn
on the occasion of his 65th birthday*

Grid-type coordination arrays, which consist of a regular array of metal ions sandwiched between two perpendicular sets of parallel ligand molecules, have been shown a great deal of interest in recent years.^[1–6] The regular spacing of metal ions and ligands results in a variety of interesting magnetic behaviors,^[6–9] and also evokes the possibility of using these complexes as molecular computing elements (quantum-dot cellular automata).^[10]

We report herein the preparation of a $[2 \times 2]$ copper(I) grid that possesses two novel features. Firstly, the geometry of this grid structure is atypical, not being readily predictable from

[*] Dr. J. R. Nitschke, M. Hutin
Department of Organic Chemistry
University of Geneva
30 Quai Ernest Ansermet, 1211 Genève 4 (Switzerland)
Fax: (+41) 22-379-3215
E-mail: jonathan.nitschke@chiorg.unige.ch
Dr. G. Bernardinelli
Laboratory of X-Ray Crystallography
University of Geneva
24 Quai Ernest Ansermet, 1211 Genève 4 (Switzerland)

[**] Financial support from the Fonds Frédéric Firmenich et Philippe Chuit, the Fonds Xavier Givaudan, and the Swiss National Science Foundation is gratefully acknowledged. We thank P. Perrottet for mass spectrometric analyses and A. Pinto for NOESY NMR spectra.



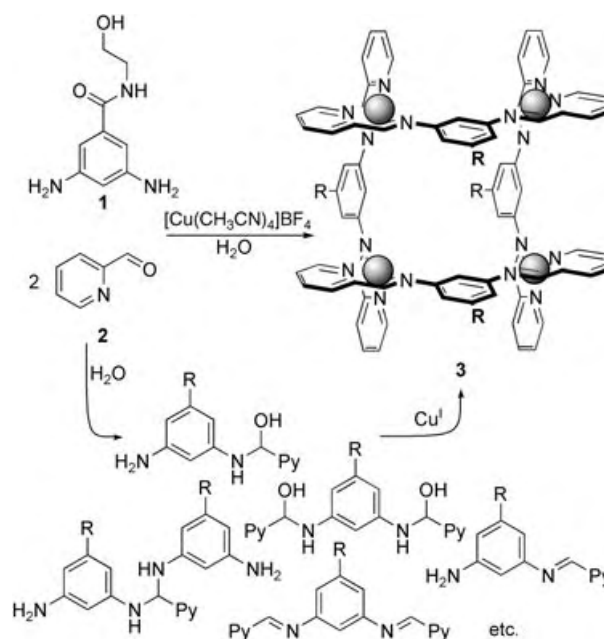
Supporting information for this article is available on the WWW under <http://www.angewandte.org> or from the author.

the “self-assembly instructions” encoded within the components.^[11] The ligands of grids generally cross at perpendicular junctions,^[6] which they cannot do in the present structure without distortion. Evidence of this distortion was noted in the crystal structure. Secondly, the self-assembly^[4,5,12,13] reaction by which this grid was synthesized took place quantitatively in aqueous solution, but was not observed to occur at all in other solvents. This observation suggests that the hydrophobic effect^[14] might play an essential role in directing the self-assembly process.

The mixture of diaminobenzamide **1** (0.024 mmol) with pyridinecarboxaldehyde **2** (0.049 mmol) in D₂O (0.7 mL) under an argon atmosphere gave a complex mixture of products, as observed by NMR spectroscopy. Within five minutes of addition, approximately 30% of **1** and **2** initially present had reacted; possible product structures are shown in Scheme 1. These products were not definitively characterized. However, signals corresponding to at least five distinct amina and imine products were noted in the ¹H NMR spectrum. These products are capable of interconversion by carbon–nitrogen bond exchange, and thus comprise a dynamic combinatorial library.^[15,16] Since diamine **1** may link two molecules of **2**, and **2** may conversely bridge two molecules of **1** in its amina form,^[16] this library could contain a limitless variety of oligomeric and cyclic structures. Our attempts to follow its evolution were hampered by the precipitation of a yellow film over the course of several hours.

The addition of [Cu(CH₃CN)₄]BF₄ (0.024 mmol) rapidly brought order to this complex mixture: the presence of Cu^I ions induced the formation of grid structure **3** (Scheme 1) as the unique product, thus templating^[17] the formation of the corresponding bisimine ligand from the dynamic library with perfect selectivity. NOESY NMR spectra indicated that the ligand conformation was as shown in structure **3**, and electrospray mass spectra demonstrated it to be tetrameric.

X-ray crystallographic analysis confirmed the presence of this tetrameric structure in the solid state (Figure 1).^[18] The complex shows a highly symmetric arrangement around a $\bar{4}$



Scheme 1. Dynamic combinatorial library generated from an aqueous solution of diamine **1** and aldehyde **2**, and the collapse of this library into grid **3** on addition of [Cu(CH₃CN)₄]BF₄. Py = 2-pyridyl, R = 2-hydroxyethylcarbamoyl. Shaded spheres represent Cu^I ions.

(*S*₄) crystallographic axis despite the presence of the flexible hydroxyethyl substituents, which are ordered by hydrogen bonds between neighboring ligands (Figure 1, right). Although they reinforce the grid structure, these hydrogen bonds are not necessary for its formation: 3,5-diaminobenzamide also generated a grid in water when used in place of **1**, despite the fact that it is incapable of forming interligand bonds within a grid-type structure.

Figure 2 shows the coordinate vectors^[19] of the ligands present in **3**, which converge at an angle of approximately 60° in an idealized ligand geometry. The coordinate vectors of other ligands in grid complexes lie naturally parallel^[1,9] or

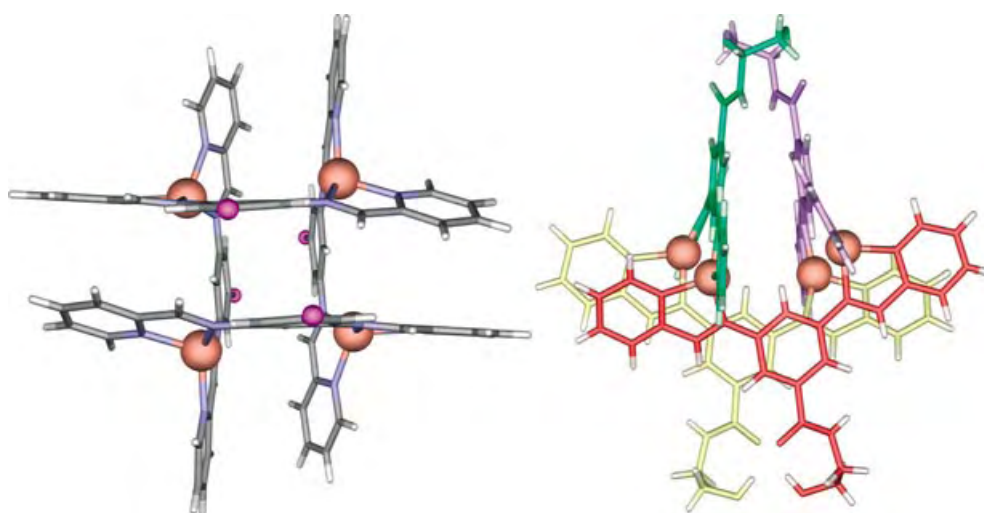


Figure 1. Views of the X-ray crystal structure of **3**. The 2-hydroxyethylcarbamoyl (–CONHCH₂CH₂OH) groups have been replaced by purple spheres in the right view for clarity. Each symmetry-equivalent ligand is shown in a different color in the view on the right.

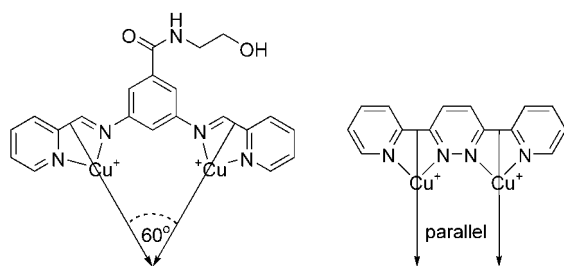


Figure 2. The coordinate vectors^[19] of the ligand present in **3** and of the prototypical grid ligand reported by Youinou et al.^[1]

diverge slightly.^[3,8] Since the geometry of the grid enforces a parallel arrangement of the ligands, distortion must occur. This distortion is exhibited as: 1) a coordination environment around copper intermediate between tetrahedral (preferred by Cu^I ions) and see-saw (as can be seen in Figure 1, right), 2) an opening of the C_{imine}-N_{imine}-C_{phenyl} angle from an ideal 120° to 127.7°, and 3) a bending (ca. 20°) from planarity of one pyridylimino group on each ligand, thus pushing the copper ions out from the square junctions formed by the ligands (Figure 1, left). These deformations imply the presence of strain, an unusual feature for a quantitatively formed self-assembled structure.

The inference of this strain was supported by the observation that **3** did not appear to be stable in solvents other than water. The formation of **3** was not observed on mixing the precursors of **3** in acetic acid, acetonitrile, acetone, benzene, chloroform, dimethyl formamide, dimethyl sulfoxide, diethyl ether, ethanol, methanol, nitromethane, pyridine, or tetrahydrofuran. When presynthesized **3** was suspended in any of the aforementioned solvents, either it did not dissolve or decomposition was observed. Thus, despite the fact that neither Cu^I ions nor imines are commonly considered to be stable in water, we were able to detect this Cu^I-linked imine complex *uniquely* in that solvent. Our previously described^[5,13] aqueous systems were stable in other solvents, and the successes of other research groups with the techniques of ligand-component self-assembly were obtained in nonaqueous solvents.^[4,12]

This solvent-dependent stability is likely to be a result of two factors. Firstly, water is a poor ligand for Cu^I ions. The compact donor orbitals of H₂O overlap poorly with the diffuse acceptor orbitals of copper(I) ions, which leads to the latter's tendency to disproportionate in aqueous solution. Imine donors, in contrast, are good ligands for Cu^I ions, so much so that this metal will template their formation in water from amines and aldehydes.^[13] The disassembly of complex **3** would be facilitated by a solvent that bound strongly to Cu^I ions, and is conversely hindered by the presence of a solvent which does not, thus stabilizing **3** in water. Secondly, non-aqueous solvents would be better able to solvate exposed ligand surfaces, and thus would not force the mixture of species derived from **1**, **2**, and Cu^I ions to collapse into the compact structure of **3**. This structure maximizes the favorable van der Waals interactions, including stacking interactions,^[20] between the ligands while minimizing the unfavorable ligand-solvent interactions.

This structure is thus held together through the cooperative interplay of three distinct self-assembly processes: the formation of strong, covalent C=N bonds, as well as weaker, dative N-Cu bonds, and finally the diffuse yet necessary "compression" applied by the hydrophobic effect.^[14] The use of the hydrophobic effect as it applies to both metals and ligands represents a new means of control within the field of metallo-organic self-assembly, thus complimenting its use in other contexts.^[21] We are continuing to investigate the ways in which an aqueous reaction medium may allow for the construction of new kinds of assemblies, as well as the novel properties that might be engendered by the presence of strain.

Experimental Section

3: Compound **1** (0.0277 g, 0.14 mmol), **2** (0.0303 g, 0.28 mmol), and water (5 mL) were added to a 50-mL Schlenk flask. The flask was then sealed, and the atmosphere was purified of dioxygen by three evacuation/argon-fill cycles. When the solution was homogeneous, [Cu(CH₃CN)₄]BF₄ (0.0446 g, 0.14 mmol) was added, which immediately dissolved to give a violet-black solution. The atmosphere was once more purified of dioxygen by three evacuation/argon-fill cycles, and the reaction was kept at room temperature overnight without stirring. Volatiles were then removed under dynamic vacuum to give **3** in a yield of 0.073 g (99%) as a violet crystalline product, which was pure by NMR spectroscopic analysis. Following the above procedure and starting with a copper concentration of 2.45 × 10⁻² M, X-ray quality single crystals (which were also used for the elemental analysis) of **3** were isolated when the solvent was decanted instead of evaporated. ¹H NMR (500 MHz, 300 K, D₂O, referenced to 2-methyl-2-propanol at 1.24 ppm as the internal standard): δ = 9.24 (s, 8H, imine), 8.22 (d, *J* = 1.7 Hz, 8H, 2,6-phenylamide), 7.94 (d, *J* = 7.7 Hz, 8H, 3-pyridyl), 7.84 (m, 12H, 4-pyridyl, 4-phenylamide), 7.77 (d, *J* = 5 Hz, 8H, 6-pyridyl), 7.26 (dt, *J* = 5.5 Hz, *J* = 1.1 Hz, 8H, 5-py), 3.95 (t, *J* = 5.5 Hz, 8H, hydroxyethylcarbamoyl), 3.74 (t, *J* = 5.5 Hz, 8H, hydroxyethylcarbamoyl); ¹³C NMR (125.77 MHz, 300 K, D₂O, referenced to the methyl groups of 2-methyl-2-propanol at 30.29 ppm as internal standard): δ = 168.1, 160.3, 149.9, 149.0, 147.6, 139.7, 137.6, 129.7, 129.6, 129.4, 118.6, 59.7, 43.1; ESI-MS: *m/z* = 436.3 [CuL]⁺, 961.2 [Cu₂L₂+BF₄]⁺, 1484.1 [Cu₃L₃+2BF₄]⁺, 2009.9 [Cu₄L₄+3BF₄]⁺; elemental analysis calcd for C₈₄H₇₆N₂₀O₈Cu₄B₄F₁₆·H₂O·CH₃CN: C 47.95, H 3.79, N 13.65; found: C 47.93, H 4.10, N 13.73.

Received: July 14, 2004

Keywords: copper · dynamic combinatorial chemistry · Schiff bases · self-assembly · template synthesis

- [1] M. T. Youinou, N. Rahmouni, J. Fischer, J. A. Osborn, *Angew. Chem.* **1992**, 104, 771; *Angew. Chem. Int. Ed. Engl.* **1992**, 31, 733.
- [2] a) L. H. Uppadine, J.-M. Lehn, *Angew. Chem.* **2004**, 116, 242; *Angew. Chem. Int. Ed.* **2004**, 43, 240; b) L. H. Uppadine, J.-P. Gisselbrecht, J.-M. Lehn, *Chem. Commun.* **2004**, 718; c) A. M. Garcia, F. J. Romero-Salguero, D. M. Bassani, J.-M. Lehn, G. Baum, D. Fenske, *Chem. Eur. J.* **1999**, 5, 1803; d) M. Ruben, E. Breuning, M. Barboiu, J.-P. Gisselbrecht, J.-M. Lehn, *Chem. Eur. J.* **2003**, 9, 291; e) U. Ziener, J.-M. Lehn, A. Mourran, M. Moller, *Chem. Eur. J.* **2002**, 8, 951; f) E. Breuning, U. Ziener, J.-M. Lehn, E. Wegelius, K. Rissanen, *Eur. J. Inorg. Chem.* **2001**, 1515.
- [3] a) J. Hausmann, S. Brooker, *Chem. Commun.* **2004**, 1530; b) A. Petitjean, N. Kyritsakas, J.-M. Lehn, *Chem. Commun.* **2004**, 1168.

- [4] S. Brooker, S. J. Hay, P. G. Plieger, *Angew. Chem.* **2000**, *112*, 2044; *Angew. Chem. Int. Ed.* **2000**, *39*, 1968.
- [5] J. R. Nitschke, J.-M. Lehn, *Proc. Natl. Acad. Sci. USA* **2003**, *100*, 11970.
- [6] M. Ruben, J. Rojo, F. J. Romero-Salguero, L. H. Uppadine, J.-M. Lehn, *Angew. Chem.* **2004**, *116*, 3728; *Angew. Chem. Int. Ed.* **2004**, *43*, 3644.
- [7] a) E. Breuning, M. Ruben, J.-M. Lehn, F. Renz, Y. Garcia, V. Ksenofontov, P. Guetlich, E. Wegelius, K. Rissanen, *Angew. Chem.* **2000**, *112*, 2563; *Angew. Chem. Int. Ed.* **2000**, *39*, 2504; b) O. Waldmann, R. Koch, S. Schromm, P. Muller, L. Zhao, L. K. Thompson, *Chem. Phys. Lett.* **2001**, *332*, 73; c) M. Ruben, E. Breuning, J.-M. Lehn, V. Ksenofontov, F. Renz, P. Guetlich, G. B. M. Vaughan, *Chem. Eur. J.* **2003**, *9*, 4422; d) V. A. Milway, V. Niel, T. S. M. Abedin, Z. Xu, L. K. Thompson, H. Grove, D. O. Miller, S. R. Parsons, *Inorg. Chem.* **2004**, *43*, 1874; e) L. Zhao, Z. Xu, H. Grove, V. A. Milway, L. N. Dawe, T. S. M. Abedin, L. K. Thompson, T. L. Kelly, R. G. Harvey, D. O. Miller, L. Weeks, J. G. Shapter, K. J. Pope, *Inorg. Chem.* **2004**, *43*, 3812; f) O. Waldmann, J. Hassmann, P. Muller, D. Volkmer, U. S. Schubert, J.-M. Lehn, *Phys. Rev. B* **1998**, *58*, 3277; g) O. Waldmann, S. Carretta, P. Santini, R. Koch, A. G. M. Jansen, G. Amoretti, R. Caciuffo, L. Zhao, L. K. Thompson, *Phys. Rev. Lett.* **2004**, *92*, 096403/1; h) O. Waldmann, L. Zhao, L. K. Thompson, *Phys. Rev. Lett.* **2002**, *88*, 066401/1; i) O. Waldmann, J. Hassmann, P. Muller, G. S. Hanan, D. Volkmer, U. S. Schubert, J.-M. Lehn, *Phys. Rev. Lett.* **1997**, *78*, 3390.
- [8] D. S. Cati, J. Ribas, J. Ribas-Arino, H. Stoeckli-Evans, *Inorg. Chem.* **2004**, *43*, 1021.
- [9] L. K. Thompson, *Coord. Chem. Rev.* **2002**, *233*, 193.
- [10] a) I. Amlani, A. O. Orlov, G. Toth, G. H. Bernstein, C. S. Lent, G. L. Snider, *Science* **1999**, *284*, 289; b) A. O. Orlov, I. Amlani, G. H. Bernstein, C. S. Lent, G. L. Snider, *Science* **1997**, *277*, 928.
- [11] J.-M. Lehn, *Supramolecular Chemistry: Concepts and Perspectives*, Wiley-VCH, Weinheim, **1995**.
- [12] a) D. A. Leigh, P. J. Lusby, S. J. Teat, A. J. Wilson, J. K. Y. Wong, *Angew. Chem.* **2001**, *113*, 1586; *Angew. Chem. Int. Ed.* **2001**, *40*, 1538; b) K. S. Chichak, S. J. Cantrill, A. R. Pease, S.-H. Chiu, G. W. V. Cave, J. L. Atwood, J. F. Stoddart, *Science* **2004**, *304*, 1308; c) L. Hogg, D. A. Leigh, P. J. Lusby, A. Morelli, S. Parsons, J. K. Y. Wong, *Angew. Chem.* **2004**, *116*, 1238; *Angew. Chem. Int. Ed.* **2004**, *43*, 1218; d) H. Houjou, A. Iwasaki, T. Ogihara, M. Kanesato, S. Akabori, K. Hiratani, *New J. Chem.* **2003**, *27*, 886; e) J. Hamblin, L. J. Childs, N. W. Alcock, M. J. Hannon, *J. Chem. Soc. Dalton Trans.* **2002**, 164; f) L. J. Childs, N. W. Alcock, M. J. Hannon, *Angew. Chem.* **2002**, *114*, 4418; *Angew. Chem. Int. Ed.* **2002**, *41*, 4244.
- [13] a) J. R. Nitschke, *Angew. Chem.* **2004**, *116*, 3135; *Angew. Chem. Int. Ed.* **2004**, *43*, 3073; b) J. R. Nitschke, D. Schultz, G. Bernardinelli, D. Gérard, *J. Am. Chem. Soc.*, in press.
- [14] a) R. Breslow, *Acc. Chem. Res.* **1991**, *24*, 159; b) S. Otto, J. B. F. N. Engberts, *Org. Biomol. Chem.* **2003**, *1*, 2809.
- [15] a) P. A. Brady, J. K. M. Sanders, *J. Chem. Soc. Perkin Trans. 1* **1997**, 3237; b) I. Huc, J.-M. Lehn, *Proc. Natl. Acad. Sci. USA* **1997**, *94*, 2106; c) L. J. Prins, P. Timmerman, D. N. Reinhoudt, *Pure Appl. Chem.* **1998**, *70*, 1459; d) B. Linton, A. D. Hamilton, *Curr. Opin. Chem. Biol.* **1999**, *3*, 307; e) J.-M. Lehn, *Chem. Eur. J.* **1999**, *5*, 2455; f) J. K. M. Sanders, *Pure Appl. Chem.* **2000**, *72*, 2265; g) G. R. L. Cousins, S.-A. Poulsen, J. K. M. Sanders, *Curr. Opin. Chem. Biol.* **2000**, *4*, 270; h) F. Hof, C. Nuckolls, J. Rebek, Jr., *J. Am. Chem. Soc.* **2000**, *122*, 4251; i) M. Albrecht, *J. Inclusion Phenom. Macrocyclic Chem.* **2000**, *36*, 127; j) E. C. Constable, C. E. Housecroft, T. Kulke, C. Lazzarini, E. R. Schofield, Y. Zimmermann, *J. Chem. Soc. Dalton Trans.* **2001**, 2864; k) I. Huc, R. Nguyen, *Comb. Chem. High Throughput Screening* **2001**, *4*, 53; l) D. M. Epstein, S. Choudhary, M. R. Churchill, K. M. Keil, A. V. Eliseev, J. R. Morrow, *Inorg. Chem.* **2001**, *40*, 1591; m) J.-M. Lehn, A. V. Eliseev, *Science* **2001**, *291*, 2331; n) S. J. Rowan, S. J. Cantrill, G. R. L. Cousins, J. K. M. Sanders, J. F. Stoddart, *Angew. Chem.* **2002**, *114*, 1528; *Angew. Chem. Int. Ed.* **2002**, *41*, 898; o) S. Choudhary, J. R. Morrow, *Methods Mol. Biol.* **2002**, *201*, 215; p) O. Ramstrom, T. Bunyapaiboonsri, S. Lohmann, J.-M. Lehn, *Biochim. Biophys. Acta* **2002**, *1572*, 178; q) O. Ramstrom, J.-M. Lehn, *Nat. Rev. Drug Discovery* **2002**, *1*, 26; r) S. Otto, R. L. E. Furlan, J. K. M. Sanders, *Curr. Opin. Chem. Biol.* **2002**, *6*, 321; s) Y. Kubota, S. Sakamoto, K. Yamaguchi, M. Fujita, *Proc. Natl. Acad. Sci. USA* **2002**, *99*, 4854; t) S. Otto, *Curr. Opin. Drug Discovery Dev.* **2003**, *6*, 509; u) Z. Grote, R. Scopelliti, K. Severin, *Angew. Chem.* **2003**, *115*, 3951; *Angew. Chem. Int. Ed.* **2003**, *42*, 3821; v) B. Brisig, J. K. M. Sanders, S. Otto, *Angew. Chem.* **2003**, *115*, 1308; *Angew. Chem. Int. Ed.* **2003**, *42*, 1270; w) E. Stulz, S. M. Scott, A. D. Bond, S. J. Teat, J. K. M. Sanders, *Chem. Eur. J.* **2003**, *9*, 6039; x) K. Severin, *Chem. Eur. J.* **2004**, *10*, 2565; y) P. T. Corbett, S. Otto, J. K. M. Sanders, *Org. Lett.* **2004**, *6*, 1825; z) S. G. Telfer, X.-J. Yang, A. F. Williams, *Dalton Trans.* **2004**, 699.
- [16] R. Nguyen, I. Huc, *Chem. Commun.* **2003**, 942.
- [17] T. J. Hubin, D. H. Busch, *Coord. Chem. Rev.* **2000**, *200*, 5.
- [18] Crystallographic data for **3**: [Cu(C₂₁H₁₉N₅O₂)₄](BF₄)₄·2-H₂O·CH₃CN; prism 0.18 × 0.18 × 0.23 mm; tetragonal, *I*₄/a (no. 88); *M*_r = 2172.3; *Z* = 4; *a* = 14.6561(3), *c* = 43.9683(14) Å, *V* = 9444.4(5) Å³; ρ_{calcd} = 1.528 g cm⁻³; $2\theta_{\text{max}}$ = 52.0°; MoK α radiation (λ = 0.71073 Å); ϕ scans of 0.5°; 37767 reflections measured at 200 K, 4601 unique reflections of which 2653 were observables ($|F_o| > 4\sigma(F_o)$); $4.4 < 2\theta < 52.0^\circ$. Data were corrected for Lorentz and polarization effects and for absorption (T_{min} , T_{max} = 0.8230, 0.8523). The structure was solved by direct methods (SIR97).^[22] All calculations were performed with the XTAL system.^[23] Full-matrix least-squares refinement based on *F* using weights of 1/ $(\sigma^2(F_o) + 0.00015(F_o^2))$ gave final values *R* = 0.036, ωR = 0.037, and *S* = 1.73(2) for 391 variables and 2914 contributing reflections. The maximum Δ/σ on the last cycle was 0.004. Min./max. residual electron density corresponded to 0.76/−0.46 e[−] Å^{−3}. Hydrogen atoms of the complex were placed in calculated positions except OH and NH groups, for which hydrogen atoms were observed and refined with restraints on bond lengths. CCDC-242577 (**3**) contains the supplementary crystallographic data for this paper. These data can be obtained free of charge via www.ccdc.cam.ac.uk/conts/retrieving.html (or from the Cambridge Crystallographic Data Centre, 12 Union Road, Cambridge CB21EZ, UK; fax: (+44)1223-336-033; or deposit@ccdc.cam.ac.uk).
- [19] D. L. Caulder, C. Brueckner, R. E. Powers, S. Koenig, T. N. Parac, J. A. Leary, K. N. Raymond, *J. Am. Chem. Soc.* **2001**, *123*, 8923.
- [20] H. Jiang, J.-M. Leger, P. Guionneau, I. Huc, *Org. Lett.* **2004**, *6*, 2985.
- [21] a) M. Ziegler, J. L. Brumaghim, K. N. Raymond, *Angew. Chem.* **2000**, *112*, 4285; *Angew. Chem. Int. Ed.* **2000**, *39*, 4119; b) M. M. Conn, J. Rebek, Jr., *Chem. Rev.* **1997**, *97*, 1647; c) J. L. Atwood, G. W. Orr, F. Hamada, S. G. Bott, K. D. Robinson, *Supramol. Chem.* **1992**, *1*, 15.
- [22] A. Altomare, M. C. Burla, M. Camalli, G. L. Cascarano, C. Giacovazzo, A. Guagliardi, A. G. G. Moliterni, G. Polidori, R. Spagna, *J. Appl. Crystallogr.* **1999**, *32*, 115.
- [23] S. R. Hall, H. D. Flack, J. M. Stewart, *XTAL 3.2 User's Manual*, Universities of Western Australia and Maryland, **1992**.

Hydrogen-Bond Lengths in Polypeptide Helices: No Evidence for Short Hydrogen Bonds**

Subrayashastry Aravinda, Saumen Datta,
Narayanaswamy Shamala,* and
Padmanabhan Balaram*

The 3_{10} helix and α helix are closely related secondary structures observed in polypeptides. The 3_{10} helix is characterized by successive $4 \rightarrow 1$ (C_{10}) hydrogen bonds (C_{10} = 10 atom hydrogen-bonding ring) of the type $C=O \cdots HN_{i+3}$, while the α helix displays a hydrogen bond of the type $C=O \cdots HN_{i+4}$ (C_{13}). The α helix is widely distributed in proteins, while the occurrence of segments of 3_{10} helix is very much less frequent.^[1] In polypeptides containing $C^{\alpha,\alpha}$ dialkylated residues, α -aminoisobutyric acid (Aib) being the prototype, both the 3_{10} and α helical structures are detected.^[2] In homooligomers of Aib, 3_{10} helices are invariably found in crystals,^[3] while in heteromeric sequences the precise helical type appears to depend on both Aib content and positioning.^[2a,d,4,5] While distinctions between 3_{10} and α helices are possible in the crystalline state, such differentiation becomes difficult in solution.^[6] Circular dichroism (CD) has been proposed for distinguishing between 3_{10} and α helix structures by using the ratio of CD bands at 222 nm and 207/208 nm.^[7] However, the use of the $[\theta]_{222}/[\theta]_{208}$ ratio has been questioned, suggesting that the distinction between 3_{10} and α helix structures by chiroptical methods may not be readily possible.^[8] The conventional interpretation of the CD spectra of helical polypeptides has been further called into question by the careful work of Kemp and co-workers, who have reported the observation of large values of $[\theta]_{222}$, which are inconsistent with those currently accepted for 100% helical structures.^[9] Kemp et al. have noted that the 222 nm $n\pi^*$ band has not “been modeled satisfactorily by theory”. The widespread use of the CD band intensities at 208 and 222 nm, in estimating helicity values quantitatively and in making qualitative distinctions between helix subtypes, underscores the impor-

tance of relating CD spectral intensities to specific peptide structural features. In addressing this issue, Dang and Hirst^[10] have used an improved theoretical method to calculate the 220 nm CD band intensities and have suggested that $[\theta]_{220}$ is extremely sensitive to main-chain hydrogen-bond length. They argue that “shortening from a conventional oxygen–nitrogen separation of about 3.0 Å to 2.8 Å or 2.7 Å is predicted to lead to a sizable enhancement of the intensity at 220 nm”, with the effect being most pronounced for α helices and less dramatic for 3_{10} and π helices. These calculations also reveal a dependence of $[\theta]_{220\text{nm}}$ on $N \cdots O$ separations in the range 3.0–3.5 Å, a factor which may contribute to the variations in band intensities in model 3_{10} and α helical peptides. With the exception of the Dang and Hirst proposal no testable explanations have been advanced for the observed variation in the 220 nm CD band intensity.

Herein we examine the distribution of hydrogen-bond parameters in high-resolution crystal structures of Aib-containing peptides to assess whether *short* hydrogen bonds are indeed observed in experimental structures. Aib-containing peptides were chosen because of the availability of a large number of accurately determined structures and the occurrence of pure α , 3_{10} , and mixed $3_{10}/\alpha$ helical structures in crystals.

The structure of *p*BrBz-(Aib)₁₀-OtBu (peptide **2**; *p*BrBz = *para*-bromobenzoyl) provides an example of a complete 3_{10} helix.^[3e] The structure of the peptide Boc-Leu-Aib-Val-Ala-Leu-Aib-Val-Ala-Leu-Aib-OMe (peptide **1**; Boc = 1,1-dimethylethoxycarbonyl (= *tert*-butyloxycarbonyl)) determined herein provides an example of a complete α helix over the length of the decapeptide. Figure 1 illustrates the molecular conformations of the two peptides and the distribution of backbone dihedral angles. The parameters for potential hydrogen-bond interactions in the two structures are compared in Table 1. The backbone dihedral angles are given in Table 2. Peptide **1** (α helix) is stabilized by seven intramolecular $5 \rightarrow 1$ hydrogen bonds while Peptide **2** (3_{10} helix) is stabilized by eight intramolecular $4 \rightarrow 1$ hydrogen bonds. The data in Table 1 suggests that for the α helix the observed range of $1 \rightarrow 5$ $N \cdots O$ separation is 2.978 Å to 3.113 Å, while for $1 \rightarrow 4$ separations in the 3_{10} helix it is 2.907 Å to 3.211 Å. Clearly, none of the observed hydrogen bonds would correspond to the *short* hydrogen bond (2.7 to 2.8 Å) used by Dang and Hirst in their theoretical computation of CD band intensities.^[10]

We have classified the hydrogen-bond patterns in the available crystal structures of Aib-containing helical peptides into $4 \rightarrow 1$ and $5 \rightarrow 1$ hydrogen bonds by using the following criteria: $N \cdots O$ separation ≤ 3.5 Å, $H \cdots O$ separation ≤ 2.6 Å, $\angle N-H \cdots O \geq 90^\circ$, $\angle C=O \cdots H \geq 90^\circ$, and $\angle C=O \cdots N \geq 90^\circ$.^[11] Table 3 summarizes the limits and mean of the hydrogen-bond parameters for the two hydrogen-bond types. Figure 2 summarizes the distribution of the parameters $N \cdots O$ separation and the angles $C=O \cdots N$ and $N-H \cdots O$. In $4 \rightarrow 1$ and $5 \rightarrow 1$ hydrogen bonds the mean hydrogen-bond lengths are 3.034 ± 0.109 Å and 3.034 ± 0.118 Å, respectively. This analysis suggests that short hydrogen bonds $N \cdots O < 2.8$ Å are extremely infrequent in polypeptide structures. While our analysis does not exclude the possibility of solvent-induced shortening of

[*] Prof. P. Balaram
Molecular Biophysics Unit
Indian Institute of Science
Bangalore—560 012 (India)
Fax: (+91) 80-2360-0683 / 0535
E-mail: pb@mbu.iisc.ernet.in

S. Aravinda, Dr. S. Datta, Prof. N. Shamala
Department of Physics
Indian Institute of Science
Bangalore—560 012 (India)
Fax: (+91) 80-2360-2602 / 0683
E-mail: shamala@physics.iisc.ernet.in

[**] This research was supported by a grant from the Council of Scientific and Industrial Research and Program Support in the area of Molecular Diversity and Design, Department of Biotechnology, India. We thank the reviewers for extremely constructive comments.

Supporting information for this article is available on the WWW under <http://www.angewandte.org> or from the author.

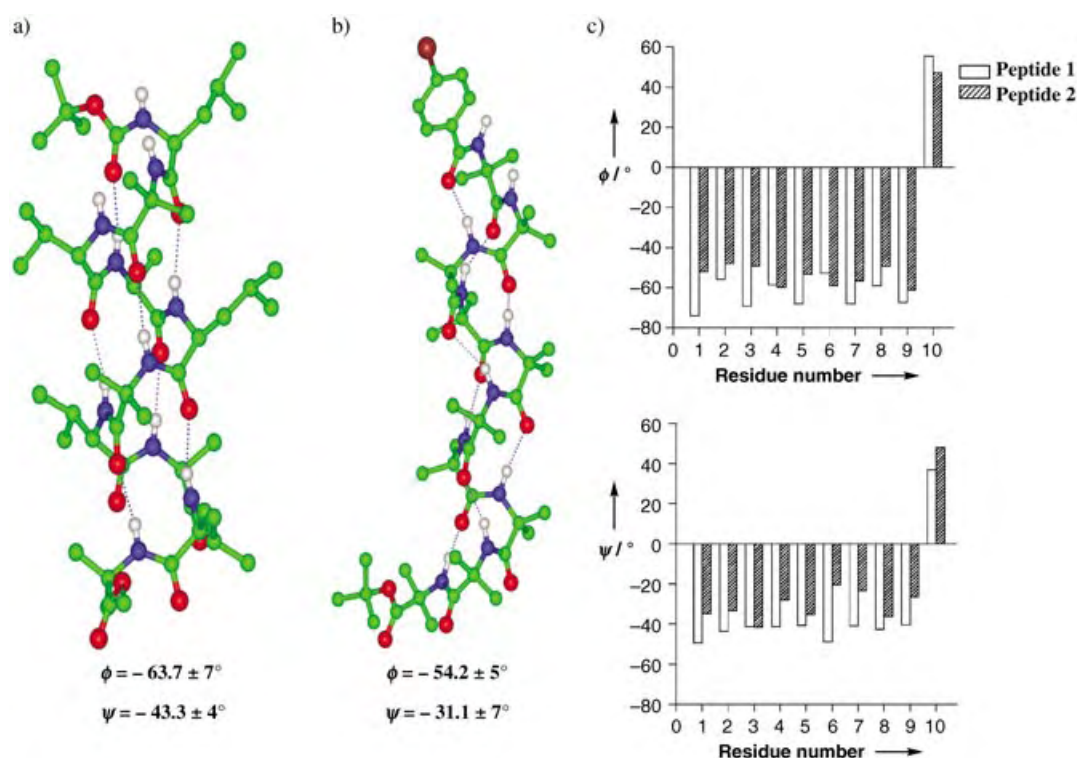


Figure 1. a) Molecular conformation of Boc-Leu-Aib-Val-Ala-Leu-Aib-Val-Ala-Leu-Aib-OMe (peptide **1**) in the crystal structure. b) Molecular conformation of pBrBz-(Aib)₁₀-OtBu (peptide **2**) in the crystal structure. All the intramolecular hydrogen bonds are shown as dotted lines; green C, red O, blue N. c) The distribution of the torsion angles in the peptide backbone ϕ, ψ observed in peptides **1** and **2**.

Table 1: Hydrogen bonds in peptides **1** and **2**.

Type	Donor	Acceptor	N...O [Å]	H...O [Å]	C=O...H [°]	C=O...N [°]	N-H...O [°]	N...O [Å]	H...O [Å]	C=O...H [°]	C=O...N [°]	N-H...O [°]
Intramolecular					Ideal α helix (peptide 1)					Ideal 3_{10} helix (peptide 2)		
4→1	N(3)	O(0)	3.559	3.104	96.7	108.5	115.4	2.945 ^[a]	2.123	127.5	131.7	159.8
4→1	N(4)	O(1)	3.200	2.779	94.9	108.4	111.8	2.975 ^[a]	2.182	131.8	136.4	153.4
4→1	N(5)	O(2)	3.401	2.920	91.7	103.5	117.3	2.979 ^[a]	2.198	118.9	126.0	151.1
4→1	N(6)	O(3)	3.221	2.855	92.9	106.9	107.5	3.179 ^[a]	2.382	119.9	125.3	154.4
4→1	N(7)	O(4)	3.393	2.923	90.3	102.4	116.3	3.020 ^[a]	2.183	122.1	126.5	164.2
4→1	N(8)	O(5)	3.283	2.884	92.3	105.7	110.3	3.211 ^[a]	2.355	129.3	130.9	173.4
4→1	N(9)	O(6)	3.390	2.932	93.4	105.6	115.3	3.057 ^[a]	2.225	130.7	133.3	163.0
4→1	N(10)	O(7)	3.235	2.782	90.9	104.5	114.5	2.907 ^[a]	2.087	122.1	128.0	159.2
5→1	N(4)	O(0)	2.978 ^[a]	2.165	149.9	156.1	157.7	4.613	3.916	136.8	143.1	140.7
5→1	N(5)	O(1)	3.113 ^[a]	2.277	157.0	159.8	163.9	4.337	3.665	135.5	143.2	137.3
5→1	N(6)	O(2)	3.071 ^[a]	2.237	147.0	151.4	163.3	4.331	3.630	142.5	149.2	140.8
5→1	N(7)	O(3)	3.005 ^[a]	2.174	155.2	159.1	162.1	4.600	4.012	129.9	138.3	128.8
5→1	N(8)	O(4)	3.014 ^[a]	2.183	147.6	152.2	162.3	4.791	4.181	135.7	142.9	131.2
5→1	N(9)	O(5)	3.048 ^[a]	2.209	154.2	157.5	165.2	5.200	4.547	125.1	131.5	136.0
5→1	N(10)	O(6)	2.986 ^[a]	2.194	146.7	154.0	153.0	4.600	3.970	128.7	136.4	133.0

[a] Acceptable hydrogen bonds.

hydrogen bonds as a factor influencing observed CD spectra, there is at present no evidence for such a phenomenon in solution. It may, therefore, be useful to reexamine the factors that contribute to the intensities of the $n \rightarrow \pi^*$ band in CD spectra of polypeptides. The extensive application of CD methods in estimating helicity in peptides and proteins emphasizes the importance of a rigorous theoretical underpinning for the analysis of peptide CD spectra. In particular

$n \rightarrow \pi^*$ band intensities may be influenced by a number of factors. The results herein suggest that short hydrogen bonds may not always be the sole contributing factor. Chiroptical distinctions between 3_{10} and α helical structures must also be tempered by the fact that many sequences can exhibit mixed hydrogen-bonding patterns and can exist in solution as equilibrium mixtures of closely related conformations.

Table 2: Torsion angles [$^{\circ}$]^[a] of peptides 1 and 2.

Peptide 1				Peptide 2			
Residue	ϕ	ψ	ω	Residue	ϕ	ψ	ω
Leu(1)	-74.1 ^[b]	-49.5	-178.0	Aib(1)	-51.9	-34.9	-178.2
Aib(2)	-55.9	-43.7	-175.7	Aib(2)	-48.2	-33.5	-177.3
Val(3)	-69.3	-41.3	176.6	Aib(3)	-49.0	-41.7	-173.2
Ala(4)	-58.5	-41.4	179.2	Aib(4)	-59.8	-28.1	-177.3
Leu(5)	-68.1	-40.7	175.4	Aib(5)	-53.2	-35.4	-173.7
Aib(6)	-52.7	-49.0	-174.9	Aib(6)	-59.0	-20.6	-178.0
Val(7)	-68.0	-40.8	177.6	Aib(7)	-56.5	-23.3	177.6
Ala(8)	-59.1	-42.7	179.1	Aib(8)	-49.3	-36.3	-177.6
Leu(9)	-67.2	-40.5	-176.9	Aib(9)	-61.2	-26.5	-172.1
Aib(10)	55.4	36.8 ^[c]	179.1 ^[d]	Aib(10)	47.3	48.0 ^[f]	176.4
Mean(9) ^[e]	-63.7 \pm 7.2	-43.3 \pm 4			-54.2 \pm 5.0	-31.1 \pm 6.9	

[a] The torsion angles for rotation about bonds of the peptide backbone (ϕ , ψ , and ω) and about bonds of the amino acid side chains (χ^1 , χ^2) as suggested by the IUPAC-IUB Commission on Biochemical Nomenclature.^[15] Estimated standard deviation $\approx 0.5^{\circ}$. [b] C'(0)-N(1)-C $^{\alpha}$ (1)-C'(1). [c] N(10)-C $^{\alpha}$ (10)-C'(10)-O(OMe). [d] C $^{\alpha}$ (10)-C'(10)-O(OMe)-C(OMe). [e] Mean value of the first nine residues. [f] The ψ value of -136.4° in ref.^[3e] corresponds to the torsion angle N(10)-C $^{\alpha}$ (10)-C'(10)-O(10).

Table 3: Summary of 4 \rightarrow 1 and 5 \rightarrow 1 hydrogen bonds in peptide helices.

	4 \rightarrow 1 hydrogen bonds				5 \rightarrow 1 hydrogen bonds			
	min	max	mean	Std	min	max	mean	Std
N \cdots O [\AA]	2.761	3.480	3.034	0.109	2.795	3.460	3.034	0.118
H \cdots O [\AA]	1.915	2.600	2.267	0.142	1.951	2.600	2.215	0.130
C=O \cdots H [$^{\circ}$]	90.7	156.0	119.7	10.5	127.5	174.3	151.0	7.6
C=O \cdots N [$^{\circ}$]	102.5	164.7	125.8	8.5	136.8	175.3	155.9	6.4
N-H \cdots O [$^{\circ}$]	114.1	173.4	150.4	14.3	121.3	178.1	158.2	9.2

Experimental Section

Peptide 1 was synthesized by conventional solution-phase procedures using a segment condensation strategy. Boc groups are used as N-terminal protecting groups and methyl ester as the C-terminal protecting groups. Peptide couplings were mediated by *N,N'*-dicyclohexylcarbodiimide (DCC) and 1-hydroxybenzotriazole.^[12] The final step involved a 3+7 coupling. Purification of the peptide was by reverse-phase medium-pressure liquid chromatography (C₁₈, 40–60 μ), using methanol–water gradients. The peptide was characterized by 500 MHz ^1H NMR spectroscopy and MALDI mass spectrometry ($[M + \text{Na}]^+_{\text{obs}} = 1089.7$; $M_{\text{calcd}} = 1067.37$) Crystals of were grown by slow evaporation of a methanol–water mixture of peptide 1. X-ray data were collected at room temperature from a dry crystal, on a CAD-4 diffractometer, using Cu $_{\text{K}\alpha}$ radiation ($\lambda = 1.5418 \text{ \AA}$). ω -2 θ scan type was used, with $2\theta = 150^{\circ}$, for a total of 7381 independent reflections. The crystal size was $0.2 \times 1.0 \times 0.2 \text{ mm}$. Space group $P2_12_12_1$, $a = 10.791(3)$, $b = 16.632(2)$, $c = 36.068(9) \text{ \AA}$, $V = 6473(3) \text{ \AA}^3$, $Z = 4$ for chemical formula $\text{C}_{52}\text{H}_{94}\text{N}_{10}\text{O}_{13}$, with one molecule per asymmetric unit. $\rho_{\text{calcd}} = 1.095 \text{ g cm}^{-3}$, $\mu = 0.064 \text{ mm}^{-1}$, $F(000) = 2320$. The structure was obtained by direct methods using SHELXS-86.^[13a] Refinement was carried out against F^2 , with full-matrix least-squares methods using SHELXL-93.^[13b] All non-hydrogen atoms were refined isotropically. The R value at the end of isotropic refinement was 0.10. The R value dropped to 0.06 after anisotropic refinement. The hydrogen atoms were fixed geometrically in idealized positions and refined in the final cycle of refinement as riding over the atoms to which they are bonded. The final R value was 0.0418 ($wR_2 =$

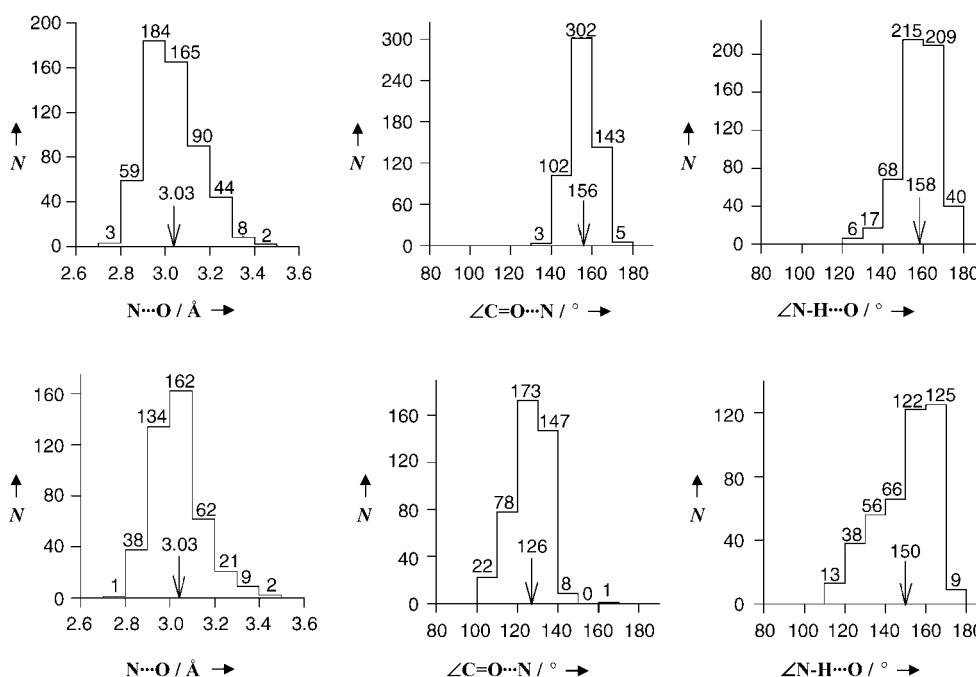


Figure 2. Distribution of N \cdots O separation, C=O \cdots N angles and N-H \cdots O angles observed in 5 \rightarrow 1 hydrogen bonds (top) and 4 \rightarrow 1 hydrogen bonds (bottom). N is the number of occurrences in the dataset.

0.113) for observed reflections 5170 with $F_o \geq 4\sigma(|F_o|)$ and 673 variables, where the data to parameter ratio is 7.7:1.0 and $S = 1.038$. The largest difference peak was $0.17 \text{ e} \text{ \AA}^{-3}$ and the largest difference hole was $-0.25 \text{ e} \text{ \AA}^{-3}$. The standard deviations in bond lengths are approximately 0.004 \AA and those of bond angles are approximately 0.3° . CCDC 243105 contains the supplementary crystallographic data for this paper. These data can be obtained free of charge via www.ccdc.cam.ac.uk/conts/retrieving.html (or from the Cambridge Crystallographic Data Centre, 12 Union Road, Cambridge CB2 1EZ, UK; fax: (+44) 1223-336-033; or deposit@ccdc.cam.ac.uk).

Data base analysis: Out of 407 sequences containing at least one Aib residue retrieved from the Cambridge Structural Database (CSD) (November 2003 release),^[14] 393 were linear and 14 were cyclic peptides. For the analysis we have used peptide sequences of length six amino acids and more. 128 sequences were used for hydrogen-bond calculation. All the N–H separations were fixed at 0.86 \AA . All the $4 \rightarrow 1$ and $5 \rightarrow 1$ hydrogen bonds were calculated. There are totally 555 (α helical) $5 \rightarrow 1$ hydrogen bonds and 429 (3_{10} helical) $4 \rightarrow 1$ hydrogen bonds in 128 sequences.

For a list of peptides, CCDC codes and references, used in the hydrogen-bond analysis see the Supporting Information.

Received: June 30, 2004

Revised: August 10, 2004

Keywords: circular dichroism · helical structures · hydrogen bonds · peptides · structure elucidation

- [1] a) D. J. Barlow, J. M. Thornton, *J. Mol. Biol.* **1988**, *201*, 601–619; b) K. A. Bolin, G. L. Millhauser, *Acc. Chem. Res.* **1999**, *32*, 1027–1033.
- [2] a) I. L. Karle, P. Balam, *Biochemistry* **1990**, *29*, 6747–6756; b) C. Toniolo, E. Benedetti, *Trends Biochem. Sci.* **1991**, *16*, 350–353; c) C. Toniolo, E. Benedetti, *Macromolecules* **1991**, *24*, 4004–4009; d) I. L. Karle, *Acta Crystallogr. Sect. B* **1992**, *48*, 341–356; e) E. Benedetti, *Biopolymers (Peptide Science)* **1996**, *40*, 3–44; f) I. L. Karle, *Biopolymers (Peptide Science)* **1996**, *40*, 157–180; g) R. Kaul, P. Balam, *Bioorg. Med. Chem.* **1999**, *7*, 105–117.
- [3] For a representative set of examples, see: a) N. Shamala, R. Nagaraj, P. Balam, *J. Chem. Soc. Chem. Commun.* **1978**, 996–997; b) E. Benedetti, A. Bavoso, B. Di Blasio, V. Pavone, C. Pedone, M. Crisma, G. M. Bonora, C. Toniolo, *J. Am. Chem. Soc.* **1982**, *104*, 2437–2444; c) A. Bavoso, E. Benedetti, B. Di Blasio, V. Pavone, C. Pedone, C. Toniolo, G. M. Bonora, *Proc. Natl. Acad. Sci. USA* **1986**, *83*, 1988–1992; d) R. Gessmann, H. Brückner, M. Kokkinidis, *Acta Crystallogr. Sect. B* **1998**, *54*, 300–307; e) C. Toniolo, M. Crisma, G. M. Bonora, E. Benedetti, B. Di Blasio, V. Pavone, C. Pedone, A. Santini, *Biopolymers* **1991**, *31*, 129–138; f) R. Gessman, H. Brückner, K. Petratos, *J. Pept. Sci.* **2003**, *9*, 753–762.
- [4] a) I. L. Karle, J. L. Flippen-Anderson, R. Gurunath, P. Balam, *Protein Sci.* **1994**, *3*, 1547–1555; b) V. Pavone, E. Benedetti, B. Di Blasio, C. Pedone, A. Santini, A. Bavoso, C. Toniolo, M. Crisma, L. Sartore, *J. Biomol. Struct. Dyn.* **1990**, *7*, 1321–1331; c) G. R. Marshall, E. E. Hodgkin, D. A. Langs, D. G. Smith, J. Zabrocki, M. T. Leplawy, *Proc. Natl. Acad. Sci. USA* **1990**, *87*, 487–491.
- [5] a) G. Basu, K. Bagchi, A. Kuki, *Biopolymers* **1991**, *31*, 1763–1774; b) G. Basu, A. Kuki, *Biopolymers* **1992**, *32*, 61–71; c) K. Otoda, Y. Kitagawa, S. Kimura, Y. Imanishi, *Biopolymers* **1993**, *33*, 1337–1345.
- [6] a) G. L. Millhauser, *Biochemistry* **1995**, *34*, 3873–3877; b) S. Mammi, M. Rainaldi, M. Bellanda, E. Schievano, E. Peggion, Q. B. Broxterman, F. Formaggio, M. Crisma, C. Toniolo, *J. Am. Chem. Soc.* **2000**, *122*, 11735–11736; c) R. A. G. D. Silva, S. C. Yasui, J. Kubelka, F. Formaggio, M. Crisma, C. Toniolo, T. A. Keiderling, *Biopolymers* **2002**, *65*, 229–243.
- [7] a) C. Toniolo, A. Polese, F. Formaggio, J. Kamphuis, *J. Am. Chem. Soc.* **1996**, *118*, 2744–2745; b) G. Yoder, A. Polese, R. A. G. D. Silva, F. Formaggio, M. Crisma, Q. B. Broxterman, J. Kamphuis, C. Toniolo, T. A. Keiderling, *J. Am. Chem. Soc.* **1997**, *119*, 10278–10285.
- [8] a) T. S. Sudha, E. K. S. Vijayakumar, P. Balam, *Int. J. Pept. Protein Res.* **1983**, *22*, 464–468; b) M. C. Manning, R. W. Woody, *Biopolymers* **1991**, *31*, 569–586; c) N. H. Andersen, Z. Liu, K. S. Prickett, *FEBS. Lett.* **1996**, *399*, 47–52.
- [9] a) P. Wallimann, R. J. Kennedy, D. S. Kemp, *Angew. Chem.* **1999**, *111*, 1377–1379; *Angew. Chem. Int. Ed.* **1999**, *38*, 1290–1292; b) P. Wallimann, R. J. Kennedy, J. S. Miller, W. Shalongo, D. S. Kemp, *J. Am. Chem. Soc.* **2003**, *125*, 1203–1220.
- [10] Z. Dang, J. D. Hirst, *Angew. Chem.* **2001**, *113*, 3731–3733; *Angew. Chem. Int. Ed.* **2001**, *40*, 3619–3621.
- [11] a) E. N. Baker, R. E. Hubbard, *Prog. Biophys. Mol. Biol.* **1984**, *44*, 97–179; b) S. Datta, N. Shamala, A. Banerjee, P. Balam, *J. Pept. Res.* **1997**, *49*, 604–611.
- [12] H. Balam, M. Sukumar, P. Balam, *Biopolymers* **1986**, *25*, 2209–2223.
- [13] a) G. M. Sheldrick *SHELXS-86*, Program for the Crystal Structure Solution, Universität Göttingen, Germany, **1986**; b) G. M. Sheldrick, *SHELXL-93*, Program for the Refinement of Crystal Structures, Universität Göttingen, Germany, **1993**.
- [14] F. H. Allen, *Acta Crystallogr. Sect. B* **2002**, *58*, 380–388.
- [15] IUPAC–IUB Commission on Biochemical Nomenclature *Biochemistry* **1970**, *9*, 3471–3479.

Asymmetric Reduction**Enantioselective Reduction of Aromatic and Aliphatic Ketones Catalyzed by Ruthenium Complexes Attached to β -Cyclodextrin*****Alain Schlatter, Mrinal K. Kundu, and Wolf-D. Woggon**

Molecular recognition of substrates by cyclodextrins is made possible by noncovalent interactions in the hydrophobic cavity of the water-soluble, cyclic sugar oligomers. Inclusion complexes of cyclodextrins^[1] and their reactions constitute one of the earliest examples of supramolecular chemistry.^[2] As a result of these unique features, cyclodextrins can be used to mediate regioselective reactions^[3] and in particular for preparing enzyme models.^[4,5]

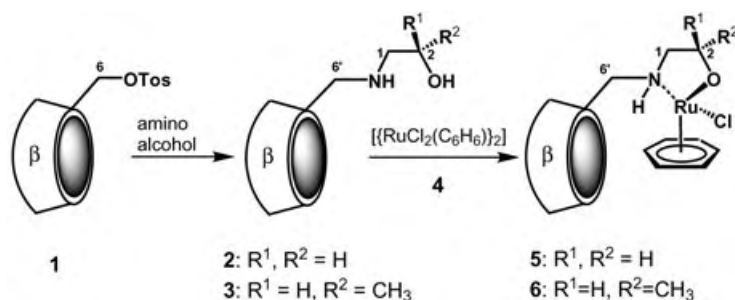
In this context, the binding properties of β -cyclodextrins have been complemented with chemically reactive subunits,

[*] A. Schlatter, Dr. M. K. Kundu, Prof. W.-D. Woggon
Department of Chemistry
University of Basel
St. Johannis-Ring 19, 4056 Basel (Switzerland)
Fax: (+41) 61-267-1102
E-mail: wolf-d.woggon@unibas.ch

[**] We thank the Swiss National Science Foundation and the Roche Foundation for supporting this research. Markus Neuburger is gratefully acknowledged for X-ray crystallographic analysis.

either by attaching functional groups such as acid–base catalysts^[3] or by linking β -cyclodextrins to metal complexes.^[4,5] In most cases superb reactivity and a very high degree of regioselectivity were observed. In contrast, enantioselective reactions with β -cyclodextrin (β -CD) as the only chiral subunit of the catalyst in general gave products with *ee* values well below 50 %. For example, the highest enantiomeric excess reported for a product of NaBH₄ reduction of an aromatic ketone in the presence of β -cyclodextrin was 24 % *ee*.^[6] Additives, such as amines^[7] or aminoboranes,^[8] improved the enantioselectivity, but only at the expense of the yield. We report herein our results on the first ruthenium–arene complexes of β -cyclodextrin-modified amino alcohols and their use in asymmetric hydrogenation reactions of prochiral ketones.

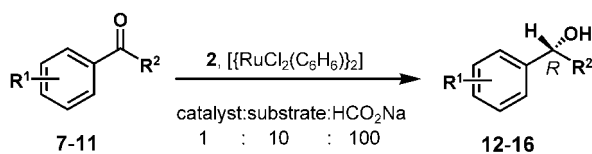
Mono(*O*-6-tosyl)- β -cyclodextrin (**1**, β -CD-Tos) is commercially available and can also be prepared by the tosylation of β -CD on a large scale.^[9] The amino alcohol linked β -cyclodextrins **2** and **3** were obtained in good yields as crystalline compounds by the treatment of **1** with an excess of the amino alcohol. $[(\text{RuCl}_2(\text{C}_6\text{H}_6))_2]$ (**4**) was prepared by a literature procedure.^[10] The formation of Ru complexes of **2** and **3** (Scheme 1) was shown to be quantitative by ¹H NMR



Scheme 1. Synthesis of Ru complexes of the amino alcohol β -cyclodextrins **2** and **3**. The structures of **5** and **6** are tentatively assigned.

spectroscopic studies (600 MHz, D₂O). For example, significant chemical-shift changes are observed between **2** and **5**: The doublets assigned to the two H atoms at C6' of **2** shift downfield by 0.56 ppm, and the triplet assigned to the H atoms at C1 of **2** shifts downfield by 0.49 ppm. The formation of the Ru complex **6** from **3** leads to the following chemical-shift changes: The signals for the two H atoms at C6' shift downfield by 0.56 ppm and 0.51 ppm, and those for the H atoms at C1 shift downfield by 0.36 ppm and 0.54 ppm.

For catalytic reactions, the Ru complexes were formed in situ and treated with ketones at room temperature under an argon atmosphere in the presence of excess sodium formate as the hydrogen source (Scheme 2). Even with β -cyclodextrin



Scheme 2. Asymmetric reduction of ketones in water.

as the only chiral unit of the Ru complex the alcohol products are formed with remarkable enantioselectivity, predominantly with the *R* configuration (Table 1). Evidently the observed *ee* values correlate with the binding constants of the ketones to β -cyclodextrin,^[11] thus reflecting the preorganization of substrates such that *Si* addition of the hydride to the carbonyl group is preferred in the reactive complex.^[11]

Table 1: Enantioselective reduction of ketones **7–11** with the catalyst **2+4** (10 mol %).

Ketone	R ¹	R ²	Alcohol ^[a]	Yield [%] ^[b]	<i>ee</i> [%] ^[c]
7	H	CH ₃	(<i>R</i>)- 12	81	12
8	H	C ₂ H ₅	(<i>R</i>)- 13	61	6
9	<i>p</i> -CH ₃	CH ₃	(<i>R</i>)- 14	67	31
10	<i>p</i> -Cl	CH ₃	(<i>R</i>)- 15	93	47
11	<i>p</i> -tBu	CH ₃	(<i>R</i>)- 16	64	47

[a] Absolute configuration based on optical rotation. [b] Yields based on GLC analysis and isolated material. [c] Enantiomeric excess determined by ¹H NMR spectroscopy (Eu(tfc)₃) (tfc = 3-(trifluoromethylhydroxymethylene)-*D*-camphorate) and HPLC analysis (chiracel OD-H).

Since it is known from work by other research groups^[12] that asymmetric reduction catalyzed by Ru/amino alcohol complexes lacking a cyclodextrin unit is largely dependent on the chirality at the carbinol carbon atom (C2), we prepared **3** by the condensation of (*S*)-(+)-1-amino-2-propanol and β -CD-Tos (**1**). Ligand **3** was isolated in 66 % yield as a white solid and was subsequently characterized by high-field NMR spectroscopy, MS(ESI), and X-ray crystal-structure analysis (Figure 1). Initial experiments with the Ru complex of **3**

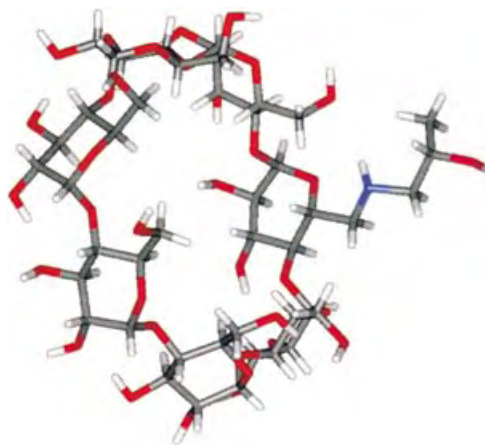


Figure 1. Structure of ligand **3** derived from X-ray crystal-structure analysis.

revealed a solubility problem in water. To avoid rather dilute conditions the transfer-hydrogenation reactions with **3** were carried out in a mixture of H₂O/DMF (3:1; see Experimental Section; DMF = *N,N*-dimethylformamide).

When the β -CD derivative **3** was used, the products were obtained with *ee* values of up to 97 % and in acceptable yields (Table 2). It is interesting to note that with **3** as a ligand for Ru, acetophenone (**7**) was reduced to (*S*)-**12** with 77 % *ee*; in

Table 2: Enantioselective reduction of ketones **7–11** with the catalyst **3+4** (10 mol %).

Ketone	R ¹	R ²	Alcohol ^[a]	Yield [%] ^[b]	ee [%] ^[c]
7	H	CH ₃	(<i>S</i>)- 12	90	77
8	H	C ₂ H ₅	(<i>S</i>)- 13	63	80
9	<i>p</i> -CH ₃	CH ₃	(<i>S</i>)- 14	69	94
10	<i>p</i> -Cl	CH ₃	(<i>S</i>)- 15	77	87
11	<i>p</i> - <i>t</i> Bu	CH ₃	(<i>S</i>)- 16	51	97

[a], [b], and [c]: see Table 1.

contrast, the Ru complex of (*S*)-1-amino-2-propanol lacking the β -cyclodextrin unit gave **12** in only $\approx 50\%$ ee in favor of the *S* isomer.^[13] Since we obtained *R* alcohols by using Ru complexes with ligand **2** and *S* alcohols with ligand **3** our results suggest a clear dominance of the chirality at C2 on the enantioselectivity.

The catalytic system described herein also enables the synthesis of ²H-enriched benzyl alcohols starting from ketones and with sodium [D₁]formate as a deuterium source for isotope labeling. Thus, ketones **7**, **8**, and **10** were reduced with 10% of **3+4** and DCO₂Na (98% D) in a H₂O/DMF mixture (3:1, 500 μ L) to give *S* deuterated alcohols **17**, **18**, and **19** in good yields and with enantioselectivities comparable to those observed with HCOONa. High-field NMR (600 MHz) spectroscopic measurements showed that ²H-labeling was as high as >97 atom % (Table 3).

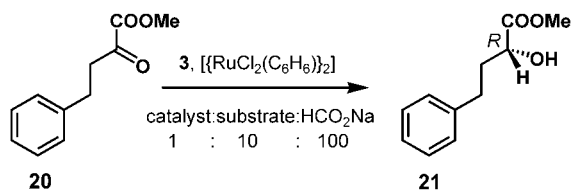
Table 3: Enantioselective reduction of ketones **7**, **8**, and **10** with the catalyst **3+4** (10 mol %) and DCO₂Na.

Ketone	R ¹	R ²	Alcohol ^[a]	Yield [%] ^[b]	ee [%] ^[c]
7	H	CH ₃	(<i>S</i>)- 17	79	77
8	H	C ₂ H ₅	(<i>S</i>)- 18	53	76
10	<i>p</i> -Cl	CH ₃	(<i>S</i>)- 19	70	87

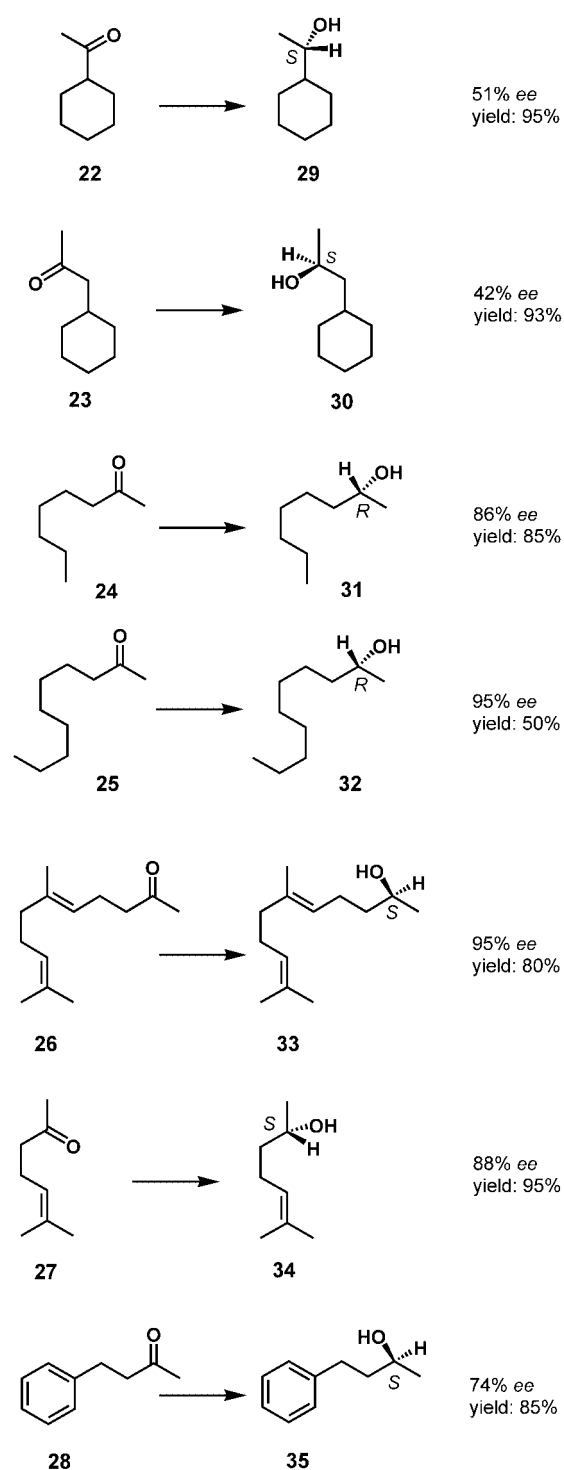
[a], [b], and [c]: see Table 1.

Further examples demonstrate the potential scope of the system. α -Ketoesters, such as **20**, are reduced quantitatively to the corresponding *R*-configured alcohols **21** with 57% ee (Scheme 3).

Also most promising were first reactions with aliphatic and unconjugated ketones. Thus, ketones **22–28** were reduced under the same conditions as described above to alcohols **29–35** in acceptable yields and with moderate to high enantioselectivity (Scheme 4).

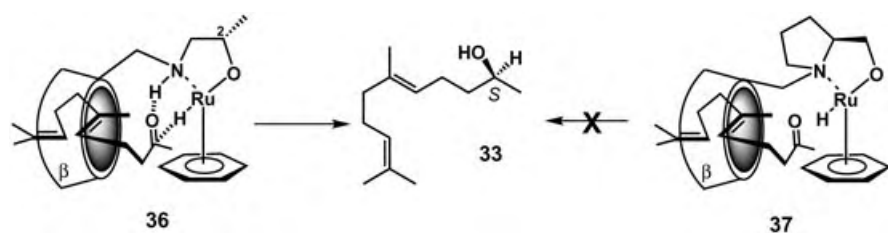


Scheme 3. Reduction of the α -ketoester **20**.



Scheme 4. Enantioselective reduction of aliphatic ketones under the conditions used for the reactions in Table 2.

The reaction mechanism of our transformations seems to resemble that suggested by Noyori and co-workers,^[11] since in contrast to **36** the cyclodextrinyl–prolinol–Ru complex **37** was completely unreactive, thus indicating the significance of the N–H group for hydrogen transfer to the carbonyl group (Scheme 5).



Scheme 5. Suggested hydrogen transfer (*Re* attack) from the Ru-hydride intermediate to geranyl acetone (**26**) encapsulated in β-cyclodextrin (see **36**); the reaction in **37** fails.

In summary, we have synthesized new water-soluble Ru complexes of β-cyclodextrin-modified amino alcohols **2** and **3** to serve as supramolecular catalysts in hydrogen-transfer reactions. Up to 97% *ee* and good to excellent yields were observed. In all cases, β-cyclodextrin plays an important role on the enantioselectivity through preorganization of the substrates in the hydrophobic cavity. This finding is particularly significant in the case of substrates such as **22–28**. Although a number of highly enantioselective Ru-based hydrogen-transfer catalysts are known,^[14] including one example that functions in water,^[15] none of these systems have been shown to reduce unconjugated ketones.

Experimental Section

Synthesis of 2: A neat solution of mono(*O*-6-tosyl)-β-cyclodextrin (265 mg, 0.20 mmol) and aminoethanol (960 mg, 15.7 mmol, 80 equiv) was stirred for 12 h at 70 °C. Water was then added (1.0 mL), and the resulting yellow solution was added dropwise to acetone (60 mL). The resulting white precipitate (245 mg) was filtered off and recrystallized from water to give pure **2** (140 mg, 59%). MS(ESI): *m/z* 1179 (*M*⁺, 100), 612 ([*M*+Na]²⁺, 72), 1201 ([*M*+Na]⁺, 67); ¹H NMR (600 MHz, D₂O): δ = 4.97–5.02 (m, 7H), 3.79–3.86 (m, 8H), 3.68–3.77 (m, 19H), 3.44–3.50 (m, 13H), 3.33 (dd, *J* = 9.60, 9.60 Hz, 1H), 2.92 (d, *J* = 10.86 Hz, 1H), 2.69 (m, 1H), 2.54 ppm (m, 2H); m.p.: decomposition > 275 °C.

Synthesis of 3: A neat solution of mono(*O*-6-tosyl)-β-cyclodextrin (300 mg, 0.23 mmol) and (*S*)-(+)-2-aminopropanol (1.4 g, 18.6 mmol, 80 equiv) was stirred for 12 h at 70 °C. Water (0.5 mL) was then added, and the resulting yellow solution was added dropwise to acetone (60 mL). The white precipitate (300 mg) was removed by filtration and recrystallized from water. The white crystals were washed with an ice-cold acetone/water mixture (1:1, 5 mL) to give pure **3** (181 mg, 66%). MS(ESI): *m/z* 1192 (*M*⁺, 100), 618.5 ([*M*+Na]²⁺, 85), 1214 ([*M*+Na]⁺, 78); ¹H NMR (600 MHz, D₂O): δ = 5.00–5.05 (m, 7H), 3.87–3.94 (m, 8H), 3.76–3.85 (m, 19H), 3.48–3.63 (m, 13H), 3.38 (dd, *J* = 9.60, 9.60 Hz, 1H), 3.02 (d, *J* = 10.86 Hz, 1H), 2.79–2.82 (m, 1H), 2.54–2.57 (m, 2H), 1.09 (d, *J* = 6.32 Hz, 3H); m.p.: decomposition > 275 °C. Crystal data for **3**: C₄₅H₇₇NO₃₅·16H₂O, orthorhombic, *P*2₁, *a* = 12.8092(4) Å, *b* = 19.6407(5) Å, *c* = 26.2645(5) Å, α = 90°, β = 90°, γ = 90°, *V* = 6696.3 Å³, *Z* = 4, ρ_{calcd} = 1.47, 85399 reflections were measured, *T* = 173 K. Data were collected with MoK_α radiation on a Bruker diffractometer (KAP-PACCD and scantype PHIOMEGA).

6 (formed in situ): MS (ESI): *m/z* = 1191 ([ligand **3**]⁺, 100), 1371 ([6-Cl]⁺, 11), 1406 ([6]⁺, 18); UV/Vis (H₂O): λ_{max} = 251 nm.

General procedure:^[16] Ligand **3** (0.01 mmol) was dissolved in H₂O/DMF (3:1, 0.5 mL), [RuCl₂(C₆H₅)₂] (**4**, 0.005 mmol) was added, and the resulting mixture was stirred for 1 h at room temperature. HCOONa (1.0 mmol) was then added, and after further stirring for 10 min the ketone (0.1 mmol) was injected. The reaction was usually

finished after 24 h at room temperature. The mixture was then extracted three times with hexane (5 mL), the combined hexane extracts were washed with water (6 mL) and dried over Na₂SO₄, and the product(s) were analyzed by GC/HPLC and/or purified by TLC. The *ee* values of the products were determined by HPLC on a chiral phase (chiracel OD-H), GC on a chiral phase (hydrodex 3P), and ¹H NMR/¹⁹F NMR spectroscopic studies of the corresponding Mosher esters.

Received: March 23, 2004

Revised: August 23, 2004

Keywords: asymmetric catalysis · cyclodextrins · reduction · ruthenium · transfer hydrogenation

- [1] a) K. Takahashi, *Chem. Rev.* **1998**, 98, 2013; b) J. Szejtli, *Cyclodextrins and their Inclusion Complexes*, Akademiai Kiado, Budapest, **1982**.
- [2] a) J.-M. Lehn, *Supramolecular Chemistry*, VCH, Weinheim, **1995**; b) *Comprehensive Supramolecular Chemistry* (Eds.: J. L. Atwood, J. E. D. Davies, D. D. MacNicol, F. Vögtle), Pergamon, Oxford, **1996**.
- [3] R. Breslow, *Acc. Chem. Res.* **1980**, 13, 170.
- [4] R. R. French, P. Holzer, M. Leuenberger, W.-D. Woggon, *Angew. Chem.* **2000**, 112, 1321; *Angew. Chem. Int. Ed.* **2000**, 39, 1267.
- [5] J. Yang, B. Gabriele, S. Belvedere, Y. Huang, R. Breslow, *J. Org. Chem.* **2002**, 67, 5057.
- [6] K. K. Park, J. W. Park, W.-J. Sim, *J. Inclusion Phenom. Mol. Recognit. Chem.* **1997**, 27, 41.
- [7] A. Deratani, E. Renard, F. Djedaini-Pilard, B. Perly, *J. Chem. Soc. Perkin Trans. 2* **1997**, 1517.
- [8] H. Sakuraba, N. Inomata, Y. Tanaka, *J. Org. Chem.* **1989**, 54, 3482.
- [9] R. R. French, J. Wirz, W.-D. Woggon, *Helv. Chim. Acta* **1998**, 81, 1521.
- [10] M. A. Bennett, A. K. Smith, *J. Chem. Soc. Dalton Trans.* **1974**, 233.
- [11] a) R. Noyori, M. Yamakawa, S. Hashiguchi, *J. Org. Chem.* **2001**, 66, 7931; b) M. Yamakawa, H. Ito, R. Noyori, *J. Am. Chem. Soc.* **2000**, 122, 1466; c) D. A. Alonso, P. Brandt, S. J. M. Nordin, P. G. Andersson, *J. Am. Chem. Soc.* **1999**, 121, 9580.
- [12] a) J. Takehara, S. Hashiguchi, A. Fujii, S. Inoue, T. Ikariya, R. Noyori, *Chem. Commun.* **1996**, 233; b) R. Noyori, *Adv. Synth. Catal.* **2003**, 1–2, 345.
- [13] D. G. I. Petra, J. N. H. Reek, J.-W. Handgraaf, E. J. Meijer, P. Dierkes, P. C. J. Kamer, J. Brussee, H. E. Schoemaker, P. W. N. M. van Leeuwen, *Chem. Eur. J.* **2000**, 6, 2818.
- [14] R. Noyori, *Angew. Chem.* **2002**, 114, 2108; *Angew. Chem. Int. Ed.* **2002**, 41, 2008.
- [15] a) H. Y. Rhyoo, H.-J. Park, Y. K. Chung, *Chem. Commun.* **2001**, 2064; b) H. Y. Rhyoo, H.-J. Park, W. H. Suh, Y. K. Chung, *Tetrahedron Lett.* **2002**, 43, 269.
- [16] The concentrations of the catalyst (10 mol%) and formate (excess) were adjusted to give a reasonable reaction time of approximately 24 h. Decreasing the catalyst and/or formate concentration led to unsuitably long reaction times. Preliminary experiments in which Ru–O was replaced by Ru–NTos revealed a sixfold increase in the rate of the reaction, thus allowing for lower catalyst loadings; results will be reported in a subsequent publication.

Drug Design

Antibacterial Aminoglycosides with a Modified Mode of Binding to the Ribosomal-RNA Decoding Site**

Boris François, Janek Szychowski,
Susanta Sekhar Adhikari,
Kandasamy Pachamuthu, Eric E. Swayze,
Richard H. Griffey, Michael T. Migawa,
Eric Westhof,* and Stephen Hanessian*

The past decade has witnessed a phenomenal advance in our understanding of the structure and function of ribosomal RNAs as they relate to the mode of action of clinically relevant antibiotics.^[1–6] The aminoglycosides are a group of well-known bactericidal antibiotics.^[7] Their widespread use in clinical practice has been curtailed as a result of their oxototoxicity, nephrotoxicity, and susceptibility to enzymatic inactivation;^[8] hence the need for careful patient monitoring in a hospital environment.^[9] By binding specifically to the bacterial decoding A site, which is responsible for fidelity during protein synthesis by monitoring correct Watson–Crick base pairing between the mRNA codon and the tRNA anticodon, aminoglycoside antibiotics increase the error rate of translation.^[10–12] Paromomycin (**1**) has been a benchmark for structural studies owing to its excellent binding affinity for the highly conserved set of nucleotides in the decoding 16S rRNA (A site) region of the 30S subunit of bacterial ribosomes (Figure 1).^[13] X-ray crystallographic studies of paromomycin complexed with the 30S subunit of

rRNA from *Thermus thermophilus*^[2] as well as with a sequence of oligonucleotides corresponding to the ribosomal A site of *E. coli*^[14] have delineated the basis for the molecular recognition.^[15]

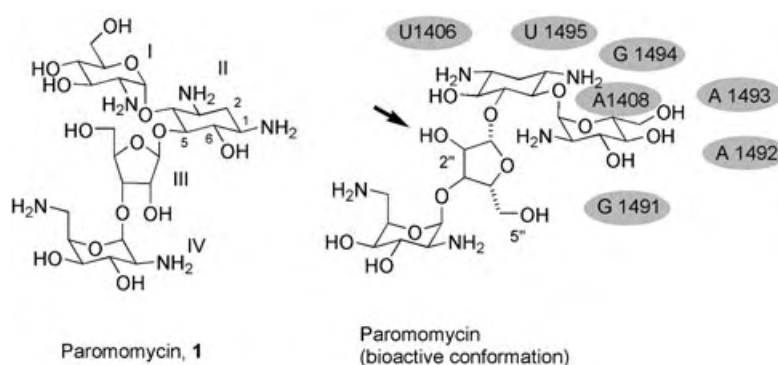


Figure 1. Structure of paromomycin, its bioactive conformation with relevant nucleotides in the A-site binding domain, and proposed site for diversification (arrow).

Crystal structures^[2,14,16,17] have shown that upon binding to the A site the four rings in paromomycin adopt an L shape, which represents its bioactive conformation. Ring I intercalates into the A site and forms two H bonds with A1408, whereas the invariant ammonium nitrogen atoms of ring II form constant interactions with A1493, G1494, and U1495. The binding of rings I and II force A1492 and A1493 to bulge out of the deep/major groove. Rings III and IV interact with the lower stem of the A site mainly through more variable charge and H-bonding interactions with neighboring nucleotides. These hallmark structural events, characteristic of all bioactive aminoglycosides that bind at the A site,^[14,16,17] are supported by the observed in vivo drug susceptibilities of several ribosomal-RNA mutants.^[18]

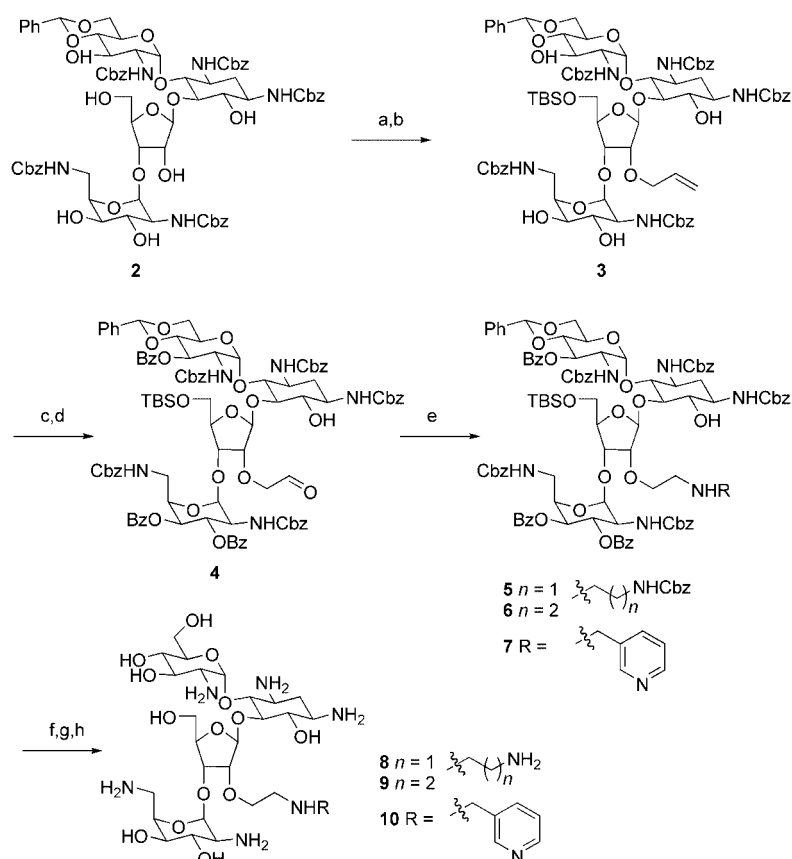
We reasoned that a structure-based design approach with a chemically modified paromomycin derivative could exploit uncharted areas of the A site, with the possible location of new modes of binding.^[19–23] Examination of the crystal structure of the paromomycin complex^[14] reveals that the hydroxy group at C2'' of ring III is favorably disposed for appropriate functional diversification (Figure 1). With this objective in mind, the main challenge was to develop methods of regioselective functionalization of the complex polyol system in paromomycin, so as to access the C2'' hydroxy group selectively.

The readily available paromomycin derivative **2**^[24] was silylated at C5'' and the product was subjected to O allylation under standard conditions (Scheme 1). Remarkably, after TBS protection of the C5'' hydroxy group, a highly regioselective allylation of the C2'' hydroxy group led to **3** in good yield. Protection of the hydroxy groups on rings II and IV by benzylation and oxidative cleavage of the allyl group afforded aldehyde **4**. Reductive amination with three representative alkyl amines gave the protected ω-(aminoalkyl) ether analogues **5–7**. Treatment with a catalytic amount of sodium methoxide in methanol afforded the corresponding

[*] B. François, Prof. E. Westhof
Institut de biologie moléculaire et cellulaire
UPR9002 CNRS, Université Louis Pasteur
15 rue René Descartes, 67084 Strasbourg Cedex (France)
Fax: (+33) 3-8841-7066
E-mail: e.westhof@ibmc.u-strasbg.fr
J. Szychowski, Dr. S. S. Adhikari, Dr. K. Pachamuthu,
Prof. S. Hanessian
Department of Chemistry, Université de Montréal
P.O. Box 6128, Station Centre-ville
Montréal, P.Q., H3C 3J7 (Canada)
Fax: (+1) 514-343-5728
E-mail: stephen.hanessian@umontreal.ca
Dr. E. E. Swayze, Dr. R. H. Griffey, Dr. M. T. Migawa
Ibis Therapeutics
2292 Faraday Avenue, Calsbad, CA 92008 (USA)

[**] We thank the NSERC and the Institut Universitaire de France for financial assistance provided to S.H. and E.W., respectively. Thanks are due to Lisa M. Risen for transcription/translation and MIC assays, and Dr. Kristen A. Sannes-Lowery for the K_D determinations. We acknowledge the European Synchrotron Radiation Facility for provision of synchrotron radiation facilities, and we thank Stéphanie Monaco and Joanne McCarthy for assistance with the use of beamlines ID14-2 and ID14-4.

Supporting information for this article is available on the WWW under <http://www.angewandte.org> or from the author.



Scheme 1. Reagents and conditions: a) TBSOTf, 2,4,6-collidine, CH_2Cl_2 , 75%; b) $\text{CH}_2=\text{CHCH}_2\text{I}$, KHMDS, THF, 70%; c) BzCl, pyridine, DMAP, 95%; d) 1. O_3 , CH_2Cl_2 , -78°C ; 2. Ph_3P , $-78^\circ\text{C} \rightarrow \text{RT}$, 80%; e) amine, NaBH_3CN , MeOH/AcOH (30:1), 90%; f) NaOMe , MeOH , 80%; g) AcOH , 80%, 60°C , 2 h; h) $\text{Pd}(\text{OH})_2/\text{C}$, H_2 , AcOH 80%, 70% (2 steps). Bz = benzoyl, Cbz = benzyloxycarbonyl, HMDS = hexamethyldisilazide, TBS = *tert*-butyldimethylsilyl.

polyols. Hydrolysis of the *O*-benzylidene acetal and the TBS ether with aqueous acetic acid, followed by catalytic hydrogenation gave the paromomycin derivatives **8–10**.

The amino ether analogues **8–10** bonded to the 16S rRNA subunit and inhibited bacterial translation/transcription (T/T)^[25] with similar potencies. This result was gratifying given our prediction from modeling studies that the C2'' position is suitable for substitution. Most rewarding, however, was that all of the substituted compounds maintained activity against Gram-positive (*S. aureus*) and Gram-negative (*E. coli*) bacteria (Table 1). Whereas in the case of **8** the addition of a

cationic side chain to the paromomycin core afforded a compound with near-identical activity to that of paromomycin, the extension of this chain by one methylene group led to a compound **9** with similar activity against *S. aureus* but diminished activity against *E. coli*. As the binding and T/T activity were largely unaffected, the diminished activity is probably a result of decreased uptake and/or increased efflux by the *E. coli* strain. Most interesting was the 3-(aminomethyl)pyridyl analogue **10**, which was slightly more potent than the parent antibiotic paromomycin against the Gram-positive *S. aureus* strain. Compound **10** was further evaluated against *Streptococcus pyogenes*, *Proteus vulgaris*, and *Klebsiella pneumoniae* strains, and was found to maintain inhibitory activity similar to that of the parent paromomycin.

Extensive studies on the nature of the C2'' tether and of the distal group have led to analogues that exhibit excellent antibacterial activities and interesting structure–activity relationships.^[26] Importantly, it might be expected that the incorporation of a large side chain could prevent resistance enzymes from modifying the compounds and rendering them inactive, which is a key element in resistance to aminoglycosides. This hypothesis was partially supported by the activity (MIC 25–50 μM) of **10** against a multidrug- and methicillin-resistant *S. aureus* (MRSA) strain (ATCC BAA-44). This activity is comparable to that observed for the semisynthetic aminoglycoside amikacin, which is modified with an N1 side chain known to combat resistance. In contrast, paromomycin, neomycin, kanamycin, tobramycin, gentamicin, sisomicin, and streptomycin were completely ineffective against MRSA. These results suggest that a C2'' substituent with an aromatic terminal group in 4,5-disubstituted aminoglycosides offers distinct advantages in the fight against the emergence of drug-resistant bacteria. However, it remains to be seen if this type of modification does in fact hinder interaction with one or more resistance enzymes, while allowing strong binding to the target RNA.

Further insight into structure-based design was gathered from X-ray cocrystal data, which revealed a new mode of binding to the decoding A site of rRNA. Crystal structures of **9** and **10** complexed with the same A-site oligonucleotide sequence of *E. coli* RNA as that used for the paromomycin structure were solved at a resolution of 2.6 Å. The two structures are isomorphous and both reveal a normal mode of

binding for rings I and II, with the characteristic bulging of A1492 and A1493, and the invariant contacts between the paromamine part (rings I and II) and A1408, or the sugar–phosphate backbone, as shown in Figure 2 for analogue **10**. An important difference is the *direct* contact between the O6 hydroxy group of the deoxystreptamine (DOS) unit and the O4 atom of U1406; the equivalent interaction is mediated by a water molecule in the case of the parent paromomycin.^[14] Furthermore, the non-Watson–Crick U1406 oU1495 base pair is

Table 1: Activities of C2''-*O*-(aminoalkyl) ether analogues of paromomycin.^[a]

Compound	16S K_D [μM]	T/T IC_{50} [μM]	<i>E. coli</i>	<i>S. aureus</i>	MIC [μM] ^[b] <i>S. pyog.</i>	<i>P. vulg.</i>	<i>K. pneum.</i>
1	0.13	0.15	5	3	3	1	1
8	0.23	0.29	6	2	nd ^[c]	nd	nd
9	0.10	0.29	25	3	nd	nd	nd
10	0.13	0.23	5	1	6	3	3

[a] For details of K_D , T/T, and MIC testing, see reference [25]. [b] Bacterial strains used: *Escherichia coli* (ATCC 25922), *Staphylococcus aureus* (ATCC 13709), *Streptococcus pyogenes* (ATCC 49399), *Proteus vulgaris* (ATCC 8427), *Klebsiella pneumoniae* (ATCC 13883). [c] nd = not determined. MIC = minimum inhibitory concentration.

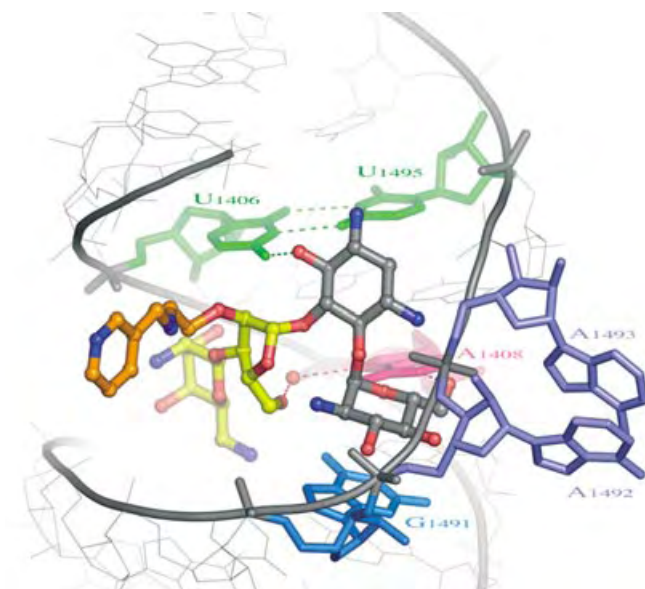


Figure 2. Top view of the complex between **10** and the A-site RNA oligonucleotide. Adenine residues A1492 and A1493 are dark blue, G1491 is paler blue, A1408 is pink, and the U1406-U1495 base pair is green. The bridging water molecule between the hydroxy group at C5'' of ring III and N7 of A1408 is also shown in pink. Note the U \cdots U pair with standard H bonds and the pseudopair of ring I and A1408.

not bifurcated as in all other aminoglycoside/A-site complexes,^[14,16,17] but instead adopts a common geometry with two direct H bonds O4 \cdots H-N3 and N3-H \cdots O2^[27] (Figure 2).

Rings III and IV of **10** are oriented very differently in the A-site complex with respect to the parent compound paromomycin (and all known 4,5-disubstituted aminoglycosides)^[14–16] (Figure 3). In the structure of both analogues **9** and **10**, there is a 40° flip about the β -D-ribofuranosyl linkage to the paromamine unit, which, together with a change in sugar pucker (from C2''-endo in paromomycin to C3''-endo in **9** and **10**) results in a 90° change in the orientation of ring IV.

The oxygen atom in ring III in **9** and **10** still forms an intramolecular H bond with the amino group at C2' of ring I, as in the paromomycin complex^[14] (Figure 4). However, the hydroxymethyl group at C5'' in **9** and **10** forms a hydrogen

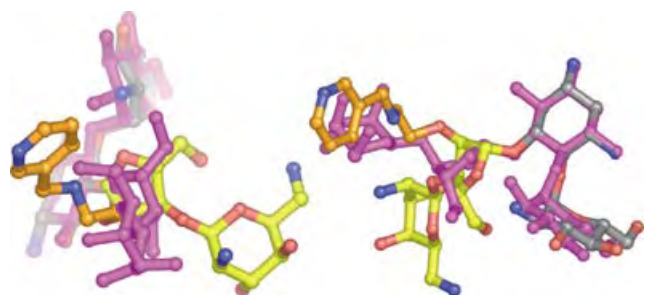


Figure 3. Superposition of paromomycin and **10** complexed to the A site with the DOS rings II superimposed. The left-hand drawing illustrates the 90° rotation of ring IV in **10** relative to that in paromomycin (magenta). The superposition on the right highlights the difference in sugar pucker of ring III from C2''-endo in paromomycin (magenta) to C3''-endo in **10**.

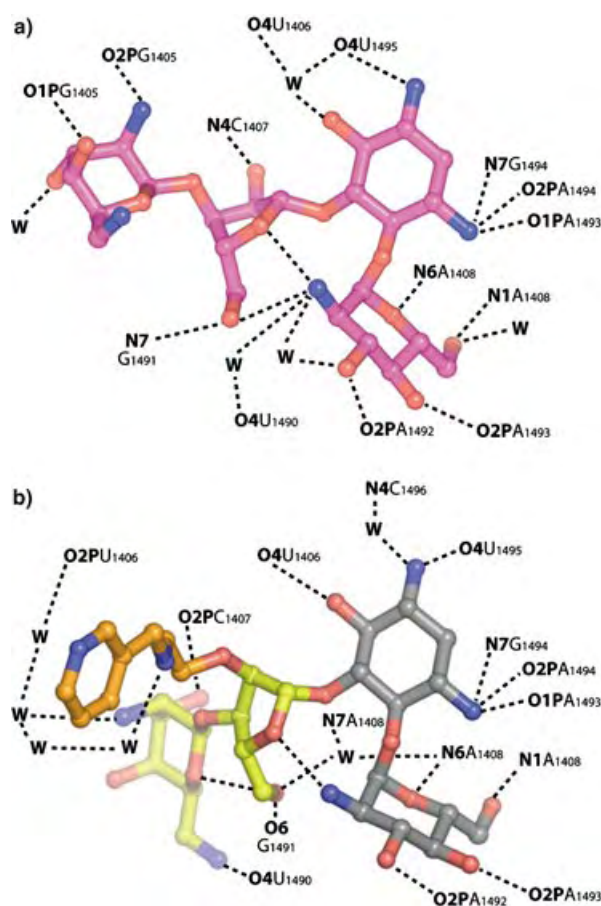


Figure 4. a) Schematic representation of the contacts between paromomycin and the RNA in the cocrystal with the A-site RNA fragment.^[14] b) Schematic representation of the direct and water-mediated contacts observed in the cocrystal of the A-site RNA fragment with **10**.

bond with O6 of G1491 instead of N7 of G1491 as in the case of paromomycin. Because of the rotation of ring III, the C5'' hydroxymethyl group forms an additional water-mediated H bond with N7 of A1408. In fact, the central A1408 residue forms three (instead of the usual two) H-bonded contacts with the aminoglycoside unit of the two analogues **9** and **10**. The new orientation of ring IV results in a new set of H-bonding interactions. Thus, a network of H bonds links rings I and IV via the C5'' hydroxymethyl group, a water molecule, and A1408.

The ether chain at C2'' with the distal amino or pyridine group in **9** and **10**, respectively, extends across the deep/major groove of the A site, points into the solvent, and forms no direct contact with the RNA (Figure 4b). Additional contacts are mediated by bridging water molecules that extend in one binding site from the aminoethyl group at C2'' to an oxygen atom of an anionic phosphate in U1406. These unprecedented conformational changes and new interactions brought about by the presence of the ether chains at C2'' of **9** and **10** result in a compactly folded aminoglycoside structure with unique binding sites (Figure 4b).

We have uncovered a new mode of binding for paromomycin analogues that contain diversely substituted amino-

alkyl ethers at C2''. Cocystal structures of compounds **9** and **10** with the A site of *E. coli* RNA revealed a new position for the C2'' substituent in the deep/major groove. The orientation of rings III and IV is dramatically changed in the bound conformation, thus resulting in a new set of intramolecular networks of H bonds. The pyridine-substituted aminoethyl ether analogue **10** of paromomycin exhibited potent inhibition of *S. aureus* and promising activity against a panel of resistant bacterial strains, including MRSA. Thus, the introduction of a novel aryl aminoalkyl functionality at C2'' of paromomycin has resulted in the discovery of an excellent first-generation lead compound for the development of new and potent bactericidal aminoglycoside analogues in this series.

Received: September 23, 2004

Keywords: aminoglycosides · antibacterial agents · bacterial resistance · drug design · rRNA

- [21] J. B.-H. Tok, W. Wong, N. Baboolal, *Bioorg. Med. Chem. Lett.* **2002**, 12, 365.
- [22] C.-H. Wong, M. Hendrix, E. S. Priestley, W. A. Greenberg, *Chem. Biol.* **1998**, 5, 397.
- [23] Y. Tor, *ChemBioChem* **2003**, 4, 919.
- [24] S. Hanessian, T. Takamoto, R. Massé, G. Patil, *Can. J. Chem.* **1978**, 56, 1482.
- [25] P. P. Kung, M. D. Casper, K. L. Cook, L. Wilson-Lingardo, L. M. Risen, T. A. Vickers, R. Ranken, L. B. Blyn, J. R. Wyatt, P. D. Cook, D. J. Ecker, *J. Med. Chem.* **1999**, 42, 4705.
- [26] Results pertaining to the medicinal chemistry of these novel analogues will be communicated separately.
- [27] N. B. Leontis, E. Westhof, *RNA* **2001**, 7, 499.

- [1] R. Berisio, J. Harms, F. Schlunzen, R. Zarivach, H. A. Hansen, P. Fucini, A. Yonath, *J. Bacteriol.* **2003**, 185, 4276.
- [2] A. P. Carter, W. M. Clemons, D. E. Brodersen, R. J. Morgan-Warren, B. T. Wimberly, V. Ramakrishnan, *Nature* **2000**, 407, 340.
- [3] J. L. Hansen, J. A. Ippolito, N. Ban, P. Nissen, P. B. Moore, T. A. Steitz, *Mol. Cell* **2002**, 10, 117.
- [4] J. L. Hansen, P. B. Moore, T. A. Steitz, *J. Mol. Biol.* **2003**, 330, 1061.
- [5] J. M. Harms, H. Bartels, F. Schlunzen, A. Yonath, *J. Cell Sci.* **2003**, 116, 1391.
- [6] D. E. Brodersen, W. M. Clemons, Jr., A. P. Carter, R. J. Morgan-Warren, B. T. Wimberly, V. Ramakrishnan, *Cell* **2000**, 103, 1143.
- [7] S. Vakulenko, S. Mobashery, *Clin. Microbiol. Rev.* **2003**, 16, 430–450.
- [8] a) C. A. Smith, E. N. Baker, *Curr. Top. Med. Chem.* **2003**, 3, 1001; b) J. Davies, *Science* **1994**, 264, 375; c) K. J. Shaw, P. N. Rather, R. S. Hare, G. H. Miller, *Microbiol. Rev.* **1993**, 57, 138.
- [9] M. P. Mingeot-Leclercq, Y. Glupczynski, P. M. Tulkens, *Antimicrob. Agents Chemother.* **1999**, 43, 727.
- [10] J. M. Ogle, D. E. Brodersen, W. M. Clemons, Jr., M. J. Tarry, A. P. Carter, V. Ramakrishnan, *Science* **2001**, 292, 897.
- [11] J. M. Ogle, A. P. Carter, V. Ramakrishnan, *Trends Biochem. Sci.* **2003**, 28, 259.
- [12] J. M. Ogle, F. V. Murphy, M. J. Tarry, V. Ramakrishnan, *Cell* **2002**, 111, 721.
- [13] D. Moazed, H. F. Noller, *Nature* **1987**, 327, 389.
- [14] Q. Vicens, E. Westhof, *Structure* **2001**, 9, 647.
- [15] For insightful NMR studies, see: a) D. Fourmy, M. I. Recht, S. C. Blanchard, J. D. Puglisi, *Science* **1996**, 274, 1367; b) S. R. Lynch, R. L. Gonzalez, Jr., J. D. Puglisi, *Structure* **2003**, 11, 43; for mass spectrometric studies, see: S. A. Hofstadler, R. H. Griffey, *Curr. Opin. Drug Discovery Dev.* **2000**, 3, 423.
- [16] Q. Vicens, E. Westhof, *Chem. Biol.* **2002**, 9, 747.
- [17] Q. Vicens, E. Westhof, *J. Mol. Biol.* **2003**, 326, 1175.
- [18] P. Pfister, S. Hobbie, Q. Vicens, E. C. Böttger, E. Westhof, *ChemBioChem* **2003**, 4, 1078.
- [19] J. Haddad, L. P. Kotra, B. Llano-Sotelo, C. Kim, E. F. Azucena, Jr., M. Liu, S. B. Vakulenko, C. S. Chow, S. Mobashery, *J. Am. Chem. Soc.* **2002**, 124, 3229.
- [20] R. J. Russell, J. B. Murray, G. Lentzen, J. Haddad, S. Mobashery, *J. Am. Chem. Soc.* **2003**, 125, 3410.

Modified Zeolites

Sequential Functionalization of the Channel Entrances of Zeolite L Crystals**

Stefan Huber and Gion Calzaferri*

Inorganic–organic host–guest systems are of great interest for designing supramolecular devices and machines.^[1] We are especially interested in artificial antenna systems that mimic natural photosynthesis. A convenient host is zeolite L, a crystalline aluminosilicate in which corner-sharing SiO_4 and AlO_4^- tetrahedra give rise to one-dimensional channels arranged in a hexagonal structure. The channels have a smallest free opening diameter of 7.1 Å and a channel-to-channel distance of 18.4 Å.^[2,3] They can be filled with suitable organic guest molecules, although only guests that can pass through the 7.1-Å opening are able to enter the channels. Pure zeolite L crystals with lengths between 30 and 7000 nm have been synthesized previously.^[4]

Due to the channel entrances, the chemical and physical properties of the base and coat of the cylindrical crystals are different. Stopcocks are molecules that can only partly enter the channels. They typically consist of a head, a spacer, and a label, as shown in Figure 1. Only the label and the spacer can enter the channels due to size restrictions,^[5] and, depending on the reactivity of the label, they can either be reversibly or irreversibly attached. While fluorescent stopcocks can be used to extract or inject electronic excitation energy from or

[*] Dipl.-Chem. S. Huber, Prof. Dr. G. Calzaferri
Department of Chemistry and Biochemistry
University of Bern
Freiestrasse 3, 3012 Bern (Switzerland)
Fax: (+41) 31-631-39-94
E-mail: gion.calzaferri@iac.unibe.ch

[**] This work was supported by the Schweizerischer Nationalfonds zur Förderung der wissenschaftlichen Forschung NFP47 (4047-057481) and by the Schweizerische Bundesamt für Energiewirtschaft (project 10441). We thank Portlandzement AG for financial support. The large zeolite L crystals were synthesized by A. Zabala Ruiz and the small ones by R. Bühler.

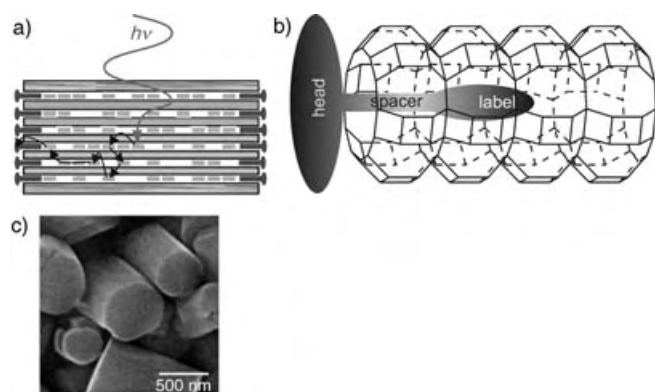


Figure 1. a) Schematic picture of a zeolite L crystal loaded with donor dye molecules and modified with acceptor stopcocks at the base. Excitation energy is channeled and focused from inside the zeolite crystal to the outside. b) Enlargement showing details of a channel, the smallest free opening of which is 7.1 Å, and the shape of a stopcock molecule. Only the spacer and label are small enough to enter the zeolite L channels; the head is too big. c) Scanning electron micrographic picture of zeolite L crystals.

into the zeolite L crystals by radiationless Förster-type energy transfer,^[6–8] others can be used to block the channel entrances against small molecules such as oxygen or water, or to hinder encapsulated dye molecules from leaving the channels.

Selective functionalization of only the channel entrances is an important topic in the development of highly organized materials, since these molecules are at the interface between the interior of a zeolite L crystal and its surroundings. We describe here a very versatile new five-step reaction principle (Figure 2), which can be summarized as follows:

- 1) Protection of the functionalizing group with a molecule that is too big to enter the channels of zeolite L. This step is necessary to ensure that the stopcock enters the channels in the desired direction.
- 2) Adsorption of the reactive stopcock at the channel entrances of the zeolite crystals.
- 3) Reaction between the adsorbed stopcock and the channel interior, which leads to irreversible fixation. The nature of the bond is not yet known, but water molecules and protons inside the channels seem to play an important role. Therefore, the bond is simply symbolized by a hook in Figure 2.
- 4) Removal of the protecting group, leaving the crystals with free functionalizing groups at the channel entrances.
- 5) Coupling of the head bearing the desired property; it can be a fluorescing dye or another molecule.

Since the delicate part of the reaction are steps 1–3, this principle allows us to synthesize a large variety of materials that would otherwise be very difficult to obtain.

This principle was demonstrated to work by functionalizing the channel ends of zeolite L crystals as follows: As a reactive stopcock, 9-fluorenylmethyl carbamate *N*-hydroxy-succinimidyl ester^[9–11] (Fmoc-NHS) was reacted with (3-aminopropyl)methoxydimethylsilane (APMS) to give **1**

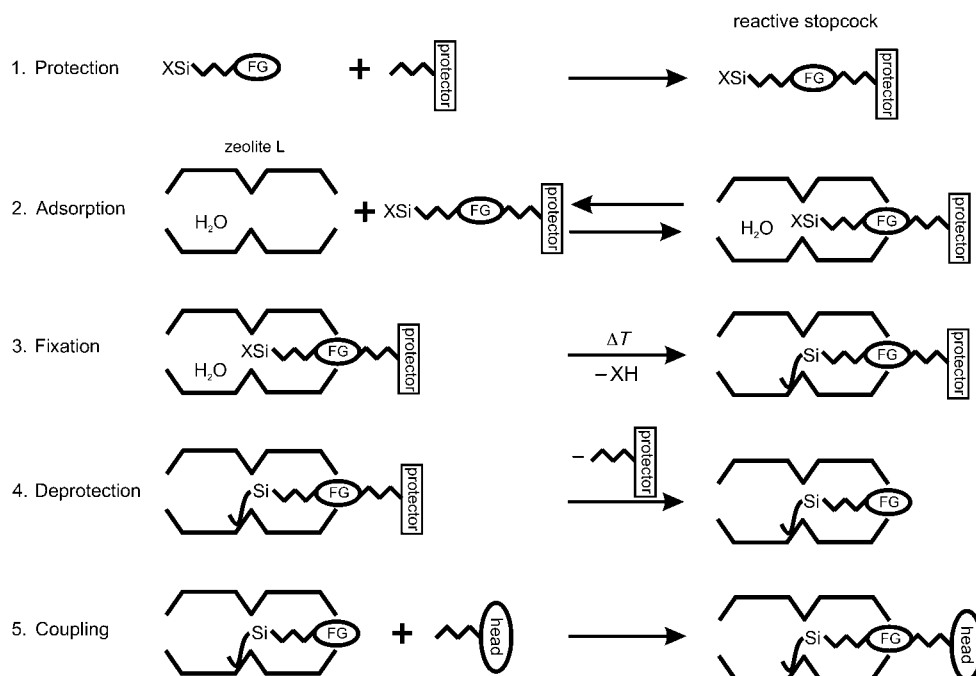
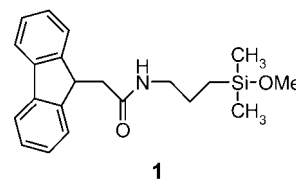


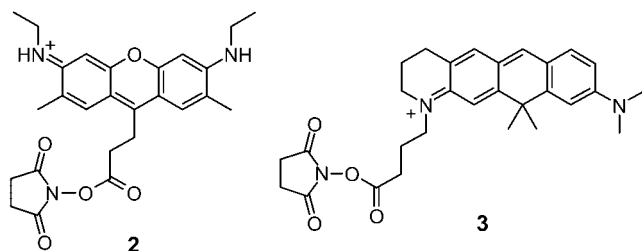
Figure 2. Reaction principle for the irreversible functionalization of the channel entrances of zeolite L crystals. FG: desired group to functionalize the channel ends; protector: the part of the molecule that is too big to enter the channels and that can be removed afterwards; XSi: the group that can penetrate the channels and bind to the zeolite L framework; head: the FG can be further reacted with a head if desired.

(FMOc-APMS). A weighed amount of zeolite L was suspended in *n*-hexane, the number of channel entrances was calculated, and the same amount of **1** was added to the suspension. Knowing the number of channel entrances per milligram of zeolite is very important, since an excess of **1** to channel entrances leads to crystals modified on the whole external surface. The stopcock molecule **1** has a hydrophobic head (FMOc) and a hydrophilic tail (methoxysilane); therefore the tail prefers to penetrate the zeolite L channels, which are hydrophilic, while the hydrophobic head prevents the molecule from entering the channels completely due to the size restriction imposed by the channel openings. The type of reaction between the methoxysilane and the interior of the zeolite channel must be investigated further. Since there are no free silanol groups inside the channels, reactions described for flat surfaces,^[12] nanoparticles,^[13] and the surface of zeolites^[14] are not very probable. However, pentacoordinate silicon oxide compounds are well known,^[15a] and pentacoordinate Al³⁺ in zeolite L has been proposed recently.^[15b]

The selectivity of the shape dependence of the adsorption was shown by performing the same reaction with FMOc-protected (3-aminopropyl)triethoxysilane (FMOc-APTES). The triethoxysilane group is too bulky to enter the channels of zeolite L under these conditions. Moreover, APTES is known to form clusters in solution, which would also hinder a selective adsorption only at the channel entrances. Therefore, the molecule is expected to adsorb all over the outer surface of the crystals, whereas the smaller stopcock **1** can adsorb selectively at the channel entrances. The same amount of zeolite was used for both modifications and therefore exactly the same amount of FMOc-APMS and FMOc-APTES. Both samples were processed as described in the Experimental Procedure giving NH₂-zeolite L.

The number of amino groups linked to the zeolite L was determined by a quantitative ninhydrin colorimetric reaction, also known as the Kaiser test,^[16] and compared to the calculated number of channel entrances. The results showed that essentially 100% of both FMOc-APMS and FMOc-APTES were attached to the zeolite, which means that every zeolite has as many amino groups on the surface as channel entrances for both reactants.

To show the spatial distribution of the amino groups on the zeolite L surface for both samples, the NH₂ groups can be marked with fluorescing dyes. Amino-reactive fluorescing dyes are used by biochemists for protein analysis and are readily available.^[17] *N*-Hydroxysuccinimidyl ester (NHS) derivatives, such as dyes **2** (ATTO520-NHS) and **3** (ATTO610-NHS), are well known to react selectively with primary amino groups in high yield, giving an amide bond.



Dye **3** was therefore coupled to the free amino group of APMS- and APTES-modified crystals. Confocal fluorescence microscopy pictures were taken of both, showing the spatial distribution of the fluorescing dye and therefore of the amino groups (Figure 3). The difference between the results

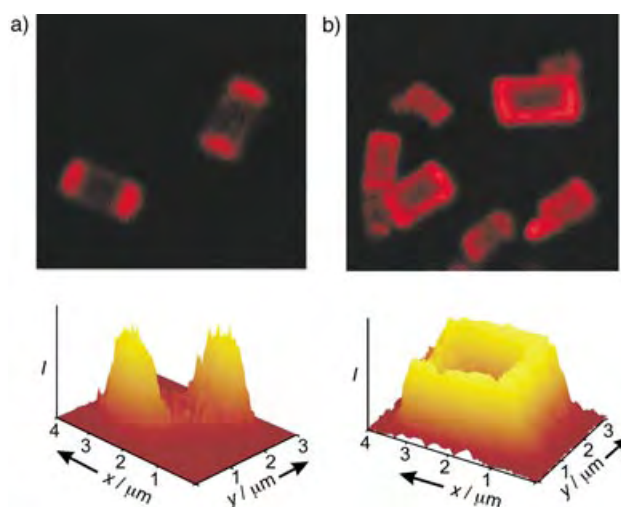


Figure 3. Confocal fluorescence microscopy pictures of zeolite L single crystals. a) Two crystals functionalized with APMS and coupled with the strongly fluorescing dye **3** (top). We also show the relative intensity distribution of one of these crystals (bottom). b) Several crystals functionalized with **3** coupled to APTES (top) and the corresponding relative intensity distribution of one of these crystals (bottom). Both samples are modified with the same amount of dye **3**, therefore the overall fluorescence intensity of the single crystals is similar.

obtained with the monomethoxysilane APMS and the triethoxysilane APTES is striking. The overall fluorescence intensity of single crystals of both samples is about the same, since the same number of amino groups is available, but the distribution of the amino groups on the zeolite surface is completely different: while FMOc-APMS is observed only at the base of the crystals, FMOc-APTES is observed to be present over the whole surface. The only way to explain this is by assuming that the smaller methoxydimethylsilyl group can enter the channels, while the more bulky triethoxysilyl cannot. Control experiments were performed by treating unmodified zeolite L crystals with dye **3**. Since there are no amino groups on the surface, one would expect the dye to be washed away completely. This is indeed the case, and no fluorescence was observed from these samples.

We found that the yield of the reaction between attached amino groups and the reactive dye is mainly determined by the size of the dye and the shape of the crystals. For dyes **2** and **3** we obtained an almost quantitative reaction with the amino groups, and hence full coverage of the channel entrances, when using crystals with a flat base and well-defined shape without any intergrowth, as shown in the SEM picture in Figure 1. The yield decreases to about 10% when zeolite L crystals with a very rough surface are used, indicating the importance of the morphology.

The excitation and emission spectra of **2**, **3**, and the near-IR-emitting dye ATTO680 (**4**) attached to the base of the

zeolite L crystals are shown in Figure 4a. (Note that the structure of **4** has not yet been revealed by the supplier). The excitation and emission spectra of **2** and **3** bound to zeolite L crystals are similar to those recorded for a dilute solution,

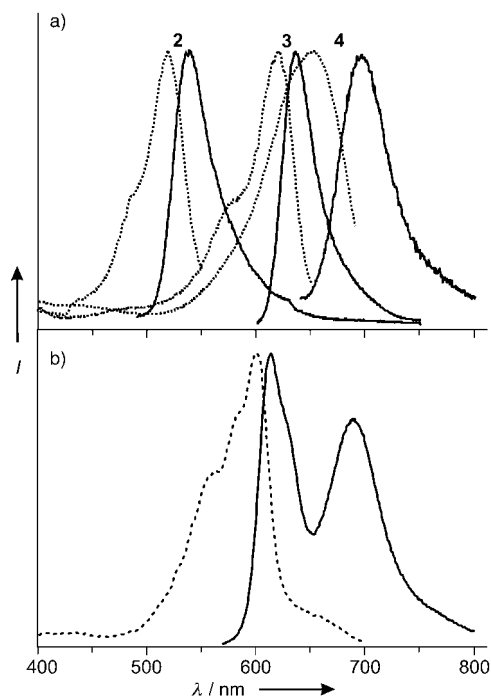


Figure 4. a) Excitation (dotted) and emission (solid) spectra of dyes **2** (ATTO520), **3** (ATTO610), and **4** (ATTO680) attached to zeolite L channel entrances. b) Excitation (dotted) and emission (solid) spectra of ATTO680, Ox⁺-zeolite L. The emission spectrum was recorded when Ox⁺ was excited selectively at 540 nm. The excitation spectrum was recorded at 720 nm, where essentially only ATTO680 emits.

showing that the dyes are present as monomers. However, the excitation spectrum of **4** is broadened and blue-shifted. Although the structure of **4** is not yet available, we can assume that its dimensions are substantially larger than those of **2** or **3**, allowing electronic interaction between dye molecules located at different channel entrances. This effect is even more pronounced when excitation and emission spectra are measured for a thick layer, in which the chances of intercrystalline electronic interactions between dye molecules bound to different crystals increase.

An additional proof to show that the amino-reactive dye is fixed on the zeolite L crystal can be obtained from energy-transfer experiments. Oxonine-loaded zeolite L (Ox⁺-zeolite L) is a strongly emitting and stable material that has its emission maximum at 615 nm. The excitation and emission spectra of Ox⁺-zeolite L were published in ref. [18]. The emission spectrum of Ox⁺-zeolite L shows a pronounced overlap with the excitation spectrum of ATTO680-zeolite L. This allows Förster-type energy transfer from Ox⁺ located inside the channels to ATTO680 at the channel entrances in an ATTO680, Ox⁺-zeolite L sample, if the distance between Ox⁺ and ATTO680 is in the range of the Förster radius. Therefore, the excitation energy absorbed inside the zeolite L

is transported spatially and focused at the channel entrances. The excitation and emission spectra of an ATTO680, Ox⁺-zeolite L sample are shown in Figure 4b. Selective excitation of Ox⁺ causes an important fluorescence of ATTO680 with a maximum at 700 nm; this is obviously due to electronic excitation energy transfer. The ATTO680 is more strongly excited due to energy transfer from Ox⁺ than by direct excitation at its absorption maximum at 660 nm, as can be seen from the excitation spectrum.

In summary, a new reaction principle for sequential functionalization of only the channel entrances of zeolite L has been developed. The reaction was demonstrated by attaching an aminomethoxysilyl group to the channel openings, which can be further used to selectively bind, for example, fluorescing dye molecules to the base of the crystals. Since amino-reactive fluorescing dyes are readily available, this allows the modification of the base of zeolite L crystals with dyes covering the whole visible and near-IR region. This has important consequences for the preparation of highly efficient antenna materials funneling the excitation energy from inside the zeolite L crystals to the channel ends, or vice versa.^[7,8] The amino groups can also be transformed into thiol groups.^[19] Such HS-zeolite L crystals are currently under investigation in our laboratory. The reaction principle is not restricted solely to zeolite L or to covalent modification with amino groups, thus opening up options for obtaining a wide range of new, functionalized zeolite-based materials, which otherwise would be very difficult, if not impossible, to obtain.

Experimental Section

Pure zeolite L crystals were synthesized and characterized as described in ref. [4]. The potassium-exchanged form was used for all experiments. The dyes **2–4** were obtained from Fluka and used as received. Confocal microscopy images were taken from zeolite L crystals having a length of about 3 μm; crystals of about 30 nm were used for the energy-transfer experiment. Fluorescence spectra were recorded on an LS 50B Perkin-Elmer luminescence spectrophotometer, and absorption spectra were measured with a Lambda 900 Perkin-Elmer UV/Vis/NIR equipment. Confocal microscopy was performed with a fluoview FV 300 (Olympus) accessory equipped with an argon-ion laser operating at 488 nm and an He/Ne laser operating at 543.5 nm.

Synthesis of FMOC-APMS (1): (3-Aminopropyl)methoxydimethylsilane (APMS, Acros, 97%; 10 μL, 8.7 mg, 0.06 mmol) and was added to 1 mL of CH₂Cl₂ (dried over CaH₂) in a Teflon tube. FMOC *N*-hydroxysuccinimide ester (FMOC-NHS, Fluka, > 98%, HPLC; 30 mg, 0.089 mmol) was dissolved in 1 mL of dry CH₂Cl₂ and added dropwise to the APMS solution. The reaction mixture was stirred at room temperature and monitored by thin-layer chromatography. After 1 h the reaction was complete, and no more free amine could be detected by a ninhydrin test.

Synthesis of FMOC-APTES: This synthesis was carried out in analogy to that of FMOC-APMS with (3-aminopropyl)triethoxysilane (APTES, Fluka, ≥ 96%, GC; 10 μL, 8.5 mg, 0.053 mmol) instead of APMS.

Synthesis of APMS-zeolite L and APTES-zeolite L: Typically, zeolite L crystals (10 mg) were suspended in 2 mL of *n*-hexane (Merck, p.a.) in a Teflon tube. The number of channel entrances was calculated and 1 equiv of either FMOC-APMS or FMOC-APTES was added to the suspension. After the suspension was sonicated for 20 min to allow the stopcock to adsorb on the zeolite L crystals, it was heated at reflux for 3 h. The suspension was then centrifuged to give

FMOC-APMS-zeolite L or FMOC-APTES-zeolite L. The crystals were suspended in 1 mL of dry DMF containing 0.2 mL of piperidine and stirred for 1 h to remove the FMOC group. After the crystals were centrifuged and washed twice with 2 mL of MeOH, APMS-zeolite L or APTES-zeolite L (NH₂-zeolite L) was obtained.

Quantification of NH₂ groups bonded to zeolite L: The amine test solution consisted of ninhydrin (Fluka, ~99%, UV; 0.5 g, 2.81 mmol) dissolved in 40 mL of *n*-butanol and 10 mL of doubly distilled water. A 2-mL aliquot of the test solution was added to 0.05 μ L, 0.025 μ L, 0.0125 μ L, and 0.005 μ L (0.3 μ mol, 0.15 μ mol, 0.075 μ mol, and 0.03 μ mol, respectively) of APMS, and the solutions were stirred at 100°C for 35 min. The absorption at 570 nm was measured for all samples against a blank containing ninhydrin solution without APMS, giving a regression line. A weighed amount of typically 1–2 mg of NH₂-zeolite L was suspended in 2 mL of the ninhydrin test solution and stirred at 100°C for 35 min. After centrifuging, the absorption of the solution was measured at 570 nm, and the number of NH₂ groups per mg of zeolite L was calculated from the regression line.

Reaction of NH₂-zeolite L with an amino-reactive dye: NH₂-zeolite L (ca. 5 mg) was suspended in 1 mL of dry acetonitrile (Merck, DNA grade). Triethanolamine (Fluka, >99%, GC; 5 μ L, 5.62 mg, 0.038 mmol) was added and the suspension was sonicated for 10 min. The amino-reactive dye (3–4 equiv relative to the NH₂ groups) was also dissolved in 1 mL of acetonitrile and added dropwise to the zeolite suspension. The dye-zeolite L was stirred for 1 h then washed twice with 2 mL of MeOH to remove excess dye. The amount of dye bound to the NH₂ groups was determined by destroying a known amount of dye-zeolite L with hydrofluoric acid and measuring the concentration of the dye by UV/Vis spectroscopy.

Synthesis of Ox⁺-zeolite L: Ox⁺ was synthesized as described in ref. [20] and inserted into zeolite L crystals by ion exchange.^[7] Further reaction with ATTO680-NHS ester was performed as described previously for empty zeolite L.

Received: June 29, 2004

Keywords: fluorescence · organic–inorganic hybrid composites · silanes · surface chemistry · zeolites

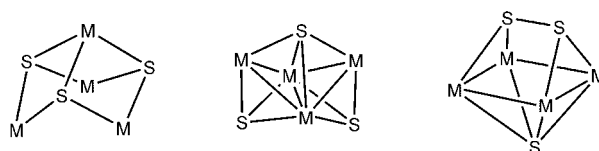
- [1] V. Balzani, A. Credi, M. Venturi, *Molecular Devices and Machines—A Journey into the Nano World*, Wiley-VCH, Weinheim, **2003**.
- [2] D. W. Breck, *Zeolite Molecular Sieves*, Wiley, New York, **1974**.
- [3] Ch. Baerlocher, W. M. Meier, D. H. Olson, *Atlas of Zeolite Framework Types*, 5th ed., Elsevier, Amsterdam, **2001**.
- [4] S. Megelski, G. Calzaferri, *Adv. Funct. Mater.* **2001**, *11*, 277.
- [5] G. Calzaferri, M. Pauchard, H. Maas, S. Huber, A. Khatyr, T. Schaafsma, *J. Mater. Chem.* **2002**, *12*, 1.
- [6] H. Maas, G. Calzaferri, *Angew. Chem.* **2002**, *114*, 2389; *Angew. Chem. Int. Ed.* **2002**, *41*, 2284.
- [7] G. Calzaferri, S. Huber, H. Maas, C. Minkowski, *Angew. Chem.* **2003**, *115*, 3860; *Angew. Chem. Int. Ed.* **2003**, *42*, 3732.
- [8] S. Huber, G. Calzaferri, *ChemPhysChem* **2004**, *5*, 239.
- [9] L. A. Carpino, G. Y. Han, *J. Org. Chem.* **1972**, *37*, 3404.
- [10] A. G. Frutos, J. M. Brockman, R. M. Corn, *Langmuir* **2000**, *16*, 2192.
- [11] A. Boeijen, J. van Ameijde, R. M. J. Liskamp, *J. Org. Chem.* **2001**, *66*, 8454.
- [12] a) S. Flink, F. C. J. M. van Veggel, D. N. Reinhoudt, *J. Phys. Org. Chem.* **2001**, *14*, 407; b) I. Haller, *J. Am. Chem. Soc.* **1978**, *100*, 8050.
- [13] T. Vossmeier, S. Jia, E. Delonno, M. R. Diehl, S.-H. Kim, X. Peng, A. P. Alivisatos, J. R. Heath, *J. Appl. Phys.* **1998**, *84*, 3664.
- [14] K. Ha, Y.-J. Lee, D.-Y. Jung, J. H. Lee, K. B. Yoon, *Adv. Mater.* **2000**, *12*, 1614.
- [15] a) R. Tacke, O. Seiler, in *Silicon Chemistry* (Eds.: P. Jutzi, U. Schubert), Wiley-VCH, Weinheim, **2003**, pp. 324–337; b) A. Devaux, C. Minkowski, G. Calzaferri, *Chem. Eur. J.* **2004**, *10*, 2391.
- [16] E. Kaiser, R. L. Colescott, C. D. Bossinger, P. I. Cook, *Anal. Biochem.* **1970**, *34*, 595.
- [17] M. Brinkley, *Bioconjugate Chem.* **1992**, *3*, 2.
- [18] M. M. Yatskou, M. Meyer, S. Huber, M. Pfenniger, G. Calzaferri, *ChemPhysChem* **2003**, *4*, 567.
- [19] C. Bresson, M.-J. Menu, M. Datiguenave, Y. Dartiguenave, *J. Chem. Research (M)* **1998**, *8*, 1919.
- [20] H. Maas, A. Khatyr, G. Calzaferri, *Microporous Mesoporous Mater.* **2003**, *65*, 233.

Cluster Compounds

Competing H–H, S–S, and M–M Bond Formation
in the “Shape-Shifting” Cluster
[Ru₄S₃(arene)₄]^{2+*}

Matthew L. Kuhlman and Thomas B. Rauchfuss*

Tetrametallic trisulfido clusters^[1] mainly adopt the *C*_{3v} “Roussin Black salt” structure,^[2,3] illustrated by the classical anion [Fe₄S₃(NO)₇][−]. This motif has recently attracted interest because M₄S₃-like fragments comprise the FeMo cofactor in nitrogenase.^[3–5] The only other M₄S₃ structure is the rare *C*_{2v} capped-butterfly seen in [Cp₂Mo₂Co₂S₃(CO)₄] (Cp = C₅H₅; Scheme 1).^[2] Herein we describe the character-



Scheme 1. Structures of M₄S₃ cluster cores; M–M bonding can vary; left: *C*_{3v} Roussin Black salt structure, middle: *C*_{2v} capped-butterfly, and right: face-capped trigonal prism (this work).

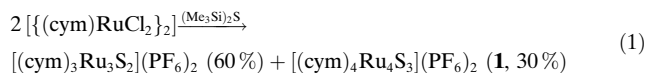
ization of a third M₄S₃ motif; this new cluster is unusual because of its structural dynamics and catalytic properties. In particular, the new M₄S₃ clusters exhibits a previously unobserved competition between S–S and M–M bonding.

[*] M. L. Kuhlman, Prof. Dr. T. B. Rauchfuss
Department of Chemistry
University of Illinois at Urbana-Champaign
Urbana, IL 61801 (USA)
Fax: (+1) 217-333-2685
E-mail: rauchfuz@uiuc.edu

[**] This research was supported by the National Science Foundation. We thank Scott Wilson and Teresa Prussak-Wieckowska for assistance with the X-ray crystallography.

Studies on this dynamic property revealed that the new clusters catalyze the reduction of protons to H_2 .

We have shown that $[(\text{cym})\text{RuCl}_2]_2$ ($\text{cym} = 4\text{-}i\text{PrC}_6\text{H}_4\text{Me}$) reacts with $(\text{Me}_3\text{Si})_2\text{S}$ to produce trigonal bipyramidal $[(\text{cym})_3\text{Ru}_3\text{S}_2]^{2+}$.^[6] We have found that this simple synthesis also affords the previously unrecognized tetrametallic species $[(\text{cym})_4\text{Ru}_4\text{S}_3]^{2+}$ ($\mathbf{1}^{2+}$). The distinctive solubility properties of $[(\text{cym})_4\text{Ru}_4\text{S}_3](\text{PF}_6)_2$ ($\mathbf{1}$) facilitates its easy isolation in 30% yield [Eq. (1)].



In MeCN solution, cluster $\mathbf{1}^{2+}$ is stable at 80°C in the presence of PPh_3 , and it is stable to UV photolysis.^[7]

The reaction stoichiometry leading to $\mathbf{1}^{2+}$ is deceptive: Ru^{II} chlorides are ostensibly converted into the corresponding Ru^{II} sulfides. The ^1H NMR data for $\mathbf{1}^{2+}$ indicate low symmetry, which is incompatible with known M_4S_3 motifs. X-ray crystallographic analysis of $\mathbf{1}$ revealed that the dication adopts a novel structure, described as a face-capped trigonal prism (Figure 1). An equilateral Ru_4 square (Ru-Ru bond $2.81 \pm 0.03 \text{ \AA}$) is capped by $\mu_4\text{-S}$ and $\mu_4\text{-S}_2$ ligands. The crystallographic result shows that $\mathbf{1}^{2+}$ formally arises via an internal reduction of two Ru^{II} to Ru^{I} concomitant with oxidative coupling of two sulfides to persulfide (S_2^{2-}). The 64-electron compound follows the 18 electron rule, although Wade's rules predict a nido cluster (9 electron pair/seven vertex).

The crystallographic analysis reveals that the four isopropyl groups are oriented towards the persulfide-containing face of the Ru_4 square, which is more spacious than the Ru_4S side. A space-filling model indicates steric crowding between the arene substituents,

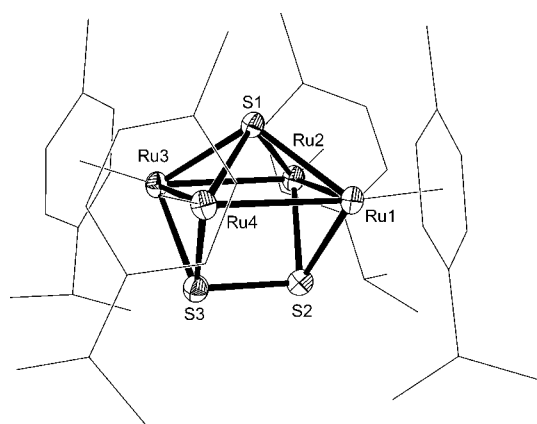


Figure 1. Molecular structure of $\mathbf{1}$. Thermal ellipsoids are set at 50% probability. Select bond lengths [Å]: Ru1-Ru2 2.782, Ru1-Ru4 2.827, Ru4-Ru3 2.776, Ru2-Ru3 2.848, S1-Ru2 2.352, S3-S2 2.109, S2-Ru2 2.281.

which would lead to restricted rotation about the ruthenium-arene bonds. Indeed, the ^1H NMR spectrum for $\mathbf{1}^{2+}$ is simple at 70°C but becomes complex at lower temperatures as arene rotation is slowed (Figure 2). At -35°C , 13 $\text{CH}_3\text{C}_6\text{H}_4i\text{Pr}$ signals are resolved (Figure 2b) 14 $\text{CH}_3\text{C}_6\text{H}_4i\text{Pr}$ signals would be consistent with seven possible atropisomers: $(\text{up})_4$, $(\text{down})_4$, $\text{trans}-(\text{up})_2(\text{down})_2$, $\text{cis}-(\text{up-}\parallel)_2(\text{down-}\parallel)_2$, $\text{cis}-(\text{up-}\perp)_2(\text{down-}\perp)_2$, $(\text{up})_3(\text{down})$, and $(\text{up})(\text{down})_3$, where up and down refer to the orientation relative to the S_2 and S faces of the Ru_4 square (see Scheme 2). The number of isomers implies that rotation of the S_2 ligand is slow on the NMR timescale, such that two $\text{cis}-(\text{up})_2(\text{down})_2$

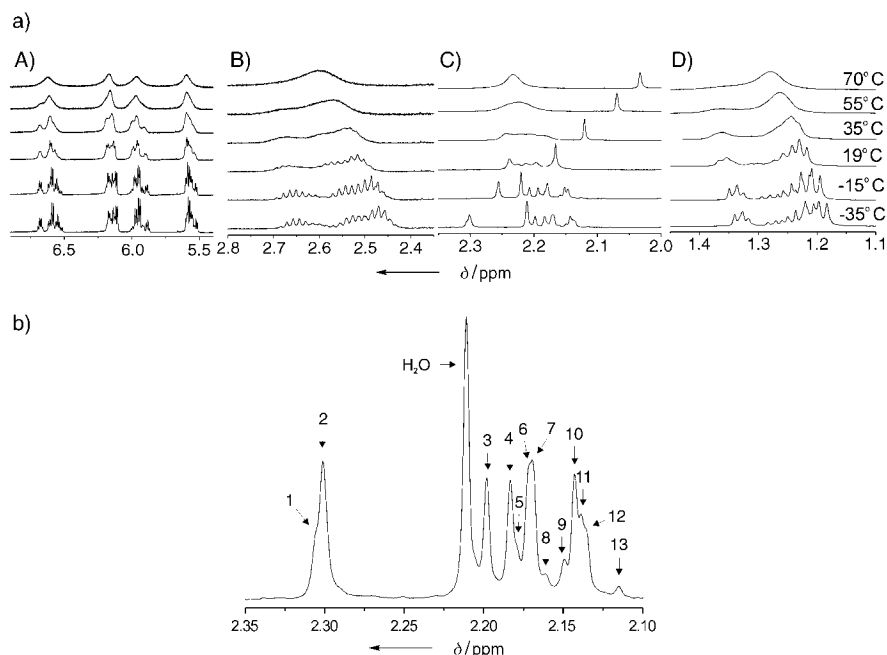
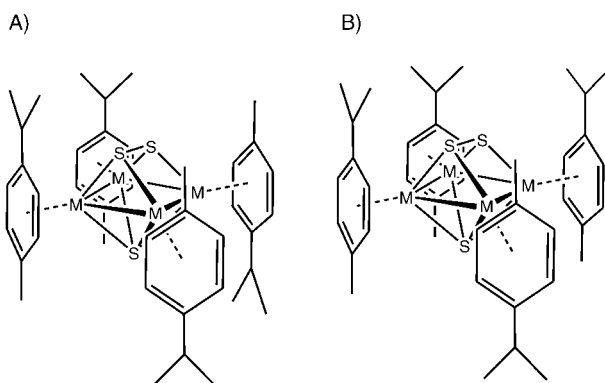


Figure 2. a) Variable temperature ^1H NMR spectra ($[\text{D}_3]\text{MeCN}$) for $\mathbf{1}$ demonstrating restricted rotation of the cym ligands. A) Aromatic region, B) methine (isopropyl), C) methyl, and D) methyl (isopropyl) of cym. b) Expansion of the $\text{CH}_3\text{C}_6\text{H}_4i\text{Pr}$ region for the -35°C spectrum, demonstrating the coexistence of several atropisomers.

isomers are implicated, those where the cisoid Me groups are parallel (\parallel ; Scheme 2) or perpendicular (\perp) to the S_2 unit. Restricted rotation of $\eta^6\text{-arene}$ ligands has rarely been detected in mononuclear complexes^[8] and never in a metal cluster. The isomerization barrier could in principle be increased through modifications in the arene ligand.

The cyclic voltammetry (CV) of $\mathbf{1}$ revealed sequential 1e^- reductions at -970 and -1270 mV (not shown; all potentials are referenced to the $\text{Ag}|\text{AgCl}$ couple). A reversible event at 790 mV is assigned to a 2e^- oxidation. Chemical reduction of $\mathbf{1}^{2+}$ with two equivalents of $[\text{Cp}^*\text{Co}]$ ($\text{Cp}^* = \text{C}_5\text{Me}_5$; $E^\circ = 1.73$ versus $\text{Ag}|\text{AgCl}$) yielded the neutral cluster $[(\text{cym})_4\text{Ru}_4\text{S}_3]$ ($\mathbf{2}^0$). The ^1H NMR spectroscopy data for this neutral species revealed a 3:1 ratio for the cym signals, which indicates idealized C_{3v} symmetry as expected for the Roussin motif, which was confirmed crystallographically (Figure 3). In contrast to other Roussin-like clusters, the apical metal atom is not connected to the other three metal centers by M-M



Scheme 2. Structures of two atropisomers of **1**, A) the *cis* || isomer and B) the (*up*)₃(*down*) isomer.

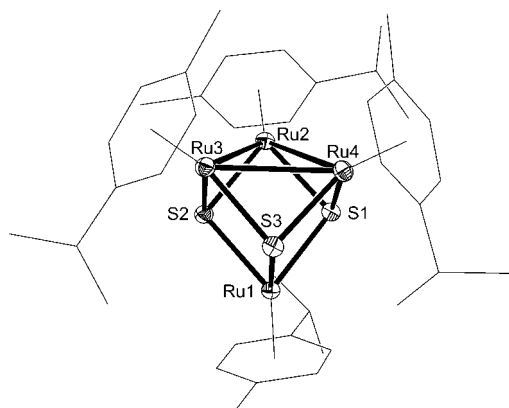
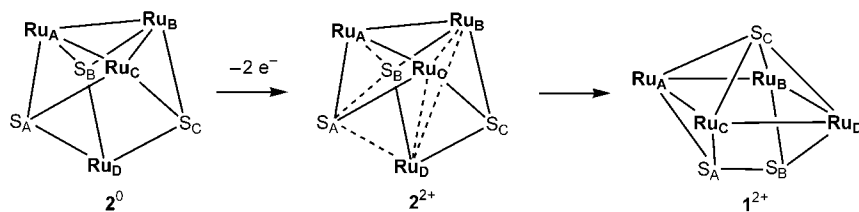


Figure 3. Molecular structure of **2**⁰ with thermal ellipsoids set at 50% probability. Select interatomic distances [Å]: Ru1...Ru2 3.620, Ru3-Ru2 3.079, Ru3-Ru4 3.059, Ru4-Ru2 3.007, Ru1-S2 2.377, Ru2-S2 2.324.

bonds. Two Ru–Ru bonds are expected in a 68e[−] M₄ cluster, thus each of the three comparably elongated Ru–Ru bonds within the Ru₃ basal plane is consistent with a bond order of 2/3. Compound **2**⁰ is formally related to the cubane [(cym)₄Ru₄S₄]^[9,10] by removal of one sulfur atom and subsequent formation of three Ru–Ru bonds.

The scan-rate dependence of the CV of **1** is consistent with a coupled electrochemical–chemical process. The reduction **1**²⁺→**1**⁺ is fully reversible, but the second reduction is not, hence this event is attributed to the rearrangement to the Roussin-like cluster **2**. At slow scan rates (20 mV s^{−1}), the initially generated **2**⁺ is fully converted into **1**⁺, indicated by the event at −970 mV. At faster scan rates (500 mV s^{−1}) separate oxidations are observed for **2**⁰→**2**⁺ and **2**⁺→**2**²⁺. The



Scheme 3. Pathway for the oxidation of **2**⁰.

scan-rate dependence suggests that the rearrangement of **2**⁺ into **1**⁺ occurs with a half-life of approximately 100 ms. A plausible pathway for rearrangement associated with the oxidation of **2**⁰ is shown in Scheme 3.

Reflecting its electron-rich character and the robustness of the Ru–S ensemble, **2**⁰ reacts efficiently with acids, such as HOTf (OTf = [CF₃SO₃][−]), to regenerate **1**²⁺. When this reaction is conducted in CH₂Cl₂ solution, **1**⁺(OTf)₂ crystallizes in near quantitative yield. Interestingly, this reaction occurs with formation of H₂ (¹H NMR: δ = 4.6 ppm in CH₂Cl₂ solution), [Eq. (2)].



Qualitative experiments suggest that **2**⁰ is a two-electron reductant since the addition of one equivalent of HOTf precipitates an approximately 50% yield of **1**⁺(OTf)₂. Thus, the implied monohydride intermediate **2**H⁺ is apparently more reactive towards HOTf than **2**⁰. Since **2**⁰ is capable of reducing protons and **1**²⁺ undergoes efficient reduction, a catalytic cycle is apparent, but the CV results were unexpected. Indeed with HOTs a catalytic current that correlates with [HOTs] is observed, but not at the expected potential of approximately *i*_{cat} = −1 V. Instead *i*_{cat} emerges in the range −0.80 to −0.60 V (Figure 4). The two new reduction events

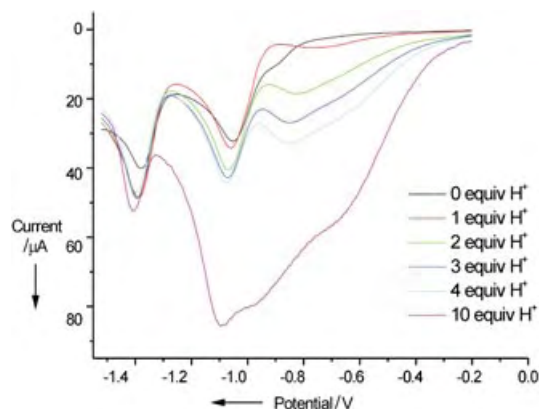


Figure 4. Voltammograms of 10^{−3} M **1** in 0.1 M Bu₄NPF₆ MeCN solution. The reductive current at approximately −800 mV can be seen to correlate with the [p-MeC₆H₄SO₃H]. Conditions: scan rate = 100 mV s^{−1}, Pt wire counter electrode, a glassy carbon electrode working electrode, Ag/AgCl reference.

observed in presence of H⁺ suggest that **1**²⁺ forms an electroactive protonated derivative, although we were unable to spectroscopically detect such a species. The two new reduction events not only increase in current with increasing [H⁺], but shift to a more negative potential with increasing [H⁺], as seen in catalytic systems.^[11,12]

In summary, new M₄S₃ clusters have been shown to exhibit “shape-shifting”, involving redox- and proton-induced conversions between C_{3v} and trigonal-prismatic structures. The parent cationic cluster is further unusual in that its arene

ligands exhibit restricted rotation owing to steric compression. The work underscores the promise of metal sulfide ensembles for hydrogen processing.

Experimental Section

1: A stirred suspension of (4.160 g, 6.8 mmol) of $[(\text{cym})\text{RuCl}_2]^{[13]}$ in warm THF (150 mL) was treated with (2.14 mL, 10.2 mmol) of $(\text{Me}_3\text{Si})_2\text{S}$. The solid slowly dissolved followed by formation of a brown precipitate. The slurry was stirred at 50 °C for 1 h. The solid was collected by filtration and washed with THF (20 mL). The dried brown powder was extracted into H_2O (100 mL) this solution was treated with KPF_6 (2.50 g 13.3 mmol) to precipitate a mixture of $[(\text{cym})_3\text{Ru}_3\text{S}_2](\text{PF}_6)_2$ and **1**. After washing this solid with CH_2Cl_2 to remove $[(\text{cym})_3\text{Ru}_3\text{S}_2](\text{PF}_6)_2$, the residue was extracted into acetone, and this solution was concentrated to 5 mL. Addition of Et_2O (80 mL) precipitated a brown powder. Yield: 1.34 g (30%). ^1H NMR (500 MHz, $[\text{D}_3]\text{MeCN}$): 1.28 (m, 6H), 2.22 (m, 3H), 2.61 (m, 1H), 6.61 (m, 1H), 6.14 (m, 1H), 5.96 (m, 1H), 5.59 ppm (m, 1H). ESI-MS: m/z 519 ($[\text{M}^{2+}]$). Elemental analysis (%) calcd for $\text{C}_{40}\text{H}_{56}\text{F}_{12}\text{P}_2\text{Ru}_4\text{S}_3$: C 36.19, H 4.25, N 0; found: C 35.74, H 4.15, N 0.28.

2⁺: A solution of $[\text{Cp}^*\text{Co}]$ (424 mg, 1.29 mmol) in THF (40 mL) was added to a stirred solution of **1** (814 mg 0.61 mmol) in MeCN (130 mL). After 1 h, the solvent was removed in vacuo, and the resulting red powder was extracted with hexane (50 mL). Dark red crystals were obtained upon concentrating and cooling the solution. Yield: 464 mg (65%). ^1H NMR (500 MHz, $[\text{D}_8]\text{THF}$): 1.22 (d, $J = 7$ Hz, 6H), 1.37 (d, $J = 7$ Hz, 18H), 1.78 (s, 3H), 2.34 (s, 9H) 2.58 (sept, $J = 7$ Hz, 1H) 2.78 (sept, $J = 7$ Hz, 3H) 4.13 (d, $J = 6$ Hz, 2H) 4.47 (d, $J = 6$ Hz, 2H) 4.80 (d, $J = 6$ Hz, 6H) 4.97 ppm (d, $J = 6$ Hz, 6H). Elemental analysis (%) calcd for $\text{C}_{40}\text{H}_{56}\text{Ru}_4\text{S}_3$: C 46.31, H 5.44, N 0; found: C 46.48, H 5.45, N 0.17.

Crystallography: Data was collected at -78°C on a Siemens Platform/CCD automated diffractometer. Data processing was performed with SAINT PLUS version 6.22. Structures were solved using direct methods and refined using full-matrix least-squares on F^2 using Bruker SHELXTL version 6.10. Hydrogen atoms were fixed in idealized positions with thermal parameters $1.5\times$ those of the attached carbon atoms. The data were corrected for absorption on the basis of Ψ -scans. CCDC-244393 and CCDC-244394 contain the supplementary crystallographic data for this paper. These data can be obtained free of charge via www.ccdc.cam.ac.uk/contents/retrieving.html (or from the Cambridge Crystallographic Data Centre, 12 Union Road, Cambridge CB2 1EZ, UK; fax: (+44) 1223-336-033; or deposit@ccdc.cam.ac.uk).

Received: July 10, 2004

Keywords: arenes · hydrogen · rearrangement · ruthenium · sulfur

- [9] H. Seino, Y. Mizobe, M. Hidai, *New J. Chem.* **2000**, 24, 907.
- [10] M. Hidai, S. Kuwata, Y. Mizobe, *Acc. Chem. Res.* **2000**, 33, 46.
- [11] I. Bhugun, D. Lexa, J.-M. Savéant, *J. Am. Chem. Soc.* **1996**, 118, 3982.
- [12] F. Gloaguen, J. D. Lawrence, T. B. Rauchfuss, *J. Am. Chem. Soc.* **2001**, 123, 9476.
- [13] M. A. Bennett, A. K. Smith, *J. Chem. Soc. Dalton Trans.* **1974**, 233.

- [1] J. R. Long, R. H. Holm, *J. Am. Chem. Soc.* **1994**, 116, 9987.
- [2] M. D. Curtis, P. D. Williams, W. M. Butler, *Inorg. Chem.* **1988**, 27, 2853.
- [3] D. Coucouvanis, J. Han, N. Moon, *J. Am. Chem. Soc.* **2002**, 124, 216.
- [4] S. C. Lee, R. H. Holm, *Proc. Natl. Acad. Sci. USA* **2003**, 100, 3595.
- [5] S. C. Lee, R. H. Holm, *Chem. Rev.* **2004**, 104, 1135.
- [6] J. R. Lockmeyer, T. B. Rauchfuss, A. L. Rheingold, *J. Am. Chem. Soc.* **1989**, 111, 5733.
- [7] A. L. Eckermann, D. Fenske, T. B. Rauchfuss, *Inorg. Chem.* **2001**, 40, 1459.
- [8] M. Nambu, D. L. Mohler, K. Hardcastle, K. K. Baldrige, J. S. Siegel, *J. Am. Chem. Soc.* **1993**, 115, 6138.

The Chemical Application of High-Resolution Electron Tomography: Bright Field or Dark Field?*

John Meurig Thomas, Paul A. Midgley,*
Timothy J. V. Yates, Jonathan S. Barnard, Robert Raja,
Ilke Arslan, and Matthew Weyland*

There are many occasions when chemists need to know detailed information pertaining to the shapes and morphology of minute (nanometer-sized) objects and the topography of nanopores. In characterizing various kinds of electronic devices ranging from quantum dots to quantum wells, in determining the structure of viruses, in visualizing the architecture of supramolecular assemblies inside eukaryotic and prokaryotic cells, and especially in the identification of nanoparticle catalysts supported on high-area nanoporous solids, it is important to know—without recourse to sectioning or other destructive techniques—the precise location, spatial

[*] Prof. Sir J. M. Thomas, Dr. P. A. Midgley, Dr. T. J. V. Yates,
Dr. J. S. Barnard, Dr. I. Arslan
Department of Materials Science and Metallurgy
University of Cambridge
Pembroke Street, Cambridge, CB2 3QZ (UK)
Fax: (+44) 1223-334-563
E-mail: jmt@ri.ac.uk
pam33@cam.ac.uk

Prof. Sir J. M. Thomas
Davy–Faraday Research Laboratory
Royal Institution of Great Britain
21 Albermarle Street, London, W1X 4BS (UK)
Fax: (+44) 207-670-2988

Dr. R. Raja
University Chemical Laboratory, University of Cambridge
Lensfield Road, Cambridge, CB2 1EW (UK)

Dr. M. Weyland
Department of Applied and Engineering Physics
Cornell University, E13 Clark Hall, Ithaca, NY 14853 (USA)

[**] The authors thank the Royal Society, the Isaac Newton Trust, the EPSRC, the IRC in Nanotechnology and the BP and FEI Companies for financial support. We also thank Dr. T. Khimyak and Prof. B. F. G. Johnson for their cooperation.



Supporting information (animation clip) for this article is available on the WWW under <http://www.angewandte.org> or from the author.

distribution, and, wherever possible, the elemental composition of such materials.^[1]

Like other, well-known forms of tomography (X-ray or positron-emission) electron tomography enables a three-dimensional (3D) picture to be computed (by using proven mathematical procedures) from a series of projected two-dimensional (2D) images taken over as wide a range of angular orientations as possible. The greater the number of distinct 2D images accumulated, the higher is the resolution of the resulting tomogram. Typically, the specimens to be investigated are imaged in a high-resolution electron microscope at a series of angular settings (see Figure 1). From such a series, the tomogram (3D picture) is reconstructed by suitable, so-called “back-projection”, as first described by Hart and others.^[2–4]

The question arises, however, as to whether the electron tomographic analysis should be performed under so-called “bright-field” (BF) or “dark-field” conditions. In BF conditions (see Figure 1), in either conventional transmission

nature of the porosity of zeolites and nanoporous silica and the distribution of finely divided noble-metal catalysts within them.^[7–11]

But when attempts are made to extend the resolution of BF electron tomography certain insurmountable, electron-optical drawbacks are encountered. The coherence of the BF signal leads to strong contrast, such as Fresnel contrast, whenever the electron wave encounters a change in refractive index, or diffraction contrast (that produce bend contours and thickness fringes) seen in crystalline specimens. In weakly scattering, noncrystalline samples, these effects are less severe and phase contrast, seen in the image by defocusing, can reveal useful detail. However, phase contrast is highly dependent on the so-called contrast transfer function of the microscope and to reveal very small structures (such as nanoparticles in mesopores, see below) it is necessary to use large defocus values. With large defocus settings, the contrast transfer function oscillates rapidly and direct interpretation of image contrast becomes impossible. For tomography, in which truly 3D samples must be examined, this problem is compounded as identical features at different heights in the specimen can show opposite contrast or no contrast at all. Using small defoci settings will not yield sufficient phase contrast to allow fine detail to be resolved above a support film or substrate, as illustrated later.

High-angle annular dark-field (HAADF) electron tomography, which is readily carried out using a scanning transmission electron microscope (STEM), suffers from none of those drawbacks.^[10,12] Electron beams scattered by the specimen to high angles conform closely to Rutherford's scattering law (where the scattered intensity is proportional to Z^2 , Z = atomic number of the scattering element) and the process is incoherent, so that the signals accumulated by a HAADF detector (Figure 1) are free from the complications arising from the contrast transfer function, adumbrated above. An authentic image of the internal structure of the specimen is thus recorded, and there are no “missing” atomic spacings (as in BF coherent imaging) arising from purely electron-optical effects. A further advantage with STEM imaging is that specimens can suffer far less beam damage during investigation (which is rather long because several images, typically 70, over an angular span of $+70^\circ$ to -70° of specimen tilt, have to be recorded).

Herein we illustrate, with two examples, the veracity of our statement that HAADF electron tomography is superior to BF electron tomography. In the first example, we focus on the bimetallic nanoparticle catalysts, $[\text{Ru}_{10}\text{Pt}_2]$, supported on mesoporous silica. Figure 2a shows images of a typical region of mesoporous silica containing this catalyst under BF conditions; and Figure 2b shows precisely the same region of the specimen recorded under HAADF conditions. Whereas under BF conditions the nanoparticles are barely visible, because of the extremely weak phase contrast, under HAADF conditions they stand out clearly because of the high amplitude, atomic number contrast.^[13]

Figure 3 shows a series of 3 nm thick slices of the tomogram (derived from images such as that shown in Figure 2b) displayed parallel to the pore axis at intervals of 5 nm—an animation of the top-to-bottom distribution of

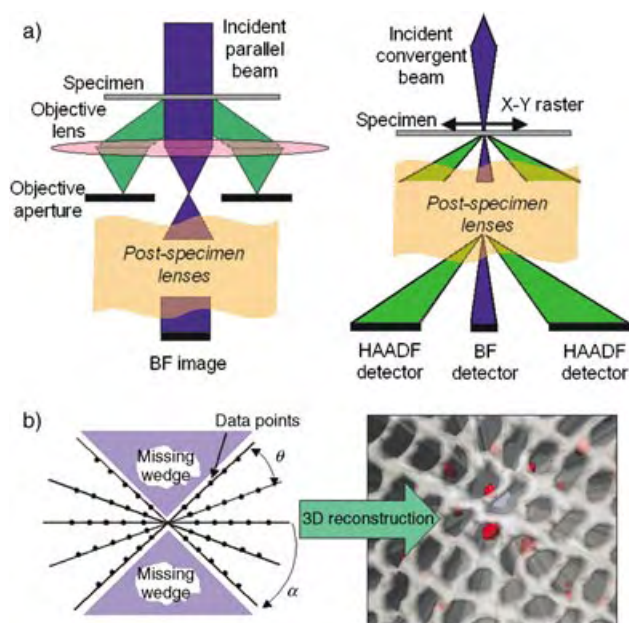


Figure 1. a) Bright field (BF) image formation in the TEM (left) and BF and high-angle annular dark-field (HAADF) image formation in the STEM (right). b) Fourier space representation (left) of the series of images, angular sampling θ , maximum tilt α , used to reconstruct a tomogram, such as that of the mesoporous catalyst (right).

(TEM) or scanning transmission (STEM) mode, the forward-scattered beam is used to construct the electron microscopic images (2D) images, whereas in the dark field conditions, it is the beams diffracted through high angles that form the images. BF imaging is the customary procedure, especially in molecular biological contexts; for example in the cryo-electron microscopic, tomographic work of Baumeister et al. a great deal of insight has been gained in visualizing the molecular organization of the cytoplasm using BF-based tomography.^[5,6] It has also been used effectively to clarify the

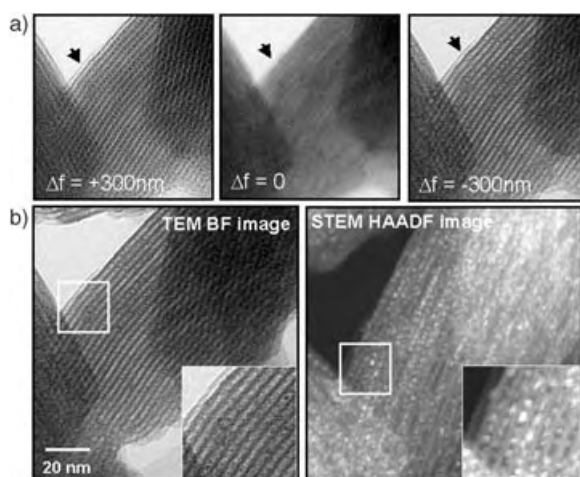


Figure 2. a) BF images, taken at three defocus values, of nanoparticle-filled mesoporous silica. b) A comparison of BF (left) and HAADF (right) images of identical areas of catalyst: nanoparticles of $[\text{Ru}_{10}\text{Pt}_2]$ invisible in BF are clearly seen in the HAADF image.

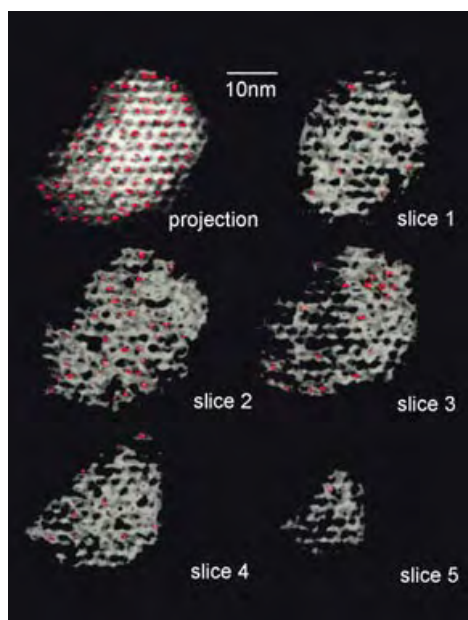


Figure 3. An axial projection of a 30 nm thick specimen and five successive 3-nm thick slices through a tomogram of silica-supported $[\text{Ru}_{10}\text{Pt}_2]$: nanoparticles (red), mesoporous silica (white).

$[\text{Ru}_{10}\text{Pt}_2]$ nanoparticles within the mesoporous silica is in the Supporting Information.

In the second example, we take a section of a Si-Ge multiple quantum-well device, recorded both under BF (Figure 4a) and HAADF (Figure 4b) conditions. Again, the benefits of dark-field imaging are clear. The BF image is dominated by coherent diffraction contrast (bend contours) and the quantum wells are barely visible. In the HAADF micrograph the diffraction contrast has disappeared and the image is dominated by thickness and atomic number contrast—the wells contain 15% Ge. Such an image contrast is ideal for subsequent tomographic analysis.

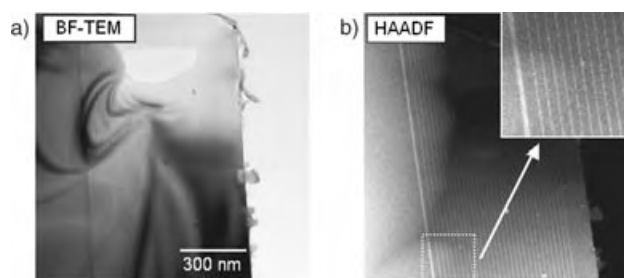


Figure 4. a) TEM BF image and b) STEM HAADF image of a Si-Ge multiple quantum well structure. Coherent diffraction effects dominate the BF image. The quantum wells are revealed clearly only in the incoherent HAADF image.

The quintessential conclusion to be drawn from this work is that when electron tomographic resolutions of 3 to 6 nm are deemed adequate, BF imaging suffices. At higher resolutions, and especially in probing nanoparticles of dimension 1 nm or less, it is imperative that HAADF tomography be employed.

Received: July 27, 2004

Published online: November 26, 2004

Keywords: electron tomography · heterogeneous catalysis · nanoparticles · scanning probe microscopy

- [1] J. M. Thomas, P. A. Midgley, *Chem. Commun.* **2004**, 1247.
- [2] R. G. Hart, *Science* **1968**, 159, 1464.
- [3] D. J. De Rosier, A. Klug, *Nature* **1968**, 217, 130.
- [4] R. A. Crowther, L. A. Amos, J. T. Finch, A. Klug, *Nature* **1970**, 226, 421.
- [5] O. Medalia, I. Weber, A. S. Frangakis, G. Gerisch, W. Baumeister, *Science* **2002**, 298, 1209.
- [6] J. M. Plitzko, A. S. Frangakis, S. Nickell, F. Forster, A. Gross, W. Baumeister, *Trends Biotechnol.* **2002**, 8, S41.
- [7] A. H. Janssen, A. J. Koster, K. P. de Jong, *J. Phys. Chem. B* **2002**, 106, 11905.
- [8] K. P. de Jong, A. J. Koster, *ChemPhysChem* **2002**, 3, 776.
- [9] U. Ziese, K. P. de Jong, A. J. Koster, *Appl. Catal. A* **2004**, 260, 71–74.
- [10] P. A. Midgley, M. Weyland, J. M. Thomas, B. F. G. Johnson, *Chem. Commun.* **2001**, 18, 907.
- [11] P. A. Midgley, J. M. Thomas, L. Laffont, M. Weyland, R. Raja, B. F. G. Johnson, T. Khimyak, *J. Phys. Chem. B* **2004**, 108, 4590.
- [12] P. A. Midgley, M. Weyland, *Ultramicroscopy* **2003**, 96, 413.
- [13] The apparent size of the nanoparticles depends on the precise imaging conditions (e.g. a larger probe size results in a “larger” particle). In reality the $[\text{Ru}_{10}\text{Pt}_2]$ particles are approximately 0.4 nm diameter.

Supramolecular Catalysis of a Unimolecular Transformation: Aza-Cope Rearrangement within a Self-Assembled Host**

Dorothea Fiedler, Robert G. Bergman,* and Kenneth N. Raymond*

Chemists have long envied the ability of enzymes to manipulate reaction energetics and specificity through steric confinement and precise functional-group interactions. The enormous rate accelerations that enzymes achieve at modest temperatures may be attributed to their high degree of complexity, and the synthetic chemist is hard pressed to create such well-constructed catalytic scaffolds. Yet in this regard, the utilization of supramolecular chemistry may have an advantage: supramolecular self-assembly facilitates the creation of large, complex structures from relatively simple precursors.^[1,2] Based on reversible weak interactions, such as hydrogen bonding or metal–ligand interactions, synthetic chemists have generated an array of self-assembled structures, diverse in architecture and composition. Some of these synthetic structures bear an internal cavity, and their interior can provide a new and very specific chemical environment, distinctly different from the exterior surroundings.^[3–6] The

development of container-like molecules into chemically useful structures is an attractive goal, and their utilization as catalytic reaction chambers can parallel the enzyme function. The rate for a bimolecular Diels–Alder reaction, for example, was reported to be significantly accelerated in the presence of a supramolecular host, owing to the increase of effective concentrations of the two substrates when bound within the same capsule.^[7,8] Major challenges are a) to develop supramolecular systems capable of catalyzing unimolecular reactions, and b) to circumvent catalyst inhibition, a problem that frequently occurs when the cavity binds the reaction product more strongly than the substrate.^[7,9] We report herein the utilization of a supramolecular metal–ligand assembly that is capable of catalyzing a unimolecular rearrangement. Simply by inclusion into a size- and shape-constrained reaction space these rearrangements are accelerated by up to three orders of magnitude compared to their background rates. Furthermore, the chemical properties of the reacting system provide an effective means of preventing product inhibition, which facilitates catalyst turnover.

Raymond and co-workers have composed supramolecular tetrahedral structures of M_4L_6 stoichiometry through self-assembly of simple metal and ligand components.^[10,11] In these assemblies the metal atoms are located at the vertices of the tetrahedron and six bis-bidentate catechol amide ligands span the edges (Figure 1). The tris-bidentate chelation of the metal centers renders them chiral (Δ or Λ), and the

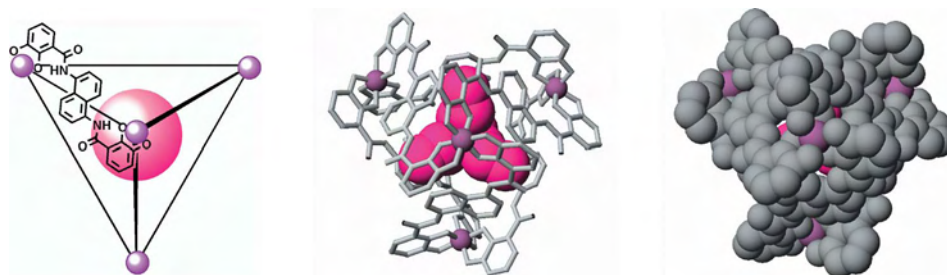


Figure 1. Left: A schematic view of the $[G \subset M_4L_6]$ (G = guest) supramolecular tetrahedral assembly, looking down the C_3 -axis. For clarity only one ligand is drawn, the other ligands are represented as sticks. Middle: CAChe model of $[NPr_4 \subset Fe_4L_6]^{11-}$, the guest molecule is shown in a space-filling view, the hydrogen atoms are omitted for clarity. Right: The same CAChe model as in the middle, now with host and guest in space filling view. This representation shows that the guest molecule is not exposed to the assembly exterior, but rather is tightly surrounded by the host.

[*] D. Fiedler, Prof. R. G. Bergman, Prof. K. N. Raymond
Department of Chemistry
University of California
Berkeley, CA 94720-1460 (USA)
Fax: (+1) 510-642-7714 (Bergman)
Fax: (+1) 510-486-5283 (Raymond)
E-mail: bergman@cchem.berkeley.edu
raymond@socrates.berkeley.edu

[**] Supported by the Director, Office of Energy Research, Office of Basic Energy Sciences, Chemical Sciences Division, of the U.S. Department of Energy under contract DE-AC03-7600098. The authors would like to thank Prof. David E. Wemmer, Dr. Anna V. Davis, Dennis H. Leung, and Emily A. Dertz for helpful discussions and suggestions, Dr. Herman van Halbeek for assistance with the 2D NMR spectroscopy, and Mathew E. Bishop for creation of the cover art.

Supporting information for this article is available on the WWW under <http://www.angewandte.org> or from the author.

mechanical coupling through the rigid ligands results in the formation of exclusively homochiral assemblies (i.e. $\Delta_4\Delta_4\Delta_4$ or $\Lambda_4\Lambda_4\Lambda_4$). By virtue of the 12^- overall charge, the assemblies are water soluble, yet they contain a flexible hydrophobic cavity of $350\text{--}500 \text{ \AA}^3$ into which they can bind a broad range of monocationic guest molecules, from alkyl ammonium cations to half-sandwich complexes.^[12,13]

In pursuing supramolecular catalysis, a chemical transformation of a cationic substrate, which is compatible with the supramolecular host, needed to be identified. The cationic 3-aza-Cope rearrangement seemed to be the ideal reaction to be carried out in the finite environment of the M_4L_6 assembly. The substrates are ammonium cations (**A**) and should bind to the cavity interior (Figure 2, top). Sigmatropic rearrangement leads to an iminium cation (**B**), which is subsequently hydrolyzed to the corresponding γ,δ -unsaturated aldehyde (**C**).

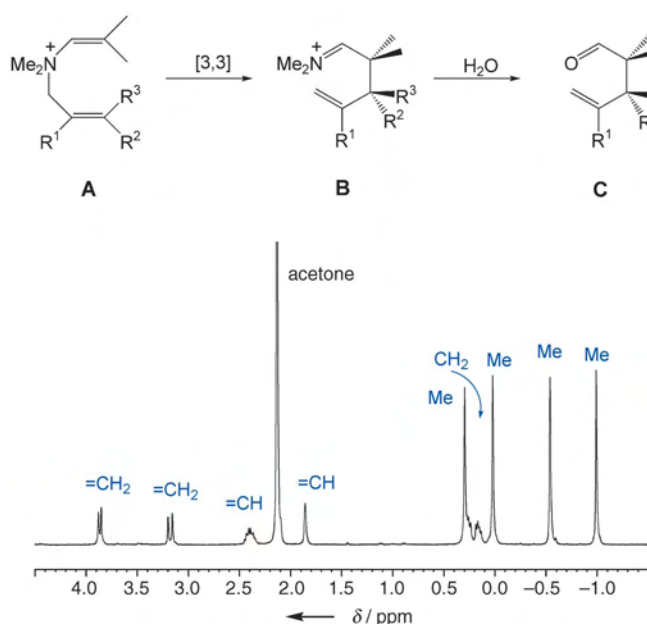


Figure 2. Top: A general reaction scheme of the 3-aza-Cope rearrangement. Starting from the enammonium cation **A**, [3,3] sigmatropic rearrangement leads to iminium cation **B**, which then hydrolyzes to the aldehyde, **C**. Bottom: ^1H NMR spectrum of $[\mathbf{1}\text{-Ca}_4\text{L}_6]^{11-}$ (**1**: R^1 , R^2 , $\text{R}^3 = \text{H}$). The observed upfield shift of guest resonance signals illustrates the close contact between host and guest.

Since neutral molecules are only very weakly bound by the supramolecular host, binding of more substrate could occur after the hydrolysis step, enabling catalytic turnover.

We explored a range of enammonium substrates **A**, diverse in size, shape, and substitution pattern (Table 1). All

Table 1: Rate constants for free (k_{free}) and encapsulated (k_{encaps}) rearrangements (measured at 50 °C) and their acceleration factors.

Substrate	R^1	R^2	R^3	$k_{\text{free}} [\times 10^{-5} \text{ s}^{-1}]$	$k_{\text{encaps}} [\times 10^{-5} \text{ s}^{-1}]$	Acceleration
1	H	H	H	3.49	16.3	5
2	Me	H	H	7.61	198	26
3	H	Et	H	3.17	446	141
4	H	H	Et	1.50	135	90
5	H	<i>n</i> Pr	H	4.04	604	150
6	H	H	<i>n</i> Pr	1.69	74.2	44
7	H	<i>i</i> Pr	H	0.37	316	854

of the substrates were encapsulated by the metal–ligand assembly, which can most easily be monitored by ^1H NMR spectroscopy. Shielding by the naphthalene moiety of the ligand scaffold causes an upfield shift of the guest resonances by $\delta = 2\text{--}3$ ppm. Enammonium cation **1** (R^1 , R^2 , $\text{R}^3 = \text{H}$), for example, quantitatively yielded the host–guest complex $[\mathbf{1}\text{-Ca}_4\text{L}_6]^{11-}$ as confirmed by NMR spectroscopy (Figure 2, bottom) and ES-mass spectrometry. To investigate whether the substrate's reactivity has been altered by encapsulation,

the rates of rearrangement were measured for the free and encapsulated enammonium cations. All rearrangements displayed clean first-order kinetics in buffered solution at 50 °C. Remarkably, the encapsulated substrates rearranged faster in all cases (Table 1). Substrate **3**, for instance, experienced 141-fold rate acceleration, once encapsulated by the supramolecular assembly. Even more dramatic is the effect on the isopropyl substituted enammonium cation **7**; binding into the host cavity resulted in a rate increase by a factor of 854. Control experiments with the free rearrangement showed no significant solvent dependence, excluding the possibility that the observed rate enhancement is simply due to the cavity's more hydrophobic environment. The prospect that the host-assembly's negative charge causes the rate acceleration was ruled out by adding salt (2M KCl) in the absence of the assembly, which did not result in a significant change in rate for the free rearrangement.

To elucidate the origin of the observed rate accelerations, the activation parameters were measured. The obtained parameters for the free rearrangement of substrate **3**, for example, are $\Delta H^\ddagger = 23.1(\pm 0.8) \text{ kcal mol}^{-1}$ and $\Delta S^\ddagger = -8(\pm 2) \text{ e.u.}$ (1 e.u. = $4.184 \text{ J K}^{-1} \text{ mol}^{-1}$). These values compare well with those reported for similar systems,^[14] and the negative entropy of activation reflects the highly organized, chairlike transition state required for the rearrangement reaction. The reaction of the encapsulated substrate $[\mathbf{3}\text{-Ca}_4\text{L}_6]^{11-}$ gave a very similar value for the enthalpy of activation, $\Delta H^\ddagger = 23.0(\pm 0.9) \text{ kcal mol}^{-1}$. The entropy of activation, however, differs remarkably by almost 10 e.u., with $\Delta S^\ddagger = +2(\pm 3) \text{ e.u.}$ (see Supporting Information). Comparable effects are observed for the other substrates.^[15]

These results imply that the host-assembly selectively binds a reactive conformation of the substrate. The space-

restrictive host cavity only allows encapsulation of a tightly packed conformation, closely resembling the conformation of the chairlike transition state. The predisposed conformers, which have already lost several rotational degrees of freedom, are selected from an equilibrium mixture of all possible conformers. Thus the entropic barrier for rearrangement decreases. This effect of preorganization becomes more significant for the larger substrates, which fit more tightly in the host cavity. For example, while an isopropyl substituent at R^2 slows down the rate of the

free reaction relative to that of the other substrates, the bulkier R^2 group effects the largest observed acceleration of the encapsulated reaction. Presumably in free substrate **7** the additional steric repulsion between the ends of the alkyl chains reduces the percentage of reactive conformations in free solution even further, therefore decreasing the rate of rearrangement. The encapsulated **7**, however, does not display a similar effect; once squeezed into the cavity, the two pendant alkyl chains are forced to be in close proximity,

and the reaction proceeds at a rate comparable to those of the other encapsulated substrates.

The effect of preorganization into a reactive conformation in the host-guest system is supported by the 2D NOESY spectrum of $[3\text{C}\text{Ga}_4\text{L}_6]^{11-}$ (Figure 3). While the unbound substrate shows no NOEs between the pendant alkyl chains, the encapsulated enammonium cation displays strong dipolar couplings between protons at the two distal ends of the molecule. Assuming a tight, chairlike conformation of the bound substrate, these correlations would be expected.^[16]

It is of interest to compare our results with the observations on the enzyme chorismate mutase, which catalyzes the unimolecular Claisen rearrangement from chorismate to prephenate, achieving rate acceleration of a factor of 10^6 relative to the uncatalyzed reaction. Even though this highly complex process is not fully understood, the factors responsible for the enzyme's catalytic efficiency include reduction of both the enthalpic and entropic barrier for rearrangement.^[17] It is proposed that a series of functional groups located at the active site stabilize the charge build-up in the transition state, which causes a decrease in enthalpy of activation.^[18] In addition, the enzyme binds the substrate in a diaxial, reactive conformation, which lowers the entropy of activation by 11–13 e.u.^[19–21] Theoretical studies by Bruice and co-workers on the chorismate rearrangement imply that the efficiency of forming near attack conformers (NACs) in the ground state can be a very important kinetic contribution.^[22,23]

Since the enzyme shows such remarkable catalytic properties, the question arose as to whether the M_4L_6 supramolecular assembly would also be able to mediate the aza-Cope rearrangement catalytically. The stoichiometric experiments had shown that in all cases of the host-mediated 3-aza-Cope rearrangement, the iminium cations **B** hydrolyzed rapidly to the corresponding aldehydes **C**, leaving behind an empty cavity.^[24] This property should enable the reaction to be carried out under catalytic conditions. Indeed, carrying out the reaction in the presence of 13 mol % catalyst relative to enammonium substrate revealed truly catalytic behavior of the supramolecular host. Raising the catalyst loading from 13 mol % to 27 mol % to 40 mol % resulted in the expected increases in rate; the observed initial rate constants at 25 °C are $k_{13\text{ mol \%}} = 0.64 \times 10^{-4} \text{ s}^{-1}$, $k_{27\text{ mol \%}} = 1.17 \times 10^{-4} \text{ s}^{-1}$, and $k_{40\text{ mol \%}} = 1.80 \times 10^{-4} \text{ s}^{-1}$ (see Supporting Information). The

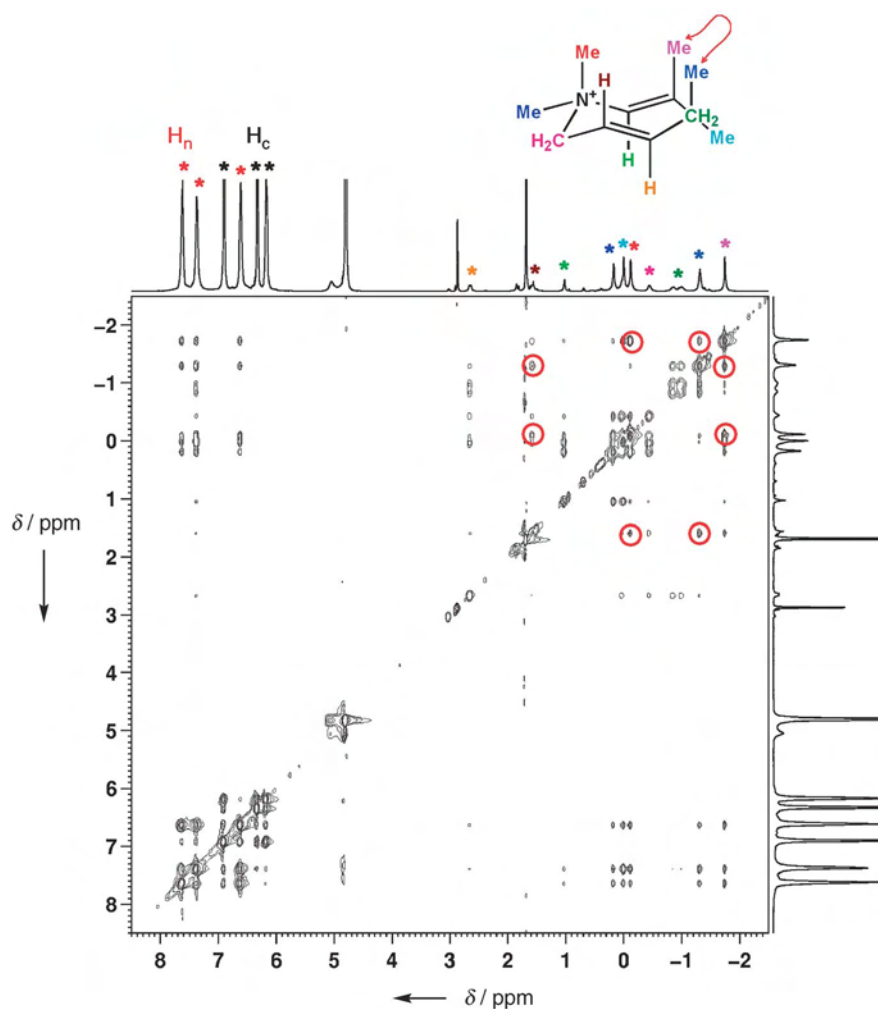


Figure 3. The 2D NOESY spectrum of $[3\text{C}\text{Ga}_4\text{L}_6]^{11-}$ in a $\text{D}_2\text{O}/\text{MeOD}$ mixture (70:30) recorded at -10°C , mixing time 100 ms. Indicated in red are selected NOEs. The correlation between Me and Me at the two distal ends of the molecule demonstrates the cavity's enforcement of a compressed and folded guest conformation. H_n = naphthyl protons, H_c = catechol protons.

idea of the supramolecular assembly providing a catalytic cavity for rearrangement is further supported by an inhibition experiment with the very strongly binding guest molecule $[\text{NET}_4]^+$. When eight equivalents of $[\text{NET}_4]^+$ were added to the reaction mixtures to block the host cavity, the catalytic activity of the supramolecular host was inhibited. Based on these results, we propose the catalytic mechanism illustrated in Figure 4: 1) A reactive conformation of the enammonium cation binds into the restricted space of the host assembly. 2) The rearrangement proceeds with significant acceleration within the boundaries of the metal–ligand assembly. 3) The rearranged product equilibrates with the bulk solution, and hydrolysis to the corresponding aldehyde enables catalytic turnover by regeneration of the empty assembly that can bind additional substrate.

These findings highlight the ability of container-like molecules to provide size- and shape-defined nanospaces, highly capable of catalysis of unimolecular organic reactions. By binding the substrates in a reactive conformation, the host assembly accelerates the rates of rearrangement by up to

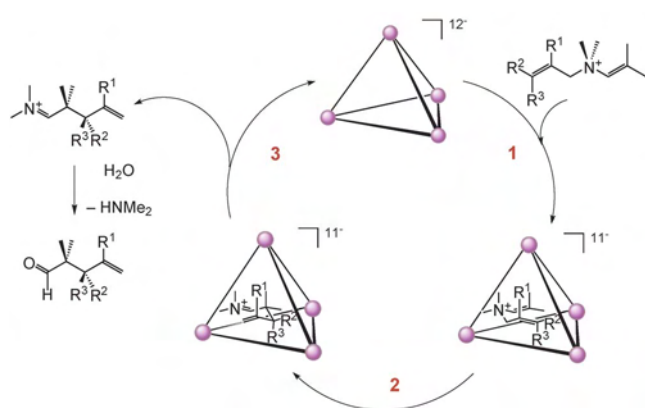


Figure 4. Proposed catalytic cycle for the cationic 3-aza-Cope rearrangement, see text for details.

three orders of magnitude. Release and hydrolysis of the rearranged product generate catalytic turnover. With this, the large potential of supramolecular assemblies as synthetically useful tools in organic chemistry becomes apparent.

Received: August 24, 2004

Published online: November 19, 2004

Keywords: cage compounds · homogeneous catalysis · host–guest systems · sigmatropic rearrangement

- [1] J. L. Atwood, J. E. D. Davies, D. D. MacNicol, F. Voegtle, J.-M. Lehn, *Comprehensive Supramolecular Chemistry*, Pergamon, Oxford, **1996**.
- [2] J.-M. Lehn, *Supramolecular Chemistry: Concepts and Perspectives*, VCH, Weinheim, **1995**.
- [3] L. Garel, J.-P. Dutasta, A. Collet, *Angew. Chem.* **1993**, 105, 1249; *Angew. Chem. Int. Ed. Engl.* **1993**, 32, 1169.
- [4] J. C. Sherman, D. J. Cram, *J. Am. Chem. Soc.* **1989**, 117, 4527.
- [5] F. Hof, S. L. Craig, C. Nuckolls, J. Rebek, Jr., *Angew. Chem.* **2002**, 114, 1557; *Angew. Chem. Int. Ed.* **2002**, 41, 1488.
- [6] W.-Y. Sun, M. Yoshizawa, T. Kusukawa, M. Fujita, *Curr. Opin. Chem. Biol.* **2002**, 6, 757.
- [7] J. Kang, J. Rebek, Jr., *Nature* **1997**, 385, 50.
- [8] J. Kang, J. Santamaria, G. Hilmersson, J. Rebek, Jr., *J. Am. Chem. Soc.* **1998**, 120, 7389.
- [9] M. Yoshizawa, Y. Takeyama, T. Kusukawa, M. Fujita, *Angew. Chem. Int. Ed.* **2002**, 114, 1403; *Angew. Chem. Int. Ed.* **2002**, 41, 1347.
- [10] D. L. Caulder, K. N. Raymond, *Acc. Chem. Res.* **1999**, 32, 975.
- [11] D. L. Caulder, C. Brückner, R. E. Powers, S. König, T. N. Parac, J. A. Leary, K. N. Raymond, *J. Am. Chem. Soc.* **2001**, 123, 8923.
- [12] D. Fiedler, D. H. Leung, R. G. Bergman, K. N. Raymond, *J. Am. Chem. Soc.* **2004**, 126, 3674.
- [13] D. H. Leung, D. Fiedler, R. G. Bergman, K. N. Raymond, *Angew. Chem.* **2004**, 116, 981; *Angew. Chem. Int. Ed.* **2004**, 43, 963.
- [14] S. Jolidon, H.-J. Hansen, *Helv. Chim. Acta* **1977**, 60, 978.
- [15] D. Fiedler, R. G. Bergman, K. N. Raymond, unpublished results.
- [16] The short mixing time of 100 ms ensures that no correlations resulting from spin diffusion are observed.
- [17] H. Gorisch, *Biochemistry* **1978**, 17, 3700.
- [18] A. Kienhofer, P. Kast, D. Hilvert, *J. Am. Chem. Soc.* **2003**, 125, 3206.
- [19] A. Y. Lee, J. D. Stewart, J. Clardy, B. Ganem, *Chem. Biol.* **1995**, 2, 195.
- [20] H. Guo, Q. Cui, W. N. Lipscomb, M. Karplus, *Proc. Natl. Acad. Sci. USA* **2001**, 98, 9032.
- [21] S. D. Copley, J. R. Knowles, *J. Am. Chem. Soc.* **1987**, 109, 5008.
- [22] S. Hur, T. C. Bruice, *J. Am. Chem. Soc.* **2003**, 125, 10540.
- [23] T. C. Bruice, F. C. Lightstone, *Acc. Chem. Res.* **1999**, 32, 127. For further discussion, see also: M. Štrajbl, A. Shurki, M. Kato, A. Warshel, *J. Am. Chem. Soc.* **2003**, 125, 10228.
- [24] In the experiments reported herein, the empty cavity refers to the host cavity containing the counterion $[\text{NMe}_4]^+$. The $[\text{NMe}_4]^+$ ion has a very weak binding constant and is easily replaced by the different substrates.

Publication Dates and Pagination 2004

Issue number	Pagination	Publication dates	
		print	online
1	1 – 130	December 22	December 17
2	131 – 260	December 29	December 19
3	261 – 380	January 5	December 29
4	381 – 530	January 16	January 14
5	531 – 646	January 26	January 21
6	647 – 764	January 30	January 27
7	765 – 910	February 6	February 2
8	911 – 1032	February 13	February 11
9	1033 – 1168	February 20	February 18
10	1169 – 1308	February 27	February 24
11	1309 – 1442	March 5	March 2
12	1443 – 1604	March 12	March 9
13	1605 – 1746	March 19	March 17
14	1747 – 1894	March 26	March 24
15	1895 – 2042	April 2	March 24
16	2043 – 2180	April 13	April 6
17	2181 – 2310	April 19	April 16
18	2311 – 2454	April 26	April 22
19	2455 – 2584	May 3	April 28
20	2585 – 2726	May 10	May 5
21	2727 – 2864	May 17	May 12
22	2865 – 2976	May 24	May 19
23	2977 – 3086	June 7	June 1
24	3087 – 3204	June 14	June 9
25	3205 – 3346	June 21	June 16
26	3347 – 3496	June 28	June 22
35	4537 – 4674	September 6	September 1
36	4675 – 4816	September 13	September 7
37	4817 – 4964	September 20	September 16
38	4965 – 5102	September 27	September 22
39	5103 – 5274	October 4	September 29
40	5275 – 5416	October 11	October 5
41	5417 – 5554	October 18	October 13
42	5555 – 5708	October 25	October 20
43	5709 – 5862	November 5	November 2
44	5863 – 6008	November 11	November 10
45	6009 – 6218	November 19	November 17
46	6219 – 6390	November 26	November 23
47	6391 – 6564	December 3	December 1
48	6565 – 6828	December 10	December 8

The complete issue was published online on the given date. Some articles were previously available in Early View.

Author Index

The entry for correspondence authors includes the complete information regarding the article. For the coauthors, the type of article and the page numbers are listed. The page numbers in square brackets refer to the German edition [*Angew. Chem.* **2004**, *116*] of *Angewandte Chemie*.

(C) = Communication (E) = Essay (H) = Highlight (L) = Correspondence (M) = Minireview (O) = Obituary
(R) = Review Article (T) = Meeting Review



- Abbenante, G. (C) 2687–2690 [2741–2744]
Abboud, K. A. (C) 345–349 [349–353],
2117–2121 [2169–2173], 6338–6342
[6498–6502]
Abd Hamid, S. B.
– Nanocatalysis: Mature Science Revisited
or Something Really New?
(M) 1628–1637 [1656–1667]
DOI: 10.1002/anie.200301684
Abdalla, M. A. (C) 3967–3970 [4057–4060]
Abdel-Rahman, A. A.-H. Corrigendum:
4389
Abraham, S. (C) 3947–3951 [4037–4041]
Abrahams, B. F.
– $[\{WS_4Cu_4(4,4'-bpy)_4\}][WS_4Cu_4I_4(4,4'-bpy)_4]_\infty$ —An Unusual 3D Porous Coordination Polymer Formed from the Pre-formed Cluster $[Et_4N]_4[WS_4Cu_4I_6]$
(C) 4741–4745 [4845–4849]
DOI: 10.1002/anie.200460076
Abrahams, B. F. (C) 6157–6160 [6283–6286]
Abrams, M. B. (C) 1955–1958 [1989–1992]
Abu-Lebdeh, Y. Corrigendum: 141
Aburel, P. S. (C) 1272–1277 [1292–1297]
Acatay, K. (C) 5210–5213 [5322–5325]
Adams, H. (C) 3938–3941 [4028–4031]
Adhikari, S. S. (C) 6735–6738 [6903–6906]
Adib, K. (C) 2918–2921 [2978–2981]
Aechtner, T. (C) 5849–5851 [5974–5976]
Aerts, A. (L) 4562–4564 [4662–4664]
Aerts, C. A. (L) 4562–4564 [4662–4664]
Afonso, C. A. M.
– Recent Advances in Chiral Resolution through Membrane-Based Approaches
(H) 5293–5295 [5405–5407]
DOI: 10.1002/anie.200460037
Afonso, C. A. M. (C) 1525–1527 [1551–1553]
Ager, D. J. (C) 2816–2819 [2876–2879]
Agnelli, F. (C) 1562–1566 [1588–1592]
Agre, P.
– Aquaporin Water Channels (Nobel Lecture)
(R) 4278–4290 [4377–4390]
DOI: 10.1002/anie.200460804
Ahlrichs, R. (C) 3823–3827 [3911–3915]
Ahn, H.-J. (C) 4940–4943 [5048–5051]
Ahrens, M. J. (C) 6363–6366 [6523–6526]
Ai, H. (C) 6323–6327 [6483–6487]
Ai, X.-C. (C) 5010–5013 [5120–5123]
Aida, T.
– A Molybdenum Crown Cluster Forms Discrete Inorganic–Organic Nanocomposites with Metalloporphyrins
(C) 6327–6331 [6487–6491]
DOI: 10.1002/anie.200460990
– Bioinspired Molecular Design of Light-Harvesting Multiporphyrin Arrays
(M) 150–158 [152–160]
DOI: 10.1002/anie.200301665
– Macroscopic Spinning Chirality Memorized in Spin-Coated Films of Spatially Designed Dendritic Zinc Porphyrin *J*-Aggregates
(C) 6350–6355 [6510–6515]
DOI: 10.1002/anie.200461431
– One-Pot Optical Resolution of Oligopeptide Helices through Artificial Peptide Bundling
(C) 4915–4918 [5023–5026]
DOI: 10.1002/anie.200460703
– Photoluminescence Properties of Discrete Conjugated Wires Wrapped within Dendritic Envelopes: “Dendrimer Effects” on π -Electronic Conjugation
(C) 2943–2947 [3003–3007]
DOI: 10.1002/anie.200353519
Ajamian, A. (M) 3754–3760 [3842–3848]
Ajayaghosh, A.
– Coiled-Coil Gel Nanostructures of Oligo(*p*-phenylenevinylene)s: Gelation-Induced Helix Transition in a Higher-Order Supramolecular Self-Assembly of a Rigid π -Conjugated System
(C) 3422–3425 [3504–3507]
DOI: 10.1002/anie.200453874
Akabane, M. (C) 6474–6479 [6636–6641]
Akai, S. (C) 1407–1410 [1431–1434]
Akasaka, T.
– Supramolecular Dynamics of Cyclic [6]Paraphenyleneacetylene Complexes with [60]- and [70]Fullerene Derivatives: Electronic and Structural Effects on Complexation
(C) 5060–5062 [5170–5172]
DOI: 10.1002/anie.200460630
Åkermark, B. (C) 1006–1009 [1024–1027],
3571–3574 [3655–3658]
Akita, M. (C) 6474–6479 [6636–6641]
Akiyama, K.
– Spin Trapping of ^{13}C -Labeled *p*-Benzynes Generated by Masamune–Bergman Cyclization of Bicyclic Nine-Membered Ene-diyne
(C) 5249–5253 [5361–5365]
DOI: 10.1002/anie.200454133
Akiyama, T.
– Enantioselective Mannich-Type Reaction Catalyzed by a Chiral Brønsted Acid
(C) 1566–1568 [1592–1594]
DOI: 10.1002/anie.200353240
Akiyama, Y. (C) 4892–4896 [5000–5004]
Akselrud, L. (C) 1088–1092 [1108–1112]
Al-Rawi, S. (C) 4366–4370 [4467–4470]
Alam, T. M. (C) 2787–2792 [2847–2852]
Alarco, P.-J. Corrigendum: 141
Alberti, A. (C) 4933–4937 [5041–5045]
Alberto, R.
– Vitamin B12 as a Ligand for Technetium and Rhenium Complexes
(C) 5025–5029 [5135–5139]
DOI: 10.1002/anie.200460923
Albrecht, M.
– Selecting Different Complexes from a Dynamic Combinatorial Library of Coordination Compounds
(C) 6662–6666 [6832–6836]
DOI: 10.1002/anie.200453975
Alcor, D. (C) 4785–4788 [4889–4892]
Alder, R. W.
– When and How Do Diaminocarbenes Dimerize?
(R) 5896–5911 [6020–6036]
DOI: 10.1002/anie.200400654
Alessi, D. R. (C) 2671–2674 [2725–2728]
Alexakis, A.
– A Highly Effective Phosphoramidite Ligand for Asymmetric Allylic Substitution
(C) 2426–2428 [2480–2482]
DOI: 10.1002/anie.200353744
Alexanian, E. J. (C) 1998–2001 [2032–2035]
Alexeev, D. (C) 5914–5918 [6040–6044]
Aliev, A. E. (C) 1225–1228 [1245–1248]
Allemand, J.-F. (C) 4785–4788 [4889–4892]
Allen, K. N.
– Structural Origin of the High Affinity of a Chemically Evolved Lanthanide-Binding Peptide
(C) 3682–3685 [3768–3771]
DOI: 10.1002/anie.200460028
Almeida, M. (C) 4049–4052 [4141–4144]
Almeida, W. P. (C) 4330–4333 [4430–4433]
Alonso, J. (C) 5510–5513 [5626–5629]
Alonso, J. L.
– The Shape of Neutral Valine
(C) 605–610 [615–620]
DOI: 10.1002/anie.200352543
Alonso, P. J. (C) 5225–5228 [5337–5340]
Alvarez, C. M. (C) 4497–4500 [4597–4600]
Alvarez-Gutiérrez, J. M. (C) 325–329 [329–333]
Àlvarez Micó, X. (C) 1400–1403 [1424–1427]
Álvarez-Rodrigo, L. (C) 3932–3935 [4022–4025]
Amann, N. (C) 1845–1847 [1881–1883]
Amatore, C.
– Imaging Concentration Profiles of Redox-Active Species with Nanometric Amperometric Probes: Effect of Natural Convection on Transport at Microdisk Electrodes
(C) 1431–1435 [1455–1459]
DOI: 10.1002/anie.200352662
Amidjojo, M. (C) 4529–4531 [4629–4631]
Amii, H. (C) 585–587 [595–597]
Amore, A. (C) 3471–3473 [3553–3555]
Amouri, H. (C) 1393–1397 [1417–1421]
An, B.-K. (C) 6346–6350 [6506–6510]
An, D. (C) 5635–5638 [5753–5756]

- An, K. (C) 2282–2285 [2332–2335]
 Anada, K. (C) 1233–1235 [1253–1255]
 Anada, M. (C) 2665–2668 [2719–2722]
 Anandhi, U. (C) 6128–6131 [6254–6257]
 Anantharaman, G. (C) 3832–3835 [3920–3923], 3842–3844 [3930–3932]
 Andersen, R. J. (C) 5946–5951 [6072–6077]
 Anderson, E. A. (C) 1998–2001 [2032–2035]
 Andreev, Yu. G. (C) 2103–2105 [2155–2157]
 Andreini, K. W. (C) 5477–5481 [5593–5597]
 Andrews, L.
 – Infrared Spectra of Indium Hydrides in Solid Hydrogen and of Solid Indane (C) 1706–1709 [1738–1741]
 DOI: 10.1002/anie.200353216
 – Significant Interactions between Uranium and Noble-Gas Atoms: Coordination of the UO_2^+ Cation by Ne, Ar, Kr, and Xe Atoms (C) 2554–2557 [2608–2611]
 DOI: 10.1002/anie.200453790
 Andrews, W. J. (C) 4788–4791 [4892–4895]
 Anet, F. A. L. (C) 2004–2008 [2038–2042]
 Angelici, R. J.
 – Synthesis and Structure of a Dimetallated Buckybowl: Coordination of One $[\text{Cp}^*\text{Ru}]^+$ Unit to Each Side of Corannulene (C) 4497–4500 [4597–4600]
 DOI: 10.1002/anie.200454225
 Anson, C. E. (C) 305–309 [309–313]
 Antesberger, J. (C) 5263–5266 [5375–5378]
 Antonietti, M.
 – Ionic Liquids for the Convenient Synthesis of Functional Nanoparticles and Other Inorganic Nanostructures (M) 4988–4992 [5096–5100]
 DOI: 10.1002/anie.200460091
 Antonietti, M. (C) 2270–2273 [2320–2323], 4345–4349 [4445–4449]
 Anwender, R.
 – Stereospecific Polymerization of Isoprene with Molecular and MCM-48-Grafted Lanthanide(III) Tetraalkylaluminates (C) 2234–2239 [2284–2289]
 DOI: 10.1002/anie.200352730
 Aoki, J. (C) 2834–2837 [2894–2897]
 Aoki, K. (C) 6691–6695 [6859–6863]
 Aoki, T. (C) 3175–3177 [3237–3239]
 Aoyagi, S. (C) 3670–3673 [3756–3759]
 Apeloig, Y. Corrigendum: 141
 Apeloig, Y.
 – The Direct Synthesis of a Silene–Organometallic Complex (C) 745–748 [763–766]
 DOI: 10.1002/anie.200353048
 Arai, H. (C) 2834–2837 [2894–2897]
 Araki, Keisuke (C) 81–84 [83–86]
 Araki, Koji
 – Design and Fabrication of a Flexible and Self-Supporting Supramolecular Film by Hierarchical Control of the Interaction between Hydrogen-Bonded Sheet Assemblies (C) 100–103 [102–105]
 DOI: 10.1002/anie.200352641
 Araujo, N. C. (C) 4193–4197 [4289–4293]
 Aravinda, S. (C) 6728–6731 [6896–6899]
 Archuleta, J. G. (C) 5658–5661 [5776–5779]
 Ardavan, A. (C) 1386–1389 [1410–1413]
 Argüello, G. A. (C) 2843–2846 [2903–2906]
 Arimoto, H. (C) 81–84 [83–86]
 Arisawa, M.
 – Cycloisomerization Promoted by the Combination of a Ruthenium–Carbene Catalyst and Trimethylsilyl Vinyl Ether, and its Application in The Synthesis of Heterocyclic Compounds: 3-Methylene-2,3-dihydroindoles and 3-Methylene-2,3-dihydrobenzofurans (C) 4063–4067 [4155–4159]
 DOI: 10.1002/anie.200454157
 Armand, M. Corrigendum: 141
 Armes, S. P.
 – Preparation of Shell Cross-Linked Micelles by Polyelectrolyte Complexation (C) 1389–1392 [1413–1416]
 DOI: 10.1002/anie.200352428
 Armitage, B. (M) 4402–4409 [4502–4510]
 Armstrong, A. R. (C) 2286–2288 [2336–2338], 4899–4902 [5007–5010]
 Armstrong, Alan
 – Amine-Catalyzed Epoxidation of Alkenes: A New Mechanism for the Activation of Oxone (H) 1460–1462 [1484–1486]
 DOI: 10.1002/anie.200301716
 Armstrong, Andrea (C) 502–505 [508–511]
 Armstrong, D. R. (C) 2135–2138 [2187–2190]
 Armstrong, G. (C) 2286–2288 [2336–2338]
 Arnaud, A. (C) 1718–1721 [1750–1753]
 Arndt, M.
 – Quantum Mechanics and Chemistry: The Relevance of Nonlocality and Entanglement for Molecules (T) 144–145 [146–147]
 DOI: 10.1002/anie.200320079
 Arndtsen, B. A.
 – Imines in Stille-Type Cross-Coupling Reactions: A Multicomponent Synthesis of α -Substituted Amides (C) 590–594 [600–604]
 DOI: 10.1002/anie.200352123
 Arriortua, M. I. (C) 977–980 [995–998]
 Arseniyadis, S. (C) 3314–3317 [3376–3379], (H) 5436–5441 [5552–5557]
 Arsequell, G. (C) 325–329 [329–333]
 Arslan, I. (C) 6745–6747 [6913–6915]
 Asanuma, H.
 – Alternating Hetero H Aggregation of Different Dyes by Interstrand Stacking from Two DNA–Dye Conjugates (C) 6522–6525 [6684–6687]
 DOI: 10.1002/anie.200460870
 Aschwanden, P. (C) 5971–5973 [6097–6099]
 Assfeld, X. (C) 3565–3568 [3649–3652]
 Assoud, A. (C) 5260–5262 [5372–5375]
 Astruc, D.
 – Synthesis of Dendritic Polyoxometalate Complexes Assembled by Ionic Bonding and Their Function as Recoverable and Reusable Oxidation Catalysts (C) 2924–2928 [2984–2988]
 DOI: 10.1002/anie.200453870
 Atkinson, C. E. (C) 1225–1228 [1245–1248]
 Atwood, J. L.
 – A New Type of Material for the Recovery of Hydrogen from Gas Mixtures (C) 2948–2950 [3008–3010]
 DOI: 10.1002/anie.200353559
 – Inner Core Structure Responds to Communication between Nanocapsule Walls (C) 5263–5266 [5375–5378]
 DOI: 10.1002/anie.200460711
 Aubry, N. (C) 4306–4311 [4406–4411]
 Auernheimer, J. (C) 6649–6652 [6818–6821]
 Auletta, T. (C) 369–373 [373–377]
 Austin, D. J.
 – Simultaneous Identification of Multiple Protein Targets by Using Complementary-DNA Phage Display and a Natural-Product-Mimetic Probe (C) 4052–4055 [4144–4147]
 DOI: 10.1002/anie.200454004
 Averbuj, C. (C) 1255–1260 [1275–1280]
 Axford, L. C. (C) 727–730 [745–748]
 Ayida, B. K. (C) 3177–3182 [3239–3244]
 Aznar, F. (C) 343–345 [347–349]
 Azumaya, I.
 – Absolute Helical Arrangement of Stacked Benzene Rings: Heterogeneous Double-Helical Interaction Comprising a Hydrogen-Bonding Belt and an Offset Parallel Aromatic–Aromatic-Interaction Array (C) 1360–1363 [1384–1387]
 DOI: 10.1002/anie.200352788



- Baba, A.
 – Catalytic Generation of Indium Hydride in a Highly Diastereoselective Reductive Aldol Reaction (C) 711–714 [729–732]
 DOI: 10.1002/anie.200352738
 – Direct Substitution of the Hydroxy Group in Alcohols with Silyl Nucleophiles Catalyzed by Indium Trichloride (C) 1414–1416 [1438–1440]
 DOI: 10.1002/anie.200353121
 Babizhetskyy, V. (C) 1979–1983 [2013–2017]
 Baccolini, G.
 – Efficient One-Pot Synthesis of Secondary Cyclic Phosphanes with Easy Regeneration of the Phosphorus-Donor Reagent Used (C) 3058–3060 [3120–3122]
 DOI: 10.1002/anie.200453820
 Bach, T.
 – Hydrogen Bond Mediated Enantioselectivity of Radical Reactions (C) 5849–5851 [5974–5976]
 DOI: 10.1002/anie.200461222
 Bachi, M. D.
 – Design and Synthesis of Endoperoxide Antimalarial Prodrug Models (C) 4193–4197 [4289–4293]
 DOI: 10.1002/anie.200453859
 Bachmann, S. (C) 5507–5510 [5623–5626]
 Back, T. G.
 – A Stereodivergent Synthesis of Virantmycin by an Enzyme-Mediated Diester Desymmetrization and a Highly Hindered Aryl Amination (C) 6493–6496 [6655–6658]
 DOI: 10.1002/anie.200461327
 – The Exceptional Glutathione Peroxidase-Like Activity of Di(3-hydroxypropyl) Selenide and the Unexpected Role of a Novel Spirodioxaselenanone Intermediate in the Catalytic Cycle (C) 1268–1270 [1288–1290]
 DOI: 10.1002/anie.200353128
 Bäckvall, J.-E.
 – Highly Compatible Metal and Enzyme Catalysts for Efficient Dynamic Kinetic

- Resolution of Alcohols at Ambient Temperature
(C) 6535–6539 [6697–6701]
DOI: 10.1002/anie.200461416
- Badjić, J. D. (C) 3273–3278 [3335–3340]
- Bae, A.-H. (C) 465–469 [471–475]
- Bae, C. (C) 2282–2285 [2332–2335]
- Bae, J. (C) 3803–3806 [3891–3894]
- Baek, K.-H. (C) 1675–1678 [1707–1710]
- Baenitz, M. (C) 112–115 [114–117]
- Baerns, M. (R) 406–446 [410–451]
- Bagdanoff, J. T. (C) 353–357 [357–361]
- Baharloo, B. (C) 5682–5685 [5800–5803]
- Bai, C.-L.
- Pt Hollow Nanospheres: Facile Synthesis and Enhanced Electrocatalysts
(C) 1540–1543 [1566–1569]
DOI: 10.1002/anie.200352956
- Baillargeon, P. (C) 349–353 [353–357]
- Baker, R. J. (C) 3852–3855 [3940–3943]
- Baker, R. T.
- Molecular and Electronic Structure of Platinum Bis(*N*-arylamino)phosphenium Complexes including [Pt(phosphane)-(phosphenium)(*N*-heterocyclic carbene)]
(C) 1955–1958 [1989–1992]
DOI: 10.1002/anie.200352326
- Bakowies, D. (C) 4055–4059 [4147–4151]
- Balaj, O. P. (C) 6519–6522 [6681–6684]
- Balaran, P.
- Hydrogen-Bond Lengths in Polypeptide Helices: No Evidence for Short Hydrogen Bonds
(C) 6728–6731 [6896–6899]
DOI: 10.1002/anie.200461127
- Balasubramanian, S.
- Templated Ligand Assembly by Using G-Quadruplex DNA and Dynamic Covalent Chemistry
(C) 1143–1146 [1163–1166]
DOI: 10.1002/anie.200353069
- Balasubramanian, S. (C) 5926–5930 [6052–6056]
- Baldauf, C. (C) 1594–1597 [1621–1624]
- Baldwin, J. E.
- Stille Coupling Made Easier—The Synergistic Effect of Copper(I) Salts and the Fluoride Ion
(C) 1132–1136 [1152–1156]
DOI: 10.1002/anie.200352979
- Balieu, S. (C) 5963–5967 [6089–6093]
- Ball, P. (E) 4842–4847 [4948–4953]
- Ballauff, M.
- Analysis of Poly(carbon suboxide) by Small-Angle X-ray Scattering
(C) 5843–5846 [5967–5970]
DOI: 10.1002/anie.200460263
 - Dendrimers in Solution: Insight from Theory and Simulation
(R) 2998–3020 [3060–3082]
DOI: 10.1002/anie.200300602
- Ballauff, M. (C) 109–112 [111–114]
- Ballester, P. Corrigendum: 141
- Ballesteros, A. (C) 325–329 [329–333]
- Balme, G.
- Pyrrole Syntheses by Multicomponent Coupling Reactions
(H) 6238–6241 [6396–6399]
DOI: 10.1002/anie.200461073
- Baltesanu, I. (C) 6519–6522 [6681–6684]
- Baltes, N. (C) 1431–1435 [1455–1459]
- Bandini, M.
- New Catalytic Approaches in the Stereoselective Friedel–Crafts Alkylation Reaction
(M) 550–556 [560–566]
DOI: 10.1002/anie.200301679
- Bandini, M. (C) 84–87 [86–89]
- Bando, Y. (C) 63–66 [65–68], 4606–4609 [4706–4709]
- Bang, D. (C) 2534–2538 [2588–2592]
- Bannenberg, T. (C) 5530–5534 [5646–5650]
- Bantignies, J.-L. (C) 203–206 [205–208]
- Bao, X.
- In Situ Assembly of Zeolitic Building Blocks into High-Order Structures
(C) 3452–3456 [3534–3538]
DOI: 10.1002/anie.200453777
 - In Situ Magnetic Resonance Investigation of Styrene Oxidation over TS-1 Zeolites
(C) 6377–6381 [6537–6541]
DOI: 10.1002/anie.200461113
- Baran, P. (C) 574–577 [584–587]
- Baran, P. S.
- Scepterin as a Potential Biosynthetic Precursor to Complex Pyrrole–Imidazole Alkaloids: The Total Synthesis of Ageliferin
(C) 2674–2677 [2728–2731]
DOI: 10.1002/anie.200453937
- Baratta, W.
- Cyclometalated Ruthenium(II) Complexes as Highly Active Transfer Hydrogenation Catalysts
(C) 3584–3588 [3668–3672]
DOI: 10.1002/anie.200454199
- Barbas III, C. F.
- Synthesis of β -Hydroxyaldehydes with Stereogenic Quaternary Carbon Centers by Direct Organocatalytic Asymmetric Aldol Reactions
(C) 2420–2423 [2474–2477]
DOI: 10.1002/anie.200353546
- Barbon, A. (C) 5328–5331 [5442–5445]
- Barbour, L. J.
- A New Type of Material for the Recovery of Hydrogen from Gas Mixtures
(C) 2948–2950 [3008–3010]
DOI: 10.1002/anie.200353559
- Barbour, L. J. (C) 5263–5266 [5375–5378]
- Bard, A. J.
- Optimization Of “Wired” Enzyme O_2 -Electroreduction Catalyst Compositions by Scanning Electrochemical Microscopy
(C) 6355–6357 [6515–6517]
DOI: 10.1002/anie.200461528
- Barder, T. E. (C) 1871–1876 [1907–1912]
- Barluenga, J.
- Diastereoselective Synthesis of Cycloheptadienol Derivatives by a Formal [5+2] Carbocyclization Reaction of $\alpha,\beta,\gamma,\delta$ -Diunsaturated (Methoxy)carbene Complexes with Methyl Ketone Lithium Enolates
(C) 5510–5513 [5626–5629]
DOI: 10.1002/anie.200460547
 - *N*-Trialkylsilylimines as Coupling Partners for Pd-Catalyzed C–N Bond-Forming Reactions: One-Step Synthesis of Imines and Azidines from Aryl and Alkenyl Bromides
(C) 343–345 [347–349]
DOI: 10.1002/anie.200352808
 - Reaction of Alkene–Zirconocene Complexes and Cyclic Enol Ethers through New Reaction Pathways
(C) 3932–3935 [4022–4025]
DOI: 10.1002/anie.200454151
 - Regioselective Postsynthetic Modification of Phenylalanine Side Chains of Peptides
Leading to Uncommon *ortho*-Iodinated Analogues
(C) 325–329 [329–333]
DOI: 10.1002/anie.200352464
- Barluenga, S. (C) 3467–3470 [3549–3552]
- Barnard, J. S. (C) 6745–6747 [6913–6915]
- Barner, J. (C) 5185–5188 [5297–5300]
- Baro, A. (C) 6547–6549 [6709–6711]
- Baron, R. (C) 4055–4059 [4147–4151]
- Barra, A.-L. (C) 1136–1139 [1156–1159], 5196–5200 [5308–5312]
- Barreau, M. A.
- Ethylene Epoxidation on Ag: Identification of the Crucial Surface Intermediate by Experimental and Theoretical Investigation of its Electronic Structure
(C) 2918–2921 [2978–2981]
DOI: 10.1002/anie.200353584
- Bartl, M. H. (C) 3037–3040 [3099–3102], 5652–5655 [5770–5773]
- Baron, O. (C) 3195–3199 [3258–3261]
- Basak, A. (C) 1417–1419 [1441–1443]
- Baskaran, D.
- Polymer-Grafted Multiwalled Carbon Nanotubes through Surface-Initiated Polymerization
(C) 2138–2142 [2190–2194]
DOI: 10.1002/anie.200353329
- Basset, J.-M.
- Cross-Metathesis of Propane and Methane: A Catalytic Reaction of C–C Bond Cleavage of a Higher Alkane by Methane
(C) 5366–5369 [5480–5483]
DOI: 10.1002/anie.200460982
- Bassil, B. S. (C) 3485–3488 [3567–3571]
- Basuli, F. (C) 3156–3159 [3218–3221]
- Batey, R. A.
- Palladium-Catalyzed [3,3] Sigmatropic Rearrangement of (Allyloxy)iminodiazaphospholines: Allylic Transposition of C–O and C–N Functionality
(C) 1865–1868 [1901–1904]
DOI: 10.1002/anie.200353284
- Batten, S. R. (C) 192–195 [194–197]
- Baudin, J.-B. (C) 4785–4788 [4889–4892]
- Bauer, J. (C) 1979–1983 [2013–2017]
- Bauer, W. (C) 2959–2962 [3019–3022]
- Baum, E. (C) 3190–3192 [3252–3255]
- Baumeister, U. (C) 4621–4625 [4721–4725]
- Baumes, L. (C) 5347–5349 [5461–5463]
- Baumgarten, M. (C) 5331–5335 [5445–5449]
- Baumgartner, T.
- The Dithieno[3,2-*b*:2',3'-*d*]phosphole System: A Novel Building Block for Highly Luminescent π -Conjugated Materials
(C) 6197–6201 [6323–6328]
DOI: 10.1002/anie.200461301
- Baumhof, P. (C) 224–228 Corrigendum: 540 [226–230 Corrigendum: 547]
- Bawendi, M. G.
- Blue Luminescence from (CdS)ZnS Core–Shell Nanocrystals
(C) 2154–2158 [2206–2210]
DOI: 10.1002/anie.200453728
- Bayer, A. (C) 5821–5823 [5945–5947]
- Bayer, J. (C) 3967–3970 [4057–4060]
- Bayer, M. J. (C) 1854–1857 [1890–1893]
- Bayley, H. (C) 842–846 [860–864], 3063–3067 [3125–3129]
- Baylies, C. J. (C) 4515–4518 [4615–4618]
- Beak, P.
- Beyond Thermodynamic Acidity: A Perspective on the Complex-Induced Proximity Effect (CIPE) in Deprotonation Reac-

- tions
(R) 2206–2225 [2256–2276]
DOI: 10.1002/anie.200300590
- Beattie, J. K.
– The Pristine Oil/Water Interface: Surfactant-Free Hydroxide-Charged Emulsions (C) 3568–3571 [3652–3655]
DOI: 10.1002/anie.200453916
- Beau, J.-M.
– Simple Synthesis of Nodulation-Factor Analogues Exhibiting High Affinity towards a Specific Binding Protein (C) 4644–4646 [4744–4746]
DOI: 10.1002/anie.200460275
- Beaulieu, P. L. (C) 4306–4311 [4406–4411]
- Bechthold, A.
– The Glycosyltransferase UrdGT2 Catalyzes Both C- and O-Glycosidic Sugar Transfers (C) 2962–2965 [3022–3025]
DOI: 10.1002/anie.200453758
- Beck, J.
– Analysis of Poly(carbon suboxide) by Small-Angle X-ray Scattering (C) 5843–5846 [5967–5970]
DOI: 10.1002/anie.200460263
- Becker, K. D. (C) 3970–3974 [4061–4064]
- Becker, R. (C) 2839–2842 [2899–2903]
- Beckhaus, R.
– Directed Reduction of Six-Membered Nitrogen Heterocycles—Selective Formation of Polynuclear Titanium Complexes (C) 1583–1587 [1609–1614]
DOI: 10.1002/anie.200353021
- Beckmann, J.
– Carbon Dioxide Fixation by the Cooperative Effect of Organotin and Organotellurium Oxides (C) 6683–6685 [6851–6853]
DOI: 10.1002/anie.200460155
- Beckwith, A. L. J.
– The Mechanism of Bu_3SnH -Mediated Homolytic Aromatic Substitution (C) 95–98 [97–100]
DOI: 10.1002/anie.200352419
- Begum, R. A. (C) 5029–5032 [5139–5142]
- Behm, M. (C) 700–704 [718–722]
- Behrens, C. (C) 1848–1851 [1884–1887]
- Beijleveld, H. (C) 369–373 [373–377]
- Bein, T.
– High-Throughput Synthesis of Phosphate-Based Inorganic–Organic Hybrid Compounds under Hydrothermal Conditions (C) 749–752 [767–770]
DOI: 10.1002/anie.200351718
- Beismann-Driemeyer, S. (R) 4014–4031 [4104–4122]
- Beissenhertz, M. K. (C) 4357–4360 [4457–4460]
- Beljonne, D. (C) 1976–1979 [2010–2013]
- Bellanda, M. (C) 3152–3155 [3214–3217]
- Bellemin-Lapponaz, S.
– A C_3 -Symmetrical Chiral Trisoxazoline Zinc Complex as a Functional Model for Zinc Hydrolases: Kinetic Resolution of Racemic Chiral Esters by Transesterification (C) 4479–4482 [4579–4582]
DOI: 10.1002/anie.200460187
- A Modular Assembly of Chiral Oxazolinylcarbene–Rhodium Complexes: Efficient Phosphane-Free Catalysts for the Asymmetric Hydrosilylation of Dialkyl Ketones (C) 1014–1017 [1036–1039]
DOI: 10.1002/anie.200353133
- Belleney, J. (C) 1718–1721 [1750–1753]
- Beller, M.
– Catalytic Markovnikov and anti-Markovnikov Functionalization of Alkenes and Alkynes: Recent Developments and Trends (R) 3368–3398 [3448–3479]
DOI: 10.1002/anie.200300616
- Development of a Ruthenium-Catalyzed Asymmetric Epoxidation Procedure with Hydrogen Peroxide as the Oxidant (C) 5255–5260 [5367–5372]
DOI: 10.1002/anie.200460528
- Enantioselective Hydrogenation of β -Ketoesters with Monodentate Ligands (C) 5066–5069 [5176–5179]
DOI: 10.1002/anie.200460190
- Bellinazzi, M. (C) 5328–5331 [5442–5445]
- Belokon, Yu. N.
– In Situ Formation of a Heterobimetallic Chiral $[(\text{Salen})\text{Ti}^{\text{IV}}]/[(\text{Salen})\text{V}^{\text{V}}]$ Catalyst for the Asymmetric Addition of TMS-CN to Benzaldehyde (C) 4085–4089 [4177–4181]
DOI: 10.1002/anie.200450301
- Ben-David, Y. (C) 5961–5963 [6087–6089]
- Bénard, M. (C) 6120–6125 [6246–6251]
- Benati, L. (C) 3598–3601 [3682–3685]
- Benedict, J. B. (C) 5328–5331 [5442–5445]
- Benkič, P. (C) 3456–3458 [3538–3540]
- Benmore, C. J. (C) 1952–1955 [1986–1989]
- Berg, T.
– When Chemistry Met Biology (T) 3750–3751 [3836–3837]
DOI: 10.1002/anie.200460998
- Berger, R.
– Do Heavy Nuclei See Light at the End of the Tunnel? (H) 398–401 [402–405]
DOI: 10.1002/anie.200301675
- Bergman, K. N. (C) 5246–5249 Corrigendum: 5721 [5358–5361 Corrigendum: 5839]
- Bergman, R. G.
– An Iridium Difluoroketene Complex: Synthesis and Isolation (C) 6366–6369 [6526–6529]
DOI: 10.1002/anie.200461402
- Carboamination: Additions of Imine C=N Bonds Across Alkynes Catalyzed by Iridozirconium Complexes (C) 5372–5374 [5486–5488]
DOI: 10.1002/anie.200461063
- Selective C–H Bond Activation by a Supramolecular Host–Guest Assembly (C) 963–966 [981–984]
DOI: 10.1002/anie.200352772
- Supramolecular Catalysis of a Unimolecular Transformation: Aza-Cope Rearrangement within a Self-Assembled Host (C) 6748–6751 [6916–6919]
DOI: 10.1002/anie.200461776
- Zirconium-Mediated Conversion of Amides to Nitriles: A Surprising Additive Effect (C) 5375–5377 [5489–5491]
DOI: 10.1002/anie.200461064
- Berkei, M. (C) 2843–2846 [2903–2906]
- Bermejo, M. R.
– A Colorimetric Approach to Anion Sensing: A Selective Chemosensor of Fluoride Ions, in which Color is Generated by Anion-Enhanced π Delocalization (C) 1962–1965 [1996–1999]
DOI: 10.1002/anie.200353148
- Bernardinelli, G. (C) 6724–6727 [6892–6895]
- Berndt, A. Corrigendum: 2737
- Bernhardt, E. (C) 4160–4163 [4254–4257]
- Berresheim, A. J. (C) 109–112 [111–114]
- Berridge, G. (C) 4637–4640 [4737–4740]
- Bertini, I.
– A Heteronuclear Direct-Detection NMR Spectroscopy Experiment for Protein-Backbone Assignment (C) 2257–2259 [2307–2309]
DOI: 10.1002/anie.200453661
- Paramagnetic Metal Ions in Ligand Screening: The Co^{II} Matrix Metalloproteinase 12 (C) 2254–2256 [2304–2306]
DOI: 10.1002/anie.200353453
- Bertozzi, C. R.
– A Strategy for Functional Proteomic Analysis of Glycosidase Activity from Cell Lysates (C) 5338–5342 [5452–5456]
DOI: 10.1002/anie.200454235
- Biomimetic Engineering of Carbon Nanotubes by Using Cell Surface Mucin Mimics (C) 6111–6116 [6237–6242]
DOI: 10.1002/anie.200460620
- Bertozzi, C. R. (C) 1355–1359 [1379–1383]
- Bertrand, G.
– Catenation of Two Singlet Diradicals: Synthesis of a Stable Tetradical (Tetradicaloid) (C) 4876–4880 [4984–4988]
DOI: 10.1002/anie.200460473
- Evidence for the Coexistence of Two Bond-Stretch Isomers in Solution (C) 4880–4883 [4988–4991]
DOI: 10.1002/anie.200460475
- Readily Available Onio-Substituted Methyleneiminium Salts: Single Precursors for a Variety of Aminocarbenes (C) 4089–4093 [4181–4185]
DOI: 10.1002/anie.200460045
- σ -Bond Stretching: A Static Approach for a Dynamic Process (C) 585–587 [595–597]
DOI: 10.1002/anie.200352944
- Besenbacher, F.
– One-Dimensional Assembly and Selective Orientation of Lander Molecules on an O–Cu Template (C) 2092–2095 [2144–2147]
DOI: 10.1002/anie.200353586
- Best, M. D. (R) 3526–3548 [3610–3632], 5736–5763 [5858–5886]
- Beswick, P. J. (C) 340–343 [344–347]
- Bethuel, Y. (C) 3327–3329 [3389–3391]
- Beyer, M. K.
– Catalytic Oxidation of CO with N_2O on Gas-Phase Platinum Clusters (C) 6519–6522 [6681–6684]
DOI: 10.1002/anie.200461215
- Bharadwaj, P. K.
– A Dodecameric Water Cluster Built around a Cyclic Quasipolar Hexameric Core in an Organic Supramolecular Complex of a Cryptand (C) 3577–3580 Corrigendum: 4390 [3661–3664 Corrigendum: 4490]
DOI: 10.1002/anie.200454002
- Bhering, D. L. (C) 3050–3053 [3112–3115]
- Bhor, S. (C) 5255–5260 [5367–5372]
- Bi, L.-H. (C) 3485–3488 [3567–3571]
- Biadene, M. (C) 4940–4943 [5048–5051]

- Bian, J. (C) 1265–1267 [1285–1287]
Bianco, A.
– Functionalized Carbon Nanotubes for Plasmid DNA Gene Delivery (C) 5242–5246 [5354–5358]
DOI: 10.1002/anie.200460437
Bickley, J. F. (C) 4193–4197 [4289–4293]
Bied, C. (C) 203–206 [205–208]
Biel, M. (C) 3974–3976 [4065–4067], (H) 6414–6416 [6574–6576]
Bigler, L. (C) 6709–6713 [6877–6881]
Bigler, P. (C) 4738–4741 [4842–4845]
Bilewicz, R.
– An Electrochemically Controlled Molecular Shuttle (C) 1668–1672 [1700–1704]
DOI: 10.1002/anie.200352528
Bill, E. (C) 4303–4306 [4403–4406]
Billingham, N. C. (C) 1389–1392 [1413–1416]
Bindl, M. (C) 1011–1014 [1029–1032]
Bindu, S. (M) 5130–5135 [5240–5245]
Binnewies, M.
– Synthesis and Functionalization of a New Kind of Silica Particle (C) 5697–5700 [5816–5819]
DOI: 10.1002/anie.200454089
Birkedal, H.
– Micrometer-Sized Spherical Assemblies of Polypeptides and Small Molecules by Acid–Base Chemistry (C) 5652–5655 [5770–5773]
DOI: 10.1002/anie.200460510
Birkner, A. (C) 2839–2842 [2899–2903]
Bischoff, D. (C) 2574–2576 [2628–2630]
Bischoff, L. (C) 3432–3436 [3514–3518]
Bister, B. (C) 2574–2576 [2628–2630]
Blackmond, D. G.
– Amplification of Enantiomeric Excess in a Proline-Mediated Reaction (C) 3317–3321 [3379–3383]
DOI: 10.1002/anie.200453997
– Physical and Chemical Rationalization for Asymmetric Amplification in Autocatalytic Reactions (C) 2099–2103 [2151–2155]
DOI: 10.1002/anie.200353086
Blake, A. J. (C) 1851–1854 [1887–1890]
Blake, M. E. (R) 5896–5911 [6020–6036]
Blanchard, J. S. (C) 1591–1594 [1618–1620]
Bleuzen, A.
– Thermally Induced Electron Transfer in a CsCoFe Prussian Blue Derivative: The Specific Role of the Alkali-Metal Ion (C) 3728–3731 [3814–3817]
DOI: 10.1002/anie.200460086
Blum, E. S. (C) 5189–5192 [5301–5304]
Blume, A.
– Self-Assembly in a Bipolar Phosphocholine–Water System: The Formation of Nanofibers and Hydrogels (C) 245–247 [247–249]
DOI: 10.1002/anie.200351731
Blundred, G. D. (C) 3562–3565 [3646–3649]
Boatz, J. A. (C) 3148–3152 [3210–3214], 5213–5217 [5325–5329], 6676–6680 [6844–6848]
Bochkarev, M. N. (C) 5045–5048 [5155–5158]
Bochmann, M.
– Arylzinc Complexes as New Initiator Systems for the Production of Isobutene Copolymers with High Isoprene Content (C) 2166–2169 [2218–2222]
DOI: 10.1002/anie.200353787
Böckmann, R. A. (C) 1021–1024 [1039–1042]
Bode, H. B. (C) 4163–4167 [4257–4262]
Boeré, R. T. (C) 502–505 [508–511]
Boese, R.
– Polymorphism of 1,3,5-Trinitrobenzene Induced by a Trisindane Additive (C) 1149–1155 [1169–1175]
DOI: 10.1002/anie.200352253
Boezio, A. A. (C) 6525–6528 [6687–6690]
Bofill, R. (C) 1991–1994 [2025–2028]
Boga, C. (C) 3058–3060 [3120–3122]
Bogár, K. (C) 6535–6539 [6697–6701]
Bøgevig, A. (C) 1109–1112 [1129–1132]
Bögge, H. (C) 4466–4470 Corrigendum: 5115 [4566–4570 Corrigendum: 5225]
Bohn, P. W.
– Nanocapillary Arrays Effect Mixing and Reaction in Multilayer Fluidic Structures (C) 1862–1865 [1898–1901]
DOI: 10.1002/anie.200353279
Boiocchi, M. (C) 3847–3852 [3935–3940]
Bolhuis, P. G. (C) 2650–2652 [2704–2706]
Bolm, C.
– C₁-Symmetric Sulfoximines as Ligands in Copper-Catalyzed Asymmetric Mukaiyama-Type Aldol Reactions (C) 5984–5987 [6110–6113]
DOI: 10.1002/anie.200460953
– Highly Enantioselective Iron-Catalyzed Sulfide Oxidation with Aqueous Hydrogen Peroxide under Simple Reaction Conditions (C) 4225–4228 [4321–4324]
DOI: 10.1002/anie.200460236
Bolskar, R. D. (C) 997–1000 [1015–1018]
Boltalina, O. V.
– C₇₄F₃₈: An Exohedral Derivative of a Small-Bandgap Fullerene with D₃ Symmetry (C) 997–1000 [1015–1018]
DOI: 10.1002/anie.200352960
Bonacchi, D. (C) 1136–1139 [1156–1159]
Bond, A. D. (C) 1959–1962 [1993–1996]
Bondyby, V. E.
– Catalytic Oxidation of CO with N₂O on Gas-Phase Platinum Clusters (C) 6519–6522 [6681–6684]
DOI: 10.1002/anie.200461215
Bonhomme, C. (C) 2801–2805 [2861–2865]
Bonhomme, F. (C) 2787–2792 [2847–2852]
Bonifazi, D. (C) 4759–4763 [4863–4867]
Bonin, M. (C) 2694–2697 [2748–2751]
Bonizzoni, M. (C) 3847–3852 [3935–3940]
Bönnemann, H. (C) 4303–4306 [4403–4406]
Bono, J.-J. (C) 4644–4646 [4744–4746]
Bonstein, T. (C) 2697–2701 [2751–2755]
Boothman, D. A. (C) 6323–6327 [6483–6487]
Borge, J. (C) 5510–5513 [5626–5629]
Börner, A.
– Enantioselective Catalysis with Chiral Phosphine Oxide Preligands (H) 5883–5886 [6007–6010]
DOI: 10.1002/anie.200460848
Bornscheuer, U. T.
– Catalytic Promiscuity in Biocatalysis: Using Old Enzymes to Form New Bonds and Follow New Pathways (M) 6032–6040 [6156–6165]
DOI: 10.1002/anie.200460416
Borovik, A. S.
– Light-Activated Transfer of Nitric Oxide from a Porous Material (C) 2806–2809 [2866–2869]
DOI: 10.1002/anie.200352881
Borovkov, V. V.
– Rationalization of Supramolecular Chirality in a Bisporphyrin System (C) 5481–5485 [5597–5601]
DOI: 10.1002/anie.200460965
Boss, S. R. (C) 2135–2138 [2187–2190]
Botman, P. N. M. (C) 3471–3473 [3553–3555]
Botoshanskii, M. (C) 745–748 [763–766]
Botta, B. (C) 4767–4770 [4871–4874]
Böttcher, C.
– The First Account of a Structurally Persistent Micelle (C) 2959–2962 [3019–3022]
DOI: 10.1002/anie.200353510
Bouchu, D. (C) 4336–4338 [4436–4438]
Boudalis, A. K. (C) 2266–2270 [2316–2320]
Boué, F. (C) 1718–1721 [1750–1753]
Bourissou, D. (C) 585–587 [595–597]
Bousquet, Y. (C) 4306–4311 [4406–4411]
Bouteiller, L.
– Aqueous Supramolecular Polymer Formed from an Amphiphilic Perylene Derivative (C) 1718–1721 [1750–1753]
DOI: 10.1002/anie.200353434
Bouwmeester, H. J. M. (C) 5069–5073 [5179–5183]
Bowman, B. J. (C) 3601–3605 [3685–3689]
Bowman, E. J. (C) 3601–3605 [3685–3689]
Bowman, W. R.
– The Mechanism of Bu₃SnH-Mediated Homolytic Aromatic Substitution (C) 95–98 [97–100]
DOI: 10.1002/anie.200352419
Bowry, V. W. (C) 95–98 [97–100]
Boyat, C. (C) 4172–4178 [4267–4273]
Boydell, A. J. (C) 5677–5679 [5795–5797]
Boydston, A. J. (C) 6336–6338 [6496–6498]
Boyle, N. A. (C) 4656–4659 [4756–4759]
Bracco, S. (C) 2792–2797 [2852–2857]
Brady, T. P. (C) 739–742 [757–760]
Braga, D.
– Reactions Between or Within Molecular Crystals (M) 4002–4011 [4092–4102]
DOI: 10.1002/anie.200301721
Brakmann, S.
– DNA-Based Barcodes, Nanoparticles, and Nanostructures for the Ultrasensitive Detection and Quantification of Proteins (H) 5730–5734 [5851–5855]
DOI: 10.1002/anie.200461112
Brand, N. R.
– Reductive Electrochemical Cyclization of a Photochromic 1,2-Dithienylcyclopentene Dication (C) 2812–2815 [2872–2875]
DOI: 10.1002/anie.200353029
Brandau, S. (C) 6667–6669 [6836–6838]
Brandt, M. (C) 2846–2849 [2906–2910]
Bräse, S.
– A Short, Atom-Economical Entry to Tetrahydroxanthones (C) 115–118 [118–120]
DOI: 10.1002/anie.200352154
Bratcher, M. S. (C) 2138–2142 [2190–2194]
Bräu, M. F. (C) 4228–4231 [4324–4327]
Braun, H. (C) 5391–5393 [5505–5507]
Braun, M.
– Titanium(IV)-Catalyzed Dynamic Kinetic Asymmetric Transformation of Alcohols, Silyl Ethers, and Acetals under Carbon Allylation

- (C) 514–517 [520–523]
DOI: 10.1002/anie.200352128
- Braunstein, P.
– An Oriented 1D Coordination/Organometallic Dimetallic Molecular Wire with Ag–Pd Metal–Metal Bonds (C) 6120–6125 [6246–6251]
DOI: 10.1002/anie.200461291
- Supramolecular, Bifurcated N–H...OC–M Bonding Explains Unusually Low ν_{CO} Frequencies in Metal Carbonyl Compounds: A Case Study (C) 5922–5925 [6048–6051]
DOI: 10.1002/anie.200461175
- Braunton, A. (C) 5507–5510 [5623–5626]
- Bravo-Zhivotovskii, D.
– The Direct Synthesis of a Silene–Organometallic Complex (C) 745–748 [763–766]
DOI: 10.1002/anie.200353048
- Bray, P. G. (C) 4193–4197 [4289–4293]
- Brechin, E. K.
– Building Molecular Minerals: All Ferric Pieces of Molecular Magnetite (C) 5772–5775 Corrigendum: 6581 [5896–5899 Corrigendum: 6743]
DOI: 10.1002/anie.200460636
- Breher, F.
– A Monomeric Organolithium Compound Containing a Free Pyramidal Carbanion in Solution and in the Solid State (C) 2521–2524 [2575–2578]
DOI: 10.1002/anie.200353308
- Breher, F. (C) 2567–2570 [2621–2624]
- Brehm, G. (C) 4360–4363 [4460–4464]
- Breinbauer, R.
– Electroorganic Synthesis on the Solid Phase using Polymer Beads as Supports (C) 2297–2299 [2347–2349]
DOI: 10.1002/anie.200352674
- The Peak of Stereochemistry: Bürgenstock 2004 (T) 2988–2989 [3048–3049]
DOI: 10.1002/anie.200460496
- The Staudinger Ligation—A Gift to Chemical Biology (M) 3106–3116 [3168–3178]
DOI: 10.1002/anie.200401744
- Breit, B.
– Iterative Deoxypropionate Synthesis Based on a Copper-Mediated Directed Allylic Substitution (C) 3790–3792 [3878–3880]
DOI: 10.1002/anie.200453990
- Stereospecific and Stereodivergent Construction of Quaternary Carbon Centers through Switchable Directed/Nondirected Allylic Substitution (C) 3786–3789 [3874–3877]
DOI: 10.1002/anie.200453991
- Breitenbruch, G. (C) 2444–2446 [2498–2500]
- Bremeyer, N. (C) 2681–2684 [2735–2738]
- Brennan, C. (C) 850–852 [868–870]
- Breuer, M. (R) 788–824 [806–843]
- Breuer, K.
– New Mass Spectrometric Methods for the Quantification of Protein–Ligand Binding in Solution (H) 22–25 [22–25]
DOI: 10.1002/anie.200301695
- Breuer, K. (C) 3922–3925 [4012–4015]
- Briand, J.-P. (C) 5242–5246 [5354–5358]
- Bridges, C. A. (C) 3562–3565 [3646–3649]
- Brigatti, K. (C) 5670–5674 [5788–5792]
- Briggs, G. A. D.
– Molecular Motion of Endohedral Fullerenes in Single-Walled Carbon Nanotubes (C) 1386–1389 [1410–1413]
DOI: 10.1002/anie.200352389
- Brinker, C. J. (C) 6169–6173 [6295–6299]
- Brinz, T. (C) 752–754 [770–773]
- Britton, R. (C) 4629–4633 [4729–4733]
- Britz, D. A. (C) 1386–1389 [1410–1413]
- Brockmann, C. (C) 454–458 [460–464]
- Broekmann, P.
– Second-Order Templatation: Ordered Deposition of Supramolecular Squares on a Chloride-Covered Cu(100) Surface (C) 1291–1294 [1311–1314]
DOI: 10.1002/anie.200352968
- Broeren, M. A. C. (C) 3557–3562 [3641–3646]
- Brookhart, M. S. (C) 2444–2446 [2498–2500]
- Brown, J. M.
– Solution Structure and Reagent Binding of the Zinc Alkoxide Catalyst in the Soai Asymmetric Autocatalytic Reaction (C) 4884–4887 [4992–4995]
DOI: 10.1002/anie.200353572
- Brown, R. S. (C) 4637–4640 [4737–4740]
- Brown, S. M. (C) 1588–1591 [1614–1617]
- Broxterman, Q. B. (C) 3152–3155 [3214–3217], 6695–6699 [6863–6867]
- Bruce, P. G.
– Structure of the Poly(ethylene oxide)–Zinc Chloride Complex (C) 2103–2105 [2155–2157]
DOI: 10.1002/anie.200353143
- TiO₂–B Nanowires (C) 2286–2288 [2336–2338]
DOI: 10.1002/anie.200353571
- Two- and Three-Dimensional Mesoporous Iron Oxides with Microporous Walls (C) 5958–5961 [6084–6087]
DOI: 10.1002/anie.200460826
- WO₃Cl₂ Nanotubes and Nanowires (C) 4899–4902 [5007–5010]
DOI: 10.1002/anie.200460334
- Brückner, A. M. (C) 4634–4637 [4734–4737]
- Brückner, C.
– Enantiomeric Resolution of a Ruffled Porphyrinoid (C) 1688–1691 [1720–1723]
DOI: 10.1002/anie.200352970
- Brückner, R.
– Total Synthesis of Xerulic Acid (C) 4523–4526 [4623–4626]
DOI: 10.1002/anie.200453729
- Bruinink, C. M. (C) 369–373 [373–377]
- Bruist, M. F. (C) 4750–4752 [4854–4856]
- Brun, M.-P. (C) 3432–3436 [3514–3518]
- Brunel, J.-M. (R) 2752–2778 [2810–2837]
- Brunelli, M. (C) 4933–4937 [5041–5045]
- Brunet, E.
– Solid-State Reshaping of Crystals: Flash Increase in Porosity of Zirconium Phosphate-Hypophosphite That Contains Polyethylenoxa Diphosphonate Pillars (C) 619–621 [629–631]
DOI: 10.1002/anie.200352711
- Brunklaus, G. (C) 4228–4231 [4324–4327]
- Brunner, B. (C) 4075–4078 [4167–4170], 4078–4081 [4170–4173]
- Brunner, H.
– A New Hydrosilylation Mechanism—New Preparative Opportunities (H) 2749–2750 [2805–2807]
DOI: 10.1002/anie.200301742
- Brunold, T. C. (C) 6716–6718 [6884–6886]
- Brustolon, M.
– Luminescent Probes of Crystal Growth: Surface Charge and Polar Axis Sense in Dye-Doped Potassium Hydrogen Phthalate (C) 5328–5331 [5442–5445]
DOI: 10.1002/anie.200453839
- Brylev, K. A. (C) 1297–1300 [1317–1321]
- Bryliakov, K. P.
– Evidence for the Formation of an Iodosylbenzene(salen)iron Active Intermediate in a (Salen)iron(III)-Catalyzed Asymmetric Sulfide Oxidation (C) 5228–5230 [5340–5342]
DOI: 10.1002/anie.200460108
- Brynda, M. (C) 2655–2658 [2709–2712]
- Bu, X. (C) 1502–1505 [1528–1531], 4753–4755 [4857–4859]
- Bu, X.-H.
– A Neutral 3D Copper Coordination Polymer Showing 1D Open Channels and the First Interpenetrating NbO-Type Network (C) 192–195 [194–197]
DOI: 10.1002/anie.200352024
- Buchini, S. (C) 3925–3928 [4015–4018]
- Buchwald, S. L.
– A Rationally Designed Universal Catalyst for Suzuki–Miyaura Coupling Processes (C) 1871–1876 [1907–1912]
DOI: 10.1002/anie.200353615
- Budisa, N.
– Prolegomena to Future Experimental Efforts on Genetic Code Engineering by Expanding Its Amino Acid Repertoire (R) 6426–6463 [6586–6624]
DOI: 10.1002/anie.200300646
- Budzelaar, P. H. M. (R) 4142–4157 [4236–4251]
- Bugaut, A. (C) 3144–3147 [3206–3209]
- Bukowski, M. R. (C) 1283–1287 [1303–1307]
- Bull, A. T. (C) 2574–2576 [2628–2630]
- Bulman Page, P. C. (C) 1685–1688 [1717–1720]
- Bulo, R. E. (C) 714–717 Corrigendum: 3748 [732–735 Corrigendum: 3834]
- Bulović, V. (C) 2154–2158 [2206–2210]
- Bundle, D. R.
– Glycosyltransferase-Catalyzed Synthesis of Thiooligosaccharides (C) 613–615 [623–625]
DOI: 10.1002/anie.200352606
- Bundle, D. R. (C) 4183–4186 [4279–4282]
- Buñuel, E. (C) 2402–2406 [2456–2460]
- Buono, F. G. (C) 2099–2103 [2151–2155]
- Burck, S. (C) 4801–4804 [4905–4908]
- Bures, F. (C) 2968–2970 [3028–3030]
- Burgert, R. (C) 3190–3192 [3252–3255]
- Bürgi, H.-B.
– Challenges in Engineering Spin Crossover: Structures and Magnetic Properties of Six Alcohol Solvates of Iron(II) Tris(2-picolylamine) Dichloride (C) 4589–4594 [4689–4695]
DOI: 10.1002/anie.200460736
- Bürgi, H.-B. (C) 4292–4295 [4392–4395]
- Burke, J. M. (C) 3061–3063 [3123–3125]
- Burke, M. D. (R) 46–58 [48–60]
- Burstein, C. (C) 6205–6208 [6331–6334]
- Bursten, B. E. (C) 2554–2557 [2608–2611]
- Burton, D. R. (C) 1000–1003 [1018–1021]
- Buryak, A. (C) 4771–4774 [4875–4878]

- Busch, S.
– Regeneration of Human Tooth Enamel
(C) 1428–1431 [1452–1455]
DOI: 10.1002/anie.200352183
- Büschel, M. G. (C) 3700–3703 [3786–3789]
- Bush, P. J. (C) 2697–2701 [2751–2755]
- Bushey, M. L. (C) 1836–1839 [1872–1875],
(M) 5446–5453 [5562–5570]
- Butcher, R. J. (C) 4513–4515 [4613–4615]
- Bütikofer, L. (C) 1698–1702 [1730–1734]
- Butterfield, S. M. (C) 724–727 [742–745]
- By, K. (C) 1117–1120 [1137–1140]
- Bykowski, D. (C) 6713–6716 [6881–6884]
- (C) 959–962 [977–980]
DOI: 10.1002/anie.200352640
- Cantrill, S. J. (C) 3273–3278 [3335–3340]
- Cao, T. (C) 2780–2783 [2840–2843]
- Cao, Z. X. (C) 975–977 [993–995]
- Capelli, S. C. (C) 3022–3025 [3084–3087]
- Caplan, N. A. (C) 1685–1688 [1717–1720]
- Cappelletti, D. (C) 5200–5203 [5312–5315]
- Cappuccio, F. E. Corrigendum: 3748
- Caps, V. (C) 5645–5649 [5763–5767]
- Carbonera, C. (C) 3136–3138 [3198–3200]
- Cárdenas, D. J. (C) 2402–2406 [2456–2460]
- Carell, T.
– Excess Electron Transfer Driven DNA
Does Not Depend on the Transfer Direc-
tion
(C) 1842–1844 Corrigendum: 2321 [1878–
1880 Corrigendum: 2373]
DOI: 10.1002/anie.200353067
- Excess Electron Transport Through DNA:
A Single Electron Repairs More than One
UV-Induced Lesion
(C) 1848–1851 [1884–1887]
DOI: 10.1002/anie.200353264
- Carl, B. (C) 1848–1851 [1884–1887]
- Carl, T. (C) 1848–1851 [1884–1887]
- Carletti, I. (C) 2551–2553 [2605–2607]
- Carlier, P. R.
– Threading the Needle: Mimicking Natural
Toroidal Catalysts
(H) 2602–2605 [2654–2657]
DOI: 10.1002/anie.200301731
- Carmona, E.
– A Measureable Equilibrium between Iri-
dium Hydride Alkylidene and Iridium
Hydride Alkene Isomers
(C) 3708–3711 [3794–3797]
DOI: 10.1002/anie.200454040
- Carpintero, M. (C) 450–454 [456–460], 454–
458 [460–464]
- Carreira, E. M.
– An Amphotericin B–Fluorescein Conju-
gate as a Powerful Probe for Biochemical
Studies of the Membrane
(C) 5181–5185 Corrigendum: 5428 [5293–
5297 Corrigendum: 5542]
DOI: 10.1002/anie.200460489
- An In Vitro Assay for Evaluation of Small-
Molecule Inhibitors of Cholesterol
Absorption
(C) 4653–4656 [4753–4756]
DOI: 10.1002/anie.200460348
- Catalytic Hydrohydrazination of a Wide
Range of Alkenes with a Simple Mn
Complex
(C) 4099–4102 [4191–4194]
DOI: 10.1002/anie.200460811
- Readily Available Biaryl P,N Ligands for
Asymmetric Catalysis
(C) 5971–5973 [6097–6099]
DOI: 10.1002/anie.200461286
- Carrell, H. L. (C) 1149–1155 [1169–1175]
- Carretero, J. C.
– Cationic Planar Chiral Palladium P,S Com-
plexes as Highly Efficient Catalysts in the
Enantioselective Ring Opening of Oxa-
and Azabicyclic Alkenes
(C) 3944–3947 [4034–4037]
DOI: 10.1002/anie.200460087
- Carrettin, S. (C) 2538–2540 [2592–2594]
- Carrot, G. (C) 1718–1721 [1750–1753]
- Carter, K. R.
– High-Resolution Soft Lithography: En-
abling Materials for Nanotechnologies
(C) 5796–5799 [5920–5923]
DOI: 10.1002/anie.200461122
- Caruso, F.
– Biofunctionalization of Fluorescent Rare-
Earth-Doped Lanthanum Phosphate Col-
loidal Nanoparticles
(C) 5954–5957 [6080–6083]
DOI: 10.1002/anie.200460856
- Caruso, R. A.
– Micrometer-to-Nanometer Replication of
Hierarchical Structures by Using a Surface
Sol–Gel Process
(H) 2746–2748 [2802–2804]
DOI: 10.1002/anie.200301747
- Casas, Jesús (C) 6528–6531 [6690–6693],
6532–6535 [6694–6697]
- Casas, Josefina (C) 862–865 [880–883]
- Casnati, A. (C) 369–373 [373–377]
- Castel, S. (C) 1811–1814 [1847–1850]
- Catone, D. (C) 1868–1871 Corrigendum:
3872 [1904–1907 Corrigendum: 3960]
- Cave, G. W. V. (C) 5263–5266 [5375–5378]
- Cavell, K. J.
– Oxidative Addition of Imidazolium Salts to
Ni⁰ and Pd⁰: Synthesis and Structural
Characterization of Unusually Stable
Metal–Hydride Complexes
(C) 1277–1279 [1297–1299]
DOI: 10.1002/anie.200353409
- Transition-Metal-Catalyzed Reactions
Involving Imidazolium Salt/N-Heterocy-
clic Carbene Couples as Substrates
(C) 3845–3847 [3933–3935]
DOI: 10.1002/anie.200454166
- Centomo, P. (C) 959–962 [977–980]
- César, V. (C) 1014–1017 [1036–1039]
- Ceulemans, A. (C) 5481–5485 [5597–5601]
- Ceyhan, B. (C) 6469–6471 [6631–6633]
- Chadwick, D. (C) 5645–5649 [5763–5767]
- Chaker, L. (R) 5896–5911 [6020–6036]
- Chakravarty, A. R.
– Cubane [Cu^{II}₄] Cluster as a Precursor for
the Preparation of a Mixed-Valent {Cu^{II}₁₂,
Cu^I₂} Core
(C) 87–90 [89–92]
DOI: 10.1002/anie.200352350
- Champion, N. (C) 320–325 [324–329]
- Champness, N. R.
– Non-Natural Eight-Connected Solid-State
Materials: A New Coordination Chemistry
(C) 1851–1854 [1887–1890]
DOI: 10.1002/anie.200352625
- Chan, E. Y. Y. (C) 1715–1718 [1747–1750]
- Chan, H.-W. (C) 1381–1385 [1405–1409]
- Chandrasekera, N. S. (C) 5386–5389 [5500–
5503]
- Chandrasekhar, S. (C) 3429–3432 [3511–
3514]
- Chandrasekhar, V. (C) 3832–3835 [3920–
3923], 3842–3844 [3930–3932], 4940–
4943 [5048–5051]
- Chandravarkar, A. (C) 4172–4178 [4267–
4273]
- Chang, A. Y. (C) 1000–1003 [1018–1021]
- Chang, H.-C. (C) 192–195 [194–197], 3269–
3272 [3331–3334]
- Chang, J.-S.
– Nanoporous Metal-Containing Nickel
Phosphates: A Class of Shape-Selective
Catalyst
(C) 2819–2822 [2879–2882]
DOI: 10.1002/anie.200353502
- Chang, S.-H. (C) 5987–5990 [6113–6116]
- Chang, Y. (C) 1397–1399 [1421–1423]
- Cabeza, J. A.
– Activation of All Bonds of a Methyl Group
Attached to an Organic Fragment
(C) 3464–3467 [3546–3549]
DOI: 10.1002/anie.200454066
- Cabrera, S. (C) 3944–3947 [4034–4037]
- Cabrol-Bass, D. (H) 6410–6412 [6570–6573]
- Caddick, S.
– Unusual Reactivity of a Nickel N-Hetero-
cyclic Carbene Complex: *tert*-Butyl Group
Cleavage and Silicone Grease Activation
(C) 5824–5827 [5948–5951]
DOI: 10.1002/anie.200460955
- Cador, O. (C) 5196–5200 [5308–5312]
- Cahard, D.
– Towards Perfect Catalytic Asymmetric
Synthesis: Dual Activation of the Electro-
phile and the Nucleophile
(R) 4566–4583 [4666–4683]
DOI: 10.1002/anie.200300635
- Cahiez, G. (C) 2968–2970 [3028–3030]
- Cai, F.-S. (C) 4212–4216 [4308–4312]
- Cai, X. (C) 2406–2409 [2460–2463]
- Calarese, D. A. (C) 1000–1003 [1018–1021]
- Calzaferri, G.
– Sequential Functionalization of the Chan-
nel Entrances of Zeolite L Crystals
(C) 6738–6742 [6906–6910]
DOI: 10.1002/anie.200461114
- Camacho, D. H. (C) 1821–1825 Corrigen-
dum: 2986 [1857–1861 Corrigendum:
3046]
- Cameron, T. S. (C) 1995–1998 [2029–2032]
- Cammack, J. K. (C) 1393–1397 [1417–1421]
- Campbell, K. (C) 5967–5971 [6093–6097]
- Campbell, T. D. (C) 1505–1507 [1531–1533]
- Campopiano, D. J. (C) 5914–5918 [6040–
6044]
- Canac, Y. (C) 4089–4093 [4181–4185]
- Canales, J. (C) 2286–2288 [2336–2338],
4899–4902 [5007–5010]
- Caneschi, A. (C) 4081–4084 [4173–4176]
- Canesi, S. (C) 4336–4338 [4436–4438]
- Cannon, D. M., Jr. (C) 1862–1865 [1898–
1901]
- Cano, J. (C) 850–852 [868–870]
- Cantat, T. (C) 6382–6385 [6542–6545]
- Canton, P.
– Generation of Size-Controlled Pd⁰ Nano-
clusters inside Nanoporous Domains of
Gel-Type Resins: Diverse and Convergent
Evidence That Supports a Strategy of
Template-Controlled Synthesis

- Chang, Y.-T.
– Solid-Phase Synthesis of Styryl Dyes and their Application as Amyloid Sensors (C) 6331–6335 [6491–6495]
DOI: 10.1002/anie.200461600
- Chapman, E. (R) 3526–3548 [3610–3632]
- Chapuis, G. (C) 2694–2697 [2748–2751]
- Charette, A. B.
– Evidence for the Structure of the Enantioactive Ligand in the Phosphine–Copper-Catalyzed Addition of Diorganozinc Reagents to Imines (C) 6525–6528 [6687–6690]
DOI: 10.1002/anie.200461920
- Charier, S. (C) 4785–4788 [4889–4892]
- Charleux, B.
– Nitroxide-Mediated Controlled Free-Radical Emulsion Polymerization of Styrene and *n*-Butyl Acrylate with a Water-Soluble Alkoxyamine as Initiator (C) 6186–6189 [6312–6315]
DOI: 10.1002/anie.200460704
- Chatterjee, D. (C) 3918–3922 [4008–4012]
- Chatzidimitriou-Dreismann, A.
– Quantum Mechanics and Chemistry: The Relevance of Nonlocality and Entanglement for Molecules (T) 144–145 [146–147]
DOI: 10.1002/anie.200320079
- Che, C.-M.
– A Practical and Mild Method for the Highly Selective Conversion of Terminal Alkenes into Aldehydes through Epoxidation–Isomerization with Ruthenium(IV)–Porphyrin Catalysts (C) 4950–4954 [5058–5062]
DOI: 10.1002/anie.200460545
- Ruthenium Nanoparticles Supported on Hydroxyapatite as an Efficient and Recyclable Catalyst for *cis*-Dihydroxylation and Oxidative Cleavage of Alkenes (C) 3303–3307 [3365–3369]
DOI: 10.1002/anie.200453703
- Cheah, K.-W.
– Green and Red Three-Photon Upconversion from Polymeric Lanthanide(III) Complexes (C) 4659–4662 [4759–4762]
DOI: 10.1002/anie.200460576
- Cheeseman, J. D. (C) 2432–2436 [2486–2490]
- Cheetham, A. K.
– Nanoporous Metal-Containing Nickel Phosphates: A Class of Shape-Selective Catalyst (C) 2819–2822 [2879–2882]
DOI: 10.1002/anie.200353502
- Chelley, S. (C) 3063–3067 [3125–3129]
- Chen, B. (Univ. Halle-Wittenberg) (C) 4621–4625 [4721–4725]
- Chen, B. (Univ. of Pennsylvania) (C) 1158–1162 [1178–1182]
- Chen, C. (C) 3571–3574 [3655–3658]
- Chen, C.-L. (C) 980–984 [998–1002]
- Chen, D. Y.-K. (C) 4312–4318 [4412–4418]
- Chen, G. Z.
– Electrochemical Preparation of Silicon and Its Alloys from Solid Oxides in Molten Calcium Chloride (C) 733–736 [751–754]
DOI: 10.1002/anie.200352786
- Chen, Jian (C) 4950–4954 [5058–5062]
- Chen, Jiehao (C) 2148–2152 [2200–2204]
- Chen, Jiutong (C) 5776–5779 [5900–5903]
- Chen, Jun
– Ni(OH)₂ Tubes with Mesoscale Dimensions as Positive-Electrode Materials of Alkaline Rechargeable Batteries (C) 4212–4216 [4308–4312]
DOI: 10.1002/anie.200460053
- Chen, Jun (C) 2017–2020 [2051–2054]
- Chen, K. (C) 2661–2665 [2715–2719]
- Chen, L. X.
– Taking Snapshots of Photoexcited Molecules in Disordered Media by Using Pulsed Synchrotron X-rays (R) 2886–2905 [2946–2966]
DOI: 10.1002/anie.200300596
- Chen, Peng (M) 4132–4140 [4224–4233]
- Chen, Peter
– Gas-Phase Reactions of the [(PHOX)IrL₂]⁺ Ion Olefin-Hydrogenation Catalyst Support an Ir^{IV}/Ir^{III} Cycle (C) 5513–5516 [5629–5632]
DOI: 10.1002/anie.200460860
- Chen, Q.
– Reply to Comment on “Growth of Large Diamond Crystals by Reduction of Magnesium Carbonate with Metallic Sodium” (L) 4700–4701 [4804–4805]
DOI: 10.1002/anie.200460857
- Chen, S. (C) 2705–2709 [2759–2763]
- Chen, W.-H. (C) 4186–4189 [4282–4285]
- Chen, X. (C) 6111–6116 [6237–6242]
- Chen, X.-G. (C) 329–334 [333–338]
- Chen, X.-M.
– Two Unprecedented 3-Connected Three-Dimensional Networks of Copper(I) Triazoles: In Situ Formation of Ligands by Cycloaddition of Nitriles and Ammonia (C) 206–209 [208–211]
DOI: 10.1002/anie.200352627
- Chen, Yi (C) 3554–3557 [3638–3641], 5335–5338 [5449–5452]
- Chen, Yongming
– Organic–Inorganic Hybrid Nanoparticles with a Complex Hollow Structure (C) 5084–5087 [5194–5197]
DOI: 10.1002/anie.200454244
- Chen, Yu (C) 4060–4063 [4152–4155]
- Chen, Z.
– Side-Wall Opening of Single-Walled Carbon Nanotubes (SWCNTs) by Chemical Modification: A Critical Theoretical Study (C) 1552–1554 [1578–1580]
DOI: 10.1002/anie.200353087
- The Smaller Fullerene C₅₀, Isolated as C₅₀C₁₀ (H) 4690–4691 [4794–4796]
DOI: 10.1002/anie.200401764
- Chenevarin, S. (C) 1155–1158 [1175–1178]
- Cheng, C.-Y. (C) 4186–4189 [4282–4285]
- Cheng, E. C.-C. (C) 4954–4957 [5062–5065]
- Cheng, F. (C) 4759–4763 [4863–4867]
- Cheng, M. (C) 3452–3456 [3534–3538]
- Chernyshov, D. (C) 4589–4594 [4689–4695]
- Chi, D. Y.
– Polymer-Supported Ionic Liquids: Imidazolium Salts as Catalysts for Nucleophilic Substitution Reactions Including Fluorinations (C) 483–485 [489–491]
DOI: 10.1002/anie.200352760
- Chin, W. S.
– Preparation of Ag₂S Nanocrystals of Predictable Shape and Size (C) 5685–5689 [5803–5807]
DOI: 10.1002/anie.200460566
- Chippindale, A. M.
– Copper(I) Cyanide: A Simple Compound with a Complicated Structure and Surprising Room-Temperature Reactivity (C) 628–630 [638–640]
DOI: 10.1002/anie.200352844
- Chivers, T.
– Complete Chalcogenation of Tin(II) Centers in an Imidotin Cluster (C) 6686–6689 [6854–6857]
DOI: 10.1002/anie.200460956
- Stable Cubic Phosphorus-Containing Radicals (C) 502–505 [508–511]
DOI: 10.1002/anie.200353108
- Chmielewski, P. J.
– Synthesis and Characterization of a Directly Linked N-Confused Porphyrin Dimer (C) 5655–5658 [5773–5776]
DOI: 10.1002/anie.200461361
- Cho, C.-W. (C) 6689–6691 [6857–6859]
- Cho, Jaehung (C) 3300–3303 [3362–3365]
- Cho, Jaephil
– A Mesoporous/Crystalline Composite Material Containing Tin Phosphate for Use as the Anode in Lithium-Ion Batteries (C) 5987–5990 [6113–6116]
DOI: 10.1002/anie.200454080
- Cho, S.-H. (C) 5503–5507 [5619–5623]
- Cho, Y.-J. (C) 1712–1714 [1744–1746]
- Choi, D. K. (C) 3053–3056 [3115–3118]
- Choi, H. J. (C) 5940–5943 [6066–6069]
- Choi, M.-G. (C) 1712–1714 [1744–1746]
- Choi, M.-S. (M) 150–158 [152–160]
- Choi, S. (C) 1158–1162 [1178–1182]
- Choi, S.-h. (C) 2382–2385 [2436–2439]
- Chou, L. J. (C) 5670–5674 [5788–5792]
- Chou, P.-T. (C) 4507–4510 [4607–4610]
- Choung, S. Y. (C) 6183–6185 [6309–6311]
- Christe, K. O.
– High-Energy-Density Materials: Synthesis and Characterization of N₅⁺[P(N₃)₆][−], N₅⁺[B(N₃)₄][−], N₅⁺[HF₂][−]·*n*HF, N₅⁺[BF₄][−], N₅⁺[PF₆][−], and N₅⁺[SO₃F][−] (C) 4919–4924 [5027–5032]
DOI: 10.1002/anie.200454242
- Polyazide Chemistry: Preparation and Characterization of As(N₃)₅, Sb(N₃)₅, and [P(C₆H₅)₄][Sb(N₃)₆] (C) 6676–6680 [6844–6848]
DOI: 10.1002/anie.200461730
- The Binary Group 4 Azides [Ti(N₃)₄], [P(C₆H₅)₄][Ti(N₃)₅], and [P(C₆H₅)₄][Ti(N₃)₆] and on Linear Ti–N–NN Coordination (C) 3148–3152 [3210–3214]
DOI: 10.1002/anie.200454156
- The [NH₃Cl]⁺ Ion (C) 5213–5217 [5325–5329]
DOI: 10.1002/anie.200460544
- Christensen, J. B. (C) 3557–3562 [3641–3646]
- Christie, A. M. (C) 2103–2105 [2155–2157]
- Christoffers, J.
– Formation of 1,4-Diketones by Aerobic Oxidative C–C Coupling of Styrene with 1,3-Dicarbonyl Compounds (C) 6547–6549 [6709–6711]
DOI: 10.1002/anie.200461406
- Christou, G.
– A Reductive-Aggregation Route to [Mn₁₂O₁₂(OMe)₂(O₂CPh)₁₆(H₂O)₂]^{2−} Single-Molecule Magnets Related to the [Mn₁₂] Family

- (C) 6338–6342 [6498–6502]
DOI: 10.1002/anie.200461551
- Giant Single-Molecule Magnets: A $\{\text{Mn}_{14}\}$ Torus and Its Supramolecular Nanotubes (C) 2117–2121 [2169–2173]
DOI: 10.1002/anie.200353352
 - Mixed Transition-Metal–Lanthanide Complexes at Higher Oxidation States: Heteronuclear Ce^{IV} – Mn^{IV} Clusters (C) 345–349 [349–353]
DOI: 10.1002/anie.200352898
- Chrostowska, A.
- First Synthesis and Characterization by Mass Spectrometry and UV-Photoelectron Spectroscopy of Methylenearene (C) 873–875 [891–893]
DOI: 10.1002/anie.200352445
- Chueh, Y. L. (C) 5670–5674 [5788–5792]
- Chun, H. (C) 971–974 [989–992], 5033–5036 [5143–5146]
- Chung, C. K. (C) 4327–4329 [4427–4429]
- Chung, M.-A. (C) 6346–6350 [6506–6510]
- Ciani, B. (C) 1991–1994 [2025–2028]
- Cichon, M. (C) 1842–1844 Corrigendum: 2321 [1878–1880 Corrigendum: 2373]
- Cini, R. (C) 5081–5084 [5191–5194]
- Cintas, P.
- The Road to Chemical Names and Eponyms: Discovery, Priority, and Credit (E) 5888–5894 [6012–6018]
DOI: 10.1002/anie.200330074
- Cioci, G. (C) 5918–5922 [6044–6048]
- Ciufolini, M. A.
- Fully Stereoccontrolled Total Syntheses of (–)-Cylindricine C and (–)-2-Epicylindricine C: A Departure in Sulfonamide Chemistry (C) 4336–4338 [4436–4438]
DOI: 10.1002/anie.200460178
- Cladis, P. E.
- Discotic Liquid Crystals: *S. Chandrasekhar* (O) 3360 [3438]
DOI: 10.1002/anie.200460918
- Clark, D. D. (C) 5181–5185 Corrigendum: 5428 [5293–5297 Corrigendum: 5542]
- Claverie, C. K. (C) 1249–1251 [1269–1271]
- Clayden, J. (C) 2135–2138 [2187–2190]
- Clays, K. (C) 5266–5268 [5378–5381]
- Clegg, W. (C) 1814–1817 [1850–1853], 3061–3063 [3123–3125]
- Clement, N. D. (C) 1277–1279 [1297–1299], 3845–3847 [3933–3935]
- Clemente, F. R. (C) 5766–5768 [5890–5892]
- Clemente-Juan, J. M. (C) 2266–2270 [2316–2320]
- Clements, D. J. (C) 1158–1162 [1178–1182]
- Clérac, R.
- A Dimeric Manganese(III) Tetradentate Schiff Base Complex as a Single-Molecule Magnet (C) 2801–2805 [2861–2865]
DOI: 10.1002/anie.200353563
 - A Three-Dimensional Ferrimagnet Composed of Mixed-Valence Mn_4 Clusters Linked by an $\{\text{Mn}[\text{N}(\text{CN})_2]_6\}^{4-}$ Unit (C) 707–711 [725–729]
DOI: 10.1002/anie.200353093
 - Thermoreversible Gels as Magneto-Optical Switches (C) 3283–3286 [3345–3348]
DOI: 10.1002/anie.200454050
- Cloke, F. G. N.
- Unusual Reactivity of a Nickel N-Heterocyclic Carbene Complex: *tert*-Butyl Group Cleavage and Silicone Grease Activation (C) 5824–5827 [5948–5951]
DOI: 10.1002/anie.200460955
- Clouet, A. (C) 4612–4615 [4712–4715]
- Clouthier, C. M. (C) 4075–4078 [4167–4170]
- Coates, G. W.
- Discrete Metal-Based Catalysts for the Copolymerization of CO_2 and Epoxides: Discovery, Reactivity, Optimization, and Mechanism (R) 6618–6639 [6784–6806]
DOI: 10.1002/anie.200460442
- Cocinero, E. J. (C) 605–610 [615–620]
- Coe-Sullivan, S. (C) 2154–2158 [2206–2210]
- Coelho, F.
- Probing the Mechanism of the Baylis–Hillman Reaction by Electrospray Ionization Mass and Tandem Mass Spectrometry (C) 4330–4333 [4430–4433]
DOI: 10.1002/anie.200460059
- Cohen, S. M.
- Self-Assembly of Two Distinct Supramolecular Motifs in a Single Crystalline Framework (C) 2385–2388 [2439–2442]
DOI: 10.1002/anie.200353520
- Cokoja, M. (C) 2299–2302 [2349–2352]
- Colby, D. A. (C) 1346–1349 [1370–1373]
- Colin, A. (C) 3283–3286 [3345–3348]
- Collings, J. C. (C) 3061–3063 [3123–3125]
- Collins, S.
- Methacrylate Polymerization using a Dinuclear Zirconocene Initiator: A New Approach for the Controlled Synthesis of Methacrylate Polymers (C) 5523–5526 [5639–5642]
DOI: 10.1002/anie.200460785
- Collison, D.
- Building Molecular Minerals: All Ferrie Pieces of Molecular Magnetite (C) 5772–5775 Corrigendum: 6581 [5896–5899 Corrigendum: 6743]
DOI: 10.1002/anie.200460636
- Collman, J. P.
- Surface-Confined Metalloporphyrin Oligomers (C) 5827–5830 [5951–5954]
DOI: 10.1002/anie.200460992
- Colonna, S. (C) 4097–4099 [4189–4191]
- Colquhoun, H. M.
- Recognition of Polyimide Sequence Information by a Molecular Tweezer (C) 5040–5045 [5150–5155]
DOI: 10.1002/anie.200460382
- Colyer, J. T. (C) 6713–6716 [6881–6884]
- Comba, P.
- Bispidine Ligand Effects on Iron/Hydrogen Peroxide Chemistry (C) 1283–1287 [1303–1307]
DOI: 10.1002/anie.200352523
- Comotti, A. (C) 2792–2797 [2852–2857]
- Comotti, M. (C) 5812–5815 [5936–5939]
- Concellón, J. M.
- Synthesis and Stereoselective Lithiation of Enantiopure 2-(1-Aminoalkyl)aziridine–Borane Complexes (C) 4333–4336 [4433–4436]
DOI: 10.1002/anie.200460120
- Concepción, P. (C) 2538–2540 [2592–2594]
- Condorelli, G. G. (C) 4081–4084 [4173–4176]
- Conejero, S. (C) 4089–4093 [4181–4185]
- Connor, S. (C) 3673–3677 [3759–3763]
- Cook, K. S. (C) 5474–5477 [5590–5593]
- Cooper, D. L. Corrigendum: 141
- Cooper, J. M. (C) 2512–2514 [2566–2568]
- Copéret, C.
- Cross-Metathesis of Propane and Methane: A Catalytic Reaction of C–C Bond Cleavage of a Higher Alkane by Methane (C) 5366–5369 [5480–5483]
DOI: 10.1002/anie.200460982
- Corain, B.
- Generation of Size-Controlled Pd^0 Nanoclusters inside Nanoporous Domains of Gel-Type Resins: Diverse and Convergent Evidence That Supports a Strategy of Template-Controlled Synthesis (C) 959–962 [977–980]
DOI: 10.1002/anie.200352640
- Corbett, A. D. (C) 2432–2436 [2486–2490]
- Cordaro, J. G. (C) 6366–6369 [6526–6529]
- Cordes, D. B. Corrigendum: 3748
- Cordonier, C. E. J. (C) 736–738 [754–756]
- Córdova, A.
- Direct Amino Acid Catalyzed Asymmetric α Oxidation of Ketones with Molecular Oxygen (C) 6528–6535 [6694–6697]
DOI: 10.1002/anie.200460295
 - Direct Catalytic Enantioselective α -Aminomethylation of Ketones (C) 6528–6531 [6690–6693]
DOI: 10.1002/anie.200460678
 - Direct Catalytic Enantioselective α -Aminoxylation of Ketones: A Stereoselective Synthesis of α -Hydroxy and α,α' -Dihydroxy Ketones (C) 1109–1112 [1129–1132]
DOI: 10.1002/anie.200353018
- Corma, A.
- Nanocrystalline CeO_2 Increases the Activity of Au for CO Oxidation by Two Orders of Magnitude (C) 2538–2540 [2592–2594]
DOI: 10.1002/anie.200353570
- Corma, A. (C) 4933–4937 [5041–5045]
- Cornia, A.
- Energy-Barrier Enhancement by Ligand Substitution in Tetrairon(III) Single-Molecule Magnets (C) 1136–1139 [1156–1159]
DOI: 10.1002/anie.200352989
- Cornish, V. W.
- Methotrexate Conjugates: A Molecular In Vivo Protein Tag (C) 1672–1675 [1704–1707]
DOI: 10.1002/anie.200352852
- Coronado, E.
- Metallic Conductivity Down to 2 K in a Polyoxometalate-Containing Radical Salt of BEDO-TTF (C) 3022–3025 [3084–3087]
DOI: 10.1002/anie.200453985
 - Polycationic Mn_{12} Single-Molecule Magnets as Electron Reservoirs with $S > 10$ Ground States (C) 6152–6156 [6278–6282]
DOI: 10.1002/anie.200460282
- Corr, S. (C) 5519–5523 [5635–5639]
- Correia, C. R. D. (C) 2514–2518 Corrigendum: 4489 [2568–2572 Corrigendum: 4489]
- Corrigan, J. F.
- Imine-Stabilized Zinc Trimethylsilylchalcogenolates: Powerful Reagents for the Synthesis of II–IV Nanocluster Materials (C) 5355–5357 [5469–5471]
DOI: 10.1002/anie.200460322
- Cortez, C. (C) 5954–5957 [6080–6083]



- Cortright, R. D. (C) 1549–1551 [1575–1577]
 Costa, A. Corrigendum: 141
 Côté, A. (C) 6525–6528 [6687–6690]
 Cotlet, M. (C) 6116–6120 [6242–6246]
 Coucouvanis, D.
 – Superclusters: A Host–Guest Complex with a Cyclic Array of Three Bridged MoFe_3S_4 Clusters (C) 5023–5025 [5133–5135]
 DOI: 10.1002/anie.200460154
 Coumans, R. G. E. (C) 4755–4759 [4859–4863]
 Couto, C. (C) 1140–1142 [1160–1162]
 Couzijn, E. P. A. (C) 3440–3442 [3522–3524]
 Cowley, A. R. (C) 628–630 [638–640]
 Cowman, M. (C) 520–523 [527–529]
 Cox, H.
 – A 1,3-Diaza-2,4-distannacyclobutane diide: Synthesis, Structure, and Bonding (C) 4500–4504 [4600–4604]
 DOI: 10.1002/anie.200460039
 Cozzi, P. G.
 – Kinetic Resolution of Epoxides by a C–C Bond-Forming Reaction: Highly Enantioselective Addition of Indoles to *cis*, *trans*, and *meso* Aromatic Epoxides Catalyzed by [Cr(salen)] Complexes (C) 84–87 [86–89]
 DOI: 10.1002/anie.200352073
 Craig, D. B. (C) 5400–5402 [5515–5517]
 Crespo, J. G.
 – Recent Advances in Chiral Resolution through Membrane-Based Approaches (H) 5293–5295 [5405–5407]
 DOI: 10.1002/anie.200460037
 Crich, D.
 – Mechanism of 4,6-*O*-Benzylidene-Directed β -Mannosylation as Determined by α -Deuterium Kinetic Isotope Effects (C) 5386–5389 [5500–5503]
 DOI: 10.1002/anie.200453688
 Crisma, M. (C) 3152–3155 [3214–3217], 6695–6699 [6863–6867]
 Croft, S. L. (C) 1381–1385 [1405–1409]
 Cronin, L.
 – Old Clusters with New Tricks: Engineering S...S Interactions and Novel Physical Properties in Sulfite-Based Dawson Clusters (C) 1817–1820 [1853–1856]
 DOI: 10.1002/anie.200352896
 Cruciani, G. (C) 4933–4937 [5041–5045]
 Cubillo de Dios, M. A. (C) 4641–4644 [4741–4744]
 Cuevas, C.
 – Total Synthesis of Natural Myriaporones (C) 1724–1727 [1756–1759]
 DOI: 10.1002/anie.200353313
 Cui, L.-F. (C) 2125–2129 [2177–2181]
 Cui, W. (C) 4791–4794 [4895–4898]
 Cui, Y. (C) 4210–4212 [4306–4308]
 Cummins, C. C.
 – Diorganophosphanylphosphinidenes as Complexed Ligands: Synthesis via an Anionic Terminal Phosphide of Niobium (C) 984–988 [1002–1006]
 DOI: 10.1002/anie.200352779
 Curran, D. P.
 – Total Synthesis of (–)-Dictyostatin: Confirmation of Relative and Absolute Configurations (C) 4634–4637 [4734–4737]
 DOI: 10.1002/anie.200460593
 Cusack, M. (C) 885–888 [903–906]
 Da Ros, P. (C) 3584–3588 [3668–3672]
 da Silva, I. (C) 3464–3467 [3546–3549]
 Dahmen, C. (C) 6649–6652 [6818–6821]
 Dähne, L.
 – Tailor-Made Polyelectrolyte Microcapsules: From Multilayers to Smart Containers (R) 3762–3783 [3850–3872]
 DOI: 10.1002/anie.200300568
 Dai, C. (C) 3061–3063 [3123–3125]
 Dai, L.-X.
 – Chiral Metal–Organic Assemblies—A New Approach to Immobilizing Homogeneous Asymmetric Catalysts (H) 5726–5729 [5846–5850]
 DOI: 10.1002/anie.200460301
 Dai, S.
 – Synthesis of a Large-Scale Highly Ordered Porous Carbon Film by Self-Assembly of Block Copolymers (C) 5785–5789 [5909–5913]
 DOI: 10.1002/anie.200461051
 Dakternieks, D. (C) 6683–6685 [6851–6853]
 Daligault, F. (C) 4078–4081 [4170–4173]
 Dalko, P. I.
 – In the Golden Age of Organocatalysis (H) 5138–5175 [5248–5286]
 DOI: 10.1002/anie.200400650
 Danheiser, R. L.
 – Natural Products and Small Rings: *Saturo Masamune* (O) 922 [940]
 DOI: 10.1002/anie.200490020
 Daniel, C. (C) 1976–1979 [2010–2013]
 Daniell, H. W. (C) 1688–1691 [1720–1723]
 Daniell, X. G. (C) 4906–4911 [5014–5019]
 Danishefsky, S. J.
 – In Pursuit of Carbohydrate-Based HIV Vaccines, Part 1: The Total Synthesis of Hybrid-Type gp120 Fragments (C) 2557–2561 [2611–2615]
 DOI: 10.1002/anie.200353625
 – In Pursuit of Carbohydrate-Based HIV Vaccines, Part 2: The Total Synthesis of High-Mannose-Type gp120 Fragments—Evaluation of Strategies Directed to Maximal Convergence (C) 2562–2565 [2616–2619]
 DOI: 10.1002/anie.200353626
 Dankers, P. Y. W. (C) 4190–4193 [4286–4289]
 Dankwardt, J. W.
 – Nickel-Catalyzed Cross-Coupling of Aryl Grignard Reagents with Aromatic Alkyl Ethers: An Efficient Synthesis of Unsymmetrical Biaryls (C) 2428–2432 [2482–2486]
 DOI: 10.1002/anie.200453765
 Danovich, D. Corrigendum: 141
 Darbre, T. (C) 4612–4615 [4712–4715]
 Dargelos, A. (C) 873–875 [891–893]
 Darses, S.
 – Tandem 1,4-Addition/Enantioselective Protonation Catalyzed by Rhodium Complexes: Efficient Access to α -Amino Acids (C) 719–723 [737–741]
 DOI: 10.1002/anie.200352518
 Das, P. (C) 5249–5253 [5361–5365]
 Daté, M.
 – Vital Role of Moisture in the Catalytic Activity of Supported Gold Nanoparticles (C) 2129–2132 [2181–2184]
 DOI: 10.1002/anie.200453796
 Datta, S. (C) 6728–6731 [6896–6899]
 Dauber, M. (C) 4597–4601 [4698–4702]
 David, O. (C) 3471–3473 [3553–3555]
 Davies, J. (C) 4193–4197 [4289–4293]
 Davis, B. G.
 – Glyco-SeS: Selenenylsulfide-Mediated Protein Glycoconjugation—A New Strategy in Post-Translational Modification (C) 828–833 [846–851]
 DOI: 10.1002/anie.200352975
 – Modular Control of Lectin Function: Redox-Switchable Agglutination (C) 3025–3029 [3087–3091]
 DOI: 10.1002/anie.200353320
 Davis, J. L. (C) 590–594 [600–604]
 Davis, J. T.
 – G-Quartets 40 Years Later: From 5'-GMP to Molecular Biology and Supramolecular Chemistry (R) 668–698 [684–716]
 DOI: 10.1002/anie.200300589
 Davis, N. (C) 4034–4037 [4126–4129]
 Davis, S. A. (C) 885–888 [903–906]
 de Bruin, B.
 – Functional Models for Rhodium-Mediated Olefin-Oxygenation Catalysis (R) 4142–4157 [4236–4251]
 DOI: 10.1002/anie.200300629
 De Feyter, S.
 – π -Conjugated Oligo(*p*-phenylenevinylene) Rosettes and Their Tubular Self-Assembly (C) 74–78 [76–80]
 DOI: 10.1002/anie.200352790
 de Hoog, P. (C) 5815–5817 [5939–5941]
 de Kanter, F. J. J. (C) 714–717 Corrigendum: 3748 [732–735 Corrigendum: 3834], 3440–3442 [3522–3524], 3474–3477 [3556–3559]
 de la Fuente, M. R. (C) 5235–5238 [5347–5350]
 de la Mata, M. J. (C) 619–621 [629–631]
 de la Torre, M. C.
 – Comments on Recent Achievements in Biomimetic Organic Synthesis (R) 160–181 [162–184]
 DOI: 10.1002/anie.200200545
 de Meijere, A.
 – A Convergent Route to Enantiomerically Pure Higher [*n*–2]Triangulanedimethanol Derivatives and [*n*]Triangulanes (*n* ≥ 7) (C) 6553–6557 [6715–6719]
 DOI: 10.1002/anie.200461166
 – Steroids and Steroid Analogues from Stille–Heck Coupling Sequences (C) 895–897 [913–915]
 DOI: 10.1002/anie.200352162
 de Meijere, A. (C) 4510–4512 [4610–4612]
 de Mello Donegá, C. (C) 3029–3033 [3091–3095]
 de Mendoza, J. (C) 196–198 [198–200]
 De Meo, C. (C) 3069–3072 [3131–3134]
 De Pol, S. (C) 511–514 [517–520]
 De Schryver, F. C.
 – π -Conjugated Oligo(*p*-phenylenevinylene) Rosettes and Their Tubular Self-Assembly (C) 74–78 [76–80]
 DOI: 10.1002/anie.200352790

- Probing the Influence of O₂ on Photo-induced Reversible Electron Transfer in Perylene-3,4,9,10-tetracarboxylic-Bisimide-Based Dendrimers by Single-Molecule Spectroscopy (C) 6116–6120 [6242–6246]
DOI: 10.1002/anie.200460560
- De Simone, J. M.
– High-Resolution Soft Lithography: Enabling Materials for Nanotechnologies (C) 5796–5799 [5920–5923]
DOI: 10.1002/anie.200461122
- de Smet, L. C. P. M. (C) 1352–1355 [1376–1379]
- de Visser, S. P. (C) 1129–1132 [1149–1152], 5661–5665 [5779–5783]
- de Wild, M. (C) 4759–4763 [4863–4867]
- de Witte, P. A. J. (C) 4045–4049 [4137–4141]
- Deacon, G. B.
– Linear Finite “Mers”—Homoleptic Polynuclear Heavy Alkaline Earth Metal Pyrazolates (C) 5218–5220 [5330–5332]
DOI: 10.1002/anie.200460628
- Debijs, M. G. (C) 5331–5335 [5445–5449]
- Decurtins, S.
– Tetrathiafulvalenes Acting as Leaving Groups: A Route to Bithiazoles (C) 4738–4741 [4842–4845]
DOI: 10.1002/anie.200460149
- Deege, A. (C) 4078–4081 [4170–4173]
- DeGrado, W. F.
– Nontoxic Membrane-Active Antimicrobial Arylamide Oligomers (C) 1158–1162 [1178–1182]
DOI: 10.1002/anie.200352791
- DeGroot, M. W. (C) 5355–5357 [5469–5471]
- Dehnen, S. (C) 305–309 [309–313]
- Dei, A.
– Thermally and Light-Induced Valence Tautomeric Transition in a Dinuclear Cobalt–Tetraoxolene Complex (C) 3136–3138 [3198–3200]
DOI: 10.1002/anie.200453944
- del Pozo, C. (C) 1724–1727 [1756–1759]
- del Río, I. (C) 3464–3467 [3546–3549]
- Del Zotto, A. (C) 3584–3588 [3668–3672]
- Deleuze, A. (C) 6680–6683 [6848–6851]
- Delgado, A. (C) 862–865 [880–883]
- Delgado, O. (C) 4629–4633 [4729–4733]
- Della Pina, C. (C) 5812–5815 [5936–5939]
- Delle Monache, G. (C) 4767–4770 [4871–4874]
- Dellis, P.
– Difluorophos, an Electron-Poor Diphosphane: A Good Match Between Electronic and Steric Features (C) 320–325 [324–329]
DOI: 10.1002/anie.200352453
- Demchenko, A. V.
– Potent, Versatile, and Stable: Thiazolyl Thioglycosides as Glycosyl Donors (C) 3069–3072 [3131–3134]
DOI: 10.1002/anie.200454047
- Demel, P. (C) 3786–3789 [3874–3877]
- Deming, T. J. (C) 5652–5655 [5770–5773]
- Demizu, Y. (C) 5360–5363 [5474–5477]
- Denegri, B. (C) 2302–2305 [2353–2356]
- Deng, Z. (C) 4068–4070 [4160–4162]
- Denison, G. M. (C) 5796–5799 [5920–5923]
- Denizot, L. (C) 3806–3810 Corrigendum: 4389 [3894–3898 Corrigendum: 4489]
- Dennis, T. J. S. (C) 1386–1389 [1410–1413]
- Depperman, E. C. (C) 3912–3914 [4002–4004]
- Députier, S. (C) 1979–1983 [2013–2017]
- Dervan, P. B.
– Design of a Sequence-Specific DNA Bisintercalator (C) 3591–3594 [3675–3678]
DOI: 10.1002/anie.200454231
- Deschamps, N. M. (C) 3076–3079 [3138–3141]
- Desiraju, G. R.
– Polymorphism of 1,3,5-Trinitrobenzene Induced by a Trisindane Additive (C) 1149–1155 [1169–1175]
DOI: 10.1002/anie.200352253
- Deutzmann, R. (C) 5933–5936 [6059–6062]
- Dewhurst, R. D. (C) 476–478 [482–484]
- Deyà, P. M. Corrigendum: 141
- Dhawan, R. (C) 590–594 [600–604]
- Di Cesare, N. (C) 5804–5808 [5928–5932]
- Di Giusto, D. A. (C) 2809–2812 [2869–2872]
- Dias, F. (C) 3307–3310 [3369–3372]
- Dias, J. C. (C) 4049–4052 [4141–4144]
- Dias, R. L. A. (C) 2109–2112 [2161–2164]
- Díaz, M. R. (C) 4333–4336 [4433–4436]
- Diebold, U. (C) 6641–6645 [6809–6814]
- Diederich, F.
– A Weak Attractive Interaction between Organic Fluorine and an Amide Group (C) 5056–5059 [5166–5169]
DOI: 10.1002/anie.200460781
- Regio- and Stereoselective Tether-Directed Remote Functionalization of C₆₀ with Derivatives of the Tröger Base (C) 1738–1740 [1770–1773]
DOI: 10.1002/anie.200453743
- Supramolecular Patterned Surfaces Driven by Cooperative Assembly of C₆₀ and Porphyrins on Metal Substrates (C) 4759–4763 [4863–4867]
DOI: 10.1002/anie.200460562
- Diele, S. (C) 4621–4625 [4721–4725]
- Diener, M. D. (C) 997–1000 [1015–1018]
- Dietiker, R. (C) 5513–5516 [5629–5632]
- Dietrich-Buchecker, C. (C) 4482–4485 [4582–4585]
- Dieudonné, P. (C) 203–206 [205–208]
- Ding, Yin (C) 6369–6372 [6529–6532]
- Ding, Yong (C) 5238–5242 [5350–5354]
- Dingenouts, N. (C) 109–112 [111–114], 5843–5846 [5967–5970]
- Dingerdissen, U. (C) 5066–5069 [5176–5179]
- Dinkelaar, J. (C) 3471–3473 [3553–3555]
- Disney, M. D. (C) 1591–1594 [1618–1620]
- Dittrich, K. (R) 788–824 [806–843]
- Dittmer, W. U. (C) 3550–3553 [3634–3637]
- Dittrich, B.
– A Simple Approach to Nonspherical Electron Densities by Using Invariants (C) 2718–2721 [2773–2776]
DOI: 10.1002/anie.200353596
- Djerassi, C.
– Chemical Safety in a Vulnerable World—A Manifesto (E) 2330–2332 [2384–2386]
DOI: 10.1002/anie.200330079
- Djordjević, A. M. (C) 3568–3571 [3652–3655]
- Dmitriev, A. V. (C) 4085–4089 [4177–4181]
- Döbler, C. (C) 5255–5260 [5367–5372]
- Dobner, B. (C) 245–247 [247–249]
- Docherty, F. T. (C) 2512–2514 [2566–2568]
- Dochnahl, M. (C) 1017–1021 [1032–1036]
- Doda, K. (C) 1588–1591 [1614–1617]
- Doerksen, R. J. (C) 1158–1162 [1178–1182]
- Doert, T. (C) 2441–2444 [2495–2498]
- Doezé, R. H. P. (C) 3138–3141 [3200–3203]
- Dohi, T. (C) 3595–3598 [3679–3682]
- Doi, M. (C) 5360–5363 [5474–5477]
- Dolbecq, A. (C) 2274–2277 [2324–2327]
- Dolder, S. (C) 4738–4741 [4842–4845]
- Domagala, S. (C) 1668–1672 [1700–1704]
- Domen, K. (C) 2955–2958 [3015–3018]
- Domingo, N. (C) 1828–1832 [1864–1868]
- Dong, L. (C) 2671–2674 [2725–2728]
- Dong, S. Corrigendum: 3749
- Dong, S.
– Large-Scale Synthesis of Micrometer-Scale Single-Crystalline Au Plates of Nanometer Thickness by a Wet-Chemical Route (C) 6360–6363 [6520–6523]
DOI: 10.1002/anie.200461013
- Donkers, R. L. (C) 2812–2815 [2872–2875]
- Donnadieu, B. (C) 2266–2270 [2316–2320]
- Donohoe, T. J.
– An Efficient Synthesis of Lactacystin β -Lactone (C) 2293–2296 [2343–2346]
DOI: 10.1002/anie.200453843
- Dordi, B. (C) 369–373 [373–377]
- Döring, S. (C) 6657–6660 [6826–6829]
- Dory, Y. L.
– Micrometer-Sized Hexagonal Tubes Self-Assembled by a Cyclic Peptide in a Liquid Crystal (C) 349–353 [353–357]
DOI: 10.1002/anie.200352259
- Dos Santos, S. (C) 4172–4178 [4267–4273]
- Dou, S.-X. (C) 4212–4216 [4308–4312]
- Dowden, J.
– Chemical Synthesis of the Second Messenger Nicotinic Acid Adenine Dinucleotide Phosphate by Total Synthesis of Nicotinamide Adenine Dinucleotide Phosphate (C) 4637–4640 [4737–4740]
DOI: 10.1002/anie.200460054
- Doyle, M. P.
– Stereoselective Synthesis of Bicyclic Pyrrolidines by a Rhodium-Catalyzed Cascade Process (C) 6713–6716 [6881–6884]
DOI: 10.1002/anie.200461722
- Drechsler, M. (C) 245–247 [247–249]
- Dressel, M. (C) 5849–5851 [5974–5976]
- Drexler, H.-J. (C) 3795–3797 [3883–3886]
- Dro, C. (C) 4479–4482 [4579–4582]
- Drury III, W. J. (C) 70–74 [72–76]
- Druzhkov, N. O. (C) 5045–5048 [5155–5158]
- Du, J. (C) 5084–5087 [5194–5197]
- Du Bois, J.
– Rh-Catalyzed Amination of Etheral C^α–H Bonds: A Versatile Strategy for the Synthesis of Complex Amines (C) 4349–4352 [4449–4452]
DOI: 10.1002/anie.200460791
- du Mont, W.-W.
– Selenol Nitrosation and Se-Nitrososelenol Homolysis: A Reaction Path with Possible Biochemical Implications (C) 3970–3974 [4061–4064]
DOI: 10.1002/anie.200453872
- Duan, H. (C) 5639–5642 [5757–5760]
- Duan, T. (C) 3190–3192 [3252–3255]
- Duan, X. (C) 4216–4219 [4312–4315]
- Duboc, C. (C) 594–597 [604–607]
- Dubrovina, N. V. (H) 5883–5886 [6007–6010]
- Dudkin, V. Y. (C) 2557–2561 [2611–2615], 2562–2565 [2616–2619]
- Dulub, O. (C) 6641–6645 [6809–6814]
- Duma, L. (C) 2257–2259 [2307–2309]

- Dumesic, J. A.
– Gold-Nanotube Membranes for the Oxidation of CO at Gas–Water Interfaces (C) 1140–1142 [1160–1162]
DOI: 10.1002/anie.200353238
– Renewable Alkanes by Aqueous-Phase Reforming of Biomass-Derived Oxygenates (C) 1549–1551 [1575–1577]
DOI: 10.1002/anie.200353050
Dumeunier, R. (C) 1588–1591 [1614–1617]
Dunbar, K. R.
– Unusual Magnetic Metal–Cyanide Cubes of Re^{II} with Alternating Octahedral and Tetrahedral Corners (C) 4912–4915 [5020–5023]
DOI: 10.1002/anie.200460614
Duplais, C. (C) 2968–2970 [3028–3030]
Dupont, J.
– On the Noninnocent Nature of 1,3-Dialkylimidazolium Ionic Liquids (H) 5296–5297 [5408–5409]
DOI: 10.1002/anie.200460431
Duprat de Paule, S. (C) 320–325 [324–329]
Dürr, C. (C) 2962–2965 [3022–3025]
Duschl, J. (C) 634–636 [644–646]
Duthie, A. (C) 6683–6685 [6851–6853]
Dutour, J. (C) 6290–6296 [6450–6456], 6296–6301 [6456–6461]
Dwek, R. A. (C) 1000–1003 [1018–1021]
Dybtsev, D. N. (C) 971–974 [989–992], 5033–5036 [5143–5146]
Dyson, P. J.
– An Octahedral Rhodium Cluster with Six Phosphine and 12 Hydride Ligands and 10 Too Few Electrons (H) 6028–6030 [6152–6154]
DOI: 10.1002/anie.200460924



- Eberlin, M. N.
– Probing the Mechanism of the Baylis–Hillman Reaction by Electrospray Ionization Mass and Tandem Mass Spectrometry (C) 4330–4333 [4430–4433]
DOI: 10.1002/anie.200460059
– Probing the Mechanism of the Heck Reaction with Arene Diazonium Salts by Electrospray Mass and Tandem Mass Spectrometry (C) 2514–2518 Corrigendum: 4389 [2568–2572 Corrigendum: 4489]
DOI: 10.1002/anie.200353076
Eberspacher, T. A. (C) 5827–5830 [5951–5954]
Echavarren, A. M.
– Cationic Gold(I) Complexes: Highly Alkynophilic Catalysts for the *exo*- and *endo*-Cyclization of Enynes (C) 2402–2406 [2456–2460]
DOI: 10.1002/anie.200353207
– The Mechanisms of the Stille Reaction (R) 4704–4734 [4808–4839]
DOI: 10.1002/anie.200300638
– Total Synthesis of Natural Myriaporones (C) 1724–1727 [1756–1759]
DOI: 10.1002/anie.200353313

- Eckert, H.
– Phosphorus Nanorods—Two Allotropic Modifications of a Long-Known Element (C) 4228–4231 [4324–4327]
DOI: 10.1002/anie.200460244
Edebrink, P. (C) 2288–2290 [2338–2340]
Edelmann, F. T.
– Fully Metalated Silsesquioxanes: Building Blocks for the Construction of Catalyst Models (C) 4603–4606 [4703–4706]
DOI: 10.1002/anie.200454094
Edin, M. (C) 6535–6539 [6697–6701]
Eelkema, R. (C) 5013–5016 [5123–5126]
Efremova, O. A. (C) 1297–1300 [1317–1321]
Egan, C. L. (C) 3138–3141 [3200–3203]
Ehlers, A. W. (C) 714–717 Corrigendum: 3748 [732–735 Corrigendum: 3834], 3440–3442 [3522–3524], 3474–3477 [3556–3559]
Ehlers, G. (C) 364–366 [368–370]
Eichhöfer, A. (C) 3823–3827 [3911–3915]
Eichhorn, B.
– [Pt@Pb₁₂]²⁻ (C) 2132–2134 [2184–2186]
DOI: 10.1002/anie.200353287
Einaga, Y.
– Reversible Photo-Switching of the Magnetization of Iron Oxide Nanoparticles at Room Temperature (C) 6135–6139 [6261–6265]
DOI: 10.1002/anie.200460964
Eisler, D. J. (C) 6686–6689 [6854–6857]
El Ashry, El S. H. Corrigendum: 4389
El Bialy, S. A. A. (C) 5391–5393 [5505–5507]
Elemans, J. A. A. W. (C) 4755–4759 [4859–4863]
Ellern, A. (C) 4497–4500 [4597–4600], 5837–5839 [5961–5963]
Elsevier, C. J. (C) 1277–1279 [1297–1299], 5530–5534 [5646–5650]
Eltepu, L. (C) 4656–4659 [4756–4759]
Emrick, T.
– Reversible Addition Fragmentation Chain Transfer (RAFT) Polymerization from Unprotected Cadmium Selenide Nanoparticles (C) 5383–5386 [5497–5500]
DOI: 10.1002/anie.200453822
Enderle, A. (C) 6649–6652 [6818–6821]
Endo, M.
– Design and Synthesis of Photochemically Controllable Caspase-3 (C) 5643–5645 [5761–5763]
DOI: 10.1002/anie.200460889
Engqvist, M. (C) 6532–6535 [6694–6697]
Enick, R. M. (C) 704–707 [722–725]
Enkelmann, V. (C) 1972–1975 [2006–2009]
Enright, G. D. (C) 2933–2936 [2993–2996]
Enthaler, S. (C) 5066–5069 [5176–5179]
Eppinger, J.
– Enzyme Microarrays: On-Chip Determination of Inhibition Constants Based on Affinity-Label Detection of Enzymatic Activity (C) 3806–3810 Corrigendum: 4389 [3894–3898 Corrigendum: 4489]
DOI: 10.1002/anie.200353623
Erhardt, M. (C) 5242–5246 [5354–5358]
Erker, G.
– Formation of a Unique *ansa*-Metallocene Framework by Intramolecular Photochemical [2 + 2] Cycloaddition of Bis(2-alkenylindenyl)zirconium Complexes

- (C) 310–313 [313–317]
DOI: 10.1002/anie.200351886
Ernst, K.-H.
– Determination of the Absolute Chirality of Adsorbed Molecules (C) 2853–2856 [2913–2917]
DOI: 10.1002/anie.200353311
Ernst, L. (C) 3970–3974 [4061–4064]
Ernsting, J. M. (C) 5530–5534 [5646–5650]
Erxleben, A. (C) 5396–5399 [5507–5511]
Escax, V. (C) 3728–3731 [3814–3817]
Eschenmoser, A. (C) 4656–4659 [4756–4759]
Escuer, A.
– Hexanuclear Manganese(III) Single-Molecule Magnets (C) 210–212 [212–214]
DOI: 10.1002/anie.200351079
Esenturk, E. N. (C) 2132–2134 [2184–2186]
Espenson, J. H.
– Phosphine-Promoted Conversion of Oxo(dithiolato)rhenium(v) into Thio(thiolatoalkyl)rhenium(v) Compounds (C) 5837–5839 [5961–5963]
DOI: 10.1002/anie.200461060
Espinete, P.
– The Mechanisms of the Stille Reaction (R) 4704–4734 [4808–4839]
DOI: 10.1002/anie.200300638
Espuña, G. (C) 325–329 [329–333]
Estrada, A. A. (C) 5087–5092 [5197–5202], 5092–5097 [5202–5207]
Etzkorn, M. (H) 26–28 [26–28]
Evans, P. A.
– Stereodivergent Construction of Cyclic Ethers by a Regioselective and Enantioselective Rhodium-Catalyzed Allylic Etherification: Total Synthesis of Gaur Acid (C) 4788–4791 [4892–4895]
DOI: 10.1002/anie.200460612
Evans, W. J.
– Expanding the LnZ₃/Alkali-Metal Reduction System to Organometallic and Heteroleptic Precursors: Formation of Dinitrogen Derivatives of Lanthanum (C) 5517–5519 [5633–5635]
DOI: 10.1002/anie.200461170
Evers, A. (C) 248–251 [250–253]
Eversfield, S. G. (C) 628–630 [638–640]



- Fabrizzi, L.
– A Colorimetric Approach to Anion Sensing: A Selective Chemosensor of Fluoride Ions, in which Color is Generated by Anion-Enhanced π Delocalization (C) 1962–1965 [1996–1999]
DOI: 10.1002/anie.200353148
– A Dimetallic Cage with a Long Ellipsoidal Cavity for the Fluorescent Detection of Dicarboxylate Anions in Water (C) 3847–3852 [3935–3940]
DOI: 10.1002/anie.200460036
– A Sleeping Host Awaken by Its Guest: Recognition and Sensing of Imidazole-Containing Molecules Based on Double Cu²⁺ Translocation inside a Polyaza Macrocyclic

- (C) 5073–5077 [5183–5187]
DOI: 10.1002/anie.200460568
- Fabretti, A. C. (C) 1136–1139 [1156–1159]
- Facchetti, A. (C) 6363–6366 [6523–6526]
- Fairbanks, A. J. (C) 828–833 [846–851]
- Fairlamb, I. J. S.
– Asymmetric Cycloisomerization of 1,6- and 1,7-Enynes by Transition-Metal Catalysts
(H) 1048–1052 [1066–1070]
DOI: 10.1002/anie.200301699
- Fairlie, D. P.
– Consecutive Cyclic Pentapeptide Modules Form Short α -Helices that are Very Stable to Water and Denaturants
(C) 2687–2690 [2741–2744]
DOI: 10.1002/anie.200352659
- Falvello, L. R. (C) 5225–5228 [5337–5340]
- Famulok, M.
– Generation and Enzymatic Amplification of High-Density Functionalized DNA Double Strands
(C) 3337–3340 [3399–3403]
DOI: 10.1002/anie.200453926
- Fan, C.-A. (C) 1702–1705 [1734–1737]
- Fan, H. (C) 3443–3445 [3525–3527], 6190–6192 [6316–6318]
- Fan, W. (C) 236–240 [238–242]
- Fan, Y. (C) 5474–5477 [5590–5593]
- Fañanás, F. J. (C) 3932–3935 [4022–4025], 5510–5513 [5626–5629]
- Farago, B. (C) 364–366 [368–370]
- Farrusseng, D. (C) 5347–5349 [5461–5463]
- Fasan, R. (C) 2109–2112 [2161–2164]
- Fasel, R.
– Determination of the Absolute Chirality of Adsorbed Molecules
(C) 2853–2856 [2913–2917]
DOI: 10.1002/anie.200353311
- Fässler, T. F.
– Endohedral Zintl Ions: Intermetallic Clusters
(M) 6242–6247 [6400–6406]
DOI: 10.1002/anie.200460427
- Fechter, E. J. (C) 3591–3594 [3675–3678]
- Fedorov, V. E.
– Rhenium–Chalcogenide–Cyano Clusters, Cu^{2+} Ions, and 1,2,3,4-Tetraaminobutane as Molecular Building Blocks for Chiral Coordination Polymers
(C) 1297–1300 [1317–1321]
DOI: 10.1002/anie.200351595
- Fedorova, E. A. (C) 5045–5048 [5155–5158]
- Feldman, A. K. (C) 3928–3932 [4018–4022]
- Feldmann, J.
– 2-Dimethylarsinothioyl Acetic Acid Identified in a Biological Sample: The First Occurrence of a Mammalian Arsenothioyl Metabolite
(C) 337–340 [341–344]
DOI: 10.1002/anie.200352740
- Feliz, M. (C) 196–198 [198–200]
- Felli, I. C. (C) 2257–2259 [2307–2309]
- Feng, L.
– A Super-Hydrophobic and Super-Oleophilic Coating Mesh Film for the Separation of Oil and Water
(C) 2012–2014 [2046–2048]
DOI: 10.1002/anie.200353381
- Feng, L. (C) 357–360 [361–364]
- Feng, P.
– Pentasupertetrahedral Clusters as Building Blocks for a Three-Dimensional Sulfide Superlattice
(C) 4753–4755 [4857–4859]
DOI: 10.1002/anie.200460386
- Three-Dimensional Frameworks of Gallium Selenide Supertetrahedral Clusters
(C) 1502–1505 [1528–1531]
DOI: 10.1002/anie.200352880
- Fenske, D.
– Syntheses and Crystal Structures of the Ag–S Cluster Compounds
[$\text{Ag}_{70}\text{S}_{20}(\text{SPh})_{28}(\text{dppm})_{10}$] (CF_3CO_2)₂ and
[$\text{Ag}_{262}\text{S}_{100}(\text{SrBu})_{62}(\text{dppb})_6$]
(C) 305–309 [309–313]
DOI: 10.1002/anie.200352351
- Synthesis and Structure of
[$\text{Ag}_{26}\text{In}_{18}\text{S}_{36}\text{Cl}_6(\text{dppm})_{10}(\text{thf})_4$][$\text{InCl}_4(\text{thf})_2$]
—A Combined Approach of Theory and Experiment
(C) 3823–3827 [3911–3915]
DOI: 10.1002/anie.200460052
- Fensterbank, L.
– Titanium-Mediated Domino Radical Cyclization/ β Elimination of Phosphine Oxides
(C) 4220–4222 [4316–4318]
DOI: 10.1002/anie.200460099
- Feresin, E. (C) 1848–1851 [1884–1887]
- Férey, G.
– A Hybrid Solid with Giant Pores Prepared by a Combination of Targeted Chemistry, Simulation, and Powder Diffraction
(C) 6296–6301 [6456–6461]
DOI: 10.1002/anie.200460592
- Férey, G. (C) 2819–2822 [2879–2882], 6285–6289 [6445–6449], 6290–6296 [6450–6456]
- Ferguson, M. J. (C) 5967–5971 [6093–6097]
- Feringa, B. L.
– Direct Visual Detection of the Stereoselectivity of a Catalytic Reaction
(C) 5013–5016 [5123–5126]
DOI: 10.1002/anie.200460822
- Feringa, B. L. (C) 1663–1667 [1695–1699]
- Ferland, J.-M. (C) 4306–4311 [4406–4411]
- Fernandes, S. A. (C) 6517–6519 [6679–6681]
- Fernandez, F. M. (C) 6541–6544 [6703–6707]
- Fernández, J. L. (C) 6355–6357 [6515–6517]
- Fernández, X. (H) 6410–6412 [6570–6573]
- Fernández-Armas, S. (C) 977–980 [995–998]
- Fernández-Carneado, J. (C) 1811–1814 [1847–1850]
- Ferreira, E. M. (C) 6144–6148 [6270–6274]
- Ferrence, G. M. (C) 1346–1349 [1370–1373]
- Ferrer, M. L.
– Metallic Nanomagnets Randomly Dispersed in Spherical Colloids: Toward a Universal Route for the Preparation of Colloidal Composites Containing Nanoparticles
(C) 6304–6307 [6464–6467]
DOI: 10.1002/anie.200460830
- Ferrier, A. (C) 3728–3731 [3814–3817]
- Fettinger, J. (C) 2132–2134 [2184–2186]
- Fey, M. (C) 2257–2259 [2307–2309]
- Fichera, A. (C) 3664–3666 [3750–3752]
- Fiedler, D. (C) 963–966 [981–984], 6748–6751 [6916–6919]
- Fiedler, H.-P. (C) 2574–2576 [2628–2630]
- Figueroa, J. S. (C) 984–988 [1002–1006]
- Filippi, A. (C) 4767–4770 [4871–4874]
- Filippou, A. C.
– Triple Bond to Lead: Synthesis and Characterization of the Plumbidyne Complex *trans*-[$\text{Br}(\text{PMe}_3)_4\text{Mo}\equiv\text{Pb}-\text{C}_6\text{H}_5-2,6\text{-Trip}_2$]
(C) 2243–2247 [2293–2297]
DOI: 10.1002/anie.200353477
- Tungsten–Lead Triple Bonds: Syntheses, Structures, and Coordination Chemistry of the Plumbidyne Complexes *trans*-[$\text{X}(\text{PMe}_3)_4\text{W}\equiv\text{Pb}(2,6\text{-Trip}_2\text{C}_6\text{H}_3)$]
(C) 6512–6516 [6674–6678]
DOI: 10.1002/anie.200461725
- Finger, I. (C) 485–490 [491–496]
- Fink, G.
– Metallocene-Catalyzed C7-Linkage in the Hydrooligomerization of Norbornene by σ -Bond Metathesis: Insight into the Microstructure of Polynorbornene
(C) 2444–2446 [2498–2500]
DOI: 10.1002/anie.200353454
- Finn, M. G.
– Cleavable Linkers for Porous Silicon-Based Mass Spectrometry
(C) 1255–1260 [1275–1280]
DOI: 10.1002/anie.200352803
- Finze, M. (C) 4160–4163 [4254–4257]
- Fischbach, A. (C) 2234–2239 [2284–2289]
- Fischer, A. (C) 2540–2543 [2594–2597]
- Fischer, A. K. (C) 4603–4606 [4703–4706]
- Fischer, C. (C) 3795–3797 [3883–3886]
- Fischer, K. (C) 1101–1104 [1121–1124]
- Fischer, M. (C) 4364–4366 [4464–4466]
- Fischer, R. A.
– AlCp^* as a Directing Ligand: C–H and Si–H Bond Activation at the Reactive Intermediate [Ni(AlCp^*)₃]
(C) 2299–2302 [2349–2352]
DOI: 10.1002/anie.200353114
- MOCVD-Loading of Mesoporous Siliceous Matrices with Cu/ZnO: Supported Catalysts for Methanol Synthesis
(C) 2839–2842 [2899–2903]
DOI: 10.1002/anie.200351166
- Fitch, A. N. (C) 6316–6319 [6476–6479]
- Fleming, F. F.
– Oxonitriles: Multicomponent Grignard Addition–Alkylations
(C) 1126–1129 [1146–1149]
DOI: 10.1002/anie.200352920
- Fleming, J. J. (C) 4349–4352 [4449–4452]
- Fleming, K. N. (C) 1728–1730 [1760–1762]
- Fleming, S. D. (C) 5328–5331 [5442–5445]
- Fletcher, G. L. (C) 856–862 [874–880]
- Flitsch, S. L.
– Profiling Primary Protease Specificity by Peptide Synthesis on a Solid Support
(C) 3138–3141 [3200–3203]
DOI: 10.1002/anie.200353367
- Flood, A. H. (C) 6486–6491 [6648–6653]
- Fokin, V. V.
– Efficiency and Fidelity in a Click-Chemistry Route to Triazole Dendrimers by the Copper(I)-Catalyzed Ligation of Azides and Alkynes
(C) 3928–3932 [4018–4022]
DOI: 10.1002/anie.200454078
- Foran, G. J. (C) 462–465 [468–471]
- Formaggio, F. (C) 3152–3155 [3214–3217], 6695–6699 [6863–6867]
- Forment-Aliaga, A. (C) 6152–6156 [6278–6282]
- Fornés, V. (C) 4933–4937 [5041–5045]
- Fornés, J. (C) 5225–5228 [5337–5340]
- Förster, G. (C) 245–247 [247–249]
- Forsyth, C. J.
– Total Synthesis and Structural Assignment of Spongidepsin through a Stereodivergent Ring-Closing-Metathesis Strategy
(C) 2148–2152 [2200–2204]
DOI: 10.1002/anie.200453663
- Foti, F. (C) 5073–5077 [5183–5187]



- Fournier, J.-H. (C) 4634–4637 [4734–4737]
 Foxon, S. P. (C) 4360–4363 [4460–4464]
 Fraanje, J. (C) 3471–3473 [3553–3555]
 Fraass, V. C. (C) 1011–1014 [1029–1032]
 Fragai, M. (C) 2254–2256 [2304–2306]
 Fragalà, I. L.
 – Anchoring Molecular Magnets on the Si(100) Surface
 (C) 4081–4084 [4173–4176]
 DOI: 10.1002/anie.200453933
 Francesch, A. (C) 1724–1727 [1756–1759]
 Francisco, J. S. (C) 3330–3333 [3392–3395]
 Franck, R. W.
 – The C-Glycoside Analogue of the Immunostimulant α -Galactosylceramide (KRN7000): Synthesis and Striking Enhancement of Activity
 (C) 3818–3822 [3906–3910]
 DOI: 10.1002/anie.200454215
 François, B. (C) 6735–6738 [6903–6906]
 Frank, D. (C) 6553–6557 [6715–6719]
 Frank, I.
 – Ultrafast Cold Reactions in the Bipropellant Monomethylhydrazine/Nitrogen Tetroxide: CPMD Simulations
 (C) 4586–4589 [4686–4689]
 DOI: 10.1002/anie.200454093
 Frantzen, A. (C) 752–754 [770–773]
 Franz, K. J. (C) 3682–3685 [3768–3771]
 Franzini, M. (H) 4837–4841 [4942–4946]
 Fréchet, J. M. J. (C) 3928–3932 [4018–4022]
 Frederick, M. O. (C) 4312–4318 [4412–4418], 4318–4324 [4418–4424]
 Freil Meyers, C. L. (C) 67–70 [69–72]
 Frenzer, G. (C) 752–754 [770–773]
 Freund, H.-J.
 – Do Quantum Size Effects Control CO Adsorption on Gold Nanoparticles?
 (C) 118–121 [121–124]
 DOI: 10.1002/anie.200352538
 Freund, H.-J. (C) 517–520 [523–526]
 Frey, W. (C) 6547–6549 [6709–6711]
 Friend, R. H. (C) 1976–1979 [2010–2013]
 Friggeri, A. (C) 1663–1667 [1695–1699]
 Frišić, T. (C) 232–236 [234–238]
 Frison, C. (C) 6120–6125 [6246–6251]
 Fröhlich, R. (C) 310–313 [313–317], 1423–1427 [1447–1451], 5694–5697 [5812–5815], 5991–5994 [6117–6120], 6662–6666 [6832–6836]
 Fron, E. (C) 6116–6120 [6242–6246]
 Frontera, A. Corrigendum: 141
 Fu, G. C.
 – A Straightforward and Mild Synthesis of Functionalized 3-Alkynoates
 (C) 3580–3582 [3664–3666]
 DOI: 10.1002/anie.200454070
 – Asymmetric Synthesis of Highly Substituted β -Lactones by Nucleophile-Catalyzed [2+2] Cycloadditions of Disubstituted Ketenes with Aldehydes
 (C) 6358–6360 [6518–6520]
 DOI: 10.1002/anie.200460698
 Fu, L.-M. (C) 5010–5013 [5120–5123]
 Fu, S.-J. (C) 4186–4189 [4282–4285]
 Fuchibe, K. (C) 1566–1568 [1592–1594]
 Fugmann, B. (C) 1381–1385 [1405–1409]
 Fujii, I. (C) 5481–5485 [5597–5601]
 Fujikawa, D. (C) 228–232 [230–234]
 Fujinami, S. (C) 334–337 [338–341], 3300–3303 [3362–3365]
 Fujisawa, K.
 – Diazeno Complexes of Copper: Synthesis, Spectroscopic Analysis, and Electronic Structure
 (C) 4944–4947 [5052–5055]
 DOI: 10.1002/anie.200460415
 Fujisawa, N. (C) 2423–2425 [2477–2479]
 Fujita, M.
 – A Palladium(II)-Clipped Aromatic Sandwich
 (C) 5936–5940 [6062–6066]
 DOI: 10.1002/anie.200460868
 – Finite, Spherical Coordination Networks that Self-Organize from 36 Small Components
 (C) 5621–5625 [5739–5743]
 DOI: 10.1002/anie.200461422
 – Kinetic Self-Assembly: Selective Cross-Catenation of Two Sterically Differentiated Pd^{II}-Coordination Rings
 (C) 5016–5019 [5126–5129]
 DOI: 10.1002/anie.200460671
 Fujita, N. (C) 465–469 [471–475], 1229–1233 [1249–1253]
 Fujitani, N. (C) 856–862 [874–880]
 Fujitsuka, M. (C) 853–856 [871–874], 2406–2409 [2460–2463], 4510–4512 [4610–4612]
 Fujiwara, N. (C) 5060–5062 [5170–5172]
 Fujiwara, Y. (C) 6474–6479 [6636–6641]
 Fukada, I. (C) 2015–2017 [2049–2051]
 Fukin, G. K. (C) 5045–5048 [5155–5158]
 Fukuda, M. (C) 2389–2391 [2443–2445]
 Fukui, K. (C) 6343–6346 [6503–6506]
 Fukui, Y. (C) 4634–4637 [4734–4737]
 Fukushima, H. (C) 3935–3938 [4025–4028]
 Fukuyasu, Y. (C) 2389–2391 [2443–2445]
 Fukuzumi, S.
 – Production of an Ultra-Long-Lived Charge-Separated State in a Zinc Chlorin-C₆₀ Dyad by One-Step Photoinduced Electron Transfer
 (C) 853–856 [871–874]
 DOI: 10.1002/anie.200352870
 Fuller, A.-M. (C) 3914–3918 [4004–4008]
 Funeriu, D. P.
 – Enzyme Microarrays: On-Chip Determination of Inhibition Constants Based on Affinity-Label Detection of Enzymatic Activity
 (C) 3806–3810 Corrigendum: 4389 [3894–3898 Corrigendum: 4489]
 DOI: 10.1002/anie.200353623
 Fürstner, A.
 – Cross-Coupling of Alkyl Halides with Aryl Grignard Reagents Catalyzed by a Low-Valent Iron Complex
 (C) 3955–3957 [4045–4047]
 DOI: 10.1002/anie.200460504
 Furumura, Yu. (C) 4490–4492 [4590–4592]
 Furuno, H. (C) 3582–3584 [3666–3668]
 Furusho, Y. (C) 966–969 [984–987]
 Furuta, H.
 – Doubly N-Confused Pentaphyrins
 (C) 2951–2955 [3011–3015]
 DOI: 10.1002/anie.200453732
 – Doubly N-Fused Pentaphyrin
 (C) 876–879 [894–897]
 DOI: 10.1002/anie.200352946
 – Inverted N-Confused Porphyrin Dimer
 (C) 5077–5081 [5187–5191]
 DOI: 10.1002/anie.200460017
 Furutachi, H. (C) 3300–3303 [3362–3365]
 Fuss, W.
 – The Photochemical *cis-trans* Isomerization of Free Stilbene Molecules Follows a Hula-Twist Pathway
 (C) 4178–4182 [4273–4277]
 DOI: 10.1002/anie.200454221
 Fyles, T. M. (C) 3461–3464 [3543–3546]
 Gabbaï, F. P.
 – A Neutral Chromium(III) Catalyst for the Living “Aufbaureaktion”
 (C) 2263–2266 [2313–2316]
 DOI: 10.1002/anie.200353040
 – Electrophilic Double-Sandwiches Formed by Interaction of [Cp₂Fe] and [Cp₂Ni] with the Tridentate Lewis Acid [(*o*-C₆F₄Hg)₃]
 (C) 5471–5474 [5587–5590]
 DOI: 10.1002/anie.200461152
 – Synthesis and Reactivity of a 1,8-Bis-(methylum)naphthalenediyl Dication
 (C) 184–187 [186–189]
 DOI: 10.1002/anie.200353011
 Gabor, B. (C) 2444–2446 [2498–2500]
 Gade, L. H.
 – A C₃-Symmetrical Chiral Trisoxazoline Zinc Complex as a Functional Model for Zinc Hydrolases: Kinetic Resolution of Racemic Chiral Esters by Transesterification
 (C) 4479–4482 [4579–4582]
 DOI: 10.1002/anie.200460187
 – A Modular Assembly of Chiral Oxazolinylcarbene–Rhodium Complexes: Efficient Phosphate-Free Catalysts for the Asymmetric Hydrosilylation of Dialkyl Ketones
 (C) 1014–1017 [1036–1039]
 DOI: 10.1002/anie.200353133
 Gademann, K.
 – A Biomimetic Route to the Peptide Alkaloid Anachelin
 (C) 3327–3329 [3389–3391]
 DOI: 10.1002/anie.200453909
 Gagliardi, L.
 – Theoretical Search for Very Short Metal–Actinide Bonds: NUIr and Isoelectronic Systems
 (C) 1573–1576 [1599–1602]
 DOI: 10.1002/anie.200353261
 Gagné, M. R.
 – Pd^{II}- and Pt^{II}-Mediated Polycyclization Reactions of 1,5- and 1,6-Dienes: Evidence in Support of Carbocation Intermediates
 (C) 3459–3461 Corrigendum: 4828 [3541–3543 Corrigendum: 4932]
 DOI: 10.1002/anie.200453913
 Gairí, M. (C) 196–198 [198–200]
 Gaisser, S. (C) 2551–2553 [2605–2607]
 Gaita-Ariño, A. (C) 6152–6156 [6278–6282]
 Gal, A. W. (R) 4142–4157 [4236–4251]
 Galeotti, M. (C) 3058–3060 [3120–3122]
 Galione, A. (C) 4637–4640 [4737–4740]
 Gambarotta, S.
 – Multimetallic Cooperative Activation of N₂
 (M) 5298–5308 [5412–5422]
 DOI: 10.1002/anie.200301669
 Gambin, D. P. (C) 828–833 [846–851]
 Gamez, P.
 – An Aromatic Anion Receptor: Anion- π Interactions do Exist
 (C) 5815–5817 [5939–5941]
 DOI: 10.1002/anie.200460486
 Gan, W. B. (C) 6331–6335 [6491–6495]

- Gao, H. (C) 1397–1399 [1421–1423], 2415–2417 [2469–2471]
- Gao, Jiali
- The Magnitude of Hyperconjugation in Ethane: A Perspective from Ab Initio Valence Bond Theory (C) 1986–1990 [2020–2024] DOI: 10.1002/anie.200352931
- Gao, Jinming
- cRGD-Functionalized Polymer Micelles for Targeted Doxorubicin Delivery (C) 6323–6327 [6483–6487] DOI: 10.1002/anie.200460800
- Gao, Pei (C) 733–736 [751–754]
- Gao, Puxian (C) 5238–5242 [5350–5354]
- Gao, S.
- Formation of Two-Dimensional Supramolecular Icelike Layer Containing (H₂O)₁₂ Rings (C) 1374–1376 [1398–1400] DOI: 10.1002/anie.200353097
- Gao, S. (C) 990–994 [1008–1012]
- Gao, X. (C) 232–236 [234–238]
- Garau, C. Corrigendum: 141
- Garbay, C.
- A Very Short Route to Enantiomerically Pure Coumarin-Bearing Fluorescent Amino Acids (C) 3432–3436 [3514–3518] DOI: 10.1002/anie.200454116
- García, F. (C) 5668–5670 [5786–5788]
- García-Granda, S. (C) 4333–4336 [4433–4436], 5510–5513 [5626–5629]
- García-Monforte, M. A. (C) 5225–5228 [5337–5340]
- García-Parajó, M. F.
- Investigation of Perylene Photonic Wires by Combined Single-Molecule Fluorescence and Atomic Force Microscopy (C) 4045–4049 [4137–4141] DOI: 10.1002/anie.200453745
- García-Zarracino, R. (C) 1507–1511 [1533–1537]
- Gardiennet, C. (C) 3565–3568 [3649–3652]
- Garipova, G. (C) 5963–5967 [6089–6093]
- Garitaonandia, J. S. (C) 977–980 [995–998]
- Garnier, P. (C) 828–833 [846–851]
- Garratt, S. (C) 2166–2169 [2218–2222]
- Garrisi, P. (C) 1136–1139 [1156–1159]
- Garstecki, P. (C) 1555–1558 [1581–1584]
- Gascon, I. (C) 6174–6177 [6300–6303]
- Gatard, S. (C) 2924–2928 [2984–2988]
- Gates, B. D. (C) 2780–2783 [2840–2843]
- Gates, D. P.
- Radical Copolymerization of a Phosphaalkene with Styrene: New Phosphine-Containing Macromolecules and Their Use in Polymer-Supported Catalysis (C) 5682–5685 [5800–5803] DOI: 10.1002/anie.200460939
- Gatteschi, D. (C) 1136–1139 [1156–1159], 4081–4084 [4173–4176], 5196–5200 [5308–5312]
- Gaunt, M. J.
- An Intramolecular Organocatalytic Cyclopropanation Reaction (C) 2681–2684 [2735–2738] DOI: 10.1002/anie.200454007
 - Enantioselective Organocatalytic Cyclopropanation via Ammonium Ylides (C) 4641–4644 [4741–4744] DOI: 10.1002/anie.200460234
- Gauthier, D. (C) 349–353 [353–357]
- Gautier, A.
- α,α -Difluoro-*H*-phosphinates: Useful Intermediates for a Variety of Phosphate Isosteres (C) 5963–5967 [6089–6093] DOI: 10.1002/anie.200460519
- Gautier, A. (C) 1588–1591 [1614–1617]
- Gazit, E.
- Inhibition of Amyloid Fibril Formation by Peptide Analogues Modified with α -Aminoisobutyric Acid (C) 4041–4044 [4133–4136] DOI: 10.1002/anie.200353565
- Gehrhus, B.
- An Insoluble Radical Anion and Dianion of a Cyclotetrasilane: Synthesis and Structure of [Si{1,2-(NEt)₂C₆H₄}]₄²⁻ and [Si{1,2-(NEt)₂C₆H₄}]₄²⁻ (C) 1124–1126 [1144–1146] DOI: 10.1002/anie.200352882
- Gehrhus, B. (C) 3474–3477 [3556–3559]
- Geier, J. (C) 2567–2570 [2621–2624], 4093–4097 [4185–4189]
- Geipel, F. (C) 3141–3144 [3203–3206]
- Geiseler, G. Corrigendum: 2737
- Gellman, S. H.
- Two Helical Conformations from a Single Foldamer Backbone: “Split Personality” in Short α/β -Peptides (C) 505–510 [511–516] DOI: 10.1002/anie.200352125
- Gemel, C. (C) 2299–2302 [2349–2352]
- Genet, J.-P.
- Tandem 1,4-Addition/Enantioselective Protonation Catalyzed by Rhodium Complexes: Efficient Access to α -Amino Acids (C) 719–723 [737–741] DOI: 10.1002/anie.200352518
- Genêt, J.-P.
- Difluorophos, an Electron-Poor Diphosphane: A Good Match Between Electronic and Steric Features (C) 320–325 [324–329] DOI: 10.1002/anie.200352453
- Geng, X. (C) 2557–2561 [2611–2615], 2562–2565 [2616–2619]
- Genov, D. G.
- Asymmetric Hydrogenation of Ketones Catalyzed by Ru^{II}-bip Complexes (C) 2816–2819 [2876–2879] DOI: 10.1002/anie.200353441
- George, M. W. (C) 5192–5195 [5304–5307]
- George, S. J. (C) 3422–3425 [3504–3507]
- Gerbi, A. (C) 5200–5203 [5312–5315]
- Gerken, M. (C) 6676–6680 [6844–6848]
- Germain, A. R. (C) 1239–1243 [1259–1263]
- Gevorgyan, V.
- A Novel 1,2-Migration of Acyloxy, Phosphatyl, and Sulfonyloxy Groups in Allenes: Efficient Synthesis of Tri- and Tetrasubstituted Furans (C) 2280–2282 [2330–2332] DOI: 10.1002/anie.200353535
- Gey, C. (H) 3998–4000 [4088–4090]
- Geyer, A.
- Coupled Hydrogen-Bonding Networks in Polyhydroxylated Peptides (C) 5789–5791 [5913–5915] DOI: 10.1002/anie.200461099
- Ghaderi, N. (C) 4880–4883 [4988–4991]
- Ghadiri, M. R.
- Single DNA Rotaxanes of a Transmembrane Pore Protein (C) 3063–3067 [3125–3129] DOI: 10.1002/anie.200453907
- Gharsa, T. (C) 6174–6177 [6300–6303]
- Ghosh, A.
- A Perspective of One-Pot Pyrrole–Aldehyde Condensations as Versatile Self-Assembly Processes (M) 1918–1931 [1952–1965] DOI: 10.1002/anie.200201603
 - Models of High-Valent Intermediates of Non-Heme Diiron Alkane Monooxygenases: Electronic Structure of a Bis(μ -oxo)diron(IV) Complex with Locally Low-Spin Metal Centers (C) 834–838 [852–856] DOI: 10.1002/anie.200351768
- Ghosh, S. K. (C) 3577–3580 Corrigendum: 4390 [3661–3664 Corrigendum: 4490]
- Ghosh, Somdatta (M) 4132–4140 [4224–4233]
- Ghosh, Suhrit (C) 3264–3268 [3326–3330]
- Giannazzo, F. (C) 4081–4084 [4173–4176]
- Gianneschi, N. C. (C) 5503–5507 [5619–5623]
- Giannis, A.
- A Fatal Affair: The Ubiquitinylation of Proteins (H) 6414–6416 [6574–6576] DOI: 10.1002/anie.200462346
 - Design, Synthesis, and Biological Evaluation of a Small-Molecule Inhibitor of the Histone Acetyltransferase Gcn5 (C) 3974–3976 [4065–4067] DOI: 10.1002/anie.200453879
 - Small Molecules, Big Plans—Can Low-Molecular-Weight Compounds Control Human Regeneration? (H) 3998–4000 [4088–4090] DOI: 10.1002/anie.200460346
 - Synthesis and Biochemical Properties of Reversible Inhibitors of UDP-*N*-Acetylglucosamine 2-Epimerase (C) 4366–4370 [4467–4470] DOI: 10.1002/anie.200453863
 - Synthesis and Biological Evaluation of an Indomethacin Library Reveals a New Class of Angiogenesis-Related Kinase Inhibitors (C) 224–228 Corrigendum: 540 [226–230 Corrigendum: 547] DOI: 10.1002/anie.200352582
- Gibson, S. E.
- A Cyclobutadiene Equivalent in the Catalytic Pauson–Khand Reaction (C) 5680–5682 [5798–5800] DOI: 10.1002/anie.200460654
- Giese, B.
- Excess Electron Transport Through DNA: A Single Electron Repairs More than One UV-Induced Lesion (C) 1848–1851 [1884–1887] DOI: 10.1002/anie.200353264
- Giesebrecht, S. (C) 2809–2812 [2869–2872]
- Giesenberger, T. (C) 5697–5700 [5816–5819]
- Giessmann, S. (C) 4603–4606 [4703–4706]
- Gil, M. P. (C) 6169–6173 [6295–6299]
- Gilardi, R. (C) 4924–4928 [5032–5036], 5658–5661 [5776–5779]
- Gilbert, T. M. (C) 1955–1958 [1989–1992]
- Gilead, S. (C) 4041–4044 [4133–4136]
- Gilje, J. W. (C) 4603–4606 [4703–4706]
- Gill, H. S. (C) 485–490 [491–496]
- Gillard, J. (C) 4306–4311 [4406–4411]
- Giménez, A. (C) 1883–1886 [1919–1922]
- Giménez-Saiz, C.
- Metallic Conductivity Down to 2 K in a Polyoxometalate-Containing Radical Salt of BEDO-TTF

- (C) 3022–3025 [3084–3087]
DOI: 10.1002/anie.200453985
- Giménez-Saiz, C. (C) 6152–6156 [6278–6282]
- Gimeno, N. (C) 5235–5238 [5347–5350]
- Ginger, D. S. (R) 30–45 [30–46]
- Giralt, E.
– A Tetraguanidinium Ligand Binds to the Surface of the Tetramerization Domain of Protein P53
(C) 196–198 [198–200]
DOI: 10.1002/anie.200352115
- Potential Peptide Carriers: Amphipathic Proline-Rich Peptides Derived from the N-Terminal Domain of γ -Zein
(C) 1811–1814 [1847–1850]
DOI: 10.1002/anie.200352540
- Girgsdies, F. (C) 112–115 [114–117]
- Giroldo, T. (C) 3588–3590 [3672–3674]
- Giunta, P. R. (C) 1505–1507 [1531–1533]
- Giuseppone, N. (C) 4902–4906 [5010–5014]
- Gladioli, S. (C) 846–849 [864–867]
- Gladysz, J. A.
– Molecular Gyroscopes: $\{\text{Fe}(\text{CO})_3\}$ and $\{\text{Fe}(\text{CO})_2(\text{NO})\}^+$ Rotators Encased in Three-Spoke Stators; Facile Assembly by Alkene Metatheses
(C) 5537–5540 [5653–5656]
DOI: 10.1002/anie.200460534
- Glaser, N. (C) 4888–4892 [4996–5000]
- Glatthaar, J. (C) 1294–1296 [1314–1317]
- Glättli, A. (C) 6312–6316 [6472–6476]
- Gleason, J. L.
– Pseudodynamic Combinatorial Libraries: A Receptor-Assisted Approach for Drug Discovery
(C) 2432–2436 [2486–2490]
DOI: 10.1002/anie.200453769
- Two Birds with One Metallic Stone: Single-Pot Catalysis of Fundamentally Different Transformations
(M) 3754–3760 [3842–3848]
DOI: 10.1002/anie.200301727
- Gleiter, R.
– Synthesis of Beltenes by Reactions of 5,6,11,12-Tetrahydrodibenzo[*a,e*]cyclo-octene with $[\text{CpCo}(\text{CO})_2]$ Derivatives
(C) 5846–5849 [5970–5973]
DOI: 10.1002/anie.200460772
- Glorius, F.
– Chiral Olefin Ligands—New “Spectators” in Asymmetric Catalysis
(H) 3364–3366 [3444–3446]
DOI: 10.1002/anie.200301752
- Efficient Asymmetric Hydrogenation of Pyridines
(C) 2850–2852 [2910–2913]
DOI: 10.1002/anie.200453942
- Organocatalyzed Conjugate Umpolung of α,β -Unsaturated Aldehydes for the Synthesis of γ -Butyrolactones
(C) 6205–6208 [6331–6334]
DOI: 10.1002/anie.200461572
- Godard, E. (C) 3722–3724 [3808–3810]
- Goddard, R. (C) 70–74 [72–76], 2850–2852 [2910–2913]
- Goddard III, W. A. (C) 4626–4629 [4726–4729]
- Goebel, M. (C) 5851–5856 [5976–5981]
- Goeldner, M.
– 1-(*o*-Nitrophenyl)-2,2,2-trifluoroethyl Ether Derivatives as Stable and Efficient Photoremovable Alcohol-Protecting Groups
(C) 2008–2012 [2042–2046]
DOI: 10.1002/anie.200353247
- Goelet, P. (C) 1672–1675 [1704–1707]
- Goeltz, J. C. (C) 5631–5635 [5749–5753]
- Göessl, I. (C) 5185–5188 [5297–5300]
- Goeta, A. E. (C) 2095–2099 [2147–2151]
- Goichi, M. (C) 2248–2251 [2298–2301]
- Golberg, D. (C) 63–66 [65–68], 4606–4609 [4706–4709]
- Golebiowski, J. (H) 6410–6412 [6570–6573]
- Göltz, P.
– Editorial: Nothing Stands Still
4–6 [4–6]
DOI: 10.1002/anie.200390640
- Editorial: The Future of Chemistry
3618–3620 [3702–3704]
DOI: 10.1002/anie.200490090
- Editorial: The Woodward–Hoffmann Rules
6568–6569 [6730–6731]
DOI: 10.1002/anie.200462590
- Golub, V. O. (C) 6169–6173 [6295–6299]
- Gómez Arrayás, R. (C) 3944–3947 [4034–4037]
- Gómez-García, C. J. (C) 3022–3025 [3084–3087]
- Gonda, J.
– The Belluš–Claisen Rearrangement
(M) 3516–3524 [3600–3608]
DOI: 10.1002/anie.200301718
- Gong, B.
– Supramolecular AB Diblock Copolymers
(C) 6471–6474 [6633–6636]
DOI: 10.1002/anie.200460472
- Gonzalez, E. (C) 834–838 [852–856]
- González, J. M. (C) 325–329 [329–333]
- González-Carreño, T. (C) 6304–6307 [6464–6467]
- González-Noya, A. M. (C) 1962–1965 [1996–1999]
- González-Roura, A. (C) 862–865 [880–883]
- Gooding, J. J. (C) 2809–2812 [2869–2872]
- Goodman, C. M. (C) 724–727 [742–745]
- Goodman, S. D. (C) 4750–4752 [4854–4856]
- Goodman, S. L. (C) 6649–6652 [6818–6821]
- Goodwin, J. C. (C) 4037–4041 [4129–4133]
- Goossen, L. J.
– Decarbonylative Heck Olefination of Enol Esters: Salt-Free and Environmentally Friendly Access to Vinyl Arenes
(C) 1095–1098 [1115–1118]
DOI: 10.1002/anie.200352357
- Gordon, H. (C) 5342–5346 [5456–5460]
- Gorelsky, S. I. (M) 4132–4140 [4224–4233]
- Gorman, C. B.
– Establishing the Molecular Basis for Molecular Electronics
(H) 5120–5123 [5230–5233]
DOI: 10.1002/anie.200301735
- Gornitzka, H. (C) 585–587 [595–597]
- Gorodetsky, B. (C) 2812–2815 [2872–2875]
- Goryunkov, A. A. (C) 997–1000 [1015–1018]
- Gösele, U. (R) 1334–1344 [1356–1367]
- Goto, E. (C) 5029–5032 [5139–5142]
- Goto, K. (C) 5019–5022 [5129–5132]
- Goto, Takayuki (C) 882–884 [900–902]
- Goto, Toshiaki (C) 2527–2530 [2581–2584]
- Gou, X.-L. (C) 4212–4216 [4308–4312]
- Goubitz, K. (C) 3471–3473 [3553–3555]
- Gourdon, A. (C) 2092–2095 [2144–2147]
- Gourzoulidou, E. (C) 450–454 [456–460], 454–458 [460–464]
- Graening, T. (R) 3230–3256 [3292–3318]
- Graetzel, M. (C) 3666–3670 [3752–3756]
- Graham, D. (C) 2512–2514 [2566–2568]
- Grainger, R. S.
– Dithiocarbamate Group Transfer Cyclization Reactions of Carbamoyl Radicals under “Tin-Free” Conditions
(C) 3445–3448 [3527–3530]
DOI: 10.1002/anie.200453600
- Greber, T. (C) 2853–2856 [2913–2917]
- Greeley, J. (C) 4296–4300 [4396–4400]
- Green, M.
– Semiconductor Quantum Dots as Biological Imaging Agents
(H) 4129–4131 [4221–4223]
DOI: 10.1002/anie.200301758
- Gregory, M. A. (C) 2551–2553 [2605–2607]
- Grenouillat, N. (C) 4644–4646 [4744–4746]
- Grepioni, F. (M) 4002–4011 [4092–4102]
- Gribkov, D. V. (C) 5542–5546 Corrigendum: 6581 [5659–5663 Corrigendum: 6743]
- Gridnev, I. D.
– Solution Structure and Reagent Binding of the Zinc Alkoxide Catalyst in the Soai Asymmetric Autocatalytic Reaction
(C) 4884–4887 [4992–4995]
DOI: 10.1002/anie.200353572
- Griesinger, C.
– The Cofactor of the Iron–Sulfur Cluster Free Hydrogenase Hmd: Structure of the Light-Inactivation Product
(C) 2547–2551 [2601–2605]
DOI: 10.1002/anie.200353763
- Griesinger, C. (C) 187–192 [189–194]
- Griffey, R. H. (C) 6735–6738 [6903–6906]
- Grigg, R. (C) 1389–1392 [1413–1416]
- Grindstaff, J. (C) 5496–5499 [5612–5615]
- Gronenberg, L. S. (C) 6713–6716 [6881–6884]
- Groth, T.
– Layer-by-Layer Deposition of Polyelectrolytes—A Versatile Tool for the In Vivo Repair of Blood Vessels
(H) 926–928 [944–946]
DOI: 10.1002/anie.200301708
- Groves, J. T.
– Anti-Markovnikov Hydrofunctionalization of Olefins Mediated by Rhodium–Porphyrin Complexes
(C) 588–590 [598–600]
DOI: 10.1002/anie.200351941
- Grubb, M. (C) 198–203 [200–205]
- Grubbs, R. H.
– The Exclusivity of Multivalency in Dynamic Covalent Processes
(C) 3273–3278 [3335–3340]
DOI: 10.1002/anie.200453963
- Gruber, M. A. (C) 1881–1882 [1917–1918]
- Grubmüller, H.
– Multistep Binding of Divalent Cations to Phospholipid Bilayers: A Molecular Dynamics Study
(C) 1021–1024 [1039–1042]
DOI: 10.1002/anie.200352784
- Grunenberg, J. (C) 2521–2524 [2575–2578]
- Grünert, W. (C) 2839–2842 [2899–2903]
- Grützmacher, H.
– “Naked” Phosphanediide Chains and their Fragmentation into Diphosphene Radical Anions
(C) 4093–4097 [4185–4189]
DOI: 10.1002/anie.200460130
- Stereochemical Control of the Redox Potential of Tetracoordinate Rhodium Complexes
(C) 2567–2570 [2621–2624]
DOI: 10.1002/anie.200353027

- Guan, Z.
– Cyclophane-Based Highly Active Late-Transition-Metal Catalysts for Ethylene Polymerization (C) 1821–1825 Corrigendum: 2986 [1857–1861 Corrigendum: 3046]
DOI: 10.1002/anie.200353226
- Gudat, D.
– Diphosphanes with Polarized and Highly Reactive P–P Bonds (C) 4801–4804 [4905–4908]
DOI: 10.1002/anie.200460003
- Guenot, P. (C) 873–875 [891–893]
- Guérin, R.
– $\text{Gd}_3\text{Si}_2\text{B}_3$: A Ternary Rare-Earth-Metal Silicide Boride Compound (C) 1979–1983 [2013–2017]
DOI: 10.1002/anie.200352468
- Guerrero, A. (C) 2166–2169 [2218–2222]
- Guerret, O. (C) 6186–6189 [6312–6315]
- Gui, L.-L. (C) 5010–5013 [5120–5123]
- Guidoni, A. G. (C) 1868–1871 Corrigendum: 3872 [1904–1907 Corrigendum: 3960]
- Guidoni, L. (C) 3286–3289 [3348–3351]
- Guidry, E. N. (C) 3273–3278 [3335–3340]
- Guillemin, J.-C.
– First Synthesis and Characterization by Mass Spectrometry and UV-Photoelectron Spectroscopy of Methyleneanesane (C) 873–875 [891–893]
DOI: 10.1002/anie.200352445
- Guiochon, G. A. (C) 5785–5789 [5909–5913]
- Guldi, D. M.
– Integrating Single-Wall Carbon Nanotubes into Donor–Acceptor Nanohybrids (C) 5526–5530 [5642–5646]
DOI: 10.1002/anie.200461217
- Gulo, F. (C) 2032–2034 [2066–2068]
- Gunari, N. (C) 1101–1104 [1121–1124]
- Gunda, P. (C) 6372–6377 [6532–6537]
- Gun'ko, Y. K. (C) 4603–4606 [4703–4706]
- Günther, R. (C) 1594–1597 [1621–1624]
- Güntherodt, H.-J. (C) 4759–4763 [4863–4867]
- Guo, M. (C) 5914–5918 [6040–6044]
- Guo, Y.-G. (C) 1540–1543 [1566–1569]
- Guo, Y.-M. (C) 4915–4918 [5023–5026]
- Guo, Z.
– Chemical Synthesis of a Skeleton Structure of Sperm CD52—A GPI-Anchored Glycopeptide (C) 1569–1573 [1595–1599]
DOI: 10.1002/anie.200353251
- Gupta, P. (C) 520–523 [527–529]
- Gutnov, A.
– Cobalt(II)-Catalyzed Asymmetric [2 + 2 + 2] Cycloaddition of Alkynes and Nitriles: Synthesis of Enantiomerically Enriched Atropoisomers of 2-Arylpyridines (C) 3795–3797 [3883–3886]
DOI: 10.1002/anie.200454164
- Ha, C. (C) 6331–6335 [6491–6495]
- Haag, R.
– Highly Branched Macromolecules at the Interface of Chemistry, Biology, Physics, and Medicine (T) 272–273 [274–275]
DOI: 10.1002/anie.200320082
- Supramolecular Drug-Delivery Systems Based on Polymeric Core–Shell Architectures (H) 278–282 [280–284]
DOI: 10.1002/anie.200301694
- Haas, C. (C) 1842–1844 Corrigendum: 2321 [1878–1880 Corrigendum: 2373]
- Haase, D. (C) 1583–1587 [1609–1614]
- Haasnoot, J. G. (C) 5668–5670 [5786–5788]
- Habicher, T. (R) 788–824 [806–843]
- Haddon, R. C. (C) 1552–1554 [1578–1580]
- Haeussler, W. (C) 364–366 [368–370]
- Hagberg, E. C. (C) 5796–5799 [5920–5923]
- Hagemann, B. (C) 5066–5069 [5176–5179]
- Hagiwara, K. (C) 6505–6510 [6667–6672]
- Hagman, P. J. (C) 3436–3439 [3518–3521]
- Hahn, F. E.
– A Dinuclear, Triple-Stranded Helicate with a Diamide-Bridged Catechol/Benzenedithiol Ligand (C) 4807–4810 [4911–4915]
DOI: 10.1002/anie.200460188
- Hahn, M. E. (C) 5800–5803 [5924–5927]
- Hahn, U. (H) 1190–1193 [1210–1213]
- Haiges, R.
– High-Energy-Density Materials: Synthesis and Characterization of $\text{N}_5^+[\text{P}(\text{N}_3)_6]^-$, $\text{N}_5^+[\text{B}(\text{N}_3)_4]^-$, $\text{N}_5^+[\text{HF}_2]^- \cdot n\text{HF}$, $\text{N}_5^+[\text{BF}_4]^-$, $\text{N}_5^+[\text{PF}_6]^-$, and $\text{N}_5^+[\text{SO}_3\text{F}]^-$ (C) 4919–4924 [5027–5032]
DOI: 10.1002/anie.200454242
- Polyazide Chemistry: Preparation and Characterization of $\text{As}(\text{N}_3)_3$, $\text{Sb}(\text{N}_3)_3$, and $[\text{P}(\text{C}_6\text{H}_5)_4][\text{Sb}(\text{N}_3)_6]$ (C) 6676–6680 [6844–6848]
DOI: 10.1002/anie.200461730
- The Binary Group 4 Azides $[\text{Ti}(\text{N}_3)_4]$, $[\text{P}(\text{C}_6\text{H}_5)_4][\text{Ti}(\text{N}_3)_5]$, and $[\text{P}(\text{C}_6\text{H}_5)_4]_2[\text{Ti}(\text{N}_3)_6]$ and on Linear Ti–N–NN Coordination (C) 3148–3152 [3210–3214]
DOI: 10.1002/anie.200454156
- Haiges, R. (C) 5213–5217 [5325–5329]
- Haigh, R. (C) 2135–2138 [2187–2190]
- Halasyamani, P. S.
– The Lone-Pair Cation I^{5+} in a Hexagonal Tungsten Oxide-Like Framework: Synthesis, Structure, and Second-Harmonic Generating Properties of $\text{Cs}_3\text{I}_4\text{O}_{11}$ (C) 5489–5491 [5605–5607]
DOI: 10.1002/anie.200460367
- Halet, J.-F.
– $\text{Gd}_3\text{Si}_2\text{B}_3$: A Ternary Rare-Earth-Metal Silicide Boride Compound (C) 1979–1983 [2013–2017]
DOI: 10.1002/anie.200352468
- Haley, M. M.
– Let the Best Ring Win: Selective Macrocyclic Formation through Pd-Catalyzed or Cu-Mediated Alkyne Homocoupling (C) 1694–1697 [1726–1729]
DOI: 10.1002/anie.200353043
- Haley, M. M. (C) 5967–5971 [6093–6097]
- Hall, D. G.
– Three-Component Sequential Aza[4 + 2] Cycloaddition/Allylboration/Retro-Sulfinyl-Ene Reaction: A New Stereocontrolled Entry to Palustrine Alkaloids and Other 2,6-Disubstituted Piperidines (C) 2001–2004 [2035–2038]
DOI: 10.1002/anie.200353152
- Hall, M. B.
– Rhodium Silyl Boryl Hydride Complexes: Comparison of Bonding and the Rates of Elimination of Borane, Silane, and Dihydrogen (C) 5474–5477 [5590–5593]
DOI: 10.1002/anie.200460430
- Halland, N. (C) 1272–1277 [1292–1297], 5507–5510 [5623–5626]
- Halper, S. R. (C) 2385–2388 [2439–2442]
- Hama, K. (C) 2834–2837 [2894–2897]
- Hamada, Y.
– Stereoselective Synthesis of *anti*- β -Hydroxy- α -amino Acids through Dynamic Kinetic Resolution (C) 882–884 [900–902]
DOI: 10.1002/anie.200353072
- Hamaguchi, T. (C) 1376–1381 [1400–1405]
- Hamai, C. (C) 1349–1352 [1373–1376]
- Hamann, H. (C) 517–520 [523–526]
- Hamashima, Y. (C) 2659–2661 [2713–2715]
- Hamilton, A. D. (C) 196–198 [198–200]
- Hamilton, E. E. (C) 3290–3292 [3352–3354]
- Hamman, S. (C) 594–597 [604–607]
- Hampe, O. (C) 3823–3827 [3911–3915]
- Hampel, F. (C) 5537–5540 [5653–5656]
- Hampel, N. (C) 5402–5405 [5518–5521]
- Han, B.
– Desulfurization of Flue Gas: SO_2 Absorption by an Ionic Liquid (C) 2415–2417 [2469–2471]
DOI: 10.1002/anie.200353437
- Pd Nanoparticles Immobilized on Molecular Sieves by Ionic Liquids: Heterogeneous Catalysts for Solvent-Free Hydrogenation (C) 1397–1399 [1421–1423]
DOI: 10.1002/anie.200352682
- Han, Q. (C) 3177–3182 [3239–3244]
- Han, S. W. (C) 1246–1249 [1266–1269]
- Han, X. (C) 6377–6381 [6537–6541]
- Hanamoto, T.
– Crystal Structure of a Dewar Benzene Derivative Formed from Fluoro(triisopropylsilyl)acetylene (C) 3582–3584 [3666–3668]
DOI: 10.1002/anie.200454174
- Hanashima, S. (C) 5674–5677 [5792–5795]
- Hancock, F. E. (C) 1685–1688 [1717–1720]
- Haneline, M. R. (C) 5471–5474 [5587–5590]
- Hanessian, S.
– Antibacterial Aminoglycosides with a Modified Mode of Binding to the Ribosomal-RNA Decoding Site (C) 6735–6738 [6903–6906]
DOI: 10.1002/anie.200462092
- Hannam, J. S. (C) 3260–3264 [3322–3326]
- Hansen, A. G. (C) 198–203 [200–205]
- Hansen, H. R. (C) 337–340 [341–344]
- Hanson, S. R. (R) 3526–3548 [3610–3632], 5736–5763 [5858–5886]
- Hao, Y. (C) 6719–6722 [6887–6890]
- Haque, S. A. (C) 1417–1419 [1441–1443]
- Hara, M.
– A Carbon Material as a Strong Protonic Acid (C) 2955–2958 [3015–3018]
DOI: 10.1002/anie.200453947
- Harada, N. (C) 3167–3171 [3229–3233]
- Harada, R. (C) 1825–1828 [1861–1864]
- Harder, S.
– The Chemistry of Ca^{II} and Yb^{II} : Astonishingly Similar But Not Equal! (C) 2714–2718 [2768–2773]
DOI: 10.1002/anie.200353557



- Harding, L. P. (C) 4515–4518 [4615–4618]
 Hardman, N. J. (C) 1955–1958 [1989–1992]
 Harling, J. D. (C) 2293–2296 [2343–2346]
 Harmer, J. (C) 2567–2570 [2621–2624],
 4093–4097 [4185–4189]
 Harmjanz, M. (C) 485–490 [491–496]
 Harriman, A.
 – Unusually Slow Charge Recombination in
 Molecular Dyads
 (H) 4985–4987 [5093–5095]
 DOI: 10.1002/anie.200301762
 Harrington, R. W. (C) 1814–1817 [1850–
 1853]
 Harris, J. R. (C) 3192–3195 [3255–3257]
 Hartig, J. R. (C) 3186–3189 [3248–3252]
 Hartline, E. L. (C) 4924–4928 [5032–5036]
 Hartmann, M.
 – Hierarchical Zeolites: A Proven Strategy
 to Combine Shape Selectivity with Effi-
 cient Mass Transport
 (H) 5880–5882 [6004–6006]
 DOI: 10.1002/anie.200406044
 Hartung, I. V. (R) 1934–1949 [1968–1984]
 Hartwich, G. (C) 3482–3485 [3564–3567]
 Hartwig, J. F.
 – Enantioselective Allylation of Aromatic
 Amines after In Situ Generation of an
 Activated Cyclometalated Iridium Catalyst
 (C) 4797–4800 [4901–4904]
 DOI: 10.1002/anie.200406026
 – Iridium-Catalyzed Intermolecular Allylic
 Etherification with Aliphatic Alkoxides:
 Asymmetric Synthesis of Dihydropyrans
 and Dihydrofurans
 (C) 4794–4797 [4898–4901]
 DOI: 10.1002/anie.200406024
 – Rhodium Silyl Boryl Hydride Complexes:
 Comparison of Bonding and the Rates of
 Elimination of Borane, Silane, and Dihy-
 drogen
 (C) 5474–5477 [5590–5593]
 DOI: 10.1002/anie.200406040
 Haruta, M.
 – A Three-Dimensional Mesoporous Titano-
 silicate Support for Gold Nanoparticles:
 Vapor-Phase Epoxidation of Propene with
 High Conversion
 (C) 1546–1548 [1572–1574]
 DOI: 10.1002/anie.200352900
 Haruta, M. (C) 2129–2132 [2181–2184]
 Harvey, I. (C) 5914–5918 [6040–6044]
 Harvey, J. N. (R) 5896–5911 [6020–6036]
 Hasegawa, M. (C) 4874–4876 [4982–4984]
 Hasegawa, T. (C) 3279–3283 [3341–3345]
 Hashimoto, H. (C) 218–221 [220–223], 221–
 224 Corrigendum: 3096 [223–226 Corri-
 gendum: 3158]
 Hashimoto, S.
 – A New Dirhodium(II) Carboxamidate
 Complex as a Chiral Lewis Acid Catalyst
 for Enantioselective Hetero-Diels–Alder
 Reactions
 (C) 2665–2668 [2719–2722]
 DOI: 10.1002/anie.200453821
 Hashimoto, Y. (C) 1559–1562 [1585–1588]
 Hashmi, A. S. K.
 – Gold Catalysis: The Benefits of N and N,O
 Ligands
 (C) 6545–6547 [6707–6709]
 DOI: 10.1002/anie.200406032
 Hatano, S. (C) 6500–6505 [6662–6667]
 Hatano, T. (C) 465–469 [471–475]
 Hauer, B.
 – Industrial Methods for the Production of
 Optically Active Intermediates
 (R) 788–824 [806–843]
 DOI: 10.1002/anie.200300599
 Haupt, E. T. K. (C) 4466–4470 Corrigen-
 dum: 5115 [4566–4570 Corrigendum:
 5225]
 Hauseler, A. (C) 2924–2928 [2984–2988]
 Hauser, A. (C) 245–247 [247–249]
 Hauser, H. (C) 4653–4656 [4753–4756]
 Hawker, C. J.
 – Efficiency and Fidelity in a Click-Chemis-
 try Route to Triazole Dendrimers by the
 Copper(I)-Catalyzed Ligation of Azides
 and Alkynes
 (C) 3928–3932 [4018–4022]
 DOI: 10.1002/anie.200454078
 Hawkins, J. M.
 – Asymmetric Catalysis in the Pharmaceu-
 tical Industry
 (E) 3224–3228 [3286–3290]
 DOI: 10.1002/anie.200330072
 Hawthorne, M. F.
 – B-Octamethyl-[12]Mercuracarborand-4 as
 Host for “Naked” Fluoride Ions
 (C) 1854–1857 [1890–1893]
 DOI: 10.1002/anie.200352899
 Hayashi, M. (C) 70–74 [72–76]
 Hayashi, S. (C) 2955–2958 [3015–3018]
 Hayashi, T.
 – Asymmetric Synthesis of Diarylmethyl
 Amines by Rhodium-Catalyzed Asymmet-
 ric Addition of Aryl Titanium Reagents to
 Imines
 (C) 6125–6128 [6251–6254]
 DOI: 10.1002/anie.200461338
 Hayashi, Y.
 – Direct Proline-Catalyzed Asymmetric α -
 Aminoxylation of Ketones
 (C) 1112–1115 [1132–1135]
 DOI: 10.1002/anie.200353085
 Hayen, A. (C) 505–510 [511–516]
 Hayes, J. F. (C) 6517–6519 [6679–6681]
 Haynes, R. K.
 – Highly Antimalaria-Active Artemisinin
 Derivatives: Biological Activity Does Not
 Correlate with Chemical Reactivity
 (C) 1381–1385 [1405–1409]
 DOI: 10.1002/anie.200352343
 Haywood, M. G. (C) 6157–6160 [6283–6286]
 Hazarika, P. (C) 6469–6471 [6631–6633]
 He, Chengjiang (C) 3571–3574 [3655–3658]
 He, Chuan
 – A Silver-Catalyzed Intramolecular Amida-
 tion of Saturated C–H Bonds
 (C) 4210–4212 [4306–4308]
 DOI: 10.1002/anie.200454243
 He, K. (C) 5834–5836 [5958–5960]
 He, Q. (C) 988–990 [1006–1008]
 Heath, J. R.
 – Molecular-Mechanical Switch-Based
 Solid-State Electrochromic Devices
 (C) 6486–6491 [6648–6653]
 DOI: 10.1002/anie.200461723
 Heath, S. L.
 – Building Molecular Minerals: All Ferric
 Pieces of Molecular Magnetite
 (C) 5772–5775 Corrigendum: 6581 [5896–
 5899 Corrigendum: 6743]
 DOI: 10.1002/anie.200460636
 – How Do Clusters Grow? The Synthesis
 and Structure of Polynuclear Hydroxide
 Gallium(III) Clusters
 (C) 4037–4041 [4129–4133]
 DOI: 10.1002/anie.200353542
 Heath, S. L. (C) 1814–1817 [1850–1853],
 6132–6135 [6258–6261]
 Heaton, B. T. (C) 90–94 [92–96]
 Hechavarria Fonseca, M. T. (C) 3958–3960
 [4048–4050], 6660–6662 [6829–6832]
 Heckmann, A. (C) 5851–5856 [5976–5981]
 Heeres, A. (C) 1663–1667 [1695–1699]
 Hegetschweiler, K.
 – Rhenium–Chalcogenide–Cyano Clusters,
 Cu²⁺ Ions, and 1,2,3,4-Tetraaminobutane as
 Molecular Building Blocks for Chiral
 Coordination Polymers
 (C) 1297–1300 [1317–1321]
 DOI: 10.1002/anie.200351595
 – Strong Ferromagnetic Interactions in
 [V₈O₁₄(H₂taci)₂]: An Unprecedented
 Large Spin Ground State for a Vanadyl
 Cluster
 (C) 3436–3439 [3518–3521]
 DOI: 10.1002/anie.200454130
 Heide, L. (C) 67–70 [69–72]
 Hein, S. (C) 5697–5700 [5816–5819]
 Heinemann, F. W. (C) 1877–1880 [1913–
 1916], 3141–3144 [3203–3206]
 Heinz, H. (C) 2239–2243 [2289–2293]
 Heinze, J.
 – Imaging Concentration Profiles of Redox-
 Active Species with Nanometric Ampero-
 metric Probes: Effect of Natural Convec-
 tion on Transport at Microdisk Electrodes
 (C) 1431–1435 [1455–1459]
 DOI: 10.1002/anie.200352662
 Heinze-Brückner, G. (C) 4466–4470 Corri-
 gendum: 5115 [4566–4570 Corrigendum:
 5225]
 Heiser, U. F. (C) 245–247 [247–249]
 Heitmann, B. (C) 5649–5651 [5767–5769]
 Hell, S. W.
 – Absolute Optical Cross Section of Individ-
 ual Fluorescent Molecules
 (C) 6646–6649 [6814–6818]
 DOI: 10.1002/anie.200461337
 Hellbach, B. (C) 5846–5849 [5970–5973]
 Heller, A. (C) 6355–6357 [6515–6517]
 Heller, B.
 – Cobalt(I)-Catalyzed Asymmetric [2 + 2 +
 2] Cycloaddition of Alkynes and Nitriles:
 Synthesis of Enantiomerically Enriched
 Atropoisomers of 2-Arylpyridines
 (C) 3795–3797 [3883–3886]
 DOI: 10.1002/anie.200454164
 Helmchen, G.
 – Regio- and Enantioselective Iridium-Cata-
 lyzed Allylic Alkylation with In Situ Acti-
 vated P,C-Chelate Complexes
 (C) 4595–4597 [4695–4698]
 DOI: 10.1002/anie.200460016
 Helmke, E. (C) 1281–1283 [1301–1303]
 Hembury, G. A. (C) 5481–5485 [5597–5601]
 Henkel, G. (C) 2843–2846 [2903–2906]
 Hennecke, U. (C) 1848–1851 [1884–1887]
 Herber, C. (C) 3790–3792 [3878–3880]
 Herbst-Irmer, R. (C) 2142–2145 [2194–
 2197], 5534–5536 [5650–5652], 6190–
 6192 [6316–6318], 6192–6196 [6318–
 6322]
 Herdtweck, E. (C) 2234–2239 [2284–2289],
 4888–4892 [4996–5000], 5530–5534
 [5646–5650]
 Herges, R. (C) 5831–5833 [5955–5957]
 Hermann, B. A.
 – Second-Order Templatation: Ordered De-
 position of Supramolecular Squares on a
 Chloride-Covered Cu(100) Surface
 (C) 1291–1294 [1311–1314]
 DOI: 10.1002/anie.200352968
 Hermann, H. (C) 2444–2446 [2498–2500]

- Hermann, T.
– Monitoring Molecular Recognition of the Ribosomal Decoding Site (C) 3177–3182 [3239–3244]
DOI: 10.1002/anie.200454217
- Hernández-Maldonado, A. J. (C) 1004–1006
Corrigendum: 2321 [1022–1024 Corrigendum: 2373]
- Hernando, J. (C) 4045–4049 [4137–4141]
- Herrera, J. M. (C) 5468–5471 [5584–5587]
- Herrmann, C. (C) 450–454 [456–460], 454–458 [460–464]
- Herz, L. M. (C) 1976–1979 [2010–2013]
- Herzog, A. (C) 1854–1857 [1890–1893]
- Hessel, V.
– Chemistry in Microstructured Reactors (R) 406–446 [410–451]
DOI: 10.1002/anie.200300577
- Hessler, E. (C) 1731–1734 [1763–1766]
- Hett, R. (C) 5933–5936 [6059–6062]
- Hettche, F. (C) 2152–2154 [2204–2206]
- Hevia, E. (C) 1709–1712 [1741–1744]
- Hibble, S. J.
– Copper(I) Cyanide: A Simple Compound with a Complicated Structure and Surprising Room-Temperature Reactivity (C) 628–630 [638–640]
DOI: 10.1002/anie.200352844
- Hickey, S. G. (C) 458–462 [464–468]
- Hiebl, K.
– Gd₂Si₂B₈: A Ternary Rare-Earth-Metal Silicide Boride Compound (C) 1979–1983 [2013–2017]
DOI: 10.1002/anie.200352468
- Hiemstra, H.
– A Staudinger Approach towards Binol-Derived MAP-Type Bidentate P,N Ligands (C) 3471–3473 [3553–3555]
DOI: 10.1002/anie.200454146
- Hill, A. F.
– Heterobimetallic C₃ Complexes through Silylpropargylidene Desilylation (C) 476–478 [482–484]
DOI: 10.1002/anie.200352693
- Hill, C. L.
– Stable, Self-Assembling, Equilibrating Catalysts for Green Chemistry (H) 402–404 [406–408]
DOI: 10.1002/anie.200301701
- Hill, R. J. (C) 1851–1854 [1887–1890]
- Hinderberger, D. (C) 4616–4621 [4716–4721]
- Hinderlich, S.
– Synthesis and Biochemical Properties of Reversible Inhibitors of UDP-N-Acetylglucosamine 2-Epimerase (C) 4366–4370 [4467–4470]
DOI: 10.1002/anie.200453863
- Hino, S. (C) 2655–2658 [2709–2712]
- Hinrichs, H. (C) 4078–4081 [4170–4173]
- Hinrichs, W.
– Old Codons, New Amino Acids (H) 1190–1193 [1210–1213]
DOI: 10.1002/anie.200301720
- Hinrichsen, O. (C) 2839–2842 [2899–2903]
- Hipler, F. (C) 2839–2842 [2899–2903]
- Hirabayashi, T. (C) 1120–1123 [1140–1143]
- Hirahara, E. (C) 6327–6331 [6487–6491]
- Hirama, M.
– A Formal Total Synthesis of (+)-Pinnatoin A (C) 6505–6510 [6667–6672]
DOI: 10.1002/anie.200461802
- Spin Trapping of ¹³C-Labeled *p*-Benzynes Generated by Masamune–Bergman Cyclization of Bicyclic Nine-Membered Ene-dienes (C) 5249–5253 [5361–5365]
DOI: 10.1002/anie.200454133
- Synthesis of the C-1027 Chromophore Framework through Atropselective Macrolactonization (C) 6500–6505 [6662–6667]
DOI: 10.1002/anie.200461428
- Hirano, R. (C) 5780–5785 [5904–5909]
- Hirao, K. (C) 2230–2234 [2280–2284]
- Hiraoka, S. (C) 3814–3818 [3902–3906]
- Hirata, Kaori (C) 3814–3818 [3902–3906]
- Hirata, Kazumasa (C) 2389–2391 [2443–2445]
- Hirata, M. (C) 1270–1272 [1290–1292]
- Hiratani, T. (C) 5943–5946 [6069–6072]
- Hiroki, Y. (C) 882–884 [900–902]
- Hirota, S. (C) 334–337 [338–341]
- Hirsch, A.
– Molecular Peapods as Supramolecular Carbon Allotropes (H) 2326–2329 [2380–2383]
DOI: 10.1002/anie.200301749
- The First Account of a Structurally Persistent Micelle (C) 2959–2962 [3019–3022]
DOI: 10.1002/anie.200353510
- Hirsch, A. (C) 1552–1554 [1578–1580]
- Hiskey, M. A.
– 3,6-Di(azido)-1,2,4,5-Tetrazine: A Precursor for the Preparation of Carbon Nanospheres and Nitrogen-Rich Carbon Nitrides (C) 5658–5661 [5776–5779]
DOI: 10.1002/anie.200460708
- Polyazido High-Nitrogen Compounds: Hydrazo- and Azo-1,3,5-triazine (C) 4924–4928 [5032–5036]
DOI: 10.1002/anie.200460366
- Hitchcock, P. B. (C) 1124–1126 [1144–1146], 4500–4504 [4600–4604], 5824–5827 [5948–5951]
- Hittinger, E. (C) 1808–1811 [1844–1847]
- Hitzbleck, J. (C) 5218–5220 [5330–5332]
- Hiyama, T.
– Nickel-Catalyzed Tandem Carbostannylation of Alkynes and 1,2-Dienes with Alkynylstannanes (C) 3448–3451 [3530–3533]
DOI: 10.1002/anie.200353649
- Hiyama, T. (C) 879–882 [897–900]
- Ho, C.-M. (C) 3303–3307 [3365–3369]
- Ho, W.-Y. (C) 1381–1385 [1405–1409]
- Höbartner, C. (C) 3922–3925 [4012–4015]
- Hochmuth, E. (C) 5933–5936 [6059–6062]
- Hoeben, F. J. M. (C) 74–78 [76–80], 1976–1979 [2010–2013]
- Hof, F. (C) 5056–5059 [5166–5169]
- Hoffmann, H. M. R.
– 8-Oxabicyclo[3.2.1]oct-6-en-3-ones: Application to the Asymmetric Synthesis of Polyoxygenated Building Blocks (R) 1934–1949 [1968–1984]
DOI: 10.1002/anie.200300622
- Hoffmann, R.
– A Claim on the Development of the Frontier Orbital Explanation of Electrocyclic Reactions (L) 6586–6590 [6748–6752]
DOI: 10.1002/anie.200461440
- Hoffmann, S. (C) 5352–5355 [5466–5469]
- Hoffmann, S. D. (M) 6242–6247 [6400–6406]
- Hoffmann-Röder, A.
– Synthesis and Properties of Allenic Natural Products and Pharmaceuticals (R) 1196–1216 [1216–1236]
DOI: 10.1002/anie.200300628
- Hoffmeister, D. (C) 2962–2965 [3022–3025]
- Hofkens, J.
– Probing the Influence of O₂ on Photo-induced Reversible Electron Transfer in Perylenediimide–Triphenylamine-Based Dendrimers by Single-Molecule Spectroscopy (C) 6116–6120 [6242–6246]
DOI: 10.1002/anie.200460560
- Höfle, G.
– Isolation, Crystal and Solution Structure Determination, and Biosynthesis of Tubulysins—Powerful Inhibitors of Tubulin Polymerization from Myxobacteria (C) 4888–4892 [4996–5000]
DOI: 10.1002/anie.200460147
- Höfle, G. (C) 4163–4167 [4257–4262]
- Hofmann, H.-J.
– Mixed Helices—A General Folding Pattern in Homologous Peptides? (C) 1594–1597 [1621–1624]
DOI: 10.1002/anie.200353249
- Hofmann, M. Corrigendum: 2737
- Hofmann, M. (C) 5402–5405 [5518–5521]
- Hofstetter, H. (C) 2395–2399 [2449–2453]
- Hofstetter, K. (C) 2163–2166 [2215–2218]
- Hofstetter, O. (C) 2395–2399 [2449–2453]
- Hogg, L. (C) 1218–1221 [1238–1241]
- Holle, S. (C) 2850–2852 [2910–2913]
- Holman, K. T.
– Isolation and Structure of an “Imploded” Cryptophane (C) 5631–5635 [5749–5753]
DOI: 10.1002/anie.200460866
- Holmes, I. P.
– Chemically Catalyzed Asymmetric Cyano-hydrin Syntheses (R) 2752–2778 [2810–2837]
DOI: 10.1002/anie.200300604
- Holthausen, M. C.
– Combined Spectroscopic and Theoretical Evidence for a Persistent End-On Copper Superoxo Complex (C) 4360–4363 [4460–4464]
DOI: 10.1002/anie.200454125
- Hom, L. G. (C) 2106–2108 [2158–2160]
- Homans, S. W.
– NMR Spectroscopy Tools for Structure-Aided Drug Design (R) 290–300 [292–303]
DOI: 10.1002/anie.200300581
- Homans, S. W. (C) 3918–3922 [4008–4012]
- Honda, Y. (C) 3044–3047 [3106–3109]
- Hong, H. (C) 2551–2553 [2605–2607]
- Hong, J. (C) 2417–2420 [2471–2474]
- Hong, J.-I.
– A Fluorescent Pyrophosphate Sensor with High Selectivity over ATP in Water (C) 4777–4780 [4881–4884]
DOI: 10.1002/anie.200453914
- Hong, K. (C) 5785–5789 [5909–5913]
- Hong, M.-C.
– Copper Complex Cation Templated Gadolinium(III)–Isophthalate Frameworks (C) 5665–5668 [5783–5786]
DOI: 10.1002/anie.200460919
- Honma, I.
– A Biopolymer Composite Material as an Anhydrous Proton-Conducting Membrane

- (C) 3688–3691 [3774–3777]
DOI: 10.1002/anie.200353176
- Hopf, H.
– Editorial: Discovering Classics or Writing, Reading, and Resonance
2046–2047 [2094–2095]
DOI: 10.1002/anie.200490045
- Höpf, H.
– A 3D Hybrid Network Containing Large Spherical Cavities Formed through a Combination of Metal Coordination and Hydrogen Bonding
(C) 1507–1511 [1533–1537]
DOI: 10.1002/anie.200352862
- Modification of 2D Water That Contains Hexameric Units in Chair and Boat Conformations—A Contribution to the Structural Elucidation of Bulk Water
(C) 3041–3044 [3103–3106]
DOI: 10.1002/anie.200453957
- Hoppe, D.
– Highly Enantiomerically Enriched Ketone Homoenolate Reagents Prepared by (–)-Sparteine-Mediated γ -Deprotonation of Achiral 1-Alkenyl Carbamates
(C) 1423–1427 [1447–1451]
DOI: 10.1002/anie.200352966
- Synthesis of Stereohomogeneous Cyclopropanecarbaldehydes and Cyclopropyl Ketones by Cycloalkylation of 4-Hydroxy-1-alkenyl Carbamates
(C) 6667–6669 [6836–6838]
DOI: 10.1002/anie.200461136
- Höppe, H. A. (C) 5540–5542 [5656–5659]
- Hori, A. (C) 5016–5019 [5126–5129]
- Horne, D. A.
– Preparation and Synthetic Applications of 2-Halotryptophan Methyl Esters: Synthesis of Spirotryprostatin B
(C) 5357–5360 [5471–5474]
DOI: 10.1002/anie.200460419
- Hörnig, J. (C) 1011–1014 [1029–1032]
- Horoszewski, D. (M) 5446–5453 [5562–5570]
- Hoshino, T.
– Deletion of the Gly600 Residue of *Allylcyclobacillus acidocaldarius* Squalene Cyclase Alters the Substrate Specificity into that of the Eukaryotic-Type Cyclase Specific to (3S)-2,3-Oxidosqualene
(C) 6700–6703 [6868–6871]
DOI: 10.1002/anie.200461523
- Hosmane, N. S. (C) 4940–4943 [5048–5051]
- Hosokawa, S. (C) 3175–3177 [3237–3239]
- Hosomi, A.
– Cascade Carbonylation Methods Leading to β -Diketones and β -Functionalized δ -Diketones
(C) 2423–2425 [2477–2479]
DOI: 10.1002/anie.200453702
- Hostettler, M. (C) 4589–4594 [4689–4695]
- Hou, J. G. (C) 6479–6482 [6641–6644]
- Houillon, F. B. (C) 6165–6169 [6291–6295]
- Houk, K. N.
– Computational Evidence for the Enamine Mechanism of Intramolecular Aldol Reactions Catalyzed by Proline
(C) 5766–5768 [5890–5892]
DOI: 10.1002/anie.200460916
- Hoveyda, A. H.
– Primo Levi's *The Periodic Table*. A Search for Patterns in Times Past
(E) 6592–6594 [6754–6757]
DOI: 10.1002/anie.200460464
- Howard, J. A. K. (C) 6553–6557 [6715–6719]
- Howorka, S.
– Stochastic Detection of Monovalent and Bivalent Protein–Ligand Interactions
(C) 842–846 [860–864]
DOI: 10.1002/anie.200352614
- Hsu, W. K. (C) 5670–5674 [5788–5792]
- Hsung, R. P.
– A Tandem Epoxidation/Stereoselective Intramolecular [4 + 3] Cycloaddition Reaction Involving Nitrogen-Stabilized Oxyallyl Cations Derived from Chiral Allenamides
(C) 615–618 [625–628]
DOI: 10.1002/anie.200352632
- Hu, A. Corrigendum: 1043
- Hu, A. (C) 2501–2504 [2555–2558]
- Hu, C.-W. (C) 5036–5040 [5146–5150]
- Hu, G. (C) 3452–3456 [3534–3538]
- Hu, J.-S. (C) 1540–1543 [1566–1569]
- Hu, Jinbo (C) 5203–5206 [5315–5318]
- Hu, Junqing
– Sn-Filled Single-Crystalline Wurtzite-Type ZnS Nanotubes
(C) 4606–4609 [4706–4709]
DOI: 10.1002/anie.200454205
- Synthesis of Crystalline Silicon Tubular Nanostructures with ZnS Nanowires as Removable Templates
(C) 63–66 [65–68]
DOI: 10.1002/anie.200352483
- Hu, Q. (C) 2259–2263 [2309–2313]
- Hu, T.-S. (C) 329–334 [333–338]
- Hu, W. (C) 6713–6716 [6881–6884]
- Hu, X.-D. (C) 1702–1705 [1734–1737]
- Hu, X.-L. (C) 1410–1414 [1434–1438]
- Hu, Xiaohong (C) 733–736 [751–754]
- Hu, Xile (C) 3156–3159 [3218–3221]
- Hu, Yong (C) 6369–6372 [6529–6532]
- Hu, Yueqing (C) 2822–2826 [2882–2886]
- Hua, F. (C) 6471–6474 [6633–6636]
- Huang, C.-Y. (C) 1000–1003 [1018–1021]
- Huang, H. (C) 5635–5638 [5753–5756]
- Huang, Jiaying (C) 5817–5821 [5941–5945]
- Huang, Jun (C) 1397–1399 [1421–1423], 2415–2417 [2469–2471]
- Huang, K. (C) 6482–6485 [6644–6647]
- Huang, L. (C) 5221–5224 [5333–5336]
- Huang, S. (C) 5635–5638 [5753–5756]
- Huang, X.
– Iterative One-Pot Synthesis of Oligosaccharides
(C) 5221–5224 [5333–5336]
DOI: 10.1002/anie.200460176
- Huang, X.-C. (C) 206–209 [208–211]
- Huang, Y.-H. (C) 990–994 [1008–1012]
- Huang, Z. (C) 5776–5779 [5900–5903]
- Hubberstey, P.
– Non-Natural Eight-Connected Solid-State Materials: A New Coordination Chemistry
(C) 1851–1854 [1887–1890]
DOI: 10.1002/anie.200352625
- Huber, G. W. (C) 1549–1551 [1575–1577]
- Huber, R. (C) 1845–1847 [1881–1883]
- Huber, S. (C) 6738–6742 [6906–6910]
- Huck, W. T. S.
– Forced Peptide Synthesis in Nanoscale Confinement under Elastomeric Stamps
(C) 4190–4193 [4286–4289]
DOI: 10.1002/anie.200460271
- Hud, N. V.
– Enzymatic Behavior by Intercalating Molecules in a Template-Directed Ligation Reaction
(C) 2004–2008 [2038–2042]
DOI: 10.1002/anie.200353155
- Hudlicky, T.
– A β -Carboline-1-one Mimic of the Anticancer *Amaryllidaceae* Constituent Pancratistatin: Synthesis and Biological Evaluation
(C) 5342–5346 [5456–5460]
DOI: 10.1002/anie.200460218
- Hudson, T. A. (C) 6157–6160 [6283–6286]
- Huffman, J. C. (C) 3156–3159 [3218–3221]
- Hughes, C. E. (C) 3443–3445 [3525–3527]
- Hughes, D. J. (C) 3025–3029 [3087–3091]
- Hughes, D. L. (C) 2166–2169 [2218–2222]
- Hugl, H. (C) 5255–5260 [5367–5372]
- Hultsch, K. C.
– Hydroamination/Cyclization of Aminoalkenes Using Cationic Zirconocene and Titanocene Catalysts
(C) 5542–5546 Corrigendum: 6581 [5659–5663 Corrigendum: 6743]
DOI: 10.1002/anie.200460880
- Humphrey, S. M. (C) 3067–3069 [3129–3131]
- Hüniger, U. (C) 1104–1107 [1125–1128]
- Hunter, C. A.
– Quantifying Intermolecular Interactions: Guidelines for the Molecular Recognition Toolbox
(R) 5310–5324 [5424–5439]
DOI: 10.1002/anie.200301739
- Hunter, D. J. B. (C) 5914–5918 [6040–6044]
- Hunter, R. (C) 1389–1392 [1413–1416]
- Hurezeanu, R. (C) 704–707 [722–725]
- Hursthouse, M. B. (C) 472–475 [478–481]
- Hüsing, N.
– Ordered Porous Nanoarchitectures with Specific Functions
(T) 3216–3217 [3278–3279]
DOI: 10.1002/anie.200460497
- Huskens, J.
– Writing Patterns of Molecules on Molecular Printboards
(C) 369–373 [373–377]
DOI: 10.1002/anie.200352767
- Hussain, F. (C) 3485–3488 [3567–3571]
- Hussey, S. L. (C) 5181–5185 Corrigendum: 5428 [5293–5297 Corrigendum: 5542]
- Hutchings, G. J.
– Heterogeneous Enantioselective Catalyzed Carbonyl- and Imino-Ene Reactions using Copper Bis(Oxazoline) Zeolite Y
(C) 1685–1688 [1717–1720]
DOI: 10.1002/anie.200352534
- Hutin, M. (C) 6724–6727 [6892–6895]
- Huynh, M.-H. V.
– 3,6-Di(azido)-1,2,4,5-Tetrazine: A Precursor for the Preparation of Carbon Nanospheres and Nitrogen-Rich Carbon Nitrides
(C) 5658–5661 [5776–5779]
DOI: 10.1002/anie.200460708
- Polyazido High-Nitrogen Compounds: Hydrazo- and Azo-1,3,5-triazine
(C) 4924–4928 [5032–5036]
DOI: 10.1002/anie.200460366
- Hwang, J.-S. (C) 2819–2822 [2879–2882]
- Hwang, Y. (C) 2282–2285 [2332–2335]
- Hyeon, T.
– Novel Synthesis of Magnetic Fe₂P Nanorods from Thermal Decomposition of Continuously Delivered Precursors using a Syringe Pump
(C) 2282–2285 [2332–2335]
DOI: 10.1002/anie.200353562



- Ibrahim, I. (C) 6528–6531 [6690–6693], 6532–6535 [6694–6697]
- Ichikawa, T. (C) 5971–5973 [6097–6099]
- Ichinohe, M. (C) 6703–6705 [6871–6873]
- Ichinose, K. (C) 2962–2965 [3022–3025]
- Iddon, P. D. (C) 1389–1392 [1413–1416]
- Iggo, J. A.
- The Complete Delineation of the Initiation, Propagation, and Termination Steps of the Carbomethoxy Cycle for the Carbalkoxylation of Ethene by Pd–Diphosphane Catalysts (C) 90–94 [92–96]
DOI: 10.1002/anie.200352369
- Iglesia, E.
- Structural and Mechanistic Requirements for Methane Activation and Chemical Conversion on Supported Iridium Clusters (C) 3685–3688 [3771–3774]
DOI: 10.1002/anie.200352703
- Ihara, H. (C) 465–469 [471–475]
- Ihata, O. (C) 717–719 [735–737]
- Ikariya, T.
- ^{13}C NMR Spectroscopic Evaluation of the Affinity of Carbonyl Compounds for Carbon Dioxide under Supercritical Conditions (C) 3719–3722 [3805–3808]
DOI: 10.1002/anie.200454190
 - Synthesis of Thermoresponsive Polyurethane from 2-Methylaziridine and Supercritical Carbon Dioxide (C) 717–719 [735–737]
DOI: 10.1002/anie.200352215
- Ikeda, Takayuki (C) 228–232 [230–234]
- Ikeda, Takuji
- The Topotactic Conversion of a Novel Layered Silicate into a New Framework Zeolite (C) 4892–4896 [5000–5004]
DOI: 10.1002/anie.200460168
- Ikeda, Y.
- ^{13}C NMR Spectroscopic Evaluation of the Affinity of Carbonyl Compounds for Carbon Dioxide under Supercritical Conditions (C) 3719–3722 [3805–3808]
DOI: 10.1002/anie.200454190
- Iki, N.
- Octalanthanide Wheels Supported by *p*-*tert*-Butylsulfonylcalix[4]arene (C) 1832–1835 [1868–1871]
DOI: 10.1002/anie.200353449
- Ikoma, T. (C) 6691–6695 [6859–6863]
- Ikonnikov, N. S. (C) 4085–4089 [4177–4181]
- Ikuma, N. (C) 3677–3682 [3763–3768]
- Ikumi, A. (C) 6180–6182 [6306–6308]
- Ikuta, H. (C) 1966–1969 [2000–2003]
- Imahori, H.
- Production of an Ultra-Long-Lived Charge-Separated State in a Zinc Chlorin– C_{60} Dyad by One-Step Photoinduced Electron Transfer (C) 853–856 [871–874]
DOI: 10.1002/anie.200352870
- Imai, Hiroaki
- Emergence of Morphological Chirality from Twinned Crystals (C) 1363–1368 [1387–1392]
DOI: 10.1002/anie.200352891
- Imai, Hiroyuki (C) 5618–5621 [5736–5739]
- Imai, N. (C) 1376–1381 [1400–1405]
- Imbert, A.
- Crystal Structure of Tricolorin A: Molecular Rationale for the Biological Properties of Resin Glycosides Found in Some Mexican Herbal Remedies (C) 5918–5922 [6044–6048]
DOI: 10.1002/anie.200460327
- Imoto, T. (C) 5780–5785 [5904–5909]
- Imperiali, B.
- Structural Origin of the High Affinity of a Chemically Evolved Lanthanide-Binding Peptide (C) 3682–3685 [3768–3771]
DOI: 10.1002/anie.200460028
- In, J.-H. (C) 2417–2420 [2471–2474]
- Inamori, K.-i. (C) 5674–5677 [5792–5795]
- Inanaga, J. (C) 3582–3584 [3666–3668]
- Inazu, T. (C) 5019–5022 [5129–5132]
- Incarvito, C. D. (C) 5474–5477 [5590–5593]
- Innocenti, P. (C) 3445–3448 [3527–3530]
- Inoue, K.
- Three-Dimensional Chiral Molecule-Based Ferrimagnet with Triple-Helical Strand Structure (C) 5618–5621 [5736–5739]
DOI: 10.1002/anie.200460867
- Inoue, K. (C) 6474–6479 [6636–6641]
- Inoue, Masayuki
- A Formal Total Synthesis of (+)-Pinnatoin A (C) 6505–6510 [6667–6672]
DOI: 10.1002/anie.200461802
 - Synthesis of the C-1027 Chromophore Framework through Atropselective Macrolactonization (C) 6500–6505 [6662–6667]
DOI: 10.1002/anie.200461428
- Inoue, Masayuki (C) 5249–5253 [5361–5365]
- Inoue, Munenori (C) 4207–4209 [4303–4305]
- Inoue, Y.
- Rationalization of Supramolecular Chirality in a Bisporphyrin System (C) 5481–5485 [5597–5601]
DOI: 10.1002/anie.200460965
- Intini, F. P. (C) 5081–5084 [5191–5194]
- Ioffe, I. N. (C) 997–1000 [1015–1018]
- Irlinger, B. (C) 1098–1100 [1119–1121]
- Irschik, H. (C) 4163–4167 [4257–4262]
- Ishida, S. (C) 4510–4512 [4610–4612]
- Ishida, T. (C) 711–714 [729–732]
- Ishihara, K. (C) 994–997 [1012–1015], 1983–1986 [2017–2020]
- Ishihara, T. (C) 1966–1969 [2000–2003]
- Ishii, K. (C) 6505–6510 [6667–6672]
- Ishii, Yasutaka
- A New Route to Lactam Precursors from Cycloalkanes: Direct Production of Nitrosocycloalkanes or Cycloalkanone Oximes by Using *tert*-Butyl Nitrite and *N*-Hydroxyphthalimide (C) 1120–1123 [1140–1143]
DOI: 10.1002/anie.200352741
- Ishii, Yusuke (C) 2702–2705 [2756–2759]
- Ishikawa, Yoko (C) 4944–4947 [5052–5055]
- Ishikawa, Yuji (C) 3167–3171 [3229–3233]
- Ishizuka, T. (C) 876–879 [894–897], 2951–2955 [3011–3015], 5077–5081 [5187–5191]
- Ismach, A. (C) 6140–6143 [6266–6269]
- Ismagilov, R. F.
- A Droplet-Based, Composite PDMS/Glass Capillary Microfluidic System for Evaluating Protein Crystallization Conditions by Microbatch and Vapor-Diffusion Methods with On-Chip X-Ray Diffraction (C) 2508–2511 [2562–2565]
DOI: 10.1002/anie.200453974
 - Minimal Functional Model of Hemostasis in a Biomimetic Microfluidic System (C) 1531–1536 [1557–1562]
DOI: 10.1002/anie.200353428
- Isobe, K.
- Activation of C–Cl and C–H Bonds by Ligated S_2^{2-} Ions: Conversion of Organic Chlorides into Organosulfur Compounds in *cis*-[$(\text{IrCp}^*)_2(\mu\text{-CH}_3)_2(\mu\text{-S}_2\text{R})$] $^+$ (C) 213–215 [215–217]
DOI: 10.1002/anie.200351792
- Isobe, M.
- An Efficient Total Synthesis of Optically Active Tetrodotoxin (C) 4782–4785 [4886–4889]
DOI: 10.1002/anie.200460293
- Itaya, K.
- Controlled Molecular Orientation in an Adlayer of a Supramolecular Assembly Consisting of an Open-Cage C_{60} Derivative and Zn^{II} Octaethylporphyrin on Au(111) (C) 3044–3047 [3106–3109]
DOI: 10.1002/anie.200453959
- Itié, J.-P. (C) 3728–3731 [3814–3817]
- Ito, Hiroshi (C) 3171–3175 [3233–3237]
- Ito, Hirotugu (C) 994–997 [1012–1015]
- Ito, M. (C) 5618–5621 [5736–5739]
- Ito, O.
- Production of an Ultra-Long-Lived Charge-Separated State in a Zinc Chlorin– C_{60} Dyad by One-Step Photoinduced Electron Transfer (C) 853–856 [871–874]
DOI: 10.1002/anie.200352870
- Ito, O. (C) 3044–3047 [3106–3109], 4510–4512 [4610–4612]
- Ito, Takeo (C) 1839–1842 [1875–1878]
- Ito, Tasuku
- Observation and Dynamics of “Charge-Transfer Isomers” (C) 1376–1381 [1400–1405]
DOI: 10.1002/anie.200353221
 - Octalanthanide Wheels Supported by *p*-*tert*-Butylsulfonylcalix[4]arene (C) 1832–1835 [1868–1871]
DOI: 10.1002/anie.200353449
- Ito, Yuki (C) 106–108 [108–110]
- Ito, Yukishige
- Synthesis of a Bisubstrate-Type Inhibitor of *N*-Acetylglucosaminyltransferases (C) 5674–5677 [5792–5795]
DOI: 10.1002/anie.200460388
- Itoh, J. (C) 1566–1568 [1592–1594]
- Iversen, B. B. (C) 700–704 [718–722]
- Iwahori, F. (C) 4763–4767 [4867–4871]
- Iwamoto, T. (C) 4510–4512 [4610–4612]
- Iwamura, H. (C) 2099–2103 [2151–2155], 3317–3321 [3379–3383]
- Izuhara, T. (C) 4207–4209 [4303–4305]



- Jacobs, P. A. (L) 4562–4564 [4662–4664]
Jacobsen, E. N.
– General Catalytic Synthesis of Highly Enantiomerically Enriched Terminal Aziridines from Racemic Epoxides (C) 3952–3954 [4042–4044]
DOI: 10.1002/anie.200460369
- Jacobsen, H.
– “Heterogeneous” Chemistry: Catalysts for Hydrogen Production from Biomass (H) 1912–1914 [1948–1950]
DOI: 10.1002/anie.200301700
- Jacobsen, N. (C) 6713–6716 [6881–6884]
- Jagannadh, B.
– Left-Handed Helical Twists in “Mixed β -Peptides” Derived From Alternating C-Linked Carbo- β^3 -Amino Acids and β -hGly Units (C) 3961–3965 [4051–4055]
DOI: 10.1002/anie.200353467
- Jäger, S. (C) 3337–3340 [3399–3403]
- Jähnisch, K.
– Chemistry in Microstructured Reactors (R) 406–446 [410–451]
DOI: 10.1002/anie.200300577
- Jain, S. S. (C) 2004–2008 [2038–2042]
- Jaitner, P. (C) 5266–5268 [5378–5381]
- Jakalian, A. (C) 4306–4311 [4406–4411]
- Jalisatgi, S. S. (C) 1854–1857 [1890–1893], 3711–3715 [3797–3801]
- James, T. D.
– Chiral Binol–Bisboronic Acid as Fluorescence Sensor for Sugar Acids (C) 3461–3464 [3543–3546]
DOI: 10.1002/anie.200454033
- Jamet, H. (C) 594–597 [604–607]
- Jamison, T. F.
– Asymmetric Catalytic Coupling of Organoboranes, Alkynes, and Imines with a Removable (Trialkylsilyloxy)ethyl Group—Direct Access to Enantiomerically Pure Primary Allylic Amines (C) 3941–3944 [4031–4034]
DOI: 10.1002/anie.200460044
- Jana, N. R.
– Shape Effect in Nanoparticle Self-Assembly (C) 1536–1540 [1562–1566]
DOI: 10.1002/anie.200352260
- Jancik, V. (C) 1419–1421 [1443–1445], 2142–2145 [2194–2197], 5534–5536 [5650–5652], 6190–6192 [6316–6318], 6192–6196 [6318–6322]
- Janda, K. D.
– Synthesis and Biological Validation of a Ubiquitous Quorum-Sensing Molecule (C) 2106–2108 [2158–2160]
DOI: 10.1002/anie.200353150
- Jang, D.-J.
– Asymmetric Double Proton Transfer of Excited 1:1 7-Azaindole/Alcohol Complexes with Anomalous Large and Temperature-Independent Kinetic Isotope Effects (C) 5792–5796 [5916–5920]
DOI: 10.1002/anie.200461102
- Jang, J.
– Fabrication of Polymer Nanofibers and Carbon Nanofibers by Using a Salt-Assisted Microemulsion Polymerization (C) 3803–3806 [3891–3894]
DOI: 10.1002/anie.200353580
- Jang, S.-H. (C) 5328–5331 [5442–5445]
- Jansen, H. (C) 714–717 Corrigendum: 3748 [732–735 Corrigendum: 3834]
- Janser, I. (C) 6662–6666 [6832–6836]
- Janshoff, A. (C) 1101–1104 [1121–1124]
- Jardin, C. (C) 1979–1983 [2013–2017]
- Jardin, R. (C) 1979–1983 [2013–2017]
- Jarjays, O. (C) 594–597 [604–607]
- Jarrosson, T. (C) 1959–1962 [1993–1996]
- Jaspars, M. (C) 337–340 [341–344]
- Jayaprakash, P. (C) 3961–3965 [4051–4055]
- Jean, Y.
– A Bis(thiophosphinoyl)methanediide Palladium Complex: Coordinated Dianion or Nucleophilic Carbene Complex? (C) 6382–6385 [6542–6545]
DOI: 10.1002/anie.200461392
- Jeannerat, D. (C) 5181–5185 Corrigendum: 5428 [5293–5297 Corrigendum: 5542]
- Jeffery, J. C. (C) 4515–4518 [4615–4618]
- Jen, A. K.-Y.
– Ordered Self-Assembly and Electronic Behavior of C₆₀–Anthrylphenylacetylene Hybrid (C) 1512–1516 [1538–1542]
DOI: 10.1002/anie.200353001
- Jennings, M. C. (C) 969–971 [987–989]
- Jeong, B.-S. (C) 2382–2385 [2436–2439]
- Jeppesen, J. O. (C) 6486–6491 [6648–6653]
- Jerabek, K.
– Generation of Size-Controlled Pd⁰ Nanoclusters inside Nanoporous Domains of Gel-Type Resins: Diverse and Convergent Evidence That Supports a Strategy of Template-Controlled Synthesis (C) 959–962 [977–980]
DOI: 10.1002/anie.200352640
- Jerga, A. (C) 2948–2950 [3008–3010]
- Jeschke, G.
– Electrostatic Site Attachment of Divalent Counterions to Rodlike Ruthenium(II) Coordination Polymers Characterized by EPR Spectroscopy (C) 4616–4621 [4716–4721]
DOI: 10.1002/anie.200460500
- Jetti, R. K. R. (C) 1149–1155 [1169–1175]
- Jeulin, S. (C) 320–325 [324–329]
- Jew, S.-s.
– Highly Enantioselective Phase-Transfer-Catalytic Alkylation of 2-Phenyl-2-oxazoline-4-carboxylic Acid *tert*-Butyl Ester for the Asymmetric Synthesis of α -Alkyl Serines (C) 2382–2385 [2436–2439]
DOI: 10.1002/anie.200353496
- Jhung, S. H. (C) 2819–2822 [2879–2882]
- Jia, W.-L. (C) 2933–2936 [2993–2996]
- Jian, F.-F. Corrigendum: 14
- Jiang, B.
– Highly Enantioselective Construction of a Chiral Tertiary Carbon Center by Alkynylation of a Cyclic *N*-Acyl Ketimine: An Efficient Preparation of HIV Therapeutics (C) 216–218 [218–220]
DOI: 10.1002/anie.200352301
- Highly Enantioselective Construction of Fused Pyrrolidine Systems That Contain a Quaternary Stereocenter: Concise Formal Synthesis of (+)-Conessine (C) 2543–2546 [2597–2600]
DOI: 10.1002/anie.200353583
- Jiang, D.-L.
– Photoluminescence Properties of Discrete Conjugated Wires Wrapped within Dendrimeric Envelopes: “Dendrimer Effects” on π -Electronic Conjugation (C) 2943–2947 [3003–3007]
DOI: 10.1002/anie.200353519
- Jiang, F.-C. (C) 990–994 [1008–1012]
- Jiang, F.-L. (C) 5665–5668 [5783–5786]
- Jiang, K. (C) 4745–4750 [4849–4854]
- Jiang, Lasheng (C) 2121–2124 [2173–2176], 3724–3728 [3810–3814]
- Jiang, Lei
– A Lotus-Leaf-like Superhydrophobic Surface: A Porous Microsphere/Nanofiber Composite Film Prepared by Electrohydrodynamics (C) 4338–4341 [4438–4441]
DOI: 10.1002/anie.200460333
- A Super-Hydrophobic and Super-Oleophilic Coating Mesh Film for the Separation of Oil and Water (C) 2012–2014 [2046–2048]
DOI: 10.1002/anie.200353381
- Responsive Aligned Carbon Nanotubes (C) 4663–4666 [4763–4766]
DOI: 10.1002/anie.200460774
- Reversible Switching between Superhydrophilicity and Superhydrophobicity (C) 357–360 [361–364]
DOI: 10.1002/anie.200352565
- Self-Assembly of Large-Scale Micropatterns on Aligned Carbon Nanotube Films (C) 1146–1149 [1166–1169]
DOI: 10.1002/anie.200351988
- Jiang, N. (C) 2230–2234 [2280–2284]
- Jiang, P.
– Surface-Templated Nanostructured Films with Two-Dimensional Ordered Arrays of Voids (C) 5625–5628 [5743–5746]
DOI: 10.1002/anie.200460539
- Jiang, P. (Toulouse) (C) 2092–2095 [2144–2147]
- Jiang, P. (Univ. of Chicago) (C) 4471–4475 [4571–4575]
- Jiang, S. (C) 329–334 [333–338]
- Jiang, T. (C) 1397–1399 [1421–1423], 2415–2417 [2469–2471]
- Jiang, Xiongwei (C) 2230–2234 [2280–2284]
- Jiang, Xiquan
– Polymer–Monomer Pairs as a Reaction System for the Synthesis of Magnetic Fe₃O₄–Polymer Hybrid Hollow Nanospheres (C) 6369–6372 [6529–6532]
DOI: 10.1002/anie.200460408
- Jiao, F. (C) 5958–5961 [6084–6087]
- Jiao, H. (R) 3368–3398 [3448–3479]
- Jiao, K. Corrigendum: 14
- Jin, H. J. (C) 1675–1678 [1707–1710]
- Jin, Xianbo (C) 733–736 [751–754]
- Jin, Xianglin (C) 5977–5980 [6103–6106]
- Jin, Y. Z. (C) 5670–5674 [5788–5792]
- Jin, Yan (C) 5635–5638 [5753–5756]
- Jin, Yongdong Corrigendum: 3749
- Jin, Z.-H. (C) 1371–1373 [1395–1397]
- Jo, H. H. (C) 1115–1117 Corrigendum: 3749 [1135–1137 Corrigendum: 3834]
- Joachim, C. (C) 2092–2095 [2144–2147]
- Job, G. E. (C) 5649–5651 [5767–5769]

- Jobic, H.
– Accelerated Diffusion of Long-Chain Alkanes between Nanosized Cavities (C) 364–366 [368–370]
DOI: 10.1002/anie.200352691
- Jockel, J. (C) 752–754 [770–773]
- Johansson, M. P.
– Au₃₂: A 24-Carat Golden Fullerene (C) 2678–2681 [2732–2735]
DOI: 10.1002/anie.200453986
- Johnson, D. W.
– Arsenic- π Interactions Stabilize a Self-Assembled As₂L₃ Supramolecular Complex (C) 5831–5833 [5955–5957]
DOI: 10.1002/anie.200461011
- Johnson, J. S.
– Catalytic Asymmetric Acylation of (Silyl-oxy)nitrile Anions (C) 2652–2655 [2706–2709]
DOI: 10.1002/anie.200353354
- Catalyzed Reactions of Acyl Anion Equivalents (H) 1326–1328 [1348–1350]
DOI: 10.1002/anie.200301702
- Johnson II, C. A. (C) 5967–5971 [6093–6097]
- Johnson-Kerner, B. L. (C) 1531–1536 [1557–1562]
- Johnsson, M.
– Host–Guest Compounds in the Family of Tellurium–Nickel Oxohalogenides (C) 4292–4295 [4392–4395]
DOI: 10.1002/anie.200460001
- Jomaa, H. (C) 251–254 [254–257]
- Jones, B. A. (C) 6363–6366 [6523–6526]
- Jones, C. (C) 4626–4629 [4726–4729]
- Jones, Cameron
– Kinetic Control over the Thermal Stability of the In–H Bond: Synthesis and Characterization of Amido Indium Hydride Complexes (C) 3852–3855 [3940–3943]
DOI: 10.1002/anie.200460304
- Jones, Cameron (C) 1277–1279 [1297–1299]
- Jones, P. G. (C) 3970–3974 [4061–4064]
- Jongen, L. (C) 3183–3185 [3245–3248]
- Jonke, S. Corrigendum: 4389
- Jonkheijm, P. (C) 74–78 [76–80], 1976–1979 [2010–2013], 3422–3425 [3504–3507]
- Joppek, W. (C) 2444–2446 [2498–2500], 6657–6660 [6826–6829]
- Jordan, P. (C) 2512–2514 [2566–2568]
- Jørgensen, K. A.
– Direct Organocatalytic Enantioselective Mannich Reactions of Ketimines: An Approach to Optically Active Quaternary α -Amino Acid Derivatives (C) 4476–4478 [4576–4578]
DOI: 10.1002/anie.200460158
- Highly Enantio- and Diastereoselective Organocatalytic Asymmetric Domino Michael–Aldol Reaction of β -Ketoesters and α,β -Unsaturated Ketones (C) 1272–1277 [1292–1297]
DOI: 10.1002/anie.200353364
- Highly Enantioselective Direct Organocatalytic α -Chlorination of Ketones (C) 5507–5510 [5623–5626]
DOI: 10.1002/anie.200460462
- Joselevich, E.
– Atomic-Step-Templated Formation of Single Wall Carbon Nanotube Patterns (C) 6140–6143 [6266–6269]
DOI: 10.1002/anie.200460356
- Chemistry and Electronics of Carbon Nanotubes Go Together (H) 2992–2994 [3052–3054]
DOI: 10.1002/anie.200301715
- Josephson, L.
– Magnetic Relaxation Switch Immunosen-sors Detect Enantiomeric Impurities (C) 2395–2399 [2449–2453]
DOI: 10.1002/anie.200352998
- Joshi, N. S. (C) 5827–5830 [5951–5954]
- Journaux, Y.
– A Cu^{II}Co^{II} Metallacyclopentane-Based Metamagnet with a Corrugated Brick-Wall Sheet Architecture (C) 956–958 [974–976]
DOI: 10.1002/anie.200352604
- Rational Design of an Enneanuclear Copper(II) Complex with a Metallacyclopentane Core (C) 850–852 [868–870]
DOI: 10.1002/anie.200352851
- Juanes, O. (C) 619–621 [629–631]
- Juarez Garcia, M.-E. (C) 4597–4601 [4698–4702]
- Juhasz, M. (C) 1543–1546 [1569–1572], 5352–5355 [5466–5469]
- Jullien, L.
– An Efficient Fluorescent Probe for Ratio-metric pH Measurements in Aqueous Solutions (C) 4785–4788 [4889–4892]
DOI: 10.1002/anie.200460557
- Jung, Da-u. (C) 6183–6185 [6309–6311]
- Jung, H.-T. (C) 6465–6468 [6627–6630]
- Jung, S. D. (C) 6346–6350 [6506–6510]
- Jung, T.
– Supramolecular Patterned Surfaces Driven by Cooperative Assembly of C₆₀ and Porphyrins on Metal Substrates (C) 4759–4763 [4863–4867]
DOI: 10.1002/anie.200460562
- Jung, Y.-G. (C) 1675–1678 [1707–1710]
- Jung, Y.-S. (C) 3479–3481 [3561–3563]
- Junge, K. (C) 5066–5069 [5176–5179]
- Junk, P. C. (C) 3852–3855 [3940–3943]
- Jux, N. (C) 5526–5530 [5642–5646]
- Kahr, B.
– Luminescent Probes of Crystal Growth: Surface Charge and Polar Axis Sense in Dye-Doped Potassium Hydrogen Phthalate (C) 5328–5331 [5442–5445]
DOI: 10.1002/anie.200453839
- Kaida, Y. (C) 5643–5645 [5761–5763]
- Kaifer, A. E.
– Cucurbit[8]uril-Mediated Redox-Controlled Self-Assembly of Viologen-Containing Dendrimers (C) 5496–5499 [5612–5615]
DOI: 10.1002/anie.200460179
- Kaim, W. (C) 3970–3974 [4061–4064]
- Kaiser, G. (C) 1959–1962 [1993–1996]
- Kaiser, S. (C) 70–74 [72–76]
- Kajita, Y. (C) 334–337 [338–341]
- Kajiwar, T.
– Octalanthanide Wheels Supported by *p*-tert-Butylsulfonfylcalix[4]arene (C) 1832–1835 [1868–1871]
DOI: 10.1002/anie.200353449
- Kakei, H. (C) 317–320 [321–324]
- Kakiuchi, K. (M) 5580–5588 [5698–5706]
- Kalindjian, S. B. (C) 5680–5682 [5798–5800]
- Kalisz, M. (C) 5468–5471 [5584–5587]
- Kalkofen, R. (C) 1423–1427 [1447–1451], 6667–6669 [6836–6838]
- Kamada, K. (C) 6505–6510 [6667–6672]
- Kambe, N.
– Nickel-Catalyzed Cross-Coupling Reaction of Alkyl Halides with Organozinc and Grignard Reagents with 1,3,8,10-Tetraenes as Additives (C) 6180–6182 [6306–6308]
DOI: 10.1002/anie.200460246
- Kamikawa, Y. (C) 1969–1972 [2003–2006]
- Kamino, T. (C) 3175–3177 [3237–3239]
- Kampf, J. W. (C) 3912–3914 [4002–4004]
- Kamura, G. (C) 2834–2837 [2894–2897]
- Kanai, Mito (C) 1386–1389 [1410–1413]
- Kanai, Motomu
– Identifying Specific Conformations by Using a Carbohydrate Scaffold: Discovery of Subtype-Selective LPA-Receptor Agonists and an Antagonist (C) 2834–2837 [2894–2897]
DOI: 10.1002/anie.200454065
- Kanazawa, T. (C) 1251–1254 [1271–1274]
- Kaneko, K. (C) 465–469 [471–475]
- Kaneko, Y. (C) 5369–5372 [5483–5486]
- Kaneno, D. (C) 2412–2415 [2466–2469]
- Kaner, R. B.
– Nanofiber Formation in the Chemical Polymerization of Aniline: A Mechanistic Study (C) 5817–5821 [5941–5945]
DOI: 10.1002/anie.200460616
- Kang, M. J. (C) 2382–2385 [2436–2439]
- Kang, M.-S. (C) 1512–1516 [1538–1542]
- Kang, S. Y. (C) 6177–6180 [6303–6306]
- Kang, Seok Ho (C) 1512–1516 [1538–1542]
- Kang, Sung Ho
– Catalytic Asymmetric Mercuriocyclization of γ -Hydroxy-*cis*-Alkenes (C) 6177–6180 [6303–6306]
DOI: 10.1002/anie.200461289
- Kang, Y. S. (C) 3053–3056 [3115–3118]
- Kanie, K. (C) 1969–1972 [2003–2006]
- Kano, D. (C) 79–81 [81–83]
- Kano, K. (C) 334–337 [338–341]
- Kanzian, T. (C) 5402–5405 [5518–5521]
- Kao, C.-I. (C) 3425–3429 [3507–3511]



- Kabanov, V. A. (C) 2378–2381 [2432–2435]
- Kadish, K. M.
– Production of an Ultra-Long-Lived Charge-Separated State in a Zinc Chlorin–C₆₀ Dyad by One-Step Photoinduced Electron Transfer (C) 853–856 [871–874]
DOI: 10.1002/anie.200352870
- Kagan, H. B.
– In Situ Formation of a Heterobimetallic Chiral [(Salen)Ti^{IV}]/[(Salen)V^V] Catalyst for the Asymmetric Addition of TMSCN to Benzaldehyde (C) 4085–4089 [4177–4181]
DOI: 10.1002/anie.200454031
- Kahne, D. (C) 67–70 [69–72], 842–846 [860–864]
- Kahnt, J. (C) 2547–2551 [2601–2605]

- Kao, H.-M.
– An Organic–Inorganic Hybrid Electrolyte Derived from Self-Assembly of a Poly-(Ethylene Oxide)–Poly(Propylene Oxide)–Poly(Ethylene Oxide) Triblock Copolymer (C) 980–984 [998–1002]
DOI: 10.1002/anie.200352243
- Kao, H.-M. (C) 4186–4189 [4282–4285]
- Kappe, C. O.
– Combinatorial Synthesis of Functionalized 1,3-Thiazine Libraries Using a Combined Polymer-Supported Reagent/Catch-and-Release Strategy (C) 621–624 [631–634]
DOI: 10.1002/anie.200352731
- Controlled Microwave Heating in Modern Organic Synthesis (R) 6250–6284 [6408–6443]
DOI: 10.1002/anie.200400655
- Kappes, M. M. (C) 3823–3827 [3911–3915]
- Kaptein, B. (C) 3152–3155 [3214–3217], 6695–6699 [6863–6867]
- Karafilidis, C. (C) 2444–2446 [2498–2500]
- Karaguni, I.-M. (C) 450–454 [456–460], 454–458 [460–464]
- Karatzali, E. (C) 3974–3976 [4065–4067]
- Karni, M. Corrigendum: 141
- Karst, U.
– Electrochemistry/Mass Spectrometry (EC/MS)—A New Tool To Study Drug Metabolism and Reaction Mechanisms (H) 2476–2478 [2530–2532]
DOI: 10.1002/anie.200301763
- Karthikeyan, S. (C) 3425–3429 [3507–3511]
- Kashida, H. (C) 6522–6525 [6684–6687]
- Kastrup, L. (C) 6646–6649 [6814–6818]
- Katayama, K. (C) 334–337 [338–341]
- Kato, Hirofumi (C) 711–714 [729–732]
- Kato, Hitoshi
– Mesopores Created by Platinum Nanoparticles in Zeolite Crystals (C) 1251–1254 [1271–1274]
DOI: 10.1002/anie.200352706
- Kato, K. (C) 3670–3673 [3756–3759]
- Kato, Takako (C) 1360–1363 [1384–1387]
- Kato, Takashi
– Supramolecular Chirality of Thermotropic Liquid-Crystalline Folic Acid Derivatives (C) 1969–1972 [2003–2006]
DOI: 10.1002/anie.200353231
- Kato, Tsuyoshi (C) 2908–2911 [2968–2971]
- Kato, Yoshio (C) 3160–3163 [3222–3225]
- Kato, Yuki (C) 1966–1969 [2000–2003]
- Katoh, T.
– Total Synthesis of (+)-Scyphostatin, a Potent and Specific Inhibitor of Neutral Sphingomyelinase (C) 4207–4209 [4303–4305]
DOI: 10.1002/anie.200454192
- Katz, A. K. (C) 1149–1155 [1169–1175]
- Katz, E. (C) 3292–3300 [3354–3362], (R) 6042–6108 [6166–6235]
- Katzin, A. M. (C) 251–254 [254–257]
- Kaufmann, G. F. (C) 2106–2108 [2158–2160]
- Kaupp, M.
– Trigonal Prismatic or not Trigonal Prismatic? On the Mechanisms of Oxygen-Atom Transfer in Molybdopterin-Based Enzymes (H) 546–549 [554–558]
DOI: 10.1002/anie.200301690
- Kauss, M. (C) 2547–2551 [2601–2605]
- Kawaguchi, H.
– Formation of an Iron(II) Carbene–Thiolato Complex by Insertion of Carbon Monoxide into an Si–C Bond (C) 1404–1407 [1428–1431]
DOI: 10.1002/anie.200352916
- Kawai, A. (C) 4892–4896 [5000–5004]
- Kawai, K.
– Two-Color Two-Laser DNA Damaging (C) 2406–2409 [2460–2463]
DOI: 10.1002/anie.200353318
- Kawai, M. (C) 6125–6128 [6251–6254]
- Kawai, T.
– A Molybdenum Crown Cluster Forms Discrete Inorganic–Organic Nanocomposites with Metalloporphyrins (C) 6327–6331 [6487–6491]
DOI: 10.1002/anie.200460990
- Kawai, T. (C) 1349–1352 [1373–1376]
- Kawakami, D. (C) 4763–4767 [4867–4871]
- Kawakami, Y. (C) 4231–4233 [4327–4329]
- Kawame, N. (C) 3677–3682 [3763–3768]
- Kawanami, T. (C) 3582–3584 [3666–3668]
- Kawano, M. (C) 5621–5625 [5739–5743]
- Kawase, T.
– Möbius Aromatic Hydrocarbons: Challenges for Theory and Synthesis (H) 4396–4398 [4496–4498]
DOI: 10.1002/anie.200460050
- Onion-Type Complexation Based on Carbon Nanorings and a Buckminsterfullerene (C) 1722–1724 [1754–1756]
DOI: 10.1002/anie.200353517
- Supramolecular Dynamics of Cyclic [6]Paraphenyleneacetylene Complexes with [60]- and [70]Fullerene Derivatives: Electronic and Structural Effects on Complexation (C) 5060–5062 [5170–5172]
DOI: 10.1002/anie.200460630
- Kayaki, Y.
– Synthesis of Thermoresponsive Polyurethane from 2-Methylaziridine and Supercritical Carbon Dioxide (C) 717–719 [735–737]
DOI: 10.1002/anie.200352215
- Kayaki, Y. (C) 3719–3722 [3805–3808]
- Kayser, M. M. (C) 4075–4078 [4167–4170]
- Kazlauskas, R. J.
– Catalytic Promiscuity in Biocatalysis: Using Old Enzymes to Form New Bonds and Follow New Pathways (M) 6032–6040 [6156–6165]
DOI: 10.1002/anie.200460416
- Pseudodynamic Combinatorial Libraries: A Receptor-Assisted Approach for Drug Discovery (C) 2432–2436 [2486–2490]
DOI: 10.1002/anie.200453769
- Ke, J.
– Sensing the Critical Point of High-Pressure Mixtures (C) 5192–5195 [5304–5307]
DOI: 10.1002/anie.200460624
- Ke, Y. (C) 5940–5943 [6066–6069]
- Keaveney, C. M. (C) 1222–1224 [1242–1244]
- Keenan, M. (C) 70–74 [72–76]
- Kegel, W. K. (C) 458–462 [464–468]
- Kehr, G. (C) 310–313 [313–317]
- Kel'in, A. V. (C) 2280–2282 [2330–2332]
- Kellermann, M. (C) 2959–2962 [3019–3022]
- Kemnitz, E.
– Amorphous Aluminum Bromide Fluoride (ABF) (C) 6653–6656 [6822–6825]
DOI: 10.1002/anie.200460491
- Kemp, D. S.
– Calibrated Calculation of Polyalanine Fractional Helicities from Circular Dichroism Ellipticities (C) 5649–5651 [5767–5769]
DOI: 10.1002/anie.200460536
- Kempe, R.
– A New Arene Synthesis—Or: How Inert Is the Cyclopentadienyl Ligand? (H) 1463–1464 [1487–1488]
DOI: 10.1002/anie.200301717
- Kennedy, A. R. (C) 1709–1712 [1741–1744]
- Kennedy, R. J. (C) 5649–5651 [5767–5769]
- Kennedy-Smith, J. J. (C) 5350–5352 [5464–5466]
- Kent, S. B. H.
– A One-Pot Total Synthesis of Crambin (C) 2534–2538 [2588–2592]
DOI: 10.1002/anie.200353540
- Kern, J.-M. (C) 2392–2395 [2446–2449]
- Kesseler, M. (R) 788–824 [806–843]
- Kessler, H.
– An Easy and Scalable Method for the Partial Alignment of Organic Molecules for Measuring Residual Dipolar Couplings (C) 1092–1094 [1112–1115]
DOI: 10.1002/anie.200352860
- Improving Implant Materials by Coating with Nonpeptidic, Highly Specific Integrin Ligands (C) 6649–6652 [6818–6821]
DOI: 10.1002/anie.200460770
- Kettler, K. (C) 251–254 [254–257]
- Kevorkiants, R. (C) 1129–1132 [1149–1152]
- Khlebnikov, A. F. (C) 6553–6557 [6715–6719]
- Khlobystov, A. N.
– Molecular Motion of Endohedral Fullerenes in Single-Walled Carbon Nanotubes (C) 1386–1389 [1410–1413]
DOI: 10.1002/anie.200352389
- Khokhar, S. S. (C) 631–633 [641–643]
- Kickelbick, G.
– Hybrid Inorganic–Organic Mesoporous Materials (H) 3102–3104 [3164–3166]
DOI: 10.1002/anie.200301751
- Kickelbick, G. (C) 5697–5700 [5816–5819]
- Kiebele, A. (C) 4759–4763 [4863–4867]
- Kieber-Emmons, M. T. (C) 6716–6718 [6884–6886]
- Kiefer, W. (C) 4303–4306 [4403–4406]
- Kijima, T.
– Noble-Metal Nanotubes (Pt, Pd, Ag) from Lyotropic Mixed-Surfactant Liquid-Crystal Templates (C) 228–232 [230–234]
DOI: 10.1002/anie.200352630
- Kikuchi, K. (C) 5618–5621 [5736–5739]
- Kilgore, U. J. (C) 3156–3159 [3218–3221]
- Kim, B. (C) 1115–1117 Corrigendum: 3749 [1135–1137 Corrigendum: 3834]
- Kim, B. J. (C) 3056–3058 [3118–3120]
- Kim, D. (C) 971–974 [989–992]
- Kim, D. B. (C) 3053–3056 [3115–3118]
- Kim, D. W. (C) 483–485 [489–491]
- Kim, E. (C) 5987–5990 [6113–6116]
- Kim, F. (C) 3673–3677 [3759–3763]
- Kim, H. (C) 5523–5526 [5639–5642]
- Kim, H.-K. (C) 1862–1865 [1898–1901]
- Kim, H. S.
– Zwitterionic Silver Complexes as Carriers for Facilitated-Transport Composite Mem-

- branes
(C) 3053–3056 [3115–3118]
DOI: 10.1002/anie.200353632
- Kim, J.
 - Direct Evidence for Oxygen-Atom Exchange between Nonheme Oxoiron(IV) Complexes and Isotopically Labeled Water (C) 2417–2420 [2471–2474]
DOI: 10.1002/anie.200353497
- Kim, J. M.
 - Dehydroxylation Route to Surface Modification of Mesoporous Silicas by Using Grignard Reagents (C) 3839–3842 [3927–3930]
DOI: 10.1002/anie.200454076
- Kim, K.
 - Metal–Organic Replica of Fluorite Built with an Eight-Connecting Tetranuclear Cadmium Cluster and a Tetrahedral Four-Connecting Ligand (C) 971–974 [989–992]
DOI: 10.1002/anie.200353139
 - Rigid and Flexible: A Highly Porous Metal–Organic Framework with Unusual Guest-Dependent Dynamic Behavior (C) 5033–5036 [5143–5146]
DOI: 10.1002/anie.200460712
- Kim, K.-C. (C) 5352–5355 [5466–5469]
- Kim, K.-S. (C) 1512–1516 [1538–1542]
- Kim, M. (C) 6177–6180 [6303–6306]
- Kim, M.-J. (C) 2382–2385 [2436–2439]
- Kim, S.
 - Radical-Mediated γ -Functionalizations of α,β -Unsaturated Carboxylic Amides (C) 5378–5380 [5492–5494]
DOI: 10.1002/anie.200460820
- Kim, S.-H. (C) 3053–3056 [3115–3118]
- Kim, S. H. (C) 739–742 [757–760], 3947–3951 [4037–4041]
- Kim, S. J. (C) 3053–3056 [3115–3118]
- Kim, S. K. (C) 3952–3954 [4042–4044]
- Kim, S. O. (C) 2417–2420 [2471–2474]
- Kim, S. Y. (C) 4777–4780 [4881–4884]
- Kim, T.-G. (C) 5987–5990 [6113–6116]
- Kim, T.-W. (C) 5231–5234 [5343–5346]
- Kim, W. (C) 6471–6474 [6633–6636]
- Kim, W. B. (C) 1140–1142 [1160–1162]
- Kim, Y. (C) 5792–5796 [5916–5920]
- Kim, Y.-S. (C) 6327–6331 [6487–6491]
- Kimmel, J. R. (C) 6541–6544 [6703–6707]
- Kimura, E. A. (C) 251–254 [254–257]
- Kimura, M. (C) 736–738 [754–756]
- Kimura, T. (C) 6350–6355 [6510–6515]
- King, G. C.
 - Enzymatic Synthesis of Redox-Labeled RNA and Dual-Potential Detection at DNA-Modified Electrodes (C) 2809–2812 [2869–2872]
DOI: 10.1002/anie.200352977
- King, P. J. (C) 5192–5195 [5304–5307]
- Kinoshita, H. (C) 1860–1862 [1896–1898]
- Kinoshita, I. (C) 213–215 [215–217]
- Kira, M.
 - The Singlet Excited State of a Stable Dialkylsilylene Is Responsible for Its Photoreactions (C) 4510–4512 [4610–4612]
DOI: 10.1002/anie.200460317
- Kiran, B. (C) 2125–2129 [2177–2181]
- Kirk, M. L.
 - Synthesis, Structure, and Magnetic Properties of a Large Lanthanide–Transition-Metal Single-Molecule Magnet (C) 3912–3914 [4002–4004]
DOI: 10.1002/anie.200454013
- Kirmani, B. A. (C) 2135–2138 [2187–2190]
- Kirmse, W.
 - Stable Singlet Carbenes—Plentiful and Versatile (H) 1767–1769 [1799–1801]
DOI: 10.1002/anie.200301729
- Kirschhock, C. E. A. (C) 3722–3724 [3808–3810], (L) 4562–4564 [4662–4664]
- Kishida, H. (C) 3171–3175 [3233–3237]
- Kita, Y.
 - Lipase-Catalyzed Domino Dynamic Kinetic Resolution of Racemic 3-Vinylcyclohex-2-en-1-ols/Intramolecular Diels–Alder Reaction: One-Pot Synthesis of Optically Active Polysubstituted Decalins (C) 1407–1410 [1431–1434]
DOI: 10.1002/anie.200353044
 - Preparation and Reactivity of 1,3,5,7-Tetrakis[4-(diacetoxyiodo)phenyl]adamantane, a Recyclable Hypervalent Iodine(III) Reagent (C) 3595–3598 [3679–3682]
DOI: 10.1002/anie.200454234
- Kitagaki, S. (C) 2665–2668 [2719–2722]
- Kitagawa, S.
 - A Neutral 3D Copper Coordination Polymer Showing 1D Open Channels and the First Interpenetrating NbO-Type Network (C) 192–195 [194–197]
DOI: 10.1002/anie.200352024
 - Expanding and Shrinking Porous Modulation Based on Pillared-Layer Coordination Polymers Showing Selective Guest Adsorption (C) 3269–3272 [3331–3334]
DOI: 10.1002/anie.200453923
 - Functional Porous Coordination Polymers (R) 2334–2375 [2388–2430]
DOI: 10.1002/anie.200300610
 - Immobilization of a Metallo Schiff Base into a Microporous Coordination Polymer (C) 2684–2687 [2738–2741]
DOI: 10.1002/anie.200352596
 - Reaction-Temperature-Dependent Supramolecular Isomerism of Coordination Networks Based on the Organometallic Building Block $[\text{Cu}^{\text{I}}_2(\mu_2\text{-BO})(\mu_2\text{-OAc})_2]$ (C) 2530–2534 [2584–2588]
DOI: 10.1002/anie.200353463
- Kitaura, R. (R) 2334–2375 [2388–2430], (C) 2684–2687 [2738–2741]
- Kitayama, H. (C) 213–215 [215–217]
- Kitova, E. N. (C) 4183–4186 [4279–4282]
- Klanner, C. (C) 5347–5349 [5461–5463]
- Klapötke, T. M. (C) 4586–4589 [4686–4689]
- Klassen, J. S.
 - Partitioning of Solvent Effects and Intrinsic Interactions in Biological Recognition (C) 4183–4186 [4279–4282]
DOI: 10.1002/anie.200353051
- Klawonn, M. (C) 5255–5260 [5367–5372]
- Klebe, G.
 - Ligand-Supported Homology Modeling of G-Protein-Coupled Receptor Sites: Models Sufficient for Successful Virtual Screening (C) 248–251 [250–253]
DOI: 10.1002/anie.200352776
- Klebe, G. (C) 251–254 [254–257]
- Klein, C. D. (C) 511–514 [517–520]
- Klein, M. L. (C) 1158–1162 [1178–1182]
- Klein-Hitpass, L. (C) 450–454 [456–460]
- Klein-Seetharaman, J. (C) 5780–5785 [5904–5909]
- Kleinke, H.
 - T-Shaped Nets of Antimony Atoms in the Binary Antimonide Hf_2Sb_6 (C) 5260–5262 [5372–5375]
DOI: 10.1002/anie.200460488
- Kleinke, K. M. (C) 5260–5262 [5372–5375]
- Kleinschmidt, V. (C) 4804–4807 [4908–4911]
- Kleist, W. (C) 1881–1882 [1917–1918]
- Klementiev, K. V. (C) 2839–2842 [2899–2903]
- Klenerman, D.
 - Individual Molecules of Dye-Labeled DNA Act as a Reversible Two-Color Switch upon Application of an Electric Field (C) 5926–5930 [6052–6056]
DOI: 10.1002/anie.200460323
- Klimowicz, M. (C) 1877–1880 [1913–1916]
- Klimpel, M. G. (C) 2234–2239 [2284–2289]
- Klinkhammer, K. W.
 - Molecular Lead Clusters—From Unexpected Discovery to Rational Synthesis (C) 6202–6204 [6328–6331]
DOI: 10.1002/anie.200461670
- Kloo, L.
 - $\text{Sb}_3(\text{GaCl}_4)_2$: Isolation of a Homopolyatomic Antimony Cation (C) 2540–2543 [2594–2597]
DOI: 10.1002/anie.200353578
- Kloth, M. (C) 3852–3855 [3940–3943]
- Knapp, C. (H) 4834–4836 [4938–4941]
- Kneisel, F. F. (C) 1017–1021 [1032–1036]
- Knemeyer, J.-P. (C) 3798–3801 [3886–3890]
- Knickerbocker, T. (C) 2780–2783 [2840–2843]
- Kniep, B. L. (C) 112–115 [114–117]
- Kniep, R.
 - $\text{Ae}[\text{Be}_2\text{N}_2]$: Nitridoberyllates of the Heavier Alkaline-Earth Metals (C) 1088–1092 [1108–1112]
DOI: 10.1002/anie.200352796
- Knobler, C. B. (C) 1854–1857 [1890–1893]
- Knobloch, B. (C) 3793–3795 [3881–3883]
- Knochel, P.
 - A General Amination Method Based on the Addition of Polyfunctional Arylmagnesium Reagents to Functionalized Arylazo Tosylates (C) 897–900 [915–918]
DOI: 10.1002/anie.200353241
 - A LiCl-Mediated Br/Mg Exchange Reaction for the Preparation of Functionalized Aryl- and Heteroarylmagnesium Compounds from Organic Bromides (C) 3333–3336 [3396–3399]
DOI: 10.1002/anie.200454084
 - An Efficient Synthesis of Diaryl Ketones by Iron-Catalyzed Arylation of Aryl Cyanides (C) 2968–2970 [3028–3030]
DOI: 10.1002/anie.200453696
 - Nucleophilic Catalysis of the Iodine–Zinc Exchange Reaction: Preparation of Highly Functionalized Diaryl Zinc Compounds (C) 1017–1021 [1032–1036]
DOI: 10.1002/anie.200353316
 - Preparation of Polyfunctional Arynes via 2-Magnesiadated Diaryl Sulfonates (C) 4364–4366 [4464–4466]
DOI: 10.1002/anie.200460417
- Knöpfel, T. F. (C) 5971–5973 [6097–6099]
- Kobayashi, N. (C) 5481–5485 [5597–5601]
- Kobayashi, Shigeya (C) 366–369 [370–373]

- Kobayashi, Shū
– Copper(II)-Catalyzed Highly Enantioselective Addition of Enamides to Imines: The Use of Enamides as Nucleophiles in Asymmetric Catalysis
(C) 1679–1681 [1711–1713]
DOI: 10.1002/anie.200353237
- Highly Diastereo- and Enantioselective Reactions of Enecarbamates with Ethyl Glyoxylate To Give Optically Active *syn* and *anti* α -Alkyl- β -Hydroxy Imines and Ketones
(C) 3258–3260 [3320–3322]
DOI: 10.1002/anie.200460165
- Stereospecific, Enantioselective Allylation of α -Hydrazono Esters by Using Allyltrichlorosilanes with BINAP Dioxides as Neutral-Coordinate Organocatalysts
(C) 6491–6493 [6653–6655]
DOI: 10.1002/anie.200461312
- Kobayashi, Susumu
– Highly Efficient Total Synthesis of (+)-Citroviral
(C) 3175–3177 [3237–3239]
DOI: 10.1002/anie.200454212
- Kobzar, K. (C) 1092–1094 [1112–1115]
- Kochi, J. K.
– Halide Recognition through Diagnostic “Anion- π ” Interactions: Molecular Complexes of Cl⁻, Br⁻, and I⁻ with Olefinic and Aromatic π Receptors
(C) 4650–4652 [4750–4752]
DOI: 10.1002/anie.200460337
- Kodama, S. (C) 2659–2661 [2713–2715]
- Kodera, M.
– Synthesis, Structure, and Greatly Improved Reversible O₂ Binding in a Structurally Modulated μ - η^2 : η^2 -Peroxodicopper(II) Complex with Room-Temperature Stability
(C) 334–337 [338–341]
DOI: 10.1002/anie.200352737
- Koert, U.
– Syntheses of Tetrodotoxin
(H) 5572–5576 [5690–5694]
DOI: 10.1002/anie.200461097
- Total Synthesis of Apoptolidin
(C) 4597–4601 [4698–4702]
DOI: 10.1002/anie.200460172
- Koftis, T. V. (C) 4312–4318 [4412–4418], 4318–4324 [4418–4424]
- Koga, Y. (C) 3582–3584 [3666–3668]
- Kogan, M. J. (C) 1811–1814 [1847–1850]
- Kögerler, P. (C) 1817–1820 [1853–1856]
- Koguchi, S. (C) 2412–2415 [2466–2469]
- Koh, J. H. (C) 3459–3461 Corrigendum: 4828 [3541–3543 Corrigendum: 4932]
- Kohl, C. (C) 1528–1531 [1554–1557]
- Köhler, F. H.
– Highly Resolved Spin-Density Distribution in the Prussian-Blue Precursors Cs₂K[Fe(CN)₆] and Cs₂K[Mn(CN)₆]
(C) 2571–2573 [2625–2627]
DOI: 10.1002/anie.200453726
- Köhler, J. (C) 2032–2034 [2066–2068]
- Köhler, Karen (C) 245–247 [247–249]
- Köhler, Klaus
– In Situ Generation of Highly Active Dissolved Palladium Species from Solid Catalysts—A Concept for the Activation of Aryl Chlorides in the Heck Reaction
(C) 1881–1882 [1917–1918]
DOI: 10.1002/anie.200353473
- Köhn, M. (M) 3106–3116 [3168–3178]
- Koide, K.
– A Mild Method for the Preparation of γ -Hydroxy- α,β -Acetylenic Esters
(C) 2525–2527 [2579–2581]
DOI: 10.1002/anie.200353400
- Kojima, T.
– A Porphyrin Nanotube: Size-Selective Inclusion of Tetranuclear Molybdenum–Oxo Clusters
(C) 1825–1828 [1861–1864]
DOI: 10.1002/anie.200353325
- Kokil, A. (C) 1808–1811 [1844–1847]
- Kokkoli, E. (L) 4558–4561 [4658–4661]
- Kolb, U. (C) 3192–3195 [3255–3257]
- Koltover, I.
– Genetic Engineering of the Nanoscale Structure in Polyelectrolyte–Lipid Self-Assembled Systems
(C) 4034–4037 [4126–4129]
DOI: 10.1002/anie.200460164
- Komanduri, V. (C) 2915–2918 [2975–2978]
- Komarov, V. Yu. (C) 2922–2924 [2982–2984]
- Komatsu, Kei (C) 4341–4345 [4441–4445]
- Komatsu, Koichi (C) 3044–3047 [3106–3109]
- Komatsu, M.
– Silica–Water Reaction Media: Its Application to the Formation and Ring Opening of Aziridines
(C) 79–81 [81–83]
DOI: 10.1002/anie.200352842
- Komiyama, M. (C) 6522–6525 [6684–6687]
- Kondo, H. (C) 1516–1520 [1542–1546]
- Kondo, J. (C) 106–108 [108–110]
- Kondo, J. N. (C) 2955–2958 [3015–3018]
- Kondo, T.
– Ru- and Rh-Catalyzed C–C Bond Cleavage of Cyclobutenones: Reconstructive and Selective Synthesis of 2-Pyranones, Cyclopentenones, and Cyclohexenones
(C) 5369–5372 [5483–5486]
DOI: 10.1002/anie.200461002
- König, B.
– Chemistry in Motion—Unidirectional Rotating Molecular Motors
(H) 1622–1624 [1650–1652]
DOI: 10.1002/anie.200301697
- Konishi, K.
– Porous Organic–Inorganic Assemblies Constructed from Keggin Polyoxometalate Anions and Calix[4]arene–Na⁺ Complexes: Structures and Guest-Sorption Profiles
(C) 2702–2705 [2756–2759]
DOI: 10.1002/anie.200453693
- Surface-Cap-Mediated Host–Guest Chemistry of Semiconductor CdS: Intercalative Cation Accumulation around a Phenyl-Capped CdS Cluster and Its Notable Effects on the Cluster Photoluminescence
(C) 5943–5946 [6069–6072]
DOI: 10.1002/anie.200461190
- Koo, B. (C) 2282–2285 [2332–2335]
- Kooijman, H. (C) 5668–5670 [5786–5788]
- Koo, E. T.
– yDNA: A New Geometry for Size-Expanded Base Pairs
(C) 5834–5836 [5958–5960]
DOI: 10.1002/anie.200461036
- Kopf, J. (C) 5406–5408 [5521–5523]
- Köppe, R. (C) 2170–2173 [2222–2225]
- Koritsánszky, T. (C) 2718–2721 [2773–2776]
- Korn, T. J. (C) 2968–2970 [3028–3030]
- Korniakov, A. (C) 520–523 [527–529]
- Kornowski, A. (C) 4774–4777 [4878–4881]
- Korshin, E. E. (C) 4193–4197 [4289–4293]
- Kortner, J. (C) 4045–4049 [4137–4141]
- Kortz, U.
– Structural Control on the Nanomolecular Scale: Self-Assembly of the Polyoxotungstate Wheel [{ β -Ti₂SiW₁₀O₃₉}]²⁴⁻
(C) 3485–3488 [3567–3571]
DOI: 10.1002/anie.200454203
- Korybut-Daszkiewicz, B.
– An Electrochemically Controlled Molecular Shuttle
(C) 1668–1672 [1700–1704]
DOI: 10.1002/anie.200352528
- Kosa, M. (C) 745–748 [763–766]
- Kosky, J. L. (C) 1836–1839 [1872–1875]
- Kosmidis, C. (C) 4178–4182 [4273–4277]
- Kostarelos, K.
– Functionalized Carbon Nanotubes for Plasmid DNA Gene Delivery
(C) 5242–5246 [5354–5358]
DOI: 10.1002/anie.200460437
- Koszinowski, K. (C) 121–124 [124–127]
- Kotani, H. (C) 853–856 [871–874]
- Kotani, M. (C) 2248–2251 [2298–2301]
- Kotha, S. (C) 1149–1155 [1169–1175]
- Kotsuki, H.
– Diels–Alder Reaction of Thiophene: Dramatic Effects of High-Pressure/Solvent-Free Conditions
(C) 2015–2017 [2049–2051]
DOI: 10.1002/anie.200353487
- Kotter, W. (C) 514–517 [520–523]
- Kou, R. (C) 6169–6173 [6295–6299]
- Koutmos, M. (C) 5023–5025 [5133–5135]
- Kowalewski, T.
– Well-Defined Carbon Nanoparticles Prepared from Water-Soluble Shell Cross-linked Micelles that Contain Polyacrylonitrile Cores
(C) 2783–2787 [2843–2847]
DOI: 10.1002/anie.200353401
- Kozak, C. M.
– Revelations in Dinitrogen Activation and Functionalization by Metal Complexes
(H) 1186–1189 [1206–1209]
DOI: 10.1002/anie.200301712
- Kozhushkov, S. I. (C) 6553–6557 [6715–6719]
- Kozioł, F. (C) 4485–4489 [4585–4589]
- Kraft, S. (C) 1583–1587 [1609–1614]
- Kragl, U. (C) 4529–4531 [4629–4631]
- Kragol, G. (C) 5839–5842 [5963–5966]
- Krahl, T. (C) 6653–6656 [6822–6825]
- Kräling, K. (C) 1842–1844 Corrigendum: 2321 [1878–1880 Corrigendum: 2373]
- Kramer, B. (C) 2446–2449 [2501–2503]
- Krämer, H.-J. (C) 1098–1100 [1119–1121]
- Krasovskiy, A. (C) 3333–3336 [3396–3399]
- Krätz, O.
– The Chemical Laboratory: Source of Progress or Chamber of Horrors?
(E) 1770–1780 [1802–1813]
DOI: 10.1002/anie.200330064
- Krause, N.
– Synthesis and Properties of Allenic Natural Products and Pharmaceuticals
(R) 1196–1216 [1216–1236]
DOI: 10.1002/anie.200300628
- Krebs, B.
– Pentanuclear Platinum(II) Macrocycles with Nucleobases
(C) 1300–1303 [1321–1324]
DOI: 10.1002/anie.200352950

- Krekberg, W. P. (C) 4296–4300 [4396–4400]
- Kremer, R. K. (C) 2032–2034 [2066–2068]
- Kremer, S. P. B. (L) 4562–4564 [4662–4664]
- Krempner, C.
- Novel Polysilanol by Selective Functionalizations of Oligosilanes (C) 5406–5408 [5521–5523]
DOI: 10.1002/anie.200460874
- Kresse, G. (C) 5546–5549 [5663–5666]
- Kressier, C. J. (C) 5997–6000 [6123–6127]
- Kretsovali, A.
- Design, Synthesis, and Biological Evaluation of a Small-Molecule Inhibitor of the Histone Acetyltransferase Gcn5 (C) 3974–3976 [4065–4067]
DOI: 10.1002/anie.200453879
- Kriebel, J. K. (C) 1555–1558 [1581–1584]
- Krieger-Beck, P. (C) 5843–5846 [5967–5970]
- Krische, M. J.
- Regio- and Stereoselective Construction of γ -Butenolides through Phosphine-Catalyzed Substitution of Morita–Baylis–Hillman Acetates: An Organocatalytic Allylic Alkylation (C) 6689–6691 [6857–6859]
DOI: 10.1002/anie.200461381
- Krishna, P. R. (C) 3961–3965 [4051–4055]
- Krishna Prasad, S.
- A Low-Molar-Mass, Monodisperse, Bent-Rod Dimer Exhibiting Biaxial Nematic and Smectic A Phases (C) 3429–3432 [3511–3514]
DOI: 10.1002/anie.200453908
- Kritikos, M. (C) 1006–1009 [1024–1027]
- Kronja, O. (C) 2302–2305 [2353–2356]
- Krossing, I.
- Noncoordinating Anions—Fact or Fiction? A Survey of Likely Candidates (R) 2066–2090 [2116–2142]
DOI: 10.1002/anie.200300620
- Kroth, H.-J. (C) 6208–6211 [6335–6338]
- Kroto, H. W. (C) 5670–5674 [5788–5792]
- Krska, S. W. (C) 5372–5374 [5486–5488]
- Krumm, M. (C) 5396–5399 [5507–5511]
- Krylov, A. I.
- 5-Dehydro-1,3-quinodimethane: A Hydrocarbon with an Open-Shell Doublet Ground State (C) 742–745 [760–763]
DOI: 10.1002/anie.200352990
- Ku, J.-M. (C) 2382–2385 [2436–2439]
- Kuang, D. (M) 4988–4992 [5096–5100]
- Kubas, G. J.
- Molecular and Electronic Structure of Platinum Bis(*N*-arylamino)phosphonium Complexes including [Pt(phosphane)-(phosphonium)(*N*-heterocyclic carbene)] (C) 1955–1958 [1989–1992]
DOI: 10.1002/anie.200352326
- Kubiak, C. P.
- Observation and Dynamics of “Charge-Transfer Isomers” (C) 1376–1381 [1400–1405]
DOI: 10.1002/anie.200353221
- Kubo, T.
- Four-Stage Amphoteric Redox Properties and Biradicaloid Character of Tetra-*tert*-butyldicyclopenta[*b,d*]thieno[1,2,3-*cd*:5,6,7-*c'd'*]diphenylene (C) 6474–6479 [6636–6641]
DOI: 10.1002/anie.200460565
- Kubota, Y. (C) 736–738 [754–756]
- Kuhlman, M. L. (C) 6742–6745 [6910–6913]
- Kuhlmann, J.
- Synthesis and Application of Fluorescence-Labeled Ras-Proteins for Live-Cell Imaging (C) 2711–2714 [2765–2768]
DOI: 10.1002/anie.200353265
- Kukolj, G. (C) 4306–4311 [4406–4411]
- Kulak, A. (C) 6691–6695 [6859–6863]
- Kumagai, N. (C) 478–482 [484–488]
- Kumamoto, K. (C) 2015–2017 [2049–2051]
- Kumar, D. (C) 1129–1132 [1149–1152], 5661–5665 [5779–5783]
- Kumar, K. (C) 3664–3666 [3750–3752]
- Kumar, S. S. (C) 4940–4943 [5048–5051]
- Kumaraswamy, S. (C) 3711–3715 [3797–3801]
- Kumazawa, K. (C) 5936–5940 [6062–6066]
- Kunai, A.
- Arynes in a Three-Component Coupling Reaction: Straightforward Synthesis of Benzoannulated Iminofurans (C) 3935–3938 [4025–4028]
DOI: 10.1002/anie.200460009
 - Distannylation of Strained Carbon–Carbon Triple Bonds Catalyzed by a Palladium Complex (C) 5052–5055 [5162–5165]
DOI: 10.1002/anie.200460189
- Kunat, M. (C) 6641–6645 [6809–6814]
- Kundu, M. K. (C) 6731–6734 [6899–6902]
- Kunst, A. (C) 5530–5534 [5646–5650]
- Kunwar, A. C.
- Left-Handed Helical Twists in “Mixed β -Peptides” Derived From Alternating C-Linked Carbo- β^3 -Amino Acids and β -hGly Units (C) 3961–3965 [4051–4055]
DOI: 10.1002/anie.200353467
- Kunz, H.
- Carbohydrate Scaffolds for Combinatorial Syntheses That Allow Selective Deprotection of All Four Positions Independent of the Sequence (C) 1104–1107 [1125–1128]
DOI: 10.1002/anie.200352919
- Kunz, W.
- A Porphyrin Dye with Monoexponential Fluorescence Intensity and Anisotropy Decay Behavior in Spherical Micelles (C) 634–636 [644–646]
DOI: 10.1002/anie.200351773
- Kunze, S. (C) 5025–5029 [5135–5139]
- Kuo, C.-T. (C) 4507–4510 [4607–4610]
- Kuo, T.-C. (C) 1862–1865 [1898–1901]
- Kurata, H. (C) 4947–4950 [5055–5058]
- Kurihara, M. (C) 5360–5363 [5474–5477]
- Kurnosov, A. V.
- New Clathrate Hydrate Structure: High-Pressure Tetrahydrofuran Hydrate with One Type of Cavity (C) 2922–2924 [2982–2984]
DOI: 10.1002/anie.200453712
- Kuroda, R.
- Noncovalent Ligand Strands for Transition-Metal Helicates: The Straightforward and Stereoselective Self-Assembly of Dinuclear Double-Stranded Helicates Using Hydrogen Bonding (C) 581–584 [591–594]
DOI: 10.1002/anie.200352833
- Kuroda, S.-i. (C) 3171–3175 [3233–3237], 4763–4767 [4867–4871]
- Kuroguchi, M. (C) 4071–4075 [4163–4167]
- Kurpejović, E. (C) 6545–6547 [6707–6709]
- Kurth, D. G. (C) 4357–4360 [4457–4460], 5639–5642 [5757–5760]
- Kurz, P. (C) 5025–5029 [5135–5139]
- Kusmann, J. (C) 4485–4489 [4585–4589]
- Kusukawa, T. (C) 5621–5625 [5739–5743], 5936–5940 [6062–6066]
- Kutzelnigg, W.
- Theoretical Chemistry: *H. C. Longuet-Higgins and J. A. Pople* (O) 2740–2743 [2796–2799]
DOI: 10.1002/anie.200460423
- Kuvychko, I. V. (C) 997–1000 [1015–1018]
- Kuwahara, S. (C) 3167–3171 [3229–3233]
- Kuykendall, T. (C) 3673–3677 [3759–3763]
- Kværnø, L. (C) 4653–4656 [4753–4756]
- Kwok, W.-M. (C) 4659–4662 [4759–4762]
- Kwon, E. (C) 4610–4612 [4710–4712]
- Kwon, O.-H. (C) 5792–5796 [5916–5920]



Laatsch, H.

- Gutingimycin: A Highly Complex Metabolite from a Marine Streptomyces (C) 1281–1283 [1301–1303]
DOI: 10.1002/anie.200352312

Labinger, J. A.

- Controversy in Chemistry: What Counts as Evidence?—Two Studies in Molecular Structure (E) 2612–2619 [2664–2672]
DOI: 10.1002/anie.200330055

Lacôte, E.

- A Radical Show (T) 4550–4551 [4650–4651]
DOI: 10.1002/anie.200461443
- Titanium-Mediated Domino Radical Cyclization/ β Elimination of Phosphine Oxides (C) 4220–4222 [4316–4318]
DOI: 10.1002/anie.200460099

Lacy, S. M. (C) 3260–3264 [3322–3326]

Ladame, S. (C) 1143–1146 [1163–1166]

Lægsgaard, E. (C) 2092–2095 [2144–2147]

Lahiri, K. (C) 1149–1155 [1169–1175]

Lakshman, M. K.

- Pd-Catalyzed Amination of Nucleoside Arylsulfonates to yield *N*⁶-Aryl-2,6-Diaminopurine Nucleosides (C) 6372–6377 [6532–6537]
DOI: 10.1002/anie.200460782

Lam, T. C. H. (C) 1715–1718 [1747–1750]

Lam, Y.-F. (C) 2132–2134 [2184–2186]

Lambert, C.

- Synthesis and Photophysics of a Neutral Organic Mixed-Valence Compound (C) 5851–5856 [5976–5981]
DOI: 10.1002/anie.200460495

Lammertsma, K.

- Dynamic Configurational Isomerism of a Stable Pentaorganosilicate (C) 3440–3442 [3522–3524]
DOI: 10.1002/anie.200353006
- 2-Phospha-4-silabicyclo[1.1.0]butane as a Reactive Intermediate (C) 3474–3477 [3556–3559]
DOI: 10.1002/anie.200454183
- The Circumambulation of a Phosphirane: Taking 9-Phenyl-9-phosphabicyclo[6.1.0]nona-2,4,6-triene for a “Walk”

- (C) 714–717 Corrigendum: 3748 [732–735 Corrigendum: 3834]
DOI: 10.1002/anie.200351855
- Lan, X. (C) 6377–6381 [6537–6541]
- Lancashire, H. N. (C) 5772–5775 Corrigendum: 6581 [5896–5899 Corrigendum: 6743]
- Lang, I. (C) 2163–2166 [2215–2218]
- Lang, J.-P.
– $\{[\text{WS}_4\text{Cu}_4(4,4'\text{-bpy})_4][\text{WS}_4\text{Cu}_4\text{I}_4(4,4'\text{-bpy})_2]\}_\infty$ —An Unusual 3D Porous Coordination Polymer Formed from the Pre-formed Cluster $[\text{Et}_4\text{N}]_4[\text{WS}_4\text{Cu}_4\text{I}_6]$ (C) 4741–4745 [4845–4849]
DOI: 10.1002/anie.200460076
- Langenberg, D. (C) 6641–6645 [6809–6814]
- Langerak, A. (C) 450–454 [456–460]
- Langner, M. (C) 5984–5987 [6110–6113]
- Laplace, A. (C) 3163–3167 [3225–3229]
- LaPlante, S. R.
– Binding Mode Determination of Benzimidazole Inhibitors of the Hepatitis C Virus RNA Polymerase by a Structure and Dynamics Strategy (C) 4306–4311 [4406–4411]
DOI: 10.1002/anie.200460326
- Laporte, C. (C) 2567–2570 [2621–2624]
- Lappert, M. F.
– A 1,3-Diaza-2,4-distannacyclobutane diide: Synthesis, Structure, and Bonding (C) 4500–4504 [4600–4604]
DOI: 10.1002/anie.200460039
- Lappert, M. F. (C) 5776–5779 [5900–5903]
- Larpernt, C.
– Macrocyclic Sugar-Based Surfactants: Block Molecules Combining Self-Aggregation and Complexation Properties (C) 3163–3167 [3225–3229]
DOI: 10.1002/anie.200353484
- Larsen, F. K. (C) 5196–5200 [5308–5312]
- Larsson, R. (C) 3716–3718 [3802–3804]
- Lash, T. D.
– Oxidative Metalation of Azuliporphyrins with Copper(II) Salts: Formation of a Porphyrin Analogue System with a Unique Fully Conjugated Nonaromatic Azulene Subunit (C) 1346–1349 [1370–1373]
DOI: 10.1002/anie.200353189
- Latos-Grażyński, L.
– Bimetallic Figure-Eight Octaphyrins Split into Four-Pyrrolic Macrocycles (H) 5124–5128 [5234–5238]
DOI: 10.1002/anie.200460645
- Lauderbach, F.
– A Trinuclear $[\text{NiFe}]$ Cluster Exhibiting Structural and Functional Key Features of $[\text{NiFe}]$ Hydrogenases (C) 3141–3144 [3203–3206]
DOI: 10.1002/anie.200353440
- Lawrence, S. C. (C) 2521–2524 [2575–2578]
- Lay, P. A.
– Biomimetic Oxidation of Chromium(III): Does the Antidiabetic Activity of Chromium(III) Involve Carcinogenic Chromium(VI)? (C) 4504–4507 [4604–4607]
DOI: 10.1002/anie.200460113
- X-ray Absorption Spectroscopic and Electrochemical Studies of $\text{Tris}(\text{catecholato}(2-))\text{chromate}(\text{v}/\text{v}/\text{III})$ Complexes (C) 462–465 [468–471]
DOI: 10.1002/anie.200352418
- Laye, R. H. (C) 6132–6135 [6258–6261]
- Layfield, R. A.
– A Manganese(II) Allyl Complex: Synthesis, Structure, and Magnetic Properties of $[\text{Li}(\text{thf})_4][\text{Mn}\{\eta^3\text{-(Me}_3\text{Si)}_2\text{C}_3\text{H}_3\}\text{-}\eta^1\text{-(Me}_3\text{Si)}_2\text{C}_3\text{H}_3\}_2]$ (C) 3067–3069 [3129–3131]
DOI: 10.1002/anie.200454008
- Le Floch, P.
– A Bis(thiophosphinoyl)methanediide Palladium Complex: Coordinated Dianion or Nucleophilic Carbene Complex? (C) 6382–6385 [6542–6545]
DOI: 10.1002/anie.200461392
- Leach, J. (C) 2512–2514 [2566–2568]
- Leadlay, P. F.
– Isolation and Characterization of Pre-rapamycin, the First Macrocyclic Intermediate in the Biosynthesis of the Immunosuppressant Rapamycin by *S. hygrosopicus* (C) 2551–2553 [2605–2607]
DOI: 10.1002/anie.200453764
- Leahy, D. K. (C) 4788–4791 [4892–4895]
- Lear, M. J.
– Spin Trapping of ^{13}C -Labeled *p*-Benzynes Generated by Masamune–Bergman Cyclization of Bicyclic Nine-Membered Ene-dynes (C) 5249–5253 [5361–5365]
DOI: 10.1002/anie.200454133
- Leardini, R. (C) 3598–3601 [3682–3685]
- Leca, D. (C) 4220–4222 [4316–4318]
- Leclair, S. (C) 349–353 [353–357]
- Lecren, L. (C) 2801–2805 [2861–2865]
- Lee, B. Y.
– Dehydroxylation Route to Surface Modification of Mesoporous Silicas by Using Grignard Reagents (C) 3839–3842 [3927–3930]
DOI: 10.1002/anie.200454076
- Lee, C.-W. (C) 4197–4200 [4293–4296]
- Lee, D. H. (C) 4777–4780 [4881–4884]
- Lee, D. S. (C) 5517–5519 [5633–5635]
- Lee, E. E. (C) 1865–1868 [1901–1904]
- Lee, E. Y. (C) 2798–2801 [2858–2861]
- Lee, G. (C) 1712–1714 [1744–1746]
- Lee, G.-H. (C) 4507–4510 [4607–4610]
- Lee, G. S. (C) 6111–6116 [6237–6242]
- Lee, H. (C) 3053–3056 [3115–3118]
- Lee, H.-K. (C) 1000–1003 [1018–1021]
- Lee, H.-L. (C) 2551–2553 [2605–2607]
- Lee, I.-R. (C) 2830–2834 [2890–2894]
- Lee, J. (C) 2382–2385 [2436–2439]
- Lee, J.-H. (C) 2382–2385 [2436–2439]
- Lee, J.-S. (C) 6331–6335 [6491–6495]
- Lee, K. (C) 1115–1117 Corrigendum: 3749 [1135–1137 Corrigendum: 3834], 1712–1714 [1744–1746]
- Lee, K.-B. (C) 1246–1249 [1266–1269], 3048–3050 [3110–3112]
- Lee, M.
– Supramolecular Crystalline Sheets with Ordered Nanopore Arrays from Self-Assembly of Rigid-Rod Building Blocks (C) 6465–6468 [6627–6630]
DOI: 10.1002/anie.200460378
- Lee, M.-R. (C) 1675–1678 [1707–1710]
- Lee, S.-g.
– Dramatic Enhancement of Catalytic Activity in an Ionic Liquid: Highly Practical Friedel–Crafts Alkenylation of Arenes with Alkynes Catalyzed by Metal Triflates (C) 6183–6185 [6309–6311]
DOI: 10.1002/anie.200460292
- Lee, S. H. (C) 5087–5092 [5197–5202], 5092–5097 [5202–5207]
- Lee, Seung-Hyun (C) 5335–5338 [5449–5452]
- Lee, Suck-Hyun
– Reversible Thermochromism in Hydrogen-Bonded Polymers Containing Polydiacetylenes (C) 4197–4200 [4293–4296]
DOI: 10.1002/anie.200453995
- Lee, V. (C) 1132–1136 [1152–1156]
- Lee, V. Y. (C) 6703–6705 [6871–6873]
- Lee, Y.-J. (C) 2382–2385 [2436–2439]
- Lee, Y.-M. (C) 2254–2256 [2304–2306]
- Lee, Y.-S. (C) 5792–5796 [5916–5920]
- Lefebvre, S. (C) 4306–4311 [4406–4411]
- Legros, J. (C) 4225–4228 [4321–4324]
- Lehmann, C. W. (C) 2850–2852 [2910–2913], 4160–4163 [4254–4257]
- Lehn, J.-M.
– Generation of Dynamic Constitutional Diversity and Driven Evolution in Helical Molecular Strands under Lewis Acid Catalyzed Component Exchange (C) 4902–4906 [5010–5014]
DOI: 10.1002/anie.200460343
- Grid-Type Metal Ion Architectures: Functional Metallosupramolecular Arrays (R) 3644–3662 [3728–3747]
DOI: 10.1002/anie.200300636
- Self-Organization of Oligomeric Helical Stacks Controlled by Substrate Binding in a Tobacco Mosaic Virus Like Self-Assembly Process (C) 3695–3699 [3781–3785]
DOI: 10.1002/anie.200353492
- Three-Level Synthetic Strategy Towards Mixed-Valence and Heterometallic $[2 \times 2]$ Gridlike Arrays (C) 240–243 [242–245]
DOI: 10.1002/anie.200352937
- Lehnert, N.
– Diazenes Complexes of Copper: Synthesis, Spectroscopic Analysis, and Electronic Structure (C) 4944–4947 [5052–5055]
DOI: 10.1002/anie.200460415
- Leigh, D. A.
– A 3D Interlocked Structure from a 2D Template: Structural Requirements for the Assembly of a Square-Planar Metal-Coordinated [2]Rotaxane (C) 3914–3918 [4004–4008]
DOI: 10.1002/anie.200353622
- A Simple General Ligand System for Assembling Octahedral Metal–Rotaxane Complexes (C) 1218–1221 [1238–1241]
DOI: 10.1002/anie.200353186
- Controlled Submolecular Translational Motion in Synthesis: A Mechanically Interlocking Auxiliary (C) 3260–3264 [3322–3326]
DOI: 10.1002/anie.200353606
- Shuttling through Anion Recognition (C) 1222–1224 [1242–1244]
DOI: 10.1002/anie.200353248
- Leitner, A. (C) 4797–4800 [4901–4904]
- Lemierre, V. (C) 873–875 [891–893]
- Lemire, C. (C) 118–121 [121–124]
- Lendlein, A. (H) 926–928 [944–946]
- Langlitz, M. (C) 5347–5349 [5461–5463]
- Lentz, D.
– Butenyl-Substituted Alkaline-Earth Metallocenes: A First Step towards Olefin Complexes of the Alkaline-Earth Metals

- (C) 6208–6211 [6335–6338]
DOI: 10.1002/anie.200460927
- Leonard, P. W. (C) 1393–1397 [1417–1421]
- Leong, K. Corrigendum: 3215
- Leoni, S. (C) 1088–1092 [1108–1112]
- Lerner, R. A. (C) 4656–4659 [4756–4759]
- Lesarri, A. (C) 605–610 [615–620]
- Lesch, B. (C) 115–118 [118–120]
- Lescouëzec, R. (C) 2571–2573 [2625–2627]
- Létard, J.-F.
- Thermally and Light-Induced Valence Tautomeric Transition in a Dinuclear Cobalt–Tetraoxolene Complex
(C) 3136–3138 [3198–3200]
DOI: 10.1002/anie.200453944
- Leumann, C. J.
- Stable and Selective Recognition of Three Base Pairs in the Parallel Triple-Helical DNA Binding Motif
(C) 3925–3928 [4015–4018]
DOI: 10.1002/anie.200460159
- Leung, D. H. (C) 963–966 [981–984]
- Leung, W.-H.
- A Water-Soluble Tetranuclear Zr^{IV} Compound Supported by the Kläui Tripodal Ligand: A Model of Zr^{IV} in Aqueous Media
(C) 1715–1718 [1747–1750]
DOI: 10.1002/anie.200353298
- Leutwyler, S. (C) 4738–4741 [4842–4845]
- Lévesque, I. (C) 885–888 [903–906]
- Levina, A. (C) 462–465 [468–471], 4504–4507 [4604–4607]
- Levine, S. (C) 4519–4522 [4619–4622]
- Lewcenko, N. A. (C) 6683–6685 [6851–6853]
- Lewis, A. K. de K. (C) 5824–5827 [5948–5951]
- Lewis, D. W.
- Pressure-Induced Hydration Effects in the Zeolite Laumontite
(C) 469–472 [475–478]
DOI: 10.1002/anie.200352364
- Lewis, W. G. (C) 1255–1260 [1275–1280]
- Ley, S. V. Corrigendum: 1043
- Ley, S. V. (C) 2681–2684 [2735–2738], 4641–4644 [4741–4744]
- Li, C. (C) 1101–1104 [1121–1124]
- Li, D. B. (C) 6709–6713 [6877–6881]
- Li, F.
- Single-Crystal Hexagonal Disks and Rings of ZnO: Low-Temperature, Large-Scale Synthesis and Growth Mechanism
(C) 5238–5242 [5350–5354]
DOI: 10.1002/anie.200460783
- Li, Guanghua (C) 2399–2402 Corrigendum: 3096 [2453–2456 Corrigendum: 3158]
- Li, Guolin (C) 853–856 [871–874]
- Li, Hongbo (C) 4937–4940 [5045–5048]
- Li, Huanjun (C) 1146–1149 [1166–1169]
- Li, J. Corrigendum: 3215
- Li, J. M. (C) 975–977 [993–995]
- Li, J. (Richland)
- Significant Interactions between Uranium and Noble-Gas Atoms: Coordination of the UO₂⁺ Cation by Ne, Ar, Kr, and Xe Atoms
(C) 2554–2557 [2608–2611]
DOI: 10.1002/anie.200453790
- Li, J. (Tokyo) (C) 100–103 [102–105]
- Li, Li (C) 5843–5846 [5967–5970]
- Li, Lidong (C) 360–363 [364–367]
- Li, Lin
- Responsive Aligned Carbon Nanotubes
(C) 4663–4666 [4763–4766]
DOI: 10.1002/anie.200460774
- Li, Linjie (C) 4745–4750 [4849–4854]
- Li, Liting (C) 4937–4940 [5045–5048]
- Li, M. (C) 5837–5839 [5961–5963]
- Li, N.-S. (C) 3033–3037 [3095–3099]
- Li, Qian (C) 6331–6335 [6491–6495]
- Li, Qihong (C) 5048–5052 [5158–5162]
- Li, S. (C) 1146–1149 [1166–1169]
- Li, S.-D.
- M₄H₄X: Hydrometals (M = Cu, Ni) Containing Tetracoordinate Planar Nonmetals (X = B, C, N, O)
(C) 1371–1373 [1395–1397]
DOI: 10.1002/anie.200353068
- Li, W.-S. (C) 2943–2947 [3003–3007]
- Li, Xi (C) 2125–2129 [2177–2181]
- Li, Xiaoyu (R) 4848–4870 [4956–4979]
- Li, Y.-Y. (C) 2409–2411 [2463–2465]
- Li, Yadong
- Colloidal Carbon Spheres and Their Core/Shell Structures with Noble-Metal Nanoparticles
(C) 597–601 [607–611]
DOI: 10.1002/anie.200352386
 - Ga₂O₃ and GaN Semiconductor Hollow Spheres
(C) 3827–3831 [3915–3919]
DOI: 10.1002/anie.200353212
 - Metastable Vanadium Dioxide Nanobelts: Hydrothermal Synthesis, Electrical Transport, and Magnetic Properties
(C) 5048–5052 [5158–5162]
DOI: 10.1002/anie.200460104
 - Thermally Stable Silicate Nanotubes
(C) 2017–2020 [2051–2054]
DOI: 10.1002/anie.200353507
- Li, Yan Corrigendum: 14
- Li, Yan (C) 329–334 [333–338]
- Li, Yi (C) 2399–2402 Corrigendum: 3096 [2453–2456 Corrigendum: 3158]
- Li, Yiwei (C) 4312–4318 [4412–4418]
- Li, Yizhi (C) 5776–5779 [5900–5903]
- Li, Zhenyu (C) 6479–6482 [6641–6644]
- Li, Zhi
- High-Throughput Measurement of the Enantiomeric Excess of Chiral Alcohols by Using Two Enzymes
(C) 1698–1702 [1730–1734]
DOI: 10.1002/anie.200353055
- Liang, C. (C) 5785–5789 [5909–5913]
- Liang, D. (L) 4562–4564 [4662–4664]
- Liang, F.-S. (C) 1562–1566 [1588–1592], 6496–6500 [6658–6662]
- Liang, H.-P. (C) 1540–1543 [1566–1569]
- Liang, K. (C) 5776–5779 [5900–5903]
- Liang, P. (C) 2690–2694 [2744–2748]
- Lichtenegger, H. C. (C) 3037–3040 [3099–3102]
- Lidin, S. (C) 4292–4295 [4392–4395]
- Lie, C. (C) 5517–5519 [5633–5635]
- Light, M. E. (C) 472–475 [478–481]
- Likos, C. N.
- Dendrimers in Solution: Insight from Theory and Simulation
(R) 2998–3020 [3060–3082]
DOI: 10.1002/anie.200300602
- Lill, R. E. (C) 2551–2553 [2605–2607]
- Lim, C. J. (C) 5378–5380 [5492–5494]
- Lim, J. E. (C) 3839–3842 [3927–3930]
- Lim, S.-J. (C) 6346–6350 [6506–6510]
- Lim, W. P. (C) 5685–5689 [5803–5807]
- Lima, J. C. (C) 1525–1527 [1551–1553]
- Lima, N. (C) 3436–3439 [3518–3521], 6132–6135 [6258–6261]
- Limberg, C.
- Intramolecular C–H Activation in Complexes with Mo–Bi Metal Bonds
(C) 2846–2849 [2906–2910]
DOI: 10.1002/anie.200353576
- Limberg, C. (C) 1283–1287 [1303–1307]
- Lin, C.-W. (C) 2940–2943 [3000–3003]
- Lin, K.-J.
- Towards Electrochemical Artificial Muscles: A Supramolecular Machine Based on a One-Dimensional Copper-Containing Organophosphonate System
(C) 4186–4189 [4282–4285]
DOI: 10.1002/anie.200454159
- Lin, L. (C) 2158–2161 [2210–2213]
- Lin, M. (C) 1986–1990 [2020–2024]
- Lin, Wenbin Corrigendum: 1043
- Lin, Wenbin
- Remarkable 4,4'-Substituent Effects on Binap: Highly Enantioselective Ru Catalysts for Asymmetric Hydrogenation of β -Aryl Ketoesters and Their Immobilization in Room-Temperature Ionic Liquids
(C) 2501–2504 [2555–2558]
DOI: 10.1002/anie.200353415
- Lin, Wenwei (C) 4364–4366 [4464–4466]
- Lin, Z. (C) 1735–1738 [1767–1770]
- Lin, Z.-Z. (C) 5665–5668 [5783–5786]
- Linclau, B.
- Enantioselective Synthesis of Tetrafluoroethylene-Containing Monosaccharides
(C) 5677–5679 [5795–5797]
DOI: 10.1002/anie.200460746
- Lindel, T.
- Modular Synthesis of Ruthenium-Labeled Diaryl Ether Peptoids
(C) 1581–1583 [1607–1609]
DOI: 10.1002/anie.200352927
- Lindeman, S. V. (C) 4650–4652 [4750–4752]
- Linden, A. (C) 3307–3310 [3369–3372]
- Lindenschmidt, A. (C) 4526–4528 [4626–4629]
- Linder, V. (C) 498–502 [504–508]
- Lindner, E. (C) 2025–2028 [2059–2062 Corrigendum: 2934]
- Lindner, P. (C) 109–112 [111–114]
- Lindsjö, M. (C) 2540–2543 [2594–2597]
- Ling, T. (C) 4312–4318 [4412–4418], 4318–4324 [4418–4424]
- Linic, S. (C) 2918–2921 [2978–2981]
- Linington, R. G. (C) 5946–5951 [6072–6077]
- Linton, D. J. (C) 2135–2138 [2187–2190]
- Lipowsky, G. (C) 4595–4597 [4695–4698]
- Lipp, J. D. (C) 3691–3695 [3777–3781]
- Lippert, B.
- Metal-Mediated Deamination of Cytosine: Experiment and DFT Calculations
(C) 5396–5399 [5507–5511]
DOI: 10.1002/anie.200460107
- Lippert, B. (C) 3793–3795 [3881–3883]
- Lipshutz, B. H.
- Copper(I)-Catalyzed Asymmetric Hydro-silylations of Imines at Ambient Temperatures
(C) 2228–2230 [2278–2280]
DOI: 10.1002/anie.200353294
- Lisdaf, F.
- Electroactive Cytochrome *c* Multilayers within a Polyelectrolyte Assembly
(C) 4357–4360 [4457–4460]
DOI: 10.1002/anie.200352804

- List, B.
- A Metal-Free Transfer Hydrogenation: Organocatalytic Conjugate Reduction of α,β -Unsaturated Aldehydes (C) 6660–6662 [6829–6832] DOI: 10.1002/anie.200461816
 - Catalytic Asymmetric Intramolecular Michael Reaction of Aldehydes (C) 3958–3960 [4048–4050] DOI: 10.1002/anie.200460578
- Liu, Biao (C) 4745–4750 [4849–4854]
- Liu, Biqian (C) 357–360 [361–364], 2012–2014 [2046–2048]
- Liu, C. (C) 5951–5954 [6077–6080]
- Liu, C.-M.
- A Unique 3D Alternating Ferro- and Antiferromagnetic Manganese Azide System with Threefold Interpenetrating (10,3) Nets (C) 990–994 [1008–1012] DOI: 10.1002/anie.200352780
- Liu, D. (C) 1158–1162 [1178–1182]
- Liu, D. R.
- DNA-Templated Organic Synthesis: Nature's Strategy for Controlling Chemical Reactivity Applied to Synthetic Molecules (R) 4848–4870 [4956–4979] DOI: 10.1002/anie.200400656
- Liu, G. (C) 2158–2161 [2210–2213]
- Liu, H. (C) 1146–1149 [1166–1169], 4663–4666 [4763–4766]
- Liu, H.-K. (C) 4212–4216 [4308–4312]
- Liu, H.-w.
- Structural Analysis of 1-Aminocyclopropane-1-Carboxylate Deaminase: Observation of an Aminyl Intermediate and Identification of Tyr294 as the Active-Site Nucleophile (C) 3425–3429 [3507–3511] DOI: 10.1002/anie.200453353
- Liu, J.-F. (C) 2409–2411 [2463–2465]
- Liu, J.-q. (C) 1287–1290 [1307–1311]
- Liu, Jianhui (C) 3571–3574 [3655–3658]
- Liu, Jianke (C) 90–94 [92–96]
- Liu, Junfeng (C) 5048–5052 [5158–5162]
- Liu, Lei (C) 2915–2918 [2975–2978]
- Liu, Lin (C) 3452–3456 [3534–3538]
- Liu, Q. (C) 6673–6675 [6841–6843]
- Liu, S. (C) 1389–1392 [1413–1416]
- Liu, S.-X. (C) 4738–4741 [4842–4845]
- Liu, Xiaogang (C) 1246–1249 [1266–1269]
- Liu, Xinyu (C) 879–882 [897–900]
- Liu, Xiumei (C) 6377–6381 [6537–6541]
- Liu, Y.
- Water-Soluble Supramolecular Fullerene Assembly Mediated by Metallobridged β -Cyclodextrins (C) 2690–2694 [2744–2748] DOI: 10.1002/anie.200352973
- Liu, Z.-L. (C) 990–994 [1008–1012]
- Liu, Zhimin (C) 1397–1399 [1421–1423], 2415–2417 [2469–2471]
- Liu, Zongwen (C) 63–66 [65–68]
- Lizcano, J. M. (C) 2671–2674 [2725–2728]
- Llebaria, A.
- Disclosing New Inhibitors by Finding Similarities in Three-Dimensional Active-Site Architectures of Polynuclear Zinc Phospholipases and Aminopeptidases (C) 862–865 [880–883] DOI: 10.1002/anie.200352241
- Lledós, A.
- A Measureable Equilibrium between Iridium Hydride Alkylidene and Iridium Hydride Alkene Isomers (C) 3708–3711 [3794–3797] DOI: 10.1002/anie.200454040
- Lloret, F. (C) 210–212 [212–214]
- Lo, S. M. F. (C) 1715–1718 [1747–1750]
- Lobana, T. S.
- Activation of C–Cl and C–H Bonds by Ligated S_2^{2-} Ions: Conversion of Organic Chlorides into Organosulfur Compounds in *cis*-[(IrCp*)(μ -CH₃)₂(μ -S₂R)]⁺ (C) 213–215 [215–217] DOI: 10.1002/anie.200351792
- Lobastov, V. A. (C) 2705–2709 [2759–2763]
- Lobo, C. V. (C) 3429–3432 [3511–3514]
- Lomoth, R.
- A Biomimetic Pathway for Hydrogen Evolution from a Model of the Iron Hydrogenase Active Site (C) 1006–1009 [1024–1027] DOI: 10.1002/anie.200353190
- Londergan, C. H. (C) 1376–1381 [1400–1405]
- Long, De-L. (C) 1817–1820 [1853–1856], 1851–1854 [1887–1890]
- Long, J. R. (C) 5940–5943 [6066–6069]
- Looper, R. E. (C) 2930–2933 [2990–2993]
- Loos, K. (C) 520–523 [527–529]
- Lopez, J. (C) 4172–4178 [4267–4273]
- López, J. C. (C) 605–610 [615–620]
- Lopez, P. (C) 3467–3470 [3549–3552]
- López, R. (C) 3307–3310 [3369–3372]
- López Nieto, J. M. (C) 2538–2540 [2592–2594]
- Lor, M. (C) 6116–6120 [6242–6246]
- Lorenz, V. (C) 4603–4606 [4703–4706]
- Lou, Z. (L) 4700–4701 [4804–4805]
- Lough, A. J. (C) 3321–3325 [3383–3387]
- Louie, J.
- Highly Active Nickel Catalysts for the Isomerization of Unactivated Vinyl Cyclopropanes to Cyclopentenones (C) 2277–2279 [2327–2329] DOI: 10.1002/anie.200353469
- Low, H. Y. (C) 5685–5689 [5803–5807]
- Löwe, H. (R) 406–446 [410–451]
- Lowery, T. J. (C) 6320–6322 [6480–6482]
- Loyaux, D. (C) 2694–2697 [2748–2751]
- Lu, A.-H. (C) 4303–4306 [4403–4406]
- Lu, H. (C) 5834–5836 [5958–5960]
- Lu, L.-De Corrigendum: 14
- Lu, S. (C) 5776–5779 [5900–5903]
- Lu, X.-B.
- Highly Active, Binary Catalyst Systems for the Alternating Copolymerization of CO₂ and Epoxides under Mild Conditions (C) 3574–3577 [3658–3661] DOI: 10.1002/anie.200453998
- Lu, Y.
- A General Route to Macroscopic Hierarchical 3D Nanowire Networks (C) 6169–6173 [6295–6299] DOI: 10.1002/anie.200460535
- Lu, Z.-L. (C) 2025–2028 [2059–2062 Corrigendum: 2934]
- Luchinat, C. (C) 2254–2256 [2304–2306], 2257–2259 [2307–2309]
- Ludwig, K. (C) 2959–2962 [3019–3022]
- Luger, P. (C) 2718–2721 [2773–2776]
- Lumbierres, M. (C) 5839–5842 [5963–5966]
- Luo, H. (C) 6169–6173 [6295–6299]
- Luo, S.-W. (C) 6719–6722 [6887–6890]
- Lusby, P. J. (C) 1218–1221 [1238–1241], 3914–3918 [4004–4008]
- Lutz, J. (C) 2163–2166 [2215–2218]
- Lutz, M. (C) 714–717 Corrigendum: 3748 [732–735 Corrigendum: 3834], 3440–3442 [3522–3524], 3474–3477 [3556–3559]
- Luy, B. (C) 1092–1094 [1112–1115]
- Lycknert, K. (C) 2288–2290 [2338–2340]
- Lyon, E. J. (C) 2547–2551 [2601–2605]
- Lyon, L. A.
- Ligand-Functionalized Core/Shell Microgels with Permselective Shells (C) 6706–6709 [6874–6877] DOI: 10.1002/anie.200461090
- 
- Ma, B.-Q.
- Formation of Two-Dimensional Supramolecular Icelike Layer Containing (H₂O)₁₂ Rings (C) 1374–1376 [1398–1400] DOI: 10.1002/anie.200353097
- Ma, Dawei
- Total Synthesis of Lepadins B, D, E, and H; Determination of the Configuration of the Latter Three Alkaloids (C) 4222–4225 [4318–4321] DOI: 10.1002/anie.200460128
- Ma, Ding
- In Situ Assembly of Zeolitic Building Blocks into High-Order Structures (C) 3452–3456 [3534–3538] DOI: 10.1002/anie.200453777
- In Situ Magnetic Resonance Investigation of Styrene Oxidation over TS-1 Zeolites (C) 6377–6381 [6537–6541] DOI: 10.1002/anie.200461113
- Ma, Hong (C) 1512–1516 [1538–1542]
- Ma, Huimin
- Donor–Donor Energy-Migration Measurements of Dimeric DsbC Labeled at Its N-Terminal Amines with Fluorescent Probes: A Study of Protein Unfolding (C) 4216–4219 [4312–4315] DOI: 10.1002/anie.200460072
- Ma, J.-A. (R) 4566–4583 [4666–4683]
- Ma, J.-F.
- A Mixed-Valence Tin–Oxygen Cluster Containing Six Peripheral Ferrocene Units (C) 2409–2411 [2463–2465] DOI: 10.1002/anie.200353359
- Ma, S.
- A 1,3-Lithium Shift of Propargylic/Allenyl Lithium and the Subsequent Transmetalation Coupling Reaction with Aryl Halides (C) 988–990 [1006–1008] DOI: 10.1002/anie.200352924
- Ma, Y. (C) 357–360 [361–364], 2012–2014 [2046–2048]
- Ma, Z. (C) 5977–5980 [6103–6106]
- McCarthy, D. (C) 5242–5246 [5354–5358]
- McDonald, R. (C) 5967–5971 [6093–6097], 6161–6165 [6287–6291]
- McDonald, R. E. (C) 3025–3029 [3087–3091]
- MacFarlane, D. R.
- Ionic Liquids as Moderators in Exothermic Polymerization Reactions (C) 5363–5366 [5477–5480] DOI: 10.1002/anie.200460575

- MacGillivray, L. R.
– Supramolecular Construction of Molecular Ladders in the Solid State (C) 232–236 [234–238]
DOI: 10.1002/anie.200352713
- McGrady, G. S.
– Agostic Interactions in d⁰ Metal Alkyl Complexes (R) 1782–1806 [1816–1842]
DOI: 10.1002/anie.200200548
- Machado, A. H. L. (C) 2514–2518 Corrigendum: 4389 [2568–2572 Corrigendum: 4489]
- McIndoe, J. S.
– An Octahedral Rhodium Cluster with Six Phosphine and 12 Hydride Ligands and 10 Too Few Electrons (H) 6028–6030 [6152–6154]
DOI: 10.1002/anie.200460924
- McKee, M. L. (C) 2843–2846 [2903–2906]
- McKenna, B. J. (C) 5652–5655 [5770–5773]
- McKenzie, K. M. (C) 2106–2108 [2158–2160], 4052–4055 [4144–4147]
- McKinlay, R. M. (C) 5263–5266 [5375–5378]
- MacKinnon, R.
– Potassium Channels and the Atomic Basis of Selective Ion Conduction (Nobel Lecture) (R) 4265–4277 [4363–4376]
DOI: 10.1002/anie.200400662
- Semisynthesis of a Functional K⁺ Channel (C) 2504–2507 [2558–2561]
DOI: 10.1002/anie.200453849
- McLain, S. E. (C) 1952–1955 [1986–1989]
- McLaughlin, L. W.
– Ru(II) Tris(bipyridyl) Complexes with Six Oligonucleotide Arms as Precursors for the Generation of Supramolecular Assemblies (C) 5808–5811 [5932–5935]
DOI: 10.1002/anie.200460399
- McMahon, R. J.
– Organic Chemistry and Education: *Orville L. Chapman* (O) 4122 [4214]
DOI: 10.1002/anie.200460954
- Macmillan, D.
– Modular Assembly of Glycoproteins: Towards the Synthesis of GlyCAM-1 by Using Expressed Protein Ligation (C) 1355–1359 [1379–1383]
DOI: 10.1002/anie.200352673
- MacMillan, D. W. C.
– Enantioselective Organocatalytic Direct Aldol Reactions of α -Oxyaldehydes: Step One in a Two-Step Synthesis of Carbohydrates (C) 2152–2154 [2204–2206]
DOI: 10.1002/anie.200453716
- The Importance of Iminium Geometry Control in Enamine Catalysis: Identification of a New Catalyst Architecture for Aldehyde–Aldehyde Couplings (C) 6722–6724 [6890–6892]
DOI: 10.1002/anie.200461851
- MacMillan, J. B. (C) 5946–5951 [6072–6077], 5951–5954 [6077–6080]
- McNally, S. J. (C) 340–343 [344–347]
- McNay, G. (C) 2512–2514 [2566–2568]
- MacNeil, S. (R) 2206–2225 [2256–2276]
- Maeda, A. (C) 3595–3598 [3679–3682]
- Maeda, Hatsuo
– Fluorescent Probes for Hydrogen Peroxide Based on a Non-Oxidative Mechanism (C) 2389–2391 [2443–2445]
DOI: 10.1002/anie.200452381
- Maeda, Hiromitsu (C) 2951–2955 [3011–3015]
- Maeda, Y. (C) 5060–5062 [5170–5172]
- Maegawa, T. (C) 3595–3598 [3679–3682]
- Maesato, M. (C) 6343–6346 [6503–6506]
- Mägerlein, W. (C) 5255–5260 [5367–5372]
- Magnet, Sophie (C) 1591–1594 [1618–1620]
- Magnet, Stéphanie (C) 6186–6189 [6312–6315]
- Magull, J. (C) 3443–3445 [3525–3527], 3832–3835 [3920–3923], 3842–3844 [3930–3932]
- Mahidol, C. (C) 866–868 [884–886]
- Mahrwald, R. (C) 4597–4601 [4698–4702]
- Mai, E. (C) 5691–5694 [5809–5812]
- Mai, Z. (C) 2012–2014 [2046–2048]
- Maier, G.
– Reaction of Atomic Silicon with Phosphane: A Matrix-Spectroscopic Study (C) 1294–1296 [1314–1317]
DOI: 10.1002/anie.200353111
- Maier, J.
– A Linear Free Energy Relationship for Gas-Solid Interactions: Correlation between Surface Rate Constant and Diffusion Coefficient of Oxygen Tracer Exchange for Electron-Rich Perovskites (C) 5069–5073 [5179–5183]
DOI: 10.1002/anie.200460081
- Maier, M. E.
– Total Synthesis of Apicularen A through Transannular Pyran Formation (C) 5821–5823 [5945–5947]
DOI: 10.1002/anie.200460760
- Maier, W. F.
– Directed Evolution of Noble-Metal-Free Catalysts for the Oxidation of CO at Room Temperature (C) 2028–2031 [2062–2066]
DOI: 10.1002/anie.200351935
- High-Throughput Method for the Impedance Spectroscopic Characterization of Resistive Gas Sensors (C) 752–754 [770–773]
DOI: 10.1002/anie.200352424
- Mainolfi, N. (C) 5680–5682 [5798–5800]
- Majdalani, A. (C) 1731–1734 [1763–1766]
- Maji, T. K. (C) 3269–3272 [3331–3334]
- Majima, T.
– Design and Synthesis of Photochemically Controllable Caspase-3 (C) 5643–5645 [5761–5763]
DOI: 10.1002/anie.200460889
- Two-Color Two-Laser DNA Damaging (C) 2406–2409 [2460–2463]
DOI: 10.1002/anie.200353318
- Makino, K. (C) 882–884 [900–902]
- Malacria, M.
– Titanium-Mediated Domino Radical Cyclization/ β Elimination of Phosphine Oxides (C) 4220–4222 [4316–4318]
DOI: 10.1002/anie.200460099
- Maleev, V. I. (C) 4085–4089 [4177–4181]
- Mallah, T. (C) 5772–5775 Corrigendum: 6581 [5896–5899 Corrigendum: 6743]
- Maltman, B. A. (C) 3138–3141 [3200–3203]
- Malysheva, N. N. (C) 3069–3072 [3131–3134]
- Mamat, C. (C) 5406–5408 [5521–5523]
- Mammi, S. (C) 3152–3155 [3214–3217]
- Manabe, S. (C) 5674–5677 [5792–5795]
- Manakov, A. Yu. (C) 2922–2924 [2982–2984]
- Mandal, B. (C) 4172–4178 [4267–4273]
- Mandal, M. (C) 2557–2561 [2611–2615], 2562–2565 [2616–2619]
- Mandl, C. P. (H) 1622–1624 [1650–1652]
- Manea, F. (C) 6165–6169 [6291–6295]
- Mangion, I. K. (C) 2152–2154 [2204–2206], 6722–6724 [6890–6892]
- Mani, G. (C) 2263–2266 [2313–2316]
- Mann, E. (C) 95–98 [97–100]
- Mann, S.
– Preparation of Higher-Order Zeolite Materials by Using Dextran Templating (C) 6691–6695 [6859–6863]
DOI: 10.1002/anie.200460146
- Promotion of Fluorapatite Crystallization by Soluble-Matrix Proteins from *Lingula Anatina* Shells (C) 885–888 [903–906]
DOI: 10.1002/anie.200353115
- Synthesis and Self-Assembly of Organoclay-Wrapped Biomolecules (C) 4928–4933 [5036–5041]
DOI: 10.1002/anie.200453868
- Manners, I.
– Isolation of [1]Ruthenocenophanes: Synthesis of Polyruthenocenylstannanes by Ring-Opening Polymerization (C) 3321–3325 [3383–3387]
DOI: 10.1002/anie.200454022
- Redox-Active Organometallic Vesicles: Aqueous Self-Assembly of a Diblock Copolymer with a Hydrophilic Polyferrocenylsilane Polyelectrolyte Block (C) 1260–1264 [1280–1284]
DOI: 10.1002/anie.200352819
- Swellable, Redox-Active Shell-Crosslinked Organometallic Nanotubes (C) 3703–3707 [3789–3793]
DOI: 10.1002/anie.200453969
- Mano, N.
– Optimization Of “Wired” Enzyme O₂-Electroreduction Catalyst Compositions by Scanning Electrochemical Microscopy (C) 6355–6357 [6515–6517]
DOI: 10.1002/anie.200461528
- Mansfield, P.
– Snapshot Magnetic Resonance Imaging (Nobel Lecture) (R) 5456–5464 [5572–5580]
DOI: 10.1002/anie.200460078
- Mansikkamäki, H. (C) 1243–1246 [1263–1266]
- Mao, C.
– A DNA Nanomachine Based on a Duplex–Triplex Transition (C) 5335–5338 [5449–5452]
DOI: 10.1002/anie.200460789
- An Autonomous DNA Nanomotor Powered by a DNA Enzyme (C) 3554–3557 [3638–3641]
DOI: 10.1002/anie.200453779
- Molecular Lithography with DNA Nanostructures (C) 4068–4070 [4160–4162]
DOI: 10.1002/anie.200460257
- Marahiel, M. A.
– Peptidyl Thiophenols as Substrates for Nonribosomal Peptide Cyclases (C) 493–498 [499–504]
DOI: 10.1002/anie.200352787
- Marby, K. A. (C) 1562–1566 [1588–1592]
- Marchetti, A. (C) 846–849 [864–867]
- Marco-Contelles, J.
– β -Lactam Synthesis by the Kinugasa Reaction

- (H) 2198–2200 [2248–2250]
DOI: 10.1002/anie.200301730
- Marder, S. R.
– Cubic Liquid-Crystalline Nanoparticles (M) 4402–4409 [4502–4510]
DOI: 10.1002/anie.200301683
- Marder, T. B.
– Structure and Phase Behavior of a 2:1 Complex between Arene- and Fluoroarene-Based Conjugated Rigid Rods (C) 3061–3063 [3123–3125]
DOI: 10.1002/anie.200453828
- Marder, T. B. (C) 5523–5526 [5639–5642]
- Margadonna, S.
– Large Lattice Responses in a Mixed-Valence Prussian Blue Analogue Owing to Electronic and Spin Transitions Induced by X-ray Irradiation (C) 6316–6319 [6476–6479]
DOI: 10.1002/anie.200460603
- Margiolaki, I. (C) 6296–6301 [6456–6461]
- Mari, A. (C) 2266–2270 [2316–2320]
- Marica, F. (C) 3565–3568 [3649–3652]
- Marigo, M. (C) 5507–5510 [5623–5626]
- Markert, C. (C) 2498–2500 [2552–2554]
- Markó, I. E.
– Efficient, Copper-Catalyzed, Aerobic Oxidation of Primary Alcohols (C) 1588–1591 [1614–1617]
DOI: 10.1002/anie.200353458
- Markov, V. Y. (C) 997–1000 [1015–1018]
- Marković, D. (C) 2928–2930 [2988–2990]
- Markovitch, G. (C) 4519–4522 [4619–4622]
- Marks, T. J.
– High-Mobility Air-Stable n-Type Semiconductors with Processing Versatility: Dicyanoperylene-3,4:9,10-bis(dicarboximides) (C) 6363–6366 [6523–6526]
DOI: 10.1002/anie.200461324
- Polynuclear Olefin Polymerization Catalysis: Proximity and Cocatalyst Effects Lead to Significantly Increased Polyethylene Molecular Weight and Comonomer Enchainment Levels (C) 4937–4940 [5045–5048]
DOI: 10.1002/anie.200460288
- Marmé, N. (C) 3798–3801 [3886–3890]
- Marrot, J. (C) 2274–2277 [2324–2327], 5468–5471 [5584–5587]
- Marsden, J. A. (C) 1694–1697 [1726–1729]
- Martens, J. A.
– Adsorption Chemistry of Sulfur Dioxide in Hydrated Na–Y Zeolite (C) 3722–3724 [3808–3810]
DOI: 10.1002/anie.200454266
- Reply (L) 4562–4564 [4662–4664]
DOI: 10.1002/anie.200460541
- Martin, R. (C) 3955–3957 [4045–4047]
- Martin, R. L.
– Molecular and Electronic Structure of Platinum Bis(*N*-arylamino)phosphonium Complexes including [Pt(phosphane)-(phosphonium)(*N*-heterocyclic carbene)] (C) 1955–1958 [1989–1992]
DOI: 10.1002/anie.200352326
- Martin, S. E. (C) 5181–5185 Corrigendum: 5428 [5293–5297 Corrigendum: 5542]
- Martin-Litas, I. (C) 2103–2105 [2155–2157]
- Martin-Matute, B. (C) 6535–6539 [6697–6701]
- Martinell, M. (C) 196–198 [198–200]
- Martinelli, J. R. (C) 1871–1876 [1907–1912]
- Martínez-Méndez, L. (C) 3464–3467 [3546–3549]
- Marty, J.-D. (C) 6174–6177 [6300–6303]
- Marumoto, K. (C) 3171–3175 [3233–3237], 4763–4767 [4867–4871]
- Maruyama, A. (C) 3595–3598 [3679–3682]
- Maruyama, T. (C) 2145–2148 [2197–2200]
- Marvaud, V.
– Reversible Photoinduced Magnetic Properties in the Heptanuclear Complex [Mo^{IV}(CN)₂(CN–CuL)₆]⁸⁺: A Photomagnetic High-Spin Molecule (C) 5468–5471 [5584–5587]
DOI: 10.1002/anie.200460387
- Marx, A.
– Bigger DNA: New Double Helix with Expanded Size (H) 1625–1626 [1653–1654]
DOI: 10.1002/anie.200301737
- Marx, D.
– Assigning Protonation Patterns in Water Networks in Bacteriorhodopsin Based on Computed IR Spectra (C) 4804–4807 [4908–4911]
DOI: 10.1002/anie.200453857
- Marx, D. (C) 6641–6645 [6809–6814]
- Masaoka, S. (C) 2530–2534 [2584–2588]
- Mase, N. (C) 2420–2423 [2474–2477]
- Maskey, R. P. (C) 1281–1283 [1301–1303]
- Maspoch, D. (C) 1828–1832 [1864–1868]
- Massa, W. Corrigendum: 2737
- Masson, O. (C) 2694–2697 [2748–2751]
- Masuno, M. N. (C) 5951–5954 [6077–6080]
- Masuo, S. (C) 6116–6120 [6242–6246]
- Masuyama, T. (C) 730–733 [748–751]
- Matarrese, R. (C) 5812–5815 [5936–5939]
- Mateu, M. G. (C) 196–198 [198–200]
- Mathew, S. P. (C) 3317–3321 [3379–3383]
- Mathonière, C.
– Reversible Photoinduced Magnetic Properties in the Heptanuclear Complex [Mo^{IV}(CN)₂(CN–CuL)₆]⁸⁺: A Photomagnetic High-Spin Molecule (C) 5468–5471 [5584–5587]
DOI: 10.1002/anie.200460387
- Matoussevitch, N. (C) 4303–4306 [4403–4406]
- Matsubara, R. (C) 1679–1681 [1711–1713], 3258–3260 [3320–3322]
- Matsubara, Y. (C) 366–369 [370–373]
- Matsuda, A. (C) 221–224 Corrigendum: 3096 [223–226 Corrigendum: 3158]
- Matsuda, H. (C) 6350–6355 [6510–6515]
- Matsuda, R. (C) 2684–2687 [2738–2741], 3269–3272 [3331–3334]
- Matsuda, Y. (C) 1825–1828 [1861–1864]
- Matsueda, Y. (C) 4490–4492 [4590–4592]
- Matsumoto, A.
– Supramolecular Control over the Stereochemistry of Diene Polymers (C) 3811–3814 [3899–3902]
DOI: 10.1002/anie.200453738
- Matsumoto, K. (C) 104–106 [106–108]
- Matsumoto, S. (C) 4610–4612 [4710–4712]
- Matsumoto, Takuya
– Kinetic and Thermodynamic Control by Chemical Bond Rearrangement on a Si(001) Surface (C) 1349–1352 [1373–1376]
DOI: 10.1002/anie.200352074
- Matsumoto, Tomoharu (C) 2527–2530 [2581–2584]
- Matsunaga, Satoshi (C) 4763–4767 [4867–4871]
- Matsunaga, Shigeki (C) 478–482 [484–488], 4493–4497 [4593–4597]
- Matsuno, H. (C) 2389–2391 [2443–2445]
- Matsuo, T. (C) 1404–1407 [1428–1431]
- Matsuoka, T. (C) 1969–1972 [2003–2006]
- Matsushita, Masayuki (C) 2106–2108 [2158–2160]
- Matsushita, Mitsunori (C) 1576–1580 [1602–1606]
- Matsushita, T. (C) 4071–4075 [4163–4167]
- Matsuzaki, H. (C) 3171–3175 [3233–3237], 4763–4767 [4867–4871]
- Matteson, D. S.
– Conversion of Alkyltrifluoroborates into Alkylchloroboranes with Tetrachlorosilane in Coordinating Solvents (C) 3056–3058 [3118–3120]
DOI: 10.1002/anie.200453690
- Matthews, C. J.
– Self-Assembly of a Spin-Coupled Octanuclear Copper(II) Circular Array from a Single-Stranded Ligand (C) 1814–1817 [1850–1853]
DOI: 10.1002/anie.200352554
- Matxain, J. M. (C) 5485–5488 [5601–5604]
- Matyjaszewski, K. (C) 2783–2787 [2843–2847]
- Matzger, A. J. (C) 3711–3715 [3797–3801]
- Mauders, B. M. (C) 5366–5369 [5480–5483]
- Mavrikakis, M.
– Strain-Induced Formation of Subsurface Species in Transition Metals (C) 4296–4300 [4396–4400]
DOI: 10.1002/anie.200454062
- Mayer, H. A. (C) 2025–2028 [2059–2062 Corrigendum: 2934]
- Mayer, M. (C) 1555–1558 [1581–1584]
- Mayor, M.
– Statistical Analysis of Single-Molecule Junctions (H) 2882–2884 [2942–2944]
DOI: 10.1002/anie.200301733
- Mayr, H.
– Electrophilic Alkylations in Neutral Aqueous or Alcoholic Solutions (C) 5402–5405 [5518–5521]
DOI: 10.1002/anie.200460812
- S_N1 Reactions with Inverse Rate Profiles (C) 2302–2305 [2353–2356]
DOI: 10.1002/anie.200353468
- Mays, J. W. (C) 2138–2142 [2190–2194], 5785–5789 [5909–5913]
- Mayser, P.
– Pityriarubins, Biologically Active Bis(indolyl)spirans from Cultures of the Lipophilic Yeast *Malassezia furfur* (C) 1098–1100 [1119–1121]
DOI: 10.1002/anie.200352549
- Mazitschek, R. (C) 224–228 Corrigendum: 540 [226–230 Corrigendum: 547]
- Mecking, S.
– Nature or Petrochemistry?—Biologically Degradable Materials (M) 1078–1085 [1096–1104]
DOI: 10.1002/anie.200301655
- Remote Substituents Controlling Catalytic Polymerization by Very Active and Robust Neutral Nickel(II) Complexes (C) 869–873 [887–891]
DOI: 10.1002/anie.200352062
- Mee, S. P. H. (C) 1132–1136 [1152–1156]
- Meetsma, A. (C) 1663–1667 [1695–1699]
- Meglio, A. (C) 4785–4788 [4889–4892]
- Meierhenrich, U. J.
– The Molecular Basis of Olfactory Chemoreception (H) 6410–6412 [6570–6573]
DOI: 10.1002/anie.200462322

- Meijer, E. J.
– Proton-Assisted Ethylene Hydration in Aqueous Solution
(C) 1660–1662 [1692–1694]
DOI: 10.1002/anie.200353103
- Meijer, E. W.
– Efficient Energy Transfer in Mixed Columnar Stacks of Hydrogen-Bonded Oligo(*p*-phenylene vinylene)s in Solution
(C) 1976–1979 [2010–2013]
DOI: 10.1002/anie.200353451
- Multivalency in the Gas Phase: The Study of Dendritic Aggregates by Mass Spectrometry
(C) 3557–3562 [3641–3646]
DOI: 10.1002/anie.200453707
- π -Conjugated Oligo(*p*-phenylenevinylene) Rosettes and Their Tubular Self-Assembly
(C) 74–78 [76–80]
DOI: 10.1002/anie.200352790
- Meijer, E. W. (C) 3422–3425 [3504–3507]
Meijerink, A.
– Temperature Antiquenching of the Luminescence from Capped CdSe Quantum Dots
(C) 3029–3033 [3091–3095]
DOI: 10.1002/anie.200353532
- Meijler, M. M. (C) 2106–2108 [2158–2160]
Meiser, F. (C) 5954–5957 [6080–6083]
Melchiorre, P. (C) 84–87 [86–89]
Melloni, A. (M) 550–556 [560–566]
Mellot-Draznieks, C.
– Hybrid Organic–Inorganic Frameworks: Routes for Computational Design and Structure Prediction
(C) 6290–6296 [6450–6456]
DOI: 10.1002/anie.200454251
- Mellot-Draznieks, C. (C) 6296–6301 [6456–6461]
Menceloglu, Y. Z.
– Tunable, Superhydrophobically Stable Polymeric Surfaces by Electrospinning
(C) 5210–5213 [5322–5325]
DOI: 10.1002/anie.200461092
- Meng, J.-C. (C) 1255–1260 [1275–1280]
Menger, F. M.
– Vesicular Latex
(C) 1265–1267 [1285–1287]
DOI: 10.1002/anie.200352936
- Menjón, B.
– A Five-Coordinate Homoleptic Organotitanium(III) Compound
(C) 5225–5228 [5337–5340]
DOI: 10.1002/anie.200460111
- Menozi, C. (C) 6680–6683 [6848–6851]
Merca, A. (C) 4466–4470 Corrigendum: 5115 [4566–4570 Corrigendum: 5225]
Mercero, J. M.
– Mono- and Multidecker Sandwich-Like Complexes of the Tetraazacyclobutadiene Aromatic Ring
(C) 5485–5488 [5601–5604]
DOI: 10.1002/anie.200460498
- Mereiter, K. (C) 3708–3711 [3794–3797]
Merino, P.
– Organocatalyzed Asymmetric α -Aminoxylation of Aldehydes and Ketones—An Efficient Access to Enantiomerically Pure α -Hydroxycarbonyl Compounds, Diols, and Even Amino Alcohols
(H) 2995–2997 [3055–3058]
DOI: 10.1002/anie.200301760
- Merkle, R. (C) 5069–5073 [5179–5183]
Merten, J. (C) 5991–5994 [6117–6120]
Merz, L. (C) 1291–1294 [1311–1314]
Merz, M. (C) 1283–1287 [1303–1307]
Mesa, J. L.
– $(\text{C}_4\text{N}_2\text{H}_{12})[\text{Fe}^{\text{II}}_{0.86}\text{Fe}^{\text{III}}_{1.14}(\text{HPO}_3)_{1.39}(\text{HPO}_4)_{0.47}(\text{PO}_4)_{0.14}\text{F}_3]$: A Fluoro-Phosphite–Hydrogenphosphate–Phosphate Iron(II,III) Mixed-Valence Organically Templated Compound
(C) 977–980 [995–998]
DOI: 10.1002/anie.200352219
- Mesbah, W. Corrigendum: 2737
Meskers, S. C. J. (C) 1976–1979 [2010–2013]
Messaoudi, A. (C) 6120–6125 [6246–6251]
Méthivier, A. (C) 364–366 [368–370]
Metz, P.
– Enantioselective Total Synthesis of the Highly Oxygenated 1,10-*seco*-Eudesmanolides Eriolanin and Eriolangin
(C) 5991–5994 [6117–6120]
DOI: 10.1002/anie.200460936
- Meyer, Arndt (C) 4629–4633 [4729–4733]
Meyer, Axel (C) 6649–6652 [6818–6821]
Meyer, B.
– A Peptidomimetic HIV-Entry Inhibitor Directed against the CD4 Binding Site of the Viral Glycoprotein gp120
(C) 2937–2940 [2997–3000]
DOI: 10.1002/anie.200353271
- Partial Dissociation of Water Leads to Stable Superstructures on the Surface of Zinc Oxide
(C) 6641–6645 [6809–6814]
DOI: 10.1002/anie.200461696
- Meyer, G.
– An Oxygen-Centered Titanium Square Embedded in a Cuboctahedron of Iodine in the Salt $\text{K}_4[\text{Ti}_4\text{O}_{12}]$
(C) 3183–3185 [3245–3248]
DOI: 10.1002/anie.200453739
- Meyer, K. (C) 3156–3159 [3218–3221]
Meyer, R. (C) 118–121 [121–124]
Mézaillies, N. (C) 6382–6385 [6542–6545]
Mezei, G. (C) 574–577 [584–587]
Meziani, M. J. (C) 704–707 [722–725]
Miah, M. A. (C) 1712–1714 [1744–1746]
Mialane, P.
– A Polyoxometalate Containing the $[\text{Ni}_2\text{N}_3]$ Fragment: Ferromagnetic Coupling in a Ni^{II} μ -1,1 Azido Complex with a Large Bridging Angle
(C) 2274–2277 [2324–2327]
DOI: 10.1002/anie.200353433
- Miao, C.-Q. (C) 1371–1373 [1395–1397]
Michalik, M. (C) 5066–5069 [5176–5179]
Michl, M. (C) 634–636 [644–646]
Micklefield, J.
– Biotransformations in Low-Boiling Hydrofluorocarbon Solvents
(C) 5519–5523 [5635–5639]
DOI: 10.1002/anie.200460082
- Micura, R.
– Genetic Control by a Natural Metabolite-Responsive Ribozyme
(H) 4692–4694 [4797–4799]
DOI: 10.1002/anie.200460233
- Triggering of RNA Secondary Structures by a Functionalized Nucleobase
(C) 3922–3925 [4012–4015]
DOI: 10.1002/anie.200460068
- Midgley, P. A.
– The Chemical Application of High-Resolution Electron Tomography: Bright Field or Dark Field?
(C) 6745–6747 [6913–6915]
DOI: 10.1002/anie.200461453
- Mielgo, A. (H) 5442–5444 [5558–5560]
Migawa, M. T. (C) 6735–6738 [6903–6906]
Miguel, D. (C) 3464–3467 [3546–3549]
Mikami, R. (C) 6135–6139 [6261–6265]
Miki, K. (C) 1857–1860 [1893–1896]
Milburn, R. R. (C) 888–891 [906–909], 892–894 [910–912]
Milios, C. J. (C) 210–212 [212–214]
Miljanić, O. S. (C) 3711–3715 [3797–3801]
Millange, F. (C) 6285–6289 [6445–6449], 6296–6301 [6456–6461]
Miller, J. J. (C) 1694–1697 [1726–1729]
Miller, L. W. (C) 1672–1675 [1704–1707]
Miller, N. (C) 4595–4597 [4695–4698]
Millet, P. (C) 4292–4295 [4392–4395]
Mills, A. M. (C) 3474–3477 [3556–3559]
Milstein, D.
– Self-Oxidation of a Phenolate Complex to a Bimetallic Stilbene Quinone
(C) 5961–5963 [6087–6089]
DOI: 10.1002/anie.200460360
- Mimna, R. (C) 4172–4178 [4267–4273]
Min, D.-H. (C) 5973–5977 [6099–6103]
Minakata, S.
– Silica–Water Reaction Media: Its Application to the Formation and Ring Opening of Aziridines
(C) 79–81 [81–83]
DOI: 10.1002/anie.200352842
- Minami, T. (C) 1251–1254 [1271–1274]
Mindiola, D. J.
– Cationic and Neutral Four-Coordinate Alkylidene Complexes of Vanadium(IV) Containing Short V=C Bonds
(C) 3156–3159 [3218–3221]
DOI: 10.1002/anie.200353210
- Minegishi, S. (C) 2302–2305 [2353–2356]
Mingotaud, C.
– A Catalytic Langmuir Film as a Model for Heterogeneous and Homogeneous Catalytic Processes
(C) 6174–6177 [6300–6303]
DOI: 10.1002/anie.200461007
- Minozzi, M.
– A Novel Tin-Free Procedure for Alkyl Radical Reactions
(C) 3598–3601 [3682–3685]
DOI: 10.1002/anie.200454245
- Mioskowski, C.
– Kinetic Resolution of Amines: A Highly Enantioselective and Chemoselective Acetylating Agent with a Unique Solvent-Induced Reversal of Stereoselectivity
(C) 3314–3317 [3376–3379]
DOI: 10.1002/anie.200453956
- Mirkin, C. A.
– Bioactive Protein Nanoarrays on Nickel Oxide Surfaces Formed by Dip-Pen Nanolithography
(C) 1246–1249 [1266–1269]
DOI: 10.1002/anie.200353203
- Control of Nanoparticle Assembly by Using DNA-Modified Diatom Templates
(C) 5500–5503 [5616–5619]
DOI: 10.1002/anie.200460905
- Multicomponent Magnetic Nanorods for Biomolecular Separations
(C) 3048–3050 [3110–3112]
DOI: 10.1002/anie.200454088
- Reversibly Addressing an Allosteric Catalyst In Situ: Catalytic Molecular Tweezers
(C) 5503–5507 [5619–5623]
DOI: 10.1002/anie.200460932
- The Evolution of Dip-Pen Nanolithography

- (R) 30–45 [30–46]
DOI: 10.1002/anie.200300608
- Mirodatos, C. (C) 5347–5349 [5461–5463]
- Mironov, Yu. V. (C) 1297–1300 [1317–1321]
- Mita, T. (C) 5249–5253 [5361–5365]
- Mitchell, C. (C) 6683–6685 [6851–6853]
- Mitchell, E. P. (C) 5918–5922 [6044–6048]
- Mitchell-Koch, J. T. (C) 2806–2809 [2866–2869]
- Mitra, D. (C) 5804–5808 [5928–5932]
- Mitsudo, T.-a.
- Ru- and Rh-Catalyzed C–C Bond Cleavage of Cyclobutenones: Reconstructive and Selective Synthesis of 2-Pyranones, Cyclopentenones, and Cyclohexenones (C) 5369–5372 [5483–5486]
DOI: 10.1002/anie.200461002
- Mitsui, K. (C) 490–492 [496–498]
- Mittendorfer, H. (C) 3922–3925 [4012–4015]
- Miura, A. (C) 74–78 [76–80]
- Miura, K. (C) 2423–2425 [2477–2479]
- Miura, M.
- Rational Ligand Design in Constructing Efficient Catalyst Systems for Suzuki–Miyaura Coupling (H) 2201–2203 [2251–2253]
DOI: 10.1002/anie.200301753
 - Synthesis of Highly Substituted 1,3-Butadienes by Palladium-Catalyzed Arylation of Internal Alkynes (C) 5063–5065 [5173–5175]
DOI: 10.1002/anie.200460409
- Miyagishi, M. (C) 3160–3163 [3222–3225]
- Miyahara, Y.
- Remarkably Facile Ring-Size Control in Macrocyclization: Synthesis of Hemicucurbit[6]uril and Hemicucurbit[12]uril (C) 5019–5022 [5129–5132]
DOI: 10.1002/anie.200460764
- Miyake, F. Y. (C) 5357–5360 [5471–5474]
- Miyake, J. (C) 3806–3810 Corrigendum: 4389 [3894–3898 Corrigendum: 4489]
- Miyake, M. (C) 3806–3810 Corrigendum: 4389 [3894–3898 Corrigendum: 4489]
- Miyamae, H. (C) 4763–4767 [4867–4871]
- Miyamoto, K. (C) 2389–2391 [2443–2445]
- Miyamura, S. (C) 366–369 [370–373]
- Miyano, S. (C) 1832–1835 [1868–1871]
- Miyasaka, H.
- A Dimeric Manganese(III) Tetradentate Schiff Base Complex as a Single-Molecule Magnet (C) 2801–2805 [2861–2865]
DOI: 10.1002/anie.200353563
 - A Three-Dimensional Ferrimagnet Composed of Mixed-Valence Mn₄ Clusters Linked by an [Mn(N(CN)₂)₆]^{4–} Unit (C) 707–711 [725–729]
DOI: 10.1002/anie.200353093
- Miyasaka, H. (C) 3171–3175 [3233–3237], 4763–4767 [4867–4871]
- Miyashita, M.
- Stereoselective Total Synthesis of the Ionophore Antibiotic Zincophorin (C) 4341–4345 [4441–4445]
DOI: 10.1002/anie.200460434
- Miyazawa, K. (C) 6553–6557 [6715–6719]
- Mizukami, F. (C) 4892–4896 [5000–5004]
- Mizuno, N.
- Efficient Hydration of Nitriles to Amides in Water, Catalyzed by Ruthenium Hydroxide Supported on Alumina (C) 1576–1580 [1602–1606]
DOI: 10.1002/anie.200353461
- Mo, Y.
- The Magnitude of Hyperconjugation in Ethane: A Perspective from Ab Initio Valence Bond Theory (C) 1986–1990 [2020–2024]
DOI: 10.1002/anie.200352931
- Mobian, P. (C) 2392–2395 [2446–2449]
- Moehle, K. (C) 2109–2112 [2161–2164]
- Mohr, F. (C) 969–971 [987–989]
- Möhwald, H.
- Photoinduced Vectorial Charge Transfer across Walls of Hollow Microcapsules (C) 360–363 [364–367]
DOI: 10.1002/anie.200352657
- Möhwald, H. (C) 4357–4360 [4457–4460], 5639–5642 [5757–5760]
- Moisan, L. (R) 5138–5175 [5248–5286]
- Molev, G. (C) 745–748 [763–766]
- Molinski, T. F.
- Enantioselective Total Synthesis of (+)-Milnamide A and Evidence of Its Autoxidation to (+)-Milnamide D (C) 5951–5954 [6077–6080]
DOI: 10.1002/anie.200461245
 - Stereochemical Assignment in Acyclic Lipids Across Long Distance by Circular Dichroism: Absolute Stereochemistry of the Aglycone of Caminoside A (C) 5946–5951 [6072–6077]
DOI: 10.1002/anie.200461158
- Moll, M. (C) 1877–1880 [1913–1916], 3141–3144 [3203–3206]
- Möller, A. (C) 3183–3185 [3245–3248]
- Monaghan, P. B. (C) 2512–2514 [2566–2568]
- Monahan, J. (C) 448–450 Corrigendum: 2986 [454–456 Corrigendum: 3046]
- Monde, K. (C) 856–862 [874–880], 1516–1520 [1542–1546]
- Monsees, A. (C) 5066–5069 [5176–5179]
- Montgomery, J.
- Nickel-Catalyzed Reductive Cyclizations and Couplings (R) 3890–3908 [3980–3998]
DOI: 10.1002/anie.200300634
- Montoya, D. P. (C) 4924–4928 [5032–5036]
- Moon, K. (C) 5496–5499 [5612–5615]
- Moore, D. R. (C) 6618–6639 [6784–6806]
- Moore, E. E. (C) 5827–5830 [5951–5954]
- Mootz, H. D. (C) 5189–5192 [5301–5304]
- Morales, G. M. (C) 4471–4475 [4571–4575]
- Moreau, C. (C) 4637–4640 [4737–4740]
- Moreau, J. J. E.
- A Better Understanding of the Self-Structuration of Bridged Silsesquioxanes (C) 203–206 [205–208]
DOI: 10.1002/anie.200352485
- Morelli, A. (C) 1218–1221 [1238–1241]
- Moretto, A. (C) 6695–6699 [6863–6867]
- Morgado, J. (C) 4049–4052 [4141–4144]
- Morgenstern, B. (C) 3436–3439 [3518–3521]
- Mori, K. (C) 3167–3171 [3229–3233]
- Mori, M.
- Arylnaphthalene Lignans through Pd-Catalyzed [2 + 2 + 2] Cycloaddition of Arynes and Diynes: Total Synthesis of Taiwanins C and E (C) 2436–2440 [2490–2494]
DOI: 10.1002/anie.200453809
- Morimoto, T.
- Evolution of Carbonylation Catalysis: No Need for Carbon Monoxide (M) 5580–5588 [5698–5706]
DOI: 10.1002/anie.200301736
- Morise, X. (C) 6120–6125 [6246–6251]
- Morita, T. (C) 3595–3598 [3679–3682]
- Morita, Y.
- A Purely Organic Molecular Metal Based on a Hydrogen-Bonded Charge-Transfer Complex: Crystal Structure and Electronic Properties of TTF-Imidazole-*p*-Chloranil (C) 6343–6346 [6503–6506]
DOI: 10.1002/anie.200460801
- Moroder, L.
- Peptide Chemistry: *Murray Goodman* (O) 3628 [3712]
DOI: 10.1002/anie.200460962
- Möröy, T. (C) 450–454 [456–460]
- Morrison, C. A.
- Dihydrogen Bonds in Solid BH₃NH₃ (C) 4780–4782 [4884–4886]
DOI: 10.1002/anie.200460096
- Mortalò, C. (C) 1136–1139 [1156–1159]
- Moskalenko, M. A. (C) 4085–4089 [4177–4181]
- Moss, J. A. (C) 2106–2108 [2158–2160]
- Mota, C. J. A.
- A DFT Study of the Acidity of Ultrastable Y Zeolite: Where Is the Brønsted/Lewis Acid Synergism? (C) 3050–3053 [3112–3115]
DOI: 10.1002/anie.200353049
- Motherwell, W. B.
- A Simple Protocol for the Modular Assembly of “Millipede” Artificial Enzymes (C) 1225–1228 [1245–1248]
DOI: 10.1002/anie.200352370
- Motoda, D. (C) 1860–1862 [1896–1898]
- Motta, A. (C) 4081–4084 [4173–4176]
- Moudrakovski, I. L. (C) 6308–6311 [6468–6471]
- Mough, S. T. (C) 5631–5635 [5749–5753]
- Moulin, E. (C) 3467–3470 [3549–3552]
- Mountford, P.
- Revelations in Dinitrogen Activation and Functionalization by Metal Complexes (H) 1186–1189 [1206–1209]
DOI: 10.1002/anie.200301712
- Mountford, P. (C) 2521–2524 [2575–2578]
- Mouri, S. (C) 228–232 [230–234]
- Moussa, Z. (C) 1268–1270 [1288–1290]
- Mozaffari-Afshar, M. (C) 517–520 [523–526]
- Mrksich, M.
- Profiling Kinase Activities by Using a Peptide Chip and Mass Spectrometry (C) 5973–5977 [6099–6103]
DOI: 10.1002/anie.200461061
- Mudring, A.-V. (C) 3183–3185 [3245–3248]
- Mueller, L. J.
- Evidence for the Coexistence of Two Bond-Stretch Isomers in Solution (C) 4880–4883 [4988–4991]
DOI: 10.1002/anie.200460475
- Mueller, U. (C) 6377–6381 [6537–6541]
- Mugesh, G. (C) 3970–3974 [4061–4064]
- Muhler, M. (C) 2839–2842 [2899–2903]
- Muir, T. W.
- Activation of an Autoregulated Protein Kinase by Conditional Protein Splicing (C) 5189–5192 [5301–5304]
DOI: 10.1002/anie.200460941
 - Photocontrol of Smad2, a Multiphosphorylated Cell-Signaling Protein, through Caging of Activating Phosphoserines (C) 5800–5803 [5924–5927]
DOI: 10.1002/anie.200461141
 - Semisynthesis of a Functional K⁺ Channel (C) 2504–2507 [2558–2561]
DOI: 10.1002/anie.200453849
- Muizebelt, I. (C) 1663–1667 [1695–1699]

- Mujica Feraud, M.-T. (C) 4597–4601 [4698–4702]
DOI: 10.1002/anie.200300641
- Mukaiyama, T.
– Explorations into New Reaction Chemistry (R) 5590–5614 [5708–5733]
DOI: 10.1002/anie.200300641
- Mukherjee, A. (C) 87–90 [89–92]
- Mulder, A. (C) 369–373 [373–377]
- Mühlaupt, R.
– Hermann Staudinger and the Origin of Macromolecular Chemistry (E) 1054–1063 [1072–1080]
DOI: 10.1002/anie.200330070
- Müllen, K.
– Arylamine-Substituted Hexa-*peri*-hexabenzocoronenes: Facile Synthesis and Their Potential Applications as “Coaxial” Hole-Transport Materials (C) 5331–5335 [5445–5449]
DOI: 10.1002/anie.200460174
- Ionic Perylenetetracarboxydiimides: Highly Fluorescent and Water-Soluble Dyes for Biolabeling (C) 1528–1531 [1554–1557]
DOI: 10.1002/anie.200353208
- Rational Design of Helical Columnar Packing in Single Crystals (C) 1972–1975 [2006–2009]
DOI: 10.1002/anie.200353245
- Superphenylene-Based Columnar Liquid Crystals (C) 755–758 [773–777]
DOI: 10.1002/anie.200352855
- Synthesis and Self-Assembly of Perylene-diimide–Oligonucleotide Conjugates (C) 3967–3970 [4057–4060]
DOI: 10.1002/anie.200353621
- Müllen, K. (C) 109–112 [111–114], 6116–6120 [6242–6246]
- Müller, A.
– Artificial Cells: Temperature-Dependent, Reversible Li⁺-Ion Uptake/Release Equilibrium at Metal Oxide Nanocontainer Pores (C) 4466–4470 Corrigendum: 5115 [4566–4570 Corrigendum: 5225]
DOI: 10.1002/anie.200453762
- Müller, O.
– Sulindac-Derived Ras Pathway Inhibitors Target the Ras–Raf Interaction and Downstream Effectors in the Ras Pathway (C) 454–458 [460–464]
DOI: 10.1002/anie.200353089
- Müller, O. (C) 224–228 Corrigendum: 540 [226–230 Corrigendum: 547], 450–454 [456–460]
- Müller, R.
– Unusual Biosynthesis of Leupyrrins in the Myxobacterium *Sorangium cellulosum* (C) 4163–4167 [4257–4262]
DOI: 10.1002/anie.200454240
- Müller, T.
– The X-ray Structure of a Vinyl Cation (C) 1543–1546 [1569–1572]
DOI: 10.1002/anie.200352986
- Müller, T. J. J.
– Novel Three-Component Reactions Based on a Heck Carbopalladation/Cyclization Domino Reaction (C) 5997–6000 [6123–6127]
DOI: 10.1002/anie.200461134
- Müller-Buschbaum, K.
– [Yb₃N(dpa)₆][Yb(dpa)₃]: A Molecular Nitride of a Rare-Earth Metal with a Yb₃N Unit (C) 5994–5996 [6120–6122]
DOI: 10.1002/anie.200460478
- Mulvaney, P. (C) 5393–5396 [5511–5514]
- Mulvey, R. E.
– Synthesis and Crystal Structure of [[nBuMg(μ-TMP)]₂] and of a Homometallic Inverse Crown in Tetranuclear [[nBuMg₂(μ-N(H)Dipp)]₂(μ₃-OnBu)]₂ (C) 1709–1712 [1741–1744]
DOI: 10.1002/anie.200353286
- Mulyani, I. (C) 4504–4507 [4604–4607]
- Munge, B. (C) 2158–2161 [2210–2213]
- Muñoz, M. P. (C) 2402–2406 [2456–2460]
- Münsch, P. (C) 3728–3731 [3814–3817]
- Munsch, T. E. (C) 742–745 [760–763]
- Murakami, M.
– Synthesis and Thermal Ring Opening of *trans*-3,4-Disilylcyclobutene (C) 4874–4876 [4982–4984]
DOI: 10.1002/anie.200460144
- Muranaka, A. (C) 5481–5485 [5597–5601]
- Murat, K. (C) 4172–4178 [4267–4273]
- Murata, M. (C) 3044–3047 [3106–3109]
- Murata, S.
– Stereoisomeric Discrimination in DNA Compaction (C) 2378–2381 [2432–2435]
DOI: 10.1002/anie.200453774
- Murata, T. (C) 6343–6346 [6503–6506]
- Murata, Yasujiro (C) 3044–3047 [3106–3109]
- Murata, Yoshihisa (C) 3175–3177 [3237–3239]
- Muratake, H.
– Total Synthesis of (±)-Nominine, a Hepatocyclic Hetisine-Type Aconite Alkaloid (C) 4646–4649 [4746–4749]
DOI: 10.1002/anie.200460332
- Murphy, P. V.
– Glycosidation Reactions of Silyl Ethers with Conformationally Inverted Donors Derived from Glucuronic Acid: Stereoselective Synthesis of Glycosides and 2-Deoxyglycosides (C) 2518–2521 [2572–2575]
DOI: 10.1002/anie.200353196
- Murugavel, R. (C) 3832–3835 [3920–3923]
- Murugesu, M. G. (C) 4207–4209 [4303–4305]
- Murny, C. A. (C) 6132–6135 [6258–6261]
- Muth, S. (C) 3192–3195 [3255–3257]
- Muthusamy, E. (C) 4928–4933 [5036–5041]
- Mutikainen, I. (C) 5815–5817 [5939–5941]
- Mutter, M.
– Switch Peptides In Statu Nascendi: Induction of Conformational Transitions Relevant to Degenerative Diseases (C) 4172–4178 [4267–4273]
DOI: 10.1002/anie.200454045
- Mynott, R. J. (C) 2444–2446 [2498–2500]
- Myrabo, R. L. (C) 1393–1397 [1417–1421]
- Nagasawa, K.
– Enantioselective Total Synthesis of Batzelladine A (C) 1559–1562 [1585–1588]
DOI: 10.1002/anie.200353200
- Nagase, S. (C) 1552–1554 [1578–1580]
- Nagayama, K. (C) 2527–2530 [2581–2584]
- Nair, G. G. (C) 3429–3432 [3511–3514]
- Nair, V.
– N-Heterocyclic Carbenes: Reagents, Not Just Ligands! (M) 5130–5135 [5240–5245]
DOI: 10.1002/anie.200301714
- Naitoh, Y. (C) 2092–2095 [2144–2147]
- Nakadai, M. (C) 1983–1986 [2017–2020]
- Nakagawa, M. (C) 2020–2023 [2054–2057]
- Nakajima, M. (C) 2665–2668 [2719–2722]
- Nakamura, Y. (C) 1679–1681 [1711–1713], 3258–3260 [3320–3322]
- Nakanishi, K.
– Chemistry and Biology of Terpene Trilactones from *Ginkgo Biloba* (R) 1640–1658 [1670–1689]
DOI: 10.1002/anie.200300601
- Natural Products and Small Rings: *Saturo Masamune* (O) 922 [940]
DOI: 10.1002/anie.200490020
- Nakanishi, Y. (C) 2530–2534 [2584–2588]
- Nakao, Y. (C) 3448–3451 [3530–3533]
- Nakasuji, K.
– A Purely Organic Molecular Metal Based on a Hydrogen-Bonded Charge-Transfer Complex: Crystal Structure and Electronic Properties of TTF-Imidazole-*p*-Chloranil (C) 6343–6346 [6503–6506]
DOI: 10.1002/anie.200460801
- Four-Stage Amphoteric Redox Properties and Biradicaloid Character of Tetra-*tert*-butyldicyclopenta[*b*:*d*]thieno[1,2,3-*cd*;5,6,7-*c'd'*]diphenalene (C) 6474–6479 [6636–6641]
DOI: 10.1002/anie.200460565
- Nakata, E.-i. (C) 1368–1371 [1392–1395]
- Nakata, K. (C) 707–711 [725–729]
- Nakatani, T. (C) 6496–6500 [6658–6662]
- Nakayama, K. (C) 5643–5645 [5761–5763]
- Nakayama, Y. (C) 4763–4767 [4867–4871]
- Nam, J. (C) 842–846 [860–864]
- Nam, J.-M. (C) 1246–1249 [1266–1269]
- Nam, W.
– Direct Evidence for Oxygen-Atom Exchange between Nonheme Oxoiron(IV) Complexes and Isotopically Labeled Water (C) 2417–2420 [2471–2474]
DOI: 10.1002/anie.200353497
- Namba, S. (C) 236–240 [238–242]
- Nancollas, G. H.
– Dissolution at the Nanoscale: Self-Preservation of Biominerals (C) 2697–2701 [2751–2755]
DOI: 10.1002/anie.200353652
- Nann, T.
– Single Quantum Dots in Spherical Silica Particles (C) 5393–5396 [5511–5514]
DOI: 10.1002/anie.200460752
- Nanni, D.
– A Novel Tin-Free Procedure for Alkyl Radical Reactions (C) 3598–3601 [3682–3685]
DOI: 10.1002/anie.200454245
- Nantz, M. H.
– Dioxazocinium Ortho Esters: A Class of Highly pH-Vulnerable Amphiphiles



Nad, S. (C) 2297–2299 [2347–2349]
Nagahama, S. (C) 3811–3814 [3899–3902]
Nagahara, T. (C) 994–997 [1012–1015]
Nagano, T. (C) 98–100 [100–102]

- (C) 1117–1120 [1137–1140]
DOI: 10.1002/anie.200352589
- Naruta, Y.
– Characterization of a Dinuclear $Mn^{V}=O$ Complex and Its Efficient Evolution of O_2 in the Presence of Water
(C) 98–100 [100–102]
DOI: 10.1002/anie.200352564
- Nasongkla, N. (C) 6323–6327 [6483–6487]
- Nastopoulos, V. (C) 2266–2270 [2316–2320]
- Natarajan, S. (R) 1466–1496 [1490–1521]
- Natile, G.
– Unusual Reactivity at a Platinum Center Determined by the Ligands and the Solvent Environment
(C) 5081–5084 [5191–5194]
DOI: 10.1002/anie.200454111
- Natsume, M.
– Total Synthesis of (\pm)-Nominine, a Hepatocyclic Hetsine-Type Aconite Alkaloid
(C) 4646–4649 [4746–4749]
DOI: 10.1002/anie.200460332
- Naumov, N. G. (C) 1297–1300 [1317–1321]
- Nava, P. (C) 3823–3827 [3911–3915]
- Navarre, L. (C) 719–723 [737–741]
- Navarro, I. (C) 862–865 [880–883]
- Nayak, S. (C) 6706–6709 [6874–6877]
- Nazaré, M.
– A Flexible, Palladium-Catalyzed Indole and Azaindole Synthesis by Direct Annulation of Chloroanilines and Chloroaminopyridines with Ketones
(C) 4526–4528 [4626–4629]
DOI: 10.1002/anie.200460122
- Neculai, A. M. (C) 1419–1421 [1443–1445], 2142–2145 [2194–2197], 6192–6196 [6318–6322]
- Neculai, D. (C) 1419–1421 [1443–1445], 2142–2145 [2194–2197], 6192–6196 [6318–6322]
- Neels, A. (C) 4738–4741 [4842–4845]
- Neffe, A. T. (C) 2937–2940 [2997–3000]
- Negishi, E.-i.
– An Efficient and General Method for the Synthesis of α,ω -Difunctional Reduced Polypropionates by Zr-Catalyzed Asymmetric Carboalumination: Synthesis of the Scyphostatin Side Chain
(C) 2911–2914 [2971–2974]
DOI: 10.1002/anie.200353429
- Highly Stereoselective Synthesis of (1*E*)-2-Methyl-1,3-dienes by Palladium-Catalyzed *trans*-Selective Cross-Coupling of 1,1-Dibromo-1-alkenes with Alkenylzinc Reagents
(C) 2259–2263 [2309–2313]
DOI: 10.1002/anie.200353022
- Negoro, R. (C) 4231–4233 [4327–4329]
- Negri, F. (C) 1972–1975 [2006–2009]
- Nehete, U. N. (C) 3832–3835 [3920–3923], 3842–3844 [3930–3932]
- Neiser, M. W. (C) 3192–3195 [3255–3257]
- Nemoto, T. (C) 317–320 [321–324]
- Neri, G. (C) 4345–4349 [4445–4449]
- Nethaji, M. (C) 87–90 [89–92]
- Netzer, F. P.
– Thermodynamically Controlled Self-Assembly of Two-Dimensional Oxide Nanostructures
(C) 5546–5549 [5663–5666]
DOI: 10.1002/anie.200460150
- Neumann, R.
– Computer-Generated High-Valent Iron–Oxo and Manganese–Oxo Species with Polyoxometalate Ligands: How do they Compare with the Iron–Oxo Active Species of Heme Enzymes?
(C) 5661–5665 [5779–5783]
DOI: 10.1002/anie.200453867
- Neumann, R. (C) 2924–2928 [2984–2988]
- Neumann, T. (C) 6197–6201 [6323–6328]
- Nevado, C. (C) 2402–2406 [2456–2460]
- Ney, J. E. (C) 3605–3608 [3689–3692]
- Ng, Y.-F. (C) 1959–1962 [1993–1996]
- Ngassa, F. N. (C) 505–510 [511–516]
- Ni, X. Corrigendum: 1043
- Ngo, H. L. (C) 2501–2504 [2555–2558]
- Nguyen, S. T. (C) 5503–5507 [5619–5623]
- Nguyen, T.-Q. (M) 5446–5453 [5562–5570]
- Ni, X. Corrigendum: 3215
- Niazov, T. (C) 4519–4522 [4619–4622]
- Nicewicz, D. A. (C) 2652–2655 [2706–2709]
- Nicolaou, K. C.
– Structural Revision and Total Synthesis of Azaspiracid-1, Part 1: Intelligence Gathering and Tentative Proposal
(C) 4312–4318 [4412–4418]
DOI: 10.1002/anie.200460695
- Structural Revision and Total Synthesis of Azaspiracid-1, Part 2: Definition of the ABCD Domain and Total Synthesis
(C) 4318–4324 [4418–4424]
DOI: 10.1002/anie.200460696
- Total Synthesis of Thiostrepton, Part 1: Construction of the Dehydropiperidine/Thiazoline-Containing Macrocyclic
(C) 5087–5092 [5197–5202]
DOI: 10.1002/anie.200461340
- Total Synthesis of Thiostrepton, Part 2: Construction of the Quinaldic Acid Macrocyclic and Final Stages of the Synthesis
(C) 5092–5097 [5202–5207]
DOI: 10.1002/anie.200461341
- Nicolas, J. (C) 6186–6189 [6312–6315]
- Nie, W.-L. (C) 310–313 [313–317]
- Niecke, E.
– Synthesis and Structure of a 1,3-Diphosphacyclobutadienediide: An Animesolytic Fragmentation of a 1,3-Diphosphetane-2,4-diyl in Solution
(C) 637–641 [647–651]
DOI: 10.1002/anie.200352746
- Niederberger, M.
– A General Soft-Chemistry Route to Perovskites and Related Materials: Synthesis of $BaTiO_3$, $BaZrO_3$, and $LiNbO_3$ Nanoparticles
(C) 2270–2273 [2320–2323]
DOI: 10.1002/anie.200353300
- Nonaqueous Synthesis of Nanocrystalline Semiconducting Metal Oxides for Gas Sensing
(C) 4345–4349 [4445–4449]
DOI: 10.1002/anie.200460610
- Nieger, M. (C) 637–641 [647–651], 4801–4804 [4905–4908]
- Nielsen, K. A. (C) 6486–6491 [6648–6653]
- Nielsen, R. J. (C) 4626–4629 [4726–4729]
- Niemeyer, C. M.
– Reversible Switching of DNA–Gold Nanoparticle Aggregation
(C) 6469–6471 [6631–6633]
DOI: 10.1002/anie.200461887
- Nierengarten, H. (C) 3695–3699 [3781–3785]
- Nierlich, M. (C) 850–852 [868–870]
- Nieto-Oberhuber, C. (C) 2402–2406 [2456–2460]
- Niikura, K. (C) 1516–1520 [1542–1546]
- Niimi, M. (C) 5369–5372 [5483–5486]
- Nijhuis, C. A. (C) 369–373 [373–377]
- Nishida, A.
– Asymmetric Total Synthesis of (–)-Nakadomarin A
(C) 2020–2023 [2054–2057]
DOI: 10.1002/anie.200453673
- Cycloisomerization Promoted by the Combination of a Ruthenium–Carbene Catalyst and Trimethylsilyl Vinyl Ether, and its Application in The Synthesis of Heterocyclic Compounds: 3-Methylene-2,3-dihydroindoles and 3-Methylene-2,3-dihydrobenzofurans
(C) 4063–4067 [4155–4159]
DOI: 10.1002/anie.200454157
- Nishida, G. (C) 6510–6512 [6672–6674]
- Nishide, H.
– Oxidative Polymerization of 2,6-Dimethylphenol To Form Poly(2,6-dimethyl-1,4-phenyleneoxide) in Water
(C) 730–733 [748–751]
DOI: 10.1002/anie.200352764
- Nishide, K. (C) 2659–2661 [2713–2715]
- Nishii, M. (C) 1969–1972 [2003–2006]
- Nishikawa, T. (C) 4782–4785 [4886–4889]
- Nishimae, Y. (C) 4947–4950 [5055–5058]
- Nishimura, S.-I.
– Antifreeze Glycoproteins: Elucidation of the Structural Motifs That Are Essential for Antifreeze Activity
(C) 856–862 [874–880]
DOI: 10.1002/anie.200353110
- Post-Translational Modifications on Proteins: Facile and Efficient Procedure for the Identification of O-Glycosylation Sites by MALDI-LIFT-TOF/TOF Mass Spectrometry
(C) 4071–4075 [4163–4167]
DOI: 10.1002/anie.200460020
- Site-Specific Introduction of Sialic Acid into Insulin
(C) 1516–1520 [1542–1546]
DOI: 10.1002/anie.200353058
- Nishimura, T. (C) 1969–1972 [2003–2006]
- Nishioka, T. (C) 213–215 [215–217]
- Nishiyama, K.
– Origin of Diastereoselection in the Hydro-silylation of Chiral *N*-Acylium Intermediates Derived from Pyroglutamic Acid
(C) 2412–2415 [2466–2469]
DOI: 10.1002/anie.200353366
- Nissinen, M. (C) 1243–1246 [1263–1266]
- Nitschke, J. R.
– Mutual Stabilization between Imine Ligands and Copper(II) Ions in Aqueous Solution
(C) 3073–3075 [3135–3137]
DOI: 10.1002/anie.200454082
- The Hydrophobic Effect as a Driving Force in the Self-Assembly of a $[2 \times 2]$ Copper(II) Grid
(C) 6724–6727 [6892–6895]
DOI: 10.1002/anie.200461308
- Nitz, M. (C) 3682–3685 [3768–3771]
- Nlate, S. (C) 2924–2928 [2984–2988]
- Noda, T. (C) 6505–6510 [6667–6672]
- Node, M.
– Total Synthesis of (–)-Galanthamine by Remote Asymmetric Induction
(C) 2659–2661 [2713–2715]
DOI: 10.1002/anie.200353636
- Noguchi, K. (C) 6510–6512 [6672–6674]
- Nolte, R. J. M. (C) 4045–4049 [4137–4141], 4755–4759 [4859–4863]
- Noltmeyer, M. (C) 4940–4943 [5048–5051]

- Nomura, M. (C) 5063–5065 [5173–5175]
Nonnenberg, C. (C) 4586–4589 [4686–4689]
Noro, S.-i. (R) 2334–2375 [2388–2430], (C) 2684–2687 [2738–2741]
North, M.
– Oxidative Synthesis of α -Amino Nitriles from Tertiary Amines (H) 4126–4128 [4218–4220]
DOI: 10.1002/anie.200301750
North, M. (C) 4085–4089 [4177–4181]
Northrup, A. B. (C) 2152–2154 [2204–2206], 6722–6724 [6890–6892]
Novak, F. (C) 2025–2028 [2059–2062 Corrigendum: 2934]
Novak, M. A. (C) 956–958 [974–976]
Novoa, J. J.
– The Origin of the Magnetic Moments in Compressed Crystals of Polymeric C₆₀ (C) 577–580 [587–590]
DOI: 10.1002/anie.200352118
Nuckolls, C.
– Assembling Dimeric π Stacks on Gold Surfaces by Using Three-Dimensional Lock-and-Key Receptors (C) 1836–1839 [1872–1875]
DOI: 10.1002/anie.200353476
– Using Hydrogen Bonds to Direct the Assembly of Crowded Aromatics (M) 5446–5453 [5562–5570]
DOI: 10.1002/anie.200301678
Nugent, A. K. (C) 3928–3932 [4018–4022]
Numata, M. (C) 3279–3283 [3341–3345]
Nyffeler, P. T. (C) 4656–4659 [4756–4759]
Nyman, M.
– [SiNb₁₂O₄₀]¹⁶⁻ and [GeNb₁₂O₄₀]¹⁶⁻: Highly Charged Keggin Ions with Sticky Surfaces (C) 2787–2792 [2847–2852]
DOI: 10.1002/anie.200353410
Nyulászi, L.
– Synthesis and Structure of a 1,3-Diphosphacyclobutadienediide: An Aniomeso-lytic Fragmentation of a 1,3-Diphosphetane-2,4-diyl in Solution (C) 637–641 [647–651]
DOI: 10.1002/anie.200352746
- Oag, R. M. (C) 5192–5195 [5304–5307]
Oaki, Y. (C) 1363–1368 [1387–1392]
Oba, M.
– Origin of Diastereoselection in the Hydro-silylation of Chiral *N*-Acyliminium Inter-mediates Derived from Pyroglutamic Acid (C) 2412–2415 [2466–2469]
DOI: 10.1002/anie.200353366
Oberbeckmann-Winter, N. (C) 6120–6125 [6246–6251]
Oberthür, M. (C) 67–70 [69–72]
Obrecht, D. (C) 2109–2112 [2161–2164]
O'Brien, D. P. (R) 6596–6616 [6760–6782]
O'Brien, T. A. (C) 345–349 [349–353]
Ochsenbein, P.
– Direct Evidence for a Furtive State in the Degradation of Carbasalatum Calcium (C) 2694–2697 [2748–2751]
DOI: 10.1002/anie.200353007
- Ochsenfeld, C.
– Ab Initio NMR Spectra for Molecular Systems with a Thousand and More Atoms: A Linear-Scaling Method (C) 4485–4489 [4585–4589]
DOI: 10.1002/anie.200460336
Oda, M.
– Arylbis(9-anthryl)methyl Cations: Highly Crowded, Near Infrared Light Absorbing Hydrocarbon Cations (C) 4947–4950 [5055–5058]
DOI: 10.1002/anie.200460480
– Möbius Aromatic Hydrocarbons: Chal-lenges for Theory and Synthesis (H) 4396–4398 [4496–4498]
DOI: 10.1002/anie.200460050
– Onion-Type Complexation Based on Carbon Nanorings and a Buckminsterful-lerene (C) 1722–1724 [1754–1756]
DOI: 10.1002/anie.200353517
– Supramolecular Dynamics of Cyclic [6]Pa-raphenylenecetylene Complexes with [60]- and [70]Fullerene Derivatives: Elec-tronic and Structural Effects on Complex-ation (C) 5060–5062 [5170–5172]
DOI: 10.1002/anie.200460630
Oda, S. (C) 3448–3451 [3530–3533]
Oderaotoshi, Y. (C) 79–81 [81–83]
Oeckler, O. (C) 5540–5542 [5656–5659]
Oehme, G. (C) 5066–5069 [5176–5179]
Ogawa, C. (C) 6491–6493 [6653–6655]
Ogino, H. (C) 221–224 Corrigendum: 3096 [223–226 Corrigendum: 3158]
Ogino, S. (C) 5063–5065 [5173–5175]
Ogliaro, F. Corrigendum: 141
Oh, N.-K. (C) 6465–6468 [6627–6630]
Oh, N. Y. (C) 2417–2420 [2471–2474]
Oh, S. J. (C) 1115–1117 Corrigendum: 3749 [1135–1137 Corrigendum: 3834]
Ohe, K.
– Polyaddition and Polycondensation Reac-tions of (2-Furyl)carbenoid as Step-Growth Polymerization Strategies: Synthe-sis of Furylcyclopropane- and Furfuryli-dene-Containing Polymers (C) 1857–1860 [1893–1896]
DOI: 10.1002/anie.200352949
Ohki, Y. (C) 2290–2293 [2340–2343]
Ohkubo, K. (C) 853–856 [871–874]
Ohmori, K. (C) 3167–3171 [3229–3233]
Ohnsmann, J. (C) 1104–1107 [1125–1128]
Ohshima, T. (C) 317–320 [321–324]
Ohshita, J. (C) 3935–3938 [4025–4028], 5052–5055 [5162–5165]
Ohtsu, H. (C) 6301–6303 [6461–6463]
Oiarbide, M. (C) 3307–3310 [3369–3372], (H) 5442–5444 [5558–5560]
Oike, H.
– One-Pot Optical Resolution of Oligopep-tide Helices through Artificial Peptide Bundling (C) 4915–4918 [5023–5026]
DOI: 10.1002/anie.200460703
Ok, K. M. (C) 5489–5491 [5605–5607]
Oka, M. (C) 5019–5022 [5129–5132]
Okamoto, Hideki (C) 736–738 [754–756]
Okamoto, Hiroshi (C) 3171–3175 [3233–3237], 4763–4767 [4867–4871]
Okamoto, K.-i. (C) 4944–4947 [5052–5055]
Okamoto, Y. (C) 366–369 [370–373]
Okano, J. (C) 2121–2124 [2173–2176], 3724–3728 [3810–3814]
Okawa, H. (C) 1825–1828 [1861–1864]
- Oku, T. (C) 966–969 [984–987]
Okuda, J.
– Micelle Formation from Amphiphilic “Cylindrical Brush”—Coil Block Copoly-mers Prepared by Metallocene Catalysis (C) 3192–3195 [3255–3257]
DOI: 10.1002/anie.200353259
Okumura, M. (C) 2129–2132 [2181–2184]
Olah, G. A.
– Structure and Mechanism in Gas-Phase Chemistry and Its Relevance to the Con-densed State: *Fulvio Cacace* (O) 1760 [1792]
DOI: 10.1002/anie.200420086
Olah, G. A. (C) 5203–5206 [5315–5318]
Oldham, N. J. (C) 828–833 [846–851]
Olenyuk, B. (C) 3591–3594 [3675–3678]
Olkowska-Oetzel, J. (C) 3823–3827 [3911–3915]
Olsen, R. A. (C) 4880–4883 [4988–4991]
O'Malley, D. P. (C) 2674–2677 [2728–2731]
O'Malley, R. (C) 3691–3695 [3777–3781]
Onaka, S. (C) 5618–5621 [5736–5739]
Onclin, S. (C) 369–373 [373–377]
O'Neill, P. M.
– Design and Synthesis of Endoperoxide Antimalarial Prodrug Models (C) 4193–4197 [4289–4293]
DOI: 10.1002/anie.200453859
Onions, S. T. (C) 1814–1817 [1850–1853]
Ono, A.
– Highly Selective Oligonucleotide-Based Sensor for Mercury(II) in Aqueous Solu-tions (C) 4300–4302 [4400–4402]
DOI: 10.1002/anie.200454172
Ono, K. (C) 2020–2023 [2054–2057]
Onoyama, G. (C) 2684–2687 [2738–2741]
Orenes, R. (C) 3273–3278 [3335–3340]
Orita, A. (C) 2121–2124 [2173–2176], 3724–3728 [3810–3814]
Orme, C. A. (C) 2697–2701 [2751–2755]
Ornatska, M. (C) 5246–5249 Corrigendum: 5721 [5358–5361 Corrigendum: 5839]
Ortmann, R. (C) 251–254 [254–257]
Osakada, K.
– Cobalt-Complex-Catalyzed Copolymeriza-tion of Ethylene with 2-Aryl-1-methylene-cyclopropanes (C) 1233–1235 [1253–1255]
DOI: 10.1002/anie.200352837
Oschkinat, H. (C) 454–458 [460–464]
Oshima, K.
– Consecutive Double 1,2-Migration of Two Different Groups in Silyl(dichloromethyl)-cuprates (C) 106–108 [108–110]
DOI: 10.1002/anie.200352828
– Phosphane-Free Rhodium Catalyst in an Anionic Micellar System for [4 + 2] Annu-lation of Dienynes (C) 1860–1862 [1896–1898]
DOI: 10.1002/anie.200353123
Osuka, A. (C) 5077–5081 [5187–5191]
Oswald, I. D. H. (C) 3914–3918 [4004–4008]
Ota, A. (C) 3670–3673 [3756–3759]
Otera, J.
– Intermittent Molecular Shuttle as a Binary Switch (C) 2121–2124 [2173–2176]
DOI: 10.1002/anie.200353534
– Rate Acceleration of the Reaction between Solid Reactants by Premixing in Solution: Application to the Efficient Syn-thesis of a [2]Rotaxane



- (C) 3724–3728 [3810–3814]
DOI: 10.1002/anie.200460062
- Tateshina Conference on Organic Chemistry (T) 2322–2323 [2376–2377]
DOI: 10.1002/anie.200420083
 - Otero, R. (C) 2092–2095 [2144–2147]
 - Ott, S.
 - A Biomimetic Pathway for Hydrogen Evolution from a Model of the Iron Hydrogenase Active Site (C) 1006–1009 [1024–1027]
DOI: 10.1002/anie.200353190
 - Ottenwaelde, X. (C) 850–852 [868–870]
 - Otto, S. (C) 1959–1962 [1993–1996]
 - Ou, Z. (C) 853–856 [871–874]
 - Oumi, Y. (C) 4892–4896 [5000–5004]
 - Ovaska, T. V. (C) 1270–1272 [1290–1292]
 - Overgaard, J. (C) 5196–5200 [5308–5312]
 - Ow-Yang, C. (C) 5210–5213 [5322–5325]
 - Oxgaard, J. (C) 4626–4629 [4726–4729]
 - Ozawa, Y. (C) 4231–4233 [4327–4329]
 - Ozeki, T. (C) 5621–5625 [5739–5743]



- Pachamuthu, K. (C) 6735–6738 [6903–6906]
- Pacholski, C. (C) 4774–4777 [4878–4881]
- Packard, G. K. (C) 2822–2826 [2882–2886]
- Padgett, M. (C) 2512–2514 [2566–2568]
- Paetzold, J. (C) 1095–1098 [1115–1118]
- Pagenkopf, B. L.
- Improving Quantum Efficiencies of Siloles and Silole-Derived Butadiene Chromophores through Structural Tuning (C) 6336–6338 [6496–6498]
DOI: 10.1002/anie.200461844
- Paik, D. H. (C) 2830–2834 [2890–2894]
- Pal, S. K. (C) 60–63 [62–65]
- Paladini, A. (C) 1868–1871 Corrigendum: 3872 [1904–1907 Corrigendum: 3960]
- Palcic, M. M. (C) 613–615 [623–625]
- Pallavicini, P.
- A Sleeping Host Awoken by Its Guest: Recognition and Sensing of Imidazole-Containing Molecules Based on Double Cu²⁺ Translocation inside a Polyaza Macrocyclic (C) 5073–5077 [5183–5187]
DOI: 10.1002/anie.200460568
- Palm, G. J. (H) 1190–1193 [1210–1213]
- Palmqvist, A. E. C.
- A Crystalline Microporous Narrow-Bandgap Semiconductor (C) 700–704 [718–722]
DOI: 10.1002/anie.200351284
- Palomo, C.
- Construction of C–S Bonds with a Quaternary Stereocenter through a Formal Michael Reaction: Asymmetric Synthesis of Tertiary Thiols (C) 3307–3310 [3369–3372]
DOI: 10.1002/anie.200453889
 - Unveiling Reliable Catalysts for the Asymmetric Nitroaldol (Henry) Reaction (H) 5442–5444 [5558–5560]
DOI: 10.1002/anie.200460506
- Palomo, J. M. (C) 5839–5842 [5963–5966]

- Pandey, R. K.
- Production of an Ultra-Long-Lived Charge-Separated State in a Zinc Chlorin–C₆₀ Dyad by One-Step Photoinduced Electron Transfer (C) 853–856 [871–874]
DOI: 10.1002/anie.200352870
- Paneque, M. (C) 3708–3711 [3794–3797]
- Panse, S. (C) 2671–2674 [2725–2728]
- Pantarotto, D. (C) 5242–5246 [5354–5358]
- Paolini, F. (R) 5896–5911 [6020–6036]
- Papageorgiou, C. D. (C) 4641–4644 [4741–4744]
- Papamtheakis, J. (C) 3974–3976 [4065–4067]
- Pape, T. (C) 4807–4810 [4911–4915]
- Papke, U. (C) 3970–3974 [4061–4064]
- Parala, H. (C) 2839–2842 [2899–2903]
- Paraskevass, I. (C) 5645–5649 [5763–5767]
- Pardy, R. B. A. (C) 5366–5369 [5480–5483]
- Parella, T. (C) 4049–4052 [4141–4144]
- Parise, J. B. (C) 2787–2792 [2847–2852]
- Park, B.
- A Mesoporous/Crystalline Composite Material Containing Tin Phosphate for Use as the Anode in Lithium-Ion Batteries (C) 5987–5990 [6113–6116]
DOI: 10.1002/anie.200454080
- Park, B. K. (C) 1712–1714 [1744–1746]
- Park, C. B. (C) 6331–6335 [6491–6495]
- Park, H.-g.
- Highly Enantioselective Phase-Transfer-Catalytic Alkylation of 2-Phenyl-2-oxazoline-4-carboxylic Acid *tert*-Butyl Ester for the Asymmetric Synthesis of α -Alkyl Serines (C) 2382–2385 [2436–2439]
DOI: 10.1002/anie.200353496
- Park, H. J. (C) 5792–5796 [5916–5920]
- Park, H. M. (C) 2282–2285 [2332–2335]
- Park, J. (C) 2282–2285 [2332–2335]
- Park, J.-G. (C) 2282–2285 [2332–2335]
- Park, J. T.
- Novel [60]Fullerene-Assisted *ortho*-Phosphonation on a Tetrairidium Butterfly Framework (C) 1712–1714 [1744–1746]
DOI: 10.1002/anie.200353290
 - Size-Dependent Magnetic Properties of Colloidal Mn₃O₄ and MnO Nanoparticles (C) 1115–1117 Corrigendum: 3749 [1135–1137 Corrigendum: 3834]
DOI: 10.1002/anie.200352400
- Park, M.-H. (C) 6465–6468 [6627–6630]
- Park, S.-E.
- Nanoporous Metal-Containing Nickel Phosphates: A Class of Shape-Selective Catalyst (C) 2819–2822 [2879–2882]
DOI: 10.1002/anie.200353502
- Park, S. Y.
- Photoswitchable Organic Nanoparticles and a Polymer Film Employing Multifunctional Molecules with Enhanced Fluorescence Emission and Bistable Photochromism (C) 6346–6350 [6506–6510]
DOI: 10.1002/anie.200461172
- Park, Sangwoo (C) 1712–1714 [1744–1746]
- Park, Sungho (C) 3048–3050 [3110–3112]
- Parola, A. J. (C) 1525–1527 [1551–1553]
- Parr, J. (C) 95–98 [97–100]
- Parsons, S. (C) 1218–1221 [1238–1241], 3914–3918 [4004–4008]
- Parvez, M. (C) 502–505 [508–511], 1268–1270 [1288–1290]
- Parviz, B. A. (C) 498–502 [504–508]
- Pasc-Banu, A. (C) 6174–6177 [6300–6303]
- Pasini, E. (C) 4193–4197 [4289–4293]
- Pasquato, L.
- Nanozymes: Gold-Nanoparticle-Based Transphosphorylation Catalysts (C) 6165–6169 [6291–6295]
DOI: 10.1002/anie.200460649
- Passmore, J.
- On the Way to “Solid Nitrogen” at Normal Temperature and Pressure? Binary Azides of Heavier Group 15 and 16 Elements (H) 4834–4836 [4938–4941]
DOI: 10.1002/anie.200401748
 - The Preparation and X-ray Crystal Structure of [(AgI₂)_n·nMF₆] (M=Sb, As): Diiodine Acting as a Donor in the Planar Polymeric [(AgI₂)_n]⁺ (C) 1995–1998 [2029–2032]
DOI: 10.1002/anie.200352969
- Patarin, J.
- Mild Methods for Removing Organic Templates from Inorganic Host Materials (H) 3878–3880 [3968–3970]
DOI: 10.1002/anie.200301740
- Patel, S. J. (C) 3941–3944 [4031–4034]
- Paterson, I.
- Total Synthesis and Configurational Assignment of (–)-Dictyostatin, a Microtubule-Stabilizing Macrolide of Marine Sponge Origin (C) 4629–4633 [4729–4733]
DOI: 10.1002/anie.200460589
- Pathak, P. (C) 704–707 [722–725]
- Patil, A. J. (C) 4928–4933 [5036–5041]
- Patil, K. (C) 1235–1238 [1255–1258]
- Patiny, L. (C) 4172–4178 [4267–4273]
- Patolsky, F. (C) 2113–2117 [2165–2169]
- Patroni, S. (C) 5073–5077 [5183–5187]
- Pattison, D. I. (C) 462–465 [468–471]
- Paulusse, J. M. J. (C) 4460–4462 [4560–4562]
- Pavam, C. H. (C) 4330–4333 [4430–4433]
- Pavlov, V. (C) 4519–4522 [4619–4622]
- Pecoraro, V. L.
- Synthesis, Structure, and Magnetic Properties of a Large Lanthanide–Transition-Metal Single-Molecule Magnet (C) 3912–3914 [4002–4004]
DOI: 10.1002/anie.200454013
- Pedrido, R. M. (C) 1962–1965 [1996–1999]
- Pedroso, E. F. (C) 956–958 [974–976]
- Pei, Z. (C) 3716–3718 [3802–3804]
- Peisach, E. (C) 3682–3685 [3768–3771]
- Peleg-Vasserman, H. (C) 745–748 [763–766]
- Peleshanko, S. (C) 5246–5249 Corrigendum: 5721 [5358–5361 Corrigendum: 5839]
- Penelle, J.
- HP-RAFT: A Free-Radical Polymerization Technique for Obtaining Living Polymers of Ultrahigh Molecular Weights (C) 1691–1694 [1723–1726]
DOI: 10.1002/anie.200353025
- Peng, L. (C) 5477–5481 [5593–5597]
- Peng, Y. (C) 3443–3445 [3525–3527], 6190–6192 [6316–6318]
- Peng, Z.
- Rational Synthesis of Covalently Bonded Organic–Inorganic Hybrids (M) 930–935 [948–953]
DOI: 10.1002/anie.200301682
- Pereda-Miranda, R.
- Crystal Structure of Tricolorin A: Molecular Rationale for the Biological Properties

- of Resin Glycosides Found in Some Mexican Herbal Remedies
(C) 5918–5922 [6044–6048]
DOI: 10.1002/anie.200460327
- Peregudov, A. S. (C) 4085–4089 [4177–4181]
- Pereira, C. L. M. (C) 956–958 [974–976]
- Pérez, M. (C) 1724–1727 [1756–1759]
- Pérez, S. (C) 5918–5922 [6044–6048]
- Periana, R. A.
– Selective Oxidation of Methane to Methanol Catalyzed, with C–H Activation, by Homogeneous, Cationic Gold
(C) 4626–4629 [4726–4729]
DOI: 10.1002/anie.200461055
- Perlepes, S. P.
– A Nonanuclear Iron(II) Single-Molecule Magnet
(C) 2266–2270 [2316–2320]
DOI: 10.1002/anie.200353147
- Hexanuclear Manganese(III) Single-Molecule Magnets
(C) 210–212 [212–214]
DOI: 10.1002/anie.200351079
- Pernice, H. (C) 2843–2846 [2903–2906]
- Perret-Aebi, L.-E. (C) 4482–4485 [4582–4585]
- Persau, C. (C) 305–309 [309–313]
- Persoons, A. (C) 5266–5268 [5378–5381]
- Péter, M. (C) 369–373 [373–377]
- Peter, M. (C) 5181–5185 Corrigendum: 5428 [5293–5297 Corrigendum: 5542]
- Peters, A. J. (C) 6486–6491 [6648–6653]
- Peters, W. (C) 1381–1385 [1405–1409]
- Peterson, B. R. (C) 5181–5185 Corrigendum: 5428 [5293–5297 Corrigendum: 5542]
- Petitjean, A. (C) 3695–3699 [3781–3785]
- Petitou, M.
– A Synthetic Antithrombin III Binding Pentasaccharide Is Now a Drug! What Comes Next?
(R) 3118–3133 [3180–3196]
DOI: 10.1002/anie.200300640
- Petkovic, H. (C) 2551–2553 [2605–2607]
- Petri, A. F. (C) 5821–5823 [5945–5947]
- Petrovic, G. (C) 4312–4318 [4412–4418], 4318–4324 [4418–4424]
- Petrushina, M. A.
– Hemibuckminsterfullerene C₃₀H₁₂: X-ray Crystal Structures of the Parent Hydrocarbon and of the Two-Dimensional Organometallic Network {[Rh₂(O₂CCF₃)₄]₃·(C₃₀H₁₂)}
(C) 5477–5481 [5593–5597]
DOI: 10.1002/anie.200460855
- Pettit, G. R. (C) 5342–5346 [5456–5460]
- Peyratout, C. S. (R) 3762–3783 [3850–3872]
- Pfaltz, A.
– Screening of Chiral Catalysts and Catalyst Mixtures by Mass Spectrometric Monitoring of Catalytic Intermediates
(C) 2498–2500 [2552–2554]
DOI: 10.1002/anie.200453844
- Synthesis of Versatile Chiral N,P Ligands Derived from Pyridine and Quinoline
(C) 70–74 [72–76]
DOI: 10.1002/anie.200352755
- Pfützer, A.
– Phosphorus Nanorods—Two Allotropic Modifications of a Long-Known Element
(C) 4228–4231 [4324–4327]
DOI: 10.1002/anie.200460244
- Pfründer, H.
– Efficient Whole-Cell Biotransformation in a Biphasic Ionic Liquid/Water System
(C) 4529–4531 [4629–4631]
DOI: 10.1002/anie.200460241
- Philippart, F. (C) 1588–1591 [1614–1617]
- Philippopoulos, A. I. (C) 6512–6516 [6674–6678]
- Phillips, A. D. (C) 2655–2658 [2709–2712]
- Phillips, D. L.
– Green and Red Three-Photon Upconversion from Polymeric Lanthanide(III) Complexes
(C) 4659–4662 [4759–4762]
DOI: 10.1002/anie.200460576
- Phillips, R. T. (C) 1976–1979 [2010–2013]
- Piao, H. (C) 2918–2921 [2978–2981]
- Piccinini, P. (C) 846–849 [864–867]
- Piccirilli, J. A.
– A Packing-Density Metric for Exploring the Interior of Folded RNA Molecules
(C) 3033–3037 [3095–3099]
DOI: 10.1002/anie.200353575
- Piccirillo, S. (C) 1868–1871 Corrigendum: 3872 [1904–1907 Corrigendum: 3960]
- Pichon, B. P. (C) 203–206 [205–208]
- Pickford, R. (C) 337–340 [341–344]
- Pierattelli, R. (C) 2257–2259 [2307–2309]
- Pierre, J.-L. (C) 594–597 [604–607]
- Piers, W. E.
– Rapidly Initiating Ruthenium Olefin-Metathesis Catalysts
(C) 6161–6165 [6287–6291]
DOI: 10.1002/anie.200461374
- Pierssens, L. J.-M. (C) 4500–4504 [4600–4604]
- Piettre, S. R.
– α,α -Difluoro-*H*-phosphinates: Useful Intermediates for a Variety of Phosphate Isosteres
(C) 5963–5967 [6089–6093]
DOI: 10.1002/anie.200460519
- Pihko, P. M.
– Activation of Carbonyl Compounds by Double Hydrogen Bonding: An Emerging Tool in Asymmetric Catalysis
(H) 2062–2064 [2110–2113]
DOI: 10.1002/anie.200301732
- Pina, F.
– Thermal and Photochemical Properties of 4',7'-Dihydroxyflavylium in Water—Ionic Liquid Biphasic Systems: A Write–Read–Erase Molecular Switch
(C) 1525–1527 [1551–1553]
DOI: 10.1002/anie.200353131
- Pineda, L. W. (C) 1419–1421 [1443–1445], 2142–2145 [2194–2197], 5534–5536 [5650–5652]
- Pines, A. (C) 6320–6322 [6480–6482]
- Pink, J. (C) 6323–6327 [6483–6487]
- Pink, M. (C) 3156–3159 [3218–3221]
- Pinkas, J. (C) 2142–2145 [2194–2197]
- Pinkerton, A. B. (C) 4327–4329 [4427–4429]
- Pinna, N.
– Nonaqueous Synthesis of Nanocrystalline Semiconducting Metal Oxides for Gas Sensing
(C) 4345–4349 [4445–4449]
DOI: 10.1002/anie.200460610
- Pinna, N. (C) 2270–2273 [2320–2323]
- Piovani, G. (C) 3847–3852 [3935–3940]
- Piper, J. L. (C) 2915–2918 [2975–2978]
- Pirani, F. (C) 5200–5203 [5312–5315]
- Pironti, V. (C) 4097–4099 [4189–4191]
- Pitt, N. (C) 2518–2521 [2572–2575]
- Pittelkow, M. (C) 3557–3562 [3641–3646]
- Pizarro, J. L. (C) 977–980 [995–998]
- Plankensteiner, K. (C) 1886–1888 [1922–1924]
- Platt, G. W. (C) 1991–1994 [2025–2028]
- Plault, L. (C) 2924–2928 [2984–2988]
- Pley, M. (C) 4168–4170 [4262–4264]
- Ploypradith, P. (C) 866–868 [884–886]
- Poirier, M. (C) 4306–4311 [4406–4411]
- Poláková, M. (C) 2518–2521 [2572–2575]
- Polet, D. (C) 2426–2428 [2480–2482]
- Poliakoff, M.
– Sensing the Critical Point of High-Pressure Mixtures
(C) 5192–5195 [5304–5307]
DOI: 10.1002/anie.200460624
- Polleux, J. (C) 2270–2273 [2320–2323]
- Porco, J. A., Jr.
– Synthesis of Azaphilones and Related Molecules by Employing Cycloisomerization of *o*-Alkynylbenzaldehydes
(C) 1239–1243 [1259–1263]
DOI: 10.1002/anie.200353037
- Total Synthesis of the Salicylate Enamide Macrolide Oximidine III: Application of Relay Ring-Closing Metathesis
(C) 3601–3605 [3685–3689]
DOI: 10.1002/anie.200460042
- Porfyrakis, K. (C) 1386–1389 [1410–1413]
- Pornsuriyasak, P. (C) 3069–3072 [3131–3134]
- Postema, M. H. D.
– A Double Ring-Closing Metathesis Approach for the Synthesis of β -C-Trisaccharides
(C) 2915–2918 [2975–2978]
DOI: 10.1002/anie.200353478
- Pötschke, D. (C) 109–112 [111–114]
- Potte, M. (C) 1528–1531 [1554–1557]
- Potter, B. V. L. (C) 4637–4640 [4737–4740]
- Poullennec, K. G. (C) 4629–4633 [4729–4733]
- Poveda, M. L. (C) 3708–3711 [3794–3797]
- Powell, G. W. (C) 5772–5775 Corrigendum: 6581 [5896–5899 Corrigendum: 6743]
- Powell, L. H. W. (C) 1249–1251 [1269–1271]
- Power, P. P.
– Synthesis and Characterization of a Quasi-One-Coordinate Lead Cation
(C) 2655–2658 [2709–2712]
DOI: 10.1002/anie.200353365
- Power-Billard, K. N. (C) 1260–1264 [1280–1284]
- Pozzi, G. (C) 6174–6177 [6300–6303]
- Prakash, G. K. S.
– Difluoromethyl Phenyl Sulfone, a Difluoromethylene Equivalent: Use in the Synthesis of 1,1-Difluoro-1-alkenes
(C) 5203–5206 [5315–5318]
DOI: 10.1002/anie.200460815
- Direct Oxidation of Azides to Nitro Compounds
(H) 26–28 [26–28]
DOI: 10.1002/anie.200301710
- Prakash, R.
– Heterolytic Cleavage of H₂ at a Sulfur-Bridged Dinuclear Ruthenium Center
(C) 1877–1880 [1913–1916]
DOI: 10.1002/anie.200453717
- Präsang, C. Corrigendum: 2737
- Prassides, K. (C) 6316–6319 [6476–6479]
- Prato, M.
– Functionalized Carbon Nanotubes for Plasmid DNA Gene Delivery
(C) 5242–5246 [5354–5358]
DOI: 10.1002/anie.200460437
- Prato, M. (C) 5526–5530 [5642–5646]

- Pretsch, E. (C) 5181–5185 Corrigendum: 5428 [5293–5297 Corrigendum: 5542]
 Prévost, N. (C) 6517–6519 [6679–6681]
 Pribisko, M. A. (C) 1955–1958 [1989–1992]
 Price, D. J.
 – One-Dimensional Magnetism in Anhydrous Iron and Cobalt Ternary Oxalates with Rare Trigonal-Prismatic Metal Coordination Environment
 (C) 472–475 [478–481]
 DOI: 10.1002/anie.200352406
 Price, D. J. (C) 1814–1817 [1850–1853]
 Prié, G. (C) 6517–6519 [6679–6681]
 Pritzkow, H. (C) 203–206 [205–208]
 Pröckl, S. S. (C) 1881–1882 [1917–1918]
 Prokop, A.
 – Iron-Containing Nucleoside Analogues with Pronounced Apoptosis-Inducing Activity
 (C) 1731–1734 [1763–1766]
 DOI: 10.1002/anie.200353132
 Proserpio, D. M. (C) 1851–1854 [1887–1890]
 Prosvirin, A. V. (C) 4912–4915 [5020–5023]
 Pu, X. (C) 4222–4225 [4318–4321]
 Puddephatt, R. J.
 – Self-Assembly in Gold(I) Chemistry: A Double-Stranded Polymer with Interstrand Auophilic Interactions
 (C) 969–971 [987–989]
 DOI: 10.1002/anie.200353127
 Pugh, M. D. (C) 4193–4197 [4289–4293]
 Pullen, A. E. (C) 3700–3703 [3786–3789]
 Puls, S. P. (C) 3037–3040 [3099–3102]
 Puentes, V. F. (C) 2538–2540 [2592–2594]
 Pyn, J. (C) 3928–3932 [4018–4022]
 Pyykkö, P.
 – Theoretical Chemistry of Gold
 (R) 4412–4456 [4512–4557]
 DOI: 10.1002/anie.200300624
 Pyykkö, P. (C) 1573–1576 [1599–1602]



- Qi, K. (C) 2783–2787 [2843–2847]
 Qi, R.-J. (C) 1410–1414 [1434–1438]
 Qian, M. (C) 2259–2263 [2309–2313]
 Qiao, Y.-F. (C) 5010–5013 [5120–5123]
 Qin, C. (C) 5036–5040 [5146–5150]
 Qiu, J.
 – Manipulation of Gold Nanoparticles inside Transparent Materials
 (C) 2230–2234 [2280–2284]
 DOI: 10.1002/anie.200352380
 Qiu, S.
 – $\text{Zn}_2[(S)\text{-O}_3\text{PCH}_2\text{NHC}_4\text{H}_7\text{CO}_2]_2$: A Homochiral 3D Zinc Phosphonate with Helical Channels
 (C) 6482–6485 [6644–6647]
 DOI: 10.1002/anie.200460724
 Qu, Da-H. (C) 2661–2665 [2715–2719]
 Qu, J. (C) 1528–1531 [1554–1557]
 Que, L., Jr.
 – Bispidine Ligand Effects on Iron/Hydrogen Peroxide Chemistry
 (C) 1283–1287 [1303–1307]
 DOI: 10.1002/anie.200352523
 – Direct Evidence for Oxygen-Atom Exchange between Nonheme Oxoiron(IV) Complexes and Isotopically Labeled Water

- (C) 2417–2420 [2471–2474]
 DOI: 10.1002/anie.200353497
 – Models of High-Valent Intermediates of Non-Heme Diiron Alkane Monooxygenases: Electronic Structure of a Bis(μ -oxo)diron(IV) Complex with Locally Low-Spin Metal Centers
 (C) 834–838 [852–856]
 DOI: 10.1002/anie.200351768
 Quebatte, L. (C) 1520–1524 [1546–1550]
 Quici, S. (C) 6174–6177 [6300–6303]
 Quiñonero, D. Corrigendum: 141
 Quitmann, C. (C) 2853–2856 [2913–2917]
 Quitmann, C. C. (C) 5994–5996 [6120–6122]



- Raab, V. (C) 4360–4363 [4460–4464]
 Raabe, G. (C) 6662–6666 [6832–6836]
 Raabe, I. (R) 2066–2090 [2116–2142]
 Rabe, J. P.
 – A Covalent-Chemistry Approach to Giant Macromolecules and Their Wetting Behavior on Solid Substrates
 (C) 5185–5188 [5297–5300]
 DOI: 10.1002/anie.200460390
 Rabideau, P. W. (C) 4497–4500 [4597–4600]
 Rabis, A. (C) 112–115 [114–117]
 Rabuka, D. (C) 1562–1566 [1588–1592]
 Rademann, J.
 – Organic Protein Chemistry: Drug Discovery through the Chemical Modification of Proteins
 (H) 4554–4556 [4654–4656]
 DOI: 10.1002/anie.200460075
 Rädler, J. O.
 – Synthesis and Self-Assembly of Perylene-diimide–Oligonucleotide Conjugates
 (C) 3967–3970 [4057–4060]
 DOI: 10.1002/anie.200353621
 Rahe, N. (C) 1842–1844 Corrigendum: 2321 [1878–1880 Corrigendum: 2373]
 Rahman, G. M. A. (C) 5526–5530 [5642–5646]
 Rainaldi, M. (C) 3152–3155 [3214–3217]
 Raineri, V. (C) 4081–4084 [4173–4176]
 Raja, R. (C) 6745–6747 [6913–6915]
 Ramakrishnan, S.
 – Aromatic Donor–Acceptor Charge-Transfer and Metal-Ion-Complexation-Assisted Folding of a Synthetic Polymer
 (C) 3264–3268 [3326–3330]
 DOI: 10.1002/anie.200453860
 Ramanan, H. (L) 4558–4561 [4658–4661]
 Rameshkumar, C. (C) 615–618 [625–628]
 Ramón, D. J. (H) 284–287 [286–289]
 Rampi, M. A.
 – Electron Transfer in a Hg-SAM//SAM-Hg Junction Mediated by Redox Centers
 (C) 3835–3839 [3923–3927]
 DOI: 10.1002/anie.200453945
 Ramsey, M. G. (C) 5546–5549 [5663–5666]
 Ramström, O.
 – Catalytic Self-Screening of Cholinesterase Substrates from a Dynamic Combinatorial Thioester Library
 (C) 3716–3718 [3802–3804]
 DOI: 10.1002/anie.200454165
 Rang, A. (C) 1291–1294 [1311–1314]

- Rannard, S. P. (C) 1389–1392 [1413–1416]
 Rao, C. N. R.
 – Metal Carboxylates with Open Architectures
 (R) 1466–1496 [1490–1521]
 DOI: 10.1002/anie.200300588
 Raptis, R. G.
 – Anion Encapsulation by Neutral Supramolecular Assemblies of Cyclic Cu^{II} Complexes: A Series of Five Polymerization Isomers, $[\text{cis-Cu}^{\text{II}}(\mu\text{-OH})(\mu\text{-pz})_n]$, $n = 6, 8, 9, 12$, and 14
 (C) 574–577 [584–587]
 DOI: 10.1002/anie.200352636
 Raptopoulou, C. P. (C) 210–212 [212–214]
 Ratera, I. (C) 5266–5268 [5378–5381]
 Ratna, B. R. (O) 3360 [3438]
 Ratner, M. A. (C) 1246–1249 [1266–1269]
 Ratovelomanana-Vidal, V.
 – Difluorophos, an Electron-Poor Diphosphane: A Good Match Between Electronic and Steric Features
 (C) 320–325 [324–329]
 DOI: 10.1002/anie.200352453
 Rauchfuss, T. B.
 – Competing H–H, S–S, and M–M Bond Formation in the “Shape-Shifting” Cluster $[\text{Ru}_4\text{S}_2(\text{arene})_4]^{2+}$
 (C) 6742–6745 [6910–6913]
 DOI: 10.1002/anie.200461264
 Rauterkus, M. J. (C) 1300–1303 [1321–1324]
 Ravoo, B. J. (C) 369–373 [373–377]
 Rayment, T.
 – In Situ Investigations into Chemical Processes by Electron-Energy-Resolved X-Ray Absorption Spectroscopy
 (C) 3691–3695 [3777–3781]
 DOI: 10.1002/anie.200353235
 Raymond, K. N.
 – Selective C–H Bond Activation by a Supramolecular Host–Guest Assembly
 (C) 963–966 [981–984]
 DOI: 10.1002/anie.200352772
 – Supramolecular Catalysis of a Unimolecular Transformation: Aza-Cope Rearrangement within a Self-Assembled Host
 (C) 6748–6751 [6916–6919]
 DOI: 10.1002/anie.200461776
 Rayner, B.
 – Use of Dynamic Combinatorial Chemistry for the Identification of Covalently Appended Residues that Stabilize Oligonucleotide Complexes
 (C) 3144–3147 [3206–3209]
 DOI: 10.1002/anie.200454041
 Ready, J. M. (C) 1270–1272 [1290–1292]
 Reddy, K. R. (C) 3961–3965 [4051–4055]
 Reed, C. A.
 – Putting *tert*-Butyl Cation in a Bottle
 (C) 2908–2911 [2968–2971]
 DOI: 10.1002/anie.200453931
 – The Strongest Isolable Acid
 (C) 5352–5355 [5466–5469]
 DOI: 10.1002/anie.200460005
 – The X-ray Structure of a Vinyl Cation
 (C) 1543–1546 [1569–1572]
 DOI: 10.1002/anie.200352986
 Reed, T. M. (C) 2806–2809 [2866–2869]
 Reedijk, J.
 – A Highly Flexible Dinuclear Ruthenium(II)–Platinum(II) Complex: Crystal Structure and Binding to 9-Ethylguanine
 (C) 5668–5670 [5786–5788]
 DOI: 10.1002/anie.200460319

- An Aromatic Anion Receptor: Anion- π Interactions do Exist
(C) 5815–5817 [5939–5941]
DOI: 10.1002/anie.200460486
- Reents, R. (C) 2711–2714 [2765–2768]
- Reetz, M. T.
- Directed Evolution as a Method To Create Enantioselective Cyclohexanone Monooxygenases for Catalysis in Baeyer–Villiger Reactions
(C) 4075–4078 [4167–4170]
DOI: 10.1002/anie.200460272
- Directed Evolution of Cyclohexanone Monooxygenases: Enantioselective Biocatalysts for the Oxidation of Prochiral Thioethers
(C) 4078–4081 [4170–4173]
DOI: 10.1002/anie.200460311
- Rehahn, M. (C) 4616–4621 [4716–4721]
- Rehder, D.
- Artificial Cells: Temperature-Dependent, Reversible Li^+ -Ion Uptake/Release Equilibrium at Metal Oxide Nanocontainer Pores
(C) 4466–4470 Corrigendum: 5115 [4566–4570 Corrigendum: 5225]
DOI: 10.1002/anie.200453762
- Reichenbach, H. (C) 4888–4892 [4996–5000]
- Reicheneder, S. (C) 4353–4357 [4453–4457]
- Reicke, A. (C) 2574–2576 [2628–2630]
- Reicke, M. (C) 3485–3488 [3567–3571]
- Reif, J. H.
- A Unidirectional DNA Walker That Moves Autonomously along a Track
(C) 4906–4911 [5014–5019]
DOI: 10.1002/anie.200460522
- Reiff, W. M. (C) 4912–4915 [5020–5023]
- Reiher, M. (C) 4360–4363 [4460–4464]
- Reilly, J. P.
- Fragmentation of Singly Charged Peptide Ions by Photodissociation at $\lambda = 157$ nm
(C) 4791–4794 [4895–4898]
DOI: 10.1002/anie.200460788
- Reimer, U. (C) 2671–2674 [2725–2728]
- Reincke, F. (C) 458–462 [464–468]
- Reiner, H. (C) 1886–1888 [1922–1924]
- Reinhoudt, D. N.
- Writing Patterns of Molecules on Molecular Printboards
(C) 369–373 [373–377]
DOI: 10.1002/anie.200352767
- Reinke, H. (C) 5406–5408 [5521–5523]
- Reiser, O.
- Surprisingly Stable Helical Conformations in α/β -Peptides by Incorporation of *cis*- β -Aminocyclopropane Carboxylic Acids
(C) 511–514 [517–520]
DOI: 10.1002/anie.200352267
- Reisman, S. E. (C) 1270–1272 [1290–1292]
- Ren, G.-M. (C) 1371–1373 [1395–1397]
- Ren, J. (C) 2661–2665 [2715–2719]
- Renaud, P. (C) 4738–4741 [4842–4845]
- Rencurosi, A. (C) 5918–5922 [6044–6048]
- Ressler, T.
- Rational Design of Nanostructured Copper–Zinc Oxide Catalysts for the Steam Reforming of Methanol
(C) 112–115 [114–117]
DOI: 10.1002/anie.200352148
- Reupohl, J. (C) 1423–1427 [1447–1451]
- Reuter, A. (C) 3550–3553 [3634–3637]
- Reutter, W. (C) 4366–4370 [4467–4470]
- Reyes, F. (C) 1724–1727 [1756–1759]
- Reymond, J.-L.
- A Combinatorial Approach to Catalytic Peptide Dendrimers
(C) 4612–4615 [4712–4715]
DOI: 10.1002/anie.200460177
- Outrunning the Bear
(H) 5577–5579 [5695–5697]
DOI: 10.1002/anie.200460313
- Ribas, X. (C) 4049–4052 [4141–4144]
- Ribas-Ariño, J. (C) 577–580 [587–590]
- Ricard, L. (C) 956–958 [974–976], 6382–6385 [6542–6545]
- Rice, C. R.
- Allosteric and Electrostatic Reprogramming of a Ditopic Ligand
(C) 4515–4518 [4615–4618]
DOI: 10.1002/anie.200460424
- Rich, J. R. (C) 613–615 [623–625]
- Richter, W. (C) 245–247 [247–249]
- Rico-Lattes, I. (C) 6174–6177 [6300–6303]
- Riedlinger, J. (C) 2574–2576 [2628–2630]
- Riendl, D. (C) 5682–5685 [5800–5803]
- Riera, V. (C) 3464–3467 [3546–3549]
- Riermeier, T. (C) 5066–5069 [5176–5179]
- Rigo, P. (C) 3584–3588 [3668–3672]
- Riis-Johannessen, T. (C) 4515–4518 [4615–4618]
- Rinderspacher, B. C. (C) 6553–6557 [6715–6719]
- Ringsdorf, H.
- Hermann Staudinger and the Future of Polymer Research Jubilees—Beloved Occasions for Cultural Piety
(E) 1064–1076 [1082–1095]
DOI: 10.1002/anie.200330071
- Rinner, U. (C) 5342–5346 [5456–5460]
- Riordan, C. G.
- Spectroscopic Elucidation of a Peroxo $\text{Ni}_2(\mu\text{-O}_2)$ Intermediate Derived from a Nickel(II) Complex and Dioxygen
(C) 6716–6718 [6884–6886]
DOI: 10.1002/anie.200460747
- Ripmeester, J. A.
- Dipeptides as Microporous Materials
(C) 6308–6311 [6468–6471]
DOI: 10.1002/anie.200460952
- Ripmeester, J. A. (C) 3310–3313 [3372–3375]
- Risatti, C. A. (C) 6671–6672 [6839–6840]
- Rissanen, K.
- Noncovalent $\pi\cdots\pi$ -Stacked Exo-Functional Nanotubes: Subtle Control of Resorcinarene Self-Assembly
(C) 1243–1246 [1263–1266]
DOI: 10.1002/anie.200353112
- Risse, T.
- Structural Changes in Nanoparticle Catalysts as Monitored by Their Magnetic Properties
(C) 517–520 [523–526]
DOI: 10.1002/anie.200352107
- Ritter, T. (C) 4653–4656 [4753–4756]
- Riveros, J. M.
- An Unusually Fast Nucleophilic Aromatic Displacement Reaction: The Gas-Phase Reaction of Fluoride Ions with Nitrobenzene
(C) 3588–3590 [3672–3674]
DOI: 10.1002/anie.200454230
- Rivière, E. (C) 850–852 [868–870], 956–958 [974–976], 2274–2277 [2324–2327]
- Roach, L. S. (C) 2508–2511 [2562–2565]
- Robinson, B. L. (C) 1381–1385 [1405–1409]
- Robinson, J. A.
- An Oxidative Phenol Coupling Reaction Catalyzed by OxyB, a Cytochrome P450 from the Vancomycin-Producing Microorganism
(C) 6709–6713 [6877–6881]
DOI: 10.1002/anie.200461278
- Using a β -Hairpin To Mimic an α -Helix: Cyclic Peptidomimetic Inhibitors of the p53–HDM2 Protein–Protein Interaction
(C) 2109–2112 [2161–2164]
DOI: 10.1002/anie.200353242
- Robson, R.
- Cubic, Hydrogen-Bonded (10,3)-*a* Networks in the Family $[\text{C}(\text{NH}_2)_3]_n[\text{N}(\text{CH}_3)_4][\text{XO}_4]$ ($\text{X} = \text{S}, \text{Cr}, \text{and Mo}$)
(C) 6157–6160 [6283–6286]
DOI: 10.1002/anie.200461678
- Rocca, M. (C) 5200–5203 [5312–5315]
- Rode, B. M.
- Prebiotic Formation of Amino Acids in a Neutral Atmosphere by Electric Discharge
(C) 1886–1888 [1922–1924]
DOI: 10.1002/anie.200353135
- Rodríguez, A. (C) 4876–4880 [4984–4988], 4880–4883 [4988–4991]
- Rodríguez, A. (C) 1724–1727 [1756–1759]
- Rodríguez, F. (C) 3932–3935 [4022–4025]
- Rodríguez-Cuamatzi, P. (C) 3041–3044 [3103–3106]
- Rodríguez-Santiago, L. (C) 5396–5399 [5507–5511]
- Rodríguez-Ubis, J. C. (C) 619–621 [629–631]
- Roemer, E. L. (C) 5658–5661 [5776–5779]
- Roesky, H. W.
- Germacarboxylic Acid: An Organic-Acid Analogue Based on a Heavier Group 14 Element
(C) 5534–5536 [5650–5652]
DOI: 10.1002/anie.200460872
- $[\text{HC}(\text{CMeNAr})_2\text{Al}_2\text{P}_4]$ ($\text{Ar} = 2,6\text{-iPr}_2\text{C}_6\text{H}_3$): A Reduction to a Formal $[\text{P}_4]^{4-}$ Charged Species
(C) 3443–3445 [3525–3527]
DOI: 10.1002/anie.200353406
- $[\text{La}(\mu\text{-S}_2)_2\text{Al}]$: A Homobimetallic Derivative of the Sulfur Crown S_8
(C) 6190–6192 [6316–6318]
DOI: 10.1002/anie.200461209
- Molecular $\{(\text{SnO})_6\}$ Trapped by Two $\{\text{R}_2\text{Si}_2\text{O}_3\}$ Fragments: X-ray Single-Crystal Structure of $[(\text{SnO})_6(\text{R}_2\text{Si}_2\text{O}_3)_2]$
(C) 3842–3844 [3930–3932]
DOI: 10.1002/anie.200454149
- Polyhedral Ferrous and Ferric Siloxanes
(C) 3832–3835 [3920–3923]
DOI: 10.1002/anie.200453740
- Preparation and Structure of the First Germanium(II) Hydroxide: The Congener of an Unknown Low-Valent Carbon Analogue
(C) 1419–1421 [1443–1445]
DOI: 10.1002/anie.200353205
- Preparation of $[\text{La}(\mu\text{-S})_2\text{MCP}_2]$ ($\text{M} = \text{Ti}, \text{Zr}$) from the Structurally Characterized Lithium Complexes $[(\text{La}(\text{SH})\text{[SLi}(\text{thf})_2]_2)]$ and $[(\text{La}[(\text{SLi})_2(\text{thf})_3])] \cdot 2\text{THF}$
(C) 6192–6196 [6318–6322]
DOI: 10.1002/anie.200461254
- Preparation of Monomeric $[\text{La}(\text{NH}_2)_2]$ —A Main-Group Metal Diamide Containing Two Terminal NH_2 Groups

- (C) 2142–2145 [2194–2197]
DOI: 10.1002/anie.200353541
- Tetranuclear Homo- and Heteroalumoxanes Containing Reactive Functional Groups: Syntheses and X-ray Crystal Structures of $[[[La(OMe)](\mu-O)(MH_2)_2]]$ (C) 4940–4943 [5048–5051]
DOI: 10.1002/anie.200460395
- Roewer, G.
– Synthesis of Amines from Imines in the Coordination Sphere of Silicon—Surprising Photo-Rearrangement of Hexacoordinate Organosilanes (C) 2441–2444 [2495–2498]
DOI: 10.1002/anie.200353267
- Rogach, A. L.
– Binary Superlattices of Nanoparticles: Self-Assembly Leads to “Metamaterials” (H) 148–149 [150–151]
DOI: 10.1002/anie.200301704
- Roger, J. (C) 1979–1983 [2013–2017]
- Roggan, S. (C) 2846–2849 [2906–2910]
- Roh, E. J. (C) 6183–6185 [6309–6311]
- Rohde, H. (C) 2243–2247 [2293–2297], 6512–6516 [6674–6678]
- Rohl, A. L.
– Luminescent Probes of Crystal Growth: Surface Charge and Polar Axis Sense in Dye-Doped Potassium Hydrogen Phthalate (C) 5328–5331 [5442–5445]
DOI: 10.1002/anie.200453839
- Rohmer, M.-M. (C) 6120–6125 [6246–6251]
- Röhr, C. (C) 869–873 [887–891]
- Rojo, J. (R) 3644–3662 [3728–3747], (C) 5808–5811 [5932–5935]
- Rojo, T.
– $(C_4N_2H_{12})[Fe^{II}_{0.86}Fe^{III}_{1.14}(HPO_3)_{1.39}(HPO_4)_{0.47}(PO_4)_{0.14}F_3]$: A Fluoro-Phosphite–Hydrogenphosphate–Phosphate Iron(II,III) Mixed-Valence Organically Templated Compound (C) 977–980 [995–998]
DOI: 10.1002/anie.200352219
- Rokita, S. E.
– Criteria for Efficient Transport of Excess Electrons in DNA (C) 1839–1842 [1875–1878]
DOI: 10.1002/anie.200353038
- Rolland, J. P. (C) 5796–5799 [5920–5923]
- Romero, F. M.
– Polycationic Mn_{12} Single-Molecule Magnets as Electron Reservoirs with $S > 10$ Ground States (C) 6152–6156 [6278–6282]
DOI: 10.1002/anie.200460282
- Romero, P. E. (C) 6161–6165 [6287–6291]
- Romero-Salguero, F. J. (R) 3644–3662 [3728–3747]
- Rominger, F. (C) 5846–5849 [5970–5973]
- Rondino, F. (C) 1868–1871 Corrigendum: 3872 [1904–1907 Corrigendum: 3960]
- Ros, M. B.
– Hydrogen-Bonded Banana Liquid Crystals (C) 5235–5238 [5347–5350]
DOI: 10.1002/anie.200460549
- Rösch, N.
– Environmental Fluctuations Facilitate Electron-Hole Transfer from Guanine to Adenine in DNA π Stacks (C) 624–627 [634–637]
DOI: 10.1002/anie.200352824
- Rosei, F. (C) 2092–2095 [2144–2147]
- Rosenbach, N., Jr. (C) 3050–3053 [3112–3115]
- Rosenbaum, C. (C) 224–228 Corrigendum: 540 [226–230 Corrigendum: 547]
- Rosenfeldt, S.
– Analysis of the Spatial Dimensions of Fully Aromatic Dendrimers (C) 109–112 [111–114]
DOI: 10.1002/anie.200351810
- Rosenfeldt, S. (C) 5843–5846 [5967–5970]
- Rosenthal, U.
– Stable Cyclopentynes—Made by Metals!? (M) 3882–3887 [3972–3977]
DOI: 10.1002/anie.200401761
- Rosi, N. L. (C) 5500–5503 [5616–5619]
- Rosner, H. (C) 1088–1092 [1108–1112]
- Rosokha, S. V. (C) 4650–4652 [4750–4752]
- Rosokha, Y. S. (C) 4650–4652 [4750–4752]
- Rosseinsky, M. J.
– New Oxidation States and Defect Chemistry in the Pyrochlore Structure (C) 3562–3565 [3646–3649]
DOI: 10.1002/anie.200453819
- Rossi, M.
– The Catalytic Activity of “Naked” Gold Particles (C) 5812–5815 [5936–5939]
DOI: 10.1002/anie.200460446
- Rössle, M. (C) 6547–6549 [6709–6711]
- Roßteuscher, T. T. J. (C) 6519–6522 [6681–6684]
- Rotello, V. M. (C) 724–727 [742–745]
- Rotger, C. Corrigendum: 141
- Röthlisberger, U.
– Green Oxidation Catalysts: Computational Design of High-Efficiency Models of Galactose Oxidase (C) 3286–3289 [3348–3351]
DOI: 10.1002/anie.200454081
- Roubeau, O. (C) 3283–3286 [3345–3348]
- Rousseau, R. (C) 4804–4807 [4908–4911]
- Routenberg Love, K. (C) 602–605 [612–615]
- Rovira, C.
– Stepwise Construction of Oligomeric 1,2-Diselenolene Platinum(IV) Complexes (C) 4049–4052 [4141–4144]
DOI: 10.1002/anie.200453761
- Rovira, C. (C) 1828–1832 [1864–1868], 5266–5268 [5378–5381]
- Rowan, A. E.
– Allosterically Driven Multicomponent Assembly (C) 4755–4759 [4859–4863]
DOI: 10.1002/anie.200460398
- Rowan, A. E. (C) 4045–4049 [4137–4141]
- Rozenberg, H. (C) 5961–5963 [6087–6089]
- Ruan, C.-Y. (C) 2705–2709 [2759–2763]
- Ruben, M.
– Color Theory in Science and Art: Ostwald and the Bauhaus (E) 4842–4847 [4948–4953]
DOI: 10.1002/anie.200430086
- Ruben, M. (R) 3644–3662 [3728–3747]
- Rubin, S. M. (C) 6320–6322 [6480–6482]
- Rubin, Y. (C) 1498–1502 [1524–1528]
- Ruchirawat, S.
– A Highly Efficient Synthesis of Lamellarins K and L by the Michael Addition/Ring-Closure Reaction of Benzylidihydroisoquinoline Derivatives with Ethoxycarbonyl- β -nitrostyrenes (C) 866–868 [884–886]
DOI: 10.1002/anie.200352043
- Ruck, R. T. (C) 5372–5374 [5486–5488], 5375–5377 [5489–5491]
- Ruckenstein, E. (C) 6471–6474 [6633–6636]
- Rudd, P. M. (C) 1000–1003 [1018–1021]
- Rudkevich, D. M.
– Emerging Supramolecular Chemistry of Gases (R) 558–571 [568–581]
DOI: 10.1002/anie.200300606
- Rudolph, M. (C) 6545–6547 [6707–6709]
- Rüegger, H. (C) 2521–2524 [2575–2578]
- Ruel, O. (C) 4785–4788 [4889–4892]
- Rufińska, A. (C) 2444–2446 [2498–2500]
- Ruhlandt-Senge, K.
– Linear Finite “Mers”—Homoleptic Polynuclear Heavy Alkaline Earth Metal Pyrazolates (C) 5218–5220 [5330–5332]
DOI: 10.1002/anie.200460628
- Ruiz, E. J. (C) 6320–6322 [6480–6482]
- Ruiz, J. (C) 2924–2928 [2984–2988]
- Ruiz-García, R. (C) 850–852 [868–870], 956–958 [974–976]
- Ruiz-Molina, D. (C) 1828–1832 [1864–1868], 5266–5268 [5378–5381]
- Ruiz-Salvador, A. R. (C) 469–472 [475–478]
- Runsink, J. (C) 6662–6666 [6832–6836]
- Runyon, M. K. (C) 1531–1536 [1557–1562]
- Russon, L. M. (C) 6372–6377 [6532–6537]
- Rust, J. (C) 2444–2446 [2498–2500]
- Ruter, S. J. T. (C) 1836–1839 [1872–1875]
- Rybak, B. (C) 5246–5249 Corrigendum: 5721 [5358–5361 Corrigendum: 5839]
- Rybtchinski, B. (C) 5961–5963 [6087–6089]
- Rychnovsky, S. D.
– Synthesis of Rimocidinolide Methyl Ester, the Aglycone of (+)-Rimocidin (C) 2822–2826 [2882–2886]
DOI: 10.1002/anie.200453697
- Ryoo, R. (C) 5231–5234 [5343–5346]
- Ryu, C. Y.
– Supramolecular AB Diblock Copolymers (C) 6471–6474 [6633–6636]
DOI: 10.1002/anie.200460472
- Ryu, I.
– Cascade Carbonylation Methods Leading to β -Diketones and β -Functionalized δ -Diketones (C) 2423–2425 [2477–2479]
DOI: 10.1002/anie.200453702
- Ryu, K.-S. (C) 5987–5990 [6113–6116]
- Rzayev, J. (C) 1691–1694 [1723–1726]



- Saaby, S. (C) 4476–4478 [4576–4578]
- Saak, W. (C) 1583–1587 [1609–1614]
- Saalfrank, J. W. (C) 2028–2031 [2062–2066]
- Sabino, A. A. (C) 2514–2518 Corrigendum: 4389 [2568–2572 Corrigendum: 4489]
- Sable, J. (C) 1672–1675 [1704–1707]
- Sachdev, H.
– Diamonds from the Pressure Cooker—Science or Science Fiction? (L) 4696–4699 [4800–4803]
DOI: 10.1002/anie.200460689
- Sadamoto, R. (C) 1516–1520 [1542–1546]
- Sadler, P. J.
– Assembly of an Oxo–Zirconium(IV) Cluster in a Protein Cleft (C) 5914–5918 [6040–6044]
DOI: 10.1002/anie.200460806

- Sadohara, H. (C) 2290–2293 [2340–2343]
 Saeki, K. (C) 2389–2391 [2443–2445]
 Saeki, N. (C) 4915–4918 [5023–5026]
 Safarowsky, C. (C) 1291–1294 [1311–1314]
 Safina, B. S. (C) 5087–5092 [5197–5202],
 5092–5097 [5202–5207]
 Sagar, P. (C) 5694–5697 [5812–5815]
 Saghatelian, A. (C) 3063–3067 [3125–3129]
 Sahakitpichan, P. (C) 866–868 [884–886]
 Sahu, S. (C) 4034–4037 [4126–4129]
 Saillard, J.-Y. (C) 1979–1983 [2013–2017]
 Saint-Aman, E. (C) 594–597 [604–607]
 Saito, G.
 – A Purely Organic Molecular Metal Based on a Hydrogen-Bonded Charge-Transfer Complex: Crystal Structure and Electronic Properties of TTF-Imidazole-*p*-Chloranil (C) 6343–6346 [6503–6506]
 DOI: 10.1002/anie.200460801
 Saito, G. (C) 3670–3673 [3756–3759]
 Saito, Kei (C) 730–733 [748–751]
 Saito, Keiji (C) 81–84 [83–86]
 Saito, S.
 – Asymmetric Direct Aldol Reaction Assisted by Water and a Proline-Derived Tetrazole Catalyst (C) 1983–1986 [2017–2020]
 DOI: 10.1002/anie.200352724
 – Chiral Molecular Recognition by Aluminum Tris(2,6-diphenylphenoxide) in an Asymmetric 1,4-Addition (C) 994–997 [1012–1015]
 DOI: 10.1002/anie.200352809
 Saito, Takahiro (C) 1414–1416 [1438–1440]
 Saito, Teruo (C) 1368–1371 [1392–1395]
 Saiz, C. G. (C) 3260–3264 [3322–3326]
 Sakaguchi, S. (C) 1120–1123 [1140–1143]
 Sakai, K. (C) 5029–5032 [5139–5142]
 Sakai, N. (C) 3677–3682 [3763–3768]
 Sakamoto, H. (C) 2684–2687 [2738–2741]
 Sakamoto, K.
 – Formation of a Stable, Lattice-Framework Disilene: A Strategy for the Construction of Bulky Substituents (C) 4610–4612 [4710–4712]
 DOI: 10.1002/anie.200460067
 Sakamoto, M. (C) 6474–6479 [6636–6641]
 Sakamoto, Satoshi (C) 6505–6510 [6667–6672]
 Sakamoto, Shigeru (C) 5621–5625 [5739–5743]
 Sakamoto, Y. (C) 5231–5234 [5343–5346]
 Sakata, M. (C) 3670–3673 [3756–3759]
 Sakata, Y. (C) 100–103 [102–105]
 Sakazaki, H. (C) 6505–6510 [6667–6672]
 Sakowski, J. (C) 251–254 [254–257]
 Salcedo, C. (C) 5963–5967 [6089–6093]
 Salem, B. (C) 2826–2830 [2886–2890]
 Salo, E. V. (C) 1821–1825 Corrigendum: 2986 [1857–1861 Corrigendum: 3046]
 Salvatella, X. (C) 196–198 [198–200]
 Samachetty, H. D. (C) 2812–2815 [2872–2875]
 Samain, E. (C) 4644–4646 [4744–4746]
 Samwer, K. (C) 3832–3835 [3920–3923]
 Sanakis, Y. (C) 2266–2270 [2316–2320]
 Sanchez-Castillo, M. A. (C) 1140–1142 [1160–1162]
 Sánchez-Quesada, J. (C) 3063–3067 [3125–3129]
 Sanders, D. (C) 752–754 [770–773]
 Sanders, J. K. M.
 – Lithium-Templated Synthesis of a Donor–Acceptor Pseudorotaxane and Catenane (C) 1959–1962 [1993–1996]
 DOI: 10.1002/anie.200353075
 Sanford, M. S. (C) 588–590 [598–600]
 Sangregorio, C. (C) 3136–3138 [3198–3200]
 Sankar, A. R. (C) 3961–3965 [4051–4055]
 Santamaría, J. (C) 485–490 [491–496]
 Santos, L. L. (C) 3708–3711 [3794–3797]
 Santos, L. S. (C) 4330–4333 [4430–4433]
 Sanz Miguel, P. J. (C) 5396–5399 [5507–5511]
 Sapountzis, I. (C) 897–900 [915–918], 2968–2970 [3028–3030], 4364–4366 [4464–4466]
 Sarikaya, M.
 – Ordered Self-Assembly and Electronic Behavior of C₆₀–Anthrylphenylacetylene Hybrid (C) 1512–1516 [1538–1542]
 DOI: 10.1002/anie.200353001
 Sarkar, T. K.
 – Bimetallic Reagents of Silicon: One-Pot Synthesis of 2,3,5-Trisubstituted Tetrahydrofurans by a Double Sakurai–Hosomi Reaction (C) 1417–1419 [1441–1443]
 DOI: 10.1002/anie.200353184
 Sartori, A. (C) 369–373 [373–377]
 Sasaki, M. (C) 4763–4767 [4867–4871]
 Sasaki, T. (C) 6500–6505 [6662–6667]
 Sasaki, Y. (C) 1251–1254 [1271–1274]
 Sass, B. (C) 3832–3835 [3920–3923]
 Sasse, F. (C) 4888–4892 [4996–5000]
 Satake, K.
 – Synthesis of a Delocalized Azepinium Ion and Investigation of Its Electrophilic Character (C) 736–738 [754–756]
 DOI: 10.1002/anie.200352794
 Satake, M.
 – Structural Revision and Total Synthesis of Azaspiracid-1, Part 1: Intelligence Gathering and Tentative Proposal (C) 4312–4318 [4412–4418]
 DOI: 10.1002/anie.200460695
 Sato, F.
 – Stereoselective Construction of Acyclic Carbon Chains by a One-Pot Coupling Process Based on Alkenyloxazoline–Titanium Complexes (C) 490–492 [496–498]
 DOI: 10.1002/anie.200352769
 Sato, I. (C) 4490–4492 [4590–4592]
 Sato, K. (C) 6343–6346 [6503–6506]
 Sato, M. (C) 1516–1520 [1542–1546]
 Sato, O. (C) 6135–6139 [6261–6265]
 Sato, Takayuki (C) 490–492 [496–498]
 Sato, Tomohiro (C) 581–584 [591–594]
 Sato, Tsutomu (C) 6700–6703 [6868–6871]
 Sato, Y.
 – Arylnaphthalene Lignans through Pd-Catalyzed [2 + 2 + 2] Cycloaddition of Arynes and Diynes: Total Synthesis of Taiwanins C and E (C) 2436–2440 [2490–2494]
 DOI: 10.1002/anie.200453809
 Satoh, T. (C) 5063–5065 [5173–5175]
 Satta, M. (C) 1868–1871 Corrigendum: 3872 [1904–1907 Corrigendum: 3960]
 Sattelmeyer, K. W. (C) 4200–4206 [4296–4302]
 Sattler, M.
 – Speeding Up Biomolecular NMR Spectroscopy (H) 782–786 [800–804]
 DOI: 10.1002/anie.200301680
 Saucède, L. (C) 4172–4178 [4267–4273]
 Sauer, M.
 – Highly Sensitive Protease Assay Using Fluorescence Quenching of Peptide Probes Based on Photoinduced Electron Transfer (C) 3798–3801 [3886–3890]
 DOI: 10.1002/anie.200453835
 Saul, S. (C) 5519–5523 [5635–5639]
 Sauvage, J.-P.
 – Light-Driven Machine Prototypes Based on Dissociative Excited States: Photoinduced Decoordination and Thermal Reoordination of a Ring in a Ruthenium(II)-Containing [2]Catenane (C) 2392–2395 [2446–2449]
 DOI: 10.1002/anie.200352522
 Sauvage, J.-P. (C) 4482–4485 [4582–4585]
 Sauvajol, J.-L. (C) 203–206 [205–208]
 Scanlan, C. N. (C) 1000–1003 [1018–1021]
 Schade, B. (C) 2959–2962 [3019–3022]
 Schaefer III, H. F. (C) 4200–4206 [4296–4302]
 Schäfer, S. (C) 2839–2842 [2899–2903]
 Schäferling, M. (C) 1735–1738 [1767–1770]
 Schakel, M. (C) 714–717 Corrigendum: 3748 [732–735 Corrigendum: 3834], 3440–3442 [3522–3524], 3474–3477 [3556–3559]
 Schalley, C. A.
 – Borromean Rings: A One-Pot Synthesis (H) 4399–4401 [4499–4501]
 DOI: 10.1002/anie.200460583
 – Second-Order Templatation: Ordered Deposition of Supramolecular Squares on a Chloride-Covered Cu(100) Surface (C) 1291–1294 [1311–1314]
 DOI: 10.1002/anie.200352968
 Schatz, M. (C) 4360–4363 [4460–4464]
 Scheel, A. (C) 3928–3932 [4018–4022]
 Scheidtman, J. (C) 752–754 [770–773]
 Scheller, F. W. (C) 4357–4360 [4457–4460]
 Schelter, E. J. (C) 4912–4915 [5020–5023]
 Schenk, H. (C) 3471–3473 [3553–3555]
 Schenk, K. J. (C) 2694–2697 [2748–2751]
 Schenker, R. (C) 6716–6718 [6884–6886]
 Schenning, A. P. H. J.
 – Efficient Energy Transfer in Mixed Columnar Stacks of Hydrogen-Bonded Oligo(*p*-phenylene vinylene)s in Solution (C) 1976–1979 [2010–2013]
 DOI: 10.1002/anie.200353451
 – π -Conjugated Oligo(*p*-phenylenevinylene) Rosettes and Their Tubular Self-Assembly (C) 74–78 [76–80]
 DOI: 10.1002/anie.200352790
 Schenning, A. P. H. J. (C) 3422–3425 [3504–3507]
 Schepers, U.
 – Polyamides as Artificial Transcription Factors: Novel Tools for Molecular Medicine? (H) 2472–2475 [2526–2529]
 DOI: 10.1002/anie.200301745
 Scherer, W.
 – Agostic Interactions in d⁰ Metal Alkyl Complexes (R) 1782–1806 [1816–1842]
 DOI: 10.1002/anie.200200548
 Scherer, W. (C) 2234–2239 [2284–2289]
 Scheschkewitz, D.
 – A Silicon Analogue of Vinylolithium: Structural Characterization of a Disilene (C) 2965–2967 [3025–3028]
 DOI: 10.1002/anie.200353347

- Scheschkewitz, D. (C) 585–587 [595–597], 4880–4883 [4988–4991]
- Schicks, J. M.
- The Coexistence of Two Different Methane Hydrate Phases under Moderate Pressure and Temperature Conditions: Kinetic versus Thermodynamic Products (C) 3310–3313 [3372–3375]
DOI: 10.1002/anie.200453898
- Schiemann, O.
- Excess Electron Transport Through DNA: A Single Electron Repairs More than One UV-Induced Lesion (C) 1848–1851 [1884–1887]
DOI: 10.1002/anie.200353264
- Schiess, P.
- Fragmentation and Inductivity: *Cyril A. Grob* (O) 4392 [4492]
DOI: 10.1002/anie.200461144
- Schindler, S.
- Combined Spectroscopic and Theoretical Evidence for a Persistent End-On Copper Superoxo Complex (C) 4360–4363 [4460–4464]
DOI: 10.1002/anie.200454125
- Schlatter, A. (C) 6731–6734 [6899–6902]
- Schlawe, D. (C) 1731–1734 [1763–1766]
- Schleth, F. (C) 313–315 [317–319]
- Schleucher, J. (C) 187–192 [189–194]
- Schleyer, P. von R.
- Aromaticity: The Alternating C–C Bond Length Structures of [14]-, [18]-, and [22]Annulene (C) 4200–4206 [4296–4302]
DOI: 10.1002/anie.200454188
 - Side-Wall Opening of Single-Walled Carbon Nanotubes (SWCNTs) by Chemical Modification: A Critical Theoretical Study (C) 1552–1554 [1578–1580]
DOI: 10.1002/anie.200353087
- Schlitzer, M.
- Farnesyltransferase Inhibitors Inhibit the Growth of Malaria Parasites In Vitro and In Vivo (C) 251–254 [254–257]
DOI: 10.1002/anie.200351169
- Schlögl, R.
- Nanocatalysis: Mature Science Revisited or Something Really New? (M) 1628–1637 [1656–1667]
DOI: 10.1002/anie.200301684
- Schlögl, R. (C) 112–115 [114–117]
- Schlörb, C. (C) 5780–5785 [5904–5909]
- Schlüter, A. D.
- A Covalent-Chemistry Approach to Giant Macromolecules and Their Wetting Behavior on Solid Substrates (C) 5185–5188 [5297–5300]
DOI: 10.1002/anie.200460390
- Schmalz, H.-G.
- Iron-Containing Nucleoside Analogues with Pronounced Apoptosis-Inducing Activity (C) 1731–1734 [1763–1766]
DOI: 10.1002/anie.200353132
 - Total Syntheses of Colchicine in Comparison: A Journey through 50 Years of Synthetic Organic Chemistry (R) 3230–3256 [3292–3318]
DOI: 10.1002/anie.200300615
- Schmelz, O. (C) 4616–4621 [4716–4721]
- Schmid, Alexander (C) 1581–1583 [1607–1609]
- Schmid, Andreas
- Coupling of Biocatalytic Asymmetric Epoxidation with NADH Regeneration in Organic–Aqueous Emulsions (C) 2163–2166 [2215–2218]
DOI: 10.1002/anie.200353338
- Schmid, W. E. (C) 4178–4182 [4273–4277]
- Schmidt, H. (C) 1883–1886 [1919–1922]
- Schmidt, H.-G. (C) 4940–4943 [5048–5051]
- Schmidt, M.
- Micelle Formation from Amphiphilic “Cylindrical Brush”—Coil Block Copolymers Prepared by Metallocene Catalysis (C) 3192–3195 [3255–3257]
DOI: 10.1002/anie.200353259
 - New Perspectives for the Design of Molecular Actuators: Thermally Induced Collapse of Single Macromolecules from Cylindrical Brushes to Spheres (C) 1101–1104 [1121–1124]
DOI: 10.1002/anie.200352845
- Schmidt, R. R. Corrigendum: 4389
- Schmidt, W. (C) 4303–4306 [4403–4406]
- Schmidtman, M. (C) 4466–4470 Corrigendum: 5115 [4566–4570 Corrigendum: 5225]
- Schmieg, J. (C) 3818–3822 [3906–3910]
- Schmitt, J.-L. (C) 4902–4906 [5010–5014]
- Schmitt, M. A. (C) 505–510 [511–516]
- Schmitt, U. W. (C) 4804–4807 [4908–4911]
- Schmitt, V. (C) 3283–3286 [3345–3348]
- Schmitz, K. (H) 2472–2475 [2526–2529]
- Schmitz, O. J. Corrigendum: 4389
- Schnakenburg, G. (C) 2243–2247 [2293–2297], 6512–6516 [6674–6678]
- Schneider, Christoph
- Scandium–Bipyridine-Catalyzed Enantioselective Addition of Alcohols and Amines to *meso*-Epoxides (C) 5691–5694 [5809–5812]
DOI: 10.1002/anie.200460786
- Schneider, Claudia (C) 4526–4528 [4626–4629]
- Schneider, Siegfried (C) 4360–4363 [4460–4464]
- Schneider, Stefan
- The $[\text{NH}_3\text{Cl}]^+$ Ion (C) 5213–5217 [5325–5329]
DOI: 10.1002/anie.200460544
- Schneider, Stefan (C) 3148–3152 [3210–3214], 4919–4924 [5027–5032], 6676–6680 [6844–6848]
- Schneider, T. (C) 4075–4078 [4167–4170]
- Schneider-Mergener, J.
- High-Content Peptide Microarrays for Deciphering Kinase Specificity and Biology (C) 2671–2674 [2725–2728]
DOI: 10.1002/anie.200453900
- Schnelle, W. (C) 1088–1092 [1108–1112]
- Schnepf, A.
- Novel Compounds of Elements of Group 14: Ligand-Stabilized Clusters with “Naked” Atoms (H) 664–666 [680–682]
DOI: 10.1002/anie.200301706
- Schnick, W.
- $\text{Ca}[\text{Si}_2\text{O}_7\text{N}_2]$ —A Novel Layer Silicate (C) 5540–5542 [5656–5659]
DOI: 10.1002/anie.200460098
- Schnöckel, H.
- $\text{Al}_{50}\text{C}_{120}\text{H}_{180}$: A Pseudofullerene Shell of 60 Carbon Atoms and 60 Methyl Groups Protecting a Cluster Core of 50 Aluminum Atoms (C) 3186–3189 [3248–3252]
DOI: 10.1002/anie.200453754
- GaAs_5 and InAs_5 : Quantum-Chemical and Experimental Investigations of Their Stability and Structure (C) 2170–2173 [2222–2225]
DOI: 10.1002/anie.200352499
 - $[\text{Ga}_{22}(\text{PrBu}_2)_{12}]$: Diversity in the Arrangement of 22 Gallium Atoms—A Unique Case in the Field of Metalloid Clusters? (C) 6549–6552 [6712–6715]
DOI: 10.1002/anie.200460776
 - $[\text{Ga}_5(\text{PrBu}_2)_{14}\text{Br}_6]^{3-}$: An Elementoid Gallium Cluster with Metalloid and Nonmetalloid Structural Elements (C) 302–305 [306–309]
DOI: 10.1002/anie.200352472
 - The Polyhedral Gallium Subhalide $[\text{Ga}_2\text{Br}_{22}] \cdot 10\text{THF}$: The First Step on the Path to a New Modification of Gallium? (C) 3190–3192 [3252–3255]
DOI: 10.1002/anie.200453786
- Schoeller, W. W. (C) 585–587 [595–597], 4876–4880 [4984–4988]
- Schoiswohl, J. (C) 5546–5549 [5663–5666]
- Schönherr, H. (C) 369–373 [373–377]
- Schooler, P. (C) 2135–2138 [2187–2190]
- Schrader, W.
- Mass Spectrometric Studies of DNA Adducts from a Reaction with Terpenoids (C) 6657–6660 [6826–6829]
DOI: 10.1002/anie.200461022
- Schranz, B. (C) 1886–1888 [1922–1924]
- Schreiber, S. L.
- A Planning Strategy for Diversity-Oriented Synthesis (R) 46–58 [48–60]
DOI: 10.1002/anie.200300626
 - Synthetic Strategy toward Skeletal Diversity via Solid-Supported, Otherwise Unstable Reactive Intermediates (C) 1681–1685 [1713–1717]
DOI: 10.1002/anie.200353466
- Schreiner, P. R. (C) 6553–6557 [6715–6719]
- Schröder, D.
- Coulomb Explosions and Stability of Multiply Charged Ions in the Gas Phase (H) 1329–1331 [1351–1353]
DOI: 10.1002/anie.200301728
- Schröder, D. (C) 121–124 [124–127]
- Schröder, M.
- Non-Natural Eight-Connected Solid-State Materials: A New Coordination Chemistry (C) 1851–1854 [1887–1890]
DOI: 10.1002/anie.200352625
- Schroer, T. (C) 3148–3152 [3210–3214], 4919–4924 [5027–5032], 5213–5217 [5325–5329], 6676–6680 [6844–6848]
- Schubert, U. S.
- Nanolithography and Nanochemistry: Probe-Related Patterning Techniques and Chemical Modification for Nanometer-Sized Devices (R) 2480–2495 [2534–2550]
DOI: 10.1002/anie.200300609
- Schuhmann, W.
- Label-Free Electrochemical Recognition of DNA Hybridization by Means of Modulation of the Feedback Current in SECM (C) 3482–3485 [3564–3567]
DOI: 10.1002/anie.200454228
- Schulte, A. (C) 3482–3485 [3564–3567]
- Schulz, F. (C) 4075–4078 [4167–4170]
- Schulze Isfort, C. (C) 4807–4810 [4911–4915]

- Schumann, H.
– Butenyl-Substituted Alkaline-Earth Metallocenes: A First Step towards Olefin Complexes of the Alkaline-Earth Metals (C) 6208–6211 [6335–6338]
DOI: 10.1002/anie.200460927
- Schuppan, J. (C) 4597–4601 [4698–4702]
- Schüth, F.
– Nanoengineering of a Magnetically Separable Hydrogenation Catalyst (C) 4303–4306 [4403–4406]
DOI: 10.1002/anie.200454222
- The Development of Descriptors for Solids: Teaching “Catalytic Intuition” to a Computer (C) 5347–5349 [5461–5463]
DOI: 10.1002/anie.200460731
- Schutkowski, M.
– High-Content Peptide Microarrays for Deciphering Kinase Specificity and Biology (C) 2671–2674 [2725–2728]
DOI: 10.1002/anie.200453900
- Schutte, S. (C) 6208–6211 [6335–6338]
- Schütz, J. (R) 5896–5911 [6020–6036]
- Schwalbe, H.
– Modulation of Compactness and Long-Range Interactions of Unfolded Lysozyme by Single Point Mutations (C) 5780–5785 [5904–5909]
DOI: 10.1002/anie.200460907
- Schwalbe, H. (C) 187–192 [189–194]
- Schwans, J. P. (C) 3033–3037 [3095–3099]
- Schwarz, H.
– Coupling of Methane and Ammonia by Dinuclear Bimetallic Platinum–Coinage-Metal Cations PtM⁺ (C) 121–124 [124–127]
DOI: 10.1002/anie.200352817
- Schweiger, A. (C) 2567–2570 [2621–2624]
- Schweizer, W. B. (C) 5056–5059 [5166–5169]
- Scialpi, R. (C) 3598–3601 [3682–3685]
- Scofield, D. M. (C) 5056–5059 [5166–5169]
- Scopelliti, R. (C) 1520–1524 [1546–1550]
- Scott, A. J. (C) 3061–3063 [3123–3125]
- Scott, J. (M) 5298–5308 [5412–5422]
- Scott, L. T.
– Methods for the Chemical Synthesis of Fullerenes (R) 4994–5007 [5102–5116]
DOI: 10.1002/anie.200400661
- Scott, L. T. (C) 5477–5481 [5593–5597]
- Scott, M. J.
– Facile Oxidative Rearrangement of Dispiro-Porphodimethenes to Nonplanar and Sheetlike Porphyrins with Intense Absorptions in the Near-IR Region (C) 485–490 [491–496]
DOI: 10.1002/anie.200352762
- Scott, T. A. (C) 5628–5631 [5746–5749]
- Scrimin, P.
– Nanozymes: Gold-Nanoparticle-Based Transphosphorylation Catalysts (C) 6165–6169 [6291–6295]
DOI: 10.1002/anie.200460649
- Scuderi, D. (C) 1868–1871 Corrigendum: 3872 [1904–1907 Corrigendum: 3960]
- Searle, M. S.
– Incremental Contribution to Protein Stability from a β Hairpin “Finger”: Limits on the Stability of Designed β Hairpin Peptides (C) 1991–1994 [2025–2028]
DOI: 10.1002/anie.200352955
- Sears, P. S. (C) 1562–1566 [1588–1592]
- Seayad, J. (R) 3368–3398 [3448–3479]
- Sebastian, M. (C) 637–641 [647–651]
- Sécheresse, F. (C) 2274–2277 [2324–2327]
- Sechi, A. (C) 3584–3588 [3668–3672]
- Seeberger, P. H.
– Aminoglycoside Microarrays To Study Antibiotic Resistance (C) 1591–1594 [1618–1620]
DOI: 10.1002/anie.200353236
- Automated Solid-Phase Synthesis of Protected Tumor-Associated Antigen and Blood Group Determinant Oligosaccharides (C) 602–605 [612–615]
DOI: 10.1002/anie.200352539
- Seeberger, S. (C) 900–903 [918–921]
- Seelan, S. (C) 1546–1548 [1572–1574]
- Seeman, N. C.
– A Protein-Driven DNA Device That Measures the Excess Binding Energy of Proteins That Distort DNA (C) 4750–4752 [4854–4856]
DOI: 10.1002/anie.200460302
- Segev, L. (C) 6140–6143 [6266–6269]
- Seiler, P. (C) 4759–4763 [4863–4867]
- Seirai, Y. (C) 1722–1724 [1754–1756]
- Sekedat, M. (C) 2504–2507 [2558–2561]
- Sekiguchi, A.
– The First Bicyclo[1.1.0]butane Dianion of Heavier Group 14 Elements (C) 6703–6705 [6871–6873]
DOI: 10.1002/anie.200461602
- Sekiguchi, T. (C) 63–66 [65–68]
- Sellmann, D. (C) 1877–1880 [1913–1916], 3141–3144 [3203–3206]
- Seo, M. S. (C) 2417–2420 [2471–2474]
- Seo, W. S. (C) 1115–1117 Corrigendum: 3749 [1135–1137 Corrigendum: 3834]
- Seppi, M. (C) 1423–1427 [1447–1451]
- Serafimov, J. M. (C) 4884–4887 [4992–4995]
- Seredyuk, V. A. (C) 1265–1267 [1285–1287]
- Sergeyev, S. (C) 1738–1740 [1770–1773]
- Sergeyev, V. G. (C) 2378–2381 [2432–2435]
- Serna, C. J. (C) 6304–6307 [6464–6467]
- Serrano, J. L.
– Hydrogen-Bonded Banana Liquid Crystals (C) 5235–5238 [5347–5350]
DOI: 10.1002/anie.200460549
- Serre, C.
– A Route to the Synthesis of Trivalent Transition-Metal Porous Carboxylates with Trimeric Secondary Building Units (C) 6285–6289 [6445–6449]
DOI: 10.1002/anie.200454250
- Serre, C. (C) 6296–6301 [6456–6461]
- Sessoli, R.
– Strong Ferromagnetic Interactions in [V₈O₁₄(H₂taci)₂]: An Unprecedented Large Spin Ground State for a Vanadyl Cluster (C) 3436–3439 [3518–3521]
DOI: 10.1002/anie.200454130
- Templating Open- and Closed-Chain Structures around Metal Complexes of Macrocycles (C) 6132–6135 [6258–6261]
DOI: 10.1002/anie.200461006
- The Magnetic Möbius Strip: Synthesis, Structure, and Magnetic Studies of Odd-Numbered Antiferromagnetically Coupled Wheels (C) 5196–5200 [5308–5312]
DOI: 10.1002/anie.200460211
- Sessoli, R. (C) 1136–1139 [1156–1159]
- Sever, M. J. (C) 448–450 Corrigendum: 2986 [454–456 Corrigendum: 3046]
- Severin, K.
– An Organometallic Chemosensor for the Sequence-Selective Detection of Histidine- and Methionine-Containing Peptides in Water at Neutral pH (C) 4771–4774 [4875–4878]
DOI: 10.1002/anie.200460808
- Combinatorial Catalysis with Bimetallic Complexes: Robust and Efficient Catalysts for Atom-Transfer Radical Additions (C) 1520–1524 [1546–1550]
DOI: 10.1002/anie.200353084
- Sevvana, M. (C) 1281–1283 [1301–1303]
- Seward, C. (C) 2933–2936 [2993–2996]
- Shah, S. P. (C) 2525–2527 [2579–2581]
- Shaik, S. Corrigendum: 141
- Shaik, S.
– Computer-Generated High-Valent Iron–Oxo and Manganese–Oxo Species with Polyoxometalate Ligands: How do they Compare with the Iron–Oxo Active Species of Heme Enzymes? (C) 5661–5665 [5779–5783]
DOI: 10.1002/anie.200453867
- Porphyrin Traps Its Terminator! Concerted and Stepwise Porphyrin Degradation Mechanisms Induced by Heme-Oxygenase and Cytochrome P450 (C) 1129–1132 [1149–1152]
DOI: 10.1002/anie.200352943
- Shaikhutdinov, S. (C) 118–121 [121–124]
- Shamala, N.
– Hydrogen-Bond Lengths in Polypeptide Helices: No Evidence for Short Hydrogen Bonds (C) 6728–6731 [6896–6899]
DOI: 10.1002/anie.200461127
- Shan, N. (C) 3938–3941 [4028–4031]
- Shandrick, S. (C) 3177–3182 [3239–3244]
- Shankar Rao, D. S. (C) 3429–3432 [3511–3514]
- Shannon, M. A. (C) 1862–1865 [1898–1901]
- Shao, J. (C) 853–856 [871–874]
- Shao, N. (C) 1569–1573 [1595–1599]
- Sharma, G. V. M.
– Left-Handed Helical Twists in “Mixed β -Peptides” Derived From Alternating C-Linked Carbo- β^3 -Amino Acids and β -hGly Units (C) 3961–3965 [4051–4055]
DOI: 10.1002/anie.200353467
- Sharma, M. (C) 3479–3481 [3561–3563]
- Sharma, P. K. (C) 1129–1132 [1149–1152]
- Sharp, P. R.
– A Gallium-Coated Gold Cluster (C) 6128–6131 [6254–6257]
DOI: 10.1002/anie.200461295
- Sharpless, K. B.
– Efficiency and Fidelity in a Click-Chemistry Route to Triazole Dendrimers by the Copper(I)-Catalyzed Ligation of Azides and Alkynes (C) 3928–3932 [4018–4022]
DOI: 10.1002/anie.200454078
- Shashidar, R. (O) 3360 [3438]
- Shashikala, I. S. (C) 3429–3432 [3511–3514]
- Shaw, R. (C) 6132–6135 [6258–6261]
- Sheeney-Haj-Idia, L. (C) 3292–3300 [3354–3362]
- Sheetz, M. P. (C) 1672–1675 [1704–1707]
- Shen, C. K. F. (C) 1498–1502 [1524–1528]
- Shen, W. (C) 4750–4752 [4854–4856]
- Shepherd, N. E. (C) 2687–2690 [2741–2744]

- Sherawat, M. (C) 3682–3685 [3768–3771]
 Sheridan, R. M. (C) 2551–2553 [2605–2607]
 Shi, B. (C) 4324–4327 [4424–4427]
 Shi, X. (C) 6482–6485 [6644–6647]
 Shibasaki, M.
 – An Efficient Synthesis of Bicyclic Amides by Intramolecular Cyclization (C) 478–482 [484–488]
 DOI: 10.1002/anie.200352750
 – Efficient Synthesis of Chiral α - and β -Hydroxy Amides: Application to the Synthesis of (*R*)-Fluoxetine (C) 317–320 [321–324]
 DOI: 10.1002/anie.200352431
 – Identifying Specific Conformations by Using a Carbohydrate Scaffold: Discovery of Subtype-Selective LPA-Receptor Agonists and an Antagonist (C) 2834–2837 [2894–2897]
 DOI: 10.1002/anie.200454065
 – Mechanistic Studies of a Reaction Promoted by the [YLi₃{tris(binaphthoxide)}] Complex: Are Three 1,1'-Bi-2-naphthol Units in a Rare-Earth–Alkali-Metal Heterobimetallic Complex Necessary? (C) 4493–4497 [4593–4597]
 DOI: 10.1002/anie.200454202
 Shibata, I.
 – Catalytic Generation of Indium Hydride in a Highly Diastereoselective Reductive Aldol Reaction (C) 711–714 [729–732]
 DOI: 10.1002/anie.200352738
 Shim, C. B. (C) 3839–3842 [3927–3930]
 Shima, S. (C) 2547–2551 [2601–2605]
 Shima, T. (C) 5537–5540 [5653–5656]
 Shimada, N. (C) 2665–2668 [2719–2722]
 Shimazaki, Y. (C) 98–100 [100–102]
 Shimizu, H. (C) 2228–2230 [2278–2280]
 Shimizu, K. H. (C) 3918–3922 [4008–4012]
 Shimizu, Kumiko (C) 2834–2837 [2894–2897]
 Shimizu, Kunio (C) 6700–6703 [6868–6871]
 Shimizu, M.
 – A Facile Stereocontrolled Approach to CF₃-Substituted Triarylethenes: Synthesis of Panomifene (C) 879–882 [897–900]
 DOI: 10.1002/anie.200353032
 Shimokawa, J. (C) 1559–1562 [1585–1588]
 Shimon, L. J. W. (C) 5961–5963 [6087–6089]
 Shimono, S. (C) 3677–3682 [3763–3768]
 Shin, I.
 – Targeted Enzyme-Responsive Drug Carriers: Studies on the Delivery of a Combination of Drugs (C) 1675–1678 [1707–1710]
 DOI: 10.1002/anie.200353204
 Shin, Y. (C) 4634–4637 [4734–4737]
 Shindo, M.
 – Electrophilic Cleavage of One Silicon–Carbon Bond of Pentacoordinate Tetraorganosilanes: Synthesis of Silalactones (C) 104–106 [106–108]
 DOI: 10.1002/anie.200352705
 Shinkai, S.
 – Helical Superstructure of Conductive Polymers as Created by Electrochemical Polymerization by Using Synthetic Lipid Assemblies as a Template (C) 465–469 [471–475]
 DOI: 10.1002/anie.200351749
 – Sol–Gel Reaction Using DNA as a Template: An Attempt Toward Transcription of DNA into Inorganic Materials (C) 3279–3283 [3341–3345]
 DOI: 10.1002/anie.200454009
 – Visible-Light-Harvesting Organogel Composed of Cholesterol-Based Perylene Derivatives (C) 1229–1233 [1249–1253]
 DOI: 10.1002/anie.200352458
 Shinohara, H. (C) 1386–1389 [1410–1413]
 Shinokubo, H.
 – Consecutive Double 1,2-Migration of Two Different Groups in Silyl(dichloromethyl)-cuprates (C) 106–108 [108–110]
 DOI: 10.1002/anie.200352828
 – Phosphane-Free Rhodium Catalyst in an Anionic Micellar System for [4 + 2] Annulation of Dienes (C) 1860–1862 [1896–1898]
 DOI: 10.1002/anie.200353123
 Shiomi, D. (C) 6343–6346 [6503–6506]
 Shiono, N. (C) 1722–1724 [1754–1756]
 Shionoya, M.
 – A Molecular Ball Bearing Mediated by Multiligand Exchange in Concert (C) 3814–3818 [3902–3906]
 DOI: 10.1002/anie.200453753
 Shipman, M.
 – A Lewis Acid Catalyzed Intramolecular [4 + 3] Cycloaddition Route to Polycyclic Systems That Contain a Seven-Membered Ring (C) 6517–6519 [6679–6681]
 DOI: 10.1002/anie.200461084
 Shirai, K. (C) 1559–1562 [1585–1588]
 Shirai, M. (C) 2230–2234 [2280–2284]
 Shirakawa, E.
 – Nickel-Catalyzed Tandem Carbostannylation of Alkynes and 1,2-Dienes with Alkynylstannanes (C) 3448–3451 [3530–3533]
 DOI: 10.1002/anie.200353649
 – Zirconium Triflate Catalyzed Direct Coupling Reaction of Lactams with Heterocyclic Arenes under Atmospheric Oxygen (C) 4231–4233 [4327–4329]
 DOI: 10.1002/anie.200460429
 Shiro, M. (C) 2665–2668 [2719–2722], 3595–3598 [3679–3682]
 Shishido, K. (C) 104–106 [106–108]
 Shoji, M. (C) 1112–1115 [1132–1135]
 Shu, C. (C) 4794–4797 [4898–4901], 4797–4800 [4901–4904]
 Shuai, X. (C) 6323–6327 [6483–6487]
 Shuai, Z. (C) 4060–4063 [4152–4155]
 Shukla, A. D. (C) 5961–5963 [6087–6089]
 Si, J. (C) 2230–2234 [2280–2284]
 Si, Y.-G. (C) 216–218 [218–220]
 Sia, S. K. (C) 498–502 [504–508]
 Sibi, M. P.
 – Enantioselective H-Atom Transfer Reactions: A New Methodology for the Synthesis of β^2 -Amino Acids (C) 1235–1238 [1255–1258]
 DOI: 10.1002/anie.200353000
 Siddick, M. M. (C) 4780–4782 [4884–4886]
 Sieber, S. A. (C) 493–498 [499–504]
 Siegel, A. (C) 498–502 [504–508]
 Sierra, M. A.
 – Comments on Recent Achievements in Biomimetic Organic Synthesis (R) 160–181 [162–184]
 DOI: 10.1002/anie.200200545
 Sies, H.
 – Ozone in Arteriosclerotic Plaques: Search for the “Smoking Gun” (H) 3514–3515 [3596–3598]
 DOI: 10.1002/anie.200460118
 Siewenie, J. E. (C) 1952–1955 [1986–1989]
 Sigel, H. (C) 3793–3795 [3881–3883]
 Sigel, R. K. O.
 – Two Metal Ions Coordinated to a Purine Residue Tolerate Each Other Well (C) 3793–3795 [3881–3883]
 DOI: 10.1002/anie.200453987
 Signoretto, M. (C) 4097–4099 [4189–4191]
 Sijbesma, R. P.
 – Reversible Mechanochemistry of a Pd^{II} Coordination Polymer (C) 4460–4462 [4560–4562]
 DOI: 10.1002/anie.200460040
 Silber, K. (C) 251–254 [254–257]
 Silva, C. (C) 1976–1979 [2010–2013]
 Simanek, E. E.
 – Synthesis and Manipulation of Orthogonally Protected Dendrimers: Building Blocks for Library Synthesis (C) 5178–5180 [5290–5292]
 DOI: 10.1002/anie.200460031
 Simmel, F. C.
 – A DNA-Based Machine That Can Cyclically Bind and Release Thrombin (C) 3550–3553 [3634–3637]
 DOI: 10.1002/anie.200353537
 Simon, A.
 – Li–Cu Exchange in Intercalated Cu₃N—With a Remark on Cu₄N (C) 2032–2034 [2066–2068]
 DOI: 10.1002/anie.200353424
 Simon, B. (H) 782–786 [800–804]
 Simon, U.
 – High-Throughput Method for the Impedance Spectroscopic Characterization of Resistive Gas Sensors (C) 752–754 [770–773]
 DOI: 10.1002/anie.200352424
 Simonsen, K. B. (C) 3177–3182 [3239–3244]
 Simonutti, R. (C) 2792–2797 [2852–2857]
 Simpson, S. A. (C) 1991–1994 [2025–2028]
 Simpson, T. J.
 – Synthesis and Incorporation of the First Polyketide Synthase Free Intermediate in Monocerin Biosynthesis (C) 727–730 [745–748]
 DOI: 10.1002/anie.200352652
 Simsek, E. (C) 5210–5213 [5322–5325]
 Sinaÿ, P.
 – Synthesis of *gem*-Difluorocarbonyl-glucose: A Step Further in Sugar Mimesis (C) 6680–6683 [6848–6851]
 DOI: 10.1002/anie.200461244
 Sinclair, G. (C) 2512–2514 [2566–2568]
 Singaram, B. Corrigendum: 3748
 Singh, H. B.
 – The Isolation and Crystal Structure of a Cyclic Selenenate Ester Derived from Bis(2,6-diformyl-4-*tert*-butylphenyl)disele-
 nide and its Glutathione Peroxidase-Like Activity (C) 4513–4515 [4613–4615]
 DOI: 10.1002/anie.200460380
 Singh, K. (C) 1149–1155 [1169–1175]
 Singh, R. (C) 5242–5246 [5354–5358]
 Singh, S. (C) 4940–4943 [5048–5051]
 Sinha, A. K. (C) 1546–1548 [1572–1574]
 Sintim, H. O. (C) 2293–2296 [2343–2346]
 Siri, O. (C) 5922–5925 [6048–6051]
 Siritwong, K. (C) 624–627 [634–637]
 Sirsch, P. (C) 5530–5534 [5646–5650]
 Sisangia, L. (C) 2293–2296 [2343–2346]
 Siuzdak, G. (C) 1255–1260 [1275–1280]

- Sivo, M. F. (C) 5081–5084 [5191–5194]
Skaff, H. (C) 5383–5386 [5497–5500]
Skouta, R. (C) 349–353 [353–357]
Slawin, A. M. Z. (C) 2103–2105 [2155–2157], 3260–3264 [3322–3326]
Sleiman, H. F.
– Self-Assembly of Cyclic Metal–DNA Nanostructures using Ruthenium Tris(bipyridine)-Branched Oligonucleotides (C) 5804–5808 [5928–5932]
DOI: 10.1002/anie.200460255
Slipchenko, L. V. (C) 742–745 [760–763]
Slootweg, J. C. (C) 3474–3477 [3556–3559]
Smarsly, B. (M) 4988–4992 [5096–5100]
Smart, B. (C) 1854–1857 [1890–1893]
Smit, B. (C) 2650–2652 [2704–2706]
Smith, J. D.
– Organosilicon Compounds: *Colin Eaborn* (O) 4978 [5086]
DOI: 10.1002/anie.200461290
Smith, M. K. (C) 476–478 [482–484]
Smith, S. C. (C) 2681–2684 [2735–2738]
Smith, W. E.
– Visual Observations of SERRS from Single Silver-Coated Silica Microparticles within Optical Tweezers (C) 2512–2514 [2566–2568]
DOI: 10.1002/anie.200352999
Snieckus, V.
– Beyond Thermodynamic Acidity: A Perspective on the Complex-Induced Proximity Effect (CIPE) in Deprotonation Reactions (R) 2206–2225 [2256–2276]
DOI: 10.1002/anie.200300590
– *ortho*-Anisylsulfonyl as a Protecting Group for Secondary Amines: Mild Ni⁰-Catalyzed Hydrodesulfonylation (C) 892–894 [910–912]
DOI: 10.1002/anie.200352634
– The Tertiary Sulfonamide as a Latent Directed-Metalation Group: Ni⁰-Catalyzed Reductive Cleavage and Cross-Coupling Reactions of Aryl Sulfonamides with Grignard Reagents (C) 888–891 [906–909]
DOI: 10.1002/anie.200352633
Soai, K.
– Asymmetric Synthesis Utilizing Circularly Polarized Light Mediated by the Photo-equilibrium of Chiral Olefins in Conjunction with Asymmetric Autocatalysis (C) 4490–4492 [4590–4592]
DOI: 10.1002/anie.200454162
Sobransingh, D. (C) 5496–5499 [5612–5615]
Sock, M. (C) 5546–5549 [5663–5666]
Sodupe, M.
– Metal-Mediated Deamination of Cytosine: Experiment and DFT Calculations (C) 5396–5399 [5507–5511]
DOI: 10.1002/anie.200460107
Soheilnia, N. (C) 5260–5262 [5372–5375]
Sohrmann, M. (C) 5181–5185 Corrigendum: 5428 [5293–5297 Corrigendum: 5542]
Soldatov, D. V.
– Dipeptides as Microporous Materials (C) 6308–6311 [6468–6471]
DOI: 10.1002/anie.200460952
Sollogoub, M.
– Synthesis of *gem*-Difluorocarbonyl-glucose: A Step Further in Sugar Mimesis (C) 6680–6683 [6848–6851]
DOI: 10.1002/anie.200461244
Solomon, E. I.
– N₂O Reduction by the μ_4 -Sulfide-Bridged Tetranuclear Cu₄ Cluster Active Site (M) 4132–4140 [4224–4233]
DOI: 10.1002/anie.200301734
Somer, M. (C) 1088–1092 [1108–1112]
Sommer, S. (C) 3195–3199 [3258–3261]
Son, D. (C) 5987–5990 [6113–6116]
Song, C. E.
– Dramatic Enhancement of Catalytic Activity in an Ionic Liquid: Highly Practical Friedel–Crafts Alkenylation of Arenes with Alkynes Catalyzed by Metal Triflates (C) 6183–6185 [6309–6311]
DOI: 10.1002/anie.200460292
Song, H. (C) 3673–3677 [3759–3763]
Song, L. (C) 1986–1990 [2020–2024]
Song, W. (C) 4663–4666 [4763–4766]
Sontag, B. (C) 5776–5779 [5900–5903]
Song, Yu (C) 2399–2402 Corrigendum: 3096 [2453–2456 Corrigendum: 3158]
Sonmez, G. (C) 1498–1502 [1524–1528]
Sontag, B. (C) 1883–1886 [1919–1922]
Sorace, L. (C) 1136–1139 [1156–1159], 3136–3138 [3198–3200]
Sordel-Klippert, M. (C) 2547–2551 [2601–2605]
Sorensen, E. J.
– Synthesis of the Furanosteroidal Antibiotic Viridin (C) 1998–2001 [2032–2035]
DOI: 10.1002/anie.200353129
Sorg, A. (C) 4523–4526 [4623–4626]
Sotiropoulos, J.-M. (C) 873–875 [891–893]
Souilivong, D. (C) 5366–5369 [5480–5483]
Sozzani, P.
– A Family of Supramolecular Frameworks of Polyconjugated Molecules Hosted in Aromatic Nanochannels (C) 2792–2797 [2852–2857]
DOI: 10.1002/anie.200353479
Spagnoli, C. (C) 520–523 [527–529]
Spagnolo, P. (C) 3598–3601 [3682–3685]
Spannenberg, A. (C) 3795–3797 [3883–3886], 5406–5408 [5521–5523]
Specht, A. (C) 2008–2012 [2042–2046]
Speiser, B.
– A Chemically Modified Platinum Electrode as a Bidentate Diamine Ligand for Forming Well-Defined, Immobilized Bis(η^1 -*P*-ether phosphane)(diamine)ruthenium(II) Complexes (C) 2025–2028 [2059–2062 Corrigendum: 2934]
DOI: 10.1002/anie.200353399
Spek, A. L. (C) 714–717 Corrigendum: 3748 [732–735 Corrigendum: 3834], 3440–3442 [3522–3524], 3474–3477 [3556–3559], 5668–5670 [5786–5788]
Spencer, J. (H) 5296–5297 [5408–5409]
Speranza, M.
– Cavity Effects on the Enantioselectivity of Chiral Amido[4]resorcinarene Stereoisomers (C) 4767–4770 [4871–4874]
DOI: 10.1002/anie.200460663
– Homolytic C α –C β Bond Cleavage in a Chiral Alkylarene Radical Cation: Effects of Asymmetric Microsolvation (C) 1868–1871 Corrigendum: 3872 [1904–1907 Corrigendum: 3960]
DOI: 10.1002/anie.200353462
Spiegel, K. (C) 3286–3289 [3348–3351]
Spielkamp, N. (C) 2850–2852 [2910–2913]
Spillmann, H.
– Supramolecular Patterned Surfaces Driven by Cooperative Assembly of C₆₀ and Porphyrins on Metal Substrates (C) 4759–4763 [4863–4867]
DOI: 10.1002/anie.200460562
Spingler, B. (C) 5025–5029 [5135–5139]
Spino, C.
– Recent Developments in the Catalytic Asymmetric Cyanation of Ketimines (H) 1764–1766 [1796–1798]
DOI: 10.1002/anie.200301686
Spivey, A. C.
– Nucleophilic Catalysis by 4-(Dialkylamino)pyridines Revisited—The Search for Optimal Reactivity and Selectivity (H) 5436–5441 [5552–5557]
DOI: 10.1002/anie.200460373
Splithoff, B. (C) 4303–4306 [4403–4406]
Splittgerber, U. (C) 4052–4055 [4144–4147]
Šponer, J. (C) 5396–5399 [5507–5511]
Šponer, J. E.
– Metal-Mediated Deamination of Cytosine: Experiment and DFT Calculations (C) 5396–5399 [5507–5511]
DOI: 10.1002/anie.200460107
Spontak, R. J.
– Redox-Active Organometallic Vesicles: Aqueous Self-Assembly of a Diblock Copolymer with a Hydrophilic Polyferrocenylsilane Polyelectrolyte Block (C) 1260–1264 [1280–1284]
DOI: 10.1002/anie.200352819
Sporer, C. (C) 5266–5268 [5378–5381]
Sreekanth, A. R. (C) 5691–5694 [5809–5812]
Sreekumar, V. (M) 5130–5135 [5240–5245]
Sreenivasulu, B. (C) 5769–5772 [5893–5896]
Srinivasan, A. (C) 876–879 [894–897], 2951–2955 [3011–3015]
Srinivasan, S. (C) 448–450 Corrigendum: 2986 [454–456 Corrigendum: 3046]
Sriramurthy, V. (C) 2669–2671 [2723–2725]
Sromek, A. W. (C) 2280–2282 [2330–2332]
Staben, S. T. (C) 5350–5352 [5464–5466]
Stach, D. Corrigendum: 4389
Stadler, F. (C) 5540–5542 [5656–5659]
Stahl, S. S.
– Palladium Oxidase Catalysis: Selective Oxidation of Organic Chemicals by Direct Dioxxygen-Coupled Turnover (R) 3400–3420 [3480–3501]
DOI: 10.1002/anie.200300630
Stahle, C. J. (C) 2004–2008 [2038–2042]
Stano, P. (C) 5181–5185 Corrigendum: 5428 [5293–5297 Corrigendum: 5542]
Staunton, E. (C) 2103–2105 [2155–2157]
Staunton, J. (C) 2551–2553 [2605–2607]
Steckel, J. S. (C) 2154–2158 [2206–2210]
Steffan, B. (C) 1883–1886 [1919–1922]
Steffensen, M. B. (C) 5178–5180 [5290–5292]
Steglich, F. (C) 112–115 [114–117]
Steglich, W.
– Pityriarubins, Biologically Active Bis(indolyl)spirans from Cultures of the Lipophilic Yeast *Malassezia furfur* (C) 1098–1100 [1119–1121]
DOI: 10.1002/anie.200352549
– Unusual Pulvinic Acid Dimers from the Common Fungi *Scleroderma citrinum* (Common Earthball) and *Chalciporus piperatus* (Peppery Bolete) (C) 1883–1886 [1919–1922]
DOI: 10.1002/anie.200352529

- Steinbach, K. (C) 2547–2551 [2601–2605]
Steinbock, O.
– Preparation of Mesoporous Silica Monoliths with Ordered Arrays of Macrochannels Templated from Electric-Field-Oriented Hydrogels
(C) 1505–1507 [1531–1533]
DOI: 10.1002/anie.200352813
- Steiner, J. (C) 302–305 [306–309], 6549–6552 [6712–6715]
Steinhart, M. (R) 1334–1344 [1356–1367]
Steiniger, F. (C) 245–247 [247–249]
Steinke, T. (C) 2299–2302 [2349–2352]
Steinmetz, H. (C) 4888–4892 [4996–5000]
Stensgaard, I. (C) 2092–2095 [2144–2147]
Stephens, E. (R) 6596–6616 [6760–6782]
Stern, F.
– Paul Ehrlich: The Founder of Chemotherapy
(E) 4254–4261 [4352–4359]
DOI: 10.1002/anie.200460632
- Stetter, J. (C) 1381–1385 [1405–1409]
Stettin, H. (C) 245–247 [247–249]
Steuerman, D. W. (C) 6486–6491 [6648–6653]
Steward, O. W. (C) 1126–1129 [1146–1149]
Stewart, K. M. (C) 5808–5811 [5932–5935]
Stiegman, A. E.
– Preparation of Mesoporous Silica Monoliths with Ordered Arrays of Macrochannels Templated from Electric-Field-Oriented Hydrogels
(C) 1505–1507 [1531–1533]
DOI: 10.1002/anie.200352813
- Stitchell, S. G. (C) 3260–3264 [3322–3326]
Stock, N.
– High-Throughput Synthesis of Phosphate-Based Inorganic–Organic Hybrid Compounds under Hydrothermal Conditions
(C) 749–752 [767–770]
DOI: 10.1002/anie.200351718
- Stöcklein, W. F. M. (C) 4357–4360 [4457–4460]
Stocks, P. A. (C) 4193–4197 [4289–4293]
Stoddart, J. F.
– Molecular-Mechanical Switch-Based Solid-State Electrochromic Devices
(C) 6486–6491 [6648–6653]
DOI: 10.1002/anie.200461723
- The Exclusivity of Multivalency in Dynamic Covalent Processes
(C) 3273–3278 [3335–3340]
DOI: 10.1002/anie.200453963
- Stojcevic, G. (C) 5523–5526 [5639–5642]
Stoltz, B. M.
– Direct Oxidative Heck Cyclizations: Intramolecular Fujiwara–Moritani Arylations for the Synthesis of Functionalized Benzofurans and Dihydrobenzofurans
(C) 6144–6148 [6270–6274]
DOI: 10.1002/anie.200461294
- Palladium-Catalyzed Oxidative Kinetic Resolution with Ambient Air as the Stoichiometric Oxidation Gas
(C) 353–357 [357–361]
DOI: 10.1002/anie.200352444
- Storey, J. M. D.
– The Mechanism of Bu_3SnH -Mediated Homolytic Aromatic Substitution
(C) 95–98 [97–100]
DOI: 10.1002/anie.200352419
- Stöber, G. (C) 302–305 [306–309], 6549–6552 [6712–6715]
Stott, N. E. (C) 2154–2158 [2206–2210]
- Stöwe, K.
– YbGaGe: Zero Thermal Expansion as a Result of an Electronic Valence Transition?
(H) 4982–4984 [5090–5092]
DOI: 10.1002/anie.200401757
- Stoyanov, E. (C) 5352–5355 [5466–5469]
Strauss, S. H.
– $\text{C}_{74}\text{F}_{38}$: An Exohedral Derivative of a Small-Bandgap Fullerene with D_3 Symmetry
(C) 997–1000 [1015–1018]
DOI: 10.1002/anie.200352960
- Strazzari, S. (C) 3598–3601 [3682–3685]
Ströbele, M. (C) 2574–2576 [2628–2630]
Strohmman, C.
– Enantiodivergence in the Reactions of a Highly Enantiomerically Enriched Silyl-lithium Compound with Benzyl Halides: Control of Inversion and Retention by Selection of Halide
(C) 1011–1014 [1029–1032]
DOI: 10.1002/anie.200352700
- Strohmeier, G. A. (C) 621–624 [631–634]
Strømgaard, K.
– Chemistry and Biology of Terpene Trilactones from *Ginkgo Biloba*
(R) 1640–1658 [1670–1689]
DOI: 10.1002/anie.200300601
- Strukul, G.
– Microencapsulated Chloroperoxidase as a Recyclable Catalyst for the Enantioselective Oxidation of Sulfides with Hydrogen Peroxide
(C) 4097–4099 [4189–4191]
DOI: 10.1002/anie.200460365
- Stucky, G. D.
– Cubic Mesoporous Frameworks with a Mixed Semiconductor Nanocrystalline Wall Structure and Enhanced Sensitivity to Visible Light
(C) 3037–3040 [3099–3102]
DOI: 10.1002/anie.200453840
- Micrometer-Sized Spherical Assemblies of Polypeptides and Small Molecules by Acid–Base Chemistry
(C) 5652–5655 [5770–5773]
DOI: 10.1002/anie.200460510
- Stucky, G. D. (C) 700–704 [718–722]
Studer, A.
– Desymmetrization of Metalated Cyclohexadienes and Application to the Synthesis of Nephrosteranic Acid
(C) 313–315 [317–319]
DOI: 10.1002/anie.200352254
- Studte, C. (C) 3786–3789 [3874–3877]
Stumpf, H. O.
– A $\text{Cu}^{\text{II}}\text{Co}^{\text{II}}$ Metallacyclopentane-Based Magnet with a Corrugated Brick-Wall Sheet Architecture
(C) 956–958 [974–976]
DOI: 10.1002/anie.200352604
- Stürmer, R. (R) 788–824 [806–843]
Su, J. (C) 5973–5977 [6099–6103]
Su, Z.-M.
– Interlocked and Interdigitated Architectures from Self-Assembly of Long Flexible Ligands and Cadmium Salts
(C) 5036–5040 [5146–5150]
DOI: 10.1002/anie.200460758
- Su, Z.-M. (C) 2409–2411 [2463–2465]
Suárez, A. (C) 3580–3582 [3664–3666]
Suárez, J. R. (C) 4333–4336 [4433–4436]
Subissati, D. (C) 4767–4770 [4871–4874]
- Subramanian, L. R.
– A Versatile Direct Approach to *ortho*-Substituted Azobenzenes from Benzotriazoles
(C) 1400–1403 [1424–1427]
DOI: 10.1002/anie.200352782
- Sucke, S. J.
– Dimeric Aminoglycosides as Antibiotics
(C) 1562–1566 [1588–1592]
DOI: 10.1002/anie.200353225
- Sudhölter, E. J. R. (C) 1352–1355 [1376–1379]
Suematsu, H. (C) 3670–3673 [3756–3759]
Suemune, H.
– Chiral Centers in the Side Chains of α -Amino Acids Control the Helical Screw Sense of Peptides
(C) 5360–5363 [5474–5477]
DOI: 10.1002/anie.200460420
- Suffert, J.
– A 4-*exo*-dig Cyclocarbopalladation/ 8π Electrocyclization Cascade: Expeditious Access to the Tricyclic Core Structures of the Ophiobolins and Aleurodiscal
(C) 2826–2830 [2886–2890]
DOI: 10.1002/anie.200453773
- Sugie, R. (C) 4490–4492 [4590–4592]
Sugimoto, A. (C) 2406–2409 [2460–2463]
Sugisaki, C. (C) 6174–6177 [6300–6303]
Sugiura, K.-i. (C) 707–711 [725–729], 2801–2805 [2861–2865], 3171–3175 [3233–3237], 4763–4767 [4867–4871]
Sugiura, M. (C) 6491–6493 [6653–6655]
Sugiyasu, K. (C) 1229–1233 [1249–1253], 3279–3283 [3341–3345]
Suh, M. P.
– A Robust Porous Material Constructed of Linear Coordination Polymer Chains: Reversible Single-Crystal to Single-Crystal Transformations upon Dehydration and Rehydration
(C) 2798–2801 [2858–2861]
DOI: 10.1002/anie.200353494
- Sulikowski, G. A.
– Total Synthesis of Apoptolidinone
(C) 6673–6675 [6841–6843]
DOI: 10.1002/anie.200461469
- Sullivan, T. P. (C) 4190–4193 [4286–4289]
Sultana, A. (C) 3722–3724 [3808–3810]
Sumiya, T. (C) 1112–1115 [1132–1135]
Summerer, D. (H) 1625–1626 [1653–1654]
Sumper, M.
– Biomimetic Patterning of Silica by Long-Chain Polyamines
(C) 2251–2254 [2301–2304]
DOI: 10.1002/anie.200453804
- Quaternary Ammonium Groups in Silica-Associated Proteins
(C) 5933–5936 [6059–6062]
DOI: 10.1002/anie.200461236
- Sun, C. (C) 2106–2108 [2158–2160]
Sun, H.-L. (C) 1374–1376 [1398–1400]
Sun, L.
– An Unusual Cyclization in a Bis(cysteinyll-S) Diiron Complex Related to the Active Site of Fe-Only Hydrogenases
(C) 3571–3574 [3655–3658]
DOI: 10.1002/anie.200453961
- Sun, L. (C) 1006–1009 [1024–1027]
Sun, Q.-Y. (C) 1352–1355 [1376–1379]
Sun, T. (C) 357–360 [361–364], 4663–4666 [4763–4766]
Sun, Xiaoming (C) 597–601 [607–611], 3827–3831 [3915–3919]
Sun, Xuping (C) 6360–6363 [6520–6523]



- Sun, Y.-P.
– Supercritical-Fluid Processing Technique for Nanoscale Polymer Particles (C) 704–707 [722–725]
DOI: 10.1002/anie.200352834
- Sunahara, T. (C) 5618–5621 [5736–5739]
- Sundén, H. (C) 1109–1112 [1129–1132], 6532–6535 [6694–6697]
- Sundermann, B. (C) 3795–3797 [3883–3886]
- Sundermann, C. (C) 3795–3797 [3883–3886]
- Sundermeyer, J.
– Combined Spectroscopic and Theoretical Evidence for a Persistent End-On Copper Superoxo Complex (C) 4360–4363 [4460–4464]
DOI: 10.1002/anie.200454125
- Sundholm, D. (C) 2678–2681 [2732–2735]
- Sunley, G. J. (C) 5366–5369 [5480–5483]
- Sünnemann, H. W. (C) 895–897 [913–915]
- Surblé, S. (C) 6285–6289 [6445–6449], 6296–6301 [6456–6461]
- Suri, J. T. Corrigendum: 3748
- Surianarayanan, M. (C) 5363–5366 [5477–5480]
- Surnev, S. (C) 5546–5549 [5663–5666]
- Süssmuth, R. D.
– Abyssomicin C—A Polycyclic Antibiotic from a Marine *Verrucosipora* Strain as an Inhibitor of the *p*-Aminobenzoic Acid/Tetrahydrofolate Biosynthesis Pathway (C) 2574–2576 [2628–2630]
DOI: 10.1002/anie.200353160
- Suter, U. W.
– Surface Structure of Organoclays (C) 2239–2243 [2289–2293]
DOI: 10.1002/anie.200352747
- Suzuki, Keisuke
– Concise Total Synthesis and Structure Assignment of TAN-1085 (C) 3167–3171 [3229–3233]
DOI: 10.1002/anie.200453801
- Suzuki, Keisuke (C) 5621–5625 [5739–5743]
- Suzuki, Koji (C) 6135–6139 [6261–6265]
- Suzuki, Masako (C) 2527–2530 [2581–2584]
- Suzuki, Masatatsu
– A Bis(μ -alkylperoxy)nickel(II) Complex as a Reaction Intermediate for the Oxidation of the Methyl Groups of the Me₂-tpa Ligand to Carboxylate and Alkoxide Ligands (C) 3300–3303 [3362–3365]
DOI: 10.1002/anie.200353637
- Suzuki, Masatatsu (C) 334–337 [338–341]
- Suzuki, Masato (C) 2834–2837 [2894–2897]
- Swager, T. M.
– Charge-Specific Interactions in Segmented Conducting Polymers: An Approach to Selective Ionoresistive Responses (C) 3700–3703 [3786–3789]
DOI: 10.1002/anie.200453896
- Swayze, E. E. (C) 6735–6738 [6903–6906]
- Sweedler, J. V.
– Nanocapillary Arrays Effect Mixing and Reaction in Multilayer Fluidic Structures (C) 1862–1865 [1898–1901]
DOI: 10.1002/anie.200353279
- Sygula, A. (C) 4497–4500 [4597–4600]
- Sygula, R. (C) 4497–4500 [4597–4600]
- Szieberth, D. (C) 637–641 [647–651]
- Szpacenko, A. (C) 613–615 [623–625]
- Szychowski, J. (C) 6735–6738 [6903–6906]
- Tachi, Y. (C) 334–337 [338–341]
- Tachibana, Y. (C) 856–862 [874–880]
- Tafi, A. (C) 4767–4770 [4871–4874]
- Taglietti, A.
– A Sleeping Host Awoken by Its Guest: Recognition and Sensing of Imidazole-Containing Molecules Based on Double Cu²⁺ Translocation inside a Polyaza Macrocyclic (C) 5073–5077 [5183–5187]
DOI: 10.1002/anie.200460568
- Taglietti, A. (C) 1962–1965 [1996–1999], 3847–3852 [3935–3940]
- Tagmatarchis, N. (C) 5526–5530 [5642–5646]
- Tago, T. (C) 730–733 [748–751]
- Taguchi, M. (C) 6135–6139 [6261–6265]
- Taguchi, Y. (C) 5369–5372 [5483–5486]
- Taira, K.
– Small-Interfering-RNA Expression in Cells Based on an Efficiently Constructed Dumbbell-Shaped DNA (C) 3160–3163 [3222–3225]
DOI: 10.1002/anie.200353445
- Takafuji, M. (C) 465–469 [471–475]
- Takagaki, A. (C) 2955–2958 [3015–3018]
- Takagi, A. (C) 1349–1352 [1373–1376]
- Takagi, Y. (C) 3160–3163 [3222–3225]
- Takahashi, M. (C) 3177–3182 [3239–3244]
- Takaishi, S.
– Visualization of Local Valence Structures in Quasi-One-Dimensional Halogen-Bridged Complexes [Ni_{1-x}Pd_x(chxn)₂Br]₂Br₂ by STM (C) 3171–3175 [3233–3237]
DOI: 10.1002/anie.200453905
- Takaishi, S. (C) 4763–4767 [4867–4871]
- Takami, T. (C) 3171–3175 [3233–3237]
- Takamizawa, S.
– Single-Crystal Adsorbents: A New Observation Field for Light Aggregates (C) 1368–1371 [1392–1395]
DOI: 10.1002/anie.200352982
- Takanashi, K. (C) 6703–6705 [6871–6873]
- Takata, M.
– Direct Observation of Bonding and Charge Ordering in (EDO-TTF)₂PF₆ (C) 3670–3673 [3756–3759]
DOI: 10.1002/anie.200454075
- Takata, Toshikazu
– A Concept for Recyclable Cross-Linked Polymers: Topologically Networked Polyrotaxane Capable of Undergoing Reversible Assembly and Disassembly (C) 966–969 [984–987]
DOI: 10.1002/anie.200353046
- Takata, Tsuyoshi (C) 2955–2958 [3015–3018]
- Takayanagi, H. (C) 1360–1363 [1384–1387]
- Takenaka, Y. (C) 2702–2705 [2756–2759]
- Takesue, H. (C) 98–100 [100–102]
- Takeuchi, D. (C) 1233–1235 [1253–1255]
- Takeuchi, M. (C) 465–469 [471–475]
- Taki, M. (C) 3160–3163 [3222–3225]
- Takikawa, Y. (C) 2290–2293 [2340–2343]
- Takui, T. (C) 6343–6346 [6503–6506], 6474–6479 [6636–6641]
- Talsi, E. P. (C) 5228–5230 [5340–5342]
- Tam, W.
– Asymmetric Induction in Ruthenium-Catalyzed [2+2] Cycloadditions between Bicyclic Alkenes and a Chiral Acetylenic Acyl Sulfonamide (C) 610–613 [620–623]
DOI: 10.1002/anie.200352555
- Tamada, O. (C) 3677–3682 [3763–3768]
- Tamaki, K. (C) 1270–1272 [1290–1292]
- Tamaruya, Y. (C) 2834–2837 [2894–2897]
- Tamasi, G. (C) 5081–5084 [5191–5194]
- Tambach, T. J.
– A Molecular Mechanism of Hysteresis in Clay Swelling (C) 2650–2652 [2704–2706]
DOI: 10.1002/anie.200353612
- Tamm, M.
– Ansa-Cycloheptatrienyl–Cyclopentadienyl Complexes (C) 5530–5534 [5646–5650]
DOI: 10.1002/anie.200460538
- Tampé, R.
– Function of the Antigen Transport Complex TAP in Cellular Immunity (R) 4014–4031 [4104–4122]
DOI: 10.1002/anie.200300642
- Tamura, R.
– Magnetic Properties of All-Organic Liquid Crystals Containing a Chiral Five-Membered Cyclic Nitroxide Unit within the Rigid Core (C) 3677–3682 [3763–3768]
DOI: 10.1002/anie.200460007
- Tamura, T. (C) 2436–2440 [2490–2494]
- Tan, W. (C) 5635–5638 [5753–5756]
- Tan, Z. (C) 2911–2914 [2971–2974]
- Tanaka, D. (C) 2530–2534 [2584–2588]
- Tanaka, F.
– Synthesis of β -Hydroxyaldehydes with Stereogenic Quaternary Carbon Centers by Direct Organocatalytic Asymmetric Aldol Reactions (C) 2420–2423 [2474–2477]
DOI: 10.1002/anie.200353546
- Tanaka, Hiroyuki (C) 6327–6331 [6487–6491]
- Tanaka, Hisaaki (C) 3171–3175 [3233–3237], 4763–4767 [4867–4871]
- Tanaka, J. (C) 6691–6695 [6859–6863]
- Tanaka, Ken
– Enantioselective Synthesis of Axially Chiral Phthalides through Cationic [Rh^I(H₈-binap)]-Catalyzed Cross Alkyne Cyclotrimerization (C) 6510–6512 [6672–6674]
DOI: 10.1002/anie.200461533
- Tanaka, Kenji (C) 1722–1724 [1754–1756]
- Tanaka, Koji
– Chemical Control of Valence Tautomerism of Nickel(II) Semiquinone and Nickel(III) Catecholate States (C) 6301–6303 [6461–6463]
DOI: 10.1002/anie.200460023
- Tanaka, M.
– Chiral Centers in the Side Chains of α -Amino Acids Control the Helical Screw Sense of Peptides (C) 5360–5363 [5474–5477]
DOI: 10.1002/anie.200460420
- Tanaka, Takeyuki (C) 5481–5485 [5597–5601]
- Tanaka, Toshihiro (C) 3811–3814 [3899–3902]

- Tanase, T.
– Linear, Redox-Active Pt_6 and $\text{Pt}_2\text{Pd}_2\text{Pt}_2$ Clusters (C) 5029–5032 [5139–5142]
DOI: 10.1002/anie.200460707
- Tanatani, A. (Kanagawa University) (C) 1360–1363 [1384–1387]
- Tanatani, A. (University of Tokyo) (C) 1559–1562 [1585–1588]
- Tang, C. (C) 2783–2787 [2843–2847]
- Tang, Jiawei (C) 5980–5984 [6106–6110]
- Tang, Jing (C) 3037–3040 [3099–3102]
- Tang, Junwang (C) 4463–4466 [4563–4566]
- Tang, R. (C) 2697–2701 [2751–2755]
- Tang, W. (C) 4312–4318 [4412–4418], 4318–4324 [4418–4424]
- Tang, Y. (C) 1389–1392 [1413–1416]
- Tangen, E. (C) 834–838 [852–856]
- Tani, F. (C) 98–100 [100–102]
- Tanigaki, K. (C) 5029–5032 [5139–5142]
- Taniguchi, M. (C) 1349–1352 [1373–1376]
- Taniguchi, N. (C) 5674–5677 [5792–5795]
- Tanimoto, K. (C) 1407–1410 [1431–1434]
- Tanino, Keiji (C) 4341–4345 [4441–4445]
- Tanino, Kenji (C) 5052–5055 [5162–5165]
- Tanner, C. (C) 4738–4741 [4842–4845]
- Tao, J. (C) 493–498 [499–504]
- Tao, N.
– Changes in the Conductance of Single Peptide Molecules upon Metal-Ion Binding (C) 6148–6152 [6274–6278]
DOI: 10.1002/anie.200460886
- Tao, Z. (C) 3425–3429 [3507–3511]
- Taquet, J.-p. (C) 5922–5925 [6048–6051]
- Tartaj, P.
– Metallic Nanomagnets Randomly Dispersed in Spherical Colloids: Toward a Universal Route for the Preparation of Colloidal Composites Containing Nanoparticles (C) 6304–6307 [6464–6467]
DOI: 10.1002/anie.200460830
- Tasiopoulos, A. J. (C) 345–349 [349–353], 2117–2121 [2169–2173], 6338–6342 [6498–6502]
- Tatsumi, K.
– A Half-Sandwich Ruthenium(II) Complex Containing a Coordinatively Unsaturated 2,6-Dimesitylphenyl Thiolate Ligand (C) 2290–2293 [2340–2343]
DOI: 10.1002/anie.200353611
- Tatsumi, T.
– A Titanosilicate That Is Structurally Analogous to an MWW-Type Lamellar Precursor (C) 236–240 [238–242]
DOI: 10.1002/anie.200352723
- Taube, D. (C) 4626–4629 [4726–4729]
- Taubert, A.
– CuCl Nanoplatelets from an Ionic Liquid-Crystal Precursor (C) 5380–5382 [5494–5496]
DOI: 10.1002/anie.200460846
- Tawa, Y. (C) 3724–3728 [3810–3814]
- Taylor, A. M. (C) 1681–1685 [1713–1717]
- Taylor, N. J. (C) 5523–5526 [5639–5642]
- Taylor, R. E.
– Enantioselective Synthesis of Cyclopropanes by Aldehyde Homologation (C) 6671–6672 [6839–6840]
DOI: 10.1002/anie.200461106
- Total Synthesis and Stereochemical Assignment of Myriaporones 1, 3, and 4 (C) 1728–1730 [1760–1762]
DOI: 10.1002/anie.200353348
- Taylor, S. J. (C) 1681–1685 [1713–1717]
- Teat, S. J. (C) 4037–4041 [4129–4133], 5196–5200 [5308–5312], 6132–6135 [6258–6261]
- Tejada, J. (C) 1828–1832 [1864–1868]
- Tejero, T. (H) 2995–2997 [3055–3058]
- Tekely, P.
– Exploiting the Joint Action of Chemical Shielding and Heteronuclear Dipolar Interactions To Probe the Geometries of Strongly Hydrogen-Bonded Silanols (C) 3565–3568 [3649–3652]
DOI: 10.1002/anie.200353339
- Telfer, S. G.
– Noncovalent Ligand Strands for Transition-Metal Helicates: The Straightforward and Stereoselective Self-Assembly of Dinuclear Double-Stranded Helicates Using Hydrogen Bonding (C) 581–584 [591–594]
DOI: 10.1002/anie.200352833
- Teplykh, A. E. (C) 2922–2924 [2982–2984]
- Terada, Y. (C) 4063–4067 [4155–4159]
- Terao, J. (C) 6180–6182 [6306–6308]
- Terasaki, O.
– Three-Dimensional Structure of Large-Pore Mesoporous Cubic $Ia3d$ Silica with Complementary Pores and Its Carbon Replica by Electron Crystallography (C) 5231–5234 [5343–5346]
DOI: 10.1002/anie.200460449
- Terni, B. (C) 2254–2256 [2304–2306]
- Tero-Kubota, S. (C) 5249–5253 [5361–5365]
- Terzis, A. (C) 210–212 [212–214]
- Tesche, B. (C) 4303–4306 [4403–4406]
- Thalladi, V. R. (C) 2780–2783 [2840–2843]
- Thallapally, P. K. (C) 1149–1155 [1169–1175]
- Tham, F. S. (C) 4089–4093 [4181–4185], 4876–4880 [4984–4988], 4880–4883 [4988–4991]
- Thauer, R. K.
– The Cofactor of the Iron–Sulfur Cluster Free Hydrogenase Hmd: Structure of the Light-Inactivation Product (C) 2547–2551 [2601–2605]
DOI: 10.1002/anie.200353763
- Thaxton, C. S. (C) 5500–5503 [5616–5619]
- Theodorakis, E. A.
– Stereoselective Total Synthesis of (–)-Borelidin (C) 3947–3951 [4037–4041]
DOI: 10.1002/anie.200460203
- Stereoselective Total Synthesis of (+)-Norrisolide (C) 739–742 [757–760]
DOI: 10.1002/anie.200352868
- Thibault-Starzyk, F.
– Two-Dimensional IR Pressure-Jump Spectroscopy of Adsorbed Species for Zeolites (C) 1155–1158 [1175–1178]
DOI: 10.1002/anie.200352754
- Thiel, W. (C) 1552–1554 [1578–1580], 2444–2446 [2498–2500]
- Thies, M. C. (C) 704–707 [722–725]
- Thivolle-Cazat, J. (C) 5366–5369 [5480–5483]
- Thomas, A. W. Corrigendum: 1043
- Thomas, F.
– How Single and Bifurcated Hydrogen Bonds Influence Proton-Migration Rate Constants, Redox, and Electronic Properties of Phenoxyl Radicals (C) 594–597 [604–607]
DOI: 10.1002/anie.200352368
- Thomas, J. A.
– Switchable Electron-Transfer Processes in a Mixed-Valence, Kinetically Locked, Trinuclear Ru^{II} Metallamacrocyclic (C) 3938–3941 [4028–4031]
DOI: 10.1002/anie.200460022
- Thomas, J. M.
– Argon and the Non-Inert Pair: Rayleigh and Ramsay (E) 6418–6424 [6578–6584]
DOI: 10.1002/anie.200461824
- The Chemical Application of High-Resolution Electron Tomography: Bright Field or Dark Field? (C) 6745–6747 [6913–6915]
DOI: 10.1002/anie.200461453
- Ultrafast Electron Crystallography: The Dawn of a New Era (H) 2606–2610 [2658–2662]
DOI: 10.1002/anie.200301746
- Thomas, R. L. (C) 3061–3063 [3123–3125]
- Thomas-Oates, J. (C) 337–340 [341–344]
- Thomassen, P. J. (C) 4755–4759 [4859–4863]
- Thomasson, K. A.
– Two Helical Conformations from a Single Foldamer Backbone: “Split Personality” in Short α/β -Peptides (C) 505–510 [511–516]
DOI: 10.1002/anie.200352125
- Thompsett, D. (C) 5645–5649 [5763–5767]
- Thompson, M. S. (C) 4791–4794 [4895–4898]
- Thordarson, P.
– Allosterically Driven Multicomponent Assembly (C) 4755–4759 [4859–4863]
DOI: 10.1002/anie.200460398
- Thorson, J. S. (C) 2962–2965 [3022–3025]
- Thorstup, P. (C) 2092–2095 [2144–2147]
- Thouin, L. (C) 1431–1435 [1455–1459]
- Tian, H.
– A Lockable Light-Driven Molecular Shuttle with a Fluorescent Signal (C) 2661–2665 [2715–2719]
DOI: 10.1002/anie.200453708
- Tian, Z. (C) 4060–4063 [4152–4155]
- Tice, J. D. (C) 2508–2511 [2562–2565]
- Tietze, L. F.
– A Highly Efficient Synthesis of the Erythrina and B-Homoerythrina Skeleton by an AlMe_3 -Mediated Domino Reaction (C) 5391–5393 [5505–5507]
DOI: 10.1002/anie.200460283
- Tillack, A. (R) 3368–3398 [3448–3479]
- Timco, G. A.
– Templating Open- and Closed-Chain Structures around Metal Complexes of Macrocycles (C) 6132–6135 [6258–6261]
DOI: 10.1002/anie.200461006
- The Magnetic Möbius Strip: Synthesis, Structure, and Magnetic Studies of Odd-Numbered Antiferromagnetically Coupled Wheels (C) 5196–5200 [5308–5312]
DOI: 10.1002/anie.200460211
- Ting, A. Y.
– A Genetically Encoded Fluorescent Reporter of Histone Phosphorylation in Living Cells (C) 2940–2943 [3000–3003]
DOI: 10.1002/anie.200353375

- Tirrell, D. A.
– Alternative Translations of a Single RNA Message: An Identity Switch of (2*S*,3*R*)-4,4,4-Trifluorovaline between Valine and Isoleucine Codons
(C) 3664–3666 [3750–3752]
DOI: 10.1002/anie.200454036
- Tissot-Crosset, K. (C) 2426–2428 [2480–2482]
- Tkachenko, O. P. (C) 2839–2842 [2899–2903]
- Tobita, H.
– Direct Evidence for Extremely Facile 1,2- and 1,3-Group Migrations in an FeSi₂ System
(C) 221–224 Corrigendum: 3096 [223–226 Corrigendum: 3158]
DOI: 10.1002/anie.200352519
- Hydrido(hydrosilylene)tungsten Complexes with Strong Interactions between the Silylene and Hydrido Ligands
(C) 218–221 [220–223]
DOI: 10.1002/anie.200352383
- Todo, H. (C) 6180–6182 [6306–6308]
- Toennies, J. P.
– Superfluid Helium Droplets: A Uniquely Cold Nanomatrix for Molecules and Molecular Complexes
(R) 2622–2648 [2674–2702]
DOI: 10.1002/anie.200300611
- Togashi, H. (C) 4300–4302 [4400–4402]
- Tohma, H.
– Preparation and Reactivity of 1,3,5,7-Tetra-*k*[4-(diacetoxyiodo)phenyl]adamantane, a Recyclable Hypervalent Iodine(III) Reagent
(C) 3595–3598 [3679–3682]
DOI: 10.1002/anie.200454234
- Tojino, M. (C) 2423–2425 [2477–2479]
- Tojo, S. (C) 2406–2409 [2460–2463]
- Tokunaga, N. (C) 6125–6128 [6251–6254]
- Tominaga, M. (C) 5621–5625 [5739–5743]
- Tomoda, S.
– Origin of Diastereoselection in the Hydro-silylation of Chiral *N*-Acyliminium Intermediates Derived from Pyroglutamic Acid
(C) 2412–2415 [2466–2469]
DOI: 10.1002/anie.200353366
- Tomović, Ž. (C) 755–758 [773–777]
- Tong, M.-L. (C) 192–195 [194–197]
- Toniolo, C.
– Direct Observation of Intramolecular Hydrogen Bonds in Peptide ₃₁₀ Helices by ^{3h}J_{N,C} Scalar Couplings
(C) 3152–3155 [3214–3217]
DOI: 10.1002/anie.200454224
- Meteoritic C^α-Methylated α-Amino Acids and the Homochirality of Life: Searching for a Link
(C) 6695–6699 [6863–6867]
DOI: 10.1002/anie.200460908
- Torii, H. (C) 1983–1986 [2017–2020]
- Törnroos, K. W. (C) 4292–4295 [4392–4395], 4589–4594 [4689–4695]
- Tosin, M. (C) 2518–2521 [2572–2575]
- Toste, F. D.
– Gold(I)-Catalyzed 5-*endo-dig* Carbocyclization of Acetylenic Dicarboxyl Compounds
(C) 5350–5352 [5464–5466]
DOI: 10.1002/anie.200460844
- Totti, F. (C) 3436–3439 [3518–3521]
- Toulmé, J.-J. (C) 3144–3147 [3206–3209]
- Touré, B. B. (C) 2001–2004 [2035–2038]
- Toyota, S.
– Macrocyclic 1,8-Anthrylene–Ethynylene Oligomers: Three-Dimensional π-Conjugated Architectures
(C) 2248–2251 [2298–2301]
DOI: 10.1002/anie.200353647
- Tramontano, A.
– A Brighter Future for Protein Design
(H) 3222–3223 [3284–3285]
DOI: 10.1002/anie.200301738
- Tramšek, M.
– The First Compound Containing a Metal Center in a Homoleptic Environment of XeF₂ Molecules
(C) 3456–3458 [3538–3540]
DOI: 10.1002/anie.200453802
- Tran, E. (C) 3835–3839 [3923–3927]
- Trapp, O. (C) 6541–6544 [6703–6707]
- Tredici, I. (C) 846–849 [864–867]
- Tremmel, P. (C) 5789–5791 [5913–5915]
- Treumann, A.
– Identification of the 5-Methylthiopentose Substituent in *Mycobacterium tuberculosis* Lipoarabinomannan
(C) 3918–3922 [4008–4012]
DOI: 10.1002/anie.200454119
- Trevisan, V. (C) 4097–4099 [4189–4191]
- Trifonov, A. A.
– C–C Coupling and C–H Bond Activation—Unexpected Pathways in the Reactions of [Yb(η⁵-C₅H₅)₂(thf)₂] with Diaza-dienes
(C) 5045–5048 [5155–5158]
DOI: 10.1002/anie.200461001
- Tröst, B. M.
– Stereocontrolled Total Synthesis of (+)-Streptazolin by a Palladium-Catalyzed Reductive Diyne Cyclization
(C) 4327–4329 [4427–4429]
DOI: 10.1002/anie.200460058
- Trushin, S. A. (C) 4178–4182 [4273–4277]
- Tsang, C.-W. (C) 5682–5685 [5800–5803]
- Tsang, S. C.
– Magnetically Separable, Carbon-Supported Nanocatalysts for the Manufacture of Fine Chemicals
(C) 5645–5649 [5763–5767]
DOI: 10.1002/anie.200460552
- Tsantrizos, Y. S. (C) 4306–4311 [4406–4411]
- Tsapatsis, M.
– On the TEM and AFM Evidence of Zeosil Nanoslabs Present during the Synthesis of Silicalite-1
(L) 4558–4561 [4658–4661]
DOI: 10.1002/anie.200460376
- Tschierske, C.
– Liquid Crystals with Complex Superstructures
(C) 4621–4625 [4721–4725]
DOI: 10.1002/anie.200460762
- Tse, M. K. (C) 5255–5260 [5367–5372]
- Tseng, H.-R. (C) 6486–6491 [6648–6653]
- Tsourkas, A. (C) 2395–2399 [2449–2453]
- Tsubota, S. (C) 1546–1548 [1572–1574], 2129–2132 [2181–2184]
- Tsuchimoto, T.
– Zirconium Triflate Catalyzed Direct Coupling Reaction of Lactams with Heterocyclic Arenes under Atmospheric Oxygen
(C) 4231–4233 [4327–4329]
DOI: 10.1002/anie.200460429
- Tsuchimoto, T. (C) 3448–3451 [3530–3533]
- Tsuda, A.
– A Molybdenum Crown Cluster Forms Discrete Inorganic–Organic Nanocompo-
- sites with Metalloporphyrins
(C) 6327–6331 [6487–6491]
DOI: 10.1002/anie.200460990
- Tsuda, S. (C) 856–862 [874–880]
- Tsuji, M. (C) 3818–3822 [3906–3910]
- Tsukahara, T. (C) 3719–3722 [3805–3808]
- Tsukruk, V. V.
– Nanofibers from Functionalized Dendritic Molecules
(C) 5246–5249 Corrigendum: 5721 [5358–5361 Corrigendum: 5839]
DOI: 10.1002/anie.200460315
- Tsuruta, H. (C) 3167–3171 [3229–3233]
- Tsutsui, S. (C) 4610–4612 [4710–4712]
- Tsutsumi, E. (C) 3044–3047 [3106–3109]
- Tsutsumi, M. (C) 5060–5062 [5170–5172]
- Tu, Y. Q.
– A Tandem Semipinacol Rearrangement/Alkylation of α-Epoxy Alcohols: An Efficient and Stereoselective Approach to Multifunctional 1,3-Diols
(C) 1702–1705 [1734–1737]
DOI: 10.1002/anie.200353177
- Tuchagues, J.-P.
– A Nonanuclear Iron(II) Single-Molecule Magnet
(C) 2266–2270 [2316–2320]
DOI: 10.1002/anie.200353147
- Tuchscherer, G. (C) 4172–4178 [4267–4273]
- Tulevski, G. S. (C) 1836–1839 [1872–1875]
- Turberfield, A. J.
– A Unidirectional DNA Walker That Moves Autonomously along a Track
(C) 4906–4911 [5014–5019]
DOI: 10.1002/anie.200460522
- Turcu, F. (C) 3482–3485 [3564–3567]
- Turnbull, W. B. (C) 3918–3922 [4008–4012]
- Turner, J. F. C.
– On the Structure of Liquid Hydrogen Fluoride
(C) 1952–1955 [1986–1989]
DOI: 10.1002/anie.200353289
- Turpeinen, U. (C) 5815–5817 [5939–5941]
- Twin, H. (C) 6517–6519 [6679–6681]
- Tykwinski, R. R.
– A Simple, One-Step Procedure for the Formation of Chiral Metallamacrocycles
(C) 5967–5971 [6093–6097]
DOI: 10.1002/anie.200461139



- Uchida, D. (C) 1360–1363 [1384–1387]
- Uchimoto, Y. (C) 1966–1969 [2000–2003]
- Ueba, M. (C) 1414–1416 [1438–1440]
- Ueda, T. (C) 5780–5785 [5904–5909]
- Uemura, D.
– Enantioselective Synthesis of the Spirotetracyclic Carbon Core of Mangelols by Using a Stereoselective Transannular Diels–Alder Strategy
(C) 81–84 [83–86]
DOI: 10.1002/anie.200351750
- Uemura, K. (C) 3269–3272 [3331–3334]
- Uemura, S.
– Polyaddition and Polycondensation Reactions of (2-Furyl)carbenoid as Step-Growth Polymerization Strategies: Synthesis of Furfurylcyclopropane- and Furfuryli-

- dene-Containing Polymers
(C) 1857–1860 [1893–1896]
DOI: 10.1002/anie.200352949
- Ueno, K. (C) 221–224 Corrigendum: 3096
[223–226 Corrigendum: 3158]
- Ueno, T.
– Size-Selective Olefin Hydrogenation by a Pd Nanocluster Provided in an Apo-Ferri-
tin Cage
(C) 2527–2530 [2581–2584]
DOI: 10.1002/anie.200353436
- Ugalde, J. M. (C) 5485–5488 [5601–5604]
- Ujaque, G. (C) 3708–3711 [3794–3797]
- Ujiie, S. (C) 1969–1972 [2003–2006]
- Ulijn, R. V. (C) 3138–3141 [3200–3203]
- Ulman, A.
– Facile Route to Ultraflat SAM-Protected
Gold Surfaces by “Amphiphile Splitting”
(C) 520–523 [527–529]
DOI: 10.1002/anie.200352249
- Ullstrup, J.
– Dynamics of Ordered-Domain Formation
of DNA fragments on Au(111) with Molec-
ular Resolution
(C) 198–203 [200–205]
DOI: 10.1002/anie.200352146
- Umani-Ronchi, A.
– Kinetic Resolution of Epoxides by a C–C
Bond-Forming Reaction: Highly Enantio-
selective Addition of Indoles to *cis*, *trans*,
and *meso* Aromatic Epoxides Catalyzed by
[Cr(salen)] Complexes
(C) 84–87 [86–89]
DOI: 10.1002/anie.200352073
- New Catalytic Approaches in the Stereo-
selective Friedel–Crafts Alkylation Reac-
tion
(M) 550–556 [560–566]
DOI: 10.1002/anie.200301679
- Ungar, G. (C) 4621–4625 [4721–4725]
- Ungaro, R. (C) 369–373 [373–377]
- Unverzagt, C.
– Synthesis of Dimeric Terpenoyl Glycoside
Side Chains from Cytotoxic Saponins
(C) 4353–4357 [4453–4457]
DOI: 10.1002/anie.200352895
- Uota, M. (C) 228–232 [230–234]
- Uoyama, S. (C) 228–232 [230–234]
- Uppadine, L. H. (C) 240–243 [242–245], (R)
3644–3662 [3728–3747]
- Urabe, D. (C) 4782–4785 [4886–4889]
- Urabe, H.
– Stereoselective Construction of Acyclic
Carbon Chains by a One-Pot Coupling
Process Based on Alkenyloxazoline–Tita-
nium Complexes
(C) 490–492 [496–498]
DOI: 10.1002/anie.200352769
- Uraguchi, D. (C) 4788–4791 [4892–4895]
- Urch, C. J. (C) 1588–1591 [1614–1617]
- Urquidí, J. (C) 1952–1955 [1986–1989]
- Uson, I. (C) 1281–1283 [1301–1303]
- Usuki, T. (C) 5249–5253 [5361–5365]
- Valbusa, U. (C) 5200–5203 [5312–5315]
- Valdés, C. (C) 343–345 [347–349]
- Valencia, G. (C) 325–329 [329–333]
- Valiyaveetil, F. I. (C) 2504–2507 [2558–
2561]
- Valleix, A. (C) 3314–3317 [3376–3379]
- van Boeckel, C. A. A.
– A Synthetic Antithrombin III Binding
Pentasaccharide Is Now a Drug! What
Comes Next?
(R) 3118–3133 [3180–3196]
DOI: 10.1002/anie.200300640
- Biopolymers: *Jacques van Boom*
(O) 5288–5289 [5400–5401]
DOI: 10.1002/anie.200461883
- van Bommel, K. J. C.
– Responsive Cyclohexane-Based Low-
Molecular-Weight Hydrogelators with
Modular Architecture
(C) 1663–1667 [1695–1699]
DOI: 10.1002/anie.200352396
- van Buuren, B. N. M. (C) 187–192 [189–194]
- van Delden, R. A. (C) 5013–5016 [5123–
5126]
- Van der Auweraer, M. (C) 6116–6120 [6242–
6246]
- van der Boom, M. E.
– Self-Oxidation of a Phenolate Complex to
a Bimetallic Stilbene Quinone
(C) 5961–5963 [6087–6089]
DOI: 10.1002/anie.200460360
- van der Pol, C. (C) 1663–1667 [1695–1699]
- van der Schilden, K. (C) 5668–5670 [5786–
5788]
- van Dijk, E. M. H. P. (C) 4045–4049 [4137–
4141]
- van Dongen, J. L. J. (C) 3557–3562 [3641–
3646]
- van Dorsselaer, A. (C) 3695–3699 [3781–
3785]
- van Erp, T. S. (C) 1660–1662 [1692–1694]
- van Esch, J.
– Responsive Cyclohexane-Based Low-
Molecular-Weight Hydrogelators with
Modular Architecture
(C) 1663–1667 [1695–1699]
DOI: 10.1002/anie.200352396
- van Genderen, M. H. P. (C) 3557–3562
[3641–3646]
- van Gunsteren, W. F.
– Are NMR-Derived Model Structures for β -
Peptides Representative for the Ensemble
of Structures Adopted in Solution?
(C) 6312–6316 [6472–6476]
DOI: 10.1002/anie.200460384
- Carbopeptoid Folding: Effects of Stereo-
chemistry, Chain Length, and Solvent
(C) 4055–4059 [4147–4151]
DOI: 10.1002/anie.200454114
- van Halbeek, H. (C) 6366–6369 [6526–6529]
- van Houselt, A. (C) 3029–3033 [3091–3095]
- van Hulst, N. F. (C) 4045–4049 [4137–4141]
- van Kasteren, S. (C) 828–833 [846–851]
- van Lagen, B. (C) 1352–1355 [1376–1379]
- van Maarseveen, J. H.
– A Staudinger Approach towards Binol-
Derived MAP-Type Bidentate P,N Ligands
(C) 3471–3473 [3553–3555]
DOI: 10.1002/anie.200454146
- van Poll, M. L. (C) 4190–4193 [4286–4289]
- Van Ryswyk, H.
– Surface-Confined Metalloporphyrin
Oligomers
(C) 5827–5830 [5951–5954]
DOI: 10.1002/anie.200460992
- Van Tendeloo, G. (L) 4562–4564 [4662–
4664]
- Vancso, G. J. (C) 369–373 [373–377]
- Vangdal, B. (C) 4589–4594 [4689–4695]
- Vanmaekelbergh, D.
– Spontaneous Assembly of a Monolayer of
Charged Gold Nanocrystals at the Water/
Oil Interface
(C) 458–462 [464–468]
DOI: 10.1002/anie.200352339
- Vanmaekelbergh, D. (C) 3029–3033 [3091–
3095]
- Vargas-Díaz, G. (C) 3041–3044 [3103–3106]
- Vasos, P. R. (C) 2257–2259 [2307–2309]
- Vattuone, L.
– Stereodynamic Effects in the Adsorption
of Ethylene onto a Metal Surface
(C) 5200–5203 [5312–5315]
DOI: 10.1002/anie.200461302
- Vaughan, G. M. B. (C) 1828–1832 [1864–
1868], 2787–2792 [2847–2852]
- Vauzeilles, B. (C) 4644–4646 [4744–4746]
- Vayssieres, L.
– Highly Ordered SnO₂ Nanorod Arrays
from Controlled Aqueous Growth
(C) 3666–3670 [3752–3756]
DOI: 10.1002/anie.200454000
- Vázquez, M. (C) 1962–1965 [1996–1999]
- Vecchi, P. A. (C) 4497–4500 [4597–4600]
- Vecchiocattivi, F. (C) 5200–5203 [5312–
5315]
- Veciana, J.
– A Molecular Multiproperty Switching
Array Based on the Redox Behavior of a
Ferrocenyl Polychlorotriphenylmethyl
Radical
(C) 5266–5268 [5378–5381]
DOI: 10.1002/anie.200454150
- A Robust Purely Organic Nanoporous
Magnet
(C) 1828–1832 [1864–1868]
DOI: 10.1002/anie.200353358
- Veciana, J. (C) 4049–4052 [4141–4144]
- Velcicky, J. (C) 1731–1734 [1763–1766]
- Verdaguer, M. (C) 3728–3731 [3814–3817],
5468–5471 [5584–5587]
- Verdier, L. (C) 2547–2551 [2601–2605]
- Verissimo, E. (C) 4193–4197 [4289–4293]
- Vescovi, A. (C) 2822–2826 [2882–2886]
- Vicente, R. (C) 210–212 [212–214]
- Vickaryous, W. J. (C) 5831–5833 [5955–
5957]
- Vickers, S. J. (C) 3938–3941 [4028–4031]
- Vidal-Gancedo, J. (C) 5266–5268 [5378–
5381]
- Vidari, G. (C) 846–849 [864–867]
- Vidlock, E. J. (C) 4052–4055 [4144–4147]
- Vidovic, D. (C) 3832–3835 [3920–3923],
3842–3844 [3930–3932]
- Vigassy, T. (C) 5181–5185 Corrigendum:
5428 [5293–5297 Corrigendum: 5542]
- Vigliotti, F. (C) 2705–2709 [2759–2763]
- Vij, A. (C) 6676–6680 [6844–6848]
- Vij, V. (C) 6676–6680 [6844–6848]
- Vijayaraghavan, R. (C) 5363–5366 [5477–
5480]
- Vilesov, A. F. (R) 2622–2648 [2674–2702]
- Villain, F. (C) 3728–3731 [3814–3817]
- Villeneuve, K. (C) 610–613 [620–623]
- Vinader, V. (C) 5677–5679 [5795–5797]
- Viney, C. (C) 3061–3063 [3123–3125]
- Vinslava, A. (C) 2117–2121 [2169–2173]
- Visser, J. (C) 4755–4759 [4859–4863]
- Vitali, F. (C) 6709–6713 [6877–6881]



Vaara, J. (C) 2678–2681 [2732–2735]
Vaidhyanathan, R. (R) 1466–1496 [1490–
1521]

- Vittal, J. J.
– Helix inside a Helix: Encapsulation of Hydrogen-Bonded Water Molecules in a Staircase Coordination Polymer (C) 5769–5772 [5893–5896]
DOI: 10.1002/anie.200460516
- Vivas, L. (C) 1381–1385 [1405–1409]
- Vlaar, M. T. (C) 3471–3473 [3553–3555]
- Vocadlo, D. J.
– A Strategy for Functional Proteomic Analysis of Glycosidase Activity from Cell Lysates (C) 5338–5342 [5452–5456]
DOI: 10.1002/anie.200454235
- Vogel, P.
– Polysulfones: Catalysts for Alkene Isomerization (C) 2928–2930 [2988–2990]
DOI: 10.1002/anie.200453897
- Vogel, U. (C) 3321–3325 [3383–3387]
- Vögtle, F.
– Highly Branched Macromolecules at the Interface of Chemistry, Biology, Physics, and Medicine (T) 272–273 [274–275]
DOI: 10.1002/anie.200320082
- Voit, B. (C) 3928–3932 [4018–4022]
- Voityuk, A. A. (C) 624–627 [634–637]
- Vollet, J. (C) 3186–3189 [3248–3252]
- Vollhardt, K. P. C.
– Anatomy of a Cyclohexatriene: Chemical Dissection of the π and σ Frame of Angular [3]Phenylene (C) 3711–3715 [3797–3801]
DOI: 10.1002/anie.200454126
- Electron Exchange Along the Tercyclopentadienyltrimetallic Scaffold: Kinetics, Equilibria, and Bond Strengths (C) 1393–1397 [1417–1421]
DOI: 10.1002/anie.200352479
- Vollmer, A. (C) 3691–3695 [3777–3781]
- von Ahsen, S.
– The Trifluoromethoxy Sulfuryl Radical, $\text{CF}_3\text{OSO}_2^\bullet$ (C) 3330–3333 [3392–3395]
DOI: 10.1002/anie.200453925
- von Mulert, U. (C) 2962–2965 [3022–3025]
- von Zelewsky, A.
– Stereoselective Synthesis of a Topologically Chiral Molecule: The Trefoil Knot (C) 4482–4485 [4582–4585]
DOI: 10.1002/anie.200460250
- Vong, B. G. (C) 3947–3951 [4037–4041]
- Voronin, V. I. (C) 2922–2924 [2982–2984]
- Voskoboev, N. V. (C) 4085–4089 [4177–4181]
- Vostrowsky, O. (H) 2326–2329 [2380–2383]
- Vourloumis, D. (C) 3177–3182 [3239–3244]
- Vrijbloed, J. W. (C) 2109–2112 [2161–2164]
- Vyskocil, S. (C) 4312–4318 [4412–4418], 4318–4324 [4418–4424]
- Wagenknecht, H.-A.
– Phenanthridinium as an Artificial Base and Charge Donor in DNA (C) 1845–1847 [1881–1883]
DOI: 10.1002/anie.200353153
- Wagler, J. (C) 2441–2444 [2495–2498]
- Wagner, A.
– Kinetic Resolution of Amines: A Highly Enantioselective and Chemoselective Acetylation Agent with a Unique Solvent-Induced Reversal of Stereoselectivity (C) 3314–3317 [3376–3379]
DOI: 10.1002/anie.200453956
- Wagner, M. (C) 2711–2714 [2765–2768]
- Wakahara, T. (C) 5060–5062 [5170–5172]
- Wakamiya, T. (C) 366–369 [370–373]
- Wakihara, M.
– A High Electrode-Reaction Rate for High-Power-Density Lithium-Ion Secondary Batteries by the Addition of a Lewis Acid (C) 1966–1969 [2000–2003]
DOI: 10.1002/anie.200353220
- Walawalkar, M. G. (C) 3832–3835 [3920–3923]
- Walde, P. (C) 5181–5185 Corrigendum: 5428 [5293–5297 Corrigendum: 5542]
- Waldmann, H.
– Asymmetric Solid-Phase Synthesis of 6,6-Spiroketal (C) 3195–3199 [3258–3261]
DOI: 10.1002/anie.200353609
- Identification of Potent Ras Signaling Inhibitors by Pathway-Selective Phenotype-Based Screening (C) 450–454 [456–460]
DOI: 10.1002/anie.200352587
- Solid-Phase Synthesis of Lipidated Peptides (C) 5839–5842 [5963–5966]
DOI: 10.1002/anie.200461150
- Synthesis and Application of Fluorescence-Labeled Ras-Proteins for Live-Cell Imaging (C) 2711–2714 [2765–2768]
DOI: 10.1002/anie.200353265
- Synthesis and Biological Evaluation of an Indomethacin Library Reveals a New Class of Angiogenesis-Related Kinase Inhibitors (C) 224–228 Corrigendum: 540 [226–230 Corrigendum: 547]
DOI: 10.1002/anie.200352582
- Waldmann, H. (C) 454–458 [460–464]
- Waldvogel, S. R.
– Highly Modular Construction of Differently Substituted Dihydrodibenzo[*a,c*]cycloheptenes: Fast and Efficient Access to Derivatives of 2,2'-Cyclo-7,8'-neolignans (C) 2446–2449 [2501–2503]
DOI: 10.1002/anie.200353597
- Walker, D. B. (C) 3914–3918 [4004–4008]
- Walker, S. D. (C) 1871–1876 [1907–1912]
- Walker, S. M. (C) 5649–5651 [5767–5769]
- Walsh, C. T.
– Characterization of NovP and NovN: Completion of Novobiocin Biosynthesis by Sequential Tailoring of the Noviosyl Ring (C) 67–70 [69–72]
DOI: 10.1002/anie.200352626
- Walsh, C. T. (C) 493–498 [499–504]
- Walsh, D. (C) 6691–6695 [6859–6863]
- Walton, D. R. M. (C) 5670–5674 [5788–5792]
- Wan, H. L.
– Laser-Induced Formation of Metal–Peroxide Linkages on the Surface of Lanthanum Sesquioxide under Oxygen (C) 975–977 [993–995]
DOI: 10.1002/anie.200351706
- Wan, L.-J.
– Pt Hollow Nanospheres: Facile Synthesis and Enhanced Electrocatalysts (C) 1540–1543 [1566–1569]
DOI: 10.1002/anie.200352956
- Wang, B. (C) 1502–1505 [1528–1531]
- Wang, Chih-Chen
– Donor–Donor Energy-Migration Measurements of Dimeric DsbC Labeled at Its N-Terminal Amines with Fluorescent Probes: A Study of Protein Unfolding (C) 4216–4219 [4312–4315]
DOI: 10.1002/anie.200460072
- Wang, Chih-Chieh
– Rhodizonate Metal Complexes with a 2D Chairlike M_6 Metal–Organic Framework: $[\text{M}(\text{C}_6\text{O}_6)(\text{bpym})(\text{H}_2\text{O})] \cdot n\text{H}_2\text{O}$ (C) 4507–4510 [4607–4610]
DOI: 10.1002/anie.200460278
- Wang, Dayang
– Directing Self-Assembly of Nanoparticles at Water/Oil Interfaces (C) 5639–5642 [5757–5760]
DOI: 10.1002/anie.200460920
- Wang, Dihua (C) 733–736 [751–754]
- Wang, Donghai (C) 6169–6173 [6295–6299]
- Wang, E.
– Large-Scale Synthesis of Micrometer-Scale Single-Crystalline Au Plates of Nanometer Thickness by a Wet-Chemical Route (C) 6360–6363 [6520–6523]
DOI: 10.1002/anie.200461013
- Wang, E.-B.
– Interlocked and Interdigitated Architectures from Self-Assembly of Long Flexible Ligands and Cadmium Salts (C) 5036–5040 [5146–5150]
DOI: 10.1002/anie.200460758
- Wang, G. (C) 357–360 [361–364]
- Wang, Haisheng (C) 5221–5224 [5333–5336]
- Wang, Hao (C) 2690–2694 [2744–2748]
- Wang, Huadong (C) 184–187 [186–189]
- Wang, Jianbo
– A Highly Stereoselective Addition of the Anion Derived from α -Diazoacetamide to Aromatic *N*-Tosylimines (C) 5977–5980 [6103–6106]
DOI: 10.1002/anie.200460730
- Wang, Joseph
– DNA-Based Amplified Bioelectronic Detection and Coding of Proteins (C) 2158–2161 [2210–2213]
DOI: 10.1002/anie.200453832
- Wang, K.
– Design of a Modular-Based Fluorescent Conjugated Polymer for Selective Sensing (C) 5635–5638 [5753–5756]
DOI: 10.1002/anie.200460371
- Wang, L. (C) 2697–2701 [2751–2755]
- Wang, L.-S.
– $[\text{SiAu}_4]$: Aurosilane (C) 2125–2129 [2177–2181]
DOI: 10.1002/anie.200353602
- Wang, M.-X.
– Synthesis, Structure, and [60]Fullerene Complexation Properties of Azacalix-[*m*]arene[*n*]pyridines (C) 838–842 [856–860]
DOI: 10.1002/anie.200351975



Wachtel, E. (C) 6140–6143 [6266–6269]
Wackerbarth, H. (C) 198–203 [200–205]
Wada, A. (C) 6510–6512 [6672–6674]
Wada, Y. (C) 4763–4767 [4867–4871]

- Wang, Mei
– An Unusual Cyclization in a Bis(cysteinyll-S) Diiron Complex Related to the Active Site of Fe-Only Hydrogenases (C) 3571–3574 [3655–3658]
DOI: 10.1002/anie.200453961
- Wang, Mingsheng (C) 3554–3557 [3638–3641]
- Wang, P. (C) 3664–3666 [3750–3752]
- Wang, Q. (C) 1126–1129 [1146–1149]
- Wang, Q.-C. (C) 2661–2665 [2715–2719]
- Wang, R.-H. (C) 5665–5668 [5783–5786]
- Wang, R.-Y. (C) 2933–2936 [2993–2996]
- Wang, S.-K. (C) 6496–6500 [6658–6662]
- Wang, Shi (C) 5940–5943 [6066–6069]
- Wang, Suning
– Luminescent 2D Macrocyclic Networks Based on Starburst Molecules: $[\text{Ag}(\text{CF}_3\text{SO}_3)]_n(\text{tdapb})$ and $[\text{Ag}(\text{NO}_3)]_n(\text{tdapb})$ (C) 2933–2936 [2993–2996]
DOI: 10.1002/anie.200353126
- Wang, T. (C) 5048–5052 [5158–5162]
- Wang, W.-W. (C) 1410–1414 [1434–1438]
- Wang, X.-L. (C) 5036–5040 [5146–5150]
- Wang, X.-S. (C) 3703–3707 [3789–3793]
- Wang, Xi (C) 4663–4666 [4763–4766]
- Wang, Xiang (C) 3601–3605 [3685–3689]
- Wang, Xinping (C) 1995–1998 [2029–2032]
- Wang, Xiqing (C) 1502–1505 [1528–1531]
- Wang, Xuefeng (C) 1706–1709 [1738–1741], 2554–2557 [2608–2611]
- Wang, Xun (C) 2017–2020 [2051–2054]
- Wang, Yi (C) 3574–3577 [3658–3661]
- Wang, Ying (C) 5203–5206 [5315–5318]
- Wang, Yuan
– A Highly Luminescent Europium Complex Showing Visible-Light-Sensitized Red Emission: Direct Observation of the Singlet Pathway (C) 5010–5013 [5120–5123]
DOI: 10.1002/anie.200454141
- Wang, Z. L.
– Single-Crystal Hexagonal Disks and Rings of ZnO: Low-Temperature, Large-Scale Synthesis and Growth Mechanism (C) 5238–5242 [5350–5354]
DOI: 10.1002/anie.200460783
- Wang, Zhaohui (C) 1972–1975 [2006–2009]
- Wang, Zhen (C) 3571–3574 [3655–3658]
- Wanner, M. (C) 3970–3974 [4061–4064]
- Wannere, C. S. (C) 4200–4206 [4296–4302]
- Ward, M. D. (C) 3938–3941 [4028–4031]
- Ward, S. A. (C) 4193–4197 [4289–4293]
- Warman, J. M. (C) 5331–5335 [5445–5449]
- Warrington, B. H. (C) 1225–1228 [1245–1248]
- Waschulowski, V. (H) 6414–6416 [6574–6576]
- Waser, J. (C) 4099–4102 [4191–4194]
- Washington, R. P. (C) 1505–1507 [1531–1533]
- Washio, T. (C) 2665–2668 [2719–2722]
- Washitake, Y. (C) 1857–1860 [1893–1896]
- Wasielowski, M. R.
– High-Mobility Air-Stable n-Type Semiconductors with Processing Versatility: Dicyanoperylene-3,4:9,10-bis(dicarboximides) (C) 6363–6366 [6523–6526]
DOI: 10.1002/anie.200461324
- Wassel, R. A. (H) 5120–5123 [5230–5233]
- Watanabe, H. (C) 6180–6182 [6306–6308]
- Watanabe, Takahito (C) 218–221 [220–223]
- Watanabe, Takumi (C) 5971–5973 [6097–6099]
- Watanabe, Y.
– Size-Selective Olefin Hydrogenation by a Pd Nanocluster Provided in an Apo-Ferri-tin Cage (C) 2527–2530 [2581–2584]
DOI: 10.1002/anie.200353436
- Waters, M. L.
– A Peptide Flavoprotein Mimic: Flavin Recognition and Redox Potential Modulation in Water by a Designed β Hairpin (C) 724–727 [742–745]
DOI: 10.1002/anie.200352527
- Watson, M. D. (C) 755–758 [773–777]
- Watson, S. J. (C) 1249–1251 [1269–1271]
- Watson, T. J. N. (E) 3224–3228 [3286–3290]
- Watt, S. W. (C) 3061–3063 [3123–3125]
- Weatherstone, S. (C) 1709–1712 [1741–1744]
- Weaver, J. V. M. (C) 1389–1392 [1413–1416]
- Webb, T. R. (C) 2843–2846 [2903–2906]
- Weber, H. B.
– Statistical Analysis of Single-Molecule Junctions (H) 2882–2884 [2942–2944]
DOI: 10.1002/anie.200301733
- Weber, M. (C) 2962–2965 [3022–3025]
- Webster, C. E. (C) 5474–5477 [5590–5593]
- Weder, C.
– Synthesis and Characterization of Cross-Linked Conjugated Polymer Milli-, Micro-, and Nanoparticles (C) 1808–1811 [1844–1847]
DOI: 10.1002/anie.200352863
- Wehlan, H. (C) 4597–4601 [4698–4702]
- Wehrmann, P. (C) 869–873 [887–891]
- Wehrspohn, R. B. (R) 1334–1344 [1356–1367]
- Wei, J. (C) 3685–3688 [3771–3774]
- Weidemann, N. (C) 6512–6516 [6674–6678]
- Weidenthaler, C. (C) 2444–2446 [2498–2500]
- Weinberg, B. D. (C) 6323–6327 [6483–6487]
- Weininger, S. J.
– Controversy in Chemistry: What Counts as Evidence?—Two Studies in Molecular Structure (E) 2612–2619 [2664–2672]
DOI: 10.1002/anie.200330055
- Weis, P. (C) 6662–6666 [6832–6836]
- Weiss, H. (C) 3691–3695 [3777–3781]
- Weiss, M. M. (C) 1270–1272 [1290–1292]
- Weisser, J. T. (C) 448–450 Corrigendum: 2986 [454–456 Corrigendum: 3046]
- Weissleder, R. (C) 2395–2399 [2449–2453]
- Weizmann, Y. (C) 2113–2117 [2165–2169]
- Weller, H.
– Site-Specific Photodeposition of Silver on ZnO Nanorods (C) 4774–4777 [4878–4881]
DOI: 10.1002/anie.200453880
- Welter, R. (C) 4479–4482 [4579–4582], 5922–5925 [6048–6051], 6120–6125 [6246–6251]
- Wemmer, D. E.
– Design of a Conformation-Sensitive Xenon-Binding Cavity in the Ribose-Binding Protein (C) 6320–6322 [6480–6482]
DOI: 10.1002/anie.200460629
- Wen, K. (C) 739–742 [757–760]
- Wender, P. A.
– Intermolecular Dienyl Pauson–Khand Reaction (C) 3076–3079 [3138–3141]
DOI: 10.1002/anie.200454117
- Wendorff, J. H.
– Nanotubes by Template Wetting: A Molecular Assembly System (R) 1334–1344 [1356–1367]
DOI: 10.1002/anie.200300614
- Weng, W. Z.
– Laser-Induced Formation of Metal–Peroxide Linkages on the Surface of Lanthanum Sesquioxide under Oxygen (C) 975–977 [993–995]
DOI: 10.1002/anie.200351706
- Wenthold, P. G.
– 5-Dehydro-1,3-quinodimethane: A Hydrocarbon with an Open-Shell Doublet Ground State (C) 742–745 [760–763]
DOI: 10.1002/anie.200352990
- Wentworth, P., Jr.
– Dihydrogen Trioxide (HOOH) Is Generated during the Thermal Reaction between Hydrogen Peroxide and Ozone (C) 4656–4659 [4756–4759]
DOI: 10.1002/anie.200460457
- Wenzel, S. C. (C) 4163–4167 [4257–4262]
- Wenzl, S. (C) 5933–5936 [6059–6062]
- Werder, M. (C) 4653–4656 [4753–4756]
- Werner, H.
– The Way into the Bridge: A New Bonding Mode of Tertiary Phosphanes, Arsanes, and Stibanes (R) 938–954 [956–972]
DOI: 10.1002/anie.200300627
- Werner, T. (C) 6547–6549 [6709–6711]
- Wernsdorfer, W.
– A Dimeric Manganese(III) Tetradentate Schiff Base Complex as a Single-Molecule Magnet (C) 2801–2805 [2861–2865]
DOI: 10.1002/anie.200353563
- Wernsdorfer, W. (C) 1136–1139 [1156–1159], 2117–2121 [2169–2173], 5772–5775 Corrigendum: 6581 [5896–5899 Corrigendum: 6743], 6152–6156 [6278–6282], 6338–6342 [6498–6502]
- Wessling, R. A. Corrigendum: 3748
- Westhof, E.
– Antibacterial Aminoglycosides with a Modified Mode of Binding to the Ribosomal-RNA Decoding Site (C) 6735–6738 [6903–6906]
DOI: 10.1002/anie.200462092
- Weston, A. J. (C) 2551–2553 [2605–2607]
- Wetzel, B. K. (C) 5400–5402 [5515–5517]
- Weuster-Botz, D.
– Efficient Whole-Cell Biotransformation in a Biphasic Ionic Liquid/Water System (C) 4529–4531 [4629–4631]
DOI: 10.1002/anie.200460241
- Weyland, M. (C) 6745–6747 [6913–6915]
- Weyrauch, J. P. (C) 6545–6547 [6707–6709]
- Wheatley, A. E. H.
– Controlling Chemoselectivity in the Lithiation of Substituted Aromatic Tertiary Amides (C) 2135–2138 [2187–2190]
DOI: 10.1002/anie.200353324
- Whisler, M. C. (R) 2206–2225 [2256–2276]
- White, C. L. I. M. (C) 469–472 [475–478]
- White, S. S. (C) 5926–5930 [6052–6056]
- Whitesides, G. M.
– An Integrated Approach to a Portable and Low-Cost Immunoassay for Resource-Poor Settings (C) 498–502 [504–508]
DOI: 10.1002/anie.200353016

- Assumptions: Taking Chemistry in New Directions
(E) 3632–3641 [3716–3727]
DOI: 10.1002/anie.200330076
- Electron Transfer in a Hg-SAM/SAM-Hg Junction Mediated by Redox Centers
(C) 3835–3839 [3923–3927]
DOI: 10.1002/anie.200453945
- Self-Assembled Aggregates of IgGs as Templates for the Growth of Clusters of Gold Nanoparticles
(C) 1555–1558 [1581–1584]
DOI: 10.1002/anie.200353161
- Shear Patterning of Microdominos: A New Class of Procedures for Making Micro- and Nanostructures
(C) 2780–2783 [2840–2843]
DOI: 10.1002/anie.200353009
- Whitney, A. M. (C) 1143–1146 [1163–1166]
- Whyman, R. (C) 90–94 [92–96]
- Wibbeling, B. (C) 6667–6669 [6836–6838]
- Wickleder, M. S.
- The Cluster Ion $[\text{Pt}_{12}\text{O}_8(\text{SO}_4)_{12}]^{4-}$
(C) 4168–4170 [4262–4264]
DOI: 10.1002/anie.200454257
- Widenmeyer, M. (C) 2234–2239 [2284–2289]
- Wider, J. (C) 2853–2856 [2913–2917]
- Widmalm, G.
- A Conformational Carbohydrate Scaffold is Present in the Short-Chain Lipopolysaccharides of *Moraxella catarrhalis*
(C) 2288–2290 [2338–2340]
DOI: 10.1002/anie.200353581
- Więckowska, A. (C) 1668–1672 [1700–1704]
- Wieder, T.
- Iron-Containing Nucleoside Analogues with Pronounced Apoptosis-Inducing Activity
(C) 1731–1734 [1763–1766]
DOI: 10.1002/anie.200353132
- Wiesner, J. (C) 251–254 [254–257]
- Wiessler, M. Corrigendum: 4389
- Wijmenga, S. S.
- NMR Spectroscopic Determination of the Solution Structure of a Branched Nucleic Acid from Residual Dipolar Couplings by Using Isotopically Labeled Nucleotides
(C) 187–192 [189–194]
DOI: 10.1002/anie.200351632
- Wilker, J. J.
- Inorganic Oxo Compounds React with Alkylating Agents: Implications for DNA Damage
(C) 3290–3292 [3352–3354]
DOI: 10.1002/anie.200353363
- Metal-Mediated Cross-Linking in the Generation of a Marine-Mussel Adhesive
(C) 448–450 Corrigendum: 2986 [454–456 Corrigendum: 3046]
DOI: 10.1002/anie.200352759
- Wilkinson, B. (C) 2551–2553 [2605–2607]
- Will, D. W. (C) 4526–4528 [4626–4629]
- Williams, D. H.
- Understanding Noncovalent Interactions: Ligand Binding Energy and Catalytic Efficiency from Ligand-Induced Reductions in Motion within Receptors and Enzymes
(R) 6596–6616 [6760–6782]
DOI: 10.1002/anie.200300644
- Williams, I. D. (C) 1715–1718 [1747–1750]
- Williams, R. M.
- A Concise Asymmetric Synthesis of the Marine Hepatotoxin 7-Epicylindrospermopsin
(C) 2930–2933 [2990–2993]
DOI: 10.1002/anie.200454208
- Williams, T. J. (C) 3076–3079 [3138–3141]
- Williams Fiori, K. (C) 4349–4352 [4449–4452]
- Willis, C. L. (C) 727–730 [745–748]
- Willis, M. C.
- Chelation-Controlled Intermolecular Hydroacylation: Direct Addition of Alkyl Aldehydes to Functionalized Alkenes
(C) 340–343 [344–347]
DOI: 10.1002/anie.200352751
- Enantioselective Suzuki Reactions: Catalytic Asymmetric Synthesis of Compounds Containing Quaternary Carbon Centers
(C) 1249–1251 [1269–1271]
DOI: 10.1002/anie.200352648
- Willner, H.
- Bis(fluoroformyl)trioxide, FC(O)OOOC(O)F
(C) 2843–2846 [2903–2906]
DOI: 10.1002/anie.200353369
- $[(\text{CF}_3)_3\text{BCP}]^-$ and $[(\text{CF}_3)_3\text{BCAs}]^-$: Thermally Stable Phosphaethynyl and Arsaethynyl Complexes
(C) 4160–4163 [4254–4257]
DOI: 10.1002/anie.200454034
- Willner, I.
- Catalytic Growth of Au Nanoparticles by NAD(P)H Cofactors: Optical Sensors for NAD(P) $^{+}$ -Dependent Biocatalyzed Transformations
(C) 4519–4522 [4619–4622]
DOI: 10.1002/anie.200460608
- Electrical Contacting of Glucose Oxidase in a Redox-Active Rotaxane Configuration
(C) 3292–3300 [3354–3362]
DOI: 10.1002/anie.200353455
- Integrated Nanoparticle–Biomolecule Hybrid Systems: Synthesis, Properties, and Applications
(R) 6042–6108 [6166–6235]
DOI: 10.1002/anie.200400651
- Long-Range Electrical Contacting of Redox Enzymes by SWCNT Connectors
(C) 2113–2117 [2165–2169]
DOI: 10.1002/anie.200353275
- Wilmer, H. (C) 2839–2842 [2899–2903]
- Wilson, C. (C) 1851–1854 [1887–1890]
- Wilson, C. C.
- Towards Designing Proton-Transfer Systems—Direct Imaging of Proton Disorder in a Hydrogen-Bonded Carboxylic Acid Dimer by Variable-Temperature X-ray Diffraction
(C) 2095–2099 [2147–2151]
DOI: 10.1002/anie.200352650
- Wilson, I. A. (C) 1000–1003 [1018–1021]
- Wilson, J. E. (C) 6358–6360 [6518–6520]
- Winkler, J. D. (C) 1158–1162 [1178–1182]
- Winner, M. (C) 1883–1886 [1919–1922]
- Winnik, M. A.
- Swellable, Redox-Active Shell-Crosslinked Organometallic Nanotubes
(C) 3703–3707 [3789–3793]
DOI: 10.1002/anie.200453969
- Winpenney, R. E. P.
- Templating Open- and Closed-Chain Structures around Metal Complexes of Macrocycles
(C) 6132–6135 [6258–6261]
DOI: 10.1002/anie.200461006
- The Magnetic Möbius Strip: Synthesis, Structure, and Magnetic Studies of Odd-Numbered Antiferromagnetically Coupled Wheels
(C) 5196–5200 [5308–5312]
DOI: 10.1002/anie.200460211
- Winssinger, N.
- Modular Asymmetric Synthesis of Pocho-nin C
(C) 3467–3470 [3549–3552]
DOI: 10.1002/anie.200454108
- Winter, M. (C) 2299–2302 [2349–2352]
- Winters, G. C. (C) 3177–3182 [3239–3244]
- Wintgens, V. (C) 1718–1721 [1750–1753]
- Wirges, B. (C) 6197–6201 [6323–6328]
- Wirmer, J. (C) 5780–5785 [5904–5909]
- Wirth, T.
- Selenocyclizations: Control by Coordination and by the Counterion
(C) 631–633 [641–643]
DOI: 10.1002/anie.200352884
- Wismach, C. (C) 3970–3974 [4061–4064]
- Wistuba, T. (C) 1283–1287 [1303–1307]
- Witholt, B. (C) 1698–1702 [1730–1734], 2163–2166 [2215–2218]
- Wittmann, V.
- Spatial Screening of Cyclic Neoglycopeptides: Identification of Polyvalent Wheat-Germ Agglutinin Ligands
(C) 900–903 [918–921]
DOI: 10.1002/anie.200352055
- Wittmann, V. (C) 187–192 [189–194]
- Wittstock, G.
- An SECM Detection Scheme with Improved Sensitivity and Lateral Resolution: Detection of Galactosidase Activity with Signal Amplification by Glucose Dehydrogenase
(C) 4170–4172 [4264–4267]
DOI: 10.1002/anie.200454261
- Wlassoff, W. A. (C) 2809–2812 [2869–2872]
- Woggon, W.-D.
- Enantioselective Reduction of Aromatic and Aliphatic Ketones Catalyzed by Ruthenium Complexes Attached to β -Cyclodextrin
(C) 6731–6734 [6899–6902]
DOI: 10.1002/anie.200460102
- Wohlert, S.-E. (C) 2962–2965 [3022–3025]
- Woithe, K. (C) 6709–6713 [6877–6881]
- Wolfbeis, O. S.
- Chameleon Labels for Staining and Quantifying Proteins
(C) 5400–5402 [5515–5517]
DOI: 10.1002/anie.200460508
- Fluorescent Imaging of Citrate and Other Intermediates in the Citric Acid Cycle
(C) 1735–1738 [1767–1770]
DOI: 10.1002/anie.200353169
- Wolfe, J. P.
- Palladium-Catalyzed Synthesis of *N*-Aryl Pyrrolidines from γ -(*N*-Arylamino) Alkenes: Evidence for Chemoselective Alkene Insertion into Pd–N Bonds
(C) 3605–3608 [3689–3692]
DOI: 10.1002/anie.200460060
- Wolfrum, J. (C) 3798–3801 [3886–3890]
- Wöll, C.
- Partial Dissociation of Water Leads to Stable Superstructures on the Surface of Zinc Oxide
(C) 6641–6645 [6809–6814]
DOI: 10.1002/anie.200461696
- Wöll, C. (C) 2839–2842 [2899–2903]
- Wolter, F. (C) 2574–2576 [2628–2630]
- Won, J. (C) 3053–3056 [3115–3118]



- Wong, C.-H.
– Dimeric Aminoglycosides as Antibiotics (C) 1562–1566 [1588–1592]
DOI: 10.1002/anie.200353225
– Reactivity-Based One-Pot Synthesis of Oligomannosides: Defining Antigens Recognized by 2G12, a Broadly Neutralizing Anti-HIV-1 Antibody (C) 1000–1003 [1018–1021]
DOI: 10.1002/anie.200353105
– Sulfatases: Structure, Mechanism, Biological Activity, Inhibition, and Synthetic Utility (R) 5736–5763 [5858–5886]
DOI: 10.1002/anie.200300632
– Sulfotransferases: Structure, Mechanism, Biological Activity, Inhibition, and Synthetic Utility (R) 3526–3548 [3610–3632]
DOI: 10.1002/anie.200300631
– Targeting RNAs with Tobramycin Analogues (C) 6496–6500 [6658–6662]
DOI: 10.1002/anie.200460558
Wong, C.-H. (C) 4656–4659 [4756–4759]
Wong, J. K. Y. (C) 1218–1221 [1238–1241]
Wong, K.-L. (C) 4659–4662 [4759–4762]
Wong, S. Y. F. (C) 1225–1228 [1245–1248]
Wong, W.-T.
– A Highly Luminescent Europium Complex Showing Visible-Light-Sensitized Red Emission: Direct Observation of the Singlet Pathway (C) 5010–5013 [5120–5123]
DOI: 10.1002/anie.200454141
– Green and Red Three-Photon Upconversion from Polymeric Lanthanide(III) Complexes (C) 4659–4662 [4759–4762]
DOI: 10.1002/anie.200460576
Wong Chi Man, M. (C) 203–206 [205–208]
Wongbuntit, S. (C) 866–868 [884–886]
Wood, J. L.
– A Mild and Efficient Synthesis of Oxindoles: Progress Towards the Synthesis of Welwitindolinone A Isonitrile (C) 1270–1272 [1290–1292]
DOI: 10.1002/anie.200353282
Wooley, K. L. (C) 2783–2787 [2843–2847]
Workentin, M. S. (C) 2812–2815 [2872–2875]
Wörth, C. C. T. Corrigendum: 4389
Wortmann, R. (C) 5851–5856 [5976–5981]
Wouters, D. (R) 2480–2495 [2534–2550]
Wozniak, K.
– An Electrochemically Controlled Molecular Shuttle (C) 1668–1672 [1700–1704]
DOI: 10.1002/anie.200352528
Wright, A. (C) 1352–1355 [1376–1379]
Wright, P. T. (C) 5680–5682 [5798–5800]
Wu, B. (C) 6673–6675 [6841–6843]
Wu, B.-L. (C) 5665–5668 [5783–5786]
Wu, Hao (C) 4324–4327 [4424–4427]
Wu, Hashen (C) 1832–1835 [1868–1871]
Wu, Jiarui (C) 4324–4327 [4424–4427]
Wu, Jishan (C) 5331–5335 [5445–5449]
Wu, M. (C) 1735–1738 [1767–1770]
Wu, P. (La Jolla) (C) 3928–3932 [4018–4022]
Wu, P. (Yokohama) (C) 236–240 [238–242]
Wu, Wei
– The Magnitude of Hyperconjugation in Ethane: A Perspective from Ab Initio Valence Bond Theory

- (C) 1986–1990 [2020–2024]
DOI: 10.1002/anie.200352931
Wu, Weize (C) 1397–1399 [1421–1423], 2415–2417 [2469–2471]
Wu, Y.-D. (C) 6719–6722 [6887–6890]
Wu, Y.-L. (C) 329–334 [333–338]
Wudl, F.
– A Red, Green, and Blue (RGB) Polymeric Electrochromic Device (PECD): The Dawning of the PECD Era (C) 1498–1502 [1524–1528]
DOI: 10.1002/anie.200352910
Wuister, S. F. (C) 3029–3033 [3091–3095]
Wulff, G.
– Molecularly Imprinted Polymers with Strong Carboxypeptidase A-Like Activity: Combination of an Amidinium Function with a Zinc-Ion Binding Site in Transition-State Imprinted Cavities (C) 1287–1290 [1307–1311]
DOI: 10.1002/anie.200352770
Wulff, J. E. (C) 6493–6496 [6655–6658]
Wurst, K. (C) 1828–1832 [1864–1868], 4049–4052 [4141–4144], 5266–5268 [5378–5381]
Würthwein, E.-U.
– A Versatile Aminobenzannulation Method Based on the Deprotonation of 2-(1-Alkynyl)benzaldimines and Similar 2-Aza-2,4-heptadienyl-6-yne: A Multistep Rearrangement Cascade (C) 5694–5697 [5812–5815]
DOI: 10.1002/anie.200461031



- Xavier, L. A. (C) 3588–3590 [3672–3674]
Xia, A.
– Donor–Donor Energy-Migration Measurements of Dimeric DsbC Labeled at Its N-Terminal Amines with Fluorescent Probes: A Study of Protein Unfolding (C) 4216–4219 [4312–4315]
DOI: 10.1002/anie.200460072
Xia, T. (C) 60–63 [62–65]
Xiao, S. (C) 6169–6173 [6295–6299]
Xiao, X. (C) 6148–6152 [6274–6278]
Xiao, Y. (C) 4519–4522 [4619–4622]
Xie, S. (C) 2547–2551 [2601–2605]
Xin, X. (C) 5238–5242 [5350–5354], 5776–5779 [5900–5903]
Xiong, R.-G. (C) 990–994 [1008–1012]
Xiong, Y. (C) 6202–6204 [6328–6331]
Xu, B. (C) 6148–6152 [6274–6278]
Xu, H. (C) 67–70 [69–72]
Xu, J. (C) 5491–5496 [5607–5612]
Xu, L. (C) 5036–5040 [5146–5150]
Xu, M. (C) 2543–2546 [2597–2600]
Xu, Q. (C) 2780–2783 [2840–2843]
Xu, Q.-F. (C) 4741–4745 [4845–4849]
Xu, R.
– Hydrogen-Bonded Helices in the Layered Aluminophosphate (C₂H₈N)₂[Al₂(HPO₄)₂](PO₄)₂ (C) 2399–2402 Corrigendum: 3096 [2453–2456 Corrigendum: 3158]
DOI: 10.1002/anie.200353118
Xu, R. (C) 6482–6485 [6644–6647]
Xue, J. (C) 1569–1573 [1595–1599]
- Yadav, V. K.
– Formal [3+2] Addition of Acceptor-Substituted Cyclopropylmethylsilanes with Aryl Acetylenes (C) 2669–2671 [2723–2725]
DOI: 10.1002/anie.200453823
Yakushijin, K. (C) 5357–5360 [5471–5474]
Yam, M. (C) 5682–5685 [5800–5803]
Yam, V. W.-W.
– Supramolecular Assembly of Luminescent Gold(I) Alkynylcalix[4]crown-6 Complexes with Planar η²,η²-Coordinated Gold(I) Centers (C) 4954–4957 [5062–5065]
DOI: 10.1002/anie.200460744
Yamada, K. (C) 6135–6139 [6261–6265]
Yamada, M. (C) 3688–3691 [3774–3777]
Yamada, T. (C) 2145–2148 [2197–2200]
Yamada, Y. M. A. (C) 4312–4318 [4412–4418], 4318–4324 [4418–4424]
Yamagiwa, N. (C) 4493–4497 [4593–4597]
Yamago, S.
– Iterative Glycosylation of 2-Deoxy-2-aminothioglycosides and Its Application to the Combinatorial Synthesis of Linear Oligoglucosamines (C) 2145–2148 [2197–2200]
DOI: 10.1002/anie.200353552
Yamaguchi, J. (C) 1112–1115 [1132–1135]
Yamaguchi, Kazuya (C) 1576–1580 [1602–1606]
Yamaguchi, Kentaro (C) 5621–5625 [5739–5743]
Yamaguchi, Tadashi (C) 1376–1381 [1400–1405]
Yamaguchi, Tatsuya (C) 6350–6355 [6510–6515]
Yamaguchi, Y.
– Synthesis and Light-Emitting Characteristics of Doughnut-Shaped π-Electron Systems (C) 366–369 [370–373]
DOI: 10.1002/anie.200352749
Yamamoto, H.
– Asymmetric Direct Aldol Reaction Assisted by Water and a Proline-Derived Tetrazole Catalyst (C) 1983–1986 [2017–2020]
DOI: 10.1002/anie.200352724
– Chiral Molecular Recognition by Aluminum Tris(2,6-diphenylphenoxide) in an Asymmetric 1,4-Addition (C) 994–997 [1012–1015]
DOI: 10.1002/anie.200352809
Yamamoto, K. (C) 6474–6479 [6636–6641]
Yamamoto, Youko (C) 3448–3451 [3530–3533]
Yamamoto, Yukio (C) 3677–3682 [3763–3768]
Yamanai, Y. (C) 5936–5940 [6062–6066]
Yamashita, K.-i. (C) 5016–5019 [5126–5129]
Yamashita, M.
– [[Pt(en)₂][PtX₂(en)₂]]₃[[MX₂X₃]] · 12 H₂O: Quasi-One-Dimensional Halogen-Bridged Pt^{II}–Pt^{IV} Mixed-Valence Compounds with Magnetic Counteranions

- (C) 4763–4767 [4867–4871]
DOI: 10.1002/anie.200460580
- Visualization of Local Valence Structures in Quasi-One-Dimensional Halogen-Bridged Complexes $[\text{Ni}_{1-x}\text{Pd}_x(\text{chxn})_2\text{Br}] \cdot \text{Br}_2$ by STM
(C) 3171–3175 [3233–3237]
DOI: 10.1002/anie.200453905
 - Yamashita, M. (C) 707–711 [725–729], 2801–2805 [2861–2865]
 - Yamato, K. (C) 6471–6474 [6633–6636]
 - Yamauchi, J. (C) 3677–3682 [3763–3768]
 - Yamauchi, Y. (C) 2389–2391 [2443–2445]
 - Yamazaki, I. (M) 150–158 [152–160]
 - Yamazaki, T. (M) 150–158 [152–160]
 - Yamochi, H. (C) 3670–3673 [3756–3759], 6343–6346 [6503–6506]
 - Yan, D.
 - Supramolecular Self-Assembly of Giant Polymer Vesicles with Controlled Sizes
(C) 4896–4899 [5004–5007]
DOI: 10.1002/anie.200460325
 - Yan, H.
 - A Unidirectional DNA Walker That Moves Autonomously along a Track
(C) 4906–4911 [5014–5019]
DOI: 10.1002/anie.200460522
 - Yan, L.-K. (C) 2409–2411 [2463–2465]
 - Yan, M. (C) 6713–6716 [6881–6884]
 - Yan, X. (C) 5980–5984 [6106–6110]
 - Yang, Changzheng (C) 6369–6372 [6529–6532]
 - Yang, Chi (C) 5010–5013 [5120–5123]
 - Yang, D.
 - $\beta^{2,3}$ -Cyclic Aminoxy Acids: Rigid and Ring-Size-Independent Building Blocks of Foldamers
(C) 6719–6722 [6887–6890]
DOI: 10.1002/anie.200454140
 - Yang, D.-S. (C) 2830–2834 [2890–2894]
 - Yang, Da (M) 4402–4409 [4502–4510]
 - Yang, Gang (C) 6377–6381 [6537–6541]
 - Yang, Guang (C) 6331–6335 [6491–6495]
 - Yang, Guangli (C) 3818–3822 [3906–3910]
 - Yang, Guoqiang (C) 4216–4219 [4312–4315]
 - Yang, H. G. (C) 5206–5209 [5318–5321], 5930–5933 [6056–6059]
 - Yang, J. W. (C) 6660–6662 [6829–6832]
 - Yang, Jerry
 - Self-Assembled Aggregates of IgGs as Templates for the Growth of Clusters of Gold Nanoparticles
(C) 1555–1558 [1581–1584]
DOI: 10.1002/anie.200353161
 - Yang, Jin (C) 2409–2411 [2463–2465]
 - Yang, Jinlong
 - Is Mayenite without Clathrated Oxygen an Inorganic Electride?
(C) 6479–6482 [6641–6644]
DOI: 10.1002/anie.200461200
 - Yang, P.
 - Platonic Gold Nanocrystals
(C) 3673–3677 [3759–3763]
DOI: 10.1002/anie.200454216
 - Yang, R. T.
 - Denitrogenation of Transportation Fuels by Zeolites at Ambient Temperature and Pressure
(C) 1004–1006 Corrigendum: 2321 [1022–1024 Corrigendum: 2373]
DOI: 10.1002/anie.200353162
 - Yang, W. (C) 4060–4063 [4152–4155]
 - Yang, Xiaohai (C) 5635–5638 [5753–5756]
 - Yang, Xiaowu (C) 6471–6474 [6633–6636]
 - Yang, Z.
 - A General Route to Macroscopic Hierarchical 3D Nanowire Networks
(C) 6169–6173 [6295–6299]
DOI: 10.1002/anie.200460535
 - Yao, J.
 - Low-Dimensional Aggregates from Stilbazolium-Like Dyes
(C) 4060–4063 [4152–4155]
DOI: 10.1002/anie.200454131
 - Yao, S. (C) 6202–6204 [6328–6331]
 - Yao, S.-L. (C) 1562–1566 [1588–1592]
 - Yao, Z.-J.
 - Parallel Fragment Assembly Strategy Towards Multiple-Ether Mimicry of Anticancer Annonaceous Acetogenins
(C) 329–334 [333–338]
DOI: 10.1002/anie.200352681
 - Yap, G. P. A. (C) 6716–6718 [6884–6886]
 - Yarasik, A. (C) 1088–1092 [1108–1112]
 - Yarmoluk, S. M. (C) 5400–5402 [5515–5517]
 - Yashima, E. (C) 1969–1972 [2003–2006]
 - Yasuda, M. (C) 711–714 [729–732], 1414–1416 [1438–1440]
 - Yates, C. M. (C) 2652–2655 [2706–2709]
 - Yates, T. J. V. (C) 6745–6747 [6913–6915]
 - Ye, B.-H. (C) 98–100 [100–102]
 - Ye, Jianping (C) 4216–4219 [4312–4315]
 - Ye, Jinhua
 - Efficient Photocatalytic Decomposition of Organic Contaminants over CaBi_2O_4 under Visible-Light Irradiation
(C) 4463–4466 [4563–4566]
DOI: 10.1002/anie.200353594
 - Ye, X.-S.
 - Iterative One-Pot Synthesis of Oligosaccharides
(C) 5221–5224 [5333–5336]
DOI: 10.1002/anie.200460176
 - Yelamagad, C. V. (C) 3429–3432 [3511–3514]
 - Yie, J. E. (C) 3839–3842 [3927–3930]
 - Yin, P. (C) 4906–4911 [5014–5019]
 - Ying, L. (C) 5926–5930 [6052–6056]
 - Yip, S.-K. (C) 4954–4957 [5062–5065]
 - Yokota, K. (C) 1566–1568 [1592–1594]
 - Yokota, W. (C) 4207–4209 [4303–4305]
 - Yokoyama, A. (C) 1360–1363 [1384–1387]
 - Yokozawa, T.
 - Absolute Helical Arrangement of Stacked Benzene Rings: Heterogeneous Double-Helical Interaction Comprising a Hydrogen-Bonding Belt and an Offset Parallel Aromatic–Aromatic-Interaction Array
(C) 1360–1363 [1384–1387]
DOI: 10.1002/anie.200352788
 - Yoo, M.-S. (C) 2382–2385 [2436–2439]
 - Yoon, D. K. (C) 6465–6468 [6627–6630]
 - Yoon, M.-H. (C) 6363–6366 [6523–6526]
 - Yoon, O. K. (C) 6541–6544 [6703–6707]
 - Yoshida, H.
 - Arynes in a Three-Component Coupling Reaction: Straightforward Synthesis of Benzoannulated Iminofurans
(C) 3935–3938 [4025–4028]
DOI: 10.1002/anie.200460009
 - Distannylation of Strained Carbon–Carbon Triple Bonds Catalyzed by a Palladium Complex
(C) 5052–5055 [5162–5165]
DOI: 10.1002/anie.200460189
 - Yoshida, J.-i. (C) 2145–2148 [2197–2200]
 - Yoshida, K. (C) 2389–2391 [2443–2445]
 - Yoshida, S. (C) 2389–2391 [2443–2445]
 - Yoshida, T. (C) 2955–2958 [3015–3018]
 - Yoshida, Y. (C) 5618–5621 [5736–5739]
 - Yoshida, Z.-i.
 - Synthesis and Light-Emitting Characteristics of Doughnut-Shaped π -Electron Systems
(C) 366–369 [370–373]
DOI: 10.1002/anie.200352749
 - Yoshikawa, I. (C) 100–103 [102–105]
 - Yoshikawa, K. (C) 2378–2381 [2432–2435]
 - Yoshimoto, S. (C) 3044–3047 [3106–3109]
 - Yoshimura, F. (C) 5249–5253 [5361–5365]
 - Yoshimura, T. (C) 228–232 [230–234]
 - Yoshizawa, M. (C) 5936–5940 [6062–6066]
 - You, W. (C) 4471–4475 [4571–4575]
 - You, X.-Z.
 - $[(\text{Tp})_8(\text{H}_2\text{O})_6\text{Cu}^{\text{II}}\text{Fe}^{\text{III}}_8(\text{CN})_{24}]^{4+}$: A Cyanide-Bridged Face-Centered-Cubic Cluster with Single-Molecule-Magnet Behavior
(C) 5940–5943 [6066–6069]
DOI: 10.1002/anie.200461515
 - Yousufuddin, M. (C) 3148–3152 [3210–3214], 6676–6680 [6844–6848]
 - Yu, B.
 - 23-Oxa-Analogues of OSW-1: Efficient Synthesis and Extremely Potent Antitumor Activity
(C) 4324–4327 [4424–4427]
DOI: 10.1002/anie.200454237
 - Yu, C.
 - Highly Ordered Mesoporous Bioactive Glasses with Superior In Vitro Bone-Forming Bioactivities
(C) 5980–5984 [6106–6110]
DOI: 10.1002/anie.200460598
 - Yu, D. (C) 5048–5052 [5158–5162]
 - Yu, H.-h. (C) 3700–3703 [3786–3789]
 - Yu, J.
 - Hydrogen-Bonded Helices in the Layered Aluminophosphate $(\text{C}_2\text{H}_8\text{N})_2[\text{Al}_2(\text{HPO}_4)(\text{PO}_4)_2]$
(C) 2399–2402 Corrigendum: 3096 [2453–2456 Corrigendum: 3158]
DOI: 10.1002/anie.200353118
 - Yu, J. (C) 6482–6485 [6644–6647]
 - Yu, L.
 - Synthesis of Diode Molecules and Their Sequential Assembly to Control Electron Transport
(C) 4471–4475 [4571–4575]
DOI: 10.1002/anie.200460110
 - Yu, S.-H.
 - Morphology Control of Stolzite Microcrystals with High Hierarchy in Solution
(C) 4745–4750 [4849–4854]
DOI: 10.1002/anie.200460090
 - Yu, W.-Y.
 - Ruthenium Nanoparticles Supported on Hydroxyapatite as an Efficient and Recyclable Catalyst for *cis*-Dihydroxylation and Oxidative Cleavage of Alkenes
(C) 3303–3307 [3365–3369]
DOI: 10.1002/anie.200453703
 - Yuan, Da-Q. (C) 5665–5668 [5783–5786]
 - Yuan, L.-H. (C) 4954–4957 [5062–5065]
 - Yuan, R.-X. (C) 4174–4745 [4845–4849]
 - Yuan, Z. (C) 4971–4200 [4293–4296]
 - Yufit, D. S. (C) 6553–6557 [6715–6719]
 - Yuki, M. (C) 1404–1407 [1428–1431]
 - Yus, M.
 - Chiral Tertiary Alcohols Made By Catalytic Enantioselective Addition of Unreactive Zinc Reagents to Poorly Electrophilic Ketones?
(H) 284–287 [286–289]
DOI: 10.1002/anie.200301696



- Zade, S. S. (C) 4513–4515 [4613–4615]
 Zähler, H. (C) 2574–2576 [2628–2630]
 Zak, M. (C) 5087–5092 [5197–5202], 5092–5097 [5202–5207]
 Zaleski, C. M. (C) 3912–3914 [4002–4004]
 Zanardi, G. (C) 3598–3601 [3682–3685]
 Zanardi, S.
 – Crystal Structure Determination of Zeolite Nu-6(2) and Its Layered Precursor Nu-6(1) (C) 4933–4937 [5041–5045]
 DOI: 10.1002/anie.200460085
 Zanghellini, E. (C) 700–704 [718–722]
 Zangrando, E. (C) 3584–3588 [3668–3672]
 Zani, G.
 – Elisabethin A: A Marine Diterpenoid Yet To Surrender to Total Synthesis (H) 4837–4841 [4942–4946]
 DOI: 10.1002/anie.200460570
 – Enantioselective Catalytic Allylation of Carbonyl Groups by Umpolung of π -Allyl Palladium Complexes (C) 846–849 [864–867]
 DOI: 10.1002/anie.200352743
 Zare, R. N.
 – Continuous Two-Channel Time-of-Flight Mass Spectrometric Detection of Electro-sprayed Ions (C) 6541–6544 [6703–6707]
 DOI: 10.1002/anie.200461240
 Zareie, M. H. (C) 1512–1516 [1538–1542]
 Zdanowska, M. (C) 74–78 [76–80]
 Zelinski, T. (R) 788–824 [806–843]
 Zemb, T. (C) 3163–3167 [3225–3229]
 Zemva, B.
 – The First Compound Containing a Metal Center in a Homoleptic Environment of XeF_2 Molecules (C) 3456–3458 [3538–3540]
 DOI: 10.1002/anie.200453802
 Zeng, H. C.
 – Creation of Intestine-like Interior Space for Metal-Oxide Nanostructures with a Quasi-Reverse Emulsion (C) 5206–5209 [5318–5321]
 DOI: 10.1002/anie.200460767
 – Self-Construction of Hollow SnO_2 Octahedra Based on Two-Dimensional Aggregation of Nanocrystallites (C) 5930–5933 [6056–6059]
 DOI: 10.1002/anie.200461129
 Zeng, X. (C) 2259–2263 [2309–2313]
 Zeng, X. B. (C) 4621–4625 [4721–4725]
 Zeni, R. J. (C) 5827–5830 [5951–5954]
 Zerbe, K. (C) 6709–6713 [6877–6881]
 Zerbe, O.
 – Surprisingly Stable Helical Conformations in α/β -Peptides by Incorporation of *cis*- β -Aminocyclopropane Carboxylic Acids (C) 511–514 [517–520]
 DOI: 10.1002/anie.200352267
 Zerbe, O. (C) 2109–2112 [2161–2164]
 Zettl, A.
 – Biomimetic Engineering of Carbon Nanotubes by Using Cell Surface Mucin Mimics (C) 6111–6116 [6237–6242]
 DOI: 10.1002/anie.200460620
 Zewail, A. H.
 – Dynamics of Ordered Water in Interfacial Enzyme Recognition: Bovine Pancreatic Phospholipase A_2 (C) 60–63 [62–65]
 DOI: 10.1002/anie.200352961
 – The Transition State of Thermal Organic Reactions: Direct Observation in Real Time (C) 2830–2834 [2890–2894]
 DOI: 10.1002/anie.200453962
 – Ultrafast Electron Crystallography of Surface Structural Dynamics with Atomic-Scale Resolution (C) 2705–2709 [2759–2763]
 DOI: 10.1002/anie.200453983
 Zhai, H.-J. (C) 2125–2129 [2177–2181]
 Zhai, J. (C) 1146–1149 [1166–1169], 4338–4341 [4438–4441]
 Zhai, Q. (C) 5635–5638 [5753–5756]
 Zhan, J. (C) 63–66 [65–68], 4606–4609 [4706–4709]
 Zhan, S. (C) 5029–5032 [5139–5142]
 Zhang, A. (C) 5185–5188 [5297–5300]
 Zhang, D.-W. (C) 6719–6722 [6887–6890]
 Zhang, De-Q.
 – A Unique 3D Alternating Ferro- and Antiferromagnetic Manganese Azide System with Threefold Interpenetrating (10,3) Nets (C) 990–994 [1008–1012]
 DOI: 10.1002/anie.200352780
 Zhang, F. (C) 4745–4750 [4849–4854]
 Zhang, F.-M. (C) 1702–1705 [1734–1737]
 Zhang, G.-Y. (C) 4212–4216 [4308–4312]
 Zhang, H.-M. (C) 1540–1543 [1566–1569]
 Zhang, H.-Y. (C) 2690–2694 [2744–2748]
 Zhang, Haiming (C) 6144–6148 [6270–6274]
 Zhang, Hong
 – Structural Analysis of 1-Aminocyclopropane-1-Carboxylate Deaminase: Observation of an Aminyl Intermediate and Identification of Tyr294 as the Active-Site Nucleophile (C) 3425–3429 [3507–3511]
 DOI: 10.1002/anie.200453353
 Zhang, Hua (R) 30–45 [30–46]
 Zhang, J. (C) 198–203 [200–205]
 Zhang, Jian-Ping
 – A Highly Luminescent Europium Complex Showing Visible-Light-Sensitized Red Emission: Direct Observation of the Singlet Pathway (C) 5010–5013 [5120–5123]
 DOI: 10.1002/anie.200454141
 Zhang, Jie-Peng (C) 206–209 [208–211]
 Zhang, Leyang (C) 6369–6372 [6529–6532]
 Zhang, Lihong (C) 1124–1126 [1144–1146]
 Zhang, Q.-F. (C) 1715–1718 [1747–1750]
 Zhang, Qianer (C) 1986–1990 [2020–2024]
 Zhang, Qiao (C) 4745–4750 [4849–4854]
 Zhang, W. (M) 5446–5453 [5562–5570]
 Zhang, X.-H. (C) 838–842 [856–860]
 Zhang, Xiaofeng (C) 3571–3574 [3655–3658]
 Zhang, Xiaomei (C) 5977–5980 [6103–6106]
 Zhang, Zhihua (C) 5685–5689 [5803–5807]
 Zhang, Zhiyu (C) 1126–1129 [1146–1149]
 Zhang, Zhongyi (C) 2012–2014 [2046–2048]
 Zhao, C. (C) 4170–4172 [4264–4267]
 Zhao, D.
 – Highly Ordered Mesoporous Bioactive Glasses with Superior In Vitro Bone-Forming Bioactivities (C) 5980–5984 [6106–6110]
 DOI: 10.1002/anie.200460598
 Zhao, G. (C) 1397–1399 [1421–1423]
 Zhao, J. (C) 3461–3464 [3543–3546]
 Zhao, L. (C) 60–63 [62–65]
 Zhao, P.-S. Corrigendum: 14
 Zhao, Q. (C) 3177–3182 [3239–3244]
 Zhao, Yong (C) 4338–4341 [4438–4441]
 Zhao, Yonghua (C) 5977–5980 [6103–6106]
 Zhao, Yue
 – Micrometer-Sized Hexagonal Tubes Self-Assembled by a Cyclic Peptide in a Liquid Crystal (C) 349–353 [353–357]
 DOI: 10.1002/anie.200352259
 Zhao, Yuxia (C) 5266–5268 [5378–5381]
 Zhao, Zhen (C) 4216–4219 [4312–4315]
 Zhao, Zongbao (C) 3425–3429 [3507–3511]
 Zheng, B. (C) 2508–2511 [2562–2565]
 Zheng, G.-L. (C) 2409–2411 [2463–2465]
 Zheng, H.
 – Self-Assembly of Interpenetrating Coordination Nets Formed from Interpenetrating Cationic and Anionic Three-Dimensional Diamondoid Cluster Coordination Polymers (C) 5776–5779 [5900–5903]
 DOI: 10.1002/anie.200460681
 Zheng, N. (C) 1502–1505 [1528–1531], 4753–4755 [4857–4859]
 Zheng, Q. (C) 1146–1149 [1166–1169]
 Zheng, Q.-Y. (C) 838–842 [856–860]
 Zheng, S.-L. (C) 206–209 [208–211]
 Zhong, W. (C) 5914–5918 [6040–6044]
 Zhou, H.-C.
 – The First All-Cyanide Fe_4S_4 Cluster: $[\text{Fe}_4\text{S}_4(\text{CN})_4]^{3-}$ (C) 5628–5631 [5746–5749]
 DOI: 10.1002/anie.200460879
 – $[(\text{Tp})_8(\text{H}_2\text{O})_6\text{Cu}^{\text{II}}\text{Fe}^{\text{III}}_8(\text{CN})_{24}]^{4+}$: A Cyanide-Bridged Face-Centered-Cubic Cluster with Single-Molecule-Magnet Behavior (C) 5940–5943 [6066–6069]
 DOI: 10.1002/anie.200461515
 Zhou, K. (C) 2017–2020 [2051–2054]
 Zhou, L. (C) 5635–5638 [5753–5756]
 Zhou, M. (R) 6596–6616 [6760–6782]
 Zhou, Q. (C) 3425–3429 [3507–3511]
 Zhou, X. (C) 5980–5984 [6106–6110]
 Zhou, Y.-F. (C) 5665–5668 [5783–5786]
 Zhou, Yong (M) 4988–4992 [5096–5100]
 Zhou, Yongfeng (C) 4896–4899 [5004–5007]
 Zhu, C. (C) 2230–2234 [2280–2284]
 Zhu, D. (C) 357–360 [361–364], 1146–1149 [1166–1169], 2012–2014 [2046–2048], 4663–4666 [4763–4766]
 Zhu, D.-B.
 – A Unique 3D Alternating Ferro- and Antiferromagnetic Manganese Azide System with Threefold Interpenetrating (10,3) Nets (C) 990–994 [1008–1012]
 DOI: 10.1002/anie.200352780
 Zhu, G. (C) 6482–6485 [6644–6647]
 Zhu, Haizhong (C) 5914–5918 [6040–6044]
 Zhu, Hongping (C) 3443–3445 [3525–3527]
 Zhu, J. (C) 1239–1243 [1259–1263]
 Zhu, L. (C) 4060–4063 [4152–4155]
 Zhu, N. (C) 4954–4957 [5062–5065]
 Zhu, N.-Y. (C) 6719–6722 [6887–6890]
 Zhu, Qingshi (C) 6479–6482 [6641–6644]
 Zhu, Qiyu (C) 2158–2161 [2210–2213]
 Zhu, Y.-J.
 – Microwave-Assisted Synthesis of Single-Crystalline Tellurium Nanorods and Nano-

- wires in Ionic Liquids
(C) 1410–1414 [1434–1438]
DOI: 10.1002/anie.200353101
- Zhu, Y. Q.
– Large-Scale Production of NbS₂ Nanowires and Their Performance in Electronic Field Emission
(C) 5670–5674 [5788–5792]
DOI: 10.1002/anie.200460447
- Zhu, Z. (C) 5040–5045 [5150–5155]
- Zhuang, Jianqin (C) 6377–6381 [6537–6541]
- Zhuang, Jing (C) 2017–2020 [2051–2054]
- Zhuang, W. (C) 4476–4478 [4576–4578]
- Ziatdinov, V. R. (C) 4626–4629 [4726–4729]
- Ziegler, T.
– A Versatile Direct Approach to *ortho*-Substituted Azobenzenes from Benzotriazoles
(C) 1400–1403 [1424–1427]
DOI: 10.1002/anie.200352782
- Ziemer, B. (C) 2846–2849 [2906–2910], 4597–4601 [4698–4702]
- Ziethe, F. (C) 245–247 [247–249]
- Ziller, J. W. (C) 1821–1825 Corrigendum: 2986 [1857–1861 Corrigendum: 3046], 5517–5519 [5633–5635]
- Zimmer, J. P. (C) 2154–2158 [2206–2210]
- Zimmermann, N. (C) 70–74 [72–76]
- Zin, W.-C. (C) 6465–6468 [6627–6630]
- Zinchenko, A. A.
– Stereoisomeric Discrimination in DNA Compaction
(C) 2378–2381 [2432–2435]
DOI: 10.1002/anie.200453774
- Zobi, F. (C) 5025–5029 [5135–5139]
- Zografos, A. L. (C) 2674–2677 [2728–2731]
- Zorn, C. (C) 511–514 [517–520]
- Zou, B.-S. (C) 5010–5013 [5120–5123]
- Zou, Y. (C) 5977–5980 [6103–6106]
- Zou, Z. (C) 4463–4466 [4563–4566]
- Zubarev, E. R.
– Supramolecular Assemblies of Starlike and V-Shaped PB–PEO Amphiphiles
(C) 5491–5496 [5607–5612]
DOI: 10.1002/anie.200460906
- Zubieta, J.
– Strong Ferromagnetic Interactions in [V₈O₁₄(H₂taci)₂]: An Unprecedented Large Spin Ground State for a Vanadyl Cluster
(C) 3436–3439 [3518–3521]
DOI: 10.1002/anie.200454130
- Zubkov, T. (C) 5961–5963 [6087–6089]
- Zuckerman, R. L. (C) 5372–5374 [5486–5488]
- Zuideveld, M. A. (C) 869–873 [887–891]
- Zuñilhof, H.
– Covalently Attached Monolayers on Hydrogen-Terminated Si(100): Extremely Mild Attachment by Visible Light
(C) 1352–1355 [1376–1379]
DOI: 10.1002/anie.200352137
- Zuleta, I. A. (C) 6541–6544 [6703–6707]
- Zumbuehl, A. (C) 5181–5185 Corrigendum: 5428 [5293–5297 Corrigendum: 5542]
- Zumstein, M. (C) 3286–3289 [3348–3351]
- Zuo, G. (C) 2277–2279 [2327–2329]
- Zuo, J.-L.
– [(Tp)₈(H₂O)₆Cu^{II}₆Fe^{III}₈(CN)₂₄]⁴⁺: A Cyanide-Bridged Face-Centered-Cubic Cluster with Single-Molecule-Magnet Behavior
(C) 5940–5943 [6066–6069]
DOI: 10.1002/anie.200461515
- Zweck, J. (C) 4228–4231 [4324–4327]
- Zweckstetter, M.
– Simultaneous Assignment and Structure Determination of Protein Backbones by Using NMR Dipolar Couplings
(C) 3479–3481 [3561–3563]
DOI: 10.1002/anie.200353588

Review Articles and Minireviews

- Schlögl, R. and **Abd Hamid, S. B.**, Nanocatalysis: Mature Science Revisited or Something Really New? 1628
- Agre, P.**, Aquaporin Water Channels (Nobel Lecture) 4278
- Choi, M.-S., Yamazaki, T., Yamazaki, I., and **Aida, T.**, Bioinspired Molecular Design of Light-Harvesting Multiporphyrin Arrays 150
- Ajamian, A., see **Gleason, J. L.** 3754
- Alder, R. W.**, **Blake, M. E.**, **Chaker, L.**, **Harvey, J. N.**, **Paolini, F.**, and **Schütz, J.**, When and How Do Diaminocarbenes Dimerize? 5896
- Antonietti, M.**, **Kuang, D.**, **Smarsly, B.**, and **Zhou, Yong**, Ionic Liquids for the Convenient Synthesis of Functional Nanoparticles and Other Inorganic Nanostructures 4988
- Armitage, B., see **Marder, S. R.** 4402
- Baerns, M.**, see **Hessel, V.** 406
- Ballauff, M.**, see **Likos, C. N.** 2998
- Bandini, M.**, see **Umani-Ronchi, A.** 550
- Beak, P.**, see **Snieckus, V.** 2206
- Beismann-Driemeyer, S.**, see **Tampé, R.** 4014
- Beller, M.**, **Seayad, J.**, **Tillack, A.**, and **Jiao, H.**, Catalytic Markovnikov and anti-Markovnikov Functionalization of Alkenes and Alkynes: Recent Developments and Trends 3368
- Best, M. D.**, see **Wong, C.-H.** 3526, 5736
- Bindu, S.**, see **Nair, V.** 5130
- Blake, M. E.**, see **Alder, R. W.** 5896
- Bornscheuer, U. T.**, see **Kazlauskas, R. J.** 6032
- Braga, D.** and **Grepioni, F.**, Reactions Between or Within Molecular Crystals 4002
- Köhn, M.** and **Breinbauer, R.**, The Staudinger Ligation—A Gift to Chemical Biology 3106
- Breuer, M.**, see **Hauer, B.** 788
- Brunel, J.-M.**, see **Holmes, I. P.** 2752
- Budisa, N.**, Prolegomena to Future Experimental Efforts on Genetic Code Engineering by Expanding Its Amino Acid Repertoire 6426
- Budzelaar, P. H. M.**, see **de Bruin, B.** 4142
- Burke, M. D.**, see **Schreiber, S. L.** 46
- Bushey, M. L.**, see **Nuckolls, C.** 5446
- Ma, J.-A.** and **Cahard, D.**, Towards Perfect Catalytic Asymmetric Synthesis: Dual Activation of the Electrophile and the Nucleophile 4566
- Chaker, L.**, see **Alder, R. W.** 5896
- Chapman, E.**, see **Wong, C.-H.** 3526
- Chen, L. X.**, Taking Snapshots of Photoexcited Molecules in Disordered Media by Using Pulsed Synchrotron X-rays 2886
- Chen, Peng**, see **Solomon, E. I.** 4132
- Choi, M.-S.**, see **Aida, T.** 150
- Coates, G. W.** and **Moore, D. R.**, Discrete Metal-Based Catalysts for the Copolymerization of CO₂ and Epoxides: Discovery, Reactivity, Optimization, and Mechanism 6618
- Peyratout, C. S.** and **Dähne, L.**, Tailor-Made Polyelectrolyte Microcapsules: From Multilayers to Smart Containers 3762
- Dalko, P. I.** and **Moisan, L.**, In the Golden Age of Organocatalysis 5138
- Davis, J. T.**, G-Quartets 40 Years Later: From 5'-GMP to Molecular Biology and Supramolecular Chemistry 668
- de Bruin, B.**, **Budzelaar, P. H. M.**, and **Gal, A. W.**, Functional Models for Rhodium-Mediated Olefin-Oxygenation Catalysis 4142
- de la Torre, M. C.**, see **Sierra, M. A.** 160
- Ditrich, K.**, see **Hauer, B.** 788
- Espinet, P.** and **Echavarren, A. M.**, The Mechanisms of the Stille Reaction 4704
- Espinet, P.**, see **Echavarren, A. M.** 4704
- Fässler, T. F.** and **Hoffmann, S. D.**, Endohedral Zintl Ions: Intermetalloid Clusters 6242
- Gal, A. W.**, see **de Bruin, B.** 4142
- Gambarotta, S.** and **Scott, J.**, Multimetallic Cooperative Activation of N₂ 5298
- Ghosh, A.**, A Perspective of One-Pot Pyrrole–Aldehyde Condensations as Versatile Self-Assembly Processes 1918
- Ghosh, Somdatta**, see **Solomon, E. I.** 4132
- Ginger, D. S.**, see **Mirkin, C. A.** 30
- Ajamian, A.** and **Gleason, J. L.**, Two Birds with One Metallic Stone: Single-Pot Catalysis of Fundamentally Different Transformations 3754
- Gonda, J.**, The Belluš–Claisen Rearrangement 3516
- Gorelsky, S. I.**, see **Solomon, E. I.** 4132
- Gösele, U.**, see **Wendorff, J. H.** 1334
- Graening, T.**, see **Schmalz, H.-G.** 3230
- Grepioni, F.**, see **Braga, D.** 4002
- Habicher, T.**, see **Hauer, B.** 788
- Hanson, S. R.**, see **Wong, C.-H.** 3526, 5736
- Hartung, I. V.**, see **Hoffmann, H. M. R.** 1934
- Harvey, J. N.**, see **Alder, R. W.** 5896
- Breuer, M.**, **Ditrich, K.**, **Habicher, T.**, **Hauer, B.**, **Keßler, M.**, **Stürmer, R.**, and **Zelinski, T.**, Industrial Methods for the Production of Optically Active Intermediates 788
- Jähnisch, K.**, **Hessel, V.**, **Löwe, H.**, and **Baerns, M.**, Chemistry in Microstructured Reactors 406
- Hartung, I. V.** and **Hoffmann, H. M. R.**, 8-Oxabicyclo[3.2.1]oct-6-en-3-ones: Application to the Asymmetric Synthesis of Polyoxygenated Building Blocks 1934
- Hoffmann, S. D.**, see **Fässler, T. F.** 6242
- Hoffmann-Röder, A.**, see **Krause, N.** 1196
- Brunel, J.-M.** and **Holmes, I. P.**, Chemically Catalyzed Asymmetric Cyanohydrin Syntheses 2752
- Homans, S. W.**, NMR Spectroscopy Tools for Structure-Aided Drug Design 290

<i>Horoszewski, D.</i> , see <i>Nuckolls, C.</i>	5446	<i>Nair, V.</i> , <i>Bindu, S.</i> , and <i>Sreekumar, V.</i> , N-Heterocyclic Carbenes: Reagents, Not Just Ligands!	5130
Hunter, C. A. , Quantifying Intermolecular Interactions: Guidelines for the Molecular Recognition Toolbox	5310	<i>Strømgaard, K.</i> and <i>Nakanishi, K.</i> , Chemistry and Biology of Terpene Trilactones from <i>Ginkgo Biloba</i>	1640
<i>Jähnisch, K.</i> , see <i>Hessel, V.</i>	406	<i>Natarajan, S.</i> , see <i>Rao, C. N. R.</i>	1466
<i>Jiao, H.</i> , see <i>Beller, M.</i>	3368	<i>Nguyen, T.-Q.</i> , see <i>Nuckolls, C.</i>	5446
<i>Kakiuchi, K.</i> , see <i>Morimoto, T.</i>	5580	<i>Noro, S.-i.</i> , see <i>Kitagawa, S.</i>	2334
Kappe, C. O. , Controlled Microwave Heating in Modern Organic Synthesis	6250	<i>Bushey, M. L.</i> , <i>Nguyen, T.-Q.</i> , <i>Zhang, W.</i> , <i>Horoszewski, D.</i> , and <i>Nuckolls, C.</i> , Using Hydrogen Bonds to Direct the Assembly of Crowded Aromatics	5446
<i>Katz, E.</i> , see <i>Willner, I.</i>	6042	<i>O'Brien, D. P.</i> , see <i>Williams, D. H.</i>	6596
<i>Bornscheuer, U. T.</i> and Kazlauskas, R. J. , Catalytic Promiscuity in Biocatalysis: Using Old Enzymes to Form New Bonds and Follow New Pathways	6032	<i>Paolini, F.</i> , see <i>Alder, R. W.</i>	5896
<i>Keßler, M.</i> , see <i>Hauer, B.</i>	788	Peng, Z. , Rational Synthesis of Covalently Bonded Organic–Inorganic Hybrids	930
Kitagawa, S. , <i>Kitaura, R.</i> , and <i>Noro, S.-i.</i> , Functional Porous Coordination Polymers	2334	<i>Petitou, M.</i> , see <i>van Boeckel, C. A. A.</i>	3118
<i>Kitaura, R.</i> , see <i>Kitagawa, S.</i>	2334	<i>Peyratout, C. S.</i> , see <i>Dähne, L.</i>	3762
<i>Köhn, M.</i> , see <i>Breinbauer, R.</i>	3106	Pyykkö, P. , Theoretical Chemistry of Gold	4412
<i>Hoffmann-Röder, A.</i> and Krause, N. , Synthesis and Properties of Allenic Natural Products and Pharmaceuticals	1196	<i>Raabe, I.</i> , see <i>Krossing, I.</i>	2066
Krossing, I. and <i>Raabe, I.</i> , Noncoordinating Anions—Fact or Fiction? A Survey of Likely Candidates ...	2066	Rao, C. N. R. , <i>Natarajan, S.</i> , and <i>Vaidhyanathan, R.</i> , Metal Carboxylates with Open Architectures	1466
<i>Kuang, D.</i> , see <i>Antonietti, M.</i>	4988	<i>Rojo, J.</i> , see <i>Lehn, J.-M.</i>	3644
<i>Ruben, M.</i> , <i>Rojo, J.</i> , <i>Romero-Salguero, F. J.</i> , <i>Uppadine, L. H.</i> , and Lehn, J.-M. , Grid-Type Metal Ion Architectures: Functional Metallosupramolecular Arrays	3644	<i>Romero-Salguero, F. J.</i> , see <i>Lehn, J.-M.</i>	3644
<i>Li, Xiaoyu</i> , see <i>Liu, D. R.</i>	4848	Rosenthal, U. , Stable Cyclopentynes—Made by Metals!?	3882
<i>Ballauff, M.</i> and Likos, C. N. , Dendrimers in Solution: Insight from Theory and Simulation	2998	<i>Ruben, M.</i> , see <i>Lehn, J.-M.</i>	3644
<i>Li, Xiaoyu</i> and Liu, D. R. , DNA-Templated Organic Synthesis: Nature's Strategy for Controlling Chemical Reactivity Applied to Synthetic Molecules	4848	Rudkevich, D. M. , Emerging Supramolecular Chemistry of Gases	558
<i>Löwe, H.</i> , see <i>Hessel, V.</i>	406	<i>Scherer, W.</i> , see <i>McGrady, G. S.</i>	1782
<i>Ma, J.-A.</i> , see <i>Cahard, D.</i>	4566	<i>Schlögl, R.</i> , see <i>Abd Hamid, S. B.</i>	1628
<i>Scherer, W.</i> and McGrady, G. S. , Agostic Interactions in d ⁰ Metal Alkyl Complexes	1782	<i>Graening, T.</i> and Schmalz, H.-G. , Total Syntheses of Colchicine in Comparison: A Journey through 50 Years of Synthetic Organic Chemistry	3230
MacKinnon, R. , Potassium Channels and the Atomic Basis of Selective Ion Conduction (Nobel Lecture)	4265	<i>Burke, M. D.</i> and Schreiber, S. L. , A Planning Strategy for Diversity-Oriented Synthesis	46
<i>MacNeil, S.</i> , see <i>Snieckus, V.</i>	2206	<i>Wouters, D.</i> and Schubert, U. S. , Nanolithography and Nanochemistry: Probe-Related Patterning Techniques and Chemical Modification for Nanometer-Sized Devices	2480
Mansfield, P. , Snapshot Magnetic Resonance Imaging (Nobel Lecture)	5456	<i>Schütz, J.</i> , see <i>Alder, R. W.</i>	5896
<i>Yang, Da</i> , <i>Armitage, B.</i> , and Marder, S. R. , Cubic Liquid-Crystalline Nanoparticles	4402	<i>Scott, J.</i> , see <i>Gambarotta, S.</i>	5298
Mecking, S. , Nature or Petrochemistry?—Biologically Degradable Materials	1078	Scott, L. T. , Methods for the Chemical Synthesis of Fullerenes	4994
<i>Melloni, A.</i> , see <i>Umani-Ronchi, A.</i>	550	<i>Seayad, J.</i> , see <i>Beller, M.</i>	3368
<i>Ginger, D. S.</i> , <i>Zhang, Hua</i> , and Mirkin, C. A. , The Evolution of Dip-Pen Nanolithography	30	<i>de la Torre, M. C.</i> and Sierra, M. A. , Comments on Recent Achievements in Biomimetic Organic Synthesis	160
<i>Moisan, L.</i> , see <i>Dalko, P. I.</i>	5138	<i>Smarsly, B.</i> , see <i>Antonietti, M.</i>	4988
Montgomery, J. , Nickel-Catalyzed Reductive Cyclizations and Couplings	3890	<i>Whisler, M. C.</i> , <i>MacNeil, S.</i> , <i>Snieckus, V.</i> , and <i>Beak, P.</i> , Beyond Thermodynamic Acidity: A Perspective on the Complex-Induced Proximity Effect (CIPE) in Deprotonation Reactions	2206
<i>Moore, D. R.</i> , see <i>Coates, G. W.</i>	6618	<i>Chen, Peng</i> , <i>Gorelsky, S. I.</i> , <i>Ghosh, Somdatta</i> , and Solomon, E. I. , N ₂ O Reduction by the μ_4 -Sulfide-Bridged Tetranuclear Cu ₂ Cluster Active Site	4132
Morimoto, T. and <i>Kakiuchi, K.</i> , Evolution of Carbonylation Catalysis: No Need for Carbon Monoxide	5580	<i>Sreekumar, V.</i> , see <i>Nair, V.</i>	5130
Mukaiyama, T. , Explorations into New Reaction Chemistry	5590	Stahl, S. S. , Palladium Oxidase Catalysis: Selective Oxidation of Organic Chemicals by Direct Dioxxygen-Coupled Turnover	3400

<i>Steinhart, M.</i> , see <i>Wendorff, J. H.</i>	1334	<i>Whisler, M. C.</i> , see <i>Snieckus, V.</i>	2206
<i>Stephens, E.</i> , see <i>Williams, D. H.</i>	6596	Williams, D. H. , <i>Stephens, E.</i> , <i>O'Brien, D. P.</i> , and <i>Zhou, M.</i> , Understanding Noncovalent Interactions: Ligand Binding Energy and Catalytic Efficiency from Ligand-Induced Reductions in Motion within Receptors and Enzymes	6596
<i>Strømgaard, K.</i> , see <i>Nakanishi, K.</i>	1640	<i>Katz, E.</i> and Willner, I. , Integrated Nanoparticle–Biomolecule Hybrid Systems: Synthesis, Properties, and Applications	6042
<i>Stürmer, R.</i> , see <i>Hauer, B.</i>	788	<i>Chapman, E.</i> , <i>Best, M. D.</i> , <i>Hanson, S. R.</i> , and Wong, C.-H. , Sulfotransferases: Structure, Mechanism, Biological Activity, Inhibition, and Synthetic Utility	3526
<i>Beismann-Driemeyer, S.</i> and Tampé, R. , Function of the Antigen Transport Complex TAP in Cellular Immunity	4014	<i>Hanson, S. R.</i> , <i>Best, M. D.</i> , and Wong, C.-H. , Sulfatases: Structure, Mechanism, Biological Activity, Inhibition, and Synthetic Utility	5736
<i>Tillack, A.</i> , see <i>Beller, M.</i>	3368	<i>Wouters, D.</i> , see <i>Schubert, U. S.</i>	2480
Toennies, J. P. and <i>Vilesov, A. F.</i> , Superfluid Helium Droplets: A Uniquely Cold Nanomatrix for Molecules and Molecular Complexes	2622	<i>Yamazaki, I.</i> , see <i>Aida, T.</i>	150
<i>Bandini, M.</i> , <i>Melloni, A.</i> , and Umani-Ronchi, A. , New Catalytic Approaches in the Stereoselective Friedel–Crafts Alkylation Reaction	550	<i>Yamazaki, T.</i> , see <i>Aida, T.</i>	150
<i>Uppadine, L. H.</i> , see <i>Lehn, J.-M.</i>	3644	<i>Yang, Da</i> , see <i>Marder, S. R.</i>	4402
<i>Vaidhyanathan, R.</i> , see <i>Rao, C. N. R.</i>	1466	<i>Zelinski, T.</i> , see <i>Hauer, B.</i>	788
<i>Petitou, M.</i> and van Boeckel, C. A. A. , A Synthetic Antithrombin III Binding Pentasaccharide Is Now a Drug! What Comes Next?	3118	<i>Zhang, Hua</i> , see <i>Mirkin, C. A.</i>	30
<i>Vilesov, A. F.</i> , see <i>Toennies, J. P.</i>	2622	<i>Zhang, W.</i> , see <i>Nuckolls, C.</i>	5446
<i>Wehrspohn, R. B.</i> , see <i>Wendorff, J. H.</i>	1334	<i>Zhou, M.</i> , see <i>Williams, D. H.</i>	6596
<i>Steinhart, M.</i> , <i>Wehrspohn, R. B.</i> , <i>Gösele, U.</i> , and Wendorff, J. H. , Nanotubes by Template Wetting: A Modular Assembly System	1334	<i>Zhou, Yong</i> , see <i>Antonietti, M.</i>	4988
Werner, H. , The Way into the Bridge: A New Bonding Mode of Tertiary Phosphanes, Arsanes, and Stibanes	938		

Essays

<i>Ball, P.</i> , see <i>Ruben, M.</i>	4842	Ringsdorf, H. , Hermann Staudinger and the Future of Polymer Research Jubilees—Beloved Occasions for Cultural Piety	1064
Cintas, P. , The Road to Chemical Names and Eponyms: Discovery, Priority, and Credit	5888	<i>Ball, P.</i> and Ruben, M. , Color Theory in Science and Art: Ostwald and the Bauhaus	4842
Djerassi, C. , Chemical Safety in a Vulnerable World—A Manifesto	2330	Stern, F. , Paul Ehrlich: The Founder of Chemotherapy	4254
Hawkins, J. M. and <i>Watson, T. J. N.</i> , Asymmetric Catalysis in the Pharmaceutical Industry	3224	Thomas, J. M. , Argon and the Non-Inert Pair: Rayleigh and Ramsay	6418
Hoveyda, A. H. , Primo Levi's <i>The Periodic Table</i> . A Search for Patterns in Times Past	6592	<i>Watson, T. J. N.</i> , see <i>Hawkins, J. M.</i>	3224
Krätz, O. , The Chemical Laboratory: Source of Progress or Chamber of Horrors?	1770	<i>Labinger, J. A.</i> and Weininger, S. J. , Controversy in Chemistry: What Counts as Evidence?—Two Studies in Molecular Structure	2612
<i>Labinger, J. A.</i> , see <i>Weininger, S. J.</i>	2612	Whitesides, G. M. , Assumptions: Taking Chemistry in New Directions	3632
Mülhaupt, R. , Hermann Staudinger and the Origin of Macromolecular Chemistry	1054		

Highlights

<i>Afonso, C. A. M.</i> , see <i>Crespo, J. G.</i>	5293	<i>Groth, T.</i> and <i>Lendlein, A.</i> , Layer-by-Layer Deposition of Polyelectrolytes—A Versatile Tool for the In Vivo Repair of Blood Vessels	926
Armstrong, Alan , Amine-Catalyzed Epoxidation of Alkenes: A New Mechanism for the Activation of Oxone	1460	Haag, R. , Supramolecular Drug-Delivery Systems Based on Polymeric Core–Shell Architectures	278
<i>Arseniyadis, S.</i> , see <i>Spivey, A. C.</i>	5436	<i>Hahn, U.</i> , see <i>Hinrichs, W.</i>	1190
Balme, G. , Pyrrole Syntheses by Multicomponent Coupling Reactions	6238	Harriman, A. , Unusually Slow Charge Recombination in Molecular Dyads	4985
Berger, R. , Do Heavy Nuclei See Light at the End of the Tunnel?	398	Hartmann, M. , Hierarchical Zeolites: A Proven Strategy to Combine Shape Selectivity with Efficient Mass Transport	5880
<i>Biel, M.</i> , see <i>Giannis, A.</i>	6414	Hill, C. L. , Stable, Self-Assembling, Equilibrating Catalysts for Green Chemistry	402
<i>Dubrovina, N. V.</i> and Börner, A. , Enantioselective Catalysis with Chiral Phosphine Oxide Preligands .	5883	<i>Hahn, U.</i> , <i>Palm, G. J.</i> , and <i>Hinrichs, W.</i> , Old Codons, New Amino Acids	1190
Brakmann, S. , DNA-Based Barcodes, Nanoparticles, and Nanostructures for the Ultrasensitive Detection and Quantification of Proteins	5730	<i>Vostrowsky, O.</i> and Hirsch, A. , Molecular Peapods as Supramolecular Carbon Allotropes	2326
Breuker, K. , New Mass Spectrometric Methods for the Quantification of Protein–Ligand Binding in Solution	22	Jacobsen, H. , “Heterogeneous” Chemistry: Catalysts for Hydrogen Production from Biomass	1912
Brunner, H. , A New Hydrosilylation Mechanism—New Preparative Opportunities	2749	Johnson, J. S. , Catalyzed Reactions of Acyl Anion Equivalents	1326
<i>Cabrol-Bass, D.</i> , see <i>Meierhenrich, U. J.</i>	6410	Joselevich, E. , Chemistry and Electronics of Carbon Nanotubes Go Together	2992
Carlier, P. R. , Threading the Needle: Mimicking Natural Toroidal Catalysts	2602	Karst, U. , Electrochemistry/Mass Spectrometry (EC/MS)—A New Tool To Study Drug Metabolism and Reaction Mechanisms	2476
Caruso, R. A. , Micrometer-to-Nanometer Replication of Hierarchical Structures by Using a Surface Sol–Gel Process	2746	Kaupp, M. , Trigonal Prismatic or not Trigonal Prismatic? On the Mechanisms of Oxygen-Atom Transfer in Molybdopterin-Based Enzymes	546
Chen, Z. , The Smaller Fullerene C ₅₀ , Isolated as C ₅₀ Cl ₁₀	4690	<i>Kawase, T.</i> , see <i>Oda, M.</i>	4396
<i>Afonso, C. A. M.</i> and <i>Crespo, J. G.</i> , Recent Advances in Chiral Resolution through Membrane-Based Approaches	5293	Kempe, R. , A New Arene Synthesis—Or: How Inert Is the Cyclopentadienyl Ligand?	1463
Dai, L.-X. , Chiral Metal–Organic Assemblies—A New Approach to Immobilizing Homogeneous Asymmetric Catalysts	5726	Kickelbick, G. , Hybrid Inorganic–Organic Mesoporous Materials	3102
<i>Dubrovina, N. V.</i> , see <i>Börner, A.</i>	5883	Kirmse, W. , Stable Singlet Carbenes—Plentiful and Versatile	1767
Dupont, J. and <i>Spencer, J.</i> , On the Noninnocent Nature of 1,3-Dialkylimidazolium Ionic Liquids	5296	<i>Knapp, C.</i> , see <i>Passmore, J.</i>	4834
<i>Dyson, P. J.</i> , see <i>McIndoe, J. S.</i>	6028	Koert, U. , Syntheses of Tetrodotoxin	5572
<i>Etzkorn, M.</i> , see <i>Prakash, G. K. S.</i>	26	<i>Mandl, C. P.</i> and König, B. , Chemistry in Motion—Unidirectional Rotating Molecular Motors	1622
Fairlamb, I. J. S. , Asymmetric Cycloisomerization of 1,6- and 1,7-Enynes by Transition-Metal Catalysts .	1048	<i>Kozak, C. M.</i> , see <i>Mountford, P.</i>	1186
<i>Fernandez, X.</i> , see <i>Meierhenrich, U. J.</i>	6410	Latos-Grażyński, L. , Bimetallic Figure-Eight Octaphyrins Split into Four-Pyrrolic Macrocycles	5124
<i>Franzini, M.</i> , see <i>Zanoni, G.</i>	4837	<i>Lendlein, A.</i> , see <i>Groth, T.</i>	926
<i>Gey, C.</i> , see <i>Giannis, A.</i>	3998	<i>Dyson, P. J.</i> and McIndoe, J. S. , An Octahedral Rhodium Cluster with Six Phosphine and 12 Hydride Ligands and 10 Too Few Electrons	6028
<i>Biel, M.</i> , <i>Wascholowski, V.</i> , and Giannis, A. , A Fatal Affair: The Ubiquitinylation of Proteins	6414	<i>Mandl, C. P.</i> , see <i>König, B.</i>	1622
<i>Gey, C.</i> and Giannis, A. , Small Molecules, Big Plans—Can Low-Molecular-Weight Compounds Control Human Regeneration?	3998	Marco-Contelles, J. , β -Lactam Synthesis by the Kinugasa Reaction	2198
Glorius, F. , Chiral Olefin Ligands—New “Spectators” in Asymmetric Catalysis	3364	Marx, A. and <i>Summerer, D.</i> , Bigger DNA: New Double Helix with Expanded Size	1625
<i>Golebiowski, J.</i> , see <i>Meierhenrich, U. J.</i>	6410	<i>Mayor, M.</i> , see <i>Weber, H. B.</i>	2882
<i>Wassel, R. A.</i> and Gorman, C. B. , Establishing the Molecular Basis for Molecular Electronics	5120	Meierhenrich, U. J. , <i>Golebiowski, J.</i> , <i>Fernandez, X.</i> , and <i>Cabrol-Bass, D.</i> , The Molecular Basis of Olfactory Chemoreception	6410
Green, M. , Semiconductor Quantum Dots as Biological Imaging Agents	4129		

Merino, P. and Tejero, T. , Organocatalyzed Asymmetric α -Aminooxylation of Aldehydes and Ketones—An Efficient Access to Enantiomerically Pure α -Hydroxycarbonyl Compounds, Diols, and Even Amino Alcohols	2995
Micura, R. , Genetic Control by a Natural Metabolite-Responsive Ribozyme	4692
Mielgo, A. , see Palomo, C.	5442
Miura, M. , Rational Ligand Design in Constructing Efficient Catalyst Systems for Suzuki–Miyaura Coupling	2201
Kozak, C. M. and Mountford, P. , Revelations in Dinitrogen Activation and Functionalization by Metal Complexes	1186
North, M. , Oxidative Synthesis of α -Amino Nitriles from Tertiary Amines	4126
Kawase, T. and Oda, M. , Möbius Aromatic Hydrocarbons: Challenges for Theory and Synthesis	4396
Oiarbide, M. , see Palomo, C.	5442
Palm, G. J. , see Hinrichs, W.	1190
Palomo, C. , Oiarbide, M. , and Mielgo, A. , Unveiling Reliable Catalysts for the Asymmetric Nitroaldol (Henry) Reaction	5442
Knapp, C. and Passmore, J. , On the Way to “Solid Nitrogen” at Normal Temperature and Pressure? Binary Azides of Heavier Group 15 and 16 Elements	4834
Patarin, J. , Mild Methods for Removing Organic Templates from Inorganic Host Materials	3878
Pihko, P. M. , Activation of Carbonyl Compounds by Double Hydrogen Bonding: An Emerging Tool in Asymmetric Catalysis	2062
Prakash, G. K. S. and Etzkorn, M. , Direct Oxidation of Azides to Nitro Compounds	26
Rademann, J. , Organic Protein Chemistry: Drug Discovery through the Chemical Modification of Proteins	4554
Ramón, D. J. , see Yus, M.	284
Reymond, J.-L. , Outrunning the Bear	5577
Rogach, A. L. , Binary Superlattices of Nanoparticles: Self-Assembly Leads to “Metamaterials”	148
Simon, B. and Sattler, M. , Speeding Up Biomolecular NMR Spectroscopy	782
Schalley, C. A. , Borromean Rings: A One-Pot Synthesis	4399
Schmitz, K. and Schepers, U. , Polyamides as Artificial Transcription Factors: Novel Tools for Molecular Medicine?	2472
Schmitz, K. , see Schepers, U.	2472
Schneppf, A. , Novel Compounds of Elements of Group 14: Ligand-Stabilized Clusters with “Naked” Atoms	664
Schröder, D. , Coulomb Explosions and Stability of Multiply Charged Ions in the Gas Phase	1329
Sies, H. , Ozone in Arteriosclerotic Plaques: Searching for the “Smoking Gun”	3514
Simon, B. , see Sattler, M.	782
Spencer, J. , see Dupont, J.	5296
Spino, C. , Recent Developments in the Catalytic Asymmetric Cyanation of Ketimines	1764
Spivey, A. C. and Arseniyadis, S. , Nucleophilic Catalysis by 4-(Dialkylamino)pyridines Revisited—The Search for Optimal Reactivity and Selectivity	5436
Stöwe, K. , YbGaGe: Zero Thermal Expansion as a Result of an Electronic Valence Transition?	4982
Summerer, D. , see Marx, A.	1625
Tejero, T. , see Merino, P.	2995
Thomas, J. M. , Ultrafast Electron Crystallography: The Dawn of a New Era	2606
Tramontano, A. , A Brighter Future for Protein Design	3222
Vostrowsky, O. , see Hirsch, A.	2326
Wascholowski, V. , see Giannis, A.	6414
Wassel, R. A. , see Gorman, C. B.	5120
Mayor, M. and Weber, H. B. , Statistical Analysis of Single-Molecule Junctions	2882
Ramón, D. J. and Yus, M. , Chiral Tertiary Alcohols Made By Catalytic Enantioselective Addition of Unreactive Zinc Reagents to Poorly Electrophilic Ketones?	284
Zanoni, G. and Franzini, M. , Elisabethin A: A Marine Diterpenoid Yet To Surrender to Total Synthesis ..	4837

Book and Website Reviews

For book reviews authors/editors, book titles, and reviewers are given, for website reviews subjects and reviewers.

Books

Biography

Enz, C. P.	No Time to be Brief	Kutzelnigg, W.	1457
------------	---------------------	----------------	------

Encyclopedia/Handbook/Reference Book

Wong, C.-H.	Carbohydrate-Based Drug Discovery	Plettenburg, O., Stilz, U.	3995
Cornils, B., A.Herrmann, W., Schlögl, R., Wong, C.-H.	Catalysis from A to Z	Stürmer, R.	1324
Hessel, V., Hardt, S., Löwe, H.	Chemical Micro-Process Engineering	de Bellefon, C.	6583
Paquette, L. A.	Chiral Reagents for Asymmetric Synthesis	Glorius, F.	1619
McCleverty, J. A., Meyer, T. J.	Comprehensive Coordination Chemistry II	Heinze, K.	3875
Meyers, R. A.	Encyclopedia of Molecular Cell Biology and Molecular Medicine	Kubinyi, H.	4689
Gasteiger, J.	Handbook of Chemoinformatics	Schneider, G.	1761
Rase, H. F.	Handbook of Commercial Catalysts	Cornils, B.	2324
Cornelis, R., Caruso, J., Crews, H., Heumann, K.	Handbook of Elemental Speciation	Karst, U.	5569
Denisov, E. T., Denisova, T. G., Pokidova, T. S.	Handbook of Free Radical Initiators	Fischer, H.	275
Messerschmidt, A., Bode, W., Cygler, M.	Handbook of Metalloproteins	Tuczek, F.	5290
Grubbs, R. H.	Handbook of Metathesis	Dörwald, F. Z.	395
Conn, P. M.	Handbook of Proteomic Methods	Wang, E. W., Bogyo, M. S.	6235
L'Annunziata, M. F.	Handbook of Radioactivity Analysis	Diehl, J. F.	1619
Gauglitz, G., Vo-Dinh, T.	Handbook of Spectroscopy	Popp, J.	2325
Schmid, R. D.	Pocket Guide to Biotechnology and Genetic Engineering	Bornscheuer, U.	1325
Kadish, K. M., Smith, K. M., Guillard, R.	The Porphyrin Handbook	Montforts, F.-P.	5431

Industrial Chemistry

Adams, D. J., Dyson, P. J., Tavener, S. J.	Chemistry in Alternative Reaction Media	Cornils, B.	2195
Mizrahi, J.	Developing an Industrial Chemical Process	Cornils, B.	3099
Aehle, W.	Enzymes in Industry	Cooper, B.	3629
Rogers, R. D., Seddon, K. R., Volkov, S.	Green Industrial Applications of Ionic Liquids	Cornils, B.	274
Hillisch, A., Hilgenfeld, R.	Modern Methods of Drug Discovery	Heinrich, N.	779
Green, M. M., Wittcoff, H. A.	Organic Chemistry Principles and Industrial Practice	Siegel, J. S.	6407

Monograph/Research Report in Analytical Chemistry

Yan, B.	Analysis and Purification Methods in Combinatorial Chemistry	Jung, G.	4552
Gübitz, G., Schmid, M. G.	Chiral Separations—Methods and Protocols	Meierhenrich, U. J.	4252
Rathore, A. S., Guttman, A.	Electrokinetic Phenomena	Schmitz, O. J.	2990
Wu, C.-S.	Handbook of Size Exclusion Chromatography and Related Techniques	Trathnigg, B.	5117
Mitchell, T. N., Costisella, B.	NMR—From Spectra to Structures	Schlörer, N.	5290

Monograph/Research Report in Biochemistry/Bioorganic Chemistry

Walsh, C.	Antibiotics	Brötz-Oesterheld, H.	2879
Atta-ur-Rahman	Bioactive Natural Products	von Nussbaum, F.	3218
van de Waterbeemd, H., Lennernäs, H., Artursson, P.	Drug Bioavailability	Grüneberg, S., Güssregen, S.	146
Testa, B., Mayer, J. M.	Hydrolysis in Drug and Prodrug Metabolism	Wehner, V.	544
Butler, A., Nicholson, R.	Life, Death, and Nitric Oxide	Mayer, B.	5724
Keinan, E., Schechter, I., Sela, M.	Life Sciences for the 21st Century	Schepers, U.	5878
Schena, M.	Microarray Analysis	Wollenberger, U.	2059
Dingermann, T., Steinhilber, D., Folkers, G.	Molecular Biology in Medicinal Chemistry	Breinbauer, R.	3510
Schliwa, M.	Molecular Motors	Baumann, C. G.	5432
Babine, R. E., Abdel-Meguid, S. S.	Protein Crystallography in Drug Discovery	Essen, L.-O.	6408
Böhm, H.-J., Schneider, G.	Protein–Ligand Interactions	Hessler, G.	146
Nielsen, P. E.	Pseudo-Peptides in Drug Discovery	Kawai, K.	5569

Monograph/Research Report in Environmental Chemistry

Scheringer, M.	Persistence and Spatial Range of Environmental Chemicals	Schüürmann, G.	1323
----------------	--	----------------	------

Monograph/Research Report in Inorganic Chemistry

Blaser, H.-U., Schmidt, E.	Asymmetric Catalysis on Industrial Scale	Stürmer, R.	2600
Steudel, R.	Elemental Sulfur and Sulfur-Rich Compounds, Vols. I and II	Breher, F.	3629
Zanello, P.	Inorganic Electrochemistry	Astruc, D.	3752
Driess, M., Nöth, H.	Molecular Clusters of the Main Group Elements	Ruck, M.	4688
Auner, N., Weis, J.	Organosilicon Chemistry V	Linti, G.	2744
Jutzi, P., Schubert, U.	Silicon Chemistry	Linti, G.	2990

Monograph/Research Report in Materials Science

Gupta, C. K.	Chemical Metallurgy Principles and Practice	Sauthoff, G.	659
Caruso, F.	Colloids and Colloid Assemblies	Schubert, H.	5434
Cawse, J. N.	Experimental Design for Combinatorial and High Throughput Materials Development	Schubert, U. S.	4123
Zana, R., Xia, J.	Gemini Surfactants	Huc, I.	4831
Laeri, F., Schüth, F., Simon, U., Wark, M.	Host–Guest Systems Based on Nanoporous Crystals	Sing, K. S. W.	4251
Poole, C. P., Jr., Owens, F. J.	Introduction to Nanotechnology	Steinhart, M.	2196
Geschke, O., Klank, H., Tellemann, P.	Microsystem Engineering for Lab-on-a-Chip Devices	Moorthy, J., Eddington, D. T., Beebe, D. J.	4393
Ajayan, P. M., Schädler, L. S., Braun, P. V.	Nanocomposites Science and Technology	Görtz, H.-H., Breiner, T.	1909
Köhler, M., Fritzsche, W.	Nanotechnology	Bockstaller, M. R.	5723
Dürr, H., Bouas-Laurent, H.	Photochromism	Uchida, K.	3362
Buchmeiser, M. R.	Polymeric Materials in Organic Synthesis and Catalysis	Fan, Q.-H.	6236

Monograph/Research Report in Organic Chemistry

Reich, S., Thomsen, C., Maultzsch, J.	Carbon Nanotubes	Guldi, D. M.	5877
Zollinger, H.	Color Chemistry	Langhals, H.	5291
Otera, J.	Esterification	Kocienski, P. J.	1183
Olah, G. A., Molnár, Á.	Hydrocarbon Chemistry	Schreiner, P. R.	1184
Gajewski, J. J.	Hydrocarbon Thermal Isomerizations	Hopf, H.	6025
Santos-Buelga, C., Williamson, G.	Methods in Polyphenol Analysis	Quideau, S.	393
Takeda, T.	Modern Carbonyl Olefination	Cornils, B.	3100
Gallego, M. G., Sierra, M. A.	Organic Reaction Mechanisms	Zipse, H.	4832
Hodgson, D. M.	Organolithiums in Enantioselective Synthesis	Goldfuss, B.	780
Chatgililoglu, C.	Organosilanes in Radical Chemistry	Clive, D. L. J.	4124
Davies, A. G.	Organotin Chemistry	Weidenbruch, M.	3753
Moss, R. A., Platz, M. S., Jones, M., Jr.	Reactive Intermediate Chemistry	Bucher, G.	3995
Rappoport, Z.	The Chemistry of Phenols	Waldvogel, S. R.	778

Monograph/Research Report in Physical/Theoretical Chemistry

Simons, J.	An Introduction to Theoretical Chemistry	Rinderspacher, B. C.	923
Brändas, E. J., Kryachko, E. S.	Fundamental World of Quantum Chemistry	Reiher, M.	3219
Puskas, J. E., Long, T. E., Storey, R. F.	In Situ Spectroscopy of Monomer and Polymer Synthesis	Abel, B.	1045
Reinhard, P.-G., Suraud, E.	Introduction to Cluster Dynamics	Hartke, B.	3099
Freeman, R.	Magnetic Resonance in Chemistry and Medicine	Gemmecker, G.	924
Trebin, H.-R.	Quasicrystals	Kreiner, G.	543
Schwerdtfeger, P.	Relativistic Electronic Structure Theory	Gagliardi, L.	2599
Buncel, E., Stairs, R., Wilson, H.	The Role of the Solvent in Chemical Reactions	Engberts, J. B. F. N.	2744

Monograph/Research Report in the History of Science

Kim, M. G.	Affinity, that Elusive Dream	Tomic, S., Vauthelin, P. M.	3362
Board on Chemical Sciences and Technologies	Beyond the Molecular Frontier Challenges for Chemistry and Chemical Engineering	Hopf, H.	394
Hargittai, I.	Candid Science III	Hopf, H.	1909
Cobb, C.	Magick, Mayhem, and Mavericks	Atkins, P.	1458

Monograph/Research Report on Catalysis

Baerns, M.	Basic Principles in Applied Catalysis	Nijhuis, X., Weckhuysen, B.	4979
Bommarius, A. S., Riebel, B. R.	Biocatalysis	Bornscheuer, U.	6584
Sen, A.	Catalytic Synthesis of Alkene–Carbon Monoxide Copolymers and Cooligomers	Bastero, A.	2880

Monograph/Research Report on Spectroscopic Methods

Pretsch, E., Tóth, G., Munk, M. E., Badertscher, M.	Computer-Aided Structure Elucidation	Bauer, W., Horn, A. H. C.	661
Gerson, F., Huber, W.	Electron Spin Resonance Spectroscopy of Organic Radicals	Korth, H.-G.	2469
Wartewig, S.	IR and Raman Spectroscopy	Reisenauer, H. P.	1761

Popular Science Book

Atkins, P.	Atkins' Molecules	Faust, R.	2059
American Chemical Society, Royal Society of Chemistry, Gesellschaft Deutscher Chemiker	Green Chemistry	Metzger, J. O.	660
Herbst, W., Hunger, K.	Industrial Organic Pigments	Erk, P.	4393
Atkinson, W. I.	Nanocosm	Zare, R. N.	3511
Doonan, S.	Peptides and Proteins	Beck-Sickinger, A. G.	2470

Text Book

Robson Wright, M.	An Introduction to Chemical Kinetics	Peeters, D.	6585
Hollas, J. M.	Basic Atomic and Molecular Spectroscopy	Smith, D.	5117
Metzler, D. E.	Biochemistry	Schwenzer, B., van Pée, K.-H.	1045
Nicolaou, K. C., Snyder, S. A.	Classics in Total Synthesis II	Fürstner, A.	20
Lewars, E. G.	Computational Chemistry	Berger, R.	4979
Parsons, A. F.	Keynotes in Organic Chemistry	Miltschitzky, S., König, B.	2196
Gross, J. H.	Mass Spectrometry	Hesse, M.	4552
Janes, B., Moore, E.	Metal–Ligand Bonding	Schindler, S.	4394
Butt, H.-J., Graf, K., Kappl, M.	Physics and Chemistry of Interfaces	Steinhart, M.	3510
Eicher, T., Hauptmann, S.	The Chemistry of Heterocycles	Nadin, A.	3876
Rao, C. N. R., Müller, A., Cheetham, A. K.	The Chemistry of Nanomaterials	Simon, U.	5723
Taylor, P., Gagan, M.	The Molecular World—Alkenes and Aromatics	Hopf, H.	6025

Websites

Biochemistry

Pohnert, G. 542

Crystallography

Bürgi, H.-B., Weber, T. 3098
Hoppe, D., Ruck, M. 6024

Environmental Chemistry

Fried, K. W., Lenoir, D. 2597

Gene sequencing

Petri, R., Schmidt-Dannert, C. 1908

Organic Chemistry

Engel, E., Kruppa, M., König, B. 6582

Muñiz, K. 2468

Spectroscopy

Schäfer, M., Schlörer, N. 2878

Obituaries

van Boeckel, C. A. A.	Biopolymers: <i>Jacques van Boom</i>	5288
Cladis, P. E., Ratna, B. R., Shashidar, R.	Discotic Liquid Crystals: <i>S. Chandrasekhar</i>	3360
Schiess, P.	Fragmentation and Inductivity: <i>Cyril A. Grob</i>	4392
Nakanishi, K., Danheiser, R. L.	Natural Products and Small Rings: <i>Saturo Masamune</i>	922
McMahon, R. J.	Organic Chemistry and Education: <i>Orville L. Chapman</i>	4122
Smith, J. D.	Organosilicon Compounds: <i>Colin Eaborn</i>	4978
Moroder, L.	Peptide Chemistry: <i>Murray Goodman</i>	3628
Olah, G. A.	Structure and Mechanism in Gas-Phase Chemistry and Its Relevance to the Condensed State: <i>Fulvio Cacace</i>	1760
Kutzelnigg, W.	Theoretical Chemistry: <i>H. C. Longuet-Higgins and J. A. Pople</i>	2740

Correspondences

Hoffmann, R.	A Claim on the Development of the Frontier Orbital Explanation of Electrocyclic Reactions	6586
Sachdev, H.	Diamonds from the Pressure Cooker—Science or Science Fiction?	4696
Ramanan, H., Kokkoli, E., Tsapatsis, M.	On the TEM and AFM Evidence of Zeosil Nanoslabs Present during the Synthesis of Silicalite-1	4558
Kirschhock, C. E. A., Liang, D., Aerts, A., Aerts, C. A., Kremer, S. P. B., Jacobs, P. A., Van Tendeloo, G., Martens, J. A.	Reply	4562
Lou, Z., Chen, Q.	Reply to Comment on “Growth of Large Diamond Crystals by Reduction of Magnesium Carbonate with Metallic Sodium”	4700
